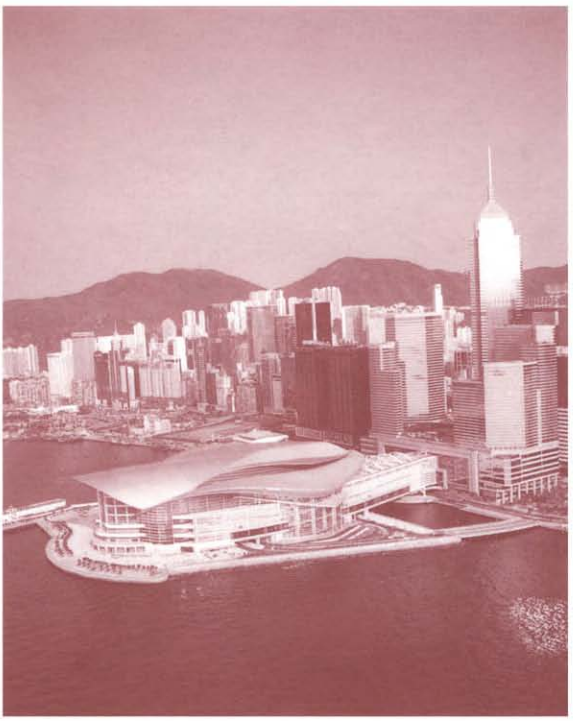
ADVANCES IN BUILDING TECHNOLOGY



A
B
T

2002

Volume I

edited by
M. Anson
J.M. Ko
E.S.S. Lam

ELSEVIER

ADVANCES IN BUILDING TECHNOLOGY

Proceedings of the
International Conference on Advances in Building Technology

4-6 December 2002, Hong Kong, China

Volume I

Elsevier Science Internet Homepage - http://www.elsevier.com

Consult the Elsevier homepage for full catalogue information on all books, journals and electronic products and services.

Elsevier Titles of Related Interest

CHAN & TENG
ICASS '99, Advances in Steel Structures.
(2 Volume Set). *ISBN: 008-043015-5*

FRANGOPOL, COROTIS & RACKWITZ
Reliability and Optimization of Structural Systems. *ISBN: 008-042826-6*

FUKUMOTO
Structural Stability Design.
ISBN: 008-042263-2

HOLLAWAY & HEAD
Advanced Polymer Composites and Polymers in the Civil Infrastructure.
ISBN: 008-043661-7

KELLY & ZWEBEN
Comprehensive Composite Materials.
ISBN: 008-042993-9

KO & XU
Advances in Structural Dynamics.
(2 Volume Set). *ISBN: 008-043792-3*

LUNDQUIST, LETERRIER, SUNDERLAND & MÅNSON
Life Cycle Engineering of Plastics: Technology, Economy and the Environment
ISBN: 008-043886-5

MAKELAINEN
ICSAS'99, Int. Conf. on Light-Weight Steel and Aluminium Structures.
ISBN: 008-043014-7

USAMI & ITOH
Stability and Ductility of Steel Structures.
ISBN: 008-043320-0

VASILIEV & MOROZOV
Mechanics and Analysis of Composite Materials. *ISBN: 008-042702-2*

WANG, REDDY & LEE
Shear Deformable Beams and Plates.
ISBN: 008-043784-2

Related Journals

Free specimen copy gladly sent on request. Elsevier Science Ltd, The Boulevard, Langford Lane, Kidlington, Oxford, OX5 1GB, UK

Advances in Engineering Software
CAD
Composites Part A: Applied Science and Manufacturing
Composites Part B: Engineering
Composite Structures
Computer Methods in Applied Mechanics and Engineering
Computers and Structures
Computer Science and Technology
Construction and Building Materials
Engineering Failure Analysis
Engineering Fracture Mechanics
Engineering Structures
International Journal of Fatigue
International Journal of Mechanical Sciences
International Journal of Solids and Structures
Journal of Constructional Steel Research
Mechanics of Materials
Mechanics Research Communications
Structural Safety
Thin-Walled Structures

To Contact the Publisher

Elsevier Science welcomes enquiries concerning publishing proposals: books, journal special issues, conference proceedings, etc. All formats and media can be considered. Should you have a publishing proposal you wish to discuss, please contact, without obligation, the publisher responsible for Elsevier's civil and structural engineering publishing programme:

Keith Lambert
Senior Publishing Editor
Elsevier Science Ltd
The Boulevard, Langford Lane
Kidlington, Oxford, OX5 1GB, UK

Phone: +44 1865 843411
Fax: +44 1865 843931
E.mail: k.lambert@elsevier.com

General enquiries, including placing orders, should be directed to Elsevier's Regional Sales Offices – please access the Elsevier homepage for full contact details (homepage details at the top of this page).

ADVANCES IN BUILDING TECHNOLOGY

Proceedings of the
International Conference on Advances in Building Technology

4-6 December 2002, Hong Kong, China

Volume I

Edited by
M. Anson
J.M. Ko
E.S.S. Lam
The Hong Kong Polytechnic University

Organized by
The Faculty of Construction and Land Use,
The Hong Kong Polytechnic University

Sponsored by
Hong Kong Institute of Construction Managers
The Association of Consulting Engineers of Hong Kong
The Hong Kong Construction Association Ltd.
The Hong Kong Institute of Architects
The Hong Kong Institution of Engineers



2002

ELSEVIER
Amsterdam – Boston – London – New York – Oxford – Paris
San Diego – San Francisco – Singapore – Sydney – Tokyo

ELSEVIER SCIENCE Ltd
The Boulevard, Langford Lane
Kidlington, Oxford OX5 1GB, UK

© 2002 Elsevier Science Ltd. All rights reserved.

This work is protected under copyright by Elsevier Science, and the following terms and conditions apply to its use:

Photocopying: Single photocopies of single chapters may be made for personal use as allowed by national copyright laws. Permission of the Publisher and payment of a fee is required for all other photocopying, including multiple or systematic copying, copying for advertising or promotional purposes, resale, and all forms of document delivery. Special rates are available for educational institutions that wish to make photocopies for non-profit educational classroom use.

Permissions may be sought directly from Elsevier Science via their homepage (http://www.elsevier.com) by selecting 'Customer Support' and then 'Permissions'.
Alternatively you can send an e-mail to: permissions@elsevier.com, or fax to: (+44) 1865853333.

In the USA, users may clear permissions and make payments through the Copyright Clearance Center, Inc., 222 Rosewood Drive, Danvers, MA 01923, USA; phone: (+1) (978) 7508400, fax: (+1) (978) 7504744, and in the UK through the Copyright Licensing Agency Rapid Clearance Service (CLARCS), 90 Tottenham Court Road, London W1P 0LP, UK; phone: (+44) 207 631 5555; fax: (+44) 207 631 5500. Other countries may have a local reprographic rights agency for payments.

Derivative Works: Tables of contents may be reproduced for internal circulation, but permission of Elsevier Science is required for external resale or distribution of such material. Permission of the Publisher is required for all other derivative works, including compilations and translations.

Electronic Storage or Usage: Permission of the Publisher is required to store or use electronically any material contained in this work, including any chapter or part of a chapter.

Except as outlined above, no part of this work may be reproduced, stored in a retrieval system or transmitted in any form or by any means, electronic, mechanical, photocopying, recording or otherwise, without prior written permission of the Publisher. Address permissions requests to: Elsevier Science Global Rights Department, at the mail, fax and e-mail addresses noted above.

Notice: No responsibility is assumed by the Publisher for any injury and/or damage to persons or property as a matter of products liability, negligence or otherwise, or from any use or operation of any methods, products, instructions or ideas contained in the material herein. Because of rapid advances in the medical sciences, in particular, independent verification of diagnoses and drug dosages should be made.

First edition 2002

Library of Congress Cataloging in Publication Data: A catalog record from the Library of Congress has been applied for.
British Library Cataloguing in Publication Data: A catalogue record from the British Library has been applied for.

ISBN: 0-08-044100-9 (2 volume set)

♾ The paper used in this publication meets the requirements of ANSI/NISO Z39.48-1992 (Permanence of Paper). Printed in the Netherlands.
The papers presented in these proceedings have been reproduced directly from the authors' 'camera ready' manuscripts. As such, the presentation and reproduction quality may vary from paper to paper.

PREFACE

The International Conference on Advances in Building Technology has been organized by the Faculty of Construction and Land Use, The Hong Kong Polytechnic University, and held in Hong Kong from December 4 to December 6, 2002. The Conference aims to provide an international forum for scientists, researchers, engineers, and other professionals to present and discuss recent research and advances in the design, construction and operation of our buildings.

The Conference also represents an initiative of a specially promoted Hong Kong Polytechnic University programme in Advanced Buildings Technology, a three-year programme which began in mid 1999. Although some hundreds of papers and reports have already been published by the Structural, Building Performance and Fire Safety Engineering teams, this Conference provides a technology transfer outlet in a more concentrated fashion for the programme as a whole.

These two volumes of proceedings contain 9 invited keynote papers, 72 papers delivered by 11 teams, and 132 contributed papers from over 20 countries around the world. These papers cover a wide spectrum of topics across the three technology sub-themes of structures and construction, environment and information technology. The variety within these categories is also wide and the Conference, therefore, provides the delegates with a good general oversight of building research advances, as opposed to the benefit, different in nature, to be gained from a specialist topic conference.

The organization of the Conference would not have been possible without the support and contributions of many individuals and organizations. We sincerely appreciate the support from the Hong Kong Institute of Construction Managers, The Association of Consulting Engineers of Hong Kong, The Hong Kong Construction Association Ltd., The Hong Kong Institute of Architects and The Hong Kong Institution of Engineers. We would like to thank the members of the International Advisory Committee for their valuable assistance, the Executive Committee, the Conference Organizing Committee, and all those who generously acted as referees. We also wish to express our gratitude to all the contributors for their careful preparation of the manuscripts. Thanks are also due to those who devoted time and effort to the organization of the Conference and publication of these Proceedings, including the secretarial staff and research students of the Faculty.

Finally, we gratefully acknowledge our pleasant cooperation with Mr. Ian Salusbury, Mr. Keith Lambert, Mrs. Lorna Canderton and Ms. Noël Blatchford of Elsevier Science Ltd. in the U.K.

M. Anson
J. M. Ko
E. S. S. Lam

This Page Intentionally Left Blank

INTERNATIONAL ADVISORY COMMITTEE

Prof. H. ADELI	The Ohio State University	*USA*
Prof. N. D. ANH	National Centre for Natural Science and Technology	*Vietnam*
Prof. C. J. ANUMBA	Loughborough University	*UK*
Prof. S. ARONI	University of California, Los Angeles	*USA*
Prof. V. ASHKENAZI	Nottingham Scientific Ltd.	*UK*
Prof. M. BETTS	The University of Salford	*UK*
Prof. B. C. BJÖRK	Swedish School of Economics and Business Administration	*Finland*
Prof. T. BOCK	Munich University of Technology	*Germany*
Prof. J. BRAUN	Purdue University	*USA*
Prof. F. CASCIATI	University of Pavia	*Italy*
Dr. J. C. S. CHANG	U.S. Environmental Protection Agency	*USA*
Prof. Y. K. CHEUNG	The University of Hong Kong	*HKSAR, China*
Prof. C. K. CHOI	Korea Advanced Institute of Science & Technology	*Korea*
Prof. K. P. CHONG	National Science Foundation	*USA*
Prof. L. L. CHRISTIANSON	University of Illinois	*USA*
Prof. A. CHRZANOWSKI	University of New Brunswick	*Canada*
Prof. A. G. DAVENPORT	The University of Western Ontario	*Canada*
Prof. A. L. DEXTER	University of Oxford	*UK*
Prof. M. EHLERS	University of Vechta	*Germany*
Prof. P. O. FANGER	Technical University of Denmark	*Denmark*
Dr. M. Q. FENG	University of California, Irvine	*USA*
Prof. J. W. FISHER	Lehigh University	*USA*
Prof. R. FLANAGAN	The University of Reading	*UK*
Prof. J. S. GERO	The University of Sydney	*Australia*
Prof. M. F. GOODCHILD	University of California, Santa Barbara	*USA*
Prof. P. L. GOULD	Washington University	*USA*
Prof. G. HANCOCK	The University of Sydney	*Australia*
Prof. M. HANNUS	Technical Research Centre of Finland-VTT	*Finland*
Prof. C. F. HENDRIKS	Delft University of Technology	*The Netherlands*
Dr. J. HODGE	Building Research Establishment Ltd.	*UK*
Prof. L. C. HOLLAWAY	University of Surrey	*UK*
Prof. T. Y. HSIEH	National Central University	*Taiwan, China*
Dr. Y. X. HU	China Seismological Bureau	*China*
Prof. G. L. HUTCHINSON	The University of Melbourne	*Australia*
Prof. Y. ITOH	Nagoya University	*Japan*
Prof. P. JONES	Cardiff University	*UK*
Dr. S. LACASSE	The Norwegian Geotechnical Institute	*Norway*
Prof. J. LEBRUN	University of Liège	*Belgium*
Prof. G. C. LEE	State University of New York at Buffalo	*USA*
Prof. D.R. LI	Wuhan University	*China*

Prof. V. C. LI	The University of Michigan	*USA*
Dr. S. C. LIU	National Science Foundation	*USA*
Prof. X. D. LIU	Huazhong University of Science and Technology	*China*
Prof. C. H. LOH	National Center for Research on Earthquake Engineering	*Taiwan, China*
Prof. L. W. LU	Lehigh University	*USA*
Prof. Q. LU	Research Institute of Tsinghua University in Shenzhen	*China*
Prof. D. McGEORGE	The University of New South Wales	*Australia*
Dr. A. MEIER	University of California, Berkeley	*USA*
Prof. U. MEIER	Swiss Federal Laboratories for Materials Testing and Research	*Switzerland*
Prof. S. MINDESS	University of British Columbia	*Canada*
Prof. J. W. MITCHELL	University of Wisconsin-Madison	*USA*
Prof. M. MOLENAAR	International Institute for Aerospace Survey and Earth Sciences	*The Netherlands*
Prof. S. NAGATAKI	Niigata University	*Japan*
Prof. A. NANNI	University of Missouri-Rolla	*USA*
Prof. S. NARAYANAN	Indian Institute of Technology, Madras	*India*
Prof. D. A. NETHERCOT	Imperial College	*UK*
Prof. B. PARK	University of Canterbury	*New Zealand*
Prof. J. RAFTERY	Oxford Brookes University	*UK*
Prof. A. Z. REN	Tsinghua University	*China*
Prof. S. P. SHAH	Northwestern University	*USA*
Prof. R. SHIBASAKI	The University of Tokyo	*Japan*
Prof. M. J. SKIBNIEWSKI	Purdue University	*USA*
Prof. G. SOLARI	University of Genova	*Italy*
Prof. T. T. SOONG	State University of New York at Buffalo	*USA*
Prof. B. F. SPENCER	University of Notre Dame	*USA*
Prof. Y. TAMURA	Tokyo Institute of Polytechnics	*Japan*
Prof. T. TANAKA	Kyoto University	*Japan*
Prof. J. H. TAY	Nanyang Technological University	*Singapore*
Prof. D. W. K. TSO	McMaster University	*Canada*
Prof. J. C. VISIER	Centre Scientifique et Technique du Batiment	*France*
Prof. G. Y. WANG	Harbin Institute of Technology	*China*
Prof. Y. Y. WANG	Institute of Earthquake Engineering	*China*
Prof. L. L. XIE	China Seismological Bureau	*China*
Prof. J. N. YANG	University of California, Irvine	*USA*
Prof. K. T. YANG	University of Notre Dame	*USA*
Prof. H. YOSHIDA	Kyoto University	*Japan*
Prof. X. T. ZHANG	Tongji University	*China*
Prof. Z. M. ZHANG	Beijing Geotechnical Institute	*China*
Prof. G. F. ZHAO	Dalian University of Technology	*China*

ORGANIZING COMMITTEE

Chairman :	**Prof. J. M. KO** The Hong Kong Polytechnic University
Secretary :	**Dr. E. S. S. LAM** The Hong Kong Polytechnic University
Members :	
Mr. F. S. Y. BONG	Maunsell Consultants Asia Ltd.
Mr. P. W. T. CHAN	The Hong Kong Construction Association Ltd.
Mrs. E. CHENG	Architectural Services Department, HKSAR Government
Mr. K. M. CHEUNG	Buildings Department, HKSAR Government
Dr. C. GIBBONS	Ove Arup & Partners Hong Kong Ltd.
Mr. M. HADAWAY	Gammon Skanska Ltd.
Mr. R. S. H. LAI	Electrical and Mechanical Services Department, HKSAR Government
Mr. D. H. M. LEE	Housing Department, HKSAR Government
Mr. P. K. W. MOK	Henderson Land Development Co. Ltd.
Mr. F. S. H. NG	Paul Y. – ITC Construction Holdings Ltd.
Mr. C. K. WONG	Meinhardt (Hong Kong) Ltd.
Mr. C. T. C. WONG	Yau Lee Construction Co. Ltd.
Mr. P. K. K. LEE	The University of Hong Kong
Prof. A. Y. T. LEUNG	The City University of Hong Kong
Prof. W. H. TANG	The Hong Kong University of Science and Technology
Prof. M. ANSON	The Hong Kong Polytechnic University
Prof. J. BURNETT	The Hong Kong Polytechnic University
Prof. Y. Q. CHEN	The Hong Kong Polytechnic University
Prof. Y. S. LI	The Hong Kong Polytechnic University
Prof. W. SEABROOKE	The Hong Kong Polytechnic University
Dr. A. K. D. WONG	The Hong Kong Polytechnic University
Prof. F. W. H. YIK	The Hong Kong Polytechnic University

EXECUTIVE COMMITTEE

Chairman :	**Prof. M. ANSON** The Hong Kong Polytechnic University
Members :	
Prof. W. K. CHOW	The Hong Kong Polytechnic University
Dr. E. S. S. LAM	The Hong Kong Polytechnic University
Dr. E. C. M. MOK	The Hong Kong Polytechnic University
Prof. C. S. POON	The Hong Kong Polytechnic University
Prof. W. SEABROOKE	The Hong Kong Polytechnic University
Dr. J. W. Z. SHI	The Hong Kong Polytechnic University
Dr. A. K. D. WONG	The Hong Kong Polytechnic University
Prof. F. W. H. YIK	The Hong Kong Polytechnic University

CONTENTS

Volume I

Preface v

International Advisory Committee vii

Organizing Committee ix

Executive Committee x

KEYNOTE PAPERS

Advances in Materials and Mechanics 3
K.P. Chong, M.R. VanLandingham and L. Sung

Advances in Concrete Technology 17
M.F. Cyr and S.P. Shah

Human Requirements in Future Air-Conditioned Environments 29
P.O. Fanger

Creating Competitive Advantage and Profits with Technology in the Construction Sector 39
R. Flanagan

Advances in IT for Building Design 47
J.S. Gero

Information Technology Support to Improved Construction Processes: Inter-Disciplinarity in Research and Practice 55
A. Marshall-Ponting, A. Lee, M. Betts, G. Aouad, R. Cooper and M. Sexton

Recent Topics in Wind Engineering Focusing on Monitoring Techniques 65
Y. Tamura and M. Matsui

A Conception of Casualty Control Based Seismic Design for Buildings 75
L-L. Xie

Thermal Radiation Effects and Their Determination in Room Fires 83
K.T. Yang

TEAM PRESENTATION

Advances in Panel Systems

Wood Frame Shear Walls with Metal Plate Connected Framework 97
R.N. Emerson

Toward Engineering Design of Gypsum Board Fire Barriers 105
O.M. Friday and S.M. Cramer

Barrier Materials to Reduce Contaminant Emissions from Structural Insulated Panels 113
J.C. Little, D. Kumar, S.S. Cox and A.T. Hodgson

Novel Microcellular Plastics for Lightweight and Energy Efficient Building Applications 121
K. Nadella, V. Kumar and W. Li

Long-Term Creep Response of Borate-Modified Oriented Strandboard 129
Q. Wu and J.N Lee

Mechanical, Physical, and Biological Properties of Borate-Modified Oriented Strandboard 137
Q. Wu, S. Lee and J.N. Lee

Commissioning and Energy Management

Re-commissioning of an Air Handling Unit 147
C. Cuevas, J. Lebrun, P. Lacôte and P. Andre

Automated Commissioning of Air-Handling Units Using Fuzzy Air Temperature Sensors 157
P.S. Lee and A.L. Dexter

Modeling of Package Air-Conditioning Equipment 165
M. Reichler, J.W. Mitchell and W.A. Beckman

Automatic Diagnosis and Commissioning of Central Chilling Systems 173
S.W. Wang

Composite Construction

Design of Simply-Supported and Continuous Beams in Steel-Concrete Composite Construction 183
P.A. Berry and M. Patrick

Innovations in Composite Slabs Incorporating Profiled Steel Sheeting 191
R.Q. Bridge and M. Patrick

Web-Side-Plate Framing Connections in Both Steel and Composite Construction 199
M. Patrick, P.A. Berry and A.T. Wheeler

Novel New Reinforcing Components for Composite Beams 207
M. Patrick and R.Q. Bridge

The Influence of Material Properties on the Local Buckling of Concrete Filled Steel Tubes 215
A. Wheeler and M. Pircher

Composites for Housing

Low-Cost, Bio-Based Composite Materials for Housing Applications 225
L.T. Drzal, A.K. Mohanty, G. Mehta and M. Misra

Durability of Pulp Fiber-Cement Composites to Wet/Dry Cycling 233
N.H. El-Ashkar, B. Mohr, H. Nanko and K.E. Kurtis

Extruded Fiber-Reinforced Composite 239
B. Mu, M.F. Cyr and S.P. Shah

Reversed In-Plane Cyclic Behavior of Post-Tensioned Clay Brick Masonry Walls for High Performance Modular Housing 247
O.A. Rosenboom and M.J. Kowalsky

An All-Natural Composite Material Roof System for Residential Construction 255
H.W. Shenton III, R.P. Wool, B. Hu, A. O'Donnell, L. Bonnaillie, E. Can, R. Chapas and C. Hong

Comparison of Optimal Designs for Stick-Frame Wall Assemblies of Different Bay Sizes 263
S. Van Dessel, A. Ismail-Yahaya and A. Messac

Earthquake Resistant Theory and Applications

A Macro-Model of RC Shear Wall for Push-Over Analysis 273
Q. Chen and J.R. Qian

Torsional Effect of Asymmetric R/C Building Structure 281
J. Dai, Y-L. Wong and M.Z. Zhang

Experimental Investigation on Axial Compressive Behavior of FRP Confined Concrete Columns 289
J. Li, J.R. Qian, and J.B. Jiang

Dynamic Properties and Seismic Response of RC Structures Characterized by Abrupt Change in Horizontal Connection Stiffness 297
J.B. Liu and Z.Y. Wang

A GIS System Integrated with Vulnerability for Seismic Damage and Loss Estimation of Hong Kong 303
H.S. Lu, Z.P. Wen, K.T. Chau and Y.X. Hu

Rules of Drift Decomposition and Drift-Based Design of RC Frames 311
W.B. Luo and J.R. Qian

Seismic Fragility Curves for Wind-Designed-Buildings in Hong Kong 319
Z.P. Wen, K.T. Chau and Y.X. Hu

A Preliminary Study of Structural Semiactive Control Using Variable Dampers 327
R.L. Yang, X.Y. Zhou and X.H. Liu

Flexible Manufacturing System in Construction

Dynamic Monitoring of the Boring Trajectory in Underground Channel for Driving Communications 335
A. Bulgakow, D. Krapivin, S. Aleksyuk and S. Pritchin

Façade Cleaning Robot 339
T. Bock, A. Bulgakow and S. Ashida

Advanced Construction Design and Technology by Robotics 343
T. Bock and K. Kreupl

Embedded System and Augmented Reality in Facility Management 351
T. Bock, H. Meden and S. Ashida

Robots for Location and Spacing of Wood 355
T. Bock, D. Parshin and A. Boulgakov

Assembly and Disassembly of Interior Wall 361
A. Hanser

MUNITEC-Fast-Connectors – Key Technology for Prefab Houses 367
F. Prochiner

Industrialized Housing

Initial Thoughts on Industrialised Solution for Low-Cost Housing in China's Rural Area 375
K. Guan and S.R. Li

Industrialized Housing Construction – The UK Experience 383
R. Howes

A Perspective of Industrialised Housing in Chongqing 391
S.R. Li

Impact on Structure of Labour Market Resulting from Large-Scale Implementation of Prefabrication 399
C.M. Tam

Priority Setting of Preferential Parameters for Home Purchase in Chongqing – An Analytic Hierarchy Process Approach 405
K.W. Wong and M. Wu

Research at the ATLSS Center on New Materials and Systems to Resist Earthquakes and Wind

Steel Moment Frame Connections that Achieve Ductile Performance 415
J.W. Fisher, J.M. Ricles, L.W. Lu, C. Mao and E.J. Kaufmann

Lateral Load Behavior of Unbonded Post-Tensioned Precast Concrete Walls 423
F.J. Perez, R. Sause, S. Pessiki and L.-W. Lu

Design of High Strength Spiral Reinforcement in Concrete Compression Members 431
S. Pessiki, B. Graybeal and M. Mudlock

Modelling and Behavior of Composite MRFs with Concrete Filled Steel Tubular Columns Subject to Earthquake Loading 439
J.M. Ricles, R. Sause, T. Muhummud and R. Herrera

The Use of Post-Tensioning to Reduce Seismic Damage in Steel Frames 447
J.M. Ricles, R. Sause, P. Rojas and M.M. Garlock

Smart Structures for Dynamic Hazard Mitigation

Stochastic Approach to Control and Identification of Smart Structures 457
J.L. Beck and K.-V. Yuen

Building Hazard Mitigation with Piezoelectric Friction Dampers 465
G.D. Chen and C.Q. Chen

A Research and Development of Smart Building Structures by Magneto-Rheological Damper 473
H. Fujitani, Y. Shiozaki, T. Hiwatashi, K. Hata, T. Tomura, H. Sodeyama and S. Soda

Structural Health Monitoring System Using Support Vector Machine 481
H. Hagiwara and A. Mita

Performance of Structures with Passive Dampers Subject to Near-Fault Earthquakes 489
W.L. He and A.K. Agrawal

Reliability and Control Performance Verification of an Actual Semi-Active Structural Control System 497
N. Kurata

Hybrid Response Control of Closely Spaced Buildings 505
G.C. Lee, M. Tong and Y.H. Wu

Model Testing of a Nonlinear Base Isolation Concept 513
D.M. McFarland, Y.M. Wang, A.F. Vakakis and L.A. Bergman

Risk Control of Smart Structures Using Damage Index Sensors 521
A. Mita and S. Takahira

Seismic Protection of Base-Isolated Structures Using Semi-Active MR Dampers 529
T. Tse and C.C. Chang

Semi-Active TLCDS using Magneto-Rheological Fluids for Vibration Mitigation of Tall Buildings 537
J.Y. Wang, Y.Q. Ni, J.M. Ko and B.F. Spencer, Jr.

Phenomenological Model of Large-Scale MR Damper Systems 545
G. Yang, B.F. Spencer, Jr., H.J. Jung and J.D. Carlson

Structural Analysis Research at the Beijing Polytechnic University

The Practical Anti-Earthquake Optimum Design of Civil Infrastructure Network System 555
Y.Y. Chen and G.Y. Wang

Earthquake Analysis of Arch Dam with Joints Including Dam-Foundation Rock Nonlinear Dynamic Interaction 563
X.L. Du and J. Tu

Earthquake Analysis of Arch Dam Including Dam-Foundation Rock Nonlinear Dynamic Interaction 571
X.L. Du, B.Y. Zhang, J. Tu and Y.H. Zhang

Stability Analysis of Large Complicated Underground Excavations 579
L.J. Tao, P.F. Li, Z.Y. Zhang, L.H. Zhang and X.L. Li

Evaluation of Ground Vibration Induced by Subway 587
L.J. Tao, X.L. Li and D.S. Zhang

Nonstationary Response of Spatial Lattice Shells Under Multiple Seismic Inputs 595
X.S. Wang, S.D. Xue and Z. Cao

Interaction Between Pile and Raft in Piled Raft Foundation 603
W.J. Wu, J.C. Chai and J.Z. Huang

The Method of Calculating the Interior Force of Soil Nails and Case Analysis 611
Q.X. Zhang, J.R. Yang and D. Huo

Structural Bamboo and Bamboo Scaffolding in Building Construction

Stability of Modular Steel Scaffolding Systems – Theory and Verification 621
A.Y.T. Chu, S.L. Chan and K.F. Chung

Recent Developments on Bamboo Scaffolding in Building Construction 629
K.F. Chung, S.L. Chan and W.K. Yu

Reliability Analysis for Mechanical Properties of Structural Bamboo 637
M. Lu, W.K. Yu and K.F. Chung

Erection of Bamboo Scaffolds and Their Recent Developments 645
F. So

Structural Design of the Bamboo Pavillion, Berlin 653
D.G. Vesey

Full Scale Tests of Bamboo Scaffolds for Design Development Against Instability 661
W.K. Yu, K.F. Chung and Y.C. Tong

CONSTRUCTION TECHNOLOGIES

Construction Technologies/Plants

Causes of Lumps and Balls in High Slump Truck-Mixed Concrete: An Experimental Investigation 671
I. Ahmad, S. Azhar and I.R. Canino

Advances in Concrete Placement Methods and Finishing Techniques for High Performance Industrial Pavements in Australia 679
P. Ashford

Review of Design and Construction Innovations in Hong Kong Public Housing 687
D.W.M. Chan and A.P.C. Chan

Static Loading Test of a Self-Balanced Approach to a Pile in the Yangtze River 695
G.L. Dai, W.M. Gong, L. Ji and Q.Z. You

The Design and Construction of Two International Finance Centre Hong Kong Station 703
C. Gibbons, A.C.C. Lee, J.M. MacArthur and C-W. Wan

The Construction of Deep and Complex Basements Under Extremely Difficult Urban Environment – 3 Representing Projects in Hong Kong 713
R.W.M. Wong

Novel Three-Step Consolidation Method to Eliminate Foundation Soil Liquefying 723
M. Xie and Z.X. Xie

Earthquake Engineering

Testing of a Transfer Plate by Pseudo-Dynamic Test Method with Substructure Technique 731
A. Chen, C.S. Li, S.S.E. Lam and Y.L. Wong

Seismic Design and Inelastic Seismic Response of Lumped Mass MDOF Dual Structure 739
J. Jing, L.P. Ye and J.R. Qian

Seismic Assessment of Low-Rise Building with Transfer Structure 747
J.H. Li, R.K.I. Su, A.M. Chandler and N.T.K. Lam

Ultimate Drift Ratio of Non-Ductile Coupling Beams 755
Z.Q. Liu, S.S.E. Lam, B. Wu and Y.L. Wong

Effect of Uncertain Evolutionary PSD Function of Seismic Excitation on Peak Response of MDOF Systems 763
S.S. Wang and H.P. Hong

Simplified Method and Parametric Sensitivity Analysis for Soil-Pile Dynamic Interaction Under Lateral Seismic Loading 771
X.C. Xiao, S.C. Chi, G. Lin and J. Alfano

FRP Composite, Retrofit and Repair Technologies Engineering

FRP Reinforced ECC Structural Members Under Reversed Cyclic Loading Conditions 781
G. Fischer and V.C. Li

Ultimate Axial Strain of FRP-Confined Concrete 789
L. Lam and J.G. Teng

Effect of Size on the Failure of FRP Strengthened Reinforced Concrete Beams 797
C.K.Y. Leung, Z.F. Chen, S.K.L. Lee and J.M. Tang

Analytical Behaviour of Concrete Beams Reinforced with Steel Rebars and FRP Rods 803
H.Y. Leung, S. Kitipornchai, R.V. Balendran and A.Y.T. Leung

Application of GFRP Rebar in Civil Structures 811
Z.J. Li and Z.J. Zhang

A Generic Structural Engineering Approach to Retrofitting RC Beams in Buildings by Adhesive Bonding Longitudinal Plates 819
D.J. Oehlers and R. Seracino

Efficiency of Strengthened R.C. Columns 827
M.A. Tahir

Rehabilitation of Reinforced Concrete Columns be External Plate Bonding 835
B. Uy

High Performance Concrete/Composites

Numerical Simulation of Thermal Cracking of Cement-Based Multi-Inclusion Composite 845
Y.F. Fu, Y.L. Wong, C.A. Tang and C.S. Poon

Applications of Copper Gangue with High Content of Fe_2SiO_4 as Cement Admixture and for Cement Production 853
Z.S. Lin, H.W. Wan, Q. Zhao and Y. Huang

Properties of Lightweight Aggregate for Lightweight Concrete Production 859
T.Y. Lo and H.Z. Cui

Preliminary Results on the Use of GFRP as an External Reinforcement for Autoclaved Aerated Concrete 865
A.M. Memari and A. Eminaga

High Performance Fibre Reinforced Concrete 873
S. Mindess and A.J. Boyd

Differential Scanning Calorimetry Study of the Hydration Products in Portland Cement Pastes with Metakaolin Replacement 881
W. Sha

Ultimate Moment Equation of Circular HSC Members 889
Y. Sun and K. Sakino

Performance Test of a Model for Predicting Strength Development of Fly Ash-Concrete 897
M.A. Tahir and P. Nimityongskul

Mixture Design for High-Performance Concrete for Slip-Form Pavement in Jiangxi Provincial National Highway 323 905
S.P. Wu, M.K. Zhou, M. Zeng and Z.X. Ouyang

Advances in the Study of Fatigue Behavior of High Performance Concrete in China 913
J-Z. Xiao and D-Y. Chen

High Performance Polymer Concrete 921
R.Y. Xiao and C.S. Chin

Study on Phosphogypsum Fly Ash Lime Solidified Material 929
M.K. Zhou, W.G Shen, S.P. Wu and Q.L. Zhao

Volume II

Preface v

International Advisory Committee vii

Organizing Committee ix

Executive Committee x

CONSTRUCTION TECHNOLOGIES (CONTINUED)

Monitoring Technologies, Damage Detection and Vibration Control

On the Local Optimal Control Counterforces in Active Controlled Structures 937
N.D. Anh and L.D. Viet

Vibration Control Elements with Advanced Cementitious Composites 945
H. Fukuyama and H. Suwada

Seismic Damage Evaluation of a 38-Storey Building Model Using Measured FRF Data Reduced Via Principal Component Analysis 953
J.M. Ko, X.T. Zhou and Y.Q. Ni

Towards Next Generation Seismic Isolation Technology 961
G.C. Lee and Z. Laing

Semi-Active Damping Device for Vibration Control of Buildings Using Magnetorheological Fluid 969
J.H.K. Lee, R.K.L. Su, P.K.K. Lee and L.C.H. Lam

Hybrid Platform for High Tech Equipment Against Traffic-Induced Vibration 977
H.J. Liu, Z.C. Yang and Y.L. Xu

Seismic Control of Adjacent Buildings Using Fluid Dampers: Experimental Study 985
X.L. Lu, Y.L. Xu and Z. Yang

Seismic Response Control of Multi-Story Buildings Using Semiactive Friction Dampers 993
C.L. Ng and Y.L. Xu

A Design of Bridge Structure Health Monitoring and Management System Based on Three-Dimensional GIS Model 1001
W.Z. Shi, P.G. Cheng, J.M. Ko and J.Y. Gong

Seismic Design Method of Structures with Active Variable Stiffness Systems 1009
B. Wu, F.T. Liu and D.M. Wei

Damage Detection of a Health Monitoring Benchmark Building Using Hilbert-Huang Spectral Analysis 1017
J.N. Yang, S. Lin and S.W. Pan

Parameter Optimization of Multi-TMDS for Wind-Excited Vibration Suppression of Tall Buildings 1025
G. Zheng, Y.Q. Ni, H. Li and Y.F. Duan

Structural Systems and Design

Steel Joists for Cost Effective Flooring System 1035
M. Aladesaye, A.M. Al-Jumaily and B. Coubray

Analysis Plane Steel Frame with Semi-Rigid Connections and Rigid-Zones with Consideration of the Second Order Effect 1043
V.Q. Anh

Post-Tensioned Concrete Floor Systems in Australia 1051
A. Charalambous, P. Ashford and R.B. Sandie

High-Tech or Mock-Tech: Structural Rationality of the High-Tech Movement in Building 1059
J.G.A. Croll

The Gammon Skanska Construction System 1073
T. Lawton, P. Moore, K. Cox and J. Clark

The Development of Factory Produced Housing 1081
J. Miles, D. Badger, J. Rose, P. Geeson and P. Donelan

Recent Research on Steel-Concrete Composite Shell Roofs 1091
J.G. Teng, H.T. Wong, Z.C. Wang and S.L. Dong

Effect of the Shear Wall Cutoff on Storey Drifts of Frame-Shear Wall Structures 1099
Q.F. Wang

Wind Engineering

Hilbert-Huang Transform for Damping Ratio Identification of Structures with Closely Spaced Modes of Vibration 1107
J. Chen and Y.L. Xu

Application of HHT Method to System Identification of Di Wang Building During Typhoon York 1115
S.W. Chen, Y.L. Xu, R.C. Zhang and G.Q. Li

Discussion on Dynamic Coefficients for Wind-Resistant Design in Single-Layer Reticulated Shells 1123
Y.Q. Li

Wind Modeling in *BLWT* and Discussion on Several Problems 1131
Y.Q. Li, Y. Tamura, A. Yoshida and A. Katsumura

Wind-Induced Dynamic Response and Wind Load Factor for Flexible Roof Structures with Medium Deformation 1139
W.J. Lou, F. Lu and B.N. Sun

The Effects of Wind-Induced Dynamic Response by Added Air Mass for Membrane Structures 1147
B.N. Sun, J.M. Wang and W.J. Lou

ENVIRONMENTAL TECHNOLOGIES

Advanced Performance Modelling

Parametrization Study on the Operating Efficiency of Air-Cooled Chillers 1157
K.T. Chan and F.W. Yu

The Design of Highly Glazed Facades and Their Environmental Impact 1165
P. Jones

Local Study of the Influence of a Numerical Thermal Manikin of the Air Flow Pattern and Temperature Field of a Space 1173
K. Kippenberg-Kretzer and P. Jones

Validation of the Simulation Models of the Double Skin Façade 1181
W.J. Stec and A.H.C. van Paassen

Modelling of a Close-Coupled Photovoltaic Heat Pump 1189
C.P. Underwood and A.D. Jones

Analysis of Natural Ventilation Effect for an Office Building Considering Moisture Absorption by Materials 1199
H. Yoshida and T. Kono

Energy /Water Conservation in Buildings

Friendly Interface and Data Transfer for Engineering Assessment of Building Design Options at Sketch Design Stage "*EnergySave*" 1209
A. Bennadji, N.M. Bouchlaghem, D. Loveday, M. Holmes, J. Shaffery, R. van Zyl and A. Hallam

The Development of a Proto-Type PV Deck-Shading System as Thermal Buffer and Electricity Generator 1217
J. Close, K.H. Lam and Y.H. Wong

Integration of Double Façades and Ventilation Systems in Buildings 1225
F. Di Maio and A.H.C. van Paassen

Mechanically Ventilated Double Skin Façades 1233
M. Kragh

Case Studies of the Application of Innovative Energy-Efficient Equipment in Buildings 1241
C.K. Lee, K.K. Lam and M.K.T. Wu

A Dynamic Model of Commercial Gas and Oil Burned Boilers 1249
Z. Liao and F. Parand

Low Energy Building Materials: An Overview 1257
A.M. Omer

Building HVAC Systems Economic Performance Evaluation Using Neural Network Method at Beginning of Design 1265
F.L. Wang, Y. Jiang and H. Yoshida

A Review of Research Concerning the Use of PCMS in Air Conditioning and Refrigeration Engineering 1273
F.Q. Wang, G. Maidment, J. Missenden and R. Tozer

Water and Energy Conservation of Rainwater Collection Systems on Building Roofs 1281
H.X. Yang, W.H. Chow and J. Burnett

The Influence of Envelope Characteristics to the Energy Behaviour of High-Rise Residential Buildings 1289
F. Yik, M. Bojic and K. Wan

Total Optimal Operation for HVAC System with Heat Source and Distribution System 1297
H. Yoshida, Y. Iguchi, I. Matsuoka and F.L Wang

Model-Based Fault Detection and Diagnosis on an Office Room 1305
B. Yu, A.H.C. van Paassen and S. Riary

The Applications of Solar Heat Transfer and Solar Electricity Transfer in Building 1313
W. Zhang and H.Z. Yuan

Fire Safety Engineering

Intumescent Fire Protection Coating Thickness for Shallow Floor Beams 1321
W. Sha and T.M. Chan

Indoor Environmental Control

The Airflow Around and Inside High-Rise Residential Buildings in Hong Kong 1331
M. Bojic, F. Yik and J. Burnett

Building Ventilation 'Health' Checks 1339
P. Jones

Application of Titanium Dioxide in Refuse Collection Point 1345
K.F. Lau, A.M.T. Suen and A.C.C. Tang

The Measurement of Surface Mass Transfer Coefficients in a Standard FLEC 1351
J.L. Niu, L.Z. Zhang and T.K. Wan

Comparison of Summer and Winter Thermal Environment in Traditional Vernacular Houses in Several Areas of Nepal 1359
H.B. Rijal and H. Yoshida

Maximizing the Ventilation Rate for Cooling Energy Reduction 1367
M. Udagawa and H. Roh

Thermal Indoor Climate as a Building Performance 1375
A.C. van der Linden, A.C. Boerstra and S.R. Kurvers

Improvements of Indoor Humidity Performance by a Novel Air-Conditioning Scheme: Chilled-Ceiling Combined with Desiccant Cooling 1383
L.Z. Zhang and J.L. Niu

Recycling Technologies

The Eco-Costs/Value-Ratio 1391
Ch.F. Hendriks, G.M.T. Janssen and J. Vogtländer

Sustainable Use of Recycled Materials in Building Construction 1399
G.M.T. Janssen and Ch.F. Hendriks

Strength of Concretes Prepared with Natural and Recycled Aggregates at Different Moisture Conditions 1407
C.S. Poon, Z.H. Shui and L. Lam

Clay-Brick Recovery from Masonry Debris by Means of a Thermal Process 1415
K. van Dijk, A. Fraaij, Ch.F. Hendriks and E. Mulder

Effective Wastewater Treatment / Recycling Technologies for Construction Industry: A Local Experience 1423
K.S.W. Wong

Balance Theory for Recycling of Construction and Demolition Wastes 1431
E.O.W. Wong and R.C.P. Yip

Improve the Quality of Construction and Demolition Waste by Separation Techniques 1439
W. Xing, H. Pietersen, Ch.F. Hendriks and P. Rem

Sustainable Building

Sustainable Bearing Structures 1449
M.J.P. Arets and A.A.J.F. van den Dobbelsteen

Delivering Sustainability Throughout the Building Process: A Study of the UK Cement and Concrete Sector 1457
J. Glass and D.N. Pocklington

Service Life Planning: Definition of Client Requirements 1467
R. Hooper, K. Bourke, J. Prior and D. Richardson

Innovations in the Design of Housing Developments in Hong Kong 1475
J.N. Horsfield, C. Gibbons, R.M.H. Yau and T.F.C. Ip

Life-Cycle Analysis and Environmental Impact Assessment of Heating and Air-Conditioning Systems 1485
M. Prek

Quantitative Evaluation of the Effects of Built-Up Geometry and Trees on Diurnal Air Temperature in Canyon-Type Courtyards 1493
L. Shashua-Bar and M.E. Hoffman

Sustainability Needs More Than Just Smart Technology 1501
A.A.J.F. van den Dobbelsteen, A.C. van der Linden and D. Klaase

Defining the Reference for Environmental Performance 1509
A.A.J.F. van den Dobbelsteen, A.C. van der Linden and C.M. Ravesloot

INFORMATION TECHNOLOGIES

Building Process Integration/Coordination

Constructing the Future 1519
T.W. Broyd

Engineering Performance Improvement Using a Hybrid Artificial Intelligence System 1527
L.M. Chang and L. Zhang

Life-Cycle Integrated Management Information System (LMIS) of Construction Project 1535
Q.H. He

Information Reuse Mechanism for a Management Information System: EPIMS 1543
Z.L. Ma, J. Yang and I. Yoshito

Mobile Communications – The Next Great Modifier of Our Homes, Workplaces and Cities 1551
B. Southwood

Online Remote Construction Management (ORCM) 1559
A. Weippert, S.L. Kajewski and P.A. Tilley

Computer-Aided-Construction-Management, A New Paradigm 1569
C.T.C. Wong, H. Mak and H. Li

Raised Floor System: A Paradigm of Future Office Building Fitout? 1577
G. Zhang, J. Yang and A.C. Sidwell

Graphics and Virtual Reality Applications

A New 3D Reconstruction Technique and Its Application in Measuring Building Quantities 1587
Y. Cao and H. Li

Virtual Planning Environment Based on Internet 1595
N.C. Chen, J.Y. Gong and D.R. Li

Modeling of Complicated Structures in a Virtual Reality Environment 1601
A.Z. Ren, Y. Wen, S.G. Li and Y. Xu

GIS/GPS Applications

A New Generation of Multi-Antenna GPS System for Landslide and Structural Deformation Monitoring 1611
X.L. Ding, D.F. Huang, J.H. Yin, Y.Q. Chen, C.K. Lau, Y.W. Yang, Y.R. Sun and W. Chen

Ultra High Resolution Remote Sensing for Urban Information Systems and 3D City Modeling 1619
M. Ehlers, J. Schiewe and M. Möller

Data Model and 3D Visualization of Underground Pipeline 1629
Q.Q. Li, Y. Yan, B.S. Yang and X.H. Hua

A Fast GPS-Based System for Survey Check of Road Alignments 1637
E. Mok

GPS Navigation and Guidance Systems for Construction Industry 1645
G. Retscher and E. Mok

The Use and Future Potential of GIS Based Approaches to Building Design and Building Management 1653
M.I. Wallace, V. Lau and C. Gibbons

An Integrated System for Slope Monitoring and Warning in Hong Kong 1661
J.H. Yin, X.L. Ding, Y.W. Yang, C.K. Lau, D.F. Huang and Y.Q. Chen

Project Management Support Systems

Decision Model for the Selection of Demolition Techniques 1671
A. Abdullah and C.J. Anumba

Developing an Expert System for Project Procurement 1681
A.P.C. Chan

Support System for Project Management and Production of Concrete Precast Elements 1689
E. Dassori and M. Frasani

A Survey Management System for Advanced Building Construction 1697
S.Y.W. Lam and C.H.W. Tang

Characterize Concrete Demand in Bored-Pile Construction Through Simulation 1705
M. Lu and K.C. Ying

Agent-Based Specification and Procurements of Construction Products 1713
E.A. Obonyo, C.J. Anumba and A. Thorpe

IVMS – An Interactive System for Improving Value Management Studies in Construction 1721
Q.P. Shen and J.K.H. Chung

Productivity Excellence Through an Integrated Construction Management System for the Building and Construction Industries 1729
P. Yan

4D-CSCW Modeling for Construction Management 1737
J.P. Zhang, M. Cao and A.Z. Ren

The Implementation of Knowledge Management and Organisational Learning in Construction Company 1745
P.X.W. Zou and C-A. Lim

A Prototype of Knowledge-Based Decision Support System for Construction Cost Management 1755
P.X.W. Zou and C.C.X. Wang

Index of Contributors I1

Keyword Index I5

This Page Intentionally Left Blank

KEYNOTE PAPERS

This Page Intentionally Left Blank

Advances in Building Technology, Volume 1
M. Anson, J.M. Ko and E.S.S. Lam (Eds.)
© 2002 Elsevier Science Ltd. All rights reserved

ADVANCES IN MATERIALS AND MECHANICS

K. P. Chong[1-2], M. R.VanLandingham[2], and L. Sung[2]

[1]Directorate for Engineering, National Science Foundation
Arlington, VA 22230, U.S.A.
[2]National Institute of Standards and Technology,
Gaithersburg, MD 20899, U.S.A.

ABSTRACT

Mechanics and materials are essential elements in all of the transcendent technologies that are the primary drivers of the twenty first century and in the new economy. The transcendent technologies include nanotechnology, microelectronics, information technology and biotechnology as well as the enabling and supporting civil infrastructure systems and materials. Research opportunities and challenges in mechanics and materials, including nanomechanics, microscopy, radiation scattering and other nanoscale metrologies, as well as improved engineering and design of materials in the exciting information age are presented and discussed.

KEYWORDS

Atomic force microscope, biotechnology, designer materials, durability, information technology, nanomechanics, nanotechnology, microelectronics, confocal microscopy, multi-scale modeling, scattering metrology, simulations.

INTRODUCTION

The National Science Foundation (NSF) has supported basic research in engineering and the sciences in the United States for a half century and it is expected to continue this mandate through the next century. As a consequence, the United States is likely to continue to dominate vital markets, because diligent funding of basic research does confer a preferential economic advantage (Wong, 1996). Concurrently over this past half century, technologies have been the major drivers of the U. S. economy, and as well, NSF has been a major supporter of these technological developments. According to the former NSF Director for Engineering, Eugene Wong, there are three *transcendental* technologies:

- Microelectronics – Moore's Law: doubling the capabilities every two years for the last 30 years; unlimited scalability; nanotechnology is essential to continue the miniaturization process and efficiency.
- Information Technology [IT] – NSF and DARPA started the Internet revolution about three decades ago; the confluence of computing and communications.
- Biotechnology – unlocking the molecular secrets of life with advanced computational tools as well as advances in biological engineering, biology, chemistry, physics, and engineering including mechanics and materials.

Efficient civil infrastructure systems as well as high performance materials are essential for these technologies. By promoting research and development at critical points where these technological areas intersect, NSF can foster major developments in engineering. The solid mechanics and materials engineering (M&M) communities will be well served if some specific linkages or alignments are made toward these technologies. Some thoughtful examples for the M&M communities are:

- Bio-mechanics/materials
- Thin-film mechanics/materials
- Wave Propagation/NDT
- Nano-mechanics/materials
- Simulations/modeling
- Micro-electro-mechanical systems (MEMS)
- Smart materials/structures
- Designer materials

Considerable NSF resources and funding will be available to support basic research related to these technologies. These opportunities will be available for the individual investigator, teams, small groups and larger interdisciplinary groups of investigators. Nevertheless, most of the funding at NSF will continue to support unsolicited proposals from individual investigator on innovative "blue sky" ideas.

The National Institute of Standards and Technology, or NIST, is a non-regulatory federal agency within the U. S. Commerce Department's Technology Administration. NIST's mission is to develop and promote measurements, standards, and technology to enhance productivity, facilitate trade, and improve the quality of life. NIST carries out its mission in four cooperative programs, the NIST Laboratories, the Baldrige National Quality Program, the Manufacturing Extension Partnership (MEP), and the Advanced Technology Program (ATP). The Baldrige National Quality Program promotes performance excellence among U. S. manufacturers, service companies, educational institutions, and health care providers by conducting outreach programs and managing the annual Malcolm Baldrige National Quality Award, which recognizes performance excellence and quality achievement. The MEP is a nationwide network of local centers offering technical and business assistance to small manufacturers, and the ATP provides co-funding of research and development partnerships with the private sector to accelerate the development of innovative technologies for broad national benefit.

Within the seven NIST Laboratories, research is conducted in support of U. S. industry that advances the nation's technology infrastructure and enables U. S. industry to continually improve products and services. Recent strategic planning efforts have lead to the development of four programmatic focus areas, which include nanotechnology, health care, information and knowledge management, and homeland security – very much along the transcendental technologies mentioned above. NIST will be working to provide distinct contributions to each of these focus areas within the framework of its mission. New funding will continue to be requested from the U. S. Congress in support of these focus areas. For the measurement laboratories, research will continue to be conducted in the development of measurement science and technology both in support of and outside of these focus areas.

NIST plays a significant role in enabling technological advances. Current project areas at NIST of particular interest to the materials and mechanics community include:

- Biomaterials
- Thin films
- Surface and Interface Characterization
- High-throughput/Combinatorial methods
- Nanoparticles and Nanocomposites
- Fire Retardant Materials and Structures
- Materials for electronics, photonics, and magnetics
- Sensor materials and systems
- Cementitious and other construction materials
- Tissue Engineering

The Center for High Resolution Neutron Scattering, or CHRNS, is a national user facility that is jointly funded by NSF and the NIST Center for Neutron Research (NCNR). The CHRNS develops and operates state-of-the-art neutron scattering instrumentation with broad applications in materials research for use by the general scientific community. When used in combination, CHRNS instruments can provide structural information on length scales from 1 nm to approximately 10 μm, and dynamic information on energy scales from approximately 30 neV (nano electron volt) to 100 meV (micro electron volt). These ranges are the widest accessible at any neutron research center in North America. The instruments are used by university, government and industrial researchers in materials science, chemistry, biology and condensed matter physics to investigate materials such as polymers, metals, ceramics, magnetic materials, porous media, fluids and gels, and biological molecules. Proposals for use of the CHRNS facilities are considered on the basis of scientific merit or technological importance. For additional information, please visit http://rrdjazz.nist.gov/programs/CHRNS/.

INFORMATION TECHNOLOGY

In addition to NSF, there is also a sense that U. S. Federal agency research support is increasingly being driven by broad systemic initiatives. One of these initiatives has been *Information Technology* (IT), listed previously as one of the *transcendental* technologies. The former President's Information Technology Advisory Committee (PITAC) advised that an "immediate and vigorous information technology research and development (R&D) effort in Information Technology be initiated. IT is essential for the United States to have economic growth and prosperity in the 21st Century." PITAC (www.ccic.gov) concluded that current U. S. Federal support for research in IT is inadequate and these current efforts also take "a short-term focus for immediate returns." PITAC recommended IT R&D with long term priorities focusing on "software development that is far more usable, reliable, and powerful; scalable information infrastructures that satisfy the demands of large numbers of users; high-end computing systems with both rapid calculation and rapid data movement; and IT education and training for the citizenry." Achieving these ends requires diversified modes of research support to foster projects of broader scope and longer duration with emphasis on projects involving multiple investigators over several years. Of most importance is the use of these new information technologies to advance critical application domains to benefit our nation and the world.

NANOTECHNOLOGY

Nanomechanics Workshop

Initiated by the senior author [KPC], with the organization and help of researchers from Brown [K.

S. Kim, et al], Stanford, Princeton and other universities, a NSF Workshop on Nano- and Micro-Mechanics of Solids for Emerging Science and Technology was held at Stanford in October 1999. The following is extracted from the Workshop Executive Summary. Recent developments in science have advanced capabilities to fabricate and control material systems on the scale of nanometers, bringing problems of material behavior on the nanometer scale into the domain of engineering. Immediate applications of nanostructures and nano-devices include quantum electronic devices, bio-surgical instruments, micro-electrical sensors, functionally graded materials, and many others with great promise for commercialization. The branch of mechanics research in this emerging field can be termed nano- and micro-mechanics of materials, highly cross-disciplinary in character. A subset of these, which is both scientifically rich and technologically significant, has mechanics of solids as a distinct and unifying theme. The presentations at the workshop and the open discussion precipitated by them revealed the emergence of a range of interesting lines of investigation built around mechanics concepts that have potential relevance to microelectronics, information technology, bio-technology and other branches of nanotechnology. It was also revealed, however, that the study of complex behavior of materials on the nanometer scale is in its infancy. More basic research that is well coordinated and that capitalizes on progress being made in other disciplines is needed if this potential for impact is to be realized.

Recognizing that this area of nanotechnology is in its infancy, substantial basic research is needed to establish an engineering science base. Such a commitment to nano- and micro-mechanics will lead to a strong foundation of understanding and confidence underlying this technology based on capabilities in modeling and experiment embodying a high degree of rigor. The instruments and techniques available for experimental micro- and nano-mechanics are depicted in Fig. 1, courtesy of K. S. Kim of Brown University.

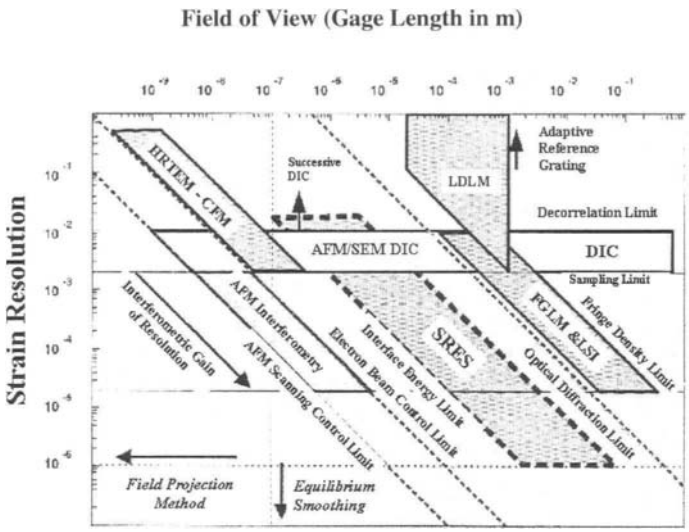


Figure 1. Instruments and techniques for experimental micro and nano mechanics [courtesy of K. S. Kim of Brown University] where

HRTEM High Resolution Transmission Electron Microscopy
SRES Surface Roughness Evolution Spectroscopy
CFTM Computational Fourier Transform Moire
FGLM Fine Grating Laser Moiré
AFM Atomic Force Microscopy
LSI Laser Speckle Interferometry
SEM Scanning Electron Microscopy
DIC Digital Image Correlation
LDLM Large Deformation Laser Moire

The potential of various concepts in nanotechnology will be enhanced, in particular, by exploring the nano- and micro-mechanics of coupled phenomena and of multi-scale phenomena. Examples of coupled phenomena discussed in this workshop include modification of quantum states of materials caused by mechanical strains, ferroelectric transformations induced by electric field and mechanical stresses, chemical reaction processes biased by mechanical stresses, and changes of bio-molecular conformality of proteins caused by environmental mechanical strain rates. Multi-scale phenomena arise in situations where properties of materials to be exploited in applications at a certain size scale are controlled by physical processes occurring on a size scale that is orders of magnitude smaller. Important problems of this kind arise, for example, in thermo-mechanical behavior of thin-film nanostructures, evolution of surface and bulk nanostructures caused by various material defects, nanoindentation, nanotribological responses of solids, and failure processes of MEMS structures. Details of this workshop report can be found by visiting http://en732c.engin.brown.edu/nsfreport.html.

Nanoscale Science and Engineering Initiatives

Coordinated by M. Roco (IWGN, 2000), NSF recently announced a second year program [NSF 01-157; see: www.nsf.gov] on collaborative research in the area of nanoscale science and engineering (NSE). This program is aimed at supporting high risk/high reward, long-term nanoscale science and engineering research leading to potential breakthroughs in areas such as materials and manufacturing, nanoelectronics, medicine and healthcare, environment and energy, chemical and pharmaceutical industries, biotechnology and agriculture, computation and information technology, improving human performance, and national security. It also addresses the development of a skilled workforce in this area as well as the ethical, legal and social implications of future nanotechnology. It is part of the interagency National Nanotechnology Initiative (NNI). Details of the NNI and the NSE initiative are available on the web at http://www.nsf.gov/nano or http://nano.gov.

The NSE competition will support Nanoscale Interdisciplinary Research Teams (NIRT) and Nanoscale Exploratory Research (NER). Nanoscale Science and Engineering Centers (NSEC) awarded in the first year (FY 2001) competition will be funded on a continuing basis. In addition, individual investigator research in nanoscale science and engineering will continue to be supported in the relevant NSF Programs and Divisions outside of this initiative. This NSE initiative focuses on seven high risk/high reward research areas, where special opportunities exist for fundamental studies in synthesis, processing, and utilization of nanoscale science and engineering. The seven areas are:

- Biosystems at the nanoscale
- Nanoscale structures, novel phenomena, and quantum control
- Device and system architecture
- Nanoscale processes in the environment
- Multi-scale, multi-phenomena theory, modeling and simulation at the nanoscale
- Manufacturing processes at the nanoscale

- Societal and educational implications of scientific and technological advances on the nanoscale

The National Nanotechnology Initiative started in 2000 ensures that investments in this area are made in a coordinated and timely manner (including participating federal agencies – NSF, DOD, DOE, DOC [including NIST], NIH, DOS, DOT, NASA, EPA and others) and will accelerate the pace of revolutionary discoveries now occurring. Current request of Federal agencies on NNI is $519 million. The NSF share of the budget is $199 million [on NSE, part of NNI].

Microscopy

In atomic force microscopy (AFM), a probe consisting of a sharp tip (nominal tip radius on the order of 10 nm) located near the end of a cantilever beam is raster scanned across the sample surface using piezoelectric scanners. Changes in the tip-sample interaction are often monitored using an optical lever detection system, in which a laser beam is reflected off of the cantilever and onto a position-sensitive photodiode. During scanning, a particular operating parameter is maintained at a constant level, and images are generated through a feedback loop between the optical detection system and the piezoelectric scanners. A schematic illustration of a scanning stylus atomic force microscope is shown in Figure 2a. In this design, the probe tip is scanned above a stationary sample, while in a scanning sample design, the sample is scanned below a fixed probe tip. Operationally, little difference exists between these two designs, because the relative motion of the tip to the sample is used to generate topographic images. Applications of AFM and other types of scanning probe microscopy continue to grow rapidly in number and include biological materials (e.g., studying DNA structure), polymeric materials (e.g., studying morphology, mechanical response, and thermal transitions), and semiconductors (e.g., detecting defects). In particular, AFM can be utilized to evaluate the surface quality of products such as paint and coating systems, contact lenses, optical components (mirrors, beamsplitters, etc.), and semiconductor wafers after various cleaning, etching, or other manufacturing processes.

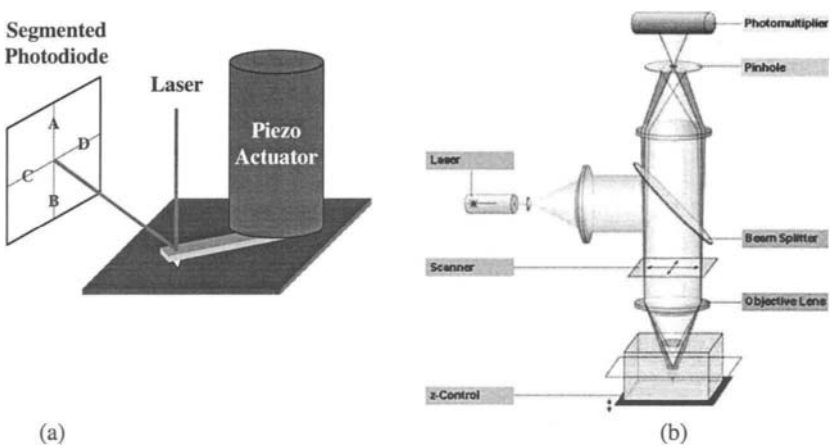


Figure 2. Schematic illustrations of (a) a scanning-probe atomic force microscope (AFM) and (b) a laser-scanning confocal microscope (LSCM).

Laser scanning confocal microscopy (LSCM) is a non-destructive, powerful tool for characterizing

the microstructure of polymeric and biological materials. In Fig. 2b, the confocal principle is illustrated. A LSCM uses coherent incident light and collects reflected or scattered light exclusively from a single plane, rejecting light out of the focal plane. The laser scanning confocal microscope scans the sample sequentially point by point and line by line and assembles the pixel information into one image. Optical slices of the specimen are thus created with high contrast and high resolution in x, y and z directions. By moving the focal plane systematically, a series of optical slices are created that can be used to construct a three-dimensional image stack that can be digitally processed. The wavelength, numerical aperture (N.A.) of the objective, and the size of the collecting pinhole in front of the detector determine the resolution in the thickness or axial direction (Corle et al., 1996). Microstructure information obtained from LSCM results can be used, for example, to model scattering properties of coating materials, which can then be compared to scattering measurements using light scattering (Sung et al., 2002).

Nanomechanics

Measurements of mechanical behavior of very small volumes of material have been enabled by the development of instruments that can sense and apply very small forces and displacements, including AFMs and nanoindenters. These devices are often capable of producing contact areas and penetration depths characterized by nanometer dimensions while also providing lateral motion capabilities for studying tribological behavior. One objective of using these devices is to provide methods for characterizing mechanical response of material systems with nanoscale spatial resolution. Such measurements can be a key to understanding technologically important material systems, including those used in magnetic storage, microelectronic and telecommunication devices. Further, these types of measurements are important in support of nanotechnology developments, e.g., nanoelectronic devices and nanostructured materials such as ultra-thin films and nanocomposites.

Nanoindentation via the AFM is performed in a non-scanning mode, termed force mode, in which the AFM probe is moved toward the sample surface, pushed into the surface, and then lifted back off of the surface (see Fig. 2a). A force-displacement curve is produced from which a force-penetration curve related to the nanoindentation process can be determined. The force applied is related to the deflection (bending) of the cantilever beam through the cantilever spring constant, and the penetration into the material is the difference between the overall vertical displacement of the cantilever and the probe tip displacement related to cantilever bending, which must be calibrated. For nanoindentation devices, shown schematically in Fig. 3a, the application of force and the measurement of displacement are often done using electromagnetic or electrostatic transducers. System compliance must be calibrated to eliminate displacement of the load frame, such that force-penetration curves are produced (see Fig. 3b). Typically, the unloading data is assumed to be primarily elastic recovery of the material and is often analyzed using a power law curve fit of the form:

$$P = \alpha \left(h - h_f \right)^m$$

where P is force, h is penetration, h_f is the penetration after unloading, and α and m are curve fitting parameters. The slope, dP/dh, taken at the point of maximum load, P_{max}, and maximum displacement, h_{max}, is the contact stiffness, S, which is used to first determine the contact depth, h_c,

$$h_c = h_{\max} - \frac{\varepsilon P_{\max}}{S}$$

here ε is a parameter related to the contact geometry, and subsequently to calculate elastic modulus,

$$E_r = \frac{\sqrt{\pi}}{2\beta}\frac{S}{\sqrt{A}}$$

where A is the contact area, which is calculated from knowledge of the tip shape and h_c, β is a parameter related to tip geometry, and E_r is the reduced or effective modulus, which is related to values of modulus and Poisson's ratio for the sample (E_s and ν_s) and indentation tip (E_i and ν_i):

$$\frac{1}{E_r} = \frac{\left(1-\nu_s^2\right)}{E_s} + \frac{\left(1-\nu_i^2\right)}{E_i}$$

Indentation hardness, H, can also be calculated as the maximum load, P_{max}, divided by the contact area, A.

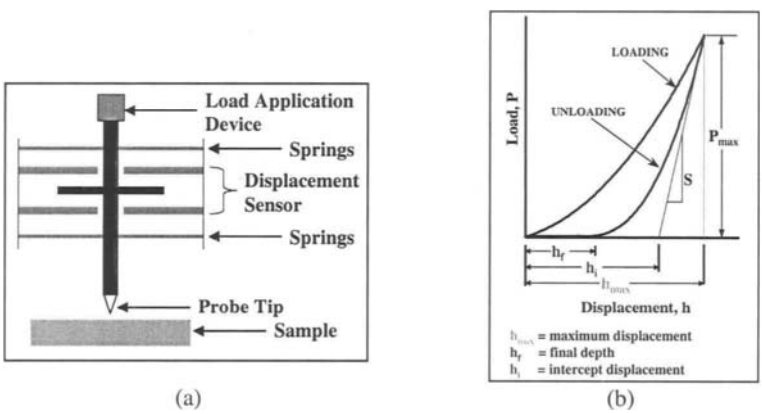


Figure 3. Schematic illustrations of (a) a nanoindentation system and (b) load-displacement or load-penetration data produced from a nanoindentation measurement, including key characteristics.

Recent advances in instrumentation have focused on improvements in sensitivity, the addition of testing capabilities, and the integration of force measurements and imaging. For nanoindentation devices, improvements in sensitivity have been made by adding dynamic capabilities to these systems, which previously have operated only in a quasi-static mode. Often, a dynamic signal with a displacement amplitude on the order of 1 nm is superimposed over a quasi-static loading history. This type of technique allows hundreds of measurements of elastic modulus and hardness to be calculated as opposed to a single measurement from a quasi-static indentation test. Also, dynamic behavior of the materials, e.g., storage and loss characteristics, can be studied, often over a range of frequencies, similar to dynamic mechanical analysis. Other additional capabilities include lateral motion and lateral force measurement capabilities for tribological studies, including scratch testing, and improvements to the control systems that allow for automated testing using a variety of user-specified loading histories.

Integration of force measurements and imaging capabilities has been made in both AFM systems and in hybrid AFM-nanoindentation devices. AFM images are now produced routinely using particular aspects of the tip-sample force interactions. Each pixel in the image represents a position on the sample at which a force-distance curve was measured. The image can then be set up to indicate changes in local tip-sample adhesion or sample stiffness, for example. However,

mechanical property measurements associated with SPM systems have significant uncertainties in the probe spring constant and tip shape, which typically render them useful only as qualitative information (VanLandingham et al., 2001). More quantitative measures of tip-sample forces can be achieved for systems that employ force transducers in combination with scanning capabilities similar to AFM. Examples of such systems include the interfacial force microscope or IFM developed at Sandia National Laboratories (Joyce & Houston, 1991) and a commercial force transducer that interfaces with many commercial AFM systems (Bhushan et al., 1996; Asif et al., 2001).

While advances in instrumentation continue, questions remain regarding uncertainties associated with measurement and calibration techniques. Current research at NIST is focused on measurement systems for calibrating micro-Newton forces. Questions regarding the use of reference materials for calibrating load-frame compliance and tip shape as well as other analysis and procedural issues persist with regard to nanoindentation measurements that must be addressed. For example, recent studies, including an interlaboratory comparison (Jennett & Meneve, 1998), have shown the calibration results to have poor reproducibility and large uncertainties.

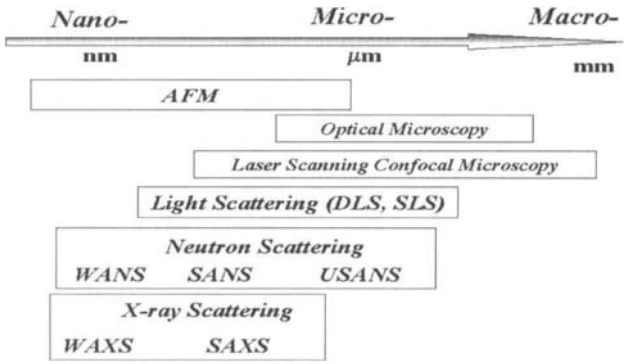


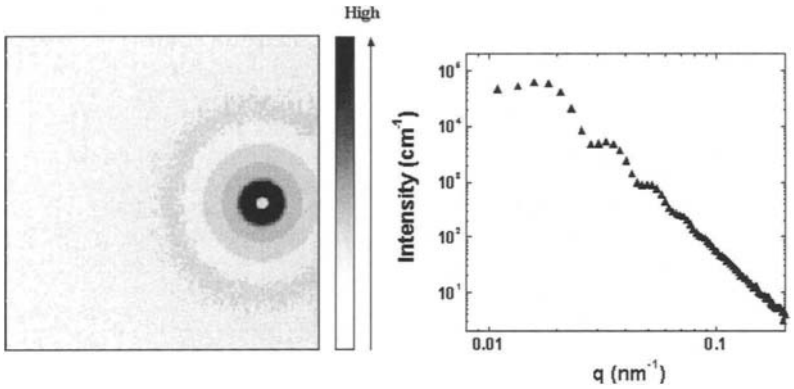
Figure 4. Capabilities of different microscopy and scattering techniques.

Scattering Metrology

Scattering metrology is widely used for characterizing nano-/ micro-domains and nano-structural features of polymers and other materials, and is a complim entary technique to microscopy tools. Many forms of radiation can be used for scattering purposes: X-rays, neutron, laser light, electrons, etc. Each has different characteristics and is used for different purposes. In general, the principle and operation of measurements is similar. However, the microstructural information generated could be different due to the different interactions between the scattering source and the materials. For example, neutron scattering is sensitive to inhomogeneities in density of nuclei in the materials, while light or X-ray scattering is sensitive to inhomogeneities in the refractive index or electron density in the materials. In this paper, we will only describe the neutron scattering method.

In Fig. 4 the relative measurable length scale using different scattering metrology and microscopy techniques are shown. The small-angle neutron and X-ray scattering methods (SANS, SAXS) are useful for polymer research (or condense matter research in general) because they probe size scales from angstrom-level to micron-level. With recently developed Ultra-SANS (USANS) instruments, the length scales using neutron scattering method can be extended to 10 μm (Drews et al., 1998).

Static light scattering (SLS) complements these techniques by focusing on the micron length scale. Dynamic light scattering (DLS) can be used for measuring diffusive motion and particle sizing in complex fluid systems from 1 nm to 5 μm. Other methods such as wide-angle neutron and X-ray scattering (WANS, WAXS) probe very local (atomic) structure on the order of a few nanometers.



(a) (b)

Figure 5. (a) A two-dimensional scattering image, and (b) the corresponding absolute scattering intensity curve as a function of the scattering wave vector q, for a polymeric system with a well-ordered structure.

The NIST Center for Neutron Research (NCNR), which maintains the leading neutron scattering facility in the U. S., offers advanced measurement capabilities for use by all qualified applicants. Information on instrumental description may be obtained at the NCNR website [http://www.ncnr.nist.gov/]. Many of its instruments rely on intense neutron beams produced by a liquid hydrogen cold neutron source (Cappelletti et al., 2001). The small angle neutron scattering (SANS) instrument is a powerful tool for characterizing nano-/ micro-domains and nanostructures of various polymeric systems as well as particles or fillers in solution or in a polymer matrix. In Fig. 5, SANS results obtained from nano-size fillers (for example: inorganic pigment) in a polymer matrix are shown. After standard calibrations and taking into account the sample transmission and film thickness, two-dimensional scattering images (see Fig. 5a) are averaged azimuthally to produce a one-dimensional absolute scattering intensity curve (see Fig. 5b) as a function of the scattering wave vector q. ($q = 4\pi\sin(\theta/2)/\lambda$, where θ is the scattering angle and λ is the wavelength). In this case, the filler has a higher neutron scattering coefficient than the polymer matrix, and the neutron scattering intensity is proportional, to the first order, to differences in the local filler concentrations within the sample. Typically the scattering intensity, I(q), can be modeled as following:

$$I(q) = I_o\, P(q)\, S(q),$$

where $P(q)$ is the form factor, and $S(q)$ is the structure factor (Higgins & Benoit, 1994). The wavelength independent part of the equation: I_o is proportional to the scattering amplitude (scattering contrast between the fillers and the polymer matrix), the number density, and the volume of the fillers. The form factor $P(q)$ comes from the intramolecular interferences and is characteristic of the size and shape of the particles. For a particle with well-defined shape, such as a spherical particle with uniform scattering density (see example of Fig. 5b) or a spherical particle with a core-shell structure, the form factor $P(q)$ can be calculated, and the size of the particles can be determined. The structure factor S(q) is related to the correlation function describing the radial distribution function between particles or micro-domains. A peak in the scattering profile at a

scattering wave vector q indicates the existence of micro-domains with a characteristic average length $d = 2\pi/q$. The microstructure/morphology information, such as the dimension of ordered domains or the correlation length of concentration fluctuations, can be determined from the intensity profile.

MODELING AND SIMULATION

The initiative *Engineering Sciences for Modeling and Simulation-Based Life-Cycle Engineering* (Program Announcement NSF 99-56) is a three-year collaborative research program by NSF and the Sandia National Laboratories (Sandia) focusing on advancing the fundamental knowledge needed to support advanced computer simulations. This collaborative initiative capitalizes on the missions of both organizations. NSF's mission is to advance the fundamental science and engineering base of the United States. Sandia has the responsibility to provide solutions to a wide range of engineering problems pertinent to national security and other national issues. It is moving toward engineering processes in which decisions are based heavily on computational simulations including meshless methods in moving boundary problems [see e.g. Boresi, Chong and Saigal, 2002]; thus, capitalizing on the available high performance computing platforms. This initiative has sought modeling and simulation advances in key engineering focus areas such as thermal sciences, mechanics and design.

The NSF Civil and Mechanical Systems (CMS) Division developed an initiative on *Model-based Simulation* (MBS), see NSF 00-26. Model-based simulation is a process that integrates physical test equipment with system simulation software in a virtual test environment aimed at dramatically reducing product development time and cost. This initiative will impact many civil/mechanical areas: "structural, geotechnicial, materials, mechanics, surface science, and natural hazards (e.g., earthquake, wind, tsunami, flooding and land-slides)." MBS would involve "combining numerical methods such as finite element and finite difference methods, together with statistical methods and reliability, heuristics, stochastic processes, etc., all combined using super-computer systems to enable simulations, visualizations, and virtual testing." Expected results could be less physical testing, or at best, better strategically planned physical testing in the conduct of R&D. Examples of the use of MBS in research, design and development exist in the atmospheric sciences, biological sciences, and the aerospace, automotive and defense industries. The manufacturing of the prototype Boeing 777 aircraft, for example, was based on computer-aided design and simulation, cutting costs and shortening production time significantly.

The NIST Center for Theoretical and Computational Materials Science (CTCMS) was established to investigate important problems in materials theory and modeling with novel computational approaches. The Center creates opportunities for collaboration where CTCMS can make a positive difference by virtue of its structure, focus, and people. It develops powerful new tools for materials theory and modeling and accelerates their integration into industrial research. The current technical focus areas include: modeling microstructure and mechanical response using object-oriented finite element analysis, micromagnetic modeling, nanofilled polymer melts, deformation of metals...etc. Detailed information can be found on the center web site at http://www.ctcms.nist.gov/programs. In addition to the current projects, the CTCMS is continuously soliciting proposals for workshops on materials theory and modeling, short-term and long-term visiting fellowship, guest researcher, and NRC postdoctoral positions, and creative and ambitious new projects in materials theory and modeling.

In the future one should expect the continued introduction of bold innovative research initiatives related to important national agenda issues such as the environment, civil and mechanical

infrastructure, the service industry and the business enterprises.

CHALLENGES

The challenge to the mechanics and materials research communities is: How can we contribute to these broad-base and diverse research agendas? Although the mainstay of research funding will support the traditional programs for the foreseeable future, considerable research funding will be directed toward addressing these research initiatives of national focus. At the request of the author [KPC], a NSF research workshop has been organized by F. Moon of Cornell University to look into the research needs and challenges facing the mechanics communities. A website with recommendations of research needs and challenges will soon be available.

Mechanics and materials engineering are really two sides of a coin, closely integrated and related. For the last decade this cooperative effort of the M&M Program has resulted in better understanding and design of materials and structures across all physical scales, even though the seamless and realistic modeling of different scales from the nano-level to the system integration-level (Fig. 6) is not yet attainable. In the past, engineers and material scientists have been involved extensively with the characterization of given materials. With the availability of advanced computing and new developments in material science, researchers can now characterize processes and design and manufacture materials with desirable performance and properties. One of the challenges is to model short-term micro-scale material behavior, through meso-scale and macro-scale behavior into long-term structural systems performance. Accelerated tests to simulate various environmental forces and impacts are needed (NSF, 1998). Supercomputers and/or workstations used in parallel are useful tools to solve this scaling problem by taking into account the large number of variables and unknowns to project micro-behavior into infrastructure systems performance, and to model or extrapolate short term test results into long term life-cycle behavior (NSF, 1998; Chong, 1999). Twenty-four awards were made totaling $7 million. A grantees' workshop was held recently in Berkeley and a book of proceedings has been published (Monteiro et al., 2001).

MATERIALS		STRUCTURES	INFRASTRUCTURE	
nano-level (10^{-9})	micro-level (10^{-6})	meso-level (10^{-3})	macro-level (10^{+0})	systems-level (10^{+3}) m
Molecular Scale	*Microns*	*Meters*		*Up to Km Scale*
*nano-mechanics	*micro-mechanics	*meso-mechanics	*beams	*bridge systems
*self-assembly	*micro-structures	*interfacial-structures	*columns	* lifelines
*nanofabrication	*smart materials	*composites	*plates	*airplanes

Figure 6. Physical scales in materials and structural systems (Boresi & Chong, 2000)

Many current NIST projects are focused on multidisciplinary and multi-scale problems, including in the areas of materials and mechanics. One successful program in the NIST Building and Fire Research Laboratory is the Service Life Prediction or SLP program, which includes partnerships with industry and other U. S. Federal Agencies. The mission of the SLP program is to greatly reduce the time-to-market for new products through the development and implementation of advanced methods and metrologies for quantitative and reliable prediction of the service life of

existing and new products. Competition within the construction materials community has drastically increased with industrial globalization. As has been the case in the high technology industries, globalization has greatly increased the competitive pressures for reducing the time-to-market for new construction materials and products. Currently, time-to-market is controlled by the time required to generate a performance history for a product, which is established through a series of time-consuming field and laboratory exposure studies, typically taking between 5 and 15 years to complete.

The methodology that is being used to reduce the time to generate these durability performance histories to months instead of years is called reliability theory and life testing analysis. This methodology has had a long and successful history of application in predicting the service life of electronic, aerospace, nuclear, and medical products, and is currently being applied in five different, but highly overlapping, project areas including: 1) appearance (the primary measure of durability for a coating system), 2) coatings and pigments, 3) composites, 4) polymeric interphases, and 5) sealants. This research effort includes implementing and developing use-inspired scientific and technical advances in methodologies and metrologies for improving and advancing the appearance, service life, and performance of polymeric construction materials. Included in this effort is an integration of materials science, metrology from nanoscale though macroscale including nanomechanics, high-throughput testing and analysis, and information management.

ACKNOWLEDGMENTS AND DISCLAIMER

The authors would like to thank their colleagues and many members of the research communities for their comments and inputs during the writing of this paper. Information on NSF initiatives, announcements and awards can be found in the NSF website: www.nsf.gov. Information pertaining to NIST can be found on its website: www.nist.gov. The opinions expressed in this article are the authors' only, not necessarily those of the National Science Foundation or the National Institute of Standards and Technology.

REFERENCES

Asif, S. A. S., Wahl, K. J., Colton, R. J., and Warren, O. L. (2001). Quantitative Imaging of Nanoscale Mechanical Properties Using Hybrid Nanoindentation and Force Modulation. *J. Appl. Phys.* **90**, 5838-5838.

Boresi, A. P. and Chong, K. P. (2000). *Elasticity in Engineering Mechanics*, John Wiley, New York.

Boresi, A. P., Chong, K. P. and Saigal, S. (2002). *Approximate Solution Methods in Engineering Mechanics*, John Wiley, New York.

Bhushan, B., Kulkarni, A. V., Banin, W., and Wyrobek, J. T. (1996). Nanoindentation and Picoindentation Measurements Using a Capacitive Transducer System in Atomic Force Microscopy. *Phil. Mag. A* **74**, 1117-1128.

Cappelletti, R.L., Glinka, C.J., Krueger, S., Lindstrom, R.A., Lynn, J.W., Prask, H.A., Prince, E., Rush, J. J., Rowe, J.M., Satija, S.K. Toby, B.H., Tsai, A., and Udovic, T.J. (2001). Materials Research With Neutrons at NIST. *J. Res. Natl. Inst. Stand. Technol.* **106**,187-230.

Chong, K. P. (1998, 1999). Smart Structures Research in the U.S. *Keynote paper, Proc. NATO Adv. Res. Workshop on Smart Structures*, held in Pultusk, Poland, 6/98, *Smart Structures,* Kluwer Academic Publ. 37-44 (1999).

Corle, T.R., and Kino, G.S. (1996). *Confocal Scanning Optical Microscopy and Related Imaging Systems*, Academic Press, San Diego.

Drews, A.R., Barker, J.G., Glinka, C.J., Agamalian, M. (1998). Development of a thermal-neutron double-crystal diffractometer for USANS at NIST. *Physica B* **241-243**, 189-191.

Higgins, J.S. and Benoit, H.C. (1994). *Polymers and Neutron Scattering*. Clarendon Press, Oxford, UK.

Interagency Working Group on Nano Science, Engineering and Technology (IWGN). (2000). *Nanotechnology Research Directions*. Kluwer Academic Publ. 37-44.

Jennett, N. M. and Meneve, J. (1998). Depth Sensing Indentation of Thin Hard Films: A Study of Modulus Measurement Sensitivity to Indentation Parameters. *Fundamentals of Nanoindentation and Nanotribology* **522**, Materials Research Society, Pittsburgh, PA, 239-244.

Joyce, S. A. and Houston, J. E. (1991). A New Force Sensor Incorporating Force-Feedback Control For Interfacial Force Microscopy. *Rev. Sci. Instrum.* **62**, 710-715.

Monteiro, P. J. M., Chong, K. P., Larsen-Basse, J. and Komvopoulos, K., eds.(2001). *Long-term Durability of Structural Materials*, Elsevier, Oxford, UK.

NSF. (1998). Long Term Durability of Materials and Structures: Modeling and Accelerated Techniques. *NSF 98-42,* National Science Foundation, Arlington, VA.

NSF. (2001). Nanoscale Science and Engineering. *NSF 01-157,* National Science Foundation, Arlington, VA.

Sung, L, Nadal, M. E., McKnight, M.E. Marx, E., and Laurenti, B. (2002). Optical Reflectance of Metallic Coatings: Effect of Aluminum Flake Orientation. *J. Coating Technology, in press.*

VanLandingham, M. R., Villarrubia, J. S., Guthrie, W. F., and Meyers, G. F. (2001). Nanoindentation of Polymers: An Overview. *Macromolecular Symposia* **167**: *Advances in Scanning Probe Microscopy of Polymers*, V. V. Tsukruk and N. D. Spencer, eds., 15-44.

Wong, E. (1996). An Economic Case for Basic Research. *Nature* **381,** 187-188.

Advances in Building Technology, Volume 1
M. Anson, J.M. Ko and E.S.S. Lam (Eds.)
© 2002 Elsevier Science Ltd. All rights reserved

ADVANCES IN CONCRETE TECHNOLOGY

M.F. Cyr and S.P. Shah

Center for Advanced Cement Based Materials,
Department of Civil Engineering, Northwestern University, Evanston, IL
60208 USA

ABSTRACT

A survey of recent advances in concrete technology, with a focus on research performed at the Center for Advanced Cement Based Materials (ACBM Center) at Northwestern University, is presented. Ultra-high-strength concrete (UHSC), with compressive strength of 200MPa, has been developed. The properties and applications of reactive powder concrete, one type of UHSC, are discussed. Fiber reinforcement is used to overcome the inherent brittleness and increase the tensile strength of concrete, especially high- and ultra-high-strength concrete. Fiber-reinforced cementitious composites can be designed for specific applications with the use of special processing techniques, such as extrusion, and hybrid fiber reinforcement. Significant reductions in drying shrinkage are achieved with a newly developed shrinkage reducing admixture. Construction costs can be reduced with the use of self-compacting concrete (SCC), which does not require vibration at placement. The design of SCC is facilitated with a newly developed rheological model. A nondestructive evaluation technique has been developed to monitor the hardening process of fresh concrete.

KEYWORDS

High-performance concrete, ultra-high-strength concrete, fibers, extrusion, shrinkage, self-compacting concrete, nondestructive evaluation

INTRODUCTION

As concrete technology developed, an initial goal was to increase its strength. High-strength concrete (HSC) columns were first used in the construction of high-rise buildings in the 1970s. The same changes that increased the strength also improved the durability and other aspects of concrete performance. The term high-performance concrete (HPC) began to be used. Today, HPC refers to concrete with many different attributes. It is produced with specifically designed matrices, often containing special chemical and mineral admixtures and fiber reinforcement. HPC performance criteria include high strength and elastic modulus, improved toughness and impact resistance, high

early-age strength, high durability—including low permeability, resistance to chemical attack and free-thaw damage—and ease of placement and compaction without segregation.

A selection of current research in HPC, with an emphasis on work performed at the Center for Advanced Cement Based Materials (ACBM) at Northwestern University, is presented. Ultra-high-strength concrete, with a compressive strength of 200 MPa, has been produced for specialized applications. The ductility of concrete, especially high- and ultra-high-strength concrete, has been enhanced with fiber reinforcement. Hybrid fiber reinforcement and special processing techniques, such as extrusion, have enabled the optimization of composite performance for specific applications. A shrinkage reducing admixture has been developed to improve shrinkage cracking resistance. A model to facilitate the design of self-compacting concrete has been developed. In addition to improving concrete performance, new nondestructive techniques have been employed to monitor the setting of fresh concrete and to assess early deterioration in hardened concrete.

ULTRA-HIGH-STRENGTH CONCRETE

The strength of brittle materials, such as concrete, is related to the porosity of the material. As the porosity decreases, the strength exponentially increases (Mindess and Young 1981). Powers and Brownyard (1948) showed that decreasing the water-to-cement (w/c) ratio reduced the porosity of the concrete, increasing the strength. This reduction in porosity also makes the concrete more durable. In addition to having a lower water-to-binder (w/b) ratio, HSC usually contains superplasticizer, and mineral admixtures, such as silica fume or fly ash. Its compressive strength is around 100 MPa compared to compressive strengths of 20-40 MPa for normal-strength concrete (Kosmatka *et al.* 2001).

Recently, special processing techniques have been used to produce concrete with even higher compressive strengths. Ultra-high-strength concrete (UHSC) can reach compressive strengths of 200 MPa. Two commonly produced UHSCs are macro-defect-free (MDF) cement and reactive powder concrete (RPC). Macro-defect free cement is a mixture of cement and a water-soluble polymer. High shear mixing causes a mechano-chemical reaction between the cement and the polymer resulting in tensile strengths of up to 200 MPa (Shah and Weiss 1998a).

Reactive powder concrete typically has a compressive strength of 200 MPa, although strengths as high as 810 MPa have been recorded (Semioli 2001). Its high strength and low porosity are obtained by optimizing particle packing and reducing water content. The mixture contains no coarse aggregates. Instead fine powders, such as sand, crushed quartz, and silica fume, with particle sizes ranging from 0.02 to 300 μm are used. The grain size distribution is optimized to increase the matrix density. Superplasticizer is used to reduce the w/b to 0.2 as compared with w/b of 0.4-0.5 for typical normal-strength concrete. Steel and synthetic fibers are typically added to improve the ductility, and a post-set heat treatment is applied to improve the microstructure.

RPC is produced commercially by two French construction companies (Semioli 2001). Béton Spécial Industriel (BSI) is produced by the Eiffage Group (EGI) in conjunction with Sika Corp., and Ductal® is made by Bouygues Construction in partnership with Lafarge Corp. Ductal® is reinforced with high-strength steel microfibers to improve ductility. It has a compressive strength of 200 MPa, a tensile strength of 8 MPa and a flexural strength of 40-50 MPa. Ductal® is 100 times more resistant to water diffusion than normal-strength concrete and 10 times more resistant than typical French HPC. It has zero shrinkage after setting and 85-95% less creep than conventional concrete. The relatively low tensile strength requires the use of prestressing in more severe applications. With Ductal®, very strong, lightweight and durable thin sections can be produced. Currently, there are plans to use Ductal® in a 120-m long, slender arch pedestrian bridge near Seoul, Korea. The bridge will consist of six post-tensioned segments with a 30-mm thick walkway. In the United States, the Federal Highway Administration (FHWA) is currently testing Ductal® in prestressed concrete girders (FHWA 2002).

BSI has been used in French nuclear power plants. The producers of RPC also see potential for its use in pipes, tunnel and canal linings, paving, floors, liquid storage structures, nuclear waste containment, and long-spanning, slender, self-supporting structures such as stadium domes.

The high strength of UHSC is due to the homogeneity and low porosity of the matrix. These same characteristics also cause the material to be extremely brittle and increase the likelihood of shrinkage cracking. Microfiber reinforcement can increase the ductility of the concrete and improve shrinkage cracking resistance. The use of shrinkage reducing admixture also improves shrinkage performance.

FIBER-REINFORCED CONCRETE

Microfiber reinforcement

Microfiber reinforcement reduces the inherent brittleness of concrete, especially UHSC. Fibers spaced at the micron scale can interact with microcracks, delaying localization and increasing the tensile strength of the matrix (Shah 1991), in ways that steel reinforcing bars with spacing at the millimeter scale cannot. In addition, microfiber reinforcement delays the age of the first visible crack and reduces the crack width in restrained shrinkage tests (Grysbowski and Shah 1990).

The performance of fiber-reinforced concrete (FRC) is governed by the ratio of the elastic modulus of the fiber to the elastic modulus of the matrix, the strength of the fiber-matrix bond, the aspect ratio (fiber length/fiber diameter) of the fiber, and the material properties of the fiber (Bentur and Mindess 1991). Different fibers types and geometries yield different composite performance. Only relatively small amounts, usually less than 1% by volume, of fiber reinforcement can be added to conventional concrete because the fibers significantly reduce the workability of the fresh concrete. At this dosage, fibers can improve shrinkage cracking resistance and slightly enhance ductility. To maximize the benefits of fibers, including increasing the tensile strength and ductility of the composite and producing a strain-hardening response, larger doses must be added to the matrix. In cement-based materials, this requires special processing techniques. These composites are referred to as high-performance, fiber-reinforced cementitious composites (HPFRCC). The relative performance of plain, normal-strength concrete, conventional FRC, and HPFRCC is shown in Figure 1.

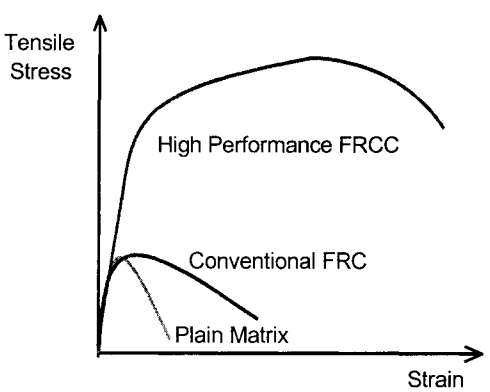


Figure 1: Tensile response of concrete, FRC, and HPFRCC.

Extruded fiber-reinforced cementitious composites

Extrusion, a common processing technique for polymers and ceramics, was recently adapted for the production of HPFRCC at ACBM (Shao and Shah 1997 and Shao *et al.* 1995). A highly viscous, dough-like mixture of cement paste and fibers (2%-10% by volume) is forced through a die to produce an element of desired cross-section. Production is continuous, and a variety of shapes, such as thin sheets for siding and roofing tiles, pipe, and cellular sections can be extruded, as shown in Figure 2. The high compressive and shear forces required to extrude the composite result in a dense matrix, a strong fiber-matrix bond and alignment of fibers in the direction of extrusion. The extruded composites are stronger and tougher than a cast composite of the same material, as shown in Figure 3 (Shah *et al.* 1998b).

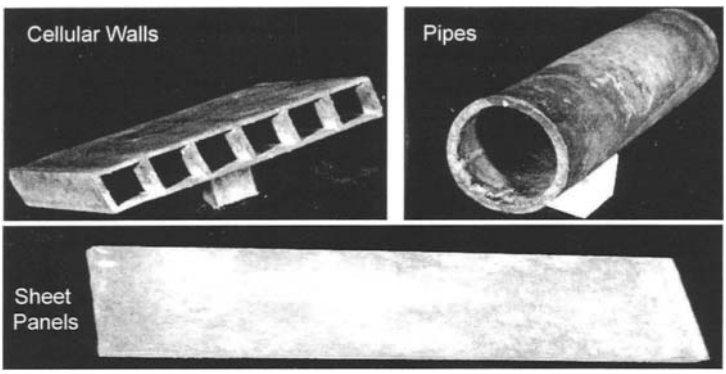


Figure 2: Extruded cross-sections.

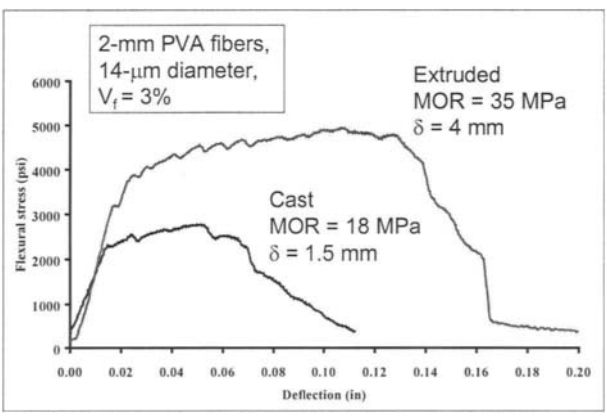


Figure 3: Flexural response of extruded and cast composites (Shah *et al.* 1998b).

Successful extrusion requires the mixture to be soft enough to flow through the extruder but stiff enough to maintain its shape after exiting the die. The highly specialized cementitious matrix has a low w/b (w/b ~ 0.25) with admixtures, and mineral additives. The rheology of the extrudate has been improved with the replacement of a portion of the cement with Class F fly ash (Peled *et al.* 2000a). The spherical fly ash particles make the paste easier to extrude. Fly ash is also less expensive and more

environmentally friendly than cement. It improves the flexural performance of fiber-reinforced extruded composites by increasing the likelihood of fiber pullout instead of fiber fracture at failure. Fly ash also improves the durability of glass-fiber-reinforced extruded composites by reducing the alkalinity of the cement matrix (Cyr *et al.* 2001)

Hybrid fiber reinforcement

Material performance can be optimized for given applications by combining different types of fiber reinforcement in hybrid fiber composites. For example, glass fibers tend to be strong but relatively brittle and form a strong fiber-matrix bond. Polyvinyl alcohol (PVA) fibers are weaker, but more ductile than glass fibers. These fibers were combined in extruded composites to produce composites that were both strong and tough with strain hardening behavior (Peled *et al.* 2000b). In addition, it was shown that a portion of the PVA fibers can be replaced with less expensive polypropylene (PP) fibers without any significant reduction in performance. The performance of extruded single-fiber composites and extruded hybrid-fiber composites is shown in Figure 4.

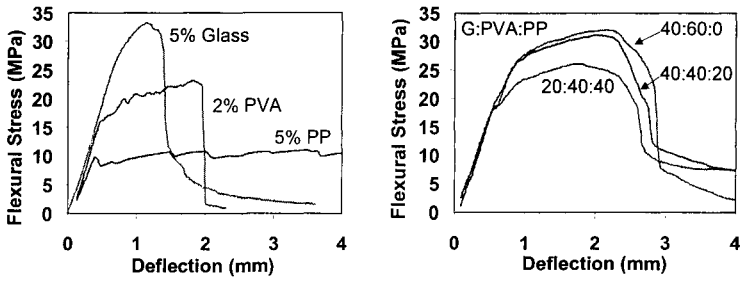


Figure 4: Flexural response of single-fiber and hybrid-fiber reinforced extruded composites. Total $V_f = 5\%$ for hybrids (Peled *et al.* 2000b).

Different size fibers can also be combined to enhance performance. Lawler (2001) found that combining 0.5% steel macrofibers (500 μm diameter, 30 mm length) with 0.5% PVA microfibers (14 μm diameter, 12 mm length) significantly improved both the pre- and post-peak performance of mortar. The microfibers bridge microcracks as they form, preventing them from coalescing and increasing the tensile strength of the composites. As the cracks grow, the steel macrofibers bridge the larger cracks, increasing the ductility of the composite. This hybrid combination also significantly reduces the permeability of cracked concrete.

SHRINKAGE REDUCING ADMIXTURES

It is well known that concrete shrinks as it dries. If the concrete is restrained, tensile stresses will develop and cracking can occur. This is of particular concern in pavements, bridge decks, and industrial floors where the volume-to-surface ratio is low. The likelihood of shrinkage cracking depends on the free shrinkage, the creep relaxation, age-dependent material properties, such as tensile strength, and the degree of restraint of the concrete. Shrinkage cracking is of greater concern in HSC where increased early-age free shrinkage, reduced creep and increased brittleness result in earlier cracking (Wiegrink *et al.* 1996). Attempts to reduce shrinkage cracking have included the use of secondary reinforcement to keep cracks from widening, the use of fiber reinforcement to prevent microcracks from coalescing, the use of expansive cement—a cement that expands during hydration creating a compressive prestress that counteracts the tensile stresses that develop under restrained shrinkage—and reducing the w/c. Research at the ACBM Center has included the development of

experimental techniques and theoretical models to assess the cracking potential due to shrinkage (Grysbowski and Shah 1990, Weiss *et al.* 1998, Shah *et al.* 1998c). In addition, a shrinkage reducing admixture (SRA) has been developed to improve the shrinkage cracking resistance of concrete (Shah *et al.* 1992).

The SRA is a propylene glycol derivative sold by Grace Construction Products as Eclipse™ that reduces free shrinkage by reducing the surface tension of water. One cause of drying shrinkage in concrete is the surface tension that develops in small pores as water evaporates (Balogh 1996). As cement reacts with water, calcium silicate hydrate (CSH) forms in water-filled spaces. These spaces are not completely filled by the CSH so a capillary pore network develops. As the water evaporates, a meniscus forms in the pores. The surface tension of the water pulls the pore walls inward causing the concrete to shrink. This phenomenon occurs pores with radii from 2.5 nm to 50 nm. The reduction in the surface tension of the water by the SRA reduces the capillary pore forces that cause shrinkage, thus reducing the drying shrinkage of the concrete.

The shrinkage reducing admixture was tested in both normal- and high-strength concrete at 1% and 2% by weight of cement (Weiss *et al.* 1998). In general, 2% SRA showed much greater improvements over mixtures without SRA than 1% SRA did. With 2% SRA, the free shrinkage at 49 days was reduced by 42% in both normal- and high-strength concrete. Because the SRA greatly reduced the free shrinkage, the age of cracking of restrained ring specimens containing SRA was increased. Rings of normal-strength concrete cracked 10 days after casting, on average. With 2% SRA, only one of the rings cracked before the end of the tests, 50 days after casting. For high-strength concrete, the mixture without SRA cracked at 3.2 days, while 2% SRA delayed cracking until 11.6 days. The rings that cracked at later ages also had much smaller cracks.

SELF-COMPACTING CONCRETE

Self-compacting concrete (SCC) is concrete that is designed to flow under its own weight. This eliminates the need for vibration, making it easy to place in dense reinforcement and complicated formwork and reducing construction time and costs. SCC must be fluid enough to fill a mold without vibration but not segregate. Viscosity agents, such as superplasticizer, and fine mineral admixtures are commonly used.

SCC is characterized by deformability, segregation resistance, and passing ability. Deformability, represented by the flow or fluidity of the SCC, is a measure of yield stress (Ozawa *et al.* 1992). It is quantified as the slump flow diameter, which is obtained from a modified slump test (Takada 2000). The segregation resistance is sufficient if the aggregates are uniformly distributed throughout the cement paste. It is evaluated using a penetration apparatus (Bui 2000). The segregation of aggregates has been modeled using Stoke's Law at the ACBM Center (Saak *et al.* 2000). The passing ability indicates how well the fresh SCC can flow through the spaces between rebar. It is measured using an L-box apparatus (Tangtermsirikul and Khayat 2000). These properties of SCC are affected by the rheology of the cement paste and the average diameter and spacing (D_{ss}) of aggregates.

To facilitate the design of SCC, a paste rheology model was developed at the ACBM Center (Bui *et al.* 2001). The goal was to determine the rheology of cement paste required to obtain SCC with sufficient deformability and segregation resistance for given aggregate properties. The paste rheology is characterized by yield stress, measured as the paste flow diameter, and the viscosity, measured with a standard rheometer. The model establishes, for given aggregate properties and doses, the minimum apparent paste viscosity, the minimum paste flow and the optimum flow-viscosity ratio required to achieve SCC with acceptable segregation resistance and deformability.

In a recent study at the ACBM Center, the parameters for the paste rheology were examined by varying the total aggregate ratio, the paste volume, the w/b, and the cement, fly ash and superplasticizer contents (Shah *et al.* 2002). These mixes had different degrees of deformability and segregation resistance. Plots of D_{ss} vs. flow diameter and D_{ss} vs. apparent viscosity were obtained for a constant average aggregate diameter (Shah *et al.* 2002). For a constant aggregate diameter and a given D_{ss}, there exists a minimum paste flow diameter below which the SCC exhibits poor deformability and a minimum viscosity below which the SCC segregates. Fresh SCC with a larger D_{ss} requires a smaller paste flow diameter and higher viscosity to achieve acceptable performance. To increase the aggregate spacing (D_{ss}), the paste volume of the mixture is increased, or the aggregate volume is decreased. This results in reduced friction between aggregates (Bui and Montgomery 1999). A higher viscosity is required to hold the aggregates together, and a smaller paste flow diameter is necessary to achieve good deformability.

NONDESTRUCTIVE EVALUATION

Nondestructive evaluation (NDE) uses stress waves to determine mechanical properties, the presence, location, and extent of damage, or the degree of hydration of concrete structures. Stress pulses are applied to the structure, and the transmission or reflection of the resulting waves or the vibration response of the structure is measured. Early NDE techniques relied on the transmission of a wave through a structure, which required access to both sides of the structure, making them inappropriate for concrete pavements or slabs. They were also unable to detect early stages of deterioration, i.e., the presence of microcracks, resulting from damage due to freeze-thaw cycling, sulfate attack, or rebar corrosion.

Recently, several new NDE techniques have been developed at the ACBM Center (Shah *et al.* 2000). These techniques are sensitive to the early stages of damage. A self-calibrating, one-sided technique, suitable for use on concrete pavements, was developed and shown to be sensitive to the presence of cracks (Popovics *et al.* 1998). The structural vibration frequency response can be tracked during test loading (Subramaniam *et al.* 1998) and was used to predict the remaining life of a specimen subjected to fatigue loading. Another newly developed technique, discussed in detail here, uses the reflection of wave energy at a steel-concrete interface to monitor the setting of fresh concrete.

A one-sided, ultrasonic technique has been developed to monitor the hardening and setting of fresh concrete (Öztürk *et al.* 1999, Rapoport *et al.* 2000, and Akkaya *et al.* 2001). The change in ultrasonic shear wave reflections over time between a steel plate and hardening concrete are measured to monitor the setting process. High-frequency, ultrasonic shear waves are transmitted through the steel plate into the fresh concrete. As the wave reaches the steel-concrete interface, a portion of it is transmitted through the concrete and the rest is reflected back to the transducer. The wave energy reflected at the steel-concrete interface is called the wave reflection factor (WRF). It depends on the differences in the acoustic impedance, the product of material density and wave velocity, of the steel and the hardening concrete. Initially, the value of the WRF is unity because the concrete is in a liquid state, which cannot transmit shear waves, so all of the wave energy is reflected at the interface. As the concrete stiffens, more of the wave energy is transmitted into the concrete and the WRF decreases. A typical WRF vs. time plot is shown in Figure 5. In the initial stage, the WRF equals one. At the end of the induction period, there is a sharp drop in the WRF as the concrete begins to harden. The WRF eventually approaches a final asymptote. The significance of this asymptote is not yet known. The WRF test setup is shown in Figure 6.

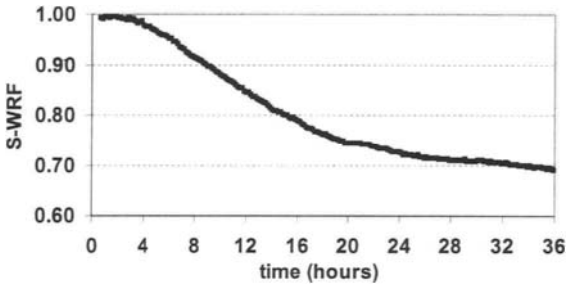


Figure 5: A typical WRF curve (Rapoport *et al.* 2000).

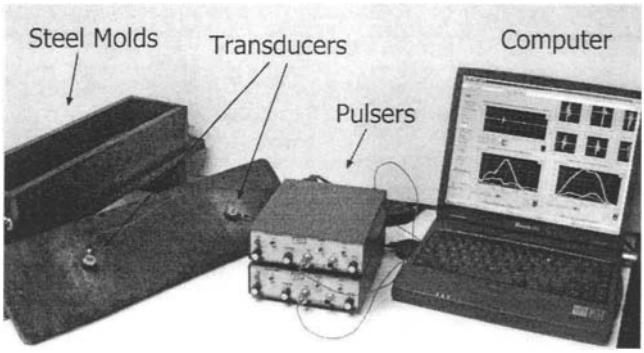


Figure 6: The WRF test apparatus.

Initial tests demonstrated the sensitivity of the WRF method to the presence of different admixtures, including accelerators, retarders, superplasticizer, and silica fume (Rapoport *et al.* 2000). WRF, pin-penetration measurements and dynamic modulus tests were performed simultaneously. The results were correlated and critical points on the WRF curve were shown to correspond to critical points in set time, temperature and dynamic modulus curves (Rapoport *et al.* 2000).

Additional work has further demonstrated the sensitivity of the technique to changes in mixture design and curing conditions and correlated the wave energy attenuation, or the inverse of the WRF, with early-age strength gain. Akkaya *et al.* (2001) measured wave energy attenuation for two different mixtures at three different curing temperatures. It is well understood that temperature affects hydration (Mindess and Young 1981). This trend is evidenced in WRF attenuation measurements. Akkaya *et al.* (2001) also compared the wave energy attenuation in mortar and concrete. Three batches of each mixture were tested. The mortar specimens showed good repeatability, while the concrete did not. The attenuation curves for mortar had the same shape and approached the same final asymptote. The shape of the attenuation curves for concrete was consistent—different stages of hydration, as indicated by distinct points on the curve, were reproduced—but each sample approached a different asymptote. This might be due to local differences in the concrete, and suggests that the homogeneity of the mixture and the final attenuation value are related.

Compressive strength tests and ultrasonic measurements were performed simultaneously to correlate wave energy attenuation with early-age strength gain (Akkaya *et al.* 2001). The results were

correlated to predict strength evolution from the change in wave energy attenuation. The relationship between strength and attenuation is linear up to three days. The linearity is not affected by changes in curing temperature or mixture design. Several tests performed outdoors demonstrated that fluctuating ambient temperatures also did not influence the linearity of the relationship between strength evolution and change in attenuation. This procedure requires the determination of one or two compressive strength values at the beginning of strength evolution—within the first day—to calibrate the strength-change-in-attenuation relationship.

CONCLUSIONS

Some of the most recent developments in concrete technology were discussed. Reactive powder concrete, one form of UHSC, has a compressive strength of 200 MPa. It is currently used in long, slender pedestrian bridges and nuclear power plants and has potential for use in pipes, tunnel linings, and nuclear waste containment. Microfiber reinforcement is used to overcome the inherent brittleness of concrete. Fiber-reinforced cementitious composites for specialized applications are produced with special processing techniques, such as extrusion, and hybrid-fiber reinforcement. Significant reductions in drying shrinkage, and thus the potential for shrinkage cracking, are achieved with the use of a newly designed shrinkage reducing admixture. The design of SCC is facilitated with a recently developed rheological model. Finally, a new nondestructive technique is used to monitor the setting and predict the strength gain of fresh concrete.

ACKNOWLEDGEMENTS

Much of the work presented here was funded by the Center for Advanced Cement Based Materials at Northwestern University. In addition, the research on extrusion is currently being funded by a grant from the National Science Foundation in support of the Partnership for Advancing Technology in Housing. The assistance of these organizations is gratefully acknowledged.

REFERENCES

Akkaya Y., Voigt, T., Kolluru, S. and Shah, S.P. (2001). Non-destructive measurement of concrete strength by an ultrasonic wave reflection method. Submitted to *RILEM Journal.*

Balogh, A. (1996). New admixture combats concrete shrinkage. *Concrete Construction.* 546-551.

Bentur, A. and Mindess, S. (1991), *Fibre Reinforced Cementitious Composites,* Elsevier Applied Science, London, UK.

Bui, V.K., Montgomery, D. (1999). Mixture proportioning method for self-compacting concrete with minimum paste volume. *Proceedings of the first RILEM Symposium on Self-Compacting Concrete.* Stockholm, Sweden. 373-384.

Bui, V.K. (2000). Penetration test of resistance to segregation. *Self-Compacting Concrete – State of the Art Report of RILEM Technical Committee 174-SCC.* ed. A. Skarendahl and O. Petersson. RILEM Report 23, 136-138.

Bui, V.K., Akkaya, Y. and Shah, S.P. (2001). A rheological model for self-consolidating concrete. Submitted to *ACI Materials Journal.*

Cyr, M.F., Peled, A. and Shah, S.P. (2001). Improving the performance of glass fiber reinforced extruded cementitious composites. *Proceedings of the 12th International Congress of the International Glassfibre Reinforced Concrete Association. GRC 2001.* ed. N. Clarke, R. Ferry. Dublin, Ireland. 163-172.

Federal Highway Administration (FHWA). (2002). A new and improved high-performance concrete. *Focus.* http://www.tfhrc.gov/focus/feb02/highperformance.htm.

Grysbowski, M. and Shah, S.P. (1990). Shrinkage cracking of fiber reinforced concrete. *ACI Materials Journal.* **87:2**, 138-148.

Kosmatka, S.H., Kerkhoff, B., Panarese, W.C. (2001), *Design and Control of Concrete Mixtures,* 14th ed., Portland Cement Association, Skokie, IL.

Lawler, J.S. (2001), *Hybrid Fiber-Reinforcement in Mortar and Concrete*, Ph.D. Thesis, submitted to Northwestern University, Evanston, IL.

Mindess, S., and Young, J.F. (1981), *Concrete,* Prentice Hall, Englewood Cliffs, New Jersey.

Ozawa, K., Maekawa, K. and Okamura, H. (1992). Development of high performance concrete. *Journal of the Faculty of Engineering. The University of Tokyo.* **3**, 381-439.

Öztürk, T., Rapoport, J., Popovics, J.S. and Shah, S.P. (1999). Monitoring the setting and hardening of cement-based materials with ultrasound. *Concrete Science and Engineering* **1**, 83-91.

Peled, A., Cyr, M.F. and Shah, S.P. (2000a). High content of fly ash (Class F) in extruded cementitious composites. *ACI Materials Journal.* **97:5**, 509-517.

Peled, A., Cyr, M. and Shah, S.P. (2000b). Hybrid fibers in high performance extruded cement composites. *Proceedings of International RILEM Symposium BEFIB'2000.* Lyon, France.

Popovics, J.S., Song, W. and Achenbach, J.D. (1998). A study of surface wave attenuation measurement for application to pavement characterization. *Structural Materials Technology III: An NDT Conference.* ed. R.D. Medlock and D.C. Laffey. Vol. 3400. International Society for Optical Engineering. Bellingham, WA. 300-308.

Powers, T.C., and Brownyard, T.L. (1948). Studies on the physical properties of hardened portland cement paste. *Bulletin 22 of the Portland Cement Association.* Chicago, IL.

Rapoport, J., Popovics, J.S., Subramaniam, K.V. and Shah, S.P. (2000). The use of ultrasound to monitor the stiffening process of portland cement concrete with admixtures. *ACI Materials Journal* **97:6**, 675-683.

Saak, A.W., Jennings, H.M. and Shah, S.P. (2001). New methodology for designing self-compacting concrete. *ACI Materials Journal.* **98:6**, 429-438.

Semioli, W.J. (2001). The new concrete technology. *Concrete International.* **23:11**, 75-79.

Shah, S.P. (1991). Do fibers increase the tensile strength of cement-based matrices? *ACI Materials Journal.* **88:6**, 595-602.

Shah S.P., Karaguler, M.E. and Sarigaphuti M. (1992). Effects of shrinkage reducing admixture on restrained shrinkage cracking of concrete. *ACI Materials Journal.* **89:3**, 289-295.

Shah, S.P. and Weiss, W.J. (1998a). Ultra high performance concrete: a look to the future. *Presented at Zia Symposium at ACI Spring Convention.* Houston, TX.

Shah, S.P., Peled, A., DeFord, D., Akkaya, Y., and Srinivasan, R. (1998b). Extrusion technology for the production of fiber-cement composites. *Sixth International Inorganic-Bonded Wood and Fiber Composite Materials Conference.* Sun Valley, Idaho.

Shah, S.P., Ouyang, C., Marikunte, S., Yang, W. and Becq-Giraudon, E. (1998c). A fracture mechanics model for shrinkage cracking of restrained concrete rings. *ACI Materials Journal.* **95:4,** 339-346.

Shah, S.P., Popovics, J.S., Subramaniam, K.V. and Aldea, C.M. (2000). New directions in concrete-health monitoring technology. *Journal of Engineering Mechanics.* **126:7**, 754-760.

Shah, S.P., Akkaya, Y. and Bui, V.K. (2002). Innovations in microstructure, processing, and properties. Accepted for publication in *Proceedings of the International Congress – Challenges of Concrete Construction.* September 2002, Dundee, Scotland.

Shao, Y., Marikunte, S. and Shah, S.P. (1995). Extruded fiber-reinforced composites. *Concrete International.* **17:4**, 48-52.

Shao, Y. and Shah, S.P. (1997). Mechanical properties of PVA fibers reinforced cement composites fabricated by extrusion processing. *ACI Materials Journal.* **94:6**, 555-564.

Subramaniam, K.V., Popovics, J.S. and Shah, S.P. (1998), Monitoring fatigue damage in concrete. *Materials Research Society Symposium Proceedings*, Materials Research Society, Warrendale, Pa. **503**, 151-158.

Takada, K. (2000). Slump flow test. *Self-Compacting Concrete – State of the Art Report of RILEM Technical Committee 174-SCC.* ed. A. Skarendahl and O. Petersson. RILEM Report 23, 117-119.

Tangtermsirikul, S. and Khayat, K. (2000). Fresh concrete properties. *Self-Compacting Concrete – State of the Art Report of RILEM Technical Committee 174-SCC.* ed. A. Skarendahl and O. Petersson. RILEM Report 23, 17-22.

Wiegrink, K., Marikunte, S. and Shah, S.P. (1996). Shrinkage cracking of high-strength concrete. *ACI Materials Journal.* **93:5**, 409-415.

Weiss, W.J., Yang, W. and Shah, S.P. (1998). Shrinkage cracking of restrained concrete slabs. *Journal of Engineering Mechanics.* **124:7**, 765-774.

This Page Intentionally Left Blank

Advances in Building Technology, Volume 1
M. Anson, J.M. Ko and E.S.S. Lam (Eds.)
© 2002 Elsevier Science Ltd. All rights reserved

HUMAN REQUIREMENTS IN FUTURE AIR-CONDITIONED ENVIRONMENTS

P. Ole Fanger, Professor, D.Sc., Hon.D.Sc.

Director, International Centre for Indoor Environment and Energy,
Technical University of Denmark, DK-2800 Lyngby, Denmark
www.ie.dtu.dk

ABSTRACT

Air-conditioning of buildings has played a very positive role for economic development in warm climates. Still its image is globally mixed. Field studies demonstrate that there are substantial numbers of dissatisfied people in many buildings, among them those suffering from SBS symptoms, even though existing standards and guidelines are met. A paradigm shift from rather mediocre to excellent indoor environments is foreseen in buildings in the 21st century. Based on existing information and on new research results, five principles are suggested as elements behind a new philosophy of excellence in the built environment: better indoor air quality increases productivity and decreases SBS symptoms; unnecessary indoor pollution sources should be avoided; the air should be served cool and dry to the occupants; personalized ventilation, i.e. small amounts of clean air, should be provided gently, close to the breathing zone of each individual; individual control of the airflow and or the thermal environment should be provided. These principles of excellence should be combined with energy efficiency and sustainability of future buildings.

KEYWORDS

Indoor air quality; Thermal comfort; Productivity; Personalized ventilation; Ventilation

INTRODUCTION

Air-conditioning of buildings has been essential for economic development in areas with warm climates or warm summers. There are numerous examples of the positive impact of air-conditioning, e.g. in eastern Asia, where over the last 30 years a remarkably strong economic growth rate has been experienced which would hardly have been possible without the widespread use of air-conditioning.

Today air-conditioning is used in many parts of the world, often in combination with heating and ventilation in HVAC systems. The image of such systems, however, is not always positive. The purpose of most systems is to provide thermal comfort and an acceptable indoor air quality for human occupants. But numerous field studies (Fisk et al., 1993; Mendell, 1993; Bluyssen et al., 1996; Lee et al., 1999; Sekhar, S.C. et al., 2000) have documented substantial rates of

dissatisfaction with the indoor environment in many buildings. One of the main reasons is that the requirements of existing ventilation standards and guidelines (ASHRAE, 1984; CEN, 1998) are quite low. The philosophy of these documents has been to establish an indoor air quality where less than a certain percentage (e.g. 15%, 20% or 30%) of people are dissatisfied with the indoor air quality, while the rest may find the IAQ barely acceptable. A similar thinking applies to the thermal environment. This philosophy behind the design of HVAC systems has led in practice to quite a number of dissatisfied persons (as predicted), while few seem to be ready to characterize the indoor environment as outstanding. At the same time numerous negative effects on human health are reported: many persons suffer from SBS (Sick Building Syndrome) symptoms (Fisk et al., 1993; Mendell, 1993, Bluyssen et al., 1996) and a dramatic increase in cases of allergy and asthma have been related to poor IAQ, especially in dwellings (Bornehag et al., 2001).

I think it is fair to say that the indoor air quality is quite mediocre in many air-conditioned or mechanically ventilated buildings, even though existing standards may be met (Lee et al, 1999; Sekhar et al., 2000). Two factors have contributed to a lowering of indoor air quality during recent decades: a general decrement in ventilation rates to save energy; and an increment in indoor air pollution sources from the many new materials and electronic processes introduced during this period. We need a paradigm shift in the new century to search for excellence in the indoor environment. Our aim should be to provide indoor air that is perceived as fresh, pleasant and stimulating, with no negative effects on health, and a thermal environment perceived as comfortable by almost all occupants. In achieving this aim, due consideration must be given to energy efficiency and sustainability. Do we have the necessary information to implement this in practice? Yes, on thermal comfort we do have a comprehensive database, while our knowledge on indoor air quality is still rather incomplete. This reflects the complexity of the interaction between indoor air quality and human comfort and health. But we do have some information on IAQ, however, as well as important new research results that will have a significant impact on the design of future air-conditioned or ventilated spaces for human occupants.

This article will discuss some principles and new research results believed to be essential for providing excellence in future indoor environments.

PRODUCTIVITY AND INDOOR AIR QUALITY

Three recent independent studies document that the quality of indoor air has a significant and positive influence on the productivity of office workers. In one study, a well-controlled normal office (field lab) was used in which two different air qualities were established by including or excluding an extra pollution source, invisible to the occupants (Wargocki et al., 1999). The two cases corresponded to a low-polluting and a non-low-polluting building as specified in the new European guidelines for the design of indoor environments (CEN, 1998).The same subjects worked for 4-1/2 hours on simulated office work in each of the two air qualities. The ventilation rate and all other environmental factors were the same under the two conditions. The productivity of the subjects was found to be 6.5% higher ($P<0.003$) in good air quality (Figure 1) and they also made fewer errors and experienced fewer SBS symptoms. This study performed in Denmark has later been repeated in Sweden with similar results (Lagercrantz et al., 2000ree different ventilation rates: 3, 10 and 30 l/s·person (Wargocki et al., 2000a). The productivity increased significantly with increased ventilation (Figure 2). The three studies involving seven experimental conditions and 90 subjects have been analysed as a whole, relating productivity to perceived air quality (Wargocki et al., 2000b). The results are presented in Figure 3 and show a significant influence of perceived air quality on productivity in offices. An improvement of perceived air quality by 1 decipol increased

productivity by 0.5%. The results of three blind studies document that improved air quality increases productivity significantly.

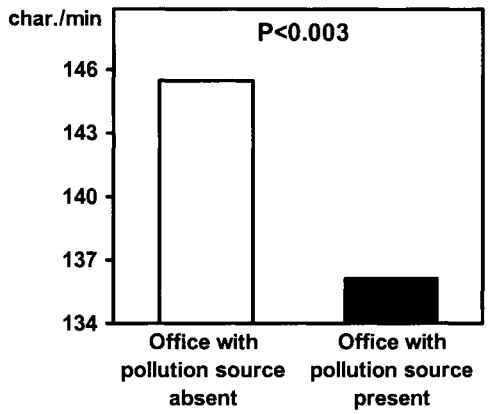


Figure 1. Impact of indoor air pollution on productivity, i.e. number of characters typed on a PC (Wargocki et al., 1999)

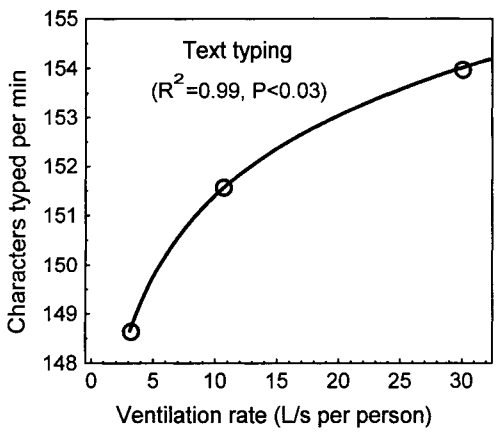


Figure 2. Impact of ventilation rate on productivity (Wargocki et al., 2000a)

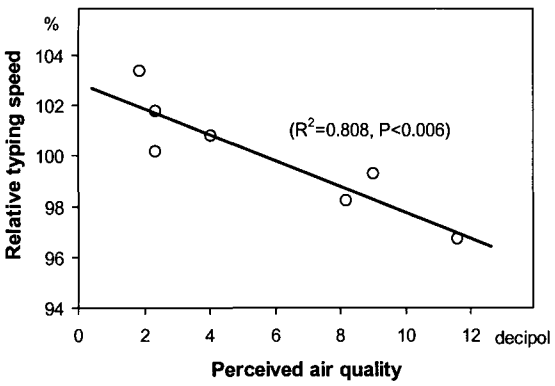


Figure 3. Relation between perceived air quality and productivity (Wargocki et al., 2000b)

POLLUTION SOURCE CONTROL AND VENTILATION

Avoiding unnecessary indoor air pollution sources is the most obvious way of improving the IAQ. Its effect on productivity and SBS symptoms has been demonstrated in the studies discussed above (Wargocki et al., 1999; Lagercrantz et al., 2000). Source control has also been used with great success outdoors and is the reason why the outdoor air quality in many cities in the developed world is much better today than it was 20 or 50 years ago.

In the new European guidelines for the indoor environment (CEN CR 1752) (CEN, 1998), there is strong encouragement to design low-polluting buildings and recommendations on low-polluting building materials are given. The same applies to ASHRAE Standard 62 (1989). Systematic selection of materials planned to be used in a building to avoid the well-known cases of SBS caused by polluting materials is common practice in several countries, e.g. in Scandinavia. Other pollution sources are electronic equipment in offices. A recent study (Bakó-Biró, Z. et al., 2002) has thus documented that personal computers can be a serious indoor pollution source. Air pollution from PCs of a common brand used for three months were found to decrease the perceived air quality and productivity significantly. Each computer had a sensory pollution source strength of 3 olfs, i.e. polluted equally as much as 3 persons. PCs and other electronic equipment provide in many cases an important pollution load requiring much extra ventilation. An obvious solution is that the PCs be modified so that their pollution load is negligible in the future. Pollution sources in the HVAC system are a serious fault, degrading the quality of the air even before it is supplied to the conditioned space. Used particle filters have been shown to degrade the perceived air quality and to contribute to SBS symptoms (Clausen, 2002). The selection of materials, components and processes, as well as maintenance of the HVAC system, should be given high priority in future.

Source control is the obvious way to provide good indoor air quality with a simultaneous decrease in the consumption of energy. But increased ventilation also improves the IAQ and decreases SBS symptoms as demonstrated by Sundell's classic field studies in 160 office buildings studies (Sundell, 1994) (Fig. 4). A multidisciplinary group pf scientists in Europe (EUROVEN) recently

reviewed the peer-reviewed literature concerning the relation between health and ventilation. The group concluded that decreasing the outdoor air supply rates below 25 L/s per person increased the risk of SBS symptoms, increases short-term sick leave and decreases procuctivity among occupants of office buildings (Wargocki et al., 2002).

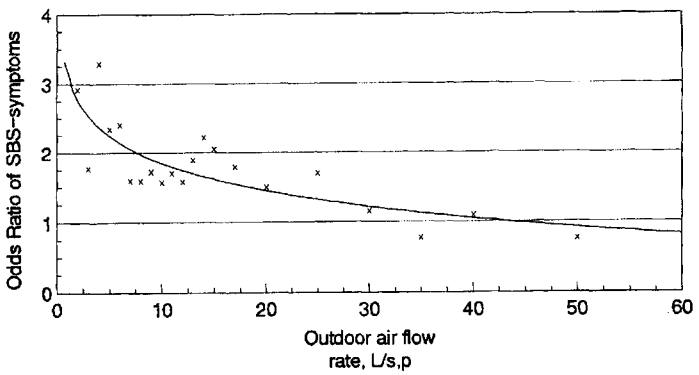


Fig. 4. SBS symptoms as a function of outdoor ventilation rate in 160 office buildings in Sweden (Sundell, 1994)

SERVE THE AIR COOL AND DRY

In ventilation standards, indoor air humidity has for decades been overlooked. It has been generally accepted that the relative humidity was rather unimportant for human beings as long as it was kept between approximately 30% and 70% (CEN, 1998; ASHRAE, 1989). This consensus stems from the fact that the humidity in the comfort range of temperatures has a minor impact on the thermal sensation of the entire human body (ASHRAE, 1992, ISO, 1993).

All existing ventilation standards and guidelines are based on the following thinking: there are certain pollution sources in a space and ventilation is required in order to dilute the chemical pollutants to a level where they are perceived as acceptable to humans. The thinking is that air is perceived exclusively by the olfactory and chemical senses and that the perception depends only on the chemical composition of the air. The implied conclusion is that the required ventilation is independent of temperature and humidity. However, a paper by Berglund and Cain indicated in 1989 that temperature and humidity have an impact on the perception of clean air in a climate chamber (Berglund and Cain, 1989).

New comprehensive studies at the International Centre for Indoor Environment and Energy have confirmed that perceived air quality is strongly influenced by the humidity and temperature of the air we inhale. People prefer rather dry and cool air. The strong effect of humidity and temperature on perceived air quality was proven in experiments where 36 subjects judged the acceptability of air polluted by different typical building materials in a climate chamber (Fang et al., 1997).

It is the effect of humidity and temperature combined in the enthalpy of the air that is essential for the perceived air quality as shown in Figure 5. The enthalpy was changed in the room while the

chemical composition of the air was constant and the thermal sensation for the entire body was kept neutral by modification of the subjects' clothing. The acceptability did not change with time, i.e. no adaptation took place.

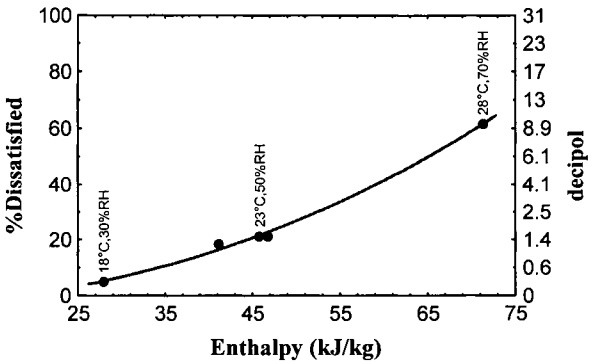


Fig. 5. Perception of clean air during whole-body exposure of persons to different levels of indoor air enthalpy (Fang et al., 1997).

The impact of enthalpy on acceptability or on perceived air quality expressed in percent dissatisfied or decipol is strong. Two other independent studies at the International Centre for Indoor Environment and Energy where approximately 70 subjects were exposed to numerous combinations of humidity and temperature on the face also showed an excellent correlation between enthalpy and acceptability (Fang et al., 1998; Toftum et al., 1998) with an even stronger impact of enthalpy.

Humans obviously like a sensation of cooling of the respiratory tract each time air is inhaled. This causes a sensation of freshness which is felt pleasant. If proper cooling does not occur, the air may be felt stale, stuffy and unacceptable. A high enthalpy means a low cooling power of the inhaled air and therefore an insufficient convective and evaporative cooling of the respiratory tract, and in particular the nose. This lack of proper cooling is closely related to poorly perceived air quality. The phenomenon is analogous to the well-known strong impact of temperature on perceived quality during intake of drinks, e.g. water or wine.

Heat loss through respiration is only around 10% of the total heat loss from the body and humidity and temperature of the inhaled air have therefore only a small impact on the thermal sensation for the human body as a whole. This is presumably why humidity has previously been overlooked. The new studies show that the local effect of temperature and humidity on the respiratory tract and therefore on perceived air quality is one order of magnitude higher than for whole-body thermal sensations. This new evidence has quite dramatic practical consequences. It is obvious that the enthalpy has a strong impact on ventilation requirements and therefore on energy consumption. Fang et al. (1999) showed thus in the most recent study that people perceive the IAQ better at 20°C and 40% RH and a small ventilation rate of 3.5 l/s·person than at 23°C and 50% RH at a ventilation rate of 10 l/s·person.

It is advantageous to maintain a moderately low humidity and a temperature that is at the lower end of the range required for thermal neutrality for the body as a whole. This will improve the perceived air quality and decrease the required ventilation. Field studies (Andersson et al., 1995; Krogstad et al., 1991) show that moderate air temperatures and humidities also decrease SBS symptoms. Moderate temperatures and humidities may furthermore result in potential energy savings, during both winter and summer. The advice is therefore: serve the air cool and dry.

SERVE THE AIR WHERE IT IS CONSUMED

In many ventilated rooms the outdoor air supplied is of the order of magnitude of 10 l/s·person. Of this air, only 0.1 l/s·person, or 1%, is inhaled. The rest, i.e. 99% of the supplied air, is not used. What a huge waste! And the 1% of the ventilation air being inhaled is not even clean. It is polluted by bioeffluents, emissions from building materials and sometimes even by ETS before it is inhaled.

According to normal engineering practice, full mixing of clean air and pollutants seems to be an ideal. With displacement ventilation systems, one may be proud of reaching a ventilation effectiveness of 1.2. What I foresee in the future are systems that supply rather small quantities of clean air close to the breathing zone of each individual. The idea is to serve to each occupant, clean air that is as unpolluted as possible by the pollution sources in the space. We would hesitate to drink water from a swimming pool polluted by human bioeffluents. Still we accept consuming indoor air polluted by human bioeffluents and other contaminants. Why not serve small quantities of high-quality air direct to each individual rather than plenty of mediocre air throughout the space? Such air may be provided by a personalized ventilation system with a terminal device close to the breathing zone (Fig. 6). The person inhales clean, cool and dry air from the core of the jet where the air is unmixed with polluted room air and has a low velocity and turbulence which do not cause draught. The position of the air terminal devide should be easily movable by each individual, who also should be able to control the airflow, its direction and its temperature. Studies on personalized ventilation have recently been published by Kaczmarczyk et al. (2002) and Cermak (2002).

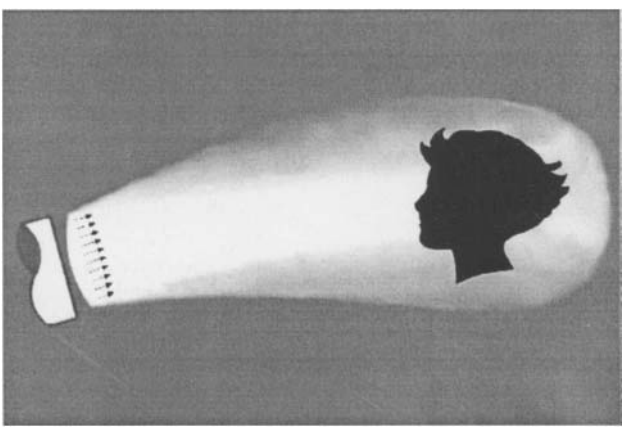


Fig. 6. The principle of personalized ventilation: small amounts of cool, dry, and clean air supplied directly and gently to a person's breathing zone

INDIVIDUAL THERMAL CONTROL

In buildings where many people occupy the same space it is difficult to provide thermal comfort for everyone at the same time .A compromise is therefore usually aimed at which satisfies most people. The PMV model (Fanger, 1970) included in ISO, ASHRAE and European standards and guidelines (ASHRAE, 1989; ISO, 1993) specifies such compromises. Due to well-known differences in preferred temperature between people, there will still be persons who are dissatisfied with the thermal environment. To accommodate these differences between people, individual thermal control is an obvious solution. This may in practice be realized by slight local heating or cooling of each individual by conduction (through seat and chair back), radiation or convection.

CONCLUSIONS

Air-conditioning of buildings has played an important role for the economic development in areas of the world with warm climates or warm summers. Still, the indoor environment in many air-conditioned buildings is rather mediocre and gives rise to frequent complaints, even though present standards are met. A paradigm shift is foreseen with a search for excellence of the indoor environment rather than the present effort to reduce dissatisfaction and complaints.

The following principles may be useful steps in realizing such a new philosophy of excellence.

- Better indoor air quality pays as it results in higher productivity and causes fewer SBS symptoms.
- Unnecessary pollution sources frequently occurring in present buildings should be avoided.
- The air should be served cool and dry for people.
- Small amounts of clean air should be served where it is consumed, i.e. by personalized ventilation close to the breathing zone of each person and individually controlled.
- Individual thermal control should be established to handle personal differences in thermal preference.

The challenge for the engineering community in the future is to combine the above principles of excellence for humans with energy efficiency and sustainability.

ACKNOWLEDGEMENT

The Danish Technical Research Council is acknowledged for its support to the International Centre for Indoor Environment and Energy.

REFERENCES

Andersson, N.H., Frisk, P., Löfstedt, B., Wyon, D.P,. 1975, *Human Responses to Dry, Humidified and Intermittently Humidified Air in Large Office Buildings*. Gävle, Swedish Building Research (D11).

ASHRAE Standard 62-1989, 1989, *Ventilation for Acceptable Indoor Air Quality*, Atlanta, USA, American Society of Heating, Refrigerating and Air-Conditioning Engineers, Inc.

ASHRAE, 2002, *Thermal Environmental Conditions for Human Occupancy*. Atlanta, GA, American Society of Heating, Refrigerating and Air-Conditioning Engineers (ANSI/ASHRAE Standard 55.2002).

Bakó-Biró, Z.m Wargocki, P., Weschler, C., Fanger, P.O., 2002, Personal comuters pollute indoor air: effects on perceived air quality, SBS symptoms and productivity in offices. In: Proceedings of Indoor Air 2002, Monterey.

Berglund, L., Cain, W.S., 1989. Perceived air quality and the thermal environment, *Proc. of IAQ'89: The Human Equation: Health and Comfort*, Atlanta, GA, American Society of Heating, Ventilating and Air-Conditioning Engineers, pp. 93-99.

Bluyssen, P.M., de Oliveira Fernandes, E., Groes, L., Clausen, G., Fanger, P.O., Valbjørn, O., Bernhard, C.A., Roulet C.A., 1996, European indoor air quality audit project in 56 office buildings, *Indoor Air*, Vol. 6, pp. 221-238.

Bornehag, C.-G. et al., 2001, Dampness in buildings and health, *Indoor Air*, **11**(2), 72-86.

CEN, 1998, *Ventilation for Buildings: Design Criteria for the Indoor Environment*, Brussels, European Committee for Standardization (CR 1752).

Cermak, R., Majer, M., Melikov, A., 2002, Measurements and prediction of inhaled air quality with personalized ventilation. In: Proceedings of Indoor Air 2002, Monterey.

Clausen, G., Alm, O., Fanger, P.O., 2002, The impact of air pollution from used ventilation filters on human comfort and health. In: Proceedings of Indoor Air 2002, Monterey.

Fang, L, Clausen, G., Fanger, P.O., 1997, Impact of temperature and humidity on perception of indoor air quality during immediate and longer whole-body exposure, *Indoor Air*, Vol. 8, No. 4, pp. 276-284.

Fang, L., Clausen, G., Fanger, P.O., 1998, Impact of temperature and humidity on the perception of indoor air quality, *Indoor Air*, Vol. 8, No. 2, pp. 80-90.

Fang, L., Wargocki, P., Witterseh, T., Clausen, G., Fanger, P.O., 1999, Field study on the impact of temperature, humidity and ventilation on perceived air quality, *Proc. of Indoor Air '99*, Vol. 2, pp. 107-112.

Fanger, P.O., 1970, *Thermal comfort – analysis and applications in environmental engineering*. Copenhagen, Danish Technical Press.

Fisk, W.J., Mendell, M.J., Daisey, J.M., Faulkner, D., Hodgson, A.T., Macher, J.M. , 1993, The California healthy building study, Phase 1: a summary, *Proc. of Indoor Air '93*, Vol. 1, pp. 279-284.

Fisk, W.J. and Rosenfeld, A.H., 1997, Estimates of improved productivity and health from better indoor environments, *Indoor Air*, Vol. 7, pp. 158-172 [Errata in *Indoor Air*, 1998, Vol. 8, p. 301].

International Organization for Standardization. 1993. *Moderate Thermal Environments - Determination of the PMV and PPD Indices and Specification of the Conditions for Thermal Comfort* (EN ISO Standard 7730).

Kaczmarczyk, J., Zeng, Q., Melikov, A., Fanger, P.O. 2002, The effect of a personalized ventilation system on perceived air quality and SBS symptoms. In: Proceedings of Indoor Air 2002, Monterey.

Krogstad, A.L., Swanbeck, G., Barregård, L. et al., 1991, *Besvär vid kontorsarbete med olika temperaturer i arbetslokalen - en prospektiv undersökning* [A prospective study of indoor climate problems at different temperatures in offices], Göteborg, Volvo Truck Corp.

Lagercrantz, L., Wistrand, M., Willén, U., Wargocki, P., Witterseh, T., Sundell, J., 2000, Negative impact of air pollution on productivity: previous Danish findings repeated in new Swedish test room, Paper submitted to *Healthy Buildings 2000.*

Lee, S.C., Chan, L.Y., Chiu, M.Y., 1999, Indsoor and outdoor air quality investigation at 14 public places in Hong Kon,. *Environment International*, **25**, 443-450.

Mendell, M.J., 1993, Non-specific symptoms in office workers: a review and summary of the epidemiologic literature, *Indoor Air*, Vol. 3, pp. 227-236.

Sekhar, S.C., Tham, K.W., Cheong, K.W., Wong, N.H., 2000, A study of indoor pollutant standard index (IPSI) and building symptom index (BSI). In: Proceedings of Healthy Buildings, **1**, 145-150.

Seppänen, O., 1999, Estimated cost of indoor climate in Finnish buildings. *Proc. of Indoor Air '99*, Edinburgh, Vol. 4, pp. 13-18.

Sundell, J., 1994, On the association between building ventilation characteristics, some indoor environmental exposures, some allergic manifestations and subjective symptom reports, *Indoor Air*, Supplement No. 2.

Toftum, J., Jørgensen, A.S., Fanger, P.O., 1998, Upper limits for air humidity to prevent warm respiratory discomfort, *Energy and Buildings*, Vol. 28, No. 1, pp. 15-23.

Wargocki, P., Wyon, D.P., Baik, Y.K., Clausen, G., Fanger, P.O. 1999, Perceived air quality, sick building syndrome (SBS) symptoms and productivity in an office with two different pollution loads, *Indoor Air*, Vol. 9, No. 3, pp. 165-179.

Wargocki, P., Fanger, P.O., 1999, Impact of ventilation rates on SBS symptoms and productivity in offices, *Proc. of DKV-Jahrestagung*, Berlin, Vol. IV.

Wargocki, P., Wyon, D.P., Sundell, J., Clausen, G., Fanger, P.O., 2000, The effects of outdoor air supply rate in an office on perceived air quality, Sick Building Syndrome (SBS) symptoms and productivity, *Indoor Air*, Vol. 10, No. 4, pp. 222-236.

Wargocki, P., Wyon, D.P., Fanger, P.O., 2000, Productivity is affected by the air quality in offices, Proc. of Healthy Buildings 2000, Vol. 1, pp. 635-640.

Wargocki, P., Sundell, J., Bischof, W., Brundrett, G., Fanger, P.O., Gyntelberg, F., Hanssen, S.O., Harrison, P., Pickering, A., Seppänen, O., Wouters, P., 2002, Ventilation and health in nonindustrial indoor environments: report from a European Multidisciplinary Scientific Consensus Meeting, *Indoor Air*, **12**(2).

Wyon, D.P., 1996, Indoor environmental effects on productivity, *Proc. of IAQ '96*, Atlanta, GA, American Society for Heating, Refrigerating and Air-Conditioning Engineers, pp. 5-15.

Advances in Building Technology, Volume 1
M. Anson, J.M. Ko and E.S.S. Lam (Eds.)
© 2002 Elsevier Science Ltd. All rights reserved

CREATING COMPETITIVE ADVANTAGE AND PROFITS WITH TECHNOLOGY IN THE CONSTRUCTION SECTOR

Roger Flanagan
School of Construction Management and Engineering
The University of Reading, Reading, RG6 6AW UK

ABSTRACT

The construction sector is often accused of a lack of investment in R&D. However, this does not reflect the huge investment made by design organisations, contractors, plant manufacturers and materials and component manufacturers in the development of their services and products. A number of countries have selected 'critical technologies' for investment over the medium to long term; these include smart materials, biomimetics, and nanotechnology. The construction sector has not been good at applying technologies from other industries, and frequently duplication of effort occurs. There must be a balance between technology push and market pull, which is reflected in enterprises' profits. New technology does not guarantee profits, but it can offer competitive advantage. The development of new products and processes cannot be divorced from the development of codes and standards.

Keywords: technology, competitive advantage, construction sector.

INTRODUCTION

This paper investigates five facets of how enterprises can create competitive advantage from technology.

1) Global drivers of change - how technology can be used to respond.
2) A technology map - how technology is shaping the future for construction enterprises in the construction sector
3) A review of construction technology strategies in selected countries.
4) New technology - some examples and how the construction sector can learn from other industries.
5) Profiting from technology.

FACET 1 GLOBAL DRIVERS OF CHANGE

Globalisation has created an interconnected and interdependent world but also an uneven one. We live in a world with a growing gulf between the haves and have-nots, the digitally rich and the digitally deprived. Economies, culture, organisations and interest groups are becoming linked together across national boundaries. Sources of saving and investment, capital markets, that were once distinct, have now become coupled together with the consequence of near-universal standards of performance of capital assets. Investors want the best they can find anywhere in the world. There is a shift from public to private sector financing of infrastructure and the utilities.

Construction sectors around the world cannot be immune from the global drivers that have an impact upon the economy and quality of life. The drivers of change for the beginning of the 21st century involve social, technological, economic, environmental and political trends; they are the factors that cannot be changed and are an inevitable result of development in the broadest sense. Their effects can be global or national.

- **Technology, knowledge and skills**
  The growing importance of technology, knowledge, and skills are now crucial with the move towards knowledge-based business with knowledge technology becoming central to all business. The level of performance of the world's best is constantly being raised as a result of innovation in communications, technology and learning. The centre of gravity in business success is shifting from the exploitation of physical assets to the realisation of the creativity and learning potential of people.

- **Globalisation - economic liberalisation and barriers to trade falling**
  Globalisation in construction can be seen with the growth in imported construction components and materials, and the increase in foreign companies working overseas. The fastest growing element in world trade is information, increasingly sent by satellite or down telephone wires. The implication of globalisation is that instead of the world being made up of a series of different economies that determine their own business conditions, the economic conditions in most parts of the world will be determined by the world economic position.

- **Demographic trends are impacting the world**
  Age distribution has significant effects on economic growth. The world's human population currently numbers about 5.8 billion people, and the figure grows by more than 80 million people each year, or around 220,000 each day. The industrialised countries face the problems of an ageing population and the implications of pensions provision, an ageing workforce, availability of human resources, and the provision of more facilities for an ageing population. In the developed world technology will provide the answer to improving productivity and wealth creation with a smaller workforce supporting more people. The developing countries give a different picture, unsustainable population growth is more of an issue. In the developing world technology will provide the means to alleviate poverty and increase competitiveness.

- **Pace of economic and technological change is accelerating**
  During the industrial revolution it took 60 years for productivity per person to double, it recently took China 10 years to achieve the same improvement. 70% of all the scientists who have ever lived are alive today. Companies must focus on service and productivity - increasing fast, flexible, customised, networked and global with clear specialisation. Rapid improvement based on continuous learning or a step-change in performance has become a critical success factor.

- **More competition**
  This will come from the developing world with the spread of literacy and the growth in the birth rate. In the next 15 years, technology will improve the literacy and skills of people in the developing world.

- **New employment patterns and organisational structures**
  New employment patterns with the old idea of the "employer and employee" becoming obsolete. No one can feel secure in the sense of lifetime employment. Only those who learn new skills will achieve long-term employability. Work is becoming less full-time; in 1994 less than 60% of employment was full time with a growth in temporary and part time workers. Service providers are growing in importance with outsourcing to specialist providers.

- **Changing client expectations**
  Customers are becoming more demanding and seeking reliability, consistency, and value for money. Ethical issues are high on customer's priorities. There is increasing need for companies to maintain public confidence in the legitimacy of their operations and business conduct - a licence to operate. Growing importance of developing community relationships by increasing participation in national and local community partnerships.

- **Growing importance of sustainability and environmental issues**
  Issues with sustainability and the greening of construction are high on the agenda of global summits. Water and other natural resources, including energy, will become more scarce and more

valuable. Over 1 billion people in the world are without safe drinking water. Almost 3 billion people (roughly half the world's population) are without adequate sanitation in developing countries. Technology has the solutions to provide safe drinking water, but the issue is at what cost.

- **New patterns of transportation**
  Traffic congestion on the roads is becoming a major issue in all big cities. Car manufacturers produce cars, irrespective of the available space on the roads. As a result, the demand for road and rail transportation in the future will be for the infrastructure to be built underground. Therefore, new technology for tunnels and ventilation systems will be required that will make the process more cost effective. Advanced Transport Telematics (ATT), is specifically concerned with improving safety and efficiency in all forms of transport and reducing damage to the environment.
- **Growth of privatisation of infrastructure and built facilities**
  In the developed world there is a shift towards privatisation of new infrastructure for roads, rail, telecommunications, water, sewerage, and power supplies.

Drivers cannot be controlled; they need to be addressed. The construction sector may be tempted to say that these will not impact their business: they would be wrong.

FACET 2 TECHNOLOGY MAP

The word 'technology' comes from the Greek 'technologia', meaning systematic treatment and describes the use of scientific knowledge for practical purposes. 'Technology' can be understood as the systematic use of knowledge usually seen in actual machines or in industry. It can also be defined as the application of the existing body of knowledge (science) to the production of goods and services; it embraces equipment, tools, techniques, materials, systems, processes, information, etc., (*Ofori, 1994*). Technology takes different forms: 'hardware', such as machinery and equipment; 'software', such as drawings and process specification; and the 'service' of technicians and professionals for tasks such as quality improvement, management and marketing know-how, process and product design. The pervasive nature of the concept of technology raises several problems in relating technology to growth (*Jeremy, 1994*).

Figure 1 shows a simplistic overview of the process and impact of technology for construction.

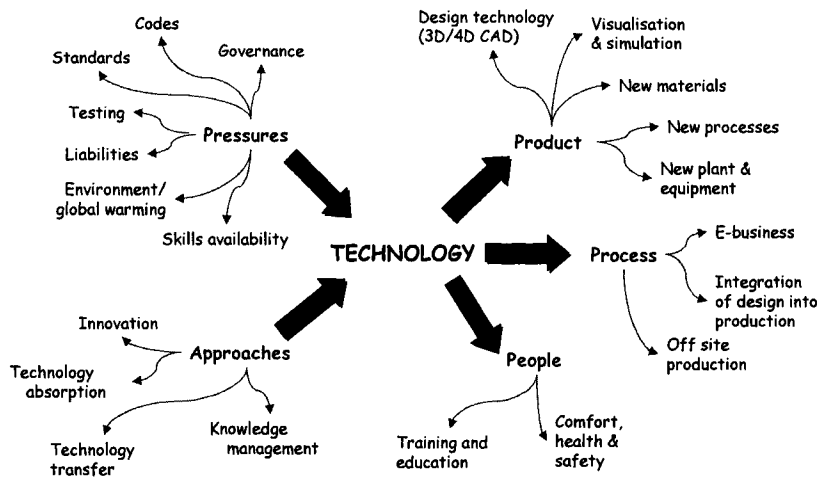


Figure 1 Technology map

- **Pressures** come from such issues as the requirement of codes and standards for new materials and products, both nationally and internationally. These should not be underestimated in importance, particularly with the liability issues and risk with new products. Similarly, governments, and even global regimes, will impose standards that must be met. New emission regulations are a good example of this.
- **Approaches** are the way in which technology is absorbed, transferred and applied, and how knowledge is 'managed'.
- The **Product** heading relates to new materials, plant and processes, such as new tunnel equipment, soil remediation, fire retardation processes and concrete pumping innovation.
- **Process** refers to the way in which business can increase competitiveness by use of information and communication technologies, off-site prefabrication and customisation of standard components.
- **People** relates to how technology can make sites safer, such as using virtual reality to simulate accidents on site; and its role in novel training and education.

FACET 3 TECHNOLOGY STRATEGIES AROUND THE WORLD

Technological developments are irreversible. The biggest question is how fast technology will change between now and say 2020, and how that change can be properly managed. Technology enables almost anything to be done; deciding what to do becomes the critical skill. Our ability to perceive and interact with complicated, remote and, either huge or tiny, abstract or concrete things will be unprecedented. Technology gives us more and more access to information, so life gets more and more chaotic. 'Information chaos' prevails and we need to help people find the information that they want, when they want it.

Many countries in the developed world are looking to the future and developing national strategies. Japan was one of the first countries to take a futures perspective, a process that is often called 'Foresight'. There are three ways to look at the future: forecasting, assessment, and foresight. Forecasting makes probabilistic predictions of future developments; assessment anticipates future societal impacts of known new and existing technologies; and foresight identifies present science and technology priorities in the light of hypothetical projections of future economic and societal developments. They each have different functions and objectives (*Gavigan and Cahill, 1997*).

Our research showed that there was a lot of duplication of research and development effort (*Flanagan et al, 2001*). There seems to be a reluctance to learn from each other. It appears to be more attractive to start new research programmes in a country rather than learning from overseas or, at industry level, learning from other industries. Figure 2 shows the potential of learning from other industries.

Table 1 shows the issues in a number of technology strategies for construction sectors in a number of countries. Our review of these strategies revealed a number of common threads. Most governments are trying to make their construction sector more competitive by leveraging competitive advantage internationally through the use of technology, becoming more efficient, and constructing to a lower unit cost. The review revealed that many of the countries have developed very similar strategies.

FACET 4 NEW TECHNOLOGIES

A number of countries have selected 'critical technologies' for investment over the medium to long term; these include smart materials, biomimetics, and nanotechnology. Embedded systems and e-business are also areas that have been selected; they are evolving very quickly and having a huge impact on the construction sector.

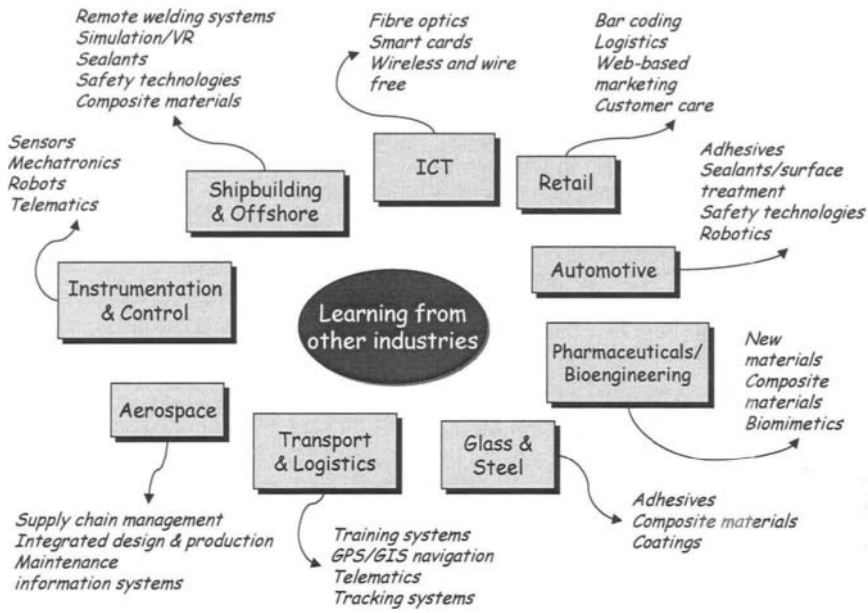


Figure 2: Learning from other industries

Table 1
CONSTRUCTION STRATEGY ISSUES AROUND THE WORLD

	Australia	Canada	Germany	Japan	Sweden	UK	USA
Intensive use of information and communication technologies	✔	✔		✔	✔	✔	✔
Development of products against market needs			✔				
Becoming a service rather than product provider						✔	✔
Process and system -orientated planning and realisation concepts			✔				
Governance, standards, and legislation	✔	✔					
Environment - embracing sustainability					✔	✔	✔
Integration and networking of all participants into all phases (feedback). Seamless industry	✔		✔				
Focus on people issues	✔			✔	✔	✔	
New construction methods				✔	✔		✔
Smart buildings and infrastructure				✔	✔	✔	
Integration of new technologies in planning, construction, and use				✔	✔	✔	
Blue sky and emerging technologies	✔	✔	✔		✔	✔	✔
Impact of new plant and equipment			✔	✔			✔
Creating competitive advantage	✔						✔

Source: Construct New South Wales, National Research Council, Bauen 21, RICE, CMB, UK Foresight reports ,CERF.

The technology of intelligent or **smart materials** uses the knowledge of a number of different technologies such as materials science, biotechnology, biomimetics, nanotechnology, molecular electronics, neural networks and artificial intelligence. These technologies are inter-related. Smart materials can be further defined as:

- Materials functioning as both sensing and actuating.
- Materials that have multiple responses to one stimulus in a co-ordinated fashion.
- Passively smart materials self-repairing or stand-by characteristics to withstand sudden changes.
- Actively smart materials utilising feedback.
- Smart materials and systems reproducing biological functions in load-bearing structural systems.

Biomimetics has been defined as 'the abstraction of good design from nature'. From the beginnings of humanity, man has been intent upon using (or abusing), and taming nature. There is a wide range of possible applications of biomimetics in building. Nature provides many examples of structures built to respond to the environment and meet the needs of the plant or animal, for example, termite towers. The fur or feathers of birds and animals are perfectly adapted for their environment and way of life. Biomimetic engineering could provide clothing that is light, responsive and strong to be used in harsh conditions on site. Mimicking nature could produce new designs in civil engineering that are lighter, stronger and adaptable to a changing environment. New adhesives, based on those produced in nature, could revolutionise the building process. Buildings could be 'glued' together, giving stronger, faster and cleaner construction techniques.

The essence of **nanotechnology** is the ability to create large structures from the bottom up, that is by starting with materials at a molecular level an building them up. The structures created – 'nanostructures' are the smallest human-made objects whose building blocks are understood from first principles in terms of their biological, chemical and physical properties. This comprehensive understanding of the make-up of nanostructures has allowed scientists to create very strong materials at a fraction of the size and weight of traditional materials. Carbon nanotubes can be constructed which are ten times the strength of steel but a sixth of its weight. Scientists can make single molecules that can behave like transistors - which makes computers the size of a sugar cube a possibility! Nanoparticles can target and kill cancer cells.

As with biomimetics and smart materials and structures, nanotechnology embraces and requires cross-disciplinary work involving physics, chemistry, biology, medicine, engineering and computer simulation. The understanding and determination of properties and processes at a molecular scale, means that nanotechnology could impact on virtually every human-made object, from cars to computer circuits, and from tissue replacements to bridges. Nanostructured ceramics, polymers and metals will have vastly improved mechanical properties. In particular, nanostructured silicates and polymers will act as contaminant scavengers to create a cleaner environment.

A number of industrial applications are beginning to emerge that exploit the newly emerging Internet capabilities of **embedded systems**. Embedded systems differ markedly from desktop systems, being fitted with just enough functionality to handle a specific application, enabling them to be produced at low-cost. Such systems have a more limited processing speed, CPU power, display capability and persistent storage capability. The challenge for developers is to produce embedded systems that are able to provide network functionality within these constraints. The future is where all electronic devices are ubiquitous and so are networked and every object, whether it is physical or electronic, is electronically tagged with information pertinent to that object. The use of physical tags will allow remote, contactless interrogation of their contents; thus, enabling all physical objects to act as nodes in a networked physical world. This technology will benefit supply chain management and inventory control, product tracking and location identification, and human-computer and human-object interfaces. In the construction sector, auto-ID technologies would have a huge impact on the supply chain, the design process, the construction process and facilities management.

FACET 5 PROFITING FROM TECHNOLOGY

The construction sector is often accused of a lack of investment in R&D: This statement does not reflect the huge investment made by design organisations, plant manufacturers and materials and component manufacturers in the development of their services and products. Whilst research and development is a good long-term investment; enterprises can only invest sums that can be justified to the shareholders. The challenge is how to measure the returns from research investment in developing technology. For example, in the manufacturing, chemical, automotive, aerospace, pharmaceutical and electronic industries, research is often laboratory-based, and results in new products or materials that can be patented. More importantly, in a less fragmented industry, such as aerospace, there are a few large clients and a small number of suppliers – BAE accounts for 60% of the UK supplier output. The aerospace industry also benefits from fixed locations, high barriers to entry and long time frames compared to the construction sector. This provides an environment in which research can be fostered. In the UK aerospace industry there are 420 SMEs, in construction there are 123,000 (DTI, UK).

The fragmentation in the construction sector does not preclude research, but makes it more difficult to quantify, justify, and to retain for competitive advantage. Therefore, construction enterprises need to balance new technology against their prime aim of maintaining sensible profit margins that show a reasonable return on the capital employed in the business. Any technology that involves high levels of risk must correspondingly carry better margins. Owners and shareholders want faster returns; construction enterprises aim to improve productivity, and correspondingly aim to increase margins, and; enterprises must balance risk and reward. With products, plant and equipment, it is easier to obtain a patent and to earn money from the application of new technology. For example, Pilkington have developed Activ™ self-cleaning glass. "Its unique dual-action uses the forces of nature to help keep the glass free from organic dirt"; this means less cleaning and better-looking windows. Hilti have developed a 'smart' drill with embedded intelligence that removes the guesswork out of drilling into different materials.

CONCLUSIONS

Technology is making a difference in construction, it is possible to leverage profit from innovation and new technology. Global drivers will put pressure on enterprises to find solutions using technology. For example, in the developed world changes in demographics will mean fewer workers leading to a skill shortage. Ultimately, there will need to be more off-site prefabrication and more mechanisation, which can be achieved through new technologies such as advances in materials science an information and communication technologies.

The importance of codes and standards should not be underestimated in the development of new technology. A new high-strength concrete will not be used unless it complies with the standard developed to cope with it, and that has been fully tested. The differences between market pull and technology push should be recognised.

Knowledge sitting on the bookshelf is of absolutely no value; this is often called 'knowing at rest'. There is a need to connect knowledge and knowing with connections between the way that people work, the way they are organised into their work, the way they get information and the way they use it.

REFERENCES

Aichholzer, G. (2000) **Delphi Austria: an example of tailoring Foresight to the needs of a small country**. Institute of Technology Assessment (ITA), Austrian Academy of Sciences on United Nations Industrial Development Organisation (UNIDO) web site http://www.unido.org/userfiles/kaufmanC/AichholzerPaper.pdf

Blind, Dr K. (2001) **Delphi As A Technology Foresight Methodology: Experiences From Germany**. Fraunhofer Institute for Systems and Innovation Research on United Nations Industrial Development Organisation (UNIDO) web site http://www.unido.org/userfiles/kaufmanC/BlindPaper.pdf

Flanagan, R. (1999) **Lessons for UK Foresight from around the world**. Construction Associate Programme, Office of Science and Technology, London.

Flanagan, R., Jewell, C.A., Larsson, B. and Sfeir, C. (2001) **Vision 2020 – Building Sweden's future**. CMB, Gothenburg, Sweden. ISBN 0 7049 12066.

Foresight (2001) **Constructing the Future**. Construction Associate programme, Built Environment and Transport Panel, Foresight, Office of Science and Technology, UK.DTI Pub 5567 3k/06/01/NP. URN 01/884

Gavigan, J.P. and Cahill E.A. (1997) **Overview of recent European and non-European National Technology Foresight studies**, Technical report TR97/02 European Commission JRC Institute for Prospective Technological Studies, Seville

Jeremy, D.J. (1994) **Technology transfer and business enterprise**. Edward Elga Publishing, UK.

Klusacek, K. (2000) **Technology Foresight In The Czech Republic**, Technology Centre, Academy of Sciences of the Czech Republic on United Nations Industrial Development Organisation (UNIDO) web site http://www.unido.org/userfiles/kaufmanC/KlusacekPaper.pdf

Kozlowski, J. (2001) **Adaptation of foresight exercises in Central and Eastern European countries** on United Nations Industrial Development Organisation (UNIDO) web site http://www.unido.org/userfiles/kaufmanC/Koslowskipaper.pdf

Ksenofontov, M. (2000) **Technology foresight in the Russian Federation: Background, modern social, economic and political context and agenda for the future**. Institute of Economic Forecasting, Russian Academy of Sciences on United Nations Industrial Development Organisation (UNIDO) web site http://www.unido.org/userfiles/kaufmanC/KsenofontovPaper.pdf

Lübeck, L. (2000) **The Swedish Technology Foresight Project: Tecknisk Framsym** on United Nations Industrial Development Organisation (UNIDO) web site http://www.unido.org/

Marsh, L., Flanagan R. and Finch, E. (1997) **Enabling technologies: a primer on bar coding for construction**. The Chartered Institute of Building, ISBN 1 85380 081 3.

Martin, B. (2001) **Technology Foresight in a rapidly globalizing economy**. Vienna, Austria: Regional Conference on Technology Foresight for CEE and NIS countries, 4-5 April 2001.

Ofori, G. (1994) Construction industry development: role of technology transfer. *Construction Management & Economics*, Spon. 379-391.

Shakeri, C. Noori, M.N. and Hou, Z. (1996) Smart materials and structures: a review. *Proceedings of the Fourth Materials Engineering Conference*, Washington DC, November 10-14, 1996. **Vol 2**, pp863-876.

United Nations Industrial Development Organisation (UNIDO) web site http://www.unido.org/

Zgurovsky, M. (2000) **Technological Foresight In Ukraine**, National Technical University of Ukraine "Kiev Polytechnic Institute" on United Nations Industrial Development Organisation (UNIDO) web site http://www.unido.org/userfiles/kaufmanC/ZurovskyPaper.pdf

Advances in Building Technology, Volume 1
M. Anson, J.M. Ko and E.S.S. Lam (Eds.)
© 2002 Elsevier Science Ltd. All rights reserved

ADVANCES IN IT FOR BUILDING DESIGN

J. S. Gero

Key Centre of Design Computing and Cognition, University of Sydney,
NSW, 2006, Australia

ABSTRACT

Computers have been used building design since the 1950s. Their first use was in structural analysis and construction planning. The use of computers in building design analysis has included extensive developments in structural analysis as well as programs for the analysis of the HVAC and environmental performance of buildings. Recently, more sophisticated analyses of environmental behaviour and the behaviour of building users have been developed and implemented. Computer graphics was developed initially in the 1960s and formed the basis of computer-aided drafting systems – called CAD systems. These early CAD systems were used during the documentation phase of building design. These CAD systems developed beyond simply drafting to modelling the geometry of the building. Today's commercial CAD systems are used at various stages in the building design process and are integrated with analysis tools. This paper briefly traces these developments before introducing current research on IT for building design that has the potential to impact the way buildings will be designed in the future. Three strands of research are presented. The first strand deals with virtual environments for designing and designing virual environments. In virtual environments the focus moves away from documents to models and from a virtual building model on a designer's computer that is then sent to other members of the design team to a building model in a virtual environment that is accessible by any authorised member of the design team anywhere at any time. The issue of designing within virtual environments is raised. The second strand deals with new ways of carrying out simulations of the behaviour of the building users rather than the behaviour of the building. The third strand deals with novel computational agent technologies and examines the potential of their use in building design.

KEYWORDS

CAD, building design, virtual environments, virtual models, simulations, design agents, computational agents

BACKGROUND

The invention of the computer goes back to the 1940s, however, their industrial use commenced only a decade later. The University of Sydney built and installed its first computer in 1953 for research purposes.

The possible use of computers in the building industry commenced with research into automating structural analysis through the development of the matrix method of frame analysis. Thus, by the late 1950s/early 1960s exceptionally unusual buildings (such as the Sydney Opera House) were having their structures analysed by computer. Standardised structural analysis programs appeared in the late 1960s and the early 1970s. Today the finite element method has the capacity to analyse virtually any building structure to a sufficient degree of accuracy. Further, the cost of analysis has dropped dramatically in the intervening 30 years. This cost reduction has been brought about by three factors: the reduction in the cost of computation, the reduction in the cost of describing the structure and the reduction in the cost of presenting the results in a coherent graphical form. The effect of this increase in ability to analyse building structures and the reduction in the cost of analysis has been to allow designers to explore a much wider range of structural forms and shapes than would have been feasible earlier.

Figure 1 shows an example of the complex three-dimensional shapes that can be readily analysed today.

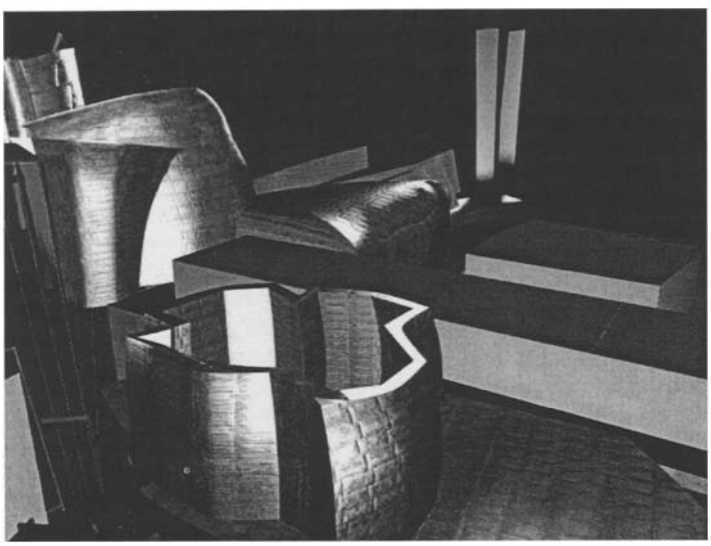


Figure 1: The Guggenheim Museum in Bilbao, Spain, designed by Frank Gehry
(model by David Ju, University of Sydney)

Following on from the developments in structural analysis were the developments in environmental analysis of buildings. These commenced with energy analysis and expanded to include a variety of other environmental factors as well as the influence of building services on the environmental performance of buildings. Today with computational fluid dynamics it is possible to model of environmental behaviour including smoke spread and fire spread in buildings.

The development by the US Navy of the PERT (Program Evaluation and Review Technique) and the later development of the CPM (Critical Path Method) based on the mathematical technique of dynamic programming provided a formalisable means construction project management that was readily computable. As a consequence this was also amongst the early applications of computers in the building industry.

In 1963 Ivan Sutherland submitted his PhD thesis titled *Sketchpad: A Man-machine Graphical*

Communications System to MIT and in it he invented interactive computer graphics. *Sketchpad* (Sutherland 1963) pioneered the concepts of interactive graphical computing, including memory structures to store objects, rubber-banding of lines, the ability to zoom in and out on the display, and the ability to make perfect lines, corners, and joints. This was the first GUI (Graphical User Interface) long before the term was coined. It also had parameterised objects. Figure 2 shows Sutherland using the system.



Figure 2: Ivan Sutherland with the *Sketchpad* system at MIT in 1963

The concepts in *Sketchpad* laid the foundation for computer-aided drafting systems for years to come. These concepts along with research on object modelling continues to provide the bases of current commercial CAD systems. More recently commercial CAD systems have begun to implement object-oriented technology that allows users a greater flexibility in their use. Most current CAD systems are world-wide web enabled, meaning that users can access them across the web.

VIRTUAL ENVIRONMENTS FOR DESIGNING

Virtual environments are computational representations of objects and spaces in "cyberspace". They fall into two distinct classes. In the first are virtual environments that are CAD models generated using the standard CAD packages. Here the focus is entirely on the CAD model that happens to be accessed in a virtual space. There are advantages in placing CAD models into virtual environments since this allows designers to collaborate asynchronously, without being co-located. One of the issues in this approach is the size of files that need to be transferred from one designer to another is generally increasingly large. This has performance effects.

The second approach is to design within a virtual environment where the model of the building is developed as it is being designed. It can then be converted into a CAD model. The advantage of this approach is the ease with which members of the design team can gain access to the design and the means by which they can communicate with each other. In general the technology that supports this is different, often having come from the distributed computer games world, and as a consequence the files that are moved around are very small and hence performance is high. Each member of the design team can be connected to the same virtual environment at the same time and can have a different view of it than any other member of the team (Maher and Gu 2001).

Figure 3 show a virtual design environment made up of objects. The virtual environment is being used by a number of designers concurrently, designers who both design within it and communicate with each other in it.

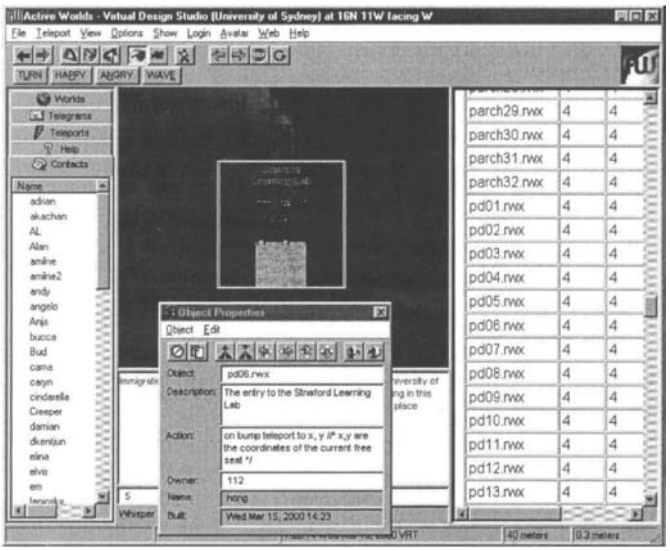


Figure 3: A virtual design environment showing objects whose information can be directly accessed

Virtual design environments offer functionality beyond CAD modelling in that all documents are treated as objects as well. So an office with all its attendant data and information content can become part of the environment (Maher and Gu 2001). Figure 4 shows a virtual environment where the office and design information is part of the environment. This opens up a variety of novel collaboration opportunities. Virtual design teams, within the overall team, can form and carry out sub-designs. Further each of the different design disciplines (architect, structural engineer, façade engineer, etc) can work on the current version of the design.

SIMULATING THE BEHAVIOUR OF BUILDING USERS

The user of buildings has been notoriously absent from most simulations of the behaviour of buildings. The behaviour of the building has been assumed to be largely independent of the users. In recent research into simulations of groups of animals Reynolds (1987) demonstrated that realistic results could be produced using simple computational agents. The "social force model" that is the result is a model of pedestrian behaviour, similar to animal flocking, used to model self-organising phenomena in crowds (Helbing and Molnár, 1995). Computer simulations have shown that the social force model is capable of realistically describing several interesting aspects of collective pedestrian behaviours (Helbing and Molnár, 1997).

A simple crowd management problem is used to illustrate the behaviour pedestrians. The problem is to design a doorway to facilitate the efficient and comfortable movement of pedestrians travelling in opposite

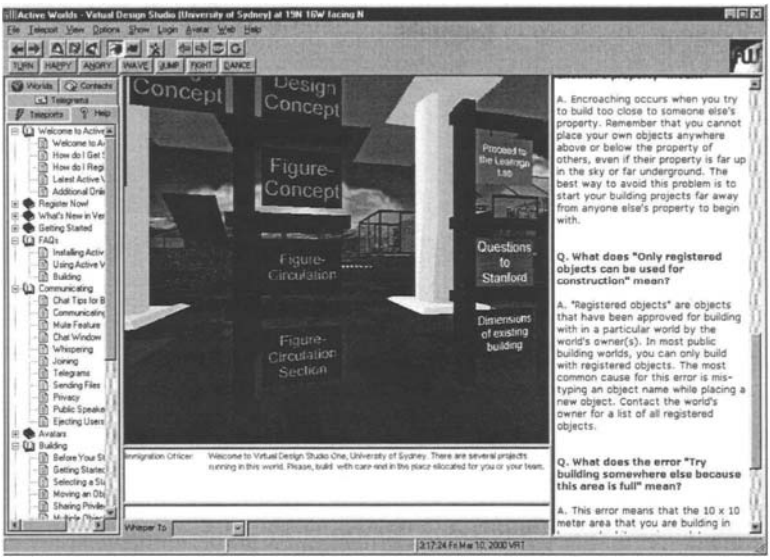


Figure 4: A virtual environment where both the design and the information about the design office are part of a single environment

directions. A pedestrian simulator was developed to evaluate doorway designs. Pedestrian movement is simulated using a microscopic model of crowd behaviour developed to account for empirically observed self-organizing phenomena. The social forces modelled in the simulations of pedestrian crowds are listed in TABL, detailed mathematical descriptions of these forces can be found in Helbing and Molnár (1995).

TABLE 1
THE SOCIAL FORCES MODELLED IN THE SIMULATIONS OF PEDESTRIAN CROWDS

	Description of social force
1.	Pedestrians are motivated to move as efficiently as possible to a destination.
2.	Pedestrians wish to maintain a comfortable distance from other pedestrians.
3.	Pedestrians wish to maintain a comfortable distance from obstacles like walls.
4.	Pedestrians may be attracted to other pedestrians (e.g. family) or objects (e.g. posters).

This model is used to simulate the behaviour of pedestrians using three different designs for the doors. The three designs are: narrow door, wide door and two separated doors. The behaviour of the pedestrians using a narrow door can be seen in Figure 5, where pedestrians moving in opposite direction block each other's paths.

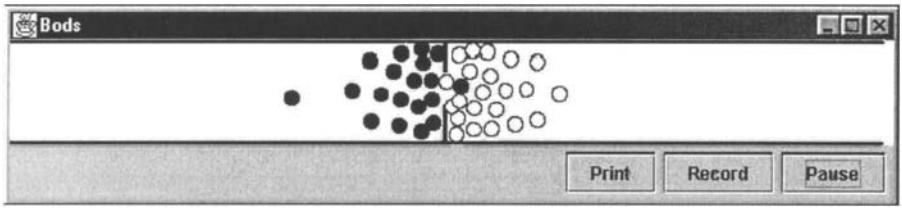


Figure 5: Simulating the behaviour of pedestrians using a narrow door (Saunders and Gero 2001)

Figure 6 shows the same pedestrians using a wide door. Here the pedestrians generate a behaviour that produces two passing streams, indicating that the size of the door is satisfactory.

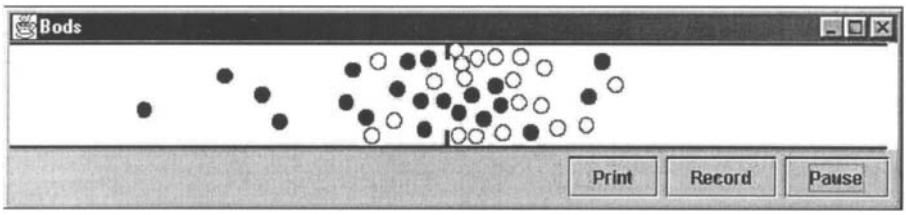


Figure 6: Simulating the behaviour of pedestrians using a wide door (Saunders and Gero 2001)

Figure 7 shows the same pedestrians using two separated doors. Here the pedestrians form two streams, one for each door. These streams are not programmed inot the system but emerge from the behaviour of each individual.

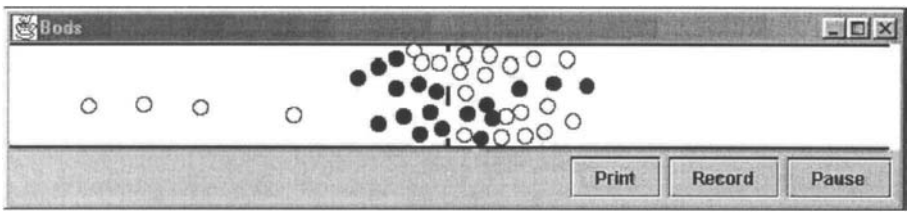


Figure 7: Simulating the behaviour of pedestrians using two doors (Saunders and Gero 2001)

DESIGNING WITH COMPUTATIONAL AGENTS

Computational agents are computer programs that are designed to exhibit a degree of autonomy and as a consequence are able to influence and change the environment within which they sit. Already many people who use the world-wide web unwittingly make use of agents during their web searches. Designing with computational agents is at the cutting edge of current design computing research. There are proposals to develop agent-based design systems (Maher and Gero 2002). These use a multi-agent system as the core of a 3D multi-user virtual world. Each object in the world is an agent in a multi-agent system. The agent model provides a common vocabulary for describing, representing, and implementing agent knowledge and

communication. The agent can sense its own environment and can generate or modify the spatial infrastructure needed for a specific collaborative or communication need of the users of the world. Each agent has five kinds of reasoning: sensation, perception, conception, hypothesizer, and action (Gero and Fujii 2000). This agent approach is derived from recent developments in cognitively-based design agents, where design is considered as a situated act (Gero 1998). The agents are developed to interact with the design and the design knowledge (Smith and Gero 2001; Saunders and Gero 2001). The agent approach to virtual worlds provides for new kinds of interaction among the elements of the virtual world representation and between individuals and project teams with the components of the virtual world that makes both the virtual environment and interactions with it dynamic.

Agents can function in three modes based on their internal processes: reflexive, reactive, and reflective (Maher and Gero 2002). Each mode requires increasingly sophisticated reasoning, where reflexive is the simplest.

Reflexive mode: here the agent responds to sense data from the environment with a preprogrammed response – a reflex without any reasoning. In this mode the agent behaves as if it embodies no intelligence. Only preprogrammed inputs can be responded to directly. Actions are a direct consequence of sense data. This mode is equivalent to the kinds of behaviors that are available in current virtual worlds.

Reactive mode: here the agent exhibits the capacity to carry out reasoning that involves both the sense data, the perception processes that manipulate and operate on that sense data and knowledge about processes. In this mode the agent behaves as if it embodies a limited form of intelligence. Such agent behavior manifests itself as reasoning carried out within a fixed set of goals. It allows an agent to change the world to work towards achieving those goals once a change in the world is sensed. Actions are a consequence not only of sense data but also how that data is perceived by the agent. The agent's perception will vary as a consequence of its experience.

Reflective mode: here the agent partially controls its sensors to determine its sense data depending on its current goals and beliefs. The agent also partially controls its perception processes depending on its current goals and beliefs and its concepts may change as a consequence of its experiences. The concepts it has form the basis of its capacity to "reflect", ie not simply to react but to hypothesize possible desired external states and propose alternate actions that will achieve those desired states through its effectors. The reflective mode allows an agent to re-orient the direction of interest by using different goals at different times in different situations (Gero and Kannengiesser 2002).

We can expect such systems to change the way we design and potentially what we design.

References

Gero J.S. (1998). Towards a model of designing which includes its situatedness, *in* H. Grabowski, S. Rude and G. Grein (eds), *Universal Design Theory,* Shaker Verlag, Aachen, 47-55.

Gero J. S. and Fujii H. (2000). A computational framework for concept formation in a situated design agent, *Knowledge-Based Systems* **13:6,** 361-368.

Gero J.S. and Kannengiesser U. (2002). The situated Function-Behavior-Structureframework, *in* JS Gero (ed.), *Artificial Intelligence in Design'02,* Kluwer, Dordrecht,. 89-104.

Helbing D. and Molnár P. (1995). Social force model for pedestrian dynamics. *Physical Review E* **51,** 4282-4286.

Helbing D. and Molnár P (1997). Self-organization phenomena in pedestrian crowds, *in* F. Schweitzer (ed.), *Self-Organization of Complex Structures: From Individual to Collective Dynamics,* London: Gordon

and Breach, London, 569 – 577.
Maher M.L. and Gero J.S. (2002). Agent models of 3D virtual worlds, *ACADIA* (to appear)
Maher, M. L. and Gu, N. (2001). 3D virtual world. *in* M. Engeli and P. Carrard (eds), *ETH World: Virtual and Physical Presence,* Karl Schwegler AG, Zurich, 146-147.
Reynolds, C. W. (1987). Flocks, herds, and schools: A distributed behavioural model, *Computer Graphics* **21:4,** 25-34.
Saunders R. and Gero J.S. (2001). Designing for interest and novelty: Motivating design agents. In *CAADFutures 2001*, B de Vries, J van Leeuwen and H Achten (eds), Dordrecht: Kluwer, 725 - 738.
Saunders R. and Gero J.S. (2001). A curious design agent, *in* JS Gero, S Chase and M Rosenman (eds), *CAADRIA'01*, Key Centre of Design Computing and Cognition, University of Sydney, 345-350.
Smith G. and Gero J.S. (2001). Situated design interpretation using a configuration of actor capabilities, *in* Gero, JS, Chase, S and Rosenman, MA (eds) (2001) *CAADRIA2001*, Key Centre of Design Computing and Cognition, University of Sydney, Sydney, 15-24.
Sutherland I.E. (1963). Sketchpad – A Man-Machine Graphical Communication System. *Proceedings of the Spring Joint Computer Conference*, Detroit, Michigan, May 1963, and *Technical Report #296,* MIT Lincoln Laboratory

Advances in Building Technology, Volume 1
M. Anson, J.M. Ko and E.S.S. Lam (Eds.)
© 2002 Elsevier Science Ltd. All rights reserved

INFORMATION TECHNOLOGY SUPPORT TO IMPROVED CONSTRUCTION PROCESSES: INTER-DISCIPLINARITY IN RESEARCH AND PRACTICE

Amanda Marshall-Ponting, Ange Lee, Martin Betts,
Ghassan Aouad, Rachel Cooper[1], Martin Sexton

School of Construction & Property Management,
University of Salford, Salford, M7 9NU, UK.
[1]School of Art and Design,
University of Salford, Salford, M7 9NU, UK.

ABSTRACT

Research and innovation in the built environment is increasingly taking on an inter-disciplinary nature. The built environment industry and professional practice have long adopted multi and inter-disciplinary practices. The application of IT in Construction is moving beyond the automation and replication of discrete mono and multi-disciplinary tasks to replicate and model the improved inter-disciplinary processes of modern design and construction practice. A major long-term research project underway at the University of Salford seeks to develop IT modelling capability to support the design of buildings and facilities that are buildable, maintainable, operable, sustainable, accessible, and have properties of acoustic, thermal and business support performance that are of a high standard. Such an IT modelling tool has been the dream of the research community for a long time. Recent advances in technology are beginning to make such a modelling tool feasible.

Some of the key problems with its further research and development, and with its ultimate implementation, will be the challenges of multiple research and built environment stakeholders sharing a common vision, language and sense of trust. This paper explores these challenges as a set of research issues that underpin the development of appropriate technology to support realisable advances in construction process improvements.

KEYWORDS

Construction process improvement; inter-disciplinarity; multi-disciplinarity; construction IT; nD modelling; trust; multi-criteria decision making.

INTRODUCTION

The building design process is complex encapsulating a great number and variety of factors - which can be social, economic and legislative - in order to satisfy the client's requirements. In fact, it is rarely the case that there will be one homogeneous client, but a number and variety of stakeholders who will be the end users of the design and its resultant product. These can include, not only the organisations and individuals who will occupy the building on a daily basis, but also those who provide it, manage it, own it, maintain it and be affected by it by its existence in their environment.

Project Context

There are increasing demands being made by multiple stakeholders for inclusion of design features such as buildability (cost and time), maintainability, sustainability, accessibility, crime deterrence and acoustic and energy performance. This diversity in stakeholder aspiration arises from increasing numbers of construction specialists who may now be involved in design. Each design parameter that these stakeholders seek to consider will have a host of social, economic and legislative constraints which often are in conflict with one another. The criteria for successful design therefore will include a measure of the extent to which all these factors can be co-ordinated and mutually satisfied to meet the expectations of all the parties involved. In this era of increasing global competition, being able to deliver value to clients - and integrated design, if this is what the market dictates - is what could set one company ahead of the competition.

The volume of information required by so many experts make it difficult for the client to visualise design changes and their impacts upon the time and cost of the project. Design adaptations which aid a client's decision-making ability in this way are also costly, time consuming and laborious. A multi-dimensional computer model, which allows the entire design and construction process to be portrayed visually, would enhance both the decision-making and construction processes, by enabling true and holistic 'what-if' analyses to be performed. This is the ultimate aim of the 3D to nD modelling research project underway at the University of Salford. Conceptually, this will involve taking 3-dimensional modelling in the built environment to an n number of dimensions.

The research seeks to develop the infrastructure, methodologies and technologies that will facilitate the integration of time, cost, buildability, accessibility, sustainability, maintainability, acoustics, crime, lighting and thermal requirements. It aims to assemble and combine the leading advances that have been made in discrete information communication technologies (ICTs) and process improvement to produce an integrated prototyping platform for the construction and engineering industries. This output will allow seamless communication, simulation and visualisation, and intelligent and dynamic interaction of emerging building design prototypes, so that their fitness for purpose for economic, environmental, building performance, and human usability will be considered in an integrated manner. It is essential to ensure that the proposed system would be durable and be compatible with new developments in IT, a far as these could be anticipated.

Project Aims and Structure

The Engineering and Physical Sciences Research Council (EPSRC) in the UK fund the 3D2nD project as a platform grant. Platform grants are a recent innovation in UK government research funding and are intended to allow longer time-scale and more fundamental basic research within leading national centres of excellence of an internationally-leading standing, into strategic research

of global importance. Salford University has secured one of the first of these grants within the Built Environment on the back of its well-established research in IT, management and environmental and design systems. The project has a large pool of senior academics from multiple disciplines within its project team. It was agreed by the project members that the nD tool should encompass people, technology, process (organisation of work), organisational relevance (business strategy/market positioning) and the business model (cost effective, capable of being developed) issues. This has led to the emergence of 5 work packages, whose interrelationships are illustrated by figure 1.

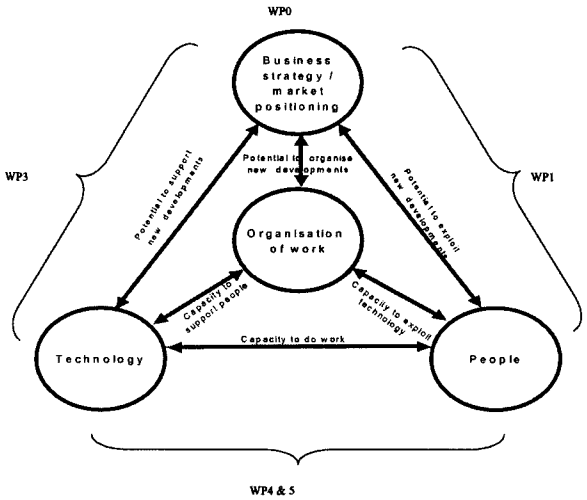


Figure 1: Work packages of the 3D2nD project

The Focus of this Paper

In view of the number and diversity of project researchers representing the requirements of construction industry stakeholders and professionals, it can be expected that gaining consensus on the characteristics of a vision for the project will be problematic and require management. Each work package inherently embodies different epistemological approaches, for example WP3's model testing will be objective and likely empirical in nature, whereas WP4's technology transfer will be more qualitative in nature and concerned with the organisational and social features and processes which will aid or inhibit the technology implementation. Should consensus be achieved and if lacking, how should it be handled so as to not jeopardise the projects' overall deliverables? This has been a key challenge for the research team in the project and is indicative of the issues associated with resolving conflicting perspectives and requirements of multiple stakeholders that the model itself will be called on to perform. As a means of exploring these trade-offs and multi-criteria maximisation issues, this early paper from the research explores how research teams might resolve these differences in approach within their own research methodology and management. Two earlier examples of multi-disciplinary research projects are examined as case studies to surface the associated risks and issues and provide some guidelines for effective inter-disciplinary research working on which this project can draw. It is argued that such inter-disciplinary approaches will increasingly become key to our broader advances in building and construction technology research and innovation.

CASE STUDY 1: AN INTERDISCIPLINARY EU-FUNDED RESEARCH NETWORK

Cooper (2002) uses the BEQUEST network, an EU concerted action with 14 partners from 6 countries, as an example of a major research exercise that illustrates the problems of multi-disciplinary working. The network's aim was to bridge discipline-based differences held by those working in the urban sustainability field to develop a shared platform for assessing sustainable urban development (SUD). This objective necessitated consensus building between the project's immediate partners, but also within the wider built environment community through its Extranet. It is of relevance to the nD modelling project because of its varied stakeholders working in the built environment field. Cooper argues (p117) that BEQUEST faced a triple challenge, because:

(1) There is no consensus of the meaning of SUD (Palmer et al 1997) or how it should be implemented;
(2) There is no agreement and little advice (Epton et al 1983) on how interdisciplinary research should be conducted, despite expressed needs to support this activity in the UK (e.g. HEFCE 2001);
(3) There is little shared experience on how to design and run effective virtual organisations, despite the rapid recognition of their appearance after the rise of the Internet

Multi- vs. Inter-disciplinary working

Cooper distinguishes between 'multi-disciplinary and 'inter-disciplinary' working (p118). The former term applies when two or more disciplines work together without stepping outside their own traditional discipline boundaries. In contrast, the latter emphasises the development of a shared perspective transcending traditional boundaries. Newell and Swan (2000) use the analogies of jigsaws and kaleidoscopes: in multi-disciplinary work, the individual pieces of the jigsaw do not change their identities as a result of being combined with other pieces, whilst with the inter-disciplinary kaleidoscope, it is not possible to establish characteristics of each individual from the whole. BEQUEST is an example of the latter as the emergent conceptual frameworks the members created transcended those owned by any one discipline making up that group (p121).

Examining and building consensus

Cooper draws attention to the 'wheel of cognate disciplines' (Eclipse Research Consultants 1997) which suggests that the closer disciplines are located to each other, the more likely they are to share a common theoretical parentage and therefore the more open their boundaries are to each other. In BEQUEST's case, the most common partner disciplines - engineering, planning and architecture - formed an arc and so it could be expected that collaboration would be fairly straightforward. However, this was not the case and Cooper argues this might be partially explained by the situated nature of professional learning and expertise: "'Legitimate peripheral participation' provides a way to speak about the relations between newcomers and old-timers and concerns the process by which newcomers become part of a community of practice" (Lave and Wenger, 1991). In BEQUEST's case, there was no newcomer-old-timer network and the collectively created shared conceptual space was still being developed.

Eclipse Research Consultants (1996) developed a self-assessment technique, PICABUE, which would gauge potential partners' individual and collective commitment to the principles

underpinning sustainability at the start of the project (Curwell et al, 1998). Eclipse embedded the principles into a simple mapping technique for ease of comparison which showed that not only were the different disciplines committed to different aspects and to greatly varying degrees, but that the partner averages increased and became more uniform between the aspects over time. This technique also allowed the 'common platform' to be established, which is a value representing the minimum amount of agreement between members. Represented as a percentage, it increased from 25% in 1996 to 45% in 2001.

New vs. Old Knowledge Production

One of the BEQUEST project deliverables was "an effective, multi-professional, international interactive networked community" to be mediated electronically over the Internet (BEQUEST 2001 p5). Pursued in this way, Cooper argues (2002 p117) that: "...the concerted action displayed some of the characteristics of a new approach to conducting global collaborative research that, in the UK at least, has very recently been given the very grand title of 'e-science'". Two defining characteristics of 'e-science' are the spatial distribution of those participating and the infrastructure, usually in the form of ICTs, which enable it. Its purpose is to achieve "world beating science through the effective use of the latest information technologies" by conducting cross-disciplinary research "at the intersection of many scientific disciplines", and that the resulting 'e-science' "will change the dynamic of the way science is undertaken" (Boyd, 2001, cited in Cooper 2002 p120).

E-science is one example of the pervasive trend towards the 'new' production of knowledge. Gibbons et al (1994) argue that the *way* in which knowledge is being produced is changing. They describe this knowledge (p 3-8) as being produced through 'mode 2 research' and some defining attributes include:

- Knowledge produced in the context of application (as opposed to problem solving using the codes of practice or a particular discipline);
- Trans-disciplinarity;
- Heterogeneity and organisational diversity (in terms of the skills and experiences brought to it);
- Social accountability and reflexivity;
- Quality control.

'New' knowledge may not show all of these characteristics, and it may not even be new: the description by Gibbons *et al* argues that innovation can occur through the reconfiguration of existing knowledge, so that it can be used in new contexts or by new users.

The expansion of the number, nature and range of communicative interactions between the different sites of knowledge production leads not only to more knowledge being produced but also to more knowledge of different kinds; not only of sharing of resources, but to their continuous configuration. Each new configuration becomes itself a potential source of new knowledge which in turn is transformed into the site of further possible configurations. The multiplication of the numbers and kinds of configurations are at the core of the diffusion process resulting from increasing density of communication...This process has been greatly aided by information technologies which not only speed up the rate of communication, but also create more new linkages. (ibid, p35). The development of communication linkages has played an important part in allowing this to occur, and this underlines the importance of the growth of the Internet and other computer-mediated communication and collaboration tools as enablers.

One of the most important conclusions Cooper (2002 p126) draws is that the BEQUEST concerted action has demonstrated that it is not necessary for all members to agree absolutely and at all times, within a research project team, for true progress to be made. What is important though, is that they are willing to negotiate openly about what they are trying to jointly achieve. The test of the validity of any group agreement will be in the reaction from other, wider stakeholders. With so little guidance on how to work effectively in inter-disciplinary groups, Cooper suggests (2002 p126) making explicit the amount of time and effort required to develop a shared perspective and that this should necessarily include trust and consensus building techniques and methods for identifying and resolving conflicts.

CASE STUDY 2: A MULTI-DISCIPLINARY UK UNIVERSITY RESEARCH PROJECT

Newell and Swan's (2000) case study is concerned with the development and maintenance of trust within a multi-disciplinary research team and the implications that this can have for inter-organisational working. The team was comprised of 4 project leaders and 4 researchers based at 3 geographically dispersed universities in the UK.

The Nature of Trust

It is generally agreed that trust is a necessary condition for co-operative behaviour among individuals, groups or organisations (Jones and George 1998) and that it facilitates the levels of communication necessary to generate learning and innovation in networked organisations (Dodgson 1993). Despite different definitions, the two central issues are that trust is about dealing with risk and uncertainty and that it is about accepting vulnerability. From their literature review, Newell and Swan (2000 p1295) conclude that a 3-fold trust typology exists:

1. Companion trust – based on goodwill judgements or personal friendships, it has an expectation of openness and honesty and although slow to develop, it is also the most resilient.
2. Competent trust – based on the perceptions of others' abilities to carry out necessary tasks, it can be driven by contextual cues – such as institution reputation. It develops more quickly, but is more fragile.
3. Commitment trust – stemming from contractual agreements between parties, the continuing existence of the contract in the absence of other trust forms makes it more resilient than competence trust.

Observer Findings

Through their in-depth analyses as invited outsider observers and team building facilitators, Newell and Swan found that the team started to break down very quickly after the project funding was received. Companion trust between two of the principal investigators (PIs) and perceptions of being able to enjoy working together led to the formation of the PI team. Temporary 'swift trust' (Meyerson et al 1996) developed based on competence cues taken from involvement on an expert panel and the quality and reputations of the universities to which each PI belonged. Crucially, in the rush to meet the proposal deadline the negotiation of the deliverables was omitted and in the light of little or no experience of working together and combined with epistemological differences of their disciplines, despite attempts to reach consensus, once work started, conflicts ensued.

The solution was to divide the project into semi-autonomous pieces which, through avoidance of conflict allowed their friendship to remain intact, but created centrifugal tensions which were later difficult to correct: this approach was agreed by everyone involved and it was often the case that the decisions made by the sub-groups would then be rejected by the other members. Newell and Swan concluded that had proper negotiations been held at the proposal stage, the group would have found that the idea would have shown itself to be unworkable. In the final phase, the research officers (ROs) got on board, but few attempts were made by the PIs to develop the informal, social coordination mechanisms and repeated changes to the project structure served to increase ambiguity and actually led to the PIs becoming less involved in the project. Disciplinary differences eroded competence trust between two of the RO s and this stared to undermine their companion trust and this eventually led to one of them leaving the project.

A Model of Trust

Newell and Swan argue that this work demonstrates how the three forms of trust interrelate and that 'it is the way in which they worked together which provides the greatest understanding of the development of trust'. The PIs and ROs differed in terms of the commitment trust demonstrated and this appeared to affect the development of companion and competence trust. As a result of their observations, they make a number of propositions which could form the basis of a model:

1. *In a low commitment trust situation, competence and companion trust are reciprocally dependent, one reinforcing the other in the same direction*
   The spiral that results can be either positive or negative: Risk among the ROs was low if the network failed to deliver its original objectives and none would be held accountable - commitment trust was low. There is little to hold the individuals together and the downward spiral develops its own momentum, which can finish with total trust and maybe group breakdown. This occurred in the RO group - 2/4 left within the first 8 months.

2. *In a high commitment trust situation, competence and companion trust are held in mutual tension such that, as one decreases, the other increases to compensate*
   Commitment trust had been established via the funding body's allocation of money which meant that, although there was high competence distrust, the same downward spiral didn't occur in the way that it had for the ROs. Also, concerted efforts were made to remain friends and confrontation was avoided - through the development of federated sub-projects. Unlike the RO situation where competence distrust reinforced companion distrust, it acted to strengthen companion trust and, consequently, led to compromises and detracted from the benefits of interdependence. Newell and Swan (p1319) argue that this demonstrates why it is important to differentiate between different types of trust as they were affected differentially by the interactions which occurred.

3. *Putting in place formal integration mechanisms will not guarantee the development of the more informal integration mechanisms which underpin the emergence of at least companion and competence trust.*
   Here, the research team did not spend enough time on social integration. Newell and Swan go further by questioning the extent to which, if at all, multi-disciplinary teams actually produce more innovative and useful knowledge, especially given their epistemological and ontological differences. Knights and Wilmott (1997) argue that the most common response to the pressures of inter-disciplinary research is 'mechanistic pooling' - each member takes a different 'slice' of the project and works with a minimum of communication with other members. This, they argue,

is the most common response because "..no time is 'wasted' in confronting differences in theoretical perspective.." and "..each member is able to maximise publication output in journals that cater for their particular specialism.." (cited in Newell and Swan 2000 p1321). Here, the research team acted in a multi-disciplinary way.

4. *The greater the variety in epistemological and ontological perspectives within a research network, the more likely the output is to be a compromise, which is actually less creative and innovative than would have been achieved within a single discipline.*
   They conclude that any examples of really creative and interdisciplinary research are likely to be the exception rather than the rule and those multi-disciplinary approaches may inhibit creation and diffusion of innovative ideas.

INTER-DISCIPLINARY APPROACHES IN 3D2ND

Taking note of the above discussion, an attempt has been made to develop consensus amongst members of the project research team on the Salford 3D2nD modelling project. A workshop was conducted in February 2002 with the whole research team to start defining the theoretical and ontological approaches for a vision for the nD tool. An electronic voting tool was used during the workshop to ascertain any participant consensus. In order to define a vision, the workshop participants explored several existing visions governing 'the future of construction IT'.

Although aspects of the existing visions can be strategically placed within the context of this project, it was clear from the results that the majority of workshop participants – 88% - wanted to develop a new collective vision of their own. The preference for an approach based and focussed both on implementation and on a blue sky approach is the crux of the project as it will dictate the type of technology that would be used and the subsequent implementation issues of the chosen technology. The majority voted for a mixture of both aspects and the voting on the ratios of this showed that, of the two most popular responses, 28% wanted a 50:50 split, but that 27% favoured 20:80. The implementation timeframe for industry was most popularly agreed at 25 years, but the question provoked the least consensus of all, with a quarter of the group thinking that some sort of implementation should be possible within 3 years. It was generally concluded from the workshop that more work would need to be done with the group to develop consensus and a shared view around the vision, but that due to the nature of the grant it would be possible to develop a range of scenarios to accommodate all of these factors, each being comprised of varying degrees of applied and blue-sky/innovative technology. The scenarios would include technology that could be utilised readily and technology/visions that could be utilised in the future, encompassing multiple timescales and a vision that would be continuously and iteratively developed so that it would harness the future direction and application of technology.

DISCUSSION

The current situation in the 3D2nD project demonstrates a relatively low level of agreement on a number of the issues voted upon in the workshop. This would be expected given the multi-disciplinary nature of the group make-up and the lack of a unanimously agreed vision at this point in time. On the 'wheel of cognate disciplines' (Eclipse Research Consultants 1997), the nD group members' disciplines are represented at almost all stages around the circle, meaning that the groups furthest from each other may never agree and that, in fact, group decisions in general would be expected to be more polarized than was the case for BEQUEST. It would be quite fair to say that in

the absence of a fully shared vision, it is human nature for individuals to try to steer a project towards their own goals and areas of expertise. However, it is also likely that with more formalised and specific goals in place, the research team will 'rally around' these. This was demonstrated by Cooper's (2002) case study of BEQUEST and the greater level of consensus demonstrated by the PICABUE assessment technique over the project's duration. It could be interesting and relevant to replicate this assessment exercise with the 3D2nD group, with some alteration to the concepts for consideration.

Newell and Swan (2000) highlighted a number of pitfalls which could be avoided through management, not only of the goals and tangible aspects, but also of the wider context and the inter-relationships of all those involved. Effective teamwork can only occur if there is a sense of ownership towards the project and its objectives by all the members of the research team. This does not mean that consensus on all aspects, by all members and at all times should be the only aim; rather than the process of striving to achieve these should help facilitate the development of factors which, in absence could bring down the project. The dominant theme in a set of case studies presented at the ISI seminar (Newell 2002) was the existence of trust, and although this may be the hardest aspect to control favourably, in the absence of consensus, if enough trust exists between members, collective goals and relationships are less likely to be lost and eroded.

Following from Coopers (2002 p118) distinction between inter- and multi-disciplinary work, it is difficult at this stage to determine which the nD project is. The project has not yet required any member to think and work beyond their discipline boundary; indeed the tool is currently envisioned as being a 'pool' for all information relating to building design and construction. The tool may take on an inter-disciplinary nature when applied to real world problems – if this is the remit – as it will be capable of more than the initial individual's inputs and should be able to cross the traditionally held discipline boundaries.

With the scarcity of previous research on how to best carry out multi-disciplinary work, an important by-product would be a paper on the management of the 3D2nD project and it mechanisms and contingencies for success and the processes by which these were achieved (or not). The encouragement of research councils to partake in research of this kind, but the ironic lack of knowledge on how to do this, highlights an area worthy of further consideration.

REFERENCES

BEQUEST (2001) Final Report 2000-1, Contract No. ENV 4 CT/97-607, EC Environment and Climate Programme (1994-1998), *Research Theme 4, Human Dimensions of Environmental Change*, University of Salford, UK.

Cooper, I. (2002) Transgressing discipline boundaries: Is BEQUEST an example of the 'new production of knowledge'? *Building Research & Information*, **30:2,** 116-129.

Curwell, S., Hamilton, A. & Cooper, I. (1998) The BEQUEST network: towards sustainable development. *Building Research and Information*, **26:1,** 56-65.

Eclipse Research Consultants (1996) *PICABUE: Mapping Commitment to Sustainable Development - A Self-assessment Technique for Policy-Makers and Practitioners*, ERC, Cambridge.

Eclipse Research Consultants (1997) *Support for Inter-disciplinary Research, workshop prepared for the Research and Graduate College, University of Salford, and for the Committee for Inter-disciplinary Environmental Studies*, University of Cambridge, ERC, Cambridge.

Egan, J., (1998) *Rethinking construction : the report of the Construction Task Force to the Deputy Prime Minister, John Prescott, on the scope for improving the quality and efficiency of UK construction.* Department of the Environment, Transport and the Regions, London.

Epton, S., Payne, R. & Pearson, A. (eds.) (1983) *Managing Interdisciplinary Research*, John Wiley & Sons, Chichester.

Gibbons, M., Limoges, C., Nowotny, H., Schwartzman, S., Scott, P. & Trow, M. (1994) *The new production of knowledge.* Sage, London.

HEFCE (2001) *Interdisciplinary Research and the RAE (Research Assessment Exercise)*, Briefing Note 14, Higher Education Funding Council (England), Bristol.

Lave, J. & Wenger, E. (1991) *Situated Learning: Legitimate Peripheral Learning*, Cambridge University Press, Cambridge.

Newell, S. (2002) Managing knowledge in project teams - some lessons from some failed projects. Seminar held at Information Systems Institute, Salford University, April 24th 2002.

Newell, S. & Swan, J. (2000) Trust and inter-organizational networking. *Human Relations*, 53 (10) pp 1287-1328.

Palmer, J., Cooper, I. & van der Vorst, R. (1997) Mapping out fuzzy buzz words – who sits where on sustainability and sustainable development. *Sustainable Development,* **5:2,** 87-93.

Swan, J., Newell, S., Scarbrough, H. & Hislop, D. (1999) Knowledge management and innovation: networks and networking, *Journal of Knowledge Management*, **3:4,** 262-275.

Advances in Building Technology, Volume 1
M. Anson, J.M. Ko and E.S.S. Lam (Eds.)
© 2002 Elsevier Science Ltd. All rights reserved

RECENT TOPICS IN WIND ENGINEERING FOCUSING ON MONITORING TECHNIQUES

Y. Tamura and M. Matsui

Department of Architecture, Tokyo Institute of Polytechnics,
Atsugi, Kanagawa, JAPAN, 243-0297

ABSTRACT

This paper presents recent results relating to wind speed monitoring, wind pressure monitoring and wind response monitoring techniques and methods. For wind speed monitoring, LDV, PIV, PTV and so on were used in laboratory tests, and Doppler sodars and GPS drop-sonde were used in atmospheric boundary layer wind measurements. For wind pressure monitoring, various applications of simultaneous multi-channel pressure measuring systems are presented, and their efficiency in research, education and practical design are demonstrated. For response monitoring, the efficiency of RTK-GPS for wind-induced responses is mainly demonstrated.

KEYWORDS

LDV, PIV, Doppler Sodar, RTK-GPS, GPS Sonde, Simultaneous Multi-channel Pressure Measuring System, POD, Extreme Pressure Distribution, Full-scale Measurement

INTRODUCTION

This paper introduces recent topics focusing on monitoring techniques in wind engineering. Techniques for monitoring wind speeds, wind pressures and building responses are introduced, such as Doppler Sodars, the Simultaneous Multi-channel Pressure Measuring System, and the Global Positioning System. Their efficient contributions and potential ability in wind engineering are demonstrated, with reference to the author's group and other researchers' recent results. It should be noted that this paper does intend to review all the relevant works and literature, so many interesting results may have been omitted.

MONITORING OF WINDS

Wind Speed Monitoring for Wind Tunnel Testing

In wind tunnel experiments, wind speed is usually measured by Pitot static tubes and hot-wire anemometers. However, optical techniques have recently been playing important roles in comprehending complex flow fields. There are two main optical techniques. One uses the optical

Doppler shift and the interference effect, and to the other obtains the loci of particles from two successive images. Both methods require seeding of tracer particles. They have several advantages, such as non-contact measurement without any disturbance and applicability even in wake regions where there are complex reverse flows. The principle of Laser Doppler Velocimetry (LDV) was first introduced by Cummins et al. (1964). This method is widely used in fluid mechanics. It is very reliable, but it provides point-wise measurement, making it difficult to obtain simultaneous spatial data. Its application to wind engineering is seen in Akins & Reinhold (1998), Havel et al. (2001), and Becker et al. (2002). Figure 1 is an example of successfully illustrated streamlines in the wake region of bluff bodies captured by LDV (Havel et al., 2001). Particle Image Velocimetry (PIV) and Particle Tracking Velocimetry (PTV) are image processing techniques that solve a spatial velocity field by carrying out synchronous photography of particles in a plane recognized by a laser light sheet that emits light for a very short duration. Particle images are acquired by Charge-Coupled Device (CCD) cameras to detect particle movements. A sophisticated method has also been used to obtain 3D flow velocity vectors, using spatial information obtained by multiple CCD cameras from different positions. However, measurement is limited to the range of the laser light sheet. Some trials for obtaining flow velocity fields around buildings with complex geometry have been carried out using a transparent material for the building models. The flow field in the space surrounded by buildings becomes very complicated, and it is difficult to apply hot-wire anemometers. PIV has advantages in measuring in such a limited space, although there are some problems to be solved, such as too high a concentration of tracer particles, failure of the laser light sheet reaching the space of interest and the laser light sheet reflecting from the model surface. Figure 2 shows an instantaneous wind velocity field inside a dome that has wide openings at the roof and side walls (Kondo et al., 2001).

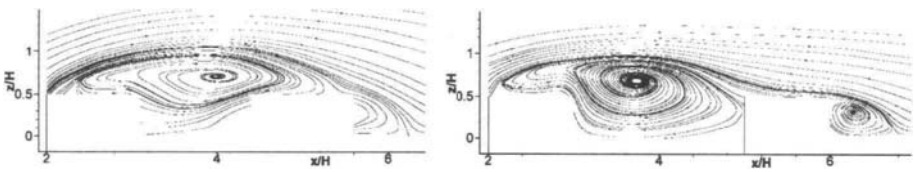


Figure 1: Streamline representation of the LDV measured mean velocity vectors for 2D cylinders. (Due to symmetry only half the plane is shown. Havel et al. 2001)

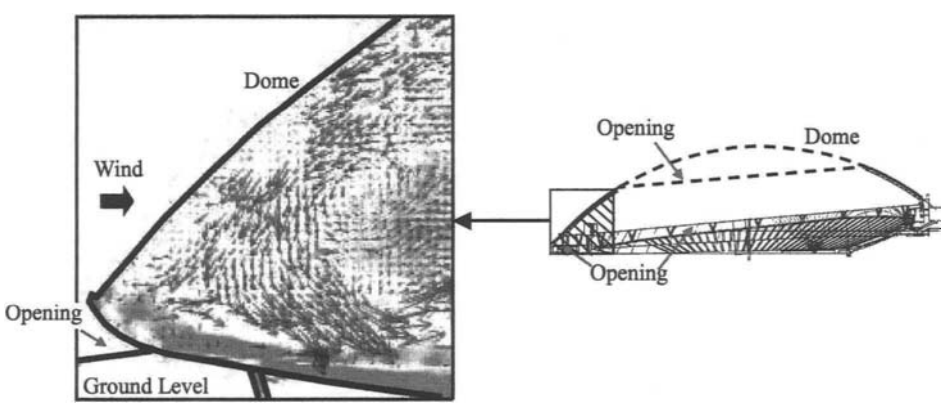
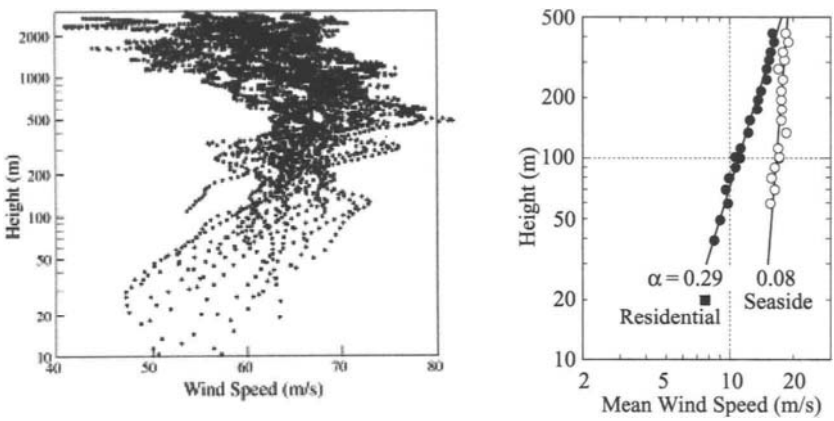


Figure 2: Instantaneous wind velocity fields in a dome measured by PIV (Kondo et al. 2001)

Wind Speed Monitoring in Atmospheric Boundary Layer

It is very important in wind-resistant structural design to accurately estimate the design wind speeds. Two topics relating to the monitoring technique are presented here: vertical wind speed profile in the atmospheric boundary layer during tropical storms such as hurricanes, cyclones and typhoons; and estimation of terrain roughness. Because of difficulties in observing extremely rare phenomena and measuring atmospheric boundary layer wind speeds at high altitudes, wind speed profiles for various terrain conditions are not well known, although almost all wind load codes specify them. Doppler radar (Hayashida et al., 1996), GPS drop-sondes (Powell et al., 1999) and Doppler sodars (Tamura et al., 1999a, 2001, Amano et al., 1999) are powerful devices for measuring atmospheric boundary layer wind profiles. Powel et al. (1999) showed wind speed profiles inside hurricanes using GPS drop-sondes as shown in Fig.3(a). Powel (2002) also obtained the normalized wind speed profiles for 14 hurricanes of 330 profiles near the eye walls. These profiles revealed some characteristics of friction at the sea surface. It is expected that a lot of useful information will be obtained from this challenging research in the near future.



(a) 10 eye-wall profiles from Hurricane Mitch (1998) (b) Seaside → 23km (Residential)→ Residential
Figure 3: Wind speed profiles measured by (a) GPS drop-sonde (Powel et al., 1999 and Powel, 2002) and (b) Doppler sodars (Tamura et al., 2001a)

To assess the design wind speed at a particular site, it is necessary to determine the variation in wind speed with terrain roughness. Wind observations at a single site provide some information on the wind speed profile, but they give no information on variations in wind speed with terrain roughness. Tamura et al. (1999a, 2001a) conducted simultaneous wind observations over two sites with different roughnesses using Doppler sodars to find a reasonable method for estimating design wind speed for a given terrain roughness. They described the results of boundary layer wind observations at seaside sites and inland sites of the main island of Japan, and discussed the change in the horizontal wind speed profiles and the reduction in wind speed at lower altitudes due to inland roughness. Mono-static Doppler sodars were used for the measurements. Figure 3(b) compares the 10min mean wind speed profiles at two sites 23km apart for sea winds during the same storms to assess the effects of terrain roughness between them. One is located in a seaside area and another is in a residential area near Tokyo. The profiles were examined as ensemble averages of several 10min mean profiles. It can be seen that, due to so-called friction, the mean wind speeds decreased at lower altitudes after the wind blew over the inland terrain roughness, and consequently the power law indices α increased considerably.

Systematic multiple-site observations were carried out by Maeda et al. (1995) to capture the wind speed

distribution over a wide area. They introduced a network of 121 anemometers installed on a transmission tower network in Kyushu, Japan. This network provides useful information on horizontal wind structures.

Terrain Roughness Monitoring with Airborne Sensors

Although the height and land use pattern of the ground surface are digitized and have been utilized as the Geological Information System (GIS), the aerodynamic effects of roughness including buildings and trees are most important in wind engineering. It has been thought to be difficult to directly measure ground roughness. Recently, a laser profiler mounted on an aircraft with a GPS and an Inertial Navigation System has been developed. This technique enables monitoring of the displacement between the ground surfaces including obstacles, and then evaluation of the terrain roughness (Kraus and Pfeifer, 1998). The measured results are obtained in the form that can be handled by a computer as a Digital Terrain Model (DTM), and is utilized for the shadow evaluation of a building condensed urban area (Yoshida et al. 2001). In wind engineering, these data can be utilized in two patterns. One is direct use of the displacement data to generate a numerical grid point to making a terrain model in boundary layer wind tunnels. The other is aerodynamic modeling of the terrain roughness (Maruyama, 1999). These are on-going studies, and results are expected in the near future.

WIND PRESSURE MONITORING AND SPATIAL DATA ANALYSIS

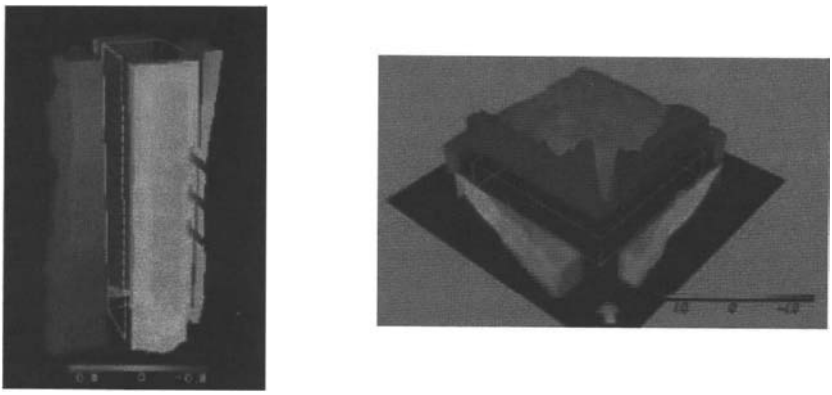
Multi-channel Wind Pressure Measuring System for Wind Tunnel Testing

The Simultaneous Multi-channel Pressure Measuring System (SMPMS) was first proposed by Fujii et al. (1986) and Ueda et al. (1994), to measure unsteady pressure fields on building models. Although its original version used 512 electronically scanned pressure sensors consisting of 32/16-port modules, every pressure tap has its own transducer without any scanning system in the current version. Animation showing the fluctuating pressure field is thought to be CFD's specialty. However, the SMPMS can provide beautiful animations showing the temporal and spatial fluctuations of the pressure fields as for the CFD results. The evidences of forming and drifting down of vortices of various sizes and shapes near the surfaces and their dynamic structures can be observed precisely. The most important advantage is that the phenomena observed by the SMPMS are the actual physical phenomena. Although SMPMS is not a recent technology, a lot of information has been obtained from the SMPMS. Here, some interesting SMPMS results are introduced.

Instantaneous pressure distributions causing extreme wind load effects

Wind pressure distributions specified for frame analyses in various wind loading codes are basically set proportional to the mean pressure distributions. However, these are quite different from the actual extreme wind pressures causing maximum load effects as in Holmes (1988, 1992), Kasperski (1992), Tamura et al.(2000). Kasperski & Niemann (1988) and Kasperski (1992) proposed the Load Response Correlation (LRC) formula to estimate the extreme pressure distributions, and Holmes (1992) and Tamura et al. (2001b) proved its validity. Figures 4(a) and 4(b) show examples of instantaneous pressure distributions on the surface of high-rise and low-rise building models.

These images give very useful information on the precise structures of fluctuating surface pressures. Based on the SMPMS data, Tamura et al. (2001c) pointed out a particular case in which the LRC formula has a limitation in its applicability. Tamura et al. (2002a) also discussed wind load combinations and extreme pressure distributions causing maximum wind forces, and clearly demonstrated the importance of considering wind force combinations even for low- or middle-rise buildings.



(a) High-rise model (b) Low-rise model

Figure 4: Instantaneous pressure distributions acting on a low-rise and a high-rise building model (Kikuchi & Hibi, 2002)

Combinations of SMPMS and POD

Proper Orthogonal Decomposition (POD) is a kind of Karhunen-Loève decomposition, which is a probabilistic expression of a method called Factor Analysis (Armit, 1968). POD is a useful tool for capturing hidden deterministic structures in random fields and for reducing information necessary to reproduce the phenomena, and it has also been used in wind engineering, e.g. Lee (1975), Best & Holmes (1983), and Kareem & Cermak (1984). When the POD technique is combined with SMPMS, its efficiency significantly increases as demonstrated by Bienkiewicz et al. (1995), Kikuchi et al. (1997), and Tamura et al. (1999b). Tamura et al. (1999b) summarized the points to note for POD analyses using SMPMS data. Their results for high-rise building models showed that the 1st and 5th modes closely relate to the vortex shedding and greatly contribute to the across-wind force, and the 2nd, 3rd and 4th principal coordinates contribute to along-wind force. Only these few of 500 modes in total can predict the wind-induced response of a high-rise building model within an error of 6%, showing an amazing reduction in necessary amount of information.

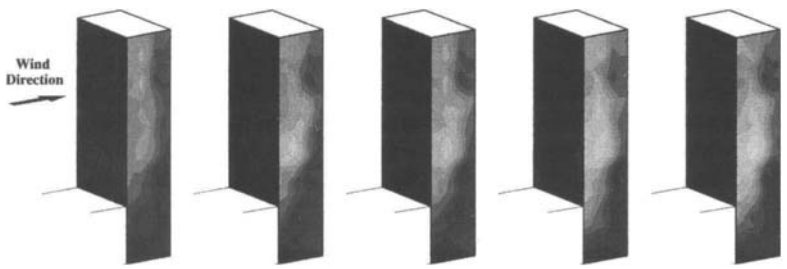
Calculations of internal forces based on SMPMS and practical applications

Information including animation based on SMPMS data showing complex temporal and spatial wind pressure fluctuations clearly demonstrates the limitation of simple wind load provisions specified in current wind load codes and the necessity of using 3D precise pressure fluctuation data for the practical design of important buildings such as long-span stadium roofs, domes or high-rise buildings. Whalen et al. (1998) proposed a wind resistant design system using electronic databases containing authorized aerodynamic data sets for various types of buildings, because of the discrepancy between the maximum load effects calculated by some major wind load codes and actual fluctuating pressures by SMPMS. SMPMS can be an efficient tool in conjunction with data processing and computer graphic techniques not only for basic academic research or educational purposes, but also for practical applications, for example Yasui et al. (1999). In practical applications, SMPMS can provide direct information on fluctuating pressures acting on building models with a sufficiently fine spacing. Internal forces or stresses in members of frames and displacements of particular points can be directly obtained by dynamic analysis of 3D frame models. Thus, errors in modeling of wind forces or lack of wind load combinations can be minimized. Taniguchi et al. (2001) directly compared the internal stresses and displacements caused by strong winds and earthquakes. Incidentally, Zhou et al. (2001) also proposed an

interactive aerodynamic database based on High Frequency Force Balance data. These trends to open web sites providing an electronic aerodynamic database may accelerate the use of direct information on pressure records obtained by SMPMS for more precise information on wind loads to realize more accurate and economic wind resistant design.

Full-scale Measurements of Fluctuating External Wind Pressures

Full-scale measurements on fluctuating pressures have been conducted since the '60s, and some sophisticated experimental studies have been conducted, such as Aylesbury Experimental House (Eaton & Mayne, 1975), Texas Tech Building (Ng & Mehta, 1990, Levitan et al., 1991), Silsoe Structures Building (Richradson et al., 1990). Some investigations have used flow visualization techniques, e.g. Banks et al. (2000). Animation of pressure fluctuation has also been carried out to visually observe actual phenomena, e.g. Hibi et al. (1994), which measured fluctuating pressures acting on a 30.4 m-high building using one hundred and fourteen pressure transducers on the walls. Figures 5(a) - 5(e) show examples of instantaneous pressure distributions acting on a full-scale building (Hibi et al., 1994).



(a) t = 131.5s (b) t = 132.5s (c) t =133.0s (d) t = 133.5s (e) t = 134.0s

Figure 5: Instantaneous pressure distributions on a 30.4m-high building (Full-scale data) (Hibi et al., 1994)

Full-scale Measurements of Internal Wind Pressures

A recent remarkable full-scale result is the measurement of internal pressures on a 120m-high office building by Kato et al. (1997). They used Highly Precise Absolute Pressure Transducers, which had a measurement range of 800-1100hPa and a resolution of 5ppm. They clearly demonstrated the variation of internal pressures with height, wind direction and so on.

RESPONSE MONITORING

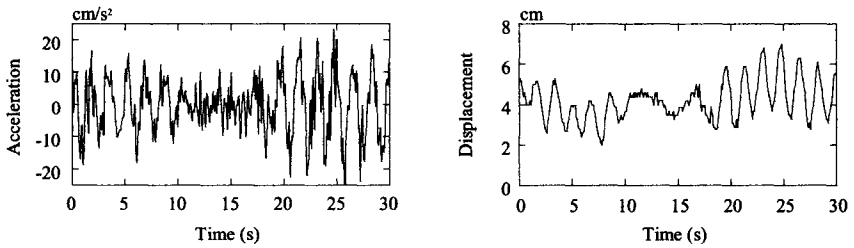
Monitoring of Displacement by RTK-GPS

Accelerometers have been commonly used for field measurements of building responses, and occasionally displacement transducers have been used. These transducers can be very useful for identifying dynamic characteristics of buildings. Tamura et al. (2002) identified the dynamic properties of a 15-story building up to the 9th mode very accurately by using the Frequency Domain Decomposition technique for ambient vibrations. Xu & Zhan (2001) measured wind-induced responses of Di Wang Tower with accelerometers and displacement transducers during a strong typhoon, and determined its dynamic components. As is well known, wind-induced responses consist of a static component, i.e. a mean value; a quasi-static component; and a resonant component. The static and

quasi-static components are difficult to measure with general accelerometers. In the past few decades, various attempts have been made to measure wind-induced responses including these components by using optical sensors or strain gauges. For example, Kobayashi (1962) used a He-Ne gas laser transmitter and a photo-cell to measure the wind-induced tip displacement of a 170m-high building. Maeda et al. (1999) utilized a CCD video camera and a target mark to measure the displacement of a power transmission tower.

Çelebi (1998) proposed using a RTK-GPS (Real-Time Kinematic Global Positioning System) for building response measurements. RTK-GPS (Leica MC1000) has a nominal accuracy of 1cm +1ppm for horizontal displacements and 2cm +2ppm for vertical displacements with a sampling rate of 10Hz (Celebi 1998, Tamura 2001d). Tamura et al. (2001d) reported that RTK-GPS could measure displacements when the vibration frequency was less than 2Hz and the amplitude was more than 2cm. Considering the static component and the first mode predominance of wind-induced responses, GPS can be a powerful tool for monitoring wind-induced responses. For this reason, many projects on monitoring of wind-induced responses of buildings and structures have been carried out, e.g. Toriumi et al. (2000), Ding et al. (2002), Kijewski & Kareem (2002), and Breuer & Konopka (2002).

Figure 6 shows an example of the temporal variation of response of a 108m-high steel tower. The RTK-GPS data consists of a static displacement of about 4cm, a slowly fluctuating quasi-static component with a period of 20s - 30s, and a resonant component with the first mode natural period of the tower: 1.8s (0.57Hz). The acceleration record seems to correspond closely to the fluctuating component of the displacement by RTK-GPS, and their power spectrum densities show very good agreement (Tamura et al., 2001d). Since the RTK-GPS measurement system can measure the static displacement, the tower deformation caused by heat stress can also be measured.



(a) Acceleration (Accelerometer) (b) Displacement (RTK-GPS)

Figure 6: Comparison of wind-induced responses of a 108m-high steel tower by accelerometer and RTK-GPS (Tamura et al., 2001d)

Stress Monitoring by Hybrid Use of FEM and RTK-GPS

Tamura et al. (2002c) developed a hybrid method for evaluating structural integrity. The tip displacement observed with the GPS was converted into structural member stresses. The conversion was based on the stiffness matrix of a finite element modeling. This concept can be developed for a future disaster prevention system consisting of an RTK-GPS monitoring system of a group of high-rise buildings in a city and a database containing analytical virtual building models having structural reality constructed in a computer.

CONCLUDING REMARKS

Recent developments and applications of various monitoring devices and techniques for detecting wind

speeds, wind pressures and wind-induced responses of buildings and structures have been briefly overviewed. Developments that we know about have mainly resulted from developments of monitoring systems and the visualization techniques. In order to understand the phenomena and their natures, a sufficient amount of accurate information is necessary. These are only supported by high quality monitoring techniques. Many of the techniques have just been introduced into the wind engineering field or are still under development, and new information will be provided in the future to deepen and widen our knowledge.

References

Akins R.E. and Reinhold T.A. (1998). Laser Doppler velocimeter measurements of separated shear layers on bluff bodies, Journal of Wind Engineering and Industrial Aerodynamics 74-76, 455-461

Amano T., Fukushima H., Ohkuma T. and Kawaguchi A. (1999). The observation of typhoon winds in Okinawa by Doppler sodar., *Journal of Wind Engineering and Industrial Aerodynamics* **83**, 11-20

Armitt J. (1968). Eigenvector analysis of pressure fluctuations on the West Burton instrumented cooling tower, *Central Electricity Research Laboratories (U.K.) Internal Report* RD/L/N114/68

Banks D., Meroney R.N., Sarkar P.P., Zhao Z. and Wu F. (2000). Flow visualization of conical vortices on flat roofs with simultaneous surface pressure measurement, *Journal of Wind Engineering and Industrial Aerodynamics* **84:1**, 65-85

Becker S., Lienhart H. and Durst F. (2002). Flow around three-dimensional obstacles in boundary layers, *Journal of Wind Engineering and Industrial Aerodynamics* **90:4-5**, 265-279

Best R.J. and Holmes J.D. (1983). Use of eigenvalues in the covariance integration method for determination of wind load effects, *Journal of Wind Engineering and Industrial Aerodynamics* **13**, 359-370

Bienkiewicz B., Tamura Y., Ham H.J., Ueda H. and Hibi K. (1995). Proper orthogonal decomposition and reconstruction of multi-channel roof pressure, *Journal of Wind Engineering and Industrial Aerodynamics* **54-55**, 369-381

Breuer P., Chmielewski T., Gorski P. and Konopka E. (2002). Application of GPS technology to measurements of displacements of high-rise structures due to weak winds, *Journal of Wind Engineering and Industrial Aerodynamics* **90**, 223-230

Celebi M. (1998). GPS and/or strong and weak motion structural response measurements -Case studies, *Structural Engineering World Congress '98, San Francisco, Conference Proceedings on CD-ROM*, T193-1

Cummins H.Z., Knable N. and Yeh Y. (1964). Observation of Diffusion Broadening of Rayleigh Scattered Light, *Phyics Review Letter* **12**, 150

Ding X.L., Chen Y.Q., Huang D.F, Xu Y.L. and Ko J.M. (2002). Measurement of Vibrations of Tall Buildings with GPS, *Structure Congress and Exposition, ASCE, Performance of Structure from Research to Design, Denver, Colorado*, 201-202

Eaton K.J. and Mayne J.R. (1975). The measurement of wind pressures on two-story houses at Aylesbury, *Journal of Industrial Aerodynamics* **1**, 67-109

Fujii K., Hibi K. and Ueda H. (1986). A new measuring system of unsteady pressures using electronically scanned pressure sensors (ESP) and its applications to building models, *Proceedings of the 9th National Symposium on Wind Engineering*, 313-318 (in Japanese)

Gerdes F. and Olivari D. (1999). Analysis of pollutant dispersion in an urban street canyon, *Journal of Wind Engineering and Industrial Aerodynamics* **82:1-3**, 105-124.

Hayashida H., Fukao S., Kobayashi T, NIrasawa H., Mataki Y., Ohtake K. and Kikuchi M. (1996) Remote sensing of wind velocity by boundary layer lader, *Journal of Wind Engineering* **67**, 39-42, (in Japanese)

Havel B., Hangan H. and Martinuzzi R. (2001). Buffeting for 2D and 3D sharp-edged bluff bodies, *Journal of Wind Engineering and Industrial Aerodynamics* **89:14-15**, 1369-1381

Hibi K., Kikuchi H. and Ueda H. (1994). Visualization of fluctuating surface pressure distribution on a

full-scale building surface, *Proceedings of Third Asian Symposium on Visualization*, 862-867
Holmes J.D. (1988). Distribution of peak wind loads on a low-rise building, *Journal of Wind Engineering and Industrial Aerodynamics* **29**, 59-67
Holmes J.D. (1992). Optimized peak load distributions, *Journal of Wind Engineering and Industrial Aerodynamics* **41-44**, 267-276
Kareem A. and Cermak J.E. (1984). Pressure fluctuations on a square building model in boundary-layer flows, *Journal of Wind Engineering and Industrial Aerodynamics* **16**, 17-41
Kasperski M. (1992). Extreme wind load distributions for linear and nonlinear design, *Engineering Structures* **14-1**, 27-34
Kasperski M. and Niemann H.J. (1988). On the correlation of dynamic wind loads and structural response of natural-draught cooling towers, *Journal of Wind Engineering and Industrial Aerodynamics* **30**, 67-75
Kato N., Niihori Y., Kurita T. and Ohkuma T. (1997). Full-scale measurement of wind-induced internal pressures in a high-rise building, *Journal of Wind Engineering and Industrial Aerodynamics* **69-71**, 619-630
Kikuchi H., Tamura Y., Ueda H. and Hibi K. (1997). Dynamic wind pressures acting on a tall building model - proper orthogonal decomposition, *Journal of Wind Engineering and Industrial Aerodynamics* **69-71**, 631-646
Kikuchi H. and Hibi K. (2002). Personal communication
Kijewski T. and Kareem A. (2002). GPS for monitoring the dynamic response of tall buildings, *Structure Congress and Exposition, ASCE, Performance of Structure from Research to Design, Denver, Colorado*, 197-198
Kobayashi S. (1962). Sway observation of tall building in strong wind (Keio Plaza Hotel Building 170m high), *Transactions of The Architectural Institute of Japan*, **192**, 33-39
Kondo K., Hongo T., Suzuki M., Tsuchiya M., Nakano R. and Hayashida K. (2001). Flow Visualization Techniques in Architectural and Civil Engineering Fields, *Journal of the Visualization Society of Japan* **21:1**, (in Japanese)
Kraus K. and Pfeifer N. (1998). Determination of terrain models in wooded areas with airborne laser scanner data, *ISPRS Journal of Photogrammetry and Remote Sensing* **53**, 193-203
Lee B.E. (1975). The effects of turbulence on the surface pressure field of a square prism, *Journal of Fluid Mechanics* **69**, 263-282
Lee S. and Kim H. (1999). Laboratory measurements of velocity and turbulence field behind porous fences, *Journal of Wind Engineering and Industrial Aerodynamics* **80:3**, 311-326
Levitan M.L., Holmes J.D., Mehta K.C. and Vann W.P. (1991). Field measurements of pressures on the Texas Tech building, *Journal of Wind Engineering and Industrial Aerodynamics* **38**, 227-234
Maeda J., Tomonobu N. and Miyazaki F. (1995) Wide area network system of wind measurement utilizing power transmission line systems, *International Symposium on cable dynamics*,
Maeda J., Imamura Y. and Morimoto Y. (1999). Wind response behaviour of a power transmission tower using new displacement measurement, *Proceedings of the 10th International Conference on Wind Engineering* **1**, 481-486
Maruyama T. (1999). Surface and inlet boundary conditions for the simulation of turbulent boundary layer over complex rough surfaces, *Journal of Wind Engineering and Industrial Aerodynamics* **81:1-3**, 311-322
Naito G., Ito Y. and Hayashi T. (1999). Strong wind features of the lower planetary boundary layer on a complex terrain, *Wind Engineering into the 21st Century, Larsen, Larose and Livesey(eds)* 281-286
Ng H.T. and Mehta K.C. (1990). Pressure measuring system for wind-induced pressures on building surfaces, *Journal of Wind Engineering and Industrial Aerodynamics* **36**, 351-360
Richardson G.M., Robertson A.P., Hoxey R.P. and Surry D. (1990). Full-scale and model investigations of pressures on an industrial/agricultural building, *Journal of Wind Engineering and Industrial Aerodynamics* **36**, 1053-1062
Powell M.D., Reinhold T.A. and Marshall R.D. (1999). GPS sonde insights on boundary layer wind

structure in hurricanes, *Wind Engineering into the 21st Century, Lasen, Larose and Livesey (eds),* 307-314

Powel M.D. (2002). (Personal communication)

Tamura Y., Suda K., Sasaki A., Iwatani Y., Fujii K., Hibi K. and Ishibashi R.(1999a). Wind speed profiles measured over ground using Doppler sodas, *Journal of Wind Engineering and Industrial Aerodynamics* **83**, 83-93

Tamura Y., Suganuma S., Kikuchi H. and Hibi K. (1999b). Proper orthogonal decomposition of random wind pressure field, *Journal of Fluids and Structures* **13**, 1069-1095

Tamura Y., Kikuchi H. and Hibi K. (2000). Wind load combinations and extreme pressure distributions on low-rose buildings, *Wind & Structures, International Journal* **3:4**, 279-289

Tamura Y., Suda K., Sasaki A., Iwatani Y., Fujii K., Ishibashi R. and Hibi K. (2001a). Simultaneous measurement of wind speed profiles at two sites using Doppler sodas, *Journal of Wind Engineering and Industrial Aerodynamics* **89**, 325-335

Tamura Y., Kikuchi H. and Hibi K. (2001b). Extreme wind pressure distributions on low-rise building models, *Journal of Wind Engineering and Industrial Aerodynamics* **89**, 1635-1646

Tamura Y., Kikuchi H. and Hibi K. (2001c). Actual pressure distributions and LRC formula, *The Fifth Asia-Pacific Conference on Wind Engineering, Kyoto, Journal of Wind Engineering* **89**, 589-592

Tamura Y., Matsui M., Pagnini L., Ishibashi R. and Yoshida A. (2001d). Measurement of wind-induced response of buildings using RTK-GPS, *Proceedings of The Fifth Asia-Pacific Conference on Wind Engineering, Kyoto, Japan*, 93-97

Tamura Y., Kikuchi H. and Hibi k. (2002a). Quasi-static wind load combinations for low- and middle-rise buildings, *Preprints of Engineering Symposium to Honor Alan G. Davenport, The University of Western Ontario*, C3-1-C3-12

Tamura Y., Zhang L., Yoshida A., Nakata S. and Itoh T. (2002b). Ambient vibration tests and modal identification of structures by FDD and 2DOF-RD Technique, *Proceedings of Structural Engineers World Congress 2002, Yokohama, Japan* (to be published)

Tamura Y., Yoshida A., Ishibashi R., Matsui M. and Pagnini L.C. (2002c). Measurement of wind-induced response of buildings using RTK-GPS and integrity monitoring, *The Second International Symposium on Advances in Wind and Structures (AWAS'02)* (to be published)

Taniguchi H., Hirose K., Watanabe Y., Gouda H. and Saitoh M. (2001). On design and construction of the roof structure of the swimming stadium for national athletic meet in Kochi, *IASS International Symposium on Theory, Design and Realization of Shell and Spatial Structures, October, Nagoya, Japan* TP172

Toriumi R., Katsuchi H. and Furuya N. (2000). A study on spatial correlation of natural wind, *Journal of Wind Engineering and Industrial Aerodynamics* **87**, 203-216

Ueda H., Hibi K., Tamura Y. and Fujii K. (1994). Multi-channel simultaneous fluctuating pressure measurement system and its applications, *Journal of Wind Engineering and Industrial Aerodynamics* **51**, 93-104

Whalen T., Simiu E., Harris G., Lin J. and Surry D. (1998). The use of aerodynamic databases for the effective estimation of wind effects in main wind-force resisting systems: application to low buildings, *Journal of Wind Engineering and Industrial Aerodynamics* **77-78** ,685-693

Xu Y.L. and Zhan S. (2001). Field measurements of Di Wang Tower during Typhoon York, *Journal of Wind Engineering and Industrial Aerodynamics* **89:1**, 73-93

Yasui H., Marukawa H., Katagiri J., Katsumura A., Tamura Y. and Watanabe K. (1999). *Journal of Wind Engineering and Industrial Aerodynamics* **83**, 277-288

Yoshida H., Ishibashi K. and Kurisaki N. (2001). A simulation of complex insolation in CBD by using airborne LIDAR data set, *Papers and Proceedings of the Geographic Information Systems, 2001* 315-319 (in Japanese)

Zhou Y., Kijewski T. and Kareem A. (2001). Aerodynamic Loads Database, *http://www.nd.edu/~nathaz/database/index.html*

Advances in Building Technology, Volume I
M. Anson, J.M. Ko and E.S.S. Lam (Eds.)
© 2002 Elsevier Science Ltd. All rights reserved

A CONCEPTION OF CASUALTY CONTROL BASED SEISMIC DESIGN FOR BUILDINGS

Li-Li Xie

College of Civil Engineering, Harbin Institute of Technology &.
Institute of Engineering Mechanics, China Seismological Bureau
Harbin, 150080, China

ABSTRACT

Earthquake disaster is still the number one among all other natural disasters, particularly, in terms of destructive power in causing deaths. Can earthquake engineers control seismic casualties through the seismic design of buildings? For this purpose, a conception of casualty control based seismic design is presented and a "two-step decision-making" method is proposed for determining the optimum seismic design intensity (or ground-motion) for controlling both seismic death and economic losses. The key problems in establishing the model are to determine the appropriate socially acceptable level of earthquake mortality and establish the corresponding objective function and /or constraint conditions for optimum seismic design intensity. Ten different grades of socially acceptable mortality are initially suggested and the final socially seismic acceptable mortality level was proposed based on a questionnaire that was carried out nationwide in China. Finally, the effect of various grades of acceptable earthquake mortality on seismic design intensity is analyzed.

KEYWORDS

Seismic Death control, Performance-based design, Seismic design criterion, Seismic vulnerability analysis, Earthquake economic loss estimation, Acceptable level for earthquake human mortality, Optimum seismic design load, Decision-making method

INTRODUCTION

Recently, with the development of Performance-Based Earthquake Engineering, it seems that control of economic losses to a reasonable level has become the main objective in determining seismic design loads (Cornell C. Allin and Helmut Krawinkler. (2000)). This may be acceptable for a developed country, but might not be appropriate for a developing country. Table 1 lists the number of human deaths and economic losses in several recent earthquakes (China Seismological Bureau (1996), Fu Zheng-xiang and Li Ge-ping (1993)). Table 1 indicates that the number of deaths is higher, but economic losses are lower in developing countries than in developed countries. For example, an earthquake of magnitude 7.1 caused deaths in Iran about 24 times those in the U.S.A, but economic loss in Iran is only about 1/3 that in the U.S.A.

TABLE 1
LIFE AND ECONOMIC LOSSES IN MAJOR EARTHQUAKE DISASTERS

Earthquake	Country	Year	Magnitude	Number of deaths	Economic loss
Haicheng	China	1975	7.3	1328	13 billions
Tangshan	China	1976	7.8	242,769	100 billions
North Iran	Iran	1997	7.1	1573	$5 billion
North Philippines	Philippines	1990	8.0	2,600	$5.3 billion
Armenia	Former USSR	1988	6.8	25,000	
Mexico	Mexico	1985	8.1	10,000	
Loma Prieta	U.S.A	1989	7.1	65	$15 billions
Northridge	U.S.A	1994	6.7	57	$151 billions
Kobe	Japan	1995	7.2	5,500	$1000 billions

It is generally accepted that the main reason causing death and injury during earthquakes is collapse of and damage to structures. How can seismic mortality be reduced at an effective cost is a central problem of seismic design of buildings (Xie Li-li (1996))? How can we control the seismic mortality through determining the seismic design load in seismic design? At present, neither seismic hazard analyses nor seismic design codes have mentioned that earthquake casualties can be quantitatively controlled by selecting seismic design load at an effective cost. The available seismic design can answer neither how great the potential mortality in a future earthquake will be, nor whether the casualty level is acceptable (Xie Li-li (1996)). In order to consider the casualty factor in determining seismic design load so as to quantitatively control casualties by adjusting design intensity, this paper specifically includes the concept of a socially acceptable level for earthquake human fatalities. For a city or a region, socially acceptable mortality is defined as a ratio of possible maximum death toll to the total population of the concerned region in a future earthquake, which can be accepted by society (Ma Yu-hong (1996)). Based on statistics of the deaths caused from historical natural disasters and devastating earthquakes (particularly the recent destructive earthquakes occurring in modern cities, such as the 1975 Haicheng, and 1976 Tangshan earthquakes, the 1988 Armenia earthquake, the 1994 Northridge earthquake, the 1995 Kobe earthquake and the 1999 Izmit earthquake in Turkey), ten grades of "acceptable" mortality are proposed in this study. After an analysis of response to a questionnaire distributed to the experts in the field of earthquake disaster prevention and officers from civil defense departments, a realistic compromise for a socially acceptable mortality level is recommended. Furthermore, a "two-step decision-making" method is developed for determining the optimum seismic design intensity conditional on reducing the earthquake fatalities. Finally, a method for determining seismic design load based on various grades of socially acceptable earthquake mortality is presented.

MODEL OF DECISION-MAKING ANALYSIS FOR SEISMIC DESIGN INTENSITY IN CONTROLLING SEISMIC FATALITIES

In the models of decision-making analysis for seismic design intensity, a reasonable objective function keeps a balance between extra cost of a structure to ensure earthquake resistance and possible earthquake losses. In quantitative form, the sum of the extra cost of construction for withstanding an earthquake and the earthquake economic losses should be at a minimum. This model of decision-making for seismic design intensity is depicted in Fig 1.

Find I to minimize

$$S(I) = C(I) + LP(I) \quad (1)$$

with constraint condition:

Numbers of fatalities $\leqslant$ socially acceptable level of mortality (2)

Figure 1. Mathematical model of optimum decision-making for seismic design

In the figure, $S(I)$ is the objective function, $C(I)$ is the extra cost of structures to resist the earthquake, $LP(I)$ is the expected earthquake economic losses of structures designed and constructed, and I is the adopted seismic design intensity for the region. The expected earthquake economic loss $LP(I)$ is a function of the design intensity I and the intensities i that are likely to happen in the region during future earthquakes. Therefore, $LP(I)$ can be expressed as:

$$LP(I) = \tau \cdot (L_1(I) + L_2(I)) \quad (3)$$

$$L_1(I) = \sum_{i=6^\circ}^{10^\circ} \sum_{j=1}^{5} P(D_j \mid I,i) \cdot l_1(D_j) \cdot W \cdot P(i) \quad (4)$$

$$L_2(I) = \sum_{i=6^\circ}^{10^\circ} \sum_{j=1}^{5} P(D_j \mid I,i) \cdot l_2(D_j) \cdot Y \cdot P(i) \quad (5)$$

Where, $L_1(I)$ is the direct economic loss due to structural damage, $L_2(I)$ is the economic loss due to the damage of contents, τ is a modified coefficient obtained from a statistical analysis and varies from 1.4 to 3.0, accounting for the indirect economic losses; for example, τ takes 1.4 for residential buildings and 3.0 for commercial and industrial buildings (Ma Yu-hong (1996)), $P(D_j \mid I,i)$ is the vulnerability matrix of buildings (Ma Yu-hong (1996)), W is the construction cost, Y is the total value of building contents, $l_1(D_j)$ and $l_2(D_j)$ are the ratio of direct economic losses of structures to W and losses of contents to Y respectively, and $P(i)$ is occurrence probability of earthquake intensity i worked out from seismic hazard analysis.

In case only objective function equation (1) is minimized, we can obtain the optimal design intensity (or **ground motion**) for assuring minimal economic losses and it can be named the **optimum economic design intensities (ground motion)**. It is apparent that the optimum economic design intensities (ground motion) can only make economic losses minimal and do nothing directly to reduce seismic mortality. However, the concept of the **optimum safe design intensity (ground motion)** is defined as the seismic design intensity or (ground motion) that can be used not only to minimize the economic losses but also to control the seismic mortality below the acceptable level. For this purpose, a "two-step decision-making" method is presented.

"TWO-STEP DECISION-MAKING" METHOD FOR DETERMINING THE OPTIMUM SAFE SEISMIC DESIGN INTENSITY TO CONTROL SEISMIC MORTALITY POTENTIAL

It has been mentioned that the optimum safe design intensity (ground motion) should be optimal in economic senses and also assure seismic mortality below the acceptable levels. In the optimum decision-making model, the equation (1) is the objective function and the controlled mortality (equation 2) is regarded as the constraint condition. The optimum safe seismic design intensity (ground motion) can be determined when both objective function and constraint condition are satisfied. It is

assumed that the optimum safe seismic intensity should ensure earthquake mortality below the socially acceptable levels for each of the "frequently occurring earthquake", "occasionally occurring earthquake" and "rarely occurring earthquake"(see Table 2). Therefore, the constraint conditions of socially acceptable mortality can be expressed as:

$$\begin{cases} RD_{I,I_{63}} \le RD_{acc,I_{63}} \\ RD_{I,I_{10}} \le RD_{acc,I_{10}} \\ RD_{I,I_5} \le RD_{acc,I_5} \end{cases} \tag{6}$$

where, I_{63} stands for intensity of a frequently occurring earthquake with exceedance probability of 63% in 50 years, I_{10} is the intensity of an occasionally occurring earthquake with exceedance probability of 10% in 50 years, I_5 is the intensity of a rarely occurring earthquake with exceedance probability of 5% in 50 years, RD_{I,I_J} is the estimated mortality caused during the earthquake of intensity I_J in a region where the buildings were designed against the earthquake of intensity I, RD_{acc,I_J} is socially acceptable mortality for the concerned region, I_J is earthquake intensity that might be considered as one of I_{63}, I_{10} and I_5.

TABLE 2.
DEFINITIONS OF THREE SEISMIC DESIGN LEVELS

Seismic design levels I_J	Probability of exceedance in 50 years	Estimated earthquake mortality caused during earthquake I_J	Acceptable mortality
Frequently occurring earthquake intensity I_{63}	63%	$RD_{I,I_{63}}$	$RD_{acc,I_{63}}$
Occasionally occurring earthquake intensity I_{10}	10%	$RD_{I,I_{10}}$	$RD_{acc,I_{10}}$
Rarely occurring earthquake intensity I_5	5%	RD_{I,I_5}	RD_{acc,I_5}

The first step in determining seismic design loads is to calculate the optimum economic intensity by minimizing the objective function, and then, substitute the obtained intensity into the inequality (4). If the inequality is satisfied, this optimum economic intensity will be the final optimum safe design intensity, otherwise, the intensity must be recalculated by finding the next minimum of the objective function and then substituting into the inequality (4); the remaining steps are the same as above. Finally, the optimum safe design intensity can be determined for a case when both objective function and constraint condition are satisfied. This method is named here as "two-step decision-making" method and is illustrated in Figure 2.

The expression of estimated mortality RD_{I,I_J} under the earthquake of intensity I_J is given as:

$$RD_{I,I_J} = f_t \cdot f_\rho \cdot \sum_{J=1}^{5} P(D_j \mid I, I_J) \cdot l_5(D_j) \cdot P(I_J) \qquad (7)$$

where, I is the design intensity, $l_5(D_j)$ is the mortality ratio corresponding to various categories D_j

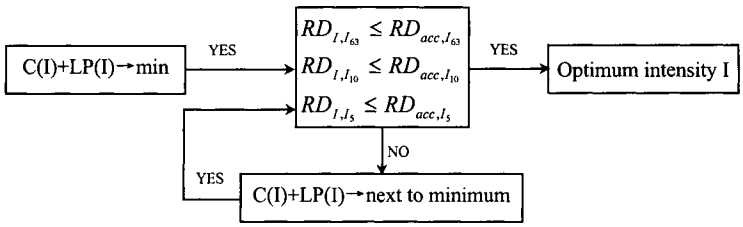


Figure 2. Two-step decision-making method for determining the optimum seismic safe intensity (ground motion)

of damage to the buildings (see Table 3), obtained from statistical data at home and abroad (Ma Yu-hong (1996)), $P(I_J)$ is the occurrence probability of intensity I_J, mainly depending on the results of seismic hazard analysis, $P(D_j \mid I, I_J)$ is the vulnerability matrix, namely the conditional probability of damage level D_j over the intensity I_J for the buildings with earthquake resistance design against intensity I, and f_ρ and f_t are the modified coefficients obtained from statistical analysis in accounting for the effects of different population density (see Table 4) and different occurrence time of earthquake on casualties (see Table 5) respectively. This is because of the fact that seismic death tolls are usually quite different with earthquake occurring in a densely populated area or in a less populated area, and whether occurring in the day time or the night. (Ma Yu-hong (1996))

TABLE 3
MORTARITY CORRESPONDING TO VARIOUS DAMAGE CATEGORIES (%)

Damage level D_j	Intact	Slight	Moderate	Extensive	Complete collapse
Mortality	0	0	0～0.1	0.01～1	2～30

TABLE 4
MODIFIED COEFFICIENT CORRESPONDING WITH POPULATION DENSITY

Population density ρ (persons/km^2)	< 50	50-200	200-500	> 500
Modified coefficient f_ρ	0.8	1.0	1.1	1.2

TABLE 5
MODIFIED COEFFICIENT CORRESPONDING TO OCCURRENCE TIME OF EARTHQUAKE

Intensity	VI	VII	VIII	IX	X
Modified coefficient f_t (night)	17	8	4	2	1.5

INFLUENCE OF SOCIALLY ACCEPTABLE EARTHQUAKE MORTALITY GRADE ON SEISMIC DESIGN INTENSITY

Different communities may make different choices in fixing an adequate level of socially acceptable earthquake mortality, according to their local social and economic situations. Therefore, the level should be flexible for various choices. In order to analyze the influence of different choices of acceptable seismic mortality on optimal safe design intensities, ten grades of socially acceptable earthquake mortality are given in Table 6. The Grade ① corresponds to the highest requirement, or the minimum level of acceptable seismic mortality and Grade ⑩ to the lowest requirement or the maximum acceptable seismic mortality .

TABLE 6
GRADE OF SOCIALLY ACCEPTABLE EARTHQUAKE MOTARITY

Intensity	VI	VII	VIII	IX	X	Intensity	VI	VII	VIII	IX	X
Grade①	1×10^{-8}	2×10^{-8}	1×10^{-7}	5×10^{-7}	2×10^{-6}	Grade⑥	2×10^{-5}	5×10^{-5}	2×10^{-4}	1×10^{-3}	$5\times10^{0^{-3}}$
Grade②	2×10^{-8}	5×10^{-8}	2×10^{-7}	1×10^{-6}	5×10^{-6}	Grade⑦	1×10^{-4}	2×10^{-4}	1×10^{-3}	5×10^{-3}	$2\times10^{0^{-2}}$
Grade③	4×10^{-8}	1×10^{-7}	4×10^{-7}	2×10^{-6}	1×10^{-5}	Grade⑧	2×10^{-4}	5×10^{-4}	2×10^{-3}	1×10^{-2}	$5\times10^{0^{-2}}$
Grade④	2×10^{-7}	5×10^{-7}	2×10^{-6}	1×10^{-5}	5×10^{-5}	Grade⑨	1×10^{-3}	2×10^{-3}	1×10^{-2}	5×10^{-2}	$2\times10^{0^{-1}}$
Grade⑤	6×10^{-6}	1×10^{-5}	2×10^{-5}	4×10^{-4}	3×10^{-3}	Grade⑩	2×10^{-3}	5×10^{-3}	2×10^{-2}	1×10^{-1}	$5\times10^{0^{-1}}$

With different acceptable mortality levels, the seismic design intensities determined by "two-step decision-making method" should be different. As a numerical example, eight cities in China are selected for determining optimum safe design intensities. For these eight selected cities, optimum safe seismic design intensities determined by the "two-step decision-making method" are shown in Table 7. From Table 7, it can be found:

1. Generally, the optimum safe seismic design intensity is increased with decrease of socially acceptable mortality grade. The lower the acceptable mortality which is adopted the higher the optimum safe design intensity required, and the more seismically resistant the designed structures will be. With increase of the grade from ① to ⑩, the corresponding optimum safe seismic design intensity will be decreased. Once an acceptable mortality ratio is chosen, the corresponding optimum safe seismic design intensity can be determined.

2. Optimum safe design intensity corresponding to different acceptable mortality levels sometimes is different from optimum economic intensity, which is conditioned on minimum economic losses only. This result means that if structures were designed to withstand optimum economic seismic intensity, constraint condition (4) can only be satisfied at rather high mortality levels.

3. The term "Basic Intensity" means the intensity or peak ground acceleration with 10% probability of exceedance in 50 years given by the existing seismic zoning map. It is widely adopted as the design intensity in the current seismic design code; however, this is with little consideration of controlling the death toll. Table 7 demonstrates that the optimum economic design intensity is generally in accordance with the Basic Intensity, but lower than the optimum safe seismic design intensity, and especially lower than the intensity required for the lower socially acceptable mortality grade. If a structure is designed to withstand only the Basic Intensity, therefore the safety of occupants cannot be guaranteed.

TABLE 7
OPTIMUM SAFE DESIGN INTENSITY DETERMINED
BY "TWO STEP DECISION-MAKING METHOD"

City		Harbin	Hangzhou	Nanjing	Dalian	Shanghai	Beijing	Xian	Xicang
Basic Intensity		6	6	7	7	7	8	8	9
Economic optimum intensity		5.5	5.5	7	7	7	8	8	9
Optimum safe design intensity	Grade ①	8	8	9	9	9	9	9	10
	Grade ②	8	8	8	8	8	9	9	9
	Grade ③	8	8	8	8	8	9	9	9
	Grade ④	8	7	8	8	8	8	8	9
	Grade ⑤	7	7	7	7	7	8	8	9
	Grade ⑥	6.5	6.5	7	7	7	8	8	9
	Grade ⑦	6.5	6.5	7	7	7	8	8	9
	Grade ⑧	5.5	5.5	7	7	7	8	8	9
	Grade ⑨	5.5	5.5	7	7	7	8	8	9
	Grade ⑩	5.5	5.5	7	7	7	8	8	9

The analysis illustrates that the influence of various grades of socially acceptable earthquake mortality on optimum safe seismic design intensity is significant. Human casualty control must be accounted for in determining seismic design load. The method presented in this paper stresses this point. It should take into account not only the need to minimize the possible economic losses but also to reduce the potential seismic mortality when determining seismic design load (or intensity) and emphasizes that the decision-makers should select carefully the socially acceptable mortality grade in determining the appropriate seismic design load.

CONCLUSIONS AND DISCUSSION

In this paper, a "two-step decision-making method" is presented for determining the optimum safe seismic design intensity in consideration of both optimal investment and controlling of seismic fatalities. The method as well as the ten recommended grades of socially acceptable seismic mortality presented in this paper intends to provide a tool by which both economic losses and life losses during earthquakes can be controlled through decision-making in determining the seismic design intensities or seismic design ground motion. It may provide a basis for government as well as building owners to formulate seismic design load (or intensity) and make an optimum balance between the economic investment and life-safe requirements.

It should be pointed out that the conception and the method developed in this paper provide only a framework for seismic design to control both economic losses and human deaths in future earthquakes. More detail of the parameters, such as socially acceptable mortality grade and several coefficients accounting for the effects of damage levels, occurrence time of earthquake and population density level on the mortality can differ from place to place and also needs to be further improved.

ACKNOWLEDGMENTS

This work was jointly funded by the Chinese National Natural Science Foundation with the Grant No.59895410 and the China Basic Research and Development Project: "the Mechanism and Prediction

of the Strong Earthquake of the Continental" under the Grant No.95130603. The authors are grateful to Professor Bruce Bolt of University of California, Berkeley, for his valuable comments.

REFERENCES

China Seismological Bureau. (1996). A compilation for earthquake losses evaluation in Chinese Mainland (in Chinese). Earthquake Publishing House. Beijing.

Cornell C. Allin and Helmut Krawinkler. (2000). Progress and Challenges in Seismic Performance Assessment. PEER CENTER NEWS. **Vol.3, No.2.**

Fu Zheng-xiang and Li Ge-ping. (1993). Studies on life losses from earthquake [M]. Earthquake Publishing House. (in Chinese). Beijing.

Ma Yu-hong. (1996). Research on performance-based seismic design load [D], Institute of Engineering Mechanics, China Seismological Bureau. (in Chinese with English summary).

Xie Li-li (1996). On the design earthquake level for earthquake resistant works [C], Proceedings of the PRC-USA Bilateral Workshop on Seismic codes. December 3-7, 1996, Guangzhou, China.

Advances in Building Technology, Volume 1
M. Anson, J.M. Ko and E.S.S. Lam (Eds.)
© 2002 Elsevier Science Ltd. All rights reserved

THERMAL RADIATION EFFECTS AND THEIR DETERMINATION IN ROOM FIRES

K. T. Yang

Department of Aerospace and Mechanical Engineering
University of Notre Dame
Notre Dame, IN 46556, USA

ABSTRACT

In fire models, especially the field fire models applied to room fires, which have received ever increasing attention and use in fire-safety engineering practice, the physical interactions among combustion, turbulence, buoyancy, and thermal radiation are accounted for in different levels of quantitative sophistication. Among these effects, radiation has apparently received the least attention and development, despite its significance in the room-fire phenomena, primarily because of the complexity in its quantitative determination. The purpose of this paper is to highlight the physical role and effects of thermal radiation in room fires, its theoretical basis, its quantitative determination, and its possible simplifications and approximations for its inclusion into the fire models.

KEYWORDS

Room fires, fire models, thermal radiation, radiative transfer

INTRODUCTION

The loss of lives and property due to unwanted fire is well recognized as a worldwide problem. In the United States alone, the annual average direct and indirect fire losses amount to approximately 10,000 lives, 100,000 severe injuries, and more than 30 billion U. S. dollars. Such losses worldwide must be several times these figures. Therefore, it is not surprising that many countries, particularly United States, Japan, Australia, Canada and several countries in Europe, have established national ongoing programs in fire research in an attempt to control and mitigate such losses. Much effort has been made in fire-research activities ranging from basic research in an attempt to understand both qualitatively and quantitatively the dynamics of the fire phenomena, to applied research dealing with the development of fire-fighting materials and equipment, and the establishment of fire codes, fire protection measures, and a rational basis for post-fire investigations.

While the significance of such research efforts in broad terms can be readily appreciated, it is however, also well appreciated that the progress of these efforts can be expected to be slow in coming, primarily because of the extreme physical complexity of the fire phenomena. They depend on the physical and chemical processes, which are complex functions of the fire ignition source, spatial geometry, and materials content, and the very large number of parameters associated with each of them. Nevertheless, there is progress, especially in the area of developing fire models to describe the fire phenomena in room fires, all based on the pertinent conservation laws of nature. While all such models have a formal theoretical structure, details in the physics and chemistry involved are described in different levels of approximations, since much of them is still not understood quantitatively or even qualitatively. It is a common practice to introduce judiciously pertinent experimental data in places in the model where no information is otherwise known or available. Most of these models have been validated, even though not sufficiently, by some limited experimental data, and are being revised and improved continuously as more physics becomes quantitatively known or as more experimental data become available. Despite all the shortcomings in the current models for room fires, they have gained some respectability in the all important fire-safety field, since room fires clearly represent the first fire hazards in inhabited buildings. In fact, the current fire models are already being used to serve several important fire-safety related functions. They offer a means of real-time control of the spread of fire and smoke in rooms, corridors and buildings, and also provide a meaningful tool for post-fire investigations. They can also be used to develop data bases for delineating fire hazards and risks based on real and hypothetical fire scenarios for rooms and buildings. It is of particular significance that such fire models are being used as the basis for developing rational fire codes for building fire-safety designs.

The first key to the development of fire models is to recognize the essential physics in the complex fire phenomena in terms of fluid mechanics, energy transfer, combustion, materials and geometry, and their mutual interactions. While the first three are truly dynamic effects, the last two can also be considered as dynamic, as the materials are being consumed in the fire, thus also altering the geometry. These effects are manifested through such individual phenomenon as fire ignition, growth, and extinction, flow with strong buoyancy and stratification, turbulence, and compressibility, and thermal radiation exchange and feedback. Fire models represent the conglomeration of approximate physical and mathematical description of each of these sub-phenomena, known as submodels, in the form of differential equations based on conservation laws such as those for mass, flow momentum, energy, and gas species. Solutions to these coupled dynamic equations, subjected to appropriate initial and boundary conditions, then lead to the determination of physical field variables such as flow velocities, temperature, and gas species which describe the evolution of the overall room-fire phenomena.

For room fires, the most difficult submodels to develop are those for combustion, turbulence, and thermal radiation, and each of them has been under intensive study in recent years with some degree of success. On the other hand, it is fair to mention that thermal radiation is probably the most neglected among the three in the current generation of fire models, and yet, it does play an equally significant role in any realistic room-fire scenarios. Radiation is strongly coupled to the high-temperature gas field resulted from the turbulent combustion process in the fire and provides a positive feedback mechanism to enhance the combustion process itself. It is also generally recognized that radiation is more responsible to fire spread in rooms and adjoining rooms as flashovers, particularly in a high-temperature environment, than the movement of hot gases. In addition, radiation does negatively impact the operation of fire-mitigation devices such as sprinklers and room structural elements. The primary reason that radiation does not receive as much attention as combustion and turbulence in the current fire models is that radiation is very sensitive to the room geometry and the nonuniform temperature and species variations, and its determination is lengthy and tedious, along with uncertain accuracy in the results. On the other hand, particularly in the current emphasis on implementing the performance-based fire codes in many developed and developing countries, there is no longer any excuse in not treating thermal radiation effects in room fires adequately in the fire

models, since it is an inherent part of the physics which would otherwise distort the fire-safety design results, if the radiation effects were not properly included. The purpose of this paper then is to promote the adequate inclusion of radiation calculations in fire models by first briefly discussing the physical role and effects of thermal radiation in room fires, followed by reviewing the theoretical basis for radiation calculations and how they are formally incorporated into the fire model. Also discussed will be the various approximation methods of incorporating simplified radiation calculations in fire models within the spirit of performance-based engineering practices. Explicit references will be cited to give an indication as to how the existing models including radiation perform as compared to available experimental data in room fires.

ROLE AND EFFECTS OF THERMAL RADIATION IN ROOM FIRES

As briefly mentioned previously, the room-fire phenomena are essentially governed by the coupled interactions among combustion, buoyancy, turbulence, and radiation. Consequently, it is difficult to discuss radiation without accounting for combustion, turbulence, and other physical effects (Yang, 1994). In room fires, the combustion phenomenon is really that of turbulent combustion, in that the flow turbulence induces mixing, which brings the reactants (fuel and oxygen molecules) together so that reactions can take place and generate heat and produce species as products of combustion. The heated gas species such as water vapor, carbon mono- and dioxides and carbon soot, which are all radiatively participating, then emit, absorb, and scatter radiation, and reach all far corners of the room. The net result is that the radiation heats up all room surfaces, producing heat sources in the gas medium, and provides a mechanism for changing local gas densities, thus resulting in additional buoyancy, which in turn further affects the behaviors of the convective flow and turbulence fields. It then enhances the turbulent combustion process and brings the entire interactions to a full circle. It is here seen that radiation acts as an intermediary for maintaining and enhancing the fire growth in the room. Therefore, despite the complexity of the role of radiation in the room-fire phenomena, no fire model can be considered truly adequate without accounting for thermal radiation and its interaction with other effects such as combustion, buoyancy, and turbulence.

From a quantitative theoretical framework, the role and effects of thermal radiation in the room-fire phenomena are known to be accommodated in a single source term in the energy equation (Siegel and Howell, 2001; Yang, 1994), which is written as the negative of the divergence of the radiative flux vector. It is also known that this energy equation is part of a set of coupled differential equations governing the dynamics and interactions in the fire phenomena, including the mass continuity equation, the flow equations, the energy equation, and the species-conservation equations (Yang, 1994). In fact, this set of governing equations forms the basis for all the fire models known as the fire field models, which, along with initial and boundary conditions and appropriate submodels, are usually solved by computational fluid dynamics (CFD) methodologies (Minkowycz et al., 1988). Examples of fire field models are UNDSAFE (Yang et al., 1994, Raycraft et al., 1990), and KAMELEON (Holen et al., 1990). Unfortunately, this deceptively simple source term to account for all radiation effects belies the fact that radiative fluxes are extremely difficult to compute, involving not only the entire physical domain of the room, but also the spatial variations of all radiation-participating species and the temperature field at every time instant into the fire. Further complications are uncertainties in the determination of radiative properties of the gas and soot mixtures and the approximate computations associated with the geometrical distribution of the radiation rays traversing the entire room. Moreover, the entire computational process for the radative fluxes must be repeated many times as the fire phenomenon evolves in time and space. Since the overall fire problem without the radiation component is already very computationally intensive for its solution, even with the available CFD solvers, there is still a need to make appropriate simplifications for the determination of the radiative fluxes. These issues will be addressed in the following sections.

THEORETICAL BASIS AND NUMERICAL METHODS FOR DETERMINING RADIATIVE FLUXES FOR ROOM FIRES

For room fires, the domain for radiation heat transfer covers basically the wall, ceiling, and floor surfaces, the surfaces of all material contents, and the volume of gas and particulate medium bounded by the solid surfaces. Also, doorways and windows, either closed or open, all play a role in the radiation heat transfer process. Once ignited, the evolving fire becomes a part of the medium in the room, where the temperature rises due to the combustion process, and heat is imparted to the rest of the room by direct radiation exchange and natural convection. In room fires, radiation exchange occurs between surface and surface, gas (including flame) and surface, and gas (including flame) and gas, and is governed by different independent physics known as radiative transfer. The easiest way to consider the propagation of radiation in a fire room is to simply look along a specific ray of radiation in a specific direction that traverses the room medium from one surface to another. At the starting point on a surface, the radiation leaving is that due to emission there and reflection of all radiation arriving at the starting surface, all in the same direction. As the radiation travels along the ray in the medium, it encounters additional emission due to the local medium temperature, absorption by the medium, and radiation scattering into and out of the ray due to soot particles from the combustion process. As a result, the original radiation intensity continues to change until it reaches the target surface, where the arriving radiation is absorbed and reflected. One inherent complexity here is that both emission and absorption are present for radiation-participating gases such as water vapor and carbon mono- and dioxides in most room fires, as they possess discrete absorption bands in the wave lengths, and such emission and absorption are also functions of local concentrations of the participating gases, in additional to the local temperatures. Furthermore, the radiation scattering is dependent on the size of the particulates in the medium. Therefore, in the calculation of variations of the radiation intensities, even along a single ray requires information on the absorption and scattering coefficients, which are the medium radiation properties. This single-ray calculation at a given solid angle characterizing the ray direction will have to be repeated for all rays spanning all the boundary surfaces in the room. The resulting accumulated local radiation intensities in all directions and the corresponding fluxes can then be resolved into the radiation fluxes in the principal directions of the chosen coordinate system. The local negative divergence of these radiation vectors then becomes the radiative heat source term in the energy equation, which is to be solved, together with other coupled equations, thus resulting in the data for the evolution of the fire dynamics phenomena of the room fires.

The radiation submodel in the fire field model is just the theoretical quantification of the determination of the radiative flux vectors and the corresponding radiative heat source based on the ray-tracing process just mentioned. Before some details are shown, it is pertinent and desirable to mention here a companion analysis needed to determine the relative geometrical positions of the chosen two surfaces which bound a particular group of rays of radiation in the fire room. In order to resolve the specific direction of a giving ray, the surfaces involved are taken to be sufficiently small so that each surface has a uniform temperature. Under this condition, it is convenient to introduce the well-known view factor or configuration factor to characterize the relative positions of any pair of surfaces in a given room. Since this factor is well discussed and tabulated in the literature (Siegel and Howell, 2001; Howell, 1982) and also in many undergraduate texts on Heat Transfer, its definition and derivation thus will not be repeated here. However, it is important to note that these view factors can be used to determine the radiation heat transfer between any pair of the surfaces with known temperatures in a black enclosure (room) with nonparticipating medium, in terms of the difference between the black-body emissions at the two surfaces at the respective temperatures in accordance with the Pranck's Law (Siegel and Howell, 2001; Modest, 1993). Furthermore, this enclosure theory for a black enclosure can be readily extended to that of a gray enclosure with gray surfaces and nonparticipating medium with prescribed emissivities in accordance with the radiosity method (Siegel and Howell, 2001). A similar role is also played by these same view factors in rooms with

radiation participating medium to characterize the geometry of radiation rays for the purpose of determining the corresponding radiation intensities and eventually the radiation flux vectors.

As mentioned previously, in the product of combustion in room fires, the water vapor, carbon mono- and dioxides, in view of their respective absorption bands, and soot particles because of their scattering properties, collectively represent a participating medium that emits, absorbs, and scatters radiation. These characteristics are determined by the equation of radiative transfer and their respective radiation properties (Siegel and Howell, 2001; Modest, 1993; Brewster, 1992). As also mentioned, the interaction of radiation with other physical effects in the room-fire dynamics manifests itself through the presence of distributed radiation heat sources in the energy equation, which can be written as

$$\rho c \frac{DT}{Dt} = -\nabla \cdot \dot{\mathbf{q}}_c - \nabla \cdot \dot{\mathbf{q}}_r \tag{1}$$

where D/Dt is the substantial derivative, - $\dot{\mathbf{q}}_c$ is the conductive flux vector, $\dot{\mathbf{q}}_r$ is the radiation flux vector, and $\nabla\cdot$ represents the scalar divergence of a vector. In the general case, the equation of radiative transfer is written as (Siegel and Howell, 2001)

$$\nabla \cdot (\mathbf{s} I_\lambda) = -(a_\lambda + \sigma_\lambda) I_\lambda + S_\lambda \tag{2}$$

where I_λ is the spectral (wave-length dependent) radiative intensity, generally expressed in terms of W/m^2 μm sr, a_λ and σ_λ are the spectral absorption and scattering coefficient, respectively, and S_λ is a source function given by

$$S_\lambda = a_\lambda I_{b\lambda}(T) + \frac{\sigma_\lambda}{4\pi} \int_0^{4\pi} I_\lambda(\mathbf{r}, \mathbf{s}') \Phi_\lambda(\mathbf{s}' \rightarrow \mathbf{s})\, d\Omega' \tag{3}$$

where $I_{b\lambda}$ is the spectral Planck function of blackbody emission, Φ_λ (s'—>s) is the phase function for scattering from s' into s, Ω' is the solid angle, and $\mathbf{r}$ is the position vector. Here the prime refers to the incoming radiation, and its relation to the ray direction s is shown in Fig. 1. By introducing an optical thickness τ_λ based on the extinction coefficient $\gamma_\lambda = a_\lambda + \sigma_\lambda$ and defined by

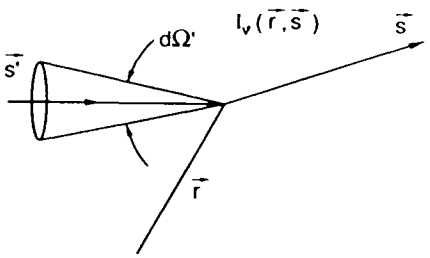


Figure 1: Geometry of radiative transfer

$$\tau_\lambda = \int_0^s \gamma_\lambda \, ds' \tag{4}$$

Eqn. 2 can be rewritten as

$$\frac{dI_\lambda}{d\tau_\lambda} + I_\lambda = (1-\omega)I_{b\lambda} + \frac{\omega}{4\pi}\int_0^{4\pi} I_\lambda(\tau_\lambda, \Omega')\Phi_\lambda(\Omega' \rightarrow \Omega)\, d\Omega' \tag{5}$$

where ω is the single-scattering albedo defined by $\sigma_\lambda / (\kappa_\lambda + \sigma_\lambda)$. Eqn. 5 can be integrated to yield the intensity

$$I_\lambda(\tau_\lambda) = I_\lambda(0)e^{-\tau_\lambda} + \int_0^{\tau_\lambda}\left[(1-\omega)I_{b\lambda}(\tau'_\lambda) + \frac{\omega}{4\pi}\int_0^{4\pi} I_\lambda(\tau'_\lambda, \Omega')\Phi_\lambda(\Omega' \rightarrow \Omega)\, d\Omega'\right] e^{-(\tau_\lambda - \tau'_\lambda)}\, d\tau'_\lambda \tag{6}$$

where $I_\lambda(0)$ is the radiation intensity leaving the boundary at s = 0 due to both emission and reflection. This equation can now be used to determine the divergence of the radiative flux vector, which is equivalent to the net out flow of radiant energy per unit volume, by integrating Eqn. 2 over the solid angle and wave lengths, resulting in

$$\nabla \cdot \dot{\mathbf{q}}_r = 4\int_0^{\infty}\left[a_\lambda e_{b\lambda} - \pi\gamma_\lambda \bar{I}_\lambda + \frac{\sigma_\lambda}{4}\int_0^{4\pi} I_\lambda(\Omega')\bar{\Phi}_\lambda(\Omega')\, d\Omega'\right] d\lambda \tag{7}$$

where $e_{b\lambda}$ is the hemispherical blackbody emissive power and the barred quantities are the average values, as given by

$$\bar{I}_\lambda = \frac{1}{4\pi}\int_0^{4\pi} I_\lambda(\Omega)\, d\Omega \qquad \bar{\Phi}_\lambda = \frac{1}{4\pi}\int_0^{4\pi} \Phi_\lambda(\Omega, \Omega')\, d\Omega \tag{8}$$

For isotropic scattering $\Phi_\lambda = \bar{\Phi}_\lambda = 1$, and Eqn. 7 takes on a simpler form

$$\nabla \cdot \dot{\mathbf{q}}_r = 4\int_0^{\infty} a_\lambda(e_{b\lambda} - \pi\bar{I}_\lambda)\, d\lambda \tag{9}$$

which can also be used for anisotropic scattering, provided that the phase function Φ_λ is independent of Ω'. Eqn. 7 is deceptively simple and in general is complicated by the fact that much additional information is needed form for its evaluation. To implement the solutions to the equation of radiative transfer, two more steps are yet to be taken. One is the evaluation of the needed gas and soot radiation

properties, and the second is the numerical solution methodology for the three-dimensional geometry in the fire room under consideration. For radiation properties of the medium in room fires (Yang, 1986; Modest,1993; Brewster, 1992), it is sufficient to deal with only those of water vapor, carbon dioxide, and soot. For these gases, the exponential wide-band model, along with provisions for overlapping bands and nonhomogeneous mixtures is of sufficient accuracy, and soot can certainly be considered as a gray medium in view of the extremely small smoke particles involved (Yuen and Tien, 1977). However, simpler gray medium models and nongray-gas models such as the weighted-sum-of-gray-gases model (Modest, 1993), have also been used. A comparison of the various nongray models for combustion products has been given by Song (1993). The second step that needs to be considered is in the calculation of radiative transfer in multidimensional spaces, primarily in accommodating the geometric complexities in evaluating the integral with respect to the solid angle in Eqn. 7. Approximate, but accurate methods are known, but are in general still rather cumbersome to use. Many versions of the classical methods such as Monte Carlo, zonal, ray-tracing, P-N, integral-evaluation and discrete ordinate methods are now available, as reviewed by Viskanta (1984) and Yang (1986), and are still being updated to broaden their utility and capability (Yuen and Takara, 1997; Fiveland, 1988; Jamaluddin and Smith, 1988). Additional new methodologies are continually being developed to improve accuracy and calculation efficiencies. Good examples are the discrete transfer method of Lockwood and Shah (1981), the radial-flux method of Chang et al. (1983), and the finite-volume method of Raithby and Chui (1990). At the present time, the common practice is simply the preference of the user, even though the multidimensional discrete-ordinate method (Fiveland, 1988) seems to be the preferred by many practitioners. Since ultimately any of these methods must be used simultaneously with the solver of the convection field in a given room fire problem, how well the radiative transfer calculations can be integrated into the convection solver has become an important issue in the selection of the method for radiation calculations. On the other hand, as the computing resources become increasingly more plentiful in both data storage and processing speed, the choice of the radiation calculation methodology may become less critical in time. For instance, the radiation source term in the unsteady energy equation can be treated as an inhomogeneous term evaluated at the last time instant where the temperatures are already known by using any of the radiative transfer methodology, and the energy equation is then solved for the unknown temperatures and species distributions at the current time instant.

So far the discussion on the theoretical basis and the numerical methodologies for including radiation calculations in the interaction phenomena in room fires has been centered on the fire field model which is more natural in assessing the significance of radiation, because of the first-principle basis in its formulation. This discussion is perhaps not complete without mentioning the zone fire models, which have been found increasing use for room and building fires for fire-risk analysis and the development of performance-based fire-safety codes. A zone model is one in which the individual flow regions with unique and distinguishable characteristics such as the flame, fire plume, ceiling layer, floor and wall layers, and regions next to windows and doorways are treated as zones. Popular zone models are, for example, CFAST (Peacock et al., 1993), FIRECAM (Yung et al., 1997), and FRESCO (Mathews et al., 1997) which have been utilized to deal with realistic room fire situations. Unfortunately, the current status of incorporating radiation effects in fire zone models is very limited, and in fact most zone models do not include radiation at all. Among some zone-model developers, there is a consensus that the critical radiation effect in room fires is in the flashover phenomenon which projects radiation heat transfer through open doorways next to the fire room and thus provides a mechanism for fire spread into the rest of a building. The critieria for flashover to occur are very *ad hoc*, and are still debated in terms of whether such criteria have the correct physical basis in radiation heat transfer.

RELEVANT APPROXIMATIONS TO ACCOUNT FOR RADIATION HEAT TRANSFER IN ROOM FIRES

While it is now recognized that there is a need to develop the best optimum method to deal with radiation in room-fire analysis in terms of accuracy and computing efficiency. One should also recognize that in real physical applications not every room-fire problem requires the full application of a complete optimum solution, even when one does exist. Simplifications in the radiation calculations in many fire-safety applications are indeed possible, and in fact are more preferable, depending on what specific information is needed. This becomes clear when one realizes that normally one is not particularly interested in actually predicting the physical fire phenomena, but will be happy to obtain information with reasonable accuracy to assess parametric effects of physical variables in specific applications for design purposes. One significant example in this regard lies in the field of fire modeling for fire-safety engineering for rooms and buildings, which are playing an ever increasingly important role in the practice and development of Performance-Based Fire Codes advocated by the majority of developed and developing nations of the world (Yang, 1999). Several such relevant and useful approximations for accommodating radiation in room-fire analysis are described:

1. As already mentioned previously, one expedient way to deal with the radiative transfer calculations for fire field-model analysis of an evolving room fire is to treat the radiation source term in the energy equation as an inhomogeneous term based on the known field variables for the previous time instant, and then to solve the coupled equations for the field variables for the current time instant. This numerical method of solution, because of its explicit nature, does require small time steps, though it is simple to use. In this method, there is no need to compute the radiation source term at every single time step. As long as the field variables do not change greatly, subject to certain prescribed variability constraint, the same source term can be used for a relatively large number of time steps without introducing any undue noticeable errors. As a result, it only needs to be updated several times throughout the fire-growth period, thus greatly reducing the radiation calculations. An example of this practice is given in the study of Chang et al. (1983) with rather good results.

2. There is a very practical and useful approximation in dealing with all the complexities for nonuniform temperatures and species distributions in the fire-room space, and it is to ignore all the effects of participating medium (Raycraft et al., 1990; Yang et al., 1994). This approximation simply reduces the full problem to one of evaluating the radiation exchange in a gray enclosure with a nonparticipating medium. In this case, the fire room consists only of boundary surfaces such as walls, ceiling and floor with prescribed emissivities, reflectivities and surface temperatures, and calculated radiation exchanges are those between surface-to-surface, and flame-to-surface pairs, taking into account the effects of shading. The flame is represented by a conveniently-chosen volume with its bounding surfaces at the flame temperature. This approxinmation, which greatly simplifies the radiation calculations, generally overpredicts the temperatures in the hot gas region in the fire room and underpredicts the temperatures in regions of low temperatures such as the floor region of the room, due to the diffusive nature of the radiation effects of the participating medium. In addition, this approximation also simplifies the combustion model, which would normally be needed for determining the heat release rates, in that it can be replaced by a prescribed heat release rate, which in turn becomes a simulation parameter for the room fire under consideration for fire-risk assessment purposes (Babrauskas and Peacock, 1992). The results from using this approximation are not strictly accurate. However, they do lead to predictable behavior as compared to that when the participating medium effect is included in the simulations. In fact, it has been found that such a simplification still leads to reasonably good results when compared to the experimental full-scale fire data even in rather complex compartments (Raycraft et al., 1990, Yang et al., 1994).

3. Another possible simplification of radiation calculations in room fires is to take advantage of the high degree of stratification of the smoke and hot-gas layers just below the ceiling, evidently because

of the strong buoyancy resulted from the fire. These layers generally are of uniform thickness throughout the room and also essentially at a uniform temperature, except possibly in a very thin region close to the ceiling in which the gas temperature drops substantially due to ceiling heat losses. Under these physical conditions, the radiation within the hot ceiling layer can be well approximated by one-dimensional radiation behaviors of a participating gas (Siegel and Howell, 2001). Further simplification is still possible if the medium that consists of hot gas mixture and soot (smoke) is taken to be a gray medium. Just as an example, if the hot smoke layer is thick, implying an optically thick medium, the radiation behavior is simply given by the optically-thick or diffusion approximation, which replaces the radiative transfer equation by a conduction-type of diffusion equation that can be be readily solved (Modest, 1993). An example of this approximation is in the study of Lloyd et al. (1979).

4. There is another approximate treatment of radiation heat transfer particularly useful in the analysis of fire phenomena by fire zone models. In the case of two-layer zone models for a room with a hot ceiling layer at a uniform temperature and an air layer below, but without a hot fire plume, radiation heat loss in the hot-layer zone can be accommodated by energy losses to the smoke-air interface, according to one-dimensional radiative heat flux calculations, which may be considered in the either optically thick or optically thin limits, depending on the instantaneous thickness of the smoke layer, and with absorption coefficients calculated from reasonably-prescribed uniform compositions of the medium mixture. The radiation heat transfer loss can then be added to the heat balance of the hot-layer zone in the energy equation of the zone. A similar adjustment can also be made for the zones that are in contact with the hot ceiling-layer zone. This procedure for incorporating radiation contribution is also applicable to a fire room with a hot fire plume zone above the fire, in which case the hot ceiling layer is treated as two separate zones, the ceiling layer away from the plume which penetrates into the ceiling layer and the plume zone itself.

There are also other radiation approximations for estimation purposes only, and are certainly more *ad hoc* than having any real rational basis. One such practice is to boast the fire heat release rates in the fire by a certain percentages to account for radiation contributions. This would inevitably increase the maximum flame temperature for a given fire (Satoh and Yang, 2000). This practice, however, is certainly not recommended unless it can be justified physically in a given situation.

CONCLUDING REMARKS

In this paper, the role and effects of thermal radiation in room fires have been described on the physical basis of the interaction of thermal radiation with strong buoyancy, turbulence, and combustion in the room-fire phenomena, and it is this interaction that governs the dynamics of fire growth and spread. Also discussed are the theoretical basis of thermal radiation itself and how it is determined quantitatively. This then becomes the formal framework to develop a radiation submodel to join the other submodels of buoyancy, turbulance, and combustion for incorporation into a fire field model based on conservation laws. The framework of the radiation submodel is extremely complex because of the complexity in obtaining the solutions to the equation of radiative transfer in the three-dimensional room space with nonuniform temperature and participating-gas and soot distributions as functions of both space and time as the fire evolves. While optimum methods for the general radiation calculations are still being sought, promising approximate calculations suitable for use in fire-safety engineering analyses can be delineated with reasonable accuracy. As more approximate methods become known, more pertinent experimental data in real fires will be needed to validate such methods so that they can be used in practice with some confidence. It is ,however, realized that large room-fire tests are extremely costly to carry out, and only slow progress in this direction is expected now and in the future.

REFERENCES

Babrauskas, V. B. and Peacock, R. D. (1992). Heat Release Rate: The Single Most Important Variable in a Fire Hazard, *Fire Safety Journal*, **18**, 255-272.

Brewster, M. Q. (1992). *Thermal Radiation Transfer and Properties*, John Wiley, New York, USA.

Chang, L. C., Yang, K. T. and Lloyd, J. R. (1983). Radiation-Natural Convection Interaction in Two-Dimensional Complex Enclosures, *Journal of Heat Transfer*, **105**, 89-95.

Fiveland, W. A. (1988). Three Dimensional radiative Heat-Transfer Solutions by the Discrete-Ordinates Method, *Journal of Thermophysics and Heat Transfer*, **2:4**, 309-316.

Holen, J., Brostrom, M. and Magnussen, B. F. (1990). Finite Difference Calculation of Pool Fires, *Proceedings of the 23rd Symposium (International) on Combustion*, The Combustion Institute, 1677-1683.

Howell, J. R. (1982). *A Catalog of Radiation Configuration Factors*, McGraw Hill, New York, USA.

Jamaluddin, A. S. and Smith, P. J. (1988). Discrete-Ordinates Solution of Radiative Transfer Equation in Non-Axisymmetric Cylindrical Enclosures, *Proceedings of the 1988 National Heat Transfer Conference*, ASME HTD **96**, 227-232.

Lockwood, F. C. and Shah, N. G. (1981). A New Radiation Solution Method for Incorporation in General Combustion Prediction Procedures, *Proceedings of the 18th Symposium (Internatioanl) on Combustion*, 1405-1414.

Mathews, M. K., Karydas, D. M. and Delichatsios, M. A. (1997). A Performance-Based Approach for Fire Safety Engineering : a Comprehensive Engineering Risk Analysis Methodology, a Computer Model, and a Case Study, *Proceedings of the 5th Symposium on Fire Safety Science*, 595-606.

Minkowycz, W. J., Sparrow, E. M., Schneider, G. E. and Pletcher, R. H. (eds.) (1988). *Handbook of Numerical Heat Transfer*, John Wiley, New York, USA.

Modest, M. F. (1993). *Radiative Heat Transfer*, McGraw Hill, New York, USA.

Peacock, R. D., Forney, G. P., Renecke, P., Portier, R. and Jones, W. W. (1993). CFAST, The Consolidated Model of Fire Growth and Smoke Transport, *Technical Note 1299*, NIST, U. S. Department of Comerce, USA.

Raithby, G. D. and Chui, E. H. (1990). A Finite-Volume Method for Predicting Radiant Heat Transfer in Enclosures with Participating Media, *Journal of Heat Transfer*, **112**, 415-423.

Raycraft, J., Kelleher, M. D., Yang, H. Q. and Yang, K. T. (1990). Fire Spread in a Three-Dimensional Pressure Vessel with Radiation Exchange and Wall Heat Losses, *Mathematical and Computer Modeling*, **14**, 795-800.

Song, T. H. (1993). Comparison of Engineering Models of Nongray Behavior of Combustion Products, *International Journal of Heat and Mass Transfer*, **16**, 3975-3984.

Siegel, R. and Howell, J. R. (2001). *Thermal Radiation Heat Transfer*, 4th edition, Taylor & Francis, Washington, D. C., USA.

Viskanta, R. (1984). Radiative Heat Transfer, *Fortschreft der Verfahrenstechnik*, **22A**, 51-81.

Yang, K. T. (1986). Numerical Modeling of Natural Convection-Radiation Interactions in Enclosures, *Proceedings of the 8th International Heat Transfer Conference*, **1**, 131-140.

Yang, K. T. (1994). Recent Development in Field Modeling of Compartment Fires, *JSME International Journal*, Ser. B, **37:4**, 702-717.

Yang, K. T. (1999). Role of Fire Field Models as a Design Tool for Performance-Based Fire-Code Implementation, *International Journal on Engineering Performance-Based Fire Codes*, **1:1**, 11-17.

Yang, K. T., Nicolette, V. F. and Huang, H. J. (1994). Field Model Simulation of Full-Scale Forced Ventilation Room-Fire Test in the HDR Facility in Germany, *Heat Transfer in Fire and Combustion Systems*, ASME HTD **272**, 13-20.

Yuen, W. W. and Takara, E. E. (1997). The Zonal Method: A Practical Solution Method for Radiative Transfer in Nonisothmal Inhomogeneous Media, *Annual Review of Heat Transfer*, **VIII**, 153-215.

Yuen, W. W. and Tien, C. L. (1977). A Simple Calculation Scheme for the Luminous-Flame Emissivity, *Proceedings of the 16th Symposium (International) on Combustion*, 1481-1487.

Yung, D., Hadjisophocleous, G. V. and Proulx, G. (1997). Modelling Concepts for the Risk-Cost Assessment Model FIRECAM and its Application to a Canadian Government Office Building, *Proceedings of the 5th Symposium on Fire Safety Science*, 619-630.

This Page Intentionally Left Blank

TEAM PRESENTATION:

ADVANCES IN PANEL SYSTEMS

This Page Intentionally Left Blank

Advances in Building Technology, Volume 1
M. Anson, J.M. Ko and E.S.S. Lam (Eds.)
© 2002 Elsevier Science Ltd. All rights reserved

WOOD FRAME SHEAR WALLS WITH METAL PLATE CONNECTED FRAMEWORK

Robert N. Emerson

School of Civil and Environmental Engineering, Oklahoma State University,
Stillwater, OK 74078-5033, USA

ABSTRACT

The vast majority of residential and light commercial structures in the United States are constructed of wood. These structures are susceptible to damage during lateral loading events. An improved shear wall system is under development that employs toothed metal plates to connect the framework of shear walls. These connectors provide moment resistant connections that transform the framework into integral moment resistant frames that assist the sheathing in resisting lateral loads. Preliminary investigations show great promise.

KEYWORDS

Engineered wood construction, wood frame shear walls, prefabricated wall panels, metal plate connections, lateral load resistance, seismic, wind

INTRODUCTION

The vast majority of homes and light commercial structures in the United States are constructed of wood. Ninety percent of new houses built in America are of woodframe construction [1]. Many of these structures reside in locations exposed to lateral forces resulting from seismic activity or high winds due to hurricanes or tornadoes. These lateral forces can cause significant damage with devastating results. While many factors lead to damage during extreme lateral loading events, inadequate shear walls result in some of the most devastating damage. Another major cost is the repair and/or replacement of non-serviceable structures associated with damage produced during lesser lateral loading events.

It is evident that the performance of wood frame shear walls directly affects the performance of wood frame structures during lateral loading events. Wood frame shear walls with increased resistance to extreme lateral loads as well as improved durability to multiple median lateral loads will save many lives and billions of dollars in repair and replacement costs. Previously proposed improvements have not been widely accepted by the building industry due to unacceptable increased costs associated with the improvements. A strong motivation for the current research is the desire and need for an improved

wood frame shear wall system that has increased performance and decreased or similar costs relative to conventional shear wall construction.

BACKGROUND

Conventional light-frame wood construction employs horizontal diaphragms and shear walls to resist lateral forces. Horizontal diaphragms are designed as horizontal beams that transfer lateral forces to the supporting shear walls. Shear walls are designed as vertical deep cantilever beams supported by the structure's foundation [2,3,4]. A typical shear wall is composed of dimension lumber framing overlaid with sheathing on one or both sides. Nails connect the framework together. The top plate is connected to the studs by end nailing. The studs are connected to the bottom plate by either toenailing or end nailing. The end studs are anchored to the foundation to resist uplift forces resulting from applied moments. The bottom plate is anchored to the foundation to resist base shear forces. The sheathing is attached to the dimension lumber framework with nails. The nails are spaced closely around the edges and spaced farther apart in the interior of the individual sheathing panels.

Conventional Wood Frame Shear Wall Behavior

Substantial research has been performed regarding the behavior, analysis, modeling, and design of conventional wood frame shear walls. The dimension lumber chords and sheathing are designed to resist applied moment and shear, respectively. However, the behavior of the system is governed by connections between the top and bottom plates and studs and connections between the sheathing and framework. Under lateral loads nailed connections between the plates and studs provide little rigidity. As a result, the framework distorts as a parallelogram. The sheathing remains rectangular and rotates as a rigid body. Relative displacement of the framework and sheathing due to racking forces is depicted in figure 1. The connections between the sheathing and framework then become the controlling factor in racking behavior. The nails connecting the sheathing to the framing resist the lateral load. Typically, failure occurs when the nail heads pull through the sheathing panel or withdraw from the framework due to large relative displacements between the sheathing and the framework at the corners of sheathing panels.

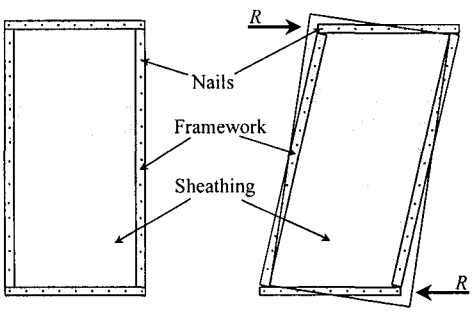


Figure 1. Conventional wood frame shear wall panel behavior due to racking forces

Tuomi and McCutcheon developed a method for calculating the racking strength of frame panels and then compared the method with experimental tests [5]. Racking strength was calculated by accounting for panel geometry, number and spacing of nails, and the lateral resistance of a single nail. The method also accounted for minimal frame resistance. Frame resistance was assumed to contribute less than ten percent of the overall racking strength. Calculated racking strength compared favorably to results from experimental testing.

Gupta and Kuo developed a model for shear wall behavior that was governed by nonlinear nail deformation but also accounted for bending and shear stiffness of the studs and sheathing, respectively [6]. They found that assuming the studs were infinitely rigid in bending gave comparable results to assuming the studs held normal bending stiffness. This confirms that the nailed connections between the plates and studs are too flexible to develop bending within the studs.

The NAHB Research Center investigated the performance of perforated shear walls [7]. Variables included in their study were narrow wall segments, reduced base restraint, and alternative framing methods. The investigation of alternative framing methods provided an interesting result. Two nearly identical perforated shear walls were tested. Both walls had a sheathing area ratio equal to 0.57 as determined from Sugiyama's empirical equation [8,9]. The control wall consisted of conventionally connected framing with moment anchors at both ends of the wall. The experimental wall with alternative framing consisted of framing connected with metal truss plate connectors at the corners and around openings. This wall also had no moment anchors to resist uplift. Even with the omission of moment anchors, the experimental wall outperformed the control wall dramatically. The experimental wall resisted 40% more lateral load and dissipated 68% more energy than the conventionally connected perforated shear wall.

Metal Plate Connected Truss Technology

Prefabricated light frame wood trusses are commonly connected with toothed metal connector plates. The trusses are designed and fabricated according to ANSI/TPI 1-1995, National Design Standard for Metal Plate Connected Wood Truss Construction [10]. Wood members are designed according to the National Design Specification for Wood Construction [11]. Guidelines for metal plate connector design regarding tooth holding, net section steel tensile capacity, net section shear capacity, and combined shear and tension capacity are presented in ANSI/TPI 1-1995.

In the past, metal plate connected trusses were modeled and designed assuming pinned connections. However, toothed metal plate connectors provide semi-rigid connections that will develop moment capacity. Noguchi investigated five models describing the moment resistance of metal plate connections [12]. These models were (i) completely elastic behavior; (ii) elastic behavior of the plate with compressive yielding of the wood member; (iii) tensile yielding of the plate with elastic behavior of the wood; (iv) plastic behavior of both the plate and wood; and (v) Edlund's model for bending moment [13]. The models were fit to experimental data and the elastic model was found to be the most conservative while the plastic model was recommended for design purposes. Kevarinmäki used both elastic and plastic models to investigate the tooth withdrawal capacity of metal plate connected truss joints subjected to bending moments [14]. O'Regan, Woeste, and Lewis developed a design method for the steel net-section of truss joints subjected to tension and moment [15]. Their design method was based on Noguchi's model where the steel is fully plastic in tension and the wood is linearly elastic in compression. O'Regan, Woeste, and Brakeman added to the design method by developing design methodology that forces steel yielding as the failure mechanism [16].

The ability to withstand repeated dynamic cyclic loading is a concern for connections in lateral load resisting systems. Emerson and Fridley investigated the tooth holding performance of toothed metal plate truss connections subjected to repeated dynamic cyclic loading [18,19]. A variety of joint configurations were tested to evaluate the effect of tooth, load, and grain orientation. Connections were subjected to a loading regime of 20, 40, and 60% of the mean maximum static load cycled at 10 Hz for 200 cycles. Dynamic stiffness degradation and residual static strength were evaluated. The connections behaved elastically when cycled at 20% of the maximum static load and experienced stiffness degradation during the 40 and 60% of maximum static load cycles. The connections maintained 100, 75, and 56% of their initial dynamic stiffness after 200 load cycles at the 20, 40, and 60% load levels, respectively. Most of the stiffness degradation occurred within the first 50 cycles and

then tapered off. After being subjected to the cyclic dynamic loading regime the connections maintained at least 87% of their mean maximum static strength.

Conclusions from Background

Conventional wood frame shear walls are designed as vertical deep cantilever beams. The sheathing provides the shear resistance. The end studs, acting as tension and compression chords, provide the bending resistance. The interior wall studs are only employed to support the sheathing. Nailed connections between the top and bottom plates and wall studs are quite flexible. This connection flexibility prevents any moment to be developed in the studs. As a result, conventional shear wall resistance is governed by the nailed connections between the sheathing and dimension lumber framework. Failure of the shear wall occurs when the nailed connections between the sheathing and framework fail due to large relative displacements between the sheathing and framework at the corners of sheathing panels. This failure mechanism prevents efficient utilization of the dimension lumber framework and dissipates little energy before significant damage to the system occurs.

Toothed metal plate connectors provide semi-rigid connections that are able to resist moment. This moment resistance has been investigated and accounted for in truss design and may be incorporated into shear wall design.

PRELIMINARY STUDIES

The potential behavior and benefits of using toothed metal plate connectors to transform underlying wood framework into moment resistant frames that are integral to the lateral force resistant system were investigated in preliminary analytical and experimental studies.

Analytical Study

Preliminary analytical studies of the proposed wall system have been performed. An 8 ft by 20 ft shear wall composed of conventional construction was employed as a model for this study. Vertical studs were positioned at 16 in. on center with double end studs, a double top plate, and a single bottom plate. Design racking forces were determined for shear walls sheathed with $^{15}/_{32}$, $^{7}/_{16}$, and $^{3}/_{8}$ in. thick structural sheathing with various nailing patterns. Design racking forces were determined using both Uniform Building Code design tables [17] and the Tuomi McCutcheon method [7]. Subsequent to calculating design racking forces it was determined how much racking force needed to be carried by the framework to reduce the sheathing thickness while maintaining overall strength. Two methods employing matrix structural analysis were used to establish reasonable limits for the design racking resistance of moment resistant frames composed of wood framework and toothed metal connector plates. First, the connections were assumed to be infinitely rigid and strong. This assumption forced failure of the wood members (end studs) and was used as an extreme upper limit to the frame's design racking strength. The design racking strength was determined assuming connection failure. Connections were designed according to ANSI/TPI 1-1995 guidelines [10] incorporating methods recommended by O'Regan, Woeste, and Lewis [15] and Kevarinmäki [14].

While differences in stiffness between the sheathing and framing were neglected, results of the preliminary analytical study are promising. An 8 ft by 20 ft shear wall with $^{15}/_{32}$, $^{7}/_{16}$, or $^{3}/_{8}$ in. thick sheathing and nails spaced at 6 in. along the panel edges has an allowable lateral load capacity of 5200, 4800, and 4400 lbs, respectively. With infinitely rigid and strong connections (unrealistic assumption), Southern Pine 2 by 4 framework has a design lateral load capacity of 640 to 2400 lbs for stud and dense select structural framing members, respectively. With connections designed according to TPI

and recommendations from previous research the design lateral load capacity of the framework was 220 lbs. If moment resistant frame design capacity is assumed directly additive to shear wall design capacity based on sheathing performance, then the *combined system* will have 4 to 55% more design lateral capacity than conventional shear walls. This range envelops the 40% increase seen in the NAHB test on one shear wall with openings reinforced with toothed metal connector plates.

Experimental Study

The relative behavior between conventional construction and the proposed system was investigated in a small-scale pilot study. A total of eight frame configurations were tested. The basic frame consisted of kiln-dried Douglas fir No.2 2x4 dimension lumber connected together with 8d common nails or 3"x3" toothed metal connector plates. Four specimens were tested for each basic frame configuration. These included bare frames and frames sheathed with 19/32" structural sheathing connected to one side of the frame with 8d common nails spaced at 4" along the perimeter. Each of theses frames was tested with and without tension anchorage between the tension chord and the support. Conventional wood frame construction was represented by an end-nailed frame with sheathing and tension anchorage. The basic test configurations are depicted in figure 2.

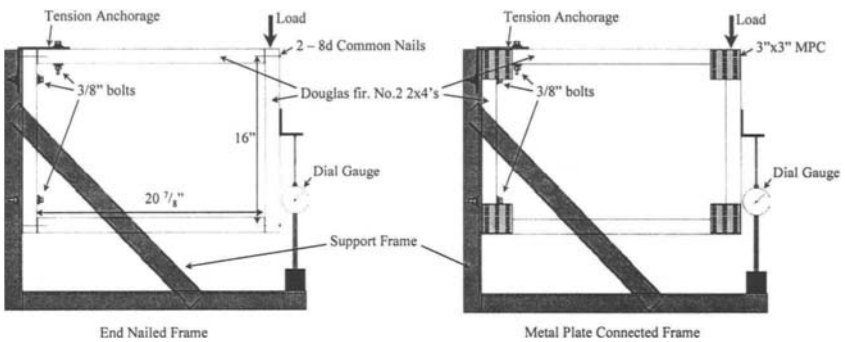


Figure 2. Basic test frames shown without sheathing

Each of the specimens was tested seven days after fabrication. Load was recorded at 0.05" displacement intervals. The test results are presented in table 1. Load-displacement plots are presented in figure 3. Elastic stiffness was calculated as the slope of the line that passes through the origin and a point representing 40% of the maximum load. The yield load was determined at the point where the load-displacement plot diverges from the line representing elastic stiffness

Table 1. Test Results of MPC Frame Pilot Study

	Elastic Stiffness (lb./in.)	Maximum Load (lbs.)	Displacement at Max Load (in.)
MPC Frame with 3x3 Plates, 19/32" Sheathing, and Tension Tie	4070	2435	1.35
MPC Frame with 3x3 Plates and 19/32" Sheathing	5770	2030	1.05
End Nailed Frame with 19/32" Sheathing and Tension Tie	2530	1850	1.1
End Nailed Frame with 19/32" Sheathing	1730	632	0.75
MPC Frame with 3x3 Plates and Tension Tie	440	392	2.05
MPC Frame with 3x3 Plates	560	368	1.85
End Nailed Frame with Tension Tie	120	145	2.35
End Nailed Frame	70	80	1.23

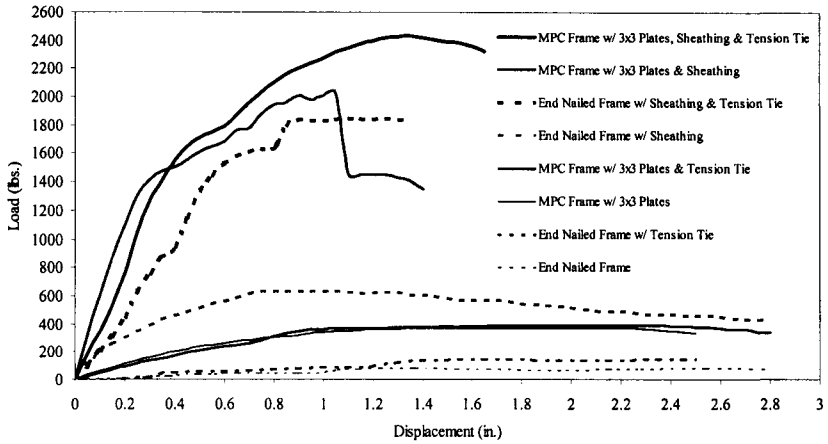


Figure 3. Load-displacement plots for test frames

The following results were derived from the pilot study tests.

1. End-nailed frames without sheathing developed virtually no lateral load resistance.

2. Metal plate connected frames without sheathing developed approximately 60% of the lateral load resistance of the end nailed frame with sheathing but without tension anchorage between the tension chord and the supports. The tension anchorage provided no benefit to the unsheathed systems because they behaved as true frames.

3. The metal plate connected frame with sheathing but without direct tension anchorage between the tension chord and the support developed 228% of the elastic stiffness and 110% of the lateral load resistance of the end-nailed frame with sheathing and tension anchorage between the tension chord and the support. The MPCs transferred tension from the tension chord into the bottom plate. The bottom plate transferred tension forces from the MPCs to the anchor bolt and support frame through cross-grain bending. This specimen displayed a sudden drop in load as a result of local tension perpendicular to the grain failure of the bottom plate between the MPCs and the support anchor.

4. The metal plate connected frame with sheathing and direct tension anchorage between the tension chord and the support developed 161% of the elastic stiffness and 132% of the lateral load resistance of the end nailed frame with sheathing and tension anchorage between the tension chord and the support.

Although the pilot study was far from definitive, it does suggest probable behavior and benefits of the proposed system. An initial concern was that stiffness of the sheathing would prevent any benefits of a more flexible underlying moment resistant frame. This concern was alleviated when both of the MPC frames with sheathing developed substantially more elastic stiffness and ultimate strength than the conventional end-nailed frames with sheathing and tension anchorage. The increased strength and stiffness provided by the metal plate connected framework should provide the following benefits to wood frame structures: (a) improved elastic and ultimate resistance to lateral loads, (b) improved

utilization of the wood framework, (c) decreased reliance on the sheathing effect, (d) improved tension anchorage to the foundation, and (e) reduced reliance on expensive tension anchorage hardware.

ONGOING RESEARCH

Current research activity is focused on preparing the foundation for the development of an engineered wood frame wall panel system integrating prefabricated metal plate connected truss technology. Design methodology for moment resistant frames integrating TPI guidelines and previous metal plate connector research recommendations are being developed and refined. The ability of the wood framework to perform as a moment resistant frame is under investigation. The behavior of the moment resistant frames covered with sheathing is being assessed. Finally, design procedures combining the lateral load resistance provided by both moment resistant frames and sheathing will be developed.

The design methodology for moment resistant frames connected with toothed metal plate connectors is a direct adaptation of procedures specified in ANSI/TPI 1-1995 [10] and recommendations of Kevarinmäki [14] and O'Regan, Woeste, and Lewis [15]. The first attempt at a design procedure for combining lateral load resistance of a moment resistant frame with that of the sheathing is an additive process. This design methodology will be refined to better represent the actual behavior of moment resistant frames and the combined systems as well.

A variety of parameters expected to affect the behavior of the wall panel system are under investigation. These include framing member stiffness, connection strength and stiffness, sheathing thickness, and wall height to width ratio. The conventional shear wall system is being tested in conjunction with the proposed wall panel system to quantify performance benefits of the experimental system.

REFERENCES CITED

[1] Portland Cement Association. 1997. "Home Builder Report of 1997."

[2] Breyer, D.E., Fridley, K.J., and Cobeen, K.E. 1998. *Design of Wood Structures, ASD.* McGraw-Hill.

[3] Stalnaker, J.J. and Harris, E.C. 1997. *Structural Design in Wood, 2nd Edition.* Kluwer Academic Publishers.

[4] Faherty, K.F. and Williamson, T.G. 1997. *Wood Engineering and Construction Handbook.* McGraw-Hill.

[5] Tuomi, R.L. and McCutcheon, W.J. 1978. "Racking Strength of Light-Frame Nailed Walls." *Journal of the Structural Division.* American Society of Civil Engineers. Vol. 104. No. ST7. pp. 1131-1140.

[6] Gupta, A.K. and Kuo, G.P. 1985. "Behavior of Wood-Framed Shear Walls." *Journal of Structural Engineering.* American Society of Civil Engineers. Vol. 111. No.8. pp. 1722-1733.

[7] McKee, S., Crandell, J., Hicks, R., and Marchman, L. (National Association of Home Builders Research Center). 1998. "The Performance of Perforated Shear Walls with Narrow Wall Segments, Reduced Base Restraint, and Alternative Framing Methods." Prepared for: The U.S. Department of Housing and Urban Development.

[8] Sugiyama, H. and Matsumoto, T. 1993. "A Simplified Method of Calculation the Shear Strength of a Plywood-Sheathed Wall With Openings II. Analysis of the Shear Resistance and Deformation of a Shear Wall with Openings." Mokuzai Gakkaishi, 39(8) pp. 924-929.

[9] Sugiyama, H. and Matsumoto, T. 1994. "Empirical Equations for the Estimation of Racking Strength of a Plywood-Sheathed Shear Wall with Openings." Summaries of Technical Papers of Annual Meeting, *Trans of A.I.J.*

[10] ANSI/TPI 1-1995. National Design Standard for Metal Plate Connected Wood Truss Construction. 1995. Truss Plate Institute. Madison, WI.

[11] ANSI/NfoPA NDS-1991 National Design Specification for Wood Construction. 1991. American Forest and Paper Association. Washington, D.C.

[12] Noguchi, M. 1980. "Ultimate Resisting Moment of Butt Joints With Plate Connectors Stressed in Pure Bending." Wood Science. Vol.12 No.3 168-175.

[13] Edlund, G. 1971. "Längdskarving av trabälkar med spikplatsforband. Byggforskningen Rapport R40. Stockholm, Sweden.

[14] Kevarinmäki, A. 1996. "Moment Capacity and Stiffness of Punched Metal Plate Fastener Joints." *In*: Proceedings of the International Wood Engineering Conference. 1:385-392.

[15] O'Regan, P.J., Woeste, F.E., and Lewis, S.L. 1998. "Design Procedure for the Steel Net-Section of Tension Splice Joints in MPC Wood Trusses." Forest Products Journal. Vol.48, No.5, 35-42.

[16] O'Regan, P.J., Woeste, F.E., and Brakeman, D.B. 1998. "Design Procedure for the Lateral Resistance of Tension Splice Joints in MPC Wood Trusses." Forest Products Journal. Vol.48, No.6, 66-69.

[17] *Uniform Building Code.* 1997. International Conference of Building Officials. Whittier, California.

[18] Emerson, Robert N. and Fridley, Kenneth J., "Resistance of Metal Plate Connections to Dynamic Loading", *Forest Products Journal*, Vol. 46, No. 5, 83-90.

[19] Emerson, Robert N. and Fridley, Kenneth J., "Probabilistic Modeling of Metal Plate Connections," Proceedings of the 7th ASCE Specialty Conference on Probabilistic Mechanics and Structural Reliability.

Advances in Building Technology, Volume 1
M. Anson, J.M. Ko and E.S.S. Lam (Eds.)
© 2002 Elsevier Science Ltd. All rights reserved

Toward Engineering Design of Gypsum Board Fire Barriers

O. M. Friday[1] and S. M. Cramer[1]

[1]Department of Civil and Environmental Engineering,
University of Wisconsin-Madison, Madison, WI, 53706, USA

ABSTRACT

Gypsum board sheathing panels are widely used throughout different building types to provide passive fire protection, but in residential construction it is the primary structural fire protection. Most fires and most fire deaths occur in residential construction so maintaining the integrity of the gypsum board fire barrier during a fire is critical to the longevity and the fire safety of the structure. Reported here is progress in a study examining the engineering properties of Type X gypsum board. Little is published concerning the engineering properties of this common construction material. The objective of this research is to measure these properties and to organize them into a rational failure theory that will allow engineering design of gypsum board fire barriers. Test were undertaken with a small oven within a test machine measuring mass loss, shrinkage, bending strength and modulus of elasticity at elevated temperatures. The research shows that near-complete calcination of the gypsum board occurs only after 60 minutes of exposure at 400°C. Only after complete calcination, where all moisture is driven off, does the bending strength approach 0. Strength appeared to decrease linearly with increasing temperature. Mass loss and modulus of elasticity exhibited similar trends with the greatest decreases occurring from 100°C to 200°C followed by more gradual decrease to 400°C. The reinforcing glass fibers play a significant stiffening and strengthening role in the long direction of sheathing panels up to 60 minutes of exposure at 300°C.

KEYWORDS

fire, gypsum, light-frame construction, wood, material properties, ASTM E119

INTRODUCTION

Problem Statement

The majority of residential construction in the United States consists of 1- and 2-family dwellings and 1 to 4 story apartment complexes, and is considered light-frame construction. This typically consists of sawn timber, engineered wood products or light gage steel as the floor and wall structural members. Engineered wood products include I-joists and trusses for floor and roof systems. Gypsum board is widely used for wall and ceiling linings and in addition to providing an enclosure surface, acoustic and fire protection are also provided. Most fire deaths in the United States each year occur in the home, with the majority of them occurring in 1- and 2- family dwellings.

Although the number of fire deaths per capita in the United States is decreasing, it is well above other industrialized nations. For example, the United States deaths per capita from fire are 20% above the European average. Fires in the United States kill many more people each year than floods, hurricanes, earthquakes, tornadoes and other natural disasters combined (United States Fire Authority 1999). Fires in homes caused 3,420 deaths, 16,975 injuries, and $5.5 billion dollars of property damage in 2000 (NFPA website). This is the result of 368,000 home fires, which represents 73% of all structural fires. Nearly 85% of the fire deaths in 2000 occurred in the home and 72% of all fire deaths occurred in 1- and 2- family dwellings. These values are representative of the previous twelve years (United States Fire Authority 1999).

The primary fire resistant strategy for residential construction is based on the use of gypsum board in certain locations to provide a passive protective membrane over wood or steel framing members. Active fire resistance systems are not customary in 1- and 2- family dwellings in the United States, so all of the fire resistance relies on the combined resistance of the structural members and the gypsum board. The gypsum board and the attachment to the framing are typically prescribed in building codes based on fire ratings achieved directly or indirectly from standard tests such as that specified in ASTM E-119.

Previous ASTM E119 tests indicate that floor/ceiling structural assemblies typically fail within minutes after the gypsum board pulls away from the ceiling structural members, allowing hot gases to flow into the plenum and ignite the wood members. It is clear from test observations that the longer the gypsum board remains intact and attached to the wall or ceiling framing members, the longer the structure will withstand the fire to which it is exposed.

It is hypothesized that if the material properties of gypsum board are known, the time and temperature conditions associated with gypsum board failure in an ASTM E-119 test or other fire condition can be computed. The significance of this research is that once the response of the gypsum board can be categorized and predicted, innovative designs that provide equivalent or superior fire safety can be designed. Costly fire testing can be used to verify proposed designs rather than serving as a trial-and-error design tool.

The objective of the research reported here was to establish the engineering properties of typical Type X gypsum board. These properties are not well established and their absence makes it impossible to conduct an engineered structural design of walls or ceilings that incorporate the structural performance of the gypsum board for either standard load or fire conditions. The research project is in-progress and our final outcomes have not yet been achieved.

Little information exists on the mechanical properties of gypsum. A series of studies have established some of the thermal properties of gypsum (Harmathy 1995 and 1983, Lawson 1977). Fuller (1990) was one investigator who examined both thermal and mechanical properties of gypsum. He established bending strength and bending stiffness of regular 13-mm (1/2-in) gypsum board at temperatures up to 140°C.

Gypsum Board Chemistry

Gypsum board generally consists of hydrous calcium sulfate with paper on either side (Lawson 1977). Different additives may be included to improve the fire resistance of the board, such as glass fibers or vermiculite. In the United States, Type X board is a fire-rated board containing glass fibers, and other additives are possible. Type X board is a generic label not specific to any particular company and is defined based only on performance as a sheathing that will provide a 60-minute load-bearing fire resistance when one 15.9 mm board is attached to each side of a wood or steel stud wall assembly (Buchanan 2001). Gypsum board undergoes calcination when exposed to temperatures above 100°C. Chemically combined water is expelled by the gypsum board between 100°C and 125°C, reducing the gypsum to plaster of paris as shown chemically in Eq. 1 (Harmathy 1995).

$$CaSO_4 \bullet 2H_2O \rightarrow CaSO_4 \bullet \tfrac{1}{2}H_2O + 1\tfrac{1}{2}H_2O \quad (1)$$

There is no information available on the rate at which this reaction occurs. With fire exposed to one side of the board, the calcination process proceeds gradually through the board thickness consuming thermal energy and limiting temperatures on the backside of the board to about 120°C. Board density and initial moisture content are important factors that influence the fire resistant capabilities of the gypsum board. The glass fibers in Type X gypsum also help retard shrinkage cracks and vermiculite also aids in this effort. Shrinkage cracks could open up and allow hot gases to flow into the cavity of a wall or floor system and ignite the structural system.

Measuring Material Properties

To predict the time to failure of gypsum board in a fire, the material properties at elevated temperatures are needed. Obviously, when complete calcination occurs the remaining plaster of paris is in powder form and no usable strength or stiffness remains. But in a fire this change does not occur immediately and the gypsum board retains structural integrity for considerable time. The properties of interest include dimensional and mass changes, and strength and stiffness losses of gypsum board at elevated temperatures. These properties were measured with an oven configured within a small-scale test machine. Through a series of bending and load-free tests, properties were measured at ambient, 100°C, 200°C, 300°C and 400°C. A high temperature linear differential induction transducer was used to measure displacements and dimensional changes of the specimen within the oven. Load tests were conducted at elevated temperatures after soak times of 15 minutes and 60 minutes at the target temperature where no load was applied. This paper is limited to presentation of the 60-minute results. A total of nine tests were conducted for each condition with at least 4 specimens obtained from cuts along the length of the panel and at least 4 specimens cut from the width of the panel. These specimens were cut from a minimum of 3 different panels. A single source of 15.9 mm thick Type X gypsum board was used for all tests. The specimens were conditioned at 21°C and 50% relative humidity for at least 30 hours prior to testing.

The test setup was configured to provide repeatable measures of material properties at different temperature exposures and not to precisely replicate conditions during a fire. Two significant differences between test conditions and fire conditions exist. First, in the tests both sides of the gypsum board specimen were exposed to the same temperature. Second, test temperatures were limited to 400°C even though much higher temperatures will likely occur in a fire. Applications of these research results must consider these factors.

TEST RESULTS

Mass and Dimensional Change Tests

According to Harmathy (1995), gypsum will expand dimensionally 0.1% from 0 to about 100°C or 200°C, and then remain somewhat constant until about 300°C. Between 300°C and 400°C it will shrink 1.3% followed by slowed shrinkage to 700°C. Our test data showed similar trends. We observed 0.1% shrinkage at 200°C and 300°C with the greatest shrinkage observed at 400°C with a value of 0.65%. Details of Harmathy's tests were not available so the differences may be due to specimen size or the heating regime used. The specimen size in our tests was 203 mm long by 51 mm wide.

Gypsum board contains approximately 21% wat er by weight and thus as calcination occurs the mass of the board is reduced. We found that after a 60-minute soak period at 100°C that only 3% of the original board weight was lost. Harmathy (1995) found the mass at 100°C reduced by about 6% of original room temperature mass, with no significant changes from 200°C through 600°C. At 200°C, we observed a 16% loss in mass that increased to 22% at 400°C (Figure 1). This observation is consistent with complete calcination and loss of all moisture.

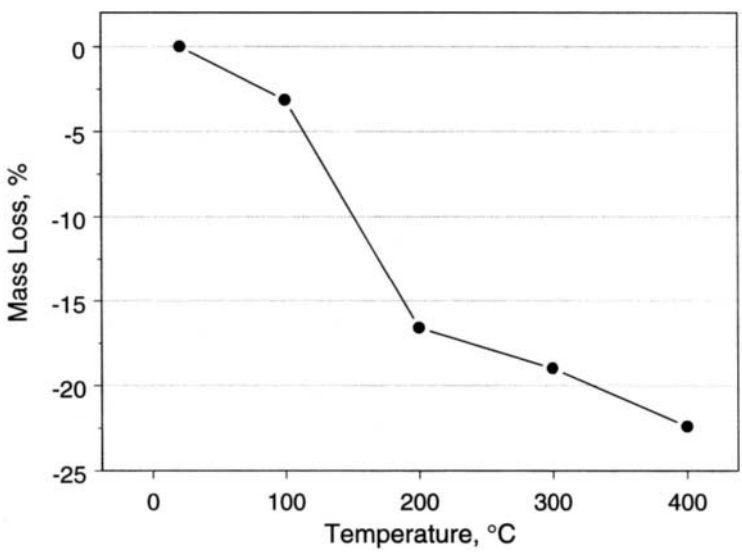


Figure 1: Mass change after 60 minutes of exposure

Tension and Bending Tests

Loads and deflections from three-point bending tests were used to evaluate modulus of elasticity and bending strength. The specimen size, 177.8 mm by 50.8 mm, was selected to meet the constraints of the test chamber, resulting in a short beam where shear deformations were significant. Shear effects were considered by assuming a fixed relationship between modulus of elasticity and shear modulus. The brittle nature and low tensile strength of the gypsum board specimens rendered tension tests impractical. All tests were conducted with the paper intact on both faces of the gypsum board as it is used in service.

The bending strength of the gypsum board specimens was defined as the maximum load achieved in the initial linear portion of the load-displacement plot. Sometimes additional load was resisted after the first crack formed but these were not considered in the initial data analysis presented here.

The strengths and bending stiffnesses of the specimens depended on the orientation of the specimen in the original gypsum board panel. When the length of the specimen coincided with the long direction, or machine direction, of the panel, the strength and stiffness were significantly higher than they were when the length of the specimen was oriented with the panel width. This distinction was reduced at higher temperatures. The glass fibers were primarily oriented in the machine direction of the panel to provide additional tensile and bending strength in the long direction.

Bending strengths at ambient conditions were in the range of 2 to 4 MPa depending on specimen direction and other factors. Figure 2 shows the average degrade in bending strength that occurs after 60 minutes of exposure at temperatures up to 400°C. As indicated by the mass loss in Figure 1, calcination is complete after 60 minutes of exposure at 400°C as all available water has been driven off. Similarly the bending strength decreases to a value close to zero after 60 minutes at 400°C. Figure 2 shows that the bending strength decreases in a near linear manner. With specimens cut from the long direction of the panel, the role of the glass reinforcing fibers is clearly revealed in Figure 2. At 300°C the strengthening influence of the glass reinforcing fibers has all but disappeared.

An apparent modulus of elasticity was computed that depended on the gross cross section. The presence of the surface paper on each face of the gypsum board results in a composite section. The separate layers most likely degrade differently as temperature exposure is increased and eventually the paper burns away completely. The gross section was used in this analysis and was assumed to be homogeneous.

The degradation of apparent modulus of elasticity relative to the ambient value to is shown in Figure 3. Ambient modulus of elasticity is in the range of 1700 to 2200 MPa. The trend of degradation is similar to that of mass loss. After 60 minutes of exposure at 200°C, the loss in modulus of elasticity in the gypsum matrix is essential complete. Sufficient adhesion to the reinforcing glass fibers continues however and it is not until exposure of 400°C that the stiffening effect of the glass fibers is completely lost.

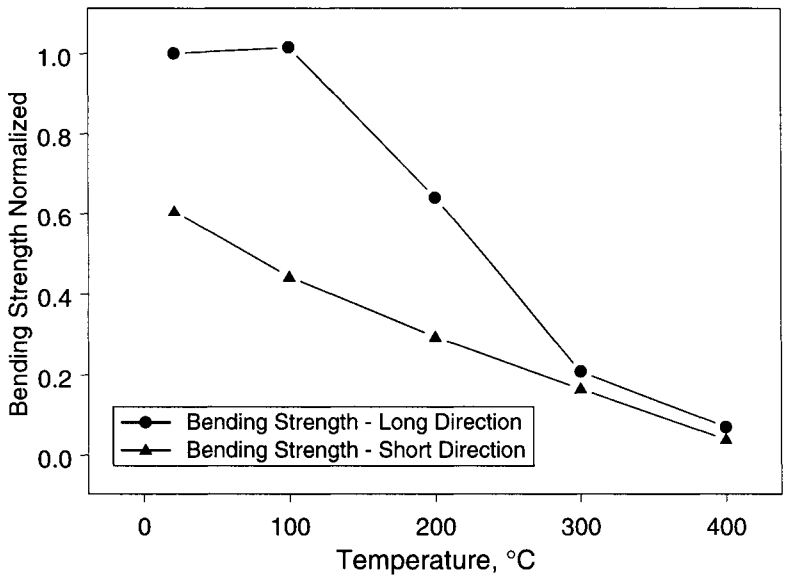


Figure 2: Degrade in bending strength after 60 minutes of exposure

Application of Test Results

To foresee the application of this research, consider a gypsum ceiling membrane attached to wood joist ceiling members. Under ambient nonfire conditions, the gypsum is held in place with screws embedded into the wood members or into a resilient channel. The gypsum experiences internal stresses that are induced from its self-weight. In addition, as the structural components of the ceiling are loaded, more stress is transferred into the gypsum board as a result of partial composite action. Different deflections of the individual ceiling joists may also induce additional stresses in the gypsum board panels that are spanning a series of joists in a continuous fashion. As heat from fire is added to this scenario, the gypsum board panel begins to shrink and the restraint of the attachments to the ceiling joists results in additional stresses. As the temperatures increase and calcination occurs, the gypsum board panel will lose stiffness and bending strength as discussed. When critical stresses are reached the gypsum board will fracture, allowing hot gases and flames to reach the wood members.

Although the described scenario is complex, it is not intractable and not unlike other structural analysis problems. With the baseline of data established from this research, structural analysis of assemblies as described above will be possible and in turn, engineering design of fire resistant barriers will also be possible.

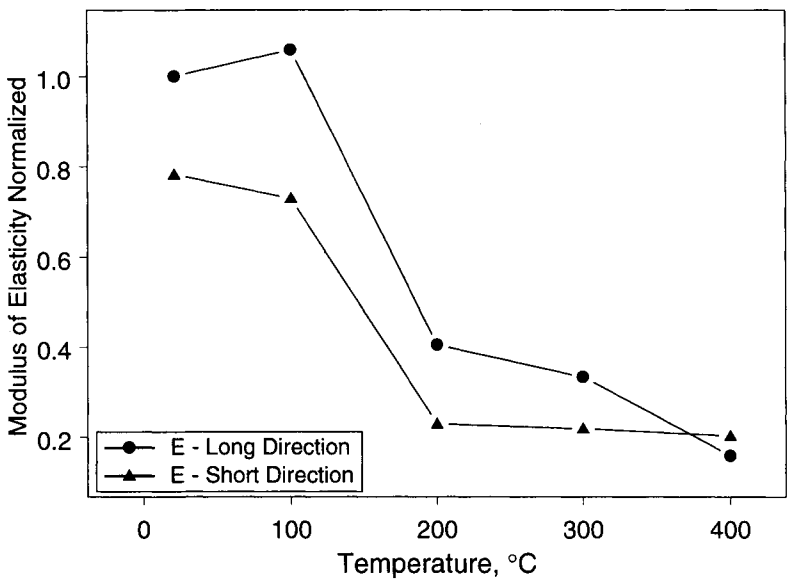


Figure 3: Degrade in modulus of elasticity after 60 minutes of exposure

CONCLUSIONS

The fire resistance of residential construction is primarily achieved through the use of gypsum board panels. The longevity of light-frame wood and steel construction in a fire depends on the maintaining the gypsum board lining over framing members. The complete loss of moisture (calcination) of the gypsum board occurred after 60 minutes of exposure at 400°C. The largest decreases in mass and shrinkage occurred between 100°C and 200°C. Bending strength, less the influence of glass reinforcing fibers, decreased linearly as temperature increased and approached 0 at 400°C. Modulus of elasticity based on an assumed homogenous section decreased the most from 100°C to 200°C. The glass reinforcing fibers played a significant stiffening role through exposure at 300°C. This research reveals the engineering properties of gypsum board such that gypsum board fire barriers can advance from simple prescriptive construction requirements to engineering design.

ACKNOWLEDGEMENTS

The authors gratefully acknowledge the support of the National Science Foundation through grant CMS-0080293 as part of the Partnership for Advanced Technologies for Housing. The assistance of US Gypsum and the technical advice of Dr. Robert White of the USDA Forest Products Lab are appreciated.

REFERENCES

Buchanan, A.H. (2001). *Structural Design for Fire Safety*, John Wiley & Sons, Ltd. Chichester, England.

Fuller, J. (1990). *Predicting the Thermo-Mechanical behavior of a Gypsum-To-Wood Nailed Connection.* Master of Science Thesis, Department of Forest Products, Oregon State University, Corvallis, OR.

Harmathy, T. (1983). Properties of building materials at elevated temperatures, *DBR Paper No. 1080 of the Division of Building Research*, National Research Council of Canada.

Harmathy, T. (1995). *The SFPE Handbook of Fire Protection, Second Edition.* National Fire Protection Association, Quincy, MA.

Lawson, J.R. (1977). An Evaluation of Fire Properties of Generic Gypsum Board Products, NBSIR 77-1265, Center for Fire Research, Institute for Applied Technology, National Bureau of Standards, Washington D.C.

National Fire Protection Association (2001). NFPA Fact Sheet: Home Fire Statistics, NFPA website, www.nfpa.org/Research/NFPAFactSheets/NFPAHomeFireStats/NFPAHomeFireStats.asp

United States Fire Authority (1999). Fire in the United States 1989-1998 (Twelfth Edition), United States Fire Authority website, www.usfa.fema.gov

Advances in Building Technology, Volume 1
M. Anson, J.M. Ko and E.S.S. Lam (Eds.)
© 2002 Elsevier Science Ltd. All rights reserved

BARRIER MATERIALS TO REDUCE CONTAMINANT EMISSIONS FROM STRUCTURAL INSULATED PANELS

J. C. Little[1], D. Kumar[1], S. S. Cox[1], and A. T. Hodgson[2]

[1]Civil & Environmental Engineering Dept., Virginia Tech, Blacksburg, VA, USA
[2]Indoor Environment Dept., Lawrence Berkeley National Laboratory, Berkeley, CA, USA

ABSTRACT

The use of Structural Insulated Panels (SIPs) to create very tight building envelopes will help reduce the environmental impact and energy use of new housing. Typically, SIPs are constructed from oriented strand board (OSB) and rigid foam in multi-layered sandwich-like structures. Although environmental and energy advantages make panelized systems very attractive, the tighter building envelopes may result in degraded indoor air quality. The potential release of volatile contaminants from SIPs must also be considered. A physically based diffusion model that predicts emissions from a single layer of vinyl flooring has recently been developed and successfully validated. A logical and promising extension of this approach is to apply the model to predict emissions from multi-layer systems such as SIPs. As a first step towards this goal, a double-layer model is developed to predict the rate of mass transfer from double-layered building material to indoor air. It is assumed that the two layers are flat homogeneous slabs, that internal mass transfer is governed by diffusion, and that the indoor air is well mixed. An analytical solution to the double-layer model is presented and used to demonstrate the potential for a thin surface barrier layer to reduce contaminant emission rates from building materials.

KEYWORDS

Air, barrier, building, contaminant, diffusion, indoor, layer, material, model, source, VOC

INTRODUCTION

One of the primary goals of the Partnership for Advancing Technology in Housing (PATH) is to cut the environmental impact and energy use of new housing by 50 percent. The use of Structural Insulated Panels (SIPs) in new construction and major renovation to create very tight building envelopes will help realize this goal. The environmental advantages of SIPs include:

- less job-site waste;
- lower energy consumption;
- greater use of fast-growth harvested farm trees rather than old-growth forests;
- reduced consumption of dimensional lumber.

These advantages make panelized systems very attractive from both environmental impact and energy use perspectives. However, degradation of indoor air quality is an important and well-documented result of tighter building envelopes and the use of engineered wood products as construction materials (Hodgson et al., 2001).

Indoor sources of volatile organic compounds (VOCs) are one determinant of residential indoor air quality (Hodgson et al., 2000). Many materials used to construct and finish the interiors of new houses emit VOCs such as formaldehyde. These emissions are a probable cause of acute health effects and discomfort among occupants (Andersson et al., 1997). Ventilation is another determinant of indoor air quality in houses (Hodgson et al., 2000). Ventilation serves as the primary mechanism for removal of gaseous contaminants generated indoors. The trend in new construction is to make house envelopes tighter. This practice improves energy efficiency by decreasing the infiltration of unconditioned outdoor air. Consequently, natural ventilation rates in new houses without supplemental forced ventilation can be relatively low with a related potential for degraded indoor air quality (Hodgson et al., 2000). In many cases, these ventilation rates may be below recommended guidelines (ASHRAE, 1989).

There have been very few investigations of VOC contamination in new houses. In one recent study (Hodgson et al., 2000), the concentrations and emission rates of VOCs were shown to be similar among 11 new manufactured and site-built houses in four different locations. This was attributed to strong similarities in construction materials and building practices. Formaldehyde, other aldehydes, and terpene hydrocarbons (HCs) were the predominant compounds. Formaldehyde concentrations had a geometric mean value for all houses of 40 ppb. Exposures to formaldehyde are of concern because formaldehyde is a potent sensory irritant and is classified as a probable human carcinogen (Lui et al., 1991; U.S. EPA, 1994). The State of California has set an allowable daily formaldehyde exposure limit of 40 μg, which equates to an indoor air concentration of just 1.6 ppb (Kelly et al., 1999). Higher molecular weight aldehydes can produce objectionable odors at low concentrations. The odor thresholds for hexanal and other aldehydes are often exceeded in new houses and may remain elevated for months after construction (Lindstrom et al., 1995; Hodgson et al., 2000). Terpene HCs are of potential concern because they react with ozone to produce ultrafine particles (Weschler and Shields, 1997). Animal studies also indicate that strong sensory irritants are formed by terpene-ozone reactions (Wolkoff et al., 2000). Wood and engineered wood products (e.g., particleboard, medium density fiberboard, plywood and OSB) are the likely major sources of aldehydes and terpene HCs in new houses (Hodgson et al., 2001).

There is a potential for houses constructed with SIPs to have degraded air quality relative to conventionally constructed houses that use fewer engineered wood products. Some SIP systems are assembled with an OSB layer on the interior facing side. OSB is a source of formaldehyde emissions approximately equivalent to phenol-formaldehyde plywoods (Kelly et al., 1999). OSB also emits pentanal and hexanal, two odorous aldehydes (Barry and Corneau, 1999). These contaminants originate in the wood drying process through the breakdown of wood tissue

(Otwell et al., 2000) and are, thus, inherent to most engineered wood products. In SIPs applications, the OSB is typically finished with a layer of gypsum board. However, gypsum board and other interior finishes may not provide an effective barrier for volatile contaminants released by OSB. The large surface area of installed SIP systems, combined with the resulting decrease in ventilation rate due to very low infiltration exacerbates the potential problem.

The ability to predict and consequently minimize the potential impact of panel systems on indoor concentrations of contaminants of concern would be extremely useful for housing technologies. Recently, a physically-based model that predicts emissions from vinyl flooring, a single-layer, diffusion-controlled VOC source, has been developed (Little et al., 1994; Little and Hodgson, 1996) and successfully validated (Cox et al., 2001a; Cox et al., 2001b; Cox et al., 2002). The model validation process achieved a much higher degree of scientific integrity than previous diffusion-controlled emission models because the three model parameters were determined in a completely independent fashion. A logical and promising extension of this approach is to apply the model to predict emissions from multi-layer systems such as SIPs. The multi-layer model will be valuable when designing new panel systems, because the emission characteristics can be predicted in advance, based on a few simple and direct measurements of the key model parameters. In addition, the model can be used to develop strategies to design panel systems in such a way as to reduce or eliminate emissions. In particular, the model could be used to optimize the required properties of suitable diffusion barriers. In this paper, the recently validated single-layer emissions model will be extended to a double-layer system. The double-layer model will then be used to investigate required barrier layer properties.

VALIDATION OF SINGLE-LAYER MODEL

In prior research, a fundamental model was developed for diffusion-controlled building material, as well as rapid procedures to measure model parameters.

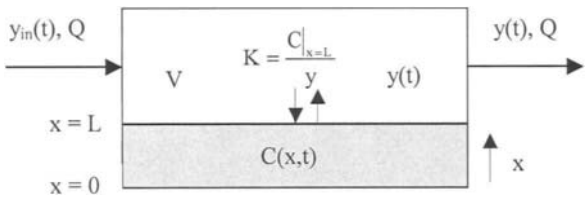


Figure 1: Schematic representation of a homogenous source in a room or chamber

The model for predicting the emission rate of VOCs from diffusion-controlled building materials is summarized in Figure 1 (Cox et al., 2002). The resulting equation for predicting the concentration of VOC in the source material is

$$C(x,t) = 2C_0 \sum_{n=1}^{\infty} \left[\frac{\exp(-Dq_n^2 t)(h - kq_n^2)\cos(q_n x)}{\left[L(h - kq_n^2)^2 + q_n^2(L + k) + h \right] \cos(q_n L)} \right] \quad (1)$$

where $h = \frac{Q}{ADK}$, $k = \frac{V}{AK}$, and the q_ns are the positive roots of $q_n \tan(q_n L) = h - kq_n^2$.

Referring to Equation 1 and Figure 1, C(x, t) is the material-phase VOC concentration, t is time, x is distance from the base of the material, y(t) is the gas-phase VOC concentration in the well-mixed chamber air, D is the concentration independent material-phase diffusion coefficient, K is the concentration independent material/air partition coefficient, Q is the volumetric flow rate of air through the chamber, V is the chamber volume, A is the exposed surface area of the material, and L is the material thickness. The initial concentration in the material (C_0) is assumed to be uniform and $y_{in}(t)$ is assumed to be zero for the entire time period.

The model was successfully validated for three VOCs found in VF (Cox et al., 2002). Model predictions were compared to gas-phase concentrations obtained during small-scale chamber tests, and to material-phase concentrations measured in the VF at the conclusion of the chamber tests. The model parameters (the initial VOC concentration in the material-phase (C_0), the material/air partition coefficient (K), and the material-phase diffusion coefficient (D)) were measured in completely independent tests (Cox et al., 2001a; Cox et al., 2001b).

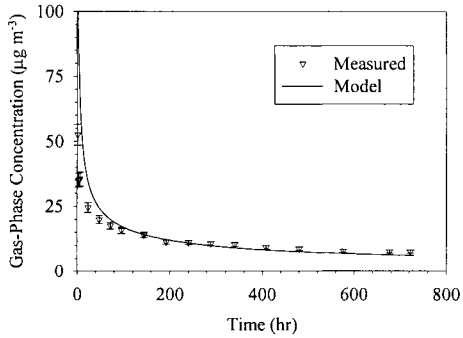


Figure 2

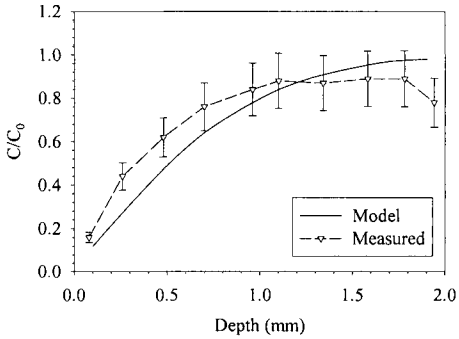


Figure 3

Figure 2 shows predicted gas-phase concentrations compared to concentrations of n-tetradecane measured in chamber experiments. Figure 3 shows the measured material-phase contaminant concentrations of n-tetradecane after 722 hours of exposure in the chamber. The model predicts the measured concentrations very well in both cases.

DEVELOPMENT OF DOUBLE-LAYER MODEL

The model for the double-layer system depicted in Figure 4 is a logical extension of the single-layer model. The diffusion equation applies to each of the layers, or

$$\frac{\partial^2 C_i}{\partial x^2} = \frac{1}{D_i}\frac{\partial C_i}{\partial t} \tag{2}$$

where i represents the specific layer, C is the material-phase concentration, D is the diffusion coefficient, t is time and x is distance as shown in Figure 4.

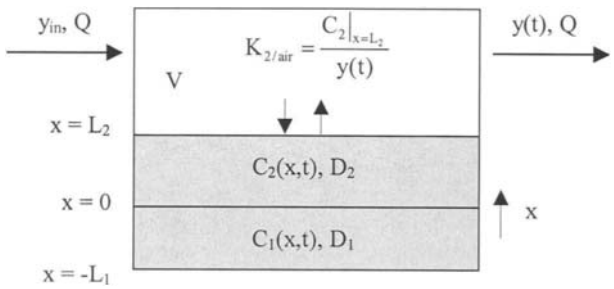


Figure 4: Schematic representation of a double-layer source in a room or chamber

The initial conditions for uniform material-phase concentrations are

$$C_1 = C_{10} \quad \text{for} \quad -L_1 \le x \le 0 \quad \text{and} \quad C_2 = C_{20} \quad \text{for} \quad 0 \le x \le L_2 \tag{3}$$

The first boundary condition is based on a mass balance about the chamber. It is assumed that the air within the chamber is in instantaneous equilibrium (partition coefficient $K_{2/air}$) with the upper surface of the top layer ($K_{2/air}\, y(t) = C_2$ at $x = L_2$). Thus,

$$V\frac{\partial y(t)}{\partial t} = -AD_2\left.\frac{\partial C_2}{\partial x}\right|_{x=L_2} - Qy(t) \tag{4}$$

where V is the volume of the chamber and Q is flow rate though the chamber. The second boundary condition assumes that the flux through the base of lower layer is zero, or

$$\left.\frac{\partial C_1}{\partial x}\right|_{x_1=-L_1} = 0 \tag{5}$$

The other two boundary conditions are obtained using the assumptions that the two layers are in interfacial equilibrium (with partition coefficient $K_{1/2} = K_{1/air}/K_{2/air}$) and that there is no loss of mass at the interface, or

$$C_1|_{x=0} = K_{1/2}C_2|_{x=0} \tag{6}$$

$$D_1\left.\frac{\partial C_1}{\partial x}\right|_{x=0} = D_2\left.\frac{\partial C_2}{\partial x}\right|_{x=0} \tag{7}$$

Using Laplace transforms, a solution is found and the inverse is obtained by the method of residues:

$$C_1 = 2\alpha\sum_{n=1}^{\infty}\left[\frac{J(q_n)\{\cos(\alpha q_n x)\cos(\alpha q_n L_1) - \sin(\alpha q_n x)\sin(\alpha q_n L_1)\}\exp(-D_2 q_n^2 t)}{q_n G(q_n)}\right] \quad (8)$$

$$C_2 = 2\sum_{n=1}^{\infty}\left[\frac{J(q_n)\{\alpha\cos(q_n x)\cos(\alpha q_n L_1) - K_{1/2}\sin(q_n x)\sin(\alpha q_n L_1)\}\exp(-D_2 q_n^2 t)}{K_{1/2} q_n G(q_n)}\right] \quad (9)$$

where

$$J(q_n) = C_{20}K_{1/2}\{h_2 - k_2 q_n^2(1-\beta)\} - (K_{1/2}C_{20} - C_{10})\{(h_2 - k_2 q_n^2)\cos(q_n L_2) - q_n \sin(q_n L_2)\} \quad (10)$$

$$\begin{aligned} G(q_n) = {} & q_n\{K_{1/2}(L_2 + 2k_2) + \alpha^2 L_1\}\sin(q_n L_2)\sin(\alpha q_n L_1) \\ & -\{K_{1/2} + (K_{1/2}L_2 + \alpha^2 L_1)(h_2 - k_2 q_n^2)\}\cos(q_n L_2)\sin(\alpha q_n L_1) \\ & -\alpha q_n\{2k_2 + L_2 + L_1 K_{1/2}\}\cos(q_n L_2)\cos(\alpha q_n L_1) \\ & -\alpha\{1 + (L_1 K_{1/2} + L_2)(h_2 - k_2 q_n^2)\}\sin(q_n L_2)\cos(\alpha q_n L_1) \end{aligned} \quad (11)$$

$$\alpha = \sqrt{\frac{D_2}{D_1}} \quad ; \quad \beta = \frac{C_{L_2}}{C_{20}} \quad ; \quad h_2 = \frac{Q}{AK_{2/air}D_2} \quad ; \quad k_2 = \frac{V}{AK_{2/air}} \quad (12)$$

and the q_ns are the roots of

$$(h_2 - k_2 q_n^2)\{K_{1/2}\tan(\alpha q_n L_1)\tan(q_n L_2) - \alpha\} + q_n\{\alpha\tan(q_n L_2) + K_{1/2}\tan(\alpha q_2 L_1)\} = 0 \quad (13)$$

Although the periodicity of the roots is complex, they can be obtained using software such as Solver in Microsoft Excel.

IMPACT OF BARRIER LAYER

The model developed can now be used to study the required properties of barrier materials used to reduce the rate of contaminant emissions from building materials. The input parameters for the model are listed in Table 1. Phenol is used as the example contaminant and the conditions employed approximate laboratory chamber experiments conducted using a sample of vinyl flooring (Cox et al., 2002).

TABLE 1
PARAMETER VALUES USED FOR CALCULATIONS

Volume of chamber, V	0.0105 m^3
Flow rate through chamber, Q	1.7×10^{-5} m^3 s^{-1}
Partition coefficient, $K_{1/air}$	120,000
Diffusion coefficient, D_1	1.2×10^{-13} m^2 s^{-1}
Initial concentration, C_{10}	2×10^8 μg m^{-3}
Surface area of VF exposed to air, A	0.0195 m^2
Thickness of VF, L_1	0.0017 m
Thickness of barrier layer, L_2	0.0002 m

To simulate a baseline scenario for the single-layer experimental VF system, the properties of layer 2 (D_2, $K_{2/air}$, and C_{20}) are set equal to those of layer 1 (D_1, $K_{1/air}$, and C_{10}). In a second scenario the surface layer has the exact same D and K values as the lower layer, but has an initial concentration of zero. In this case, the barrier layer acts as a buffer to reduce the initial peak in the chamber concentration. Finally, to simulate the properties of a diffusion barrier, D_2 is decreased by a factor of 10. The series of results is shown in Figure 5. Decreasing D of the barrier layer results in a significant drop in gas-phase concentration.

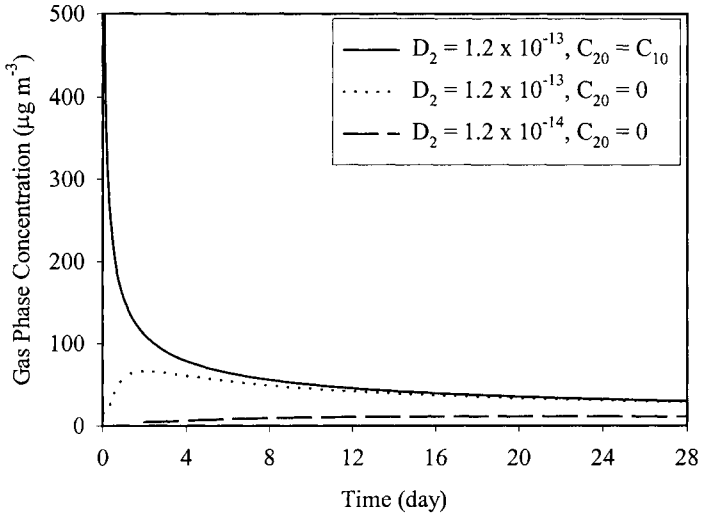


Figure 5: Effect on gas-phase concentration of decreasing D_2 of barrier layer

CONCLUSIONS

The results suggest that thin barrier layers can be used to reduce the rate of emissions from diffusion-controlled materials, including SIPs. The model provides a means to predict the combined effect that diffusion barriers and material transport properties have on overall emission rates. Note that while the emission rate is reduced, the same amount of mass is ultimately emitted, unless the initial material-phase contaminant concentration could itself be decreased. The double-layer model should prove useful in predicting the source/sink behavior of other layered building materials. It will also be used to validate the more mathematically complex multi-layer model that is currently being developed to predict contaminant transport through SIPs. Although the single-layer version of this model has been validated, experimental work has yet to be done to formally validate the double-layer model.

ACKNOWLEDGEMENTS

Financial support was provided by the National Science Foundation (NSF) through an NSF CAREER Award (Grant No. 9624488) and an NSF PATH Award (Grant No. 0122165).

REFERENCES

Andersson, K., Bakke, J.V., Bjorseth, O., Bornehag, C.-G., Clausen, G., Hongslo, J.K., Kjellman, M., Kjaergaarrd, S., Levy, F., Molhave, L., Skerfving, S. and Sundell, J. (1997). TVOC and Health in Non-industrial Indoor Environments *Indoor Air* **7**, 78-91.

ASHRAE. (1989). Standard 62, Ventilation for Acceptable Indoor Air Quality, American Society of Heating, Refrigeration and Air-Conditioning Engineers.

Barry, A. and Corneau, D. (1999). The Impact of Wood Composite Panel Products such as OSB, Particleboard, MDF and Plywood on Indoor Air Quality *Indoor Air 99, Proceedings of the 8th International Conference on Indoor Air Quality and Climate* **5**, 129-134.

Cox, S.S., Hodgson, A.T. and Little, J.C. (2001a). Measuring Concentrations of Volatile Organic Compounds in Vinyl Flooring *Journal AWMA* **51**, 1195-1201.

Cox, S.S., Little, J.C. and Hodgson, A.T. (2002). Predicting the Emission Rate of Volatile Organic Compounds from Vinyl Flooring *Environmental Science & Technology* **36**, 709-714.

Cox, S.S., Zhao, D.Y. and Little, J.C. (2001b). Measuring Partition and Diffusion Coefficients of Volatile Organic Compounds in Vinyl Flooring *Atmospheric Environment* **35**, 3823-3830.

Hodgson, A.T., Rudd, A.F., Beal, D. and Chandra, S. (2000). Volatile Organic Compounds Concentrations and Emission Rates in New Manufactured and Site-built Houses *Indoor Air* **10**, 178-192.

Hodgson, A.T., Beal, D. and McIlvaine, J. (2001). Sources of Formaldehyde, other Aldehydes and Terpenes in a New Manufactured House *Indoor Air* – In press.

Kelly, T.J., Smith, D.L. and Satola, J. (1999). Emission Rates of Formaldehyde from Materials and Consumer Products found in California Homes *Environmental Science and Technology* **33**, 81-88.

Lindstrom, A.B., Proffitt, D. and Fortune, C.R. (1995). Effects of Modified Residential Construction on Indoor Air Quality *Indoor Air* **5**, 258-269.

Little, J. C. and Hodgson, A. T. (1996). A Strategy for Characterizing Homogeneous, Diffusion-controlled, Indoor Sources and Sinks *Standard Technical Publication 1287, American Society for Testing and Materials* 294-304.

Little, J. C., Hodgson, A. T., and Gadgil, A. J. (1994). Modeling Emissions of Volatile Organic Compounds from New Carpets *Atmospheric Environment* **28**, 227-234.

Lui, K.-S., Huang, F.-Y., Hayward, S.B., Wesolowski, J. and Sexton, K. (1991). Irritant Effects of Formaldehyde Exposure in Mobile Homes *Environmental Health Perspectives* **94**, 91-94.

Otwell, L.P, Hittmeier, M.E., Hooda, U., Yan, H., Wei, S. and Banerjee, S. (2000). HAPs Release from Wood Drying *Environmental Science and Technology* **34**, 2280-2283.

U.S. EPA. (1994). Review Draft of the Health Effects Notebook for Hazardous Air Pollutants. Environmental Protection Agency, Air Risk Information Support Center, (Contract N. 68-D2-0065).

Weschler, C.J. Shields, H.C. (1997). Potential Reactions Among Indoor Pollutants *Atmospheric Environment* **31**, 3487-3495.

Wolkoff, P., Clausen, P.A., Wilkins, C.K. and Nielsen, G.D. (2000). Formation of Strong Airway Irritants in Terpene/Ozone Mixtures *Indoor Air* **10**, 82-91.

Advances in Building Technology, Volume 1
M. Anson, J.M. Ko and E.S.S. Lam (Eds.)
© 2002 Elsevier Science Ltd. All rights reserved

NOVEL MICROCELLULAR PLASTICS FOR LIGHTWEIGHT AND ENERGY EFFICIENT BUILDING APPLICATIONS

Krishna Nadella, Vipin Kumar[1], and Wei Li

Department of Mechanical Engineering
Box 352600
University of Washington
Seattle, WA 98195-2600

ABSTRACT

This paper presents thick microcellular plastics for lightweight, energy efficient building applications. The technology is capable of reducing polymer density and thermal conductivity, while increasing its specific strength. The resulted plastic materials can significantly contribute to reducing the house construction time, energy consumption, maintenance cost, and risk of injury during construction. The proposed thick microcellular plastics are produced in a batch process. In this research, a systematic study of various process variables is conducted using a two-stage, sliding-level design of experiment approach. The preliminary results have shown that the foamed thick ABS sheets have clearly defined skins and foamed core structures. 70% relative density reduction has been achieved.

KEYWORDS

Microcellular plastics, polymer processing, building material, plastic foam, design of experiment

INTRODUCTION

Microcellular Plastics refer to closed-cell thermoplastic foams with a very large number of very small bubbles. Typically, the cells are of order 10 micrometers in diameter, and there are 10^8 or more cells per cubic centimeter (cm^3) of the foam. The idea to introduce such small bubbles in plastics was first introduced by Suh *et al* (1982, 1984) as a means to reduce the density of solid plastics, and thus to save on material costs in applications where the full mechanical properties of solid plastics were not needed. Being a foam material, the microcellular polymers have inherited beneficial characteristics such as lightweight and low thermal conductivity. The bubbles inside the polymers are in very small scales and therefore the materials maintain reasonably high tensile and shear strength. These

[1] Corresponding author: vkumar@u.washington.edu

characteristics offer an excellent solution to many of the problems encounter in the current construction practice. Particularly, thick microcellular polymer sheet can be used in advanced panel systems to reduce house construction time and maintenance cost, cut energy consumption, reduce the risk of injury during construction, and improve the durability of the houses.

A house consists of many panels such as walls, roofs, floors, doors, and windows. The manufacture and thermal properties of these panels directly affect the construction time, energy consumption, and thus the cost of new houses. In order to reduce construction time and achieve better thermal properties, various advanced panel systems have been developed. These include precast concrete, tilt-up concrete panel, structural insulated panel system (SIPS), and insulated concrete foam (ICF). These systems often consist of a sandwich type of structure in which a foamed core is used with a layer of other materials on each side. Fig. 1 shows an example SIP system where the sheathing material used is compressed wood.

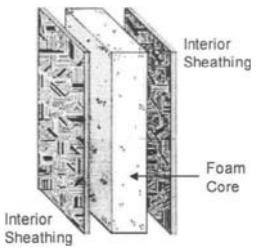


Figure 1: A schematic of an advanced panel system.

Although the concept of advanced panel systems has the potential to reduce the house construction time and thus the cost of new houses, currently available panel systems have not been widely accepted. In order to meet the requirements of home construction, the materials used for advanced panel systems have to be lightweight, reasonably strong, and easy to manufacture. Another important characteristic of such panel system is high surface quality. Good surface quality of panels can reduce large amount of interior work, which accounts for a major portion of the selling price of an average new house.

Foam materials are lightweight and low thermal conductive. However, currently available construction foam materials usually have low strengths. The sandwich type of panel systems helps increase the overall strength of the structures. But the sheathing materials used usually have poor surface quality. More often, the interior side of the walls need large amount of finish work. Recently, carbon fiber reinforced precasts and composite panels have been developed. Such panels are low cost, lightweight, and have the potential to be used as a "stand-alone" construction component. However, this type of panels has to be used together with insulation and still needs interior finish work.

The long-range objective of this research is to develop an industrially viable technology of manufacturing thick microcellular polymer sheets (6 mm–10 mm) that can be used in advanced panel systems. The proposed microcellular technology is capable of reducing polymer density and thermal conductivity while increasing its specific strength. The resulted polymer materials can significantly contribute to reducing the house construction time and maintenance cost, cutting energy consumption, reducing the risk of injury during construction, and improving the durability of the houses.

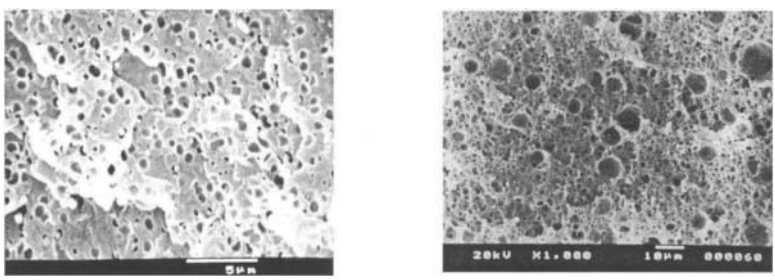
This paper presents the proposed thick microcellular sheet manufacturing process. A two-stage, sliding-level design of experiment approach is used to study the effects of various process variables on

the microstructure of the polymer sheet. Preliminary results have shown that thick ABS sheets can be foamed and the structure has clearly defined skins and a foamed core. 70% relative density reduction has been achieved in this preliminary study.

MICROCELLULAR PLASTICS

The basic solid-state microcellular process is a two-stage batch process. In the first stage, the polymer is placed in a pressure vessel with a high-pressure and non-reacting gas. This step is usually conducted at room temperature. Over time, the gas diffuses into the polymer, and attains a uniform concentration throughout the polymer specimen. When this specimen is removed from the pressure vessel and brought to the atmospheric pressure, a "supersaturated" specimen that is thermodynamically unstable due to the excessive gas dissolved into the polymer is produced. In the second stage, the specimen is heated to what is termed the foaming temperature. This step is typically carried out in a heated bath with temperature control. The dissolved gas lowers the glass transition temperature of the polymer (Zhang & Handa, 1998) and the foaming temperature needs only to be above the glass transition temperature of the gas-polymer system in order for the bubbles to nucleate and grow. Since the polymer is still in a solid state, the foams thus produced are called "solid-state foams" to distinguish them from the conventional foams that are produced in an extruder from a polymer melt. Details of the batch process can be found in Kumar & Weller (1994), where the polycarbonate-CO_2 system is described.

Fig. 2 (a) shows a CPET microcellular foam with a 26% reduction of density. The size of the cells is of the order of 1 micrometer and the cell density is estimated to be 10^{13} cells per cm^3. Fig. 2 (b) shows a PVC microcellular foam produced by the solid-state process. Here we find a bimodal distribution of the bubble size, with the bubble diameters clustered around 2 and 10 micrometers. The density of the PVC specimen was 40% of the solid PVC. A unique feature of the microcellular process is that a solid, unfoamed skin can be created as an integrated part of the process (Kumar &Weller, 1994). A brief overview of microcellular polymers can be found in Kumar (1993).



(a) (b)

Figure 2: (a) Microcellular CPET (originally 1 mm thick) with a relative density of 74% (or a density reduction of 26%). The cell density is estimated to be 10^{13} per cm^3, while the average cell diameter is approximately one micrometer. (b) The cells in this 40% Relative Density PVC example (originally 1.5 mm thick) are bi-modal in diameter distribution; some are about 10 micrometer and most about two micrometer.

It was recognized that although the batch process could be used to study new systems and characterize mechanical properties, the potential of these novel materials could not be realized unless the process could be scaled up for mass-production. An extrusion process to produce microcellular filaments was developed by Park and Suh (1992). At the University of Washington, a semi-continuous process to

produce rolls of microcellular foams from rolls of polymer film was developed by Kumar and Schirmer (1995,1997) while Seeler et al (1996) demonstrated the feasibility of producing a net-shape part in a sintering process based on saturating and foaming polycarbonate powder. Meanwhile, further innovations in extrusion based microcellular processing have been reported from Japan (Shimbo et al, 1998) and Germany (Seibig et al, 2000). Thus, the race to develop industrial processes and reap the potential benefits of microcellular foams was on in the U.S., Europe, Canada, and Japan.

The end product of this research is envisioned to be an industrial-scale commercial "batch" process, which will produce, for example, 1.2 m × 2.4 m (about 4 ft × 8 ft) microcellular sheets of desired thickness and density. These sheets will have a microstructure that is tailored to the strength and stiffness requirements. The microcellular process has the capability to control material density distribution across the thickness and to create a solid skin of desired thickness that is integral to the foam itself. These materials will be the new, lightweight building blocks for future house construction.

EXPERIMENT DESIGN

In this research, a preliminary experimental study is being conducted to study the feasibility of producing thick microcellular sheets and the effects of various process variables. The ABS-CO_2 gas polymer system is chosen for this study. The batch process described above is used to create flat sheets that are 12.5 mm thick. The primary characteristics of interest include the skin thickness and the average density of the core. In additions, it is also of interest to control the bubble size distribution through the control of the gas concentration profile and/or the temperature profile. The equipment used in the experiment includes a hot press and a high-pressure vessel.

The process variables are examined in order to determine a set of potentially significant ones for further study. High and low priorities are assigned to the variables. Table 1 summarizes the results. The first four variables in the table have a high priority and will be systematically studied.

TABLE 1
VARIABLES THAT COULD AFFECT THE QUALITY
OF THICK MICROCELLULAR SHEET FOAMING PROCESS

No	Parameters	Priority
1	Saturation pressure	High
2	Temperature of platens (Foaming temperature)	High
3	Desorption time	High
4	Thickness of starting material	High
5	Force exerted by the platens	Low
6	Foaming time	Low
7	Shim thickness	Low
8	Environmental temperature during desorption	Low
9	Environmental pressure during desorption	Low
10	Composition of raw material	Low
11	Saturation temperature	Low
12	Humidity of the environment	Low

Hot press foaming is a complicated process. There is interdependency among the process variables to achieve desirable results. For example, to obtain a foamed structure, the foaming temperature is dependent on the saturation pressure. This interdependency can be observed in Fig. 3. In general, if the saturation pressure is low, the foaming temperature has to be high. Without a foamed structure, the experiment does not provide useful information on relative density and skin thickness. Therefore,

conventional design of experiment, in which the settings of process variables are independently chosen, does not provide an efficient experiment plan, because they result in data points outside of the interest area or considerably smaller response area to be explored. In this study, a two-stage, sliding-level design of experiment approach (Li, et al, 2001) is used to resolve the parameter interdependency problem. In this experiment, the foaming temperature is chosen as a "slid factor" whose settings will be determined based on those of other variables. Table 2 shows the settings the process variables. The saturation pressure and desorption time are chosen as three-level variables, and the starting thickness of the unfoamed sheet as two-level variable. The foaming temperature will be determined for each of the combinations of the factor levels.

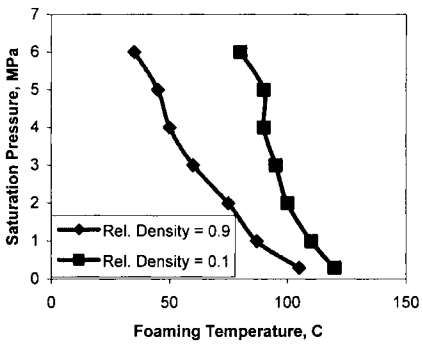


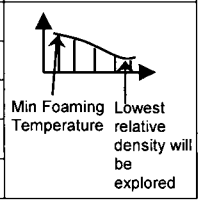
Figure 3: The interdependency between foaming temperature and saturation pressure.

TABLE 2
FACTORS AND THEIR LEVELS IN THE DESIGN OF EXPERIMENT

Factors	Levels		
	1	2	3
Saturation Pressure	1 MPa	3 MPa	5 MPa
Desorption Time	0	1	2
Starting Thickness of Unfoamed Sheet	3/16"	7/16"	--
Foaming Temperature (Temperature of Platens)	Five levels of foaming temperature at each combination of factor levels in the matrix for the above three factors		

As shown in in Table 3, given any setting of the other three variables, the maximum and minimum foaming temperatures have to be found first. These two temperatures will yield the maximum and minimum possible relative density for different pressures. For the ABS material, the minimum foaming temperature for a given saturation pressure can be estimated by using Chow's equation. The maximum foaming temperature, on the other hand, is not easy to find. Fortunately, prior experience can help with the search. For example, the maximum foaming temperature is known to be close to the glass transition temperature T_g of unsaturated ABS. It decreases as the saturation pressure increases. Once the maximum foaming temperature is determined, another three levels of temperature will be chosen equally spaced within the two extreme temperatures. Since there will be five temperature data points for each setting of other variables, the maximum and minimum temperatures do not have to be exact. Based on the above design, the total number of experiments to be conducted is 3*3*2*5 = 90.

TABLE 3
DESIGN MATRIX OF THE EXPERIMENT

Saturation Pressure (p)	Desorption Time (t)	Thickness (h)	Foaming Temperature (T)	Relative Density (ρ)
1	1	1	T_{11} T_{12} T_{13} T_{14} T_{15}	
1	2	1	T_{21} T_{22} T_{23} T_{24} T_{25}	
1	3	1	T_{31} T_{32} T_{33} T_{34} T_{35}	
1	1	2	T_{41} T_{42} T_{43} T_{44} T_{45}	
...	...	...	...	

PRELIMINARY RESULTS

Preliminary experiments are conducted with 0.25" thick ABS sheets using the hot press foaming process. The resulting foamed boards have the desired structure with a relative density of 30% (thus a 70% density reduction) and a final thickness of 0.385". The surfaces of the sheet are unfoamed skins and the core is uniform microcellular foam. Figures 4, 5, 6 and 7 show micrographs of the cross-section of 30% relative density ABS sheet at different magnifications. Fig. 4 is a low magnification image showing the unfoamed skin, the skin-core transition area, and the foamed core on the ABS sample. Fig. 5 shows a close up view of the skin, which is about 400 μm thick. The image of the skin-core transition area in Fig. 6 shows a gradual change from solid material near the surface on the left to the microcellular bubbles towards the core on the right. Fig. 7 shows the uniformly nucleated microcellular bubbles in the core. The size of the microcellular bubbles is in the range of 2 – 10 μm. The result of the preliminary experiments is very encouraging. It demonstrates that it is possible to not only create an ideal thick microcellular polymer sheet with desired density reduction and foam structure, but also maintain the flatness and smoothness on the surface of the board to make them viable for construction panel applications.

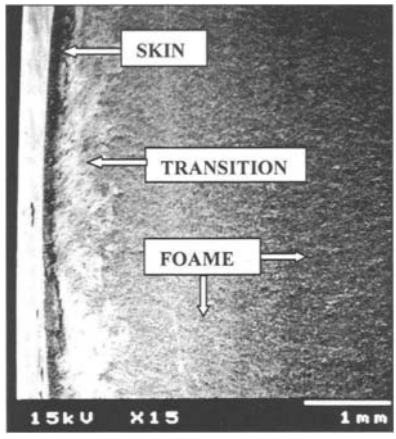


Figure 4: 30% relative density ABS sample showing skin, transition area and core.

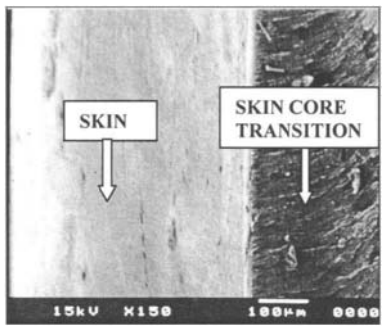


Figure 5: 30% relative density ABS sample showing close up of skin and skin-core transition area.

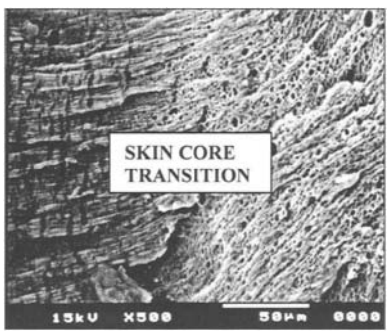


Figure 6: 30% relative density ABS sample micrograph showing close up of skin-core transition area.

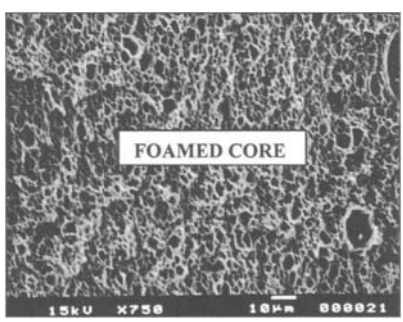


Figure 7: 30% relative density ABS sample micrograph showing foamed core.

SUMMARY

This paper presents thick ABS microcellular sheets technology for lightweight, energy efficient building applications. A systematic study of various process variables is being conducted using a two-stage, sliding-level design of experiment approach. The preliminary results have shown that the foamed ABS sheet has clearly defined skins and foamed core structures. 70% relative density

reduction is achieved. In general, the proposed technology is expected to be capable of reducing polymer density and thermal conductivity while increasing its specific strength. The resulted polymer materials can significantly contribute to reducing the house construction time and maintenance cost, energy consumption, and risk of injury during construction and improving the durability of the houses. The work presented in this paper is preliminary results of a long-range research in developing an industrially viable industrial process. Future work includes the study of gas polymer interaction to reduce the gas saturation time, investigation on other gas-polymer systems, and optimization of the processes.

Acknowledgement

The authors wish to acknowledge the United States National Science Foundation for the financial support of this study under Grant No. CMS-0122055.

References

1. Kumar V. and Schirmer H.G. (1997). A Semi-Continuous Process to Produce Microcellular Foams. **US patent 5,684,055**, issued November 4, 1997.
2. Kumar V. and Weller J.E. (1994). A Model for the Un-foamed Skin on Microcellular Foams. **Polymer Engineering and Science: Vol. 34,** pp. 169-173.
3. Kumar V. and Weller J.E. (1994). Production of Microcellular Polycarbonate using Carbon Dioxide for Bubble Nucleation. **ASME Journal of Engineering for Industry: Vol. 116,** pp. 413-420.
4. Kumar V., and Schirmer H. G. (1995). Semi-Continuous Production of Solid State PET Foams. **Society of Plastics Engineers Technical Papers: Vol. XLI**, pp. 2189-2192.
5. Kumar, V., (1993). Microcellular Polymers: Novel Materials for the 21st Century. **Progress in Rubber and Plastics Technology: Vol. 9,** No. 1, pp. 54-70.
6. Li W., Hu S.J., and Ni J., (2001). On-line Quality Estimation in Resistance Spot Welding. **ASME Journal of Manufacturing Science and Engineering: Vol. 122,** pp. 511-512.
7. Martini, J. Waldman F.A., and Suh N.P. (1982). The Production and Analysis of Microcellular Foam. **SPE Tech. Papers: XXVIII,** pp. 674-676
8. Martini-Vvedensky J.E., Suh N.P., and Waldman F.A. (1984). U.S. Patent # 4,473,665.
9. Park C. B. and Suh N. P., (1992). Extrusion of Microcellular Filament: A case Study of Axiomatic Design. **ASME Winter Annual Meeting, Anaheim, CA: MD-Vol. 38**, pp. 69-91.
10. Seeler K.A., Billington S.A., Drake B.D. and Kumar V. (1996). Net-Shape Forming of Sintered Microcellular Foam Parts. **1996 ASME Cellular and Microcellular Materials: MD-Vol. 76**, pp. 65-70.
11. Seibig B., Huang Q., and Paul D. (2000). Design of a Novel Extrusion System for Manufacturing Microcellular Polymer. **Cellular Polymers: Vol. 19, No. 2**, pp. 93-102.
12. Shimbo M., Nishid, K., Nishikawa S., Sueda T., and Eriguti M. (1998). Foam Extrusion Technology for Microcellular Foams. **Porous, Cellular and Microcellular Materials: MD-Vol. 82, V. Kumar, Ed.,** pp. 93-98.
13. Zhang Z. and Handa Y. P. (1998). An In-Situ Study of Plasticization of Polymers by High-Pressure Gases. **Journal of Polymer Science: Part B: Polymer Physics: Vol. 36,** pp. 977-982.

Advances in Building Technology, Volume 1
M. Anson, J.M. Ko and E.S.S. Lam (Eds.)
© 2002 Elsevier Science Ltd. All rights reserved

LONG-TERM CREEP RESPONSE OF BORATE-MODIFIED ORIENTED STRANDBOARD

Qinglin Wu and Jong N. Lee

School of Renewable Natural Resources
Louisiana State University, Baton Rouge, LA 70803, USA

ABSTRACT

Creep performance of zinc and calcium borate-modified OSB was assessed under both constant and varying moisture conditions. The influence of initial borate content, wood species, and stress level on the creep deformation was studied. Under the constant moisture condition, there was practically no difference in creep for boards at various borate levels for both types of borate. The creep data were fitted well with a spring-dashpot model. Predicted fractional creep validated the current adjustment factor up to a 30-year duration under a constant moisture content level. Under the varying moisture condition, large creep deflection developed due to the mechano-sorptive effect. The effect of borate on wood deformation became significant for both zinc and calcium borate OSB, indicating a reduced load carrying capacity of the OSB at higher borate levels. This result indicates the need for studying long-term duration of load properties of the modified OSB under combined mechanical and moisture loadings.

KEYWORDS

Borate, creep, mechano-sorptive, modeling, OSB, stress level, termite, wood composites

INTRODUCTION

Borate-modified oriented strandboard (OSB) has been developed to combat Formosan Subterranean Termite (FST) infestation on wood buildings in the southern United States (Laks and Manning 1995, Wu et al. 2002). One large uncertainty on the use of the product is its long-term structural performance under sustained loading conditions. It has been shown that boards bonded with both phenolic and isocyanate adhesives displayed a reduction in bending strength upon the incorporation of borate. Thus, durability issues of borate-modified OSB will arise both

in load-bearing (e.g., OSB shear wall, roof, and I-beams) and non-load bearing (e.g., OSB siding and sheathing) situations. Because the chemical is an inorganic salt, it diffuses throughout the wood with moisture movement (LeVan and Winandy 1990). In some situations, such as roofs, elevated temperatures and humidity changes cause shifts in the equilibrium moisture content (MC) of the wood. As the moisture moves, so does the inorganic salt. This cycling could cause migration of the salt within the wood. At each new site, the acidic salt can cause wood degradation. It is well-known that cyclic MC changes accelerate creep due to mechano-sorptive (MS) effect. In the presence of borate chemicals, creep may be further accelerated and degradation of other mechanical properties becomes more pronounced.

Creep studies on untreated structural wood composite panels were well documented (Laufenberg 1988, McNatt and Laufenberg 1991, and Fridley et al. 1992). Various analytical models have also been proposed to describe the observed behavior under combined mechanical and moisture loading (Ranta-Maunus 1975, Fridley et al. 1992). However, creep data on treated OSB are completely lacking and the applicability of the creep models to describe its time-dependent behavior has yet to be evaluated. This work forms part of a larger project on investigating long-term durability of borate-modified OSB from southern wood species. The specific objective of this study was to investigate the creep response of the modified OSB as influenced by wood species, borate type, borate content level, moisture cycling, and other panel processing variables.

MATERIAL AND METHODS

Panel production and sample preparation

The details of panel manufacturing are presented in Wu et al. (2002). In brief, green boards from eight southern wood species were selected for the study. These species included ash (Fraxinus spp.), cottonwood (Populus spp.), cypress (Taxodium distichum L.), elm (Ulmus americana L.), locust (R. pseudoacacia L.), pecan (Carya spp.), red oak (Quercus spp.), and southern pine (Pinus taeda L.). The boards were cross-cut into 152-mm sections, which were flaked to produce 76-mm long flakes using a disc flaker. The flakes were dried to 2-3% MC and screened to eliminate fines prior to panel manufacturing. The wood flakes were used to manufacture single species of OSB for zinc borate (ZB) and mixed hardwood and southern pine OSB for calcium borate (CB).

During the panel manufacturing, certain amounts of dry wood flakes, liquid phenol formaldehyde resin, wax, and borate were blended together. The loading rates for resin and wax were 4 and 1% based on the oven-dry wood weight. There were one type of ZB and two types of CB with two different particle sizes. The borate was loaded at several levels to achieve target BAE (Boric Acid Equivalent) levels (Wu at al. 2002). The formed mats were hot pressed in a single opening press with a regulated platen temperature of 200°C for 5 minutes. The target thickness and panel density were 12.7 mm and 0.75 g/cm^3, respectively. Tests were done to determine basic panel properties as shown in Wu et al. (2002). Creep samples were cut from the experimental panels. The samples were conditioned. Their weight and dimension were measured for the determination of sample density prior to the creep measurements. Four samples from each board type were randomly selected to test their static bending modulus of rupture (MOR). The mean MOR value from each group was used to determine actual stress levels (SLs) for the creep test.

Creep testing

A twenty-four position loading frame for constant load creep tests was constructed (Figure 1). The frame has two levels with twelve samples at each level arranged side by side. Each sample was supported and dead weight (lead) was applied to the sample at the central point of the span with a pneumatic loading device for loading and unloading. One linear variable differential transducer (LVDT) was used to measure sample deflections at each level. During measurements, each LVDT was traveling to individual samples with a miniature carriage on two precision stainless steel rods. One reference plate was set on each level for positioning the LVDT before each measurement. The deflection data (D in Figure 1) were collected through a Strawberry-Tree DataShuttle card controlled by a specially designed Visual Basic program. The program enables a three-way communication with the WorkBench program (data acquisition) and Microsoft Excel (data processing) using dynamic data exchange tools (Figure 1). During testing, the loading frame was placed in a climate-controlled laboratory. Stress levels equivalent to 15%, 25%, and/or 40% of the MOR of each board type were applied to the specimens. Several unloaded samples from each board type were used to monitor sample MC and thickness change.

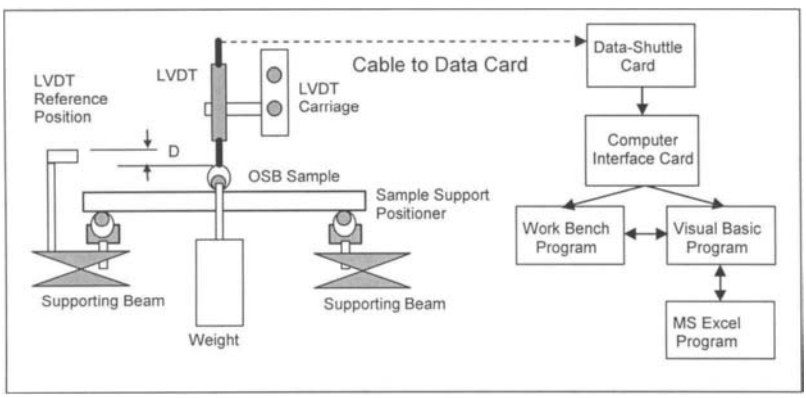


Figure 1. A Schematic of the Loading Frame and Data Acquisition System for Creep Testing

Data reduction and modeling

The measured deflection data were converted to strain using the geometric relationship for three point bending. The effect of sample thickness swelling (TS) on measured deflection during moisture cycling was accounted in the strain calculation. A four-element spring and dashpot model was used to fit the measured creep data under constant MC condition (Pierce and Dinwoodie 1977). The model, consisting of elastic (e), viscoelastic (k), and viscoplastic (v) deformations, has the following form:

$$\varepsilon_{Creep}(t) = \varepsilon_e + \varepsilon_K + \varepsilon_V = \frac{\sigma}{K_e} + \frac{\sigma}{K_k}\left\{1 - \exp\left[-\frac{K_k t}{\eta_k}\right]\right\} + \frac{\sigma t}{\eta_V} \quad (1)$$

where, ε represents deformation, t is time, σ is the applied stress, K_e is the elastic spring constant, K_k and η_k are the spring constant and viscosity for the viscoelastic deformation, and η_r

is the viscosity of dashpot for the viscoplastic deformation. A nonlinear curve fitting technique was employed to determine the model parameters (Pierce and Dinwoodie 1977). The model parameters were then used to predict creep, recovery strain, and fractional creep over an extended time period (i.e., 30 years).

To model the mechano-sorptive effect under changing MC condition, an additional element was added to the creep model (Equation 1) following the approach proposed by Fridley (1990). The MS element has a form (Fridley et al 1992):

$$\varepsilon_{ms}(t_\omega) = \frac{\sigma}{\mu'_{ms}} |\Delta\omega| [1 - \exp(-B_\omega t_\omega)] \tag{2}$$

where, $\Delta\omega = \omega_e - \omega_i$ with ω_e as the final equilibrium MC and ω_i as initial MC, μ'_{ms} is viscosity of the MS element, σ is applied stress, t_ω is elapsed time for MC change, and B_ω is a constant related to the time required for reaching moisture equilibrium. Equation 1 can be rewritten with the MS element as:

$$\varepsilon_{Total}(t) = \frac{\sigma}{K_e} + \frac{\sigma}{K_k}\left\{1 - \exp\left[-\frac{K_k t}{\eta_k}\right]\right\} + \frac{\sigma t}{\eta_V} + \frac{\sigma}{\mu'_{ms}} |\Delta\omega| [1 - \exp(-B_\omega t_\omega)] \tag{3}$$

to describe the total strain under combined mechanical and moisture loading. The MS component was actually modeled by first determining the MC factor B_w in Equation 2. This was done by fitting the measured MC data as a function of time with the exponential function. The MS strain was obtained by subtracting the predicted creep component from the total strain. Assuming a piece-wise linear relationship between MS strain and MC change in a given time step, the coefficient, μ'_{ms}, was determined through a linear regression analysis.

RESULTS AND DISCUSSION

Creep strain

Typical creep curves at the 40% stress level are shown in Figure 2 for zinc borate OSB. The data represent an average of four replicate samples for each board type. The sample MC remained about 6% throughout the test period. For both southern pine and mixed hardwood OSBs, the observed creep was generally higher at the higher borate loading levels. This is very obvious for zinc borate modified hardwood OSB shown in Figure 2B. However, a statistical analysis on instantaneous, total, and permanent plastic strains from various species indicated an insignificant effect of the borate level on the creep deflection. The effect of load level on the observed creep strain is shown in Figure 3 for single species OSB from southern pine (A) and red oak (B). Compared with data at the 15% SL, the increase in the strain at the 40% SL was mainly due to the initial elastic strain for both species. Thus, the creep behavior at the SLs used was basically linear. This is true regardless the borate type and its content level. The effect of wood species on creep under the influence of load level, borate type and content was also inconsistent among the species. OSB made of mixed hardwoods and calcium borate showed smaller strain than those of southern pine. This was mainly due to the difference in the initial moduli of the panels, which were influenced largely by panel density and other processing variables. Therefore, the creep behavior of borate-treated OSB under constant MC conditions was not practically different from those of untreated controls.

The four-element creep model (Equation 1) fitted the individual creep data set well (Lines in Figures 2 and 3). The model parameters varied with borate type, borate content level, and wood species. The model parameters allow predicting creep performance of the OSB under similar loading and environmental conditions.

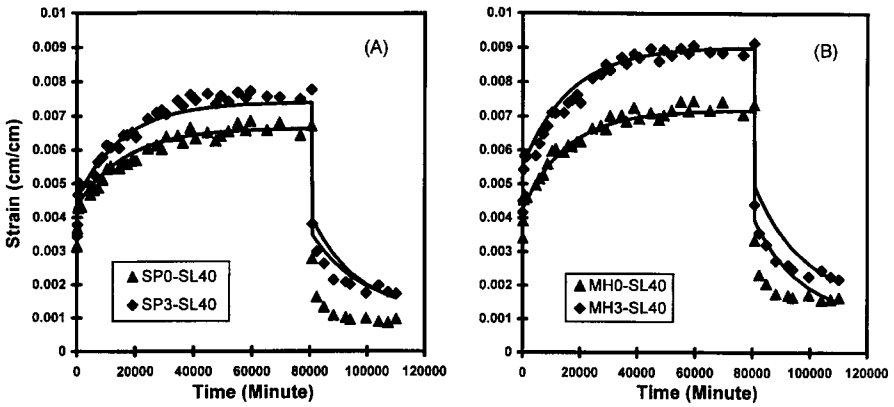


Figure 2. Creep Response of Zinc-Borate Modified OSB under the 40% Stress Level. A) Southern Pine with BAE= 1.78% for SP3 and B) Mixed Hardwoods with BAE=1.72% for MH3. The Lines Show The Predicted Values By The Model (Equation 1).

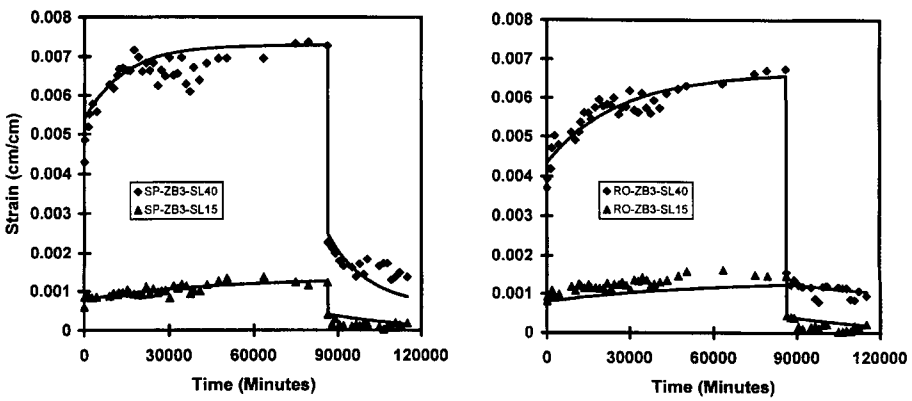


Figure 3. Effect of Load Level on Creep Response of Zinc Borate Modified OSB from Southern Pine (Left) and Red Oak (Right) under the 40% and 15% Stress Levels. BAE=1.95% for SP and 1.265% for RO. The lines show the predicted values by the creep model (Equation 1).

Figure 4 shows predicted fractional creep for southern pine and red oak OSB at various borate levels. The predicted fractional creep under the specific test condition meets the recommended level in the national design standards for wood construction (NFPA 1991). Thus, the current

design practice can be applied to borate-modified OSB up to a 30-year service period. After 30 years, a rapid increase of the fractional creep was predicted at both of the stress levels.

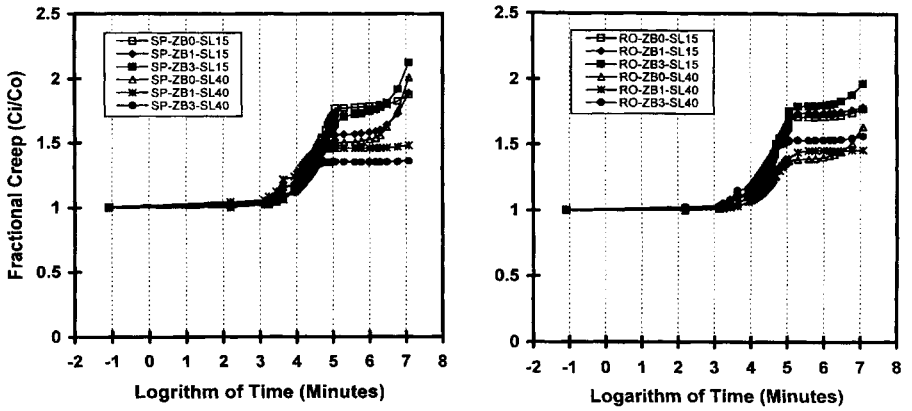


Figure 4. Predicted Fractional Creep for Single-Species OSB from Southern Pine (Left) and Red Oak (Right) under the 15% and 40% Stress Levels. BAE= 1.95% SP-ZB3, 0.89% SP-ZB1, 1.265% for RO-ZB3 and 0.39% for RO-ZB1.

Mechano-sorptive Strain

Typical plots showing time-dependent fractional deflection under varying MC conditions are shown in Figure 5. Tests consisted of an 18-day creep under a constant MC (8%), a 27-day wetting (from 8% to 23% MC), and a 12-day drying (from 23% to 12.5% MC) under load. The mean maximum MC reached during the wetting cycle was somewhat lower from the mixed hardwood group compared with the southern pine group.

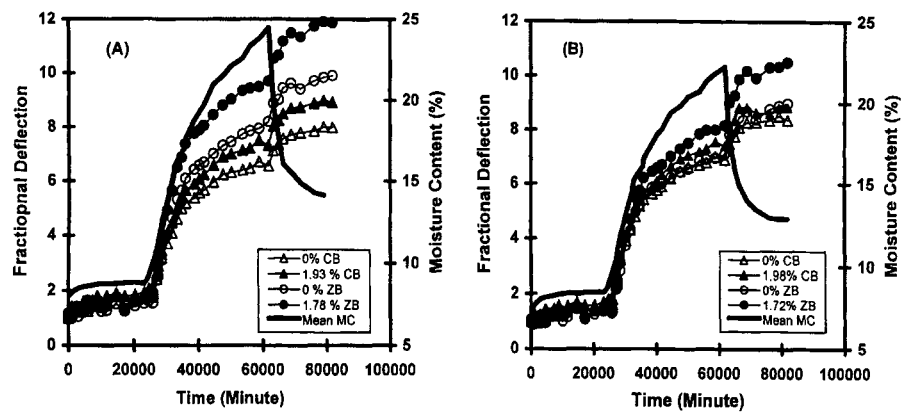


Figure 5. Mechano-sorptive Response (Fractional Deflection) of Zinc and Calcium Borate Modified OSB from Southern Pine (A) and Mixed Hardwoods (B) under the 25% Stress Level.

Creep at 8% MC developed in a regular manner. MC increases and decreases under load led to large deflections in all groups (i.e., MS effect). The effect of borate on the fractional deflection is obvious, considering difference between treated and untreated groups for either ZB or CB OSB. The control groups for ZB and CB OSB showed a significant difference in creep deflection. This was due to difference of initial panel modulus between the groups as those boards were made separately.

Significant TS occurred during testing especially for CB treated OSB. The TS had a significant negative effect on the deformation. Figure 6 shows predicted strain using Equation 3 based on model parameters from each group (ZB or CB) under the same stress level. For both zinc and calcium borates, all treated groups showed a significant larger strain compared with the control group. CB showed a larger negative effect on the deformation than ZB due to its effect on swelling. The increased creep deformation will definitely affect long-term load carrying capacity of the modified product under varying moisture conditions. Thus, a proper account of the MS effect on long-term duration of load behavior of treated OSB has to be made. Further testing and modeling on the MS deformation of the OSB are still on-going.

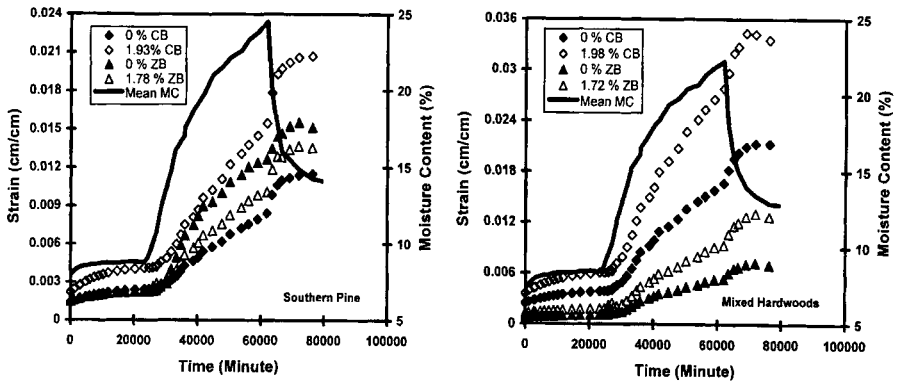


Figure 6. Mechano-Sorptive Response (Predicted Strains) of Zinc and Calcium Borate Modified OSB from Southern Pine (A) and Mixed Hardwoods (B) under the 25% Stress Level.

CONCLUSIONS

Creep behavior of borate-modified OSB was investigated under controlled environments. The experimental work was carried out with OSB made of zinc and calcium borate. A four-element spring-dashpot model was used to fit the creep data under constant moisture condition. The model was combined with an MS element to predict measured strain under varying MCs. There was practically no difference in creep for boards at various borate levels under the constant moisture condition. Predicted fractional creep validated the current adjustment factor up to 30-year duration under a constant moisture content level. However, the added borate led to a significant larger deformation under varying moisture condition due to the mechano-sorptive effect and the deteriorating effect of borate on the thickness swelling properties of the OSB. This

indicates the need for studying long-term duration of load properties of treated OSB under combined mechanical and moisture loadings.

ACKNOWLEDGMENTS

This material is based upon work supported by the National Science Foundation under Grant No. 0080248. Any opinions, findings, and conclusions or recommendations expressed in this material are those of the authors and do not necessarily reflect the view of the National Science Foundation.

REFERENCES

Fridley, K. J., R.C. Tang, and L.A. Soltis. 1992. Creep behavior model for structural lumber. J. of Structural Engineering 118(8):2261-2277.

Fridley, K.J. 1990. Load-duration behavior of structural lumber: effect of mechanical and environmental load histories. Ph.D. Dissertation, Auburn University. 316 pp.

Laks, P.E., and M.J. Manning. 1995. Preservation of wood composites with zinc borate. IRG/WP 95-30074. Intl. Res. Group on Wood Pres., Stockholm, Sweden.

Laufenberg, T. L. 1988. Composite products rupture under long-term loads: a technology assessment. In Proc. 22nd International Particleboard /Composite Materials Symposium, T. M. Maloney Ed. Washington State University, Pullman, WA. pp. 247-256.

LeVan, S.L. and J.E. Winandy. 1990. Effects of fire retardant treatments on wood strength: a review. Wood Fiber Sci. 22(1):113-131.

McNatt, J.D., and T. L. Laufenberg. 1991. Creep and creep-rupture of plywood and oriented strandboard. In Proc. of International Timber Engineering Conference, London, England. pp. 3457-3464.

National Forest Products Association (NFPA). 1991. National design specifications for wood construction. AFPA. Washington D.C.

Pierce, C.B., and J.M. Dinwoodie. 1977. Creep in chipboard. Part 1. Fitting 3- and 4-element response curves to creep data. J. Materials Sci. 12:1955-1960.

Ranta-Maunus. 1975. The viscoelasticity of wood at varying moisture content. Wood Sci. Technol. (9):189-205.

Wu, Q., S. Lee, and J. N. Lee. 2002. Mechanical, physical, and biological properties of borate-modified oriented strandboard. In Proc. International Conference on Advances in Building Technology. Hong Kong. December 4-6, 2002.

Advances in Building Technology, Volume 1
M. Anson, J.M. Ko and E.S.S. Lam (Eds.)
© 2002 Elsevier Science Ltd. All rights reserved

MECHANICAL, PHYSICAL, AND BIOLOGICAL PROPERTIES OF BORATE-MODIFIED ORIENTED STRANDBOARD

Qinglin Wu, Sunyoung Lee, and Jong N. Lee

School of Renewable Natural Resources
Louisiana State University, Baton Rouge, LA 70803, USA

ABSTRACT

Borate-modified oriented strandboard (OSB) was manufactured using zinc and calcium borate to provide resistance to Formosan Subterranean Termites (FSTs). Mechanical, physical, and biological properties of the product were evaluated. It was shown that static bending properties of the OSB were affected little at the room condition by the added borate. The internal bond strength was, however, generally smaller at the higher borate loading levels. Thickness swelling (TS) under the 24-hour water soaking increased with increased borate content, especially for calcium borate. Part of the borate leached out under the water soaking condition due to the glueline washing and decomposition of the borate to form less water-soluble boric acid. The use of borate with a smaller particle size helped reduce TS and leaching rate significantly. Laboratory no-choice termite tests indicated that both zinc and calcium borate modified OSB resisted FSTs well. Thus, termite resistant OSB with required mechanical and physical performance could be successfully developed using southern wood species. This technology will allow more OSB producers to manufacture chemically modified OSB to meet increasing market demands.

KEYWORDS

Borate, leaching, treated wood composites, stiffness, strength, swelling, termites

INTRODUCTION

The Formosan Subterranean Termites (FSTs) pose a growing threat to all structural wood materials in residential construction. The species is one of the most aggressive and voracious insects in the world, eating cellulose - a main component of wood material. FSTs cause over $1

billion structural damage per year in the United States, with a large portion of that in Louisiana (Henderson and Dunaway 1999, Ring1999.) Chemical treatments of wood members with chromated copper arsenate (CCA) and borate have been shown to be effective against the termites (Laks 1988, Barnes et al. 1989). Structural lumber and plywood can be successfully treated after manufacturing (e.g., pressure treatments with CCA). Structural composite panels such as oriented strandboard (OSB), however, cannot be pressure-treated once it is made into panel form due to its large swelling characteristics. The product is made of wood flakes glued with a thermal-setting resin. It is widely used as sheathing, flooring, and I-joist materials in light-frame wood construction, replacing more traditional plywood. Thus, alternative techniques for protecting OSB against FSTs have to be developed.

Work has been done to combine powder borate with wood flakes during the manufacturing of OSB to provide termite resistance of the finished products (Laks et al. 1988; Laks et al. 1991; Sean et al. 1999). However, information on the effect of wood species, borate type, borate particle size, initial borate content level, and other panel processing variables on long-term durability of borate-treated OSB is still missing. The information is highly desired for developing durable structural panels for residential construction using southern wood species.

This project was conducted to incorporate powder borate into OSB furnish in order to provide required biological performance characteristics of OSB. The objectives of this work were to investigate the effects of wood species, borate type and content on short-term loading stiffness and strength, swelling, water leaching, and biological performance of the product. Long-term structural performance of the modified OSB under sustained loading conditions is discussed in other related publications.

MATERIAL AND METHODS

Panel Manufacturing and Testing

Green boards from eight southern wood species were selected from a local sawmill in south Louisiana. These species included ash (Fraxinus spp.), cottonwood (Populus spp.), cypress (Taxodium distichum L.), elm (Ulmus americana L.), locust (R. pseudoacacia L.), pecan (Carya spp.), red oak (Quercus spp.), and southern pine (Pinus taeda L.). The boards were cross-cut into 152-mm sections, which were flaked to produce 76-mm long flakes using a disc flaker. The flakes were dried to 2-3% moisture content. They were screened to eliminate fines and stored in polyethylene bags until needed. The wood flakes were used to manufacture single species of OSB for zinc borate (ZB) and mixed hardwood and southern pine OSB for calcium borate (CB).

During the panel manufacturing, certain amounts of dry wood flakes, liquid phenol formaldehyde resin, wax, and borate were blended together. The loading rates for resin and wax were 4 and 1% based on the oven-dry wood weight. There were one type of zinc borate ($2ZnO3B_2O_33.5H_2O$) and two types of calcium borate ($Ca_2B_6O_{II}5H_2O$) with two different particle sizes. Both types of borate are considered as water insoluble at room temperature. The loading rates for zinc borate were 0 (control), 0.5, 1, and 3% based on dry flake weight in the panel. The loading rates for calcium borate were 0 (control), 0.75, 1.5, 3, and 4.5%. Several

single species panels with zinc borate were made with addition of PEG, $H(OCH_2CH_2)_{n>4}OH$, to study its effect on panel properties. The formed mats were hot pressed in a single opening press with the regulated platen temperature of 200°C for 5 minutes. The target thickness and panel density were 12.7 mm and 0.75 g/cm^3, respectively. Two replicate panels at each borate level were made. Samples were taken from each panel to test its chemical content. Each sample was ground to pass through a 20-mesh screen with a Wiley mill. Approximately 5 g oven-dry wood meal was extracted under acid condition for 2 hours at boiling temperature. After extraction, the wood meal was filtered out and the liquid filtrate was analyzed with an Inductively Coupled Plasma (ICP) spectrograph. The percent of boron in the sample was calculated based on the oven-dry weight of wood meal. The result was expressed as boric acid equivalent (BAE)

Tests were conducted to determine the panel's static bending stiffness and strength, internal bond (IB) strength, and thickness swelling (TS) according to the American Society for Testing and Materials standard D1037-96 (ASTM 1998). Water leaching experiments were done to evaluate the leachability of the modified products. Laboratory no-choice tests were conducted according to the American Wood Preservation Association (AWPA) Standard E1-97, Standard Method for Laboratory Evaluation to Determine Resistance to Subterranean Termites (AWPA 1997) to evaluate termite resistance of the products.

RESULTS AND DISCUSSION

Mechanical Properties

The specific modulus of elasticity (static bending modulus/sample specific gravity) was affected little at room condition (i.e., 5% moisture content at 70°F temperature) by borate up to the 3.5% BAE level (Figure 1A for zinc borate and Figure 2A for calcium borate).

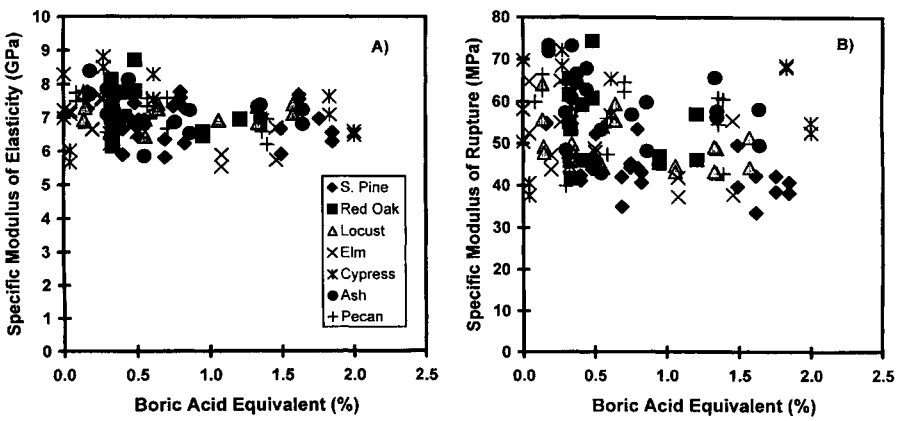


Figure 1. Bending Properties of Zinc Borate OSB (A: Bending Modulus of Elasticity/Specific Gravity and B: Bend Modulus of Rupture/Specific Gravity)

There was some reduction for the specific modulus of rupture (i.e., bending strength/sample specific gravity) at higher borate loading levels (Figure 1B for zinc borate and Figure 2B for calcium borate), indicating a negative effect of borate on panel strength. Wood species and borate type had an insignificant influence on both properties as shown in the graphs.

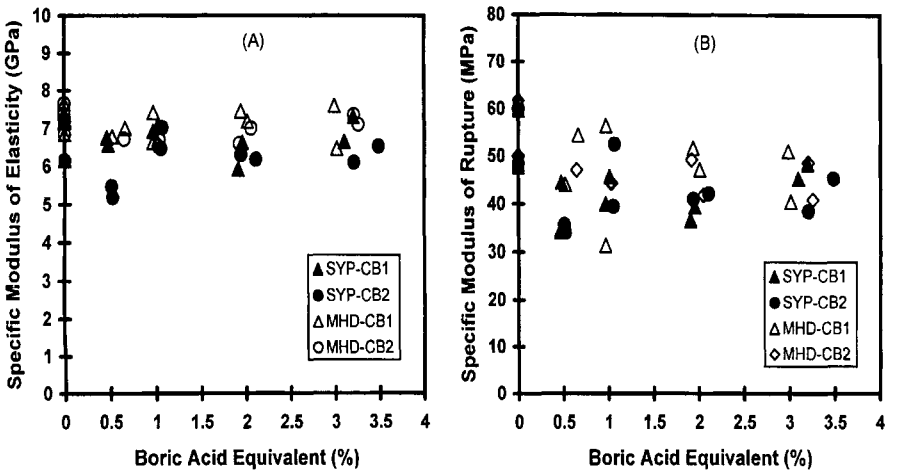


Figure 2. Bending Properties of Calcium Borate OSB (A: Bending Modulus of Elasticity/Specific Gravity and B: Bend Modulus of Rupture/Specific Gravity)

The effect of borate on the specific IB strength varied with borate type and wood species. Zinc borate generally showed less negative effects on the IB values (Figure 3A), compared with calcium borate (Figure 3B) for hardwood OSB. Southern pine OSB showed an IB reduction at higher BAE levels for both zinc and calcium borates. For calcium borate, the particle size had some influence on the IB strength. At a comparable BAE level, CB2, which had a smaller particle size, led to a higher IB strength compared with boards made of CB1, which had a larger particle size. For both types of borate, acceptable bending stiffness, strength, and IB values (based on the industry standard) can be achieved.

Physical Properties

Thickness swelling from the 24-hour water soaking (Figure 4) generally increased with borate content in the panel for both ZB and CB OSB, indicating a negative effect of borate on the panel properties under high moisture content levels. For the given exposure condition, ZB-modified OSB had a smaller TS than CB OSB at a comparable BAE level. Borate particle size had a significant influence on the swelling properties. Calcium borate with a larger particle size (CB1) had large TS, especially at the higher BAE levels. However, reducing the particle size of the chemical (CB2) helped bring the thickness welling to a stable and acceptable level (Figure 4B). Wood species had a large influence on TS for single species OSB with ZB. The single species hardwood OSB had relatively smaller TS.

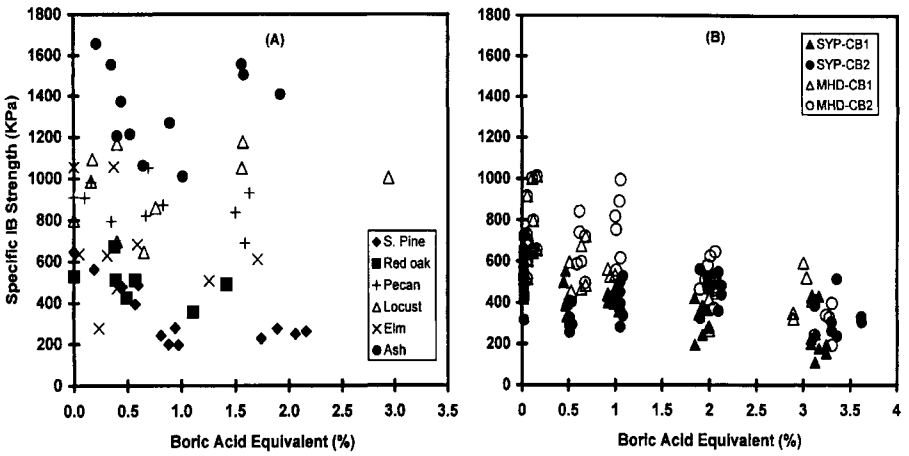


Figure 3. Internal Bond Strength of Zinc (A) and Calcium (B) Borate OSB. The Value Shown Represents A Ratio of Internal Bond Strength and Sample Specific Gravity.

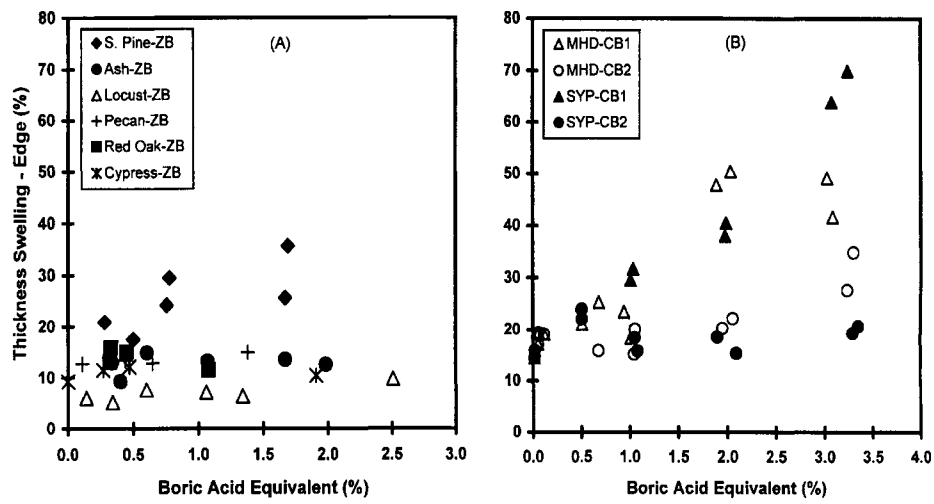


Figure 4. A Comparison of the 24-hour Water Soaking Thickness Swelling Properties of Zinc (A) and Calcium (B) Borate OSB.

A significant amount of borate leached out under the water soaking condition (Figure 5). The leaching of the OSB occurred upon the initial water exposure, and the leaching rate decreased as the leaching time increased. Wood species, borate type, initial BAE level, and sample TS

significantly influenced the leaching rate. This was due to a combined effect of water washing on the glueline under the swelling condition and decomposition of the borate to form a more water-soluble chemical (i.e., boric acid). Calcium borate with a smaller particle size (CB2) helped reduce sample thickness swelling and leaching rate. There was no consistent effect of polyethylene glycol (PEG) on zinc borate leaching. Thus, boron fixation with other chemical agents is necessary for borate-modified OSB under the extreme water exposure condition. Protection of the panel from direct water exposure can help reduce this problem significantly. A unified method specifying sample size and exposure condition for testing the leachability of treated wood composite materials is highly needed.

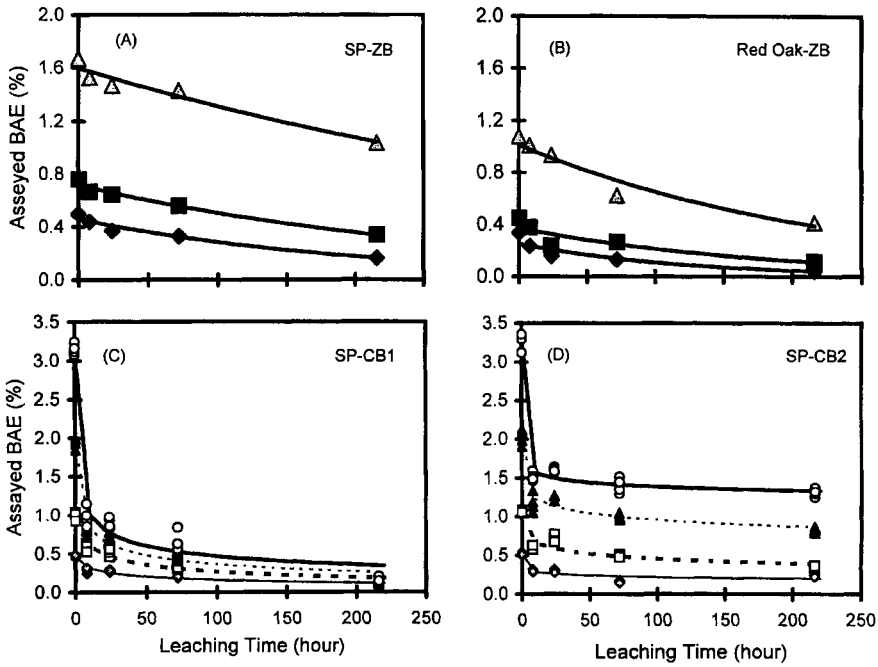


Figure 5. Leaching Properties of Zinc (A and B) and Calcium (C and D) Borate OSB.

Biological Performance

Laboratory no-choice termite tests indicated that both zinc and calcium borate modified OSB resisted FSTs well (Figure 6 and Table 1 for ZB OSB). As the borate loading increased, termite mortality rate (Figure 6A) increased and wood sample weight loss (Figure 6B) decreased. At the higher borate levels, there was little damage on wood samples, showing a significant deterring effect of boron on termites. The observed weight loss in these samples was due to loss of volatile materials in the samples. A similar behavior was seen for calcium borate OSB. Wood species showed an insignificant effect. There were strong correlations among the visual damage rating as

stipulated in the AWPA standards (AWPA 1997), wood sample weight loss, and termite mortality. The established correlations among the three variables allow predicting FST damage and mortality based on visual rating for treated OSB at various borate levels.

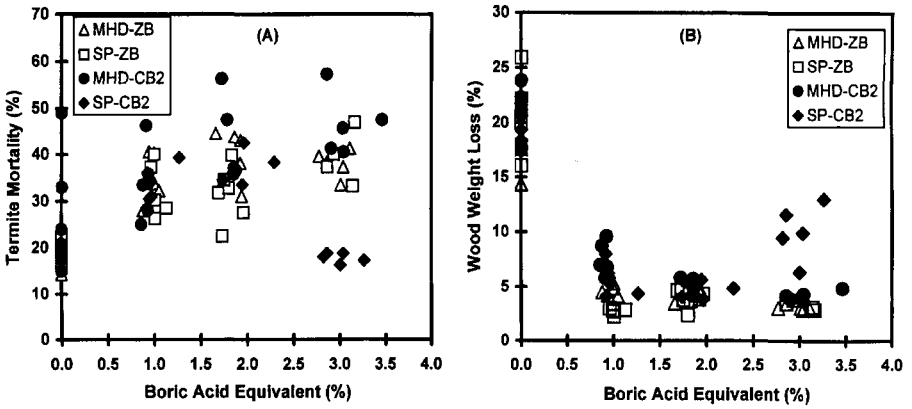


Figure 6. Termite Resistance Properties of Zinc and Calcium Borate OSB. A) Termite Mortality and B) Wood Sample Weight Loss.

Table 1. Results of Laboratory Termite Tests for Zinc-Borate Modified OSB from Southern Pine and Mixed Hardwoods.

Wood Species	Zinc Borate Weight [1] (%)	Sample Density (g/cm^3)	Visual Damage Rating [2,3] (1-10)	Wood Weight Loss (%)	Termite Mortality (%)
Mixed Hardwood	0	0.74	2.96c	16.48a	17.50b
	1.5	0.69	8.54b	4.58b	34.95a
	3.0	0.59	8.52b	4.17b	40.05a
	4.5	0.71	9.54a	3.08b	37.95a
Southern Pine	0	0.74	2.36c	21.02a	19.50b
	1.5	0.72	9.80a	2.70b	32.45a
	3.0	0.70	8.86b	3.84b	32.25a
	4.5	0.67	9.18ab	3.51b	37.00a

[1] Target weight percentage based on dry flake weight used for manufacturing the board.
[2] 1 showing the most amount of damage and 10 showing the least amount of damage.
[3] Each mean represents five replicates. Means within each column followed by the same letter are not significantly different based on the Tukey's multiple range tests at the 5% significance level.

CONCLUSIONS

Borate-modified OSB using southern wood species was manufactured and their performance characteristics were evaluated according to the industry test standards. The results of this study

indicated that termite-resistant structural OSB with desired mechanical and physical performance could be successfully developed with a right combination of wood species, borate type and content, and other processing variables. The results provide comparative properties between zinc and calcium borate modified OSB and an alternative treating method for structural OSB (i.e., using calcium borate). This technology will allow more OSB producers to manufacture chemically modified OSB to meet increasing market demands.

ACKNOWLEDGMENTS

This material is based upon work supported by the National Science Foundation under Grant No. 0080248. Any opinions, findings, and conclusions or recommendations expressed in this material are those of the authors and do not necessarily reflect the view of the National Science Foundation. The authors also wish to thank several wood products, resin, and chemical companies for their material and technical support.

REFERENCES

American Society for Testing Materials (ASTM). 1998. Standard test methods for evaluating properties of wood-based fiber and particle panel materials, D 1037-96a. Philadelphia, Pa.

American Wood Preservation Association (AWPA). 1997. Standard Method for Laboratory Evaluation to Determine Resistance to Subterranean Termites, E1-97. AWPA, Woodstock, MD.

Barnes, H.M., T.L. Amburgey, L.H. Williams, and J.J. Morrell. 1989. Borates as wood preserving compounds: The status of research in the United States. IRG/WP/3542. International Research Group on Wood Preservation, Stockholm.

Henderson, G., and C. Dunaway. 1999. Keeping Formosan termites away from underground telephone lines. Louisiana Agriculture 42:5-7.

Laks, P.E. 1988. Wood preservations – looking ahead. The Construction Specifier: 10:61-69.

Laks, P.E., B.A. Haataja, R.D. Palardy, and R.J. Bianchini. 1988. Evaluation of adhesives for bonding borate-treated flakeboards. Forest Prod. J. 38(11/12):23-24.

Laks, P.E., X. Quan, and R.D. Palardy.1991. The effects of sodium octaborate and zinc borate on the properties of isocyanate-bonded waferboard. In Proc. Adhesives and Bonded Wood Symposium (C.Y. Hse and B. Tomita, eds.) FPRS. PP. 44-57.

Ring, D. 1999. Need for integrated pest management of the Formosan Subterranean Termite. Technical Note, LSU Agricultural Center. 3 pp.

Sean, T., G. Brunnett, and F. Cote. 1999. Protection of oriented strandboard with borate. Forest Prod. J. 49(6):47-51.

TEAM PRESENTATION:

COMMISSIONING AND ENERGY MANAGEMENT

This Page Intentionally Left Blank

Advances in Building Technology, Volume 1
M. Anson, J.M. Ko and E.S.S. Lam (Eds.)
© 2002 Elsevier Science Ltd. All rights reserved

Re-commissioning of an Air Handling Unit

Cristian CUEVAS*, Jean LEBRUN*, Patrick LACÔTE, Philippe ANDRE**

*University of Liège – Laboratory of Thermodynamics
**Fondation Universitaire Luxembourgeoise – Department of Environmental Monitoring

1. Presentation of the building and HVAC system

The building, the Administrative Center of the Walloon Ministry of Equipments and Transport (CA-MET), is designed for a one thousand occupants and is made of 13 modules representing together 15 000 m^2 of gross floor area. Each module can be subdivided in three sections (figure 1, 2) :

1. The southern building
2. The atrium (or the interior street)
3. The northern building



Figure 1 : General view of the CA-MET in Namur, Belgium

The division appears different for the central module, which constitutes a "welcome area" for the whole building. Most of the useful area of the building consists in offices distributed on four rows (two in each building, separated by a corridor) and three to five levels.

The CA-MET building is characterized by a complex HVAC plant made of the following components:

- Centralized production of heating and cooling using :
  - 3 boilers (operating in cascade)
  - 2 chillers (reciprocating compressors with air condensers) situated at both ends of the building

- Heating and cooling power is distributed through collectors to 14 substations (figure 4). Most of the substations, divided in northern and southern parts are feeding two building modules. In each substation, distribution of heat is organized from local collectors who are feeding the different entities connected thereto.

- In each substation, the AHU's feeding the offices and the atrium are connected to each other in that a fraction of the air extracted from the offices is ventilated in the atrium. The part that is not injected in the atrium AHU's is re-circulated in the offices or extracted through the toilets. Ventilation in the atrium is happening at constant flow rate (CAV system) while ventilation in the offices is made through a VAV system. A constant fresh air flow rate is furthermore provided in the office. Figure 2 shows a schematic diagram of a coupled offices-atrium AHU. Some rooms (meeting-rooms) are provided with fan-coils which ventilate air, pre-heated at 20° C.

- ´ The Air Handling Units are made of the following components: mixing box, filter, heating coil, cooling coil (not present in the fan coils AHU's), humidifier, fan

- Energy is distributed in the room by means of radiators (heating) and VAV boxes (cooling and ventilation). Thermostatic valves or VAV terminals provide a local control.

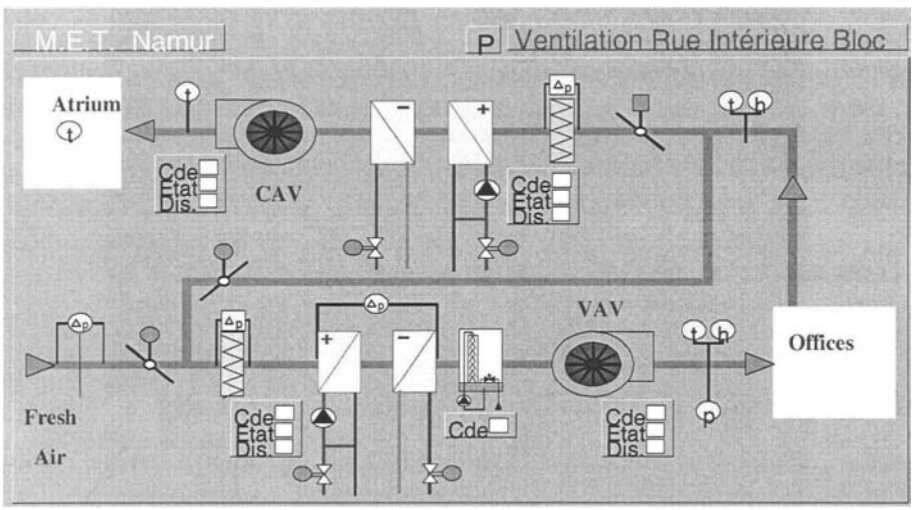


Figure 2 : Schematic of typical offices-atrium AHU's.

The Building Energy Management system is controlling both the Air Handling Units and the radiators heating circuits. For AHU's, the strategy consists in controlling the valve of the heating or cooling coil in order to modify the supply air temperature according to the return air and the outside air temperature conditions.
The control is thus performed following two steps :
- Return temperature set point calculation (including summer weather compensation)

- Supply air temperature set point calculation from the difference between return temperature measurement and its set point (including winter weather compensation).
- Valves signal control (by a classical PI algorithm).

In order to assume a minimum air flow rate into the offices whatever the opening of the VAV terminals, speed of the fan is regulated in order to keep a constant static pressure at the its outlet.

For radiators heating circuits, control is changing the water flow rate depending upon both the external conditions (temperature) and the internal climate (reflected by a room temperature sensor).

2. MEASUREMENTS

The AHU studied was the GP Bs1, which supplies air to the modules B and C. Figure 2 shows a schematic of the AHU, which supplies an airflow rate varying between 8600 and 18900 m^3/h.

A constant part of this air flow rate (3400 m^3/h) is fresh air; the (variable) remaining part is recirculation air. The non-recirculated part of the air, extracted from the offices, is used to feed the atrium AHU GP Bs2.
During the tests presented here, the AHU GPBSs2 was cut off, in order to make easier the study only the performance of GPBs1.

In air side, the following variables were measured:

ΔP_{hx} : Pressure drop through the heat exchangers, Pa
$P_{st,AHU}$: AHU exhaust air static pressure, Pa
$T_{exhaust\ AHU}$: AHU exhaust air temperature, °C

Movable pressure transducers were installed in parallel with existing ones. Their locations are indicated in Figure 3 . It can also be seen in that figure that the static pressure used by the fan control ($P_{st,AHU}$) is located just after an elbow.

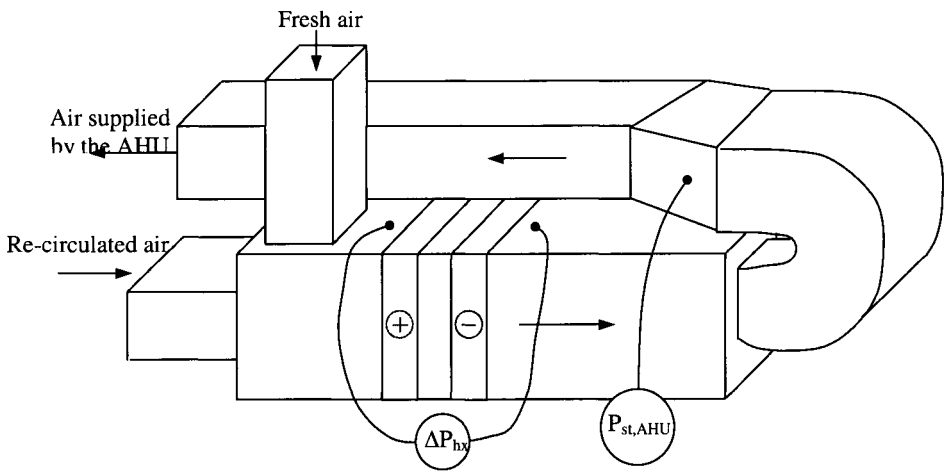


Figure 3: Location of the pressure sensors

In the water side, the movable measuring points were:

$T_{w,su,cc,GPBs1}$: Cooling coil supply temperature GPBs1, °C

$T_{w,ex,cc,GPBs1}$: Cooling coil exhaust temperature GPBs1, °C

$M_{w,cc,GPBs1}$: Cooling coil water mass flow rate, kg/s

The cooling coil water flow rate was measured using transit time flow meter, which was located just after the derivation of the main water network to the cooling coil.

3.RESULTS AND ANALYSIS OF THE MEASUREMENTS

3.1.Air handling unit fan control performance

The air handling unit fan control regulates the AHU exhaust pressure. It must stay constant at the set point fixed by the monitoring system, which ensures a good performance of the terminal units. In this case, it was fixed to 400 Pa.

Figure 4 and 5 show an example of test made in order to check the fan control system.

At the beginning of the test the AHU return temperatures is 21 °C.

At 14:13 h the radiators are turned on in order to heat the offices of the modules B and C. After 2 hour 40 min. the return temperature has only increased of 3 K, which is not yet enough for the test considered.

In order to speed-up the temperature increase, the fresh air valve is closed at 15:50 h and then the heating coil of the AHU is opened to 100 % at 16:35 h.

Due to the temperature increase, all VAV boxes are opening in such a way to increase the airflow rate, which makes that the fan speed has also to increase, in order to cope with the exhaust pressure set point, as it can be seen in Figure 4. According to the results shown in Figure 5, the fan control is able to keep the value fixed by the monitoring system.

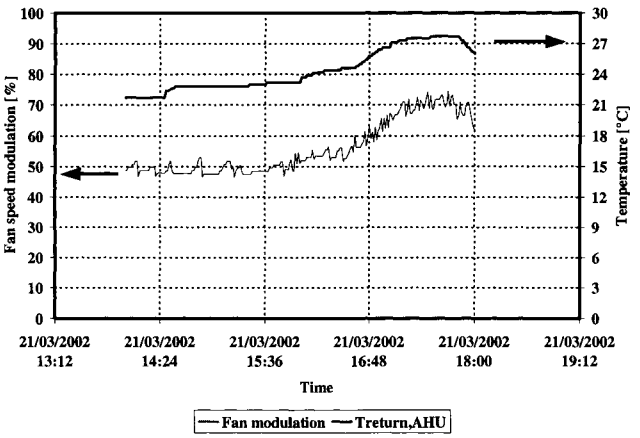


Figure 4: AHU fan control performance

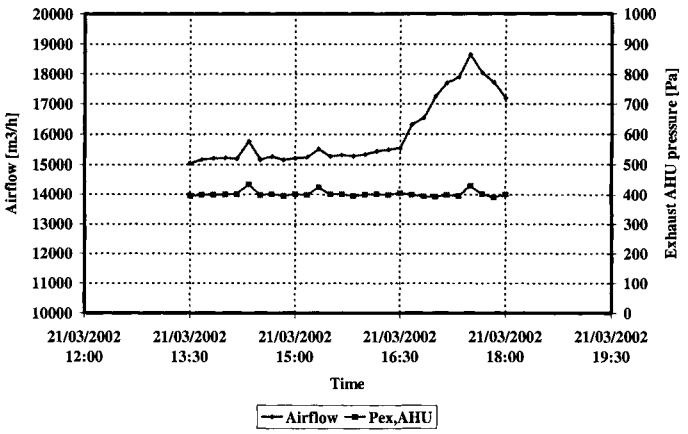


Figure 5: Fan speed modulation

3.2 Air handling unit cooling coil performance

The cooling coil imposes the exhaust AHU temperature. This heat exchanger works with a variable water flow, controlled by a solenoid valve. It regulates the water flow rate to keep the AHU exhaust temperature at the value fixed by the monitoring system. In this case, the law imposed by the monitoring system is calculated according to the AHU return temperature, as

shown in Figure 6. In the actual case, the control is working without seasonal compensation because of the external temperature is lower than 20°C (Andre et al. 2000).

According to the measurements, when the AHU return temperature is higher than 22 °C, the set point of the AHU exhaust temperature is 14°C. For AHU return temperatures between 20 and 22°C, there is a linear relationship between the control temperature and the return temperature. At return temperatures lower than 20°C the control temperature is fixed at 35 °C.

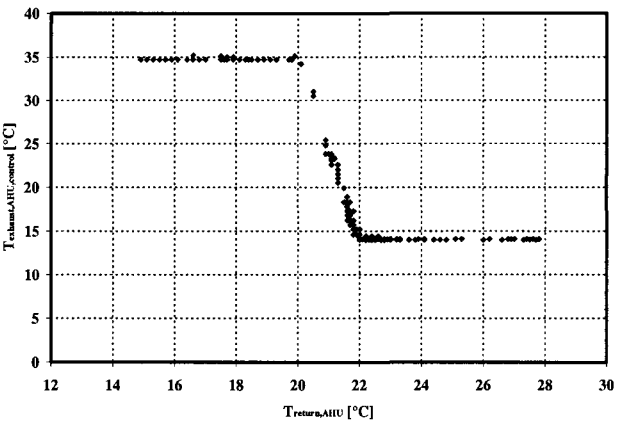


Figure 6: Control law of the AHU exhaust temperature

Time variations of temperatures and water flow rate are presented in Figure 7.

The solenoid valve modulates the water flow rate between 0 and 5.4 l/s (nominal value).

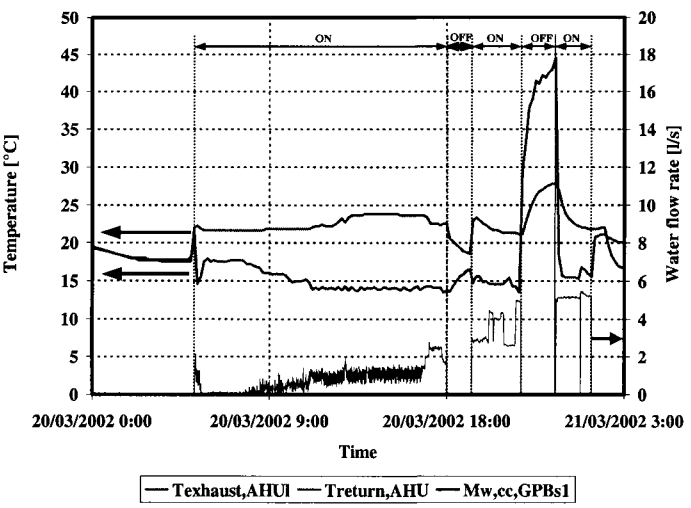


Figure 7: Modulation of the water mass flow in the cooling coil

The cooling coil model proposed by Ding et al. (1991) was used to verify the performance of the heat exchanger. The model has two parameters to be identified: the water and the air side heat transfer coefficients respectively. The identification was done in this case on the basis of cooling coil capacities *given by the manufacturer*. A total of 60 data points were used in this identification. All the values given by the manufacturer correspond to wet regime. The water flow rates and air flow rates covered by these points are shown in Figure 8. The two dry steady state regimes (point 1 and 2) selected from the recordings are also indicated.

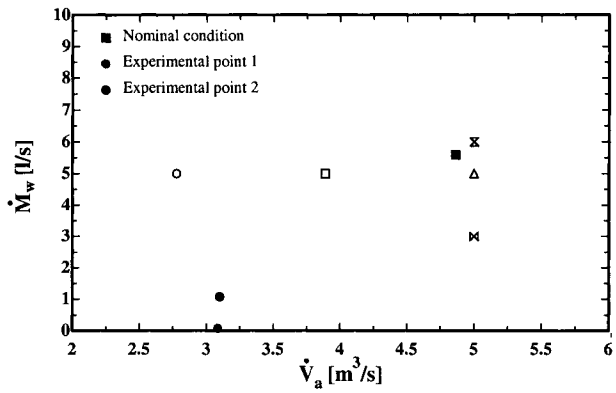


Figure 8: Range covered by the manufacturer data

The results of this modeling are presented in Figure 9: most of the values are predicted with an accuracy of ±7 %, except for two points, where the error reaches -12 %. One of these two points was not included in the regression analysis: it is the nominal regime.

No further parametric adjustment was done; the model was then supposed to underestimate the nominal cooling.

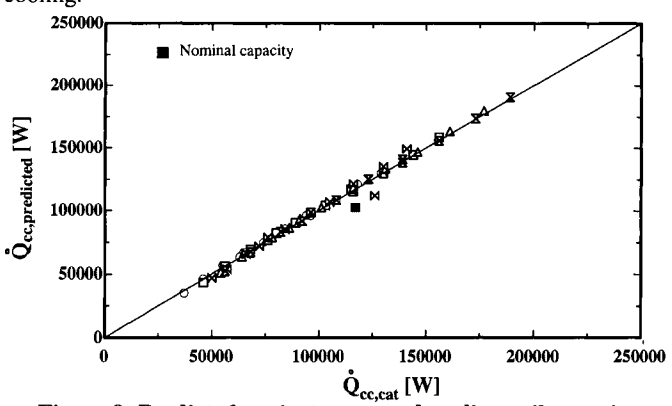


Figure 9: Predicted against measured cooling coil capacity

Table 1 gives the results of the modeling for the two steady state periods already selected. Cooling powers are predicted (in dry regime), with errors of -0.2 and +7 %, respectively. This agreement is very good. But it has to be so for the first regime: when one of the capacity flow rate is very low, the heat exchanger effectiveness has to stay very near to 100 % and there is no more room for any simulation mistake!

The second point is still satisfactory, but an error analysis should still be made in order to estimate the corresponding heat transfer coefficient uncertainty.

We may conclude that the cooling coil performances are in the expected range, but other tests at higher power would be welcome in order to confirm this diagnosis.

Table 1 Cooling coil capacity

Point	$\dot{Q}_{cc,measured}$ [W]	$\dot{Q}_{cc,model}$ [W]
1	3677	3671
2	23890	25603

4. CONCLUSIONS

The commissioning of the AHU permits us to conclude that the summertime problem of high temperatures is probably not due to bad performances of the AHU.

This was verified in different ways:

- The air supplied for the AHU corresponds to the design value and the fan control performance is good;
- The AHU exhaust temperature was always kept to the set point value, which confirms the good performance of the cooling coil, at least in the conditions considered.

Other tests should still be done at higher cooling powers to confirm these results.

In the mean time, the commissioning of the central control system has shown that the air pressure set point was fixed to a much too low value, making impossible a satisfactory behavior of the VAV boxes, but that is another story...

5. REFERENCES

Andre, Ph.; Lacôte, P.; Lebrun, J.; Dewitte, J.; Georges, B. "QG-MET building in Namur: Identification of typical errors, evaluation of their influence on energy consumption using simulation and proposals for automatic detection". IEA Annex 34 working document, Liège meeting, April 2000.

Ding X., Eppe J. P., Lebrun J. and Wasacz M. 1991. "Cooling Coil Models to Be Used in Transient and/or Wet Regimes. Theoretical Analysis and Experimental Validation". System Simulation in Building, December 3-5, pp. 405-441.

This Page Intentionally Left Blank

Advances in Building Technology, Volume 1
M. Anson, J.M. Ko and E.S.S. Lam (Eds.)
© 2002 Elsevier Science Ltd. All rights reserved

AUTOMATED COMMISSIONING OF AIR-HANDING UNITS USING FUZZY AIR TEMPERATURE SENSORS

P.S. Lee and A.L. Dexter

Department of Engineering Science, University of Oxford, Oxford, OX1 3PJ, UK

ABSTRACT

Measurement errors can result in faults being incorrectly diagnosed during commissioning. One of the main causes of errors is the use of a single or multi-point sensor to measure the average value of a spatially distributed variable whose distribution changes at different operating conditions. In such cases, the problem is not the accuracy of the sensor itself, but estimation bias. The paper describes a new approach to automating the commissioning of air-handling units based on the use of fuzzy air-temperature sensors whose outputs indicate the measurement uncertainties. The fuzzy sensors are developed from data obtained by simulating the air temperature and flow around the sensing element(s) using a computational fluid dynamics package. The data obtained during commissioning are analysed automatically using generic fuzzy reference models, which describe the behaviour of the air-handling unit when it is operating correctly and when particular faults are present. To assess the benefits of using the fuzzy sensors, automated commissioning tests are performed on the cooling coil subsystem of an air-handling unit. Experimental results are presented, which show that the use of a fuzzy mixed air temperature sensor can reduce the number of false alarms and lead to a more precise diagnosis of any faults.

KEYWORDS

Bias errors, fuzzy sensors, fault diagnosis, automated commissioning, air-conditioning systems

INTRODUCTION

For some time, there has been interest in automating the process of commissioning HVAC control systems, Dexter et al. (1993). Early work, Haves et al. (1996), demonstrated that data collected during manually controlled commissioning tests could be analysed using expert rules. An automatic commissioning tool, which analyses the test data using a model-based fault diagnosis scheme, has also been developed, Ngo & Dexter (1998).

Schemes for automating the commissioning of air-handling units (AHUs) are usually based on measurements provided by the temperature and flow sensors, which are connected to the building

energy management and control system. The accurate measurement of the average temperature of the air flowing down a large duct is extremely difficult as there can be significant variations in the temperature and velocity over the cross-section of the duct, Carling & Isakson (1999). Errors arising from the spatial variations are difficult to avoid, particularly if the spatial distribution changes with operating conditions, because the problem is not the accuracy of the sensor itself but estimation bias. Such errors can result in either low sensitivity to faults, imprecise diagnosis or unacceptably high false alarm rates. The presence of these measurement errors is one of the main barriers to the practical application of schemes for automatically commissioning air-conditioning systems, Dexter & Pakanen (2001).

A measurement of the mixed air temperature is often used when commissioning the sub-systems of AHUs. This measurement is particularly problematic because space restrictions often result in the mixed air temperature sensor being located very close to the outlet of the mixing-box where there can be significant stratification, Robinson (1999). Even commercial averaging sensors can produce large errors if they are used downstream of a mixing-box, Lee & Dexter (2001b).

A number of ways of dealing with sensor bias have been proposed. The sensor bias can be estimated and eliminated, Wang & Wang (1999). This approach requires a large number of temperature and flow sensors to be installed, assumes that the bias is constant or slowly varying and is computationally demanding. Alternatively, the detection threshold can be adjusted to take sensor bias into account. The main difficulty of this approach is the selection of an appropriate value for the threshold, Carling (2002). Too high a value reduces the fault sensitivity too much; too low a value causes too many false alarms. The effects of sensor bias can be incorporated into the reference models used by the diagnosis scheme, Lee & Dexter, (2001a). This approach avoids false alarms but can produce highly ambiguous results, especially if a constant, worst-case, bias is assumed, Ngo & Dexter (1999). Another approach is to use other available measurements to estimate the measured variable, Lee et al. (1997). The main weakness of this approach is that estimates based on the outputs of other sensors may exhibit even greater bias because the estimation will be sensitive to modelling errors as well as the biases on the other sensors.

There is widespread interest in the development of smart sensors, which make better use of other sources of information and provide an indication of their accuracy and reliability. Previous work has shown that the fusion of measurements and *a priori* information can reduce measurement errors, Filippidis (1996). Sensor fusion is an attractive option in this area of application because many other sources of information are already available through the building energy management system. Fuzzy approaches to sensor fusion, Mauris et al. (1996), have been shown to have particular strengths in complex and highly uncertain systems, Perrot et al. (1996).

The paper describes a new approach to automating the commissioning of air-handling units based on the use of a fuzzy mixed air temperature sensor. The fuzzy sensor, Schodel (1994), is developed using a fuzzy identification scheme and training data obtained by simulating the air temperature and flow around the sensing element(s) with a computational fluid dynamics package. The fuzzy sensor removes the bias errors and provides an indication of the uncertainty associated with the air temperature measurement at the current operating conditions. Sensor fusion is used to reduce the measurement uncertainty. Fuzzy reference models, which take account of sensor bias, are identified using the output from the fuzzy sensor together with training data generated by both CFD and conventional lumped-parameter simulations. The reference models, which provide a semi-qualitative description of the plant behaviour when it is fault-free and when particular faults are present, are incorporated into a fuzzy model-based fault diagnosis scheme, Dexter & Ngo (2001). The results of automated commissioning tests performed on a laboratory test rig are presented.

DEVELOPMENT OF A FUZZY MIXED-AIR TEMPERATURE SENSOR

A CFD package is used to simulate, in two dimensions, the mixing of two air streams in a mixing-box for a range of outside and return air temperatures, positions of the sensor and positions of the dampers in the mixing-box. A fuzzy model, which relates the true mixed air temperature to the output from a six-point averaging sensor mounted downstream of the mixing-box, is identified using a fuzzy identification scheme, which takes "frequency of occurrence" into account, Ridley et al. (1988), and simulation data obtained at a wide range of the operating conditions. Figures 1 to 2 show the output generated by the fuzzy sensor at two different measured temperatures (287K and 292K).

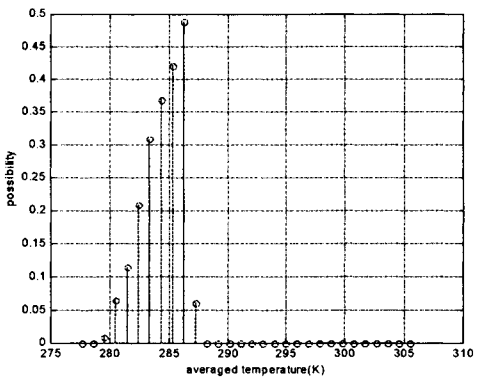


Figure 1: Fuzzy sensor output when the measured mixed air temperature is 287K

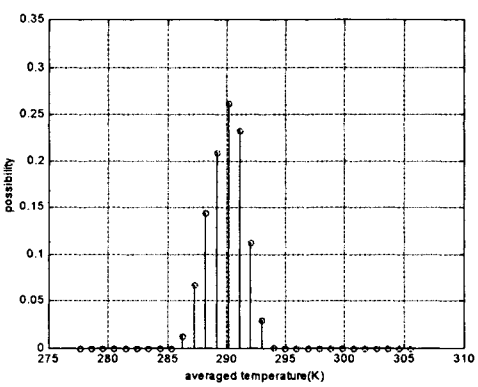


Figure 2: Fuzzy sensor output when the measured mixed air temperature is 292K

The results show that there is significant uncertainty associated with the estimate of the average temperature in both cases and that the averaging sensor generates a biased estimate of the mixed air temperature.

A version of the fuzzy sensor, which uses the return damper position as an auxiliary input, has also been developed to reduce the levels of uncertainty associated with estimating the average mixed air temperature. The results of an earlier study showed that the size of the bias error is related to the position of the dampers, Lee & Dexter (2001a). Figures 3 to 5 show the output generated by the fuzzy sensor for three different positions of the return dampers when the measured temperature is 287K.

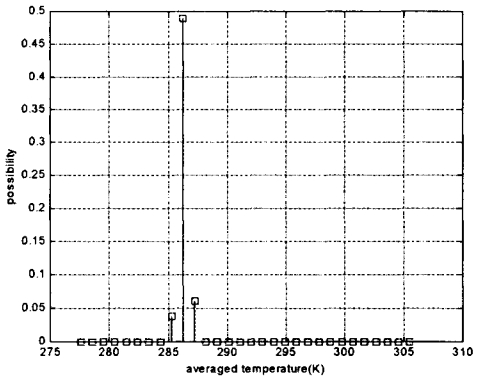


Figure 3: Fuzzy sensor output when the measured mixed air temperature is 287K and the return damper angle is 20 degrees

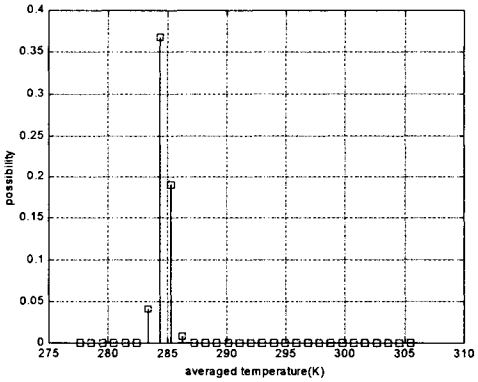


Figure 4: Fuzzy sensor output when the measured mixed air temperature is 287K and the return damper angle is 45 degrees

The results demonstrate that knowledge of the damper angle reduces the uncertainty associated with estimating the average mixed air temperature, when the return damper is less than half open. The results also show that the uncertainty and the bias vary with damper angle.

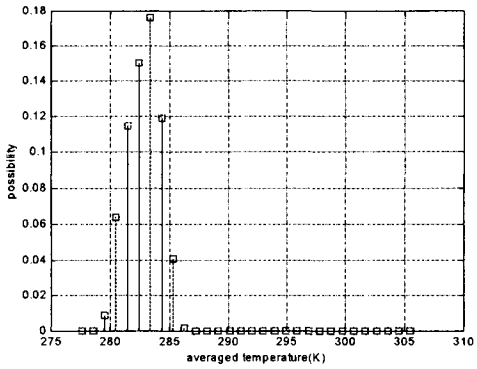


Figure 5: Fuzzy sensor output when the measured mixed air temperature is 287K and the return damper angle is 70 degrees

GENERATION OF THE REFERENCE MODELS

The test data collected during commissioning are analysed by comparing the observed behaviour to the behaviour predicted by a set of fuzzy reference models. The fuzzy reference models relate the temperature difference across the coil to the position of the control valve, the air flow rate, and the on-coil air temperature and humidity. The mixed air temperature sensor is used as a proxy for the on-coil air temperature.

The reference models are identified using training data obtained from a lumped-parameter model of the chilled water, cooling coil subsystem and from the output of the fuzzy mixed air temperature sensor. To obtain generic reference models, which can be used for commissioning a class of chilled-water cooling coils, nine different designs of cooling coil subsystems are simulated over a range of operating conditions, when there are no faults present and when various faults have occurred, Dexter & Ngo (2001). The output of the fuzzy mixed air temperature sensor is combined with the data obtained from the cooling coil simulations using the following procedure. Data from the CFD simulation of the mixing-box is used to identify those values of the mixed air temperature measured by the averaging sensor that correspond to the particular value of the average mixed air temperature used in the lumped-parameter simulation. The outputs of the fuzzy sensor, which correspond to the largest and smallest values measured by the averaging sensor, are then included in the training data.

COMMISSIONING THE COOLING COIL SUBSYTEM IN AN AIR-HANDLING UNIT

The commissioning tests are performed on the cooling coil subsystem of the laboratory air-handling unit shown in Figure 6. During the commissioning test, the cooling coil valve is automatically stepped through a pre-specified series of values from its fully closed to its fully open position. The commissioning software checks whether steady-state operating conditions have been achieved before it moves on to the next step in the sequence, Ngo & Dexter (1998). The test is performed for two different positions of the mixing-box dampers: when the recirculation damper is nearly closed (return damper angle = 18°) and when it is half open (return damper angle = 45°). The AHU operates at its full design air flow rate throughout the tests. The mixed air temperature, which is used as a proxy for the

on-coil temperature, is measured using either a commercial averaging sensor or the fuzzy sensor with the auxiliary input (the return damper angle). A commercial averaging sensor is used to measure the supply air temperature, which is used as a proxy for the off-coil air temperature. The on-coil relative humidity is assumed to be 50% as no measurement was available. Six fuzzy reference models are used for the diagnosis: correct operation (no faults), leaky valve, fouled coil, valve stuck closed, valve stuck midway and valve stuck open. Tables 1 to 3 show the results obtained from the automated commissioning tests for two different positions of the mixing-box dampers. The symbol " c " indicates correct operation; " f " indicates fouled coil; " l " indicates leaky valve; " cf " indicates either correct operation or fouled coil; " cl " indicates correct operation or leaky valve; and "cfl" indicates either correct operation or fouled coil or a leaky valve.

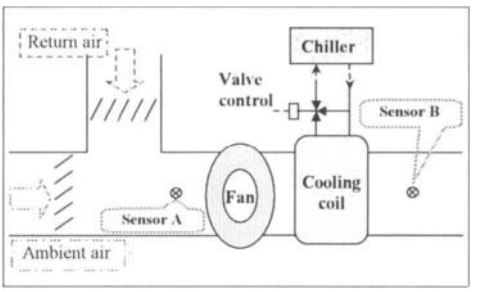


Figure 6: The air-handling unit.

The results of the commissioning test using the fuzzy sensor to measure the mixed-air temperature are analysed using the generic reference models of the cooling coil subsystem described in the previous section (reference models A). The reference models do not take the damper angle into account. When the commercial averaging sensor is used to measure the mixed-air temperature, the reference models are trained using data obtained only from the lumped-parameter simulation. It is assumed either that there are no bias errors (reference models B) or that the bias errors are less than $\pm 2^{o}C$ (reference models C).

TABLE 1
RESULTS OF AN AUTOMATED COMMISSIONING TEST IN AN OCCUPIED BUILDING WHEN NO FAULTS WERE PRESENT

Mixed Air Temperature Measurement	Reference Models	Return Damper Angle	
		18°	45°
		Largest Least Ambiguous Belief	
Fuzzy Sensor	A	cf 2.6%	cf 3.9%
Averaging Sensor	B	cf 0.4%	cl 2.6%
Averaging Sensor	C	cfl 63.3%	cfl 71.0%

Table 1 shows the results obtained when no faults were present in the cooling coil subsystem. When the return damper is nearly closed, the use of the fuzzy sensor produces slightly higher levels of belief in correct operation or fouled coil compared to diagnosis based on the averaging sensor and the type B reference models. The results are less ambiguous than those produced by diagnosis based on the averaging sensor and the type C reference models at both damper angles.

Table 2 shows the results obtained when the cooling coil control valve was leaking (20% of the valve control signal). At both positions of the return damper, the use of the fuzzy sensor results in lower values of belief in a leaky valve than are obtained using the averaging sensor and the references models that assume there is no sensor bias (type B reference models). However, when the damper is nearly closed, the fuzzy sensor does produce a far less ambiguous result than is obtained with the averaging sensor and type C reference models.

TABLE 2
RESULTS OF AN AUTOMATED COMMISSIONING TEST IN AN OCCUPIED BUILDING WHEN THE COOLING COIL CONTROL VALVE WAS LEAKING

Mixed Air Temperature Measurement	Reference Models	Return Damper Angle	
		18°	45°
		Largest Least Ambiguous Belief	
Fuzzy Sensor	A	l 2.1%	l 5.7%
Averaging Sensor	B	l 2.6%	l 22.1%
Averaging Sensor	C	cfl 16.8%	l 5.6%

The size of the bias errors depends on the difference between the return air temperature and the ambient air temperature. If commissioning takes place when the building is unoccupied and the cooling load is negligible, the return air temperature will be lower, and the effect of the bias errors on the results will be greater. Table 3 shows the results of an automated commissioning test when no faults were introduced into the cooling coil subsystem and the building was unoccupied. The use of the fuzzy sensor avoids the false alarm, which is generated when the return damper is nearly closed and the averaging sensor and the type B reference models are used. The results of the diagnosis using the fuzzy sensor are less ambiguous than those, which are obtained with the averaging sensor and the type C reference models, when the return damper is half open.

TABLE 3
RESULTS OF AN AUTOMATED COMMISSIONING TEST IN AN UNOCCUPIED BUILDING WHEN NO FAULTS WERE PRESENT

Mixed Air Temperature Measurement	Reference Models	Return Damper Angle	
		18°	45°
		Largest Least Ambiguous Belief	
Fuzzy Sensor	A	cf 8.5%	c 0.3%
Averaging Sensor	B	f 0.4%	cl 0.9%
Averaging Sensor	C	cf 9.8%	cfl 36.2%

CONCLUSIONS

Fuzzy sensors can eliminate bias errors and provide an indication of the uncertainty associated with air temperature measurements in ducts. Automated commissioning of AHUs based on fuzzy air temperature sensors can reduce the number of false alarms or result in a more precise diagnosis. However, bias errors can sometimes increase the belief in a fault. For example, when the measured mixed air temperature is larger than the actual mixed air temperature, and the valve is leaking, the apparent temperature difference across the coil will be larger than expected and the evidence of a leaky valve will be greater.

Acknowledgements

Miss P S Lee would like to acknowledge the financial support provided by the Rhodes Trust.

References

Carling P. and Isakson P. (1999). Temperature Measurement Accuracy in an Air-handling Unit Mixing Box. Trans. 3rd International Symposium on HVAC, ISHVAC '99. Shenzhen, PRC, 922-928.

Carling P. (2002). Comparison of Three Fault Detection Methods based on Field Data of an Air-Handling Unit. *Trans. ASHRAE* 108:1.

Dexter A.L, Haves P. and Jorgensen D.R. (1993). Automatic Commissioning of HVAC Control Systems. CD ROM of technical papers presented at Clima 2000 World Congress, London, UK.

Dexter A.L. and Ngo D. (2001). Fault Diagnosis in HVAC Systems: a Multi-step Fuzzy Model-based Approach. *Int. J. of HVAC&R Research* 7:1, 83-102.

Dexter A.L. and Pakanen J. (2002). Demonstrating Automated Fault Detection and Diagnosis Methods in Real Buildings. *VTT Building Technology*, Finland.

Filippidis A. (1996). Data Fusion using Sensor Data and A Priori Information.*Control Engineering Practice* 4:1, 43-53.

Haves P., Jorgensen R., Salsbury T.I. and Dexter A.L. (1996). Development and Testing of a Prototype Tool for HVAC Control System Commissioning. *Trans. ASHRAE* 102:1, 483-491.

Lee P.S. and Dexter A.L. (2001a). Generating Fuzzy Reference Models for Fault Diagnosis when Sensor Bias is the Main Uncertainty. Proc. UK Workshop on Computational Intelligence, Edinburgh, 28-34.

Lee P.S. and Dexter A.L. (2001b). A Fuzzy Approach to Fault Diagnosis in the Presence of Sensor Bias. Proc. IEEE Conference FUZZ'01, Melbourne, Australia.

Lee W-Y, Park C., House J.M and Shin D.R. (1997). Fault Diagnosis and Temperature Sensor Recovery for an Air-handling Unit. *Trans. ASHRAE* 103:1.

Mauris G., Benoit E. and Foulloy L. (1996). The Aggregation of Complementary Information via Fuzzy Sensors. *Measurement* 17:4, 235-249.

Ngo D. and Dexter A.L. (1998). Automatic Commissioning of Air-conditioning Plant, Proc. Control '98, IEE Conf. Pub. 455:2, 1694-1699.

Ngo D. and Dexter A.L. (1999). A Robust Model-based Approach to Diagnosing Faults in Air-handling Units. *Trans ASHRAE* 105:1.

Perrot N., Trystram G., Le Guennec D. and Guely F. (1996). Sensor Fusion for Real-time Quality Evaluation of Biscuit during Baking. Comparison between Bayesian and Fuzzy Approaches. J. *of Food Engineering* 29, 301-315.

Ridley J.N., Shaw I.S. and Kruger J.J. (1988). Probabalistic Fuzzy Models for Dynamic Systems. *Electronic Letters* 24:14, 890-892.

Robinson K.D. (1999). Mixing Effectiveness of AHU Combination Mixing/Filter Box with and without Filters. *Trans. ASHRAE* 105:1.

Schodel H. (1994). Utilization of Fuzzy Techniques in Intelligent Sensors. *Fuzzy Sets and Systems* 63, 271-292.

Wang S.W. and Wang J.B. (1999) Law-Based Sensor Fault Diagnosis and Validation for Building Air-conditioning Systems, *Int. J. of HVAC&R Research* 5:4, 353-378.

Advances in Building Technology, Volume I
M. Anson, J.M. Ko and E.S.S. Lam (Eds.)
© 2002 Elsevier Science Ltd. All rights reserved

MODELING OF PACKAGE AIR-CONDITIONING EQUIPMENT

M.Reichler[1] J.W. Mitchell[2] W. A. Beckman[2]
[1] Graduate student, Solar Energy Laboratory
[2] Professor, Mechanical Engineering Department
University of Wisconsin, Madison, Wisconsin, 53717, USA

ABSTRACT

A model for package air-conditioning units that can accurately replicate equipment performance data is described in this paper. The model is suitable for use in building energy simulation programs. The performance of each component is described with mechanistic models using the Engineering Equation Solver (EES) software package (Klein and Alvarado (1999). Generally available manufacturer catalog data are employed to determine the model parameters. Using characteristic parameters based on manufacturer's performance data allows extrapolation of performance data to different operating conditions. The method has been successfully used to predict the full load performance of package air-conditioning systems over the range of operating conditions.

KEYWORDS: Air-conditioning, modeling, performance, prediction, simulation

INTRODUCTION

In the design of an air-conditioning system it is important to evaluate the energy performance of different alternatives. Computer simulations are a convenient method, but models that predict the performance under all operating conditions are required. The goal of this paper is to describe a model of a package air-conditioning system that is suitable for use in such simulations. The model uses available manufacturer catalog data to allow extrapolation over a wide range of operating conditions.

Package air-conditioning systems and central air-conditioning systems are both used in buildings. Typically, central air-conditioning systems are used for large buildings and package units for small buildings or zones. Package air conditioners, which are self-contained units that provide the cooling, heating, and circulation of the conditioned air, are the subject of this work. The cooling of the airflow is provided by a vapor compression cycle using either a reciprocating or scroll compressor. The cooling coils are direct expansion coils in which the refrigerant directly cools the circulating air. The condenser is air-cooled. The components in package units from different manufacturers are basically the same, which allows a general model to be developed. The available cooling capacity of common package units ranges from about 10 to 1000 kW and the circulation airflow rate covers a range from 400 to 40,000 l/s. Package units are equipped with a supply fan and, if needed, an additional return air fan. Thus, package units cover a wide range of applications.

Manufacturers of package air-conditioning units supply catalogs that contain detailed performance information. The total cooling capacity, the sensible cooling capacity and the power draw are given as functions of ambient temperature and return air temperature and humidity, and volumetric flow rate of the supply air. The model that is developed uses this generally available catalog information together with separate catalog information for the compressor that includes the refrigerant flow rate and power draw as a function of inlet and outlet pressure.

In developing the system model, the different components of a standard air-conditioning system (compressor, evaporator, condenser, and expansion valve) were modeled. One modeling approach considered was the use of polynomial curve fits. Although the characteristics of a component are readily represented with this method, the resulting equations have no physical meaning and prediction outside the range of the fitted data may be inaccurate. Engineering models that describe the behavior of a component were also considered. However, these require detailed knowledge on many parameters such as the geometric specifications, fin efficiencies, and other quantities that are not generally given in manufacturer catalogs. A semi-mechanistic modeling technique was therefore chosen in order to avoid the problems of uncertain extrapolation and to utilize the available information. Models for the components were developed that contain the basic engineering relations underlying the performance, with values of the parameters obtained by fitting the model to the catalog data.

COMPONENT MODELS

A single stage vapor compression cycle, consisting of a compressor, condenser, expansion valve, and evaporator, was used as the basis for the model. It was assumed that the refrigerant leaving the evaporator was saturated vapor and the refrigerant leaving the condenser was saturated liquid. With these assumptions the thermodynamic state points were calculated using basic engineering principles.

Compressor Model

The power and mass flow rate through the compressor were predicted using the clearance volumetric efficiency model of McQuiston and Parker (1988). The clearance volumetric efficiency is defined as the ratio of the actual mass flow rate of the refrigerant through the compressor to that theoretically possible. The theoretically possible mass flow rate assumes that the displacement volume is fully filled with refrigerant vapor at the suction inlet state. The clearance volumetric efficiency was calculated as:

$$\eta_V = \frac{\dot{m}_{r,act}}{\dot{m}_{r,th}} = \left(1 + C - C \cdot \left(\frac{p_{dis}}{p_{suc}}\right)^{1/n}\right) \cdot \frac{v_{suc}}{v_a} \cdot \frac{RPM}{\overline{RPM}} \tag{1}$$

and the corresponding compressor power draw was calculated as:

$$P_{th} = \dot{m}_{r,act} \cdot \left(\frac{n}{n-1}\right) \cdot p_{suc} \cdot v_{suc} \cdot \left[\left(\frac{p_{dis}}{p_{suc}}\right)^{n-1/n} - 1\right] \tag{2}$$

Jaehnig (1999) proposed introducing a pressure drop parameter and a combined compressor efficiency to account for motor and mechanical inefficiencies and for heat transfer in the compressor. The suction pressure and combined efficiency were determined as:

$$p_{suc} = p_{evap} \cdot (1 - \Delta p) \tag{3}$$

$$\eta_{comb} = \frac{P_{th}}{P_{act}} = a + \frac{b}{p_{suc}} \qquad (4)$$

Using this formulation, four model parameters are required to model a compressor: the clearance factor C, a pressure drop parameter Δp, and parameters a and b for the compressor efficiency. These four parameters are obtained by fitting the compressor model to compressor performance data.

The compressor model was validated using data from two different manufacturers over a capacity range from 4 to 52 kW. The minimum information required is five data points chosen as combinations of low and high values for the operating variables (condensing and evaporating temperature) and one other data point within this range. The effect of using fourteen data points in the fitting process was also evaluated.

Figure 1 shows the fit of power data to the compressor model. Using five data points, the mean RMS-error for the power draw was 3.9 %, and that for the mass flow rate was 2.6 %. With fourteen data points spread over the whole range, the RMS-error for the power draw was decreased to 2.9 % and that for the mass flow rate to 2.0 %. Increasing the number of points increased the accuracy only slightly.

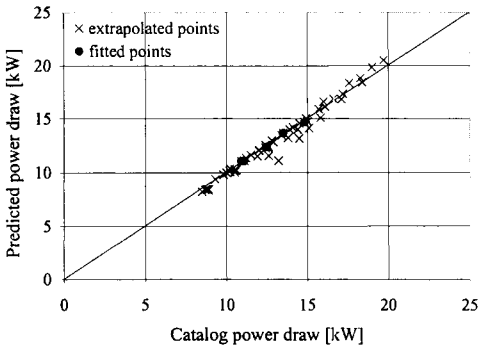


Figure 1: Predicted compressor power draw compared to catalog values

Cooling Coil Model

The modeling technique of Rabehl (1997) was used for the cooling coil (evaporator) and the condenser. In this approach, the overall heat transfer coefficient is related to the mass flow rates using fundamental heat and mass transfer correlations with heat exchanger specific parameters. These parameters depend on heat exchanger geometry and flow arrangement and are determined by fitting the system model to catalog data. With the overall heat transfer coefficient determined, the effectiveness-NTU approach was used to predict performance. The prediction is good and extrapolation is possible since generally valid fundamental heat and mass transfer relations are used (Rabehl (1997)). The condenser model uses the same approach as the cooling coil, but with different relations, and is described separately.

For the direct expansion coil the heat exchanger analogy method (Braun et al. (1989)) was employed. In this approach, a wet coil is analyzed using the effectiveness-Ntu heat exchanger equations for a sensible heat exchanger with the refrigerant flow inside the tubes represented by an equivalent flow of saturated air, and with enthalpy used as the driving force instead of temperature. Heat transfer calculations are made for both totally dry and totally wet operation. If the air entering dew point

temperature is higher than the tube surface temperature at the entrance, the coil is totally wet. Otherwise, the coil is partially wet and the performance is approximated depending on which calculation yields the higher heat transfer rate. The error in using the maximum heat transfer rate of the two conditions is usually less than 5 % (Braun et al. (1989)).

The overall heat transfer coefficient for the cooling coil was calculated as the resistance between the refrigerant flow and the inside of the tube wall in series with that between the finned tube surface on the outside and the air stream. The resistance due to conduction through the tube was neglected. For the heat transfer coefficient between the outside surface and the air stream, the correlation of Zhukauskas (Incropera and DeWitt (1996)) was used:

$$Nu_D = C_0 \cdot Re_D^m \cdot Pr^{0.36} \cdot \left(Pr / Pr_s \right)^{0.25} \tag{5}$$

where C_0 and m are specific values that depend on the heat exchanger configuration. Rearranging the equations and introducing a convection coefficient correction factor C_f for wet coil operation (Brandemuehl (1992)) allowed the following equation for the overall conductance-area product to be obtained:

$$(\eta_0 hA)_a = C_f \cdot C_1 \cdot k_a \cdot \left(\frac{\dot{m}_a}{\mu_a} \right)^{C_2} \cdot Pr_a^{0.36} \cdot \left(Pr_a / Pr_{a,s} \right)^{0.25} \tag{6}$$

where η_o is the overall efficiency of the surface and the correction factor C_f is determined by

$$C_f = 1.07 \cdot u_a^{0.101} \text{ with } u_a \text{ in [m/s]} \tag{7}$$

A single correlation that describes the convection coefficient for boiling inside tubes over the complete range of quality was not available. Rabehl (1997) combined an empirical heat transfer correlation with that developed by Pierre (1955) (ASHRAE Fundamentals (1997).

$$(hA)_r = C_3 \cdot k_r \cdot \left[\left(\frac{\dot{m}_r}{\mu_r} \right) \cdot \Delta h_r \right]^{0.45} \tag{8}$$

The direct expansion coil model incorporates the three model parameters C_1, C_2, and C_3. The range of C_2 is between 0.4 and 0.8 (Incropera and de Witt (1998)). Setting the parameter C_2 to a fixed value of 0.5 allowed an accurate prediction of performance. Figure 2 compares the predicted and catalog heat transfer rate for a number of different cooling coils.

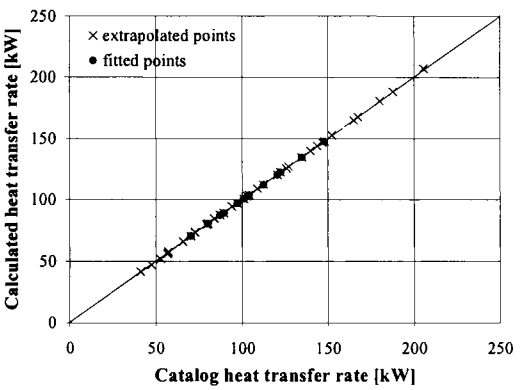


Figure 2: Predicted evaporator heat transfer rate compared to catalog values

Condenser Model

The condenser coil was modeled using the effectiveness-NTU method for sensible heat exchangers. In a condenser, the superheated refrigerant vapor discharged from the compressor is first cooled down, condenses when it reaches the dew point temperature, and then is subcooled before it exits. A detailed condenser model would require correlations for these three different regions. It was assumed that the refrigerant leaving the condensing coil was saturated liquid, and therefore a heat transfer correlation was not required for the subcooling region. The sensible heat transfer in the superheated region is usually small and was taken into account by including it in the overall heat transfer area coefficient product. The refrigerant flow was thus treated to be an isothermal phase change.

As with the direct-expansion coil, the condenser was modeled with two convective resistances, one on the inside of the tubes where condensation of the refrigerant occurs and the other one on the outside exposed to the air stream. The same heat transfer correlation as for the direct expansion coil, but with different coefficients, was used to determine the airside heat transfer area coefficient product.

$$(\eta_0 hA)_a = C_4 \cdot k_a \cdot \left(\frac{\dot{m}_a}{\mu_a}\right)^{C_5} \cdot \mathrm{Pr}_a^{0.36} \cdot \left(\mathrm{Pr}_a / \mathrm{Pr}_{a,s}\right)^{0.25} \tag{9}$$

Inside the tubes, a correlation for condensation in horizontal tubes was found to work best (Rohsenow (1998)):

$$h_c = F \cdot \left[\frac{g \cdot \rho_f \cdot (\rho_f - \rho_g) \cdot k_f^3 \cdot h_{fg}}{D \cdot \mu_f \cdot (T_{sat} - T_s)}\right]^{0.25} \tag{10}$$

where F is a coefficient that is a function of the tube circumference that is covered by refrigerant. The coefficient F was assumed constant. An additional parameter C_6 was introduced that contains all of the constants in equation 10.

$$(\mathrm{hA})_r = C_6 \cdot \left[\frac{\rho_{f,r} \cdot (\rho_{f,r} - \rho_{g,r}) \cdot k_{f,r}^3 \cdot h_{fg,r}}{\mu_{f,r} \cdot (T_{sat} - T_s)}\right]^{0.25} \tag{11}$$

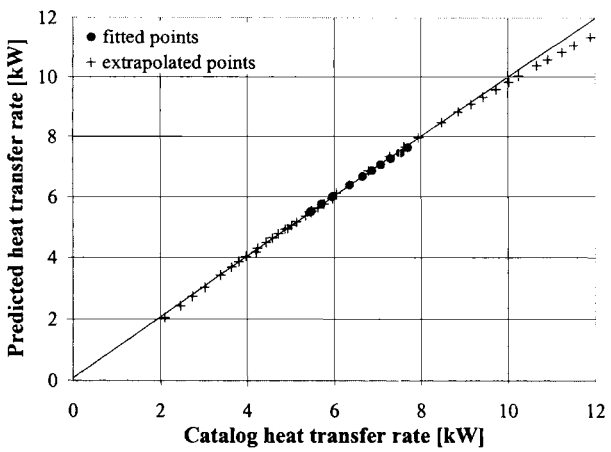


Figure 3: Predicted condenser heat transfer rate compared to catalog values

The model for the condensing coil was validated using condensing coil catalog performance data for a number of coils. Figure 3 shows the predicted coil performance versus the catalog coil performance.

System Model

The compressor, cooling coil, and condenser models described in the preceding sections were coupled together and modeled using EES. In fitting the system model to data, the compressor parameters (C, Δp, a, and b) need to be determined first from compressor performance data. This allows the thermodynamic state points inside the vapor compression cycle to be calculated. Catalog information available for package units generally consists of the capacity (sensible and total) and the compressor power draw as functions of the air temperature entering the condenser, the dry and wet bulb air temperature entering the evaporator, and the air flow rate through the evaporator. Because performance data for the condenser and evaporator separately are not given, system data are used to determine the heat exchanger parameters.

The air conditioner model was validated for units from three manufacturers that used the refrigerant R-22. The ability of different data sets to extrapolate performance was evaluated. It was found that data points that were combinations of high and low values for each of the operating point parameters yielded the best fit.

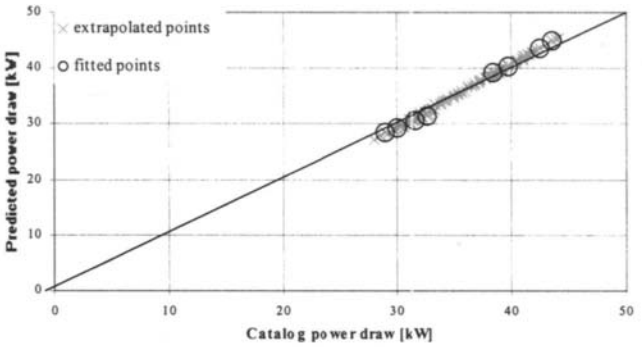


Figure 4: Predicted compressor power draw compared to catalog values

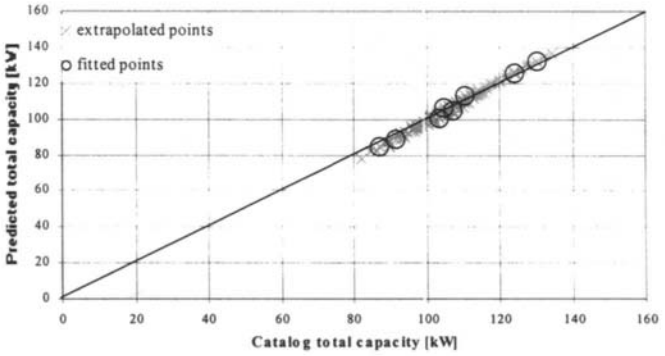


Figure 5: Predicted total capacity compared to catalog values

For the four operating parameters (circulation flow rate, ambient temperature, and supply air dry and wet bulb temperature), 16 data points chosen as indicated were found to be satisfactory. The improvement obtained using data sets with more points within the range of low and high values was not significant. Figures 4, 5, and 6 show the performance prediction for the power draw, the total capacity, and the sensible capacity, respectively, for a units with a nominal 105 kW capacity. The error was less than 3.3 % for the power prediction, less than 2.3 % for the total capacity, and less than 3.2 % for the sensible capacity.

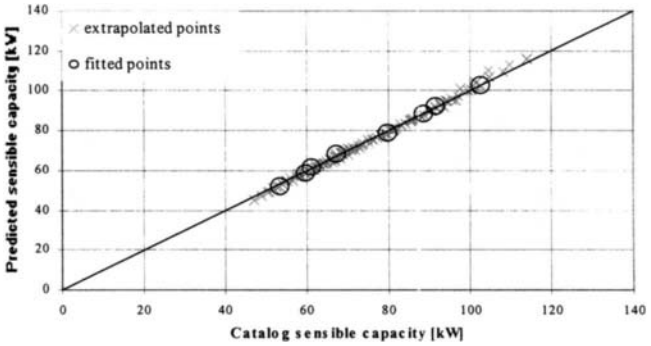


Figure 6: Predicted sensible capacity compared to catalog values

CONCLUSIONS

A model for package air-conditioning equipment was developed that predicts the full load performance (power draw, total and sensible capacity) for different operating conditions. The model is based on semi-mechanistic component models that are interconnected to form the system model.

The semi-empirical model for the compressor contains four parameters that are obtained in a fitting process to performance data. The model is applicable to both reciprocating and scroll compressors. Compressor performance was predicted to within 5 % of manufacturer's catalog data. The condenser and evaporator are modeled using the effectiveness-NTU method. Each heat exchanger model contains three characteristic parameters obtained by fitting the model to system data. The condenser model predicted the performance within 3.9 % and that for the evaporator model was within 1.8 %.

Fitting the characteristic parameters with only a portion of the catalog data set allowed an accurate prediction over the entire range of catalog data. Data points that were combinations of high and low values for each of the operating point parameters (e.g. flow rate and temperatures) produced a good fit. With four operating parameters, 16 data points were found to be satisfactory. Using more data points within the range of low and high values did not significantly improve the performance prediction.

The ability of the model to predict performance was evaluated using data for three package units. The overall prediction of performance was within 3.3 % over the entire operating range. The model allows simulation of the power and capacity of package units outside the range of the fitted data.

NOMENCLATURE

a, b	parameter for compressor efficiency
C	clearance factor
C_0	coefficient in heat transfer correlation
$C_{1..9}$	heat exchanger parameters
C_f	coefficient in heat transfer correlation
D	tube diameter
Δhr	enthalpy difference in condensation
Δp	pressure drop parameter
F	coefficient in condensation correlation
η_0	fin efficiency
η_{comb}	combined efficiency
η_v	volumetric efficiency
g	gravitational constant
h_c	convection coefficient
h_{fg}	enthalpy of vaporization
hA	overall conductance area product
k	thermal conductivity
m	exponent in heat transfer correlation
$\dot{m}$	mass flow rate
μ	dynamic viscosity
n	polytropic exponent
Nu_D	Nusselt number
P	power
p	pressure
Pr	Prandtl number
Re_D	Reynolds number
ρ	density
RPM	motor speed
T	Temperature
u	velocity
v	specific volume
va	specific volume before compression

Subscripts

a	air
act	actual
dis	discharge
evap	evaporator
f	liquid
g	vapor
r	refrigerant, at refrigerant temperature
s	at surface temperature
sat	saturated
suc	suction
th	theoretical

REFERENCES

American Society of Heating, Refrigeration and Air-Conditioning Engineers (ASHRAE), *1997 ASHRAE Handbook Fundamentals*, American Society of Heating Refrigeration and Air-Conditioning Engineers, Atlanta, GA.

Brandemuehl, M.J. et al. (1992), *HVAC2 Toolkit Algorithms and Subroutines for Secondary HVAC Systems Energy Calculations*, American Society of Heating Refrigeration and Air-Conditioning Engineers, Atlanta, GA

Braun, J.E., Klein S.A., and Mitchell, J.W. (1989), "Effectiveness Models for Cooling Towers and Cooling Coils", ***ASHRAE Transactions*, Vol 95, Pt 2**

Incropera, F.P., and de Witt, D.P. (1998), *Introduction to Heat Transfer*, John Wiley & Sons, New York, NY

Jaehnig, D. (1999), *A Semi-Empirical Method for Modeling Reciprocating Compressors in Residential Refrigerators and Freezers*, MS Thesis, University of Wisconsin

Klein, S.A. and Alvarado, F.L. (1999), *EES – Engineering Equation Solver*, F-Chart Software, Middleton, WI

McQuiston, F.C., Parker J. D. (1988), *Heating, Ventilating and Air Conditioning Analysis and Design*, 3rd edition, John Wiley & Sons, New York

Rabehl, R.J., Mitchell, J. W., and Beckman, W. A. (1999), *Parameter Estimation and the Use of Catalog Data in Modeling Thermal System Components*, **Intl J of HVAC&R Research,** Vol 5, No. 1

Rohsenow, R.M., Hartnett, J.P., and Young, I. C. (1998), *Handbook of Heat Transfer*, 3rd edition, McGraw Hill, New York

Advances in Building Technology, Volume 1
M. Anson, J.M. Ko and E.S.S. Lam (Eds.)
© 2002 Elsevier Science Ltd. All rights reserved

AUTOMATIC DIAGNOSIS AND COMMISSIONING OF CENTRAL CHILLING SYSTEMS

Shengwei Wang

Department of Building Services Engineering
Faculty of Construction and Land Use, The Hong Kong Polytechnic University, Hong Kong

ABSTRACT

A strategy is developed to automatically diagnose and evaluate the BMS sensors and building refrigeration systems during commissioning or periodical check (re-commissioning). The strategy evaluates soft sensor faults (biases) by examining and minimizing the weighted sum of the squares of the concerned mass and/or steady state energy balance residuals represented by the corrected measurements over a period, on the basis of the measurements downloaded from BMS. A Genetic Algorithm is employed to determine the global minimal solution to the multimodal objective function. This paper presents the strategy and examples of application.

KEYWORDS

Chilling system, Building Management System, Sensor fault, Commissioning, Fault diagnosis

INTRODUCTION

Proper commissioning of BMS is a prerequisite for the successful application of the Building Management Systems (BMS) [1]. In engineering practice, all sensors (measurements) should be checked against calibrated instruments at the normal operation conditions manually on site [1,2]. They also need to be checked periodically during operation. This involves large amount of labor and time costs, and may encounter difficulties in practice [3,4,5]. On site checking of some sensors can be difficult and even impossible.

The accuracy of the on site manual checking is limited also. Besides, sensor faults, particularly the soft ones (drifts or biases), might be undetected due to ignorance or other reasons, such as the inadequate thermal contact between thermistor and medium to be monitored. It is, therefore, highly desirable to develop some convenient methods for assessing the health states of the monitoring sensors. Application of such FDD methods would help to ease the burdens and difficulties in on site manual sensor check during the commissioning or re-commissioning of BMS.

On sensor faults in HVAC systems, Usoro et al. [6] studied the detection and diagnosis of an abrupt bias in a room temperature sensor using a model-based method. Stylianou and Nikanpour [7] also used a model-based method to detect soft sensor fault aiming at making sure that the measurements were reliable when monitoring the performance of a laboratory chiller. Lee et al. [8] investigated the detection and automatic recovery of a faulty supply air temperature sensor in AHU. Recently, the

authors of this paper developed a "law-based" strategy for the fault detection, diagnosis and evaluation (FDD&E) of the temperature sensors and flow meters in building refrigeration plants [9,10].

The law-based sensor FDD&E strategy is based on the fundamental mass and (steady state) energy conservation (balance) relationships in statistics. These relationships are easy to build and their validity is absolute and independent of plant performance degradations and change of working conditions. Sensor bias values are estimated basically by minimizing the weighted sum of the squares of the corrected residuals of each of the involved balances. On this basis, a software package in prototype is developed to evaluate the BMS sensors automatically on a personal computer using the measurements recorded in a period, downloaded from BMS, during BMS sensor commissioning or periodical check. This paper presents the basic principle and approach of the sensor FDD&E method, the structure of the software, and the examples of the application of the software in central chilling systems.

OUTLINE OF STRATEGY

Basic Principle of Strategy

Figure 1 shows the schematic of a typical central chilling system and its monitoring instruments commonly used in large HVAC systems. In principle, heat balance and mass balance exist in each control volume. Using the measurements from the sensors shown in Figure 1, the residuals (unbalances) of the mass and heat balances for the control volumes can be presented in Equation (1)-(4). Equation (1)-(4) refer to the mass balance and the heat balance of the control volume B, the heat balance of the control volume C (physical redundancy) and the heat balance of the control volume A, respectively. Where, *Ix* or *I(x)* equals to 1 if its corresponding sensor is in use, otherwise it equals to zero.

$$\hat{r}_M^{[i]} = \hat{M}_b^{[i]} + \hat{M}_{bp1}^{[i]} I_{bp1}^{[i]} + \hat{M}_{bp2}^{[i]} I_{bp2}^{[i]} - \sum_{j=1}^{N} \left[\hat{M}^{[i]}(j) I^{[i]}(j) \right] \tag{1}$$

$$\hat{r}_B^{[i]} = \rho c_{pw} \sum_{j=1}^{N} \left[I_{bp1}^{[i]} I^{[i]}(j) \hat{M}^{[i]}(j) \left(\hat{T}_s^{[i]}(j) - \hat{T}_{sb}^{[i]} \right) \right] \tag{2}$$

$$\hat{r}_C^{[i]} = \left(\hat{T}_{rb}^{[i]} - \hat{T}_{rch}^{[i]} \right) I_{bp2}^{[i]} \tag{3}$$

$$\hat{r}_A^{[i]} = \rho c_{pw} \left\{ \hat{M}_b^{[i]} \left(\hat{T}_{rb}^{[i]} - \hat{T}_{sb}^{[i]} \right) - \sum_{j=1}^{N} \left[\hat{M}^{[i]}(j) I^{[i]}(j) \left(\hat{T}_{rch}^{[i]} - \hat{T}_s^{[i]}(j) \right) \right] \right\} \tag{4}$$

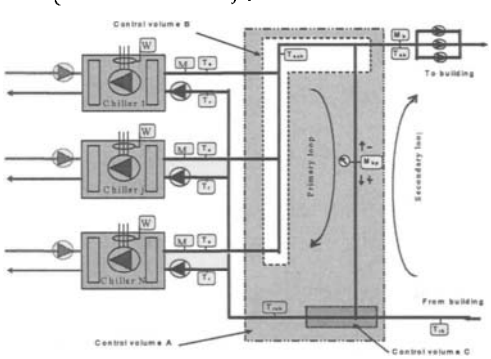


Figure 1: Schematic of primary-secondary refrigeration system

In ideal case, these residuals should be equal to zero when there are no heat losses, thermal storage and water leakage associated with the control volumes. Unfortunately, perfect balance can never be achieved using the realistic measurement data for any system due to various errors in measurements, such as biases, drifts, noises and failures. Any sampled measurement ($\hat{x}^i$) consists of three components: true value of the process variable (x^i), sensor bias (δx) and random noise ($\nu_x{}^i$), as shown by the measurement model, Equation (5). When the raw measurements in the equations (1)-(4) are corrected by eliminating the sensor biases from the raw measurements as represented by equations (6) and (7), the balance residual should be reduced significantly if not to zero.

The basic idea of the strategy is that the best estimates of the sensor biases are these values of δx, that minimize the sum of the squares of the balance residuals over certain period when the raw measurements are corrected using the values (δx) as presented by Equation (8).

$$\hat{x}^i = x^i + \delta x + \nu_x{}^i \tag{5}$$

$$x^i \cong \hat{x}^i - \delta x \tag{6}$$

$$r^{[i]} = r(\hat{x}^{[i]} - \delta_x) \tag{7}$$

$$\text{minimize}\Big|_{\delta_x} \sum_i \left(r^{[i]}\right)^2 \;;\; [r^{[i]} = r_M^{[i]}, r_C^{[i]}, r_B^{[i]}, r_A^{[i]}] \tag{8}$$

Basic and Robust FDD&E Schemes

Based on the concept presented by equation (8), four estimator are developed to evaluate the biases of chilled water flow meters, biases of relative supply water temperatures, bias of building return temperature sensor and biases of building supply flow meter and temperature sensors respectively. The sequence of their application is illustrated in Figure 2 (as basic scheme).

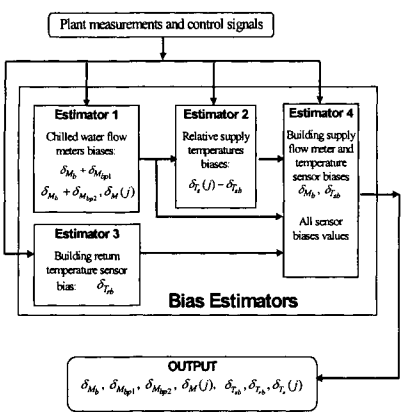


Figure 2: Basic FDD&E scheme for refrigeration plants

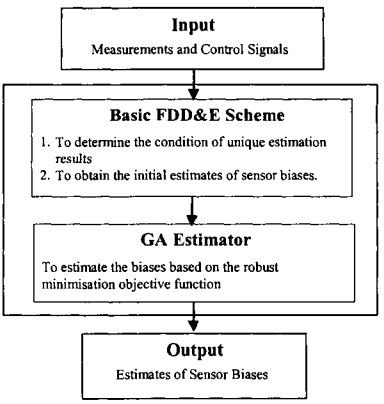


Figure 3: Robust scheme for sensor fault detection, diagnosis and estimation

As the mass and heat balance residuals for the control volumes are minimized individually in the basic scheme, and outputs of estimators are used as the known parameters of the other estimators. The uncertainty of the estimation might be accumulated. The estimation errors of an estimator used earlier might be amplified by the other estimators used later. Tests using data from existing refrigeration systems and simulation show that the robustness of the basic scheme might not be

satisfactory in some cases. To overcome this problem, a robust scheme is developed, which minimizes systematically the heat balance residuals of the control volume A and B. A Genetic Algorithm (GA) is employed to cope with the minimization problem of multiple variables.

Figure 3 illustrates the overall structure of the robust FDD&E scheme. It employs the basic FDD&E scheme and a robust GA Estimator. The GA Estimator is designed to estimate the biases of the building supply flow meter and temperature sensor (δ_{M_b}, $\delta_{T_{sb}}$), and the chiller supply temperature sensors ($\delta_{T_s}(j)$). The biases of the chiller flow meters and the building return temperature sensor ($\delta_M(j)$, δ_{Trb},) are estimated by the basic scheme. The GA Estimator estimates δ_{M_b}, $\delta_{T_{sb}}$ and $\delta_{T_s}(j)$ by minimizing the sum of the mean squares of the normalized corrected residuals of the control volume A and control volume B heat balances, as shown in Equation (14). Where, $\dot{r}_A^{[i]}$, $\dot{r}_B^{[i]}$ are the normalized corrected residuals at the instant *[i]*, which are normalized against the number of the chillers operating.

$$\text{minimise}_{\delta_x}\left(\frac{\dot{S}r_{sq.A}}{n_A}+\frac{\dot{S}r_{sq.B}}{n_B}\right);\quad [\delta_x=\delta_{M_b},\ \delta_{T_{sb}},\ \delta_{T_s}(j),\ j=1,\ldots,\ N] \tag{9}$$

where,

$$\dot{S}r_{sq.A}=\sum_i(\dot{r}_A^{[i]})^2 \tag{10}$$

$$\dot{S}r_{sq.B}=\sum_i(\dot{r}_B^{[i]})^2 \tag{11}$$

In the robust scheme, the basic scheme is employed not only to estimate the biases of the individual chiller and bypass flow meters and the building return temperature sensor, but also to assist the GA Estimator in two ways. First, the basic scheme is used to check whether a unique set of estimates can be obtained based on the collected measurement data. Secondly, the basic scheme is used to produce a set of initial estimates, which are then used to determine and narrow the search space of the GA Estimator. A fitness function (*f*), Equation (17), is defined, which is the reciprocal of the objective function of the original minimization problem (Equation (14))

$$f=f\left(\delta_{M_b},\delta_{T_{sb}},\delta_{T_s}(j)\right)=1\Big/\left(\frac{\dot{S}r_{sq.A}}{n_A}+\frac{\dot{S}r_{sq.B}}{n_B}\right) \tag{12}$$

STRUCTURE OF SOFTWARE

Overview of Software

The software consists of three modes: *Preparation*, *FDD&E programs*, and *Presentation*. The *Preparation* mode is designed for users to input necessary information for configuring and running the FDD&E programs. The FDD&E programs are a series of sensor bias estimators, the corresponding confidence estimators, and the routines for generating data for presenting the results. Execution (*Running* mode) of those programs is the core of the package. The *Presentation* mode allows users to review the FDD&E results. The results include the estimates of the sensor biases, the confidence intervals for the estimates, and the statistics of the balance residuals based on the raw and corrected measurement data.

Preparation Mode

The *Preparation* mode is divided into two stages, while two different kinds of information are requested. Stage I concerns the refrigeration plant configuration and sensor installation condition on

which the selection and configuration of the appropriate FDD&E programs are based. Stage II asks for the information regarding the measurement data collected for examination.

□

The program enters Stage I first if the relevant system and sensor information has not been specified before, or, if re-specifying is necessary. On completion of this stage, the program enters Stage II. If the information required in Stage I has been available in the software from previous runs, the user can enter Stage II directly.

The required specifications regarding the refrigeration plant include the types of the chilled water distribution system, the number of chillers in the plant, the number of chiller types, the specifications of each chiller type, etc. This information is used for selecting the FDD&E programs. Sensor installation conditions are required also for selecting and configuring appropriate FDD&E programs. Figure 4 shows an example of the windows designed as the interface for the users to select the sensors installed in the chilling systems.

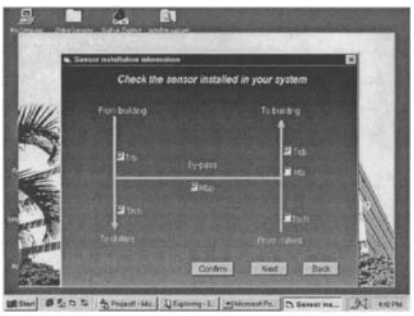


Figure 4: A window for specifying the installation condition of the sensors

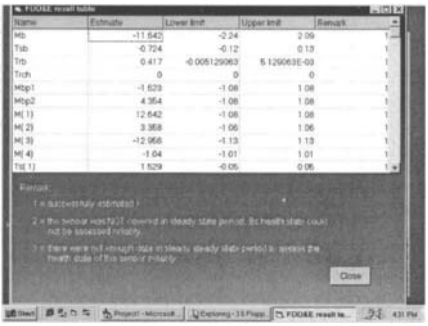


Figure 5: A window presenting sensor bias estimates and the confidence intervals



Figure 6: A window showing the statistics of the balance residuals

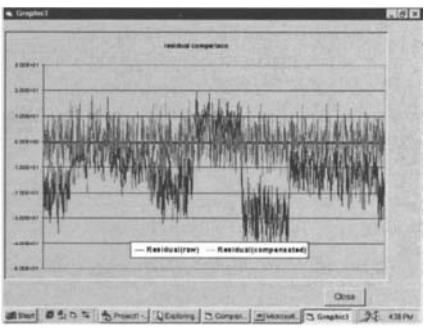


Figure 7: A window showing the time series of the raw and corrected flow balance

After the information about a refrigeration system and the sensor installation conditions have been specified, a program makes decisions accordingly on what FDD&E programs (estimators) should be used, and configures the selected programs into a proper execution sequence. A bank of 12 sensor bias estimators and the GA estimator, the corresponding confidence estimators and post data processing routines have been developed for all the possible sensor installation conditions.

The second preparation stage also asks for the information regarding the collected measurement data. It is required that the collected data have been prepared in a data file with given format. The software will check if the data file is in the format required.

Running Mode

On entering this mode, the software checks the availability of the files that record the required information regarding the system and sensor conditions and the properly manipulated measurement data. If the preparation is complete, the three batch files created in the preparation stage are activated to run. Otherwise, the user will be prompt to re-enter the preparation mode.

At the end of the running mode, three types of files are generated after running estimation programs. The first type is the one that records the estimated biases of the examined sensors. The second type is the one that records the confidence intervals for all the estimated sensor biases. The third type is the one that records the statistical quantities and the time series of the raw and the corrected balance residuals.

Presentation Mode

In the *Presentation* mode, the user can view the FDD&E results through graphic interfaces. The three types of files resulting from the Running mode are further processed. The final results are presented to user in two tables. One table (see Figure 5) shows the values of the estimated sensor biases and confidence intervals. The second table (see Figure 6) shows the statistics of the raw and corrected balance residuals. Time series of the raw and corrected residuals of individuals can also be viewed graphically as shown in Figure 7, when it is selected on the second table.

EXAMPLE OF CASE STUDY

An example of applying the software to an existing building central chilling system of five chillers is presented. The system has the same configuration as the system in Figure 1 except that the common return water temperature measurement (T_{rch}) is not available. The measurement data from the monitoring sensors are recorded in BMS, which are then retrieved from the central computer station. Data of several intermittent days within one month is collected. Sensor faults (biases) are introduced to three of the chilled water temperature sensors (i.e., biases introduced into T_{sb}, $T_s(2)$ and $T_s(3)$ are 1.5°C, -1.0°C and 1.5°C respectively). Prior to introducing these faults, check and calibration of the temperature sensors in the refrigeration plant are conducted. Table 1 presents the output of the robust FDD&E scheme based on the collected measurement data. The biases introduced to the three temperature sensors are successfully diagnosed. The largest error of the three estimates is 0.25°C ($\delta_{T_{sb}}$).

The estimated biases of the bypass chilled water flow meter (negative direction, δ_{Mbp2}), the chilled water flow meters of chiller 2, 3, and 5 ($\delta_M(2)$, $\delta_M(3)$, $\delta_M(5)$) turn out to be significant. For chiller 2, 3, and 5, the biases are more than ten percent of the measured values. The remaining four chilled water flow meter biases are negligible, considering the measurement uncertainties of the flow meters. Since there is no other simple method to compare accurately the flow meter bias estimation results with the actual unknown condition, the chilled flow rate measurements before and after correction are compared with each other and with the historical commissioning data.

TABLE 1 Bias estimates of the sensor in an existing refrigeration plant

Sensor	$M(1)$	$M(2)$	$M(3)$	$M(4)$	$M(5)$	M_b	M_{bp1}	M_{bp2}
Bias Estimate (L/s)	3.2	17.9	17.7	6.8	17.0	-4.9	-2.2	16.8
Sensor	$T_s(1)$	$T_s(2)$	$T_s(3)$	$T_s(4)$	$T_s(5)$	T_{sb}		
Bias Estimate (°C)	-0.08	1.10	-1.47	0.14	0.27	1.75		
Sensor	$T_r(1)$	$T_r(2)$	$T_r(3)$	$T_r(4)$	$T_r(5)$			
Bias Estimate (°C)	-0.24	-0.11	0.04	0.24	0.08			

The balance residuals are the effective indicators for validating the results of bias estimates. Two examples of the balance residuals using the raw measurements and corrected measurements are presented for comparison. The raw flow balance residual indicates the existence of the flow meters biases as shown in Figure 8. The raw residual deviates apparently from zero. This indicates that some, if not all, of the flow meters are biased.

It has been carefully checked if chilled water flowed through any of the evaporators of the idle chillers, by tracing the individual supply and return temperatures. The rising rate of each of those temperature measurements was found normal after the chillers were shut down. This indicates that there was no bypass flow through the evaporators. There cannot be any other reason why some of the chilled water disappeared or was generated. Therefore, the violation of the law of mass conservation by the raw flow measurements presents the clear evidence that the flow meters must have problems. On the other hand, the corrected flow balance residual varies randomly around zero approximately. Of the raw residual, the mean and the standard deviation are -9.01 and 21.4 litres per second, respectively. Of the corrected residuals, they are 0.04 and 7.45 litres per second.

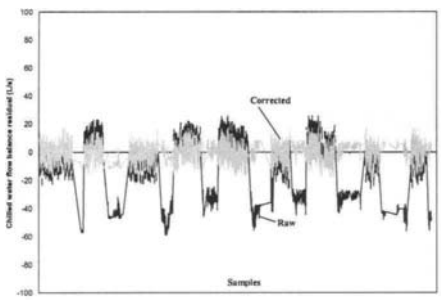


Figure 8: Raw and corrected chilled water flow balance residuals

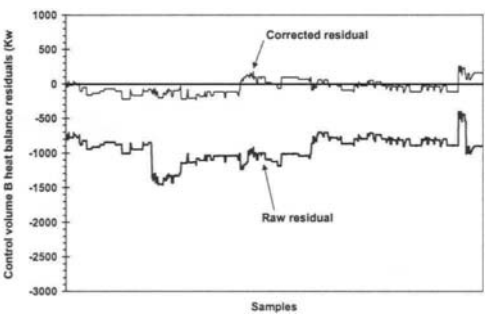


Figure 9: Comparison of the control volume B heat balance residuals (normalized)

Similar to the flow balance residual, the heat balance residuals also indicate the existence of the biases of the associated sensors. The raw and the corrected heat balance residuals of the control volume B are shown in Figure 9. It can be seen that the raw heat balance residuals of the control volume deviate from zero severely. Obviously, the main reason was that three large temperature sensor biases were introduced. After the raw measurements have been corrected with the obtained bias estimates, the large biases in the balance residuals diminished.

CONCLUSIONS

The balance residuals are sensitive indicators of the existence of flow meter and temperature sensor biases. Analysis of the residuals under various operating conditions of the chilling systems and minimization of the sum of the squares of the corrected balance residuals make it possible to locate biased sensors and to estimate the magnitudes of the biases.

In Building Management Systems, there are enormous data stored. It is very convenient for the users to download some data and evaluate the BMS measurements in a computer in commissioning stage or any time during normal operation. When no significant error is detected by the software, the engineer may not need to spend too much effort to check or calibrate the sensors frequently because the measurement quality is ensured. When there is significant error reported by the software, the engineers can focus their effort to check the faulty sensors reported. As remote monitoring via Internet is becoming a regular function of BMS nowadays, the automatic commissioning software provides a means for remote check and diagnosis of the BMS sensors.

ACKNOWLEDGEMENT

The research work of presented in the paper is supported by a grant from the Research Grants Council of the Hong Kong SAR.

REFERENCES

1. Pike P. G. and Pennycook K. 1992. Commissioning of BEMS - A code of practice. AH 2/92. BSRIA.
2. Pike P.G. (1994) BEMS Performance Testing, BSRIA
3. Bilas F., Bourdouxhe J.P., et al. 1997 "Commissioning Of A Centralized Cooling Plant", CLIMA 2000, Brussels. P292.
4. Haves P. Salsbury T.I, Jorgensen D.R. and Dexter A.L. 1996. Development and Testing of A Prototype Tool for HVAC Control System Commissioning, ASHRAE Transactions, 102(1), 467-475
5. Ngo D. and Dexter A.L. 1998. Automatic Commissioning of Air-conditioning Plant, Proceedings of The 1988 International Conference on Control, Pt2, 1690-1699
6. Usoro, P.B., L.C. Schick and S. Negahdaripour. 1985, An Innovation-Based Methodology for HVAC System Fault Detection. *Journal of Dynamics systems, Measurement, and Control. Transactions of the ASME*, 107: 284-285.
7. Stylianou, M. and D. Nikanour. 1996. Performance Monitoring, Fault Detection, and Diagnosis of Reciprocating Chillers. *ASHRAE Transactions,* 102(1): 615-627.
8. Lee, W.Y., J.M. House and D.R. Shin. 1997. Fault Diagnosis and Temperature Sensor Recovery for An Air-Handling Unit. *ASHRAE Transactions,* 103(1): 621-633.
9. Wang S. and J.B. Wang 1999. Law-Based Sensor Fault Diagnosis and Validation for Building Air-conditioning Systems. *Int. J. of HVAC&R Research*, 5(4): 353-380.
10. Wang S.W. and Wang J.B. 2002. Automatic Sensor Evaluation in BMS Commissioning of Building Refrigeration Systems, Automation in Construction, V11(1), pp59-73.

TEAM PRESENTATION:

COMPOSITE CONSTRUCTION

This Page Intentionally Left Blank

Advances in Building Technology, Volume 1
M. Anson, J.M. Ko and E.S.S. Lam (Eds.)
© 2002 Elsevier Science Ltd. All rights reserved

DESIGN OF SIMPLY-SUPPORTED AND CONTINUOUS BEAMS IN STEEL-CONCRETE COMPOSITE CONSTRUCTION

P.A. Berry and M. Patrick

Centre for Construction Technology & Research,
College of Science, Technology & Environment, University of Western Sydney, Locked Bag 1797, Penrith South DC, NSW 1797, Australia

ABSTRACT

Steel-concrete composite beams in Australia are predominantly designed as simply-supported with web-side-plate steel connections, which has some structural limitations. The inevitable slope discontinuity at internal supports can cause wide cracks, whilst its remedy, sufficient tension reinforcement to control cracking, can overload the cleat of the web-side-plate connection, which is in corresponding compression.

Continuous composite beams offer better crack control and lower deflections, even when the depth of the steel section is less than that required for the equivalent simply-supported beam. Innovative design methods for continuous and semi-continuous composite beams have recently been developed which eliminate the need for iterative approaches and allow accurate preliminary sizing of members. This paper reviews the design of simply-supported and continuous composite beams in Australia, highlighting the benefits of continuous construction with two typical design examples.

KEYWORDS

Composite beam, continuous composite beam, semi-continuous composite beam, composite connection, web-side-plate connection, end plate connection.

INTRODUCTION

Current Australian practice is to support composite beams with web-side-plate connections, which are assumed to behave as nominally pinned joints. If the connections do behave as pins, the resulting high end rotations can cause unacceptable cracking of the concrete surface and there are a number of composite carparks in Australia that are excessively cracked due to inadequate reinforcement over the connection (Patrick *et al.* 2002). Conversely, typical levels of crack control reinforcement may invalidate the pinned joint assumption and can lead to compressive forces in the cleat that exceed the current Australian design limit for web-side-plate connections (Berry *et al.* 2000).

Recent design guidelines (Berry *et al.* 2001a), which supplement AS 2327.1 (Standards Australia 1996), have demonstrated the benefits of continuous composite beams. Continuous composite beams may be defined in the broadest sense to refer to any composite member (beam or cantilever) subject to negative curvature at one or more of its supports. Continuity in a composite beam may be achieved either with internal supports, or by the use of suitable connections within a frame. In the latter case, this paper is limited to rigid connections in braced frames, and in order to limit the rotation demand on the connection, the design moment capacity at the critical positive moment cross-section is limited to $0.85\phi M_{bv}^{+}$ (Steel Construction Institute 1998).

COMPOSITE CONSTRUCTION

Classification of Connections

A composite connection must have adequate strength, ductility, and stiffness at the strength limit state. These three attributes form the basis of a useful classification system for both the bare steel and composite states, as shown in Figure 1.

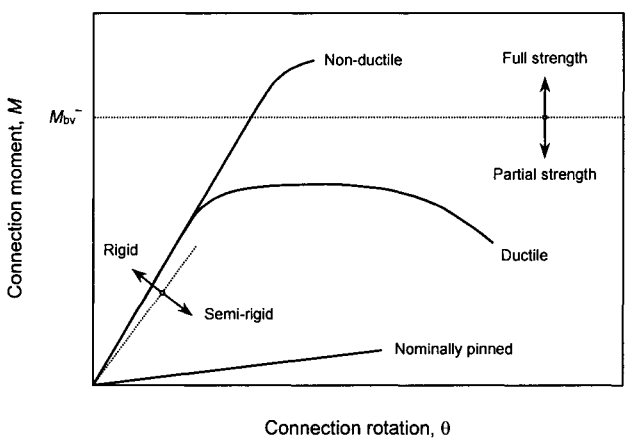


Figure 1: Classification of Connections (adapted from Steel Construction Institute 1998)

Types of Framing

Three different types of framing can be defined by the requirements of global analysis (British Standards Institution 1994) and the corresponding connections that are applicable.

1. *Simple*. Only equilibrium need be considered in the global analysis. Simple framing uses only nominally pinned connections.
2. *Continuous*. Both equilibrium and the structural properties of the member need to be considered in the global analysis. Any connections that are not nominally pinned must be full-strength rigid connections, so that the connection properties do not affect the member behaviour.
3. *Semi-continuous*. The structural properties of the connections also need to be considered in the global analysis. For the purposes of this paper, which excludes semi-rigid connections, semi-continuous framing may use partial-strength rigid connections in addition to those permitted for continuous framing.

DESIGN FACTORS

Simply-supported beams

The bending moment diagram for a simply-supported beam depends solely on satisfying equilibrium for the given applied loads and is unaffected by the variation of other design parameters. The designer has little scope for creative input into the design process. Given the steel beam and concrete slab details, it is possible to determine directly the minimum degree of shear connection at each potentially critical cross-section that is required to satisfy the strength limit state (Patrick & Dayawansa 1998).

Simply-supported beams, although very efficient at satisfying strength requirements, do not perform well under serviceability conditions. The end rotations are high, which can cause unacceptable cracking over internal supports, and the deflections frequently govern the design, negating the benefits of efficiency at the strength limit state. It is not uncommon for only 70% of the strength capacity to be utilised under ultimate loads.

Continuous beams

For continuous and semi-continuous beams, the bending moment diagram must satisfy compatibility as well as equilibrium. Varying the relative stiffness and strength of each cross-section can therefore be used in conjunction with moment redistribution to produce different design options. Innovative design charts have recently been developed that allow designers to obtain accurate preliminary designs for a range of parameters in order to find the optimum solution (Berry *et al.* 2001b).

The degree of shear connection at the peak positive moment cross-section, β_m^+, may be varied within the range $0.5 \le \beta_m^+ \le 1$. It is most economical to use $\beta_m^+ = 0.5$: increasing the degree of shear connection above this level leads to decreasing returns in composite strength. Based on the values given in Table A4 of the Composite Beam Design Handbook (Australian Institute of Steel Construction and Standards Australia 1997), for typical universal beams (310 UB – 610 UB), 50% shear connection ($\beta_m^+ = 0.5$) produces 70% of the maximum composite benefit ($\phi M_{bc}^+ - \phi M_s^+$).

The designer may also choose the desired level of reinforcement: the suggested practical range that satisfies minimum crack control requirements is $0.75\% \le p_r \le 1.5\%$. In general, it is most economical to use $p_r = 0.75\%$, but there may be situations in which the overall structural depth is the governing factor. Based on the values given in Charts G2.1 – G2.4 of the Composite Structures Design Booklet DB2.1 (Berry *et al.* 2001a), increasing the reinforcement from the minimum value of $p_r = 0.75\%$ to the suggested maximum value of $p_r = 1.5\%$ increases the load-carrying capacity on average by 20% for a semi-continuous composite beam and by 10% for a continuous beam.

The design of continuous and semi-continuous composite beams is rarely governed by deflections, which means they perform well under serviceability conditions. By the very nature of continuity, the end rotations are low, which minimises any cracking over internal supports. Economics and ease of construction are often raised as factors in support of simply-supported composite beams, but this perception may not be soundly based. A partial depth end plate connection requires no more fabrication in terms of drilling and welding than a web-side-plate connection and, since the one set of bolts connect adjacent beams, the total number of bolts required during erection may be halved. A rigorous cost-benefit analysis, including the cladding savings of reduced floor-to-floor heights, may show that continuous and semi-continuous composite beams should be the preferred construction option.

DESIGN PROCEDURE FOR CONTINUOUS BEAMS

Geometry

It is assumed that the general layout is known, including details of the:

- *beam* (length and spacing to adjacent beams);
- *concrete* (grade and depth of slab); and,
- *profiled steel sheeting* (type and orientation of ribs).

Loads

It is assumed that all design loads, together with their stage of application, are known. The one exception at the outset of design is the beam self-weight, which can typically be approximated by a uniformly distributed load in the range 0.5 – 1 kN/m.

Supports in the Composite State

The supports in the composite state must be either pinned or rigid, since semi-rigid connections are beyond the scope of this paper. Rigid composite supports rely on symmetry for properly anchored negative moment reinforcement, and therefore should normally only be used at internal supports.

Rigid supports may be either partial-strength or full-strength, which correspond to *semi-continuous* and *continuous* framing respectively. Semi-continuous framing relies on high levels of moment redistribution and requires a 0.85 positive moment capacity reduction factor to be applied in design, to minimise the rotation demand at the supports (Steel Construction Institute 1998).

Degree of Positive Moment Shear Connection

Partial shear connection is permitted for critical cross-sections in positive moment regions, so the designer may choose the desired degree of shear connection at the peak positive moment cross-section, β_m^+, such that

$$0.5 \leq \beta_m^+ \leq 1 \tag{1}$$

Level of Negative Moment Reinforcement

The designer may choose the desired level of reinforcement, within certain limits. One of the requirements for crack control in AS 3600 (Standards Australia 2001) equates to $p_r = 0.75\%$ for N12 reinforcing bars, which represents a suitable minimum, and 1.5% has been chosen as a convenient maximum for the purposes of preliminary design. Therefore,

$$0.75\% \leq p_r \leq 1.5\% \tag{2}$$

If a beam is relatively short and heavily loaded, levels of reinforcement towards the higher end of this range will be required to satisfy the stiffness requirements for a rigid connection.

Initial Member Sizing

Semi-continuous and continuous beams are more likely to be governed by strength than deflection, which means that the strength charts can provide accurate member sizing. The charts are based on

fully built-in beams with complete shear connection at the peak positive moment cross-section. In other cases, approximate solutions can be obtained by making the following adjustments before using the charts (Figure 2):

- for propped cantilevers, increase the beam span by 15%; and,
- for partial shear connection ($\beta_m^+ = 0.5$), increase the loads by 10%.

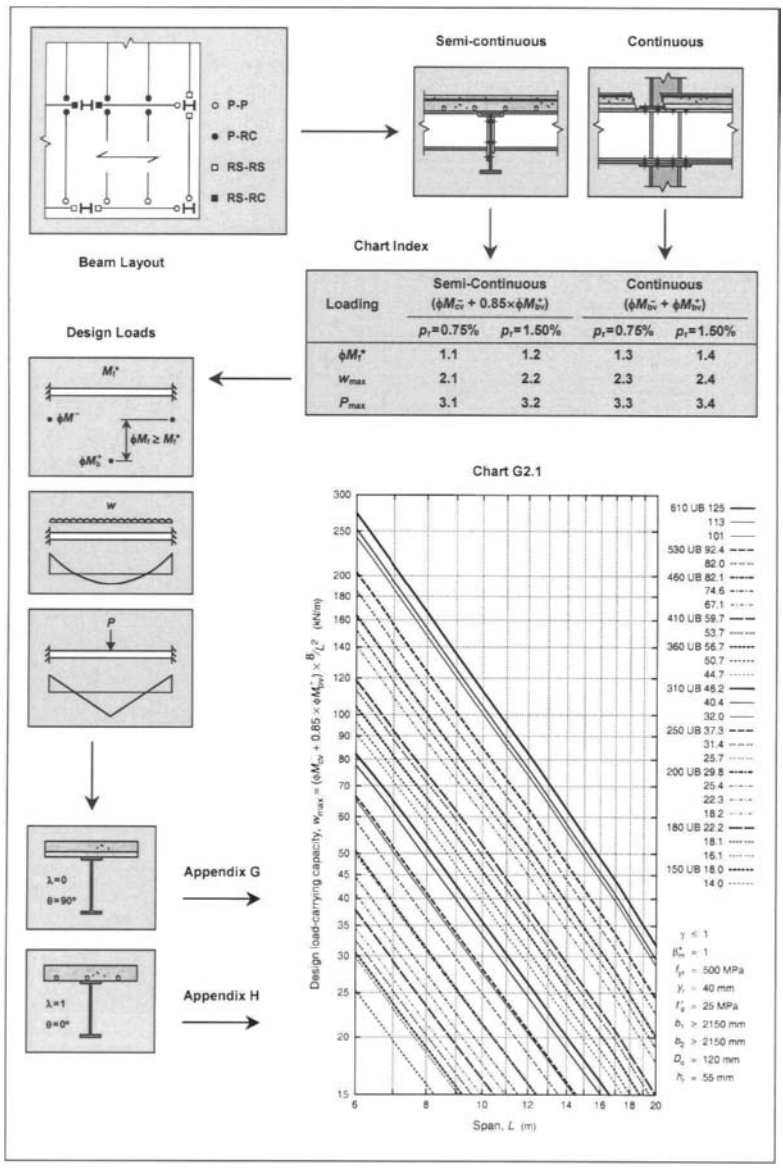


Figure 2: Design Flowchart for Continuous Composite Beams (after Berry *et al.* 2001b)

DESIGN EXAMPLES

Secondary Beam in a Carpark

Two semi-continuous beam options have been added to the simply-supported secondary beam 'B1' from scheme 1C of the BHP Design Guide for Economical Carparks (Watson *et al.* 1998), as shown in Figure 3. Not only has the beam size been reduced from a 460 UB 74.6 to a 360 UB 50.7 in each case, but the incremental deflection, which governed the simply-supported design, has also reduced by 40% and 25% for the unpropped and propped options respectively. The detailed design calculations are given in Berry *et al.* (2001a).

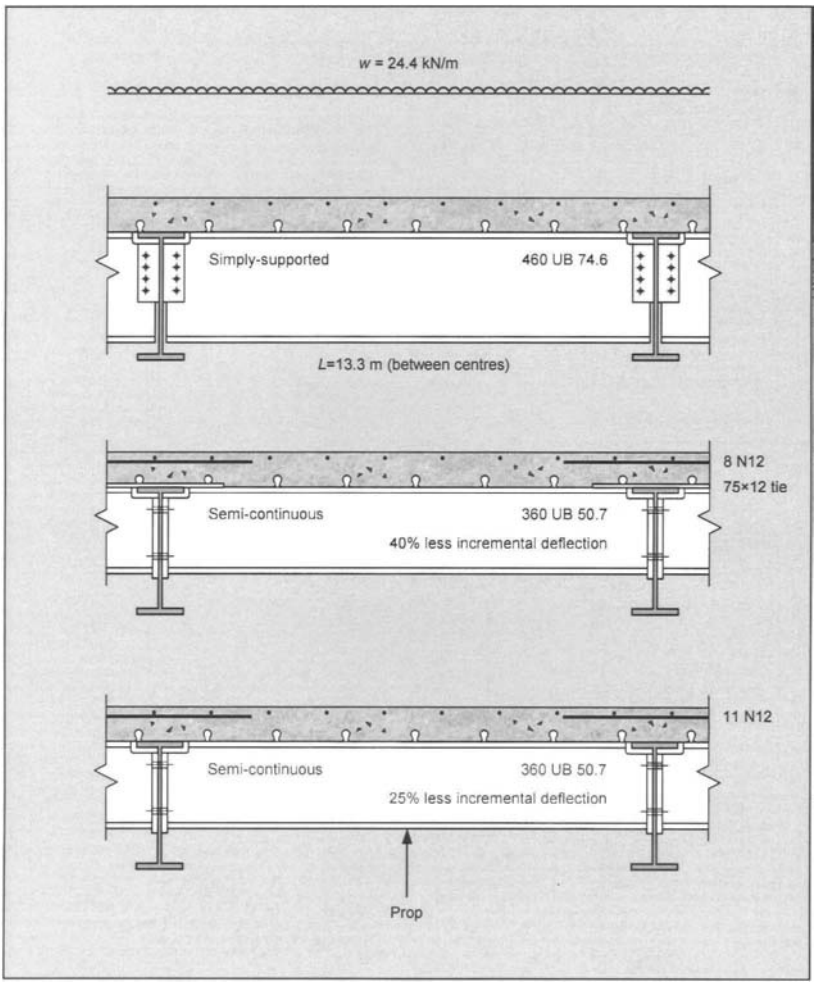


Figure 3: Secondary Beam in a Carpark

Primary Beam in a Carpark

A semi-continuous and a continuous beam option have been added to the simply-supported primary beam 'PB1' from scheme 1C of the BHP Design Guide for Economical Carparks (Watson *et al.* 1998), as shown in Figure 4. Again, continuous construction has resulted in significantly smaller beam sizes, while the total deflection, which was the governing factor in the simply-supported design, still reduced by 50% and 25% for the semi-continuous and continuous options respectively.

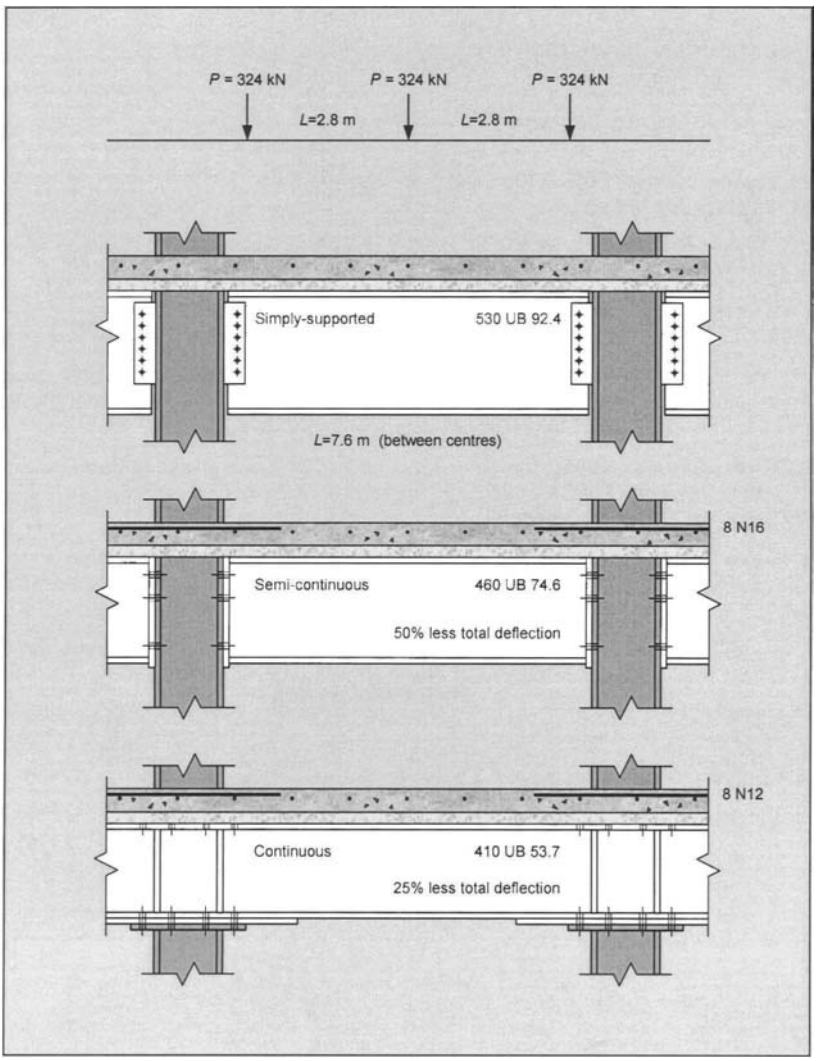


Figure 4: Primary Beam in a Carpark

CONCLUSIONS

Continuous composite beams have significant advantages compared to simply-supported composite beams, particularly with regard to serviceability performance. Continuous composite beams offer better crack control and lower deflections, even when the depth of the steel section is less than that required for the equivalent simply-supported beam. Continuous beams provide the designer with greater scope to vary design parameters, such as positive moment shear connection and negative moment reinforcement levels, to find the optimum solution for each situation. The perception that simply-supported composite beams have economic and construction benefits may be overemphasized. A rigorous cost-benefit analysis may show that continuous and semi-continuous composite beams should be the preferred construction option.

REFERENCES

Australian Institute of Steel Construction and Standards Australia (1997). *Composite Beam Design Handbook (SAA HB–1997)*, Sydney.

Berry, P.A., Bridge, R.Q., Patrick, M. and Wheeler, A.T. (2000). *Design Booklet DB5.1, Design of the Web-Side-Plate Steel Connection*, Ed. 1, OneSteel Market Mills, Sydney.

Berry, P.A., Bridge, R.Q. and Patrick, M. (2001a). *Design Booklet DB2.1, Design of Continuous Composite Beams with Rigid Connections for Strength*, Ed. 1, OneSteel Market Mills, Sydney.

Berry, P.A , Patrick, M. and Bridge, R.Q. (2001b). Development of Design Charts for Continuous and Semi-Continuous Composite Beams, *Proceedings, The First International Conference on Steel and Composite Structures (ICSCS'01)*, 14-16 June, Pusan, Korea, 369-376.

British Standards Institution (1994). *Eurocode 4: Design of Composite Steel and Concrete Structures, Part 1.1. General Rules and Rules for Buildings (together with United Kingdom National Application Document)*, DD ENV 1994-1-1, London.

Patrick, M., Berry, P.A. and Wheeler, A.T. (2002). Web-Side-Plate Framing Connections in both Steel and Composite Construction. *Proceedings, Advances in Building Technology*, 4-6 December, Hong Kong.

Patrick, M. and Dayawansa, P.H. (1998). Design of Continuous Composite Beams for Bending Strength. *Proceedings, Australasian Structural Engineering Conference*, Auckland.

Standards Australia (1996). *AS 2327.1–1996: Composite structures, Part 1: Simply supported beams*, Sydney.

Standards Australia (2001). *AS 3600–2001: Concrete Structures*, Sydney.

Steel Construction Institute (1998). *Joints in Steel Construction: Composite Connections*, SCI Publication 213, The Steel Construction Institute (in association with The British Constructional Steelwork Association), Ascot, United Kingdom.

Watson, K., Cottam, J. and Dallas, S. (1998). *Economical Carparks - A Design Guide*, Ed. 1., BHP Integrated Steel, Sydney.

Advances in Building Technology, Volume 1
M. Anson, J.M. Ko and E.S.S. Lam (Eds.)
© 2002 Elsevier Science Ltd. All rights reserved

INNOVATIONS IN COMPOSITE SLABS INCORPORATING PROFILED STEEL SHEETING

R.Q. Bridge and M. Patrick

Centre for Construction Technology & Research, College of Science, Technology & Environment, University of Western Sydney, Kingswood, NSW 2747, Australia,

ABSTRACT

The use of structural steel decking as a dual formwork/reinforcement system in Australian building practice has developed steadily since the 1960's. The pressure to improve conventional construction practices and to reduce construction time and overall cost coupled with competition from a number of manufacturers has led to new technological developments, the emergence of new applications, the development of new design methods and the improved education of design engineers.

KEYWORDS

Composite slab; design; friction; mechanical resistance; shear; standards; steel decking; tests.

INTRODUCTION

Non-composite, cellular steel decking originated in the USA in the early 1930's for constructing light-weight floors with in-floor services in steel-frame buildings, which led to the development of structural steel decking as we know it today (Dallaire, 1971). As part of this development, a less steel-intensive deck which acted compositely with the hardened concrete on account of steel reinforcing mesh welded to the decking, first appeared in 1950. Even more economical embossed decks were first developed in the 1960's (Viest, 1997) and composite slabs are now the preferred flooring alternative for steel-frame buildings in most developed countries. Despite its success in steel-frame buildings, steel decking has long been perceived as a "short-span (7-15 ft) construction, unsuitable to the longer spans of a concrete frame" (Dallaire, 1971). Several of the new developments described herein will eventually allow the Australian decks to be used structurally in concrete-frame

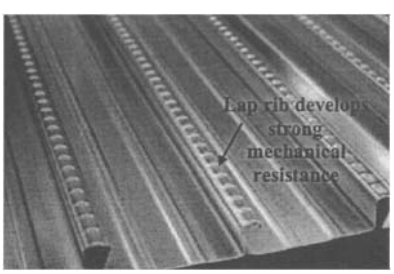


Fig. 1 An Australian Structural Steel Deck

buildings without any span restrictions applying (Patrick, 1998).

Composite slab construction has a long history of successful use in Australia, dating back to the mid-1960's. At that time there were no embossments on the dovetail ribs of the steel decking, Bondek, and the bond between the galvanised steel and concrete was principally achieved by chemical adhesion of the cement paste to the zinc coating. The major Australian decks now all include an asymmetric lap rib like that shown in Fig. 1 for Bondek II. It is now known that this type of rib develops strong mechanical resistance with hardened concrete, even if the rib is unembossed, although embossments are still very beneficial. An innovative small-scale test, developed by the authors, shows this. This and other innovations concerning composite slab behaviour and design are described herein.

STRUCTURAL DECKING - COMBINED FORMWORK/REINFORCEMENT SYSTEM

As steel decking can serve dual roles as both the formwork and as the main longitudinal tensile reinforcement in the bottom face of the slab, economic advantages should result compared with using removable formwork systems. In the case of short-span composite slabs typical of steel-frame buildings constructed unpropped, the large cross-sectional area of the decking, or more specifically its large tensile capacity, cannot normally be utilised efficiently in design for the composite stage. In this situation, the economic viability of the system is often governed by the formwork stage. Steel decking in its conventional trapezoidal form can also significantly reduce the strength of the shear connection between the steel beam and the slab, thereby reducing the efficiency of the composite beam.

For structural steel decking to be an advanced, efficient system, it must at least be possible for the decking to also be utilised efficiently during the composite stage. Neither should the decking impinge unduly on the performance of the composite member. Decks that develop strong mechanical resistance allow its tensile capacity to be well utilised in long-spanning or heavily-loaded situations. Otherwise, end anchorage is required, which may not be a practical or an economic proposition.

COMPOSITE SLAB CONSTRUCTION

Structural steel decking is produced with a wide variety of cross-section profiles. In the USA, there is a move to treat decking generically during the composite stage, in a bid to eliminate the need for standard slab testing. However, the amount of mechanical resistance they each develop with the concrete, which largely determines how effectively a deck can be used as longitudinal reinforcement in a slab, varies enormously depending on the decking profile and its features (see Fig. 2). The major American, British and European Standards for composite slabs, i.e. ANSI/ASCE 3-91, BS 5950: Part 4: 1994 and Eurocode 4: Part 1.1, permit any deck to be used compositely, irrespective of the amount of mechanical resistance it develops. However, the failure mode of a slab can be significantly affected by the strength (and ductility) of the shear connection (Patrick, 1989). This is at least recognised in Eurocode 4.

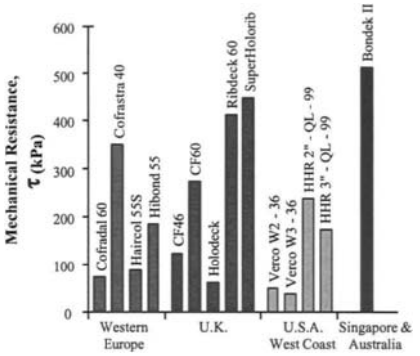


Fig. 2 Mechanical resistance developed by different steel decks (Patrick, 1990a)

The decks with very low mechanical resistance cannot be used in long spans. They can still be used without penalty in short spans and designed using the empirical shear-bond method (ASCE 3-91, BS5950: Part 4: 1994) even though their behaviour may be brittle. If the behaviour is ductile, i.e. if

the mechanical resistance is sufficiently high, then the more advanced partial shear connection strength theory (Patrick, 1990b, Bode and Sauerborn, 1991, Patrick and Bridge, 1994) may be used as an alternative design method. Partial shear connection strength theory has many significant advantages over the empirical shear-bond theory used in BS 5950: Part 4. The strength and ductility of the mechanical resistance that the steel decking develops in the hardened concrete is known which improves the understanding of the design engineer; the loading arrangement and termination of the decking ends can be directly included; and small-scale tests can be used to derive design values for the major parameters used in the strength model.

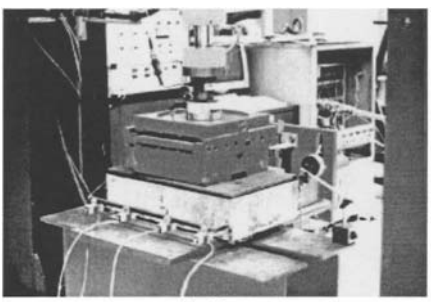
COMPOSITE SLABS INCORPORATING STRUCTURAL STEEL DECKING

Although designers of composite slabs often focus on the determination of shear-bond capacity, for the Australian decks which can develop strong, ductile mechanical resistance, there are many other issues that should be of equal importance to the designer. Some of these are touched upon in this section.

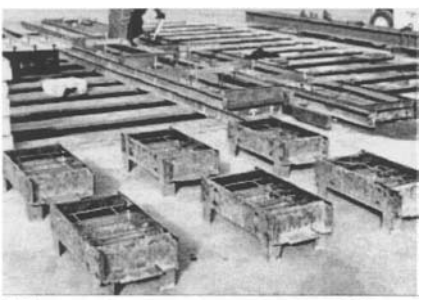
Structural Testing

Detailed reports have been prepared which explain the tests that were conducted on nine composite slabs incorporating Bondek II structural steel decking. The basis for the tests, performed on slabs and Slip-Block™ Test specimens, has been fully documented after a detailed review of BS 5950: Part 4: 1982 (Patrick, 1991). The test results have been examined in detail (Patrick, 1994), and are briefly discussed in the analysis of test results that follows. All of these tests were concerned with the strength limit states of shear-bond or longitudinal slip, and flexure. A separate experimental investigation has been made into the effects of vertical shear, another important strength limit state (Patrick, 1993). This investigation showed that the design provisions for vertical shear in BS 5950: Part 4 and Eurocode 4: Part 1.1 are incorrect (Johnson, 1994).

Six slabs were tested in strict accordance with BS 5950: Part 4: 1982 to develop the shear-bond relationship (m and k values) to be used in design for a particular bare metal thickness t_b = 0.75 mm. Therefore, these slabs were designed to fail by longitudinal slip. Partial shear connection strength theory, and prior knowledge of the shear connection performance of the decking obtained from the Slip-Block™ Test, made this possible. It was necessary to limit the span of each of these test slabs so that they would not fail by flexure. The Slip-Block™ Test set-up is shown in Fig. 3(a), while a group of typical test specimens is shown prior to being poured in Fig. 3(b), and the test procedure is described elsewhere (Patrick, 1990b, 1994; Standards Australia, 1997).



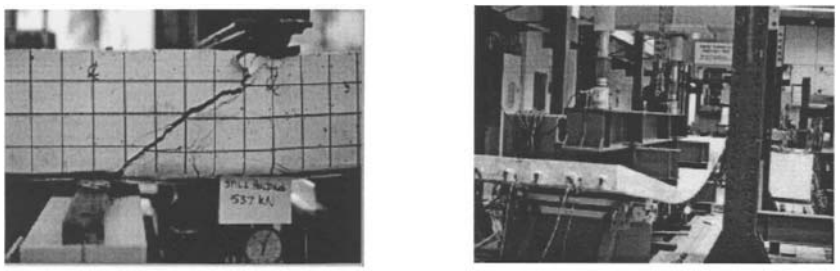
(a) Test set-up



(b) Test specimens as companions to slabs

Fig. 3 The Slip-Block™ Test

Fourteen simply-supported composite slabs were tested for vertical shear (Patrick, 1993). These are the first-known tests of their kind. The slabs were designed such that they could not fail by longitudinal slip if loaded at any location between the supports. Diagonal splitting failure was observed in some of the tests when loaded very close to the supports (see Fig. 4(a)). Flexural failure occurred if they were not loaded close to the supports. A slab could experience very large deflections in excess of span/30 in order to fracture the steel decking (see Fig. 4(b)).



(a) Diagonal splitting failure (b) Flexural failure

Fig. 4 Vertical Shear and Flexural Slab Tests

Analysis of Test Results for Design

The results from testing over eighty Slip-Block™ Test specimens have been used to derive a design relationship between mechanical resistance τ (kPa), bare metal thickness t_b (mm) and concrete compressive strength f'_c (MPa), viz. $\tau = 88\sqrt{(t_b f'_c)}$. The strength model assumed using partial shear connection strength theory which includes support friction is explained elsewhere (Patrick, 1989). The results of the Slip-Block™ Test gave accurate predictions of the slab strengths gained in the tests. Accurate prediction of the ultimate strength of slabs that failed by either longitudinal slip or flexure is illustrated by Fig. 5(a). The results in Fig. 5(b) illustrate the importance of including frictional resistance developed at the support in the strength prediction.

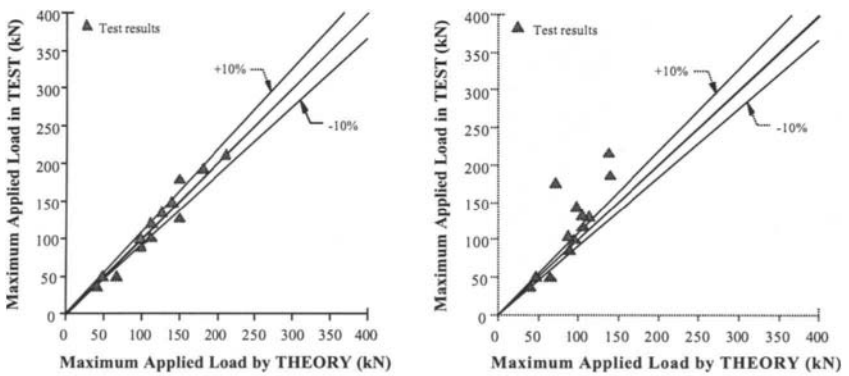


Fig. 5 Strength Predictions Using Partial Shear Connection Strength Theory (Patrick, 1994)

It can be seen from this latter figure that the strength of some of the slabs cannot be explained if friction is ignored. Support friction can have a significant effect on the strength of composite slabs when the decking passes over supports, which is the normal case in steel-frame building construction (Johnson, 1994; Johnson and Anderson, 1993; Bode and Minas, 1997).

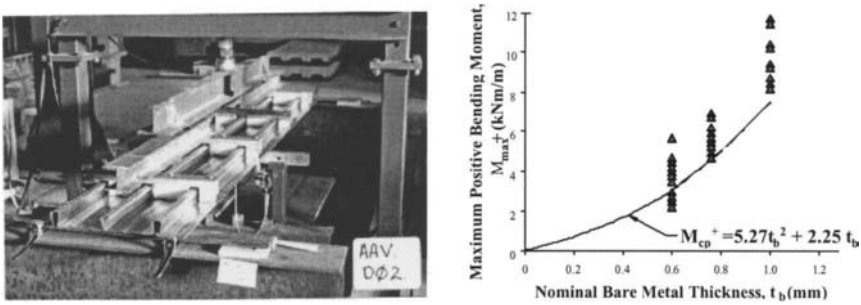
STRUCTURAL STEEL DECKING AS PERMANENT FORMWORK

Structural Testing

Extensive structural testing of the Bondek steel decking in single and multiple span arrangements has been performed in order to model the behaviour of the decking during the formwork stage. Simple design rules have been developed for calculating design action effects, design ultimate moments of resistance, design end shear resistance, effective bending stiffness and minimum bearing lengths under uniformly-distributed loading conditions. Some tests were also performed using concentrated loads, while all the tests were conducted in the absence of any wet concrete. Thus the decking can be designed using a consistent approach through the whole construction process, ignoring any increase in strength due to the stabilising effect of wet concrete.

The tests were performed in accordance with British Standard BS 5950: Part 4: 1982, which has subsequently been superseded by BS 5950: Part 4: 1994. The 1982 edition of BS 5950: Part 4 allowed the strength of the decking to be determined by testing. This option was taken with regard to both strength and deflection since it had been determined that the analytical methods in BS 5950: Part 4: 1982 were not appropriate for Bondek and resulted in unconservative designs. This is on account of the complex, undesirable behaviour of the lap joint which causes the decking to exhibit such effects as flange curling (with associated amplified lateral flange displacements and pan lifting), warping of lap joint flanges (consistent with shear lag effects), distortional buckling, moment softening, etc.

Reference is made in BS 5950: Part 4: 1994 to Section 7 of BS 5950: Part 6: 1995 to determine the strength and stiffness of the steel decking during the formwork stage. These testing provisions are essentially the same as those referred to in BS 5950: Part 4: 1982. The tests comprised: mid-span bending under distributed loading (21 tests); bending at a support under distributed loading (13 two-span and 10 three-span tests); shear at an end support (12 tests); and point-loading tests (20 tests).



(a) Mid-span bending test (b) Design relationship and test results

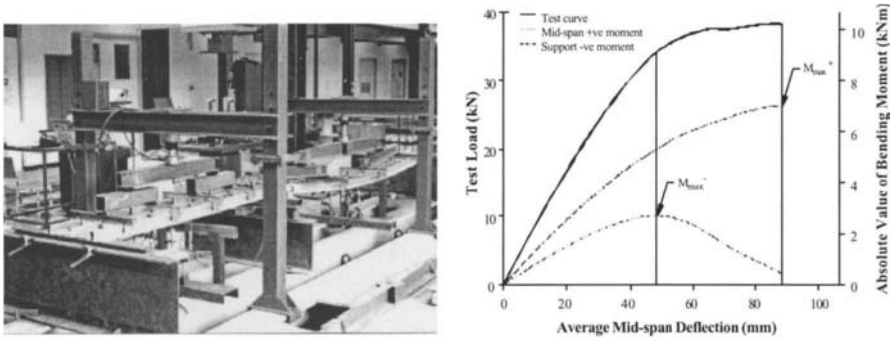
Fig. 6 Design Ultimate Positive Moment of Resistance

Analysis of Test Results for Design

Forty-four test results were available to determine the design ultimate positive moment of resistance M_{cp}^+. Some of these came from mid-span bending tests (see Fig. 6(a)). The design relationship

between M_{cp}^{+} and bare metal thickness t_b is shown in Fig. 6(b) along with the test results. The maximum positive bending moments obtained in the tests were used. This was also the case for the multi-span tests (see Fig. 7(a)) in which moment-softening was exhibited at internal supports (see Fig. 7(b)).

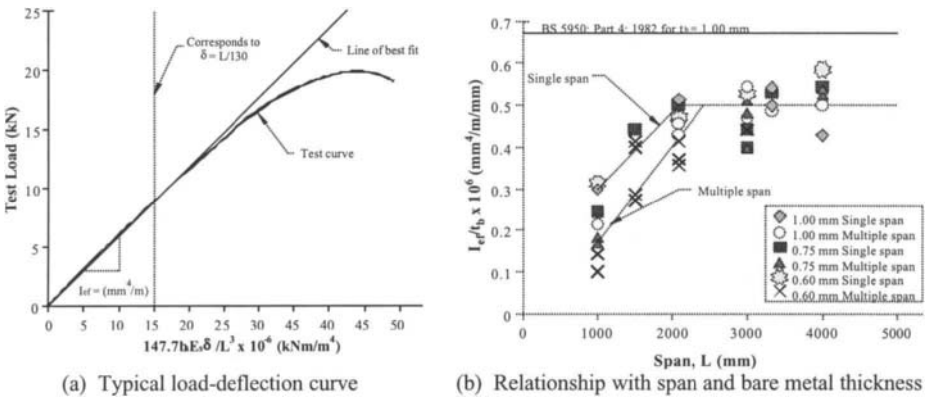
The tests for bending at a support under distributed loading (see Fig. 7(a)) revealed that the continuous spans effectively became simply-supported due to substantial moment-softening of the support regions prior to the maximum positive bending moment being reached in the mid-span regions (see Fig. 7(b)). The sheets tended to shed load suddenly when the maximum positive moment was reached. Therefore, the design ultimate negative moment of resistance is assumed to equal zero, i.e. $M_{cp}^{-} = 0$.



(a) Bending at a support test *(b) Support softening*

Fig. 7 Design Ultimate Negative Moment of Resistance

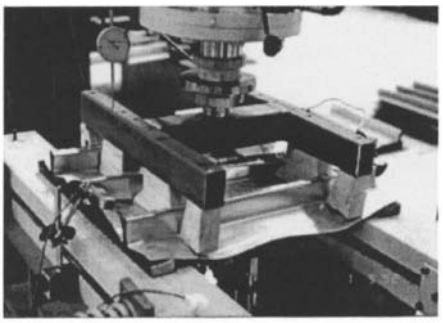
Estimates for the effective bending stiffness $E_s I_{ef}$ were determined from the slope of the linear-elastic portion of the load-deflection curves for the forty-four tests mentioned above (see Fig. 8(a)). The assumptions made were that the decking had a constant section, response was linear-elastic up to a mid-span deflection of span(L)/130, and $E_s = 210$ GPa. Linear regression analysis of the test data gave the relationships shown in Fig. 8(b) for single- and multiple-span situations. It can be noticed that the minimum and maximum spans tested were 1000 and 4000 mm, respectively.



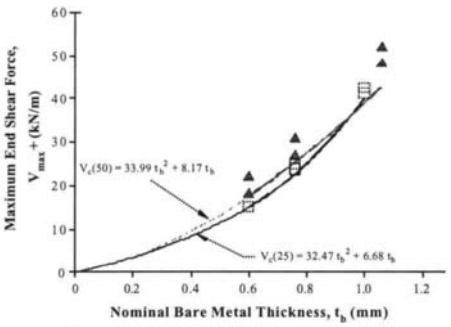
(a) Typical load-deflection curve (b) Relationship with span and bare metal thickness

Fig. 8 Effective Bending Stiffness

The relationship between design end shear capacity V_c and bare metal thickness t_b (see Fig. 9(b)) was determined from the end shear tests (see Fig. 9(a)). Two end bearing lengths of 25 and 50 mm were investigated. It was found that the bearing length had only a small effect on the shear capacity at a simple support.



(a) End shear test



(b) Relationships with bare metal thickness

Fig. 9 Design End Shear Resistance

Relationships were also derived for the design ultimate point load (P_u) that could be applied in pans away from the decking edge. Span (L) and bare metal thickness (t_b) had a significant effect on the strength of the decking when supporting point loads. The load must be applied over an area of at least 100×100 mm^2, and at least one screw fastener must be placed in the lap joint at each mid-span location. Maximum spans were derived so that a point load of 2.3 kN can be supported with a load factor of 1.5, although for t_b =1.0 mm, L was limited to the maximum span tested (3250 mm).

NEW DEVELOPMENTS

The Centre for Construction Technology and Research at the University of Western Sydney has been developing a new long-spanning composite steel-concrete floor system called TRUSSDEK™ (OneSteel Reinforcing, 2001) in conjunction with a leading Australian company OneSteel Reinforcing. TRUSSDEK™ is a patented, ultra-lightweight, permanent combined formwork and reinforcement system incorporating light steel trusses with a structural deck that offers unrivalled spanning capabilities compared with other steel decking systems in Australia and is the winner of the prestigious 2001 Australian Design Award™. The product and its use on a project are shown in Fig. 10.

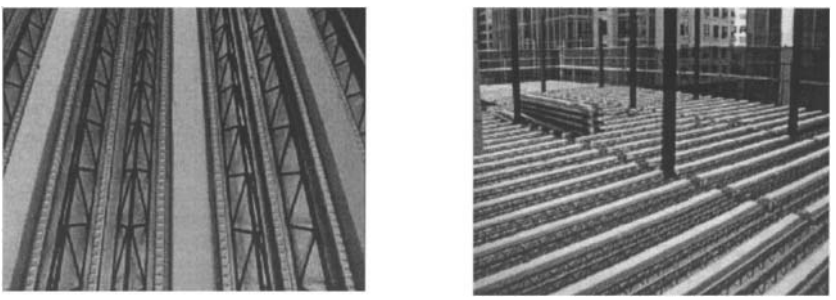


Fig. 10 TRUSSDEK™ long-spanning floor construction system

CONCLUSIONS

Structural steel decking has advanced as a dual formwork/reinforcement system in Australian building practice. Decks with strong mechanical resistance and ductile behaviour have been developed. Some innovative concepts and testing that have allowed these developments to occur have been described.

REFERENCES

ASCE 3-91 (1994). *Standard for the Structural Design of Composite Slabs*. American Society of Civil Engineers, New York.

BHP Structural Steel (1998). *Composite Structures Design Manual - Design of Composite Slabs for Strength.* Design Booklet DB3.1, May.

Bode, H. and Minas, F. (1997) Composite Slabs with and without End Anchorage under Static and Dynamic Loading. *Conference Report*, International Conf. on Composite Construction - Conventional and Innovative, IABSE, Innsbruck, Sept.

Bode, H. and Sauerborn, I. (1991). Partial Shear Connection Design of Composite Slabs. *Proceedings*, 3rd Int. Conf. Steel-Concrete Composite Structures, ICCS-3, Fukuoka, Japan, 467- 472.

BS 5950: Part 4: 1982. *Structural Use of Steelwork in Building, Part 4. Code of Practice for Design of Floors with Profiled Steel Sheeting*. British Standards Institution, London.

BS 5950: Part 4: 1994. *Structural Use of Steelwork in Building, Part 4. Code of Practice for Design of Design of Composite Slabs with Profiled Steel Sheeting*. British Standards Institution, London,

BS 5950: Part 6: 1995. *Structural Use of Steelwork in Building, Part 6. Code of Practice for Design of Light Gauge Profiled Steel Sheeting*. British Standards Institution, London.

Dallaire, E.E. (1971). Cellular Steel Floors Mature. *Civil Engineering*, ASCE, July, 70-74.

Eurocode 4: (1994). *Design of Composite Steel and Concrete Structures, Part 1.1. General Rules and Rules for Buildings (United Kingdom National Application Document).* DD ENV 1994-1-1: 1994, British Standards Institution, London.

Johnson, R.P. (1994). *Composite Structures of Steel and Concrete, Volume 1: Beams, Slabs, Columns, and Frames for Buildings*. 2nd ed., Blackwall Scientific Publ. London.

Johnson R.P. and Anderson, D. (1993). *Designers' Handbook to Eurocode 4, Part 1.1: Design of Composite Steel and Concrete Structures*. Thomas Telford, London.

OneSteel Reinforcing (2001). *Trussdek Span Charts.* OneSteel Reinforcing, Sydney, Australia

Patrick, M., (1989). Design of Continuous Composite Slabs - The Issue of Ductility. *AISC Steel Construction Journal*, **23:3**, 2-10.

Patrick, M. (1990a). The Slip Block Test — Experience with Some Overseas Profiles (Part A). *BHP Melb. Res. Labs Report*, MRL/PS64/90/021, June.

Patrick, M. (1990b). A New Partial Shear Connection Strength Model for Composite Slabs. *AISC Steel Construction Journal*, **24:3**, 2-17.

Patrick, M. (1991). Proposed Bondek II Composite Slab Tests to British Standard BS 5950: Part 4: 1982. *BHP Melb. Res. Labs Report*, BHPRML/PS64/91/029, Jan., 1991.

Patrick, M. (1993). Testing and Design of Bondek II Composite Slabs for Vertical Shear. *AISC Steel Construction Journal*, **27:2**, 2-26.

Patrick, M. (1994). *Shear Connection Performance of Profiled Steel Sheeting in Composite Slabs.* PhD Thesis, School of Civil Engineering, Univ. of Sydney.

Patrick, M., (1998). The Application of Structural Steel Decking to Commercial and Residential Buildings, *Malaysian Structural Steel Association Convention*, Dec.

Patrick, M. and Bridge, R.Q. (1994) Partial Shear Connection Design of Composite Slabs. *Engineering Structures Journal*, **16:4**, 348-362.

Standards Australia (1997*). Methods of Test for Elements of Composite Construction, Method 1: Slip-Block Test*. Proposed Standard, BD/32-0090-203, Oct.

Viest, I.M. (1997). Studies of Composite Construction at Illinois and Lehigh, 1940-1978. *Proceedings, Composite Construction in Steel and Concrete III*, ASCE, Irsee, 1-14.

Advances in Building Technology, Volume 1
M. Anson, J.M. Ko and E.S.S. Lam (Eds.)
© 2002 Elsevier Science Ltd. All rights reserved

WEB-SIDE-PLATE FRAMING CONNECTIONS IN BOTH STEEL AND COMPOSITE CONSTRUCTION

M. Patrick, P.A. Berry and A.T. Wheeler

Centre for Construction Technology & Research, College of Science, Technology & Environment, University of Western Sydney, Kingswood, NSW 2747, Australia,

ABSTRACT

The web-side-plate connection is by far the most common connection used in Australia to support simply-supported steel or composite beams in steel building frames. It is also used extensively in other developed countries, although it is known by different names and its details may vary to some degree.

An up-to-date, detailed review was made of Australian and overseas research and design practice for the web-side-plate steel connection. This led to an extensive series of new Australian tests being undertaken on the connection using a novel test rig, and an improved design model being developed for the connection in the bare steel state. This allowed some significant restrictions to be removed that applied at the time to the Australian limit-state design method for the steel connection.

In composite construction, longitudinal reinforcement located in the concrete slab over the connection, which is needed for crack control, can cause significant compressive force to develop in the cleat. The effect of this force has normally been ignored in design, irrespective of its potential magnitude. This can cause problems in practice under both serviceability and ultimate load conditions, which can only be avoided if the behaviour of the web-side-plate composite connection is better understood and appropriate design rules are developed. Preliminary results from several types of tests undertaken for this purpose are presented and briefly discussed. Future work is also described.

KEYWORDS

Web-side-plate connection; single-plate connection; fin plate; steel connection; composite connection.

INTRODUCTION

The web-side-plate steel connection is used to connect steel or composite beams to a supporting member or element such as a steel beam, a steel column or a concrete core wall. The type of construction envisaged is shown in Figure 1, noting that the uncoped primary and coped secondary

steel beams shown could equally be elements of composite beams if shear connectors and a concrete slab were located on top of the steel beams. It has been assumed to qualify as being suitable for simple construction according to AS 4100 (Standards Australia 1998).

When the web-side-plate steel connection is used with composite beams, the longitudinal reinforcement in the slab can lead to continuity, thus developing a resultant compressive force in the cleat. In this instance, the connection is referred to as a web-side-plate composite connection. The compressive force in the cleat can affect the behaviour of the connection at ultimate load. Design rules developed by Berry et al. (2001) place an upper limit on the compressive force developed in the cleat at ultimate load, and provided that this condition is met, the connection may be treated as a web-side-plate steel connection. Design rules that allow for composite action are currently under development.

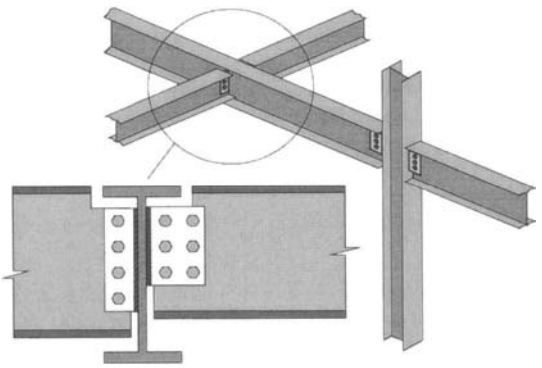


Figure 1: Typical construction using the web-side-plate steel connection

WEB-SIDE-PLATE STEEL CONNECTION

Review of Research and Design Practice

An up-to-date, detailed review has been made of Australian and overseas research and design practice for the web-side-plate steel connection (Berry, et al. 2000b). This led to an extensive series of new Australian tests being undertaken on the connection using a novel test rig, and an improved design model for the bare steel connection being developed. Moreover, the rotation capacity or ductility of the connection was found to be much greater than previously believed. This allowed some significant restrictions to be removed that applied at the time to the limit-state Australian design method for the connection (Hogan & Thomas 1994). Some significant advantages that followed, which lead to economic improvements, are that much more flexible beams may be supported by the connection (allowing much longer spans), much smaller welds are required, and fewer bolts and/or thinner cleats may be used in equivalent situations. Also, thicker cleats than were previously allowed may be specified, whereby the large additional strength of double-column bolt groups over single-column groups can be utilised leading to shallower connections with improved rotation capacity. Australian design engineers now use the improved design method (Berry et al. 2000a) and associated software.

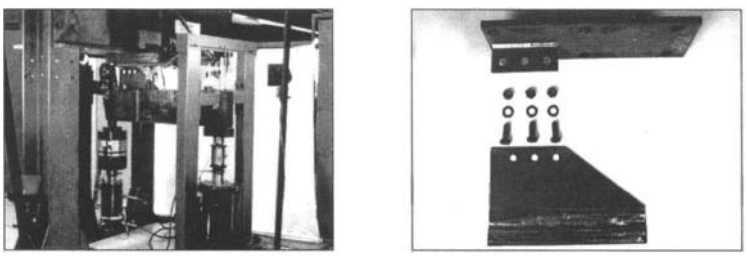
Test Program

A highly innovative program of laboratory testing was undertaken to study the moment-rotation behaviour of the web-side-plate steel connection, and to gain values for key parameters used in the

design model when the connection is attached to a rigid support (Berry et al. 2000a). The test rig that was used is unique, and it allowed over 50 tests to be performed to study the effect of major parameters such as plate thickness, steel grade and different bolt group arrangements. Moreover, the rig was also designed to simulate the conditions experienced for the web-side-plate composite connection - see Figure 4. It is planned in the future that other innovative types of tests will be performed to greatly reduce the need for testing full-scale composite connections, the results from which other researchers have previously depended too heavily upon.

In previous work in Australia, the web-side-plate steel connection has been tested in the rigid support condition using a relatively complex procedure of lowering the free end of a long steel beam attached by the connection to a column (Pham & Mansell 1982, Patrick et al. 1986). Xiao et al. (1994) and other overseas researchers have performed tests on the web-side-plate composite connection, although only small numbers of tests have been performed, typically in a conventional cruciform arrangement involving twin cantilever steel beams connected to a continuous composite slab. Patrick et al. (1986) have explained some of the technical limitations with tests of this type. The economic disadvantage is obvious, and largely explains why so few tests have been performed; a problem it seems is common to connection testing. Also, the compressive force in the steel part of the connection has not been measured, and nor can it necessarily be determined accurately from the test results, even though this is a critical consideration during the modelling and design of the connection components. Ren (1995) claims to have performed the first tests of their type on several other types of bare steel connections (e.g. double angle cleats) to investigate the effect of axial compressive force on moment-rotation response. Ren attempted to simulate the conditions experienced by a steel connection at a support in the hogging moment region of a continuous composite beam. A test rig was devised whereby a vertical force was applied at the end of a steel beam which could be rotated and fixed in one of four possible positions, ranging from a cantilever (no axial force with the beam horizontal) through to a column (no bending with the beam vertical). Otherwise, the load was applied at either 30 or 60 degrees to the longitudinal axis of the steel beam. A disadvantage with this system is that the ratio of axial force to shear force effectively remains constant during a test, and is not affected by the behaviour of the connection, which it would be in a beam in a real structure.

The special test rig shown in Figure 2(a) was developed which uses small plate specimens like that shown in Figure 2(b) to simulate a web-side-plate connection subjected to rotation in either the bare steel or composite states. Shear force is assumed to not significantly affect the response and is not applied during the test. The test specimens do not incorporate a steel beam or a concrete slab, whereby the cost and time associated with their construction and testing is very considerably reduced. Therefore, it is possible to conduct a comparatively large number of tests, and thus systematically examine the effect that different variables have on moment-rotation response.



(a) Overview of moment-rotation test rig (b) Typical test specimen components

Figure 2: Special moment-rotation test rig and typical unassembled test specimen

WEB-SIDE-PLATE COMPOSITE CONNECTION

Review of Research and Design Practice

Overseas researchers are currently focussing their attention on the development of composite connections or joints that can be used with semi-continuous or continuous composite beams (Anderson 2000, Kemp & Nethercot 2000, Crisinel & Kattner 2000). The behaviour of the web-side-plate composite connection has previously been investigated in full-scale tests (Xiao et al. 1994), and a design method has been proposed for predicting moment capacity using the results of six tests (Ahmed et al. 1997). However, like some other types of connections that do not permit the compressive force in the bottom flange of the steel beam to be transmitted directly through the connection, its moment capacity and rotational stiffness are low. Some modifications have been made to the web-side-plate composite connection, which involve the use of a contact plate, or an angle, placed between the bottom flange and the support, in order to improve the strength and stiffness (Ahmed et al. 1997, Bode & Kronenberger 1996, Robertson 1997). However, the primary objective of this investigation will be to study the web-side-plate composite connection as it is constructed in practice in many composite buildings in Australia. Modifications to the connection to improve performance for use with continuous composite beams are beyond the scope of the investigation.

Limited studies have been made into the behaviour of the web-side-plate composite connection, and adequate design models do not exist, the connection normally being designed ignoring composite action and treating it as an ordinary web-side-plate steel connection. Design models are needed to address serviceability design issues, particularly crack control, as well as strength.

Australian Construction Practice

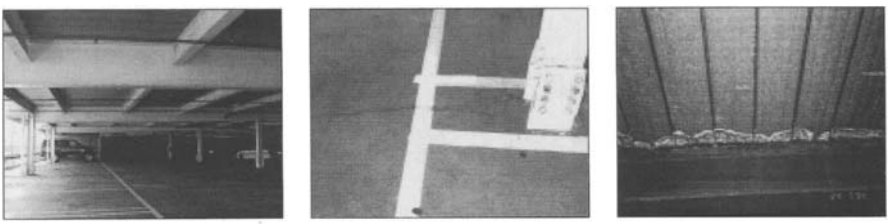
Extensive use is made of composite construction in multi-storey buildings in developed countries. Australian Standard AS 2327.1 addresses the design of simply-supported composite beams, and most composite beams in Australian buildings take this form. This is because the design calculations are simple to perform, and the web-side-plate steel connection can be used in the steel frame, which is simple to fabricate and erection of the structural steel is rapid.

An important restriction has been placed on the use of the new, improved design method for the web-side-plate steel connection (Berry et al. 2000b), viz.: the compressive force that develops in the cleat at the strength limit state must not exceed 15 percent of its nominal squash load, i.e. $0.15 f_{yi} t_i d_i$, where these variables are the yield stress, thickness and overall depth of the cleat, respectively. Larger compressive forces may adversely affect the moment-rotation response of the connection, which is critical in design. No guidance is given to designers using the improved method if the compressive force in the cleat exceeds this limit. Then they do not have a design model to use.

In a floor of a building comprising simply-supported composite beams, compressive force develops in the cleats wherever the concrete slab extends between adjacent ends of the composite beams, and continuity of longitudinal reinforcement in the slab causes the reinforcement to be in tension over the connections. The limit placed on the maximum compressive force that may act on the cleat of a web-side-plate connection directly affects the maximum amount of longitudinal reinforcing steel that may be placed in the concrete slab.

Cracking of the concrete slab needs to be controlled in composite buildings where durability is important such as in multi-storey carparks. There are cases in Australia of composite carparks that are excessively cracked due to an inadequate amount of reinforcement in the slab over the web-side-plate connections. Some of them are in disrepair despite still being used (see Figure 3). Cracking can also cause concern in buildings with brittle floor finishes, or where the cracks can form directly along lines

of shear connectors raising questions about the integrity of the shear connection. Again, this is a common occurrence in Australian composite buildings incorporating web-side-plate steel connections. Temporary propping of the supporting steelwork during construction greatly increases the chance of excessive cracking occurring, and normally the concrete cracks immediately the props are removed. If the quantity of reinforcing steel is small and it yields at the same time the props are removed, then the crack widths become uncontrollable. Even in unpropped construction, normal drying shrinkage of the concrete during the early life of a floor in a building can cause excessively wide cracks to form over web-side-plate connections at the beam ends. In order to control cracking, there needs to be a sufficient quantity of longitudinal reinforcement over the connections.



(a) Open-deck layout (b) Excessively wide cracks (c) Corrosion of steel

Figure 3: Australian carpark constructed with web-side-plate connections

The latest Australian design guidance on controlling cracking in concrete slabs of continuous composite beams (Berry et al. 2001) indicates that, typically, the tensile capacity of the reinforcement will be greatly in excess of 15 percent of the cleat squash load. Clear examples of this situation can readily be taken from an Australian design guide for carparks (Watson et al. 1998), that requires additional reinforcement to be placed over the web-side-plate connections to provide crack control. Typically, the tensile capacity of the additional bars alone is more than four times the limit placed on the maximum cleat compressive force. Moreover, in designs involving the largest web-side-plate connections, the compressive force in the cleat could be in excess of 100 tonnes. Therefore, new design rules are needed to cater for greater compressive force in the cleat if cracking is to be controlled. The problem cannot be simply overcome by increasing the thickness and/or yield stress of the cleat, and therefore its squash load, to enable the connection to be designed ignoring composite action. This is because the beam web or the bolt group would then become the component that controls the moment-rotation response of the connection rather than the cleat. An upper limit on the compressive force is necessary using the current design model.

It follows from above that design rules for the web-side-plate composite connection are required with some urgency, viz.: (a) design engineers who choose to comply with the limit on cleat compressive force and use light amounts of reinforcement will continue to experience excessively wide cracks, and therefore problems associated with poor durability and aesthetics; while (b) those who ignore the limit by using large amounts of reinforcement needed for crack control, may be well outside the scope of the existing design model, and risk premature or sudden structural failure of the connections and therefore the beams.

New Australian design rules for more substantial types of composite connections, including partial strength and full strength versions, have recently been developed (Berry et al. 2001). However, many situations will still require the web-side-plate composite connection to be widely used in various parts of a composite floor. For example, it is likely to continue to be the preferred alternative for composite secondary beams, or where the beam ends frame into building edges and logically remain simple supports.

Test Program

The test rig shown in Figure 2(a) has been designed to also simulate the behaviour of the web-side-plate composite connection by allowing a steel pin to be inserted into the rig as explained by Figure 4.

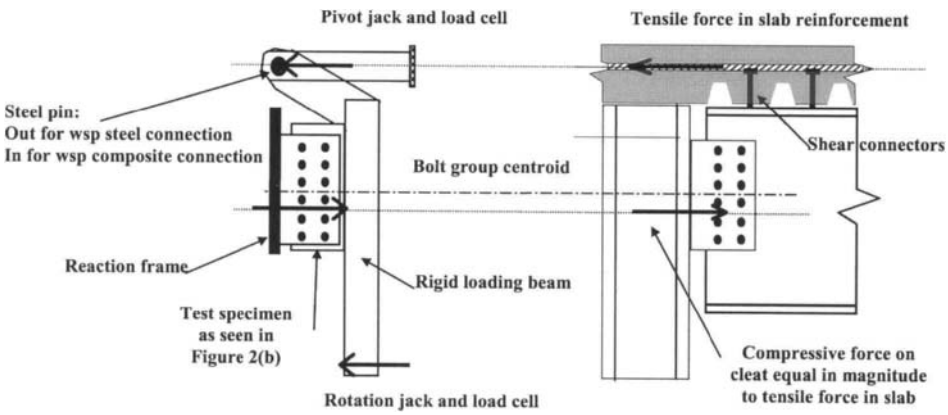
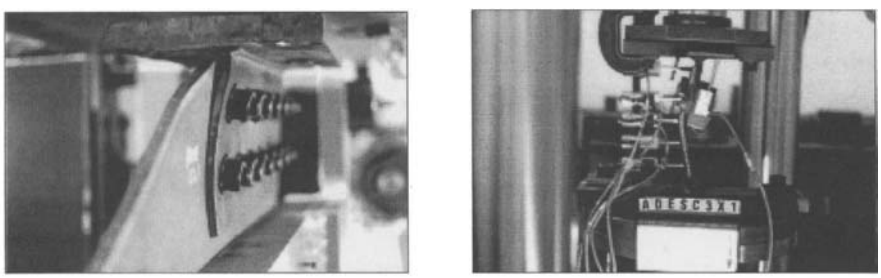


Figure 4: Testing of the web-side-plate composite connection

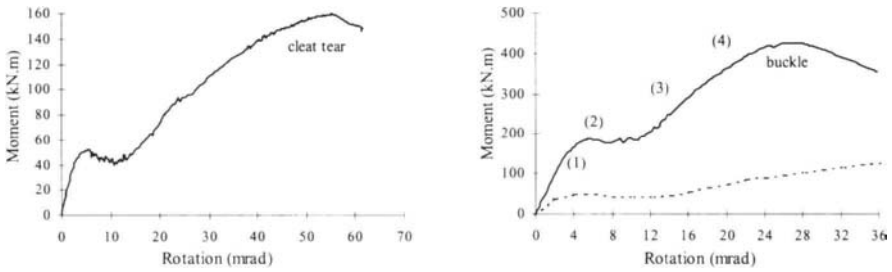
When large compressive force acts with the steel pin engaged, the connection could buckle as seen in Figure 5(a). Other small-scale tests like that shown in Figure 5(b) have also been performed to investigate the complex interaction between the cleat, beam web and bolt group.



(a) Buckled specimen in moment-rotation test rig (b) Buckled bolted web and cleat strip

Figure 5: Tests involving buckling of web-side-plate connection

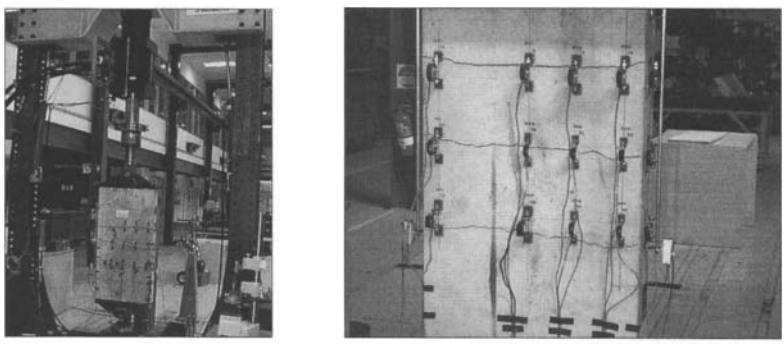
Some preliminary test results have already been obtained using the test rig shown in Figures 2(a) and 4, with the pin engaged to simulate the situation for a web-side-plate composite connection. Referring to Figures 6(a) and (b), which came from tests on web-side-plate steel and composite connections, respectively, with a 6×2 bolt group, the 300 MPa grade cleat and web plates were both 10 mm thick. Part of the same bare steel curve is shown dashed in Figure 6(b). It can be seen that both the secant stiffness and moment capacity were significantly increased in the composite connection, while rotation capacity was greatly reduced. Also in this test on the composite connection, the compressive force on the cleat reached 988 kN, which explains the change in failure mode from a cleat tear to a cleat/web buckle, cf. Figure 6(a).



(a) Web-side-plate steel connection (6×2) (b) Web-side-plate composite connection (6×2)

Figure 6: Comparison of results from steel and composite web-side-side plate tests

Another special test rig shown in Figure 7(a) has also already been built to investigate the development of cracking in concrete or composite slabs under direct tension (Adams & Patrick 1998). For example, the test specimens (see Figure 7(b)) can represent a composite slab incorporating profiled steel sheeting situated in the vicinity of a secondary-to-primary beam connection. In this region, tension is created from secondary-beam end rotation. The sheeting spans perpendicular to the secondary beams, and therefore to the direction of the tensile force. Control of cracking in this region is of particular concern due to the discontinuity in the concrete created by the sheeting ribs.



(a) Overview of test rig (b) Typical test specimen

Figure 7: Direct tension tests on reinforced composite slab

CONCLUSIONS

New Australian research has led to improvements in the design of the web-side-plate steel connection, and as a consequence, also of the simply-supported beams they support.

A number of composite buildings in Australia that have been constructed using the web-side-plate connection have had excessively wide cracks develop in the concrete slabs. This is because the beams have been designed as simply-supported without any consideration being given to this serviceability issue. The compressive force that develops on the connection when the slab is continuous, which can reduce its shear capacity and ductility, has also been ignored. Further research, supported by the results of a carefully-planned experimental program using the types of tests described in the paper, is required

before the web-side-plate composite connection can also be designed with sufficient confidence to avoid problems in practice.

REFERENCES

Adams, J.C. and Patrick, M. (1998). *Testing of the Web-Side-Plate Semi-Rigid Composite Connection*, Proc. Australasian Structural Engineering Conference (ASEC-98), Auckland, 133-140.

Ahmed, B., Li, T.Q. and Nethercot, D.A. (1997). Design of Composite Finplate and Angle Cleated Connections, *J. Construct. Steel Research,* **41**, 1-29.

Anderson, D. (2000). *European Recommendations for the Design of Composite Joints*, Theorie und Praxis im Konstruktiven Ingenieurbau (Festschrift zu Ehren von Prof. Dr.-Ing. Helmut Bode), Ibidem-Verlag, Stuttgart, 457-464.

Berry, P.A., Bridge, R.Q., Patrick, M. and Wheeler, A.T. (2000a). *Design Booklet DB5.1, Design of the Web-Side-Plate Steel Connection*, Ed. 1, OneSteel Market Mills.

Berry, P.A., Bridge, R.Q., Patrick, M. and Wheeler, A.T. (2000b). *Design Booklet SDB5.1, Supplement - Web-Side-Plate Steel Connection Improved Design Method*, Ed. 1, OneSteel Market Mills.

Berry, P.A., Bridge, R.Q. and Patrick, M. (2001). *Design Booklet DB2.1, Design of Continuous Composite Beams with Rigid Connections for Strength*, Ed. 1, OneSteel Market Mills.

Bode, H. and Kronenberger, H.J. (1996). *Behaviour of Composite Joints and their Influence on Semi-Continuous Composite Beams*, Composite Construction in Steel and Concrete III, Proc. Engineering Foundation Conference, Irsee, Germany, ASCE, 766-779.

Crisinel, M. and Kattner, M. (2000). *A Design Method for Braced Steel Frames Comprising Semi-Continuous Composite Joints*, Proc. Engineering Foundation Conf., Composite Construction IV, Vol. 1, M1: Composite Systems I.

Hogan, T. J. and Thomas, I. R. (1994). *Design of Structural Connections*, 4th Edition, Australian Institute of Steel Construction, Sydney.

Kemp, A.R. and Nethercot, D.A., *Satisfying Ductility Criteria in Continuous Composite Beams*, Proc. Engineering Foundation Conf., Composite Construction IV, Vol. 1, T1: Composite Beams, May, 2000.

Patrick, M., Thomas, I.R. and Bennetts, I.D. (1986). Testing of the web-side-plate connection, *Australian Welding Research,* AWRA Report P6-1-87.

Pham, L. and Mansell, D.S. (1982). Testing of standardised connections, *Australian Welding Research,* AWRA Report P6-22-81.

Ren, P. (1995). *Numerical modelling and experimental analysis of steel beam-to-column connections allowing for the influence of reinforced-concrete slabs*, Swiss Federal Institute of Technology, Lausanne, Thesis No. 1369.

Robertson, B.W. (1997). *Semi-continuous Composite Beams*, BE Thesis, Dept. Civil, Mining and Environmental Engineering, University of Wollongong.

Standards Australia (1998), *AS 4100-2000: Steel Structures*, Sydney.

Watson, K.B., et al. (1998). *Economical Carparks - A Design Guide*, 1st Ed., BHP Integrated Steel.

Xiao, Y., Choo, B.S. and Nethercot, D.A. (1994). Composite connections in steel and concrete. I. Experimental behaviour of composite beam-to-column connections, *J. Construct. Steel Research,* **31**, 3-30.

Advances in Building Technology, Volume 1
M. Anson, J.M. Ko and E.S.S. Lam (Eds.)
© 2002 Elsevier Science Ltd. All rights reserved

NOVEL NEW REINFORCING COMPONENTS FOR COMPOSITE BEAMS

M. Patrick and R.Q. Bridge

Centre for Construction Technology & Research, College of Science, Technology & Environment, University of Western Sydney, Kingswood, NSW 2747, Australia

ABSTRACT

Several novel new reinforcing components have been developed in Australia to improve detailing of the shear connection in composite beams. By using these components: unsatisfactory failure modes are suppressed; the amount of reinforcement required for longitudinal shear resistance is significantly reduced compared with conventional detailing; design is simplified; and installation of reinforcement on site is much easier and faster. Rules developed for design engineers to detail beams incorporating the new products are described in detail in the paper.

One type of component has been developed to prevent a special type of longitudinal shear failure from occurring in the concrete flange of secondary composite edge beams when profiled steel sheeting is laid transverse to the longitudinal axis of the steel beam. It is now mandatory in Australian Standard AS 2327.1 "Simply-Supported Composite Beams" to provide reinforcement for this purpose. A method for designing this reinforcement is proposed for the first time. Another type of component was developed to prevent a similar type of longitudinal shear failure in primary composite beams with widely-spaced shear connectors. A further two types of components have been developed for use in any primary and secondary composite internal or edge beams where the other types of components are not required. All the components can be used in either continuous or simply-supported composite beams, as described in the paper.

KEYWORDS

Composite beam; shear connector; longitudinal shear; reinforcing steel.

INTRODUCTION

The shear connection of a composite beam comprises the five components shown in Figure 1. They can all influence the behaviour of the shear connection, and can be considered to include the shear connectors, profiled steel sheeting, slab reinforcement (including longitudinal bars if beams are continuous), concrete slab and steel beam top flange.

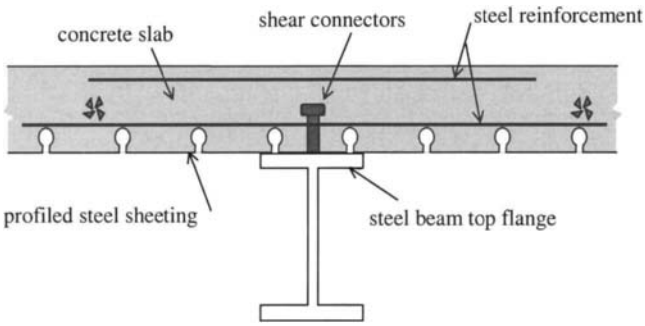


Figure 1: Components of the shear connection of a composite beam

Three new, patented reinforcing components have been developed in Australia to ensure that design engineers can detail economical longitudinal shear reinforcement in the presence of profiled steel sheeting. Otherwise, it is possible that non-composite beams, or even other forms of construction, will be more economical. The new components are described, and were designed to be used with automatically welded, headed studs, which are the only type of shear connector referred to in AS 2327.1 (Standards Australia 1996) that may be attached directly through profiled steel sheeting.

The strength design method given in AS 2327.1 requires that the shear connection is "ductile", which can be assessed by knowing the shape of the load-slip curves from push-out tests, and also the magnitude of the slips required along typical composite beams at ultimate load. No specific guidance is given to designers on either of these matters in AS 2327.1. However, Eurocode 4, Part 1.1 (British Standards Institution 1994) requires ductile shear connectors to have a slip capacity of at least 6 mm. Ductile and brittle behaviour of the shear connection, as well as the assumed model for design in AS 2327.1, are shown diagrammatically in Figure 2. A feature of this model for the Australian shear connection covered by AS 2327.1 is that it reaches its design shear capacity, f_{ds}, with very little slip (in practice, typically 2 to 4 mm) and maintains it indefinitely (typically 8 to 10 mm).

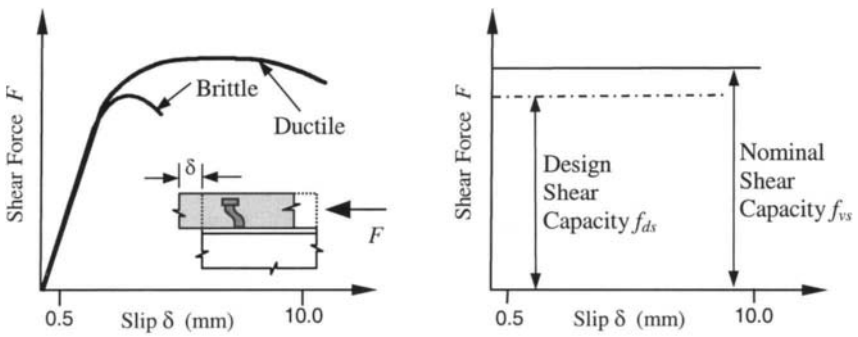
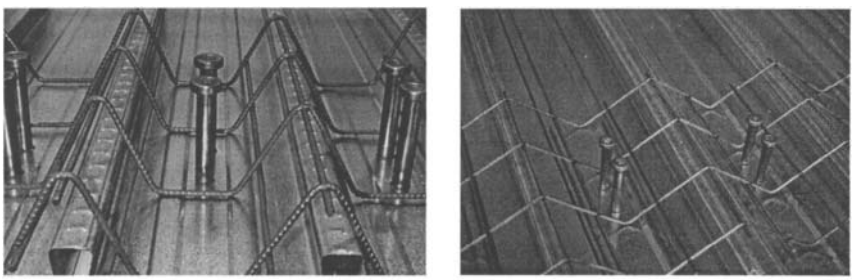


Figure 2: Load-slip behaviour of the shear connection

WAVE-FORM REINFORCEMENT – RIBS PERPENDICULAR

Rib Shearing Failure Mode

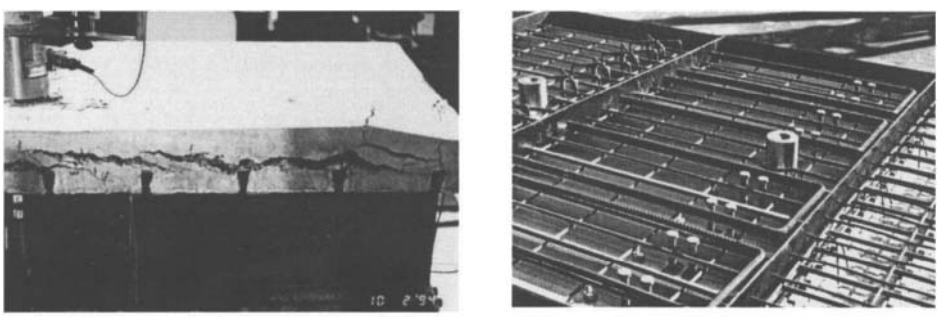
A patented wave-form reinforcing component, DECKMESH™ (OneSteel Reinforcing 2001), has been developed to prevent rib shearing failure in composite edge beams when profiled steel sheeting is laid transverse to the longitudinal axis of the steel beam, and welded-stud shear connectors are fastened directly through the sheeting. This brittle failure mode involves horizontal cracks that form in the concrete ribs between the tops of the steel sheeting ribs in pans where there are shear studs, while the failure surface locally avoids the studs by passing over their heads. It is now mandatory in AS 2327.1 to reinforce against rib shearing failure, in certain circumstances, which is referred to therein as Type 4 longitudinal shear failure. The product has to date been developed for use with BONDEK II and CONDECK HP (see Figure 3), but can potentially be used with many other profiles including those with wide steel ribs, e.g. Patrick (2001).



(a) DECKMESH™ -B for BONDEK II (b) DECKMESH™-C for CONDECK

Figure 3: DECKMESH™ longitudinal shear reinforcement

A more detailed account of the development of DECKMESH™ to reinforce against rib shearing failure is given by Patrick (2000). The severe delamination of the cover slab of the composite beam occurred as a result of a rib shearing failure over each pan along the beam which were all fitted with shear connectors. At the end of the test, the maximum slip had only reached 2.5 mm. It is worth noting that the horizontal cracks did not penetrate to the far side of the slab. The beam was detailed in accordance with BS 5950: Part 3.1 (British Standards Institution 1990) and Eurocode 4, Part 1.1 as seen in Figure 4(b). While the heavy, 16 mm diameter U-bars successfully controlled longitudinal splitting, they could not prevent rib shearing failure, and in fact possibly weakened the failure surface.



(a) Type 4 rib shearing failure (b) U-bars required by some Standards

Figure 4: Rib shearing failure in edge beams detailed using BS 5950 and Eurocode 4

The situations when Type 4 shear surfaces must be reinforced are described in Clause 9.8.1 of AS 2327.1. The product DECKMESH™, shown in Figure 3, can be used to reinforce a Type 4 shear surface in a beam incorporating either BONDEK II or CONDECK HP without requiring design calculations. DECKMESH™ should only be used when the sheeting ribs are deemed perpendicular to the longitudinal axis of the steel beam. Some out-of-alignment of the sheeting ribs (up to about 15 degrees) can be accommodated by either twisting the DECKMESH™ panels around slightly (CONDECK HP option) or off-setting them by up to 150 mm (BONDEK II option).

Designing Against Rib Shearing Failure

Tests have shown that rib shearing failure is caused by a flexural crack that initiates in the concrete at the top of the sheeting rib on the opposite side to where the compressive force in the slab thrusts on the shear connectors (point A in Figure 5). The crack propagates horizontally across the top of the concrete rib, locally passing over the top of the welded studs, as shown in Figure 5. Tests have also shown that the slab must be reinforced over a width of at least 400 mm in order to suppress the failure mode completely. Clause 9.8 of AS 2327.1 requires four reinforcing wires or bars to be placed on each side of the concrete rib, with a maximum centre-to-centre spacing of 150 mm measured in the transverse direction. Correspondingly, it will be assumed that the effective width of the slab, b_{eff}, with respect to resisting rib shearing failure, normally equals 600 mm in edge beams, and is centred about the steel beam, except when the concrete flange outstand on one side of the beam is less than 300 mm measured from the vertical centreline of the steel beam.

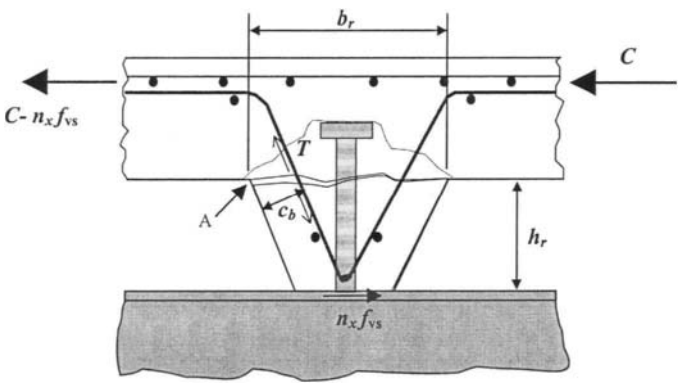


Figure 5: Design of wave-form reinforcement to prevent rib shearing failure

It is proposed that reinforcement like that shown in Figure 5 is not required to control rib shearing failure provided the cracking moment of the concrete rib is not exceeded, viz.:

$$n_x f_{vs} h_r \leq f'_{cf} b_{eff} b_r^2 / 6 \qquad (1)$$

where –

n_x = number of welded studs per pan;
f_{vs} = nominal shear capacity of a welded stud in accordance with AS 2327.1;
h_r = overall height of profiled steel sheeting ribs;
f'_{cf} = flexural tensile strength of concrete determined in accordance with AS 3600 (Standards Australia 2001);
b_{eff} = effective width of concrete rib resisting rib shearing failure (≤ 600 mm); and
b_r = width across top of concrete rib.

It follows that when Eqn. 1 is not satisfied, rib shearing reinforcement is required. With four bars placed on each side of a concrete rib containing shear connectors, and ignoring any inclination of the reinforcement to the horizontal plane, it can be shown that the diameter of each wire or bar, d_b, must be such that:

$$d_b \geq \sqrt{\frac{n_x f_{vs} h_r}{2.8 \phi f_{sy} (b_r - c_b) k_b}} \qquad (2)$$

where –

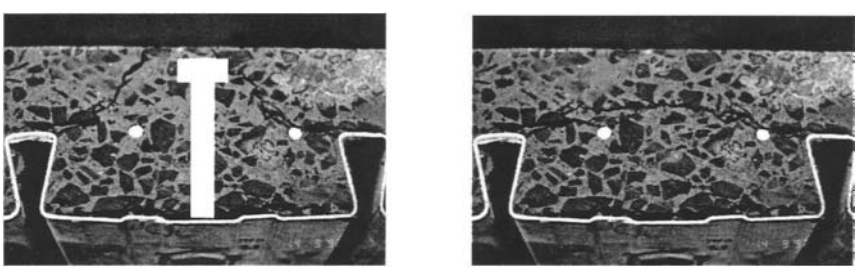
f_{sy} = design yield stress of steel reinforcement (=500 MPa in AS 3600);
ϕ = capacity factor for bending of concrete rib (=0.8 in AS 3600);
c_b = concrete cover measured from nearest edge of sheeting rib to centre of bar (see Figure 5); and
k_b = bar anchorage factor, which equals 1.0 if the bars can develop f_{sy} across the horizontal failure surface, but is otherwise less than 1.0.

When the design of the product is based on the results of structural tests involving the actual profiled steel sheeting to be used, such as has been the case for DECKMESH™ with BONDEK II and CONDECK HP, then bars of a lesser diameter than given by Eqn. 2 may be used.

WAVE-FORM REINFORCEMENT – RIBS PARALLEL

As recognised in AS 2327.1, a Type 3 longitudinal shear surface may form instead of a Type 2 surface if the steel sheeting ribs on at least one side of the steel beam run parallel to the steel beam. If the nearest rib is sufficiently close to the shear connectors, the failure surface first passes to the top of the rib instead of to the base of the slab, i.e. the failure surface will form along the path of least resistance.

In Figures 6(a) and (b) the different features of a potential Type 3 failure surface are shown. The failure surface in the region of a shear connector is shown in Figure 6(a) passing over the top of the connector, then down to the top of each adjacent sheeting rib. If the shear connectors are well spaced apart along the steel beam (which is parallel to the sheeting ribs), then it is possible that the shear surface will become approximately horizontal in the regions between the connectors, passing directly between the tops of the sheeting ribs as shown in Figure 6(b). The narrower the width of the concrete rib and the greater the tension in the shear connectors, then the more likely that this will occur. A horizontal shear surface like that in Figure 6(b) has been observed in tests when the shear connectors were so short that they did not even protrude above the tops of the sheeting ribs (Veldanda & Hosain 1992).



(a) Shape of shear surface in region of stud (b) Shape of shear surface away from stud

Figure 6: Possible Type 3 longitudinal shear surfaces (Patrick 2001)

It follows that various parameters can affect the shape of a Type 3 longitudinal shear surface. Limited account has been taken of this in AS 2327.1 to date. Moreover, if the shear surface takes the form shown in Figure 6(a), then horizontal reinforcing bars placed transverse to the steel beam will pass through the shear surface and therefore be effective in resisting longitudinal shear. However, in regions where the shear surface is effectively horizontal (Figure 6(b)), then wave-form reinforcement like that shown in Figure 7 is required.

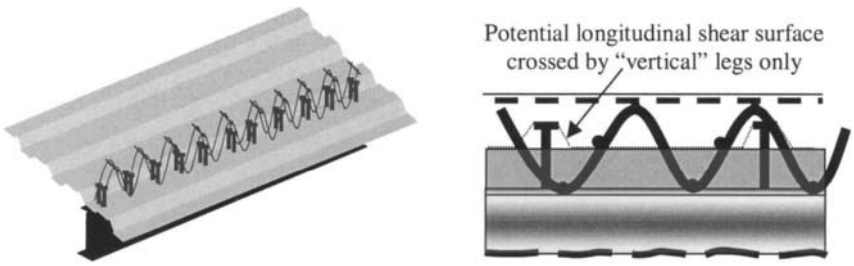
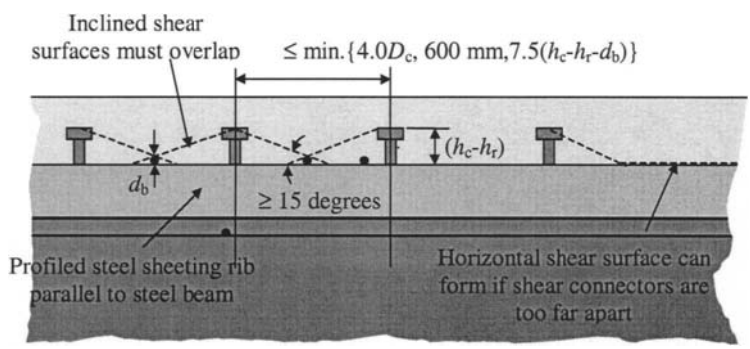


Figure 7: Possible Type 3 longitudinal shear reinforcement for well-spaced shear connectors and narrow concrete ribs with sheeting ribs parallel to steel beam

In view of the discussion above, it is proposed that an additional requirement must be satisfied when determining the maximum longitudinal spacing of shear connectors in accordance with Clause 8.4.1(b) of AS 2327.1. This requirement applies if the profiled steel sheeting on at least one side of the steel beam is deemed parallel to the steel beam, and therefore a Type 3 longitudinal shear failure is possible. The requirement is explained diagrammatically by Figure 8, and is particularly relevant to primary beams. The objective of this rule is to ensure that only conventional Type 1 (vertical) or Type 3 (see Figure 6(a)) shear surfaces can form. Therefore, horizontal bars placed transverse to the steel beam will be effective as longitudinal shear reinforcement. Otherwise, waveform reinforcement like that shown in Figure 7 is required, in order to cross the horizontal shear surface that can form in the region between shear connectors. This rule may sometimes necessitate either using more-closely-spaced single shear connectors rather than pairs of connectors, or increasing the overall height of the connectors.



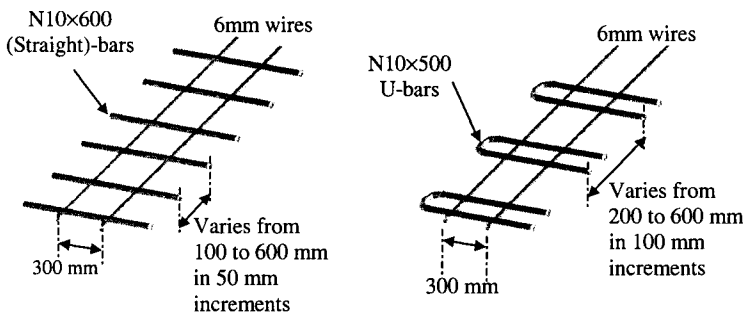
Note: In the transverse direction it is assumed that the crack angle can be much sharper so that the width of the concrete rib does not control the longitudinal stud spacing.

Figure 8: Maximum longitudinal spacing of shear connector groups when formation of a Type 3 shear surface is possible

TRANSVERSE REINFORCEMENT

Improved Detailing

A new reinforcing component STUDMESH® (OneSteel Reinforcing 2001) has been specially developed to overcome problems with designing and detailing horizontal Type 2 and 3 longitudinal shear reinforcement (see Figure 9). The practice of tying individual transverse bars to other reinforcement in order to reinforce these shear surfaces, even if done reasonably simply, is costly and labour intensive and should be avoided whenever possible. STUDMESH® is produced in N10 (i.e. Normal ductility, 10 mm diameter), 500 MPa reinforcing bar because it is more economical to anchor small diameter bar rather than using larger N12 or N16 bar. Also, the light 6 mm longitudinal wires to which the N10 bars are attached assist in the anchorage of the transverse bars, further reducing the total mass of the product. Cutting panels of mesh across their shorter dimension into 2.4 metre long strips comprising four transverse bars to form fully-anchored Type 2 or 3 reinforcement is an improvement to using ordinary bars. However, there is wastage of the steel when it is cut, and also, mesh is normally only available with wires in standard diameters, which further reduces its efficiency in many cases. Using STUDMESH® can significantly reduce the mass of the reinforcement, and also the labour required during construction (since it doesn't have to be cut into strips) compared with using mesh.



(a) SMS Series STUDMESH® for internal beams, and edge beams with a wide outstand

(b) SMU Series STUDMESH® version for edge beams with a narrow outstand

Figure 9: STUDMESH® as Type 2 or 3 Reinforcement

Reinforcement that crosses a shear surface must be fully anchored on both sides of the crack for the shear-friction model to be valid. Rules for the anchorage of straight deformed bars, and welded-wire mesh with ribbed wires, are given in Section 13 of Australian Standard AS 3600. However, recourse has also been made to Eurocode 2, Part 1 (British Standards Institution 1992) to determine suitable anchorage details for STUDMESH®. A provisional patent has been lodged for the product.

Standard Solutions

Tables of standard solutions for STUDMESH® have been published by Patrick (2001). Solutions are given for 19 mm diameter welded studs spaced at 100 to 600 mm centres. Significant savings of over 30 percent can be made in the mass of the reinforcing steel by choosing STUDMESH® instead of mesh, but the market price of the different products should also be considered before making a final decision. The solutions for primary beams, for which the sheeting ribs are deemed parallel to the steel beam, cannot be used unless the stud height, h_c, is increased enough to satisfy the requirements in Figure 8. Otherwise, wave-form reinforcement is required in accordance with Figure 7.

CONCLUSIONS

The shear connector types permitted in AS 2327.1 all exhibit ductile load-slip behaviour reaching magnitudes of slip required along typical composite beams at ultimate load. When used in conjunction with the current types of Australian profiled steel sheeting with narrow re-entrant steel ribs, the strength of shear studs is the same as the strength in a solid slab provided the shear connection is detailed in accordance with AS 2327.1.

A patented wave-form reinforcing component DECKMESH™ has been developed and is now in use in Australia. It is designed to prevent rib shearing failure from occurring in composite edge beams when profiled steel sheeting is laid transverse to the longitudinal axis of the steel beam. While designed specifically for the Australian types of profiled steel sheeting, tests have shown that its use in slabs incorporating trapezoidal profiled steel sheeting prevents rib shearing failure and results in a ductile load-slip performance rather than the brittle performance observed in tests without this wave-form reinforcing component. A simple method for designing the wave-form reinforcement has been presented for the first time in the paper. The method can be applied to internal beams, as well as edge beams, if the concrete ribs are narrow. Another patent-pending type of waveform reinforcement may be required in primary composite beams if the shear connectors are widely spaced along the steel beam. A new patent-pending reinforcing component STUDMESH® has been specially developed to overcome problems with designing and detailing Type 2 and 3 shear surfaces. The practice of tying individual transverse bars to other reinforcement in order to reinforce these shear surfaces, even if done reasonably simply, is costly and labour intensive. This new component is an improvement on using ordinary reinforcing bars or pieces of cut mesh. It comes in a range of standard sizes to cover most applications and the anchorage length requirements are automatically satisfied.

REFERENCES

British Standards Institution (1990). *BS 5950: Part 3: Section 3.1: Code of Practice for Design of Simple and Continuous Composite Beams*, London.

British Standards Institution (1992). *Eurocode 2: Design of Concrete Structures, Part 1 – General Rules and Rules for Buildings*, DD ENV-1992-1-1.

British Standards Institution (1994). *Eurocode 4: Design of Composite Steel and Concrete Structures, Part 1.1. General Rules and Rules for Buildings (together with UK National Application Document)*, DD ENV 1994-1-1: 1994, London.

OneSteel Reinforcing (2001). *DECKMESH™ & STUDMESH® – Composite Slab Shear Reinforcement Solutions.*

Patrick, M. (2000). Experimental Investigation and Design of Longitudinal Shear Reinforcement in Composite Edge Beams, *Journal of Progress in Structural Engineering and Materials*, **2:2**, April-June, 196-217.

Patrick, M. (2001). *Design of the Shear Connection of Simply-Supported Composite Beams, Composite Structures Design Manual - Design Booklet DB2.1*, OneSteel Market Mills.

Standards Australia (1996). *AS 2327.1-1996: Composite Structures - Simply Supported Beams*, Sydney.

Standards Australia (2001), *AS 3600-2001: Concrete Structures*, Sydney.

Veldanda, M.R. and Hosain, M.U. (1992). Behaviour of Perfobond Rib Shear Connectors: Push-out Tests, *Canadian Journal of Civil Engineering*, **19:1**, 1-10.

Advances in Building Technology, Volume I
M. Anson, J.M. Ko and E.S.S. Lam (Eds.)
© 2002 Elsevier Science Ltd. All rights reserved

THE INFLUENCE OF MATERIAL PROPERTIES ON THE LOCAL BUCKLING OF CONCRETE FILLED STEEL TUBES

A. Wheeler and M. Pircher

Centre for Construction Technology and Research, College of Science, Technology and Environment, University of Western Sydney, NSW, 2747 Australia

ABSTRACT

Extensive studies have been conducted on thin walled concrete filled steel tubes, subjected to predominantly axial loading. However, limited documented research has been carried out into the behaviour of these sections subjected to pure flexure. The University of Western Sydney is currently carrying out an extensive investigation which includes both numerical and experimental studies into flexural behaviour of concrete filled tubes.

In this paper the effect of material properties of the circular hollow sections, with an emphasis on the effect of the yield stress on the on the local buckling of the tube when subjected to flexural actions, is investigated numerically. The study looks at both the bare steel tube and the concrete filled tube to determine the effect of the concrete infill on the flexural behaviour of the tube. The investigation is conducted using the finite element method, with a numerical model developed to simulate experimental work being carried out at the University of Western Sydney.

KEYWORDS

Buckling Capacity, Tubes, Concrete Filled, Flexural Loading

INTRODUCTION

The use of concrete filled steel tubes in the construction industry continues to increase as an economical alternative to traditional construction methods. The system utilises the compressive strength of the concrete, while the steel tube provides tensile capacity under flexural loading. The tube also provides the necessary formwork for construction. Current practice employs concrete filled tubes in members subjected to predominantly axial loads (columns). Consequently, extensive research into the axial behaviour of concrete filled tubes exists (O'Shea & Bridge, 2000). However, for tubes subjected to flexural loading, limited documented research exists (Shilling, 1965 and Sherman, 1976). An investigation into the flexural behaviour of concrete filled tubes is currently being carried out at the Centre for Construction Technology and Research, University of Western Sydney, in which concrete filled tubes subjected to pure bending are being investigated.

The current work takes into account imperfections (Wheeler & Pircher, 2002) and focuses on the behaviour of the composite system as well as on the behaviour of the individual components. The concrete infill in a steel tube limits the deformations of the steel tube in bending such as ovalisation and inward buckling and thus increases the capacity of such members. This paper will report on the studies performed to determine the influence of the yield stress of the steel tube on the buckling behaviour. Tubes with D/t–ratios (diameter to thickness ratios) in the range from 40 to 110 have been investigated numerically and the buckling behaviour of these tubes with and without concrete infill has been recorded. While the results presented in this paper are generated using a numerical model, the paper will also demonstrate that the model accurately predicts results obtained in an experimental programme carried out at the University of Western Sydney.

FINITE ELEMENT ANALYSIS

The finite element analysis carried out in this paper was conducted using the ABAQUS finite element analysis package (HKS, 1998). To accurately predict the behaviour of the tube, a model was developed that represented a section of tube subjected to four-point bending. This method enabled studies to be carried out on a section of tube subjected to constant moment with no shear. The model also replicated experimental tests being carried out at the University of Western Sydney.

In this study both bare steel tubes and concrete filled steel tubes were considered. The model of the tube is shown in Figure 1. Symmetries at mid-span and in the longitudinal direction reduce the model to one quarter of the beam. The elements used for the analysis were four-noded shell elements with nine integration points through the thickness. To negate local effects at the support and loading points, resulting from loading, a pair of stiff diaphragms were placed at the loading points. The accuracy of the model, in particular for modelling of the local buckling effects, was further improved by refining the mesh in the compression region of constant moment zone. To instigate the buckling of the tube, imperfections based on eigen-modes were super-imposed on the perfect geometry, with a magnitude of one percent of the wall thickness.

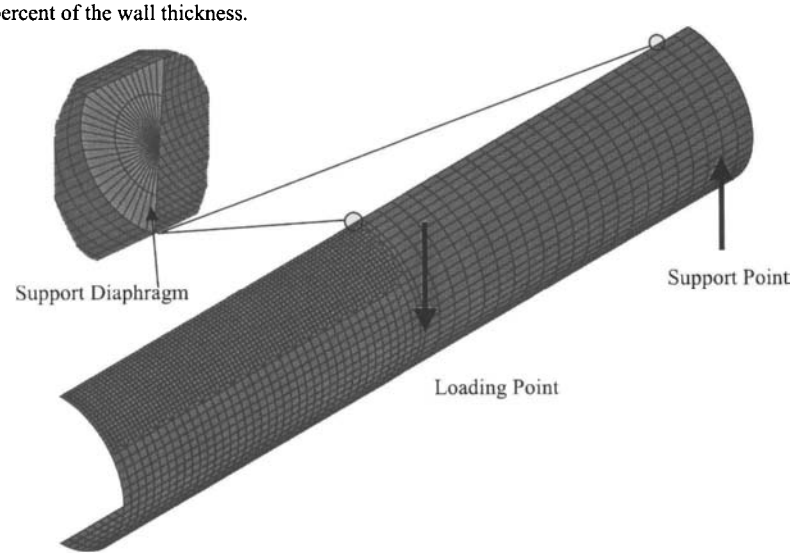


FIGURE 1 FINITE ELEMENT MODEL

The behaviour of the bare steel tube subjected to flexural loading has been studied by Wheeler *et al* (1999). This study looked primarily at the effect of imperfections on the buckling behaviour of the tubes. However, it was observed that prior to buckling considerable ovalisation occurred within the initially circular cross-section. Consequently one of the major effects of the concrete infill was assumed to be to prevent any ovalisation. The infill was assumed to also prevent any inward buckles forming along the tube. To model the effect of the concrete infill on the behaviour of the tube incompressible springs placed with in the section, allowing outward deformations but limiting any inward deformations. The element type used for the springs were two dimensional with a high stiffness in compression and zero stiffness in tension.

The accuracy of the model is demonstrated in Figure 2, were the experimental results for a 406 mm tube (solid line) is compared to the results for the same tube generated using the finite element model (dashed line). Also shown in the figure are the load levels at which yielding commences, the limit imposed by AS 4100 and the theoretical load when the section is fully plastic.

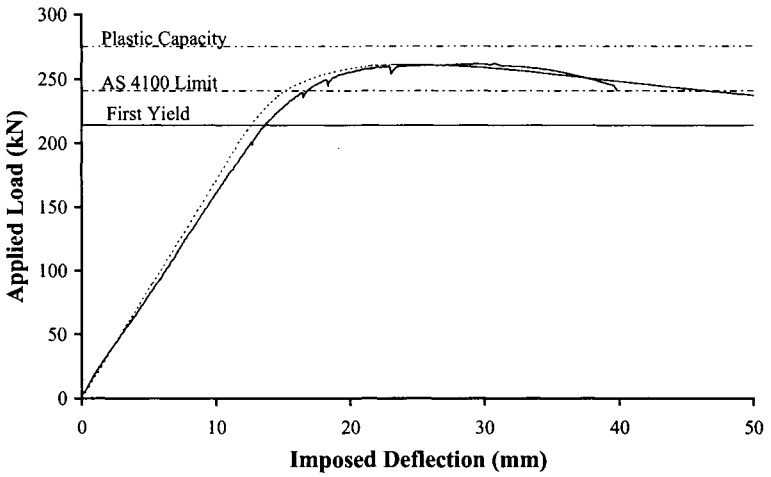


FIGURE 2 ABAQUS MODEL VS EXPERIMENTAL RESULTS

The match between the numerical and experimental results is close, with the initial stiffness and the peak loads demonstrating a good correlation. The variation in stiffness as the load increases is explained by the fact that the numerical model uses a bi-linear elastic plastic material relationship, while the true material properties are generally non-linear.

GEOMETRY AND MATERIAL PROPERTIES

The geometry of the tubes selected for this investigation was limited to D/t ratios that are generally used in the structural building industry. All tubes in this study had an equal wall thickness of $t = 6.4$ mm, with the span of the load introduction points adjusted to maintain a constant span to depth ratio. The diameter (D) and the D/t–ratios for the tubes investigated are given in Table 1.

The material properties of commercially available steel tubes vary significantly, depending on both the geometry and the process used in manufacturing the tube. The stress-strain behaviour for typical cold-formed tubes are generally highly non-linear with no clear yield point and yield plateau. However, this

paper focuses on the effect of the yield stress on the local buckling of tubes. Thus, a perfectly elastic-plastic stress strain curve will be used for the steel tubes.

TABLE 1
TUBE DIAMETERS

D	D/t
219	34
457	71
710	111

BARE STEEL TUBE

Initial analyses were carried out to determine the behaviour of the tube without the presence of the concrete infill. Firstly the classic elastic buckling load (M_{Buckle}) for each tube was determined using an eigenmode-extraction and perfect tube geometry. Secondly, seven analyses were performed on the same tube with varying material properties to determine the influence of the yield-stress. In these analyses the yield stress of the tube material was varied between 200 MPa to 800 MPa with geometric non-linearity being considered. The moment-deflection behaviour for these tubes are presented in Figure 2, Figure 3 and Figure 4 for the 219 mm, 457 mm and 710 mm tubes respectively. The moment has been normalised against the elastic buckling moment (M_{Buckle}), and the deflection at mid span (Δ) has been normalised using the wall thickness of the tube.

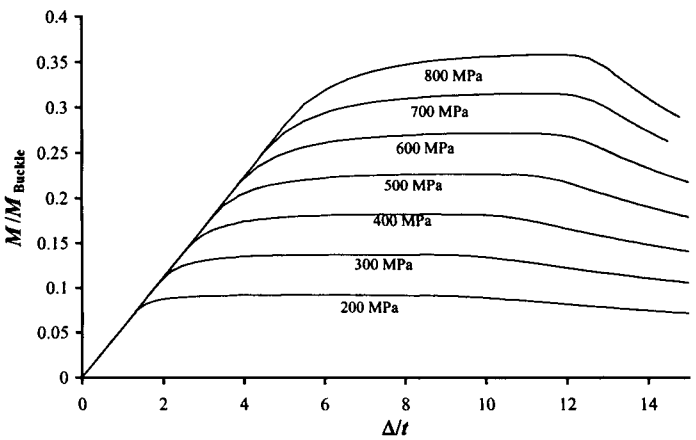


FIGURE 3 BARE STEEL D=219 MM

Figure 3 depicts the results for a 219 mm tube, in this case the D/t is considered to be low at a value of approximately 34. The behaviour of the tube for all yield stresses selected behaves as would be expected for a compact section, with an increase in moment capacity until plastic section capacity is approached. The moment then remains stable until the onset of local plastic buckling at large strains, resulting in a reduction of the moment capacity.

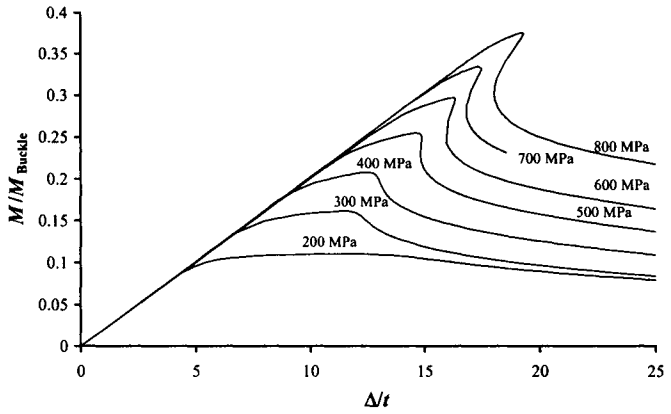


FIGURE 4 BARE STEEL D = 457 mm

As the *D/t* ratio is increased the tube behaviour varies significantly depending on the yield stress as shown in Figure 4. In this case the load-deflection curves for a 457 mm tube is presented with a *D/t* ratio of approximately 71. For low yield stresses (≤ 200MPa), the behaviour is similar to the compact sections with a long yield plateau followed by a gradual reduction in moment capacity. However, as the yield stress increases the tube behaviour becomes more dependent on local buckling effects with significant buckling occurring. As the yield stress increase the effect of the local buckling on the post buckling behaviour increases with significant snap back being observed for the higher yield stresses.

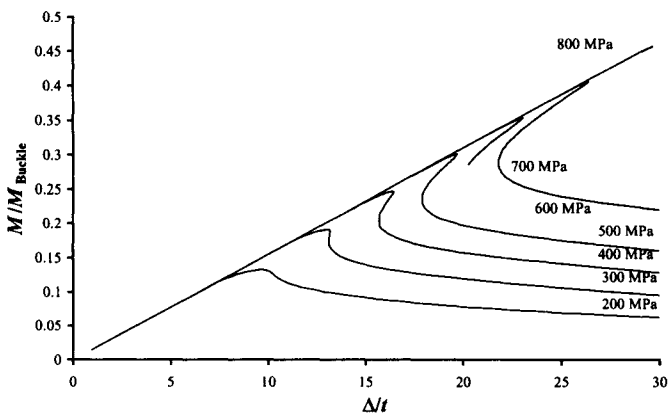


FIGURE 5 BARE STEEL D = 710 mm

Figure 5 presents the moment-displacement behaviour for a 710 mm-diameter tube with a *D/t* ratio of approximately 111. In this case the tube would be considered to be either non-compact or slender (AS4100, 1998), with the formation of local buckles having a distinct effect on the post buckling behaviour of the tubes. It is shown that even for low yield stresses (300 MPa) significant losses in the moment capacity can be observed with the onset of local buckling.

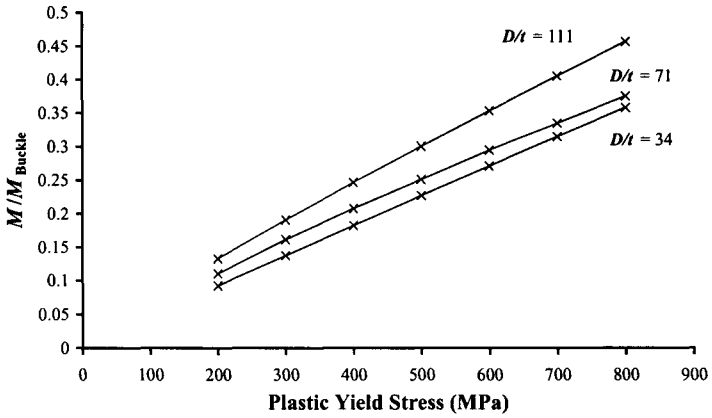


FIGURE 6 PEAK MOMENT TO YIELD STRESS – TUBE ONLY

In Figure 6 the buckling moments versus the yield stresses of the three considered tubes are shown. In each case the relationship between the buckling moment and the yield stress is very close to linear. However, the slopes vary significantly between the three tubes. This figure supports the assumption made in most standards that the relationship between the buckling moment and the nominal yield stress is linear. For example, the definition for section slenderness in the Australian standard AS 4100 (SA, 1998) is defined as

$$\lambda_s = \left(\frac{d_o}{t}\right)\left(\frac{f_y}{250}\right) \tag{1}$$

In the Australian standard a tube is considered to be compact if is λ_s is less that 50, and slender if λ_s is greater than 120. While this formula may be sufficient for most materials, at the extremes it may be un-conservative. For example, the slenderness λ_s for the tube with d = 219mm equals λ_s =109 which classifies this tube as non-compact. However, the analysis results shown in Figure 3 suggest that the section is in fact compact.

CONCRETE FILLED TUBE

In studying the effect of the concrete infill on the steel tube, it was assumed that the concrete within the tube has cracked and that there is no longitudinal interaction such as friction or mechanical interlocking. Consequently, the concrete infill makes no direct contribution to the flexural strength. It is recognised that frictional forces and mechanical interlocking will increase the flexural capacity of the concrete filled tube. However, this will be the subject of further studies.

Subjecting the bare steel tube to flexural action results in the cross-sectional deformations, with a decrease in depth and a corresponding increase in the width of the section. Such a deformation is referred to as "*ovalisation*". Wheeler et al. (1999) demonstrated that this ovalisation decreases the buckling capacity of the tube. By including the concrete infill in the tube, the cross-sectional shape of the tube is retained, thus preventing any significant ovalisation. The concrete infill also prevents any inward buckles from forming, causing the buckles to form in the shape of a buckling mode with higher associated buckling moments thus increasing the bending capacity of the tube.

Analyses corresponding to those carried out on the bare steel tube were repeated with the simulated concrete infill. In all cases a significant increase in the flexural capacity of the tube was observed.

Typical results are shown in Figure 7, where the dashed line is the response of the bare steel tube while the solid line represented the concrete filled tube. Beside the increase in critical moment a significant change in the post-buckling behaviour was observed. The change became more pronounced for higher yield stresses of the considered tubes and can be characterised as an increase in ductility of the system due to the concrete infill.

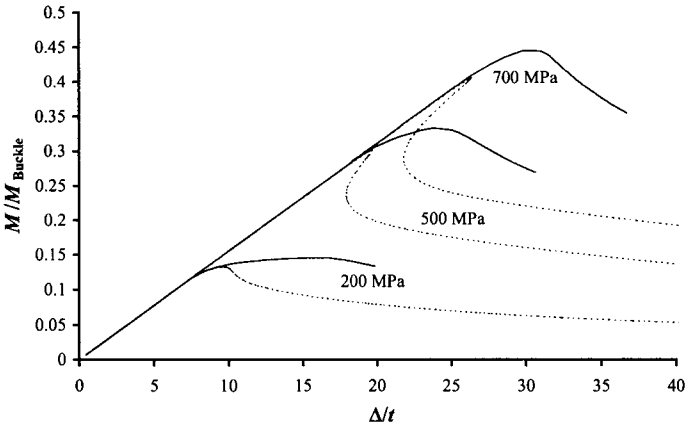


FIGURE 7 EFFECT OF CONCRETE INFILL ON FLEXURAL BEHAVIOUR

The overall effect of the concrete infill on the tube behaviour is shown in Figure 8, with the ratio of buckling moment to elastic buckling moment is plotted against the yield stress of the tubes. For the bare steel tubes as well as for the concrete-filled tubes, the relationships between the yield stress and the buckling moment is very close to linear. From this figure it is also evident that the effect of the concrete infill is related to the *D/t* ratio, with larger increases in moment capacity between the bare and concrete filled tubes observed for the tubes with higher *D/t* ratios. For the *D/t* of 71 at 200 MPa the capacities differ by one percent while for 800 MPa the difference increases to 10 percent.

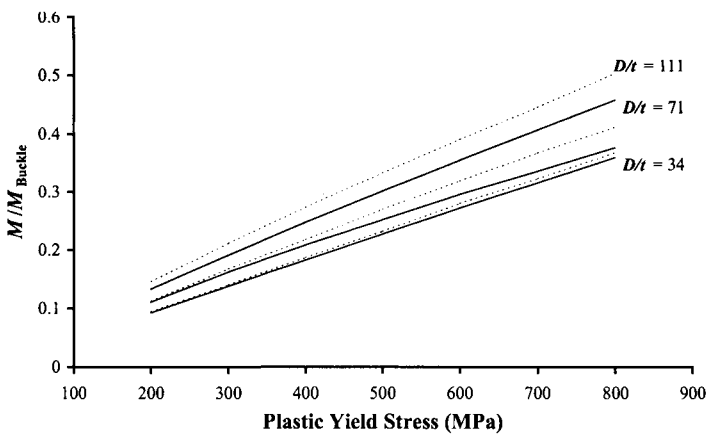


FIGURE 8 PEAK MOMENT TO YEILD STRESS - CONCRETE FILLED TUBE

CONCLUSION

The accuracy of the numerical model used in this paper was demonstrated with excellent correlation between the experimental and numerical results. This accuracy of the finite element model suggests that parametric studies may be used in lieu of expensive experimental tests to predict the effect of material properties on the buckling behaviour of thin wall tubes

In this paper the influence of the yield stress in concrete filled steel tubes on the buckling behaviour in pure bending was investigated. It was found that there are significant increases in the flexural capacity of steel tubes when filled with concrete, these increase include both the stiffening of the section and the realisation of higher buckling loads. The gain in strength is directly related to the yield stress. However, the *D/t* ratio also influences this relationship, with higher stresses experienced in the tubes with lower *D/t* ratio's and higher increases in capacity due to concrete infill observed for the more thin-walled members investigated for this paper.

REFERENCES

HKS (1998). *ABAQUS/Standard Users Manual, Version 5.8*. Hibbit, Karlsson and Sorensen , Inc.

O'Shea M.D. and Bridge R.Q. (2000). Design of Thin-walled Concrete Filled Tubes. *Journal of Structural Engineering, ASCE*, **126**(11), 1295-1303.

SA (1998), *AS 4100-1998: Steel Structures*, Standards Australia, Sydney.

Sherman D.R. (1976) Tests of Circular Steel Tubes in Bending. *Journal of the Structural Division, ASCE*, **102**(11), 2181-2195.

Schilling, C.G., "Buckling Strength of Circular Tubes", *Journal of the Structural Division*, American Society of Civil Engineers, Vol 91, No. 5, 1965, pp. 325-348.

Wheeler A.T., Pircher M., Bridge R.Q. (1999). Modelling of Thin-walled Tubular Sections Subjected to Pure Bending. *Proceeding, The Thirteenth Australian Compumod Users' Conference*, Melbourne Australia, 33.1-33.11.

Wheeler A. and Bridge R.Q. (2000). Thin-walled Steel Tubes Filled with High Strength Concrete in Bending. *Proceedings, Engineering Foundation Conference, Composite Construction IV*, Banff, Canada.

Wheeler A. and Pircher M. (2002). Measured Imperfections in Six Cold-Formed Thin-Walled Steel Tubes. *Research Report CCTR: 001*, Centre of Construction Technology & Research, University of Western Sydney

TEAM PRESENTATION:

COMPOSITES FOR HOUSING

This Page Intentionally Left Blank

Advances in Building Technology, Volume 1
M. Anson, J.M. Ko and E.S.S. Lam (Eds.)
© 2002 Elsevier Science Ltd. All rights reserved

LOW-COST, BIO-BASED COMPOSITE MATERIALS FOR HOUSING APPLICATIONS

L.T. Drzal, A. K. Mohanty, G. Mehta, M. Misra

Composite Materials and Structures Center
Dept of Chemical Engineering and Materials Science
Michigan State University, East Lansing, Michigan, USA , 48824

ABSTRACT

In an on-going project, sponsored by the National Science Foundation, to develop bio-based composite materials for the next generation of American housing panel applications, a group of researchers at Michigan State University are striving to generate eco-friendly greener composite materials for structural applications. The objective of this research is to determine if bio-composites designed and engineered from natural/bio-fibers and blends of polyester resin and derivitized soybean oil can replace existing glass fiber-polyester composites for use in housing structures. Bio-composites provide environmental gains, reduced energy consumption, lighter weight, insulation and sound absorption properties, elimination of health hazards and reduce dependence on petroleum based and forest product based materials. A three cornered approach including the use of engineered natural fibers, polymer resin modification and development of a new high volume continuous manufacturing processes(Bio-Composite Sheet Molding Compound Panel-BCSMCP) is required to achieve the objective of producing an affordable alternative construction material for the housing industry of the 21st century .

KEYWORDS

Housing Panels, Biocomposites, Unsaturated Polyester Resins, Derivitized soybean oil

INTRODUCTION

Contemporary housing needs are challenging designers and builders to utilize more inventive materials in order to provide housing that are environmentally benign and at the same time provides for the requisite occupant environment and operating efficiency. Increasing attention is turning to bio-based materials from renewable resources. The future for bio-based building materials is bright (Figure 1, ref.1) and several new agricultural natural fiber-based building materials are already making

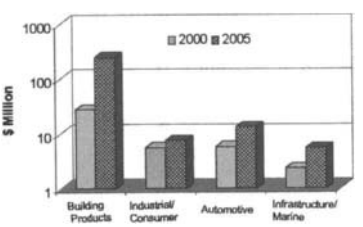


Figure 1: Growth Outlook For Bio-based Composites by Application in United States, 2000-2005

their mark in the building industry. Natural fiber composites (bio-based composite materials) are economical commodity composites that have useable structural properties at relatively low cost. The manufacture, use and replacement of conventional building materials (e.g. petroleum-based plastics, glass fibers, etc.) are becoming priorities because of the growing environmental consciousness[2]. There is a growing interest in the use of natural/bio-fibers as reinforcing components for thermoplastics and thermosets. Advantages of natural fibers over traditional reinforcing fibers such as glass and carbon are: low cost, low density, acceptable specific properties, ease of separation, enhanced energy recovery, CO_2 sequesterization and biodegradability. Although thermoplastics have the added advantage of recyclability, thermosets have the necessary mechanical properties for use as structural bio-composites. Bio-composites derived from natural fibers and traditional thermoplastics or thermosets are not fully environmentally friendly because matrix resins are non-biodegradable. However these bio-composites do now maintain a balance between economics and environment allowing them to be considered for applications in the automotive, building, furniture and packaging industries.

The use of reinforced thermoset composites by automakers has nearly doubled in the last decade, and is expected to increase 47 percent during the next five years[3] through 2004. The majority of resins

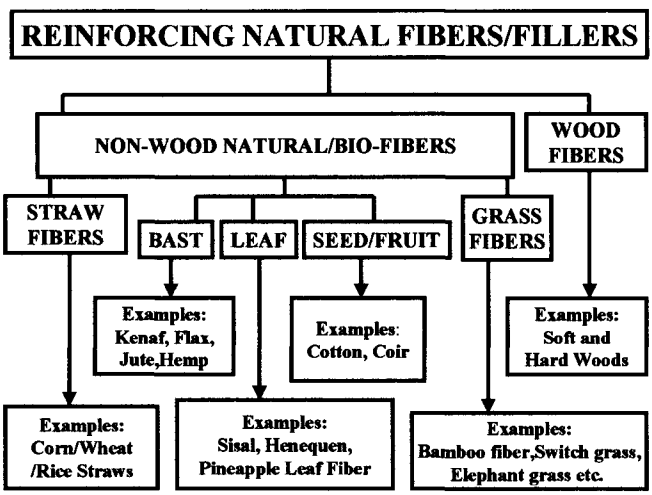


Figure 2: Broad classification of Natural/Bio-fibers: Strong potential reinforcing fibers in designing bio-composites for Building Products Industry

used in the composite industry are thermosets[4]. About 65% of all composites produced currently for various applications; use glass fiber and polyester or vinyl ester resins. Unsaturated polyester (USP) resins are widely used, thanks to a relatively low price, ease of handling and a good balance of mechanical, electrical and chemical properties. Natural fibers have recently made a comeback in FRP (fiber reinforced plastics) to replace glass fiber in many applications such as automotive and building products. The engine and transmission covers of *Mercedes-Benz* transit buses now contain polyester resin reinforced with natural fiber[5]. Natural fiber reinforced polyester composites have received much commercial success in the infrastructure area primarily for low cost housing applications.

There is, however, a major drawback associated with the application of bio-fibers for reinforcements of organic matrix resins. Due to the presence of hydroxyl and other polar groups on the surface and

throughout bio-fibers, moisture absorption can be high which leads to poor wettability by the matrix resin and weak interfacial bonding between fibers and hydrophobic matrices. In order to develop composites with better mechanical properties, it is necessary to impart hydrophobicity to biofibers by suitable chemical treatments[6].

The mechanical behavior of fiber, the types of fiber (non-woven, woven, short/long fibers), the nature of matrix, and fiber-matrix adhesion play vital role in controlling the properties of composites. This paper gives an overview of natural fiber reinforced polyester composites highlighting the future aspects of such bio-based composite materials in building applications.

REINFORCING NATURAL/BIO-FIBERS

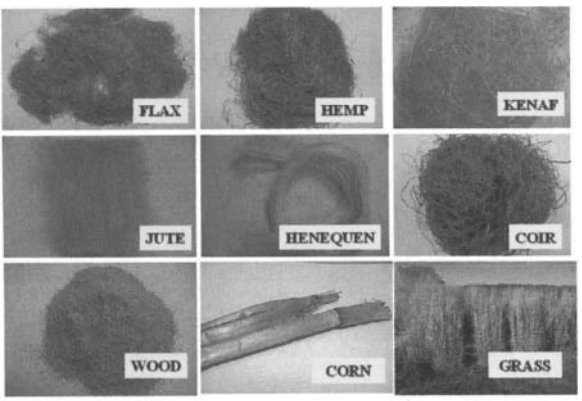


Figure 3. Various Sources for BioFibers.

Plastics, by themselves are not fit for load bearing application due to their lack of strength, stiffness and dimensional stability. However fibers possess high strength and sufficiently stiffness but cannot be used for load bearing applications because of their fibrous structure. In fiber-reinforced composites, the fibers serve as reinforcement by giving the strength and stiffness to the structure. Bio-fibers may be classified in two broad categories: Non-wood fibers and Wood fibers (Fig.2). Interest in the use of non-wood cellulose fibers in plastic composite structures has increased rather dramatically in recent years. The non-wood bast (from the stem part of the plant) fibers are poised to be utilized to a greater extent than wood fibers in bio-composite housing structures. The best-known examples are: (i) bast fibers: flax, ramie, kenaf/mesta, hemp and jute (ii) Leaf fibers: sisal, pineapple leaf fiber (PALF), and henequen (iii) seed fibers: cotton; fruit fibers: coconut fiber i.e. coir. (Fig.3) All natural fibers (wood and non-wood) are lingo-cellulosic in nature with the basic components being cellulose and lignin (Fig.4). The density (g/cm^3) of natural fibers (varies from ~1.2-1.5) is much less than that of E-glass (2.55); the specific strength of natural fibers is quite comparable to glass fibers. The elastic modulus and specific modulus[7] of natural fibers are comparable or even superior to E-glass fibers (Table 1 and Fig.5).

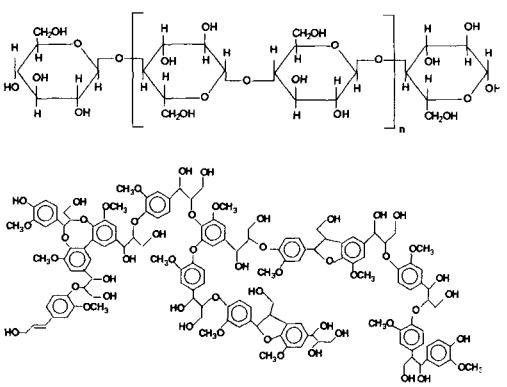


Figure 4: Structure of Cellulose (shown top) and lignin (shown bottom): basic constituents of natural fibers

POLYESTER RESIN MATRIX POLYMERS FOR BIO-COMPOSITES

The polyester resins, because of their versatility and low cost, are widely used in polymer composites. Polyester resins are classified (Scheme 1) as: (i) ortho resins, (ii) isoresins, (iii) bisphenol-A-fumarates, (iv) chlorendics, and (v) vinyl ester. Ortho-resins, known as general-purpose polyester resin, are based on phthalic anhydride, maleic anhydride and glycols (Scheme 2). Ortho-resin is the least expensive among all the polyester resins. The solutions of unsaturated polyesters and styrene vinyl monomers (reactive diluents) are known as unsaturated polyester (UP) resins. Considerable work has been reported on the synthesis, characterization, and curing behavior of UP resins[8]. The curing reaction of UP is a free-radical chain growth polymerization between reactive diluents styrene and UP resin. A wide range of peroxides, azo and azine compounds can be used as initiators, depending on the curing temperature. For room temperature curing as in the case of hand-lay-up structures, methyl ethyl ketone peroxide (MEKP) is used; for moderate temperature curing benzyl peroxide is used. For high temperature processing, di-t-butyl peroxide or t-butyl perbenzoate is used. A mixture of initiators is used when a large temperature increase is expected. To accelerate the decomposition of peroxides, some metal compounds, tertiary amines, and mercaptans can be used. Cobalt naphthenate (CoNp) and cobalt octanoate (CoOc) are the most widely used accelerators.

Table 1: Modulus comparison of E-glass and some important Natural Fibers (after ref.6 and partially modified)

Fiber Type	Density (g/cm^3)	Elastic Modulus (GPa)	Specific modulus
E-glass	**2.55**	**73**	**29**
Hemp	**1.48**	**70**	**47**
Flax	**1.4**	**60-80**	**43-57**
Jute	**1.46**	**10-30**	**7-21**
Sisal	**1.33**	**38**	**29**
Coir	**1.25**	**6**	**5**
Cotton	**1.51**	**12**	**8**

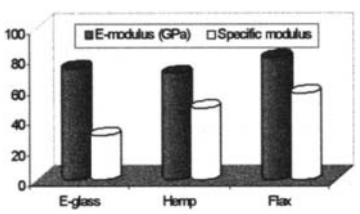
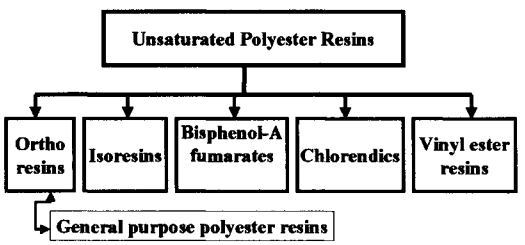
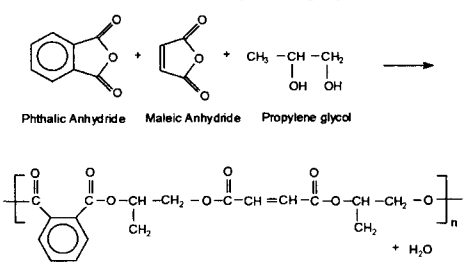


Figure 5: Modulus and Specific modulus: E-glass vs. some Natural Fibers



Scheme 1: Unsaturated Polyester resins--Classifications



Scheme 2

OUR APPROACHES TO STRUCTURAL BIO-BASED COMPOSITE MATERIALS FOR HOUSING APPLICATIONS

Natural fiber composites are emerging as a realistic alternative to glass-reinforced composites. While they can deliver the same performance for lower weight, they can also be 25-30 percent stronger for the same weight. Research success from our lab.-scale experiments of our group[9-11] has shown that it is possible to produce bio-composites with properties that can compete with glass fiber reinforced composites. Natural fiber (NF) unsaturated polyester (UP) composites show lower density, equal flexural modulus, comparable flexural strength but relatively poor impact strength as compared to a glass fiber (GF) composites[12]. Our three-pronged approach to designing superior strength (Fig.6) bio-composites for housing structures includes:

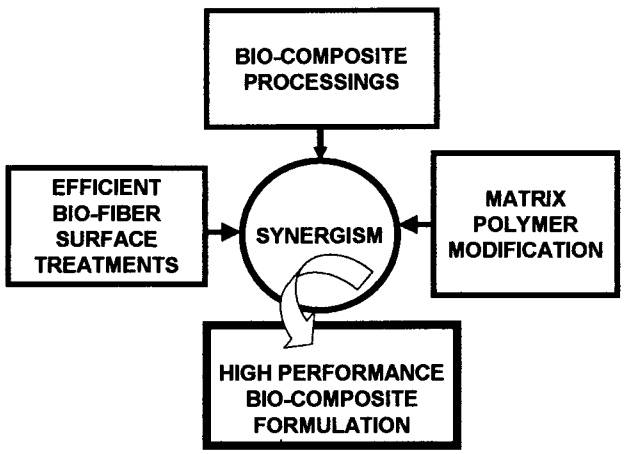


Figure 6: Design of superior strength Bio-Composite-Approaches

- An efficient (low cost but effective) bio-fiber surface treatment
- Matrix modification (Blending with functionalized vegetable oil)
- New, property-enhancing bio-composite process - - Sheet Molding Manufacturing.

Bio-fiber treatments and Design of "Engineered Natural/Bio-fibers"

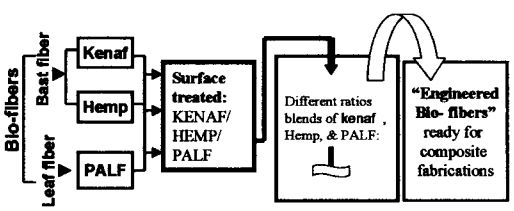


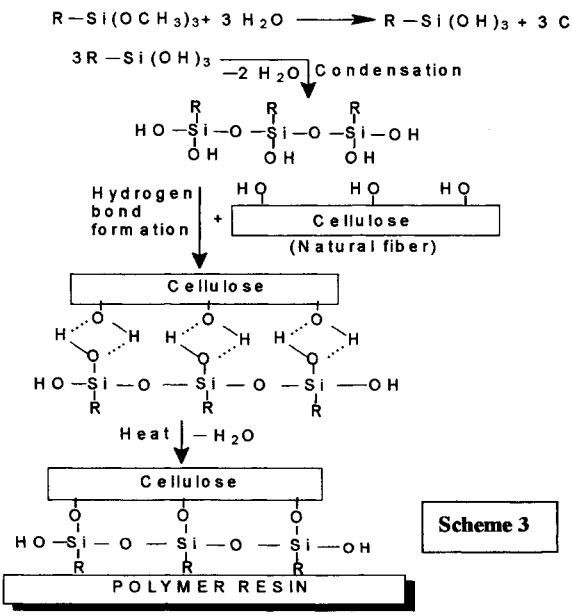
Figure 7: Design of Engineered Natural/Bio-fiber

Design of "Engineered Natural/Bio-fiber" is schematically represented in Fig.7. Engineered bio-fibers" are defined as a blend of surface treated bast (e.g. Kenaf, Hemp) and a leaf fiber (e.g. Pineapple leaf fiber, PALF). Selection of blends of bio-fibers is also based on the fact that the correct blend achieves an optimum balance in mechanical properties. The Kenaf and/or Hemp based composites exhibit excellent tensile and flexural properties, while leaf fiber (PALF) composites give the best impact properties of the composites. A blended composition of two bast and one leaf fiber is selected to achieve a balance of flexural and impact properties of the targeted bio-composites. Alkali treatment (AT) of natural fibers appears to be a very promising treatment, having the right combination of surface chemical and structural benefits along with low cost. The alkali treatment enhances the biofiber surface roughness, causes surface fibrillation and thus drastically improves

fiber-matrix adhesion. An increase in strength for bio-composites can also be achieved through the use of silane treatment. However, the choice of the correct silane coupling agent and treatment conditions all play a vital role in achieving superior strength composites. A general compatibilization mechanism for silane treated natural cellulose fiber and polymer resin composites is represented in Scheme 3.

Matrix modification (Blend of polyester resin and derivitized vegetable oil)

Unsaturated polyester resin is petroleum-based and is not eco-friendly. Attempts are in progress in our group to replace polyester resin with vegetable oil based resins. Through successful blending of petroleum-based polyester resin and derivitized soybean oil we are developing a number of bio-based



Scheme 3

resins for producing bio-composites. Combining a suitable reinforcement with a properly modified resin blend of polyester and vegetable oil will result in a novel bio-composite material. The incorporation of derivitized vegetable oil into polyester resins can improve the toughness of the resin and the resulting bio-composites. The content of derivitized vegetable oil and varying curing agent composition will affect the overall performance of the materials. Optimally maximizing the concentration of derivitized soybean oil under accurate curing conditions and incorporating suitably surface treated natural fibers will launch a new generation of eco-friendly bio-composites for housing applications.

Bio-Composite Processing

Bio-composites can now compete with glass-polyester composites both on a cost and performance basis. Most of the existing results on bio-composites are based on hand-lay-up labscale fabrication techniques. However the success of a high volume processing technique will be necessary to produce bio-composites in composite panels for housing applications economically. We have created a unique new process for fabrication of bio-composites. This process is similar to the Sheet Molding Compound (SMC) process but is a new and necessary approach for bio-composites.

SMC type of materials are often used in semi-structural components. The short production cycle times and the excellent surface appearance of some grades make it attractive as a panel material. Stronger SMC type material can be developed, mainly by incorporating high fiber contents. A schematic representation of a high volume bio-composite processing in making bio-composites from chopped

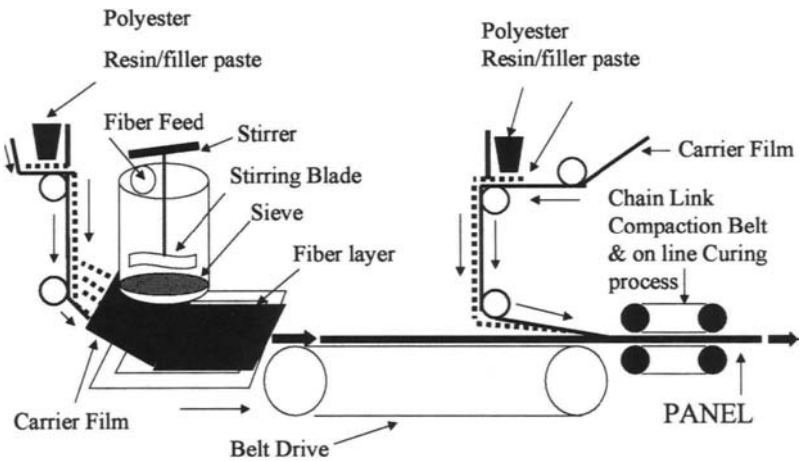


Figure 8: Schematic of Continuous Bio-Composite Sheet Molding Compound Panel (BCSMCP) Manufacturing Process being developed at Michigan State University

natural/bio-fiber and polyester resin or resin/filler paste is shown in Fig.8. Polyester resin in combination of $CaCO_3$ filler is required to be blended with biofibers to produce structural quality low cost housing panels.

CONCLUSIONS

New environmental regulations and societal concerns have triggered the search for new products and processes that are compatible with the environment. The incorporation of bio-resources into composite materials can reduce dependency on petroleum reserves. American market studies clearly identify the potential impact and opportunities for natural fiber composites. Natural fiber composites have the potential for major applications in building products. The majority of such applications include natural fiber-thermoplastic composites for applications like decking, window/siding/railing, flooring, furniture and automotive interiors. The vast majority of this market volume deals with wood fiber and remainder is comprised of non-wood agricultural natural fibers like kenaf, hemp and flax. Wood-fibers cannot impart the required strength for paneling applications, so our efforts target to use non-wood bast and leaf-based natural fibers. Natural fiber – thermoset composites show improved mechanical properties over thermoplastic-based bio-composites and such properties are required for paneling applications. In the U.S., current housing panels made from glass fiber – polyester composite contains ~10-20% glass fiber. Since natural fibers are less expensive (~ 25-30 cents/lb. in North America) than both glass fiber and PE resin, incorporation of the maximum permissible amount of inexpensive natural fibers into the composite structure would not only provide immense economical benefit, but also would result in housing structures with maximum permissible content of renewable resource based natural fibers. The impact/stiffness balance of bio-composites needs to be solved through the combination of bio-fibers (hybrid of bast and leaf fibers) and matrix modification through blending with derivitized vegetable oil. The future for bio-composites ("GREENER" than exiting

glass composites) is bright because of the shortage of landfill availability, difficulty in recyclability of fiber glass composites, and the uncertainty of petroleum price/availability. Achieving this unique balance of mechanical properties and environmental benefits will create new markets for bio-composites for 21st century building product applications.

ACKNOWLEDGEMENTS

Financial support was [provided from the National Science Foundation (NSF) under Partnership for Advancing Technologies in Housing (PATH), 2001 Award # 0122108.

REFERENCES

1. Harris, T. (2001). Trends In New Filler And Reinforcement Technologies For Plastic Composites, *Conference on Functional Fillers*, San Antonio, TX.
2. Mohanty, A. K., Misra, M.. and Hinrichsen, G. (2000) *Macromol. Mater. Sci.* **276/277, 1**.
3. *Composite Week Newsletter*, (2000) **10(2)**.
4. *Composites Technology*, (2000).
5. *DaimlerChrysler HighTech Report* (1999), **88**.
6. Mohanty, A. K. , Misra, M. and Drzal, L. T., (2001) *Polym. Interf.* **8(5), 313**.
7. Brouwer, W. D., (2000). Natural Fiber Composites: Where Can Flax Compete with Glass ?, *SAMPE Journal*, **36(6), 18.**
8. M. Malik, V. Choudhary, I. K. Varma, J. Macromol. Sci. – Rev. Macromol. Chem. Phys; C40 (2&3), 139 (2000).
9. Mohanty, A. K. , Misra, M. and Drzal, L. T., (2001). Surface Modification of Natural Fibers to Improve Adhesion As Reinforcements for Thermoset Composites, *Proceedings of the 24th Annual Meeting of the Adhesion Society – Adhesion Science for the 21st Century"* **418-420**.
10. Mohanty, A. K. , Misra, M. and Drzal, L. T., (2001). Environmentally Benign Powder Impregnation Processing And Role Of Novel Water-Based Coupling Agents In Natural Fiber-Reinforced Thermoplastic Composites, *Polymer Preprint – Polymer Chemistry Division*, ACS, **42(2), 31**.
11. Belchler, L., Drzal, L. T., Misra, M. and Mohanty, A. K. (2001) Natural Fiber Reinforced Thermoset Composites: Studies on Fiber-Matrix Adhesion of Aligned Henequen Fiber – Epoxy Composites *Polymer Preprint – Polymer Chemistry Division*, ACS, **42(2), 73**.
12. Schloesser, T., (2000). Natural Fiber Composites in Automotive Applications, *3rd International Symposium- Bioresource Hemp & other fiber crops*, Wolfsburg, Germany.

Advances in Building Technology, Volume 1
M. Anson, J.M. Ko and E.S.S. Lam (Eds.)
© 2002 Elsevier Science Ltd. All rights reserved

DURABILITY OF PULP FIBER-CEMENT COMPOSITES TO WET/DRY CYCLING

N.H. El-Ashkar[1], B. Mohr[1], H. Nanko[2], and K.E. Kurtis[1]

[1]School of Civil and Environmental Engineering, Georgia Institute of Technology, Atlanta, GA, 30332-0355, USA
[2]Institute of Paper Science and Technology, Atlanta, GA, 30318-5794, USA

ABSTRACT

To ensure satisfactory long-term performance, focused research is required to more completely understand the moisture-related durability of natural fiber-reinforced cement-based materials. The results presented here are part of a comprehensive investigation to examine both the initial state of the fiber-cement matrix bond and the changes in the bond, and resulting mechanical performance of the composite, that occur due to moisture fluctuations. In this early phase of an extensive and systematic investigation, the appropriateness of a proposed environmental exposure test program is examined. Results show that the initial curing period should be extended beyond eight days for both the control samples and those samples subjected to wet/dry cycling to minimize the influence of continued cement hydration during environmental exposure.

KEYWORDS

cement, composite, concrete, durability, fiber, housing, paper, pulp

1.0 INTRODUCTION

Depending on their application, fiber-cement materials can offer a variety of advantages over traditional construction materials:

- As compared to wood, fiber-cement products offer improved dimensional stability, moisture resistance, decay resistance, and fire resistance.
- As compared to masonry, fiber-cement products enable faster, lower cost, lightweight construction.
- As compared to cement-based materials without fibers, fiber-cement products may offer improved toughness, ductility, and flexural capacity, as well as crack resistance and "nailability".

An alternative to more expensive steel fiber-, glass fiber-, and synthetic polymer fiber-reinforced cement products, wood fibers are well-suited for reinforcing cement-based materials because of their high strength-to-cost ratio, availability, renewability and recyclability, and non-hazardous nature [MacVicar *et al.*, 1999]. Increasing regulations surrounding the use of asbestos fiber reinforced materials has also prompted the growing interest in wood fiber-cement composites for construction. The growing

worldwide acceptance and use of fiber-cement products in residential construction and the continuing development of new products have caused the industry to describe fiber-cement materials as "tomorrow's growth product" [Kurpiel, 2000].

Yet, despite continuing interest in the development of load-bearing or structural fiber-cement composites, the primary applications of this class of material remain non-structural. This is in part due to concerns about the degradation of fiber-cement composites. One issue of continuing concern is the effect of swelling of the fibers in the presence of moisture, and the effects of such swelling on composite performance over time. American Concrete Institute (ACI) Committee 544 "Fiber Reinforced Concrete" has identified moisture-related durability of natural fiber-reinforced cement-based materials as an area requiring focused research to ensure satisfactory long-term performance of such materials.

A comprehensive research plan is underway to improve understanding of the implications of fiber swelling/shrinking on the composite system – the changes that occur in the fiber, surrounding brittle matrix, and the performance of the composite as a whole. The objectives of this research are:

1) to assess the effects of repeated wetting and drying (rain and heat) cycles on dimensional changes of wood fibers, physical bonding at the fiber/cement paste interface, and bond strength between the fiber and matrix, and
2) to assess if improved bonding can be produced through tailoring the fiber processing for this application. (Specifically, the processes to be examined, individually and in combination, include fibrillation, bleaching, and pre-drying.)

Research to achieve these objectives is ongoing and includes both microstructural characterization by scanning electron microscopy and mechanical testing using both traditional flexural testing as well as specialized samples prepared assess fiber/matrix bonding. Here, the results of some initial work in this investigation to assess the proposed environmental exposure regimen are presented.

2. EXPERIMENT

2.1 Materials and Sample Preparation

Pulp fiber reinforced mortar bar samples, 1x1x4in. (2.54x2.54x10.16cm), were prepared with water-to-cement ratio of 0.60 and sand-to-cement ratio of 1. The cement used was commercially available Type I cement. The sand used was a natural siliceous sand (FM=1.80), obtained from Brown Brothers Quarry in Junction City, Georgia USA. Unbleached softwood (Slash Pine) kraft pulp was used without beating as fiber reinforcement at 1% fiber volume fraction in the mortar. Mortars were mixed in a 1.5L-capcity Hobart mixer at 120 rpm.

2.2 Exposure

All of the samples were cured in a saturated lime solution at room temperature for four days. After this initial curing period, the samples were divided into three groups and subjected to three different aging/exposure conditions. One group of samples was allowed to air cure at room temperature and humidity (RH = 60±5%) for one more day and was tested at 5 days of age. A second group was allowed to air cure, after the initial 4-day moist curing period, and was subsequently tested at 8 days of age. A third group was exposed to 10 cycles of wetting and drying in an environmental chamber (Thermotron Model SE-1200-3-3) over a 74-hour period. These samples were tested just after their environmental exposure, at an age of 8 days.

In the environmental chamber, the samples were kept for 2h 55min at 60° F (16°C) and 85% RH. Over a 30-minute period, the temperature was increased at a rate of 1.33°F/min (0.74°C/min) to 100°F (33°C) and the humidity was decreased at a rate of 2.17%/min to 20%; these conditions were held for 2h

55min. Over a 60-minute period, the environmental conditions were cycled to 60° F and 85% RH at rates of 0.67°F/min (0.37°C/min) and 1.08%RH/min, respectively, completing one wet/dry cycle. The selection of the "hold" period of 2h 55 min is based upon ASTM C 1185-99 and the selection of the rates is based upon the capabilities of the environmental chamber. A representation of these exposure conditions is shown in Figure 1.

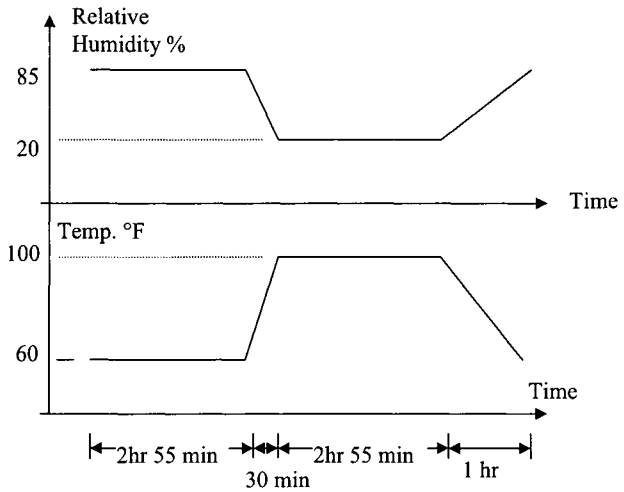


Figure 1: Schematic representing a single wet/dry cycle.

2.3 Test Method

Center-point flexure tests were performed on the mortar beams using a span of 3 in. (7.62 cm). The span-to-depth ratio of 3 was chosen to comply with ASTM C 348-97 and C 293-94. Tests were performed in triplicate using a 22-kip screw driven test frame (Satec model 22EMF). The deflection was captured using an electronic deflectometer, placed under the center point of the beam. The test was controlled using the deflection control system to better capture the post-peak behavior of the beams.

3.0 RESULTS AND DISCUSSION

Load-deflection curves for all three groups of samples are shown in Figure 2. Average behavior for each sample type is shown in Table 1. The results show that the average peak load is moderately increased due to age in the sample tested at 8 days without environmental exposure as compared to the sample tested at 5 days, also without environmental exposure. The average peak loads carried by these samples were 864 and 813 psi (5.96 and 5.61 MPa), respectively. A larger (46 %) increase in peak strength, as compared to the samples tested at 5 days, is seen in the data for the samples tested after 8 days and after being subjected to wet/dry cycling. This result was not expected, but it is proposed that this increased strength is due to accelerated cement hydration in a warm moist environment. Thus, this peak strength data can be seen to represent a change in the matrix with environmental exposure and time.

While peak load capacity may have increased with wet-dry cycling, toughness was found to decrease. The average post-peak toughness for the samples tested at 5 days, 8 days, and 8 days with wet/dry cycling were 1.176, 1.175, and 1.104 lb.in. (132.9, 132.8, and 124.7 N·mm), respectively. This 6% decrease in toughness observed between the samples tested at 8 days with and without environmental exposure may be due to increased matrix strength and perhaps increased matrix/fiber bond strength, which in turn changes the behavior of the composite in flexure. It is proposed that the increased strength of the fiber-cement bond causes the failure mode to result, to a greater extent, from fiber breakage rather than fiber pullout. These competing effects (i.e., increasing bond strength with continued cement hydration during aging and possible decreasing bond strength during wet/dry cycling) can make data interpretation challenging.

These results show that to isolate the effect of wet/dry cycling, the curing period and environmental exposure should be altered. First, the control samples should be continuously moist cured until testing. Second, samples should be cured for a longer period prior to wet/dry cycling, to minimize the effect of continued cement hydration during the environmental exposure.

TABLE I
SUMMARY OF RESULTS FROM FLEXURAL TESTING

Specimen Type	Curing Time (days)	Age at Testing (days)	Number of Wet/dry Cycles	Average Flexural Strength (psi)	Post-peak Toughness (lb.in.)
1	4	5	0	813	1.176
2	4	8	0	864	1.175
3	4	8	10	1188	1.104

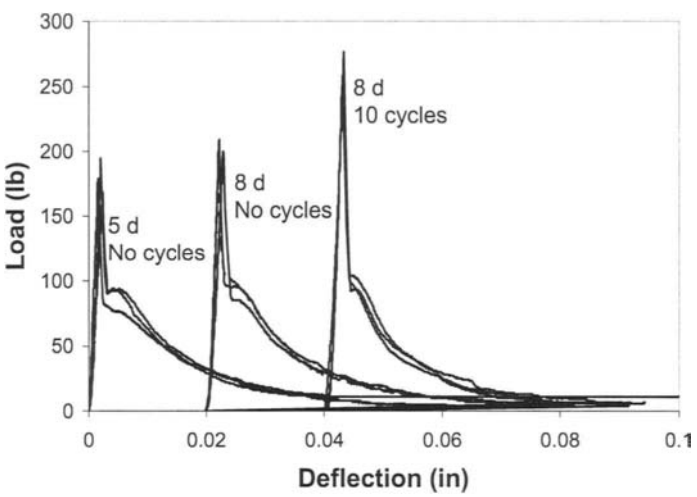


Figure 2 Load-deflection curves for samples cured for 5 and 8 days without wet/dry cycling and those cured for 4 days and subsequently subjected to 10 wet/dry cycles over a 4-day period.

4.0 CONCLUSIONS

This investigation shows that the wet/dry cycling employed here can result in improved flexural strength, which is likely due to the increase in the degree of hydration of the cement-based matrix during the environmental exposure. However, post-peak toughness is decreased as a result of the wet/dry cycling employed and this is believed to reflect changes occurring at the fiber/matrix interface. Therefore, to assess the effect of environmental exposure cycles on composite performance, data analysis should focus on the post-peak region of the load-deflection curve.

More than one factor may contribute to the observed decrease in toughness with environmental exposure. The loss in toughness may be due to fiber/matrix debonding during the wet/dry cycling and also due to the increased fiber/matrix bond strength due to continued cement hydration. Thus, it is recommended that control samples be moist cured until the day of testing and that the samples subjected to wet/dry cycling be moist cured for a more extended period prior to environmental exposure. Both of these measures are intended to reduce the effect of the bonding strength. Research is ongoing to identify appropriate conditions (i.e., curing times, exposure periods, temperature, relative humidity) for this environmental exposure.

ACKNOWLEDGEMENTS

The authors gratefully acknowledge support from U.S. National Science Foundation award CMS-0122068, which is part of an initiative co-sponsored by the Partnership for Advancing Technologies in Housing (PATH) as well as support from the Institute for Paper Science and Technology seed grant program and PATHWAYS program.

REFERENCES

American Concrete Institute Committee 544 (1996) "State-of-the-Art Report on Fiber Reinforced Concrete", Manual of Concrete Practice, ACI 544-1R96, Farmington Hills, MI.

American Society for Testing and Materials (1994) "Flexure Strength of Concrete (Using Simple Beam with Center-Point Loading)," *ASTM Spec. Tech. Publ. C 293.*

American Society for Testing and Materials (1997) "Flexure Strength of Hydraulic Cement Mortars," *ASTM Spec. Tech. Publ. C348.*

American Society for Testing and Materials (1999) "Standard Test Methods for Sampling and Testing Non-Asbestos Fiber-Cement Flat Sheet, Roofing and Siding Shingles, and Clapboards," *ASTM Spec. Tech. Publ. C 1185.*

Kurpiel, F. (2000) "Fiber-cement siding is tomorrow's growth product," *Wood Technology*, November.

MacVicar, R.; Matuana, L.M.; and Balatinecz, J.J. (1999) "Aging Mechanisms in cellulose fiber reinforced cement composites", *Cement and Concrete Composites*, **V.21**, 189-96.

This Page Intentionally Left Blank

Advances in Building Technology, Volume 1
M. Anson, J.M. Ko and E.S.S. Lam (Eds.)
© 2002 Elsevier Science Ltd. All rights reserved

Extruded Fiber-Reinforced Composite

B. Mu, M. F. Cyr and S. P. Shah

Center for Advanced Cement Based Materials, Northwestern University,
2145 Sheridan Road, Evanston, IL 60208, USA

ABSTRACT

In this study, high performance fiber-reinforced cementitious composites (HPFRCC) were produced using the extrusion technique. The reinforcing effects of three types of short fibers, glass, polyvinyl alcohol (PVA) and polypropylene (PP), and combinations of these fibers were tested. The mechanical properties and durability of extruded composites with high percentage of class F fly ash were also studied. It was found that the flexural performance of extruded composites can be controlled and optimized using hybrid fibers. The durability of glass-fiber composites was greatly improved by the addition of fly ash. A widely applicable rheological constitutive model was selected based on the experimental observations.

KEYWORDS

Fiber-reinforced concrete, Extrusion, Rheology, Fibers, Fly ash, Viscosity, ACBM

EXTRUSION

High performance fiber-reinforced cementitious composites (HPFRCC) exhibit increased tensile strength, enhanced toughness, and sometimes, a strain-hardening response. The amount of fiber reinforcement needed to achieve this behavior is higher than what can typically be added to conventional cast-in-place concrete. Special processing techniques are required to produce HPFRCC. Recently, extrusion technology has been adapted for the production of HPFRCC at the Center for Advanced Cement Based Materials (ACBM Center) at Northwestern University.

Extruded elements are formed by forcing a highly viscous, dough-like mixture of cement paste and fibers through a die of desired cross-section. The composites are formed under high shear and high compressive forces, producing a compact matrix with a good fiber-matrix bond and fiber alignment in the direction of extrusion. The ACBM center research group at Northwestern University started the trials to produce extruded HPFRCC (Shao *et al.* 1995). They have successfully extruded a variety of products including sheets, tubes and cellular shapes. Their research shows that extruded HPFRCC are much stronger and tougher than that made by traditional casting methods. This improvement can be attributed to the achievement of low porosity and good interfacial bond in HPFRCC under the high

shear and compressive stresses during extrusion process (Shao and Shah 1996). Their findings and methodology have been adopted and verified by many other researchers (Stang and Pedersen 1996; Li and Mu 1998).

The relation of the modulus of elasticity of the fibers to the modulus of elasticity of the cement matrix influences the mechanical performance of the composite (Bentur and Mindess 1990). High-modulus; high-strength fibers that have a strong bond with the cement matrix can be used to increase composite strength, and low-modulus fibers that have a weaker bond with the cement matrix can be used to enhance composite ductility. Hybrid composites containing two or more fiber types can be considered to control the properties of HPFRCC by taking advantage of both high-modulus; high-strength and low-modulus fibers. The combination of the advantages of hybridization and the extrusion process enables the production of a large range of composite performance and the design of a specific composite performance.

Properly designed extrudate rheology, which controls both internal and external flow properties, is essential for successful extrusion. If the rheology is not correct, defects like lamination and surface tearing can occur during extrusion. Such extrusion defects could be reduced or eliminated with the use of a rheological model in the design of a HPFRCC mixture. The model could predict if the rheology of the matrix is appropriate for extrusion.

The mechanical properties of extruded HPFRCC containing several fiber types, along and in hybrid combinations were studied. The fibers included low elastic modulus PP fibers, as well as strong and stiff glass and PVA fibers. The flexural performance of composites containing large amounts of fly ash was examined. The durability of glass-fiber composites with and without fly ash was also examined. Based on the experimental observations of the fresh extrudate, a differential viscoelastic constitutive model was selected for the future description of the extrusion process.

PROPERTIES OF EXTRUDATES

Special processing techniques, such as extrusion, can enhance the benefits of fiber reinforcement and matrix. Short reinforcing fibers and mineral admixtures have been shown to increase strength and toughness of traditional cement-based composites. Figure 1 (Peled *et al.* 1999) shows that an extruded fiber-reinforced composite is stronger and more ductile than an identical cast fiber-reinforced composite. The effects of different reinforcing fibers and fly ash on the mechanical properties and durability of the extruded HPFRCC were investigated. The mechanical properties were characterized by flexural performance. Specimens were subjected to accelerated aging to assess durability.

The basic mixture proportions, by volume, of the composites were 43% Type I OPC, 12% silica fume, 1% superplasticiser, and 1% rheological enhancer, with a water/cement ratio of 0.24. When fly ash was added to the matrix, it replaced 70%, by volume, of the cement. The basic mixture proportions for composites containing fly ash were 30% Class F fly ash, and 13% cement, with remaining ingredients at the same proportions.

The cementitious matrices were reinforced with glass, PP and PVA fibers, individually and in hybrid combinations. The glass, PVA, and polypropylene fibers have strengths of 3500, 1900, and 700 MPa, respectively, and elastic moduli of 71, 41, and 5 GPa, respectively. The glass-fiber and polypropylene-fiber composites were prepared with a fiber volume fraction (V_f) of 5%. The PVA-fiber composite was prepared with a V_f of 3% because it was difficult to mix and achieve good dispersion of PVA fibers at higher volumes. The hybrid fiber composites were examined by preparing various combinations of glass, PP and PVA fibers (glass/PP/PVA): 20:80:0, 20:40:40, 40:20:40, 40:0:60. The

total V_f in the hybrid combinations was 5%. The influence of fly ash on durability was studied in 5% glass-fiber reinforced composites only.

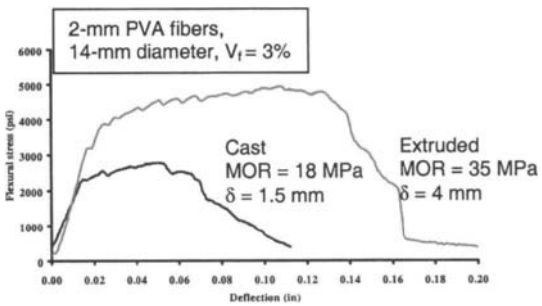


Figure 1: Flexural behavior of extruded HPFRCC and traditional cast FRC (Peled *et. al.* 1999).

Thin sheet specimens, 4mm x 25mm, were extruded using a laboratory-scale ram extruder. After extrusion, the specimens were covered with plastic to set for three days. Then, they were moist cured for 28 days at room temperature and 100% relatively humidity (RH). To evaluate long term durability of glass-fiber composites one batch of specimens was placed in an 80°C water batch for six week after a 28-day moist cure to accelerate aging. Prior to testing, the specimens were removed from the curing or aging environment and stored at 22°C, 50% RH for 24 hours to allow surface moisture to evaporate.

The three-point bend flexural tests were performed on an MTS machine with a 445 N load cell. The span of the extruded specimen was 101.6 mm. The test was conducted under stroke control at the rate of 0.0114 mm/sec. The modulus of rupture and area under the stress-deflection curves, referred to here as the toughness, were calculated. The toughness was calculated up to 20% of the maximum stress in the post-peak region, except from composites containing polypropylene, where the toughness was calculated to a deflection of 10 mm. The test results presented are an average of at least 5 specimens. Typical stress-deflection curves representing the flexural behavior of individual composites are chosen for comparison.

Effect of Hybridization

Hybrid composites containing two or more fiber types can be considered to optimize the desired properties of composites by taking advantage of the properties of each fiber. Figure 2 shows the flexural response of 100% glass, 100% PVA and 100% PP fiber composites with V_fs of 5%, 2%, and 5%, by volume, respectively. The relatively brittle behavior of the glass-fiber composite is clear in this figure.

PP fibers have a lower elastic modulus than the cementitious matrix and a relatively poor fiber-matrix bond, while glass fibers have a higher elastic modulus than the cementitious matrix and a relatively strong fiber-matrix bond. Figure 3 presents the flexural response of the 100% PP composite and the hybrid composite with a 20:80 glass/PP ratio, both with a V_f of 5%. When only 20% of the PP fibers are replaced with glass fibers, the strength of the composite increases by about 60%. However, the increase in toughness is quite small. It has been shown that further replacement of PP fibers with glass fibers will lead to a decrease in toughness but an increase in strength (Peled *et al.* 2000).

The performance of hybrid composites of various combinations of glass, PP, and PVA fibers with a total V_f of 5% is shown in Figure 4. Replacing half of the PP fibers in the 20:80 glass/PP hybrid with PVA fibers (glass/PP/PVA 20:40:40) significantly increases both the strength and toughness of the

composite, producing a strain hardening response. Further replacement of some of the remaining PP fibers with glass fibers, 40:20:40 glass/PP/PVA composite leads to a greater improvement in flexural performance of the composite. Moreover, the 40:20:40 and 40:0:60 glass/PP/PVA hybrid combinations exhibit flexural strengths similar to the 100% glass fiber composite but show a significant improvement in toughness. It can be concluded that performance of extruded composites can be controlled and optimized with different hybrid combinations.

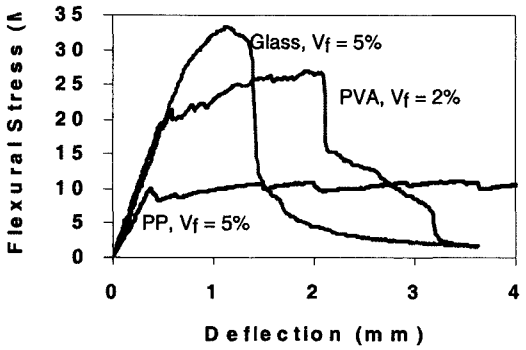


Figure 2: Flexural response of composites with different fiber types (Peled *et al.* 2000).

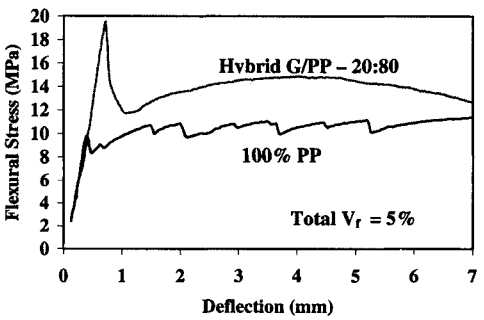


Figure 3: Flexural response of 100% PP fiber compared with glass/PP (20:80) hybrid composite (Peled *et al.* 2000).

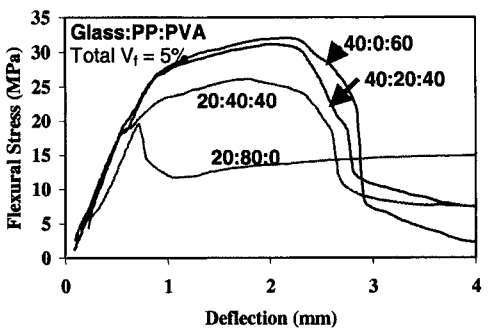
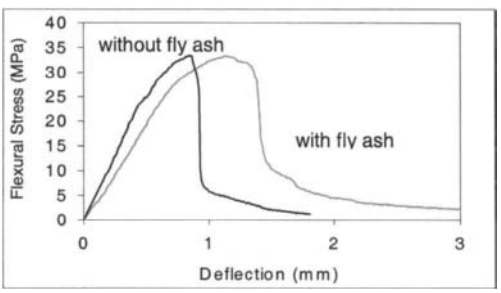


Figure 4: Flexural response of hybrid composite (Peled *et al.* 2000).

Effect of Fly Ash

Class F fly ash can replace cement in extruded composites. Its round particle morphology serves as a rheological aid. It is less expensive and more environmentally sound than cement. Fly ash also improves the mechanical performance of extruded composites, especially those containing glass fibers (Peled *et al.* 2000b). The replacement of 70% of the cement, by volume, with fly ash in a glass-fiber extruded composite increases the strength by 10% and the toughness by 50%, as shown in Figure 5 (Cyr *et al.* 2001). This improvement in performance might be a result of an increase in porosity with the addition of fly ash, which weakens the bond strength enough to increase fiber pullout at failure (Peled *et al.* 2000b).

Fly ash also improves the durability of extruded glass-fiber composites. Glass fibers, even those designed to be alkali resistant, may degrade in the alkaline environment of a cementitious matrix. Fly ash lowers the alkalinity of the matrix (Peled *et al.* 2000b) reducing the possible fiber degradation. Strength is maintained with aging and the reduction in toughness is only 30% when fly ash is added to the matrix, ash shown in Figure 6.



gure 5: Flexural performance of glass-fiber composites with and ithout fly ash after 28-day moist cure. V_f=5% (Cyr *et al.* 2001)

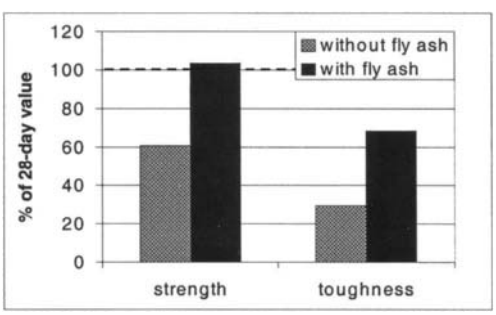


Figure 6: Change in strength and toughness of glass-fiber composites with and without fly ash after accelerated aging. V_f=5% (Cyr *et al.* 2001)

RHEOLOGY OF FRESH HPFRCC IN AN EXTRUDER

The rheology of the fresh HPFRCC is essential to the success of extrusion. If the rheology of the fresh HPFRCC is not ideal, defects will form during extrusion. To facilitate the extrusion process of the

HPFRCC, a study of the rheological behavior of the extrudate is required. Considering the deformation rate is small (described as a small Deborah number: <1), Li et al. (1999) employed the retarded-motion expansion constitutive model for analysis and obtained some preliminary results. However, the retarded-motion expansion was restricted to a small deformation rate. A more widely applicable nonlinear viscoelastic constitutive model is desired. The selected model should be able to describe the normal stress differences of the extrudates observed in the extrusion process.

To develop a suitable constitutive model, both the viscosity and elastic properties of the fresh HPFRCC were studied using two self-designed rheometers. One was a coaxial cylinder rheometer based on a screw extruder (Rheocord 9000, HAAKE), and the other was a cone-and-plate rheometer based on a torsion-compression Material Testing Machine (MTS 858 Table Top System). For the coaxial cylinder rheometer, two cylinders were installed at the head of the extruder. The extrudate was packed between the two coaxial cylinders. The extruder recorded the rotation speeds and the corresponding torques. From these data, the viscosities of the extrudate were calculated. The cone-and-plate rheometer was used to study the elastic properties of the extrudate. During the test, the cone was rotated with the MTS fixture and the plate was kept stationary. Under displacement control the MTS provided a compressive force to keep the cone and the plate in contact. From this compressive force, the elastic material parameter was obtained.

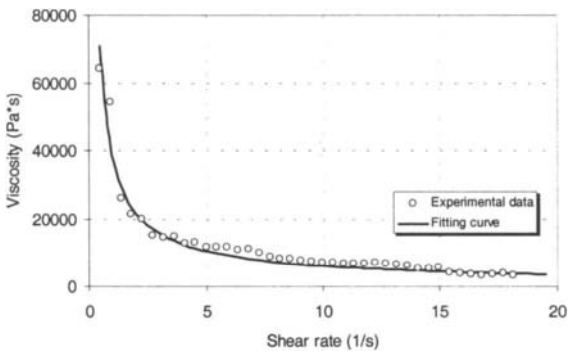


Figure 7: Viscosity and shear rate relationship of the fresh HPFRCC

The experimental results from the coaxial cylinder rheometer and the cone-and-plate rheometer are shown in Figure 7 and 8, respectively. The mixture proportions of the extrudate were cement:slag:sand-1:sand-2:water = 1:1:0.39:0.26:0.60, where sand-1 and sand-2 are silica sand with diameters of 600~300 μm and 150~90 μm, respectively. The mixture was reinforced with 2% PVA fibers. Figure 7 shows that this cementitious flow exhibits a shear thinning response. The curve fitting of the experimental data results in a power law fluid, $\eta(\dot{\gamma}) = m\dot{\gamma}^{n-1}$, with m = 37500 and n = 0.2, where $\eta(\dot{\gamma})$ is viscosity and $\dot{\gamma}$ is shear rate, respectively. The compressive force increases with the shear rate, as shown in Figure 8. This implies that the elastic material parameter is not only a function of the compressive force but also a function of the shear-thinning viscosity.

One model that explains the above experimental observations well is the White-Metzner model (White and Metzner 1963) given by

$$\tau = -\eta(\dot{\gamma})(\gamma_{(t)} + \frac{1}{G}\tau_{(t)}) \tag{1}$$

where G is a constant modulus and $\eta(\dot{\gamma})$ is an arbitrary function to describe the shear rate dependent viscosity. τ and $\gamma_{(1)}$ are stress tensor and rate of strain tensor, respectively. $\tau_{(1)}$ is the convected time derivative of the stress tensor. In the cone-and-plate rheological experiment (simple shear), Eq. (1) can be expressed as

$$G = \frac{\pi R_0^2 m^2 \dot{\gamma}^{2n}}{F} \tag{2}$$

where R_0 is the diameter of the cone and F is the compressive force.

The selected constitutive model gives a reasonable description of the observed behavior in the simple steady shear case. Since it is a differential constitutive model, it is not limited to small deformation gradients as are the linear viscoelastic models, or to small slowly changing deformation rates, as is the retarded-motion expansion model. There are only three unknown material parameters, m, n, and G, all of which can be obtained with standard rheometers. So, the White-Metzner model is applicable for simulating the extrusion of HPFRCC.

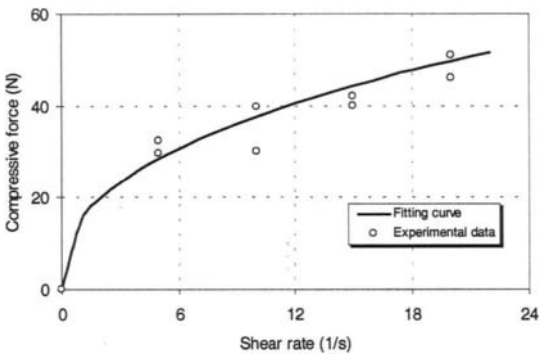


Figure 8: Compressive force and shear rate relationship of the fresh HPFRCC

FUTURE WORK

Future research will be the development of extruded HPFRCC suitable for residential construction applications, particularly advanced panel systems. Future work will focus on batch composition, development of cross-sections, and material testing.

New composites will be reinforced with different types of fibers, including glass, polypropylene, PVA and cellulose, and hybrid fiber combination, to tailor performance for specific applications. These composites will be developed with a high fly ash content to reduce cost, to improve ductility, and to make production more ecological. The effect of fiber movement and particle sizes on extrusion will be studied through a rheological analysis of the composites. Theoretical modeling will be used to guide the manufacture of extrudates with different cross-sections, including cellular and corrugated sheets.

Material testing will focus on determining extruded composite characteristics important to residential construction applications. Impact test will be highly emphasized. Its results will be employed to describe nailability of the extrudates. Impact wave propagation and fracture resistance of the extrudats will be modeled.

ACKNOWLEDGEMENT

This work is being funded by a grant from the National Science Foundation in support of the Partnership for Advancing Technologies in Housing (PATH), a presidential initiative to accelerate the creation and use of advanced technologies to improve the quality, durability, environmental performance, energy efficiency and affordability of housing in the US. Prof. Peter C. Chang, Program Director at Structural Systems and Hazards Mitigation at Division of Civil and Mechanical Systems at National Science Foundation is gratefully acknowledged.

References

Balaguru P. and Shah S. P. (1992). *Fiber Reinforced Cement Composites,* McGraw-Hill, New York.

Bentur A. and Mindess S. (1990). *Fiber Reinforced Cementitious Composites*, Elsevier Applied Science, UK.

Cry M. F., Peled A., and Shah S. P. (2001) Improving Performance of Glass Fiber-Reinfroced Extruded Composites. Proceedings of the 12th International Glassfiber Reinforced Concrete Congress GRC 2001 eds. N. Clarke and R. Ferry. Dublin, Ireland 143-172.

Li Z., and Mu B. (1998). Application of Extrusion for Manufacture of Short Fiber Reinforced Cementitious Composite, *Journal of Materials in Civil Engineering, ASCE*, **10**, 2-4.

Li Z., Mu B., and Chui S. (1999). Rheology Behavior of Short Fiber-Reinforced Cement-Based Extrudate, *Journal of Engineering Mechanics, ASCE*, **125:5**, 530-536.

Peled A., Cyr M., and Shah S. P. (2000). Hybrid Fibers in High Performance Extruded Cement Composites. *Proceedings of International RILEM Symposium BEFIB'2000.* Lyon, France.

Peled A., Cyr M., and Shah S. P. (2000b). High Content of Fly Ash (Class F) in Extruded Cementitious Composites. *ACI Materials Journal*, **97:5**, 509-517.

Peled A., Akkaya Y., and Shah S. P. (1999). Extruded Fiber-reinforced Cement Composites Containing Fly Ash. *Proceedings: 13th International Symposium on the Use and Management of Coal Combustion Products (CCPs).*ed. S.S. Tyson, B.R. Stewart, G.J. Deinhart. American Coal Ash Association, Orlando, FL. 32-1 – 32-16.

Stang H. and Pederson C. (1996). HPFRCC-extruded Pipes, Materials for the New Millennium, K. P. Chong, ed., *Proceedings of the 4th Materials Eng. Conference*, Washington, D. C., **2**, 261-270.

Shao Y., Marikunte S. and Shah S. P. (1995). Extruded Fiber-Reinforced Composites, *Concrete International* **17:4**, 48-52.

Shao Y., and Shah S. P. (1996). High Performance Fiber-Cement Composites by Extrusion Processing, Materials for the New Millennium, K. P. Chong, ed., *Proceedings of the 4th Materials Eng. Conference*, Washington, D. C., **2**, 251-260.

White J. L. and Metzner A. B. (1963). *J. Appl. Polym. Sci.*, **7**, 1867-1889.

Advances in Building Technology, Volume 1
M. Anson, J.M. Ko and E.S.S. Lam (Eds.)
© 2002 Elsevier Science Ltd. All rights reserved

REVERSED IN-PLANE CYCLIC BEHAVIOR OF POST-TENSIONED CLAY BRICK MASONRY WALLS FOR HIGH PERFORMANCE MODULAR HOUSING

Owen A. Rosenboom, Graduate Research Assistant

Mervyn J. Kowalsky, Assistant Professor

Department of Civil Engineering, North Carolina State University, Raleigh, NC, 27695, USA

ABSTRACT

Initial experimental results of a research program aimed at investigation of post-tensioned clay masonry walls for high performance modular housing are presented. A series of five large scale reversed cyclic tests on double-wythe clay brick masonry walls are discussed. Each of the five walls contain different details with the objective being to identify the characteristics of each such that choices depending on required performance can be made. The basic behavioral mechanism that is a characteristic of unbonded post-tensioned masonry walls is discussed, followed by details of the performance of each test. Results indicate that walls with unbonded post-tensioning steel performed best in terms of deformation capacity, and strength degradation. Particularly good performance was achieved by confining the compression toe regions of unbonded walls.

KEYWORDS

Post-tensioned masonry, confined masonry, seismic design, cyclic wall response, in-plane wall response.

RESEARCH OBJECTIVE, MOTIVATION AND METHODS

The primary objective of the research described in this paper is to conduct fundamental research into the behavior of pre-stressed clay masonry walls that will then lead into a new modular housing technique that will advance the goals of the Partnership for Advancing Technology in Housing (PATH) program. The PATH program (http://www.pathnet.org) represents a partnership between industry, government, and researchers aimed at achieving the four goals listed below. Of the four PATH program goals, the research conducted at NC State specifically addresses goals one and two. Although it is difficult to quantify, it is also envisioned that strides in the third and fourth goals shown below would be made, particularly over the long term.

1. Reduce the risk of life, injury, and property destruction from natural hazards by at least 10% and reduce residential construction work illness and injuries by at least 20%.
2. Improve durability and reduce maintenance costs by 50%
3. Cut the environmental impact and energy use of new housing by 50%.

4. Reduce the monthly cost of new housing by 20% or more.

Specifically discussed in this paper is the behavior of post-tensioned clay brick masonry walls under seismic conditions. As discussed in the introduction, the motivation for the use of post-tensioning in clay brick masonry walls revolves around enhanced construction efficiency, cost, and most importantly, lateral force performance. Although the emphasis here is on seismic behavior, the details used could be readily employed in regions of low to moderate seismicity, as well advancing the behavior due to other lateral loads such as wind.

The methods used in this research center around five components that together form the first phase of a larger research project on the topic. A project website, http://www4.ncsu.edu/~kowalsky, may be accessed by the reader for complete details on all aspects of the research. The five components in this phase one research are as follows: (1) Literature review and evaluation of the most promising details to employ in the design of post-tensioned masonry walls and assessment of current design approaches. (2) Development of an analysis and design algorithm for the displacement-based design of post-tensioned clay masonry walls. (3) Reversed cyclic testing of a series of five large scale post-tensioned clay brick masonry walls. (4) Evaluation of displacement-based design parameters and revision of analysis and design algorithm. (5) Identification of Phase 2 research needs. In this paper, components 3, and 5 are discussed.

EXPERIMENTAL PROGRAM

Test Specimen Details

As part of the study described in this paper, a series of five large scale cantilever walls were tested in the Constructed Facilities Laboratory (CFL) at North Carolina State University (NCSU). All five walls were double wythe walls 1.22m long, 305mm thick and 2.44m tall to the center of seismic force as shown in Fig. 1. The walls were constructed from standard cored clay brick masonry units measuring 57mm high, 92mm wide, and 194mm long. All of the walls were post-tensioned with 3 equally spaced 25mm diameter dywidag bars as shown in Fig. 1. Test unit one represented the 'control' specimen and contained a fully grouted wall cavity. The tendons were unbonded, and no additional reinforcement was placed in the wall. Test unit two was the same as test unit one with the exception that confinement plates were placed in the compression toe regions of the wall to enhance the compression strain capacity. Test unit three was also the same as test unit one, with the exception that 4#4 grade 60 ASTM A706 mild reinforcing bars were placed near the end regions of the wall to provide some additional energy dissipation capacity. These mild reinforcing bars extended 914mm above the footing level and were unbonded over a length of 152mm below the footing interface and 457mm above the footing interface. Special considerations were needed in the design of this wall as too little reinforcing steel would not provide sufficient benefit, and too much would result in a large amount of residual deformation after cyclic loading. Test unit four was also the same as test unit one with the exception that the post-tensioning bars were bonded to the wall. The final test specimen was different from the first in that the wall was ungrouted, and as a result, the post-tensioning bars not laterally restrained. All five walls were post-tensioned with a target total force of 1000kN. The test matrix shown in Table 1 provides details of all 5 test units.

Design Approach

The pre-stress force for the walls was determined using a displacement-based design approach. It was stipulated that the pre-stress force in the walls should provide sufficient moment capacity to limit the wall drift ratio to 2% under the design level earthquake, which was obtained from the IBC for Charleston, SC (ICBO, 2000). For details regarding the displacement-based design approach, the reader is referred to Kowalsky et al (2003).

Test Setup, Instrumentation, and Load History

The test setup utilized is shown in Fig. 1. The walls were tested in single bending via a 980kN MTS hydraulic actuator mounted on one side to the strong wall, and at the test specimen via a cast in place concrete loading stub. A guidance frame (not shown in Fig. 1 for clarity) was used to provide out of plane lateral restraint. Instrumentation consisted of load cells to measure pre-stress force and actuator force, a string potentiometer to measure wall displacement, linear potentiometers to measure the profile of the crack at the wall base as well as wall curvature, and electrical resistance strain gages on test unit 3 to measure strain in the

supplemental mild steel. The loading history for all five test specimens was identical and followed a pattern of reversed cyclic loading at increasing levels of drift ratio. At each drift ratio, the wall was cycled three times in each direction. The applied load history was based on the ACI recommendations for frame testing (ACI, 2002).

Test One Results - (Grouted, Unbonded, Unconfined)

Test unit one represents the 'control' specimen. During the course of this test, it was observed that the behavioral mechanism by which such a wall deforms is one of 'rocking', which is consistent with observations made by Laursen and Ingham (2000a,b) on post-tensioned concrete masonry walls. At a drift ratio of 0.2%, a crack formed at the base of the wall. Once this cracked formed, no further flexural cracking was observed, which is as expected given the absence of bond between masonry and steel post-tensioning steel. Cycling continued without any further observation of damage until a drift ratio of 0.5% when initial signs of crushing of masonry on the compression toe region was noted. Once the masonry started to crush, the extent of damage extended into the core region of the wall as the masonry was unconfined. At a drift ratio of 2.75% the maximum lateral force capacity of 327kN was achieved. The wall was cycled to a drift ratio of 6.5% with some gradual strength degradation. A photo of the test unit at 6.5% drift is shown in Fig. 2a, while the force-displacement hysteretic response is shown in Fig. 3a. From Fig. 2a, note the rather extensive damage to the compression toe regions, however, the remainder of the wall above this region remained largely crack free. The integrity of the masonry above the plastic hinge region is very important from the perspective of achieving a stable compression strut as will be noted in the discussion of tests four and five

From the force-displacement hysteretic response of Fig. 3a, there are two characteristics that must be noted. First, the unbonded post-tensioned system is largely self correcting as residual displacement is close to zero for the majority of the load history. This observation is consistent with the observations made for post-tensioned concrete (Priestley et al., 1999) and post-tensioned concrete masonry (Laursen and Ingham, 2000a,b). Second, the amount of energy dissipation is rather limited, however, this is not a considered to be a fatal flaw as the lateral strength is generally dependable without strength degradation until a drift ratio of 3.75%. Furthermore, test unit three will investigate the use of mild steel as a means for supplemental energy dissipation.

Test Two Results - (Grouted, Unbonded, Confined)

Test unit two was identical to test unit one, with the exception of the addition of galvanized steel plates to the mortar bed joints in the bottom five courses of masonry. Application of confinement plates to masonry was first proposed by Priestley and Bridgeman (1974). The initial behavior of the test specimens was identical to that of test unit one. Initial crushing was noted at the same drift ratio of 0.5%. Beyond initial crushing, however, the behavior of the wall changed dramatically. Whereas unit one started significant strength degradation after 3.75% drift, the confinement of unit two stabilized the compression toe region allowing the wall to achieve a drift ratio of 10% without significant strength degradation. By stabilizing the compression toe region, the diagonal compression strut was able to sustain much higher levels of lateral deformation until finally, the compression toe region degraded, forcing the compression strut resultant outside of the confined region at a drift ratio of 11.3%. Fig. 2b represents the test specimen at a drift ratio of 6.75%. Compared to test unit one, very little damage is noted in the compression toe regions. The test specimen at 11.3% drift ratio is shown in Fig. 2c. Note the diagonal shear crack that formed parallel to the compression strut once the compression strut resultant migrated outside of the confined region. It is likely that the wall could have sustained even higher deformations had the confinement plates extended further into wall core; however, the need to achieve a drift ratio higher than 11.3% is unlikely. The force-displacement hysteretic response is shown in Fig. 3b. Note the very stable loops with little residual deformation or loss of strength. The overall energy dissipation is rather low, consistent with the observation of test unit one.

Test Three Results - (Grouted, Unbonded, Unconfined, Supplemental Mild Steel)

The purpose of test unit three was to investigate the possibility of increasing the energy dissipation while retaining the desirable characteristics of little residual deformation of walls one and two. This test unit was identical to test unit one with the exception of the presence of mild steel to act as supplemental energy dissipation. Such an approach has been utilized for post-tensioned concrete structures (Priestley et al., 1999) and post-tensioned steel structures (Christopoulos et al., 2002), (Ricles et al., 2001) with some success. In order to determine the amount of mild steel to be placed in the wall, the following process was utilized: (1) Size mild

steel such that applied PT force will be sufficient to return the mild steel strain to zero at zero column drift. This step ensures that the residual deformation of the wall will be kept to a minimum. It is important to note that the total PT force will vary as a function of applied lateral deformation, and that at high lateral drift, there is the potential for significant loss of pre-stress force. As a result, the initial pre-stress force should not be used to determine the compressive clamping force to return the mild steel to zero strain, but rather, the reduced PT force that can be expected at higher levels of response. (2) Determine the required length to debond the mild steel based on a pre-determined limit for mild steel tension strain. Due to the single large base crack, if the mild steel is not debonded, it is expected that the bars will rupture rather early on due to the high stress concentration at the base. Based on the kinematic relationship between wall drift ratio and base crack size, it is straightforward to determine the amount of debonded length that is required to keep the strain in the mild steel below an acceptable level. In the case of this test specimen, at a drift ratio of 6%, a base crack of 51mm is expected based on a neutral axis depth of 150mm. If it is desired to keep the strain in the mild steel below 8.5%, then the required debonded length is 610mm (51mm/0.085)

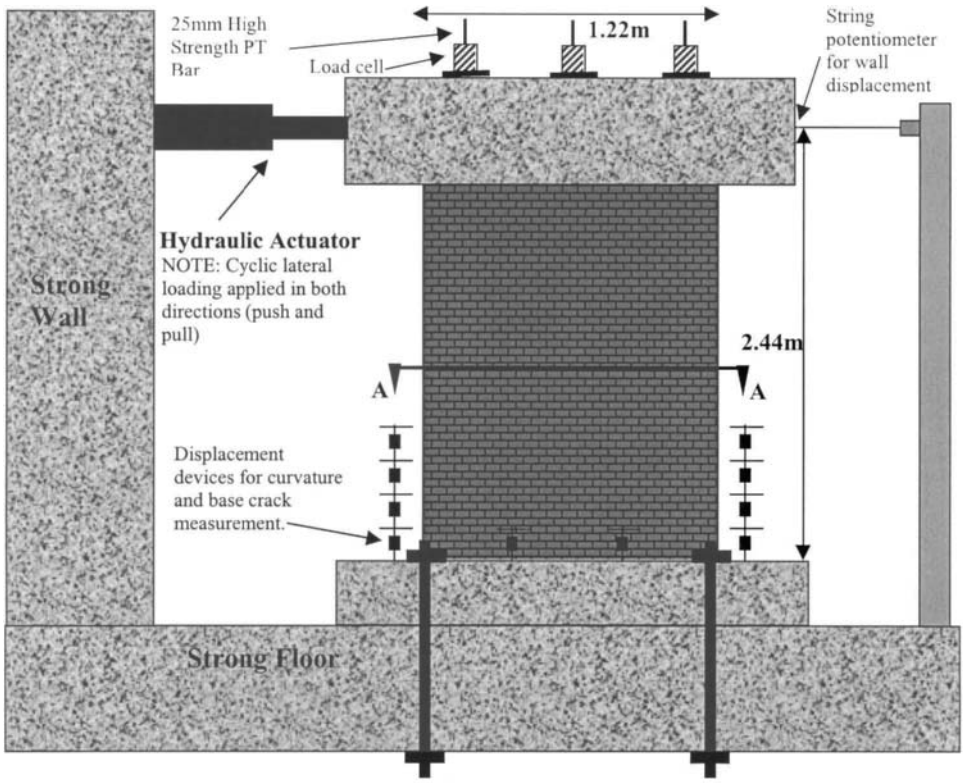
Just as the previous two tests, test three started in a similar manner. The base crack was observed to open at a drift ratio of 0.2%. Initial crushing was noted at a drift ratio of 0.35%. Fig. 2d represents a photo of the test specimen at a drift ratio of 6.5% which compares favorably to Fig. 2a for the control wall. The force-displacement hysteretic response is shown in Fig .3c. When compared to the control wall, it is noted that significant strength degradation did not occur until a drift ratio of 5.0%. It is also noted that the energy dissipated in the walls is greater than that from the control specimen. Since the wall was unconfined, once the masonry starts to crush, there is a rather rapid degradation of strength. Application of confinement would certainly enhance the performance of this configuration, however, the added benefit may not out way the added effort for designing and constructing this configuration.

Test Four Results - (Grouted, Bonded, Unconfined)

The goal of test four was to most closely mimic the behavior of a conventionally reinforced wall. In doing so, the PT bars were fully bonded along the length of the wall after applying the PT force. Although it was expected that this wall would be damaged more than the unbonded walls, it was still expected to achieve similar deformation capacity. Unfortunately, that was not the case. Unlike the previous three walls, in addition to the base crack, minor flexural cracks due to the bond stresses between PT steel and masonry occurred at a drift ratio of 0.2%. These cracks were spaced at 250mm. Further loading resulted in masonry crushing at 1.0% drift. Soon after, at a drift ratio of 1.75%, vertical cracks were noted at the positions of the PT bars. These cracks occurred due to exceedance of the bond stress capacity between PT duct and surrounding grout. As the bond stresses increased resulting in vertical cracks, the behavioral mechanism started to shift away from flexural deformation back to the rocking mechanism observed in the previous three tests. Significant strength degradation was noted after 3% drift ratio, and at a drift ratio of 3.75% (Fig. 2e) damage was extensive in the wall. Due to this rather extensive damage, the diagonal compression strut was unable to stabilize, resulting in wall failure. The force-displacement hysteretic response for the wall is shown in Fig. 3d, and although there is higher energy dissipation than the control wall, the level of damage, reduced deformation capacity, and quick loss of strength rendered the performance of this wall poor.

Test Five Results - (Ungrouted, Unbonded, Unconfined)

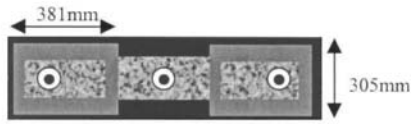
The final test of the series was the simplest to construct, and the motivation for this test stemmed from simplicity of the configuration. Unfortunately, this turned out to be the poorest performing configuration. Although it behaved initially just as tests one through three, this configuration suffered a diagonal shear failure on a plane parallel to diagonal compression strut at drift ratio of only 1% (Fig. 2f). Due to the lack of a grouted core, it became impossible for a diagonal compression strut to form in the wall, and as a result, the rocking deformation was not achievable. Laursen and Ingham observed similar behavior in partially grouted concrete masonry walls (Laursen and Ingham, 2000a,b). The force displacement hysteretic response is shown in Fig. 3e. It is clear that such a configuration is not for anything but the lowest seismic regions.



(a) Elevation of test specimen



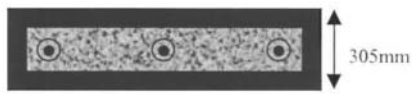
(b) Cross Section A-A for Test 1 (GROUTED, UNCONFINED, wall with UNBONDED tendons)



(c) Cross Section A-A for Test 2 (GROUTED, CONFINED, wall with UNBONDED tendons)



(d) Cross Section A-A for Test 3 (GROUTED, UNCONFINED, wall with UNBONDED tendons and SUPPLEMENTAL mild steel)



(e) Cross Section A-A for Test 2 (GROUTED, UNCONFINED, wall with BONDED tendons)

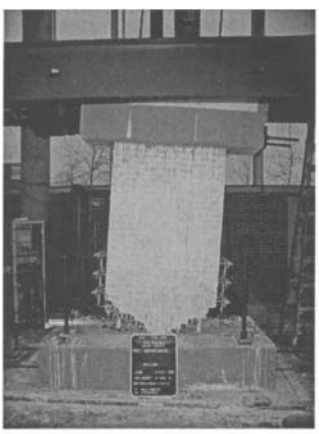


(f) Cross Section A-A for Test 1 (UNGROUTED, UNCONFINED, wall with UNBONDED tendons)

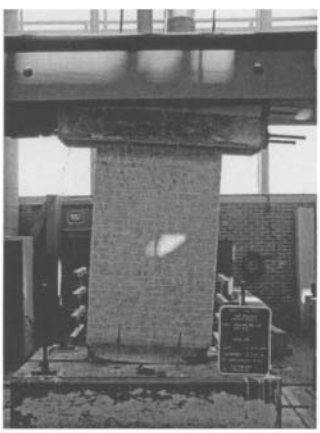
Fig. 1 Test Setup and Specimen Details

Table 1 Test matrix and specimen details

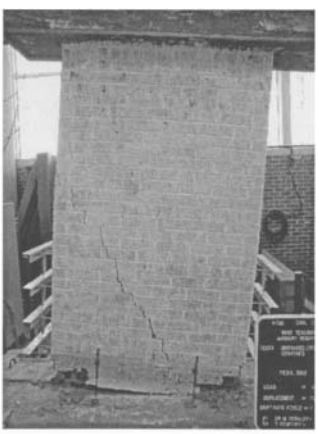
Test #	Initial PT Force (kN)	Mild Steel	Confinement	Grouted	Bonded	$f'm$ (Mpa)
1	983	No	No	Yes	No	22.2
2	962	No	3mm thick plates @ 67mm vertical spacing. fy=269MPa.	Yes	No	25.5
3	944	4#4 Grade 60 ASTM A706, fy = 408MPa	No	Yes	No	25.5
4	840	No	No	Yes	Yes	25.5
5	986	No	No	No	No	25.5



(a) Test 1: 6.5% Drift Ratio



(b) Test 2: 6.5% Drift Ratio



(c) Test 2: 11% Drift Ratio



(d) Test 3: 6.5% Drift Ratio



(e) Test 4: 3.75% Drift Ratio



(f) Test 5: 1% Drift Ratio

Fig. 2 Photos of test specimens during testing at various drift ratios

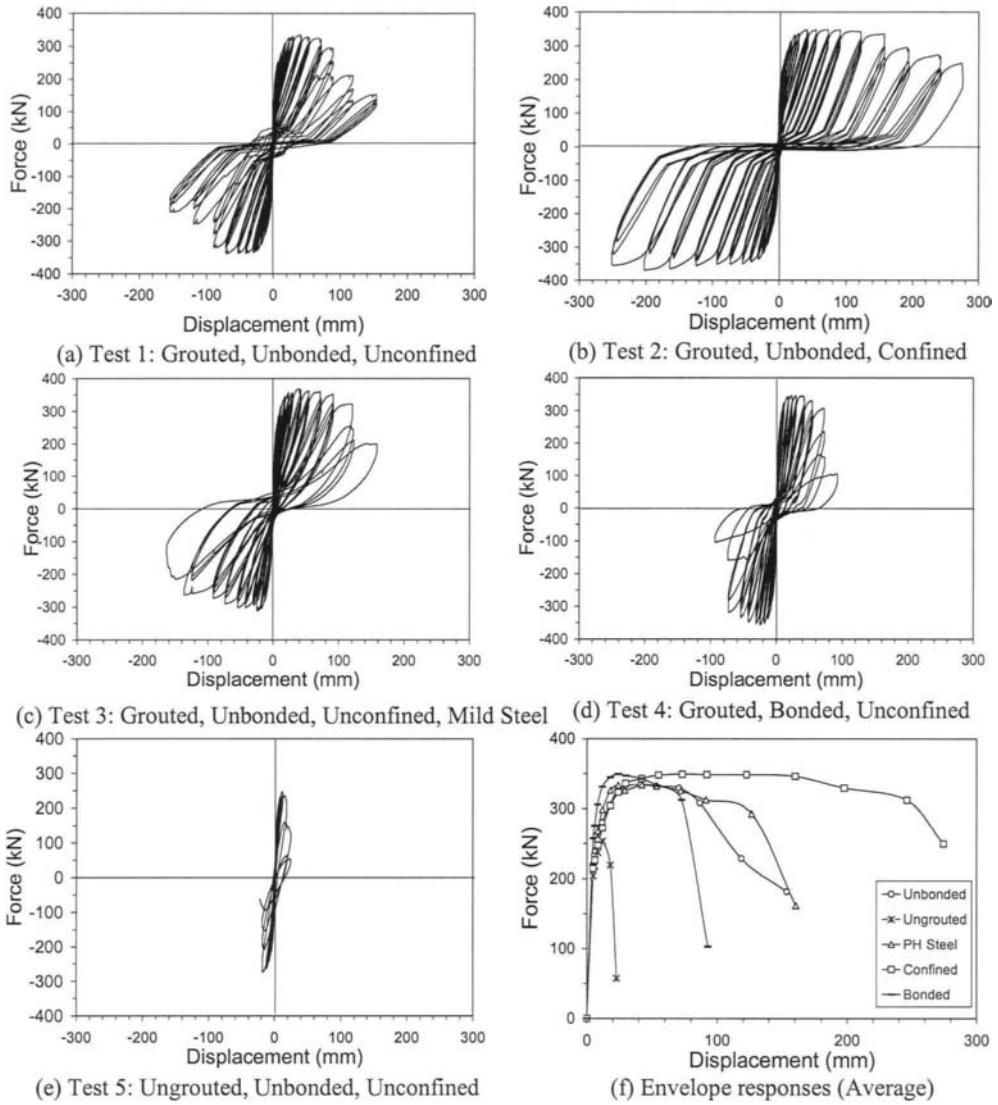


Fig. 3 Force-displacement responses

PLANS FOR FUTURE RESEARCH

For a complete discussion of Phase I research, the reader is referred to (Rosenboom and Kowalsky, 2002), (Kowalsky et al., 2003). The second phase of the program is currently underway and involves the following components: (1) Shake-table testing of the most promising configuration from Phase I, namely, grouted, confined, unbonded walls. (2) Large-scale (cyclic and dynamic) testing and analysis of post-tensioned clay masonry walls with window openings. (3) Large-scale cyclic testing and analysis of "L" and "T" cross-section walls. (4) Development of cyclic section analysis software for analysis and design of post-tensioned walls. The

third phase of the research will concentrate on practical applications and design details, namely, floor and roof diaphragm to wall connections and integration of non-structural components.

CONCLUSIONS

Based on the initial results, the following tentative conclusions are advanced. (1) Application of post-tensioning to clay masonry walls provides benefits similar to what has been observed for pre-cast concrete. (2) Walls with unbonded tendons performed best in terms of strength, deformation capacity, and strength degradation. (3) Application of galvanized steel confinement plates results in a marked effect on wall deformation capacity due to the ability of the plates to confine the compression toe region and stabilize the diagonal compression strut required for the wall rocking mechanism to develop.

ACKNOWLEDGEMENTS

The authors would like to acknowledge the support of the National Science Foundation (NSF) through grant #0080210. In addition, the support of North Carolina State University, Department of Civil Engineering is appreciated. Several local industry members are also thanked: Eric Johnson of the Carolinas Brick Association, Cody Cress of General Shale for material donations, Danks Burton of Pinnacle Masonry for mason's labor support, and John Little and Gary Rhodes of AmeriSteel. We would also like to thank Jerry Atkinson, the technician at the Constructed Facilities Laboratory at NC State without whom this work would not have been possible.

REFERENCES

American Concrete Institute (1999) "Acceptance Criteria for Moment Frames Based on Structural Testing" *ACI Provisional Standard.*

Christopoulos C., Filiatrault A., Uang C-M (2002). "Post-tensioned energy dissipating connections for steel frames". *Journal of Structural Engineering,* ASCE 2002.

International Code Council (2000) "International Building Code"

Kowalsky, M.J., Ewing, B.D. and Rosenboom, O.A. (2003) "Displacement-Based Design of Post-Tensioned Masonry Wall Buildings", ASCE Structures Congress, June, 2003.

Laursen, P., and Ingham J.M. (2000). "Cyclic In-Plane Structural Testing of Prestressed Concrete Masonry Walls, Volume A: Evaluation of Wall Structural Performance." *School of Engineering Report No. 599,* Department of Civil and Resource Engineering, University of Auckland, New Zealand.

Laursen, P., and Ingham J.M. (2000). "Cyclic In-Plane Structural Testing of Prestressed Concrete Masonry Walls, Volume B: Data Resource." *School of Engineering Report No. 600,* Department of Civil and Resource Engineering, University of Auckland, New Zealand.

Priestley and Bridgeman (1974) "Seismic Resistance of Brick Masonry Walls" *Bulletin of the New Zealand National Society for Earthquake Engineering,* Vol. 7, No. 4, December, pp167-187.

Priestley M.J.N, Sritharan S., Conley J.R., Pampanin S. (1999). "Preliminary Results and Conclusions from the PRESSS Five-Story Precast Concrete Test Building", *PCI Journal,* Vol. 44, No. 6, pp42-67

Ricles J.M., Sause R., Garlock M, Zhao C. (2001). "Post-tensioned seismic-resistant connections for steel frames", *Journal of Structural Engineering,* ASCE Vol. 127, No.2, pp113-121.

Rosenboom, O.A. and Kowalsky, M.J. (2002) "Reversed In-Plane Cyclic Behavior of Post-Tensioned Clay Brick Masonry Walls" Submitted to the *ASCE Journal of Structural Engineering.*

Advances in Building Technology, Volume 1
M. Anson, J.M. Ko and E.S.S. Lam (Eds.)
© 2002 Elsevier Science Ltd. All rights reserved

An All-Natural Composite Material Roof System for Residential Construction

H. W. Shenton III[1], R. P. Wool[2], B. Hu[1], A. O'Donnell[2], L. Bonnaillie[2], E. Can[2], R. Chapas[2] and C. Hong[2]

1-Department of Civil and Environmental Engineering, University of Delaware, Newark, Delaware, USA 19716
2-Department of Chemical Engineering and the Center for Composite Materials, University of Delaware, Newark, Delaware, USA 19716

ABSTRACT

In a collaborative effort between researchers from the Departments of Chemical Engineering and Civil and Environmental Engineering at the University of Delaware, work in underway to develop an all-natural composite material roof system for residential construction. The roof will be fabricated using innovative composite materials made from soy-oil based resins and all-natural fibers. The all-natural composites are significantly less expensive than traditional polymer-based composites and are environmentally friendly. The composite resin is derived from soy-oil, a plentiful, renewable crop, and the fibers are by-products or waste from other seasonal crops. The research will involve design and optimization of the composite material for the roof, development of an integral weather protection layer for the roof, and structural design, analysis and testing of the roof system. The preliminary design of the roof is a sandwich structure configuration, with top and bottom face sheets, periodically spaced webs, and a foam core. Tests are currently underway of the first unit beam section of the roof.

KEYWORDS

Composite material, fiber, natural, resin, roof, sandwich structure, seismic, soy oil, testing, wind

INTRODUCTION

Traditional composite materials are made from a petroleum-based matrix resin such as epoxy, vinyl-ester, or polyester, and a reinforcement of synthetic fibers such as glass, carbon, or aramid. These traditional composites can be quite expensive, are non-biodegradable, and depend upon our rapidly depleting petroleum reserves. In the

Affordable Composites from Renewable Resources (ACRES) program, headed by Professor Richard P. Wool at the University of Delaware, genetically engineered soybean oil and other plant oils have been made amenable to polymerization using a broad range of chemical routes (Williams and Wool, 2000). Using soy-based resins and natural fibers, the ACRES program has produced all-natural composite materials that have mechanical properties that are comparable to certain polymer-based composites and also some natural woods.

All-natural composites are environmentally friendly for a number of reasons. The composite resins are derived from soy beans, a seasonal crop that is already grown in large quantities in the United States. Inexpensive natural fibers such as hemp, flax, jute, and kenaf, are also seasonal crops grown specifically for the fiber, or are byproducts of other crops. These materials are renewable, biodegradable, and recyclable. When used as a substitute for conventional wood in low-rise commercial or residential construction, the composite system will reduce the demand on natural wood and its resulting deforestation. Finally, at the end of their useful life cycle, the composite materials can be ground up and used as low-cost filler for other thermosetting composites.

Recently, in a collaborative effort between the ACRES program and the Department of Civil and Environmental Engineering at the University of Delaware, researchers are exploring the use of all-natural composites in residential construction. With funding from the National Science Foundation, Partnership for Advanced Technology in Housing (PATH) program, the interdisciplinary research team is working to develop an advanced all-natural composite material roof system for residential construction. The composite roof fulfills the four main goals of the PATH program by, (1) reducing the monthly cost of housing through the roof's inherent insulation capability, (2) improving durability and reducing maintenance costs with the development of an integral weather protection layer (thus eliminating the need for shingles), (3) reducing environmental impact with the use of the all-natural composite materials, and (4) reducing the risk of life, injury and property destruction through the monolithic, ground based fabrication process.

Presented in the paper is a brief overview of the ongoing research effort. The all-natural composites are first described. Next, the concept for the composite roof is introduced, along with an outline of the work completed to date. Finally, a general discussion of the potential benefits of the all-natural composites is presented, with particular emphasis on the advantages for seismic and hurricane resistant design.

ALL-NATURAL COMPOSITES

Soybean oil is a naturally occurring triglyceride. Triglycerides are composed of three fatty acids connected by glycerol through ester linkages. The fatty acids in soyoil have zero to three double bonds. These double bonds are not suitable for polymerization but can be activated by different reactions. In the ACRES program, the chemically modified oils have been converted into a range of high-performance materials including plastics, rubbers, foams, and composite liquid molding resins. Several patent disclosures have been filed on these novel materials. Of the several chemical routes investigated by the ACRES group, at least ten have yielded materials that can be successfully used as matrix materials for polymer composites (Wool et al., 1998). These resins have been combined with synthetic fibers like glass and natural fibers like hemp and flax to make composites. In August 1999, the John Deere Company, an international supplier of farm equipment,

announced their first fleet of harvesters that include parts made with ACRES soy-based resins.

The properties of composites made using ACRES resins have been found to be equivalent to those of synthetic-resin-based composites with similar reinforcement. Further development and commercialization of the ACRES resins and composites will serve three important purposes: (1) help the agricultural community through the use of a crop that is produced on a large scale in the United States; (2) help reduce the depletion of petroleum feedstock; and (3) in housing applications, help reduce reliance on natural wood and the resulting deforestation. Because of the very low cost of the soyoil from which the resins are derived, projections for the ACRES resins suggest a price half that of comparable vinyl-ester resins. This will represent a significant cost saving that comes with no sacrifice in properties and performance.

Combining the soy-based resins with natural fibers yields an all-natural composite material. The choice of natural fibers is numerous and includes hemp, jute, flax, kenaf and even chicken feathers. Many of these fibers are waste or by-products of seasonal crops, which normally have little practical use and in many cases are simply destroyed. These fibers are renewable, biodegradable and recyclable.

Preliminary studies have already been conducted by the ACRES group on selected all-natural composite materials (Williams and Wool, 2000). Presented in Table 1 are the tensile and flexural properties of two different all-natural composites, one a random, chopped flax fiber in the soy-based resin and the other, an oriented hemp fiber in the soy-based resin. Also shown in Table 1 are typical properties for two common softwoods, Douglas Fir and Cedar. Note that the all-natural composites have a tensile modulus lower than that of Douglas Fir, but about equal to the modulus of certain types of Cedar. Tensile strengths are lower than that of Cedar, but only by 20 to 30%. The flexural modulus of the all-natural composites are again lower than that of Douglas Fir, but very comparable to that of Cedar. The flexural strength, on the other hand, is about equal to the average strength of Douglas Fir.

Table 1: Comparison of Tensile and Flexural Properties of Various Materials

Material	Specific Gravity	Tensile Modulus[a] (ksi)	Tensile Strength[a] (ksi)	Flexural Modulus[a] (ksi)	Flexural Strength[a] (ksi)
Flax/soy oil matrix[b]	~1	680-870	4,4	610-650	8.8-9.3
Hemp/soy oil matrix[c]	~1	640	5.1	390	5.1-7.4
Douglas Fir[d]	0.48	1160-1940	15.5	1160-1940	6.8-13.1
Cedar[d]	0.50	640-1700	6.7-11.5	640-1700	4.2-12.8

[a]tensile properties for composites determined in accordance with ASTM D3039; flexural properties in accordance with ASTM D790; [b]random chopped fiber; 30-40% fiber content; [c]two layers placed at 0/90 degree to each other, 20% fiber content; [d]from Wood (1999)

It should be noted that while the results presented in Table 1 are encouraging, they do not in anyway depict the full potential of the all-natural composite material, since the materials tested for that study were not designed or optimized with the specific objectives

for the roof system in mind. Nevertheless, the data does suggest that stiffness and not strength will govern the design of an all-natural composite structure. This has been found to be the case in other applications of composite materials to the civil infrastructure (e.g., in bridges).

COMPOSITE ROOF DESIGN

The objective of the NSF funded research is to develop a monolithic composite roof system for residential construction that is fabricated from low-cost, all-natural composite materials. The all-natural composite roof system will be designed to carry normal and in-plane loads, have a durable weather protection surface, and offer intrinsic insulation. The specific objectives are to (1) design and optimize the soy-based resin, all-natural composite material for roof applications; (2) develop and test a weather protection layer that is integral to the composite roof; and (3) design, analyze, and test the roof structural system.

The roof will be fabricated with a foam core, all-natural composite top and bottom face sheets, and all-natural composite ribs/webs. Two different proposed designs are shown in Figure 1. On the left in Figure 1 is the "rafter-core" design, in which foam cores run longitudinally from the roof ridge to the eave; on the right in Figure 1 is the "waffle-core" design, in which the foam cores form a honeycomb structure. The exterior face sheet will be fabricated with an integral weather protection layer, thus eliminating the need for shingles, tiles, or other conventional roofing material. In many ways, the roof is a hybrid system, similar to a conventional stressed-skin panel and a structural insulated panel (SIP), combined.

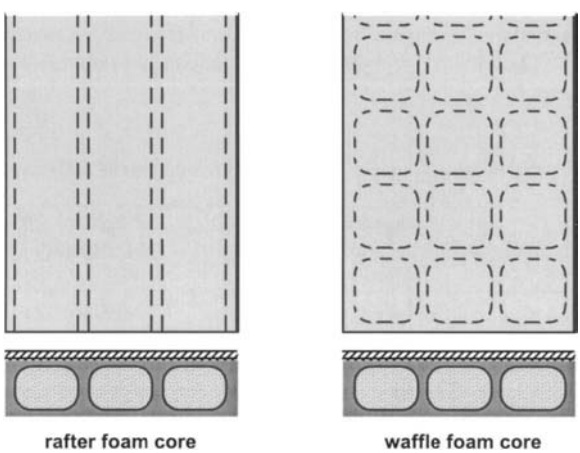


Figure 1: Two design concepts for the roof system - rafter foam core(left) and waffle foam core(right).

At least initially, the foam cores will be made of commercially available synthetic foam; however, the ACRES program is also working to develop an all-natural foam for use in the roof system.

Manufacturing

Minimizing the cost of fabrication of the roof and simplifying the manufacturing process are both very important goals in developing the roof system. It is envisioned that the roof will be fabricated as one single unit, or in very large components that will be bolted together in the field. Components will be fabricated using the Vacuum Assisted Resin Transfer Molding (VARTM) process. VARTM is a very flexible and inexpensive manufacturing process that has been used successfully in the past to create very large composite parts. The process does not require expensive one-of-a-kind molds, in fact, it is expected that the formwork for the roof will be constructed of plywood and framing materials. The nature of the composites is such that the roof will be air cured. As envisioned, the components could be fabricated in a plant and shipped by truck to the construction site, or, for larger new housing developments, fabricated on site in a temporary manufacturing facility.

Preliminary Design and Tests

The initial phase of the research has involved design of the composite material, and design and fabrication of a reduced-scale beam section of the "rafter-core" design. The current composite design uses Flax-Mat 85/15-20, produced by Cargill Limited (85% flax by volume, chopped, random orientation, 20 oz/yd^2 density and 0.25" thick) and Acrylated Epoxidized Soybean Oil (AESO) resin (Knot, et al, 2001). This is not an optimum design and work will be continuing to tailor the resin and fiber system for the roof application.

Presented in Figure 2 is a schematic of the reduced-scale beam section from the rafter-core design. The beam has a length of 3.5 ft, depth of 3.5 inches and width of 8 inches. The cross-section of the beam is a unit section of the rafter design roof. Based on the

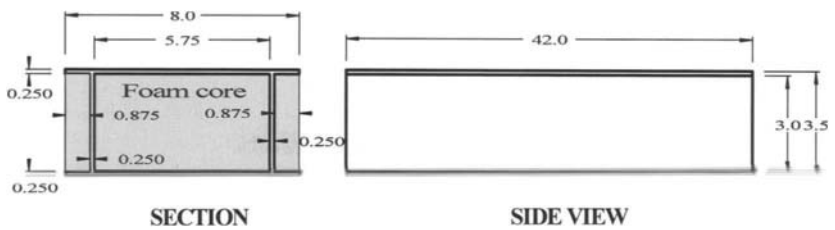
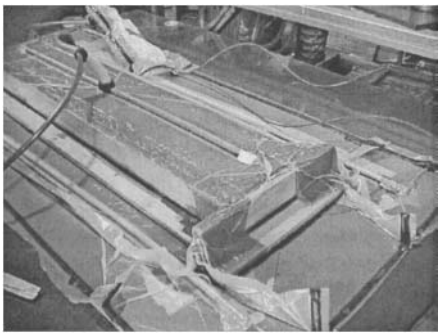
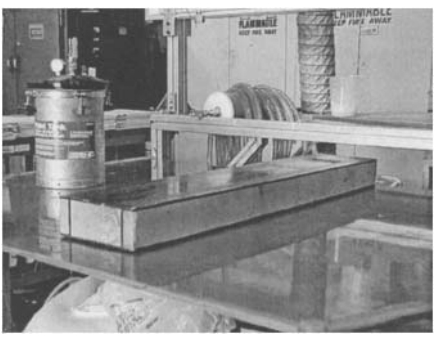


Figure 2. Reduced-scale unit beam of rafter-core roof design (units in inches).

material properties, the theoretical ultimate moment capacity of the beam is 6x10^4 in-lb. The beam will be tested under four point bending. Strains will be measured at several locations on the top and bottom surface of the beam, as will deflections. The tests will be used to measure the elastic flexural stiffness of the section, the yield and ultimate strength of the beam, the post-yield behavior and the failure mode. The data from the test will be analyzed and used to design the next, larger beam specimen, and also to calibrate a finite



(a.) Unit beam during fabrication



(b.) Completed beam

Figure 3. First unit beam

element model of the beam. Presented in Figures 3(a) and 3(b) are photographs of the beam during fabrication and the completed beam.

Tests will be conducted on smaller unit beam sections of the roof, of increasing size and length, as the composite material and section details are optimized, and the manufacturing process is refined. Reduced-scale tests will also be conducted of the "waffle-core" roof design. Ultimately, a large full panel section of the roof will be fabricated and tested to failure. Tests will be conducted for normal and in-plane loads acting on the roof.

SEISMIC AND HURRICANE RESISTANT DESIGN

The use of low-cost, all-natural composite materials should open the door for alternatives in design, fabrication and manufacturing in residential construction, that may lead to improved performance during earthquakes and hurricanes.

Traditional polymer-based composite materials typically have a high strength-to-weight ratio when compared to conventional materials (e.g., steel, concrete, and wood). Referring to Table 1, the non-optimal all-natural composites developed to date have a lower strength-to-weight ratio than typical woods; however, the real benefit of composites comes from being able to optimize the section details and to provide

reinforcement where it is most needed. All-natural composite materials hold the potential for being able to create new structural members that are lighter, stronger and more durable than conventional wood members, which should translate into improved seismic and wind resistance of the structure. Another benefit of the randomly oriented fiber composite is the quasi-isotropic nature of the material: the complexity and design constraints that arise with grain direction in conventional woods would be eliminated with the composite material.

Flexibility in manufacturing should also lead to improved wind and seismic response of structures built from all-natural composites. Relatively large, monolithic components (e.g., walls, floors, rooms or entire homes) can be shop fabricated using VARTM and bolted or bonded together in the field. This should reduce the number of critical connections in the structure, a particular area of vulnerability for any structure. In addition, the manufacturing process can also open the door for more free-form design of the structure, for improved seismic and hurricane performance.

CONCLUSIONS

In a collaborative effort between researchers from the Departments of Chemical Engineering and Civil and Environmental Engineering of the University of Delaware, work is underway to develop an all-natural composite material roof for residential construction. The roof will be fabricated from innovative fiber reinforced composite materials made from soy-oil based resins and natural fibers. These low-cost, environmentally friendly materials offer great potential for their use in low-rise commercial and residential construction. The current project is focusing on the roof structure; however, other components such as walls, floors or entire homes could also be fabricated using the new composites. Work will be continuing to optimize the composite material for the roof system, to develop an integral weather protection layer for the roof, and to design, analyze and test sections of the roof and full-scale roof panels.

ACKNOWLEDGEMENTS

Funding for this work has been provided by the National Science Foundation under grant CMS-0122076. The authors would like to thank the NSF for their support.

REFERENCES

Khot, S. N., Lascala, J.J., Can, E., Morye, S.S., Williams, G.I., Palmese, G.R., Kusefoglu, S.H., and Wool, R.P. (2001), "Development and Application of Triglyceride-Based Polymers and Composites," Journal of Applied Polymer Science, Vol. 82, 703-723.

Williams, G.I. and Wool, R.P. (2000) "Composites from Natural Fibers and Soy Oil Resins," *Applied Composite Materials*, Vol 7, pp 421-432.

Wood Handbook, Forest Products Laboratory Technical Report FPL-GTR-113, Madison, WI, 1999.

Wool, R. P. S. Kusefoglu, R. Zhao, G. R. Palmese, and S. Khot (1998). "High Modulus Polymers and Composites from Plant Oils" (filed April 28,1998). Patent Application 09/067,743, PCT filed October 20, 1998.

Advances in Building Technology, Volume I
M. Anson, J.M. Ko and E.S.S. Lam (Eds.)
© 2002 Elsevier Science Ltd. All rights reserved

COMPARISON OF OPTIMAL DESIGNS FOR STICK-FRAME WALL ASSEMBLIES OF DIFFERENT BAY SIZES

S. Van Dessel[1], A. Ismail-Yahaya[2], and A Messac[3]

[1] School of Architecture, Rensselaer Polytechnic Institute, Troy, NY 12180, USA
[2] Department of Mechanical, Aerospace, and Nuclear Engineering, Rensselaer Polytechnic Institute, Troy, NY 12180, USA
[3] Department of Mechanical, Aerospace, and Nuclear Engineering, Rensselaer Polytechnic Institute, Troy, NY 12180, USA

ABSTRACT

This paper aims to demonstrate a typical optimization process that is applicable to the design of stick-frame structures. A 10-meter load-bearing wall is optimized considering different bay sizes with the objective of minimizing the use of wood. The results of our study indicate that the amount of wood needed to build a single story wall increases dramatically at bay sizes larger than about 90 cm. This seems to correlate well with common notions that framing systems that use smaller lumber dimensions spaced at shorter distances are more efficient than heavy timber systems. The efficiency of such light framing systems however does not seem to be affected significantly when decreasing bay size to very small dimensions. This may suggest that more efficient manufacturing procedures can be more instrumental if we wish to decrease the cost of similar wall assemblies.

KEYWORDS

Design, Optimization, Frame, Wall, Wood, Bay

INTRODUCTION

Worldwide, an estimated fifty-five percent of trees cut for non-fuel uses are being used for making buildings [Roodman D. and Lenssen N., 1995]. While buildings can be constructed in various ways, stick-frame technology currently remains the most common way for making structures from wood. Being able to determine relative efficiencies for various types of framing systems may therefore have important economic and environmental consequences. In light of the above, this paper aims to demonstrate a typical optimization process that is applicable to the design of stick-frame structures. A single story 10-meter long wall composed of typical wood members and exposed to both vertical and

lateral forces is being optimized. Optimal dimensional parameters were calculated for bay sizes ranging from 10m (1bay) to 0.20m (50 bays). Our interest here was to determine how efficiency changes with decreasing bay size for stick-frame wall assemblies. The total volume of wood needed to build the various walls was adopted as measure of efficiency. The total volume represents the sum of the volume of vertical, horizontal, and the infill members as expressed in Equation 1 (figure 1). Three cases were considered: In Case a, it is assumed that both vertical and horizontal wood members have the same dimensions and are placed in one plane (Figure 2a). This configuration conforms to current practice in the US. In Case b it is assumed that the vertical and horizontal members remain of the same dimensions, however the top member is rotated 90° accommodating a more optimum structural placement for that member (Figure 2b). In Case c both vertical and horizontal members were allowed to evolve independent from each other (Figure 2c). All three designs were assumed to be loaded in the same way. A uniformly distributed load was applied to the top member. This load was assumed to come from a flat roof 6 meters deep and 10 meters in length, half of this load was applied to the wall being studied. A lateral wind load was further applied to the wall enclosure. Roof and wind loads were calculated according to the international building code. The deflection for each member was constrained to *l*/360 of the member's length, this upper limit was used for all three cases. The upper bound for lumber size was set at 30 cm, while the lower bound was set at 1mm. The material was assumed to be solid wood. All joints within the frame were considered to be pinned connections. A more detailed description of the optimization follows.

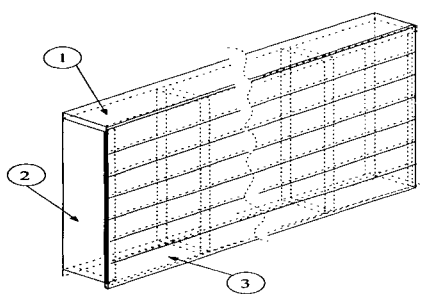


Figure 1: Stick-frame

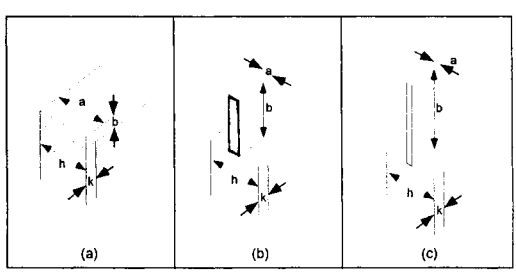


Figure 2: Three member-geometry cases

Nomenclature

Parameter	Value	Units
V	Volume	m^3
a,b,c,d,h,k	Wood dimensions	m
δ_{max}	Maximum deflection	m
n	Number of bays	
m =20	Number of in-fills	
L	Total length of the building	m
H	Total height of the building	m
D	Total width/span of the building	m
E = 14 GPa	Modulus of elasticity of the wood	Pa
σ_b =180MPa	Allowable stress wood	Pa
I	Moment of Inertia	m^4
S	Section Modulus	m^3
DL	Dead load	N/m^2
RL	Roof load	N/m^2
L_r	Live load	N/m^2
P_f	Snow load	N/m^2
W	Wind load	N/m^2
g =9.81	Gravitational force	m/s^2

**Note: Values are omitted if the parameters are design variables.

Design Objectives

An optimal design is defined as the structure having the least volume, while satisfying strength and geometrical requirements. The volume, *V*, of the structure is computed as follow:

$$V = 2abL + (n+1)(H-2b)hk + HdL \tag{1}$$

Design Constraints

1. Geometry constrain

For the design to stay connected, the following equations are applied.

$$nl = L \tag{2}$$
$$mc = H \tag{3}$$

The length of *k* must be less than the length of *h*.

$$k \le h \tag{4}$$

2. Deflection

a) Deflection of Component 1

$$\text{Maximum deflection, } \left(\delta_{max}\right)_1 = \frac{5q_1 l^4}{384EI_1} \text{ (m)} \tag{5}$$

The deflection is limited to: *span length* /360

$$(\delta_{\max})_1 \leq \frac{l}{360} \tag{6}$$

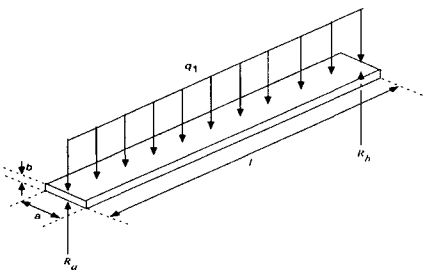


Figure 3: Component 1

b)Deflection of Component 2

$$\text{Maximum deflection, } (\delta_{\max})_2 = \frac{5q_2(H-2b)^4}{384EI_2} \text{ (m)} \tag{7}$$

The deflection is limited to: *span length*/360

$$(\delta_{\max})_2 \leq \frac{H-2b}{360} \tag{8}$$

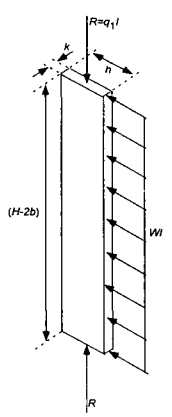


Figure 4: Component 2

c) Deflection of Component 3

The maximum deflection of the infill is computed by modeling the infill as a beam. The force over the area is modeled as a distributed force over the length by multiplying the distributed force by the infill width.

$$\text{Maximum deflection, } (\delta_{\max})_3 = \frac{5q_3 l^4}{EI_3} \text{ (m)} \tag{9}$$

The deflection is limited to: *span length*/360

$$(\delta_{\max})_3 \le \frac{l}{360} \tag{10}$$

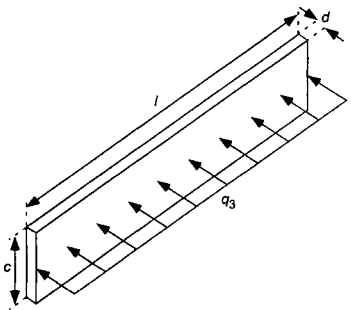


Figure 5: Component 3

3. Euler buckling

To prevent buckling, the reaction force, R, needs to be less than the critical force for buckling, P_{cr}, which can be computed using AFPA formulas

$$P_{cr} = \sigma_{allow} A = \sigma_{allow} hk \tag{11}$$

$$\sigma_{allow} = \begin{cases} F_c; \ 0 \le (H-2b)/k \le 11 \\ F_c\left[1 - \frac{1}{3}\left(\frac{(H-2b)/k}{K_c}\right)^4\right]; \ 11 \le (H-2b)/k \le K_c \\ \frac{0.3E}{\left((H-2b)/k\right)^2}; \ K_c \le (H-2b)/k \le 50 \end{cases} \tag{12}$$

Design constraint to be satisfied:

$$R \le P_{cr} \tag{13}$$

4. Side Constraints

Component 1:

$$1mm(0.0394") \le a,b \le 30.48cm(12") \tag{14}$$

Component 2:

$$1mm(0.0394") \le h,k \le 30.48cm(12") \tag{15}$$

Component 3:

$$c = \frac{H}{m} = 0.12m \tag{16}$$

$$1mm(0.0394") \le d \le 30.48cm(12") \tag{17}$$

Optimization Problem Statement:

$$\min\ V = 2abL + (n+1)(H-2b)hk + HdL \tag{18a}$$

Subject to:

$$nl = L \tag{18b}$$
$$mc = H \tag{18c}$$
$$k \le h \tag{18d}$$
$$(\delta_{\max})_1 \le \frac{l}{360} \tag{18e}$$
$$(\delta_{\max})_2 \le \frac{H-2b}{360} \tag{18f}$$
$$(\delta_{\max})_3 \le \frac{l}{360} \tag{18g}$$
$$R \le P_{cr} \tag{18h}$$
$$1mm(0.0394") \le a,b \le 30.48cm(12") \tag{18i}$$
$$1mm(0.0394") \le d \le 30.48cm(12") \tag{18j}$$
$$1mm(0.0394") \le h,k \le 30.48cm(12") \tag{18k}$$

The following additional case specific constraints are applied:

Case a

$$a = h \tag{19a}$$
$$b = k \tag{19b}$$

Case b

$$a = k \tag{20a}$$
$$b = h \tag{20b}$$

There are no additional constraints for Case c.

RESULTS and DISCUSSION

Table 1 provides the optimal results for the three different scenarios. Figures 6, 7, and 8 represent changes in wood volumes with increasing numbers of bays for Cases a, b, and c, respectively. As might be expected, the result for Case c indicates that the design with more independent wood sizing yields the most optimal solution. Our results show that the volume of wood needed in Case c is approximately 10 % less than for Case a, and the results in Case b used about 5% less wood relative to Case a.

TABLE 1
OPTIMUM RESULTS FOR STICK-FRAME WALL

	n	a(m)	b(m)	h(m)	k(m)	l(m)	d(m)	Vol.(m^3)
Case a	30.0000	0.0877	0.0462	0.0877	0.0462	0.3333	0.0066	0.5280
Case b	30.0000	0.0446	0.0857	0.0857	0.0446	0.3333	0.0066	0.4977
Case c	28.0000	0.0215	0.0431	0.0899	0.0463	0.3571	0.0070	0.4464

Traditional wood light framed buildings in the US use dimension lumber of approximately 2x4 inches or 5 by 10 cm [Allen E., 1999]. The maximum spacing distance for these is typically 40 to 60 cm (16' to 24") depending on loading conditions and height of the studs [Ching F., 1991]. From Table 1 we can see that the design of Case a yields almost the actual dimension of such traditional design for both vertical and horizontal members of the frame. The common spacing distances of 40 to 60 cm (16 to 25 bays for our 10-meter wall) also correlates well with the results presented in Figure 6a. In general, the results for all 3 cases indicate that the use of wood starts to increases dramatically at n-values between 12 and 14, this represents a bay size of approximately 90 cm. For n-values starting at about 14 and higher, results further indicate that the optimal designs for each of these different n-values are very close to each other. Any solution within this range is relatively close to the optimum solution.

CONCLUSIONS

In this initial study we have developed a means to design and evaluate optimal dimensional parameters for load bearing single story timber walls utilizing optimization approaches. The results of our study indicate that the amount of wood needed to build a single story wall increases dramatically at bay sizes larger than about 90 cm. This seems to correlate well with common notions that framing systems that use smaller lumber dimensions spaced at shorter distances are more efficient than heavy timber systems. The efficiency of such light framing systems however does not seem to be affected significantly when decreasing bay size to very small dimensions. This may suggest that more efficient manufacturing procedures can be more instrumental, if we wish to decrease cost of similar wall assemblies.

ACKNOWLEDGEMENTS

Financial support from the National Science Foundation (Award No. CMS-0122022, Directorate for Engineering, Division of Civil and Mechanical Systems) and the US Department for Housing and Urban Development is much appreciated.

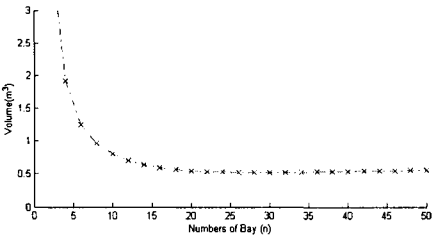


Figure 6: Optimal solutions for Case a

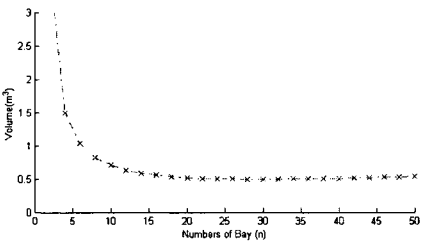


Figure 7: Optimal solutions for Case b

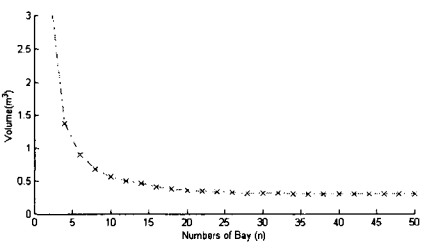


Figure 8: Optimal solutions for Case c

REFERENCES

Allen E. (1999), Fundamentals of Building Construction, Materials and Methods. third edition. John Wiley and Sons, Inc.

Ching F. (1991), Building Construction Illustrated, second edition, Van Nostrand Reinhold

Roodman D. and Lenssen N. (1995), A Building Revolution: How Ecology and Health Concerns Are Transforming Construction, *Worldwatch Paper 124*

TEAM PRESENTATION:

EARTHQUAKE RESISTANT THEORY AND APPLICATIONS

This Page Intentionally Left Blank

Advances in Building Technology, Volume 1
M. Anson, J.M. Ko and E.S.S. Lam (Eds.)
© 2002 Published by Elsevier Science Ltd.

A MACRO-MODEL OF RC SHEAR WALL FOR PUSH-OVER ANALYSIS*

Chen qin Qian jiaru

Department of Civil Engineering, Tsinghua University,
Beijing, 100084, CHINA

ABSTRACT

Reinforced concrete shear wall is a kind of main vertical structural element of high-rise buildings to resist earthquakes. In order to perform push over analysis in the displacement-based seismic design of buildings, a simple, rational macro-model of shear wall is developed in this paper. The macro-model is composed of two kinds of element: concrete column element and concrete membrane element. In push-over analysis the shear wall is divided into layers along its height, and the wall panel is divided into columns. Two adjacent layers are connected by a rigid beam. There are only three degrees of freedom for one layer. A method called single degree of freedom compensation is adopted to solve the ill-conditioned equations, by which a complete capacity curve can be obtained. Experimental study of four shear wall specimens was carried out and the specimens were analyzed by the developed program. The analytical results have good agreement with the test results.

KEYWORDS

Shear wall, Macro-model, Push-over analysis, Column element, Membrane element, MCFT, Ill-conditioned equations

INTRODUCTION

In order to perform the displacement-based seismic design and push-over analysis of building structures, a simple and rational analytical model of shear wall should be developed. Various shear wall models have been proposed such as: beam model (Park Y.K 1987), spring macro-model (Linde P. 1994), braced wide-column analogy (Koumousis V.K. 1992). A macro-model which simulates the continuity model is developed in this paper. The degree of freedom of the model is condensed, and constitutive relation of cracked concrete is interpreted in the model, these make the calculation process much easy. The complete capacity curve can be obtained by using a method called single degree of freedom compensation to solve ill-conditioned equations. Comparison of the experimental data and the push-over analysis results verifies the accuracy of the proposed macro-model and the reliability of

*Supported by the National Natural Science Foundation of China (Grant No. 59895410)

$d_0, -d_0$ or 0), and the modified equilibrium equations: $P = (K_g + C)\Delta$ can be solved stably. The true solution can be obtained after iterative calculation of the modified equilibrium equations. Forced iteration approach is adopted to resolve the equilibrium equations after the stiffness matrix reaches negative condition.

So complete capacity curve of RC shear wall can be obtained by push-over analysis.

EXPERIMENT VERIFICATION

Specimens

Four isolated RC shear wall specimens (SW-1~SW-4) were tested to verify the shear wall model developed in this study. SW-1 and SW-2 were rectangular section, SW-3 was I section and SW-4 was T shape section. The details of specimens are shown in Fig.5.

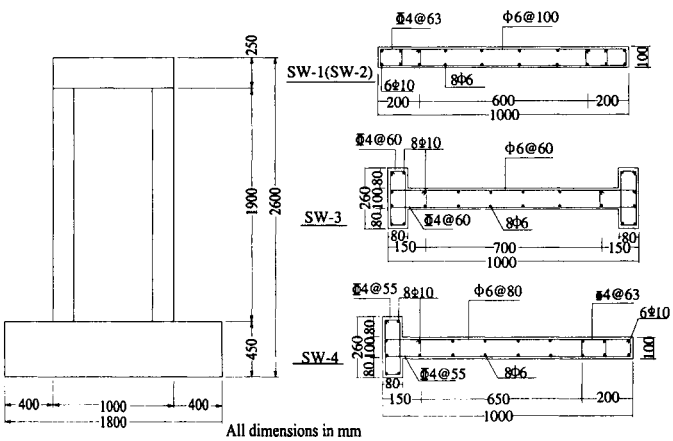


Fig. 4 Details of specimens

The concrete cubic strength of specimens f_{cu} was 25.2Mpa, 22.9Mpa, 34.1Mpa and 34.4Mpa respectively. The yield strength f_y of reinforcement with diameter of 4mm, 6mm and 10mm was 631.7Mpa, 451.7Mpa and 395Mpa respectively.

The boundary zone of specimens was confined with stirrups and the wall panel was reinforced with distributed reinforcements. The degree of confinement of stirrups is measured with the stirrup characteristic-value λ_v, which is:

$$\lambda_v = \rho_v \cdot f_y / f_c \tag{16}$$

where ρ_v is the volumetric ratio of stirrup, f_c is the concrete compressive strength and f_c=0.67 f_{cu}. For SW-1~SW-3, λ_v was 0.26, 0.28 and 0.25 respectively. For SW-4 λ_v of rectangular boundary zone and flanged boundary zone was 0.19 and 0.25 respectively.

Strains of vertical reinforcements in boundary zones were measured with strain gauges. Lateral displacement along the wall height was measured. Test data were recorded with the computer-based data acquisition system.

The specimens were subjected to a constant vertical load and cyclic lateral load at the top. The axial

the analysis methodology.

MODEL DESCRIPTION

The macro-model developed in this study is composed of two kinds of element: concrete membrane element which models the plane stress state of wall panel, and concrete column element which analogies tension or compression state of boundary zone respectively. Fig. 1 illustrates the modeling of shear wall in which the shear wall is divided into 5 layers and the wall panel is divided into 4 columns. Two column elements represent a boundary member to fit the different shape of the boundary member, such as rectangular section, flanged section or barbell section. In total, the wall shown in Fig.1 is modeled with 20 concrete column elements and 20 concrete membrane elements.
Two basic assumptions are adopted in the model: the cross section of shear wall remains plane section after deformation, and the stress in horizontal direction is equal to 0, i.e., $\sigma_x = 0$. By the plane section assumption, it is considered that there is a rigid beam between two adjacent layers. For one rigid beam there are three degrees of freedom at the center point: $\{u^g \quad v^g \quad w^g\}$, i.e., horizontal displacement, vertical displacement and rotation respectively. According to the assumption $\sigma_x = 0$, the strain in horizontal direction of any point in a membrane element is the same: $\varepsilon_x = \alpha$. If the wall panel is divided into k columns, the unknown numbers of horizontal strain for one layer of membrane element is $\{\alpha_1, \alpha_2 \cdots \alpha_k\}$. Then the total unknown numbers of one layer of membrane element is 3+k.

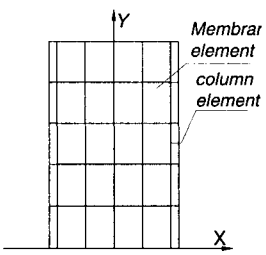


Fig.1 Macro-model of RC shear wall

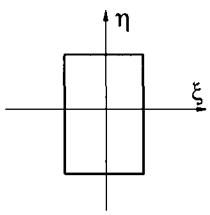


Fig. 2 Coordinate system of membrane element

STIFFNESS MATRIX OF MODEL

Membrane Element

Fig.2 shows the local coordinate system of the membrane element. The displacement pattern of any point in membrane element is the following:

$$u = a_0 + a_1\eta + a_2\eta^2 + a_3\eta^3 + a_4\xi \tag{1a}$$

$$v = b_0 + b_1\eta + b_2\xi + b_3\eta\xi \tag{1b}$$

in which u is the horizontal displacement, v is the vertical displacement, ξ and η is the horizontal and vertical normal coordinate value of this point respectively; $a_0, a_1, a_2, a_3, a_4, b_0, b_1, b_2, b_3$ are the parameters to be determined. By derivating the displacement pattern and transferring the normal coordinate system (ξ, η) to global coordinate system (X,Y) the strains of membrane element of any point can be obtained:

$$\varepsilon = [B]\mu \tag{2}$$

in which the matrix $[B]$is the shape function matrix. The stiffness matrix K^e of membrane element can be got by virtual work theory:

$$K^e = \int_e B^T DBtdxdy \tag{3}$$

in which $[D]$is the stress-strain relation matrix of membrane element, t is the thickness of membrane element, i.e., the thickness of wall panel.

Layer of Membrane Element

The relationships of displacement increment between layer membrane element and membrane element can be obtained by their geometrical relations (Fig. 3):

$$\begin{bmatrix} du_1 \\ du_2 \\ dv_1 \\ dv_2 \\ dw_1 \\ dw_2 \\ d\alpha \end{bmatrix} = \begin{bmatrix} 1 & 0 & 0 & 0 & 0 & 0 & \cdots & 0 & \cdots \\ 0 & 0 & 0 & 1 & 0 & 0 & \cdots & 0 & \cdots \\ 0 & 1 & -l_i & 0 & 0 & 0 & \cdots & 0 & \cdots \\ 0 & 0 & 0 & 0 & 1 & -l_i & \cdots & 0 & \cdots \\ 0 & 0 & 1 & 0 & 0 & 0 & \cdots & 0 & \cdots \\ 0 & 0 & 0 & 0 & 0 & 1 & \cdots & 0 & \cdots \\ 0 & 0 & 0 & 0 & 0 & 0 & \cdots & 1 & \cdots \end{bmatrix} \begin{bmatrix} du_1^g \\ dv_1^g \\ dw_1^g \\ du_2^g \\ dv_2^g \\ dw_2^g \\ \cdots \\ d\alpha_i \\ \cdots \end{bmatrix} \tag{4}$$

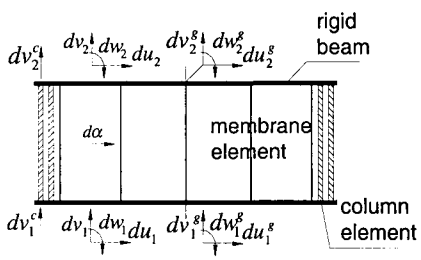


Fig.3 Displacement sketch of a layer

in which l_i is the distance between the center point of the membrane element and the center point of the rigid beam. Eqn. 4 can be marked as:

$$[du] = [B^g][du^g] \tag{5}$$

in which matrix $[du]$is displacement increment of membrane element, matrix $[du^g]$ is the displacement increment of layer of membrane element, $[B^g]$is the transfer matrix between the two kinds of displacement increment.

The relationships between the force increment and the displacement increment of the layer membrane element in the global coordinate system are:

$$[dX^g] = \left(\sum_k B^{g^T} K^e B^g \right) [du^g] \tag{6}$$

In which $dX^g = \{dX_1^g \quad dY_1^g \quad dM_1^g \quad dX_2^g \quad dY_2^g \quad dM_2^g \quad d\bar{X}_1 \quad d\bar{X}_2 \quad \cdots \quad d\bar{X}_n\}$, the parameter $d\bar{X}_i$ is the horizontal force of the membrane element corresponding to ε_x. By the assumption σ_x=0, $d\bar{X}_i$=0. The stiffness matrix of the layer of membrane element K_l can be obtained:

$$K_l = \sum_k B^{g^T} K^e B^g \tag{7}$$

Eqn. 6 can be expressed by block matrices:

$$\begin{Bmatrix} dX \\ 0 \end{Bmatrix} = \left[\begin{array}{c|c} K_{11} & K_{12} \\ \hline K_{21} & K_{22} \end{array}\right] \begin{Bmatrix} du \\ d\alpha \end{Bmatrix} \tag{8}$$

Resolve Eqn. 8 can get the strain increments $d\alpha$ of this layer:

$$d\alpha = -K_{22}^{-1} K_{21} du \tag{9}$$

From Eqn. 8 and Eqn. 9:

$$dX = K_m du \tag{10}$$

in which: $K_m = K_{11} - K_{12} K_{22}^{-1} K_{21}$, $dX = \{dX_1^g \;\; dY_1^g \;\; dM_1^g \;\; dX_2^g \;\; dY_2^g \;\; dM_2^g\}^T$, $du = \{du_1^g \;\; dv_1^g \;\; dw_1^g \;\; du_2^g \;\; dv_2^g \;\; dw_2^g\}$. The stiffness matrix of layer of membrane element K_m has been developed. The number of DOF of layer membrane element has been condensed from 3+k to 3.

Column Element

Two unknown numbers of displacement in the vertical direction at the two ends of column element are the only two degrees of freedom of the element. From the plane section assumption, the displacement of column element can be determined by the displacement of the rigid beam. The geometrical relationship of the two kinds of displacement is (Fig. 3):

$$du_c = \begin{bmatrix} 0 & 1 & -l_c & 0 & 0 & 0 \\ 0 & 0 & 0 & 0 & 1 & -l_c \end{bmatrix} du \tag{11}$$

Eqn. 11 can be marked as: $du_c = B_c du$, in which B_c is the shape function matrix of column element; du has the same meaning as Eqn. 10, l_c is the distance between the center of column element and the center point of rigid beam. The element stiff matrix of column element is:

$$K_c = B_c^T \begin{bmatrix} s & -s \\ -s & s \end{bmatrix} B_c \tag{12}$$

in which s is the tensile or compressive stiffness parameter, which can be determined by the constitutive relation.

Stiffness Matrix of Layer

The stiffness matrix of layer of the model is the sum of the stiffness matrices of membrane elements and column elements:

$$K_{layer} = K_m + \sum_4 K_c \tag{13}$$

in which 4 means there are 4 column elements in one layer.

CONSTITUTIVE RELATION OF MODEL

Constitutive Relation of Membrane Element

For the vertical and horizontal reinforcements are uniformly distributed in the wall panel, concrete membrane element is considered as a kind of continuous and uniform material composed of steel and concrete. Stress-strain relation matrix of this material is:

$$[D]=[D_c]+\sum_2[D_s] \tag{14}$$

in which $[D_c]$ is the stress-strain relation matrix of concrete; $[D_s]$is the stress-strain relation matrix of steel in one direction; $\sum_2[D_s]$means the sum of the stress-strain relation matrices of steel in horizontal and vertical directions.

Before cracking, concrete can be considered as an isotropic linear material. The modified compression field theory (MCFT) (Vecchio F.J. 1986, 1989, 1993) is adopted to determine the cracked concrete constitutive relations. The theory treats cracked reinforced concrete in terms of average stress and average strain, with the directions of principal stress and principal strain, and reflects the compression softening effects and tension stiffening effects. The relations of MCFT are formulized in complete curves.

The perfect elastic-plastic constitutive relation is used for the stress-strain relation of reinforcement embedded in concrete before concrete cracking. The experimental results (Abdeldjelil B. 1994) indicated that the constitutive relation of reinforcement embedded in concrete was different from that of bare reinforcement after concrete cracking, and the effect of crack should be considered. Based on the analysis of experiment data the linear strengthen constitutive relation for reinforcement in cracked concrete is adopted in this paper.

Constitutive Relation of Column Element

There are two kinds of boundary zone of shear wall: confined and unconfined. The stress-strain curve equations for confined concrete and for plain concrete suggested by Guo Z.H.(1999) were adopted. The longitudinal reinforcement is considered as perfect elastic-plastic material.

CALCULATION PROCESS

The equilibrium equations of push-over analysis of a structure are:

$$P=K_g\Delta \tag{15}$$

in which K_g is the global stiffness matrix, P and Δ is load and displacement field respectively. Before the peak of $P-\Delta$ relation curve, the stiffness matrix K_g is positive. After the peak, it is negative. The equilibrium equations are easy to be solved if the stiffness matrix is positive. When the $P-\Delta$ curve approaches its peak, the equations are ill-conditioned. A method called single degree of freedom compensation (SDFC) proposed by Zou J.L.(2001) is approached to solve ill-conditioned linear equations. The global stiffness matrix K_g should be decomposed into LDL^T style before the equilibrium equations are resolved by SDFC. The main concept of SDFC is to introduce a compensation value d_0 to keep stability of the resolution, so every diagonal element of matrix D is big enough. Then matrix K_g is modified to K_g+C (C is a diagonal matrix whose elements are

load ratio of specimens was 0.44, 0.21, 0.31 and 0.31 respectively. All specimens were designed with strong shear and weak bending and failed in flexure.

Comparison of Analytical and Experimental Results

To perform push-over analysis, each specimen was divided into 11 layers along the height, its wall panel was divided into 8 columns. In total there were 88 concrete membrane elements and 44 concrete column elements and 33 unknown numbers.

Complete process push-over analysis program of RC shear wall developed by this study was used to perform the analysis.

Lateral force-top displacement curves, i.e., capacity curves, of specimens obtained by experiment and push-over analysis are given in Fig. 5. The experimental results are skeleton curves of lateral force-top displacement hysteresis loops of specimens.

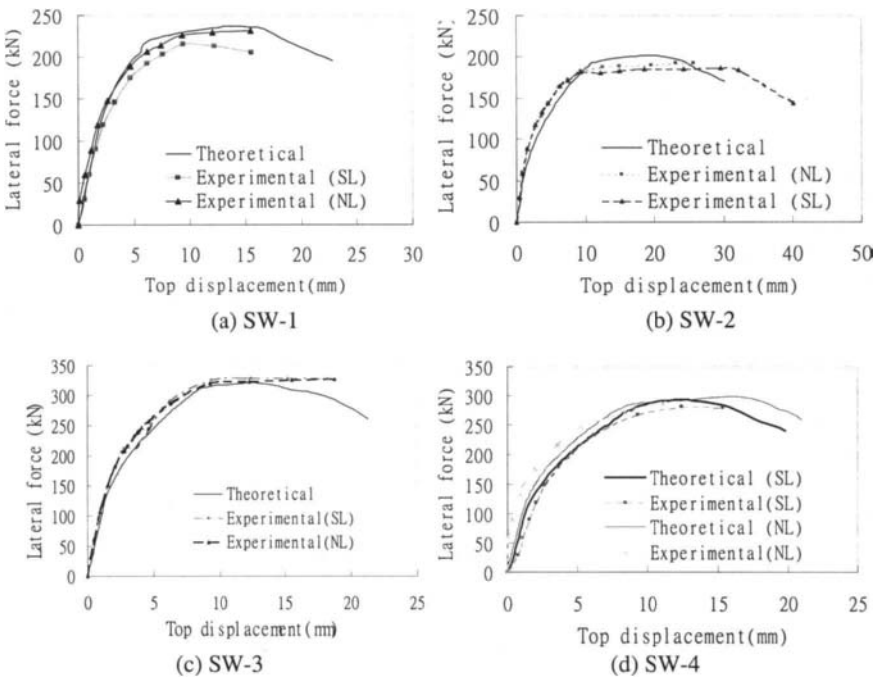


Fig. 5 Analytical and experimental lateral force-top displacement curves of specimens
(Note: the SL and NL mean the south loading and north loading respectively)

Table 1 lists the analytical and experimental maximum horizontal loads, i.e., the ultimate strength of specimens. The difference of two results is less than 10%. Table 1 also shows the displacement ductility ratios and the ultimate rotations of specimens. The displacement ductility ratio μ and the ultimate rotation θ are defined as:

$$\mu = \Delta u / \Delta y \tag{17a}$$

$$\theta = \Delta u / H \tag{17b}$$

in which, Δy and Δu are the yield and the ultimate lateral displacement at the top of specimen respectively, H is the displacement measure height.

From the comparison, the push-over analysis by using the macro-model provides a good estimate of the capacity curve of shear wall.

TABLE 1
COMPARISON OF ANALYTICAL AND EXPERIMENTAL ANALYSIS

Specimens		Ultimate lateral force (kN)		μ		θ	
		Exp	Ana	Exp	Ana	Exp	Ana
Sw-1	S	215.8	237.2	3.21	4.13	1/118	1/95
	N	232.1		3.68		1/119	
Sw-2	S	185.6	201.8	8.6	6.45	1/49	1/56
	N	192.9		5.58		1/72	
Sw-3	S	328.2	321.4	4.23	4.48	1/101	1/87
	N	326.1		4.35		1/99	
Sw-4	S	282.0	293.2	3.48	3.96	1/120	1/94
	N	286.4	297.9	2.92	3.43	1/166	1/110

(Note: S and N mean the loading direction of south and north respectively, Exp and Ana means the experimental and analytical results respectively.)

CONCLUSIONS

Membrane element and column element are used to simulate the wall panel and the boundary zone of RC shear wall respectively in the proposed macro-model. The model has advantages of finite element but the degree of freedom is greatly condensed. At the same time the constitutive relation derived from MCFT makes the analysis of cracked concrete very easy. The complete capacity curve of RC shear wall can be obtained by adopting single degree of freedom compensation approach. The macro-model of shear wall developed in the study is proved by comparison of experiment results and analytical results.

REFERENCES

Abdeldjelil B. and Hsu T.T.C. (1994). Constitutive Laws of Concrete in Tension and Reinforcing Bars Stiffened by Concrete. *ACI Structural Journal* 91:4, 465-474

Guo Z.H. (1999). *Theory of Reinforced Concrete*, Tsinghua University, Beijing, PRC.

Koumousis V.K. and Peppas G.A. (1992). Stiffness Matrices for Simple Analogous Frames for Shear Walls Analysis. *Computers and Structures* 43:4, 613-633

Linde P. and Bachmann H. (1994) Dynamic Modeling and Design of earthquake-resistant Walls. *Earthquake Engineering and Structural Dynamics* 23:12, 1331-1350

Park Y.H. and Reinhorm A.M. (1987). Inelastic Damage Analysis of RC Frame-shearwalls Structures. In: *National Center for Earthquake Engineering Research*, State University of New York at Baffalo, Baffalo, USA

Vecchio F.J. and Collins M.P. (1986) The Modified Compression-Field Theory for Reinforced Concrete Elements Subjected to Shear. *ACI Structural Journal* 83:2, 219-231

Vecchio F.J. (1989) Nonlinear finite Element Analysis of Reinforced Concrete Membranes. *ACI Structural Journal* 86:1, 26~35

Vecchio F.J. and Collins M.P. (1993). Compression Response of Cracked Reinforced Concrete. *Journal of Structural Engineering* 119:12 , 3590~3610

Zou JL. (2001). *3D RC frame structure full-range pushover analysis*. Ph.D. thesis, Tsinghua University, Beijing, P.R.C.

Advances in Building Technology, Volume 1
M. Anson, J.M. Ko and E.S.S. Lam (Eds.)
© 2002 Published by Elsevier Science Ltd.

TORSIONAL EFFECT OF ASYMMETRIC R/C BUILDING STRUCTURE

Junwu DAI[1] Yuk-Lung WONG[2] and Minzheng ZHANG[1]

[1]Institute of Engineering Mechanics, China Seismological Bureau, China
[2]Department of CSE, The Hong Kong Polytechnic University, Hong Kong

ABSTRACT

This paper is composed by the following investigations: 1) Using the time-history response of the base shear-torque of 3 asymmetric RC single-story-building systems under a set of earthquake simulation tests on shake table, both of the advantages and shortcomings of the base shear-torque (BST) surface (J.C. De La Llera and A.K. Chopra) established on the assumption of idealized force-displacement relationship are checked. 2) Based on the experimental results and the assumption of the bi-linear force-displacement relationship, a more reasonable and effective analytical model, the state space of base shear-torque is developed for estimation of the seismic performance particularly the torsional effects of the RC asymmetric structures.

KEY WORDS

earthquake simulation test, torsional, asymmetric, seismic response, inelastic, shear-torque relationship

BACKGROUND AND OBJECTIVES

It has been observed repeatedly in strong earthquakes that the presence of asymmetry in the plan of a structure makes it more vulnerable to seismic damages. There are reports of extensive damages to buildings that are attributed to excessive torsional responses caused by asymmetry in earthquakes such as the 1972 Managua earthquake, the 1989 Loma Prieta earthquake, the 1995 Kobe earthquake and the 1999 Chi-Chi earthquake. Although torsion has been recognized as a major reason for poor seismic performance of asymmetric buildings and many studies have been done on this topic, the analytical and experimental studies on the inelastic seismic response of asymmetric buildings do not have a long history. Recently, De La Llera and Chopra (1995) developed a simple model for analysis and design of asymmetric buildings based on the assumption of idealized elasto-plastic force-displacement relationship. Each story of the building is represented by a single super-element in the simplified model. In this method, the story shear and torque interaction surface (Kan and Chopra 1981, Palazzo and Fraternali 1988, De La Llera and Chopra 1995) is used as an important component. The story shear and torque (SST) surface is basically the yield surface of the story due to the interaction between story shear and torque. Each point inside the surface represents a combination of story shear and torque that the story remains elastic. On the other hand, each point on the surface represent a combination of shear and torque that leads to the yielding of the story. How realistic is such a model to represent the behavior of ductile frame buildings in seismic regions is a subject that requires further investigation.

The objective of this paper presented here are: 1) to check the limitations of the story shear-torque surface based on the assumption of the idealized force-displacement relationship with the experimental

results earthquake simulation tests on 3 asymmetric single-story structures and 2) to develop it to the more realistic three state spaces based on the bi-linear force-displacement relationship.

SHEAR-TORQUE RELATIONSHIP

There are three reinforced concrete single-story-building structures are designed to cater for the research objectives. All experiments are carried out on a single-axial shake table installed by MTS in HK Polytechnic University. Design detailing, instrumentations and ground excitations used in experiments have been described in reference [2].

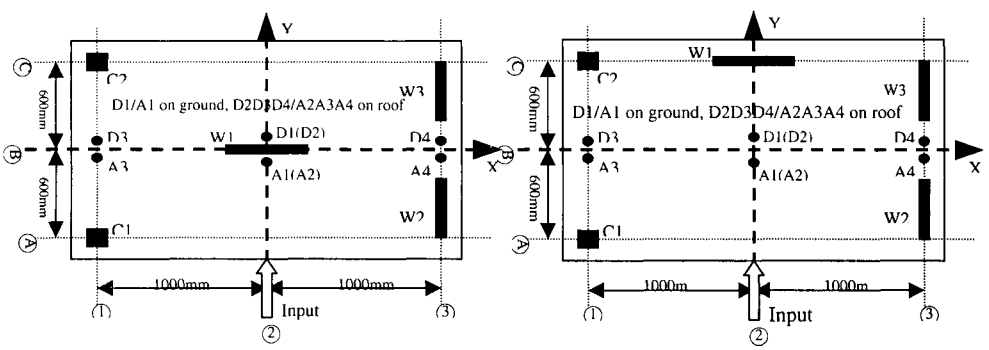


Fig.1 Specimen Configuration & Instrumentation

Verification of the shear-torque relationship

Based on the assumption of idealized force-displacement relationship of structural members, J.C. De Le Llera and A.K. Chopra (1995) developed a useful and effective method for understanding of fundamental issues on seismic torsional phenomena of asymmetric structures. The most important component of this approach is the use of the idealized yield base shear-torque (BST) surface of the studied system. As examples, abovementioned 3 model structures studied in earthquake simulation tests are used to examine both of the validity and the shortage of the idealized yield BST surface here for understanding of the real seismic behavior of asymmetric systems correctly.

According to the method of reference [3] developed, the BST surfaces of the 3 asymmetric model structures are founded respectively based on the assumption of idealized force-displacement relationship while only single-directional ground excitation is considered, shown in fig. 8 for convenience of comparison. The displacement-based approach that T. Paulay (2000) established is used in the determination of the stiffness of structural members. From fig.2, obviously, it can be found that the BST surface of specimen2 expanded uniformly on the basis of specimen1 while for that of specimen3, it is skewed and extended to the 1st and 3rd quadrant relatively. In fact, due to the strength of concrete used in the fabrication of specimen2 is higher than that of in specimen1, the strength of structural members in specimen2 is uniformly increased. Together with the wall w1 being arranged at the outer edge of specimen2 comparing with specimen1, the entire shear-torque resistant capacity is correspondingly increased in specimen2 than that of specimen1. The result is the space covered by the BST surface of

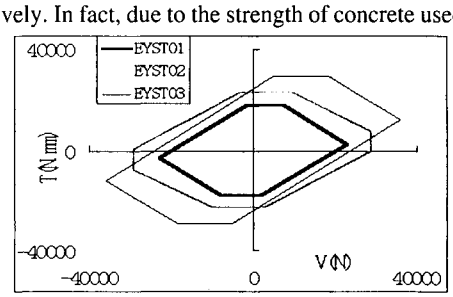


Fig.2 Comparison of BST surfaces of 3 model structures

specimen2 is larger than that of specimen1. Similarly, the higher strength of concrete and the reinforcement ratio used in specimen3 particularly in walls than that of in specimen1, intensified the strength eccentricity and simultaneously increased the entire shear-torque resistant capacity of specimen3. The associated consequence is that the BST surface of specimen3 is skewer and larger than that of specimen1. This figure illustrates the different seismic capacity among different model structures directly. From the area covered by the BST surface of each specimen, it can roughly predict that the seismic behavior of each specimen will be changed differently in a certain way.

In fact, there is no available method currently can be used to record the base shear and torque response directly in shake table tests but it is an easy thing to measure both of the acceleration and displacement response. In addition, because the roof plate of the 3 single-story model structures all performed as rigid body in experiments. Therefore, the rotational acceleration and the twist angle of the floor used to describe the torsional response can be determined directly from the lateral acceleration and displacement response based on the kinetic theory about rigid body. Further, the base torque response can be easily obtained. Associated base shear can be determined directly from the inertia force related lateral acceleration response.

The comparison between abovementioned theoretical results (solid line signifies the idealized BST surface of each specimens) and the experimental response (dotted area) in terms of the time history of the base shear-torque of each specimen is shown in fig.3~fig.5. Each sub-figure dictates one case of ground excitation. For example, A0.14g, E0.30g, L0.37g and N0.91g signify the time history response of base shear-torque in the case of ground excitation with intensity of artificial wave 0.14g, El Centro-NS component 0.30g, Loma Prieta record 0.37g and North Ridge record 0.91g, respectively.

From fig.3~fig.5, the following conclusions can be inferred:

1) For most cases of the intensity of ground motions are not higher than about 0.47g, the time history response of the base shear-torque does not or only lightly exceed the area the BST surface encircled. But it exceeds the boundary of the BST surface greatly in cases of the intensity of ground motions higher than about 0.47g for all 3 model structures. These facts tell the truth that the assumption of the idealized force-displacement relationship is only roughly reasonable for evaluation of the most common concrete structures in region with potential lower to moderate seismic intensity. However, for other relatively more important structures particularly those located in region with higher potential seismic intensity, more reasonable models such as bi- or tri-linear force-displacement relationship based strength/stiffness degradation/harden model should be used case to case. Correspondingly, the idealized BST surface should be developed further to be more realized bi- or tri-state spaces model to estimate the seismic performance (torsional effects) of asymmetric

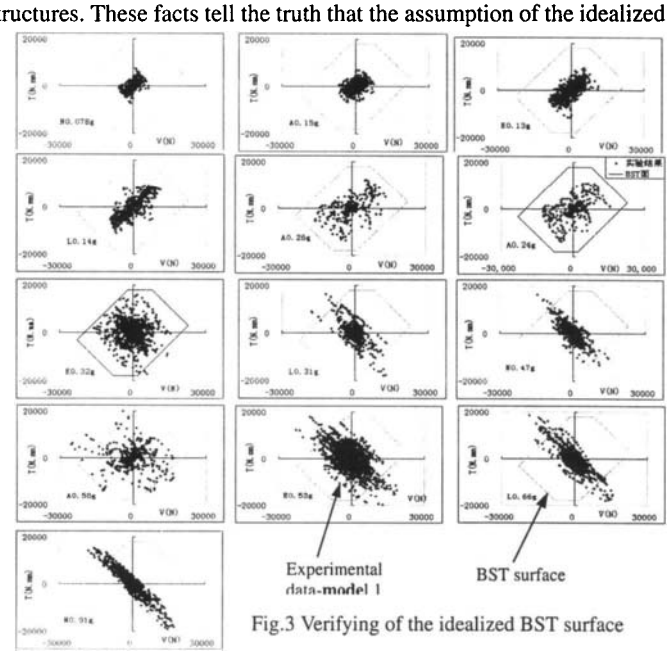


Fig.3 Verifying of the idealized BST surface

structures in a more general sense.

2) With the increase of the intensity level of the ground excitations, the time history response of the base shear-torque tends to be developed to the longest inclined side of the BST surface. From the definition of the BST surface according to reference [3], these two longest inclined sides signify the mechanism of other lateral resistant planes (the left column even the central wall planes) are damaged when the strongest right wall plane remains linear elastic. The experimental observation proved the fact that the damage sequence of all 3 specimens are started from the right column plane to the right wall plane at last although there are obvious difference among the seismic damage type of them. These experimental results testified that the theoretical results are reasonable. Therefore, the idealized BST surface can be used to estimate the seismic damage sequence of asymmetric structures roughly.

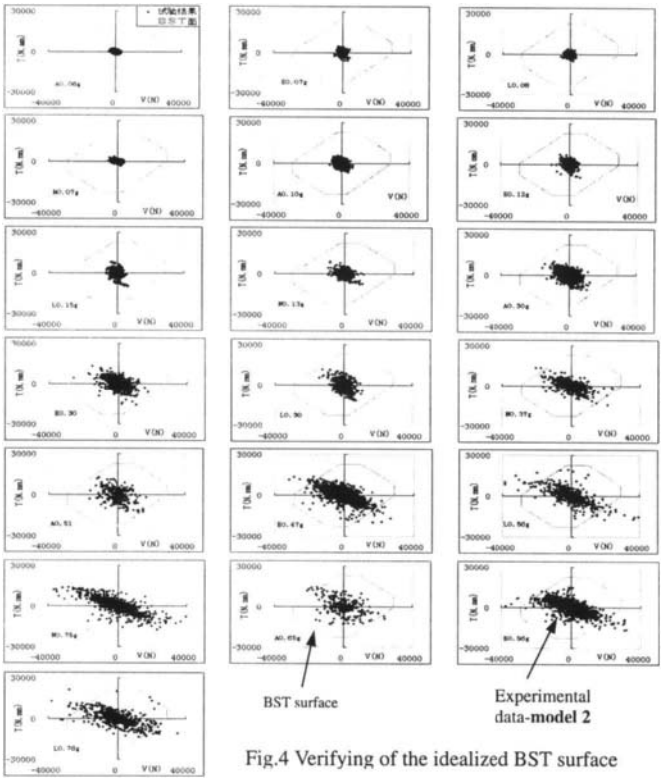


Fig.4 Verifying of the idealized BST surface

3) On the other hand, the trends of the time history of the base shear-torque lean to the longest sides of the BST surface illustrate effects of the change of the stiffness eccentricity to the seismic behavior of the model structure. That is, at the onset of the damage of the left column and central wall plane, the stronger right wall plane still remains linear elastic. Inevitably, the stiffness center shifts to the stronger right wall plane, intensified the stiffness eccentricity of the model structure. This phenomenon explains that although the stiffness eccentricity does not affect the shape of the BST surface, it really influences the developing trends of the time history response of the base shear-torque. In other words, the larger of the stiffness eccentricity is, the smaller of the possibility that the stronger members near the stiffness center are damaged will be and, the larger of the possibility that the weaker members far away from the stiffness center are damaged will be. The consequence is the larger of the possibility of the serious unbalanced damage occurring will be.

4) In most experimental cases, there is no pure torsional damage observed from the responses of the base shear-torque, i.e., only in few cases of model1 and model3, the torque resistance are exceeded lightly. In model2, such phenomena are never found. This fact illustrates, on one hand, the possibility of the occurring of the pure twist damage will be very small even for structures with larger eccentricity such as the model structures here studied. On the other hand, it shows that the location change of the central wall w1 improves the entire torque resistance directly and makes the coupling response more uniform and simultaneously, it tells the fact of the effects of the structural members in the orthogonal direction is

un-negligible when the seismic resistant capacity in one principal direction of the structure is studied and vice versa.

State space of base shear-torque relationship

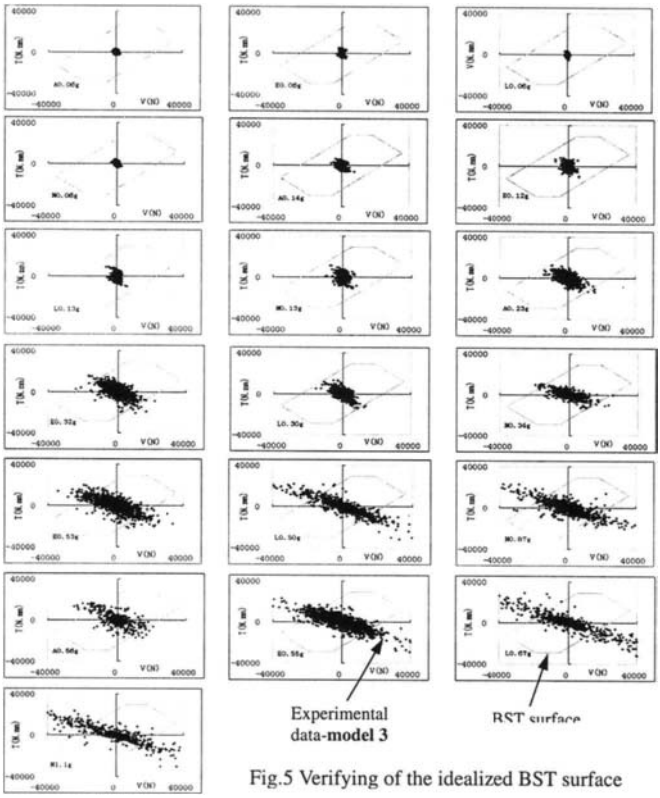


Fig.5 Verifying of the idealized BST surface

In fact, the degradation type of bi- and tri-linear force-displacement relationship should be more suitable than the idealized elasto-plastic one for most cases of reinforced concrete building structures in seismic ductility design. This conclusion can be verified directly from the comparison of the abovementioned experimental response and the idealized BST surface shown in fig.3~5. Then, correspondingly, the single space surrounded by the BST surface can be developed to 2 or 3 state spaces signifying respectively the elastic, inelastic even collapsed state of the related structural system. In other words, for evaluating the seismic performance of asymmetric RC structures realistically, the ultimate BST surface in the idealized model should be developed to nonlinear space(s) of the base shear-torque responses. The first space signifies the elastic response while the second space represents the inelastic characteristics when yield damage occurred in structure, and the third space means that the shear-torque response exceeds the ultimate capacity of the system. The boundary between the first and the second space describes a kind of critical state that the yielding damage initiates in system. Whilst, the boundary between the second and the third space should theoretically signify that the system begins to collapse.

As example, abovementioned specimen2 (bi-directional asymmetry with 3 lateral resistant planes along the y-direction of ground excitations) here is used to show how the 3 state-spaces model for evaluation of the seismic response of the base shear-torque is established. From the experimental data for the yielding strength f_y of the reinforcement used in the model system shown in table 1 respectively, the yield boundary dividing the elastic and the inelastic response spaces can be determined according to the method that De La Llera and A.K. Chopra established, i.e., its' location is completely same to that of the BST surface in the idealized model but they have quiet different meaning. Using the similar way and the ultimate strength f_u shown in table 1, the eight vertices of the collapse boundary can be easily determined based on the following formulas[3]:

$$x_1 = V_{y0}^* \qquad y_1 = V_{y0}^* x_p^* + T_\perp^*(1-\hat{V}_x^*) \qquad x_2 = V_{yu}^* + V_{yc}^* \qquad y_2 = T_0^* - T_\perp^* \hat{V}_x^*$$

$$x_3 = V_{yu}^* - V_{yc}^* \qquad y_3 = T_0^* - T_\perp^* \hat{V}_x^* \qquad x_4 = -V_{y0}^* \qquad y_4 = -V_{y0}^* x_p^* + T_\perp^*(1-\hat{V}_x^*)$$

$$x_5 = -x_1 \ , \ x_6 = -x_2 \ , \ x_7 = -x_3 \ , \ x_8 = -x_4$$
$$y_5 = -y_1 \ , \ y_6 = -y_2 \ , \ y_7 = -y_3 \ , \ y_8 = -y_4 \qquad (1)$$

where, in a more general sense, the symbol "*" signifies two kinds of critical state: the onset of yielding and reaching at the ultimate strength. If the structure system just starts to be damaged (reaches its yield strength), parameters in the above formulas have the same meanings with those of in the idealized BST surface. If the structural response reaches the maximum capacity of the system, these parameters can be determined based on the ultimate strength of structural members. As shown in fig.6, structural parameters controlling the response state space of the studied system are explained as,

1). $\hat{V}_x^* = V_x / V_{x0}^*$ is the normalized base shear along x-direction, while $V_{x0}^y = \sum_{i=1}^{M} f_{yxi}$ and $V_{x0}^u = \sum_{i=1}^{M} f_{uxi}$ are the yielding and ultimate lateral resistant capacities along the x-direction of the studied system respectively, in which, f_{yxi} and f_{uxi} are the corresponding yield and ultimate strength of the ith lateral resistant plane, and M is the number of the lateral resistant planes along x-direction. If the earthquake actions along the x-direction (besides slong the y-direction) should be taken into account, i.e., $V_x \neq 0$, the shape of the state space would be changed with the change of the value of V_x. Otherwise, if only single-directional earthquake excitation is studied, i.e., $V_x=0$, the effects of this item should be ignored.

2). $V_{y0}^y = \sum_{i=1}^{N} f_{yyi}$ and $V_{y0}^u = \sum_{i=1}^{N} f_{uyi}$ are the lateral yield and ultimate capacity of the system along y-direction, f_{yyi} and f_{uyi} are the lateral yield and ultimate strength of the lateral resistant planes, respectively. N is the number of the lateral resistant planes along y-direction. The value of V_{y0}^y and V_{y0}^u determine the span of the state space of base shear-toque on the shear axial. $V_{y0}^u - V_{y0}^y$ directly gives out the improvable space of the shear capacity of the structural system after yielding.

3). V_{yc}^y and V_{yc}^u are the lateral yield and ultimate capacity of the resistant plane passing through the center of mass. Generally, this parameter represents the sum of the resistant capacity of all lateral planes closing to the center of mass. From fig.6, it is obvious that the increase of the value $V_{yc}^u - V_{yc}^y$ means the increase of the possibility that the pure torsional mechanism will occur after yielding.

4). $T_0^y = \sum_{i=1}^{N} \left| f_{yyi} x_i \right| + \sum_{i=1}^{M} \left| f_{yxi} y_i \right|$ and $T_0^u = \sum_{i=1}^{N} \left| f_{uyi} x_i \right| + \sum_{i=1}^{M} \left| f_{uxi} y_i \right|$, respectively, define the torsional capacity of the system when pure twist yield and ultimate damage will be occurring. These two parameters control the maximum and minimum coordinates of the two critical boundaries along the torque axial. Moreover, the improvement of the torsional capacity of the system after yielding is also controlled by the value $T_0^u - T_0^y$.

5). $T_\perp^y = \sum_{i=1}^{M} \left| f_{yxi} y_i \right|$ and $T_\perp^u = \sum_{i=1}^{M} \left| f_{uxi} y_i \right|$ are

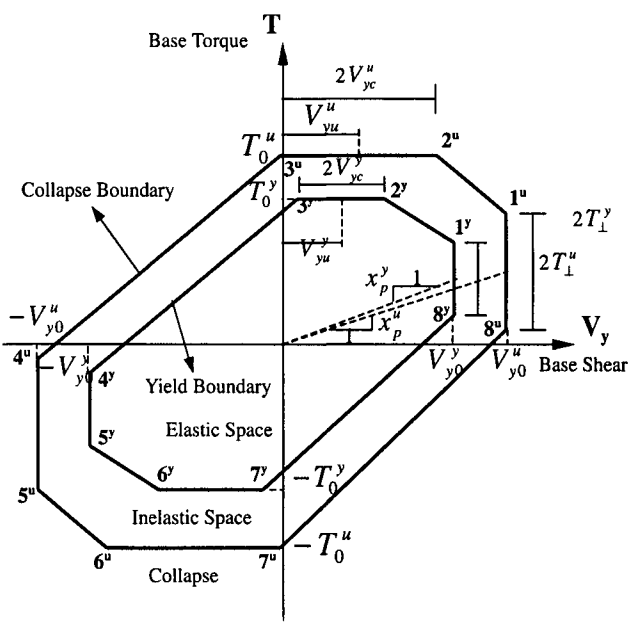


Fig.6 Structural parameters controlling the state space of base shear-torque

contribution of the torsional capacity provided by the orthogonal lateral planes at the level of initiating yield and collapse respectively. The possibility of the pure shear mechanism should be increased with the increase of the value $T_{\perp}^{u} - T_{\perp}^{y}$ particularly during the stage of inelastic response.

6). $x_p^y = \sum_{i=1}^{N} f_{yyi} x_i / V_{y0}^y$ and $x_p^u = \sum_{i=1}^{N} f_{uyi} x_i / V_{y0}^u$ determine the strength eccentricity of the system at two damage levels: before yielding and at the initiating of collapse, respectively. They signify independently the degree of the strength eccentricity on the two critical levels. Here, x_p^y is considered to be a constant during the elastic stage while x_p^u is also defined as a critical value at the instant of initiating collapse although the strength eccentricity is varied from x_p^y to its' maximum value, and then decreased to x_p^u with the increase of the intensity of the ground excitations gradually during the inelastic stage.

7). $V_{yu}^y = \sum_{\substack{i=1 \\ i\neq 2}}^{N} (f_{yyi} x_i / |x_i|)$ and $V_{yu}^u = \sum_{\substack{i=1 \\ i\neq 2}}^{N} (f_{uyi} x_i / |x_i|)$, at two levels: before yielding and at the initiating of collapse, respectively, define the degree of the unbalanced strength distribution at the two sides of the center of mass. The variation of the value $V_{yu}^u - V_{yu}^y$ shows the change of the possibility of the occurring of the pure shear mechanism. A maximum value of V_{yu} between V_{yu}^y and V_{yu}^u is also expected. Corresponding with the change of the strength eccentricity, this peak value should represent the state of some weaker structural members being damaged on one side of the center of mass while remaining elastic on the other side of the CM. Fig.6 does not show the peak value directly.

From the determination of the two critical boundary of the torsional-lateral coupling system, it can be inferred that the seismic response of the base shear-torque is naturally divided into 3 regions that represent respectively the linear elastic state, nonlinear state and the destroyed collapse state. The two critical boundaries, which signify the initiating yield and collapse, can be established independently based on the yield strength and the ultimate strength of structural members. This model can be directly used to estimate both of the overall seismic capacity and the developing trends of the time history response of the system base shear-torque to strong earthquakes even without complicated nonlinear analysis.

Fig.7 shows the comparison of the theoretical state space of the base shear-torque with the experimental results. The time-history shear-torque response of the bi-directional asymmetric single-story RC system in

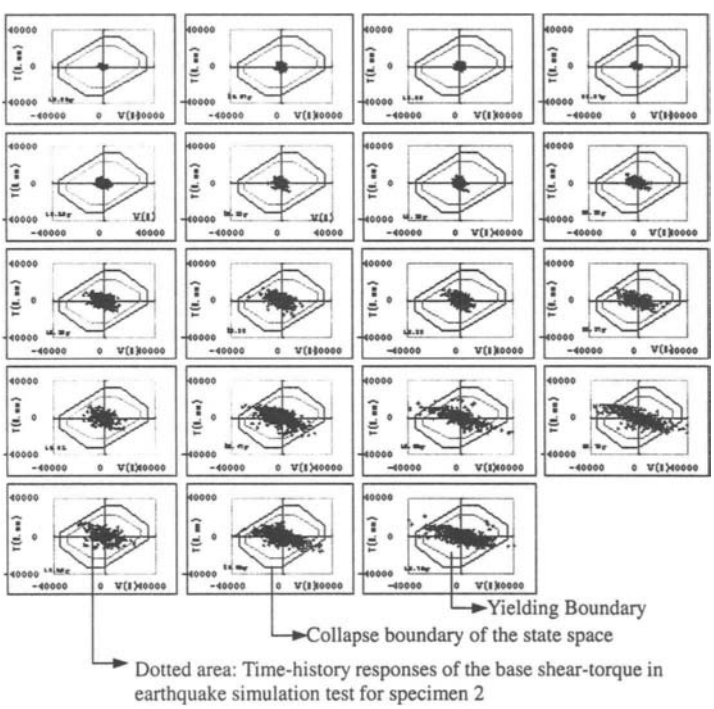


Fig.7 comparison of the theoretically established state space of the base shear-torque with experimental results

19 cases of ground excitations illustrates highly consistency with the state space established based on the assumption of the bi-linear force-displacement relationship. Such consistency is unreachable only by using the BST surface based on the idealized elasto-plastic assumption.

CONCLUDING REMARKS

In summary, the shake table tests provided useful data references for theoretical studies on seismic torsional effects of asymmetric building structures. Through the comparison between the experimental and the theoretical results, the following conclusions can be obtained:

1) Although the BST (base shear-torque) surface established on the assumption of idealized force-displacement relationship can be roughly used to estimate the seismic performance of asymmetric systems, it will bring obvious error on the prediction of the nonlinear response when the studied structure suffered strong earthquakes.
2) Therefore, based on the assumption of the bi-linear force-displacement relationship and the displacement-based method to determine the stiffness, the state space signifying the base shear-torque relationship is developed to describe the entire seismic capacity of the asymmetric systems. It shows high consistency with the experimental results. Therefore, it is no doubt a reliable model that can be directly used to estimate not only the entire seismic capacity but also the potential seismic damage may occur in the studied systems, even without relying on any complicated numerical analysis. It can be seen, this model will be very convenient and useful in evaluation of the lateral-torsional coupling effects of asymmetric structures particularly in the preliminary stage of design, retrofitting and research.

It should be noted that abovementioned conclusions are obtained on the basis of the experimental results of single story building structure. Their reliability and universality should be checked further with real seismic records or earthquake simulation tests for multi-story and high-rise building.

References

1. Dai Junwu, Yuklung Wong and Minzheng Zhang, *Torsion Response of Reinforced Concrete Building under Shaking Table Test*. Advances In Structural Dynamics, 2000, Vol. II, pp859-865.
2. Dai Junwu, *Research on nonlinear seismic performance of asymmetric RC building structure*, Ph.D. thesis, Institute of Engineering Mechanics, China Seismological Bureau, 2002,
3. De la Llera, J.C., Chopra, A. K., *Understanding the Inelastic Seismic Behaviour of Asymmetric Plan Buildings*, J. Earthquake Engineering & Structural Dynamics, 1995, v.24, pp.549-572.
4. De la Llera, J.C., Chopra, A. K., *Inelastic Behaviour of Asymmetric Multistory Buildings*, J. Structural Engineering, 1996, v.122, no.6, pp.597-606.
5. Guo Xun, Yuk-lung Wong and Yuan Yifan, *Investigation of Seismic Response of Soil site in HK*, HKIE Transactions, 2000, Vol. 7, No. 3.
6. Kan, C.L. and Chopra, A.K., *Torsional coupling and earthquake response of simple elastic and inelastic systems*, J. structural Division, ASCE, 1981, v.107, pp.1569-1588.
7. Minzheng Zhang, *Problem study on the application of the similitude law in earthquake simulation test*, Earthquake Engineering and Engineering Vibration, 1997.6, Vol.17, No.2.
8. Palazzo, B. and Fraternali, F., *Seismic ductility demand in buildings irregular in plan: A new single story nonlinear model*, Proceedings of the 9th World Conference on Earthquake Engineering, Tokyo-Kyoto, Japan, 1988, Vol.V, V-43 to V-48.
9. Paulay, T., *Displacement-based design approach to earthquake-induced torsion in ductile buildings*, Engineering Structures, 1997, Vol.19, No.9, pp.699-707.
11. Paulay, T., *Torsional mechanisms in ductile building systems*, Earthquake Engineering and Structural Dynamics, 1998, Vol.27, pp.1101-1121.
12. Paulay, T., *Understanding torsional phenomena in ductile systems*, Bulletin of the NZ Society for Earthquake Engineering, 2000, Vol.33, No.4, pp.403-420.

Advances in Building Technology, Volume 1
M. Anson, J.M. Ko and E.S.S. Lam (Eds.)
© 2002 Published by Elsevier Science Ltd.

EXPERIMENTAL INVESTIGATION ON AXIAL COMPRESSIVE BEHAVIOR OF FRP CONFINED CONCRETE COLUMNS

Li Jing [1], Qian Jiaru [1] and Jiang Jianbiao [2]

[1] Dept. of Civil Engineering, Tsinghua University, Beijing
[2] Beijing Texida Technical Limited Company, Beijing

ABSTRACT

In this paper axial compression test results of 29 Fiber Reinforced Polymer (FRP) confined concrete columns and 2 reference plain concrete columns are introduced. Most of column specimens were confined with Carbon Fiber Reinforced Polymer (CFRP) sheet and some of specimens were hybrid confined with both CFRP sheet and Glass Fiber Reinforced Polymer (GFRP) sheet. The influences of FRP sheet layer, section height to width ratio, initial compressive ratio and FRP type on the axial compressive behavior of FRP confined concrete columns are investigated. Based on the experimental results equations of complete stress-strain curve and the parameters of equations are proposed for CFRP sheet confined concrete.

KEYWORDS

FRP confined concrete column, axial compressive behavior, complete stress-strain curve equation

PREFACE

One of the effective approaches to upgrade strength and ductility of concrete columns is to confine the column with FRP sheet, see Karbhari & Gao (1997), Yu (2001), Lam & Teng (2001), Zhao, Xie and Dai (2001). The method of confinement is to wrap concrete columns with FRP sheet, use epoxy resin to bond layers of FRP and to bond FRP sheet with the surface of column. Thus FRP confined column is formed as shown in Fig.1.

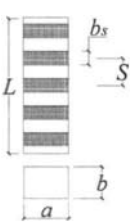


Figure 1:
FRP confined column

The objectives of this paper were to study the compressive behavior of FRP confined concrete columns subjected to concentric axial compressive loads and to develop complete stress-strain curve equations for CFRP confined concrete.

TEST PROGRAM

Specimen Details

Thirty-one specimens including 29 FRP confined columns and 2 reference plain concrete columns were tested. All specimens were cast in 6 groups. Four groups were square cross section columns and two groups were rectangular cross section columns. Four parameters were varied: 1) the degree of confinement provided by FRP, 2) cross section dimensions, 3) initial axial compressive force before specimens were wrapped with FRP sheet, and 4) confinement material. All specimens were plain concrete column to neglect the influence of longitudinal reinforcements and stirrups on confinement. Two types of FRP sheet were used: CFRP and GFRP. The material properties of CFRP and GFRP are listed in Table 1.

A parameter called FRP characteristic value λ_{FS} is adopted to measure the degree of confinement provided by FRP. The FRP characteristic value accounts for the effect of FRP layer-wrapped, tension strength and thickness of FRP sheet, dimensions of cross section of specimen, axial compressive strength of plain concrete. It can be computed as:

$$\lambda_{FS} = \frac{V_{FS}}{V_C}\frac{f_{FS}}{f_c} = \frac{2(a+b)n_S t_S}{ab}\cdot\frac{f_{FS}}{f_c} \tag{1}$$

Where: V_{FS} and V_C are the volume of FRP sheet and the volume of concrete column specimen respectively, n_s and t_s are the layer-wrapped and thickness of FRP sheet, a and b are the length and width of cross section of the specimen, f_{FS} is the tension strength of CFRP or GFRP and f_c is the axial compression strength of concrete. For specimens hybrid confined with both CFRP and GFRP, the value of λ_{FS} is the sum of λ_{CFS} and λ_{GFS} calculated with Eqn.1. The layer-wrapped is defined as the ratio of the area of FRP sheet to the vertical surface area of specimen. With the definition, the layer-wrapped of the specimen shown in Fig.1 is 0.5. The 1-layer-wrapped means that allover the vertical surface of the specimen is wrapped with 1-layer FRP sheet.

Some specimens were loaded with an initial compressive force before they were wrapped with FRP. The initial compressive ratio n_p is adopted to measure the magnitude of initial force, which is defined as the ratio of the initial axial compressive force N to the produce of column cross section area ($a \times b$) and f_c. Specimens of group 2,3 and 4 were loaded with the initial compressive ratio n_p of 0.22, 0.46 and 0.3 respectively. The initial force was applied by prestressing steel cables. To avoid the local destroy and bending failure, the steel cable were symmetrically prestressed. The real force applied to the specimen was measured with force sensors. The prestressing facilities are schematically shown in Fig.2.

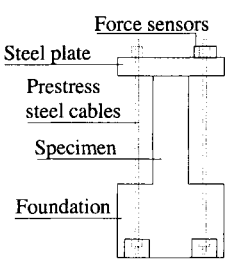


Figure 2:
Prestressing facilities

The details of each specimen are listed in Table 2.

TABLE 1
MATERIAL PROPERTIES OF FRP SHEET

FRP sheet type	Tension strength f_{FS} (MPa)	Tension module E (GPa)	Thickness t_s (mm)	Ultimate tension strain
CFRP	4013	241	0.111	16650×10^{-6}
GFRP	2777.1	97	0.169	28630×10^{-6}

TABLE 2
DETAILS OF SPECIMENS

Group No	Specimen No	Dimension (mm)	f_c	n_p	FRP sheet type	Layer -wrapped	λ_{FS}
1	Z1-0	200×200×600	25.4	0	CFRP	-	0
	Z1-1					0.5	0.18
	Z1-2					1	0.37
	Z1-3					1.5	0.55
	Z1-4					2	0.74
	Z1-6					3	1.11
	Z1-4a		29.3			2	0.63
2	Z2-0	200×200×600	29.3	0.22	CFRP	-	0
	Z2-1					0.5	0.16
	Z2-2					1	0.31
	Z2-4					2	0.63
	Z2-6					3	0.94
3	Z3-1	200×200×600	26.6	0.46	CFRP	0.5	0.19
	Z3-2					1	0.38
	Z3-3					1.5	0.58
	Z3-4					2	0.77
	Z3-6					3	1.15
4	Z4-1	300×200×600	31.7	0.3	CFRP	0.5	0.17
	Z4-2					1	0.34
	Z4-3					1.5	0.50
	Z4-4					2	0.67
	Z4-5					3	1.01
	Z4-6	300×200×600	27.9	0.3	CFRP, GFRP	1, 1	0.55
	Z4-7					2, 2	1.09
5	Z5-1	400×200×900	26.7	0	CFRP	4/3	0.32
	Z5-2					8/3	0.64
	Z5-3				CFRP, GFRP	1, 1/3	0.33
6	Z6-1	300×300×900	28.3	0	CFRP	13/9	0.33
	Z6-2					3	0.68
	Z6-3				CFRP, GFRP	1, 4/9	0.33
	Z6-4					2, 1	0.69

Test Instrumentation

The axial deformation was measured with two couples of linear variable displacement transducer located on the symmetrical surfaces of specimen. One couple of transducer recorded the relative movement between the upper and lower load plates. One couple of transducer recorded the relative movement between two sections with 400mm spacing. The horizontal strains of FRP were measured with strain gauges. The gauges were located at the mid-height section of the specimen. The distributions of the gauges are shown in Fig.3. The specimens were tested by monotonically increasing concentric axial compressive load in a 5000KN capacity compressive testing machine. Fig.4 shows the photo of test setup. All of data were collected using a computer-based data acquisition system.

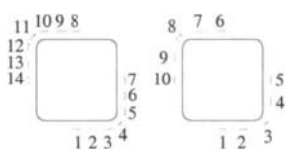


Figure 3: Location of strain gauges

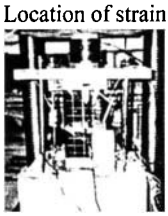


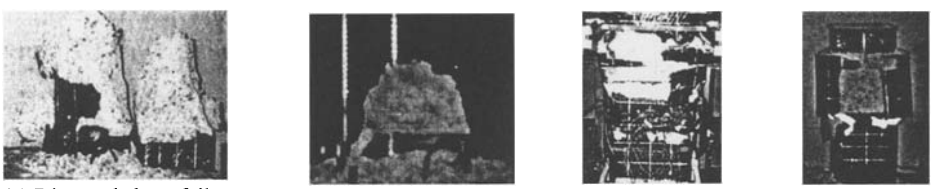
Figure 4: Photo of test setup

EXPERIMENTAL RESULTS AND ANALYSES

Process of Destroy and Failure Modes

The measured axial compressive force-displacement curve was linear when the axial force was less than about half of the strength of specimen. When the curve reached its peak or started turn to level, concrete crack voice could be heard. Finally the rupture of FRP sheet characterized the failure of confined specimens.

Failure modes of FRP confined concrete column specimens can be classified into two types: diagonal shear failure and compression failure. If λ_{FS} was small, the specimen failed in shear as shown in Fig. 5(a). On the contrary, the specimen failed in compression and the failure surface was similar to a pyramid as shown in Fig.5(b). The force-displacement curve corresponding to compression failure is plump near the turning corner, and the descending branch was higher than that corresponding to diagonal shear failure. The FRP sheet of most specimens was broken at the corner of specimen. The rupture mode of FRP sheet was related to λ_{FS} and n_p. If λ_{FS} and n_p were smaller, the rupture was fluffy and unorderly by tearing out, on the contrary, it was straight like cut by scissors, as shown in Fig.5(c) and 5(d).



(a) Diagonal shear failure

Figure 5: Failure modes of concrete and FRP sheet of specimen

Test Results

Fig.6 shows $\sigma/\sigma_0-\varepsilon/\varepsilon_0$ curves of all specimens, where σ and ε are measured axial stress and strain respectively, σ_0 and ε_0 are peak stress and peak strain of plain concrete respectively. For specimens of group1 and 2, the maximum average stress (i.e., the maximum load divided by section area) of the reference column specimen is taken as the peak stress (σ_0) respectively. For other specimens the average value of σ_0/f_c of two reference columns is taken to calculate the peak stress (σ_0) of plain concrete. For all specimens, the average peak strain (0.002) of two reference column specimens is taken as the peak strain (ε_0) of plain concrete.

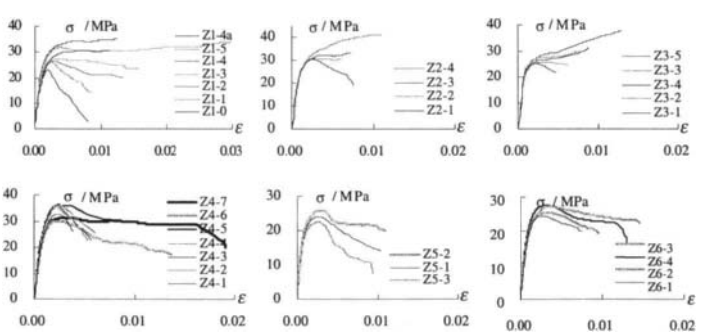


Figure 6: $y(\sigma/\sigma_0)-x(\varepsilon/\varepsilon_0)$ curves of specimens

Three types of curve shape can

be distinguished. (1) The curve has an ascending branch (before the peak of curve) and a descending branch (after the peak of curve). (2) The curve has an ascending branch and a horizontal branch. (3) The curve has two ascending branches, the slope of the latter branch is much less. Most of curves are type 1.

The main test results are listed in Table 3. In the table, f_{cc} and ε_{cc} are peak stress and peak strain. The peak point refers to the turning point for type 2 curves and type 3 curves. f_{ccu} is the ultimate stress corresponding to the end point for type 3. ε_{ccu} is the ultimate compressive strain which is defined as the strain corresponding to the residual stress of $0.6f_{cc}$ or the failure strain for type 2 and type 3. The average ultimate strain (0.004) of two reference columns is taken as the ultimate strain (ε_{cu}) of plain concrete for all specimens.

TABLE 3
TEST RESULTS

Group No	Specimen No	f_{cc} (MPa)	f_{cc}/σ_0	ε_{cc} ($\times 10^{-6}$)	$\varepsilon_{cc}/\varepsilon_0$	f_{ccu} (MPa)	f_{ccu}/σ_0	ε_{ccu} ($\times 10^{-6}$)	$\varepsilon_{ccu}/\varepsilon_{cu}$
1	Z1-0	23.02	1.0	2005	1.0			4501	1.13
	Z1-1	26.57	1.15	2296	1.13			8317	2.08
	Z1-2	26.54	1.15	3041	1.52			13388	3.35
	Z1-3	27.33	1.18	3458	1.74			15571	3.89
	Z1-4	30.38	1.31	6424	3.21	30.56	1.32	11765	2.94
	Z1-6	31.87	1.38	3745	1.87	33.97	1.46	29897	7.47
	Z1-4a	34.30	1.26	6532	3.27	34.44	1. 30	12417	3.10
2	Z2-0	27.20	1.0	2000	1.0			3600	0.90
	Z2-1	31.66	1.16	2628	1.31			7599	1.90
	Z2-2	32.40	1.19	5050	2.52	32.40	1.19	6070	1.52
	Z2-4	34.13	1.25	7026	3.51	34.13	1.26	8687	2.17
	Z2-6	40.14	1.48	7802	3.90	41.35	1.52	10905	2.73
3	Z3-1	25.33	1.14	2254	1.13			4769	1.19
	Z3-2	25.80	1.16	2572	1.29			6186	1.55
	Z3-3	27.64	1.24	3687	1.84	29.87	1.34	7622	1.91
	Z3-4	26.69	1.20	3312	1.66	31.09	1.40	8870	2.22
	Z3-6	29.24	1.31	4618	2.31	37.66	1.69	12985	3.25
4	Z4-1	33.24	1.17	1963	0.98			3095	0.77
	Z4-2	35.56	1.26	2148	1.07			4466	1.12
	Z4-3	35.75	1.26	2191	1.10			5292	1.32
	Z4-4	36.13	1.29	2416	1.21			5746	1.44
	Z4-5	36.03	1.28	2445	1.22			10090	2.53
	Z4-6	30	1.12	3588	1.22			11019	2.75
	Z4-7	31.24	1.16	2447	1.58			21443	5.36
5	Z5-1	24.05	0.90	2555	1.28			10439	2.61
	Z5-2	25.91	0.97	3215	1.61			11515	2.88
	Z5-3	22.60	0.85	2286	1.16			9812	2.45
6	Z6-1	24.53	0.98	2246	1.12			6134	1.54
	Z6-2	27.27	1.09	3588	1.79			14625	3.66
	Z6-3	25.49	1.02	3273	1.64			9553	2.39
	Z6-4	27.53	1.10	3334	1.67			12980	3.25

Influence Factors

FRP characteristic value λ_{FS}

The effect of λ_{FS} on the $\sigma/\sigma_0-\varepsilon/\varepsilon_0$ relationships of FRP confined concrete is obvious, as seen from Table 3, Fig.6 and Fig.8. The following conclusions can be obtained under the condition of $0 \le \lambda_{FS} < 1.1$. (1) The larger λ_{FS} is, the larger f_{cc}, f_{ccu}, ε_{cc} and ε_{ccu} are. (2) The initial stiffness of FRP confined concrete columns is larger than that of plain concrete columns. The larger λ_{FS} is, the larger initial stiffness is. (3) The descending branch of $\sigma/\sigma_0-\varepsilon/\varepsilon_0$ curve becomes more and more flat with the increasing of λ_{FS}. When λ_{FS} is large enough, the curve does not have descending branch.

Initial axial compressive ratio n_p

Initial axial compressive ratios n_p of group 1, 2 and 3 specimens are 0, 0.22 and 0.46 respectively. Comparing $\sigma/\sigma_0-\varepsilon/\varepsilon_0$ curves of group 1, 2 and 3 with about the same λ_{FS}, it is found that the larger n_p is, the flatter the descending branch is. Most specimens of group 2 and 3 do not have descending branch. For they had had initial lateral deformation before they were wrapped, the FRP sheet had more capacity to deform (i.e., FRP sheet provided more lateral confinement) after the turning point of $\sigma/\sigma_0-\varepsilon/\varepsilon_0$ curve than those with $n_p=0$.

Section length to width ratio λ_{ab}

FRP characteristic value λ_{FS} doesn't include the influence of section length to width ratio. Comparing $\sigma/\sigma_0-\varepsilon/\varepsilon_0$ curves of group 1, 4 and 5 specimens with λ_{ab} of 1.0, 1.5 and 2.0 with about the same λ_{FS}, the larger λ_{ab} is, the less f_{cc} and ε_{ccu} are.

FRP type

Comparing σ/σ_0 -$\varepsilon/\varepsilon_0$ curves of Z4-4 with Z4-6, Z4-5 with Z4-7 as shown in Fig.6, the second branch of the curve for specimens hybrid confined with both CFRP and GFRP is relatively higher, and the ultimate strain is larger. The results show that combining with GFRP to CFRP, especially allover the vertical surface of column was wrapped with GFRP, benefits deformation and ductility capacity, for the tension module of GFRP is less than that of CFRP and the ultimate tension strain is larger than that of CFRP.

EQUATION OF COMPLETE STRESS-STRAIN CURVE FOR CFRP CONFINED CONCRETE

Shape of Curves

As mentioned before, there are three types of stress-strain curve shape for CFRP confined concrete as shown in Fig.7. The coordinates in Fig.7 are defined as:

$$x=\frac{\varepsilon}{\varepsilon_{cc}}, \quad y=\frac{\sigma}{f_{cc}} \tag{2}$$

All curves have two branches. The first branch is the ascending branch, the shape of which can be described

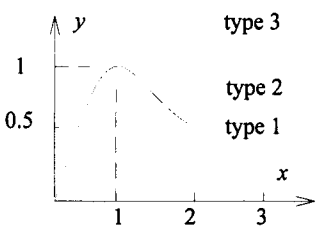


Figure 7: Three types of complete stress strain curve for CFRP confined concrete

with a single equation that will be presented below. The shape of the second branch is related to the value of λ_{FS} and the critical value λ_{FS0}. If $\lambda_{FS} < \lambda_{FS0}$, the curve shape is type 1. If $\lambda_{FS} = \lambda_{FS0}$, the curve shape is type 2. If $\lambda_{FS} > \lambda_{FS0}$, the curve shape is type 3. From experimental data, the critical value λ_{FS0} depends on n_p and λ_{ab}, i.e.:

$$\lambda_{FS0} = \frac{0.8(1-n_p)}{2-\lambda_{ab}} \tag{3}$$

Suggested Equation of Stress-strain Curve

The form of equation for plain concrete suggested by Sargin (1971) is adopted for the ascending branch of stress-strain curve of CFRP confined concrete, and a linear equation is adopted for the second branch, i.e.:

$$x \le 1: \quad y = \frac{a'x}{1+(a'-2)x+x^2} \tag{4}$$

$$x > 1: \quad y = \beta'(x-1)+1 \tag{5}$$

Five parameters are needed to define an equation of complete stress-strain curve of FRP confined concrete: peak stress f_{cc}, peak strain ε_{cc}, ultimate stress f_{ccu}, the ascending branch parameter a' and the second branch parameter β'. According to the experimental data under the condition of $0 \le \lambda_{FS} < 1.1$, $0 \le n_p < 0.5$ and $1 \le \lambda_{ab} < 2$, Eqn.(6)~Eqn.(9) are proposed to calculate f_{cc}, f_{ccu}, ε_{cc}, ε_{ccu}.

$$f_{cc}/f_c = 0.38\lambda_{FS}+1 \tag{6}$$

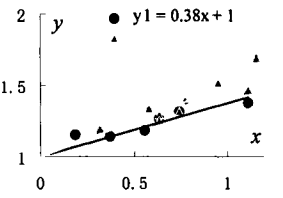
$$f_{ccu}/f_c = 0.51\lambda_{FS}+1 \tag{7}$$

$$\varepsilon_{cc}/\varepsilon_0 = 1.75\lambda_{FS}+1 \tag{8}$$

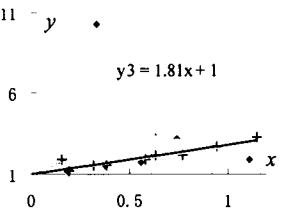
$$\varepsilon_{ccu}/\varepsilon_{cu} = \begin{cases} 4.76\lambda_{FS}+1, & n_p \le 0.2 \\ 1.81\lambda_{FS}+1, & n_p > 0.2 \end{cases} \tag{9}$$

Eqn.(6) and Eqn.(7) are compared with tests in Fig.8(a), and Eqn.(8) and Eqn.(9) are compared with tests in Fig.8(b).

a' and β' are the parameters used to adjust the shape of the ascending branch and the second branch of stress-strain curve respectively. The FRP characteristic value λ_{FS} is selected to identify the curve shape so that the parameters a' and β' are recommended in Eqn.(10) and Eqn.(11).



(a) $y1(f_{ccu}/\sigma_0)$, $y2(f_{cc}/\sigma_0)$–$x(\lambda_{FS})$



(b) $y1(\varepsilon_{cc}/\varepsilon_0)$, $y2(\varepsilon_{ccu}/\varepsilon_{cu}, n_p \le 0.2)$, $y3(\varepsilon_{ccu}/\varepsilon_{cu}, n_p > 0.2)$–$x(\lambda_{FS})$

Figure 8: The influence of λ_{FS} on f_{cc}, f_{ccu}, ε_{cc} and ε_{ccu}

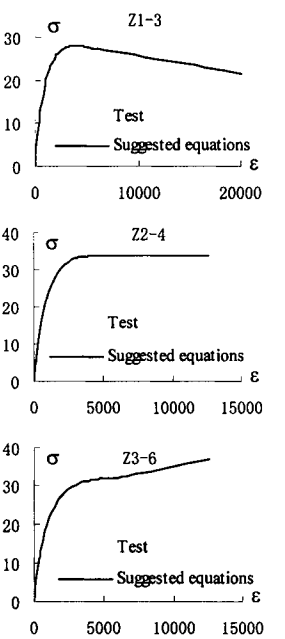


Figure 9: Comparison of σ(Mpa)-ε($\times 10^{-6}$) curves charted by test and by suggested equations

$$a' = 2(2.56\lambda_{FS} + 1) \tag{10}$$

$$\beta' = \begin{cases} \text{type 1}: -0.25(\lambda_{FS} - \lambda_{FS0})^2 + 0.17(\lambda_{FS} - \lambda_{FS0}) \\ \text{type 2}: 0 \\ \text{type 3}: 0.20(\lambda_{FS} - \lambda_{FS0}) \end{cases} \tag{11}$$

Using the above equations, the complete stress-strain curve of CFRP confined concrete can be described. The stress-strain curves of Z1-3 (type 1), Z2-4 (type 2) and Z3-6 (type 3) suggested by Eqn.(4) ~Eqn.(11) are charted in Fig.9, and the curves obtained from the test data are also drawn. It can be seen from Fig.9 that the relative curves have a good agreement. The equations recommended in this study to describe the behavior of CFRP confined concrete are suitable.

CONCLUSIONS

Concrete confined with FRP sheet is advantage to its strength, deformation and ductility. The strength and the ultimate strain of FRP confined concrete columns can be 1.6 and 7 times of those of plain concrete columns.

The effect of FRP on the strength and deformation of concrete columns is related to the degree of confinement, cross section dimensions, initial axial compressive ratio, and confinement material.

Two type failure modes of concentric axial loaded FRP confined concrete columns are diagonal shear failure and compression failure. The failure mode mostly depends on the characteristic value λ_{FS} of the column.

The stress-strain curve of CFRP confined concrete is classified into three types. A series of equations are obtained to describe the three type curves. Parameters of the equations are suggested by experimental data of this study.

REFERENCE

Karbhari V.M. and Gao Y. (1997). Composite Jacketed Concrete under Uniaxial Compression-Verification of Simple Design Equation. *Journal of Materials in Civil Engineering, ASCE* **9:4**, 185-193.

Sargin M. (1971). *Stress-Strain Relationships for Concrete and the Analysis of Structural Concrete Sections*. Canada

Lam L. and Teng J.G. (2001). A New Stress-strain Model for FRP-confined Concrete. *FRP Composites in Civil Engineering*, **Vol.I, J.-G. Teng (Ed.)**, 283-291.

Yu Qing. (2001). Investigation on Stress-strain Relationship of FRP Confined Concrete under Axial Compression. *Magazine of Industry Structure,* **31:4**, 18-25.

Zhao Tong, Xie Jian and Dai Ziqiang. (2001). Experimental Investigation on Full Stress-strain Curve of CFRP Confined Concrete. *Magazine of Structure Construction,* **30:7**, 32-38.

Advances in Building Technology, Volume 1
M. Anson, J.M. Ko and E.S.S. Lam (Eds.)
© 2002 Elsevier Science Ltd. All rights reserved

DYNAMIC PROPERTIES AND SEISMIC RESPONSE OF RC STRUCTURES CHARACTERIZED BY ABRUPT CHANGE IN HORIZONTAL CONNECTION STIFFNESS

Liu Jingbo[1] and Wang Zhenyu[1]

[1]Department of Civil Engineering, Tsinghua University, Beijing, 100084, China

ABSTRACT

More and more concrete structures characterized by abrupt change in stiffness are built because of requirements of building appearance and functions. Obviously, dynamic properties and seismic response of this kind of structure are very different from common structures. It is very interesting to discuss the design concept, analysis methods and other details of this kind of structure. Dynamic properties and seismic response of concrete structure characterized by abrupt change in horizontal connection stiffness are studied systematically in this paper. General mechanic concepts and analysis methods of this kind of structure are introduced firstly. Then for Putian Center of Radio, Film and TV example, complicated mode shapes and stress concentration resulted from abrupt change in horizontal connection stiffness are revealed. Moreover, effects of different connective plans located in place of abrupt change in horizontal connection stiffness on structure dynamic properties and seismic response are discussed. These effects are analyzed by FE numerical experiments. Finally, some useful suggestions are proposed which may be used as a reference in engineering.

KEYWORDS

abrupt change, concrete structures, dynamic properties, seismic response, connection stiffness, stress concentration

INTRODUCTION

It is very important that building structural systems have reasonable stiffness distribution. Strong stress and plastic deformation concentration because of partly weakening or abrupt change in stiffness should be avoided. However, abrupt change in horizontal or vertical stiffness usually exists because of the demand of architectural function and style in practice. In general, we must pay more attention to not only structural member's stress and deformation located in place of abrupt change in stiffness, but also the change of dynamic properties caused by abrupt change in stiffness. The design method of transfer beams or stories located in place of abrupt change in vertical stiffness has been studied by many authors. But few studies on abrupt change in horizontal stiffness have been performed. In fact, abrupt change in horizontal stiffness will lead to marked change of dynamic properties and acute stress and

deformation concentration of structure members. In this paper, general problems of such structure dynamic analysis are discussed firstly. Then effects on structure dynamic properties and seismic responses are studied which caused by different connective plans located in place of abrupt change in horizontal stiffness. The effects are analyzed by finite element numerical experiments based on project of Putian Center of Radio, Film and TV, China. Methods and conclusions in this paper are referenced to such structure dynamic response analysis and optimization of seismic design.

GENERAL PROBLEMS OF DYNAMIC RESPONSE ANALYSIS

Two problems must be considered when we study seismic analysis of RC structure characterized by abrupt change in horizontal connection stiffness. The two problems consist of characteristics and selection of mode shapes, and acute stress concentration located in place of abrupt change in horizontal connection stiffness.

Mode superposition time history analysis and response spectra analysis are usually to be used in structural aseismic analysis. Enough number of mode shapes should be selected in order to reflect structure major dynamic properties. Few mode shapes are needed for structures characterized by reasonable stiffness distribution. However, only few mode shapes used in calculation will result in large extent of error for structures characterized by abrupt change in horizontal connection stiffness. The major reason lies in differences between mode shapes' curve. The structure characterized by abrupt change in horizontal connection stiffness has marked characteristics of mode shapes, such as many hybrid, interlocked and torsional modes. An uniform formula which can be used to determine number of mode shapes used in calculation is not given in this paper. But two principles are suggested for determining number of mode shapes used in calculation. One is that entirely deformation should be reflected in selected mode shapes, the other is that complicated mode shapes including hybrid, interlocked and torsional modes should be used in calculation. The last principle is specified for structures characterized by abrupt change in horizontal connection stiffness.

Stress concentration located in place of abrupt change in horizontal connection stiffness under horizontal earthquake motion can be given by finite element method. But small size element distribution in place of abrupt change in horizontal connection stiffness must be used in order to get precision results. We also pay attention to determination of member's stiffness located in place of abrupt change in connection stiffness. Small stiffness demand is given base on earthquake energy dissipation and slight stress concentration, which will result in large structure horizontal displacement. On the other hand, large stiffness demand is given based on small horizontal displacement, which will result in low energy dissipation capability and acute stress concentration. The above problems will be discussed in detail in following paper by numerical experiments based on project of Putian Center of Radio, Film and TV, China.

NUMERICAL CALCULATION

Structure and Finite Element Model

Putian Center of Radio, Film and TV, China is a multifunctional high-rise building. The total building area of the project is about 13560 square meters. It consists of main building and skirt building. Standard floor of the building is shown in figure 1. The building's plane layout is two connected polygonal tubes. The main building is composed of two stories underground and fifteen stories aground, which has frame-shear-wall structural system. The big tube of the main building is 59.4 meter high, while the small tube of the main building is 69.3 high including a turret. The first story aground is 4.8 meter high and the standard story height is 3.6 meter.

Characteristics of abrupt change in horizontal connection stiffness are marked because of connection of the big tube and the small tube of the main building, as shown in figure 1. Plate and beam members are used where the big tube is transferred to the small tube. Obviously, abrupt change in horizontal connection stiffness has considerable effects on structure dynamic properties, and most of important is acute stress concentration located in place of the connection of the big tube and the small tube under earthquake motion. In order to research this problem, the structure is simulated by means of discrete finite elements. Floor slabs and shear walls are simulated by discrete plate elements, while beams and columns are simulated by beam elements. Then we get the calculating model of finite element shown in figure 2.

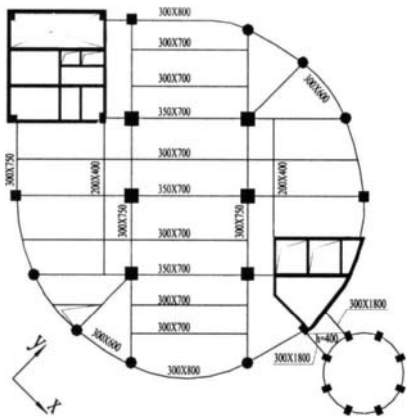


Figure 1: standard story planar graph

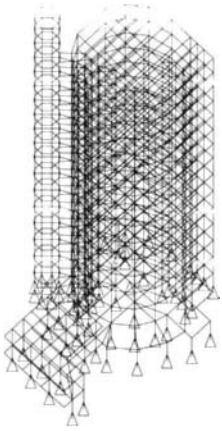


Figure 2: structural finite element modal

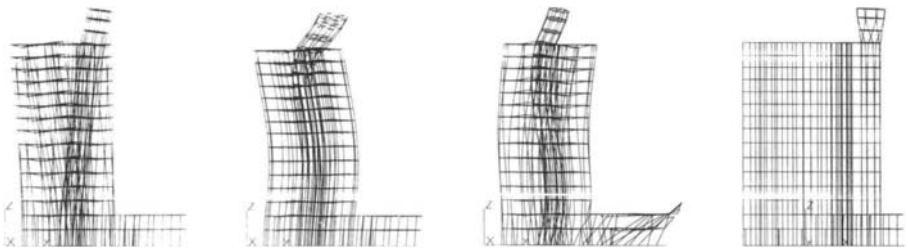
Structure Dynamic Properties

In order to research effects caused by abrupt change in horizontal connection stiffness on structural dynamic properties, mode shapes calculation of the structure is performed firstly. The first tenth natural frequencies and periods are given in table 1. We can discriminate natural period in coordinate direction and natural period of torsional vibration. Fundamental natural period in x direction is 1.339 second, and 1.482 second in y direction. Similarly, fundamental natural period of torsional and vertical vibration are respectively 0.854 and 0.226 second.

TABLE 1
THE FIRST TENTH NATURAL FREQUENCIES AND PERIODS OF THE STRUCTURE

Mode shape	1	2	3	4	5	6	7	8	9	10
Frequency(Hz)	0.675	0.747	1.172	2.452	2.904	3.505	3.803	4.015	4.430	4.659
Period(s)	1.482	1.339	0.854	0.408	0.344	0.285	0.263	0.249	0.226	0.215

We find many kinds of complex and partly mode shapes of the structure which include relative movement of the big tube and the small tube, partly torsion and so on. These mode shapes are caused by abrupt change in horizontal connection stiffness. Some mode shape graphs are shown in figure 3, which clearly illustrate relative movement, partly torsion and translation.



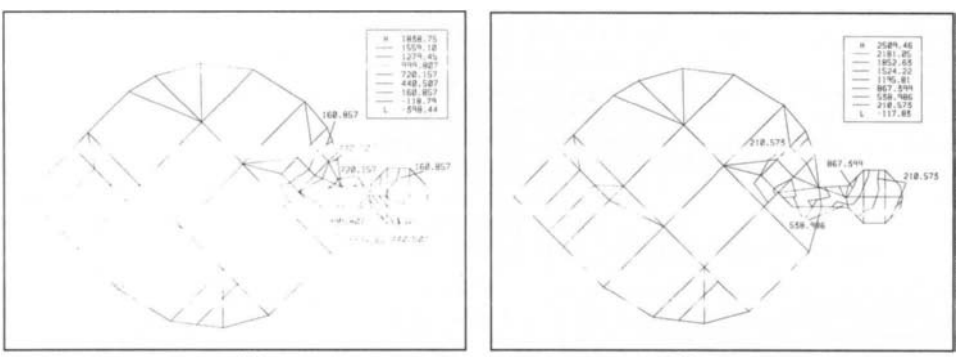
3rd mode(y-z plane) 6th mode(y-z plane) 7th mode(y-z plane) 12th mode(x-z plane)

Figure 3: Some mode shapes of the structure

Horizontal Seismic Response Analysis

Response spectra method is used to calculate horizontal seismic response of the structure in this paper. The first 30th mode shapes including the complex mode shapes caused by abrupt change in horizontal connection stiffness are considered to ensure level of accuracy. Stiffness in y direction is lower than that in x direction, so only seismic response of the structure in y direction is discussed in this paper.

Calculating results illustrate that horizontal displacement is major deformation and torsional deformation is very small under earthquake motion in y direction. The top floor's horizontal displacement is about 0.0244 meter and the maximum displacement between adjacent floors is 0.00196 meter which located in the 17th floor of the small tube. The magnitude contours of stress in plane of floor slabs are shown in figure 4. Distributions of magnitude contour clearly illustrate acute stress concentration located in the connection of the big tube and the small tube. The maximum shearing stress and the positive stress in x and y directions are respectively 1177.00 KN/m^2、1838.75 KN/m^2 and 2509.46KN/m^2. Most of important, places which turn up these maximum values are all located in connection of the big tube and the small tube.



(a) σ_x (b) σ_y

Figure 4: Magnitude contour distribution of positive stress of 15th floor slabs

Acute stress concentration located in place of abrupt change in horizontal connection stiffness is revealed in extent of elasticity. It can be inferred that members located in place of abrupt change in horizontal connection stiffness will possibly become key members of energy dissipation, when the structure go through nonlinear range under strong earthquake motion. Therefore a key problem is how to handle the connection of members in the place. Effects of different connective members on structure

seismic response will be studied by finite element numerical experiments in following paper. Obviously, the big tube isn't connected to the small tube when stiffness of the connection members is infinitely small, which becomes another structure plan.

COMPARISONS OF DIFFERENT CONNECTIVE PLANS

Structure Plan of Separated Tube

Because of acute stress concentration caused by abrupt change in horizontal connection stiffness, the possibility of removing the connective members is easily considered. The calculating results illustrate that structure plan of two independent tubes without connectivity improves dynamic properties and reduce dynamic response of the big tube. The small tube's fundamental natural period and maximum displacement under horizontal earthquake motion and wind loading are given in table 2. At the same time, the above values of the connected tubes are also given in table 2.

TABLE 2
COMPARISON OF DIFFERENT STRUCTURE PLANS

Name	Fundamental natural period(s)	Maximum displacement under earthquake motion(m)	Maximum displacement under wind loading(m)
The small tube	3.179	0.0585	0.1196
The connected tubes	1.482	0.0244	0.0222

The independent small tube has smaller stiffness and longer natural period than those of the connected tubes, as shown in table 2. Moreover, maximum displacement of the small tube under horizontal wind loading is unaccepted. In other words, the small tube must not be built independently and the connective members can't be removed.

Comparisons of Different Stiffness of the Connective Members

We have demonstrated that the connective members can't be removed, but there is a key problem about how to choose stiffness of the connective members. In general, stiffness variety of the connective members has considerable effects on natural period, horizontal displacement and stress concentration of the structure. Three kinds of stiffness of the connective members are used to calculate the structure seismic response in y direction in this paper, as shown in table 3.

TABLE 3
COMPARISONS OF DIFFERENT STIFFNESS OF THE CONNECTIVE MEMBERS

Stiffness of the connective members		Enlarging stiffness by 100 times	Design stiffness	Neglecting stiffness of the connective floor slabs
Fundamental Natural period (s)		1.476	1.482	1.491
Maximum displacement under earthquake motion (m)		0.0240	0.0244	0.0257
Maximum stress in plane of the connective floor slabs (KN/m^2)	σ_x	2548.02	1838.75	——
	σ_y	2845.44	2509.46	——
	τ_{xy}	1076.83	1177.00	——
Maximum stress of the connective beams (KN/m^2)		250.46	1949.63	7543.52

Results given in table 3 show that there isn't marked influence on structure fundamental natural period and maximum horizontal displacement if stiffness of the connective members is limited to certain range. The above results are given based on the fact that stiffness of the big tube is much larger than that of the small tube. By comparison, stiffness variety of the connective members has important influence on inner forces of the connective members. The increment of the connective members' stiffness maybe gives rise to acute stress concentration because of the increment of allocated earthquake loading. In regard to neglecting stiffness of the connective floor slabs, the maximum stress has great increase because the connective beams must resistant earthquake loading independently.

CONCLUSIONS

Dynamic properties and seismic response of RC structure characterized by abrupt change in horizontal connection stiffness are studied in this paper. Different structure plans and stiffness of the connective members are discussed based on finite element numerical experiments. Finally, we can get some conclusions as followed.

The structure characterized by uniform stiffness distribution has advantages of clear and definite transmission channel of earthquake loading. By contrast, the structure characterized by abrupt change in horizontal connection stiffness has disadvantages of complex mode shapes and acute stress concentration under earthquake motion.

The number of mode shapes in calculation must be selected carefully in seismic response analysis by method of response spectra analysis. Complex and partly mode shapes caused by abrupt change in horizontal connection stiffness must be contained in calculation. In addition, denser discrete elements located in place of abrupt change in horizontal connection stiffness should be used to ensure accuracy of stress field.

Stiffness of the connective members should be determined carefully in design. In general, stiffness of the connective members should be limited to a certain range. It will lead to acute stress concentration if stiffness of the connective members increases blindly. Moreover, there isn't obvious influence on structure horizontal displacements and fundamental natural period under earthquake motion.

This paper is limited to discuss linear elastic behaviors of RC structure characterized by abrupt change in horizontal connection stiffness. Nonlinear behaviors of the structure under strong earthquake motion will be studied in other papers.

References

Jingbo Liu and Yong Wang.(2000). Dynamic properties and seismic response of high-rise building with podium. *China Journal of Building Structures* **21:2,** 36-43

Jingbo Liu, etal.(2001). Preliminary study on seismic responses of large-span brick and concrete mixed structures. *China Earthquake Engineering and Engineering Vibration* **21:4,** 67-72

Jumin Shen, etal.(2000), *Aseismic Engineering*, China Architecture and Building Press

Kunyao Huang, etal.(2001). Influence of the connection stiffness on seismic response of the double-tower connected tall building. *China Journal of Building Structures* **22:3,** 22-26

Advances in Building Technology, Volume 1
M. Anson, J.M. Ko and E.S.S. Lam (Eds.)
© 2002 Elsevier Science Ltd. All rights reserved

A GIS SYSTEM INTEGRATED WITH VULNERABILITY FOR SEISMIC DAMAGE AND LOSS ESTIMATION OF HONG KONG

H.S. Lu[1], Z.P. Wen[1], K.T. Chau[2] and Y.X. Hu[1]

[1]Institute of Geophysics, China Seismological Bureau, Beijing, China
[2]Department of Civil and Structural Engineering, The Hong Kong Polytechnic University, Kowloon, Hong Kong, China

ABSTRACT

Estimation of damage and loss of a region due to earthquakes is of primary importance for disaster planning, mitigation and rehabilitation purposes. For regions of moderate seismicity, like Hong Kong, the social awareness of the potential risk of infrequent but high consequence events is very low. In this paper, a GIS is integrated with a simple vlnerability for reinforced concrete structures for estimating the seismic damage and loss for Hong Kong both in terms of deterministic scenario earthquake and probabilistic earthquake risk. This system is the first of this kind for Hong Kong. Two urban districts in Hong Kong, Tsim Sha Tsui East and Wanchai, are chosen for our preliminary analysis. Digital map developed by the Lands Development Department is adopted and modified, while the building inventory was initially supplied by Centaline Property Agency Limited which was subsequently updated and expanded for our purposes to include, building usage, number of story, and damage probability matrix. The evaluation of seismic hazard in the areas has been performed using the scenario earthquake and probabilistic approach. Earthquake intensity and response spectrum are used as input. The vulnerability of buildings is estimated by means of theoretical approach based on the modal response analysis. Seismic risk and loss are evaluated corresponding to 63%, 10% and 2% probability of exceedence in 50 years. Distribution of earthquake damage and loss under different ground motions are presented and managed by relational database management system in GIS. In addition, empirical formulas have been adopted to yield direct economic losses for both the deterministic and the probabilistic approach.

KEYWORDS

GIS, Vulnerability, Scenario earthquake, Risk, Hong Kong, Seismic damages, Loss, Digital map

INTRODUCTION

In the last few decades, civil engineering structures in many big cities become denser than ever due to the rapid population and economic growth. If earthquake hits such a metropolitan area, it may lead to catastrophe. The aftermath of the 1995 Kobe earthquake provides a vivid example on the problems associated with a densely populated city under the attack of a strong earthquake. For big cities like Kobe and Hong Kong, the seismic risk assessment and management is only feasible by using GIS based system, which should incorporate all inventory of buildings and lifelines. Such system can be

used for prediction of future earthquake damage and loss, therefore it can support the seismic risk management by government agencies and by insurance companies Tasumi et al. (1992).

Using GIS, a program called RADIUS has been resulted from an initiative of the United Nation's International Decade for Natural Disaster Reduction (IDNDR) with financial assistance from the Japanese Government. This program has been carried out for seismic risk assessment of nine different cities worldwide (Ababa in Ethiopia; Antofagasta in Chile; Bandung in Indonesia; Guayaquil in Ecuador; Izmir in Turkey; Tashkent in Uzbekistan; Skopje in Macedonia; Tijuna in Mexico; and Zigong in China). In USA, the most popular GIS based system is the HAZUS99, which was originally proposed by the Federal Emergency Management Agency (FEMA, 1999). Such system has also been found useful in assessing seismic risk in other countries, such as Turkey. The evaluation of seismic damages in HAZUS99 bases primarily on ACT-13 (ATC, 1985) through the use of damage probability matrix.

Although HAZUS99 has been found useful in USA and other some countries, it cannot be used directly for the case of Hong Kong. One main problem is that the available vulnerability matrices in the HAZUS99 are not suitable for Hong Kong. In particular, there are for 16 different building types and, according to different story number, these are further subdivided into 36 building categories. According to this system 1-3 story buildings are identified as "low-rise", 4-7 story buildings are identified as "mid-rise", and 8 story or up buildings are identified as "high-rise". In Hong Kong, over 90% of the buildings are more than 8 stories. Probably, buildings over 26 stories in Hong Kong will be considered as "high-rise". Even so, many of these so-called buildings are of different structural forms and different design philosophy. Another issue of using HAZUS99 GIS system is that it is location dependent. That is, all local digital maps and building inventory are unique for different locations. Therefore, there is no such thing as simply modify the existing HAZUS99 system from USA to Hong Kong. All GIS programming has to be started from scratch.

In view of this, there is no advantage of using HAZUS99 system over any other system. More importantly, the vulnerability matrices of building available from HAZUS99 cannot be used. Thus, in this study a new GIS system (HKEHAS) is developed for Hong Kong. Limited by time and resources constraint, the present study only cover two districts in Hong Kong, namely, Wanchai and Tsim Sha Tsui (TST) East. These two areas are chosen because there are many different variety of buildings within these two areas. They include old pre Second World War buildings, medium age and mid-rise residential buildings (from 10 to 20 stories), mid-rise to high-rise new commercial buildings (including the tallest building in Hong Kong—The Central Plaza), sport stadium, temples and churches, markets, museums and schools.

Regarding the calculation of the seismic vulnerability of existing buildings in Hong Kong, there is a high uncertainty involved. All Hong Kong buildings are designed according to wind loads, while no special attention paid to reinforcement detailing. Typical new commercial and residential buildings are highly non-symmetric in both vertical stiffness distribution and structural forms, due to architectural requirement and the use of transfer-plate system to open up lower floor space for shopping mall or parking. The demand and capacity curve concept used in HAZUS99 assumes all buildings as single-degree-of-freedom (SDOF) oscillators, which is clearly too restrictive for most Hong Kong buildings. At this moment, it seems that no reliable and mature mathematical models available for estimating the earthquake resistance of buildings built according to wind code with no seismic provisions. Clearly, much works need to be done in this area.

In this study, we do not attempt to solve this complicated problem completely. Instead, a very simple approach developed by Yin (1995) will be adopted. The main feature of such approach is that the vulnerability of the structures depends on the total sectional areas of load bearing columns and shear wall. For the case of Hong Kong, the stiffness and ductility of wind-designed buildings can be taken into account appropriately. Another beauty of the present approach is that the local "high-rise" buildings are modeled more realistically as multi-degree-of-freedom (MDOF) oscillators, instead SDOF oscillators. A n-story building will be modeled as a n-DOF oscillator. The maximum seismic shear demand at

each story level can be estimated and checked against the story shear capacity, estimated from the total load-bearing sections of columns and walls. For simplicity, only a small number of building classifications have been used here.

Nevertheless, the present study provides the first preliminary seismic risk and loss analyses using a GIS based system for Hong Kong. In addition, the present approach is quite compatible that applied to the seismic damage-loss estimation and disaster mitigation of many mainland Chinese cities, such as Urumqi (the capital of the Xinjiang Uygur Autonomous Region). The only differences arise from the vulnerability calculation and building categorization. One of the beauties of the GIS system is that the building inventory can be changed with time, the property price as well as the population can be revised, and, more importantly, a more accurate prediction for the damage probability matrix can be incorporated at any time. It is hoped that the present study can provide a framework for future seismic risk and loss assessment and management of Hong Kong.

FRAMEWORK OF SEISMIC DAMAGE AND LOSS ESTIMATION

Seismic hazard and risk are related but distinct concepts that need explanation. In earthquake engineering, hazard is related the probability of exceeding certain level of ground motion at a site, while risk is the probability of damage of a building exposed to and subjected to such hazard. If a building is more vulnerable to earthquake attack, it is more likely to suffer damages during earthquake. In mathematical terms, we have (Hu, 1998; Hu et al., 1996):

$$SR = SH(P/I) * \sum [VUL(D/I) * (DL(D) + SL(D)) * (1 + ID) * EXP] \quad (1)$$

where

EXP = exposure or everything subject to the attack of the earthquake (e.g. all items in natural, man-made, engineering and social environments);

SR= seismic risk in terms of damage-loss of the exposure;

SH(P/I) = seismic hazard on the exposure, in terms of probability P of the earthquake intensity I;

VUL(D/I) = vulnerability of the exposure, in terms of probability of damage D for intensity I;

DL(D) = direct loss-damage transfer matrix, as a function of damage D;

SL(D) = secondary or induced loss of the exposure item, as a function of damage D;

ID = indirect loss due to DL and SL (e.g. number of injury, number of death and monetary loss);

* = convolution operator or matrix multiplication;

Σ = summation over all items of exposure in an area.

However, the risk analysis conducted in the present study concerns only buildings and considers only direct economic loss due to building damage. The comprehensive frame of damage and loss estimation methodology can be outlined in Figure 1. As shown in Fig.1, the framework of risk analysis includes three components: seismic hazard (including the site condition), exposure inventory (or buildings), and vulnerability analysis (structural behavior). The final damage stages of large amount of buildings of different categories at different site conditions can be presented and managed by a GIS, which will be discussed in later section.

First, the building inventory is classified into different categories. Once the ground motion parameters are chosen, the corresponding vulnerability matrices will be assigned to each building category according to the risk level specified, far or near field earthquake, ground parameters, and site condition. For seismic load input, we can use either probabilistic or deterministic approaches. Each of these will be discussed briefly next.

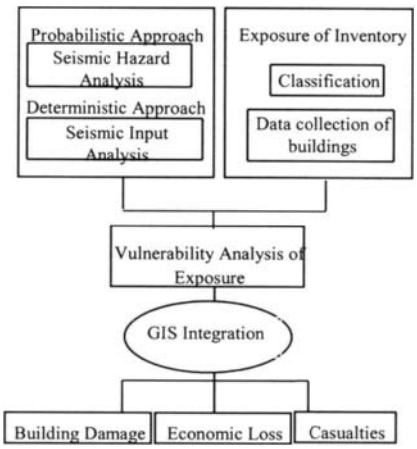


Figure 1: Seismic loss Calculation Flowchart

SEISMIC RISK BY DETERMINISTIC SCENARIO EARTHQUAKES

For scenario earthquake input, one has to assume the location, magnitude, and focal mechanism of an earthquake. The attenuation relation for either intensity or ground motions should also be input, together with the local site characteristics period and soil conditions. A response spectrum associated with the estimated macroseismic intensity or magnitude of shaking should also be included. The probability distribution of building damage at different levels can be determined by considering the structural response modeled by MDOF oscillators. In the present study, we follow the most commonly adopted 5-lvevl of damages stages. These damage stages are shown in Fig. 2.

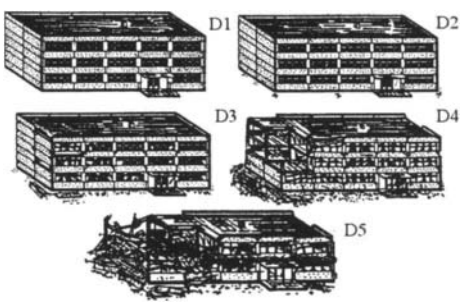


Figure 2: Five levels of damage stages, defined as: D1=none; D2=slight; D3=moderate; D4=extensive; and D5=complete.

The user can either create an event based on a historical earthquake epicenter, create an event from a map of potential source zones around Hong Kong, or create a scenario event by selecting a completely arbitrary epicenter. To help the user, we have input the potential seismic sources around Hong Kong in our GIS, together with the maximum creditable earthquake magnitude (see Fig. 3). Then, the

ground-shaking hazard is displayed as an intensity map over the studied region for a prescribed scenario earthquake. For a given event, attenuation relation by Wang et al. (1988) is used to calculate ground shaking macroseismic intensity.

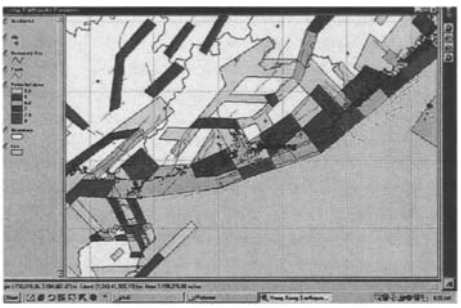


Figure 3: Potential seismic sources displayed in our GIS system HKEHAS.

Seismic vulnerability analysis

The reliability of a seismic risk analysis depends mainly on the vulnerability analysis for buildings. In this study, we modify Yin's (1995) method to obtain the damage probability matrices $P(D_j|I)$ in terms of intensity I, allowing for variations of local site conditions. The site-specific design response spectrum and inelastic building capacity was developed to describe the building damage (Wen et al, 2002). In particular, with the estimated ground shaking or macroseismic intensity and given soil condition, a simple model is used to estimate distribution of the ductility factor μ, which is estimated from the ratio of story yield shear to inter-story seismic shear. Note that $\mu > 1$ for inelastic deformation of buildings. The full details of this method are referred to Wen et al. (2002). These predicted nonlinear responses of building are used to obtain probability of the extent of damage to buildings. These damage estimates are expressed in terms of the probability $P(D_j|I,SC)$ that building is in one of the five damage states: none, slight, moderate, extensive, and complete damage. Sometimes, it is more information to express the probability of damages in a cumulative from:

$$P^*(D \geq D_j) = 1 - \sum_{i=1}^{j-1} P(D_i / I, SC) \tag{2}$$

The plots of $P^*(D \geq D_j)$ are normally referred as fragility curves.

Estimation of economic losses method

After completing the vulnerability analysis by combining the inventory and hazard, direct loss due to building damage, economic loss and casualties can be evaluated. In particular, the preliminary economic losses from the earthquake can be calculated by simple summing all building loss in the region. The losses are the results of combining the PDM (probability damage matrices), damage ratio, and values of the buildings. The expected economic loss of the buildings is obtained by

$$EL = \sum_{I} \sum_{D_j} P[D_j|I,SC] \cdot b_s(D_j) \cdot B_s \tag{3}$$

where $P[D_j|I,SC]$ is probability of building experiencing damage state D_j for intensity I and on the site condition SC; b_s is mean damage factor (percent) for building experiencing the damage state D_j. In the present study, the mean damage factors for none, slight damage, moderate, extensive and complete

damages are set as 0%, 7.5%, 25%, 55%, 100% respectively, following Ying (1995). The value of the building B_s depends on the market price of the building inventory, which can be adjusted easily in our GIS system HKEHAS.

Estimation of human casualties

The estimation of human casualties in seismic events is one of the main objectives of seismic risk studies. Deaths and injuries are perhaps the most important to government. Protection of life is a primary function of a government and a prime incentive for undertaking hazard reduction. For most civilized societies, it is normally unacceptable to tolerate a very high fatality rate due to any earthquake event. Unfortunately, the ability to predict casualties is not as good as in the case of damage and direct economic loss. Data on which rational, systematic estimates can be made are very sparse (NRC, 1989). There are various ways to predict the number of casualties. One approach is that casualty rates are tied empirically to the damage states of buildings. This methodology can be used on the condition that there are detailed population distributions in the buildings available. Other approach to predict the casualty is to use historical rates of casualties per unit of population for wood-frame dwellings and extrapolated such data for other types of construction. In this way, a city-wide casualty rate can be established from previous earthquake data (Fu and Li, 1993). In the present work, since no detailed population distributions within each category of building are available for Wanchai and TST East, the estimation of fatality is carried out by means of methodologies developed Fu and Li (1993) based on the total population in the studied region. It is assumed that there are only two conditions of casualty from earthquake disaster, i.e., $m_j = 1,2$ corresponding to the conditions of the injuries and deaths respectively. The expected earthquake casualty $R(m_j)$ can be calculated form casualty probability matrix by:

$$R(m_j) = \sum_I P[m_j|I] \cdot B_p \tag{4}$$

where $P[m_j|I]$ is casualty probability matrix and B_p is total population in the region of study. Based on Yin (1995), the following values have been assumed for the injured at various seismic intensity: 5.4×10^{-4}(VI), 53×10^{-4}(VII), 460×10^{-4}(VIII), 4000×10^{-4}(IX); for death rate at various seismic intensity: 0.14×10^{-4}(VI), 3.1×10^{-4}(VII), 48×10^{-4}(VIII), 680×10^{-4}(IX).

SEISMIC RISK BY PROBABILISTIC ANALYSIS

The second type of risk analysis uses a probabilistic approach. The probabilities for various levels of loss being exceeded are estimated. It is important to realize that a particular loss data may result from earthquakes of different characteristics, for example, from a nearby earthquake of moderate size or from a distant earthquake of larger magnitude. Except for the initial phase of analysis, the loss produced by probabilistic seismic hazard is estimated using a procedure similar to scenario earthquake estimate, and therefore the details will not be repeated here. Only main differences will be discussed.

Probabilistic seismic hazard analysis provides a framework in which the uncertainties in size, location, and rate of recurrence of earthquakes can be avoided and results presented in a more rational manner to provide a more complete picture of the seismic hazard (Kramer, 1996). In the probabilistic approach, ground shaking may be characterized by response spectrum. The methodology includes ground shaking at three different hazard levels: 63%, 10% and 2% probability of being exceeded in 50 years. These probabilities of exceedance correspond to a return period of 50, 475 and 2475 years respectively.

In the present study, the probability distribution of building damage among different damage states for reinforced concrete structures are given as a function of response spectrum. The equivalent static force

method is used to estimate the ductility factor distribution of different types of buildings at a specified probability. Similar to the scenario case, the distributions of ductility factor for none, slight, moderate, extensive and complete damages to building are denoted by $P[D_j|S_a(T)]$, with the only difference being using response spectrum as input. Similarly, the probable damage to buildings can be expressed as exceedance probability $P^*(D \geq D_j)$. The estimation of economic loss is again very similar and can be given as

$$EL = \sum_{D_j} P[D_j|S_a(T)] \cdot b_s(D_j) \cdot B_s \tag{5}$$

where $P[D_j|S_a(T)]$ is probability of building experiencing damage state D_j in case of ground shaking $S_a(T)$; and all other parameters are the same as those given for equation (3).

Again, the data can be used for predicting deaths and injuries are very sparse, and considerable judgment is necessary in organizing available information to estimate casualties. There is no reliable and well accepted relation between casualty rate and probabilistic response spectrum which specifies the level of seismic hazard since the casualty rate must also depend on the structural response. In this study, we will simply correlate the designed peak ground acceleration to macroseismic intensity by using empirical relation adopted by CSB. It should be pointed that the conversion is very crude, and it is intended to yield some ideas only.

HKEHAS—A GIS SYSTEM FOR RISK ASSESSMENT

For hazard and disaster mitigation and management, there is a need to manage all data of potential damages in a graphical and user-friendly way for planning. Geographical Information System (GIS) has been a popular choice for seismic risk management, as it has been used for HAZUS99 and other systems. In the present study, ArcView GIS system of the ESRI was used since the digital map of the Hong Kong is available under software. All programming is made primarily using "Avenue" of ArcView. We will not, however, discuss the architecture as well as the development of our system HKEHAS (stands for Hong Kong Earthquake Hazard Analysis System).

A total of 1431 buildings have been included in our database system within Wanchai and TST East. All building data include the story number, the year of building, the usage of the building, and the site condition. Buildings are classified as residential, commercial, school, hotel, and museum. For residential buildings, 3 sub-categories are 1-7, 8-16 and 17-50 story; for commercial buildings, 3 sub-categories are 1-16, 17-40 and 41-80 story; for hotels, 2 sub-categories are 4-16 and 17-50. Therefore, a total of ten categories of buildings are used. More idealized categorization should consider the structural responses of buildings under seismic loads. With the limited knowledge on how Hong Kong buildings may perform under seismic attack, we cannot classify our buildings according to structural performance or damage potentials. Further works are required in this direction.

More detailed parametrical studies have been done, but we also aware of the fact that there is large uncertainty regarding the vulnerability of existing buildings in Hong Kong. Thus, these analyses will not be discussed here. In fact, the most important contribution of the present work lies on the introduction of a new GIS system for Hong Kong. Once a more reliable theoretical model is developed for estimating the vulnerability matrix of the existing Hong Kong buildings, the system can be updated by simply replacing the old vulnerability matrix with a more reliable one.

CONCLUSIONS

This paper has briefly described a procedure for calculating regional damage, loss and casualty, integrating information on regional earthquake hazard, site condition, building inventories, population inventories, and building damage functions by a new GIS system under the ArcView platform. Applica-

tion of the procedure to Wanchi and TST East in Hong Kong has provided preliminary results that show the potential of the present GIS system—HKEHAS. This system provides the first ever GIS based system for seismic risk management for Hong Kong, and which will be extremely useful for policy maker of government and insurance companies in the future.



Figure 4: A typical display of the probable damage distribution for Wanchai

ACKNOWLEDGEMENTS

The research was supported by ASD funding of the Hong Kong Polytechnic University through Project A214—Earthquake Risk Assessment and Reliability Analysis Using GIS. We are grateful to Centaline Property Agency limited for providing a preliminary database for Hong Kong building inventory.

REFERENCES

ATC (Applied Technology Council) (1985). Earthquake Damage Evaluation data for California (ATC-13) Redwood City, CA.

FEMA (Federal Emergency Management Agency) (1999). Earthquake Loss Estimation Methodology, HAZUS 99: Technical Manual. Washington, D.C.

Fu Z. and Li G. (1993). *Report on Casualties Due to Earthquakes.* Seismological Press.

Hu, Y. (1998). *Earthquake Disaster Mitigation & Engineering Seismology.* IUGG/SSB International raining Course on Continental Earthquakes and Seismic Hazard, 70pp., Beijing, China.

Hu Y., Liu S.C. and Dong W.M. (1996). *Earthquake Engineering.* E & FN SPON, Chapman & Hall.

Kramer S.L. (1996). *Geotechnical Earthquake Engineering.* New Jersey: Prentice-Hall

NRC (National Research Council) (1989). Estimating losses from further earthquakes. (Washington, DC: National Academy Press)

Tasumi Y., Sugimoto M. and Seya. H. (1992) A seismic damage evaluation system for buildings. *Proc. 10th World conference of Earthquake Engineering.*

Wang S.Y., Liu H.Y., Wang Y.C. and Wu C.Y. (1988). The attenuation relationship for ground shaking parameters in the region of southern China. *Publication as Theme of Earthquake Research for Northern Hainan Island.* Seismological Press (in Chinese), 1988, 284-293.

Wen Z.P., Hu Y.X. and Chau K.T. (2002). Site effect on vulnerability of high-rise shear wall-buildings under near and far field earthquakes. Submitted to *Soil dynamics and Earthquake Engineering.*

Yin Z. (1995). *The Method of Seismic Damage and Loss Prediction.* Beijing: Seismological Press (in Chinese).

Advances in Building Technology, Volume 1
M. Anson, J.M. Ko and E.S.S. Lam (Eds.)
© 2002 Published by Elsevier Science Ltd.

RULES OF DRIFT DECOMPOSITON AND DRIFT-BASED DESIGN OF RC FRAMES *

Luo Wenbin Qian Jiaru

Department of Civil Engineering, Tsinghua University
Beijing, 100084, CHINA

ABSTRACT

In this paper, a drift-based design approach for RC frames is presented. Introducing the collapse mechanism factor χ as a pivotal indicator of the desirable collapse mechanism, the rules of drift decomposition are developed. By decomposing the target drift of the structure, the deformability demands of the columns and beams are determined. For detailing the columns and beams to meet the deformation demands, the $\theta_c^u - n - \lambda_{sv}$ diagram and $\mu_{b\delta} - \varepsilon_{cu} - \lambda_{sv}$ relations are proposed.

KEYWORDS

Drift decomposition; Drift-based design; Deformability; RC frame

INTRODUCTION

As is known, the displacement-based design approach begins with establishing a target displacement which is consistent with the selected performance objectives of the structure subjected to the expected intensity level of earthquake, and the capacity of the structure should conform to the anticipated target displacement or drift. It is now believed that the inter-storey drift ratio is a preferable performance criterion of RC frames. However, in realistic practice of the displacement-based seismic design of RC frames, three key issues must be solved. One is to predict the target drift ratio of the frame. The second

* Supported by the National Natural Science Foundation of China (No. 59895410)

is to determine the relationship between the drift ratio and the deformation of each member. The third is to ensure the deformability of members to meet the deformability demand when the frame reaches the target drift ratio.

The objectives of this study are to establish the drift decomposition rules for RC frame, and to develop the deformability design method for columns and beams. Then a drift-based design procedure is proposed.

TARGET DRIFT OF FRAME

For multi-storey frames, assuming that the anti-flexural point of beam or column is located at its mid-span or its mid-height, the inter-storey drift can be represented by the deformation of a typical beam/column sub-assemblage. As shown in Figure 1, the drift ratio θ of the frame is defined as the ratio of the inter-storey drift to the height of the storey, as follows:

$$\theta = \delta / h \tag{1}$$

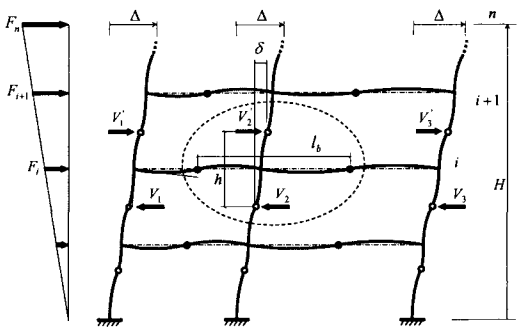


Figure 1: drift of frame and sub-assemblage

Based on the analysis of extensive experimental database of beam/column sub-assemblage, Priestley (1998) suggested an expression for the yield drift ratio θ_y in the form:

$$\theta_y = 0.5 \cdot \varepsilon_y \cdot (l_b / h_b) \tag{2}$$

in which, ε_y is the yield strength of longitudinal reinforcement of beam, l_b and h_b is the span length and the section depth of beam respectively. From Eqn.(2), the yield drift δ_y can be obtained.

Then the target drift ductility ratio μ_δ can be estimated as:

$$\mu_\delta = \delta_u / \delta_y \tag{3}$$

where δ_u is the target drift corresponding to the selected performance objectives. Many researches have been focused on the determination of the target drift or the target displacement, more detailed discussion can be found in Whittaker (1998).

RULES OF DRIFT DECOMPOSITION

Components of drift

Figure 2 shows that the drift of RC frames is the sum of drift due to the deformation of related beams, columns and joint, and the drift is composed of elastic drift and inelastic drift. Each of them could be expressed as:

$$\delta_y = \delta_b^y + \delta_c^y + \delta_{jV} \tag{4}$$

$$\delta_p = \delta_b^p + \delta_c^p + \delta_{js} \tag{5}$$

where δ_y and δ_p are yield drift and inelastic drift respectively, δ_b^y and δ_c^y are the contribution of elastic deformation of beam and column to δ_y, δ_b^p and δ_c^p are the contribution of inelastic deformation of beam and column to δ_p, δ_{jV} and δ_{js} are the contribution of shear deformation of joint core and bond slip of longitudinal reinforcements in core region to δ_y and δ_p respectively. The contribution of each component depends on the relative stiffness, relative strength and deformability of the beam, column and joint core.

Target Ductility Ratio of Members

According to the definition, the contribution of column and beam deformation to the target drift ductility ratio of the frame could be expressed as:

$$\mu_{c\delta} = \frac{\delta_c^y + \delta_c^p}{\delta_c^y} \Rightarrow \delta_c^p = (\mu_{c\delta} - 1)\delta_c^y \tag{6}$$

$$\mu_{b\delta} = \frac{\delta_b^y + \delta_b^p}{\delta_b^y} \Rightarrow \delta_b^p = (\mu_{b\delta} - 1)\delta_b^y \tag{7}$$

Given

$$\alpha_b \equiv \frac{\delta_b^y}{\delta_y}, \alpha_c \equiv \frac{\delta_c^y}{\delta_y}, \alpha_{js} \equiv \frac{\delta_{js}}{\delta_p} \tag{8}$$

Substituting Eqns. (6) and (7) into Eqn. (5), gives:

$$\delta_p = \frac{(\mu_{b\delta} - 1)\alpha_b + (\mu_{c\delta} - 1)\alpha_c}{(1 - \alpha_{js})}\delta_y \tag{9}$$

The drift ductility ratio of the frame can be written as:

$$\mu_\delta = \frac{\delta_y + \delta_p}{\delta_y} = 1 + \frac{(\mu_{b\delta} - 1)\alpha_b + (\mu_{c\delta} - 1)\alpha_c}{(1 - \alpha_{js})} \tag{10}$$

Defining the collapse mechanism factor χ to indicate the contribution ratio of column plastic deformation to beam plastic deformation:

$$\chi \equiv \frac{\delta_{cp}}{\delta_{bp}} = \frac{(\mu_{c\delta} - 1)\alpha_c}{(\mu_{b\delta} - 1)\alpha_b} \tag{11}$$

For RC frames designed according to the requirements of "Code for seismic design of buildings" (GBJ50011), with column overstrength factor η_c of 1.4, analytical results reveal that the collapse mechanism factor χ is about 0.24 when drift ductility ratio reaches 4. Based on a series of analysis, the relations between the collapse mechanism factor and column overstrength factor at different ductility levels are shown in Figure 3.

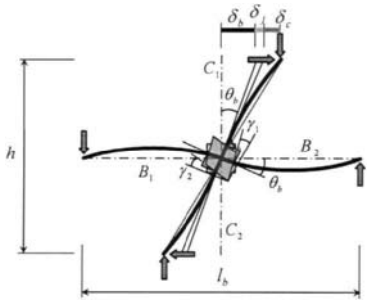


Figure 2: Drift decomposition of beam/column assemblage

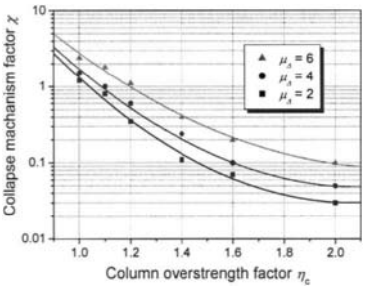


Figure 3: Relationship of $\chi - \mu - \eta_c$

The contribution of column and beam to the drift ductility ratio is obtained by substituting Eqn. (11) into Eqn. (10):

$$\mu_{c\delta} = 1 + \frac{(1-\alpha_{js})}{(1+1/\chi)\alpha_c}(\mu_\delta - 1) \tag{12}$$

$$\mu_{b\delta} = 1 + \frac{(1-\alpha_{js})}{(1+\chi)\alpha_b}(\mu_\delta - 1) \tag{13}$$

Clearly, Eqns. (12) and (13) show that the relationship between the contribution of members and the drift ductility ratio of frame is related to $\alpha_b, \alpha_c, \alpha_{js}$ and η. For a code based beam/column assemblage, the test results indicated that $\alpha_b = 56\%$, $\alpha_c = 19\%$, $\alpha_{js} = 13\%$. In this case, for the above mentioned frame with $\chi = 0.24$, the ductility ratio demand of beams would be:

$$\mu_{b\delta} = 1 + (1 - 0.13)(\mu_\delta - 1)/0.69 = 1.26\mu_\delta - 0.26 \tag{14}$$

It is found that the collapse mechanism factor χ, which depends on the column overstrength factor and drift ductility of the frame, is a very important parameter for determining the ductility demand and target deformability. Practically, coefficients α_b and α_c can be calculated by the elastic analysis, and α_{js} could approximately be taken 10% for normally proportioned beam-column joint.

DEFORMABILITY DESIGN OF MEMBERS

After the collapse mechanism factor χ is selected according to the expected collapse mechanism, with the target drift ductility ratio of the assemblage, the ductility demand of columns and beams can be evaluated by Eqns. (12) and (13).

Deformability of column and $\theta_c^u - n - \lambda_{sv}$ equations

According to the ductility demand of column $\mu_{c\delta}$ and the yield drift of column δ_c^y in the form of

$$\delta_c^y = \phi_{cy} h_c^2 / 3 \tag{15}$$

the target drift ratio of column θ_c^u is given by:

$$\theta_c^u = \frac{\mu_{c\delta}\delta_c^y}{h_c} = \frac{\mu_{c\delta}\phi_{cy}h_c}{3} \tag{16}$$

where ϕ_{cy} is the yield curvature of column section, h_c is the clear height of column.

The deformability of RC columns mainly depends on the axial compression ratio and transverse reinforcement, which is expressed by $\theta_c^u - n - \lambda_{sv}$ relations in this study. As shown in Eqn. (17), Luo & Qian (2001a) suggested an empirical expression based on the statistic analysis of the column test database, which collected hundreds of RC column test results worldwide. For columns in the database, the axial compression ratio ranged from 0 to 0.9 and the characteristic value of transverse reinforcement was 0.05~0.35. To establish Eqn.(17), the ultimate drift of column was taken as the drift corresponding to the point of strength decreasing 15% from peak strength.

$$\theta_c^u = \left(200 - 100\lambda_{sv} \frac{40}{1+10n} \sqrt{\frac{A_{co}}{A_g}} \right)^{-1} \tag{17}$$

where n is the axial compression ratio, defined as $n = N_c / f_c bh$, N_c is the axial compression force, f_c is the axial compression strength of concrete, b and h are the width and depth of column section respectively. λ_{sv} is the characteristic value of transverse reinforcement, $\lambda_{sv} = \rho_{sv} f_{yh} / f_c$. ρ_{sv} is the volumetric ratio of transverse reinforcement. A_g and A_{co} are the column gross section area and the confined core area respectively.

From Eqn.(17), the characteristic value of transverse reinforcement is obtained:

$$\lambda_{sv} = \left(\frac{200 - 1/\theta_c^u}{100} \right) \left(\frac{1+10n}{40} \right) \sqrt{\frac{A_g}{A_{co}}} \tag{18}$$

Figure 4 illustrates the above equation by $\theta_c^u - n - \lambda_{sv}$ diagram, by which the required characteristic value of transverse reinforcement of column with different axial compression ratio and with different drift ratio can be determined. For instance, a column with cross section dimensions of 800mm×800 mm, cover thickness of 25 mm, C40 concrete and transverse reinforcement yield strength of 310Mpa, the required λ_{sv} values are listed in table 1.

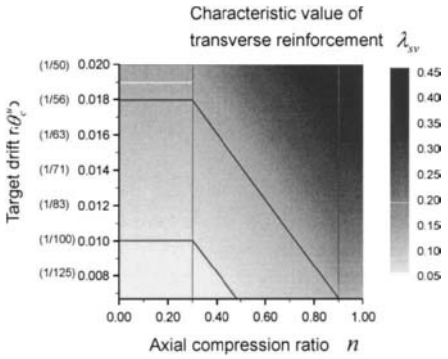


Figure 4: $\theta_c^u - n - \lambda_{sv}$ diagram for RC column

TABLE 1 REQUIREMENTS OF TRANSVERSE CONFINEMENT λ_{sv}

Target drift ratio of columns θ_c^u	Axial compression ratio n					
	0.4	0.5	0.6	0.7	0.8	0.9
1/100	0.15	0.18	0.21	0.24	0.27	0.30
1/120	0.13	0.15	0.17	0.19	0.22	0.24
1/150	0.08	0.09	0.11	0.12	0.14	0.15

Deformability of beam and $\mu_{b\delta} - \varepsilon_{cu} - \lambda_{sv}$ ***relations***

The deformation capacity of RC beams directly depends on the ultimate compression strain of concrete, while the ultimate compression strain mainly depends on the characteristic value of transverse reinforcement.

To assure deformation capacity of beams, there is a need to determine the required ultimate compression strain of confined concrete and then to numerically calculate the transverse reinforcement requirement. The former could be obtained as shown in Eqn. (19). More detailed sources could refer to Luo and Qian (2001).

$$\varepsilon_{cu} = \frac{1.7\varepsilon_{sy}(A_s - A_s')f_y}{k_1 f_c b h_b}\left[1 + (\mu_{b\delta} - 1)\frac{l_b^2}{3l_p(l_b - l_p/2)}\right] \tag{19}$$

In which ε_{sy} is the yield strain of the longitudinal reinforcement of the beam. l_p is the equivalent plastic hinge length. The coefficient k_1, as mentioned by Yie (2000), has the commendatory value listed in Table 2.

TABLE 2 THE VALUES OF COEFFICIENT k_1

Concrete strength	≤C50	C60	C70	C80
k_1	0.797	0.774	0.746	0.713

Applying relations between ultimate compression strain of confined concrete and characteristic value of transverse reinforcement proposed by Qian and et al. (2001), and with a little transfer, the requirement of transverse reinforcement is:

$$\lambda_{sv} = (\varepsilon_{cu} \times 10^3 - 4.2)/28.6 \tag{20}$$

DRIFT BASED DESIGN PROCEDURE FOR RC FRAMES

The procedure of drift based design for RC frames consists of the following steps:

(1) Designate the inter-storey drift demand δ_u or target drift ratio θ_u for the frame.
(2) Calculate the yield drift θ_y, and determine the required drift ductility ratio μ_δ.
(3) Determine the coefficient α_b and α_c by means of elastic analysis. Evaluate the collapse mechanism factor χ consistent with the expected yield and collapse mechanism. Estimate the required drift ductility ratio of column $\mu_{c\delta}$ and beam $\mu_{b\delta}$ using Eqns. (12) and (13).
(4) Perform the deformability design of columns by application of $\theta_c^u - n - \lambda_{sv}$ diagram.
(5) Detailing design of beams using $\mu_{b\delta} - \varepsilon_{cu}$ equations and $\varepsilon_{cu} - \lambda_{sv}$ relations.

DISCUSSION AND CONCLUSIONS

The drift based design approach developed in this study provides the designers a practical method for proportioning the RC frame which has been designed to resist minor earthquake without structural element and non-structural element damage. As an initial indicator in this proposed approach, the target drift ratio of the structure is designated according to the performance objects of the structure subjected to moderate or severe earthquakes.

In this approach, the collapse mechanism factor χ is a pivotal indicator of the desirable collapse mechanism of the frame and it manages the distribution of plastic deformation among the components. The factor χ can be straightforward treated as a function of column overstrength factor and drift ductility ratio. For a RC frame, using the rules of drift decomposition to determine the ductility demand of components according to the target drift ductility ratio of the frame, then the $\theta_c^u - n - \lambda_{sv}$ diagram and $\mu_{b\delta} - \varepsilon_{cu} - \lambda_{sv}$ relation can be respectively employed in proportioning the columns and beams to meet the drift and ductility demand.

REFERENCES

Priestley M.J.N. (1998). Displacement based approaches to rational limit states design of new

structures, *Proceedings of the XI ECEE - Invited lectures*, Paris, 317-335.

Qian J.R. and Luo W.B. (2001). Displacement Based Seismic Design of Building Structures, *Building Structures* **31:4,** 3-6.

Whittaker A, Constantinou M and Tsopelas P. (2001). Displacement estimates for performance -based seismic design, *Journal of Structural Engineering* ASCE **124:8,** 905-912.

Luo W.B. and Qian J.R. (2001). Drift Based Design of RC Frame Sub-assemblages, *Reports of Research Advance in Displacement Based Seismic Design*, Department of Civil Engineering at Tsinghua University, Beijing.

Lu X.L., Guo Z.X. and Wang Y.Y. (2001). Experimental Study on Seismic Behaviour of Beam -column Sub-assemblages in RC Frame, *Journal of Building Structures* **22:1,** 2-7.

Yie L.P. (2000). *Concrete Structures and Masonry Structures*, Tsinghua University, Beijing.

Qian J.R., Zhou D.L. and Cheng L.R. (2001). Axial compression behaviour of concrete confined with general stirrups, Accepted by *Journal of Tsinghua University*.

Advances in Building Technology, Volume 1
M. Anson, J.M. Ko and E.S.S. Lam (Eds.)
© 2002 Elsevier Science Ltd. All rights reserved

SEISMIC FRAGILITY CURVES FOR WIND-DESIGNED-BUILDINGS IN HONG KONG

Z.P. Wen [1], K.T. Chau [2], and Y.X. Hu [1]

[1]Institute of Geophysics, China Seismological Bureau, Beijing, China
[2]Department of Civil and Structural Engineering, The Hong Kong Polytechnic University, Kowloon, Hong Kong, China

ABSTRACT

This paper presents a simple analytical method to generate seismic fragility curves for low-rise to high-rise buildings in Hong Kong. In particular, the seismic vulnerability is assumed proportional to the sectional areas of the column and shear walls of the structure. Three wind-code-designed buildings were selected as examples for the present analysis, namely a 6-story school building by the Architectural Services Department, and a 21-story residential building at Mei Foo Sun Chuen and a 40-story residential building of the Hong Kong Housing Authority (HKHA). Instead of using intensity, seismic hazard is prescribed in terms of peak ground acceleration (PGA) in the present study. The adopted response spectra are site-dependent and depend on whether the design earthquakes are near field or far field. The seismic responses of buildings are analyzed using the equivalent static force approach for multi-degree-of-freedom-oscillators, expressed in terms of the fundamental site period and epicentral distances. The ductility distribution of buildings is then formulated as a log-normal distribution. Finally, the vulnerability of the structure is given as fragility curves. The results indicate that damage probability is highly sensitive to the number of story or building height, structural scheming, and functional usage of the buildings; other parameters such as site condition and epicentral distance are equally crucial to the structural seismic vulnerability. The conclusion should also be expected for other wind-designed buildings in Hong Kong and other parts of the world.

KEYWORDS

Fragility curves, Tall-buildings, Epicentral distance, Site condition, Near field and far field earthquakes, PGA input

INTRODUCTION

As reviewed by Docle et al. (1994), the most commonly adopted seismic input for vulnerability analysis is the macroseismic intensity (e.g. the Modified Mercalli Intensity or MMI). Less often, the seismic input is expressed in terms of ground motion parameters such as peak ground acceleration (PGA) or velocity (PGV). In the loss estimation methodologies, such as ATC-13 (ATC=Applied Technology Council) and FEMA-177 (FEMA=Federal Emergency Management Agency) used in the USA, inten-

sity instead of PGA is still being used as the earthquake hazard. However, there is a recent trend of adopting PGA instead of intensity to quantify seismic hazard. In the last decade, many seismic codes in the world have been changed from specifying hazard in terms of intensity to specifying hazard in terms of PGA. For example, the newest Chinese seismic code GB 50011-2001 has adopted PGA contour map as hazard input comparing to the old code GBJ11-89 using intensity contour map as hazard input. In the newest seismic hazard evaluation methodology HAZUS99 (HAZUS=Hazards U.S.), PGA has been adopted as the hazard input. However, the most commonly used measure of the site hazard remains the macroseismic intensity in the vulnerability analysis of buildings, due to the lack of reliable PGA hazard map in many parts of the world.

For historical and pragmatic reasons, MMI has been used as ground-shaking measure in most earthquake loss studies conducted in the past. This procedure was popular in early loss studies because multiple, instrumental records of ground shaking were not available to correlate motion levels to damage. Even today, strong motion records at a particular site of a severely damaged building are rare. Thus, it remains difficult to statistically correlate damage distribution of buildings to PGA, PGV or response spectrum. Another reason is that intensity levels are partly defined by means of building damage data, it seems straightforward conceptually to predict future damage levels on the basis future expected intensity levels.

Despite all these obvious reasons, there are, however, conceptual and practical difficulties with the use of intensity as the principal hazard parameter in earthquake risk assessment. Intensity scales are essentially non-quantitative scales, using only a discrete scale system. Thus, intensity does not provide a satisfactory basis for the estimation of future losses (Coburn and Spence, 1992). The input parameters for the vulnerability analysis should be compatible with those from earthquake hazard analysis, which is typically in terms of PGA. By considering the frequency characteristics of ground motions, this paper further analyzes the effects of site condition and epicentral distance on fragility curves of low-rise to high-rise reinforced concrete (RC) wind-designed buildings in terms of PGA.

Past earthquake records clearly demonstrate that the effect of site conditions and source-to-site distance on damage probability distribution of buildings is very significant. Even in the 1920s, people realized from the damage data of buildings in the 1923 Kanto earthquake that rigid structures suffered heavier damage on the rigid ground and flexible structures suffered heavier damage on flexible ground. Similar observations on selective damages include those induced damages during the 1952 Kern earthquake of USA, the 1977 Vrancea earthquake of Romania, the 1985 Mexico earthquake, and the 1989 Loma Prieta earthqauke of USA (Hu, 1988; Hu et al., 1996). In general, short stiff structures suffer heavier damage under near field moderate earthquake; while, on the contrary, tall flexible structures suffer more damage under far field large earthquakes. Thus, the damages are highly selective in terms of both the fundamental frequency of structures and the frequency content of ground shaking. So both the frequency and amplitude characteristics of ground motions should be considered when the vulnerability analysis and loss estimation are conducted. This is precisely the aim of the present study.

FRAGILITY CURVES FOR VARIOUS SITES AND EPICENTRAL DISTANCES

The overall framework for evaluating the fragility curves of the building consists of three stages: input ground motion, seismic response analysis and probability distribution of building damage among different damage states. The PGA is resulted from seismic hazard assessment. The effect of soil condition and distance on ground motions is described by characterized period of ground motion. The structural responses are calculated by equivalent lateral force method. The probability distributions of

damage states of building are predicted by damage functions, through the estimated ductility.

Input ground motions

It is known that local soil condition and seismic wave propagation can alter response spectra significantly. Therefore, an accurate modeling of ground motion should consider the frequency characteristics of ground motions. The dependence of response spectra on ground conditions is recognized in many earthquake-resistant design codes throughout the world (Paz, 1994; IAEE, 1996). For many years, the shape dependence of response spectrum on soil condition, at least approximately, was accounted for by using peak ground acceleration to scale down or up the design spectra in different frequency range (Newmark and Hall, 1982). Examination of the records from many earthquakes reveals that the distance of the recording station from seismic source can cause big difference in the spectral shapes at the rock stratum (Mohraz, 1992). The effects of both site condition and distance on shapes of response spectra are considered by in ATC-3, Romanian, Canadian and the building code for China when defining design spectra (site-dependent and earthquake-dependent spectra). In this study, the normalized response spectra S_a given in GBJ 11-89 are used (5% damping):

$$S_a(T)=\begin{cases} 2.2a_{\max}(5.5T+0.45) & \text{for } T\le 0.1\,\text{sec} \\ 2.2a_{\max} & \text{for } 01.<T\le T_g \\ 2.2a_{\max}\left(\dfrac{T_g}{T}\right)^{0.9} & \text{for} T_g<\mathrm{T}\le 3.0\ \text{sec} \end{cases} \tag{1}$$

where T_g is given in GBJ 11-89 for various site categories and epicentral distances (i.e. far or near field earthquake); and a_{max} is the median of mean PGA expected at a site from seismic hazard analysis. To account for uncertainty, log-normal distribution of PGA is usually assumed.

Seismic shear of story

Applying the equivalent lateral force method, the shear force Q_x at the x-story is given by summing all lateral seismic forces above that story as

$$Q_x=\sum_{i=x}^{n}\frac{G_iH_i}{\sum_{j=1}^{n}G_jH_j}S_a(T)G_{eq}(1-\delta_n)+S_a(T)G_{eq}\delta_n \tag{2}$$

where $S_a(T)$ is the site-dependent response spectrum give in (2), which is derived from seismic hazard specified in terms of PGA $a_{\max}$; G_{eq} is the total equivalent weight of a structure; H_i and G_i are the height and weight at level i respectively; n is the total number of stories of the building; and δ_n is the additional seismic action coefficient which is intended to account approximately for the higher mode contributions and can be found from GBJ 11-89. In using the response spectrum at a site, the fundamental period T of the building is needed, and for the present case of RC frame/shear wall building we can estimate T (in s) by the following empirical formula (Guo, 1990):

$$T=0.33+0.00069\frac{H^2}{\sqrt[3]{B}} \tag{3}$$

where H and B are the height and length of the building (in m)along the shaking direction.

Distributions of ductility factor in terms of PGA

The capacity of each story is evaluated in terms of the yield shear force. For shear wall structures and frame structures with shear wall, the yield story shears are, respectively (GBJ 11-89)

$$Q_{yx} = 0.2F_C A_{wx} \text{ and } Q_{yx} = 0.25F_C A_{wx} \tag{4}$$

where F_C is compressive strength of concrete and A_{wx} is sectional area of shear walls which are parallel to the earthquake action in the x-story. Then, the yield shear coefficient of each story is calculated as:

$$R_x = \frac{Q_{yx}}{Q_x} \tag{5}$$

where Q_x and Q_{yx} are defined in (2) and (4) respectively. Many studies show that, in the case of multi-story frame structure with shear walls, nonlinear deformation will concentrate at the weakest stories (Newmark and Roseblueth, 1971; Yin et al., 1981), which corresponds to the minimum R_x among all stories. Note that the yield shear coefficient relates not only to the strength of the structure, but also to the characteristics of the seismic input. The next step to estimate the story ductility factor in terms of the minimum R_x, and subsequently to building damages. The story with minimum yield shear coefficient experiences the maximum deformation and the maximum ductility factor. By using the equivalent energy criterion (Veletsos and Newmark, 1960), the structural ductility may be evaluated from the following formula:

$$\mu_0 = \begin{cases} \dfrac{1+R^2}{2R^2} & R \le 1 \\ \dfrac{1}{R} & R > 1 \end{cases} \tag{6}$$

where R is the minimum yield story shear coefficient calculated from (5). This empirical formula can further be refined by adding correction factors C_i (i=1,2,...,5) (Yin, 1995):

$$\overline{\mu} = \mu_0\left(1 + \sum C_i\right) \tag{7}$$

How to apply these correction factors are discussed in Wen et al. (2002) and will not be reported here.

Naturally, a higher maximum mean ductility factor $\overline{\mu}$ also implies a more severely damaged building. But, due to the uncertainties involved in the estimation of seismic hazard as well as in the analysis of structural response, the ductility as well as the damage state is better represented in terms of probability distribution function. In particular, both the peak ground acceleration and seismic capacity of structures are often found satisfying a log-normal probability distribution versus the input ground parameters (Shibata, 1980; Kircher et al., 1997; Yamaguchi and Yamazaki, 2001; Yin et al., 1985). By analyzing 3120 cases of elastic-plastic seismic responses, Yin et al. (1985) suggested the following log-normal distribution for μ :

$$f(\mu) = \frac{1}{\sqrt{2\pi}\xi\mu} \exp\left[-\frac{(\ln\mu - \lambda)^2}{2\xi^2} \right] \tag{8}$$

where

$$\lambda = \ln\bar{\mu} - \frac{1}{2}\xi^2 \quad \text{and} \quad \xi^2 = \ln\left(1 + \frac{\sigma^2}{\bar{\mu}^2}\right) \tag{9}$$

In these equations, $\bar{\mu}$ and σ are respectively the maximum mean value estimated from (7) and the standard deviation of the ductility factor of the stories. In this study, we assume that the uncertainty of the ductility factor mainly comes from the seismic hazard. Thus, the value of $\sigma / \bar{\mu}$ is taken from that of the attenuation relationship on peak ground acceleration. Note that this ductility distribution depends on the structural characteristics as well as the input ground motions through the calculation of $\bar{\mu}$ and variance. Using the threshold values of the ductility factor as integration limits, the probability of various damage states for a given ground motion can be integrated. For frame structures with shear walls, the threshold ductility factors for the onset of slightly damage, moderate damage, extensively damage and completely damage states are taken as 1.0,1.5,3.0 and 5.0 respectively (Yin, 1995).

Fragility curves

Identifying the relationship between ground shaking and distribution of damage is essential to vulnerability analyses (Hu, 1998). There are several ways in which this relationship about distribution of damage may be expressed and evaluated. One method for expressing the distribution of damage is to use damage probability matrix (DPM) which was introduced by Whitman et al. (1973) and DPM were developed in ATC-13 for 42 building classes for California (ATC, 1985). Fragility curves introduced by Kennedy et al. (1980) and Kircher and McCann (1983) provide essentially the same information as DPM does. Each curve gives the probability that the indicated damage states is equaled or exceeded as a function of the intensity of ground shaking, such as those in FEMA-177 (FEMA, 1989).

FRAGILITY CURVES FOR LOW-RISE TO HIGH-RISE BUILDINGS IN HONG KONG

In this study, three types of buildings are considered: a 40-story with RC frame apartment building of the HKHA, which contains a thick RC transfer plate located between upper apartment and lower department store or parking area; a 21-story RC frame/shear building of Mei Foo Sun Chuen in Hong Kong, which was built in 1960s and consists of two lower levels of car park and 19 levels of upper residential block; and a 6-story RC government primary school. All these building are designed according to the Hong Kong wind code with no seismic provision.

The fragility curves are constructed at various levels of PGA in different site conditions (I, II, III, IV) and epicentral distance (near or far). In this paper, we only show those plots for near field earthquakes in Figs. 1-3 due to page limit. The vulnerability of these buildings depends on the site condition as well as on the building types. In general, we also observe that high-rise buildings with longer fundamental period are more vulnerable from far field earthquakes than from near field earthquakes, and on soft site than on stiff site.

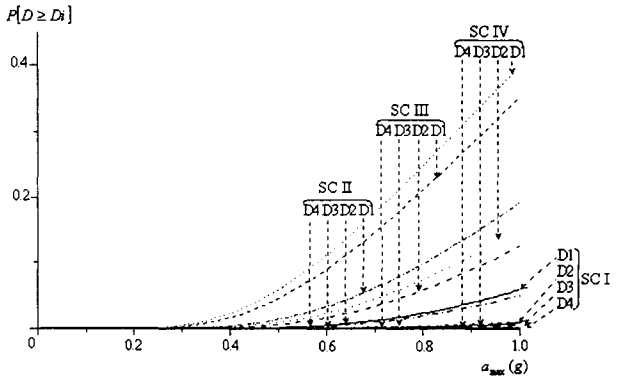


Figure 1: The fragility curves for the 6-story government school under near field earthquakes

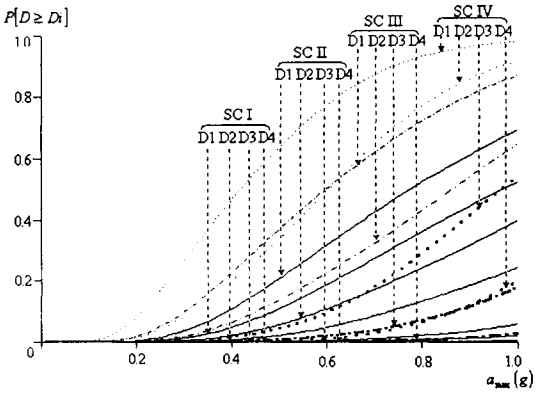


Figure 2: The fragility curves for the 42-story HKHA building under near field earthquakes

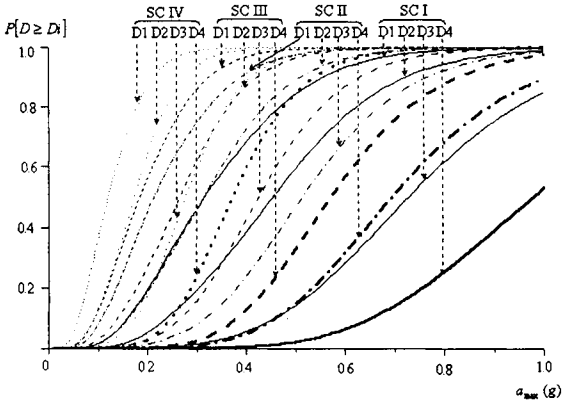


Figure 3: The fragility curves for the 21-story Mei Foo building under near field earthquakes

DISCUSSION AND CONCLUSION

We have proposed a simple model to consider the seismic vulnerability of a 6-story school, a 21-story residential building and a 42-story HKHA residential building, under various PGA input and site conditions. All these buildings are designed in compliance with the Hong Kong wind code with no seismic provisions. The fragility curves are given in terms of probability of various damage state or above versus the input PGA for various site conditions. The input acceleration spectrum is adopted from GBJ 11-89 and is site- and epicentral distance-dependent. The yield shear of each story of the building is checked against the shear force induced by various ground excitations to yield the probability of damages. The yield shear is assumed proportional to the total cross-sectional area of columns and walls at each level, while the seismic shear force is calculated based on an equivalent force method on a multi-degree-of-freedom-oscillator. In addition, the weight distribution and fundamental period of the building have also been incorporated into the fragility analysis. Uncertainty in both hazard and structural response is incorporated through an assumed log-normal distribution of the ductility of the building subject to certain ground motions.

For near field earthquakes, Figs. 1-3 demonstrate that the 6-story government school designed by the Architectural Services Department is the strongest against potential seismic shakings. The weakest building against earthquake attack is the 21-story Mei Foo Sun Chuen building, while the seismic performance of the 42-story HKHA building is between the 6-story school and the 42-story HKHA building. According to the HK wind code, if no topographic effect is considered, the design wind pressure for the 6-story school is from 1.2 to 2.2 kPa, that for 21-story building is from 1.2 to 3.0 kPa, and that 42-story building is 1.2 to 3.5 kPa. By enforcing a top floor drift of 1/500 in serviceability state under wind load, the bending stiffness EI of a typical Hong Kong building versus height L (in m) can be approximated as (Koo et al, 2002):

$$EI = 500(0.001256175L^2 + 0.2480387L - 0.45484)L^3B \tag{10}$$

where B is the width of the building in m. Therefore, the stiffness (or the net sectional area of the columns) increases nonlinearly with the number of story of the building, but the seismic shear force also increases nonlinearly with height. Figures 1-3 illustrate that the medium-rise building is more vulnerable to seismic attack than both low-rise and high-rise buildings. In addition, we also find that site condition and epicentral distance play an important role in building damage and earthquake loss estimation, especially at high PGA. This conclusion should be true for buildings in other region of moderate seismicity in the world, at where buildings were designed according to wind loads instead of seismic loads.

ACKNOWLEDGEMENTS

The research was fully supported by ASD Project A202 and A214 of the Hong Kong Polytechnic University. Their support is gratefully acknowledged. The authors would like to thank Mr. Philip Kwok the Buildings Department of Hong Kong SAR Government in providing building information.

REFERENCES

Applied Technology Council (ATC) (1985). *ATC-13: Earthquake damage evaluation data for California.* Applied Technology Council, Redwood City, CA.

Coburn A. and Spence R. (1992). *Earthquake Protection.* Wiley, Chicheste.

Dolce M., Zuccaro G., Kappos A. and Coburn A.W. (1994). Report of the EAEE working group 3: vulnerability and risk analysis. *Proceedings of 10th European Conference on Earthquake Engineering*, 4, Vienna, Austria, 3049-3077

Federal Emergency Management Agency (FEMA) (1989). *Estimating Losses From Future Earthquakes*. FEMA –177, National Research Council (NRC), Washington, D.C.

Gou J.W. (1990). *Seismic Design of Building*. Beijing: High Education Press.

Hu Y.X. (1988). *Earthquake Engineering*. Beijing: Seismological Press (in Chinese), 1988; pP60-61.

Hu, Y.X. (1998). *Earthquake Disaster Mitigation & Engineering Seismology*. IUGG/SSB International Training Course on Continental Earthquakes and Seismic Hazard, 70pp., Beijing, China.

Hu Y.X., Liu S.C. and Dong W.M. (1996). *Earthquake Engineering*. E & FN SPON.

IAEE. (1996). *Earthquake Resistant Regulations a Word List*. International Association for Earthquake Engineering, Tokyo, Japan.

Kennedy R.P., Cornell C.A., Campbell R.D., Kaplan S. and Perla H.F. (1980). Probabilistic seismic safety study of an existing nuclear power plant. *Nuclear Engineering and Design* 59, 315-338.

Kircher C.A. and McCann M.W. (1983). *Appendix A: Development of seismic fragility curves for sixteen types of structures common to cities of the Mississippi Valley region*, J.R. Benjamin & Assoc., Mountain View, Calif.

Kircher C.A., Nassar A.A., Kustu O. and Holmes W.T. (1997). Development of building damage functions for earthquake loss estimation. *Earthquake Spectra* 13(4), 663-682.

Koo K.K., Chau K.T., Yang X., Lam, S.S. and Wong Y.L. (2001). Soil-pile-structure interactions under SH waves. *Earthquake Engineering and Structural Dynamics*, 2000, accepted, in press.

Mohraz B. (1992). Recent studies of earthquake ground motion and amplification. *Proceedings of 10th World Conference on Earthquake Engineering*, Spain, 1992, Vol.11, pp. 6695-6704.

Newmark N.M. and Hall W.J. (1982). *Earthquake Spectra and Design*. Berkeley: Earthquake Engineering Research Institute.

Newmark N.M. and Rosenblueth E.A. (1971). *Fundamentals of Earthquake Engineering*. New Jersey: Prentice-Hall.

Paz M. (1994). *International Handbook of Earthquake Engineering, Codes, Programs, and Examples*. Chapman & Hall.

Shibata A. (1980). Prediction of the probability of earthquake damage to reinforced concrete building groups in a city. *Proceedings of the Seventh World Conference on Earthquake Engineering* 1980, Istanbul, Vol. 4, 395-402.

Veletsos A.S. and Newmark N.M. (1960). Effect of inelastic behavior on the response of simple systems to earthquake motions. *Proceedings of the second World Conference of Earthquake Engineering*, Vol.2, 1960.

Wen Z.P., Hu Y.X. and Chau K.T. (2002). Site effect on vulnerability of high-rise shear wall-buildings under near and far field earthquakes. *Soil dynamics and Earthquake Engineering*, accepted, in press.

Whitman R.V., Reed J.W. and Hong S.T. (1973). Earthquake damage probability matrices. *Proceedings of 5th World Conference on Earthquake Engineering 1973*, Rome, Italy.

Yamaguchi N. and Yamazaki F. (2001). Estimation of strong motion distribution in the 1995 Kobe earthquake based on building damage data. *Earthquake Engineering and Structural Dynamics* 30, 787-801.

Yin Z. (1995). *The Method of Seismic Damage and Loss Prediction*. Beijing: Seismological Press (in Chinese).

Yin Z.Q. Li S. and Sun P. (1981). Elasto-plastic earthquake responses of multi-story frames structures. *Earthquake Engineering and Engineering Vibration* 1(2), 56-77.

Yin Z.Q., Li S. and Sun P. (1985). Relation between story displacement and yield strength in multi-story framed structures and problem of controlling displacement to prevent collapse. *Earthquake Engineering and Engineering Vibration* 5(1), 33-44.

Advances in Building Technology, Volume 1
M. Anson, J.M. Ko and E.S.S. Lam (Eds.)
© 2002 Elsevier Science Ltd. All rights reserved

A PRELIMINARY STUDY OF STRUCTURAL SEMIACTIVE CONTROL USING VARIABLE DAMPERS

R. L. Yang[1], X.Y. Zhou[1] and X. H. Liu[2]

[1] Institution of Earthquake Engineering, China Academy of Building Research, Beijing 100013, China
[2] Electronic Information Center, Ministry of Information Industry, Beijing 100846, China

ABSTRACT

It's well known that the semiactive control system is very attractive due to a large control force capacity, a small power demand and its inherent stability. As a classical example the semiactive variable damper is widely used, however, the latest research results show that its performance still need to be further studied. In this paper based on the theory of a SDOF vibration-isolation system under harmonic excitation, the basic conditions and limits of the applicability of viscous variable dampers are discussed. As a numerical example a six-story base-isolated frame is considered. According to the qualitative analysis and numerical simulation, two basic conclusions are drawn. They include: (1) Only far from the resonance may reductions in both the displacement and acceleration responses be possible for structures with viscous variable dampers; (2) The effectiveness of viscous variable dampers on reducing the response of structures depends on the characteristics of the ground motion that excites structures. In contrast to that of passive dampers, the effect of variable dampers is only slightly improved.

KEYWORDS

Semiactive variable dampers, fluid viscous dampers, OTE algorithm, structural control, hybrid base-isolated system, seismic excitations

1 INTRODUCTION

Similar to the natural evolution of species, vibration control techniques have a development process from a low-grade phase to a high-grade phase, i.e., from passive control systems to active/semiactive control systems. In recent years, considerable interests are shifted to semiactive control systems because of a broad dynamic adjustable range, a small power demand and its inherent stability. As a basic type of semiacive devices, semiactive variable dampers have been widely adopted. Nevertheless, the latest research results have shown that further attention should be paid to its efficiency.

In an extensive analytical and experimental study, Symans and Constantinou[1] developed and tested a two-stage damper and a variable semiactive fluid damper. For two dampers, different algorithms were used. Their study included a single-stoery frame and a three-stoery frame under different seismic excitations. The results indicated that while variable dampers significantly reduced the response as compared to the case with no control, no reduction was observed when compared to the same device acting as a passive damper with the upper limit of the damping of corresponding variable damper. As a result their study indicates that the use of semiactive dampers in structures is inefficient in some cases when compared to passive systems. To probe into the influence of supplemental damping and structural period on the seismic response of structures, Sadek and Mohraz[2] used six-SDOF structures with periods 0.2, 1.0, 1.5, 2.0, 2.5, and 3.0s respectively, and a structural damping ratio 0.05. Two supplemental passive dampers with damping ratios 0.05 and 0.40 were considered. 20 horizontal accelerograms were chosen. The average responses for the 20 records for the six structures showed for rigid structures (structures with periods below 1.5s) increasing the supplemental damping ratio decreased both the relative displacement and the absolute acceleration, whereas for flexible structures (structures with periods beyond 1.5s) increasing the supplemental damping ratio decreased the relative displacement but increased the absolute acceleration. Sadek and Mohraz made such a conclusion: Variable dampers can be effective in reducing the acceleration response in flexible structures,such as base-isolated and tall buildings, where an increase in the damping adversely affects the acceleration response. Variable dampers, however, are not effective for rigid structures as compared to passive dampers.

Inspired by these research results, the authors' latest study demonstrates for structures with variable dampers there is a dependency of the attained reduction in response on the characteristics of the ground motion that excites the structure. Referring to the transmissibility relation of an SDOF vibration-isolation system under support excitation[3], there are some basic features: If the ratios of the disturbance frequency to the fundamental frequency of structures are below $\sqrt{2}$, increasing the damping ratio decreases both the relative displacement and the absolute acceleration, whereas if that is beyond $\sqrt{2}$, increasing the damping ratio decreases the relative displacement but increases the absolute acceleration. Therefore, for structures with variable dampers under harmonic loadings, only is the ratio of the disturbance period to the fundamental period below $\sqrt{2}$, it's possible to achieve reductions in both the relative displacement and the absolute acceleration responses. Despite seismic excitations which contain a broad rang of frequency spectrum are very complicated compared to harmonic excitations, a qualitative analysis, referring to the corresponding results of harmonic loadings, is possible.

The authors, recently, presented a new general control strategy-OTE strategy in which the control operation is considered from the viewpoint of the relations of the motion of structures, the exciting force and the control operation. Based on the OTE strategy, all the control operations in the process of leaving/approaching balancing-position should suppress the motion of structures, however, in the process of approaching balancing-position should be kept at a slightly suppressive level. OTE algorithm, including the continuous control and the discrete control, which combines OTE strategy and fuzzy control theory, is capable of acquiring an ideal result.

Based on OTE algorithm, a discrete control by means of setting the damping into a high/low binary state is used in this paper. The numerical example studies the reducing-vibration performance of a six-stoery base-isolated frame with a hybrid seismic isolation system, i.e., isolators with supplemental variable dampers, and verifies the authors' viewpoints.

2 HYBRID ISOLATION SYSTEM

The ideal of protecting a building from the damaging effects of an earthquake by introducing some type of support that isolates it from the shaking ground is an appealing one, and many mechanisms to achieve this result have been invented successively. Although the early proposals may be traced back to 100 years, it's in recent years that base isolation has become a practical technique for earthquake-resistant design. Despite wide variation in detail, there are two basic types of isolation systems: elastometric bearings (which are predominantly natural rubber) and sliders. The mostly widely adopted system is the former, which introduce a layer of low lateral stiffness between the structure and the foundation. With this isolation layer the structure has a natural period that is much longer than its fixed-base natural period. The deformation of the isolated structure primarily occurs in the isolation layer, and the superstructure basically shows itself a rigid behavior. Considering the case in further earthquakes that occur close to seismic-isolated structures, a certain level of damping is beneficial to suppress the responses of structures[4-6]. Therefore a hybrid isolation system - isolators with variable dampers is studied in order to illustrate the efficiency of using variable dampers (Figure1).

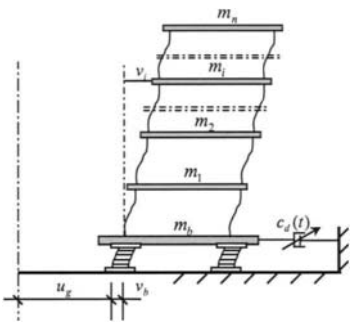


Figure 1: Multistory Hybrid Base-Isolated Structure

Assume that $\mathbf{M}$、$\mathbf{C}$、$\mathbf{K}$ are , respectively, the mass, damping and stiffness matrices of the superstructure, with n-degrees-of-freedom, m_b is the mass of the base, k_b is the total stiffness of isolators, $c_d(t)$ is the total instantaneous damping of viscous variable dampers, u_g、v_b and $\mathbf{v}$ are the ground acceleration, the relative base displacement with respect to the ground, the relative floor displacement with respect to the base respectively, $\mathbf{r}$ is a column of ones and $\mathbf{0}$ of zeros, m is the total mass of the superstructure. For this hybrid isolation system the equations of motion are as follows:

$$\mathbf{M}^*\ddot{\mathbf{v}}^* + \mathbf{C}^*\dot{\mathbf{v}}^* + \mathbf{K}^*\mathbf{v}^* = -\mathbf{M}^*\mathbf{r}^*\ddot{u}_g \qquad (1)$$

where $\mathbf{M}^* = \begin{bmatrix} m+m_b & \mathbf{r}^T\mathbf{M} \\ \mathbf{Mr} & \mathbf{M} \end{bmatrix}$, $\mathbf{C}^* = \begin{bmatrix} c_d(t) & \mathbf{0}^T \\ \mathbf{0} & \mathbf{C} \end{bmatrix}$, $\mathbf{K}^* = \begin{bmatrix} k_b & \mathbf{0}^T \\ \mathbf{0} & \mathbf{K} \end{bmatrix}$, $\mathbf{r}^* = \begin{bmatrix} 1 \\ \mathbf{0} \end{bmatrix}$, $\mathbf{v}^* = \begin{bmatrix} v_b \\ \mathbf{v} \end{bmatrix}$.

3 APPLICATION OF OTE ALGORITHM

According to OTE strategy, the damping function isn't always in favor of pushing the structure to go back to the balancing position. The characteristics of the damping function combining with the detailed motive trend of structures require being analyzed carefully. If the structure is departing from the balancing position, the instantaneous damping of variable dampers should be kept at a higher level and suppresses this trend; if the structure is approaching the balancing position, the instantaneous damping of variable dampers should be kept at a lower level and suppresses this trend slightly. Therefore in order to examine the efficiency of using variable dampers a simple on-ff control model was chose for variable dampers in this paper (Table 1).

TABLE 1
CONTROL CONDITIONS BASED ON OTE ALGORITHM

Algorithm	Control conditions	
OTE	If $x_b\dot{x}_b > 0$, then $c_d = c_{d\max}$ (ON)	If $x_b\dot{x}_b < 0$, then $c_d = c_{d\min}$ (OFF)

4 NUMERICAL EXAMPLE

A six-stoery base-isolated frame is considered as the numerical example to examine the efficiency of using variable dampers. Assume that all the floor masses are $m_i = 100$ ton, all the floor stiffnesses $k_i = 3\times10^5$ kN/m; the superstructure is with a damping ratio of 5 per cent in its fundamental period, and with a damping matrix proportional to its own stiffness matrix; the base mass is $m_b = 140$ ton; the stiffness of isolators is $k_b = 9\times10^3$ kN/m, and its damping is attached to the semiacive viscous damper; the lower and upper limits of the damping of the attached damper are 100 and 900kN.s/m respectively. All the isolators are expressed as linear models, and the fundamental period of the base-isolated frame is 1.82s.

In order to evaluate the ratio of the disturbance period to the fundamental period of the base-isolated frame, the predominant period of the acceleration response spectrum may be considered as a reference. Such a reference is approximate but meaningful by its physical meaning. It's enough to explain the authors' viewpoints. Two input records are as follows: (a) Luquan accelerogram(Luquan, Yunan, China, April 19, 1985, Station: Zhuanlong, Orientation: E-W, the predominate period of the acceleration spectra: 0.15s), (b) A S60E accelerogram synthesized by combining the two components of horizontal motion recorded at SCT during Sep.19,1985, Mexico City earthquake(the predominate period of the acceleration response spectrum: 2.0s). The numerical simulation considers three cases: off (the min. damping), on (the max. damping) and on-off control (damping adjustable). During the calculation the seismic-isolated frame is assumed to behave elastically at all times.

Figure 2 presents the peak responses of the base-isolated frame under two different seismic excitations. It's clear that

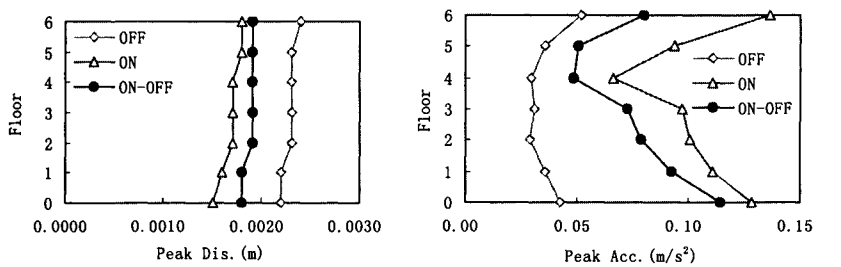
- Since the predominate period of the acceleration response spectrum of Luquan accelerogram is far below the fundamental period of the seismic-isolated frame (a non-resonant condition), an increase in the damping ratio further decreases the displacement response but increases the acceleration response.
- Since the predominate period of the acceleration response spectrum of Mexico City accelerogram is close to the fundamental period of the seismic-isolated frame (a resonant

condition), an increase in the damping ratio further decreases both the displacement response and the acceleration response.

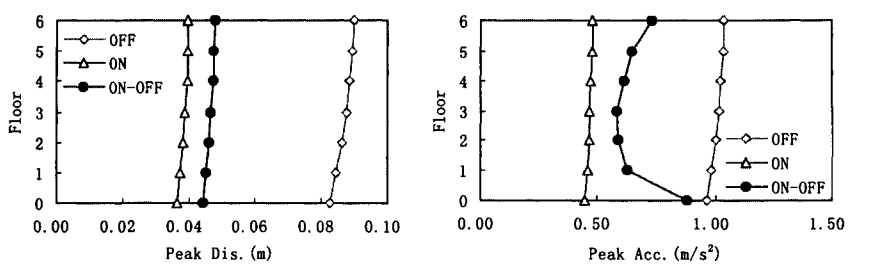
This phenomenon is consistent with the corresponding characteristics of a SDOF vibration-isolation system subjected to harmonic excitations[7].

No matter what an algorithm is adopted, the potential effect of any semiactive control system by adjusting the damping is, undoubtfully, interposed between that of the corresponding passive control system by using the min. or max. damping. The results seen in Figure 2 also imply that

- Under non-resonant conditions, the improvement of both the displacement and acceleration response can be gained simultaneously. The semiactive variable dampers are possible to achieve reductions in both the displacement and acceleration response. However, because of small peaks of the responses the use of variable dampers is not valuable.
- Under resonant conditions, an increase in the damping is always beneficial to suppress the responses of structures. Therefore passive control systems with high damping coefficient are more suitable. The efficiency of using variable dampers is questionable.



(a) Luquan record



(b) Mexico record

Figure 2: The peak response of the base-isolated structure

5 CONCLUSIONS

Based on OTE algorithm, the efficiency of using semiactive variable dampers is studied thoroughly in this paper. There are some basic conclusions as follows

a) Only under non-resonant conditions is using semiactive variable dampers possible to improve the control effects slightly compared to passive dampers.
b) The effectiveness of viscous variable dampers on reducing the response of structures depends on the characteristics of the ground motion that excites structures.

On the basis of known research results the authors find that considering the characteristics of the ground motion is necessary in order to study the efficiency of using variable dampers. As an index the ratios of the disturbance frequencies to the fundamental frequencies of structures is of consequence rather than the periods of structures.

6 LMITATIONS AND THE APPLICABLE RANGE

Semiactive variable dampers involved in this paper are primarily fluid viscous dampers, i.e., the damping forces are only correlative with the velocity (zero stiffness, irrespective to the displacement). Since only under the condition far from the resonance is using variable dampers possible to improve the control effects, variable dampers can be effective only in tall buildings or base-isolated structures. Meanwhile it should be pointed out that TMDs(tuned mass dampers) and TLCDs with varying-damping devices, based on the theory of dynamic absorbers, are exceptional.

REFERENCES

[1] Symans M.D. and Constantinou M.C. (1995). *Development and Experimental Study of Semi-Active Fluid Damping Devices for Seismic Protection of Structures.* Rep. No. NCEER-95-0011, State Univ. of New York at Buffalo, Buffalo, N.Y.

[2] Sadek F. and Mohraz B. (1998). Semiactive Control Algorithms for Structures with Variable Dampers. *Journal of Engineering Mechanics* **124:9,** 981-990

[3] Chopra A.K. (1995). *Dynamics of Structures: Theory and Applications to Earthquake Engineering.* Prentice Hall, New Jersey

[4] Kelly J. M. (1997). *Earthquake-Resistant Design with Rubber (Second Edition).* Springer, London, UK

[5] Nagarajaiah S. (1994). Fuzzy Controller for Structures with Hybrid Isolation System. *Proceedings of 1st World Conference on Structural Control* **2:** TA2 -67—TA2 -76

[6] Hussain S.M. and Retamal E. (1994). A Hybrid Seismic Isolation System-Isolators with Supplemental Viscous Dampers. *Proceedings of 1st World Conference on Structural Control* **3:** FA2 -53—FA2 -62

[7] Paz M. (1997). *Structural Dynamics: Theory and Computation (Fourth Edition).* Chapman&Hall, New York

TEAM PRESENTATION:

FLEXIBLE MANUFACTURING SYSTEM IN CONSTRUCTION

This Page Intentionally Left Blank

Advances in Building Technology, Volume 1
M. Anson, J.M. Ko and E.S.S. Lam (Eds.)
© 2002 Elsevier Science Ltd. All rights reserved

DYNAMIC MONITORING OF THE BORING TRAJECTORY IN UNDERGROUND CHANNEL FOR DRIVING COMMUNICATIONS

Prof. Dr. Eng. sc. tech. Alexej Bulgakow
Faculty of Architecture, Munich University of Technology
Arcisstr. 21, D-80333 München, Germany
Dr. Eng. Dimitry Krapivin, Dipl. Eng. Sergej Aleksyuk, Dr. Eng. Sergej Pritchin
Faculty of Mechatronik, South Russian State Technical University
Proswestchenja Str. 132, 346428 Novotcherkassk, Russia

ABSTRACT

This paper deals with high precision directional boring of underground channels, including programmable curved trajectories for enclosed digging driving communications and other purposes.

KEYWORDS

Underground channel, dynamic monitoring, driving communications.

As the working tool for boring in soft anisotropic soils a cone is taken, which is imparted a revolving motion whose angular velocity is ω_{pr}, its impact frequency f. The impact makes the revolving cone penetrate into the soil along the screw trajectory. The cone thus revolves around its symmetry axis OO_1 with angular velocity $\omega_к$ (Fig. 1) in such a way that the above axis OO_1 itself oscillates

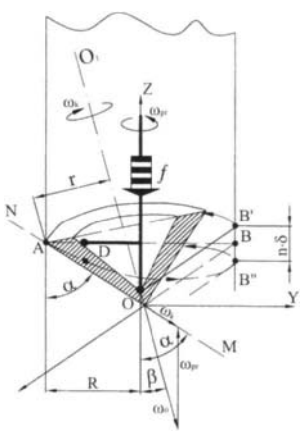


Figure 1

eccentrically around O_Z at an angular velocity ω_0 at β angle.
Acted by various factors the conditions of oscillating motion of OO_1 axis can change in such a way that the apex of the cone is displaced from the axis of the so, the canal symmetry and takes port in oscillating motion as well, its parameters being e and Δh to O_Z axis (Fig. 2). Here, the cone slips and performs friction work while its constituent OA is displaced from NM line during its turn at some angle φ to $O_2\,O_3$ at an angular velocity ω_e.

The above parameters of this motion are found following the calculation of point O_2 location, based on the principle of the least action. With uniform distribution of the normal force

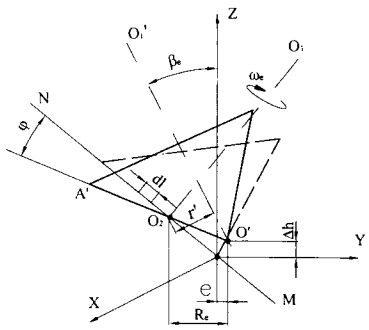


Figure 2

longitudinally the generating line of OA, the elementary work of the friction force F on $d\ell$ element will be $dA = F \cdot V \cdot d\ell$,
where $V = \omega_\varepsilon \cdot S$ - linear rate of $d\ell$ element, S – the distance of $d\ell$ element up to NM.

Total work of friction forces is

$$A = \frac{F}{2} \cdot \omega_e \cdot \frac{\cos\beta \cdot \sin\varphi}{\sin(\beta - \alpha)} \cdot \left[(L - \ell)^2 + \ell^2\right].$$

The minimum of the function A will be at $\frac{dA}{d\ell} = 0$ or with $\ell = \frac{L}{2}$, where L=OA, i. e. when the cone constituent slips along the well face relatively to point O_2 located in the middle of cone constituent.
The slip appearance will make point A shift from the screw line B'AB". The coordinates of it point A can be derived as

$$x = (R - e) \cdot \cos\omega_{pr} t; \qquad x = (R - e) \cdot \sin\omega_{pr} t; \qquad z = n \cdot \delta,$$

where n - number of impacts,
δ - permeating in a direction of operation of impacts.

R-e value is found from $R - e = \frac{\omega_k}{\omega_{pr}} \cdot r$,
where r is the greatest cone diameter.

Thus, dynamic monitoring of the trajectory of a working cone motion is carried out by means of defining angular velocities ω_e, ω_{pr} and analysis of the amplitude readings of impacts. These indications can be used to control the directed cone motion. The shift value e at every turn can change with varying ω_{pr} and redistributing the number of impacts around the face perimeter.
When boring the channel in a uniform medium e=const. In a particular case, if e=0, the motion parameter relation is observed

$$h[n] = \frac{\omega_\kappa \cdot r}{\omega_{pr}} \cdot \sin\beta, \qquad (1)$$

Where h[n] is boring length in the preset direction within n impact - h=nδ, β is the angle of screw line

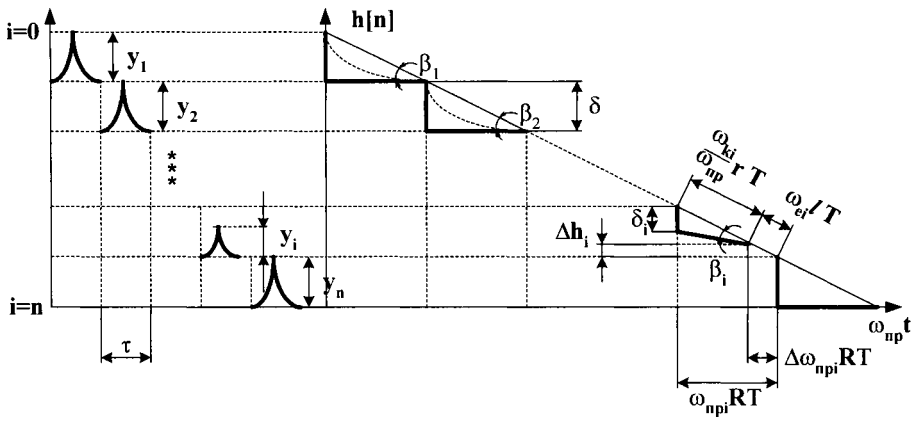


Figure 3

inclination. Figure 3 show the plane projection of a screw line for a turn.

Impact of duration τ=T and amplitude y make line B'AB" to be formed, which consists of curved portions of separate tunneling for every impact, thus resulting in screw line inclination at β angle.

If the medium is nonuniform, the parameter relationship in (1) is violated. Thus, in figure 3 at i-th stage impact amplitude $y_i << y_n$, impact duration $\tau_i < T$, by Δh_i decreases $\delta_i < \delta$, the angle $\beta_i < \beta$ changes and there appears eccentricity e_i. All the above can result in trajectory deviation due to variation of dynamic properties of tunnelling process.

To correct this deviation operatively one must have a self – adjusting system of automatic controlling the direction, which is effective if the anisotropy of medium acts casually. The system shown figure 4 has as a source of data gauge 1 of the amplitude of impact, gauge 2 of angular velocity of cone turn $\omega_к$, gauge 3 of the angle of drive rotation velocity, a discrete correlator, a controlled filter, adaptive regulator. To find the dynamic properties of the system consisting of a drive feeding set, penetrating cone with a striker, a pulse transient function as a sequences of coordinates is being synthesized in a controlled filter as:

$$W_0 = W(0)\,,\ W_1 = W(\tau)\,,\ W_2 = W(2\cdot\tau)\,,\ W_n = W(n\cdot\tau).$$

These values enter the RAM on OS_1 - OS_n.

Standard values ω^*_0–ω^*_n are recorded on OS^*_1 – OS^*_n to put programmable trajectory into ROM.
On the delay line a periodic signal is put from the input unit, which is proportional to the centered correlation input – output function. Thus, the following expression is obtained on the adder output:

$$K^{*0}_{xy}(\tau) = T_m \cdot \sum_{i=0}^{n} W(i\cdot T_m)\cdot K^0_y\cdot(\tau - iT_m)\,.$$

The difference is put to the comparator:

$$\varepsilon = K_{xy}^{0*}(\tau) - K_{xy}^{0}(\tau),$$

By adjusting the coefficients they ten fd to make it minimal. Extreme regulators are used to make the process of impact function estimate automatic.

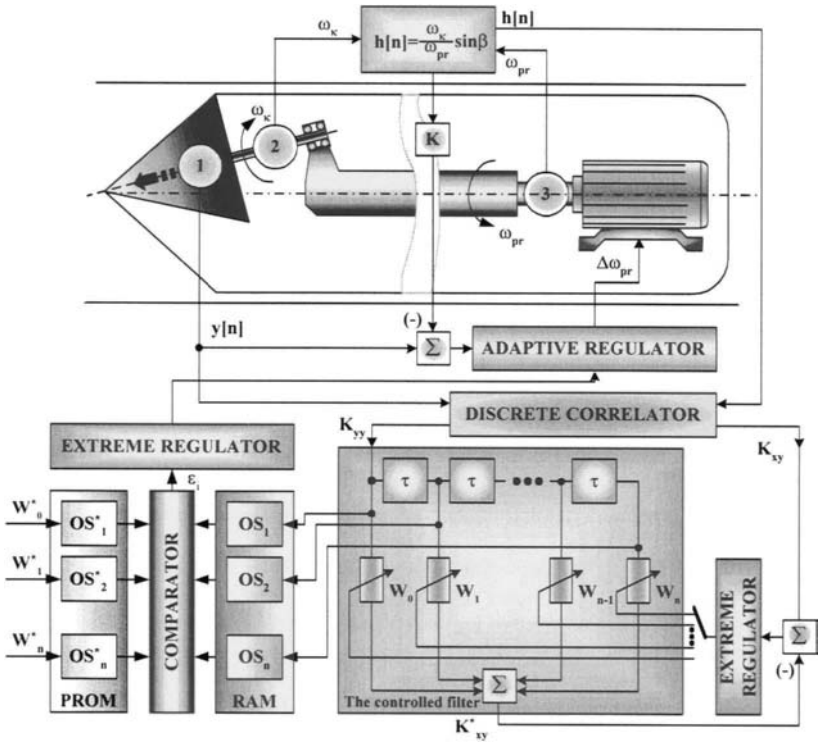


Figure 4

Thus, the procedure of trajectory monitoring envisages a complete analysis of dynamic system properties taking into account stochastic character of effect. This method of driving uses intensifying impact effects for probing anisotropic properties at the face and controlling the process of direction correction.

Advances in Building Technology, Volume 1
M. Anson, J.M. Ko and E.S.S. Lam (Eds.)
© 2002 Elsevier Science Ltd. All rights reserved

Façade Cleaning Robot

Thomas Bock, Alexej Bulgakow, Shigeki Ashida
The Chair for Realization and Informatics of Construction
The Faculty of Architecture, Technical University of Munich
Arcisstr. 21 80333 Munich, Germany
Tel. +49-89-289-22100 Fax. +49-89-289-22102
Email: thomas.bock@bri.ar.tum.de : bulgakow@bri.ar.tum.de : ashida@bri.ar.tum.de

Abstract

Considering all available basic conditions, a semiautomatic façade cleaning robot can be best implemented for technical, organizational and economic reasons. All cleaning processes are executed by means of a service robot. The robot is controlled and adjusted by just one operator. The cleaning quality remains constantly excellent and the cleaning efficiency is increased significantly.

Keywords: Cleaning Robot, Façade cleaning, Semiautomatic, Vacuum suction, Nacelle traveling, Skyscraper

Introduction

Skyscrapers have to fulfill above all a representative function for the companies. The status of a façade surface and the entire appearance plays a particularly important role. The environmental leads to intensive contamination of facades, and modern building materials react quite differently to weather influences. Even high-quality natural stone facades do not remain spared from visible signs of pollution. Facades must be cleaned regularly, and the cleaning cycle can last for decades. Nevertheless the demand of the facades must be kept by the cleaning processes within maintainable boundaries. The higher the degree of pollution is, the more intensive the cleaning agents and instruments must be.
The first skyscraper with anodized aluminum facades was built in the seventies. Such facades were offered at that time as maintenance-free, and cleaning was not judged to be necessary, because the anodicl oxide coating is hard and weatherproof. Commercial criteria were a further aspect. Experience showed however that facades anodized and got dirty by weathering. A further important argument for cleaning was not considered, i.e. that the dirtier the façade, the greater is the corrosion load. In addition contamination increases the original surface area making it more absorptive so that larger quantities of aggressive air impinge on the surface. That can lead within several years to corrosion of facade surface to the extent that the original immaculate appearance cannot be repaired.
Cleaning anodized facades therefore is recommended for the following reasons:

- for good appearance
- to remove the chemical load by removing contamination
- to remove iridescence
- preservation of value

Implementation concept

Considering all available basic conditions, a semiautomatic cleaning version as described below is best implemented for technical, organizational and economic reasons. The robot is accommodated thereby on a nacelle of the traveling unit, adjusted during the whole cleaning process until completion and with the transfer of a worker (figures 1 – 2).

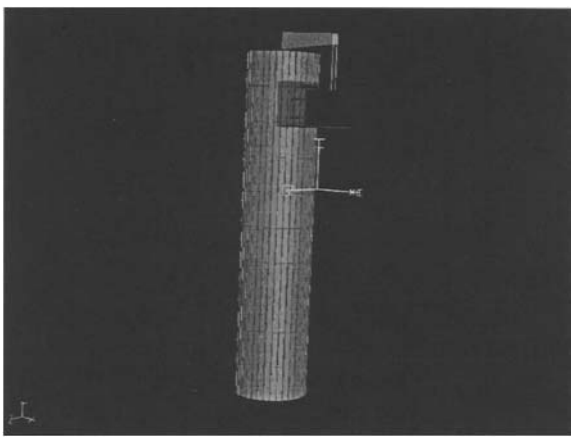


Fig. 1. Nacelle of the traveling Unit

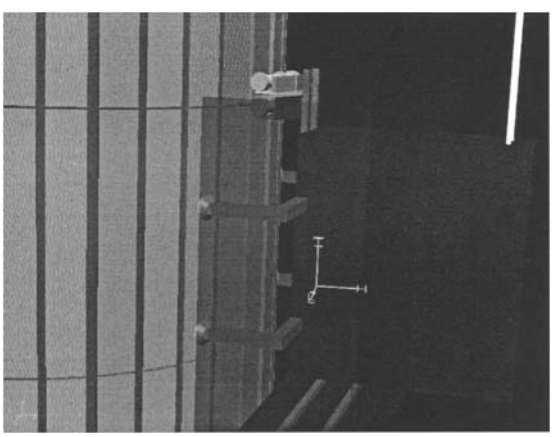


Fig. 2. Fixing of the Robot on the facade surface with Vacuum Suction Cups

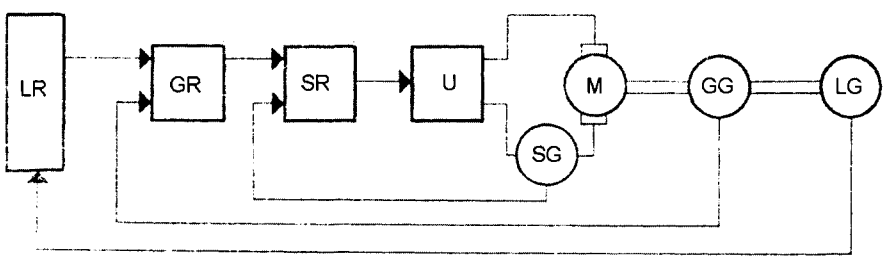
The function of the worker exists in the monitoring of the cleaning process and in the execution of the cleaning of the facade surface zones difficult to access by hand. The latter enables a simplification of the robot system and thus a cost saving.
The robot can be used also at surfaces of other types, e.g. for window surface cleaning.

Technical data of the facade cleaning robot

Type of cleaning	Brushes
Brush size	Length: 300 mm Thickness: 50 mm
Drive	Automatic guidance of the cleaning heading
Heading pressure	Manual adjusts
Dressing plant	Negative pressure system
Capacity	4,0 kW
Cleaning performance	50 m²/h
Advantages	Small personal expenditure Good and safe cleaning quality
Weight	75 kg

Application of the cleaning operation

When an electromechanical system consisting of power supply, motors, transmissions is designated for the cleaning drive, it brings the cleaning brushes into motion. The main parameters of the drive are performance, speed, precision, controllability, dimensions, weight and price. The special feature of electric drives is that they are of small dimensions, easy to control, of high precision, maximum efficiency and reliability (fig. 3).
Regardless of their relatively low performance and quite high price, electric motors are the best fit for cleaning robots of facades.



LR ; Position regulator, GR ; Speed regulator, SR ; Power regulator,
U ; Converter, M ; Motor,
LG ; Position sensor, GG ; Speed sensor, SG ; Power sensor

Fig. 3. Main Scheme of electrical operation

Application of the robot platform

The platform of the robot is equipped with a pneumatic drive. The vacuum cups serve mainly to maintain the contact pressure of the robot to the surface during the cleaning process. Additionally they permit a progressive movement up and down along the facade. The robot is held by the wire rope of the traveling unit. The vacuum force is kept normally as a function of

the entire mass of the robot, either by the degree of the vacuum or by the number of suction cups. These adjustments are made before beginning the work and do not need to be corrected during the job.

Completely differently adaptive vacuum cups are possible. At the fig. 4 an appropriate structural variant is represented. The vacuum cup consists of the pneumatic cylinder (1), the lower part of which is a suction cup in the form of an open vacuum chamber (2). The vacuum chamber is through the connecting piece (3) is connected to a vacuum source. The entire device is connected by the coupling (5) to the lifting machine. The axle (4) forms a link connection to the piston rod (6) of the cylinder. The vacuum chamber additionally has a valve (7) which connects to the atmosphere. Between the housing of the pneumatic cylinder and the coupling the torsion spring (8) is placed. When releasing the instruction for touching the object, the valve is closed, and in the vacuum chamber a vacuum is created by the compressor. If the load (e.g. because of wind conditions) exceeds the nominal value, the housing of the pneumatic cylinder shifts downward relative to the coupling, the torsion spring stretches, and the piston space of the cylinder becomes larger, so that the vacuum in the vacuum chamber corresponding to the load of the robot increases. The suction force increases, and the holding of the robot in position becomes more reliable. The greater the difference between the nominal and the actual value of the load, the larger the shifts of the housing of the cylinder, the volume of the piston space and thus the suction force of the grip arm.

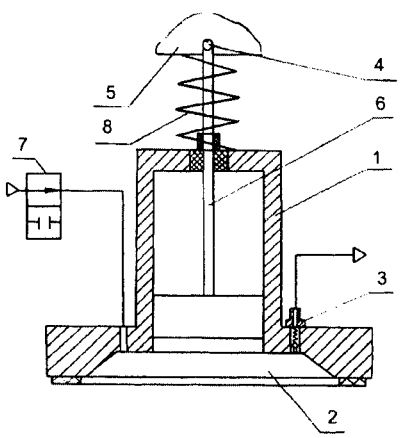


Fig. 4. Adaptable Vacuum Sucker

Conclusion

Considering all of available basic conditions of technical, organizational and economic constraints, semiautomatic cleaning version can be best implemented. The cleaning process is executed by the robot. The check of the process and adjusting the robot are implemented by an operator. The second worker can be saved. The quality of the surface remains constant and the cleaning efficiency increases significantly.

Advances in Building Technology, Volume 1
M. Anson, J.M. Ko and E.S.S. Lam (Eds.)
© 2002 Elsevier Science Ltd. All rights reserved

ADVANCED CONSTRUCTION DESIGN AND TECHNOLOGY BY ROBOTICS

Prof. Dr. Dipl. Eng. Thomas Bock
Dipl. Eng. Klaus Kreupl

Faculty of Architecture, Munich University of Technology
Arcisstr. 21, D-80333 München, Germany

ABSTRACT

When a single client needs a building the normal procedure usually produces low quality. The establishment of big general contractor-companies or powerful clients leads to a loss of price transparency and variety of building types. The robot-oriented construction method will allow to satisfy all requirements of all parties who are involved in construction and achieve a robot-oriented building market. This will increase productivity and profitability because the robot-oriented construction process is characterized by minimized construction time, high variety and flexibility of design. This process will lead to more complex and coordinated building systems and will need an integrated design method to fulfil any functional requirements and regional building codes. Joining will be a key technology to reduce time of assembly. Due to the high working speed of robots, even small elements can be assembled quickly on-site . This results in a high design flexibility and minimized construction time. A robot oriented building block system requires well defined conditions, which can be achieved by the prefabrication of value added and highly finished small blocks, that have to be only finally assembled on-site. Especially if finish operations can be reduced through high degree of prefabrication the construction cost can be decreased – or profitability of buildings can be increased. Installations such as ducts and pipes can be integrated in building elements. In the early design and conception phases all conditions of construction have to be defined in their physical and geometrical quality. With a clear product hierarchy, the advantages of Industrial Robotics in the controlled environment of factories for mass-production of small and value added elements can be used thus on-site construction time can be reduced.

KEYWORDS

Robot-oriented construction, building processes, building systems, Integrated Design Method, Joining Operations, Design Flexibility, Prefabrication Systems, Robotic Assembly Systems, Product Hierarchy.

1. INTRODUCTION

Although the building industry doesn't reach the degree of automation and rationalisation which is common in other industries (e.g. the automobile industry), there are many singular implementations in use with a remarkable technological level. Industrial automated processes are only implemented in the

production of components in stationary prefabrication plants (e.g. masonry and concrete elements) in order to obtain high-quality results (Dalacker, 1997). Irregular demand, great variety and high capital costs in construction require similar strategies as already applied in the manufacturing industry. The shorter the time span between contract signing and utilization of the building the cheaper the financing of the project. Therefore robot oriented manu-facturing requires standardized planning, production and assembly systems (Bock 1988).
An overall hightech construction method for buildings would offer many benefits: Increasing quality of product and proceeding, less construction time, lower prices or higher profitability, so why are these potentials not used? The reason is, that all current solutions are isolated applications. So "Robot Oriented Construction" has to consider all relevant levels of a building project: Beginning with the market conditions and contactors structures, leading over the project organisation concerns, and finally reaching the production and assembly methods – everything has to be redesigned in view of automatisation.

2. GLOBAL STRATEGY FOR ROBOT-ORIENTED CONSTRUCTION – TRANSITION OF BUILDING MARKET TOWARDS ROBOT-ORIENTED CONSTRUCTION

Normally when a client needs a building, he will ask a company, for which architects and engineers are working, for the design, planning and disposition of the construction project. Later one or more builders will be assigned to execute the construction works (figure 1).
A major disadvantage of this model is the way of defining the quality. Since there is no sufficient quality control of works between company and builder even though specifications are usually listed. Due to the fast development of science and technology, building related specifications of up to date technology is hardly available especially to small builders. The smaller the builder is, the less successful is the definition and control of quality. Since technological know-how is related to production technology which is varying from one company to other, the quality of the building as a product is differently decided by each builder. Furthermore the architect is sometimes not aware of the state of the art of technology. This dilemma can be seen at the fact that former tasks of architects are now executed by specialized engineers. This development supported the establishment of large general contractors offering turn-key-system in construction (figure 2).
If the client is confronted to few large contractors which decide the quality and guaranty of the building, he can only choose between some companies and there is no transparency of prices. Figure 3 shows powerful public or private clients which also run their own planning office. In this case, the client can partly influence the producer, but the producer will always decide the variety of building types for the production and construction of large projects. The robot-oriented building and construction system will allow to satisfy the requirements of all parties that are involved in construction. Due to the inherent character of robotic technology, all standards of soft- and hardware have to be well defined. Suppliers have to provide the geometrical and physical qualities of building elements that are required for robot-oriented construction method (figure 4).

TRANSITIONS OF BUILDING MARKET TOWARDS ROBOT-ORIENTED CONSTRUCTION
FIGURE 1

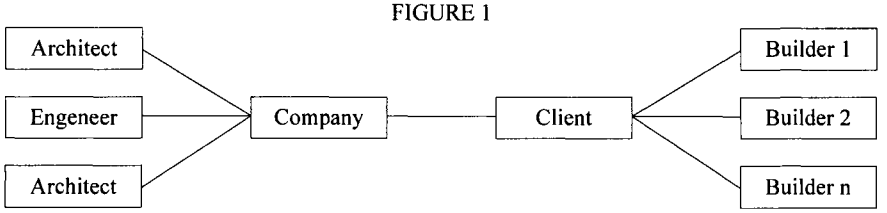


FIGURE 2



FIGURE 3

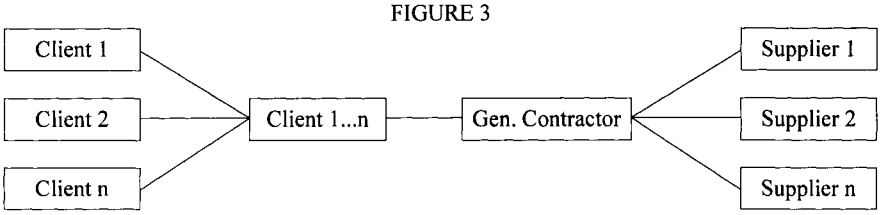
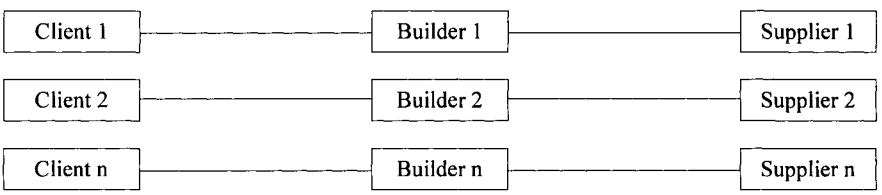


FIGURE 4



This robot-oriented building market will be achieved, if the following 15 parameters can be simultaneous fulfilled without excluding each other.

3. PARAMETERS OF ROBOT-ORIENTED CONSTRUCTION

1. Flexibility
2. Definition of cost
3. Clear marketability
4. Definition of price
5. Guaranty of price
6. Transparency of price
7. Homogeneity of production
8. Continuity of production
9. Definition of quality
10. Control of Quality
11. Transparency of quality
12. Standardization
13. Definition of construction period and time
14. Control of construction time
15. Transparency of construction time

a. Increase of Productivity and Profitability

Productivity of construction industry can be increased through production of highly differentiated building elements which are suited for many function. A major improvement in Robot-Oriented Construction is the reduction of on-site construction time through higher working speed and almost 24 hours working hour a day. For example, it takes a mason about 1 to 1½ hours to construct 1 m^2 of masonry. The same job, a robot could do 10 to 50 times faster. Thus the cost of the building will increase because the building can be utilized shortly after it has been ordered or purchased.

b. The Transition of Building Processes Towards Robot-Oriented Construction

The traditional building process is characterized by a long construction period, which is resulting in a lower profitability of the building and therefore uncertain prices but a big variety and flexibility of

design (figure 5). The rationalized construction process is characterized by typification of planning and well defined supply system already before the contract is signed thus reducing the construction time but also limiting variety and flexibility of design through the use of large sized elements (figure 6). The industrialized construction process is characterized by a reduced construction time thus allowing higher profitability and security of price through homogeneous and continuous production of mass-produced building elements (figure 7). But this model is weak for fluctuations of the building market. The robot-oriented construction process will be characterized by minimized construction time, high variety and flexibility of design. The flexibility of software allows the production to adjust to fluctuations in demand. This system requires a certain product hierarchy which results in well defined and specially designed building elements for robotic construction (figure 8).

FIGURE 5

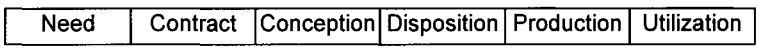


FIGURE 6

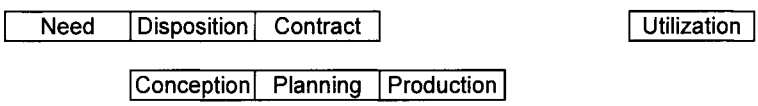


FIGURE 7

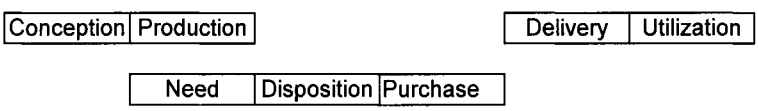
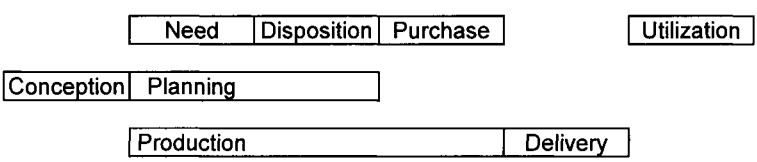


FIGURE 8



c. Planning of Building Systems and Coordination of Building Systems

The more advanced and industrialized a construction process is the more important the design stage becomes, since most building elements are designed and produced before the construction of a building is ordered. The accuracy of subsystems vary: The low accuracies of foundation works are insufficient for other construction works and the higher accuracy of floor wall or installation assemblies are not required for earth works. Different categories of accuracies should be defined for different construction works, considering with compliant interfaces of building sub-system. This is also true for the production of complex elements which are composed by e.g. wood, plastic, steel section whose tolerances also vary, affecting each other and therefore they have to be compliantly coordinated. Due to the increased complexity of modern building compared to the ancient building this kind of coordination of subsystem is required.

d. Integrated Design Method

Building systems should not only be designed for robot-oriented construction but also for usual maintainability, reliability, stability, serviceability, safety and aesthetics. This requires the coordination of production-related engineers with planners and architects. The robot oriented design of small standardized, functional and material elements are required for robotic construction in order to adjust to any project. This requires the modular coordination of smallest elements of building kit as well as modularization of robot software. Specifications and building systems have to be designed as kits which consist of highly differentiated parts which fulfill any functional requirements and regional building codes.

e. Importance of Joining Operations in Construction

In construction more than 2/3 of the production time is used for some kind of assembly operation (DIN 8593 "FUEGEN"). Therefore efficiency of construction can be mostly increased if building elements are designed for automatic assembly.

f. Increase of Construction Efficiency and Design Flexibility

Due to the high working speed of robots, even small elements can be assembled quickly on-site . This results in a high design flexibility and minimized construction time (figures 9 and 10).

FIGURE 9
COMPARISON OF ON-SITE AND FACTORY PRODUCTION TIMES OF CONSTRUCTION

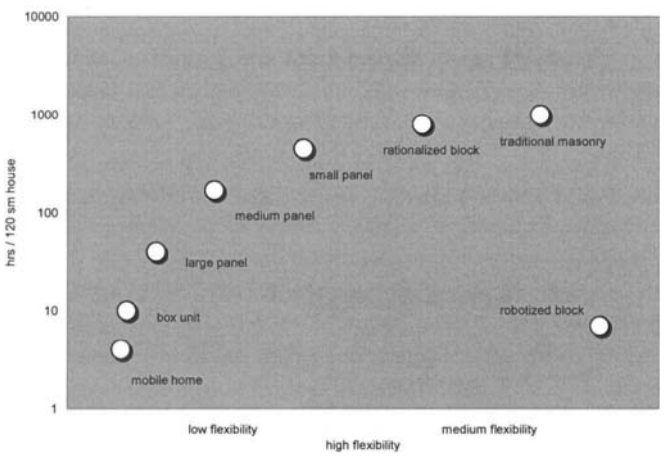
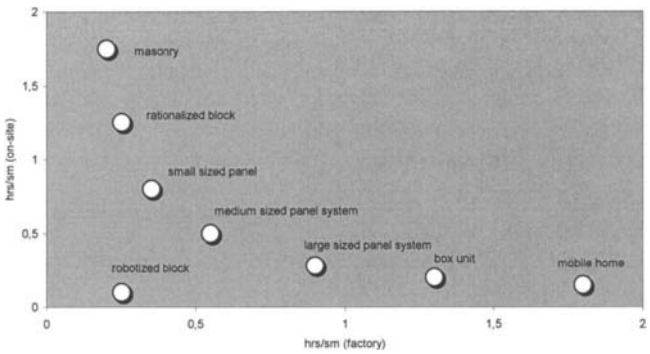


FIGURE 10
DESIGN FLEXIBILITY



g. Increase of Construction Speed and Design Flexibility

Most commonly used prefabrication systems are based on the following principle of building production: Building elements, that are as large as possible and as prefabricated as possible, are centrally produced and finally assembled on-site. The basic idea is to minimize on-site construction operations. All existing prefabrication systems are based on this principle, which is economically oriented in order to improve quality of production and increase productivity of construction.

Among existing prefabrication systems, the box unit system allows the highest reduction of on-site construction time. The size of the box unit is decided by the conditions of transport. Other prefabrication systems consist of elements and parts that are transported to the site for further processing.

As most prefabrication systems, especially the box unit system incorporates the problem of low flexibility in time. Conventional building systems which are almost produced on-site offer an increased flexibility in time and in design. Changes in design can be realized at a later time since the size of elements and parts is smaller and allows later adjustments – during construction phases.

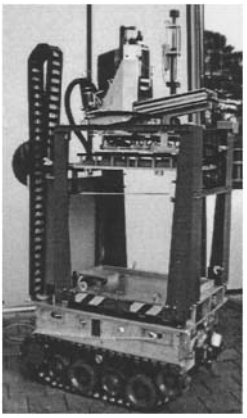
This disadvantage of prefabrication systems might be a reason for the stagnating market share of 10% to 20% of all construction of housing.

Through robotic technology we can combine the advantage of traditional and flexible building systems and prefabrication systems:

- Small building elements can be prefabricated centrally and shipped to the site where assembly robots construct the building at an increased assembly speed.
- The size of the building elements does not necessarily have to be large since the working speed of robots is many times faster and robots can work 3 shifts a day.

Figure 11 shows a robotic assembly system.

FIGURE 11
PROTOTYPE OF A MOBILE INTERIOR ROBOT
(FELDMANN, KOCH 2000)



The advantage of the robotized block system is increased design flexibility and easy material transportations even on narrow streets and over small bridges.
The centralized prefabrication of small block-like building elements enables the following on-site production:

- higher investments of production facilities due to long-term and continuous production
- free from bad environmental conditions (weather)
- homogeneous working conditions
- high level of organization
- due to minimized on-site construction building materials and elements are less damaged
- highly prefabricated and finished elements can be assembled on-site

A robot oriented building block system requires well defined conditions, which can be achieved by the prefabrication of value added and highly finished small blocks, that have to be only finally assembled on-site. Especially if finish operations can be reduced through high degree of prefabrication the construction cost can be decreased – or profitability of buildings can be increased. Installations such as ducts and pipes can be integrated in building elements.

h. Physical and Geometrical Definition of all Elements

During early design and concepting phases, a three dimensional space is created in which the positions of all parts are well defined. All conditions of construction have to be defined in their physical and geometrical quality.

i. Clear Product Hierarchy

The clearer the product hierarchy becomes, the easier robots can be implemented in construction. In order to rationalize construction building kits, they are split up into well defined hierarchical levels. This means a product is subdivided into sub-products according to robot-oriented requirements. If a project is realized an hierarchy of all the building parts , elements and groups necessary for the project can be shown. On construction sites, we can see all kinds of parts, elements sections and material that are transported to the site and further processed there. But in case of robotic construction, the site is just the final production stage of building production. Prefabricated, value added, small elements are

shipped and installed on-site before the building is utilized. In this case, advantages of Industrial Robotics in the controlled environment of factories for mass-production of small and value added elements can be used thus on-site construction time can be reduced (figures 12 and 13).

FIGURE 12
PRODUCT STRUCTURE OF CONVENTIONAL CONSTRUCTION

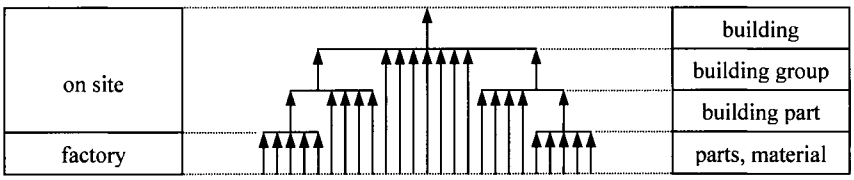
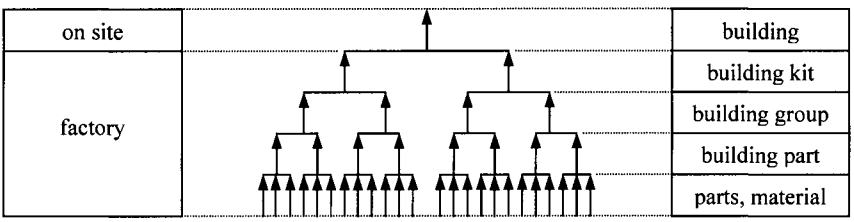


FIGURE 13
PRODUCT STRUCTURE OF ROBOT ORIENTED CONSTRUCTION



4. CONCLUSION

An overall hightech construction method for buildings would offer many benefits for every party involved in building construction processes (clients, building industry, planners): Increasing quality of product and proceeding, less construction time, lower prices or higher profitability.
These potentials could only be used, if all levels of construction processes (the market structures, planning and building systems, design methods and product integration), could be aligned with the concerns of automation.

REFERENCES

Bock, Th., *Robot Oriented Design*, Shokokusha, Tokio, May 1988.

Bock, Th., Kreupl, K., Herbst, J. *"Planning aids for enhancing the implementation of a mobile robot on the construction site"*, proceedings of the 17th International Symposium on Automation and Robotics in Construction, ISARC, September 2000.

Dalacker, M. "Entwurf und Erprobung eines mobilen Roboters zur automatisierten Erstellung von Mauerwerk auf der Baustelle", *Schriftenreihe Planung, Technologie, Management und Automatisierung im Bauwesen*, Band 1, Fraunhofer IRB Verlag, Stuttgart, 1997.

Feldmann, K., Koch, M. *"Development of an Open and Modular Control System for Autonomous Mobile Building Robots with Flexible Manipulators"*, proceedings of the 17th International Symposium on Automation and Robotics in Construction, ISARC, September 2000.

Advances in Building Technology, Volume 1
M. Anson, J.M. Ko and E.S.S. Lam (Eds.)
© 2002 Elsevier Science Ltd. All rights reserved

Embedded System and Augmented Reality in Facility Management

Thomas Bock, Helga Meden, Shigeki Ashida
The Chair for Realization and Informatics of Construction
The Faculty of Architecture, Technical University of Munich
Arcisstr. 21 80333 Munich, Germany
Tel. +49-89-289-22100 Fax. +49-89-289-22102
Email: thomas.bock@bri.ar.tum.de : helga.meden@bri.ar.tum.de : ashida@bri.ar.tum.de

Abstract

The functions of facilities often have to be optimised regarding all requirements. To optimise effectively, we must analyse the present situation and refer to optimising future requirements.
For each aspect of facility management, we should use real time data, and not store data which are sometimes never used anymore.
For integrating real time data systematically, 3D scanning is simple and the best, but there are still some difficulties in such methods.
We can employ an embedded system with RFID (Radio Frequency Identification) and AR (augmented reality) system with mobile computers. With this combination, we have the following possibilities of;

- Fast and easy grasp of the basic data of facilities through RFID and virtual realizing with AR
- Visual comparison between the basic data and the present situation, and the adjustment of data
- The ability to see through obstacles
- Simulation of consequences

Both, RFID and AR systems, are already existing products, offered as mobile or wearable devices in the market.

Keywords: Facility Management, Embedded System, RFID (Radio Frequency Identification), Augmented Reality, Mobile Computers, Recognizing

1. Introduction

Facility Management is one of the disciplines, used in Architecture for the past 25 years in the US-market, 20 years in the Netherlands and Great Britain and about 10 years in Germany. Facility management aims at more effectiveness in using facilities at their maximum function at any time for any intention, instead of reconstructing a new building. Facility Management is more than a management of facilities, but a management of the function and services in facilities.
Function means convenience, satisfaction, safety, pleasure by facilities, which are for example rooms, walls, furniture, lights, machinery, papers (information) and others.
These functions should be always adapted to suit present requirements, when users change, organizations or the environment has to be rearranged. Sometimes it is better a total change of facilities in the case of new technology. Of course facilities must be maintained of waste and breakdown.
To optimising the functions of facilities effectively, the present situation and findings consolidated in the future.
3D scanning with AR is one of the best methods, but there are still some technical and practical difficulties in achieving such method. It is sometimes expensive, inexact and time for scanning is required. It is also still hard to carry or wear the equipment easily. Therefore an accepted technique with visual 3D only scanning all facilities concerned is not practical at the moment. We must change the functions of facilities when requirements change. The cost for these changes must be minimized by manager in achieving the maximum function and performance.

2. Identification technology

RFID (Radio Frequency Identification) is a popular identification method. A chip is embedded in each object containing its specific data as registered. The scanner for this system is in most of cases easy to carry or wear. AR (Augmented Reality) itself with wearable computers has also already been popular. One such application needs trials of AR for 3D scanning.
It seems becoming possible, but still many devices are required for recognizing self-position. At the moment it is better to fix the scanning position for easy and exact scanning.

3. Concept of mobile management

Our work is trying to adopt an embedded system using RFID and AR with mobile computers for recognizing of facilities.
All specific facilities data are initially registered and a RFID chip embedded. If more detail data must be stored, the identification is related to a data bank automatically (Fig. 1). The manager does not need to search, compare and select the data.

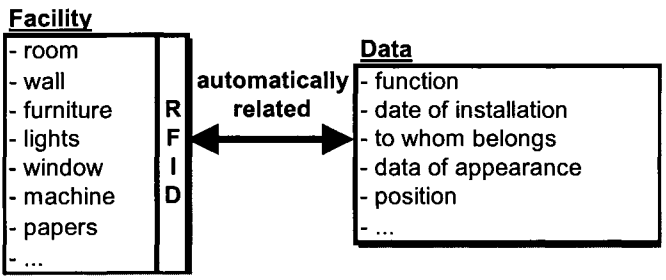


Fig. 1: Embedded data

With RFID, instead of using a bar code, all facilities within radio reach identified at one time. The manager can also take invisible objects into account. Furthermore a RFID chip can be embedded in the facility without disturbing the aesthetic appearance.
The ability of RFID for rewriting is important as well. The visual situation, which means position, wearing, shape, colour and others, is shown virtually with AR. The manager adjusts his/her position of view, and compare with the real present situation. Then the difference is rewritten on RFID system. (Fig. 2)
These devices are easy to carry, even to wear when more convenient. The manager can move to all related areas light on footwork. He/She can collect quickly only the necessary data for facilities under consideration, and the data are transferred for analysis between requirement and action. Only the necessary data, which are not expensive in quantity, are handled.
In case immediate action is required, fast and suitable decisions can be made just in time and place, because all relevant data are carried or worn by him/her. It is also possible to confer with a different person, who is in different place at the same moment, though a mobile communication tool to make better decisions whenever it is necessary.

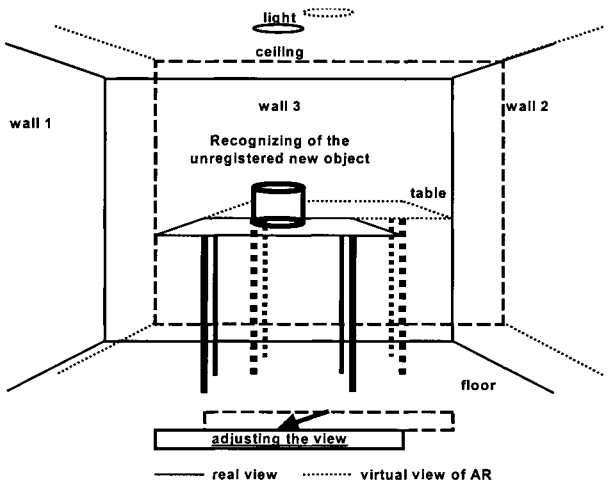


Fig. 2: Concept of recognizing and adjustment

4. Enhanced capacity by AR

With AR, it is also possible to show invisible objects. An object behind some obstacle, something inside the facility, pipes or ducts above the ceiling, electrical or communication cables under the floor, reinforcement in the walls.
A helpful view for consideration becomes visible with AR as well. The temperature, humidity, airflow, direction and level of lighting, smell, sound and others can be surveyed visually by the manager.
In the case there are some different ways to meet a requirement, the manager can compare or confirm the effect of each action through virtual simulation with AR. It is possible to select the best action, and also check the need for materials or new facilities.

5. Future work

This trial is still just a concept, and we must think furthermore about the realization. The best concrete systems should be created and combined.
Of course its efficiency must be confirmed with some case study or practical adoption, if this survey method as to be used in Facility Management. It should not only be used to analyse an existing situation, but also included as part of a total system of management if it is to be used effectively. We will create such a facility management system with RFID and AR recognizing system.

6. Conclusion

There are exciting possibilities for the Facility Management discipline through its development of AR and RFID embedded systems. Practical trials are in work; results will be published.

This Page Intentionally Left Blank

Advances in Building Technology, Volume 1
M. Anson, J.M. Ko and E.S.S. Lam (Eds.)
© 2002 Elsevier Science Ltd. All rights reserved

ROBOTS FOR LOCATION AND SPACING OF WOOD

Prof. Dr. Eng. Thomas Bock
Faculty of Architecture, Munich University of Technology
Arcisstr. 21, D-80333 München, Germany
Dr. Eng. Dimitry Parshin
Faculty of Mechatronik, South Russian State Technical University
Proswestschenja Str. 132, 346428 Novotcherkassk, Russia
Dipl. Oec. Aleksei Boulgakov
Faculty of building technology, Moscow State Building University
Kedrowstr. 14, H. 3, of. 405, 117036 Moscow, Russia

ABSTRACT

Construction is of great interest for usage of wood processing robotics. The structure, kinematic and dynamic models of robots for material location and spacing as well as wood processing have been considered in the paper. Taking into account specific features and dynamic characteristics of robots, recommendations on movements planning and forming laws of control have been given. In conclusion recommendations for obtaining accurate measuring data and on the composition of robot software have been provided.

KEYWORDS

Robots, wood, location, spacing, dynamic models, kinematics.

1. INTRODUCTION

When producing elements of prefabricated wooden houses a great deal of work on location and spacing of wood and shaping of holes, recesses, decorative patterns is done. The project's individual peculiarities require the application of technological equipment with quick readjustment and opportunity to prepare control programs on the model during a short period of time. While solving this problem much attention is paid to the robotization of the operations mentioned above and the creation of robotic systems. The successful solution of robotization tasks is first connected with the development of original kinematic structures and competent structural analysis. One more significant problem of robotization of wood processing operations is setting the trajectory for cutting tool movement and provision of its purposeful movement along these trajectories with definite orientation.

2. ROBOT STRUCTURE, KINEMATIC AND DYNAMIC MODELS

When producing elements of prefabricated wooden houses a great deal of work on location and spacing of wood and shaping of holes, recesses, decorative patterns is done. The projects individual peculiarities require the application of technological equipment with quick readjustment and opportunity to prepare control programs for a model duping a short period of time.

The analysis of jobs connected with the location and spacing of wood as well as the shaping of holes and decorative patterns has shown that in the basis of the robotic system there should be a rectangular 3-coordinate gantry robot (fig.1). This cell provides the working tool movement in the plane of a working table as well as lifting, lowering and pressing of the tool. The second cell is an orienting working head providing changes in the tool position relative to the working plane or its rotation around the axis *Z*. The main kinematic relations defining the nature of the wood processing robot motions are presented by the system of the form

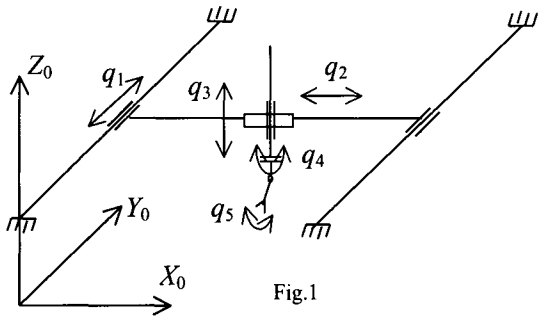


Fig.1

$$x(t) = q_1(t) + l\sin(q_4(t))\sin(q_5(t));$$
$$y(t) = q_2(t) + l\cos(q_4(t))\sin(q_5(t));$$
$$z(t) = q_3(t) + l\cos(q_5(t)),$$

where $q_i(t)$ are generalized robot's coordinates, l is the length of the end link.

The laws for changing the tool phase coordinates $x(t), y(t), z(t)$ and its orientations $\theta(t), \gamma(t)$ are determined by shape and view of the pattern being fulfilled. The angle θ specifies the tool pitch relative to the plane XY, and the angle γ - the direction of the inclination being read from the axis *X*. The values of these parameters their laws of change in time are formed at the stage of planning robot motions. The kinematics of orienting degrees of freedom have been chosen so that the tool pitch angles θ and the pitch directions γ are given separately by the degrees of freedom q_5 and q_4: $\theta(t) = q_5(t), \gamma(t) = q_4(t)$. In this case the laws of the generalized coordinates changes of the transportable degrees of freedom are described by the following ratios:

$$q_1(t) = x(t) - l\sin(\theta(t))\cos(\gamma(t));$$
$$q_2(t) = y(t) - l\sin(\theta(t))\sin(\gamma(t));$$
$$q_3(t) = z(t) - l\cos(\theta(t)).$$

To simplify the controlling functions and increase the accuracy of tool positioning a special-purpose orienting head has been developed, whose rotation axis of the last degree of freedom has been brought onto the plane of tool cutting. While rotating it allows the centre of the tool coordinate system on the rotation axis q_4 to be retained and obtain the main kinematic ratios of a simple kind:

$$[x(t), y(t), z(t), \theta(t), \gamma(t)] = [q_1(t), q_2(t), q_3(t), q_4(t), q_5(t)].$$

Dynamic models have been used to control robots and develop control programs. For translational degrees of freedom in the basis of dynamic models the equation for the forces balance is used

$$\sum m_i \cdot \ddot{x} = F_e - \sum F_j,$$

where m_i are the weights of movable parts; F_e - control force of degrees of freedom; F_j - disturbing effects incorporating frictional forces in movable parts of the mechanism and load forces on the working tool. The control force F_e is connected with a moment *M*. on the drive by the ratio $F_e = M \cdot i_r \cdot G / r$, where i_r is the drive gear ratio; *G* is the gear box efficiency; *r* is an effective radius of the mechanism transforming rotational motions into translatory ones. The drive dynamics for each degree of freedom in the models is presented in a linearized form by the system of equations

$$\alpha(s) = \frac{k_m}{s(T_m s + 1)} u(s),$$

where α is the angle of the motor shaft turn; u is the motor control voltage.

The degree of freedom along the coordinate Z has a double function. One is connected with tool lifting and lowering and the other with creating the necessary pressing force on the working surface. When a resolved force control is applied to the drive Z coordinate, the relationships connecting the moment and control voltage have been incorporated in the model:

$$M_m(s) = \frac{k_m s(Js + f)}{s(T_m s + 1)} \cdot u_m(s),$$

where J, T_m, k_m are inertia, a time constant and the gain factor of the drive.

3. MOVEMENT PLANNING AND CONTROL

The specific feature of controlling robots for location and spacing of wood is the necessity of forming programmed trajectories of cutting tool movement. On this basis the prediction of displacements according to the coordinates is made and control voltages for each of them are determined. At the foundation of the programmed robot control is the principle of setting movement trajectories for a cutting tool and movement program with help of the pattern being performed with the CorelDraw vector graphic editor. While composing patterns their accurate scaling in a special file is provided, this file is then used as an assigning file while carrying out control. On the pattern for material location and spacing or for performing decorative cutting the coordinates of the initial point, and the starting point of the process trajectory are assigned, transition lines between closed figures of the pattern are assigned as well. While processing each figure pattern scanning with digitization step T and read-out of information about the coordinates of the next positioning $x[kT+1], y[kT+1]$ are fulfilled. After the coordinates having been obtained control voltages are determined $u_x[kT+1]$ and $u_y[kT+1]$, and motion speeds along the coordinates x and y during the next control step are calculated as well. In order to reduce the effect of quantization as a control means in the interval $t_n \le t \le t_{n+1}$ we choose:

$$u[t_n] = 0.5[u(t_n) + u(t_{n+1})].$$

This ensures minimization of maximal deviation $\bar{u}[t_n]$ from the true value when changes $u(t)$ take place. When applying graphical means for setting movement trajectories there appears necessity to build algorithms ensuring the proper tool orientation at each point of the trajectory. To solve this problem different kinds of interpolation have been analysed and in the algorithms of robot control a parabolic interpolation in the interval $[(n-1)T, (n+1)T]$ is selected as a basic one. In this case for the time moment $t = (n+1)T$ a predictive calculation of coordinates for the point of tool position is made and according to the coordinates of three points coefficients of an interpolating equation are defined:

$$\begin{bmatrix} a_0 \\ a_1 \\ a_2 \end{bmatrix} = \begin{bmatrix} x^2[(n-1)T] & x[(n-1)T] & 1 \\ x^2[nT] & x[nT] & 1 \\ x^2[(n+1)T] & x[(n+1)T] & 1 \end{bmatrix}^{-1} \cdot \begin{bmatrix} y[(n-1)T] \\ y[nT] \\ y[(n+1)T] \end{bmatrix}$$

Next the obtained values of coefficients a_i are checked:

$$y[(n+1)T] = a_0 + a_1 x[(n+1)T] + a_2 x^2[(n+1)T]$$

and in case of identify the angle of normal to the trajectory in the point $t[(n+1)T]$ is calculated

$$\theta[(n+1)T] = 0.5\pi - \text{arctg}(2a_0 x[(n+1)T] + a_1 .$$

After determining the vector of tool position and orientation and the vector of generalized coordinates $\overline{q}[(n+1)T]$ for the next step of control the values of tool motion speeds $\dot{x}$, $\dot{y}$ and the angular speed of rotation θ are calculated. The accuracy of development of the movement trajectory depends on the accuracy of fulfilling the task mentioned above. The simplest algorithm is the linear dependence

$$v_x[(n+1)T] = (x[(n+1)T] - x[nT])/T$$
$$v_y[(n+1)T] = (y[(n+1)T] - y[nT])/T$$
$$\omega_\theta[(n+1)T] = 2\pi(\theta[(n+1)T] - \theta[nT])/360 \cdot T$$

To perform high-quality patterns we have incorporated high precision control algorithms. For this purpose the trajectory of tool movement is interpolated by a polynomial of the third degree and according to the interpolating function $S_n(T)$ the derivative $\dot{S}_n[(n+1)T]$ is determined. The obtained derivative values are applied for calculating generalized speeds:

$$v_x[(n+1)T] = \dot{q}_1[(n+1)T] = V_0 \cos(\text{arctg}(\dot{S}_n[(n+1)T]))$$
$$v_y[(n+1)T] = \dot{q}_2[(n+1)T] = V_0 \sin(\text{arctg}(\dot{S}_n[(n+1)T]))$$
$$\omega_\theta[(n+1)T] = \dot{q}_4[(n+1)T] = (\dot{S}_n[(n+1)T] - \dot{S}_n[nT])/T$$

Taking into account the fact that during the functioning of control algorithm we can form sampled-data functions $q[nT]$ describing the trajectories of links movement, then to determine derivatives in the points of tool movement trajectory it is advantageous to use control algorithms for the model. While simulating the process of motion differentiation of digital sequences is presented as a sum of the kind:

$$\dot{q}[n] = T^{-1} \sum_{k=1}^{m} K^{-1} \nabla^k q[n] = \sum a_i q[n-i],$$

where $\nabla q[n] = q[n] - q[n-1]$ - inverse difference; m - number of terms of a degree series; $a_i = (-1)^i \sum_{i=0}^{m} K^{-1} C_k^i$; C_k^i - binomial coefficients.

Besides the control method considered on the graphical model it is necessary to include algorithms of programmed control by the path reference point into mathematical calculations and software. In this case reference points $P[x, y]$ and angles of tool orientation in each of them are assumed. Taking into account these values we form the data base to develop the laws of generalized coordinates changes.

Motions planning is thus fulfilled on the basis of interpolation with cubic splines: $S_3(t) = \sum_{k=0}^{3} a_k t^k$.

Coefficients a_k are calculated in each section of interpolation having assumed that the trajectory is continuous and smooth. Planning of the robot's movement is carried out taking account of limitations in degrees of freedom which are preset with reference to the table of limit values for each coordinate $q_i^{\min} \le q_i \le q_i^{\max}$.

The authenticity of the measured parts is of great importance for control. In the encoding position sensors being used there may be abnormal short-term imperfect data that can lead to short-term limit accelerations and deviations from the trajectory. The casual character of some changes of these sensors makes us to introduce predictive and correcting algorithms of simple calculating structure into the algorithms of robot control. In the applied algorithms, expected values of position along the coordinates for the period of change T are predicted in each control step with help of m degree polynomial. Meanwhile we apply algorithms of single prediction, which are based on the Lagrangian interpolating polynomial

$$P(t) = \frac{1}{\tau^m} \sum P_{k-i} \prod_{j=0}^{m} \frac{k\tau + \tau r}{j-i} + \frac{M_{m+1}}{(m+1)!} \prod_{j=0}^{m} (k\tau + j\tau) \ ,$$

where k=1,2,3 - prediction steps.

The analysis of prediction errors has shown that algorithms of double prediction should be applied for robots and values at three points (m=3) are to be taken. For convenience in usage of predictive expressions and reductions of calculations it is better to use a recurrent form of the analysis.
A robot software solves the following problems: analog and discrete information about the parameters of robot condition is obtained, interface with drivers of analog inputs and outputs, output of discrete and analog control signals, formation of technological and emergency information, data display in real time. The programs can function in the environment of Windows and other versions and use all features of this environment. Drivers for data exchange are formed as dynamic libraries DLL. The software includes robot models, which allow to carry out check of algorithm operation.

4. CONCLUSION

The material is prepared on the basis of the authors' research, which was carried out while developing robotic systems for wood processing. The presented kinematic structure, algorithms of motions planning and control have been investigated on the models. Computer simulation of robot motions has shown the effectiveness of the described methods and algorithms. The obtained simulation results were applied while developing and designing robots for cutting and spacing of wood.

This Page Intentionally Left Blank

Advances in Building Technology, Volume 1
M. Anson, J.M. Ko and E.S.S. Lam (Eds.)
© 2002 Elsevier Science Ltd. All rights reserved

ASSEMBLY AND DISASSEMBLY OF INTERIOR WALL

Dipl-Eng. Albrecht Hanser

Technical University Munich, chair of building realization + -informatics, Prof. T. Bock
Arcisstrasse 21, D 80333 München, albrecht.hanser@bri.ar.tum.de

Abstract

Flexible extension walls - watched on a long-term-use - have lower costs and are more economical and especially more variable compared to convenient post-and- beam-structures. Because room requirements – mainly in office and administration building – change faster and faster, an extensive potential on future markets for these technologies exists

Keywords

Flexibility, Economic Efficiency, Non-supporting removable wall-unity, Media- and electric wiring, Put-and-slide-technology, Relocate systems, Cost, Different Elements,



Figure 1: The non-supporting removable wall-unity

Present situation

Flexibility
A higher and higher flexibility of the floor plan is expected in office- and commercial building as in house building. The change of users or function often results in the wish redesigning the existing

spatial pattern. A basic floor plan flexibility is often possible and implemented by dividing the load-bearing building surface from non-structural separation walls and ceilings. A well known system of this type of walls is a wooden or metal post-and-beam-structure with mineral fibre filling and plasterboard panelling. By using this building system it is difficult to realize variations in different room structures and subdivisions by self building. Once they are cheaper to produce and to install but in the end they cause much difficulty in redesigning. They are not flexible and actually not reusable. There are reusable, demountable partition systems available, usually to expensive and to much trouble to construct.

Economic Efficiency

All partners in the construction business know exactly what construction cost means. Very often we think and act only in this kind of category.

The reason for this is the existence of two different types of budget. One for construction and a second for consequential costs during the life cycle, which are even managed by two different teams. Feedback between the two will rarely occur. So at the end of a life cycle for a building, nobody is able to find out the real cost situation which has been followed after construction time, of a product incorporated in the building. We cannot find out what the savings could have been, , even if we had constructed in prefabricated and modular systems.

Indeed thinking in a complex overall view, we realize the advantages for prefabricated and relocatable partitions are:

- Connections with its components, seperations in floor- and ceiling-areas are close in cost of these construction types.
- The finishes of gypsum board partition-walls, assembled on site, do not have the same standard of quality as industrial prefabricated partitions. Prefabricated partitions need no new coatings for 30 years. Conventional gypsum boards need it after 5 years.
- If prefabricated partitions get relocated, the difference in investment cost becomes obvious. A prefabricated partition incurs 40% of its former construction cost, while a conventional partition, which has to be demolished and reconstructed almost completely new, incurs 220%. Beyond a doubt, the payout-return depends on type of construction prefabrication and the number of relocations.
- Recovery and cleaning up belong to an ecological and economical overview; in this context reusable systems offer advantages. Savings of material and avoidance of waste have no exceeding fees for supervised dumps. These charges have been growing constantly in recent years.

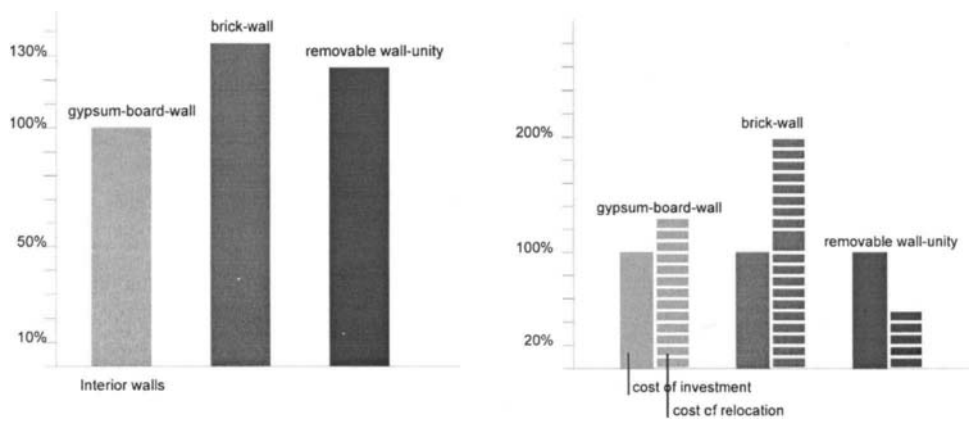


Figure 2: interior walls: cost of investment and relocation

Aim of the project

It was valid to develop a non-supporting removable wall-unity, which allows adaptable, fast and disassembling room-splitting.
Next to the standard components we have to develop elements for the connection at the existing support structure, elements for passages and doors, for windows on the inside and other glazing structures.
Media- and electric wiring are components of the removable wall-unity. The elements are delivered prefabricated and manageable on the construction site.
The connection to the available support structure is created with a wiring mechanism (Justix); the coupling of the elements and also the management of media and electric to work with a put-and-slide-technology.

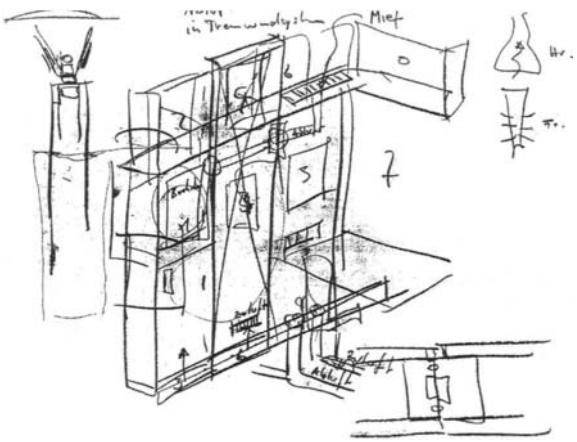


Figure 3: First sketch

Development

The system must be:
- "More than a wall", which means integrated media, such as TV, phone, flat screen, switches, bus, safe, mini-bar, shelf-systems, cupboards, completely connected up;
- Demountable and reusable without damaging the existing solid construction;
- With finish-surface on both sides, in complete lightweight construction;
- Suitable for two persons to handle and install
- Located in price between the plaster board/ post-and-beam-structures and the conventional wall systems.
- Simple construction and long-term use

Beside separating for offices, administration or housing the wall unit is supposed to serve as a room divider, half height screen wall or fair stand.
Put on wheels it can even become a mobile office wall.

One of our aims is to see the wall not only as a separating element between two areas, but to include additional functions such as screen lights, mini-bars, shelf-boards, integrated air-conditioners, even a PC or printer can be hidden in the wall;

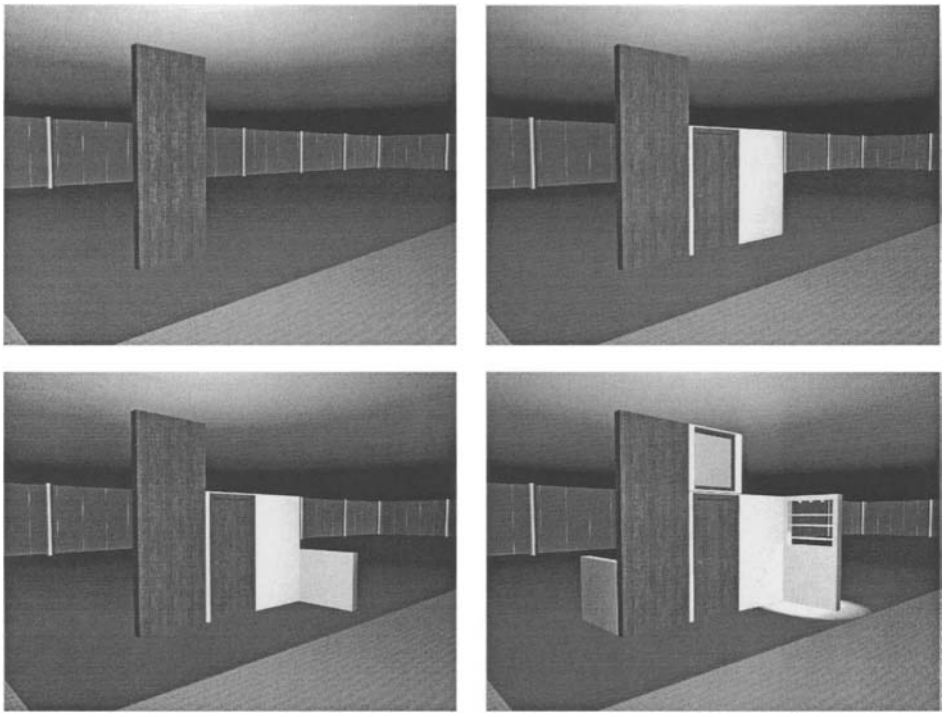


Figure 4: Simulation of the elements

Elements

Surface finished, easy-to-handle modules are basic for interior wall surfaces.
Elements are:
- Full room heightelements (size depending on height of the ceiling, standard sizes)
- Door high elements (height 210 cm)
- Elements fitting above door high elements (size depending on height of the ceiling)
- Elements for easy zoning, separating areas (height 105 cm)
- Special elements

Construction

The substructure for the single module is to be a ring-like frame. Panel materials for wall surfaces such as wooden panels, plasterboard, glass etc. serve as frame bracing, and wooden profiles but also special formed plates can be the frame material.
The connection to the load bearing wall construction and to the ceiling is designed as edging board, and the gap between the bottom of the wall and the floor is covered by a clipped baseboard. A dovetail-like joint with integrated plugs for power and data supply connects the single elements to one another and to the load bearing walls.
The single modules, therefore, are coupled by fitting and pushing the connecting elements together. The stack design is variable.

Door high elements and end elements are connected in the same way. A special processing of the frame profiles makes it possible to carry the prefabricated electronic wires through the element.
The contact from element to element becomes possible through the connecting modules just mentioned. The necessary fitting in to the surrounding construction could be succeeded by vertical adjustable foot construction, which there are two for each wall panel. After connecting the elements the foot adjustor is screwed up and pressed against a connecting profile. The gap arising at the bottom of the wall can be used for supplementary wires – especially for wire systems, that can only be added later (phone, networks). A clip on profile covers the open bottom area as a baseboard. There must be sound and fire technical measures on the surface, in the stack area and in the base and ceiling area.

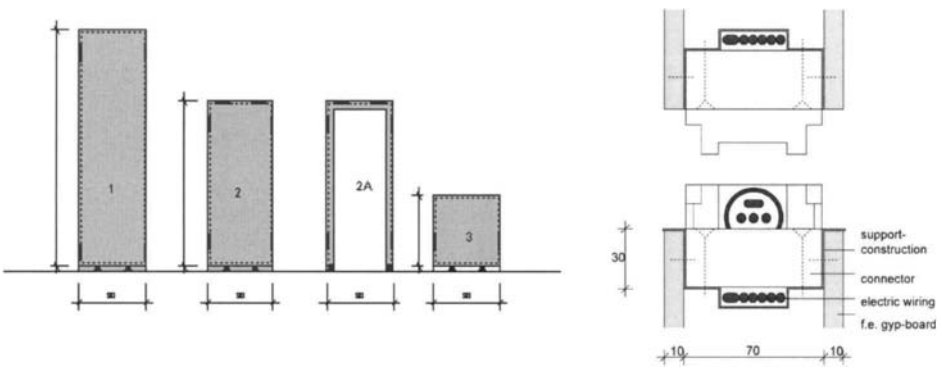


Figure 5: The elements; dimension: 90cm wide, 300cm, 210cm, 90cm high; the connecting system

Fabricating prototypes

Currently parallel extensive tests are taking place using prototype wall modules to transfer the practiced knowledge gained.

Conclusion

The system shown in this paper will find place between the low cost but not reusable gypsum board partition-walls and the industrial prefabricated partitions, which are very expensive. The combination between a prefabricated high tech system, affordable and economical, usable as flexible elements for different tasks are the main advantages of the new system.

References

Studiengemeinschaft Fertigbau (1987): Trennwandsysteme

Tichelmann / Pfau (2000): Entwicklungswandel Wohnungsbau, Vieweg, Wiesbaden

Diverse Herstellerunterlagen(1999, 2000, 2001, 2002): Lindner, Knauf, Item, Dorma, Häfele, Strähle, Hettich, u.a.

This Page Intentionally Left Blank

Advances in Building Technology, Volume 1
M. Anson, J.M. Ko and E.S.S. Lam (Eds.)
© 2002 Elsevier Science Ltd. All rights reserved

MUNITEC-FAST-CONNECTORS - KEY TECHNOLOGY FOR PREFAB HOUSES

Dipl. Eng. Frank Prochiner
Faculty of Architecture, Technical University of Munich, Germany

ABSTRACT

Most leading manufacturers of timber housing confirm that developments leading to a greater degree of prefabrication, and thus a shorter construction period, would significantly improve the sales of this type of building. Today, the carcass structure of so-called prefabricated houses can be erected in an extremely short period, but the subsequent fitting out can easily take a further 4 –6 weeks because of the division of work between different trades that are often dependent on each other. The site assembly of complete, large-scale elements that require no further processing is something virtually unknown at present.

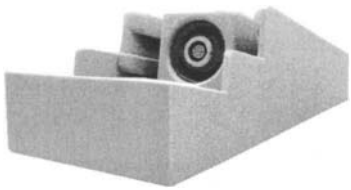
KEYWORDS

Prefabrication, house, connector, process, construction, connection system.

The automobile industry provides a good example of the way an assembly process can be divided between a number of construction groups and suppliers and carried out concurrently or in an efficient sequential manner. Crucial in this respect is the coordination of the various working interfaces between different trades. This includes a strict compliance with manufacturing tolerances and the development of a simple connection system for all elements. Similarly, the advantages of any assembly system will be fully felt only if the connections can be made without the presence on site of various specialists. As part of a project being conducted at the University of Technology in Munich and supported by the Federal German Ministry for Education and Research, a quick, plug in connection unit is being developed that will facilitate the erection of housing in record time. It should be possible in future to take a building into occupation after only 24 working hours; in other words, three days after the commencement of construction. The first day would be taken up by the actual assembly work, the second day by the fitting out and finishing, and the third day by the occupants moving in.
The new quick-connection unit, for which a patent has been applied, will allow a simultaneous coupling not only of the building elements, but of all the systems integrated within them, , such as heating and electrical installations and control networks. The units are fixed to the end faces of the building elements that are to be connected.

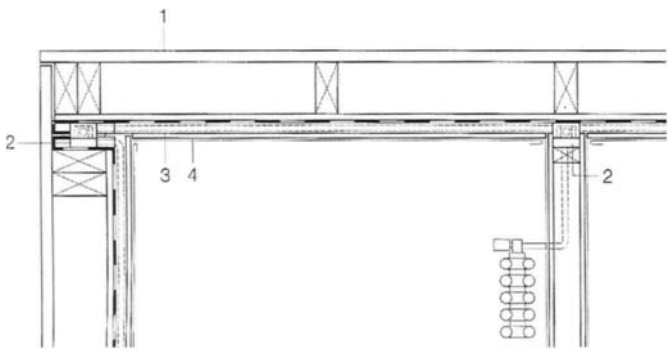
Where a number of runs for different media have to be linked, the connection
units can be installed in a row. Where there are no installations in two adjoining elements, the connecting units will serve solely as a means of mechanical jointing. In collaboration with partners in industry, plugs and sockets have been developed for all kinds of media, including electricity, telephones, data lines, TV, and also liquid media such as heating runs. Further developments are foreseen for waste and soil pipes.
When two wall elements are pushed together, the quick-connection units provide a rough centring for the actual plug-in link. The self centring geometry of the plug then ensures a safe

connection. The connectors permit the coupling to be executed from the side or the rear, in which case the service runs can be installed in the inner skin of the wall or in the wall itself. On



MUNITEC-Fast-Connector

inserting the connectors, their wedges haped geometry causes the elements to be pressed together against the sealing strips. The dead load of the wall element thus ensures a good seal. All heating and electrical runs are installed in the walls and on the underside of the floors, so that the depth of the floor finishings is not a factor in this respect. The ends of the circuits in the walls simply have to be plugged into a central vertical services shaft.

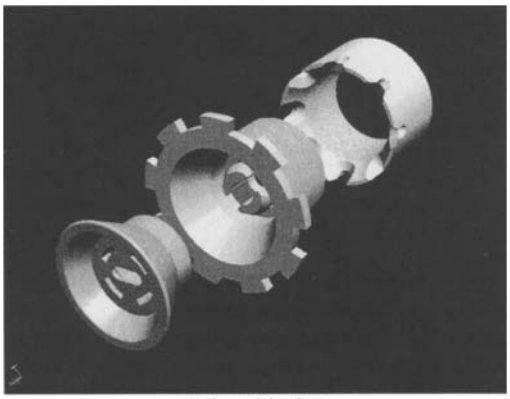


External wall connection – internal wall connection

1 – wall construction depends on manufacturer; 2 – Munitec-fast-connector; 3 – installation zone, integrated in Pavatex panel; 4 – plasterboard, wallpaper and paint finished

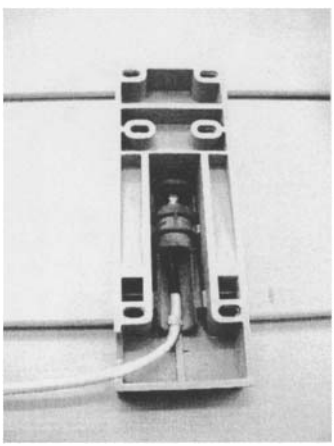
This system reveals a number of advantages over traditional forms of construction and assembly.
• It is faster: the construction period is reduced to three days; service installations are prefabricated and incorporated more swiftly; and building firms are less dependent on the weather and time of year.
• It is more economical: the shorter assembly period represents a big potential cost saving; and life-cycle costs are reduced as a result of the simple method of removal and disposal.
• It ensures a higher level of quality: all components and services are installed at works to a constant quality level and with comprehensive quality controls; and the risk of accidents on site is reduced.

• It is environmentally friendly: building sites are cleaner; waste products are avoided on site; and the reuse of components is simplified by the scope provided for a damage-free dismantling and removal of elements.
An adjustable foot serves to position the individual wall elements on the concrete floor slab. A threaded member integrated in the foot allows the wall unit to be raised and



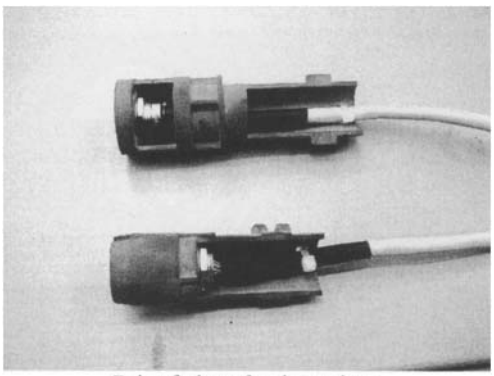
Adjustable foot

Lowered until it is precisely in position. This is indicated by a sound signal from an electronic spirit level on the top of the wall. To facilitate a parallel execution of the work by the various trades, all service installations should be prefabricated to as great an extent as possible, so that these can simply be laid in the wall, floor or roof elements by the respective timber construction firm.
In the case of the electrical installation, a patented system is available – a cable harness or premoulded wiring system – that simply needs to be plugged in, in a similar technique to that used in the car industry. The planning data are coordinated in a special computer program, which also prepares a wall diagram showing the actual cable runs. The ready-wired plugs can be simply clipped into the quick-connection unit. To avoid too many transfer points between the individual building elements ,the cable runs are distributed in the wall with the aid of a newly developed subdistribution system. The conventional distribution box is



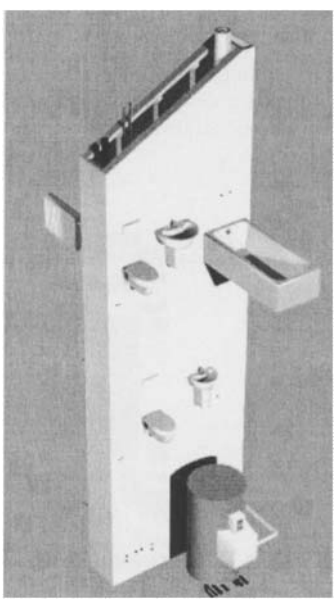
Backview of the MUNITEC fast connector with plugged in connector for data.

replaced by a power installation box (PIB).A simple coding system ensures that runs cannot be plugged into the PIB in the wrong position. In this way, the whole process of wiring up and making connections is obviated, saving time, and allowing the work to be executed by non-electricians.



Pair of plugs for data wires.

If the pipe runs for the heating installation are installed in the inner skin of the wall as heating coils, it will be possible to obviate the need for radiators entirely. Wall heating panels of this kind make sense especially in low-energy buildings. They provide a pleasant radiant heat and are not visible. In contrast to buildings erected in traditional forms of construction ,the installation of heating coils at works avoids damage to pipes and potential leaks. A 30 mm sheet of fibreboard laid on the inner face of the structural wall elements serves as the plane for the installation. This layer allows chases to be cut for the simple fixing of electrical, water and heating runs. At the same time, the fibreboard improves the sound and thermal insulation of the wall.



The central services core is prefabricated complete for all storeys of the building and hoisted into position on site by crane. The entire sanitary installation will possibly be incorporated in it, as well as the vertical distribution cables and runs for the electrical installation and heating.
The vertical shaft will be fitted with the appropriate connection units on all faces that abut walls. It is also conceivable that entire construction groups such as the boiler for the heating, or the sanitary fittings can be plugged in via an appropriate connector. Using this connection technology, it would be possible to achieve a new quality in building in the future. In a system analogous to that found in vehicle construction ,subcontractors and suppliers of components would work collaboratively to provide large system modules. This would also open up new perspectives for the export of prefabricated housing. At present, manufacturers and assembly firms work largely on a regional basis because of the transport costs involved and the fact that site work can require the presence of a trained assembly team for between 2 and 6 weeks. The use of a plug-in system of connection units would reduce the time required for assembly and finishing work to only 2 –3 days. Countries like Japan that are heavily dependent on the import of timber for construction purposes could order entire prefabricated housing kits. Similar markets exist in eastern Europe as well. Emergency shelters for disaster or crisis areas could also be provided in fully functioning form within a short time.
An important aspect of this system is the absolutely damage-free dismantling process once the building has served its useful life. Components or entire buildings can be reused or returned to the manufacturer for recycling – an important aspect when one considers that the building industry holds the record at present for
the creation of waste and the consumption of raw materials.
The use of quick-connection, plug-in technology need not be restricted to the building sector, however. The principle could be adapted for application in many different areas where, together with mechanical connections, service, supply or signal runs have to be linked. Easy maintenance by means of a simple exchange of
units could result, for example, in defect telephone boxes not requiring the services of qualified engineers or electricians to repair them at the place of installation. They could be simply unplugged and replaced with a new unit by service staff. Repairs and maintenance could then be carried out by qualified personnel under more pleasant conditions in the workshop.

This Page Intentionally Left Blank

TEAM PRESENTATION:

INDUSTRIALIZED HOUSING

This Page Intentionally Left Blank

Advances in Building Technology, Volume 1
M. Anson, J.M. Ko and E.S.S. Lam (Eds.)
© 2002 Elsevier Science Ltd. All rights reserved

INITIAL THOUGHTS ON INDUSTRIALISED SOLUTION FOR LOW-COST HOUSING IN CHINA'S RURAL AREA

Guan Kai and Li Shirong

Research Centre for International Construction Economics and Management,
Chongqing University
Shapingba, Chongqing, 400045, PR China

ABSTRACT

This paper deals with the industrialised solution for low-cost housing in China's rural areas. The paper firstly focuses on materials used for frames, roofs, floors, walls and ceilings. It then analyses the requirement and the construction methods for each material on fireproofing, antisepsis and waterproofing. Based on the analysis it also gives some suggestions on the detailed connections of the structural components and the surrounding components. From the structural engineer's point of view, this paper analyses the general load supporting system and the basic principles on the disposition of the structural components in both horizontal and vertical directions. It also gives an introduction an the normal steel components on the size, component, connection and methods of antisepsis and fireproofing. The last part of the paper deals with manufacture and site construction for industrialised housing in China.

KEYWORDS

Cold-formed steel frame, design, industrialised housing, China, construction, low-cost housing, poverty

THE BACKGROUND OF THE RESEARCH

The housing for poor people or low-income people is a mayor problem that every government must face. Because of the huge population and the undeveloped economy in China, it is especially a serious social problem. The traditional construction methods used for hundred of years can't fit the modern needs due to the consideration of sustainability, low-cost, quick and easy construction, high quality, easy maintenance and possibility to move. There is a need to find new approaches to solve these problems.

In addition, looking at the huge rural area in China, there are still many people who cannot afford normal housing. It's especially difficult for the people living in a mountainous area or some old, weak and disabled peasants who are less able to work.

In order to provide low cost, good quality and sustainable housing for those poor people in rural areas in China, the Chongqing University (China), in cooperation with South Bank University (UK), has set up a research team in 2000. The research team has been given financial support from both the British Council

and the China of the Foreign Expert Bureau for three years (from 2001 to 2003). The research team has finished the first stage work so far which was to survey the current rural housing situation, the rural people's need and the local building resources in the rural area. This paper is mainly based on this research project.

THE TARGET GROUP IN THE RESEARCH

Not all the people living in rural area are the target group for the research. The determination of the target group is based on the policies of some local government towards poor housing in rural areas. Each year, for example, the local government provides a certain amount of money to help those people to build new houses. It focuses on those people who live in the caves and the mountain regions and have poor living conditions. There are five types:

(1) Those people who live in the mountain regions where the altitude is over 1000 metres, and also very cold with poor living conditions;
(2) Those people who live in the remote mountain regions, which are far from villages (more than 3 km). The investment for infrastructure is too big and can not to be solved in a short time;
(3) Those people who live in the regions where endemic is very difficult to cure;
(4) Those people who live in the regions where 70% of the cultivated lands slopese more than 25 degree, and lean soil less than 15 cm in depth, and the outputs of foodstuff per hectare are not more than 2kg;
(5) Those people who live in the regions where there are no water supply facilities and it is very difficult to get water without walking more than 1km and climbing is more than 100 metres.

THE PRINCIPLES OF THE SOLUTION

The aim of the research is to find a way to build low cost, easy to build and maintain, good quality and sustainable houses for the poor people in rural areas in west China. To meet the general requirement, some principles to focus the research are listed as follows:

- The layout of the house must fit the needs of the poor people's real life
- The house should keep a traditional Chinese character
- Local materials and resources should be used as much as possible
- The construction should be easy, quick and economical
- The building materials should best be manufactured locally and be usable by less skilled people
- The house should be sustainable with lower environmental impact
- The house should be cheap and affordable

THE RESULT OF THE FIRST STAGE WORK

After the first stage of the research, some useful information on housing in China's rural areas was obtained and this information is most important for the next stage of the research work.

The Cost of the House

Clay-brick and pre-stressed reinforced concrete boards are widely used to build houses in rural areas. The cost of the house is usually around 200~300 Yuan per square meter. The cost difference mainly depends on the local building products and local transport conditions.

The cost items of the house in rural area are building material costs and construction costs. The land for a farmer's house in rural area can be used after the application is accepted by the local town authority. The local rural people help each other to build houses. The construction costs then usually cover the food and accommodation for these people and the owner also invites several skilled workers to guide the work. The detailed items and the percentage of each element of work are listed in table 1.

TABLE 1
THE DETAILED COST ITEMS

Item Name	Percentage	Sub-item Name	Percentage
Building Material cost	90%	Walls	25%
		Roof & floors	30%
		Doors & windows	15%
		Foundation	20%
Construction cost	10%		

Table 1 shows the normal costs for a two-story brick-concrete house in China's rural area. If the building materials and the floors are different, the percentage of each item should be quite different. For example, to build a one story brick-concrete house, the percentage of the foundation and the roof & floors will drop while the percentage of other items will increase.

Based on the initial investigation, some initial thoughts come out for the housing design, namely:

- Looking for cheap materials to build walls, floors and roof
- Using light weight materials to reduce the load and the cost of the foundation
- Adopting new construction technology to shorten the construction period

The Local Building Resources

The investigation found that the local resources to be used could be straw, bamboo, stone and sugar cane.

In most parts of South-west China, rice is the main crop in rural area. Only 5% of the straw are used for animal food and then most of them are burned.

Bamboo is the most popular plant in South-west China in the rural areas. Normally people use bamboo for crafts such as basket or other commodities and it has not been used in housing in recent years. Bamboo grows much faster than wood and has high strength in the vertical direction. Another advantage of bamboo is its very cheap price of 0.12 Yuan per kg for retail.

Stone is easy to get for the people living in mountain areas and highlands. Even today it is still widely used for the foundation or walls of the houses. It is almost free to local people who find stone on the mountain. The only cost is to transport and shape it but people in rural areas usually do this themselves.

Sugar cane can be found in the countryside in the western part of China but not over the whole area. There is potential to use sugar cane as a building material in the future.

The number of people living in a house

The number of people living in a house is one of the key issues in the research and it is different from the number of people in a family, because some people in the family usually go out to work and don't live in

the house. It has been found that most of the poor families have up to 4 people. Due to the poor conditions in the poor areas, some young people in the families usually leave the area.

THE INITIAL THROUGHT ABOUT THE SOLUTION

After the first stage of work some thoughts exist on the industrialised solution for the housing for poor people in rural area in China. This will be the main content of the next stage of work once proved to be practical and effective.

The design

The conceptual design is based on the real rural life need listed in the report of the survey on rural housing. However, the flat has a toilet and kitchen which will give much more improvement to people's life in rural areas.

The dimension of the kitchen is 3 meters in width and 4.2 meters in length, while the dimension of each room are almost uniform, about 3.6 meters in width and 4.2 meters in length. One of the reasons for doing so is that local people like a big kitchen and big rooms so that they can put some firewood in the kitchen and some working tools in rooms. Another reason is that the more uniform the dimensions are, the more convenient the manufacture and construction is.

Figure 1 shows the lay out for a house, for a couple. If there is more than a couple living in the house, the lay out can be changed as shown in Figure 2.

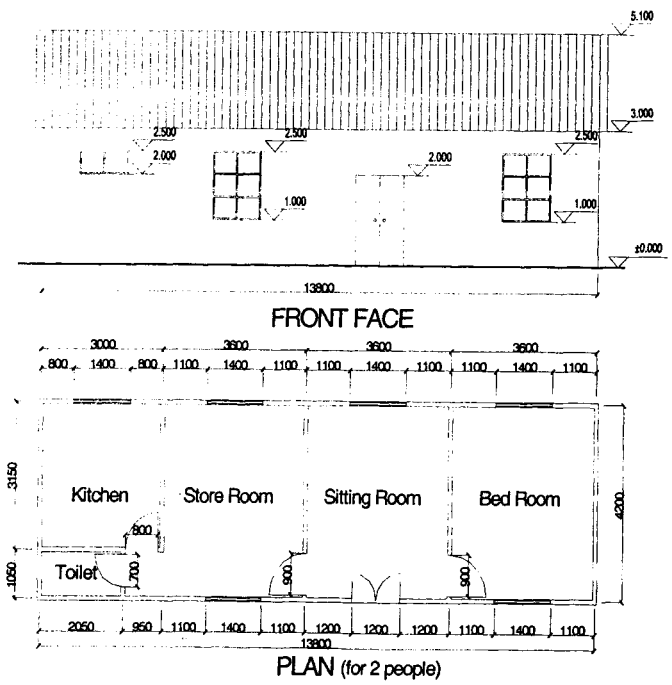


Figure 1 Lay out for two people (a couple)

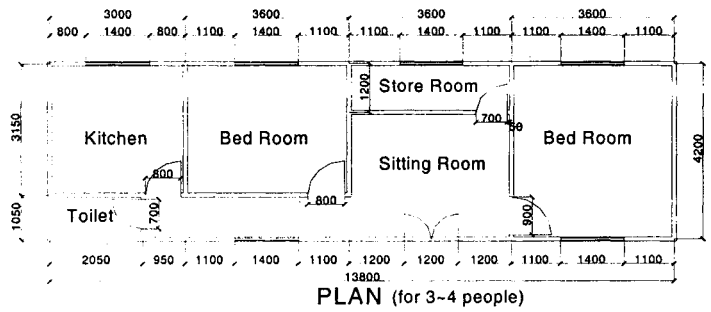


Figure 2 Lay out for 3-4 people

The lay outs shown in Figure 1 and 2 are for up to 4 people living together. If there are more than 4 people living in the house, a dwelling unit can be easily added to fit the need. On the same way, more dwelling units can be continually added for more people living together.

The wall and roof

The wall and roof are the main costs for housing. If the costs for walls and roof can be controlled successfully the total costs to build a house can be greatly reduced.

The best way to reduce the costs of walls and roof in rural area is to use straw board or bamboo board. build it. The techniques of making this board, with different thickness and different strength has already been researched.

The suggested combined board for the project is shown in Figure 3.

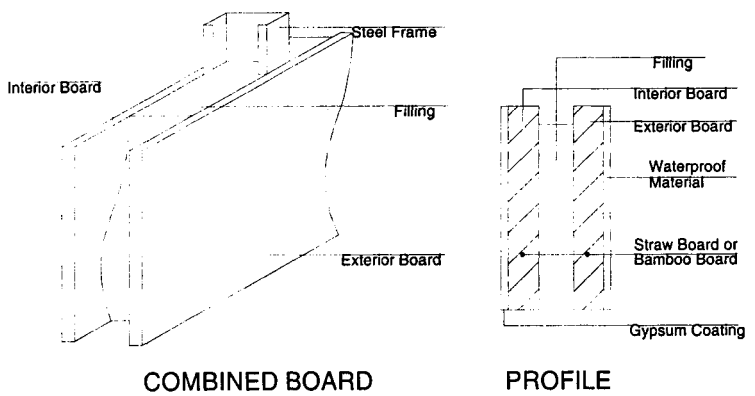


Figure 3 The housing structure

As shown in Figure 3, the interior and exterior boards can be made from straw or bamboo, shaped at high temperature and high pressure. The byproduct of the board such as the bamboo leaves and straw can be used as a filling material after it has been dried, pressed and shaped. This filling material can bring benefit both at taking full use of local resources and getting better thermal performance and sound insulation. The gypsum coating on the interior surface can help the house to be dry and comfortable. Asphaltum or paint can be used as a waterproof material on the exterior surface. The suggested thickness of these coatings is 5mm.

This board is cheap, strong, light-weight, has good performance and is local resource based.

The structure and the foundation

There are two choices of load-bearing systems identified in the research.

The first is the load-bearing wall system making some external wall and internal wall act as load-bearing to stand the vertical load. The advantage of this system is simplicity and low cost, but the disadvantage is to increase the thickness of the board to ensure that the board has enough strength to stand the load. Probably it is difficult for the local farmers to manufacture the board with simple facilities.

The second system is to use a steel frame to stand both vertical and horizontal loads and non load-bearing walls to enclose the house. The advantage is a high strength frame and board made of minimal thickness. However, the disadvantage of the system is that the cost may be higher than the load-bearing wall system.

Of these two systems, the steel frame system is more responsible. Considering overall costs, though the steel frame system will cost more than the board system, this board can be cheaper, the manufacture and construction can be easier and the equipment in the factory can be simpler and cheaper. Therefore, a steel frame system is considered as a possible solution.

Hot-formed steel is used because it cheap and has been widely used to build structures. Steel poles and beams are necessary to build a basic frame shown in Figure 4.

In this way, the house could be built to provide enough resistance at a affordable cost.

The sizes and sections of the steel elements are carefully designed to obtain the structure with best economic performance. L section hot formed steel is the primary material for the structure because of it's low cost and low skill needed to form it.

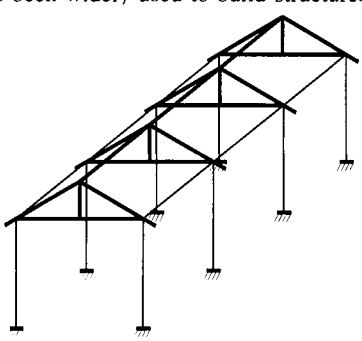


Figure 4 The structure

For resistance to rust of the steel frame, it is suggested to use paint because it is cheap, easy to get in rural area and low skill required.

Stone is a good material for the foundation because it's cheap and easy to find in rural areas. In some areas, such as the north west of China, stone may be difficult to find. Concrete should then be the

foundation material. The steel poles are counter sunk into the stone foundation and cement concrete is used to secure them in place.

The financial support

If the cost of the house is kept below 200 Yuan per square meter, the total cost of the house should be no more than 11,500 Yuan. Even though this is a low cost house it is still a great deal of money for the local farmers and financial support is very important in the project. For poor people there are two ways to have their own houses.

The first is to obtain government financial support. For poor people, the Chinese government has a poverty support plan every year. The central government and local government will give special money to homeless people to get their house on the plan, at about 10,000~15,000 Yuan for each family. In Chongqing, for example, the policy is that the government pays 90% of the money and the farmer pays the rest.

The second way is to get support from other organisations. For example, the World Bank and the Asia Development Bank have fund for poor people support every year.

CONCLUSION - THE FUTURE RESEARCH

The following will be the key activities for the next stage of the research:

- Collecting detailed information from some organisations which are good at using bamboo or straw to make building materials and ensuring that there should be no technical problems on our solution.
- Setting up supply chain in both China and abroad focusing on building materials.
- Developing the detailed design, including the detailed structure, building services and connections.
- Doing further research on the local climate, people's income and related local government policy.
- Looking for possible organisations to give financial support for the poor people in rural area.

This Page Intentionally Left Blank

Advances in Building Technology, Volume 1
M. Anson, J.M. Ko and E.S.S. Lam (Eds.)
© 2002 Elsevier Science Ltd. All rights reserved

INDUSTRIALIZED HOUSING CONSTRUCTION – THE UK EXPERIENCE

R. Howes

Professor in Construction Management
Chairman of the Innovation and Research Committee, Construction Industry Council, UK

ABSTRACT

The historical development of industrialized housing in the United Kingdom is outlined and key milestone developments have been identified. Past mistakes have been analysed, together with the affect that this has had on the progress of advances in building technology associated with domestic house construction. The circumstances relating to the renaissance of industrialized housing have been highlighted, leading to the current state of development. The paper analyses the benefits to be derived from industrialized housing over traditional house construction, assuming favourable circumstances. Attention has been given to problems and pitfalls to be avoided in order not to repeat mistakes that have manifested themselves in the past. The paper concludes with an assessment of potential future developments and draws attention to the need for acceptance by the construction industry and future homebuyers of industrialized housing.

KEYWORDS

Industrialized, system, traditional, frame, panel, steel, concrete, timber.

INTRODUCTION

The need to provide affordable, sustainable and functionally competent housing is fundamental to the living standards and well being of individuals and families throughout the World. The United Kingdom is no exception and there has been a long history of housing shortages and substandard housing. A common perception is that the UK housing system has failed to provide adequate housing for low-income households and the generally poor maintenance of the housing stock, particularly at the low end, Gann et el (1997). A major problem is the cost of land and the limited availability of affordable urban sites especially in the South East of England. The British Government has been slow in releasing land for housing and the cost of cleaning up brown field sites has led to a situation where the demand for housing far out paces the supply. This situation has been exacerbated by skill shortages in traditional building trades and escalating wage rises. The quality of construction and the lack of design innovation have resulted in higher than necessary life cycle costs and the premature decline in the condition of property leading to higher expense to rectify defects.

In Japan, USA and Europe savings of up to 30% in cost and time have been claimed by the introduction of industrialized housing techniques where housing is constructed in factories using standard components, Fairs (1998). This has the advantage of reducing construction activity and time on site and provides the potential to assure quality and guarantee in use performance.

The introduction of prefabricated industrialized housing is not new and there have been many public and private initiatives over the past 80 years to implement industrialized techniques in support of the need to meet increasing housing demand. None of these initiatives have led to an identifiable progressive development of industrialized housing and as a consequence it only represents a small percentage of the total UK market. This paper is intended to trace the historical development of industrialized housing in the UK with the objective of identifying successes and failures for the purpose of establishing what needs to be done to increase the potential of future attempts to produce houses using factory based manufacturing.

HISTORICAL DEVELOPMENT

The review traces the development of industrialized housing and aims to identify significant systems and their degree of success or failure. It has been stated that standardization applied to building technology was borrowed from manufacturing and the intention was to increase precision and gain efficiency through repetition and continuous improvement, Finnimore (1989). These concepts were developed and it was proposed that houses should be prefabricated in factories and then transported to the site for fast assembly.

The first attempt to introduce industrialized housing occurred because of labour and material shortages caused by the First World War. Subsequent to the publication of the Tudor Report in 1918 a series of committees were established to investigate the potential for implementing new ways of building that did not rely on bricklaying, carpentry and joinery. The Committee for Standardization and New Methods of Construction was tasked with the role of looking into the potential for standardization in state aided housing schemes. In 1919 the Addison Housing Programme replaced traditional construction with pre-cast concrete and steel that employed unskilled labour. Further development work took place and principles where established for social housing, which led to the Homes Fit for Heroes Programme in 1921. Approximately 30,000 steel and concrete prefabricated homes where built and additional strains were placed on the construction industry due to a lack of proper planning or control. Unfortunately these housing programmes suffered from serious defects associated with cracking, leaking and corrosion, which were never resolved. This initiative provided the first example of hastily prepared designs that where not properly thought through and tested. The consequences manifested themselves in costly repairs and poor living environments, which gave industrialized housing a bad name.

It was not until immediately after the Second World War that industrialized housing was revisited. War damage and neglect had created a major housing crisis, which was addressed by the introduction of prefabricated homes first designed in 1944. The Portal House was based on a lightweight steel frame, however due to the shortage of steel it was never put into production. Instead manufacturers adapted the design using timber frames and aluminium clad in asbestos wall panels and roof sheets, Vale (1995). A major development occurred when the Arcan Group amalgamated the resources of materials suppliers and engineering companies to produce a range of designs and 41,000 temporary homes were provided, Gear (1967). These dwellings proved to be extremely robust and there are still examples that have survived and provide homes over 55 years after their manufacture, thus providing an important demonstration of the longevity of non-traditional construction methods.

After the Second World War the Cornish and Airy systems were designed based on small pre-cast concrete panels that could be man handled without the use of cranes, Ministry of Works (1948). It was soon established that the system incurred heavy labour costs and was found to be uneconomic resulting in a rapid decline in use. In 1948 a study by the Ministry of Works established that large pre-cast panel industrialized systems were more economical and Wates were the first UK company to produce a system using room sized load bearing external cladding panels. The Reema system followed, which combined the external and internal cladding surfaces into one load-bearing panel that was linked to internal pre-cast load

bearing panels. Hence this was the start of the large panel pre-cast housing systems that dominated public housing in the UK for the next 20 years. In comparison the Reema system required less man-hours to produce than the Wates system and 20,000 houses were built using this method up to 1962.

Due to two successive World Wars the majority housing stock in the early 1950's was old, lacked amenities and was in an advanced state of decay and disrepair. The British Government initiated a housing policy of slum clearance to provide land for new homes, especially in city and urban areas. It was decided that public housing redevelopment would rely heavily on system building for both high-rise and low-rise development. In London 34% of new housing was built using an industrialized system and this figure was exceeded by County Boroughs and New Towns who achieved 44% and 43% respectively. In the 1950's the London County Council (LCC) developed a policy to employ new technologies and it instigated the use of system building in its Post War General Needs Programme, Walker (1953). Throughout the 1950's it became increasingly clear that industrialized housing would need to be used in order to meet the large demand for new homes brought about by the regeneration of the UK's industrial base, especially in the Midlands and the South. The British Government invested money into research and development aimed at deriving economy of scale through standardized components that could be used in buildings designed to a common dimensional framework. The aim was to enforce the design of public housing through a prescribed set of dimensions that in turn allowed the use of standard components, Ministry of Works (1948). Unfortunately, the commercial sponsors of the various industrialized systems ignored this initiative and to some extent the potential advantage was lost.

Towards the end of the 1950's attention turned to the severe shortage of new public housing in inner cities. The use of confined sites resulted in the need to increase the density of housing and the obvious solution was the adoption of high-rise designs. Hence, the birth of large scale inner city housing estates dominated by tower blocks. The British Government's research into industrialized building was not restricted to housing. Consortiums of local authorities were set up to produce designs for schools, hospitals and other public buildings using a national system of interchangeable components. The majority of systems developed where steel framed and used a variety of cladding components. In contrast the design of public housing was left mainly to the commercial sector that, in general, favoured the use of large pre-cast concrete panel systems.

Bison was one of the first British large pre-cast systems that were designed for tower blocks between 8 and 20 storeys. The pre-cast panels integrated external and internal finishes, services and fixings and were produced in factories and transported to the site. Because of the high demand the LCC decided to explore the possibility of adapting pre-cast panel systems from elsewhere in Europe and this resulted in the use of the Danish Nielson System being licensed to Taylor Woodrow Anglian. Other foreign systems where also used, including the Camus system. Two notable British manufactured systems where 12m Jesperson developed in 1963 by Laing and Wates Modular , which used site based factories to reduce transportation costs. Typically public housing estates comprised of 500-600 dwellings. The Larsen Nielson system alone accounted for 182 residential tower blocks constructed for the LCC.

Increasing prosperity in the UK economy of the 1960's created the view that standards of social housing were not keeping pace with the development of the economy and an investigation into desirable housing standards was implemented. The outcome was the Parker Morris Report, entitled "Homes for Tomorrow" which concluded that the quality of social housing was not keeping pace with living standards and it advised that more space and amenities be provided and new guidelines were drawn up for dwellings.
During the mid 1960's the UK construction industry was at the centre of the modernization of the nation's housing and infrastructure. In 1965 Government policy decreed that an annual programme of 500,000 new homes should be in place by 1970. Housing production continued to rise from 1966 to 1972 when house completions in system building averaged 30% of all public housing and it peaked in 1970 at 41%, Housing

Statistics GB (1972). In contrast to the public sector, private housing continued to use traditional building construction, mainly for two storey dwellings in suburban and rural and rural areas. Low to medium rise apartment developments were adopted in inner cities.

THE DECLINE

A defining event occurred in 1968 when a gas explosion on an upper floor of a Larsen Nielson system built tower block at Ronan Point in London, led to a progressive collapse of all twenty two floors of one corner of the building, killing and injuring those residents in that part of the building. The subsequent investigation into the collapse revealed a major design fault in that the walls and floors were not structurally tied together. Huge public expenditure was necessary to carry out remedial works to make other tower blocks safe. It was also revealed that in Denmark this system was not built over six storeys and in the USA this type of construction was banned over 6 storeys. The resulting scandal did much to destroy British public confidence in high-rise residential accommodation.

Critics pointed to the fact that system building solutions were born out of crisis and stated that political ideologies bypassed the need for proper research, development and testing of designs and their continual improvement over time, Russell (1981). Russell cited 'Homes for Heroes' , the post war 'prefabs' and the large panel systems of the 1960's and blamed a lack of long term planning, which was aided and abetted by politicians and civil servants. The 1967 economic crisis effectively curtailed expenditure on housing and questions were raised about the efficiency and desirability of high-rise residential blocks. In the early 1970's it was realized that the system building stock was expensive to build and there were emerging problems of technical deficiency and social behaviour and well being. As a result system public house building was abandoned in the UK in favour of low-rise high density traditional construction.

During the 1970's and 1980's the problems associated with large panel concrete systems began to reveal themselves. Common defects were the spalling and cracking of panels and water barriers incorporated in the panel joints were not adequate to stop in ingress of rainwater. Further, the panels suffered serious condensation destroying internal decoration and creating a damp living environment. Window frames rotted and services, including lifts, suffered breakdowns. Social problems created vandalism and abuse of the buildings and the resultant cost of renovation and repairs placed a heavy additional burden on public expenditure. Many local authorities decided to cut their losses by demolishing many of the worst affected tower blocks after just 10-20 years of use. The sell off of public housing by the Thatcher Government resulted in all the best housing being purchased by tenants. However, many of the worst developments are still being maintained by local authorities to satisfy social housing need. These events have been well publicized and the British public is extremely sceptical of system building. The general public perception equates to images of the worst forms of architectural design with social deprivation, poor engineering and shoddy workmanship.

DEVELOPMENTS POST 1970

An alternative to constructing traditional low rise load bearing masonry dwellings is the use of timber frame construction. Supported by the increasing supply of domestic plantation softwood, timber frame became a viable alternative to fill the gain left by the abandonment of large panel construction. Timber frame housing increased the speed of construction and improved thermal insulation. It also provided traditional brick and tile elevations, which were aesthetically pleasing to the public. Technology 'know-how' was borrowed from the USA, Sweden and Canada and the British Timber Research and Development Association conceptualized and developed design recommendations. There was growing acceptance of this

technique until a disastrous BBC World in Action programme that produced a damning report of the poor workmanship adopted by Barratts, a major UK house builder specializing in timber framed housing. The report could not fault the basic design principles or the best practice adopted overseas, however it did reveal poor working practices and a complete failure in site management in quality control procedures. The outcome resulted in a rapid down turn in the sale of timber framed houses. Unlike the large panel systems that were fundamentally flawed, timber frame systems made a comeback in the early 1990's and these are now accepted as an efficient and quality means to produce housing to an acceptable standard.

Steel framed systems such as CLASP and NENK were produced in the 1960's and were applied mainly to low rise schools, libraries and other public buildings, but these also suffered defects and failures e.g. inability to limit the spread of fire. There were limited attempts to produce steel frame housing systems but these never caught on, mainly due to cost and poor aesthetic design. The decreasing price of steel and developments in design technology in the mid 1990's led to system building using lightweight cold rolled steel. McDonald's, the global fast food chain were able to demonstrate the advantages of lightweight steel systems in terms of speed of construction, quality and cost. It was quickly realized that this system could be effectively adapted to produce affordable housing.

LESSONS LEARNED

System building in the UK has suffered major failures; by far the worst was that of the large-scale panel systems in the 1960's. The British public still holds the general view that system building represents the worst of modern architecture and defects resulting in poor life cycle performance, Russell (1981). Construction professionals are still sceptical about the implementation of systems and there is a strong body of opinion that considers previous system house building to be a series of misguided attempts to introduce higher levels of construction design and manufacturing techniques. As a consequence, there has been no consistent development of system building in the UK over the past 85 years. Instead the subject has been revisited twice as the result of two World Wars and once to solve a peace time housing crisis, which resulted in almost total failure after a period of 20 years commencing in the 1950's. The main lessons to be learned from the UK experience are listed below, however underlying these is the need for a long term strategic development plan for system built housing, backed by sufficient innovation, research and development:

- The design should be subject to full value analysis, where aesthetic, performance and cost factors are given detailed consideration in the context of the planned life cycle. The selected design should be engineered and tested by means of prototypes in order to assure design quality and performance through rigorous testing procedures;
- Solutions should be sustainable in that they require low embodied and in-use energy, as well as using materials that can be recycled on completion of the life cycle;
- Systems should be open and flexible in order that standard components are based on a common approach to dimensional co-ordination. Thus interchangeability between components provides for greater design flexibility and aesthetic appearance;
- Advantages offered by standardization and economy of scale should be fully exploited; and
- New components and fabrications require independent accreditation regarding their quality and functional performance. They must also comply with the minimum standards set by building regulations and codes of practice;

CURRENT HOUSE BUILDING PRACTICE IN THE UK

New housing in the UK is produced primarily by the private sector for purchase by homeowners. Most of this construction is traditionally based on load bearing brick and block cavity walls, nevertheless timber framed has gained ground in this sector. For higher rise apartments in city centres, traditional construction in steel and concrete is in common use. Social housing is provided by housing associations and it is mainly traditionally constructed. Advances have been made in the use of timber-framed systems and there has been innovation involving the use of steel frames and concrete walling. Public housing in the UK has progressively diminished to the point where it is non-existent apart from a limited number of sheltered housing projects to accommodate old people. In the suburbs and rural areas houses are normally built to a maximum of three storeys as detached, semi-detached and terraced units. In city areas flats and apartments are normally provided up to six storeys and in a minority of cases where land is extremely expensive, high rise will be employed utilizing structural frames and cladding systems. It may therefore be concluded that the construction of housing can be classified into two prime categories, namely 'traditional' and 'system'. These categories can be further subdivided as shown in Figures 1 and 2. Although system built housing is very much in the minority there is a growing body of opinion in the UK that it offers the potential to build more efficient and better quality homes at an affordable price.

Progressive development of steel framed systems since the 1970's have lead to the advent of cold rolled lightweight steel framed panel and modular systems. This has enabled lightweight modules to be designed and constructed for feasible transportation from the factory to site by road. There are five major manufacturers of these units in the UK. Much of this production has been geared to restaurants and hotels, but recent pilot housing projects such as Murray Grove in London have proved that this technology can be successfully applied to housing.

Innovation and research into the production of timber framed housing dates back over fifty years. Houses produced in kits have been a commercial success and this has encouraged further investment. Recently development has concentrated on fabrication away from the site in factories and the feasible construction of timber framed construction above three storeys. Modular construction has proved to be economically feasible for the construction of low-rise hotels and this approach is now being developed for application in the social housing sector. Timber systems are more established than steel systems and will see further ongoing development.

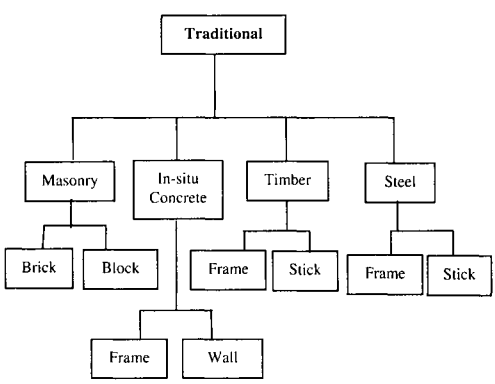


Figure 1: Classification of Traditional House Construction
Source: Kaluarachchi, Howes and Tah 2000

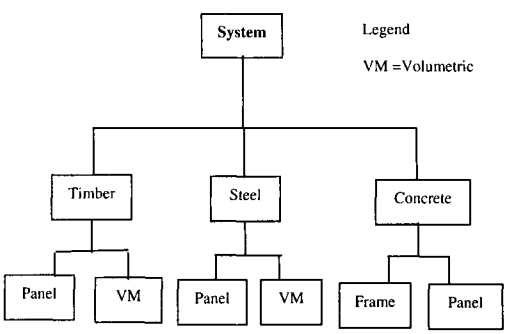


Figure 2: Classification of System House Construction
Source: Kaluarachchi, Howes and Tah 2000

Building on experience gained experience gained from Europe, concrete systems have been developed. These are primarily panel and frame based systems that are pre-cast in factories using casting batteries or extrusion machines. Because they are relatively heavy, volumetric construction appears not to be a feasible option. Developments in the finishing and insulation of external walls provide more design flexibility and better thermal performance. Concrete systems claim to be robust requiring only limited life cycle maintenance.

Although a wide variety of housing systems are available in the UK none of these have achieved the potential advantages of economy of scale. Traditional house building still dominates the market, but there are problems due to the cost of construction and a lack of traditional craftsmen such as bricklayers, carpenters, plumbers and plasterers. Currently there is a serious housing shortage in the UK and the number of new homes being built has dropped to only 162,900 in 2001, the lowest number for decades. Statistics released in April 2002 have shown that house prices had risen by 3.8% in March 2002, pushing the average price above £100,000. Pressures are now building for the introduction of system built homes to provide affordable quality housing for public sector workers, teachers, nurses and police officers who cannot afford to purchase housing in inner city areas.

POTENTIAL DEVELOPMENTS

The construction of housing can be considered as a largely repetitive process, involving a range of components and materials, which can be constructed in a variety of ways to produce an infinite range of designs. Traditional construction relies heavily on the effective integration of the various trades in a sequential process to achieve production on site. Research indicates that 80% of building work and repairs are of a repetitive nature, Environment Committee Report (1996). Under such circumstances there is scope to rationalize and advance the quality of house building through the use of systems based standardized components and processes where continual improvement can be facilitated. A wide range of choice and flexibility can be achieved through the use of a carefully selected supply chain to provide the materials and components necessary to support factory-based assembly. To achieve this, the construction of housing under factory conditions must be seen as a total process using integrated teams, Environment Committee Report (1996), Gann (1996). The Egan Report "Rethinking Construction" and the follow up report "Accelerating Construction" points towards the high level of waste occurring in labour, materials and the misuse of equipment which is making houses too expensive. As a consequence low income groups are being precluded from owning their own homes, Egan (1998), Strategic Forum (2002). Egan also points towards lessons that can be learned from manufacturing and the utilization of integrated supply chains.

Important progress has already been made in the production of system housing demonstration projects and prototypes. Indications are that quality has improved and construction times have been dramatically reduced, however the cost is still too high. Further development needs to take place to improve designs and to provide more flexibility and choice for house purchasers. Manufacturing efficiency requires improvement and potential purchasers need convincing that modern factory produced homes really are superior and are better value for money than the traditional alternative. Better co-operation within the industry and the acceptance of a range of standard products and components will considerably assist price reduction by means of economy of scale. A reduction in construction time can be achieved by adopting multiple assembly lines in order that modules can be constructed concurrently. At the same time site works can be scheduled so that rapid erection can commence once modules, panels, floors and roof assemblies are delivered from the factory.

CONCLUSION

The UK has experienced over 80 years of spasmodic activity in the development and use of industrialized housing. Periods of high activity have been brought about by two World Wars, which reduced available manpower, created considerable damage to the housing stock through bombing and diverted attention away from essential maintenance and repair. The most significant period of industrialized housing occurred in the 1960's, which was brought about by increased prosperity and the need to improve living standards. Political, economic and social pressure together with the misconception that living standards could be improved by untried and inadequately tested technology, directly contributed towards the major failure of concrete panel system tower blocks and urban housing estates. The public was devastated by the scandals, failures and waste associated with system building during this period and great scepticism still exists. This effectively killed off system building in the UK from the late 1970's to the mid 1990's. The exception has been the development of timber frame housing systems and kits, although this area suffered a major set back due to the BBC's World in Action programme on Barratt House Builders.

Important research and development sponsored by forward thinking clients such as McDonalds, British Airports Authority, Travel Lodge and supermarket chains eg Asda have proved that factory based construction technology can produce superior buildings for the same, and in some cases less cost, with the added bonus of much faster construction times. The demonstration and prototype-industrialized housing projects have affectively proved that the new system based technology can be transferred to housing. The UK Construction Industry now has reached the stage were new system housing has the potential to satisfy the huge demand for home ownership at an affordable price. It is now the responsibility of the wider construction industry, housing associations, building societies and banks to embrace and further develop this technology to meet the needs of future homeowners and society in general. Success or failure will be driven through private demand and not through a state housing programme. Unlike on previous occasions referred to earlier in this paper, new industrialized building technology has been carefully developed and thoroughly tested and it has been shown to be sound. In conclusion there would seem to be a promising future for system building in the UK.

REFERENCES

Egan, J.,The Construction Task Force, (1998), *Rethinking Construction*, DETR, London.
Environment Committee Report, (1996), *Housing Need*, Vol.1,Report Session 1995-96.
Fairs, M., (June 1998), *Evolve or be Damned*, Building Design, p6.
Finnimore, B., (1989), *Houses from the Factory*, Rivers Oran Press, London.
Gann, D., (1996), *Construction as a Manufacturing Process*?, Vol 14, pp 437-450, Journal of Construction Management and Economics, SPON.
Gann, D., et el, (December 1997), *Mission Statement – Flexibility and Choice in Meeting Occupants' Housing Needs,* RSA, SPRU University of Sussex.
Gear A. M. and Associates, (1967), *The Arcon Group 1943-67*, Report.
Housing Statistics Great Britain 1964-72, (1972), HMSO.
Ministry of Works, (1948), *Post War Building Studies*, No 45, HMSO.
Russell, B., (1981), *Building Systems Industrialisation and Architecture*, John Wiley & Sons, London.
Strategic Forum, (2002), *Accelerating Change*, DTI, London.
Vale, B., (1995), Prefabs; *A History of the UK Temporary Housing Programmes*, Chapman and Hall, London.
Walker, H., (1953), *Prefabrication 1*, p32.

Advances in Building Technology, Volume 1
M. Anson, J.M. Ko and E.S.S. Lam (Eds.)
© 2002 Elsevier Science Ltd. All rights reserved

A PERSPECTIVE OF INDUSTRIALISED HOUSING IN CHONGQING

Li Shirong

Research Centre for International Construction Economics and Management
Chongqing University
Shapingba, Chongqing, 400045, PR China

ABSTRACT

The aim of the paper is to provide a better understanding of Chongqing's features and the potential for promoting industrialised housing in this region. It first reviews the current development for industrialised buildings abroad. It then focuses on the features of Chongqing, the importance, the potential and the advantages for promoting industrialised housing in Chongqing. It also introduces an international cooperation project in Chongqing.

KEYWORDS

Housing, industrialised housing, China, Chongqing, construction industry, manufacture

DEVELOPMENT OF INDUSTRIALISED HOUSING

Industrialised housing development abroad

In 1950s, due to the damage made in the Second World War, there was a great demand for houses in Europe. Therefore, in order to settle the problem, many industrialised houses were assembled, which are still standing. There were complete, standard and systematic housing system in Europe. Ten years later, the wave of industrialised housing spread all over the European countries and soon to USA, Canada, Japan and other developed countries.

With the continual enhancement of science and technology in recent years, the demand for houses came through a phase of "Pay attention to: Quantity-Quantity & Quality-Quality First-Individualisation, diversification, high qualify environment". At the same time, the production of industrialised houses in many western countries reached its climax. As it is well known, Sweden is one of the most advanced countries developing industrialised housing, and 80% of the country's houses adopt generally a housing system based on universally available parts. In USA, there are 34 professional companies producing modular construction parts now. In the UK, the Egan Report in 1998 further pushes this new trend. Currently, the study of the production of industrialised housing in the UK has paid more attention to the flexibility and design variation of housing systems, in order to widen the adoptable coverage and to bring

in the scale effect (Prewer, 2001).

Although industrialised housing has been developed in the past 40 years, the speed is slow. The main reasons include the techniques, user's understanding and economic conditions. For example, during the 1960s and 1970s, the UK built many industrialised residential buildings with concrete panels, which many people don't like. Therefore, even today when people hear about industrialised housing they are negative (Shirong, 2002).

To shorten the construction period is not the only objective of implementing industrialized housing. Within the report 'Rethinking Construction' provided by UK key clients who appointed by the British government in 1998, it is clearly stated the objectives to be achieved within the British construction industry through innovation, implementation, industrialized production are (Egan, 1998):

- To reduce cost 10%
- To shorted the time 10%
- To improve the predictability 20%
- To reduce the defect rate 20%
- To reduce the accident rate 20%
- To improve the production rate 10%
- Eventually, to improve the profit rate 10%

Therefore, the main purpose of industrialized housing is to absorb the principles developed in the manufacture industry into the construction industry. Thus, it is hoped to change the traditional construction methods and lead the housing industry to the development of industrialization, standardization, integration and information technology. This is a kind of revolution within the construction industry. Obviously, the principles of implementing industrialized housing are to achieve standardization through modules, and then to achieve industrialization through standardization. An example shows the importance of using an industrialised housing system. There are about 3,000 spare parts for making a car, while there are about 40,000 for building a house (Shirong, 2002). Due to the complication of building houses, it is important to use standardised parts with a manufactured approach for the building of houses. It is an important approach to improve quality and efficiency in the construction industry.

The common interesting in housing development

From a global market perspective, the following are some common interesting in housing development:

- In housing development, some key issues become more and more important, such as the quality, function and efficiency of construction, thinking of people, environment protection and sustainable development.
- There is a new revolution in construction approach focusing on manufacture-based construction.
- Partnering, project management and supply chain logistics are the key issues for success in this revolution.
- Industrialisation, Standardisation, integration and information technology are key factors for developing industrialised housing.
- Transferring the production approach of manufacturing industry into the construction industry is the breach in the traditional approach construction in order to achieve and achieving the objectives of the innovation revolution.
- The new challenges in the new century requires rethinking of the construction approach in order to meet the requirements from society in terms of high quality, zero defects, reduced waste, high speed and high efficiency, as well as sustainable development and environment protection.

- The lack of technology for industrialised housing affected the development in the past, while today the industrialised housing system has to be promoted to overcome the challenges.
- Although for many years, there were been different type of structures in industrialised housing systems, the light-steel frame structure seems to have more advantages particularly with today's requirements in sustainable development and environment protection.

THE IMPORTANCE FOR USING INDUSTRIALISED HOUSING IN CHONGQING

Compared with other major cities in China, it is more urgent and important for Chongqing to develop industrialised housing. The technology and management level in Chongqing's housing industry is comparatively lower than in other major cities in China. Along with lack of experienced human resources within the local housing industry and the low level of industrialization, it is more difficult for Chongqing to further develop the industry and to grasp the opportunities. How to adjust the industry structure, change the construction methods and fully use local resources to realize the objectives of industrialized housing and restructure the related industries is the key problem for Chongqing in the new century. Therefore, to implement the industrialized housing can not only meet the requirement of central government, but also comply with the current conditions in Chongqing.

Accelerating the development of Chongqing's construction industry

Meeting the great housing demand in Chongqing

Due to the use of standardized and manufacture-based components, procurement and production of large scale become possible which could speed up the housing production process.

Due to the huge population (30 million), the average floor space per head in Chongqing is below the national level. With the quick economic development, the demand for houses in Chongqing now is up to about 20 million square metres per year (Chongqing Construction Industry Yearbook, 2000). Although the housing sector in Chongqing has been developed in Chongqing since 1980s, it still can not meet the requirement of the society. For example, the average floor space per head for housing was 3.12 square metres in 1980, 7 square metres in 1995, and 11.59 square metres in 2001. The rapid development of urbanisation in Chongqing further increases the demand for housing in Chongqing. Based on the city planning for 2010 and 1020, the urban population will account for 37% in 2010 and 47% in 2020.

Improving construction productivity in Chongqing

Currently, traditional approaches are still being used in housing construction in Chongqing. Construction productivity in Chongqing is lower than the average level of the country and even lower than the level of western part of China, much lower than in Beijing, Tianjin and Shanghai, as shown in Figure 1.

In addition, due to the change of production when using industrialised housing approach, majority of building components could be made in factories that will improve the quality. In Chongqing, the skills of construction employees are relatively low because a large number of construction workers in Chongqing are from rural areas. Until the end of 2000, the total number of construction workers in Chongqing was 1 million but about 75% of the total number were farmers. The other three cities are much smaller than in Chognqing, such as Beijing: 14.7%, Tianjin: 32.7%, Shanghai: 24.9% (China Statistical Yearbook, 2001).

Speeding up housing construction in Chongqing

One of the main advantages of using industrialised housing is to speed up the construction process and

greatly reduce the site work that also avoids the outside affects for construction. It is great desire for both developers and users to speed up housing construction in Chongqing. It happens for some customers that they have to wait for 2 years to get their new houses although they pay before. In addition, Chongqing has about 800,000 people who should be relocated due to Three-Gorge Project. In 1998, for example, about 70,319 people were relocated in Chongqing, costing almost 3 billion yuan. The total floor space was 2.25 million square metres.

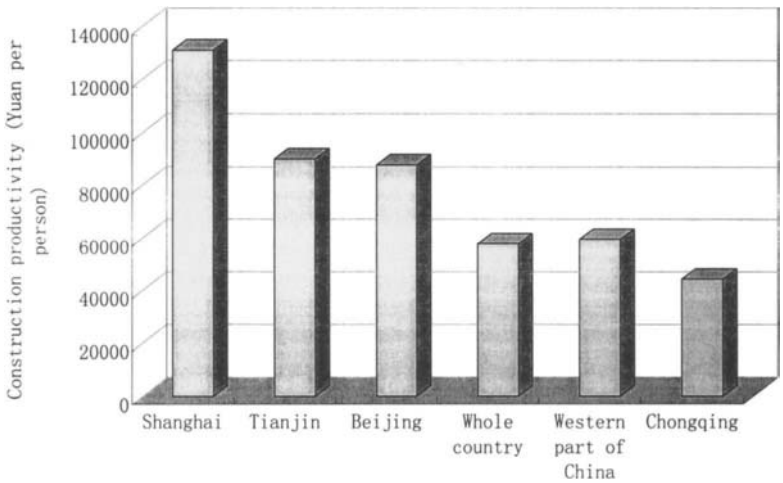


Figure 1 Construction productivity in some cities (2000)

Setting up production base for building materials in Chongqing

Though construction industry has been one of the key industries in Chongqing, the variety and the size of building materials and products are still very small. For example, about 80 percent of building materials and products for fitting out used in Chongqing are produced from other cities.

Besides, there are a lot of industrial and agricultural wastes materials in Chongqing that can be used in the production of building materials, and this'll do good to environment protection of Chongqing.

Chongqing has strong steel production, but there is small amount steel used in building structure in Chongqing.

Chongqing is also one of the key districts in agriculture with abundant agricultural byproducts which can be used for producing building materials such as light boards.

Restructuring manufactures and introducing new products

Chognqing is an old industry city with many heavy industry manufactures, such as steel and shipbuilding. Restructuring industries is one of the key tasks for Chongqing government. Many state-owned enterprises in Chongqing need to introduce new products, such as Chongqing Steel and Chuandong Shipyard. Many state-owned enterprises with traditional industry products have low productivity. For example, in 2000, the industry productivity in Chongqing was 31252 Yuan per head, while it was 63878 in Beijing, 52425 in Tianjin and 82327 in Shanghai.

Introducing foreign funds and technology to Chognqing

Economic development needs money. For many years, Chongqing has the shortage of foreign investment. For example, in 2000, FDI was 1.98 billion yuan in Beijing, 1.76 billion yuan in Tianjin, 2.84 billion yuan in Shanghai, but only 240 million yuan in Chongqing. As a lot of new technology and products will be involved in the carrying out of industrialized housing, we can introduce these and other experience from advanced countries, and may cooperate with them in setting up factories.

Re-employment of people

The promotion of industrialized housing can not only bring along many relevant industries, but also produce some new industries, which can solve the re-employment of people who are out of work. Economic reforms in Chognqing have brought about many people out of work (about 400,000 people), while the revolution in construction process with manufacture-based approach will bring new industries, particularly building materials. This will provide opportunities for unemployed people in Chongqing for new job.

Benefit for environment protection and sustainable development

With the carrying out of industrialized housing, construction site work and waste of construction materials can be reduced; some waste materials can be recycled; and new green and light materials can be put into use. All of these act a positive part in environment protection and sustainable development of Chongqing.

THE MAIN ADVANTAGES FOR USING INDUSTRIALISED HOUSING IN CHONGQING

- Chongqing's market environment provides a basis for promoting industrilaised housing in Chongqing (municipal city, Gorge project, western part of China, key economic areas along Yangze River).
- Great demand for housing in Chongqing provides huge market for industrialised housing.
- Abundant resources in Chongqing provides basic condition for establishing building material manufactures.
- Sufficient labour force in Chongqing makes it possible for establishing manufactures.
- Existing shipyard in Chongqing provides the site for housing manufacture.
- The transportation network in Chognqing (including roads, railways, and water roads) provides a good condition for establishing supply chain.

In a word, Chongqing has the potential for being one of the main manufacture centres for industrialised housing in China.

AN INTRODUCTION TO INDUSTRIALISED HOUSING IN CHONGQING

A joint research team was established at the end of 1999, including the members from UK, Hong Kong and Chongqing. The main members are from three universities (South Bank University from UK, Hong Kong Polytechnic University from Hong Kong, and Chongqing University from Chongqing). Research work has been under taken since then.

Project objectives

An industralised housing system is to be established in Chongqing, which includes housing industry and other industries such as steel, metal, building material, real estate, decoration, manufacture, environment, environment protection and information technology. This system is aimed at research on serial technologies of industralised housing and the base establishment and directed by the basic ideas of technology innovation service system. In this system the serial technologies of industralised housing serves as the main body of innovation and the goal is to establish the base for industralised housing in Chongqing.

Principles for development industralised housing system in Chongqing

The following main principles are the key drivers for the project:

- Technology transfer in the form of appropriate industrialized building systems will be adapted to conform with local requirements.
- The use of locally available material and human resources will determine the type of system to be developed.
- The proposed system must be within the potential skill capability of local professionals, technicians and operators, after they receive some training courses.
- The system will supply sufficient freedom to allow variety in design.
- The system will be suitable for local environmental condition. Energy consumption will be a major consideration. Priorities will be focused on the internal environmental factors including: air quality, damp proofing, acoustic insulation, as well as temperature and humidity control.
- The design of the dwellings will be determined by the production cost and maintenance cost.
- Quality and fitness for purpose will be considered according to cost and affordability.
- Waste will be minimized in the process and recognition will be given to issues concerning sustainability.
- Safety performance improvement will be focused on the quality control of factory production, which are the spare parts for the dwellings.
- Time will be saved and progress will be accelerated since more parts do not have to be pre-fabricated on site.

Possible systems

There would appear to be three basic approaches to industrialized steel construction, namely:

- High rise using a hot rolled steel frame to support modular or panel units consisting of lightweight cold rolled sections.
- Lightweight cold rolled steel framed panels intended for construction up to around eight stories.
- Load-bearing modular units stacked one on the other up to six stories.

Pre-fabricated bathroom and kitchen pods could be used in all three categories.

Of the three approaches, the second appeared to offer the most flexibility. It could be extended to high-rise construction through the use of hot rolled principal structural frames and could be adapted to small-scale production by using the kind of portable bending equipment.

Work stages

There are three main stages in this project, including research on technology and system, prototype, demonstration.

The first stage includes:

- Understanding local conditions.
- Analysis and valuation of industralised housing systems used in practice, finding out both advantages and disadvantages of these systems, and determining suitable systems for further analysis.
- Designing new system.

The second stage includes:

- Setting up partnering (including government, research organisations, industry people).
- building the prototype.
- Testing and showing.

The third stage includes:

- Establishing key manufactures.
- Building houses for demonstration.

The key technologies for the project

- The establishment of structure system of houses, which is suitable for industralised housing and local conditions in Chongqing which includes the index such as structure type, size and height
- The establishment of standard and specification
- New technology of building material
- The product upgrade of other relative industries. How to make the needed production for the industrialised housing by the utilization of the production ability of mental, steel and shipbuilding industries and the importation of new product and production line
- The material supply chain which is gradually formed for the housing industrialization
- The establishment of industrialised housing base which is the objectives at the first stage and the key jobs of the project

Main features of the project

Firstly due to the involvement of many different fields and departments, the project has the following characters:

- **One** significant character --- a system engineering
- **Two** important aspects --- production systems development, demonstration project
- **Three** parties' joint effort --- Government, enterprise and research organization
- **Four** approaches --- research and innovation, communication, demonstration and training
- **Five** assurances--- policies, funding, personnel, land and time

Just because of the above characters, there is specialty in the implementation of the project. However, the following must be mutually agreed for implementing the project:

- The government is the leader
- The enterprises are the main players
- The research organizations are the supporting bodies

From above the implementation of the project is big system engineering involving multi directions, multi levels, multi objectives and multi stages. As government is concerned, it involves construction, economy

and agriculture commission, planning science and environment protection departments; As the enterprise is concerned, it involves the bodies such as design, consulting, developer, contractor, supplier and manufacturer; As the research organization is concerned, it involves the university and design institute; As the industry is concerned, it involves architecture, real estate, material, mental, fabrication and service.

Therefore to ensure the effective implementation of the project, a project team including government, research organization and enterprise must be established. And in the team the work of each body shall be clearly clarified, project organization shall be realistic and functional so that the advantage and resource of each participant can be fully taken and exploited.

CONCLUSION - KEYS TO SUCCESS

- It is important for Chongqing government to realise the potentials for promoting industrialized housing project in Chongqing. It is not only to improve building sector but also to improve other related industries. Compared with other cities, Chongqing has more potential for promoting this work.
- The publics should have a better understanding of industrialised housing because they are the main forces for promoting this work. Without their understanding, the work is difficult to carry out. Education and training are important approaches for reaching this objective.
- It is also important for all parties to the project to know their roles and responsibilities in implementing the project. They should also clearly see their benefits from this project. Without their understanding, it is difficult to carry out. Among them, government is a key party to make this project happen in Chongqing. The benefits that local government achieves are huge, including promoting the development of Chongqing construction industry and other related industries, helping restructuring industries.
- The most advantages for international cooperation is to attract foreign funding and introduce overseas advanced technology and management skills.
- The possibility for carrying out this project depends upon the government's active attitude, good cooperation among all parties.
- Industrialised housing systems are new in China. Many cities are eager to set up the system. Early action will bring a lot of benefits.

References

Chongqing Construction Commission (2001), *Chongqing Construction Industry Year Book*, Chongqing Publishing House, China.
Egan John. (1998), *Rethinking Construction*, DETR, UK
Genfang Wang. (2001), Perspective of Chongqing Housing Development, *Journal of Chongqing Jianzhu University*, 23:3, 6-10, China.
Ministry of Construction (2000), *China Construction Industry Yearbook*, China Construction Industry Publishing House, China.
National Bureau of Statistics (2001), *China Statistical Yearbook*, *China Statistic Press*, China.
Prewer John. (2001), Innovation and development in moudular industrialised housing, *Journal of Chongqing Jianzhu University*, 23:3, 55-66, China.
Chirong, Li. (2001), *Journal of Chongqing Jianzhu University*, 23:3, 34-42, China.
Steel Construction Institute (2000), *Value and benefits assessment of modular construction*, Steel Construction Institute, UK.
Steel Construction Institute (1999), *Modular Construction Using Light Steel Framing, An Architect's Guide*, Steel Construction Institute, UK.

Advances in Building Technology, Volume 1
M. Anson, J.M. Ko and E.S.S. Lam (Eds.)
© 2002 Elsevier Science Ltd. All rights reserved

IMPACT ON STRUCTURE OF LABOUR MARKET RESULTING FROM LARGE-SCALE IMPLEMENTATION OF PREFABRICATION

C M Tam

Department of Building & Construction, City University of Hong Kong,
83 Tat Chee Avenue, Kowloon Hong Kong

ABSTRACT

The construction industry of Hong Kong is characterized by labour intensive trades such as plastering, tiling, concreting, steel bar fixing, formwork erection and bamboo scaffolding, which are considered by the public as dirty and hazardous. Traditionally, the industry has found difficulties in recruiting appropriate workers. The Construction Industry Training Authority (CITA) has set the entrance requirement of trainees at Form 3 school leavers, the lowest standard in the territory. Over the years, CITA has helped relieving the social pressure by offering these youngsters a training opportunity. In recent years, the industry has also helped to absorb the surplus labour supply, especially of the low technology sector when most of the manufacturing industries have been moving from the Hong Kong Special Administration Region (HKSAR) back to the Mainland since early 80's. The construction industry offers employment opportunities to the new immigrants from the Mainland who lack modern skills to survive in the new economy of the territory. However, this scenario is put under threat as prefabrication has become more widely accepted by the industry. Akin to the manufacturing sector, prefabrication will encourage the shifting of site casting work to factory casting in the PRC. Recent studies by the authors have indicated that the labour demand can be reduced by as much as 40%.

KEYWORDS

Construction Labour Supply, Labour Market, Prefabrication.

INTRODUCTION

The free market economy will drive capitalists to move the place of production from the costly regions to places with a lower cost of manufacturing (Lipsey and Steiner1978). The manufacturing industry has followed strictly this doctrine and hence, most factories from Hong Kong have moved to the Mainland and this has triggered the historically high unemployment rate of 6.7% in early 2002. Fortunately, the construction industry, whose products are for local consumption only, still remains very labour intensive. Owing to the public's strong objection to the importation of labour, construction workers are mainly drawn from local residents, providing a good employment opportunity to the Hong

Kong citizens. Currently, there are about 300,000 construction workers (including the interior decoration trades) recorded, contemplated least affected by the shift of factories to the Mainland.

Most of the construction trades have their strict and hard boundaries which workers will not or cannot cross over and hence induces inflexibility both for workers in seeking continuous employment and for employers in labour deployment (Tam et al 2001). This results in the lack of continuous employment for workers due to the daily pay arrangement of the workforce. The entrenched tradition of labour subcontracting is seen as an effective cost control and reduction measure in response to the cyclical nature of the construction industry (Gray and Flanagan 1989). However, this practice has been criticized by the industry and the public in general for the induced poor safety records and unacceptable quality performance.

As a result, the use of prefabrication has been strongly advocated recently in the industry, as it can help to improve site safety by providing a cleaner and tidier site environment, enhance quality by producing elements under the factory conditions and eliminate site malpractices. Further, factory production can reduce wastage and encourage re-cycling of construction waste, leading to environment protection and sustainability of the industry.

IMPEDIMENTS TO WIDE ADOPTION OF PREFABRICATION

However, prefabrication bears some limitations. Firstly, the modular units may bring about monotonous designs, which are strongly opposed by town planners and architects. Secondly, the prevailing high-rise building structures in Hong Kong lead to connection and jointing problems and concerns on structural integrity. Thirdly, the water and weather tightness at joints (rains come with typhoons in Hong Kong) also imposes barriers in the wide adoption of prefabrication.

The Hong Kong Housing Authority has adopted small scale prefabrication since 1988 (Cheung et al 2002). The prefabricated elements include precast façade units, staircases, drywall and semi-precast floor planking. Their experience in using prefabrication is positive in terms of quality, time, safety; some good responses are listed as follows:

- Site tidiness is obviously improved resulting in reduction in site accidents;
- The speed of construction can be improved by converting some critical site casting activities into precasting works;
- The external outlook of building structures can be varied by changing the combinations of modular units;
- The in-situ grouted joints can minimize the occurrence of water leakage;
- The quality of prefabrication units is much improved. The former quality breakdowns like the de-lamination of external mosaic tiles and water leakage along external window frames have been seldom recorded.

STIMULUS TO PREFABRICATION DUE TO NEW CONSTRUCTION TECHNOLOGY

As regards structural integrity, the new developments in high strength concrete and structural lightweight concrete can, to certain extent, overcome some structural difficulties. Modular flat units can be designed to sit upon each other and lumped together to form a tower block, which are supported by cast in-situ structural cores and tie beams.

This new development gives ways to the wide adoption of prefabrication. Consequently, this poses an intense threat to the local labour market. With the extensive use of prefabrication, it is anticipated that

large numbers of site workers will be replaced with factory workers at the prefabrication yards. Further, some trades will diminish while some new trades may emerge. This shifting of work nature will induce significant impact on the existing labour market structure, as well as training provisions.

STUDY OF THE IMPACT ON THE LOCAL LABOUR MARKET

The authors have conducted interviews with the key staff of the major contractors to identify the impact on the labour market resulting from the widespread use of prefabrication. Eight interviewees, all at directorate levels of six major building contractors who have a market share of more than 50% of the local building industry market were met and interviewed. Prior to the interviews, information requisition forms were designed and distributed to the six contractors to collect the necessary data. Existing labour consumption data was collected from the standard information requisition forms. In the interviews, buildings with a high degree of prefabrication (70% of elements by prefabrication) were postulated and used as the basis to work out the labour consumption.

The results of the study are summarized as follows:

Comparison of Site Worker Consumption

Summarizing from the interviews, the total manpower for the prevailing residential tower block and the proposed new highly prefabricated tower block are derived. Table 1 shows the comparisons of the average site manpower requirements for the two.

TABLE 1
Comparison of HB/NCB and SPC on Site Labour Consumption

In Labour-days / Tradesmen	Average per Existing Residential Unit	Average per New Highly Prefabricated Residential Unit	Difference per unit
Foreman	1.24	0.71	-(0.53)
Assistant foreman	1.39	0.94	-(0.45)
Coolie	2.47	3.17	0.7
Steel Fixer	4.21	3.42	-(0.79)
Formworker	2.61	0.60	-(2.01)
Concretor	1.20	0.07	-(1.13)
Lightweight Partition Fixer	0.43	0.00	-(0.43)
Plasterer	5.24	1.65	-(3.59)
Joiner	0.40	0.15	-(0.25)
Metal Worker	0.27	0.35	0.08
Painter	1.73	0.60	-(1.13)
Electrician	2.00	0.94	-(1.06)
Plumber	1.36	0.54	-(0.82)
Joint Filling Worker	0.18	2.37	2.19
General Labour	5.24	1.17	-(4.07)
Mechanics	1.83	1.40	-(0.43)
Total:	31.79	18.08	-(13.71)

Truck Driver Consumption

With the widespread adoption of prefabrication, there will be a great demand on local transportation. As a result, the need for truck drivers will increase. Table 2 summarizes the truck driver consumption.

TABLE 2
Comparison of HB/NCB and SPC on Truck Drivers Consumption

	Driver-days Required per Existing Residential Unit	Driver-days Required per New Highly Prefabricated Residential Unit	Difference per unit (in Driver-days)
Truck Drivers*	2.98	3.82	0.84

*Assume each truck driver can manage two round trips per day

For a typical residential tower block, there will be a reduction of site workers of 43%, a terrifying figure to the local construction workers. The decision to promote prefabrication will become a political rather than a technical or managerial problem.

RECOMMENDATIONS ON PREVENTING FROM DRAINING OFF OF JOBS

One of the ways to retain construction jobs is to set up prefabrication yards within the Hong Kong SAR by:

Offer of Cheap Land for Prefabrication Yards

The Hong Kong SAR government can encourage contractors to set up prefabrication yards within the Hong Kong region by offering land with low rental fees.

Contractual Arrangements

To facilitate building control and to ensure that the use of materials and construction methods coupled with the performance of the finished products do comply with the Hong Kong Building Regulations, the large developers, especially the public clients, can mandate that all prefabrication yards must be located within the Hong Kong SAR or located in a place acceptable to them.

CONCLUSIONS

The shift from the current high percentage of site casting to prefabrication designs will definitely affect the local labour consumption. The study has revealed that there could be a 43% reduction in site labour consumption if the move is realized. The figure may have been exaggerated as some minor trades such as setters-out, scaffolders, marble-layers, project management staff and etc., which should remain unaffected, were not counted in the model. Although the cut in jobs seems alarming, the move towards a more advanced building technology for public housing construction is a worldwide trend, which is inevitable. If prefabrication is not widely adopted, the competitiveness of the construction industry in Hong Kong in terms of productivity, time, quality and safety performance will suffer.

References

Gray, C and Flanagan, R. (1989), The Changing Role of Specialist and Trade Contractors. The Chartered Institute of Building, Ascot.

Lipsey R.G. and Steiner P.O. (1978) Economics. Fifth Edition, Harper & Row, Publishers, Inc., N.Y.

S O Cheung, Thomas K L Tong, and Tam C.M., (2002) "Site Pre-cast Yard Layout Arrangement Through Genetic Algorithms" Journal of Automation in Construction, Vol. 11, No. 1, pp. 35-46.

Tam C.M., Tong T.K.L., Cheung S.O. and Chan A.P.C. (2001) "Genetic Algorithm Model in Optimising Labour Utilization" Journal of Construction Management and Economics, UK., Vol. 19, No. 2, pp.207-215.

This Page Intentionally Left Blank

Advances in Building Technology, Volume 1
M. Anson, J.M. Ko and E.S.S. Lam (Eds.)
© 2002 Elsevier Science Ltd. All rights reserved

PRIORITY SETTING OF PREFERENTIAL PARAMETERS FOR HOME PURCHASE IN CHONGQING – AN ANALYTIC HIERARCHY PROCESS APPROACH

K.W. Wong [1] and M. Wu [2]

[1] Department of Building and Real Estate, Faculty of Construction and Land Use
The Hong Kong Polytechnic University, Kowloon, Hong Kong
[2] Department of Building, School of Design and Environment
The National University of Singapore, 4 Architecture Drive, Singapore, 117566

ABSTRACT

Chongqing, being the fourth metropolis ranked after Beijing, Shanghai, and Tianjin, is one of the most important cities in the western part of Mainland China. It is situated on the Yangtze River, 2500 kilometres from the coastal city of Shanghai. Chongqing, with a population about 32.5 million, has developed rapidly in recent years due mostly to major economic and infrastructure developments, including the "three gorges" project.

A prominent problem in the real estate market in Chongqing is the high vacancy rate of commodity housing. According to the Chongqing Construction Committee (2000), 1.1 million square metres of residential commodity housing have remained unsold by the end of 1999. By contrast, around a hundred thousand workers and their families were living in quarters with less than 4 square metres per capita. Thirty percent of housing unit lacked basic facilities such as kitchens and lavatories (Chongqing Municipal Bureau, 1999). A mismatch between housing demand and supply is the key to the dilemma of housing vacancies, though low affordability contributes to part of the problem, as the economic situation of the households in Chongqing has experienced continuing improvment during recent years. A Housing Preference Expert System, which contains parameters with priority vectors, are urgently needed as a tool to assist the developers to supply marketable residence, and to help homebuyers to select suitable houses.

This paper reports the preliminary findings from stage 1 of a collaborative study on affordable housing conducted by a tripartite research team from The Hong Kong Polytechnic University, the Chongqing

University, and the South Bank University. The overall research objectives are to use the concept of industrialized affordable housing to examine the feasibility and viability of its use, and to design suitable types of industrialized affordable housing for use in Chongqing, by maximising the use of indigenous resources from the region. At this stage, an investigation has been carried out to identify the basic characteristics of the construction industry in Chongqing and to set the scene for the housing research. This focuses on the priority of parameters regarding potential buyers' preference, by using an analytic hierarchy process approach.

KEYWORDS

Industrialized Housing, Analytic Hierarchy Process, Chongqing.

INTRODUCTION

Chongqing as a Key City in the Western Part of China

Chongqing is positioned strategically at the gateway to western China, bridging the western part and the coastal region (Wong, et. al., 2001). As China's most populated city, it has an area of 82.4 thousand square k.m., is 470 km long from East to West, 450 km wide from North to South, and has a total population of 32.5 million. According to the Mayor of Chongqing, the city is important in the western part of China for its rich mineral resources, its huge market, and its cheap labour (Bao, 2000). The technology, human resources, and industrial setting in Chongqing are comparatively more advanced than other cities.

There are three attributes that distinguish Chongqing from the rest of western China. Firstly, Chongqing is the sole and biggest central metropolis, being directly controlled by the central government and equipped with a highly developed infrastructure. Secondly, being situated at the upper stream of the Yangtze River, Chongqing is an excellent economic centre for transportation facilities. Thirdly, the Three Gorges Project requires the migration of one million people and the reconstruction of hundreds of towns, which will create an enormous market to encourage the development of industrialized housing in Chongqing. More than 20 provinces, in terms of capital, technology, and managerial skills, will assist the Three Gorges Project. Completion of the project will bring fundamental improvements to the supply and distribution of hydroelectric power, which in turn will benefit all industries.

Problems Encountered in the Chongqing Housing Market

One of the main problems in Chongqing's real estate market is the high vacancy ratio caused by a huge housing demand, and poor affordability. This mismatch between supply and demand is explained below.

Huge housing demand

The total amount of housing floor space sold in 1998 was 4.2 million square metres, which amounted to 4.186 billion RMB. Housing units amounting to 2.5 billion yuan were sold to individual families and the remainder was sold to work units (China Municipal Publishing House, 2000). Up to now there are still 8,000,000 families who are classified as living under difficult conditions in Mainland China (China Municipal Bureau, 2000).

The estimated demand for commodity housing in the Chongqing urban area during the year 2000 amounted to 6 million sq.m. (Chongqing Construction Committee, 2000).

High vacancy ratio

The real estate market in Chongqing has become more agile in recent years yet a considerable number of housing units in the market remain unsold, possibly due to lack of a proper feasibility study before the development stage.

	Item	Total
1998	Housing Under Construction (million sq.m)	12.24
	Housing Newly Completed (million sq.m)	5.96
	Housing Sold (million sq.m)	4.21
	Housing Unsold (million sq.m)	1.17
1999	Housing Under Construction (million sq.m)	12.68
	Housing Newly Completed (million sq.m)	4.29
	Housing Sold (million sq. m)	4.34
	Housing Unsold (million sq. m)	1.12

Source: Chongqing Construction Committee, 2000

Figure 1: Housing Supply in Chongqing 1998 - 1999

Figure 1 shows that the unsold number of housing units in Chongqing remained about the same from 1998 to 1999. In 1999, 12.68 million sq.m. of housing was under construction and only 4.29 million sq.m. was completed, of this total 1.12 million sq.m. remained unsold (Chongqing Construction Committee, 2000). Clearly a mismatch exists between supply and demand because of affordability and quality issues.

This mismatch between housing demand and supply is the key to the dilemma of housing vacancy, though low affordability contributes to part of the problem, as the economic situation of the households in Chongqing has experienced continuing improvement during recent years. To help alleviate the mismatch problem, the Housing Preference Expert System (HPES), with appropriate parameters and priority vectors, can be used to assist developers to supply marketable residence, and to assist homebuyer to select their suitable houses.

RESEARCH

Objectives

- To determine the priority vector for each parameter of the proposed Housing Preference Expert System.
- To scrutinize the factors that affect homebuyers' behavior in China.

Methodology

- Identify the housing experts in Chongqing.
- Invite the housing experts to complete an investigation form.
- Use an Analytic Hierarchy Process (AHP) approach to calculate the priority vector of each parameter.

ANALYTIC HIERARCHY PROCESS (AHP)

The Analytical Hierarchy Process is an analytical tool using a deductive approach. It is a systematic procedure to represent the elements of any problem, and is particularly useful for solving complex problems, which are in the state of 'fuzziness'. It organizes the basic rationality by breaking down a problem into its smaller constituent parts and then calls for only simple pair-wise comparison judgments, to develop priorities in each hierarchy.

One should note that to design an analytic hierarchy, like the structuring of a problem by any other method, is more of an art than a science. It necessitates substantial knowledge of the system in question. A very strong aspect of the AHP is that the knowledgeable individuals who supply judgments for the pair-wise comparisons usually also play a prominent role in specifying the hierarchy.

SETTING UP WEIGHTINGS FOR THE RESIDENCE CRITERIA

Structuring a Decision-making Hierarchy

The prioritization problem has been broken down into a hierarchy of interrelated decision levels, each of which involves a number of factors. Level 1 describes the objective (goal) in the decision-making problem whilst Level 2, 3, and 4 contain factors that are perceived as important attributes affecting the level 1 decision. Level 5 gives the decision alternatives. The factors have been distilled from a comprehensive literature review of housing preferences.

Formation of a Pair-wise Comparison Matrix

Housing experts in Chongqing were invited to make a pair-wise judgment for the selected factors. Each pair-wise comparison involved assigning the priority factor with respect to the other factors on a rational scale. The scale used in this study is based on the recommendations from Saaty (1991).

Consistency of Priorities

The results of the pair-wise comparison matrix were examined for consistency of priorities by using the following formula:

The Index of Consistency (C.I.) = (λ_{max} -n) / (n-1)

(Note: n= number of factors for pair-wise comparison, and λ_{max} = largest eigenvalue for size matrix)

Consistency Ratio (C.R.) = C.I. / Random Consistency (n)

Size of Matrix	1	2	3	4	5	6	7	8	9	10
Random Consistency	0.00	0.00	0.58	0.90	1.12	1.24	1.32	1.41	1.45	1.49

Figure 2: Random Consistency for Different Matrix Sizes (Saaty, 1982)

THE PRIORITY VECTOR OF RESIDENCE PREFERENCE PARAMETERS

Totally six experts on housing issues in Chongqing completed the questionnaire. They comprised one general manager and one director from the China Construction Science & Technology (Chongqing) Corporation, two senior architects from the Chongqing Municipal Architecture Design Institute, and two professors from the Chongqing University.

The overall housing preference parameters' priority vectors

Level 1 Matrix							
	A & S	Facility	Trans.	Price	Environ.	Decor.	P.M.
Architecture & Structure	1	1	1/3	1/5	1/4	1	1/2
Facility	1	1	1/3	1/5	1/4	1	1/2
Transportation	3	3	1	3/5	3/4	3	3/2
Price	5	5	5/3	1	5/4	5	5/2
Environment	4	4	4/3	4/5	1	4	2
Decoration	1	1	1/3	1/5	1/4	1	1/2
Property Management	2	2	2/3	2/5	1/2	2	1
Priority Vector	0.059	0.059	0.176	0.294	0.235	0.059	0.118

Figure 3: Results of Priority Vectors

Figure 3 provides the consolidated pair-wise comparison results from the housing experts, and Table 1 and Table 2 provide the breakdown details.

Table 1
Pair-wise Comparison Matrix

	Housing preference – pair-wise comparison matrix	**Priority vector**
Architecture & Structure	$7\sqrt{}$ 1 x 1 x 1/3 x 1/5 x 1/4 x 1 x 1/2 = $7\sqrt{}$ 0.0083 = 0.5043	0.5043 / 8.5778 = 0.059
Facility	$7\sqrt{}$ 1 x 1 x 1/3 x 1/5 x 1/4 x 1 x 1/2 = $7\sqrt{}$ 0.0083 = 0.5043	0.5043 / 8.5778 = 0.059
Transportation	$7\sqrt{}$ 3 x 3 x 1 x 3/5 x 3/4 x 3 x 3/2 = $7\sqrt{}$ 18.225 = 1.5139	1.5139 / 8.5778 = 0.176
Price	$7\sqrt{}$ 5 x 5 x 5/3 x 1 x 5/4 x 5 x 5/2 = $7\sqrt{}$ 651.0416 = 2.5232	2.5232 / 8.5778 = 0.294
Environment	$7\sqrt{}$ 4 x 4 x 4/3 x 4/5 x 1 x 4 x 2 = $7\sqrt{}$ 136.53 = 2.0185	2.0185 / 8.5778 = 0.235
Decoration	$7\sqrt{}$ 1 x 1 x 1/3 x 1/5 x 1/4 x 1 x 1/2 = $7\sqrt{}$ 0.0083 = 0.5043	0.5043 / 8.5778 = 0.059
Property Management	$7\sqrt{}$ 2 x 2 x 2/3 x 2/5 x 1/2 x 2 x 1 = $7\sqrt{}$ 1.0667 = 1.0093	1.0093 / 8.5778 = 0.118
	Total = 8.5778	1.0000

Table 2
Multiplication of the Matrix by the Priority Vector

Architecture & Structure	(1x0.0059)+(1x0.0059)+(1/3x0.176)+(1/5x0.294) +(1/4x0.235)+(1x0.059)+(1/2x0.118)=	0.413
Facility	(1x0.0059)+(1x0.0059)+(1/3x0.176)+(1/5x0.294) +(1/4x0.235)+(1x0.059)+(1/2x0.118)=	0.413
Transportation	(3x0.059)+(3x0.059)+(1x0.176)+(3/5x0.294) +(3/4x0.235)+(3x0.059)+(3/2x0.118)=	1.236
Price	(5x0.059)+(5x0.059)+(5/3x0.176)+(1x0.294) +(5/4x0.235)+(5x0.059)+(5/2x0.118)=	2.061
Environment	(4x0.059)+(4x0.059)+(4/3x0.176)+(4/5x0.294) +(1x0.235)+(4x0.059)+(2x0.118)=	1.649
Decoration	(1x0.0059)+(1x0.0059)+(1/3x0.176)+(1/5x0.294) +(1/4x0.235)+(1x0.059)+(1/2x0.118)=	0.413
Property Management	(2x0.059)+(2x0.059)+(2/3x0.176)+(2/5x0.294) +(1/2x0.235)+(2x0.059)+(1x0.118)=	0.825
	Largest eigenvalue for size matrix λ_{max} =	7.01

The results of the pair-wise comparison matrix from Table 1 and Table 2 were examined for consistency of priorities:

$$\text{The Index of consistency (C.I.)} = (\lambda_{max} - n) / (n-1)$$

$$= (7.01-7) / (7-1) = 0.01 / 6 = 0.0017$$

$$\text{Consistency Ratio (C.R.)} = \text{C.I.} / \text{Random Consistency (n)}$$

$$= 0.0017 / 1.32 = 0.0013$$

The value should be in the region of 0.1 or less. Since the consistency ratio in this case is at 0.0013, which is less than 0.1, the judgment is proved to be numerically consistent. A similar approach could be used to determine the priority vectors of sub-parameters at the other levels.

CONCLUSIONS

The priority setting of preferential parameters for home purchase in Chongqing was determined as follows (priority vector): price (2.061), environment (1.649), transportation (1.236), property management (0.825), architecture & structure (0.413), facility (0.413) and decoration (0.413).

To conclude, the Analytic Hierarchy Process (AHP) approach can be used as an effective analytical tool to determine complex issues, such as preferential parameters for home purchase. With appropriate parameters and priority vectors, a Housing Preference Expert System (HPES) could be developed, to assist potential homebuyers to select suitable properties. However, caveat is that such an analysis will very much depend on the comprehensiveness of the literature review to determine the appropriate parameters to be adopted in the study, and the professional judgment of the experts asked to make the pair-wise comparisons. An obvious limitation of this approach is that there is a certain degree of subjectivity in prioritising the parameters. Finally, it is recommended that similar studies be conducted in other major cities in China Mainland, so that comparisons between major cities and regions could be made in the future.

ACKNOWLEDGEMENTS

The Hong Kong Polytechnic University's Institutional Research Fund funds this study. The research title is 'A Study of Manufactured Affordable Housing in Chongqing', and the Project Account Code is G – YC 32.

REFERENCES

Bao Xu Ding (2000) Western Exploration Hundreds of Questions, *Chongqing Municipal Party Committee Propaganda Department* (in Chinese).
China Municipal Bureau (2000) 2000 *China Statistical Yearbook* (in Chinese).

China Municipal Publishing House (2000) *PRC real Estate Statistical Year Book.*

Chongqing Construction Committee (2000) *Chongqing Construction Industry Report in Year 2000.*

Chongqing Municipal Bureau (1999) *Chongqing Statistical Yearbook* (in Chinese).

Li Ye Heng Zheng Estate (2000) *Report on Housing Demands at 1999 Chongqing Trade Fair of Real Estate.*

Saaty, T.L. (1980) *The Analytic Hierarchy Process*, McGraw-Hill.

Saaty, T.L. (1982) The Analytic Hierarchy Process: A New Approach to Deal with Fuzziness in Architecture, *Architectural Science Review*, Vol.25, No.3, September, pp. 64-69.

Saaty, T.L. (1997) A Scaling Method for Priorities in Hierarchical Structures, *Journal of Mathematical Psychology*, Vol.15, pp.234-281.

Saaty, T.L., & Beltran, M. (1980) Architectural Design by the Analytic Hierarchy Process, *Design Methods and Theories*, Vol. 14, Nos. 3/4, pp. 124-134.

Saaty, T.L. & Erdener, E. (1979) A New Approach to Performance Measurement - The Analytic Hierarchy Process, *Design Methods and Theories*, Vol. 13, No. 2, pp. 64-72.

Saaty, T.L., & Vargas, L. (1991) The Logical of Priorities, *Kluwer Nijhoff Publishing.*

Shen, Q.P. & Lo, K.K. (1999) Priority Setting in Maintenance Management – An Analytic Approach, *The Hong Kong Polytechnic University*, 62 pp.

Wong, K.W., Hui, C.M., Li, S.R., Howes, R., & Wu, M. (2001) A Study of Manufactured Affordable Housing in Chongqing, Research Monograph, *The Hong Kong Polytechnic University*, 77pp.

TEAM PRESENTATION:

RESEARCH AT THE ATLSS CENTER ON NEW MATERIALS AND SYSTEMS TO RESIST EARTHQUAKES AND WIND

This Page Intentionally Left Blank

Advances in Building Technology, Volume 1
M. Anson, J.M. Ko and E.S.S. Lam (Eds.)
© 2002 Elsevier Science Ltd. All rights reserved

STEEL MOMENT FRAME CONNECTIONS THAT ACHIEVE DUCTILE PERFORMANCE

John W. Fisher[1], J.M. Ricles[1], Le-Wu Lu[1], C. Mao[1], Eric J. Kaufmann[1]

[1]ATLSS Engineering Research Center, Lehigh University, 117 ATLSS Drive, Bethlehem, PA 18015-4729, USA

ABSTRACT

An extensive research program was conducted at the ATLSS Center, Lehigh University, to investigate the causes of brittle failures observed in welded connections during the 1994 Northridge earthquake and ways to improve their ductility. Tests on pre-Northridge connection details verified several weak links in the connection design and fabrication. Full-scale connection tests were carried out to develop improved details for welded unreinforced connections. These test results are presented, along with recommendations to insure ductile connection performance.

KEYWORDS

Continuity plates, ductility, fracture, inelastic rotation, notch toughness, panel zone, weld access hole, welded moment connection.

INTRODUCTION

The 1994 Northridge earthquake in California resulted in widespread damage to welded beam-to-column connections in moment resisting framed structures in the Los Angeles area [1]. The moment connection used in these structures was the popular welded flange and bolted web type with beam flanges welded to the column flange with full penetration groove welds with backing bars and the beam web is bolted to a shear tab. This connection was "prequalified" as a ductile connection based on the results of tests on moderate size laboratory specimens [2], and had been widely adopted since the late 1960's. Shortly after the earthquake damage was found in more than 100 low- and high-rise buildings in the Los Angeles area.

This paper summarizes the results of a comprehensive research program that was conducted at Lehigh University following the 1994 Northridge earthquake. This research program included investigations to study causes of the connection fractures that occurred during the earthquake as well as experimental and analytical studies to develop improved performance of welded connections under inelastic cyclic loading.

FAILURE ANALYSIS OF FRACTURED PRE-NORTHRIDGE CONNECTIONS

Following the 1994 Northridge earthquake a survey of 1290 floor-frames in 51 steel buildings was conducted by Youssef at al. [1]. The buildings were from a variety of locations in Los Angeles, of different sizes, frame configuration and construction type.

Youssef et al. [1] reported that the most common form of damage found was partial or complete fracture of the beam flange groove welds. Damage to the base metal was found to occur most frequently as a fracture of the column flange adjacent to the beam bottom flange weld. The observed column flange and weld fracture patterns strongly suggested that the damage was related to the condition at the weld root. The welded joints appeared to be brittle, with little evidence of inelastic behavior in the weldment or base metal. The fractures were attributed to a variety of other factors, including the weld process, quality of workmanship, base metal properties, and connection design [3].

A study was undertaken at Lehigh University [4] in order to characterize the origin of the fracture and material properties of failed connections. A detailed analysis was performed of 19 fractures removed from five different buildings damaged during the Northridge earthquake. The fracture surfaces of all of the samples were analyzed in order to characterize the fractures. The size and source of the originating defect was recorded.. The details are presented by Kaufmann et al. [4]. Cleavage fracture was found to be the mechanism of crack propagation in all of the samples regardless of crack propagation path. Brittle fracture initiated close to the mid-width of the weld at the column centerline usually from a weld root incomplete fusion flaw arising from entrapped slag or porosity at the back-up bar.

Another common factor among all of the fractured connections that were studied is that the welds were deposited with E70T-4 electrodes which were in common use. Fracture toughness tests of weld metal removed from sixteen connection samples, other damaged building connections and laboratory tests [4,5] have consistently shown that the E70T-4 weld metal provides a low level of fracture toughness. Figure 1 shows CVN values of various self-shielded, flux core electrode E70T-4, E70T-7, E71T-8 and E70TG-K2 and E7018 a shielded-metal-arc electrode.

The dynamic fracture toughness, K_{ID}, of the weld metal obtained by applying the correlation $K_{ID} = \sqrt{0.64E(CVN)}$, to the Charpy V-notch data, where E and CVN are the modulus of elasticity (in MPa), and the measured Charpy V-notch energy (in Joules). Weld metal compact tension tests of E70T-4 weld metal tested statically and at intermediate loading rates similar earthquakes [4] provided fracture toughness of 52 to 54 MPa $\sqrt{m}$. A strain shift rate of $0.75T_S$ shows good agreement between the lower bound dynamic toughness and the intermediate rate K_{1C} tests. This indicated that E70T-4 weld metal toughness at intermediate loading rates was 50 MPa$\sqrt{m}$ to 75 MPa$\sqrt{m}$ at room temperature [4].

PRE-NORTHRIDGE CONNECTION TESTS AND OTHER PRIOR STUDIES

Following the Northridge earthquake, numerous experimental studies were conducted to investigate the various aspects that were believed to be associated with the failures observed in the pre-Northridge connection and to improve connection performance. Two full-scale beam-and-column assemblies with a "pre-Northridge" connection detail were dynamically tested. The column was a W14x311 made of A572 Gr. 50 steel. It was supported by a pin at its bottom and a roller at its top. The beam was an A36 steel W36x150 section, with a flange yield strength equal to 262 MPa. The beam was connected to the column at mid-height. Dynamic load cycles were applied at the free end of the beam by two actuators.

The first specimen tested was Specimen A-1, which was typically pre-Northridge practice. The second specimen, Specimen A-2, was the same as Specimen A-1, but with the back-up bar and weld tabs removed and a 9.5-mm reinforcing fillet weld (E71T-8) added to its weld root. E70T-4 was used as the filler metal in both specimens. The groove welds were ultrasonically tested. In both specimens ten A325 bolts, 25.4-mm in diameter, were used to connect the beam web to a shear tab.

The applied beam load-beam tip displacement responses of Specimens A-1 and A-2 are shown in Figure 2. Specimen A-1 fractured at the bottom flange connection in a brittle manner. The cracks started at the root of the weld, extended into the column flange and caused a divot type fracture (Figure 3). The maximum bending moment achieved in the beam during the test was only $0.87M_p$. The fracture occurred

when both the beam and column were still in the elastic range. The applied stress at the groove welds was approximately 262 MPa. The critical value for the stress intensity K is about 58 MPa$\sqrt{m}$. This value is compared with the estimated weld fracture toughness (point A-1) in Figure 4. Also shown are the results of static tests on other large-size connection specimens fabricated with E70T-4 welds [10] that fractured without significant yielding of the beam.

The removal of the back-up bars in Specimen A-2 slightly improved the connection performance, but brittle fracture of the flange welds again led to failure. Other than the limited yielding at the weld access holes, the connection behaved elastically when the welds of the top and bottom flanges fractured almost simultaneously during reversed loading. The fracture surface was confined entirely in the weld. The maximum bending moment resisted by the connection was $0.92M_p$. The inferior performance of Specimens A-1 and A-2, with E70T-4 filler metal, was mainly due to the low fracture resistance of the E70T-4 weld metal. A Charpy V-notch fracture toughness of 27 Joules at $-29^{\circ}C$ was imposed by the AISC in 1997 [6].

Since the Northridge Earthquake several experimental studies were conducted in an attempt to develop improved details for ductile welded unreinforced moment connections. These studies included 13 tests conducted by Lu et al. [7], Stojadinovic et al. [8], and Engelhardt [9]. The test specimens consisted of a beam-to-column exterior connection, where the beam and column sections ranged in size from W24x68 to W36x150 and W14x120 to W14x455, respectively. The complete penetration groove beam flange welds were made for all specimens using the E70TG-K2 electrode, except for Specimen A3 tested by Lu et al. which used an E7018 electrode. The bottom flange the backing bar was removed; the root of the weld was gouged rewelded and reinforced with a fillet weld using the E71T-8 electrode. On the top flange the backing bar was left in place and the bottom side facing the column was reinforced with an E71T-8 fillet weld. In the two tests by Lu et al. and the one test by Engelhardt, both the top and bottom flange backing bars were removed. The beam webs of all of the specimens were bolted, except for the tests by Lu et al. which had the beam webs attached to the column flange with a groove weld. All specimens had continuity plates, except Specimen NSF3. The access holes for the specimens are shown in Figure 5 and represented typical fabrication practice.

All of the specimens developed inelastic deformation in both their beams and panel zones, except for two specimens tested by Stojadinovic et al. [8] and Specimen NSF3 tested by Engelhardt which had strong panel zones. A summary of the total plastic story drift, θ_p, developed in the specimens and the contribution from the beam and panel zone is given in Figure 5. Of the 13 tests, only one successfully achieved a plastic rotation of 0.03 radians or more. The typical failure mode in all of the specimens was a fracture in the base metal of the beam flange that originated at the access hole. Some of the specimens developed a through thickness crack that was a low-cycle fatigue failure [10].

NEW STUDIES TO IMPROVE CONNECTION DUCTILITY

The numerous causes that contributed to the poor performance of moment connections motivated additional analytical and experimental studies by the authors which were conducted under the second phase of the SAC Steel Project [11]. In these studies the effects that various connection details have on inelastic cyclic performance of welded unreinforced moment connections were investigated. The details investigated included: (1) geometry and size of the weld access hole, (2) beam web attachment, and (3) panel zone capacity. The analytical study involved a parametric study using nonlinear finite element models of a welded moment flange connection [12]. These design details were verified by testing 11 full-scale specimens, and shown to produce ductile connections.

Test Program

The experimental study consisted of six exterior moment connections and five interior moment connections. All of the specimens had complete penetration beam flange groove welds using the E70TG-

K2 filler metal. The top flange backing bar was left in place, and a fillet weld reinforcement was provided between the backing bar and the column flange. The beam bottom flange backing bar was removed, back gouged and reinforced with a fillet weld. The beam web attachment detail, panel zone strength, and use of continuity plates were varied among the specimens.

Specimens T1 to T6 were exterior connections. The beam and column were A572 Gr. 50 W36x150 and W14x311 sections. The beam web attachment and panel zone strength were the main variables. Five different beam web attachment details were tested. Specimen T1 beam web was welded directly to the column flange with a groove weld and supplementary fillet weld around the shear tab. In Specimen T2, the weld details are the same as T1 except no supplementary fillet weld. In Specimen T3, a fillet weld connected the shear tab. In Specimen T4, the beam web was bolted to the shear tab. Specimens T1 through T4 had continuity plates, but no doubler plates because their panel zone strength satisfied the 1997 AISC Seismic Provisions. Specimens T5 and T6 had stronger panel zones. Specimen T5 was similar to Specimen T1 except that it had a 12mm thick doubler plate in the column panel zone and no continuity plates. Specimen T6 was also similar, except that it had a 12 mm doubler plate and a heavy shear tab welded to the column face and no continuity plates. The shear tab and welds for Specimen T6 were designed to resist the plastic moment capacity of the beam web. The design of the doubler plates for Specimens T5 and T6 was based on the AISC LRFD provisions, but the panel zone was designed to resist the expected beam capacity $M_{pe}=1.1M_p$, as opposed to $0.8M_{pe}$ per AISC [6].

The interior connection specimen consisted of two W36x150 A572 Grade 50 beams with either a W14x398 A572 Grade 50 column (Specimens C1, C2, and C5) or a W27x258 A572 Grade 50 column (Specimens C3 and C4). Specimens C1, C3, and C5 did not have continuity plates. The W14x398 column section (Specimen C1, C2, and C5) has a 72- mm thick flange and a flange width-to-thickness ($b_{f,col}/t_{f,col}$) ratio of 5.83. The W27x258 section, having a 45-mm thick flange, was selected as the column for Specimens C3 and C4 because the ($b_{f,col}/t_{f,col}$) ratio for the section is 8.06.

The test setup for both exterior and interior connections was designed to simulate the boundary conditions of a beam-to-column connection in a MRF subjected to lateral loading. The ends of the beams were pin connected to rigid links using cylindrical bearing to simulate beam points of inflection in the prototype frame. The base of the column was pinned to the laboratory floor. At the top of the column a pair of parallel horizontal actuators were pin connected to the column to impose story drift to the specimen. Lateral bracing was provided and conformed to the requirements of the 1997 AISC Seismic Provisions. Each specimen was instrumented with strain gages and displacement transducers.

Test Results

The normalized beam moment at the column face-total plastic connection rotation (M/M_p - θ_p) relationship for two exterior connections is shown in Figure 6, where M_p is the plastic beam moment capacity based on measured material properties and section dimensions. The behavior of the exterior connection specimens varied, depending on the web attachment detail and strength of the panel zone.

Specimen T1 developed 2% total story drift when cracks formed at the fusion line of the beam web groove weld at the top and bottom of the web. While yielding occurred in the beam, along with minor local beam flange buckling, extensive yielding occurred in the panel zone. Consequently, the M/M_p-θ_p response showed a progressive increase in capacity with each cycle, until at 5% story drift fracture of the beam bottom flange occurred. In Specimen T2 the beam top flange fractured at the fusion line of the groove weld during the second cycle of 4% total story drift. The omission of the supplemental fillet weld in Specimen T2 reduced the ductility of the connection. Specimen T3 had the fillet welded shear tab separate from the column face, which led to a fracture of the beam bottom flange base metal at 3% total story drift. The fillet weld was not strong enough to resist the moment in the beam web. In Specimen T4, slip occurred in the bolted shear tab. This lead to a fracture of the beam top flange in the HAZ at 4% total story drift. During the testing of Specimen T5, which had a stronger panel zone, yielding developed in the panel zone followed by yielding of the beam flanges and web, before significant local buckling of the

beam flanges and web occurred at 3% total story drift. The beam bottom flange fractured at a total story drift of 6% in the region of local flange buckling. Specimen T6 did not fracture, and the test was stopped at a total story drift of 6%. The performance of the access hole was exceptional since in all of the specimens no cracking or fractures were observed to have initiated in the access hole region.

The behavior of the interior connection specimens were all similar, where pronounced yielding occurred in the beam flanges and web, leading to local flange and web buckling (see Figure 7). The location was about one-half the beam depth from the face of the column. After local beam buckling the capacity of the specimens then began to deteriorate with further cyclic displacements. A fracture of the beam flange eventually occurred in all specimens except Specimen C4. The maximum panel zone inelastic deformation occurred when specimen peak capacity developed. The total story drift at which flange fracture occurred ranged from 4% to 6%. The fracture in Specimen C5, which had the composite slab and shear studs welded to the beam top flange, occurred suddenly in the east beam at a shear stud located 533 mm from the column face where cyclic local buckling developed.

A summary of the contribution of the beam, column and panel zone to the total maximum plastic story drift θ_p for each specimen is given in Figure 8. These results are based on the last successful cycle that was achieved prior to fracture, or termination of the test. With the exception of Specimen C5, specimens that had dominant beam plastic rotation exceed the total plastic rotation of the specimens that had mainly panel zone deformation. Only the specimens with either the complete penetration groove welded beam web and supplement fillet welds or the heavy shear tab fillet welded to the beam web achieved a maximum plastic rotation of at least 0.03 radians.

CONCLUSIONS AND DESIGN RECOMMENDATIONS

Based on the research presented, the following conclusions and design recommendations are given.

1. Full-scale dynamic cyclic tests of pre-Northridge connections show failure modes similar to those observed in the field. Brittle fracture developed in the elastic range of response from flaws in the low toughness E70T-4 weld metal and geometric conditions.

2. In the connection tests with a notch tough filler metal and access holes with conventional geometry, ductile fracture initiating at weld access hole was observed, degrading the performance of the connection. The modified access hole geometry shown in Figure 8 was found to result in good performance and has been adopted by FEMA 350.

3. The web attachment detail can significantly affect the ductility of a connection which has been fabricated using a notch tough filler metal. A beam web attachment detail consisting of a complete penetration groove welded web and supplemental fillet welds around the beam shear tab, or a heavy shear tab welded to the column with a complete penetration groove weld and fillet welded to the beam web produced the best results.

4. Test specimens with a weak panel zone and notch tough filler metal developed significant inelastic shear deformation in the panel zone and increased the plastic strain demand on the beam web welds. Better performance was achieved when the panel zone strength was based on the web alone.

5. Shear studs welded to the beam flange in the region of inelastic cyclic local flange bucking caused cracks to initiate and deteriorate plastic rotation. Test results also indicate that continuity plates are not always required. All specimens without continuity plates and shear studs had a plastic story drift greater than 0.041 radians.

ACKNOWLEDGMENTS

This research described in this paper was supported by grants from the U.S. National Science Foundation, the National Institute of Standards, the SAC Joint Venture, and the Pennsylvania Infrastructure Technology Alliance.

REFERENCES

[1] Youssef, N. F. G, Bonowitz, D., and Gross, J. L., "A Survey of Steel Moment Resisting Frame Buildings Affected by the 1994 Northridge Earthquake," NIST, Report No. NISTIR 5625, 1995, Gaithersburg, MD.

[2] Popov, E. P., and Pinkney, R. B., "Cyclic Yield Reversal in Steel Building Connections," *Journal of the Structural Division*, ASCE, Vol. 95, No. ST3, 1969, pp. 327-353.

[3] Campbell, H.H., "The Northridge Fractures: Are We Learning the Right Lessons?" *Civil Engineering*, March, 1995.

[4] Kaufmann, E.J., Fisher, J.W., Di Julio Jr. R.M., and Gross, J.L., "Failure Analysis of Welded Steel Moment Frames Damaged in the Northridge Earthquake," National Institute of Standards and Technology, Report No. NISTIR 5944, January, 1997.

[5] Xue, M., Kaufmann, E. J., Lu, L-W, and Fisher, J. W., "Achieving Ductile Behavior of Moment Connections-Part II," Modern Steel Construction, June, 1996.

[6] AISC, "Seismic Provisions for Structural Steel Buildings," AISC, Chicago, Illinois, 1997.

[7] Lu, L.W, Xue, M., Kaufmann, E. J. and Fisher, J. W., "Cracking, Repair And Ductility Enhancement of Welded Moment Connections." *Proceedings, NEHRP Conference and Workshop on Research on the Northridge, California Earthquake of January 17, 1994*, Vol. III, 1997, pp. 637-646, Los Angeles.

[8] Stojadinovic, B., Goel, S., Lee, K., Margarian, A.G., Ghoi, J.H., "Parametric Tests on Unreinforced Steel Moment Connections," *Journal of Structural Engineering*, ASCE, Vol. 126, No. 1, 2000, pp. 40-49.

[9] Engelhardt, M., "Cyclic Testing of Welded Unreinforced Moment Connections," Unpublished report, University of Texas, Austin, 2000.

[10] Barsom, J., "Failure Analysis of Welded Beam to Column Connections," Report No. SAC/BD-99/23, SAC Joint Venture, Sacramento, California, 1999.

[11] Ricles, J. M., Mao, C., Lu, L.W. and Fisher, J.W., "Development and Evaluation of Improved Ductile Welded Unreinforced Flange Connections," Report No. SAC/BD-00/24, SAC Joint Venture, Sacramento, California, 2000.

[12] Mao, C., Ricles, J., Lu, L-W, Fisher, J. W., "Effect of Local Details on Ductility of Welded Moment Connections," *Journal of Structural Engineering,* Vol. 127, No. 9, Sept. 2000.

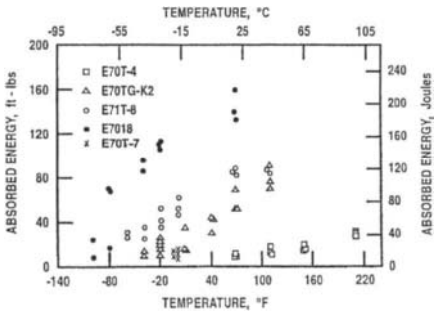


Figure 1 CVN test data for various filler metals [6]

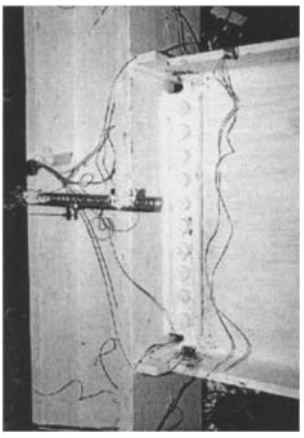
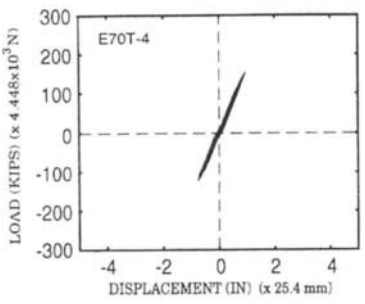
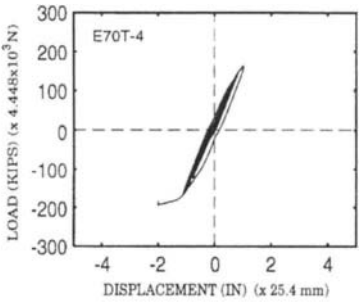


Figure 3 Beam flange weld fracture, Specimen A-1



(a) Specimen A-1



(b) Specimen A-2

Figure 2 Applied load-beam tip displacement response

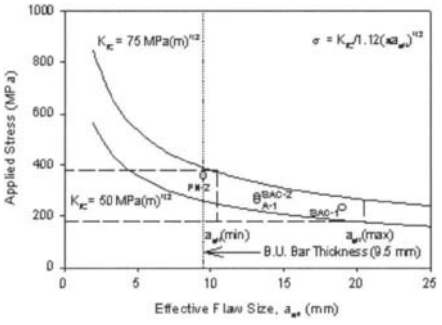


Figure 4 Critical applied stress vs. effective flaw depth
for E70T-4 WSMF Connections

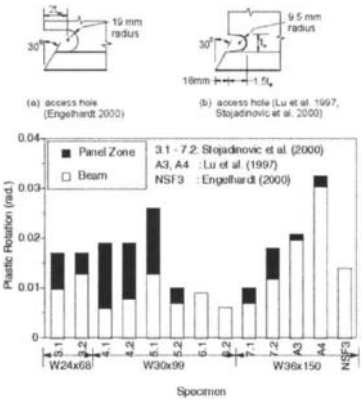


Figure 7 Interior Specimen C4 at completion of testing connection test



Figure 5 Summary of plastic story drift of prior Post-Northridge

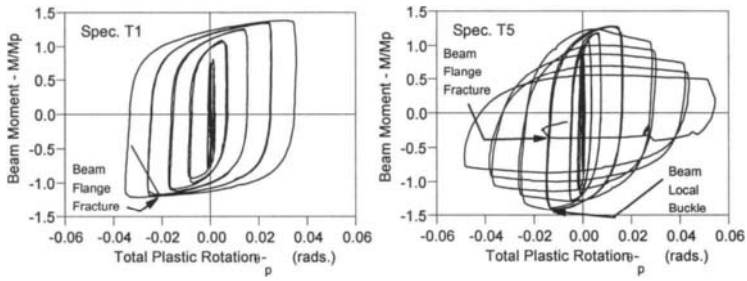


Figure 6 Exterior connection beam moment-plastic rotation response for a weak and strong panel zone

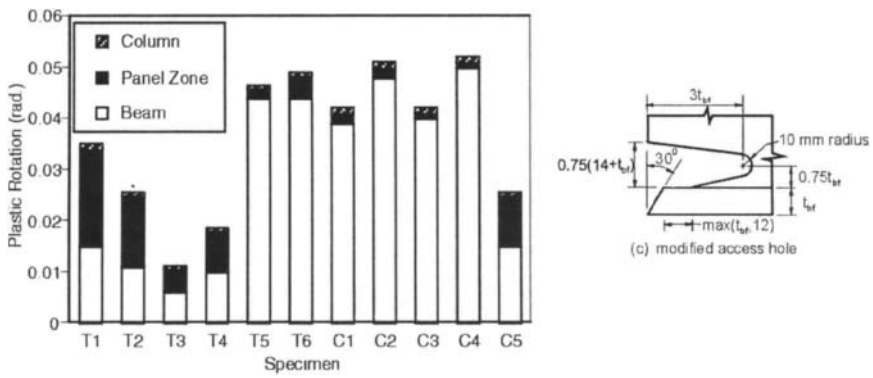


Figure 8 Test specimen plastic story drift

Advances in Building Technology, Volume 1
M. Anson, J.M. Ko and E.S.S. Lam (Eds.)
© 2002 Elsevier Science Ltd. All rights reserved

LATERAL LOAD BEHAVIOR OF UNBONDED POST-TENSIONED PRECAST CONCRETE WALLS

F.J. Perez, R. Sause, S. Pessiki, and L.-W. Lu

ATLSS Research Center, Department of Civil and Environmental Engineering, Lehigh University, Bethlehem, PA 18015, USA

ABSTRACT

Unbonded post-tensioned precast walls are constructed by post-tensioning precast panels across horizontal joints with the post-tensioning steel unbonded to the panels over a significant portion of its length. The lateral load behavior of these walls differs significantly from that of conventional cast-in-place reinforced concrete walls and precast concrete walls designed to emulate cast-in-place walls. An unbonded post-tensioned wall can be designed with strength and initial stiffness similar to those of a conventional cast-in-place reinforced concrete wall. In addition, however, the unbonded post-tensioned wall can be designed to undergo significant nonlinear lateral drift without significant damage. The nonlinear behavior results from the opening of gaps along the horizontal joints. Subsequent closing of these gaps, as a result of the post-tensioning, results in a self-centering behavior that eliminates residual lateral drift. The paper reports on the experimentally and analytically observed lateral load behavior of unbonded post-tensioned precast concrete walls. The limit states in the behavior are outlined. Results of monotonic and cyclic lateral load tests of large-scale wall specimens are presented and compared with analytical results. Conclusions regarding the suitability of the observed behavior are given.

KEYWORDS

Walls, Precast, Unbonded, Prestressed, Concrete, Seismic, Earthquake

INTRODUCTION

Past earthquakes have demonstrated the superior seismic performance of buildings with reinforced concrete walls as the primary lateral load resisting system (Fintel, 1995). However, the provisions of current U.S. building codes limit the use of precast concrete walls as a primary lateral load resisting system in seismic regions. Precast concrete systems that can be designed in the U.S. under current building codes use connections made with cast-in-place concrete, and the resulting wall emulates a cast-in-place wall. However, these emulative precast walls do not have all the economic advantages of precast construction as a result of the cast-in-place concrete and expensive details in the connections.

Alternative non-emulative precast seismic structural systems have been developed that take advantage of natural discontinuities at the connections of precast systems. In the U.S., these alternative systems have been the focus of the PRESSS (PREcast Seismic Structural Systems) program, initiated in 1990. PRESSS research has shown that the use of unbonded post-tensioned connections of precast elements results in precast concrete systems with excellent load-deformation hysteretic behavior (Cheok et al., 1993, MacRae et al., 1994, Priestley et al., 1993). An analytical study of the seismic response of unbonded post-tensioned precast concrete walls with horizontal joints was carried out at Lehigh University by Kurama et al. (1999). These unbonded post-tensioned precast walls are constructed by post-tensioning precast wall panels across horizontal joints at the floor levels (Figure 1). Grout is used between the joints for construction tolerances. The analytical study shows that, as a result of unbonding, large nonlinear lateral drifts can be achieved in a wall without yielding or fracturing the post-tensioning steel. Dynamic analysis results indicate that unbonded post-tensioned precast walls have large flexural ductility and self-centering capacity without sustaining significant damage and excessive drift under moderate-to-severe earthquakes.

An experimental program to verify the results of this analytical study is currently underway at Lehigh University. This paper discusses the behavior of unbonded post-tensioned precast concrete walls subjected to static monotonic and cyclic lateral loads. The experimental results obtained to date are compared with results obtained using the analytical model developed by Kurama et al. (1996).

BEHAVIOR

This paper reports on the experimentally and analytically observed lateral load behavior of unbonded post-tensioned precast concrete walls. The walls considered in this study are shown schematically in Figure 1. Each wall is comprised of six one-story precast panels that are connected along horizontal joints using unbonded post-tensioned steel, which is anchored at the roof and within the foundation (Figure 1(a)). The bottom panel has regions that are confined, as shown in Figure 1(b). This confinement enables the base panel to sustain the large compressive strains that develop as a result of gap opening displacements that develop along the base of the wall due to lateral loads.

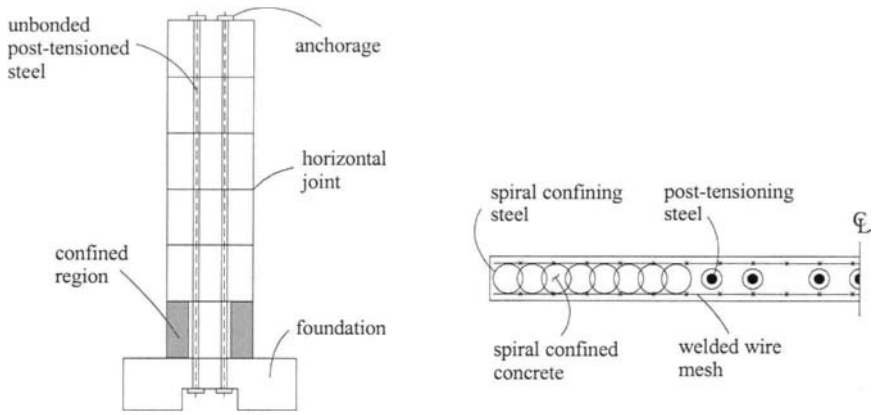


Figure 1: Unbonded post-tensioned wall.

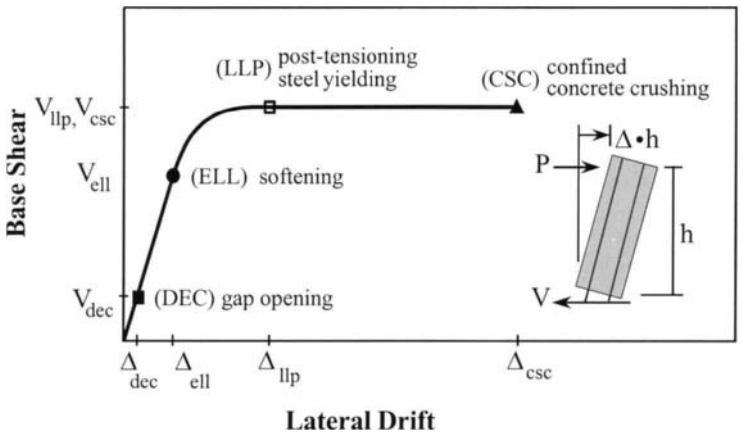


Figure 2: Lateral load behavior of unbonded post-tensioned walls.

As shown in Figure 2, the lateral load behavior of unbonded post-tensioned walls is characterized by several limit states: (1) decompression at the base of the wall; (2) significant reduction in lateral stiffness (i.e., softening) due to gap opening in flexure along the wall-to-foundation connection; (3) yielding of the post-tensioning steel; (4) base shear capacity; and (5) crushing of confined concrete. The limit states are described below.

Decompression at the base of the wall occurs when the overturning moment at the base of the wall causes one end of the wall to begin to decompress. Under a specified lateral load distribution, decompression of the wall can be related to a specific level of base shear and lateral drift, V_{dec} and Δ_{dec} respectively. Decompression is accompanied by the *initiation* of gap opening along the horizontal joint between the base panel and the foundation. The point on the base-shear-lateral-drift response of a wall when the lateral stiffness of the wall begins to reduce significantly is called the effective linear limit. This reduction in lateral stiffness (called softening) is caused by significant gap opening along the horizontal joint between the base panel and the foundation. The base shear and lateral drift corresponding to the effective linear limit are denoted as V_{ell} and Δ_{ell} respectively. Softening usually occurs in a smooth and continuous manner in a precast wall with unbonded post-tensioned horizontal joints (Kurama et al., 1999). Hence, the term *effective* linear limit is used to describe this point on the base-shear-lateral-drift relationship.

Yielding of the post-tensioning steel occurs when the strain in the steel reaches the linear limit of the steel. The base shear and lateral drift corresponding to the linear limit strain of the post-tensioning steel are denoted as V_{llp} and Δ_{llp}. Since the post-tensioning steel is unbonded, this limit state is reached after large nonlinear lateral drift has occurred, providing the wall with significant drift capacity before significant inelastic deformation develops (Kurama et al., 1999). Failure of the wall occurs when the confined concrete at the base of the wall fails in compression. Thus the drift capacity of the wall is controlled by the compression strain capacity of the confined concrete. Figure 1 refers to spiral confined concrete, although other confining reinforcement details may be used. The base shear and lateral drift corresponding to failure of the confined concrete are denoted as V_{csc} and Δ_{csc}. In a well-designed wall Δ_{csc} is significantly larger than Δ_{llp}. Also, the base shear capacity of the wall is V_{llp}, which is approximately equal to V_{csc}. Thus, in a well-designed wall, the base shear capacity is governed by axial-flexural (overturning) capacity of the wall, rather than the shear sliding capacity.

EXPERIMENTAL PROGRAM

An experimental program is currently underway at Lehigh University to study the behavior of unbonded post-tensioned precast concrete walls with horizontal joints under static monotonic and cyclic lateral loads. The walls considered in this study are 5/12-scale models of a 6-story full-scale wall similar to that shown in Figure 1. An elevation view of the test set-up is shown schematically in Figure 3. At the base is a large precast concrete foundation with a manhole (not shown) to provide access to the inside of the foundation, where the post-tensioning bars (shown dashed) are anchored. The test specimen is comprised of four wall panels, a loading block, and two extension panels. The bottom two panels have confinement on both ends of the wall, as shown by the shaded regions in Figure 4. The confinement is the same as that shown in Figure 1(b). It is noted that the confinement in the second panel is provided to preserve its integrity and thus make it reusable throughout the test program.

The loading block, which rests on the fourth panel, is used to apply gravity and lateral loads. The gravity load is applied by stressing an external bar on either side of the wall using a hydraulic cylinder. The gravity load remains constant throughout the experiment. The lateral load actuator is connected to the loading block at a height of 7.14 m from the base of the wall. This height represents the resultant of a triangular inertia force profile with zero load at the base and the maximum load at the roof. The two extension panels above the loading block provide a total unbonded height of 9.91 m, which is the unbonded height of the full-scale 6-story wall, scaled by 5/12.

The effect of five parameters on the flexural behavior of the walls is investigated. As summarized in Table 1, these parameters are: (1) area of post-tensioning steel, A_p; (2) initial stress in post-tensioning steel, f_{pi} (normalized with respect to the maximum stress of the post-tensioning steel, f_{pu}); (3) initial stress in concrete due to post-tensioning, $f_{ci,p}$; (4) eccentricity of post-tensioning steel, e_p; and (5) confining reinforcement details in the base panel. To date, Tests 1 and 2 have been performed (See Table 1) to compare the effects of monotonic versus cyclic loading on the flexural behavior of the walls. Results from these tests are discussed next.

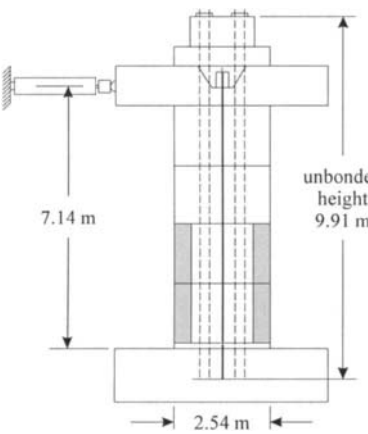


Figure 3: Test set-up.

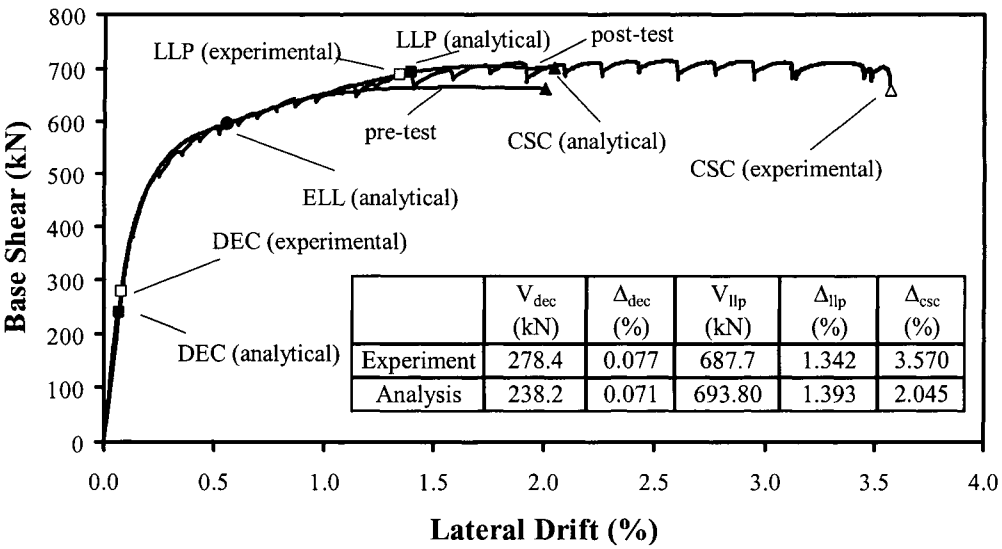
TABLE 1
EXPERIMENTAL PARAMETER STUDY

Test	Loading	A_p (mm^2)	f_{pi}/f_{pu}	$f_{ci,p}$ (N/mm^2)	e_p (mm)	Confinement Type	Confinement Ratio (%)	
							Volumetric	Area
1	monotonic	4839	0.59	6.07	508	spirals	7.3	-
2	cyclic	4839	0.59	6.07	508	spirals	7.3	-
3	cyclic	2419	0.59	3.03	508	hoops	-	1.75
4	cyclic	4839	0.295	3.03	508	hoops	-	1.75
5	cyclic	2419	0.59	3.03	127	hoops	-	1.75

EXPERIMENTAL RESULTS

Figure 4 shows three plots of base shear versus lateral drift for Test 1. The base shear corresponds to the lateral load applied by the horizontal actuator shown in Figure 3. The lateral drift is taken as the horizontal displacement at the level of the actuator, divided by the height of the actuator relative to the base of the wall (i.e., 7.14 m). The two smooth plots in Figure 4 are obtained analytically using the wall model proposed by Kurama et al. (1996). The third plot, with the repeated load drops, is the experimental results. Each load drop is a result of a temporary halt in the loading of the specimen. The analytical result plotted with the darker line is from a pre-test prediction. It can be seen that the analytical model predicts the results quite accurately in the elastic range and through the effective linear limit point (ELL). However, the peak base shear and the lateral drift at failure do not agree. After Test 1 was completed, post-tensioning steel samples were tested in tension to obtain the stress-strain behavior of the material. These samples were taken from bars that did not yield during the test. It was observed that the yield strength of the post-tensioning steel was 15 percent larger than the pre-test model. A post-test analytical model was created from the pre-test model by increasing the post-tensioning steel yield strength, and the analysis was repeated. The post-test analytical result is shown in the lighter curve in Figure 4. It can be seen that (except for the lateral drift at failure) there is an excellent correlation between the wall analytical model and the experimental result. The values obtained for various key limit states from the second analytical model and the experiment are shown in tabular form in Figure 4.

At this time, two explanations are proposed for the difference in the lateral drift at failure (i.e., lateral drift corresponding to crushing of spiral confined concrete, Δ_{csc}). First, the strain capacity of the confined concrete in the experiment may be larger than the strain capacity in the analytical model, which was obtained using the stress-strain relationship for confined concrete proposed by Mander et al. (1988). Second, the compressive strain demand in the concrete, as a function of the lateral drift of the wall, may be smaller in the experiment than in the analytical model. That is, the model, which assumes plane sections in the concrete, overestimates the compressive strains at the base of the wall, and thus predicts an early failure when compared to the experiment.



	V_{dec} (kN)	Δ_{dec} (%)	V_{llp} (kN)	Δ_{llp} (%)	Δ_{csc} (%)
Experiment	278.4	0.077	687.7	1.342	3.570
Analysis	238.2	0.071	693.80	1.393	2.045

Figure 4: Comparison of analytical and experimental results for Test 1.

The base shear-lateral drift results for Tests 1 and 2 (see Table 1) are plotted in Figure 5. Test 1 was conducted under a static monotonic lateral load, while Test 2 was performed under a static cyclic lateral load. As shown in Figure 5 and in Table 2, the lateral load results for the two tests are in good agreement. Test 2 shows that an unbonded post-tensioned precast concrete wall exhibits a nearly nonlinear elastic load-deformation response with a small amount of energy dissipation per cycle of loading. Before yielding of the post-tensioning steel, the nonlinearity results from gap opening that occurs between the base panel-to-foundation connection as the precompression due to prestressing is overcome by the moment due to lateral load. In addition, it can be observed that the wall exhibits excellent self-centering behavior. The self-centering capacity of the wall is only slightly compromised when it is loaded past yielding of the post-tensioning steel. Therefore, preliminary experimental results indicate that an unbonded post-tensioned precast concrete walls exhibit cyclic lateral load behavior that make them good candidates for use in earthquake-resistant building structures.

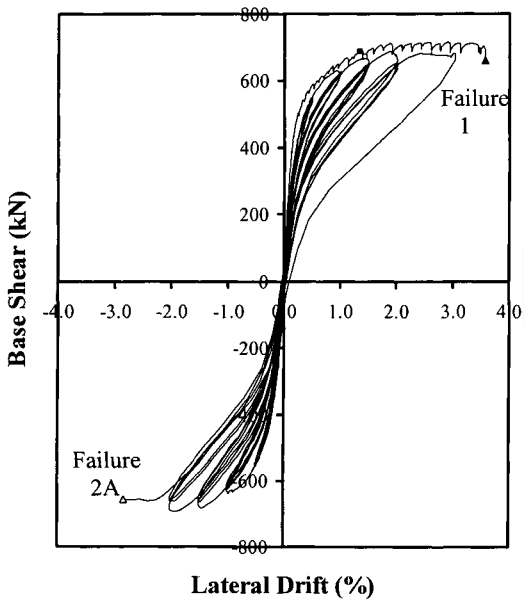


TABLE 2
EXPERIMENTAL RESULTS

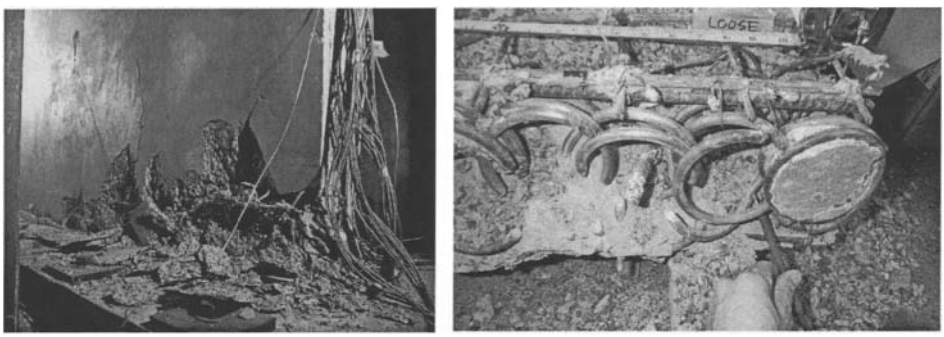
Test	V_{dec}	Δ_{dec}	V_{llp}	Δ_{llp}	Δ_{csc}
1	278.4	0.077	687.7	1.342	3.570
2	290.1	0.117	671.0	1.437	2.828

Figure 5: Experimental results under monotonic and cyclic lateral loads.

FAILURE MODES

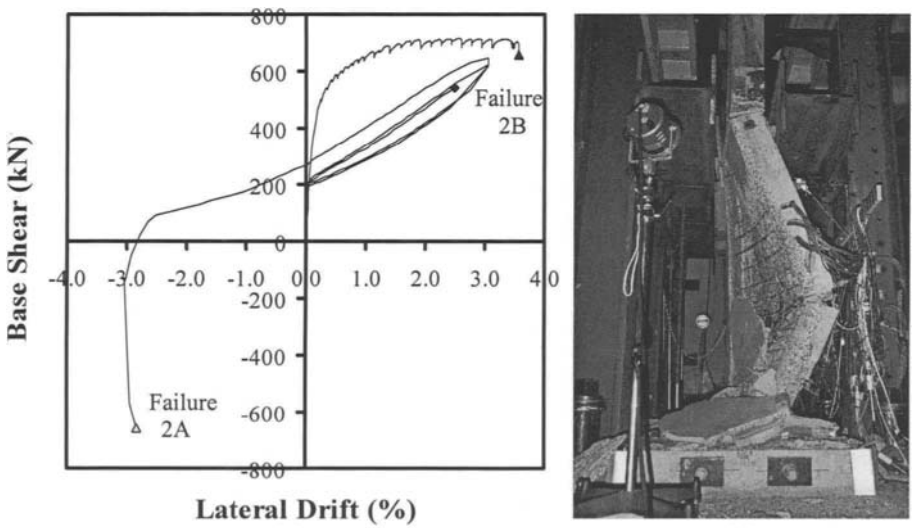
An unbonded post-tensioned precast concrete wall that is well designed and adequately detailed is expected to fail when the confined concrete at the base of the wall fails in axial-flexural compression. This failure occurs when the confining steel fractures and the lateral confining pressure in the confined concrete is lost. As noted earlier, the lateral drift when crushing of the confined concrete occurs is denoted as Δ_{csc}. This limit state is shown in Figure 5 for Tests 1 and 2 and is labeled as "Failure 1" and "Failure 2A," respectively. The observed failure at the base of the wall for Test 1 is shown in Figure 6. Figure 6(a) shows the base panel after failure. After excavating the concrete at the base of the compression edge of the wall, it was observed that the spirals fractured in the through-thickness direction of the wall, as shown in Figure 6(b). The same mode of failure was observed for Test 2 (Failure 2A). After Failure 2A occurred at one end of the wall for Test 2, the specimen was loaded in the opposite direction for additional cycles, as shown in Figure 7(a) until that side of the wall failed (labeled "Failure 2B"). As shown in Figure 7(b), Failure2B was a sudden local buckling failure of the

confined concrete region of the base panel. It is important to emphasize that only the confined concrete region buckled, while the rest of the base panel did not, as shown in Figure 7(b) by the shiny vertical conduit which remained attached to the unbuckled portion of the panel. This failure mode can be explained as follows. During Test 2, as the wall was subjected to cyclic lateral loads, numerous short diagonal cracks formed in a narrow vertical band along the height of the base panel. These cracks formed adjacent to the vertical conduit shown in Figure 8(b), which was the outermost conduit, next to the highly confined region (see also Figure 1(b)). The development of these cracks ultimately permitted the confined concrete region to act independently from the rest of the wall. As a result, the confined region, which was carrying the compressive load, buckled after it was no longer restrained from buckling by the rest of the wall. This mode of failure is undesirable as the gravity load capacity of the wall is jeopardized. Therefore, the reinforcing steel in the base panel is being redesigned to better control cracking and to prevent this mode of failure.



(a) (b)

Figure 6: Observed failure mode for Test 1.



(a) (b)

Figure 7: Second failure mode observed for Test 2.

CONCLUSIONS

This paper reports on the experimentally and analytically observed lateral load behavior of unbonded post-tensioned precast concrete walls. The limit states that characterize the lateral load behavior are outlined. Results of monotonic and cyclic lateral load tests of large-scale wall specimens are presented and compared with analytical results. The results show that the limit states that characterize the lateral load behavior occur as anticipated in the design of the walls and at force and drift levels predicted by the analytical model, except that the experimentally observed drift capacity significantly exceeds the drift capacity predicted by the analytical model. The results demonstrate that unbonded post-tensioned precast walls can be designed to undergo significant nonlinear lateral drift without significant damage, and to retain their ability to self-center, thereby eliminating residual lateral drift. The cyclic lateral load behavior of the walls is nearly nonlinear elastic, with only a small amount of energy dissipation per cycle of loading. As a result, larger lateral drifts can be expected under earthquake loading. However dynamic analysis results (Kurama et al. 1999) show that these walls can be designed to avoid sustaining excessive drift under moderate-to-severe earthquakes.

ACKNOWLEDGMENTS

This research is funded by the National Science Foundation (NSF) under Grant No. CMS-9612165 as part of the PREcast Seismic Structural Systems (PRESSS) program. The support of NSF program director S.C. Liu is gratefully acknowledged. The research is also supported by the Pennsylvania Infrastructure Technology Alliance through a grant from the Pennsylvania Department of Community and Economic Development. Numerous individuals from the U.S. Precast Concrete Industry have also provided assistance. The opinions, findings, and conclusions in this paper are those of the authors and do not necessarily reflect the views of those acknowledged herein.

REFERENCES

Cheok, G., Stone, W., and Lew, H. (1993). Model Precast Concrete Beam-to-Column Connections Subject to Cyclic Loading. *PCI Journal*, Precast/Prestressed Concrete Institute **38:4,** 80-92.

Fintel, M. (1995). Performance of Buildings with Shear Walls in Earthquakes of the Last Thirty Years. *PCI Journal*, Precast/Prestressed Concrete Institute **40:3,** 62-80.

Kurama, Y., Pessiki, S., Sause, R., Lu, L. W., and El-Sheikh, M. (1996). Analytical Modeling and Lateral Load Behavior of Unbonded Post-Tensioned Precast Concrete Walls. Research Report No. EQ-96-02, Department of Civil and Environmental Engineering, Lehigh University, Bethlehem, PA.

Kurama, Y., Pessiki, S., Sause, R., and Lu, L. W. (1999). Seismic Behavior and Design of Unbonded Post-Tensioned Precast Concrete Walls. *PCI Journal*, Precast/Prestressed Concrete Institute **44:3,** 72-89.

MacRae, G., and Priestley, M. (1994). Precast Post-Tensioned Ungrouted Concrete Beam-Column Subassemblage Tests. Report No. PRESSS – 94/01, Department of Applied Mechanics and Engineering Sciences, Structural Systems, University of California, San Diego, CA.

Mander, J., Priestley, M., and Park, R. (1988). Theoretical Stress-Strain Model for Confined Concrete. *Journal of Structural Engineering*, American Society of Civil Engineers **114:8**, 804-1826.

Priestley, M., and Tao, J. (1993). Seismic Response of Precast Prestressed Concrete Frames with Partially Debonded Tendons. *PCI Journal*, Precast/Prestressed Concrete Institute **38:1**, 58-69.

Advances in Building Technology, Volume 1
M. Anson, J.M. Ko and E.S.S. Lam (Eds.)
© 2002 Elsevier Science Ltd. All rights reserved

DESIGN OF HIGH STRENGTH SPIRAL REINFORCEMENT IN CONCRETE COMPRESSION MEMBERS

Stephen Pessiki[1], Benjamin Graybeal[2] and Michael Mudlock[3]

[1] Department of Civil and Environmental Engineering, Lehigh University
Bethlehem, PA 18015, USA
[2] PSI Inc., FHWA Turner-Fairbank Highway Research Center
Mclean, VA 22101, USA
[3] Simpson, Gumpertz & Heger Inc., Arlington, MA 02474, USA

ABSTRACT

Current provisions of the ACI 318 Code and AASHTO Design Specification limit the nominal yield stress of spiral reinforcement for compression members to 414 MPa (60 ksi). A procedure for the design of high strength spiral reinforcement for compression members is described. The procedure utilizes useable stress values, rather than nominal yield stress values, for spiral design. To evaluate the design procedure, concentric axial load tests were performed on six spirally reinforced concrete compression members with spiral reinforcement yield stress values ranging from 538 MPa (78 ksi) to 1345 MPa (195 ksi), and useable stress values ranging from 545 MPa (79 ksi) to 1131 MPa (164 ksi). It was found that, for the compression member geometries and material properties treated in this study, the proposed design procedure satisfactorily predicted the behavior of the compression members made from spirals with useable stress values up to 758 MPa (110 ksi).

KEYWORDS

compression, concrete, confinement, design, high strength steel, spiral reinforcement

INTRODUCTION

In current U.S. practice, spiral reinforcement in compression members is designed so that, should the compression member be overloaded, confinement by the spiral reinforcement provides enough strength enhancement to the concrete core to replace the strength lost by the spalling of the concrete cover. For a given compression member cross-section, a higher strength concrete requires a greater amount of confinement. Current provisions of the ACI 318 Building Code Requirements for Structural Concrete (1995) and the American Association of State Highway and Transportation Officials LRFD Bridge Design Specifications (1994) limit the spiral reinforcement yield stress to 414 MPa (60 ksi). As concrete strengths have increased over the years, the required amount of spiral reinforcement has also increased. To satisfy

the need for a greater amount of spiral reinforcement, either the use of larger diameter spiral wires or decreased pitch can be employed. However, fabrication problems and concrete placement difficulty based on practical spacing limits and code requirements may result. One alternative to the above practices is to use higher strength spiral reinforcement (in excess of current code provisions), wherein a smaller amount of higher strength spiral steel is used to provide a given required amount of confining pressure to the concrete. This paper presents a procedure for the design of high strength spiral reinforcement and the results of tests to evaluate this procedure. Complete details of the research presented in this paper are given in Graybeal and Pessiki (1998) and Mudlock and Pessiki (1999).

BACKGROUND

In the early 1900's Considère (1903) found that the compressive strength of concrete was increased by transverse confining pressure. This confining pressure, whether active (i.e. applied externally by a pressurized fluid) or passive (i.e. created by lateral expansion of the axially compressed concrete against a confining material), worked to resist the lateral expansion of concrete as it was loaded axially. Richart, Brandzaeg, and Brown (1934) presented Eqn.1 to describe the relationship between the unconfined concrete strength f_{co}, lateral pressure $f_{2\text{-}2}$, and the confined concrete strength f_{c2}:

$$f_{c2} = f_{co} + 4.1 f_{2-2} \tag{1}$$

Richart et al. also proposed Eqn. 2 to relate the longitudinal strain at the confined concrete strength, ε_{c2}, to the confined strength, f_{c2}, the unconfined strength, f_{co}, and the corresponding unconfined longitudinal strain, ε_{co}:

$$\varepsilon_{c2} = \varepsilon_{co}\left(5\frac{f_{c2}}{f_{co}} - 4\right) \tag{2}$$

Eqns. (1) and (2) are used as part of the proposed design procedure.

Current Design Requirements

The ACI 318 Code and the AASHTO Design Specification both state that the nominal concentric axial load capacity, P_o, of a reinforced concrete compression member is given by:

$$P_o = 0.85 f_{co}\left(A_g - A_{st}\right) + A_{st} f_y \tag{3}$$

where A_g is the gross cross-sectional area of the compression member, A_{st} is the area of the longitudinal reinforcement, and f_y is the yield stress of the longitudinal reinforcement. The volumetric ratio of spiral reinforcement in a compression member, ρ_{sp}, defined as the ratio of the volume of the spiral to the volume of the concrete core, is computed as:

$$\rho_{sp} = \frac{4A_{sp}}{d_{sp}s} \tag{4}$$

where the spiral wire cross-sectional area, pitch, and out-to-out diameter are A_{sp}, s, and d_{sp}, respectively. The confining pressure $f_{2\text{-}2}$ which is applied to the concrete core by spiral reinforcement is calculated as:

$$f_{2-2} = \frac{1}{2}\rho_{sp} f_{sp} \tag{5}$$

where f_{sp} is the stress in the spiral reinforcement. Spiral reinforcement is designed according to the philosophy that the strength reduction caused by spalling of the concrete cover should equal the strength gain of the concrete core due to confinement. In design codes, this leads to the following equation for the required amount of spiral reinforcement:

$$\rho_{sp} \geq 0.45 \frac{f_{co}}{f_{sy}} \left(\frac{A_g}{A_{core}} - 1 \right) \tag{6}$$

In Eqn. (6), the stress in the spiral reinforcement, f_{sp}, is assumed to equal f_{sy}, the yield stress of the spiral reinforcement.

PROPOSED DESIGN PROCEDURE

In the proposed design procedure, spiral reinforcement design is based upon a useable stress $f_{sp2,dsgn}$ instead of the nominal yield stress of the spiral reinforcement. The proposed design procedure provides a means to calculate the useable strain $\varepsilon_{sp2,dsgn}$ in the spiral reinforcement, which in turn is used to determine the useable stress from the stress-strain curve of the particular spiral wire.

Step 1 in the procedure determines the level of confined compressive strength $f_{c2,dsgn}$ required for the core concrete in the compression member. Using an approach consistent with the ACI 318 Code and AASHTO Design Specification, this core strength enables the member to carry the same axial load after the loss of the concrete cover that it carried prior to concrete cover failure:

$$f_{c2,dsgn} = \frac{f_{co}(A_g - A_{st})}{A_{core}} \tag{7}$$

where A_{core} is the area of the core concrete. Step 2 calculates the confining pressure, $f_{2\text{-}2,dsgn}$, which is required for the core concrete to reach its desired strength. From Eqn. (1), $f_{2\text{-}2,dsgn}$ is calculated as:

$$f_{2-2,dsgn} = \frac{1}{4.1}(f_{c2,dsgn} - f_{co}) \tag{8}$$

Step 3 determines the longitudinal strain $\varepsilon_{c2,dsgn}$ using Eqn. (9), which is taken from Eqn. (2):

$$\varepsilon_{c2,dsgn} = \varepsilon_{co} \left(5 \frac{f_{c2,dsgn}}{f_{co}} - 4 \right) \tag{9}$$

Step 4 determines the transverse strain in the concrete core, $\varepsilon_{ct2,dsgn}$, which occurs at fracture of the spiral reinforcement. The value of $\varepsilon_{ct2,dsgn}$ is calculated as:

$$\varepsilon_{ct2,dsgn} = 0.41\varepsilon_{c2,dsgn} - 0.105\varepsilon_{co} \tag{10}$$

The development of Eqn. (10) is discussed in Graybeal and Pessiki (1998). In Step 5, from strain compatibility, the useable strain in the spiral reinforcement $\varepsilon_{sp2,dsgn}$ is the same as the transverse strain in the concrete core $\varepsilon_{ct2,dsgn}$. This relationship applies at all strains, including those at spiral fracture. This relationship is expressed as:

$$\varepsilon_{sp2,dsgn} = \varepsilon_{ct2,dsgn} \tag{11}$$

Thus the value of useable strain is determined by the compression member geometry and concrete material properties. The useable strain is not dependent upon the stress-strain curve of the particular spiral wire that is used. The chosen spiral wire must possess sufficient ductility to achieve this strain value.

Step 6 determines the useable stress $f_{sp2,dsgn}$ from the useable strain $\varepsilon_{sp2,dsgn}$ and the stress strain curve for the particular spiral wire under consideration. Thus, while the useable strain is independent of the stress-strain curve of the spiral, the useable stress does depend upon the stress-strain curve. The ideal situation is to utilize the stress-strain curve of the spiral in its in-situ, or spiraled, state. However, it is more likely that only a stress-strain curve from a tension test of an unspiraled wire will be available, which may not accurately represent the behavior of the spiraled wire. In this case, the value obtained may need to be modified in order to ensure a proper design. This is discussed more fully in Mudlock and Pessiki (1999).

Step 7 determines the required volumetric ratio of spiral reinforcement $\rho_{sp,dsgn}$ from Eqn. (12), which is a rearranged form of Eqn. (5).

$$\rho_{sp,dsgn} = \frac{2f_{2-2,dsgn}}{f_{sp2,dsgn}} \tag{12}$$

Finally, Step 8 computes the required pitch, s_{dsgn}, from Eqn. (13), which is a rearranged form of Eqn. (4).

$$s_{dsgn} = \frac{4A_{sp}}{d_{sp}\rho_{sp,dsgn}} \tag{13}$$

EXPERIMENTAL PROGRAM

Concentric axial load compression tests were performed to evaluate the design procedure presented above. The test program, described in Table 1, included six 356 mm (14 in.) diameter compression member specimens made with six different spiral wires. Each specimen was designed using an unconfined concrete compressive strength of 55.2 MPa (8.0 ksi). The nominal yield stress of the spiral reinforcement varied from 538 MPa (78 ksi) to 1345 MPa (195 ksi), and the useable stress varied from 545 MPa (79 ksi) to 1131 MPa (164 ksi). The specimens all measured 1.42 m (56 in.) in height and had a 51 mm (2 in.) concrete cover to the outside of the spiral reinforcement.

The design procedure described above was used to design the spiral for each specimen. The calculation of useable strain proceeded as follows. First, $f_{c2,dsgn}$ was calculated from Eqn. (7) as 109 MPa (15.8 ksi). From Eqn. (8), the confining pressure $f_{2\text{-}2,dsgn}$ was calculated as 13.0 MPa (1.88 ksi). Next, $\varepsilon_{c2,dsgn}$ was calculated by Eqn. (9) as 0.0158, and $\varepsilon_{ct2,dsgn}$ was calculated from Eqn. (10) to be 0.0062. Finally, Eqn. (11) was used to obtain a value for $\varepsilon_{sp2,dsgn}$ equal to 0.0062. This was the useable strain value used in the design of the specimens. The useable stresses $f_{sp2,dsgn}$ were determined for each wire at that strain, and Eqns. (12) and (13) were used to calculate $\rho_{sp,dsgn}$ and finally the spiral pitch s_{dsgn}.

Extra spiral reinforcement was provided in each specimen over one diameter of height from each end. The test region was the portion of the specimen between the more heavily confined end regions. Two wires were bundled to create the spiral in specimens14-A' and 14-B'. This is shown in Table 1, where n_{sp} is the number of wires in the bundle. Four 12.7 mm (0.5 in.) diameter mild steel longitudinal reinforcement held the spiral in position during fabrication. Each specimen was tested under concentric axial compression in a 22.2 MN (5000 kip) capacity universal testing machine. Twelve electrical resistance strain gages were used to monitor strains in both the spiral and longitudinal reinforcement within the test region, and linear

TABLE 1
DESCRIPTION OF TEST SPECIMENS

Specimen		Spiral Reinforcement						
I.D.	d_c (mm)	$f_{sy,nom}$ (MPa)	$f_{sp2,dsgn}$ (MPa)	d_{sw} (mm)	n_{sp}	A_{sp} (mm^2)	s (mm)	ρ_{sp} %
14-A'	356	538	545	8.9	2	124	41	4.76
14-B'	356	738	717	8.9	2	124	54	3.62
14-C'	356	834	745	8.9	1	62	28	3.48
14-D'	356	965	758	8.9	1	62	29	3.42
14-E'	356	1345	1131	9.1	1	65	44	2.29
14-F'	356	1276	1110	10.9	1	93	62	2.34

variable differential transformer displacement transducers were used to measure overall axial shortening. Based on material testing, the unconfined concrete compressive strength f_{co} for the Series 2 tests was taken as 52.1 MPa (7.55 ksi), and the axial concrete strain corresponding to the unconfined concrete strength, ε_{co}, was taken as 0.0027. Due to a fabrication error, Specimen 14-B' failed prematurely during testing in the heavily confined region at the top of the specimen. The results from this specimen are excluded from the remaining discussions.

RESULTS AND DISCUSSION

The axial load-axial shortening response of each specimen is shown in Figure 1. Failure of all eight specimens was defined by rupture of one or more turns of wire of the spiral reinforcement and a subsequent loss of confining pressure on the concrete core. This resulted in a significant decrease in the load carrying capacity of the specimen. However, two observations indicate that the failures were not due to the spiral reinforcement reaching its ultimate strain as caused by lateral expansion of the core. First, for all specimens, the measured strain in the spiral reinforcement just before failure was less than one-third of the spiral strain at ultimate stress, ε_{su}. Typically, the maximum strains measured during the tests were less than 0.01. Second, for most of the specimens, multiple spiral fractures occurred simultaneously along a well defined inclined plane throughout the test region. This suggests that the plane formed first, and that the spirals fractured as a result of relative movement of the concrete along this plane.

Longitudinal Strains

Tables 2 and 3 show the experimentally obtained values and design values of ε_{c2}, and Table 4 shows the ratio of these two values, $R(\varepsilon_{c2})_{exp/dsgn}$. The experimental value $\varepsilon_{c2,exp}$ was obtained as the average measured strain in the longitudinal reinforcement at failure. Table 4 shows that the experimental values exceeded the design values in every case except Specimen 14-A', where the value of $R(\varepsilon_{c2})_{exp/dsgn}$ was 0.97. This indicates that the design procedure gives a reasonable to conservative prediction of longitudinal strain at failure.

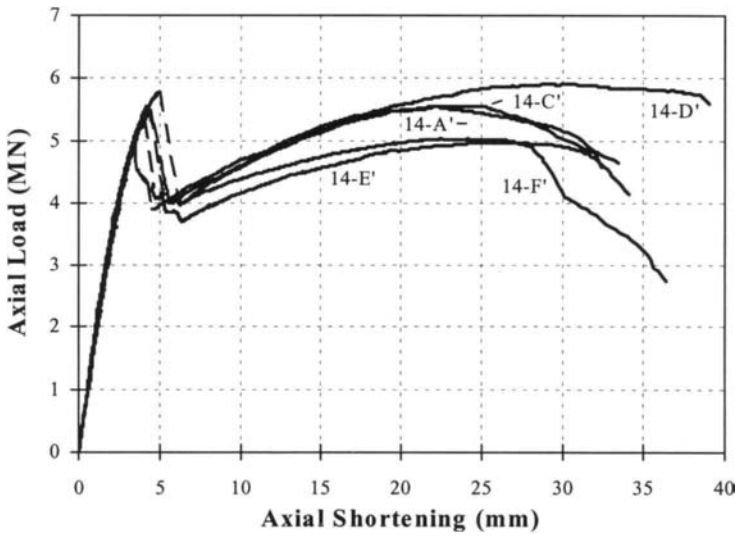


Figure 1: Axial load-axial shortening responses

Spiral Strains and Stresses

Tables 2 and 3 show the experimentally obtained and design values of ε_{sp2}, and Table 4 shows the ratio of these two values $R(\varepsilon_{sp2})_{exp/dsgn}$. Table 4 shows that, in all cases, the measured strains were equal to or greater than the design values. Tables 2, 3 and 4 show similar results for the experimental and design values of f_{sp2}. From the foregoing results, it is clear that the design procedure provides a reasonable to conservative estimate of the values of the spiral strains and stresses, and thus a reasonable to conservative estimate of the confining pressure provided by the spiral reinforcement.

Confined Concrete Strength

An experimental value for the increase in compressive strength of the confined concrete core, $\Delta f_{c12,exp}$ was computed from the experimental results. This experimental value is compared to the design value of the increase in strength of the concrete core, $\Delta f_{c12,dsgn}$. Tables 2 and 3 show the values of $\Delta f_{c12,exp}$ and $\Delta f_{c12,dsgn}$, and Table 4 shows the ratio of these values, $R(\Delta f_{c12})_{exp/dsgn}$. Table 4 shows that Specimens 14-A', 14-C' and 14-D' either achieved or exceeded the design values of core strength enhancement based on the spiral design useable stress. For these specimens, $R(\Delta f_{c12})_{exp/dsgn}$ ranged from 1.00 to 1.14. In contrast, the core strength enhancement in Specimens 14-E' and 14-F' fell approximately 20 percent below the design values.

Table 3 also shows the Richart et al. predicted values of $\Delta f_{c12,Rich}$, and Table 4 shows $R(\Delta f_{c12})_{exp/Rich}$, which is the ratio of $\Delta f_{c12,exp}$ to $\Delta f_{c12,Rich}$. Table 4 shows that Specimens 14-A' and 14-C' satisfied the Richart et al. prediction of increased compressive strength of the concrete core. Specimen 14-D' nearly satisfied the prediction, falling short by only 5 percent. However, Specimens 14-E' and 14-F' achieved only 67 percent and 69 percent of the Richart et al. predictions. Thus Specimens 14-A',14-C' and 14-D' exhibited experimental core strength increases consistent with the stresses observed in the spiral steel, but Specimens 14-E' and 14-F' did not. This suggests that the Richart et al. equation may have a limit on its range of applicability for higher strength steels.

TABLE 2
SUMMARY OF DESIGN VALUES

I.D.	$\varepsilon_{c2,dsgn}$	$\varepsilon_{sp2,dsgn}$	$f_{sp2,dsgn}$ (MPa)	$\Delta f_{c12,dsgn}$ (MPa)
14-A'	0.0158	0.0062	545	53.2
14-C'	0.0158	0.0062	745	53.1
14-D'	0.0158	0.0062	758	53.2
14-E'	0.0158	0.0062	1131	53.1
14-F'	0.0158	0.0062	1110	53.2

TABLE 3
SUMMARY OF EXPERIMENTAL VALUES

I.D.	$\varepsilon_{c2,exp}$	$\epsilon_{sp2,exp}$	$f_{sp2,exp}$ (MPa)	$f_{c2,exp}$ (MPa)	$\Delta f_{c12,exp}$ (MPa)	$\Delta f_{c12,Rich}$ (MPa)
14-A'	0.0153	0.0063	545	105.4	53.4	53.2
14-C'	0.0219	0.0063	752	105.9	53.8	53.6
14-D'	0.0344	0.0091	917	112.8	60.7	64.3
14-E'	0.0231	0.0122	1338	94.1	42.1	62.8
14-F'	0.0206	0.0086	1310	95.4	43.3	62.8

TABLE 4
RATIOS OF KEY VALUES

I.D.	$R(\epsilon_{c2})_{exp/dsgn}$	$R(\epsilon_{sp2})_{exp/dsgn}$	$R(f_{sp2})_{exp/dsgn}$	$R(\Delta f_{c12})_{exp/dsgn}$	$R(\Delta f_{c12})_{exp/Rich}$
14-A'	0.97	1.02	1.00	1.00	1.00
14-C'	1.39	1.02	1.01	1.01	1.00
14-D'	2.18	1.47	1.21	1.14	0.95
14-E'	1.46	1.97	1.18	0.79	0.67
14-F'	1.30	1.39	1.18	0.81	0.69

CONCLUSIONS

The conclusions of this research are as follows:

1. The proposed design procedure provides satisfactory spiral designs for spiral steels with useable stress values up to 758 MPa (110 ksi). This conclusion is applicable to the specimen geometries and material strengths treated in this research.

2. From the conclusion above, it follows that current design requirements that limit the design yield stress of spiral reinforcement in compression members to 414 MPa (60 ksi) may be modified to permit higher stresses. Spiral steel stresses in excess of 414 MPa (60 ksi) can be used to design spiral reinforcement in compression members similar to the specimens treated in this research.

3. Three key relationships used in the design procedure provide acceptable results for the design purposes. First, Eqn. (9) (Eqn. (2) from Richart et al.) provides reasonable to conservative estimates of the longitudinal strain at failure. Second, Eqn. (10), the tangent dilation ratio relationship proposed by Graybeal et al., provides reasonable to conservative estimates of transverse strains in the concrete, and thus strains in the spiral reinforcement at failure. Third, Eqn. (8) (Eqn. (1) from Richart et al.) which relates confining pressure to axial strength enhancement, is valid for compression members made with useable stress values up to 758 MPa (110 ksi).

ACKNOWLEDGMENTS

This research was funded by the Precast/Prestressed Concrete Institute, through a Daniel P. Jenny Fellowship, and by the Center for Advanced Technology for Large Structural Systems at Lehigh University. Additional support was provided by Concrete Technology Corporation, Sumiden Wire Products Corporation, Florida Wire and Cable, Inc., and Neturen Co., Ltd. The findings and conclusions presented in this report are those of the authors.

REFERENCES

ACI Committee 318. (1995). *Building Code Requirements for Structural Concrete (ACI 318-95) and Commentary (ACI 318R-95),* American Concrete Institute, Farmington Hills, MI, USA.

AASHTO. (1994). *AASHTO LRFD Bridge Design Specifications,* American Association of State Highway and Transportation Officials, Washington, D.C., USA, First Edition.

Graybeal, B.A., and Pessiki, S. (1998). *Confinement Effectiveness of High Strength Spiral Reinforcement in Prestressed Concrete Piles.* Report No. 98-01, Center for Advanced Technology for Large Structural Systems, Lehigh University, 164 pp.

Mudlock, M., Pessiki, S. (1999). *Design of High Strength Spiral Reinforcement for Prestressed Concrete Piles.* Report No. 99-12, Center for Advanced Technology for Large Structural Systems, Lehigh University, 134 pp.

Considère, A. (1903). Rèsistance à la compression du bèton armè et du bèton frettè. *Gènie Civil,* 1903.

Richart, F.E., and Brown, R.L. (1934). *An Investigation of Reinforced Concrete Columns.* University of Illinois Bulletin, Vol. XXVI, No. 40, 94 pp.

Advances in Building Technology, Volume 1
M. Anson, J.M. Ko and E.S.S. Lam (Eds.)
© 2002 Elsevier Science Ltd. All rights reserved

MODELING AND BEHAVIOR OF COMPOSITE MRFs WITH CONCRETE FILLED STEEL TUBULAR COLUMNS SUBJECT TO EARTHQUAKE LOADING

J.M. Ricles[1], R. Sause[1], T. Muhummud[1], R. Herrera[1]

[1]Department of Civil and Environmental Engineering, Lehigh University,
117 ATLSS Drive, Bethlehem, PA 18015-4729, USA

ABSTRACT

In conjunction with the U.S.-Japan Cooperative Research Program in Earthquake Engineering on Composite and Hybrid Structures, analytical studies on the seismic behavior of steel moment resisting (MRFs) with concrete filled steel tubular (CFT) columns were performed. The CFT columns consisted of normal strength concrete with a high strength steel tube. In these studies the seismic performance of this type of composite structure was investigated using a fiber element in order to account for non-linear behavior due to material yielding, local buckling, and concrete cracking and crushing. Using the IBC 2000 provisions several frames were designed and analyzed. It was found that the frames are likely to perform adequately under both the design level and maximum considered earthquakes.

KEYWORDS

composite construction, concrete filled steel tubular column, earthquake, high strength steel, nonlinear analysis, structural steel.

INTRODUCTION

Composite construction is becoming more common for designing the structural systems of buildings. This is due to the numerous advantages that composite construction offers, including: the inherent mass, stiffness, damping, and economy of reinforced concrete; and the speed of construction, strength, long-span capability, and light weight of structural steel. Composite structures for buildings often include steel moment resisting or braced frame systems with steel-concrete composite columns to help control lateral drift. The composite columns may be structural shapes encased in reinforced concrete (SRC), or circular or rectangular concrete filled steel tubes (CFT). CFT columns have advantages over SRC columns because the steel tube serves as formwork and offers confinement to the concrete, thus improving its ductility. Additionally, the concrete infill delays the local buckling of the rectangular steel tubes and increases the flexural stiffness of the column. This enables the inter-story drift requirements to be met.

This paper presents the results of research that was conducted in conjunction with the U.S.-Japan Cooperative Research Program in Earthquake Engineering on Composite and Hybrid Structures. A composite moment resisting frame (MRF) was designed with high strength CFT columns. The members and connections of the structure were modeled to account for the effects of local buckling, concrete crushing and cracking, connection deformations, as well as P-delta effects. The results of static pushover and non-linear time history analysis involving the design basis earthquake (DBE) and maximum considered earthquake (MCE) records are presented.

PROTOTYPE FRAME

Description of Frame

The six-story five-bay frame shown in Figure 1 was designed as a special MRF in accordance with the International Building Code (IBC) 2000 provisions (*"International"* 2000). Drift was found to control the design of the MRF. The dimensions of the frame were based on the U.S.-Japan theme structure (Goel and Yamanouchi 1992). The beams were A992 steel wide flange sections with a nominal 345 MPa yield strength. The CFT columns were high strength steel tubes (with a nominal 552 MPa yield strength) filled with a 55 MPa nominal strength concrete. The beam-to-column moment connections are shown in Figure 2, and consisted of split tees that were fillet welded (in the field) to the beam flanges and bolted to the column. No shear tab was used. The design of these connections was based on the research conducted by Peng et al. (2001), which demonstrated that good strength and ductility can be developed with this detail under inelastic cyclic loading. The members were proportioned in order to satisfy a weak beam-strong column design in accordance with FEMA Provisions (FEMA 2000). The required column moment capacity was based on the expected plastic beam moment developing at a distance of one-third the beam depth from the end of the tee stems in the connection. The inflection points in the column were assumed to be located at the far end of the column above and below the joint when determining the required column moment capacity.

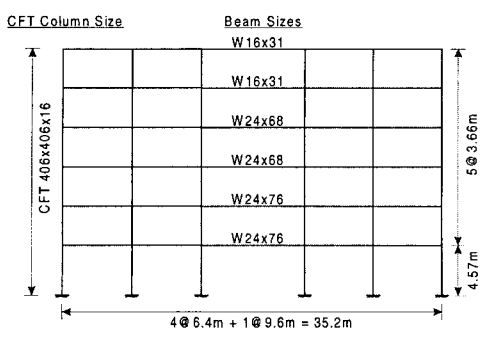


Figure 1: MRF with CFT columns.

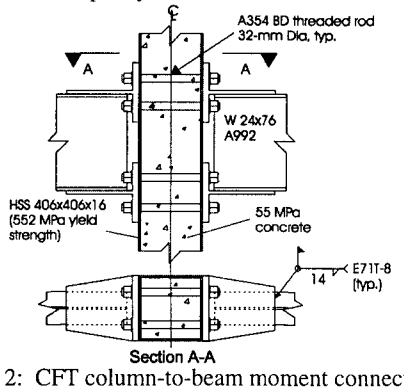


Figure 2: CFT column-to-beam moment connection.

Modeling of Frame

The frame was analyzed using the DRAIN-2DX computer program (Prakash et al. 1993, Herrera et al. 2001). To account for the possibility of concrete crushing, concrete cracking, steel yielding, and steel local buckling (which can lead to a deterioration of stiffness and strength under cyclic loading) the CFT columns in the frame were modeled using a fiber element, as shown in Figure 3. The cross section of the column was discretized using 22 fibers (12 for the concrete and 10 for the steel). Fibers with local buckling incorporated into their stress-strain relationship were located at the ends of the

column, as shown in Figure 3(b), to account for the effects of any local buckling that may occur in the steel tube, particularly at the base of the ground floor column where a plastic hinge is expected to form (Varma et al. 2001). Shear springs were prescribed to transfer the transverse shear through the plastic hinge zone. The stress-strain curves for the steel and concrete fibers were developed using the results of finite element analysis of the CFT section under monotonic axial load to account not only for the effects of local buckling in the steel tube wall but also confinement on strength, stiffness and ductility of the concrete. Representative steel and concrete fiber stress-strain curves are shown in Figure 3(c), where the cyclic unloading and reloading rules adopted for the analysis are illustrated. Existing test data was used to validate the CFT column model, with representative results shown in Figure 4.

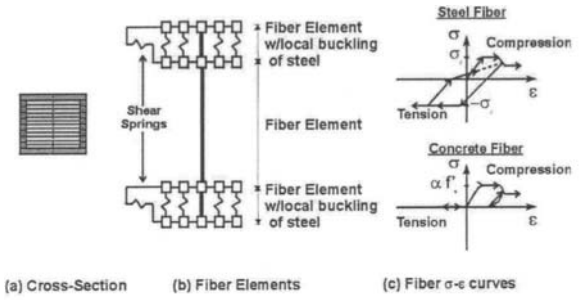


Figure 3: Modeling of CFT columns.

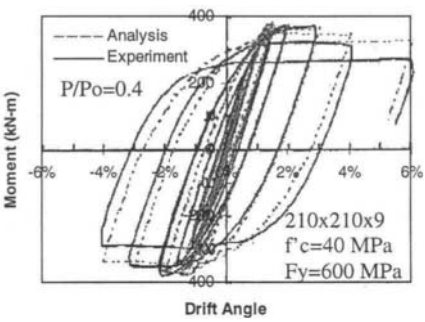


Figure 4: Comparison of CFT column analysis and experimental results.

The wide flange steel beams were modeled using steel fibers located in the plastic hinge region of the beam to capture the effects of cyclic yielding, strain hardening, and local buckling. Outside the plastic hinge region the beam was modeled using an elastic beam element. The cyclic stress-strain relationship for the fibers was based on experimental data from Ricles et al. (2002). A comparison of the moment-plastic rotation cyclic response predicted by the beam model and test data is shown in Figure 5. The connection was carefully modeled to account for flexibility and any inelastic behavior that may develop. A set of master and slaved nodes was used to define the panel zone kinematics that considered the depth of the column and beams at the joint, as shown in Figure 6. The shear-deformation relationship for the panel zone was defined by specifying the properties of the two parallel rotational springs ($k_{\gamma 1}$ and $k_{\gamma 2}$) shown in Figure 6. Tests on CFT panel zones conducted by Koester (2000) were used to define the spring properties. A comparison of measured panel zone cyclic behavior with predicted response is shown in Figure 7.

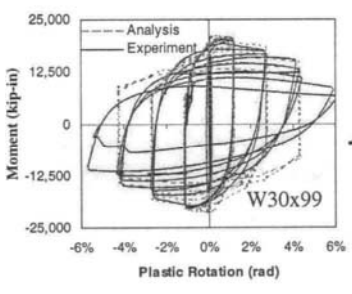


Figure 5: Analysis of beam with local buckling.

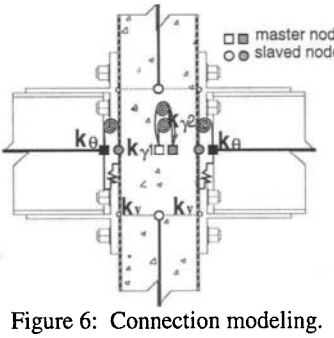


Figure 6: Connection modeling.

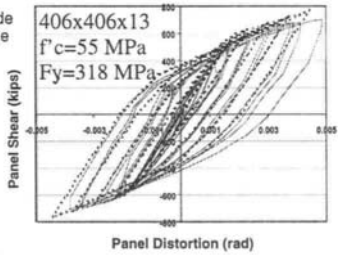


Figure 7: Comparison of analysis and experimental results.

The rotational and transverse flexibility of the tee stems was considered through the use of a rotational (k_θ) and transverse spring (k_v) at each beam-column interface as shown in Figure 6. The properties of the tee-stem springs were based on research conducted by Peng et al. (2001) on split-tee moment connections. P-delta effects from the interior gravity frames were incorporated into the frame model using a leaning column (not shown in Figure 1).

ANALYSIS RESULTS

Static Pushover Analysis

The frame model was used to perform a nonlinear static pushover analysis of the composite MRF. The lateral loads were distributed over the height of the frame in accordance with the IBC 2000 provisions. Figure 8 shows the relationship between the normalized base shear and the roof drift index (RDI). The normalized base shear is defined as the base shear divided by the seismic dead weight of the building, W, whereas the RDI is the roof displacement divided by the building height. The analysis results indicated that the frame first yields at a base shear of 0.15W at the fifth floor beams at a corresponding RDI of 1.1%. The maximum overstrength of the MRF is 3.29 (0.23W) at a corresponding RDI of 2.3%, where the overstrength is defined as the base shear divided by the IBC 2000 design base shear. In the static pushover that maximum story drift was 5.26% and occurred at the first story. The inelastic deformations in the structure are concentrated in all the floor beams and at the base of the ground floor columns. The panel zones in the interior columns at the first and second floors developed minor inelastic response, illustrating that they are relatively strong in shear compared to the demand imposed on them.

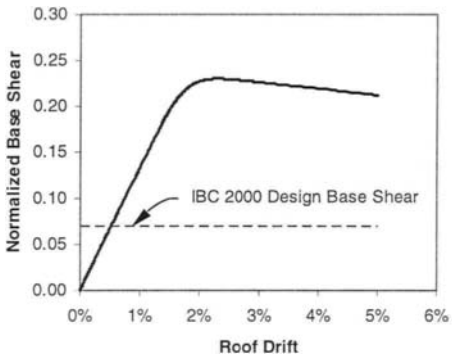


Figure 8: Static pushover results.

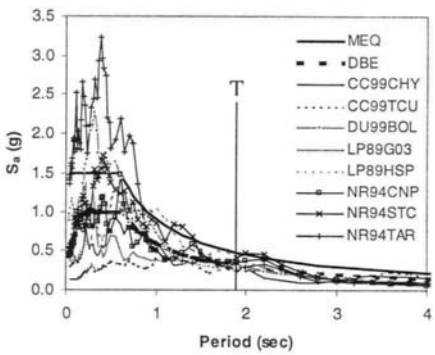


Figure 9: Response spectra.

Time History Analysis

Nonlinear time history analyses were conducted using an ensemble of eight earthquake records. The eight earthquake records are summarized in Table 1. Two sets of analyses were conducted. The first set involved scaling the eight earthquake records to the Design Basis Earthquake (DBE) and evaluating the response of the frame to these scaled records. The scale factor for each record was determined using the IBC 2000 design response spectrum as the target spectra and the scaling procedure developed by Somerville (1997). The second set of analysis involved scaling the same eight earthquake records to the Maximum Considered Earthquake (MCE) and evaluating the response of the frame to these scaled records. The scale factors corresponding to the MCE were determined using the IBC 2000 maximum considered earthquake response spectrum in conjunction with the procedure of Somerville (1997). The IBC 2000 design and maximum considered earthquake response spectra are

compared to the response spectra for the eight un-scaled records in Figure 9. The scale factors for each record corresponding to the DBE and MCE are summarized in Table 1. The IBC 2000 DBE has a return period range from 300 to 600 years in areas of high seismicity (approximately a 8% to 16% probability of exceedance in 50 years) while the MCE has a 2% probability of exceedance in 50 years (2/50). The fundamental elastic period, T_1, of the frame was 1.93 seconds.

TABLE 1
TIME HISTORY ANALYSIS RESPONSE RESULTS

Ground Motion (name, year, component)	Design Basis Earthquake				Max. Considered Earthquake			
	Scale Factor	Max. Roof Disp. (mm)	Max. IDI (%)	Max. Base Shear (%W)	Scale Factor	Max. Roof Disp. (mm)	Max. IDI (%)	Max. Base Shear (%W)
Chi-Chi 1999, CHY036-W	1.04	518	3.7	24.3	1.55	582	4.4	25.4
Chi-Chi 1999, TCU123-N	1.34	480	2.3	25.2	2.01	662	3.4	26.9
Duzce 1999, BOL000	1.08	392	2.4	25.8	1.61	523	4.1	26.9
Loma Prieta 1989, G03090	1.49	578	2.9	25.5	2.24	833	4.1	25.6
Loma Prieta 1989, HSP000	0.95	430	2.7	26.4	1.42	709	4.3	26.9
Northridge 1994, CNP196	1.27	581	3.1	25.1	1.91	906	5.0	25.9
Northridge 1994, STC180	0.89	501	3.1	26.2	1.33	636	4.0	27.7
Northridge 1994, TAR360	1.09	450	4.1	28.1	1.64	653	4.5	28.7

Table 1 summarizes the maximum roof displacement, inter-story drift (IDI), and base shear for both sets of analysis. It can be seen that the response increases for the MCE compared to the DBE. Furthermore, the maximum base shear developed during the DBE and MCE both exceed that developed in the static pushover (0.23W). This effect is due to the participation of the higher vibration modes in the response to the earthquake excitation.

The maximum story drifts at each floor level are shown in Figure 10, where the mean and mean plus one standard deviation are noted. The mean plus one standard deviation results are approximately the 84th percentile, assuming that the results are lognormal distributed. The results in Figure 10 indicate there is a greater drift developed in the upper floors for this design, particular under the MCE. The maximum mean and mean+standard deviation for the maximum drift are 2.9% and 3.6%, respectively, for the DBE, and 4.0% and 4.5%, respectively, for the MCE. FEMA 273 (1997) recommends that the drift not exceed 2.5% and 5.0% under the DBE and MCE, respectively. Although under the DBE the drift exceeded 2.5% in some analysis, a stability analysis indicated that the structure was not on the verge of collapse, and the plastic rotation demand on the members was not excessive.

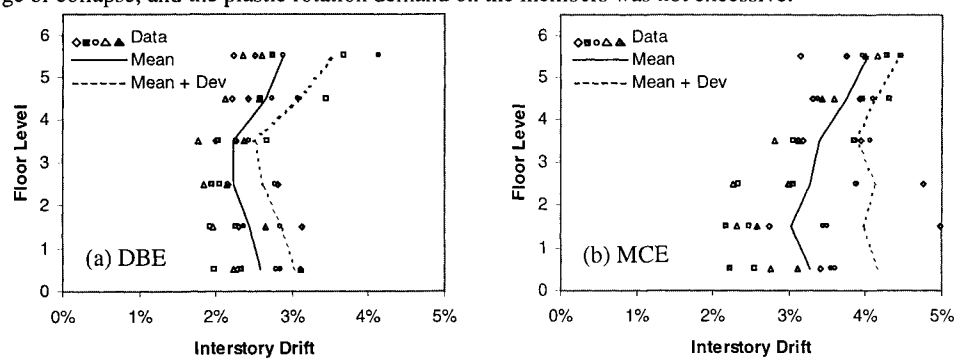


Figure 10: Maximum inter-story drift for various earthquakes.

The maximum plastic rotation in the beams at each floor level is shown in Figure 11, where also the mean and mean plus one standard deviation are shown. Figure 11 indicates statistically that the maximum plastic beam rotation develops in the upper floors for this design, although under the MCE a first-floor beam developed 4.79% radians of plastic rotation. The maximum mean and mean+standard deviation of maximum plastic rotation are 1.6% and 2.1% radians, respectively, for the DBE, and 2.7% and 3.0% radians, respectively, for the MCE. Tests by Peng et al. (2001) indicated that split-tee connections could enable a plastic rotation in excess of 5.0% radians to develop in the beam under cyclic loading before failure. An examination of the hysteretic stress-strain response of the fibers in the plastic hinge zone indicated that the beam flanges developed local buckling, however the web did not develop enough appreciable local buckling to cause any appreciable degradation in beam capacity.

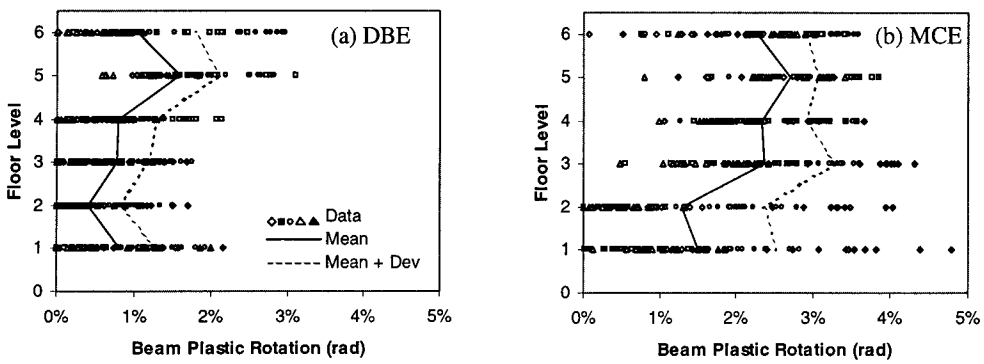


Figure 11: Maximum beam plastic rotation for various earthquakes.

The maximum plastic rotation in the columns at each floor level is shown in Figure 12, where also the mean and mean plus one standard deviation are shown. Yielding in the columns occurred only at the base of the ground floor columns. The maximum mean and mean+standard deviation of maximum plastic rotation are 1.1% and 1.7% radians, respectively, for the DBE, and 1.8% and 2.7% radians, respectively, for the MCE. An examination of the hysteretic stress-strain response in the plastic hinge zone indicated that both the flanges and webs developed local buckling, however the latter did not develop an appreciable amount to cause any significant amount of degradation in column capacity. Because of concrete cracking, however, there was degradation in the column elastic flexural stiffness. The fact that the columns yielded only at the base at the ground floor indicates that the approach used to proportion the column and beam sizes ensured a weak beam-strong column design. The accumulative plastic strain in the ground floor columns was less than that to cause low cycle fatigue failure for high strength CFT columns (Varma et al. 2001).

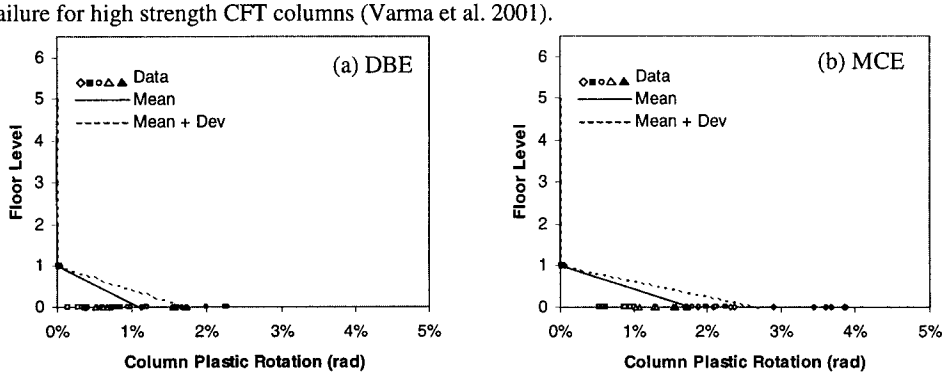


Figure 12: Maximum column plastic rotation for various earthquakes.

The maximum plastic shear deformation in the panel zones at each floor level is shown in Figure 13, where also the mean and mean plus one standard deviation are shown. Yielding in the panel zones occurred at only the first and second floors. The maximum mean and mean+standard deviation of panel zone maximum plastic deformation are 0.13% and 0.14% radians, respectively, for the DBE, and 0.15% and 0.17% radians, respectively, for the MCE. An examination of the hysteretic stress-strain response of the panel zones with plastic deformation indicated that they developed the onset of inelastic response, and had significant reserve strength (i.e., they did not achieve their ultimate capacity).

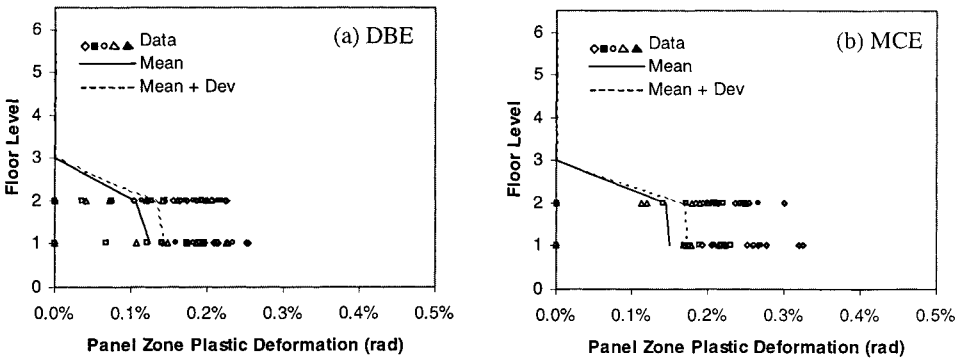


Figure 13: Maximum panel zone plastic rotation for various earthquakes.

The tee stems were found to remain elastic throughout all of the time history analyses.

SUMMARY AND CONCLUSIONS

A steel MRF with high strength CFT composite columns was designed and analyzed for response to the Design Basis and Maximum Considered Earthquakes. The modeling of the CFT columns and steel beams involved the use of fiber elements to account for nonlinearities due to steel yielding, local buckling, concrete cracking and crushing. Joint flexibility and nonlinearities were considered by modeling the panel zones and connection elements. Based on the results of the analysis, and a comparison of the demand with resistance of test specimens, it appears that the frame performed satisfactory. An experimental program is currently in progress at Lehigh University involving large-scale testing of steel MRFs with CFT columns subject to earthquake loading. The test results will provide data to verify the analysis results.

ACKNOWLEDGEMENTS

The research reported herein was supported by the National Science Foundation (Dr. Shih-Chi Liu cognizant program official), by a grant from the Pennsylvania D.C.E.D. through the PITA program, and a scholarship to the third author through the Royal Thai Government. The opinions expressed in this paper are those of the authors and do not necessarily reflect the views of the sponsors.

REFERENCES

American Institute of Steel Construction (1997) "Seismic Provisions For Structural Steel Buildings," Chicago, Illinois.

FEMA (1997) "NEHRP Guidelines for the Seismic Rehabilitation of Buildings," *Report No. FEMA 273*, FEMA, Washington, D.C.

FEMA (2000) "Recommended Seismic Design Criteria for New Steel Moment-Frame Buildings," *Report No. FEMA 350*, FEMA, Washington, D.C.

Goel, S. and K. Yamanouchi (1992) "Recommendations for U.S.-Japan Coop. Research Program – Phase 5: Composite and Hybrid Structures," Report No. UMCEE 92-29, Department of Civil and Environmental Engineering, University of Michigan, Ann Arbor, Michigan.

Herrera, R., Sause, R., and J. Ricles, (2001) "Refined Connection Element (Type 05) for DRAIN-2DX, Element Description and User Guide," ATLSS Report No. 01-07.

"International Building Code" International Code Council (ICC) (2000) Falls Church, Virginia.

Koester, B. (2000) " Panel Zone Behavior of Moment Connections Between Rectangular Concrete-Filled Steel Tubes and Wide Flange beams" Ph. D. Dissertation, Department of Civil and Environmental Engineering, University of Texas, Austin, Texas.

Peng, S.W., Ricles, J.M., and L.W. Lu, (2001) "Seismic Resistant Connections for Concrete Filled Column-to-WF Beam Moment Resisting Frames," ATLSS Engineering Research Center, Report No. 01-08, Lehigh University, Bethlehem, Pennsylvania.

Prakash, V., Powell, G., and S. Campbell, (1993). "DRAIN-2DX Base Program Description and User Guide, Version 1.10," Report No. UCB/SEMM-93/17 & 18, Structural Engineering Mechanics and Materials, Department of Civil Engineering, University of California, Berkeley, California.

Ricles, J.M., Mao, C., Lu, L.W., and J.W. Fisher, (2002) "Inelastic Cyclic Testing of Welded Unreinforced Moment Connections," Journal of Structural Engineering, ASCE, Vol. 128, No. 4.

Somerville, P. (1997). "Development of Ground Motion Time Histories for Phase 2 of the FEMA/SAC Steel Project," Report No. SAC/BD-97/04.

Varma, A.H., Ricles, J.M., Sause, R., and L.W. Lu, (2001) "Seismic Behavior, Analysis, and Design of High Strength Square Concrete Filled Steel Tube (CFT) Columns," ATLSS Engineering Research Center, Report No. 01-02, Lehigh University, Bethlehem, Pennsylvania.

Advances in Building Technology, Volume 1
M. Anson, J.M. Ko and E.S.S. Lam (Eds.)
© 2002 Elsevier Science Ltd. All rights reserved

THE USE OF POST-TENSIONING TO REDUCE SEISMIC DAMAGE IN STEEL FRAMES

J. M. Ricles[1], R. Sause[1], Pedro Rojas[1], and M. M. Garlock[1]

[1]Department of Civil and Environmental Engineering, Lehigh University,
117 ATLSS Drive, Bethlehem, PA 18015-4729, USA

ABSTRACT

A post-tensioned friction damped connection for earthquake resistant steel moment resisting frames (MRFs) is introduced. The connection includes friction devices with post-tensioned high strength strands running parallel to the beam. The connection has excellent ductility, minimizes inelastic deformation to the components of the connection, requires no field welding, and returns the structure to its pre-earthquake position. Inelastic analyses were performed on a 6-story, 4-bay post-tensioned steel MRF to study its response to strong ground motions. Results show good energy dissipation, strength, and ductility in the post-tensioned system. The analyses indicate that the seismic performance of a post-tensioned steel frame can exceed that of a frame with conventional moment resisting connections.

KEYWORDS

earthquake, moment resisting connection, moment resisting frame, nonlinear analysis, post-tensioning, seismic damage mitigation, structural steel.

INTRODUCTION

The inadequate performance of steel moment resisting frames (MRFs) in recent earthquakes has caused much concern. During the 1994 Northridge Earthquake, many steel-framed buildings suffered unexpected premature fractures in their welded beam-to-column connections. The conventional earthquake resistant steel moment connection is composed of full penetration welds between the beam flanges and the column face, with the beam web bolted to a shear tab extending from the column. The occurrence of premature fractures in the beam flange welds between the beams and columns indicates an immediate need to revise current design and construction standards.

As an alternative to welded construction the authors developed a post-tensioned friction damped moment connection (PFDC) for use in seismic resistant steel MRFs. The connection utilizes high strength steel strands that are post-tensioned after friction devices are installed (Figure 1(a)). The post-tensioning strands run through the column, and are anchored outside the connection region (Figure

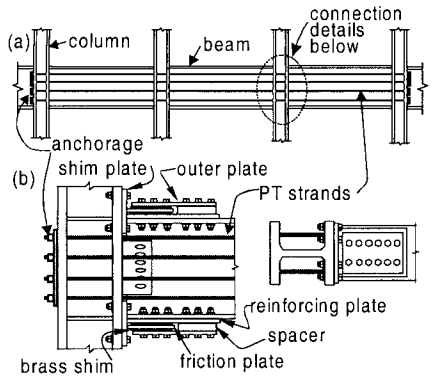


Figure 1(a) Schematic elevation of one floor of a frame with PFDCs and (b) connection details.

1(b)). A properly designed PFDC has several advantages: (1) field welding is not required; (2) the connection is made with conventional materials and skills; (3) the connection has an initial stiffness similar to that of a typical welded connection; (4) the connection is self-centering without residual deformation, thus the MRF will not have residual drift after an earthquake if significant residual deformation does not occur at the base of the ground floor columns; and (5) the beams and columns remain essentially elastic while the friction plates provide energy dissipation.

This paper describes the details, behavior, and analytical studies of a steel MRF with PFDCs. Experimental test results were used to calibrate a fiber element connection model, which was in turn used to analyze a 6-story, 4 bay steel MRF with PFDCs. Nonlinear static pushover and seismic time history analysis were performed on the frame model and compared to the response of the same MRF with standard fully restrained welded connections (FR MRF).

POST-TENSIONED FRICTION DAMPED CONNECTION

Connection Details

The post-tensioned high strength strands run parallel to the beam and are anchored outside of the connection. Due to the initial post-tensioning force applied to the strands, the beam flanges are compressed against the column flanges (Figure 1(a)). As shown in Figure 1(b), reinforcing plates are placed on the beam flanges in order to limit beam compression yielding and thus, to minimize structural damage. Shim plates are placed between the column flange and the beam flanges so that only the beam flanges and reinforcing plates are in contact with the column. This enables good contact to be maintained between the beam flanges and column face, while protecting the beam web from yielding under bearing.

Friction devices are located at the beam flanges, consisting of a friction plate sandwiched by two brass shim plates that are inserted between the beam flange reinforcing plate and an outer plate. All plates are bolted to the beam flanges. Long slotted holes are drilled through the friction plate. The shim plate is bolted to the column flange and serves as a tee flange that the friction plate is attached to. Friction is generated when the beam flanges and outer plate slide against the stationary friction plate when the beam rotates about the center of rotation situated at the mid-depth of the reinforcing plates (see Figure 2 insert). The brass shim plates are used to produce a stable friction force and to control the energy capability of the PFDC (Grigorian et al. 1993, Petty 1999). A shear tab with slotted holes is bolted to the beam web and welded to the column flange to transmit the shear forces.

Flexural Behavior

The moment-relative rotation (M-θ_r) curve for a PFDC when subjected to cyclic loading is shown in the schematic given in Figure 2. The behavior is characterized by a gap opening and closing at the beam-column interface. The total moment resistance of the connection is provided by the moment due

to the initial post-tensioning force in the strands, friction force, and an additional force developed due to elongation of the strands. For simplicity, the post-tensioned forces are assumed to be acting at the centroidal axis of the beam while the friction forces are assumed to be acting at the mid-depth of top and bottom friction plates.

Under applied moment, the connection initially behaves as a fully restrained connection, where the initial stiffness is similar to that of a fully restrained welded moment connection when θ_r is equal to zero (events 0 to 2 in Figure 2). Once the magnitude of the applied moment reaches the moment resistance due to the initial post-tensioning force in the strands, decompression of the beam from the column face occurs. The moment at which this occurs (event 1) is called the decompression moment. The applied moment continues to increase between events 1 and 2 as the rotation of the beam is restrained by the resistance of the friction component. At event 1 the friction force is minimal and increases gradually up to its maximum value at point 2, which is the point of incipient rotation. The maximum value of the friction force is computed using classical friction Coulomb's theory.

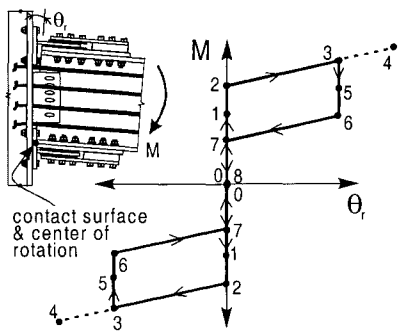


Figure 2. Moment-relative rotation behavior.

The stiffness of the connection after gap opening is associated with the elastic axial stiffness of the post-tensioned strands. With continued loading, the strands elongate producing an additional force, which contributes to resist the total applied moment. Yielding of the strands eventually may occur at event 4. Upon unloading (event 3), θ_r remains constant. At event 5, the friction force is zero. Between events 5 and 6 the friction force changes direction and starts increasing until reaching its maximum value at event 6. Between events 6 and 7, the beam rotates until the beam top flange is back in contact with the shim plate, but not compressed. Between events 7 and 8 the value of the friction force decreases with the beam being compressed against the shim plates and M equal to zero at event 8. A complete reversal in the applied moment will result in a similar connection behavior occurring in the opposite direction of loading, as shown in Figure 2. Because a residual friction force exists at event 8, the forces in the system are indeterminate until event 2 is again reached. Thus, there is no clear point of decompression on the curve following the first half-cycle.

As long as the strands remain elastic, and there is no significant beam yielding, the post-tensioning force is preserved and the connection will self-center upon unloading (i.e., θ_r returns to zero rotation upon removal of the connection moment and the structure returns to its pre-earthquake position). The energy dissipation capacity of the connection is related to the force developed between the friction surfaces.

Main Design Considerations

The connection behavior described above is the basis for the design of a PFDC. Preliminary design considerations were developed using experimental results and nonlinear static pushover analyses of beam-column subassemblies (Garlock et al. 2002), in addition to nonlinear time history analysis of MRFs with PT connections having top and seat angles (Ricles et al. 2001). For design it was assumed that the connection developed a resistance of at least $0.93M_p$ (where M_p is the plastic nominal moment of the beam) corresponding to a relative rotation, θ_r, of 0.0225 radians. The connections were designed with a moment of at least $0.60M_p$ when gap opening becomes imminent.

ANALYTICAL MODELING OF A PFDC

Description of Model

The computer program DRAIN-2DX (Prakash et al. 1993) was used to develop a model of the PFDC and the associated beams and columns of the MRF. This computer program is well suited for this purpose since it accounts for geometric and material non-linearities in static and dynamic two-dimensional structural analysis. A brief description of the model is presented. More detailed information on the modeling of PFDCs is given in Rojas (2002).

The beams and columns are modeled using fiber elements. Each fiber element is divided into a number of segments along the element length. Only one segment is used in those elements were elastic behavior is expected. The cross-section of each segment is comprised of several fibers. A material stress-strain relationship, a cross sectional area, and a distance from the longitudinal reference axis of the member characterize each fiber. The beam fiber elements adjacent to the columns are used to model connection gap opening. The fibers of the beam cross section initially in contact with the shim plates are assigned a stress-strain relationship that has stiffness in compression, but none in tension. Fibers are omitted from the cross section not in contact with the shim plates.

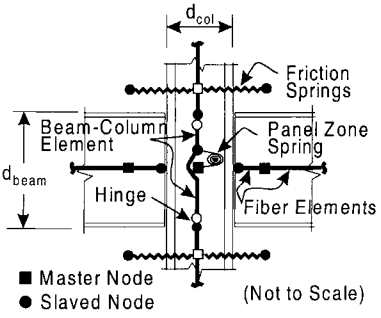


Figure 3. Post-tensioned friction damped connection analysis model.

To properly account for the depth of the beam and the size of the panel zone in the connection region, it was necessary to utilize a set of master-slave nodes as shown in Figure 3. The flexibility of the panel zone was modeled by placing a rotational spring with moment-rotational characteristics determined from the shear stiffness and strength of the panel zone. The strands were modeled using truss elements. The friction components were modeled with spring elements having a bilinear force deformation relationship.

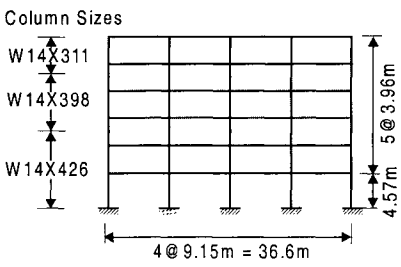
A model was also developed for the FR MRF. Beams, columns, and panel zones were modeled as described in the model with PFDCs. However, one of the limitations of DRAIN-2DX is that it cannot model local buckling of members. To overcome this difficulty Herrera (2001) developed a fiber element to include the effects of local buckling. Ojeda and Muhummud (2002) implemented a beam plastic hinge model that includes strength degradation and strain hardening in order to model beam local buckling. P-delta effects from the interior gravity frames were incorporated into the FR MRF and MRF with PFDC models using a leaning column.

SEISMIC BEHAVIOR OF A MRF WITH PFDCS

Description of Frames

To study the seismic behavior of steel frames with PFDCs, a 6-story perimeter MRF with 4 bays was designed as a special MRF (SMRF) in accordance with the 2000 International Building Code (IBC 2000) provisions (ICC 2000). The beam and column sections were designed based on the following assumptions: 1) connections were assumed to be rigid; 2) the structure is an office building located on stiff soil in the Los Angeles area; 3) the design accelerations were determined using the deterministic limit of the site-specific procedure; and 4) A992 steel was used. The resulting member sizes are shown

in Figure 4. Two frame models were created with these members where one model had rigid connections and the other had PDFCs. The PFDCs were designed for $0.93M_p$ in the first three stories and increased to M_p in the last three stories corresponding to a θ_r=0.0225 radians. The reinforcing plates were 1778 mm long. Figure 4 shows the initial post-tensioning (T_o) and friction forces (F_f) provided in the MRF with PFDCs. Additional details can be found in Rojas (2002).



Beam Sizes	T_o - kN	F_f - kN
W24X76	1659	539
W30X108	2190	712
W30X108	2190	712
W36X150	2753	688
W36X160	3022	756
W36X160	3022	756

Figure 4. Frame used in analytical study.

Static Pushover Analysis

A nonlinear static pushover analysis of both frames was conducted. The lateral loads were distributed over the height of the frame in accordance with the IBC 2000 provisions. Figure 5 shows the relationship between the normalized base shear and the roof drift index (RDI) for both frames. The normalized base shear is the base shear divided by the seismic dead weight of the building, W. The analysis results for the FR MRF show that first yielding occurs when the applied base shear is 0.14W at a corresponding RDI of 0.93%. The maximum overstrength of the FR MRF is 3.16 (0.21W) at a corresponding RDI of 2.45%. The overstrength is defined as the base shear divided by the IBC 2000 design base shear. This value is close to the one anticipated in the IBC 2000 code (3.00) for SMRF systems. The maximum interstory drift index (IDI) was 5.91% and occurred at the first story. The inelastic behavior in the structure is concentrated at the girders of all floors and at the base of the ground floor columns. Panel zone yielding also occurred in most of the interior columns of the frame.

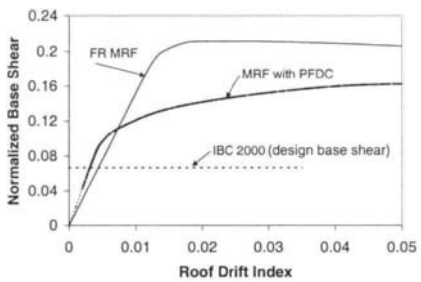


Figure 5. Static pushover results.

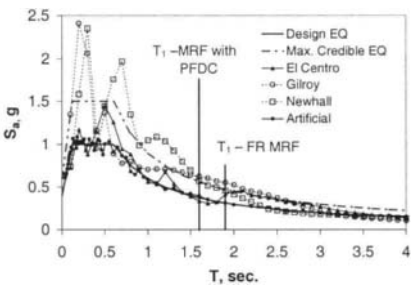


Figure 6. Response spectra.

The frame with PFDCs has a larger initial stiffness than the FR MRF due to the reinforcing plates. Gap opening becomes imminent at a base shear of 0.098W, corresponding to a RDI of 0.5%. After gap opening, the lateral stiffness of the MRF with PFDCs decreases. In the MRF with PFDCs, first yielding occurs at the base of the ground floor columns when the applied base shear is 0.12W and the RDI is 0.97%. The maximum overstrength of the MRF with PFDCs is 2.42 (0.162W) when the RDI is 5%. The maximum interstory drift was 5.45% and occurred at the second story. The maximum connection relative rotation, θ_r, was 0.055 radians and occurred at the first floor. Beam compression yielding at the end of the reinforcing plates begins when the RDI is 1.67%. The panel zones remain elastic.

Time History Analysis

Nonlinear dynamic time history analyses were conducted using an ensemble of four accelerograms to investigate the seismic behavior of the MRF with PFDCs and the FR MRF. These accelerograms include three records classified as ground motions with 10% probability of exceedance in 50 years (10/50) according to the SAC project (Somerville 1997) and an artificial ground motion generated to be compatible with the IBC 2000 design response spectrum for the seismicity conditions noted previously. The SAC records are: (1) a scaled component rotated 45° from fault normal of the 1940 Imperial Valley Earthquake recorded at El Centro, CA; (2) a scaled component rotated 45° from fault parallel of the 1994 Northridge Earthquake recorded at Newhall, CA; and (3) a scaled component rotated 45° from fault normal of the 1989 Loma Prieta recorded at Gilroy, CA. The peak ground accelerations for the three SAC ground motions and the artificial ground motion were 0.46g, 0.66g, 0.67g, and 0.40g, respectively.

Figure 6 shows the IBC 2000 design and maximum credible earthquake response spectra, as well as the response spectra of the four ground motions. The IBC 2000 design response spectrum has approximately a 10% probability of exceedance in 50 years while the IBC 2000 maximum credible earthquake response spectrum has a 2% probability of exceedance in 50 years. Scale factors for the three SAC ground motions were computed (according to the procedure described by Somerville (1997)) using the IBC 2000 response spectra as the target spectra and compared with the scale factors provided by Somerville (1997). From these new scale factors it was concluded that the as-scaled El Centro ground motion may be classified as approximately a 10/50 ground motion, even though at some period ranges it exceeds the IBC 2000 design spectrum. The as-scaled Newhall and Gilroy ground motions lie between the 2/50 and 10/50 ground motions, with the Newhall ground motion closer to a ground motion with a 2% probability of being exceeded in 50 years (2/50). However, it is interesting to note that between 1.7 and 3.0 seconds, the as-scaled Gilroy ground motion exceeds the as-scaled Newhall ground motion. The fundamental elastic period, T_1, of the frames are 1.87 and 1.60 seconds for the FR MRF and MRF with PFDCs, respectively.

Table 1 presents a summary of the seismic response for both frames. It can be seen that the MRF with PFDCs develops a smaller magnitude of displacement response than the FR MRF for the artificial and El Centro ground motions. The maximum residual IDI is negligible in both frames. Both frames perform satisfactorily for this ground motion, having minimal yielding.

TABLE 1
RESPONSE OF MRF WITH PFDCS AND FR MRF

Ground Motion	$\theta_{r,\max}$ (rads)	Max. Roof Disp. (mm)		Max. IDI (%)		Max. Base Shear (%W)		Max. Res. IDI (%)	
		MRF-PFDC	FR-MRF	MRF-PFDC	FR-MRF	MRF-PFDC	FR-MRF	MRF-PFDC	FR-MRF
Artificial	0.0168	303.0	365.4	1.50	2.01	17.7	23.1	0.06	0.09
El Centro	0.0222	432.7	456.7	2.31	2.63	17.1	25.3	0.20	0.50
Newhall	0.0232	521.1	478.0	2.67	2.55	19.0	25.8	0.05	0.24
Gilroy	0.0347	673.3	640.5	3.51	3.06	17.3	24.6	0.07	0.70

The response envelope of lateral displacement and story shear for the MRF with PFDCs and the FR MRF to the El Centro ground motion is shown in Figure 7(a). It can be seen that the maximum floor displacements in the MRF with PFDCs is less than the FR MRF. Also, the maximum story shears are shown in Figure 7(b) to be less for the frame with PFDCs. The roof displacement time-history is given

in Figure 7(c). The girders and panel zone remain elastic in the MRF with PFDCs. The FR MRF has significant permanent deformation in the lower stories. Inelastic deformation developed at the base of the ground floor columns, and the girders and panel zones in almost all stories of the FR MRF. The maximum residual displacement for the MRF with PFDCs is 19.5 mm while for the FR MRF it is 47.3 mm (see Figure 7(d)). The residual deformation in the MRF with PFDCs is due to some inelastic hinging at the base of the ground floor columns. This can be avoided by using a PFDC at the base of the ground floor columns (beyond the scope of this paper).

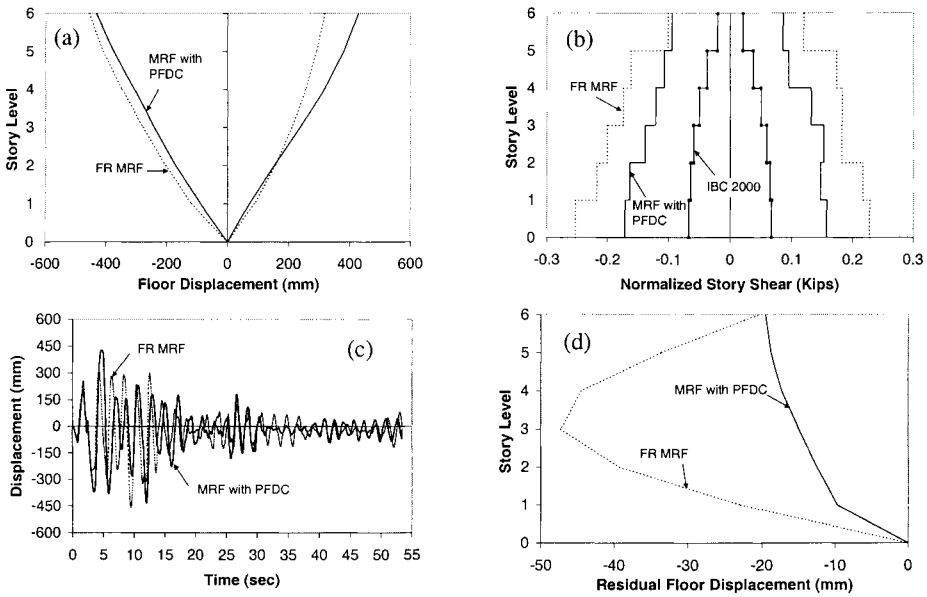


Figure 7. Response of frames to El Centro earthquake.

In the cases studied the MRF with PFDCs did not always develop a smaller magnitude of maximum drift response to the selected ground motion, as seen in Table 1. However, even in the cases where the FR MRF exhibited a smaller magnitude of response, the MRF with PFDCs exhibited superior behavior that included self-centering capability with minimal inelastic deformation to the main structural components of the system. Therefore, after a major earthquake the MRF with PFDCs will have little damage and its post-earthquake position will be very close to the undeformed configuration. The maximum values for θ_r in Table 1 are close to the design value of 0.0225 radians except the Gilroy record (which is however larger than the design earthquake).

SUMMARY AND CONCLUSIONS

An innovative connection for seismic resistant design of steel structures that requires no field welding has been presented. Combining friction devices with high strength post-tensioned steel strands results in a connection with excellent ductility and an initial stiffness that is similar to fully welded moment resisting connections. In addition, the connection has a self-centering capability, resulting in minimal permanent interstory drift in a building following a severe earthquake. Adequate design of reinforcing plates in beam flanges and doubler plates in panel zones will avoid damage in these elements. The frame however must be properly designed to avoid permanent rotational deformation at the base of the

ground floor columns. An analytical model was presented that was based on fiber elements. Results from the analytical studies indicate that moment resisting frames with PFDCs may perform better than moment resisting frames with conventional welded moment connections.

ACKNOWLEDGEMENTS

The research reported herein was supported by the National Science Foundation (Dr. Ken Chong and Dr. Ashland Brown cognizant program officials) and by a grant from the Pennsylvania DCED through the PITA program. The opinions expressed in this paper are those of the authors and do not necessarily reflect the views of the sponsors.

REFERENCES

Garlock, M., Ricles, J., and Sause, R. (2002). "Experimental Studies on Full-Scale Post-Tensioned Seismic-Resistant Steel Moment Connections," *Proceedings of the 7th U.S. National Conference on Earthquake Engineering (NCEE), Boston, MA.*

Grigorian, C.E., Yang, T.S., and Popov, E.P. (1993). "Slotted Bolted Connection Energy Dissipators," Earthquake Spectra, 9(3), pp. 491-504.

Herrera, R., Sause, R., and Ricles, J. (2001). "Refined Connection Element (Type 05) for DRAIN-2DX, Element Description and User Guide," ATLSS Report No. 01-07.

ICC (2000) "International Building Code" International Code Council (ICC), Falls Church, VA.

Ojeda, J. and Muhummud, T. (2002). "Beam Strength Degradation Model for DRAIN-2DX," ATLSS report in progress.

Petty, G.D. (1999). "Evaluation of a Friction Component for a Post-Tensioned Steel Connection," M.S. Thesis, Lehigh University, 328pp.

Prakash, V., Powell, G., and Campbell, S., (1993). "DRAIN-2DX Base Program Description and User Guide, Version 1.0," Report No. UCB/SEMM-93/17 & 18, Structural Engineering Mechanics and Materials, Department of Civil Engineering, University of California, Berkeley, CA.

Ricles, J., Sause, R., Garlock, M, and Zhao, C. (2001). "Post-Tensioned Seismic Resistant Connections for Steel Frames," *Journal of Structural Engineering,* ASCE, 127(2), 113-121.

Rojas, P. (2002). "Seismic Analysis and Design of Post-Tensioned Friction Damped Connections for Steel Moment Resisting Frames," *Ph.D. Dissertation*, Civil and Environmental Engineering Dept., Lehigh University, Bethlehem, PA.

Somerville, P. (1997). "Development of Ground Motion Time Histories for Phase 2 of the FEMA/SAC Steel Project," Report No. SAC/BD-97/04.

TEAM PRESENTATION:

SMART STRUCTURES FOR DYNAMIC HAZARD MITIGATION

This Page Intentionally Left Blank

Advances in Building Technology, Volume 1
M. Anson, J.M. Ko and E.S.S. Lam (Eds.)
© 2002 Elsevier Science Ltd. All rights reserved

Stochastic Approach to Control and Identification of Smart Structures

James L. Beck and Ka-Veng Yuen

Division of Engineering and Applied Science, California Institute of Technology

ABSTRACT. To fully exploit new technologies for response mitigation and structural health monitoring, improved design methodologies are desirable. In this paper, a stochastic framework is presented for robust control and identification of structural systems under dynamical loads, such as those induced by wind or earthquakes. A reliability-based stochastic robust control approach is used to design the controller for an active or semi-active control system. Feedback of the incomplete response at earlier time steps is used, without the need for any state estimation. The optimal controller is chosen by minimizing the robust failure probability over a set of possible models for the system. Here, failure means excessive levels of one or more response quantities representative of the performance of the structure and the control devices. When calculating the robust failure probability, the plausibility of each model as a representation of the system's dynamic behavior is quantified by a probability distribution over the set of possible models; this distribution is initially based on engineering judgment but it can be updated using Bayes' Theorem if dynamic data become available from the structure. For this purpose, a probabilistic system identification technique is presented for model updating using incomplete noisy measurements only. This method allows for updating of the uncertainties associated with the values of the parameters controlling the dynamic behavior of the structure by using only one set of stationary or nonstationary response data. This updated probabilistic description of the system can be used to modify the controller for improved performance of the system. It can also be used for structural health monitoring. An example is presented to illustrate the proposed stochastic framework for identification and control of smart structures.

KEYWORDS: Bayesian inference, model updating, robust control, robust reliability, smart structures, system identification.

1 STOCHASTIC RESPONSE ANALYSIS

Consider a linear model of a structural system with N_d degrees-of-freedom (DOFs) and equation of motion:

$$\mathbf{M}(\boldsymbol{\theta}_s)\ddot{\mathbf{x}}(t) + \mathbf{C}(\boldsymbol{\theta}_s)\dot{\mathbf{x}}(t) + \mathbf{K}(\boldsymbol{\theta}_s)\mathbf{x}(t) = \mathbf{T}\cdot\mathbf{f}(t) + \mathbf{T}_c\cdot\mathbf{f}_c(t) \tag{1}$$

where $\mathbf{M}(\boldsymbol{\theta}_s)$, $\mathbf{C}(\boldsymbol{\theta}_s)$ and $\mathbf{K}(\boldsymbol{\theta}_s)$ are the $N_d \times N_d$ mass, damping and stiffness matrix, respectively, parameterized by the structural model parameters $\boldsymbol{\theta}_s$ for the system; $\mathbf{f}(t) \in \mathbb{R}^{N_f}$ and $\mathbf{f}_c(t) \in \mathbb{R}^{N_{fc}}$ are the external excitation and control force vector, respectively, and $\mathbf{T} \in \mathbb{R}^{N_d \times N_f}$ and $\mathbf{T}_c \in \mathbb{R}^{N_d \times N_{fc}}$ are their distribution matrices. A control law is given later that specifies $\mathbf{f}_c$ by feedback of the measured output.

The uncertain excitation $\mathbf{f}(t)$ could be earthquake ground motions or wind forces, for example, and it is modeled by a zero-mean stationary filtered white-noise process described by

$$\begin{aligned} \dot{\mathbf{w}}_f(t) &= \mathbf{A}_{wf}(\boldsymbol{\theta}_f)\mathbf{w}_f(t) + \mathbf{B}_{wf}(\boldsymbol{\theta}_f)\mathbf{w}(t) \\ \mathbf{f}(t) &= \mathbf{C}_{wf}(\boldsymbol{\theta}_f)\mathbf{w}_f(t) \end{aligned} \tag{2}$$

where $\mathbf{w}(t) \in \mathbb{R}^{N_w}$ is a Gaussian white-noise process with zero mean and unit spectral intensity matrix; $\mathbf{w}_f(t) \in \mathbb{R}^{N_{wf}}$ is an internal filter state and $\mathbf{A}_{wf}(\boldsymbol{\theta}_f) \in \mathbb{R}^{N_{wf} \times N_{wf}}$, $\mathbf{B}_{wf}(\boldsymbol{\theta}_f) \in \mathbb{R}^{N_{wf} \times N_w}$ and $\mathbf{C}_{wf}(\boldsymbol{\theta}_f) \in \mathbb{R}^{N_f \times N_{wf}}$ are the parameterized filter matrices governing the properties of the filtered white noise. A vector $\boldsymbol{\theta}$ is introduced, which combines the structural model and excitation model parameter vectors, i.e. $\boldsymbol{\theta} = [\boldsymbol{\theta}_s^T, \boldsymbol{\theta}_f^T]^T \in \mathbb{R}^{N_\theta}$. The dependence on $\boldsymbol{\theta}$ will be left implicit hereafter in this section.

By introducing the state vector $\mathbf{y}(t) = [\mathbf{x}(t)^T, \dot{\mathbf{x}}(t)^T]^T$, (1) can be rewritten in state-space form as:

$$\dot{\mathbf{y}}(t) = \mathbf{A}_y\mathbf{y}(t) + \mathbf{B}_y\mathbf{f}(t) + \mathbf{B}_{yc}\mathbf{f}_c(t) \tag{3}$$

where $\mathbf{A}_y = \begin{bmatrix} \mathbf{0}_{N_d \times N_d} & \mathbf{I}_{N_d} \\ -\mathbf{M}^{-1}\mathbf{K} & -\mathbf{M}^{-1}\mathbf{C} \end{bmatrix}$, $\mathbf{B}_y = \begin{bmatrix} \mathbf{0}_{N_d \times N_f} \\ \mathbf{M}^{-1}\mathbf{T} \end{bmatrix}$ and $\mathbf{B}_{yc} = \begin{bmatrix} \mathbf{0}_{N_d \times N_{fc}} \\ \mathbf{M}^{-1}\mathbf{T}_c \end{bmatrix}$. Here, $\mathbf{0}_{a \times b}$ and $\mathbf{I}_a$ denote the $a \times b$ zero matrix and $a \times a$ identity matrix, respectively.

In order to allow more choices of the output to be fed back or to be controlled, an output vector $\mathbf{y}_f \in \mathbb{R}^{N_{yf}}$ is introduced that is modeled by the following state equation:

$$\dot{\mathbf{y}}_f(t) = \mathbf{A}_{yf}\mathbf{y}_f(t) + \mathbf{B}_{yf}\mathbf{y}(t) \tag{4}$$

where $\mathbf{A}_{yf} \in \mathbb{R}^{N_{yf} \times N_{yf}}$, $\mathbf{B}_{yf} \in \mathbb{R}^{N_{yf} \times 2N_d}$ are the matrices that characterizes the output filter. Note that the output vector can represent many choices of feedback. For example, it can handle displacement, velocity or acceleration measurements if the matrices $\mathbf{A}_{yf}$ and $\mathbf{B}_{yf}$ are chosen appropriately. Accelerations can be obtained approximately by passing the velocities in the state vector through a filter with the transfer function $H_d(s) = \omega_0^2 s(s^2 + \sqrt{2}\omega_0 s + \omega_0^2)^{-1}$: This filter can approximate differentiation very accurately if ω_0 is chosen larger than the upper limit of the frequency band of interest. On the other hand, one can model the sensor dynamics for displacements or velocities measurements by using a low-pass filter with the transfer function $H_l(s) = \omega_0^2(s^2 + \sqrt{2}\omega_0 s + \omega_0^2)^{-1}$.

If the full state vector $\mathbf{v}(t) = [\mathbf{w}_f(t)^T, \mathbf{y}(t)^T, \mathbf{y}_f(t)^T]^T$ is introduced, then (2) - (4) can be combined as follows:

$$\dot{\mathbf{v}}(t) = \mathbf{A}\mathbf{v}(t) + \mathbf{B}\mathbf{w}(t) + \mathbf{B}_c\mathbf{f}_c(t) \tag{5}$$

where the matrices $\mathbf{A}$, $\mathbf{B}$ and $\mathbf{B}_c$ are given by

$$\mathbf{A} \equiv \begin{bmatrix} \mathbf{A}_{wf} & \mathbf{0}_{N_{wf} \times 2N_d} & \mathbf{0}_{N_{wf} \times N_{yf}} \\ \mathbf{B}_y\mathbf{C}_{wf} & \mathbf{A}_y & \mathbf{0}_{2N_d \times N_{yf}} \\ \mathbf{0}_{N_{yf} \times N_{wf}} & \mathbf{B}_{yf} & \mathbf{A}_{yf} \end{bmatrix}, \quad \mathbf{B} \equiv \begin{bmatrix} \mathbf{B}_{wf} \\ \mathbf{0}_{2N_d \times N_w} \\ \mathbf{0}_{N_{yf} \times N_w} \end{bmatrix} \text{ and } \mathbf{B}_c \equiv \begin{bmatrix} \mathbf{0}_{N_{wf} \times N_{fc}} \\ \mathbf{B}_{yc} \\ \mathbf{0}_{N_{yf} \times N_{fc}} \end{bmatrix} \tag{6}$$

By treating $\mathbf{w}$ as constant over each subinterval $[k\Delta t, k\Delta t + \Delta t)$, where Δt is the sampling time interval that is small enough to capture the dynamics of the structure, (5) yields the following discrete-time equation:

$$\mathbf{v}[k+1] = \bar{\mathbf{A}}\mathbf{v}[k] + \bar{\mathbf{B}}\mathbf{w}[k] + \bar{\mathbf{B}}_c\mathbf{f}_c[k] \tag{7}$$

where $\mathbf{v}[k] \equiv \mathbf{v}(k\Delta t)$, $\bar{\mathbf{A}} \equiv e^{\mathbf{A}\Delta t}$, $\bar{\mathbf{B}} \equiv \mathbf{A}^{-1}(\bar{\mathbf{A}} - \mathbf{I}_{N_{wf}+2N_d+N_{yf}})\mathbf{B}$ and $\bar{\mathbf{B}}_c \equiv \mathbf{A}^{-1}(\bar{\mathbf{A}} - \mathbf{I}_{N_{wf}+2N_d+N_{yf}})\mathbf{B}_c$, and $\mathbf{w}[k]$ is Gaussian discrete white noise with zero mean and covariance matrix $\boldsymbol{\Sigma}_w = \frac{2\pi}{\Delta t}\mathbf{I}_{N_w}$.

Assume that discrete-time response data, with sampling time interval Δt, is available for N_o components of the output state, that is, the measured output is given by

$$\mathbf{z}[k] = \mathbf{L}_o\mathbf{v}[k] + \mathbf{n}[k] \tag{8}$$

where $\mathbf{L}_o \in \mathbb{R}^{N_o \times (N_{wf}+2N_d+N_{yf})}$ is the observation matrix and $\mathbf{n}[k] \in \mathbb{R}^{N_o}$ is the uncertain prediction error which accounts for the difference between the actual measured output from the structural system

and the predicted output given by the model defined by (7); it includes both modeling error and measurement noise. The prediction error is modeled as a stationary Gaussian discrete white noise process with zero mean and covariance matrix $\boldsymbol{\Sigma}_n$; this choice gives the maximum information entropy (greatest uncertainty) in the absence of any additional information about the unmodeled dynamics or output noise.

Now, choose a linear control feedback law using the current and the previous N_p output measurements,

$$\mathbf{f}_c[k] = \sum_{p=0}^{N_p} \mathbf{G}_p \mathbf{z}[k-p] \tag{9}$$

where $\mathbf{G}_p, p = 0, 1, \ldots, N_p$ are the gain matrices, which will be determined in the next section. It is worth noting that if the matrices $\mathbf{G}_p, p = 0, \ldots, N_p^\star$ ($N_p^\star < N_p$) are fixed to be zero, the controller at any time step only utilizes output measurements from time steps that are more than $N_p^\star \Delta t$ back in the past. Furthermore, by choosing a value of $N_p^\star$ such that $N_p^\star \Delta t$ is larger than the reaction time of the control system (data acquisition, online calculation of the control forces and actuator reaction time), it is possible to avoid any instability problem caused by time-delay effects.

Substituting (9) into (7):

$$\mathbf{v}[k+1] = (\bar{\mathbf{A}} + \bar{\mathbf{B}}_c \mathbf{G}_0 \mathbf{L}_o)\mathbf{v}[k] + \bar{\mathbf{B}}\mathbf{w}[k] + \bar{\mathbf{B}}_c \sum_{p=1}^{N_p} \mathbf{G}_p \mathbf{z}[k-p] + \bar{\mathbf{B}}_c \mathbf{G}_0 \mathbf{n}[k] \tag{10}$$

Now, define an augmented vector $\mathbf{U}_{N_p}[k]$ as follows:

$$\mathbf{U}_{N_p}[k] \equiv [\mathbf{v}[k]^T, \mathbf{z}[k-1]^T, \ldots, \mathbf{z}[k-N_p]^T]^T \tag{11}$$

Then, (10) can be rewritten as follows:

$$\mathbf{U}_{N_p}[k+1] = (\bar{\mathbf{A}}_u + \bar{\mathbf{B}}_{uc})\mathbf{U}_{N_p}[k] + \bar{\mathbf{B}}_u \bar{\mathbf{f}}[k] \tag{12}$$

where

$$\bar{\mathbf{f}}[k] \equiv [\mathbf{w}[k]^T \quad \mathbf{n}[k]^T]^T \tag{13}$$

and $\bar{\mathbf{A}}_u$, $\bar{\mathbf{B}}_u$ and $\bar{\mathbf{B}}_{uc}$ are given by

$$\bar{\mathbf{A}}_u \equiv \begin{bmatrix} \bar{\mathbf{A}} & \mathbf{0}_{(N_{wf}+2N_d+N_{yf})\times N_p N_o} \\ \mathbf{L}_o & \mathbf{0}_{N_o \times N_p N_o} \\ \mathbf{0}_{(N_p-1)N_o \times (N_{wf}+2N_d+N_{yf})} & \mathbf{I}_{(N_p-1)N_o} \quad \mathbf{0}_{(N_p-1)N_o \times N_o} \end{bmatrix}$$

$$\bar{\mathbf{B}}_{uc} \equiv \begin{bmatrix} \bar{\mathbf{B}}_c \mathbf{G}_0 \mathbf{L}_o & \bar{\mathbf{B}}_c \mathbf{G}_1 & \cdots & \bar{\mathbf{B}}_c \mathbf{G}_{N_p} \\ \mathbf{0}_{N_p N_o \times (N_{wf}+2N_d+N_{yf}+N_p N_o)} & & & \end{bmatrix}, \qquad \bar{\mathbf{B}}_u \equiv \begin{bmatrix} \bar{\mathbf{B}} & \bar{\mathbf{B}}_c \mathbf{G}_0 \\ \mathbf{0}_{N_o \times N_w} & \mathbf{I}_{N_o} \\ \mathbf{0}_{(N_p-1)N_o \times N_w} & \mathbf{0}_{(N_p-1)N_o \times N_o} \end{bmatrix} \tag{14}$$

Therefore, the covariance matrix $\boldsymbol{\Sigma}_u \equiv E[\mathbf{U}_{N_p}[k]\mathbf{U}_{N_p}[k]^T]$ of the augmented vector $\mathbf{U}_{N_p}$ is readily obtained:

$$\begin{aligned} \boldsymbol{\Sigma}_u &= (\bar{\mathbf{A}}_u + \bar{\mathbf{B}}_{uc})\boldsymbol{\Sigma}_u(\bar{\mathbf{A}}_u + \bar{\mathbf{B}}_{uc})^T + \bar{\mathbf{B}}_u \boldsymbol{\Sigma}_{\bar{f}} \bar{\mathbf{B}}_u^T \\ \boldsymbol{\Sigma}_{\bar{f}} &= \begin{bmatrix} \boldsymbol{\Sigma}_w & \boldsymbol{\Sigma}_{wn} \\ \boldsymbol{\Sigma}_{wn}^T & \boldsymbol{\Sigma}_n \end{bmatrix} \end{aligned} \tag{15}$$

where $\boldsymbol{\Sigma}_{\bar{f}}$ denotes the covariance matrix of the vector $\bar{\mathbf{f}}$ in (13). Note that (15) is a standard stationary Lyapunov covariance equation in discrete form. The system response is a stationary Gaussian process with zero mean and covariance matrix that can be readily calculated using (15). These properties are used to design the optimal robust controller for the structure.

2 OPTIMAL CONTROLLER DESIGN

The optimal robust controller is defined here as the one which maximizes the robust reliability (Papadimitriou et al. 2001) with respect to the feedback gain matrices in (9), that is, the one which minimizes the robust failure probability for a structural model with uncertain parameters representing the real structural system. Failure is defined as the situation in which at least one of the performance quantities (structural response or control force) exceeds a given threshold level. This is the classic 'first passage problem', which has no closed form solution. Therefore, the proposed method utilizes an approximate solution based on Rice's 'out-crossing' theory.

2.1 *Conditional Failure Probability*

Use $\mathbf{q}[k] \in \mathbb{R}^{N_q}$ to denote the control performance vector of the system at time $k\Delta t$. Its components may be structural interstory drifts, floor accelerations, control forces, etc. The system performance is given by $\mathbf{q}[k] = \mathbf{P}_0\mathbf{U}_{N_p}[k] + \mathbf{m}[k]$, where $\mathbf{P}_0 \in \mathbb{R}^{N_q \times (N_{wf}+2N_d+N_{yf}+N_pN_o)}$ is a performance matrix which multiplies the augmented vector $\mathbf{U}_{N_p}$ from (11) to give the corresponding performance vector of the model. In order to account for the unmodeled dynamics, the uncertain prediction error $\mathbf{m} \in \mathbb{R}^{N_q}$ is introduced because the goal is to control the system performance, not the model performance; it is modeled as discrete white noise with zero mean and covariance matrix $\mathbf{\Sigma}_m$.

For a given failure event $F_i = \{|q_i(t)| > \beta_i \text{ for some } t \in [0,T]\}$, the conditional failure probability $P(F_i|\boldsymbol{\theta})$ for the performance quantity q_i based on the structural model and excitation model specified by $\boldsymbol{\theta}$ can be estimated using Rice's formula:

$$P(F_i|\boldsymbol{\theta}) \approx 1 - \exp[-\nu_{\beta_i}(\boldsymbol{\theta})T] \tag{16}$$

where $\nu_{\beta_i}(\boldsymbol{\theta}) = \frac{\sigma_{\dot{q}_i}}{\pi\sigma_{q_i}} \exp(-\frac{\beta_i^2}{2\sigma_{q_i}^2})$ is the mean out-crossing rate for the threshold level β_i, and where σ_{q_i} and $\sigma_{\dot{q}_i}$ are the standard deviations for the performance quantity q_i and its derivative $\dot{q}_i$, respectively. In implementation, $\dot{q}_i$ must be included in $\mathbf{y}_f$ in (4) if it is not already part of $\mathbf{y}$.

Now consider the failure event $F = \cup_{i=1}^{N_q} F_i$, that is, the system fails if any $|q_i|$ exceeds its threshold β_i. Since the mean out-crossing rate of the system can be approximated by $\nu = \sum_{i=1}^{N_q} \nu_{\beta_i}$ (Veneziano et al. 1977), the probability of failure $P(F|\boldsymbol{\theta})$ of the controlled structural system is given approximately by

$$P(F|\boldsymbol{\theta}) \approx 1 - \exp[-\sum_{i=1}^{N_q} \nu_{\beta_i}(\boldsymbol{\theta})T] \tag{17}$$

where N_q denotes the number of performance quantities considered.

2.2 *Robust Failure Probability*

No matter what technique is used to develop a model for a structural system, the values of the structural model parameters that best represent the system are always uncertain to some extent. Furthermore, the excitation model is uncertain as well. Therefore, a probabilistic description is used to describe the uncertainty in the model parameters $\boldsymbol{\theta}$ defined earlier. Such probability distributions can be specified using engineering judgement or they can be obtained using system identification techniques. This leads to the concept of the robust failure probability given by the theorem of total probability (Papadimitriou et al. 2001):

$$P(F|\Theta) = \int_{\boldsymbol{\Theta}} P(F|\boldsymbol{\theta})p(\boldsymbol{\theta}|\Theta)d\boldsymbol{\theta} \tag{18}$$

which accounts for modeling uncertainties in deriving the failure probability. This robust failure probability is conditional on the probabilistic description $p(\boldsymbol{\theta}|\Theta)$ of the parameters that is specified over the set of possible models Θ. Since this high-dimensional integral is difficult to evaluate numerically, an asymptotic expansion is utilized (Papadimitriou et al. 1997). Denote the integral of interest by $I = \int_{\boldsymbol{\Theta}} e^{l(\boldsymbol{\theta})}d\boldsymbol{\theta}$, where $l(\boldsymbol{\theta}) = \ln[P(F|\boldsymbol{\theta})] + \ln[p(\boldsymbol{\theta}|\Theta)]$. The basic idea is to fit a Gaussian density centered at the 'design point' at which $e^{l(\boldsymbol{\theta})}$, or $l(\boldsymbol{\theta})$, is maximized. It is assumed here that there is a unique design point; see Au et al. (1999) for a more general case. Then, this integral is approximated by

$$I \equiv P(F|\Theta) \approx (2\pi)^{\frac{N_\theta}{2}} \frac{P(F|\boldsymbol{\theta}^\star)p(\boldsymbol{\theta}^\star|\Theta)}{\sqrt{\det \mathbf{L}(\boldsymbol{\theta}^\star)}} \tag{19}$$

where $\boldsymbol{\theta}^\star$ is the design point at which $l(\boldsymbol{\theta})$ has a maximum value and $\mathbf{L}(\boldsymbol{\theta}^\star)$ is the Hessian of $-l(\boldsymbol{\theta})$ evaluated at $\boldsymbol{\theta}^\star$. The optimization of $l(\boldsymbol{\theta})$ to find $\boldsymbol{\theta}^\star$ can be performed, for example, by using MATLAB subroutine 'fmins'.

The proposed control design can be summarized as follows: By solving (15), the covariance matrix of the structural response can be obtained. Then, the robust failure probability can be calculated using the asymptotic expansion formula in (19) along with (16) - (17). The optimal robust controller is obtained by minimizing the robust failure probability over all possible controllers parameterized by their gain matrices, which again can be performed, for example, using MATLAB subroutine 'fmins'.

3 SYSTEM IDENTIFICATION

The optimal controller can be readily updated when dynamic data $\mathbf{Z}_{1,N}$ is available from the system (Beck and Katafygiotis 1998; Yuen et al. 2002). Here, $\mathbf{Z}_{m,p}$ denotes the set of the measurements from time $m\Delta t$ to $p\Delta t$. In this case, Bayes' Theorem is used to get an updated PDF (probability density function) $p(\boldsymbol{\theta}|\mathbf{Z}_{1,N}, \Theta)$ that replaces $p(\boldsymbol{\theta}|\Theta)$ in (18) and hence the updated robust failure probability $p(F|\mathbf{Z}_{1,N}, \Theta)$ (Papadimitriou et al. 2001) is minimized to obtain the optimal control gains.

Using Bayes' Theorem, the expression for the updated PDF of the parameters $\boldsymbol{\theta}$ given some measured response $\mathbf{Z}_{1,N}$ is:

$$p(\boldsymbol{\theta}|\mathbf{Z}_{1,N}, \Theta) = c_1 p(\boldsymbol{\theta}|\Theta) p(\mathbf{Z}_{1,N}|\boldsymbol{\theta}, \Theta) \tag{20}$$

where c_1 is a normalizing constant such that the integral of the right hand side of (20) over the domain of $\boldsymbol{\theta}$ is equal to unity. The factor $p(\boldsymbol{\theta}|\Theta)$ in (20) denotes the prior PDF of the parameters and is based on previous knowledge or engineering judgement. As long as it varies smoothly over the parameter space Θ, $p(\mathbf{Z}_{1,N}|\boldsymbol{\theta}, \Theta)$ is the dominant factor on the right-hand side of (20) and the prior PDF has little influence. To evaluate this factor, a recently developed approach (Yuen et al. 2002) is used that can handle stationary or nonstationary response. This approach is based on the approximation:

$$p(\mathbf{Z}_{1,N}|\boldsymbol{\theta}, \Theta) \simeq p(\mathbf{Z}_{1,N_p}|\boldsymbol{\theta}, \Theta) \prod_{k=N_p+1}^{N} p(\mathbf{z}(k)|\boldsymbol{\theta}, \Theta, \mathbf{Z}_{k-N_p,k-1}) \tag{21}$$

where the conditional probabilities depending on more than N_p previous data points are approximated by conditional probabilities depending on only the last N_p data points. The validity of this approximation was verified by numerous simulations. The factors $p(\mathbf{Z}_{1,N_p}|\boldsymbol{\theta}, \Theta)$ and $p(\mathbf{z}(k)|\boldsymbol{\theta}, \Theta, \mathbf{Z}_{k-N_p,k-1}), k = N_p + 1, ..., N$ can be calculated using fundamental time series theory (Yuen et al. 2002).

4 ILLUSTRATIVE EXAMPLE

A three-bay four-story structural frame (Figure 1) with an active mass damper on the roof is used to demonstrate the proposed framework. Mass is assumed uniformly distributed over the floor slabs and along the columns, but the mass per unit length of the slabs is twice as much as that of the columns. The stiffness-to-mass ratio is taken as $EI_{c1}/m = 1.25 \times 10^5 \mathrm{m}^4\,\mathrm{sec}^{-2}$, where m is the mass per unit length of the columns. Furthermore, $[EI_{c2}, EI_{c3}, EI_{c4}] = [0.9, 0.8, 0.7]EI_{c1}$. The rigidity of the slab is taken to be $EI_s/m = 2.00 \times 10^6 \mathrm{m}^4\,\mathrm{sec}^{-2}$. The first four natural frequencies of the structure are 4.108Hz, 11.338Hz, 17.26Hz and 21.50Hz. Rayleigh damping is assumed, so the damping matrix $\mathbf{C}$ is given by $\mathbf{C} = \alpha_m \mathbf{M} + \alpha_k \mathbf{K}$, where $\mathbf{M}$ and $\mathbf{K}$ are the mass and stiffness matrices of the system; and $\alpha_m = 0.376\,\mathrm{sec}^{-1}$, $\alpha_k = 2.07 \times 10^{-4}$ sec, which gives 1.0% damping for the first two modes.

Assume that absolute accelerations measurements are available at the 2^{nd} and 4^{th} DOFs for 30 sec with a sampling frequency 200 Hz. These data are simulated using the actual model with 10% rms noise added. Furthermore, assume that the system is subjected to a white noise ground motion with spectral intensity $S_{f0} = 1.0 \times 10^{-3} \mathrm{m}^2\,\mathrm{sec}^{-3}$.

In order to have better scaling, the rigidities are parameterized as follows: $EI_j = \theta_j \widetilde{EI}_j, j = 1, 2, 3, 4$, where EI_j denotes the j^{th} story rigidity and $\widetilde{EI}_j$ is its nominal value. The rigidity parameters θ_j are

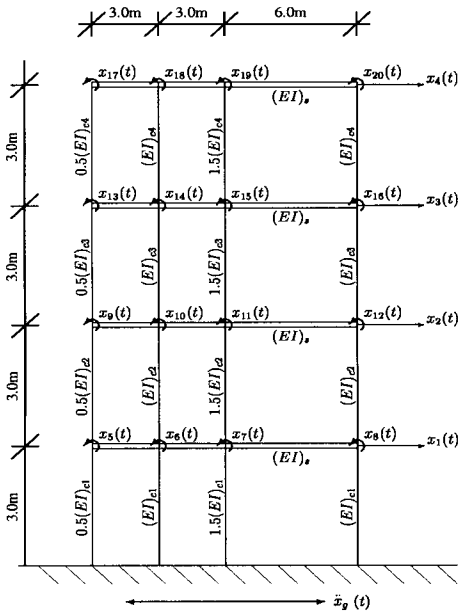


Figure 1: Four-story structural frame.

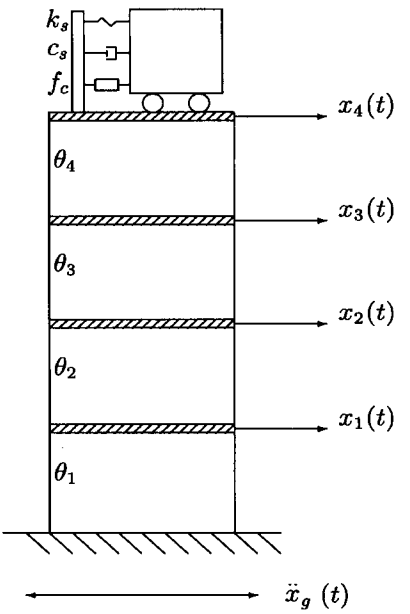


Figure 2: Structure-actuator model.

considered unknown and are determined by identification. Table 1 shows the exact values and the identified rigidity parameters and damping ratios for the two classes of models. Note that the damping ratios are presented in percentages. Table 2 shows the corresponding frequencies for the actual and the optimal models.

Table 1: Optimal structural parameters for the model class representing the structural frame.

Parameter	θ_1	θ_2	θ_3	θ_4	ζ_1	ζ_2	ζ_3	ζ_4
Exact	—	—	—	—	1.000	1.000	1.296	1.537
Identified	0.908	0.987	0.881	1.040	1.128	0.563	2.342	0.623

Table 2: Natural frequencies (in Hz) of the best model in each class.

Mode	f_1	f_2	f_3	f_4
Actual	4.108	11.34	17.26	21.50
Identified	4.158	11.35	17.40	21.02

The updated PDF of the rigidity parameters is used for calculating the robust failure probability in the controller design. First, the identified model is used to design the stiffness and damping of the AMD (active mass damper). The AMD mass M_s is chosen to be 10% of the mass of the building and the AMD stiffness and damping parameters are taken as: $k_s/M_s = 500\,\text{sec}^{-2}$ and $c_s/M_s = 15.0\,\text{sec}^{-1}$ to give a natural frequency and damping ratio approximately equal to that of the identified fundamental mode of the structure.

In Dyke et al. (1995), hydraulic actuators are modeled as follows: $\dot{f}_c = A_f f_c + B_f \dot{x}_a + B_{fu} u$, where f_c is the control force applied by the actuator; $\dot{x}_a$ is the actuator velocities; u is the signal given to the actuator; and A_f, B_f and B_{fu} are given by $A_f = -\frac{2\beta k_a}{V}$, $B_f = -\frac{2\beta A^2}{V}$ and $B_{fu} = \frac{2\beta A k_q}{V}$, where β

is the bulk modulus of the fluid; k_a and k_q are device constants; V is the characteristic hydraulic fluid volume of the actuator; and A is the cross-sectional area of the actuator. Here, these parameters are taken from Dyke et al. (1995): $2\beta k_a/V = 66.7\,\text{sec}^{-1}$, $2\beta A^2/V = 250$ N/m, $2\beta A k_q/V = 1670\text{Nsec}^{-1}$. The structure-actuator system is shown schematically in Figure 2.

The output vector $\mathbf{y}_f$ in (4) is comprised of: $\mathbf{y}_f = [f_c, \tilde{f}_c, \tilde{\tilde{f}}_c]^T$, where $\tilde{f}_c$ and $\tilde{\tilde{f}}_c$ are the state vectors for a low-pass filter with input f_c that approximates differentiation of f_c. Note that $\tilde{\tilde{f}}_c$ is used to estimate the out-crossing rate of the control force and it is not used in the control system feedback. The full state vector equation is:

$$\dot{\mathbf{v}}(t) = \mathbf{A}\mathbf{v}(t) + \mathbf{B}w + \mathbf{B}_c u \tag{22}$$

where $\mathbf{v} = [\mathbf{x}^T, \dot{\mathbf{x}}^T, \mathbf{y}_f^T]^T$; w is the ground motion; and u is the signal given to the actuator which is discussed in more detail later. The matrices $\mathbf{A}$, $\mathbf{B}$ and $\mathbf{B}_c$ are given by

$$\mathbf{A} = \begin{bmatrix} \mathbf{0}_{5\times5} & \mathbf{I}_5 & \mathbf{0}_{5\times3} \\ -\mathbf{M}^{-1}\mathbf{K} & -\mathbf{M}^{-1}\mathbf{C} & \mathbf{M}^{-1}\mathbf{A}_{12} \\ \mathbf{A}_{21} & & \mathbf{A}_{22} \end{bmatrix}$$
$$\mathbf{B} = -[0,0,0,0,0,1,1,1,1,1,0,0,0]^T, \quad \mathbf{B}_c = [\mathbf{0}_{1\times10}, B_{fu}, 0, 0]^T \tag{23}$$

where $\mathbf{A}_{12}$ and $\mathbf{A}_{21}$ and $\mathbf{A}_{22}$ are given by

$$\mathbf{A}_{12} = \begin{bmatrix} & \mathbf{0}_{3\times3} & \\ -1 & 0 & 0 \\ 1 & 0 & 0 \end{bmatrix}, \mathbf{A}_{21} = \begin{bmatrix} \mathbf{0}_{1\times8} & -B_f & B_f \\ & \mathbf{0}_{2\times10} & \end{bmatrix}, \mathbf{A}_{22} = \begin{bmatrix} A_f & 0 & 0 \\ 0 & 0 & 1 \\ \omega_c^2 & -\omega_c^2 & -\sqrt{2}\omega_c \end{bmatrix}, \omega_c = 10.0\text{Hz} \tag{24}$$

In analogy with (5), (22) can be transformed to the discrete-time augmented state equation (7) where $\bar{\mathbf{A}} \equiv e^{\mathbf{A}\Delta t}$, $\bar{\mathbf{B}} \equiv \mathbf{A}^{-1}(\bar{\mathbf{A}} - \mathbf{I}_{13})\mathbf{B}$ and $\bar{\mathbf{B}}_c \equiv \mathbf{A}^{-1}(\bar{\mathbf{A}} - \mathbf{I}_{13})\mathbf{B}_c$.

The absolute acceleration measurements at the 2^{nd} and 4^{th} DOF are modeled by

$$\mathbf{z}[k] = -\mathbf{L}_o\mathbf{M}^{-1}\mathbf{K}\mathbf{x}[k] - \mathbf{L}_o\mathbf{M}^{-1}\mathbf{C}\dot{\mathbf{x}}[k] + \mathbf{n}[k] \tag{25}$$

where $\mathbf{L}_o$ is an observation matrix which picks up the second and fourth row and $\mathbf{n}[k]$ is discrete white noise with zero mean and standard deviations 0.01g, which models the prediction error, i.e. measurement noise, the differentiator errors and modeling error.

The signal given to the AMD actuator is given by

$$u[k] = \mathbf{G}_1\mathbf{z}[k-1] + \mathbf{G}_2\mathbf{z}[k-2] \tag{26}$$

so the controller feeds back only the previous two time steps. Here, the gains $\mathbf{G}_p \in \mathbb{R}^{1\times2}, p = 1, 2$ are design parameters. Substituting (25) and (26) into the discrete-time augmented state equation, one can obtain the augmented vector equation:

$$\mathbf{U}[k+1] = \bar{\mathbf{A}}_u\mathbf{U}[k] + \bar{\mathbf{B}}_u\bar{\mathbf{f}}[k] \tag{27}$$

where $\mathbf{U}[k] = [\mathbf{v}[k]^T, \mathbf{z}[k-1]^T, \mathbf{z}[k-2]^T]^T$; $\bar{\mathbf{f}} = [w[k], \mathbf{n}[k]^T]^T$; and $\bar{\mathbf{A}}_u$ and $\bar{\mathbf{B}}_u$ are given by

$$\bar{\mathbf{A}}_u = \begin{bmatrix} \bar{\mathbf{A}} & & & \bar{\mathbf{B}}_c\mathbf{G}_1 & \bar{\mathbf{B}}_c\mathbf{G}_2 \\ -\mathbf{L}_o\mathbf{M}^{-1}\mathbf{K} & -\mathbf{L}_o\mathbf{M}^{-1}\mathbf{C} & \mathbf{0}_{2\times3} & \mathbf{0}_{2\times2} & \mathbf{0}_{2\times2} \\ & \mathbf{0}_{2\times13} & & \mathbf{I}_2 & \mathbf{0}_{2\times2} \end{bmatrix}, \quad \bar{\mathbf{B}}_u = \begin{bmatrix} \bar{\mathbf{B}} & \mathbf{0}_{13\times2} \\ \mathbf{0}_{2\times1} & \mathbf{I}_2 \\ \mathbf{0}_{2\times1} & \mathbf{0}_{2\times2} \end{bmatrix} \tag{28}$$

Then, the covariance matrix $\mathbf{\Sigma}_u$ of the augmented vector is the solution of the following Lyapunov equation in discrete form: $\mathbf{\Sigma}_u = \bar{\mathbf{A}}_u\mathbf{\Sigma}_u\bar{\mathbf{A}}_u^T + \bar{\mathbf{B}}_u\mathbf{\Sigma}_{\bar{f}}\bar{\mathbf{B}}_u^T$, where $\mathbf{\Sigma}_{\bar{f}}$ is the covariance matrix of $\bar{\mathbf{f}}$. The threshold levels for the interstory drifts, actuator stroke and the actuator acceleration are 1.0cm, 20cm and 1.0g, respectively. The optimal gain coefficients are found to be $\mathbf{G}_1 = [0.271, 0.305]$ and $\mathbf{G}_2 = [-0.395, -0.350]$. Tables 3 and 4 show the performance quantities, including the interstory drifts, AMD actuator stroke (x_s) and control force (f_{cn}), for the cases of a random excitation sample and the 1940 El Centro earthquake record, respectively. In these tables, σ denotes the rms value of a quantity. It can be seen that the interstory drifts are significantly reduced in both cases when the AMD is installed.

Table 3: Performance quantities under random excitation sample.

Performance quantity	Threshold	Uncontrolled	Controlled
σ_{x_1} (m)	—	0.0072	0.0022
$\sigma_{x_1-x_2}$ (m)	—	0.0073	0.0022
$\sigma_{x_2-x_3}$ (m)	—	0.0061	0.0020
$\sigma_{x_3-x_4}$ (m)	—	0.0037	0.0015
$max\|x_1\|$ (m)	0.01	0.0222	0.0091
$max\|x_1 - x_2\|$ (m)	0.01	0.0217	0.0086
$max\|x_2 - x_3\|$ (m)	0.01	0.0212	0.0084
$max\|x_3 - x_4\|$ (m)	0.01	0.0133	0.0056
σ_{x_s} (m)	—	—	0.0075
$\sigma_{f_{cn}}$ (g)	—	—	0.1256
$max\|x_s\|$ (m)	0.20	—	0.0288
$max\|f_{cn}\|$ (g)	1.00	—	0.4990

Table 4: Performance quantities under 1940 El Centro earthquake record.

Performance quantity	Threshold	Uncontrolled	Controlled
σ_{x_1} (m)	—	0.0012	0.0005
$\sigma_{x_1-x_2}$ (m)	—	0.0013	0.0005
$\sigma_{x_2-x_3}$ (m)	—	0.0010	0.0005
$\sigma_{x_3-x_4}$ (m)	—	0.0006	0.0003
$max\|x_1\|$ (m)	0.01	0.0053	0.0037
$max\|x_1 - x_2\|$ (m)	0.01	0.0053	0.0037
$max\|x_2 - x_3\|$ (m)	0.01	0.0043	0.0032
$max\|x_3 - x_4\|$ (m)	0.01	0.0024	0.0020
σ_{x_s} (m)	—	—	0.0018
$\sigma_{f_{cn}}$ (g)	—	—	0.0236
$max\|x_s\|$ (m)	0.20	—	0.0125
$max\|f_{cn}\|$ (g)	1.00	—	0.1693

References

Au, S. K., C. Papadimitriou, and J. L. Beck (1999). Reliability of uncertain dynamical systems with multiple design points. *Structural Safety 21*, 113–133.

Beck, J. L. and L. S. Katafygiotis (1998). Updating models and their uncertainties. I: Bayesian statistical framework. *Journal of Engineering Mechanics 124(4)*, 455–461.

Dyke, S. J., B. Spencer, Jr, P. Quast, and M. K. Sain (1995). Role of control-structure interaction in protective system design. *Journal of Engineering Mechanics 121(2)*, 322–338.

Papadimitriou, C., J. L. Beck, and L. S. Katafygiotis (1997). Asymptotic expansions for reliability and moments of uncertain systems. *Journal of Engineering Mechanics 123(12)*, 1219–1229.

Papadimitriou, C., J. L. Beck, and L. S. Katafygiotis (2001). Updating robust reliability using structural test data. *Probabilistic Engineering Mechanics 16(2)*, 103–113.

Veneziano, D., M. Grigoriu, and C. A. Cornell (1977). Vector-process models for system reliability. *Journal of Engineering Mechanics 103(EM3)*, 441–460.

Yuen, K.-V., J. L. Beck, and L. S. Katafygiotis (2002). Probabilistic approach for modal identification using non-stationary noisy response measurements only. *Earthquake Engineering and Structural Dynamics 31(4)*, 1007–1023.

Advances in Building Technology, Volume 1
M. Anson, J.M. Ko and E.S.S. Lam (Eds.)
© 2002 Elsevier Science Ltd. All rights reserved

BUILDING HAZARD MITIGATION WITH PIEZOELECTRIC FRICTION DAMPERS

G. D. Chen[1] and C. Q. Chen[1]

1. Department of Civil Engineering, University of Missouri-Rolla, Rolla, MO 65409-0030, USA

ABSTRACT

Semi-active piezoelectric friction dampers have been recently introduced to reduce the peak responses of buildings. They are regulated in real time with applied voltages according to a simple yet effective control algorithm that combines the viscous and nonlinear Reid damping mechanisms. This paper is aimed at further addressing some performance-related issues such as the stick and sliding features of a friction damper, optimum ratio of Reid and viscous damping in the control algorithm, performance comparison with Coulomb dampers, and optimal placement of friction dampers in a multi-story building. Numerical simulations of a single- and a 20- story building (statistical analysis under 10 earthquake ground motions) indicate that Coulomb dampers are effective when the external excitation on the building is known a *prioror*. Semi-active friction dampers, however, are effective in response reduction of a building subjected to excitations of various intensities. They have been applied to effectively mitigate the responses of buildings under both near-fault and far-field ground motions. The optimum ratio of control gain factors for the Reid and viscous damping is equal to $2/\pi$ times the excitation frequency. The application of piezoelectric actuators in civil engineering relies upon the distribution effect of multiple dampers. A sequential sub-optimal procedure for damper placement is developed for practical applications. Due to their adaptability to external disturbances, semi-active dampers can greatly enhance the multi-objective performance of buildings under multi-level excitations and will play an important role in performance-based engineering.

KEYWORDS:

Piezoelectric actuators, active friction dampers, semi-active friction dampers, Coulomb dampers, seismic effectiveness, performance evaluation, near-fault effect, performance-based engineering

INTRODUCTION

Friction dampers guarantee the dissipation of energy by friction and therefore do not cause instability of a structure being controlled. In this paper, piezoelectric actuators are used to modulate the clamping force of a fiction damper to make the damper adaptive to external disturbances. Such a device is referred to as a piezoelectric friction damper. Piezoelectric materials offer such unique features as effectiveness over wide frequency bands, high-speed actuation, low power consumption, simplicity,

reliability, and compactness as demanded in civil engineering applications (Housner *et al.*, 1994). However, these materials work under a small strain level and therefore are limited in their loading capacity. To generate a sufficient control force with piezoelectric materials in civil engineering applications must rely on the distribution effect of many actuators.

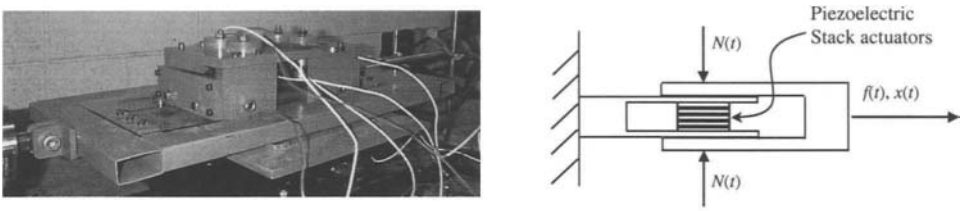
Piezoelectric friction dampers have recently been used to mitigate the peak responses of elastic and inelastic buildings (Chen and Chen, 2000; 2002) under dynamic loading. A new control algorithm has been developed to command friction dampers. It has been demonstrated very effective in suppressing the harmonic responses of single-story structures and seismic responses of multi-story buildings. In this paper, some issues related to the control algorithm and optimal placement of multiple dampers in a building are addressed.

SEMI-ACTIVE PIEZOELECTRIC FRICTION DAMPERS

A prototype damper and its schematic representation are shown in Figure 1. The schematic consists of two U-shaped bodies, one sliding against the other. The outer body is assumed to be rigid. The clamping force, $N(t)$, acting on the sliding surfaces is controllable with four PZWT100 stack actuators. Each actuator consists of 24 discs with 0.02 in. thick each; they are connected mechanically in series and electrically in parallel. The clamping force on two friction surfaces is determined by

$$N(t) = N_{pre} + \frac{4EAd_{33}V(t)}{h} \tag{1}$$

in which N_{pre} is the pre-load on the stack actuators required for the generation of the passive friction force, E is the Young's Modulus of the PZWT material, A is the area of cross section of the stacks, h is the thickness of each layer, d_{33} is the piezoelectric strain coefficient and $V(t)$ is the applied voltage on the stack actuators. When $V(t)$ in Eqn.1 is equal to zero, the clamping force is constant ($=N_{pre}$) and it corresponds to a passive Coulomb friction damper. When N_{pre} is negligible, the clamping force is proportional to the applied voltage $V(t)$, which is fully adaptive to the feedback of the damper slippage and thus corresponds to an active friction damper. When both pre-load and voltage are applied, the damper is semi-active and requires less energy than an active damper to operate.



(a) Prototype (b) Schematic representation

Figure 1: A piezoelectric friction damper

Control Algorithm

For a damper installed in the i^{th} story of a building, a semi-active control strategy is proposed to regulate the damper with an applied voltage such that the following friction force is generated:

$$f_i(t) = \begin{cases} 2\mu N_{pre} sgn[\dot{x}_i(t)], & when\ e|x_i(t)| + g|\dot{x}_i(t)| \le N_{pre} \\ 2\mu e|x_i(t)|sgn[\dot{x}_i(t)] + 2\mu g \dot{x}_i(t), & when\ e|x_i(t)| + g|\dot{x}_i(t)| > N_{pre} \end{cases} \quad (2)$$

in which e and g are positive gain factors, $|x_i(t)|$ and $|\dot{x}_i(t)|$ are respectively the absolute values of the drift and drift rate of the i^{th} building story, μ is the coefficient of friction and $sgn[\ ]$ represents the sign of the argument in the bracket. Note that the factor of *2* is used to account for two friction surfaces. The first expression represents the passive damper mechanism when structural responses are relatively small. When structural responses become significant, the active damper mechanism represented by the second expression is activated. Eqn. 2 indicates that, for relatively large structural responses, the active component of the proposed semi-active control strategy essentially combines both the viscous and the non-linear Reid damping mechanisms, which has been proved to be more effective than individual damping mechanisms (Chen and Chen, 2000).

Optimum Gain Factor Ratio

The active component of the proposed semi-active control strategy involves two gain factors, e and g, representing the weighting effect on the Reid and viscous damping mechanisms. Since the Reid damping force reaches its maximum when the viscous damping force is zero, there must exist an optimum gain ratio, e/g, which corresponds to the minimal responses of a structure under the same maximum control force. Consider the single-story frame structure with mass, natural frequency, and damping ratio respectively equal to $m=2.92\ kN\text{-}sec^2/m$, $\omega_0=3.47\ Hz$, *and* $\xi=1.24\%$ (Soong, 1990). The structure is controlled with an active friction damper ($N_{pre}=0$). The proposed control algorithm is homogeneous to the first degree and is linearized, leading to an equivalent structure-damper system:

$$\begin{aligned} &m\ddot{x}(t) + m2\xi\omega_0\dot{x}(t) + m\omega_0^2 x(t) + C_e\dot{x}(t) = F_0 \sin(\omega t) \\ &C_e = \mu g(1 + 2e/\pi g\omega) \end{aligned} \quad (3)$$

in which C_e is the damping coefficient of the equivalent viscous damper for the active control force (Chen and Chen, 2000a). The active control force in the second expression of Eqn. 2 (i=1) can then be approximately represented by the stead state response from Eqn. 3 and its maximum value is

$$f_{1\max} = \mu g A\sqrt{\omega^2 + (e/g)^2} \quad (4)$$

where A is the displacement amplitude of the structure described by Eqn. 3. After solving for μg from Eqn. 4 and plugging it into C_e of Eqn. 3, the equivalent damping coefficient C_e can be expressed as a function of f_{1max}, A, and e/g, and A satisfies the following equation:

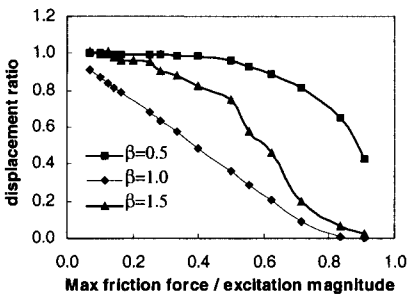
$$[(1-\beta^2)^2 + (2\xi\beta)^2]\left(\frac{Am\omega_0^2}{F_0}\right)^2 + 4\xi\beta\frac{f_{1\max}}{F_0}\frac{1 + 2e/\pi g\omega}{\sqrt{1 + (e/g\omega)^2}}\frac{Am\omega_0^2}{F_0} + \frac{f_{1\max}^2}{F_0^2}\frac{(1 + 2e/\pi g\omega)^2}{1 + (e/g\omega)^2} - 1 = 0 \quad (5)$$

in which β is the ratio of excitation and natural frequencies. When f_{1max} is constant, A can be solved from the above equation as a function of e/g as well as structural and excitation parameters. The displacement amplitude reaches its minimum value when e/g is approximately equal to $2\omega/\pi$. To obtain a real solution for A in Eqn. 5, the maximum control force must satisfy

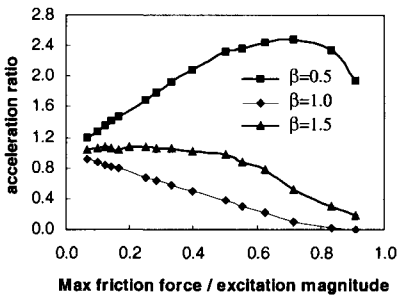
$$f_{1\max}/F_0 \le \sqrt{(1-\beta^2)^2 + (2\xi\beta)^2}\ /\left|1-\beta^2\right|\sqrt{1 + 4/\pi^2} \quad (6)$$

Roles of Passive and Active Mechanisms in the Proposed Control Algorithm

The same single-story frame structure is studied. When Coulomb damping is considered, the displacement and acceleration ratio of the controlled and uncontrolled structure are respectively shown in Figures 2(a, b). Their corresponding ratios when active damping is considered are presented in Figures 3(a, b), respectively. It can be observed from Figure 2 that, as the friction force increases or the excitation decreases, the displacement of the structure controlled with a Coulomb damper always decreases. However, its associated acceleration increases when β is smaller than *1.0* since the stick nature of the friction damper results in a sudden movement at the beginning of sliding stages. On the other hand, Figure 3 indicates that the reduction in both displacement and acceleration is nearly independent of the intensity of excitation due to the adaptability of an active damper.

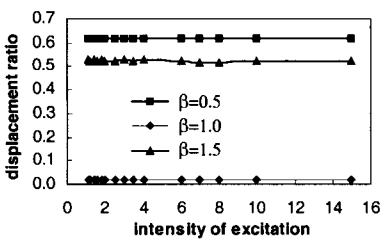


(a) Reduction in displacement

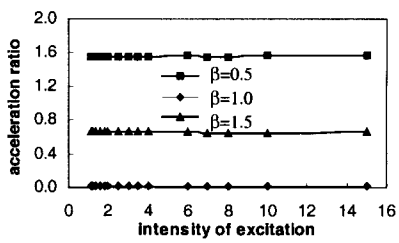


(b) Reduction in acceleration

Figure 2: Performance of a Coulomb friction damper



(a) Reduction in displacement



(b) Reduction in acceleration

Figure 3: Performance of an active damper with the proposed algorithm

In building designs, both story drift and acceleration are important measures of building performance. Therefore, it would be beneficial to implement a semi-active control strategy for performance-based designs of buildings that are subjected to dynamic loads with uncertainties in magnitude and phase.

OPTIMAL PLACEMENT OF DAMPERS IN MULTI-STORY BUILDINGS

The 20-story steel frame structure and 10 earthquake ground motions studied by Ohtori *et al.* (2000) are used to demonstrate the distribution and seismic effectiveness of piezoelectric friction dampers. For practical applications, a heuristic approach is taken to develop a simple and effective procedure for damper placement. The optimum gain factor ratio, *e/g*, is determined with the average dominant frequency ($\omega_u \cong$ *4.73 rad/sec*) of the uncontrolled displacement responses under the 10 earthquake

inputs. The gain factor g is taken to be 1.9×10^5 *N-sec/m* to ensure that the dampers can generate the maximum friction force nearly equal to their capacity (*93.1 kN*) without saturation under the earthquake excitations. The pre-load N_{pre} is selected to provide a friction force equal to *10%* of the damper capacity. This algorithm is implemented in MATLAB (Chen and Chen, 2002).

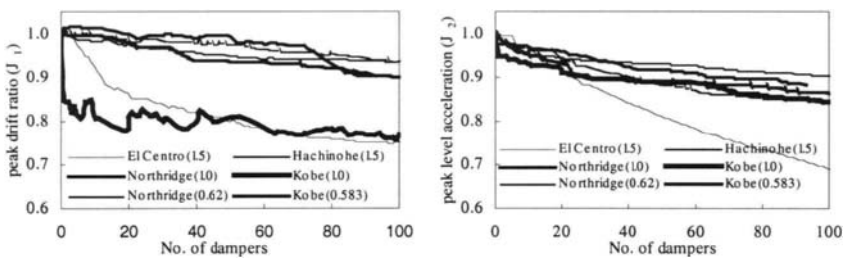
The following sequential procedure is used for the sub-optimal placement of dampers in a building:

Step 1. Select an optimization index such as peak story drift or peak floor acceleration of the building.

Step 2. Place one or several dampers on the structure toward the reduction of the optimization index. Specifically, place one damper on each permissible location of the building and evaluate the performance index. If the index is reduced with the installation of the damper at various locations, the damper is placed at the location corresponding to the maximum reduction. If adding one damper at a time cannot further reduce the performance index, two or more dampers should be placed on the structure simultaneously.

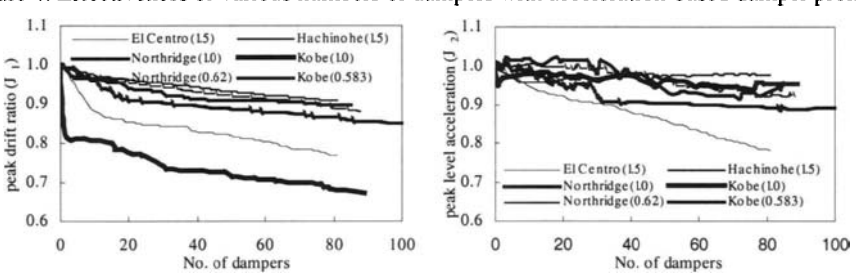
Step 3. Repeat Step 2 until all the dampers have been placed on the structure.

The peak story drift and the peak floor acceleration are used as potential optimization indices to facilitate the placement of dampers. To determine which index is more effective in reducing the overall building responses, both peak story drift and peak acceleration of the building under six earthquake ground motions are presented in Figures 4(a, b) and 5(a, b) as the number of dampers on the structure increases. It can be observed from Figure 4 that the use of peak floor acceleration as an optimization index results in comparable reduction in both acceleration and drift of the structure except for the Kobe earthquake. On the other hand, if the peak drift ratio is used as an index as indicated in Figure 5, it is very difficult to reduce the peak floor acceleration simultaneously. Sometimes it even increases the acceleration as illustrated in Figure 5(b). Therefore, it is recommended that the peak floor acceleration be used as the optimization index for optimal damper placement.



(a) Peak drift ratio (b) Peak floor acceleration

Figure 4: Effectiveness of various numbers of dampers with acceleration-based damper profiles



(a) Peak drift ratio (b) Peak floor acceleration

Figure 5: Effectiveness of various numbers of dampers with drift-based damper profiles

Figures 4 and 5 indicate the comparable reductions in both story drift and floor acceleration under the Northridge earthquake of different modification factors of 62% and 100%. However, under the Kobe earthquake, dampers can suppress significantly more story drift under the high excitation (100%) than that under the low excitation (58.3%). This result implies the occurrence of substantial plastic deformation at several locations under the 100%Kobe earthquake. Considering various earthquakes of the same intensity, e.g. 150%El Centro vs. 62%Northridge earthquake, it is observed from Figures 4 and 5 that both story drift and floor acceleration can be reduced more effectively under the El Centro earthquake than those under the Northridge earthquake. Those under the 150%Hachinohe are mitigated slightly less effectively than under the 58.3%Kobe earthquake. In general, a structure subjected to far-field ground motions, such as the El Centro earthquake, can be more easily controlled with dampers than that under near-fault ground motions such as the Northridge and Kobe earthquakes. However, it is not difficult to control the excessive inelastic story drift of a structure under strong near-fault earthquakes such as the 100%Kobe.

To select the optimal distribution of the 80 dampers over the building height for overall performance under various earthquakes, six damper profiles were determined using the proposed sequential procedure with the peak floor acceleration as the optimization index. Each profile corresponds to one of the six earthquake inputs used in Figures 4 and 5. These profiles were then employed to calculate the peak accelerations at all floors of the building subjected to the 10 earthquake excitations (Ohtori *et al.*, 2000). The maximum value of the peak accelerations at all floors was normalized with that of the uncontrolled structure under each of the 10 earthquake excitations. The statistical characteristics of the 10 samples for peak acceleration ratio (r_a) such as the maximum value [$max(r_a)$], average ($\bar{r}_a$), and standard deviation [$s(r_a)$] are shown in Table 1. It can be observed from the table that Profile8 has the lowest maximum and average accelerations. The standard deviation associated with this profile is also very small, indicating the consistent damper performance under the 10 earthquake ground motions. Thus, Profile8, determined under the Northridge earthquake, achieves the best overall performance in reducing the peak floor acceleration of the structure. The 80 dampers in this case are distributed along the building height from top to bottom as: [26, 1, 3, 0, 7, 0, 0, 1, 7, 0, 7, 5, 4, 2, 1, 0, 6, 1, 0, 9].

TABLE 1
PEAK ACCELERATION RATIOS WITH 10% CAPACITY FROM THE PASSIVE COMPONENT

Damper Profile	$max(r_a)$	$\bar{r}_a$	$s(r_a)$
Profile3 (150%El Centro EQ)	1.111	0.882	0.122
Profile6 (150%Hachinohe EQ)	0.985	0.891	0.059
Profile8a (62%Northridge EQ)	1.085	0.882	0.110
Profile8 (100%Northridge EQ)	**0.989**	**0.878**	**0.081**
Profile10a (58.3%Kobe EQ)	1.004	0.885	0.085
Profile10 (100%Kobe EQ)	1.067	0.882	0.104

PERFORMANCE OF PASSIVE, SEMI-ACTIVE, AND ACTIVE FRICTION DAMPERS

To understand the pre-load effect on the damper performance, the statistical characteristics similar to those in Table 1 under the Northridge earthquake are given in Table 2 for various N_{pre}. It can be clearly seen from the table that all statistical characteristics of the peak floor acceleration increases as the pre-load increases. This means less effectiveness of dampers in reducing the structural acceleration when the percentage of the passive friction force increases in the proposed semi-active strategy. Similarly, more pre-load on the passive component of the semi-active damper results in the increasing maximum and average peak drift ratio. On the other hand, Table 2 indicates that the required maximum active

control force (normalized by the total building weight, 1.09×10^5 *kN*) significantly drops as the pre-load increases. In conclusion, the introduction of more passive friction force in the semi-active friction dampers significantly degrades the performance of the dampers but reduces the active control force. To maintain the effectiveness of dampers with reasonable power demand, a pre-load corresponding to 10% of the damper capacity was used in the previous section.

TABLE 2
PERFORMANCE COMPARISON BETWEEN ACTIVE AND SEMI-ACTIVE DAMPERS

Damper Profile	Response Quantity	$max(r)$	$\bar{r}$	$s(r)$
Profile8b (N_{pre}⇒0% capacity) (active)	Story drift ratio	0.957	0.877	0.718
	Acceleration ratio	0.944	0.872	0.044
	Control force ($\times 10^{-4}$)	8.186	4.228	2.099
Profile8 (N_{pre}⇒10% capacity) (semi-active)	**Story drift ratio**	**0.962**	**0.875**	**0.078**
	Acceleration ratio	**0.980**	**0.878**	**0.081**
	Control force ($\times 10^{-4}$)	**7.470**	**3.362**	**2.174**
Profile8d (N_{pre}⇒30% capacity) (semi-active)	Story drift ratio	0.976	0.860	0.095
	Acceleration ratio	1.428	0.976	0.191
	Control force ($\times 10^{-4}$)	5.339	1.799	1.827
Profile8f (N_{pre}⇒50% capacity) (semi-active)	Story drift ratio	0.982	0.854	0.100
	Acceleration ratio	2.255	1.211	0.481
	Control force ($\times 10^{-4}$)	4.164	0.847	1.422

To compare the performance between Coulomb dampers and semi-active friction dampers, Table 3 lists the statistical characteristics of the peak story drift and peak floor acceleration ratios associated with the optimal damper placement, Profile8, determined under the Northridge earthquake. For passive dampers, different levels of friction forces have been used in numerical simulations. It is seen from Table 3 that the maximum values of both story-drift and floor acceleration ratios can be reduced more by semi-active dampers. As the friction force of Coulomb dampers increases, both the maximum and average drifts decreases and their standard deviation increases due to stick effects. All the statistical quantities of the floor acceleration substantially increase with the friction force of Coulomb dampers, indicating degrading performance. These results indicate that semi-active dampers outperform Coulomb dampers for the multi-level earthquake design of buildings.

TABLE 3
PERFORMANCE COMPARISON BETWEEN SEMI-ACTIVE AND PASSIVE DAMPERS

Control Strategy	Response Quantity	$max(r)$	$\bar{r}$	$s(r)$
Semi-active (N_{pre}⇒10% capacity)	**Story drift ratio**	**0.962**	**0.875**	**0.078**
	Acceleration ratio	**0.980**	**0.878**	**0.081**
Passive (N_{pre}⇒10% capacity)	Story drift ratio	1.012	0.932	0.078
	Acceleration ratio	1.036	0.938	0.074
Passive (N_{pre}⇒50% capacity)	Story drift ratio	0.986	0.833	0.101
	Acceleration ratio	2.249	1.173	0.431
Passive (N_{pre}⇒100% capacity)	Story drift ratio	0.964	0.778	0.109
	Acceleration ratio	4.224	1.850	0.994

The optimum ratio of control gain factors, e/g, was derived from a single-story building subjected to harmonic loading. To see how sensitive the dampers' performance is to the change of the gain factor ratio, Table 4 shows the statistical results of peak story-drift and peak acceleration ratios when ±10%

uncertainties in the determination of the gain factor ratio is introduced. Clearly, it is observed that the changes in maximum and average story-drift ratios or acceleration ratios are all within 1%. The optimum ratio of two gain factors derived in this study is thus valid for the practical design of dampers.

TABLE 4
PERFORMANCE SENSITIVITY TO OPTIMUM GAIN FACTOR RATIO

Excitation Frequency	Response Quantity	$max(r)$	$\bar{r}$	$s(r)$
$0.9\omega_u$	Story drift ratio	0.965	0.880	0.076
	Acceleration ratio	0.978	0.880	0.081
$1.0\omega_u$	**Story drift ratio**	**0.962**	**0.875**	**0.078**
	Acceleration ratio	**0.980**	**0.878**	**0.081**
$1.1\omega_u$	Story drift ratio	0.959	0.870	0.082
	Acceleration ratio	0.980	0.874	0.079

CONCLUDING REMARKS

Based on the extensive numerical simulations in this study, it is concluded that Coulomb dampers can be designed to effectively reduce the dynamic responses of a building when the intensity of an external disturbance exerted on the building is known during the design period. Semi-active friction dampers, however, are effective in response reduction of a building subjected to excitations of various intensities. The proposed algorithm is effective in mitigating the inelastic responses of buildings under near-fault ground motions. The optimum ratio of control gain factors for the Reid and viscous damping is equal to $2/\pi$ times the excitation frequency. The application of piezoelectric actuators in civil engineering relies upon the distribution effect of multiple dampers. The proposed sequential procedure for damper placement is very efficient.

ACKNOWLEDGEMENTS

This study was sponsored by the U.S. National Science Foundation under Award No. CMS-9733123 with Drs. S. C. Liu and P. Chang as Program Directors. The results, opinions and conclusions expressed in this paper are solely those of the authors and do not necessarily represent those of the sponsor.

REFERENCES

Chen, G. D. and Chen, C. C. (2000). Behavior of Piezoelectric Friction Dampers under Dynamic Loading. *Proc. SPIE Symposium on Smart Structures and Materials: Smart Systems for Bridges, Structures, and Highways*, Newport Beach, CA, Vol. **3988**, 54-63.

Chen, G. D. and Chen, C. C. (2002). Semi-Active Control of the 20-Story Benchmark Building with Piezoelectric Friction Dampers. *Journal of Engineering Mechanics*, ASCE (accepted for publication).

Housner, G. W., Soong T. T. and Masri, S. F. (1994). Second Generation of Active Structural Control in Civil Engineering. *Proc.1st World Conference on Structural Control*, Los Angeles, CA, Panel: 3-18.

Ohtori, Y., Christenson, R. E. and Spencer, Jr., B. F. (2000), "Benchmark control problems for seismically excited nonlinear buildings", *http://www.nd.edu/~quake/nlbench.html.*

Soong T.T. (1990). *Active Structural Control: Theory & Practice*, Longman & Scientific Technical, New York.

Advances in Building Technology, Volume 1
M. Anson, J.M. Ko and E.S.S. Lam (Eds.)
© 2002 Elsevier Science Ltd. All rights reserved

A RESEARCH AND DEVELOPMENT OF SMART BUILDING STRUCTURES BY MAGNETO-RHEOLOGICAL DAMPER

H. Fujitani [1], Y. Shiozaki [2], T. Hiwatashi [3], K. Hata [4], T. Tomura [4], H. Sodeyama [5] and S. Soda [6]

[1] Department of Structural Engineering, Building Research Institute
Tsukuba, Ibaraki 305-0802, Japan
[2] Nishimatsu Construction Co. Ltd. (Visiting Researcher of Building Research Institute)
Tsukuba, Ibaraki 305-0802, Japan
[3] TOA Technical Research Institute (Visiting Researcher of Building Research Institute)
Tsukuba, Ibaraki 305-0802, Japan
[4] Central Research & Development Division, Bando Chemical Industries, Ltd.
Ashihara-dori, Hyogo-ku, Kobe 652-0882, Japan
[5] Manager, Test & Research Department, Sanwa Tekki Corporation
Naka-okamoto, Kawachi-machi, Tochigi 329-1192, Japan
[6] Department of Architecture, School of Science & Engineering, Waseda University
Okubo, Shinjuku-ku, Tokyo 169-8555, Japan

ABSTRACT

Magneto-rheological damper (MR damper) has been expected to control the response of building structures in recent years, because of its large force capacity and variable force characteristics. Authors developed some MR dampers and conducted shaking table tests for the improvement the performance of building structures subjected by earthquake. A three-story large-scaled test frame supposing both base-isolated and normal structure was developed. As for base-isolated building, 40kN Magneto-Rheological damper was installed at base-isolation. The effectiveness of MR damper and proposed control algorithm was verified. In the other hand, a new Magneto-Rheological fluid is also developed in order to apply to the MR damper. The new MR fluid had a good property concerning the settlement of particles in dampers. The settlement was one of serious problems to be solved in handling of MR fluid in case of controlling the earthquake response of building structures. Fourth author developed a new MR fluid, which keeps the particles in the fluid adequately enough for usual use of MR damper

KEYWORDS

MR Fluid, MR damper, Test frame, Shaking table test, Semi active control, Base-isolation, Earthquake response control

INTRODUCTION

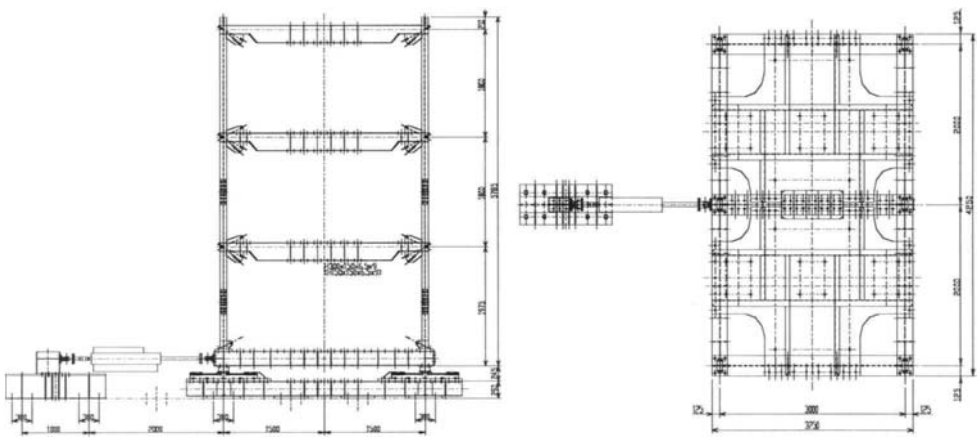
The Building Research Institute (BRI) of Japan and the U.S. National Science Foundation (NSF) initiated the U.S.-Japan Cooperative Research Program on Auto-adaptive Media (Smart Structural Systems) in 1998 (Otani et al (2000)), under the aegis of the U.S.-Japan Panel on Wind and Seismic Effects of the U.S.-Japan Cooperative Program in Natural Resources. At the Joint Technical Coordinating Committee (JTCC) meeting, research items and plans were discussed in detail for three research thrusts: (1) structural systems, (2) sensing and monitoring technology, and (3) effecter technology.

BRI planned a series of large-scale tests to verify some smart systems developed in this project. The effectiveness of "Semi-active control by MR dampers", "Damage detection system" and "Rocking energy dissipation system" was confirmed. This paper outlines the development of MR fluid and MR damper, the characteristics of the large-scale test frame and test results of response control of base-isolated building by MR damper.

LARGE-SCALE TEST OF RESPONSE CONTROL BY MR DAMPER

The passive control has a limitation of damping effect to a certain range with frequency and input level in general. Semi-active control reduces both response displacements and accelerations. MR damper generates damping force, which does not depend on the piston speed so much (Fujitani et al (2000)). The target of this subject is to improve the safety and functionality and habitability by controlling the response displacements and accelerations by using MR dampers. For this purpose, a MR damper and a control algorithm have been developed and their validity is discussed by an analytical study and shaking table tests.

The basic test frame used for the large-scale test is a 3-story steel frame (Figure 1). It is 3m (1 span) x 4m (2m x 2 span) in plan and 6m high, weighs a total of 20.23 ton (including the weight of the 1st floor), and has a natural period of about 0.546 sec. (TABLE 1). The shaking table of the National Research Institute for Earth Science and Disaster Prevention (NIED) was used. The shaking table has a maximum displacement of 22 cm, a maximum velocity of 75 cm/s, and a maximum weight of 500 ton.



(a) Central frame of span direction (b) First floor of base isolation system

Figure 1: Test frame for response control by MR dampers

TABLE 1
DATA OF TEST FRAME

(a) Masses (ton),(b) Stiffness and Elastic displacement of the frame,(c) Characteristics as base-isolation

Roof	4.67
3rd Floor	4.78
2nd Floor	4.78
1st Floor	6.00
Total	20.23

	Stiffness(kN/cm)	Elastic Displacement(cm)
3F	27.6	1.74
2F	28.4	3.00
1F	35.4	2.27

Stiffness(kN/cm)	1.01
Friction Force(kN)	0.692
Damping Coefficient(kNs/cm)	0.0333
Damping Ratio	0.037
Natural Period(sec)	2.84

DEVELOPMENT OF MR FLUID

Trial product of MR fluid "#230", which was made on an experimental basis by the fourth and fifth authors of this paper, was applied for MR damper. The "#230" is oil-based fluid, and has a good stability. Properties of "#230" are shown in TABLE 2.

TABLE 2
PROPERTIES OF MR FLUID "#230"

Properties	#230
Base fluid	Oil
Density	$3.3*10^3$ kg/m^3
Stability *)	Approximately 98%(by volume) after $2*10^4$ min.

*):Stability(%)=V(t) / V(0) *100
V(t):sedimental volume after t min
V(0):original sedimental volume

DEVELOPMENT OF MR DAMPER

Design of MR damper

The sixth author of this paper developed a MR damper. The design of the bypass-flow-type MR damper for base isolation used in the experiment is shown in Figure 2 and TABLE 3. It is composed of three parts: bypass-flow and pressure chambers and a reservoir. In bypass-type hydraulic dampers

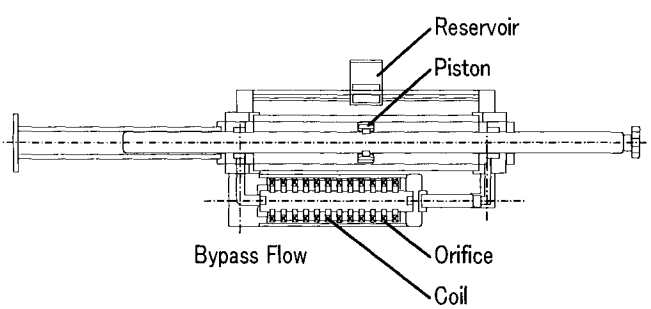


Figure 2: Structure of MR damper

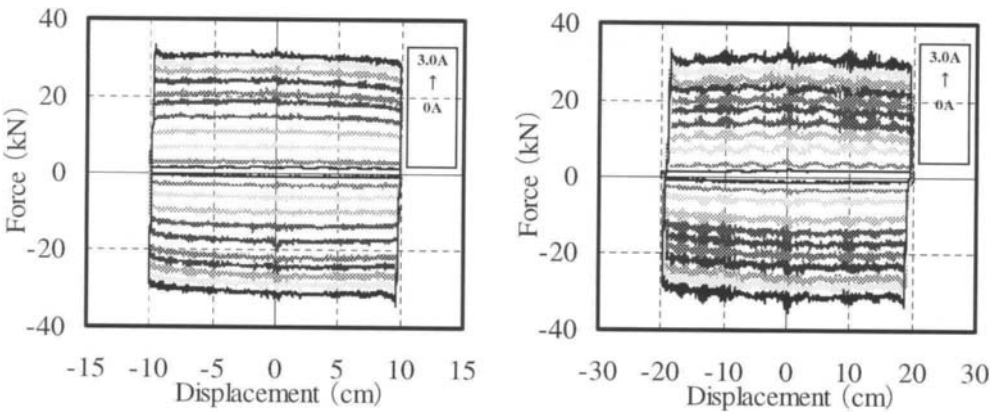
TABLE 3
DESIGN SPECIFICATION

Max.Force		40kN
Stroke		±295mm
Cylinder Bore		φ90mm
Orifice	Section	Outer diameter φ48mm
		Gap 3.0mm
	Length	420mm
Electromagnet	Inductance	37.4mH×3
	Resistance	12Ω×3
	Max.Current	3A
MR fluid		Bando:#230

such as this, the cylinder is divided into two pressure chambers by a piston with rubber O-rings. The bypass flow portion is a passage for MR fluids connecting two pressure chambers. The bypass flow portion has an orifice for effectively magnetizing the fluid. The uniform magnetic field is applied perpendicularly to the MR fluid flow at the annular orifice. The thermal expansion due to the temperature rise of the MR fluid is absorbed by the reservoir.

Mechanical characteristic of MR damper by cyclic loading

Cyclic loading tests were conducted to clarify the performance of the MR damper. Figure 3 shows the force-displacement relationship. The electric current to the electromagnet was set at the constant value at 0A～3A in the 0.3A interval. The hysteretic loop shows like rigid-plastic characteristics caused by friction force of MR fluid with magnetic field. The force increases almost proportionally for the increase in the electric current. Figure 4 shows the force-velocity relationship. The velocity is the maximum velocity of piston in case of sinusoidal loading in this figure. This figure also shows that the force increases almost proportionally for the increase in the electric current and the force does not depend on the piston velocity so much.



(a) 0.1Hz, 10cm, 6.28cm/sec (b) 0.1Hz, 20cm, 12.56cm/sec

Figure 3: Force-displacement relationship of MR damper

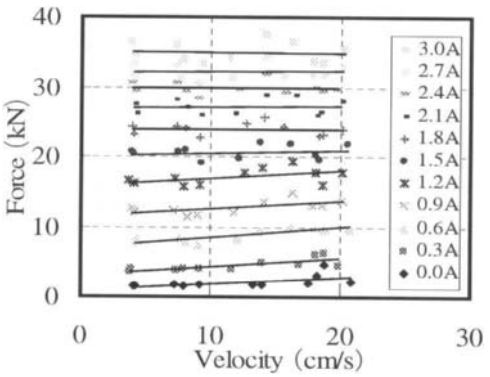


Figure 4: Force-velocity relationship of MR damper

SHAKING TABLE TEST

Testing Facilities

The base-isolation system is constituted of six roller bearings with four laminated rubber bearings (Photo 1). The laminated rubber bearing gives the restoring force, and the roller bearing supports the vertical load. The input wave for the shaking table test were sweep sinusoidal wave, white noise wave, and five earthquake waves of El Centro 1940 NS, Hachinohe 1968 NS, JMA Kobe 1995 NS and Taft 1952 EW standardized at a maximum velocity of 50cm/s. Figure 5 shows the performance of the shaking table.

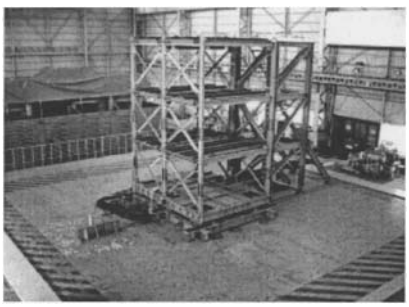


Photo 1: Test frame

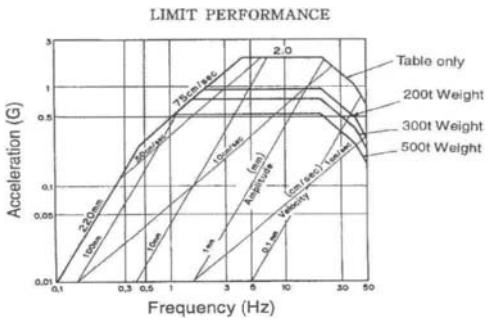


Figure 5: Performance of the shaking table

Control System

The measurement and control system in the shaking table test is shown in Figure 6. Accelerometers, transducers for measuring displacement and strain gauges were installed at each part of the test frame, and the data were recorded. There were 256 recording channels, and the data sampling was 2kHz. The data were recorded by an EWS for the measurement, which served as D/A converter of input waveform to the shaking table. The control signal incorporated the signal from the sensor in the amplifier, and it took in a voltage signal output from the amplifier to the A/D converter of the control PC. The control signal of electric current supplied to the MR damper was output from the D/A converter of the control PC to the high-speed DC power supplies.

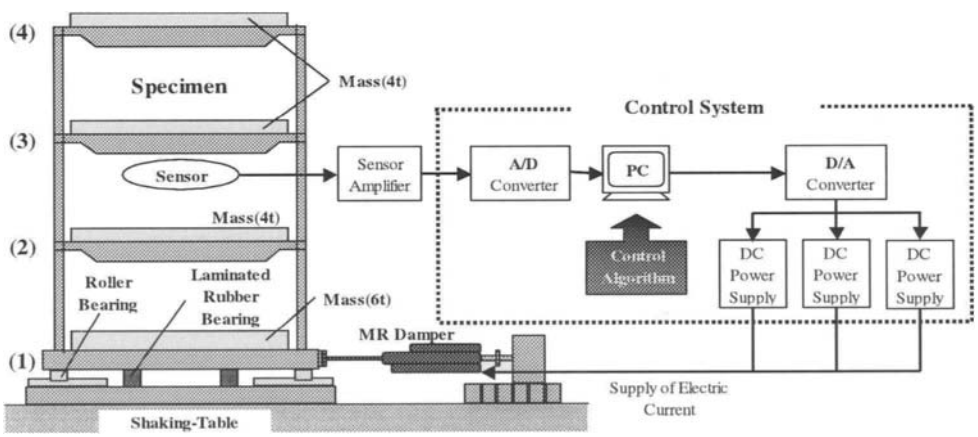


Figure 6: Control system

Control Algorithm

Although response displacements are reduced with passive dampers, response accelerations may become larger. Thus, the following two control objectives were considered.

(1)To reduce response displacement by semi-active control as much as by a passive damper.

(2)To reduce absolute acceleration response by semi-active control to less than that achieved by a passive damper.

The second author proposed a very simple semi-active control algorithm formulated in Eqn. 1 and shown in Figure 7, which aims the above two control objectives (Shiozaki et al. (2002)), by considering the base-isolated structure to be a one-degree-of-freedom system. In Eqn. 1, F is force of MR damper, k is the stiffness of base-isolation, u is relative displacement of base-isolation, ω is natural circular frequency, λ_{opt} is optimized constant.

$$F = \begin{cases} \mathrm{sgn}(\dot{u})k\left(\sqrt{\left(\dfrac{\lambda_{opt}\dot{u}}{\omega}\right)^2 + u^2} - |u|\right) & (u\dot{u} \geq 0) \\ k\dfrac{\lambda_{opt}\dot{u}}{\omega} & (u\dot{u} < 0) \end{cases} \tag{1}$$

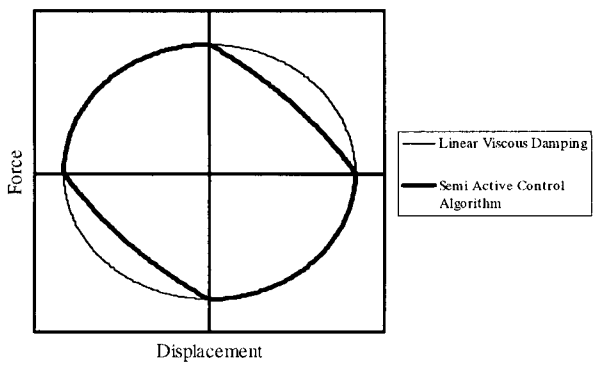


Figure 7: Concept of semi-active control

TEST RESULTS

Figures 8.1-8.3 show the maximum response accelerations of each story of test frame subjected to earthquake excitation of El Centro 1940 NS 50cm/sec, with constant electric current applied to MR damper. Applying high ampere of electric current reduced the maximum response displacements; in other hand, the maximum response accelerations became larger.

Figures 9.1-9.3 show the maximum response accelerations of each story of test frame controlled by proposed semi-active algorithm, comparing with those of passive control as shown in Figure 7. The maximum values of accelerations are reduced at about largest 20% compared with those of passive control. The RMS values of accelerations are reduced at about largest 30% compared with those of passive control. The efficacy of the proposed semi-active control is sufficiently demonstrated.

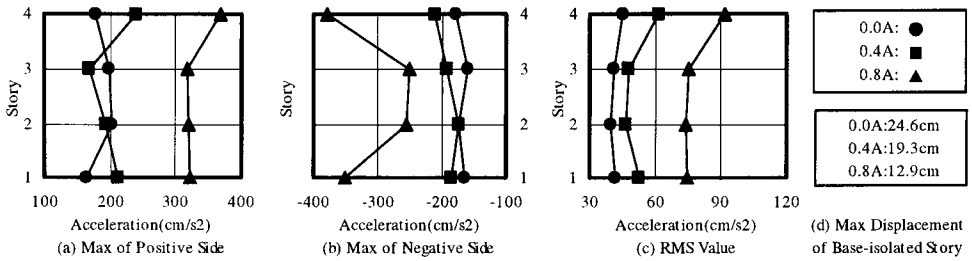


Figure 8.1: Response Acceleration of each story in comparison among three constant electric current values of 0.0A, 0.4A, 0.8A (El Centro 1940 NS 50cm/sec)

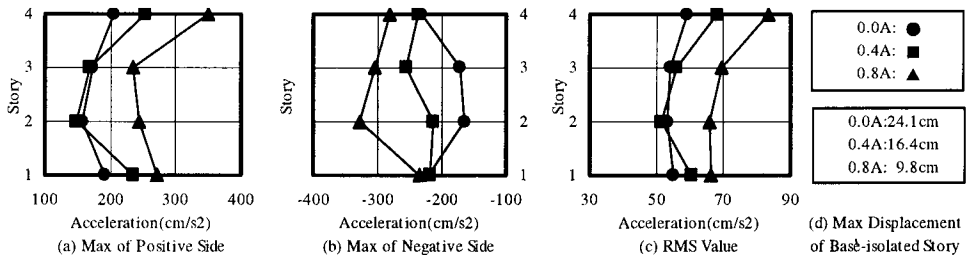


Figure 8.2: Response Acceleration of each story in comparison among three constant electric current values of 0.0A, 0.4A, 0.8A (Hachinohe 1968 NS 50cm/sec)

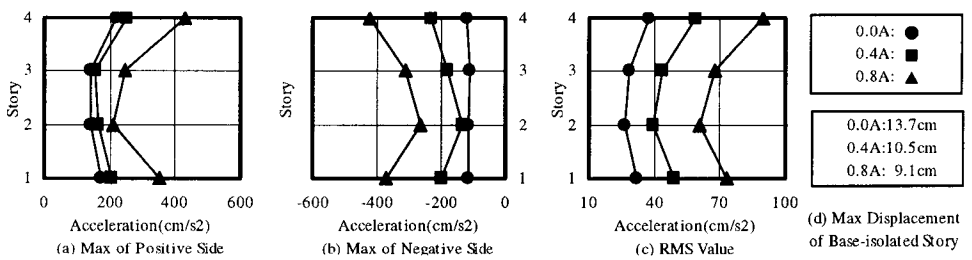


Figure 8.3: Response Acceleration of each story in comparison among three constant electric current values of 0.0A, 0.4A, 0.8A (JMA Kobe 1995 NS 50cm/sec)

CONCLUSIONS

The MR fluid showed the good results in the point of view that the force-displacement relationship of the MR damper is like rigid-plastic characteristics caused by friction force. The basic viscosity is low enough so that the MR damper generates small force without electric current. Authors have to evaluate the performance of the MR fluid to resist against the settlement of articles.

MR damper developed for this large-scale test showed the good results, too. The force-displacement relationship shows that the MR damper responds quickly to the inversion of the movement of the piston.

The maximum values of response accelerations are reduced by proposed semi-active control at about largest 20% compared with those of passive control. The RMS values are reduced at about largest 30% compared with those of passive control. The effectiveness of the semi-active control for the passive control was clarified.

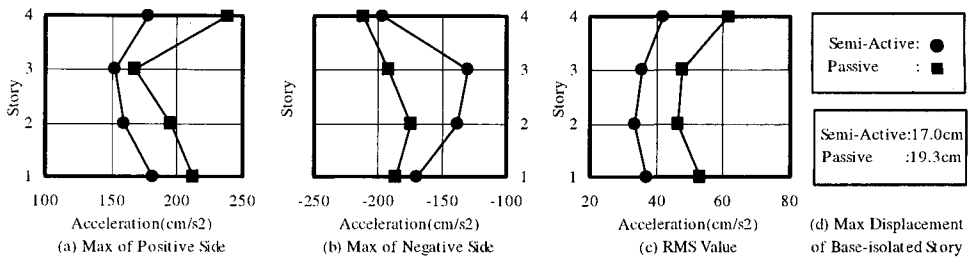


Figure 9.1: Response Acceleration of each story in comparison between proposed semi-active control and passive control (El Centro 1940 NS 50cm/sec)

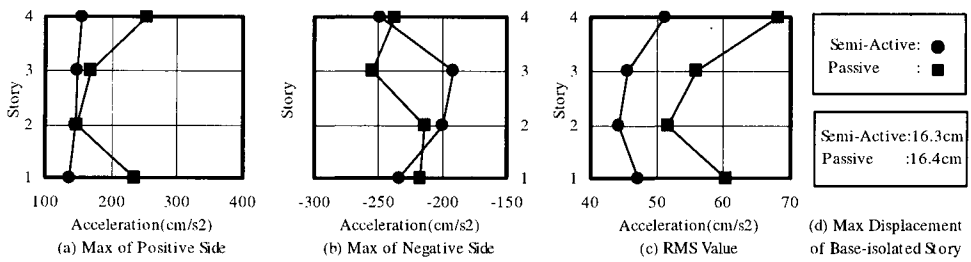


Figure 9.2: Response Acceleration of each story in comparison between proposed semi-active control and passive control (Hachinohe 1968 NS 50cm/sec)

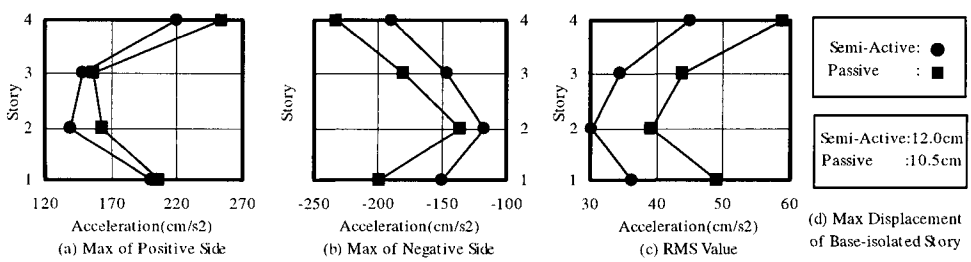


Figure 9.3: Response Acceleration of each story in comparison between proposed semi-active control and passive control (JMA Kobe 1995 NS 50cm/sec)

Acknowledgement

This work has been carried out under the US-Japan cooperative structural research project on Smart Structural Systems. The authors wish to thank the members of ER/MR working group of the project for their fruitful discussions and thank Mr. Chikahiro Minowa of NIED. This research was partly supported by 2001 Grant-in-Aid for Scientific Research (B).

References

Fujitani H., et al. (2000). Dynamic Performance Evaluation of Magneto-Rheological Damper, Proceedings of Advances in Structural Dynamics 2000, Vol.1, pp.319-326.

Otani S., et al. (2000). Development of Smart Systems for Building Structures (Invited paper), Proc.of SPIE's 7th. International Symposium on Smart Structures and Materials, Paper No. 3988-01

Shiozaki Y. et al. (2002). Study of response control by MR Damper for base-isolated building, Proc. of 3WCSC.

Advances in Building Technology, Volume 1
M. Anson, J.M. Ko and E.S.S. Lam (Eds.)
© 2002 Elsevier Science Ltd. All rights reserved

STRUCTURAL HEALTH MONITORING SYSTEM USING SUPPORT VECTOR MACHINE

Hiromi Hagiwara and Akira Mita

Department of System Design Engineering, Keio University
3-14-1 Hiyoshi, Kohoku-ku, Yokohama 223-8522, Japan

ABSTRACT

A structural health monitoring system for a building structure utilizing Support Vector Machine (SVM) is proposed. The SVM is a new machine learning technique for pattern recognition. In our proposed system, modal frequencies of a structure are used for pattern recognition. As our system does not require modal shapes, typically only two vibration sensors detecting an input signal and an output signal for a structural system are enough to define damage. Changes in moral frequencies normalized by original modal frequencies before suffering any damage are used as feature vectors for feeding into the SVMs. The proposed system is capable of identifying the damaged locations even when multiple stories suffered damages.

KEYWORDS

Damage assessment, support vector machine, health monitoring, machine learning, modal frequency

1. INTRODUCTION

Many methods and approaches for health monitoring of a structure have been proposed targeting at reducing the maintenance cost or improving the structural performance. In those methods or approaches, one of the critical issues is the number of sensors available for monitoring. Though it is theoretically possible to obtain the detailed health information of a structure using unlimited number of sensors, it is not the case for most practical situations. The possible financial allocation for a structural health monitoring system is not so large and should be lower than the expected merit by introducing the system. For example, there is little rationale at this point to install a health monitoring system that measures acceleration of all floors.

The purpose of this study is to propose a new structural health monitoring system that can obtain the detailed damage information from the minimum number of sensors by utilizing the SVM. The feature vectors fed to the SVMs are formed based on the physical relationship between damages and modal frequency changes. The relationship is established by a sensitivity analysis.

2. SUPPORT VECTOR MACHINE

The Support Vector Machine (SVM) is a mechanical learning system introduced by Vapnik and his co-workers. The SVM uses a hypothesis space of linear functions in a high dimensional feature space[1), 2)]. The simplest SVM model is the so-called Linear SVM (LSVM). It works only for the case where data are linearly separable in the original feature space. Hence, applicable problems in the real-world are limited. In the early 1990s, nonlinear classification in the same procedure as LSVM became possible by introducing a nonlinear function called a kernel function, without being conscious of the mapped high-dimensional space. The machine extended to nonlinear feature spaces is called Nonlinear SVM (NSVM).

In what follows, we assume a training sample S consisting of vectors $\boldsymbol{x}_i \in R^n$ with $i = 1,...,N$.

$$S = ((\mathbf{x}_1, y_1),...,(\mathbf{x}_N, y_N)) \tag{1}$$

Each vector $\boldsymbol{x}_i$ belongs to either of two classes and thus is given a label $y_i \in \{-1,1\}$. The pair of $(\boldsymbol{w},b)$ defines a hyper-plane of equation

$$(\mathbf{w} \cdot \mathbf{x}) + b = 0 \tag{2}$$

This hyperplane is named separating hyperplane (see Fig.1 (a)).

We now need to establish the optimal separating hyperplane (OSH) that divides S leaving all the points of the same class on the same side while maximizing the margin which is the distance of the closest point of S (see Fig.1 (b)). This closest vector $\mathbf{x}_i$ is called the support vector.

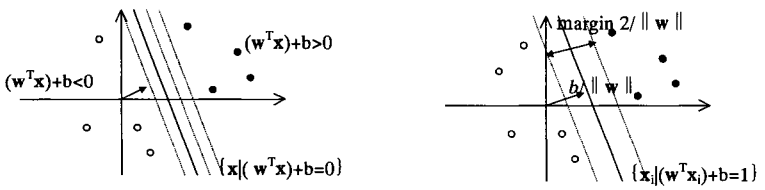


Figure 1: (a) separating hyperplane (b) OSH (the dashed lines in (b) define the margin)

For the reasons mentioned above, the OSH $(\boldsymbol{w},b)$ can be determined by solving an optimization problem defined by

$$\begin{aligned} &\text{minimize} \quad \text{margin } d(\mathbf{w}) = \frac{1}{2}(\mathbf{w} \cdot \mathbf{w}), \\ &\text{subject to} \quad y_i((\mathbf{w} \cdot \mathbf{x}_i) + b) \geq 1, \quad i = 1,2,...,N \end{aligned} \tag{3}$$

The resulting SVM is called Hard Margin SVM. However, applicable problems are still limited. In order to relax the situation, we allow a small number of misclassified feature vectors. The previous analysis (Eqn.3) is generalized by introducing N nonnegative variables $\xi = (\xi_1, \xi_2, ..., \xi_N)$ such that

$$\begin{aligned} &\text{minimize} \quad \text{margin } d(\mathbf{w}) = -\frac{1}{2}(\mathbf{w} \cdot \mathbf{w}) + C\sum \xi_i, \\ &\text{subject to} \quad y_i((\mathbf{w} \cdot \mathbf{x}_i) + b) \geq 1 - \xi_i, \quad i = 1,2,...,N, \ \xi \geq 0. \end{aligned} \tag{4}$$

This SVM defined by Eqn. 4 is called Soft Margin SVM. The purpose of the term $C\Sigma\ \xi_i$, where the

sum is for i=1,2, ...,N is to keep under control the number of misclassified vectors. The parameter C can be regarded as a regularization parameter. The OSH tends to maximize the minimum distance $1/w$ for small C, and minimize the number of misclassified vectors for large C.

We described the case of linear decision surfaces in the above. To allow much more general decision surfaces, we have to introduce nonlinear transformation to a set of original feature vectors $\boldsymbol{x}_i$ into a high-dimensional space by a map $\mathbf{F}:\mathbf{x}_i \mapsto \mathbf{z}_i$ as in Fig. 2. Then a linear separation becomes possible in the high-dimensional space there. However the computation of inner products $(\mathbf{F}(\mathbf{x})\cdot\mathbf{F}(\mathbf{x}_i))$ in a high-dimensional space is prohibitively time-consuming. Therefore, we are interested in cases where these expensive calculations can be significantly reduced by using a kernel function which satisfies the Mercer's theorem such that

$$(\mathbf{F}(\mathbf{x})\cdot\mathbf{F}(\mathbf{x}_i)) = K(\mathbf{x},\mathbf{x}_i) \tag{5}$$

The polynomial kernel and the Gaussian kernel are typical kernel functions. Each kernel function is shown in the following formula.

$$K(\mathbf{x},\mathbf{x}_i) = (\mathbf{x},\mathbf{x}_1)^d \quad \text{(polynomial kernel)} \tag{6}$$

$$K(\mathbf{x},\mathbf{x}_i) = \frac{\exp(-\|\mathbf{x}-\mathbf{x}_1\|)^2}{\sigma} \quad \text{(Gaussian kernel)} \tag{7}$$

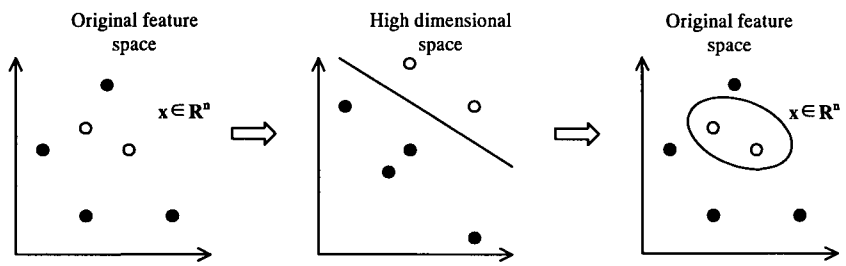


Figure 2: Nonlinear SVM

3. DAMAGE DETECTION IN A BUILDING USING SVM

3.1 Relation between stiffness change and natural frequency change

A natural frequency change associated with a certain mode does not provide any spatial information of any structural damage. However, multiple natural frequency changes may provide the information on the location of damaged stories.[3), 4)]

In a multi-mass shear system shown in Fig.3, the equilibrium equation for an undamped structure is given by

$$\left(-\omega_r^2[M]+[K]\right)\{\phi\}_r = \{0\} \tag{8}$$

where r = 1,2, ...,N, $[M]$ and $[K]$ = mass and stiffness matrices, respectively. $\{\phi\}_r$ = r-th mode shape corresponds to the natural frequency ω_r and is normalized by $\{\phi\}_r^T[M]\{\phi\}_r = 1$.

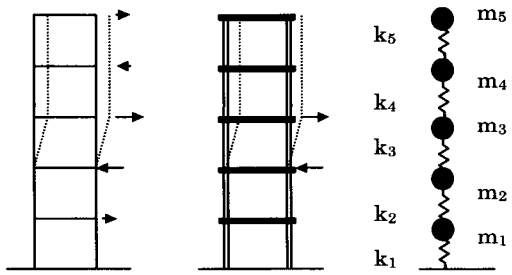


Figure 3: Multi-mass shear system

The sensitivity coefficient of the r-th natural frequency in terms of k_{ij} is defined by the derivative of Eqn.8 with respect to k_{ij} [3].

$$\frac{\partial \omega_r}{\partial k_{ij}} = \frac{1}{2\omega_r} \{\phi\}_r^T \frac{\partial [K]}{\partial k_{ij}} \{\phi\}_r \tag{9}$$

If we take into consideration the symmetry of stiffness matrix, the sensitivity coefficients of the natural frequencies can be rewritten as

$$\frac{\partial \omega_r}{\partial k_{ij}} = \begin{cases} \frac{1}{\omega_r} \phi_{ir} \phi_{jr}, & i \neq j \\ \frac{1}{2\omega_r} \phi_{ir}^2, & i = j \end{cases} \tag{10}$$

where $\{\phi\}_{ir}$ is i -th component of the r-th mode.

This equation for the natural frequencies may be expanded into first-order Taylor's series. The resulting series represents the change in natural frequency as

$$\Delta \omega_r = \sum_{i=1}^{N} \sum_{i=1}^{N} \frac{\partial \omega_r}{\partial k_{ij}} \Delta k_{ij} \tag{11}$$

For the multi-mass shear system, when the i-th story stiffness is reduced, only k_{ii}, $k_{(i-1)(i-1)}$, $k_{i(i-1)}$ and $k_{(i-1)i}$ are altered in the stiffness matrix. Hence, Eqn.11 is simplified into

$$\frac{\Delta \omega_r}{\omega_r} = \frac{\Delta k_i}{2\omega_r^2} \left(\phi_{ir} - \phi_{(i-1)r}\right)^2 \tag{12}$$

We define the i-th vector of natural frequency change associated with the i-th story stiffness change in Eqn.12 as.

$$\{\gamma_i\} = \left[\frac{\Delta \omega_{1i}}{\omega_1}, \frac{\Delta \omega_{2i}}{\omega_2}, \ldots, \frac{\Delta \omega_{Ni}}{\omega_N} \right] \quad (i = 1,2,\cdots,N) \tag{13}$$

where $\Delta \omega_{ri}$ is i–th component of the r-th natural frequency. The vectors have typical patterns depending on the location of damaged story. In this study, the above vectors of natural frequency change are used as the basis of feature vectors.

Under the assumption that the 5-mass shear system model consists of the same stiffness and the same mass at each story, vectors defined by Eqn. 13 are typically plotted in Fig.4. The stiffness of each story is varied from 95% to 15% of the original stiffness for simulating damages. From Fig.4, we could observe the vectors are showing characteristic shapes depending of the location of damage. This fact indicates us recognition of damage location may be possible from these vectors.

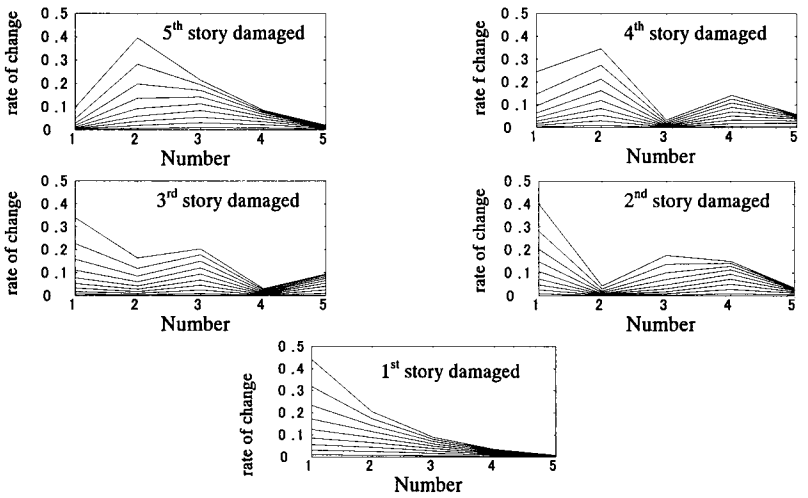


Figure 4: Basis of feature vectors

3.2 Support vector machines for 5-story building

The number of classes that should be distinguished by the SVMs is 6. Therefore, we need six SVMs defined by undamaged (SVM0), 1st story damaged (SVM1), 2nd story damaged (SVM2), 3rd story damaged (SVM3), 4th story damaged (SVM4) and 5th story damaged (SVM5). The feature vector is slightly modified from the vector defined by Eqn. 13. The vector is normalized so that the minimum component is set to zero. As the feature vectors can not be classified using LSVM, a Gaussian kernel function is used to introduce the NSVM. In addition, slack variables are used for softening the condition.

The parameters to be determined for each NSVM are σ as in Eqn.7, and C as in Eqn.4. These parameters are determined to minimize misclassified data. The list of the parameters used for SVM is shown in Table.1. The *l-o-o* (leave-one-out bounds) shown in Table.1 represents the probability that the data does not exist in a margin ($0<f<1$). Thus, after tuning the SVM to classify the data into two classes by the boundary of $f=0$ (correctness=100%), discernment accuracy becomes good as *l-o-o* is close to 100%. The column SV represents the number of support vectors. It is observed that about half of the training feature vectors should be used as support vectors for each classification.

The SVM0 that classifies the data of undamaged structure is shown in the top of Table 1. This SVM can be used to know whether any damage exists in the structure. The SVM5 shown in the next line of Table 1 classifies the data with some damage in the 5th story. Therefore, this SVM finds the case when the damage is expected in the 5th story. Other SVMs have similar meaning.

TABLE 1
SVM FOR DAMAGE DETECTION OF THE 5-STORY BUILDING

SVM	σ	C	SV	l-o-o[%]
SVM0	60	20	21	88.5
SVM5	90	90	45	81.3
SVM4	90	80	48	83.3
SVM3	90	80	47	82.3
SVM2	90	80	48	86.5
SVM1	90	80	48	78.1

3.3 Performance evaluation

In the following, ■ indicates it is damaged. ▒ it may be damaged, and ■ it is undamaged. By observing outputs from each SVM (as shown Fig.5 (b)), we can judge whether the structure is damaged or not. And if it is damaged, the SVM will tell the location. Moreover, the magnitude of an output represents the distance from the margin.

The performance of SVMs was tested using 46 feature vectors generated by a simulation. In Fig.5, The data No. 1 is for an undamaged structure. The next 9 data (No.2~10) are those with damage in the 1st story. The story stiffness is reduced to 95% to 15% of the original stiffness with a pitch of 10%. The next 9 data are similarly for the 2nd story damage. The last 9 data are for the 5th story damage.

The SVM0 is observed to give correct outputs for all data sets. However, SVM2 to SVM5 failed to give correct outputs for the damage with 95% stiffness. In addition, the outputs are in the margin for 35%, 25%, 15% stiffness data sets.

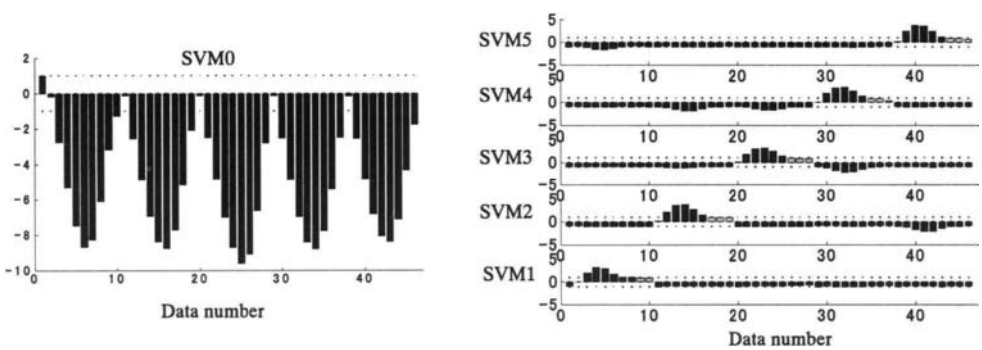


Figure 5: Damage detection using simulated data

Using the SVMs taught for single story damage, the possibility of detecting the damage in multiple stories was evaluated. Assuming both the 3rd story and the 5th story are damaged as listed in Table 2, outputs from the SVMs were plotted in Fig. 6. The outputs shown in Fig.6 indicate that the proposed

SVMs can detect the multiple damages. However, accuracy is less for small stiffness reduction and for very large stiffness reduction as was the case for single damage story.

TABLE 2
DATA NUMBER FOR CASES WITH DAMAGE IN 3RD AND 5TH STORIES

The 3rd story \ The 5th story	$0.9k_0$	$0.8k_0$	$0.7k_0$	$0.6k_0$	$0.5k_0$
$0.9k_0$	No.1	No.2	No.3	No.4	No.5
$0.8k_0$	No.6	No.7	No.8	No.9	No.10
$0.7k_0$	No.11	No.12	No.13	No.14	No.15
$0.6k_0$	No.16	No.17	No.18	No.19	No.20
$0.5k_0$	No.21	No.22	No.23	No.24	No.25

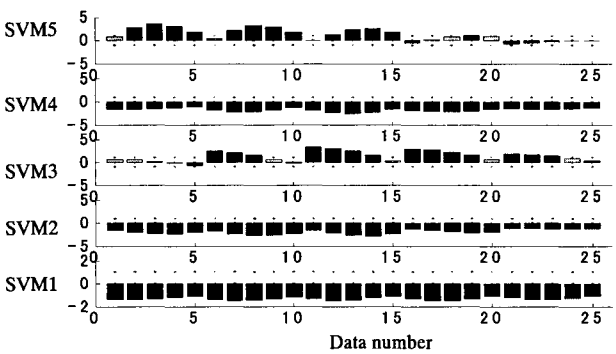


Figure 6: SVM outputs for damaged structure in 3rd and 5th stories

4. EXPERIMENTAL VERIFICATION

A series of experiments were performed to verify the performance of our proposed approach. The model structure is depicted in Fig. 7(a). The damage was introduced by replacing columns by weak columns. By replacing two columns (Fig. 7(b)), the story stiffness is reduced to 60% of the original stiffness. Although acceleration sensors are installed at all stories, only the top sensor and the bottom sensor were used for obtaining modal frequencies. The modal frequencies were calculated from time histories of the vibration experiment by applying the subspace identification method.

Fig.8 shows the outputs from the SVMs. Fig. 8 (a) shows the results for cases with single story damage. Fig. 8 (b) gives the results for cases in which two stories are damaged. The combinations are (0, 0)(no damage), (1st,2nd), (1st,3rd), (1st,4th), (1st,5th), (2nd,3rd), (2nd,4th), (2nd,5th), (3rd,4th), (3rd,5th), (4th,5th). From these figures, we may conclude that the method is indeed applicable to realistic problems. However, the existence of uncertainty due to the sensor noises degraded the accuracy compared to the simulated ones.

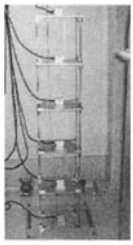
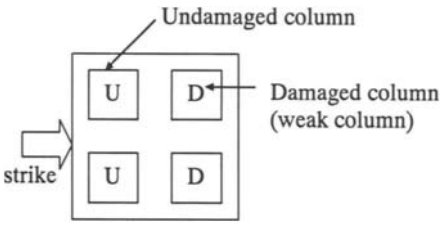
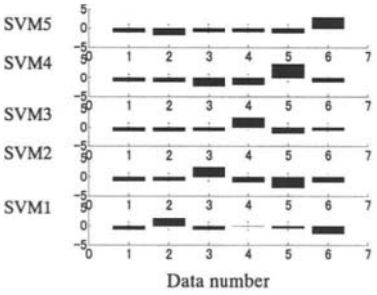


Figure 7: (a) Model structure



(b) Plan of damaged story
(Story stiffness is 60% of the original)



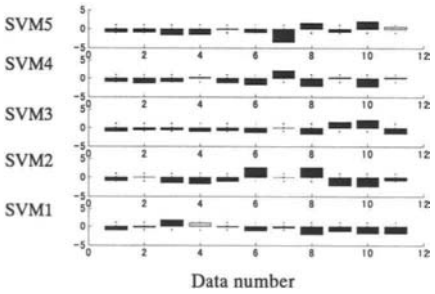


Figure 8: (a) Single story damage

(b) 2 stories damage

5. CONCLUDING REMARKS

A structural health monitoring system for a building structure utilizing Support Vector Machine (SVM) was proposed. The proposed system uses modal frequencies of a structure as feature vectors fed to the SVMs for pattern recognition. As our approach does not require modal shapes, minimum number of sensors is necessary for detecting the damage. Typically only two vibration sensors detecting an input signal and an output signal for a structural system are enough to define modal frequencies. The SVMs taught by the data with single damage in a story was found to be also capable of detecting the damage in multiple stories.

6. REFERENCES

1) Vapnik, V.N. (1995). *The Nature of Statistical Learning Theory*, Springer.
2) Christianini, Nello and John Shawe-Taylor (200). *An Introduction to Support Vector Machines*.
3) Zhao, J. and T. DeWolf (1999). Sensitivity Study for Vibrational Parameters Used in Damage Detection. *J. of Structural Engineering, ASCE*, vol.125, NO.4,410-416.
4) Morita, K., M. Teshigawara, H. Isoda, T. Hamamoto and A. Mita (2001). Damage Detection Tests of Five-Story Frame with Simulated Damages. *Proc. of the SPIE* vol.4335, Advanced NDE Methods and Applications.

Advances in Building Technology, Volume 1
M. Anson, J.M. Ko and E.S.S. Lam (Eds.)
© 2002 Elsevier Science Ltd. All rights reserved

PERFORMANCE OF STRUCTURES WITH PASSIVE DAMPERS SUBJECT TO NEAR-FAULT EARTHQUAKES

W. L. He[1] and A.K. Agrawal[2]

Graduate Student Researcher[1] and Assistant Professor[2], Department of Civil Engineering, The City College of New York, New York, NY 10031.

ABSTRACT

In this paper, performance of passive viscous and friction dampers subject to near-fault ground motion velocity pulses for elastic and inelastic structures has been investigated through numerical simulations. The objective of the investigation is to determine the guidelines for types of structures where a passive damper may be effective in reducing damages during a near-fault ground motion. Simulation results show that viscous dampers are most effective around $T/T_g \approx 1$ for elastic structures, whereas they are most effective for inelastic structures in range of natural periods $T/T_g < 1.0$ when both the input energy and hysteretic energy (damage) decrease and dissipated viscous energy increases. Passive friction dampers have good performance for elastic structures around $T/T_g \approx 1$ where input energy decreases and energy dissipated by the damper increases. For inelastic structures with μ=4, friction dampers have good performance in the range of for $0.3 < T/T_g < 2$.

KEYWORD: Near-fault ground motions, long period velocity pulses, passive viscous dampers, passive friction dampers, supplemental energy dissipation systems, structural response control

INTRODUCTION

The traditional approach for seismic hazard mitigation is to design structures with sufficient strength capacity and the ability to deform in a ductile manner. Such design philosophy is based on the assumption that the structure dissipates input seismic energy as hysteretic energy through damage to structural members. Observations during recent seismic destructive events show that displacement ductility ratios higher than 4 imply unacceptable levels of damage to the structure. An alternative to the traditional seismic design is the use of supplemental energy dissipation devices. The objective of using these devices is to dissipate or reduce the input seismic energy of the structures. If a structure is equipped with energy dissipation devices, the primary members of structures are expected to be protected during strong earthquakes, since a part of the energy input from ground motion will be dissipated by the supplementary energy dissipation elements. Iwan (1980) investigated the input energy dissipated due to the inelastic deformation during earthquakes by approximating the inelastic energy spectrum with an elastic structure using an equivalent viscous damping and an equivalent

natural period. The concept of input energy and energy balance in structures was systematically investigated by Uang and Bertero (1990). Fajar and Vidic (1994) constructed the E_H/E_I spectra, where E_H is the hysteretic energy (damage) and E_I is the input energy, for inelastic structures as a function of the damping, the ductility factor and the hysteretic behavior of the structures. Recently, Goel (1997) and Fu and Kasai (1998) discussed the idea of energy balance for designing supplementary passive energy devices. In this paper, the energy transfer between supplemental energy dissipation devices and hysteresis actions in structural members, and the performance of supplemental energy dissipation devices in preventing damage to the structural members is investigated.

MATHEMATICAL FORMULATION

Consider a single-degree-of-freedom (SDOF) system with the governing equation

$$\ddot{x}(t)+2\zeta\omega\dot{x}(t)+f_r(x)+u=-\ddot{x}_g(t) \tag{1}$$

where $x(t)$, $\dot{x}(t)$ and $\ddot{x}(t)$ are the relative displacement, velocity and acceleration of the structure, respectively, ζ is inherent viscous damping ratio, ω is the natural frequency of the structure, $f_r(x)$ is the restoring force per unit mass (e.g., $f_r(x)=\omega^2 x$, if the structures is in elastic range), u is unit mass control force, and $\ddot{x}_g(t)$ is the earthquake ground motion. For passive energy dissipation systems that are functions of the velocity across the damper, the control force u is given as

$$u(t)=c\dot{x} \tag{2}$$

Likewise, the control force for a pure Coulomb friction damper is given is given as

$$u=\mu N(t)\,\mathrm{sgn}(\dot{x}) \tag{3}$$

where μ is the coefficient of friction and N(t) is the normal force across the damper. For passive friction dampers, N is constant and it is variable for semi-active friction dampers [e.g., He et al (2002a)]. The control force in Equations (2) or (3) is a function of structural response, which depends on the characteristics of earthquake ground motions. Therefore, the performance of passive energy dissipation devices depends on the nature of earthquake ground motions. By assuming the initial displacement and velocity of the structure to be zero, multiplying Eq.(1) by dx and integrating it from time t_0 to t_1, the energy balance from time $t_0=0$ to t_1 is obtained as

$$\left[\frac{1}{2}\dot{x}^2\right]_{t=t_1}+\left[\int_0^{t_1} f_r\dot{x}\,dt\right]+\left[\int_0^{t_1} 2\zeta\omega\dot{x}^2\,dt\right]+\left[\int_0^{t_1} u\dot{x}\,dt\right]=\left[-\int_0^{t_1}\ddot{x}_g\dot{x}\,dt\right] \tag{4}$$

The terms in brackets in the left side of equation are kinetic energy, strain energy, damping energy, and control force energy, respectively. The term in the right hand side is the input seismic energy. In Eq.(4), various energy terms are expressed in per unit mass of the structure. It is noted that the energy terms in equation (4) are for relative energy, which is inappropriate for long period structures. However, it has been pointed out by Uang and Bertero (1990) that the use of relative energy form is valid for structures in realistic period ranges. For any supplemental velocity dependent damper in Eq.(2), the fourth term in Eq.(4) is always positive definite for any positive value of c. A similar argument applies for the friction damper in Eq.(3) since $N(t) > 0$. Hence, such systems are always dissipative in nature and they continuously dissipate energy.

Consider a Single-Degrees-of-Freedom (SDOF) elastic-perfectly-plastic structure in Eq.(1) equipped linear viscous damper in Eq (2) or a friction damper in Eq. (3). For a general hysteretic energy dissipation system, the nonlinear damper force can be represented by the Bouc-Wen model,

$$u(t)=\alpha K_e x(t)+(1-\alpha)K_e u_y z(t) \tag{5}$$

where x(t) is the displacement across the damper, K_e is a reference stiffness, α is a parameter controlling post-yielding stiffness, u_y is the value of yield displacement and z(t) is a dimensionless hysteretic quantity given by

$$u_y \dot{z} + \gamma |\dot{x}(t)| z |z|^{n-1} + \beta \dot{x}(t) |z|^n - A\dot{x}(t) = 0 \tag{6}$$

where β γ n, A are dimensionless quantities that control the shape of the hysteretic loop. Equations (5) and (6) can be used to model various types of nonlinear energy dissipation systems. For example, appropriate values of parameters β, γ, n and A can be selected to model the elasto-plastic type of hysteretic loops of viscoelastic elements. For a pure Coulomb type of friction damper, the rigid plastic behavior can be simulated by assuming A = 1, α = 0, u_y a sufficiently small quantity and $K_e u_y = \mu N$. Hence, a general form of hysteretic controller that represents a wide variety of elastic-plastic behavior can be written as

$$u(t) = \varepsilon \cdot (\ddot{x}_g)_{\max} z(t) \tag{7}$$

where $\varepsilon = \left| u / \ddot{x}_{g\,\max} \right|$ is the ratio of magnitude of control force to the peak shaking force per unit mass generated by ground motion, and u is the magnitude of the control force.

The efficiency of the supplement energy dissipation devices depends on the structures, frequency content and energy distribution of ground motions and energy dissipation mechanism of passive dampers. Since parameters of ground motions are highly stochastic in nature, no attempt has been made to perform rigorous statistical analysis using a large samples of ground motions. Instead of using a large number of ground motions, a closed-form approximation which is demonstrated to be capable of capturing kinematic characteristics of near-fault ground motion pulses has been recently proposed by the authors [He and Agrawal (2002b)]. In this formulation, the predominant velocity pulse in near-fault ground motions has been modeled by decaying sinusoidal functions,

$$\dot{x}_g = s e^{-\zeta_g \omega_g t} \sin \omega_g \sqrt{1-\zeta_g^2}\, t \tag{8}$$

where ζ_g is the ground motion decaying factor, ω_g is the predominant frequency of the pulse of ground motions, and s is the initial amplitude of the pulse. Expressions for acceleration for the velocity pulses in Eq.(8) can be obtained by differentiating Equation (8), i.e.,

$$\ddot{x}_g = s e^{at} [a \sin bt + b \cos bt] \tag{9}$$

where the coefficient a and b are obtained as

$$a = -\zeta\ \omega_p\ ;\ b = \omega_g \sqrt{1-\zeta_g^2} \tag{10}$$

The displacement u_g of the pulse can be obtained by integrating Equation (8) as follows

$$x_g = \frac{s e^{at}}{\omega_g^2} [a \sin bt - b \cos bt] + \frac{sb}{\omega_g^2} \tag{11}$$

Makris and Chang (1998) have modeled near-fault ground motions pulses by three distinct types of pulses, e.g., Type A, Type B and Type C_n. The authors have investigated the pulses in several ground motions recorded during Northridge, Kobe, Turkey and Chi-Chi earthquakes, and have demonstrated that actual ground motion pulses behave like decaying sinusoidal waveforms rather than distinct types of pulses modeled by Type A, Type B and Type C_n. The correlation of the decaying sinusoidal formulation with recorded ground motions pulses has been demonstrated in He and Agrawal (2002).

In this paper, a ground motion pulse with peak acceleration of 0.5g, a decay ratio of $\zeta_g = 0.2$ and $\omega_g = 2\pi$ (i.e., $T_g = 1.0$ sec) is used to study the effectiveness of passive dampers.

STRUCTURE WITHOUT DAMPERS

A SDOF elastic-perfectly-plastic structure with inherent viscous damping ratio of 5% and the natural period of the elastic structure varying from 0.05 to 5 s subject to the velocity pulse in Eq.(8) is investigated. The plots of seismic input energy of the structure with displacement ductility μ=1, 2, 3, 4, 6 and 8 are shown in Figure 1(a). In this figure, μ=1 represents the elastic structure. The input energy of SDOF inelastic systems is approximately independent of the strength of the structure in short (i.e., T < 0.25 sec.) and long (T > 2.5 sec.) period ranges, since the plots for structures with different ductilities almost coincide. The peak of the input energy spectrum corresponds to the predominant period T_g of the ground motions and it shifts slightly towards smaller periods as the ductility is increased. Input energy increases slightly with ductility for structures with $T/T_g < 0.7$ and it decreases with ductility ratio for longer period structures.

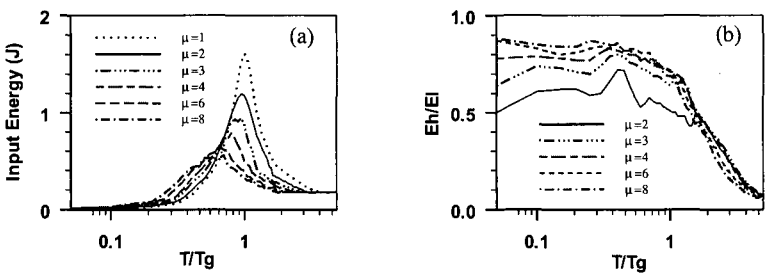


Figure 1 (a) Input Energy; (b) Eh/EI ratio of Structures Without Dampers.

The input energy is completely dissipated by viscous damping at the end of the ground motion in an elastic structure. The total input energy is partly dissipated by viscous damping mechanism and partly through hysteretic damage to the structure during inelastic deformation. Figure 1(b) shows the plots of E_H/E_I ratio for the inelastic structure with different ductilities, where E_H is the hysteretic energy of the structure and E_I is the input energy. It is observed that the E_H increases with μ from 2 to 4 and the increase in E_H (i.e., damage to the structure) is smaller for $\mu > 4$ for structure in the period range $T/T_g < 1$. The E_H/E_I ratio is approximately stable for $T/T_g < 1$ for a given ductility demand μ. This characteristics of the E_H/E_I spectra is similar to that of presented by Fajar and Vidic (1994). For structures with $T/T_g > 1$, the E_H/E_I ratio decreases gradually to zero for all displacement ductilities since the present study uses relative input energy.

EFFECTS OF PASSIVE VISCOUS DAMPER

The SDOF structures with displacement ductilities of μ=1 and 4 are assumed to be equipped with supplemental passive viscous damper in Eq. (2). Two cases of supplemental dampers are designed such that the total damping ratios (i.e., supplemental +inherent) of the structure are 15% and 30%. Such design of dampers is practical using commercially available passive dampers. Figure 2 shows input energy spectra of the structures with μ=1 and 4. It is observed from Figure 2(a) that the input energy decreases significantly as the viscous damping is increased for elastic structures of natural

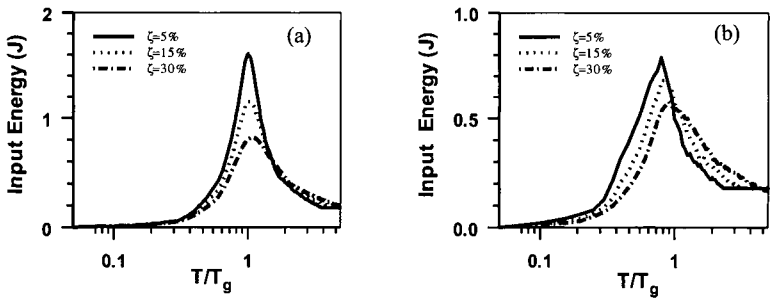


Figure 2: Input energy spectra of the structure with supplemental viscous dampers: (a) μ=1; (b) μ=4.

period around T_g, i.e., $T/T_g \approx 1$. For the inelastic structure with μ=4, it is observed from Figure 2(b) that the peak input energy without any supplemental damper is 0.8 J as compared to 1.6 J for the elastic structure. The reduction in input seismic energy for the inelastic structure without dampers is achieved at the expense of damage to the structure. An increase in damping ratio of the inelastic structure through supplemental viscous dampers has a lesser effect in reducing the peak input energy. In fact, increasing the damping ratio of the inelastic structure reduces the input energy for structures with $T/T_g < 1$ and it increases the input energy for long period structures with $T/Tg > 1.0$.

Figure 3 shows plots for hysteretic and viscous energy dissipated for the inelastic structure with μ=4 equipped with supplemental viscous damper. It is observed from Figure 3(a) that the viscous dampers are most effective in reducing hysteretic damage to the structures of natural periods $T/T_g < 1.5$. For longer period structures with periods $T/T_g > 1.5$, supplemental viscous dampers dissipate more viscous energy [as shown in Figure 3(b)] since the input energy is also increased because of addition of viscous dampers [as shown in Figure 2(b)]. They are, however, ineffective in reducing hysteretic

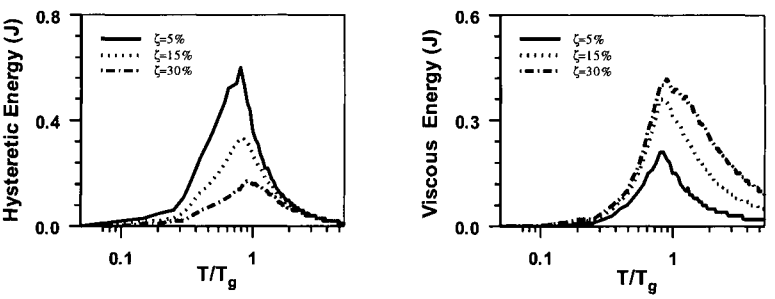


Figure 3: Hysteretic and viscous energy spectra for the inelastic structure with original displacement ductility μ=4.

damage to the longer period ($T/T_g < 1.5$) inelastic structure, as shown in Figure 3(a). Viscous dampers are most effective for structures in the range of natural periods $T/T_g < 1.0$ when both the input energy and hysteretic energy (damage) decrease and dissipated viscous energy increases.

Figure 4 shows the displacement ductility spectra of the elastic (μ=1) and the inelastic (μ=4) structures with supplemental viscous dampers. It is observed from Figure 4(a) that the supplemental viscous dampers can more effectively reduce the displacement of elastic structures in the period range 0.3< T/T_g < 2, although displacements decrease in the entire period range of $0 \leq T/T_g \leq 5$. For inelastic structures with μ = 4, supplemental viscous dampers are more effective for structures in the range of T/T_g < 1, as shown in Figure 4(b). It is further observed from Figure 4(b) that supplemental dampers with total structural damping ratio (inherent + supplemental) of 30% are capable of reducing the displacement ductility of structures with T/Tg = 0.6 from μ=4 to approximately μ=1.25, implying that the structure will undergo significantly smaller damage than the original structure. For long period structures with T/Tg > 1.0, the displacement ductility decreases to 3 and 2.5 for 15% and 30% damping ratios, respectively. The effects of supplemental viscous dampers on the acceleration of elastic and inelastic structures has also been investigated. It has been observed that the acceleration decreases for all period ranges except for a slight increase in long period ranges (T/T_g > 1) for elastic structures. For inelastic structures, an increase in damping ratio increases the acceleration of the structure in all period ranges.

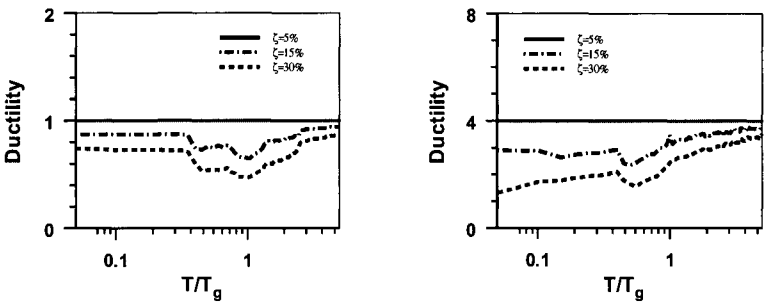


Figure 4: Displacement ductility spectra of the structure with viscous dampers: (a) elastic structure (μ=1); (b) inelastic structure (μ=4).

EFFECTS OF PASSIVE FRICTION DAMPERS

Next, a coulomb friction damper is used as a supplemental damping device in a SDOF structure with displacement ductility μ=1 and μ=4. The friction damper is installed in a building with 5% inherent viscous damping and sliding force ε =10% and 20% of the maximum seismic inertial force. Figure 5 shows input energy spectra for elastic and inelastic structures with supplemental friction dampers. It is observed from Figure 5(a) that the friction damper is effective in reducing input seismic energy significantly for T/T_g < 2 for the elastic structures. However, the input energy increases slightly for T/T_g > 2. For inelastic structures in Figure 5(b), the friction damper reduces the input seismic energy for T/T_g < 1 (more predominantly around $T/T_g \approx 1$) and it increases the input energy for T/T_g > 1. Since the energy is dissipated both by friction damper and inelastic behavior (hysteretic) of structure, a comparative study is done for the two types of hysteretic energy dissipation mechanisms in Figure 6. Fig 6(a) shows hysteretic energy dissipated by the friction damper for both elastic and inelastic structures. For the elastic structure, significant amount of hysteretic energy is dissipated by the friction damper. However, the hysteretic energy doesn't increase significantly by increasing the friction force from ε = 10% to 20%. This may happen because of sticking in the friction damper at the higher friction force. For the inelastic structure, a higher amount of energy is dissipated by the larger frictional force. Figure 6(b) shows the energy dissipated because of inelastic behavior of the structure. It is observed that the hysteretic energy (damage) decreases drastically as friction force is increased,

clearly indicating a lesser degree of damage in the structure using a larger friction force. The friction damper is more effective in reducing hysteretic damage to the structure for $0.3 < T/T_g < 2$.

Figure 7(a) and (b) show displacement ductility spectra for elastic (μ=1) and inelastic (μ=4) structures. For a comparative study, ductility spectra for viscous dampers with total damping of 15% and 30% are also shown in these figures. It is observed from Figure 7(a) that friction dampers are more effective than viscous dampers for long period elastic structures. For inelastic structures (μ=4), while friction

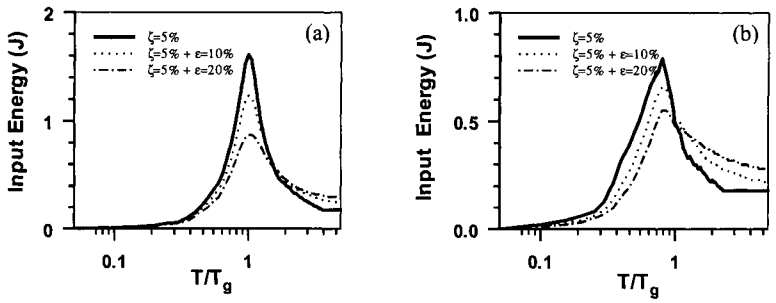


Figure 5: Input Energy spectra of structure with friction damper: (a) elastic structures (μ=1); (b) Inelastic structures (μ=4).

dampers are effective over the period range of $0.2 < T/T_g < 5$, viscous dampers are more effective for $T/T_g < 1$. Through acceleration spectra for elastic and inelastic structures for both friction damper and viscous dampers, it has been observed that acceleration of structures with friction damper is generally higher than those of structure with viscous dampers.

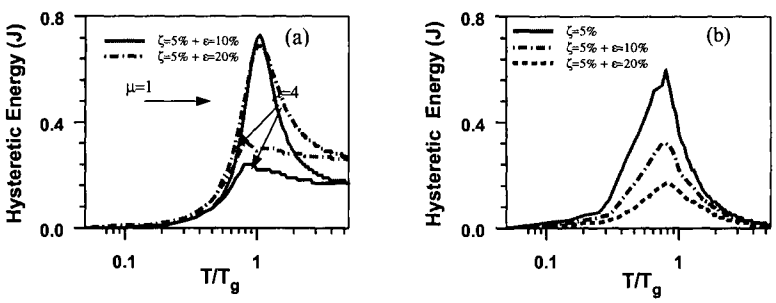


Figure 6: Hysteretic energy dissipated by: (a) Friction damper; (b) Structural damage (μ=4).

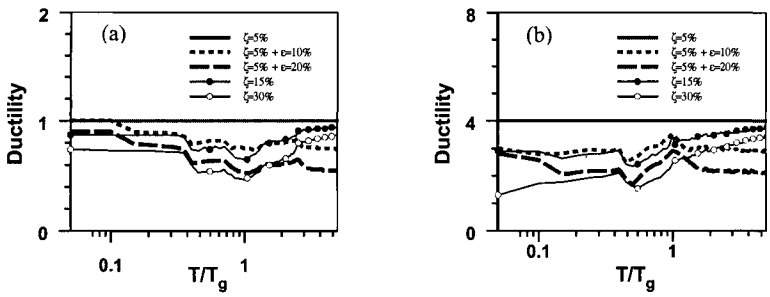


Figure 7: Displacement ductility spectra of the structure with friction dampers: (a) Elastic structure (μ=1); (b) Inelastic structure (μ=4).

CONCLUSIONS

In this study, the performance of the supplemental energy dissipation devices for a SDOF elastic or elastic-perfectly-plastic structure subject to near-fault velocity pulses is investigated. By adding the supplement energy dissipation devices, the input energy and the hysteretic energy dissipated by the structure, which is directly related to the damage of the structure, as well as the displacement ductility are investigated in detail. For elastic structure, viscous dampers are most effective around $T/T_g \approx 1$, whereas they are most effective for inelastic structures in range of natural periods T/Tg < 1.0 when both the input energy and hysteretic energy (damage) decrease and dissipated viscous energy increases. Passive friction dampers have good performance for elastic structures around $T/T_g \approx 1$ where input energy decreases and energy dissipated by the damper increases. For inelastic structures with μ=4, friction dampers have good performance in the range of for 0.3 <T/T_g <2. The present investigation is a preliminary effort to address the design of passive supplement dampers from input seismic energy point of view. More detailed investigation, including the verification using actually recorded ground motion is underway and it will be reported in future publications.

ACKNOWLEDGMENT

The research presented in this paper is sponsored by the Grant Number CMS 0099895 by the National Science Foundation.

REFERENCES

Fajfar P and Vidic T. (1994), Consistent inelastic design spectra: hysteretic and input energy. *Earthquake Engineering and Structural Dynamics*, **23**, 523-532.

Fu, Y. and Kasai, K. (1998). Comparative study of frames using viscoelastic and viscous dampers. *J. Struct. Eng.*, **124:5**, 513–552.

Goel, R. K. (1997). Seismic response of asymmetric systems: Energy based approach. *J. Struct. Eng.*, **123:11**, 1444–1453.

He, W.-L. and Agrawal, A.K. (2002a). A Novel Semi-Active Friction Controller for Linear Structures Against Earthquakes. Accepted for publication in *Journal of Structural Engineering*, ASCE.

He, W.-L. and Agrawal, A.K. (2002b). A closed-form approximation of near-fault ground motion pulse for flexible structures. Submitted to ASCE *Journal of Engineering Mechanics*.

Iwan, W. D. (1980). Estimating inelastic response spectra from elastic spectra. *Earthquake Eng. Struct. Dyn.* **8**: 375–388.

Uang C.M., Bertero V.V. (1990), Evaluation of seismic energy in structures. *Earthquake Engineering and Structural Dynamics*. **19**: 77-90.

Advances in Building Technology, Volume 1
M. Anson, J.M. Ko and E.S.S. Lam (Eds.)
© 2002 Elsevier Science Ltd. All rights reserved

RELIABILITY AND CONTROL PERFORMANCE VERIFICATION OF AN ACTUAL SEMI-ACTIVE STRUCTURAL CONTROL SYSTEM

Narito KURATA

Kobori Research Complex, Kajima Corporation,
KI Building, 6-5-30, Akasaka, Minato-ku, Tokyo 107-8502, Japan

ABSTRACT

In the past 15 years, active and semi-active structural control systems have been applied to actual buildings and bridges. However, a reliability of these systems was not discussed enough in previous stages. This can be secured by a system's health monitoring function and a fail-safe function in unpredicted emergency cases. In this paper, the reliability and control performance about the following practice are presented. After the theoretical and experimental study, a semi-active structural control system using a continuous-variable semi-active hydraulic damper with a maximum damping force of 1,000 kN, was applied to an actual 5-story building in 1998. A consideration of health monitoring for the system, fail-safe function, treatment at the time of power failure and trouble of the sensor, control device, computer and communication system, etc., are required. A forced vibration test was carried out to recognize the required functions. These results show the effectiveness of system's functions. Finally, it is presented that the reliability of the system will be secured as well as the control performance.

KEYWORDS

semi-active structural control, semi-active hydraulic damper, reliability, fail-safe, health monitoring, power failure

INTRODUCTION

In the semi-active structural control systems, a large control force can be obtained only by adjusting the characteristics of the control device itself with a small external energy supply. This enables a structural control system to be realized that is highly effective over the range from small to large earthquakes, and that is highly reliable and economical. With this in mind, the research of a semi-active control has been carried out actively from the middle of the 1990's (Kobori, 2000; Spencer, 2000; Soong and Spencer, 2000). For example, Kurata et al. (1998) and Matsunaga et al. (1998) have developed a semi-active hydraulic damper with a maximum damping force of 2000 kN and demonstrated the effectiveness of this semi-active control system through simulation analyses of a semi-actively controlled building in severe earthquakes. Spencer, Jr. et al. (1996, 1998) proposed a Magneto-rheological (MR) fluid damper for the semi-active structural control and developed a full-scale damper. Dyke et al. (1996) and Jansen and Dyke (2000) developed a control algorithm for investigating the use of the MR dampers. Furthermore, there have been three applications of an on-off variable hydraulic device to two actual buildings (Kobori et al. 1991; Kobori, 2000) and a bridge (Patten et al. 1999), and an application of a multi-stage variable hydraulic damper to a base isolated building (Yoshida and Fujio, 2000).

We developed a continuously variable semi-active hydraulic damper (SHD) that can produce a maximum damping force of 1000 kN with an electric power of 70 watts, and installed it with a computer system in an actual five-story building in 1998 (Kurata et al. 1999, 2000; Kurata, 2001) after basic studies (Kurata et al. 1994, 1998). This was the world's first application of the semi-active structural control system to civil structure in terms of the following two points.

(i) Application of a continuously variable semi-active control device;

(ii) Full support for large earthquakes. It satisfied the following criteria for an input motion equivalent to the "large earthquake" referred in design of high-rise buildings in Japan. Here, the criteria are that the structures should be elastic and that the story drift angle should be within 1/200.

For this application, consideration of health monitoring for the system, fail-safe function, treatment at the time of power failure and trouble of the sensor, control device, computer and communication system, etc., are required. In this paper, the reliability of this semi-active structural control system is discussed. Detail of a system's health monitoring system and a fail-safe semi-active control are described. After the system installation, a forced vibration fail-safe test for the building with semi-active control was carried out. In the test case, the electrical power supply for the 1st floor SHDs was cut off during the semi-active control in the forced vibration. These results show the effectiveness of system's fail-safe functions. Finally, it is presented that the reliability of the system will be secured as well as the control performance.

SEMI-ACTIVE STRUCTURAL CONTROL SYSTEM

The office building in which the SHD system is installed is a five-story steel structure with PC curtain walls and a basement, and it is located in Shizuoka City, Japan. A configuration of the SHD system is shown in Figure 1. The system consists of velocity sensors, SHDs, computers and an uninterruptible power supply unit. The sensors, which are placed on each floor, measure the absolute acceleration and are able to output the absolute velocity by the analog integration. The eight SHDs are installed transversely between a steel brace and a beam on each story from the first to the fourth on both gable sides. The computers are placed in the control room on the first floor. The elasto-plastic steel dampers are installed in the longitudinal direction.

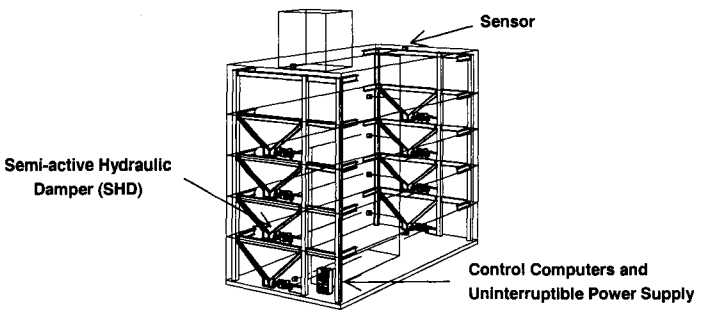


Figure 1: Semi-active damper system configuration

A full-size SHD that can produce a maximum damping force of 1000 kN with an electric power of only about 70W has been developed (see Figures 2 and 3). It is compact and requires no special installation space, so the required number of them can easily be installed in a building. It comprises a flow control valve, a check valve and an accumulator. A relief valve that opens at a set pressure is installed in parallel with the flow control valve, so that the load cannot cause the design stress of the SHD to be exceeded. It is activated, and this restricts the damping force to 900 kN when an excessive command is given. Furthermore, a solenoid valve that opens in case of an interruption of the electrical service is provided as a fail-safe to an unexpected system fault or power failure. When it opens, the oil flows through the orifice and the SHD works as a passive damper.

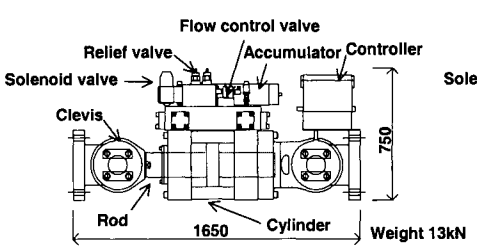


Figure 2: Outline of SHD

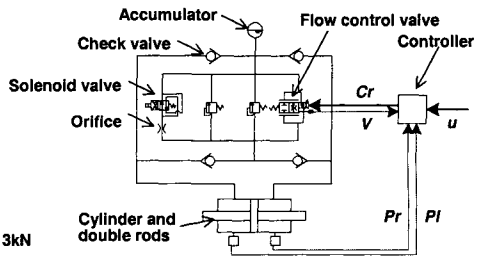


Figure 3: Hydraulic circuit of SHD

The functions of system management, control computation and command transmission are assigned to four computers in the control room on the 1st floor. It is possible to achieve real-time control with a 5-millisecond sampling time with high reliability. The control procedure is as follows: (i) the sensors measure the building's responses; (ii) the computer calculates the damping force command to minimize the response based on the measured data; and (iii) the SHDs generate the damping forces according to the computer's command. By this control procedure, the damping force is optimized and the semi-active control system can achieve a high response reduction performance that is not obtained with a passive device.

The damping force fvi of the i-th SHD can be expressed by the following equation.

$$f_{vi} = \begin{cases} f_{\max} \cdot sign(v_i) & u_i \cdot v_i > 0, \quad |u_i| > f_{\max} \\ c_{\max} \cdot v_i & u_i \cdot v_i > 0, \quad \left|\frac{u_i}{v_i}\right| > c_{\max}, \quad |u_i| \le f_{\max} \\ c_i(t) \cdot v_i = u_i & u_i \cdot v_i > 0, \quad \left|\frac{u_i}{v_i}\right| \le c_{\max}, \quad |u_i| \le f_{\max} \\ 0 & u_i \cdot v_i \le 0 \end{cases} \tag{1}$$

where u_i is the damping force command from the computer to the i-th SHD and v_i is the i-th SHD's velocity. $f_{\max}$ and $c_{\max}$ are the upper limit values of the damping force and the damping coefficient of the SHD, respectively. They were determined through a dynamic loading test (Kurata et al. 1999). The damping force command u_i is the optimal control force, which is designed to minimize the building's response by using the relative velocity feedback law based on a Linear Quadratic Regulator (LQR). The optimal control force is:

$$U(t) = \{u_i(t)\}^T = -G_{j,k} X(t) \quad , j=1,10; \; k=1,15 \tag{2}$$

where $G_{j,k}$ is the velocity feedback gain. The index j and k, which are the variable gain number, relates response level and fail-safe mode, respectively.

HEALTH MONITORING AND FAIL-SAFE SEMI-ACTIVE CONTROL

The computer system configuration is shown in Figure 4. The required function of the control system is real-time control and system management. The former contains control trigger determination, real time computation with several milliseconds and communication between the SHD and computers. The latter contains measurement of a lot of information, health monitoring of the system, fail-safe, and emergency alarm. Each function was realized by a separate computer. A control computer (Con-C) determines the damping force command to the SHD from the building's response measured by the sensors and outputs it to the communication computer (Com-C) with a sampling time of five milliseconds. One Com-C outputs the damping force command to four SHDs. A management computer (Man-C) monitors the condition of each SHD and communication situation of each computer, and

determines whether or not it is normal. If there is a fault with the system, the fail-safe function corresponding to each abnormal mode becomes effective and an alarm is sent through the telephone line to the remote computer (Rem-C) located in the Kobori Research Complex, Akasaka, Tokyo. The sampling time of the Man-C is 0.02 seconds. The remote operation of the Man-C and the starting and shutdown of the whole system can be done from the Rem-C. Furthermore, the control can be continued, even if the function of the Man-C is lost. The computers are in real time monitoring the health of the sensors, the SHDs and all communication lines. At the same time, the SHDs and the computers have a self-diagnosis function and a mutual surveillance function. It is possible to make the fail-safe function corresponding to various abnormalities work effectively by these health monitoring.

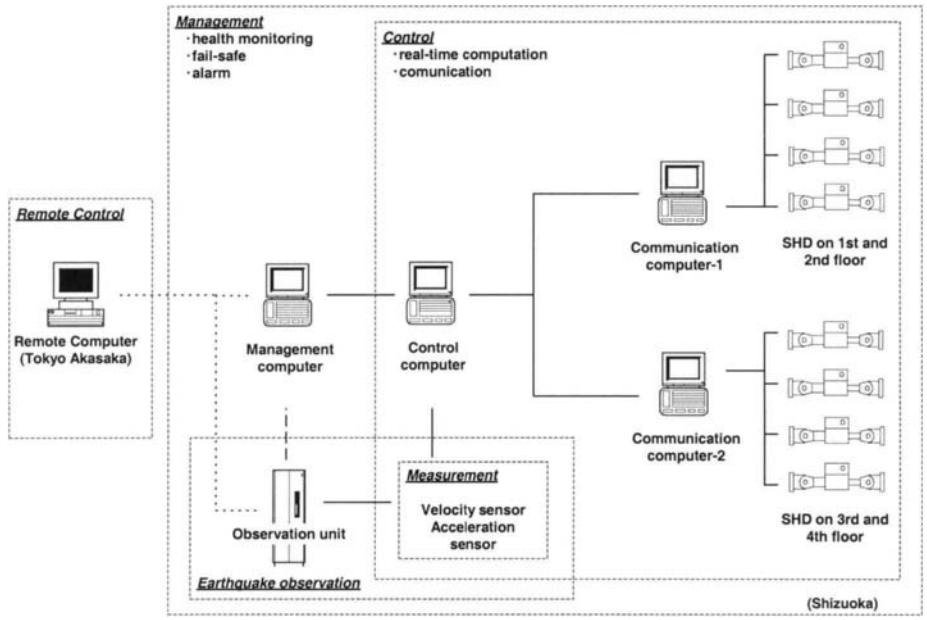


Figure 4: Computer system configuration

Waiting, control and fail-safe system modes are provided. Usually, in the waiting mode, all the SHDs function as passive dampers. Then, the semi-active control mode starts when the trigger by the control computer turns ON. Next, it returns in the waiting mode when an earthquake finishes and the trigger turns OFF. The trigger turns ON when the first floor acceleration exceeds five cm/sec^2. The fail-safe mode is set for emergency situations. Table 1 shows the semi-active control under fail-safe modes. The SHDs corresponding to an abnormal part changes to a passive damper for every floor unit and optimal semi-active çontrol using variable gains is carried out under this situation. Accordingly, this system secures high control performance as a hybrid structural control system, even if the power supply is cut off. The conditions of the SHD's hydraulic circuits are the same in the waiting mode and the fail-safe mode. However, all the SHDs are in the passive condition in the waiting mode.

TABLE 1

FAIL-SAFE SEMI-ACTIVE CONTROL

State	Number of semi-active controlled stories	Gain	Story			
			1	2	3	4
Semi-active control	4	$Gj_{,1}$	S	S	S	S
Fail-safe semi-active control	3	$Gj_{,2}$	S	S	S	P
		$Gj_{,3}$	S	P	S	S
		$Gj_{,4}$	S	S	P	S
		$Gj_{,5}$	P	S	S	S
	2	$Gj_{,6}$	S	S	P	P
		$Gj_{,7}$	S	P	S	P
		$Gj_{,8}$	S	P	P	S
		$Gj_{,9}$	P	S	S	P
		$Gj_{,10}$	P	S	P	S
		$Gj_{,11}$	P	P	S	S
	1	$Gj_{,12}$	S	P	P	P
		$Gj_{,13}$	P	S	P	P
		$Gj_{,14}$	P	P	S	P
		$Gj_{,15}$	P	P	P	S
Passive control	–	–	P	P	P	P

FORCED VIBRATION FAIL-SAFE TEST

A forced vibration fail-safe test for the building using an exciter was carried out to recognize an actual fail-save functions of this system. A large-scale synchronous exciter with a maximum force of 100 kN was used. This exciter generates a sinusoidal force by rotating two pairs of eccentric masses. It was placed at the center of the building's roof floor, and a transverse forced excitation was applied. The tests were carried out under a constant excitation force amplitude. Displacement sensors were placed transversely on each floor from the basement to the roof at both ends. In addition, sensors for semi-active control were placed in each floor as shown in Figure 1. For each SHD, the damping force command u, the hydraulic pressures Pl and Pr at the inside left and right parts of the cylinder, and the actual valve opening V of the flow control valve and the control current Cr, shown in Figure 3, were measured. A constant harmonic excitation force of 16 kN with a frequency of 1.46 Hz was applied to the semi-active controlled building. In the test case, the electrical power supply for the 1st floor SHDs was cut off during the semi-active control in the forced vibration. The damping force and the valve opening of the SHD located on the 1st and 3rd floor, and the velocity at the roof floor, are shown in Figure 5. At the same time, two SHDs located on the 1st floor switched to the fail-safe passive state. The opening of the flow control valve went to zero, the orifice was activated and the passive damping force generated. However, other SHDs continued to be semi-actively controlled. The velocity at the roof floor became large a little after the switching.

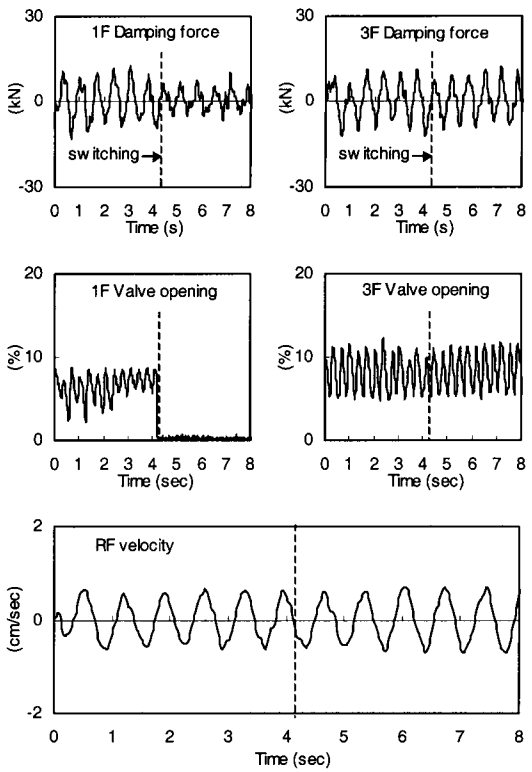


Figure 5: Forced vibration fail-safe semi-active control test

CONCLUSIONS

In this paper, the reliability of a semi-active structural control system is discussed. First, the outline of a building with Semi-active Hydraulic Damper (SHD) system was presented. Next, the health monitoring and fail-safe semi-active control was described. Then, the actual fail-safe performance of this system was confirmed through the forced vibration test. The elements that composed the SHD system demonstrated the specified performance and the whole system operated well. Finally, it is presented that the reliability of the system will be secured as well as the control performance.

ACKNOWLEDGEMENTS

The author would like to express his gratitude to Messrs. Y. Matsunaga, N. Niwa and H. Midorikawa of Kajima Corporation, and to Kawasaki Heavy Industry Ltd. for developing the SHD system.

REFERENCES

Dyke S.J. and Spencer Jr. B.F. (1996). Seismic response control using multiple MR dampers. *Proc., 2nd Int. Workshop on Struct. Control*, 163-173.

Jansen L.M. and Dyke S.J. (2000). Semiactive control strategies for MR dampers: comparative study. *J. Engrg. Mech.*, ASCE, **126:8**, 795-803.

Kobori T. et al. (1991). Shaking Table Experiment and Practical Application of Active Variable Stiffness (AVS) System. *Proc., 2nd Conf. on Tall Buildings in Seismic Regions*, 213-222.

Kobori T. (2000). Stream of structural control for large earthquakes - Semiactive control system -. *Proc., 2nd European Conf. on Struct. Control*, in press.

Kurata N. et al. (1994). Shaking table experiment of active variable damping system. *Proc., 1st World Conf. on Struct. Control* **2**, USC Publications, TP2 108-117.

Kurata N. et al. (1998). Semi-active damper system in large earthquakes. *Proc. 2nd World Conf. on Struct. Control* **1**, Wiley, West Sussex, U.K., 359-366.

Kurata N. et al. (1999). Actual seismic response controlled building with semi-active damper system. *Earthquake Engrg. Struct. Dyn.* **28**, 1427-1447.

Kurata N. et al. (2000). Forced vibration test of a building with semi-active damper system. *Earthquake Engrg. Struct. Dyn.* **29**, 629-645.

Kurata N. (2001). Actual seismic response control building with semi-active damper system. *Proc. Struct. Congr. 2001*, ASCE, CD-ROM.

Matsunaga Y. et al. (1998). Development of actual size semi-active hydraulic damper for large earthquake. *Proc., 2nd World Conf. on Struct. Control* **2**, Wiley, West Sussex, U.K., 1615-1622.

Patten W. N. et al. (1999). Field test of an intelligent stiffener for bridges at the I-35 Walnut Creek Bridge. *Earthquake Engrg. Struct. Dyn.* **28**, 109-126.

Soong T.T. and Spencer Jr. B.F. (2000). Active, Semi-active and hybrid control of structures. *Proc., 12th World Conf. on Earthquake Engrg.*, No. 2834.

Spencer Jr. B.F. et al. (1996). Magnetorheological dampers: a new approach to seismic protection of structures. *Proc. Conf. on Decision and Control,* 676-681.

Spencer Jr. B.F. et al. (1998). "Smart" dampers for seismic protection of structures: a full-scale study. *Proc., 2nd World Conf. on Struct. Control* **1**, Wiley, West Sussex, U.K., 417-426.

Spencer Jr. B.F. (2000). Advanced in semi-active control of civil engineering structures. *Proc., 2nd European Conf. on Struct. Control*, in press.

Yoshida K. and Fujio T. (2000). Semi-active base isolation control of a building using variable oil damper. *Proc., 3rd Int. Workshop on Struct. Control*, World Scientific, Singapore, 567-575.

Advances in Building Technology, Volume 1
M. Anson, J.M. Ko and E.S.S. Lam (Eds.)
© 2002 Elsevier Science Ltd. All rights reserved

HYBRID RESPONSE CONTROL OF CLOSELY SPACED BUILDINGS

George C. Lee, Mai Tong[1] and Yihui Wu[2]

(1) Multidisciplinary Center for Earthquake Engineering Research,
State University of New York at Buffalo, Buffalo, NY 14261, USA
(2) Maguire Group Inc., 225 Chapman St. Providence, RI 02852, USA

ABSTRACT

Seismic retrofit of buildings in urban centers often encounters the challenge of limiting the displacement between closely spaced buildings in addition to acceleration reduction. Recent advances in energy dissipation technologies have enabled structural engineers to control deformational responses to desired levels. However, in order to handle responses of various magnitude, particularly those associated with large inelastic deformations, energy dissipation devices are not effective. This paper describes a hybrid control strategy for reducing building seismic responses. By switching between damping and stiffness devices, the control system is adaptive to different levels of building displacements. An example of controlling the roof displacement of two closely spaced buildings is given to compare the tradeoff of the control effect using a combination of passive damping with/without variable stiffness.

KEYWORDS

Semi-active control, effective damping, structural responses, response reduction.

PASSIVE DAMPING DEVICES AND THEIR APPLICATIONS IN BUILDING SEISMIC PROTECTION

The use of energy dissipation devices (EDD), in particular the use of viscous dampers, as a retrofit strategy for building structures has increased in recent years. Some design procedures for EDD are available in FEM 273/274 *"Guidelines for the Seismic Rehabilitation of Buildings"* and FEMA356, "*Prestandard and commentary for the seismic rehabilitation of buildings*". Design of dampers under performance based design considerations have also been studied (Elhassan et al, 1998).

The current practice typically follows a linear elastic response analysis approach, as described in FEMA guidelines. In FEMA 273, the corresponding effective damping due to the added supplemental energy dissipation devices is to be calculated according to the formula:

$$\beta_{eff} = \beta + \frac{\sum_j C_j \cos^2 \theta_j \phi_{rj}^2}{2\omega \sum_i \left(\frac{w_i}{g}\right) \phi_i^2} \qquad (1)$$

where C_j is the damping constant of device j, θ_j is the angle of inclination of device j to the horizontal direction, ϕ_{rj} is the first mode relative displacement between the ends of device j in the horizontal direction, ω is the fundamental frequency of the rehabilitated building including the stiffness of the velocity dependent devices, w_i is the reactive weight of floor level i, and ϕ_i is the first mode displacement at floor level i.

The effective damping β_{eff} is then used to modify the design spectrum coefficient B_s (short period design spectral coefficient) and B_1 (long period design spectral coefficient). Figure 1 shows the changes of the level of design spectrum as the effective damping is increased.

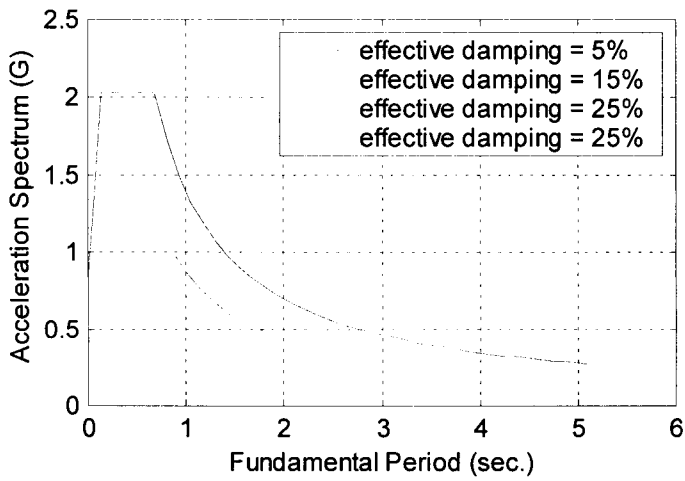


Figure 1: Acceleration Spectrum for LA area per FEMA 273/356

Figure 1 is based on an assumption of 5% design damping. For destructive earthquakes, most structures will experience inelastic deformation, in which structures will have undergone of their ductility capacity to various degrees. Response reduction factors in design codes typically reflect such effect (Bertero, 1986, 1991). The equivalent damping from the ductility will largely overpass that of the energy dissipation devices. As it is shown in Figure 1, when the effective damping level increases, the same percentage increase of damping will produce less response reduction. On the other hand, as structural responses enter the inelastic range, the fundamental period will increase, which will result in reduced acceleration response, but increased displacement response. Therefore, displacement response level will be the major concern for large earthquakes.

COMBINED RSPM AND PASSIVE DAMPING HYBRID CONTROL SYSTEM

The Real-time Structural Parameter Modification (RSPM) technology is a semi-active nonlinear control system for reducing structural seismic responses (Liang, Tong and Lee, 1999a,b; Lee et al, 1997). This semi-active nonlinear system can effectively reduce seismic responses, especially when the objective is to reduce displacement or story drift. A combined RSPM and passive damping control approach can achieve better seismic reduction than the passive damping alone. The combined system can reduce the acceleration response very effectively because of the added damping. Figure 2 shows this hybrid system which consists a passive damper and a controlled stiffness unit. The passive damper will always contribute to the dissipation of energy of the system which the stiffness unit the deformation reaches a threshold value—termed as the open distance. If the relative displacement (the absolute value) is larger than the open distance, the stiffness unit will contribute to reduce the response. If, at any instant, the displacement (absolute value) becomes smaller than the threshold, the RSPM nonlinear stiffness will be automatically switched off. It will be switched on only when the displacement exceeds the threshold, and the RSPM control mechanism is activated only when the stiffness is engaged. The devices are combined in pairs of a tension and a compression units working as a push-and-pull set.

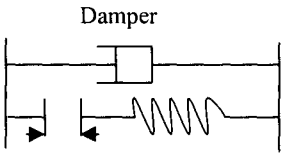


Figure 2: Combined RSPM and passive damping hybrid control system

This hybrid control system has been studied and designed fro two adjacent existing buildings in LA. The weaker building is a seven story steel structure (Building I) with full moment resisting connections. The seismic retrofit problem is to avoid collision of this building with the much stiffer adjacent building II. The gap between these two buildings at the roof level is only six inches (see Figure 3). The combined RSPM and passive damping devices are considered for implementation between the two buildings at the roof level A secondary requirement of this retrofit project is to reduce the acceleration response level, for which pure damping device can be effectively used. The combined RSPM and damping approach therefore is developed to take advantage of their respective strengths.

The hybrid system consists of a linear viscous damper with C=6kips/inch, which is able to provide 30% critical damping for the structure. RSPM is controlled in seven different open distances (1,1.5, 2.0, 2.5, 3.0, 4.0, 5.0 inch) and eight stiffness levels (10, 20, 50, 100, 150, 200, 300, 500 kips/inch). Ground motions used in the analysis include the San Fernando earthquake and Kobe earthquake. The San Fernando earthquake ground acceleration is considered as the design earthquake. Under this excitation, the roof displacement response reaches up to 7.41 inches if without any response control devices.

Figure 4 shows the different roof response levels under different control schemes. Figure 5 shows the roof displacement response and acceleration response for the different level of controlled open distance under Kobe earthquake. It is seen that the displacement and acceleration responses have a tradeoff effect. As the open distance increases, the acceleration response will be reduced more effectively in the tradeoff of the displacement response reduction.

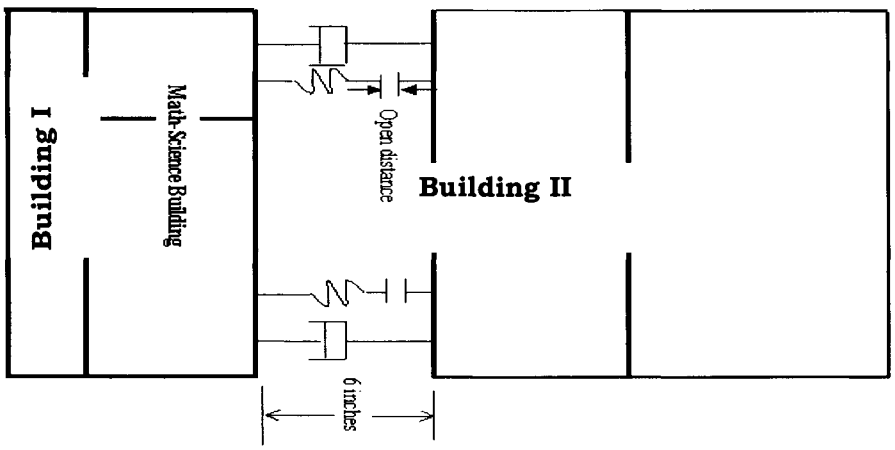
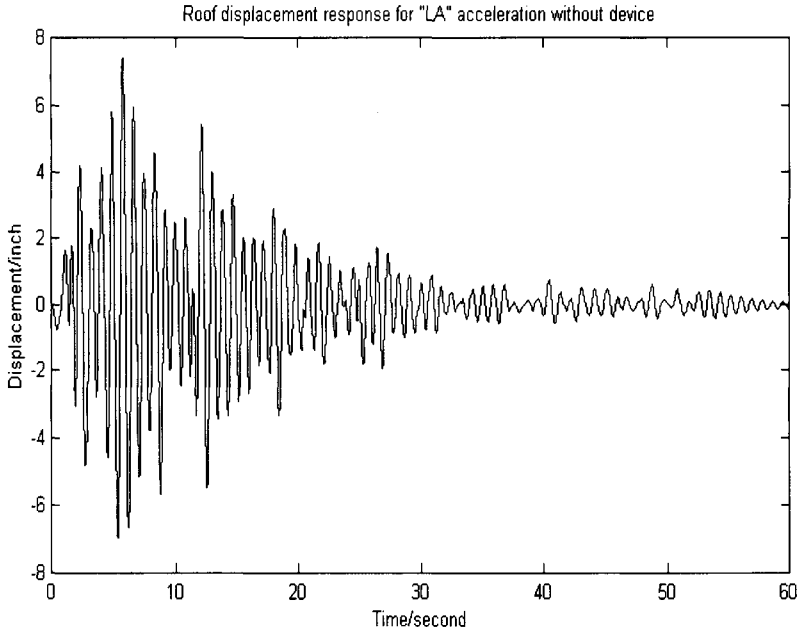
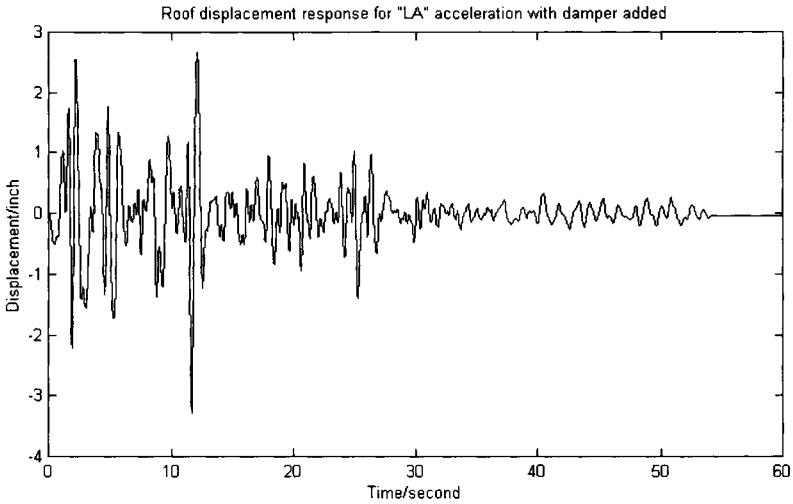


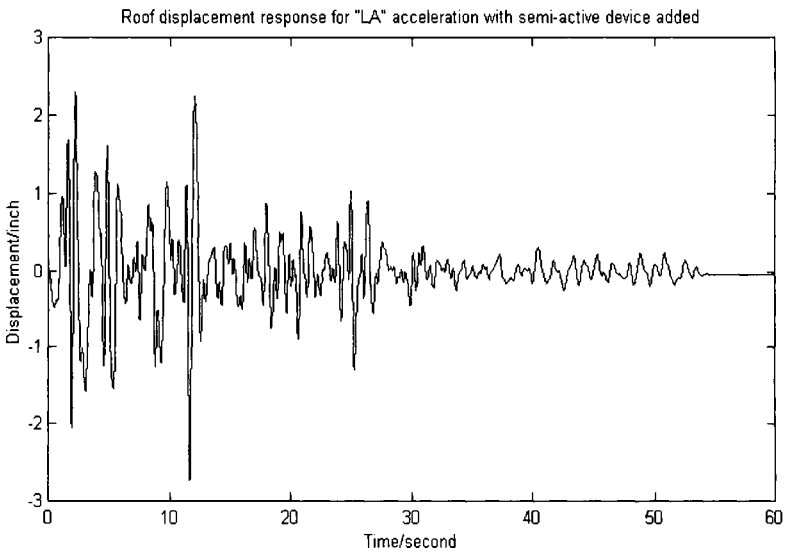
Figure 3: Application to two adjacent buildings



4 (a) No device

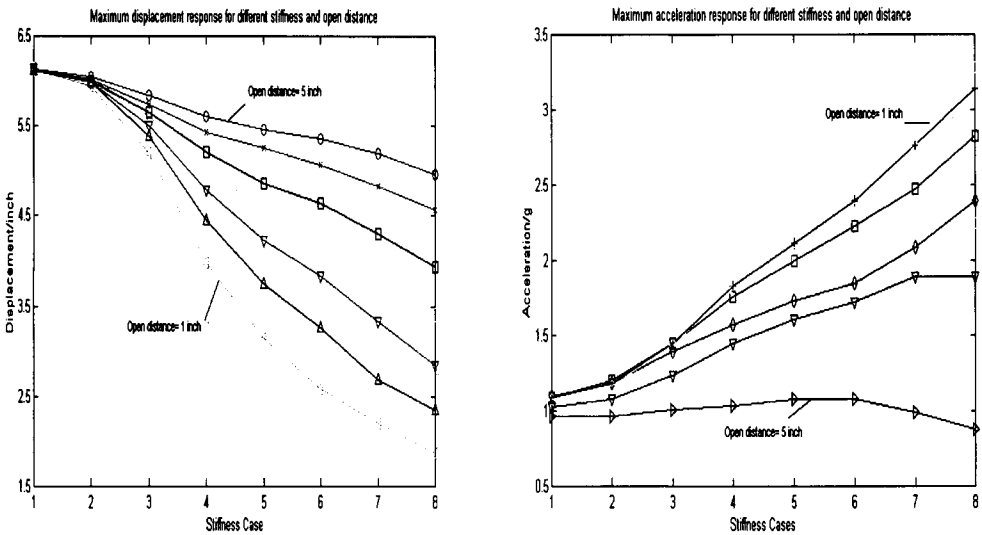


4 (b) Pure damping



4 (c) Combined RSPM

Figure 4: Roof displacement response



(a) displacement response (b) acceleration response

Figure 5: Roof response reduction

COMPARISON OF DAMPING AND HYBRID CONTROL EFFECTS FOR INELASTIC STRUCTURAL RESPONSE

To compare the effectiveness of the hybrid system under various ductility demands, a single DOF nonlinear model with perfect plastic stiffness and 5% hardening spring is considered. The mass and linear stiffness of the spring are equivalent to the UCLA math science building. A 4% of critical damping is assumed for the structure. The bare structure is subject to ductility demands of 1-2 for post yield, 3-10 for life safety level and 10-16 for near collapse stage. An equivalent effective damping of 5% to 40% is added. The nonlinear time history analysis is carried out under the same design earthquake ground acceleration used in the linear analysis, but the amplitude is scaled to match the ductility demand levels of the bare structure (that is at each ductility demand level, the acceleration record is scaled up to the level to produce the corresponding ductility demand for the bare structure). The response reduction with pure damping is illustrated in Figure 6. As the ductility demands increases, the damping effectiveness decreases. It can be seen from Fig.6, for the same 15% pure damping, the structural response is reduced by about 15% for ductility demand of 15, 20% for ductility demand of 10, and 30% for ductility demand of 2.

In a separate comparison of the response reduction effect with combined RSPM and passive damping device, three RSPM stiffness levels of 10%, 20% and 30% of the structural stiffness are considered respectively. A 15% effective passive damping ratio is assumed for the hybrid system. The open distance is selected as 50% of the yield displacement. The results are illustrated in Figure 7. The response reduction (dashed line) of the 15% pure damping is also shown in the figure. It can be seen that the hybrid system has more response reduction than pure damping only. The response reduction effect increases as the ductility demand increases until 10. Higher RSPM will result in more response reduction. In the near

collapse stage of ductility demand (11-16), because the RSPM stiffness is limited to less than 30% of the total stiffness, the response reduction effect become smaller. Overall, the most effective response reduction is in the life safety range (3-10).

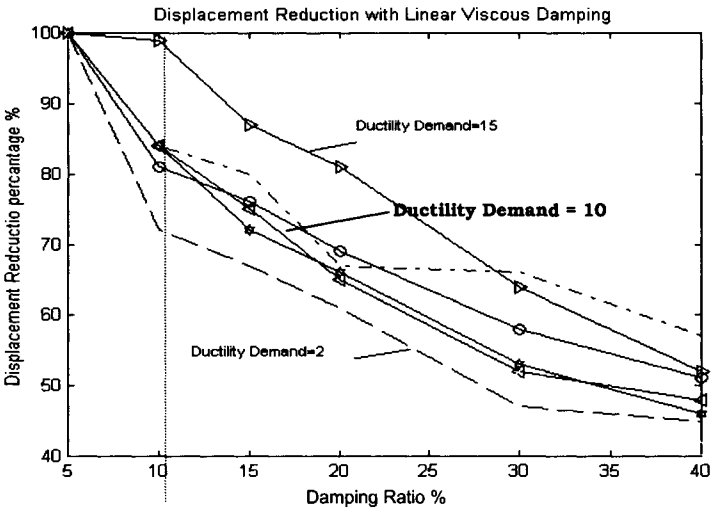


Figure 6. Nonlinear displacement reduction under combined damper

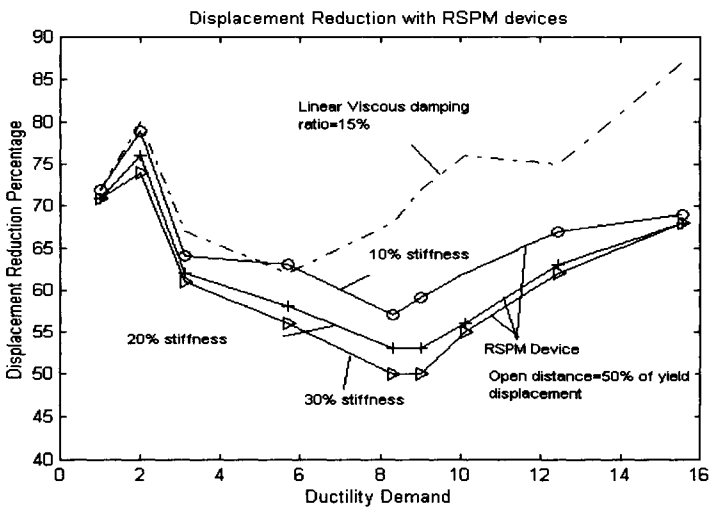


Figure 7: Nonlinear displacement reduction under combined RSPM

CONCLUSION

A combined RSPM and passive damping control system approach takes advantage of the RSPM effectiveness in reducing displacement and acceleration by passive damping. It can be used to effectively reduce the displacement and acceleration. By optimizing the control parameter, the roof displacement of s building (I) can be reduced effectively and the acceleration response can also be controlled at the same time. Inelastic response analysis indicates that the combined RSPM and passive damping hybrid control system can have 20% more response reduction for 15% damping and 30% stiffness level. The system has the greatest reduction in the ductility demand range of 5 to 10, which is the life safety performance ductility range for most building structures. In general, the nonlinear stiffness part of the RSPM technology alone can provide damping up to 30%; however, the size and capacity are normally balanced with other considerations such as the level of damping and the capacities of the supporting load bearing structural members.

ACKNOWLEDGEMENT

This study is performed by a grant from the National Science Foundation through the Multidisciplinary Center for Earthquake Engineering Research (Grant No. ECC-9701471).

REFERENCES

Bertero, V. V. (1986). Evaluation of Response Reduction Factors Recommended by ATC and SEAOC. *Proceedings of the 3rd US National Conference on Earthquake Engineering*, 1663-1673.

Bertero V. V. (1991). Design Guidelines for Ductility and Drift Limits: Review of State-of-the-Practice and State-of-the-Art in Ductility and Drift-Based Earthquake-Resistant Design of Buildings. UCB/EERC No.91/15.

Bunce, B.T. (1970). *Two and Three Dimensional Modeling and Dynamic Analysis of the Five Story Math-science Addition.* Master Thesis, UCLA, 1970.

Elhassan, R.M., Hart, G.C. and Liu, X. (1998). Viscous dampers in performance-based seismic rehabilitation of buildings. *Structural Engineering World Wide*, Sponsored by SEI-ASCE (CD-Rom), 1998.

Lee, G.C., Tong, M., Liang, Z., Houston, B., Taylor, S. Clinard, R.L., Tomita, K. and Gottwald, W. (1997). Structural Vibration Reduction with ISMIS Control Technology. *Proceedings of the 68th Shock and Vibration Symposium.*

Liang, Z., Tong, M. and Lee, G.C. (1999a). A Real-time Structural Parameter Modification (RSPM) Approach for Random Vibration Reduction: Part I - Principle. *J. Probabilistic Engineering*, June 1999, Vol. 14, 349-362.

Liang, Z., Tong, M. and Lee, G.C. (1999b). A Real-time Structural Parameter Modification (RSPM) Approach for Random Vibration Reduction: Part II - Experimental Verification. *J. Probabilistic Engineering*, Vol. 14, 362-385.

Advances in Building Technology, Volume 1
M. Anson, J.M. Ko and E.S.S. Lam (Eds.)
© 2002 Elsevier Science Ltd. All rights reserved

MODEL TESTING OF A NONLINEAR BASE ISOLATION CONCEPT

D. Michael McFarland[1], Yumei Wang[2], Alexander F. Vakakis[3] and Lawrence A. Bergman[1]

[1]Department of Aeronautical and Astronautical Engineering,
University of Illinois, Urbana, IL, 61801, USA
[2]Department of Civil and Environmental Engineering,
University of Illinois, Urbana, IL, 61801, USA
[3]Division of Mechanics, National Technical University of Athens,
GR–157 10 Zografos, Athens, Greece

ABSTRACT

We present a unique response reduction strategy for complex structures subjected to base or ground shock-induced vibrations. The primary focus of our efforts has been the development of a new type of passive nonlinear shock isolation system for protection of flexible structures that effectively and robustly isolates the structure from transient ground motions. The proposed design is based on the concept of nonlinear localization whereby induced vibrational energy is passively confined to a preassigned secondary system and away from the primary structure to be isolated. In this paper, we demonstrate the performance of the system using a simple, spatially one-dimensional model. The structure to be isolated is a two-degree-of-freedom system, which is weakly and linearly coupled to a single-degree-of-freedom intermediate or secondary system. This, in turn, is connected to ground through a hardening spring which, here, is produced by the parallel combination of two linear springs, one having a clearance nonlinearity. The structural system to be protected is weakly coupled to an intermediate system consisting of a subfoundation and linear spring which is tuned to a mode of the structural system. A clearance spring acts to excite the appropriate nonlinear normal mode, the clearance being a design parameter which determines the onset of nonlinear behavior as a function of the input to the system. The performance of the system is examined for pulse-type inputs using simulation.

KEYWORDS

Base isolation, nonlinear dynamics, nonlinear normal mode, mode localization

INTRODUCTION

The vulnerability of flexible structures to large-magnitude shock inputs is well documented. Various methods have been proposed, and in some cases implemented, through which the reliability of these structures can be enhanced. Implementations include passive isolation systems and auxiliary damping devices, while proposed solutions include various manifestations of active and semi-active protective systems. Generally speaking, active systems have not been readily embraced due to considerations such as reliability, power requirements and cost, and semi-active systems are still in the research stage, while passive devices and systems have been employed for many years with great success despite some performance limitations that we seek to address with this technology.

The primary focus of our efforts has been the development of a new type of passive nonlinear shock isolation system for protection of flexible structures that, when implemented, effectively and robustly isolates the structure from transient ground motions, thus reducing the potential for damage and extending useful life. The proposed design is based on the concept of nonlinear localization whereby induced vibrational energy is passively confined to a preassigned secondary system and away from the primary structure to be isolated. We show that such a robust nonlinear localization phenomenon can be effected by: (a) tuning the shock isolation system so that a 1:1 internal resonance exists between the secondary substructure and a mode of the primary structure; and (b) inducing a strongly localized nonlinear normal mode in which vibration is predominantly confined to the secondary substructure. In this paper, we demonstrate the performance of the system using a simple, spatially one-dimensional model.

PROBLEM STATEMENT

A conventional base isolation system consists of linear stiffness and damping elements arranged to permit relative motion between the ground and a building's foundation. Its tuning is limited to the adjustment of the values of these components with the goal of decoupling the structure to be isolated from the ground supporting it. This decoupling can be achieved by making the stiffness of the foundation very small, with the result that small disturbances may produce large displacements while larger ground motions may use up all the travel available in the isolation system without adequately protecting the primary structure. On the other hand, a linear isolation system sized to function properly in response to a strong ground input may be too stiff and highly damped to offer the desired protection (decoupling) during a lesser disturbance. The design process typically includes trading off the reduction of "rattle space" to simplify utility connections, the minimization of the absolute accelerations of the superstructure to preserve occupant comfort and confidence, and the minimization of inter-story displacements to limit potentially damaging shear stresses.

The design goals for the system we propose are the same, but the introduction of an additional, nonlinear degree of freedom offers new options in meeting them. In particular, it becomes possible to preferentially direct energy to an auxiliary mass and confine it there by designing the isolation system so that the entire structure has a nonlinear normal mode of vibration in which motion is effectively limited to this degree of freedom. It will be seen that this tuning can be achieved through the linear components of the isolation system, leaving the nonlinear elements (a clearance and an additional linear stiffness) as additional parameters which may be adjusted to improve the overall response. One use of this additional capability is to create a structural system that responds appropriately to both large and small ground motions.

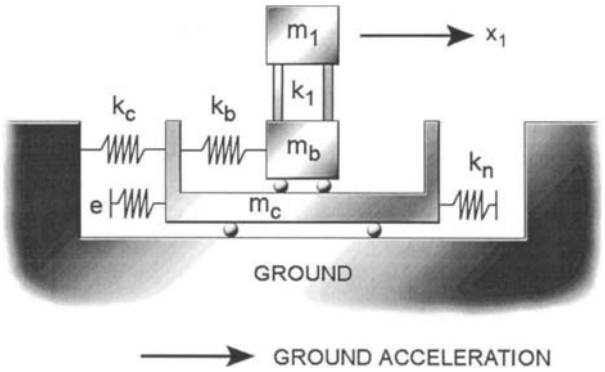


Figure 1: Nonlinear base isolation system with SDOF superstructure.

MECHANICAL MODEL AND ANALYSIS

The nonlinear base isolation system to be analyzed is shown schematically in Figure 1. The structure to be isolated is a two-degree-of-freedom system, which is weakly and linearly coupled to a single-degree-of-freedom intermediate or secondary system. This, in turn, is connected to ground through a hardening spring which, here, is produced by the parallel combination of two linear springs, one having a clearance nonlinearity. The structural system consisting of the foundation m_b, superstructure m_1 and column stiffness k_1 is weakly coupled to the subfoundation m_c through the spring k_b. The intermediate system consisting of the subfoundation m_c and linear spring k_c is tuned to a mode of the structural system. The clearance spring k_n acts to excite the appropriate nonlinear normal mode, while the clearance e is a design parameter which determines the onset of nonlinear behavior as a function of the input to the system.

Equations of Motion

We denote the restoring force provided by the nonlinear spring-gap element by

$$f_n(y_c) = \begin{cases} k_n(y_c - e), & y_c > e, \\ k_n(y_c + e), & y_c < e, \\ 0, & \text{otherwise} \end{cases} \tag{1}$$

and adopt the convention that x represents displacement with respect to a fixed reference frame, y, displacement with respect to the ground, and z, displacement with respect to the base mass m_b. Hence

$$x = y + x_g = z + y_b + x_g \tag{2}$$

and the equations of motion of the structure may conveniently be written as

$$\ddot{y}_c = \frac{1}{m_c}[-(c_c + c_b)\dot{y}_c + c_b\dot{y}_b - (k_c + k_b)y_c + k_b y_b - f_n] - \ddot{x}_g, \tag{3}$$

$$\ddot{y}_b = \frac{1}{m_b}[-c_b\dot{y}_b + c_b\dot{y}_c + c_1\dot{z}_1 - k_b y_b + k_b y_c + k_1 z_1] - \ddot{x}_g \tag{4}$$

plus an equation representing the dynamics of the superstructure,

$$m_1\ddot{z}_1 + c_1\dot{z}_1 + kz_1 = -m(\ddot{x}_g + \ddot{y}_b). \tag{5}$$

The input to the system in all cases examined here was a ground acceleration shock pulse of amplitude A_g and duration T_g. This ground motion was further assumed to be either a rectangular pulse,

$$\ddot{x}_g(t) = \begin{cases} A_g, & 0 < t < T_g, \\ 0, & \text{otherwise}, \end{cases} \tag{6}$$

or a half-sine pulse,

$$\ddot{x}_g(t) = \begin{cases} A_g \sin \dfrac{\pi t}{T_g}, & 0 < t < T_g, \\ 0, & \text{otherwise}, \end{cases} \tag{7}$$

both of which provide a large amount of energy to the system in a short time.

Numerical Simulation

The response of the system was simulated using Matlab and Simulink, where the isolation system was represented by a detailed block diagram while the building was described by the state-space model

$$\dot{\xi} = \mathbf{A}\xi + \mathbf{B}\mathbf{u}, \tag{8}$$

$$\eta = \mathbf{C}\xi + \mathbf{D}\mathbf{u} \tag{9}$$

with

$$\xi = \begin{Bmatrix} z_1 \\ \dot{z}_1 \end{Bmatrix}, \quad \mathbf{A} = -\mathbf{A}_1^{-1}\mathbf{A}_2, \quad \mathbf{B} = \mathbf{A}_1^{-1}\mathbf{B}_1, \quad \mathbf{C} = \mathbf{I}, \quad \mathbf{D} = \mathbf{0} \tag{10}$$

where

$$\mathbf{A}_1 = \begin{bmatrix} c_1 & m_1 \\ m_1 & 0 \end{bmatrix}, \quad \mathbf{A}_2 = \begin{bmatrix} k_1 & 0 \\ 0 & -m_1 \end{bmatrix}, \quad \mathbf{B}_1 = \begin{Bmatrix} -m \\ 0 \end{Bmatrix}, \quad u = \ddot{x}_g. \tag{11}$$

No difficulty was encountered in solving these equations numerically using either fixed-step or adaptive integrators (e.g., Matlab's functions `ode4` and `ode45`, respectively). Numerical results obtained using Matlab were compared to the analytical solution for a simpler, SDOF model exhibiting the same sort of dead-band nonlinearity to verify that the potentially abrupt change in stiffness associated with the subfoundation mass m_c contacting the spring k_n posed no unusual numerical problems. In general, the adaptive integrator performed well, and it was used for all the simulations reported herein. The fixed-time step solver was found to be considerably slower for these equations, but has the advantage that its output is more amenable to some forms of post-processing.

TUNING ALGORITHM

The design of the isolation system begins with knowledge of the superstructure mass and stiffness, m_1 and k_1. The masses of the base, m_b, and the intermediate subsystem, m_c, are then chosen. These are in principle arbitrary but in any given application the total foundation and auxiliary mass will be expected to lie in a range familiar to designers; here we have chosen m_b for compatibility with existing experimental apparatus, then selected m_c as a practical fraction of the total mass of the isolated structure. Tuning of the isolation system is then accomplished through the selection of appropriate values of the springs k_c, k_b and k_n. This process is simplified by fixing the ratios of the other two stiffnesses to k_c, that is, by setting

$$k_b = \frac{1}{10} k_c, \tag{12}$$

$$k_n = 10 k_c. \tag{13}$$

TABLE 1
PHYSICAL PARAMETERS OF MODEL SYSTEM

Superstructure	
m_1	0.2 kg
k_1	3500 N/m
c_1	0 N/m/s

Base	
m_b	0.3 kg
k_b	583.1 N/m
c_b	0 N/m/s

Intermediate System	
m_c	0.2 kg
k_c	5831 N/m
c_c	0 N/m/s
k_n	58310 kg
e	Variable

The first of these equations reflects the requirement that the coupling between the intermediate SDOF system and the base mass be weak, and allows us to use a very simple formula to determine the single remaining parameter, k_c.

The desired response of the complete structure to ground motion is a mode in which vibration is almost entirely confined to the intermediate subsystem—a localized mode in which the base and superstructure participate very little. With the above assumption of weak coupling, and assuming for the moment that the displacement of the intermediate mass with respect to ground is smaller than the gap e so that the nonlinear element may be ignored, an approximate expression for the resonant frequency of the isolator's degree of freedom is seen to be

$$\omega_c = \sqrt{k_c/m_c}. \tag{14}$$

The determination of k_c, and hence k_b and k_n, is thus reduced to the specification of the resonant frequency ω_c. On physical grounds, this is chosen to be equal to the frequency of the first mode in which the base-superstructure combination would experience significant inter-story displacements. Considering the linear system consisting of masses m_b and m_1 and the spring k_1, but neglecting k_b, we can readily compute its natural frequencies. The lowest of these will be zero, corresponding to a rigid-body mode, but the second will be non-zero and will correspond to the mode to which we seek to tune the isolator. Denoting these frequencies

$$\tilde{\omega}_0 = 0, \quad \tilde{\omega}_1 > 0, \tag{15}$$

we can state the tuning condition as

$$\omega_c = \tilde{\omega}_1, \tag{16}$$

from which we immediately obtain

$$k_c = m_c \tilde{\omega}_1^2. \tag{17}$$

The values in Table 1 were calculated using this algorithm. The only parameter of the isolation system not now uniquely determined is the clearance e, the effect of which will be investigated below.

An experiment is planned which will utilize existing hardware to the extent practical while demonstrating the efficacy of the proposed isolation system and tuning algorithm. The values shown in Table 1 have been selected for the experimental structure to be used. These reflect previously identified or readily available components and are consistent with the tuning criteria for the isolator as outlined above. The most significant departure from similitude to a realistic civil structure is in the relatively large base mass m_b. This will be mollified in later experiments by increasing the number of floors in the superstructure and, thus, its total mass. However, the present values are adequate for proof-of-concept work, and the SDOF superstructure is retained here for simplicity.

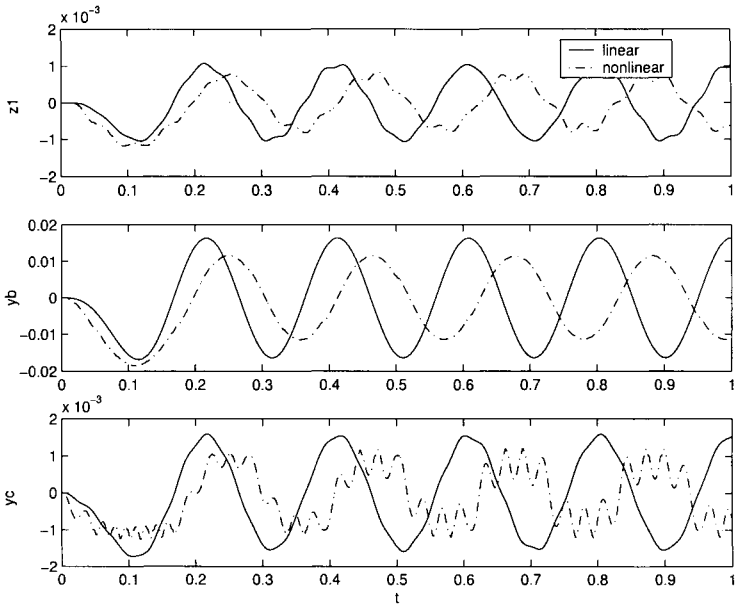


Figure 2: Time responses of the linear ($k_n = 0$) and nonlinear ($k_n = 58310$ N/m, $e = 0.001$ m) systems.

SIMULATION RESULTS

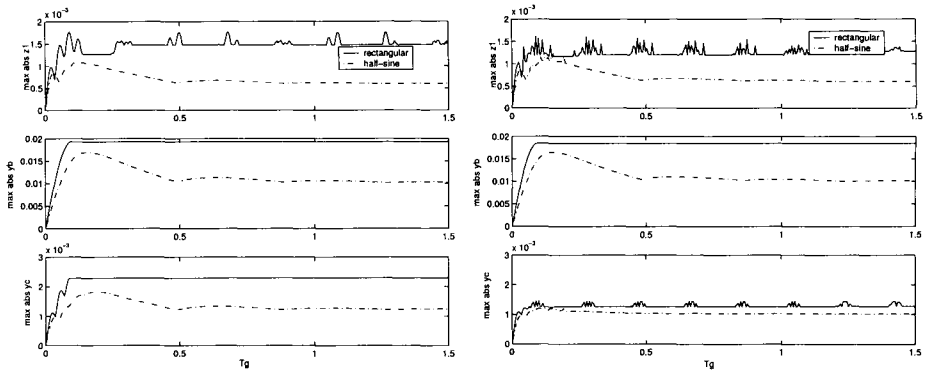
With the isolation system tuned as just described, a number of numerical simulations were made to assess its potential effectiveness. This section presents some typical results of these runs, then summarizes the influence of the design parameter e, the clearance between the spring k_n (tied to ground) and the intermediate mass m_c.

Time Histories of Response

Time history results from two cases are shown in Fig. 2, and clearly demonstrate the existence of the desired localized mode in the nonlinear system. The larger response plotted in this figure is that of the linear system obtained when $k_n = 0$. It depicts the interaction of three nonlocalized modes; the intermediate degree of freedom introduced by the isolator is ineffective in limiting the response of the superstructure. In the other simulation results shown on the same axes, the nonlinear spring coefficient has been returned to its nominal value of $k_n = 58310$ N/m and the clearance set to $e = 0.001$ m (a large gap in that it is approximately two-thirds of the peak value of y_c from the linear analysis). The response plots indicate the isolator is beginning to function as intended, with the building and base mass moving less than in the linear case while the intermediate mass m_c responds more strongly than before and with additional, higher-frequency motion.

Shock Spectra

In order to compare the simulation results obtained with different nonlinear isolation system designs, we have found it useful to adopt the familiar concept of the *shock spectrum* of a mechanical system (Meirovitch, 1986), in which the maximum value of a response quantity is plotted against the shock pulse duration T_g. Conventionally, both pulse duration and response amplitude are normalized with respect to



(a) Linear system ($k_n = 0$)

(b) Nonlinear system ($k_n = 58310$ N/m, $e = 0.001$ m)

Figure 3: Shock spectra of responses to rectangular and half-sine ground accelerations.

combinations of the system parameters, but in dealing with nonlinear systems it is more convenient to work directly with dimensional quantities.

The shock spectra for the two systems of the previous section are shown in Fig. 3. In each case, two curves are plotted for each of the three degrees of freedom, corresponding to rectangular and half-sine shocks. Those familiar with the classical shock spectra of an SDOF system will notice these are less smooth due to the modal interactions of the multiple degrees of freedom present. The isolator's effectiveness can be seen most clearly by comparing the peak superstructure responses at several values of the pulse duration. With the clearance used here ($e = 0.001$ m), the response spectrum resulting from the half-since shock is almost the same for the nonlinear system as for the linear. However, the peak response z_1 due to the rectangular pulse is significantly reduced for all pulse durations. Although not shown by these plots, a similar response improvement occurs for the half-sine input when the clearance is reduced or the shock amplitude increased.

Effect of the Isolator Clearance

With the other design parameters fixed, the clearance (gap) e is still available with which to optimize the response of the isolated structure. Its influence is indicated in Fig. 4, where the maximum value of the shock spectra are plotted against e. In constructing these plots, the amplitude of the ground acceleration was held constant at $A_g = 1$ g. In an actual application, there is a minimum level of ground motion that must occur before the nonlinearity comes into play, and the larger the gap is made the greater this ground acceleration threshold becomes. In general, however, it can be said that there is an optimum gap from the standpoint of reducing the response of the isolated structure and its base to strong ground motions, although for the present problem it appears that optimum lies outside the range of Fig. 4.

CONCLUSION

A novel base isolation system depending for its operation on the tuning and excitation of a highly localized nonlinear mode has been described and demonstrated through numerical simulations. Isolation is

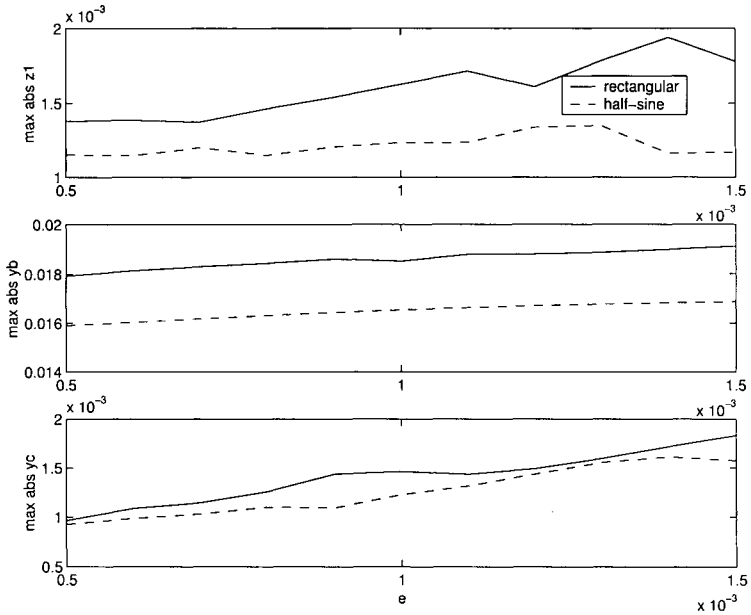


Figure 4: Effect on the maximum value of the shock spectrum of varying the clearance e.

achieved by confining response energy to an auxiliary mass, vibration of which dominates this localized mode. An effective tuning algorithm has been reviewed and the influence of the remaining free design parameter, a clearance, has been investigated through the computation of shock spectra.

REFERENCES

Gendelman O. (2001). Transition of energy to a nonlinear localized mode in a highly asymmetric system of two oscillators. *Nonlinear Dynamics* **25:1–3**, 237–253.

Ma X., Nayfeh T.A., Vakakis A.F. and Bergman L.A. (2000). Experimental verification of shock reduction achieved through non-linear localization. *Journal of Sound and Vibration* **230:5**, 1177–1184.

Meirovitch L. (1986). *Elements of Vibration Analysis*, 2nd ed., McGraw-Hill, New York.

Vakakis A.F. (2001). Shock isolation through the use of nonlinear energy sinks. Submitted to the *Journal of Vibration and Control.*

Vakakis A.F., Kounadis A.N. and Raftoyiannis I.G. (1999). Use of non-linear localization for isolating structures from earthquake-induced motions. *Earthquake Engineering and Structural Dynamics* **28**, 21–36.

Vakakis A.F., Manevitch L.I., Mikhlin Y.V., Pilipchuk V.N., Zevin A.A. (1996). *Normal Modes and Localization in Nonlinear Systems*, John Wiley & Sons, New York.

Advances in Building Technology, Volume I
M. Anson, J.M. Ko and E.S.S. Lam (Eds.)
© 2002 Elsevier Science Ltd. All rights reserved

RISK CONTROL OF SMART STRUCTURES USING DAMAGE INDEX SENSORS

Akira Mita and Shinpei Takahira

Department of System Design Engineering, Keio University
3-14-1 Hiyoshi, Kohoku-ku, Yokohama 223-8522, Japan

ABSTRACT

Simple and inexpensive passive sensors that can monitor the peak strain or displacement of a critical structural member were developed. The developed sensors have an ability to quickly assess the degree of damage in a structure when a checkup is needed. The sensors need no power supply for monitoring. The peak values can be retrieved wirelessly if desired. In addition, they can be easily modified to measure other damage indexes such as maximum acceleration and force. The mechanism to memorize the peak strain or displacement values relies on the pure plastic extension of sensing section. The pure plastic extension of the sensing section is made possible by introducing elastic buckling. The peak value is detected by measuring a change in electric resistance, inductance or capacitance. In addition, introduction of an LC circuit into the sensor enabled wireless retrieval of the data. Theoretical and experimental studies exhibit the feasibility of the developed sensors for structural health monitoring of smart structures.

KEYWORDS

Damage index, smart structure, health monitoring, peak sensor, wireless, damper

INTRODUCTION

A health monitoring system is getting strong attention for controlling or reducing risks associated with natural hazards such as large earthquakes. This trend has been accelerated after the 1994 Northridge Earthquake and the 1995 Hyogo-Ken Nanbu (Kobe) Earthquake[1]. Both occurred in the populated areas so that many infrastructures and engineered buildings experienced unexpected damages. For example, many steel buildings suffered sever damages mainly at their beam-column joints. It was a

surprising fact that the damages were not identified until removing fire-protection coatings on beam-column joints. In most cases, it was not possible to find the correct degree of the damages by a simple eye-inspection of the structure surface because there were no major visible damages.
One of the key issues raised was the difficulty to find and quantify damages in piles and foundations of a building. If the building were inclined or tilted, it would be rather easy to notice the structural damage. However, as was the case for beam-column joints in steel structures, a simple eye-inspection can not identify the damages in piles and foundations in most cases. Even when the damage was identified to be in a pile system, it is necessary to excavate soils around the foundation for accurate assessment. Thus, an efficient health monitoring system for piles and foundations is indeed useful.

In the course of developing a health monitoring system for steel structures, piles and others, it was found that the current sensor and network technologies had certain limitations for proper assessment. For example, nondestructive damage assessment of beam-column joints in a tall steel building is very difficult without removing coating materials for fire-protection. Evaluation of embedded piles is further difficult since excavation of foundation soil is necessary for installing sensors. Though several nondestructive methods were proposed, no single method could satisfy all the requirements for correct assessment of damages.

In addition to the beam-column steel joints and piles, damper devices for smart structures are becoming sources of needs for health monitoring systems. Typical building structures equipped with damper devices are depicted in Fig. 1. The number of devices installed into a tall steel building may easily exceed one hundred. The current inspection practice depends solely on eye-inspections so that a certain number of wall panels covering damper devices have to be removed when the building is hit by a large earthquake. This inspection work will be not only time-consuming but also costly.

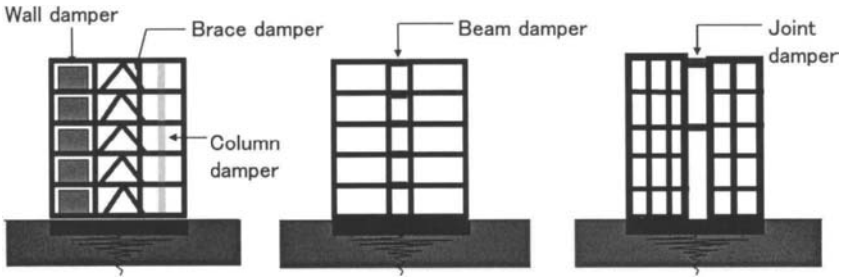


Figure 1: Smart structures with dampers

For a conventional building structure, introducing sensors to detect damages may not be practical as the damage scenario is complicated due to high degree of nonlinearity and statical indeterminacy. However, a smart structure that is equipped with passive or active dampers as shown in Fig. 1 has a clearer scenario for the damage. The input power due to earthquakes or strong winds is guided to be absorbed by dampers. Therefore, installing sensors to identify the condition of dampers may become feasible. For a ten-storey building, we may need to know the health of one hundred dampers for assuring the structural health. As a realistic and economical means, employing damage index sensors

to the dampers will be attractive if the cost for sensors is reasonable. A damage index is defined as a physical value that is well correlated to a critical damage in a structure. Typical damage indexes include peak strain, peak displacement, peak acceleration, story drift, absorbed energy, accumulated plastic deformation, and so on. They will only memorize the indexes that are well correlated to the damage without any electrical power supply. Therefore, the maintenance cost for such sensor systems is minimal.

In the past few years, several peak strain sensors have been proposed and developed. The peak strain sensor is one of the most promising damage index sensors. The TRIP (TRansformation Induced Plasticity) steel was used as a sensor head as it is magnetized when large strain is applied[2]. However, the TRIP sensor may not be reused once the sensor experiences a large strain. In addition, detection of the magnetization level is rather difficult. In another research, the relationship between the electric resistance change and the peak strain was studied for CFGFRP (Carbon Fiber Glass Fiber Reinforced Plastics)[3]. It was concluded that the change of the electric resistance in the CFGFRP material would be well correlated to the peak strain. This feature is unique as the material itself can function as a sensor. Unfortunately, however, the electric resistance is correlated not only to the peak strain but also to the residual strain so that isolation of the peak strain is difficult. In the other studies, the electric resistance of SMA (Shape Memory Alloys) was used in the hope of using it as a peak strain sensor[4]. However, the characteristics of the sensor output was not so simple.

In this paper, a new concept is presented to memorize the peak strain or the peak displacement. The mechanism utilizes elastic buckling of a thin wire. In addition, the memorized value can be retrieved wirelessly.

MECHANISM OF DAMAGE INDEX SENSOR

One of the most useful damage indexes is the peak strain. In the following, the mechanism of a sensor that can memorize the peak strain is explained. Although the mechanism is to memorize the maximum strain only, the same mechanism is applicable to obtain other damage indexes with minor modifications. The ideal response of a peak strain sensor is plotted in Fig. 2 compared with a conventional strain sensor. The peak strain sensor keeps the peak strain value even when the strain in the object material is released. This feature can be realized by using a material that has a pure plastic response against applied load for a sensor element. We propose to use the elastic buckling of a thin wire to introduce such plastic response as shown in Fig. 3.

In Fig. 3, the right end of a thin wire is attached to a conductive block. The left side of the wire is sandwiched by a conductive block resulting in a certain level of friction force. At the initial phase, no tension is applied to the wire. When the left block is pulled to the left direction, the wire will be stretched. Under the condition that the tension force in the wire reaches beyond the static friction force, the wire is pulled out from the left conductive block. When the tension force is removed, the wire may keep the extended length if the static friction force is larger than the elastic buckling force for the extended wire. Thus the peak strain is obtained by measuring the length of the wire. If the wire is electrically resistive, the length is linearly related to the change of the electric resistance.

A slightly different mechanism is shown in Fig. 4. In this case, the plastic behavior is achieved by a

variable element such as a variable capacitor, a variable inductor or a variable resistance. Therefore, the length of the thin wire in this case is unchanged except for elastic elongation. The plastic deformation is kept in the variable element by utilizing the inherent friction. The sensor is sensitive in only one direction. In the opposite direction, the sensor is insensitive by the buckling of the thin wire.

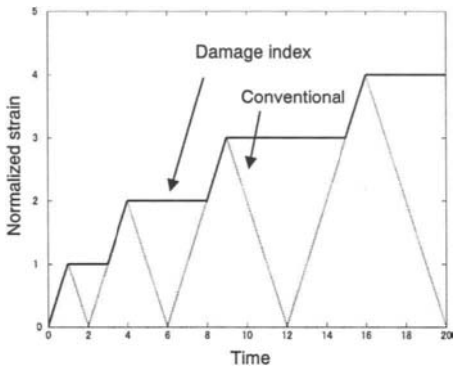


Figure 2: Ideal response of damage index sensor



Figure 3: Mechanism of memory using elastic buckling of a thin wire

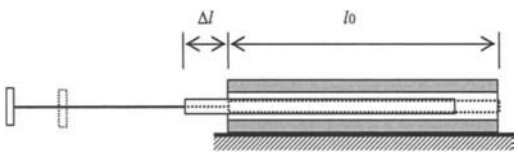


Figure 4: Mechanism of a damage index sensor consisting of a variable element and a thin wire

The buckling force P_{cr} to induce the first buckling mode in a thin wire with fixed-end boundary conditions at both ends and of its length of l is given by

$$P_{cr} = \frac{4\pi^2 EI}{l^2} \tag{1}$$

where E is Young's modulus and I is the moment of inertia of an area. The corresponding buckling stress and strain in the wire are given by

$$\sigma_{cr} = \frac{4\pi^2 EI}{l^2 A}, \quad \varepsilon_{cr} = \frac{4\pi^2 I}{l^2 A} \tag{2}$$

where A is the cross sectional area of the wire. The condition required for the peak strain sensor is to keep this buckling force smaller than the static friction force so that the extended length of the wire should be kept. In addition, the buckling strain should be as small as possible since it is associated with the maximum elastic strain induced in the sensor. The elastic component in the response of the sensor should be minimized.

For a peak strain sensor depicted in Fig. 2 of its initial length l_0 for the resistant wire, the output from the sensor as a change of resistance ΔR is given by.

$$\frac{\Delta R}{R_0} = \frac{\Delta l}{l_0} + 2\nu \frac{\Delta l^e}{l_0} \tag{3}$$

where ν is Poisson's ratio. The increase of the length is divided into two components.

$$\Delta l = \Delta l^e + \Delta l^p \tag{4}$$

The superscript e represents elastic elongation. The superscript p indicates the component associated with plastic or permanent elongation beyond the friction force. The typical but exaggerated response of the sensor is shown in Fig. 5. In this figure, the dynamic friction coefficient was assumed to be half of the statical friction coefficient. The buckling stress was assumed to be negligibly small. In the segment 1 in Fig. 5, only elastic elongation occurs until the stress in the thin wire exceeds the static friction force. In the segment 2, the friction is reduced to the dynamic friction. The increase of the resistance is due to the plastic elongation. In the segment 3, the elastic elongation is reduced to zero. In the segment 4, the thin wire is buckled so that the same output is kept.

For a peak strain sensor using a variable capacitor and a thin wire depicted in Fig. 4, the expected response is slightly different from the above. The response is typically given by

$$\frac{\Delta C}{C} = \frac{\Delta l}{l_0} \tag{5}$$

where C is capacitance. From Eqn. 5, it is clearly understood that the response of this sensor is only due to the change of variable element and not due to the elastic deformation of the thin wire. A simulated response of the sensor consisting of a thin wire and a capacitor is depicted in Fig. 6. In the segment 1, due to the static friction force, the sensor will not give any output before exceeding a certain strain where the resulting stress becomes larger than the static friction. In the segment 2, the tension force is larger than the dynamic friction force so that the variable capacitor changes its capacitance. In the segment 3, the tension force is removed from the thin wire so that the capacitance is kept at the maximum value.

The damage indexes are obtained by measuring changes in resistance, capacitance or inductance. Although the simplest configuration would be using a variable resistor, the use of a variable capacitor or a variable inductor has an additional benefit, that is, wireless retrieval capability. When a variable capacitor or a variable inductor is used, the sensor can be easily modified to form a closed LC circuit by adding an inductor or a capacitor. When an LC circuit consisting of a capacitor C and an inductor

L exists, the natural frequency of the circuit is given by

$$f = \frac{1}{2\pi\sqrt{LC}} \tag{6}$$

This natural frequency can be detected without touching the wire. The simplest way to measure the frequency would be using a dip meter. A dip meter generates radio waves of various frequencies and detects the frequency at which the energy is dipped by the nearby LC circuit. The frequency at which the energy is absorbed can be considered to be the natural frequency of the nearby sensor. The desired peak strain or displacement value is therefore retrieved wirelessly from the measured natural frequency. This feature is extremely useful, when the sensor should be covered by a fire-protection material or a cosmetic wall.

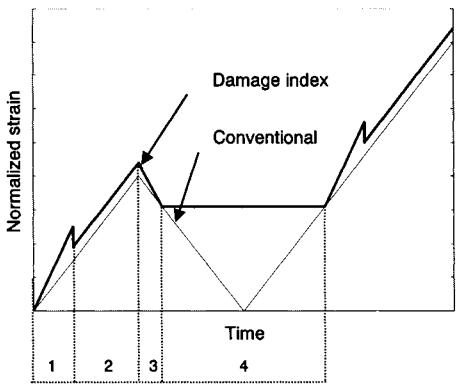


Figure 5: Simulated response of damage index sensor using a resistant thin wire

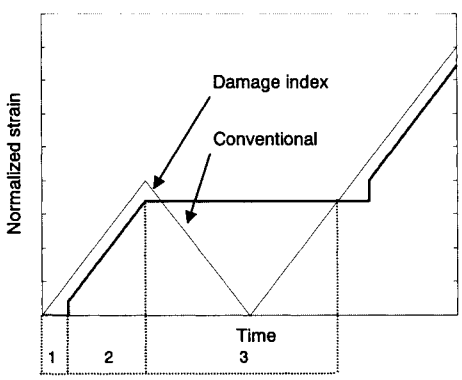


Figure 6: Simulated response of a damage index sensor using a variable capacitor and a thin wire

EXPERIMENTAL VERIFICATION

In the following experiment, a peak strain sensor consisting of a thin wire and a variable capacitor depicted in Fig. 4 was chosen for verification as shown in Fig. 7.

A variable capacitor used here is depicted in Fig. 8. It is made of two aluminum cylinders that are separated by a non-conductive material as a separator. Therefore, the capacitance of this system can be varied by changing the overlapping length of two aluminum cylinders. The measured initial capacitance was 217 pF. An inductor added to the variable capacitor to form a closed LC circuit was measured to be about 25 μH. Therefore, the natural frequency of the prototype sensor at its initial condition is 2.16 MHz at its initial position. The buckling wire is made of a fluorocarbon line to assure high Young's modulus. The diameter of the wire is 219 μm. The output was compared with the data taken by the laser sensor. The data were retrieved in the form of natural frequency change.

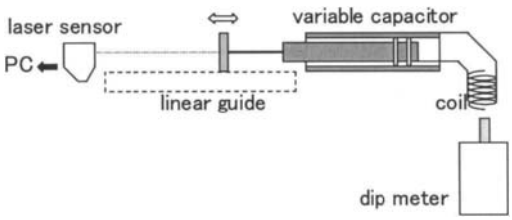


Figure 7: Experimental setup

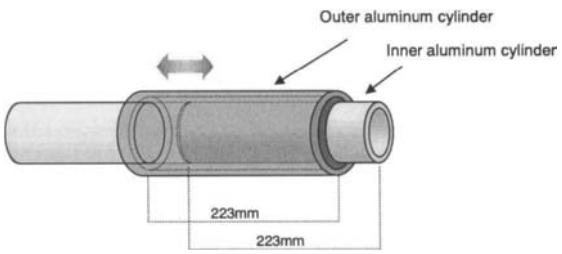


Figure 8: Variable capacitor consisting of aluminum cylinders

The measured results are shown in Fig. 9. From this figure, it is clearly shown that the peak response is indeed memorized. The response was measured using a dip meter. The initial position corresponds to 2.1637 MHz. The largest value of the peak strain sensor in Fig. 9 corresponds to 2.4177 MHz. If this sensor is bonded to a material with the initial sensor length of 400 mm, the range tested here corresponds to 0 μstrain to 52,750 μstrain. As the mechanism employed here is very flexible, the measurement range can be easily narrowed or widened by changing the length of variable capacitor and the length of wire. The size of the sensor can be as small as a conventional strain gauge or as large as the largest displacement sensor. The mechanism employed here to memorize the peak strain or displacement value can be extended to memorize other physical values such as force, stress, acceleration, velocity, accumulation of plastic deformation and so on.

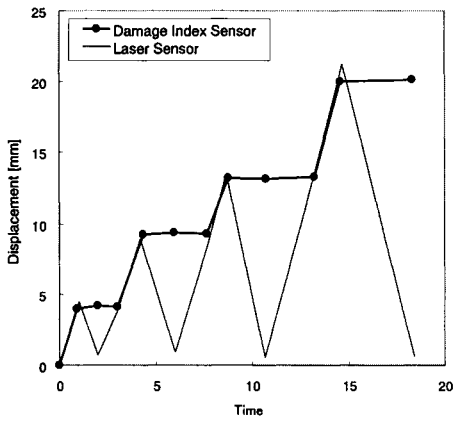


Figure 9: Response of damage index sensor

CONCLUDING REMARKS

A damage index is defined as a physical value that can be well correlated to a critical damage in a structure. Typical damage indexes include peak strain, peak displacement, peak acceleration, absorbed energy, accumulated plastic deformation, and so on. A mechanism of simple and inexpensive passive sensors that can monitor such damage indexes was developed. The mechanism to memorize the damage indexes relies on the pure plastic deformation of the sensing section. The pure plastic deformation of the sensing section is made possible by introducing a thin wire that is easily buckled by a small compressive force. The change in the length of the sensing section is detected by a change in resistance, inductance or capacitance. The sensors need no power supply for monitoring. In addition, introduction of an LC circuit into the sensor enabled wireless reading of the damage index. The damage index sensors are the most promising tools for controlling risks associated with natural hazards for smart structures with passive or active dampers by assessing the quantitative health conditions within a reasonable cost.

REFERENCES

1. Mita, A. (1999). Emerging Needs in Japan for Health Monitoring Technologies in Civil and Building Structures. *Proc. Second International Workshop on Structural Health Monitoring*, Stanford University, Sept. 8-10, 56-67.
2. Westermo, B.D. and L. Thompson (1994). Smart Structural Monitoring: A New Technology. *International Journal of Sensors*, 15-18.
3. Muto, N., H. Yanagida, T. Nakatsuji, M. Sugita, Y. Ohtsuka and Y. Arai (1992). Design of Intelligent Materials with Self-Diagnosing Function for Preventing Fatal Fracture. *Smart Materials and Structures*, **1**, 324-329.
4. Kakizawa, T. and S. Ohno (1996). Utilization of Shape Memory Alloy as a Sensing Material for Smart Structures,. *Proc. Advanced Composite Materials in Bridges and Structures*, 67-74.

Advances in Building Technology, Volume 1
M. Anson, J.M. Ko and E.S.S. Lam (Eds.)
© 2002 Elsevier Science Ltd. All rights reserved

Seismic Protection of Base-isolated Structures Using Semi-active MR Dampers

T. Tse[1], and C.C. Chang[2]

[1] Research Assistant, Department of Civil Engineering, Hong Kong University of Science and Technology, Clear Water Bay, Kowloon, Hong Kong.
[2]Associate Professor, Department of Civil Engineering, Hong Kong University of Science and Technology, Clear Water Bay, Kowloon, Hong Kong.

ABSTRACT

Magnetorheological (MR) damper is one semi-active device that shows a great potential for vibration suppression and hazard mitigation of civil structures. One special advantage of the damper is that its damping characteristics can be adaptively and quickly altered by a varying magnetic field. This semi-active damper has been shown to be more effective than passive dampers in reducing the seismic response of flexible structures with a dominant natural period of 1.5 sec or more. Examples of these structures include base-isolated structures, cables of long-span bridges and tall buildings. In this study, the effectiveness of MR dampers for seismic protection of base-isolated structures is investigated. The damper is commanded by an inverse Bouc-Wen model together with a linear quadratic regulator (LQR) algorithm. An elevated highway bridge, modeled as a 2-degree-of-freedom system, is used to illustrate the effectiveness of the MR damper in protecting a base-isolated structure.

KEYWORDS

MR damper, Based-isolated Structure, Inverse Dynamic Model, LQR, Semi-active Control

INTRODUCTION

Magnetorheological (MR) damper is a newly developed semi-active device that shows great promises for civil engineering applications. The damper utilizes special characteristics of the MR fluid that possesses magnetically controllable yield strength and can reversibly change from free-flow to semi-solid in milli-seconds. This semi-active damper has been shown to be more effective than passive dampers in reducing the seismic response of flexible structures with a dominant natural period of 1.5 sec or more. A clipped-optimal control algorithm proposed by Dyke et al. (1996) has been adopted to

adjust the command voltage of the MR damper (Dyke et al. 1996, Dyke et al. 1998, Johnson et al. 2000). Analytical and experimental studies demonstrated that the MR damper, used in conjunction with the clipped optimal control algorithm, was effective for controlling a multi-story building model.

Alternatively, Chang and Tse (2001) proposed an inverse dynamic model to command the MR damper. The inverse dynamic model could directly estimate voltage that needed to be input into the damper in order to produce a desired damper force. The inverse dynamic model was derived from the Bouc-Wen model based on the following two assumptions: (i) the external displacement is much larger than the internal displacement, and (ii) the MR fluid always behaved in the post-yielding region. Under these assumptions, it was possible to directly link the damper force to the command voltage. Experimental and numerical results showed that the inverse model can provide a smoother tracing of target force as compared with the clipped-optimal model.

In this study, the effectiveness of MR damper for seismic protection of base-isolated structure is investigated. The damper is commanded by an inverse Bouc-Wen model together with a linear quadratic regulator (LQR) algorithm. An elevated highway bridge modeled as a 2-degree-of-freedom system is used to illustrate the effectiveness of MR damper in protecting this bridge under three different ground excitations: the El Centro, the Northridge, and the Kobe earthquake.

BOUC-WEN HYSTERESIS MODEL

A phenomenological model proposed by Spencer et al. (1997) to portray the hysteretic behavior of a prototype MR damper was shown to be accurate over a wide range of operation. The governing equations of the model are:

$$f = c_1\dot{y} + k_1(x - x_0) \tag{1}$$

$$\dot{y} = \frac{1}{c_0 + c_1}\left[\alpha z + c_0\dot{x} + k_0(x - y)\right] \tag{2}$$

$$\dot{z} = -\gamma|\dot{x} - \dot{y}|z|z|^{n-1} - \beta(\dot{x} - \dot{y})|z|^n + A(\dot{x} - \dot{y}) \tag{3}$$

$$\alpha = \alpha_a + \alpha_b u \tag{4}$$

$$c_0 = c_{0_a} + c_{0_b} u \tag{5}$$

$$c_1 = c_{1_a} + c_{1_b} u \tag{6}$$

$$\dot{u} = -\eta(u - v) \tag{7}$$

where x is the external displacement of the MR damper; f is the force generated by the MR damper; y is the internal displacement of the damper; c_0 and c_1 control the viscous damping at large and low velocities, respectively; k_0 and k_1 represent the stiffness at large velocity and the accumulator stiffness, respectively; x_0 is the initial displacement of spring k_1 associated with the nominal damper force due to the accumulator; α is a parameter associated with the evolutionary variable z; γ, β and A are the hysteresis parameters for the yield element; u and v are the output of a first-order voltage filter and the command voltage, respectively. The optimal values of the 14 parameters (k_0, k_1, γ, β, A, n, x_0, α_a, α_b, α_c, c_{0_a}, c_{0_b}, c_{1_a}, c_{1_b}, and η) were determined by solving a constrained nonlinear optimization with experimental data of a prototype MR damper. While large-scale MR dampers that are capable of producing forces in the order of 20 tons are currently under study, the force ranges for commercially available MR dampers are too small for practical application. For numerical demonstration, Erkus et al. (2002) suggested multiplying some of the parameters by a modification

factor MF to scale up the force of the prototype MR damper. The parametric values and the MF factor used in this study are summarized in Table 1. By setting the MF factor at 1264, the force range of the MR damper will be in the order of a few hundred tons.

INVERSE DYNAMIC MODEL

It has been suggested that the force generated by MR damper cannot be directly commanded. Only the voltage v supplied to the current driver for the MR damper can be directly changed. A clipped-optimal control algorithm proposed by Dyke et al. (1996), based on acceleration feedback, is thus used along with MR damper to approximately generate the optimal control force f_c. The command voltage is determined based on how the damper force f compared with the desired control force f_c,

$$v = v_{max} H[(f_c - f)f] \tag{8}$$

where v_{max} is the maximum voltage to the current driver associated with saturation of the magnetic field in the MR damper and $H(\bullet)$ is the Heaviside step function. However it was found that the force generated by the MR damper using the clipped algorithm oscillated about the target control force. This was primarily due to the switching of voltage at either its minimum or maximum value.

Chang and Tse (2001) proposed an approximate formula based on the Bouc-Wen hysteretic model with the following two assumptions: (i) the external displacement x was much larger than the internal displacement y; and (ii) the evolutionary variable z was assumed to be equal to its ultimate hysteretic strength z_u (Spencer 1986), i.e.,

$$z \cong z_u = \mathrm{sgn}(\dot{x} - \dot{y})\left(\frac{A}{\gamma + \beta}\right)^{1/n} \cong \mathrm{sgn}(\dot{x})\left(\frac{A}{\gamma + \beta}\right)^{1/n} \tag{9}$$

Based on these two assumptions, the damper force f can then be approximated as,

$$f \cong \frac{(c_{1_a} + c_{1_b} u)}{(c_{0_a} + c_{1_a}) + (c_{0_b} + c_{1_b})u}\left[(\alpha_a + \alpha_b u)z_u + (c_{0_a} + c_{0_b} u)\dot{x} + k_0 x\right] + k_1(x - x_0) \tag{10}$$

The evolutionary variable z is found to be equal to the ultimate hysteretic strength for most regions. This suggests that the MR fluid operates in its post-yielding region for most of the time. There is some discrepancy for forces at low velocity, which is attributed to the second assumption where no intermediate values are allowed for z. The discrepancy however does not affect the control performance since the force magnitudes in these regions are small and the time duration is short.

It can be seen from Eqn. 10 that the damper force is a function of the voltage filter output u, the external displacement x and velocity $\dot{x}$. If the magnitude of the damper force f is specified (i.e. optimal control force f_c determined from control algorithm), Eqn. 10 can be rearranged to a quadratic function in u:

$$p_2 u^2 + p_1 u + p_0 = 0 \tag{11}$$

$$p_2 = c_{1_b}\alpha_b z_u + c_{0_b} c_{1_b}\dot{x} \tag{12}$$

$$p_1 = (c_{1_a}\alpha_b + c_{1_b}\alpha_a)z_u + (c_{0_a} c_{1_b} + c_{1_a} c_{0_b})\dot{x} + c_{1_b} k_0 x + (c_{0_b} + c_{1_b})[k_1(x - x_0) - f] \tag{13}$$

$$p_0 = c_{1_a}\alpha_a z_u + c_{0_a} c_{1_a}\dot{x} + c_{1_a} k_0 x + (c_{0_a} + c_{1_a})[k_1(x - x_0) - f] \tag{14}$$

It is seen that u at any time instance can be solved rather easily and the corresponding command voltage v can then be numerically obtained from Eqn. 7. Two experiments were conducted to illustrate how the damper forces could be commanded to trace desired target forces. Results showed that this inverse model could provide a smoother tracing of target forces as compared to the clipped algorithm.

NUMERICAL EXAMPLE

Modeling of elevated highway bridge

An elevated highway bridge modeled as a 2-degree-of-freedom system (see Fig. 1) proposed by Erkus et al. (2002) is used here to illustrate the effectiveness of the MR damper. The MR damper is rigidly connected between the pier and the bridge deck. The equations of motion for this system and the MR damper are

$$\boldsymbol{M}_s\ddot{\boldsymbol{s}} + \boldsymbol{C}_s\dot{\boldsymbol{s}} + \boldsymbol{K}_s\boldsymbol{s} = \boldsymbol{\Gamma}\mathrm{f_c} - \boldsymbol{M}_s\Lambda\ddot{\mathrm{s}}_g \tag{15}$$

where $\boldsymbol{s}$ and $\ddot{\mathrm{s}}_g$ are the displacement vector of the building model and the earthquake ground acceleration, respectively; $\mathrm{f_c}$ is the control force; $\boldsymbol{\Gamma}$ and Λ represent the location of the MR damper and the excitation, respectively; and $\boldsymbol{M}_s$, $\boldsymbol{C}_s$ and $\boldsymbol{K}_s$ are the mass matrix, the damping matrix and the stiffness matrix with the following values:

$$\boldsymbol{M}_s = 10^3\begin{bmatrix}100 & 0\\ 0 & 500\end{bmatrix}\ \mathrm{kg};\quad \boldsymbol{C}_s = 10^3\begin{bmatrix}321.6 & -196\\ -196 & 196\end{bmatrix}\ \mathrm{N\cdot sec/m};\quad \boldsymbol{K}_s = 10^6\begin{bmatrix}23.5 & -7.7\\ -7.7 & 7.7\end{bmatrix}\ \mathrm{N/m}$$

For semi-active control, the mass and the stiffness matrices remain the same, while the damping coefficient of bearing c_2 is set to 0. The state-space form of Eq. 16 is

$$\dot{\boldsymbol{x}} = \boldsymbol{A}\boldsymbol{x} + \boldsymbol{B}\mathrm{f_c} + \boldsymbol{E}\ddot{\mathrm{s}}_g \tag{16}$$

where $\boldsymbol{x}$ is the state vector. The matrices $\boldsymbol{A}$, $\boldsymbol{B}$, and $\boldsymbol{E}$ can be written as,

$$\boldsymbol{A} = \begin{bmatrix}\boldsymbol{0} & \boldsymbol{I}\\ -\boldsymbol{M}_s^{-1}\boldsymbol{K}_s & -\boldsymbol{M}_s^{-1}\boldsymbol{C}_s\end{bmatrix};\quad \boldsymbol{B} = \begin{bmatrix}\boldsymbol{0}\\ \boldsymbol{M}_s^{-1}\boldsymbol{\Gamma}\end{bmatrix};\quad \boldsymbol{E} = -\begin{bmatrix}\boldsymbol{0}\\ \Lambda\end{bmatrix}; \tag{17a-c}$$

The control force $\mathrm{f_c}$ depends on the gain matrix $\boldsymbol{G}$ as follows,

$$\mathrm{f_c} = -\boldsymbol{G}\boldsymbol{x} \tag{18}$$

The gain matrix $\boldsymbol{G}$ is a constant matrix depending on the control algorithm used.

Control Algorithm

In this study, the linear-quadratic regulator (LQR) algorithm is used for the semi-active control. The control force $\mathrm{f_c}$ is so determined that it minimizes the following quadratic objective function,

$$\mathrm{J} = \int_0^\infty (\boldsymbol{x}^{\mathrm{T}}\boldsymbol{W}\boldsymbol{x} + \mathrm{f_c}^{\mathrm{T}}\boldsymbol{R}\mathrm{f_c})\mathrm{dt} \tag{19}$$

where $\boldsymbol{W}$ and $\boldsymbol{R}$ are the weighting matrices. By adjusting these weighting matrices, one can reduce the structural responses with different objectives, such as reducing the pier displacement, the deck displacement, or the inter-story drift. The weighting matrices used in this study are assumed to be,

$$\boldsymbol{W} = \frac{1}{2}\begin{bmatrix} rk_1 + k_2 & -k_2 & 0 & 0 \\ -k_2 & k_2 & 0 & 0 \\ 0 & 0 & rm_1 + m_2 & -m_2 \\ 0 & 0 & -m_2 & m_2 \end{bmatrix}; \quad R=10^{-9} \tag{20a,b}$$

where k_1 (=15.8 MN/m) and k_2 (=7.7 MN/m) are the stiffness of pier and deck respectively; m_1 (=100 tons) and m_2 (=500 tons) are the mass of pier and deck respectively; the weighting parameter r defines the relative importance of the pier and the deck responses. A larger value of r would decrease the pier response and a smaller value would decrease the deck response.

Numerical Results

To quantify the control effect, three performance indices are introduced.

$$J_1 = \max(s_1); \; J_2 = \max(s_2); \; J_3 = \max(s_2 - s_1) \tag{21a-c}$$

where s_1 and s_2 are the pier and the deck displacement respectively. The weighting parameter r is set to be 0.1, which means the deck response is to be minimized. The time increment is set to be 0.005 sec. It is also assumed that an ideal actuator that can produce exactly the desired control forces specified by the control algorithm is available for comparison. Assume that the elevated bridge is excited by ground motion of three earthquakes: the El Centro, the Northridge and the Kobe.

Figures 2-4 show the simulation results for the three different ground excitations. It can be seen from the figures that the inter-story drift $s_1 - s_2$ is substantially reduced. Also the responses of the bridge controlled by the ideal actuator nearly coincide with those controlled by the MR damper. The MR damper forces are seen to coincide with the forces of the ideal actuator for all three earthquakes. These results demonstrate that the inverse dynamic model can be used effectively for commanding the MR damper in the control application. The three performance indices for the bridge under the three earthquake excitations are summarized in Table 2. Although the pier response J_1 appears to increase slightly under the El Centro and the Kobe earthquake, it can be seen clearly that the deck response J_2 and the drift between the deck and the pier J_3 are both reduced significantly for all three earthquakes. The control effect of installing an MR damper between the deck and the pier is quite vividly demonstrated in this example.

CONCLUDING REMARKS

The effectiveness of MR dampers for seismic protection of base-isolated structures is investigated in this study. The damper is commanded by an inverse Bouc-Wen model together with a linear quadratic regulator (LQR) algorithm. This inverse Bouc-Wen model provides a direct relationship between the target control force computed from the LQR algorithm and the required voltage input to the damper. An elevated highway bridge, modeled as a 2-degree-of-freedom system, is used to illustrate the applicability of the MR damper. Results show that the MR damper can effectively reduce the deck response and the drift between the deck and the pier without significantly increase the pier response.

ACKNOWLEDGEMENT

This work is supported by the Hong Kong Research Grant Council Competitive Earmarked Research Grant HKUST 6218/99E.

REFERENCE

Chang, C.C. and Tse, T. (2001). A Bouc-Wen Based Inverse Dynamic Model for Ccommanding MR Dampers. Submitted to *Earthquake Engineering and Structural Dynamics*.

Dyke, S.J., Spencer, Jr. B.F., Sain, M.K., and Carlson, J.D. (1996). Modeling and Control of Magnetorheological Dampers for Seismic Response Reduction. *Smart Materials and Structures*, **5**, 565-575.

Dyke, S.J., Spencer, Jr. B.F., Sain, M.K., and Carlson, J.D. (1998). Experimental Study of MR Dampers for Seismic Protection. *Smart Materials and Structures: Special Issue on Large Civil Structures*. **7:5**, 693-703.

Erkus, B., Abe, M., and Fujino Y. (2002). Investigation of Semi-active Control for Seismic Protection of Elevated Highway Bridges. *Engineering Structures*, **24:3**, 281-293.

Johnson, E.A., Christenson, R.E. and Spencer, Jr. B.F. (2000). Semiactive Damping of Cables with Sag." Proceedings of the International Conference on *Advances in Structural Dynamics*, Eds. J.M. Ko and Y.L Xu, 13-15 Dec. 2000, Hong Kong, Elsevier Service Ltd. Vol. I, 327-334.

Spencer Jr., B.F., Dyke, S.J., Sain, M.K. and Carlson, J.D. (1997). Phenomenological Model for Magnetorheological Dampers. *Journal of Structural Engineering*, ASCE, **123:3**, 230-238.

Spencer, Jr., B.F. (1986). *Reliability of Randomly Excited Hysteretic Structures*. Springer-Verlag, New York.

TABLE 1
PARAMETERS FOR THE MR DAMPER

Parameter	Value	Parameter	Value
MF	1264	α_a	140 MF N/cm
c_{0_a}	21 MF N·sec/cm	α_b	695 MF N/cm·V
c_{0_b}	3.5 MF N·sec/cm·V	γ	363 cm^{-2}
k_0	46.9 MF N/cm	β	363 cm^{-2}
c_{1_a}	283 MF N·sec/cm	A	301
c_{1_b}	2.95 MF N·sec/cm·V	n	2
k_1	5.0 MF N/cm	η	190 sec^{-1}
x_0	14.3 cm		

TABLE 2
PERFORMANCE INDICES J_1, J_2, AND J_3 OF THE ELEVATED HIGHWAY BRIDGE

	J_1 (cm)			J_2 (cm)			J_3 (cm)		
	No Control	Ideal	MR	No Control	Ideal	MR	No Control	Ideal	MR
El Centro	6.91	7.99	8.08	20.05	8.26	8.33	13.73	2.03	1.95
Northridge	18.03	17.62	16.68	52.80	18.86	18.85	34.89	4.53	4.81
Kobe	16.77	25.93	22.73	42.75	25.46	26.21	29.92	6.00	7.20

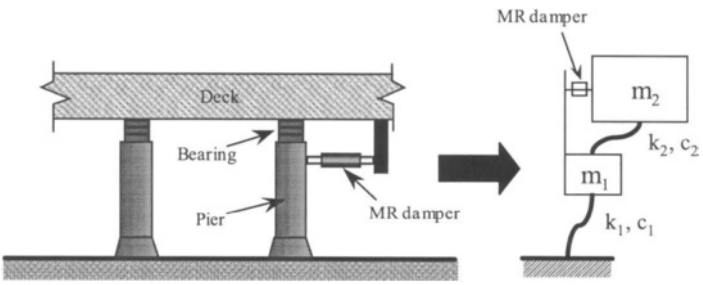


Figure 1: The elevated bridge and its mathematical model

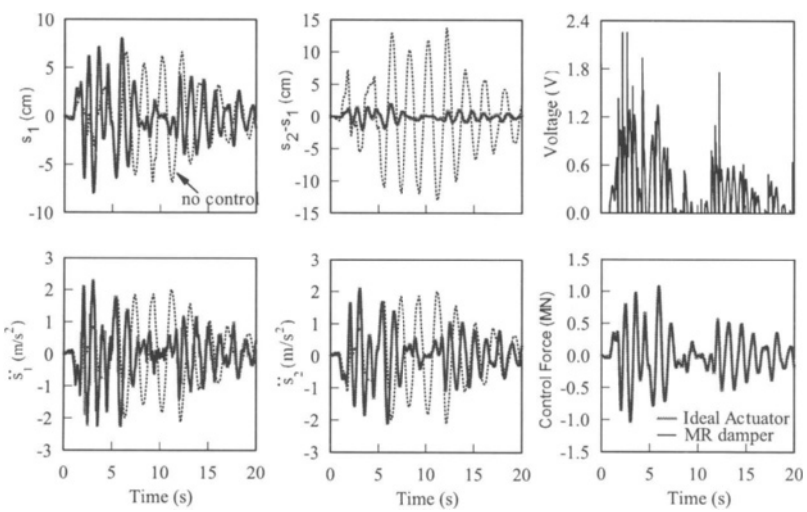


Figure 2: Results under the El Centro ground excitation

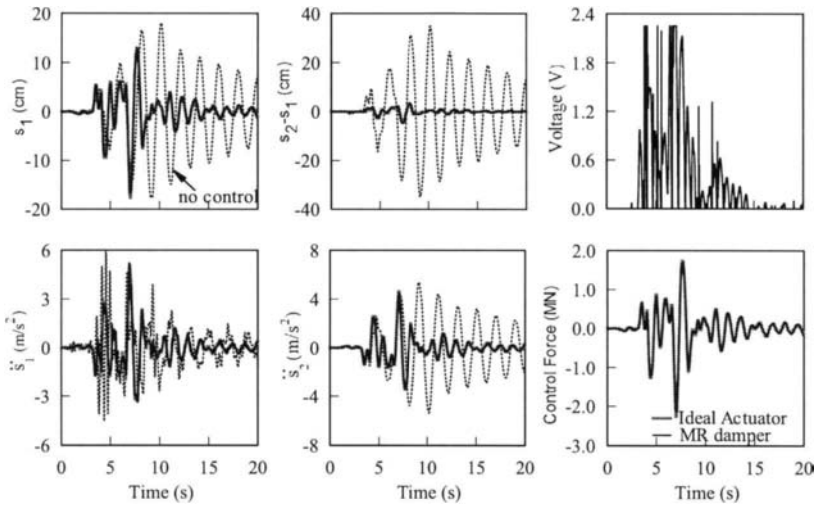


Figure 3: Results under the Northridge ground excitation

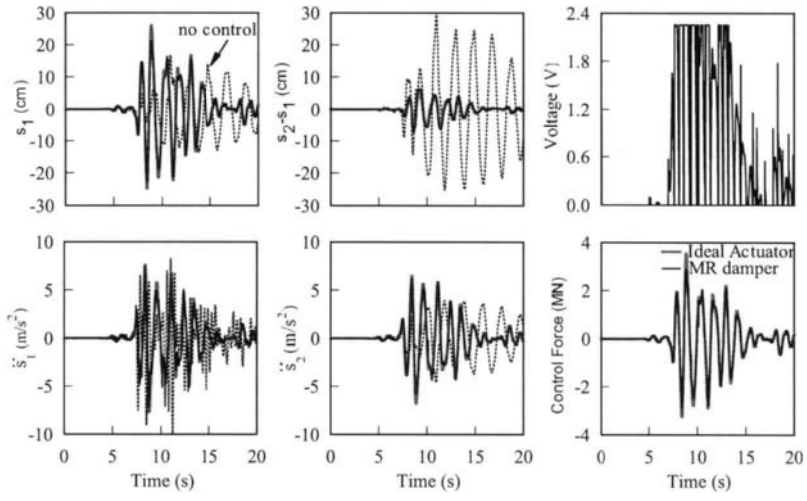


Figure 4: Results under the Kobe ground excitation

Advances in Building Technology, Volume 1
M. Anson, J.M. Ko and E.S.S. Lam (Eds.)
© 2002 Elsevier Science Ltd. All rights reserved

SEMI-ACTIVE TLCDS USING MAGNETO-RHEOLOGICAL FLUIDS FOR VIBRATION MITIGATION OF TALL BUILDINGS

J. Y. Wang[1], Y. Q. Ni[1], J. M. Ko[1], B. F. Spencer, Jr.[2]

[1]Department of Civil and Structural Engineering, The Hong Kong Polytechnic University, Hung Hom, Kowloon, Hong Kong
[2]Department of Civil and Environmental Engineering, University of Illinois at Urbana-Champaign, Urbana, Illinois 61801, USA

ABSTRACT

A semi-active tuned liquid column damper using magneto-rheological fluid (MR-TLCD) is proposed for wind-induced vibration mitigation of high-rise buildings. The magneto-rheological (MR) fluids can reversibly change from a free-flowing, linear viscous fluid to a semi-solid with controllable yield strength in milliseconds when exposed to a magnetic field. They are used as damping fluids to devise semi-active MR-TLCDs with alterable fluid viscosity. The sharply alterable fluid viscosity results in adjustable and controllable damping forces that achieve real-time structural vibration control. By applying a magnetic field to the MR fluid at the bottom part of a U-shaped tube, the damping effects of an MR-TLCD can be changed continuously through altering the magnetic field strength. Making use of the equivalent linearization technique, a stochastic response analysis for tall buildings incorporating semi-active MR-TLCDs subjected to random wind excitation is formulated. A 50-storey tall building using MR-TLCDs for wind-induced vibration mitigation is considered as a case study. The control effectiveness using MR-TLCDs is evaluated by comparing the RMS acceleration and deflection of the structure with an MR-TLCD damping system and with a conventional TLCD system.

KEYWORDS

Tuned liquid column damper (TLCD), magneto-rheological (MR) fluid, tall building, wind-induced excitation, random response analysis, vibration mitigation.

INTRODUCTION

The tuned liquid column damper (TLCD) is a supplemental energy dissipation system that relies on the motion of the liquid column in a U-shaped tube to counteract the action of external forces acting on the structure. Due to its cost-effectiveness, simplicity in installation, and low maintenance costs, the TLCD has attracted significant interest for researchers and engineers (Xu et al. 1992; Belendra et al. 1995, 1999).

The dynamic property and damping effect for conventional TLCDs are determined from the geometric construction of the liquid column. Therefore, the damping coefficient is unchangeable. However, the wind and earthquake forces are random in nature, and the extent and frequency content of the external forces acting on a structure are different at different times. In this sense, a damping-variable TLCD is desirable to achieve optimal damping under various load conditions, for example, using a controllable valve to adjust the TLCD orifice opening (Yalla et al. 2001).

In this study, a semi-active tuned liquid column damper using magneto-rheological fluid (MR-TLCD) is proposed, as shown schematically in Figure 1. The essential characteristic of MR fluids is their ability to reversibly change from a free flowing, linear viscous liquid to a semi-solid having a controllable yield strength in milliseconds when exposed to a magnetic field. By adjusting the strength of the applied magnetic field, the yield stress of the MR fluid, and thus the controllable damping of the MR-TLCD, can be developed.

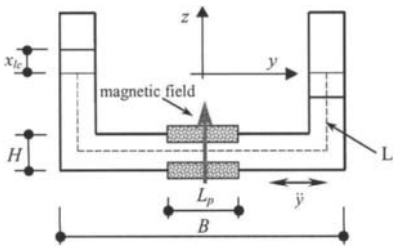


Figure 1: Schematic of MR-TLCD

STRUCTURAL SYSTEM WITH MR-TLCDS

A high-rise building is generally considered as a lumped-mass system with n degrees-of-freedom (DOF) corresponding to the n floor stories. Wind loading in the along-wind direction is applied to discrete lumped masses. To derive the analytical formulation, the case of installing p MR-TLCDs on selected floors is considered. It is assumed that the wind load does not act on the dampers directly.

Mechanics of MR Fluid in a Rectangular Duct

As shown in Figure 2, the motion of the MR fluid between fixed poles can be modeled by the parallel-plate model (Yang et al. 2002), The pressure drop developed along a pressure-driven flow can be assumed as the sum of a viscous component Δp_η and a component Δp_τ due to the field-dependent yield stress (Phillips 1969; Jolly et al. 1999).

$$\Delta p = \Delta p_\eta + \Delta p_\tau = \frac{12\eta Q L_p}{h^3 w} + \frac{c\tau_y L_p}{h} \tag{1}$$

where L_p, h and w are the length, depth and width of the flow between the fixed poles; Q is the volumetric flow rate; η is the field-independent viscosity and τ_y is the yield stress developed by the applied field; c is a function of the flow velocity and has a value ranging from 2.07 to 3.07 (Spencer et al. 1998; Yang et al. 2002).

The head loss and the pressure drop are related through

$$h_p = \frac{\Delta p}{g\rho} = \frac{12\eta Q L_p}{g\rho h^3 w} + \frac{c\tau_y L_p}{g\rho h} \tag{2}$$

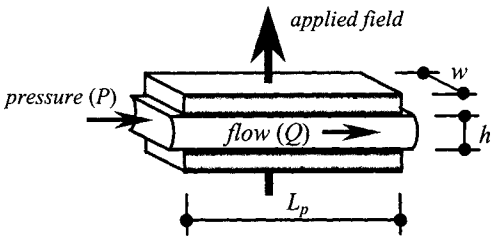


Figure 2: Operational model for pressure-driven fluid

The first term in the previous equation is the head loss due to the viscosity, which can be expressed as

$$h_{pv} = \frac{\delta_v V^2}{2g} \tag{3}$$

in which the head loss coefficient δ_v is obtained by

$$\delta_v = \frac{48}{\mathrm{Re}_H (1+\frac{h}{w})^2}\frac{L_p}{h}, \qquad \mathrm{Re}_H = \frac{2\rho V(w+h)}{\eta w h} \tag{4}$$

where Re_H is the Reynold number for rectangular duct. Then the total head loss along the complete fluid column can be computed from

$$h_w = \frac{\delta V^2}{2g} + \frac{c\tau_y L_p}{g\rho h}, \quad \delta = \frac{48}{\mathrm{Re}_H (1+\frac{h}{w})^2}\frac{L}{h} + \sum_j \zeta_j \tag{5}$$

where δ is referred as the overall head loss coefficient, V is the fluid velocity, ζ_j is the coefficient of minor loss, including elbows and orifices.

Governing Equation of MR-TLCD

The governing equation of an MR-TLCD is given by

$$\rho A L\ddot{x}_{lc} + \frac{1}{2}\rho A\delta|\dot{x}_{lc}|\dot{x}_{lc} + \frac{c\tau_y AL_p}{h}\frac{\dot{x}_{lc}}{|\dot{x}_{lc}|} + 2\rho A g x_{lc} = -\rho AB\ddot{y} \tag{6}$$

where A, L and B denote the cross-sectional area, the total length, and the horizontal length of the liquid column; ρ is the liquid density; and $\ddot{y}$ is the acceleration of the structure. The MR-TLCD has a natural frequency of $\omega_{lc} = \sqrt{2g/L}$, which is not affected by the applied field.

It is noted that the above governing equation is nonlinear. To simplify the computation, the equivalent linearization technique is adopted in dealing with the nonlinear damping terms. Let the equivalent linearized equation be

$$\rho A L\ddot{x}_{lc} + c_{lc}\dot{x}_{lc} + 2\rho A g x_{lc} = -\rho AB\ddot{y} \tag{7}$$

Assuming that the external excitation can be modeled as a zero-mean stationary Gaussian process, the equivalent damping coefficient, c_{lc}, can then be derived by minimizing the mean square value of the equation error (Iwan & Yang 1972; Wen 1980):

$$c_{lc} = \sqrt{\frac{2}{\pi}}\rho A \delta \sigma_{\dot{x}_{lc}} + \sqrt{\frac{2}{\pi}}\frac{c\tau_y A L_p}{h\sigma_{\dot{x}}} \tag{8}$$

The corresponding equivalent damping ratio is

$$\xi_{lc} = \frac{c_{lc}}{2\rho A L \omega_{lc}} = \frac{1}{2\sqrt{\pi g L}}(\delta\sigma_{\dot{x}} + \frac{c\tau_y L_p}{\rho h \sigma_{\dot{x}}}) \tag{9}$$

where $\sigma_{\dot{x}}$ is the standard deviation of the fluid velocity. Since the value of $\sigma_{\dot{x}}$ is unknown *a priori*, an iterative procedure is necessary in the analysis.

Analytical Model

By taking the motion of dampers as the control force, the governing equations for vibration of the coupled MR-TLCD-structure system can be expressed as

$$M_j \ddot{y}_j + C_j \dot{y}_j + K_j y_j = F_j(t) + F_{dj}(t) \qquad (j = 1,2,\cdots,n) \tag{10}$$

$$m_{lc,q}\ddot{x}_{lc,q} + c_{lc,q}\dot{x}_{lc,q} + k_{lc,q}x_{lc,q} = -\lambda_q m_{lc,q}\ddot{\bar{y}}_q \qquad (q = 1,2,\cdots,p) \tag{11}$$

where M_j, C_j, K_j, $F_j(t)$ are the mass, damping, stiffness, and external force of the structure at the jth floor; $m_{lc,q}$, $c_{lc,q}$, $k_{lc,q}$ are the mass, equivalent damping, and stiffness of the qth MR-TLCD, respectively. The control force of the qth MR-TLCD, which is installed at the jth floor, is obtained as

$$F_{dj}(t) = m_{lc,q}(\frac{1}{\lambda_q}((1.0-\lambda_q{}^2)\ddot{x}_{dq} + 2\xi_{dq}\omega_{dq}\dot{x}_{dq} + \omega_{dq}^2 x_{dq}))^T, \quad \lambda_q = \frac{B_q}{L_q} \tag{12}$$

In the frequency domain, the responses can be written as

$$[S_r(\omega)] = [H(i\omega)][S_F(\omega)][H^*(i\omega)]^T \tag{13}$$

in which, the transfer function matrices corresponding to cases without and with the dampers being installed are

$$[\tilde{H}(i\omega)] = diag[\omega_1^2 - \omega^2 + 2i\xi_1\omega_1\omega \quad \omega_2^2 - \omega^2 + 2i\xi_2\omega_2\omega \quad \cdots \quad \omega_n^2 - \omega^2 + 2i\xi_n\omega_n\omega] \tag{14}$$

$$[H(i\omega)] = ([\tilde{H}(i\omega)]^{-1} - [\Phi]^T[m_{lc}][D][\tilde{H}_d(i\omega)][\Phi])^{-1} \tag{15}$$

where $[\tilde{H}_d(i\omega)]$ is the transfer function matrix of MR-TLCDs,

$$[\tilde{H}_d(i\omega)] = diag\left[\frac{\lambda_1\omega^2}{\omega_{d1}^2 - \omega^2 + 2i\xi_{d1}\omega_{d1}\omega} \quad \frac{\lambda_2\omega^2}{\omega_{d2}^2 - \omega^2 + 2i\xi_{d2}\omega_{d2}\omega} \quad \cdots \quad \frac{\lambda_p\omega^2}{\omega_{dp}^2 - \omega^2 + 2i\xi_{dp}\omega_{dp}\omega}\right] \tag{16}$$

and $[D]$ denotes the factor of the control force having a form of

$$D_q = \frac{1}{\lambda_q}((\lambda_q{}^2 - 1)\omega^2 + \omega_{dq}^2 + 2i\xi_{dq}\omega_{dq}\omega) \qquad (q = 1,2,\cdots,p) \tag{17}$$

The response quantities of displacement spectrum at jth DOF can be calculated by

$$\tilde{S}_{y,j}(\omega) = \{\Phi\}_j[\tilde{H}(i\omega)][\overline{M}]^{-1}[\Phi]^T[S_F(\omega)][\Phi]([\overline{M}]^{-1})^T[\tilde{H}^*(i\omega)]\{\Phi\}_j^T \quad \text{(without dampers)} \tag{18}$$

$$S_{y,j}(\omega) = \{\Phi\}_j [H(i\omega)][\overline{M}]^{-1}[\Phi]^T [S_F(\omega)][\Phi][[\overline{M}]^{-1}]^T [H^*(i\omega)]\{\Phi\}_j^T \quad \text{(with MR-TLCDs)} \tag{19}$$

The root-mean-square (RMS) displacement responses are

$$\tilde{\sigma}_{y,j}^2 = \int_0^{+\infty} \tilde{S}_{y,j} d\omega \quad \text{(without dampers)} \tag{20}$$

$$\sigma_{y,j}^2 = \int_0^{+\infty} S_{y,j} d\omega \quad \text{(with MR-TLCDs)} \tag{21}$$

Similarly, the root-mean-square (RMS) acceleration responses can be obtained from

$$\tilde{\sigma}_{\ddot{y},j}^2 = \int_0^{+\infty} \omega^4 \tilde{S}_{y,j} d\omega \quad \text{(without dampers)} \tag{22}$$

$$\sigma_{\ddot{y},j}^2 = \int_0^{+\infty} \omega^4 S_{y,j} d\omega \quad \text{(with MR-TLCDs)} \tag{23}$$

The effectiveness of the MR-TLCD in mitigating the wind-induced vibration is quantified using the following indicators:

$$\alpha_{y,j} = (1 - \frac{\sigma_{y,j}}{\tilde{\sigma}_{y,j}}) \times 100, \quad \alpha_{\ddot{y},j} = (1 - \frac{\sigma_{\ddot{y},j}}{\tilde{\sigma}_{\ddot{y},j}}) \times 100 \tag{24}$$

Wind Load Spectrum

The spectrum of longitudinal turbulence proposed by Davenport (1961) has been used to simulate the wind loading in this study. The cross-spectral density representation of along-wind force in the frequency domain is given as

$$S_{F,ij}(\omega) = \rho_a^2 C_D^2 V_{10}^2 A_i A_j (\frac{z_i z_j}{100})^{\alpha} coh(z_i, z_j, \omega) \frac{S(\omega)}{2\pi} \tag{25}$$

where the coherence function, $coh(z_i, z_j, \omega)$, reflecting the spanwise correlation of the fluctuating force, is calculated by

$$coh(z_i, z_j, \omega) = \exp(-\frac{C_z \cdot \omega \cdot (z_i - z_j)}{2\pi V_{10}}) \tag{26}$$

The wind velocity spectral density is given by

$$S(\omega) = 8\pi K_D V_{10}^2 \frac{n^2}{\omega(1+n^2)^{4/3}}, \quad n = \frac{600\omega}{V_{10}\pi} \tag{27}$$

in which K_D is the ground coarse coefficient; α is a power-law exponent; C_D is the drag coefficient; C_z is the exponential decay constant; ρ_a is the air density; ω is circular frequency in rad/s; V_{10} is the mean wind velocity at 10 m above the ground; z_i and z_j are heights of ith and jth nodes; A_i; and A_j are the equivalent projection areas at z_i and z_j, respectively.

NUMERICAL EXAMPLE

A 50-storey building, 162m in height, is used as an example to demonstrate the effectiveness of MR-TLCD system in mitigating wind-induced vibration. The total mass of the building, $\tilde{M}$, is 27,774 ton.

Modal properties obtained from a three-dimensional finite element model in the along-wind direction are listed in Table 1. Damping ratios for all modes are assumed to be 4.0%. The first three modes, which contribute over 85% in the along-wind vibration are taken into account in the analysis. Two cases, i.e., installation of one MR-TLCD on the top-floor and one at the top and another at the 25th floor, are considered. The following values of the MR-TLCD and wind loading parameters have been adopted in this example: ρ=2500kg/m^3, c=2.1, δ=30, λ=0.9, L_p=0.5m, h=0.3m, ρ_a=1.28kg/m^3, α=0.19, V_{10}=45.3 m/s, K_D=0.02, C_D=1.2, C_z=10.

Tables 2 and 3 give the mitigation indicators at the top floor when the mass ratio ($\mu = m_{lc} / \tilde{M}$) is equal to 1.0% and 2.5%, respectively. The corresponding frequency ratio ($\mu_f = \omega_{lc} / \omega$) is set to be 1.0 and 0.95. It is noted when no magnetic field is applied, i.e. $\tau_y = 0$, the damper(s) has little effect. As the magnetic field, consequently the fluid yield stress, increases, a larger response reduction is achieved. However, it should be pointed out that there exists an optical value to make the MR-TLCD have an ideal performance. The installation of the second MR-TLCD at the 25th floor contributes a little in vibration mitigation.

Figure 3 shows the displacement and acceleration spectra of the building with an MR-TLCD installed on the top. The resonant peak responses are significantly reduced. Figures 4 and 5 illustrate the

TABLE 1
MODAL PROPERTIES OF BUILDING

Mode order	1	2	3	4	5
f(Hz)	0.216	0.940	2.278	3.941	5.932
ω (rad/s)	1.355	5.904	14.314	24.762	37.269
Mass factor (%)	66.82	13.08	5.51	3.11	1.92

TABLE 2
DISPLACEMENT AND ACCELERATION MITIGATION INDICATORS (μ=1.0%, μ_f=1.0)

	$p=1$			$p=2$		
τ_y	$\alpha_{y,51}$	$\alpha_{\ddot{y},51}$	ξ_{lc}	$\alpha_{y,51}$	$\alpha_{\ddot{y},51}$	ξ_{lc}
0.0	1.11	4.58	0.003	0.73	4.35	0.003
10.0	9.57	17.17	0.020	10.46	18.94	0.020
20.0	14.06	23.94	0.039	14.88	25.64	0.039
40.0	16.44	27.48	0.078	16.98	28.73	0.079
60.0	16.03	26.75	0.114	16.47	27.83	0.116
100.0	14.02	23.59	0.181	14.38	24.53	0.183

TABLE 3
DISPLACEMENT AND ACCELERATION MITIGATION INDICATORS (μ=2.5%, μ_f=0.95)

	$p=1$			$p=2$		
τ_y	$\alpha_{y,51}$	$\alpha_{\ddot{y},51}$	ξ_{lc}	$\alpha_{y,51}$	$\alpha_{\ddot{y},51}$	ξ_{lc}
20.0	18.20	28.32	0.041	19.73	31.64	0.043
40.0	27.34	43.91	0.098	28.50	47.06	0.103
60.0	30.63	50.55	0.161	31.22	52.80	0.166
80.0	31.55	52.91	0.220	31.94	54.68	0.226
100.0	31.62	54.49	0.275	31.92	55.01	0.281
150.0	30.65	52.38	0.397	30.87	53.63	0.403

displacement and acceleration root-mean-square (RMS) response profiles. The MR-TLCD is found to be capable of reducing responses along the entire height of the building. However, the reduction is not uniformly distributed.

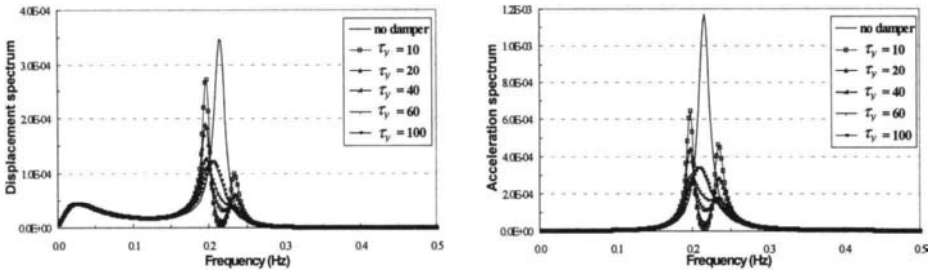


Figure 3: Displacement and acceleration spectra (p=1, μ=1.0%, μ_f=1.0)

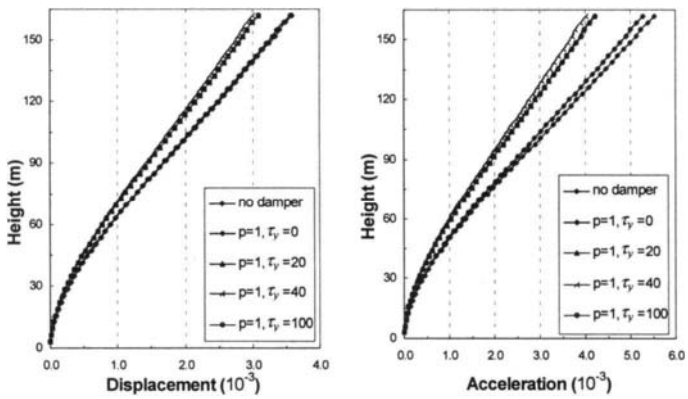


Figure 4: RMS displacement and acceleration response profiles (μ=1.0%, μ_f=1.0)

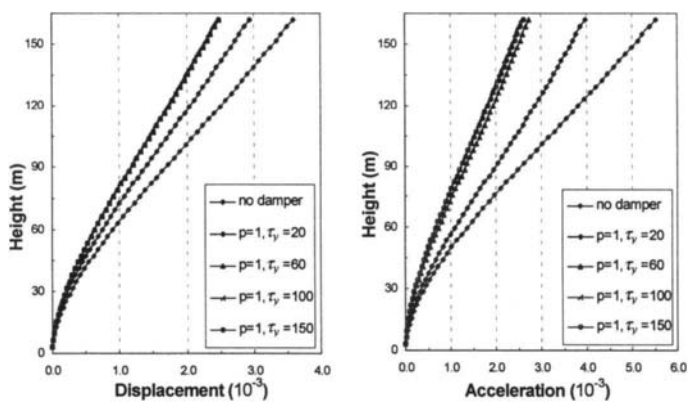


Figure 5: RMS displacement and acceleration response profiles (μ=2.5%, μ_f=0.95)

CONCLUSION

A semi-active tuned liquid column damper using magneto-rheological fluid (MR-TLCD) is proposed in the present study. Making use of the equivalent linearization technique, a random response analysis for an MR-TLCD-structure system under stochastic wind excitation is conducted. Numerical analysis of a 50-storey building demonstrates that using a larger mass ratio provides a larger reduction in vibration response and MR-TLCDs are able to supply the optimal damping requirement facilely. Further study aims to evaluate the effectiveness of MR-TLCDs for structures with varying dynamic characteristics and to use MR-TLCDs in hybrid damping systems, as well as to develop a real-time control strategy for semi-active seismic response mitigation.

ACKNOWLEDGEMENTS

The work presented in this paper was supported by a grant from The Hong Kong Polytechnic University through the Area of Strategic Development Programme (Research Centre for Urban Hazard Mitigation). This support is gratefully acknowledged.

References

Balendra T., Wang C.M. and Cheong H.F. (1995). Effectiveness of tuned liquid column damper for vibration control of towers. *Engineering Structures* **17:9,** p668-675.

Balendra T., Wang C.M. and Rakesh G. (1999). Effective of TLCD on various structural systems. *Engineering Structures* **21,** 291-305.

Davenport A.G. (1961). The application of statistical concepts to the wind loading of structures. *Proc., Inst. of Civil Engineer* **19,** 449-472.

Iwan W.D. and Yang I.M. (1972). Application of statistical linearization techniques to nonlinear multidegree-of-freedom systems. *Journal of Applied Mechanics* **39,** 545-550.

Jolly M.R., Bender J.W. and Carlson J.D. (1999). Properties and applications of commercial magnetorheological fluids. *Journal of Intelligent Material Systems and Structures* **10,** 5-13.

Phillips R.W. (1969). Engineering applications of fluids with variable yield stress, PhD Thesis, University of California, Berkeley, USA.

Spencer Jr. B.F., Yang G., Carlson J.D. and Sain M.K. (1998). Smart dampers for seismic protection of structures: a full-scale study. *Proceedings of 2nd World Conference on Structural Control* **1,** Kyoto, Japan, 417-426.

Wen Y.K. (1980). Equivalent linearization for hysteretic systems under random excitation. *Journal of Applied Mechanics* **47,** 150-154.

Yalla S.K., Kareem A. and Kantor J.C. (2001). Semi-active tuned liquid column dampers for vibration control of structures. *Engineering Structures* **23,** 1469-1479.

Yang G., Spencer Jr. B.F., Carlson J.D. and Sain M.K. (2002). Large-scale MR fluid dampers: modeling and dynamic performance considerations. *Engineering Structures* **24,** 309-323.

Xu Y.L., Samali B. and Kwok K.C.S. (1992). Control of along-wind response of structures by mass and liquid dampers. *Journal of Engineering Mechanics* **118:1,** 20-39.

Advances in Building Technology, Volume 1
M. Anson, J.M. Ko and E.S.S. Lam (Eds.)
© 2002 Elsevier Science Ltd. All rights reserved

PHENOMENOLOGICAL MODEL OF LARGE-SCALE MR DAMPER SYSTEMS

G. Yang,[1] B.F. Spencer, Jr.,[1] H.J. Jung,[2] and J.D. Carlson[3]

[1] Department of Civil and Environmental Engineering, University of Illinois at Urbana-Champaign
205 North Matthews Ave., Urbana, IL 61801, USA

[2] Dept. of Civil Engineering, Korea Advanced Institute of Science and Technology,
Taejon 305-701, Korea

[3] Material Division, Lord Corporation, 111 Lord Drive, Cary, NC 27512, USA

ABSTRACT

Magnetorheological (MR) dampers are one of the most promising new devices for structural vibration mitigation. Because of their mechanical simplicity, high dynamic range, low power requirements, large force capacity, and robustness, these devices have been shown to mesh well with demands and constraints of earthquake and wind engineering applications. Quasi-static models of MR dampers have been investigated by researchers. Although useful for damper design, these models are not sufficient to describe the MR damper behavior under dynamic loading. This paper presents a new dynamic model of the overall MR damper system which is comprised of two parts: (i) a dynamic model of the power supply, and (ii) a dynamic model of the MR damper. Because previous studies have demonstrated that a current-driven power supply can substantially reduce the MR damper response time, this study employs a current driver to power the MR damper. The operating principles of the pulse-width modulated current driver, and an appropriate dynamic model are provided. Subsequently, MR damper force response analysis is performed, and a phenomenological model based on the Bouc-Wen model is proposed to predict the MR damper behavior under dynamic loading. This model accommodates the MR fluid stiction phenomenon, as well as fluid inertial and shear thinning effects. Compared with other types of models based on the Bouc-Wen model, the proposed model has been shown to be more effective, especially in describing the force roll-off in the low velocity region, force overshoots when velocity changes in sign, and two clockwise hysteresis loops at the velocity extremes.

KEYWORDS: MR dampers, Smart damping devices, Hysteresis model, Parameter estimation, System identification, Rheological technology

INTRODUCTION

MR fluid dampers are new semi-active devices that utilize MR fluids to provide controllable damping forces. These devices overcome many of the expenses and technical difficulties associated with semi-active devices previously considered (Carlson and Spencer 1996; Yang 2001). Recent studies have

shown that the semi-active dampers can achieve the majority of the performance of fully active systems, thus allowing for the possibility of effective response reduction during both moderate and strong seismic activity (Dyke et al. 1996; Spencer et al. 2000). For these reasons, significant efforts have been devoted to the development and implementation of MR devices. Indeed, the first full-scale implementation of MR dampers in building was realized in the National Museum of Emerging Science and Innovation of Tokyo, Japan in 2001. In this building, two 30-ton MR fluid dampers built by the Sanwa Tekki Corporation were installed between the 3rd and 5th floors; the MR fluid inside the damper is manufactured by the Lord Corporation.

To investigate the salient features of large-scale MR devices, a 20-ton MR fluid damper has been designed and built (Carlson and Spencer 1996; Yang et al. 2002). At that time, this device constituted the largest MR damper ever produced. Fig. 1a shows the schematic of the MR damper tested in this paper. Detail information about this damper can be found at Yang (2001). Fig. 1b shows the experimental setup at the University of Notre Dame for this large-scale MR fluid damper.

Because of quasi-static models of MR dampers are not sufficient to describe the damper nonlinear behavior under dynamic loading (Yang 2001; Yang et al. 2001, 2002), this paper presents a new dynamic model of the overall MR damper system which is comprised of two parts: (i) a dynamic model of the power supply, and (ii) a dynamic model of the MR damper. Because previous studies have demonstrated that a current-driven power supply can substantially reduce the MR damper response time (Yang et al. 2001), a dynamic model of the pulse-width modulated current driver is provided. Subsequently, MR damper force response analysis is performed, and a phenomenological model based on the Bouc-Wen model is proposed to predict the MR damper behavior under dynamic loading. This model accommodates the MR fluid stiction phenomenon, as well as inertial and shear thinning effects. Experimental verification has shown that the proposed dynamic model of the MR damper system predicts the experimental results very well.

DYNAMIC MODEL OF CURRENT DRIVERS

Previously study has demonstrated that the exponential current response in damper coil when driven by a voltage source is insufficient for many practical applications (Yang et al. 2000, 2002). Several approaches can be considered to decrease the response time of the MR damper's electromagnetic circuit. One of them is to use a current driver instead of a voltage-driven power supply. The schematic of the current driver based on a PWM amplifier are given in Fig. 2. Usually, a PI controller is employed in the feedback loop to regulate the duty cycle based on the error between the measured and desired current. Assuming that the duty cycle is proportional to the controller output u_c and that u_c is not satu-

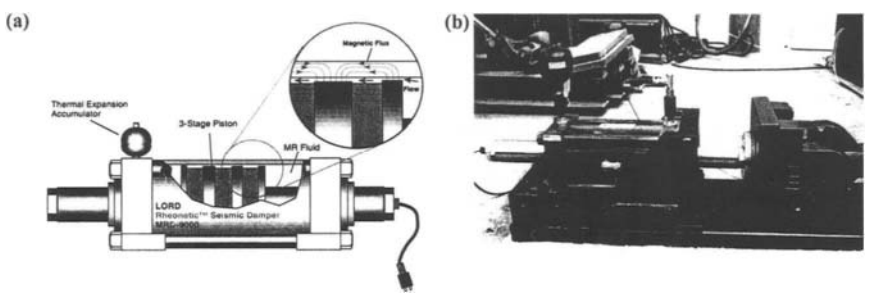


Figure: 1 (a) Schematic of the large-scale 20-ton MR fluid damper; (b) experimental setup

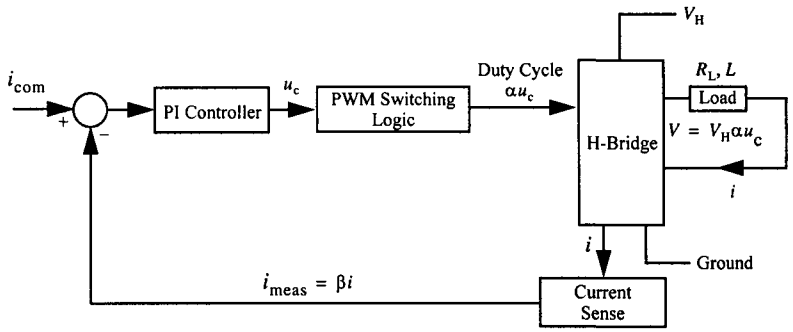


Figure: 2 (a) Schematic of the current driver based on the PWM servo amplifier

rated, the governing equation for current driver is given as (Yang 2001)

$$\frac{L}{\beta\gamma}\frac{d^2 i}{dt^2} + \frac{(R_L + \beta\eta)}{\beta\gamma}\frac{di}{dt} + i = \frac{i_{com}}{\beta} + \frac{\eta}{\beta\gamma}\frac{di_{com}}{dt} \tag{1}$$

where $\gamma = \alpha K_i V_H$; $\eta = \alpha K_p V_H$; i_{com} = reference input signal; β = sensitivity of the current sensing; and K_p, K_i = controller proportional and integral gains. The steady state current is given by

$$I_s = \frac{i_{com}}{\beta} \tag{2}$$

which depends only on the input reference signal i_{com} and the sensitivity of the current sensing β. The load resistance R_L and the bus voltage V_H have no effect on the steady state current.

Fig. 3 shows a typical current driver response to a step reference signal. At the beginning of the response, the error signal is large. The power supply applies maximum voltage to facilitate the current increase. The current increase follows the same path as that of the 100% duty cycle. As the current increases, the error signal decreases. The controller output u_c is no longer saturated, and the current is governed by Eq. (1). The controller regulates the current to a steady state current of i_{com}/β. As compared with the exponential current response using a voltage source, the current driver can substantially reduce the current response time which is readily seen in Fig. 3. To experimentally verify the effectiveness of the current driver, currents in the 20-ton MR fluid damper coil (connected in series) due to a step input command generated by both a constant voltage power supply and a current driver are compared. The experimental results are shown in Fig. 4 (Yang et al. 2002). The constant voltage case corresponds to the scenario where a voltage-driven power supply is attached to the damper coils. The time constant L_0/R_0 for the coils of the 20-ton MR fluid damper arranged in series is 0.3 sec. Therefore, as shown in Fig. 4, it takes about 1 sec for the current to achieve 95% of the final value, which is unacceptable for most of civil engineering applications. Alternatively, using a current driver, the 5% error range is achieved within 0.06 sec.

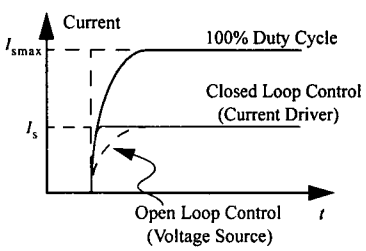


Figure: 3 Current driver response under a step reference signal

Based on Eq. (1), the dynamic model of the current driver used in the experiment is identified. The transfer function between the input reference signal i_{com} and current i is given by (Yang et al. 2001; Yang 2001)

$$i(s) = \frac{1001.45s + 1016.1}{s^2 + 503.7s + 508.05} i_{com}(s) \qquad (3)$$

A comparison between the measured and predicted current is provided in Fig. 5; close agreement is observed.

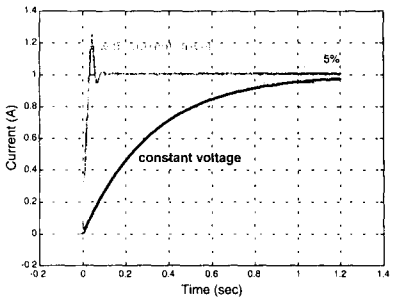


Figure: 4 Comparison between the coil current driven by constant voltage and current driver (Yang et al. 2002)

DYNAMIC MODEL OF MR DAMPERS

In this section, following the MR damper force response analysis, a phenomenological model of MR dampers based on the Bouc-Wen hysteresis model is proposed, which accommodates the MR fluid stiction phenomenon, as well as inertial and shear thinning effect. The experimental verification of the proposed model under various types of input current and loading conditions is also provided.

MR damper force response analysis

For the purposes of this discussion, the damper response in Fig. 6a can be divided into three regions. At the beginning of region I, the velocity changes in sign from negative to positive, the velocity is quite small and flow direction reverses. At this stage, the MR damper force is below the yield level, and the MR fluid operates mainly in the pre-yield region, i.e., not flowing and having very small elastic deformation. After the damper force exceeds the yield level, a damper force loss occurs during the transition from the pre-yield to post-yield region due to the stiction phenomenon of MR fluids (Pignon et al. 1996; Powell 1995; Weiss et al. 1994), resulting in an overshoot type of behavior in force. By definition, stiction is a particle jamming or a mechanical restriction to flow that is highly dependent upon both particle size and shape, as well as the prior electric field and flow history of the material. The illustration of stiction phenomenon is shown in Fig. 6b, which is similar to the Coulomb friction. As shown in this figure, the MR fluid stress increases in the pre-yield region when strain increases. As the strain exceeds the critical strain, the MR fluid changes from pre-yield to post-yield region and begins to flow; consequently, the elastic stress is released, and stress loss is observed (Weiss et al. 1994; Pignon et al. 1996). Note that due to the stiction phenomenon, the displacement measurement lags the command signal during the force transition from the pre-yield to the post yield region, as shown in Fig. 6a. Because the

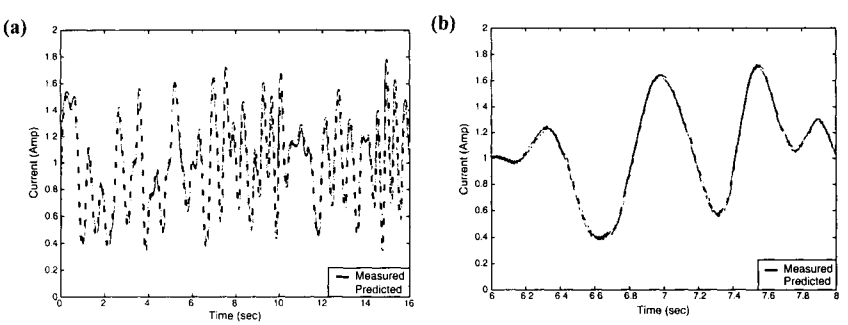


Figure: 5 (a) Comparison between the measured and predicted current; (b) detailed comparison in current fast-changing region

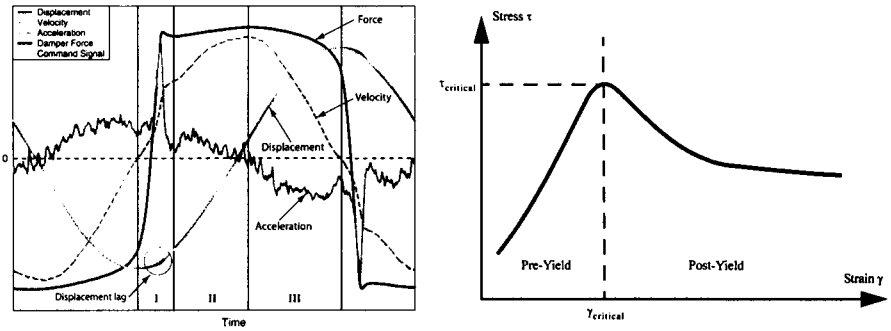


Figure: 6 (a) MR damper force response analysis; (b) Illustration of stiction phenomenon of MR fluids (Weiss et al. 1994)

servo controller uses displacement feedback, the controller tends to command a large valve opening to facilitate the damper movement. Therefore, a substantial increase in acceleration is observed. After the damper force exceeds the yield level, the acceleration quickly drops to its normal sinusoidal trajectory, as shown at the end of region I. Because the fluid inertial force is related to the acceleration, an additional force overshoot due to the dynamics of the experimental setup may be introduced, and may increase the degree of force overshoot caused by the stiction phenomenon of MR fluids. However, the experimental results have been shown that the force overshoot resulting from the inertial force is much smaller than the force due to the stiction phenomenon. This indicates that the stiction phenomenon dominates the force overshoot (Yang 2001).

In region II, the velocity continues to increase while still remaining positive. Therefore, the plastic-viscous force increases, and a damper force increase is observed.

In region III, the velocity decreases. The damper velocity approaches zero at the end of this region, and the plastic viscous force drops more rapidly due to the fluid shear thinning effect. Therefore, a force roll-off is observed. Note that the stiction phenomenon or the damper force loss after yielding is irreversible (Powell 1995), the force overshoot does not occur in this region; therefore, two clockwise loops are observed in the force-velocity plot.

Dynamic model of MR dampers

Two types of dynamic models of controllable fluid damper have been investigated by researchers: non-parametric and parametric models. Ehrgott & Masri (1992) and Gavin (1996) presented a non-parametric approach employing orthogonal Chebychev polynomials to predict the damper resisting force using the damper displacement and velocity information. Chang & Roschke (1998) developed a neural network model to emulate the dynamic behavior of MR dampers. However, the non-parametric damper models are often quite complicated. Gamato & Filisko (1991) proposed a parametric viscoelastic-plastic model based on the Bingham model. Wereley et al. (1998) developed a nonlinear hysteretic biviscous model, which is an extension of the nonlinear biviscous model having an improved representation of the pre-yield hysteresis. Spencer et al. (1997) proposed a mechanical model based on the Bouc-Wen model.

Based on the damper response analysis presented in the previous section, a phenomenological model considering the MR fluid stiction phenomenon, as well as inertial and shear thinning effects. The schematic of the model is shown in Fig. 7. The damper force is given by

$$f - f_0 = m\ddot{x} + c(\dot{x})\dot{x} + kx + \alpha z \tag{4}$$

where the evolutionary variable z is governed by

$$\dot{z} = -\gamma|\dot{x}||z|^{n-1} - \beta\dot{x}|z|^n + A\dot{x} \tag{5}$$

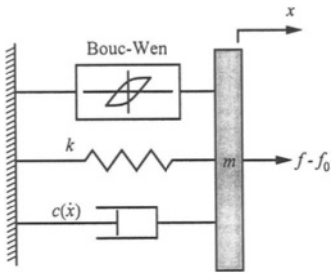


Figure: 7 Proposed phenomenological model of MR dampers

In this model, m = equivalent mass which represents the MR fluid stiction phenomenon and inertial effect; k = accumulator stiffness and MR fluid compressibility; f_0 = damper friction force due to seals and measurement bias; and $c(\dot{x})$ = post-yield plastic damping coefficient. To describe the MR fluid shear thinning effect which results in the force roll-off of the damper resisting force in the low velocity region, the damping coefficient $c(\dot{x})$ is defined as a mono-decreasing function with respect to absolute velocity $|\dot{x}|$. In this paper, the post-yield damping coefficient is assumed to have a form of (Yang et al. 2001)

$$c(\dot{x}) = a_1 e^{-(a_2|\dot{x}|)^p} \tag{6}$$

where a_1, a_2 and p are positive constants.

To determine a model which is valid under the fluctuating input current, the functional dependence of the parameters on the input current must be determined. Since the fluid yield stress is dependent on input current, α can then be assumed as a function of the input current i. Moreover, from the experiment results, a_1, a_2, m, n, and f_0 are also functions of the input current. In order to obtain the relationship between the input current i and damper parameters α, a_1, a_2, n, m and f_0, the damper was driven by band-limited random displacement excitations with a cutoff frequency of 2 Hz at various constant current levels. A constrained nonlinear least-squares optimization scheme based on the trust-region and preconditioned conjugated gradients (PCG) methods is then used. The results are shown in Table 1. A linear piecewise interpolation approach is utilized to estimate these damper parameters for current levels which are not listed in the above table. The rest damper parameters which are not varied with input current are chosen to be $\gamma = 25179.04\ \mathrm{m}^{-1}$, $\beta = 27.1603\ \mathrm{m}^{-1}$, $A = 1377.9788\ \mathrm{m}^{-1}$, $k = 20.1595$ N/m, and $p = 0.2442$. Note that a first order filter needs to be used to accommodate the dynamics involved in the MR fluid reaching rheological equilibrium

$$H(s) = \frac{31.4}{s + 31.4} \tag{7}$$

Table 1. Damper parameters at various current levels under random displacement excitation

Current (A)	α (10^5 N)	a_1 (N · sec/m)	a_2 (sec/m)	m (kg)	n	f_0 (N)
0.0237	1.3612	4349000	862.03	3000	1.000	1465.82
0.2588	2.2245	24698000	3677.01	11000	2.0679	2708.36
0.5124	2.3270	28500000	3713.88	16000	3.5387	4533.98
0.7625	2.1633	32488000	3849.91	18000	5.2533	4433.08
1.0132	2.2347	24172000	2327.49	19500	5.6683	2594.41
1.5198	2.2200	38095000	4713.21	21000	6.7673	5804.24
2.0247	2.3002	35030000	4335.08	22000	6.7374	5126.79

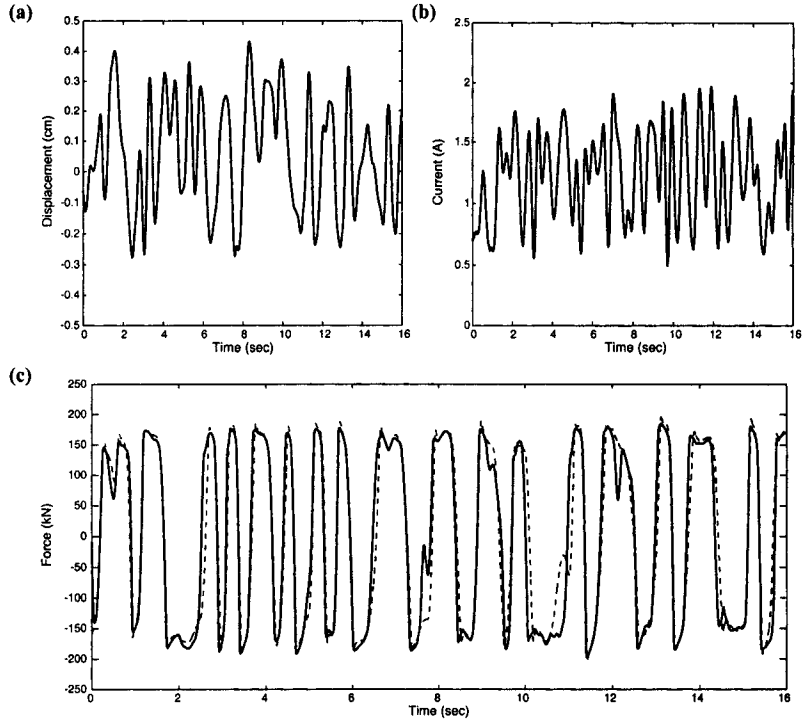


Figure: 8 Comparison between predicted and experimentally-obtained damper responses under random displacement excitation with random input current, (a) displacement vs. time; (b) current vs. time; (c) force vs. time

Fig. 8. provides the comparison between the predicted force and experimental data when the damper is subjected to a fluctuating current input. In this test, a band-limited random displacement excitation is applied. The displacement excitation and input current is also shown in Fig. 8. Excellent agreement is observed between the experimental and model responses.

CONCLUSIONS

Magnetorheological (MR) fluid dampers provide a level of technology that has enabled effective semi-active control in a number of real world applications. This paper provides fundamental insight into the dynamic behavior of a 20-ton MR damper capable of providing semi-active damping for full-scale civil engineering applications. A phenomenological model based on the Bouc-Wen hysteresis model is proposed to describe the dynamic behavior of this large-scale MR damper. The model considers the MR fluid stiction phenomenon, as well as shear thinning and inertial effects, which are observed in the experimental data. Moreover, experimental result shows that use of a pulse-width modulated current driver can dramatically reduce the MR damper response time. The operational principle of the current driver is also discussed, and its dynamic model is given. This dynamic model is then combined with the phenomenological model proposed for the MR damper to obtain the dynamic model of the overall MR damper system. The predicted results compare well with the experimental data, and effective predic-

tions are obtained. This model provides a new tool for analysis and synthesis of structures employing such large-scale MR dampers.

ACKNOWLEDGEMENT

The authors gratefully acknowledge the support of this research by the National Science Foundation under grant CMS 99-00234 (Dr. S.C. Liu, Program Director).

REFERENCES

Carlson J.D. and Spencer Jr. B.F. (1996). Magneto-Rheological Fluid Dampers for Semi-active Seismic Control. *Proc. 3rd International Conference on Motion and Vibration Control*, vol. 3, Chiba, Japan, pp. 35–40.

Chang C.C. and Roschke P. (1998). Neural Network Modeling of a Magnetorheological Damper. *J. of Intelligent Material Systems and Structures* **9**, 755–764.

Dyke S.J., Spencer Jr. B.F., Sain M.K. and Carlson, J.D. (1996). Modeling and Control of Magnetorheological Dampers for Seismic Response Reduction. *Smart Materials and Structures* **5**, 565–575.

Ehrgott R.C. and Masri S.F. (1992). Modeling the Oscillatory Dynamic Behavior of Electrorheological Materials in Shear. *Smart Materials and Structures* **1**, 275–285.

Gamota D.R. and Filisko F.E. (1991). Dynamic Mechanical Studies of Electrorheological Materials: Moderate Frequencies. *J. of Rheology* **35**, 399–425.

Gavin H.P., Hanson R.D. and Filisko, F.E. (1996). Electrorheological Dampers, Part 2: Testing and Modeling. *J. of Applied Mechanics* ASME **63:9**, 676–682.

Pignon F., Magnin A. and Piau J-M. (1996). Thixotropic cOlloidal Suspensions and Flow Curves with Minimum: Identification of Flow Regimes and Rheometric Consequences. *J. Rheology* **40:4**, 573–587.

Powell J.A. (1995). Application of a Nonlinear Phenomenological Model to the Oscillatory Behavior of ER Materials. *J. Rheology* **39:5**, 1075–1094.

Spencer Jr. B.F., Dyke S.J., Sain M.K. and Carlson. J.D. (1997). Phenomenological Model of a Magnetorheological Damper. *J. of Engineering Mechanics* ASCE **123:3**, 230–238.

Spencer Jr. B.F., Johnson E.A. and Ramallo J.C. (2000). "Smart" Isolation for Seismic Control. *JSME International Journal* JSME **43:3**, 704–711.

Weiss K.D., Carlson J.D., and Nixon D.A. (1994). Viscoelastic Properties of Magneto- and Electrorheological Fluids. *J. Intelligent Material Systems and Structures* **5:11**, 772–775.

Wereley N.M., Pang L. and Kamath G.M. (1998). Idealized Hysteresis Modeling of Electrorheological and Magnetorheological Dampers. *J. of Intelligent Material, Systems and Structures* **9:8**, 642–649.

Yang G., Ramallo J.C., Spencer Jr. B.F., Carlson J.D. and Sain M.K. (2000). Large-Scale MR Fluid Dampers: Dynamic Performance Considerations. *Proceedings of International Conference on Advances in Structure Dynamics*, Hong Kong, China. pp. 341–348.

Yang G., Jung H.J., and Spencer Jr. B.F. (2001). Dynamic Modeling of Full-Scale MR Dampers for Civil Engineering Applications. *US-Japan Workshop on Smart Structures for Improved Seismic Performance in Urban Region*, Seattle, WA., Aug. 14. pp. 213–224.

Yang G. (2001). *Large-scale magnetorheological fluid damper for vibration mitigation: modeling, testing and control*. Ph.D dissertation, University of Notre Dame, IN.

Yang G., Spencer Jr. B.F., Carlson J.D. and Sain M.K. (2002). Large-Scale MR Fluid Dampers: Modeling, and Dynamic Performance Considerations. *Engineering Structures* **24**:309–323.

TEAM PRESENTATION:

STRUCTURAL ANALYSIS RESEARCH AT THE BEIJING POLYTECHNIC UNIVERSITY

This Page Intentionally Left Blank

Advances in Building Technology, Volume 1
M. Anson, J.M. Ko and E.S.S. Lam (Eds.)
© 2002 Elsevier Science Ltd. All rights reserved

THE PRACTICAL ANTI-EARTHQUAKE OPTIMUM DESIGN OF CIVIL INFRASTRUCTURE NETWORK SYSTEM

Chen Yanyan[1] and Wang Guangyuan[2]

[1] College of Civil Engineering, Beijing Polytechnic University
Beijing, 100022, P.R.China
[2] College of Civil Engineering, Harbin Polytechnic University
Harbin, 150090, P.R.China

ABSTRACT

The optimum anti-earthquake design of civil infrastructure system (CIS) is a problem with numerous variables, complex constraints and high dimensions. In this paper, we try to alleviate the difficulty by dividing the design into two stages, i.e. system optimization and structure optimization. Taking the structure design load or reliability as bridge, the two stages are joined together. Considering the future loss expectation, the global optimum objective is to minimize the total investment cost (the sum of system original cost and future loss expectation). Through changing the system optimum variables into fewer discrete ones, an effective optimum method for CIS anti-earthquake design is suggested.

KEYWORDS

Anti-earthquake optimum design, civil infrastructure system, Reliability, Life-cycle cost

INTRODUCTION

Many civil infrastructure system (CIS) are large building-lifeline interrelated systems. It includes various kinds of buildings and lifeline segments and can be modeled as a network of interconnected nodes and links. It's important to undertake anti-earthquake design for the system because seismic damages may cause extraordinary loss. In the meantime, there is clearly a need for an optimum design procedure that is able to strike an acceptable compromise between safety and economy.

In the past, structure optimum design is often independent and only aims at minimum cost. And the optimized variable is the structure dimension, with which it is difficult to express system loss

expectation. In this paper, the optimum design of CIS is divided into two stages, system optimization and structure optimization, that is:

(1) system optimization design: i.e. optimization of structure design intensity. The optimization objective is:

$$W_S[\bar{x}_n(I_{dn})] = C_S[\bar{x}_n(I_{dn})] + M_S(\bar{x}_n) + L_S[\bar{x}_n(I_{dn})] \rightarrow \min \quad (1)$$

Here, structure design intensity I_{dn} is taken as the parameter to represent the nth structure anti-earthquake level. $\bar{x}_n$ is the design vector of the nth structure. W_S is CIS lifecycle cost, which includes system initial cost C_S, maintenance cost M_S and loss expectation L_S. Because routine maintenance cost is irrelevant to the structure anti-earthquake level, so it may be omitted in the anti-earthquake design.

(2) structural optimum design: i.e. optimization of structure design vector. The optimization objective is:

$$C_n[\bar{x}_n(I^*_{dn})] \rightarrow \min \quad (2)$$

Here, I^*_{dn} is the optimum design intensity got in the first stage. C_n is the cost of the nth structure.

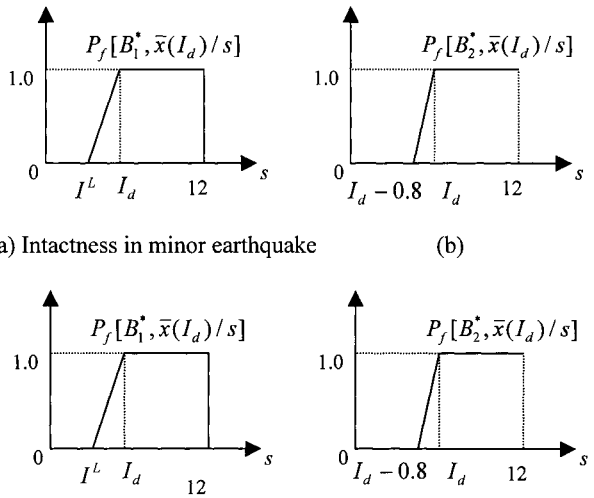
THE COMPONENT VULNERABILITY ANALYSIS

In the building design code of P.R.China (1994), five damage states are considered for building structure. If the ith damage states is denoted by B_i, then there is

$[B_1, B_2, B_3, B_4, B_5]$=[intactness, minor damage, medium damage, major damage, collapse]

According to the three-level anti-earthquake design norm in the design code of P.R.China (1994), which requires the structure to be intact ($=B_1$) under minor earthquake (written as I^L, lower by 1.55 degree than design intensity I_d), repairable($=B_3$) under medium earthquake (equal to I_d), not collapse($=B_4$) under strong earthquake(written as I^U, higher by 1 degree or so than I_d), building structure is designed under design intensity (written as I_d). So under the single failure mode, for

given earthquake intensity s, the probability of the structure with design intensity I_d being damaged over (more seriously than) B_i state (written as $P_f[B_i^*, \bar{x}(I_d)/s]$) can be shown in fig.1 (Wang guangyuan, 1999).



(a) Intactness in minor earthquake (b)

(c) Repairable in medium earthquake (d) Not collapse in strong earthquake

Fig.1: The damage probability curve of structure for different intensity s

Fig.1 (a), fig.1 (c), fig.1 (d) correspond to the three-level anti-earthquake design norm separately, while fig1. (b) is decided approximately by fig1. (a) and fig.1(c).

Depending on the probability curve of the biggest earthquake intensity in design terms, the structure damage probability $P_f[B_i^*, \bar{x}(I_d)]$ can be obtained from

$$P_f[B_i^*, \bar{x}(I_d)] = \int_0^{12} f_s(s) P_f[B_i^*, \bar{x}(I_d)/s] ds \tag{3}$$

Here, $f_s(s)$ is the probability density function of the biggest earthquake intensity in design terms.

It can easily be seen that, the structure damage probability $P_f[B_i^*, \bar{x}(I_d)]$ is only a function of design intensity and damage degree, and has no relationship with the design dimension vector.

Suppose the component in CIS has only two states, connective and failure. Failure often happens only

when building structure being damaged over B_3 level. Then the connective reliability R of building structure component can be described by

$$R = R(I_d) = 1 - P_f[(B_3^*, \bar{x}(I_d)] \tag{4}$$

For the link component (lifeline segment), we can suppose the damage-place number conforming to Poisson distribution, then the component connective reliability can be described by

$$R = R(\bar{x}) = 1 - e^{-\alpha l} \tag{5}$$

Here, α is the damage rate (the number of damage places per unit length), which is related with design vector $\bar{x}$, l is the link component length.

THE SYSTEM LIFECYCLE COST

The key problem of system anti-earthquake optimum design is the decision on the appropriate objective function. According to discussion above, the objective should be minimizing system life-cycle cost, which includes system original cost C_S and future loss expectation L_S. The system original cost could be expressed by the following formula:

$$C_S = \sum_{n=1}^{N_1} C_n[\bar{x}_n(I_{dn})] + \sum_{n=1}^{N_2} C_n(\bar{x}_n) \tag{6}$$

Here, $C_n[\bar{x}(I_{dn}]$ is the cost of the nth building component with design intensity I_{dn}, N_1 is the number of the buildings in the system . $C_n(\bar{x}_n)$ is the cost of the nth lifeline segment component with design vector $\bar{x}_n$, N_2 is the number of the lifeline segment components.

In fact, there will be different design vectors under the same design intensity, which means, there will be different cost under the same design intensity. But the optimum design should be the most economic design, i.e. $C_n[\bar{x}(I_{dn}]$ should be the lowest cost $C_{\min,n}[\bar{x}(I_{dn}]$. Approximately, in the practical application, we can take the cost of a reasonable plan with design intensity I_{dn} as $C_{\min,n}[\bar{x}(I_{dn})]$.

Under the earthquake action, the loss expectation L_S of CIS could be divided into two parts, one

results from the component structural damage, the other results from system service interruption, which can be described by

$$L_S = L^{(e)} + L^{(s)} \tag{7}$$

Here, $L^{(e)}$ is the structural loss expectation resulted from the component structural damage, $L^{(s)}$ is the system loss expectation resulted from system service interruption.

$L^{(e)}$ is the sum of all component structural loss expectation, through the component vulnerability analysis, $L^{(e)}$ can be described by

$$L^{(e)} = \sum_{n=1}^{N_1} L_n^{(e)}(\mathrm{I}_{\mathrm{dn}}) + \sum_{n=1}^{N_2} L_n^{(e)}(\bar{x}_n) \tag{8}$$

For the building structure

$$L_n^{(e)}(\mathrm{I}_{\mathrm{dn}}) = \sum_{i=1}^{5} P_{fn}^{(e)}(B_i, I_{dn}) D_{ni}^{(e)} \tag{9}$$

Here, $L_n^{(e)}(I_{dn})$ is the structural loss expectation of the nth component, $P_{fn}^{(e)}(B_i, I_{dn})$ is the probability of the nth building component designed under intensity I_{dn} in damage state B_i, $D_{ni}^{(e)}$ is the structural loss of the nth structure in damage state B_i.

$L_n^{(e)}(\bar{x}_n)$ is the structural loss expectation of the nth lifeline component with design vector $\bar{x}_n$. For the lifeline segment, the damage degree is often expressed by the damage rate (the number of damage places per unit length). Then the component loss expectation can be determined by

$$L_n^{(e)}(\bar{x}_n) = \int_0^{\lambda_n(\bar{x}_n)l_n} D_n^{(e)}(m)dm \tag{10}$$

Here, m is the variable of expectation number of damage places. $\lambda_n(\bar{x}_n)$ is the damage rate expectation of the nth component with design vector $\bar{x}_n$. $D_n^{(e)}$ is the component loss of the nth structure, which is the function of damage-place number.

The system loss is resulted from the failure in connection from source nodes to terminal nodes, which

can be expressed as:

$$L^{(s)} = \sum_{k=1}^{K} L_k^{(s)} = \sum_{k=1}^{K} (1 - R_S^{(k)}) D_k^{(s)} \tag{11}$$

Here, $L_k^{(s)}$ is the system loss expectation of the kth source-terminal pair. K is the number of source-terminal pairs. $D_k^{(s)}$ is the system loss of the kth source-terminal pair when system service being interrupted. $R_S^{(k)}$ is the connective reliability of the kth source-terminal pair, which can be obtained by Monte Carlo simulation or Analysis algorithm(Li Guiqing,1994).

Then the anti-earthquake optimum objective of CIS is:

$$W_S = C_S + L_S^{(e)} + L_S^{(s)} \rightarrow \min \tag{12}$$

THE PRACTICAL OPTIMUM ANTI-EARTHQUAKE DESIGN FOR CIS

The global optimum anti-earthquake design of CIS is to find the optimum design intensity I_d for each building component and design vector $\bar{x}$ for each lifeline segment component to minimize the system lifecycle cost subject to the system original cost constraints and system function constraints.

In design practice, the design intensity can be taken as discrete values. In any case, the reasonable designs of the lifeline segment are relatively few because of the limits to structure type, function, flux and coded spare part size. So in system optimum design, depending on the earthquake risk analysis, component importance, function requirement and so on, the designer can choose several possible discrete values of design intensity for each building and several possible design vectors for each lifeline segment. Combining every possible selection through enumeration, and computing system objective and constraints in each possible combination, then the optimum result meeting system global optimization requirements can be chosen. Of course, other discrete variable optimization algorithms, such as GA can be taken. Finally, under optimum design intensity, minimum cost design or traditional design of the structure can be undertake.

EXAMPLE

To check the application of the proposed method, an underground pipeline network to be built is considered here. The simplified network model is shown in fig.2.

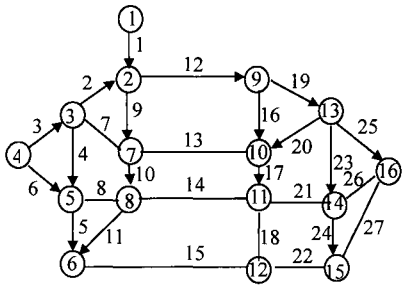


Fig.2: a pipeline network

The optimum design of the network can be made through the following procedure:

a. Decide the importance of components.

b. Decide some relatively reasonable design intensity values for the plant building and pumping plant building or design vectors (here we only consider the joint type variables) for each pipeline segment components according to their importance, requirement of function, seismic risk analysis of the region and so on.

c. Calculate the corresponding original cost, damage probability and future structural loss expectation of each component under various design intensity values or design vectors.

d. Combine every possible selection through enumeration, and computing system objective and constraints in each possible combination.

e. Under the original cost constraint, joint type (flexible joint or rigid joint) for each lifeline segment and optimum design intensity for pumping plant building can be decided to minimize the system lifecycle cost.

f. Under optimum design intensity, minimum cost design of the structure can be made for the pumping plant building. The optimum result is that pipeline [1][2][3][4][5][6][14][15][22][23][27] use flexible joints, the design intensity of water plant building and pump building are 9 and 8 separately.

CONCLUSION

A two-stage optimization method is presented for CIS anti-earthquake design. A simplified method for component and system seismic risk analysis is suggested. The optimum objective allowing for future loss expectation can meet the requirement of system global optimization. Through changing the system optimum variables into fewer discrete ones, the anti-earthquake optimum design of CIS becomes simple and practical.

References:

1. Ministry of construction department of P.R.China. (1994). *Design code of civil engineering*, Press of the Earthquake, Beijing, P.R.China
2. Wangguangyuan.(1999), Practical Methods of Optimum Aseismic Design for Engineering Structure and System, Building Factory Press, Beijing, P.R.China
3. Li Guiqing, Huo Da &Wang Dongwei. (1994), *The Anti-earthquake Reliability Analysis of Urban Civil engineering network system*, Press of the Earthquake, Beijing, P.R.China

Announcement

Thanks for the sponsor of China Natural Science Fund Committee.

Advances in Building Technology, Volume 1
M. Anson, J.M. Ko and E.S.S. Lam (Eds.)
© 2002 Elsevier Science Ltd. All rights reserved

Earthquake Analysis of Arch Dam with Joints Including Dam-Foundation Rock Nonlinear Dynamic Interaction

Xiuli Du[1] Jin Tu[2]

[1]Department of Science and Technology, Beijing Polytechnic University,
No. 100, Pingleyuan Road, Beijing 100022, China
[2] China Institute of Water Resources and Hydropower Research,
No.20, Chegongzhuan Road, Beijing 100044, China

ABSTRACT

The influence of contraction joints in arch dams on the seismic response analysis under strong earthquake is all very obvious. Existing models simulating the contact process of joints used in the seismic response analysis of arch dams, such as Fenves' model and Dowlings' model, are based on the penalty parameter method. It is difficult to determine the penalty parameters and in addition, the effect of dam-foundation dynamic interaction has not yet been considered in the analyses methods by the models stated above, and it is difficult to consider the two effects together by the frequency domain methods. Therefore, a combination method in the time domain of the explicit FEM and a transmitting boundary have been proposed for the earthquake analysis of arch dams by X.L., Du et al (2002). In this paper, the first effect stated above is studied by introducing a contact force model into the combination method. Finally, some results have been obtained by using this approach for the designed Xiaowan arch dam with maximum height of 292m in China.

KEYWORDS

Arch Dam, Foundation, Contraction Joint, Dynamic Interaction, Nonlinear Seismic Response

INTRODUCTION

The influences of energy radiation in an infinite foundation on the seismic response of arch dams have been studied by O. Maeso, J. Dominguez (1993), J. Dominguez O. Maeso (1993), H.Tan and A.K. Chopra (1995a, b) through the combination method of BEM and FEM in frequency domain, which is not suitable for nonlinear problems and is complicated in calculation. Taking consideration of the effect of faults and cracks existing in near-field foundation on the seismic response of arch dams, X.L. Du et al (2002) studied the nonlinear seismic response of arch dam-foundation systems by use of the explicit FEM and a transmitting boundary in the time domain. In this way some advantages are very obvious for solving nonlinear problems with large degrees of freedom due to the uncoupling feature. As far as the influence of simulating the opening and closing of contactable

joints in arch dams on the seismic response of the arch dams during strong earthquake is concerned, some developments have been achieved. D. Row and V. Schricker (1984) proposed a contact element model with two nodes. G.L. Fenves, S. Mojthahedi and R.B. Reimer (1989) used a block contact element model without thickness. M.J. Dowling (1989) presented a three parameter contact model with rotational angle spring, transational spring and its position. The models mentioned above are based on the penalty parameter method. J.F. Hall (1996) used a smear crack method for simulating the influences of contactable joints on the seismic response of arch dams, which is suitable for simulating the stress response of arch dams. In this paper, based on the method suggested by X.L. Du et al (2002), a dynamic contact force model proposed by J.B. Liu, S. Liu and X.L. Du (1999) is used to analysis the seismic responses of arch dams with contactable joints, meanwhile, the energy radiation in infinite foundation and the local topographical and geological features in the near-field foundation are also considered.

WAVE MOTION SIMULATION METHOD

From the explicit FEM, the equation of motion in the j direction at any node i in the discrete model of arch dam-foundation systems can be written as

$$m_i \ddot{u}_{ij} + \sum_{l=1}^{n_e} \sum_{k=1}^{n} c_{ijlk} \dot{u}_{lk} + R_{ij} = F_{ij} \tag{1}$$

Where, m_i is the mass of the node i, $\ddot{u}_{ij}$ is the acceleration of j direction at the node i, $\dot{u}_{lk}$ is the velocity in k direction at some node l which is around the node i and belongs to the same element with the node i, R_{ij} and F_{ij} are the restoring force and external force in j direction at the node i respectively, c_{ijlk} is the damping influence coefficient of k direction at the node l on j direction at the node i, n_e is the nodal number related to the node i, n is the number of degrees of freedom, R_{ij} may be determined by an elastic-plastic constitutive model. If R_{ij} is an elastic restoring force, it is expressed by

$$R_{ij} = \sum_{l=1}^{n_e} \sum_{k=1}^{n} k_{ijlk} u_{lk} \tag{2}$$

In which, u_{lk} is the displacement in k direction at the node l, k_{ijlk} is the stiffness coefficient of k direction at the node l on j direction at the node i. By introducing an explicit integration formula with the accuracy of 2-order ($O(\triangle t^2)$) given by X.J. Li, et al (1992), we have

$$u_{ij}^{t+\Delta t} = \left(F_{ij}^{t} - R_{ij}^{t} - \sum_{l=1}^{n_e} \sum_{k=1}^{n} c_{ijlk} \dot{u}_{lk}^{t} \right) \Delta t^2 / 2m_i + u_{ij}^{t} + \Delta t \cdot \dot{u}_{ij}^{t} \tag{3}$$

$$\dot{u}_{ij}^{t+\Delta t} = \dot{u}_{ij}^{t} + \Delta t \left(F_{ij}^{t+\Delta t} - R_{ij}^{t+\Delta t} + F_{ij}^{t} - R_{ij}^{t} \right) / 2m_i - \left(\sum \sum c_{ijlk} \left(u_{lk}^{t+\Delta t} - u_{lk}^{t} \right) \right) / 2m_i \tag{4}$$

DYNAMIC CONTACT FORCE MODEL

A contactable interface S is shown in Fig.1, the two side surfaces of S are called S^+ and S^-, they are coincident with each other, and assuming that S is a smooth curve or curve surface. The finite element nodes between S^+ and S^- are a pair of nodes. The sliding deformation along the direction of

interface of the contactable joints is too little to be considered. Hence, the contact process between the surfaces of the contactable joints may be simulated by the contact process between the two nodes of the pairs of nodes.

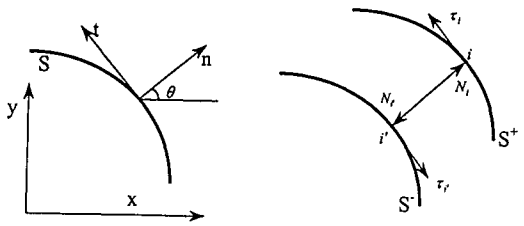


Fig1:Model with Joints and Two Side of Contactable Interface

For any pair of nodes, i and i', the node i is located on the side of S^+ and the node i' is located on the side of S^-, $\vec{N}_i$ and $\vec{\tau}_i$ are a normal contact force and a tangential contact force, respectively. Here, it is assumed that $\vec{n}$ in the normal direction to S^+ is positive. From the formula (3), by neglecting the effects of damping force, the displacement in j direction at the node i can been written as

$$u_{ij}^{t+\Delta t} = ((F_{ij}^t + N_{ij}^t + \tau_{ij}^t) - R_{ij}^t)\Delta t^2 / 2m_i + u_{ij}^t + \Delta t\dot{u}_{ij}^t \tag{5}$$

In which, N_{ij} and τ_{ij} are a projection of $\vec{N}_i$ and $\vec{\tau}_i$ on j direction, respectively. From the motion of equilibrium equations of j direction at the node i at time t, it can be known that $u_{ij}^{t+\Delta t}$ can not be got directly from the formula (5) in which N_{ij}^t and τ_{ij}^t are the functions of motion state at the time t and the time t+△t and unknown because $u_{ij}^{t+\Delta t}$ is unknown. Usually, the formula (5) may be solved by the iteration method. Fortunately, because of the characteristic of the explicit method, the tedious iterative process may be avoided through determining the contact state between the interfaces of the contactable joints at the time t. For convenience to derive, the formula (5) is written as:

$$u_{ij}^{t+\Delta t} = \bar{u}_{ij}^{t+\Delta t} + \Delta u_{ij}^{t+\Delta t} + \Delta v_{ij}^{t+\Delta t} \tag{6}$$

$$\bar{u}_{ij}^{t+\Delta t} = (F_{ij}^t - R_{ij}^t)\Delta t^2 / 2m_i + u_{ij}^t + \Delta t\dot{u}_{ij}^t \tag{7}$$

$$\Delta u_{ij}^{t+\Delta t} = N_{ij}^t / M_i \tag{8}$$

$$\Delta v_{ij}^{t+\Delta t} = \tau_{ij}^t / M_i \tag{9}$$

$$M_i = 2m_i / \Delta t^2 \tag{10}$$

Similarly, for the node i' there are the formulas as follow:

$$u_{i'j}^{t+\Delta t} = \bar{u}_{i'j}^{t+\Delta t} + \Delta u_{i'j}^{t+\Delta t} + \Delta v_{i'j}^{t+\Delta t} \tag{11}$$

$$\bar{u}_{i'j}^{t+\Delta t} = (F_{i'j}^t - R_{ij}^t)\Delta t^2 / 2m_{i'} + u_{i'j}^t + \Delta t\dot{u}_{i'j}^t \tag{12}$$

$$\Delta u_{i'j}^{t+\Delta t} = N_{i'j}^t / M_{i'} \tag{13}$$

$$\Delta v_{i'j}^{t+\Delta t} = \tau_{i'j}^t / M_{i'} \tag{14}$$

$$M_{i'} = 2m_{i'} / \Delta t^2 \tag{15}$$

$$N_{ij}^t = -N_{i'j}^t \tag{16}$$

$$\tau_{ij}^{t} = -\tau_{i'j}^{t} \tag{17}$$

Next, the computation methods for N_{ij}^{t} and τ_{ij}^{t} are introduced, respectively.

Computation of N_{ij}^{t}

N_{ij}^{t} is dependent on the contact state between the interfaces of the contactable joints. By the geometric conditions of not intruding into each other, there is

$$\vec{n}_i^T \cdot (\vec{u}_{i'}^{t+\Delta t} - \vec{u}_i^{t+\Delta t}) = 0 \tag{18}$$

The formula (18) represents the normal contact condition between the pair of the nodes i and the node i'. While to satisfy

$$\vec{n}_i^T \cdot (\vec{u}_{i'}^{t+\Delta t} - \vec{u}_i^{t+\Delta t}) \geq 0 \tag{19}$$

The contacting occurs between the nodes i and the node i', otherwise, the node i and the node i' keep separating. When separation between the node i and the node i' occurs, we have

$$N_{ij}^{t} = N_{i'j}^{t} = 0 \quad , \quad \tau_{ij}^{t} = \tau_{i'j}^{t} = 0 \tag{20}$$

$$u_{ij}^{t+\Delta t} = \bar{u}_{ij}^{t+\Delta t} \quad , \quad u_{i'j}^{t+\Delta t} = \bar{u}_{ij}^{t+\Delta t} \tag{21}$$

When the contact between the node i and the node i' occurs, there is the formula (18). Substituting formula (6) and (11) into formula (18), we have

$$\vec{n}_i^T \cdot (\vec{\bar{u}}_{i'}^{t+\Delta t} + \Delta\vec{u}_{i'}^{t+\Delta t} + \Delta\vec{v}_{i'}^{t+\Delta t} - \vec{\bar{u}}_i^{t+\Delta t} - \Delta\vec{u}_i^{t+\Delta t} - \Delta\vec{v}_i^{t+\Delta t}) = 0 \tag{22}$$

Because the displacement in the normal direction induced by the tangential force is zero, we have

$$\vec{n}_i^T \cdot \Delta\vec{v}_i^{t+\Delta t} = \vec{n}_i^T \cdot \Delta\vec{v}_{i'}^{t+\Delta t} = 0 \tag{23}$$

Substituting formula (23) into formula (22), we obtain

$$\vec{n}_i^T \cdot \left(\Delta\vec{u}_i^{t+\Delta t} - \Delta\vec{u}_{i'}^{t+\Delta t}\right) = \vec{n}_i^T \cdot \left(\Delta\vec{\bar{u}}_{i'}^{t+\Delta t} - \Delta\vec{\bar{u}}_i^{t+\Delta t}\right) \tag{24}$$

and we can define

$$\Delta_{1i} = \vec{n}_i^T \cdot \left(\Delta\vec{u}_i^{t+\Delta t} - \Delta\vec{u}_{i'}^{t+\Delta t}\right) = \vec{n}_i^T \cdot \left(\Delta\vec{\bar{u}}_{i'}^{t+\Delta t} - \Delta\vec{\bar{u}}_i^{t+\Delta t}\right) \tag{25}$$

Substituting formule (8) and (13) into formula (24) again, we obtain

$$\vec{N}_i^t = \left(M_i M_{i'} / \left(M_i + M_{i'}\right)\right)\Delta_{1i} \cdot \vec{n}_i \tag{26}$$

Computation of τ_{ij}^{t}

When the contact between node i and node i' occurs, the sliding between node i and node i'

along the tangential direction may or may not be generated or not be generated. When there is no relative sliding, a static friction state is generated. When there is relative sliding, the dynamic friction state is generated. μ_s and μ_d are the static friction coefficient and the dynamic friction coefficient, respectively.

For the static friction state, we have

$$\vec{t}_i^{\,T} \cdot \left(\vec{u}_i^{t+\Delta t} - \vec{u}_{i'}^{t+\Delta t}\right) = \vec{t}_i^{\,T} \cdot \left(\vec{u}_i^{t} - \vec{u}_{i'}^{t}\right) \tag{27}$$

Where, $\vec{t}_i$ is the tangential vector at the node i on S^+. Substituting formula (6), (11) into formula (27), we have

$$\vec{t}_i^{\,T} \cdot \left(\bar{\vec{u}}_{i'}^{t+\Delta t} + \Delta\vec{u}_{i'}^{t+\Delta t} + \Delta\vec{v}_{i'}^{t+\Delta t} - \bar{\vec{u}}_i^{t+\Delta t} - \Delta\vec{u}_i^{t+\Delta t} - \Delta\vec{v}_i^{t+\Delta t}\right) = \vec{t}_i \cdot \left(\vec{u}_{i'}^{t} - \vec{u}_i^{t}\right) \tag{28}$$

Noting the condition, $\vec{t}_i^{\,T} \cdot \Delta\vec{u}_{i'}^{t+\Delta t} = \vec{t}_i \cdot \Delta\vec{u}_i^{t+\Delta t} = 0$, and assuming that $\Delta_{2i} = \vec{t}_i^{\,T} \cdot \left[\left(\bar{\vec{u}}_{i'}^{t+\Delta t} - \bar{\vec{u}}_i^{t+\Delta t}\right) - \left(\vec{u}_{i'}^{t} - \vec{u}_i^{t}\right)\right]$, from formula (28), we can obtain

$$\vec{t}_i^{\,T} \cdot \left(\Delta\vec{v}_i^{t+\Delta t} - \Delta\vec{v}_{i'}^{t+\Delta t}\right) = \Delta_{2i} \tag{29}$$

Substituting formula (9) and (14) into formula (29), we have

$$\vec{\tau}_i^{t} = -\vec{\tau}_{i'}^{t} = \left(M_i M_{i'} / \left(M_i + M_{i'}\right)\right)\Delta_{2i} \cdot \vec{t}_i \tag{30}$$

For the dynamic contact state, we have

$$\left|\vec{\tau}_i^{t}\right| = \mu_d \left|\vec{N}_i^{t}\right| \tag{31}$$

During the calculation process, it is first assumed that the friction state between node i and node i' is the same as the former time step. If the friction state at the former time step is static, $\vec{\tau}_i^{t}$ can be solved by formula (30), then, the assumption is examined

$$\left|\vec{\tau}_i^{t}\right| \le \mu_s \left|\vec{N}_i^{t}\right| \tag{32}$$

If the formula (32) is not satisfied, $\left|\vec{\tau}_i^{t}\right|$ is calculated by formula (31), the sign of $\vec{\tau}_i^{t}$ is determined by Δ_{2i}. If the contact state between the node i and the node i' is dynamic, the next sufficient and necessary conditions are observed

$$\text{If } \operatorname{sgn}(\Delta 2i) = 1,\ \vec{t}_i^{\,T} \cdot (\vec{u}_{i'}^{t+\Delta t} - \vec{u}_i^{t+\Delta t}) > \vec{t}_i \cdot (\vec{u}_{i'}^{t} - \vec{u}_i^{t}) \tag{33}$$

$$\text{If } \operatorname{sgn}(\Delta 2i) = -1,\ \vec{t}_i^{\,T} \cdot (\vec{u}_{i'}^{t+\Delta t} - \vec{u}_i^{t+\Delta t}) < \vec{t}_i \cdot (\vec{u}_{i'}^{t} - \vec{u}_i^{t}) \tag{34}$$

The calculation accuracy of the dynamic contact force model has been verified by some typical examples with an analytic solution case in the research work of J.B. Liu, S. Liu, and X.L. Du (1999). In the dynamic contact force model, only the equilibrium conditions of mechanics and the contact conditions of geometry are considered. It is also suitable for the contact problems with nonlinear material media.

For a three-dimensional problem, S is a curved surface. The tangential sliding direction in the

tangential plane at any contact point at t time is unknown. Therefore, the tangential sliding direction at any contact point should firstly be determined, then, the tangential friction force is determined by the same method as that for the two-dimensional problem. The tangential sliding direction at the time t can be determined through neglecting the friction force at the time t.

ANALYSIS EXAMPLE OF THE SEISMIC RESPONSE OF AN ARCH DAM WITH JOINTS

Xiaowan arch dam with a height of 292m will be located at the upper reach of the Lanchuang River in Yunnan province in China, the descriptions of the finite element model of the arch dam-foundation system and the earthquake input are seen in Ref. Given by X.L. Du et al (2002)

The four different kind of analytical case considered here are illustrated in Table.1. For simplicity, the influence of arch dam-reservoir water dynamic interaction was modeled through added mass with neglect of the compressibility of reservoir water. The influences of gravity load, temperature load, hydrostatic load, and sediment load have been considered. Five strips of joints are set up in the arch dam for Case A, C, D.

TABLE 1
THE FOUR DIFFERENT KINDS OF ANALYTICAL CASES

Case	Water Lever	Strips of Joints	Bottom Crack
A	Low water lever	5	Without
B	Low water lever	Without	Without
C	Normal water lever	5	With
D	Normal water Lever	5	Without

The Influence of the Contraction Joints on the Seismic Response of the Arch Dam

The comparison of X direction stresses and Z direction stresses at the different heights on the surface of the arch dam with joints and without joints are shown in Table.2 and Table.3 respectively. It can be seen that the effect of the joints make X direction stresses (approximate arch stresses) lower obviously, Z direction stress (Cantilever stresses) increase roughly.Table.4 shows the maximum degree of opening for the joints for the case A. Table 5 shows the maximum dynamic stresses at the different heights on the surface of the crown cantilever given by the paper method. The maximum opening on the upstream and downstream surfaces of the joints are shown in Table 6.

TABLE 2
THE INFLUENCES OF TRANSVERSE JOINTS TO STRESSES OF X DIRECTION IN MAIN LOCATION (MPa)

Location			Dam Crest			Mid Dam	Dam Bottom
			Left Abutment	Crown	Right Abutment	Crown	Crown
Maximum	Case A	US	1.21	0.76	-0.17	-1.69	0.44
		DS	0.42	0.75	0.63	-0.18	--
	Case B	US	1.20	2.20	-0.28	-1.45	0.30
		DS	0.47	3.10	0.68	-0.50	--
Minimum	Case A	US	-0.33	-6.10	-1.88	-6.23	-1.96
		DS	-0.43	-5.69	-0.18	-2.86	--
	Case B	US	-0.20	-6.02	-1.76	-5.96	-2.05
		DS	-0.42	-5.70	-0.14	-2.80	--

Note: US =Upstream Surface, DS =Downstream Surface

TABLE 3
THE INFLUENCES OF TRANSVERSE JOINTS TO STRESS OF Z DIRECTION IN MAIN LOCATION (MPa)

Location			Dam Crest			Mid Dam	Dam Bottom
			Left Abutment	Crown	Right Abutment	Crown	Crown
Maximum	Case A	US	0.16	1.07	-0.67	-1.40	2.75
		DS	-0.58	0.31	0.07	0.79	--
	Case B	US	0.15	1.10	-0.64	-1.30	2.50
		DS	-0.58	0.05	0.10	0.75	--
Minimum	Case A	US	-1.08	-2.01	-2.17	-5.25	-6.99
		DS	-1.36	-0.93	-0.47	-2.68	--
	Case B	US	-1.00	-1.60	-2.12	-5.25	-7.20
		DS	-1.35	-0.84	-0.47	-2.75	--

Note: US =Upstream Surface, DS =Downstream Surface

TABLE 4
THE MAXIMAL OPENING DEGREE OF JOINTS (mm)

Location	Joint 1	Joint 2	Joint 3	Joint 4	Joint 5
US	4.06	4.67	11.05	3.56	8.65
DS	5.05	3.65	10.25	4.22	6.21

Note: US =Upstream Surface, DS =Downstream Surface

TABLE 5
EFFECTS OF RADIANT DAMPING TO MAXIMAL DYNAMIC STRESS (MPa)

Altitude	Location	Arch stress	Cantilever Stress
▽1210	US	3.186	1.176
	DS	1.900	0.827
▽1170	US	3.034	1.559
	DS	2.008	1.654
▽1130	US	2.579	1.750
	DS	1.761	1.958
▽1090	US	2.024	1.664
	DS	1.450	1.774
▽1050	US	1.441	1.646
	DS	1.215	1.361
▽1010	US	0.883	2.055
	DS	0.960	1.347
▽975	US	0.818	3.460
	DS	0.639	1.382
▽953	US	1.409	5.196
	DS	0.359	1.378

TABLE 6
EFFECTS OF RADIANT DAMPING TO THE OPENING DEGREE OF JOINTS (mm)

Case	Location	Joint 1	Joint 2	Joint 3	Joint 4	Joint 5
A	US	5.05	3.65	10.25	4.22	6.21
	DS	4.06	4.67	11.05	3.56	8.65
B	US	0.70	0.00	0.00	0.09	0.75
	DS	0.47	0.67	0.98	0.04	0.00

Note: US =Upstream Surface, DS =Downstream Surface

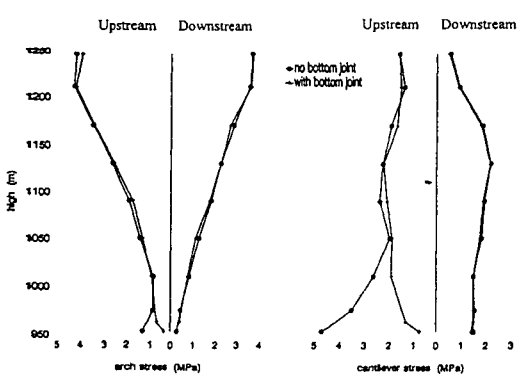


Fig.2 Arch and Cantilever Stress at Crown of Arch Dam with and without Bottom Crack

The Influence of Bottom Joint on the Seismic Response of Arch Dam

A strip of joint at the bottom of the dam was set up for comparison of the influence of the bottom joint on the seismic responses of arch dams. The comparison between dynamic arch and cantilever stresses at the crown of the arch dam with bottom joint and without bottom joint for the normal level of water is shown in Fig.2. It can be seen that the bottom joint makes the cantilever dynamic stresses lower as would be expecting.

CONCLUSION

In this paper, a calculation method has been established for solving the nonlinear seismic responses of the arch dam-foundation systems by combining the dynamic contact force model with the explicit FEM. As an example, the influences of contraction joints and bottom joints on the seismic response of Xiaowan arch dam are calculated by the use of the proposed method in this paper, and some results are obtained for reference to engineering design.

ACKNOWLEDGEMENTS

The study was supported by CNSF grant (No. 59739180)

REFERENCES:

1. Dominguez, J., and Maeso, O. (1993). "Earthquake Analysis of Arch Dams, II . Dam-Water-Foundation Interaction." *J. Eng. Mech.*, ASCE, 119(3), 513-530.
2. Dowling, M. J. (1987). "Nonlinear Seismic Analysis of Arch Dams." *Report No. EERL-87/03*, Earthquake Engineering Research Laboratory, California Institute of Technology, Pasadena, California..
3. Du, X. L., Zhang, B. Y., Tu, J. and Zhang, Y. H. (2002). "Earthquake Analysis of Arch Dam Including Dam-Foundation Nonlinear Dynamic Interaction." International Conf. On Advances in Building Technology.
4. Fenves, G. L., Mojthahedi, S., and Reimer, P. B. (1989). "ADAD-88: A Computer Program for Nonlinear Earthquake Analysis of Concrete Arch Dams." *Report No. UCB/EERC-89/12*, Earthquake Engineering Research Center University of California, Berkeley, California.
5. Hall, J. F. (1996). "Efficient Nonlinear Seismic Analysis of Arch Dams-Smeared Crack Arch Dam Analysis." *California Institute of Technology, Pasadena, California*, April.
6. Li, X. J., Liao, Z. P., and Du, X. L. (1992). "An Explicit Finite Difference Method for Viscoelastic Dynamic Problem." *Earthquake Engineering and Engineering Vibration*, 12(4), 74-80.
7. Liu, J. B., Liu, S., and Du, X. L. (1999). "A Method for the Analysis of Dynamic Response of Structure Containing Non-Smooth contactable Interfaces." *ACTA Mechanic Sinica* (English Series), 15(1), 63-72.
8. Maeso, O., and Dominguez, J (1993). "Earthquake Analysis of Arch Dams, I , Dam-Foundation Interaction." *J. Eng. Mech.*, ASCE, 119(3), 496-512.
9. Row, D., and Schricker, V. (1984). "Seismic Analysis of Structures With Localized Nonlinearities." *Proc. 8th WCEE.*, San Francisco, California.
10. Tan, H., and Chopra, A. K. (1995a). "Earthquake Analysis of Arch Dams Including Dam-Water-Foundation Rock Interaction." *Earthquake Eng. Struct. Dyn.* , 24(11), 1453-1474.
11. Tan, H., and Chopra, A. K. (1995b). "Dam-Foundation Rock Interaction Effects in Frequency-Response Function of Arch Dams." *Earthquake Eng. Struct. Dyn.* , 24(11), 1475-1489.

Advances in Building Technology, Volume 1
M. Anson, J.M. Ko and E.S.S. Lam (Eds.)
© 2002 Elsevier Science Ltd. All rights reserved

Earthquake Analysis of Arch Dam Including Dam-Foundation Rock Nonlinear Dynamic Interaction

Xiuli Du[1] Boyan Zhang[2] Jin Tu[2] Yanhong Zhang[2]

[1]Department of Science and Technology, Beijing Polytechnic University,
No. 100, Pingleyuan Road, Beijing 100022, China
[2] China Institute of Water Resources and Hydropower Research,
No.20, Chegongzhuan Road, Beijing 100044, China

ABSTRACT

An analysis method in the time domain is proposed by combining the explicit finite element method and the transmitting boundary, and by using a dynamic analysis method the static responses of arch dams is solved and a combination method is also proposed to calculate the nonlinear responses of arch dams under the actions of static and dynamic load. The influences of the arch dam-foundation dynamic interaction with energy dispersion and its local material nonlinear and non-homogeneous behavior on the seismic response of arch dams have also been studied for the designed Xiaowan arch dam with maximum height of 292m in China.

KEYWORDS

Arch dam, Foundation Rock, Nonlinear Dynamic Interaction, Earthquake

INTRODUCTION

Prof. R.W. Clough (1973) developed one of the earliest computer programs, ADAP, based on the finite element method for calculating the seismic response of arch dams, in which a massless foundation rock model with fixed boundaries was adopted and the influences of impounded water on the seismic response of arch dams were not considered. Based on ADAP, J. S. –H. Kuo (1982) and Y. Ghanaat and R.W. Clough (1989) studied the influences of the hydrodynamic effects with added mass approximation on the seismic response of arch dams and developed a computer program EADAP. In order to consider the hydrodynamic effects of impounded water with compressibility and the reservoir boundary absorption effects, a substructure technique in the frequency domain was developed by J.F. Hall and A.K. Chopra (1983) and K. –L. Fok (1986a, 1986b, 1986c,, 1987). O. Maeso and J. Dominguez (1993) and J. Dominguez and O. Maeso (1993) used the boundary element method in the frequency domain for considering the arch dam-foundation rock dynamic interaction and the travelling-waves effects of arch dam systems under the action of the harmonic seismic motion input. H. Tan and A.K. Chopra (1995a, b) also used the boundary element method to calculate the foundation impedance matrix and developed a substructure technique considering the foundation

rock-arch dam dynamic interaction, impounded water with compressibility-arch dam dynamic interaction and the reservoir boundary absorption effects. There are still the some difficulties to consider the foundation rock-arch dam dynamic interaction and the effects of the local nonlinear and non-homogenous behavious in foundation rock in the meanwhile. It is the reason that the methods used for analysis of the arch dam-foundation rock dynamic interaction in the frequency domain are not suitable to the problem with nonlinear behavious. In this paper, an analytical technique in the time domain has been proposed for considering the foundation rock-arch dam dynamic interaction and the nonlinear effects of materials mentioned above.

At present, there are mainly the two classes of method to simulate scattering wave propagation in infinite media, the one class satisfies all the differential equations of motion and the radiation conditions at infinite region in the exterior of discrete models exactly, such as the boundary element method. They couple in space and time, and are usually formulated in the frequency domain, in which the shortcomings are that computing costs are high and it is difficult to simulate the local nonlinear and non-homogeneous features in the foundation near structures. The other class satisfies approximately the non-reflection condition at the artificial boundary of the finite discrete models to be used to simulate the effects of infinite foundation, in which the assumption of outgoing plane waves is mostly made, such as a transmitting boundary suggested by Z.P. Liao et al (1984), an absorbing boundary suggested by R. Clayton and B. Engquist (1977), a viscous boundary suggested by J. Lysmer and R.L. Kuhlemeyer (1969), they are all local non-coupling in space and time, and have the advantages for solving of the near field wave motion problems with local nonlinear behaviors. J.P. Wolf (1986) compared the accuracy of these artificial boundary methods for the simple one-dimensional case and pointed out that the well-known viscous boundary and the transmitting boundary lead to good accuracy. Due to the feature of multi-times transmitting, the high-order transmitting boundary methods lead to good accuracy for two-and-three dimensional cases also.

In this paper, an analysis method in the time domain used for computing the seismic responses of arch dams with consideration of the dam-foundation rock dynamic interaction and the local nonlinear behavior in the near-field foundation rock has been developed by combining the explicit finite element method with the transmitting boundary proposed by Z.P. Liao, et al (1984). It is noticed that there is a high frequency unstable phenomenon at artificial boundaries by use of the transmitting boundary. A method to eliminate the phenomenon has been proposed by Z.P. Liao (1996), in which the damping forces of media are related to the stiffness of media. Therefore, Rayleigh damping assumption was used here.

FUNDAMENTAL APPROACH

In this paper, an arch dam-foundation system is divided into an interior region with dam body and its adjacent near-field foundation with important local topographical and geological features and an infinite far-field foundation region with homogenous and linear features. The interior region is meshed by using the finite element method. The infinite exterior region is simulated by setting a set of artificial boundaries to simulate the propagation of outgoing scatter waves from the interior region to the infinite exterior region. The motions of the nodes of the discrete finite element model in the interior region are calculated by the explicit finite element method and the motions of the nodes at the artificial boundaries are solved by the transmitting boundary. The detailed introduction on the accuracy and the efficiency of the transmitting boundary can be seen in the references given by Z.P. Liao (1996). Next, the brief descriptions of the explicit finite element method are given.

From the explicit FEM, the motion of equation of j direction at any node i in the discrete model of arch dam-foundation systems can be written as

$$m_i \ddot{u}_{ij} + \sum_{l=1}^{n_e} \sum_{k=1}^{n} c_{ijlk} \dot{u}_{lk} + R_{ij} = F_{ij} \tag{1}$$

Where, m_i is the mass of the node i, $\ddot{u}_{ij}$ is the acceleration of j direction at the node i, $\dot{u}_{lk}$ is the velocity of k direction at the node l which is around the node i and belongs to the same element with the node i, R_{ij} and F_{ij} are the restoring force and the external force of j direction at the node i respectively, c_{ijlk} is the damping influence coefficient of k direction at the node l on j direction at the node i, n_e is the nodal number related to the node i, n is the number of freedom degree, R_{ij} may be determined by an elastic-plastic constitution model.

If R_{ij} is an elastic restoring force, it is expressed by

$$R_{ij} = \sum_{l=1}^{n_e} \sum_{k=1}^{n} k_{ijlk} u_{lk} \tag{2}$$

In which, u_{lk} is the displacement of k direction at the node l, k_{ijlk} is the stiffness coefficient of k direction at the node l on j direction at the node i.

Assuming that the damping force of any direction at the node i is only relative to itself velocities at the node i, thus

$$\begin{cases} c_{ijlk} = 0 & l \neq i \\ c_{ijlk} = c_{ij} & l = i \end{cases} \tag{3}$$

When $c_{ij} = c_{ik} = c_i$, the formula (1) may by written as

$$m_i \ddot{u}_{ij} + c_i \dot{u}_{ij} + R_{ij} = F_{ij} \tag{4}$$

It is known that formula (4) is a special example of formula (1), this is, when the damping force is only relative to the velocity of the node i and every direction damping coefficient is the same, there is the formula (4). Substituting the central difference formulations for acceleration and displacement into the formula (4), the explicit integration formula of Eq. (4) can by obtained. Generally, the assumption from the formula (1) to the formula (4) is not reasonable. Thus, an explicit integration formula can not be obtained by introducing the central difference method. X.J. Li, et al (1992) derived a explicit integration formula with the accuracy of 2-order ($O(\triangle t^2)$), which can be expressed as

$$u_{ij}^{t+\Delta t} = \left(F_{ij}^t - R_{ij}^t - \sum_{l=1}^{n_e} \sum_{k=1}^{n} c_{ijlk} \dot{u}_{lk}^t \right) \Delta t^2 / 2m_i + u_{ij}^t + \Delta t \cdot \dot{u}_{ij}^t \tag{5}$$

$$\dot{u}_{ij}^{t+\Delta t} = \dot{u}_{ij}^t + \left(F_{ij}^{t+\Delta t} - R_{ij}^{t+\Delta t} + F_{ij}^t - R_{ij}^t \right) \Delta t / 2m_i - \left(\sum_{l=1}^{n_e} \sum_{k=1}^{n} c_{ijlk} \left(u_{lk}^{t+\Delta t} - u_{lk}^t \right) \right) / 2m_i \tag{6}$$

The formulations introduced above is conditional stable, the determination of the time step Δt is seen in Ref. Given by X.J.Li, et al (1992).

COMPUTING OF THE COMBINATIVE RESPONSES OF ARCH DAM-FOUNDATION SYSTEMS DURING STATIC LOADS AND EARTHQUAKE

In this paper, the faults, cracks etc are treated as elastic-plastic media with a nonlinear constitutive relation with Druker-Prager Cap model adopted here. The nonlinear seismic response of arch dams is related to the static response of ones subjected by static loads. Such as self-weight, impound water and sediment etc. A techniquefor calculating the static responses by the dynamic method has been adopted here, in which the static loads are regarded as the step loads exerted at the initial time and the artificial damping are exerted during the step loads. Because the attenuation phenomenon of outgoing scattering waves in the infinite domain can not be considered in the transmitting boundary, the constrained effect of the stiffness supplied by the infinite domain for the finite model of the near-field medium is neglected. While the elastic restore behavior of the artificial boundaries of the finite model is needed in order to keep the equilibrium of the calculation model, the transmitting boundary may lead to drift instability. In order to overcome the instability, a constrained artificial boundary on which the elastic coefficients are given by experiences is introduced for computing the static response of the problem.

APPLICATION TO ARCH DAM-FOUNDATION SYSTEMS

The proposed method is used to calculate the seismic dynamic responses of an arch with height of 292 m called as Xiaowan arch dam located in the upper reach of the Lanchuang River in Yunnan province in China. The design earthquake intensity for the arch dam is IX degree with a horizontal peak acceleration of 0.290g, while the vertical peak acceleration is 2/3 of the horizontal one. The finite element model containing the arch dam and the foundation region to be calculated has the total element number of 20107 and the total nodal number of 22878, and there are the material kinds of 22 in the model. The sketch of the finite element discrete model except the artificial boundary region is shown in Fig.1. The altitude at the top of the dam is 1245 m. The arc length at the top of the dam is 935 m, the thickness at the top of the dam is 12 m, and the thickness at the bottom of the dam is 73 m. The dynamic elastic modulus is 27.3GPa, the density is 2400 N/m^3, and the Poisson ratio is 0.189 in the concrete of dam body. The material constants in the foundation region are shown in Table 1. Here, the dynamic elastic modulus is 1.3 times the static elastic modulus. For simplicity, the influence of arch dam-reservoir water dynamic interaction was modeled through added mass with neglect of the compressibility of reservoir water. The acceleration histories of incident seismic waves are shown in Fig.2 (incident S waves for stream-wise component and cross-stream component, incident P wave for vertical component). In the model the most liked fault location apart from the dam heel is also considered with a nonlinear constitutive relation with Druker-Prager Cap model adopted here. In the fault, the two groups material parameters are given out according to the distance from the valley site. In group 1, the static elastic modulus is 3500 MPa, the Poisson ratio is 0.3, the density is 1900 N/m^3, the friction coefficient f=1.00, the cohesive force C=0.5 MPa. In group 2, the static elastic modulus is

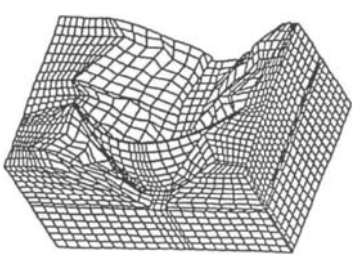


Fig.1 Finite Element Discrete Model of Xiaowan Arch Dam-foundation

1400 MPa, the Poisson ratio is 0.31, the density is 1900 N/m^3, the friction coefficient f=0.85, the cohesive force C=0.35 MPa. In the finite element discrete model, the minimum element size is 3 m, Δt is determined as 0.0004 second according to the computational requirements given by X.J.Li, et al (1992). The stress and displacement fields induced by gravity load, temperature load and hydrostatic load of normal water lever are considered during the calculation process of seismic action.

TABLE 1
MATERIAL CONSTANTS OF THE FOUNDATION REGION MEDIA (SI units)

Group No.	Density (N/m^3)	Dynamic elastic modulus ($\times 10^{11}$Pa)	Poisson ratio	Group No.	Density (N/m^3)	Dynamic elastic modulus ($\times 10^{11}$Pa)	Poisson's ratio
1	2630.00	0.3250	0.2200	12	2630.00	0.2210	0.2600
2	2630.00	0.2600	0.2500	13	2630.00	0.7150	0.3000
3	1900.00	0.4550	0.3000	14	2630.00	0.2990	0.2300
4	1900.00	0.1820	0.3100	15	2630.00	0.3250	0.2200
5	2000.00	0.5070	0.3000	16	2630.00	0.2600	0.2500
6	2630.00	0.1170	0.2650	17	2630.00	0.2860	0.2400
7	1900.00	0.2600	0.3000	18	2630.00	0.3380	0.2100
8	1900.00	0.1326	0.3100	19	2630.00	0.2730	0.2500
9	1900.00	0.3900	0.3500	20	2630.00	0.2470	0.2500
10	1900.00	0.7150	0.3000	21	2630.00	0.2340	0.2500
11	1900.00	0.1040	0.2900				

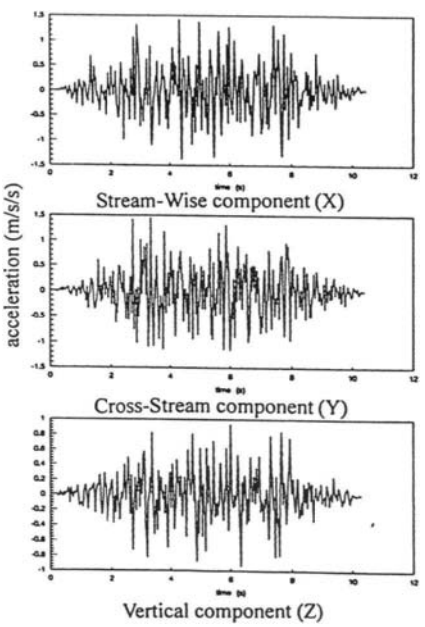


Fig.2 Incident Seismic Waves of Xiaowan Arch Dam

The comparison between the proposed method and the conventional method

The arch and cantilever peak dynamic stress absolute values at the different heights of the crown cantilever calculated by the proposed method and the conventional method are shown in Table2 and Table3. We can see that the peak dynamic stresses obtained by the proposed method with consideration of energy dispersion in infinite foundation through the transmitting boundaries are more less than the ones obtained by the conventional method with the assumptions of a massless foundation with fixed boundaries and uniform input seismic motion along the interface of dam-foundation on an average. The principal stresses of the upstream and downstream surfaces at the top altitude near the abutments are illustrated in Table 4. It can be seen that the maximum principal stresses by the two methods are roughly identical. The minimum principal stress absolute values by the proposed method are obviously larger than the ones by the conventional method.A and B represent the results of the conventional method and the proposed method here, respectively.

TABLE2
DYNAMIC ARCH STRESS OF CROWN CANTILEVER OF XIAOWAN ARCH DAM (MPa)

Altitude (m)		▽1210	▽1170	▽1130	▽1090	▽1050	▽1010	▽975	▽953
Upstream	B	4.18	3.47	3.05	2.39	1.83	1.11	0.79	1.25
	A	4.70	4.02	3.28	2.53	1.85	0.95	0.51	0.72
Downstream	B	3.38	2.39	1.62	1.10	0.80	0.77	0.41	0.26
	A	3.80	2.88	2.25	1.83	1.27	0.85	0.46	0.29

TABLE3
DYNAMIC CANTILEVER STRESS OF CROWN CANTILEVER OF XIAOWAN ARCH DAM (MPa)

Altitude (m)		▽1210	▽1170	▽1130	▽1090	▽1050	▽1010	▽975	▽953
Upstream	B	1.29	1.86	2.19	2.32	1.92	2.57	3.43	4.82
	A	1.32	2.52	2.92	2.77	2.45	2.58	3.52	4.36
Downstream	B	0.94	2.03	2.26	2.04	1.83	1.51	1.55	1.65
	A	1.15	2.21	2.44	2.16	1.87	1.72	2.52	3.09

TABLE4
DYNAMIC PRINCIPAL STRESSES NEAR THE ABUTMENTS (MPa)

			Right Abutments	Left Abutments
Upstream surface	Maximum	A	1.82	1.40
		B	1.93	1.13
	Minimum	A	-0.13	-0.12
		B	-1.85	-1.14
Downstream surface	Maximum	A	2.10	1.80
		B	1.49	1.56
	Minimum	A	-0.10	-0.08
		B	-1.53	1.17

The effects of the fault

In order to study the effects of the fault with the different type of mechanical behavious, comparison calculations have been carried out for the two foundation models with the fault with linear and nonlinear behavious. The results are illustrated in Table 5 and Table 6, respectively. It can be seen that with consideration of the nonlinear behavious of the fault, the influences on the arch and cantilever stresses at the different parts upstream and downstream of the crown cantilever are less. The reason may be reason that the fault located not at the dam heel is not across the interface between the arch dam and the rock foundation.

TABLE5
NONLINEAR AND LINEAR EFFECTS OF THE FAULT ON PEAK SYNTHETICAL ARCH STRESS OF CROWN CANTILEVER OF XIAOWAN ARCH DAM (MPa)

Altitude (M)		▽1210	▽1170	▽1130	▽1090	▽1050	▽1010	▽975	▽953
Upstream	Linear Fault	11.45	11.25	10.38	9.04	7.64	5.75	3.64	1.58
	Nonlinear Fault	11.61	11.09	10.32	9.17	7.74	5.88	3.70	1.57
Downstream	Linear Fault	8.42	6.04	4.86	4.18	3.21	2.15	1.32	1.63
	Nonlinear Fault	8.77	6.28	4.99	4.20	3.11	1.99	1.24	1.53

TABLE6
NONLINEAR AND LINEAR EFFECTS OF THE FAULT ON PEAK SYNTHETICAL CANTILEVER STRESS OF CROWN CANTILEVER OF XIAOWAN ARCH DAM (MPa)

Altitude (M)		▽1210	▽1170	▽1130	▽1090	▽1050	▽1010	▽975	▽953
Upstream	Linear Fault	2.36	3.64	4.42	4.62	4.72	4.12	3.30	8.59
	Nonlinear Fault	2.58	3.87	4.55	4.66	4.77	4.26	3.29	8.52
Downstream	Linear Fault	1.35	2.79	3.33	3.42	3.70	5.35	9.10	10.26
	Nonlinear Fault	1.40	2.79	3.41	3.56	3.79	5.25	8.95	10.11

CONCLUSION

Some conclusions for the analysis of the seismic responses of the Xiaowan arch dam can be drawn as follows:

1. Allowing for energy dispersion in the infinite foundation and the effects of non-uniform motion at the dam base along the canyon, the arch and cantilever stresses in the central and upper part of the arch dam are obviously reduced by (20%~40%).

2. The influence of the fault with nonlinear behavious on the seismic stresses in the arch dam is very little.

ACKNOWLEDGEMENTS

This research has been supported by CNSF grant (No.59739180).

REFERENCES

1. Clayton, R., and Engquist, B. (1977). "Absorbing Boundary Conditions for Acoustic and Elastic Wave Equations." *BSSA*, 67(6), 1529-1540.
2. Clough, R. W., Raphael, J. M., and Mojtahedi, S. (1973). "ADAP-A Computer Program for static and Dynamic Analysis of Arch Dams." *Report No. EERC 73-14*, Earthquake Engineering Research Center, University of California, Berkeley, California
3. Dominguez, J., and Maeso, O. (1993). "Earthquake Analysis of Arch Dams II . Dam-Water-Foundation Interaction." *J. Eng. Mech.*, ASCE, 119(3), 513-530.
4. Fok, K. -L., and Chopra, A. K. (1986a). "Earthquake Analysis of Arch Dams Including Dam-Water Interaction, Reservoir Boundary Absorption and Foundation Flexibility." *Earthquake Eng. Struct. Dyn.*, 14(2), 155-184.
5. Fok, K. -L., and Chopra, A. K. (1986b). "Frequency Response Functions for Arch dams: Hydrodynamic and Foundation Flexibility Effects." *Earthquake Eng. Struct. Dyn.,* 14(5), 769-795.
6. Fok, K. -L., and Chopra, A. K. (1986c). "Hydrodynamic and Foundation Flexibility Effects in Earthquake Response of Arch Dams." *J. Struct. Eng.*, ASCE, 112, 1810-1828.
7. Fok, K. -L., and Chopra, A. K. (1987). "Water Compressibility in Earthquake Response of Arch Dams." *J. Struct. Eng.*, ASCE, 113(5), 958-975.
8. Ghanaat, Y., and Clough, R. W. (1989). "EADAP Enhanced Arch Dam Analysis Program, User's Manual." *Report No. UCB/EERC-89/07*, Earthquake Engineering Research Center, University of California, Berkeley, California.
9. Hall, J. F., and Chopra, A. K. (1983). "Dynamic Analysis of Arch Dams Including Hydrodynamic Effects." *J. Eng. Mech.*, ASCE, 109(1), 149-167.
10. Kuo, J. S. -H. (1982). "Fluid-Structure Interaction: Added Mass Computations for Incompressible Fluid." *Report No. UCB/EERC-82/09*, Earthquake Engineering Research Center, University of California, Berkeley, California.
11. Li, X. J., Liao, Z. P., and Du, X. L. (1992). "An Explicit Finite Difference Method for Viscoelastic Dynamic Problem, Earthquake Engineering and Engineering Vibration." 12(4), 74-80 (In Chinese).
12. Liao, Z. P. (1996). "An Introduction to Wave Motion Theories in Engineering." Beijing, China, Academić Press, 165-322 (In Chinese).
13. Liao, Z. P., Wong, H. L., Yang, B. P. and Yuan, Y. F. (1984). "A Transmitting Boundary for the Numerical Simulation of Elastic Wave Propagation." *Soil Dyn, Earthq. Eng.,* 3(4), 174-183.
14. Lysmer, J., And Kuhlemeyer, R. L. (1969). "Finite Dynamic Model for Infinite Media." *J. Eng. Mech. Div.*, ASCE, 95(4), 859-877.
15. Maeso, O., and Dominguez, J. (1993). "Earthquake Analysis of Arch Dams, I . Dam-Foundation Interaction." *J. Eng. Mech.*, ASCE, 119(3), 496-512.
16. Tan, H., and Chopra, A. K. (1995). "Earthquake Analysis of Arch Dams Including Dam-Water-Foundation Rock Interaction." *Earthquake Eng. Struct. Dyn.*, 24(11), 1453-1474 .
17. Tan, H., and Chopra, A. K. (1995). "Dam-Foundation Rock Interaction Effects in Frequency-Response Functions of Arch Dams." *Earthquake Eng. Struct. Dyn.*, 24(11), 1475-1489 .
18. Wolf, J. P. (1986). "A Comparison of Time-Domain Transimitting Boudaries." *Earthq. Eng. Struct. Dyn.*, 14(4), 655-673.

Advances in Building Technology, Volume 1
M. Anson, J.M. Ko and E.S.S. Lam (Eds.)
© 2002 Elsevier Science Ltd. All rights reserved

Stability Analysis of Large Complicated Underground Excavations

Tao Lianjin[1] Li Panfeng Zhang Zhuoyuan[2], Zhang Lihua[3] and Li Xiaolin[1]

College of Architecture and Civil Engineering, Beijing Polytechnic University, Beijing, 100022, China
Institute of Engineering Geology, Chengdu University of Technology, Chengdu, 610059, China
Civil Engineering Department, North China Institute of Technology, Sanhe, China

ABSTRACT

Based on field investigation and data analysis, the geostress field is fitted to a three-dimension model and then a model to evaluate the stability of powerhouses is built and computed. Some suggestions are proposed based on the analysis.

KEY WORDS

underground powerhouses, surrounding rockmass, discontinuities, stability analysis, numerical modeling

INTRODUCTION

The planed Xiluodu Hydropower station is at the third stage of the principal stream of Jinshajiang River between Panzhihua City and Yibin City. The station is located in the deep downcutting valley at the border of Leibo County, Sichuan Province and Yongshan County, Yunnan Province as shown in Fig. 1.

According to the feasibility design scheme, underground powerhouses are adopted and all of the powerhouses are located along the two banks in the deep downcutting valley. The underground chambers mainly include three large chambers, i.e. main chamber with

size 436×33.8×57.4m, alternative chamber 43×17×31.6m and the tailrace 300×26×93.5m. The three main chambers are all located in the Permian Emei Mountain Basalt strata. As a whole, the rock mass quality is quite sound and the geostress is medium. However many discontinuities can be found such as interlayer shearing belts, intrastratal shearing belts, joints and protogenesis joints and discontinuities caused by epigenetic recreation. Especially the intrastratal shearing belts randomly distributing in the strata, make the rock mass strength and quality worse. The powerhouses are characterized by their large cross-section, complicated space intersection. Therefore it is very important to properly assess the effects of discontinuities and interaction of chambers.

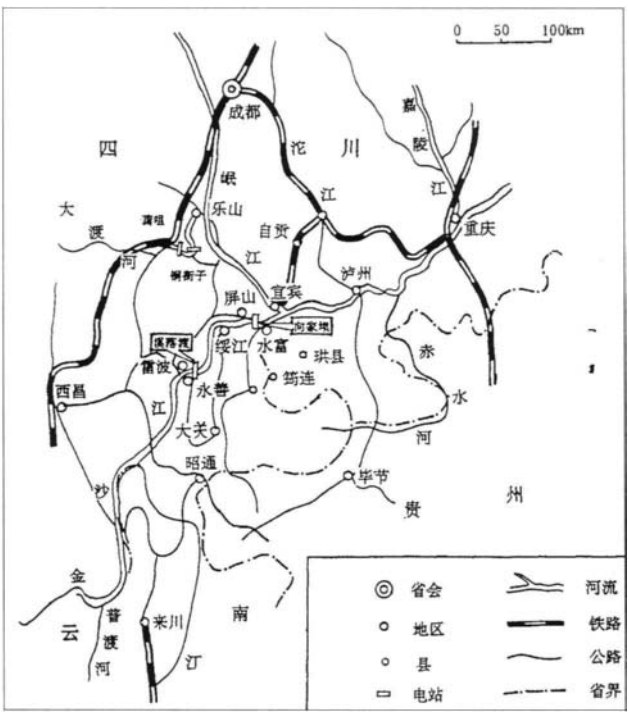


Figure 1 The sketch illustrating the location of Xiluodu Hydropower Station

GEOSTRESS FIELD FITTING

Geological Conditions

The three underground chambers(turbine, transformer and tail water chamber) on both bank located in Permian Emei Mountain Basalt strata P2 β 4 to P2 β 6. The rock mass

quality is quite sound. However because of several times of active tectonism, many discontinuities can be found in the rockmass at the damsite. Especially the intrastratal shearing belts randomly distributing in the strata, worsen the rockmass strength and quality.

Three types of structural plane mainly distributed surrounding the underground powerhouse zone are described as follows:

Interlayer shearing belts(C for short): Interlayer shearing belts, as consequence of the interface in the tectonic rebuilding process of terrane, are the I class structural plane at dam site and extend continuously and steadily. They are gently inclined and the tilt angle is between 4 and 6 degrees. Intrastratal shearing belts (Lc for short): Intrastratal shearing belts, a suite of tectonic shearing plane distributing in terranes, are the II class structural plane. There exist a lot of intrastratal shearing belts in rock mass and some of them are bad in the view of engineering geology. Steep dip joints (J for short): The joints with steep dip angle and distributing widely and randomly in dam site, are the III class structural planes. The trace length of joints in the rock mass surrounding the powerhouses is about 2~4 meters; some of the joints are quite long and so they are called long joints.

Geostress measurement

So far a lot of geostress measurements have been carried out in the dam area, which includes six groups Kaiser effects in lab, 18 groups of stress relief borehole in-situ measurements and 6 groups of hydraulic fracturing measurements. The measurement points distribute at the bottom of the valley and in the shallow rockmass along the valley bank.

All the results are analyzed and compared with each other, which shows considerable derivation both in amount and orientation. Moreover due to limited measuring samples available, it is far insufficient to satisfy the demand of stress and deformation analysis of the excavations. It is therefore necessary to make further analysis to the original stress field and then fit it by fitting and simulating the generation process of the stress field with the approach of tectonic theory.

For this purpose, a 3-D finite element model is built to model the generation of the stress field as shown in Figure 2.

According to structural geology analysis, the present stress field is the result of deep down cutting of the valley. Therefore only the three-phase down cutting process and the main rockmass features are considered. The finite element model consists of 11842 elements and 51807 nodes.

The results of the general stress distribution are: the direction: middle stress – almost horizontal; the maximum and minimum are nearly flat; the amount: the maximum stress is 14~18 MPa in the left bank and 16~20 MPa in the right bank, the middle stress is 10~15 MPa, the minimum stress is little different in both banks, 4~6 MPa.

The modeling results have ideal consistency with the in-situ measurements in value, and some derivation in stress orientation, which has been corrected, based on the stress measurement and tectonic analysis.

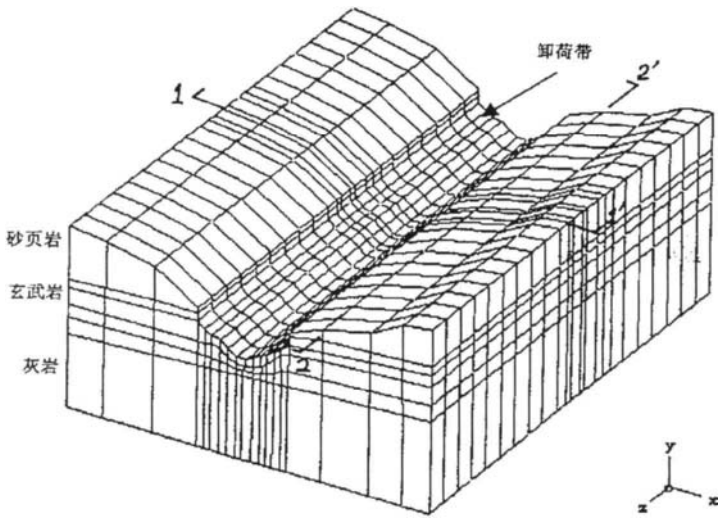


Figure 2 Finite element model to analyzing the initial stress field

TABLE 1

COMPARISON OF MEASURED AND MODELED GEOSTRESS RESULTS IN THE RIGHT BANK

Measuring point number	σ_1 (MPa)		σ_2 (MPa)		σ_3 (MPa)	
	measured	modeled	measured	modeled	measured	modeled
$\sigma_{45\text{-}1}$	15.9	16.3	10.0	12.5	5.37	5.4
$\sigma_{45\text{-}2}$	18.4	17.5	15.8	13.8	4.23	5.2
$\sigma_{45\text{-}3}$	18.2	17.0	12.3	12.8	6.51	5.7
$\sigma_{45\text{-}4}$	20.5	18.2	15.5	13.9	6.73	5.5
$\sigma_{45\text{-}5}$	18.2	17.6	12.7	12.5	6.05	5.4
$\sigma_{45\text{-}6}$	17.3	17.4	15.6	13.7	5.01	5.3

FINITE ELEMENT MODEL FOR THE UNDERGROUND EXCAVATIONS

In order to eliminate the boundary effects, the size of the 3-D model is: 840m long in Z direction, orientation N70° W; 425m wide in X direction, orientation S20° W; 300m high in Y direction. The model is divided into 16275 3-D elements, 67923 nodes. The upper load on the model is the gravitational load and the boundary load in the horizontal direction is determined by the geostress fitting results. The uniform distributed loads σ_1、

σ_3 are applied at 17MPa and 5MPa respectively. Due to the considerably large elastic modulus and brittle failure mode of the basalt, it is assumed that the rockmass is in elastic condition. However approximate yielding and failure analysis is made with elastic stress. The effects of the discontinuities are modeled by the strength equivalent approach. The computational parameters are listed in table 2.

TABLE 2 MECHANICAL PROPERTIES OF THE ROCKMASS

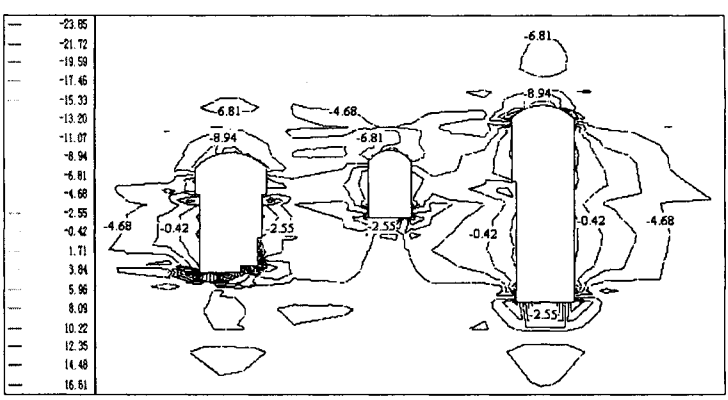
Rock type	Deformation modulus (MPa)	Poisson ration	Density (MN/m^3)	Cohesion (MPa)	Friction angle (^{0})	Tensile strength (MPa)
Compact basalt	13500	0.2	0.0285	2.5	55	0.2
Dotted basalt	13200	0.205	0.028	2.4	53	0.2
Porphyritic basalt	13000	0.208	0.027	2.35	52	0.2
Breccia latite	11000	0.21	0.0268	1.7	50	0.15
Discontinuities	2000	0.27	0.026	0.25	43	0
Limestone	12000	0.212	0.0265	1.8	50	0.18

RESULTS ANALYSIS

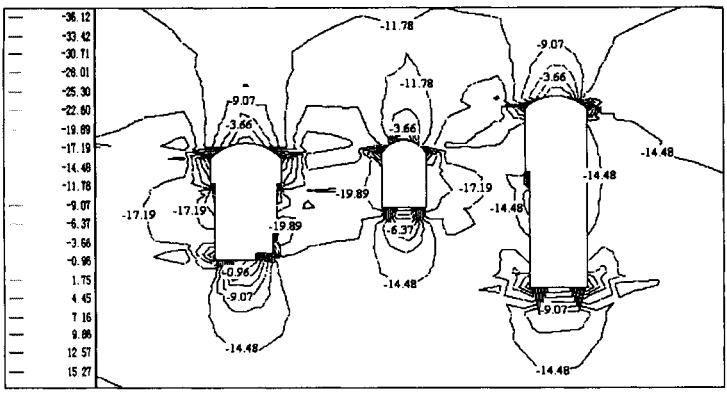
The above-mentioned model was analyzed with an FEM package 3D-σ and the excavation steps follow the design scheme.

The induced secondary stress after excavation

The distribution of secondary stress in the cross section located at No. 1 turbine is shown in Figure 3



(a) Contour of horizontal stress σ_{xx}

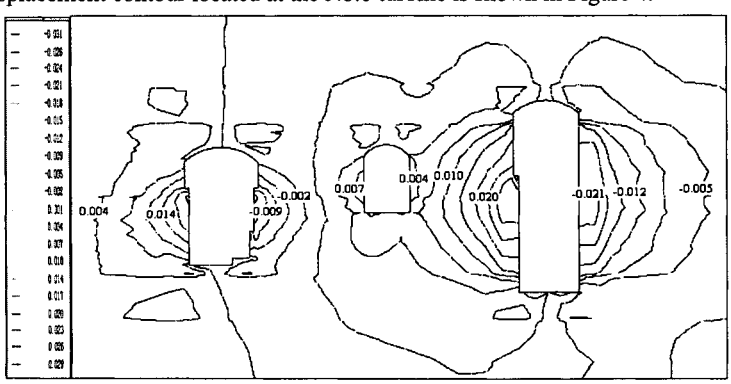


(b) Contour of vertical stress σ_{yy}

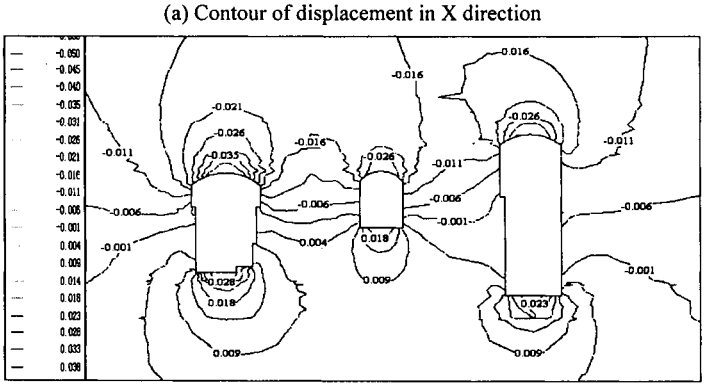
Figure 3 Stress distributions after excavation

The displacement

The displacement contour located at the No.1 turbine is shown in Figure 4.



(a) Contour of displacement in X direction



(b) Contour of displacement in Y direction

Figure 4 Displacement distributions in a typical cross section

The displacement value at some typical points is listed in Table 3

TABLE 3
DISPLACEMENT AT SOME TYPICAL POINTS IN THE CENTERLINE CROSS SECTION LOCATED AT TURBINE NO.1 (unit: cm)

Point No	Disp X	Disp Y	Point No	Disp X	Disp Y	Point No	Disp X	Disp Y
1	0.15	-4.38	7	-0.03	3.403	13	-1.37	0.183
2	0.45	-2.07	8	-0.052	3.414	14	-0.9	0.22
3	1.35	-0.25	9	-0.006	3.056	15	-0.8	-0.02
4	1.45	0.21	10	-0.08	1.666	16	-0.15	-2.07
5	1.783	0.004	11	-0.60	1.416			
6	0.2735	1.2371	12	0.8287	-0.973			

The failure zone

The failure zone is enclosed by the Coulomb-Mohr failure criteria. Figure 5 shows the failure zone in cross section located at No. 1 turbine room. The following features can be seen: (1) The shape of the failure zone at different cross section is similar; (ii) There exists considerable failure zone around the excavations, serious damage at the floor and sidewalls, the failure zone is deep in the sidewall. It should be noticed that the failure zone may connect between the alternator room and the tailwater chamber along the interlayer shearing belt C3; (iii) The damage degree and the shape of the failure zone of the surrounding rock are controlled by the discontinuities (interlayer shearing belts and intrastratal shearing belts).

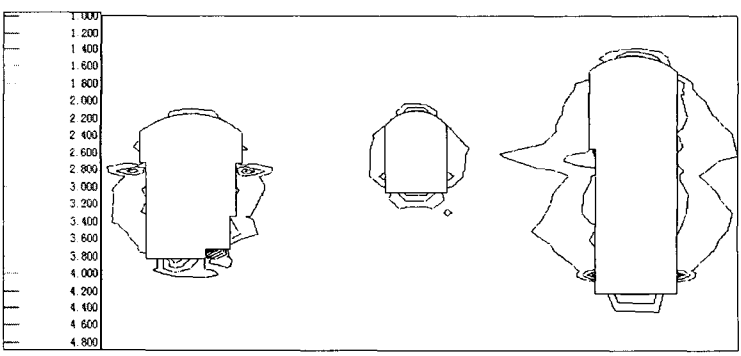


Figure 5 Failure zone around the excavations at cross section in turbine No.1

CONCLUSIONS AND SUGGESTIONS

Based on geological investigation, geostress measurement and fitting, 3-D finite element analysis, the following conclusions and suggestions may be drawn:

(1) There exists stress concentration after excavation with maximum 36.04 MPa at tailwater chamber; there is also some tensile stress zone in the surrounding rock unfavorable to the stability of powerhouses.

(2) Displacement: The maximum horizontal displacements are 1.78 cm and 1.59 cm at the sidewall of main turbine chamber; 0.90 cm and 0.25 cm at the sidewall of main alternator chamber; 2.29 cm and 2.07 cm at the sidewall of tailwater chamber. The maximum vertical displacements are 4.38 cm at the crown of the main turbine chamber; 2.96 cm at the alternator chamber; 3.69 cm at the tailwater chamber.

(3) Failure zone: There exists different failure zones around the excavations. The main turbine chamber: serious damage in the floor but the failure range is small; the damage in the sidewall is slight but deep. The failure zone between the main alternator chamber and the tailwater chamber almost connect, which is the result of the effects of the high sidewall of the tailwater chamber to the main alternator chamber, and the results of the discontinuities.

(4) The effects of the discontinuities: all the discontinuities, especially those exposed during excavation, have significant effects on the stress distribution, displacement and the failure zone of the surrounding rock.

REFERENCES

1. Chengdu Institute of Hydropower Investigation and Design, Feasibility research report on Xiluodu Hydropower, Jinshajiang River, 1998
2. Chengdu Institute of Hydropower Investigation and Design, Outline and guideline of feasibility study on Xiluodu Hydropower, Jinshajiang River, 1999
3. Hu Bin, Zhang Zhuoyuan and Tao Lianjin, Statistical analysis of geostress measurements in deeply downcutting valley, J of Geohazards Prevention and Geoenvironment Protection, 2001(3)
4. Hu Bin, Zhang Zhuoyuan and Tao Lianjin, Variation feature of geostress in a deep downcutting valley, J of World Earthquake Information, 2001(2)

ACKNOWLEDGEMENTS

This research is supported by the Young Talented Teacher Program of the Ministry of Education of China, the Natural Science Foundation of Beijing, the project of Beijing New SciTech Star and the Geohazard Prevention Openlab Foundation.

Advances in Building Technology, Volume I
M. Anson, J.M. Ko and E.S.S. Lam (Eds.)
© 2002 Elsevier Science Ltd. All rights reserved

Evaluation of Ground Vibration Induced by Subway

Tao Lianjin [1], Li Xiaolin [1] and Zhang Dingsheng [2]

[1] College of Architecture and Civil Engineering, Beijing Polytechnic University
Beijing, 100022, China
[2] Beijing Design Institute of City Construction

ABSTRACT

Based on field monitoring and wheel-rail model analysis, a finite element model is built to evaluate the vibration in the subway tunnels between subway stations. A spring and viscous boundary is adopted in the model and transient approach is used to model the dynamic effects of the train with ANSYS. The simulation results show good consistency with the monitored data in situ, and the following conclusions are drawn according to the analysis and monitoring:

(1) The horizontal vibration just above the tunnel is minimum and the vertical vibration is maximum;
(2) The vertical ground vibration caused by subway train is more noticeable than the horizontal one;
(3) On the ground, the vibration decreases with the increase of the distance away from the subway tunnel, and that the attenuation in the vertical direction is faster than in horizontal direction.

KEYWORDS

ground vibration, wave transmission, finite element model

1. INTRODUCTION

The subway circuit in a city generally passes through the downtown area where the building is multitudinous. The embedded depth of subway tunnel is generally shallow, and the vibration that the running subway train gives rise to will be delivered to the lining through the track structure, and be delivered to the ground through the rock soil medium outside the lining structure, causing the ground vibration. This kind of vibration will influence building on the ground. At present, the environment problem initiated by engineering construction is arousing more and more attention.

In recent years, the environment questions such as vibration caused by subway are more and more noticeable owing to the great development of city tube traffic systems. It is meaningful to evaluate the effects of subway vibration to the environment.

2. CURRENT RESEARCH

The research on vibration caused by the subway chiefly includes two aspects at present: (1) vehicle-track system dynamics model, and finding the exciting force the running subway train erects on the subway tunnel by computing [1][2]. (2) from dynamic model of tunnel structure-strata, obtaining the kinetic equation of the model, and adopting a numerical method to solve the equation and so obtaining the response of the whole model. Wang Fengchao[5], Zhang Yue and Pan Changshi [6] and Sun Juns [7] made some progress in this aspect.

3. COMPUTING MODEL AND RESULTS

3.1. General Engineering Situation

The soil in Beijing generally can be divided into miscellaneous filling soil (1~3m), clay silt, silty clay, sand soil (total thickness $>$ 20 meters) and cobble. Because the embedded depth of subway tunnel does not generally surpass 10 meters, it is considered that the subway tunnel passes through clay silt, silty clay, and sand soil. The tunnel cross section in the region between subway stations is a rectangle, and reinforced concrete lining is used. A sketch of the tunnel cross section is shown in figure 1.

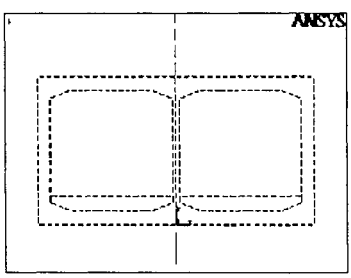


Fig. 1. Tunnel cross section

3.2. Effect of Impact of Train wheel to The Track

According to the testing data of Pan Changshi [7] to the vibration in a Beijing subway tunnel , we used spectral analysis to obtain the expression for the acceleration of the rail bottom:

$$x(t) = \sum_{k=-N/2}^{N/2} (A_k \cos k\omega t + B_k \sin k\omega t) \tag{1}$$

Where

$$A_k = \frac{2}{N}\sum_{j=0}^{N-1} x_j \cos\frac{2\pi kj}{N} \tag{2}$$

ω---- circle frequency, $\omega = \dfrac{2\pi}{N\Delta t}$

N ---- number of sampling, $N = 2048$

$$B_k = \frac{2}{N}\sum_{j=0}^{N-1} x_j \sin\frac{2\pi kj}{N} \tag{3}$$

Δt ----time interval for sampling, $\Delta t = \dfrac{s}{300}$

The model of interaction between a simplified wheel system of the subway train and the rail is shown in figure 2.

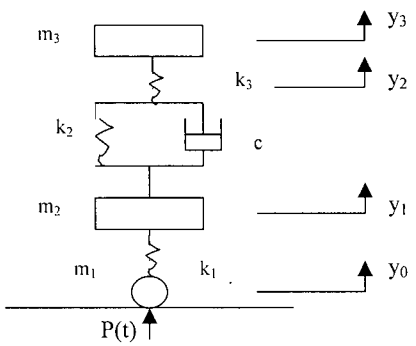


Fig 2. The interaction model of wheel and rail

In Fig. 2, m_1 = 1700.0 Ns^2/m, m_3 = 9050.3 Ns^2/m, $k_1 = 2.45\times10^6$ N/m, $k_3 = 1.90757\times10^6$ N/m, $c = 0.240884\times10^6$ Ns/m. The interaction force is marked as $P(t)$, the balance seat coordinates of m_1, m_2, k_3, m_3 are marked as y_0, y_1, y_2, y_3. According to the D'Alembert principle, the differential equation of motion of the train wheel system can be attained as follows:

$$\begin{aligned} P(t) = 125500 + \sum_{k=-N/2}^{N/2} & \{[128.0669A_k - 165.7383(k\omega)^2 \bullet F_k - 24.7128(k\omega)^3 \bullet E_k \\ & + 0.1119(k\omega)^4 \bullet F_k + 0.0103(k\omega)^5 \bullet E_k]\cos k\omega t \\ & + [128.0669B_k - 165.7383(k\omega)^2 \bullet E_k - 24.7128(k\omega)^3 \bullet F_k \\ & + 0.1119(k\omega)^4 \bullet E_k + 0.0103(k\omega)^5 \bullet F_k]\sin k\omega t\} \end{aligned} \quad (N) \tag{4}$$

where, A_k, B_k are coefficients. The vertical train load can be calculated from the expression:

$$F(t)=\frac{K \bullet n \bullet N \bullet P(t)}{L} \qquad \text{(N/m)} \tag{5}$$

In this expression,

K ---- coefficient of correction
N --- -number of double wheel of each railway carriage
n ---- number of railway carriages
L ---- length of the subway train

The dynamic load induced by the subway train can be obtained when N=5, n=2, L=5*19.2=96m, K=1. We simplified the result, and produced the load-time curve as shown in figure 3.

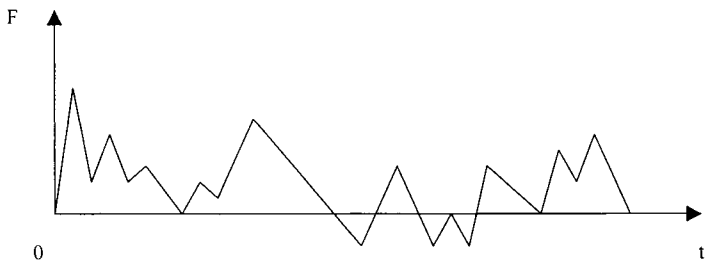


Fig 3. Load-time curve of wheel to rail

3.3. Computational Model and Method

3.3.1. Geometry model

The computational model is shown in figure 4.

Analyzing the vibrating influence question that the subway train causes, is strictly a 3-D question, which would require a long time for the computer to perform. When it is simplified to a 2D plane strain question, the time spent on computing can be shortened greatly, and the precision can still satisfy the engineering needs[8][9].

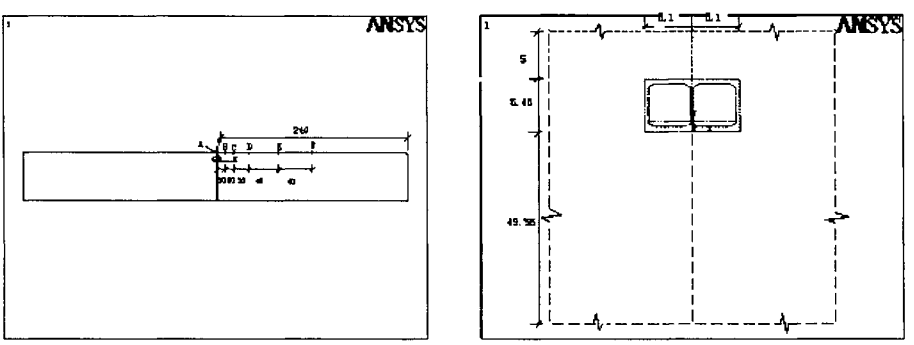


Fig. 4. Subway tunnel geometry model and its partly enlarged view

3.3.2. The computing parameters

The subway railway roadbed is of the crushed stone railway roadbed, and is considered as linear elastic material. The computing parameters are:
Young's modulus:E=1.3 × 10^3 MPa Poisson ratio:μ = 0.2 Density:ρ = 2000 Kg / m^3

The reinforced concrete lining is considered as linear elastic. The computing parameters are:
Young's modulus:E=2.1 × 10^4 MPa Poisson ratio:μ = 0.2 Density:ρ = 2400 Kg / m^3

The surrounding soil is considered as linear elastic. The computing parameters are:
Young's modulus:E=30 MPa Poisson ratio:μ = 0.3 density:ρ = 2000 Kg / m^3

3.3.3. Computational method

The finite element method with ANSYS is adopted. The Newmark time integral method at dispersed time points was used to solve the above-mentioned equation. The dynamic load shown in figure 2 is adopted as the computing load, and initial stress and the gravity load of all the structure are considered. The analysis time is 7 seconds, the length of step time is 0.05 second, and 140 steps were computed. The 8 nodes plane quadrilateral isoparametric element was adopted. The number of the elements was 2420, having 7413 nodes. An elasticity boundary condition was adopted at the two sides and at the bottom of the model.

The finite element mesh is shown in figure 5.

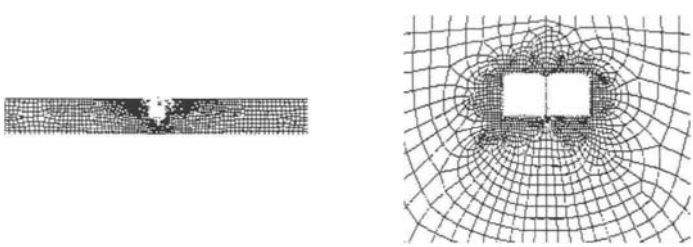


Fig. 5. The finite element mesh (whole and the close-up central part)

3.4. Part of Computational Results and the Analysis

3.4.1. Part of computational results

Six reference points were chosen in computing: A, B, C, D, E and F. The positions of each reference point are shown in figure 4. The vibrations in horizontal direction and vertical direction are computed respectively.

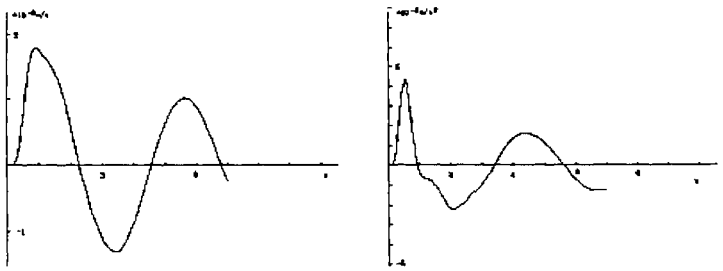


Fig. 6. Velocity-time curve (left) and acceleration-time curve (right) at point A

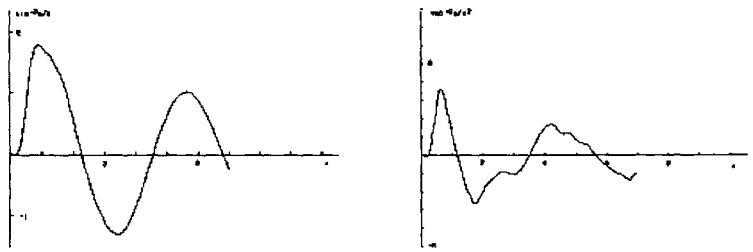


Fig. 7. Velocity-time curve (left) and acceleration-time curve (right) at point E

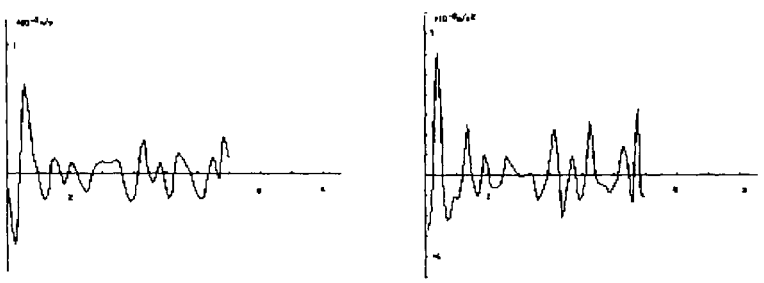


Fig. 8. Velocity-time curve (left) and acceleration-time curve (right) at point A

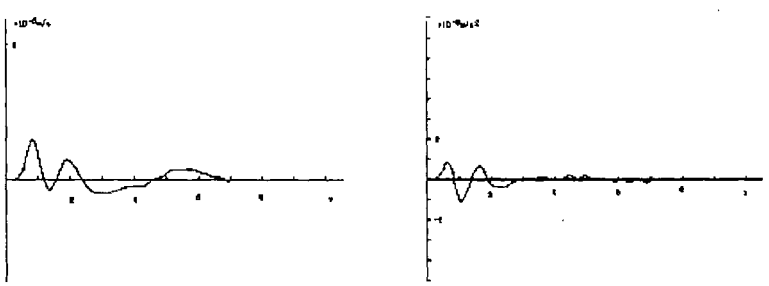


Fig. 9. Velocity-time curve (left) and acceleration-time curve (right) at point E

The maximal values of the results at each reference point are shown in in figure 10 and 11.

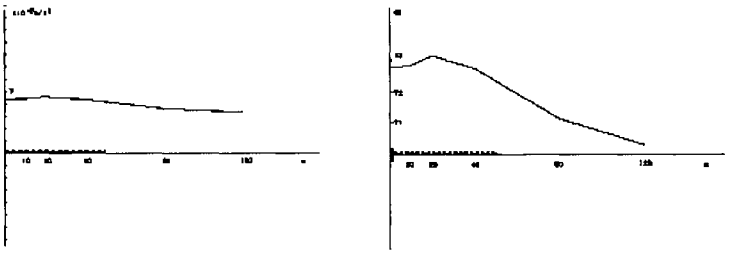


Fig.10. The relationship of the maximal acceleration values between horizontal direction and distance

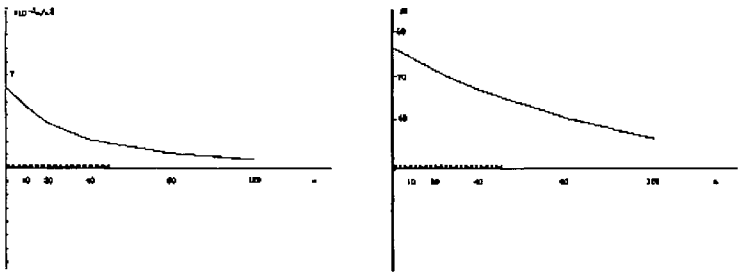


Fig.11. The relation of the maximal acceleration values of vertical direction and distance

4. CONCLUSIONS

According to the results given above, some conclusions can be drawn:

1. The horizontal vibration of the ground just above the subway tunnel is the minimum, while the vertical direction vibration is maximum;

2. The vertical vibration caused by the subway train is more significant than the vibration in the horizontal direction;

3. The ground vibration attenuates to some extent with increase of the distance from the subway tunnel, and attenuation of vibration in the vertical direction is faster than in horizontal direction.

Acknowledgements

This research is supported by the Young Talented Teacher Program of the Ministry of Education of China, the Natural Science Foundation of Beijing and the Project of Beijing New

References

[1] Zhang Yue, Bai Baohong. (2000). The method of identifying train vibration load acting on subway tunnel structure. *Journal of Vibration and Shock* **19:3**, 68-76

[2] Li Dewu, Gao Feng. (1999). In-situ measurement and frequency-spectrum analysis for the traffic vibration of foundationstructure of the tunnel. *Journal of Gansu Sciences* **11:1**, 52-54

[3] Liu Weining, Xia He, Guo Wenjun. (1996). Study of vibration effects of underground trains on surrounding environments. *Chinese Journal of Rock Mechanics and Engineering* **15**, 586-593

[4] Chen Shi, Xu Guobin,Gao Ri. (1998). Dynamic analysis of the impact of train vibration acting on the structure along the railway. *Journal of Northern Jiaotong University* **22:4**, 57-60

[5] Wang Fengchao, Xia He, Zhang Hongru. (1999). Vibration effects of surrounding buildings. *Journal of Northern Jiaotong University* **23:5**, 45-48

[6] Zhang Yue, Bai Baohong, Pan Changshi. (1997). Evaluation of the impact of subway train vibration acting on surroundings. *Control for yawp and vibration* **2**, 37-41

[7] Sun Jun. (1996). *Theory and practice of underground engineering design*, Science and Technology Publishing House of Shanghai

[8] DRJ·Irving. Zheng Guoping, Liu Zhong, Xu Jiali translated. (1989). *Theory and application of finite element method of plastic mechanics*, Weapon Industry Publishing House

[9] Pan Changshi, Zhang Mi, Wu Hongqing. (1995). *Numerical method of tunnel mechanics*, Railway Publishing House of China

Advances in Building Technology, Volume 1
M. Anson, J.M. Ko and E.S.S. Lam (Eds.)
© 2002 Elsevier Science Ltd. All rights reserved

NONSTATIONARY RESPONSE OF SPATIAL LATTICE SHELLS UNDER MULTIPLE SEISMIC INPUTS

X.S. Wang, S.D. Xue and Z. Cao

The College of Architecture and Civil Engineering
Beijing Polytechnic University, Beijing 100022, China

ABSTRACT

This paper presents a nonstationary random vibration study of spatial lattice shells under multi-support and multi-dimensional seismic excitations. The multi-dimensional pseudo excitation method for random vibration analysis of structures is first developed. It is found that the derived method is particularly suitable for random vibration analysis of long span spatial structures, which are usually characterized with closely spaced natural frequencies and coupled vibration modes. Based on the method, a computer program is developed. The seismic performance of a spatial lattice shell under different earthquake inputs is investigated. Some observations are made. It is shown that the developed method is a highly efficient algorithm, which can easily solve the nonstationary problem of large structures under multi-support and multi-dimensional seismic excitations.

KEYWORDS

Random vibration, nonstationary, seismic response, lattice shell, spatial structure, pseudo excitation method, multiple seismic inputs, multi-support earthquake excitation, 3-D random analysis.

INTRODUCTION

Lattice shell is a type of popular spatial structure. At present, lattice shells have been widely used in the construction of long span sports buildings, exhibition halls, and hangars, etc. The potential social and economical influence and impacts resulting from the failure of this type of structure make it mandatory that special care be taken in the design of lattice shells, in which the seismic performance of the structure is an important concern. In recent years, dynamic analyses of lattice shells to earthquake excitations have been performed by many researchers (Cao and Zhang 2000; Shen *et al* 2000). However, most of the studies in the past focused only on single-dimensional and deterministic analysis. Since lattice shell is a type of spatial structure whose vibrations are dominated by both horizontal and vertical motion, its seismic performance to multiple earthquake inputs needs to be investigated. To this end, this paper presents a nonstationary random vibration analysis of lattice shells subjected to multi-support and multi-dimensional earthquake excitations.

The earthquake ground motion can be regarded as a random process (Houser 1947). At present, random vibration analysis method has been widely accepted for analyzing the stochastic responses of structures to earthquake excitations. Many scholars engaged in random vibration study of structures in past few years (Gasparini 1979; Harichandran and Vanmarcke 1986). Recently, structural responses to multiple seismic excitations have attracted much attention by researchers (Li 1998; Lopez *et al* 2000). Two major methods, response spectrum method and random analysis method, have been investigated. However, it is found that these methods are difficult to apply to practical large structures due to their considerable computation efforts. In order to reduce the computational effort, the cross-correlation items between the participant modes are generally neglected, i.e., the accurate CQC method is approximately replaced by the SRSS method (Clough and Penzien 1993). However, this is acceptable only for structures with small damping and sparsely spaced eigen-frequencies. For most spatial structures, it is well known that the participant frequencies are often closely spaced and the vibration modes may couple together. Therefore, the SRSS method may produce large errors. Recently, Lin *et al* (1993; 1994) proposed a highly efficient algorithm called the Pseudo Excitation Method (PEM). This method is a fast and accurate CQC algorithm, in which all the cross-correlation terms between the participant modes are involved, therefore, it is more suitable for dynamic analysis of structures which are characterized with closely spaced natural frequencies and coupled vibration modes. Using the concept of PEM, a multi-dimensional pseudo excitation method was further developed by Xue *et al* (2000) in order to investigate the random responses of lattice shells under multi-component seismic excitations. However, in the researches of Xue *et al* (2000), the seismic excitations were assumed to be stationary and no phase lags between the excitations were taken into account. In this paper, the multi-dimensional pseudo excitation method is further developed for nonstationary random vibration analysis of structures under multi-support and multi-dimensional earthquake excitations, in which the phase lags between the excitations have been involved. The formulation is first derived. Then, a random vibration analysis is performed for a spatial lattice shell to investigate its seismic performance under multiple seismic input, from which some conclusions are drawn.

FORMULATION

Selecting a global coordinate system O-XYZ with Z-axis vertically upwards. The system is assumed to be static relative to the center of the earth. For a lumped mass structure having P ground joints and N free joints, the equation of motion can be expressed by

$$\begin{bmatrix} M_{ss} & 0 \\ 0 & M_{mm} \end{bmatrix} \begin{Bmatrix} \ddot{U}_s + \ddot{U}_r \\ \ddot{U}_m \end{Bmatrix} + \begin{bmatrix} C_{ss} & C_{sm} \\ C_{ms} & C_{mm} \end{bmatrix} \begin{Bmatrix} \dot{U}_r \\ 0 \end{Bmatrix} + \begin{bmatrix} K_{ss} & K_{sm} \\ K_{ms} & K_{mm} \end{bmatrix} \begin{Bmatrix} U_s + U_r \\ U_m \end{Bmatrix} = \begin{Bmatrix} 0 \\ P_m \end{Bmatrix} \tag{1}$$

where $[M_{ss}]$, $[C_{ss}]$, $[K_{ss}]$ are, respectively, mass, damping, and stiffness matrices of the structural free joints; $[M_{mm}]$, $[C_{mm}]$, $[K_{mm}]$ are, respectively, mass, damping, and stiffness matrices of the ground joints; $[C_{sm}]$, $[C_{ms}]$ and $[K_{sm}]$, $[K_{ms}]$ are respectively coupled damping and stiffness matrices between the structural free joints and ground joints; $\{U_s\}$ and $\{U_r\}$ are respectively the quasi-static and quasi-dynamic displacement vectors caused by the ground motion; $\{U_m\}$ is the enforced displacement vector of the ground joints; $\{P_m\}$ represents the forces exerted on the structure by ground motion. After simplification (Lin *et al* 1994; 2000), Eqn. 1 becomes

$$[M_{ss}]\{\ddot{U}_r\} + [C_{ss}]\{\dot{U}_r\} + [K_{ss}]\{U_r\} = -[M_{ss}]\{\ddot{U}_s\} \tag{2}$$

$$\{U_s\} = -[K_{ss}]^{-1}[K_{sm}]\{U_m\} \tag{3}$$

Substituting Eqn. 3 into Eqn. 2 leads to

$$[M_{ss}]\{\ddot{U}_r\}+[C_{ss}]\{\dot{U}_r\}+[K_{ss}]\{U_r\}=[M_{ss}][K_{ss}]^{-1}[K_{sm}]\{\ddot{U}_m \tag{4}$$

Assuming the earthquake wave reaches the jth ground joint (X_j, Y_j) at $t = T_j$

$$T_j = (X_j \cos\theta + Y_j \sin\theta)/v \tag{5}$$

where v is the equivalent phase velocity of the earthquake wave, θ is the angle between v direction and X-axis direction. Thus, the acceleration of ground joints can be expressed by

$$\{\ddot{U}_m(t)\}=[G(t)]\{\ddot{U}_g(t) \tag{6}$$

where $[G(t)]$ is a specified time-lags envelope function matrix; $\{\ddot{U}_g(t)$ is a time-lags zero-mean-valued stationary random process vector

$$[G(t)]=\begin{bmatrix} G_1(t) & & & & \\ & \ddots & & 0 & \\ & & G_j(t) & & \\ & 0 & & \ddots & \\ & & & & G_p(t) \end{bmatrix} \tag{7}$$

$$[G_j(t)]=\begin{bmatrix} g_x(t-T_j) & & 0 \\ & g_y(t-T_j) & \\ 0 & & g_z(t-T_j) \end{bmatrix} \tag{8}$$

$$\{\ddot{U}_g(t)\}=[\ddot{U}_{g1}(t) \quad \cdots \quad \ddot{U}_{gj}(t) \quad \cdots \quad \ddot{U}_{gp}(t)]^T \tag{9}$$

$$\{\ddot{U}_{gj}(t)\}=[X(t-T_j) \quad Y(t-T_j) \quad Z(t-T_j)]^T \tag{10}$$

In practical calculation, we usually assume that $g_x(t) = g_y(t) = g_z(t) = g(t)$, $g(t) = 0$ when $t < 0$. For linear structure with orthogonal damping matrix, the structural responses are usually determined by mode-superposition scheme, the displacement of structural free joints $\{U_r\}$ can be expressed as the linear composition of the first q mode shapes ($q << 3n$)

$$\{U_r\}=\sum_{j=1}^{q}\{\phi_j\}\mu_j=[\Phi]\{\mu\} \tag{11}$$

Eqn. 4 can be decomposed into

$$\{\ddot{\mu}\}+diag[2\xi_j\omega_j]\{\dot{\mu}\}+diag[\omega_j^2]\{\mu\}=[\beta]\{\ddot{U}_m\} \tag{12}$$

where ξ_j and ω_j are, respectively, the jth damping ratio and frequency of the jth mode; $[\beta]=[\Phi]^T[M_{ss}][K_{ss}]^{-1}[K_{sm}]$, in which the following relation is utilized

$$[\Phi]^T[M][\Phi]=[I] \tag{13}$$

The input power spectral density matrix can be written as

$$[S_{\ddot{U}_m\ddot{U}_m}]=[G(t)]^*[S_{\ddot{U}_g\ddot{U}_g}][G(t)]^T \tag{14}$$

$$\begin{aligned}\left[S_{\ddot{U}_g\ddot{U}_g}(\omega)\right]&=\begin{bmatrix}[I]_3 e^{i\omega T_1}\\ [I]_3 e^{i\omega T_2}\\ \vdots\\ [I]_3 e^{i\omega T_p}\end{bmatrix}\begin{bmatrix}S_{xx}(\omega) & S_{xy}(\omega) & S_{xz}(\omega)\\ S_{yx}(\omega) & S_{yy}(\omega) & S_{yz}(\omega)\\ S_{zx}(\omega) & S_{zy}(\omega) & S_{zz}(\omega)\end{bmatrix}\left[[I]_3 e^{-i\omega T_1} \quad [I]_3 e^{-i\omega T_2} \quad \cdots \quad [I]_3 e^{-i\omega T_p}\right]\\ &=[V]^*[S(\omega)][V]^T\end{aligned} \tag{15}$$

where $[I]_3=\begin{bmatrix}1 & 0 & \\ & 1 & \\ 0 & & 1\end{bmatrix}$; $[S(\omega)]$ is the power spectral density matrix of three-dimensional earthquake inputs; Considering the coherence between ground motions, $[S(\omega)]$ is a Hermitian's matrix. According to the spectral decomposition scheme of the Hermitian matrix, $[S(\omega)]$ can be decomposed into

$$[S(\omega)]=\sum_{j=1}^{r}\alpha_j\{\psi_j\}^*\{\psi_j\}^T \tag{16}$$

where r is the rank of the matrix $[S(\omega)]$; α_j and $\{\psi_j\}$ are respectively the jth eigenvalue and normalized eigenvector of $[S(\omega)]$. Substituting Eqns. 15 and 16 into Eqn. 14 gives

$$[S_{\ddot{U}_m\ddot{U}_m}]=\sum_{j=1}^{r}[G(t)]^*[V]^*\alpha_j\{\psi_j\}^*\{\psi_j\}^T[V]^T[G(t)]^T \tag{17}$$

According to the principle of pseudo excitation method, taking a pseudo ground acceleration vector

$$\{\ddot{U}_{m_j}(t,\omega)\}=\sqrt{\alpha_j}[G(t)][V]\{\psi_j\}e^{i\omega t} \tag{18}$$

The solution for Eqn. 11 under the pseudo excitation $\{\ddot{U}_{m_j}(t,\omega)$ is given by

$$\{\ddot{U}_{r_j}(t,\omega)\}=\int_0^t[\Phi][h(t-\tau)][\beta]\sqrt{\alpha_j}[G(\tau)][V]\{\psi_j\}e^{i\omega\tau}\,d\tau \tag{19}$$

where

$$[h(t-\tau)]=diag[h_i(t-\tau)] \tag{20}$$

$$h_i(t-\tau)=\frac{1}{\omega_{di}}e^{-\xi_i\omega_i(t-\tau)}\sin\omega_{di}(t-\tau) \tag{21}$$

in which $\omega_{di}=\omega_i\sqrt{1-\xi_i^2}$. According to the concept of pseudo excitation method, the power spectral density matrix for structural quasi-dynamic displacement is developed by

$$\left[S_{U_r U_r}(t,\omega)\right]=\sum_{j=1}^{r}\left\{U_{r_j}(t,\omega)\right\}^{*}\left\{U_{r_j}(t,\omega)\right\}^{T} \tag{22}$$

The quasi-static displacement vector can be obtained by substituting Eqn. 18 into Eqn. 3,

$$\left\{U_{s_j}(t,\omega)\right\}=-\left[K_{ss}\right]^{-1}\left[K_{sm}\right]\int_0^t\left(\int_0^{t'}\left[G(\tau)\right]\left[V\right]\sqrt{\alpha_j}\left[F_m\right]\left\{\psi_j\right\}e^{i\omega\tau}\,d\tau\right)dt' \tag{23}$$

Then, the power spectral density matrix for structural quasi-static displacement is given by

$$\left[S_{U_s U_s}(t,\omega)\right]=\sum_{j=1}^{r}\left\{U_{s_j}(t,\omega)\right\}^{*}\left\{U_{s_j}(t,\omega)\right\}^{T} \tag{24}$$

The power spectral density of total displacement is written as

$$\left[S_{U_{ss}U_{ss}}(t,\omega)\right]=\sum_{j=1}^{r}\left\{U_{ss_j}(t,\omega)\right\}^{*}\left\{U_{ss_j}(t,\omega)\right\}^{T} \tag{25}$$

$$\left\{U_{ss_j}(t,\omega)\right\}=\left\{U_{s_j}(t,\omega)\right\}+\left\{U_{r_j}(t,\omega)\right\} \tag{26}$$

The power spectral density matrix for internal forces can be obtained through translation matrix $\left[Z_N\right]$

$$\left[S_{NN}(t,\omega)\right]=\sum_{j=1}^{r}\left\{N_j(t,\omega)\right\}^{*}\left\{N_j(t,\omega)\right\}^{T} \tag{27}$$

$$\left\{N_j(t,\omega)\right\}=\left[Z_N\right]\left\{U_{ss_j}(t,\omega)\right. \tag{28}$$

It can be easily verified that Eqns. 22, 24, 25 and 27 are mathematically identical to expressions given by conventional CQC method.

The time-dependent variance for internal force of the *i*th member can be assessed by corresponding component of $\left[S_{NN}(t,\omega)\right]$

$$\sigma_{N_i}^2(t)=\int_{-\infty}^{+\infty}S_{N_iN_i}(t,\omega)d\omega \tag{29}$$

The mean value of peak response can be estimated by the variance (Jiang and Hong 1984).

ANALYSIS

To study the seismic performance of spatial lattice shells under multiple nonstationary seismic excitations, a double-layer cylindrical lattice shell is selected for the random vibration study. Figure 1 shows a finite element model of the structure, where B_S and B_X represent respectively the upper and the lower chord members in B direction; Z_S and Z_X represent respectively the upper and the lower chord members in L direction. The boundary supports of the lattice shell are assumed to be fixed hinge joints. The structural parameters are taken as follows: span length L=30 m; width B=25 m; shell thickness d=1.0 m; the ratio of depth to span f/B=0.3; the basic grid size is taken as 2×2 m. The members are modeled as bar elements in the analysis. The roof load is taken as 1kN/m^2. All the loads and self-weights of the members are treated as lumped masses concentrated at the joints.

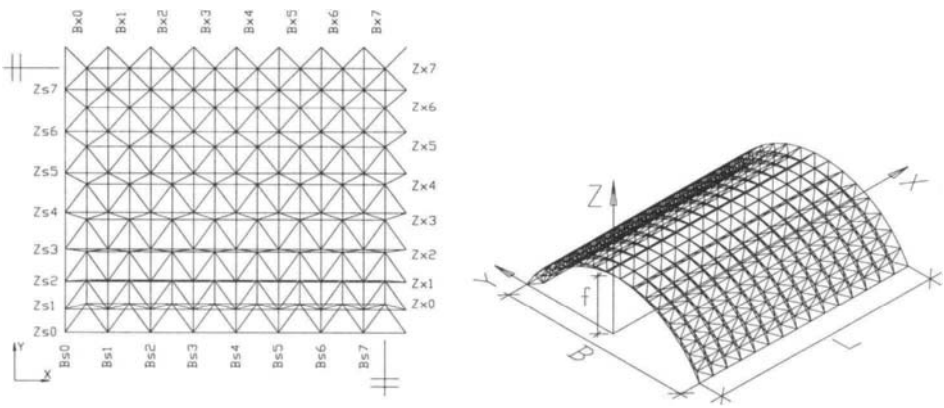


Figure 1 Finite element model of double-layer cylindrical lattice shell

The earthquake power spectrum for horizontal ground motion is represented by revised Kanai-Taijimi expression (Clough and Penzien 1993)

$$S_{xx}(\omega)=S_{yy}(\omega)=\frac{\omega_g^4+4\xi_g^2\omega_g^2\omega^2}{(\omega_g^2-\omega^2)^2+4\xi_g^2\omega_g^2\omega^2}\cdot\frac{\omega^4}{(\omega_f^2-\omega^2)^2+4\xi_f^2\omega_f^2\omega^2}S_0 \tag{30}$$

where ω_g is the natural ground frequency; ξ_g is the damping ratio of the ground; S_0 is the intensity parameter; ξ_f, ω_f are revised parameters; generally, it is taken that $\xi_f=\xi_g$, $\omega_f=0.1-0.2\omega_g$ (Chen *et al* 1999). The earthquake power spectrum for vertical ground motion is considered to have similar spectral distribution of Eqn. 30, but the parameters is modified as suggested by the authors (Xue *et al* 2000; Wang *et al* 2001), $\omega_{gV}=1.58\omega_{gH}$; $\xi_{gV}=\xi_{gH}$; $S_{0V}=0.281S_{0H}$.

The cross-spectrum between the excitations are assumed to have the form: $S_{xy}(\omega)=\sqrt{S_{xx}(\omega)S_{yy}(\omega)}$ (Huang and Liu 1987); $S_{xz}(\omega)=0.6\sqrt{S_{xx}(\omega)S_{zz}(\omega)}$; $S_{yz}(\omega)=0.6\sqrt{S_{yy}(\omega)S_{zz}(\omega)}$ (Xue *et al* 2000). The following envelope function is adopted (Amin and Ang 1968)

$$f(t)=\begin{cases}(t/t_1)^2 & 0\le t<t_1\\ 1 & t_1\le t\le t_2\\ e^{-c(t-t_2)} & t>t_2\end{cases} \tag{31}$$

The parameters used for the input spectra are respectively: ξ_g=0.8; ω_{gH}=15.71 rad/s; S_{0H}=8.6409 cm^2/s^3; $t_1=1.2$; $t_2=9.0$; $c=0.5$; assuming $\theta=0$, v=500, 1000, 2000, 3000 m/s.

Based on the formulation, a computer program has been developed for nonstationary random vibration analysis of lattice shells under multiple seismic inputs. The random responses of the double-layer cylindrical lattice shell are obtained using the developed program. Some of the results are shown in Figures 2 to 5, respectively, where the response of dynamic internal force represents the mean value of peak response. Following observations can be drawn from the results:

(1) From Figures 2 and 3 we can observe that the seismic responses under three-dimensional

earthquake inputs (XYZ input) are always greater than those under single-dimensional earthquake input (Y input), whether or not the phase lags are considered.

(2) The results shown in Figure 4 indicate that stationary input produces larger seismic responses than nonstationary input.

(3) It is observed from Figure 5 that the change of wave speed may result in significant different responses in different members, indicating the effects of phase lags between excitations. It is also observed that the earthquake wave with low speed may produce quite larger responses in some members (see member 18 in Figure 5).

(4) The analyses of the example show that the developed method is a highly efficient algorithm, which can easily solve the nonstationary problem of large structures under multi-support and multi-dimensional seismic excitations.

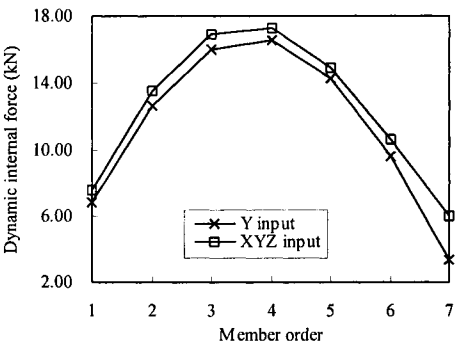


Figure 2 Dynamic internal force of Bx4 (nonstationary without phase lag, $v=\infty$)

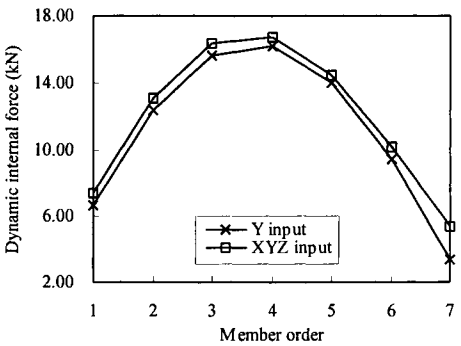


Figure 3 Dynamic internal force of Bx4 (nonstationary with phase lag, v=500m/s)

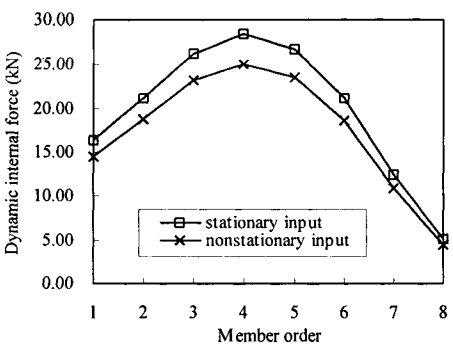


Figure 4 Dynamic internal force of Bs7 (XYZ input, without phase lag)

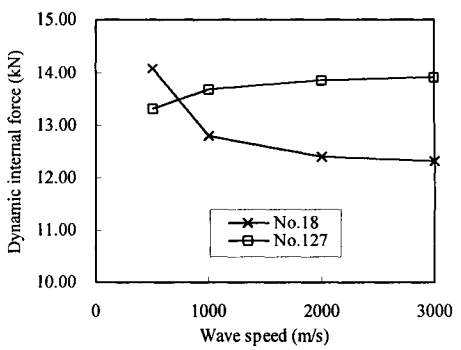


Figure 5 Dynamic internal force of member 18 and 127 at nonstationary XYZ input

CONCLUSIONS

A nonstationary random vibration study of spatial lattice shells under multi-support and multi-dimensional seismic excitations has been performed in this paper. The multi-dimensional pseudo excitation method for random vibration analysis of structures was developed. It is found that the

derived method is particularly suitable for random vibration analysis of long span spatial structures, which are usually characterized with closely spaced natural frequencies and coupled vibration modes. Based on the method, a computer program has been developed. The seismic performance of a cylindrical lattice shell under different earthquake inputs was investigated. Some observations were made. It is shown that the developed method is a highly efficient algorithm, which can easily solve the nonstationary problem of large structures under multi-support and multi-dimensional seismic excitations.

ACKNOWLEDGEMENTS

The authors are grateful for the support from the National Natural Science Foundation of China.

REFERENCES

Amin M. and Ang A. (1968). Nonstationary Stochastic Models of Earthquake Motions. *J. Engineering Mechanics Division, ASCE.* **94:EM2,** 559-584.

Cao Z. and Zhang Y.G. (2000). A Study on the Seismic Response of Lattice Shells. *International Journal of Space Structures*, **15:3&4**, 243-247.

Chen G.X, Jin Y.B. and Zai J.M. (1999). A Simple Method of Random Earthquake Response Analysis for High-Rise Buildings. *Journal of Nanjing Architectural and Civil Engineering Institute.* No.1 (Sum No.48), 29-37.

Clough R.W. and Penzien J. (1993). *Dynamics of Structures.* McGraw-Hill, Inc., 2nd ed., New York.

Gasparini D.A. (1979). Response of MDOF Systems to Nonstationary Random Excitation. *J. Engineering Mechanics, ASCE.* **105:EM1,** 13-28.

Harichandran R.S. and Vanmarcke E.H. (1986). Stochastic Variation of Earthquake Ground Motion in Space and Time. *J. Engineering Mechanics, ASCE*, **112:2,** 154-175.

Houser G.W. (1947). Characteristics of strong motion earthquakes. *Bull. Seism. Soc. Am.*, **37**, 17-31.

Huang Y.P. and Liu J. (1987). The Spatial Correlation of Two Horizontal Direction Earthquake. *Journal of Harbin Architectural and Civil Engineering Institute.* **3**, 10-14.

Jiang J.R. and Hong F. (1984). Conversion Between Power Spectrum and Response Spectrum and Artificial Earthquakes. *Earthquake Engineering and Engineering Vibration.* **4:3,** 89-94.

Li H.N. (1998). *Theoretical Analysis and Design of Structures to Multiple Earthquake Excitations.* Science Press, Beijing.

Lin J.H., Williams F.W. and Zhang W.S. (1993). A New Approach to Multiphase-Excitation Stochastic Seismic Response. *Microcomputers in Civil Engineering.* **8,** 283-290.

Lin J.H., Zhang W.S. and Williams F.W. (1994) Pseudo-excitation Algorithm for Nonstationary Random Seismic Responses. *Engineering Structures.* **16:4,** 270-276.

Lin J.H., Zhong W.X. and Zhang Y.H. (2000). Seismic Analysis of Long Span Structures by Means of Random Vibration Approach. *Journal of Building Structures.* **21:1,** 29-36.

Lopez O.A., Chopra A.K. and Hernandez J.J. (2000). Critical Response of Structures to Multicomponent Earthquake Excitation. *Earthquake Engineering and Structural Dynamics*, **29**, 1759-1778.

Shen Z.Y., Zhou D. and Gong M. (2000). Analysis of the Tower-column Element and Cable Element as Well as the Dynamic Properties for Cable-stayed Reticulated Shell Structures. *Journal of Tongji University* **28:2,** 128-133.

Wang X.S., Xue S.D. and Cao Z. (2001). Review and Prospects of the Research on Multi-components Earthquake Excitation for Structures (I): Seismic Inputs. *World Information on Earthquake Engineering.* **17:4,** 27-33.

Xue S.D., Li M.H., Cao Z. and Zhang Y.G. (2000). Random Vibration Analysis of Lattice Shells Subjected to Multi-dimensional Earthquake Inputs. *Advances in Structural Dynamics*, Vol. I, JM Ko and YL Xu (Eds.), Hong Kong, 777-784.

Advances in Building Technology, Volume I
M. Anson, J.M. Ko and E.S.S. Lam (Eds.)
© 2002 Elsevier Science Ltd. All rights reserved

INTERACTION BETWEEN PILE AND RAFT IN PILED RAFT FOUNDATION

W. J. Wu[1], J. C. Chai[2] and J. Z. Huang[3]

[1]College of Architecture and Civil Engineering, Beijing Polytechnic University, Beijing, China
[2]Department of Civil Engineering, Saga University, Saga, Japan
[3]Wuhuan Chemical Engineering Corporation, Wuhan, China

ABSTRACT

The interaction between pile and raft in a piled raft foundation has been investigated by model test and finite element analysis. A method is presented to predict the complete load-settlement response of a piled raft foundation in soft clay from those of its component parts, the pile and the raft, based on interaction between pile and raft. The efficiency of a piled raft foundation and independent partial-safety factors for pile and raft in a piled raft foundation are also discussed.

KEYWORDS

piled raft, foundation, soft clay, model test, bearing capacity, finite element method

INTRODUCTION

Being one of the most sensitive clays, Ariake clay has a natural water content of 70% to 150% and has a thickness of 10 to 30m in the Saga Plain, Northern Kyushu, Japan. In this plain, most of the lightweight structures have been constructed on end bearing piles supported by a gravel layer below the soft clay layer. In this case, a large differential settlement between structure and surrounding ground can occur because of subsidence due to ground water pumping. In order to mitigate the differential settlement, a floating type of piled raft foundation is found to be a suitable alternative, since the floating pile can settle with the surrounding ground (Wu and Miura 1995). However, there is no design standard in Japan for a piled raft foundation in soft clay.

The most important thing in designing the piled raft foundation is to consider the interaction between pile and raft. Some design procedures based on elastic or non-linear elastic analysis are proposed (Randolph, 1983; Clancy and Randolph, 1993; 1996; etc). However, the mechanism of the

interaction between pile and raft are not fully understood. In order to consider these factors in design, more researches are needed. In this study, laboratory tests were carried out for investigating the behavior of a piled raft foundation in soft clay. Numerical analysis (FEM) was conducted to study the interaction between the pile and raft. This indicates that due to interaction between pile and raft, the bearing capacity of a piled raft foundation will be less than the sum of the bearing capacities of piles and raft taken separately. A simple approach is presented to predict the behavior of a piled raft foundation in soft clay, based on the interaction between the pile and raft. Finally, the bearing capacity of piled raft foundation and independent partial-safety factors for pile and raft in a piled raft foundation are also discussed.

INTERACTION BETWEEN PILE AND RAFT

Laboratory Test

The model ground for the laboratory test was made of Ariake clay in a concrete soil tank with a bottom area 1.5mx1.5m and a depth, 1.0m. Sampling of Ariake clay took place at a depth of 2m in the suburb of Saga City, Japan. The physical properties of the clay are as follows: w_L=89%, I_P=50, w_n=147%. Ariake clay in a slurry state was placed in the tank. A uniform pressure of 5kPa was applied over the entire area and maintained for about 5 months for consolidation (Miura et al, 1995).

The model pile was made of timber with a diameter ($2r_p$) of 25mm. The length (L) of the pile varied from 125mm to 375mm with a length to diameter ratio ($L/2r_p$) of 5 to 15. The model raft was made of transparent plastic plate. In this case, the conduct condition between raft and soil can be checked easily. The diameter ($2r_r$) of the raft ranged from 75 to 225mm, which resulted in a raft radius to pile radius ratio (r_r/r_p) of 3 to 9. For the piled raft model, a load cell was mounted on top of the pile to measure the load transferred to the pile.

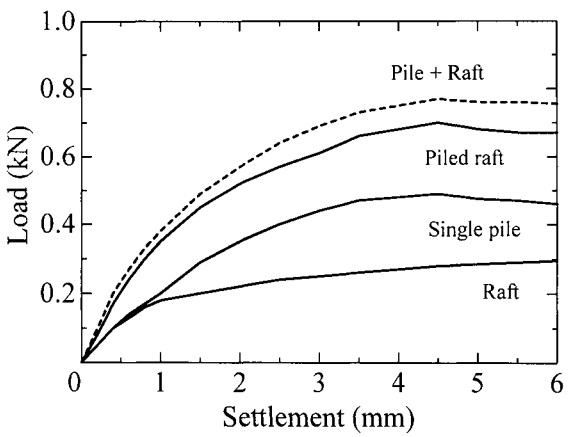


Figure 1: Load settlement diagram for model pile in soft clay

The model pile was installed in the model ground and was left for 28 days to allow the recovery of the disturbed zone around the pile. Three types of model test were carried out: (a) single pile, (b) raft only, and (c) piled raft system. The load was applied by dead load. The time interval between

load increments was 30min. for each test, 10 to 20 load increments were applied. For the piled raft system, the load transferred to the pile was monitored by a load cell mounted on top of the pile. The settlement was measured by dial gages.

The load-settlement curves of model pile, raft and piled raft are presented in Figure 1. To compare the behavior of pile, raft, and piled raft, a load-settlement curve of (P+R) is also plotted in this figure, which is drawn by adding up the load-settlement curves for the pile and raft. It can be seen in Figure 1 that the curve for the piled raft (PR) and curve for (P+R) show a similar trend, but (PR) curve indicates less capacity than the (P+R) curve. Figures 2, 3 show the normalized load-normalized settlement responses of a single pile and a pile in piled raft system, raft only and raft in piled raft system, respectively.

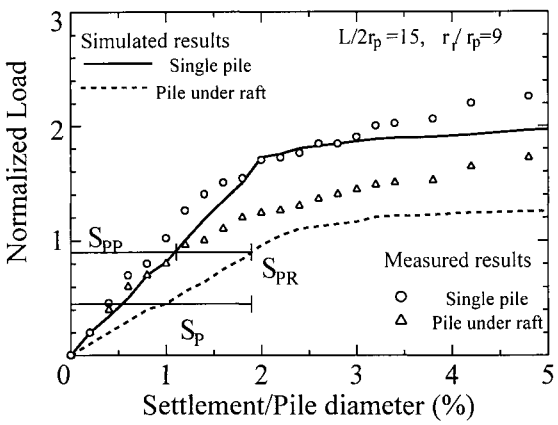


Figure 2: Load-settlement curves for pile

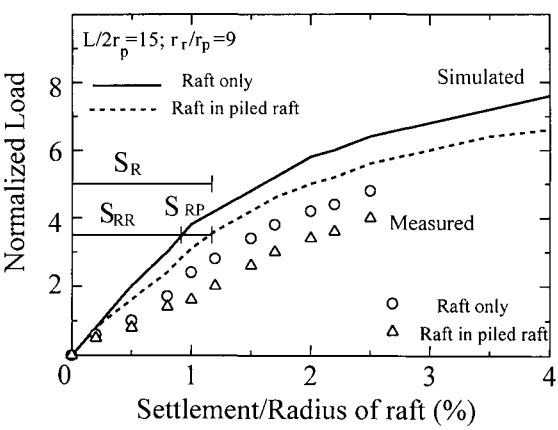


Figure 3: Bearing stress-settlement curves for raft

Numerical Analysis

For FE analysis, an eight node quadrilateral element with reduced integration scheme is used. The sub-stepping technique with error control is adopted to integrate the elasto-plastic stress-strain relationship. To illustrate the effectiveness of the numerical method used, a circular plate on a uniform foundation is analyzed and compared with the theoretical value. The foundation is assumed weightless and with an isotropic initial stress of 10 kPa and represented by a modified Cam clay model. The model parameters and the initial stress condition are estimated to represent the behavior of the model ground. The behavior of soil is represented by a modified Cam clay model. The soil parameters are λ =0.29, κ =0.03, and the coefficient of permeability, k, is determined from 1-D consolidation test results: k=1.1x10^{-4}m/day and initial void ratio, e_0=2.3. The friction parameter M, and Poisson's ratio, υ , are determined empirically: M=1.2, υ =0.3. Model pile and raft are assumed as elastic material.

The numerical results are shown in Figures 2, 3 with the results of model tests. Both measured and numerical results indicate that the curve of pile (raft) in the piled raft system shows larger settlement under any given load than for the single pile (raft only). In piled raft system, due to interaction, the load transmitted by the pile causes an additional settlement on the raft (S_{RP}) and in a similar manner; the stress from the raft to the soil generates an additional pile displacement (S_{PR}). At given load, the settlement of pile, S_P (or raft, S_R) in piled raft is the sum of the settlement (S_{PP}, S_{RR}) due to their own loads and those (S_{PR}, S_{RP}) due to stresses from the raft (or pile). Fig. 4 shows the shear strain and shear stress level contours of piled raft system (L/2r_p=15; r_r / r_p =9), at a settlement of 2% of raft radius. This settlement is about 18% of pile diameter, which implies that the soil/pile interface strength is mobilized at a much smaller value of settlement.

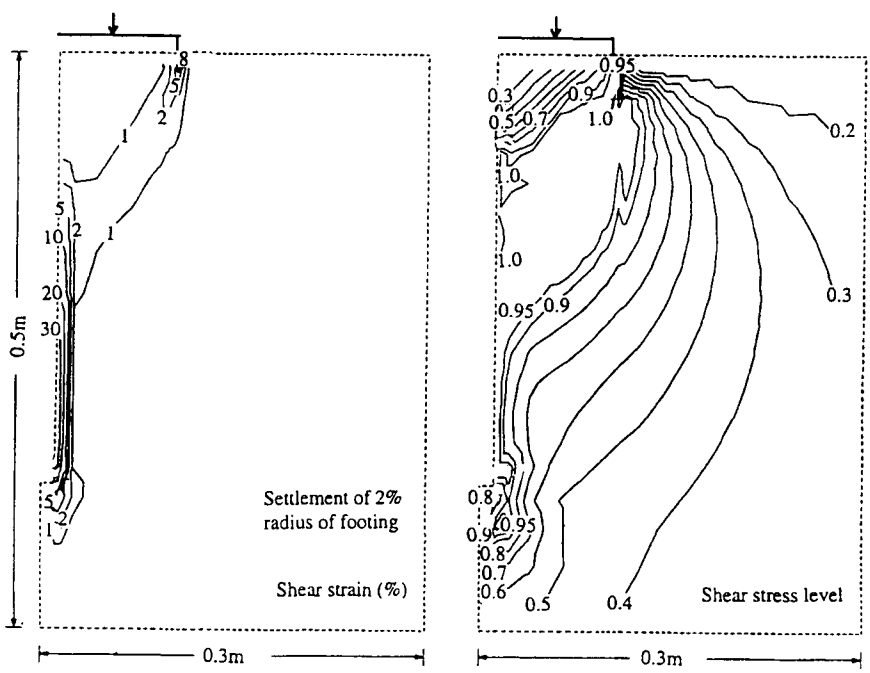


Figure 4: Shear strain and shear stress level contours for piled raft

Pile Raft Interaction

Due to the interaction between pile and raft, the total resistance of piled raft system will be less than the sum of the resistance of single pile and raft. Figures. 2 and 3 compare the resistance of single pile and raft with those in piled raft system, respectively. It can be seen that due to interaction, the bearing stress is reduced. Firstly, the effect of raft on pile behavior is to reduce the relative movement at soil/pile interface, and therefore the mobilized resistance is also reduced. This effect is most significant for that part of the pile close to the raft. As shown in Figure 4, at a depth of about the raft radius, the shear strain is less than 1%, which indicates the small relative movement at the soil/pile interface. For a given raft and pile radius ratio, r_r/r_p, the pile efficiency increases with the increase of the pile length. Then, the effect of pile on raft behavior is that the pile will drag the soil adjacent to it to move downward, which will reduce the mobilized bearing resistance under the raft. It has been found that this effect is mainly a function of r_r/r_p ratio. The larger the r_r/r_p, the less the effect of the pile on raft bearing resistance is as shown in Figure 5. The efficiency of the piled raft system is defined as the bearing resistance of piled raft system over the sum of single pile and raft resistances, which is also shown in Figure 5. The efficiency of a piled raft system is an index to show the degree of pile raft interaction. The larger the r_r/r_p ratio, the more effective is the system because the bearing resistance will be mainly controlled by the raft. For a fixed r_r/r_p ratio, the efficiency is slightly increasing with an increase of $L/2r_p$ ratio.

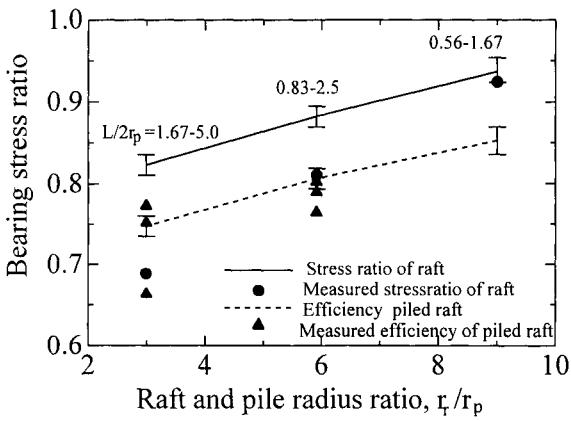


Figure 5: Efficiency of raft and piled raft

LOAD-SETTLEMENT RESPONSES OF PILED RAFT SYSTEM

The load-settlement responses of foundations can be approximated by a hyperbola. Based on the hyperbolic relations, the prediction of the load-settlement response of a piled raft foundation is discussed as follows. Eqns. 1 and 2 can express the load versus settlement responses for the single pile and the raft foundation, respectively,

$$S_{PP}=P_P/\{k_P(1-(P_P/P_{Pu}))\} \quad (1)$$

$$S_{RR}=P_R/\{k_R(1-(P_R/P_{Ru}))\} \quad (2)$$

where k_P (Randolph, 1983) and k_R (Madhav, 1980) are the initial slopes of the load-settlement curves of pile and raft, respectively. P_{Pu}, and, P_{Ru} are the ultimate bearing capacities of the pile and raft, respectively. Eqns. 1 and 2 were rewritten in incremental form as follows (Madhav et al, 1993):

$$\Delta S_{PP}=\Delta P_P/\{k_P(1-(P_P/P_{Pu}))^2\} \quad (3)$$

$$\Delta S_{RR}=\Delta P_R/\{k_R(1-(P_R/P_{Ru}))^2\} \quad (4)$$

As mentioned previously, the settlements of pile and raft in the piled raft foundation are the sum of the settlements due to their own loads and those due to stresses from the raft and the pile, respectively (Figures 2, 3). It is assumed that the pile or raft settlements due to their own loads or stresses and the interaction effects are proportional to these settlements. The average incremental settlement of the raft, ΔS_{RP}, due to an increment of load in the pile, ΔP_P, is $\Delta S_{RP}=I_{RP}\times S_{PP}$. The average incremental settlement of the pile, ΔS_{PR}, due to increment of stress, transmitted by the raft to the soil, is $\Delta S_{PR}=I_{PR}\times S_{RR}$, where, I_{RP} and I_{PR} are the interaction coefficients, respectively (Clancy and Randolph, 1993).

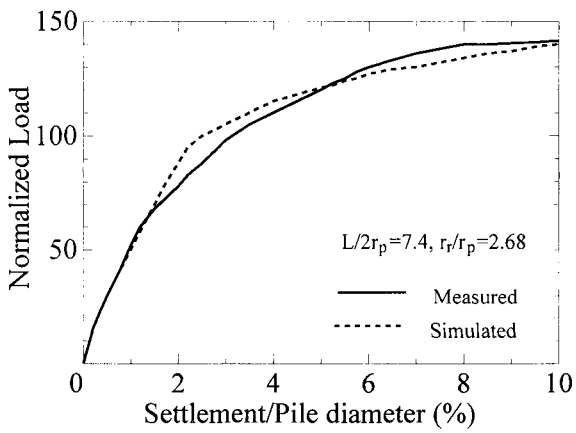


Figure 6: Measured and predicted results

In the piled raft foundation, the load on the piled raft, P_{PR}, is shared by the pile and the raft, making each share P_P and P_R ($P_{PR}=P_P+P_R$). The incremental load versus incremental settlement responses for the pile and the raft in piled raft foundation can be expressed as Eqns. 5 and 6, respectively.

$$\Delta S_P=\Delta P_P/\{k_P(1-(P_P/P_{Pu}))^2\}+I_{PR}\times\Delta P_R/k_R \quad (5)$$

$$\Delta S_R=\Delta P_R/\{k_R(1-(P_R/P_{Ru}))^2\}+I_{RP}\times\Delta P_P/k_P \quad (6)$$

Because the settlement increment for the pile and the raft in the piled raft foundation are the same, it is possible to show the relation by this form $\Delta S_P=\Delta S_R$. Solving Eqns. 5, 6, the incremental settlement of the piled raft and the loads shared by the pile and raft are obtained, and by integrating the incremental settlement the complete load settlement response of the piled raft can be determined. The test results are compared with the predicted ones obtained by the above approach as shown in

Figure 6. It shows that there exists a good agreement between the measurement and the prediction.

BEARING CAPACITY AND SAFETY FACTOR

The capacity of a piled raft foundation can be estimated from the summation of the calculated capacities of pile and raft by introducing an efficiency factor, η. It has been found that the efficiency factor, η ranges from 0.7 to 0.9.

Figure 7 shows the load-settlement curves of an idealized piled raft foundation. The ultimate bearing capacity of piled raft foundation R_{PRu}, ultimate bearing capacity of raft R_{Ru}, and ultimate bearing capacity of pile R_{Pu} are shown by AD, AB, AC in this figure, respectively. If we take a safety factor F=3, the allowable bearing capacity will be EF. The bearing capacity of pile that corresponds to this and the bearing capacity of the raft are not LK and IJ, respectively, but in fact they will be EG and EH respectively. It can be concluded that $F_R \neq F_P$ then the differential safety factor should be adopted. When the total safety factor 3 is considered, the pile safety factor and raft safety factor should be proposed separately on the basis of total load on the piled raft foundation. The allowable bearing capacity of the piled raft foundation, Ra, can be calculated by the following equations.

$$Ra=\eta\,(R_{Pu}+R_{Ru})/F \tag{7}$$

and

$$Ra=\eta\,(R_{Pu}/F_P+ R_{Ru}/F_R) \tag{8}$$

where, F is the safety factor of the piled raft; F_P and F_R are partial safety factors for pile and raft, respectively. Miura et al (1993) pointed out that in the usual case F is equal to 3, F_P=1.5 to 2 and F_R>3.

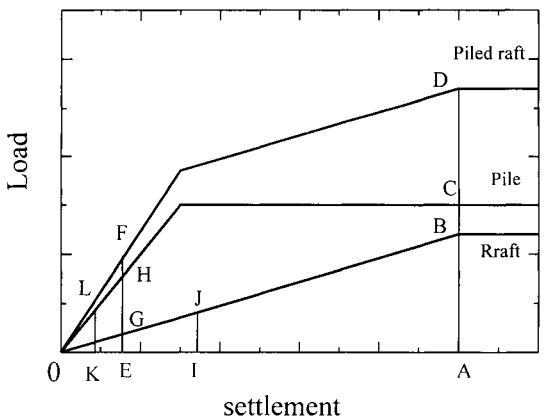


Figure 7: Idealized load vs. settlement response for pile, raft and piled raft

CONCLUSIONS

Based on the above test results and analysis, the following conclusions are summarized:

The model test and numerical analysis results indicate that due to pile raft interaction, the resistance of piled raft system is less than the sum of the resistances of pile and raft considered separately. This interaction is expressed as a piled raft system efficiency factor which is a function of raft/pile radius ratio, r_r/r_p.

The test and analysis results show that the ultimate bearing capacity of piled raft foundation can be estimated from the summation of the calculated capacities of pile and raft modified by the efficiency factor.

A method to predict the load-settlement responses of a piled raft foundation is presented based on the interaction between pile and raft. The predicted result compares well with the measured one.

Independent partial-safety factors for pile and raft foundation were discussed. If the total safety factor 3 is considered for the piled raft foundation, the safety factor for the pile in the piled raft foundation is proposed to be 1.5 to 2.

ACKNOWLEDGEMENT

The authors would like to express their sincere gratitude to professor N. Miura (Saga University, Japan) and Professor M. R. Madhav (Indian Institute of Technology, Indian), for their continuous guidance.

References

Clancy P. and Randolph M. F. (1993). An Approximate Analysis Procedure for Piled Raft Foundations, *International Journal for Numerical and Analytical Methods in Geomechanics,* **17:12,** 849-869.

Clancy P. and Randolph M. F. (1996). Simple Design Tools for Piled Raft Foundations, *Geomechanics,* **46:2,** 313-328

Madhav M. R. (1980). Settlement and Allowable Pressures for Rigid or Annular Footings, *Indian Geotechnical Journal,* **23:4,** 113-118.

Madhav M. R., Miura N. and Wu W. J. (1993). Settlement and Efficiency of Piled Raft Foundation, *The 28th Japan National Conference on SMFE*, 1647-1648.

Miura N., Wu W. J., Madhav M. R. and Nagaike S. (1993). Settlement Behavior and Bearing Capacity of Piled Raft Foundations, *Reports of Faculty of Science and Engineering, Saga University*, **22:1,** 143-149.

Miura N., Wu W. J., Nakamura R. and Ichinose T. (1995). Experimental Study on Skin Resistance of Pile in Soft Clay, (in Japanese), *JSCE, Journal of Geotechnical Engineering,* **517:3-31**, 63-72.

Randolph M. F. (1983). Design of Piled Raft Foundation, *Proc. Intl. Symposium on Recent Developments in Laboratory and Field Tests and Analysis of Geotechnical Problems*, 525-537.

Wu W. J. and Miura N. (1995), Vertical Loading Test for Evaluating Skin Resistance of Timber Pile in Clay, (in Japanese), *Tsuchi-to-Kiso,* **43:5,** 40-42.

Advances in Building Technology, Volume 1
M. Anson, J.M. Ko and E.S.S. Lam (Eds.)
© 2002 Elsevier Science Ltd. All rights reserved

THE METHOD OF CALCULATING THE INTERIOR FORCE OF SOIL NAILS AND CASE ANALYSIS

Zhang Qinxi[1] Yang Jingrong[2] Huo Da[1]

[1] The College of Architectural and Civil Engineering, Beijing Polytechnic University, Beijing, 100022, China
[2] Institute of Geography Science and Natural Resource, The Chinese Academy of Science, Beijing, 100101, China

ABSTRACT

On the basis of analyzing the current methods in the technical codes of the PRC, this paper discusses a reasonable design approach for soil-nailing and put forwards a new design method, especially a more reasonable method of calculating the interior forces in soil nails.
To check the reliability of the proposed method, an in-situ measuring test has been performed in an excavation project 10 meters deep, and the measurement results show that the method proposed in this paper can achieve most satisfactory results.

KEYWORDS

excavation, soil-nailing, design method, interior forces in nails, in-situ test, case analysis

1 INTRODUCTION

Because of the advantages such as lower price, faster construction speed, and the absence of heavy construction machines, soil-nailing, as a kind of retaining structure in deep foundation pits, has been widely used in Beijing. Due to the complexity of the interaction mechanism between nails and soils, the estimation of the interior force in nails during the working process has not been ideally solved so far. At the same time, the estimation of interior force in nails is very important for soil-nailing design. So, it is meaningful to study and discuss how to better calculate the interior force in nails.

2 CURRENT METHODS FOR ESTIMATING THE INTERIOR FORCE IN NAILS

In China, the methods for estimating the interior forces in nails are all based on the active earth pressure theory (Rankine or Coulomb's). That is to say, the maximum force in a nail is equal to earth pressure times the area on which a nail acts, which can be seen in Fig.1and Eqn.1.

$$T=PaSvSh/\cos\theta \tag{1}$$

where:
T=the maximum interior force in soil nails, kN
Sv and Sh=the vertical and horizontal space between nails, m
θ =the angle between nails and horizontal level, degree
Pa=working earth pressure, kPa.

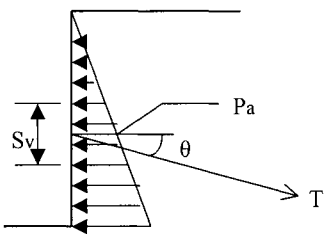


Fig.1 Model of calculating T

There are two methods to calculate the working pressure Pa at present in China, which are as follows.

2.1 Triangular Model[1]

It is supposed that the distribution of the working earth pressure is triangular as Fig.2 (a) shows:

$$Pa=\xi P_A \tag{2}$$

where:
P_A= active earth pressure of Rankine, kPa
ξ =coefficient of discount, see Eqn.3

$$\xi=tg[(\beta+\phi)/2]\{1/tg[(\beta+\phi)/2]-1/tg\beta\}/tg^2(45^\circ-\phi/2) \tag{3}$$

where:
β =the angle of slope(see Fig.3), degree
ϕ =the friction angle of soils, degree

2.2 Trapezium Model[3]

The supposed distribution of Pa is shown in Fig.2 (b). Where Pm is the maximum value of Pa and Pm can be determined according to the following stipulations:

(1) For sands and silts , C/(γ H) ≤0.05:

$$Pm=0.55Ka\,\gamma\,H \tag{4}$$

(2) For cohesive soils, C/(γ H) >0.05:

$$Pm=Ka\,[1-2C/(\gamma\,H\sqrt{Ka})]\,\gamma\,H$$

$$\text{and} \quad 0.2\,\gamma\,H \leq Pm \leq 0.55Ka\,\gamma\,H \tag{5}$$

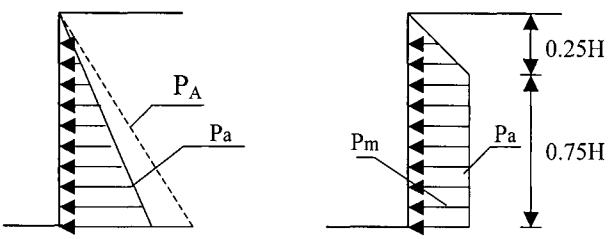
where:

γ =unit weight, kN/m^3

H =depth of foundation pit, m

Ka=coefficient of active earth pressure of Rankine

C=cohesion of soils, kPa



(a) (b)

Fig.2 Two models of Pa in China

2.3 Problems Existing in the Two Models Above

(1) For the triangular model, Pa increases linearly with depth, so the nail which bears maximum force is at the bottom, but in-situ measurement tests show that this is not true. Further more, the discount coefficient ξ lacks any basis in theory;

(2) The trapezium model can not reflect the fact that Pa decreases with the decrease of β. So the interior force in nails calculated based on this model are not reasonable, especially when β is small.

3 A NEW METHOD OF CALCULATING THE INTERIOR FORCE IN SOIL NAILS

According to the analysis above and to avoid the vagueness of earth pressure, a new method called sliding wedge-mass limit analysis is proposed for estimating the interior force in nails[2].

Suppose that the failure zone is a plane and the angle between the failure plane and horizontal plane is (β + φ)/2 (see Fig.3), we can get safety factor K from the equilibrium equation of wedge ABC:

$$K=[T\cos(\alpha+\theta)+T\sin(\alpha+\theta)\,tg\,\phi+W\cos\alpha\,tg\,\phi+CLSh]/W\sin\alpha \tag{6}$$

then:

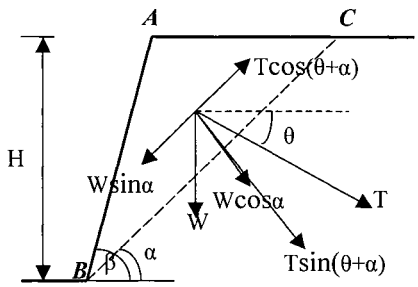


Fig.3 Model of wedge-mass analysis

$$T=[KW\sin(\alpha+\theta)-CLS_h-W\cos\alpha\,tg\phi]/[\cos(\alpha+\theta)+\sin(\alpha+\theta)tg\phi] \quad (7)$$

where:
K=safety factor
T=the total force provided by nails, kN
W=the weight of wedge ABC, kN
L=the length of failure plane, m
S_h=the horizontal space of nails, m
α =the angle between the failure plane and horizontal plane, $\alpha=(\beta+\phi)/2$ (see Fig.3) , degree
θ =the angle between nails and horizontal plane, degree
To get the interior force of each nail, we can work out the horizontal and vertical space between nails based on experience and soil properties, so we get "n", the number of rows along vertical, and refer to Fig.2 (b), we may suppose that the force in each row of nails are equal. So the interior force in each row of nails is:

$$T_i=T/n \quad (8)$$

where:
T_i= the interior force in each row of nails, kN
n= the number of rows along vertical direction

4 CASE ANALYSIS

To check the reliability of the method proposed above, an in-situ test has been made in a deep foundation pit from Oct. to Nov. in 2001. The measurement results are introduced as follows.

4.1 General Situation

Beijing Hai-Run International Apartment is located in Jiangtai Road, Chaoyang District, Beijing. The building complex includes 5 tower blocks with 17~28 stories and 1 public building with 2~3 stories. There is a large underground parking lot with 2 stories under the whole building complex. The depth of the foundation pit is 9.75 m, the area of excavation is about 10000m^2.

According to the geological survey report, properties of the soil layers in the field are summarized in Table1.

TABLE 1
GEOTECHNICAL PROPERTIES OF DIFFERENT SOILS IN THE CONSTRUCTION FIELD

Name of soil	Depth (m)	Thickness (m)	γ (kN/m³)	C (kPa)	Φ (degree)
Fill (silty clay)	0~2	2	20	15	15
Silty clay or clayey silt	2~10	8	20	20	25
Medium sand	10~13	3	20	0	32
Silty clay	13~17.5	4.5	20	20	20

According to the geological survey report, the underground water level is at 2~4m under the ground level. So dewatering wells surrounding the foundation pit are designed to lower the water level.
According to the technical codes concerned in China, the soil nails are designed as shown in Fig.4 and Table 2 .

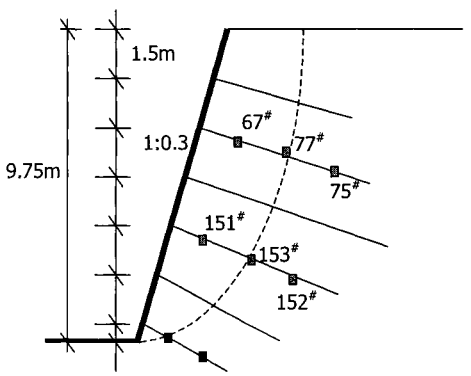


Fig.4 Location of measurement points

TABLE 2
PARAMETERS OF SOIL NAILS

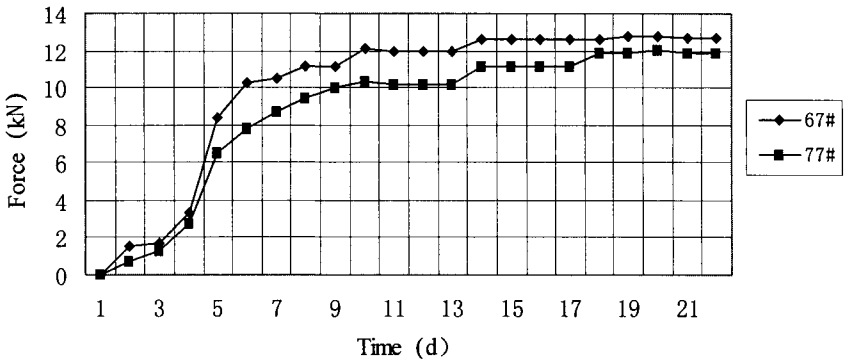
No. of row	Length (m)	Steel bar	Diameter of nails(mm)
1	7	1Φ16	110
2	8	1Φ16	110
3	9	1Φ18	110
4	7	1Φ18	110
5	6	1Φ22	110
6	5	1Φ22	110

4.2 In-situ Measure Test Plan

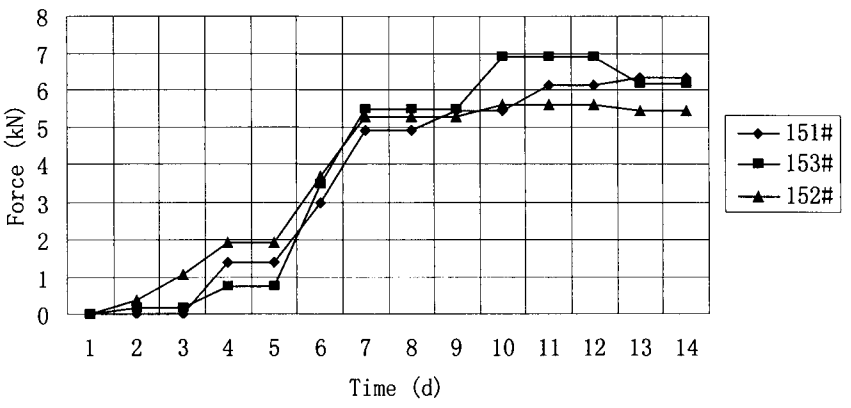
It is planed to embed 8 pieces of steel bar stress-meter in nails, and the location of these measurement points are shown in Fig.4. Due to the changes of construction plan, 6 pieces of stress-meter are embedded actually, and their locations are shown in Fig.4. There is 1 stress-meter (75#) failed during test due to its quality.

4.3 Analysis of Test Results

Throughout the whole excavation process, the interior force in nails is measured every one day. The test results are shown in Fig. 5.



(a) 67#、77# Force~Time curves



(b) 151#、153# 、152# Force~Time curves

Fig.5 Force~Time curves of the measurement points

Fig.5 shows that:

(1) The interior force in the second row nails is about 12kN, smaller than the designed interior force 21.72 kN;

(2) The interior force in 4th row nails is about 6 kN, much smaller than the designed interior force 68.82 kN.

Table3 shows the results calculated with different methods, it shows that the method proposed in this paper is closest to the measurement results.

TABLE 3
RESULTS GETTING FROM DEFERENT METHODS (Unit: kN)

Location of nails	Model [1]	Model [2]	Method proposed by authors	Results measured
The second row	23.7	91.4	10	11.87~12.68
The fourth row	47.5	91.4	10	5.44 ~ 6.32

5 CONCLUSIONS

From above analysis and measurement results, we derive some conclusions as follows:

(1) The forces in soil nails are very small generally; the methods of earth pressure are not able to estimate the interior forces in nails correctly;

(2) In-situ measurement tests and calculations show that the method proposed in this paper can achieve very satisfactory results;

(3) The concept of earth pressure may not be suitable for soil nails, and the development of new methods is very important.

References

Ministry of Construction, PRC. (1999), *Technical Specification for Retaining and Protection of Building foundation Excavations,* Press of Construction Industry, Beijing, China

Q.X.Zhang. (1999). Designing Soil Nailing by Sliding Sphenoid-Mass Equilibrium Method. *Foundation Engineering* **9:1**,32-39.

Z.Y.Chen. (1997). *Specification for Soil Nailing in Foundation Excavations,* Press of China Association for Engineering Construction Standardization, Beijing, China

This Page Intentionally Left Blank

TEAM PRESENTATION:

STRUCTURAL BAMBOO AND BAMBOO SCAFFOLDING IN BUILDING CONSTRUCTION

This Page Intentionally Left Blank

Advances in Building Technology, Volume 1
M. Anson, J.M. Ko and E.S.S. Lam (Eds.)
© 2002 Elsevier Science Ltd. All rights reserved

STABILITY OF MODULAR STEEL SCAFFOLDING SYSTEMS — THEORY AND VERIFICATION

Chu A.Y.T.[1], Chan S.L.[2] and Chung K.F.[2]

[1]*Buildings Department, Hong Kong, China*
[2]*Department of Civil and Structural Engineering, the Hong Kong Polytechnic University, Hong Kong, China*

ABSTRACT

In the design of modular steel scaffolding systems, it is always difficult to assess the instability behaviour of these systems as the effective length coefficient of each member depends on many factors: number of bays, storey height, joint stiffness between steel scaffolding frames, and bracing details. This paper presents the investigation on both the structural modelling and the stability analyses of modular steel scaffolding systems. Based on the second order non-linear analysis approach, a finite element model was developed, and physical tests were carried out to provide test data to verify the findings of the theoretical work obtained from the finite element modelling.

KEYWORDS

Stability analysis, effective length coefficient, column buckling, modular steel scaffolds

INTRODUCTION

Modular steel scaffolding systems have the advantages of easy fabrication, installation and dismantling. However, major problems are encountered in designing such modular steel scaffolding systems (Yen 1993) as most of the steel design codes consider building frames with beams and columns in conventional framing systems and configurations, and thus, their provisions are not strictly applicable to steel scaffolding frames. In general, collapses of steel scaffolding frames are usually accompanied by large deformations with material yielding. The deformations of these steel frames increase the lateral deflections (P-δ effect) of the posts, and, at the same time, increase the drift due to the applied load (P-Δ effect) of the entire structures. These preceding P-δ and P-Δ effects do not frequently occur in most building frames, but this can happen in modular steel scaffolding systems under large vertical loads as such destabilizing effects reduce the buckling resistances of these steel scaffolding systems significantly. According to Lightfoot and Oliveto (1977), experimental results showed that for articulated structures of a minimal and lightweight nature such as falsework, the stability of the whole and the elements of the structure was suspected when using effective lengths normally associated with permanent works. The design of steel scaffolding systems should be based on experiments with judgement, rather than standard design rules.

The objective of this paper is to investigate the instability behaviour of modular steel scaffolding systems. Moreover, experiments on similar steel scaffolding systems are carried out to provide test results to verify the findings of the theoretical work obtained from the finite element model. Through the application of an advanced integrated design and analysis software, NIDA, it is not necessary to pre-determine the effective lengths of the members in these systems as they are analysed nonlinearly. Unlike the eigenvalue analysis which only provides an upper bound solution, the load-carrying capacities of these systems are evaluated using the load-deflection path tracing technique. Consequently, the use of the empirical Merchant-Rankine formula is not needed.

ASSUMPTIONS

In order to study the structural behaviour of modular steel scaffolding systems, the following assumptions are made for the theoretical study (Chu, 1994 and Peng, 1994):

- The jack bases and the sleeve connections joining between modular steel scaffolding frames are assumed to be pinned supports and rigid joints respectively.
- The cross sections of the steel members are symmetrical about both the principal x and y axes.
- The structures are primarily under vertical loads while a horizontal notional force of 1% of the vertical loads is also applied according to codified design rules (BS5950, 2000).

Figure 1 presents the typical form and dimensions of the steel frames adopted in modular steel scaffolding systems.

STRUCTURAL FORMULATION

The structural analysis software NIDA is adopted to analyse the structural behaviour of modular steel scaffolding systems. Second-order elastic analyses with geometrical non-linearity are performed; all materials are assumed to be linear elastic. The analysis on of the elements of the modular systems is based on the self-equilibrium concept (Chan, 1992 and Chan & Zhou, 1998) in which the internal moment balances the external moment at the mid-span of the elements, as shown in Figure 2. The condition can be achieved by the following equations:-

For compatibility

At $x = -L/2$; $\dot{v} = \theta_1$

At $x = L/2$; $\dot{v} = \theta_2$

At $x = \pm L/2$; $v = 0$

For equilibrium

At $x = 0$; $$E I \ddot{v} = P v + \frac{M_2 + M_1}{L}\left(\frac{L}{2} + x\right) - M_1 \qquad [1]$$

At $x = 0$; $$E I \ddot{v} = P \dot{v} + \frac{M_2 + M_1}{L} \qquad [2]$$

where

$E I$	EI is the flexural rigidity;
M_1 and M_2	are the applied nodal moments at nodes 1 and 2;
L	is the undeformed member length;
v	is the lateral displacement with the dots on its top representing a differentiation with respect to the distance along element length, x; and
θ_1 and θ_2	are the nodal rotations at two ends.

A fifth order polynomial for the lateral displacement is assumed as follows:

$$v = a_0 + a_1 x + a_2 x^2 + a_3 x^3 + a_4 x^4 + a_5 x^5 \qquad [3]$$

By eliminating the coefficients in Equation [3], the lateral displacement can be expressed as follows:

$$v = [\, N_1 \quad N_2 \,]\, [\, L\,\theta_1 \quad L\,\theta_2 \,]^T \qquad [4]$$

in which the shape functions, N_1 and N_2 are given by

$$N_1 = A / H_1 + B / H_2$$

$$N_2 = A / H_1 - B / H_2$$

Refer to Chan and Zhou (1998) for detailed expressions of parameters A, B, H_1, H_2 and θ.

Using the same procedure for y axis and similar equations for three dimensional analysis, the displacement function for z axis can be evaluated and its displacement function, v, in Equation 3 is replaced by ($v + v_0$) in which v_0 is given by

$$v_0 = v_{m0} (1 - t^2) \qquad [5]$$

$$t = 2 x / L \qquad [6]$$

where v_{m0} is the deflection at mid-span of the element and t is a non-dimensional parameter.

With the displacement functions in Equation 5 and the revised form allowing for the initial imperfection in Equation 6, the tangent and secant stiffness relations can be obtained via a standard energy equation:-

$$M_1 = \frac{EI}{L}\left[c_1(\theta_1 + \theta_2) + c_2(\theta_1 - \theta_2)\right]$$

$$M_2 = \frac{EI}{L}\left[c_1(\theta_1 + \theta_2) - c_2(\theta_1 - \theta_2)\right]$$

TANGENT STIFFNESS MATRIX AND NUMERICAL PROCEDURE

The tangent stiffness matrix relates the incremental change in forces to a corresponding change in displacements and the tangent stiffness matrix can be formulated via a standard energy equation (Lightfoot and Oliveto,1977). The formulation of the analysis method is simple and the method follows a standard finite element procedure with only minimal amount of mathematical manipulation.

Both the load-deflection curve and the load-stress path for the structure analysed can be obtained by the derived elements using a numerical scheme suggested by Chan. With these plots, the load levels at which the deflection limit and the induced stress being equal to the yield strength can be determined. This load is of great interest to practising engineers, and it depends on the yield strength of materials used. It should be noted that the load calculated by the proposed non-linear theory is significantly different from the loads predicted by conventional linear analysis.

EXPERIMENTAL RESULTS

Three single storey double bay modular steel scaffolding systems were tested to provide data for comparison with the theoretical results obtained from the finite element method. The test specimens comprise of two 1930 mm × 1219 mm steel scaffolding frames which are positioned at 1819 mm apart with two cross-bracings at two planes. The jack extensions at the bases and the U-heads are adjusted so that the overall height of the specimens is 2025 mm. The specimens are mounted onto a loading frame and set in a vertical position. An axial compression load is applied progressively with a 50 ton hydraulic jack until unloading occurs. Figure 3 illustrates the general test set-up, and also the overall view of the test specimens. After the test, a proportion of the failed frame is taken out to perform a tensile test in order to determine the mechanical properties of the frame. Typical deflected shapes of the test specimens are shown in Figure 4. Large horizontal displacements were observed out of the plane of the modular units while little displacement was measured in the direction of the plane. Table 1 summarises the test results of the three test specimens.

TABLE 1
LOADING TESTS ON SPECIMENS

Test	Dimensions			Maximum Applied load per leg, P_{max}	Maximum Applied stress, σ	Yield strength, σ_y	σ / σ_y
	D (mm)	t (mm)	A (mm^2)	(kN)	(N/mm^2)	(N/mm^2)	
1	43.2	2.63	335.2	60.6	180.8	412	0.44
2	43.2	2.63	336.0	63.5	188.8	399	0.47
3	43.35	2.76	351.9	66.1	187.8	409	0.46

It was shown that due to high slenderness in the steel members, the members are working at less than 50% of the yield strength. Moreover, the test results also suggested that substantial restraints were provided to the test specimens by the knee braces through fixings, and also by the loading beam through attachments.

RESULTS FROM FINITE ELEMENT METHOD

A three dimensional finite element model was established to study the structural behaviour of the modular steel scaffolding systems using NIDA, as shown in Figure 5. In order to provide realistic evaluation on the load carrying capacities of the systems, initial imperfection in the form of the first eigenmode of the system was provided in the model, also shown in Figure 5. The maximum out-of-straightness in the steel members was assigned to be *1/1000* of the overall system height. Due to the presence of restraints in both the jack bases and the loading beam, finite element models with four different boundary conditions with different degrees of both positional and rotational restraints onto the systems were analysed. The predicted deformations of the systems are presented in Figure 6 together with respective predicted load carrying capacities.

It is shown that while both the '*Pinned-Fixed*' condition and the '*Pinned-Pinned*' condition over-estimate the load carrying capacities significantly, the '*Free-Pinned*' condition is considered not to be sufficient. The '*Free-Fixed*' condition is found to give a load carrying capacity of 56.9 kN which compares favourably with the test results of 60.6 kN. Moreover, the predicted deformation at failure also follows broadly with the observed deformation of the test specimens.

In reality, the loading beam is considered to provide certain amount of positional restraints to the top of the steel scaffolding frames while the jacket base cannot provide fully fixed rotational restraints to the bottom of the frames. As shown in the finite element results, these two partial restraints somehow provide certain restraining effects to the test specimens which may be best approximated as the '*Free-Fixed*' condition.

CONCLUSIONS

This paper presents the investigation on both the structural modelling and the stability analyses of modular steel scaffolding systems. Based on the second order non-linear analysis approach, a finite element model was developed, and physical tests were carried out to provide test data to verify the findings of the theoretical work obtained from the finite element modelling. The instability behaviour of modular steel scaffolding systems was successfully modelled through the non-linear analysis using *NIDA*. Both the deformation and the load carrying capacities of the systems from the non-linear analysis are found to agree well with the experimental results. However, any external positional and rotational restraints will affect the structural behaviour of these systems significantly, and these restraining effects should be incorporated into the finite element model carefully to yield safe and reliable results.

REFERENCES

British Standard Institution (2000). *BS5950, Part 1 Structural Use of Steelwork in Buildings*, BSI, London, England.

Chan S.L. (1992). Large Deflection Kinematics Formulation for Three Dimensional Framed Structures, *Comp. Methods in Appl. Mech. and Engineering*, 95, 17-36.

Chan S.L. and Zhou Z.H. (1998). On the development of a robust element for second-order 'non-linear integrated design and analysis (NIDA)'. *Journal of Constructional Steel Research*, 47, 169-190.

Chu Y.T. (1994). *A Study on Elastic Stability of Steel Scaffolding*, thesis submitted to the Department of Civil and Structural Engineering, the Hong Kong Polytechnic University for partial fulfilment for the Degree of Master of Science in Civil Engineering.

Lightfoot E. and Oliveto G. (1977). The Collapse Strength of Tubular Steel Scaffold Assemblies. *Proceeding of Institution of Civil Engineers*, Part 2, June, 311-329.

Peng J.L. (1994). *Analysis Models and Design Guidelines for High Clearance Falsework Systems*. Ph.D. dissertation, School of Civil Engineering, Purdue University, West Lafayette, Ind.

Yen T. (1993). *Research in Preventing Collapses of Modular Steel Falsework in Construction.* Res. Rep., Council of Labor Affairs, Taipei, Taiwan.

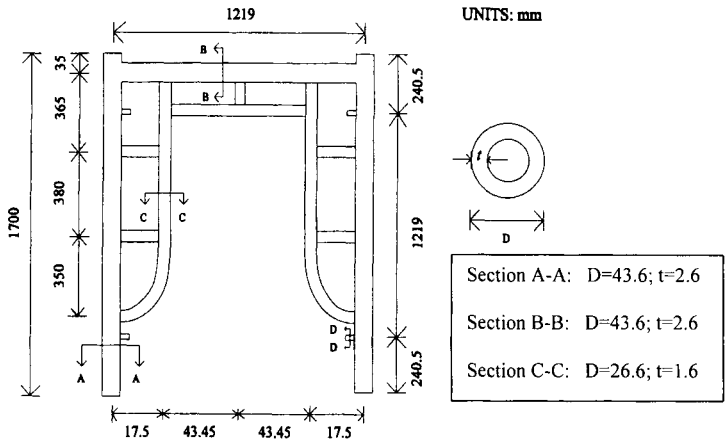


Figure 1: Typical form and dimensions of modular steel scaffolding frame

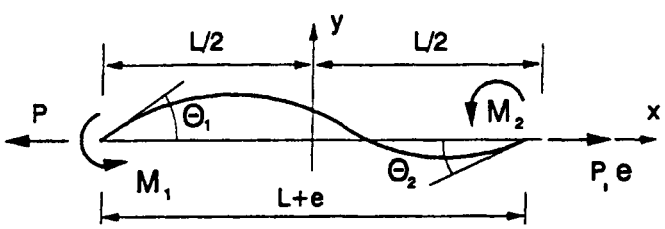


Figure 2: Basic force versus displacement in high order beam element

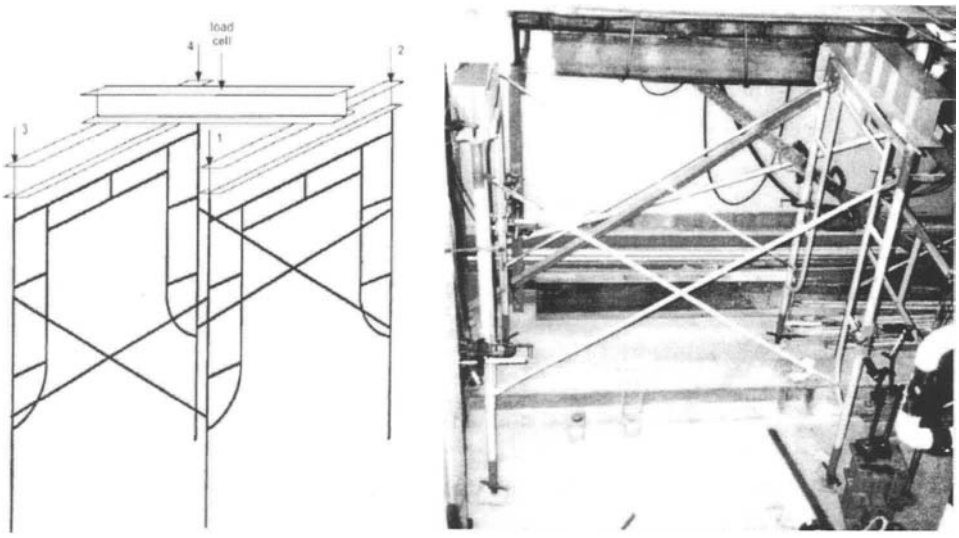


Figure 3: General view of test set-up for modular steel scaffolding systems

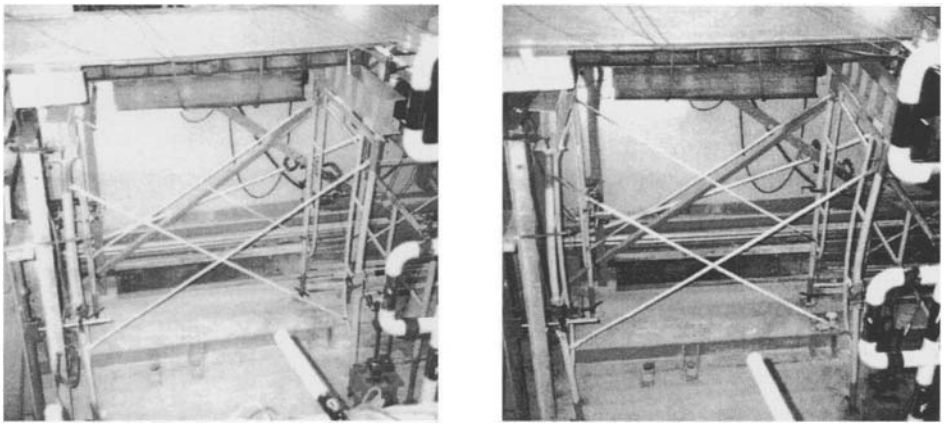
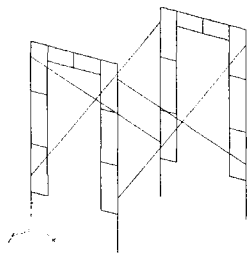
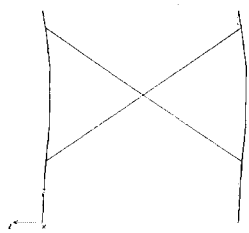


Figure 4: Typical failure mode in modular steel scaffolding systems – column buckling





Eigenvalue mode

Figure 5: Geometry and initial imperfection of the finite element model

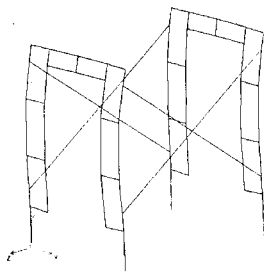
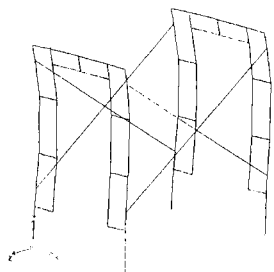
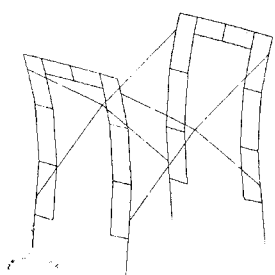
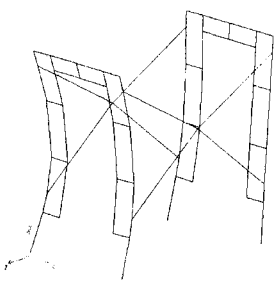
Case A *Boundary condition: Pinned-Fixed*  P_{max} = 76.4 kN	*Case B* *Boundary condition: Pinned-Pinned*  P_{max} = 73.1 kN
Case C *Boundary condition: Free-Fixed*  P_{max} = 56.9 kN	*Case D* *Boundary condition: Free-Pinned*  P_{max} = 33.8 kN

Figure 6: Numerical results obtained from non-linear analyses using *NIDA*

Advances in Building Technology, Volume I
M. Anson, J.M. Ko and E.S.S. Lam (Eds.)
© 2002 Elsevier Science Ltd. All rights reserved

RECENT DEVELOPMENTS ON BAMBOO SCAFFOLDING IN BUILDING CONSTRUCTION

K.F. Chung, S.L. Chan and W.K. Yu

Department of Civil and Structural Engineering, the Hong Kong Polytechnic University, Hung Hom, Kowloon, Hong Kong

ABSTRACT

Bamboo scaffolds have been used in China for over a few thousand years, and both the basic framing systems and the erection methods for bamboo scaffolds in building construction were established through practice about two thousand years ago. Bamboo scaffolds provide temporary access, working platforms for workers and supervisory staff, and also prevents construction debris from falling onto passers-by. In order to promote the effective use of bamboo scaffolds in building construction, a research and development project titled '*Bamboo Scaffolds in Building Construction*' was undertaken at the Research Center for Advanced Technology in Structural Engineering of the Hong Kong Polytechnic University in 1999. This paper aims to present the major deliverables and findings of the project.

KEYWORDS

Bamboo scaffolds, green construction, structural bamboo, mechanical properties, design development.

INTRODUCTION

Bamboo scaffolds have been widely used in construction applications in South East Asia, in particular, Hong Kong for many years. Because of their high adaptability and low construction cost, bamboo scaffolds can be constructed in different shapes to follow any irregular architectural features of a building within a comparatively short period of time. In general, bamboo scaffolds are mainly used to provide access of workers to different exposed locations to facilitate various construction and maintenance process. Besides widely erected on construction sites, bamboo scaffolds are also used in signage erection, decoration work, demolition work and civil work.

In 1999, a research and development project titled '*Bamboo Scaffolds in Building Construction*' was undertaken at the Research Center for Advanced Technology in Structural Engineering (*RCATISE*) of the Hong Kong Polytechnic University with the support of the International Network of Bamboo and Rattan (*INBAR*). This was a high-level contracted research project on the technology transfer of bamboo scaffolding, and the primary objective was to promote the effective use of bamboo scaffolds in building construction.

SCOPE OF WORK

This paper aims to present major deliverables and findings derived from the project, and three major tasks are undertaken as follows:

Task 1 ***Dissemination of Established Bamboo Scaffolding Technology***
To promote the effective use of bamboo scaffolding in building construction through dissemination of technical information. Both the established knowledge and the proven practice of bamboo scaffolding in Hong Kong have been formalized and documented:

Task 1A Design Guide entitled '*Design of Bamboo Scaffolds*' covering material requirements, typical usage, structural principles and safety requirements for structural engineers.

Task 1B Erection Manual entitled '*Erection of Bamboo Scaffolds*' covering material selection, typical configurations with details, and erection procedures for scaffolding practitioners.

Task 2 ***Development of Engineered Bamboo Scaffolding Systems***

Task 2A To develop engineered bamboo scaffolding for typical applications with improved structural forms through advanced analysis and design.

Task 2B To establish connection resistances of conventional and engineered connections for practical design of bamboo scaffolds.

Task 3 ***General Technical Information of Structural Bamboo***
In order to facilitate wide engineering applications of bamboo, a document titled '*Engineering and Mechanical Properties of Structural Bamboo*' is compiled to provide general technical information on bamboo as a constructional material.

DISSEMINATION OF ESTABLISHED BAMBOO SCAFFOLDING TECHNOLOGY

Task 1A Design Guide

A '*Design Guide*' is complied [1] which comprises of the following chapters:

- Chapter 1 introduces the background on structural bamboo and also on bamboo scaffolds commonly used in South East Asia, in particular, in Hong Kong and the Southern China, namely, the Single Layered Bamboo Scaffold (SLBS) and the Double Layered Bamboo Scaffold (DLBS) as shown in Figures 1 and 2 respectively. The modern design philosophy based on limit states is also presented.
- Chapter 2 presents an experimental investigation [2] on the mechanical properties of two bamboo species, namely *Bambusa Pervariabilis* (or Kao Jue) and *Phyllostachys Pubescens* (or Mao Jue), which are commonly used in access scaffoldings in the South East Asia, in particular, in Hong Kong and the Southern China. Based on systematic compression and bending testing on a large number of test specimens, characteristic values of both the strengths and the Young's moduli of each bamboo species for limit state structural design are provided for practical design [3].
- In general, column buckling is considered to be one of the critical modes of failure in bamboo scaffolds, leading to overall structural collapse. Chapter 3 presents the design development of a limit state design method against column buckling of structural bamboo. A total of 72 column buckling tests for both Kao Jue and Mao Jue are executed [4] to provide test data, and a design method against column buckling for both Kao Jue and Mao Jue is proposed for general design.

- Chapter 4 presents an experimental investigation on the connection resistances in bamboo scaffolds where the connections are formed using either bamboo strips or plastic strips [5]. After statistical analysis, the characteristic connection resistances of the beam-column connections and the column splices with Kao Jue and Mao Jue are presented for practical design.
- Chapter 5 presents the basic configurations of typical bamboo scaffolds using both Kao Jue and Mao Jue, namely, the Single Layered Bamboo Scaffold (SLBS) and the Double Layered Bamboo Scaffold (DLBS). The results of a parametric study on the structural behaviour of bamboo scaffolds with different practical arrangements of lateral restraints are presented, and recommendations on the effective length coefficients for posts in both SLBS and DLBS with different practical arrangements of lateral restraints are also provided.
- Chapter 6 presents the general design principles of bamboo scaffolds. The design procedures of a number of typical structural bamboo members and scaffolding systems are fully presented through worked examples [6]. Moreover, the design of both SLBS and DLBS are also presented with careful consideration of various arrangements of lateral restraints for practical applications.

With the availability of rational and scientifically based design methods, structural engineers are encouraged to take the advantage offered by bamboo to build light and strong bamboo scaffolds to achieve enhanced economy and buildability.

Task 1B Erection Manual

An '*Erection Manual*' is complied [7] which comprises of the following chapters:

- Chapter 1 presents the advantages of bamboo scaffolds in building construction, and a number of practical issues such as field tests, loading requirements, safety and inspection are also presented.
- Chapter 2 introduces basic understandings on the structural forms of bamboo scaffolds, as shown in Figures 3 and 4, together with relevant requirements on supports against overall stability.
- Chapter 3 describes a total of seven types of common bamboo scaffolds, and they are fully illustrated with photographs in Chapter 4.
- Chapter 5 illustrates the structural forms and the erection sequences of various bamboo scaffolds.
- Chapter 6 introduces the basic forms of fastenings with plastic strips between bamboo members, and tightening sequences of knots for members in practical orientations are also illustrated.

With the establishment of the structural forms of the bamboo scaffolds through structural design, the conventional erection techniques are thus rationalized and simplified.

DEVELOPMENT OF ENGINEERED BAMBOO SCAFFOLDING SYSTEMS

Task 2A To develop engineered bamboo scaffolding

In order to achieve overall structural stability of the bamboo scaffolds with high structural efficiency, lateral restraints should be provided at close intervals whenever feasible. However, due to site restrictions such as availability of strong supports in proximity, it may not be practical or even possible to provide lateral restraints in every main post – main ledger connection of the bamboo scaffolds. In the absence of sufficient lateral restraints, the effective length of bamboo columns will be larger than their member lengths between ledgers, reducing the axial buckling resistance of the bamboo columns significantly. Thus, it is necessary to provide design guidance on practical arrangements of lateral restraints.

An advanced non-linear finite element analysis using *NIDA* was carried out to investigate the column buckling behaviour of bamboo scaffolds. Both SLBS and DLBS with practical arrangements of lateral restraints are examined [8], and the configurations of the systems are presented in Figure 5. Both the local buckling of bamboo posts between ledgers and the global instability of the entire structures with practical lateral restraints are accurately incorporated as shown in Figure 6. Based on the results of the parametric studies, a set of design rules for both SLBS and DLBS was proposed for practical support conditions. Moreover, a total of four full-scale tests on double layered bamboo scaffolds were carried out [9], and they provide test data for the calibration of the proposed design methods.

Task 2B Connection resistances of conventional and engineered connections

In order to enable bamboo scaffolds to compete directly with metal scaffolds, it is necessary to rationalize the existing bamboo scaffolding systems with simple, standardized and reliable connections for quick installation. In the past, bamboo strips were commonly used to form knots in joining members together while plastic strips are widely used instead after 1970s. The major advantage of plastic strips is quick erection of bamboo scaffolds by hands with only simple tools. However, the strength and stiffness of these connections depend primarily on the skills of the workers, and these connections tend to be weakened over time due to weathering on both the plastic strips and the bamboo members. It is highly desirable to develop reliable engineered connections for bamboo scaffolds with prolonged usage. An experimental investigation was carried out to establish connection resistances of conventional and engineered connections for practical design of bamboo scaffolds, and full details of the experimental investigation are presented in the Technical Report '*Connections in Bamboo Scaffolds*' [5]. The investigation may be divided into the following two parts:

Part I Conventional connections using bamboo and plastic strips

- Destructive tests on practical beam-column connections with typical member configurations, as shown in Figure 7. Material tensile tests on both bamboo and plastic strips were also carried out.

Part II Engineered connections using steel bolts and screws

- Destructive tests on beam-column connections with steel strips, wooden wedges and screws, as shown in Figure 8.
- Destructive tests on column-column connections with steel bolts and screws, as shown in Figure 8.

A number of different connection configurations were proposed, and connections using plastic strips, steel wires, steel bars, thin gauge steel strips, steel couplers, nails, and self drilling self tapping screws were made as samples. For those connections with high buildability and sufficient strength and stiffness, destructive tests were carried out to assess their structural adequacy, and material tests were also performed as appropriate. The results of all the test series are fully presented in the Technical Report [5] together with statistical analysis.

BAMBOO AS A CONSTRUCTIONAL MATERIAL

Task 3 General technical information of structural bamboo

In order to facilitate wide engineering applications of bamboo, a document titled '*Engineering and Mechanical Properties of Structural Bamboo*' is compiled [10]. The document aims to provide general technical information to readers who are considering to use bamboo as a constructional materials, to help their understanding on bamboo and to select the most suitable species for their purposes. It also covers relevant and up-to-date technical guidance to structural engineers to exploit bamboo as load bearing structural members.

CONCLUSIONS

This paper presents the major deliverables and findings of a research and development project which aims to provide technical solutions against various hinderances of wide applications of bamboo scaffolds. With the availability of modern design methods and engineering data of the mechanical properties of structural bamboo, engineers are encouraged to take the advantage offered by bamboo to build light and strong scaffolds to achieve enhanced economy and buildability.

ACKNOWLEDGEMENTS

The research project is supported by both the Research Committee of the Hong Kong Polytechnic University Research (Project No. G-V849), and the International Network for Bamboo and Rattan (Project No. ZZ04). The authors would like to thank Professor J.M. Ko of the Hong Kong Polytechnic University and Professor J.J.A. Janssen of the Eindhoven University of Technology, co-chairmen of the Steering Committee of the INBAR project, for their general guidance and technical advice. The technical support from the Construction Industry Training Authority of the Government of Hong Kong Special Administration Region on erection of bamboo scaffolds is also gratefully acknowledged.

REFERENCES

1. Chung K.F. and Chan S.L.: *Bamboo Scaffolds in Building Construction. Design of Bamboo Scaffolds.* Joint Publication, the Hong Kong Polytechnic University and International Network for Bamboo and Rattan (in press).
2. Chung K.F. and Yu W.K.: *Mechanical properties of structural bamboo for bamboo scaffolding.* Engineering Structures 24 (2002): 429-442.
3. Chung K.F., Yu W.K. and Chan S.L.: *Mechanical properties and engineering data of structural bamboo.* Proceedings of International Seminar 'Bamboo Scaffolds in Building Construction' - An Alternative and Supplement to Metal Scaffolds, May 2002, pp1-23.
4. Yu W.K., Chung K.F. and Chan S.L.: *Column buckling of structural bamboo.* Engineering Structures (submitted for publication).
5. Chung K.F., Yu W.K. and Ying K.: *Connections in Bamboo Scaffolds.* Research Centre for Advanced Technology in Structural Engineering, the Hong Kong Polytechnic University, 2002.
6. Chung K.F., Chan S.L. and Yu W.K.: *Practical design of bamboo scaffolds.* Proceedings of International Seminar 'Bamboo Scaffolds in Building Construction' - An Alternative and Supplement to Metal Scaffolds, May 2002, pp65-88.
7. Chung K.F. and Siu Y.C.: *Bamboo Scaffolds in Building Construction. Erection of Bamboo Scaffolds.* Joint Publication, the Hong Kong Polytechnic University and International Network for Bamboo and Rattan (in press).
8. Chan S.L. and Chung, K.F.: *Stability design of hollow timber section - bamboo.* Proceedings of International Seminar 'Bamboo Scaffolds in Building Construction' - An Alternative and Supplement to Metal Scaffolds, May 2002, pp55-64.
9. Yu W.K., Chung K.F. and Tong Y.C.: *Full scale tests of bamboo scaffolds for design development against instability.* Proceedings of International Conference on Advances in Building Technology, December 2002, Hong Kong (in press).
10. Chan S.L. and Xian X.J.: *Engineering and Mechanical Properties of Structural Bamboo.* Research Centre for Advanced Technology in Structural Engineering, the Hong Kong Polytechnic University, 2002 (in press).



Figure 1: Typical bamboo scaffold – *Single Layered Bamboo Scaffold (SLBS)*



Figure 2: Typical bamboo scaffold – *Double Layered Bamboo Scaffold (DLBS)*

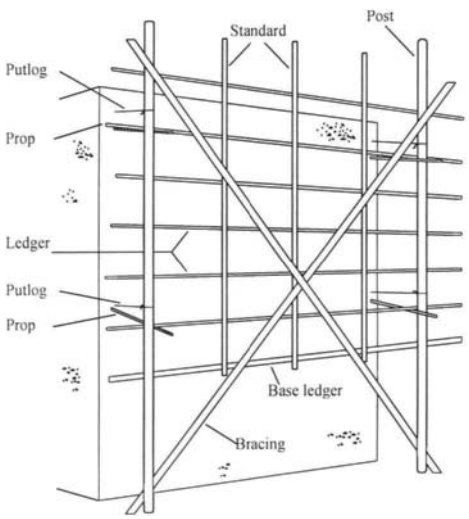


Figure 3: Typical configuration of *SLBS*

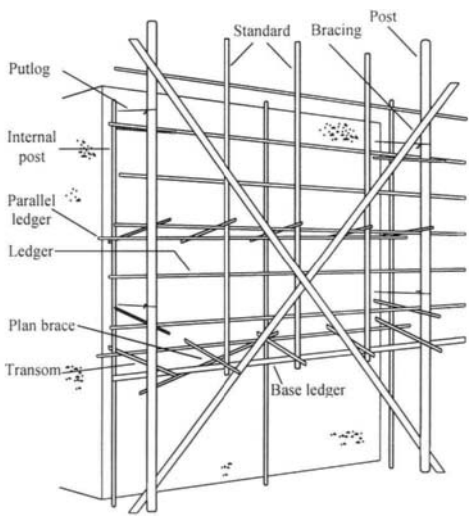
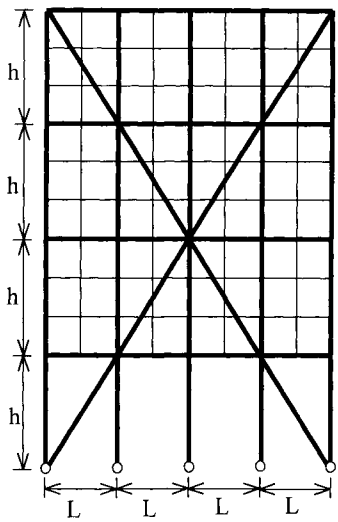


Figure 4: Typical configuration of *DLBS*

a) *SLBS* using Mao Jue

L = 1.5m ~ 2.4m
h = 1.8m ~ 2.25m

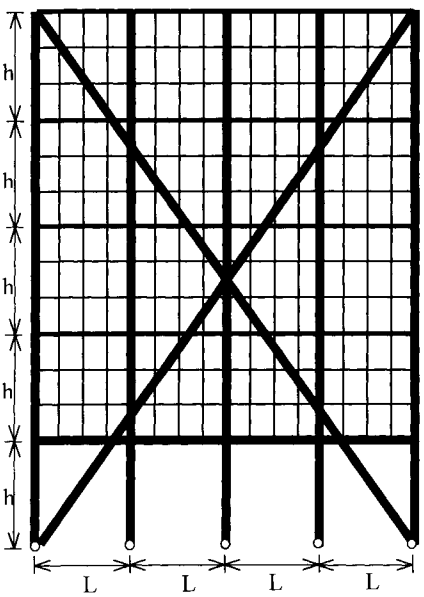
Member	Member type
Main post	*Mao Jue*
Base ledger	*Mao Jue*
Standard	*Kao Jue*
Ledger	*Kao Jue*
Diagonal	*Mao Jue*

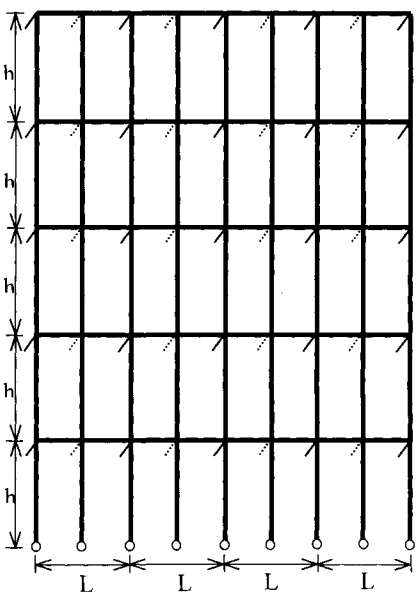


b) *SLBS* using Kao Jue

L = 1.2m ~ 1.8m
h = 1.8m ~ 2.25m

All members using Kao Jue.





c) *DLBS* using Mao Jue and Kao Jue

L = 1.5m ~ 2.4m
h = 1.8m ~ 2.25m

Lateral restraints connected to main posts of outer layer.

Lateral restraints connected to ledgers.

Outer layer	Member type
Main post	*Mao Jue*
Base ledger	*Mao Jue*
Standard	*Kao Jue*
Ledger	*Kao Jue*
Diagonal	*Mao Jue*

All members in the Inner layer and transoms using Kao Jue.

Figure 5: Typical configurations of *SLBS* and *DLBS*

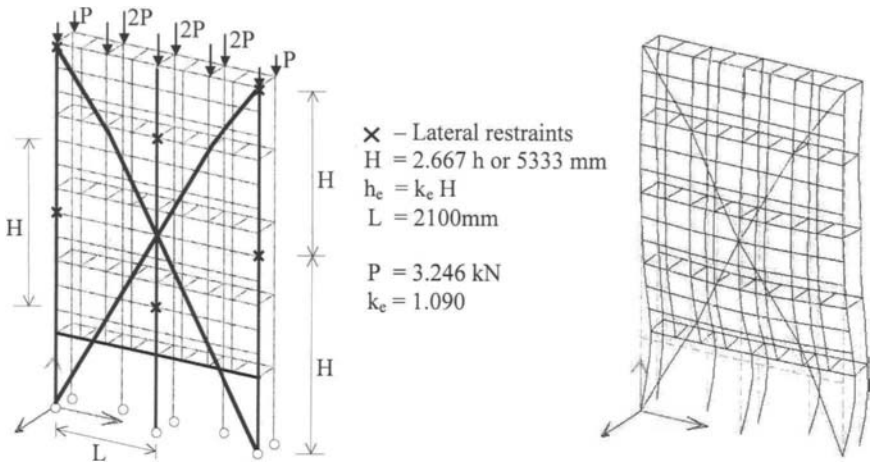
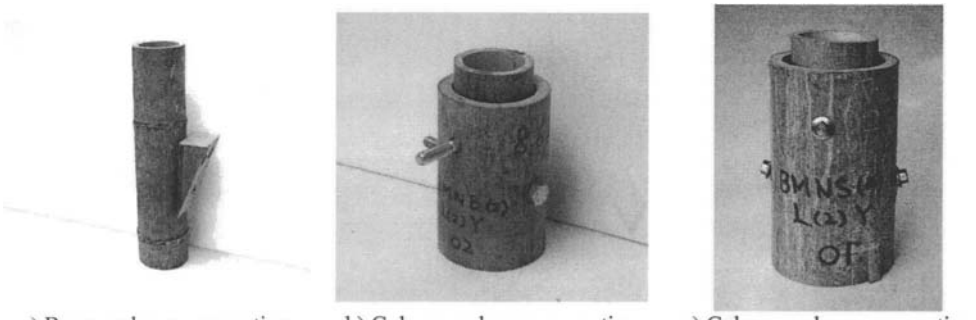


Figure 6: Advanced non-linear analysis with NIDA on *DLBS* under practical supports



a) Bamboo strips b) Plastic strips

Figure 7: Conventional beam-column connections



a) Beam-column connection using wooden wedge and steel screws

b) Column-column connection using steel bolts

c) Column-column connection using steel screws

Figure 8: Engineered connections

Advances in Building Technology, Volume 1
M. Anson, J.M. Ko and E.S.S. Lam (Eds.)
© 2002 Elsevier Science Ltd. All rights reserved

RELIABILITY ANALYSIS FOR MECHANICAL PROPERTIES OF STRUCTURAL BAMBOO

Ming Lu, W.K. Yu and K.F. Chung

Department of Civil and Structural Engineering, the Hong Kong Polytechnic University, Hung Hom, Kowloon, Hong Kong

ABSTRACT

Some of the bamboo species are very stiff and strong, hence are considered as ideal natural structural materials suitable for many construction applications, such as low-rise houses, short span footbridges, long span roofs and assess scaffolds. On the other hand, bamboo - a natural non-homogenous organic substance, often exhibits large variations of physical properties along the length of its members, such as external and internal diameters, dry density and moisture content. While structural engineers expect variations in the mechanical properties of bamboo, they tend to accept that the mechanical properties of bamboo are likely to be more consistent than those of concrete, probably similar to structural timber.

This paper presents a series of experimental investigations on structural bamboo species, together with a neural network (NN) based approach for sensitivity analysis and reliability analysis of the experimental data. Through an optimized NN model for characterizing the mechanical properties from the physical ones for Mao Jue using the pilot test results, we have gained insight on how physical properties of bamboo influence the compressive strength and Young's modulus of structural bamboo. Further, the NN model also serves as a "virtual lab" for carrying out controlled experiments and conducting reliability analysis on the mechanical properties of bamboo. The NN-produced 5^{th} percentile compressive strength is compared against present knowledge on structural Mao Jue, coming close to the characteristic value of Mao Jue obtained in previous findings. This new NN-based approach, as a reliable and cost-effective means to study structural bamboo, can facilitate structural engineers to understand the properties of structural bamboo and design bamboo structures at a known level of confidence against failure.

KEYWORDS

Structural bamboo, basic mechanical properties, neural networks, computer modeling, design development.

INTRODUCTION

Bamboo is a good natural structural material, and there are over 1500 different botanical species of bamboo in the world. Some of the bamboo species are considered to be effective structural materials for many construction applications such as structural members in low-rise houses, short span foot bridges, long span roofs and construction platforms in countries with plentiful bamboo resources. In general, it is considered that the mechanical properties of bamboo are likely to be at least similar, if not superior, to those of structural timber. Furthermore, as bamboo grows very fast and usually takes three to six years to harvest, depending on the species and the plantation, there is a growing global interest in developing bamboo as a substitute of timber in construction. It is generally expected that the effective use of structural bamboo will mitigate the pressures on the ever-shrinking natural forests in developing countries, and thus, facilitate the conservation of the global environment.

On the other hand, bamboo - a natural non-homogenous organic substance, often exhibits large variations of physical properties along the length of its members, such as external and internal diameters, dry density and moisture content. While structural engineers also expect variations in the mechanical properties of bamboo, they tend to accept that the mechanical properties of bamboo are likely to be more consistent than those of concrete, and probably similar to structural timber. So far, a major constraint to the development of bamboo as a modern construction material is the lack of mechanical properties and engineering data for structural bamboo. Moreover, there were only limited design rules available for the general design of structural bamboo, and further design development is highly desirable to provide guidance on the structural behaviour of bamboo members under practical loading and support conditions.

Bamboo scaffolds

Bamboo scaffolds have been used in building construction in China for over a few thousand years. Nowadays, in spite of open competition with many metal scaffolding systems imported from all over the world, bamboo scaffolds remain to be the preferred systems for access in building construction in Hong Kong and the neighbouring areas, according to Fu [1].

As reported by So and Wong [2], bamboo scaffolds are commonly employed in building construction to provide temporary access, working platforms for construction workers and supervisory staff. Owing to their high adaptability and low construction cost, bamboo scaffolds can be constructed in any layout to follow various irregular architectural features of a building within a comparatively short period of time. Moreover, they are also erected to prevent construction debris from falling onto passers-by. In 1995, an industrial guide on safety of bamboo scaffolds was issued by the Hong Kong Construction Association [3]. Typical usage of bamboo scaffolds in building construction in Hong Kong [4] include:

- Single Layered Bamboo Scaffolds (SLBS) for light duty work. It is highly adaptable to site conditions with both easy erection and dismantling.
- Double Layered Bamboo Scaffolds (DLBS) with working platform for heavy duty work. It provides safe working platforms for construction activities to be carried out at heights.
- Signage erection, decoration work, demolition work and civil work [5].

Recent research in structural bamboo

Structural bamboo has been traditionally used in China, Philippines, India, and Latin America for centuries, but little research was reported in the past. Recent scientific investigations on bamboo as a construction material were reported by Au *et. al.* [6] in Hong Kong, and also by Janssen in 1981 [7] in Holland. A large amount of data of the mechanical properties for various bamboo species all over the world were also reported by Janssen in 1991 [8]. While these sets of data provide typical values of

compressive, bending and shear strengths of various bamboo species, no characteristic strengths for structural design were provided. A series of experimental studies on structural bamboo were reported by Arce-Villalobos in 1993 [9] and practical connection details for bamboo trusses and frames were also proposed and tested. Moreover, Gutierrez in 1999 [10] conducted a recent study on the traditional design and construction of bamboo in low-rise housing in Latin America, and innovative applications of bamboo in building construction in India was also reported by INBAR [11]. More recently, Amada *et. al.* [12] classified bamboo as a smart natural composite material with optimized distribution of fibers and matrices, both across cross sections and along member lengths, in resisting environmental loads in nature.

EXPERIMENTAL INVESTIGATIONS

In order to promote the safe use of structural bamboo, we carried out a series of experimental investigations on the mechanical properties of two bamboo species, namely, *Bambusa Pervariabilis* (or Kao Jue) and *Phyllostachys Pubescens* (or Mao Jue). Selection of the two bamboo species for study is attributed to their common use in Hong Kong and the Southern China as bamboo scaffolds. The mechanical properties for both Kao Jue and Mao Jue are investigated [13,14,15], aimed to establish basic design data (like characteristic strength) for evaluating their basic compression and bending capacities of structural bamboo. Due to the variations of physical properties in structural bamboo, it is necessary to carry out a large number of tests to assess the variations of the test results, and to provide engineering data based on statistical analysis of the test results. For details of the testing procedures, please refer to the INBAR documents compiled by Janssen [16,17].

PILOT STUDY ON SHORT BAMBOO MEMBERS UNDER COMPRESSION

A pilot study was first carried out to examine the variation of compressive strength against the following physical properties of bamboo members:

- External diameter, D ,
- Wall thickness, t , (both D and t are used to evaluate cross-sectional area, A)
- Dry density, ρ , and
- Moisture content, *m.c.*

Some of these physical parameters vary significantly along the length of bamboo members, and it is highly desirable to establish any correlation between the physical and the mechanical properties of bamboo members. Three dry bamboo members were tested, and all of them were mature with an age of at least three years and no visual defect. The height to diameter ratio of the short bamboo members was kept approximately at two, and the maximum height of the short members was 150 mm.

Figure 1 illustrates the general set-up of the compression tests, and both the applied loads and the axial shortening of the test specimens were measured during the tests. Two failure modes, namely *End bearing* and *Splitting*, were identified, as also shown in Figure 1. It was found that most specimens failed in *End Bearing*, especially for those specimens with high moisture contents. As the moisture content decreased, cracks along fibers were often induced, leading to *Splitting*.

Figure 2 presents the variations of the physical properties along the length of the bamboo members for Mao Jue. The variations of the ultimate compressive strengths and the Young's modulus against compression can also be found in Figure 2 for comparison.

For Mao Jue, two observations are made:

1. The physical properties of the three members are found to be significantly different from one anther. From the bottom to the top of the members, the external diameter typically decreases from 80 mm to 50 mm. The wall thickness varies from 10 mm at the bottom to 6 mm at the top of the members.
2. Contrary to the physical properties, the mechanical properties of the three members are found to be broadly similar. The compressive strength is found to be 50 N/mm^2 at the bottom of the members and increases steadily to 70 N/mm^2 at the top. The Young's modulus against compression is found to vary steadily from 5 kN/mm^2 to 10 kN/mm^2 from the bottom to the top of the members.

In brief, representative values of mechanical properties may be obtained through systemic testing on Mao Jue regardless of large variations in external diameter, wall thickness and dry density. Chung and Yu [18] conducted systemic testing on Mao Jue and obtained the characteristic values of both the compressive strengths and the Young's modulus of Mao Jue as given in Table 1. It should be noted that the characteristic values of the mechanical properties of Mao Jue are shown to be superior to common structural timber, and probably also to concrete. The material partial safety factor for structural bamboo, γ_m , is proposed to be 1.5.

SENSITIVITY AND RELIABILITY ANALYSIS THROUGH NN MODELING

The back-propagation neural network (BPNN) has been researched and applied as a convenient decision-support tool in a variety of application areas in civil engineering [19]. The BPNN is also successfully applied to analyze the relationship between the physical and the mechanical properties for Mao Jue. A total of 40 pilot test data are complied and used to train a neural network model under control of 10 randomly selected test data. The NN has 4 input parameters (i.e. external diameter, wall thickness, moisture content and dry density) and 2 output values (i.e. compressive strengths and corresponding Young's Modulus). The internal architectural and the learning parameters of NN are determined using an optimized NN modeling approach suggested in Lu and Shi (2002) [20] as: four hidden nodes are on the one hidden layer, the learning rate is equal 0.5 and the momentum term is equal 0.25, the initial random seed is equal to 60, and the number of learning iterations is equal to 19387. The trained NN model is further validated with an independent production set of 8 records, representing eight additional experimental tests.

The Monte Carlo simulation based sensitivity analysis [19] was conducted on the validated NN model and the results are shown in Figure 3. The horizontal axis represents the relative input sensitivity, that is, the output response (negative or positive in it own unit of measure) with a change of 10% relevant range in an input parameter. The vertical axis is the baseline corresponding to no output response or zero change in output. Five short vertical bars correspond to each input parameter, representing respectively the five percentiles (10^{th}, 25^{th}, 50^{th}, 75^{th}, and 90^{th}) from left to right and reflecting the central trend, the spread and the shape of the observed slope data distribution obtained from simulation. It is observed both the diameter and the dry density of Mao Jue exhibit a positive correlation with compressive strength and Young's modulus while the thickness exhibits a negative correlation. The sensitivity of moisture content is found to be not as significant as the other parameters, which is due to the relatively small range of moisture content in the pilot test data.

Next, the NN model serves as a "virtual lab" for carrying out controlled experiments and conducting reliability analysis on the mechanical properties of Mao Jue and evaluating its design data. Over 1000 specimens for each typical combination of diameter-thickness dimensions at a constant moisture content of 20% were simulated by querying the NN model, with the dry density as a random variable uniformly distributed over the range from 600 to 850 kg/m^3. Figure 4 presents the results of the reliability analysis of compressive strength, showing that the compressive strength at fifth percentile is

about 49 N/mm^2 regardless of the moisture content and the dimension combination. Note that the simulated compressive strength is found to be close to the corresponding characteristic compressive strength obtained from the systematic laboratory tests (44 N/mm^2 as read from Table 1).

CONCLUSIONS

A pilot study was carried out to examine the variation of compressive strength against the following physical properties of bamboo members, i.e. external diameter (D), wall thickness (t) dry density (ρ), and moisture content (*m.c.*). Some of these physical parameters vary significantly along the length of bamboo members, and it is highly desirable to establish any correlation between the physical and the mechanical properties of bamboo members.

The back-propagation neural network (BPNN) has been successfully applied to analyze the relationship between the physical and the mechanical properties (i.e. compressive strengths and corresponding Young's Modulus) for Mao Jue. A total of 40 pilot test data were complied and used to train a neural network model under the control of 10 randomly selected test data. The internal architectural and learning parameters of NN were decided using an optimized NN modeling approach. Following further validation of the trained NN model with an independent production set, the sensitivity and reliability analyses were performed on the NN model to (1) gain insight on how physical properties of bamboo influence its compressive strength and Young's modulus, and to (2) facilitate the design of bamboo structures at a known level of confidence against failure. This new NN-based approach has been proven to be a reliable and cost-effective means for studying mechanical properties of structural bamboo and facilitating the development of associated design methods.

ACKNOWLEDGEMENTS

The research project leading to the publication of this paper is supported by the International Network for Bamboo and Rattan (Project No. ZZ04), and also by the Research Committee of the Hong Kong Polytechnic University Research (Project No. G-V849). The authors would like to thank Professor J.M. Ko of the Hong Kong Polytechnic University and Professor J.J.A. Janssen of the Eindhoven University of Technology, Co-chairmen of the Steering Committee of the INBAR project, for their general guidance and technical advice.

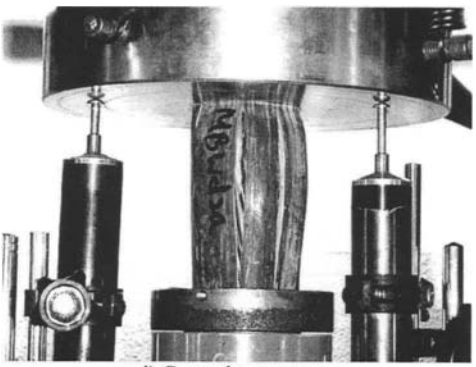
REFERENCES

1. Fu, W.Y. (1993). *Bamboo scaffolding in Hong Kong*. The Structural Engineer, Vol. 71, No. 11, pp202-204.
2. So, Y.S. and Wong, K.W. (1998). *Bamboo scaffolding development in Hong Kong – A critical review*. Proceedings of the Symposium on 'Bamboo and Metal Scaffolding', the Hong Kong Institution of Engineers, October 1998, pp63-75.
3. The Hong Kong Construction Association (1995). *Practice Guide for Bamboo Scaffolding Safety Management*. Labour and Safety Committee.
4. Chung, K.F. and Siu, Y. C. (2002). *Bamboo Scaffolds in Building Construction: - Erection of Bamboo Scaffolds*. Joint Publication, the Hong Kong Polytechnic University and International Network for Bamboo and Rattan (in press).
5. Tong, A.Y.C. (1998). *Bamboo Scaffolding - Practical Application*. Proceedings of the Symposium on 'Bamboo and Metal Scaffolding', the Hong Kong Institution of Engineers, pp43-62.

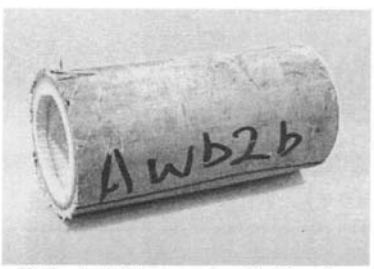
6. Au, F., Ginsburg, K.M., Poon, Y.M., and Shin, F.G. (1978). *Report on study of bamboo as a construction material.* The Hong Kong Polytechnic.
7. Janssen, J.J.A. (1981). *Bamboo in building structures.* Ph.D. thesis, Eindhoven University of Technology, Holland, 1981.
8. Janssen, J.J.A. (1991). *Mechanical properties of bamboo*, Kluwer Academic Publisher.
9. Arce-Villalobos, O. A. (1993). *Fundamentals of the design of bamboo structures.* Ph.D. thesis, Eindhoven University of Technology, Holland.
10. Gutierrez, J.A. (1999). *Structural adequacy of traditional bamboo housing in Latin-America.* Technical Report No. 321-98-519. Laboratorio Nacional de Materiales y Modelos Estructurales, Universidad de Costa Rica, Costa Rica.
11. INBAR (1999). Society for Advancement of Renewable Materials and Energy Technologies, *Technical Report on 'Buildings with bamboo arch roof at Harita Ecological Institute - A review report and recommendations for design upgradation'*, International Network for Bamboo and Rattan, Beijing, China.
12. Amada, S., Munekata, T., Nagase, Y., Ichikawa, Y., Kirigai, A. and Yang, Z. (1997). *The mechanical structures of bamboos in viewpoint of functionally gradient and composite materials.* Journal of Composite Materials, Vo. 30, No.7, 1997, pp800-819.
13. Yu, W.K. and Chung, K.F. (2000a). *Qualification tests on Kao Jue under compression and bending.* Technical Report, Research Centre for Advanced Technology in Structural Engineering, the Hong Kong Polytechnic University.
14. Yu, W.K. and Chung, K.F. (2000b). *Qualification tests on Mao Jue under compression and bending.* Technical Report, Research Centre for Advanced Technology in Structural Engineering, the Hong Kong Polytechnic University.
15. Yu, W.K. and Chung, K.F. (2001). *Mechanical properties of bamboo for scaffolding in building construction.* Proceedings of International Conference on Construction, Hong Kong, June 2001, pp262-272.
16. Janssen, J.J.A. (1999a). *An international model building code for bamboo.* The International Network for Bamboo and Rattan (draft document).
17. Janssen, J.J.A. (1999b). *INBAR standard for determination of physical and mechanical properties of bamboo.* The International Network for Bamboo and Rattan (draft document).
18. Chung, K.F. and Yu, W.K. (2002). *Mechanical properties of structural bamboo for bamboo scaffoldings.* Engineering Structures, 24, pp429-442.
19. Lu, M., AbouRizk, S.M. and Hermann, U.H. (2001). *Sensitivity analysis of neural networks in spool fabrication productivity studies.* Journal of Computing in Civil Engineering, ASCE, Vol. 15, No. 4, 2001, pp299-308.
20. Lu, M. and Shi, W.Z. (2002). *Optimized Neural Network Model for Characterizing Geographical Terrain Slope.* Journal of Computing in Civil Engineering, ASCE, accepted

TABLE 1 Proposed mechanical properties for structural bamboo

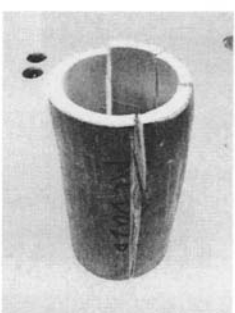
Phyllostachys Pubescens (Mao Jue)	Dry (under 5% *m.c.*)	Wet (over 30% *m.c.*)
Characteristic compressive strength, $f_{c,k}$ (N/mm^2) (at fifth percentile)	117	**44**
Design compressive strength, $f_{c,d}$ (N/mm^2) (γ_m = 1.5)	78	29
Design Young's Modulus against compression, $E_{c,d}$ (kN/mm^2) (average value)	9.4	6.4



i) General test set-up



ii) Typical failure mode - End bearing



iii) Typical failure mode – Splitting

Figure 1: Compression test

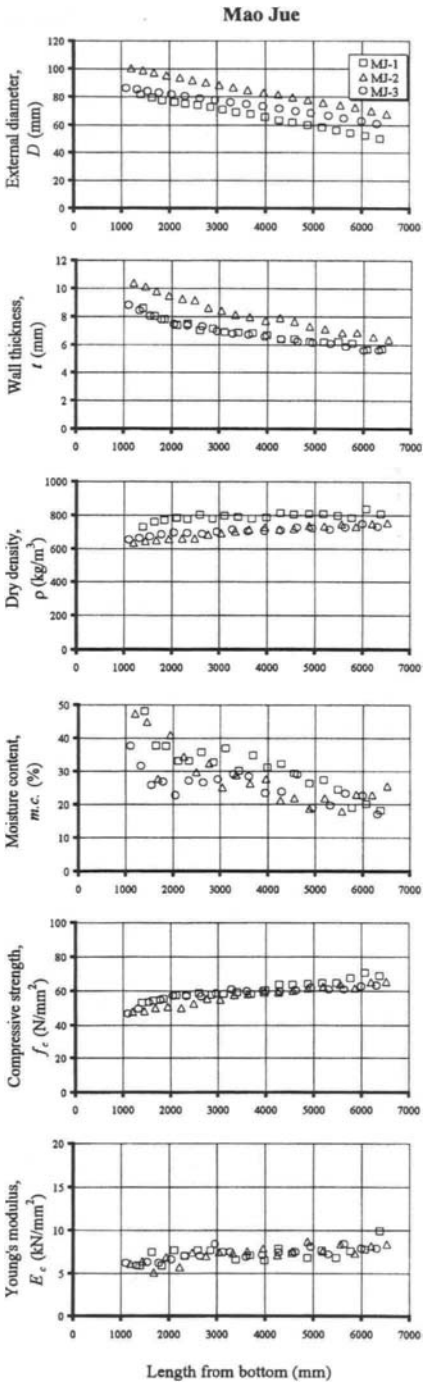
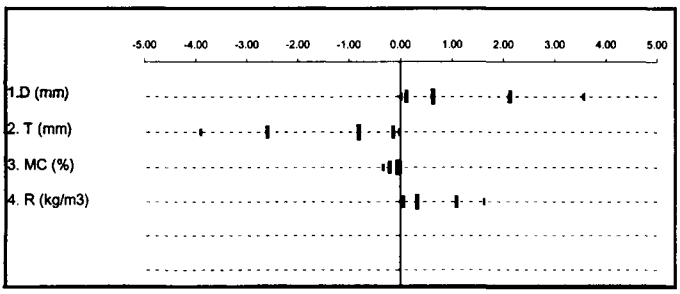


Figure 2: Variations along bamboo length

(a) Output "Compressive Strength"



(b) Output "Young's Modulus"

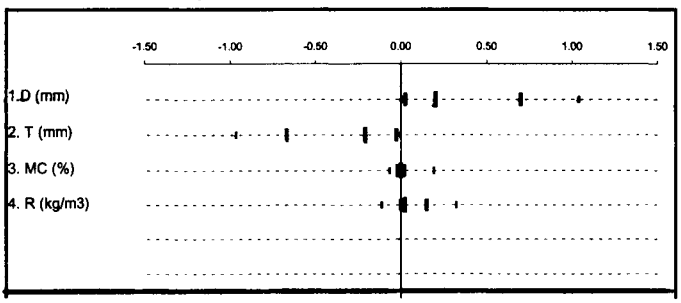


Figure 3: Neural Networks Generalized Input Sensitivity

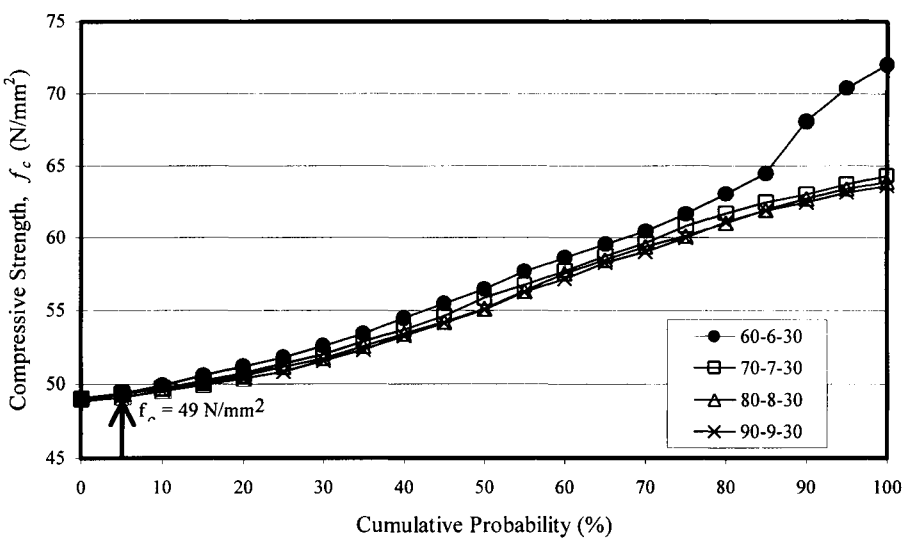


Figure 4: Reliability Analysis of Compressive Strength through Monte-Carlo simulation on the Trained NN model.

Advances in Building Technology, Volume 1
M. Anson, J.M. Ko and E.S.S. Lam (Eds.)
© 2002 Elsevier Science Ltd. All rights reserved

ERECTION OF BAMBOO SCAFFOLDS AND THEIR RECENT DEVELOPMENTS

Mr. Francis So

Wui Loong Scaffolding Works Co., Ltd.

SYNOPSIS

Bamboo scaffold has a long history of application in the construction industry in Hong Kong and Mainland China. Bamboo material is environmental-friendly and low-cost. It has been widely used in the construction of new buildings, renovation, repair works, slope maintenance and neon signage works. Basically, it is a kind of temporary working platform and a means of access and egress for workers at height. However, the trend of substantial increased in height of building, Bamboo scaffold has been partly substituted at the bottom level by Metal scaffold or Metal Bamboo Matrix System Scaffolds in some projects to provide better foundation of overall scaffolding structure.

INTRODUCTION

Most of the construction operations require the use of scaffolding and material is an important factor which affects the competitiveness as well as its overall investment.

Most experienced engineers and contractors in Hong Kong prefer using bamboo instead of steel in scaffolding works because it is easier to fabricate, light so that load on supports like steel brackets can be smaller, environmental-friendly and more economical. In addition, its characteristics of significant deflection before failure offer sufficient warning to the users that cannot be found in steel scaffolding.

COST EVALUATION

Bamboo is much cheaper than steel sections. The cost of a bamboo member of 6m length is about HK$10, compared with a steel circular hollow section of similar size of HK$80.

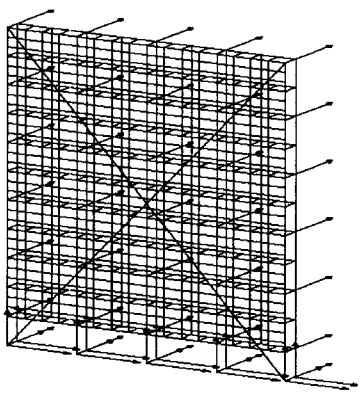
STRENGTH AND STIFFNESS

The design strength for typical bamboo species *Phyllostachys pubescens* is 40 N/mm2, which is the lower end of the average value of the design stress of bamboo because of its high variation. Compared to steel of grade 43, bamboo has a smaller design strength and Young's modulus of elasticity, which are two major basic parameters for engineering materials.

TABLE 1
COMPARISON OF ENGINEERING PROPERTIES BETWEEN STEEL AND BAMBOO

Material	Specific Density	Design stress (MPa)	E_t (GPa)	Poisson's ratio
Bamboo	0.8	40 - 60	12	0.35
Steel	7.8	275	205	0.3

Note : Bamboo specimen is Phyllostachys pubescens and steel grade is S275 or grade 43



With the above data, structural analysis is carried out using computer model for bamboo scaffolding system for checking the stability of the complete system and buckling strength of individual members.

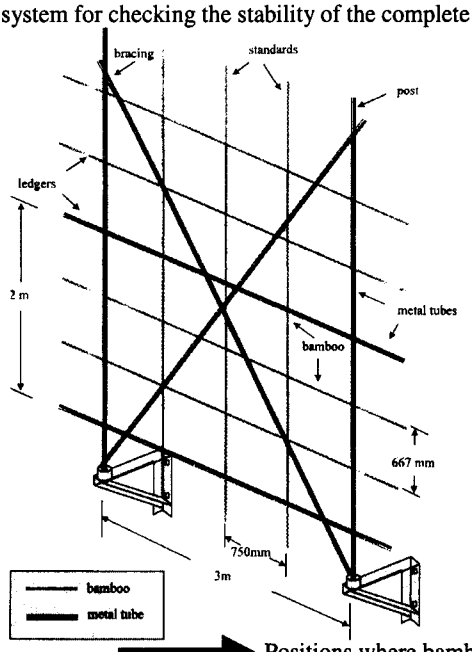


Figure 1: External layer for MBMSS

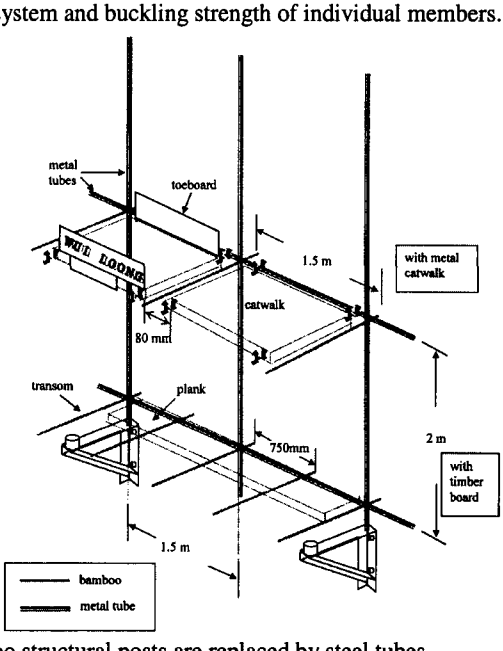


Figure 2: Internal layer for MBMSS

Positions where bamboo structural posts are replaced by steel tubes

Owing to the difficulty in obtaining larger size and stronger bamboo posts and to the failure of bamboo itself due to various reasons such as degradation, natural disasters, destruction by other trade works, etc., the author developed a new system called the Metal Bamboo Matrix System Scaffolds (MBMSS). To increase the load carrying capacity of the system, the heavily loaded members can be replaced by steel circular sections. The system was further analyzed and checked by Professor S.L. Chan and Dr. K.F. Chung of the Hong Kong Polytechnic University for structural adequacy.

The replacement of partly bamboo structural posts by steel tubes can strengthen the stability of overall scaffolding structure. However, the financial burden to such huge investment for the whole building has limited the application of this mixed scaffolding structure partly. (most popular at one half or a third of the overall height of building instead)

In fact, light duty scaffolding structures such as traditional drama shed, neon signage or suspended working platform are still the first choice for bamboo scaffold as compare to structures like residential building etc. It is not easy to find the application of metal or mixed scaffolding on those light duty scaffolding structures.



Photo 1: Metal Bamboo Matrix System Scaffolds (MBMSS) can provide better supporting load for the scaffolding structure at the top and an ideal place for anchorage of safety harness at the connection of metal tubes.



Photo 2: The most popular usage of bamboo scaffolding in new building under construction for formwork fixing and plastering



Photo 3: The usage of bamboo scaffolding in renovation works of old building.

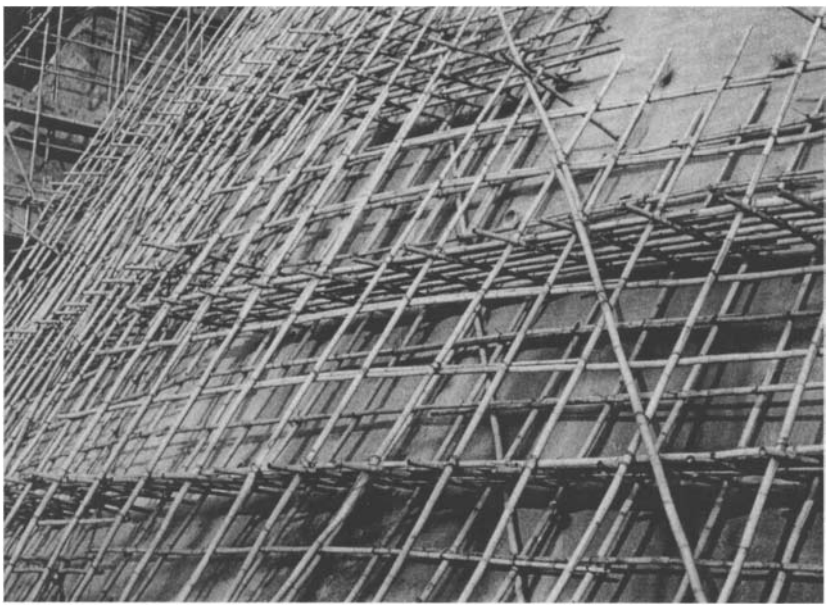


Photo 4: Bamboo scaffolding application in slope maintenance



Photo 5: Bamboo scaffolding application in neon signage installation



Photo 6: Suspended bamboo scaffolding working platform

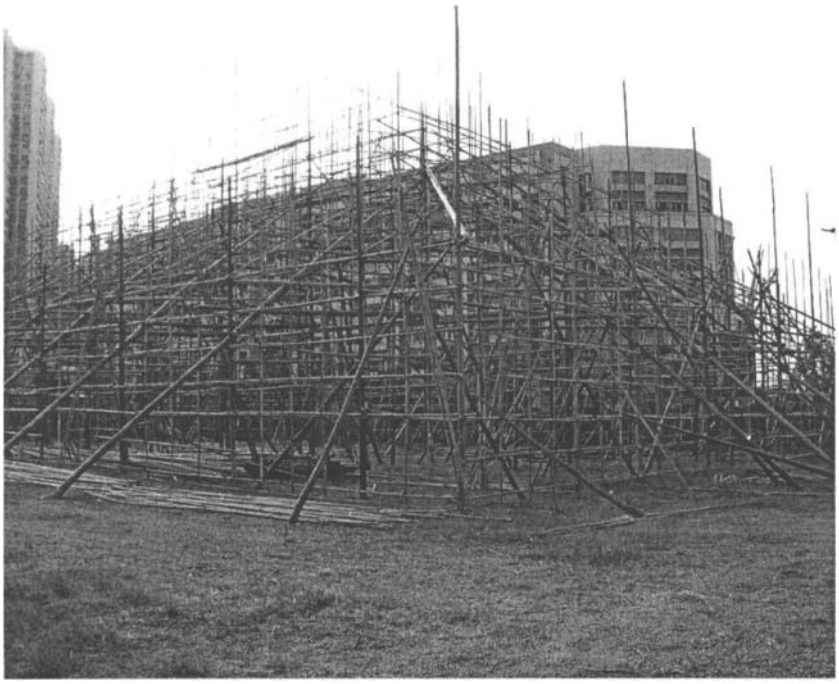


Photo 7: Bamboo scaffolding application in traditional Chinese drama shed

SAFETY ISSUE

Bamboo scaffolding has a public image of being prone to collapse, causing higher casualties than steel scaffolding, which is, in fact, subject to flaw. There have been many instances of collapse in steel scaffolding around the world. For instance, there are more than 100 reported cases per annum in UK as revealed in the engineering journals. In Hong Kong, there were 2 known cases of metal scaffolding collapse during the construction stage of the KCRC West Rail Project.

The layman often has the impression that bamboo scaffolding is less safe than steel scaffolding and think that "Even when steel scaffold collapses, we cannot do much about it since we have used the strongest building material-steel". When using bamboo scaffolding, the layman may wonder why steel, a stronger material, is not used instead. I am not a defender of bamboo, but to criticize the application of traditional bamboo scaffold as unsafe and contributing to the high accident rate is really a biased, irresponsible and unprofessional allegation. It should not be made by any sensible man in construction industry. To distort the usage of bamboo in scaffolding has only one excuse – "This method is not westernized".

From the engineering point of view, safety depends on the calculated factors of safety, quality control and site practice since stronger material normally has lesser dimensions and construed as more slender in this competitive world.

CONCLUSIONS

The existence of bamboo scaffold remains as the first option of choosing scaffolding structure by contractors due to its popularity, highly competitive in economical consideration and greater flexibility. With the emphasis of safety in construction industry in Hong Kong, the quality of bamboo material to sustain high durability becomes extremely important for high-rise building construction. Therefore, the mixed system scaffolding that metal tubes serve as structural support can relieve any worries arise from the safety of scaffold caused by intentional damages by other workers and self-degradation itself. On the other hand, the usage of bamboo scaffolding structures on light duty works such as signage installation and drama shed can demonstrate this craft and art, must be inherited continuously to attract public interests.

ACKNOWLEDGEMENT

The author acknowledges the valuable comments of Professor S.L. Chan on the draft of this paper.

This Page Intentionally Left Blank

Advances in Building Technology, Volume 1
M. Anson, J.M. Ko and E.S.S. Lam (Eds.)
© 2002 Elsevier Science Ltd. All rights reserved

STRUCTURAL DESIGN OF THE BAMBOO PAVILLION, BERLIN

David G Vesey

Ove Arup & Partners Hong Kong Limited

ABSTRACT

A small theatre pavillion was constructed in Berlin in August 2000 and then in Hong Kong in November as part of an Arts Festival jointly organised by the Haus der Kulturen der Welt and the Hong Kong Institute of Contemporary Culture. The Architect was Rocco Yim with Arup Hong Kong providing the Structural Design and Gammon as Builders. The design required the use of this traditional material in new ways to provide a light and elegant structure. Large sizes of bamboo were sourced in China, traditional joints were tested and relatively new types of joint devised.

KEYWORDS

Bamboo, Engineered Structure, Traditional material used in a modern way, Pavillion, Joints, Testing

INTRODUCTION

As part of the Millennium celebrations the Hong Kong Institute of Contemporary Culture and the Haus der Kulturen der Welt of Berlin jointly hosted a festival called "One Vision Two Cities, Festival 2000 Hong Kong In Berlin and Berlin in Hong Kong" The first half of the festival was held in Berlin in August 2000 and the second part held in Hong Kong in November.

Part of the Festival included the construction of a bamboo theatre artwork showing contemporary usage and artistic interpretations of this structural material so traditional in Chinese culture.

The vision of Rocco Yim, the Architect was to have a more open structure than the traditional bamboo lattice work of closely spaced horizontal and vertical members. In order to achieve this the structural design is interesting in that it combines the traditional material and method of jointing bamboos with modern structural technology using fabricated structural steel connections and high strength bracing cables.

The Pavillion uses traditional Chinese bamboo construction methods. It is in the form of an open theatre building, see figures 1, 2. It was erected in an ornamental pool at the Haus der Kulturen der Welt in Berlin where it stood from July 2000 to Spring 2001. The design was re-enacted at the Tamar Site in Hong Kong in November.

The Pavillion won the 2002 Award for Members work Outside of Hong Kong, given by the Hong Kong Institute of Architects.

BAMBOO AS A STRUCTURAL MATERIAL

Bamboo has been widely used in Hong Kong and China for scaffolding because of its light weight, structural efficiency and cost. It is still the material of choice for many Hong Kong Projects, see

figure 3. It is also used for quite large temporary buildings at various festivals in Hong Kong, see figures 4, 5. It is used for housing in various parts of the world. The Architect Simon Velez has used it to produce some large and beautiful buildings in South America as described in the book "Grow your own House" published by Vitra Design Museum.

The bamboo for the Pavillion was sourced from Guan Xi in Southern China. Large poles over 120mm diameter and 8m long were required. They were treated in Hong Kong and shipped to Hamburg.

A team from Australia had designed and built a bridge over the river Spree in Berlin as part of a previous festival organized by Haus der Kulturen der Welt, see figure 6.

STRUCTURE

The bamboo theatre artwork is an open ended pitched roof structure occupying a footprint plan area of 22m by 22m. It consists of transverse frames of bamboo and is about 9m high at its highest point, the roof ridge. Poles at a pitch of about 25° span from the ridge onto the inner upper ends of side rakers and thence onto outward sloping palisade walls. The palisade walls form convex curves in plan and the roof poles fan outward from the ridge to match, see figures 1, 2, 7. The whole bamboo artwork springs from structural steel "shoes", which in turn sit on concrete plinths founded on the strong base of an ornamental pool, see figure 8. A timber floor is supported separately from the pool base.

Loads arise from the self weight of the bamboo and from wind pressure on the open lattice bamboo framework. The forces which can arise during storms or typhoons govern the design.

Although the bamboo theatre artwork was a temporary sculpture it was quite large and the public could walk and sit under it. It was to be constructed generally using traditional materials and jointing methods. This led to requirements for the design as follows:

- The artwork is a temporary structure and public safety must be ensured.
- As an artwork it is important to realize the Artist's vision
- Bamboo constructions have been successfully used for many years but are difficult to analyse and design precisely. This is recognized in Hong Kong and such structures are permitted without normal buildings approval so long as they are constructed by experienced bamboo masters.

The structural design method, or philosophy, needs to respect these requirements. The approach taken was therefore:

- Define the structural system, loadpaths and structural diagrams and illustrate these clearly with sketches, see figure 9.
- Adopt reasonable minimum loads for the artwork, for example do not design for roof access, other than the point load of an adventurous youth!
- Carry out relatively simple and clear calculations to establish reasonable member design forces and structural behaviour.
- Compare design forces with calculated bamboo pole capacities.
- Substantiate required connection joint capacities with simple load tests.
- Carry out and record a trial erection.

JOINTS AND CONNECTIONS

The bamboo jointing method was of particular interest because the German Building Authorities required a quite rigorous justification.

In the past traditional bamboo joints were made by soaking strips of bamboo and lashing around the poles. The arrangement and number of lashes was decided by the bamboo master based on experience and rules of thumb. More recently galvanized mild steel wire was used and today the lashing material is a 6mm wide flat strip of black polypropylene – polyethylene (PP-PE).

Initially a series of load tests were carried out on joins made with the PP-PE ties, and these satisfied strength requirements. However concerns on fire resistance were raised and led to a change to use mild steel wire ties. Further tests were also carried out on these. See figure 10, 11.

The base connection joint was made using a short steel tube welded to a base plate, see figure 8. The large ends of the bamboo poles were grouted into these sockets. Where required fin plates were also attached to these steel shoe to allow the tension cables to be anchored. The tops of the poles forming the walls were connected in pairs to increase lateral stability under the loads from bracing cables, see figure 12. Figure 13 shows connection between the roof and palisade walls.

CONSTRUCTION

A trial erection was carried out in June 2000 in Hong Kong and provided a useful learning experience for the design and construction team. Photographs and video recordings were sent to Berlin to assist the Proof Engineer in demonstrating the feasibility to the Building Authorities. The trial erection helped to confirm that additional pairs of guy cables from the ridge to ground at each end were not required. See figure 14. Figure 15 shows the Pavillion during the opening ceremony in Berlin.

ACKNOWLEDGEMENTS

Rocco Design Ltd: The Architects

Gammon Construction Ltd: Who supplied the bamboo, tested joints and built the pavilion.

World Pacific Scaffolding Works Ltd: The specialist bamboo erectors.

Ove Arup & Partners Hong Kong Ltd: Who carried out structural analysis and design, devised and supervised joint tests and liased with HKW in Berlin.

Haus Der Kulturen Der Welt: Who organized the Berlin end.

Bugler und Jaeck: Who provide the structural proof engineering service in Berlin.

Festival of Vision Hong Kong Berlin: Who organized the Festival at the Hong Kong end.

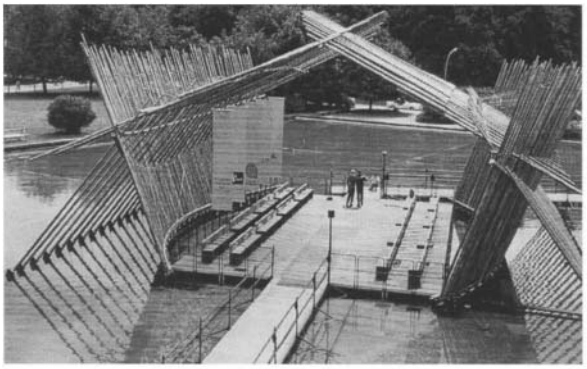


FIGURE 1

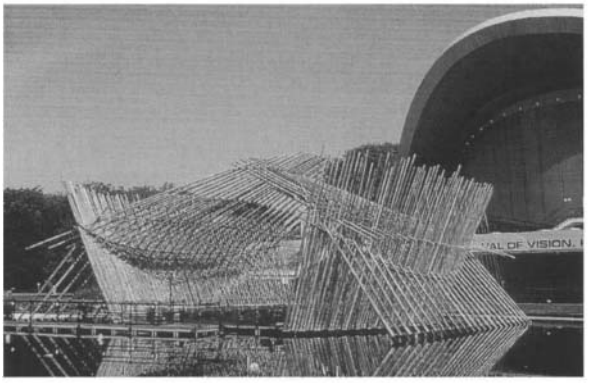


FIGURE 2

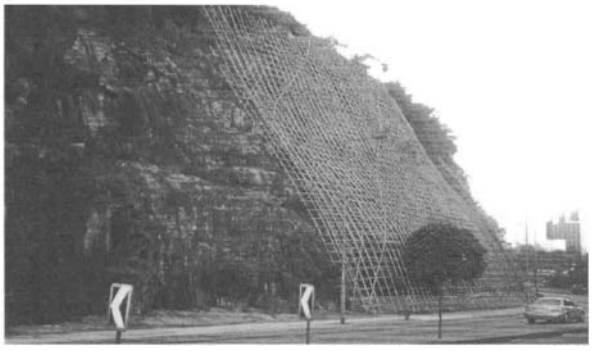


FIGURE 3



FIGURE 4

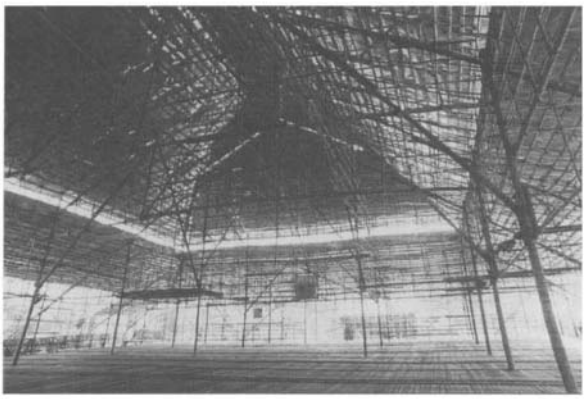


FIGURE 5

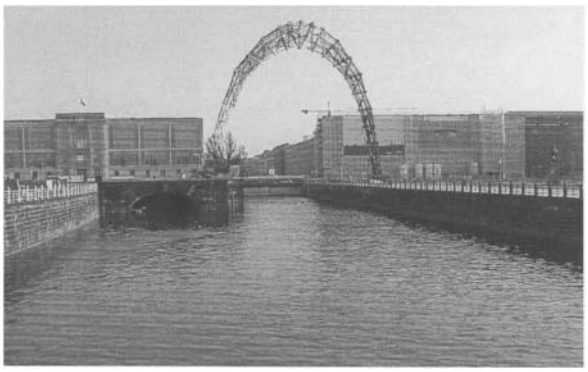


FIGURE 6

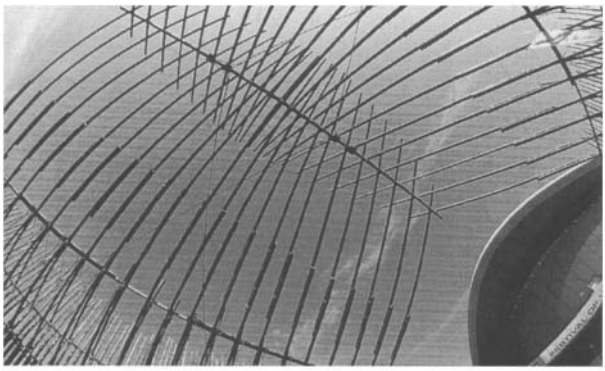


FIGURE 7

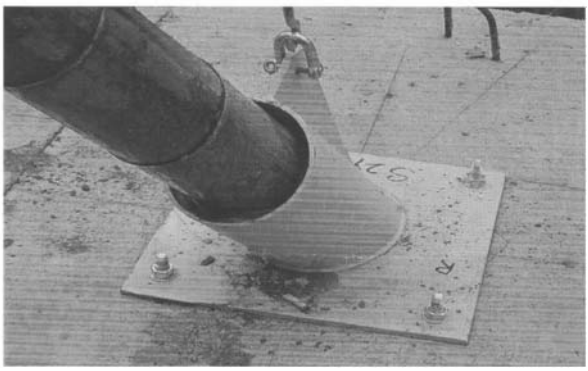


FIGURE 8

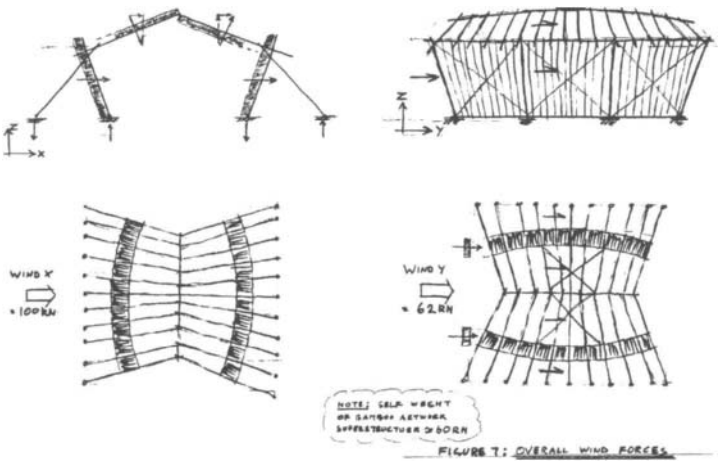


FIGURE 9

FIGURE 7: OVERALL WIND FORCES

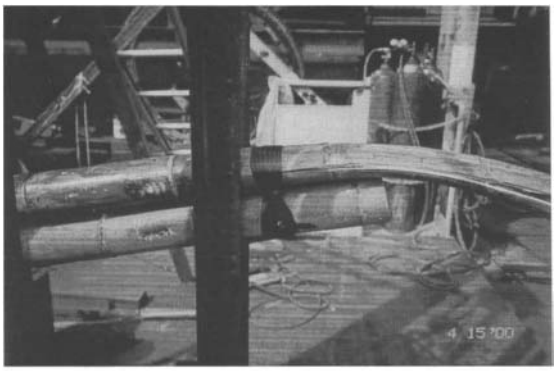


FIGURE 10

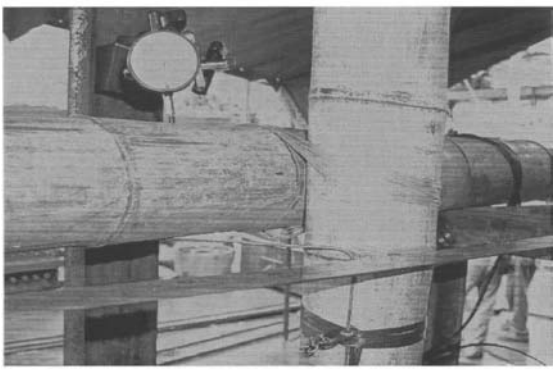


FIGURE 11

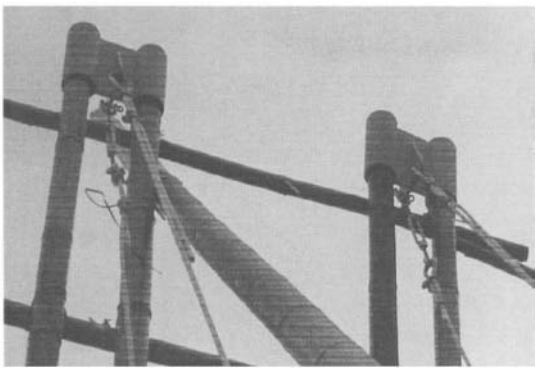


FIGURE 12

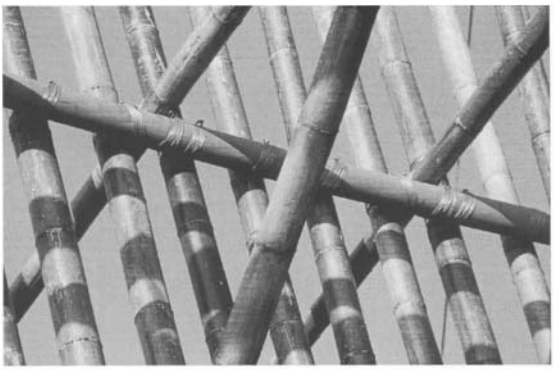


FIGURE 13

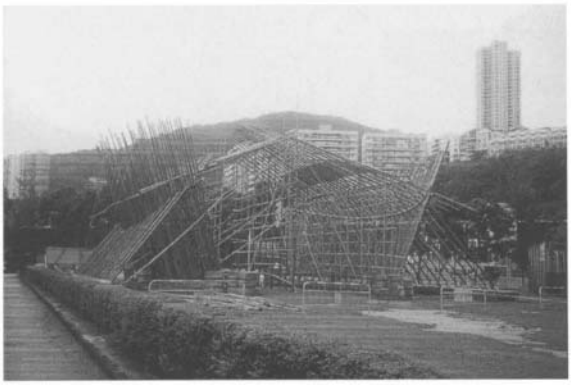


FIGURE 14

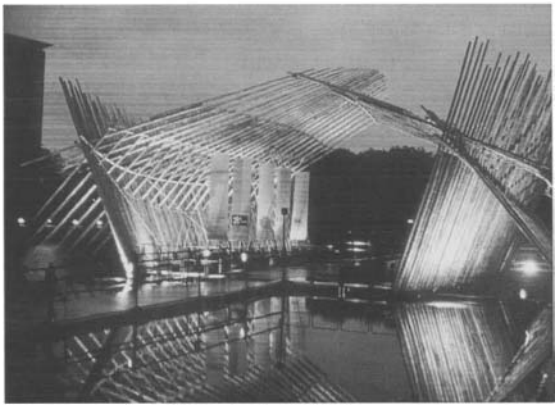


FIGURE 15

Advances in Building Technology, Volume 1
M. Anson, J.M. Ko and E.S.S. Lam (Eds.)
© 2002 Elsevier Science Ltd. All rights reserved

FULL SCALE TESTS OF BAMBOO SCAFFOLDS FOR DESIGN DEVELOPMENT AGAINST INSTABILITY

Yu WK.[1], Chung KF.[1] and Tong YC.[2]

[1] *Department of Civil and Structural Engineering, the Hong Kong Polytechnic University, Hung Hom, Kowloon, Hong Kong*
[2] *Construction Industry Training Authority, Aberdeen, Hong Kong.*

ABSTRACT

Bamboo scaffolding is widely used in construction in the South East Asia, in particular, the Southern China and Hong Kong for many decades. However, bamboo scaffolds are generally erected by scaffolding practitioners based on their intuition and experiences without any structural design. In order to standardize the design and erection of bamboo scaffolds and to improve the safety of bamboo scaffolds, a research and development program to promote the effective use of structural bamboo was carried out. As part of the program activities, four full-scale bamboo scaffolds were built and tested to failure in order to examine the structural behaviour of bamboo scaffolds in site condition. The load carrying capacities of these bamboo scaffolds with different member configurations and lateral restraint arrangements were assessed and compared against practical load requirements and support conditions. Details of the full-scale tests and their test results are presented in this paper.

KEYWORDS

Bamboo scaffolds, structural bamboo, bamboo columns, full-scale tests, load proportion

INTRODUCTION

Bamboo scaffolds are widely used in construction in the South East Asia, in particular, the Southern China and Hong Kong for many decades. It is believed among Chinese that the first bamboo scaffold was built some 5000 years ago while the basic framing systems and the erection methods were established through practice about two thousand years ago. Bamboo scaffolds are traditionally erected by specialized scaffolding practitioners without any structural design, the structural adequacy and thus the safety of the bamboo scaffolds depend primarily on the skills of individual practitioners. The knowledge is passed onto young workers through an apprentice system, mostly through on-the-job training.

Bamboo scaffolds

Bamboo scaffolds provide temporary access, working platforms for construction workers and supervisory staff, and also prevent construction debris from falling onto passers-by. Figures 1 and 2

illustrate typical applications of bamboo scaffolds in Hong Kong [1], namely, Single Layered Bamboo Scaffolds (SLBS) and Double Layered Bamboo Scaffolds (DLBS) respectively. Both Kao Jue and Mao Jue are commonly used as the vertical members, or the posts, and the horizontal members, or the main ledgers, in bamboo scaffolds. They are light enough for one person to handle a single member at a time. Due to the ease of handling, bamboo scaffolds are erected and dismantled quickly; compared to steel scaffolds, where installation and dismantling take the same amount of time, bamboo scaffolds can be dismantled in one tenth of the time it takes to install. No machinery, power-driven tools and tightening equipment are required as only simple hand tools and nylon or wire ties are used.

Consequently, in spite of open competition with many metal scaffolding systems imported from all over the world, bamboo scaffold remains to be one of the most preferred access scaffolding systems in building construction in Hong Kong and the neighbouring areas. At present, the typical height of bamboo scaffolds is 15 m, and installation of steel bracket supports at regular intervals allows full coverage of the height of a building.

In Hong Kong, the usage of DLBS [2] is to provide access and safe working platforms for workers to carry out simple or *'light duty'* construction activities, such as plastering, and the construction load at each working platform should not be less than 1.5 kPa for design purpose [3].

Structural bamboo

As bamboo columns are natural non-homogenous organic materials, large variations of physical properties along the length of bamboo members are apparent: external and internal diameters, dry density and moisture content. Two bamboo species, namely Kao Jue and Mao Jue, are commonly used in access scaffolds in Hong Kong. A pilot study was carried out by Chung and Yu [4] to examine the variation of compressive strength against various physical properties along the length of bamboo culms for both Kao Jue and Mao Jue. Moreover, systematic test series with a large number of compression and bending tests were also executed [5,6] to establish characteristic values of both the strengths and the Young's moduli of each bamboo species for limit state structural design. As shown in Table 1, both Kao Jue and Mao Jue are good constructional materials with excellent mechanical properties against compression and bending.

OBJECTIVES AND SCOPE OF STUDY

In order to achieve overall structural stability of bamboo scaffolds with high structural efficiency, lateral restraints should be provided at close intervals. However, in practice, it may not be practical or even possible to provide lateral restraints to all connections between the posts and the main ledgers of the bamboo scaffolds. In the absence of sufficient lateral restraints, the effective length of bamboo columns will be larger than their member lengths between ledgers, and thus, the axial buckling resistances of the bamboo columns are reduced significantly.

Consequently, four full-scale bamboo scaffolds were built and tested to failure in order to examine the structural behaviour of bamboo scaffolds with practical lateral restraint configurations. The load carrying capacities of these bamboo scaffolds with different lateral restraint configurations will be assessed and compared against practical load requirements. Details of the full-scale tests and their test results are presented in this paper.

TEST PROGRAM

A total of four 6 m wide by 9 m high DLBS were erected in the Aberdeen Centre of the Construction Industry Training Authority, a statutory public body of the of Hong Kong SAR. The first two tests were performed on DLBS with typical configurations commonly erected in building sites in Hong

Kong, where Kao Jue and Mao Jue were used as the main posts of the inner and the outer layers respectively. The only difference between the first two tests was the number of putlogs provided to the posts of the outer layer. The first two tests were designated as *MJ3R* and *MJ2R* as both of them used Mao Jue as the posts of the outer layers, but with three and two putlogs provided to Mao Jue respectively. Refer to Figure 3 for details of the lateral restraint arrangements. For easy reference, the lateral restraint arrangement with three putlogs per post (over a height of 9 m) is referred as the full restraint condition while that with two putlogs per post is referred as the practical restraint condition.

In the third and the fourth full scale tests, it was decided to use Kao Jue as the posts of the outer layers with three and two lateral restraints provided to Kao Jue, and thus, they were designated as *KJ3R* and *KJ2R* respectively. Such bamboo scaffolds were considered to be useful in situations where there was only one kind of structural bamboo available. All bamboo scaffolds were loaded with sand-bags at the top level working platform in close proximity of the central posts, and the reaction forces at the bottom of both the inner and the outer central posts of the DLBS were measured using load cells. The general view of the test specimens is presented in Figure 4.

In order to provide practical results for general application, all bamboo culms were air-dried for at least 3 months before testing in order to allow the bamboo members to achieve typical moisture contents commonly found in practice. Moreover, after each test, at least three short bamboo culms were cut out from the failed members, and compression tests on these short culms were carried out to evaluate their compressive strengths. The length of each compression test specimen was about twice the external diameter of the bamboo culm, but not larger than 75 and 150 mm for Kao Jue and Mao Jue respectively.

TYPLICAL LOAD CARRYING CAPACITIES OF BAMBOO SCAFFOLDS

From the four tests, the structural performance of all the DLBS was found to be satisfactory in terms of strength and deformation. Despite of large deformation in the posts (Kao Jue) due to axial buckling and flexural failure in the main ledgers (Kao Jue) over supports under large hogging moment, the scaffolds were found to be able to sustain additional loading without global collapse, as shown in Figure 5a. Moreover, two typical modes of failure were identified as shown in Figure 5b and 5c, namely, the overall buckling of Kao Jue between two working platforms and the slippage of the post – main ledger connection.

The failure load in test *MJ3R* was found to be 4.07 kN with apparent buckling of Kao Jue in the inner layer. As the effective loaded area of each post is equal to 1.5 m × 0.3 m or 0.45 m^2, the load carrying capacity of the DLBS with Mao Jue as posts and three lateral restraints per post is equal to 9.04 kPa.

Similarly, the failure load in test *MJ2R* was found to be 2.86 kN with apparent buckling of Kao Jue in the inner layer, and thus, the load carrying capacity of the DLBS with Mao Jue as posts and two lateral restraints per post is equal to 6.35 kPa.

For tests *KJ3R* and *KJ2R*, the failure loads were found to be 2.98 and 2.53 kN respectively, and thus, the load carrying capacities of the DLBS with Kao Jue as posts and with three and two lateral restraints per post are equal to 6.62 and 5.62 kPa respectively.

TESTS RESULTS AND DISCUSSIONS

Table 2 summarizes the load carrying capacities of the bamboo scaffolds. As the safe load carrying capacities in tests *MJ3R* and *MJ2R* are found to be 5.65 and 3.98 kPa respectively, a 30% reduction in the safe load carrying capacities of the typical DLBS should be allowed for when the full lateral restraint condition is modified to the practical restraint condition. Moreover, as the safe load carrying

capacities in tests *KJ3R* and *KJ2R* are found to be 4.14 and 3.51 kPa respectively, there is only 15% reduction in the safe load carrying capacity when the full restraint condition is modified to the practical restraint condition. Consequently, it is shown that the reduction in the safe load carrying capacity of DLBS due to the change of lateral restraint arrangement is related to the member configurations of the bamboo scaffolds.

It should be noted that as the minimum load requirement for a *'light duty'* assess scaffold is 1.5 kPa (unfactored), all of the four bamboo scaffolds are shown to be structurally adequate to support two fully loaded working platforms. Only the bamboo scaffold in test *MJ3R* is shown to be structurally adequate to support three fully loaded working platforms.

In order to examine the load distribution between the end and the central posts, the support reactions of the central posts in both the inner and the outer layers were measured, and the support reactions are summarized in Table 3. For test *MJ3R*, it is found that only 40% of the applied load (from the top working platform) is resisted by the central inner and the central outer posts. There is a significant spreading of loads from the central posts to the end posts through connected ledgers and diagonals. Similar conclusions may be drawn in test *KJ3R* as about 50% of the applied load is distributed away from the inner and the outer central posts.

Furthermore, it is interesting to compare the load distribution between the inner and the outer posts. Table 3 shows that in test *MJ3R*, due to the high in-plane stiffness of the outer layer provided by Mao Jue as posts and diagonals, the support reaction of the outer post is 2 to 2.75 times to that of the inner post. However, in test *KJ3R*, the support reactions of the inner and the outer posts are practically the same. Consequently, the applied loads may be conservatively assumed to be equally distributed between the inner and the outer layers of bamboo scaffolds.

Last but not the least, although the bamboo scaffolds were declared to be failed when buckling of bamboo members was apparent, it should be noted that there was no overall collapse of the bamboo scaffolds even after all the sand-bags were placed (i.e. a total of 60 sandbags with each of them weighted 20 kg); though significant local deformation in one or two bamboo members was observed. Consequently, it is shown that as the configuration of the bamboo scaffolds allows many members to be connected through standards and ledgers, loading will always be effectively re-distributed away from any failed member, and thus, the bamboo scaffolds can take up additional loads after local failure, i.e. *multiple load paths with high structural redundancy*. This is one of the most important features of bamboo scaffolds in providing sufficient safety margin against overall structural failure. Meanwhile, lateral restraints to the bamboo scaffolds should always be sufficient and secure. Otherwise, the load carrying capacities of bamboo scaffolds will be reduced considerably.

It should be noted that the load carrying capacities of bamboo scaffolds depend on the following:

- mechanical properties of bamboo culms,
- member configurations of bamboo scaffolds including bracing members,
- support conditions of bamboo scaffolds including lateral restraint arrangements,
- buckling of bamboo columns, and
- resistances of post – main ledger connections.

For details of rational design and erection of bamboo scaffolds, refer to the design guide [7] and the erection manual [8] jointly published by the Research Centre for Advanced Technology in Structural Engineering of the Hong Kong Polytechnic University and the International Network for Bamboo and Rattan, INBAR. The results obtained from the four full-scale tests have been used to calibrate the design rules proposed in the design guide.

CONCLUSIONS

Based on the full-scale tests of four Double Layered Bamboo Scaffolds (DLBS), the typical bamboo scaffolds are shown to be structurally adequate to support two to three *'light duty'* working platforms. Due to the high structural redundancy in bamboo scaffolds, loading will be effectively re-distributed away from any failed member, and thus, the bamboo scaffolds can take up additional loads after local failure in bamboo members. This is one of the most important features of bamboo scaffolds in providing sufficient safety margin against overall structural failure.

Through rational design and erection, bamboo scaffolds will be transformed into modern building systems with high structural safety and buildability. They will continue to serve the construction industry in Hong Kong and the neighbouring areas with reliable and innovative applications.

ACKNOWLEDGEMENTS

The research and development project leading to the publication of this paper is partially supported by the International Network for Bamboo and Rattan (Project No. ZZ04), and also by the Research Committee of the Hong Kong Polytechnic University Research (Project No. G-V849). The authors would like to thank Professor J.M. Ko of the Hong Kong Polytechnic University and Professor J.J.A. Janssen of the Eindhoven University of Technology, co-chairmen of the Steering Committee of the INBAR program, for their general guidance and technical advice. Moreover, the authors would like to express their gratitude to the Construction Industry Training Authority for the execution of the tests. Technical advice on practical erection of bamboo scaffolds from Mr Y.C. Siu is also gratefully acknowledged.

REFERENCES

1. Tong, Albert Y.C. (1998). *Bamboo scaffolding - Practical Application.* Proceedings of the Symposium on '*Bamboo and Metal Scaffolding*', the Hong Kong Institution of Engineers, October 1998, pp43-62.
2. Labour Department of the Government of Hong Kong, 1995. *Code of practice for scaffolding safety*: Factory Inspectorate Division.
3. *BS5973: 1993: Code of practice for assess and working scaffolds and special scaffold structures in steel*: the British Standards Institution.
4. Chung KF and Yu WK. (2002). Mechanical properties of structural bamboo for bamboo scaffoldings. *Engineering Structures* 24, 429-442.
5. Yu WK. and Chung KF. (2000). *Qualification tests on Kao Jue under compression and bending.* Technical Report, Research Centre for Advanced Technology in Structural Engineering, the Hong Kong Polytechnic University.
6. Yu WK. and Chung KF. (2000). *Qualification tests on Mao Jue under compression and bending.* Technical Report, Research Centre for Advanced Technology in Structural Engineering, the Hong Kong Polytechnic University.
7. Chung KF. and Chan SL. (2002). *Bamboo Scaffoldings in Building Construction: Design of Bamboo Scaffolds.* Joint Publication, the Hong Kong Polytechnic University and International Network for Bamboo and Rattan (in press).
8. Chung KF. and Siu YC. (2002). *Bamboo Scaffoldings in Building Construction: Erection of Bamboo Scaffolds.* Joint Publication, the Hong Kong Polytechnic University and International Network for Bamboo and Rattan (in press).

TABLE 1 Proposed mechanical properties for structural bamboo

	Kao Jue		Mao Jue	
	Dry	Wet	Dry	Wet
Characteristic compressive strength, $f_{c,k}$ (N/mm^2) (at fifth percentile)	79	35	117	44
Design compressive strength, $f_{c,d}$ (N/mm^2) ($\gamma_m = 1.5$)	53	23	78	29
Design Young's Modulus against bending, $E_{b,d}$ (kN/mm^2) (average value)	22.0	16.4	13.2	9.6

TABLE 2 Summary of test results

Test	Measured P_i with apparent column buckling (kN)	Load carrying capacity (factored) (kPa)	Safe load carrying capacity (unfactored) (kPa)
MJ3R	4.07	9.04	5.65
MJ2R	2.86	6.36	3.98
KJ3R	2.98	6.62	4.14
KJ2R	2.53	5.62	3.51

TABLE 3a Summary of measured support reactions in test *MJ3R* – Initial loading

Total applied load P_T		P_o	P_i	P_o (corrected)	P_i (corrected)	$P_o + P_i$	$\frac{P_o + P_i}{P_T}$	$\frac{P_o}{P_i}$
(kg)	(kN)	(kN)	(kN)	(kN)	(kN)	(kN)		
0	0	1.233	0.147	0.000	0.000	0.000	-	-
250	2.45	1.818	0.499	0.585	0.352	0.937	0.38	1.66
330	3.24	2.096	0.656	0.863	0.509	1.372	0.42	1.70
410	4.02	2.300	0.730	1.067	0.583	1.650	0.41	1.83
490	4.81	2.754	0.776	1.521	0.629	2.150	0.45	2.42
570	5.59	3.023	0.804	1.790	0.657	2.447	0.44	2.72
650	6.38	3.265	0.887	2.032	0.740	2.772	0.43	2.75

TABLE 3b Summary of measured support reactions in test *KJ3R*– Initial loading

Total applied load P_T		P_o	P_i	P_o (corrected)	P_i (corrected)	$P_o + P_i$	$\frac{P_o + P_i}{P_T}$	$\frac{P_o}{P_i}$
(kg)	(kN)	(kN)	(kN)	(kN)	(kN)	(kN)		
0	0	0.545	0.102	0.000	0.000	0.000	-	-
240	2.35	0.822	0.510	0.277	0.408	0.685	0.29	0.68
320	3.14	1.229	0.769	0.684	0.667	1.351	0.43	1.03
400	3.92	1.562	0.992	1.017	0.890	1.907	0.49	1.14
480	4.71	1.729	1.437	1.184	1.335	2.519	0.53	0.89
560	5.49	2.042	1.558	1.497	1.456	2.953	0.54	1.03
640	6.28	2.311	1.743	1.766	1.641	3.407	0.54	1.08

Notes: P_T = Total applied load due to the self-weight of sand-bags.
P_o = Measured reaction of the post (Mao Jue or Kao Jue) at the outer layer.
P_i = Measured reaction of the post (Kao Jue) at the inner layer.



Figure 1: Single Layered Bamboo Scaffold (SLBS)

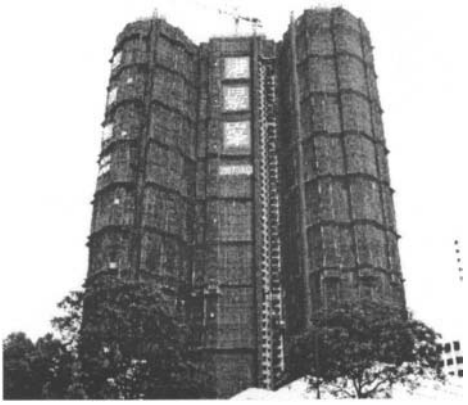
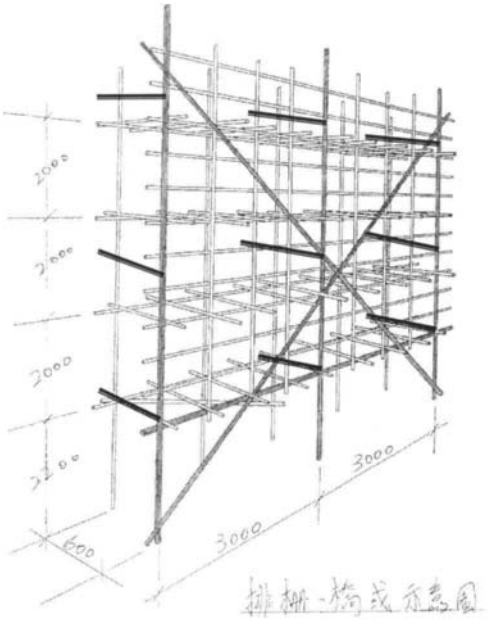
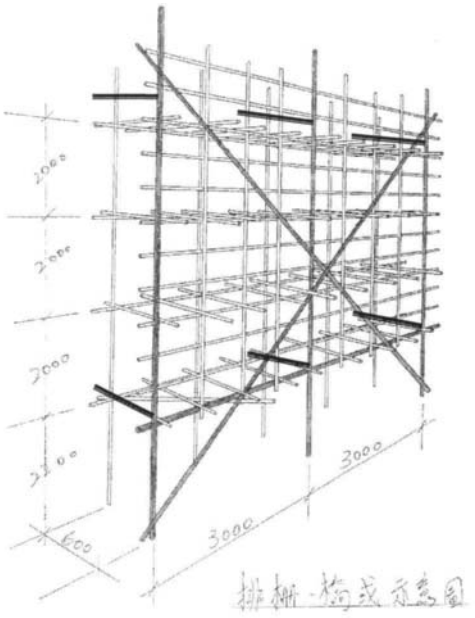


Figure 2: Double Layered Bamboo Scaffold (DLBS)



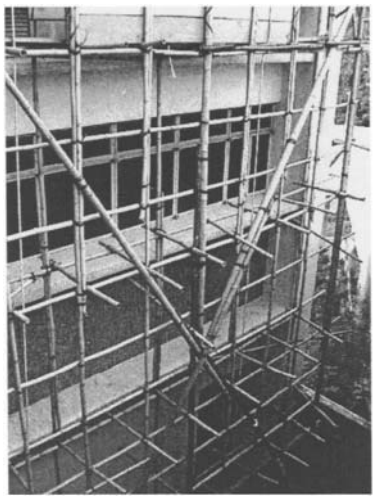
a) Three putlogs per post are provided



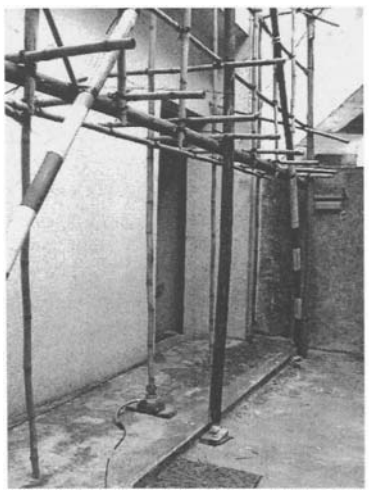
b) Two putlogs per post are provided

Figure 3: General layout of DLBS with typical lateral restraint arrangements

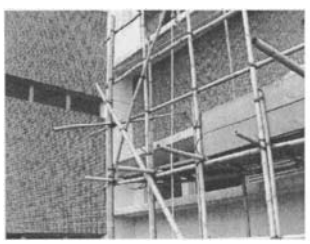
Remarks: ═══ denotes the position of a putlog
Outer layer: main posts at a horizontal spacing of 3.0 m and main ledgers at a vertical spacing of 2.0 m.
Inner layer: main posts at a horizontal spacing of 1.5 m and main ledgers at a vertical spacing of 2.0 m.
Diagonals: Mao Jue was used.



a) Typical arrangement of DLBS



b) Supports to posts

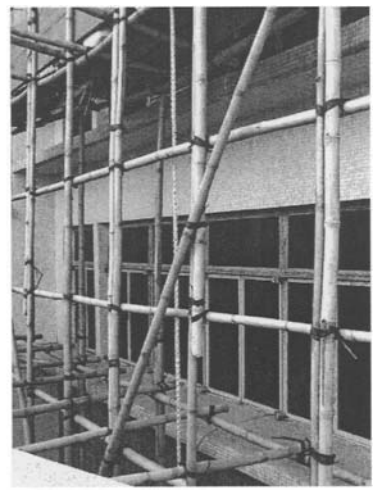


c) Typical arrangement of a putlog

Figure 4: General view of DLBS



a) Flexural failure of main ledgers initiating load re-distribution at large deformation – Test *MJ2R*



b) Buckling of a Kao Jue (inner layer) – Test *KJ2R*



c) Slippage in a post-main ledger connection – Test *MJ2R*

Figure 5: Typical failure modes in DLBS

CONSTRUCTION TECHNOLOGIES:

CONSTRUCTION TECHNOLOGIES/PLANTS

This Page Intentionally Left Blank

Advances in Building Technology, Volume 1
M. Anson, J.M. Ko and E.S.S. Lam (Eds.)
© 2002 Elsevier Science Ltd. All rights reserved

CAUSES OF LUMPS AND BALLS IN HIGH SLUMP TRUCK-MIXED CONCRETE: AN EXPERIMENTAL INVESTIGATION

Irtishad Ahmad, Salman Azhar and Ivan R. Canino

Department of Civil and Environmental Engineering,
Florida International University, Miami, Florida, USA

ABSTRACT

In high slump truck-mixed concrete, mostly used for drilled shafts (deep foundation system for heavy loads), lumps and balls typically the size of a lemon to a baseball, are frequently found. Such lumps and balls jeopardize the structural integrity of concrete by forming weakened zones and by increasing the potential for soil intrusion. Florida Department of Transportation (FDOT) requires that the concrete should be free from lumps. Hence when lumps are found, concrete batches are to be rejected consequences of which may cause disruption of work, costly rework, and loss of valuable time. Occurrences of lumps and balls must be avoided to ensure the best interest of all the parties involved – the concrete producer, contractor and the client. This experimental study was conducted to find the causes of lumps and balls formation in high slump truck-mixed concrete and to develop procedures to avoid them. Experiments were conducted at the CSR Rinker Concrete Plant in Miami, Florida and 17 concrete batches were tested. The testing variables were the materials discharge rate, truck load, headwater content and mixing revolutions. It was found that using standard discharge rate and truck load, a headwater content of 30-40% and 80-100 initial mixing revolutions at a speed of 12 rpm could produce lumps-free concrete. On the basis of these experiments, a set of remedies is suggested and recommendations are made for further experimentation.

KEYWORDS

High slump concrete, Truck-mixed concrete, Lumps and balls, Concrete uniformity, Concrete mixing

INTRODUCTION

While ready mixed concrete can be produced in a number of ways, the most common production methods are the *central-mixed concrete* and the *truck-mixed concrete.* In the United States, the overwhelming majority of ready mixed concrete producers use truck-mixed concrete due to its low capital cost and greater coverage area. Truck mixing allows more flexibility to a concrete producer to produce customized specifications concrete (NRMCA 2002).

In the truck mixed concrete, all raw ingredients are charged directly in the truck mixer. Most or all water is usually batched at the plant. The mixer drum is turned at charging (fast) speed during the loading of the materials. There are three production techniques for truck mixed concrete:

Concrete mixed at the job site: While traveling to the job site the drum is turned at agitating speed (slow speed). After arriving at the job site, the concrete is completely mixed. The drum is then turned for 70 to 100 revolutions, or about five minutes, at mixing speed to ensure uniform mixing.

Concrete mixed in the yard: The drum is turned at high speed or 12-15 rpm for 50 revolutions. This allows a quick mixing of the batch. The concrete is then agitated slowly while driving to the job site.

Concrete mixed in transit: The drum is turned at medium speed or about 8 rpm for 70 revolutions while driving to the job site. The drum is then slowed to agitating speed till it reached the job site.

Mixing concrete in a truck is different from mixing it in a central batch plant. Mixing blades in a plant lift and drop the concrete. Width limitations on truck mixers dictate the use of spiral blades that first move the concrete down towards the head end of the drum then back up the central axis towards the discharge end. Therefore, concrete mixed in a truck mixer is normally not as uniform as concrete from a central batching plant (Gaynor 1996).

The non-uniformity of truck mixed concrete causes the development of *head packs* and *concrete balls*. Head packs refer to sand streaks that appear when discharging the final portions of the concrete. Head packs are produced when sand is loaded before coarse aggregates. The sand packs in the head of the drum and breaks loose after about half the load has been discharged. Usually the head pack goes unnoticed because the sand gets mixed into the concrete before it reaches the chute. Despite the absence of visual clues, head packs are undesirable because they cause variations in slump, air content, and strength. Head packs can be avoided by loading sand and cement together after 50-75% of the coarse aggregates and water has been charged in the truck (Gaynor 1996).

Concrete balls are round lumps of cement, sand and coarse aggregates, typically the size of a lemon to a baseball. Such lumps and balls jeopardize the structural integrity of hardened concrete by forming weakened zones and by increasing the potential for soil intrusion. Moreover, they reduce the freeze-thaw resistance of hardened concrete. Their occurrence usually indicates problems with batching and mixing, such as improper batching sequencing or not enough revolutions of the mixing drum (Suprenant 1992). Gaynor (1996) indicates that in low-slump concrete (2-3 inch slump), the concrete balls are usually grinded during mixing operation. However, in high slump concrete (over 6 inch slump), such balls doesn't breakup due to high fluidity of concrete. Hence a special loading and mixing sequence is desirable for high slump concrete to produce lumps-free concrete.

RESEARCH OBJECTIVES AND SIGNIFICANCE

Florida Department of Transportation (FDOT) Standard Specifications for Road Bridge Construction (2000) section 346-7.4.1 requires that concrete should be free from lumps and balls of cementations material. When lumps and balls are found, concrete batches are to be rejected, consequences of which may cause disruption of work, costly rework and loss of valuable time. This research was conducted with the objective of determining the reasons for the formation of lumps and balls in high slump truck mixed concrete and to find the remedies to avoid them. The production of lumps-free concrete is in the best interest of all parties involved in the project, i.e. the concrete producer, contractor and the client. There is very little published material available on this topic, hence this research paper is expected to be a valuable source of information for the concrete producers.

METHODOLOGY

The uniformity of truck-mixed concrete depends on a number of factors such as the Mixing sequence, Mixing time, Charging and mixing speed, Discharge rate (speed at which the materials are charged into the mixing truck through chute), Concrete load (total volume of concrete), Initial revolutions (number of revolutions of truck mixer after addition of materials but before slump adjustment), and Headwater content (water added to the mixer before the addition of materials). The first three factors have been extensively studied by a number of researchers (Gaynor 1996; Suprenant 1992; Gaynor and Mullarky 1975) and standardized by different organizations such as FDOT. Hence the other four factors were selected as variables for this research. All the experimentation was carried out at CSR Rinker Concrete Plant in Miami, Florida, USA.

Concrete Mix Design

FDOT standard mix design for drilled shafts (Class 4: #06-0281) was used throughout the study. The mix proportions are shown in Table 1.

TABLE 1
MIX PROPORTIONS FOR FDOT CLASS IV CONCRETE (PER CUBIC YARD)

Cement (Type I)	298 lbs	Coarse aggregates	1667 lbs	Superplasticizer	23.8 oz
Slag	447 lbs	Fine aggregates	1053 lbs	Total water content	308 lbs
Slump	7-9 inch	Compressive strength	4000 Psi	Air content	3.6%

Concrete Truck Mixer Specifications

A single 10 cubic yards truck mixer was used throughout the study. The truck had a drum volume of 473 ft^3, an agitating speed of 2-6 rpm, mixing speed of 12-16 rpm and water storage capacity of 80 gallons. The truck mixer was manufactured by McNeilus Inc. (Model KX6-414) and approved by National Ready Mix Concrete Association (NRMCA).

Mixing Sequence

The standard mixing sequence adopted by CSR Rinker concrete plant was used in this study. The details are as follows:

1. With the drum rotating at charging mode (2-4 rpm), headwater and admixtures were introduced.
2. Next the discharging of coarse and fine aggregates into the truck was initialized.
3. While this process continued, cementitious materials were ribbon fed into the aggregates stream. The aggregates continued to discharge in the truck during the whole process (even when the cementitious materials were finished).
4. Finally, the tail water was added.

The truck mixed the concrete using a certain number of initial revolutions at a mixing speed of 12 rpm. This was followed by slump water adjustment (the concrete was initially batched for a slump of 3" as the computerized batching program is designed for this slump) to increase the concrete slump up to 7-9 inch. That water is termed as *jobsite allowable.* Additional 30 revolutions were given at mixing speed (12 rpm) after each addition of jobsite allowable water until the desired slump was achieved.

Experimental Details

The experimentation was conducted in two phases. In the first phase, discharge rate, concrete load and the headwater content were taken as variables. While in the second phase, headwater content and

initial revolutions were selected as the variables. The following tests were carried out in each phase: *Slump test, Air content test and the Density test.* The standard ASTM testing procedures were followed. The concrete was passed through a 2.5 inch sieve to collect concrete lump and balls and then discharged into another empty truck as illustrated in Figure 1. The size and number of lumps and balls were recorded for each batch and selected samples were sent to the laboratory for sieve analysis to determine their composition.



Figure 1: Test arrangement to collect concrete lumps and balls

TEST RESULTS

The test results are summarized in Table 2. The effect of each variable on the number of lumps formed is explained below:

Discharge Rate

Figure 2a shows the relation between the discharge rate and the number of concrete lumps. It is evident from the figure that the optimum discharge rate to minimize concrete lumps is 200 lbs/sec. Hence this discharge rate was used throughout further experimentation.

Concrete Load

The relation between the concrete load and the number of lumps (normalized to load size) came out to be linear as depicted in Figure 2b. This is very straightforward as the smaller concrete load would have less number of concrete lumps and balls. The loads of 3 yd^3 and 5 yd^3 are not commercially feasible and hence rejected. Since the normalized number of lumps between the loads of 7 yd^3 and 9 yd^3 were same, it was decided to select 9 yd^3 as the optimum concrete load.

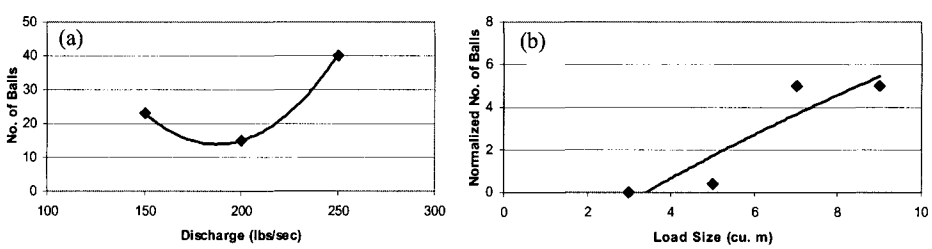


Figure 2: Effect of discharge rate and concrete load on number of concrete lumps and balls

TABLE 2
SUMMARY OF TEST RESULTS

Set	Load	Initial Rev.	Head Water	Discharge Rate	Slump	Air Content	Density	Number of Lumps and Balls						
	(yds^3)		(%)	(lbs/sec)	(inch)	(%)	(lbs/ft^2)	1"-2"	3"-4"	5"-6"	7"-8"	9"-10"	>10"	Total
A (Phase I)	9	40	90	150	7.8	2.00	142.0	5	6	4	7	1	0	23
	9	N.A.^	90	200	8.3	2.00	140.8	4	8	3	0	0	0	15
	9	N.A.^	90	250	8.5	2.00	142.0	6	7	8	9	5	5	40
B (Phase I)	3	48	90	200	8.0	2.25	139.6	0	0	0	0	0	0	0
	5	N.A.^	90	200	7.5	2.00	141.2	0	2	0	0	0	0	2
	7	38	90	200	7.5	2.00	140.4	7	5	12	11	0	0	35
	9	31	90	200	7.5	2.00	140.8	8	9	15	8	2	3	45
C (Phase I)	9	40	81*	200	7.8	2.25	140.4	0	2	3	3	0	1	9
	9	35	78*	200	8.5	2.50	140.0	6	7	17	6	2	6	44
	9	35	68*	200	8.0	2.00	141.2	1	2	1	1	0	0	5
	9	49	64*	200	7.5	2.50	140.0	0	0	0	0	0	0	0
D (Phase II)	9	55	50	200	8.3	3.20	140.6	9	13	11	2	3	2	40
	9	55	30	200	8.8	2.80	141.6	1	4	0	1	0	0	6
	9	55	20	200	9.0	2.80	141.0	3	3	3	0	0	1	10
E (Phase II)	9	55	30	200	8.8	2.80	141.6	1	4	0	1	0	0	6
	9	75	30	200	8.8	2.60	140.6	1	2	2	2	0	0	7
	9	100	30	200	8.5	2.50	141.6	0	0	0	0	0	0	0

* designed headwater ratios were 80%, 75%, 70% and 65%, respectively. Figures in Table show actually measured percentages.
^ N.A.: not available or not recorded.

Headwater Content and Initial Revolutions

After the first two set of experiments in Phase I, it was realized that the headwater content and initial revolutions could have a combined effect on the number of lumps. Hence in the next three sets, these factors were tested by keeping one as a constant and varying the other. The data for concrete batches with 10 or less number of lumps is plotted in Figure 3 using an average curve (approximated by eyeballing). Since 10 or less number of lumps in a 9 yd^3 load are very minimal, such concrete was considered as fairly uniform. The initial revolutions are plotted on the horizontal axis as they are usually specified in the specifications.

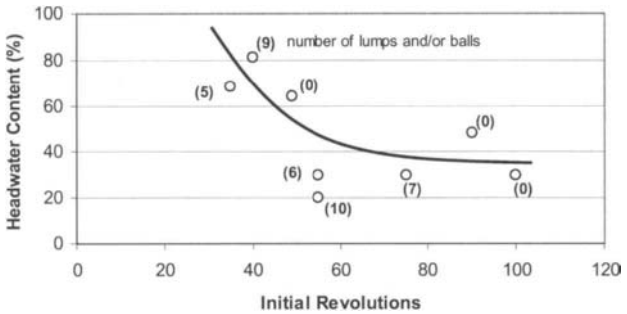


Figure 3: Combined effect of headwater content and initial revolutions on reduction of lumps and balls

It is clear from Figure 3 that with increasing numbers of initial revolutions, the headwater content can be decreased in order to produce lumps-free concrete. However, the headwater content should not be less than 25%, as the lower headwater resulted in head packs. It was further observed that the size of concrete lumps was smaller when lower headwater content was used with greater number of initial revolutions. The optimum headwater content was found to be between 30%-40% with initial revolutions ranging between 80 to 100.

Composition of Concrete Lumps

A visual inspection of lumps and balls indicated that they made up of cement, coarse and fine aggregates. The composition of most of the lumps and balls seemed to be uniform with few exceptions where dry sand and coarse aggregates were found in the center of the lump. This might be due to too low headwater content followed by low number of initial revolutions.

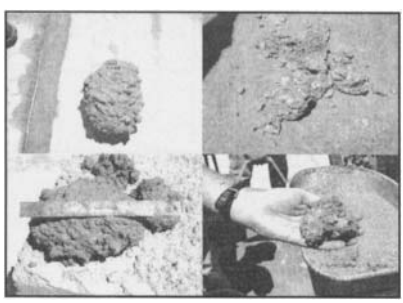


Figure 4: Composition of concrete lumps and balls

A representative number of samples of concrete lumps and balls were taken from different sets of batches and sent to the laboratory for sieve analysis. The results are shown in Figure 5.

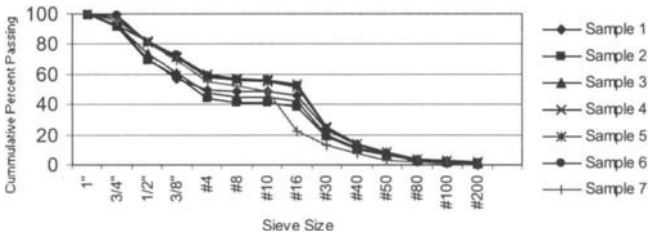


Figure 5: Sieve analysis of concrete lumps and balls

The sieve analysis indicates a gap grading with concentration of small size coarse aggregates, fine sand and cement. This is very obvious as these materials are more prone to form lumps and balls in the presence of water. The percentage of cement and water in the samples could not be determined due to the limited scope of experiments.

The size of concrete lumps varied between 1 inch to 14 inch and most bathes showed a combination of various sizes. However, smaller lumps were found in batches with low headwater and more initial revolutions. This is due to the fact that less headwater reduces the chances of cement and sand to form clutches and if formed, high initial revolutions break them. Figure 6 shows the different sizes of concrete lumps and balls found in a particular batch.

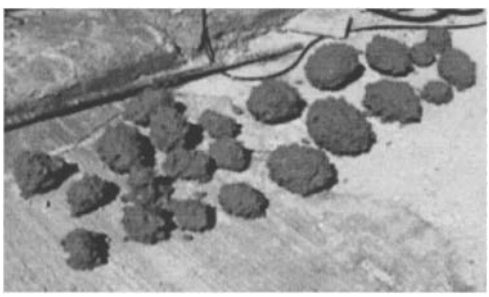


Figure 6: Lumps and balls found in a concrete batch

Concrete Batches with Lumps and Balls

Based on the interviews conducted with concrete plant managers and supervisors, the following actions could be taken to break lumps and balls in concrete, if allowed by the client and contractor.

1. If the concrete lumps are large, rotate the concrete drum at charging speed for 2-3 minutes and then at mixing speed for 3-5 minutes. This action could break the large lumps and makes concrete more uniform.

2. If small size concrete balls are found, sieve the concrete before discharging it on the chute. However, this action could not be taken if the concrete is directly pumped from the truck.

CONCLUSIONS

Based on the results of this study, the following conclusions can be drawn.

1. Headwater content and initial revolutions have a combined effect on the number of lumps and balls produced. A low headwater content followed by higher number of initial revolutions could minimize or even eliminate concrete lumps. The optimum combination was found to be 30-40% headwater with number of initial revolutions between 80-100 at a speed of 12 rpm.

2. The optimum discharge rate was found to be 200 lbs/sec.

3. The concrete load does not have a great effect on the number of lumps and balls produced. A load of 9 yd^3 was found to be commercially viable.

4. Mixing sequence has an effect on the formation of lumps and balls. A different mixing sequence could produce different results even if other factors are controlled.

5. If allowed by the client and contractor, the larger concrete lumps can be broken by rotating the drum at charging speed for 2-3 minutes and then at mixing speed for 3-5 minutes. Smaller balls could be sieved before discharging into the chute.

RECOMMENDATIONS

This research study was conduced with the aim to identify different factors that produce lumps and balls in high slump concrete. Due to the high cost of experimentation, only one set of data was collected for each factor. This may produce erroneous results hence further testing for each factor is recommended before any solid conclusions are drawn. Moreover, different concrete plants use different mixing sequences; hence more plants should be studied to support the results of this research.

ACKNOWLEDGEMENTS

The authors highly appreciate the support and help of following individuals during this research: *Dr. Sastry Putcha, Mr. Ken Blanchard, Mr. Leigh Merkert* and *Ms. Robbin Dano* from Florida Department of Transportation; *Mr. Jerry Haught* from CSR Rinker Concrete Plant, Miami, Florida; and *Dr. John Sobanjo* from Florida State University, Tallahassee, Florida.

REFERENCES

Florida Department of Transportation (FDOT). (2000). Standard Specifications for Road Bridge Construction. [online]. http://www11.myflorida.com/specificationsoffice/. Accessed on June 09, 2002.

Gaynor, R.D. (1996). Avoiding Uniformity Problems in Truck-Mixed Concrete. *Concrete Journal* **August 1996**, 570-572.

Gaynor, R.D., and Mullarky, J.I. (1975). Mixing Concrete in a Truck Mixer. *Publication No. 148. National Ready Mix Concrete Association* (NRMCA), Maryland 20910.

NRMCA (National Ready Mix Concrete Association). (2002). Ready Mix Concrete. [online] *http://www.nrmca.org*. Accessed on June 09, 2002.

Suprenant, B.A. (1992). Mixing Concrete in the Truck Takes Proper Procedures. *Publication #J921112*, The Aberdeen Group, UK.

Advances in Building Technology, Volume 1
M. Anson, J.M. Ko and E.S.S. Lam (Eds.)
© 2002 Elsevier Science Ltd. All rights reserved

ADVANCES IN CONCRETE PLACEMENT METHODS AND FINISHING TECHNIQUES FOR HIGH PERFORMANCE INDUSTRIAL PAVEMENTS IN AUSTRALIA

Peter Ashford

Faculty of Architecture, Building and Planning, University of Melbourne, Parkville, 3010, Australia

ABSTRACT

The quality and overall performance of concrete industrial floor slabs has improved dramatically as a result of technological advances in concrete supply, placement methods, the finishing process, curing and joint sealants. Placement and finishing techniques have improved substantially in recent years with larger area pours now resulting in a reduction in construction time. Client expectations for a high quality, hard wearing concrete industrial floor slab with long term performance and minimal maintenance costs has become the norm. Both designers and contractors now require specialised expertise to achieve these results. In order to improve the quality of industrial floors it has been necessary to establish working relationships between engineers, developers and the concrete contractors. This close relationship allows communication between the parties and provides a mutual understanding of all the issues associated with the design and construction methods to be employed.

KEYWORDS

High performance pavements, Vibrating screeds, Laser screeds, Scraping straight edges, Bump cutters, Ride on helicopters, Panfloats, Burnish finish, Surface tolerances, Flatness and Levellness.

INTRODUCTION

This paper reviews the most current practices in Australia for construction of high performance industrial pavements. The different floor pouring / placement methods associated with fabric reinforced, steel fibre reinforced and post-tensioned designs are highlighted together with levelling techniques and the degree of burnish finish achieved. The paper investigates through a series of six case studies, a comparison of construction methods and pour types including, long strips, double width strips with removable rails and large area pours together with floor tolerances.

The size of the pour areas and shape thereof often predetermine the choice of both the vibrating screed equipment and trowelling equipment necessary to achieve the slab finish required whilst maintaining surface tolerances. The case studies represent a variety of pour sizes and shapes and indicate the

selection of equipment used by a range of specialist concrete. The paper concludes with a "Table of Characteristics and Comparisons" with an indication of future directions, developments and trends.

CONSTRUCTION TECHNIQUES & EQUIPMENT

Pouring Methods

- Pour widths, pour lengths, and the set up of reinforcement once documented and detailed, usually predetermine the concrete placement method.
- Direct placement from the truck for low slump, low shrinkage concrete.
- Reinforcement chaired up and inspected prior to the pour, but direct placement not possible.
- The alternative is to chair up reinforcement progressively but cover is suspect.
- Hence the advantage of steel fibre reinforced slabs.
- Concrete pumps with placement booms provide an efficient method of placing concrete for both post-tensioned and steel reinforced slabs when the reinforcing has been set up prior to the pour.
- However, with limited roof heights, the horizontal reach of placement booms is limited.

Established Levelling Techniques

- The plan shape and pour area size has a major impact on the levelling techniques used during construction. The traditional "Long Strip" layout requires accurate set up and levelling of the edge formwork with hand screeds or mechanical beam type vibrating screeds used to level the surface.
- Double width long strips with a removable intermediate rail are more efficient since the pour area can be doubled and construction time thereby reduced. Removable rails can also be used on large area pours.
- Large area pours with dimensions in excess of 25m (approx.) in each direction can be levelled by taking spot levels (optical or laser) on the concrete surface at regular grids (up to 3.6m) and then power floated between the spot levels. Floor tolerances expected with this method of construction are perhaps + or – 4mm in 3.0m at best. The alternative would be to use a removable intermediate rail which would require the vibrating screeds to span 12.5m (their upper limit) and floor tolerances would be unlikely to be improved. To achieve higher levels of flatness and levelness a laser guided hydraulic driven mobile cutting and vibrating screed can be used.

Slab Specifications for Finish & Tolerances

- Various trowelling techniques are used to produce either a light, medium or heavy burnish finish. Early trowelling with panfloats followed by trowelling with the standard blades and continually working the surface over an extended period which results in a hard wearing, abrasive resistant, burnish finish, (often referred to as "black concrete").
- Australian specifications typically call for a slab to be constructed within + or – 3mm in 3.0m with a cross fall not compounding over 10m and not to exceed 5mm from RL and a differential across all joints of + or – 1mm maximum. More recently however, larger buildings have been specified using the " American Standard Specifications for Tolerances for Concrete Construction and Materials, ACI #117R-90 ". This covers the specification and measurement of F_F (floor flatness) and F_L (floor levelness) values for concrete slabs.

Equipment Overview

The equipment used and the procedures to be adopted for placement, screeding and finishing varies significantly from contractor to contractor in accordance with their available equipment, crew size, quality of surface finish required, their expertise and their specialisation in constructing particular pour area types. Recent improvements in placement, finishing methods and concrete technology have

allowed the pour size and joint spacing to be increased without comprising finish, flatness or overall cost. The range of equipment currently used includes:

- Optical and laser levels
- Hand screeds
- Power trowels (magic screeds)
- Scraping straightedges and bullfloats
- Mechanical vibrating screeds, solid steel sections or truss type vibrating screeds
- Laser guided hydraulic driven mobile cutting, levelling and vibrating screeds
- Pan floats (pizza pans) for walk-behind and ride-on trowels
- Single blade walk behind helicopter trowels , double and triple blade ride ons

CASE STUDIES

For comparative purposes, the project highlights were covered in the following order:

- Project description / pour areas
- Specifications / floor finish and tolerances
- Concrete placement method
- Screeding and levelling techniques / equipment
- Trowelling equipment / finishing / duration
- Difficulties experienced and comments

Each case study is complimented by two digital images which highlight the specific project features.

1. " Country Road " Clothing Distribution Warehouse

- The total floor area of 5,200 m^2 was divided into 18 long strip pours each 50m long by varying widths up to 5.85m. Pouring commenced on completion of the exterior cladding with areas up to 290m^2 per pour. This was the first burnish finish fibre reinforced slab constructed in Victoria.
- A hard wearing burnish finish was specified for both the racking and order collation areas. Tolerances were specified at + or – 3mm in 3.0m with a cross fall no compounding over 10m and not to exceed 5mm from RL with + or –1mm across joints. The constructed slab met these requirements and was checked using an "F meter " at F_F 70 and F_L 40.
- The concrete was placed direct from the truck chute, having reversed down the long strips.
- Truss type vibrating screeds were used and traversed the length of the strip. Edge formwork comprised of timber with a 50 x 4mm steel flat nailed vertically onto the timber so that the top edge was some 10mm above the timber. Optical levels to within 2mm were taken at 900mm centres along the steel edge. A 2.4m wide bump cutter was used across the strips to remove any surface irregularities.
- Twin blade ride-on power trowels commenced early with panfloats, followed by approximately 4 hrs. of helicopter blade trowelling with the blade angle progressively increasing as time passed. At this stage the concrete was quite dark in colour, characteristic of a burnish finish. The machines were equipped with two containers of aliphatic alcohol (a set retarder), which was sprayed onto the surface to adjust non-uniform setting rates. A chlorinated rubber spray on curing compound was applied immediately after the trowelling had ceased. The typical 290m^2 long strips took on average 9 hrs. to complete.
- Some steel fibres were exposed on the surface with occasional fibre tearout at the saw cut joints. The combination of a relatively dry mix design and the fibre reinforcement made the concrete difficult to work.



Figure.1 Truss vibrating screed, FRC slab

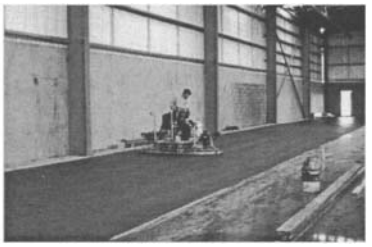


Figure.2 Ride on power trowel, long strip

2. " QP2 " A Supermarket Chain High Bay Warehouse and Distribution Centre

- The warehouse comprised a 9 storey high bay racking system with a 500mm thick ground slab to support the superstructure. This slab covered 7,730m^2 and was poured in 8 stages, covering 46m x 168m with each pour approximately 23m wide x 42m long (966m^2).The "distribution centre" slabs were 180mm thick and post-tensioned. This area covered some 15,200m^2 in 8 adjacent pours each approximately 38m x 50m ,(1,900m^2 each pour).
- The above slabs were specified to have a hard wearing burnish finish. Tolerances were specified at + or – 3mm in 3.0m with all levels not to exceed 5mm from RL. (Achieved F_F 50, F_L 40)
- Both slab types were poured using concrete pumps with placement booms. The post-tensioned slab of 1900m^2 required the use of 2 pumps and 2 vibrating screeds.
- Double and triple width pour strips were necessary to screed these large areas. Truss type vibrating screeds were used in both cases, each utilising removable rails set to the correct height / levels The rails were removed on completion of the screeding and localised rectification works done. The screeds spanned up to 11.5m to achieve the pour widths required. Optical levelling of the supporting steel edge piece to within 2mm was done at 1.2m centres. Long handle 3.0m wide scraping straightedges were used in the transverse direction to take out surface irregularities.
- The post-tensioned slab required the use of two, twin blade and one, triple blade ride-on power trowels and several walk behind machines . Early panfloat trowelling was followed by 3 hrs. of helicopter blade trowelling which achieved the light burnish finish as specified. Each slab pour required a double size crew with an average 14 hrs. to complete
- A continuous supply of concrete for the 500m^3 "high bay " slab pours, often extended the completion time. Concrete placement and vibration was difficult with closely spaced large diameter reinforcing bars in both the top and bottom of the 500mm slab. Cold and windy conditions extended the trowelling requirements.



Figure.3 Removable rails, double width strip



Figure.4 Initial trowelling with panfloats

3. " Chiffley Drive " Paper Distribution Warehouse

- A combination of reinforced and post-tensioned concrete designs with total floor area of 12,000m^2. Reinforced slabs 250mm thick poured in long strips from 9.0-13.5m wide with saw cuts on 6m x4.5m grid and maximum pour area 785m^2. Post-tensioned slabs 180mm thick with ducts at 1500mm crs. each way with both movement and construction joints. Maximum pour area 2088m^2.
- The slab was specified to be a hard burnish finish with floor tolerances of + or -4mm in 3.0m and not more than 5mm from datum. Achieved + or – 3mm in 3.0m.
- Concrete was placed using 2 placement boom concrete pumps with 2 separate concrete crews.
- The concrete was compacted with immersion vibrators, roughly shovelled level and then spot optical levels taken to suit the power float (magic screed) with a 3.6m blade utilised to screed and float the concrete surface. Permissible floor tolerances made this screeding and levelling technique more economical and faster in contrast to using long hand screeds. A long handle 3.6m wide scraping straightedge was used in the transverse direction.
- 4 walk behind power trowels with panfloats commenced at 5 hrs. and were followed by up to 5 twin blade ride-on power trowels with helicopter blades and pans. With 2 concrete crews of 8, the final trowelling ceased at 12 hrs. with a spray on curing compound applied immediately thereafter.
- The slabs was completed with a large concrete crew utilising basic equipment as the slab tolerances were not difficult to achieve. Optical levels were taken over distances up to 50m.



Figure.5 Power float, large area pour

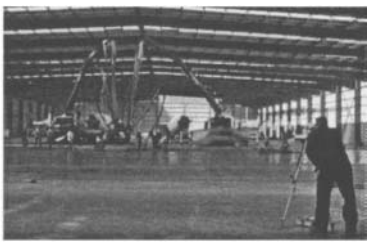


Figure.6 Two concrete pumps, optical levels

4. " Penguin Books " Warehouse

- The slab was redesigned to a steel fibre reinforced slab 180mm thick. The total floor area was 21,000m^2 poured in 21 stages on a 3 wide x 7 long grid pattern. Pours in the 11m high racking area were 870m^2 each (28m x 31m)
- A hard wearing burnish finish was specified. Floor tolerances were specified by the supplier of the man-up turret trucks (14m lift). The specification required a 6mm maximum difference in elevation of any 2 points 2.4m apart in the direction of truck travel and a 2mm maximum difference in elevation of any 2 points across the aisle at the outside of the load wheel path. There was a 1.5mm maximum difference in elevation of any 2 points 300mm apart in the load and steer wheel path. An F_F 50 slab was considered adequate to meet these requirements. Over the 9 areas poured in the high rack area, the averages achieved were F_F 70 and F_L 60. A comparative optical level grid survey was carried out at 2m centres with < 2mm variance.
- The fibre reinforced concrete was placed directly from the chute with two trucks being able to discharge at once.
- A Somero laser screed was used to cut, screed and vibrate the concrete. A uniform head of concrete in front of the screed was no longer required and the screeding time was significantly less, resulting in substantial labour savings and the ability to level / screed much larger areas of concrete. Long handle 2.4m wide scraping straightedges were used in the transverse direction to take out surface irregularities. Edge formwork was checked with a laser level at 1.5m centres.

- Two walk behind and two ride-on power trowels were used to finish the slab. Initial trowelling with panfloats commenced 4 hrs. after the first concrete delivery. At 6 hrs. the pans were removed and helicopter blades continued with the slab starting to burnish up at 7hrs. The slab was completed at 9 hrs. and sprayed immediately with a curing compound.
- The concrete was placed with a 28m wide working face (the full width of the pour) which created some relatively cold faces when there were delays in truck deliveries. This had a direct effect on the trowelling and subsequent work required on the slab surface where fresh and older concrete occur, side by side. . Consistent concrete deliveries and uniform setting rates must be maintained. With 6 pours per week, the concreter's progress was restricted by the slower progress of the roof and wall cladding.

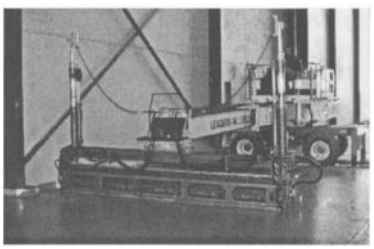


Figure.7 Somero laser screed, large area pour



Figure.8 Direct concrete placement

5. " Tsusho " Toyota Spare Parts Warehouse

- This fabric reinforced concrete slab 175mm thick covered an area of 25,000m^2 and was poured in 24 stages. The pours were approximately 34m long x 30m wide (1020m^2).
- Tolerances specified at + or – 3mm in 3.0m, within + or -5mm from RL and 2mm differential across joints. An optical survey on completion indicated slab tolerances were within 1.5mm.
- Placement was by concrete pump with a hydraulic boom arm and required two set up positions to cover the area. Two trucks fed the concrete pump.
- Levelling completed by laser screed set up on ladder tracks which were supported on large 4 legged stools which neatly fitted in between the reinforcing mesh grid. A long handle 2.4m wide scraping straightedge were also used. Achieved F_F 60 F_L 50 tolerances.
- Walk behind and ride-on power trowels with panfloats and blades completed the hard burnish finish within 11 hrs.
- Each slab pour area was sofcut sawed at 8 hrs. to a depth of 40mm to divide the area into 4 panels. Danley flat plate dowels 50 x10 at 600mm crs in prefabricated cages were located under these saw cuts with a 55mm high crack inducer detailed. At 24 hrs. the joint was recut to 50mm and additional cuts made to reduce the panel areas to 7.5m x 5.6m. Pour joints were constructed with Danley 6mm thick diamond plate dowels at 600mm crs.

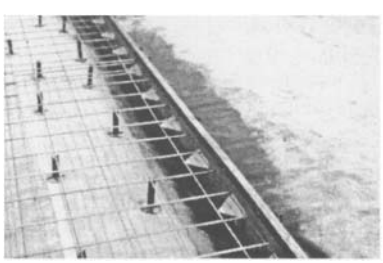


Figure.9 Danley diamond dowel joint



Figure.10 Laser screed, ladder rails & stools

6. " Toll Holdings " Transportation Distribution Warehouse

- The total floor area covered 31,680m^2 and was poured in 20 stages on a 2 wide x 10 long grid pattern. Each pour measured approximately 36m x 44m (1,584m^2). The slab was 160mm thick post-tensioned with ducts at 2.1m centres each way. On completion of the stressing, the 900mm wide edge strip between the slab and external precast walls was poured.
- The specification was extremely brief and called for a standard burnish finish. Floor tolerances were specified at minimum F_F 50 and F_L 40. After each pour, an "F" meter was run over the floor in lines around the perimeter. Average readings for the slabs completed were F_F 62 and F_L 50.
- The slabs were poured using a concrete pump with a placement boom. The hydraulic arm could not reach beyond 27m, so 9-10m of flexible rubber pump hose supported on timber blocks had to be attached to the end of the pump arm in order to reach the 36m wide pour.
- Screeding and levelling was done using a Somero laser screed. Heavy duty aluminium removable ladder rail tracks were set up on stools above the tendon ducts, these extended the full width of the pour and included a ramp section to pass over the edge formwork. A long handle 3.6m wide scraping straightedge was used to smoothen out minor surface irregularities. The laser screed used two passes to achieve the tolerances required. Timber edge formwork had a 30 x 5 steel edge plate nail fixed at 450mm centres and checked for level at 1.2m centres using a laser level with circular bubble on the staff.
- Three, twin blade ride-on power trowels were used to finish the slab. Initial trowelling with panfloats commenced 4.5 hrs. after the first concrete delivery. At 6.5 hrs, helicopter blades were used with the slab starting to burnish up at 8hrs. The slab was completed at 13 hrs. with a crew of 12. " F " meter readings were taken prior to the slab being sprayed with a curing compound.
- Additional immersion vibrators were required to ensure adequate compaction of the concrete under the tendon ducts (normally the laser screed is sufficient). Setting up the 10m of rubber hose extension to the pump slowed down the concrete placement process.

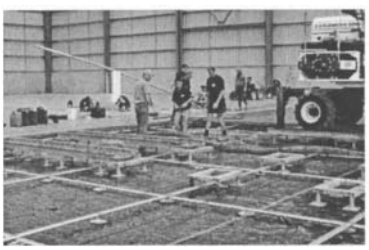


Figure.11 Laser screed on post-tensioned slab

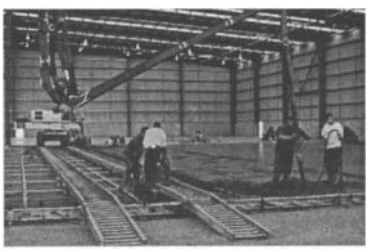


Figure.12 Ladder tracks & concrete pump

SUMMARY & CONCLUSIONS

The concrete contractors in Australia, have in recent years, imported a wide range of equipment best suited to meet their own specialised construction method. The variety of equipment purchased, enables the contractors to meet the surface finish and surface tolerance specifications particular to their market sector. There remains significant market segmentation within the industrial ground slab concrete industry. This is particularly noticeable with those contractors who have imported expensive laser screed equipment and now only construct large area pours to F_F and F_L requirements / specifications.

The six case studies represent a range of slab pour types, levelling and finishing techniques adopted in Australia, but it is still primarily the engineer who dictates the pour area / layout. Pour areas around or in excess of 1000 m^2 are becoming the norm with the traditional large concrete crews being replaced by the use of laser guided screed equipment. A summary Table 1. follows.

Table 1.
Characteristics & Comparison of Case Studies

CASE STUDY NO.	TOTAL FLOOR AREA SQ.M.	CONC. POUR AREA SQ.M.	POUR AREA TYPE/ METHOD	SLAB DESIGN	PLACE-MENT METHOD	TOLER-ANCES (Achieved)	SURF-ACE FINISH	LEVELS & SCREED TYPE	TROWEL METHOD & FINISHING
1	5,200	290	Long strip	Steel fibre	Direct from truck	3mm/3m 5mm RL 1mm joint (F_F 70 F_L40)	Hard burnish	Optical Truss vibrating screed	Ride-on panfloats Ride-on blades
2	7,730	966	Double strip	Steel rein.	Concrete pump	3mm/3m 5mm RL (F_F50 F_L40)	Hard burnish	Optical 2 Truss vibrating screeds	Ride-on panfloats Ride-on blades
3	12,000	2,088	Large area	Post-tension & Steel rein.	Concrete pump	4mm/3m 5mm RL (3mm/3m)	Hard burnish	Optical Power floats	Ride-on panfloats Ride-on blades
4	21,000	870	Large area	Steel fibre	Direct from truck	F_F 50 F_L 40 (F_F70 F_L60)	Hard burnish	Laser Laser vibrating screed	Ride-on panfloats Ride-on blades
5	25,000	1,020	Large area	Steel rein.	Concrete pump	3mm/3m 5mm RL 2mm joint (F_F60 F_L50)	Hard burnish	Laser Laser vibrating screed	Walk behind panfloats
6	31,680	1,584	Large area	Post-tension	Concrete pump	F_F 50 F_L 40 (F_F62 F_L50)	Standard burnish	Laser Laser vibrating screed	Ride-on panfloats Ride-on blades

COMMENTS ON TABLE 1. Characteristics and Comparison of Case Studies

Although there is no correlation between tolerances specified in (mm/3.0m and within RL) to (F_F and F_L) tolerances, measurements and verification of actual tolerances achieved are normally carried out over the slabs using an " F " meter.

ACKNOWLEDGEMENTS

The author would like to acknowledge the support and assistance from the Building Contractors, Project Managers, Engineers, Consultants and Concrete Contractors, for access to sites and documentation.

Building Contractors / Project Managers
Baulderstone Hornibrook, Vaughan Constructions, Pritchard Builders, Griffin Project Management, Hansen Yuncken

Engineers and Consultants
CSR Construction Services, Scott Wilson Irwin Johnston, The O'Neill Group, Ancon Beton P.L. John McGovern, Structural Systems

Concrete Contractors
Anglo Italian Concrete, V&G Concrete, Decco Constructions.

Advances in Building Technology, Volume I
M. Anson, J.M. Ko and E.S.S. Lam (Eds.)
© 2002 Elsevier Science Ltd. All rights reserved

REVIEW OF DESIGN AND CONSTRUCTION INNOVATIONS IN HONG KONG PUBLIC HOUSING

Daniel WM Chan[1] and Albert PC Chan[2]

[1] Research Fellow, Department of Building & Real Estate, The Hong Kong Polytechnic University, Hung Hom, Kowloon, Hong Kong, China
[2] Associate Professor, Department of Building & Real Estate, The Hong Kong Polytechnic University, Hung Hom, Kowloon, Hong Kong, China

ABSTRACT

Public housing has exhibited a profound impact on the social and economic development of Hong Kong. During the past few decades, the Hong Kong Housing Authority (HKHA) has been committed to the construction of a substantial number of high-rise public residential blocks to meet its target housing demand. In order to cope with such a massive public housing development, the concept of 'construction process re-engineering' has been applied to these projects, especially in the significant improvements in production times and costs without compromising quality.

This paper presents a review of the current innovations in the design, construction and management of high-rise public housing towers in Hong Kong. These innovations include: (1) standardization of block designs and construction sequences; (2) large panel steel formwork systems; (3) precast concrete facade elements; (4) extensive use of prefabricated building components; and (5) submission of alternative tenders for shorter project durations. It was suggested that considerable efforts should be dedicated to the research, development and dissemination of advances in building technology (e.g. modularization and prefabrication), coupled with innovations in project delivery and management principles (e.g. project partnering and strategic alliance).

KEYWORDS

Design innovations, construction technologies, construction process re-engineering, public housing, Hong Kong.

INTRODUCTION

Public housing has brought a significant influence on the social and economic development of Hong Kong. The public housing programme is one of Hong Kong's prides over its history and has developed into one of the most cohesive and far-sighted programmes in the Asia-Pacific Region. The Hong Kong Housing Authority (HKHA) controls one of the world's largest public housing stocks, comprising 1,005,869 flats in 361 housing estates/courts as at 31 March 2001 (HKHA, 2001), amounting to house a population of 3,235,200. With its planned public housing production programmes extending into the 21st century, the Government's commitment to housing construction will continue to grow. In order to cope with such an extensive public housing programme, current strategies in relation to design principles and construction technologies applied to the public housing projects are reviewed and discussed, especially in the context of expediting the construction process, minimizing the construction cost and enhancing the quality levels of constructed facilities.

CURRENT INNOVATIONS FOR ENHANCING PROJECT PERFORMANCE

'Process Re-engineering' is a new production philosophy of proven value in the manufacturing industry (Mohamed and Yates, 1995). The initial popularity and apparent success of this new production philosophy in manufacturing has instigated researchers and practitioners to apply its concepts to the construction industry. It aims to achieve substantial improvements in production times and costs without lowering quality.

An attempt was particularly made to provide some useful insights for shortening construction durations in these public housing projects. This improvement in construction time performance can be accomplished by re-engineering the design and construction processes. It was confirmed through face-to-face interviews with the construction professional staff of the HKHA and project managers of leading building contractors, that there is considerable potential for more time savings if such major changes are introduced in the '***superstructure***' construction. Therefore, the following innovations are currently employed in pubic housing construction in Hong Kong, for accelerating the construction process which mainly focus on reducing the time for superstructure erection.

Standardization of Block Designs, Construction Sequences and Durations

Speed of construction is obviously important in achieving the expeditious rate of building and development required to meet the unprecedentedly enormous housing programme in Hong Kong. To enhance the buildability of project design, the Hong Kong Housing Department (the executive arm of HKHA) introduced a new series of standard block designs (Harmony Types 1, 2, 3 and New Cruciform Type) in the early 1990s to house some one million people by the end of the decade. Its architects and engineers carried out detailed investigations into optimizing construction programmes, leading to in-house standard norms and related guidelines for construction durations for each of the standard block designs, with specific breakdowns for piling and building contracts, as indicated in Table 1.

Moreover, face-to-face interviews with senior construction professionals of the HKHA, together with a series of case study projects under construction, reached a consensus agreement on construction progamming. It was manifested from the observations on their master construction programmes that the major construction activities of a public housing block can be classified into several fundamental primary work packages, as illustrated in Figure 1. Their detailed definitions can be sought in Chan and Kumaraswamy's (1999) publication. Standard construction sequences for these projects can lead to a shorter delivery time on the basis of an optimum resource allocation.

TABLE 1
SCHEDULE OF EXPECTED CONSTRUCTION PERIODS OF STANDARD PUBLIC HOUSING BLOCKS
(AS OF 15 OCTOBER 1996)

Type of block	Number of storeys	Piling contract		Building contract		Total construction duration
		Without caps (months)	With caps (months)	With caps (months)	Without caps (months)	(months)
Harmony 1	41	6	9	29	26	35
Harmony 2	41	6	9	29	26	35
Harmony 3	30	6	9	25	22	31
New Cruciform	38	6	9	28	25	34
Concord 1	41	6	9	29	26	35
Concord 2	31	6	9	26	23	32

To further promote the constructability, the block designs are more 'spacious' and of a standard module form. They also take account of a number of important factors, including the need to offer a flexibility in the flat mix while maintaining consistently high standards of quality in construction and detail. The standard modular flat designs have been developed which incorporate more standard prefabricated building components and work details, as well as an efficient and simple construction sequence, so as to minimize labour content on-site and speed up the construction process

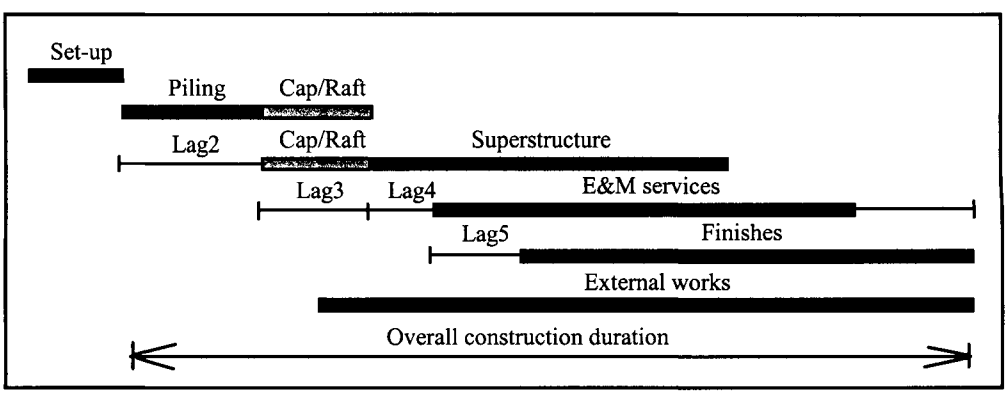


Figure 1: Typical master construction programme for standard public housing blocks

Large Panel Steel Formwork Systems

Due to the high costs of labour, market forces have driven more and more mechanization (or mechanized methods of construction) into the international construction industry (Wong and Yau, 1999). A high level of mechanization is also applied to the public housing construction industry of Hong Kong. To expedite flat production and for better quality control, the building contractors are mandatorily required to use large panel steel wall forms for wall erection and table forms for floor slab

construction since the mid-1990s. This mandatory method could only be achieved by employing tower cranes to lift the heavy metal formwork. Since the reinforced concrete superstructure constitutes the most critical activity in the construction programme, the speed and efficiency provided by large panel metal formwork, as assisted by the site cranage provided by tower cranes, has significantly helped in completing projects nearer to the original schedule.

Most of the building contractors have found that the construction of each typical floor in a single Harmony Type 1 block can be accelerated from a 8-day working cycle in the early 1990s to a 6-day cycle in the mid-1990s with the wall elements lying on the critical path, specially if the design is directed towards the use of prefabricated elements and large panel steel formwork systems. Subsequent 'trial' studies indicated that casting cycles per floor of each block can be further reduced to 4 days (see Table 2), and thus compressing the original standard schedule for superstructure erection (26 months) of a standard Harmony Type 1 block of 40 domestic floors by 4 months (Chan, 1998).

TABLE 2
FOUR-DAY WORKING FLOOR CYCLE FOR A TYPICAL HARMONY DOMESTIC BLOCK

Activity	Duration
1. Install precast facade; fix reinforcement and concealed conduits to wall	1 day
2. Install large panel wall form; pour concrete to wall	1 day
3. Strike large panel wall form; install semi-precast concrete slab (for domestic areas); erect aluminum slab form (for corridor and lift lobby)	1 day
4. Fix concealed conduits and reinforcement to topping slab; pour concrete to topping slab	1 day
Typical floor cycle time :	**4 days**

In order to achieve such a 4-day construction cycle, it was also suggested to place concrete to typical floors by pump in view of relieving the expected high workload demand on tower crane for other site operations. It was recommended to provide a concrete placing boom at each floor under construction to pour concrete through distribution pipelines to any required position across the whole floor (pump rate of 60 m^3/hour to over 120m high above ground). There should be one tower crane and one concrete boom placer for each block, together with precast plank (slab) yards, precast facade yards and concrete batching plants operated on-site to ensure a continuous workflow among them. Another benefit accruing from employing metal formwork is that contractors can re-use their own sets of steel formwork for future projects. System formwork can be much more widely adopted if flat dimensions are modularized. Furthermore, high strength concrete and steel reinforcement are also recommended because of not only saving overall material costs but also the reduction in structural member sizes.

Precast Concrete Facade Elements

The use of prefabrication techniques has marked a turning point in the construction industry. Advantages include less time and reliance on site labour, easier site inspection, as well as greatly improved design details and quality control. With the labour shortages prevalent in the building industry, prefabrication together with the greater use of standardization and modular flat design are now the essential principles in the design of standard domestic blocks in Hong Kong (Chan, 1998).

As a result, another innovation in the Hong Kong public housing construction is the introduction of precast concrete facade elements for the Harmony and Concord block series, which has been highly recommended by the Housing Department since 1991. In order to achieve a finish with better quality,

these elevation facades are often cast at site precasting yards complete with cast-in aluminum window frames and mosaic tiles. Though the adoption of precast facades will necessitate an increase in the initial capital investment of contractors, this can be set off by savings in in-situ formwork for the facade elements in the long run and also by the higher quality of finished concrete elements. The use of precast facades now becomes mandatory in all Harmony Block and Concord Block building contracts.

There are two kinds of methods to install the precast facades with bay windows i.e. pre-installation and post-installation. Pre-installation lies on the critical path of the construction programme and hence affects the floor cycle time, whereas post-installation is not critical but facade connections between wall and slab would have to be made very carefully in order to ensure water-tightness and overcome leakage problems. Much more use of precasting and off-site prefabrication should be encouraged for reducing construction durations and maintaining consistently high quality standards of the products.

Increasing the Extent of Prefabrication of Building Components

To expedite the construction programmes and enhance the quality levels of finished concrete products, the dependence on wet finishing trades has been significantly reduced. The HKHA has increased the large scale use of factory produced building components for standard types of housing blocks since the mid-1990s to ensure consistency in the standard of the major finishing and fitting materials. Apart from facade panels, other prefabricated products now being used widely include semi-precast concrete floor slabs, staircases, lightweight concrete partition walls, fabric reinforcements, aluminium windows, cooking bench and sink units, kitchen and bathroom doorsets, and stainless steel collapsible entrance gates (Chan, 1998). A more recent 'trial' project of using prefabricated bathroom units was carried out at Tseung Kwan O Area 73A Phase 2 Project and confirmed successful (HKHA, 2001). Modular packaging is also employed more extensively e.g. rebar in many situations is designed to be delivered pre-assembled for rapid fixing on-site.

The quality of precast elements is usually higher than that of the constructed in-situ components. However, their site assembly is more sensitive to poor quality control, for example, at the joints when connecting components. As is common to all prefabrication, most of the work is conducted in the factory, leaving little to be done on-site. This increases the likelihood of more efficient, high-quality and faster construction being achieved (Rosenfeld, 1994). Unlike the traditional methods of construction, these prefabricated components have a higher inherent quality, as well as more accurate profiles and dimensions so that fast-track construction will not be at the expense of poor quality.

Alternative Tenders for Reduced Construction Durations

In order to shorten standard construction periods, the HKHA is launching trials on different tendering methods, including (1) offering competent contractors more opportunities for proposing their own construction methods and solutions with 'shorter' construction durations (e.g. with a 4-day floor cycle) during the tender process – the Alternative Tender B which was first introduced in 1995 (HKHA, 2001); (2) negotiated fast-track contracts with prominent contractors for shorter completion periods; negotiated contracts encourage flexibility and early consideration of construction issues in the design process; and (3) selective tendering – awarding the contract to a contractor who has exhibited effective site management and supervision over the previous projects, as well as a proven track record of outstanding performance (Chan ,1998). Hence, tenders are either given financial incentives or a higher chance for winning future building contracts, to develop innovative construction techniques for faster construction schedules, but of course without compromising quality and safety.

Another new strategy proposed by the HKHA for shortening construction durations is an increased use of 'value engineering' in construction projects which would lead to more design-and-build contracts, particularly for a type of home purchase scheme (the Private Sector Participation Scheme, PSPS) where the building contractors may be responsible for both the design and construction of a new housing block (HKHA, 2001). This scheme has been introduced since 1978 and a number of measures have been implemented to encourage faster construction and building quality enhancement for new projects. For instance, the construction periods can be reduced by overlapping the design phase and construction phase, as well as by enhancing the buildability of project design (Rowlinson, 1999). Other innovative alternatives in construction procurement methods in the industry may also be considered in addition to the traditional type of contracts.

SUMMARY

This paper reviewed various current strategies for improving project performance of public housing in terms of time, cost and quality, by means of 're-engineering' a series of design and construction processes. These strategies embrace standardization of block designs and construction sequences, mandatory use of large panel steel formwork systems, precast concrete facade elements and other standardized prefabricated building components. Other processes that need to be 're-engineered' include the submission and evaluation of alternative tenders for a shorter project delivery from contractors.

To conclude, all these major technological improvements, coupled with advances in the current design and management strategies, have been observed to be effective in upgrading the present quality levels of concrete products and finishes, while variations in design work and project delays have been minimized. Chan and Kumaraswamy (2002) recently consolidated from their research study a series of technological and managerial strategies for reducing the typical floor cycle time for a standard public housing block design and hence compressing the overall project duration.

As the largest provider of housing in the Region, the HKHA is in a pioneering position of generating momentum for the introduction of a wide variety of innovative construction methods (e.g. Jump-form system formwork covering central core walls and other domestic structural walls for all wings of the building in floor cycles of 4 days), industrialized building components (e.g. modularization and prefabrication), and modern management principles (e.g. project partnering and strategic alliance) into the industry as the future core direction for building construction. Indicative site photos are given in Appendix 1 for further illustration.

REFERENCES

Chan, D.W.M. (1998). *Modelling Construction Durations for Public Housing Projects in Hong Kong.* PhD thesis, The University of Hong Kong, Hong Kong.

Chan, D.W.M. and Kumaraswamy, M.M. (1999). Modelling and predicting construction durations in Hong Kong public housing. *Construction Management and Economics*, 17(3), 351-362.

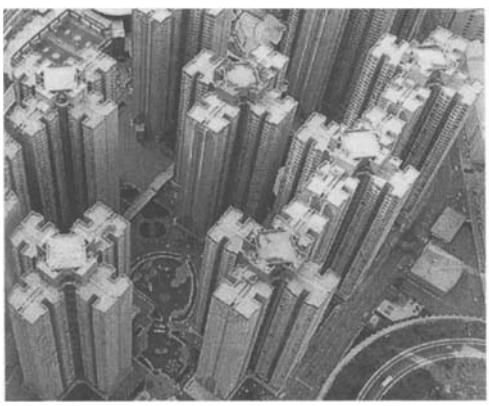
Chan, D.W.M. and Kumaraswamy, M.M. (2002). Compressing construction durations: Lessons learned from Hong Kong building projects. *International Journal of Project Management*, 20(1), 23-35.

Choi, J.C.W. (1998). *A Comparative Study on Architectural Design between the Harmony Block and Concord Block.* BSc(Hons) dissertation, The Hong Kong Polytechnic University, Hong Kong.

Construction and Contract News (2001). Public housing – Precast construction. *Construction and Contract News*, April 2001, Issue No. 2, China Trend Building Press Ltd., Hong Kong, 42-51.

HKHA (1999). *Annual Report 1998/1999*, Hong Kong Housing Authority (HKHA), Hong Kong.
HKHA (2001). *Annual Report 2000/2001*, Hong Kong Housing Authority (HKHA), Hong Kong.
Mohamed, S. and Yates, G. (1995). Re-engineering approach to construction: A case study. *Proceedings of the 5th East Asia-Pacific Conference on Structural Engineering and Construction*, 25-27 July 1995, Gold Coast, Queensland, Australia, 775-780.
Rosenfeld, Y. (1994). Innovative construction methods. *Construction Management and Economics*, 12(6), 521-541.
Rowlinson, S. (1999). "Chapter 2: A definition of procurement systems", In *Procurement Systems – A Guide to Best Practice in Construction* (edited by Steve Rowlinson and Peter McDermott), E & FN Spon, London, UK, 27-53.
Wong, A.K.D. and Yau, A.S.K. (1999). Public housing construction in Hong Kong: From building traditionally to the era of rationalization. *Group Proceedings: Group 1 – Construction*, The Hong Kong Institution of Engineers (HKIE), 2(1), 11-17.

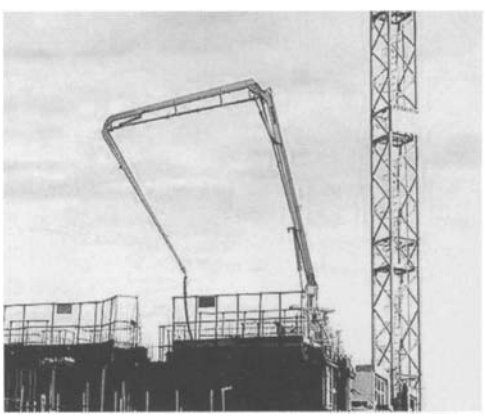
APPENDIX 1



Standard Harmony block design of four wings
(HKHA, 1999, p.33)



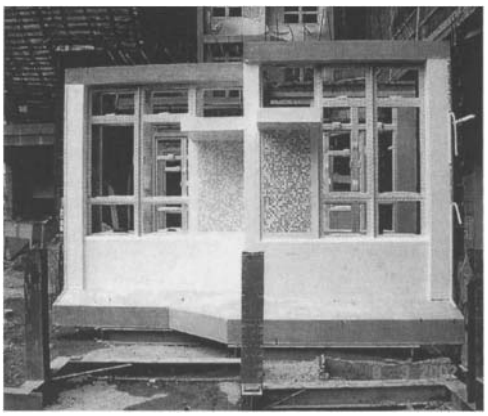
Large panel steel wall form
(HKHA, 1999, p.36)



Tower crane and concrete boom placer
(Construction and Contract News, 2001, p.42)



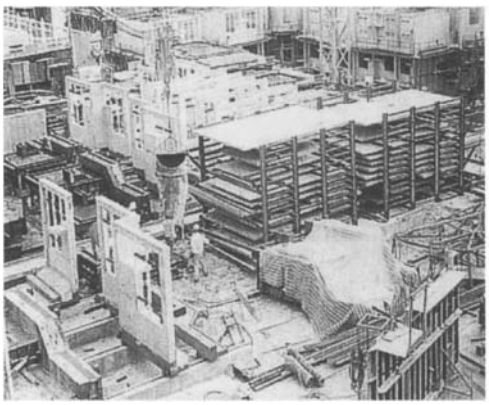
Concrete batching plant on-site
(Construction and Contract News, 2001, p.50)



Complete precast concrete façade element
(Construction and Contract News, 2001, p.45)



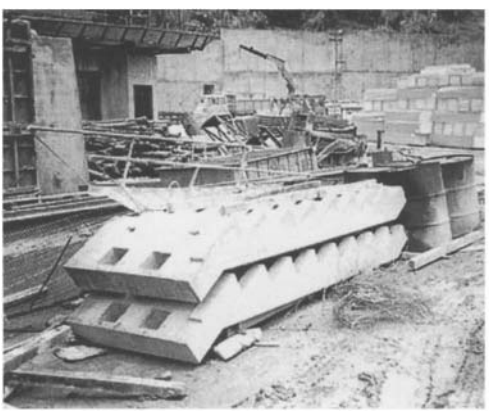
Semi-precast concrete floor slab panel
(Construction and Contract News, 2001, p.43)



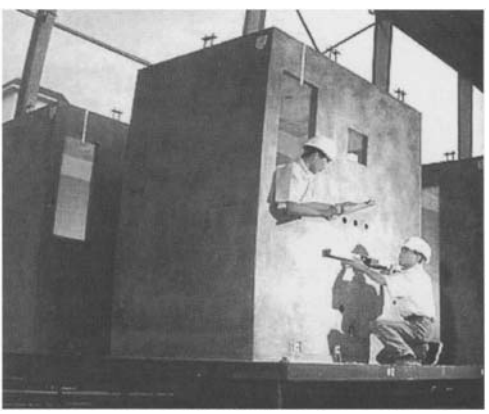
Precast concrete façade and slab yards
(Construction and Contract News, 2001, p.44)



Jump-form system formwork for central core wall
(Choi, 1998, p.89)



Precast concrete staircases (Choi, 1998, p.38)



Prefabricated bathrooms (HKHA, 2001, p.34)

Advances in Building Technology, Volume 1
M. Anson, J.M. Ko and E.S.S. Lam (Eds.)
© 2002 Elsevier Science Ltd. All rights reserved

STATIC LOADING TEST OF A SELF-BALANCED APPROACH TO A PILE IN THE YANGTZE RIVER

Dai Guoliang[1] Gong Weiming[1] Ji Lin[2] You Qinzhong[2]

1College of Civil Engineering, Southeast University, Nanjing, Jiangsu province, China
2Commander Department of Runyang yangtze River Highway bridge, Zhenjiang, Jiangsu province, China

ABSTRACT

Pile foundations are increasingly applied to the rapid development of long-span bridges in our country. In any kind of pile foundation a static loading test must be undertaken to determine the ultimate compressive bearing capacity of a single pile under criterion GBJ7-89. The Beicha bridge test pile of the Runyang Highway Yangtze River Bridge located in the Yangtze River between Zhenjiang and Yangzhou, whose ultimate bearing capacity is up to 40,000 kN, is hardly possible to test in conventional methods. The self-balanced method (Osterberg, Load-cell) is a new static load test method, almost not limited by testing sites and ultimate bearing capacity, which can directly determine the ultimate side resistance and tip resistance. This paper discusses the method successfully applied to the test pile, instrumented with strain gauges and the method for converting the results of the self-balanced test to the conventional loading test results is put forward, which suits the design method. The results also indicate the method will have expanding prospects for testing bridge piles under conditions of high bearing capacity and for special testing sites.

KEYWORDS: static load test, self-balanced test, side resistance, tip resistance, conversion method

1 INTRODUCTION

Pile foundations have been increasingly applied with the rapid development of long-span bridges in our country. In any kind of pile foundation a pile static loading test must be undertaken in order to determine the ultimate bearing capacity of a single pile under criterion GBJ7-89. The ultimate bearing capacity of the tested pile, located in the Yangtze River, is up to 40,000 kN. So a conventional static load test would have been prohibitively costly and, also difficult to arrange in the available time and

space. Hence, the self-balanced method (Osterberg, Load cell) was selected. This is almost not limited by the test sites and ultimate bearing capacity, and can directly determine the ultimate side resistance and tip resistance. This paper describes the method, which was successfully applied in the test pile, and a method converting the results of the self-balanced test to the traditional loading test results is put forward, which suits the design process well. The results indicate the method will also have very good prospects in testing bridge piles under the conditions of high bearing capacity and for special testing sites.

2 MAIN TEST RESULTS

2.1 Principles of Self-balanced Test

The self-balanced technique incorporates a sacrificial hydraulic jack-like device (load-cell) placed at or near the base of the pile to be tested. When hydraulic pressure is increased, the load-cell expands, pushing the shaft upward and the base downward. The upward movement of the load-cell top plate is the movement of the shaft at the loading cell location and it is measured by means of displacement transducers extending from the loading cell top plate to the ground surface. The downward movement of the load-cell base plate is also measured by means of displacement transducers extending from the load-cell bottom plate to the ground surface. It is important to realize that the upward and downward load movements are not equal. The upward load movement is governed by shear resistance characteristics of the soil or rock or both along the upper part of the shaft, whereas the shear resistance of the soil or rock or both along the lower part of the shaft and the compressibility of the soil or rock or both, below the pile toe, govern the downward load movement. At the start of the test the pressure in the load-cell is 0 and the load-cell assembly carries the self-weight of the pile at the location of the load-cell structurally. The test consists of applying load increments to the pile by incrementally increasing the pressure in the load-cell and recording the results upward and downward displacements. The first pressure increments transfer the pile self-weight from the assembly to the load-cell fluid. The load-cell load determined from the hydraulic pressure reading at completed transfer is the self-weight value and it is reached at minimal movement (i.e., separation of the load-cell plates). When the full self-weight of the pile has been transferred to the pressure in the load-cell, a further increase of pressure expands the load-cell; that is, the top plate moves upward and the bottom plate moves downward.

2.2 Test procedure

The test pile diameter is 1.5 m, 89 m in length and with 8 soil-rock interfaces. Every interface is instrumented with four strain gauges. The load-cell location is 10 m away from the pile toe. Load tests were carried out generally in accordance with JTJ 024-85: Specifications for Design of ground and Foundation of Highway bridges and Culverts, in detail as follows:

(1) load increment

Each load increment was 1/15 of estimated ultimate bearing capacity; that is: 5330kN, 8000kN, 10670kN, 13300kN, 16000kN, 18670kN, 21340kN, 24000kN, 26670kN, 29340kN, 32000kN, 34670kN, 37340kN, 40000kN.

(2) displacement observation

Displacement was measured at 5, 10, 15, 30, 45, 60 minutes in the first hour, every 30 minutes after the first hour (under the control of computer).

(3) stable standard

Each load increment was maintained until the rate of movement did not exceed 0.1 mm in every

one hour and lasted for two times within 1.5 hours.

(4) determination of pile ultimate bearing capacity

1) for clay, powder soil and sandy soil

$$Q_u = \frac{Q_{uT} - W}{\gamma} + Q_{uB} \quad (1)$$

Where Q_u is the ultimate compressive bearing capacity; Q_{uT} is the ultimate bearing capacity of upward pile shaft; Q_{uB} is the ultimate bearing capacity of downward pile; W is the weight of upward pile shaft; γ is the coefficient of upward pile side resistance. For clay and powder soil, γ is 0.8, while for sandy soil the value is 0.7.

2) for rock

$$Q_u = Q_{uT} + Q_{uB} \quad (2)$$

2.3 Test results

2.3.1 Pile movement versus applied load

Figure 1 presents the results of movements of top plate and bottom plate of load-cell. From the figure the upper and lower piles don't reach their ultimate bearing capacity. When the load reaches the maximum 20 000 kN, the elastic deformation of pile–soil system below the load-cell is 3.94mm(The settlement of the bottom plate when loading reached 20 000kN minus the residual settlement the bottom plate when unloading is up to 0), while its plastic deformation is 11.89mm(the residual settlement the bottom plate), and the elastic deformation of pile–soil system along the load-cell is 1.47mm(The settlement of the top plate when loading reached 20 000kN minus the residual settlement of the top plate when unloading is up to 0), while its plastic deformation is 3.09mm(the residual settlement the top plate). At the same time the compressive deformation is 3.09mm (the displacement of top plate of the load-cell minus the displacement of pile head when loading reached 20 000kN). So the ultimate compressive bearing capacity is calculated as:

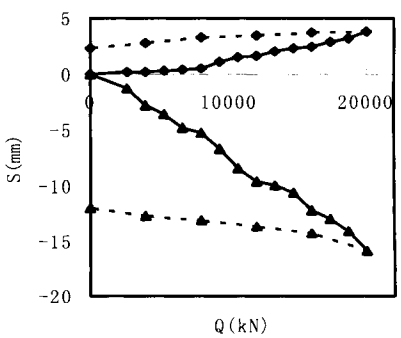


Figure 1: Pile movement versus applied load

$$Q_u \geq \frac{20000 - \pi \times 0.75^2 \times 89 \times 24.5}{0.8} + 20000 = 40180 \text{ kN} \quad (3)$$

2.3.2 Load distribution along pile

The strains measured within the pile by the strain gauges are used to estimate the load transferred along the pile to the soil, rock socket, and rock mass below the pile tip. Figure 2 is a plot of load

distribution along the pile with the applied load. The distribution is the same as that of the conventional, that is, the axial force generally decreases with an increase in depth away the load-cell because of the effect of soil resistance, while axial force in the load-cell location is maximal. The load distribution along the pile when unloading is approximately the same as the loading. When unloading until 0, every section has some axial force because there still exist the compressive deformation and the soil resistance along the pile.

2.3.2 side resistance distribution along pile

Side resistance between two sections is obtained by the division of the area of surface between the two sections and the minus of axial force of the two sections, subtracting the self-weight of pile shaft between the two sections in the upper part of pile. Figure 3 represents the side resistance distribution along the pile. Judging from figure 3, the side resistance of every section increases generally with the increase of applied load. The side resistance near the load-cell first comes into effect. At the same time, it is can be concluded that the side resistance has transferred the load into other soil layer before it reaches its ultimate value.

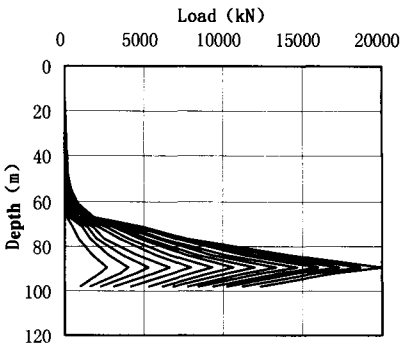


Figure 2: Load distribution

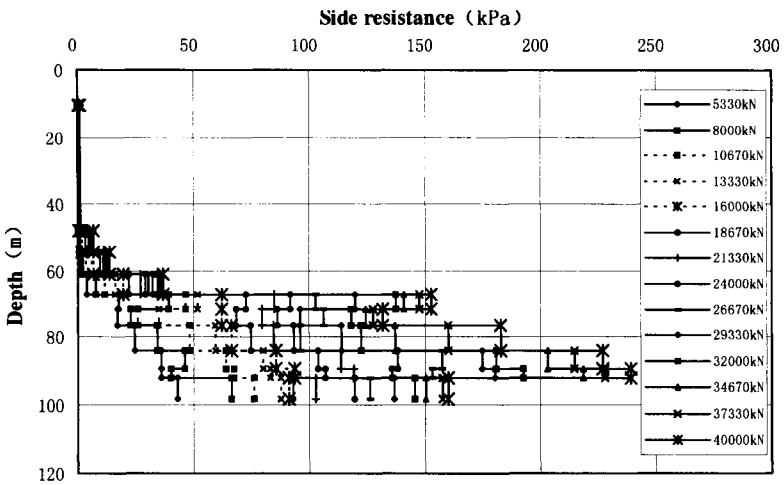
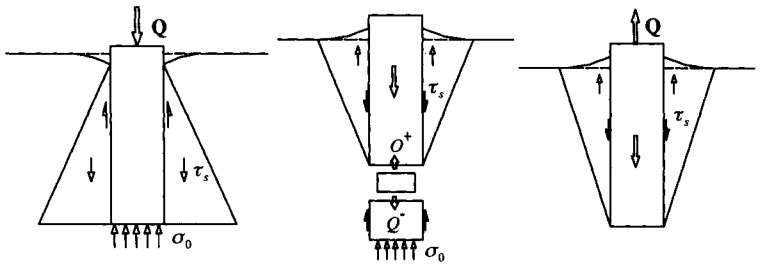


Figure 3: Side resistance distribution

3 CONVERSION TO CONVENTIONAL RESULTS

The bearing behavior of a self-balanced pile is different to that of compressive pile and tensile piles. The behaviors of load transfer of the three types of piles are shown in figure 4.



(a) compressive pile (b) self-balanced pile (c) tensile pile

Figure 4: Load transfer behavior

The displacements of the top and bottom plates of the load-cell are measured and the strains are also measured by strain gauges (see Figure 5) in the self-balanced test. The axial force distribution is obtained by calculating strains and sectional stiffness of pile. Therefore the side resistance distribution can be derived. So the equivalent pile head load-displacement can be obtained in terms of the relationship with side resistance and pile-soil displacement, and the relationship with load and displacement of a bottom plate of load-cell. In this analysis, assumptions are made as follows:

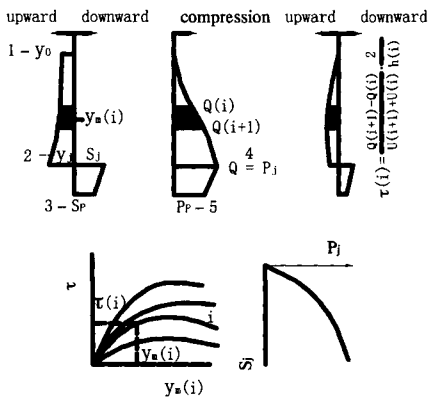


Figure 5: Relationship between axial force and side resistance and displacement

1—pile head displacement; 2—displacement of load-cell; 3—pile tip displacement; 4—load-cell force; 5—pile tip axial force.

(1) The stress-strain relationship of the pile material is elastic;

(2) Each sectional strain can be obtained from axial forces in the upper and lower sections of the unit and average sectional stiffness.

(3) The relationship between load-displacement of pile base and of side resistance and pile-soil displacement are the same as those for the conventional tests.

The upper pile shaft is divided into n units, where axial force and displacement at unit i is represented by P(i) and S(i) respectively in the self-balanced method. Their values can be expressed as follows:

$$P(i) = P_j + \sum_{m=i}^{n} f(m)\{U(m)+U(m+1)\}h(m)/2 \tag{4}$$

$$S(i) = S_j + \sum_{m=i}^{n} \frac{P(m)+P(m+1)}{A(m)E(m)+A(m+1)E(m+1)}h(m) = S(i+1) + \frac{P(i)+P(i+1)}{A(i)E(i)+A(i+1)E(i+1)}h(i) \tag{5}$$

where P_j is the axial force in the pile at unit i=n+1(load-cell force); S_j is the displacement of the pile at unit i=n+1 (the displacement of bottom plate of load-cell); f(m) is the side resistance between pile-soil interface at unit m (between units i~n) (upward is plus); U(m) is the perimeter of the pile at unit m; A(m) is the sectional area of the pile at unit m; E(m) is the elastic modulus of the pile; h(m) is the length of unit m.

$S_m(i)$, the midpoint displacement of unit i, can be expressed as follows:

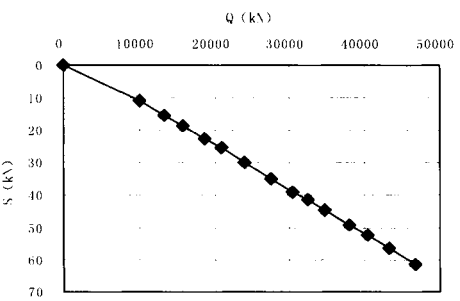


Figure 7: Equivalent load-displacement curves

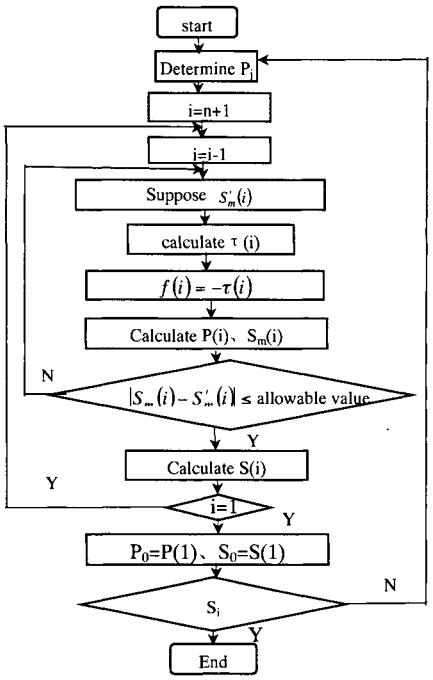


Figure 6: the flow chart of calculation

$$S_m(i) = S(i+1) + \frac{P(i)+3P(i+1)}{A(i)E(i)+3A(i+1)E(i+1)} \cdot \frac{h(i)}{2} \tag{6}$$

Substitute equation (4) into equation (5) and (6), can obtain:

$$S(i) = S(i+1) + \frac{h(i)}{A(i)E(i)+A(i+1)E(i+1)} \cdot \left\{2P_j + \sum_{m=i+1}^{n} f(m)[U(m)+U(m+1)]h(m) + f(i)[U(i)+U(i+1)]\frac{h(i)}{2}\right\} \tag{7}$$

$$S_m(i) = S(i+1) + \frac{h(i)}{A(i)E(i)+3A(i+1)E(i+1)} \cdot \left\{2P_j + \sum_{m=i+1}^{n} f(m)[U(m)+U(m+1)]h(m) + f(i)[U(i)+U(i+1)]\frac{h(i)}{4}\right\} \tag{8}$$

when i=n,

$$S(n) = S_j + \frac{h(n)}{A(n)E(n)+A(n+1)E(n+1)}\left\{2P_j + f(n)[U(n)+U(n+1)]\frac{h(n)}{2}\right\} \tag{9}$$

$$S_m(n) = S_j + \frac{h(n)}{A(n)E(n) + 3A(n+1)E(n+1)} \left\{ 2P_j + f(n)[U(n) + U(n+1)] \frac{h(n)}{4} \right\} \quad (10)$$

Using the equations (3)～(10) and the relationship between τ (i) and y_m(i), f(i) can be expressed as a function of $y_m(i)=S_m(i)$. Thus τ (i) can be obtained and f(i) can be derived through relationship $f(i) = -\tau(i)$. P_j can be obtained through the relationship of P_j and S_j. Therefore, 2n equations about S(i) and S_m(i) can be set up. Figure 6 represents the flow chart.

Figure 7 is the plot of conversion of the test pile into equivalent pile head load-displacement curve.

4 CONCLUSIONS

(1) In this paper the self-balanced pile test method was successfully applied to a pile of Beicha bridge of the Yunyang Highway Yangtze River Bridge, with an ultimate compressive bearing capacity up to 40,000 kN and locating in the Yangtze river, which is hardly possible for a conventional test. This method can determine the side resistance and base resistance and the curves of load-displacement. The results indicate the method will also have excellent prospects in bridge piles tests under conditions of high bearing capacity and testing sites, which are difficult for conventional pile tests to be performed.

(2) A method converting the self-balanced test results to conventional test results is put forward based on three assumptions. The converted results are of benefits to the designer.

Reference

[1] Jori Osterberg (1989). New device for load testing driven piles and drilled shaft separates friction and end bearing. Piling and Deep Foundations.，421～427

[2] 前田良刀(1996). 第二东名东海大府高架桥工区における壁基础原位置载. 基础の工，5：60～66

[3] Ulrich Vollenweder (1997). Prufung nach dem pfahfusspresserfahren. Zurich:Journey of ETH, 6:42～53

This Page Intentionally Left Blank

Advances in Building Technology, Volume 1
M. Anson, J.M. Ko and E.S.S. Lam (Eds.)
© 2002 Elsevier Science Ltd. All rights reserved

THE DESIGN AND CONSTRUCTION OF TWO INTERNATIONAL FINANCE CENTRE HONG KONG STATION

Gibbons C.[1], Lee A.C.C.[1], MacArthur J.M.[2], Wan C-W.[1]

[1]Ove Arup & Partners, Hong Kong, [2] Ove Arup & Partners, London

ABSTRACT

Two International Finance Centre (IFC Tower) due for completion in mid 2003 will be the tallest building in Hong Kong and 5th tallest in the world at 420m high. It is located on the harbour front of the Central District, the business centre of Hong Kong. This paper describes the some of the geotechnical design considerations, the structural design development and construction of the tower. Specifically, the paper addresses the large diameter cofferdam solution which was adopted for the foundation; the lateral response of the structure; the issues influencing the floor system; and the detailed design of the megacolumn and outrigger lateral stability system. The paper also addresses construction-led aspects of the design adopted to reduce the construction time of the tower.

KEYWORDS

Tall Building, Composite Construction, Outriggers, Construction-led Design.

INTRODUCTION

The IFC Tower forms part of Hong Kong Station Development on the Central Reclamation Hong Kong. Developers of the site are Central Waterfront Properties (CWP) - a joint venture between Sun Hung Kai Properties Ltd, Henderson Land Development Co Ltd, Bank of China Group Investment Ltd and the Hong Kong & China Gas Co Ltd. The Mass Transit Railway Corporation (MTRC) is also a development partner of the joint venture company. Architects for the project are Cesar Pelli & Associates and Rocco Design Limited with Ove Arup & Partners (Arup) providing structural and geotechnical engineering consultancy services. Mechnical and electrical consultancy services were provided by J. Roger Preston Ltd.

The tower comprises 88 storeys with a basement level of -32.0mPD and a level to the top of the roof feature of +420.0mPD. The general footprint of the tower is 57m x 57m. Towards the top, a series of

staggered step-backs reduce the plan dimensions to 39m x 39m at roof level. In all, it provides a gross floor area over 180,000m^2 of grade A office accommodation. Figure 1 shows a model of the tower on completion. One of the main requirements of the brief was to provide open plan floors and to incorporate a large degree of flexibility in order that the requirements of major tenants (such as financial institutions) could be accommodated.

The tower is just one element of a major new commercial development in central Hong Kong. The development as a whole provides office, retail, hotel and serviced apartment accommodation and accommodates Phase 2 of the MTRC Hong Kong Airport Railway Station in the 5 level basement below. It also houses major transportation facilities for the local bus companies together with several floors of car parking. The total constructed floor area of the Hong Kong Station Development amounts to 650,000 square metres.

The Main Contractor for the tower, and the remainder of the development, was a joint venture (ESJV) between E. Man and Sanfield Contractors. The steelwork for the tower was awarded in two stages - both as nominated subcontracts. The steel for the megacolumns below 6/F level (5,000 tonnes) was fabricated and installed by NKK Corporation of Japan. The steelwork for the tower above 6/F (19,000 tonnes) was awarded to a joint venture (NSJV) between NKK Corporation and Sumitomo Corporation.

The construction of the raft commenced in January 2000. At the time of writing, June 2002, the central core was constructed to level 82/F.

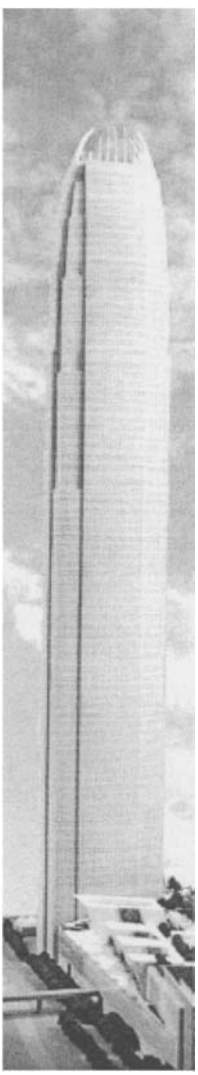


Figure 1: model of completed tower

TOWER CONFIGURATION

The basic plan configuration of a typical floor is shown in figure 3. The core at ground level is 29m x 27m with perimeter walls 1.5m and 1.25m thick. The size of the core was essentially driven by the need to maximise the efficiency of the vertical transportation system to serve the tower. The core is of conventional reinforced concrete - studies had shown that there was a significant cost advantage compared to steel and steel/composite alternatives. Initial cost studies were also conducted on core designs comprising grade 60 (28-day cube strength in N/mm^2), grade 80 and grade 100 concrete. These revealed that no great advantage was gained by changing from the grade 60 option, as savings in lettable floor space did not significantly compensate for the additional cost and construction implications of using a higher grade.

The fundamental requirement for flexible office layouts, and the desire to maximise the panoramic views, necessitated that the perimeter structure should be kept to a minimum. This led to an outrigger lateral stability solution employing eight main megacolumns (two per face) with small secondary columns in the four corners. The outriggers mobilised the columns directly without the need for transfer through a belt truss system. A less accentuated belt truss system was incorporated into these floors, however, to accept the heavy plant room floor loadings, and transfer the secondary corner column loads (as described below) into the megacolumns.

Studies showed that three outrigger levels were required, these were located at the levels R2/F to 33/F, R3/F to 55/F and R4/F to 67/F. As the

triple floor height steel outrigger trusses coincided with refuge and double mechanical floor levels, their locations were effectively a compromise between the optimum structural arrangement and constraints imposed by vertical planning and lift zoning. In any event, the system was effective in that the amount of structure occupying useable floor area was minimised.
The small corner columns support gravity load only. There are three ones of such columns, each extending a maximum of 20 storeys, which are supported off transfer trusses at each of the outrigger levels. The loads for the secondary columns are effectively 'collected' by these trusses and transferred to the megacolumns.

At the higher levels, where the corners of the floor plate are stepped back, these columns are removed with the floor plate cantilevering from the megacolumns. Consideration was also given to the removal of these secondary columns throughout. However, it was concluded that the cost of the additional weight of floor steel involved, and the likely problems associated with tolerances of large cantilever floor systems, warranted that these small columns 300x 300mm should remain.

GEOLOGY AND FOUNDATION DESIGN

The geology in the vicinity of the tower is fairly typical of Hong Kong. Grade III granite, having a permissible bearing capacity of 5MPa, is found approximately 35 metres below ground level although it shelves off steeply to the west of the tower footprint. Above this are layers of decomposed granite and alluvium, and over the top 20 metres there is a layer of fill, the land only having been reclaimed three years earlier. Dynamic compaction had been carried out on certain areas of the fill to enable diaphragm walling to take place. With a total tower load of 5,200MN, foundations obviously had to be taken to rock head.

Surrounding the tower is a five level basement with a low-level commercial podium built above it. The southern most wall of the basement box also forms part of the adjacent Hong Kong Station Phase 1 structure. With trains under operation, it was essential that movements in this vicinity should be kept to a minimum. To achieve this top down methods of construction were adopted for the general basement construction outside the footprint of the tower which enabled potential movements to be minimised.

In order to optimise the construction programme, it was considered appropriate for the tower to be built using a more conventional bottom up technique. The initial foundation solution envisaged 2.5 metre diameter bored piles, belled out to 3 metres. A large diameter cofferdam, encompassing the plan form of the tower, would then be constructed using diaphragm walling techniques to enable excavation down to the pile cap level. This would enable the cap to be cast in open excavation and the whole tower constructed from the pile cap level within the cofferdam. The circular (compression ring) nature of the cofferdam eliminated the need for internal props to provide lateral support the excavation.

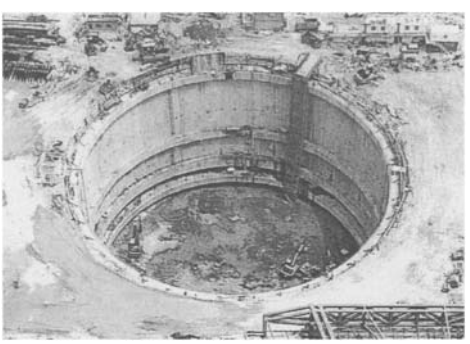


Figure 2: Excavation within the temporary cofferdam

Consequently excavation within the cofferdam could be carried out unhindered (figure 2). The cofferdam provided very stiff lateral support and consequently further ensured that the ground movements were kept to a minimum, particularly with respect to the operational MTRC tunnels running alongside the development.

The foundation sub-contractor Bachy Soletanche Group proposed an alternative foundation solution which was adopted in the final works. With a reasonably constant rock head level (as determined from site investigation) it was proposed to construct the 61.5 metre diameter cofferdam down to bedrock using a 1.5 metre thick diaphragm wall keyed into the rock. Using three reinforced concrete ring beams, and lowering the external water table by eight metres, excavation could then take place to rock head level and the pile cap/raft be cast bearing directly on rock, thus omitting the need for bored piling. Conditions on site proved to be slightly different from those anticipated, with a localised depression to the South East of the footprint of the rock head level down to a depth of approximately 55 metres, a depth too great to allow open excavation in this area. In order to overcome this a mixed foundation solution was adopted. Over much of the area the original raft solution was adopted. Mass concrete fill was then used locally, between rock head level and the underside of the cap, in the areas where the rock head sloped away. Locally, at the location of deepest rock, barrettes were installed from ground level to transfer the pile cap/raft loads to the bearing stratum, use also being made of the cofferdam panels to transfer vertical load.

Construction of the tower commenced in earnest in January 2000 with the first pour of the 6.5m thick reinforced concrete raft. With a total concrete volume of almost 20,000 cubic metres for the entire raft, it was considered not feasible to cast the raft in one continuous pour. The first pour was 5,000 cubic metres in volume and covered the entire area of the cofferdam. A further eight pours each covered half the area of the cofferdam, with the vertical construction joints rotated on plan through 90 degrees for each successive layer. A final capping layer comprising 3000 cubic metres of concrete, again covered the entire area of the cofferdam in a single pour.

LATERAL RESPONSE

Wind tunnel studies were performed on the tower by Rowan Williams Davies & Irwin Inc. (RWDI) in accordance with the Hong Kong Buildings Department Practice Note PNAP 150. This included topographical studies, a force balance assessment of the loads and monitoring of cladding pressures. A second confirmatory wind tunnel study was undertaken by Cermak Peterka Peterson (CPP). The two studies agreed to within 6%.

Studies highlighted the dominance of crosswind response for this particular building. The resulting global characteristic base bending moments and base shears in the orthogonal directions were 19,000MNm and 128MN. The combination factors used in the derivation of diagonal design forces were $\pm 0.79Fx \pm 0.79Fy$.

The predicted period of the building is 9.1 seconds, which accords quite well with the simple H/46 approximation. Lateral accelerations were predicted and compared against the NBCC, ISO and Davenport Criteria for occupancy comfort. In doing this a variable structural damping was built into the analysis equivalent to 0.8% percent at 1year return events, varying linearly to 2.0% for 50 year return events. Under these conditions the most critical accelerations, in terms of impact on human comfort, occurred in the 5-10 year return typhoon event range. The accelerations were however deemed acceptable for office occupancy in Hong Kong without the need for supplementary damping.

The lateral deflections under wind loading, including the second order P-delta effects of gravity load, were H/450 in the orthogonal direction and H/380 in the diagonal, where H is the height of the building above pile cap level.

FLOOR SYSTEM

Above the 6/F the tower comprises typical office floors and trading floors, with a design imposed loading of (3+1)kPa and (4+1)kPa respectively. Below 6/F level the floors are reinforced concrete - commensurate with the podium and basement construction. Initial designs were conducted to compare prestressed concrete and composite steel/concrete floor systems for the floors above 6/F. The concrete solution comprised a 275mm post-tensioned slab with 2000mm x 650mm deep perimeter reinforced concrete band beams. The composite schemes comprised 125mm thick slabs acting compositely with permanent decking supported at up to 3m intervals on a variety of steel beam options. Although studies showed that the cost of the concrete floor was slightly less, and that the anticipated cycle times for the two systems were similar, the additional costs for the columns and foundations due to the increased dead loading showed that, overall, the composite solution was preferable.

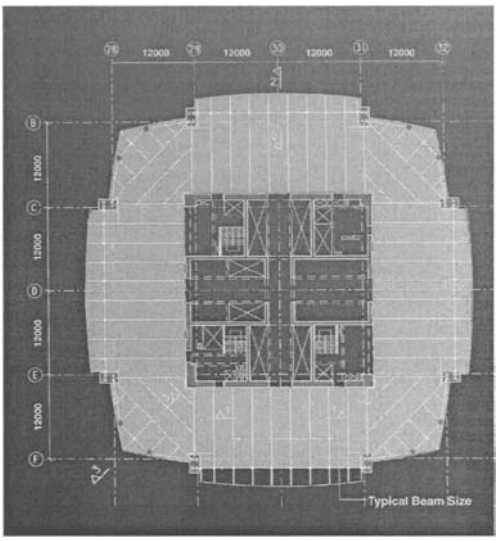


Figure 3: Typical floor framing

The typical floor-to-floor height is 4.2m with a dimension from underside of ceiling to the top of floor slab of 1.2m. A number of composite floor solutions were investigated which offered varying degrees of service/structure integration. Of these, asymmetric fabricated tapered beam and composite truss solutions presented the lightest (though not necessarily the cheapest) solutions. Such systems were, however, not favoured due to the need for maximum flexibility in the layout of main and tenant services within the floor. The solution that was adopted comprised 460mm deep steel secondary beams spanning (11.4m to 13.5m) from the core to 900mm deep primary girders spanning 24m between the main columns. One of the key features of the layout of the floor was the inclusion of a significant diagonal beam which, in conjunction with the primary girder on the main faces, provided a continuous 'tension ring' around the floor plate. This was deemed necessary to enhance robustness and provide direct buckling restraint to the columns. This peripheral primary beam arrangement provided a zone around the core where services could be installed beneath the steel beams requiring only small penetrations through the main primary girder for minimal services which needed to access the building perimeter. The 24m primary girder comprised an asymmetric fabricated section and was structurally continuous with the megacolumns.

The limiting criterion for the design of the floor system was the vertical inter-storey deflection limits at the facade of 20mm. In achieving this limit, the effects of potential differential shrinkage and long term creep effects of the primary beams on adjacent floors, were considered in addition to

patterned imposed load. These effects along with the axial shortening of the core and columns were incorporated in the construction presets to ensure that the building was constructed within acceptable tolerance.

The weight of floor beam steel is 36 kg/m^2 based on gross constructed floor area.

MEGACOLUMNS

The megacolumns comprise composite steel/concrete in which the steel elements are encased with reinforced concrete. Table 1 presents a summary of the columns sizes at various heights in the building together with details of steel content. Extensive studies were carried out to establish the most appropriate form of the columns in terms of cost and buildability and to optimise the size and steel/concrete ratios.

Concrete encasement was adopted to enable the maximum use of steel in the form of reinforcement rather than the less cost-effective use of structural sections. Reference 1 describes initial studies that were performed to investigate the optimum proportions of those elements that contribute to the lateral stiffness of the tower. This included an assessment of the optimum proportions of the steel and concrete in the megacolumns (as the proportions of the core walls and outrigger elements) to minimise the initial capital structural cost of the tower. In addition, reference 1 describes subsequent optimisation studies that were performed considering the value of the useable floor space occupied by the structure.

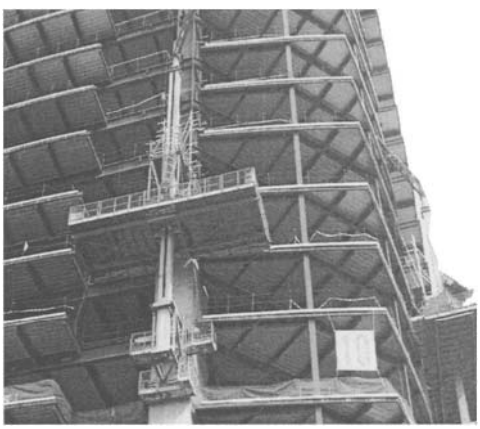


Figure 4: Column Climbform system

One key issue was the need to maximise the buildability of the megacolumns. As a consequence, the structural steel component was split into a number of sub sections that could be lifted and connected with ease. In addition, it was considered at the outset the concrete encasement of the megacolumns would be formed using self climbing formwork (figure 4). This latter initiative effectively removed the reliance on the cranes in lifting column formwork between floor levels, thereby maximising their efficiency in lifting structural steel components and reinforcement. The formwork system effectively comprised hinged forms that wrapped around the column. Prior to jumping to the next floor, the form were unfolded to form a single plane on the façade side of the column. The formwork could then climb without interfering with the pre-installed main structural steel elements. Following the passage of the form, a few light trimming steel members could be then added to complete the floor framing immediately adjacent to the column and façade.

TABLE 1

MEGACOLUMN SCHEDULE

Level	overall dimensions	no. of sub-stanchions	Averaged weight of steel (tonne/m)	Percentage of reinforcement bar	Design effective length (m)	concrete grade
B5 to 6/F	2.3m x 3.5m	6	9.7	4.0 %	30.3	60D
6/F to 32/F	2.3m x 3.5m	3	2.7	3.5 %	24.0	60D
33/F to 52/F	1.85m x 3m	2	1.1	3.0 %	19.2	60D
53/F to 69/F	1.4m x 2.6m	2	0.9	3.0 %	14.8	45D
70/F to 77/F	1.2m x 0.9m	1	0.6	2.0 %	12.8	45D
78/F to Roof	1m x 0.75m	1	0.5	2.0 %	8.9	45D

The effect of the megacolumn buckling and restraints provided by the floor diaphragms was a key consideration given the massive nature of the columns and the relatively thin nature of the individual floor diaphragms. A second order non-linear analysis was undertaken to investigate the interaction of the spring stiffness of the floor diaphragms and the column buckling. This enabled the effective length of the column to be determined and quantified the forces to be resisted by the floor diaphragms (see table 1). The inclusion of a continuous substantial primary beam tie connecting all the megacolumns facilitated the mobilisation of the floor diaphragms in providing the necessary column restraint. It should be noted that this perimeter tie also enhanced the overall robustness of the tower.

The Contract for the structural steelwork was split into two parts in order to gain an overall programme advantage.

The steelwork in the megacolumns up to 6/F level formed one contract, with all the steel above that level forming the larger follow-on steelwork contract. In the initial contract, the steel in the megacolumns was installed by mobile cranes from ground floor level into the temporary cofferdam. The optimisation studies had shown that there were significant commercial advantages in increasing the stiffness of the columns in this first contract over and above that required for strength. It effectively minimised the stiffness requirement, and hence the impact on the tower cranes (of lower capacity than the mobile cranes), in the follow-on contract.

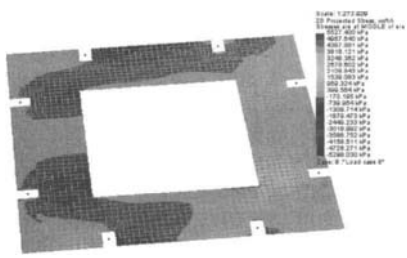


Figure 5: Finite Element analysis of floor diaphragms to assess stiffness and resulting forces in resisting column buckling.

Hence a construction-led optimisation of proportioning of structural material. The total weight of steel in the megacolumns is equivalent to 49kg/m² over the gross constructed floor area of the tower.

OUTRIGGERS

At the outset it was apparent that, in order to satisfy the access requirements in and around the mechanical floors, a steel outrigger system would be required. A punched concrete wall type outrigger was considered, however, this provided insufficient stiffness given the openings that had to be accommodated.

The steel truss outriggers pass through, and are cast within, the core walls. Optimisation studies had suggested that the axial stiffness ratios for the bottom, middle and upper outriggers should be 1 : 0.81 : 0.64 respectively (ref 1). Initially, it was considered that only the top and bottom booms of the outriggers would pass through the core - the longitudinal shears between the booms being resisted by the reinforced concrete of the core walls. However, due to the need for large openings through the core wall to accommodate the requirement for significant M&E access, it became apparent that a steel truss would be required to supplement the strength and stiffness of the perforated core.

In the analysis of the outrigger system, a detailed assessment of the local deformations at the core wall/outrigger interface was made, with the stiffness of the overall lateral stability system modified accordingly. Extensive analysis was carried out to assess the precise characteristics of the interface between the steel truss and concrete wall components to ensure strain compatibility - thereby minimising the potential for cracking in the core. The analysis took into account the flexural stiffness of the shear studs and anchorage that were used to transmit the forces from the outriggers to the concrete core. From the analysis it was found that to achieve compatibility of strain, it was necessary to restrict the stress in the shear studs to half their design capacity – essentially restricting the flexural performance of the studs to the elastic range, thereby maximising stiffness.

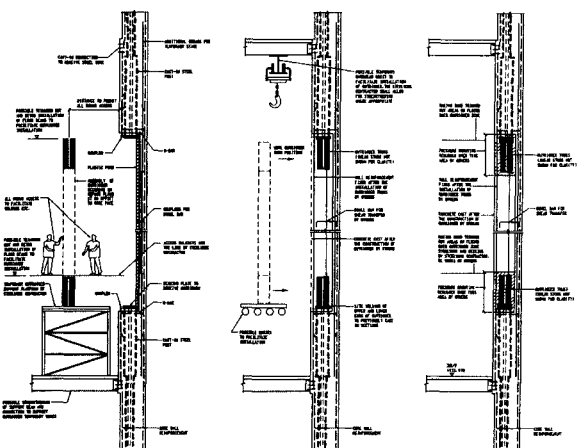


Figure 6: Conceptual stages of outrigger retro-installation

One of the key issues concerning steel outriggers in composite tall building construction, particularly where such large outriggers are required, is their potential impact on the construction programme. The core of such buildings can be constructed with relative speed and efficiency using a climbform system. Typical cycle times achieved on the core were 3-4 days. Clearly, stopping the climbform at the outrigger levels to permit the steelwork contractor to install the outrigger is not conducive to optimising continuity of labour usage, or minimising the construction programme.

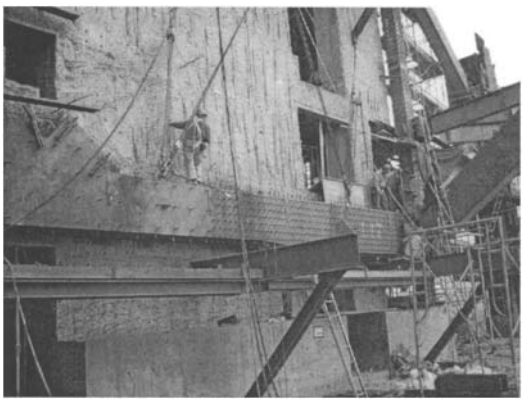


Figure 7: Retro-installation of steel outrigger within the core wall

Figure 6 shows conceptually, the retro-outrigger installation approach adopted on the tower. Stage 1 involved reducing the outer core wall thickness from (typically) 1000mm to 300mm over the full height of the outrigger zone. Above the outrigger zone, the wall thickness reverts to (typically) 1000mm. Although this involved an adjustment to the climbform system at the locations of the change in wall thickness, it did permit the climbform to pass through the outrigger zone in advance of steelwork installation. In Stage 2, and with the climbform continuing to construct the upper levels, the outrigger elements were located in position and assembled. Figure 7 shows the partial installation of the outrigger within the zone corresponding to the thinned core wall. Stage 3, with the welding of the outrigger completed, the core wall was retro-concreted. This included a 100mm thick grouted layer at the top of the outrigger zone at the interface with the widened section of the wall. Figure 8 shows a view of the tower during construction with the climbform progressing beyond the outrigger zone and the partially completed steel outrigger.

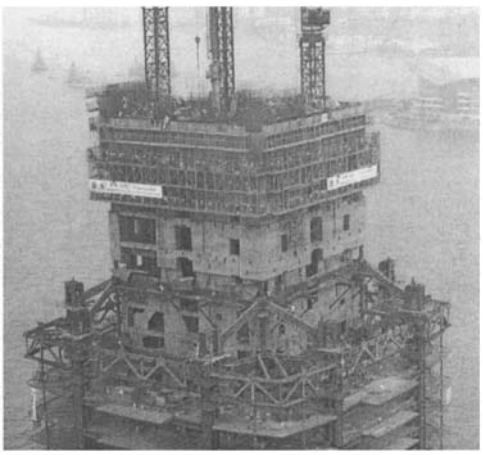


Figure 8: Climbfrom construction of the core progressing prior to completion of the steel outriggers.

DIFFERENTIAL AXIAL SHORTENING

One key considerations is the differential shortening between the core and the perimeter columns during the construction of the tower and the long term effects post completion. This is particularly important in composite tall buildings in which the deformation characteristics of the steel intensive columns and the large core can be markedly different. Prior to construction a number of specific

material tests were carried out to quantify the modulus and shrinkage characteristics of the proposed concrete mix. This was necessary because of the limited data available on the precise characteristics of grade 60 concrete incorporating 25% PFA. From these studies, Arup undertook a comprehensive study to quantify the differential shortening and the necessary pre-sets to be built into the construction of vertical elements.

The outrigger connections to the megacolumns incorporated a series of packing shims at the contact surfaces. This enabled the outriggers to be effective during construction to enable the tower to resist any typhoon winds that may have occurred. In addition, it allowed the packing shims to be removed, or added, as required (with the assistance of small jacks) to enable differential movements between the outrigger and columns to occur during construction. Using this approach, it effectively prevented the build-up of very large internal forces that would otherwise have been generated in the event that the outrigger and columns were rigidly, and permanently, connected together from the outset.

CONCLUSIONS

This paper has presented a brief overview of some of the design and construction-led innovations that have been adopted in the construction of the IFC Tower, the tallest building in Hong Kong.

REFERENCES

1. Chan, C.M., Gibbons, C., MacArthur, J.M., *"Structural Optimisation of the North East Tower, Hong Kong Sation"*, Fifth Int. Conf. on Tall Buildings, Hong Kong, Dec. 98.
2. Gibbons, C., Lee, A.C.C., MacArthur, J.M., "The Design of the North East Tower, Hong Kong Station", *Fifth Int. Conf. on Tall Buildings,* Hong Kong, Dec. 98.

Advances in Building Technology, Volume 1
M. Anson, J.M. Ko and E.S.S. Lam (Eds.)
© 2002 Elsevier Science Ltd. All rights reserved

The construction of deep and complex basements under extremely difficult urban environment – 3 representing projects in Hong Kong

Raymond W M Wong

Division of Building Science & Technology, City University of Hong Kong

ABSTRACT

Hong Kong is famous for its congested urban environment and hilly topography, which impose enormous constraints in the construction of buildings. Cases like constructing very tall buildings, either of residential or non-residential nature, up to 50 or even 60 storeys high, and in close proximity of MTR tunnels, near sensitive slopes, or in the middle of an old town area, are very common. Such building examples are often consisting of very deep basement, with depth sometimes more than 20m.

The author has identified 3 project cases in recent Hong Kong which can best illustrate the mentioned features. These projects include the redevelopment of the Lee Gardens Hotel, the construction of the Festival Walk and the construction of the Cheung Kong Center. The author wishes to generalize these 3 projects, each has applied rather unique and innovative concepts and techniques in construction, and highlight how engineers and constructors in Hong Kong tackle such extreme situations and have the jobs neatly accomplished.

KEYWORDS

Basement construction, difficult construction environment, common construction problems and solutions

INTRODUCTION

Deep basements are becoming very popular as buildings constructed higher and higher in Hong Kong. Numerous engineering problems are likely to be encountered as construction works are going deeper and deeper down into the ground. Engineers and builders have to face a lot of problems such as the existence of complicated sub-soil, overcoming of tremendous soil pressure, the provision of complicated temporary support works, working in congested underground or sensitive nearby environment. In particular in most modern development projects, the scale of construction tends to be growing bigger and bigger, that makes planning and construction of deep basement become much more difficult and complex.

At the same time, the construction of deep basement is very expensive, time consuming, inconsistent and sensitive to the quality of planning and management of individual projects. The most important of all, such works are highly hazardous, both to human operatives working within and the life and properties of third parties that within the vicinity. Though very technical or engineering in nature it seems, to implement jobs of that level of complexity is of no doubt associated with quite a lot of managerial challenges. Such as, in the preparation of a highly efficient working programme,

monitoring and rectifying the progress of works in case problems arising, or in resources planning where materials, labours and plant equipment are involved.

From the construction point of views, there are many methods to construct large-scaled and deep basement. Deep basement can be constructed using some traditional ways such as cut and fill or bottom up methods. These methods are very effective when dealing with certain jobs which is simpler in nature. On the other hand where basement is going deeper and the surrounding environment getting more complex and sensitive, bottom up method may be a more appropriate option to construct (Fig. 1).

Under typical urban environment, the situation where a basement is to be constructed can be very complex. Scenario such as working in congested site (Fig. 2), working very close to sensitive buried structure (eg. adjacent to a section of railway tunnel), or the site is located close to relatively unstable slope, are common examples that can be found everywhere in Hong Kong. Or, in certain cases, the design of a basement structure is very deep, the size of the basement is exceptionally large, sub-soil condition is very complicated, are again typical situations that make basement construction becomes very difficult.
Besides, there are situations where a new basement is required to construct simultaneously to replace an old one. Or due to the requirement of working under fast-track schedule, some basement works need to be carried out at the same time with the new foundation or even with part of the future superstructure. This will create very difficult coordination problems that involve various contractors and complicate the contractual position of the entire job. The process to make decision arriving at the best solution is of no doubt an agony journey for both engineers and builders.



Fig. 1 – Very large basement job with top-down and bottom up approach working at the same time

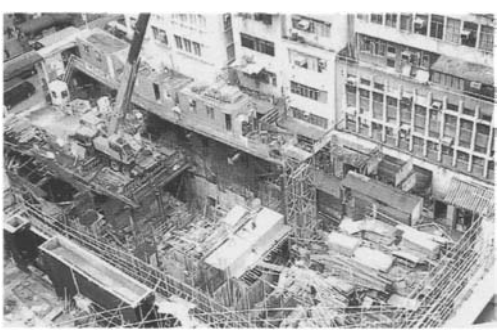


Fig. 2 – Example of basement constructed in very congested down-town environment

The main objective of this paper is to find a solution for the mentioned problems for there should be no absolute cure or one-step formula for construction works of such scale and complexity. Most often, the extent and scale of work for complex basement projects are usually very broad with a huge contract sum. It is difficult to compare alternatives base on previous data or project cases. Accurate cost analysis or work study is difficult to carry out either for there is almost without standard ground to make comparisons. Every project, though look relatively similar from certain indicating factors, is in fact unique in itself. A great number of random and uncontrollable variances are likely to arise during the courses of work. This makes planning and scheduling almost cannot be exact. The actual effectiveness of works is highly depended on the as-constructed site environments. Besides, the quality of the management and the executing parties, as well as the problems solving ability of the frontline personnel, also seriously affects the performance and effectiveness of works.

By the use of 3 recent basement projects, the writer tries to bring up some very representing project cases and demonstrate how works can be arranged to fit in such complicated environment and have the job accomplished in a safe and efficient manner.

LEE GARDEN REDEVELOPMENT PROJECT

The project located in a 5,750 m^2 site, which was abutted on 3 sides to small roads from 12 to 20m wide, and the remaining side adjoining a 17-storey residential building of 35 years old. In addition to the congested environment, the project also required to demolish the 22-storey Lee Garden Hotel, with a 2-level basement structure in it. In the redevelopment, a new 50-storey office building, constructed in structural steel with a RC core, together with a 4-level basement, was to be built. There were quite a number of difficulties to be overcome in the project. For example, almost all the new foundations and the required ground strengthening and permanent basement supporting works had to be carried out in the old basement before it could be demolished. As a result the old basement could only be demolished in small sections to allow for room and to cope with other associated works. At the same time when part of the basement was being demolished and cleared, temporary or sometime permanent supporting structures have to be built as soon as possible to infill the void until the old basement was completely replaced by the new. In order to gain more time, provisions were also made for the construction of the future building including the central core in RC as well as part of the new basement constructed in top-down method. Due to such constraints, it is comprehensible that limited mechanical plant could be used during the entire process.

Difficulties and Uniqueness

Though project of this kind is not exactly uncommon in Hong Kong, the following features, however, still make the project quite unique and thus imposed certain technical difficulties.

- A 2-level old basement structure covered the entire site area was to be demolished.
- A 4-level basement of the same size was to be built to replace the old, on top of which is a 5-level podium structure. This made the site extremely lack of working space.
- Due to the old basement could not support those heavy equipments (like the RCD) which were required for the construction of the foundation. Hand-dug caissons were thus used in this case.
- Because of the inevitable sectioning and phasing arrangement involved in the demolition of the old basement and to replace it with a new structure, complicated planning and construction jointing provisions were required (see attached demolition phasing plan).
- Part of the future building structure was carried out at the same time while doing the major substructure works. This included the construction of the foundation and raft for the central core of the future tower.
- The congested environment made storage and transportation arrangement within site very difficult. At a result of this, huge temporary loading platforms were provided at different locations (required to relocate from time to time) in order to store the steel stanchions, to station mobile cranes or other excavating machines etc.

Demolition of the Old Basement and Construction of the Substructure

In order to have the old basement demolished and replaced by the construction of a new, as well as to make way and facilitate the construction of the new 50-storey tower block, the following works were being carried out.

Demolition support and ground stabilization

- A series of temporary supporting system in the form of a steel strut frame was erected before various stages of basement demolition.
- A grouted wall was formed along the site perimeter down to 3m below bedrock level (av. 25m deep) as a means of ground water control.
- Demolish part of the basement slab along the perimeter wall to give way for the construction of hand-dug caissons, which were used later as cut-off wall for the new basement structure. Totally 244 caissons of 1.2m diameter were constructed for the purpose.

Construction of new foundations

- Hand-dug caissons were formed as foundation for the future building within the old basement. Totally 49 caissons with diameter ranging from 1.6m to 5.0m were constructed.
- The central part of the old basement was demolished to provide working space for the carrying out of the foundation and raft for the future building core.
- Hand-dug caissons and the caisson raft were constructed to support the central core of the new building. Excavation and construction of the 5m diameter caissons was done at the bottom of a 800m^2 pit that formed after the demolition of the center part of the old basement (Fig. 3).

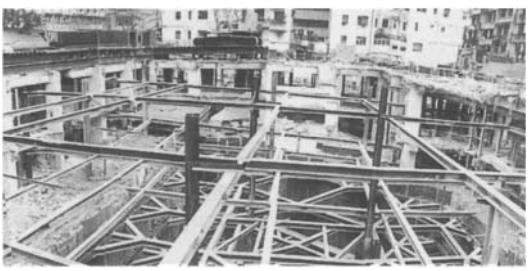


Figure 3 – A pit formed further down from the partly demolished old basement structure for the construction of the foundation and raft for the future building tower.



Figure 4 – Layout showing the extremely complicated construction phasing as seen at the peak period.

Changing over and provisional works for the new building

- Part of the old basement structure along the perimeters was demolished to allow space to build the capping beam on top of the caisson wall.
- Similarly, part of the old basement structure was demolished to provide room for the erection of steel stanchions as column support to future building. These columns could enable the superstructure be constructed at the same time with the basement that was built using top-down method.
- The building core was constructed from the raft up to ground level. Since there was very limited working space within the central pit, traditional timber formwork was used in the construction of the core. The core would act later as a lateral support for the ground floor slab which served also as a separating plate to facilitate the construction of the top-down basement.
- Demolish the remaining old basement, section by section, and covered the space immediately with the new ground floor slab. Phasing and junctioning arrangement was the most difficult part of work here (Fig. 4).

Construction of the Basement

The basement was constructed using top-down method. In order to allow excavated material could be removed conveniently, two outlet points were provided on site. A grab lifter was set up on top of one of the outlets for the removal of spoil. As usual top-down construction does, excavation started from the top level downward until it reached a depth of about 5m where it would be shored and strutted. Basement slab would then be constructed with connection made to the central core, steel columns and the caisson wall using couplers. The works repeated until it reached the bottom level of the basement where the caisson caps and other ground beams were finally constructed.

THE FESTIVAL WALK

The Festival Walk, situated on a 21,000 sq m site on a stump of a small hill near the Kowloon Canton Railway (KCR) and the Mass Transit Railway (MTR) stations. The project exhibited a lot of

complications during the course of its construction, basically inherited from the special nature of the job such as its unfavorable topographical and geotechnical environment, working within the railway and tunnel lines of two very busy railway networks, the requirements of constructing a very large building with exceptionally deep basement, as well as some access problems.

Topography and Geology of Site

The site is situated on a narrow terraced strip of land along the Tat Chee Avenue (TC Av.), which measured about 290m x 80m in size. The existing ground levels vary from +29mPD to +36mPD along the west boundary on TC Av. side, and from +19mPD to +26mPD along the east boundary on the KCR and Kowloon Tong (KT) Station side. In order to cope with the aerial height restriction requirements and to achieve the development potential allowed under the condition of sale of the site, there is 4 levels of basement and 3 levels of semi-basement in the development, with the deepest level being some 36m below TC Av. Completely decomposed granite was encountered at ground level, with the presence of many corestones. Rockhead on the TC Av. side varied between 6m to 65m deep. At the northern portion of site, bedrock was very close to the surface, but sloping downward to about 60m deep near the KT Station. The MTR tunnels run directly through the center of the site, thus confined the geometrical design of the sub-structure. As a result, the lowest excavation levels to the north and south of the tunnels are at -1mPD and +8mPD respectively, with the section above the MTR tunnels not exceeding +13mPD so as to ensure at least 3m cover above the tunnel structures.

Site Formation and diaphragm wall construction

The site formation contract required the contractor to excavate and remove the soil material on the terraced site from averaged +34.5mPD on TC Av. side down to +19.5mPD on the KT Station side. This involved initially a total of about 180,000 cu m of excavation.
To support the sides of the excavation, a 1.2m thick diaphragm wall was constructed around the site perimeter as well as along the MTR tunnels as a cut-off between the basement and the tunnel structure. The walls generally extended to the rockhead, which varied between 6m and 65m below ground level. Due to the shallow-laying of bedrock, the toe of the diaphragm wall in many locations were formed well above the final formation level of the basement. Underpinning works to extend the wall down to the final level were thus required, which would be carried out in parallel with the construction of the top-down basement in the following contract.

Since chiseling was not allowed within 10m of MTR tunnels, "stitch drilling" was being used to overcome underground obstructions before the forming of the diaphragm walls. This was done by drilling a series of 450mm diameter holes in row, so that any boulder or corestone could later be cut into fragments small enough to be removed by grab. Site formation works were in general phased from the north to south. The main reason was to maintain an entrance/exit point, which situated at the south-western corner of the site, for the removal of the overall 460,000 cu m excavated spoil efficiently during the course of the site formation and basement construction processes.

Phasing and Removal of Spoil

Site formation works were carried out in roughly 6 phased, unsymmetrical sections, according to the convenience of cutting and dividing of the complicated building layout with construction jointings. The main strategy in the scheduling of site formation was to have the northern portion completed as the earliest possible, so that this portion could hand over to the main contractor for the construction of the basement and superstructure. The reason is straight forward, a circular ramp leading to the basement carpark is located here. With the circular ramp completed, it could be used as the access for vehicle to enter into the basement which constructed using top-down method. Without which, the last phase of formation on the southern tip of site could not be carried out in full scale. By that time, the only entrance/exit into the site was still in the southern tip.



Figure 5 – Entrance arrangement from ground level into the top-down basement.

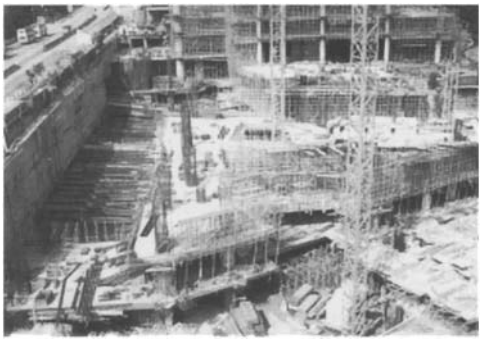


Figure 6 – A complicated junction where various major phasing sections of the superstructure and basement meet

Construction of the Basement Structure

Based on the initial formation level on +19.5mPD, there are 4 levels of full basement and 3 levels of semi-basement to be constructed. As for all top-down basement construction, the first floor plate to be constructed is important for it signifies the commencement of the basement work by providing the separating plate and lateral strut such that basement excavation can be started from there on. In this project, the first plate was located on the +19.5mPD level (Fig. 5). The basement construction also followed the 6-phased arrangement in conjunction roughly with the site formation sequences (Fig. 6). Instead of working with the basement and superstructure at the same time The superstructure was constructed in an advanced stage from the 1st and 2nd portions in staggered section onwards. This was to accommodate enough working room until the basement excavation could be started in a more efficient manner, as well as to allow the additional weight of the upper structure to balance the buoyancy effect during the excavation. With the first two to three levels of the top structure being maintained at its typical cycle, an entrance point to the basement below was then formed at the edge of position between portion 2 and 3.



Figure 7 – The portion of the basement slab located above the MTR tunnel tubes. Note the thickened slab serving as a transfer membrane spanning over the tunnel and the steel stanchion for the support of the basement structure during top-down construction



Figure 8 – The lateral support system erected during the basement excavation process to stabilize the existing MTR pedestrian entrance/ventilation shaft which is located on the right side of the photo

From this entrance point, excavation to the basement and the construction of the semi-basement structure above the +19.5mPD plate proceeded simultaneously according to the preliminary 6-phased arrangement, again, in staggered sections with the separation of carefully located construction jointing. For the lowest 4 levels of basement with headroom averaged at 3.2m that used as parking spaces for private car, part of which were excavated and constructed using a "Double Bit" method. This could produce a higher headroom such that excavation could be done using normal-sized excavating

machines, as well as to allow the entrance of dumping vehicles for removal of spoil. To provide the required protection to the MTR tunnels and to prevent heaving while large volume of soil was being removed, some of the basement slabs, especially those around the MTR tunnels, were deliberately thickened for the purposes (Fig. 7).

There were some locations where the progress of the basement construction works had been significantly interrupted. At the northern edge and the adjoining corner along the TC Av. where the rockhead was laying shallowly well above the final formation level of the lowest basement, the toe of the diaphragm wall panels had to be extended further downward until it reached the final level below the lowest basement. This was done by in-situ underpinning method. Sections of the diaphragm wall panels were constructed after the removal of the bedrock, layer by layer, with vertical junctions being connected by the provision of steel couplers. This section being interrupted measured about 100m. To allow for the continual progress to the upper structure and to stabilize the effect of isolating this part of the basement structure, a row of steel strut was erected, which provided the lateral support between the diaphragm wall and the base plate at the +19.5mPD level.

Another major area of interruption came from the works around the MTR pedestrian entrance and ventilation shaft. This sensitive structure was initially protected by a row of in-situ bore piles. A 4-layered temporary steel strut and shoring system was erected to stabilize the structure while excavation proceeded (Fig. 8).

CHEUNG KONG CENTER (Redevelopment of the previous Hilton Hotel)

The project situated in a 9,650m^2 site in the down-town area of Central. The new building is a 62-storey composite structure, with a 22m x 27m reinforced concrete inner core encased in a 47 m x 47m external steel frame, together with a 6-level basement that constructed over the 2-level old basement of Hilton Hotel.

Demolition and Foundation

The previous Hilton Hotel was to be demolished at the commencement of the project. After the site was cleared, the works that followed were the construction of the diaphragm walls and the bored foundation for the new building. All the diaphragm walls employed in the project were of 1.2m thick reinforced concrete. The perimeter walls helped to support and stabilize the ground during the construction of the new basement, as well as to act as the permanent basement wall. There was a 37m-diameter shaft pit formed in the middle of the site for the construction of the core wall for the future tower. Large diameter bored piles were used as foundation for the new building. The bored piles were basically in two standard sizes. Eight of the piles were 6m in diameter and dug manually for supporting the superstructure. 20 piles for the support of the 6-level basement structure were of 1.5m diameter and dug mechanically using grabs and chiselling method.

Forming a 37m-diameter shaft pit and the construction of the core wall

Before the carrying out of the basement construction using a top-down method, the first major work below ground was to construct the central core of the main building tower, the foundation of which rested on bedrock about –28m from ground level. Instead of constructing the central core in a top-down manner, the core was built bottom up. This could be done by the forming of a pit large enough to house the core structure and its foundation (Fig. 9). A pit was thus formed with the sides supported by panels of 1.2m-thick RC diaphragm wall. When the pit was excavated down to the required formation level, a 5m-deep RC raft was constructed as foundation for the core. The core wall on the lowest basement was constructed on top of the raft (Fig. 10).



Figure 9 – A 37m dia. shaft and eight 6.5m dia. manual-dug caissons were formed to construct foundation raft for the 62-storey building



Figure 10 – The construction of the core wall using a jump-form system inside 37-m dia. shaft.

Construction of the basement

After the completion of the bored piles, steel stanchion was erected on top of each pile at its formation level as support to the basement slabs during the construction process using a top-down sequence. In order to allow the core wall and the structural frame to proceed to a safe separating distance, the ground floor slab was cast after the core wall had been completed up to the 9^{th} level. With the temporary diaphragm wall that formed the 37m-diameter shaft gradually being demolished, the basement slab bound by the 8 super-columns was cast and connected to the core wall structure as soon as a stage of excavation completed. This made the basement structure at the center very rigid and from thereon, excavation to the sides continued, with the central part acting as a base to shore-support the newly excavated sides (Fig. 11). The floor system in the basement was of flat slab design with dropped panel around column heads. Average slab thickness was 400mm.

As a means to expedite the progress in the basement construction, the "double-bit" method was adopted (Fig. 13). The principle of this method is to have 2 levels of the basement excavated at a same time. At the bottom of the excavated, then cast the slab of the lower basement. And from this level, usual floor form would be erected and have the upper basement slab cast afterward. The basement further below would be repeated using the same principle. Temporary shores were installed in certain positions to stabilize the sides due to the depth of the excavation in the double bit. To facilitate the removal of large volume of excavated materials, several temporary openings were formed on the basement slab so that the excavated soil could be removed by lifting grabs, excavating machines or dumper truck entering into the basement through temporary ramp within the basement (Fig. 12).



Figure 11 – Center portion of the basement acting as a base to support the excavated sides during the top-down process.



Figure 12 – One of the openings formed inside the basement slab for the purpose of spoil removal. Temporary ramp would be erected in this opening to allow dumping vehicles entering into the basement for the purpose.



Figure 13 – Another openings for spoil removal. The construction of the intermediate slab using "Double Bit" method can be observed.

CONCLUSION

Besides the 3 cases as referred to in this paper, there are countless other similar basement projects being executed recently in Hong Kong. A brief summary listing some of the commonality of these projects can be drawn as a conclusion to finalize the discussion here.

- Basements of this kind are usually very big (say up to 10,000m^2) and very deep (below 20m).
- Majority of the basements are constructed in a top-down manner. Some other methods such as combining top-down and bottom up, or combining open-cut and top-down arrangement, can sometimes be seen.
- Complicated coordination problems and teething arrangement often exist between various major contracts or other major building works.
- Layout planning especially in phasing and sectioning of the job forms a very important consideration mastering the success of the project.
- Dynamic layout arrangement is usually required for the removal of the excavated spoil from the basement. This may involve the forming of temporary ramp, provision of special equipment, or the taking over of part of the completed building as temporary access in an advanced stage.
- Diaphragm walling is the most common cut-off provision being used.
- System formwork can hardly be applied for most basement jobs due to access problems as well as the confined working condition inside the excavated.
- Constructing the basement in "double bit" arrangement is becoming common.
- Protection and safety measures in particular to the life and property of third parties are highly concerned in basement jobs. Accident in this area is maintained at a relatively very low rate.
- Progress of work can hardly be predicted or monitored accurately due to the existence of numerous unforeseeable problems during the construction process.

From the investigator's point of view the suggestion to improve such situations may be quite simple. Engineers and builders in Hong Kong should have sufficient experience in handling these kinds of complicated basement jobs. Enhancement in the following areas may be simple and straight-forward solutions to improve the performance of such projects.

- Spend more resources to improve house-keeping works on site (e.g. better ventilation, lighting, access provision or tidier working place, remember it is working within basement).
- Lengthen the duration of the construction period where possible. Differences between fast track and quality should find a balance.
- Improve planning and supervision quality, other than just rely on software and log record.

As for most construction jobs, technicality is often the least of the problem. On the other hand, human factors, planning and management concerns are the most determining issues in reality. This is even more factual for basement project.

REFERENCE

RAMOND W M WONG, A Review on Common Technology Employed for the Construction of Buildings in HK, 1st International Structural Engg & Construction Conference, Hawaii, USA, 2001.

RAMOND W M WONG, Construction of a Semi-buried Building – A Super-sized Shopping Mall: The Festival Walk, Megacities 2000 Conference, Dept. of Architecture, University of HK, 2000.

DAVID SCOTT & GOMAN HO, Design and Construction of 62-Storey Cheung Kong Center, Symposium on Tall Bldg Design & Construction Technology, Beijing, 1999.

M J TOMLINSON, Lateral Support of Deep Excavations, Proceedings of The Institution of Civil Engineers, 1970.

G N GILLOTT AND JAMES C K LAM, Construction of Site Formation and Foundation Works in Building Projects, Building Construction in Hong Kong, Building Departments, HKSAR, 1998.

G J TAMARO, Deep Foundations in the Urban Environment, Habitat and the High-Rise, Council on Tall Building and Urban Habitat, Dutch Council on Tall Buildings, Amsterdam, 1995.

This Page Intentionally Left Blank

Advances in Building Technology, Volume I
M. Anson, J.M. Ko and E.S.S. Lam (Eds.)
© 2002 Elsevier Science Ltd. All rights reserved

NOVEL THREE-STEP CONSOLIDATION METHOD TO ELIMINATE FOUNDATION SOIL LIQUEFYING

Min Xie, Zhengxun Xie

Nanjing Gulou Town Construction Develop Company,
Nanjing, 210016, China

ABSTRACT

This paper introduces a novel three-step method to consolidate liquescent foundation soil. The three steps are: first, drain the ground water to lower the underground water level by drilling well points; second, inject clay solutions into the soil through these well points, drain water again, and repeat this process several times; third, use machine to tamp the ground by shocking and compressing. The key to this method: before the first step is carried out, a thin waterproof wall of clay concrete is to be built around the foundation plane. Because all the materials (clay solutions and low-grade concrete) used in this technology are very cheap, the engineering cost is lower than, and the efficiency higher than, those of the usual consolidation methods, such as the heavy tamping (dynamic compaction) method, the sand or granulate stone compaction stake method, dry jet mixing method, etc.. The safety and reliability of this method has also been proved. In Haikou city (Hainan China), there is a real project example, in which the liquescent foundation soil has been consolidated by this novel method. The geological features of the project area are very bad due to the three geological faults. The geological formation there is composed of soft clay and loose sand, and high underground water level of this area makes the situation even worse. Despite all these difficulties, the consolidation method has been successfully applied.

This paper is organized in 5 parts:

(1) Background of the researching subject
(2) Basic principles of the method
(3) The detailed measures taken (consolidation scheme)
(4) A real project example
(5) Conclusions

KEYWORDS

Foundation, Liquefying, Water Flow Consolidation, Clay Solution Cementing, Compressing Consolidation

1. BACKGROUND OF THE RESEARCHING SUBJECT

There're many similarities between the Los Angeles Earthquake (Jan. 1994, USA) and the Kobe-Osaka Earthquake (Jan. 1995, Japan). The hypocenters were located directly beneath both cities, and both earthquakes caused horrible damage. What troubled the earthquake experts most was not the collapses of those modern buildings, but the extensive destruction of major expressways, rail lines, and bridges, etc. Without the availability of roads, the rescue work was hard to carry out, and thousands of lives were lost because of the delay. In the Kobe-Osaka Earthquake, the expressway system along the area of Kobe, Osaka and Nagoya was severely destroyed, and nearly half of Japan's economy was paralyzed, causing great loss. Consider the reasons why the expressways were damaged so greatly. In several places, the geological structures are really bad, the cracking and sinking of the land is hard to resist, but these areas can sometimes be avoided in the reconstruction by proper layout and path selection. What threatens the road most is the liquefying of the road foundation over large areas. In construction practice, general methods such as the stake foundation method, the deep mixing method, and the transfer soil method are used to prevent foundation from liquefying. But these methods are very expensive and work consuming, which limit them from wide application. Even in those developed countries such as USA and Japan, engineers hesitate to apply these methods. Besides, in the region where underground water level is high and loose sand layer is thick, even if stakes are used to consolidate the foundation, the effects are still not satisfactory. The initial earthquakes will gradually liquefy the soil between stakes, subsequent major earthquake and following earthquakes will put down the stakes, thus invalidating the consolidation method. Currently, many scholars and engineers are trying to find the countermeasure to eliminate the liquefying of large areas of soil foundation. The author began to pay attention to this problem after reviewing the Kobe-Osaka Earthquake, and has made a breakthrough after several years of exploring,

2. BASIC PRINCIPLES OF THE METHOD

To prevent foundation soil from liquefying, the research must be based on the preconditions of soil liquefying. As is well known, the two preconditions are high underground water level, and low clay content in the sand. And the discriminant is as follows:

$$\begin{cases} N_{63.5} < N_{cr} \\ N_{cr} = N_O[0.9 + 0.1(ds - dw)]\sqrt{3/\rho_c} \end{cases} \tag{1}$$

Where:

$N_{63.5}$: Measured value of model penetration test for liquefying soil

N_{cr}: The critical number of model penetration test for liquefying soil, variable according to earthquake magnitude

N_O: The standard number of model penetration test for liquefying soil

ds: The depth of test point of penetration for liquefying soil (m)

dw: The depth of underground water level (m)

ρ_c: The percentage of clay particles

If the underground water level can be restrained, or the clay content of sand can be increased, then the critical number of model penetration tests N_{cr} can be greatly decreased, and the possibility of foundation soil liquefying will be eliminated. This is the most simple and most ideal method. Solely depending on increasing the density of foundation soil and enhancing the measured number of model penetration tests $N_{63.5}$, it is hard to eliminate foundation liquefying, and it is also not economic. For example, in coastal area, underground water level dw is about 2.0m. The practical depth of model

penetration test point of loose sand is set at 15.0m, and suppose the clay content of sand ρ_c is below 3%, then the computed critical number of model penetration test $N_{cr} = 2.2N_0 = 22$. But the surveyed $N_{63.5}$ of normal loose sand is mainly between 6 and 10, therefore, it is very difficult to acquire the ideal number of model penetration test (>22) by solely tamping and compressing, besides, the cost is very high.

If through the using of some techniques, the underground water level can be lowered, or even controlled forever, and the clay content can be increased from lower than 3% to 6%, then it is easy to meet the requirements for eliminating foundation liquefying. First, if the underground water level can be lowered or controlled forever, then the density of loose sand will be enhanced during the draining process, thus the number of model penetration test is increased. This is the procedure of water flow consolidation. Second, after the underground water level is lowered, then dw is close to ds, or even greater than ds, consequently outside the liquefying conditions, and the current N_{cr} is equal or smaller than N_o (set as 10). The number of model penetration tests can now be met with ease. Third, if ρ_c can be increased from lower than 3% to around 6%, then N_{cr} will be $N_o/\sqrt{2} = 0.7N_o$, and the number of model penetration test is easier to meet. The loose sand, which has been consolidated by the procedure of clay solution cementing, also contributes greatly to eliminating liquefying. At last, if the foundation soil is compressed by tamping and compressing, then it will be safer and liquefying is more reliably eliminated.

3. THE DETAILED MEASURES TAKEN (CONSOLIDATION SCHEME)

1) Build Waterproof Wall

To control the underwater level effectively, a waterproof wall must be built around the effective control area of the construction foundation. Theoretically speaking, a waterproof wall only need hold back water and not sustain load, therefore it can be built using cheap low-grade concrete. The thickness of the waterproof wall is approximately 600mm, depending on the convenience of construction, and its depth is determined by the desired control depth. Generally the wall should reach the waterproof layer below the loose sand layer. The construction materials are mixed with clay, coal fly ash and grits, and the intensity is about C5. If necessary, a little cement can also be added, so as to make low-grade concrete.

2) Drain Soil Water Through Well Points

Set well points on a 10.0m×10.0m grid, and drain water from the foundation soil through these well points.

3) Inject Clay Solution Into Well Points

Inject high pressure clay solution (can also be made from the drilling mud, or mixture of clay powder, coal fly ash and water) from the well points into the loose sand layer. The quantity of solution (clay content) are determined by different needs.

4) Drain Water Again

Drain the water again, so as to make the consolidation process and the cementing process simultaneous.

5) Tamping And Compressing By Machines

Tamping and compressing follows, in order to eliminate the holes and bumps in the crust surface.

6) Check And Approve

Check the project by a light penetration test and load test, obtain the survey data, compare with the design requirements, and then decide whether to accept or not.

4. A REAL PROJECT EXAMPLE

1) Project Information

A real application relates to the Chengli Fruit Vintage Factory, which takes up an area of 62,692.00m^2, and has a building area of 23,792.00m^2. For a light factory, the floor board load requirement is 250kPa.

2) Geological Conditions

The project is located in Fourth Period Alluvium. The area is geologically located in the triangle forward by the Qiongya big fault, the South Dujiang small fault, and the Qiongshan seismic belt. There are 10 layers in the soil from the surface to 15m below. The layers are thin, discontinuous, and appear interlaced. The sixth layer of silt is lentoid, and its thickness varies from 0 to 7.0m. The surveyed number of model penetration test $N_{63.5}$ of three loose sand layers was around 6.0; the underground water level is about 2.0m, and the stratum's allowable bearing strength fk varies from 70kPa to 210kPa, and there is no solid layer available to bear stakes.

3) Measures Taken

(1) Construct Waterproof wall:

Drill and place stakes (diameter of ϕ600), deep into the sixth and seventh layers (waterproof mud layer), The depth is 12.0m. Construct a waterproof wall using low-grade concrete, and its intensity is C5.

(2) Drain water through well points

Well points are set on a 10.0m$\times$10.0m grid, the diameter of well points is ϕ100, and depth 8.0m. The steel bar cage can be used repeatedly. If adopting the light well points drainage method, the cost will be even less.

(3) Inject clay solution

The clay solution is a mix of clay powder, coal fly ash and water. The quantity of the clay solution should make sure that the clay content of all the three sand layers reaches 6%.

(4) Tamping and compressing

A heavy bulldozer (more than 100kw) was used three times for compression.

(5) Quality control (The author will write a special summary on details of this subject)

(a) Underground water level check

(b) Number of model penetration test check, or take light penetration test and load test.

(6) Economic benefits

Compared with the tamping method, approximately ¥350,000 was saved. Compared with the rock filling stake method, ¥200,000 was saved; compared with the jet cementing method, the saving is approximately ¥2,760,000. What is the most important is that the reliability is superior to that of any other method, and the satisfactory results will be permanent.

5. CONCLUSIONS

1) Theoretical analysis and practical engineering trials prove that the three-step method, novel technique to eliminate foundation liquefying, is of the highest reliability, the easiest to carry out, and the cost is the most economic.

2) The research and improvements on the special instruments (high-pressure mud pumps, valves, squirt gun, and water pipes) will further promote the effectiveness of this method.

References:

1. Design code for Structure Foundation GBJ789
2. Seismic Design code of Building Structure GBJ11-89

This Page Intentionally Left Blank

CONSTRUCTION TECHNOLOGIES:

EARTHQUAKE ENGINEERING

This Page Intentionally Left Blank

Advances in Building Technology, Volume I
M. Anson, J.M. Ko and E.S.S. Lam (Eds.)
© 2002 Elsevier Science Ltd. All rights reserved

TESTING OF A TRANSFER PLATE BY PSEUDO-DYNAMIC TEST METHOD WITH SUBSTRUCTURE TECHNIQUE

A. Chen[1], C.S. Li[1], S. S.E. Lam[1] and Y.L. Wong[1]

[1]Department of Civil and Structural Engineering, The Hong Kong Polytechnic University

ABSTRACT

A pseudo-dynamic testing system is developed with the incorporation of the substructure technique. Newmark-α method is used to perform the numerical integration. The pseudo-dynamic system has been implemented to study the seismic response of a transfer plate in a 18-story high-rise building. Structural system comprises a transfer plate at the first floor with evenly spaced columns below, and shear walls above the transfer. A test specimen in ¼-scale was used to model the ground floor, transfer plate and the second floor. All the upper stories were simulated numerically. Pseudo-dynamic tests were conducted using three types of time-history records. When subject to an El-Centro earthquake record with maximum acceleration at 32%g, the shear wall remained undamaged whereas the transfer plate was severely damaged. The experimental study has indicated that the transfer plate system has insufficient strength to resist possible strong earthquake action.

KEYWORDS

Pseudo-dynamic test method, Substructure, Experiment, Transfer plate, Seismic, Time-history, High-rise building

INTRODUCTION

Pseudo-dynamic test method is an experimental technique for simulating the time-history response of structural members. It combines the realism of shaking table tests with the economy and convenience of quasi-static testing. Compared with the shaking table test, it has many advantages. It enables the testing of large-scale specimens. This is especially important for reinforced concrete members as we can observe the propagation of cracks and progress of failure. Concentrated mass can also be easily assumed, whereas in the shaking table tests additional loading blocks have to be used. In the last thirty years, many researches have been conducted to develop this method. Among others, Mahin and Shing (1985) and Takanashi and Nakashima (1987) have provided detail description of the method. Nakashima *et al* (1992) have also developed a system capable of performing real-time pseudo-dynamic tests. Development in recent years has already made the pseudo-dynamic testing method a reliable experimental tool. To facilitate the testing

of a multi-degree-of-freedom system, a pseudo-dynamic testing system was developed and verified (Chen *et al* 2000). It is the objective of this study to extend the capability of the system to include the substructure technique. The newly developed system is also used to study the seismic response of a transfer plate system when subject to the earthquake action.

SUBSTRUCTURE TECHNIQUE

Equilibrium condition of a dynamic system is expressed while considering inertia force, damping, resistance and applied force as

$$Ma + Cv + R = f \tag{1}$$

M and C are the mass and damping matrix respectively. f is the applied load vector. a and v represent the acceleration and velocity vector respectively. Using the substructure technique, the resisting force R can be separated into two components.

$$R = r + \overline{K}d \tag{2}$$

r is the experimental component to be modeled by the test specimen. $\overline{K}d$ is the analytical component to be simulated numerically (Nakashima *et al* 1990). $\overline{K}$ is the stiffness matrix and d is the displacement vector.

In a pseudo-dynamic test, the applied load f is expressed in the form of a time-history record. As a result, Equation (1) has to be solved using an integration scheme. Newmark Method was first introduced to provide accurate and stable solution (Mahin and Shing, 1985). Shing *et al* (1991) applied implicit time integration, whereas Bursi *et al* (1994) introduced an integration scheme with adaptive time steps. In this study, a Newmark-α method (Hilber *et al* 1977) is used to perform the numerical integration. For a general multi-degree-of-freedom system and without substructure, algorithm of the pseudo-dynamic test can be expressed in the following form.

$$Ma_{i+1} + (1+\alpha)Cv_{i+1} - \alpha Cv_i + (1+\alpha)R_{i+1} - \alpha R_i = (1+\alpha)f_{i+1} - \alpha f_i \tag{3}$$

$$d_{i+1} = d_i + \Delta t v_i + \Delta t^2[(\frac{1}{2} - \beta)a_i + \beta a_{i+1}] \tag{4}$$

$$v_{i+1} = v_i + \Delta t[(1-\gamma)a_i + \gamma a_{i+1}] \tag{5}$$

The subscripts i and i+1 indicate two consecutive time increments at time t_i and t_{i+1} respectively. Δt is the time interval or $(t_{i+1}-t_i)$. α, β and γ are parameters governing numerical properties of the algorithm. To incorporate the substructure technique, Equation (3) is modified in considering Equation (2).

$$Ma_{i+1} + (1+\alpha)Cv_{i+1} - \alpha Cv_i + (1+\alpha)r_{i+1} - \alpha r_i + \overline{K}(1+\alpha)d_{i+1} - \overline{K}\alpha d_i = (1+\alpha)f_{i+1} - \alpha f_i \tag{6}$$

After some mathematical manipulation using Equations (4) to (6), we have

$$[\overline{M} + \Delta t^2 \beta \overline{K}(1+\alpha)]d_{i+1} = g_{i+1} - \Delta t^2 \beta (1+\alpha) r_{i+1} \tag{7}$$

Where

$$g_{i+1} = \overline{M}[d_i + \Delta t v_i + \Delta t^2(\frac{1}{2} - \beta)a_i] + \Delta t^2 \beta[(1+\alpha)f_{i+1} - \alpha f_i - Cv_i - (1+\alpha)(1-\gamma)C\Delta t a_i + \alpha r_i + \overline{K}\alpha d_i] \quad (8)$$

and

$$\overline{M} = M + (1+\alpha)C\Delta t\gamma \quad (9)$$

Equation (7) represents an implicit expression, since r_{i+1} depends on d_{i+1}. An iterative solution procedure is implemented in the manner described as follows.

Considering an approximate solution at iteration k,

$$[\overline{M} + \Delta t^2 \beta \overline{K}(1+\alpha)]d_{i+1}^{(k)} = g_{i+1} - \Delta t^2 \beta(1+\alpha)r_{i+1}^{(k)} + e_{i+1}^{(k)} \quad (10)$$

Here, the superscript k represents the results obtained from the k^{th} iteration. Assuming a converged solution is obtained at iteration k+1,

$$[\overline{M} + \Delta t^2 \beta \overline{K}(1+\alpha)](d_{i+1}^{(k)} + \Delta d_{i+1}^{(k)}) = g_{i+1} - \Delta t^2 \beta(1+\alpha)(r_{i+1}^{(k)} + \Delta r_{i+1}^{(k)}) \quad (11)$$

$\Delta d^{(k)}_{i+1}$ and $\Delta r^{(k)}_{i+1}$ are the corrections at the k^{th} iteration. Subtracting Equation (11) from Equation (10), we obtain the displacement corrections $\Delta d^{(k)}_{i+1}$.

$$K^* \Delta d_{i+1}^{(k)} = -e_{i+1}^{(k)} \quad (12)$$

with

$$K^* = \overline{M} + \Delta t^2 \beta(1+\alpha)K' + \Delta t^2 \beta(1+\alpha)\overline{K} \quad (13)$$

K' and $\overline{K}$ are stiffness matrices of the test specimen and the analytical component respectively. Improved solution at the end of the k^{th} iteration is given by

$$d_{i+1}^{(k+1)} = d_{i+1}^{(k)} + \Delta d_{i+1}^{(k)} \quad (14)$$

$$r_{i+1}^{(k+1)} = r_{i+1}^{(k)} + \Delta r_{i+1}^{(k)} \quad (15)$$

The iterative procedure is repeated until all the corrections are less than the tolerance. The pseudo-dynamic test continues with progressive increase in the time domain, t ,via the time increment Δt.

TEST SPECIMEN OF A TRANSFER PLATE SYSTEM

Figure 1 shows a high-rise building having 17 typical floors and a single story podium. Structural system at typical floors comprises a simple shear wall system with no lintel beams connecting the shear walls.

Floor slabs are 160mm thick. The shear walls are supported by a 1500mm thick transfer plate, and below the transfer are evenly spaced columns of 900mm square. The high-rise building has been designed according to non-seismic provisions.

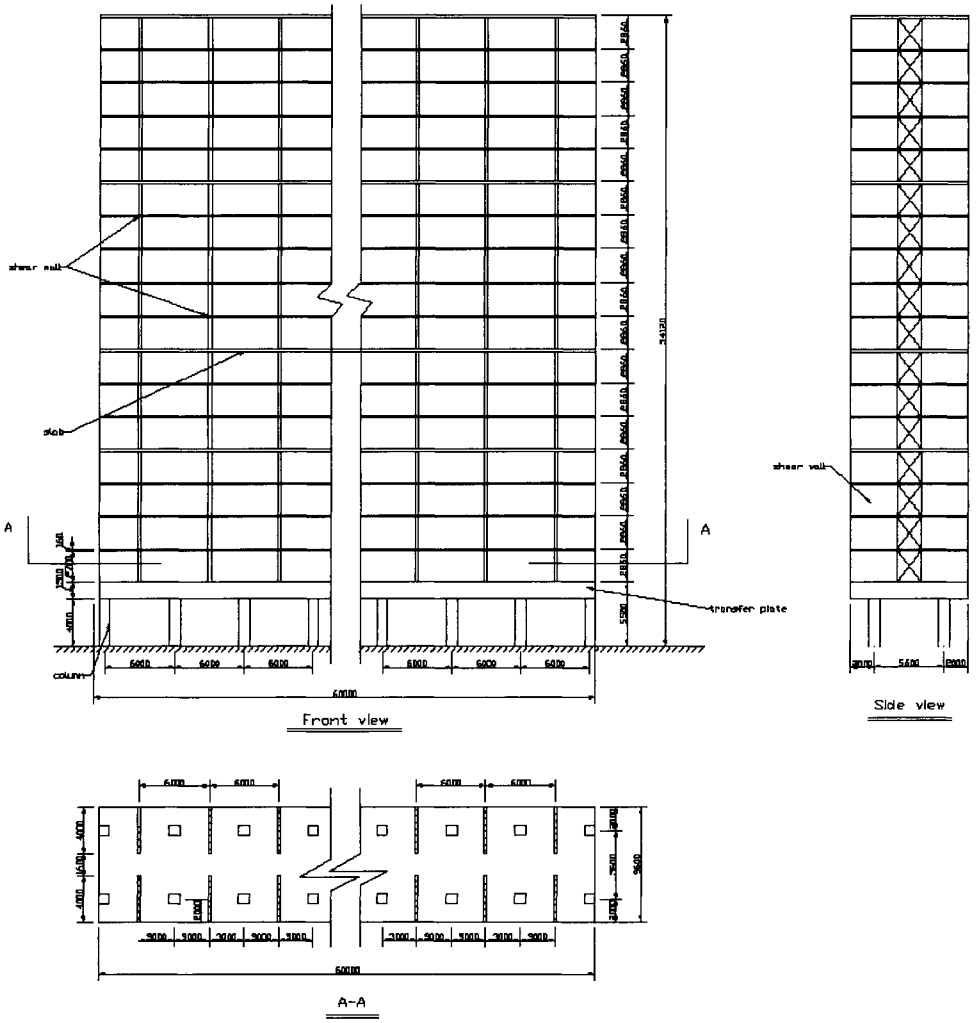


Figure 1. 18-story building with a transfer plate at the first floor.

In applying the pseudo-dynamic test method with substructure technique, upper stories of the high-rise building were simulated numerically as shown in Figure 2. A ¼-scale specimen was fabricated to represent the transfer plate and second floor of the building. Further simplifications were made in considering symmetries of the structure in both directions. Lateral displacements were applied at the first

and second floors through two actuators. Normal strength concrete with maximum aggregate size at 10mm was used and the measured cube strengths f_{cu} are tabulated in Table 1. High yield deformed bars (f_y=460MPa) and mild steel bars (f_y=250MPa) were used for the main reinforcement and links respectively. To prevent the columns from failure before the transfer plate, the columns were strengthened by epoxy-grouting.

Table 1. Measured cube strength of concrete.

Member	Cube strength (MPa)
Columns	42.9
Transfer plate	41.1
Shear wall	32.9
1st floor slab	32.9

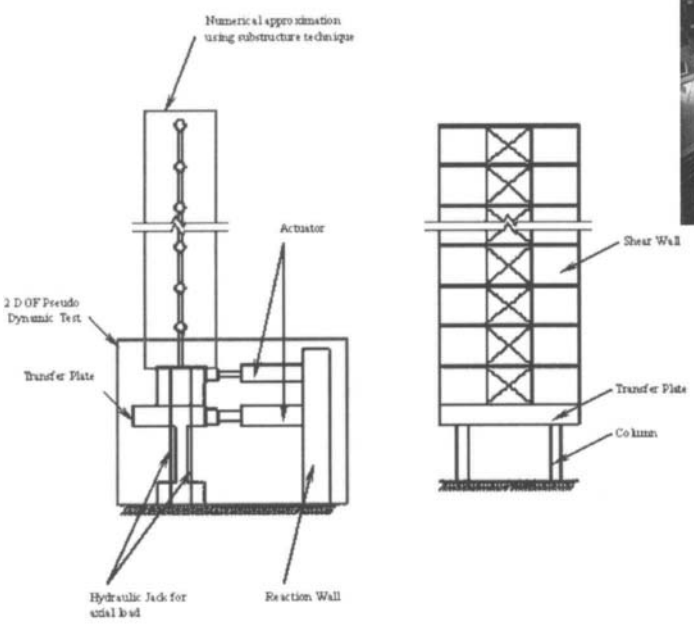


Figure 2. Setup of the pseudo-dynamic test

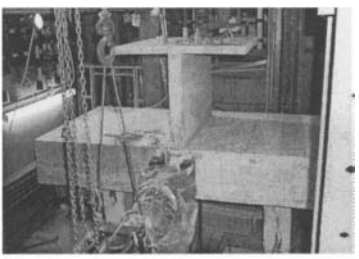


Figure 3. Test specimen

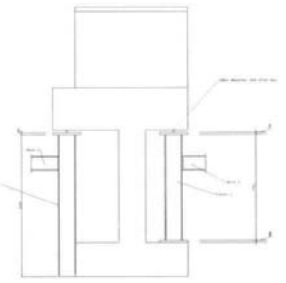


Figure 4. Roller supports

Figure 3 shows the test specimen. Strain gauges were installed to measure the strains in the reinforcements and concrete. Displacement transducers were installed to record the deformations. Constant axial loads acting on the transfer plate and the columns were applied through two manually controlled hydraulic jacks. To restrain rotation of the transfer plate during application of the lateral displacements, four steel columns

were used to act as roller supports as shown in Figure 4. The roller supports were installed after the application of the axial loads.

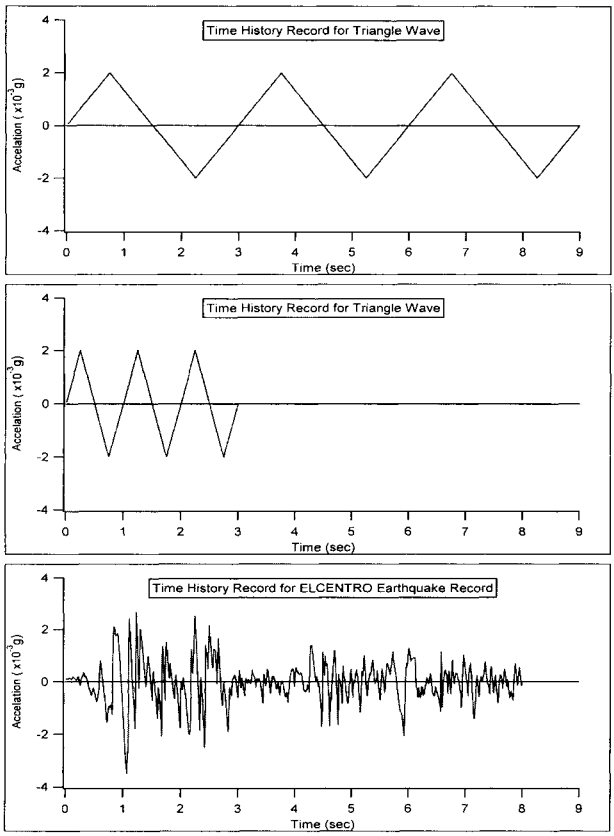


Figure 5. Time-history records

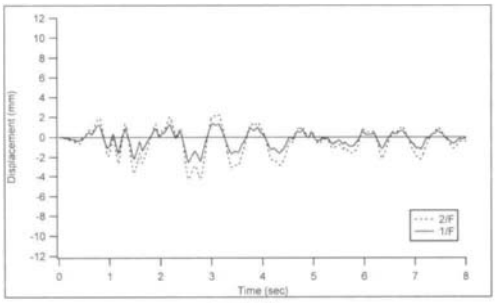
To estimate the initial stiffness at the two floors of the test specimen, lateral displacement was applied to one of the floors while the actuator at the other floor was fixed against any lateral movement. All the upper floors were assumed to have the same stiffness as the second floor, and were simulated numerically via substructure technique. Damping ratio of all the floors was assumed to be at 5%.

In simulating the seismic action, three types of loading histories were considered as shown in Figure 5, namely triangular waves and the El-Centro earthquake record. All the records were compressed according to the similitude rule. The two triangular waves were used to estimate response of the transfer plate within the elastic range. Finally, a series of El-Centro earthquake records with increasing magnitude of acceleration was applied.

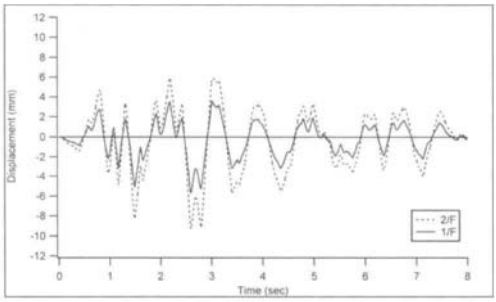
EXPERIMENTAL RESULTS AND DISCUSSIONS

Figure 6 shows the lateral displacements at the transfer level ("1/F") and the second floor ("2/F") when subject to the El-Centro earthquakes with maximum acceleration at 16%g and 32%g. The two responses at 16%g and 32%g are virtually in proportional to each other. There appears to be no appreciable change in the lateral stiffness of the two floors. In the course of the experiment, no crack was observed on the shear wall. This indicates that the responses were generally elastic.

Figure 7 shows the deflection at the centre of the transfer plate when subject to the El-Centro earthquakes with maximum acceleration at 16%g and 32%g. There was substantial increase in the central deflection.

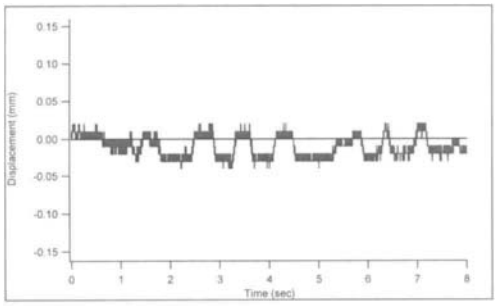


(a) 16%g

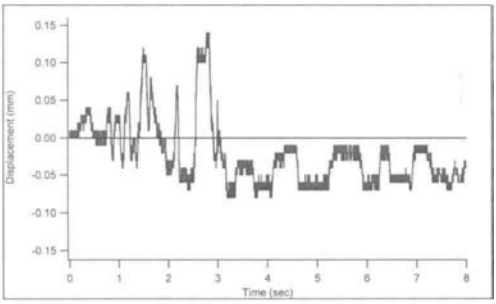


(b) 32%g

Figure 6. Lateral displacement at the 1/F and 2/F when subject to El-Centro earthquakes



(a) 16%g



(b) 32%g

Figure 7. Deflection at the center of the transfer plate when subject to El-Centro earthquakes



Figure 8. Cracking pattern viewed from below

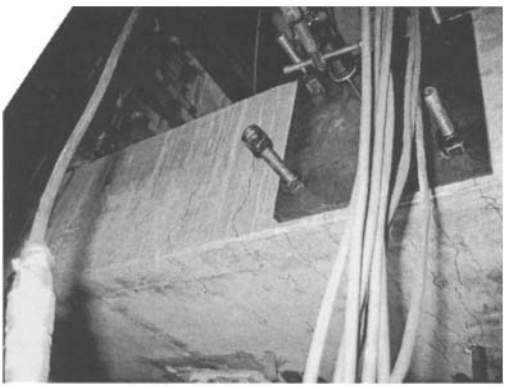


Figure 9. Cracking pattern viewed from one end

When subject to 32%g earthquake, there was considerable cracking at the bottom of the transfer plate at the vicinity below the shear wall. Figures 8 and 9 show the cracking patterns at the bottom of the transfer

plate. All the cracks are flexural in nature and propagated along the length of the shear wall. It is worth noticed that at the initial application of the axial force through the hydraulic jacks, some cracks were also found at the bottom of the transfer plate. In general, when the maximum acceleration of the earthquake increased, new cracks were observed with more extensive coverage.

CONCLUSIONS

A pseudo-dynamic testing system is developed to examine the seismic performance of a transfer plate. Newmark-α method is used to perform the numerical integration and substructure technique is applied. A test specimen in ¼-scale was used to represent lower stories of a 18-story building. Pseudo-dynamic tests were conducted using three types of time-history records. Test results have indicated that the shear walls remained elastic throughout the loading histories, whereas the transfer plate was severely damaged when subject to an El-Centro earthquake record with a maximum acceleration at 32%g. The experimental study has indicated that the transfer plate system has insufficient strength to resisting strong earthquake action.

ACKNOWLEDGEMENT

The writers are grateful for the financial support from the Research Grant Council of Hong Kong through a RGC research grant (RGC no: PolyU 5026/98E) and The Hong Kong Polytechnic University (Project no: G-V853).

REFERENCES

Bursi, S.O., Shing P.S.B. and Zorica R.G. (1994). Pseudodynamic Testing of Strain-softening Systems with Adaptive Time Steps. *Earthquake Engineering and Structural Dynamics*, **23**, 745-760.

Chen A., Lam S.S.E. and Wong Y.L. (2000). Verification of a pseudodynamic testing system. *Proceedings of the Int. Conf. on Advances in Structural Dynamics*, Hong Kong, **2**, 851-858.

Hilber H.M., Hughes T.J.R. and Taylor R.L. (1977). Improved Numerical Dissipation for Time Integration Algorithm in Structural Dynamics. *Earthquake Engng & Structural Dynamics*, **20**, 283-292.

Mahin, S.A. and Shing P.S.B. (1985). Pseudodynamic Method for Seismic Testing. *J. St. Eng. ASCE*, **111(7)**, 1482-1503.

Nakashima et al (1990). Integration Technique for Substructure Pseudodynamic Test. *Proceedings 4th US National Conference Earthquake Engineering*, Palm Springs, CA II, 515-524.

Nakashima M., Kato H. and Takaoka E. (1992). Development of Real-time Pseudodynamic Testing. *Earthquake Engineering and Structural Dynamics*, **21**, 79-92.

Shing P.B. and Mahin S.A. (1984), *Pseudodynamic Test Method for Seismic Performance Evaluation: Theory and Implementation*, University of California, Berkeley, California, USA.

Shing, P.B., Vannan M.T. and Cater E. (1991). Implicit Time Integration for Pseudodynamic Tests. *Earthquake Engineering and Structural Dynamics*, **20**, 551-576.

Takanashi K. and Nakashima M. (1987). Japanese activities on on-line testing. *J. Eng. Mech. ASCE*, **113**, 1014-1032.

Advances in Building Technology, Volume 1
M. Anson, J.M. Ko and E.S.S. Lam (Eds.)
© 2002 Elsevier Science Ltd. All rights reserved

SEISMIC DESIGN AND INELASTIC SEISMIC RESPONSE OF LUMPED MASS MDOF DUAL STRUCTURE*

Jie Jing[1], Lieping Ye [1], Jiaru Qian[1]
[1]Department of Civil Engineering, Tsinghua University, Beijing 100084, China

ABSTRACT

Based on the concept of seismic control, dual structure systems aiming at improving the shortcoming of traditional seismic structures was proposed for seismic design model by the second author. The seismic design performance objectives at different earthquake levels were previewed first in this paper. Under small earthquake and moderate earthquake levels, the elastic response spectrum method and equal cyclic energy criteria are adopted respectively to determine the parameters of the secondary structure in the dual seismic structure system. The inelastic seismic response under the severe earthquakes showed that the structure designed based on the suggested method had a suitable seismic performance.

KEYWORDS

Seismic design, dual structure system, energy concept, inelastic seismic response, performance objective levels

INTRODUCTION

In traditional seismic structure, the demand for the structure stiffness, stability, energy absorption ability is usually satisfied by the structure itself, which results in an uncertain seismic performance, especially the damage and inelastic deformation of some important structure elements are very serious under moderate and severe earthquakes and the repairing expense may be very high. With the development of seismic control method, researchers proposed the concept of Damage Controlled Structures (DCS) (J.J.Connor, et al, 1997), which makes use of the energy dissipation of secondary

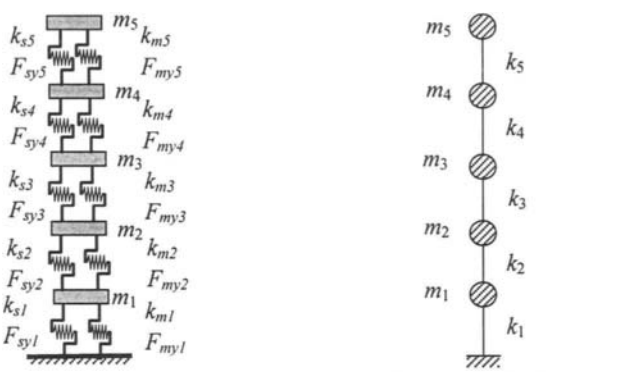
* This research is supported by Chinese national natural science foundation. No. 59895410.

structure to protect primary structure (original structures) and reduces the repairing expense. After Kobe earthquake, the design using DCS became a trend (Akira Wada, et al, 1997). In the new version Chinese Building Seismic Design Code (CBSDC: GB50011-2001), the energy dissipation building structure is adopted.

Recently, the performance-based seismic design had become widely accepted. The structure seismic performance should be designed or predicted for different earthquake levels. But the current seismic design code does not suggested. In CBSDC: GB50011-2001, element design and the limit elastic story drifts are demanded at the small earthquakes level, while reinforcement detailing requirements are presented to prevent collapse of the structure.

The second author of this paper put forward the concept of dual seismic structure system, which is used as the design model for passive controlled seismic structure. In dual seismic structure system, primary structure withstands loads at service limit state; secondary structure dissipates earthquake input energy (L.P. Ye, 2000).

This paper is focused on the seismic design based on the performance-based design concept for lumped dual seismic MDOFS structures with middle-long initial period, i.e. $T_g<T_0<5T_g$, where T_0 is the initial period of the structure, T_g is the site predominant period. The elastic response spectrum method is adopted to determine the stiffness of secondary structure under small earthquake, while equal cyclic energy criteria is adopted to determine yielding strength of secondary structure under moderate earthquake. The seismic performance of the structure under severe earthquakes is calculated to check the design results.



(a) Dual structure (b) Corresponding single structure

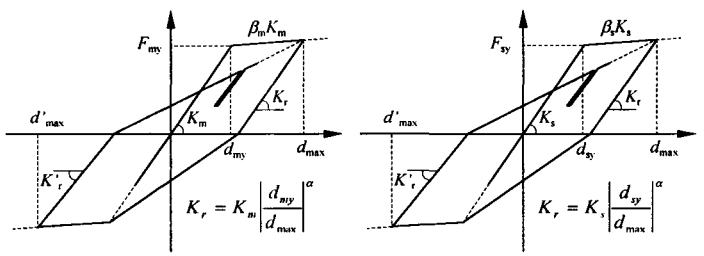
Figure 1: Analysis model

DUAL SEISMIC STRUCTURE SYSTEM AND ITS SEISMIC OBJECTIVES

Analysis Model and Parameters

The analysis model for dual seismic structure system used in this paper is shown as Figure 1(a). Figure

1(b) shows the corresponding single structure model, in which the structure parameters is same as the primary structure in the dual structure. The main parameters of the model are: (1)The mass distribution is uniform along height (m_i=m); (2)The story initial stiffness is uniform (k_{si}=k_s, k_{mi}=k_m); (3) The Clough degraded bilinear hysteresis model (Figure 2), which is fit for reinforced structures, is adopted both for primary structure and secondary structure. In the hysteresis model, the post-yielding stiffness equals to zero, and the degraded stiffness factor α equals to 0.4; (4). Mass proportional Damping is considered in analysis, the damping coefficient h=0.05m. Elcentro NS, Hachinohe NS and Kobe NS earthquake records are used for excitation input. Considering the earthquake design level 8° in CBSDC: GB50011-2001, the peak acceleration A_{max} takes 70Gal, 200Gal and 400Gal corresponding to small, moderate and severe earthquakes, respectively. The elastic and inelastic time history analysis was based on program package CANNY developed by K. N. Li.

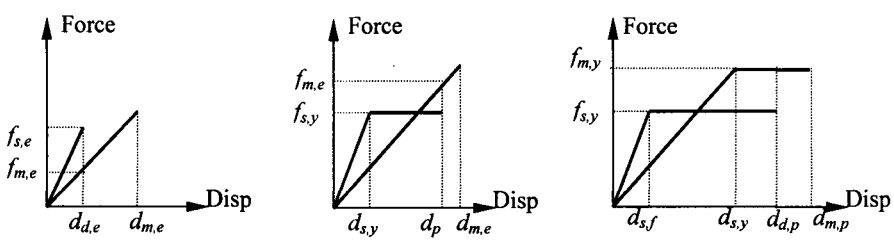


(a) Hysteresis model of primary structure (b) Hysteresis model of secondary structure

Figure 2: Hysteresis model

Seismic Objectives of DUAL STRUCTURE SYSTEM

According to the seismic demand under different earthquake levels, the seismic performance objectives of primary and secondary structure for dual structure are suggested as: (1) Primary and secondary structure remain in elastic stage at small earthquake level (Figure 3(a)). (2) Secondary structure yields but primary structure remains elastic or just reaches yielding critical state at moderate earthquakes level (Figure 3(b)). (3). Under severe earthquakes, primary and secondary structure are both in inelastic stage, but the damage of the secondary structure is some more serious than the primary structure (Figure 3(c)).



(a) under small earthquake level (b) under moderate earthquake level (c) under severe earthquake level

Figure 3: Seismic objectives of dual structure system

SEISMIC DESIGN OF DUAL STRUCTURE SYSTEM

Definition of Structural Parameters

$d_{m,e}$: maximum elastic displacement of the corresponding single structure at small and moderate earthquakes levels;

$d_{d,e}$: maximum elastic displacement of dual structure at small earthquake level. It is chosen as seismic objective for dual structure under small earthquake;

$d_{d,p}$: maximum displacement of dual structure at moderate earthquakes level. It is chosen as seismic objective for dual structure under moderate earthquake;

$F_{m,e}$: maximum elastic force response of the corresponding single structure under small and moderate earthquakes;

$F_{d,e}$: maximum elastic force response of dual structure system under small earthquake, $F_{d,e}=f_{m,e}+f_{s,e}$;

$f_{m,y}$: yielding strength of primary structure;

$f_{s,y}$: yielding strength of secondary structure;

T_m: initial period of the corresponding single structure;

T_d: initial period of the dual structure;

K_m: equivalent elastic stiffness of the corresponding single structure or primary structure in dual structure;

K_s: equivalent elastic stiffness of secondary structure in dual structure;

α_K: stiffness ratio of secondary structure to primary structure, $\alpha_K=K_s/K_m$;

α_d: maximum displacement ratio of dual structure to the corresponding single structure at small earthquake level, $\alpha_d=d_{d,e}/d_{s,e}$;

η_d: maximum displacement ratio of dual structure to the corresponding single structures at moderate earthquake level;

$\alpha_{s,f}$: ratio of yielding strength of secondary structure to the maximum elastic force response in the corresponding single structure;

μ_s: equivalent ductile factor of secondary structure, i.e. the ratio of the maximum displacement of dual structure to the yielding displacement of secondary structure;

The displacement Response of DUAL STRUCTURE SYSTEM at small earthquake level

Based on the elastic response spectrum method of CBSDC: GB50011-2001, the displacement response can be determined as:

The corresponding single structure,

$$d_{m,e}=\frac{F_{m,e}}{K_m}=\frac{\alpha_1\cdot G_{eq}}{K_m}=\frac{\left(\frac{T_g}{T_m}\right)^{0.9}\alpha_{\max}G_{eq}}{K_m} \tag{1}$$

Dual structure,

$$d_{d,e}=\frac{F_{d,e}}{K_m+K_s}=\frac{\left(\frac{T_g}{T_d}\right)^{0.9}\alpha_{\max}G_{eq}}{K_m+K_s} \tag{2}$$

The maximum displacement ratio α_d can be determined as:

$$\alpha_d = \frac{d_{d,e}}{d_{s,e}} = \left(\frac{K_m}{K_m + K_s}\right)^{0.55} = \left(\frac{1}{1+\alpha_K}\right)^{0.55} \tag{3}$$

From above Eqn.3, the stiffness K_s of the secondary structure can be obtained as,

$$K_s = \left(\left(\frac{1}{\alpha_d}\right)^{\frac{1}{0.55}} - 1\right) \cdot K_m \tag{4}$$

The relationship between the story stiffness k and structure equivalent stiffness K is shown in Eqn.5. Because the corresponding single structures and dual structure system are both lumped structures, following relation can be obtained,

$$\frac{k_s}{k_m} = \frac{K_s}{K_m} \tag{5}$$

Thus, with the known α_d, the stiffness ratio α_k can be expressed as:

$$\alpha_k = \frac{k_s}{k_m} = \frac{K_s}{K_m} = \left(\frac{1}{\alpha_d}\right)^{\frac{1}{0.55}} - 1 \tag{6}$$

TABLE 1
CALCULATION EXAMPLES UNDER SMALL EARTHQUAKE LEVEL

α_d	Stories	α_K(Eqn. 6)	$d_e \cdot \alpha_d$ (CANNY)	$d_e \cdot \alpha_d$ (Predition)	Difference (%)
0.7 (ElcentroNS T_0=1.05s)	1	0.9127	5.586mm	6.542mm	-14.6
	2		5.423mm	6.042mm	-10.2
	3		5.055mm	5.235mm	-3.4
	4		4.052mm	4.444mm	-8.8
	5		2.450mm	2.883mm	-15.0
0.8 (KobeNS T_0=1.439s)	1	0.5004	11.54mm	11.376mm	1.4
	2		9.938mm	10.16mm	2.2
	3		8.455mm	8.2mm	3.1
	4		7.418mm	6.806mm	9.0
	5		4.31mm	4.454mm	-3.2
0.9 (HachinoNS T_0=1.82s)	1	0.2111	9.626mm	8.951mm	7.5
	2		8.24mm	7.989mm	3.1
	3		8.027mm	7.328mm	9.5
	4		7.125mm	7.526mm	-5.3
	5		4.724mm	5.231mm	-9.7

Table 1 shows the comparison of prediction displacement response based on above design method to time history analyzed results for the dual structure at small earthquake level. Three initial period structures are analyzed: 1.05s, 1.439s and 1.82s. The design objective is chosen as α_d=0.7, 0.8 and 0.9, respectively. It could be seen that the difference between the prediction and analyzed results is acceptable for practical design.

The displacement Response of DUAL STRUCTURE SYSTEM at moderate earthquake level

Known from Figure 3(b), primary structure remains elastic while secondary structure yields under moderate earthquake level. Based on equal cyclic energy criteria proposed by the second author (L. P. Ye, 2001), the energy dissipation capacity of secondary structure of dual structure equals to the energy dissipation demand of the corresponding single structures. The derivation is:

E_D, the dissipated energy demand for secondary structure for displacement objective $\eta_d d_{m,e}$ of dual structure:

$$E_D = (1-\eta_d)\cdot d_{m,e}\cdot\frac{1}{2}\cdot(\eta_d F_{m,e} + F_{m,e}) = \frac{1}{2}(1-\eta_d{}^2)F_{m,e}d_{m,e} \tag{7}$$

E_C, energy dissipation capacity of secondary structure:

$$E_C = f_{s,y}\cdot\frac{f_{s,y}}{K_s}\cdot\frac{1}{2} + f_{s,y}(d_{d,p} - d_{s,y}) + 4\beta\cdot f_{s,y}(d_{d,p} - d_{s,y}) \tag{8}$$

Where β, the hysteresis energy dissipation factor, usually equals to 0.33 for RC structures. Let Eqn.7=Eqn.8, following result can be obtained:

$$\alpha_{s,f} = \frac{1-\eta_d{}^2}{(4.64 - 3.64/\mu_s)\eta_d} \tag{9}$$

Based on above Eqn.9, the ratio of yielding strength $\alpha_{s,f}$ will be obtained when μ_s and η_d is given.

Figure 4 gives the response results comparison of dual structure system under the moderate earthquake for μ_s=2 and varying displacement objective ratio η_d. It could be seen from Figure 4 that the average analyzed results have a reasonable agreement with prediction value of the suggested method.

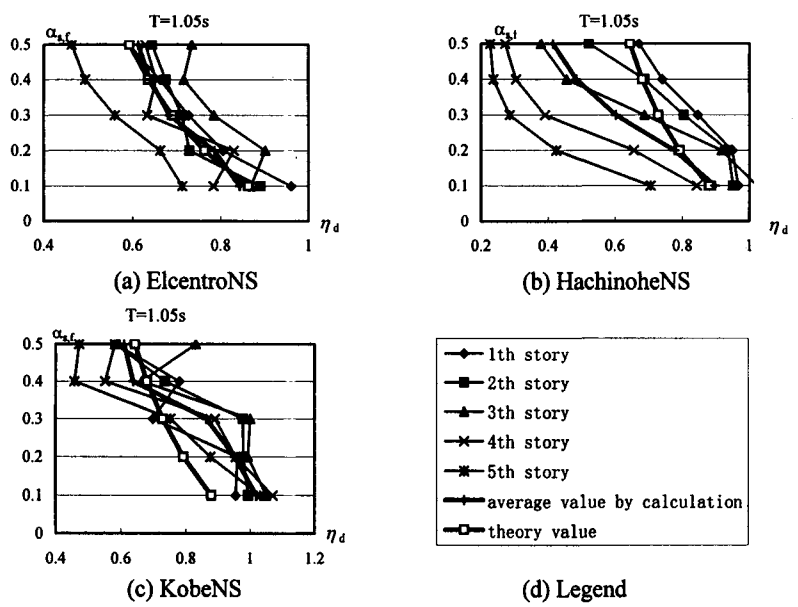
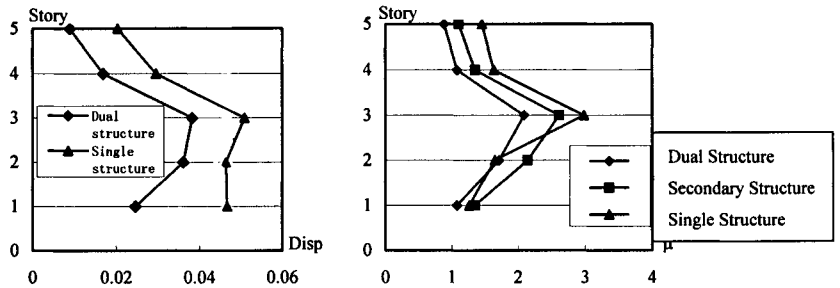


Figure 4: the effects of dual structure system under the moderate earthquakes

THE MAXIMUM INELASTIC RESPONSE OF DUAL STRUCTURE SYSTEM UNDER SEVERE EARTHQUAKE LEVEL

Based on the stiffness and yielding strength determined under the small and moderate earthquake levels previously, displacement responses of dual structure, with the design parameters α_K=1.25, $\alpha_{s,f}$=0.4 and μ_s =2, under the severe earthquake level are shown in Figure 5(a). Compared with the corresponding single structure, the story displacement response was reduced about 16~40%. Figure 5(b) shows the ductility factors. It can be seen that the ductility factor of primary structure was much decreased compared with the corresponding structure. And the ductility factor of secondary structure was within a reasonable value and also some smaller than that of the corresponding structure.



5(a) Displacement 5(b) Ductile factor μ

Figure 5: the effects of dual structure system under the major earthquakes

CONCLUSIONS

The following conclusions are obtained based on suggestion and analysis of this paper:

(1) It is available adopting dual structure system to resist earthquakes.

(2) The stiffness K_s of secondary structure can be determined by elastic response spectrum at the design objective of small earthquakes.

(3) The yielding strength $f_{s,y}$ of secondary structure can be determined by equal cyclic energy criteria at moderate earthquake level.

(4) The structural performance under severe earthquakes level is acceptable when the objective parameters are properly chosen.

REFERENCE

Akira Wada, et al. (1997). Seismic Design Trend of Tall Steel Buildings After the Kobe Earthquake, Japan

National Standard Building Seismic Design Code operating panel. (2001). *Building Seismic Design Code*. GB50011-2001, Beijing

Jie Jing. (2000). Applications in High-rise Buildings about Dual Seismic Structure Systems, *16th Structural Proceedings of Tall Buildings*, Shanghai, China

J.J.Connor, et al, (1997). Damage-Controlled Structures. I: Preliminary Design Methodology for

Seismically Active Regions, *Journal of Structural Engineering*, 1997.4, 423-431
L.P. Ye. (2000). Dual Seismic Structure Systems, *Building Structure*, 2000.4
L.P. Ye. and S. Otani. (1999) Maximum Seismic Displacement of Inelastic Systems Based on Energy Concept, *Earthquake Engineering and Structure Dynamics*, 1999 (6), 1483-1499
L.P. Ye. et al. (2001). Equal cyclic energy criteria and its application in the seismic and damping design. *The 5th Chinese-Japanese Structural Technique Communion*, 515-522, Xi'an, China
SEAOC Vision 2000 Committee. (1995). Performance-based Seismic Engineering, *Report Prepared by Structural Engineering Association of California,* Sacramento, California, U.S.A

Advances in Building Technology, Volume 1
M. Anson, J.M. Ko and E.S.S. Lam (Eds.)
© 2002 Elsevier Science Ltd. All rights reserved

SEISMIC ASSESSMENT OF LOW-RISE BUILDING WITH TRANSFER STRUCTURE

J.H. Li[1], R.K.L. Su[1], A.M. Chandler[1] and N.T.K.Lam[2]

[1] Department of Civil Engineering, The University of Hong Kong,
Pokfulam Road, Hong Kong, SAR, PRC
[2] Department of Civil & Environmental Engineering, The University of Melbourne,
Parkville, Victoria 3052, Australia

ABSTRACT

An overview of the structural performance of a transfer structure in Hong Kong under potential seismic actions is presented. A hypothetical but realistic low-rise building model has been developed with 7 storey reinforced concrete frame structure and reinforced concrete transfer beams at first floor. Structural design has been based on the British Standard BS8110 and local practices. Parametric analyses of the moment-curvature relationship of each component have been conducted. By adopting the displacement-based (DB) approach, various seismic assessment methodologies, including response spectrum analysis (RSA), manual calculation and pushover analysis (POA) have been carried out. The deformations induced by the predicted seismic actions in Hong Kong are compared with those arising from POA in terms of average lateral drift ratios and maximum inter-storey drift ratios of the building. Factors influencing the performance of transfer structures are highlighted and discussed. This paper also provides a general indication of seismic vulnerability of common low-rise transfer structures in regions of low to moderate seismicity.

KEYWORDS

Earthquakes, wind, transfer, low-rise buildings, spectral, displacement, drift, soil

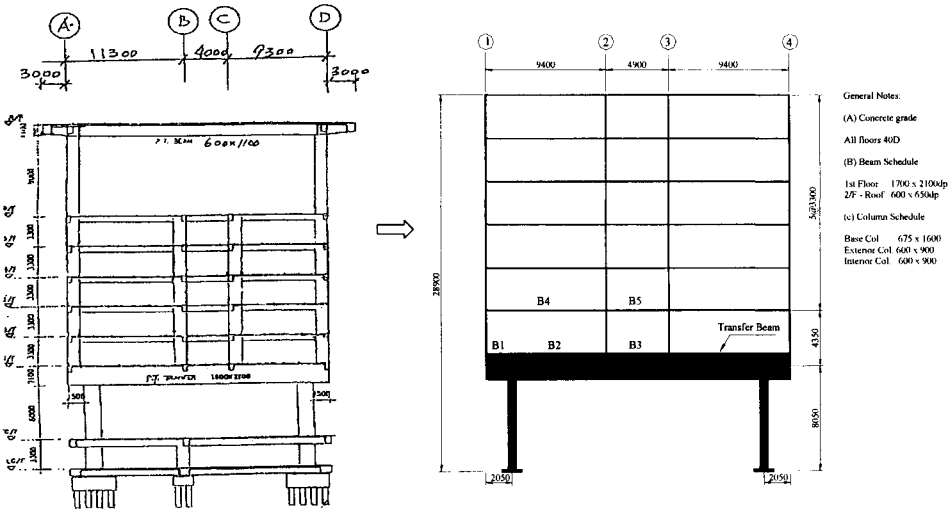
INTRODUCTION

Unlike other countries, transfer structures are widely used in Hong Kong, for both low-rise and high-rise buildings, in order to provide flexibility in different architectural or commercial usages above and below the transfer structures. As for low-rise transfer buildings, column type structures above the transfer structures (usually transfer deep beams) are transferred via the beam to the column type structures below. It is, however, well known by seismic engineers (Scott *et al.*, 1994, Pappin *et al.*, 1999) that under cyclic earthquake loads, concentrated stresses and large lateral displacement demands may occur at a locations where there is significant change in stiffness. Critical review of the design and construction practices of those kinds of transfer structures is urgently required. In the present study,

static pushover analysis for the idealised transfer structure in Hong Kong has been carried out to identify the critical failure mechanism and to determine the pre- and post-elastic load-displacement behaviour of the structure. A displacement-based procedure has been used to assess the capacity of the structure to accommodate the strength and displacement demand generated by the soil surface response.

STRUCTURAL DETAILS OF THE 7 STOREY TRANSFER BEAM BUILDING

A hypothetical but realistic two-dimensional 7 storey reinforced concrete structure model (as shown in Figure 1) has been developed with reference to a Hong Kong school building. This model is a low-rise framed structure of 28.9m high, 23.7 width and 6 floors with a transfer beam (TB) in its first floor. Base columns are assumed to be fully fixed at ground level. Detail schedules of columns and beams are shown in Figure 1. The idealized building has been designed for the distribution of loads given in Table 1 and the design wind load derived in accordance with the Hong Kong Wind Design Code for a 50 year Return Period. It is found that the design is controlled by the loading combination case with respect to dead load and live load only. From the distribution of moments, axial forces, and shear forces generated by program ETABS Version 7.22 (Habibullah *et al.*, 1999), designs of those beams above 1st floor and between gridline ① and gridline ② are the same as B4 (see Figure 1b), those above 1st floor and between gridline ② and gridline ③ are the same as B5 (see Figure 1b).



(a) Hong Kong School Building (b) Design Model

Figure 1: Example transfer building

DUCTILITY CAPACITY OF COLUMNS AND BEAMS

The moment curvature analyses for columns and beams have been conducted using the computer program RESPONSE (Collins *et al.*, 1997). The results indicate that at ultimate axial loading condition, the columns including the base columns and the frame columns have nearly reached their design ultimate inelastic strength, whilst the beams still have a large range of curvature ductility. Therefore columns are likely to be more vulnerable than beams under certain loadings. The idealized moment curvature relationship for the base columns at ultimate axial loading, utlised for the subsequent push over analysis, is shown in Figure 2. This 675 x 1600 rectangular column is reinforced along the section by 6 layers of totally 28 nos. 40mm diameter high tensile steel reinforcement. The column is confined

by 10mm diameter circular hoops at a uniform spacing of 300mm centres. An independent check (based on Priestley, 1995; Priestley & Calvi, 1997; Kowalsky *et al.*, 1995) has been undertaken to assess the limiting curvatures in base columns, which gives the ultimate curvature ϕ_u of value 5 rad/1000 m, and the effective (notional) yield curvature ϕ_y of value 2 rad/1000. This leads to a curvature ductility of 2.5, which is in good agreement with the results from the RESPONSE analysis. For the limitation of the length of the paper, only the result of Moment-Curvature relationship of base column has been shown in graphical form (see Figure 2). The detailed results of all columns and beams have been given in Table 2.

TABLE 1
DISTRIBUTION OF LOADS

Load		Roof Level		Typical Floor		1st Floor	
UDL	DL	68		53		120	
(kN/m)	LL	8		11		11	
Point	Gridline	DL	LL	DL	LL	DL	LL
Load at	①	282	35	212	53	212	53
Each	②	429	54	322	80	322	80
Floor	③	429	54	322	80	322	80
(kN)	④	282	35	212	53	212	53

Note: DL = Dead Load, LL = Live Load

SEISMIC ASSESSMENT OF BUILDING

Modified lateral stiffness of the building

It is not straightforward to determine the actual stiffness of reinforced concrete as it depends on a number of factors including the dynamic stiffening, aging, steel ratio and extent of cracks in concrete under tensile loads. Typical elastic modulus of concrete can be determined either from codes of practice or from uni-axial compressive test at 40% and 10% of ultimate axial load, respectively (Lee *et al.*, and BSI, 1985). In addition, the elastic modulus of reinforced concrete may be slightly increased by 10% to 20% due to the presence of reinforcement. It was pointed out by Priestley (1998) and by Priestley and Kowalsky (1998) that section stiffness may not be considered as a fundamental section property. The stiffness of the section would be altered by changes in axial load ratio or flexural reinforcement content, due to the non-linear behaviour of the reinforced concrete and the variation of the effective sectional area for cracked sections. The stiffnesses of vertical members have therefore been modified herein, under ultimate conditions, with the factors applied to the stiffness of column and beam being 0.8 and 0.5, respectively. These factors were derived according to design values presented in the above references, modified appropriately to allow for the relatively low levels of seismic displacement demand. The natural periods are 1.40sec, 0.43sec, and 0.25sec for mode 1, mode 2, and mode 3, respectively.

Ductility and drift demand of the building

Response spectra analysis based on the modal superposition method is restricted to linear elastic analysis. This analysis can simulate the maximum response of joint displacements and member forces due to a specific ground motion loading without carrying out the lengthy integration process. There are computational advantages in using the response spectrum method of seismic analysis for prediction of displacement and member forces in structural systems. The method involves the calculation of only the maximum values of the displacement and member forces in each mode using smooth design spectra that are the average of several earthquake motions.

By using the modified stiffness model as well as assuming 5% and 3% viscous damping, a detailed response spectrum analysis (RSA) was implemented herein using the computer package ETABS (1999). Rock and soil acceleration response spectra (shown in Figure 3) as used in the RSA were generated by Sheikh (2001) based on the Shau Kei Wan reclamation site with soil depth of 52m, for different return periods, near-field and far-field events. It is found that the 2500-year return period far-field event is the critical case affecting the structures. Therefore only the corresponding drift results for the building will be presented in the following sections due to the limitation of the length of this paper.

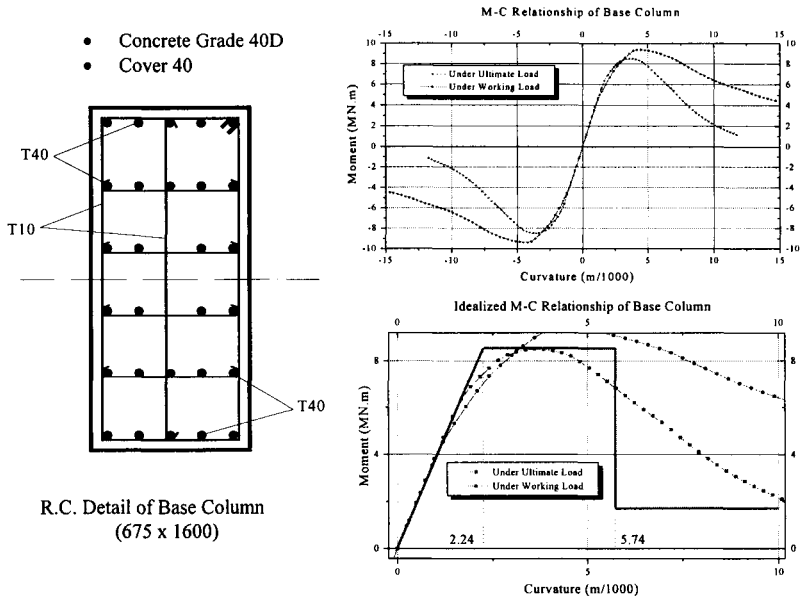


Figure 2: Idealized moment curvature relationship

TABLE 2
SUMMARY OF THE MOMENT-CURVATURE ANALYSES

Member (refer to Figure 1)	Load Condition	Effective (notional) Yield Curvature ϕ_y (rad/1000 m)		Ultimate Yield Curvature ϕ_u (rad/1000 m)		Curvature Ductility Ratio ϕ_u/ϕ_y		Ultimate Moment Capacity (MNm)	
Columns									
Base	Ultimate Axial Load (=17MN)	2.24		5.74		**2.56**		8.0	
Exterior	Ultimate Axial Load (=7MN)	4.2		9.82		**2.34**		2.0	
Interior	Ultimate Axial Load (=7MN)	3.77		9.07		**2.41**		1.7	
Beams									
	Axial Force	Positive	Negative	Positive	Negative	Positive	Negative	Positive	Negative
B1	0	1.5	2.03	19.76	22	13.17	10.84	1	12.46
B2	0	2.34	1.91	15.84	22.49	6.77	11.77	42.34	23.31
B3	0	2.68	13.76	7.07	22.51	2.64	1.64	37.33	3.61
B4	0	8.36	9.48	92.16	27.43	11.02	2.89	0.836	1.68
B5	0	6.0	6.0	76.67	76.67	12.78	12.78	0.18	0.18

Note: The R.C. arrangements of columns and beams are symmetric and asymmetric, respectively, about their principal geometric axes.

The elastic seismic displacement demand profiles determined by RSA are shown in Figure 4b, and corresponding interstorey drift ratios are shown in Figure 5. Comparisons of the results for one mode only with those for all modes indicate that higher mode effects can be ignored when analyzing the low-rise building. The maximum seismic roof displacement is 144mm and gives a 1/200 average drift ratio. At effective height, taken according to Priestley (1995) as 0.75h, the displacement demand computed as determined by RSA is 108mm giving an effective drift ratio of 1/268. The displacement at TB level is 16mm and gives the drift ratio in base column of 1/500.

The displacement spectrum at a notional 5% critical damping is normally provided from seismic hazard studies. However Wong (2000) and Su *et al.* (2002) find that damping value for typical buildings in Hong Kong is approximately 0.5-0.7%. Considering the moderate shaking intensity for a 2500-year earthquake event in Hong Kong, 3% damping ratio might be taken for the RSA of buildings in Hong Kong. Therefore for this case, the displacement demand is multiplied with a scale factor of around 1.2. The revised displacement demand and drift demand of 3% damping are shown in Figure 4b and Figure 5, respectively.

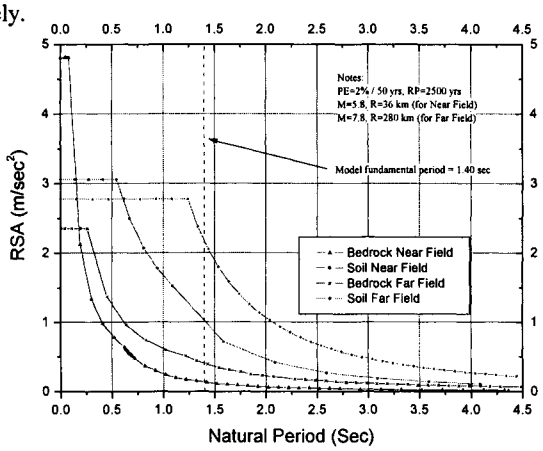


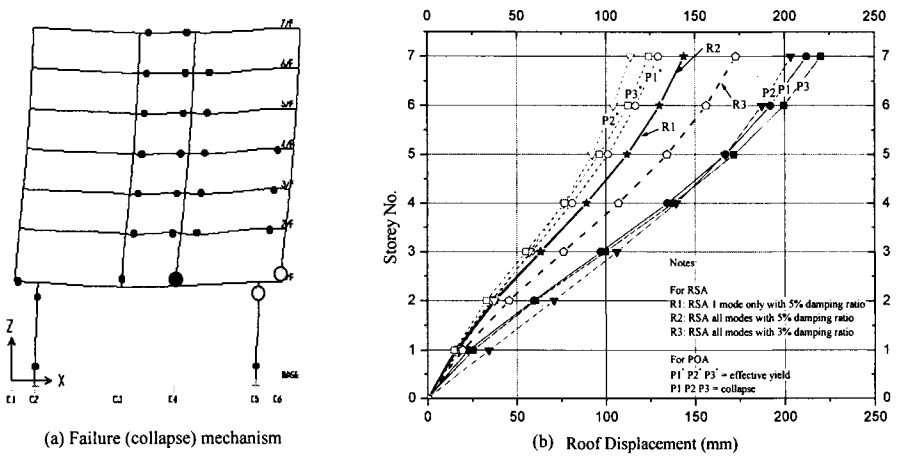
Figure 3: Response spectral acceleration (5% damping) for Hong Kong rock and soil sites

Overall ductility and drift capacity of building

As an alternative to manual calculation, the displacement capacity of building structures as a whole may be obtained by static POA (Calvi and Pavese, 1995; Park, 1996; Krawinkler and Seneviratna, 1998; Mwafy and Elnashai, 2001). POA is a simple tool for evaluating the behaviour of structures responding into the inelastic range under lateral loading. Essentially, a lumped mass single-degree-of freedom (SDF) system is created and under lateral loading the correct ratio of its mass and initial stiffness is determined such that initial period of vibration matches the fundamental natural period of vibration of the original multi-degree-of-freedom (MDOF) model. The initial natural period matching will automatically result in the response displacement time-histories at any point on the MODF structure that is proportional to that of the SDOF model, provided that the response is governed by a single fundamental mode. The linear and nonlinear behaviours are sensitive to the chosen pattern of lateral load. The load patterns adopted may not give good estimates of dynamic interstorey drift ratios over the entire height, since different load patterns may induce different localized yield mechanisms in a structure, and furthermore the demands will depend on the frequency characteristics of the ground motion and hence determine which, if any, of those localized mechanisms will activated and amplified in an earthquake. Bearing in mind the above considerations, it is herein recommended that three load patterns are selected for carrying out such POA. The first loading pattern (P1) is determined by iteration such that its shape is proportional to the deflections shape of the building throughout the elastic range of response. The second load pattern (P2) attempts to capture the soft storey effect and

provides an essentially constant loading above the TB level, being linearly decreased to zero from the TB to ground level. The third load pattern (P3) attempts to capture the higher mode effects and is proportional to the SRSS combination interstorey shear obtained from RSA discussed above.

Program ETABS (Habibullah *et al*, 1999) has been used to accomplish the POA described above. The roof displacement profiles at effective (notional) yield limit and ultimate limit are shown in Figure 4b, and interstorey drift ratios at each stage are shown in Figure 5. It is found that the ultimate roof displacements, which are sensitive to different load patterns, range from 204mm to 220mm, and those at TB level range from 23mm to 34mm. Load pattern (P2) gives the smallest ultimate roof displacement capacity, but gives the largest displacement at TB level. Pattern (P3) gives the smallest value of 23mm at TB level, which is in very close agreement with the value 22mm predicted by hand calculation for ultimate axial load. The displacement ductility capacity for all load patterns is rather low and less than 2. This indicates that selecting only one load pattern as the POA is not enough to predict the critical case, and hence two patterns (P2 and P3 described above) are recommended. Displacement at effective height is 157mm at ultimate condition.



(a) Failure (collapse) mechanism

(b) Roof Displacement (mm)

Figure 4: Displacement profiles under different seismic loadings

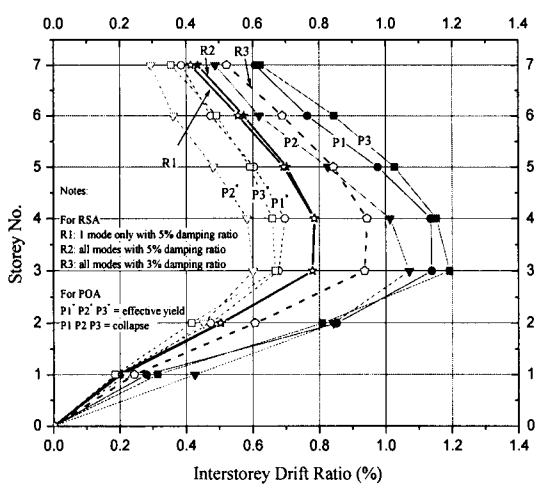


Figure 5: Interstorey drift ratios under different seismic loadings

Comparison of seismic demand with capacity

The comparison of the maximum interstorey drift demand and capacity over the entire height of the building is an effective way to identify any local distortional effect and hence any local overloading at particular floor levels. The RSA reveals that a relatively high seismic interstorey drift demand occurs at 3rd and 4th floor rather than at roof level, at effective height, or at TB level. The maximum lateral displacement demand at TB level as determined in the RSA is 16mm corresponding to a 2500-year return period, far-field earthquake at soil site. The ultimate displacement capacity from POA is 23mm, which agrees well with the value of 22mm estimated by using manual calculation. When comparing the maximum expected seismic displacement demand with capacity, a safety margin of 1.4 can be found. Also the same safety margin value of 1.4 is attained when comparing the lateral displacement demands with the ultimate displacement capacities at roof level and effective height respectively. Hence the building has a relative low probability of ultimate collapse in the form of a soft storey failure under seismic action in Hong Kong. But the drift demand will exceed the smallest drift capacity by POA under P2 at the upper part of the building (see Figure 5) if we take the 3% as the analysing damping ratio, and therefore local damages (short span beams shown in Figure 4a) of the upper part of structure may occur.

It is found that all the displacement shapes from POA are similar to those predicted by RSA. This result matches with Krawinkler and Seneviratna (1998) who highlighted the fact that the deflection profiles obtained by POA and by dynamic analysis are closely correlated for low-rise structures. The results clearly reveal that the POA described above can produce reliable results for situations where higher mode effects are minor and the soft storey effects are slight.

CONCLUSIONS

This paper has provided, for the first time in Hong Kong, a rigorous and comprehensive structural seismic assessment of a typical low-rise transfer structure designed to local codes and practices.

The major conclusions of this study are as follows:

1. Design of a low-rise building in Hong Kong is controlled by dead load rather than wind load, which is different from the high-rise building. Therefore it is not meaningful when assessing the capacity of those types of building to simply compare the seismic displacement demand with those from the design wind load.
2. Structural seismic assessment for Transfer Structures in Hong Kong requires specific account to be taken of the acute lack of ductility arising in columns supporting the transfer beam (TB) as well as the frame columns above TB level. Failure mechanism (refer to Figure 4a) shows that the short spanned beams connecting columns are prone to form plastic hinges, and therefore reach this ultimate capacity and collapse finally. Concerns on the design of those beams should be given.
3. POA procedure is sufficient to assess the displacement capacity of a low-rise building since the deflection shapes produced match well with those from the RSA due to minor higher mode effects, whilst for high-rise building POA is not recommended (Su. *et al.*, 2001). It is also found that only one load pattern to predict the critical displacement and drift capacities of building is not enough. Two loading patterns, namely uniform loading pattern (P2) and SRSS loading pattern (P3), are recommended herein.
4. The acute lack of ductility of Hong Kong transfer structures, at both member and global levels indicates that the ratio of ultimate and notional yield displacement capacities (~2) is relatively low. The possibility of sudden brittle-type failures of those columns of such structures, under excessive seismic displacements, is therefore a matter of some concern.
5. Comparisons among those inter-storey drift ratios from various analyses indicate that detailed local checks are required when assessing the performance of a low-rise transfer building rather than only focusing concern on the roof level, the effective height level and the TB level.

6. The building has a low probability of ultimate collapse in the form of a soft storey failure under seismic action in Hong Kong when taking the damping ratio as 5%, but damages may occur at upper parts of the building (especially to short span beams) if the damping value is reduced to 3%.

ACKNOWLEDGEMENTS

The methodology described in this paper forms part of the outcome of a major strategic research programme to address seismic risk in Hong Kong. The Hong Kong programme, directed by the second and third authors, has been undertaken at the University of Hong Kong since 1998, as has received continuous funding from the Research Grants Council (RGC) under grants HKU7023/99E and HKU7002/00E. The authors wish to thank the RGC for their generous support.

References

Building Development Department (1983) *Code of Practice on Wind Effects: Hong Kong – 1983*, Government of Hong Kong, Hong Kong

British Standards Institution (BSI) (1985). *Code of Practice for Design and Construction* (BS8110 Part 2), *British Standard, Structural Use of Concrete.*

Calvi, G.M. and Pavese, A. (1995). Displacement Based Design of Building Structures. *European Seismic Design Practice*, Balkema, Rotterdam, 127-132.

Collins, M.P. and Mitchell D. (1997) *Prestressed Concrete Structures*, Response Publications, Canada.

Habibullah, A. (1999), *ETABS (version 7.22) Three Dimensional Analysis of Building Systems, User's Manual*, Computers & Structures Inc.

Krawinkler, H. and Seneviratna, G.D.P.K. (1998). "Pros and cons of a pushover analysis of seismic performance evaluation", Engineering Structures, **20**(4-6), 452-464.

Lee, P.K.K., Kwan, A.K.H. and Zheng, W. (2000). "Tensile strength and elastic modulus of typical concrete made in Hong Kong", *Transactions of Hong Kong Institution of Engineers*, **7**(2), 35-40.

Mwafy, A.M. and Elnashai, A.S. (2001). "Static pushover versus dynamic collapse analysis of RC buildings", *Journal of Engineering Structures*, 23(5), 407-424.

Pappin, J.W., Kwok, M.K.Y. and Chandler, A.M. (1999). Consideration of Extreme Seismic Events in the Design of Structures in Hong Kong. *Proceedings of Conference on Construction Challenges into the Next Century*, 98-105.

Priestley, M.J.N. (1995). Displacement-Based Seismic Assessment of Existing Reinforced Concrete Buildings. *Proceedings of the Fifth Pacific Conference of Earthquake Engineering*, Melbourne, 225-244.

Priestley, M.J.N. and Calvi, G.M. (1997). "Concepts and procedures for direct displacement-based design and assessment", *Proceedings of the Workshop on Seismic Design Approaches for the 21st Century,* June 1997, Slovenia.

Priestley, M.J.N. and Kowalsky M.J.(1998) Aspects of Drift and Ductility Capacity of Rectangular Cantilever Structural Walls, *Bulletin of the NZNSEE,* **31:4,** 246-259.

Priestley, M.J.N. (1998) Brief Comments on Elastic Flexibility of Reinforced Concrete Frames and Significance of Seismic Design, *Bulletin of the NZNSEE* , **31:4,** 246-259.

Scott, D.M., Pappin, J.W. and Kwok, M.K.Y. (1994) Seismic Design of Buildings in Hong Kong, *Transactions of the Hong Kong Institution of Engineers.* **1:2,** 37-50.

Sheikh, M.N. (2001). *Simplified Analysis of Earthquake Site Response with Particular Application to Low and Moderate Seismicity Regions, MPhil Thesis*, The University of Hong Kong

Su R.K.L, Chandler A.M, Lam N.T.K. and Li J.H. (2000) Motion induced by distant earthquakes: the assessment of transfer building structures. *International conference on Advances in Structural Dynamics (ASD2000)*, the Hong Kong Polytechnic University, **1**:249-256

Su R.K.L, Chandler A.M and Li J.H. (2002) *Dynamic testing and modeling of existing buildings in Hong Kong* (submitted to Transactions of HKIE)

Wong J.C.K. (2000) *Identification of non-linear damping of tall buildings by random decrement, PhD Thesis*, City University of Hong Kong, Hong Kong, PRC

Advances in Building Technology, Volume 1
M. Anson, J.M. Ko and E.S.S. Lam (Eds.)
© 2002 Elsevier Science Ltd. All rights reserved

ULTIMATE DRIFT RATIO OF NON-DUCTILE COUPLING BEAMS

Z.Q. LIU[1], S.S.E. LAM[2], B. WU[3] and Y.L. Wong[2]

[1]School of Civil Engineering, Harbin Institute of Technology, Harbin, China
[2]Department of Civil and Structural Engineering, The Hong Kong Polytechnic University, Hong Kong
[3]Department of Civil Engineering, South China University of Technology, Guangzhou, China

ABSTRACT

Seismic performance of coupling beams designed according to non-seismic provisions is examined. Coupling beam specimens in 1/4 scale were tested under cycles of end shear. Characteristics of the specimens include high main reinforcement ratio, about 3-4%, and large spacing of links with 90-degree hooks. Based on the test data, 140mm is recommended to be the optimal spacing of links. Furthermore, coupling beams must not be heavily reinforced. Since this would lead to substantial reduction in the displacement ductility and ultimate drift ratio. Finally, an empirical relationship is proposed to estimate the ultimate drift ratio of non-ductile coupling beams.

KEYWORDS

Reinforced concrete, Coupling beams, Seismic, Non-ductile, Ultimate drift ratio, Ductility

INTRODUCTION

Coupling beams are commonly used in high-rise buildings to link up the shear walls. Seismic performance of coupling beams has been an area of strong research interest (Paulay 1971). Paulay and Binney (1974) and Barney *et al* (1980) examined the use of diagonal bars as the main reinforcements. Tassios *et al* (1996) and Harries *et al* (2000) studied the performance of different types of coupling beams. However, there exists very few research studies related to the seismic performance of coupling beams designed according to non-seismic requirements. In our earlier study (Liu *et al* 2002), cyclic load tests were carried out on 5 coupling beam specimens designed according to non-seismic design requirements. Characteristics of the specimens include high main reinforcement ratio, about 3-4%, and large spacing of links with 90-degree hooks. As a result, such coupling beams are non-ductile with limited ductility. Subsequent to the earlier study, two new specimens were prepared and tested. It is the

objective of this study to combine our test data with those obtained by others to develop an empirical relationship to predict the ultimate drift ratio of non-ductile coupling beams.

EXPERIMENTAL SETUP

Two coupling beam specimens (specimens L-1 and L-2) in 1/4 scale were prepared and tested in this study. Reinforcement details of these two specimens were designed so that comparisons can be made with two other specimens (specimen L-A and L-D) reported in the previous study (Liu *et al* 2002). Figure 1 shows the reinforcement details. Furthermore, all the links used in the specimens have 90-degree hooks.

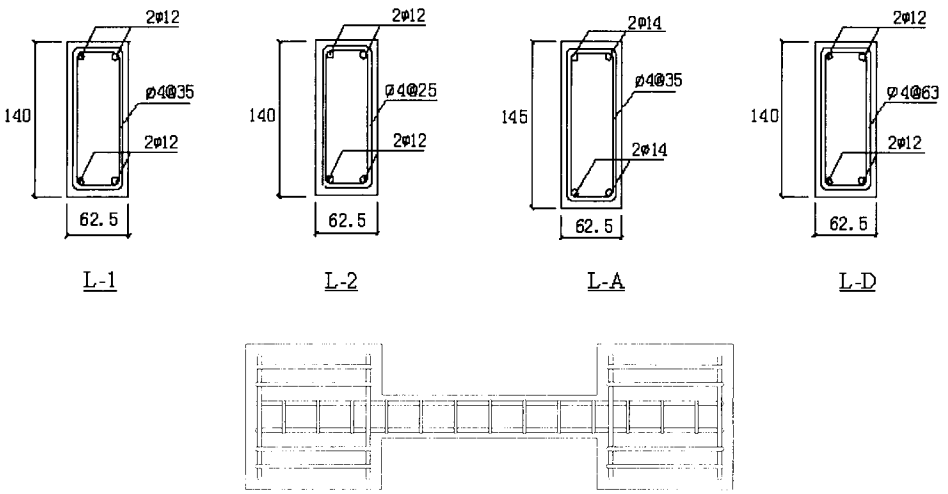


Figure 1. Reinforcement details of the specimens

Basic characteristics of the specimens are shown in Table 1. B, H, h and L are the breadth, overall depth, effective depth and clear span of a specimen. λ is the shear span ratio and is defined as half clear span divided by the effective depth of a specimen. A_{st} is the main reinforcement, and ρ is the amount of A_{st} expressed as a fraction of the cross-sectional area. Transverse reinforcement ratio is defined as A_{sh}/S_tB. A_{sh} is the total area of links in the transverse direction of bending and S_t is the spacing of links.

Table 1. Basic characteristic of the specimens

Specimen	BxH (mm)	h (mm)	L (mm)	λ	A_{st}	ρ	Links	A_{sh}/S_tB
L-1	62.5×140	124	750	3.0	2Φ12	2.92%	Φ4-2legs@35	1.15%
L-2	62.5×140	124	750	3.0	2Φ12	2.92%	Φ4-2legs@25	1.61%
L-A	62.5×145	128	750	2.9	2Φ14	3.85%	Φ4-2legs@35	1.15%
L-D	62.5×140	124	750	3.0	2Φ12	2.92%	Φ4-2legs@63	0.64%

Normal strength concrete with maximum aggregate size at 5mm was used in this study. The measured

average compressive strength f_{cu} of specimens L-1 and L-2 is 38.1MPa and 37.3MPa for specimens L-A and L-D. The measured yield strength and ultimate strength of the reinforcement are tabulated in Table 2. Φ12 and Φ14 are deformed bars, whereas Φ4 is a round bar.

Table 2. Mechanical properties of reinforcements (MPa)

Specimens	Reinforcement	Yield stress	Ultimate strength
L-1 and L-2	Φ12 bars	386	582
	Φ4 steel wire	284	391
L-A and L-D	Φ12 bars	393	590
	Φ14 bars	422	630
	Φ4 steel wire	273	374

Tests were conducted using an existing loading frame installed in the Harbin Institute of Technology. Figure 2 shows the loading apparatus. The test setup represents typical loading condition in a coupling beam in that the coupling beam is subject to end shears. A load cell was installed to measure the shear load. Transducers were used to measure the relative displacements between the top and bottom stubs and the displacements within the plastic hinges.

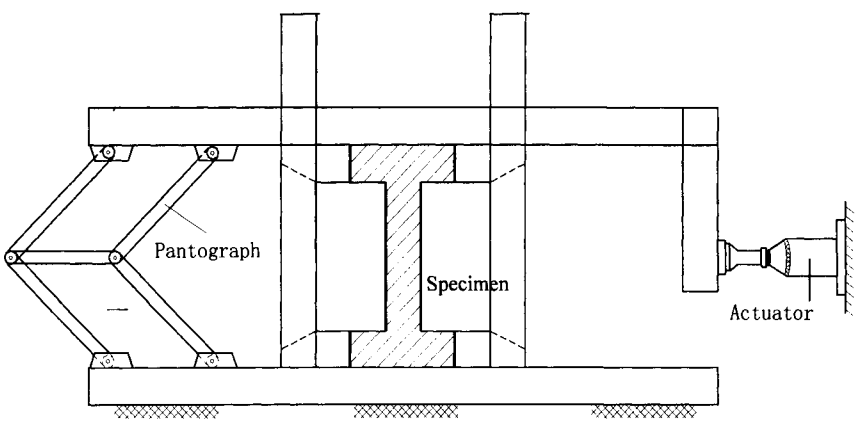


Figure 2. Setup of the loading apparatus

The specimens were subject to a series of positive and negative loading cycles. Firstly, shear load was applied (the first push cycle) until obvious reduction in stiffness was observed. The corresponding displacement was denoted as U1. Two complete cycles of push-pull loading were performed to achieve the targeted displacement δ at δ=U1. The loading cycles continued with progressive increase in the targeted displacement, i.e. δ=U2, δ=U3, and so on. The loading cycles terminated when there was more than 20% drop in the load-carrying capacity from the maximum.

TEST RESULTS

When subject to cycles of push-pull loading, failures of all the specimens were due to shear. Figure 3 shows conditions of the specimens at failure. Formation of cracks in specimens L-1 and L-2 are similar to each other. In the first few loading cycles, flexural cracks were found within the plastic hinges at the

two ends. Subsequently, shear cracks developed with spalling of the concrete cover within the plastic hinges. No obvious opening of the 90-degree hooks was observed in the tests.

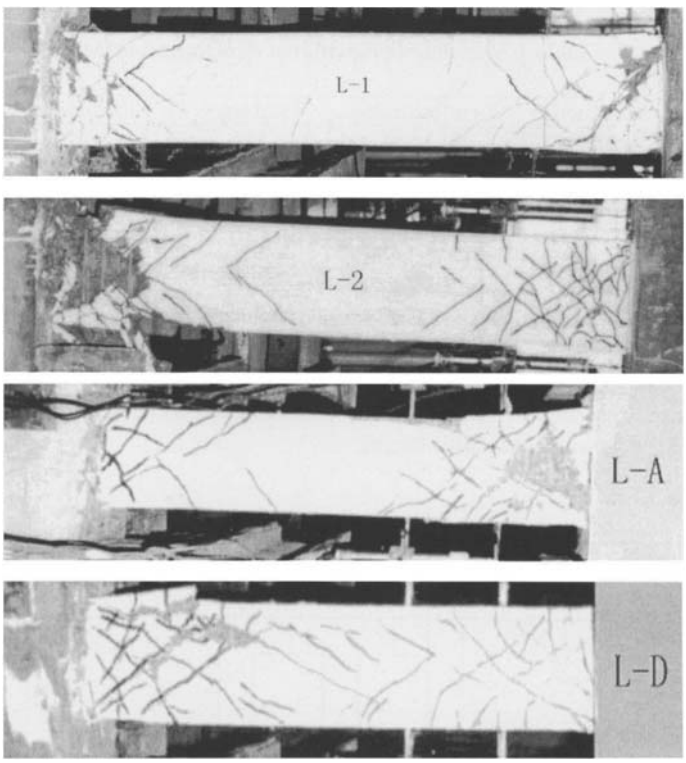


Figure 3. Modes of failure of the specimens

At the advanced stage of the loading history, deformations of all the specimens were mainly due to shear. Similarly, many inclined cracks were observed when approaching failure. However, for specimens L-1 and L-2 having smaller spacing of links, cracks were found to be concentrated at the two ends. On the contrary, the cracking pattern of specimen L-D (having the largest spacing of links) was more extensive and covers over the whole length of the beam.

HYSTERESIS BEHAVIOR

Figure 4 shows the hysteresis loops of the specimens. P is the shear load acting on a specimen. Test results are summarized in Table 3. For specimens L-1 and L-2, these are obtained from the negative envelops. For specimens L-A and L-D, these are estimated by taking the average of the values obtained from the positive and negative envelops. Yield condition is defined according to Figure 5. Failure load and displacement at failure are the corresponding values at 20% drop in the load-carrying capacity from the maximum. Displacement ductility factor is the ratio of the displacement at failure to the yield displacement. Ultimate drift ratio is the ratio of the relative displacement at the two ends of a beam at

failure against the clear span of the beam.

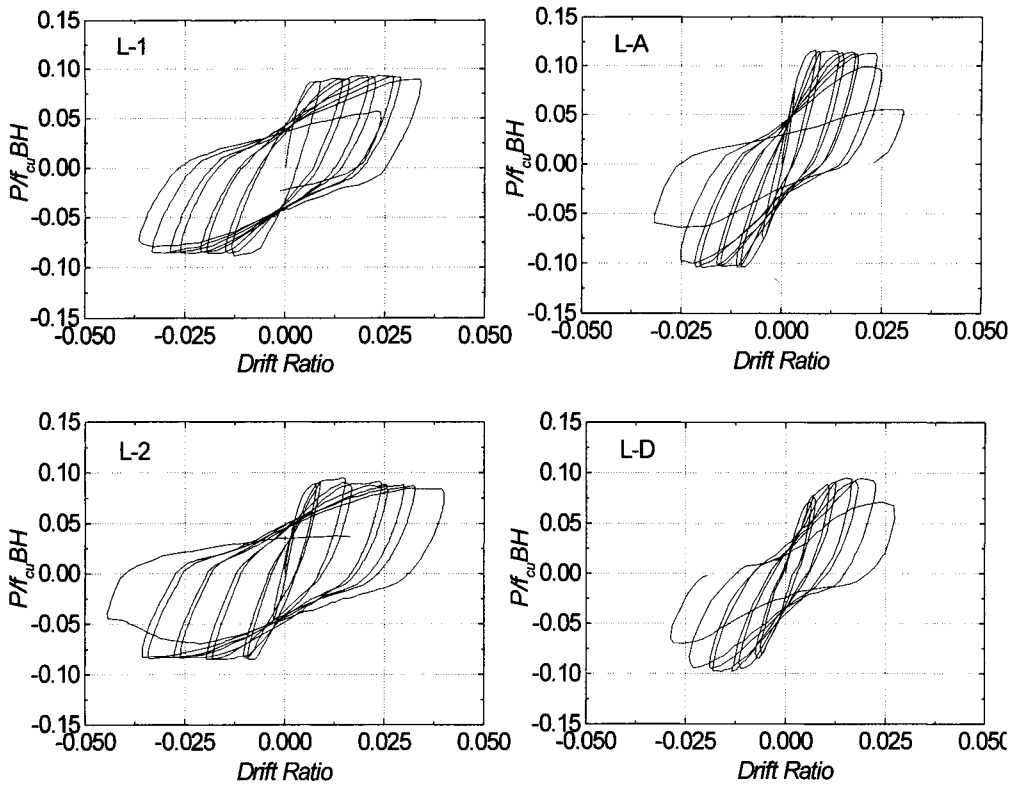


Figure 4. Hysteresis behavior

Table 3. Test results

Specimen	L-1	L-2	L-A	L-D
Yield load P_y (kN)	26.85	26.44	32.28	25.7
Yield displacement Δ_y (mm)	4.18	4.48	4.28	5.03
Ultimate load P_m (kN)	30.30	30.00	37.23	31.01
Ultimate displacement Δ_m (mm)	12.45	12.20	6.52	12.55
Failure load P_u (kN)	23.62	22.64	29.79	24.53
Displacement at failure Δ_u (mm)	27.87	28.67	20.04	19.66
Ultimate drift ratio	1/26.9	1/26.2	1/37.4	1/38.1
Displacement ductility factor	6.67	6.40	4.68	3.91

Apart from having different spacing of links, specimens L-1, L-2 and L-D have the same reinforcement details. When the spacing of links is reduced from 63mm (specimen L-D) to 35mm (specimen L-1), the ultimate drift ratio increases by 42% and the displacement ductility factor by 71%. However, when the spacing of links is further reduced to 25mm (specimen L-2), there is no obvious gain in either the ultimate drift ratio or displacement ductility factor. This indicates that the optimal spacing of links could be around 140mm (i.e. 4x35mm in full scale).

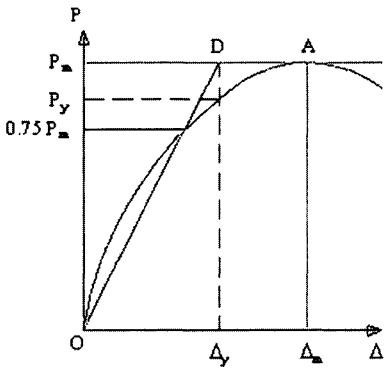


Figure 5. Definition of yielding

Main reinforcements in specimens L-A is 32% more than that specified in specimen L-1. This leads to a 23% increase in the ultimate load P_m. However, there is substantial reduction in both the ultimate drift ratio and displacement ductility factor by 28% and 30% respectively. This demonstrates the use of heavily reinforced beams may serious reduce the ductility and is therefore undesirable for seismic resistance.

EMPIRICAL RELATIONSHIP FOR ULTIMATE DRIFT RATIO

In order to develop an empirical formula to predict the ultimate drift ratio of non-ductile coupling beams, test data obtained from this study are correlated with those obtained by others. Basic properties of the selected test data are summarized in Table 4. There are 13 test data, of which 7 are obtained from this study.

Table 4. Test data

Specimen	BxH (mm)	h (mm)	L (mm)	λ	ρ	A_{sh}/S_tB	Ultimate drift ratio	Reference
L-1	62.5×140	124	750	3.0	2.92%	1.15%	1/26.9	Present study
L-2	62.5×140	124	750	3.0	2.92%	1.61%	1/26.2	Present study
L-A	62.5×145	128	750	2.9	3.85%	1.15%	1/37.4	Liu *et al* (2002)
L-D	62.5×140	124	750	3.0	2.92%	0.64%	1/38.1	Liu *et al* (2002)
L-C1	75×140	124	625	2.5	3.65%	1.15%	1/31.4	Liu *et al* (2002)
L-C2	75×140	124	625	2.5	3.65%	1.15%	1/28.6	Liu *et al* (2002)
L-E	100×150	124	875	3.5	5.47%	1.12%	1/31.7	Liu *et al* (2002)
C2	102×169	159	423	1.33	0.70%	1.10%	1/21.9	Barney *et al* (1980)
C5	102×169	159	423	1.33	0.70%	1.10%	1/22.5	Barney *et al* (1980)
C7	102×169	159	847	2.66	0.70%	1.10%	1/19.6	Barney *et al* (1980)
CB-1A	130×500	484	500	0.52	0.36%	1.03%	1/20.5	Tassios *et al* (1996)
CB-1B	130×300	284	500	0.88	0.61%	1.03%	1/19.0	Tassios *et al* (1996)
B3	182×300	267	750	1.40	1.29%	0.55%	1/39.8	Pam *et al* (2002)

In comparing the test data of specimens C2, C5 and C7, influence of the shear span ratio λ to the ultimate drift ratio appears to be of secondary importance. For lightly reinforced specimens CB-1A and CB-1B and for heavily reinforced specimens L-C1, L-C2 and L-E, the shear span ratio λ has minor effect on the ultimate drift ratio. Therefore, the shear span ratio λ is not considered as a parameter in

the empirical relationship.

Based on the observations obtained from the various test results, the main reinforcement ratio ρ and the transverse reinforcement ratio A_{sh}/S_tB are identified as the controlling factors affecting the ultimate drift ratio θ. After examining several mathematical expressions, an empirical relationship is proposed to be in form of

$$\theta = \frac{A_{sh}}{s_t B}(0.0516 - 0.0095\rho + 0.0009\rho^2) \quad (1)$$

Equation (1) is obtained using the nonlinear regression technique. Figure 6 plots the variation of the ultimate drift ratio against the main reinforcement ratio ρ. Figure 7 shows the correlation between the predicted values and the experimental data. Also presented in dotted lines is the 10% error zone. The experimental data generally fall within 10% of the values predicted by the empircial relationship, Equation (1), indicating reasobably accurate predictions can be obtained by Equation (1). Lastly, applicable range of the empirical relationship is limited to normal strength concrete and with the lateral reinforcement ratio within the range of $0.5\% < A_{sh}/S_tB < 1.6\%$.

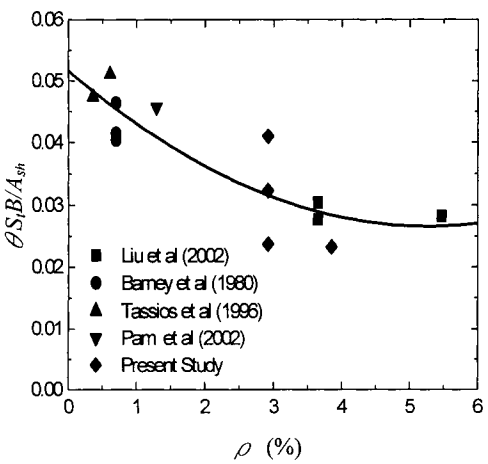


Figure 6. Variation of θ against ρ

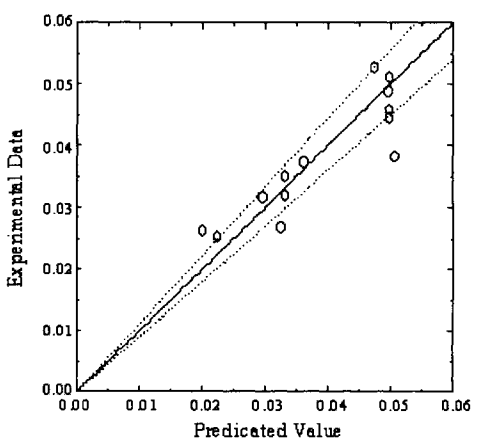


Figure 7. Prediction of ultimate drift ratio

CONCLUSIONS

Coupling beam specimens in 1/4 scale designed according to non-seismic design provisions were tested under cycles of shear loads. Characteristics of the specimens include high main reinforcement ratio, about 3-4%, and large spacing of links with 90-degree hooks. Based on the test data, 140mm is recommended to be the optimal spacing of links. Furthermore, coupling beams must not be heavily reinforced. Since this would lead to substantial reduction in the displacement ductility and ultimate drift ratio.

Combined with the test data obtained by others, an empirical relationship is proposed to estimate the ultimate drift ratio of non-ductile coupling beams. Applicable range of the empirical relationship should be limited to normal strength concrete and with the lateral reinforcement ratio within the range of $0.5\% < A_{sh}/S_tB < 1.6\%$.

ACKNOWLEDGEMENT

The authors are grateful to the financial supports from the Research Grants Council of Hong Kong (RGC No: PolyU 5038/99E).

REFERENCES

Barney G.B., Shiu K.N., Rabba B.G., Fiorato A.E., Russell H.G. and Corle W.G. (1980). *Behavior of Coupling Beams under Load Reversals*. Research and Development Bulletin RD068.01, PCA, Research and Development/Construction Technology Laboratories.

Harries K.A., Gong B. and Shahrooz B.M. (2000). Behavior and Design of Reinforced Concrete, Steel, and Steel-Concrete Coupling Beams. *Earthquake Spectra*, **16(4)**, 775-799.

Liu Z.Q., Lam S.S.E. and Wu B. (2002). Seismic Performance of Non-ductile Coupling Beams. *Proceedings of the Structural Engineering World Congress (SEWC 2002)*, Oct 9-12, 2002, Yokohama, Japan.

Pam H.J., Su R.K.L., Lam W.Y., Li J., Au F.T.K., Kwan A.K.H. and Lee P.K.K. (2002). Designing Coupling Beams and Joints in Concrete Buildings for Improved Earthquake Resistance. *Proceedings of Recent Developments in Earthquake Engineering*, HKIE Structural Division, 17 May 2002, 91-105.

Paulay T. (1971). Coupling beams of reinforced concrete shear walls. *Journal of Structural Division, ASCE*, **97(3)**, 843-861.

Paulay T. and Binney J.R. (1974). Diagonally reinforced coupling beams of shear walls. Paper no 26, *ACI Publication SP-42*, **2**, 579-598.

Tassios T. P., Moretti M. and Bezas A. (1996). On the Behavior and Ductility of Reinforced Concrete Coupling Beams of Shear Walls. *ACI Structural Journal*, **93(6)**.

Advances in Building Technology, Volume 1
M. Anson, J.M. Ko and E.S.S. Lam (Eds.)
© 2002 Elsevier Science Ltd. All rights reserved

EFFECT OF UNCERTAIN EVOLUTIONARY PSD FUNCTION OF SEISMIC EXCITATION ON PEAK RESPONSE OF MDOF SYSTEMS

S.S.Wang and H.P. Hong

Department of Civil and Environmental Engineering, University of Western Ontario, London, Canada, N6A 5B9

ABSTRACT

Seismic excitation is inherently non-stationary with respect to time and frequency. The non-stationary excitation or process is commonly characterized by the evolutionary power spectral density (PSD) function which may be represented by a time modulating function and a PSD function of a stationary process. The present study describes an analysis procedure for evaluating probability that the peak response of a multi-degree-of-freedom system to non-stationary excitation exceeds a specified level. The analysis considers that the parameters controlling the evolutionary PSD function are uncertain. This uncertain arises from the consideration that a structural system is designed to withstand all potential earthquake threats. The model used for the PSD function of the stationary process is the Kanai-Tajimi model and the exponential modulating function is employed for the time modulating function. Parametric studies are carried out using the proposed procedure for assessing the adequacy of the so-called complete quadratic combination rule that is commonly employed in aseismic design.

KEYWORDS

Peak response, Probability, Non-stationary excitation, complete quadratic combination rule, evolutionary power spectral density function.

INTRODUCTION

The combination rules with the response spectra are often used to evaluate the peak responses of multi-degree-of-freedom (MDOF) linear systems subjected to ground motions. The response spectra are usually obtained by the mean or mean plus one standard deviation of the normalized response spectra of a suite of ground motions and the ground motion parameters such as peak ground acceleration. Such spectra may have different probability of exceedance since the peak responses at different periods are not fully correlated. If the uniform hazard spectra (UHS) which have equal

probability of exceedance at different periods are taken place, the adequacy of use of the combination rules to evaluate the peak responses of MDOF should be verified. Recently, it has been found that the peak response of MDOF systems to stationary ground motions calculated by the complete quadratic combination (CQC) rule with the UHS may be conservative or unconservative depending on the modal periods and contributions of each mode (Hong and Wang 2002). However, the ground accelerations are non-stationary with respect to both time and frequency. The effect of the non-stationary excitation on the use of the CQC rule with UHS to estimate the peak response of MDOF systems was considered in this study. The analysis was carried out by modeling the non-stationary excitation as the evolutionary power spectral density (PSD) function with uncertain parameters. In particular, the Kanai-Tajimi model with exponential modulating function was used to define the evolutionary PSD function. The first-passage probability distribution developed by Vanmarcke (1975, 1976) was used to represent the probability distribution of the peak responses. A set of UHS to non-stationary ground accelerations was established. Using the obtained UHS, the probability associated with the peak responses of MDOF systems to non-stationary ground motions evaluated by the CQC rule was assessed. Details of analysis procedure and the obtained results were given in the following section.

NON-STATIONARY EXCITATION AND STRUCTURAL RESPONSES

Non-stationary Excitation

The non-stationary ground motion may be characterized with an evolutionary PSD function that consists of a time modulating function $A(t)$ and a PSD function of stationary process $G_x(\omega)$ (Priestley 1967). The evolutionary PSD function (one-sided), $G_x(\omega,t)$, can be expressed as:

$$G_x(\omega,t) = |A(t)|^2 G_x(\omega), \tag{1}$$

The Kanai-Tajimi PSD function employed in this study takes the following form (Tajimi 1960)

$$G_x(\omega) = \frac{\omega_g{}^4 + 4\xi_g{}^2\omega_g{}^2\omega^2}{\left(\omega_g{}^2 - \omega^2\right)^2 + 4\xi_g{}^2\omega_g{}^2\omega^2} G_0, \tag{2}$$

where ω (rad/sec) is the frequency, G_0 is the intensity of the ideal white noise; ω_g (rad/sec) is the filter frequency that determines the dominant range of input frequencies; the damping coefficient ξ_g is a parameter that indicates the shape of the power spectral density.

The exponential modulating function adopted in this study can be written as (Shinozuka and Sato 1967):

$$A(t) = A_0(e^{-b_1 t} - e^{-b_2 t}), \quad b_2 > b_1, \tag{3}$$

where the b_1 and b_2 are dependent on the strong motion duration, T_0, and the fraction of rise time, ε; and the scaling factor A_0 which equals $1/\max(e^{-b_1 t} - e^{-b_2 t})$ is used in the present study.

Structural Responses to Non-stationary Ground Motion

Consider a linear MDOF system with ω_i and ξ_i denoting the frequency and damping ratio of the i-th mode subjected to a non-stationary ground acceleration with evolutionary PSD function $G_x(\omega, t)$. The response $R(t)$ of the system is also a non-stationary random process with its one-sided evolutionary PSD function, $G_R(\omega,t)$, given by:

$$G_R(\omega,t) = \sum_i^n \sum_j^n C_i C_j M_i(\omega,t) M_j^*(\omega,t) G_x(\omega), \tag{4}$$

where C_i is the effective participation factor of i-th mode; the asterisk denotes the complex conjugate; and $M_i(\omega,t) = \int_0^t h_i(\tau) A(t-\tau) e^{-i\omega\tau} d\tau$, where $h_i(\tau) = \frac{1}{\omega_i\sqrt{1-\xi_i^2}} e^{-\xi_i\omega_i\tau} \sin\left(\omega_i\sqrt{1-\xi_i^2}\,\tau\right)$.

PROBABILISTIC ANLYSIS OF PEAK RESPONSE

Statistics of Random Variables

To represent the uncertainty in seismic excitation for all potential earthquake events, the model parameters ω_g, ξ_g and G_0 in Kanai-Tajimi PSD function and the parameters T_0 and ε controlling the time modulating function were considered as random variables. The statistics of ω_g, ξ_g, G_0, and T_0 given by Vanmarcke and Lai (1980, 1982) and the statistics of ε provided by Balendra et. al (1991) were adopted. The recommended statistics of these parameters were shown in Table 1.

TABLE 1
STATISTICS OF MODEL PARAMETERS IN KANAI-TAJIMI PSD FUNCTION

Model parameter	Mean	Coefficient of variation	Standard deviation	Distribution type
ω_g (rad/sec)	19.06	0.427	8.139	Gamma
ξ_g	0.316	0.427	0.135	Lognormal
G_0 (cm^2/sec^3)	35.32	2.454	86.675	Lognormal
ε	0.159	0.58	0.092	Uniform
τ (sec)	10.09	0.90	9.081	Gumbel

Probability of Exceedance of Peak Response

Consider a linear system subjected to non-stationary ground acceleration with the evolutionary PSD function $G_x(\omega, t)$ given Eqn. 1. The probability that the peak response of the system, R, is within the prescribed barriers $\pm r$ during $(0, t)$, $L_R(r,t)$, can be found in the literature (Vanmarcke 1975, 1976). The parameters in $L_R(r,t)$ depend on the first three moments of peak response, which are related to the evolutionary PSD function of peak response. Since the evolutionary PSD function of ground motion depends on a set of random variables **X**, $L_R(r,t)$ is also conditioned on **X**. To emphasize the conditional relation, the notation $L_{R|X}(r,t)$ is employed to replace $L_R(r,t)$.

The unconditional probability that the peak response exceeds the prescribed barriers $\pm r$ during $(0, t)$, $P_e(r)$, can be evaluated by FORM using (Madsen et. al 1986):

$$P_e(r) = \int_{\Omega} \left(1 - L_{R|X}(r,t)\right) f_{\mathbf{X}}(\mathbf{x}) dz d\mathbf{x} = \int_{g \le 0} \phi(z) f_{\mathbf{X}}(\mathbf{x}) dz d\mathbf{x}, \tag{5}$$

where Ω denotes the domain of $\mathbf{X}$, $f_{\mathbf{X}}(\mathbf{x})$ represents the joint probability density function of $\mathbf{X}$,

$$g = z - \Phi^{-1}\left(1 - L_{R|X}(r,t)\right), \tag{6}$$

represents an auxiliary limit state function, $\phi(\bullet)$ is the standard normal probability density function, and $\Phi^{-1}(\bullet)$ is the inverse of the standard normal distribution function $\Phi(\bullet)$.

Fractile of Peak response

Given an evolutionary PSD function and structural parameters, Eqns. 5 and 6 can be used to calculate the probability that the (absolute value of) peak response is less than a specified value. Alternatively, the peak response corresponding to a specified probability of exceedance P_{Te} or a target reliability index β_T, r_T, can be carried out iteratively. The fractiles of the peak response for a series of SDOF systems with a range of natural periods of vibration and damping ratios can be used to form the response spectra. These response spectra can be viewed as the UHS since they have equal probability of exceedance P_{Te}, and the seismic risk was reflected by considering the uncertainty in the parameters of evolutionary PSD function.

Note that for practical applications, rather than using the fractile of MDOF systems r_T, the modal combination rules with peak modal responses obtained from the response spectra are commonly employed. Since the CQC rule is most widely used in aseismic design, the study is focused on the verification of adequacy of using this rule with UHS to evaluate the peak responses of MDOF systems.

NUMERICAL ANALYSIS

Peak Response of SDOF System with Equal Probability of Exceedance

For establishing the UHS, the probability of non-exceedance levels, $1\text{-}P_{Te}$, were set as 0.57 and 0.84 (i.e., $\beta_T = 0.177$ and 1). The obtained results for the non-stationary excitation represented by (N) were shown in Figure 1. Comparisons of these fractiles to the 0.57- and 0.84-fractile of peak responses to stationary excitation represented by (S) were also shown in Figure 1. This figure indicates that the peak responses obtained for stationary excitation are different from those for non-stationary excitation. This is expected because the ground accelerations are modulated by time modulating function. Note that the magnitude of the peak response to non-stationary ground acceleration depends on the scaling factor A_0 of the time modulating function. Using the results given in the figure it can be shown that the ratios of the responses and the ratios of the logarithmic of responses between any two curves at different frequencies are not constant. The logarithmic of these ratios are slightly different as well. These imply that the peak responses at different natural frequencies are not fully correlated. Therefore, the peak responses cannot be represented accurately by the product of or the logarithmic of product of a deterministic function of the natural frequency and a random variable.

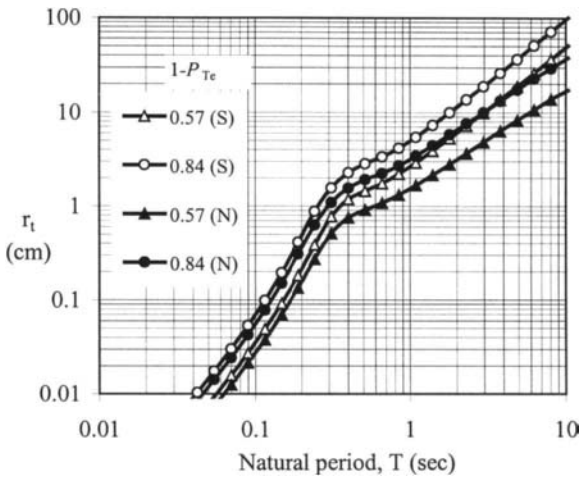


Figure 1: Peak response of SDOF systems to stationary and non-stationary excitation

Probability of Peak Response of Two-degree-of-freedom System

For a linear two-degree-of-freedom (2DOF) system, the peak response denoted by r_a can be calculated by CQC rule using the following expression (Der Kiureghian 1981, Chopra 2000):

$$r_a = \left((C_1 r_{1T})^2 + 2\rho_{12} C_1 C_2 r_{1T} r_{2T} + (C_2 r_{2T})^2\right)^{1/2}, \tag{7}$$

where r_{1T} and r_{2T} denoting the peak modal responses with the specified probability of exceedance P_{Te} can be obtained directly from the UHS shown in Figure 1 at ω_1.and ω_2; and ρ_{12} is the correlation coefficient given by Der Kiureghian (1981); C_1 and C_2 represent the effective participation factors. The Eqn 7 can also be written as:

$$r_a = \left((1-\zeta)^2 + \mathrm{sgn}(C_1 C_2) 2\rho_{12}(1-\zeta)\zeta + \zeta^2\right)^{1/2} r_{ABS}, \tag{8}$$

where sgn( ) returns the sign of the argument and $\zeta = |C_2 r_{2T}| / r_{ABS} = |C_2 r_{2T}| / (|C_2 r_{2T}| + |C_1 r_{1T}|)$ represents the contribution of the second mode.

By simple mathematical manipulation, it can be shown that given the value of ζ the probability that the peak response of the 2DOF system exceeds r_a can be evaluated using Eqn. 8 independent of the actual value of the r_{ABS}, except that r in Eqn. 5 is replaced by r_a. Note that by assigning different values of ζ from 0 to 1, different percentage of the contribution due to each mode to the system can be obtained. In particular, ζ equal to zero and one means the system is SDOF system with natural frequency equal to the ω_1 and ω_2, respectively.

Consider a 2DOF structure with T_1 = 0.2 sec and T_2 = 0.1 sec. The reliability indices β of peak responses exceeding r_a calculated using Eqn 8 were shown in Figure 2. The β for stationary ground motions were also shown in the figure. The figure indicates that β vary with ζ and β_T. The β is almost identical to β_T when ζ is close to 0 or 1; otherwise it is distinctively differ from β_T. This

suggests that when the contribution due to one of modes is dominant the use of CQC rule with the UHS is adequate which is expected. However, if the contributions of both modes to the system response are significant, the use of the CQC rule with UHS could lead to different safety levels. For this 2DOF system, the CQC rule under- and over-estimates the peak response of the system for $\mathrm{sgn}(C_1C_2) > 0$ and $\mathrm{sgn}(C_1C_2) < 0$, respectively.

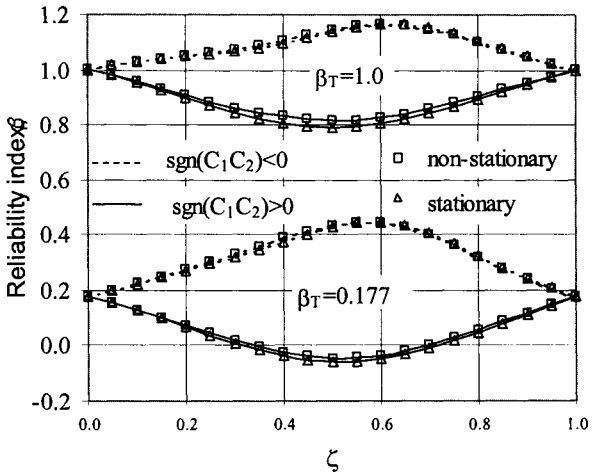


Figure 2 Reliability index of the peak response of 2DOF system using CQC rule with the UHS

Based on the above, it may be concluded that use of the CQC rule with the UHS may lead to conservative or unconservative results. To quantify such error, the ratio between the peak response r_a estimated by the CQC rule and the (1-P_{Te})-fractile peak responses, r_T, η, was calculated and shown in Figures 3a and 3b. To investigate the influence of the modal periods, other two 2DOF systems with T_1 = 0.2 sec and T_1/T_2 = 1.2, and T_1 = 1.5 sec, T_1/T_2 = 2.0 were also considered. The results for stationary ground motions were shown in the figures. These results indicate that the peak response to non-stationary ground motions obtained using CQC rule with the peak modal response from the UHS may not be adequate. It may over- or under- estimate, depending on the modal contribution and the natural periods of the structures. The conclusions for non-stationary excitations are similar to those for stationary excitations. However, the over- and under-estimation for the former seems to be larger than that for the latter.

In general, it seems that the errors (i.e., absolute value of 1-η) appear to be larger for the cases with $\mathrm{sgn}(C_1C_2)<0$ than for the cases with $\mathrm{sgn}(C_1C_2)>0$. The under- or over-estimation are less than about 10% and 20% if the modal contribution is less than 10% and 20% of the absolute sum of the effective modal peak response, respectively. However, CQC rule may lead to severe errors in other cases.

CONCLUSIONS

The probability analysis of the peak response was carried out using non-stationary evolutionary random vibration analysis to investigate the effect of uncertain non-stationary of seismic excitation on peak response of MDOF systems. In the analysis, the uncertainty in seismic excitation due to all potential earthquakes was considered using non-stationary PSD function with uncertain parameters.

Further, the adequacy of using CQC rule with the modal responses from the ordinates of the uniform hazard spectra was assessed.

The results show that the use of CQC rule with the modal responses obtained from the UHS is adequate if the peak responses of MDOF system are dominated by the response of one mode. However, if the contributions of different modes to the peak responses of a MDOF system are about equally significant, the use of CQC rule with the UHS leads to significant under- or over-estimation of the peak response. Such under- or overestimation depends on the modal periods of the system, and the effective modal participation factors.

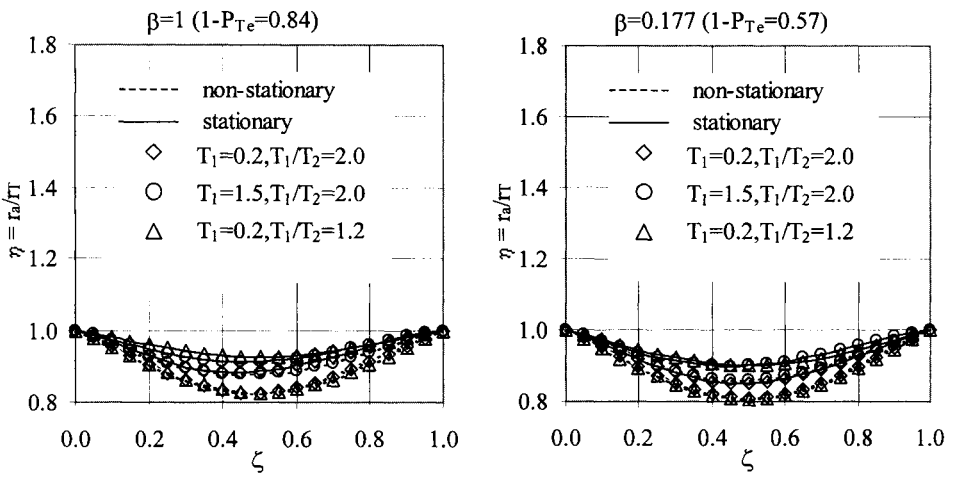


Figure 3a Ratio of the peak response of the CQC rule to the (1-P_{Te}) fractile response, sgn(C_1C_2)>0

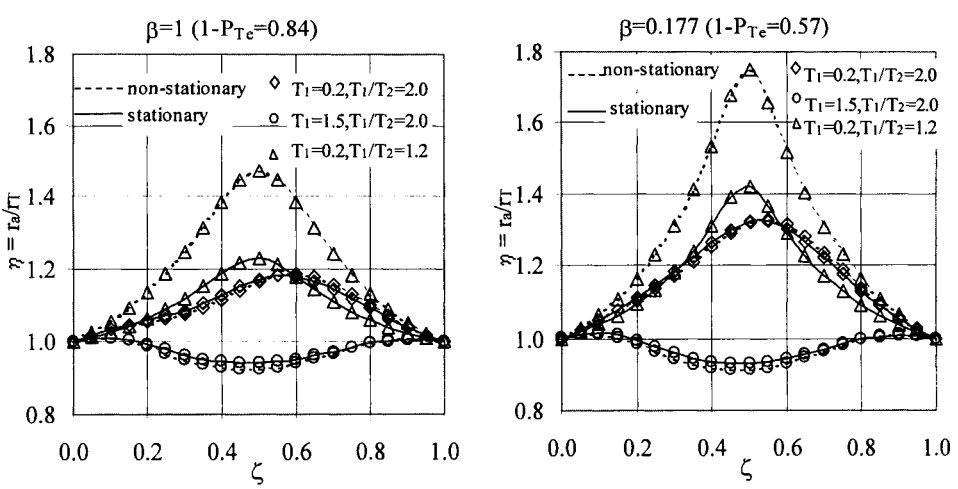


Figure 3b Ratio of the peak response of the CQC rule to the (1-P_{Te}) fractile response, sgn(C_1C_2)<0

ACKNOWLEDGEMENTS

The financial support of the Natural Science and Engineering Research Council of Canada is gratefully acknowledged.

REFERENCES

Balendra T, Quek ST and Teo YP. (1991) Time-variant reliability of linear oscillator considering uncertainties of structural and input model parameters. *Probabilistic Engineering Mechanics* **6:1**,10-17.

Chopra AK. (2000) *Dynamics of structures: Theory and application to earthquake engineering*, Prentice-Hall, Englewood Cliffs, New Jersey.

Der Kiureghian A. A response spectrum method for random vibration analysis of MDOF systems, *Earthquake Engineering and Structural Dynamics*, 1981, **9**: 419-435.

Hong HP, Wang SS (2002) Probability analysis of peak response of MDOF systems with uncertain PSD function. *Earthquake Engineering and Structural Dynamics* (in process).

Lai SP. (1982) Statistical characterization of strong motions using power spectral density function. *Bulletin of the Seismological Society of* America **72:1**, 259-274.

Madsen HO, Krenk S, Lind NC. (1986). *Methods of structural safety*, Prentice-Hall, Englewood Cliffs, N. J.

Priestley M.B. (1967). Power spectral analysis of non-stationary random process. *Journal of Sound and Vibration* **6:1**, 86-97

Shinozuka M. and Sato Y. (1967) Simulation of nonstationary random processes. *Journal of Engineering Mechanics Division ASCS* **93:EM1**, 11-40.

Tajimi H. (1960) A statistical method of determining the maximum response of a building structure during an earthquake, *Proceedings, Second Word Conference on Earthquake Engineering*, **2**, 782-796 Tokyo, Japan.

Vanmarcke EH, Lai SP. (1980) Strong-motion duration and RMS amplitude of earthquake records, *Bulletin of the Seismological Society of America*, **70:4**, 1293-1307.

Vanmarcke EH. (1976) *Structural response to earthquakes, in Seismic Risk and Engineering Decision* (Eds. Lomnitz, C. and Rosenblueth, E.), Elsevier Scientific Publishing Company, Amsterdam.

Vanmarcke EH. (1975) On the distribution of the first-passage time for normal stationary random process, *Journal of Applied Mechanics*, **42:Ser. E**, 215-220.

Advances in Building Technology, Volume 1
M. Anson, J.M. Ko and E.S.S. Lam (Eds.)
© 2002 Elsevier Science Ltd. All rights reserved

Simplified Method and Parametric Sensitivity Analysis for Soil-Pile Dynamic Interaction under Lateral Seismic Loading

Xiaochun Xiao [1] Shichun Chi[1] Gao Lin [1] John Alfano[2]

[1.] Department of Civil Engineering, Dalian University of Technology, Dalian, 116023, P.R.China
[2.] Department of Civil and Environmental Engineering Cornell University, Ithaca, NY, 14850, USA

ABSTRACT

Pile foundation for buildings erected on soft soil sites are often subjected to lateral loading induced by wind, sea wave and earthquakes. In many cases, the horizontal loads at the pile head usually constitute the primary constraint that affects the deformation of underlying piles or pile groups, so the behavior of lateral loaded pile has great significant for pile foundation design. In this paper, a simplified model based on Beam on Nonlinear Dynamic Winkler Foundation (BNDWF) for soil-pile dynamic interaction analysis under lateral loading is presented, and the corresponding computer program (NASPI) is developed using the *Wilson-θ* method. Through comparisons with the rigorous Finite Element analysis in time domain, it is shown that the model is simple and effective. Sensitivity analysis of the parameters including the effect of pile-soil stiffness ratio, pile slenderness ratio and earthquake excitation level has been performed. The statistical results indicate that the pile-soil stiffness ratio play the most important role in the soil-pile interaction.

KEYWORDS

Soil-pile dynamic interaction, BNDWF, lateral seismic loading, parametric sensitivity

INTRODUCTION

The response of piles and their load carrying capacity depends on the soil-pile interaction. Pile foundations of different type of structure are often subjected to lateral loading induced by the environment acting such as wind, sea wave and earthquakes. The lateral loads exerted at the pile head are basic factor that governs the response of single pile or pile groups. Since the early 1960s, many researchers have concerned themselves with piles undergoing dynamic lateral loads. Quite variety methods such as field tests, laboratory tests, numerical analyses have been performed.

Field experiments were initially conducted in the early 1960s by Matlock and Reese. As pointed out by Meymand, field experiment has the advantage that take into consideration in-site stress conditions, however seismic loads can be neither realistically nor easily reproduced. Matlock first completed his tests on laterally loaded piles in soft clays (Matlock 1962) and published a set of design *p-y* (resistance-deflection) curves at various depths. Novak was the first who attempted to analyze the dynamic response of single pile using continuum theory in frequency domain. He modeled the pile as an assembly of beam elements and their soil reactions were obtained based on a plane strain condition assumption (infinitely long pile). Nogami *et al.* developed closed-form solution for vertical and horizontal modes of vibration of an end-bearing pile by making use of rigorous three-dimensional theory in time domain. To obtain analytical closed-form solution, George Gazetas *et al.* used dynamic Winkler model with realistic frequency-dependent 'springs' and 'dashpots' to account for pile-soil-pile interaction. At same time many researchers studied pile vibration using finite element method or boundary element method in time domain and frequency domain.

In our research, a simplified model based on Beam on Nonlinear Dynamic Winkler Foundation (BNDWF) for soil-pile dynamic interaction under lateral seismic loading is presented. The validity of this simplified model is calibrated by comparing the results with those of Finite Element Method (FEM). Sensitivity analysis of the factors which affect the response of soil-pile system such as pile soil stiffness ratio, pile slenderness ratio and design earthquake level was examined. The calculation results indicate that pile soil stiffness ratio is the most sensitive one among these factors.

OUTLINE OF SIMPLIFIED MODEL AND METHOD

The single pile is modeled as a beam based on BNDWF. To develop the governing equation, the beam is discretized into a series of N-1 discrete beam elements with a total of N nodes. Element analysis, each beam element is considered individually as forces acting at the nodes, and it cause displacements and rotations of the nodes. The element model is shown in figure 1, and the relationship between nodal forces and nodal displacements given by:

$$\{F\}^e = [k_p]^e \{\Delta\}^e \tag{1}$$

where, $[k_p]^e$ is pile element stiffness, $\{F\}^e$ and $\{\Delta\}^e$ are forces and nodal displacements vectors for the same element, $\{F\}^e = [F_i \quad F_{i+1}]^T = [y_i \quad M_i \quad y_{i+1} \quad M_{i+1}]^T$, $\{\Delta\}^e = [\Delta_i \quad \Delta_{i+1}]^T = [u_i \quad \theta_i \quad u_{i+1} \quad \theta_{i+1}]^T$. The soil reaction has been modeled with a spring and dashpot element connected at each node along the

pile. A graphical representation of soil element is shown in the middle part of figure 1. The terms, as pictured, are m_i, the lumped mass of the beam element at node i, k_{si}, the spring stiffness representing the soil modulus of deformation at node i, c_{si}, the damping coefficient of the soil at node i. This model gives the soil reaction shown in the following equation:

$$F_i = \begin{Bmatrix} y_i \\ M_i \end{Bmatrix} = \begin{Bmatrix} k_{si}u_i + c_{si}\dot{u}_i + m_i(\ddot{u}_i + \ddot{u}_{g_i}) \\ 0 \end{Bmatrix} \tag{2}$$

The $k_{si}u_i$ term is the spring force, the $c_{si}\dot{u}_{si}$ term is the damping force of the dashpot, the $m_i(\ddot{u}_i + \ddot{u}_g)$ term is the inertial force of the pile, the $\ddot{u}_{g_i}$ term is the acceleration due to an earthquake, but other dynamic forces such as wind or wave loads can also be used.

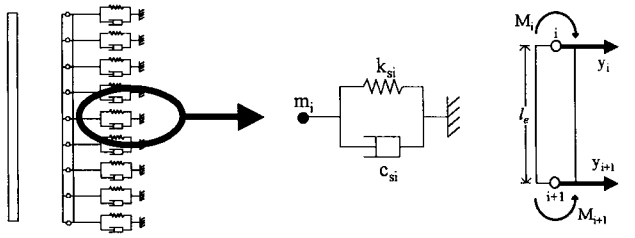


Figure 1: Discretized soil and beam elements

The k_{si}, c_{si} of every node can be calaulated as follows:

$$k_{si} = E_s A \quad \text{and} \quad c_{si} = A\sqrt{\rho E_s} \tag{3}$$

where, ρ is the soil density and A is the area of nodal control. The soil modulus of deformation E_s can be solved through the following simple equation:

$$E_s = 2(1+\mu)\times G \tag{4}$$

where, μ is definied as the soil Poisson's ratio, G is the soil dynamic shear modulus, The current shear modulus (G) is related to the initial shear modulus (G_0) through a function of the shear strain (γ). The Hardin-Drnevich model is used in our research and is represented as follows:

$$\frac{G}{G_0} = \frac{1}{1+\frac{\tilde{\gamma}_i}{\gamma_r}} \tag{5}$$

where the effective shear strain across an element is $\tilde{\gamma}_i \approx 0.65(\gamma_i)_{\max}$ and (γ_r) is a reference shear strain value. After the first computational iteration, the shear modulus changes and has to be recalculated.

In order to calculate the initial shear modulus (G_0), the empirical equations will be used. The equation

differs depending on the soil type. In this research project only a single, homogeneous layer of sand is considered. The empirical equation for sand is:

$$G_0 = \frac{3270(2.97-e)^2}{1-e} \times \sqrt{\sigma_0'} \tag{6}$$

where, σ_0' is the average of the principle stresses, and e is the voids ratio. G_0 and σ_0' are in units of kiloPascals (kPa). As Equation 5 shows, the shear modulus is dependent on the principle stresses. Since the stress level changes with depth, a different shear modulus will have to be computed for each node. The largest principle stress is approximated as $\sigma_1 \approx \rho g x$, x is depth from the ground surface. The smallest principle stress is approximated as $\sigma_3 \approx K_y \sigma_1$, where $K_y = \mu/(1-\mu)$ and μ is definied as the soil static Poisson's ratio. The intermediate principle stress σ_2 is taken to be equal to σ_3. All three principle stresses are then averaged to calculate σ_0'.

GOVERNING EQUATION AND SOLUTION METHODOLOGY

The simplified form of the governing equation for the whole system is represented as:

$$[K]\{\Delta\}+[C]\{\dot{\Delta}\}+[M_p]\{\ddot{\Delta}\}=-[M_p]\{\ddot{u}_g\} \tag{7}$$

where, $[K]$, $[C]$ and $[M_p]$ are global stiffness matrix, global damping matrix and mass matrix of pile respectively. $[K]=[k_s]+[k_p]$, and $[k_s]$ is soil spring stifness matrix. The $\{\Delta\}$, $\{\dot{\Delta}\}$, and $\{\ddot{\Delta}\}$, are the displacement, velocity, and acceleration vectors respectively. This research employs the *Wilson-θ* Method (Clough, R. 1996) for numerical integration of the equation (7), and θ=1.4 guarantees unconditional stable convergence. Once solutions for lateral displacements are found, they will be substituted into element equation to find the resulting shear forces and bending moments in the pile.

VERIFICATION OF SIMPLIFIED MODEL

Basing on above mentioned theory, a FORTRAN code with name of NASPI was developed. In the code, there are two main loops run through the program for calculating the outputs. The first loop begins with the dynamic calculations that constitute the *Wilson-θ* Method. The step-by-step integration method of the dynamic equation is accomplished as the acceleration, velocity, and displacement of each node are calculated for each earthquake time-step. After the final time-step, the loop completes and the soil modulus is recalculated for the dynamic condition. The dynamic calculations are then iterated until the convergence criteria are met.

In the FEM code, the system that consists of pile and surrounding soil is idealized as an assemblage of 3D finite elements. At the each node there are three translational degrees of freedom. The deformation of the pile, including bending, will be derived from these nodal translational displacements and element stresses. To accommodate the flexibility of pile under lateral loading, the piles are modeled as H_{11}, a kind of incompatible 3D element, which is improved from eight-node isoparametric hexahedral elements by adding 3 initial nodes. The incompatible element can be similarly dealt with the common eight-node isoparametric hexahedral elements after the condensation, but when to calculate the element stresses, the initial nodes' contribution will be taken into consideration. The pile will be

regarded as linear elastic during the whole seismic responses, and for soil, equivalent linear method will be adopted in FEM analysis. This method for modeling nonlinear hysteretic behavior of soil was developed by Idriss and Seed (1968) *et al.* Because of its simplicity, it is the most popular method for site response analysis today. The fundamental assumption of the method is that a spring-dashpot model may approximate the dynamic response of a nonlinear hysteretic material satisfactorily if the properties of such model are chosen appropriately (i.e., strain level dependency of these material properties).

A simple sample problem is input to the program and the output is compared with FEM for test the validity of the NASPI code. A single end-bearing pile is modeled as a prismatic, cylindrical beam with a length of 15 meters and a diameter of 0.6 meters. The pile has a modulus of deformation of 25,000 MPa, a density of 2,400 $^{kg}/_{m}{}^{3}$, and a Poisson's ratio of 0.142. The pile head is flush with the ground surface and free to rotate and translate. The soil is modeled as a single, homogeneous layer of sand with a density of 2,000 $^{kg}/_{m}{}^{3}$, a voids ratio of 0.65, a static Poisson's ratio of 0.37, and a reference strain of 0.001. The input earthquake is the part of El Centro type shown in figure 2. The duration is 8.0 seconds with a time-step of 0.01. It has a design level of 0.2g for this problem. Since the response of pile head is most important in design, the displacement; shear force and bending moment time history of pile head are shown in figure 3, 4 and 5 respectively.

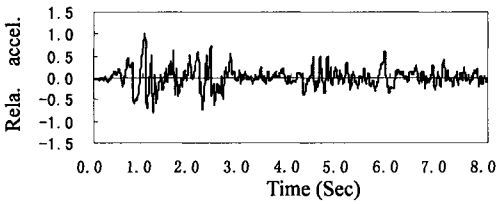


Figure 2: Input earthquake time history

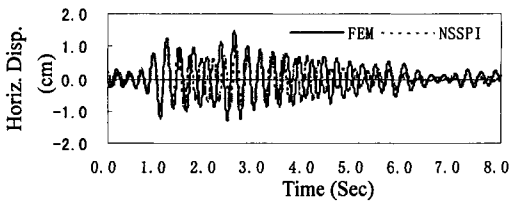


Figure 3: Comparison of pile head displacement time histories for NASPI and FEM

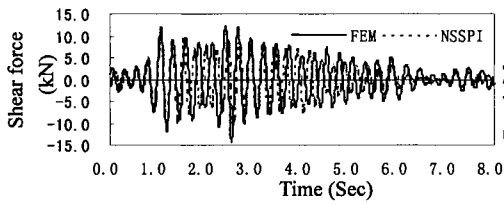


Figure 4: Comparison of pile head shear force time histories for NASPI and FEM

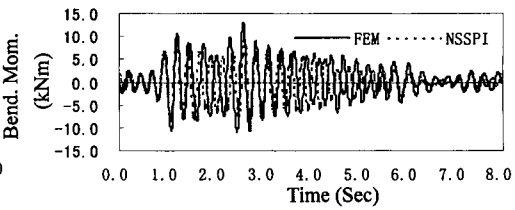


Figure 5: Comparison of pile head bending moment time histories for NASPI and FEM

Figure 3 shows the horizontal displacements of the pile head over the entire duration of the earthquake. The solid line represents the FEM analysis and the dashed line represents the output of NASPI. Initially, the two methods match up quite well for the small amplitudes of motion. As the amplitude increases, the results for NASPI fall slightly below that of the FEM analysis. This would indicate a

slight overestimation of the soil stiffness. As the amplitude begins to decrease, NASPI does so more rapidly than FEM. This would indicate a slight underestimation of the damping coefficients in NASPI. These observations are not of significant importance at this point. The results for the two codes match up well enough to consider the NASPI code valid. Slight variations are to be expected due to the simplicity of the NASPI code as well as other approximations used in the solution process. For the purpose of this research, these calculations show that NASPI works properly. Similar comparisons can be made in considering the shear force and bending moment experienced by the pile head (figures 4 and 5).

PARAMETRIC SENSITIVITY ANALYSIS

Gazetas (1984) is earlier researcher to study effects of dimensionless parameters in frequency domain. He studied single piles undergoing vertical seismic loading, and believed "such results would be useful not only for developing an improved understanding of the mechanics of the problem and checking the accuracy of sophisticated solutions, but also for making preliminary design estimates in practice". The parameters of importance in this study were E_p/E_s (the pile-to-soil stiffness ratio), L/D (the slenderness ratio of the pile), and f/f_1 (the frequency ratio of excitation function to fundamental frequency of the soil). Thus, a parametric study using NASPI in time domain, would illustrate the usefulness of the code developed herein as well as the importance of various input factors. The input parameters to NASPI could be varied such that studies of E_p/E_s and L/D could be conducted. The effects of varying the design earthquake level a_i/g were also considered. Each parameter was considered at 3 different levels indicative of a high, middle, and low range for that particular parameter. Each level is shown in table 1. If a study were to consider every possible combination of levels and parameters, a total of $3\times3\times3=27$ trials would have to be conducted. However, these 27 trials can be adequately represented by only 9 trials where each parameter is tested three times as shown in Table 2.

TABLE 1
CALCULATION TRIALS AND RESULTS

factor / level	L/D (A)	E_p/E_s (B)	a_i/g (C)
1	10	23.8	0.1
2	20	94.3	0.2
3	40	312.5	0.4

The horizontal acceleration and bending moment in the pile head were chosen as the objective functions since they are used as the inputs for what would be the base excitation of the superstructure and the constraint values for the pile design respectively. Once parameters were collected, the values for acceleration and moment were all normalized relative to the maximum value for each. The normalized values corresponding to the three trials involving each level were summed. This process was also completed for comprehensive target value that is a weighted average of the acceleration and moment for each trial and presented in Table 2. The weighted average coefficients are determined according to the cost of superstructure and pile foundation. In this research they are valued 2/3 and 1/3 roughly.

TABLE 2
CALCULATION TRIALS AND RESULTS

factor / trial	L/D (A)	E_p/E_s (B)	a_i/g (C)	Max. Horiz. Acceleration		Max. Bending Moment		Results for Comprehensive Target Values
				real (m/s^2)	Norm (%)	Real (kN m)	Norm (%)	
1	1	1	1	0.379	11.21	444	0.34	7.59
2	1	2	2	1.740	51.48	25700	19.92	40.96
3	1	3	3	3.380	100.00	129000	100.00	100.00
4	2	1	2	0.844	24.97	794	0.62	16.85
5	2	2	3	2.200	65.09	12200	9.46	46.61
6	2	3	1	1.720	50.89	33000	25.58	42.45
7	3	1	3	0.525	15.53	979	0.76	10.61
8	3	2	1	1.310	38.76	9340	7.24	28.25
9	3	3	2	1.945	57.54	17900	13.88	42.99

TABLE 3
STATISTICAL ANALYSIS FOR COMPREHENSIVE VALUES

Factor	S	Dof	T	F-value	Critical values		Sensitivity	Rank
					$F_{0.05}$	$F_{0.01}$		
A	716.27	2	358.13	3.52	19.00	99.00	*	3
B	4428.01	2	2214.01	21.77	19.00	99.00	**	1
C	1467.49	2	733.75	7.21	19.00	99.00	*	2
Tolerance	203.42	2	101.71					
Sum	6815.20	8						

Note: The F-value is defined in reference (Chen, K. 1996).
The symbols *, **, *** represent insensitive, sensitive and very sensitive respectively.

A statistical analysis for comprehensive target values was conducted and presented in table 3. The F-values for each factor are computed as shown in the above table. The F-value is calculated using the different levels as mere data points. The magnitude of the level is not important, and thus the sensitivity is independent of the differences in level sizes. Depending on F-value relative to the critical values, the sensitivity of comprehensive values is determined. For $F<F_{0.05}$, the factor is said to be insensitive. For $F_{0.05}<F<F_{0.01}$, the factor is sensitive. For $F>F_{0.01}$, the factor is very sensitive. From this table, it has been determined that comprehensive values are sensitive to changes in stiffness ratio. These results correspond well with the qualitative analysis.

CONCLUSIONS

NASPI presents an alternative method for evaluating soil-pile interactions, which is an important step to properly evaluating the soil-pile-superstructure interactions in design practice. NASPI meets the goals of being both simple and efficient, thus it is a valuable tool in practical preliminary design. The

use of NASPI in the parametric study of three important dimensionless parameters: slenderness ratio, stiffness ratio, and earthquake design level, shows that output results are most sensitive to the stiffness ratio.

REFERENCES

Chen, K. (1996) *Experiments Design and Analysis*, Tsinghua Univ. Publishing House, Beijing.

Clough, R., Penzien, J. (1996). *Dynamics of Structures*, 2nd Edition, McGraw-Hill, New York

Fan, K., *et al.* (1991) "Kinematic Seismic Response of Single Piles and Pile Groups," *Journal of Geotechnical Engineering, ASCE*, **(117)12,** 1860-1879.

Gazetas, G. (1984). "Seismic Response of End-bearing Single Piles," *Soil Dynamics and Earthquake Engineering*, **3(2),** 82-93.

Gazetas, G., *et al.* (1991) "Dynamic Interaction Factors for Floating Pile Groups," *Journal of Geotechnical Engineering, ASCE,* **117(10),** 1531-1548.

Gazetas, G., et al. (1995) "Simple Methods for the Seismic Response of Piles Applied to Soil-Pile-Bridge Interaction," *Proceedings, 3rd International Conference on Recent Advances in Geotechincal Earthquake Engineering and Soil Dynamics*; Vol. III, pp. 1547-1556.

Lok, M.H. (1999) "Numerical Modeling of Seismic Soil-Pile-Superstructure Interaction in Soft Clay," *Ph.D. Thesis*, Univ. of California, Berkeley.

Markis N., Gazetas, G. (1992) "Dynamic Pile-Soil-Pile Action. Part II: Lateral and Seismic Response", *Earthquake Engineering and Structure Dynamic*, **21(2),** 145-162.

Matlock, H. & Reese, L. C. (1960). "Generalized solutions for laterally loaded piles", *Journal of Soil Mechanics and Foundation Division, ASCE,* **86:SM5**, 63-91

Matlock, H. (1962) "Correlations for Design of Laterally Loaded Piles in Soft Clay", A Report to Shell Development Company, Houston, Texas, Engineering Science Consultants.

Meymand, P.J. (1998) "Shaking Table Scale Model Tests of Nonlinear Soil-Pile-Superstructure Interaction in Soft Clay," *Ph.D. Thesis*, Univ. of California, Berkeley.

Nogami, T., *et al.* (1988) "Time domain flexural response of dynamically loaded piles," *Journal of Engineering Mechanics Division, ASCE*, **114(9),** 1512-1525.

Nogami, T., *et al.* (1992) "Nonlinear Soil-Pile Interaction Model for Dynamic Lateral Motion," *Journal of Geotechnical Engineering, ASCE,* **118(1),** 89-106.

Novak, M. (1974). "Dynamic Stiffness and Damping of Piles", *Can. Geotech. J.*, **11(4)**, 574-598.

Novak, M. (1977). "Soil-Pile Interaction", *Proc. 6th World Conf. Earthquake Eng.*, New Delhi, **IV**, 97-102.

Prakash, S. (1981). *Soil Dynamics*, McGraw-Hill, Inc. US, 220-270.

Winkler, E. (1867). "Die Lehre von der Elastizitat und Kestigkeit," Verlag, 182.

CONSTRUCTION TECHNOLOGIES:

FRP COMPOSITE, RETROFIT AND REPAIR TECHNOLOGIES

This Page Intentionally Left Blank

Advances in Building Technology, Volume 1
M. Anson, J.M. Ko and E.S.S. Lam (Eds.)
© 2002 Elsevier Science Ltd. All rights reserved

FRP REINFORCED ECC STRUCTURAL MEMBERS UNDER REVERSED CYCLIC LOADING CONDITIONS

Gregor Fischer, Victor C. Li
ACE-MRL, Department of Civil and Environmental Engineering, University of Michigan

Abstract

This paper reports on an investigation of FRP reinforced ECC flexural members with respect to their load-deformation behavior, residual deflection, damage evolution and failure mode. The paper briefly reviews particular aspects of conventional FRP reinforced concrete members, such as interfacial bond strength, flexural crack formation, composite deformation behavior, and brittle failure mode and presents a comparison to FRP reinforced ECC under reversed cyclic loading conditions. The combination of structural FRP reinforcement and ECC matrix in flexural members is characterized by a non-linear elastic response with stable hysteretic behavior, small residual deflections and ultimately gradual compression failure. Compatible deformations of FRP reinforcement and ECC lead to low interfacial bond stress and prevent composite disintegration by bond splitting and cover spalling. Flexural stiffness and strength as well as crack formation and widths in FRP reinforced ECC members are found effectively independent of interfacial bond properties due to the tensile deformation characteristics of the cementitious matrix.

Keywords: ECC, FRP reinforcement, composite, interfacial bond, deformation compatibility, damage tolerance

Introduction

Conventional FRP reinforced concrete members are typically over-reinforced and designed to fail in compression of concrete rather than by tensile rupture of the FRP reinforcement. Consequently, FRP reinforced concrete members possess relatively low ductility due to the brittle failure mode of concrete in compression as compared to tensile yielding of reinforcement in properly designed steel reinforced concrete members. Concepts to overcome this deficiency include ductile compression failure of concrete by providing confinement reinforcement or utilizing fiber reinforced concrete (Naaman and Jeong, 1995; Alsayed and Alhozaimy, 1999) as well as hybrid FRP reinforcement with inherent ductility (Harris et al., 1998). These concepts may provide a more gradual failure mode under monotonic loading conditions as compared to tensile failure of FRP reinforcement, however, under reverse cyclic loading conditions are unable to maintain their energy dissipation capabilities due to the unrepeatable nature of their inelastic deformation mechanism, i.e. concrete crushing, fiber pullout, or partial tendon rupture.

This paper presents results of an investigation on the effect substituting brittle concrete with a ductile, fiber reinforced cementitious composite in combination with structural FRP reinforcement under reverse cyclic loading conditions. This engineered cementitious composite (ECC) represents one type of

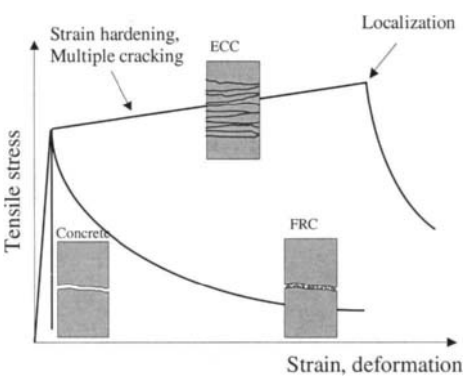


Figure 1 Schematic stress-strain behavior of cementitious matrices in tension

high performance fiber-reinforced cement composites (HPFRCC), which are designed with the intent of obtaining a high toughness composite material with pseudo strain-hardening and multiple cracking properties. While concrete in tension fails in a brittle manner upon reaching its cracking strength, ECC undergoes a strain-hardening phase analogous to that of metals (Fig.1). Beyond formation of first cracking in the cementitious matrix, ECC is designed to increase its composite tensile stress up to strain levels on the order of several percent. In contrast to localized deformation in concrete and conventional FRC (Fig.1), ECC accommodates imposed tensile deformations by formation of uniformly distributed multiple cracking with small individual crack widths (<200μm).

The interaction of elastic reinforcement and ductile cementitious matrix with respect to interfacial bond mechanisms, composite damage evolution, member deformation capacity, and failure mode are experimentally verified and contrasted to FRP reinforced concrete. The combination of elastic FRP reinforcement and ductile ECC takes advantage of the material properties of the constituent materials and more importantly of their synergistic interaction. In particular, the interfacial bond mechanism in FRP reinforced ECC is affected by this interaction, where compatible tensile deformations of reinforcement and matrix on a macro-scale prevent relative slip and therefore reduce activation of interfacial bond stress (Fischer and Li, 2002).

Material composition and properties

The ECC matrix used in this particular study utilized 1.5%-Vol. of Polyethylene fibers, which are added during the mixing procedure and randomly oriented in the hardened composite. The cementitious matrix in ECC consists of cement, sand (maximum particle size 0.3mm), water, superplasticizer, and common admixtures to enhance the fresh properties of the composite.

Material properties obtained from this composition are a tensile first cracking strength of 4.5MPa at 0.01% strain and an ultimate tensile strength of 6.5MPa at approximately 4% strain (Fig.2a). In compression, ECC has a lower elastic stiffness compared to concrete as well as larger strain at reaching its compressive strength due to the lack of large aggregates. The compressive strength of this particular version of ECC was 80MPa. Beyond ultimate, the compressive stress drops to approximately $0.5f'_c$ with subsequently descending stress at further increasing deformation (Fig.2b).

Concrete utilized coarse aggregates (maximum particle size 10mm), cement, water, and superplasticizer to enhance the fresh properties of the mix. The compressive strength of concrete used in this study was 50MPa at a strain of 0.2% (Fig.2b).

The longitudinal reinforcement of the specimens investigated in this study was provided by Aramid-FRP with a ribbed surface geometry similar to that of conventional steel reinforcement. The material properties according to the specifications of the manufacturer are a tensile elastic modulus of 54GPa, average tensile strength of 1800MPa, and tensile strain capacity of 3.8%.

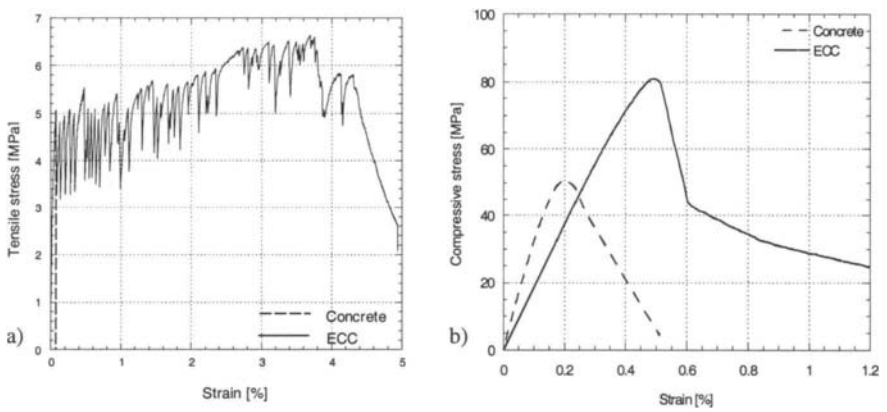


Figure 2 Stress-strain behavior of concrete and ECC in a) tension and b) compression

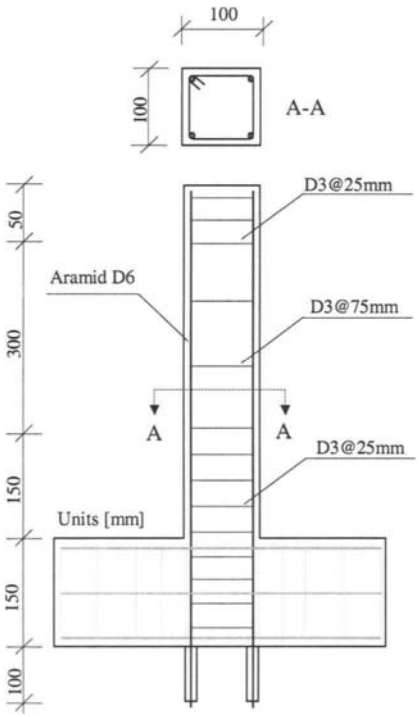


Figure 3 Specimen configuration

Specimen configuration and testing procedure

In this paper, results from tests of four different specimen configurations are presented, which were longitudinally reinforced with four FRP bars (Ø6mm), arranged symmetrically relative to both axes (Fig.4). These specimens were designed to exceed the compressive strength of the cementitious matrix prior to rupture of the FRP reinforcement. The experimental tests presented herein contain an R/C control specimen with transverse reinforcement (S-1), an R/ECC specimen with transverse reinforcement (S-2), an R/ECC specimen without transverse reinforcement (S-3), and an R/ECC specimen without transverse reinforcement and additional sand coating (S-4). The specimen configurations are summarized in Table 1.

The load-deformation response of FRP reinforced ECC flexural members is experimentally investigated and compared to FRP reinforced concrete using small-scale cantilever beams with 500mm height and square cross-sectional dimensions of 100mm (Fig.3). In order to provide cantilever type loading conditions, a rigid transverse beam was integrally cast with the cantilever base. Lateral loading was applied at the top of the cantilever through a loading frame equipped with a 100kN capacity actuator according to a displacement controlled loading sequence.

Load-deformation response

The load-deformation response of the tested specimens, FRP reinforced concrete as well as FRP reinforced ECC, is predominantly characterized by non-linear elastic behavior with relatively small residual deflections. As intended, failure is initiated by inelastic deformations of concrete in specimen S-1 and ECC in specimens S-2, S-3, and S-4. Ultimate failure occurred in all considered cases by reinforcement rupture due to reverse cyclic loading conditions and resulting damage on the longitudinal reinforcement under compression. The apparent differences between FRP reinforced concrete and FRP reinforced ECC in terms of load-deformation response, damage evolution, and deflection capacity are established in detail by comparing specimens S-1 and S-2. Furthermore, the behavior of specimens S-3 and S-4 is compared to specimen S-2 in order to investigate the influence of reinforcement detailing and interfacial bond properties on FRP reinforced ECC members.

Flexural cracking in specimens S-1 (R/C, with transverse reinforcement) and S-2 (R/ECC, with transverse reinforcement) occurred at relatively small flexural loads and deflections, which are for all practical purposes insignificant compared to service and ultimate deflections.

Beyond initiation of flexural cracking and at increasing drift levels, the formation of further flexural cracks is limited in specimen S-1 due to interfacial bond properties and stress transfer length between FRP reinforcement and concrete, resulting in a relatively large crack spacing of approximately 100mm (Fig.5). Therefore, imposed specimen deflections are accommodated by relatively large crack widths. The crack spacing in specimen S-2 is significantly smaller at all drift levels (Fig.5) especially at the cantilever base and similar to the crack spacing observed in this particular version of ECC in direct tension (10mm), suggesting that flexural crack formation is

effectively independent of the interaction with the FRP reinforcement. The formation of bond splitting cracks in specimen S-1 and the lack thereof in specimen S-2 further indicate differences in the respective composite deformation mechanism. While the strain lag between reinforcement and concrete at a crack location causes relative slip and radial stresses exceeding the matrix tensile strength as indicated by significant formation of bond splitting cracks, compatible deformations between reinforcement and ECC in the multiple cracking stage prevent significant bond stress and relative slip.

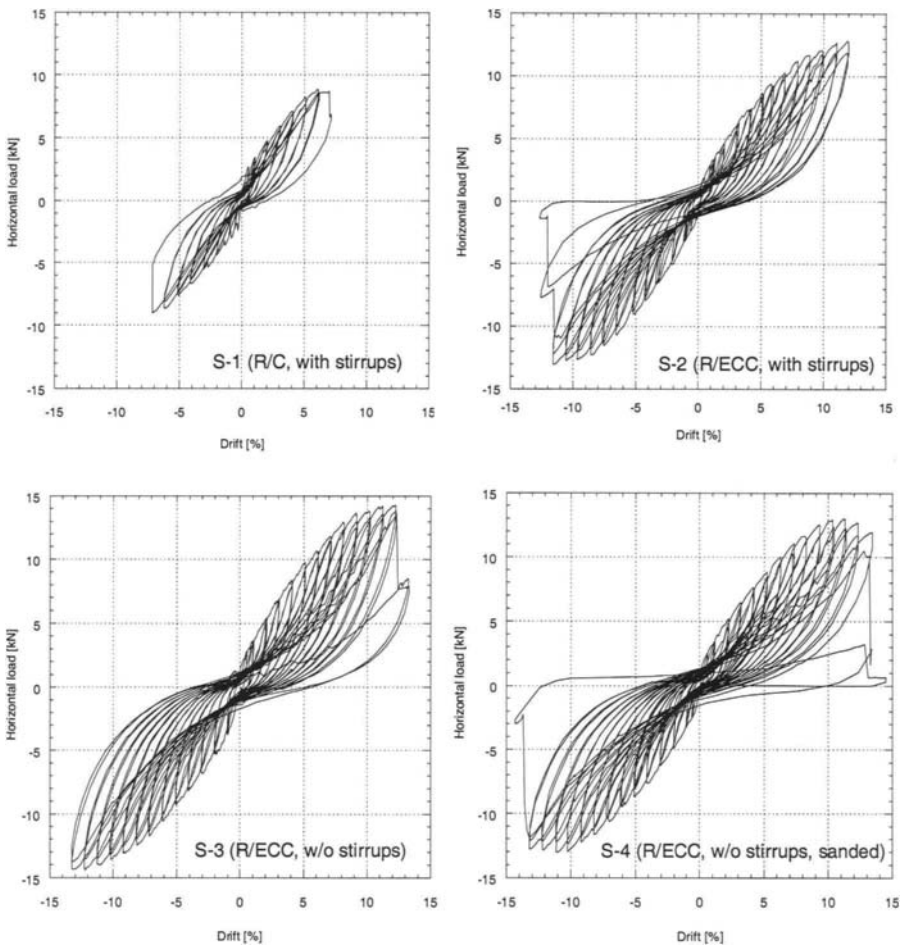


Figure 4 Load-deformation response of tested specimens

At further increasing deflection, the load-deformation behavior of specimens S-1 and S-2 is characterized by a progressive reduction of flexural stiffness at increasing applied load. A linear portion of the response cannot be clearly identified, which is due to inelastic deformations in the cementitious matrices in tension (flexural crack formation) and compression (gradual crushing). Furthermore, progressing interfacial bond failure and bond splitting cracks in specimen S-1

contribute to stiffness reduction and increasing non-linearity of the load-deformation response. Disintegration of the FRP reinforced concrete composite by crushing and bond splitting induces severe damage to the FRP reinforcement and partial rupture occurs at 7% drift and ultimate load of approximately 9kN (Fig.4).

In specimen S-2, flexural cracking continuously initiates up to relatively large deflections (7% drift), beyond which flexural stiffness reduction is influenced by ECC inelastic deformations under compression. The transition between these phases is indicated by noticeable plateau in the load-deformation curve beyond 7% drift (Fig.4). Ultimately, excessive compressive strain in ECC lead to damage in the FRP reinforcement and subsequent rupture at 12% drift and ultimate shear force of approximately 13kN. Similar to specimen S-1, the nominal tensile strength of the reinforcement is not exceeded at this point, however, damage induced by compressive and transverse deformations considerably reduces the tensile capacity.

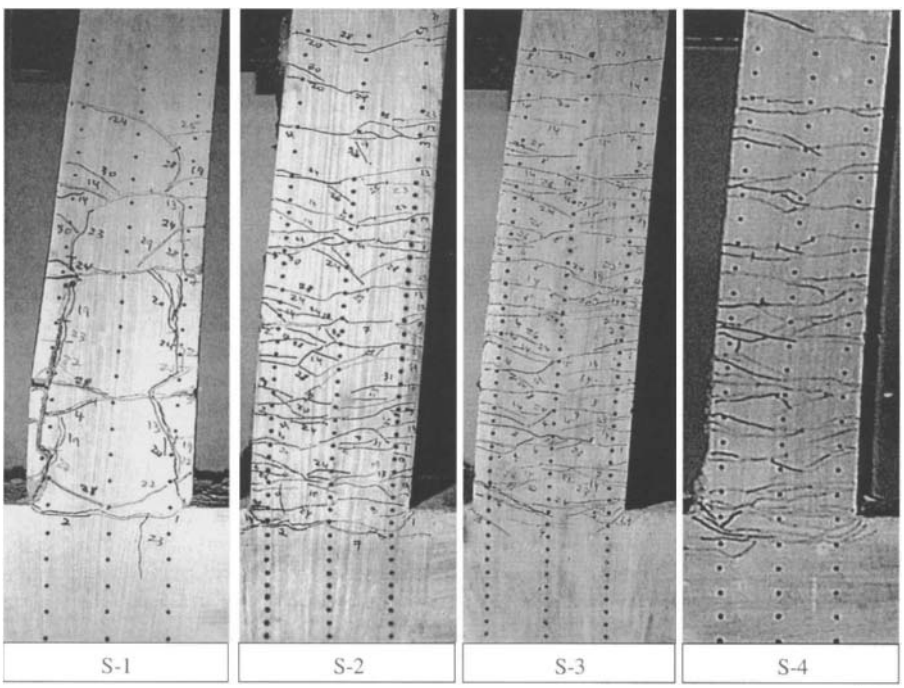


Figure 5 Deflected shape and damage pattern of specimens at 7% drift

Residual deflection and energy dissipation

The behavior of specimens S-1 and S-2 in terms of residual deflection and energy dissipation (Fig.6) is compared at increasing drift levels. In this paper, residual deflection is characterized by the ratio of permanent deflection after unloading and maximum deflection experienced at a given drift level. Energy dissipation is represented by the equivalent damping ratio, defined as the energy dissipated during a complete loading cycle normalized by the elastic energy stored in the member at a given drift level (Chopra, 1995).

Flexural crack formation primarily affects the specimen behavior at small drift levels in terms of residual deflection and energy dissipation. Incomplete crack closure after unloading at small drift levels significantly contributes to the residual deflection of specimens S-1 and S-2, which show

relatively large residual deflection ratios at 0.5% drift. At increasing drift levels, this ratio declines in both specimens and reaches a minimum of approximately 0.2, however, at different drift levels. Minimum residual deflection in S-1 is observed at 3% drift and in S-2 at 6% drift, which roughly coincides with flexural crack saturation in both specimens, respectively. In specimen S-1, additional inelastic deformation mechanisms, such as bond splitting, spalling and compression failure, succeed this phase particularly beyond 5% drift, thus the residual deflection ratio increases rapidly. In specimen S-2, flexural crack saturation is achieved at approximately 7% drift, beyond which the residual deflection ratio remains constant at 0.2 due to a stable flexural deformation mechanism. At deflections above 10% drift, crushing of ECC and rotational sliding constitute a major change in the deformation mechanism, resulting in a considerable increase in residual deflection ratio.

The energy dissipation characteristics of both specimens show trends very similar to those described for the residual deflection ratio. In both specimens, the equivalent damping ratio at small drift levels is primarily affected by flexural crack formation and reaches their respective minimum at flexural crack saturation, beyond which it remains constant due to internal friction along the crack planes and increases slightly at further damage by matrix crushing, spalling or rotational sliding occurs.

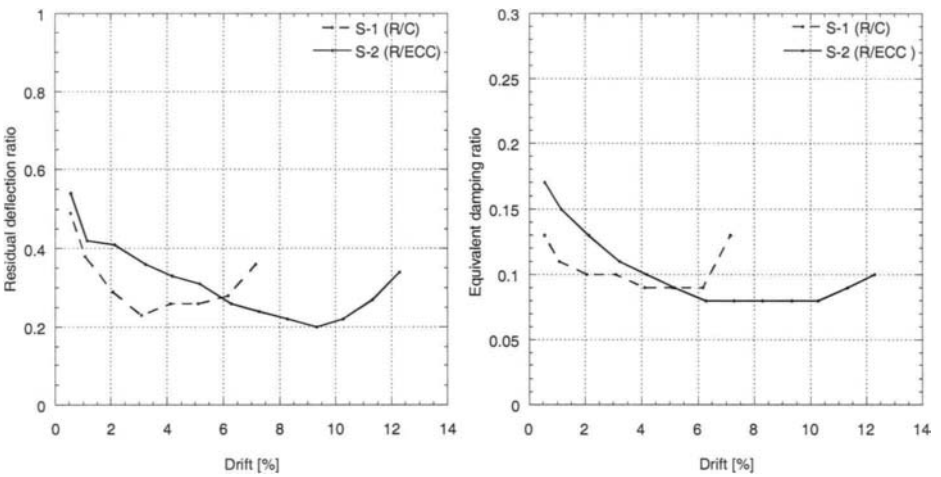


Figure 6 Residual deflection and equivalent damping in specimens S-1 and S-2

These observations suggest that flexural crack formation and saturation as well as damage induced by compression have major influence on residual deflection and equivalent damping characteristics of FRP reinforced members. While at drift levels prior to flexural crack saturation FRP reinforced ECC (S-2) shows larger residual deflection due to the larger number of flexural cracks compared to FRP reinforced concrete (S-1), it is able to maintain its flexural deformation mode beyond saturation with small residual deflections up to relatively large drift levels.

Transverse reinforcement

The comparison of specimen S-2 (R/ECC, with transverse reinforcement) (Fig.4) and S-3 (R/ECC, w/o transverse reinforcement) (Fig.4) indicates higher ultimate strength and deflection of specimen S-3 without transverse reinforcement. In view of identical longitudinal reinforcement in both specimens, this suggests that the presence of stirrups in specimen S-2 contributes to tensile strength reduction in the FRP reinforcement leading to premature failure. Inspection of specimen S-2 after completion of the test gives evidence supporting this assumption. Rupture of FRP exclusively

occurred at the intersection with stirrups, which locally constrained and punctured the longitudinal reinforcement. The experimentally obtained flexural strength of specimen S-3 is nearly identical to that predicted and therefore, its ultimate strength is considered optimal at given material properties of reinforcement and matrix. Lateral support and confinement of FRP reinforcement in S-3 is entirely provided by ECC. In contrast to a discrete lateral support in members with conventional stirrups, the longitudinal reinforcement is continuously supported, confined, and protected in the ECC matrix without intermittent restraint. The comparison of specimens S-2 and S-3 suggests that transverse reinforcement should not be used in FRP reinforced ECC flexural members if shear strength requirements permit. Although transverse reinforcement is usually found to enhance effective compressive strength and strain capacity of cementitious materials (concrete, ECC), which is advantageous in compression controlled members, its damaging effect on FRP reinforcement is detrimental. From the experimental results obtained in this study it is found that the self-confining effect of ECC is sufficient to prevent reinforcement buckling and assure ductile compressive failure, such that additional confinement reinforcement is not necessary.

Interfacial bond strength

The modification of the FRP reinforcement surface by additional sand coating does not positively affect the load-deformation behavior of specimen S-4 (R/ECC, w/o transverse reinforcement, sand coating) (Fig.4) compared to S-3 (R/ECC, w/o transverse reinforcement) (Fig.4). Maximum crack widths are identical prior to localization of cracking and ultimately, flexural crack spacing and distribution are similar in both specimens, however, in specimen S-4 local crack spacing at the cantilever base is found slightly smaller and localization of cracking is to some extent delayed. The increased crack density at the cantilever base weakens the compressive strength of the matrix and promotes the formation of a rotational sliding plane, which negatively affects flexural stiffness and strength of specimen S-4.

The comparison of specimens S-3 and S-4 with respect to load-deformation behavior and flexural crack formation confirms the assumption that the composite deformation characteristics of reinforced ECC members are effectively independent of the interfacial bond properties, provided that sufficient development length is available or external anchorage is supplied.

Conclusions

The response of FRP reinforced flexural members to reversed cyclic loading conditions indicates non-linear elastic load-deformation behavior with relatively small residual deflections. While the overall load-deformation behavior of FRP reinforced concrete and ECC show similarities, detailed differences have been established in terms of their composite deformation mechanism, damage evolution and ultimate deflection capacity.

Deformation compatibility between FRP reinforcement and ECC is found to effectively eliminate interfacial bond stress and relative slip in the multiple cracking deformation regime, preventing bond splitting and spalling of ECC cover. In contrast, incompatible deformations between reinforcement and concrete cause loss of interfacial bond and composite action resulting in damage to the reinforcement and limited deflection capacity of the FRP reinforced concrete member.

While the increased flexural strength of FRP reinforced ECC compared to reinforced concrete is mainly attributed to the compressive strength of ECC, the deflection capacity is fundamentally affected by improved composite interaction. The load-deformation response of FRP reinforced ECC is dominated by flexural deformation up to relatively large drift levels and crack formation is found effectively independent of interfacial bond properties. Inelastic deformation of ECC in compression lead to flexural stiffness reduction and ultimately gradual mode of failure, however, also induced compressive strain and tensile strength reduction in the FRP reinforcement.

Despite the ductile deformation behavior of ECC in direct tension, FRP reinforced ECC members do not have significant energy absorption capacity compared to conventional steel reinforced members. Flexural crack formation is the primary dissipating mechanism and therefore, cannot be repeatedly utilized.

Acknowledgements
The research described in this paper has been supported by a grant from the National Science Foundation (CMS-0070035) to the ACE-MRL at the University of Michigan. This support is gratefully acknowledged.

References

Alsayed, S.H., Alhozaimy, A.M. (1999), "Ductility of concrete beams reinforced with FRP bars and steel fibers", Journal of Composite Materials, Vol.33, No.19, pp.1792-1806

Chopra, A.K. (1995), "Dynamics of Structures – Theory and applications to Earthquake Engineering", Prentice-Hall, Inc.

Fischer, G., Li, V.C. (2002), "Influence of matrix ductility on the tension-stiffening behavior of steel reinforced Engineered Cementitious Composites (ECC)", ACI Structural Journal Vol.99, No.1, January-February 2002, pp104-111

Harris, H.G., Samboonsong, W, Ko, F.K. (1998), "New ductile FRP reinforcing bar for concrete structures", ASCE Journal for Composites for Construction, Vol.2, No.1, February 1998, pp.28-37

Naaman, A.E., Jeong, S.M. (1995) "Structural ductility of concrete beams prestressed with FRP tendons", *Non-metallic (FRP) Reinforcement for Concrete Structures*, Proceedings of the Second International RILEM Symposium (FRPRCS-2), E&FN Spon, London

Tables

Specimen	Composite	Surface	Reinforcement ratio		Ultimate strength	
			$\rho_{longitudinal}$	$\rho_{transverse}$	Predicted	Experimental
S-1	R/C	ribbed	1.13	0.57/ 0.19	9.5	9.0
S-2	R/ECC	ribbed	1.13	0.57/ 0.19	14.2	12.5
S-3	R/ECC	ribbed	1.13	-	14.2	14.3
S-4	R/ECC	ribbed, sanded	1.13	-	14.2	13.0

Table 1 Summary of specimen configurations

Advances in Building Technology, Volume 1
M. Anson, J.M. Ko and E.S.S. Lam (Eds.)
© 2002 Elsevier Science Ltd. All rights reserved

ULTIMATE AXIAL STRAIN OF FRP-CONFINED CONCRETE

L. Lam and J.G. Teng

Department of Civil and Structural Engineering
The Hong Kong Polytechnic University, Hong Kong, China

ABSTRACT

External confinement by the wrapping of FRP sheets (or FRP jacketing) provides a very effective method for the retrofit of reinforced concrete (RC) columns subject to either static or seismic loads. For the reliable and cost-effective design of FRP jackets, an accurate stress-strain model is required for FRP-confined concrete. Central to such a model is the determination of the ultimate condition of FRP-confined concrete which is reached when the FRP ruptures. This ultimate condition is characterized by two parameters: the ultimate axial strain and the corresponding stress level which may or may not be the ultimate strength of the FRP-confined concrete (i.e. the axial compressive strength). This paper presents a new equation for the ultimate axial strain of FRP-confined concrete on which there has been much uncertainty and considerable controversy. Both the stiffness and the actual ultimate condition of the FRP jacket are explicitly accounted for in this new equation. The theoretical basis and performance of the equation are discussed in detail. The paper also suggests confined cylinder tests as a standard type of tests to determine the efficiency factor of a particular FRP product in confinement applications, defined as the ratio between the actual hoop rupture strain of FRP in FRP-confined concrete and the ultimate tensile strain from material tests generally conducted using flat coupons.

KEYWORDS

Concrete, FRP, Confinement, Stress-Strain Model, Ultimate Strain, Ultimate Condition

INTRODUCTION

One important application of FRP composites in civil engineering is as a confining material to concrete in the retrofit of existing reinforced concrete (RC) columns by the provision of an FRP jacket in the form of FRP wraps or prefabricated FRP shells. As the main function of the FRP jacket is to provide confinement to the concrete, the reinforcing fibres are mainly or only present in the hoop direction, so the jacket has little longitudinal stiffness. That is, the jacket can be simplified as a unidirectional material providing only hoop resistance to any expansion of the concrete. The ultimate condition of such FRP-confined concrete is reached when the FRP ruptures due to hoop tensile stresses; failure of insufficient vertical lap joints is excluded from consideration here. It is with this type of FRP-confined concrete that this paper is concerned. Concrete-filled FRP tubes for new construction also make use of FRP confinement but they differ somewhat in behaviour as a result of the substantial longitudinal stiffness possessed by the tube.

For the reliable and cost-effective design of FRP jackets, an accurate stress-strain model is required for FRP-confined concrete. Over the last few years, a number of stress-strain models have been proposed. These models can be classified into two categories: (a) design-oriented models, and (b) analysis-oriented models. Stress-strain models of the first category are in closed-form expressions, with key parameters directly based on test results. They are suitable for direct application in design calculations by hand and/or spreadsheets. On the other hand, stress-strain models of the second category are aimed at accurate predictions using an incremental numerical procedure. These models are particularly suitable for incorporation in computer-based numerical analysis such as a nonlinear finite element analysis. A detailed discussion of these models can be found in Monti (2001), Teng et al. (2002) and Lam and Teng (2002a).

Central to any stress-strain model for FRP-confined concrete is the determination of the ultimate condition of FRP-confined concrete which is reached when the FRP ruptures. This ultimate condition is characterized by two parameters: the ultimate axial strain and the corresponding stress level which may or may not be the ultimate strength of the FRP-confined concrete (i.e. the axial compressive strength). There are two major deficiencies in existing stress-strain models including the authors' recent design-oriented model (Lam and Teng 2001, 2002b, Teng et al. 2002) and both are closely associated with the definition of the ultimate condition of FRP-confined concrete. First, the stiffness of the FRP jacket has not been properly accounted for by existing design-oriented models in predicting the ultimate condition of confined concrete, although analysis oriented models do not suffer from this problem. The stiffness of the FRP jacket in fact controls the stress-strain response of FRP-confined concrete, particularly the ultimate axial strain (referred to simply as the ultimate strain hereafter), as shown in this paper. If the confinement effect of the FRP jacket on the ultimate strain is accounted for only through the confinement ratio (i.e., the ratio between the maximum confining pressure and the compressive strength of unconfined concrete) as in a number of existing design-oriented models (e.g. Karbhari and Gao 1997, Miyauchi et al. 1999, Lam and Teng 2002b), different expressions are needed for the ultimate strain for different types of FRP due to their different stiffnesses (Lam and Teng 2002b). Second, when calculating the maximum confining pressure in both design- and analysis-oriented models, it has been commonly assumed that FRP rupture occurs when the hoop stress in the FRP jacket reaches the tensile strength determined from material tests, with the only exception being Xiao and Wu's (2000) model. This assumption is however not valid according to observations made in tests on FRP-wrapped concrete cylinders. The hoop strain reached in FRP at rupture can be much lower than the ultimate tensile strain of FRP from material tests (Lam and Teng 2002a). The omission of this important aspect of behaviour in existing models results in uncertainty in defining the ultimate condition of FRP-confined concrete. A more detailed discussion of the limitations of existing stress-strain models for FRP-confined concrete can be found in Lam and Teng (2002a).

This paper is concerned with the ultimate axial strain of FRP-confined concrete which is one of the two parameters defining the ultimate condition of FRP-confined concrete. By explicitly accounting for the stiffness of the FRP jacket and the actual condition of FRP rupture in FRP-confined concrete, a unified equation is presented for concrete confined by different types of FRP materials. The theoretical basis and performance of the equation are also discussed in detail.

THEORETICAL BASIS

In studies on actively confined and steel-confined concrete, the axial strain at the compressive strength of confined concrete ε_{cc} has been shown to relate linearly to the confinement ratio (Richart et al. 1929, Candappa et al. 2001). Based on this approach, in several design-oriented models for FRP-confined concrete (e.g. Karbhari and Gao 1997, Miyauchi et al. 1999, Lam and Teng 2002b), the confinement effect of the FRP jacket on the ultimate strain of FRP-confined concrete ε_{cu}, which in most cases is equal to ε_{cc}, is accounted for only through the confinement ratio. A deficiency of this approach is that the stiffness of the FRP jacket is not properly accounted for. This deficiency can be explained by examining

the predictions of an analysis-based model in which the stiffness of the jacket is an inherent factor in determining the interaction between the FRP jacket and the concrete core.

TABLE 1
PROPERTIES OF CONFINING MATERIALS FOR RESULTS SHOWN IN FIGURE 1

Confining material	Elastic modulus (MPa)	Rupture or yield stress (MPa)	Rupture or yield strain (%)	Thickness of confining jacket (mm)
Steel	2×10^5	300	0.15	4
CFRP	2.35×10^5	3530	1.5	0.34
GFRP	23100	462	2.0	2.6

Figure 1 shows three stress-strain curves predicted by the analysis-oriented model developed by Speolstra and Monti (1999) for concrete cylinders confined by three different confining materials: steel, CFRP and GFRP. The compressive strength of the unconfined concrete is 35 MPa while the diameter of the cylinder is 152 mm. The three materials have typical properties as given in Table 1; the thicknesses were assumed values which lead to the same ultimate tensile capacity in the hoop direction and thus the same maximum confining pressure but different jacket stiffnesses. Figure 1 shows clearly that the predicted stress-strain response, particularly the ultimate strain, depends strongly on the stiffness of the FRP jacket. The compressive strength also depends on the stiffness of the jacket, but this dependence is much weaker within the practical range of FRP material properties, which supports the stiffness-independent approach widely-adopted for compressive strength (e.g. Lam and Teng 2002c). These conclusions from the analysis-oriented model are believed to be valid also for real FRP-confined concrete, because any significant inaccuracy of the model is in the concrete but the results were obtained for the same concrete and the behaviour of concrete is reasonably well approximated in the model from limited previous comparisons (Yuan et al. 2001).

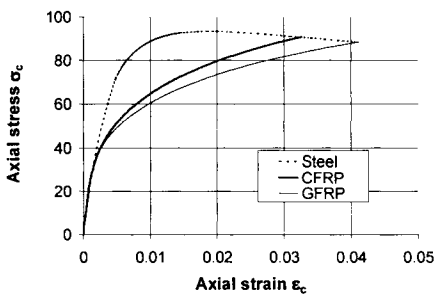


Figure 1 Stress–strain curves predicted by Spoelstra and Monti's (1999) model

The dependence of the ultimate strain of FRP-confined concrete on the stiffness of the confining jacket can also be shown by examining the constitutive model for concrete under a triaxial state of stress proposed by Ottosen (1979). This model is based on non-linear elasticity, with the properties of concrete being represented by the secant values of elastic modulus and Poisson's ratio. It has been adopted by the CEB-FIP Model Code 1990 (CEB-FIP 1993). The basic equations of the model are

$$\varepsilon_1 = \frac{1}{E_{sec}}\left[\sigma_1 - \nu_{sec}(\sigma_2 + \sigma_3)\right] \tag{1a}$$

$$\varepsilon_2 = \frac{1}{E_{sec}}\left[\sigma_2 - \nu_{sec}(\sigma_1 + \sigma_3)\right] \tag{1b}$$

$$\varepsilon_3 = \frac{1}{E_{sec}}[\sigma_3 - \nu_{sec}(\sigma_1 + \sigma_2)] \tag{1c}$$

where E_{sec} = secant modulus of elasticity and ν_{sec} = secant Poisson's ratio. For confined concrete, ε_1 = ε_c = axial strain of concrete, ε_2 = ε_r = radial (lateral) strain of concrete = ε_3 = ε_θ = circumferential strain of concrete, σ_1 = σ_c = compressive stress of concrete, and σ_2 = σ_3 = σ_r = lateral confining pressure. In this paper, compressive stresses and strains in concrete are taken as positive, while for the FRP, tensile stresses and strains are taken to be positive. The following equation can be obtained from Eqn. 1:

$$\varepsilon_c = -\frac{\varepsilon_r}{\nu_{sec}} + \frac{(1 - \nu_{sec} - 2\nu_{sec}^2)\sigma_r}{\nu_{sec} E_{sec}} \tag{2}$$

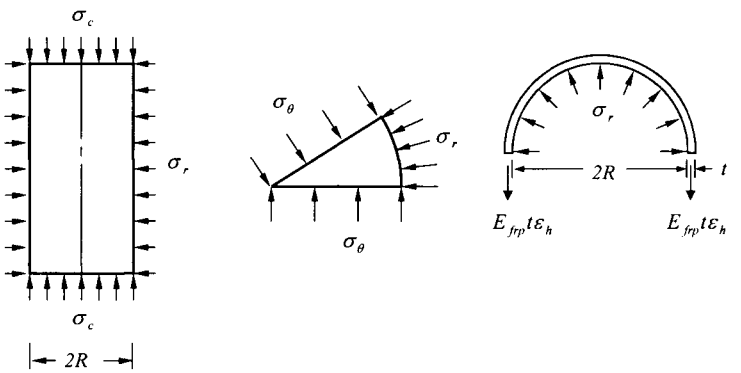


Figure 2 Confinement of concrete by an FRP jacket

The confining action of FRP to concrete is illustrated in Figure 2 where all the stresses are shown in their positive directions. The lateral confining pressure provided by FRP at any stage of loading is given by

$$\sigma_r = \frac{E_{frp} t \varepsilon_h}{R} \tag{3}$$

where E_{frp} and t = elastic modulus in the hoop direction and total thickness of the FRP jacket respectively, R = radius of the concrete core, and ε_h = hoop tensile strain in the FRP and = $-\varepsilon_r$ due to the difference in sign convention between the FRP jacket and the concrete core. Under the ultimate condition of FRP rupture, ε_r = ε_{ru} = $-\varepsilon_{h,rup}$, where ε_{ru} is the ultimate lateral strain of the confined concrete and $\varepsilon_{h,rup}$ is the hoop rupture strain of the FRP. The secant modulus of elasticity of concrete under the ultimate condition is given by (Ottosen 1979)

$$E_{sec\,u} = \frac{E_{sec\,o}}{1 + 4(A-1)x} \tag{4}$$

where $E_{sec\,o}$ = secant modulus of elasticity at the compressive strength of unconfined concrete and = $f_{co}^{'} / \varepsilon_{co}$ with $f_{co}^{'}$ being the compressive strength of unconfined concrete and ε_{co} being the axial strain at $f_{co}^{'}$; A = 2 for a parabolic stress-strain curve; and x is given by $x = \sqrt{J_2} / f_{co}^{'} - 1/\sqrt{3}$ with J_2 being the second invariant of the deviatoric stress tensor under the ultimate condition. Substituting Eqns. 3 and 4 into Eqn. 2 for the ultimate condition, the following expression (Lam and Teng 2002d) can be obtained:

$$\frac{\varepsilon_{cu}}{\varepsilon_{co}} = \frac{\varepsilon_{h,rup}}{\nu_{sec\,u}\varepsilon_{co}} + \frac{(1 - \nu_{sec\,u} - 2\nu_{sec\,u}^2)(1 + 4x)}{\nu_{sec\,u}} \left(\frac{E_{frp} t}{E_{sec\,o} R}\right)\left(\frac{\varepsilon_{h,rup}}{\varepsilon_{co}}\right) \tag{5}$$

where ε_{cu} = ultimate strain of the confined concrete, and $\nu_{sec\,u}$ = secant Poisson's ratio of the confined concrete under the ultimate condition. The term $E_{frp}t/E_{sec\,o}R$ is the confinement stiffness ratio, representing the stiffness ratio between the FRP jacket and the concrete core (Lam and Teng 2002d).

PROPOSED EQUATION

Equation 5 shows clearly the dependence of the ultimate strain of FRP-confined concrete ε_{cu} on the confinement stiffness ratio and the strain capacity of FRP at hoop rupture. The secant Poisson's ratio of FRP-confined concrete under the ultimate condition, $\nu_{sec\,u}$, also depends strongly on the confinement stiffness ratio (Lam and Teng 2002d). Thus, the ultimate strain of FRP-confined concrete ε_{cu} can be predicted using the following equation:

$$\varepsilon_{cu}/\varepsilon_{co} = c + k_2\left(\frac{E_{frp}t}{E_{sec\,o}R}\right)^{\alpha}\left(\frac{\varepsilon_{h,rup}}{\varepsilon_{co}}\right)^{\beta} \tag{6}$$

where c = normalised ultimate strain of un-confined concrete, k_2 = strain enhancement coefficient, and α and β are exponents to be determined. The effects of the secant Poisson's ratio $\nu_{sec\,u}$ and the parameter x are reflected by the choice of appropriate values for α, β and k_2. This equation explicitly accounts for the stiffness and the actual ultimate condition of the jacket, and may thus be referred to as a stiffness-based equation. If both α and β are taken as unity, then Eqn. 6 reduces to

$$\varepsilon_{cu}/\varepsilon_{co} = c + k_2\frac{f_{l,a}}{f_{co}'} \tag{7}$$

where $f_{l,a}$ is the actual maximum confining pressure given by

$$f_{l,a} = \frac{E_{frp}t\varepsilon_{h,rup}}{R} \tag{8}$$

so that the ultimate strain is directly and only related to the actual confinement ratio $f_{l,a}/f_{co}'$ as ε_{co} is generally taken as a constant.

DETERMINATION OF α AND β

The two exponents, α and β, can be determined using test results from the open literature (Lam and Teng 2002d). In Lam and Teng (2002d), a database containing the test results of 81 plain concrete circular specimens wrapped with FRP is presented. Different types of FRP, namely, carbon FRP (CFRP), aramid FRP (AFRP) and glass FRP (GFRP) were used in these tests. The CFRP used included normal CFRP with high strength carbon fibres and HM CFRP with high modulus carbon fibres. The database includes results of the ultimate lateral strain ε_{ru}, ultimate axial strain ε_{cu} and compressive strength of confined concrete f_{cc}'. Most of the specimens were reported with corresponding FRP material properties from flat coupon tests (e.g. ASTM D3039 1995). For the rest, FRP properties from the manufacturers were reported.

Figure 3 shows plots of the strain enhancement ratio against the actual confinement ratio from the test database (Lam and Teng 2002d) for CFRP wraps and AFRP wraps respectively. In these diagrams and elsewhere in the paper, ε_{co}, which is the strain at the compressive strength of unconfined concrete, is taken as 0.002. A linear relationship clearly exists in both cases but the two trend lines are very different (Figure 3). These diagrams indicate that the strain enhancement ratio can be related to the confinement ratio for a given type of FRP, but separate expressions are needed for different types of FRP due to their difference in stiffness (Lam and Teng 2002b, Teng et al. 2002). To achieve a unified expression for the

ultimate strain of FRP-confined concrete, the confinement stiffness ratio needs to be reflected, which means that the exponents, α and β, cannot both be unity.

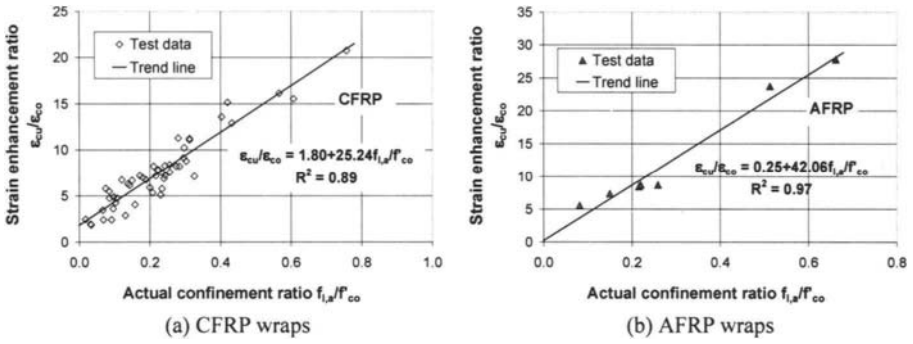


Figure 3 Strain enhancement ratio versus actual confinement ratio

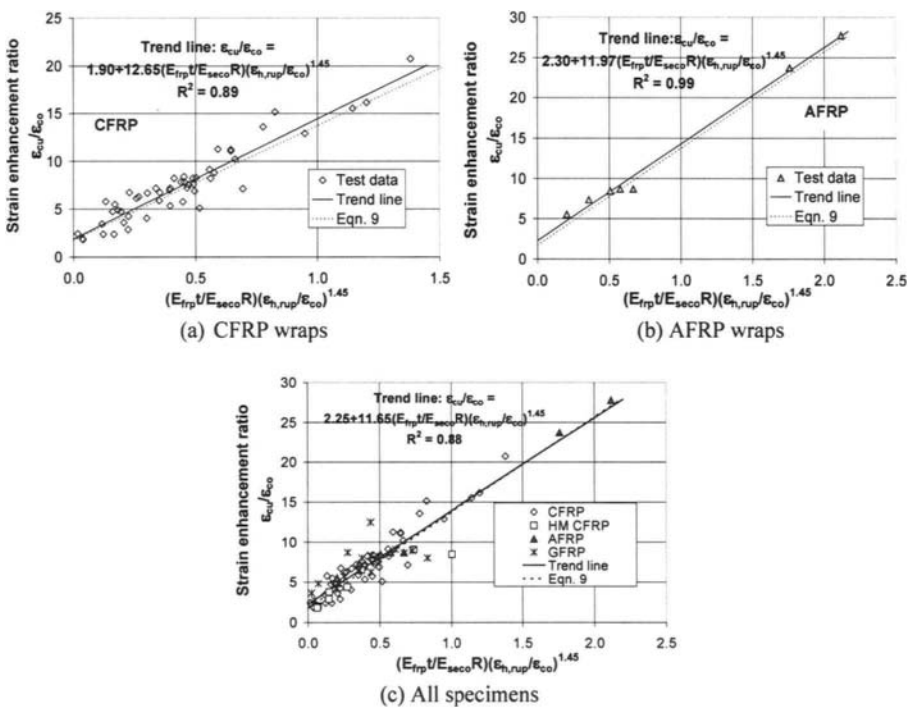


Figure 4 Performance of proposed equation for the ultimate strain of FRP-confined concrete

Figure 4 shows comparisons of the test data with the following equation with the various coefficients of Eqn. 6 carefully calibrated from the test data (Lam and Teng 2002d):

$$\varepsilon_{cu}/\varepsilon_{co} = 1.75 + 12\left(\frac{E_{frp}t}{E_{seco}R}\right)\left(\frac{\varepsilon_{h,rup}}{\varepsilon_{co}}\right)^{1.45} \tag{9}$$

Figures 4a and 4b show that when plotted separately, similar trends are observed for CFRP and AFRP wraps. When all test data are plotted together (Figure 4c), the data points of HM CFRP wraps and GFRP wraps also fall near the trend line and the predictions of Eqn. 9, although the data points of GFRP wraps are rather scattered. Eqn. 9 therefore provides a unified expression for the ultimate strain of FRP-confined concrete that is accurate for different types of FRP.

FRP EFFICIENCY FACTOR

The application of Eqn. 9 requires the FRP hoop strain at rupture which cannot be taken to be the tensile strain from material tests, generally conducted using flat coupons following an acceptable standard (e.g. ASTM D-3039 1995). For most of the test specimens in the database, the FRP material properties were obtained by the researchers from flat coupon tensile tests. For the 51 CFRP-wrapped specimens, the ratio of the actual FRP hoop rupture strain ($\varepsilon_{h,rup}$) in FRP-confined concrete to the FRP rupture strain from flat coupon tests (ε_{frp}), defined as the FRP efficiency factor, is 0.583 on average (Lam and Teng 2002d). Making use of this efficiency factor, the ultimate strain of FRP-confined concrete can be expressed as

$$\varepsilon_{cu}/\varepsilon_{co} = 1.75 + 5.5\left(\frac{E_{frp}t}{E_{seco}R}\right)\left(\frac{\varepsilon_{frp}}{\varepsilon_{co}}\right)^{1.45} \tag{10}$$

This equation requires the user to know only the tensile strain ε_{frp} from flat coupon tests. It is worth noting that with this average efficiency factor of 0.583 for CFRP-wrapped concrete, the compressive strength equation proposed in Lam and Teng (2002c) for FRP-wrapped concrete derived mainly from test data of CFRP-wrapped specimens based on the flat coupon tensile strength and the alternative equation proposed in Lam and Teng (2002d) based on the actual hoop rupture strain of FRP provide almost identical predictions. The former equation is given by

$$\frac{f_{cc}^{'}}{f_{co}^{'}} = 1 + 2\frac{f_l}{f_{co}^{'}} \tag{11}$$

where f_l is the nominal maximum confining pressure which can be obtained using Eq. 8 with $\varepsilon_{h,rup}$ replaced by ε_{frp}, while the latter equation is given by

$$\frac{f_{cc}^{'}}{f_{co}^{'}} = 1 + 3.3\frac{f_{l,a}}{f_{co}^{'}} \tag{12}$$

For other types of FRP, insufficient information exists to define this efficiency factor with confidence. Even for CFRP-confined concrete, there is a considerable scatter in the efficiency factor deuced from test results (Lam and Teng 2002d). The present authors therefore recommend that for cost-effective and safe designs, a small number of FRP-confined cylinder tests, analogous to plain cylinder tests, be conducted to determine the efficiency factor of a particular FRP product in confinement applications. For this purpose, a standard confined cylinder test method should be formulated. FRP manufacturers can then supply the results of such tests as part of their product information. If this information is not available from the manufacturer, the user should conduct these tests instead.

CONCLUSIONS

This paper has been concerned with the ultimate axial strain of FRP-confined concrete. A stiffness-based ultimate strain equation has been presented for concrete confined by wrapped FRP with fibres only or mainly in the hoop direction. The theoretical basis and performance of the equation have been described in detail. The stiffness and the actual ultimate condition of the FRP jacket are explicitly accounted for in

the equation so that it is accurate for different types of FRP as shown through comparisons with existing test data. For the application of this equation in design, the FRP efficiency factor (ratio between the actual hoop rupture strain of FRP in FRP-confined concrete to the tensile rupture strain from material tests) needs to be established. For this purpose, confined cylinder tests have been suggested as a standard type of tests to supply this information.

ACKNOWLEDGEMENTS

Both authors wish to thank the Research Grants Council of Hong Kong SAR (Project No: PolyU 5064/01E) and The Hong Kong Polytechnic University for their financial support.

REFERENCES

ASTM D3039/D3039M –95 (1995). Standard Test Method for Tensile Properties of Polymer Matrix Composites Materials, *Annual Book of ASTM Standards*, Vol. 14.02.

CEB-FIP (1993) *CEB-FIP Model Code 1990: Design Code*, Thomas Telford, London, UK.

Candappa, D.C., Sanjayan, J.G., and Setunge, S. (2001). Complete Triaxial Stress-Strain Curves of High-Strength Concrete. *Journal of Materials in Civil Engineering, ASCE*, **13:3**, 209-215.

Karbhari, V.M., and Gao, Y. (1997). Composite Jacketed Concrete under Uniaxial Compression–Verification of Simple Design Equations. *Journal of Materials in Civil Engineering, ASCE*, **9:4**, 185-193.

Lam, L. and Teng, J.G. (2001). A New Stress-Strain Model for FRP-Confined Concrete. *Proceedings, International Conference on FRP Composites in Civil Engineering*, Hong Kong, China, pp. 283-292.

Lam, L. and Teng, J.G. (2002a). Stress-Strain Models for Concrete Confined by Fiber-Reinforced Polymer. *Proceedings, 17th Australasian Conference on the Mechanics of structures and Materials*, Gold Coast, Queensland, Australia, pp. 39-44.

Lam, L. and Teng, J.G. (2002b). *Stress-Strain Models for FRP-Confined Concrete*, Research Centre for Advanced Technology in Structural Engineering, The Hong Kong Polytechnic University.

Lam, L. and Teng, J.G. (2002c). Strength Models for FRP-Confined Concrete. *Journal of Structural Engineering, ASCE*, **128:5**, 612-623.

Lam, L. and Teng, J.G. (2002d). Design-Oriented Stress-Strain Model for FRP-Confined Concrete. To be published.

Miyauchi, K., Inoue, S., Kuroda, T., and Kobayashi, A. (1999). Strengthening Effects of Concrete Columns with Carbon Fiber Sheet. *Transactions of The Japan Concrete Institute*, **21**, 143-150.

Monti, G. (2001). Confining Reinforced Concrete with FRP: Behavior and Modeling. *Proceedings, Workshop on Composites in Construction: a Reality*, Capri, Italy, July 2001.

Ottosen, N.S. (1979). Constitutive Model for Short-Time Loading of Concrete. *Journal of the Engineering Mechanics Division, ASCE*, **105**, 127-141.

Richart, F.E., Brandtzaeg, A. and Brown, R.L. (1929). *The Failure of Plain and Spirally Reinforced Concrete in Compression*, University of Illinois Engineering Experimental Station, Bulletin No. 185, Urbana, Illinois, USA.

Spoelstra, M.R. and Monti, G. (1999). FRP-Confined Concrete Model. *Journal of Composites for Construction, ASCE*, **3:3**, 143-150.

Teng, J.G., Chen, J.F., Smith, S.T. and Lam, L. (2002). *FRP-Strengthened RC structures*, John Wiley & Sons, Ltd., UK.

Xiao, Y. and Wu, H. (2000). Compressive Behavior of Concrete Confined by Carbon Fiber Composite Jackets. *Journal of Materials in Civil Engineering, ASCE*, **12:2**, 139-146.

Yuan, X.F., Lam, L., Teng, J.G. and Smith, S.T. (2001). FRP-Confined RC Columns under Combined Bending and Compression: a Comparative Study of Concrete Stress-Strain Models. *Proceedings, International Conference on FRP Composites in Civil Engineering*, Hong Kong, China, pp. 749-758.

Advances in Building Technology, Volume 1
M. Anson, J.M. Ko and E.S.S. Lam (Eds.)
© 2002 Elsevier Science Ltd. All rights reserved

EFFECT OF SIZE ON THE FAILURE OF FRP STRENGTHENED REINFORCED CONCRETE BEAMS

Christopher K.Y. LEUNG[1], Zhongfan CHEN[2], Stephen K.L. LEE[3], Jianmao TANG[3]

[1]Department of Civil Engineering, and [3]Advanced Engineering Materials Facility
Hong Kong University of Science and Technology,
Clear Water Bay, Kowloon, HONG KONG
[2]Department of Civil Engineering, Southeast University, Nanjing, CHINA

ABSTRACT

The bonding of fiber reinforced plastic (FRP) plates is an effective and efficient method to improve the bending capacity of concrete beams. In the literature, various design methodologies have been proposed and several of them have been found to compare well with test data or to provide reasonable lower bounds. However, almost all the experimental data are obtained from laboratory-size specimens that are several times smaller than members in real structures. On close examination, different design methodologies exhibit significantly different trends of load capacity vs member size. With no test results on larger specimens, it is not possible to determine which approach is more appropriate for designing real size members. In this investigation, geometrically similar reinforced concrete beams with steel ratio of 0.01, and depth ranging from 0.2 m to 0.8 m were prepared. Some RC beams were tested as control while others were retrofitted with 2 to 8 layers of Carbon fiber reinforced plastic (CFRP) sheets to achieve the same CFRP/concrete area ratio. All the beams were tested to failure to investigate the variation of failure load with member size. The results of the present investigation are expected to provide useful information for (i) the extrapolation of small specimen results to large members of practical size, and (ii) the checking of theoretical models for design.

KEYWORDS

Reinforced Concrete, Fiber Reinforced Plastics, Structural Retrofitting, Experimental Testing

INTRODUCTION

After years in service, many concrete structures have deteriorated and are in need of repair. In some cases, due to change of usage, members need to be strengthened through retrofitting to provide a load carrying capacity higher than that of the original design. For the flexural strengthening of concrete beams, the bonding of fiber reinforced plastic (FRP) plate to the tensile side has been shown to be an effective means (Saadatmanesh and Ehsani, 1991, Triantafillou and Plevris, 1992, Meier et al, 1993,

Arduini et al, 1997). Besides extensive laboratory studies, the application of FRP to strengthen beams in real structures has also been reported by Meier (1995) and Tan (1997).

For the widespread use of FRP strengthening in practice, a comprehensive design guideline is required. Any design guideline should include a method to accurately predict the failure load of the strengthened member. In the literature, various approaches have been proposed for failure prediction of FRP strengthened members. Some approaches (Teng et al, 2000) are based on the direct fitting of experimental data. Others (El-Mihilmy and Tedesco, 2001 , Raoof and Hassanen, 2000) are based on analytical models, and test data are employed to verify the theoretical prediction. In any case, the full verification of design models relies on the availability of experimental data covering a wide range of design variables. Most available data in the literature, however, are obtained from laboratory-size specimens, that are much smaller than members in real structures. For example, out of the 127 test results on flexural strengthening from 23 studies collected by Bonacci and Maalaj (2001), over 80 of them were obtained from specimens with depth of 300 mm or less. There are only 15 results with beam depth of 400mm or above, and the largest beam was 574mm in depth (with only data from one test). In real structures, beam members are rarely below 400 mm in depth, and very often deeper than 600 mm. Therefore, very few available existing data are representative of real members.

To see the effect of size on member strength, the best way is to calculate the normalized ultimate moment M/bd^2 for sections with similar reinforcement ratio but different size. In Fig.1 below, theoretical prediction of the size effect are carried out with 5 different models (El-Mihilmy and Tedesco, 2001, Oehlers, 1992, Raoof and Hassanen, 2000, Teng et al, 2001, Ziraba et al. 1994). In the analysis, geometrically similar beams 220, 440, 660 and 880 mm in depth are considered. The beam length (L), is 12 times the depth. Loading is applied at one-third points along the span. The steel reinforcement ratio is 1%. The width of the FRP plate (E=235 GPa) is the same as the beam, and the plate thickness is 0.2% the beam depth. The cut-off point of the plate is at a distance L/12 from the support. For each curve, the normalized failure moment (M/bd^2) (Here, d is taken to be the total beam depth, as the FRP is glued to the bottom) is further normalized with its value for the 220 mm depth beam. The predicted trend of failure load vs size can then be easily compared. From Fig.1, it can be seen that the different models show significantly different effects of member size.

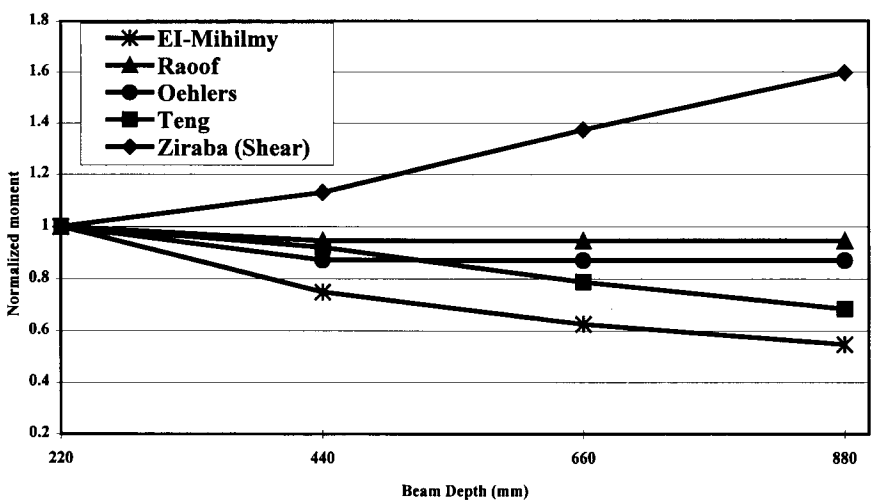


Figure1 Effect of Size on the Normalized Failure Moment of FRP retrofitted Beams

Note that each of these models has been compared with a significant number of experimental data for small specimens, with reasonable agreement achieved. However, even if we empirically 'calibrate' each model (e.g. by multiplying the predicted value with an empirical constant) to give similar results for laboratory size specimens (at 220 mm depth), the predicted failure moment for large members can differ a lot. We suspect that the increasing trend predicted by Ziraba et al.'s model is an artifact of the model, but even if this curve is taken out, the other models still show significant differences. The implication is very clear: experimental results on large members are necessary for the proper validation of design models for flexural failure of strengthened beams.

TESTING PROGRAM

Specimen Design, Preparation and Testing

To study the effect of size on the bending behaviour of FRP strengthened beams, nine reinforced concrete beams were prepared in three different sizes: 75mm (width) x 200mm (depth) x 2m (length), 150 mm x 400 mm x 4 m and 300 mm x 800 mm x 7.5 m. For all the beams, high yield steel reinforcement (σ_y=460 MPa) was employed and the thickness of cover (c) to the tensile reinforcement was 0.075d. The tensile steel reinforcement ratios in the beams (A_s/bh, where h = d-c) were respectively 1.13%, 1.09% and 1.13%. Also, all beams were over-reinforced in shear to ensure that failure would occur under bending. During testing, the loading spans for the three types of beams were respectively 1.8m, 3.6m and 7.2 m. 4 point loading was carried out, with loading applied at one-third points along the loading span. All the specimens were prepared at the same time, with concrete from a ready mix supplier. The design strength of the concrete (f_{cm}) was 30 MPa. Considering standard deviation of concrete, the mean strength should be close to 40 MPa. When the beams were tested, compression strength was also determined with concrete cubes. The average cube strength was found to be 47 MPa.

After the reinforced concrete beams were prepared and cured for over a month, 6 of the beams (2 for each size) were strengthened with bonded carbon fiber reinforced plastic (CFRP) strips. The Young's modulus of the CFRP is 235 GPa while its strength is 4.2 GPa. The CFRP is supplied in the form of a flexible sheet (0.11mm in thickness) with impregnated resin. In the retrofitting process, the bottom surface of the concrete beam was first roughened with a needle gun. A primer was then applied onto the concrete surface. Alternate layers of resin and CFRP were applied under the required thickness was attained. Note that the applied resin contains a hardener and will cause the CFRP sheet to harden and bond strongly to the concrete. For the three beam sizes, 2, 4 and 8 layers of CFRP were applied, and they were cut off at 0.2m, 0.4m and 0.8m from each support respectively. The width of CFRP was the same as the width of the beam. At least 7 days was allowed for the resin to attain maximum strength before testing of the beams were carried out.

All tests were performed with a Dartec loading system of 250 tonne capacity. In all specimens, strain gauges have been installed on both the steel reinforcements and CFRP sheet to monitor the failure process during the test. Besides the applied load, the displacement at mid-span was also measured with a LVDT. For some of the beams, the complete testing was videotaped to capture the damage processes leading to final failure.

Test Results

As mentioned above, a lot of information has been obtained from each individual test. Complete analysis of all the experimental data is still in progress and will be reported in an upcoming publication. In this short paper, we will only focus on the normalized moment for beams of various sizes, the maximum strain measured on the FRP and the percentage increase in load capacity due to strengthening. The experimental values are summarized in Table 1 below.

TABLE 1
EXPERIMENTAL RESULTS FOR BEAMS OF VARIOUS SIZES

Member	Type	Section Dimensions	Load Capacity (kN)	Max. FRP Strain ($\times 10^{-6}$)	M/bd^2 (N/mm^2)	% Increase in Load Capacity
SB1	Control	200 mm (d) x 75 mm (b)	61.02	-	6.102	-
SB2	Strengthened		69.56*	6634*	6.956*	14.0*
SB3	Strengthened		75.74	9737	7.574	24.1
MB1	Control	400 mm (d) x 150 mm (b)	212.02	-	5.301	-
MB2	Strengthened		274.14	7752	6.854	29.3
MB3	Strengthened		272.54	6976	6.813	28.5
LB1	Control	800 mm (d) x 300 mm (b)	822.78	-	5.142	-
LB2	Strengthened		1017.56	6400	6.360	23.7
LB3	Strengthened		1033.00	6673	6.456	25.5

* For specimen SB2, there was a problem with the surface preparation, so the CFRP debonded prematurely, with no concrete sticking to its surface. The result is hence an underestimate for the load capacity of a properly retrofitted beam.

From the above table, the effect of member size on the normalized moment can be observed. When going from the smallest to the largest member, (M/bd^2) decreases by roughly 15%. This size effect is considered quite moderate, considering the fact that the largest specimen is four times the size of the smallest one. In all members, failure was associated with debonding of the FRP from the bottom of the beam. The debonded region was not confined to one side of the beam but extended through the middle span. After testing, the failure surface of the FRP was inspected, and only a thin layer of stuck concrete was found. From our experience, this type of failure was induced by the opening of flexural cracks in the middle of the beam, rather than by stress concentrations near the plate cut-off point. Indeed, in the test on the largest beam, we were able to capture the failure sequence with a video camera. On replaying, it was clear that interfacial failure first started below a flexural crack near one of the loading points, and then propagated towards the end of the bonded plate.

The maximum strain measured on the FRP also suggested the presence of a size effect. Since the magnitude of measured strain also depends on the location of the gauge relative to the flexural cracks, the comparison of maximum strain between various members cannot be considered exact. However, a clear qualitative trend can be observed from the results. With a smaller specimen, it was possible for the FRP to reach a higher strain before failure. This observation is consistent with the size effect on normalized moment of the beam.

A very interesting observation from our result is that the size effect also exists for normal reinforced concrete members that are not strengthened. Indeed, if we consider the percentage increase of load capacity through FRP strengthening, the intermediate member exhibits the highest improvement, while the large and small members show about the same increase. Note that the tensile reinforcement ratio in the intermediate member was a bit smaller than the other two beams. The amount of added FRP reinforcement was hence relatively higher. This may partially explain the higher strengthening ratio. Overall, if one considers the percentage of load increase for members of all three sizes, the size effect is not too significant.

CONCLUSION

In this paper, the effect of member size on the load carrying capacity of FRP strengthened reinforced concrete beams is studied. The result shows that the size effects on the normalized moment of strengthened beams and percentage improvement in load capacity are quite moderate. To our knowledge, this investigation is the first ever study of its kind. It provides useful results for (i) extrapolation of laboratory results to real structural members, and (ii) checking of theoretical models. Based on the test data, any correct theoretical model for FRP debonding failure should not exhibit a large effect of size on the failure load.

REFERENCES

M. Arduini, A. Di Tommaso and A. Nanni (1997) Brittle Failure in FRP Plate and Sheet Bonded Beams. *ACI Structural Journal*, **94(4)**, 363-370.

J.F. Bonacci and M. Maalaj (2001). Behavioral Trends of RC Beams Strengthened with Externally Bonded FRP. ASCE Journal of Composites in Construction, **5**(2), 102-113.

M.T. El-Mihilmy and J.W. Tedesco, J.W. (2001). Prediction of Anchorage Failure for Reinforced Concrete Beams Strengthened with Fiber-Reinforced Polymer Plates. *ACI Structural Journal*, **98**(3), 301-314.

U. Meier, M. Deuring, H. Meier, and G. Schwegler, G. (1993). CFRP Bonded Sheets. *In*: *Fibre-Reinforced Plastic (FRP) Reinforcement for Concrete Structures: Properties and Applications*, edited by A. Nanni, Elsevier Science, Amsterdam, The Netherlands.

U. Meier (1995) Strengthening of Structures using Carbon Fibre/Epoxy Composites. *Construction & Building Materials*, **9**, 341-353.

Oehlers, D.J. (1992). Reinforced Concrete Beams with Plates glued to their Soffits. ASCE Journal of Structural Engineering, **118**(8), 2023-2038.

M. Raoof and M.A.H. Hassanen (2000). Peeling Failure of Reinforced Concrete Beams with Fibre-Reinforced Plastic or Steel Plates Glued to their Soffits. *Proceedings of the Institution of Civil Engineers: Structures and Buildings*, **140**, 291-305.

H. Saadatmanesh and A.M. Malek (1998). Design Guidelines for Flexural Strengthening of RC Beams with FRP Plates. *ASCE Journal of Composites for Construction*, **2**(4), 158-164.

K.H. Tan (1999). Towards a Cost-Effective Application of FRP Reinforcement in Structural Rehabilitation. *In: Proceedings of the Seventh East Asia-Pacific Conference on Structural Engineering and Construction*, Kochi, Japan, 65-73.

J.G. Teng, J.F. Chen, S.T. Smith and L. Lam. (2001). FRP Strengthened RC Structures. John Wiley & Sons, West Sussex, U.K.

T. C. Triantafillou and N. Plevris (1992). Strengthening of RC Beams with Epoxy Bonded Fibre Composite Materials. *Materials and Structures* **25**, 201-211.

Y.N. Ziraba, M.H. Baluch, I.A. Basunbul, A.M. Sharif, A.K. Azad and G.J. Al-Sulaimani (1994). Guidelines towards the Design of Reinforced Concrete Beams with External Plates. *ACI Structural Journal*, **91**(6), 439-646.

This Page Intentionally Left Blank

Advances in Building Technology, Volume 1
M. Anson, J.M. Ko and E.S.S. Lam (Eds.)
© 2002 Elsevier Science Ltd. All rights reserved

ANALYTICAL BEHAVIOUR OF CONCRETE BEAMS REINFORCED WITH STEEL REBARS AND FRP RODS

H. Y. Leung, S. Kitipornchai, R. V. Balendran and A. Y. T. Leung

Department of Building and Construction, City University of Hong Kong,
Tat Chee Avenue, Kowloon, Hong Kong

ABSTRACT

Reinforced concrete (RC) beam embedded with steel reinforcement usually gives a ductile behaviour but low strength whereas use of fibre-reinforced-plastic (FRP) rods provides a higher ultimate strength but limited ductility. It is thus thought that a combined use of steel rebars and FRP rods in concrete beam can offer a ductile and strong performance. To verify this, an analytical model is generated. The model computes the flexural behaviour of concrete members reinforced with conventional steel reinforcing bars and novel FRP rods. The model implementation is based on the use of the true stress-strain relationships for plain concrete, steel rebar and FRP rod. The main variable considered in this study is arrangement/depth of steel rebars and FRP rods. This paper presents some particular findings from the model. Most results are also compared with that of concrete beam reinforced only with steel rebars.

KEYWORDS

Concrete, RC beam, reinforcement, steel rebar, FRP rod, flexural strength

INTRODUCTION

Reinforced concrete (RC) beam embedded with conventional steel reinforcement usually gives a ductile behaviour but low strength whereas use of novel fibre-reinforced-plastic (FRP) rods provides a higher ultimate strength but limited ductility. Instead of exploring new materials as reinforcement so as to enhance the performance of reinforced concrete beam, it is thought that a mix use of steel rebars and FRP rods in concrete beam can offer a ductile and strong performance. Tentatively, concrete beams reinforced with both steel rebars and FRP rods exhibit one of the following flexural failure modes:

1. Concrete crushing occurs before steel yields and FRP breaks.
2. Steel yields followed by concrete crushing while FRP remains intact.
3. Steel yields followed by steel breaks while FRP remains intact.
4. Steel yields followed by FRP snaps.

These failure modes depend largely on the material properties of the ingredients and the configuration of the beam section. It is apparent that the first failure mode occurs only in over-reinforced sections. Since the aim of this study is to investigate the effect of addition of FRP rods into the steel-reinforced section, the latter three failure modes are desired. In this paper, an analytical model is generated to compute the flexural behaviour of concrete section reinforced with conventional steel reinforcing bars and novel FRP rods. Some results, including the strains, neutral axis depth, moments and curvatures, are discussed.

ANALYSIS & ASSUMPTIONS

A simple analytical procedure is developed to calculate the strains and stresses in concrete and reinforcements, moment and curvature in a rectangular concrete cross section reinforced with steel rebars and FRP rods. The procedure, which is derived from force equilibrium and strain compatibility, is applicable to conventional steel reinforced sections, FRP reinforced sections, as well as concrete sections reinforced with a combination of steel rebars and FRP rods. Fig. 1 shows the rectangular concrete beam section used in this study. The basic assumptions made include (1) linear strain distribution across the depth of section, (2) no bond slip of reinforcement, (3) reinforcement stress can be obtained from its stress-strain relationship, (4) tension concrete ignored, (5) shear deformation neglected and (6) failure of section is defined by either concrete crushing or reinforcement snapping.

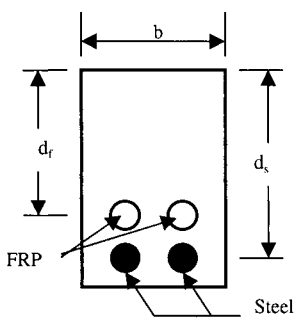


Figure 1: Beam cross section

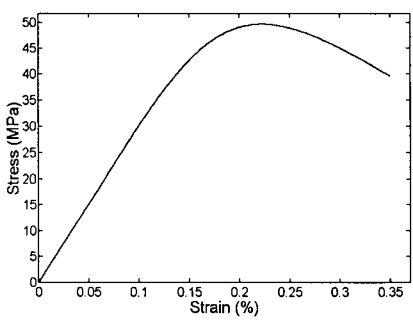


Figure 2: Stress-strain curve for concrete in compression

STRESS-STRAIN RELATIONSHIPS

Concrete in compression

The nonlinear stress-strain model of concrete in compression developed by Almusallam & Alsayed (1995) is used. This model was found to fit well the experimental results for normal strength and high strength concretes. In the model, the relationship between concrete stress (σ_c) and concrete strain (ε_c) is expressed by Eqn. 1.

$$\sigma_c = \frac{(K - K_p)\varepsilon_c}{\left[1 + \left(\frac{(K - K_p)\varepsilon_c}{\sigma_0}\right)^n\right]^{\frac{1}{n}}} + K_p\varepsilon_c \qquad (1)$$

where K = initial slope of the curve; K_p = final slope of the curve; σ_0 = reference stress; and n = curve-shape parameter. The equations of all these model parameters are listed in Appendix. Fig. 2 shows a stress-strain curve of compression concrete where the ultimate concrete strength $\sigma_c^{'} = 50\,\text{MPa}$. As can be seen in Fig. 2, the stress-strain curve terminates at an assumed strain value of 0.0035.

Tensile steel embedded in concrete

The stress-strain curve of steel reinforcing bars embedded in concrete is assumed to be bi-linear and was modelled by Wang & Hsu (2001). The relationship between steel stress (σ_s) and steel strain (ε_s) can be expressed by the following two equations (Eqn. 2 and Eqn. 3):

$$\text{for } \varepsilon_s \le \varepsilon_n \qquad \sigma_s = E_s \varepsilon_s \tag{2}$$

$$\text{for } \varepsilon_s > \varepsilon_n \qquad \sigma_s = \sigma_y \left[(0.91 - 2B) + (0.02 + 0.25B)\frac{\varepsilon_s}{\varepsilon_y} \right] \tag{3}$$

where E_s = elastic modulus of steel; σ_y = yield stress of steel; B = stress parameter; ε_y = strain of steel at yield; and ε_n = strain of steel at average stress when initial yielding occurs. All the model parameters are again given in the Appendix. This model, unlike others, accounts for the fact that the stresses in the steel bars between concrete cracks will be less than the yield stress at the cracks. An averaged value of steel stress across the cracks is thus adopted.

To facilitate generating a curve, some parameters are assumed and they include the breadth of concrete section (b = 200 mm); depth of steel rebars (d_s = 300 mm); area of steel (A_s = 157 mm^2); yield stress (σ_y = 420 MPa); and elastic modulus (E_s = 200 GPa). The resulting curve is shown in Fig. 3.

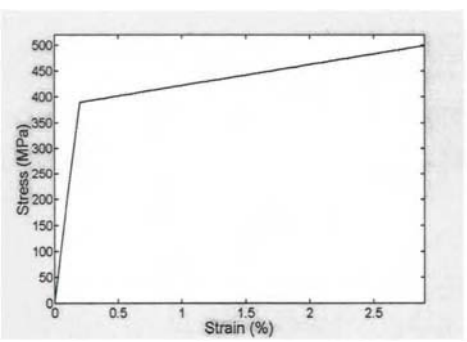


Figure 3: Stress-strain curve for steel

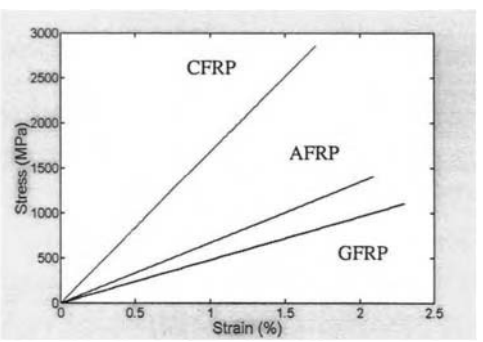


Figure 4: Stress-strain curve for FRP

Tensile FRP rod

The relationship of FRP stress (σ_f) and FRP strain (ε_f) under tension is assumed to be linear and is defined by Eqn. 4 and Eqn. 5.

$$\text{for } \varepsilon_f \le \varepsilon_f^u \qquad \sigma_f = E_f \varepsilon_f \tag{4}$$

$$\text{for } \varepsilon_f > \varepsilon_f^u \qquad \sigma_f = 0 \tag{5}$$

where E_f denotes the elastic modulus of FRP.

The three common FRPs used in construction industry are C(carbon)FRP, A(aramid)FRP and G(glass)FRP, and some of their properties (values obtained from Leung & Burgoyne, 2001) are given in Table 1. Using these values, the stress-strain curves for the three FRPs can then be generated and they are illutrated in Fig. 4.

TABLE 1
PROPERTIES OF FRPS

Materials	CFRP	AFRP	GFRP
Elastic modulus E_f	168 GPa	67 GPa	48 GPa
Ultimate strain ε_f^u	0.017	0.021	0.023

DERIVATIONS

A strain incremental technique is used in the derivation of different parameters. The strain in the extreme fibre of concrete (ε_c^{top}) is increased in a fixed increment, from zero to the ultimate (failure) strain value, to generate the moment-curvature relationship. Fig. 5 shows the distributions of strain and stress across the cross section.

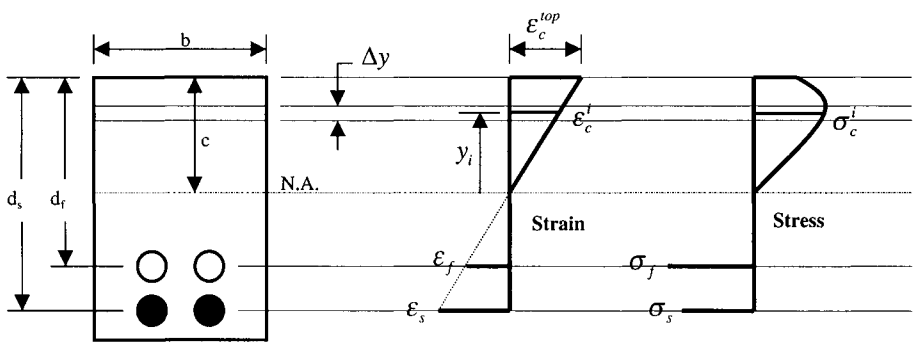


Figure 5: Strain and stress distributions

Once the value of ε_c^{top} is determined, a value of c is assumed. The compression concrete is divided into slices. Strains in the i^{th} compression concrete slice (ε_c^i), FRP rods (ε_f) and steel rebars (ε_s) are then calculated, in terms of ε_c^{top}, by the following three equations (Eqns. 6 to 8):

$$\varepsilon_c^i = \varepsilon_c^{top} \times \left(\frac{y_i}{c} \right) \tag{6}$$

$$\varepsilon_f = \varepsilon_c^{top} \times \left(\frac{d_f - c}{c} \right) \tag{7}$$

$$\varepsilon_s = \varepsilon_c^{top} \times \left(\frac{d_s - c}{c} \right) \tag{8}$$

where y_i is the distance of the i^{th} concrete slice measured from the neutral axis; c is the depth of neutral axis; d_f and d_s are the depth of FRP rods and steel rebars respectively. The stresses in the i^{th} concrete slice (σ_c^i), FRP rods (σ_f) and steel rebars (σ_s) are found from the corresponding stress-strain curves.

The concrete compressive force (F_c) is determined by summation of the product of elemental stress and the corresponding elemental area ($b \times \Delta y$) over the entire compression concrete portion. It is expressed by Eqn. 9.

$$F_c = \sum_i \left(\sigma_c^i \times b \times \Delta y \right) \tag{9}$$

The tensile FRP force (F_f) and steel force (F_s) are found by multiplying the FRP stress by the FRP area (A_f) and the steel stress by the steel area (A_s) respectively (Eqns. 10 and 11).

$$F_f = \sigma_f \times A_f \tag{10}$$

$$F_s = \sigma_s \times A_s \tag{11}$$

Equilibrium of internal forces is imposed by using Eqn. 12:

$$F_c = F_f + F_s \tag{12}$$

If the above equation is not satisfied, the location of the neutral axis (c) is adjusted until force equilibrium is achieved.

The internal resisting moment (M) is then calculated by summing the moments of all internal forces about the neutral axis, and it can be expressed, by Eqn. 13, as follows:

$$M = \sum_i \left(\sigma_c^i \times b \times \Delta y \right) y_i + F_f \times \left(d_f - c \right) + F_s \times \left(d_s - c \right) \tag{13}$$

As indicated by Eqn. 14, the curvature (κ) is also found by dividing the extreme concrete fibre strain by the neutral axis depth.

$$\kappa = \frac{\varepsilon_c^{top}}{c} \tag{14}$$

A small increment on ε_c^{top} is applied and the procedure repeats. The analysis terminates when ε_c^{top} goes beyond 0.0035.

RESULTS & DISCUSSION

To generate analytical results from the above procedure, some material and geometric parameters are assumed. To do this, the model parameters used in generating the curves in Fig. 2 and Fig. 3 are adopted, GFRP is chosen as the internal reinforcement and its properties are obtained in Table 1. It should be noted that a breaking strain of 10% is imposed for tensile steel rebars embedded in concrete. Assumed that $A_f = A_s$, the single variable left is the depth of GFRP rods (d_f) and its value is altered so as to investigate its effect on the flexural behaviour of the beam section (as shown in Fig. 1). Some analytical results are generated and are shown in Figs 6 to 10.

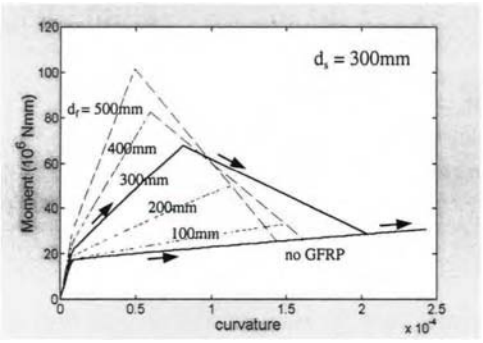


Figure 6: Moment against curvature

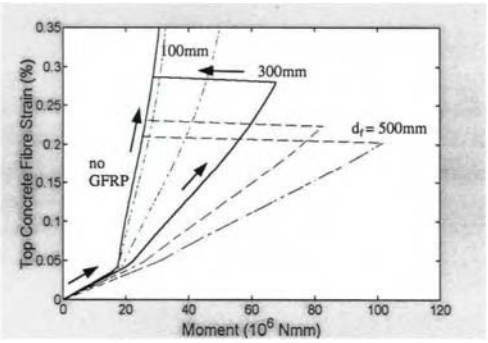


Figure 7: Concrete strain against moment

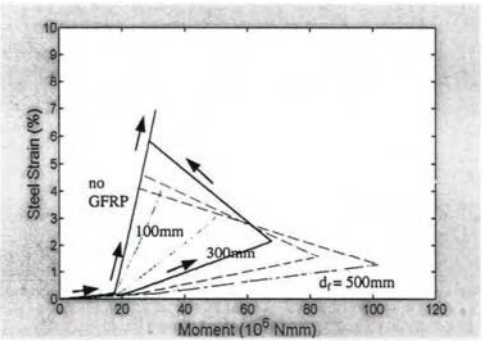


Figure 8: Steel strain against moment

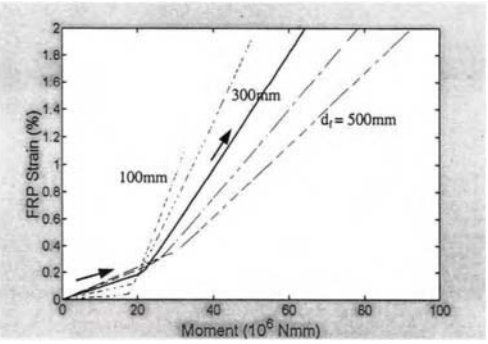


Figure 9: GFRP strain against moment

Fig. 6 shows the variation of moment against curvature for different values of d_f, the curve for no GFRP is also plotted. Since under-reinforced section is adopted, all different sections show occurrence of steel yielding. From the figure, it is clear that the beam section, with no GFRP, becomes a conventional steel-reinforced section and its moment-curvature relationship is bi-linear. Notice that when GFRP rods are added, the initial stiffness and the yield moment seem to increase slightly. When larger value of d_f is adopted, the resisting moment increases in a faster way and higher peak value is resulted. When the two curves with $d_f = 100mm$ and $d_f = 200mm$ are considered, they show an increase up to a peak and then stop. The two curves generally show a similar shape of the steel-reinforced section, except the increase in moment capacity and reduction in ductility. From Figs 7 to 9, it can be seen that the strains of steel bars and GFRP rods for

$d_f = 100mm$ and $d_f = 200mm$ are smaller than their corresponding ultimate strain values, while the concrete strain increases rapidly to 0.0035. This demonstrates that concrete crushing occurs before steel or FRP snaps. For the remaining three curves, a reverse situation is found; reinforcement breaks before concrete crushing occurs. As can be seen in Figs 8,9 and 10, the variation of steel strain remains in its plastic range while GFRP rods have reached its breaking point at failure. This explains the abrupt drop in moment-curvature relationship for $d_f = 300mm$, $d_f = 400mm$ and $d_f = 500mm$, as indicated in Fig. 6. It should also be noted that when larger value of d_f is used, the decrease in moment is more rapid. After GFRP rods have broken, the beam section contains only steel rebars and the moment-curvature curve for steel-reinforced section is followed.

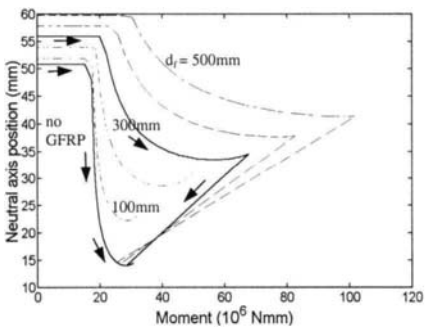


Figure 10: Neutral axis depth against moment

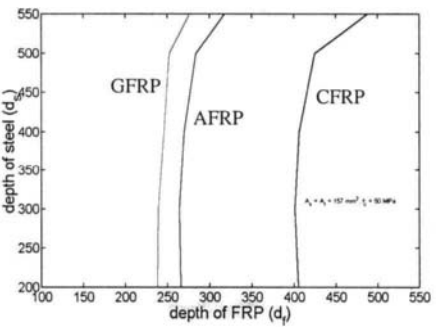


Figure 11: d_s versus d_f

It is interesting to study the neutral axis depth for section containing both kinds of reinforcements. As can be seen in Fig. 10, when no GFRP is used, the neutral axis remains fairly constant. Upon loading, it shifts upward when yielding of steel occurs. The neutral axis slightly goes downward when the section is about reaching its failure, this is explained by the fact that a reduction in concrete stress after its peak value and an increase in stresses in tensile reinforcement give rise to an increase in neutral axis depth. A similar situation is found when the depth of GFRP rods is not large ($d_f = 100mm$ and $d_f = 200mm$). When d_f is further increased, an abrupt upward shift in neutral axis is expected since the failure is governed by snapping of GFRP. Once the GFRP loses its action, the neutral axis depth must be reduced to balance the force between compression concrete and remaining steel rebars.

A similar analysis can be carried out for AFRP and CFRP using values in Table 1. Instead of plotting the strains, neutral axis depths, moments and curvatures, an interaction diagram for different failure modes is produced in Fig. 11. Three different curves are plotted for the three FRPs. Each curve represents the condition that concrete crushing and breaking of FRP rods break simultaneously. The area to the left of the curve indicates that concrete crushing occurs prior to snapping of FRP while the area to the right suggests FRP breaks followed by concrete crushing.

The current investigation provides some results on concrete flexural members reinforced with a mix of tension reinforcements, but there are limitations from a practical point of view. Firstly, it is rare to have steel rebar snapped at ultimate state as the breaking strain of steel is very much in excess of that for FRP. Besides, d_f greater than 300 mm is not common in daily practice. However, these two conditions are considered for the completeness of study.

CONCLUSIONS

From the analytical results, it is possible to conclude that:

1. Failure of steel-reinforced section with adddition of FRP rods is usually governed by concrete crushing or FRP snapping. The steel breaking failure mode is rare.
2. When steel rebars and FRP rods are employed, concrete crushing is usually accompanied by small value of FRP depth whereas breaking of FRP is normally the case for large value of FRP depth.
3. When FRP snaps, the beam section returns to the conventional steel-reinforced section.
4. Interaction diagram, which shows different failure modes, is produced.

REFERENCES

Almusallam T.H. and Alsayed S.H. (1995). Stress-strain relationship of normal, high-strength and lightweight concrete. *Magazine of concrete research* **47:170,** 39-44.

Wang T. and Hsu T.T.C. (2001). Nonlinear finite element analysis of concrete structures using new constitutive models. *Computers and Structures* **79**, 2781-2791.

Leung H.Y. and Burgoyne C.J. (2001). Analysis of FRP-reinforced concrete beam with aramid spirals as compression confinement. *Proceedings of the International Conference on Structural Engineering, Mechanics and Computation Cape Town, South Africa, edited by A. Zingoni,* Elsevier. **1,** 335-342.

APPENDIX

1. *Model parameters for concrete in compression*

$$n = -\frac{\ln 2}{\ln\left(\frac{\sigma_1}{\sigma_0} - \frac{K_p}{K - K_p}\right)}$$

$$\sigma_1 = \sigma_c'\left[\left(\frac{\varepsilon_1}{\varepsilon_0}\right) - \left(\frac{\varepsilon_1}{\varepsilon_0}\right)^2\right]$$

$$\varepsilon_1 = \frac{\sigma_0}{K - K_p}$$

$$\sigma_0 = 5.6 + 1.02\sigma_c' - K_p\varepsilon_0$$

for $\sigma_c' \le 55$ MPa

$$K_p = 5470 - 375\sigma_c'$$

for $\sigma_c' > 55$ MPa

$$K_p = 16398.23 - 676.82\sigma_c'$$

$$K = 3320\sqrt{\sigma_c'} + 6900$$

$$\varepsilon_0 = \left(0.2\sigma_c' + 13.06\right)\times 10^{-4}$$

where the ultimate compressive strength of concrete (σ_c') is in MPa.

2. *Model parameters for tensile steel rebars embedded in concrete*

$$\varepsilon_n = \varepsilon_y(0.93 - 2B)$$

$$B = \frac{(\sigma_{cr}/\sigma_y)^{1.5}}{\rho}$$

$$\rho = \frac{A_s}{bd_s} \ge 0.5\%$$

$$\sigma_{cr} = 0.31\sqrt{\sigma_c'}$$

where σ_c' and the cracking strength (σ_{cr}) are in MPa.

Advances in Building Technology, Volume I
M. Anson, J.M. Ko and E.S.S. Lam (Eds.)
© 2002 Elsevier Science Ltd. All rights reserved

APPLICATION OF GFRP REBAR IN CIVIL STRUCTURES

Z.J. Li[1] and Z.J. Zhang[2]

[1]Assoc. Prof., Dept. of Civil Engineering
[2]Grad. Student, Dept. of Civil Engineering
The Hong Kong University of Science & Technology
Clear Water Bay, Hong Kong

ABSTRACT:

The bonding properties between GFRP rebar and concrete are tested and analyzed to ensure feasible application of GFRP rebar in concrete structures. It is found that the bonding strength between GFRP bar and concrete is comparable with that between steel rebar and concrete. Also when there is special surface treatment, the bonding can be significantly improved. Then concrete beams with GFRP rebar embedded as reinforcement are tested and analyzed. It is found that the bonding is acceptable, and the bending capacity is larger using GFRP rebar, except that serviceability is difficult to satisfy.

KEYWORDS

GFRP, bond property, concrete structure, beam, bending

INTRODUCTION

Composites have been introduced into civil engineering structures mainly in the last decade. The application of composites in structural concrete mainly has three forms, FRP bars (tendons), sheets and composite tubes. Compared with conventional steel reinforcement, composite or fiber reinforced plastic (FRP) offers some excellent advantages. They are non-corrosion, non-magnetic, lightweight , and they have excellent handling property, high specific strength, availability in long lengths avoiding the need for lapping, and good fatigue and creep characteristics.

Nanni (1993) analyzed behavior and a design method for concrete beams with different concrete strengths, different kinds of FRP and different reinforcement ratios. Nanni et al (1996) systematically introduced components, and studied the behavior and applications of anchorage systems for FRP tendons. Dolan and Burke (1996) studied the behavior of concrete flexural members prestressed with pretensioned FRP tendons.

GFRP rebar has the advantages of high strength/weight ratio, corrosion resistance, and is also economical comparing with CFRP. Furthermore, when used as a prestressing tendon, its low Young's Modulus brings the unique benefit of lower prestress loss. Its disadvantages include non-ductility, instability at high

temperature, etc. However, by carefully selecting the application situation and methodology, GFRP materials can be very useful in civil engineering structures.

In this study, the push-out method is adopted for studying the bonding property between GFRP rebar and concrete, and the results are found to be satisfactory. Then, the four-point bending test is carried out to study the effect of GFRP rebar as conventional reinforcement. It is found that bonding between GFRP rebar and concrete is acceptable but the serviceability problem prevents the full utilization of GFRP's high ultimate tensile strength.

BOND PROPERTY STUDY

The bond between the composite rod and concrete was studied using the push-out test method, developed by Li et al (1998). The material used is GFRP rod with a glass fiber volume ratio of 67% and Young's Modulus of 51 GPa, and one the diameter is 8 mm. As shown in Table 1, six different formulas are used, with 2 kinds of GFRP rod: one has a smooth surface and the other is sand blasted on the surface. On addition, specimens of formula 1 with smooth surface steel bar were tested as control specimens.

TABLE 1
FORMULAS USED FOR SPECIMEN PREPARATION

		Water	cement	sand	PVA	CEP	Metakaolin	Silicon fume	Slag
1	Plain mortar matrix (cement+sand, w/c=35%, c/s=1:1	0.35	1	1					
2	PVA powder modified matrix (1%) (cement+sand+PVA, w/c=35%, c/s=1:1	0.35	1	1	0.01				
3	Cellulose Ether Powder modified (0.2% of methocel added)	0.35	1	1		0.002			
4	cement+sand+silica fume (replace 5% of cement with s.f.)	0.35	0.95	1				0.05	
5	cement+sand+metakaolin (replace 5% of cement with metakaolin)	0.35	1	1			0.05		
6	cement+sand+slag (replace 50% of cement with slag)	0.35	0.5	1					0.5

A typical load push-out curve as a function of displacement is shown in Figure 1. The load curve shows a linear-elastic stage, a nonlinear ascending stage, then a sudden drop followed by a stable constant force stage. This indicates that the push-out process includes interfacial crack propagation phenomenon.

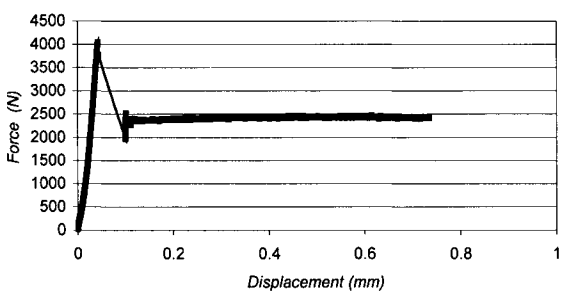


Figure 1: A typical push-out load curve as a function of displacement

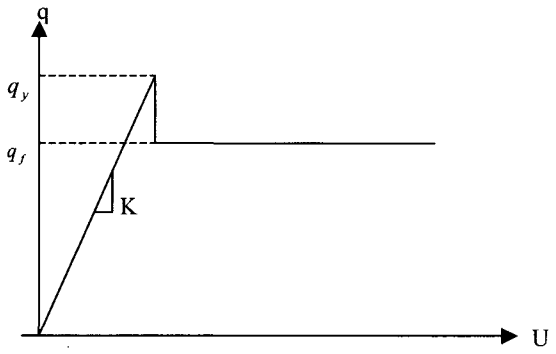


Figure 2: Constitutive model for interfacial shear force

Figure 2 shows the simplified constitutive model for the interfacial bonding stress between GFRP rod and cement mortar.

Calculation of the interfacial bonding stress was carried out using equations 1 to 5

$$\begin{cases} U^* = U(L) = \dfrac{P^* - q_f a}{E_s A \omega}\coth[\omega(L-a)] + \dfrac{P^* - 0.5 q_f a}{E_s A} a & (1) \\ q_f = \dfrac{\omega P^*_{\max}}{a\omega + \sinh[\omega(L-a)]\cosh[\omega(L-a)]} & (2) \\ q_y = q_f \cosh^2[\omega(L-a)] & (3) \\ \tau_y = \dfrac{q_y}{2\pi R} & (4) \\ \tau_f = \dfrac{q_f}{2\pi R} & (5) \end{cases}$$

where,
U: rebar displacement;
P: push force at x = L;
q: shear force per unit length acting on the rebar;
q_f: frictional shear force per unit length;
q_y: interfacial yield parameter;
a: debonding length;
L: rebar embedment length;
A: rebar cross-sectional area;
R: rebar radius;

$$\omega = \sqrt{\frac{k}{E_s A}}$$

Since the only unknown is the debonding length, a, its solution will result in the length of the debonded zone at the peak load, $P^*_{\max}$. After obtaining the value of the debonding length, a, the frictional shear bond

strength q_f and the value of q_y were determined. Then bonding strength measures τ_y and τ_f were calculated, as shown in Table 2 and Table 3.

TABLE 2
RESULTS FOR THE SMOOTH GFRP ROD AND SMOOTH STEEL ROD

Mix Formula	*W*	τ_y *(MPa)*	τ_f *(MPa)*
Formula 1	14.44	6.63	6.1
Formula 2	26.85	5.32	4.07
Formula 3	26.72	7.00	5.29
Formula 4	33.91	8.47	5.48
Formula 5	27.60	8.06	6.04
Formula 6	29.55	8.30	5.98
Formula 1 with Steel rod	7.98	7.33	6.85

TABLE 3
RESULTS FOR THE SAND BLASTED GFRP ROD

Mix Formula	*w*	τ_y*(MPa)*	τ_f*(MPa)*
Formula 1	49.89	17.50	13.64
Formula 2	44.78	10.63	7.14
Formula 3	20.75	10.02	8.84
Formula 4	30.35	19.69	16.26
Formula 5	27.51	16.25	14.07
Formula 6	42.38	18.41	15.34

As shown in Table 2, the silica fume modified matrix had the maximum bond strength, which was comparable to that of the control specimen, with a smooth-surface steel rod in plain cement mortar.

It can be seen in Table 3 that GFRP rod with the sand blasting surface treatment has improved bonding with cement mortar, increasing from 67% to 196%. It can be concluded that GFRP rod with proper surface treatment can significantly improve the bonding property and hence can be utilized as normal reinforcement in concrete structures.

GFRP as normal reinforcement

Beam specimens with dimensions of 100 x 150 x 2000 mm were prepared for the 4-point bending test with an effective cross section depth d = 120 mm. Two Φ8mm sand-blasted GFRP rebars were embedded in the concrete beam as reinforcement, with a reinforcement area A_{frp} of 100.5 mm^2.

The four-point bending test arrangement at Material Testing System (MTS) is shown in Figure 3. Strain gauges are attached to the surface of the concrete beam, and two Linear Variable Differential Transducers (LVDTs) are used to measure the deflection at the bottom of the beams in the pure bending region.

Figure 4 shows the schematic layout of the test specimen, with S = 600 mm, and L = 1800 mm.

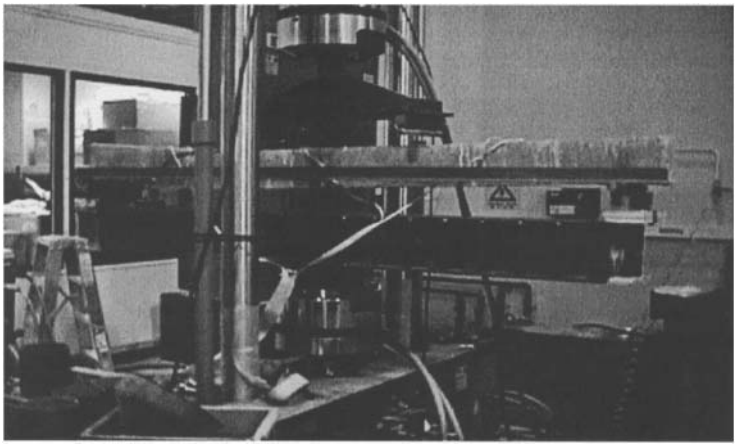


Figure 3: Set up of 4-point bending test

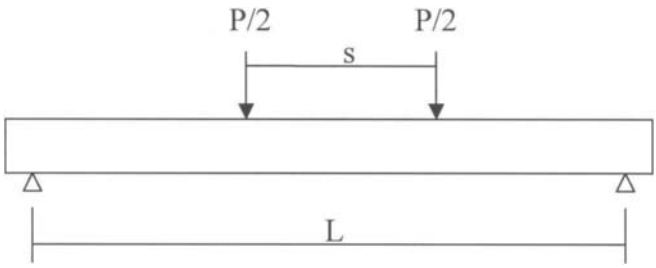


Figure 4: Schematic layout of test specimen

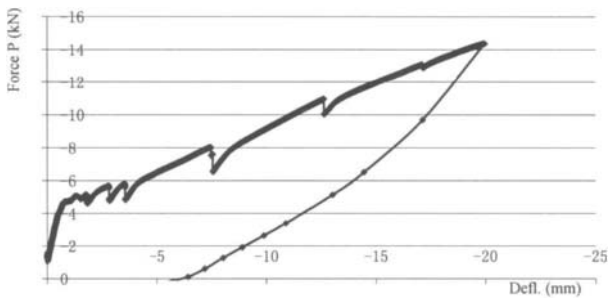


Figure 5: Force vs deflection curve for beam specimen 1

The force vs deflection relationship of beam specimen 1 is shown in Figure 5. It is loaded in deflection control mode until its deflection reaches 20 mm, and then unloaded. The maximum deflection to load span ratio is 1/82, which is far beyond the serviceability requirement. It is observed that several main cracks occurred in the pure bending region, with their depths extending to over ¾ of the beam depth. This

implies that the bonding between GFRP rebar and concrete is acceptable, otherwise the beam would have failed. The turning point where the slope changes rapidly indicates the occurrence of a crack at the bottom surface of the beam where tensile stress exceeds the ultimate tensile strength of the concrete. This turning point has a value of force P as about 5 kN.

The several sudden drops in the force vs deflection curve may be caused by some partial failure in the bonding between GFRP rebar and concrete. Since the sand blasted on the GFRP rebar surface is not quite uniform, at some weak position the sand can separate from the rebar causing partial debonding, which is also observed in the push-out test.

The strain vs Time curve in Figure 6 shows the same characteristic as that of the force vs deflection curve.

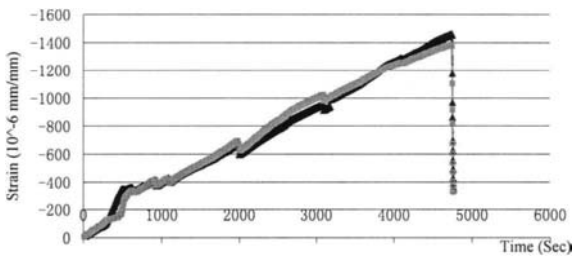


Figure 6: Strain on bottom of beam vs time for beam specimen 1

Another two specimens were tested using deflection control mode until failure occurred. Figure 7 shows the force vs deflection curve for beam specimen 2, which is quite similar to that of beam specimen 1. The turning point is at a force of about 5 kN, as is the case for beam specimen 1. The maximum deflection to load span ratio is 1/61, which is even larger than beam specimen 1. The failure mode is in shear, where the concrete cover burst out due to partial debonding between GFRP rebar and concrete, as can be seen in Figure 8.

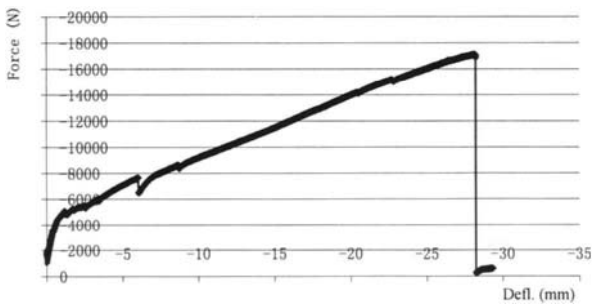


Figure 7: Force vs deflection curve of beam specimen 2

Beam specimen 3 has a behavior similar to that of beam specimens 1 and 2. The maximum deflection to load span ratio is 1/49, which is the largest among the three. Shear failure occurs and the ultimate load P_u is 19.9 kN.

All three specimens show a similar crack propagation manner. The first crack appears in the pure bending region, and then in this region several cracks subsequently occur. The bending cracks continue to extend upward, as long as the beam is still capable of carrying loading. The occurrence and propagation of shear crack leads to shear failure, and part of the concrete below the shear crack at the bottom side of the beam debonds from the GFRP bar and bursts out.

Bending Capacity Calculation

If we assume bonding between GFRP and concrete is satisfactory, and fcu is 40 MPa, and f_{frp} is 1100 MPa, hence Mu is calculated as 11kN•m, and the corresponding Pu is 36.7 kN

Shear Capacity Calculation

Similarly, we can get the shear capacity Vu = 10.7 kN, corresponding Pu = 21.4 kN

With the assumptions, shear capacity is shown to be less than bending capacity, so is aspect controls and the failure mode is a shear failure, and this agrees with the test result. The prediction of shear failure load Pu = 21 kN is close to the test results, and the difference in values may be caused by non-uniformity of specimens, inaccurate assumptions, inaccuracy in calculation method, etc.

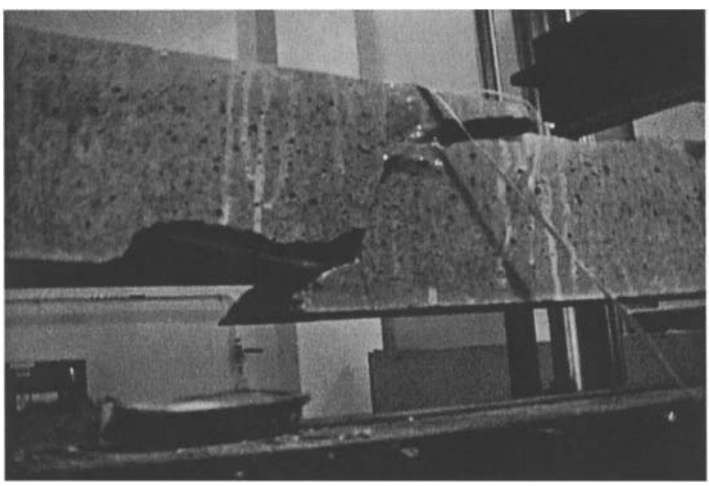


Figure 8: Shear failure of beam specimen 2 (shear crack)

CONCLUSION

The bonding between GFRP rebar and concrete is comparable to that between steel bar and concrete. And the bond property can be significantly improved using proper surface treatment of the GFRP rebar. This, in a sense, ensures the possible application of GFRP rebar as reinforcement for concrete structures.

Due to the low elastic modulus of GFRP rebar, concrete beams with GFRP as reinforcement usually have lower flexural rigidity, so the serviceability requirement usually controls the design. Some possible ways to overcome this limitation on the usefulness of GFRP, are to carefully control the application situation to avoid the serviceability problem. Combination of GFRP reinforcement and steel reinforcement, adopting prestressing system to solve the serviceability problem are two possibilities.

References:

Chaallal, O. and Benmokrane, B. (1996). Fiber-Reinforced Plastic Rebars for Concrete Applications. *Composites*: Part B, 27B, 245-252.

Dolan C.W. and Burke C.R. (1996). Flexural Strength and Design of FRP Prestressed Beams. *Advanced Composite Materials in Bridges & Structures – 2 nd International Symposium*, Canadian Society of Civil Engineers, Montreal, Quebec, Canada, 383-390.

Larralde, J. and Silva-Rodriguez, R. (1993). Bond and Slip of FRP Rebars in Concrete. *Journal of Materials in Civil Engineering*, **5:1**, 30-40.

Li, Z.J., Xu, M.G. and Chui, N.C. (1998). Enhancement of rebar (smooth surface)-concrete bond properties by matrix modification and surface coatings. *Magazine of Concrete Research*, **50:1,** 49-57.

Maheri, M.R. (1995). An improved method for testing unidirectional FRP composites in Tension. *Composite Structures*, v33, 27-34.

Mirmiran, A. (2001) Innovative combinations of FRP and traditional materials. *FRP Composites in Civil Engineering, CICE 2001*, v2, 1289-1298.

Mulu Muruts and Ludovit Nade, Laminated Galss Fiber Reinforced Plastic (GFRP) Bars in Concrete Structures. [online].
Available: http://www.vbt.bme.hu/phdsymp/2ndphd/proceedings/muruts.pdf

Nanni A. (1993). *Fiber-reinforced-plastic (FRP) reinforcement for concrete structures : properties and applications,* Elsevier , Amsterdam ; New York, USA

Nanni A. Bakis C.E., O'Neil E., and Dixon T.O. (1996). Performance of FRP Tendon-Anchor Systems for Prestressed Concrete Structures. *PCI Journal*, **41:1**, 34-44

Uomoto, T. (2001). Durability of FRP reinforcement as concrete reinforcement. *FRP Composites in Civil Engineering, CICE 2001*, v1, 85-96.

Advances in Building Technology, Volume 1
M. Anson, J.M. Ko and E.S.S. Lam (Eds.)
© 2002 Elsevier Science Ltd. All rights reserved

A GENERIC STRUCTURAL ENGINEERING APPROACH TO RETROFITTING RC BEAMS IN BUILDINGS BY ADHESIVE BONDING LONGITUDINAL PLATES

Deric J. Oehlers and Rudi Seracino
Department of Civil and Environmental Engineering, The University of Adelaide
Adelaide, South Australia, SA5005, Australia

ABSTRACT

Retrofitting reinforced concrete structures by adhesive bonding steel or FRP plates to their surfaces is an efficient and inexpensive form of rehabilitation that is rapidly gaining in importance. The main problem with adhesive bonding plates to reinforced concrete is the very weak tensile strength of the concrete that allows premature debonding of the plate that can occur even before the serviceability loads are reached. There has been published much research on premature debonding, particularly for tension face plates, from which have been developed: design rules of thumb; analyses based on stress concentrations; and those based on fracture mechanics. Much of this research may appear to be confusing for structural engineers as they are often not based on a structural engineer's understanding of the familiar behaviour of reinforced concrete. In this paper, a new, simple and generic structural engineering approach is described for designing plated structures that are based on the fundamental principles and mechanisms of behaviour familiar to structural engineers who design reinforced concrete structures. It will be shown that this new approach can be applied to longitudinal plates: of any material type such as FRP or steel; of any size; of any cross-section such as flat plates, angle sections and U-sections; and that are adhesively bonded to any position such as the tension face, compression face and sides of the RC beams or slabs.

KEYWORDS

Retrofitting, rehabilitation, plating, reinforced concrete, beams, slabs, FRP plating, steel plating.

INTRODUCTION

Many non-structural engineering researchers appear to make the problem of retrofitting reinforced concrete buildings by adhesive bonding longitudinal plates sound extremely complex and outside the scope of understanding of structural engineers. This is wrong. It is shown in this paper that the fundamental understanding that structural engineers have of the behaviour of reinforced concrete structures is essential to the understanding of the plated RC structure, and allows a simple generic design approach to be developed and used. In this paper, the retrofitting of an internal continuous beam in an RC

building is used as an illustration. At first, the variety of materials that can be used is discussed, this is followed by the structural engineering reasons for choosing the positions of the longitudinal plates, which is then followed by a description of the structural engineering debonding mechanisms and where they occur. The paper is concluded with an application of a design approach.

MATERIAL AND SECTIONAL DUCTILITY

The material behaviour of the plate affects the structural behaviour of the plated section. Structural engineers are familiar with the behaviour of steel as shown in Fig.1 which in its elastic range is relatively stiff (E_s) after which there is a large ductile plateau before the onset of strain hardening at very high strains. Hence, if a steel plate is designed to yield prior to debonding then the plated section will behave in a ductile fashion and moment redistribution can occur. In contrast, fibre reinforced polymer (FRP) is a linear elastic material that is relatively flexible, then fractures without any material ductility. Hence in an FRP plated beam, the force in the FRP plate keeps increasing until crushing of the concrete or debonding, so that the curvature at failure is relatively low allowing little if any moment redistribution.

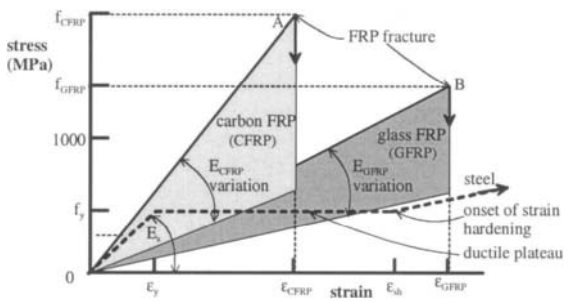


Figure 1: Plate material properties

LONGITUDINAL PLATE POSITIONS

Probably the most common form of longitudinal plating is to adhesively bond plates to the tension faces of continuous beams as shown in Fig.2, so that the internal lever arm of the axial plate force is maximised. However as structural engineers well know, the addition of tension reinforcement reduces the sectional ductility which imposes a limit to the amount of strengthening that can occur. Furthermore, tension face plates are prone to debonding due to the interaction of the plate stress fields with those of the tension reinforcing bars, such that debonding occurs at the level of the tension reinforcement.

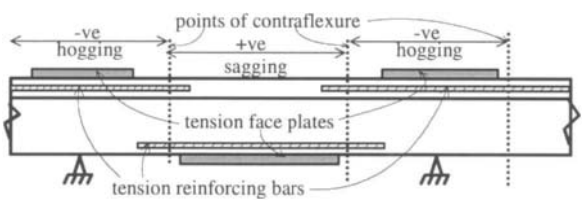


Figure 2: Tension face plates

An alternative approach is to adhesively bond plates to the sides as in Fig.3. These plates are less prone to debonding as they are less likely to interact with the tension reinforcing bar stress fields, so that the plane

of debonding occurs in the concrete adjacent to the adhesive layer and not at the level of the tension reinforcing bars. Furthermore, side plates have less of an effect on the sectional ductility particularly when there are deep side plates as in A in Fig.3, in which case the sectional ductility may increase. It may also be worth noting that sides plates can also increase the shear capacity.

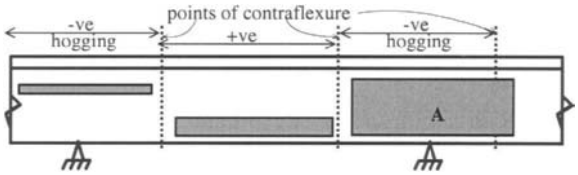


Figure 3: Side plates

PREMATURE DEBONDING MECHANISMS

An example of a retrofitted beam is shown in Fig.4. This beam reached its moment capacity at large rotations even though some debonding cracks were visible. The aim of the structural engineer is to ensure that premature debonding of the plate does not occur to such an extent as to weaken the structure or reduce its ductility. The following three major debonding mechanisms have been identified.

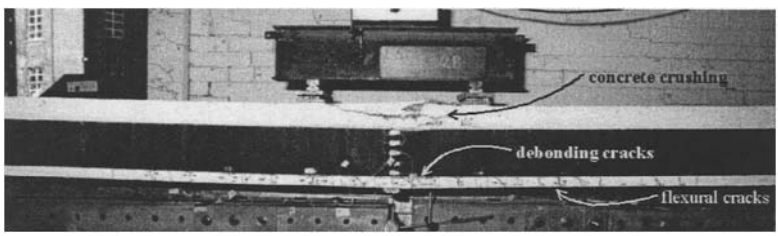


Figure 4: Retrofitted beam

Plate End (PE) Debonding

An example of plate end (PE) debonding is shown in Fig.5. The stress concentrations due to the termination of the plate induce cracks that start at the plate end and propagate inwards, gradually at first and then rapidly until complete debonding occurs at which the strains in the plate reduce to zero so that the beam now acts as unplated.

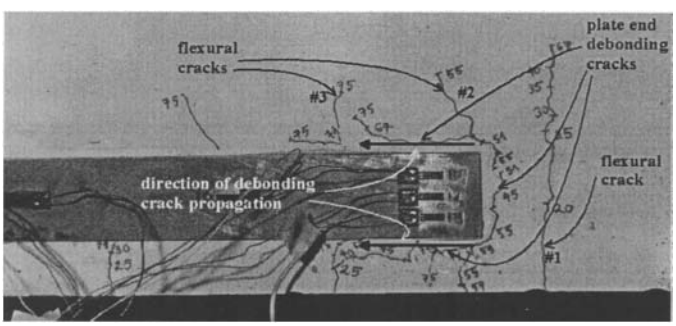


Figure 5: Plate end debonding of a steel side plate

The mechanism of PE debonding is illustrated in Fig.6 for a tension face plate, where it can be seen in Fig.6(a) that the curvature of the plated beam induces a moment M_c and axial force P_a in the plate. These stress resultants M_c and P_a, caused by the curvature of the beam induce the plate/concrete interface forces in Fig.6(a) and stresses in Fig.6(b) and (c) that result in debonding. Hence a simple solution to preventing PE debonding is to terminate the plate at a point of contraflexure where the curvature is zero. Sometimes it may not be possible to terminate the plate at a point of contraflexure due to envelopes induced by variations in load. In which case, the plates can be terminated in regions of low moment, where the section apart from tensile cracking can be assumed to be elastic; design rules are available for tension face plates (Oehlers and Moran 1990), side plates (Oehlers 2000), angle sections (Nguyen et al 1998) and compression face plates (Mohamed Ali et al 2002) to ensure that premature debonding does not occur. It can be seen that PE debonding controls the extent of plating, that is the length of plate required.

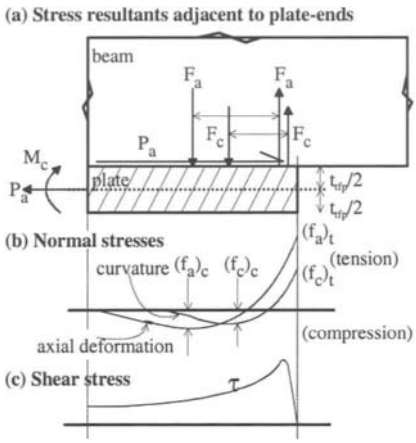


Figure 6: Plate end debonding mechanism

Intermediate Crack (IC) Debonding

Intermediate crack (IC) debonding of a tension face plate is shown in Fig.7. The interface IC debonding cracks propagate from the intercept of the intermediate cracks, induced by combinations of applied flexural or shear forces, with the longitudinal plate. The IC debonding cracks propagate towards the plate ends gradually joining up until a large length of plate between the plate ends has separated from the beam. Hence, to all intents and purposes the plate has debonded even though the plate ends may still be attached, as the plate contribution is now negligible.

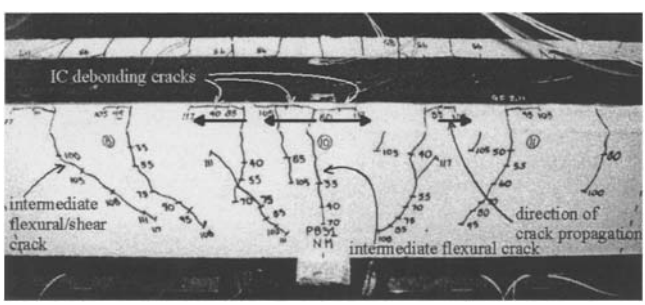


Figure 7: IC debonding of tension face plate

The mechanism of IC debonding is illustrated in Fig.8. To accommodate the formation of the flexural intermediate crack adjacent to the plate requires infinite strains in the plate which of course cannot occur, so that the strains are relieved by the formation of the interface IC debonding cracks. Much research has been done on IC debonding (Teng et al 2002). For example it has been shown the stress at which debonding occurs is proportional to $\sqrt{(E_p\sqrt{f_c})/t_p}$ where E_p and t_p are the plate stiffness and thickness respectively; so that thin stiff plates are less likely to debond and IC debonding will usually start in regions of maximum flexure. Therefore, the thickness of a steel plate can be adjusted so that yield will occur before IC debonding, so that the cross section fails in a ductile mode that allows moment redistribution. In contrast, FRP plates will debond whilst still elastic, often at a stress of about 30% of the ultimate FRP strength, so that failure tends to be brittle and little moment redistribution can occur. It can be seen that IC debonding controls the flexural strength and ductility.

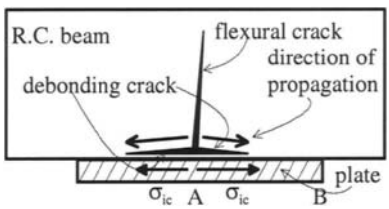


Figure 8: Mechanism of intermediate crack debonding

Critical Diagonal Crack (CDC) Debonding

Critical diagonal crack (CDC) debonding is due to the vertical shear displacement across a critical diagonal crack as shown in Fig.9(a) for a beam without stirrups and in Fig.9(b) for a beam with stirrups. The debonding crack propagates catastrophically from the intercept of the diagonal crack with the plate to the plate end. Tests have clearly shown that the longitudinal plates debond before the stirrups can be stretched so that debonding occurs at the strength of the concrete beam without stirrups. However these tests have also shown that the longitudinal plates inhibit the formation of the critical diagonal crack. Hence a lower bound to the shear load at which debonding occurs V_{cdc} is the shear strength of the beam without stirrups V_{uc} (Zhang 1997) and the contribution from the stirrups V_{us} is negligible or zero.

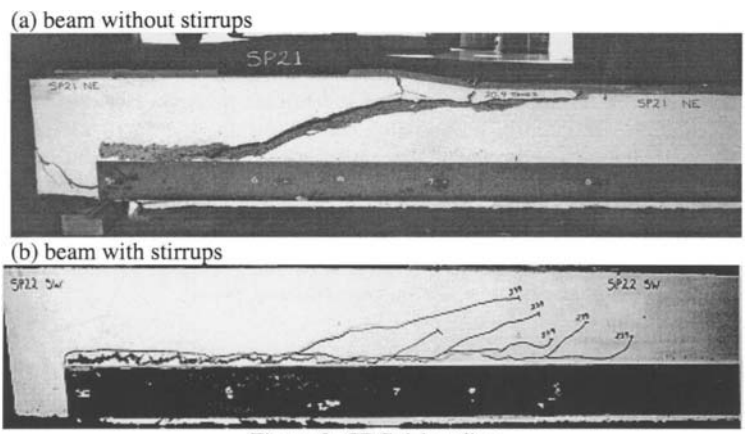


Figure 9: CDC debonding

If a shear capacity greater than V_{uc} is required for the longitudinally plated region, then methods of analysis are available for determining the vertical shear load to cause a longitudinal plate to debond V_{cdc}, which depends on whether the plate is attached to the tension, side or compression face (Jansze 1997; Mohamed Ali et al 2001, 2000, 2002). The method of analysis is illustrated in Fig.10 for a side plated beam. For each possible position of a diagonal crack, it is necessary to determine the shear load to cause the diagonal crack to develop V_{cr} and the shear resistance against sliding across this diagonal crack V_u. The intercept as in Fig.10 defines both the position of the critical diagonal crack and the vertical shear to cause debonding V_{cdc}. It is worth noting in Fig.10, that for each position of the diagonal crack, the resistance to sliding depends on the IC debonding resistance across the diagonal crack P_{ic} in the top half of the figure. It can be seen that CDC debonding relies on the IC debonding strength but IC debonding is not the same as CDC debonding as IC debonding depends on axial deformations in the plate whilst CDC debonding depend on shear deformations in the RC beam.

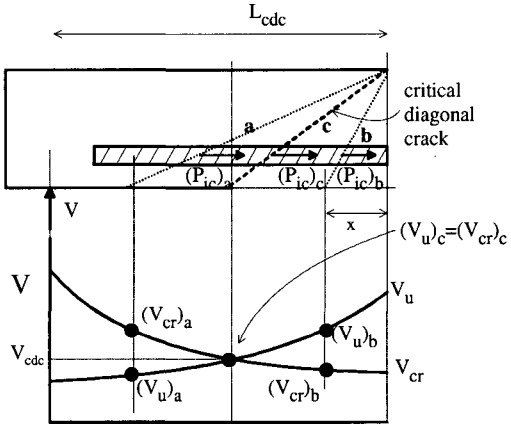


Figure 10: Analysis of CDC debonding resistance

OCCURRENCE OF DEBONDING MECHANISMS

The distribution of the major debonding mechanisms are illustrated in Fig.11(a) for tension face plates. It can be seen that IC debonding initiates in the regions of maximum moment, where the strains in the plate are at their largest, and propagate towards the plate ends. IC debonding controls the flexural capacity and flexural ductility and hence the ability of the beam to redistribute moment. CDC debonding depends on the vertical shear capacity, ignoring the contribution due to stirrups, and hence is often more likely to occur in the negative or hogging regions where the vertical shear is at its highest and where often stirrups are required. Hence in slabs where stirrups are rarely used, CDC debonding is unlikely to affect design as most slabs are designed for V_{uc} only. In contrast in the negative regions of continuous beams where the vertical shear is at its highest and where stirrups are required then it may not be possible to adhesively bond plates. PE debonding always occurs at the plate ends and propagate inwards and can be simply prevented by terminating the plate near to a point of contraflexure.

Sometimes the plates are placed or terminated in the compression face as in Fig.11(b). In which case in the compression face zones, IC debonding cannot occur but CDC and PE debonding can occur as shown. The same debonding mechanisms also apply to side plates beams as in Fig.11(c). Hence it can be seen that these are generic debonding mechanisms.

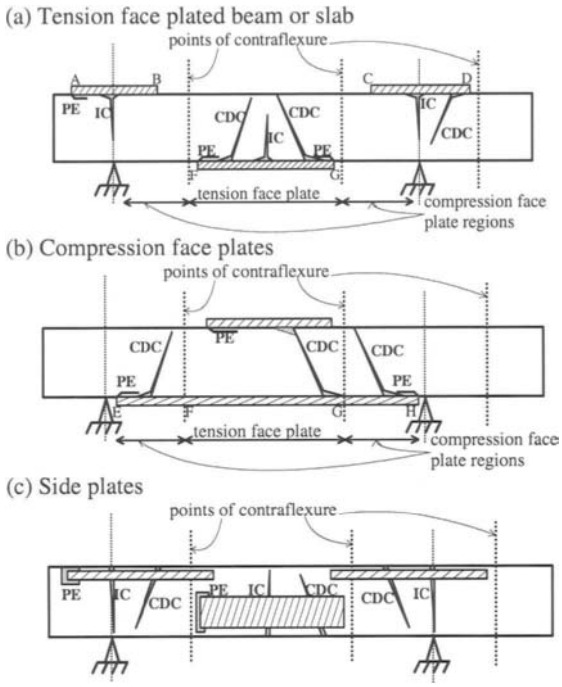


Figure 11: Distribution of debonding mechanisms

APPLICATION OF DESIGN APPROACH

The continuous member in Fig.12 is used to illustrated the generic plating approach.

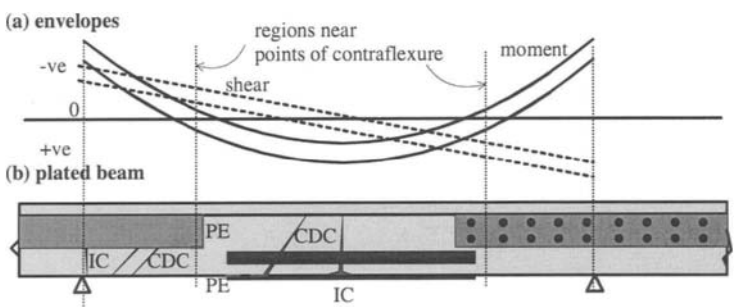


Figure 12: Generic plating approach

Let us first assume that the continuous member in Fig.12 is a slab and hence does not have stirrups, so that the vertical shear capacity is V_{uc} which is the shear resistance of the critical diagonal crack of the unplated section. The addition of plates will inhibit the formation of the critical diagonal crack which will increase the vertical shear capacity to V_{cdc}, the shear load to cause CDC debonding. V_{cdc} is now both the shear load to cause debonding as well as the shear capacity of the plated slab. Hence CDC debonding is unlikely to occur anywhere along the slab, just as long as the new design shear load due to retrofitting

does not exceed V_{cdc} which is the likely scenario. PE debonding can be prevented by terminating the plates in regions of low moment so this should also not be a problem. Hence this leaves IC debonding which can occur at the positions of maximum moment in both the -ve and +ve regions. FRP plates are usually the preferred option due to their ease of application and handling and durability. These can be used in both the –ve and +ve regions if little or no moment redistribution is required. If, however, the -ve regions are required to redistribute moment to the positive region then steel plates may be the preferred option in the –ve regions as the steel plates can be designed to yield before IC debonding. Hence there is a possibility that the final design will use both steel and FRP plates.

Let us now assume that the continuous member in Fig.12 is a beam and hence does have stirrups so that the vertical shear capacity is now $V_{uc} + V_{us}$ which is the shear resistance of the unplated section. As with the slab, plate end debonding can be prevented by terminating the plate at the point of contraflexure. In the +ve region the vertical shears here are relatively small, compared with those in the –ve region, so that V_{us} may be relatively small. Just as long as $V_{cdc} < V_{uc} + V_{us}$ of the +ve region, then CDC debonding may not occur particularly as tests have shown that plating can increase V_{cdc} to twice V_{uc}. However, in the –ve region it may not be possible to prevent CDC debonding due to the high value of V_{us} in which case it may be necessary to bolt the plates as shown. As with the slabs, IC debonding and its effect on ductility may control where FRP and steel plates are used.

REFERENCES

Jansze W. (1997). *Strengthening of RC members in bending by externally bonded steel plates.* PhD Thesis, Delft University of Technology.

Mohamed Ali M.S. Oehlers, D.J. and Bradford, M.A. (2000). Shear peeling of steel plates adhesively bonded to the sides of reinforced concrete beam. *Proc. Instn Civ. Engrs Structs & Bldgs*, **140,** 249-259.

Mohamed Ali M.S. Oehlers D.J. and Bradford M.A. (2001). Shear peeling of steel plates bonded to the tension faces of RC beams. *ASCE Journal of Structural Engineering.* **Vol.127 No.12,** 1453-1460.

Mohamed Ali M.S., Oehlers D.J. and Bradford M.A. (2002). Interaction between flexure and shear on the debonding of RC beams retrofitted with compression face plates. Accepted by *Journal of Advances in Structural Engineering.*

Nguyen N.T., Oehlers, D.J., and Bradford, M.A. (1998). Models for the flexural peeling of angle plates glued to R.C. beams. *Journal of Advances in Structural Engineering.* **Vol. 1 No.4,** 285-298.

Oehlers D. J. and Moran J. P. (1990). Premature failure of externally plated reinforced concrete beams. *Journal of the Structural Division of the ASCE*, **Vol. 116, No. 4**, 978-995.

Oehlers D.J., Nguyen, N.T. and Bradford, M.A. (2000). Retrofitting by adhesive bonding steel plates to the sides of R.C. beams. Part 1: Debonding of plates due to flexure. *Journal of Structural Engineering and Mechanics, An International Journal,* **Vol.9, No.5**, 491-504.

Teng J.G. Chen J.F. Smith S.T. and Lam, L. (2002). *FRP strengthened RC structures.* Wiley, Oxford, UK.

Zhang J.P. (1997). Diagonal Cracking And Shear Strength Of Reinforced Concrete Beams. *Magazine of Concrete Research.* **Vol.49, No.178**, 55-65.

Advances in Building Technology, Volume 1
M. Anson, J.M. Ko and E.S.S. Lam (Eds.)
© 2002 Elsevier Science Ltd. All rights reserved

EFFICIENCY OF STRENGTHENED R. C. COLUMNS

Prof. Dr. M. Akram Tahir

University of Engineering and Technology, Lahore-Pakistan.

ABSTRACT

An experimental study was conducted, in which a large number of full-scale models of columns were cast and later strengthened by preparing different types of surface conditions between the existing and added concrete. The core was encased in the jacket cast from fresh concrete by placing properly tied additional reinforcement in the jacket. Five types of surface condition were studied during the strengthening program. The other parameters of the study were the strengths of concrete and steel both in the core and jacket. It was interesting to note that surface conditions of existing concrete had little effect on the strength of strengthened columns in case load was applied concentrically. However, in case of eccentrically loaded columns, the surface conditions resulting in poor bond showed drastic decrease in strength as compared to those providing better bond between old and new concrete. Another interesting fact was noted that for the efficient strengthening of the columns the strength of the two materials in the jacket should be at least equal to or greater than those of the respective core materials.

KEYWORDS:

Strengthening, eccentrically loaded columns, full-scale models, concrete jacket, surface conditions.

INTRODUCTION

During renovation of buildings often it becomes necessary to strengthen the existing columns in order to increase their load carrying capacity. The strengthening becomes inevitable due to increase in the service loads or loss of member strength. The strengthening is provided by adding an additional section, termed as jacket, around the existing column section, named as core. Additional longitudinal bars that are properly tied are provided in the jacket. The bond between the surfaces of core and jacket-concretes has sharp influence on the integrity of the strengthened column. The core is subjected to the stresses prior the strengthening is done where as the jacket has to take the share of load by transition. The strength of the materials in core and jacket is usually different. These factors make the problem of strengthening a bit more complex. In this study a number of columns were cast and strengthened. Two concretes with nominal strengths of 21 MPa and 28 MPa were used during casting and strengthening operations with two grades of steel i.e., 280 MPa and 420 MPa. The details of the test program are presented in the following section.

EXPERIMENTAL PROGRAM

A number of full-scale models were cast, strengthened, and tested to destruction. The main variables of the study were the strength of concrete and steel in the core and jacket, the eccentricity of loading, and surface condition of the core concrete. The test program was completed in three series. First of all a pilot study was conducted on 75-mm square sections strengthened to 150-mm square sections. The concrete was made using coarse river sand as fine aggregate; 12-mm maximum size crushed lime stone aggregate, and ordinary Portland cement. The concrete mixtures were designed for two grades with nominal strengths of 21 MPa and 28 MPa. Two grades of deformed mild steel with nominal yield strength of 280 MPa and 420 MPa were used as reinforcement. The columns were cast using molds in vertical direction. The columns were cured for twenty-eight days and then left for weathering for quite a some time. The test program was completed in three different series. The details are presented.

The Pilot Program

The concrete mixtures were designed for nominal strengths of 21 and 28 MPa at 28 day. Five surface conditions of the old concrete, as listed in the following, were prepared before strengthening during the pilot test program:

S1. The same old dried surface without cleaning was used for strengthening.
S2. The cover was removed of the old steel reinforcement before strengthening.
S3. The old surface was cleaned thoroughly before strengthening the section.
S4. The surface was painted and aged before strengthening.
S5. The surface was prepared wet by using cement water.

The columns were cast, cured, and then left for aging in weather. These columns were later strengthened with the five surface conditions of old concrete. The strengthened columns were cured and then tested to destruction by applying both concentric and eccentric loads. The characteristics of the columns cast and tested during the pilot study are reported in Table 1.

Table 1
THE COLUMNS CAST IN PILOT STUDY

S,No	Old Section (Core)				New Section (Jacket)			
	b, h mm	f'_c MPa	f_y MPa	A_s	b, h mm	f'_c MPa	f_y MPa	A_s
1	75	21	280	4#4	150	21	280	6#4
2	75	21	280	4#4	150	21	420	6#4
3	75	21	280	4#4	150	28	420	6#4
4	75	21	420	4#4	150	28	280	6#4
5	75	28	280	4#4	150	21	420	6#4
6	75	28	420	4#4	150	21	280	6#4

Note: The length of the columns was 2 m. Twenty-two columns were cast in this part of the program. The main reinforcement in core and jacket sections were tied properly using #3 bar-square ties spaced at 75 mm and 150 mm respectively.

Results of The Pilot Test Program

Table 2
EXPERIMENTAL STRENGTHS OF THE COLUMNS LISTED IN TABLE 1.

Sr. No	P, kN (e=0 mm)					P, kN (e= 50mm)				
	S1	S2	S3	S4	S5	S1	S2	S3	S4	S5
1	774	776	774	774	764	321	331	311	264	324
2				843					321	
3				950					367	
4	936			929		386	415		321	
5				914					364	
6				860					307	

The strengthened columns were cured and later tested to destruction in a 100-Ton Buckton universal testing machine. The machine may accommodate 4m long columns. It can be observed from the tabulated results that surface conditions of old concrete have little influence whatsoever on the load carrying capacity of the strengthened columns where the load was applied concentrically. The strength results of the columns listed at serial no. 1 confirm this fact when loaded concentrically. However, in case of eccentric loading, severe segregation occurred at the interface of the old and new concretes for the surface condition S4, where the old surface was painted and put for aging before strengthening. The most effective surface condition for strengthening was S2, where the old concrete cover was removed prior the strengthening was performed.

FULL SCALE MODELS

The tests on full-scale models were carried out in two series. In the first of the series, twenty-two 100x100 mm columns were cast and later strengthened to 200 x 200 mm. The height of the columns

TABLE 3
DETAILS OF THE COLUMNS CAST AND TESTED DURING 2ND SERIES.

S. No	Old Section		New Section		P, kN, e= 50mm		P, kN, e= 100mm	
	f'_c MPa	f_y MPa	f'_c MPa	f_y MPa	S1	S4	S1	S4
11	21	280	21	280	587	507		
12	21	280	21	420	653	570		
13	21	420	21	420	667	590		
14	21	420	21	280	604	534		
15	21	280	28	280	713		397	280
16	21	280	28	420	780		456	336
17	28	280	21	280	626		355	265
18	28	280	21	420	674		415	305
19	28	420	21	420	680			
20	28	420	21	280	607			

was fixed at 2500 mm. The materials used in this series were same as those employed in the pilot study. The combinations of two concrete mixtures with nominal strengths of 21 and 28 MPa were used in core and jacket. The details of the columns and experimental strengths are reported in Table 3

The comparison of axial strengths of the columns tested in series 2 is depicted in Fig.1. It is interesting to note that strength reduces appreciably with the reduction in strengths of jacket steel and concrete. The concrete strength is less effective than steel strength in enhancing the load carrying capacity of the strengthened columns

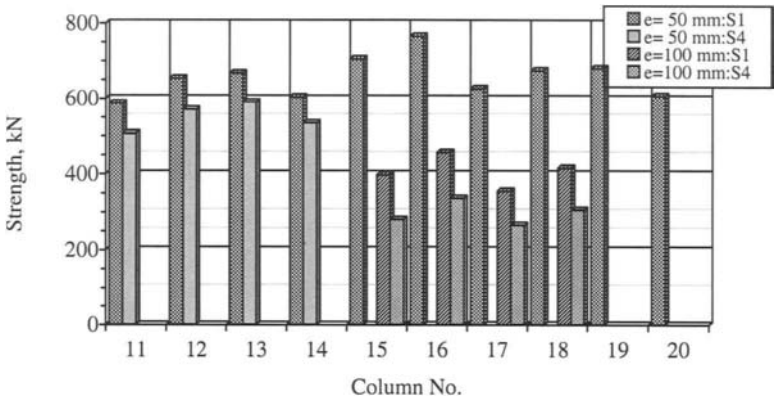


Figure 1. Ultimate strength of the columns tested in series 2.

Another set of ten columns was cast and strengthened in the third series. The length of these members was 3000 mm and core size was 150 mm square and jacket size was 300 mm square. The reinforcement in core was 4#6 bars and that in jacket was 6#4 bars. The concrete of the same two nominal strengths, 21 and 28 MPa was used in core as well as in jacket. The same reinforcement of the two nominal grades, 280 MPa and 420 MPa, was used. The details of the columns are given in Table 4 and the test results are reported in Figure 2.

TABLE 4

THE DETAILS OF THE COLUMNS CAST AND TESTED DURING SERIES 3.

Sr. No	Old Section 150x150 mm			Strengthened Section 300x300 mm		
	f'_c MPa	f_y, MPa	Reinforcement	f'_c MPa	f_y, MPa	Reinforcement
21	21	280	4#6	21	280	6#4
22	21	280		21	420	
23	21	420		21	420	
24	21	420		21	280	
25	21	280	4#6	28	280	6#4
26	21	280		28	420	
27	28	280	4#6	21	280	6#4
28	28	280		21	420	
29	28	420		21	420	
30	28	420		21	280	

The length of the columns was 3000 mm and they were strengthened with surface condition S5. These columns were properly tied to avoid bulging of longitudinal steel. The tabulated concrete and steel strengths are nominal. The loading eccentricity was kept constant at 150 mm.

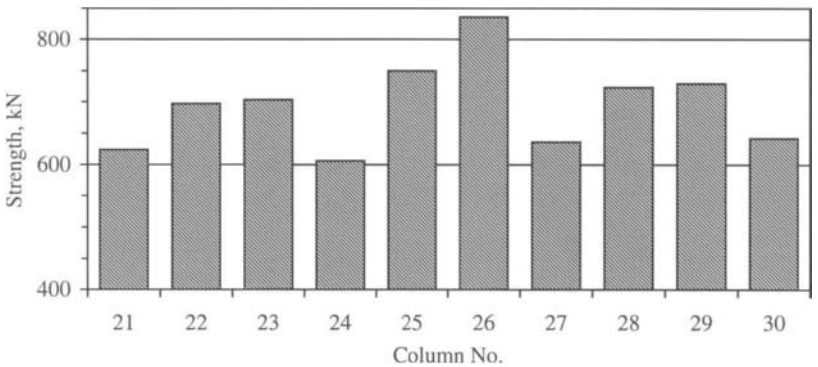


Figure 2. The axial strengths of the series 3 columns loaded with eccentricity=150 mm

DISCUSSION OF THE RESULTS

A very interesting picture emerges as the axial strengths of various columns are compared. The results of the two series are compared with respect to the change in strengths of steel and concrete both in core and jacket. The comparisons for series 2 tests are presented in Figure 3. It can be noted from Figure 3a and 3b that change in strength of steel or concrete in core does not affect the strength of strengthened column appreciably. For example, compare the strengths of the two columns, in each of the pairs (11,14), (12,13), (17, 20) and (18,19). The jackets of the two columns in each pair are cast from the same set of materials. The core of the two is also cast from the same concrete. The steel reinforcement, however, in the core of the two columns in each pair is different. It can be seen that increasing yield strength of core steel from 280 MPa to 420 MPa does not enhance the strength of the columns appreciably. The change is merely in the range of 1 to 3%. A similar picture is emerged from the comparison of the two columns in each of the pairs; (11,17), (12,18), (13,19) and (14,20). The two columns in each pair are cast from identical materials except that the concrete in the cores of the two is of different strength. It can be confirmed from Figure 3b, that increasing strength of core concrete from 21 MPa to 28 MPa does not affect the strength of column significantly. The change in strength is in the range of 1 to 6%, with an average of 3%. Similar trends can be observed from Figure 4, which confirm that core strength is not that important for eccentrically loaded strengthened columns.

However, an increase in either concrete- or steel-strength of jacket appreciably enhances the strength of strengthened column. These comparisons are based on the steel strength in jacket and are depicted in Figure 3c and those on concrete strength of jacket are shown in Figure 3d. It can be observed from Figure 3c, that strengths of the columns increase in the range of 7-12% when strength of reinforcement is changed from 280 MPa to 420 MPa. Similarly the increase in strength of jacket concrete from 21 MPa to 28 MPa enhances the strength of column by 20%. Similar observations can be made from Figure 4c and d. It may be noted that increase in the strength of jacket concrete is more effective than that of steel in increasing the load carrying capacity of the strengthened columns.

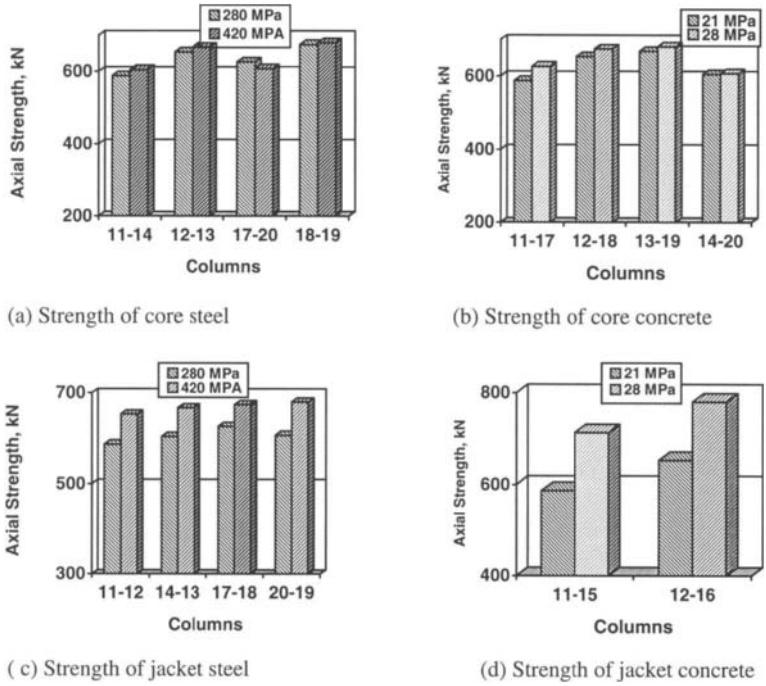


Figure 3. Comparison of strengths based on concrete and steel strengths in core and jacket. (Results from series 2.)

Another important observation made from the comparison of series 2 test results is that surface condition S4 causes a sever reduction in the strength of strengthened columns when loaded eccentrically. This reduction is more pronounced when eccentricity is increased from 50 mm to 100 mm. Compare the drop in strength of the columns with surface conditions S1 and S4, at serial numbers 11 to 14 and 15 to 18 as shown in Figure 1. The surface condition of old concrete, i.e.,, interface between core and jacket is an important parameter of strengthening. If a perfect bond is not established between the old and new concretes, a sever segregation is observed at testing time when load is applied eccentrically. This effect becomes more and more pronounced with increase in loading

CONCLUSIONS

Two important conclusions can be drawn from the results observed in this study. Firstly the ultimate strength of concrete and yield strength of steel in jacket should be kept at-least equal to the strengths of the two materials used in core for an efficient strengthening of existing columns. It means that use of stronger materials in jacket makes the strengthening more efficient. Secondly, there should be a perfect bond between old and new concretes at the interface of core and jacket to avoid segregation of concrete during load application. The surface of old concrete should be prepared thoroughly before the strengthening operations are carried out. It may be noted, however, that there is quite a sharp difference between the test conditions and the actual situation in buildings where the columns would have be strengthened. In these tests, the core and jacket were simultaneously stressed whereas in real

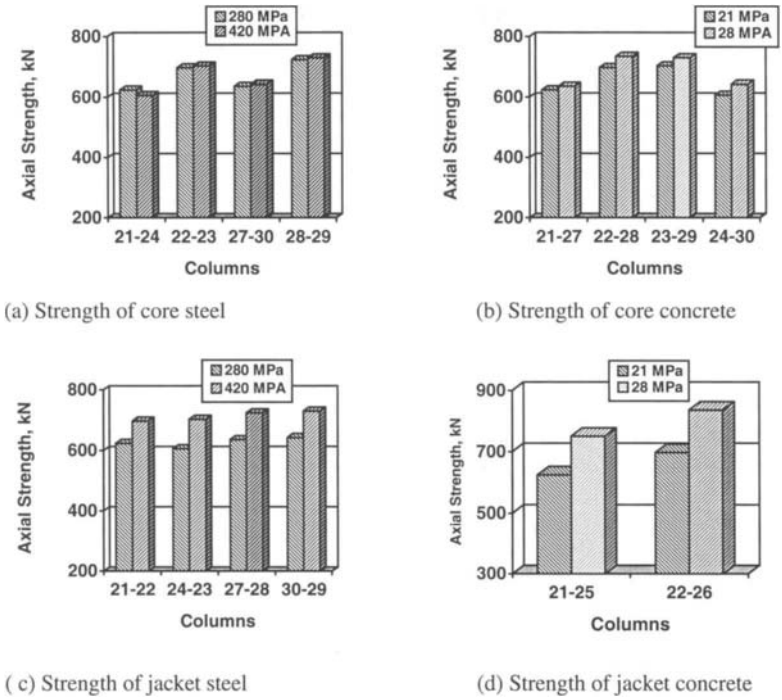


Figure 4. Comparison of strengths based on concrete and steel strengths in core and jacket (Results from series 3.)

buildings the core would be stressed prior the strengthening process would have been carried. Therefore it would be necessary to provide some stress transfer mechanism between old and new concrete sections. It may be provided in the form of the shear bolts, by surface roughening or by providing epoxy coating on the surface of existing section.

ACKNOWLEDGEMENTS

The author is highly indebted to the Directorate of Research, Extension, and Advisory Services of the University of Engineering and Technology, Lahore, for funding this piece of research work.

This Page Intentionally Left Blank

Advances in Building Technology, Volume 1
M. Anson, J.M. Ko and E.S.S. Lam (Eds.)
© 2002 Elsevier Science Ltd. All rights reserved

REHABILITATION OF REINFORCED CONCRETE COLUMNS BY EXTERNAL PLATE BONDING

B. Uy[1]

[1]School of Civil and Environmental Engineering, The University of New South Wales, Sydney, NSW 2052, AUSTRALIA

ABSTRACT

Rehabilitating reinforced concrete elements using external steel plates has been applied to both beams and slabs in bridge and building construction over the last two decades. The effect of applying external steel plates increases the strength of beams and slabs. This technique can also be applied to reinforced concrete columns to increase their strength with a minimal increase in the cross-sectional dimensions of the member. This paper presents an experimental programme used to ascertain the behaviour of both short and slender columns. These columns had steel plates bonded to them by the use of both bolting or gluing and bolting. A simplified theoretical model based on composite construction techniques is then presented and calibrated with the experiments to determine the strength increase and recommendations for further research are then made. Furthermore, recent research on the compressive behaviour of carbon fibre reinforced plastic (CFRP) plates and their effects on rehabilitating reinforced concrete elements is also discussed.

KEYWORDS

buckling, columns, composite structures, concrete structures, rehabilitation

INTRODUCTION

Rehabilitation or retrofitting of reinforced concrete structures often provides a more logical and economical alternative than demolition or replacement. This has been made evident with the many applications where steel plating has been used to increase both the stiffness and strength of existing reinforced concrete slabs and beams. To further increase the range of applicability of steel plate bonding, research into the retrofitting of reinforced concrete columns needs to be carried out as illustrated in Figure 1. The advantages of this include increasing both the strength and stability of a column without a significant increase in cross-sectional dimensions. Reinforced concrete columns may need to be strengthened for a number of reasons, which may be due to increasing the gravity load on a structure, or upgrading a structure for lateral loading such as wind or earthquake.

This paper presents an experimental and analytical study to consider the effects of steel plate bonding on the strength and stability of reinforced concrete columns. The experiments involved testing both short and slender columns. A series of theoretical models is then presented and calibrated with the experiments for determining the axial and flexural strengths. The paper concludes with suggestions for further research into the rehabilitation and retrofitting of concrete structures in particular in relation to the use of carbon fibre reinforced plastic plating.

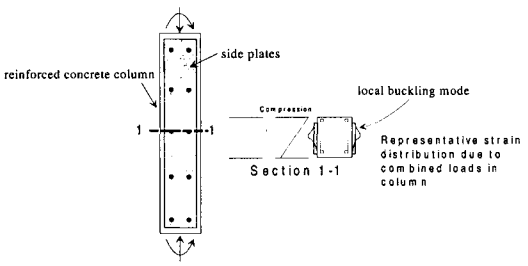


Figure 1: Application of CFRP plates to reinforced concrete columns

EXPERIMENTS

This paper will present the results of two series of experiments. Two series of experiments were conducted on short reinforced concrete columns to assess the increase in both axial stiffness and strength obtained by plate bonding. The concrete in these two series was exactly the same. A model to assess the axial stiffness and strength is then presented and calibrated with the experimental results. The following section outlines the two series of tests conducted. All of the plain reinforced concrete specimens were designed according to the Australian Standard for Concrete Structures, AS3600-1994, (Standards Australia, 1994).

Test Series 1

This set of tests consisted of constructing six identical reinforced concrete columns of 150 x 150 mm in cross-section, which were all of 450 mm in length. Each of these columns contained minimal longitudinal reinforcement consisting of four deformed Y12 bars and was detailed with sufficient lateral ties. Two plain specimens were tested and denoted as Plain 1 and Plain 2. Two specimens were tested with plates bolted to their sides and were denoted as Bolted 1 and Bolted 2. A final set of columns was tested with plates glued and bolted to their sides and these specimens were denoted Glued & Bolted 1 and Glued & Bolted 2. For this series of tests, plate coupons were tested in tension to establish their yield strength and elastic modulus, which are summarised in Table 1. Furthermore, a series of concrete cylinders were tested in compression to establish their mean compressive strength as summarised in Table 2.

Test Series 2

This set of tests also considered six identical reinforced concrete columns of 150 x 3000 mm of 815 mm in length. Again each of these columns was reinforced with minimal longitudinal reinforcement and detailed with sufficient lateral ties. This diagram also shows the location and extent of stiffeners used to initiate failure of the columns away from the ends of the specimen. The difference in these tests was that they were bonded with steel plates on only two opposite sides. Again two plain

specimens were tested and denoted as Plain 1 and Plain 2, two specimens were tested with plates bolted to their sides and denoted as Bolted 1 and Bolted 2 and two specimens with plates glued and bolted to their sides were denoted Glued & Bolted 1 and Glued & Bolted 2. Also concrete cylinders were tested in compression and steel plate coupons were tested in tension to assess their stress-strain characteristics, which are again summarised in Tables 1 and 2 respectively.

TABLE 1
STEEL COUPON EXPERIMENTS

Series	Nominal Plate Thickness (mm)	Nominal Plate Width (mm)	Elastic Modulus ($x10^3$ N/mm^2)	Yield Stress (N/mm^2)
Mean	3	24	200	285

TABLE 2
CONCRETE CYLINDER TESTS

Series	Cylinder Diameter (mm)	Age at Testing (days)	Compressive Strength (N/mm^2)
Series 1	150	106	54
Series 2	150	106	54

TABLE 3
REINFORCING TESTS

	Nominal Diameter (mm)	Nominal Area (mm^2)	Yield Stress (N/mm^2)	Ultimate Stress (N/mm^2)
Mean	12	113	478	594

Short Column Tests

The short column tests, which included both Test Series 1 and 2, were conducted under pure compression in a Denison 5,000 kN capacity servo-controlled testing machine. The column ends were set in large steel plates and cast in high strength mortar to ensure uniform loading conditions and thus uniform compression loading. The short column tests were designed so that the ends were fully fixed, which virtually eliminated any second order effects from developing.

RESULTS

The following section outlines the results of each of the test series as well as summarising the results of the material property tests.

Test Series 1

The results of these tests are summarised in Table 4. The comparisons of axial strength show one that by the application of bolting a 16% increase in axial strength is achieved whereas gluing and bolting achieves a 32 % increase in axial strength. There is very little difference in axial stiffness created by steel plate bonding, although it seems to lie between 0 and 20 %. Failure modes of these columns are

illustrated in Figure 2 which highlights local buckling of the steel plates and local crushing of the concrete.

TABLE 4
SERIES 1 COMPARISONS

Type	N_u Strength (kN)	N_u Average (kN)	Relative Value
Plain 1	1031		
Plain 2	1125	1078	1.00
Bolted 1	1251		
Bolted 2	1255	1253	1.16
Glued and Bolted 1	1359		
Glued and Bolted 2	1476	1418	1.32



Figure 2: Failure mode of short steel plated reinforced concrete column

Test Series 2

Results from the second series of tests were slightly different from those of Test Series 1 and the comparisons of axial strength are summarised in Table 5. Firstly, two plain samples were tested and these gave a base strength for the reinforced concrete member. Now the glued and bolted specimens achieved a lower strength than the specimens, which were bolted only, with an 11% and 20% increase respectively.

TABLE 5
SERIES 2 COMPARISONS

Type	N_u Strength (kN)	N_u Average (kN)	Relative Value
Plain 1	2214		
Plain 2	1828	2021	1.00
Bolted 1	2374		
Bolted 2	2476	2425	1.20
Glued and Bolted 1	2252		
Glued and Bolted 2	2229	2240	1.11

THEORETICAL MODEL

In order to be able to predict the strength of externally plated reinforced concrete columns, a theoretical model is proposed. The axial strength of the steel plated reinforced concrete columns is determined by employing the principle of superposition, which yields the following equation

$$N_u = N_{uc} + N_{ur} + N_{us} \tag{1}$$

where the concrete contribution to the axial strength is

$$N_{uc} = \alpha f_c A_c \tag{2}$$

where α is the factor associated with compression of the columns. The factor based on back analysis of the reinforced concrete columns was determined to be approximately 0.70 for Series 1 and Series 2. The reasons for this supposedly lower concrete strength can be explained by the fact that the cross-sections had a significantly large cover are compared with core area and thus this concrete suffered from premature spalling. The reinforcing steel contribution is given by

$$N_{ur} = f_{yr} A_r \tag{3}$$

The contribution of the steel plate was calculated as

$$N_{us} = f_{ys} A_s \tag{4}$$

when local buckling did not occur, or a reduced strength was used which was dependent on the local buckling strength, so that

$$N_{ol} = f_{ol} A_s \tag{5}$$

where the critical stress is given by

$$f_{ol} = \frac{\pi^2 E_s I_s}{A_s L_{bb}^2} \tag{6}$$

This buckling load may be higher if the adhesive restricts the steel plate from buckling out of plane. However in Series 2 the glue may have promoted buckling at a much earlier stage due to creating some initial imperfections. The steel plate undergoes a restrained buckling mode, which essentially reduces the effective length. An adequate buckling model assumes the plates are clamped at the bolt locations, however the unloaded edges are assumed to be free, which is essentially a column buckling approach with fixed ends.

COMPARISONS

The model developed for axial strength is compared with the experimental results of test Series 1 and 2. For both Series the concrete strength used a factor of 0.70 for the concrete cylinder strength as discussed previously. Tables 6 and 7 show the comparisons between the experiment and theory for the axial strengths. One can see that the model is very accurate in predicting the axial strength. The ratio of experimental to predicted strength is shown to be greater than 1.0 in all cases, thus showing

that the model is conservative. The mean value for this ratio was 1.06 and 1.09 for Series 1 and 2 respectively, with a standard deviation of 0.08 in both cases. In both Series 1 and Series 2 plate buckling governed the strength of the steel plating, and this was substantiated by the experiments where plate buckling was noted to be one of the failure modes.

In addition to comparing the test results with the theoretical model proposed, it was also compared with the suggested ultimate strength and design strengths from the Australian Standards for Concrete Structures, AS3600. Tables 6 and 7 shows the ratio of the experimental strength to predicted ultimate strength, as well as the ratio of experimental to assumed design strength.

The AS3600 model was used with nominal strengths, so that the nominal concrete compressive strength was 40 MPa and the nominal reinforcing steel strength was 400 MPa as ordered. The nominal yield strength for the steel plate was taken as 250MPa. This comparison therefore resulted in some interesting observations. If one was to use the AS3600 strength model with nominal strengths, a mean value of 1.02 and 1.06 was established with a standard deviation of 0.11 and 0.08 respectively for Test Series 1 and 2.

If one compares the experimental strengths with the design strengths as suggested by AS3600, a standard deviation of 1.70 and 1.78 with a corresponding standard deviation of 0.32 for both test series. This shows that for design, the AS3600 model will certainly provide a factor of safety of approximately 2.5, by the time load factors are introduced.

TABLE 6
AXIAL STRENGTH COMPARISONS (SERIES 1)

Specimen	$N_{u.Experiment}$ (kN)	N_{uc}	N_{ur}	N_{us}	$N_{u.Predicted}$ (kN)	Ratio= ($N_{u.Experiment}$/ $N_{u.Predicted}$)	Strength Ratio (AS3600)	Design Ratio (AS3600)
Plain #1	1031	815	216	0	1031	1.00	1.09	1.82
Plain #2	1125	909	216	0	1125	1.00	1.19	1.98
Bolted #1	1251	849	216	163	1228	1.02	0.90	1.49
Bolted #2	1255	849	216	163	1228	1.02	0.90	1.50
Glued and Bolted #1	1359	849	216	163	1228	1.11	0.97	1.62
Glued and Bolted #2	1476	849	216	163	1228	1.20	1.06	1.76
					Mean	1.06	1.02	1.70
					Standard Deviation	0.08	0.11	0.32

TABLE 7
AXIAL STRENGTH COMPARISONS (SERIES 2)

Specimen	$N_{u.Experiment}$ (kN)	N_{uc}	N_{ur}	N_{us}	$N_{u.Predicted}$ (kN)	Ratio= ($N_{u.Experiment}$/ $N_{u.Predicted}$)	Strength Ratio (AS3600)	Design Ratio (AS3600)
Plain #1	2214	1890	324	0	2214	1.00	1.22	2.05
Plain #2	1828	1504	324	0	1828	1.00	1.01	1.69
Bolted #1	2374	1697	324	52	2073	1.15	1.05	1.76
Bolted #2	2476	1697	324	52	2073	1.19	1.10	1.83
Glued and Bolted #1	2252	1697	324	52	2073	1.09	1.00	1.67
Glued and Bolted #2	2229	1697	324	52	2073	1.08	0.99	1.65
					Mean	1.09	1.06	1.78
					Standard Deviation	0.08	0.08	0.32

CARBON FIBRE PLATING IMPLICATIONS

Recent studies on the compressive behaviour of carbon fibre plates restrained by a rigid medium have shown that these plates are more susceptible to local instability than steel plates, due to the high level of anisotropy which is existent in unidirectional plates, (Uy and Aw, 2001 and Uy and Yang, 2001). Further experiments have also shown that due to the very low transverse stiffness and strength, small out of plane deformations of the plate in compression can lead to transverse splitting which is a highly undesirable failure mode. Further experiments of these plates when used in conjunction with reinforced concrete columns should be conducted to assess the suitability of this material for rehabilitation purposes.

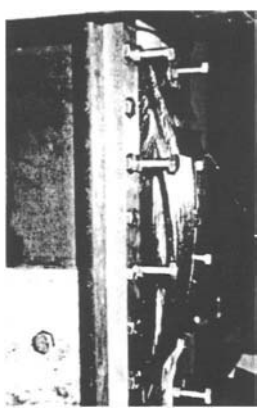


Figure 3: Failure mode of carbon fibre reinforced plastic plating under compression

CONCLUSIONS

This paper has presented a benchmark set of tests for reinforced concrete columns bonded with steel plates under axial flexural loading. The paper has illustrated that bonding steel plates to reinforced concrete columns can increase both the stiffness and strength of the member. Both bolting and gluing and bolting were investigated. Bolting steel plates was shown to produce a higher strength and stiffness than the control specimens. Gluing and bolting also produced an increase in strength and stiffness and in the case of the slender columns, this was totally effective in eliminating local buckling and slip and thus allowing full composite action to be achieved. A theoretical model has also been presented to determine the axial stiffness and strength. This model was calibrated with sufficient accuracy with the test results and in all cases the model is shown to be conservative. However further research is required before this approach could be adopted in design as only a limited amount of specimens were tested. Furthermore, given the growing use of fibre reinforced plastic plates in retrofitting concrete structures, further tests should be conducted using these forms of plates.

ACKNOWLEDGEMENTS

The author would like to thank Ms. Caroline Raleigh and Messrs Ian Bridge, Bob Rowlan, Richard Webb and Philip Yeadon all formerly of the Faculty of Engineering, University of Wollongong for assisting in undertaking the experimental programme presented in this paper. This project was sponsored by the Australian Research Council Small Grants Scheme.

REFERENCES

Standards Association of Australia, *SAA Concrete Structures Code*, SAA, Sydney, Australia, 1994, AS3600-1994.

Uy, B. and Aw, K. (2001) Local buckling of carbon fibre plastic (CFRP) plates restrained by a rigid medium, *Proceedings of the First International Conference of FRP in Civil Engineering, Hong Kong, December,* pp. 723-728.

Uy, B. and Yang, T. (2001) Local Buckling of anisotropic plates restrained by concrete, *First Asian Pacific Congress on Computational Mechanics, Sydney, November,* pp. 279-284.

CONSTRUCTION TECHNOLOGIES:

HIGH PERFORMANCE CONCRETE/COMPOSITES

This Page Intentionally Left Blank

Advances in Building Technology, Volume 1
M. Anson, J.M. Ko and E.S.S. Lam (Eds.)
© 2002 Elsevier Science Ltd. All rights reserved

NUMERICAL SIMULATION OF THERMAL CRACKING OF CEMENT-BASED MULTI-INCLUSION COMPOSITE

Y.F. Fu[1], Y.L. Wong[1], C.A. Tang[2]and C.S. Poon[1]
[1]Department of Civil & Structural Engineering, Hong Kong Polytechnic University
[2]Lab of Numerical Test of Material Failure, Northeastern University, Shenyang, China

ABSTRACT

A newly developed 2-*D* mesoscopic thermoelastic damage (MTED) model is used to study the thermal stress field and associated fracture in a cement-based composite with multiple circular inclusions at high temperatures. It is found that the thermal stress field and the associated cracking are dominated by the interaction of inclusions, and the heterogeneity. The macrocracks occur firstly between the two inclusions which have the shortest distance apart if coefficient of thermal expansion (CTE) of the inclusion is greater than that of matrix. The resistance of inclusion with higher strength against crack is also found. The MTED model yields a good agreement between the proposed numerical simulations and the available experimental results.

KEYWORDS

Thermal stress; Thermal induced cracking; Irregular inclusion; Numerical simulation; Heterogeneity

INTRODUCTION

When a cement-based composite material is subjected to elevated temperatures, the difference in thermal deformations of the cementitious matrix and the aggregate inclusions induces thermal stresses and possibly cracking in the material. Previous investigations [Venecanin, 1990; Khoury,1992] have shown that the greater the mismatch in the mechanical and thermal properties between the matrix and the inclusion, the more significant the reduction of strength, elasticity modulus, and durability of concrete would be. The deteriorations of these properties were mainly due to the thermal induced cracking. Venecanin (1990) experimentally studied the effects of thermal incompatibility of concrete components (TICC) by measuring their CTE, and the CTE heterogeneity of aggregate inclusions. The results showed that TICC was one of the reasons for thermal cracking. Kristensen and Hansen (1994) lent a support to the Venecanin's view in their investigation of the thermal cracking of cement paste and concrete using ultrasonic pulse velocity techniques. Their experimental results indicated that cement paste and concrete could be damaged by internal cracking due to differential stresses at differential temperature between core and surface of specimen. Later, based on the fracture mechanics and micromechanics approaches, an analytical

model (Sumarac et al., 1998) was proposed to study the reduction of elastic modulus with temperatures due to the mismatch in the CTE between mortar and aggregate, assuming a uniform distribution of cracks. Recently, both analytical modeling and numerical simulation (Hsueh, et al., 2001) were used to analyze residual thermal stresses and CTE in two-phase composites. It was found that the predicted CTE of a two-phase material was dependent on the Young's modulus ratio and the difference between the CTE of the two phase-materials. If the intergranular phase had a greater CTE than that of the grain, the intergranular phase and the grain would be stressed in tension and hydrostatic compression, respectively. Although the studies on the thermal stress and the thermal crack have been conducted numerically or experimentally, the studies of the thermal cracking processes – the initiation, propagation and linkage of crack in concrete at elevated temperatures is still limited.

As observed in experiments (Tijissens et al., 2001; Mier et al., 1997), concrete is a highly heterogeneous material that can be quantified in three levels: macroscale, mesoscale and microscale. The heterogeneity is an indispensable reason to cause the concentration stress and local failure (Brandt, 1996; Hsu, 1963). At room temperature, the effects of heterogeneity on the fracture processes in concrete have been reported in literatures. However, the previous studies do not consider the effects of heterogeneity among the phase materials of concrete on the stress development and cracking process under high temperatures. The complex structure of concrete is unable to be described by an analytical model. The process of thermal cracking of heated concrete has not been visually demonstrated till now.

This paper presents a series of numerical studies to quantify/qualify the effects of the interaction and CTE of multi inclusions on the thermal stresses and associated cracking in a cement-based composite. Consequently, a more realistic thermal stress field and the thermal cracking in meso-structure can be observed visually and dynamically by the newly developed mesoscopic thermoelastic damage (MTED) model (Fu et al., 2002).

NUMERICAL METHOD

Brief Outline Of Mesoscopic Thermoelastic Damage (MTED) Model

The cement-based composite is made of two phase materials (matrix and inclusion), each of which at mesoscale is heterogeneous. The interface bonding between the matrix and the inclusion is assumed to be perfect. A statistical Weibull Distribution is used to describe the heterogeneity of the phase material using a homogeneity index. The mechanical properties (such as strength, elastic modulus and Poisson ratio) are randomly allocated to each representative volume element (RVE) to account for the inherent variability in the phase material, using the Monte-Carlo method.

In this study, we implicitly assume that the macroscopic mechanical behavior of the composite is a result of the growth of microcracks, and is captured in the damage evolution law for RVE. A smeared crack concept is adopted to construct the constitutive law of RVE. The crack is not considered as a discrete displacement jump, but rather a variation in the mechanical properties according to a continuum law, such as damage mechanics. A separation function of damage is deduced to describe the softening process of the material. A full description of the MTED model is available in the paper (Fu et al., 2002). The schematic of the thermoelastic behavior law of the material is shown in Fig.1. It is assumed that the stress-strain relationship of a RVE is linearly elastic till its peak-strength is reached, and thereafter follows an abrupt drop to its residual strength. Under compression, RVE remains a residual strength after peak-strength; whereas, under tension, the residual strength of RVE is equal to zero. Parameters S and S_r are used to denote the uniaxial compressive/tensile strength and residual strength; ε^0, ε_0 are the initial thermal strain and the strain corresponding to the peak strength of RVE, respectively. This model is able to capture the complete

thermal cracking processes including the initiation, propagation and linkage of cracks. In the present study, the CTE and mechanical properties of the matrix and inclusions are considered to be independent of temperature variations.

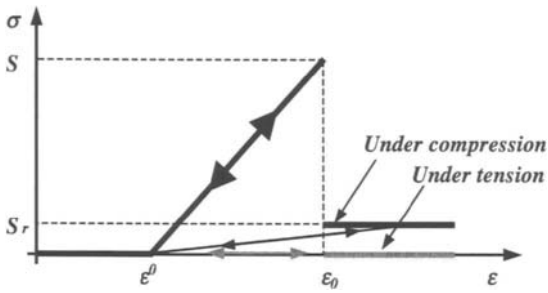


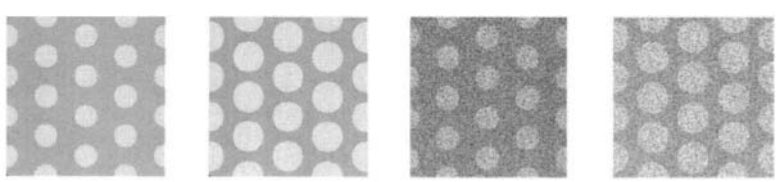
Fig.1 Constitutive relation of RVE

Numerical Specimens

Four numerical square specimens with different thermal and geometrical properties (see Table.1) are presented here to simulate the thermal induced cracking process in the composite with multi-inclusions. Specimen no.1 and no.2 with multi circular inclusions of same CTE (see Fig.2) are set to investigate the influence of the interaction between inclusions on the thermal stress field, and the only variable is the inclusion diameter. The proportion of the inclusions in Specimens no.1 and no.2 are 28.3% and 50.2%, respectively. For the former, the diameter of inclusion is 15mm. For the latter, the diameter of inclusion is 20mm. Specimens no.3 and no.4 (see Fig.2) are similar to those of Specimens no.1 and no.2 respectively, except the former ones have a higher degree of heterogeneity (h=3 in matrix and inclusions). All specimens are subjected to uniform temperature field changes (steady state) ranging from 20°C till 620°C, at an increment of 10°C.

TABLE.1
MATERIAL PROPERTIES OF SPECIMENS NO.1 TO 4

Parameter		Value	
		Matrix	Inclusion
Homogeneity index (h)	Specimen no.1 and no.2	300	300
	Specimen no.3 and no.4	3	3
Mean elastic modulus (MPa)		60000	100000
Mean compressive strength (MPa)		200	300
Poisson Ratio		0.25	0.20
Coefficient of thermal expansion (/°C)	Specimens no.1 to no.4	1.0E-5	1.1E-5
Temperature increment (°C)		10	10
Tension cutoff		0.1	0.1
Frictional angle (°)		30	30
Dimension (mm)	Specimen no.1	100×100	Φ15
	Specimen no.2		Φ20
	Specimen no.3		Φ15
	Specimen no.4		Φ20



(a) Specimen no.1 (b)Specimen no.2 (c) Specimen no.3 (d) Specimen no.4

Fig.2 Numerical models

NUMERICAL RESULTS AND DISCUSSION

Thermal Stress Field

Effects of interaction of inclusions

In case of Specimen no.1 with multi inclusions of 15mm diameter, a diamond-shaped region surrounded by the inclusions (see Fig.3a) is chosen to explain the influence of the arrangement of inclusions. In this region, the distance between the inclusions ***A*** and ***B*** is larger than that between the inclusions ***C*** and ***D***. Consequently, in the sub-region Ψ_1 the stress in the *X*-direction is smaller than 0, $\sigma_x<0$, and in the *Y*-direction is larger than 0, $\sigma_y>0$; whereas in the sub-region Ψ_2 the stress in the *X*-direction is larger than 0, $\sigma_x>0$, and in the *Y*-direction is smaller than 0, $\sigma_y<0$ (as shown in Fig.3c). In the locally enlarged pictures of the principal stress contours of the sub-regions Ψ_1 and Ψ_2

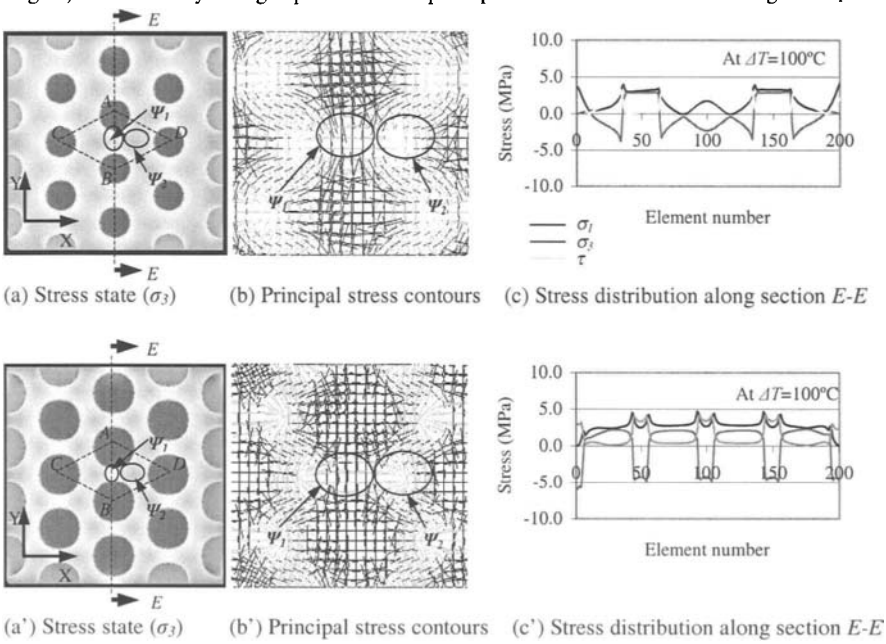


Fig.3 Thermal stress field in Specimens no.1 and no.2

(see Fig.3b), a dark line is a trajectory of a maximum principal stress and a light is the trajectory of the minimum principal stress. It is evident that the values of all principal stresses approach zero in the sub-region Ψ_2, but the principal stresses in the sub-region Ψ_1 have the highest value in the whole matrix (see Fig.3c). There are six sub-regions of low stress like Ψ_2 around each inclusion in the composite. Hence, the elements in Ψ_1 have higher probability of failure than those in Ψ_2. Similar stress states in Ψ_1 and Ψ_2 are observed in Specimen no.2 with larger multi inclusions of 20mm diameter (see Fig.3a', 3b'). The calculated results have a good agreement with those reported in the literature (Hsueh et al., 2001; Hsu, 1963). The results from Specimen no.2 further prove that the stress induced by the cross-effect of the inclusions is one of the reasons to cause the stress concentration. From Fig.3c and Fig.3c', it is found that the principal stresses between the inclusions ***A*** and ***B*** are increased by 20%. Such also occurs between the inclusions ***A*** and ***C***, or ***C*** and ***B***, or ***B*** and ***D***, or ***D*** and ***A***.

Consequently, the stress concentration occurred in the matrix due to the cross-effect of multi inclusions makes the elements in the matrix more prone to fail.

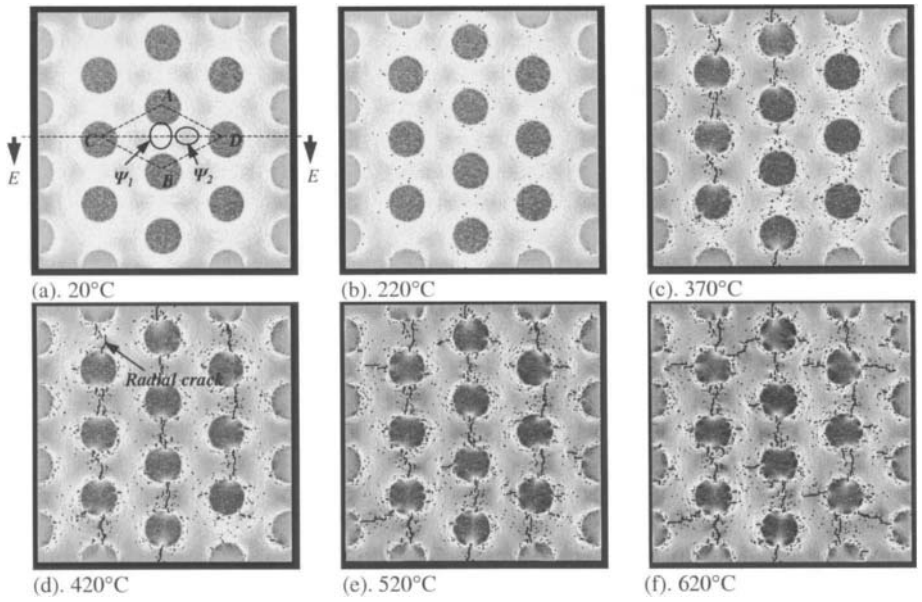


Fig.4 Thermal cracking process of Specimen no.3

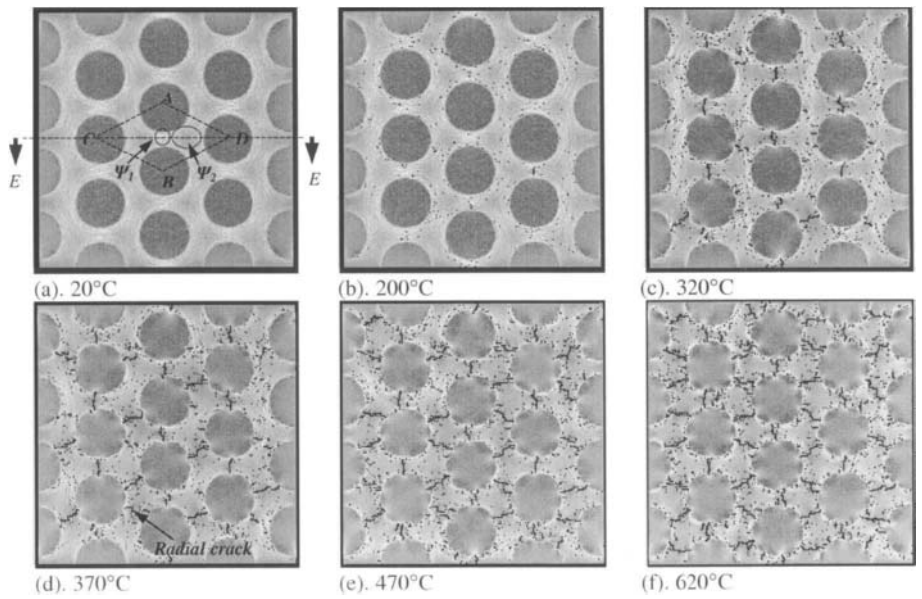
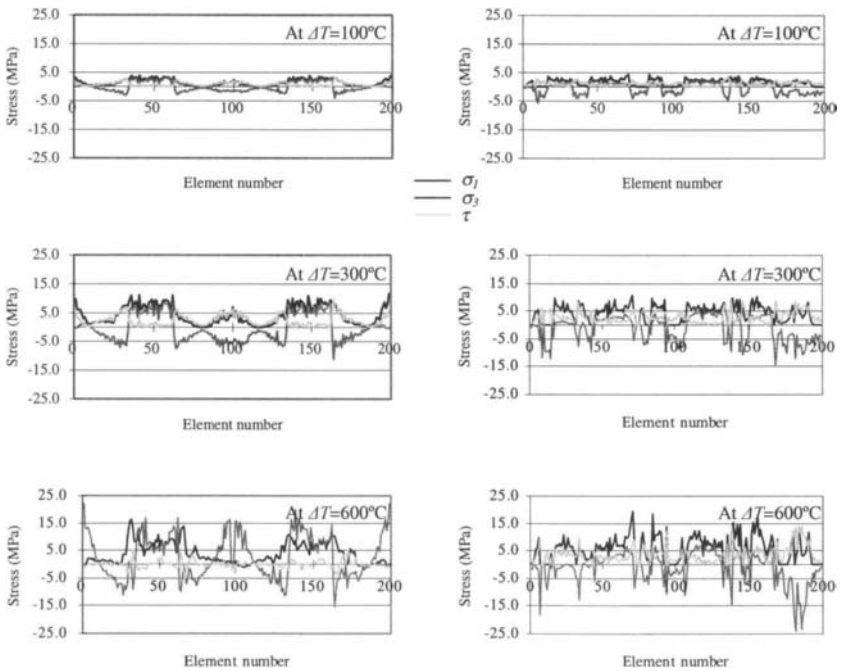


Fig.5 Thermal cracking process of Specimen no.4

Effects of heterogeneity

Fig.4a shows the thermal stress field of Specimen no.3 that has heterogeneous matrix and inclusions. Gray scale indicates minimum principal stress values. Comparing the stress distribution along the mid-section *E-E* of Specimen no.3 (Fig.6a) with that of Specimen no.1 with homogeneous phase materials (Fig.3c), it is very clear that heterogeneity causes local fluctuation of stresses in matrix and inclusion even before crack initiates (see Fig.6a), even though their macroscopic thermal stress fields are same from the view point of statistics. With increasing the temperatures, the number of the broken elements is also increased. Due to this reason, the degree of the stress fluctuation becomes severe (see Fig.6a). With the increase of number of the damaged elements, the original stress distribution is changed. For example, at temperature increment of 620°C (see Fig.4f), the high stresses have been transferred to the tips of the irregular cracks, whose distributions are closely associated with the change in the heterogeneous mesostructure. This transfer of thermal stress field with the variation of mesostructure cannot be easily observed in experiments.



(a) Specimen no.3 (b) Specimen no.4

Fig.6 Thermal stress distribution along mid-section *E-E* of Specimens no.3 and 4

Thermal Fracture

Effects of interaction of multi inclusions

The cross-effect on stresses between the two neighborhood inclusions makes the elements in sub-region Ψ_1 more prone to fail. The commence of crack development is largely dependent on the distance between any given two inclusions. For example, for Specimen no.3, when the elements around the inclusions firstly reach their strength, cracks begin to develop at the interface of the matrix and the inclusion, and then propagate towards to the middle of the two neighborhood

inclusions (see Fig.4). For Specimen no.4 with larger inclusions, cracks are firstly formed in the middle of the two neighborhood inclusions which have the shortest distance apart, rather than at the interface of the matrix and the inclusion, and then propagate towards the two neighborhood inclusions (see Fig.5b). As the diameter of inclusions increases, the distance between ***A*** and ***C***, or ***C*** and ***B***, or ***B*** and ***D***, or ***D*** and ***A*** in Specimen no.4 reduces (see Fig.5). As a result, inclined cracks making an angle of about 30° to the horizontal line are developed (see Fig.5e-f) instead of the horizontal cracks occurred in Specimen no.3 with smaller circular inclusions (as shown in Fig.4e-f).

Effects of heterogeneity

In case of Specimen no.3, a diffused damage initially appears randomly in the whole region of the matrix at temperature of 220°C (see Fig.4b). It means that the failure of an element is dependent both on the thermal induced local stress and on the strength of the element. The strength distribution of the elements is mainly dependent on the heterogeneity at meso-scale. Under the same stress field, the elements with a higher ratio of the stress to the strength have higher probability to fail than those with a lower ratio. Consequently, the shape of the crack path is irregular, rough and bifurcate.

Another interesting phenomenon can be observed from Fig.4 and Fig.5. The crack development is resisted by an inclusion with high elastic modulus and strength. When the tip of a radial crack touches an inclusion with higher elastic modulus and strength, the inclusion obstructs the radial crack propagation. For example, in case of Specimen no.3, after the radial cracks coalesce between two-neighborhood inclusions linking up in the *Y*-direction, they do not propagate when the tips of the cracks approach such an inclusion (see Fig.4c-f). Instead, the radial cracks in the *X*-direction begin to initiate and propagate, since the stresses have been redistributed and transferred into the tips of these horizontal cracks. Thus the inclusion can play an important role to (i) resist further propagation of crack, (ii) consume more energy required by failure, and (iii) dictate the redistribution of the stresses. These results are consistent with the viewpoints in the literature (Kristensen et al., 1994) that thermal cracking probably travel in all directions in mortar due to the presence of aggregate in concrete.

The numerical results also reveal that discontinuous cracks grow simultaneously at the poles of the different inclusions. Increasing number of such cracks eventually result in the irregular radial cracks, length of which is greater than the direct distance between the two corresponding inclusions because of the irregular path of crack. It lastly impairs the cohesive properties of the bond phase material (matrix). From the observation of the thermal fracture processes, it appears that heterogeneity can be used to interpret the randomization of crack origin and crack shape. It can also be used to explain the reason of local thermal fracture.

CONCLUSIONS

In this paper, a newly developed mesoscopic thermoelastic damage model (MTED) has been implemented to numerically simulate the thermal stress field and the crack formation, extension and coalescence in a cement-based multi-inclusions composite at elevated temperatures. From the results presented in this study, some main conclusions are summarized as follows.

1. The thermal stress field being studied is focused on the effects of thermal mismatch and the arrangement of inclusions. When the CTE of inclusion is larger than that of the matrix, the inclusion and the matrix are subjected to statistically hydrostatic compression and a combination of compression and tension, respectively. A high stress region is induced at the interface between the matrix and the inclusion by the thermal mismatch, and in the area between any two-neighborhood inclusions with the shortest distance apart.

2. The initiation and path of cracks depend on the heterogeneity at meso-scale. When the CTE of inclusion is larger than that of matrix, the interaction of inclusions is another factor affecting the thermal cracking. The cracks form, propagate and coalesce firstly along direction between the two inclusions which have the shortest distance apart. When the inclusion diameter increases, the cross-effect of stress concentration around the two neighborhood inclusions increases the probability of failure of the elements locating between these two inclusions. However, when the strength of the inclusion is higher than that of matrix, the inclusion can prevent the further propagation of the cracks to a certain extent.

In this paper the temperature-dependent properties (strength, elastic modulus and CTE) of each component material of the composite at high temperatures, which can substantially affect the thermal cracking, have not been quantified. Further work on this direction will be conducted. Nevertheless, the numerical study by using the proposed MTED model offers an understanding of the thermal stress redistribution and cracking process of a cement-based composite, from which various mechanisms of thermal induced stresses and associated cracking have been identified.

REFERENCE

Venecanin SD. (1990). Thermal incompatibility of concrete components and thermal properties of carbonate rocks *ACI Materials Journal* **87:6**, 602-607.
Khoury A. (1992). Compressive strength of concrete at high temperatures: a reassessment. *Magazine of Concrete Research* **44:161**, 291-309.
Kristensen L, Hansen TC. (1994). Cracks in concrete core due to fire or thermal heating shock. *ACI Materials Journal* **91:5**, 453-459.
Sumarac D, Krasulja M. (1998). Damage of plain concrete due to thermal incompatibility of its phases. *International Journal of Damage Mechanics* **7**, 129-142.
Hsueh CH, Becher PF, Sun EY. (2001). Analysis of thermal expansion behavior of intergranular two-phase composites. *Journal of Materials Science* **36**, 255-261.
Tijissens MGA, Sluys LJ, Giessen EVD. (2001). Simulation of fracture of cementitious composites with explicit modeling of microstructural features, *Engineering Fracture Mechanics* **68**, 1245-1263.
Van Mier, Jan GM. (1997). *Fracture Processes of concrete: assessment of material parameters for fracture models*. CRC Press, U.S.A
Brandt AM. (1995). *Cement-based composites: Materials, Mechanical Properties and performance*. E& FN Spon, UK
Bažant ZP, Kaplan MF. (1996). *Concrete at high temperatures: Material properties and mathematical models*, Longman House, UK
Hsu Thomas TC. (1963). Mathematical analysis of shrinkage stresses in a model of hardened concrete, *ACI Journal,* 371-390.
Fu YF, Wong YL, Tang CA, Poon CS. (2002). Thermal induced stress and associated cracking in cement-based composite at elevated temperatures – Part I: Thermal cracking around single inclusion. *Submitted to Cement and Concrete Composite.*
Neville AM. (1993). *Properties of concrete*, 3rd Ed., Longman House, UK
Goltermann P. (1995). Mechanical predictions on concrete deterioration. Part 2: Classification of crack partterns, *ACI Materials Journal* **92:1**, 58-63.

ACKNOWLEDGEMENTS

The materials presented in this paper are some of the findings of the G-V848 research project entitled "Thermal Stress and Associated Damage in Concrete at Elevated Temperatures", of The Hong Kong Polytechnic University funded by the research Grants Council. The project is also partly supported by the NNSF of China (No.50174013).

Advances in Building Technology, Volume 1
M. Anson, J.M. Ko and E.S.S. Lam (Eds.)
© 2002 Elsevier Science Ltd. All rights reserved

APPLICATIONS OF COPPER GANGUE WITH HIGH CONTENT OF Fe_2SiO_4 AS CEMENT ADMIXTURE AND FOR CEMENT PRODUCTION

Lin Zongshou Wan Huiwen Zhao Qian Huang Yun

School of Materials and Engineering, Wuhan University of Technology , Wuhan,Hubei,P.R.China,430070

Abstract:

Copper gangue (CG) is an inactive industrial waste generated from a copper refinery. Making good use of this waste will be beneficial to the sustainable development of society. In this study, the copper gangue was firstly used as a cement admixture. The results showed that with the replacement of 5~25% CG, 3-day and 28-day strengths decreased by 5~32%. However the long-term strength of the specimens with 10% CG, especially after the samples cured for 3 months, approached that of plain mortar. Its mechanism was studied by electron probe microanalyzer (EPM), and the results indicated that a small quantity of $Fe(OH)_3 \cdot nH_2O$ slowly formed from Fe_2O_3 in the presence of $Ca(OH)_2$, and accordingly the hardened cement paste became more dense. Secondly, the CG as iron material for cement production was also researched. Optical microscope analyses showed that CG containing Cu, Zn, Ti, Mn, Ag etc microelements, can decrease clinker burning temperature and liquid viscosity, and enhance migration of the CaO and SiO_2. A blended admixture with low content of CaF_2-$CaSO_4 \cdot 2H_2O$ could take a partial mineralization effect and further benefits the clinker burning.

Key words:

Industrial waste, Copper gangue, Cement admixture, Microelement

1. Introdution

Copper residue is an industrial waste that is discharged by a copper refinery. In order to extract some useful metals, a cooling technology for removing residue is introduced by slowly cooling (48h) rather than quickly cooling so that some metals ions grow. Such copper residue contains 4~5% copper, 1.01g/t gold, 24g/t silver and 42% magnetite. After one more flotation for copper and magnetic by extraction of iron, the discharged residue is called copper gangue (CG). But CG grains mostly are in the range 0.037~0.10mm and contain a large amount of water. CG still contains approximately 48% fayalite (mostly Fe_2SiO_4) and 28% fine crystal magnetite (mostly Fe_2O_3 and less FeO), while copper content is only 0.3~0.4%.

It is well known that raw material containing high iron oxide can be used as an alterative material for cement production. Because iron oxide can form liquid phase in clinker burning, the addition of

CG can enhance migration of the CaO and SiO_2, and benefit the clinker sintering forming calcium aluminoferrite [1]. J.O.Odigure's researches [2-5] showed that abrasive slurry containing high metallic particles (Fe^{3+}, Fe^{2+}, Fe) content, could significantly improve the clinker mineral chemical composition, morphology and phase ratio. The kinetics of chemical reactions in hardening cement mortar produced from the raw mix containing metallic particles, differ from those of ordinary Portland cement using raw materials of natural origin.

This research is aimed at investigating the influence of CG used as a cement admixture on cement mortar strength and the influence of CG used as a raw material on cement clinker mineral morphology. It will be helpful to the recycling and reuse of this industrial waste.

2. Experiment

2.1 Chemical composition and microanalysis of CG

The chemical composition and mineral analysis of CG are presented respectively in Tables 1 and 2. The X-ray diffraction pattern of is shown in Fig.1, which indicates that the mineral components of CG are mainly composed of Fe_2SiO_4, Fe_2O_3, FeO and a small quantity of amorphous SiO_2.

SiO_2	Al_2O_3	Fe_2O_3	CaO	MgO	SO_3	LOI*
34.84	2.99	52.42	4.27	4.14	/	-2.36

LOI*—Loss on ignition

Table 1 Chemical composition of CG (mass %)

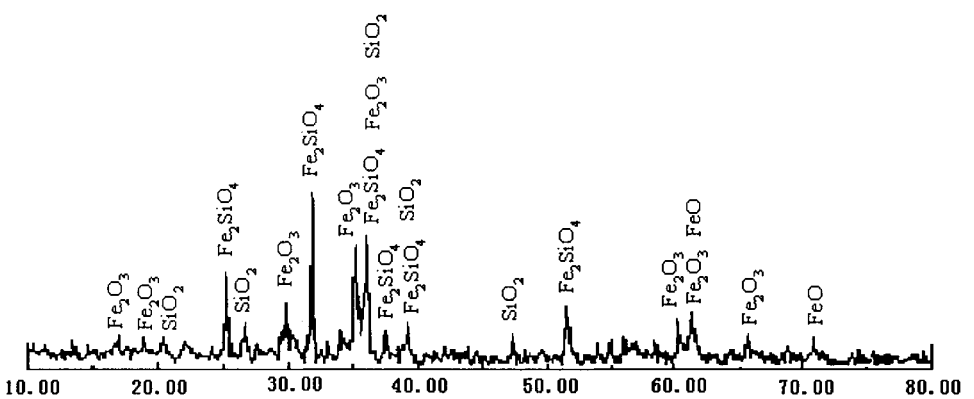


Fig. 1 X-ray diffraction pattern of the CG

Magnetite	Fayalite	Amorphous silicate	Hematite & limonite	Feldspar & kaolinite	Brass & matte
30.2	47.8	14.7	2.8	2.5	0.7

Table 2 Mineral composition of CG (mass %)

2.2 CG used as cement admixture

The CG was dried and manually dispersed. Portland cement (surface area 300m^2/kg) was provided by Jinyue cement plant, the chemical composition of the clinker is shown in Table 3. CG substitution percentages by weight relative to cement were 0%, 5%, 10%, 15%, 20% and 25%, respectively. All samples were mixed for 6h in an automatic blender and then normal consistency and setting time were measured according to GB 1346-92 (Chinese standard). Specimens for testing mechanical strength, after demoulding, were cured in water 28 days at 20±2℃and then cured to prescribed ages in the ambient conditions. Compressive strengths were measured according to GB 175-92. CG substitution ratios and physical properties of cement are presented in Table 4.

SiO_2	Al_2O_3	Fe_2O_3	CaO	MgO	f_{CaO}	LOI*
19.52	5.80	4.81	62.66	2.11	2.27	0.44

LOI*—Loss on ignition

Table 3 Chemical composition of clinker (mass %)

N	CG substitution ratio (mass %)	Setting times (min)		Normal consistency	Compressive strength (MPa. After days)			
		Initial	Final	(%)	3	28	90	360
1	0	104	195	29.0	25.6	52.3	68.4	69.3
2	5	125	210	28.6	24.2(0.95)	50.2(0.96)	68.0(0.99)	68.7(0.99)
3	10	138	220	28.0	22.1(0.86)	46.8(0.89)	68.7(1.01)	70.6(1.02)
4	15	155	245	27.5	20.3(0.79)	42.5(0.81)	65.3(0.95)	66.5(0.96)
5	20	168	250	27.0	18.7(0.73)	38.6(0.74)	63.0(0.92)	61.8(0.89)
6	25	176	270	26.4	17.3(0.68)	35.5(0.68)	58.9(0.86)	58.1(0.84)

*( )—strength ratio, which is the ratio of the strength of various sample to that of sample 1 at the same age.

Table 4 CG substitution ratios (mass %) and physical properties of cement

In order to study the influence of the Fe_2SiO_4 and Fe_2O_3 into CG on mechanical strength of cement and avoiding interfere with the iron phase contained in Portland cement, the following experiments were carried out. (1) Incorporating 25% CG in white Portland cement to make paste sample A. (2) At the same condition, 25% CG in Portland cement to make paste sample B (curing 3 months, curing system as before). (3) Their microstructure and composition were studied using EPM (Figs. 2 and 3).

2.3 CG used as raw material for cement production

The raw materials used for the experiments were limestone, clay, coal, gypsum, fluorite and CG. For the making of coal ash, coal was put in an earthen box and burnt in an electric furnace using silicon-heating elements. The burning temperature was 1200℃, with a duration of 6h at the maximum temperature. Coal ash content was 25.8%. The compositions of the raw materials are presented in Table 5. The compositions of the raw mixes were determined (shown in Table 6). The dried raw materials mixed in the required proportion were ground to a fineness of 6 to 8 mass % residue on an 80-μm size mesh using a laboratory ball-mill. They were then watered and manually pressed into a Φ10×30mm column. Those columns were dried and burnt in an electric furnace using silicon-heating elements. The burning temperature was gradually raised to 1450℃, the rate of rise of temperature was controlled to 200~250℃/h, with a duration of 45 min at the maximum temperature. The clinkers were cooled in the air. The clinker samples were analyzed with an optical microscope and the microstructural images are shown in Figs. 4 and 5. The result determined of the free CaO is shown in Table 6. The produced clinker and 4% gypsum were ground approaching a surface area of $310m^2/kg$. The mechanical strengths of the clinkers, determined by the above method, are presented in Table 6.

Table 5 Chemical composition of raw materials

Material	Oxides contents, mass %							
	SiO_2	Al_2O_3	Fe_2O_3	CaO	MgO	SO_3	CaF_2	LOI*
Limestone	5.64	1.65	0.76	48.50	1.77			40.38
Clay	63.48	13.76	5.93	2.25	1.62			9.60
CG	34.84	2.99	52.52	4.27	4.14			-2.36
Gypsum	0.26	0.25	0.06	32.56	0.18	45.88		19.80
Fluorite	25.22	1.08	0.09	1.71	0.50		65.73	5.41
Coal ash	54.20	29.14	7.84	3.45	0.47			

LOI*—Loss on ignition

Table 6 Composition of raw mix and compressive strength of cement

N	Composition of raw mix , mass %							f_{CaO} (mass %)	Compressive strength (MPa)	
	Limestone	Clay	Iron powder*	CG	Gypsum	Fluorite	Coal*		After 3days	After 28days
7	79.41	7.84	1.92	0	0	0	10.83	2.52	28.0	56.1
8	78.34	7.37	0	3.46	0	0	10.83	2.08	27.8	56.7
9	75.27	7.03	0	3.49	2.64	0.74	10.83	1.75	29.4	60.2

Iron powder*— chemical agent containing Fe_2O_3 98.5%.

Coal*—laboratory should use coal ash, 10.83×25.8%.

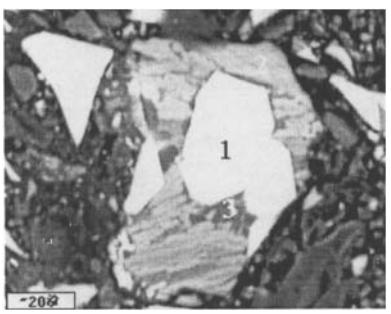


Fig. 2 EPM photograph of the sample A
1-Fe_2O_3 2,3-Fe_2SiO_4

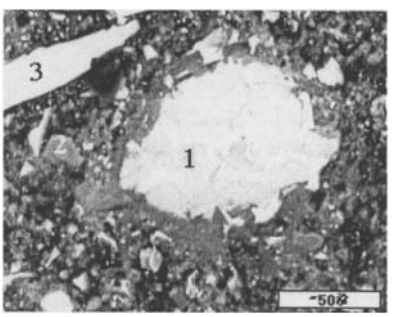


Fig. 3 EPM photograph of the sample B
1-C_2S 2-$Ca(OH)_2$ 3-Fe_2SiO_4

3. Results and discussion

3.1 Petrographic features of the CG

The mineral analyses of Table 2 show that CG comprises mainly fayalite, magnetite and amorphous silicate minerals. From Fig. 1, it is clear that the diffraction peaks of Fe_2SiO_4, Fe_2O_3, FeO and SiO_2. EPM (Fig. 2) show that Fe_2O_3 particle is partially wrapped in Fe_2SiO_4. The grains of CG are distributed mostly in the range 0.037~0.10mm with tough surface and dense structure. Its density is 5.20g/cm^3.

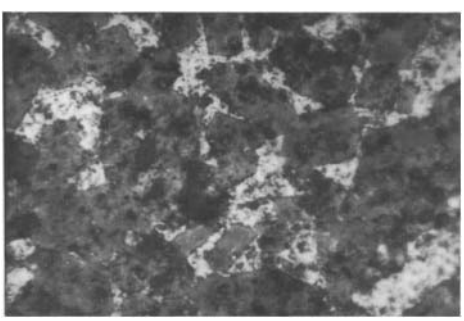


Fig. 4 Optical photograph of sample 7

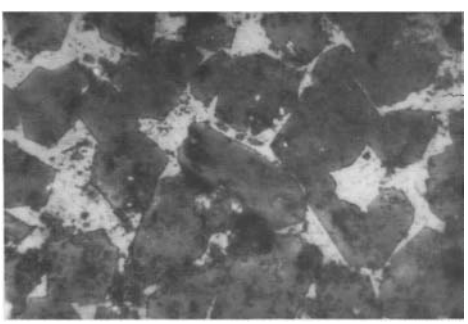


Fig. 5 Optical photograph of sample 8

3.2 The influence of CG used as admixture on strength of the cement

Table 4 shows that if the setting time of the cement is prolonged normal consistency of the cement decreased gradually with the increase of CG substitution. The effect of CG on the mechanical

properties was remarkable. An investigation was made over a period of one year. It is found that the CG substitution led to a decrease of strength, and the higher the replacement, the lower the compressive strength. To increase understanding of the influence of the CG substitution on strength, the strengths at various ages are expressed in term of the strength ratio, which is presented in bracket of Table 4. It can be seen that the strength ratios of 3-day and 28-day were approximately equal at the same substitution ratio, and both reduce from 0.95(or 0.96) with 5% CG to 0.68 with 25% CG. However the strength ratios at 3 months and 1 year increased, even exceeding the control group and reached 1.02 within the substitution ratio was 10% CG. This implies that the CG has a positive effect on the long-term strength.

It is easy to understand that cement strength decreased with the increase of CG due to its inactivity. The long-term strength increase was related probably to Fe_2O_3 and FeO, which is contained in CG. The interactions between the oxides and the cement matrix could be that $Fe(OH)_3 \cdot nH_2O$ gradually form through the reaction of Fe_2O_3 in the presence of $Ca(OH)_2$. Even in the atmosphere, FeO can also slowly form $Fe(OH)_3 \cdot nH_2O$ in a solution of $Ca(OH)_2$ [6]. The volume of $Fe(OH)_3 \cdot nH_2O$ is much bigger than that of Fe_2O_3 and FeO, and thereby hardened cement paste becomes more compact. Fig. 3 shows that there is still a small quantity of unhydrated C_2S after curing for 3 months and the strength hence further increased after 3 months. Fig. 2 shows that a part of Fe_2O_3 was wrapped in Fe_2SiO_4. By composition analyses of bare Fe_2O_3 particles using EPM, the results showed that the chemical composition around the Fe_2O_3 particles differed obviously from those of Fe_2O_3 particles in the centre. This implies that a small quantity of $Fe(OH)_3 \cdot nH_2O$ probably formed on the surface of the Fe_2O_3 particles. When the samples were kept in the atmosphere for 1 year, a little $Fe(OH)_3 \cdot nH_2O$ was continuously formed increasing local stress and $Fe(OH)_3 \cdot nH_2O$ lost nH_2O increasing pore ratio. These factors resulted in only a slight decrease of the one-year compressive strengths with high content of Fe_2SiO_4 and Fe_2O_3. This phenomenon will be continuously observed.

3.3 The influence of CG on mineral composition and microstructure of clinker

Table 6 shows that 2.52% free CaO existing in sample 7 was higher than in samples 8 and 9. It indicated that CG helped clinker burning, because CG contains Cu, Zn, Ti, Mn, Ag etc microelements, which can decrease burning temperature of clinker and liquid viscosity [7]. In sample 9, free CaO was of its lowest content, indicating that CaF_2-$CaSO_4 \cdot 2H_2O$ partially shared mineralization effect, greatly accelerating sintering reaction [8]. The results showed that CG used as raw material for cement production is not disadvantageous to cement strengths. An Optical photograph of sample 7 (Fig.4) shows the predominance of hexagonal alite crystals 30~40 μ m in length, and minerals partially eroded and containing about 50% alite. Sample 8 (Fig.5), which was burnt in the same condition, has larger uniform size alite crystals predominantly 50~60 μ m in length, profile of alite clarity and containing over 55% alite. This could be attributed to early formation of a large quantity of liquid phase and consequently enhanced migration of the CaO and SiO_2.

4. Conclusion

When the CG was used as a cement admixture, the early strengths of the cement decreased with the increase of CG, however the long-term strengths of the cement, especially after 3 months, clearly increased. Analyses of EPM show that there was probably $Fe(OH)_3 \cdot nH_2O$ slowly forming through the reaction between Fe_2O_3 and water in the hardened cement paste.

CG substitution percentage by weight of cement should be controlled below 20%, as the compressive strengths at 1 year incorporating more than 20% CG decreased lightly.

CG used as a raw material, due to the Cu, Zn, Ti, Mn, Ag etc microelements contained can decrease clinker burning temperature and liquid viscosity, with advantage to clinker burning. A little CaF_2-$CaSO_4 \cdot 2H_2O$ added to raw meal, is of further benefit to clinker burning.

Reference

[1] F.M.Lea. (1984). The Chemistry of Cement and Concrete, third ed., China construction industry publishing company
[2] J.O.Odigure. (1996). Mineral composition and microstructure of clinker from raw mix containing metallic particles. Cem. Concr. Res. **26:8,** 1171-1178.
[3] J.O.Odigure. (1996). Kinetic modelling of cement raw mix containing iron particles and clinker microstructure. Cem. Concr. Res. **26:9,** 1435-1442.
[4] J.O.Odigure. (1997) Preparation of cement raw mix containing metallic particles. Cem. Concr. Res. **27:11,** 1641-1648.
[5] J.O.Odigure. (2001) Optimization of cement mortar strength from raw mix containing metallic particles. Cem. Concr. Res. **31:1,** 51-56.
[6] Cai Shaohua. (1999) Inorganic Chemistry of Elements, second ed., Zhongshan university publishing company
[7] Wang yanmou et al. (1985) Beijin International Congress on the Cement and Concrete, beijin.
[8] W.A.Kleem and I.Jawed. (1980) Seventh International Congress on the Chemistry of Cements, Paris.

Advances in Building Technology, Volume 1
M. Anson, J.M. Ko and E.S.S. Lam (Eds.)
© 2002 Elsevier Science Ltd. All rights reserved

PROPERTIES OF LIGHTWEIGHT AGGREGATE FOR LIGHTWEIGHT CONCRETE PRODUCTION

Tommy Y. Lo, H.Z. Cui

Department of Building & Construction
City University of Hong Kong

ABSTRACT

The increasing demands for the speed of construction and the greater use of prefabrication units in the building industry have urged the need for exploring new innovative construction materials. The adoption of lightweight aggregate concrete in prefabrication of structural panels for building works can minimize the foundation load, reducing the size of structural members, speeds up the construction program and has better control on material quality. All lightweight aggregates are porous in nature that water absorption is much greater than normal weight aggregate. The great absorption rate of aggregate will lowers the water content at the aggregate/cement paste interface and affects critically the mix design, workability of fresh lightweight concrete. Since characteristic of lightweight aggregate varies with the production plants, operation and the raw material used in the production process, the surface characteristic, size and pore structure of the lightweight aggregate differs from one type to the others. Surface topography and pore distribution of the aggregate surface dominate the water absorption characteristic of the aggregate, affect critically the properties of the resulting lightweight aggregate concrete and the bonding with the cement matrix. This paper presented a detail study on the physical properties of a locally available lightweight aggregate made from expanded clay. Density and strength of the lightweight aggregate of different density ranges and their relationship with water absorption characteristic and internal microscopic were examined.

KEYWORDS

Lightweight aggregate, porosity; strength, water absorption, microstructure

1. INTRODRUCTION

The adoption of lightweight aggregate concrete in prefabrication of structural panels for building works can minimize the foundation load, reducing the size of structural members, speeds up the construction program, achieving better quality control and provides a green building construction environment. In other part of the world, high-rise buildings have been built with structural lightweight aggregate concrete [LWAC]. The 42 storeys Prudential Life Building in Chicago and the famous "Nordhordland" bridge are good examples of the applications of structural LWAC (1). A cost model of an eight-storey height office building compared the construction cost of using LWC and NWC reinforced concrete finding that a LWC building could save 1½ week in the construction period. Although the cost of LWAC is 5% higher than traditional normal weight concrete, the overall cost saved 4% (2).

However, the lightweight concrete currently adopted in Hong Kong is limited to non-structural applications (3,4). The available type of ready mixed lightweight concrete is limited to foam concrete or polystyrene bean concrete. Although research finding indicated that structural lightweight concrete with density below 1600kg/m^3 can be made with a locally available expanded clay lightweight aggregate (5), the development on the use of structural LWAC is hindered by the lack of research data on concrete properties, in particular the long-term durability characteristics. Moreover, overseas experience may not apply to Hong Kong because properties of the LWAC vary with the type and characteristic of the lightweight aggregate use.

2. MATERICALS

The LWA used in this experimental work is a lightweight expanded clay aggregate [LECA] produced by bloating clay under high temperature firing of over 1200°C in the rotary kiln [Figure 1 & 2]. Because of the porous nature of the aggregate core, it is extremely light in weight and the insulation property is good. The aggregate is stable, inert to acid corrosion, not attacked by fungi, non-absorbent and frost resistant.



Figure 1: General view of coarse LECA (10mm size)

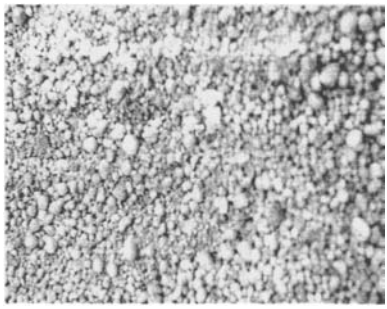


Figure 2: General view of fine LECA

3. RESEARCH SIGNIFICANCE

This paper presented the results on the physical properties, internal microstructure and water absorption of a locally available LECA aggregate. The finding is crucial in understanding the characteristic of LECA aggregate for the development of prefabricating structural lightweight members.

4. RESULTS AND DISCUSSIONS

Bulk density and strength

Most of the lightweight aggregates [LWA] are cellular in structure; the bulk densities are considerably less than those of normal weight aggregate [NWA]. As seen in table 1, 5mm, 14mm and 25mm sizes LECA aggregate were compared. The measured bulk density ranging between 450-850kg/m^3 was only ¼ to ½ the density of NWA. The oven-dry density also fall within the standard ranges of 400~1200kg/m^3 for fine lightweight aggregates and 250~1000kg/m^3 for coarse aggregate (6).

Strength and density of lightweight aggregate varies with the type of aggregate, source of raw materials and production method. Aggregates can be strong and hard or weak and fragile depending on the shape and size of aggregate. Microscopically speaking, it is related to the volume and distribution of the micro pores and whether the pores are inter-connected within the aggregate. Shell thickness is also one of the controlling factors. Simple tube compressive strength was used to examine the average strength of lightweight aggregate. Detail of the tube strength equipment was given in figure 3 (7). Results of the tube strengths of the LECA aggregate are presented in figure 4 and co-related with the bulk densities. Aggregate with a density of 450kg/m^3, 650kg/m^3 and 850kg/m^3 achieved tube strength of 35kN, 50kN and 65kN respectively. In general, aggregate with low bulk densities achieves low tube strengths.

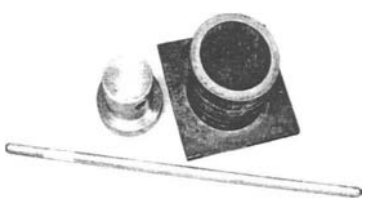


Figure 3 : Equipment for Tube strength determination

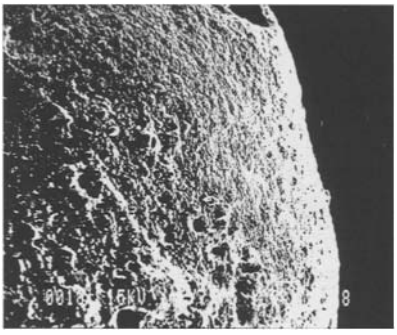


Figure 4 : Surface topography of a typical lightweight aggregate

Microstructure and water absorption of aggregate

Figure 4 shows the surface topography of a typical LECA aggregate. It is seen the aggregate is round with a rough surface texture. The porous surface of the aggregate is good in forming a mechanical bond with the surrounding mortar enhancing the aggregate/cement pastes interface, and reduces the formation of micro-cracks inside the concrete matrix (8).

Water absorption of the porous lightweight aggregates is generally higher than the normal weight aggregate. Finding from past research (9) suggested that seventy percent of the 23-h water absorption took place within the first 30s of absorption. Water absorption rate also differ significantly between cut and whole aggregates. The 1-h water absorption rate of the cut sample was 58% higher than that of whole aggregate. The great variation in water absorption rate was attributed to the presence of an outer shell that controls the ingress of water and the number of voids and fissures that appeared in the

aggregate core, pore size and its distribution within the aggregate core affects critically the density, water absorption and strength of the resulting concrete (7).

The cross-sections of the aggregate microstructure were shown in Figs 5,6 and 7. The microstructure of the 3 grades of aggregate with densities 450kg/m^3, 600kg/m^3 and 850kg/m^3 were compared. For aggregate with density 850kg/m^3, it is seen that micro pores were evenly distributed throughout the aggregate particles and were not inter-connected with each other. Comparing to the aggregate of density 450kg/m^3, the internal microstructure composed with large inter-connected voids and fissures. In general, the number of inter-connected pores increases with the decrease in bulk density of aggregate.

Water absorptions of the 3 grades of aggregate were compared and results were shown in Figure 8. It indicated that the initial absorption of 6mm aggregate was greater than that of 25mm. The absorption rate of 14mm aggregate was the lowest. Around 50-65% of the 24 hours absorption took place at the first few minutes. The absorption increases with time but the absorption ranking was the same. The finding confirmed with past research result by Swamy (9). Moreover, the absorption rate was irrelevant to the size of aggregate.

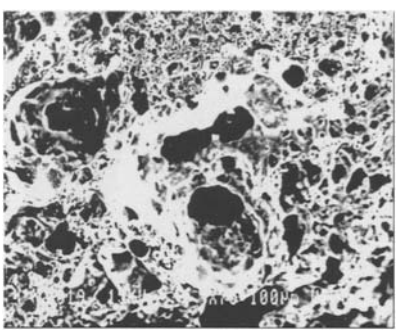


Figure 5: Lightweight Aggregate (Density 450 kg/m^3)

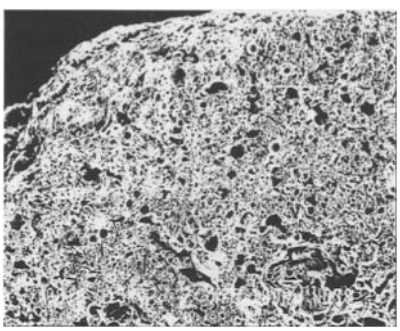


Figure 6: Lightweight Aggregate (Density 600kg/m^3)

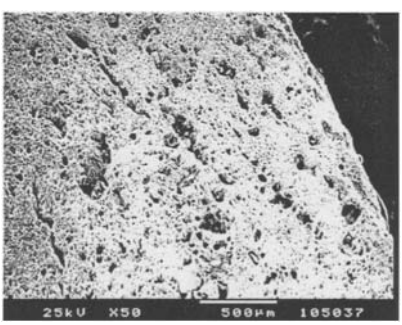


Figure 7: Lightweight Aggregate (density 850 kg/m^3)

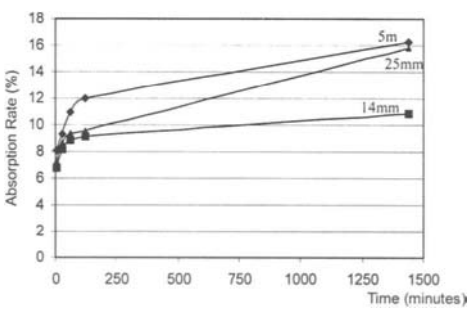


Figure 8: Water absorptions of the lightweight aggregates

Table 1 summarized the pore distribution of the 3 aggregate samples with different density. It is seen that the majority of the pore are sized between 1µm to 100µm for all three density graded aggregate. When the total volume of micro pore increases, the aggregate density decrease. This also explains why water absorption of cut (or fragmented) aggregate was greater than that of whole aggregate. When the

lightweight aggregate broken, the number of open pores increases leading to a larger water absorption rate of the absorption. Therefore, a thick and dense aggregate shell is necessary in ensuring the blockage of water path passing into the aggregate core.

TABLE 1
PORE SIZE AND THE VOLUME DISTRIBUTION WITHIN CORE OF LIGHTWEIGHT AGGREGATE

Aggregate Density (kg/m^3)	Aggregate size	Pore Distribution				
		<0.01 μm	0.01-1μm	1-10 μm	10-100 μm	>100 μm
400	25 mm	0.3	87.4	728.6	171.8	7.9
600	5 mm	0.4	36.8	652.3	156.5	3.9
800	14 mm	0.2	53.5	459.6	102.1	4.5

* Above data is the average of ten samples

It is also interesting to note that the density of aggregate does not necessarily directly related to the size. For example, the density of the 5mm aggregate was greater than that of the 25mm aggregate but was lower than the density of a 14mm aggregate. This phenomenon can be explained by the presence of substantial amount of large pore (>100μm) within the 25mm sized aggregate.

5. CONCLUSION

Based on the findings, the following conclusions can be drawn:

1) Pores size of the locally available LECA aggregates mainly ranged between 1 μm to 100 μm.
2) When the total volume of micro pore decreases, the aggregate density increase.
3) The initial water absorption is 50-65% of the 24 hours absorption
4) Tube strength of aggregates is related to the pores volume and bulk density. The aggregate strength decreases with the increase of total pore volume within the aggregate core.
5) The number of inter-connected pores increases with the decrease in bulk density of aggregate.

6. ACKNOWLEDGEMENT

The work described in this paper was fully supported by a grant from the Research Grants Council of the Hong Kong Special Administrative Region, China [Project No. CityU 1037/01E]

7. REFERENCES

1. CEB-FIP. (2000). Lightweight Aggregate Concrete, part 3, International Federation for Structural Concrete..
2. Institution of Structural Engineers. (1987). "LWAC Guide: lightweight aggregate", *Institution of Structural Engineers/Concrete Society,* p.11-31. London..

3. Lo, T. Y. (1992). "The Application of Lightweight Precast Wall Systems to Housing Block of Hong Kong." *The Third International Symposium on Noteworthy Applications in Concrete Prefabrication.* Singapore, 13-15 July, (p95-101).
4. Lo, T. Y. (1995), "Lightweight Concrete - A Challenge in Housing Construction," Proceedings of XXIII IAHS World Housing Congress, Excellence in Housing : Prospects and Challenges in the 'Pacific' Century, Vol. 2, Singapore. 25-29 Sept.
5. Lo, Y, Gao, X. F. and Jeary, A. P. (1999), Microstructure of Pre-wetted Aggregate on Lightweight Concrete," Building and Environment. Vol. 34. No. 6.
6. BS3797. (1990) *Specification for lightweight aggregates for concrete.* Part 2, BSI, London. U.K.
7. GB 2839-81. (1981) *National Standard for Production of Lightweight Expanded Clay Aggregate,* People Republic of China.
8. Mays G C & Barnes R A. (1991) Performance of Lightweight Aggregate Concrete Structures in Services Royal Military Coll of Science, *Structural Engineers* Vol 69, No. 20, 351-361, 15 Oct.
9. Swamy, R.N. and Lambert, G.H. (1981). "The microstructure of Lytag aggregate", *Journal of Cement Composite and Lightweight Concrete,* Vol. 3, No. 4, Nov. pp.273-282.

Advances in Building Technology, Volume 1
M. Anson, J.M. Ko and E.S.S. Lam (Eds.)
© 2002 Elsevier Science Ltd. All rights reserved

PRELIMINARY RESULTS ON THE USE OF GFRP AS AN EXTERNAL REINFORCEMENT FOR AUTOCLAVED AERATED CONCRETE

Ali M. Memari* and Ayca Eminaga*

*Department of Architectural Engineering, The Pennsylvania State University
104 Engineering A, University Park, Pennsylvania, USA

ABSTRACT

The bond strength between Glass Fiber Reinforced Polymer (GFRP) sheets and Autoclaved Aerated Concrete (AAC) surface is investigated. Specimens made of two small AAC blocks attached together with two strips of GFRP are pulled apart by using a hydrolic jack. Bond length is a variable in the study. The results show that the bond strength between AAC and GFRP is comparable to that between Carbon FRP and normal concrete surface.

KEYWORDS

Fiber reinforced polymer, autoclaved aerated concrete, bond strength, external reinforcement.

INTRODUCTION

Although Autoclaved Aerated Concrete (AAC) products have been used in Europe and several other countries in Asia and the Middle East for a few decades, this lightweight concrete has been introduced in the U.S. market primarily since 1995. According to Woodard *et al.* (1999), "This new building material combined the advantage of wood and cement products – it could be cut, drilled, and nailed like wood while maintaining high strength, excellent durability, thermal insulation, sound insulation, and fire resistance. Subsequently, it gained rapid acceptance in Europe and throughout the world." There is good optimism for the growth of AAC in the U.S. market. Chusid (1999) predicts that if the announced plans for a few more factories realize, "there will be three million cubic yards of annual capacity in North America within the next two to three years, equivalent to over 150 million square of wall, floor and roofs and enough for an estimated 10,000 to 15,000 buildings per year." Currently, the primary use of AAC in the U.S. is in the form of masonry blocks, wall and floor panels, and lintels. Panels and lintels are reinforced to carry superimposed loads. Three of the key references on AAC are Wittmann (1983), Wittmann (1992), and Aroni *et al.* (1993). The book by Wittmann (1983) includes a bibliography chapter on AAC that lists 492 documents on AAC. Even though many publications exist on AAC, only a fraction of the studies have addressed structural aspects.

Unlike Normal Weight Concrete (NWC), one of the deficiencies associated with the use of steel bars to reinforce AAC elements is the weakness of the bond between the steel surface and the surrounding AAC. According to Aroni *et al.* (1993), because of the low alkali reserve and high porosity of AAC, reinforcement should be covered with anti-corrosion material (such as protective bituminous coating). According to Hanecka (1992), because of corrosion protection coating, the bond properties and their effects on the response of AAC members under load are not sufficiently understood. Aroni *et al.* (1993) clearly mentions the deficiency: "The bond strength between the reinforcement and AAC is much lower than that in normal concrete." Because of such a problem, the anchorage of reinforcement cannot be provided by bond, and therefore, cross bars welded to longitudinal reinforcement must be used. In such cases, the anchorage is provided by the bearing of the cross bars against the AAC. The pullout strength of longitudinal bars is limited by the smaller of the spot weld capacity of cross bar-longitudinal reinforcement connections and bearing capacity of the cross bar-AAC interface (Boutros and Saverimutto 1997). Therefore, practically the bond strength between steel and AAC is ignored. However, according to Aroni *et al.* (1993), if any bond strength is to be allowed in design, the capacity has to be verified by a pullout test based on RILEM Recommendation AAC 8.1.

In an effort to find an alternative reinforcement system or an approach for supplemental reinforcement (in addition to what is usually provided in precast AAC members), this paper explores the possibility of using Fiber Reinforced Polymers (FRP) as an externally applied reinforcement. Before the experimental program is described, a brief background on the use of FRP on NWC and the basis for the experimental study reported here is mentioned.

BACKGROUND ON THE USE OF FRP ON NWC AND THE BASIS FOR THE EXPERIMENTAL STUDY

Over the past decade, FRP composites have evolved as reliable alternative reinforcing products for repair and rehabilitation of aging concrete and masonry structures. Currently, three types of fibers, namely, carbon, aramid, and glass are widely manufactured, which when the fibers are embedded in a polymeric resin (matrix), the composites are referred to, respectively, as CFRP, AFRP, and GFRP. From the three types of composites, CFRP provides the largest strength and is commonly used to strengthen existing reinforced concrete members. Given that AAC is a weaker material then NWC, the use of high strength CFRP is not justified (Vadovic 2000) and therefore, GFRP was determined to be suitable for use with AAC in this study.

The effectiveness of using externally bonded FRP composites to strengthen concrete beams has been well established. The primary objective of this study is to investigate the suitability of externally bonded GFRP composites to be used for AAC lintels and floor and wall panels. However, before experiments on beams and wall panels are carried out, the characteristics of the bond between the externally applied GFRP sheets and AAC surface should be determined. Several investigators have performed such studies for bond characteristics between CFRP and NWC. Maeda *et al.* (1997) used two small concrete blocks (100 mm x 100 mm in cross section) that were attached together with 50 mm wide strips of CFRP on two sides of the blocks, but with a gap between the blocks. The tension force to the CFRP was applied by pulling two steel rebars that were inside the concrete prisms. In that study, bond length and concrete strength was varied and the resulting data provided information on the variation of bond strength with bond length and concrete strength in addition to strain distribution. Brosens and Van Gemert (1997) have also performed tension tests on two concrete prisms (150 mm x 150 mm x 300 mm) attached with CFRP laminates on two opposite sides. Tensile force is applied on steel plates glued on the other sides (opposite to CFRP sheets) of the prisms. During the displacement controlled tests, information on the applied load, relative movement of the prisms and the strains of the

CFRP were taken. In that study, too, the bond length and concrete strength were varied. Representative results from these studies will be compared with the results of AAC tests reported in this paper.

EXPERIMENTAL PROGRAM

The diagram of the test setup for this study is shown in Figure 1. The test specimen consists of two AAC prisms (100 mm x 100 mm x 275 mm) connected together by two GFRP strips, which are attached to two opposite faces of the AAC prisms. In order to apply tension to the GFRP strips, a loading jack is placed between the two AAC blocks such that it can push them apart. The loading jack, which is operated by a hydraulic pump, has a 88 kN capacity.The test specimen is loaded in a load controlled manner. The load on the specimen is obtained from reading the pressure recorded. Displacements of the prisms are recorded using potentiometer and also an oscilloscope connected to the potentiometer. Figure 2 shows a photograph of the test setup. In the first part of the study reported here, only bond length was varied. The GFRP strips used had a width of 50 mm, but the bond length was varied from 50 mm to 200 mm at 50 mm increments.

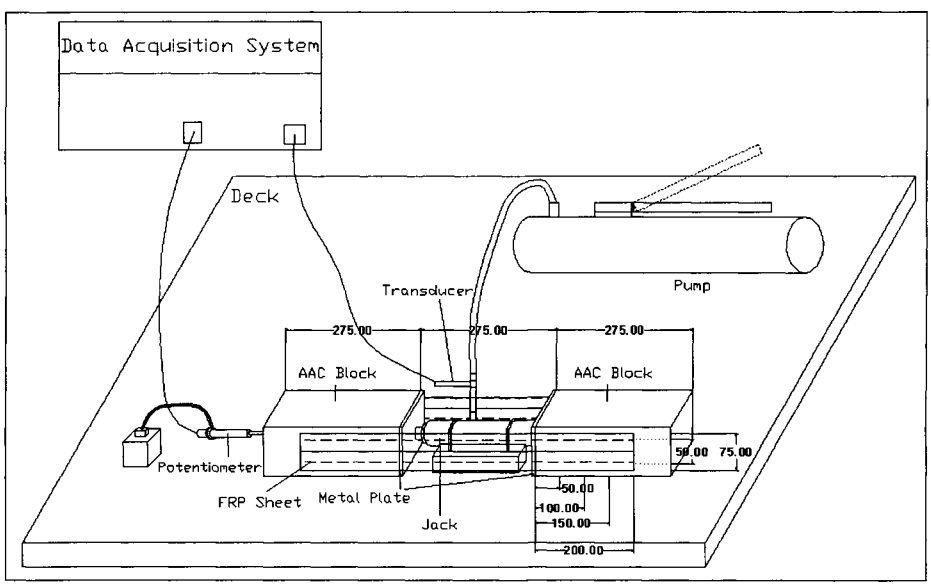


Figure 1: Illustration of test set up (dimensions are in mm).

The AAC used, which was produced by a HEBEL plant in the state of Georgia in US and now owned by Babb International, Inc., Matrix PAAC Division, had a nominal compressive strength of 5 MPa and a unit weight of 720 kg/m^3. The GFRP used is manufactured by Master Builders, inc. and is designated MBrace EG 900 E-glass fibers, which according to Tysl (2000), is more economical compared to carbon or aramid FRP for use with AAC. The matrix (resin) used consists of MBrace Primer, MBrace Putty, and MBrace Saturant.The EG 900 material used is unidirectional, weighs 900 grams/m^2, and has a strength of 525 N/mm of width. Table 1 shows the matrix of specimen configurations used in this

part of the study. For each bond length, three tests were performed. Further tests are ongoing (but not reported here) to investigate the effects of GFRP width and the AAC compression strength.

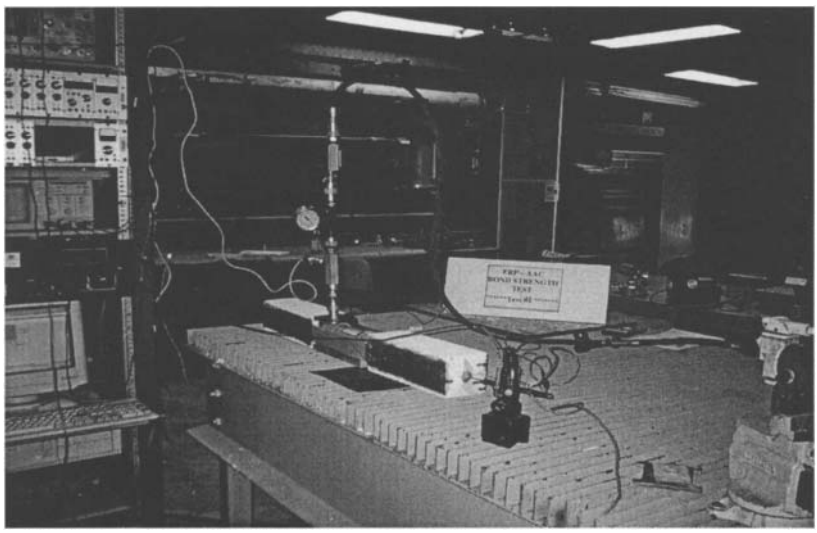


Figure 2: A photograph of the test set up of specimen d1.

TABLE 1
Specimen Configurations and Experimental Results

Specimen	Bond Width	Bond Length	Bond Area	Failure Load	Failure	Bond Strength
	mm	mm	mm2	(Fu)	Displacement	(Fu/BA)
			(2*BW*BL)	KN	mm	Mpa
a1	50.00	50.00	5000.00	11.14	2.44	2.16
a2	50.00	50.00	5000.00	10.70	2.41	2.07
a3	50.00	50.00	5000.00	10.93	1.80	2.12
b1	50.00	100.00	10000.00	13.795*	2.48	1.335*
b2	50.00	100.00	10000.00	14.40	1.97	1.39
b3	50.00	100.00	10000.00	12.77	3.84	1.24
c1	50.00	150.00	15000.00	17.53	2.08	1.13
c2	50.00	150.00	15000.00	14.76	3.36	0.95
c3	50.00	150.00	15000.00	16.36	3*	1.06
d1	50.00	200.00	20000.00	17.69	3.79	0.86
d2	50.00	200.00	20000.00	18.00	2.19	0.87
d3	50.00	200.00	20000.00	17.13	3.27	0.83

*; Data could not be received. So assumptions are made regarding to other similar specimens to plot result graphs.

TEST RESULTS AND DISCUSSION

The results of the tests are listed in Table 1 and also plotted in Figures 3 to 5. Moreover, photographs of typical failure modes are shown in Figures 6 to 9 (one for each bond length). As can be seen in Figure 3, an increase in bond length does not necessarily lead to an increase in bond strength. This result has also been reached in the Maeda *et al.* (1997) study. Looking at the photographs of failed specimens helps the understanding of the behavior. Figure 6 shows the mode of failure of specimen a3 with a bond length of 50 mm. As can be seen, the failure is not a bond failure; rather, it is a shear failure in the AAC prism. Figure 7 shows the typical failure mode for specimens b1 to b3 with a bond length of 100 mm. The failure mode here seems to be a combination of bond failure and shear failure. The same type of failure can be seen in Figure 8 for specimens c1 to c3. However, Figure 9 shows a pure bond failure for the longest (200 mm) bond length used.

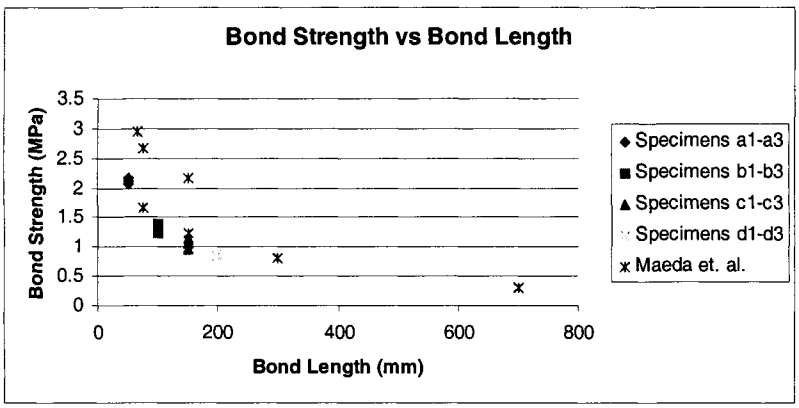


Figure 3: Graph of bond strength versus bond length.

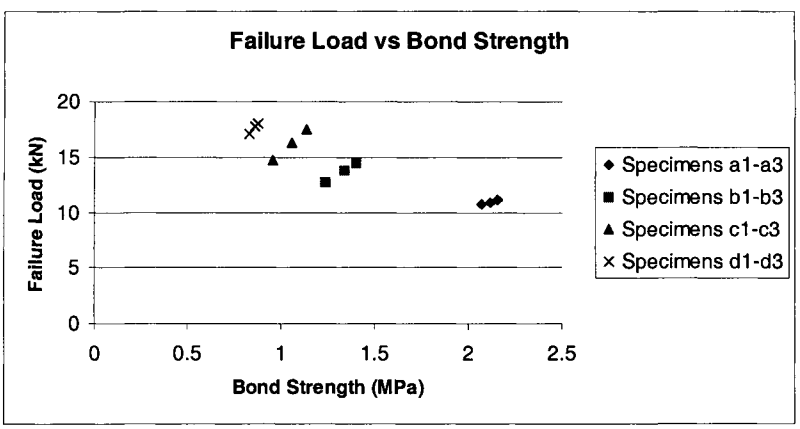


Figure 4: Graph of failure load versus bond strength.

The plotted results in Figure 3 show that bond strength between GFRP and AAC surface for longer contact surface approaches 0.83 MPa (for bond length of 200 mm) from a high value of 2.16 MPa for the short bond length of 50 mm. It should be noted that the bond strength values are only nominal values obtained by diving the failure load by the bond area (on two faces) regardless of the mode of failure. For practical situations, where the FRP sheet is applied rather continuously at the bottom of a beam, the bond strength to be expected is then the value close to that for the longest bond length, i.e., approximately 0.83 MPa. According to the study by Maeda *et al.* (1997) as shown in Table 2, bond strength between CFRP and NWC varies from 0.31 to 2.94 MPa with bond strength decreasing with increasing bond length. A significant observation here is that this range of bond strength is very close to that obtained in this study. Of course, tests on the use of GFRP on NWC will be conducted as a follow-up in this study to confirm this conclusion. Yet another observation is that while the ratio of an average bond strength for long bond lengths (0.75 MPa) from Maeda *et al.* (1997) study to the NWC compressive strength (say 43.3 MPa) is 0.017, the ratio from this study is 0.83/5.0 or 0.166, or 10 times larger. This is another reason for the suitability of the use of GFRP as an external reinforcement of AAC flexural members.

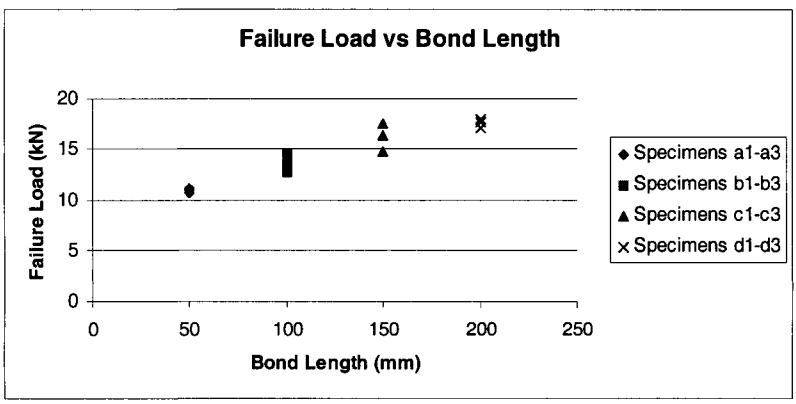


Figure 5: Graph of failure load versus bond length.

TABLE 2.
Experimental Results of *Maeda et. al. (1997)*

Bond Length(mm)	Ultimate Load (kN)	Average Bond Strength (MPa)
75	11.6	1.67
150	18.4	1.23
300	23.9	0.8
75	20	2.67
150	14.6	0.97
65	19.1	2.94
150	32.5	2.17
700	20	0.31

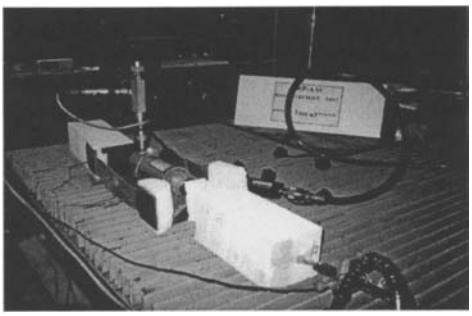


Figure 6: Failure of specimen a3.

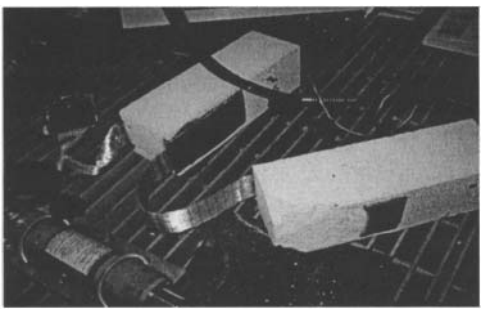


Figure 7: Failure of specimen b2.



Figure 8: Failure of specimen c3.

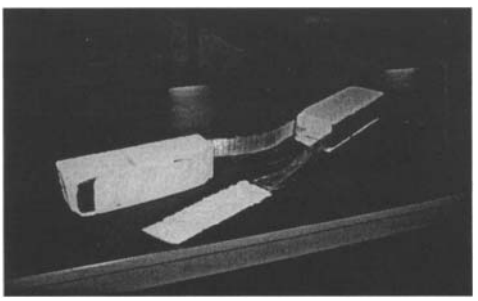


Figure 9: Failure of specimen d2.

CONCLUSION

The study has shown that the bond strength between AAC and GFRP is comparable to that between NWC and CFRP. This shows the stability of GFRP sheet to be used as an external reinforcement on NWC. Further tests are needed, however to establish the characteristics of bond and strength enhancement when GFRP sheets are applied to beams and panels for use under flexural conditions.

ACKNOWLEDGEMENT

The materials for this study were donated by Babb International, Inc. and Master Builders, Inc. and Cyprus Fulbright Commision has provided a fellowship for the second author for an M.S. Degree in Architectural Engineering at Penn State University. All contributions are gratefully acknowledged.

REFERENCES

Aroni, S., de Groot, G. J., Robinson, M. J., Svanholm, G. and Wittmann, F. H., (1993). *Autoclaved Aerated Concrete Properties, Testing, and Design – RILEM Recommended Practice*, RILEM Technical Committees 78-MCA and 51-ALC, E & FN SPON.

Boutros, M. and Saverimutto, L., (1997). Anchorage Capacity of Reinforcing bars in Autoclaved Aerated Concrete Lintels, *Materials and Structures*, **Vol. 30, No. 203**, pp. 552-555.

Brosens, K. and Van Gemert, D., (1997). Anchoring Stresses Between Concrete and Carbon Fibre Reinforced Laminates, *Proceedings of the 3rd International Symposium on Non-metallic (FRP) Reinforcement for Concrete Structures*, **Vol. 1 Oct. 1997**, pp. 271-278.

Chusid, M., (1999). Building with Autoclaved Aerated Concrete, *Masonry Construction*, **January 1999**, pp. 24-27.

Hanecka, K. (1992). The Bond Stresses of AAC and Slips of Reinforcement Bars, *Advances in Autoclaved Aerated Concrete*, Wittmann (Ed.), Balkema, Rotterdam, pp. 181-186.

Maeda, T. Asano, Y., Sato, Y., Ueda, T. and Kakuta, Y. (1997). A Study of Bond Mechanism of Carbon Fiber Sheet, *Proceedings of the 3rd International Symposium on Non-metallic (FRP) Reinforcement for Concrete Structures*, **Vol. 1 Oct. 1997**, pp. 279-286.

Tysl, S. (2000). Master Builders, Inc., Personal Communications.

Vadovic, M. (2000). Gannett Fleming, Inc., Personal Communications.

Woodard, J, Barnett, R., and Schmidt, S., (1999). Design and Utilization of Autoclaved Aerated Concrete Masonry, *Proceedings, 8th North American Masonry Conference*, **June 6-9, 1999**, Austin, Texas, pp. 335-345.

Wittmann, F. H., (1983). *Autoclaved Aerated Concrete, Moisture and Properties*, (Ed.), Proceedings of the RILEM International Symposium on Autoclaved Aerated Concrete, Lausanne, Switzerland, March 1982, Elsevier,

Wittmann, F. H., (1992). *Advances in Autoclaved Aerated Concrete*, (Ed.), Proceedings of the 3rd RILEM International Symposium on Autoclaved Aerated Concrete, Zurich, Switzerland, 14-16 October 1992, A.A. Balkema, Rotterdam.

Advances in Building Technology, Volume 1
M. Anson, J.M. Ko and E.S.S. Lam (Eds.)
© 2002 Elsevier Science Ltd. All rights reserved

HIGH PERFORMANCE FIBRE REINFORCED CONCRETE

S. Mindess[1] and A.J. Boyd[2]

[1] Department of Civil Engineering, University of British Columbia, Vancouver, British Columbia, V6T 1Z4, Canada
[2] Department of Civil and Coastal Engineering, University of Florida, Gainesville, Florida, 32611, USA

ABSTRACT

Since its introduction in the late 1960s, fibre reinforced concrete (FRC) has become an increasingly common building material. It is estimated that, in North America, over 15% of the concrete produced now contains fibres of some kind. At present, almost all of the FRC is used in relatively "low level" applications: slabs-on-grade, control of plastic shrinkage, fibre shotcrete for repairs and tunnel linings, and so on. However, there are still very few truly *structural* applications of FRC; it is rarely used in conjunction with conventional steel reinforcement to improve the mechanical behaviour of concrete in civil engineering structures. As well, fibres are still most commonly used with relatively low strength concretes. In the present work, the use of fibres with both high strength concrete (HSC) and steel reinforcement is described. It is shown that with conventionally reinforced HSC, the fibres improve the post-peak behaviour of the system. Under impact loading, fibres greatly improve the toughness of the composite, particularly when the concrete is subjected to uniaxial or biaxial confinement; fibres may also change the mode of failure, from brittle shear fracture to more ductile flexural failure in both beams and plates.

KEYWORDS

Fibre reinforced concrete, plates, beams, impact loading, uniaxial confinement, biaxial confinement, steel reinforcement.

INTRODUCTION

Plain concrete is a brittle material, strong in compression, but with very low tensile stress and strain capacities. In traditional concrete construction, continuous steel reinforcing bars are used to carry the tensile and shear forces in concrete structures, and to provide some degree of ductility (or energy absorption capacity). However, since about 1970, *fibre reinforced concrete* (FRC) has become an increasingly common building material. The short, discrete, randomly distributed fibres bridge across the microcracks that develop as the concrete is subjected to stress (due to loading, drying shrinkage, thermal changes, and so on), and may impart considerable *"pseudo-ductility"* to the concrete. Thus, the FRC may continue to carry significant stresses at deflections far beyond those required to crack the plain matrix; that is, it acquires *post-peak load carrying capacity.*

Currently in North America, it is estimated that about 15% of the concrete that is placed contains fibres of some type. The majority of the FRC is used in what might be termed "low-level" (i.e., non-structural) applications: for control of plastic shrinkage cracking, in slabs-on-grade, for fibre shotcrete tunnel linings, and for repair of damaged concrete. There are still very few truly structural applications of FRC, in which it is used in conjunction with conventional reinforcing bars to help carry the design loads and deformations. Moreover, fibres are still most commonly used with relatively low strength (ordinary) concretes.

In the present work, the use of fibres with both high strength concrete (HSC) and steel reinforcement is described, with particular reference to recent experimental work carried out at the University of British Columbia. It is shown that, with conventionally reinforced HSC, fibres greatly improve the post-peak behaviour of the system. Under impact loading, fibres greatly improve the toughness of the composite materials, particularly when the specimens are subjected to lateral confinement; in these cases, the fibres may also lead to a change in the mode of failure.

COMPRESSION

Plain concrete fails in a relatively brittle manner. For HSC ($f'_c > 70$ MPa), it exhibits nearly elastic behaviour up to a stress of about 0.7 f'_c; at higher stress levels its behaviour becomes increasingly nonlinear as the microcracks which have developed begin to coalesce, leading eventually to failure. The addition of fibres to a high strength matrix has little effect on f'_c, though it tends to increase somewhat the stress level at which the σ-ε curve becomes noticeably nonlinear. However, by bridging across the cracks, the fibres lead to multiple cracking and hence the ability of the FRC to exhibit much greater strains at failure. For fibre volumes less than about 1.5%, the fibres simply lead to the formation of more (and finer) cracks, and consequently to a greater toughness. For higher fibre volumes, however, a ductile mode of failure occurs, characterized by the development of a few inclined shear cracks. The effects of high volumes of various fibres in a HSC matrix ($f'_c = 70$ MPa) are shown in Fig. 1.

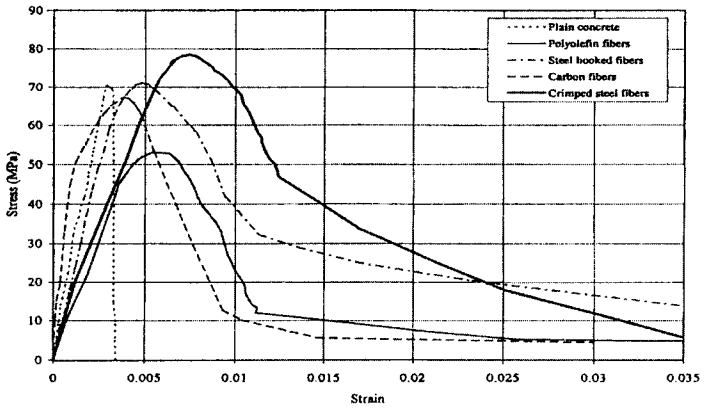


Figure 1(a): Stress-strain curves for HSC at 2.0% by volume of fibres (adapted from Campione and Mindess (1999)).

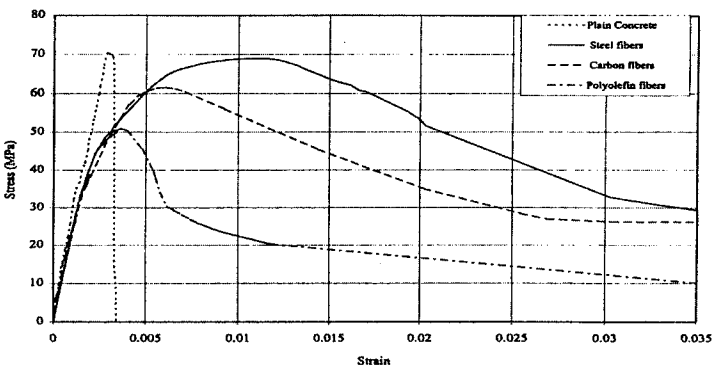


Figure 1(b): Stress-strain curves for HSC at 3.0 percent by volume of fibers (adapted from Campione, Mindess and Zingone, (1997)).

The slight reduction in strength at the highest fibre volumes is due to the difficulty of compacting the concrete fully at such fibre volumes. For similar volumes of carbon fibres, greater reductions in strength were observed, again due to difficulties in compaction, though the increases in toughness were about the same as those found with the steel fibres (Campione *et al.*, 1999b).

The real advantage of using high volume FRC, however, comes when the fibres are combined with conventional steel reinforcement. (Campione et al., 1997; Campione and Mindess, 1999; Campione et al, 1999b; Campione and Mindess, 2000; Campione, et al. 1999). When FRC cylinders containing more than 2% by volume of fibres were reinforced with spiral steel reinforcement, a number of effects were noted:

- Both the ultimate strength and the corresponding strain were increased;
- Beyond the peak load, the failure of the specimen was characterized by successive yielding of the steel spirals at different sections. This occurred because the fibres were able to carry the load transferred to the matrix when a spiral ruptured, as may be seen in Fig.2.

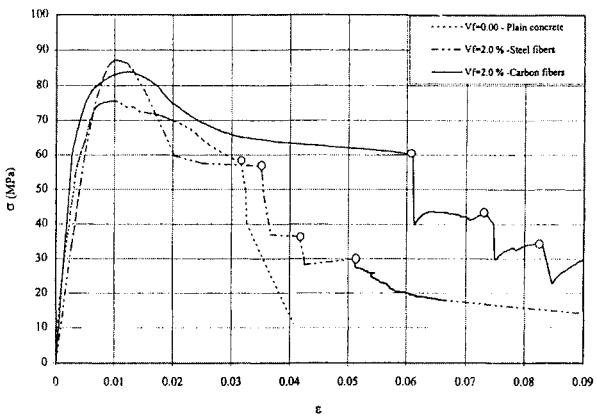


Figure 2: Stress-strain curves for confined HSC at different fiber volumes spiral reinforcement ρ=0.02592 -o failure of steel spirals. (adapted from Campione and Mindess, 1999).

- Thus, the combination of FRC and steel spirals may lead to a considerable increase in the specimen ductility (or ability to absorb energy).
- The maximum strain corresponding to the failure of the steel spirals increased.
- The concrete cover over the spiral steel exhibited less spalling; primarily, spalling was confined to the regions of rupture of the spiral steel.

Fibres combined with spiral steel reinforcement were also found to be very effective under *cyclic* compressive loading. In these tests, specimens similar to those described above were tested under cyclic loading, between 90% of the ultimate stress and 10% of the ultimate stress, to obtain the complete envelope of the cyclic $\sigma-\varepsilon$ behaviour, as shown in Fig.3.

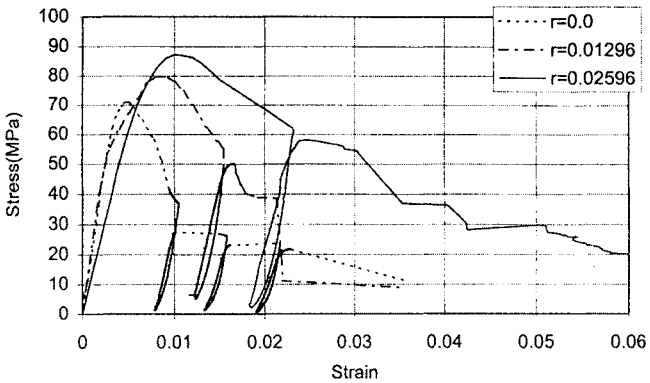


Figure 3: Cyclic stress-strain curves for confined HSC with 2.0% by volume of hooked steel fibers and different steel spiral volumes (Campione et al., 1999a)

The envelope of the cyclic loading curves corresponds closely to that of the monotonic σ–ε curve (measured on a companion specimen). In addition,

- The failure strain under cyclic loading between two fixed stress levels depends only on the maximum stress level in the matrix;
- The toughness of the material under cyclic loading is higher than that under monotonic loading.

FLEXURE

As in the case of compression, the addition of high fibre volumes also increases the residual (post-cracking) strength and energy absorption capacity (toughness) of high strength concrete beams. Under cyclic loading (Campione *et al.*, 2000) showed that FRC with a fibre volume of 3% could withstand very high strains without significant losses in strength. At even higher fibre volumes (≈3.8%), Balaguru and Franklin (1999) showed that steel FRC could withstand approximately 75% of the ultimate load at large deflections, even under reverse cyclic loading. This has obvious implications for concrete structures in severe seismic areas.

High fibre volumes are particularly effective in increasing the shear capacity of high strength, conventionally reinforced beams (Campione and Mindess, 1999; Campione *et al.*, 2000a; Campione *et al.*, 2000b). Although there was no particular increase in the load carrying capacity of the FRC beams compared to those made with a plain concrete matrix, the brittle compressive failure of plain concrete over-reinforced beams was transformed to a "ductile" compressive failure. However, the current provisions for calculating ductility factors appear not to be suitable for FRC reinforced beams.

IMPACT

Both plain concrete and FRC are highly strain rate sensitive materials, with their apparent strengths increasing with increasing strain rates. However, we are still unable to predict their behaviour under impact or dynamic loading on the basis of static tests. Also, because of the inherent difficulties in carrying out properly instrumented impact tests, the available experimental data are often *artifacts* of the particular testing system and specimen geometry employed. Nonetheless, there are enough data reported to permit the following general observations to be drawn:

- The addition of fibres to concrete increases the measured impact strength. The increase obtained in a particular test depends upon the fibre volume, fibre geometry , and matrix strength.
- As with plain concrete, the fracture energy (toughness) of FRC is increased under impact loading (Banthia *et al.*, 1994).
- The strain rate sensitivity of FRC increases both with increasing fibre content and fibre aspect ratio. This is generally attributed to the strain rate sensitivity of the fibre-matrix bond strength (Naaman and Gopalaratnam, 1983).
- Adding fibres to the concrete matrix will significantly improve the bond between the concrete and conventional steel reinforcing bars (Yan and Mindess, 1991; Yan and Mindess, 1994). The composite becomes more ductile, absorbs more energy, and exhibits a higher ultimate bond stress.

The effects of fibres can be particularly dramatic when the FRC is subjected to multiaxial loading. As shown in detail by Sukontasukkul (2001) and Sukontasukkul *et al.* (2001).

- When compression specimens are confined laterally, the mode of failure changes from the usual shear cone appearance to a columnar or vertical splitting type. Both the strength and strain at peak load are increased.
- For beams and plates, an increased lateral confining stress gradually changes the mode of failure from flexure to shear. Both the strength and toughness increase with increasing confinement.
- Higher confining stresses and higher fibre contents permit more impact energy to dissipate through the specimens, and at the same time permit the specimens to absorb more energy.

CONCLUSIONS

The combination of high strength concrete, high fibre volumes and conventional reinforcement can lead to dramatic improvements in the mechanical behaviour of concrete members, for both static and dynamic loading conditions. Despite the higher *material* costs of such systems, both the structural properties and durability of concrete structures can be greatly improved. As yet, the available building codes do not make it easy to exploit these improved properties, since most codes are based entirely on *strength* considerations, and do not take into account the *toughness* of the material. It can only be hoped that the codes will soon reflect the advances made in enhancing the properties of cement-based composite materials, so that this new generation of construction materials can be exploited to their full extent.

REFERENCES

Balaguru P. and Franklin H.S. (1999). 'High Performance User-Friendly Fiber Reinforced Composite Under Cyclic Loading', in: Reinhardt H.W and Naaman A.E. (eds.), *High Performance Fiber Reinforced Cement Composites (HPFRCC3)*, RILEM Publications, S.A.R.L.: 225-238.

Banthia N., Chokri C., Ohama Y. and Mindess S. and (1994). Fiber Reinforced Cement-Based Composites Under Tensile Impact. *Advanced Cement-Based Materials* **1:3**, 131-141.

Campione G., La Mendola L. and Zingone G. (2000). 'Flexural-Shear Interaction in High Strength Fibre Reinforced Concrete Beams' in: Rossi P. and Chanvillard (eds.), *Fibre-Reinforced Concretes (FRC) – BEFIB' 2000*, Proceedings of the Fifth International RILEM Symposium, RILEM Publications, S.A.R.L.: 451-460.

Campione G. and Mindess S. (1999a). 'Compressive Toughness Characterization of Normal and High-Strength Fiber Concrete Reinforced with Steel Spirals', in: Banthia N. MacDonald C. and Tatnall P. (eds), *Structural Applications of Fiber Reinforced Concrete*, ACI SP-182, American Concrete Institute, Farmington Hills, Michingan: 141-161.

Campione G. and Mindess S. (1999b). 'Fibers as Shear Reinforcement for High Strength Reinforced Concrete Beams Containing Stirrups', in: Reinhardt H.W and Naaman A.E. (eds.), *High Performance Fiber Reinforced Cement Composites (HPFRCC3)*, RILEM Publications, S.A.R.L.: 519-529.

Campione G. and Mindess S. (1999c). 'The Flexural Behavior of Over-Reinforced High Strength Concrete Beams Containing Fibers', in: Reinhardt H.W and Naaman A.E. (eds.), *High Performance Fiber Reinforced Cement Composites (HPFRCC3)*, RILEM Publications, S.A.R.L.: 509-518.

Campione G. and Mindess S. (2000). 'Size Effect in Compression of High Strength Fibre Reinforced Concrete Cylinders Subjected to Concentric and Eccentric Loads', in: Wittmann F.H. (ed.), *Materials for Building and Structures, EUROMAT99*. Wiley-VCH, 6, 86-91.

Campione G. and Mindess S. (2001). Behaviour of Normal Weight and Lightweight Fibre Reinforced Concrete in Compression', in: Banthia, N. Sakai K. and Gjaru O.E. (eds.), *Proceedings, Third International Conference on Concrete Under Severe Conditions (CONSEC '01)*. University of British Columbia, Vancouver, B.C.: **2:1274-1286**.

Campione G., Mindess S. and Banthia N. (2000). 'Monotonic and Cyclic Flexural Behaviour of Medium and High Strength Fibre Reinforced Concrete', in: Rossi P. and Chanvillard (eds.), *Fibre-Reinforced Concretes (FRC) – BEFIB' 2000*, Proceedings of the Fifth International RILEM Symposium, RILEM Publications, S.A.R.L.: 461-470.

Campione G., Mindess S. and Zingone G. (1997). 'Failure Mode in Compression of Fibre Reinforced Concrete Cylinders with Spiral Steel Reinforcement', in: Brandt A.M., Li V.C. and

Marshall I.H. (eds.), *Brittle Matrix Composites 5*, Woodbend Publishing Limited, Cambridge and Bigraf, Warsaw: 123-132.

Campione G., Mindess S. and Zingone G. (1999a). 'Behavior of Fiber Concrete Reinforced with Steel Spirals under Cyclic Compressive Loading', in: Azizinamini A. Darwin D. and French C. (eds.), *High Strength Concrete*, First International Conference sponsored by United Engineering Foundation, Inc., American Society of Civil Engineers: 136-148.

Campione G., Mindess S. and Zingone G. (1999b). Compressive Stress-Strain Behaviour of Normal and High-Strength Carbon-Fiber Concrete Reinforced with Steel Spirals. *ACI Materials Journal* **96:1**, 27-34.

Naaman A.E. and Gopalaratnam V.S. (1983). Impact Properties of Steel Fibre Reinforced Concrete in Bending. *International Journal of Cement Composites and Lightweight Concrete* **5:40**, 225-233.

Sukontasukkul P. (2001). *Impact Behaviour of Concrete Under Multiaxial Loading*. Ph.D. Thesis, University of British Columbia, Vancouver, Canada.

Sukontasukkul P., Mindess S., Banthia N. and Mikami T. (2001). Impact Resistance of Laterally Confined Fibre Reinforce Concrete Plates. *Materials and Structures (RILEM)* **34**, 612-618.

Yan C. and Mindess S. (1991). Bond Between Concrete and Steel Reinforcing Bars Under Impact Loading. *Brittle Matrix Composites 3*, 184-192.

Yan C. and Mindess S. (1994). Bond Between Epoxy Coated Reinforcing Bars and Concrete Under Impact Loading. *Canadian Journal of Civil Eng.* **21:1**, 89-100.

Advances in Building Technology, Volume 1
M. Anson, J.M. Ko and E.S.S. Lam (Eds.)
© 2002 Elsevier Science Ltd. All rights reserved

DIFFERENTIAL SCANNING CALORIMETRY STUDY OF THE HYDRATION PRODUCTS IN PORTLAND CEMENT PASTES WITH METAKAOLIN REPLACEMENT

W. Sha

School of Civil Engineering, The Queen's University of Belfast, Belfast
BT7 1NN, UK

ABSTRACT

The hydration products in Portland cement pastes mixed with metakaolin (MK) replacement have been examined using differential scanning calorimetry (DSC). The amounts of calcium hydroxide remaining in the pastes after long ages were evaluated in particular by measuring the enthalpy of its decomposition. Reasonable agreements are demonstrated between the results from the present work and previous studies by other investigators.

KEYWORDS

Hydration products, thermal analysis, fly ash, metakaolin, Portland cement, calorimetry.

INTRODUCTION

Recent years have seen a significant amount of research on the use and properties of cement and concrete mixed with cement replacement materials. These include pulverised fuel ash (pfa, or fly ash), condensed silica fume (csf, or microsilica), ground granulated blast furnace slag (ggbs) and metakaolin (MK). The large quantity of literature published in this area has been accompanied by an increased use of these replacement materials in construction [Sindu (2000)], mostly because of environmental and economical benefits. Increased use of cement replacement materials has also been driven by the requirement for enhanced durability.

In 1999, the author and his colleagues used differential scanning calorimetry (DSC) to study the hydration products in Portland cement (PC) paste [Sha et al. (1999)]. This was extended to PC with metakaolin [Sha & Pereira (2001a)], pulverised fuel ash [Sha & Pereira (2001b)] and slag [Sha & Pereira (2001c)] replacements. The present work is a continuation of the research by Sha & Pereira (2001a), but concentrates on hydration after longer times. Specifically, the longer times are for ages

beyond 230 and 190 days for the PC with 20% and 30% metakaolin, respectively. Results are also compared with previous data for samples at shorter ages.

The work in Sha et al. (1999) involves using DSC in an investigation of the thermal behaviour of hydration products in Portland cement as a function of age. The two-step loss of water from calcium silicate hydrate, dehydroxylation of calcium hydroxide, and decarbonation of calcium carbonate contribute respectively to the three major endothermic peaks in the DSC curves. Peaks due to the formation of ettringite and iron-substituted ettringite, C_4AH_{13} and Fe_2O_3 solid solution were also found.

The work in Sha & Pereira (2001a) has demonstrated that DSC analysis can be used to trace the hydration process of cement with metakaolin replacement. The pozzolanic reaction of metakaolin and its effect on cement hydration can be monitored. The technique, combined with theoretical analysis based on reaction stoichiometry, can contribute to the understanding of these processes.

In Sha & Pereira (2001b), hydration products in normal Portland cement mixed with 30% fly ash were analysed. The phases detected include calcium silicate hydrate, iron-substituted ettringite, C_4AH_{13}, calcium hydroxide, calcium carbonate and amorphous phases in fly ash. In addition, ggbs powder was investigated, revealing peaks due to the crystallisation of the amorphous phases. Due to their relatively preliminary nature and the limit of article space, the results of the powders and pastes were not closely correlated, and some of the experimental results remained unexplained with regard to their hydration/pozzolanic processes, or the resulting engineering implications. At the then stage of the research development in the area, there was a lack of proper understanding of the implications of the DSC testing results on engineering properties particularly at early ages. The result presented could not possibly give a full meaningful interpretation of the role of fly ash or slag in concrete, although there was a catalogue of data that may prove crucial in the course of further research. Chemical analyses of quenched samples either side of peak temperatures was expected to help in understanding the mechanisms involved. Unfortunately, there was some wrong assignments of the DSC peaks in Sha & Pereira (2001a,b).

The work reported in Sha & Pereira (2001c) involves an investigation of the thermal behaviour of hydration products in ggbs. The two-step loss of water from calcium silicate hydrates and dehydroxylation of calcium hydroxide ($Ca(OH)_2$) contribute, respectively, to the two major peaks in the DSC curves. Peaks due to the formation of ettringite and Fe_2O_3 solid solution were also found. The crystallisation peaks from amorphous phases in the ggbs are also significant in the DSC thermograms.

The DSC used in these studies has high temperature sensitivity, but the accuracy of the enthalpy measurement is limited to approximately 20% relative error. Compared to other analytical methods, DSC measurement of phases is fast, but the identification of phases relies on previous knowledge of their decomposition or transformation temperatures and enthalpies.

There has been other work, by de Silva & Glasser (1990, 1992, 1993), Frías & Cabrera (2001), Frías et al. (2001), Kinuthia et al. (2001), Murat (1983), Pera & Ambroise (1998), Péra et al. (1998, 2001), and Serry et al. (1984).

MATERIALS

The work reported in this paper was carried out on the same pastes as used in Sha & Pereira (2001a), using the same procedure and apparatus. Therefore, the experimental details will not be repeated here, for which Sha et al. (1999) and Sha & Pereira (2001a,b,c) can be consulted. The chemical

composition, phase analysis, fineness and some other physical properties of metakaolin and cement are given in Table 1. The water/solid ratio is 0.45.

TABLE 1
CHEMICAL COMPOSITION AND SOME PHYSICAL PROPERTIES OF CEMENT AND METAKAOLIN

Compound	Cement	Metakaolin
SiO_2	21.8	54.8
Al_2O_3	4.2	41.2
Fe_2O_3	2.5	0.57
CaO	65.1	0.02
MgO	-	0.31
Na_2O	0.13	0.04
K_2O	0.72	2.27
TiO_2	-	0.01
SO_3	2.4	2.4
Loss on ignition	-	0.8
Specific gravity	3.15	2.52

RESULTS AND DISCUSSION

20% Metakaolin

Samples were analysed at two ages, 230 and 420 days, after storing continuously under water at 20°C from one day after mixing (Figure 1). A number of peaks are shown in the curve.

It has been established by a range of different authors, that the reaction of MK with CH, either as added CH or from hydrating PC, produces C-S-H gel and C_4AH_{13} and, often at a rather later stage, C_2ASH_8. At long curing periods (beyond 28 days) hydrogarnet (C_3AH_6) may develop particularly at elevated temperatures. At high MK:CH, or MK:PC, C_2ASH_8 is favoured relative to C_4AH_{13}. If carbonation occurs or carbonate is available, which is often the case, carboaluminates, $C_3A.0.5C\underline{C}.0.5CH.H_{11.5}$ and/or $C_3A.C\underline{C}.H_{11}$, form together with C_4AH_{13}. In addition, if sulphate is available in the system, this is normally the case, ettringite forms rapidly, within the first few hours. Gehlenite hydrate, C_2ASH_8, is often not crystalline in its initial stages of formation. It normally shows a weight loss band on thermogravimetry analysis (TGA) and an exotherm on differential thermal analysis (DTA) at 160–200°C, C_4AH_{13} and related carboaluminate phases at 220–280°C and hydrogarnet at 350–400°C. Ettringite usually loses its water at 80–130°C and C-S-H gel, although it loses its water over a wide temperature range, loses the greatest proportion of its water between 120 and 160°C. The DSC measures the energy change of these dehydration or dehydroxylation reactions rather than the weight loss (TGA) or differential temperature (DTA). The transformations, however, occur in the same temperature regions, in the same way that those for $Ca(OH)_2$ and $CaCO_3$ do.

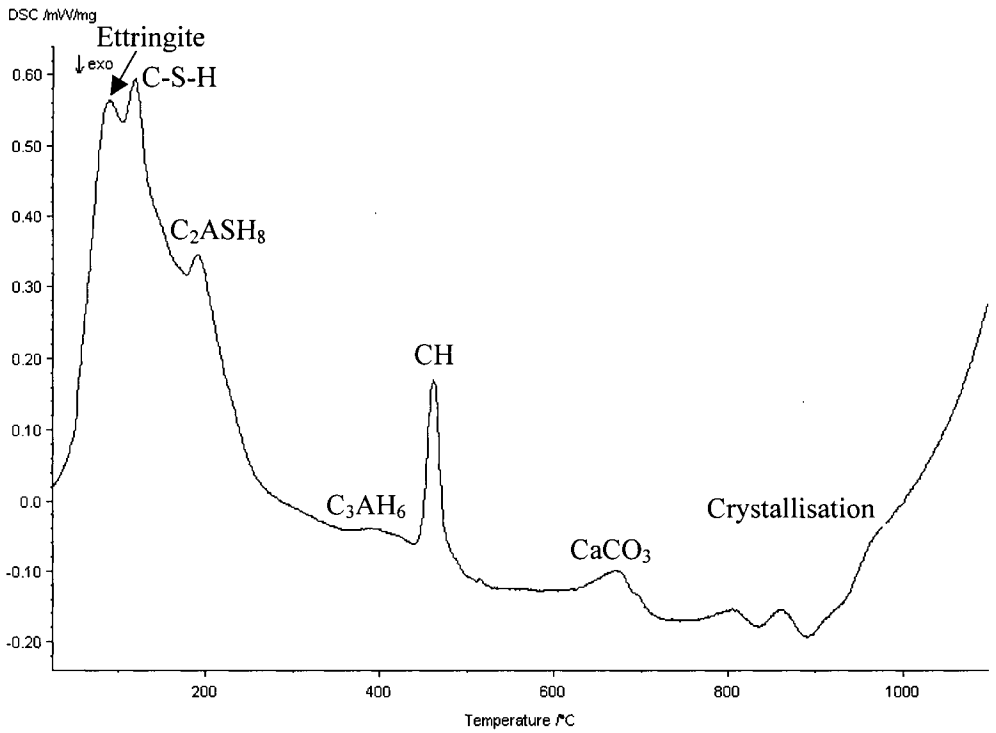


Figure 1: Differential scanning calorimetry curve of Portland cement paste with 20% metakaolin at 230 days

It was found that there was no significant change between the two ages studied, indicating that no significant reaction had occurred, including in particular the pozzolanic reaction. Calculation showed that with 15% or higher metakaolin replacement, there should be no calcium hydroxide left in the system after hydration and pozzolanic reactions are complete [Sha & Pereira (2001a)]. The large amount of calcium hydroxide ($Ca(OH)_2$, or CH) remaining in the samples was not surprising, however. Reaction products are formed in such a way that they inhibit further reaction. For example in concrete with only PC as binder, after many years of PC hydration there is still unhydrated PC remaining. Wild & Khatib (1997) conclude that replacement levels of PC by MK considerably in excess of 15% would be required to fully consume all the CH in MK-PC pastes and mortars. This is based on their hypothesis that an inhibiting layer of reaction product is formed on the MK particles. This is also discussed in Kinuthia et al. (2001). Considering that there is no calcium hydroxide after similar age in cement with 30% metakaolin replacement (see next section), it appears that the theory used in the calculations is essentially valid but the coefficients need to be adjusted. The amount of calcium hydroxide, 24 J/g, is equivalent to 2.4% of the paste, or 4.2% of the original amount of cement. This is lower than the values reported by Frías & Cabrera (2000), but the overall trend for the change of CH amount with age is in agreement with Sha & Pereira (2001a). The same qualitative comparison can be made with work by Wild & Khatib (1997), although the DSC work did not reveal the drop of CH content at around 14 days [Sha & Pereira (2001a)]. The lower CH level found in this work compared to the literature [Wild & Khatib (1997), Frías & Cabrera (2000)] should be related with the different materials and mixes used. It is difficult however to separate the influence of different metakaolin and cement compositions, different physical properties of the materials, and different water/solid ratio.

Calculating enthalpy values for combined adjacent peaks was applied to the peaks previously identified as from crystallisation of the amorphous materials [Sha & Pereira (2001a)]. The double crystallisation peak starts to appear in samples at 52 days, but the total enthalpy remains the same until 420 days, averaged at 43±5 J/g.

30% Metakaolin

For PC paste with 30% metakaolin replacement, samples at two ages were analysed, 190 and 380 days (Figure 2). As for 20% metakaolin, data for earlier ages were given in Sha & Pereira (2001a). The paste with 30% metakaolin exhibited significant acceleration of the speed and degrees of the pozzolanic reaction. Figure 3 shows DSC thermograms for pastes at the ages of 2, 24, 38 and 73 days, respectively. The separation of the crystallisation peak is complete after 38 days (Figure 3), half of the age for this in the paste with 20% metakaolin. In addition, the peak corresponding to the decarbonation of $CaCO_3$ starts to grow large at an earlier age. There is an overlap of peaks at this region, with possible additional contribution from solid-solid transformations [Bhatty (1991)]. Therefore, the obvious dual peak phenomenon in this temperature range may be attributed to this transformation. It is also interesting to note the significant peaks corresponding to gehlenite hydrate and C-S-H, at 24 days (Figure 3). These continue to increase with longer age, overlapping to cause the large peak in the curve for 73 days (Figure 3). As gehlenite hydrate and C-S-H are both pozzolanic reaction products from MK, this difference from the behaviour of 20% metakaolin paste is as expected. Figure 4 shows the variation of peak temperature as a function of age.

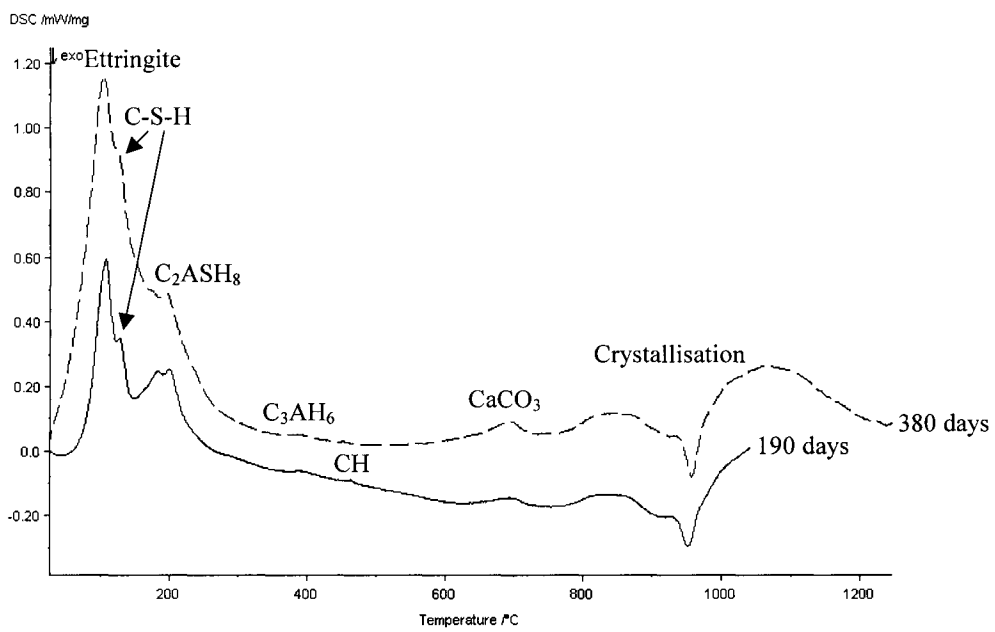


Figure 2: Differential scanning calorimetry curves of Portland cement paste with 30% metakaolin at 190 days (solid line) and 380 days (dashed line)

There is no significant change apart from the complete disappearance of the calcium hydroxide peak after 380 days, from the absence of CH peak in Figure 2. There is a peak for the sample after 190 days, but it is very small and almost invisible in the printed DSC curve.

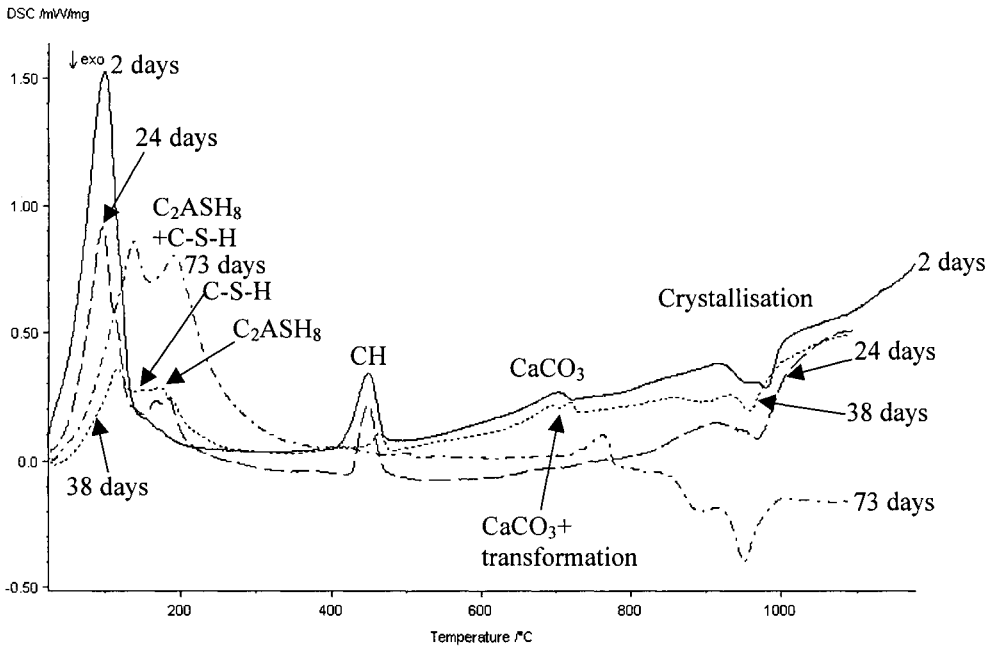


Figure 3: DSC thermograms from hardened paste containing 30% metakaolin replacement at 2 (solid line), 24 (long dashed line), 38 (short dashed line) and 73 days (dash dot line)

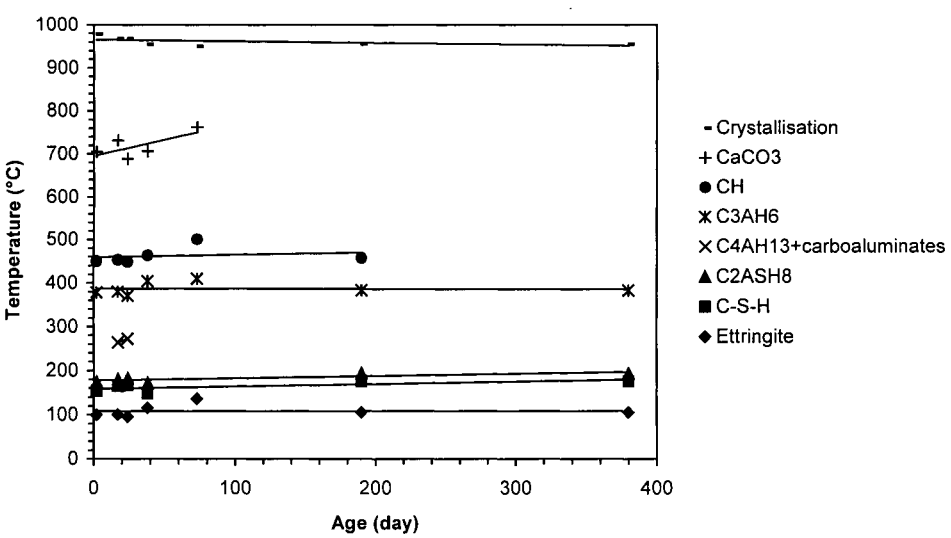


Figure 4: DSC peak temperatures from the mix with 30% metakaolin replacement

The increase of metakaolin level from 20% to 30% replacements pushes up the crystallisation temperatures. The average total enthalpy from the crystallisation peaks for ages of 73, 190 and 380 days is 106±8 Joule per gram of sample.

CONCLUSIONS

Differential scanning calorimetry analysis showed that in cement paste with 20% metakaolin replacement, the amount of calcium hydroxide after 230 and 420 days hydration remains the same, 2.4% of the paste. With 30% metakaolin replacement, there is only a minute quantity of calcium hydroxide after 190 days, and this completely disappears after 380 days.

ACKNOWLEDGEMENT

The author thanks Professor P.A.M. Basheer for discussion and the provision of concrete laboratory facilities.

REFERENCES

Bhatty J.I. (1991). A Review of the Application of Thermal Analysis to Cement-admixture Systems. *Thermochimica Acta* **189:2**, 313–350.

de Silva P.S. and Glasser F.P. (1990). Hydration of Cement Based on Metakaolin Thermochemistry. *Advances in Cement Research* **3:2**, 167–177.

De Silva P.S and Glasser F.P. (1992). Pozzolanic Activation of Metakaolin. *Advances in Cement Research* **4:16**, 167–178.

Desilva P.S and Glasser F.P. (1993). Phase Relations in the System CaO-Al_2O_3-SiO_2-H_2O Relevant to Metakaolin-calcium Hydroxide Hydration. *Cement and Concrete Research* **23:3**, 627–639.

Frías M. and Cabrera J. (2000). Pore Size Distribution and Degree of Hydration of Metakaolin-cement Pastes. *Cement and Concrete Research* **30:4**, 561–569.

Frías M. and Cabrera J. (2001). Influence of MK on the Reaction Kinetics in MK/lime and MK-blended Cement Systems at 20°C. *Cement and Concrete Research* **31:4**, 519–527.

Frías M., Sánchez de Rojas M.I. and Rivera J. (2001). The Effects of Temperature on the Formation of Hydrogarnet in Matrices Made with Metakaolin/lime Mixtures. *Seventh CANMET/ACI International Conference on Fly Ash, Silica Fume, Slag and Natural Pozzolans in Concrete* (SP 199-43), vol. 2, 22–27 July 2001, Chennai (Madras), India, ed: V.M. Malhotra, pp. 757–768.

Kinuthia J.M., Bai J., Wild S. and Sabir B.B. (2001). Thermogravimetric Analysis of Portland Cement-metakaolin-PFA Blends. *Modern Building Materials, Structures and Techniques*, The Seventh International Conference, 16–18 May 2001, Lithuania, Abstract Proceedings, p. 55.

Murat M. (1983). Hydration Reaction and Hardening of Calcined Clays and Related Minerals, I-Preliminary Invstigation on Metakaolinite. *Cement and Concrete Research* **13:2**, 259–266.

Pera J. and Ambroise J. (1998). Pozzolanic Properties of Metakaolin Obtained from Paper Sludge. *Sixth CANMET/ACI International Conference on Fly Ash, Silica Fume, Slag and Natural Pozzolans in Concrete* (SP178-52), vol. 2, Bangkok, ed: V.M. Malhotra, pp. 1007–1020.

Pera J., Bonnin E. and Chabannet M. (1998). Immobilization of Wastes by Metakaolin-blended Cements. *Sixth CANMET/ACI International Conference on Fly Ash, Silica Fume, Slag and Natural Pozzolans in Concrete* (SP178-52), vol. 2, Bangkok, ed: V.M. Malhotra, pp. 997–1006.

Péra J., Ambroise J. and Chabannet M. (2001). Transformation of Wastes into Complementary Cementing Materials. *Seventh CANMET/ACI International Conference on Fly Ash, Silica Fume, Slag and Natural Pozzolans in Concrete* (SP 199-26), vol. 2, 22–27 July 2001, Chennai (Madras), India, ed: V.M. Malhotra, pp. 459–475.

Serry M.A, Taha A.S, El-Hemaly S.A.S. and El-Didamony H. (1984). Metakaolin-lime Hydration Products. *Thermochimica Acta* **79**, 103–110.

Sha W., O'Neill E.A. and Guo Z. (1999). Differential Scanning Calorimetry Study of Ordinary Portland Cement. *Cement and Concrete Research* **29:9**, 1487–1489.

Sha W. and Pereira G.B. (2001a). Differential Scanning Calorimetry Study of Ordinary Portland Cement Paste Containing Metakaolin and Theoretical Approach of Metakaolin Activity. *Cement and Concrete Composites* **23:6**, 455–461.

Sha W. and Pereira G.B. (2001b). Differential Scanning Calorimetry Study of Normal Portland Cement Paste with 30% Fly Ash Replacement and of the Separate Fly Ash and Ground Granulated Blast-furnace Slag Powders. *Seventh CANMET/ACI International Conference on Fly Ash, Silica Fume, Slag and Natural Pozzolans in Concrete*, Supplementary Papers, 22–27 July 2001, Chennai (Madras), India, compiled: M. Venturino, pp. 295–309.

Sha W. and Pereira G.B. (2001c). Differential Scanning Calorimetry Study of Hydrated Ground Granulated Blast-furnace Slag. *Cement and Concrete Research* **31:2**, 327–329.

Sindu J. (2000). Pfa in Runways. *Concrete* **34:8**, 46–47.

Wild S. and Khatib J.M. (1997). Portlandite Comsumption in Metakaolin Cement Pastes and Mortars. *Cement and Concrete Research* **27:1**, 137–146.

Advances in Building Technology, Volume 1
M. Anson, J.M. Ko and E.S.S. Lam (Eds.)
© 2002 Elsevier Science Ltd. All rights reserved

ULTIMATE MOMENT EQUATION OF CIRCULAR HSC MEMBERS

Y. Sun and K. Sakino

Department of Architecture, Graduate School of Human Environment Studies,
Kyushu University, Hakozaki 6-10-1, Fukuoka, 812-8581, JAPAN

ABSTRACT

It has been widely accepted that confinement of concrete by transverse reinforcement is effective in upgrading deformation capacity of high strength concrete (HSC). In order for structural engineers to conduct reasonable design of confined HSC members, they are of fundament importance 1) to make clear correlation between the amount of transverse steels and the mechanical properties (e.g. ultimate moment capacity, etc) of the confined member, and 2) to develop a sound design method that can take into account effects of primary structural factors, particularly of confinement by transverse steels.

Purpose of this paper is to propose a simple design equation for computing ultimate flexural strength of circular confined HSC or NSC (normal-strength concrete) members. The emphasis is placed on HSC members. The proposed design equation has a very simple mathematical expression so that structural engineer can conduct the complicated calculation of the ultimate moment of confined concrete members by hand. Another significant feature of the proposed design equation is that it can take into account effects of circular transverse steels on the ultimate moment of confined circular members. Experimental results of confined concrete columns available are used to verify validity of the proposed equation. The predicted ultimate moments agreed very well with the measured ones, which implies that the proposed design equation could provide a powerful tool for structural engineer to appropriately and directly calculate the ultimate moment of a circular HSC member.

KEYWORDS

Circular concrete member, high-strength concrete, confined concrete, confinement effect, circular steel tube, ultimate moment, confinement design

INTRODUCTION

Due to its high load-carrying capacity and durability, HSC has recently gained increasing use in high-rise building structures and highway constructions. To promote use of HSC in structures located on seismic regions, prevention of brittle failure mode of the HSC becomes an important issue.

Confinement of concrete by transverse reinforcement is effective in enhancing ductility of the HSC.

Traditionally, the transverse spirals or hoops have been widely used to confine concrete members, and their beneficent effects on the mechanical behavior of concrete members have been studied by many researches as reviewed in the ACI state of art report [ACI, 1997]. Nevertheless, there has not yet been a reliable and comprehensive design method enabling structural engineers to simply compute the ultimate capacities of confined HSC columns. Particularly true is this for the circularly confined HSC columns due to lack of information on the ultimate flexural behavior of circular columns.

The authors have conducted an integrated experimental and analytical studies of mechanical behavior of circularly confined HSC columns, aiming at setting up a rational design method for the ultimate capacities of the circular columns. In the authors' previous experimental works [Sun and Sakino, 1999, 2000], the test columns were confined by circular steel tubes with various thickness in lieu of common circular hoops, to quantitatively study confinement effect of circular transverse reinforcement on the mechanical properties of the "pure" confined concrete. Based on their experimental data, the authors have developed an unified stress-strain model for the circularly confined concrete [Sun and Sakino, 2001]. This confinement model has been proved applicable to the concrete confined by conventional circular hoops, the concrete confined by circular steel tubes, and the concrete in circular CFT column. Furthermore, as the first step toward simplification of ultimate capacity design for the circular HSC columns, Sun and Sakino [2001] have also proposed a equivalent rectangular stress block for the compressed concrete in a circular column section and a design procedure to predict ultimate capacities of circularly confined HSC columns. However, as can be seen later, that method involves the use of complicated expressions and still needs help of a computer.

To overcome these shortcomings in the previous design method, this paper propose a much simpler design equation for computing the ultimate flexural strength of circularly confined HSC members. The mathematical expression of the proposed design equation, which defines the correlation between the axial load and the ultimate moment for a given circular column, is developed by utilizing the rectangular equivalent stress block proposed by the authors [Sun and Sakino, 2001]. Study of this paper will focus on circular columns confined by steel tube. Development of the design equation for calculation of ultimate moment of the columns confined by common circular hoops is in progress, and will be reported in near future.

OUTLINE OF EQUIVALENT RECTANGULAR STRESS BLOCK

Interaction diagram between the axial load N and the ultimate moment (referred to as N-M interaction diagram hereafter) is usually adopted to compute the flexural strength of concrete columns. Generally, for a given column, the N-M interaction diagram can be obtained by conducting flexural analysis, i.e., by computing the moment-curvature response of the column section under various levels of axial load. If a sound stress-strain model for the confined concrete is assumed, the flexural analysis can give fairly accurate prediction of the flexural strength, in which confinement effect of transverse steels can be taken into account. This general approach, however, is very tedious and needs help of a computer program, since it involves an iterative procedure to find the depth of the neutral axis for the internal forces to balance the external applied load.

On the other hand, if the stress state of the compressed concrete at the peak moment can be simplified, it is possible to simplify the calculation procedure of the N-M interaction diagram. By conducting parametric study of flexural response for circularly confined columns, the authors have proposed an equivalent rectangular stress block to replace the actual stress state for the compressed concrete in a circular column section as the first step toward simplification of flexural strength calculation [Sun and Sakino, 2001]. Figure 1 shows outline of the proposed stress block for the circularly confined concrete. As shown in Figure 1, the equivalent stress block has width of αD_c and depth of βX with uniform stress f_{cc}, where D_c is the diameter of core concrete, X is the depth of the neutral axis, and f_{cc} ($=K f_P$) is the strength of confined concrete. Utilizing the stress block, the axial compressive force N_B and the first moment M_B sustained by the concrete at ultimate state can be calculated as follows:

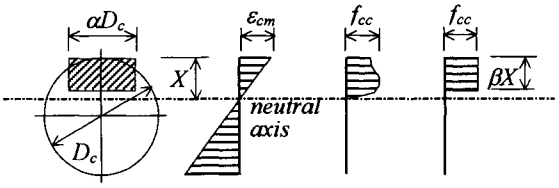


Figure 1: Equivalent rectangular stress block for the compressed concrete in a circular column

$$N_B = \alpha\beta K f_p D_c X, \qquad M_B = \alpha\beta K f_p D_c X\left(\frac{D_c}{2} - \frac{\beta}{2}X\right) \tag{1}$$

where α and β are the stress block parameters, K is the strength enhancement ratio of confined concrete, f_p is the unconfined concrete strength, D_c is the diameter of concrete core, and X is the depth of the neutral axis. Based on the theoretical results concerning with the flexural behavior of circularly confined concrete columns, the authors have developed mathmatical expressions to compute the stress block parameters α and β in forms of

$$\alpha\beta = A(K, X_n) - B(K, X_n)\frac{f_p}{42}, \quad \frac{\beta}{2} = C(K, X_n) - D(K, X_n)\frac{f_p}{42} \tag{2}$$

where

$$A(K, X_n) = \frac{0.723 + 0.061K}{0.112 + X_n}X_n, \quad B(K, X_n) = \frac{0.048K^{-2}}{0.072K^{-1.5} + X_n}X_n \tag{3}$$

$$C(K, X_n) = (0.476 + 0.051K)\left(1 - 0.132X_n{}^2\right), \quad D(K, X_n) = 0.017\left[1 - (0.024 + 0.187K)X_n{}^2\right] \tag{4}$$

in which X_n is the normalized depth of the neutral axis. The strength enhancement ratio K of concrete confined by circular steel tube can be obtained by applying famous Richart formula as follow

$$K = \frac{f_{cc}}{f_p} = 1 + 4.1\frac{2}{D/t - 2}\frac{f_{yt}}{f_p} \tag{5}$$

where f_{cc} is the confined concrete strength, f_{yt}, t, and D are the yield strength, thickness, and outside diameter of the steel tube, respectively.

FEATURES OF THE ULTIMATE *N-M* INTERACTIVE DIAGRAM

To investigate features of the ultimate *n-m* interactive curve for circularly confined concrete columns and get fundamental information for development of design equation, parametric flexural study was conducted. Figure 2 shows details of the sample section as well as varying ranges of the main variables. As obvious in Figure 2, parametric study covered a wide range of concrete strength and steel amount, which implies the wide applicability of the to be proposed design equation in terms of the concrete strength and the amount of longitudinal bars.

To compute the ultimate *n-m* interactive curve using the equivalent stress block, they are assumed that

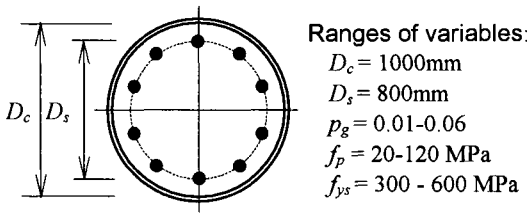
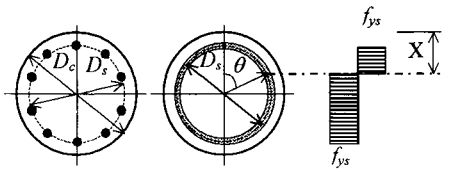


Figure 2: Details of the sample column section



(a) longitudinal bars (b) equivalent steel tube (c) stress distribution

Figure 3: Concept of the equivalent axial steel tube of the longitudinal bars

1) the tensile strength of concrete can be neglected, 2)the concrete sustained axial force as well as moment can be replaced by those of the stress block shown in Figure 1, 3) the longitudinal bar is a rigid-plastic material, and 4) the longitudinal bars can be replaced with an equivalent axial steel tube having identical reinforcement area (see Figure 3).

Based on these assumption, the calculation procedure for ultimate *N-M* interaction diagram doesn't involve iterative calculation, and can be summarized as follows.

1) Calculate the strength enhancement ratio K of confined concrete by substituting D/t ratio and yield strength f_{yt} of the steel tube and the unconfined concrete strength f_p, into Eq. 5.
2) Give an initial value (e.g. 0.02π) to θ, the radial angle of the section and calculate the normalized depth of the neutral axis X_n by Eq. 6.

$$X_n = X/D_c = 0.5(1 - D_s \cos\theta / D_c) \tag{6}$$

where D_c is the diameter of confined core concrete, and D_s is the distance between the centroids of the longitudinal bars. (see Figure 3)

3) Calculate the stress block parameters $\alpha\beta$ and $\beta/2$ from Eq. 2 through Eq. 4 and compute the axial force N_B and moment M_B sustained by the concrete by using. 1
4) Based on the last two assumptions above mentioned, the axial force N_s and moment M_s sustained by longitudinal bars can be calculated as

$$N_s = \frac{f_{ys} p_g D_c^2 (2\theta - \pi)}{4}, \quad M_s = \frac{f_{ys} p_g D_c^2 D_s \sin\theta}{4} \tag{7}$$

where f_{ys} and p_g are the yield strength and the steel ratio of the longitudinal bars, respectively.

5) The normalized axial force n as well as the normalized moment m corresponding to the given radial angle θ are then given by

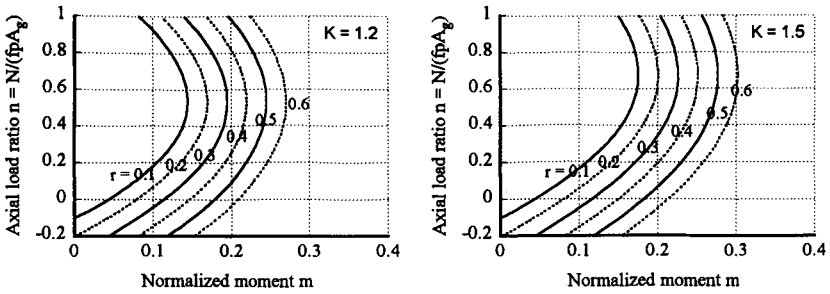


Figure 4: Examples of the calculated *n-m* interactive diagrams of the sample columns

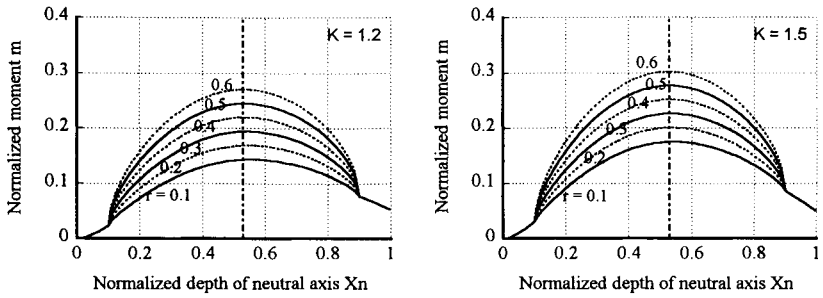


Figure 5: Relationships between the normalized neutral axis depth *Xn* and the moment m

$$n = \frac{N_B + N_s}{A_g f_p} = \frac{4}{\pi}\alpha\beta \bullet K \bullet X_n + \frac{1}{\pi}\frac{f_{ys}\rho_g}{f_p}(2\theta - \pi) \tag{8}$$

$$m = \frac{M_B + M_s}{A_g D_c f_p} = \frac{4}{\pi}\alpha\beta \bullet K \bullet X_n\left(\frac{1}{2} - \frac{\beta}{2}X_n\right) + \frac{1}{\pi}\frac{f_{ys}\rho_g}{f_p}\frac{D_s}{D_c}\sin\theta \tag{9}$$

6) The normalized ultimate *n-m* interaction diagram can be completely determined by incrementing θ till θ = π, and repeating the calculation step 2) through step 5) above.

Figure 4 plots several ultimate *n-m* interactive curves of the sample column section obtained utilizing the calculation procedure described above, while Figure 5 shows relationships between the normalized ultimate moment *m* and the neutral axis depth. In Figures 4 and 5, the confinement effect of circular steel tube is represented by the strength enhancement ratio K of confined concrete as defined by Eq. 5, and the factor *r* expresses the normalized steel ratio of the longitudinal bars and is given by $r = f_{ys}\rho_g / f_p$.

From Figures 4 and 5, one can observe the following features for the ultimate *n-m* interactive curves of circularly confined concrete columns:

1) For a circular column confined by the steel tube with a specific K value, the *n-m* interactive curves expand outwards as increment of the amount of longitudinal bars. On the other hand, the normalized moment *m*, as a function of the axial load ratio *n*, tends to reach its maximum at a axial load level that is nearly independent of the amount of longitudinal bars.
2) The axial load ratio n_o at the peak point of each *n-m* interactive curve increases with the K value, while the peak moment m_o at each *n-m* interactive curve increases as increment of both the K value

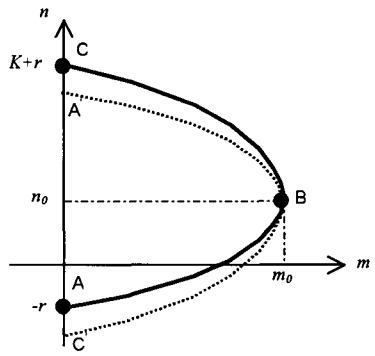


Figure 6: Idealization of the ultimate *n-m* interactive diagram

and the amount of longitudinal bars.

3) Regardless of the confinement degree (i.e. the K value) and the amount of longitudinal bars, each ultimate *n-m* curve reaches its peak moment as the normalized neutral axis depth X_n is between 0.52 through 0.55 with a mean value of 0.53.

PROPOSAL OF A DESIGN EQUATION

The calculation method using the equivalent stress block does really simplify the computation of flexural strength for the circularly confined members as compared with the method using the general flexural analysis. However, this method is still complicated as can be seen from Eq. 2 through Eq. 4. To provide a simpler and more powerful tool enabling structural engineers to more quickly and reasonably conduct the confinement design, a design equation is developed in this section.

Based on the results of parametric study described in the previous section, the ultimate *n-m* interactive curve can be idealized as the curve ABC shown in Figure 6. Obviously, to represent the features observed in the ultimate *n-m* interactive diagrams, the design equation, which defines the relationship between the normalized moment m and the axial load ratio n, should satisfy the following conditions:

$$\begin{aligned} m|_{n=-r} &= 0, & m|_{n=K+r} &= 0 \\ m|_{n=n_0} &= m_0, & \left.\frac{\partial m}{\partial n}\right|_{n=n_0} &= 0 \end{aligned} \tag{10}$$

where m_0 and n_0 are the peak moment of each *n-m* curve and the corresponding axial load ratio, respectively.

The four conditions given by Eq. 10 can determine a single cubic curve, but a cubic curve containes four constants, which might results in new complexity. By carefully analyzing the ABC curve shown in Figure 6, one can find that dividing the *n-m* curve into two parts, the ascending portion AB and the descending part BC, will result in a much simpler expression for the *n-m* curve. In fact, the AB curve can be taken as the ascending half of a parabola ABA', while the BC curve as the descending half of a parabola C'BC.

Considering that the both parabolas, ABA' and C'BC, have the line defined by $n=n_0$ as their common symmetric axis, the mathematical expression for the ultimate *n-m* curve can be simply written as follow:

$$m = \begin{cases} m_0\left[1-\left(\dfrac{n-n_0}{n_0+r}\right)^2\right], & n \le n_0 \\ m_0\left[1-\left(\dfrac{n-n_0}{n_0+K+r}\right)^2\right], & n > n_0 \end{cases} \tag{11}$$

The two parabolas defined by Eq. 11 are continuous at the peak point. Apparently, the proposed design equation is a two-parameter model. Only if the peak moment m_0 and the corresponding axial load ratio n_0 are given, one can completely determine the ultimate *n-m* curve.

As described in the previous section, each *n-m* curve reaches its peak as the normalized depth of neutral axis is between 0.52 and 0.55 with a mean value of 0.53 regardless of the values of both K and r. Hence, substituting X_n=0.53 into Eq. 3 and Eq. 4, and then Eq. 8 and Eq. 9, one can obtain close approximations for m_0 and n_0. Noting that as X_n=0.53,

$$\theta \approx \frac{\pi}{2} \;\Rightarrow\; \sin\theta \approx 1.0$$

exists, and by conducting regression analysis on the approximations of m_0 and n_0, the following expressions were derived to compute m_0 and n_0:

$$\begin{aligned} n_0 &= \frac{1}{\pi}\left(0.1K^2 + 1.3K - 2.2K^{-1}f_p \times 10^{-3}\right) \\ m_0 &= \frac{1}{\pi}\left[0.31K + (0.61K - 0.85)f_p \times 10^{-3} + r\frac{D_s}{D_c}\right] \end{aligned} \tag{12}$$

It can be seen from Eq. 11 and Eq. 12 that the proposed design equation enables structural engineers to calculate the ultimate flexural strength by hand.

VERIFICATION OF THE DESIGN EQUATION

The experimental results of bending tests by Sun and Sakino [2000] are used to validate the proposed design equation. The previous tests comprised of eleven columns made of HSC. These columns were confined in circular steel tubes having inner diameter of 250mm and five kinds of wall thickness varying between 1.2mm and 4.5mm. The concrete strengths were 55.4MPa and 89.2MPa. In each column, the longitudinal steel was ten D13 deformed bars (12.7mm diameter) placed uniformly along the perimeter with 25mm of cover to the steel centroids to give a steel ratio of 2.54%.

The circular steel tubes were fabricated by welding folded steel plate having the targeted thickness at laboratory. The steel tubes were used only to confine concrete rather than to directly sustain the axial stress due to external loads.

Table 1 lists the experimental outlines of these test column along with the measured ultimate moments as well as the calculated results. For comparison, the theoretical predictions based on the stress block are also given in Table 1. It can be seen that the theoretical moments obtained by the proposed design equation agree very well with the experimental results, having the same accuracy as the calculated results by the equivalent stress block.

TABLE 1: OUTLINES OF THE PREVIOUS TESTS AND PRIMARY RESULTS

Column	fp (MPa)	t (mm)	fyt (MPa)	K	n	Mexp (kNm)	Mc1 (kNm)	ratio	Mc2 (kNm)	ratio
No.1	55.4	1.15	297	1.20	0.2	87.0	83.9	1.037	84.3	1.032
No.2		1.15	297	1.20	0.4	110.9	103.9	1.067	105.0	1.056
No.3		2.2	308	1.40	0.4	126.1	112.3	1.122	113.7	1.110
No.4		2.2	308	1.40	0.7	145.0	120.7	1.201	120.6	1.202
No.5	89.2	1.15	297	1.13	0.2	111.2	114.1	0.974	110.5	1.006
No.6		1.55	290	1.17	0.2	110.0	115.3	0.954	110.6	0.995
No.7		1.55	290	1.17	0.3	131.7	135.6	0.971	130.6	1.008
No.8		3.1	304	1.35	0.5	173.0	170.3	1.016	171.2	1.011
No.9		3.1	304	1.35	0.7	175.0	168.3	1.040	169.4	1.033
No.10		4.5	375	1.58	0.5	198.3	189.7	1.046	189.8	1.045
No.11		4.5	375	1.58	0.7	211.0	201.7	1.046	202.0	1.045
							Mean	1.043	Mean	1.049
							St. Dev.	0.071	St. Dev.	0.061

Note: n = axial load ratio
Mexp = the measured ultimate moments
Mc1 = the calculated moment based on the proposed design equation
Mc2 = the calculated moment by the equivalent stress block
Ratio = the measured moment / the calculated moment

CONCLUSIONS

A simple design equation has been proposed in this paper to calculate the ultimate flexural strength of concrete columns retrofitted by circular steel tubes. The Proposed design equation has a very simple expression and can take into account confinement effect of steel tubes on the flexural strength. Because of its simplicity and comprehensiveness, the proposed design equation can provide a powerful tool enabling structural engineers to conduct rational retrofitting design for the existing concrete columns.

REFERENCES

ACI 441R-96. (1997). *High-Strength Concrete Columns: State of the Art*, ACI Structural Journal, May-June, pp. 323-335.

Sun Y. and Sakino K. (1999). *Axial Behavior of the HSC Confined by Circular Steel Tubes*, Procs. of the JCI, Vol. 21, No. 3, pp. 589-594. (in Japanese)

Sun Y., et al. (1999). *Axial and Flexural Behavior of Confined HSC Columns*, Procs. of the Annual Convention of the AIJ, Vol. 3, pp. 763-770.(in Japanese)

Sun Y. and Sakino K. (2000). *A Comprehensive Stress-Strain Model for High-Strength Concrete Confined by Circular Transverse Reinforcement*," Procs. of the 6th ASSCS-2000 International Conference on Composite Structures, Los Angeles.

Sun Y. and Sakino K. (2001). *Simplified Design Method for Ultimate Capacities of Circularly Confined High-Strength Concrete Columns.* The ACI special Publication SP193, pp.571-585.

Advances in Building Technology, Volume 1
M. Anson, J.M. Ko and E.S.S. Lam (Eds.)
© 2002 Elsevier Science Ltd. All rights reserved

PERFORMANCE TEST OF A MODEL FOR PREDICTING STRENGTH DEVELOPMENT OF FLY ASH-CONCRETE

Tahir M. A.[1] and Nimityongskul P.[2]

[1]Professor, Department of Civil Engineering, University of Engineering and Technology, Lahore, Pakistan
[2]Program Coordinator, Structures and Construction Program, School of Civil Engineering, Asian Institute of Technology, Bangkok, Thailand.

ABSTRACT

The main features of a model that takes into account the chemical composition and physical properties of the binder materials for predicting strength development of fly ash-concrete are discussed. The model is based on the Feret's Law enriched by the concept of maximum paste thickness. The performance of the model is tested using the strength data from an experimental program in addition to the data adopted from several researchers. The model predictions agree very well with the experimental data. In an extensive theoretical study the sensitivity of the model to the changes in chemical composition of cement and fly ash is also evaluated. It is found that the model performance is just in line with the accepted principles of the hydration and pozzolanic chemistry.

KEYWORDS:

Strength, chemical composition, fineness, fly ash, hydration, maximum paste thickness, pozzolana.

INTRODUCTION

Tahir and Nimityongskul (1998) presented a model for predicting strength development of fly ash-concrete. The model bases its predictions on the chemical composition and fineness of both the Portland cement and fly ash incorporated in the concrete. Further, it considers the effect of aggregate content and grading on the strength development of concrete. The model was calibrated and validated using data from a huge experimental program conducted at AIT (Tahir, 1998) in addition to the data adopted from several researchers around the globe. The nature of the data involved in calibration and validation made the model site independent and it could be used for design of fly ash concrete mixtures quite confidently. In this study the performance of the model is tested in view of the established facts from the chemistry of hydration and pozzolanic reactions. The chemical compositions of the cement and fly ash are varied within the practical limits and influence is evaluated on the strength development of concrete. The selected material compositions are adopted from published data.

THE MODEL

The model is described briefly; the detailed derivation of the model has been presented elsewhere (Tahir, 1998). The model predicts the strength on the basis of the four Bogue Compounds in Portland cement and four major oxides in the fly ash, namely CaO, SiO_2, Fe_2O_3, Al_2O_3, and the alkali contents of the binder, in terms of the equivalent Na_2O. In the following a brief outline of the model is presented, the detailed derivation of the model are presented elsewhere. The strength development of a fly ash concrete is based on the modified Feret's Law (De Larrard and Tondat, 1993) as given below:

$$f_c'(t) = A\ \Lambda^B \left[\frac{V_h(t)}{V_c + V_f + V_w + V_v}\right]^2 \tag{1}$$

where

$$V_h(t) = V_h(28) + \Delta V_h(t) \tag{2}$$

In which $V_h(28)$ denotes the solid volume of hydrated pasted at the age of 28-day and $\Delta V_h(t)$ denotes the change in the former with time. The solid volume at any age t, $V_h(t)$), is expressed in terms of Hyd_i and Poz_i, the hydraulic and pozzolanic parameters, r_W and r_F, the physical parameters and NaEq, the sodium equivalent of the mixture, as

$$\begin{aligned} V_h(t) = {} & \alpha \log\frac{t}{28} + \sum_{i=1}^{6}(\beta_i + \beta_i' \log\frac{t}{28})\,Hyd_i + \sum_{i=1}^{4}(\gamma_i + \gamma_i' \log\frac{t}{28})\,Poz_i \\ & + (a + a' \log\frac{t}{28})\,r_W + \sum_{i=1}^{2} b_i + b_i' \log\frac{t}{28})\,[r_F]^{\frac{1}{i}} + (c + c' \log\frac{t}{28})\,NaEq \end{aligned} \tag{3}$$

$$V_h(t) = \sum_{i=1}^{6}\beta_i\,Hyd_i + \sum_{i=1}^{4}\gamma_i\,Poz_i + a\,r_W + \sum_{i=1}^{2} b_i\,[r_F]^{\frac{1}{i}} + c\,NaEq \tag{4}$$

$$\Delta V_h(t) = (\alpha + V_h(28)) \log\frac{t}{28} \tag{5}$$

The 6-hydration parameters have been defined as follows:

$$Hyd_1 = \Omega_C \frac{C_2S}{C_2S + C_3S} x \frac{C_3A}{G_C} \quad ; \quad Hyd_2 = \Omega_C \frac{C_2S}{C_2S + C_3S} x \frac{C_4AF}{G_C}$$

$$Hyd_3 = \Omega_C \frac{0.994\,C_2S}{G_C} \quad ; \quad Hyd_4 = \Omega_C \frac{C_3S}{C_2S + C_3S} x \frac{C_3A}{G_C}$$

$$Hyd_5 = \Omega_C \frac{C_3S}{C_2S + C_3S} x \frac{C_4AF}{G_C} \quad \text{and} \quad Hyd_6 = \Omega_C \frac{0.75\,C_3S}{G_C} \tag{6}$$

in which C_3A, C_2S, C_3S and C_4AF denote the weights of the four Bogue Compounds respectively from the cement per unit volume of the concrete mixture, G_C denotes the density of cement and Ω_C denotes the fineness index of the Portland cement which can be obtained from the Blaine surface areas of the Portland cement used and a reference cement, F_c and F_{co}. F_{co} is taken equal to300 m^2/kg.

$$\Omega_C = \sqrt{\frac{F_C}{F_{CO}}} \tag{7}$$

The four pozzolanic parameters are defined in the following; when $SiO_2 < S_d$:

$$Poz_1 = \Omega_F \frac{2.85\,SiO_2}{G_F} x \frac{1.321\,CaO}{CH_p}$$

$$Poz_2 = \Omega_F \frac{2.85\,SiO_2}{G_{CF}} x \frac{0.215\,C_2S + 0.487\,C_3S - 0.305\,C_4AF}{CH_p}$$

$$Poz_3 = \Omega_F \frac{Al_2O_3}{G_{CF}} \quad \text{and} \quad Poz_4 = \Omega_F \frac{Fe_2O_3}{G_{CF}} \tag{8}$$

in which G_F and Ω_F respectively denote the density and fineness index of fly ash. The latter is defined in terms of the fineness of fly ash used, F_F, and that of a reference fly ash, F_{Fo}, as follows:

$$\Omega_F = \left[\frac{F_F}{F_{FO}}\right]^{1/3} \tag{9}$$

where F_{F0} is taken equal to 300 m^2/kg. The symbols CaO, SiO_2, Al_2O_3 and Fe_2O_3 denote the weights per unit volume of concrete of the calcium oxide, silica, alumina and ferric oxide respectively from the fly ash. The symbols CH_P and S_d appearing in the above expressions respectively denote the net calcium hydrate available for taking part in the pozzolanic reaction and the silica demand of the mixture. The two are calculated as follows:

$$CH_p = 1.321\ CaO + 0.215\ C_2S + 0.487\ C_3S - 0.305\ C_4AF \tag{10}$$

$$S_d = 0.541\ CH_p \tag{11}$$

The four parameters Poz_1 to Poz_4 are defined in the following; when $SiO_2 \geq S_d$:

$$Poz_1 = 1.541\ \Omega_F\ S_{co}\ \frac{1.321\,CaO}{G_F}$$

$$Poz_2 = 1.541\,\Omega_F\ S_{co}\ \frac{0.215\,C_2S + 0.487\,C_3S - 0.305\,C_4AF}{G_{CF}}$$

$$Poz_3 = \Omega_F\ S_{co}\ \frac{Al_2O_3}{G_{CF}} \quad \text{and} \quad Poz_4 = \Omega_F\ S_{co}\ \frac{Fe_2O_3}{G_{CF}} \tag{12}$$

in which, S_{co} denoted the silica coefficient and is defined as follows:

$$S_{co} = \left[\frac{SiO_2}{S_d}\right]^{0.2} \tag{13}$$

The symbol G_{CF} appearing in the above equations denotes the density of that material, which takes part in the hydration reaction from the fly ash and Portland cement, to produce pozzolanic $C_3S_2H_3$:

$$G_{CF} = 0.649\ G_C + 0.351\ G_F \tag{14}$$

The only chemical parameter is equivalent sodium content of the mixture NaEq, expressed as:

$$NaEq = NaEq(OPC) + NaEq(FA) \tag{15}$$

Where NaEq(OPC) and NaEq(FA) denote the weights of the alkali oxides from Portland cement and ash. The two alkali oxides (Na_2O and K_2O) are expressed as equivalent of Na_2O. The two physical parameters water-binder ratio, r_W and fly ash-cement ratio, r_F are defined as:

$$r_W = \frac{W}{C+F} \tag{16}$$

$$r_F = \frac{F}{C} \tag{17}$$

Where W, C and F denote the weights of water, cement and fly ash respectively per unit volume of concrete. The values of the 29 constants in Eqn. 2 are given in the following table. These values were determined by calibrating the model from a versatile data.

Constant	β_1	β_2	β_3	β_4	β_5	β_6	γ_1	γ_2	γ_3	γ_4
Value	-26.2	22.9	2.49	6.66	-5.76	1.06	.169	.025	.594	.279
Constant	β'_1	β'_2	β'_3	β'_4	β'_5	β'_6	γ'_1	γ'_2	γ'_3	γ'_4
Value	-24	12.2	1.49	15.57	-6.42	-.90	.0022	.0435	.436	-.087
Constant	a	a'	b_1	b_2	b'_1	b'_2	c	c'	α	
Value	-.0351	.937	-.321	.0656	-.0138	.0344	3.27e-4	-6.7e-5	-.0171	

PERFORMANCE TEST

The model was calibrated and validated using data from a large number of researchers from several countries around the globe. The details of the data have been published by Tahir (1998). The scatter of the predicted and test data is plotted in Figure 1. It can be seen that model predictions agree very closely to the experimental observations. In addition to this a performance test was run on the model using Portland cements and fly ashes of various chemical compositions. The solid volume resulting from the hydration and pozzolanic reactions was computed from the strength data of the mixtures. It was estimated by the model. The trends were tested and compared with the standard norms of the chemistry of hydration and pozzolanic reactions.

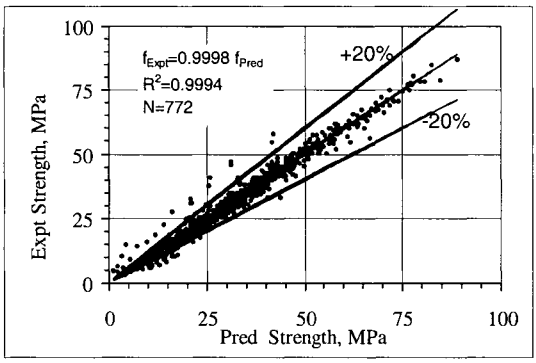


Figure 1. Scatter of model predictions and experimental data

Once the calibration and validation of the model was performed, the performance of the model was tested using Portland cements and fly ashes of different chemical compositions and fineness. In the first part of the performance test a Portland cement of constant composition was used with fly ashes of different compositions. The properties of a partial list of the binders are given in Tables 1 and 2.

TABLE 1

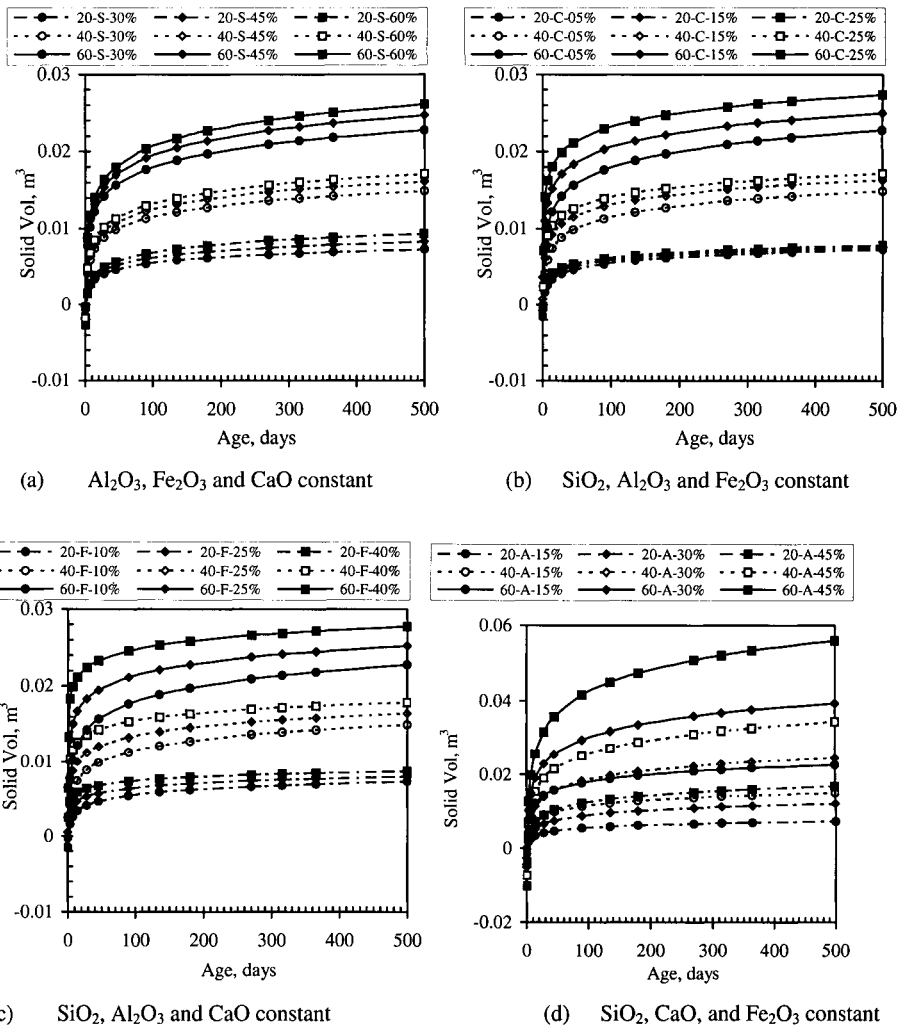
VARIATION OF OXIDE CONTENTS OF FLY ASH CONSIDERED IN THE PERFORMANCE TEST

ID	%SiO_2	%Al_2O_3	%Fe_2O_3	%CaO	%Na_2O	%K_2O	Remarks
S-20%	20						Variation
S-40%	40	15	10	5	2.0	1.9	of
S-60%	60						SiO_2
C-05%				5			Variation
C-15%	30	15	10	15	2.0	1.9	OF
C-25%				25			CaO
F-10%			10				Variation
F-25%	30	15	25	5	2.0	1.9	of
F-40%			40				Fe_2O_3
A-15%		15		5			Variation
A-30%	30	30	10	5	2.0	1.9	of
A-45%		45		5			Al_2O_3

TABLE 2

PROPERTIES OF THE CEMENT CONSIDERED IN THE PERFORMANCE TEST

$\%C_2S$	$\%C_3S$	$\%C_3A$	$\%C_4AF$	$\%Na_2O$	$\%K_2O$	Surface Area
20	55	10	10	0.17	0.50	300 m^2/kg



(a) Al_2O_3, Fe_2O_3 and CaO constant

(b) SiO_2, Al_2O_3 and Fe_2O_3 constant

(c) SiO_2, Al_2O_3 and CaO constant

(d) SiO_2, CaO, and Fe_2O_3 constant

Figure 2. Change in pozzolanic solid volume due to variation in oxide composition of fly ash.

However, the rate of change of the solid volume with age is much slower compared to that caused by the same variation in the silica content. It can be observed from the figure that the higher the calcium content of the ash, the earlier the pozzolanic reaction starts contributing to the solid volume. The change in the solid volume is nonlinear with the change in calcium content of ash. For all replacement

ratios, an increase in Fe_2O_3 content of ash causes an increase in the solid volume. The influence of Al_2O_3 on the pozzolanic reaction is shown in Fig 2d. The solid volume increases appreciably with an increase in alumina content of the ash. It can be noted that for the same increase in the two oxide contents, Al_2O_3 produced the solid volume about five times more than that produced by Fe_2O_3. This phenomenon is just in line with the observed facts from the hydraulic and pozzolanic behavior of the low and high calcium fly ashes

In the second part of the performance test the Bogue's compounds are varied as shown in Table 3. The properties of ash used with these cements are listed in Table 4. The results of this study are shown in Fig. 3.

TABLE 3

VARIATION IN THE MAIN COMPOUNDS OF THE CEMENT CONSIDERED IN THE PERFORMANCE ANALYSIS

ID	$\%C_2S$	$\%C_3S$	$\%C_3A$	$\%C_4AF$	$\%Na_2O$	$\%K_2O$	Remarks
C3S=50%	30	50	8	9	0.17	0.5	Variation
C3S=45%	30	45	8	9	0.17	0.5	of
C3S=40%	30	40	8	9	0.17	0.5	C_3S
C2S=30%	30	50	8	9	0.17	0.5	Variation
C2S=25%	25	50	8	9	0.17	0.5	of
C2S=20%	20	50	8	9	0.17	0.5	C_2S
C3A= 8%	30	50	8	7	0.17	0.5	Variation
C3A=10%	30	50	10	7	0.17	0.5	of
C3A=12%	30	50	12	7	0.17	0.5	C_3A
C4AF=5%	30	50	8	5	0.17	0.5	Variation
C4AF=7%	30	50	8	7	0.17	0.5	of
C4AF=9%	30	50	8	9	0.17	0.5	C_4AF

TABLE 4

PROPERTIES OF THE FLY ASH CONSIDERED IN THE PERFORMANCE ANALYSIS

$\%SiO_2$	$\%Al_2O_3$	$\%F_2O_3$	%CaO	$\%Na_2O$	$\%K_2O$	Surface Area
29.2	19.2	13.2	23.4	2.00	1.90	300 m^2/kg

It can be observed from Figure 3 that an increase in C_4AF causes increase in solid volume and strength at all ages. On the other hand an increase in C_3A reduces the solid volume of hydration, which means that an increase in C_3A causes reduction in the strength of hydrated paste at all ages. This observation is in line with the established facts of the hydration chemistry. The increase in C_3S or C_2S causes increase in solid volume of hydration at all ages. However, the change caused by C_2S variation is more pronounced at later ages as compared to that caused by C_3S. This observation is again in line with the established facts of hydration chemistry.

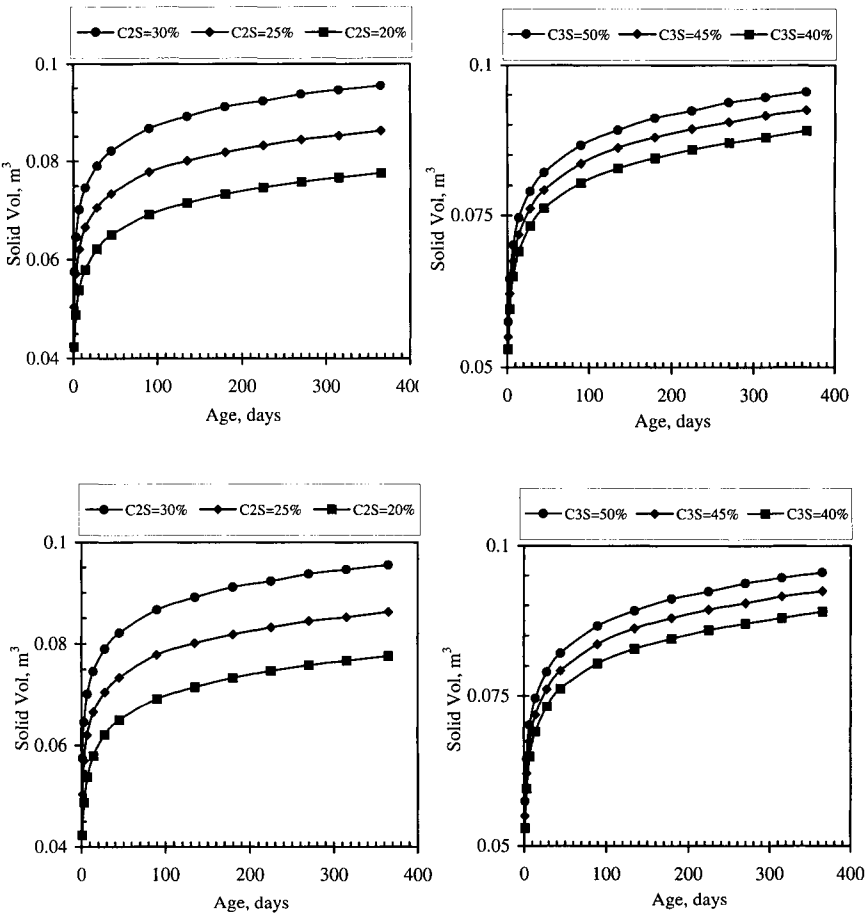


Figure 3. Change in solid volume due to variation in compound composition of cement.

CONCLUSIONS

The quality of calibration and validation of the presented model is found quite satisfactory and the predicted strengths agree closely to the experimental strengths. It has been observed from the performance tests on the model that an increase in SiO_2, CaO and Fe_2O_3 results in increase of strength at all ages and the relationship is quite similar for the three oxides. However, the change in Al_2O_3 content affects the strength in quite a different way. It is further seen that an increase in C_3A content of cement results in decrease of strength at al ages, which is a confirmation of the basic fact of the chemistry of hydration and pozzolanic reactions. The model predictions further confirm that an increase in C_4AF causes increase in the solid volume of hydration and hence in strength of hardened

paste. All the tests and observations confirm the site independence of the model and hence it can be used confidently in designing mixtures incorporating fly ash of variable characteristics.

REFERENCES

Tahir, M. A. and Nimityongskul, P., (1998). "Model for Predicting 28-day Strength of Fly ash-Concrete", *Proceeding of Japan Concrete Institute*, Vol. 20, No. 2, pp. 139-144.

Tahir, M. A., (1998). "Model for Predicting Strength Development of Concrete Incorporating Fly ash of Variable Chemical Composition and Fineness", *Doctoral Dissertation,* AIT, Bangkok.

De Larrard, F. and Tondat, P., (1993). "Sur la contribution de la topologie du squelette granulaire a la resistance en compression du beton.", *Materials and Structures*, Vol. 26, pp. 505-516, (In French).

Advances in Building Technology, Volume 1
M. Anson, J.M. Ko and E.S.S. Lam (Eds.)
© 2002 Elsevier Science Ltd. All rights reserved

MIXTURE DESIGN FOR HIGH-PERFORMANCE CONCRETE FOR SLIP-FORM PAVEMENT IN JIANGXI PROVINCIAL NATIONAL HIGHWAY 323

Wu Shaopeng[1,2] , Zhou Mingkai[1] , Zeng Ming[1] and Ouyang zhengxiang[1]

[1]Key Laboratory for Silicate Materials Science and Engineering Ministry of Education, Wuhan University of Technology, Wuhan 430070,China
[2]College of Transportation, Southeast University, Nanjing 210096,China

ABSTRACT

Raw materials such as Ninguo ordinary Portland cement (produced by Anhui province), crushed lime stone, Fengcheng fly ash, mixture additive, etc were used in optimizing the design of mix proportions for slip-form paving cement concrete pavement in Jiangxi provincial national highway 323. Experimental results indicated that these raw materials could fully meet the engineering requirements and the slip-form paving cement concrete had good workability and mechanical properties. And, it was economically reasonable and feasible. This was proved with the achievement of more than 90 kilometers of highway and 20,000m^3 cement concrete. The proposed methods for controlling and adjusting mix proportions are helpful for practical highway construction projects.

KEYWORDS: Slip-form paving, Optimizing design, Mixture proportion, Workability

1. INTRODUCTION

Slip-form paving cement concrete is a special pavement material. Its mix proportions are central to one of the pivotal constructional techniques in ensuring high-performance slip-form paving cement concrete pavements in a high-grade highway. The technical requirements for mix proportions of cement concrete pavement for National Highway 323 are as follows: Firstly, it has suitable workability. The slump of fresh cement concrete is less than 5 cm, and it should match the speed of paving and meet the capacity of mechanical vibration. Secondly, it should have excellent mechanical properties. Bending strength after 28 days is 5.2MPa, and the structural bending strength should not be less than 4.5MPa. Thirdly, it should have good durability. The service life of the slip-form paving cement concrete pavement is required to be 10 years longer than that of an ordinary concrete pavement. Lastly, it should be economically reasonable and feasible. In this study, many attempts have been tried to fulfill the above requirements for highway construction, and a satisfactory result was achieved on a practical project.

2.RAW MATERIAL

The ordinary Portland cement(32.5 degree) was produced by the Ningguo cement works, Anhui province. A middle coarse river sand was employed as fine aggregate while a 531.5mm crushed limestone as coarse aggregate. Fengcheng Class II dry fly ash was used as mineral admixture. The chemical additives were used Type FDN-R water-reducer and Type JS-2 water reducer and retarder, which were produced Hubei and Hunan, respectively.

3. MIXTURE PROPORTION DESIGN

3.1MIXTURE PROPORTIONS

To achieve the mixture proportions for slip-form paving cement concrete it was first necessary to determine its water/cement ratio and sand ratio. There is an empirical formula to calculate water/cement ratio, which designs mixture proportions mainly in terms of bending strength. But the mixture proportion should be adjusted by the accumulated experience. In fact, water to cement ratio has a greater influence on compressive strength on than bending strength to a certain extent. Except for cement type and aggregate factor, cement content is the most significant factor affecting the bending strength of cement concrete. Sand rate of slip-form paving cement concrete is higher than that in ordinary cement concrete, so as to ensure the adhesion and compactness of cement concrete. There is an optimum sand ratio for a specific aggregate and water to cement ratio, with which the best properties of cement concrete can be achieved. According to our experience, when total volume of cement mortar, including cement, water, sand and air void, was 0.55~0.59m^3 in each cubic meter at concrete, the comprehensive properties were much better. Of course, the experimental result was decisive. Based on the engineering demands, the primary mix proportions requirements are shown in table 1.

TABLE 1
TECHNICAL REQIREMENT OF MODIFIED SLIPFORM PAVEING CEMENT CONCRETE NATIONAL HIGHWAY 323

Strength requirement	Setting time	Slump	Workability
Bending strength after 18 days is more than 5.2 MPa	Initial setting time is 6-7 hours and final setting time is 8-10 hours at 20.	The slump of fresh cement concrete was less than 6cm. Constructional slump is more than 2cm.	Excellent adhesion and workability, no weeping

The design of mixture proportions is based on experience based parameter and formulae. In order to agree with the requirements for bending strength and relevant technical properties, experiments were carried out to test and adjust mixture proportions in the lab. The results are showed in table 2.

TABLE 2

TEST-EXPERIMENTAL MIXTURE PROPORTION RESULTS

NO.	Water cement ratio	Sand ratio (%)	Mixture additive (%)	Material content of per cubic meter (kg/m^3)				
				Cement	Fly ash	Water	Sand	Stone
1	0.41	36	JS-2 1.2	300	80	156	687	1220
2	0.42	36	FDN-R 1.5	300	80	159	687	1220
3	0.445	36	FDN-R_1 1.0	300	80	169	666	1245
4	0.43	36	FDN-R 1.4	320	50	159	692	1229
5	0.43	36	JS-2 1.2	320	50	159	692	1229
6	0.44	36	FDN-R_1 1.0	320	50	163	692	1229
7	0.41	36	FDN-R 1.4	280	100	156	689	1225
8	0.46	36	FDN-R_1 1.0	280	100	175	688	1222
9	0.426	36	JS-2 1.2	280	100	162	688	1222
10	0.49	38	JS-2 1.2	280	60	167	747	1218
11	0.466	38	FDN-R 1.4	280	60	158	747	1218
12	0.51	38	FDN-R 1.4	280	60	174	747	1218
13	0.45	36	FDN-R 1.4	300	80	169	685	1218
14	0.48	36	FDN-R 1.4	280	60	163	706	1254
15	0.46	36	FDN-R 1.4	260	100	167	697	1238
16	0.44	36	FDN-R 1.4	390	0	172	691	1212
17	0.43	36	FDN-R 1.4	350	60	176	671	1194
18	0.42	36	FDN-R 1.4	350	60	171	671	1194

3.2 EXPERIMENTAL RESULTS

Experimental results are showed in Table 3.

TABLE 3

EXPERIMENTAL PROPORTIONS OF THE MIX OF TABLE 2

NO.	Slump mm			Bending strength MPa			Workability
	Initial	1/2h	1h	3d	7d	28d	
1	140	20		5.18	4.81	5.70	Good adhesion, little bleeding
2	60	30		5.51	5.29	5.62	Good adhesion, little bleeding
3	75	30	10	5.00	4.88	6.40	Good adhesion, little bleeding
4	160	35	15	5.78	6.87	6.92	Good adhesion, little bleeding

5	150	40	10	5.44	5.91	5.61	Excellent adhesion, little bleeding
6	75	20		5.53	6.22	6.40	Good adhesion, little bleeding
7	165	105	60	5.33	6.64	6.83	Excellent adhesion, no bleeding
8	50	25		4.42	5.53	7.20	Excellent adhesion, no bleeding
9	65	25		5.00	5.73	5.80	Excellent adhesion, no bleeding
10	35	15			5.27	4.90	Good adhesion, little bleeding
11	55	25		4.91	5.24	6.07	Good adhesion, little bleeding
12	65	35		4.13	4.78	6.00	Good adhesion, little bleeding
13	65	30	25	3.01	4.53	5.50	Good adhesion, little bleeding
14	55	30	30	3.35	4.48	5.10	Common adhesion, a little bleeding
15	75	40	20	3.00	3.71	5.40	Good adhesion, little bleeding
16	60	20		3.65	4.18	5.80	Common adhesion, bleeding
17	55	25		2.61	4.06	5.00	Excellent adhesion, little bleeding
18	90	45	35	3.00	4.34	5.20	Excellent adhesion, little bleeding

Firstly, workability: the orthogonal test analysis showed that primary factors influencing the slump was the additive and cement content next, and then water to cement ratio.
Secondly, bending strength: the most important factor influencing strength was cement content, water to cement ratio next, and then cement type. Cement content had the greatest influence among them. During the construction of slip-form paving cement concrete, water cement ratio, water content and cement content were strictly controlled. It is important to use a water-reducing agent and air-entraining agent properly. Based on the research results, the constructional mixture proportions were as follows.

TABLE 4
RECOMMENDED MIXTURE PROPORTION

Cement	Fly ash	Water	Sand	Broken stone	Mixture additive.
300	60	151	704	1225	JS-2 4.32

3.3 ADJUST AND CONTROL MIXTURE PROPORTION

Mixture proportion test and adjusting, including workability of fresh mixing cement concrete, air void content, density and strength was done to make these relevant standards meet the requirement.

3.3.1 ADJUST MIXTURE PROPORTION

Firstly, according to the recommended mixture proportion, the feasibility test was conducted, and raw materials, adhesion of the fresh concrete, bleeding and surface status of the concrete were taken into account. The result in table 5 showed that the fresh concrete had good workability.

TABLE 5
TESTING RESULT OF FRESH-MIXING CEMENT CONCRETE

Item	Slump (mm)	Density (kg/m^3)	Air void content (%)	Workability
Initial	60	2390	5.0	Excellent adhesion, little bleeding
1/2h	35	2410	4.3	Excellent adhesion, little bleeding
1h	25	2420	3.9	Excellent adhesion, no bleeding

Secondly, the air void content was determined. The air void content of freshly mixed cement concrete was measured based on Test JTJ 053-94. It agreed with the requirement for freeze-resisting properties as to the air content and met the pavement engineering need. Thirdly, the mixture proportion of freshly mixed cement concrete was adjusted. The mixture proportion test assumed the density method in this study. The density of fresh-mixing cement concrete was 2390 kg/m^3 after vibrating, which was less than designing density. Because of the bleeding, a conversion coefficient was used as follows.

$$\beta=R_1/R_2 2390/2444=0.978 \quad (1)$$

$$ScSd\times\beta \quad (2)$$

Mixture proportions after adjusting are as shown table 6.

TABLE 6
MIXTURE PROPORTION AFTER ADJUSTING

Cement	Fly ash	Water	Sand	Broken stone	Mixture additive
293	59	148	688	1198	JS-2 4.3

Lastly, the bending strength was determined. The beam samples were made based on the relevant standards. In this test, the water content was kept constant, but the water to cement ratio was increased or decreased 0.05, respectively. Two groups of samples were tested for determining bending strength. The results are shown in table 7. Test result agreed to the requirement.

TABLE 7
TEST RESULT OF BENDING STRENGTH

Type	Bending strength after 7 days (MPa)	Bending strength after 28 days (MPa)
W/C = 0.42	5.28	6.40
W/C = 0.47	5.15	6.20
W/C = 0.37	5.50	6.50

3.3.2CONTROL CONSTRUCTIONAL MIXTURE PROPORTION

It is necessary to adjust and control mixture proportion according to ambient temperature, transport distance, raw materials, especially water content of the aggregates, proportion of sand and crushed stone after mixing. The purpose is to ensure mixture proportion parameters fulfill the design

requirements for concrete workability, bending strength and durability.

Firstly, raw materials on site must be tested when they are received. Slip-form paving is mechanized construction as a large scale. During construction, cement, sand, crushed stone and mixture additives are tested regularly. Only qualified material can enter the site. It was necessary to adjust mixture to meet constructional requirements when the quality of qualified material fluctuated. The regular test result of Hailuo P42.5 Portland cement showed that its quality fluctuated only slightly and the properties remained stable. Properties of fly ash were up to standard except for color changes. Water-reducer content varied a little with single mixture additive. The calculation system broke down easily with higher injection of mixture additive. Screening tests indicated that modulus of fine sand and the grading of 5-16mm of crushed stone varied greatly, but other relevant standards qualified.

Secondly, the precision of the mixing system was calibrated regularly. The precision of slip-form paving cement concrete is required to the higher than that of ordinary cement concrete and be calibrated before construction. Measuring error requirements were as follows: cement±1%, fly ash±2%, crushed stone ±2%, water±1% mixture additive±2%. If the measuring error was out of the requirement, the measuring system had to be re-calibrated during construction. If the automatic measuring system broke down, the pavement construction had to be stopped until the breakdown was fixed. When a trial batch was used on the 323-highway construction site, bleeding was found in the pavement. The reason was that the error of the binding material system beyond the requirement limits. The measuring system for chemical additives easily broke down or went out of control for low contents and complex composition. So it was important to test and calibrate that measuring system.

Thirdly, the quantity of the sand, crushed limestone and water were adjusted according to the moisture contents of sand and crushed stone, fineness modulus of sand and gradation of aggregate. Moisture contents of the raw materials varied with weather conditions, locations and exposure time etc., hence, the moisture contents of these materials had to be kept monitored. Sand ratio and fineness modulus differs for different batches. Sand ratio was adjusted when fineness modulus varied obviously. Increasing sand ratio was based on pavement requirement. Sand ratio for slip-form paving cement concrete, fineness modulus, water content of raw material and stone proportions were tested every day before mixing in 323 Engineering. The tests were performed by professional quality inspectors. On the construction site on Highway 323, the mix proportions were adjusted according to slump changes. With these measures, the quality of the pavement was further improved.

Lastly, the mixture proportions were adjusted according to paving conditions on site. The quality of the slip-form paving depends on weather conditions, pavement conditions, concrete delivering distance. So it is necessary to adjust mixing parameters according to paving condition to ensure high-quality of pavement. The 323 Engineering experienced all sorts of strict tests, including high-temperature, long-distance transportation and bad constructional conditions. When the transporting distance was about 18km and the temperature in summer was 47, the slump of cement concrete reduced quickly. In order to improve the slump and to meet the slump requirement of more than 20mm on site, a water-reducing agent was accordingly added. Dense mortar layer on the pavement surface was 2 to 4mm thick. In order to ensure the quality of cement concrete, a finer aggregate was chosen, and the reducing-water agent content was increased and the water content reduced accordingly. Transporting assembly line had to be organized well, avoiding traffic jam and breakdown.

Freshly mixed cement concrete conformed to the requirement for slip-form paving by testing and controlling the constructional mixture proportion. Acceptance quality of the pavement engineering approached a good level and achieved complete success.

4. CONCLUSIONS

4.1 The concrete prepared with Niangua ordinary Portland cement, crushed limestone, Fengcheng class II fly ash and water-reducers was able to meet the requirements for slip-form paving construction in Jiangxi Provincial National Highway 323.

4.2 The cement concrete prepared based on the mixture proportions in table 6 exhibited suitable workability, excellent mechanical properties and economy.

4.3 The mixture proportion designed for the slip-form paving concrete in Highway 323 engineering had been firstly used in slip-form paving construction of Jiangxi Province. These satisfactory results were achieved is proved by the completion of the qualified construction projects including more than 90 kilometers of highway and 20 thousands cubic meters cement concrete.

References

[1].Rongqing Yan (1997). Paving Machine And Constructional Technology Of Slip-form Paving Cement Concrete. People's Communications Press Of China(Beijing)

[2]Daoyuan Zhu(1999). Multi-statistical Analysis And Software, Southeast University's Press Of China(Nanjing)

[3]Chuhang Wu(2000), Paving Construction And New Technology Of Cement Concrete, People's Communications Press Of China(Beijing)

This Page Intentionally Left Blank

Advances in Building Technology, Volume I
M. Anson, J.M. Ko and E.S.S. Lam (Eds.)
© 2002 Elsevier Science Ltd. All rights reserved

ADVANCES IN THE STUDY OF FATIGUE BEHAVIOR OF HIGH PERFORMANCE CONCRETE IN CHINA

XIAO Jian-Zhuang and CHEN De-Yin

Department of Building Engineering, Tongji University, Shanghai 200092 P.R. China

ABSTRACT

With the wide application of high performance concrete in civil engineering, in such as high-speed railroads, maglev transrapid, offshore platforms and super high-rise buildings, the fatigue behavior of high performance concrete has had more and more attention by civil engineers. Based on the investigations reported in relevant home references, using the comparative analysis method, the fatigue behavior of high performance concrete is reviewed and the factors affecting fatigue behavior are studied, including fatigue damage mechanism analysis, fatigue failure characteristic and fatigue concept design. Finally some suggestions on the fatigue-resistance of high performance concrete are given.

KEY WORDS

High performance concrete, fatigue test, fatigue behavior, fatigue design, number of cycles, cumulative damage

HIGH PERFORMANCE CONCRETE

Concrete, since the 19th century, has developed rapidly from plain concrete to reinforced concrete, pre-stressed concrete, and special concrete into which additives are added. Although the new members in the family of concrete----high strength concrete and high performance concrete [1], came into use only a few years ago, as they meet the demands of suitable strength and excellent durability in structures, they will be used widely in civil engineering in the future.

FATIGUE PROBLEMS ON STRUCTURES OF HIGH PERFORMANCE CONCRETE

Under repeated load, many structures in civil engineering have collapsed suddenly, in which the stress is less than the design value. This is called fatigue failure [2]. Since World War II, many such accidents have occurred. Before the 1970's, the fatigue problems of concrete structures were not paid so much attention as steel structures. This is because fatigue failure occurred infrequently when the permissible stress method was adopted in structural design. But with the development and wider application of

concrete structures, fatigue damage can not be ignored in some structures under repeated load, especially for some important structures in a condition of high stress, such as high-speed railroads, maglev transrapid, offshore platforms and super high-rise buildings. Therefore, several scholars in China have carried out many tests and conducted research on the fatigue behavior of concrete. It should be pointed out that although high performance concrete or high strength concrete is not mentioned in much literature, as the relevant performance of the concrete used in the tests approaches or reaches the basic behavior of high performance concrete such as high strength, good fluidity, or excellent durability, they can be effectively considered as high performance concrete.

FATIGUE TESTS ON HIGH PERFORMANCE CONCRETE

Different methods are used in classifying fatigue tests. For example, fatigue tests can be classified as low-cycle fatigue tests and high-cycle fatigue tests according to number of cycles. Because the stress level in low-cycle fatigue tests is high, the tests are called fatigue tests under high stress, while high-cycle fatigue tests are called fatigue tests under low stress. Fatigue tests may also be classified as constant-amplitude loading tests and variable-amplitude loading tests [3] which can be sub-classified as one stage constant-amplitude, multi-stage constant-amplitude, incremental stages loading and so on. For this aspect of loading status, the fatigue tests are classified as under compression, tension, flexure, flexure and shear. The main fatigue tests in China in recent years are listed and described in Table 1. Based on those advances in the study of the problems of fatigue performance of high performance concrete nowadays is put forward in this paper.

FACTORS AFFECTING FATIGUE BEHAVIOR OF HIGH PERFORMANCE CONCRETE

Effect of Admixtures

The common mechanism of fatigue failure of concrete is described as follows. There are subtle defects such as subtle cracks, holes, low-strength interfaces or impurities. When the defects are subjected to loading, a stress concentration is produced. Under repeated load, damage emerges and accumulates so much so that structures fail. Fatigue failure is a process of cumulative damage. But adding some special admixtures such as silicon ash, and fly ash and others can reduce initial defects in concrete. The admixtures can prevent cracks from emerging and developing, and the fatigue behavior of the concrete is raised. Another kinds of admixture are fibers, including steel fiber, carbon fiber and polypropylene fiber. These fibers can be included singly or mingled. The fatigue behavior of high strength concrete is improved markedly by mixing proper contents of steel fiber [4]. The reason is obtained easily. Under repeated load, the initial defects in concrete develop into tiny cracks and stress concentrations appear at the tip of tiny cracks. However the cracks are stopped by the intersections with steel fibers. At the same time stress concentration is released by steel fibers. So fatigue behavior is improved. But when the number of cycles increases further, the ability of steel fibers holding cracks is limited so that cracks expand across steel fibers and finally the concrete fails from cumulative damage exceeding the limit value. It is suggested in the test [5] that the compressive strength of steel

TABLE 1
MAIN TESTS ON FATIGUE PERFORMANCE IN CHINA

Investigator	Strength (MPa)	Mixture of concrete	Size (mm^3)	Feature	Type
Wu Peigang Zhao Guangyi Bai Liming	76.4 84.7 77.6	Water cement ratio:0.330 Sand cement ratio: 1.204 Stone cement ratio:2.458 Water reducer:0.010	Prism $70.7^2 \times 212.1$ $100^2 \times 300$	S_{max}=0.80,0.75,0.70 0.65 S_{min}=0.10 f=0.10Hz Constant-amplitude	Axial compression
Ju Yang Fan Chengmou	30	Water cement ratio: 0.5 Sand cement ratio: 2.213 Sand cement ratio: 2.213 Fiber ratio: 0.012	Cylinder specimens Effective size: 100×250	S_{max}=0.75,0.65 S_{min}=0.05 f=7.5Hz Variable-amplitude	Axial compression
Wu Peigang Zhao Guangyi Zhan Weiwei	73.7 65.7 77.9 83.9 69.9	Water cement ratio: 0.33 Sand cement ratio: 1.204 Stone cement ratio: 2.458 Water reducer: 0.010	Prism: $100^2 \times 100$ $100^2 \times 400$ $100^2 \times 400$	S_{max}=0.90,0.80,0.75 0.70,0.65,0.60 S_{min}=0.10 f=5, 10, 15Hz	Tension (Split axial, bending tension)
Li Yongqiang Chen Huimin	51.74	Water cement ratio:0.40 Sand cement ratio:1.16 Stone cement ratio:.47	Prism: $100^2 \times 515$	S_{max}=0.9,0.8,0.75, 0.675,0.6,0.5 S_{min}=0.09,0.08, 0.075,0.0675, 0.06,0.05, f=10Hz	Flexure
Yan Yun Sun Wei	80 100 120	Water cement ratio: 0.28 Silicon / cement: 0.20 Fiber ratio: 0.015	Prism: $100^2 \times 400$	S_{max}>0.8 or<0.8 S_{min}=0.1 S_{max} f=5-7Hz,or15-20Hz	Flexure
Zhao Shunbo Zhao Guofan Huang Chengkui	38.3-48.5	Mixed with shear steel-typed steel fiber, the maximum grain size:10mm, NF-B water reducer, the shear steel fiber, steel fiber reinforced pre-stressed concrete beams	Beam: 150×300×2300 Shear-span ratio: 1.75	S_{max}=0.6 S_{min}=0.1 S_{max} f=8-10Hz	Flexure and shear
Yu Maohong Zhan Junhai Don Wenshan Zhang etc.	25.0	Water cement ratio: 0.5 Sand cement ratio: 4	Thin-walled cylinder tube, Φ115×330 δ=20	τ / σ =0.45,0.25, σ =-10MPa f=4Hz	Compression and torsion

Note: S_{max}, S_{min}—the maximum stress σ_{max}/f_c and the minimum stress σ_{min}/f_c under fatigue load
σ_{max}, σ_{min}—the stress of upper limit and lower limit, MPa

fiber concrete under static loading is closed to that of normal strength concrete, but there are obvious differences in fatigue behavior, such as fatigue life. The fatigue life of steel fiber concrete is 7.9-13.7 times that of concrete without steel fibers. It is also proved by the test that steel fiber is effective in aspects of fatigue behavior in reinforced pre-stressed concrete beams [6].

When part of the cement is replaced with silicon ash in high strength concrete [4], variation happens in structures due to the characteristics of the interfacial zone between aggregate and matrix. The effect of silicon ash and fly ash eliminates tropism and enrichment of the crystal of $Ca(OH)_2$. The boundary between interface and matrix blurs and this means the weakness of the interface is alleviated or disappears. So the interfacial bond between aggregate and cement is strengthened and interface failure will be avoided when loading is applied. Thus, the fact that silicon ash has an overall effect on fatigue

behavior can be explained by the reduction in amount and size of the initial cracks.

The following conclusions can be obtained from the comprehensive analysis of test results described in Table 1. There have different effects improving fatigue behavior depending on the different admixtures used. Steel fiber is effective for confining the prolongation of cracks especially, while silicon ash is good at reducing the source of cracks. Carbon fiber has good rigidity with poor toughness and polypropylene fiber is the other way round. Under the same conditions, carbon fiber improves the fatigue behavior of concrete more effectively than polypropylene fiber. But if fiber and silicon ash are intermixed, fatigue behavior is improved greatly because they make full use of their respective advantages and make up for each other's shortcomings. In the test [4], it is suggested that when the number of cycles is the same, high strength concrete in which the same ratio of silicon and steel fiber are mixed can increase 2 times in strength, and when the level of stress is the same, the number of cycles is increased over 10 times. If carbon fiber and polypropylene fiber are mixed together, a superimposed effect exists and fatigue behavior is improved greatly because the polypropylene fiber increases the tenacity of concrete and carbon fiber improves the ability to resist load. When the volume content of carbon fiber and polypropylene fiber reach 0.015 and 0.009 respectively, fatigue life [7] can be increased by up to 10 times that of pure concrete.

Effect of Loading

The effect of loading is referred to as the effect of stress level and sequence of loading. Generally, when its stress level is high, fatigue life is short; and when stress level is low, fatigue life is long. However, there are different opinions about the exact relationship between them. For example, one researcher thinks that single logarithm relationship exists [8], and others think that double logarithm relationship exists [9].

The varieties of fatigue behavior affected by stress level mostly lie in the way of cracks develop and the speed of cumulative damage. When the stress level is low, at the beginning of stage, cracks are few and short. With the cycles increasing, these cracks develop steadily or increase slowly. With a number of cycles increasing further yet, new cracks emerge so much so that structures fail due to new cracks and old cracks intersect and run through. When its stress level is high, at the early stage there are more cracks. With number of cycles increasing further, old cracks develop continuously and new cracks also emerge rapidly. Eventually the cracks intersect and become so wide that the structures fail. As for high strength concrete, it is suggested by the test [10] that under high stress, the fatigue life of high strength concrete is greater than that of normal strength concrete under the same conditions, while under a low stress level, normal strength concrete has a longer life.

The effect of the sequence of variable-amplitude loading on fatigue behavior is different. The loading history in which the early stress level is lower (or higher) and the late stress level is higher (or lower) is often referred to. Different load sequences are mainly attributed to transformation of cumulative damage. According to this idea, controlling the number of early stress level cycles is very important. When the cycles are less than a critical number, the subtle cracks in concrete tend to close back; otherwise the subtle cracks tend to develop. It is inferred from the tests [11, 12] that when the number of cycles at low (or high) stress levels at the early stage is less than the critical number, the surplus fatigue life improves much more than the corresponding life when it only remains in high (or low) stress level.

Relationships Between Admixtures Effects and Loading

The effect of admixtures on fatigue behavior is related to the sequence of loading. This conclusion is obtained from the relationships between the varieties and content of admixtures and the sequences of loading. Fatigue behavior is obviously increased when the proper content is controlled according to various stress levels. Also a critical number for the early stress level exists depending on the various

loading regimes. The critical number is related to the behavior of concrete. It is concluded from the test [7] that when fibers are intermixed, corresponding to a certain stress level, the flexure fatigue behavior is improved as the content increases. In the study [6] on the shear fatigue behavior of concrete with fiber, it is clear that steel fibers are effective in controlling the development of cracks while the function of steel fibers is also related to the cyclic characteristics. In the tests under variable-amplitude loading [11, 12], the low-high loading sequence, fatigue life improves as long as under low stress, the number of cycles do not exceed a critical number. The critical number is different for various concrete. The detailed relationship will need to be studied further. From the above descriptions, it can be deduced that fatigue behavior is affected by the inner characteristics of the concrete and the exterior factors of loading.

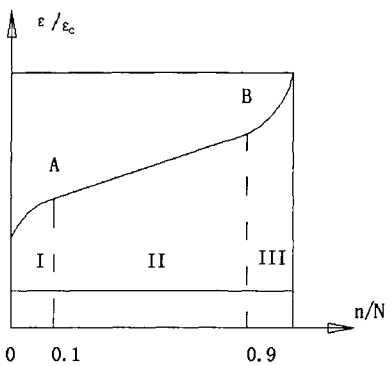


Figure 1: The ideal curve of the three-phrased fatigue deformation development

FATIGUE DEFORMATION OF HIGH PERFORMANCE CONCRETE

Fatigue Deformation Characteristics

First, under repeated load, fatigue failure takes a long time, but at the moment of failure, it is brittle. Moreover the internal force is complex and it is more appropriate to relate fatigue failure with deformation. As for high performance concrete and high strength concrete, when failure happens, the brittleness is obvious and ductility is weak. Second, during the course of cumulative damage, damage is usually measured by deformation and elastic modulus. Finally many tests suggest that the characteristics of fatigue deformation of concrete under repeated load are similar [13]. With stress level and number of cycles increasing, the longitudinal fatigue deformation increases. A three-phased law described by the ideal curve line in Figure 1 has been proposed. In the figure, the phase of deformation develops rapidly before point A and longitudinal strain increases slowly after that. The second phase is the relatively steady phase. This phase also fits the normal working phase of concrete structures under repeated load. The longitudinal strain varies as a linear function as the number of cycles increases. This phase ends of point B. After B, the failure phase is entered. The longitudinal strain increases sharply, develops rapidly and failure occurs.

Criterion of Fatigue Failure

Deformation of concrete under repeated load demonstrates general characteristics and its durability behavior of a concrete structure declines as a result of cumulative damage. Although the final failure has not emerged, the durability has reduced so much that structures are not in a safe condition any longer. Based on this, the deformation due to cumulative damage is looked as the criterion to judge

fatigue failure. This indicates [14] that when the residual strain of high strength concrete reaches 35% longitudinal total strain while the number of cycles is up to 85% of the total number of cycles, high strength concrete has lost the ability to resist repeated load. Under repeated load [6], the failure characteristics for oblique section in beams is that when oblique cracks have appeared under static loading, the strain in the shear-compression zone at the tip of the individual oblique cracks mostly comes up to the ultimate compressive strain.

FATIGUE DESIGN OF HIGH PERFORMANCE CONCRETE

Fatigue design of concrete can be divided into conventional fatigue design and fatigue design based on probability.

Conventional Fatigue Design

The size of the section of members is designed according to static loading and the fatigue check is carried out at the critical points in the section. Based on the requirement for structure design, it is necessary for the structural resistance to be greater than the internal force. The internal force is a function of repeated load, while the resistance of the structure is a function based on the fatigue strength. So in the study of conventional fatigue design, the first thing is to determine fatigue strength. Fatigue strength can be acquired by fatigue tests on the concrete under the basic constant-amplitude repeated load.

The relationship between stress and number of cycles at failure (S-N) needs to be obtained and the fatigue limit diagram needs to be considered to obtain the relationship between the effect of constant-amplitude and variable-amplitude. A series of studies on fatigue behavior of concrete under conditions of tension, compression, flexure, shear, and torsion have been carried out, it is rarely reported that relationships among them are found. The fatigue limit diagram is such a chart [3] that describes the relationship between cyclic loading regimes. From the chart, variable-amplitude loading can be transformed to constant-amplitude loading in order to acquire fatigue strength. However in this field, the studies so far are insufficient and are affected by the randomness of the date. So further study needs to be carried out to obtain the correct fatigue limit curve.

Fatigue Design Based on Probability

Nowadays, although reliability is considered in fatigue design, the design still actually depends on combination of experience and probability. Two problems that need to be solved are for given reliability how to calculate the critical number and for given critical number how the reliability can be checked. Most of the research abroad and at home is mainly focused on the distribution of random variables and the relationship of S-N under certain distributions.

CONCLUSIONS

1) Both similarities and differences are found in the fatigue performance of normal concrete and high performance concrete.
2) The factors affecting fatigue behavior of high performance concrete, including the different varieties and contents of admixtures, are related to certain stress level and the sequence of loading.
3) In the study of fatigue behavior of normal strength concrete, fatigue strength is mostly focused upon. While for high performance concrete, the deformation characteristics can be seen as important and should be investigated under repeated load.
4) Study of the fatigue behavior of high performance concrete should be combined with the research

on its durability.

5) Admixtures, including silicon ash, fly ash, steel fiber, carbon fiber and polypropylene fiber, can enhance the fatigue behavior of high performance concrete. However further study is needed.

REFERENCES

[1]Yves Malier. (1992). *High performance concrete from material to structure*. E and FN SPON

[2]Guo Zhenhai. (1999). *The theory of reinforced concrete* . Press of Tinghua University

[3]Xu Hao. (1988). *Fatigue Strength*. Press of High Education

[4]Sun Wei and Yan Yun.(1994). Study on the impact and fatigue performance and mechanism of high strength concrete and steel fiber reinforced high strength concrete. *Journal of Chinese Civil Engineering* 27:5, 20~27.

[5]Deng Zongcai.(2000). Study on compressive behavior of steel fiber reinforced concrete. *Building Structures* 30:9,53~55.

[6]Zhao Shunbo, Zhao Guofan and Huang Chengkui.(2000). Research on the shear fatigue behavior for steel fiber reinforced prestressed concrete beams. *Journal of Chinese Civil Engineering* 33:5, 35~39.

[7]Zhang Shaobo, Hua Yuan and Jiang Zhiqing.(1998). Experimental study on flexural fatigue behavior of hybrid fiber reinforced concrete. *Journal of Mechanics in Engineering*, 59~63(supplement)

[8]ACI Committee 215. (1974). Considerations for design of concrete structures subjected to fatigue loading. *Jounal of ACI* 30:2, 97~121.

[9]Shi Xiaoping, Yao Zukang, Li Hua and Gu Minhao.(1990). Study on flexural fatigue behavior of cement concrete. *Journal of Chinese Civil Engineering* 23:3, 11~22.

[10]Zhao Guangyi , Wu Peigang and Zhan Weiwei.(1993). The fatigue behavior high-strength concrete under tension cyclic loading. *Journal of Chinese Civil Engineering* 26:6, 13~19.

[11]Ju Yang and Fan Chengmou.(1995). Enhancement action in fatigue of steel fiber reinforced concrete. *Journal of Chinese Civil Engineering* 28:3, 66~77.

[12]Ju Yang and Fang Chengmou.(1995). Fatigue action of steel fiber concrete under variable-amplitude axial compressive loading. *Journal of Harbin University of Architecture and Engineering* 28:3, 77~82.

[13]Ou Jinping and Lin Yanqing.(1999). Experimental study on performance degradation of plain concrete due to high-cycle fatigue damage. *Journal of Chinese Civil Engineering* 32:5,15~22.

[14]Wu Peigang, Zhao Guangyi and Bai Liming.(1994). Fatigue behavior of high strength concrete under compressive cyclic loading. *Journal of Chinese Civil Engineering* 27:3, 33~40.

[15]Li Yongqiang and Che Huimin.(1998). A study on the cumulative damage to plain concrete due to flexural fatigue. *Journal of the Science of Railway in China* 19:2, 52~59.

[16]Yu Maohong, Zhao Junhai, Don Wenshan, Zhang Chunyan and Zhang Ning.(1998). Experimental studies on the fatigue strength of concrete under the complex stress state. *Journal of Xi'an Jiaotong University* 32:3, 89~92.

This Page Intentionally Left Blank

Advances in Building Technology, Volume I
M. Anson, J.M. Ko and E.S.S. Lam (Eds.)
© 2002 Elsevier Science Ltd. All rights reserved

HIGH PERFORMANCE POLYMER CONCRETE

R Y Xiao and C S Chin

Department of Civil Engineering, University of Wales Swansea, UK SA2 8PP

ABSTRACT

This paper presents experimental investigation and analysis of high performance polymer concrete (HPP) in which volume fraction of fibres was varied. Test results indicate that both compressive, tensile strength of concrete could be increased with the inclusion of fibre. Moreover, the use of fibres to improve the shear resistance has also been shown to be very effective for beams. HPP fibres have significantly increased the ultimate shear strength of reinforced concrete beam.

KEYWORDS: high performance polymer (HPP); superplasticizer; compressive strength; flexural strength; cylinder splitting strength; shear strength; design formulae.

INTRODUCTION

Cementitious materials in the form of concrete are attractive for use as construction materials since they can be readily molded and complex shapes may be fabricated. Concrete lends itself to a variety of innovative designs as a result of its many desirable properties. Concrete is brittle and weak in tension; these characteristics have limited its use. The development of fibre reinforced concrete has provided a technical basis for improving these deficiencies [(1)].

The main reason for the growing interest in the contribution of fibres in cement-based materials is the desire to increase the tensile properties of the basic matrix. However recent developments made polypropylene fibres the most widely used fibre in concrete, with the UK usage for 1995 estimated at 1000 tonnes. Polypropylene fibre provides a simple effective and economical means, even in small quantities, have dramatic effect on suppression of early cracking and thereby eliminate the main causes of weakness [(2)].

Goldfein [(3)] firstly suggested polypropylene fibres as an admixture to concrete in 1965 for the construction of blast-resistant buildings for the U.S. Corps of Engineers. His work comprised the incorporation of fibres in mortar and neat cement. This research gave the incentive for the early trials on polypropylene film fibre in concrete by Shell International Chemical Co. Ltd. who gave the material the name Caricate [(4)]. For centuries, man has attempted to reinforce concretes with various types of fibres. There are biblical references to the use of straw fibers in the molding of bricks. Later, the Roman Empire used hair fibres in structural mortars. Today, fibres are used in concrete to minimize cracking. Cracking happens in concrete when external stress exceeds strain capacity. By increasing concrete's strain capacity, stresses from intrinsic and external forces can be better managed. Fibre reinforcement redistributes stress in concrete and therefore cracking can be minimized [(5)].

The concept of using traditional steel and polypropylene fibres as reinforcement is not new, it is well known that both flexural and ductility of concrete could be increased with the inclusion of fibre. Moreover, the use of fibres to improve the shear resistance has also been shown to be very effective for beams. Handling steel fibres for concrete mixing may cause construction hazardous while traditional polypropylene fibres tend to form bundles in the concrete mixing if the volume ratio is high which will affect the strength contribution.

These are the reasons why that the new generation of HPP has been designed and produced. This type of fibre has the similar to that of steel fibres and could also be bent and has dents on its surface. Clearly, this will increase its workability in the concrete also improve its bond strength with the mortar of concrete. HPP fibre is extruded from 100% virgin polypropylene and mechanically deformed in a proprietary shape to maximize anchorage for reinforcement in cementitious composites. S-152 High Performance Polymer fibre is manufactured as a coarse filament with an engineered contoured profile. HPP fibre, because of the low modulus, provides good toughness response for large crack openings. Typical relevant properties of HPP fibres are shown in Table 1 [5].

TABLE 1

HPP FIBRE PHYSICAL PROPERTIES

PROPERTIES	VALUE
Specific Gravity	0.91
Nominal Filament Diameter	0.9mm
Fibre Length	50 mm
Aspect ratio	55.6
Deformation Spacing	3 /cm
Elastic Modulus	3.5 kN / mm^2
Ultimate Elongation	15 %
Water Absorption	0

RESEARCH SIGNIFICANCE

The research reported in this paper shows the effect of HPP fibres in improving the compressive strength, tensile strength and shear capacity of concrete. The test results obtained prove that HPP fibre could improve material properties and clearly increase the shear strength of the reinforced concrete beams Combination of minimum links and fibre reinforcement forms an effective system of shear reinforcement in a structural member. Experimental results suggest a simple means of predicting the flexure, cylinder splitting strength, and ultimate shear strength of fibre reinforced concrete beam. The paper presents useful data on material properties of fibre reinforced concrete, particularly for test data separating fibre contents.

TEST PROGRAM

Ordinary Portland cement, HPP fibres, crushed gravel with maximum size of 6mm coarse aggregate, beach sand and tap water were mixed to make the concrete. The specimens were cast from two different mixes. Mix A had cement: water: sand: coarse aggregate (6mm) ratio of 1: 0.52: 1.83: 3.25 and Mix B had a cement: water: sand: coarse (6mm) aggregate ratio of 1:0.51: 1.61: 2.57. A variety of mixers have been used in practice, some requiring an adjustment to the existing equipment, some none at all. Previous research has shown that he tumble form of mixer is a good way of mixing the fibres. The absence of blades in the tumble mixer helped to ensure good fibre distribution in the mixture. The aggregates, sand, and cement were added with water and mixed for three minutes. The polypropylene fibres were then evenly sprinkled over the surface, and mixing resumed for three minutes. Finally, superplaticizers were poured to the mix without pre-mixed with other admixtures.

6 non-reinforced beams (100 x 100 x 500mm), 48 cubes (6 x 6 x 6in), 10 cylinders (6 x 12in) and 12 reinforced beams (120 x 150 x 1000mm) were cast from each batch of mix. All specimens

were cast perpendicular to the testing direction were then removed from the molds and stored in air at room temperature after 24 hours until testing at 30 days of age.

PRESENTATION OF TEST RESULTS

TABLE 2
RESULTS OF CUBE, CYLINDER AND BEAM TESTS

Beams	Fibres content	Web steel	Concrete strength			First shear crack strength	Ultimate shear strength
			Compressive strength	Cylinder splitting tensile strength	Modulus of rupture		
	%		N/mm^2	N/mm^2	N/mm^2	N/mm^2	N/mm^2
Mix Type A							
N1	-	No	40.95	2.74	4.38*	1.47	1.51
NF1	0.8	No	46.79	3.02	4.28*	1.78	1.97
W1	-	Yes	40.95	2.74	4.38*	1.88	1.91
WF1	0.8	Yes	46.79	3.02	4.28*	1.97	2.60
Mix Type B							
N2	-	No	40.86	2.47	4.34†	1.54	1.66
NF2	0.8	No	45.79	2.98	3.86†	1.54	1.72
NF3	1.0	No	45.53	2.26	5.01†	1.60	1.75
NF4	1.2	N0	43.46	2.40	5.66†	1.91	2.02
W2	-	Yes	40.86	2.47	4.34†	2.40	2.58
WF2	0.8	Yes	45.79	2.98	3.86†	2.58	2.71
WF3	1.0	Yes	45.53	2.26	5.01†	2.58	2.71
WF4	1.2	Yes	43.46	2.40	5.66†	2.58	2.72

Compressive Strength

Nine cubes had no fibres and twenty-seven cubes had HPP fibres of varying amount (0.8%, 1.0%, 1.2%) were cast to make more effective comparison between plain concrete and fibrous concrete reinforced by HPP fibres. Three cubes were tested for each batch of mixes to obtained the average value. The compressive strength increase with the percentage of fibres but there is a drop in compressive strength as percentage of fibres is over 1%; however the figure shows that the compressive strength is still higher than that of plain concrete. This can be concluded that HPP fibres have increased the compressive strength of concrete. The results from the cube crushing tests are shown in Table 2.

Flexural Strength

The flexural strength for fibrous concrete that contained 0.8 per cent of HPP fibres is slightly lower than that plain concrete. This applied to flexural test for both Mix Type A and B. However the flexural strength is increased when 1.0 and 1.2 per cent of HPP fibres were added. The flexural strength increased to a maximum value of 30% for beam that contained 1.2 per cent of HPP fibres. The failure pattern of the samples highlighted the benefit of inclusion of fibres. The plain sample failed with a sudden brittle where as the fibrous samples failed in more ductile manner.

Cylinder Splitting Strength

The cylinder splitting strength is increased by 20% when 0.8 per cent of HPP fibres were added to the mix. But the splitting strength is decrease when more than 0.8 per cent of HPP fibres were added. The splitting strength for cylinder that contained 1.0 and 1.2 per cent of HPP fibres became close to the plain cylinder. This may be explained that 0.8 per cent of HPP fibres had increased the splitting strength to the maximum value of 20%. The failure pattern of the samples that were similar to the samples used in flexural beam tests again highlighted the properties of fibrous concrete. The test results can be seen in Table 2.

RELATIONSHIP BETWEEN COMPRESSIVE AND TENSILE STRENGTH

The compressive strength of concrete is its property commonly considered in structural design but for some purposes the tensile strength is of interest [6]. It is possible to form an empirical relationship between the compressive strength and the tensile strength of the concrete. The relationship however is not directly proportional because as the compressive strength increases the tensile strength increases at different rate. A number of ratios have been suggested but they are all subjected to variation by a number of factors. As the tensile strength is so small it is much more sensitive to variation in constituents and production. The amount of fine and coarse aggregate and the overall grading of the aggregate can also affect the ratio.

Eight cylinders and four beams of different fibre contents have been tested. The test results obtained from the flexure and cylinder splitting tension test suggest two empirical relationship between compressive and indirect tensile strength of the fibrous concrete as follows:

$$f_t = 0.21 * (f_{cu})^{2/3} * \left(\frac{1}{V_f}\right)^{0.45} \quad (1) \qquad f_f = 0.398 * (f_{cu})^{2/3} * V_f^{0.85} \quad (2)$$

where f_f = Flexure strength of fibrous concrete, N/mm^2
f_t = Cylinder splitting strength of fibrous concrete, N/mm^2
f_{cu} = Characteristic strength of fibrous concrete, N/mm^2
V_f = Percentage of fibres added into the mix, %

Figure 1: Relation between tensile strength and compressive strength and percentage of fibres

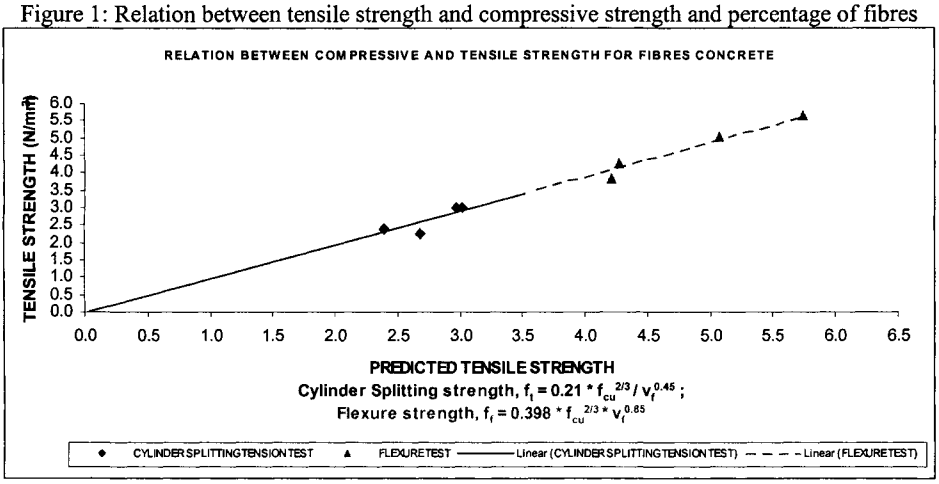


Figure 1 shows good straight-line correlation between the tensile strength obtained from both flexure and cylinder splitting tension test and the suggested equation stated above. The comparison between test results and predicted strength using equation (1) and (2) are shown in Table 3.

TABLE 3
COMPARISON OF TEST RESULTS FOR PREDICTED AND EXPERIMENTAL TENSILE STRENGTH

Specimen	Fibres percentage	Tensile strength	Predicted tensile strength	$\left(\frac{Experimental}{Predicted}\right)$ (Tensile strength)	
	%	N/mm^2	N/mm^2		
Mix Type A					
AC1 [C]	-	2.74	-	-	
AC2 [C]	0.8	3.02	3.01	1.00	
AF1 [F]	-	4.38	-	-	
AF2 [F]	0.8	4.28	4.27	1.00	
Mix Type B					
BC1 [C]	-	2.47	-	-	
BC2 [C]	0.8	2.98	2.97	1.00	
BC3 [C]	1.0	2.26	2.68	0.84	
BC4 [C]	1.2	2.40	2.39	1.00	
BF 3 [F]	-	4.34	-		
BF 4 [F]	0.8	3.86	4.21	0.92	
BF 5 [F]	1.0	5.01	5.07	0.99	
BF 6 [F]	1.2	5.66	5.74	0.99	
[C] Cylinder		Mean		0.96[C]	0.98[F]
[F] Flexure Beam		Standard Deviation		0.08[C]	0.04[F]

PREDICTION OF ULTIMATE SHEAR STRENGTH

As Ref. [9], the development of a general simple formula to predict the shear strength of fibres reinforced concrete beams is critical to the successful application of fibres as shear reinforcement in practice. However, from the test results reported here, it appears that the splitting tensile and the flexural strength are the important material parameters that reflect the ultimate shear strength.

From the previous report [9], parameters that influence the ultimate shear strength other than flexure and splitting strength are the shear span-effective depth ratio and the reinforcement ratio. It is not possible to include the effect of beam size in this formula because all tests were on a single beam size. However, computational studies seem to indicate similar shear strength predicted when beams of different size scale were entered. But, ultimate shear strength reduces with the beam size particularly the beam depth; that is, larger beams are proportionately weaker than smaller beam [8]. If so, an additional factor indicating dependence on effective depth of the beam must be included. Thus, the shear strength of a fibre reinforced concrete beam are expressed as:

$$f_v = (0.368) * (f_f * f_t)^{5/6} * \left(\frac{1000 * A_s}{b_v * a_v * d^{0.6}} \right)^{1/3} \qquad (3)$$

where f_v = Predicted ultimate shear strength of fibre reinforced concrete beam;
f_f = Flexure strength of fibrous concrete, N/mm^2;
f_t = Cylinder splitting tensile strength, N/mm^2;
A_s = Area of tension steel provided, mm^2;
b_v = Width of the beam, mm;

a_v = Shear span, mm;

As proposed by Sharma [10], the ultimate shear strength of a fibres reinforced concrete beam with web reinforcement can be expressed as

$$v_{nf} = f_v + f_s \tag{4}$$

where v_{nf} = Nominal shear strength of fibres reinforced concrete section in combined bending and shear, N/mm^2;

f_v = Ultimate shear strength of the fibrous concrete, N/mm^2;

f_s = Shear strength due to web reinforcement, N/mm^2.

Shear strength due to web reinforcement f_s can be evaluated by using equation (5) as proposed in BS 8110 [11],

$$f_s = \left(\frac{0.95 * f_{yv}}{b_v}\right) * \left(\frac{A_{sv}}{S_v}\right) \tag{5}$$

where f_{yv} = Characteristic strength of links

b_v = Breadth of the section, mm;

A_{sv} = Total cross-section of links at the neutral axis, at a section, mm^2;

S_v = Spacing of links along the member, mm.

Figure 2 shows good straight-line correlation between the ultimate shear strength and the predicted ultimate shear strength through the origin. To show that equation (3) give a reasonable estimate of the ultimate shear strength of fibres reinforced concrete beams, results from this investigation are compared in Table 4. All the beams with fibres reinforcement are used in the correlation. The ratio of experimental to predicted shear strength is calculated. There is a definite trend, as shown in Table 4, that fibres reinforcement in beams increase the ultimate shear strength of beams

Figure 2: Relationship between ultimate shear strength and material and geometrical properties. (Unit for horizontal axis are in $N^{5/3} / mm^{2/3}$)

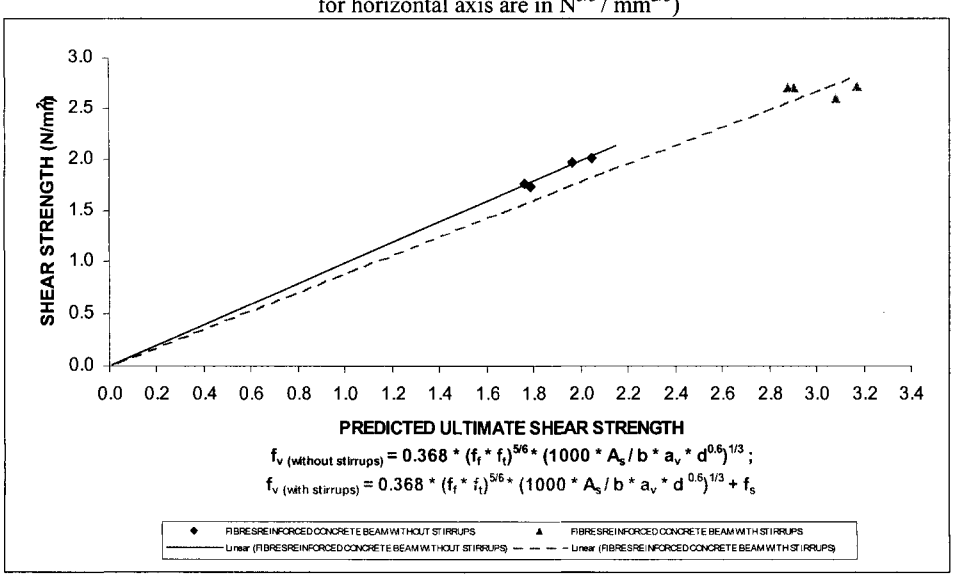


TABLE 4
COMPARISON OF TEST RESULTS OF BEAMS FAILING IN SHEAR

Beam No.	$\left(\frac{a}{d}\right)$	Fibre content	Ultimate shear strength (USS)		Percentage increase of USS	Predicted USS	$\left(\frac{Experimental}{Predicted}\right)$ (USS)
			With fibres	Without fibres			
		%	N/mm^2	N/mm^2	%	N/mm^2	
Mix Type A							
N1	2.57	-		1.51	-		
NF1	2.57	0.8	1.97		30.5	1.96	1.00
W1	2.57	-		1.91	-		
WF1	2.57	0.8	2.60		36.1	3.08	0.84
Mix Type B							
N2	2.57	-		1.66	-		
NF2	2.57	0.8	1.72		3.6	1.78	0.97
NF3	2.57	1.0	1.75		6.0	1.76	1.00
NF4	2.57	1.2	2.02		21.7	2.05	0.98
W2	2.57	-		2.58	-		
WF2	2.57	0.8	2.71		13.0	2.90	0.93
WF3	2.57	1.0	2.71		13.0	2.88	0.94
WF4	2.57	1.2	2.72		14.0	3.17	0.86
					Mean		0.94
					Standard Deviation		0.06

CONCLUSIONS

From the experimental observations reported in this paper, the following conclusions can be drawn:

1) Polypropylene fibres (S-152) are effectively in increasing the compressive, tensile, and shear capacity of concrete.
2) Flexural strength increased with fibre percentage, as there was a 30 per cent increase in tensile strength for the 1.2 per cent fibres beam while the splitting tension test has a 20 per cent increase in tensile strength with the 0.8 per cent HPP fibres cylinder but decrease in tensile strength was observed with the 1.0 and 1.2 per cent fibres cylinder. The increase in splitting strength with fibre percentage however was less well defined. Anyway, the failure pattern of the all the samples highlighted the benefit of the inclusion of HPP fibres. The plain sample failed with a sudden brittle failure where as the fibrous samples failed in more ductile manner. This shows that HPP fibres can reduce crack widths and prevent brittle failure of concrete. The results from both tests were used to generate empirical formulae, relating the compressive and tensile strengths of the fibrous concrete.
3) However, HPP fibres have significantly increased the ultimate shear strength of reinforced concrete beam. As reported by Sharma [11], for a practical solution, tests have shown that a combination of minimum links and HPP fibre forms an effective system of shear reinforcement in a structural member. With these combinations, HPP fibres have changed the failure mode of the specimen beams from shear to flexure failure. Fibres reinforced concrete beams have more ductility and significant amount of energy absorption than normally reinforced concrete beams. The presences of polypropylene fibres (S-152) in concrete restrict propagation of cracks and allow more uniform cracking. Reasonable estimation shear strength of HPP fibres reinforced concrete beams can be made by using the semi empirical equation derived.

References

(1) J. J. Beaudoin, "Fibre-Reinforced Concrete", *Canadian Building Digest*, CBD-223, originally published April 1982.

(2) Ir. Trevory Gregory, One-Day Seminar on Fibre Reinforced Concrete, Concrete and Steel Structures Into the 21st Century, 5th May 1995.

(3) Goldfein, S., "Fibrous Reinforcement for Portland Cement", Modern Plastics, 1965, 156-159 (April).

(4) D. J. Hannant, "Fibre Cements and Fibre Concretes", John Wiley & Sons.

(5) Synthetic Industries, Fibre Reinforced Concrete Division, Copyright 1999.

(6) A. M. Neville, "Properties of Concrete", Fourth edition, Longman.

(7) P. J. F. Wright, " Comments on an Indirect Tensile Test on Concrete Cylinders ", Magazine of Concrete Research (London), V.7, No. 20, July 1955, pp. 87-96.

(8) Kong & Evans, "Reinforced and Prestressed Concrete", Third edition.

(9) Victor C. Li, Robert Ward, and Ali M. Hamza, "Steel and Synthetic Fibers as Shear Reinforcement" *ACI Structural Journal* / September – October 1992, 89-M54, pg. 499-508.

(10) A. K. Sharma, "Shear Strength of Steel Fiber Reinforced Concrete Beams", *ACI Structural Journal* / July – August 1986, 83-56, pg. 624-628.

(11) British Standards Institution, BS 8110-1:1997:Concrete Design, Section 2 & 3, Code of Practice for Design and Construction.

Advances in Building Technology, Volume 1
M. Anson, J.M. Ko and E.S.S. Lam (Eds.)
© 2002 Elsevier Science Ltd. All rights reserved

STUDY ON PHOSPHOGYPSUM FLY ASH LIME SOLIDIFIED MATERIAL

Zhou Mingkai[1] Shen Weiguo[1] Wu Shaopeng[1,2] Zhao Qinglin[1]

1. Key Laboratory for Silicate Materials Science and Engineering Ministry of Education, Wuhan University of Technology, Wuhan 430070,
2. College of Transportation, Southeast University, Nanjing 210096

ABSTRACT

A new type of solidified material mainly composed of phosphogypsum, fly ash and lime was prepared in this study. Its mix proportions were optimized. The test results suggested that the ratio of phosphogypsum and fly ash at 1 : 1 and the content of the lime solidified material 6~8% was the optimum mix proportion. This kind of solidified material could be used as road base course material when its compacting ratio is 93~96%. It could also be used as sub-base material when its compacting ratio is around 93%. Crushed stone stabilized with it could be used as road base material. The microstructure of this kind of materials was observed with SEM and the mechanism of strength formation is discussed.

KEYWORDS: Phosphogypsum, Fly ash, Solidified material, Road base

1. INTRODUCTION

Recycling of solid waste is significant to sustainable development. Phosphogypsum and fly ash are the vital solid waste sources in China. Large amounts of them are left without treatment. The lime-fly ash road base material has been widely used in China. But its early age strength was very low [1,2], and this limited its extensive usage. The development of a new type of solidified material is described in this study. The solidified material is mainly composed of phosphogypsum, fly ash and lime. Its strength at early age was much higher than that of the ordinary lime-fly ash road base materials. It can be used as road base material and sub-base material. It can also be used as road base filling material. When stabilized with crushed rock it can be used as road base material.

2 MATERIALS AND TEST METHODS

2.1 MATERIALS

Phosphogypsum was obtained from Xianfan Liming Chemistry Ltd and the fly-ash from Xiangfan lignite power station. The stabilizer was made of lime and 10% of additive. The crushed rock was obtained from Xianshan stone plant, Xangfan, Hubei province.

TABLE 1:CHEMICAL AND MINERALOGICAL COMPOSITIONS OF THE RAW MATERIALS (w%)

materials	chemical composition								
	SiO_2	Fe_2O_3	Al_2O_3	CaO	MgO	TiO_2	SO_3	P_2O_5	IL
PG	3.62	0.05	0.08	31.57	0.17	0.06	42.48	1.05	19.88
FA	6.20	5.98	6.70	8.50	1.80	0.49	—	—	3.50
ST	1.42	0.13	0.38	87.79	1.64	1.80	4.05	—	4.05

Notes: PG-phosphogypsum; FA-fly ash; ST-stabilizer

2.2 TEST METHODS

Tamping test of phosphogypsum-fly ash-lime solidified material was carried out conforming to the specifications of test method T0804-94, which was published by the Ministry of Communication of China. The unconfined compressive strength was carried out conforming to test method T0804-94. The phosphogypsum-fly ash-lime solidified material was shaped within a $\Phi 5.0\times5.0cm^3$ mould while the phosphogypsum-fly ash-lime solidified material stabilized crushed rock was shaped within a $\Phi 10\times10cm^3$ mould.

3 RESULT AND DISCUSSION

The effect of the composition of phosphogypsum-fly ash-lime solidified material on the dry density and strength of the solidified material was studied. And the suitable mixture proportions of phosphogypsum-fly ash-Lime solidified material were optimized by means of the 7 days strength. By providing silica and calcium oxide respectively, fly ash and lime also play an important role in the solidified material. In this paper it described how the crushed rock stabilized with phosphogypsum-fly ash-lime solidified material was prepared as road base material.

3.1 THE PROPORTION OF THE PHOSPHOGYPSUM-FLY ASH-LIME SOLIDIFIED MATERIAL

In this test the effect of mix proportions and the influence of stabilizer on the strength of phosphogypsum-fly ash-lime solidified material was studied. The content of stabilizer varied from 4:96 to 10:90. The testing cylinder was made with compactness ratio of 96%. The phosphogypsum-fly ash-lime solidified material was stabilized with ashed lime stabilizer, slaked lime on quick lime. The strength and maximum dry density of phosphogypsum-fly ash-lime solidified material with different proportions are listed in table 2.

TABLE 2: MIX PROPORTION TEST OF PG-FA-QL SOLIDIFIED MATERIAL

No	ST : PG : FA	γ_{dm}(g/cm^3)	W_{pt}(%)	R_{7d}(MPa)
1-1	8 : 20 : 72	1.401	18.34	2.56
1-2	8 : 30 : 62	1.446	17.62	2.76
1-3	8 : 40 : 52	1.464	16.35	3.13
1-4	8 : 50 : 42	1.487	16.21	3.24
1-5	8 : 60 : 32	1.491	16.21	3.19
1-6	8 : 70 : 22	1.498	15.76	3.10
1-7	8 : 80 : 12	1.493	14.91	3.04
1-8	4 : 50 : 46	1.487	16.21	2.01
1-9	6 : 50 : 44	1.487	16.21	2.76
1-10	10 : 50 : 40	1.487	16.21	2.65
*1-11	8 : 0 : 92	1.312	19.30	0.90

Notes: ST-stabilizer; *: ST is slaked lime; +: ST is quicklime; γ_{dm}-Maximum dry density Notes; W_{pt}-Optimum water content; R_{7d} is compressive strength

Table 2 show that the maximum dry density of the phosphogypsum-fly ash-lime solidified material increased with the increase of the phosphogypsum content since the phosphogypsum has a density higher than that of the fly ash. When the ratio of fly ash and phosphogypsum was about 1:1, the phosphogypsum-fly ash-lime solidified material had the highest strength. When the stabilizer content of phosphogypsum-fly ash-lime solidified material was about 6% the solidified material obtained the highest strength. From the results we can preliminarily concluded that the suitable proportion is the ratio of fly ash and phosphogypsum of about 1:1 and the stabilizer content about 8~9%.

3.2 COMPACTNESS RATIO OF THE PHOSPHOGYPSUM-FLY ASH-LIME SOLIDIFIED MATERIAL

The phosphogypsum-fly ash-lime solidified material is a material with high porosity. The porosity was dependent on the forming pressure and compacting work while the products (specimens) were made. Porosity can govern the properties of the materials, especially affecting material strength. High porosity will result in low material strength, whereas decreasing porosity can enhance material strength. The cylindrical specimens of this study were compacted to the compactness ratio of 93% and 96%. The strengths at 7 and 28 days are listed in table 3.

TABLE 3: PG-FA-QL SOLIDIED MATERIAL'S COMPRESSIVE STRENGTH AT DIFFERDNT COMPACTION RATIO

No	ST : PG : FA	93% compaction ratio	96% compaction ratio
		R_{7d}/R_{28d}(Mpa)	R_{7d}/R_{28d}(MPa)
2-1	8 : 30 : 62	1.57/2.21	2.76/3.75
2-2	8 : 40 : 52	1.89/2.34	3.13/4.97
2-3	8 : 50 : 42	2.04/2.85	3.24/4.86
2-4	8 : 60 : 32	1.97/2.67	3.19/4.51

Table 3 shows that the strength of the phosphogypsum-fly ash-lime solidified material with the compactness ratio of 96% had a much higher strength than that with the compactness ratio of 93%. This strength is satisfactory when the material is used as road base material or sub-base material. If the compactness ratio of the phosphogypsum-fly ash-lime solidified material is below 93%, it can only be used as road base filling material.

3.3 PHOSPHOGYPSUM-FLY ASH-LIME SOLIDIFIED MATERIAL STABILIZED CRUSHED ROCK

The base course material of high grade road must have a great deal of aggregate as framework. we use the phosphogypsum-fly ash-lime solidified material to stabilize crushed rock. The compactness ratio was 98%. The test result of the strength is listed in table 4.

TABLE 4: COMPRESSIVE STRENGTH OF CRUSHED ROCK STABILIZED BY ST-PG-FA MATERIAL AND LIME FLY ASH

No	Mix proportion ST : FA : PG : CS	γ_{md}/(g/cm^3)	W_{pt}/ (%)	R_{7d}/ (MPa)	Cv/ (%)
3-1*	5 : 30 : 65	1.880	9.90	0.823	5.81
3-2+	5 : 30 : 65	1.885	9.90	0.995	3.88
3-3	5 : 30 : 65	1.885	9.90	1.100	7.82
3-4	5 : 10 : 20 : 65	1.887	9.50	1.200	5.38
3-5	5 : 15 : 15 : 65	1.890	9.40	1.480	8.84
3-6	5 : 20 : 10 : 65	1.891	9.30	1.680	6.85

Notes: ST-stabilizer; *: ST is slaked lime; +: ST is quicklime;
γ_{dm}-Maximum dry density Notes; W_{pt}-Optimum water content

The strength of the phosphogypsum-fly ash-lime solidified material stabilized crushed rock was about 40~100% higher than that of the lime-fly ash stabilized crushed rock. The strength of this material is about the range of the standard of "Lime-Fly ash Solidified Materials" of Ministry of Communication of China. Hence, it can be used as road base material for various grades of highway.

3.4 THE MECHANISM OF STENGTH FORMATION

When the lime was added into fly ash, the pozzolana reaction took place. The reaction can be qualitatively described as fellow [3].

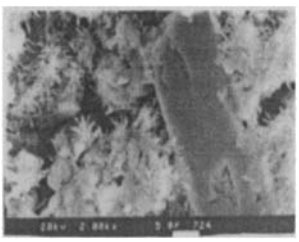
$$xCa(OH)_2+SiO_2+nH_2O \rightarrow xCaO\cdot SiO_2\cdot (n+x)H_2O$$

$$yCa(OH)_2+Al_2O_3+nH_2O \rightarrow yCaO\cdot Al_2O_3\cdot (n+y)H_2O$$

When there is plenty of phosphogypsum ($Ca_2SO_4.2H_2O$), the product $yCaO\cdot Al_2O_3\cdot (n+y)H_2O$ was substituted by AFt. The phosphogypsum hastened the pozzolana reaction also. So the strength of the phosphogypsum-fly ash-lime solidified material is much higher than that of the lime-fly ash road base material[4].

$$3Ca(OH)_2+Al_2O_3+3CaSO_4\cdot 2H_2O+26H_2O\rightarrow 3CaO\cdot Al_2O_3\cdot 3CaSO_4\cdot 32H_2O$$

The SEM images of the phosphogypsum-fly ash-lime solidified material show the microstructure of material and the crystal of phosphogypsum.



a. MICROSTRUCTURE OF MATERIAL



b. FLAKY CRYSTAL OF PHOSPHOGYPSUM

Fig 1: SEM PICTUREOF 28d PG-FA-QL BINDER

The phosphogypsum-fly ash-lime solidified material is a material with a large number of pores. The morphology of the phosphogypsum is flake-like crystal[1] while AFt is needle-like crystal[5], according to the SEM images. The fractional force between phosphogypsum grains is larger than that between fly ash grains. This also contributed to the strength formation also.

4 SUMMARY AND CONCLUSIONS

A suitable proportion for the phosphogypsum-fly ash-lime solidified material was a ratio of fly ash to phosphogypsum at 1:1 and a stabilizer content was about 8~9%.

The strength of the phosphogypsum-Fly Ash-Lime Solidified Material with a compactness ratio of 96% had a much higher strength than that with a compactness ratio of 93%. A 96% one can be used as road base material or sub-base material. Materials with a compactness ratio of 93% and below can only be used as road base filling material.

The strength of the phosphogypsum-fly ash-lime solidified material stabilized crushed rock was about 40~100% higher than that of lime-fly ash stabilized crushed rock. This strength reached the required range of lime-fly ash solidified materials of the standard of the Ministry Communication of China. Hence, it can be used as road base material for various grades of highway.

When there is sufficient plenty phosphogypsum($Ca_2SO_4.2H_2O$), the product of $yCaO\cdot Al_2O_3\cdot (n+y)H_2O$ was substituted by AFt. The phosphogypsum hastens the pozzolanic reaction also. So the strength of the phosphogypsum-fly ash-lime solidified material was much higher than the lime fly-ash road base material. The fractional force between phosphogypsum grains is also larger than that between the fly ash grains. This also contributed to the strength formation.

References

[1]Hou Changjun, Huo Danqun, ect. Performance and application of **Phosphogypsum** [J]. Chemistry industry and mine technology, 1997, 26 (2): 50-52

[1] Fu Buojie, Chen Liding, Yu Xiubo, ect. The new trait and countermesure of china environment[J]. Environment Science, 2000, 21 (5): 104-106

[2] Caijun Shi, Robert L. Day, etc. Chemical activation of Blended cement made with lime and natural pozzolans[J]. Cement and Concrete Research, 1993, 23(6):1389-1395

[3]Weiping Ma, Paul W. Brown, etc. Hydrothermal Reactions of fly ash with $Ca(OH)_2$ and $CaSO_4$ $2H_2O$[J]. Cement and Concrete Research, 1997, 27(8):1237-1248

[4]P. K. Mehta. Scanning elector micrographic studies of effringife formation[J]. Cement and Concrete Research, 1976, 6(2):169-181

CONSTRUCTION TECHNOLOGIES:

MONITORING TECHNOLOGIES, DAMAGE DETECTION AND VIBRATION CONTROL

This Page Intentionally Left Blank

Advances in Building Technology, Volume 2
M. Anson, J.M. Ko and E.S.S. Lam (Eds.)
© 2002 Elsevier Science Ltd. All rights reserved

ON THE LOCAL OPTIMAL CONTROL COUNTERFORCES IN ACTIVE CONTROLLED STRUCTURES

N.D. Anh[1], L.D.Viet[2]

[1] Institute of Mechanics, 264 Doi can, Hanoi, Vietnam
[2] Hanoi National University, 334 Nguyen Trai, Hanoi, Vietnam

ABSTRACT

The paper presents a so called local feedback-feedforward control law to find local optimal magnitude and location of control counterforces to reduce undesired vibrations in active controlled structures. Using information on state response and a part of external excitations, the counterforces are applied to structures in such a way to minimize the local performance index. Numerical simulations are carried out for a two-degree-of-freedom structural system. The comparison between performance indexes shows the effectiveness of local feedback-feedforward control to the classical linear quadratic regulator control.

KEYWORD: *Structural Control, Local Optimal Feedback-Feedforward Control, Local Optimal Location of Counterforces.*

1. INTRODUCTION

In recent years much progress and new concepts have been achieved in the development of structural control in reducing the response during excessive vibrations due to environmental disturbances, see, for example, [5-8, 11,12]. Since the objective is to reduce the structural response due to external disturbances, one may expect that the control problem would be more simplified if both structural response variables and external disturbances could be measured during structural motion. But, in many practical situations, one is unable to measure the external excitation while the structural response can often be measured. Many new and interesting control strategies and concepts have been proposed to overcome this difficulty, see, for example, [1-4, 9-10, 13]. The control of structure motions can be done by various means. Among them active control [14] is one of promise aspects which uses the control counterforces produced by actuators to balance or reduce the energy of the environmental loading. There are some basic problems in the active control such as control law, magnitude and location of the control counterforces. The latter problem is investigated in the paper. Some components of the external excitation are assumed to be known. The problem identifying external excitations will be investigated latter by using identification algorithm [1]. Using information on state response and a part of external excitations, the counterforces are applied to structures in such a way to minimize the so called local performance

index. Numerical simulations are carried out for a two-degree-of-freedom structural system and show the effectiveness of local feedback-feedforward control to the classical linear quadratic regulator control.

2. GLOBAL OPTIMAL FEEDBACK-FEEDFORWARD CONTROL

Suppose that the controlled structure is modeled by a multi-degree-of-freedom system, whose state equation is described in the form

$$\begin{cases} \dot{z}(t) = Az(t) + Bu(t) + Hf(t), \\ z(0) = z_0, \end{cases} \tag{1}$$

where $z(t) = [x(t) \quad \dot{x}(t)]^T$ is the 2n-dimensional state vector, the superscript ^{T} indicates vector or matrix transpose, A is the 2n × 2n system matrix, u(t) is the m-dimensional control force vector, f(t) is an r-vector representing external excitation, B and H are 2n × m and 2n × r location matrices specifying the locations of controllers and external excitations in the state-space, respectively. The control force u(t) is to be chosen in such a way that a global performance index J, defined as

$$J = \int_0^{t_f} [z^T(t)Qz(t) + u^T(t)Ru(t)]dt, \tag{2}$$

is minimized. In the above, the time interval $[0,t_f]$ is defined to be longer than that of the external excitation, Q and R are weighting matrices, Q is a 2n×2n positive semi-definite matrix and R is a mxm positive definite matrix. Their magnitude depends on the relative importance attached to the state variables and to the control forces in the minimization procedure. The global feedback-feedforward control law is taken as [11]

$$u(t) = G_z z(t) - R^{-1}B^T p(t) \tag{3}$$

where G_z is determined as

$$G_z = -R^{-1}B^T P \tag{4}$$

P is a solution of the Riccati equation

$$PA - PBR^{-1}B^T P + A^T P + Q = 0 \tag{5}$$

and p(t) is determined from the differential equation

$$\begin{cases} \dot{p}(t) - (PBR^{-1}B^T - A^T)p(t) + PHf(t) = 0, \\ p(t_f) = 0 \end{cases} \tag{6}$$

It is seen from (3), (6) that the control law requires the full knowledge of state response and the excitation force. Thus, the control is called as global FB-FW control.

3. LOCAL OPTIMAL FEEDBACK-FEEDFORWARD CONTROL

The full knowledge of state response and excitation force required in global FB-FW control may be unrealized in practical application to large structures. For that purpose consider so called local FB-FW control problems in each of which a local optimal control force is to be determined for one excitation force component, $f_i(t)$. Denote

$$u(t) = \sum_{j=0}^{r} u^j(t), \tag{7}$$

$$z(t) = \sum_{j=0}^{r} z^j(t), \tag{8}$$

where z^0 and z^i, i=1,2,..,r, are 2n-dimensional vectors, which satisfy the differential equations, respectively,

$$\begin{cases} \dot{z}^0(t) = Az^0(t) + Bu^0(t), \\ z^0(0) = z_0, \end{cases} \tag{9}$$

$$\begin{cases} \dot{z}^i(t) = Az^i(t) + Bu^i(t) + H_i f_i(t), \\ z^i(0) = 0 \end{cases} \tag{10}$$

where H_i is the ith column vector of matrix H. The local optimal control forces $u^j(t)$, j =0,1,..r, are chosen to minimize the local performance indexes

$$J_j = \int_0^{t_f} [z^{jT}(t)Qz^j(t) + u^{jT}(t)Ru^j(t)]dt. \tag{11}$$

Thus, the local optimal control forces are determined as

$$u^0(t) = G_z z^0(t) \tag{12}$$

$$u^i(t) = G_z z^i(t) + G_i f_i(t) \qquad (i=1,2..r) \tag{13}$$

where G_z is found from (4), G_i are column vectors which will be determined latter. Substituting (13) into (10) yields

$$z^i(t) = \int_0^t exp[(A + BG_z)(t-s)](BG_i + H_i) f_i(s)ds. \tag{14}$$

Denote

$$T_i(t) = \int_0^t exp[(A + BG_z)(t-s)]Bf_i(s)ds, \tag{15}$$

$$V_i(t) = \int_0^t exp[(A + BG_z)(t-s)]H_i f_i(s)ds. \tag{16}$$

Thus, one gets

$$z^i(t) = T_i(t)\, G_i + V_i(t). \tag{17}$$

Substituting (17) into (13) yields

$$u^i(t) = [G_z\, T_i(t) + If_i(t)]G_i + G_z V_i(t) \tag{18}$$

where I denote the m × m identity matrix. Substituting (17) and (18) into (11) gives

$$\begin{aligned} J_i = & \int_0^{t_f} (G_i^T T_i^T + V_i^T) Q (T_i G_i + V_i)\, dt + \\ & \int_0^{t_f} [G_i^T (G_z T_i + If_i)^T + (G_z V_i)^T] R [(G_z T_i + If_i) G_i + G_z V_i]\, dt \end{aligned} \tag{19}$$

The necessary condition for minimum of J_i is

$$\frac{\partial J_i}{\partial G_i} = 0 \tag{20}$$

or,

$$2\int_0^{t_f} \{(G_i^T T_i^T + V_i^T) Q T_i + [G_i^T (G_z T_i + If_i)^T + (G_z V_i)^T] R (G_z T_i + If_i)\} dt = 0 \tag{21}$$

Denote:

$$S_i = \int_0^{t_f} [T_i^T Q T_i + (G_z T_i + If_i)^T R (G_z T_i + If_i)]\, dt \tag{22}$$

$$W_i = \int_0^{t_f} [V_i^T Q T_i + (G_z V_i)^T R (G_z T_i + If_i)]\, dt \tag{23}$$

Using (21)-(23), one has

$$G_i = -((S_i)^{-1})^T W_i^T \tag{24}$$

Thus, the local optimal feedback-feedforward control law is determined as (4), (7), (12), (13), (15), (16), (22)-(24) with the corresponding performance index

$$J_L = \int_0^{t_f} [(\sum_{j=0}^{r} z^{j^T}(t)) Q (\sum_{j=0}^{r} z^j(t)) + \sum_{j=0}^{r} (u^{j^T}(t)) R (\sum_{j=0}^{r} u^j(t))]\, dt. \tag{25}$$

The effectiveness of the local optimal feedback-feedforward control proposed above will be illustrated in the next section.

4. NUMERICAL SIMULATION

Consider a model in Fig.1 taken from Soong [11]

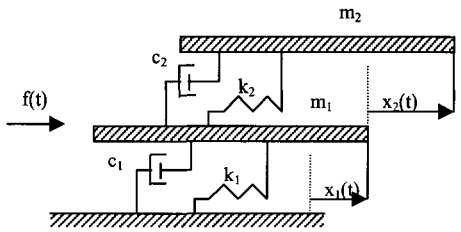


Fig.1. Two-degree-of-freedom structural system

The state equation of uncontrolled two-story structural system has the form

$$\dot{z}(t) = Az(t) + Hf(t)$$

where

$$z(t) = \begin{bmatrix} x_1(t) \\ x_2(t) \\ x_3(t) \\ x_4(t) \end{bmatrix}, A = \begin{bmatrix} 0 & 0 & 1 & 0 \\ 0 & 0 & 0 & 1 \\ -0.5 & 0.25 & -0.02 & 0.01 \\ 0.25 & -0.25 & 0.01 & -0.01 \end{bmatrix}, H = \begin{bmatrix} 0 & 0 \\ 0 & 0 \\ 1 & 0 \\ 0 & 1 \end{bmatrix}$$

$x_1(t)$ is the relative displacement of the first floor with respect to foundation and $x_2(t)$ is the relative displacement of the second floor with respect to first floor. A wind-type excitation is expressed by

$$f(t) = \begin{bmatrix} 10 \\ 3 \end{bmatrix} \sin \omega t + \begin{bmatrix} 1 \\ 5 \end{bmatrix} \sin 2\omega t + \begin{bmatrix} 1 \\ 7 \end{bmatrix} \sin 3\omega t + \begin{bmatrix} 1 \\ 4 \end{bmatrix} \sin 4\omega t$$

where ω = 0.309. This value of ω is close to the first frequency of the structure. The first component of the external excitation is assumed to be known. The time duration of action of the external excitation is T=[0,50]. The control to be applied to the structure is assumed to be of the form Bu(t), where u(t) is a scalar. Two cases are considered:
Case A: B^T=[0,0,1,0], control applied at first floor only
Case B: B^T=[0,0,0,1], control applied at second floor only
The weighting matrices are chosen as:

$$Q = \begin{bmatrix} 1 & 0 & 0 & 0 \\ 0 & 1 & 0 & 0 \\ 0 & 0 & 0 & 0 \\ 0 & 0 & 0 & 0 \end{bmatrix}, R = 100$$

Three methods are used to control:
- LQR control
- Local Feedback-feedforward control (LFB-FF)
- Global Feedback-feedforward control (GFB-FF)

In case A and B, counterforces are scalars. Because only the first component of the external excitation is known, so the values of matrix G_z and column vector G_1 are:

$$Case\,A: \quad G_z = [-0.0316 \quad -0.0057 \quad -0.2404 \quad -0.2143], G_1 = [-0.6578]$$

$$Case\,B: \quad G_z = [0.0044 \quad -0.0449 \quad -0.0920 \quad -0.2929], G_1 = [-0.5519]$$

The histories of relative displacements are shown from Fig.2 to Fig.4. The maxima of relative displacements and counterforces, the performance indexes J are compared in Table 1.

TABLE 1
MAXIMUM RESPONSE AND MAXIMUM COUNTERFORCE

		Counterforce	1st floor displacement	2nd floor displacement	Performance index ($\times 10^5$)
Uncontrolled			332.07	515.58	34
Case A	LQR	16.19	96.64	134.53	8.132
	LFB-FF	15.74	66.97	85.97	6.39
	GFB-FF	15.8	40.12	58.86	5.156
Case B	LQR	13.25	83.17	91.69	4.436
	LFB-FF	13.03	58.98	51.48	3.132
	GFB-FF	9.42	46.51	39.52	2.375

From Table 1, in comparison between performance indexes, one can see that local FB-FF control proposed is more efficient than LQR control. We also note that, because equation (6) is solved backwards from the terminal time t_f then control force of global FB-FF control is not equal zero at initial time. So, although global FB-FF control has the least performance index but it is infeasible in many structural control situations. Besides, in comparison between case A and case B, the counterforce in case A is larger than in case B but the displacements in case A are larger than case B. So, it is more efficient to place the controller on the second floor than on the first. It is noted that when f(t)=0, the solution of local feedback-feedforward control will return the solution of LQR control. So, LFB-FF control is more general than LQR control.

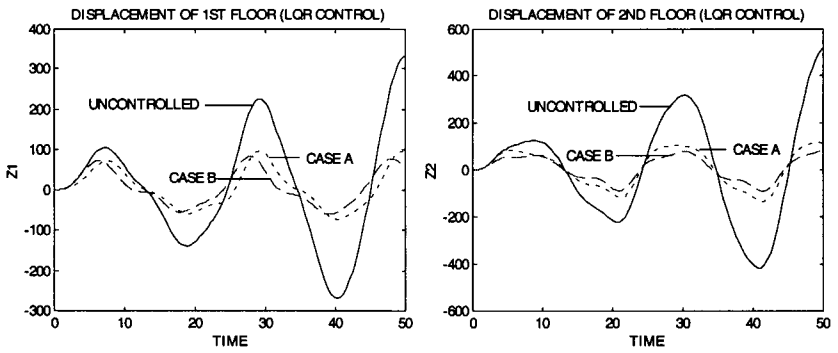


Fig.2. Displacements (LQR control)

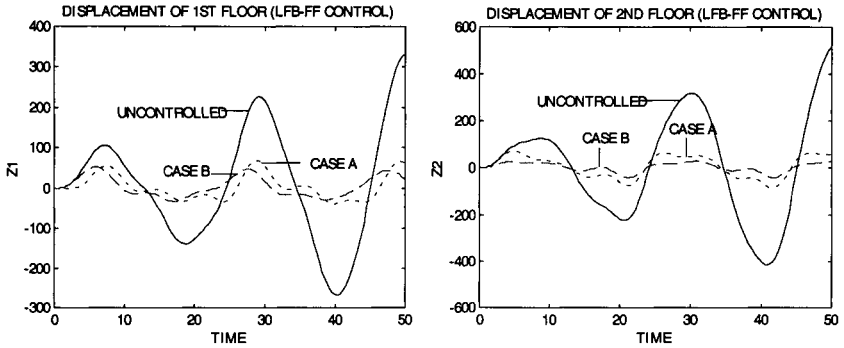


Fig.3. Displacements (local feedback-feedforward control)

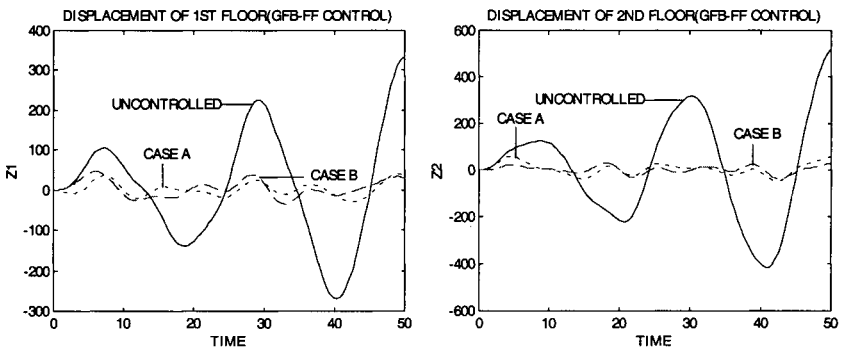


Fig.4. Displacements (global feedback-feedforward control)

5. CONCLUSION

In recent years, active control is one of the promising aspects which uses the control counterforces produced by actuators to balance or reduce the energy of the environmental loading. There are some basic problems in the active control such as control law, magnitude and location of the control counterforces. This paper use local feedback-feedforward control to find local optimal magnitude and location of counterforces. The comparison between local FB-FF control and LQR control shows the good effect of local FB-FF control. The results look promising and encourage further extending. The combination of the LFB-FF control proposed with the identification algorithm (Anh [1]) will be applied in the future to the case where the external forces are unknown.

REFERENCE

[1]. Anh N.D. (2000), An identification algorithm for feedback active control, *Proc. of 3rd International Workshop on Structural Control, Champ-Sur-Marne, July* 6-8, Eds. F Casciati and A. Martelli, p 27-38.

[2]. Casciati F., Faravelli L. and Yao T. (1996), "Control of Nonlinear Structures Using the Fuzzy Control Approach", *Nonlinear Dynamics,* vol.11, 171–187.

[3]. Del Grosso A., Zucchini A. (1995), Bounded state active control of structures: a set- theoretic approach, *Smart Material and Structures*, Vol 4, A15-A24.

[4]. Faravelli L., Venini P. (1994), Active structural control by neural networks, *J. of Structural Control*, vol. 1, N 1-2, 79-102.
[5]. Fujino. Y, Soong T.T. and Spencer B.F. (1996), "Structural Control: Basic Concepts and Applications," *Proc. ASCE Structures Congress XIV*, Chicago, Illinois, 1277–1287.
[6]. Housner G. W., Bergman L. A., Caughey T.K., Chassiakos A. G., Claus R. O., Masri S. F., Skelton R. E., Soong T. T., Spencer B. F., and Yao J. T. P. (1997), Structural Control: Past, Present and Future, *ASCE, J. Engrg. Mech.*, 123(9), 897-958.
[7]. Ko J. M., Chen Y., Zheng G., Ni Y. Q. (2000) Experimental study of vibration mitigation of a stayed-cable using non-linear hysteretic dampers, *Proc. of Int. Conf. on Advances in Structural Dynamics, Eds. J. M. Ko and Y. L. Xu,* Elsevier Science Ltd, Oxford, UK, vol.2, 1325-1332.
[8]. Kobori T., (1998), "Mission and perspective towards future structural control research", *Proc. of 2nd World Conf. in Struct. Control*, vol.1, Kyoto, Japan, 25-34.
[9]. Lee S. K., Kozin F. (1986), Bounded state control of structures with uncertain parameter, *ASCE, Dynamic Response of Structures*, 788-794.
[10]. Rodellar J., Barbat A. H., Martin-Sanchez D. K. (1986), Predictive control of structures, *ASCE, J. Engrg. Mech.*, 113, 797-817.
[11]. Soong T. T. (1990), *Active Structural Control: Theory and Practice*, John Wiley and Sons, Inc., New York.
[12]. Spencer B.F. and Sain M.K. (1997), "Controlling buildings: A new frontier in feedback", *IEEE Control Systems Magazine: Special Issue on Emerging Technologies*, 17(6), 19-35.
[13]. Spencer B.F., Sain M. K., Won C. H., Kaspari D.C., Jr. and Sain P. M. (1994), "Reliability-Based Measures Of Structural Control Robustness," *Struct. Safety*, vol. 15, 111–129.
[14]. Yao, J.T.P. (1972), "Concept of Structural Control," *ASCE J. Struct. Div.*, vol.. 98, 1567–1574.

Advances in Building Technology, Volume 2
M. Anson, J.M. Ko and E.S.S. Lam (Eds.)
© 2002 Elsevier Science Ltd. All rights reserved

VIBRATION CONTROL ELEMENTS WITH ADVANCED CEMENTITIOUS COMPOSITES

H. Fukuyama[1] and H. Suwada[2]

[1] Department of Structural Engineering, Building Research Institute
1 Tatehara, Tsukuba, Ibaraki 305-0802, JAPAN

[2] National Institute for Land and Infrastructure Management, MLIT
1 Tatehara, Tsukuba, Ibaraki 305-0802, JAPAN

ABSTRACT

Structural performance of the vibration control elements made by steel bar and advanced fiber reinforced cementitious composites was experimentally observed. These vibration control elements will be applied for reducing damage as well as response of RC structures under the performance based design system. Since stiffness of RC structures is relatively higher than that of steel structures, stiffer vibration control elements compared to the conventional one mainly applied for steel structures are required for reducing the seismic response of RC structures drastically. The advantage of the vibration control elements is selective structural performance, strength, stiffness, and ductility, by changing configuration, bar arrangements and type of materials used. The experimental results indicate that elemental ductility is much increased with decreasing damage when the advanced cementitious composites are applied to the vibration control elements. It means cementitious damper for structural control is available which has merit in performance and cost.

KEYWORDS

Advanced cementitious composites, Damage free, Damage reduction, RC building structures, Restoring force characteristics, Vibration control elements

INTRODUCTION

In researching methods to enhance safety, reparability and durability of concrete structures the authors have developed some types of advanced cementitious composites that have a high ductility and at the same time are able to reduce damage through formation and dispersion of micro cracks. Advanced cementitious composites with 1 to 2 % of short fibers by volume mixed with a mortar matrix show a strain hardening property as well as a multiple micro-cracking property. The stress in these composites does not decreases until the strain increases to about 1 to 2 % after the first crack appears under a

tensile stress following which multiple cracks appear. Some fibers have material properties similar to concrete confined by lateral reinforcing bars in which their compressive stress gently decreases after attaining the maximum compressive strength. Therefore, the failure mechanism, ductility, hysteresis, and damage of reinforced concrete (RC) members can be appropriately controlled. Moreover, stiffness and strength can be easily controlled by the configuration of members. It may therefore be possible to assemble vibration control elements using advanced cementitious composites such that they are more effective than conventional vibration control devices in controlling seismic response of buildings. As part of an effort to get a better understanding of the properties of advanced cementitious composite, a structural test with cyclic lateral force loading on cement members with different bar arrangements and cementitious materials to examine their hysteresis property.

BACKGROUND OF THE RESEARCH

In order to deal with recent global environmental issues, such as energy saving and waste minimization, it is imperative to increase the longevity of short-lived buildings subject to the conventional model of repetitive demolish and build. A fundamental improvement in structural durability is indispensable for increasing longevity of buildings. Additionally, technological advancements are required which make it possible to control and, even, prevent damage and deterioration caused by external loadings such as a large-scale earthquake during the service life of buildings. Only then will it be possible to secure the continuous use of buildings with simple repair works or preferably without any repair works after a large-scale earthquake.

This demand for control and prevention of damage against a large-scale earthquake has emerged after the Hyogoken-Nanbu Earthquake (Kobe Earthquake) in 1995, when many buildings that had protected human lives had to be demolished and reconstructed due to the large cost of extensive repair works. This underscores the importance of the concept of life cycle cost by which it is not enough just to consider general structural performances such as safety and serviceability, but also reparability of structures as well.

At present, seismic retrofit is being applied to the existing structures worldwide. However, the seismic design is based on the principle of protection of human lives but not necessarily the prevention of damage. Therefore, it is possible that in the near future buildings are severely damaged in a large-scale earthquake and the huge repair cost could turn into a serious social problem. Furthermore, a large number of buildings constructed during the period (1960s-1970s) of high economic growth are now reaching a phase of reconstruction. Therefore, it is imperative to expeditiously develop new technology for extending the lives of these buildings while at the same time reducing reconstruction costs and minimizing waste.

To sum up, there is a growing demand for structures with long service lives and are relatively free from collapse and damage.

VIBRATION CONTROL ELEMENTS FOR DAMAGE REDUCTION

Fig. 1 shows an independent wall member used as a vibration control element by its energy absorption, for reducing response displacement of an entire structure thereby reducing damage of each component in the structure. Since wall members built of advanced cementitious composites have high stiffness, high strength and ductility, they can efficiently absorb energy through small deformations. Then they are suitable damper for RC structures with high stiffness. The stiffness and strength of a wall element built of advanced cementitious composites can be easily changed by varying the configuration, bar

arrangement, and type of materials used in composites. Moreover, these elements are built of cement materials that can be molded freely. Thus, it is possible to design energy absorption elements whose properties and configurations are optimized to any given structure. By using these elements in nonstructural wall that are normally disregarded in structural design, the performance of a building can be enhanced with minimal or no change to the original design. Another advantage is that these elements are more cost effective than conventional energy absorption devices.

In these elements reinforcing bars are mainly expected to absorb energy as in conventional energy absorption elements used in concrete structures. The introduction of advanced cementitious composites will assist in securing a better integration of reinforcing bars in the matrix so that vibration control members will exhibit an enhanced, more effective energy absorption performance and at the same time be capable of undergoing large deformations. More specifically, advanced cementitious composites prevent brittle failures, such as shear failure, bond-splitting failure, and anchorage failure, even after the reinforcing bars have yielded. On many occasions vibration control elements undergo rotational deformations within a frame and thus experience large compressive forces. The use of advanced cementitious composites is expected to prevent brittle compressive failure as well.

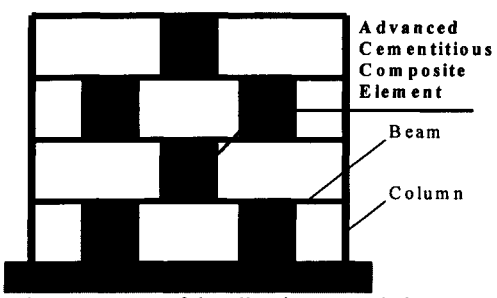


Figure 1 Image of the vibration control element

OUTLINE OF TESTS

Test Specimens

The specimens used in the tests are representative of independent wall members. The dimensions and bar arrangements of the test specimens are shown in Figure 2 and Table 1, respectively. Variables in the tests are bar arrangement and type of cementitious material used. The three types of bar arrangements used are: Type 1- Main reinforcing bars arranged in parallel, with shear reinforcement; Type 2 - Main reinforcing bars arranged in an X-shape, without shear reinforcement; and Type 3 - Main reinforcing bars arranged in an X-shape, with shear reinforcement by auxiliary reinforcing bars (4-D6) arranged in parallel. Screw-ribbed re-bars were used for main reinforcement and were tied directly to a loading steel plate by rock nuts. Three types of cement materials were used: mortar, PE-HPFRCC, and PS-HPFRCC. The mortar had a water-cement ratio of 45 %, and a sand-cement ratio of 40 %. Mortar with an identical mix proportion was mixed with 1 % polyethylene fibers by volumetric ratio in the case of PE-HPFRCC while 1% polyethylene fibers and 1% steel cords by volumetric ratio were mixed for PS-HPFRCC. Test specimens were named according to the type of material, MO for mortar, PE for PE-HPFRCC and PS for PS-HPFRCC and the type of bar arrangements, 1, 2, or 3, following the material designation with a hyphen in between. For example, MO-1 is a test specimen made of mortar and having a Type 1 bar arrangement.
Material properties and the stress-strain relation of HPFRCC are shown in Table 2 and Figure 3,

respectively. Tensile tests and cyclic tension-compression tests on HPFRCC were conducted following the method described in Sato, Fukuyama & Suwada (2001). The loading on the compressive side in the cyclic tension-compression tests was limited to 1/3 of the maximum compressive strength.

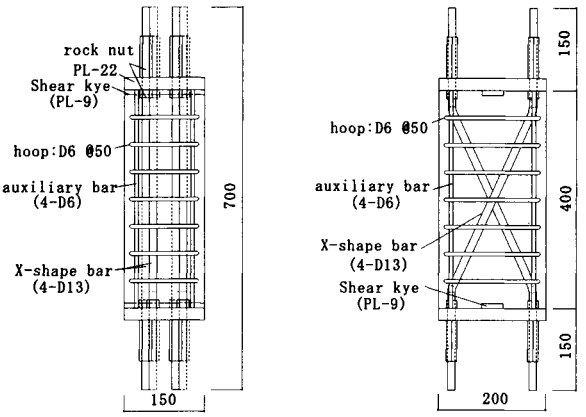


Figure 2 Configuration and bar arrangement of specimens (in case of bar arrange type-3)

Table 1
TEST SPECIMENS

Name of specimen	Cross section	Type of bar arrangement	Main bar	Hoop	Cementitious material
MO-1	150×200 (mm)	1	4-D13(parallel)	2-D6@50	mortar
PE-1					PE-HPFRCC
PS-1					PS-HPFRCC
MO-2		2	4-D13(X-shaped)	None	mortar
PE-2					PE-HPFRCC
PS-2					PS-HPFRCC
MO-3		3	4-D13(X-shaped)	2-D6@50	mortar
PE-3					PE-HPFRCC

Table 2
MATERIAL PROPERTIES

Cementitious material	Compressive strength N/mm^2	Young's modulus N/mm^2	Steel bar	Yield stress N/mm^2	Yield strain μ
mortar	78.0	1.83×10^4	D13	342	1892
PE-HPFRCC	55.1	1.77×10^4	D6	425	2474
PS-HPFRCC	54.5	1.82×10^4			

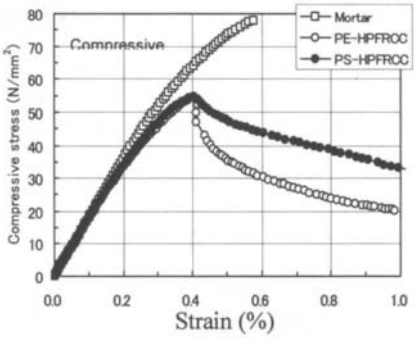
Test Methods

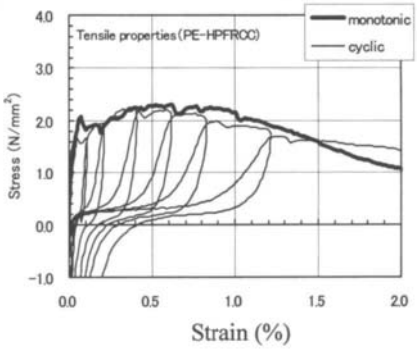
The load was applied under anti-symmetrical moment condition using the loading equipment in Building Research Institute. Cyclic load was applied under a displacement control. An initial axial force was not introduced but an axial jack was used to restrain any axial elongation resulting from rotation at the end of the specimen.

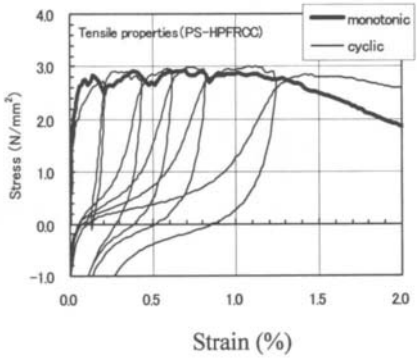
TEST RESULTS

Hysteresis Properties

Figure 4 shows the relation between average shear stress, lateral force divided by cross section (150 x 200 mm), and angle of rotation of the member, lateral deflection divided by specimen height (400mm), hereinafter referred to as the τ - R relation, for each test specimen.







The Type 1 specimens showed hysteresis properties that were remarkably much better for the specimens with advanced cementitious composites. MO-1, with only a regular mortar, showed a decrease in strength as a base collapsed when the main reinforcing bars yielded at R = 0.03 radian. On the other hand, PE-1 and PS-1 showed steady hysteresis properties without any decrease in strength until R was equal to 0.067 radian and 0.093 radian, respectively. On the whole, there was little difference between PE-1 and PS-1; however, compared to PE-1, the strength of PS-1 tended to increase with deformation even after flexural yielding. PS-1 showed a smaller number of shear cracks with narrower width and a smaller amount of shear deformation (a larger amount of rotational deformation) than PE-1. Judging from the state of ultimate failure and changes in crack width, it is considered that the strength of PS-1 increased due to the larger additional axial tension acting on PS-1. The better performance of HPFRCC demonstrated the effect of shear reinforcement and effect of restraint on the compressive side.

In the case of Type 2 specimens, without shear reinforcement, when each test specimen attained its maximum strength, a diagonal shear crack widened abruptly along an X-shaped main reinforcing bar, as if it split a compressed strut formed on the member, following which the strength decreased rapidly. There was an obvious difference in ductility according to the type of material with HPFRCC showing by far the superior behavior and PS-2, in particular, showing steady hysteresis properties until R was $\pm$0.04 radian.

As for Type 3 specimens, the strength of PE-3 increased with deformation more remarkably than for MO-3. This may be the result of the difference in axial compression force, similar to the difference seen between PE-1 and PS-1 in Type 1 specimens. All Type 3 specimens showed a reversed S-shaped hysteresis curve and not a spindle-shaped curve that shows superior energy absorption ability. A possible explanation for this lower performance is considered to be the opening of cracks (caused by slip of main reinforcing bars) along a critical section. Another reason is that in the tests, an axial jack

was used to restrain deformations cased by rotation in the axial direction and this lead to an excessive increase in the shear force on one of the compressive struts of the members. In fact, one of the specimens using mortar lost strength at a relatively small deformation, as the base collapsed and cracks occurred along one of the struts. The results of the tests show that HPERCC was most effective for both tensile and compressive resistance mechanisms.

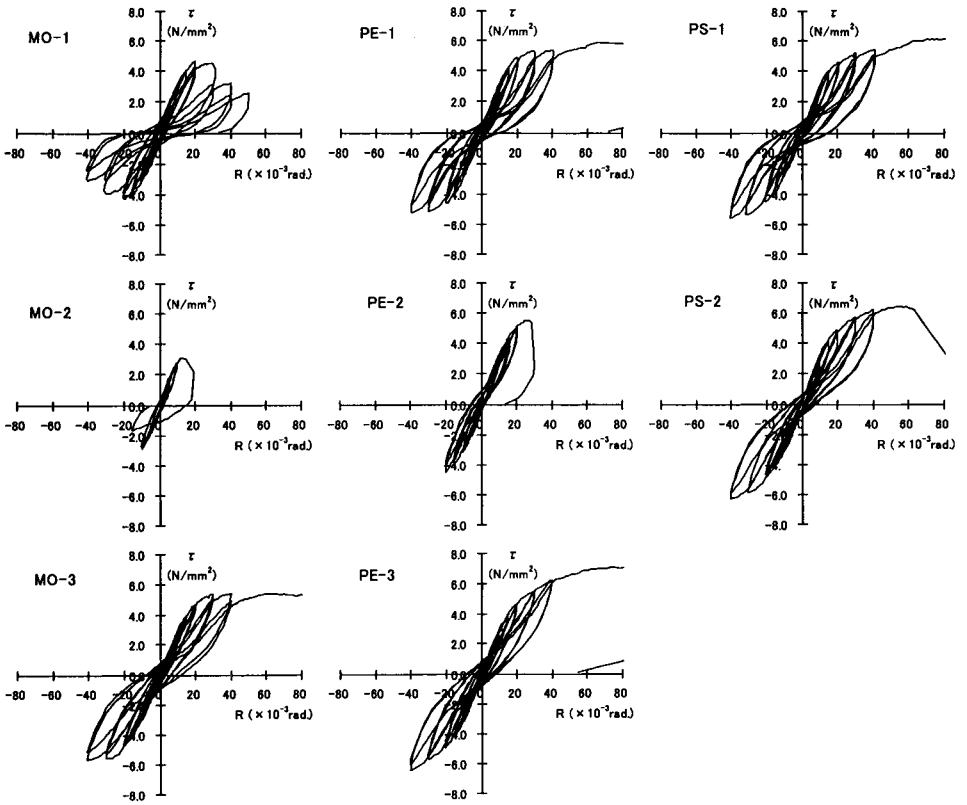


Figure 4 Relationships between average shear stress(τ) and deflection angle(R)

Damage Properties

Figure 5 shows the state of ultimate failure. Figure 6 shows the relation between maximum shear crack width and deflection angle of members (hereinafter referred to as the Wcr-R relation) at the peak of each cycle. These photos and figures clearly indicate that occurrence of cracks is greatly influenced by bar arrangement and material type. All Type 1 specimens with main reinforcing bars arranged in parallel and with shear reinforcement showed 45-degree diagonal cracks all over the members resulting in a truss-like stress transfer for resisting the input shear force. On the other hand, Type 2 specimens showed a crack only along an X-shaped main reinforcing bar, which ultimately developed into a crack that seemed to split members diagonally. The occurrence of cracks in Type 3 specimens was intermediate between Type 1 and Type 2, implying that damage properties can be controlled through shear reinforcement using auxiliary bars with X-shaped main reinforcing bars. Test specimens using HPERCC seemed to have been significantly damaged at a first glance as was apparent by the

appearance of cracks traced with a marker. In reality, as the changes in cracking width showed, micro cracks dispersed (to form multiple cracking), which made visual inspection difficult.

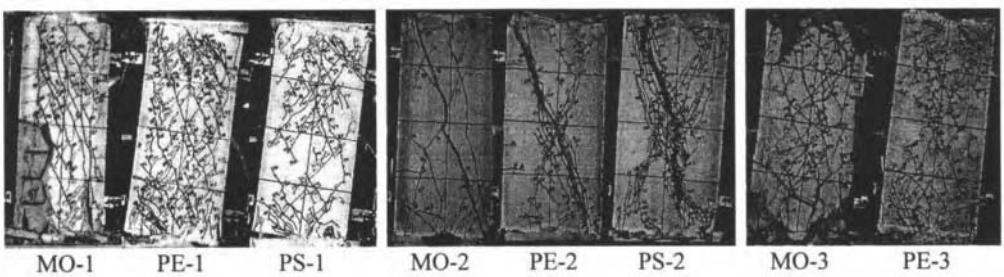


Figure 5 Final failure patterns

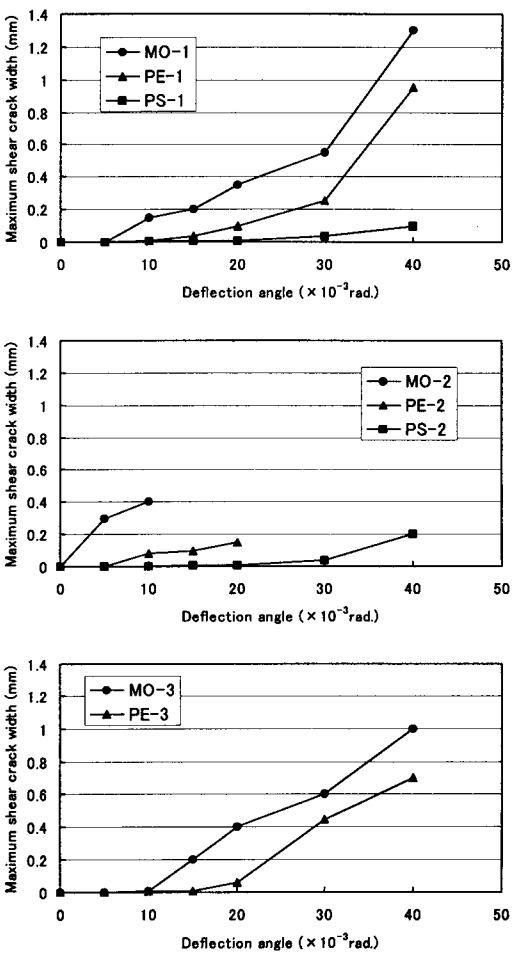


Figure 6 Maximum shear crack width—deflection angle relationships

Fluctuating Axial Compression by Deformation Restraint

In the tests the axial elongation caused by rotation was restrained using a jack in the axial direction. Consequently, an additional, fluctuating axial compression acted on test specimens. Figure 7 shows the relation between axial force ratio (axial stress / compressive strength on cementitious materials) and the deflection angle of members, hereinafter referred to as the η -R relation, at the peak of each cycle. The additional axial compression caused by restraining the axial deformation lead to an increase of 0.36 in the axial ratio.

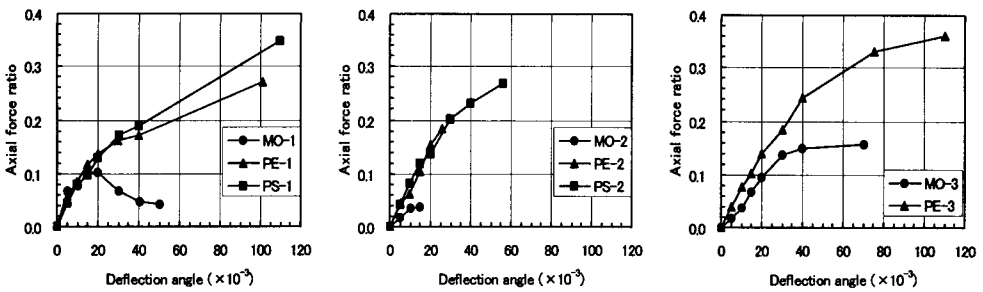


Figure 7 Axial force ratio - deflection angle relationships

CONCLUSION

Cyclic loading tests were carried out on independent wall members with different bar arrangements and cementitious materials in order to determine if the application of HPFRCC to concrete members is effective in controlling their failure mechanism, ductility, hysteresis properties, and damage. The findings obtained from the tests are:

(1) Using HPFRCC, steady hysteresis properties can be obtained up to relatively large deformations if the deformation caused by rotation is restrained. It will act as a cementitious damper for structural control.

(2) Using HPFRCC, the opening in cracks can be prevented and damage can be reduced.

References

Fukuyama H., Sato Y., Li V.C., Mtsuzaki Y. and Mihashi H.(2000): Ductile Engineered Cementitious Composite Elements for Seismic Structural Application, Proceedings of the 12th World Conference on Earthquake Engineering (12WCEE), New Zealand Society of Earthquake Engineering, #1672/6/A

Fukuyama H. and Kuramoto H. (2001). Smart Concrete – Ductile Concrete, Concrete Journal, Japan Concrete Institute, Vol.39, No.1, 104-109 (in Japanese)

Sato Y., Fukuyama H. and Suwada H. (2001). A Proposal of Tension-Compression Cyclic Loading Test Method for Ductile Cementitious Composite Materials, Journal of Structural and Construction Engineering, Architectural Institute of Japan, No.539, 7-12 (in Japanese)

Suwada H., Fukuyama H. and Iso M. (2001). Development of Ductile Fiber Reinforced Cementitious Composites for High Performance Structures, Proceedings of the Japan Concrete Institute, Vol.23, No.3, 133-138 (in Japanese)

Advances in Building Technology, Volume 2
M. Anson, J.M. Ko and E.S.S. Lam (Eds.)
© 2002 Elsevier Science Ltd. All rights reserved

SEISMIC DAMAGE EVALUATION OF A 38-STOREY BUILDING MODEL USING MEASURED FRF DATA REDUCED VIA PRINCIPAL COMPONENT ANALYSIS

J. M. Ko, X. T. Zhou, Y. Q. Ni

Department of Civil and Structural Engineering,
The Hong Kong Polytechnic University, Kowloon, Hong Kong

ABSTRACT

This paper presents an experimental study on seismic damage evaluation of a 38-storey tall building model using measured frequency response function (FRF) data and neural network technique. The 1:20 scale structural model was tested on a shaking table by exerting successively enhanced ground earthquake excitations to generate trifling, moderate, severe and complete (nearly collapsed) damage, respectively. A total of 27 accelerometers were instrumented on the structure for the measurement of FRFs in healthy state and after incurring each of the damage scenarios. A multi-layer neural network with FRF data as input variables is configured and trained for damage occurrence and extent detection in the structure. In order to circumvent the difficulty of huge dimension of input vector when using full-size FRF data with neural network, principal component analysis (PCA) is introduced to compress the size of FRFs, and the projection of measured FRFs onto the most significant principal components is finally used instead of raw FRF data as neural network input for damage identification. The results show that this approach can indicate the structural damage condition with high fidelity.

KEYWORDS

High-rise building, seismic damage evaluation, frequency response function, principal component analysis, neural network.

INTRODUCTION

Structural damage detection using measured frequency response functions (FRFs) has been widely studied (Roitman et al. 1992; Lew 1995; Wang et al. 1997; James et al. 1998; Thyagarajan et al. 1998; Sampaio et al. 1999; Lee and Shin 2002). Since natural frequencies and mode shapes are indirectly-measured test data, they could be contaminated by measurement errors as well as modal extraction errors, and provide less information than FRF data. In this sense, it is more reasonable and reliable to use directly-measured FRF data for structural damage detection, especially for structures with closely spaced modes. On the other hand, artificial neural networks (ANNs) have been a promising

computation tool for damage identification due to their strong capabilities such as pattern recognition and classification, data interpretation, function approximation, etc. The use of measured FRF data with ANNs for structural damage detection was reported in the literature. For example, Wu et al. (1992) addressed the damage detection of a three-storey frame by using selected frequency points of response spectrum as input to a neural network. Chaudhry and Ganino (1994) used frequency response data over a specified frequency range to train a neural network for delamination identification in a beam structure. Manning (1994) trained a neural network using active member transfer function information to classify damage and predict damage extent. Rhim and Lee (1995) studied damage detection using a neural network with input data being transfer functions of auto-regressive model. Luo and Hanagud (1997) used FRF data obtained from PVDF sensors to train a neural network for delamination detection. However, a bottleneck remaining for the use of FRF data with ANNs is the huge size of FRF data. The direct use of full-size FRF data will lead to the neural network with a large number of input nodes, which may also result in the problem of training convergency and computational efficiency. If only using partial FRF data, improper selection of data points from frequency windows may lead to a loss of important information. It is known that using the FRF data in the vicinity of resonant frequencies is not necessary to provide the most reliable damage detection. In order to circumvent the above difficulty, Zang and Imregun (2001) recently proposed a novel approach to compress FRF data for damage detection application. Based on principal component analysis (PCA), they obtained size-reduced projection of measured FRFs on significant principal components and used such compressed FRFs as ANN input variables for structural damage detection.

This paper reports an experimental study on seismic damage evaluation of tall building structures based on a combined use of measured FRF data and ANN technique. A 1:20 scale 38-storey tall building model was tested on a shaking table by incurring successively enhanced ground earthquake excitations to generate trifling, moderate, severe and complete (nearly collapsed) damage, respectively. After experiencing each damage scenario, the structure was subjected to a low-intensity white-noise random excitation and a total of 27 accelerometers were deployed along the structure height to collect acceleration responses in both east-west and south-north directions. According to the distribution of the sensors, the structure is divided into nine regions along the vertical direction. For each region, at least one FRF is measured for the intact structure and for each of the damage scenarios, and a four-layer feed-forward neural network is trained to predict the damage occurrence and extent in this region. The compressed FRF data, obtained by the projection of the raw FRF on 13 principal components, are used as input variables to train the neural network. In order to quantitatively assess damage extent for each scenario, the output of the neural network is designated to be a value between 0 and 1, indicating the damage level.

FRF REDUCTION USING PCA

Principal Component Analysis

Principal component analysis (PCA) can be viewed as a classical method of multivariate statistical analysis for achieving a dimensionality reduction (Jolliffe 1986; Dunteman 1989). Usually, a small set of uncorrelated variables is much easier to understand and use in further analysis for damage detection than a larger set of correlated variables (Worden and Manson 1999). Using an orthogonal projection, the original set of variables in an N-dimensional space is transformed into a new set of uncorrelated variables, the so-called principal components (PCs), in a P-dimensional space such that $P<N$. Namely, it seeks to project the high-dimensional data into a new low-dimensional set of Cartesian coordinates $(z_1, z_2, \cdots, z_P)$. The new coordinates have the following property: z_1 is the linear combination of the original x_i with maximal variance, z_2 is the linear combination which explains most of the remaining variance and so on. If the N-coordinates are actually a linear combination of P ($<N$) variables, the first

P principal components will completely characterize the data and the remaining (N–P) will be zero. The calculation can be described as follows: Given original data set $\{x\}_i = \{x_{1i}, x_{2i}, \cdots, x_{Mi}\}$, i=1, 2, ···, N, form the covariance matrix $[C]$

$$[C] = \sum_{i=1}^{N} \{x\}_i \{x\}_i^T \tag{1}$$

and perform singular value decomposition for $[C]$

$$[C] = [A][\Lambda][A]^T \tag{2}$$

where $[\Lambda]$ is diagonal. The transformation to principal components is then

$$\{z\}_i = [A]^T (\{x\}_i - \{\bar{x}\}) \tag{3}$$

where $\{\bar{x}\}$ is the vector of means of the x-data. From the point of view of dimension reduction, the PCA works by discarding those linear combinations of the data which contribute least to the overall variance or range of the data set.

FRF Reconstruction

In order to determine how many principal components are enough for reserving the most information of original FRF data, FRF reconstruction using only a few principal components will be conducted firstly. The projection of the original FRF matrix $[H(\omega)]_{M\times N}$, which has M rows of FRFs and each with N frequency points, onto the N principal components is given by

$$[P]_{M\times N} = [H(\omega)]_{M\times N}[A]_{N\times N} \tag{4}$$

The projection matrix $[P]$ and the principal components matrix $[A]$ can be portioned into two sub-matrices with P important principal components and (N–P) remaining principal components as

$$\begin{aligned} [P]_{M\times N} &= [[P_1]_{M\times P} \vdots [P_2]_{M\times(N-P)}], \\ [A]_{N\times N} &= [[A_1]_{N\times P} \vdots [A_2]_{N\times(N-P)}]. \end{aligned} \tag{5}$$

The FRF matrix now can be reconstructed for P principal components only

$$[H_R] = [P][A]^T = [[P_1]_{M\times P} \vdots [P_2]_{M\times(N-P)}][[A_1]_{N\times P} \vdots [A_2]_{N\times(N-P)}]^T \approx [P_1]_{M\times P}[A_1]^T_{P\times N} \tag{6}$$

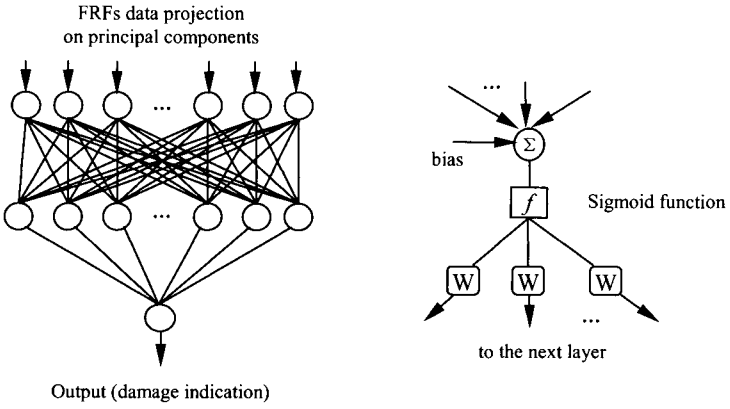
Representation of Damage Feature

After dividing the principal components matrix $[A]$ into two sub-matrices, the projection of the original FRF matrix $[H(\omega)]_{M\times N}$ onto the first P principal components is regarded as damage feature and taken as input to neural network

$$[P]_{M\times P} = [H(\omega)]_{M\times N}[A_1]_{N\times P} \tag{7}$$

NEURAL NETWORK BASED DAMAGE IDENTIFICATION

Figure 1 illustrates the multi-layer feed-forward neural network employed in this study. One neural network is configured and trained for each of the nine structural regions to indicate the damage state in the corresponding region. The compressed FRF relevant to the region, represented by the projection of raw FRF onto a number of principal components, is taken as input to the neural network.



(a) Network topology (b) Connections at a typical node

Figure 1: Neural network configuration for damage identification

EXPERIMENTAL DESCRIPTION

The tested model is a 1:20 scale 38-storey tall building structure. Its overall dimensions are 2.370 m long, 2.160 m wide and 6.515 m high. For the convenience of damage location, the structure is divided into nine regions along the vertical direction as shown in Figure 2, each consisting of 4~5 stories. The scaled model simulates the prototype tall building structure well. It is constructed with bottom floors (No. 1 ~ No. 3), transfer plate, typical floors (No. 4 ~ No. 38) and top machine floors (No. 39 ~ No. 42). Most elements in the prototype structure are simulated in the model without simplification except for the top equipment stories. In the model structure, sizes of the concrete beams, columns, slabs and walls are strictly fabricated according to the similitude law. The section and number of reinforcement are designed to meet the requirement of reinforcement ratio used in the prototype structure.

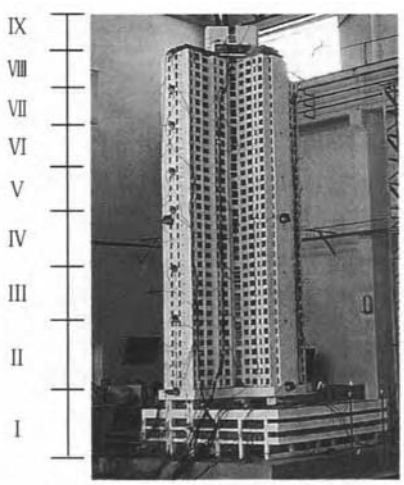


Figure 2: Tested model of a 38-storey tall building

The structure was tested on a 5m×5m, 6-DOF shaking table by exerting successively enhanced earthquake waves. Accordingly, it incurred seismic destroy extending from trifling, moderate, serious damage till to catastrophic one. A total of 27 accelerometers are instrumented uniformly along the height, to track acceleration responses at east-west and south-north directions. After the earthquake excitation at each level, a 20-minute white-noise random excitation was applied to measure the FRFs under each level of damage. Due to the limitation of power supply, the 20-minute white-noise random excitation is divided into 6 segments, each with about 3 minutes, exerting on the base of the tested model. The sampling frequency of all accelerometers is taken as 100 Hz in the testing. The loading level of random excitations is considerably low. So the structure can be regarded to hold the original damage state during the random excitations.

ANALYSIS AND RESULTS

Compression of FRFs

In order to determine the appropriate number of principal components (PCs) which can retain the most information of original FRFs and meanwhile reduce the dimensionality considerably, reconstruction of FRFs using different numbers of principal components based on Eq. (6) is firstly conducted. Figures 3, 4 and 5 show the reconstruction results of FRFs at the floor C34 for the intact structure and moderate damage case, using 5, 13 and 30 principal components respectively. It is seen that the reconstructed FRF using only 5 PCs deviates considerably from the original one, whereas for the cases of using 13 and 30 PCs, this deviation is negligible. The reconstructed and original FRFs are almost identical for the latter two cases. As a trade-off between retaining the most original information and reducing the dimensionality farthest, the reconstructed FRFs using 13 PCs are regarded as damage indicators in the present study.

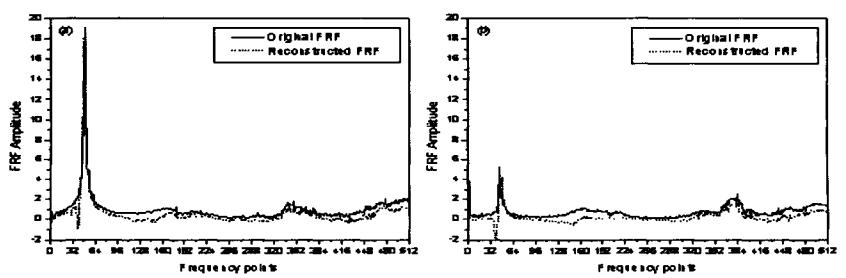


Figure 3: Reconstruction of FRFs using 5 PCs: (a) intact structure; (b) moderate damage case

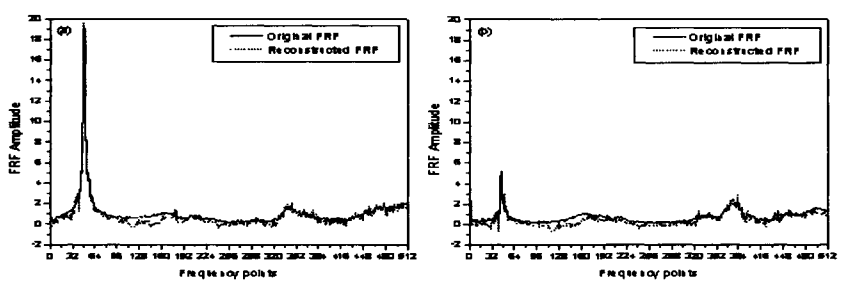


Figure 4: Reconstruction of FRFs using 13 PCs: (a) intact structure; (b) moderate damage case

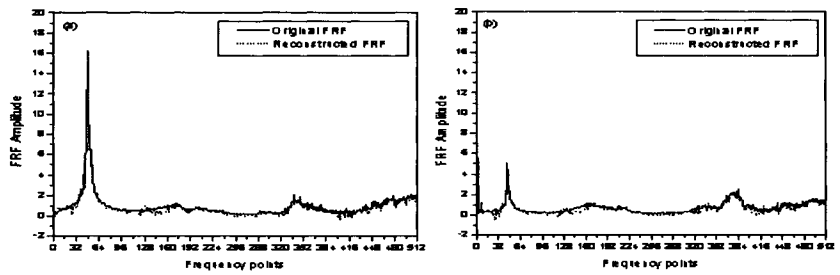


Figure 5: Reconstruction of FRFs using 30 PCs: (a) intact structure; (b) moderate damage case

Damage Identification Results

In the damage identification using neural network for each structural region, the compressed FRF, which is obtained by the projection of the measured FRF from the relevant region onto 13 principal components, is taken as input to the neural network. A four-layer neural network configuration is employed and trained with back-propagation (BP) algorithm. The two hidden layers take 15 and 18 neurons respectively, and the output layer has only one node that indicates damage severity of the specified region. To quantitatively evaluate the five damage scenarios, the target output of the neural network at training phase is designated as a definite value, while the actual output at testing phase is classified into a tolerant range, as indicated in Table 1.

A total of 500 training samples and 500 testing samples are selected from the measured FRFs which are more or less polluted by noise. No overlap exists between the training and testing samples. If and only if the output value of one testing sample lies in the tolerant range of the corresponding damage scenario, we account the testing sample as being correctly identified. Table 2 summarizes the identification results of all damage scenarios for 100 testing samples, obtained from the FRF measured at the floor C34 (7th structural region). In this table, the identification accuracy (percentage) is defined as the ratio of the number of correctly identified samples to the number of total testing samples (100). Figure 6 illustrates the output results of the neural network for all damage scenarios by using FRF data measured at the floor C34, where N, T, M, S and C denote the testing samples of no damage, trifling damage, moderate damage, serious damage and completely damaged scenarios, respectively. It is seen that for the overwhelming majority of testing samples, the predicted output results lie in the respective tolerant ranges. This concludes that the constructed neural network can predict the relative damage severity with high fidelity. The neural network identification results using compressed FRFs measured from other structural regions are also obtained but not presented in this paper due to the limit space. A similar consequence is achieved from those results.

TABLE 1
NEURAL NETWORK TARGET OUTPUT AND TOLERANT OUTPUT

Damage scenarios	Target output	Tolerant output
No damage (N)	0.1	< 0.2
Trifling damage (T)	0.3	$0.2 \sim 0.4$
Moderate damage (M)	0.5	$0.4 \sim 0.6$
Serious damage (S)	0.7	$0.6 \sim 0.8$
Completely damaged (C)	0.9	> 0.8

TABLE 2
IDENTIFICATION ACCURACY FOR ALL DAMAGE SCENARIOS

Damage Scenarios	Number of testing samples	Number of correctly identified samples	Identification accuracy (%)
No damage (N)	100	97	97
Trifling damage (T)	100	87	87
Moderate damage (M)	100	91	91
Serious damage (S)	100	87	87
Completely damaged (C)	100	92	92

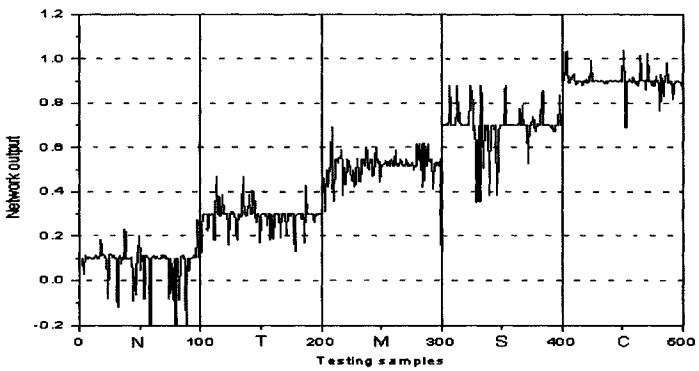


Figure 6: Output values of neural network

CONCLUSIONS

A combined use of frequency response function (FRF) data and neural network technique for seismic damage detection of tall building structures has been studied in this paper. The applicability of the proposed method has been experimentally verified by using a 38-storey tall building model. The model structure was tested on a shaking table to suffer from trifling, moderate, severe and complete (nearly collapsed) damage, respectively. The FRFs of the structure after each damage scenario was measured and the compressed FRFs through principal component analysis (PCA) were used as input variables to neural networks for structural damage identification. The identification results show that: (i) The PCA technique is powerful tool for reducing the dimensionality of measured FRFs. The reconstructed FRFs using a few principal components coincide well with the raw FRFs; (ii) Introducing the PCA technique for dimension reduction greatly facilitates the configuration and training of neural networks with FRF data as input variables; (iii) The proposed method can indicate the structural damage occurrence and relative severity region-by-region with high fidelity.

ACKNOWLEDGEMENTS

The work presented in this paper was supported by The Hong Kong Polytechnic University under the grant G-V856 and through the Area of Strategic Development Programme (Research Centre for Urban Hazard Mitigation). These supports are gratefully acknowledged.

References

Chaudhry Z. and Ganino A.J. (1994). Damage detection using neural networks: an initial experimental study on debonded beams. *Journal of Intelligent Material Systems and Structures* **5**, 585-589.

Dunteman G.H. (1989). *Principal Components Analysis*. London: New Delhi.

James G.H., III, Zimmerman D.C. and Mayes R.L. (1998). Experimental study of frequency response function (FRF) based damage assessment tools. *Proceedings of the 16th International Modal Analysis Conference*, Santa California, 151-157.

Jolliffe I.T. (1986). *Principal Component Analysis*. New York: Springer-Verlag.

Lee U. and Shin J. (2002). A frequency response function-based structural damage identification method. *Computers and Structures* **80**, 117-132.

Lew J.-S. (1995). Using transfer function parameter changes for damage detection of structures. *AIAA Journal* **33**, 2189-2193.

Luo H. and Hanagud S. (1997). Dynamic learning rate neural training and composite structural damage detection. *AIAA Journal* **35**, 1522-1527.

Manning R.-A. (1994). Structural damage detection using active members and neural networks. *AIAA Journal* **32**, 1331-1333.

Rhim J. and Lee S.W. (1995). A neural network approach for damage detection and identification of structures. *Computational Mechanics* **16**, 437-443.

Roitman N., Viero P.E., Magluta C., Batista R.C. and Rosa L.F.L. (1992). Identification of offshore platform structural damage using modal analysis techniques. *Mechanical Systems and Signal Processing* **6**, 287-295.

Sampaio R.P.C., Maia N.M.M. and Silva J.M.M. (1999). Damage detection using the frequency-response-function curvature method. *Journal of Sound and Vibration* **226**, 1029-1042.

Thyagarajan S.K., Schulz M.J., Pai P.F. and Chung J. (1998). Detecting structural damage using frequency response functions. *Journal of Sound and Vibration* **210**, 162-170.

Wang Z., Lin R.M. and Lim M.K. (1997). Structural damage detection using measured FRF data. *Computer Methods in Applied Mechanics and Engineering* **147**, 187-197.

Worden K. and Manson G. (1999). Visualization and dimension reduction of high-dimension data for damage detection. *Proceedings of the 17th International Modal Analysis Conference*, Kissimmee, Florida, 1576-1585.

Wu X., Ghaboussi J. and Garrett J.H., Jr. (1992). Use of neural network in detection of structural damage. *Computers and Structures* **42**, 649-659.

Zang C. and Imregun M. (2001). Structural damage detection using artificial neural networks and measured FRF data reduced via principal component projection. *Journal of Sound and Vibration* **242**, 813-827.

Advances in Building Technology, Volume 2
M. Anson, J.M. Ko and E.S.S. Lam (Eds.)
© 2002 Elsevier Science Ltd. All rights reserved

TOWARDS NEXT GENERATION SEISMIC ISOLATION TECHNOLOGY

George C. Lee and Zach Liang

Multidisciplinary Center for Earthquake Engineering Research
State University of New York at Buffalo, Buffalo, NY 14261, USA

ABSTRACT

Seismic isolation modeled as a single degree-of-freedom (S-DOF) system has been successfully applied to vibration reduction of equipment and structures in the fields of mechanical and aerospace engineering for many decades. More recently, the civil engineering profession has gradually introduced the technology for seismic protection of infrastructure systems (buildings, bridges, nonstructural components, lifeline systems, etc.) against strong earthquake ground motions. It has evolved as a specialty area in earthquake engineering, known as (structural) base isolation (as versus shock and vibration isolation). The application of base isolation technology in civil engineering therefore has stemmed from S-DOF models traditionally used in the mechanical/defense/aerospace industry. However, a large number of civil engineering structures are complex multiple degree-of-freedom (M-DOF) systems. Recent developments in structural dynamics, computing and experimental capacities have shown that there are shortcomings of using over-simplified S-DOF based seismic isolation design practice for civil engineering structures. This paper advances the concept of developing the next generation seismic isolation technology for civil engineering structures based on M-DOF models by first pointing out a number of key issues current technology does not address, followed by the suggestion of a hybrid semi-active/passive base isolator system to indicate future goal of developing intelligent seismic isolation bearings.

KEYWORDS

base isolation principles, M-DOF systems, semi-active/passive, intelligent bearings

1. INTRODUCTION

Base isolation is generally regarded as a relatively matured technology in earthquake engineering. Many buildings and bridges have been installed with seismic isolation bearings in many regions of the world. The isolation technique has also been shown to be reliable, inexpensive, and effective in many other applications. Most of the successful applications are to those structures and equipment that can be modeled by a single degree-of-freedom model. In many civil engineering structures, the responses due to earthquake ground motions cannot be adequately modeled by a S-DOF system. This paper addresses

some key issues in current state-of-practice in seismic isolation design based on more appropriate M-DOF models. An "intelligent seismic isolation bearing" is proposed to deal with issues identified in order to better control the performance of base isolated structures. This proposed system is considered to be the first attempt towards the development of intelligent seismic isolation bearing system for civil engineering applications.

2. SOME KEY DESIGN ISSUES OF BASE ISOLATION

In the following, a few important design issues for base isolation are briefly outlines. Many of them should be considered by using M-DOF models.

Ground Motions

Using proper input excitations is an important issue in earthquake engineering design. This is true not only for seismic isolation purposes. However, the matter of considering the ground motion direction has not been given adequate attention in the past (Lee and Liang, 1998). Using a given ground motion record with different incident, the maximum and minimum peak responses of a given structure can be considerably different. This may be explained by using two horizontal earthquake ground motion components. Since any seismic ground motions can be projected onto a pair of Cartesian coordinate axes, denoted by x_g" and y_g", the peak values of the projected time histories will be different for different sets of projections. It follows that the resulting peak values of the structural responses will also be different. Choosing different Cartesian coordinate is equivalent to choosing different incident angle of the earthquake motion direction. By using an earthquake-record in the standard "normal/parallel" directions will not likely yield the worst case of response calculation. In addition, it is not well understood that the seismic incident will affect the design of response magnification devices such as the base isolators caused by "directional or cross effect." Penzien and Watabe (1975) defined principal axes of ground motions as a pair of mutually $\perp$ axes about which the cross correlation function of x_g" and y_g" equals to zero. This defines a special incident angle of a given ground motion for which engineers have a method to calculate structural responses. It is not a criterion of choosing the incident for maximum structural responses because the seismic responses of a structure depend on both the ground excitation and the dynamic properties of the structure itself. This fundamental issue is often misunderstood or ignored by many engineers by assuming that using the ground motions defined by Penzien will automatically yield maximum structural response for the purpose of design. This is a misinterpretation of the original concept of Penzien. Lopez et al. (2000) had suggested a formula to modify the existing CQC3 method to calculate the maximum peak response based on design spectrum in the period domain, which has great advantage of accuracy and simplicity. However, it cannot be used for performance based design, where time domain responses are necessary.

Design Response Spectra

In seismic isolation design based on response spectrum, the general guiding principle is to achieve lower acceleration of the superstructure by providing adequate longer period of a structure, for a given damping ratio (Kelly, 1993). If, for a certain reason, the period cannot be shifted to a longer value, more damping may be used to lower the acceleration. This guiding principle is very approximate and should not be used for all cases. For example, reduction of superstructure acceleration can only be achieved when the dominant frequency of the ground motion is 41% greater than the fundamental frequency. Furthermore, the reduction of superstructure acceleration should not be the sole criterion of base isolation. In many cases, reduction of base shear and/or bearing displacement is more important. For different performance

objectives, different design parameters and different approaches are needed. They often require the consideration of M-DOF models.

Near Field Effect and Bearing Displacement

The design of isolation bearings is importantly related to the velocity pulses because of the large displacement and the structural responses (observed in recent large earthquakes). They are the results from both the nature of excitations and the dynamic behavior of the isolation system. To actually reduce the bearing displacement, we may use non-linear bearing to modify the phase different of the motion of the superstructure and the base as far from 180^0 as possible. Or, we may introduce structural control technologies to modify the responses of the structure. To consider these methods properly, again, M-DOF models should be used.

Role of Large Damping

Large damping can be introduced in isolation systems to reduce the resonant amplitude of structural response. However, the isolation should not be designed to have a resonance to begin with. In the design-response-spectrum approach, large damping is introduced to reduce the acceleration (actually, only the pseudo acceleration can be reduced). Large damping is also thought to be helpful to reduce the bearing displacement by many. However, bearing displacement is difficult to be reduced if linear restoring and damping force are used (see Kelly 1999 and Hall 1999).

Cross Effect

One of the challenging areas in structural dynamics of base-isolated structures is the "cross effect" or "directional coupling." The authors have been pursuing a study to quantify the dynamic responses of structures in the perpendicular direction of loading (Lee and Liang, 1998). There are several factors contributing to this special response of dynamically loaded structures. The authors believe that the cross effect can be very large in base isolated structures if the isolation system is not properly designed. In general, when a system does not have the same pair of principal axes in the horizontal directions, along the vertical axis and/or at different loactions of sub-structures, horizontal input in one direction will cause response in its perpendicular horizontal direction. Structures with initial imperfections in geometry and/or unsymmetrical distribution of mass and damping properties can further magnify the cross effect. In most cases, we typically cannot treat base isolated structures as S-DOF systems or as decoupleable M-DOF systems. For example, certain isolation bearings only have one pair of cross-sectional principal axes in one of the three mutually $\perp$ directions. The combined structure-bearing system will certainly have response couplings under dynamic loading. The challenge is not about their existence but their magnitude. We need to quantify them in order to properly design the seismic isolation as well as other response modification systems for structures.

3. REAL-TIME STRUCTURAL PARAMETER MODIFICATION FOR BASE ISOLATION SYSTEMS

In the previous section, we briefly discussed four of the important issues that should be considered in developing a new generation of seismic isolation technology. Some issues require fundamental research in structural dynamics both theoretically and experimentally. In order to proceed with the improvement of present day seismic isolation technology, the authors advocate the use of a hybrid control scheme to improve the performance and to provide fail-safe capacity in base isolation applications. In the remainder of the paper, this new concept will be described. It represents the beginning of a new generation of seismic isolation design, primarily based on M-DOF system models (Lee and Liang, 2002).

As pointed out earlier, one of the shortcomings in current base isolation design is the possibility of underestimating the bearing displacement and the inefficiency of the "linear bearing." We suggest the application of real-time structural parameter modification (RSPM) technology together with passive base isolators. RSPM is a special kind of semi-active control technology, containing sensory, decision-making and execution components, assembled as a single device (function switch) to provide "switching" functions to extend the capacity of a passive device. RSPM uses less power to control solenoid valves to modulate the stiffness and viscosity of the function switch, which in turn varies the dynamic behavior of the passive isolators, changing the stiffness and damping from linear to nonlinear variables. Kobori et al. (1993) introduced the concept of semi-active control to earthquake engineering applications. Liang et al. (1999) introduced the function switch device in vibration and shock isolation. Ruan (1997) discussed the possibility of using the RSPM technology for building base isolations. In the following, we first discuss the advantages and limitations of using passive nonlinear base isolation, followed by describing the approach of using the RSPM technology to obtain optimal nonlinear responses of the bearings.

Nonlinear Base Isolation

Using linear isolation bearing, the motion of the structure is 180^0 out of phase with the ground motion. This will result in large bearing displacement. If this phase difference can be modified to either greater or smaller than 180°, the bearing displacement will be reduced.

Large linear damping can shift the phase angle, but the amount is insignificant. Therefore, introducing large nonlinear damping to the passive base isolation is a reasonable approach. In addition, if an isolated building can be modeled as a linear SDOF system, damping force has a 90^0 phase difference from the restoring force. In linear MDOF system, the change of phase difference will not be significant. By using nonlinear isolators, the phase difference can be greatly changed. This suggests that we can modulate the restoring forces in developing the nonlinear base isolators.

Figure 1 shows the normalized bearing displacements, as a comparison between linear and nonlinear isolation bearings. Here, normalized plots are used for the purpose of comparison. It is clearly seen the phase difference. One of the reasons that the displacement of nonlinear bearing can be considerably smaller, from this figure, that the phase difference is modulated. In this example, the linear damping force is calculated by using a constant 30% damping ratio. The nonlinear curve is obtained from a constant slope roller bearing (linear restoring force) together with viscous damping force and constant restoring nonlinear force, as well as friction nonlinear damping forces (Lee and Liang, 2002). The response spectrum of this new type of slope roller bearing does not have notable peak responses because a constant slope with angle 2^0 to 3^0 is used to achieve a constant restoring force. For this configuration, the acceleration of the superstructure is almost a constant.

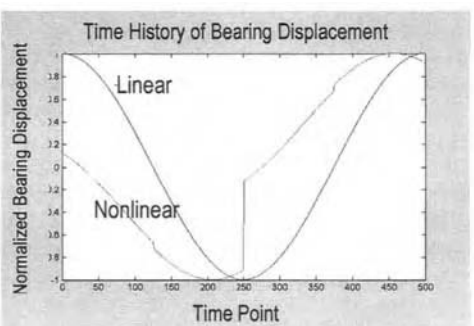


Figure 1: Linear and Nonlinear Bearing Displacements

Figure 2 shows the energy dissipation loops, where the nonlinear loop can dissipate about twice the energy than the linear loop. Figure 3(a) shows typical experimental result of the bearing displacement under the Kobe earthquake excitation, where the peak-to-peak value is about 4 inches. Figure 3(b) shows a separate experimental result of the nonlinear slope-roller bearings, where the peak-to-peak value is less than 1.5 inch. The reduction of bearing displacement of the nonlinear system is rather significant, although the latter is still large.

There are several other issues regarding the design parameters for nonlinear seismic isolation. They will not be described in this concept paper due to length limit.

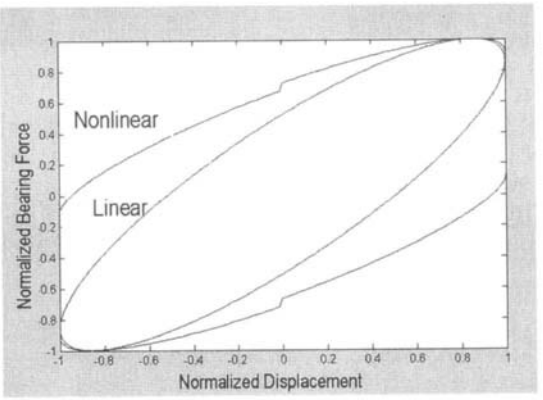


Figure 2: Linear and Nonlinear Bearing Constitution Loop

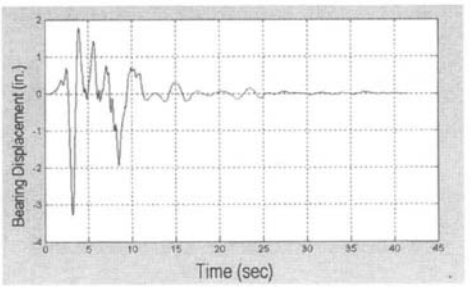


Figure 3(a): Displacement of linear bearing

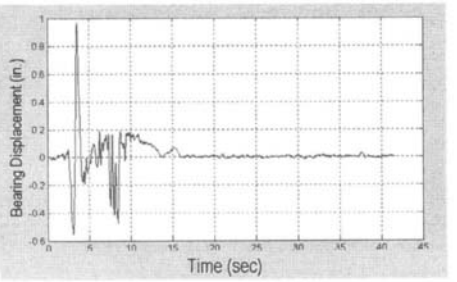


Figure 3(b): Displacement of nonlinear bearing

An Intelligent Base Isolation System

As an example of developing intelligent base isolators, a semi-active control element is added to a passive seismic isolation system, which is considerably more economical than using an active control system in order to achieve the same objective.

The RSPM technology mentioned earlier can vary the stiffness and damping coefficients of a passive bearing. With a given external excitation, the variable stiffness and damping device can generate appropriate restoring and damping forces. Figure 4 shows displacement that using RSPM to simulate the nonlinear bearing. It is seen that this semi-active control system can closely simulate the desired nonlinear displacement. In this simulation, the RSPM performs a switching function that adds or disconnects a pair of stiffness to the main bearing stiffness. By suddenly drop (disconnect) the added stiffness, the result shown in Figure 4 can be achieved.

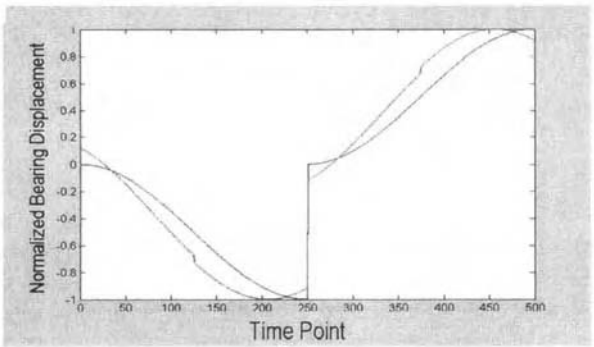


Figure 4: Passive and RSPM nonlinear bearing displacements

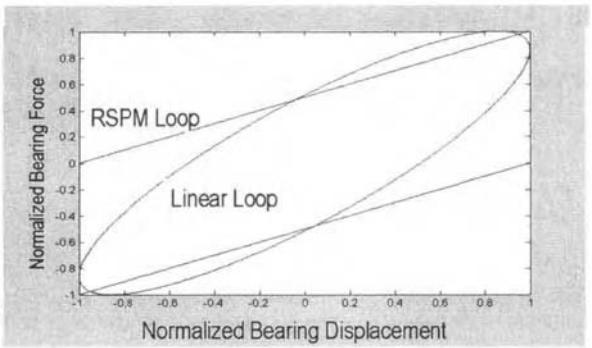


Figure 5: Linear and RSPM bearing constitution loop

Figure 5 is the comparison of energy dissipation between the RSPM technology and linear bearing. It is seen that the RSPM-controlled isolation can absorb significantly more energy than does the linear bearing. In fact, the former technology can achieve the maximum energy dissipation by using two functional switches in the push-pull pair (see Liang et al., 1999).

Figures 4 and 5 are normalized plots which cannot indicate the effectiveness of how to use RSPM to adaptively vary the bearing parameters. This is a rather complex issue that will not be explained in this paper (see Liang et al., 1999).

Figure 6(a) shows a simulated example of the responses of the RSPM-controlled base isolations. The excitation is Mexico earthquake, whose long period can make bearing displacement quite large. As a comparison, we also plot the bearing displacement by using a 50% linear damping. It is seen that a significant reduction can be achieved. In figure 6(b), we also plot the comparison of the resulted base shears. It is seen that the base shear of RSPM-controlled isolation system is significantly reduced, too.

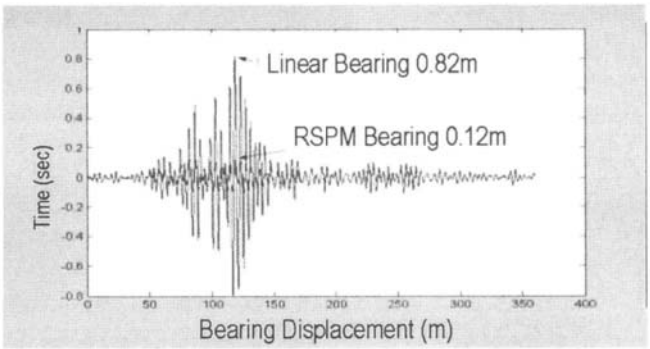


Figure 6(a): Comparison of bearing displacement

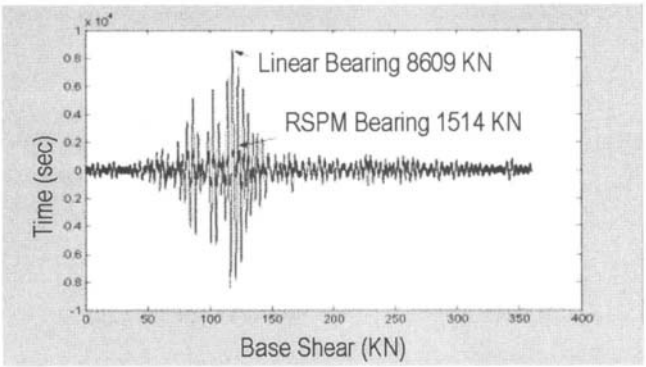


Figure 6(b) Comparison of base shear

SUMMARY

Advances in theoretical analyses and experimental observations in structural dynamics, coupled with the maturity and experiences in the earthquake engineering profession, have suggested the opportunity to begin the development of next generation seismic isolation technology for civil engineering applications at the Multidisciplinary Center for Earthquake Engineering Research (MCEER). This paper is an attempt

to summarize some of the key issues that should be addressed through M-DOF theoretical modeling and experimental studies. Although the concept of an intelligent seismic isolation system is proposed, the objective of the paper is to describe the vast area of research opportunities towards the development of next generation of seismic isolation technologies for earthquake engineering applications.

ACKNOWLEDGEMENT

This study is supported jointly by the National Science Foundation (Grant No. ECC-9701471) and the Federal Highway Administration (Contract No. ETFH61-98-C-00094). The work of RSPM-controlled base isolation is partially contributed by Dr. S. Ruan.

REFERENCES

American Association of State Highway and Transportation Officials (2000) *Guide Specifications for Seismic Isolation Design.*

Hall, J. (1999) "Discussion: the role of damping in seismic isolation," *Earthquake Engineering and Structural Dynamics*, 28, 1717-1720.

Kelly, J. M. (1993) "Current development on isolation of civil buildings in the United States," Isolation, Energy Dissipation and Control of Vibrations of Structures, *Proc. of the International Post-SMIRT Conference Semina,r* Capri, Italy, August, 1993.

Kelly, J. M. (1999) "The role of damping in seismic isolation," *Earthquake Engineering and Structural Dynamics,* 28 3-20.

Kobori, T. M. Takahashi, T. Nasu, N. Niwa, and K. Ogasawara (1993) "Seismic response controlled structure with active variable stiffness system," *Earthquake Engineering and Structural Dyanmics*, Vol. 22 pp 925-941.

Lee, G.C. and Z. Liang (1998) "On cross effects of seismic responses of structures," *Engineering Structures*, Vol . 20, Nos. 4-6, pp 503-509.

Lee, G. C. and Z. Liang (2002) "Design considerations of bridge isolation bearings for large displacements," 81th TRB Annual Meeting, Washington, DC, Jan. 13-17, 2002.

Liang, Z., M. Tong and G.C. Lee (1992) "Complex modes in damped linear dynamic systems," *The International Journal of Analytical and Experimental Modal Analysis*, 7(1), 1-20.

Liang, Z., M. Tong and G.C. Lee (1999) "A real-time structural parameter modification approach for random vibration reduction, Part I: principle," *Journal of Probabilistic Mechanics*, 14: 349-362.

Liang, Z., M. Tong and G.C. Lee (1999) "A real-time structural parameter modification approach for random vibration reduction, Part II: experimental verification," *Journal of Probabilistic Mechanics*, 14: 363-381.

Lopez, O.A., A.K. Chopra and J.J. Hernandez (2001) "Evaluation of combination rules for maximum response calculation in multicomponents seismic analysis," *Earthquake Engineering and Structural Dynamics*, 30: 1379-1398.

Penzien, J. and M. Watabe (1975) "Characteristics of 3-dimensional earthquake ground motion," *Earthquake Engineering and Structural Dynamics*, 3: 365-374.

Ruan, S. (1997) "Animated control of base isolation systems," Ph.D. dissertation, University at Buffalo, New York.

Advances in Building Technology, Volume 2
M. Anson, J.M. Ko and E.S.S. Lam (Eds.)
© 2002 Elsevier Science Ltd. All rights reserved

SEMI-ACTIVE DAMPING DEVICE FOR VIBRATION CONTROL OF BUILDINGS USING MAGNETORHEOLOGICAL FLUID

Joseph H. K. Lee[1], Ray K. L. Su[2], Peter K. K. Lee[2], Louis C. H. Lam[1]

[1]Department of Construction,
Hong Kong Institute of Vocational Education (Tsing Yi), Hong Kong
[2]Department of Civil Engineering,
The University of Hong Kong, Hong Kong

ABSTRACT

Recent studies show that semi-active vibration control systems using Magnetorheological (MR) dampers have most of the good characteristics of passive and active control systems. Their applications in mitigating dynamic effects produced by seismic and wind loads on civil engineering structures are quite promising. In this paper a new form of semi-active damping device using MR Fluid for vibration control of structures is proposed. A model of the proposed MR damping device was developed. This paper presents the results of the studies as well as proposals on further research on the MR damping device including experimental tests and control strategies so that the potential of its applications in seismic and wind-induced vibration control of structures can be further explored.

KEYWORDS

Magnetorheological fluid, MR fluid, damping device, semi-active vibration control, control strategy.

INTRODUCTION

A significant amount of research on vibration control and civil engineering application has been conducted in the past decade. Four basic categories of control systems were identified and definitions

were given in Housner *et al* (1997), namely, passive, active, hybrid, and semi-active control systems. Passive control systems, such as base isolation, metallic yield dampers, viscoelastic dampers, viscous wall, friction dampers, tuned mass dampers, tuned liquid dampers, employ supplemental devices, which respond to the motion of the structure to dissipate vibration energy in the structural system. They do not require external power source. The energy in a passive control system cannot be increased by the passive control devices. Active control systems, such as active tendon system, active bracing system, active tuned mass damper, active mass drivers, operate by using external energy supplied by actuators to generate forces on the structure in a prescribed manner, in accordance with the response of the system measured with physical sensors. The generated forces can result in adding or dissipating energy. They normally require a significant amount of power for the operation. Hybrid control systems combine two or more passive and active control systems to reduce the responses of a structure. There are two main systems: the hybrid mass damper systems and the active base isolation system. Semi-active control systems may be considered as a class of active control systems that require relatively small amount of external energy sources, or as controllable passive devices, yet they have most of the good characteristics of passive and active control systems. The following damping devices belong to the semi-active control systems: variable-orifice fluid dampers, controllable friction dampers, and controllable fluid dampers which include the magnetorheological (MR) fluid dampers and the electrorheological (ER) fluid dampers. Semi-active control devices do not add mechanical energy to the structure. Semi-active systems, especially the MR dampers, perform significantly better than passive devices and may achieve, or may even outdo, the performance of fully active systems. Semi-active control systems also do not induce adverse effects on the stability of the structure. The potential of applications of semi-active vibration control systems in civil engineering is quite promising

THE NEW PROPOSED SEMI-ACTIVE DAMPING DEVICE USING MR FLUID

Magnetorheological (MR) fluid dampers were investigated in recent years and promising results of mitigating dynamic effects on buildings have been achieved. Most of the MR dampers studied belong to the valve mode in the control of fluid flow. A new shear mode damping device using MR fluid is proposed and developed herein. The proposed damping device consists of two 10 mm thick steel plates placed parallel to each other with a gap of 15 mm in between. This gap is filled with MR fluid. Another steel plate, which can slide freely between the two parallel plates, is immersed in the fluid to a depth of about 30 mm. The width of the sliding plate in contact with the MR fluid is 50 mm. Details of the damping device are shown in Figure 1. A coil is placed at the lower part of the device in between the two parallel plates to produce an electromagnetic circuit. When an electric current passes through the coil, a magnetic field is generated, which in turn, generates a resisting force against the movement of the sliding plate. The force generated is due to the change of yield stress of the MR fluid. Only a current of less than two amperes is required. Damping forces that vary with the magnitude of the induced magnetic field passing through the MR fluid are generated. Thus vibration control can be achieved when the applied current is regulated by a suitable feedback control algorithm.

MR fluids contain suspensions of micro-sized particles that can be easily magnetized. When a magnetic field passes through the fluid, the suspended particles align with the direction of the field like chains, which obstruct the movement of the fluid within the area. Thus the yield stress of the fluid is altered and can be controlled by the magnetic field applied to it. This is a major favourable characteristic of the MR fluid. The free-flowing, viscous fluid can be changed to a semi-solid to solid stage in milliseconds when varying magnetic field passes through it. MR fluids also have other favourable properties of high strength, fast response time, low viscosity, maintain stable condition over a wide range of temperature and are insensitive to impurities. Furthermore, they only need minimal power to operate. Silicon steel is used and considered satisfying the requirements of high magnetic permeability and saturation. MR Fluid MRF-132LD produced by Lord Corp. is used. It has the following properties: the dynamic shear yield stress is less than 45 kPa; the range of operating temperature is from -40^0 to 150^0C; the plastic viscosity is from 0.25 to 0.9 Pa-sec; there is no effect on most chemical impurities; the required response time is just a few milliseconds; the required current is only 1 to 2 Ampere when a 12 V DC power supply is used. All these properties are favourable to damping devices for vibration control.

SHEAR FORCES IN THE PROPOSED MR DAMPING DEVICE

For a flowing MR fluid with an applied magnetic flux, the Bingham's equations may be used (Mark 1998), the fluid stress is given by $\tau = \tau_y(H) + \eta \dot{\gamma}$

where $\dot{\gamma}$ = fluid shear rate, $\tau_y(H)$ = yield stress induced by the magnetic field, η = plastic viscosity at no applied magnetic field.

The actual behavior of MR fluid departs slightly from the Bingham model. MR fluid shows non-Newtonian behavior even with no applied magnetic field. Nevertheless, the Bingham model still provides a useful basis for the design of MR damping devices. The shear force developed in the shear mode device is $F = F_\eta + F_\tau = \frac{\eta V_R A}{g} + \tau_y(H)A$

where V_R = relative velocity of the plates, A = shear area $\approx 2 L_p w$, L_p and w = length and width of the contact area respectively, g = gap width of the flow channel between the plates.

ELECTROMAGNETIC CIRCUIT DESIGN AND FINITE ELEMENT ANALYSIS

The design of electromagnetic circuit requires the optimization of magnetic field energy in the fluid gap and minimization of the magnetic flux loss in other areas of the circuit. There should be adequate steel areas so as to keep the magnetic field intensity low. Design procedure (Lord 1999) involves the determination of the magnetic flux density B_f in the MR fluid to give the required yield stress τ_o. B_f can

be obtained from the τ_0-B_f curve of the MR fluid, and in turn the magnetic field intensity H_f in the fluid can then be determined from the B-H curve of the fluid.
For continuity of magnetic flux, $\phi_i = \phi j = \phi_k = ...$and $\phi = B_f A_f = B_s A_s$, where A_f and A_s are effective areas of the fluid and the steel respectively; and B_s is the magnetic flux density in the steel. Thus B_s can be calculated from $B_s = \phi / A_s = B_f A_f / A_s$. From the B-H curve of the steel, the magnetic field intensity H_s in the steel can be determined.

In a magnetic circuit, NI = $\oint Hdl$, where NI is the number of amp-turns required in the coil.

Thus NI = $\sum HiLi = H_f g + H_s L_s$, where g = total gap width filled with the fluid, and L_s = Length of the segment of the circuit through the steel, by assuming uniformly distributed magnetic flux across the effective areas and no losses incurred.

The electromagnetic circuit design and the configuration of the MR damping device have been verified using the finite element computer program, COSMOS/M. Results of the two-dimensional finite element analysis indicate that there are losses and non-uniform distribution of fluxes at junctions and boundaries, especially at the parallel steel plates. Results of the finite element computer analysis showing the non-uniform distribution of the magnetic flux and the MR fluid are shown in Figure 2. From the equations in the previous paragraph and assuming uniform flow of magnetic flux across the areas with no loss of flux, the calculated magnetic flux densities are 0.56 Tesla at the MR fluid and sliding steel, 1.65 Tesla at the parallel plates, and 0.62 Tesla at the coil. The results from the finite element analysis are 0.43, 1.3 and 0.68 Tesla at the corresponding locations respectively. The losses of flux vary at different locations.

MECHANICAL MODEL OF THE PROPOSED MR DAMPING DEVICE

It is required to have a mechanical model to predict the measured responses and the behaviour of the damping device. The Bouc-Wen model (Wen 1976) has been used extensively to simulate nonlinear hysteretic system. The mechanical model developed by Yi and Dyke *et al.* (2001), based on the Bouc-Wen model, for shear mode MR damper is considered suitable and is adopted herein for the damping device. The model is shown in Figure 3. In this model, the force in the system consists of two parts, the non-hysteretic component and the hysteretic component, as follows:

$$p = c_o \dot{x} + \alpha z$$

where z = a hysteretic variable and depends on the time history of the response; x = displacement of the device; c_o = damping coefficient, α = a parameter and is a function of the input current.
The following differential equation containing x and z must be satisfied:

$$\dot{z} = -\lambda_1 |\dot{x}| z |z|^{n-1} - \lambda_2 \dot{x} |z|^n + \lambda_3 \dot{x}$$

The parameters of c_o, α, λ_1, λ_2, λ_3, and n control the scale and general shape of the hysteresis loop and

the smoothness of the force-displacement curve. The parameters can be adjusted so as to match the measured response of the system from experiments.

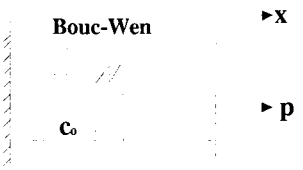


Figure 3 - Mechanical Model of the MR Damping Device

The response time of the MR damping device is an important factor affecting the performance of the device. Yang *et al.* (2002) indicated that the use of a current driver instead of a voltage-driven power supply could reduce the response time of a MR damper significantly and proved to be effective in practice. It can be shown that the governing equation for the current i in the coil, and the desired current i_d, using current driver is $L\frac{d^2i}{dt^2} + R\frac{di}{dt} + \mu i = \mu i_d$

The time required to reach the desired current i_d is $t_1 = \frac{2L}{R\beta}(\pi - \tan^{-1}\beta)$

where L = coil inductance, R = coil resistance, μ = proportional gain, $\beta = \sqrt{[(2\gamma L)/R^2 - 1]}$.
Due to the existence of residual magnetic field in the steel plates, Yang *et al.* (2002) indicated that the response time required to reduce the force in the MR damper to its minimum value was much longer than that required to increase the force in the upward direction. This phenomenon is not desirable. In order to reduce the response time when the force decreases, the current in the coil was recommended to be back-driven. Therefore, a negative current was introduced to demagnetized the steel before the current was set back to zero. It was shown that the back-driven current approach could significantly reduce the response time to an acceptable level. The back-driven current approach and a current driver are adopted in this project. Using this method, regular steel with higher carbon content may be used for the damping device instead of low carbon steel.

CONTROL STRATEGY

Dyke *et* al. (1996, 1997) has proposed a clipped-optimal control strategy based on acceleration feedback for MR dampers. Dyke and Spencer (1996) have extended the control algorithm to control MR dampers installed at different floors of a multi-storey structure. Similar research has been conducted by Yoshida and Dyke *et al.* (2001), and also Yi and Dyke (2001). It has been proved that the proposed control strategy was effective. The principles of this control algorithm are adopted herein for the nonlinear semi-active damping devices. A summary of the control strategy is given below. For a multi-storey structure with n number of damping devices, the equations of motion are as follows:

$$\mathbf{M}\ddot{\mathbf{x}} + \mathbf{C}\dot{\mathbf{x}} + \mathbf{K}\mathbf{x} = -\mathbf{M}\mathbf{R}\ddot{x}_g + \mathbf{H}\mathbf{p}$$

$$\dot{\mathbf{z}} = \mathbf{A}\mathbf{z} + \mathbf{B}\mathbf{p} + \mathbf{C}\ddot{x}_g \qquad \mathbf{y} = \mathbf{D}\mathbf{z} + \mathbf{E}\mathbf{p} + \mathbf{F}\mathbf{v}$$

Where $\ddot{x}_g$ = one dimensional ground acceleration; $\mathbf{p}$ = vector of measured forces in the n damping devices = $[p_1, p_2, \ldots p_i, \ldots p_n]$, and each force is calculated from the mechanical model based on the Bouc-Wen model as discussed above; $\mathbf{R}$ = a unit vector; $\mathbf{H}$ = a matrix depends on the locations of the dampers; $\mathbf{z}$ = state vector; $\mathbf{y}$ = vector of measured responses, such as measured acceleration at certain locations, measured displacements of the damping devices and the measured control forces; $\mathbf{v}$ = measurement noise vector; $\mathbf{A}$, $\mathbf{B}$, $\mathbf{C}$, $\mathbf{D}$, $\mathbf{E}$ and $\mathbf{F}$ are matrices in terms of $\mathbf{M}$, $\mathbf{C}$, $\mathbf{K}$, $\mathbf{R}$, and $\mathbf{H}$.

In order to produce a desired control force p_{di} in each MR damping device, n force feedback loops are required. The vector of the desired control forces is $\mathbf{p_d} = [p_{d1}, p_{d2}, \ldots p_{di}, \ldots p_{dn}]^T$

To determine the value of $\mathbf{p_d}$ from values of $\mathbf{p}$ and $\mathbf{y}$, a linear optimal controller $\mathbf{K_c}(s)$ is required, through the Laplace transform L{ }, as follows:

$$\mathbf{p_d} = L^{-1}\left\{-\mathbf{K_c}(s)L\left\{\begin{matrix}\mathbf{y}\\ \mathbf{p}\end{matrix}\right\}\right\}$$

The Linear Quadratic Gaussian, H_2/LQG strategies can be used to obtain $\mathbf{K_c}(s)$. Acceleration feedback control strategies, instead of full state feedback strategies or velocity feedback strategies, are adopted.

The relative structural displacements and velocities at the MR damping devices determine the response of the MR damping devices. The force generated by each MR damping device depends on the command current applied to the current driver of the damping device. By comparing the measured force to the desired force, the command signal for the command current is determined so as to generate the corresponding desired optimal control force p_{di} in each MR damping device.

Based on the modified clipped-optimal control algorithm developed by Yoshida and Dyke *et al.* (2001) and the use of a current driver, when the measured force, p_i, is smaller in magnitude than the desired force, p_{di}, $|p_{di}| > |p_i|$ the command current to drive the MR damping device is set to $i_i = I_{ci}$, and the magnitude of the control force increases, otherwise, when the measured force is larger than the desired force, $|p_{di}| < |p_i|$, the command current is back-driven and then set to zero.

When the measured force and the command force have opposite signs, the command current is also back-driven and then set to zero.

$$i_i = I_{ci} H(\{p_{di} - p_i\} p_i) \qquad I_{ci} = \begin{cases} a_i p_{di} & for\ p_{di} \le p_{\max} \\ I_{\max} & for\ p_{di} > p_{\max} \end{cases}$$

Where H( ) is the Heaviside step function, p_{max} is the maximum force produced by the control device and a_i is a factor showing the relationship between the command current I_{ci} and the desired force p_{di}.

Various building structural models, consist of steel members as columns and beams; and steel plates as slabs, for experimental verification of vibration control have been designed, with MR damping devices to be installed. Optimum locations of damping devices in the model will then be established so as to mitigate the dynamic effects of seismic and wind vibration. Vibration tests on building models with MR damping devices installed will be performed on a shake table to simulate earthquake excitation. Wind tunnel tests will also be performed to simulate wind excitation.

CONCLUSION

A new form of semi-active shear mode MR damping device is introduced. Results of studies on the configurations of the device and the magnetic field distributions in the device under a controlled electric current are presented. Further research including experimental tests and control strategies necessary for further development of the device has also been proposed and discussed. Preliminary results have shown that the proposed damping device will provide a positive and practical alternative for mitigating dynamic effects in buildings due to wind and earthquake loads.

ACKNOWLEDGEMENT

The work described in this paper has been fully supported by the URC (University Research Committee) of The University of Hong Kong through Seed Funding for Basic Research (2002-2003).

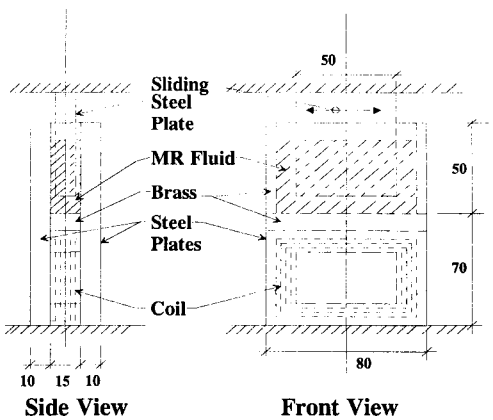


Figure 1 - MR Damping Device Details
All dimensions in millimeters unless otherwise noted

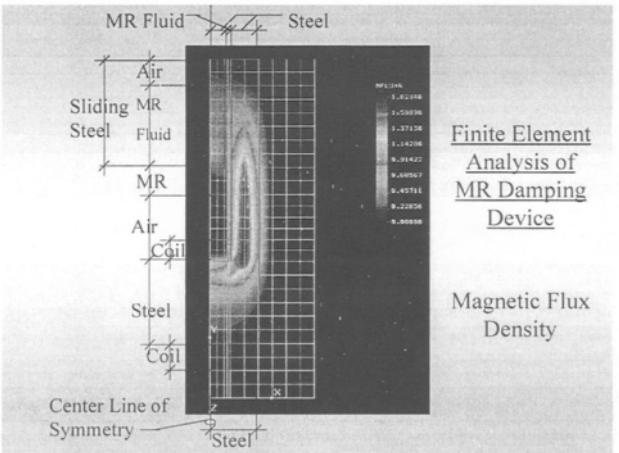


Figure 2

REFERENCES

Dyke, S.J., Spencer Jr., B.F., Sain, M.K. and Carlson, J.D. (1996). Modeling and Control of Magnetorheological Dampers for Seismic Response Reduction. *Smart Materials and Structures: Special Issue on Large Civil Structures* **5**, 565-575

Dyke, S.J., Spencer Jr., B.F., Sain, M.K. and Carlson, J.D. (1997). An Experimental Study of MR Dampers for Seismic Protection. *Smart Materials and Structures: Special Issue on Large Civil Structures.* **7**, 693-703.

Dyke, S.J., Spencer Jr. (1996). Seismic Response Control Using Multiple MR Dampers. *Proc. of the 2nd International Workshop on Structural Control. Hong Kong.* 163-173.

Housner, G.W., Bergman, L.A., Caughey, T.K., Chassiakos, A.G., Claus, R.O., Masri, S.F., Skelton, R.E., Soong, T.T., Spencer, B.F., Yao, J.T.P. (1997). Structural Control: Past, Present, and Future. *Journal of Engineering Mechanics Division,* ASCE **123**, 897-971.

Mark, R., Jolly, M.R., Jonathan, W., Bender, J.W., and Carlson, J.D. (1998). Properties and Applications of Commercial Magnetorheological Fluids. *SPIE 5th Annual Int. Symposium on Smart Structures and Materials, San Diego, CA,* March 1998.

Lord Materials Division. (1999). Magnetic Circuit Design. *Engineering Note.*

Wen, Y.K. (1976). Method of Random Vibration of Hysteretic Systems. *Journal of Engineering Mechanics Division,* ASCE **102:EM2**, 249-263.

Yang, G., Spencer Jr., B.F., Carlson, J.D., Sain, M.K. (2002). Large-scale MR Fluid Dampers: Modeling, and Dynamic Performance Considerations. *Engineering Structures,* **24**, 309-323.

Yi, F., Dyke, S.J., Caicedo, J.M., and Carlson, J.D. (2001). Experimental Verification of Multi-Input Seismic Control Strategies for Smart Dampers. *Journal of Engineering Mechanics*, ASCE **127:11,** 1152-1164.

Yoshida, O., Dyke, S.J., (2001). Seismic Control of a Nonlinear Benchmark Building Using Smart Dampers. *Journal of Eng. Mechanics: Special Issue on Struct. Control Benchmark Problem*, ASCE.

Advances in Building Technology, Volume 2
M. Anson, J.M. Ko and E.S.S. Lam (Eds.)
© 2002 Elsevier Science Ltd. All rights reserved

HYBRID PLATFORM FOR HIGH TECH EQUIPMENT AGAINST TRAFFIC-INDUCED VIBRATION

H.J.Liu[1,2], Z.C. Yang[1,2] and Y.L. Xu[1]

[1]Department of Civil and Structural Engineering, The Hong Kong Polytechnic University, Hung Hom, Kowloon, Hong Kong
[2]Department of Aircraft Engineering, Northwestern Polytechnic University, Xi'an 710072, China

ABSTRACT

This paper presents an experimental study of using a hybrid platform to mitigate vibration of a batch of high tech equipment installed in a building subject to nearby traffic-induced ground motion. A three-story building model and a hybrid platform model are designed and manufactured. The hybrid platform is mounted on the building floor through passive mounts and controlled actively by an electromagnetic actuator with velocity feedback control strategy. A series of shaking table tests are then performed on the building model without the platform, with the passive platform of different parameters, and with the hybrid platform. The experimental results demonstrate that hybrid platform is very effective in reducing the velocity response of a batch of high tech equipment in the building subject to nearby traffic-induced ground motion if dynamic properties of the platform and control feedback gain are selected appropriately.

KEYWORDS

Experimental study, high tech equipment, nearby traffic-induced ground motion, hybrid platform.

INTRODUCTION

With rapid advancement in high tech equipment such as that used for the production of semiconductors and optical microscopes, vibration criteria for high tech facilities (buildings), in which high tech equipment is installed, become more and more stringent (Gordon, 1991). One of the major sources of vibrations of concern in relation to high tech facilities is nearby road and rail traffic-induced ground motion. Thus, to ensure the high quality of ultra-precision products, it is imperative to find effective and efficient ways to reduce velocity response of a batch of high tech equipment in a modern high tech facility against nearby traffic-induced ground motion.

Using passive mounts (spring-damper systems) to isolate individual high tech equipment from building floor vibration is a very common practice in high tech equipment industry. To reduce vibration to a sufficient level, the frequency of the passive mount is expected to be as low as possible but the passive mount of low frequency will result in excessive drift. The passive mount of very low frequency may

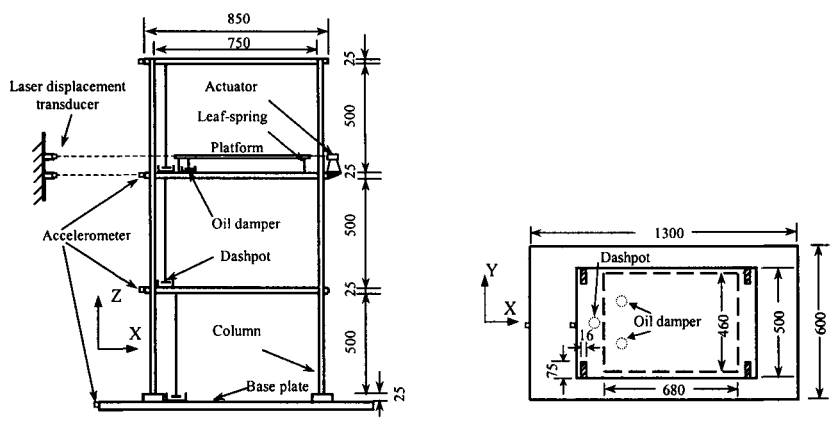
also lead to static instability of high tech equipment. To overcome these problems, a hybrid control by coupling active actuators with passive mounts to prevent individual high tech equipment from building floor vibration has been recently investigated (Nakamura et al, 1999; Yoshioka et al, 2001). However, most of the previous studies take the building floor vibration as a direct excitation to high tech equipment. Dynamic interaction between the building and the high tech equipment either passively isolated or hybrid-controlled is not considered.

This paper thus carries out an experimental study to examine the effectiveness of a hybrid platform for mitigating the vibration of a batch of high tech equipment installed in a building subject to nearby traffic-induced ground motion. A three-story building model and a hybrid platform model are designed and manufactured. The hybrid platform is mounted on the building floor through passive mounts and controlled actively by an electromagnetic actuator of velocity feedback control. A series of shaking table tests are then performed on the building model without the platform, with the passive platform of different parameters, and with the hybrid platform.

EXPERIMENTAL ARRANGEMENT

Building Model and Platform Model

The building model used in the experiment was designed and built as a three-storey shear building. The steel frame of the building model consisted of three rigid plates and four flexible columns (see Fig.1). The overall dimension of the building model was measured at 1575mm x 850mm x 500mm. The four columns of the building model were eventually welded to a thick steel plate that was in turn bolted into a shaking table. The building model motion was restricted in the x-direction only, leading to a planar frame in the x-z plane for the investigation. To properly simulate the inherent energy dissipation capacity of the real building, the small dashpots were installed between every two floors.



(a) Elevation (Unit: mm) (b) Plane (Unit: mm)

Figure 1: Configuration of model building and platform

To reduce velocity response of a batch of high tech equipment installed in a building subject to ground motion, high tech equipment is now to be installed on the hybrid platform rather than on the building floor. Therefore, the control performance of the platform is assessed by comparing its absolute velocity with that of the corresponding building floor without the platform under the same traffic-induced ground motion. The platform was mounted on the second floor of the building model through two leaf

springs. The platform was clamped on the leaf spring using three steel clamps: one fixed in the middle of the leaf spring and two designed movable in opposite direction to change the horizontal stiffness of the platform. Two shear type oil dampers were designed and installed between the platform and the second floor of the building model. Different damper damping coefficients could be achieved. An electromagnetic exciter JZK-5 was selected as an actuator to control the platform. The maximum force which could be generated by the actuator was 50 N. The force exerted on the platform by the actuator was measured using a load cell installed between the actuating rod of the actuator and the platform.

Ground Motion and Instrumentation

The experiments were carried out on the shaking table of the Hong Kong Polytechnic University. The traffic-induced ground motion was simulated using a uniformly modulated nonstationary random process (Yang and Agrawal, 2000). As the shaking table used was a seismic simulator and the building model was light, the maximum simulated ground acceleration was taken as 0.06g to ensure the normal operation of the seismic simulator, where g is the acceleration due to gravity in m/s^2. Such high ground acceleration may not be subjected by high tech facilities in real situation. However, since the linear building and platform and the linear control algorithm are concerned in this experiment, the normalized velocity responses of both the building and platform obtained from the experiment still provide a good indication of the performance of hybrid platform. Fig.2 shows the ground acceleration time-history generated by the shaking table to reproduce the nearby traffic-induced ground motion and recorded by the accelerometer installed on the surface of shaking table in the horizontal direction. The duration of the simulated ground motion was 15 seconds. The dominant frequency of the simulated ground motion ranged from 6 Hz to 35 Hz. The sampling frequency of the ground acceleration time histories was 100 Hz.

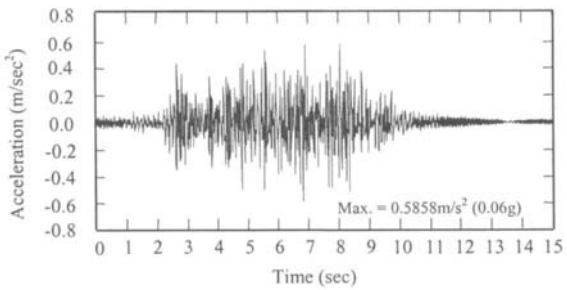


Figure 2. Compressed ground acceleration time history used in experiment

Each building floor was equipped with one B&K 4370 accelerometer in the x-direction (see Fig.1). Two Keyence LK-503 laser displacement transducers were used to measure the absolute horizontal displacement responses of both the platform and the second floor of the building (See Fig.1). The difference between the two displacement responses gave the platform drift. The signal from each B&K 4370 accelerometer was transferred to the B&K 2635 signal conditioner by which the acceleration signal could be amplified and/or converted into velocity signal using the built-in electronic circuit. The signal from the signal conditioner was then passed to a dSPACE DS1005 real-time simulator system. The displacement signal from the laser displacement transducer was also transferred to the dSPACE DS1005 real-time simulator system and sampled at 100 Hz. A power amplifier YE587 was used to provide the power to the electromagnetic exciter. The power amplifier was controlled by the dSPACE real-time simulator system. The hybrid control of the platform in this experiment was realized by using the dSPACE real-time simulator system together with the MATLAB/Simulink program on the host computer via Real Time Interface (RTI).

DYNAMIC PROPERTIES AND HYBRID CONTROL

Dynamic Properties

The natural frequencies, mode shapes, and modal damping ratios of the building model without platform were identified experimentally. The first three natural frequencies of the building model were 8.64 Hz, 25.29Hz, and 38.91 Hz. The platform can be seen as a single degree of freedom system in the x-direction. The mass of the platform together with the six clamps and two worms were weighed as 20.5 kg. For a given position of the two movable clamps and a given gap of the oil damper and with the actuator being switched off, the natural frequency and damping ratio of the platform were identified. The given position of the two movable clamps was designated in terms of the distance between the two movable clamps. The distance was selected in this investigation as 100mm (refer to D1), 250mm(refer to D2), and 300 mm (refer to D3). The gap of the oil damper was selected as 1mm (refer to C3), 2mm (refer to C2), and 3mm (refer to C1), respectively. If the gap of the oil damper exceeded 6mm, the piston of the damper did not touch any oil, leading to a no damper case (refer to C0). The natural frequencies and damping ratios of the platform were identified from the transfer functions using the bandwidth method for a series of the clamp position and the damper gap and listed in Table 1.

TABLE 1
IDENTIFIED NATURAL FREQUENCIES AND DAMPING RATIOS OF THE PLATFORM

Clamp distance D(mm)	Disk gap d(mm)	Natural frequency (Hz)	Damping ratio(%)
100	1	6.15	12.70
	2	6.15	10.53
	3	6.05	8.07
	No damper	5.66	6.04
250	1	8.20	7.15
	2	8.20	6.75
	3	8.01	6.17
	No damper	7.91	4.94
300	1	11.8	4.97
	2	11.8	4.55
	3	11.7	3.76
	No damper	11.7	3.76

Hybrid Control

For the active control, there was always a trade-off between the response reduction and the control power required. In the present work, the maximum driving force that could be generated by the electromagnetic actuator was 50N. From a practical point of view, it is difficult, if not impossible, to measure the response of all the building floors and the platform. The sub-optimal control strategy was adopted in the experiment. The sub-optimal control strategy used only the absolute velocity of the platform as a feedback variable. By trial and error, a nominal feedback control gain between the selected feedback velocity response of the platform and the control force of the actuator was determined as 640 N.s/m. Then, the feedback control gain used in the experiment changed from 20% to 100% of the nominal feedback control gain at an interval of 20%.

EXPERIMENTAL RESULTS AND ANALYSIS

Building without Platform and with Passive Platform

The building model without the platform was first tested under the nearby traffic-induced ground motion as shown in Fig.2. Fig. 3a displays the velocity response time history of the second floor of the building without the platform. The measured maximum and rms velocity responses of the second floor are 90.04mm/s and 26.13mm/s, respectively. For the case of the building without the platform, high tech equipment is supposed to be installed on the second floor of the building. Thus, the measured velocity response of the second floor of the building without platform provides a basis for the evaluation of the effectiveness of the platform by comparing it with the velocity response of the platform.

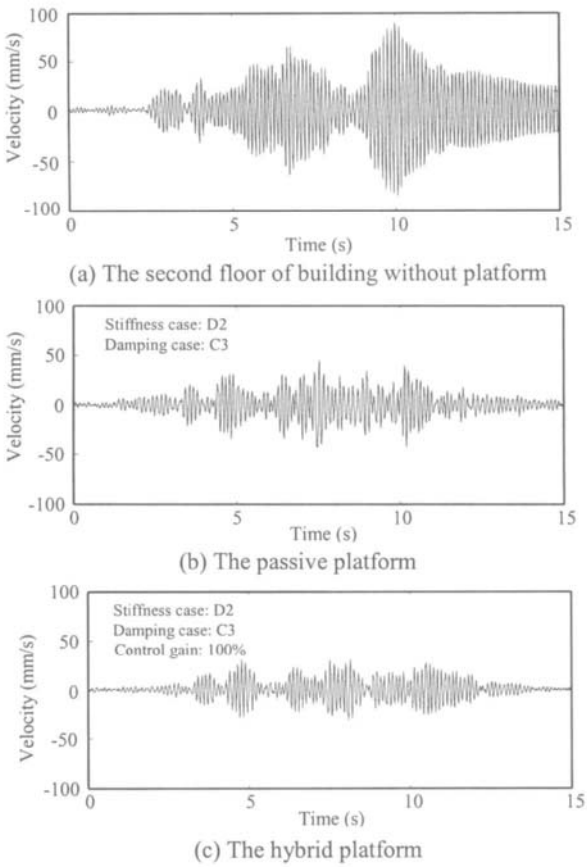


Figure 3. Comparison of absolute velocity response time histories

The building model with the passive platform presented and with the actuator switched was then tested under the traffic-induced ground motion selected. The stiffness of the passive platform varied from case D1 to case D3 in an ascending order, and the damping ratio of the passive platform altered from case C0 to case C3 also in an ascending order. There were a total of 12 test cases. The measured absolute velocity response of the passive platform was then divided by the absolute velocity response of the second floor of the building without platform to obtain the normalized velocity response (velocity response ratio) of the passive platform.

Depicted in Fig.4 are the normalized maximum velocity responses of the passive platform against the frequency and damping of the platform. The normalized maximum velocity response less than one indicates that the response of the passive platform is less than that of the second floor of the building without platform, that is, the velocity response of high tech equipment is reduced. It can be seen that except for stiffness case D3, all the normalized maximum velocity responses of the passive platform are less than one. The maximum velocity response of high tech equipment can be reduced to as low as 36% of the corresponding second floor velocity response of the building without platform. It is also seen that the platform of smaller stiffness has lower velocity response and larger velocity response reduction. Fig. 4 also shows a trend that larger damping ratio of the passive platform produces larger velocity response reduction for high tech equipment.

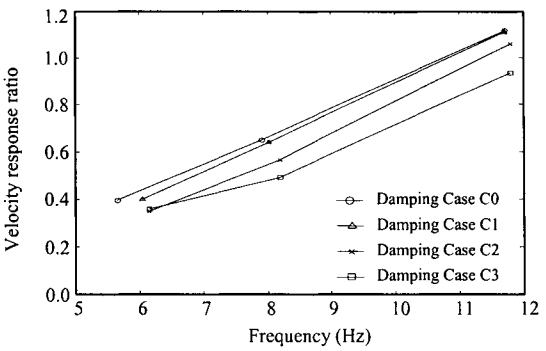


Figure 4. Normalized maximum velocity response of platform

Fig. 3b displays the velocity response time history of the passive platform with case D2 for its stiffness and case C3 for its damping ratio under the same traffic-induced ground acceleration as shown in Fig.2. It clearly demonstrates that the velocity response of the passive platform is much smaller than that of the second floor of the building without the platform as shown in Fig.3a. The maximum and rms velocity responses of the passive platform are 44.38 mm/s 11.64 mm/s only, leading to 51% and 55% reduction, respectively. This signifies that if high tech equipment is installed on the passive platform, its velocity response to traffic-induced ground motion via the building floor will be much smaller than that if it is directly installed on the building floor.

Building with Hybrid Platform

The building model with the hybrid platform was finally tested under the traffic-induced ground motion selected. For a given platform stiffness and damping ratio, the velocity feedback control gain of the hybrid platform varied from 20% to 100 % of the nominal control gain of 640 N.s/m at an interval of 20%. There were a total of 60 test cases. The measured absolute velocity response of the hybrid platform was then divided by the absolute velocity response of the second floor of the building without the platform to obtain the normalized velocity response (velocity response ratio) of the hybrid platform.

Plotted in Fig. 3c is the time history of velocity response of the hybrid platform with stiffness case D2, damping case C3, and 100% control gain. The maximum and rms velocity responses of the hybrid platform are 31.22 mm/s and 9.30 mm/s, respectively. The maximum and rms velocity responses of the hybrid platform are only 35% and 36% of the corresponding response of the second floor of the building without the platform. It is also smaller than the absolute velocity response of the passive platform by 30 % for the maximum response and by 20% for the rms response.

Fig.5 shows variations of the normalized maximum velocity response of the hybrid platform with control gain for three stiffness cases from D1 to D3 and one damping case C3. It is seen from Fig.5 that as the stiffness of the platform decreases from case D3 to case D1, the velocity response of the passive platform reduces from 94% to 36% of the second floor velocity response of the building without the platform. The velocity response of the hybrid platform at 100% control gain reduces from 65% to 24 % of the second floor velocity response of the building without the platform, and from 69% to 67% of the velocity response of the passive platform. These results demonstrate the effectiveness of the passive platform and the superior performance of the hybrid platform over the passive platform.

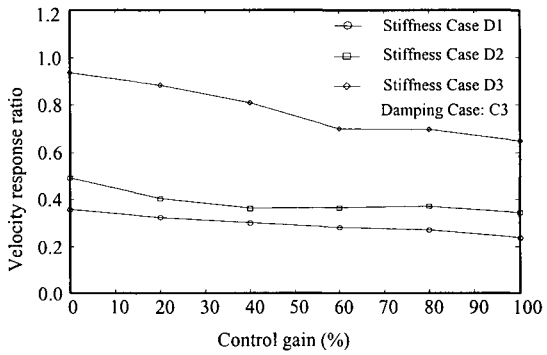


Figure 5. Normalized maximum velocity response of hybrid platform vs. control gain & stiffness

While the use of hybrid platform can significantly reduce the velocity response of high tech equipment, it can also reduce the drift of the platform compared with the passive platform. Fig. 6 shows variations of the normalized rms drift (drift ratio) of the platform with control gain for three stiffness cases from D1 to D3 and one damping case C3. The rms drift of the hybrid platform plotted in Fig.6 is normalized by the rms drift of the corresponding passive platform. It is seen that with the increase of control gain, the drift of the hybrid platform decreases. The drift of the hybrid platform can be reduced to 61%, 54%, and 49% of the drift of the corresponding passive platform for stiffness case D1, D2 and D3, respectively. The significant reduction of the platform drift benefits the practical use of the hybrid platform. The high performance of the hybrid platform is attributed to the control force or control power provided by the actuator. Fig.7 shows variations of the maximum control force with control gain for the building under the selected ground motion of peak acceleration of 0.06g and for the platform of three stiffness cases from D1 to D3 and one damping case C3. It is seen that with the increase of control gain, the velocity response and drift of the hybrid platform are reduced as shown in Figs. 5 and 6, but the required control force increases as shown in Fig.7. It is also seen that the platform of higher stiffness needs larger control force. However, it was found that the control power required was not significantly larger in the case of higher control gain or larger control force.

CONCLUSIONS

An experimental study has been carried out to examine the effectiveness of a hybrid platform for mitigating the vibration of a batch of high tech equipment installed in a building subject to nearby traffic-induced ground motion. A series of shaking table tests have been performed on a three-story building model without the platform, with the passive platform of different parameters, and with the hybrid platform of velocity feedback control. The experimental results demonstrated that the passive platform is effective in reducing the velocity response of high tech equipment in the building subject to nearby traffic-induced ground motion if the stiffness of the platform is small. The hybrid platform is

more effective than the passive platform in reducing both the velocity response of a batch of high tech equipment and the drift of the platform, in particular when the stiffness of passive platform is high.

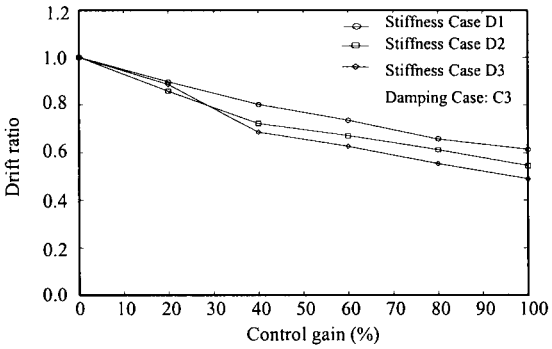


Figure 6. Normalized RMS drift of hybrid platform vs. control gain & stiffness

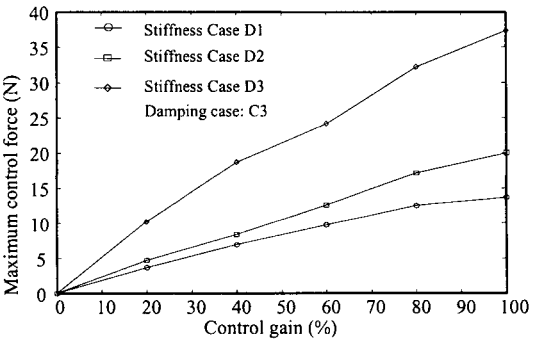


Figure 7. Maximum control force vs. control gain & stiffness

ACKNOWLEDGEMENTS

The writers are grateful for the financial support from the Hong Kong Polytechnic University through its Area of Strategic Development Programme in Structural Control.

REFERENCES

Gordon, C.G. (1991). Generic criteria for vibration sensitive equipment. *Proc. SPIE 1619*, 71-85.

Nakamura, Y. Nakayama, M., Masuda, K., Tanaka, K., Yasuda, M. and Fujita, T.(1999). Development of 6-DOF microvibration control system using giant magnetostrictive actuator. *Proc. SPIE 3671,* 229-240.

Yang, J. N. and Agrawal, A.K.(2000). Protective systems for high-technology facilities against microvibration and earthquake. *J. Struct. Eng. and Mech.* **10**(6): 561-567.

Yoshioka, H., Takahashi, Y., Katayama, K., Imazwa, T. and Murai, N.(2001). An active microvibration isolation system for hi-tech manufacturing facilities. *J. Vib. and Acoustics, ASME* 123: 269-275.

Advances in Building Technology, Volume 2
M. Anson, J.M. Ko and E.S.S. Lam (Eds.)
© 2002 Elsevier Science Ltd. All rights reserved

SEISMIC CONTROL OF ADJACENT BUILDINGS USING FLUID DAMPERS: EXPERIMENTAL STUDY

X.L.Lu[1], Y.L. Xu[2] and Z. Yang[1]

[1]Research Institute of Structural Engineering and Disaster Reduction, Tongji University, Shanghai 200092, China
[2]Department of Civil and Structural Engineering, The Hong Kong Polytechnic University, Hung Hom, Kowloon, Hong Kong

ABSTRACT

A comprehensive experimental investigation on dynamic characteristic and seismic response of adjacent buildings linked by fluid dampers is carried out using a 4m x 4m seismic simulator. Two building models are built as one five-story steel frame 5m high and the other six-story steel frame 6m high. The fluid dampers connecting the two building models are of linear force-velocity property. The control performance of fluid dampers is assessed through the comparison of dynamic characteristic and seismic response of the adjacent buildings linked by fluid dampers with those linked by rigid rods or without any connections. The effects of the number, location, and linking pattern of fluid dampers on control performance are then investigated. The experimental results show that the installation of fluid dampers can significantly reduce the seismic responses of both buildings. The number, location, and linking pattern of fluid dampers should be considered properly to achieve good control performance.

KEYWORDS

Seismic response control, adjacent buildings, fluid damper, rigid rod, seismic simulator.

INTRODUCTION

Buildings in a modern city are often built closely to each other because of limited land available and centralized services preferable. Most of these buildings are separated without any structural connections. Some of adjacent buildings are linked by sky bridges at several locations to provide a horizontal transportation system for access to the two buildings. Some of adjacent buildings are rigidly connected by stiff plates or beams at a few locations to enhance the lateral stiffness of the buildings. The concept of linking adjacent buildings using passive dampers, semi-active dampers, or active dampers has been thus proposed to improve their seismic resistant performance.

Westermo (1989) analytically investigated the seismic behavior of adjacent buildings connected by hinged rigid links. Kobori et al.(1988) developed bell-shaped hollow connectors to link adjacent buildings in a complex. Zhang and Xu (2000) presented a framework for estimating modal damping ratios and stochastic seismic responses of adjacent buildings connected by fluid dampers. Apart from

passive control, Seto and Matsumoto (1996) suggested using active actuators to connect a group of buildings and investigated how to prevent spillover problem. Xu and Zhang (2002) presented a closed form solution for seismic response of adjacent buildings with LQG controllers. Christenson et al (1999) investigated the semi-active control of adjacent buildings using modern smart dampers with a clipped-optimal control strategy.

The experimental investigations of adjacent buildings linked by passive control devices are very limited. Xu et al. (1999) experimentally investigated dynamic characteristic and response of adjacent buildings connected by fluid dampers. The experimental was, however, conducted by applying a harmonic excitation in one direction only. As a continuing investigation, this paper thus performs a series of experiments of adjacent buildings linked by fluid dampers on a 4m x 4m seismic simulator. The experimental arrangement, including the design of two large-scale building models and the instrumentation, is introduced. The performance of fluid dampers is then assessed through the comparison of seismic responses of the adjacent buildings linked by fluid dampers with those linked by rigid rods or without any connections. Effects of the number, location, and linking pattern of fluid dampers on control performance are also investigated.

EXPERIMENTAL ARRANGEMENT

Two building models of 1:4 length scale were designed and built. Building 1 was constructed as a symmetric single-bay six-story steel frame while Building 2 was made as a symmetric single-bay five-story steel frame (see Fig. 1). The overall dimensions of Building 1 were 1.95m×1.95m in plane and 6.0m in elevation while Building 2 had a dimension 2.0m×1.08m in plane and 5.0m in elevation. The story height for each building was 1.0m. The two building models were set on the shaking table side by side with a distance of 637mm for the installation of fluid dampers. Fluid dampers used in the experiment were 1.5x 4 d-series linear fluid dampers with a 102 mm stroke and a maximum damping force of 8900 N, designed and manufactured by Taylor Devices Inc., USA. The d-series fluid dampers were extensively calibrated and tested by Constantinou and Symans (1993). The damping coefficient of the used fluid damper at zero frequency was about 15.41 N.s/mm.

The experiments were carried out on a six-degree-freedom seismic simulator of the State Key Laboratory for Disaster Reduction in Civil Engineering at Tongji University in Shanghai, China. The shaking table was manufactured by the MTS corporation, USA, with the size 4.0m×4.0m in plane and the maximum specimen weight 250KN. The simulated seismic motion can be generated in two horizontal directions and one vertical direction simultaneously with the maximum accelerations of 1.2g, 0.8g, and 0.7g, respectively. A total of 23 accelerometers were arranged in the two buildings to measure their absolute acceleration responses in the x-, y-, and z-directions and their absolute angular acceleration responses about the z-axis. The locations of the accelerometers are indicated in Fig. 1. The dynamic displacement responses of both buildings were obtained from the measured acceleration response time histories through double integration with a proper filter. Subsequently, the relative dynamic displacement of each floor to the shaking table was acquired by subtracting the shaking table displacement from the absolute floor displacement. A total of 6 fluid dampers were available and each fluid damper was installed together with a load cell to measure damper damping force. The signals from all the sensors were directly sent to the data acquisition/processing system of the MTS seismic simulator. The sampling period was 0.01 second for all the tests.

TEST CASES

The whole experiment in this study was divided into 4 phases with 22 cases. Phase 1 is mainly to assess the performance of fluid dampers through the comparison of seismic responses of the adjacent

buildings linked by fluid dampers with those linked by rigid rods or without any connections. Each fluid damper or rigid rod was connected to a building through a hinge. In this phase, the two buildings without any connections were first tested under the El Centro 1940 N-S ground motion of 0.2g peak acceleration in the x-direction only (Case 1) and then under the El Centro ground motions of 0.1g, 0.08g, and 0.06g peak accelerations in the x-, y- and z-directions correspondingly (Case 4). The two buildings were then connected by two rigid rods at the 5th floor at an oblique (45^{o}) angle and tested under the El Centro ground motion in the x-direction only (Case 2) and then under the three directional El Centro ground motions (Case 5). Finally, the two rigid rods were replaced by two fluid dampers at the same position to connect the two buildings, which were also tested under the El Centro ground motion in the x-direction only (Case 3) and then under the three directional El Centro ground motions (Case 6).

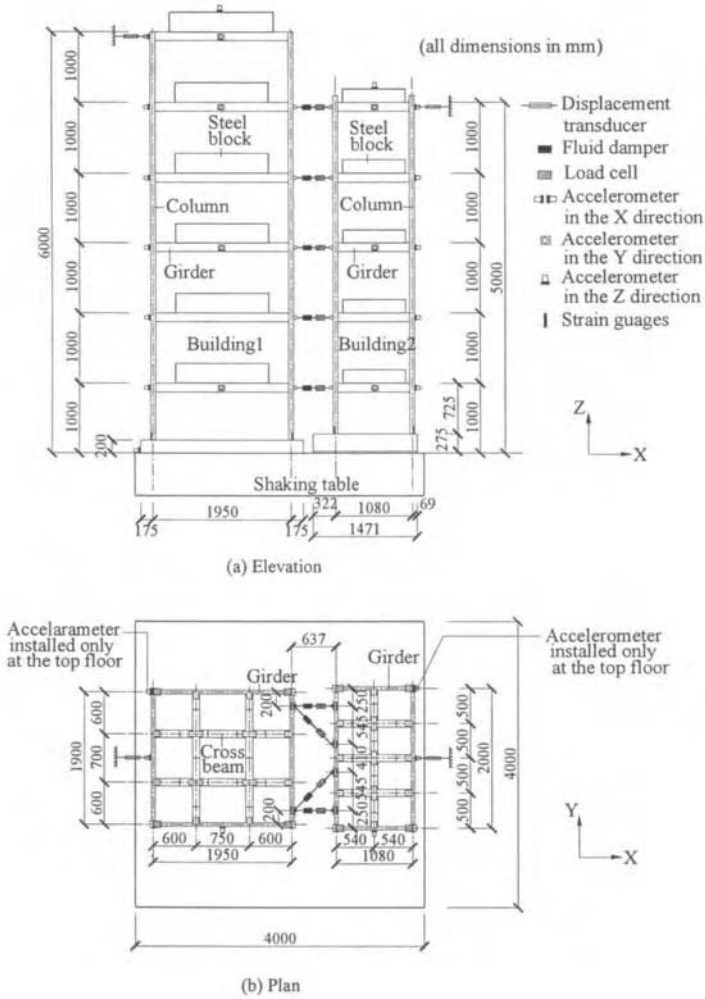


Figure 1: Configuration and instrumentation of adjacent buildings with fluid dampers

Phase 2 is mainly to investigate effects of the number, location, and linking pattern of fluid dampers on control performance. There were a total of 8 cases in Phase 2. In Case 7 to Case 11, the two buildings were connected by two parallel fluid dampers per floor at the 1st floor only (Case 7), at the 3rd floor

only (Case 8), at the 5th floor only (Case 9), at the 2nd and 4th floors (Case 10), and at the 1st and 3rd and 5th floors (Case 11) under the El Centro ground motion of 0.2g peak acceleration in the x-direction only. In Case 12 to Case 14, the two buildings were connected by two oblique dampers per floor at the 5th floor only (Case 12), at the 2nd and 4th floors (Case 13), and at the 1st and 3rd and 5th floors (Case 14) under the El Centro ground motions of 0.2g and 0.16g peak accelerations in the x- and y-directions, respectively. Because of space limitation, only part of the work involved in phase 1 and phase 2 is presented in this paper.

PERFORMANCE OF FLUID DAMPER

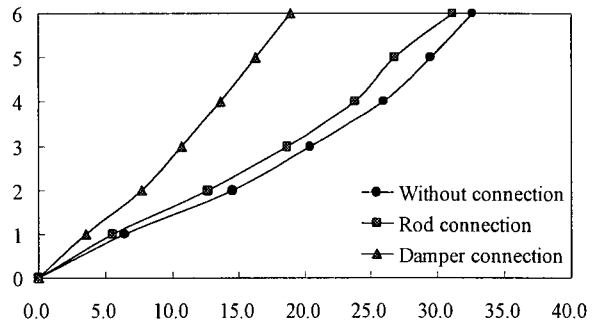
Dynamic Characteristics

To identify the natural frequencies and modal damping ratios of the two buildings with and without connections, a 0.07g white noise ground motion was inputted into the shaking table to excite the two buildings. The recorded acceleration responses were then processed to obtain the transfer functions, from which the natural frequencies and modal damping ratios were estimated. In the x-direction, the first three natural frequencies of Building 1 without any connections were 1.86 Hz, 5.86 Hz, and 9.77 Hz while the first three natural frequencies of Building 2 without any connections were 3.42 Hz, 10.35 Hz and 16.02 Hz, respectively. For the two buildings pin-connected by the two rigid rods at the 5th floor and at a 45° angle, the first three natural frequencies of Building 1 were the same as those of Building 2 with the values of 2.34 Hz, 5.76 Hz, and 9.86Hz, respectively. This result implies that the two buildings are strongly coupled in the x-direction. For the two buildings connected by two fluid dampers at the same position as the two rigid rods, the first three natural frequencies dominated by Building 1 were 2.05 Hz, 5.86 Hz, and 9.77 Hz while those dominated by Building 2 were 3.71 Hz, 10.55 Hz, and 16.02 Hz, respectively. Evidently, the installation of the fluid dampers only slightly changed the first natural frequency of each building while remaining the higher frequencies almost unchanged. The retention of the natural frequencies of the unlinked buildings is especially desirable for the adjacent buildings that have already been built and need to be strengthened. The more important result is that with the installation of fluid dampers, the first modal damping ratio dominated by Building 1 was increased from 1.78% to 7.14% and that dominated by Building 2 was enhanced from 1.67% to 10.80%. For the rigid rod connection, the modal damping ratios changed only slightly compared with the buildings without any connections.

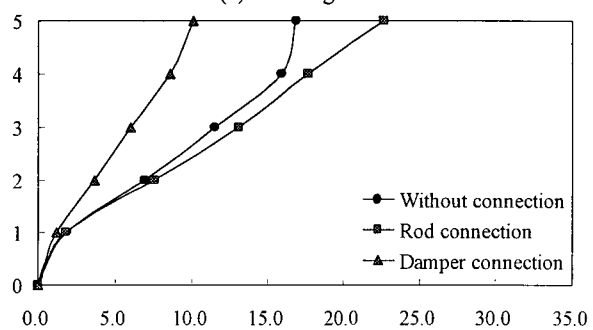
Seismic Response to One Directional Excitation

The seismic responses of the two buildings with and without connections presented in this section were obtained under the El Centro ground motion of 0.2g peak acceleration in the x-direction only. The seismic responses obtained from the recorded time-histories included the maximum and root-mean-square (RMS) relative displacement response, the maximum and RMS absolute acceleration response, and the maximum and RMS story drift. Because of space limitation, only a small part of results can be presented in this section. Figs. 2a and 2b depict variations of the maximum relative displacement responses of the two buildings to the shaking table with building height. It is seen that with the rigid rod connection, the maximum relative displacement responses of Building 1 are only slightly reduced while those of Building 2 are actually increased significantly at the top floor by 33.8 % compared with the building without connection. With the fluid dampers installed, the maximum relative displacement responses of both buildings are considerably reduced with the maximum reduction by 42.1 % at the top of Building 1 and by 40.6 % at the top of Building 2. These results are consistent with the changes in the measured modal damping ratios and natural frequencies. As for the maximum story drifts of the two buildings, with the rigid rod connection the maximum story drifts of Building 2 were actually increased by up to 62.0 % except for the 1st floor. The maximum story drifts of Building 1 were increased at the 3rd and 6th floors but reduced at the 1st, 2nd, and 4th floors. For the two buildings connected by the two fluid dampers, the maximum story drifts of both buildings were significantly reduced with the

maximum reduction by 44.4 % for Building 1 and by 55.4 % for Building 2 at the 2nd floor. The above results clearly demonstrate the effectiveness of fluid dampers in reducing the seismic responses of both buildings.



(a) Building 1



(b) Building 2

Figure 2: Variations of maximum relative displacement responses with building height

Seismic Response to Three Directional Excitations

The two buildings with and without connections were also tested under 3-D El Centro excitations with 0.1g, 0.08g and 0.06g peak accelerations in the x-, y- and z-directions, respectively. It was found that the seismic responses of both buildings in the z-direction were very small and seemed not to affect the seismic responses of both buildings in the x- and y-directions. In the x-direction, it was found that the measured seismic responses of the two buildings with and without connections were almost proportional to those under the x-directional El Centro excitation described in the last section. The fluid dampers were quite effective in reducing the seismic responses of both buildings whereas the rod connections enlarged the maximum relative displacement response of Building 2 and slightly reduced the maximum relative displacement response of Building 1.

In the y-direction, it was found that the installation of fluid dampers remarkably reduced the seismic responses of Building 2 but only slightly abated that of Building 1. The rod connections could not reduce the seismic response of Building 1 and only slightly reduced that of Building 2. For the two building models investigated, the connection of the two buildings by either rigid rods or fluid dampers under the y-directional excitation introduced some small torsional vibration to both buildings. Compared with the rod connection, the fluid dampers induced much less torsional response to the buildings. Though the use of fluid dampers to connect the two symmetric buildings may introduce

some small torsional vibration when the ground motion in the y-direction, it may be able to reduce excessive torsional vibration for two buildings of irregular shape but it needs further investigation.

EFFECTS OF DAMPER NUMBER AND LOCATION

Parallel Arrangement of Dampers

To investigate effects of the number and location of fluid dampers on control performance, the two buildings were connected by two parallel fluid dampers per floor at the 1st floor only (Case 7), at the 3rd floor only (Case 8), at the 5th floor only (Case 9), at the 2nd and 4th floors (Case 10), and at the 1st and 3rd and 5th floors (Case 11). The 0.07g white noise ground motion was first used to identify the natural frequencies and modal damping ratios for each case. The El Centro ground motion of 0.2g peak acceleration was then inputted into the shaking table in the x-direction to record seismic responses of the two buildings.

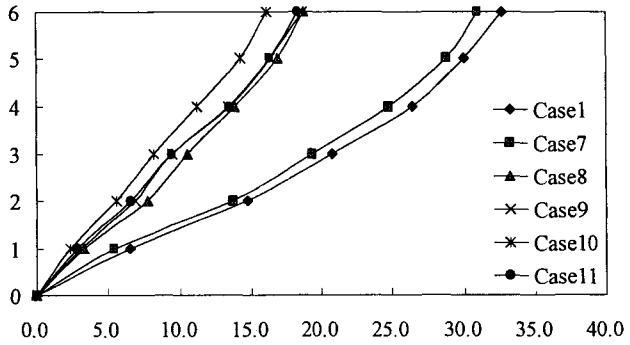
In Case 7 where the two fluid dampers were installed at the 1st floor, the first three natural frequencies dominated by either building remained almost the same as those of the building without any connection. The first three modal damping ratios dominated by Building 1 were moderately increased but those dominated by Building 2 changed slightly compared with the building without connection. When the two dampers was moved to the 3rd floor (Case 8), the 2nd natural frequency of Building 1 could not be clearly identified from the transfer function while the first three natural frequencies dominated by Building 2 were changed slightly. The identified first modal damping ratios dominated by Building 1 and Building 2 were 9.14% and 15.5%, respectively. The higher modal damping ratios were not easy to be identified because the measured transfer function became flat around the higher natural frequencies. In Case 9 where the two dampers were installed at the 5th floor, the first three natural frequencies dominated by either building changed slightly compared with those without connection. However, the first modal damping ratio dominated by either building was significantly increased to more than 8%. The results from Case 7 to Case 9 clearly demonstrate the effects of damper location on the dynamic characteristics of the two buildings. When the number of dampers were increased to 4 (Case 10) and 6 (Case 11), the two buildings were strongly coupled and the first natural frequency of both buildings became the same of 2.25 Hz for Case 10 and 2.34 Hz for Case 11. The first modal damping ratios of the buildings were increased to above 6.78% in Case 10 and 6.90 % in Case 11. No higher natural frequencies and modal damping ratios could be identified.

Figures 3a and 3b depict the maximum relative displacement responses of Building 1 and Building 2, respectively, against building height for each case under the El Centro ground motion of 0.2g peak acceleration in the x-direction. For Building 1, the most effective arrangement of fluid dampers is either Case 10 using four fluid dampers or Case 8/Case 9 using two dampers only. The maximum relative displacement response of the top floor is reduced by 50.6 % in Case 10 and by 42.4 % in Case 8. For Building 2, the most effective arrangement is Case 8 where only the two dampers were arranged at the 3rd floor. The maximum relative displacement response of the top floor is reduced by 52 %. It is interesting to see that the use of more dampers (Case 11) may not achieve larger vibration reduction for Building 2. This may be because the damping coefficient of dampers used in the tests is not optimal for Case 11.

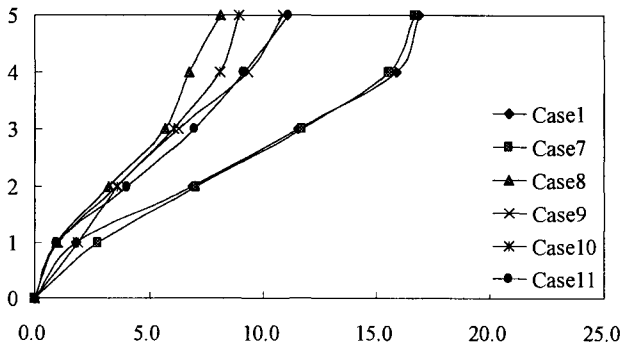
Oblique Arrangement of Dampers

This section examines the two buildings connected by two oblique dampers per floor at the 5th floor only (Case 12), at the 2nd and 4th floors (Case 13), and at the 1st and 3rd and 5th floors (Case 14). In such arrangements, not only the effects of damper number and location but also the effects of damper damping coefficient on control performance could be examined. This is because when a fluid damper

was arranged at an angle of 45^0 to the building motion, its original damping coefficient would be reduced by 50% in the direction of building motion.



(a) Building 1



(b) Building 2

Figure 3: Effects of number and location of fluid dampers

The first three natural frequencies and modal damping ratios dominated by either building in the x-direction or the y-direction in Case 12 were the same as those in Case 3. For the two buildings connected at the 2^{nd} and 4^{th} floors (Case 13), the first natural frequency dominated by Building 1 in the x-direction had a slight change to 2.05 Hz and the higher natural frequencies had almost no change compared with the building without connection. The first modal damping ratio dominated by Building 1 had an increase to 6.75 %. For Building 2, only the first natural frequency could be clearly identified as 3.71 Hz and the corresponding modal damping ratio was 7.68%. In the y-direction, the natural frequencies and modal damping ratios identified from Case 13 were close to those from Case 12. When the two buildings were linked at the 1^{st}, 3^{rd}, and 5^{th} floors (Case 14), the first natural frequency of both buildings became the same of 2.05 Hz but the higher natural frequencies could not be accurately identified. The first modal damping ratio was 10.8% for Building 1 and 11.9% for Building 2. Compared with Case 11 in which the two buildings were connected at the 1^{st}, 3^{rd}, and 5^{th} floors but with parallel arrangement of dampers, one may find that the first modal damping ratio of either building with oblique arrangement of dampers was considerably increased. This confirms that the damper damping coefficient used in Case 11 was not optimal.

Corresponding to the changes in natural frequencies and modal damping ratios, the most effective arrangement of fluid dampers for Building 1 and Building 2 was Case 14 in the x-direction. The maximum relative displacement response of the top floor of Building 1 was reduced by 49.6% for

Building 1 and 49.1% for Building 2. The reduction of RMS relative displacement response was even larger. In the y-direction the three cases gave almost the same control performance. The maximum relative displacement response of the top floor was reduced by 8.9 % for Building 1 and 51.6% for Building 2.

CONCLUSIONS

A comprehensive experimental investigation on dynamic characteristic and seismic response of adjacent buildings linked by fluid dampers has been carried out on a 4m x 4m seismic simulator using a five-story steel frame 5 m high, a six-story steel frame 6 m high, and a few Taylor fluid dampers. The experimental results showed that the installation of fluid dampers of proper parameters could significantly increase the modal damping ratios and reduce the seismic responses of both buildings while remaining the natural frequencies of both buildings almost unchanged. The seismic performance of adjacent buildings linked by fluid dampers was more superior than that of the adjacent buildings linked by rigid rods. The number, location, and linking pattern of fluid dampers should be properly selected in order to achieve good control performance. For the two buildings investigated, two fluid dampers installed at the 3rd floor gave the best performance. The use of more dampers did not necessarily achieve larger vibration reduction. The oblique damper arrangement could reduce the seismic responses of both buildings in two directions but it could introduce some torsional effects.

ACKNOWLEDGEMENTS

The writers are grateful for the financial supports from the National Natural Science Foundation of China through an NNSF grant (50025821) and the Hong Kong Polytechnic University through an internal research grant and its Area of Strategic Development Programme. The writers also very much appreciate the help from Mr Craig Winters of Taylor Devices, Inc., USA, in providing the fluid dampers and useful information for the writers.

REFERENCES

Christenson R.E., Spencer, B.F., and Johnson, E.A. (1999). Coupled building control using active and smart damping strategies. *Proc. 5th Int. Conf. on Application of Artificial Intelligence to Civil Engng. and Struct. Engng.*, Oxford, UK, 187-195.

Constantinou M.C. and Symans M.D. (1993). Experimental study of seismic response of buildings with supplemental fluid dampers. *The Structural Design of Tall Buildings*, 2, 93-132.

Kobori T., Yamada T., Takenaka Y., Maeda Y., and Nishimura I. (1988). Effect of dynamic tuned connector on reduction of seismic response: application to adjacent office buildings. *Proc. of the Ninth World Conference on Earthquake Engineering*, Vol.V, Tokyo-Kyoto, Japan, 773-8.

Seto T. and Matsumoto Y.(1996). A structural vibration control method of flexible buildings in response to large earthquakes and strong winds. *Proc. 2nd Int. Workshop on Struct. Control*, Hong Kong, 490-496.

Westermo B. (1989). The dynamics of interstructural connection to prevent pounding. *Earthquake Engng. Struct. Dyn.*, 18, 687-99.

Xu Y.L., Zhan S., Ko J.M., and Zhang W.S. (1999). Experimental investigation of adjacent buildings connected by fluid damper. *Earthquake Engng. Struct. Dyn.*, 28, 609-631.

Xu, Y.L. and Zhang, W.S. (2002). Closed form solution for seismic response of adjacent buildings with LQG controllers. *Earthquake Engng. Struct. Dyn.*, 31(2), 235-259.

Zhang W.S. and Xu Y.L.(2000). Vibration analysis of two buildings linked by Maxwell model-defined fluid dampers. *J Sound and Vibration*, 233, 775-796.

Advances in Building Technology, Volume 2
M. Anson, J.M. Ko and E.S.S. Lam (Eds.)
© 2002 Elsevier Science Ltd. All rights reserved

SEISMIC RESPONSE CONTROL OF MULTI-STORY BUILDINGS USING SEMIACTIVE FRICTION DAMPERS

C.L. Ng and Y.L. Xu

Department of Civil and Structural Engineering, The Hong Kong Polytechnic University, Hung Hom, Kowloon, Hong Kong

ABSTRACT

This paper presents an investigation on the seismic response control of multi-story buildings using semi-active friction dampers (SAFD) in conjunction with the ordinary braces. Piezoelectric materials are used to control the clamping force of a friction damper so as to regulate the slip force of the damper through simple feedback of stick or slip status of the damper. The performance of SAFD in suppressing structural vibration is assessed by considering first a single-story building under white noise excitation and then a multi-story building under El-centro seismic ground motion. The responses of the buildings with SAFD are compared with those of the buildings without control and with passive friction dampers (PFD). The simulation results demonstrate the effectiveness of semi-active friction dampers and the robustness and adaptability of the buildings with SAFD to different excitation intensities and damper parameters.

KEYWORDS

Multi-story building, seismic response, semi-active friction damper, control algorithm, parametric study, comparison.

INTRODUCTION

Passive friction damper (PFD) is one of the widely accepted energy dissipating devices for vibration control of civil engineering structures. Not only the performance of passive friction dampers in abating seismic response of structures has been verified by numerous experimental and analytical studies, but also they have been implemented into many real buildings and structures of a variety of configurations in the past twenty years. Pall and Marsh (1982) developed the friction devices for X-bracing in frame structures, which were further put in practical application by Pall and Pall (1993) in the aseismic design and construction of some new buildings and retrofitting of existing buildings. An efficient numerical modeling for Pall friction device was described by Filiatrault and Cherry (1989) who proposed a simplified design procedure for the friction damped braced frames in 1990 leading to a greater acceptance of the design.

As the friction dampers are operated in passive nature, a specific slip force should be decided so as to optimize the reduction of structural vibration for particular ground excitation. However, the slip force preset based on one ground excitation may not be optimal parameter for another excitation. In this connection, semi-active friction dampers (SAFD) of which the slip force can be adjusted in real time may be able to overcome the problem and further enhance the efficacy of friction devices. Akbay and Aktan (1991) and Kannan et al (1995) proposed an actively regulated friction slip braces where the pre-specified clamping load was regulated by a fixed increment in response to the stick and slip status of the damper. A similar device was considered by Dowdell and Cherry (1994) by employing two semi-active control algorithms, the off-on control scheme and the continuously variable amplitude friction damper scheme.

Most of previous studies on semi-active friction dampers employed hydraulic actuators to regulate the clamping forces of dampers. This paper suggests using piezoelectric materials as an actuator to regulate the slip force of the damper through a simple feedback of damper motion status. The control algorithm adopted in the study was suggested by Akbay and Aktan which attempts to reverse the sticking and sliding status of the damper at the friction interface by reducing or increasing the slip force by one pre-specified increment at fixed time intervals to initiate early energy dissipation. This control algorithm is preferred due to the advantage that only local feedback information is sufficient to achieve the feedback control of structure, which is also motivated from both economical and practical points of view. The performance of SAFD in suppressing structural vibration is assessed by considering first a single-story building under white noise excitation and then a multi-story building under El-centro seismic ground motion in this paper. The responses of the buildings with SAFD are then compared with those of the buildings without control and with passive friction dampers.

FORMULATION AND ANALYTICAL PROCEDURE

Equation of Motion of Friction Damped Buildings

Consider an n-story building in which m friction dampers of each connected in series with an elastic axial member are installed in selected story units as shown in Fig. 1. The system is idealized as an n-degree-of-freedom linear system and is subjected to one-dimensional ground acceleration $\ddot{x}_g$. The equation of motion of the system is given by

$$\mathbf{M}\ddot{\mathbf{x}} + \mathbf{C}\dot{\mathbf{x}} + \mathbf{K}\mathbf{x} = -\mathbf{M}\mathbf{l}\ddot{x}_g + \mathbf{B}\mathbf{u} \tag{1}$$

where $\mathbf{M}$, $\mathbf{C}$, and $\mathbf{K}$ are the $n \times n$ mass, damping and stiffness matrices of an n-story unbraced frame, respectively; $\mathbf{x} = [x_1, x_2, \ldots, x_n]^T$ is the n-dimensional lateral displacement vector relative to ground; $\dot{\mathbf{x}}$ and $\ddot{\mathbf{x}}$ are the velocity vector and acceleration vector, respectively; $\mathbf{l}$ is the $n \times 1$ unit vector denoting the influence of the horizontal ground acceleration $\ddot{x}_g$ to the masses; $\mathbf{B}$ is the $n \times m$ matrix describing the locations of semi-active friction dampers; and $\mathbf{u} = [u_1, u_2, \ldots, u_m]^T$ is the m-dimensional control force vector depending on the sticking and slipping status of the damper as follows:
(i) If the i^{th} damper is sticking, $|u_i| \leq S_i$

$$u_i = \bar{k}_i (d_i - e_i) = \bar{k}_i z_i \tag{2}$$

$$\bar{\mathbf{K}} = \mathrm{diag}[\bar{k}_1, \bar{k}_2, \ldots, \bar{k}_m] \tag{3}$$

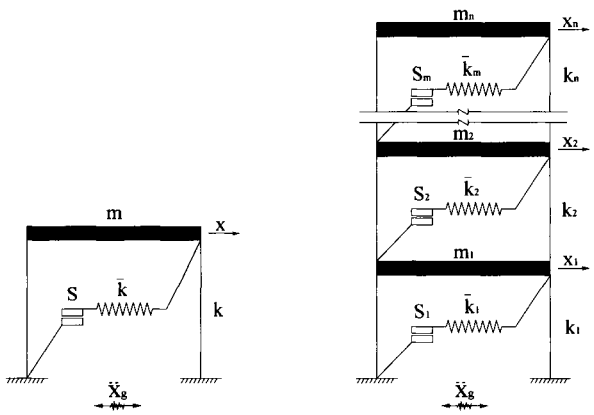
in which $\bar{k}_i$ is the i^{th} element of the lateral diagonal brace stiffness matrix $\overline{\mathbf{K}}$; d_i and e_i are the inter-story drift and lateral slip deformation of friction damper on the i^{th} story, respectively; z_i denotes the elastic lateral deformation of the brace; and S_i is the lateral slip force of the i^{th} friction damper.
(ii) If the damper is slipping, $|u_i|>S_i$

$$u_i = S_i \, \mathrm{sgn}(z_i) \tag{4}$$

$$\mathrm{sgn}(z_i) = \begin{cases} 1 & \text{if } z_i > 0 \\ -1 & \text{if } z_i < 0 \end{cases} \tag{5}$$

where the lateral brace force is tensile if $\mathrm{sgn}(z_i)$ is positive and vice versa. When the aforementioned damped brace system is operated passively, the lateral damper slip force S_i is fixed. However, in respect to semi-active control, if the damper slips in the previous decision interval, the slip force is raised to achieve more energy dissipation. On the other hand, if slippage does not take place in the previous decision interval, the slip force is lowered to come into slipping stage and invoke the energy dissipation. Therefore, the slip force S_i is regulated by a constant slip load increment ΔS_i with time and is given by,

$$S_i(t_i) = \begin{cases} S_i(t_{i-1}) - \Delta S_i & \text{(sticking)} \\ S_i(t_{i-1}) + \Delta S_i & \text{(slipping)} \end{cases} \tag{6}$$



(a) Single-story model (b) Multi-story model

Figure 1: Schematic diagrams of friction damper-building systems

Numerical Simulation

Equation of motion of friction damped system expressed by Eq. 1 can also be written in incremental form as

$$\mathbf{M}\Delta\ddot{\mathbf{x}} + \mathbf{C}\Delta\dot{\mathbf{x}} + \mathbf{K}\Delta\mathbf{x} = -\mathbf{M}\mathbf{I}\Delta\ddot{x}_g + \mathbf{B}\Delta\mathbf{u} \tag{7}$$

Based on the Wilson-θ method, the incremental pseudo-static equilibrium equation is given by

$$\hat{\mathbf{K}}\hat{\Delta}\mathbf{x} = \hat{\Delta}\mathbf{P} \tag{8}$$

where

$$\hat{\mathbf{K}} = \mathbf{K} + \frac{6}{\tau^2}\mathbf{M} + \frac{3}{\tau}\mathbf{C} \tag{9}$$

$$\hat{\Delta}\mathbf{P} = \theta\Delta\mathbf{P} + \theta\mathbf{B}\Delta\mathbf{u} + \mathbf{M}(\frac{6}{\tau}\dot{\mathbf{x}} + 3\ddot{\mathbf{x}}) + \mathbf{C}(3\dot{\mathbf{x}} + \frac{\tau}{2}\ddot{\mathbf{x}}) \tag{10}$$

$$\Delta\mathbf{P} = -\mathbf{M}\mathbf{I}\Delta\ddot{x}_g \tag{11}$$

$$\tau = \theta\Delta t \tag{12}$$

As explained in Eqs. 2 and 4 that the control force vector $\mathbf{u}$ is a function of displacement vector $\mathbf{x}$. However, it can be observed from Eqs. 8 and 10 that the pseudo-displacement increment vector $\hat{\Delta}\mathbf{x}$ is a function of control force increment vector $\Delta\mathbf{u}$. Therefore, successive iterations should be employed in solving Eq. 8.

Definition of Key Parameters

To find beneficial parameters of dampers for achieving the maximum reduction of seismic response of the passively controlled building through parametric studies, the stiffness ratio λ and the slip force ratio β are defined as,

$$\lambda = \frac{\bar{k}_i}{k_i}; \qquad \beta = \frac{S_i}{N_i} \tag{13}$$

in which $\bar{k}_i$ and k_i are corresponding to the lateral brace stiffness and the lateral frame stiffness of the i^{th} story unit; S_i is the slip force of the i^{th} friction damper; and N_i is the maximum lateral force in the brace on the i^{th} story under the applied ground excitation where no slippage of the dampers are expected. For studying the performance of semi-active friction damped system with the selected control algorithm, two more parameters, that is, the decision time interval t_d and the slip load increment ΔS_i should be defined, in which the slip load increment is related to the slip force increment ratio as

$$\alpha = \frac{\Delta S_i}{S_i} = \text{Slip force increment ratio} \tag{14}$$

Clearly, the slip force ratio equal to zero represents the case of the building without any brace and control while the slip force ratio equal to one stands for the braced building without control.

COMPUTATION RESULTS

To demonstrate the application of the control method and to examine the performance of semi-active friction dampers, computation results are obtained and presented. Two building models are considered: a single-story building and an eight-story building.

Single-story Building

The single-story building is assumed to have a mass of 345.6×10^3 kg, a lateral frame stiffness of 6.8×10^5 kN/m, and a 2% structural damping ratio. The building is subjected to white noise ground

acceleration over a 5 sec duration as shown in Fig.2, of which the time step is 0.001 sec and the root mean square (RMS) acceleration is 0.632 m/s^2. The RMS drift response of the building is computed with stiffness ratio λ ranging from 0.5 to 5 and illustrated in Figs.3 to 6. It is seen from Fig.3 that the seismic response of the building can be significantly reduced with PFD, compared with the building without PFD ($\beta = 0$) and the building with brace only ($\beta = 1$). There is an optimal slip load for PFD associated with a minimum RMS drift for a given stiffness ratio.

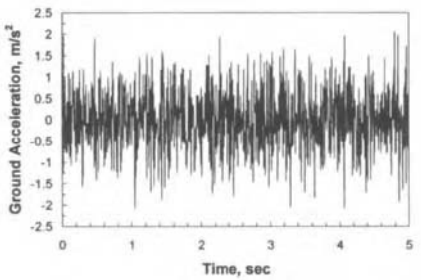


Figure 2: White noise ground excitation

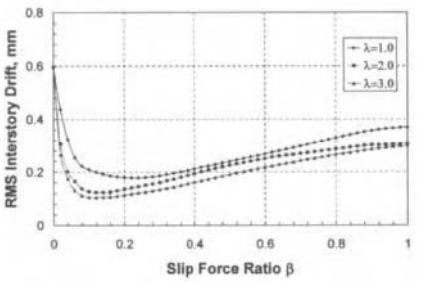


Figure 3: Variation of RMS drift for PFD

Fig. 4 shows a comparison of the RMS drift of the building between PFD and SAFD with λ=1.0, α=0.01, and t_d=0.001. It is demonstrated that the PFD system is sensitive to the preset slip force while the performance of the semi-active friction damper is almost independent of the preset slip force. Practically, the actual slip force in a damper may deviate from the preset slip force due to uncertainties in installation and environmental changes. Thus, the SAFD system demonstrates its robustness: the steady control performance can be guaranteed even though the slip force is changed. However, the maximum drift reduction using the SAFD system is slightly less than that using the PFD system around the optimal slip force.

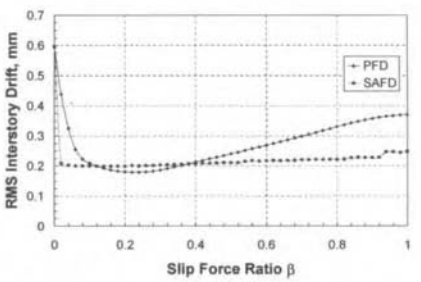


Figure 4: Comparison of PFD and SAFD

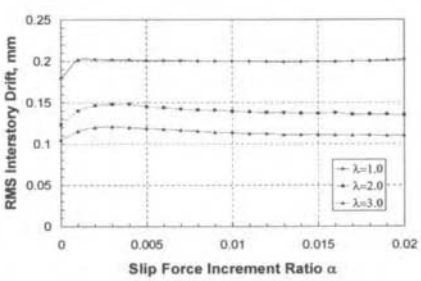


Figure 5: Variation of RMS drift for SAFD

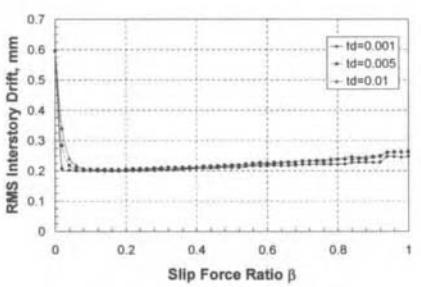


Figure 6: Effect of decision time interval

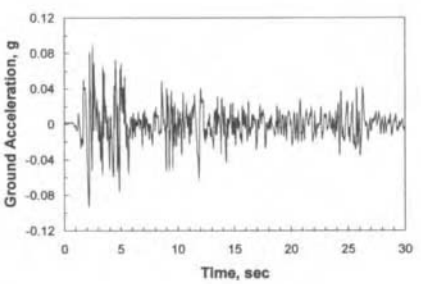


Figure 7: 30% of El Centro earthquake

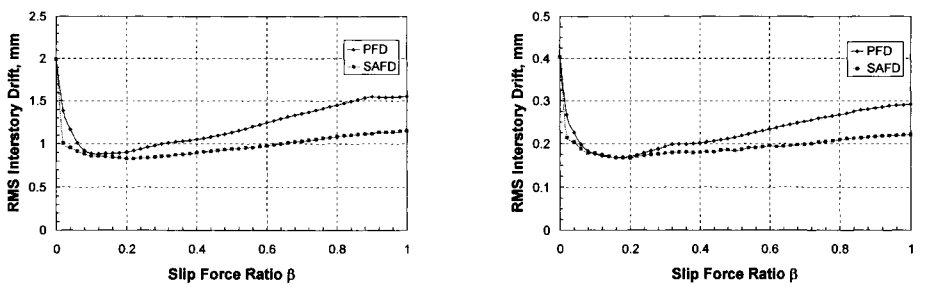
The sensitivity of SAFD to the slip force increment ratio and the decision time interval is illustrated in Figs. 5 and 6 respectively. It can be observed that the performance of semi-active friction damper is quite steady when the slip load increment ratio α is above 0.002. The RMS drift reduction achieved by the semi-active friction damper is slightly less than that by the passive friction damper with the optimal slip force but such difference becomes smaller when the stiffness ratio is higher. Fig. 6 demonstrates that the performance of the SAFD remains almost unchanged when different decision time interval t_d is implemented.

Eight-story Building

A shear-type eight-story building model with the following properties is considered. The mass and stiffness are identical for every story unit with $m_i=345.6\times10^3$ kg and $k_i=6.8\times10^5$ kN/m. The modal damping ratio of 2% is assumed for the first and second vibration mode of the unbraced building where the corresponding first two natural frequencies are 1.30 Hz and 3.86 Hz. The El Centro earthquake ground acceleration scaled to 30% of its original intensity (see Fig. 7) is used as the base excitation. It is supposed that one friction damper is mounted on every story. The stiffness of brace connected to the friction damper is considered to be identical for every story unit. The stiffness ratio chosen in the computation is $\lambda=1$, and the first and second natural frequencies of the braced building are then shifted to 1.84 Hz and 5.46 Hz, respectively. The present slip force distribution for the friction dampers along the height of the building is selected according to the maximum drift distribution of the braced building under the selected earthquake excitation.

$$S = S_1[1 \quad 0.95 \quad 0.89 \quad 0.80 \quad 0.68 \quad 0.54 \quad 0.38 \quad 0.20]^T \tag{15}$$

where S_1 is the slip force for the friction damper at the first story, which is now taken as S_i in Eq. 13 together with N_1 replacing N_i for the multi-story building. This distribution is also applied to the building with semi-active friction dampers initially and then is changed with the slip force increment ratio $\alpha=0.001$.



(a) 1st floor (b) 8th floor

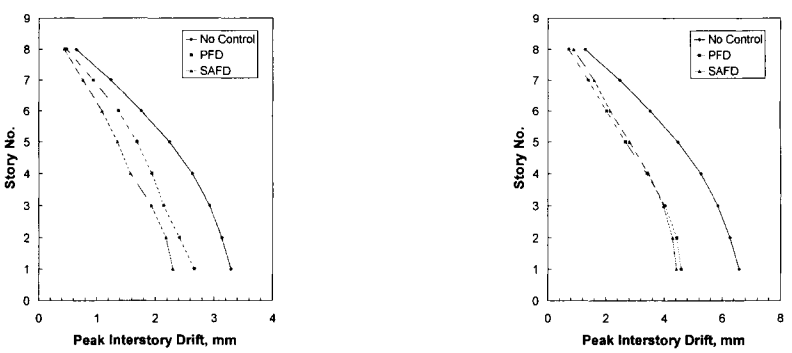
Figure 8: Comparison of RMS drift between PFD and SAFD

Displayed in Figs. 8a and 8b are the RMS drift of the building with passive and semi-active friction dampers against slip force ratio for the first floor and the eighth floor, respectively. It is seen that for the eight story building, the SAFD can not only achieve larger response reduction but also keeps its robustness: less sensitive to the preset slip force. This characteristic of slip force insensitivity enhances the actual application of semi-active friction dampers.

To investigate the sensitivity of both PFD and SAFD to the change of ground excitation, the drift responses of the building under 15% El Centro earthquake are computed using the optimal slip force found in the case of 30% El Centro earthquake. Table 1 lists the peak drifts x_p and RMS drifts x_{rms} of three systems: (i) braced building without control; (ii) braced building with passive friction dampers; and (iii) braced building with semi-active friction dampers. These results are also presented in Figs. 9a and 9b. The results manifest that both the PFD system and the SAFD system are effective in reducing seismic responses of the building. However, when the intensity of ground motion is changed, the control performance of the PFD decreases. The reduction of peak responses achieved by SAFD is larger than that by PFD under 15% El Centro earthquake. The reason for such phenomenon is that the slip forces of SAFD are continuously regulated to low enough slip forces to initiate the energy dissipation which cannot be performed in PFD system which are particularly designed for higher seismic intensity. Although the peak response alleviation achieved by SAFD system under 30% El Centro earthquake is not absolutely improved in comparison with that by PDF system of optimal slip force, the SAFD system can perform further reduction near the end of the earthquake duration (see Fig. 10). As a result, the RMS drifts x_{rms} of the building with SAFD are smaller than that with PFD.

TABLE 1
PEAK AND RMS DRIFTS OF EIGHT-STORY BUILDING

	15% El Centro earthquake						30% El Centro earthquake					
	No Control		Passive		Semi-Active		No Control		Passive		Semi-Active	
Story no.	x_p (mm)	x_{rms} (mm)	x_p (mm)	x_{rms} (mm)	x_p (mm)	x_{rms} (mm)	x_p (mm)	x_{rms} (mm)	x_p (mm)	x_{rms} (mm)	x_p (mm)	x_{rms} (mm)
1	3.29	0.78	2.66	0.60	2.30	0.48	6.59	1.56	4.60	0.98	4.42	0.85
2	3.14	0.75	2.41	0.58	2.18	0.46	6.27	1.50	4.44	0.93	4.29	0.80
3	2.93	0.70	2.14	0.54	1.93	0.42	5.86	1.39	4.04	0.86	3.99	0.74
4	2.63	0.62	1.94	0.50	1.57	0.38	5.27	1.24	3.41	0.76	3.46	0.66
5	2.24	0.53	1.68	0.41	1.35	0.32	4.48	1.05	2.68	0.65	2.81	0.55
6	1.76	0.41	1.37	0.32	1.09	0.25	3.53	0.83	2.03	0.51	2.15	0.44
7	1.24	0.29	0.94	0.22	0.76	0.18	2.48	0.57	1.40	0.36	1.60	0.32
8	0.64	0.15	0.48	0.11	0.44	0.10	1.29	0.29	0.73	0.19	0.89	0.18



(a) 15% El Centro earthquake (b) 30% El Centro earthquake

Figure 9: Peak drifts of eight-story building under different earthquake intensities

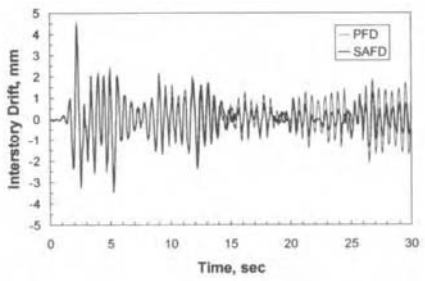


Figure 10: Time history of drift of 1st floor under 30% El Centro earthquake

CONCLUSIONS

The application of semi-active friction dampers to reduce seismic response of multi-story buildings has been investigated in this paper. The computation results demonstrate that the semi-active friction dampers have no obvious advantage in reducing the peak drifts comparing with the passive friction dampers designed with optimal slip forces. However, the semi-active friction dampers demonstrate a dominant adaptability in abating the seismic response of buildings under ground motion of different intensities. Moreover, the insensitivity characteristics of semi-active friction dampers to preset slip force, slip force increment, and decision time interval enable them to displace passive friction dampers in real applications.

ACKNOWLEDGEMENT

The writers gratefully acknowledge the financial supports from the Hong Kong Polytechnic University through a postgraduate scholarship to the first writer.

REFERENCES

Akbay Z. and Aktan H.M. (1991). Actively regulated friction slip braces. *Proc. 6th Canadian Conference on Earthquake Engng*, Toronto, 367-374.

Filiatrault A. and Cherry S. (1989). Efficient numerical modeling for the design of friction damped braced steel plane frames. *Can J Civil Engng.*, **16:3**, 211-218.

Kannan S., Uras H.M. and Aktan H.M. (1995). Active Control of Building Seismic Response by Energy Dissipation. *Earthquake Engng. Struct. Dyn.* **24**, 747-759.

Dowdell D.J. and Cherry S. (1994). Semi-Active Friction Dampers for Seismic Response Control of Structures. *Proc. 5th US National Conference on Earthquake Engng.*, Chicago, 819-828.

Pall A.S. and Marsh C. (1982). Response of Friction Damped Braced Frames. *J. Struct. Div. ASCE*, 1313-1323.

Pall A.S. and Pall R. (1993). Friction Dampers Used fro Seismic Control of New and Existing Buildings in Canada. *ATC-17-1 Seminar on Seismic Isolation, Passive Energy Dissipation, and Active Control*, San Francisco, California, 557-568.

Advances in Building Technology, Volume 2
M. Anson, J.M. Ko and E.S.S. Lam (Eds.)
© 2002 Elsevier Science Ltd. All rights reserved

A DESIGN OF BRIDGE STRUCTURE HEALTH MONITORING AND MANAGEMENT SYSTEM BASED ON THREE-DIMENSIONAL GIS MODEL

W.Z. Shi[1], P.G. Cheng[1,2,3], J.M. Ko[1], J.Y. Gong[2]

[1]Faculty of Construction and Land Use
The Hong Kong Polytechnic University, Kowloon, Hong Kong;
[2]LIESMARS of Wuhan University, Wuhan, Hubei, China, 430079;
[3]East China Geologic Institute, Fuzhou, Jiangxi, China, 344000

ABSTRACT

Geographical Information System (GIS) is a computer system for capturing, storing, managing, and analyzing spatial data. GIS has been applied in many areas to deal with the geographic distribution of spatial features, such as natural resources management, urban planning, calamity monitoring and others. Currently, most of the GIS applications are based on two-dimensional (2D) vectors or images and are weak in handling three-dimensional (3D) spatial information. Although structural health monitoring information for bridges can be partially managed by 2D GIS, it would be much more efficient with a 3D GIS. This paper presents a design of structural health monitoring and management system for bridges based on 3D GIS. A discussion on the implementation of the design and analysis of the technique are also presented.

KEYWORDS

Three-dimensional data model, Geographical Information System (GIS), bridge, structural healthy monitoring system

INTRODUCTION

Structural health monitoring works provide valuable information in the evaluation of structure integrity, durability and reliability. Taking the monitoring data and bridge location information of Ting Kua Bridge in Hong Kong as our research objects, we have established a prototype of GIS-based structural health monitoring and management system. This system integrates large commercial database, GIS and network techniques. The system can run on Local Area Network or Internet. GIS software is used to manage regional map on which locations of bridges are indicated, and location information about sensors. It also provides users an interactive interface between user and the system. Large database system, such as SQL Sever, is used to manage huge dataset captured from the sensors (Shi, 2002). However, 2D GIS are limited in showing the bridge 3D graph, sensors location at bridge, and health of bridge structures. In recent years, 3D GIS have been developed and applied in many domains,

such as urban planning, ocean, mine and so on. It is obvious that 3D GIS can manage bridge health monitoring information more efficiently than 2D GIS. In this paper, we analyses the necessity design a Bridge Structural Health Monitoring And Management System (BSHMAMS) based on 3D GIS. Secondly, we compare the similarities and the differences between a CAD-based bridge model and a 3D GIS data model. Thirdly, we proposed a conceptual framework of the BSHMAMS. Fourthly, The integration technique of GIS, VR and the Internet is put forward to implement the system development, and the system functions were discussed. Lastly, some conclusions are given.

DEMOND ON A 3D GIS MODEL

Currently, most commercial GIS packages are 2D. Thus 3D spatial objects are simplified and represented two dimensionally by points, lines, and polygons in vector or raster data structures. Although these 2D data are in digital forms and can be handled efficiently, however many 3D applications are either impossible or unable to demonstrate the potential GIS.

In the BSHMAMS, some kinds of information, such as, bridge location map, bridge drawing, sensor position in the bridge, structure monitoring data coming from sensors and the analysed result, attribute (health) about the bridge bodies, should be managed efficiently. See table 1, these data have different features, such as graphic, non-graphic, static, dynamic, very large data. GIS is adopted to manage graphic information such as the map (bridge location), bridge (body) drawing, and locations of sensors, visualize the bridge structures health in special method such as colour, texture. In 2D GIS, some information could not be represented, because all the spatial information is projected into horizontal level or profile. For example, it is impossible if users want to see the bridge bodies, bridge structures, and sensors in different direction, or to view the scene of the bridge location. 3D GIS have the ability to manage 3D spatial information and can overcome the above problems; so it is necessary to establish bridge structural health monitoring system based on 3D GIS model.

TABLE 1

DATA FEATURES TABLE ABOUT BRIDGE STRUCTURE HEALTH INFORMATION

Data item name	Dynamic	Static	Graphic	Non-Graphic	Very large
Bridge location (map)		✔	✔		
Bridge body information		✔	✔	✔	
Sensor information		✔	✔	✔	
Capture data	✔			✔	✔
Analysis result	✔			✔	
Bridge structure health	✔		✔		

COMPARISON BETWEEN CAD AND 3D GIS MODELS

Features Analysis of CAD

Computer Aided Design (CAD) is a computer technology system, which used widely to design drawing of machine, construction, engineering and production. The products that can be designed are from airplane to CMOS chip. Geometrical modeling and 3-D geometric representations, which can represent surfaces and solids of 3-D objects, were developed and applied for decades in Computer Aided Design (CAD) and computer graphics systems. However, in CAD packages, the geometric description of objects is of the first priority; while non-spatial information, especially, GIS topologic and attribute information, is not considered. This identifies the most significant difference between CAD systems and GIS.

The designed objects in CAD are regularly shaped, and can be described by 3-D geometric representations with predefined primitives, such as boxes, cylinders, spheres and others. In CAD, the design works is very detail for bridge engineering. A suspension bridge, for example, although the main structures are fewer such as anchor, tower pier, main cable, cable band, suspender, deck, beam and girder and so on, but the detailed structures are very complex and thousands of drawings are needed to describe the detailed structures. Except for the design view scene, the design works include from the three-dimensional scene to the dimension of an accessory. The main structures of a suspension bridge are seen in figure1.

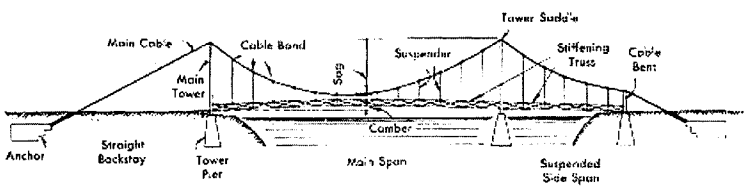


Figure 1: Suspension bridge main structures

3D GIS Model

3D geometric representations provide geometric descriptions of objects for storing, geometric processing, displaying, and management of 3-D spatial data by computers in GIS. In real worlds, there are some regular manual constructions, such as buildings, bridges, dams and so on; but in some applications, such as digital mapping, geosciences, and ocean engineering, the objects are so called free forms. In GISs, the regular and irregular objects should be represented. For this purpose, some 3D geometric representations have already been proposed. According to the geometric characterizations of data structures, 3-D geometric representations are classified into two groups, namely surface based and volume based representation.

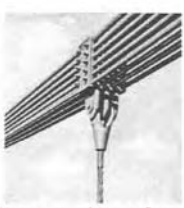
Surface based 3D geometric representations depict geometric characteristics of objects by using micro surface cell or surface primitives. There are four popular and important surface based representations, namely grids, shape models, facet models, and boundary representations. Grids, shape models and facet models are suited for describing objects surfaces with irregular shapes, and Boundary representation (B-reps) could represent not only

regularly shaped objects such as building, bridge and machine part, but also freeformed surfaces like car body surfaces, and terrain models. Volume based geometric representations describe the interior of objects by using solid information, instead of surface information. With these representations, solid information of objects can be presented, analyzed and visualized. There are four kinds of representations, such as binary arrays, needle models, octrees, and Constructive Solid Geometry models (CSG). The former three representations are capable of representing objects with irregular shapes and CSG representations are suited very well for describing regularly shaped objected.

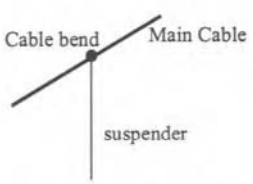
Obviously, it is impossible to design a data model that is suitable for all kinds of 3D applications. We should design a special 3D spatial data model based on the characteristics of objects in the applications.

Transferring CAD Model into 3D GIS

CAD is suited for describing regular objects and emphasizing the details and geometric dimension of objects. 3D GIS models are more complex than CAD model. It could not only describe the regular and irregular objects, but also insist the geometric relationship among objects and the attributes. If a CAD model is transferred into GIS model, generalization should be made when using 3D GIS model to describe the objects and the attribute should be transferred at the same time. See figure 2, for example, (a) is close-up view of main cable, cable bend and suspender, and (b) is the general GIS model about (a), and this model comprise of three objects i.e. main cable, suspender and a node. It is obvious that simplified works have been made to implement the model transformation. In 3D GIS model, cylinders with different diameter can be used to describe the main cable and the suspender, and spheres can be used to describe the cable bend. The B-reps and the CSG are suited for representing the bridge bodies, and the grid and TIN could be used to describe terrain model of the bridge location.



(a) Close-up view of main cable, cable bend and suspender



(b) Representation in GIS

Figure 2: Model generalization

CONCEPTUAL FRAMEWORK DESIGN

The system objective of the BSHMAMS is to establish a data management, analysis and visualization system based on 3D GIS model. The system could be run in Internet, and has the functions of 3D visualization and interaction to the graphic and attribute information, database management ability to the captured data from the sensors, and the analysis ability to the structural health monitoring data. In the Server-side, 3D models of bridge and the location map should be established; captured data database should be created, and the structural health analysis module should be provided. In Client-side, users can view the 3D scene of bridge and

terrain in different azimuth, interact on the model and further retrieve the attribute or monitoring data of selected objects in the model.

Large Relationship Database Management System (RDBMS), such as SQL Sever or Oracle, is an effective tool of data management. The RDBMS based on Client/Server architecture provides more efficient means to manage and share very large data. So we can use them to manage huge dataset captured from the sensors. For example, in the Sever-Side, by using the data input and database maintain module, the captured data that come from data capturing system of the bridge monitoring system, can be imported into the central database termly, and the period data are backup. The create database scheme, which one days' capture data creating a daily database, is very conveniently to create database, database backup and restore, and retrieve data from database. 3D GIS are the powerful tools to integrate and to manage different sources of spatial data and attribute data. We can use it to manage the scene of bridge location map, the 3D model of bridge body, and the sensors in the bridge model. Conceptual design of the system is illustrated in figure 3.

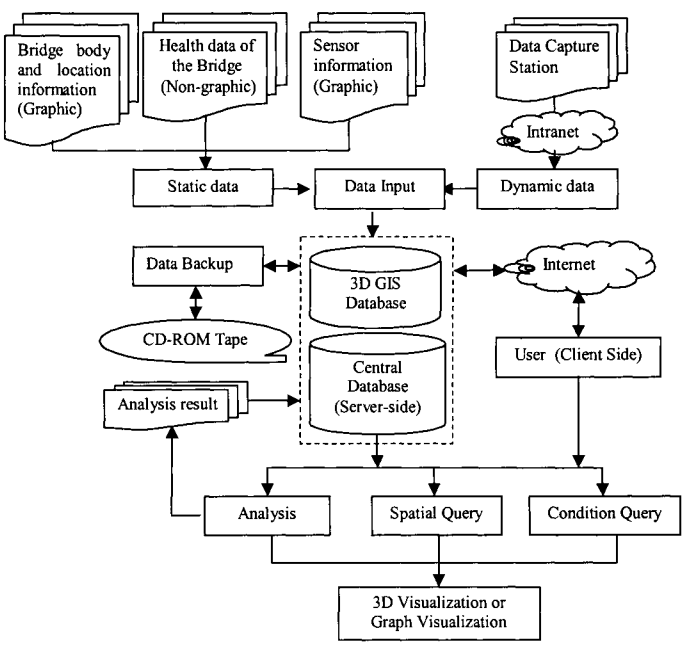


Figure 3: System conceptual design

The capture data acquired from typical sensors are firstly transmitted from the data capture station to user's computer via Internet or Intranet techniques. Under the control of user with control program, the transmitted data are pre-processed, including data classification, data filtering, etc. The pre-processed data are reorganized according to sensor ID and channel ID into a dynamic database that can be updated dynamically. The data in the dynamic database can be updated automatically with a regular interval. Users can also manually update it in both time interval and data amount. Following this process, the existing data in the database will be backup and replaced regularly by new data.

Analysis module can access the dynamic database and make special analysis, such as frequency analysis of captured data, structural health monitoring, damage detection, fatigue analysis and so on. Some analysis results, especially statistics results, can be stored in an analysis results database (ARD) for long-term use. The static information, such as original structural information and sensor system information, are stored in a static database (SD). The entire dynamic database, static database and analysis database are compose of the central database in Server-side.

Visualization program include 3D visualization of spatial information and the graph visualization of the time and frequency domain information of structural response and environmental loading data from the databases.

SYSTEM IMPLEMENTATION MECHANISM

For implementing this system, we can adopt the integration technique of GIS, VR and the Internet. This integration mechanism can be implemented through the use of Virtual Reality Modelling Language (VRML), an ISO standard for describing interactive 3D objects and worlds to be experienced on the World Wide Web. Through VRML, in conjunction with Java and HTML, GIS, VR and the Internet can be combined in different ways to support Web-based modelling, visualization and analysis. In such integration, GIS provides rather rich spatial data, VR helps to visualize the large volume of data in a rather realistic format, and the Internet facilitates information dissemination. There are two basic applications to deploying GIS or any other complex, data driven applications on the Internet: server-side and client-side applications.

The sever-side application, having main software and databases on the server side that are linked with the Web server through a Common Gateway Interface (CGI) script, significantly simplify development, deployment and maintenance of the Internet GIS software. The results transmitted to a Web client are in standard HTML formats that can be viewed in any browser. The disadvantages of server-side are associated with limited user interface and poor performance. Client-side solutions typically are implemented by augmenting the Web browser in the form of plug-in, ActiveX or Java. The primary advantages of client-side solutions are the abilities to enhance the user interface and improve performance. In summation, both methods should be considered complementary rather than competitive in practice. Hence the integration of client- and server-side solutions, typically in the form of Java and CGI, is a better approach. It can provide not only a user-friendly interface by use of Java but also a powerful data processing server by using CGI-linked exiting GIS functions. In general, complex spatial data processing task are performed on the server side, while tasks of user interaction and the system controlling are carried out on the client-side.

For satisfying the above integration plan, we can adopt the three-tier Client/Server pattern. This pattern consists of three components: the Client, the Server and the middleware. See figure 4. The client side provides Web pages embedded with Java applets. The user then submits the request in the form of Unique Resource Locator (URL) to the server via a CGI program. After receiving the URL request from Java-based client, the application server extracts all the necessary parameters, processes them, and delivers the results in HTML-compatible format to the client for displaying. The result could be 3D VRML model or a 2D map. The interaction with VRML worlds can now be realized by interface Java or JavaScript with VRML 2.0. Two methods are used for the interaction, namely using Script node in

VRML and the External Authoring Interface (EAI). We can use the EAI method for a flexible interaction with the VRML scene generated by the 3D visualization module. For the graph visualization of the capture data, frequency data and the attributes of the interest objects, we can use JDBC technique to access the central database. After retrieving the wanted data (data package), use Java applets to visualize the data in client.

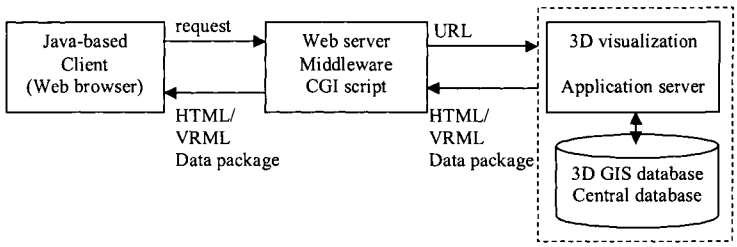


Figure 4: Three-tier Client/Server architecture

SYSTEM FUNCTIONS

Considering the system architecture, functional requirements of the BSHMAMS base on 3D GIS Model, there are several mainly functions: data input, data management, database backup and restore, data analysis, data query and visualization. Their implementation mechanisms are discussed in the section of the conceptual framework design.

Data input module are used to continuously import the source data into the centralized database via Intranet, and input the graphic and attribute information of the BSHMAMS into the system by using GIS software directly or transferred from CAD model.

In data management module, the capture data and the analysis result are managed by RDBMS, and the graph and attribute information are managed by GIS software. All the information are spatially maintained and integrated in unique information systems in sever side.

Database backup and restore module can backup the dynamic database into the secondary storage devices, such as CD-ROM, and restore it when user want to retrieve the data.

Spatial query include: query attribute by 3D VRML interface, and query graph by attributes.

Data analysis includes frequency domain analysis of captured data, statistical calculation, etc. It can be implemented by advanced language program in server side.

Visualization includes 3D Visualization of the bridge scene; different types of graphic display of captured data, visualization of frequency domain analysis and so on.

CONCLUSIONS

This paper presented a design of the prototype of the BSHMAMS based on 3D GIS model. Based on our design work, we can get following conclusions.

- It is necessary and feasible to establish the BSHMAMS based on 3D GIS model based on a view of technical solutions and method.
- 3D GIS model is more efficient to manage 3D spatial information, and can enrich the visualization of bridge scene and interaction between users and the system.
- The integration of the techniques, such as GIS, VR and the Internet is a better solution scheme about these systems running in Internet.
- In the course of CAD model transferring into 3D GIS model, generalization should be made and attribute should be transferred at the same time.
- SQL Server database can be used to manage the very large quantity data. The create database scheme that One days' capture data creating a daily database has some advantages.

System design is the first steps for developing the overall System, and further work is to implement this system. The integration of the technologies will be applied, such as GIS, VR and the Internet, the transformation from CAD model into GIS 3D model, and the interaction between user and system in VRML scene. The implementation of this system will finally improve the efficiency of bridge structural health monitoring and management system.

ACKNOWLEDGEMENTS

This work was supported by the research project granted from The Hong Kong Polytechnic University (Project No.1.31.37.87A5), and the Funded By Open Research Fund Program of LIESMARS (WKL (01) 0302).

REFERENCES

Bergmeister K., Santa U. (2000), Global Monitoring Concepts for Bridge, In Nondestructive Evaluation of Highways, Utilities, and Pipeline IV, A. Emin Aktan, Stephen R.Gosselin, Proceedings of **SPIE Vol. 3995**, 266-275, SPIE, Newport Beach, USA,

Gong J.H and Lin H. (2001). Study on Distributed Virsual Geo-Environment. Journal of Image and Graphics **6(A):9**, 879-885

Huang B., Jiang B. and Lin H. (2001). An integration of GIS, visual reality and the Internet for visualization, analysis and exploration of spatial data. INT.J. Geographic Information Science **15:5,** 439-456.

K. Y. Wong, C. K. Lau, A. R. Flint (2000). Planning and Implementation of the Structural Health Monitoring System for Cable-Supported Bridges in Hong Kong, In Nondestructive Evaluation of Highways, Utilities, and Pipeline IV, A. Emin Aktan, Stephen R.Gosselin, Proceedings of SPIE **Vol. 3995** 266-275, SPIE, Newport Beach

Lau C.K. and Wong K.Y. (1997). Design, construction and monitoring of the three key cable-supported bridge, Structures in the new minllennium, Lee(ed.), 105-115, Rotterdam, 1997

R.X. Li (1994). Data Structures and Application Issues in 3D Geographoic Information Systems. GEOMATICA **48:3**, 209-223

She T. H. (1999). A Geographic Information System (GIS)-Based Bridge Management System. Computer-Aided Civil and Infrastructure Engineering **14(1999),** 417-427

Shi W.Z., Cheng P.G., Ko J.M., Liu C., Development of GIS-Based Bridge Structural Health Monitoring and Management System, In NDE and Health Monitoring of Aerospace Materials and Civil Infrastructures, Proceeding of **SPIE Vol.4704** (to be published)

http://www.inventionfactory.com/history/RHAbridg/sbtd/

Advances in Building Technology, Volume 2
M. Anson, J.M. Ko and E.S.S. Lam (Eds.)
© 2002 Elsevier Science Ltd. All rights reserved

SEISMIC DESIGN METHOD OF STRUCTURES WITH ACTIVE VARIABLE STIFFNESS SYSTEMS

Bo Wu Fen-tao Liu De-min Wei

(Department of Civil Engineering, South China University of Technology, Guangzhou 510640, P. R. of China)

ABSTRACT

It has been demonstrated that active variable stiffness (AVS) systems may be effective for response control of building structures subjected to earthquake excitations. The dynamics of structures with AVS systems are highly nonlinear because the stiffness of each story unit, in which the AVS system is installed, varies as a function of time. Hence, the classical seismic design method for linear structures, such as the mode-superposition response-spectrum method, is not feasible to structures with AVS systems. In this paper, a seismic design method based on the approximate mode superposition (AMS) approach suggested by the authors (Wu et al., 2001) is proposed for building structures equipped with AVS systems. First, the AMS approach for structures with AVS systems is briefly introduced. Then, the accuracy of this approach for estimating the maximum interstorey shear forces of structures is investigated through extensive numerical simulations, and some revision is given to the approach, in order to improve the simulation precision. Simulation results indicate that the revised AMS approach is effective in estimating the maximum interstorey shear forces in structures with AVS systems. Subsequently, the distribution of the maximum interstorey shear forces between structural members and AVS systems are discussed. Finally, a seismic design method based on the AMS approach is primarily presented for building structures equipped with AVS systems.

KEYWORDS

seismic design, semi-active control, active variable stiffness system, mode superposition

INTRODUCTION

It has been demonstrated that so-called active variable stiffness (AVS) systems, introduced originally by Kobori at the end of the 1980s, may be effective for response control of structures subjected to earthquake excitations. Owing to the advantage of not requiring the input of extensive power and energy, the AVS systems have received considerable attention in recent years. Extensive efforts have been devoted to the theoretical and practical development of AVS systems. Different control strategies for the AVS systems have been investigated by, for example, Kobori et al. (1990), Kobori and Kamagata (1992), Kamagata and Kobori (1994), Yang et al. (1994, 1996), Yamada and Kobori (1995) and Nasu et al. (2001). Such systems have also been tested experimentally and installed on a full-scale test building in Japan (Kobori

et al., 1990, 1991a and 1991b).

The AVS systems consist of stand-by bracings attached to selected storey units of building structures, and the locking and unlocking devices. During the earthquake ground motion, some of the bracings may be locked at a particular time instant, to increase the stiffnesses of the corresponding story units. The locking and unlocking of different bracings at each time instant are regulated by a control algorithm in order to reduce the structural responses to an earthquake. One of the control algorithms proposed by Kobori and Kamagata is based on engineering insight as follows. Since the locking of bracings increases the stiffness restoring force, the bracings should be locked if the interstorey drift, $x(t)$, and its velocity, $\dot{x}(t)$, are both positive or both negative, i.e., $x(t)\dot{x}(t) > 0$. On the other hand, if $x(t)$ and $\dot{x}(t)$ are in the opposite direction (different sign), i.e., $x(t)\dot{x}(t) < 0$, then bracings should be unlocked. Such a control algorithm is quite effective, so it is adopted in the study described in this paper.

The dynamics of structures with AVS systems are highly nonlinear. Hence, a classical seismic design method for linear systems is not applicable to active variable stiffness structures. At present, the seismic design of structures equipped with AVS systems is always conducted using a time-history analysis method, which is inconvenient to engineers. The purpose of this paper is to present a simple design method for building structures with AVS systems, which is based on the approximate mode superposition (AMS) approach that was suggested by the authors and has been proven to be effective in estimating the maximum displacements relative to the ground and the maximum interstorey drifts in structures equipped with AVS systems (Wu et al., 2001). In this paper, the AMS approach is briefly introduced first. Then, the accuracy of this approach for estimating the maximum interstorey shear forces in structures is investigated through extensive numerical simulations, and some revision is given to the approach, in order to improve the simulation precision. Simulation results indicate that the revised AMS approach is effective in estimating the maximum interstorey shear forces in structures with AVS systems. Subsequently, the distribution of the maximum interstorey shear forces between structural members and AVS systems is discussed. Finally, a seismic design method based on the AMS approach is primarily presented for building structures equipped with AVS systems.

APPROXIMATE MODE SUPERPOSITION (AMS) APPROACH

The equation of motion for an n-story building structure equipped with AVS systems in selected storey units and subject to a horizontal ground acceleration $\ddot{x}_g(t)$ can be written as:

$$M\ddot{X} + C\dot{X} + KX + HU(t) = -MI\ddot{x}_g(t) \tag{1}$$

in which M、C and K are $(n \times n)$ mass, damping and stiffness matrices of the uncontrolled structure, respectively, X is an n vector with the jth element x_j being the displacement of the jth floor relative to the ground, I is a column vector of "ones"; H is a constant matrix depending on the locations of the AVS systems, and $U(t)$ is a control vector with the jth element $u_j(t)$ being:

$$u_j(t) = g_j(t)\Delta k_j(x_j - x_{j-1}) \quad j > 1; \qquad u_j(t) = g_j(t)\Delta k_j x_j \quad j = 1 \tag{2}$$

where Δk_j is the additional stiffness of stand-by bracings of the AVS system installed in the jth story unit. If there is no AVS system installed in the jth story unit, then $\Delta k_j = 0$ and $u_j(t) = 0$.

The control strategy for the structure with AVS systems is one of the control algorithms proposed by Kobori and Kamagata as follows:

if $j > 1$ and $(x_j - x_{j-1})(\dot{x}_j - \dot{x}_{j-1}) \geq 0$: $g_j(t) = 1$; if $j = 1$ and $x_j\dot{x}_j \geq 0$: $g_j(t) = 1$

if $j > 1$ and $(x_j - x_{j-1})(\dot{x}_j - \dot{x}_{j-1}) < 0$: $g_j(t) = 0$ if $j = 1$ and $x_j\dot{x}_j < 0$: $g_j(t) = 0$

The mode shape matrix Φ_s, mode circular frequency vector ω_s, and mode damping ratio vector ξ_s of the uncontrolled structure are, respectively, expressed as:

$$\Phi_s = [\phi_{s1},\ldots,\phi_{si},\ldots,\phi_{sn}],\quad \omega_s = [\omega_{s1},\ldots,\omega_{si},\ldots,\omega_{sn}]^T,\quad \xi_s = [\xi_{s1},\ldots,\xi_{si},\ldots,\xi_{sn}]^T \tag{3}$$

in which ϕ_{si}、ω_{si} and ξ_{si} are, respectively, the natural mode vector, circular frequency and damping ratio of the i th mode for the uncontrolled structure.

Consider the condition that all the stand-by bracings in the structure are locked. Here, the mass and damping matrices of the controlled structure are equal to M and C in Eq.(1), respectively, but the stiffness matrix of the controlled structure should be a sum of K in Eq.(1) and an additional stiffness matrix $\Delta K_{\max}$, which is of the same form as K except that k_j is replaced by the additional stiffness Δk_j. Now the mode shape matrix and the mode circular frequency vector are, respectively, given as:

$$\Phi_c = [\phi_{c1},\ldots,\phi_{ci},\ldots,\phi_{cn}],\qquad \omega_c = [\omega_{c1},\ldots,\omega_{ci},\ldots,\omega_{cn}]^T \tag{4}$$

Suppose the displacement response of the structure with AVS systems can be approximated by a linear combination of several natural modes: $X \approx \sum_{r=1}^{l} q_r(t)\phi_{sr}$ $(l \le n)$. Introducing the expression of X into Eq.(1) and then premultiplying each term in this equation by ϕ_{si}^T gives:

$$\phi_{si}^T M\sum_{r=1}^{l}\phi_{sr}\ddot{q}_r(t) + \phi_{si}^T C\sum_{r=1}^{l}\phi_{sr}\dot{q}_r(t) + \phi_{si}^T(K+\Delta K)\sum_{r=1}^{l}\phi_{sr}q_r(t) = -\phi_{si}^T MI\ddot{x}_g(t) \tag{5}$$

in which ΔK is the additional stiffness matrix due to the stand-by bracings of AVS systems equipped in the structure. If all the stand-by bracings in the structure are locked, ΔK is equal to $\Delta K_{\max}$; on the other hand, if all the stand-by bracings are unlocked, ΔK is a null matrix. If some stand-by bracings are locked and the others are unlocked, ΔK is range from a null matrix to $\Delta K_{\max}$.

Utilizing the orthogonality property of the natural mode vectors of the uncontrolled structure, Eq.(5) can be written as:

$$\ddot{q}_i(t) + 2\xi_{si}\omega_{si}\dot{q}_i(t) + \frac{\phi_{si}^T(K+\Delta K)\sum_{r=1}^{l}\phi_{sr}q_r(t)}{\phi_{si}^T M\phi_{si}} = -\gamma_i\ddot{x}_g(t) \tag{6}$$

in which $\gamma_i = \phi_{si}^T MI / \phi_{si}^T M\phi_{si}$ is the modal participation factor of the i th mode.

Suppose the controlled structure vibrates only in the i th mode. Now only two states exist for all the stand-by bracings in the structure: locked simultaneously or unlocked simultaneously (He and Feng, 2000). When all the stand-by bracings are unlocked $(q_i(t)\dot{q}_i(t) < 0)$, ΔK is equal to a null matrix and Eq.(6) may be further written in a simplified form:

$$\ddot{q}_i(t) + 2\xi_{si}\omega_{si}\dot{q}_i(t) + \omega_{si}^2 q_i(t) = -\gamma_i\ddot{x}_g(t) \tag{7}$$

On the other hand, when all the stand-by bracings are locked $(q_i(t)\dot{q}_i(t) > 0)$, ΔK is equal to $\Delta K_{\max}$. In such a case, replacing the elements of Φ_s, in the third term on the left-hand of Eq.(6), approximately by the corresponding elements of Φ_c gives:

$$\ddot{q}_i(t) + 2\xi_{si}\omega_{si}\dot{q}_i(t) + \omega_{ci}^2 q_i(t) = -\gamma_i\ddot{x}_g(t) \tag{8}$$

Eqs.(7) and (8) may be regarded as two special cases of a SDOF active variable stiffness structure that is:

$$\ddot{q}_i(t) + 2\xi_{si}\omega_{si}\dot{q}_i(t) + \omega_{si}^2 q_i(t) + \frac{\omega_{ci}^2 - \omega_{si}^2}{2}(1 + sign(q\dot{q}))q_i(t) = -\gamma_i\ddot{x}_g(t) \tag{9}$$

in which $sign(\bullet)$ denotes symbol function.

Referring to the equivalent relationship between the SDOF structure with AVS system and the so-called special linear structure, which is determined according to the principle that the peak point on the steady-state displacement amplitude-excitation frequency curve of the latter structure is in good agreement with that of the former structure (Wu et al., 2001), Eq.(9) may be approximately expressed as:

$$\ddot{q}_i(t) + 2\xi^* \omega_m \dot{q}_i(t) + \omega_m^2 q_i(t) = -\gamma_i \ddot{x}_g(t) \tag{10}$$

in which $\omega_m^2 = \omega_{si}^2(1+\eta_e)$, $\xi^* = \xi_e + \xi_{si}$, and η_e and ξ_e are related to $\alpha = (\omega_{ci}{}^2 - \omega_{si}{}^2)/\omega_{si}{}^2$ and ω_{si}. In this way, the ith modal coordinate $q_i(t)$ can be determined by solving Eq.(10), and then the displacement response of the n-story structure equipped with AVS systems can be approximately determined by $X \approx \sum_{r=1}^{l} q_r(t)\phi_{sr}$.

REVISION OF THE AMS APPROACH

Based on the AMS approach, the maximum interstorey shear force $V_{j\max}$ of the jth story unit of the structure equipped with AVS systems can be written as:

$$V_{j\max} = \max\left|F_j + F_{j+1} + \cdots + F_n\right| \tag{11}$$

in which $F_j = m_j[\sum_{r=1}^{l} \ddot{q}_r(t)\varphi_{srj} + \ddot{x}_g(t)]$ is the seismic action at the jth-floor level, m_j is the mass of the jth floor, and φ_{srj} is the jth element of the rth mode vector ϕ_{sr}.

Extensive numerical simulations, using the time-history analysis method and the AMS approach, are carried out for structures equipped with AVS systems and subjected to different artificial earthquake excitations listed in Table 1. Simulation results indicate that the maximum interstorey shear force of each storey unit may be effectively estimated by the AMS approach with some revision --- multiplying the maximum interstorey shear force of each storey unit determined by Eq.(11) with modification parameter β. Here β is given as:

$$\beta = \begin{cases} 0.0285n + 1.4764 & \textit{Top floor} \\ 0.0239n + 1.2461 & \textit{Other floors} \end{cases} \qquad (5 \le n \le 12) \tag{12}$$

Consider a 5-story building with the following properties. The mass and stiffness of each storey unit are identical with $m_j = 100$ t and $k_j = 4.87 \times 10^4$ kN/m, respectively, for $j = 1,2,.....,5$. A Rayleigh damping matrix is adopted, and the damping ratio in the first and the second modes is specified by ξ_{s1}=ξ_{s2}=0.05. Suppose one AVS system is installed in every storey unit, where the additional stiffness of stand-by bracings is $\Delta k_j = k_j = 4.87 \times 10^4$ kN/m. The 30 artificial earthquakes listed in Table 1 are used as the input excitations. Using the revised AMS approach with coefficient β, the maximum interstorey shear forces of each storey unit under 30 artificial earthquakes are obtained. For comparison, corresponding results using the time-history analysis method are also obtained. Assume Q is the ratio of the maximum interstorey shear force of each storey unit using the time-history analysis method to that using the revised AMS approach. Simulation results of Q corresponding to different storey units and different artificial earthquakes are shown in Figure 1.

Next, a 12-storey building with the following properties is considered. The mass and stiffness of each storey unit are identical with $m_j = 400$ t and $k_j = 4.4 \times 10^5$ kN/m, respectively, for $j = 1,2,.....,12$. A Rayleigh damping matrix is adopted, and the damping ratio in the first and the second modes is specified

TABLE 1
PARAMETERS OF ARTIFICIAL EARTHQUAKES

Site	Dominating period of site (s)	Number of earthquakes	Average peak Ground acceleration (gal)	Standard deviation of peak ground acceleration (gal)
Class II	0.3	10	253.94	25.46
Class II	0.3	10	127.78	9.46
Class III	0.4	10	67.9	5.18

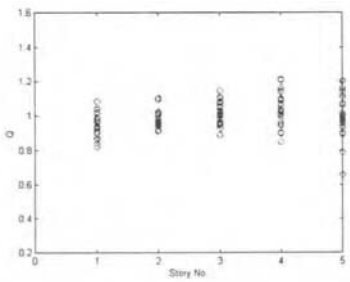


Figure 1 Five-story structure

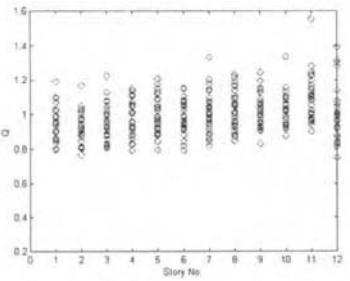


Figure 2 Twelve-story structure

by $\xi_{s1}=\xi_{s2}=0.05$. Suppose one AVS system is installed in every storey unit, where the additional stiffness of stand-by bracings is $\Delta k_j = k_j = 4.4\times10^5$ kN/m. The 30 artificial earthquakes listed in Table 1 are used as the input excitations. Using the revised AMS approach with coefficient β, the maximum interstory shear forces of each storey unit under 30 artificial earthquakes are obtained. For comparison, corresponding results using the time-history analysis method are also obtained. Simulation results of Q corresponding to different storey units and different artificial earthquakes are shown in Figure 2.

It is observed from Figures 1 and 2 that the value of Q fluctuates around 1.0. Among the total 150 data in Figure 1, 117 data (78.0%) are within the range of [1.0/1.1, 1.0/0.9], and 139 data (92.7%) are within the range of [1.0/1.15, 1.0/0.85]. Further, among the total 360 data in Figure 2, 229 data (63.6%) are within the range of [1.0/1.1, 1.0/0.9], and 297 data (82.5%) are within the range of [1.0/1.15, 1.0/0.85]. Hence, the maximum interstorey shear force of each storey unit may be approximately estimated using the revised AMS approach with an error mostly less than 10%.

In order to improve the simulation precision of the AMS approach for maximum interstorey shear forces of structures with AVS systems, another equivalent relationship between the SDOF structure with AVS system and the so-called special linear structure may be established, according to a new principle that the peak point on the steady-state acceleration amplitude-excitation frequency curve of the latter structure is in good agreement with that of the former structure. Again, Eq.(9) may be approximately expressed as Eq.(10), and $\omega_m^2 = \omega_{si}^2(1+\eta_e)$, $\xi^* = \xi_e + \xi_{si}$, but now η_e and ξ_e should be given as:

$$\eta_e = (0.0315\alpha - 0.0233)\omega_{si} + 0.3788\alpha + 0.1113 \tag{13}$$

$$\xi_e = (0.0002\alpha^2 - 0.0015\alpha + 0.0007)\omega_{si} - 0.0056\alpha^2 + 0.0403\alpha + 0.0282 \tag{14}$$

in which $\alpha = (\omega_{ci}^{\ 2} - \omega_{si}^{\ 2})/\omega_{si}^{\ 2}$.

Extensive numerical simulations, using the time-history analysis method and the AMS approach based on the new equivalent relationship, are carried out for structures equipped with AVS systems and subjected to different artificial earthquake excitations listed in Table 1. Simulation results indicate that the maximum interstorey shear force of each storey unit may be further effectively estimated by multiplying

the corresponding result of each storey unit determined by Eq.(11) with modification parameter β, but now β should be rewritten as:

$$\beta = \begin{cases} 0.0270n + 1.2911 & \textit{Top floor} \\ 0.0250n + 1.1025 & \textit{Other floors} \end{cases} \qquad (5 \le n \le 12) \qquad (15)$$

Consider the above two example structures again. Simulation results of Q, which is the ratio of the maximum interstorey shear force of each storey unit using the time-history analysis method to that using the revised AMS approach, corresponding to different storey units and different artificial earthquakes are, respectively, shown in Figure 3 and Figure 4 for the 5-storey and 12-storey buildings.

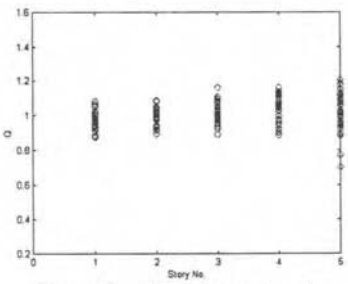


Figure 3 Five-storey structure

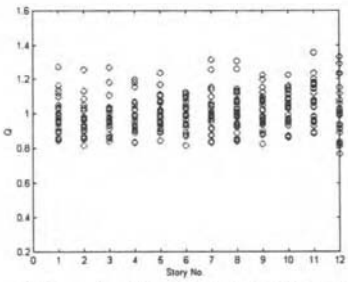


Figure 4 Twelve-storey structure

Among the total 150 data in Figure 3, 126 data (84.0%) are within the range of [1.0/1.1, 1.0/0.9], and 147 data (98.0%) are within the range of [1.0/1.15, 1.0/0.85]. Further, among the total 360 data in Figure 4, 244 data (67.8%) are within the range of [1.0/1.1, 1.0/0.9], and 308 data (85.6%) are within the range of [1.0/1.15, 1.0/0.85]. Comparing Figure 1 and Figure 2, it can be seen that the simulation precision of the revised AMS approach, based on the new equivalent relationship, is better than that based on the old equivalent relationship.

DISTRIBUTION OF MAXIMUM INTERSTORY SHEAR FORCE

At any time instant, the interstorey shear force of the j th storey unit of the structure equipped with AVS systems is balanced by the interstorey damping force, the stiffness restoring force $k_j(x_j - x_{j-1})$ related to the structural members, and the additional stiffness restoring force related to the AVS system installed in the j th floor, which are equal to $\Delta k_j(x_j - x_{j-1})$ and 0 for locked and unlocked stand-by bracings, respectively.

Figure 5 shows the time-history curves of the interstorey shear force, the stiffness restoring force and the additional stiffness restoring force for the base floor of the aforementioned five-storey example structure subjected to a certain artificial earthquake. It is observed from this figure that: (1) At any time instant, the sum of the stiffness restoring force and the additional stiffness restoring force is approximately equal to the interstorey shear force, so the effect of interstorey damping force on balancing the interstorey shear force is quite limited. In this way, the interstorey shear force may be approximately distributed between the structural members and the AVS system according to their lateral stiffnesses. Here, the stiffness of the structural members is constant at any time instant, but the stiffness of the AVS system varies with the locking and unlocking of stand-by bracings. (2) The maximum stiffness restoring force and the maximum additional stiffness restoring force occur at almost the same time as the maximum interstorey shear force, so the former two forces may be approximately determined by distributing the latter force according to the lateral stiffnesses of the structural members and the AVS system.

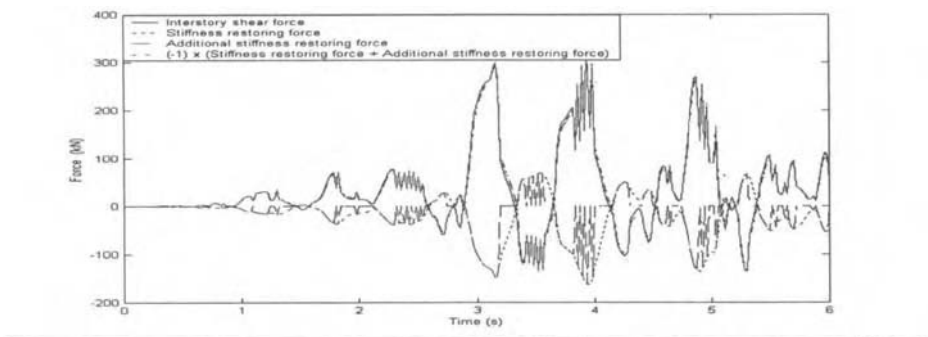


Figure 5 Time-history curves

SEISMIC DESIGN METHOD OF STRUCTURES WITH AVS SYSTEMS

Based on the revised AMS approach and referring to the seismic design procedure for uncontrolled structures, the seismic design method of structures with AVS systems may be summarized as:

(1) Using the AMS approach, the nonlinear equation of motion of the structure with AVS systems is transformed into a set of uncoupled linear equations as shown in Eq.(10).

(2) Using the acceleration response spectrum with large damping ratio in the Seismic Design Code of China (GB50011-2001), $V_{ij\max}(j=1,2,\cdots,n)$, the maximum interstorey shear force of the j th storey unit for the i th mode, is determined.

(3) According to the *square-root-of-sum-of-squares* (SRSS) rule for modal combination, the maximum interstorey shear force of the j th story unit is primarily determined as $V_{j\max}^{*}=\sqrt{\sum_{i=1}^{I}V_{ij\max}^{2}}$.

(4) Using the modification parameter of β shown in Eq.(15), the maximum interstorey shear force of the j th storey unit is further determined as $V_{j\max}=\beta V_{j\max}^{*}$.

(5) According to the lateral stiffnesses of the structural members in the j th floor and the AVS system installed in the same floor, $V_{j\max}$ is distributed between the structural members and the AVS system.

(6) Combining the stiffness restoring force and the additional stiffness restoring force with other load effects, the detail design of the structural members and the AVS systems may be carried out.

CONCLUDING REMARKS

The following conclusions may be drawn from the study reported here.

1. The maximum interstorey shear force of each storey unit in structures with AVS systems may be estimated using the revised AMS approach with parameter of β shown in Eq.(12), based on the equivalent relationship between the SDOF structure with AVS system and the so-called special linear structure presented by Wu et al., 2001.

2. The simulation precision of the maximum interstorey shear force of each storey unit of structures with AVS systems may be improved using the revised AMS approach with parameter of β shown in Eq.(15), based on the new equivalent relationship between the SDOF structure with AVS system and the so-called special linear structure presented in this paper.

3. The maximum interstorey shear force of the j th storey unit of the structure with AVS systems may be approximately distributed between the structural members in the j th floor and the AVS system installed in the same floor, according to their lateral stiffnesses. The maximum stiffness restoring force and the maximum additional stiffness restoring force of the j th floor occur at almost the same time as the maximum interstorey shear force of the same floor.

4. The seismic design method for structures with AVS systems presented in this paper is similar to that for uncontrolled structures, so it is convenient to engineers for practical structural design applications.

ACKNOWLEDGEMENT

This research was supported by the National Natural Science Foundation of China through grant 59895410.

REFERENCES

1. He Y. A. and Feng D. P. (2000). Research on multi-mode optimal control method for active variable stiffness structural system. *Report of Project Supported by the National Natural Science Foundation of China under grant 59895410 (Part 7.3)*, 33-39 (in Chinese)
2. Kamagata S. and Kobori T. (1994). Autonomous adaptive control of active variable stiffness systems for seismic ground motion. *Proc. 1st World Conf. on Struct. Control*, Los Angeles, CA, Vol.2, TA4-33-TA4-42
3. Kobori T. *et al.* (1990). Experimental study on active variable stiffness system-active seismic response controlled structure. *Proceedings of the 4th World Congress Council on Tall Buildings & Urban Habitat*, 561-572
4. Kobori T. *et al* (1991a). Shaking table experiment and practical application of active variable stiffness (AVS) system. *Proc. 2nd Conf. on Tall Buildings in Seismic Regions, 55th Regional Conf.*, 213-222
5. Kobori T. *et al.* (1991b). Dynamic loading test of real scale steel frame with active variable stiffness device. *Journal of Structural Engineering*, 37B, 317-328
6. Kobori T. and Kamagata S. (1992). Active variable stiffness system-active seismic response control. *Proc. U.S.-Italy-Japan Workshop/Symp. on Struct. Control and Intelligent Sys.*, Elsevier Science, New York, 140-153
7. Nasu T., Kobori T., Takahashi M., Niwa N. and Ogasawara K. (2001). Active variable stiffness system with non-resonant control. *Earthquake Engineering and Structural Dynamics*, Vol.30, 1597-1614
8. Wu B., Liu F. T. and Wei D. M. (2001). Approximate mode decomposition method for structures with active variable stiffness systems. *Report of Project Supported by the National Natural Science Foundation of China under grant 59895410 (Part 7.3)*, 29-36 (in Chinese)
9. Yamada K. and Kobori T. (1995). Control algorithm for estimating future responses of active variable stiffness structure. *Earthquake Engineering and Structural Dynamics*, Vol.24, 1085-1099
10. Yang J. N., Wu J. C. and Li Z. (1996). Control of seismic-excited buildings using active variable stiffness systems. *Engineering Structures*, Vol.18, No.8, 589-596
11. Yang J. N., Li Z. and Wu J. C. (1994). Control of seismic-excited buildings using active variable stiffness systems. *Proc. 1994 Am. Control Conf.*, IEEE, Piscataway, NJ, 1083-1088

Advances in Building Technology, Volume 2
M. Anson, J.M. Ko and E.S.S. Lam (Eds.)
© 2002 Elsevier Science Ltd. All rights reserved

Damage Detection of A Health Monitoring Benchmark Building Using Hilbert-Huang Spectral Analysis*

Jann N. Yang, Silian Lin and Shuwen Pan

Department of Civil & Environmental Engineering, University of California, Irvine, CA. 92697, USA.

ABSTRACT

Based on the Hilbert-Huang spectral analysis, a system identification and damage detection approach is proposed and applied to the ASCE structural health monitoring benchmark structure. The cases analysed involve the damage detection and assessment in the weak direction of the test structure using a 4-DOF linear shear-building model. In this approach, the structural parameters, including stiffness and damping before and after damage are identified first and then the location and severity of the damage are assessed by a comparison. The effect of measurement noises has been taken into account. Simulation results demonstrate that the accuracy of the proposed method in identifying the structural damages is very plausible, and it represents a new and viable system identification and damage detection approach for linear structures.

KEYWORDS

Structural Health Monitoring, System Identification, Damage Detection, Data Analysis Techniques, Hilbert Transform, Frequency-Time Decomposition.

INTRODUCTION

For structural health monitoring, appropriate data analysis techniques are needed to interpret the measured data and to identify the state of the structure and its damage after a severe event, such as earthquake. Various data analysis techniques have been available in the literature for the health monitoring of linear structures [e.g., Chang (1997, 1999, 2001)]. In order to facilitate a comparison of available techniques on the common basis, the ASCE Task Group on Structural Health Monitoring has established a benchmark problem recently. The benchmark structure is a 4-story building model and the corresponding analytical models have been developed [Johnson, et al (2001)]. The disturbances are assumed to be unknown random uncorrelated forces (white noise processes) applied to each floor of the building. Damage is introduced into the structure by removing braces in the analytical model. Only acceleration measurements are available and each

* This research is supported by the National Science Foundation through Grant No. CMS-98-07855.

acceleration measurements are also polluted by uncorrelated noise. Details of the benchmark problem are given in [Johnson, et al (2001)], and various different approaches have been presented [e.g., Beck et al (2001), Yang et al (2001), Dyke et al (2000)].

In this paper, a new approach based on the Hilbert-Huang spectral analysis [Huang et al (1998)] is proposed and applied to the damage identification and assessment of the benchmark structure. In this approach, the cross-correlation functions of the measured floor acceleration responses are first decomposed into different modal components using the Empirical Mode Decomposition (EMD) method and band-pass filters [Yang et al (2001)]. Then, the Hilbert transform is applied to each modal component to obtain the time-dependent (instantaneous) phase angles, frequencies and amplitudes. All the natural frequencies and damping ratios can be identified using only a single measurement. When the acceleration responses at all floors are measured, the mode shapes and the stiffness and damping matrices can be identified using the proposed approach. Based on a comparison of the stiffness of each story unit prior to and after damage, the damage locations and severities can be identified. Simulation results are presented for the damage patterns in the weakest direction of the benchmark structure using a 4-DOF linear shear building available in [Johnson, et al (2001)].

CROSS CORRELATION FUNCTION AND MODAL CONTRIBUTION

The equation of motion of an n DOF structure can be expressed as

$$\mathbf{M}\ddot{\mathbf{X}}(t) + \mathbf{C}\dot{\mathbf{X}}(t) + \mathbf{K}\mathbf{X}(t) = \mathbf{F}(t) \tag{1}$$

in which $\mathbf{X}(t) = [x_1, x_2, \ldots, x_n]^T$ = n-displacement vector, $\mathbf{F}(t)$ = n-excitation vector, and $\mathbf{M}$, $\mathbf{C}$ and $\mathbf{K}$ are $(n \times n)$ mass, damping and stiffness matrices, respectively. With the assumption of the existence of normal modes, the displacement and acceleration responses can be decomposed into n real modes,

$$\mathbf{X}(t) = \sum_{j=1}^{n} \mathbf{\Phi}_j q_j(t) \quad ; \quad \ddot{\mathbf{X}}(t) = \sum_{j=1}^{n} \mathbf{\Phi}_j \ddot{q}_j(t) \tag{2}$$

in which $\mathbf{\Phi}_j$ is the jth modal vector, and $q_j(t)$ is the jth modal coordinate. Substituting Eq.(2) into Eq.(1) and using the orthogonal properties of mode shapes, one can decouple Eq.(1) into n modes

$$\ddot{q}_j + 2\zeta_j\omega_j\dot{q}_j + \omega_j^2 q_j = \mathbf{\Phi}_j^T\mathbf{F}(t)/m_j^* \tag{3}$$

in which ω_j = jth modal frequency, ζ_j = jth modal damping ratio, and m_j^* = jth modal mass. When the excitation $\mathbf{F}(t)$ is a stationary white noise vector, the cross-correlation function of the floor responses, denoted by $R_{rs}(\tau)$, can be obtained as

$$R_{rs}(\tau) = E[\ddot{x}_r(t)\ddot{x}_s(t+\tau)] = \sum_{j=1}^{n} \phi_{rj}\,\alpha_{sj}\, e^{-\zeta_j\omega_j\tau} \sin(\omega_{dj}\tau + \theta_{sj}) \tag{4}$$

in which ϕ_{rj} is the rth element of the jth modal vector $\mathbf{\Phi}_j$, $\omega_{dj} = \omega_j(1-\zeta_j^2)^{1/2}$ is the jth damped modal frequency, θ_{sj} is the phase lag, and α_{sj} a positive constant. For simplicity of analysis, the time difference τ will be denoted by t and Eq. (4) will be expressed as follows,

$$R_{rs}(t) = \sum_{j=1}^{n} R_{rs,j}(t) = \sum_{j=1}^{n} |\phi_{rj}|\,\alpha_{sj}\, e^{-\zeta_j\omega_j t} \cos(\omega_{dj}t + \theta_{sj} + \frac{3\pi}{2} + \varphi_{rj}) \tag{5}$$

in which

$$R_{rs,j}(t) = B_{rs,j}\, e^{-\zeta_j\omega_j t} \cos(\omega_{dj}t + \theta_{sj} + \frac{3\pi}{2} + \varphi_{rj}) \tag{6}$$

and

$$B_{rs,j} = |\phi_{rj}|\alpha_{sj}; \qquad \varphi_{rj} = \begin{cases} \pm 2m\pi, & \text{if } \phi_{rj} \geq 0 \\ \pm(2m+1)\pi, & \text{if } \phi_{rj} < 0 \end{cases} \tag{7}$$

In Eqs.(5)-(7), $R_{rs,j}(t)$ is the contribution from the jth mode, referred to as the jth modal contribution. The cross-correlation function $R_{rs}(t)$ will be decomposed into modal contributions $R_{rs,j}(t)$ (j = 1, 2, ..., n) using the Empirical Mode Decomposition (EMD) method and band-pass filters. Then, the Hilbert transform will be applied to each modal contribution $R_{rs,j}(t)$ in Eq.(6) to determine the modal frequency ω_j, the modal damping ratio ζ_j, and the mode shape vector $\boldsymbol{\Phi}_j$ (with ϕ_{rj} as the rth element). Assuming that the mass matrix M in Eq. (1) is known, the generalized masses m_j^* can be obtained as

$$\boldsymbol{\Phi}^T\mathbf{M}\boldsymbol{\Phi} = \text{diag}\,(m_1^*, m_2^*, ..., m_n^*) \tag{8}$$

in which $\boldsymbol{\Phi}$ is the modal matrix consisting of the modal vector $\boldsymbol{\Phi}_j$ as the jth column. After determining m_j^*(j =1, 2, ..., n), the modal stiffness k_j^* and the modal damping c_j^* can be obtained as

$$k_j^* = m_j\,\omega_j^2; \text{ and } c_j^* = 2m_j\zeta_j\omega_j \tag{9}$$

Since $\boldsymbol{\Phi}^T\mathbf{K}\boldsymbol{\Phi} = \text{diag}\,(k_1^*, k_2^*, ..., k_n^*)$ and $\boldsymbol{\Phi}^T\mathbf{C}\boldsymbol{\Phi} = \text{diag}\,(c_1^*, c_2^*, ..., c_n^*)$, the stiffness matrix **K** and the damping matrix **C** in Eq. (1) can be identified as

$$\mathbf{K} = \boldsymbol{\Phi}^{-T}\text{diag}\,(k_1^*, k_2^*, ..., k_n^*)\,\boldsymbol{\Phi}^{-1}; \quad \mathbf{C} = \boldsymbol{\Phi}^{-T}\text{diag}\,(c_1^*, c_2^*, ..., c_n^*)\,\boldsymbol{\Phi}^{-1} \tag{10}$$

For a shear-beam building model, the stiffness of each story unit can be obtained from **K**.

HILBERT-HUANG TRANSFORM

Suppose x(t) is a general measured signal such as the cross-correlation functions $R_{rs}(t)$ in Eq. (5). The Hilbert transform (HT) of x(t), denoted by $\tilde{x}(t)$, is given by

$$\tilde{x}(t) = HT[x(t)] = \int_{-\infty}^{+\infty} \frac{x(\tau)}{\pi(t-\tau)}\,d\tau \tag{11}$$

where $\tilde{x}(t)$ can be computed numerically using the efficient Fast Fourier transform [Huang et al (1998, 1999)]. The analytical signal Y(t) of x(t) is expressed as

$$Y(t) = x(t) + \underline{i}\,\tilde{x}(t) = A(t)\,e^{\underline{i}\,\theta(t)} \tag{12}$$

in which A(t) is the instantaneous amplitude, $\theta(t)$ is the instantaneous phase angle, and $\underline{i} = (-1)^{1/2}$. The instantaneous frequency $\omega(t)$ of the signal is obtained as

$$\omega(t) = d\theta(t)/\,dt \tag{13}$$

From Eqs.(11)-(13), there is only a single frequency ω at any time t, if the general signal x(t) is processed through the Hilbert transform. On the contrary, for a general signal x(t) at any time t, there is a distribution of frequencies at that time rather than just a single frequency. Consequently, to obtain a meaningful decomposition of a signal in the frequency-time domain, it was proposed by Huang et al (1998) to first decompose the signal x(t) into m Intrinsic Mode Functions (IMFs) using the EMD method. Then, the Hilbert transform is applied to each IMF to form a meaningful frequency-time decomposition of a general signal, referred to as the Hilbert-Huang spectral analysis. Such an approach will be used herein to detect the damage in the benchmark building.

The method of Empirical Mode Decomposition (EMD) will be used to decompose the cross-correlation function $R_{rs}(t)$ into "Intrinsic Mode Functions" (IMFs) that admit well-behaved Hilbert transform. The procedure of EMD is to construct upper and lower envelopes of the signal by spline fitting, and the average (mean) of both envelopes are computed. Then, the signal is subtracted from the mean, referred to as the

sifting process. By repeating the sifting process until the resulting signal becomes a monocomponent, i.e., one up-crossing (or down-crossing) of zero will result in one local peak (or trough). Such a monocomponent signal admits a well-behaved Hilbert transform and it is referred to as an IMF. The original signal is then subtracted from the IMF, and the repeated sifting process is applied to the remaining signal to obtain another IMF. The process is repeated to obtain m IMFs, i.e.,

$$R_{rs}(t) = \sum_{j=1}^{m} c_{pj}(t) + r_p(t) \tag{14}$$

in which $c_{pj}(t)$ for $j = 1,...,$ m are IMFs of $R_{rs}(t)$, and $r_p(t)$ is the residue, which is the mean trend (or a constant) of the signal. Such a process is referred to as the Empirical Mode Decomposition (EMD) method. The IMFs obtained from the sifting process described above may contain more than one frequency, which is not the modal contribution $R_{rs,j}(t)$. During the sifting process in EMD, one can also impose an intermittency frequency, denoted by ω_{int}, so that the resulting IMF will not contain any frequency components smaller than ω_{int}. By successive applications of the EMD method with intermittency frequency in respective range of modal frequencies, it is possible to extract the modal contribution $R_{rs,j}(t)$ as described e.g., in Yang et al (2000a,b, 2001), i.e.,

$$R_{rs}(t) \approx \sum_{j=1}^{n} R_{rs,j}(t) + \sum_{j=1}^{m-n} c_{pj}(t) + r_p(t) \tag{15}$$

Another alternative approach is to use the band-pass filter and EMD method to extract the modal contribution $R_{rs,j}(t)$ in Eq.(15) as follows: From the Fourier spectrum of $R_{rs}(t)$, the approximate frequency range for each natural frequency, i.e., $\omega_{jL} < \omega_j < \omega_{jH}$ ($j = 1, 2, ..., n$) can be determined. $R_{rs}(t)$ is processed through the band-pass filter with a frequency band $\omega_{jL} < \omega_j < \omega_{jH}$. The resulting time history is then processed through EMD, and the first IMF is quite close to the jth modal contribution $R_{rs,j}(t)$. Repeating the same procedures for $j = 1, 2, ..., n$, one obtains $R_{rs,j}(t)$ in Eq.(15).

Taking the Hilbert transform of $R_{rs,j}(t)$, denoted by $\tilde{R}_{rs,j}(t)$, and forming the analytical function, one obtains for $\zeta_j << 1$ and $\zeta_j << \omega_j$,

$$Y_{rs,j}(t) = R_{rs,j}(t) + i\,\tilde{R}_{rs,j}(t) = A_{rs,j}(t)\exp[i\,\theta_{rs,j}(t)] \tag{16}$$

$$A_{rs,j}(t) = B_{rs,j}\, e^{-\zeta_j \omega_j t} \tag{17}$$

$$\theta_{rs,j}(t) = \omega_{dj} t + \theta_{sj} + \frac{3\pi}{2} + \varphi_{rs,j} \tag{18}$$

where Eqs.(5)-(7) have been used. From Eqs.(17)-(18), one obtains

$$\ln A_{rs,j}(t) = \ln B_{rs,j} - \zeta_j \omega_j t \tag{19}$$

$$\omega_{rs,j}(t) = \frac{d}{dt}\theta_{rs,j}(t) = \omega_{dj} \tag{20}$$

IDENTIFICATION OF STRUCTURAL PARAMETERS

For the identification of natural frequencies ω_j and damping ratios ζ_j for $j = 1, 2, ..., n$, only one cross-correlation (or auto-correlation) function is sufficient. The procedures are described in the following. For small ζ_j, it follows from Eq.(18) that the damped natural frequency ω_{dj} can be obtained from the slope of the phase angle $\theta_{rs,j}(t)$ vs. time t plot, whereas $-\zeta_j\omega_j$ can be estimated from the slope of the decaying amplitude $\ln A_{rs,j}(t)$ vs. time t plot, Eq.(19). For the general case in which ζ_j is not small, both $\theta_{rs,j}(t)$ and $\ln A_{rs,j}(t)$ are not linear functions of time t. In this case, it was proposed in Yang et al (2000a,b, 2001)

to use linear least-square fit procedures to estimate the natural frequencies and damping ratios as follows: (i) The plot of the phase angle $\theta_{rs,j}(t)$ vs. time t is fitted by a straight line using the linear least-square fit procedure. This straight line is referred to as the least-square straight line for the phase angle. Then, the slope of the straight line is ω_{dj}, (ii) The plot of the decaying amplitude $\ln A_{rs,j}(t)$ vs. time t is fitted by a straight line using the linear least-square fit procedure. This straight line is referred to as the least-square straight line for the decaying amplitude. Then, $-\zeta_j\omega_j$ is estimated from the slope of the straight line, (iii) With ω_{dj} and $-\zeta_j\omega_j$ estimated from (i) and (ii), ω_j and ζ_j can be computed using $\omega_{dj} = \omega_j(1-\zeta_j^2)^{1/2}$. As will be demonstrated later in the benchmark example, ω_{dj} can be estimated from step (i) above without any problem. However, when ζ_j is large, the oscillation of $\ln A_{rs,j}(t)$ around the linear least-square line may be significant, so that the slope $-\zeta_j\omega_j$ may be sensitive to the range of time interval used for the linear least-square fit. In this case, we propose to process $\ln A_{rs,j}(t)$ through the EMD to obtain the residue, denoted by $r_{Apj}(t)$. Since the residue represents the mean trend of $\ln A_{pj}(t)$, it is fitted by a straight line using the linear least-square fit procedure. Then, the slope $-\zeta_j\omega_j$ can be estimated from the linear least-square line.

To identify the mode shapes, damping matrix and stiffness matrix, the response time histories at all DOF should be measured. It follows from Eqs.(7) and (19) that the ratio of the absolute value of the modal elements ϕ_{rj} and ϕ_{mj} (r, m = 1, 2, ..., n) can be identified as

$$\left|\phi_{rj}\right| / \left|\phi_{mj}\right| = \exp[A'_{rs,j}(t_0) - A'_{ms,j}(t_0)] \tag{21}$$

in which $A'_{rs,j}(t_0)$ and $A'_{ms,j}(t_0)$ are, respectively, the magnitudes at the time $t = t_0$ of the least-square straight lines for the decaying amplitudes $\ln A_{rs,j}(t)$ and $\ln A_{ms,j}(t)$ obtained previously. Further, the differences between the phase angle $\varphi_{rs,j}$ of the modal element ϕ_{rj} and that of ϕ_{mj} follow from Eq.(18) as

$$\Delta\varphi_{r\,m,j} = \varphi_{rs,j} - \varphi_{ms,j} = \theta'_{rs,j}(t_0) - \theta'_{ms,j}(t_0) \tag{22}$$

in which $\theta'_{rs,j}(t_0)$ and $\theta'_{ms,j}(t_0)$ are, respectively, the magnitudes of the least-square straight lines for the phase angles $\theta_{rs,j}(t)$ and $\theta_{ms,j}(t)$ at the time $t = t_0$ obtained previously. The value of $\Delta\varphi_{r\,m,j}$ above is either $\pm 2m\pi$ or $\pm(2m+1)\pi$, see Eq.(7). With the aid of Eq.(7), the sign of ϕ_{rj} relative to ϕ_{mj} can be determined. Thus, both the absolute values and signs of all elements relative to an arbitrary element in the jth modal vector $\mathbf{\Phi}_j$ have been determined. Repeating the same procedures for all modal contributions j = 1, 2, ..., n, the modal matrix $\mathbf{\Phi}$ can be identified. Finally, the stiffness and damping matrices **K** and **C** can be obtained from Eq.(10).

BENCHMARK RESULTS

The approach described previously is applied to the noisy acceleration data provided by the benchmark problem. To obtain a reasonable estimate of cross spectral density functions, a total of 400 seconds of stationary response data with a sampling rate of 1000Hz is used, after removing the beginning transient parts (first 3 seconds). This allows for 47 averages in computing the cross spectral density functions. The reference floor response is selected to be the acceleration of the fourth floor, i.e., s = 4 in Eq.(4), so that all the modes can be observed in the data. A representative cross spectral density function and the corresponding cross correlation function of the 4th and 1st floors of the undamaged structure are shown in Fig.1.

The EMD method and band-pass filters with bandwidths $\omega_{jL} \le \omega_j \le \omega_{jH}$ (j = 1, 2, 3, 4) are applied to the cross correlation functions of the undamaged structure in Fig.1(b) to obtain the modal components $R_{14,j}(t)$

with ω_{1L} = 7Hz, ω_{1H} = 12Hz, ω_{2L} = 24Hz, ω_{2H} = 27Hz, ω_{3L} = 36Hz, ω_{3H} = 40Hz, ω_{4L} = 46Hz and ω_{4H} = 50Hz. The decomposed modal responses of the cross correlation function in Fig.1 (b) are shown in Fig.2. Due to the phase shift of band-pass filters, the beginning segments in Fig.2 do not represent the free decay characteristics. Hence, a small segment at the beginning will be removed. Then, the Hilbert transform is applied to each modal response to obtain the instantaneous phase angle $\theta_{rs,j}(t)$ and amplitude $A_{rs,j}(t)$. The plots of $\ln A_{rs,j}(t)$ and $\theta_{rs,j}(t)$ versus time t for the first modal response in Fig.2(a) are presented in Fig.3 as dotted curves. These dotted curves are fitted by solid straight lines using the linear least-square procedure. Following the identification procedures presented previously, the first natural frequency ω_1 and damping ratio ζ_1 can be determined from the slopes of two solid lines in Fig.3. Choosing a time instance t_0 in the middle of the range of the solid straight line in Fig.3, i.e., t_0 = 2.5 seconds, one obtains $A'_{rs,j}(t_0)$ and $\theta'_{rs,j}(t_0)$ from Fig.3. Repeating the same procedures for each modal response, the mode shape vector $\mathbf{\Phi}_j$ and modal matrix $\mathbf{\Phi}$ can be identified.

The identified natural frequencies and damping ratios for the undamaged and damaged structures (damage patterns 1 and 2 of Case 1) are presented in Table 1 as denoted by "Id.". Also shown in Table 1 are the theoretical values, as denoted by "Th.", for comparison. The theoretical damping ratio for each mode is 1%. For the damage pattern 1, all braces in the first story unit are removed, whereas for the damage pattern 2, all braces in both the first and third story units are removed. As observed from Table 1, the estimated natural frequencies and damping ratios are quite accurate. Assuming that the mass matrix is known, the stiffness matrix **K** and damping matrix **C** have been estimated. The stiffness in each story unit is computed based on the shear-beam model. The identified results for the stiffness in each story unit, denoted by k_1, k_2, k_3 and k_4, respectively, are presented in Table 2. Also shown in Table 2 are the theoretical values for comparison. From the identified stiffness in each story unit presented in Table 2, the damage locations and damage severities have been detected and identified quite accurately.

CONCLUSIONS

Based on the Hilbert-Huang spectral analysis, a method of system identification and damage detection is proposed and applied to the ASCE benchmark building model. All the natural frequencies and damping ratios of the structure can be identified with only one measurement of the acceleration response that may be polluted by noises. When the acceleration responses at all DOF are measured, the modal matrix, stiffness matrix and damping matrix can be identified assuming that the mass matrix is known. Damages in the structure can be identified by a comparison of the stiffness in each story of the building prior to and after the damage event. Simulation results demonstrate that the proposed method is quite accurate in identifying the structural damages, including the damage locations and severities. The method is shown to be quite effective for the system identification and damage detection of structural health monitoring.

REFERENCES

Beck, J.L., Katafygiotis, L.S., Yuen, K.-V., and Lam, H.-F. (2001). Damage Detection for a Benchmark Structure Using One-Step and Two-Step Probabilistic Approach. *Proc. 3rd Inter. Workshop on Structural Health Monitoring,* 478-487. Sept. 11-13, Stanford, CA.

Chang, F.-K., ed. (1997, 1999, 2001). *Structural Health Monitoring*, Proc. 1st, 2nd and 3rd International Workshop on Structural Health Monitoring, Stanford University, Stanford, CA. CRC Press.

Dyke, S.J., Caicedo, J.M. and Johnson, E.A. (2000). Monitoring of a Benchmark Structure for Damage Identification. *Proc. 14th Engineering Mechanics Conference (EM2000),* Austin, Texas.

Huang, N.E., Shen, Z., Long, S.R., Wu, M.C. and Shih, H. H., et al. (1998). The Empirical Mode Decomposition and Hilbert Spectrum for Nonlinear and Nonstationary Time Series Analysis. *Proc. Royal Society of London Series*, **A454**, 903-995.

Huang, N.E., Shen, Z. and Long, S.R. (1999). A New View of Nonlinear Water Waves: The Hilbert Spectrum. *Annu. Rev. Fluid Mech.*, **31**, 417-457.

Johnson, E.A., Lam, H.F., Katafygiotis, L.S., and Beck, J.L. (2001). A Simulated Data Benchmark Problem in Structural Health Monitoring. *Proc. 3rd Inter. Workshop on Structural Health Monitoring,* Sept. 11-13, Stanford, CA. pp.467-477; also http://wusceel.civil.wustl.edu/ asce.shm/.

Yang, J.N., and Lei, Y. (2000a). Identification of Civil Structures with Nonproportional Damping. *Smart Structures and Materials 2000: Smart Systems for Bridges, Structures & Highways,* Proc. of SPIE, Vol. **3988**, 284-294. Newport Beach , CA.

Yang, J.N., and Lei, Y. (2000b). Identification of Tall Building Using Noisy Wind Vibration Data. *Advances in Structural Dynamics,* Vol.**II**, 1093-1100. Elsevier Science Ltd., *Proc. International Conf. On Advances in Structural Dynamics, Hong Kong.*

Yang, J.N., Lei, Y. and Huang, N.E. (2001). Damage Identification of Civil Engineering Structures Using Hilbert-Huang Transform. *Proc. 3rd Inter. Workshop on Structural Health Monitoring,* 544-553. Sept. 11-13, Stanford, CA.

TABLE 1: IDENTIFIED NATURAL FREQUENCIES AND DAMPING RATIOS

Mode	Undamaged			Damage Pattern 1			Damage Pattern 2		
	Frequency (Hz)		Damping (%)	Frequency (Hz)		Damping (%)	Frequency (Hz)		Damping (%)
	Th.	Id.	Id.	Th.	Id.	Id.	Th.	Id.	Id.
1	9.41	9.39	1.09	6.24	6.25	1.17	5.82	5.83	1.01
2	25.54	25.41	1.16	21.53	21.51	1.04	14.89	14.88	1.03
3	38.66	38.59	1.05	37.37	37.35	0.88	36.06	36.02	1.10
4	48.01	48.13	1.03	47.83	47.81	1.12	41.35	41.37	1.00

TABLE 2: STIFFNESS PARAMETER OF EACH STORY UNIT FOR CASE 1

Stiffness	Theoretical Values			Identified Values		
	No Damage	Damage Pattern 1	Damage Pattern 2	No Damage	Damage Pattern 1	Damage Pattern 2
k_1 MN/m	67.90	19.68	19.68	67.71	19.02	20.26
k_2 MN/m	67.90	67.90	67.90	68.58	68.38	67.36
k_3 MN/m	67.90	67.90	19.68	68.25	68.38	19.21
k_4 MN/m	67.90	67.90	67.90	67.35	66.91	68.42

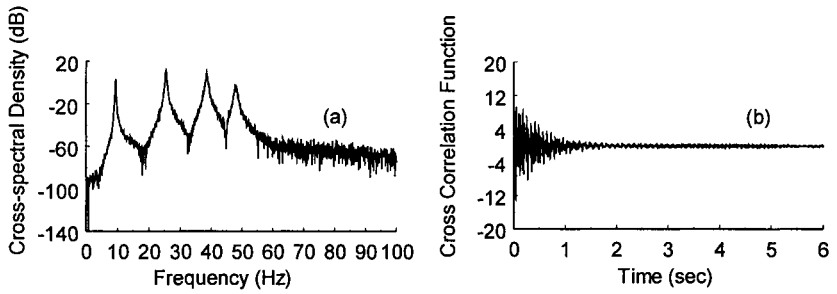


Fig. 1: Cross-spectral density, (a), and cross-correlation function, (b), of undamaged structure.

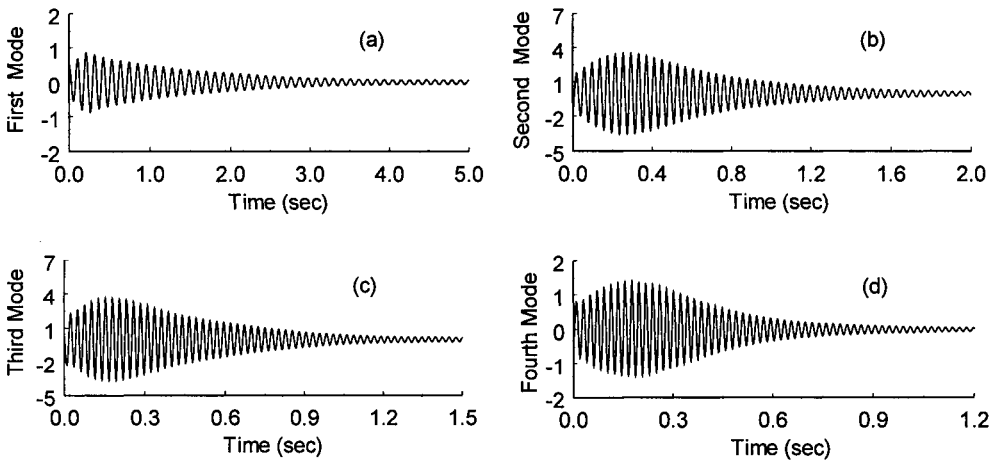


Fig.2: Modal decomposition of cross-correlation function in Fig.1

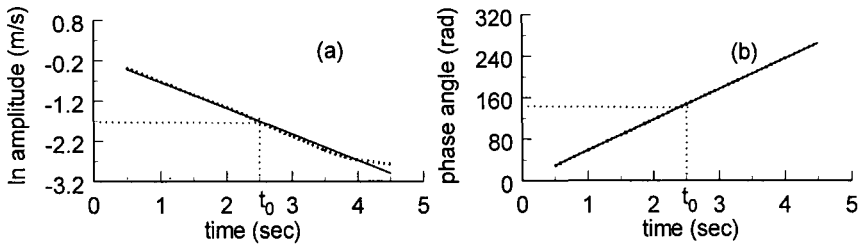


Fig.3: Time-dependent amplitude and phase angle of first modal response;
(a) $\ln A_{rs,j}(t)$ vs. t, and (b) $\theta_{rs,j}(t)$ vs. t.

Advances in Building Technology, Volume 2
M. Anson, J.M. Ko and E.S.S. Lam (Eds.)
© 2002 Elsevier Science Ltd. All rights reserved

PARAMETER OPTIMIZATION OF MULTI-TMDS FOR WIND-EXCITED VIBRATION SUPPRESSION OF TALL BUILDINGS

G. Zheng, Y. Q. Ni, H. Li, Y. F. Duan

Department of Civil and Structural Engineering, The Hong Kong Polytechnic University, Hung Hom, Kowloon, Hong Kong

ABSTRACT

Owing to shortage in the supply of land in Hong Kong, buildings in the urban areas of Hong Kong are often built to be tall and slender. Mitigation of wind-induced vibration by using supplemental damping devices has been required in design of some slender tall buildings to satisfy stringent criteria resulting from Hong Kong's typhoon wind climate. Tuned mass/liquid dampers (TMDs/TLDs) provide a cost-effective means for this purpose. This paper describes a study on optimizing the parameters of multiple tuned mass dampers (multi-TMDs) for wind-excited vibration suppression of high-rise buildings. Based on three-dimensional finite element model for design analysis of tall buildings, a reduced-order lumped mass MDOF model with the same modal properties as original model is developed for multi-TMDs design. By dividing the building-damper system as two sub-structures, transfer functions of the building with multi-TMDs attached at arbitrary stories are explicitly derived, and random vibration response of the building-damper system is accurately expressed by adopting appropriate wind force spectrum and accounting for spatial correlation of the excitation. With these analytically derived formulations, the genetic algorithm is then applied to search optimal parameters of the multi-TMDs that achieve maximum response suppression for the building. The damper parameters concerned include the stiffness, mass and damping. A case study of an actual 50-story tall building using multi-TMDs for wind-excited response mitigation is given as an example.

KEYWORDS

Multiple tuned mass dampers (multi-TMDs), tall building, wind excitation, vibration suppression, parameter optimization, genetic algorithm.

INTRODUCTION

Tuned mass dampers (TMDs) have been widely used in high-rise buildings worldwide for wind- and earthquake-induced vibration mitigation (McNamara 1977; Kwok 1984; Ueda et al. 1992; Kwok and Samali 1995; Kitagawa and Midorikawa 1998; Breukelman and Haskett 2001). The TMD consists of a mass, a spring and a viscous damper attached to a vibrating main system. By tuning natural frequency of the TMD close to natural frequency of the main system, the vibration energy is dissipated through the damping of the TMD. One of the disadvantages of a single TMD system is its high sensitivity to

fluctuation in natural frequency of the structure and/or that in damping ratio of the TMD. The effectiveness of a TMD is decreased significantly by mis-tuning frequency or off-optimum damping. As a result, the use of multiple tuned mass dampers (multi-TMDs) has been proposed for improving the control effectiveness and robustness (Yamaguchi and Harnpornchai 1993; Abe and Fujino 1994; Igusa and Xu 1994; Kareem and Kline 1995; Jangid and Datta 1997; Rana and Soong 1998). In the majority of existing studies on multi-TMDs, the primary system was assumed to vibrate in a single mode and idealized as a mode-generalized SDOF model. However, tall buildings usually exhibit multi-mode dynamic response under the action of wind or seismic loading. Multi-TMDs have been shown effective in controlling multiple structural modes (Rana and Soong 1998).

In this paper a method for parameter optimization of multi-TMDs for controlling multi-mode structural response of tall buildings under random wind excitation is presented by using the genetic algorithm, and its application to a 50-storey building in Hong Kong is described. Based on the accurate analysis model for structural design, a reduced-order lumped mass MDOF model is formulated for multi-TMDs design. Making use of sub-structuring, transfer functions of the building-damper system are explicitly derived, and the root-mean-square response expression is further obtained by considering appropriate wind force spectrum and accounting for spatial correlation of the excitation. The genetic algorithm is then implemented to search optimal parameters of the multi-TMDs that achieve maximum structural response reduction. In the case study, the wind excitation spectrum used is determined according to the Hong Kong Code of Practice on Wind Effects and the wind profile suggested by the Hong Kong Building Department.

FORMULATION

Wind Force Spectrum

The mean wind speed profile can be approximated either by a logarithmic law or a power law, i.e.,

$$V(z)=\frac{1}{k}V^{*}\ln\frac{z}{z_0} \quad \text{or} \quad V(z)=V_g\left(\frac{z}{\delta}\right)^{\alpha} \tag{1a, b}$$

A power exponent of 0.19, i.e., $\alpha = 0.19$ is suggested for the mean wind profile at general terrain in the Hong Kong Building Department Notes for Wind Tunnel Tests. The wind pressure is related to the wind speed by

$$P=\frac{1}{2}\rho V^2 \tag{2}$$

According to the Code of Practice on Wind Effects (1983) for Hong Kong, the wind pressure at 250 m or above is 4.3 kN/m^2 at general terrain. The wind speed at the height of 250 m or above is obtained as

$$V(250) = 81.96 \text{ m/s} \tag{3}$$

The mean wind profile is determined by

$$V(z) = V(250)\times(z/250)^{0.19} \tag{4}$$

and the mean wind velocity at 10 m height is

$$V_{10} = 44.46 \text{ m/s} \tag{5}$$

The wind velocity spectrum is taken as Davenport spectrum with the expression (Davenport 1961)

$$W(f) = 4k\bar{v}^2(10)\frac{x^2}{f(1+x^2)^{4/3}} \tag{6}$$

$$x = L_v^{*}\cdot f/\bar{v}(10) \tag{7}$$

where k is the coefficient about the ground surface coarse, being 0.02 for open sea area; $\bar{v}(10)=V_{10}$ is

the mean wind speed at 10 m height above the ground; L_v^* is the integral length scale, generally taken as 1200; f is frequency in Hz.

The coherence function between two points at different heights is taken as the expression

$$coh(f) = \exp(-\frac{C_z \cdot f \cdot \Delta z}{V_{10}}) \tag{8}$$

where the constant C_z is taken as 10; Δz is the vertical distance between the two concerned points; V_{10} is the mean wind speed at 10 m height and is taken as 44.46 m/s in the present study. Then the co-spectrum of the wind velocity on a tall building at height i and height j is

$$W_{ij} = coh(f) \cdot \sqrt{W_{ii} W_{jj}} = \exp(-\frac{10 f \cdot \Delta z_{ij}}{44.46}) \cdot \sqrt{W_{ii} W_{jj}} \tag{9}$$

The co-spectrum of wind load is obtained by

$$S_{Wij} = \rho^2 C_{D,i} C_{D,j} A_i A_j \overline{v}_i \overline{v}_j W_{ij} \tag{10}$$

in which the coefficient ρ is taken as 1.28 kg/m^3; C_D = 1.2; and the factor A representing the equivalent projection area along wind direction at heights i and j is taken as 1 in the present study. So,

$$S_{Wij} = 1.28^2 1.2^2 A^2 \overline{v}_i \overline{v}_j W_{ij} = 2.3593\, \overline{v}(z_i)\, \overline{v}(z_j) \exp(-\frac{10 f \cdot \Delta z_{ij}}{44.46}) W(f) \tag{11}$$

Response of Building without Multi-TMDs

For a tall building with arbitrary stories, the governing equation of motion can be expressed as

$$\boldsymbol{M}\ddot{\boldsymbol{x}}(t) + \boldsymbol{C}\dot{\boldsymbol{x}}(t) + \boldsymbol{K}\boldsymbol{x}(t) = \boldsymbol{F}(t) \tag{12}$$

where $\boldsymbol{M}$, $\boldsymbol{C}$, $\boldsymbol{K}$ are the mass, damping and stiffness matrices of the building, respectively, which are usually obtained from the finite element model for structural design analysis. Based on modal analysis of the finite element model, the structural response $\boldsymbol{x}(t)$ can be expressed in modal coordinates as

$$\boldsymbol{x} = R_1\{\boldsymbol{\varphi}_1\} + R_2\{\boldsymbol{\varphi}_2\} + \cdots + R_N\{\boldsymbol{\varphi}_N\} = [\boldsymbol{\Phi}]_{N\times N}\{\boldsymbol{R}\}_{N\times 1} \tag{13}$$

where $[\boldsymbol{\Phi}]$ are mode shape matrix obtained from modal analysis; $\{\boldsymbol{R}\}$ is modal coordinate vector. By substituting Eq. (13) into Eq. (12) and then left-multiplying Eq. (12) with $[\boldsymbol{\Phi}]^T$, we get

$$[\overline{\boldsymbol{M}}]\{\ddot{\boldsymbol{R}}\} + [\overline{\boldsymbol{C}}]\{\dot{\boldsymbol{R}}\} + [\overline{\boldsymbol{K}}]\{\boldsymbol{R}\} = [\boldsymbol{\Phi}]^T\{\boldsymbol{F}\} = \{\overline{\boldsymbol{F}}\} \tag{14}$$

where

$$[\overline{\boldsymbol{M}}] = [\boldsymbol{\Phi}]^T[\boldsymbol{M}][\boldsymbol{\Phi}], \quad [\overline{\boldsymbol{C}}] = [\boldsymbol{\Phi}]^T[\boldsymbol{C}][\boldsymbol{\Phi}], \quad [\overline{\boldsymbol{K}}] = [\boldsymbol{\Phi}]^T[\boldsymbol{K}][\boldsymbol{\Phi}] \tag{15a, b, c}$$

are all diagonal matrices under the assumption of proportional viscous damping.

The transfer function in modal coordinates is obtained as

$$\begin{aligned} \boldsymbol{H}_s(\omega) &= \left[-\omega^2 \overline{\boldsymbol{M}} + i\omega \overline{\boldsymbol{C}} + \overline{\boldsymbol{K}}\right]^{-1} \\ &= \left[\boldsymbol{Diag}(\omega_1^2 - \omega^2, \cdots, \omega_N^2 - \omega^2) + i\, \boldsymbol{Diag}(2\zeta_1\omega_1\omega, \cdots, 2\zeta_N\omega_N\omega)\right]^{-1} \end{aligned} \tag{16}$$

Therefore the response co-spectrum in modal coordinates is

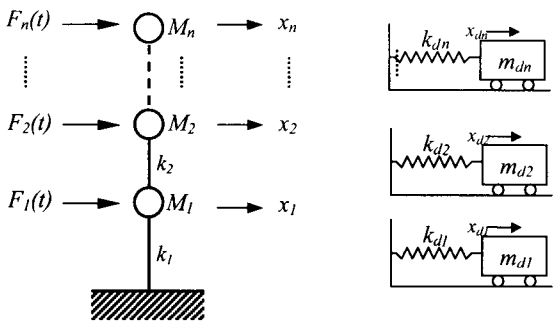
$$\boldsymbol{S}_r^M = \boldsymbol{H}_S^*(\omega)\boldsymbol{S}^{MF}\boldsymbol{H}_S^T(\omega) \tag{17}$$

where $\boldsymbol{S}^{MF}$ is the wind load co-spectrum in modal coordinates, defined as

$$\boldsymbol{S}^{MF} = \boldsymbol{\Phi}^T \boldsymbol{S}_W \boldsymbol{\Phi} \tag{18}$$

The response co-spectrum in physical coordinates is obtained by

$$\boldsymbol{S}_X = \boldsymbol{\Phi}\boldsymbol{S}_r^M\boldsymbol{\Phi}^T \tag{19}$$



(a) Substructure of building (b) Substructure of multi-TMDs

Figure 1: Model of building-damper system

Response of Building with Multi-TMDs

When the building is attached with multi-TMDs, the whole system can be considered with two sub-structures as shown in Fig. 1: one is the original building with additional forces due to building-TMD interaction and the other is the multi-TMDs subjected to forces due to building-TMD interaction.

The governing equation of motion of the building substructure is as follows

$$[\overline{\boldsymbol{M}}]\{\ddot{\boldsymbol{R}}\}+[\overline{\boldsymbol{C}}]\{\dot{\boldsymbol{R}}\}+[\overline{\boldsymbol{K}}]\{\boldsymbol{R}\}=[\boldsymbol{\Phi}]^T\{\overline{\boldsymbol{F}}'(t)\} \tag{20}$$

where

$$\{\overline{\boldsymbol{F}}'(t)\}=\{\boldsymbol{F}(t)\}+\{\boldsymbol{F}_D(t)\} \tag{21}$$

in which $\{\boldsymbol{F}_D(t)\}$ is the vector of interactive forces applied to the building by the tuned mass dampers. It has the expression

$$\{\boldsymbol{F}_D(t)\}=\{k_{d1}x_{d1}+c_{d1}\dot{x}_{d1},\ k_{d2}x_{d2}+c_{d2}\dot{x}_{d2},\ \cdots\ k_{dn}x_{dn}+c_{dn}\dot{x}_{dn}\}^T \tag{22}$$

where k_{dj} and c_{dj} (j=1, 2, ···, n) are the stiffness and viscous damping coefficient of the jth TMD. Substituting Eqs. (21) and (22) into Eq. (20) and applying Laplace transformation yield

$$[\boldsymbol{H}(\omega)]^{-1}\{\widetilde{\boldsymbol{R}}(\omega)\}=[\boldsymbol{\Phi}]^T[\widetilde{\boldsymbol{F}}(\omega)]+[\boldsymbol{\Phi}]^T[\boldsymbol{d}]\{\widetilde{\boldsymbol{x}}_d(\omega)\} \tag{23}$$

where

$$[\boldsymbol{d}]=\boldsymbol{Diag}[k_{d1}+ic_{d1}\omega\quad k_{d2}+ic_{d2}\omega\quad\cdots\quad k_{dn}+ic_{dn}\omega] \tag{24}$$

$$[\boldsymbol{H}(\omega)]^{-1}=\boldsymbol{Diag}[\omega_1^2-\omega^2+2i\zeta_1\omega_1\omega\quad\omega_2^2-\omega^2+2i\zeta_2\omega_2\omega\quad\cdots\quad\omega_N^2-\omega^2+2i\zeta_N\omega_N\omega] \tag{25}$$

in which ω_j's (j=1, 2, ···, N) are the natural frequencies of the building without TMDs.

The governing equation of motion of the TMD substructure is as follows

$$[\boldsymbol{M}_d](\{\ddot{\boldsymbol{x}}\}+\{\ddot{\boldsymbol{x}}_d\})+[\boldsymbol{C}_d]\{\dot{\boldsymbol{x}}_d\}+[\boldsymbol{K}_d]\{\boldsymbol{x}_d\}=0 \tag{26}$$

Applying Laplace transformation to Eq. (26) yields

$$([\boldsymbol{K}_d]-\omega^2[\boldsymbol{M}_d]+i\omega[\boldsymbol{C}_d])\{\widetilde{\boldsymbol{x}}_d(\omega)\}=\omega^2[\boldsymbol{M}_d]\{\widetilde{\boldsymbol{x}}(\omega)\} \tag{27}$$

from which it follows that

$$[\widetilde{\boldsymbol{x}}_d(\omega)]=[\boldsymbol{H}_d]\{\widetilde{\boldsymbol{x}}(\omega)\}=[\boldsymbol{H}_d][\boldsymbol{\Phi}]\{\widetilde{\boldsymbol{R}}(\omega)\} \tag{28}$$

where

$$[\boldsymbol{H}_d]=\boldsymbol{Diag}[h_{d1}\quad h_{d2}\quad\cdots\quad h_{dn}] \tag{29}$$

$$h_{dj} = \frac{\omega^2}{\omega_{dj}^2 - \omega^2 + 2i\zeta_{dj}\omega_{dj}\omega} \qquad (j=1, 2, \cdots, n) \tag{30}$$

in which $\omega_{dj} = \sqrt{k_{dj}/m_{dj}}$ and $\zeta_{dj} = c_{dj}/(2m_{dj}\omega_{dj})$ are the frequency and damping ratio of the jth TMD.

Substituting Eq. (28) into Eq. (23) obtains

$$\{\tilde{\boldsymbol{R}}(\omega)\} = \tilde{\boldsymbol{H}}_d(\omega)[\boldsymbol{\Phi}]^T\{\tilde{\boldsymbol{F}}(\omega)\} \tag{31}$$

where

$$\tilde{\boldsymbol{H}}_d(\omega) = \left[[\boldsymbol{H}(\omega)]^{-1} - [\boldsymbol{\Phi}]^T[\boldsymbol{d}][\boldsymbol{H}_d][\boldsymbol{\Phi}]\right]^{-1} \tag{32}$$

The spectrum expression of Eq. (31) is

$$[\tilde{\boldsymbol{S}}_R(\omega)] = [\tilde{\boldsymbol{H}}_d(\omega)][\boldsymbol{\Phi}]^T[\boldsymbol{S}_F(\omega)][\boldsymbol{\Phi}][\tilde{\boldsymbol{H}}_d^*(\omega)] \tag{33}$$

and thus the response spectrum of the TMD-controlled structure at degree j is obtained as

$$\tilde{S}_{Xjj}(\omega) = \{[\boldsymbol{\Phi}]_{j,1:end}\}^T[\tilde{\boldsymbol{S}}_R(\omega)]\{\boldsymbol{\Phi}_{j,1:end}\} \tag{34}$$

PARAMETER OPTIMIZATION

The RMS responses at degree j of the building without and with multi-TMDs can be obtained by

$$\sigma_j^2 = \int_0^{+\infty} \{[\boldsymbol{\Phi}]_{j,1:end}\}^T[\boldsymbol{S}_R(\omega)]\{[\boldsymbol{\Phi}]_{j,1:end}\}d\omega \tag{35}$$

$$\tilde{\sigma}_j^2 = \int_0^{+\infty} \{[\boldsymbol{\Phi}]_{j,1:end}\}^T[\tilde{\boldsymbol{S}}_R(\omega)]\{[\boldsymbol{\Phi}]_{j,1:end}\}d\omega \tag{36}$$

The ratio between the RMS responses at degree j is defined as

$$\gamma_j = \frac{\int_0^{+\infty} \{[\boldsymbol{\Phi}]_{j,1:end}\}^T[\tilde{\boldsymbol{S}}_R(\omega)]\{[\boldsymbol{\Phi}]_{j,1:end}\}d\omega}{\int_0^{+\infty} \{[\boldsymbol{\Phi}]_{j,1:end}\}^T[\boldsymbol{S}_R(\omega)]\{[\boldsymbol{\Phi}]_{j,1:end}\}d\omega} \tag{37}$$

The TMD system can be optimized to minimize γ_j, which indicates a local optimal TMD system and is referred to as reduction index. A global optimal TMD system is defined by the one that minimizes a weighted sum of γ_j. In the present study, the genetic algorithm (GA) is adopted to search the optimal parameters, including the frequency, damping ratio of each TMD when constrain of gross mass of the multi-TMDs is given, to achieve the maximum response reduction. Description of the philosophy of GA for parameter identification is escaped herein due to the limited space. Some implementation points of this technique for the present problem will be addressed in the following case study.

CASE STUDY

A 162m-high 50-storey building is now under construction in Hong Kong. The initial design of this building was found to not satisfy the wind-resistant requirement prescribed in the Hong Kong design code, and therefore use of multi-TMDs as supplemental damping devices in this building was studied. The total mass of the building is 27,774 ton. Modal properties obtained from a three-dimensional finite element model in the along-wind direction are given in Table 1. Damping ratios for all modes are assumed to be 4.0%. The first two modes, which contribute over 80% in the along-wind response are taken into account in the analysis. The TMDs are only allowed to be installed at the top floor and the 25th floor (facility installation storey). As a result, two TMDs, one at the top-floor and the other at the 25th floor, are considered in the present study.

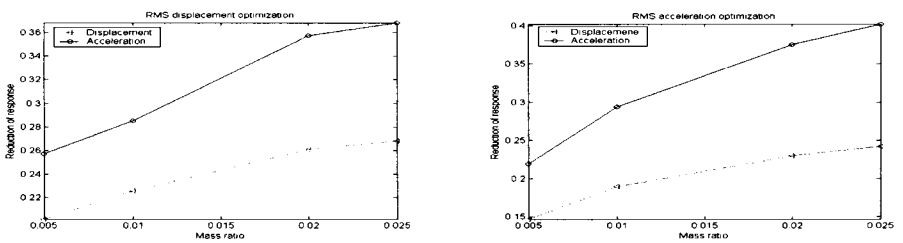
TABLE 1
MODAL PROPERTIES OF 50-STOREY BUILDING

Mode order	1	2	3	4	5
f (Hz)	0.216	0.940	2.278	3.941	5.932
ω (rad/s)	1.355	5.904	14.314	24.762	37.269
Mass factor (%)	66.82	13.08	5.51	3.11	1.92

Two strategies for parameter optimization are conducted with the objectives to maximize reduction of the root-mean-square displacement and acceleration at the top floor, respectively. In the optimization search by GA, the range of the frequencies of TMDs is set as 0.7 times the first modal frequency to 1.3 times the second modal frequency of the building, i.e., 0.151 to 1.222 Hz. The damping ratio of each TMD is set between 0 and 0.2. It is found that the convergence speed of GA for displacement and acceleration reduction optimization is fairly rapid. Usually 60 generations can provide acceptable result with a group size of 10, while 120 generations are used in the present study.

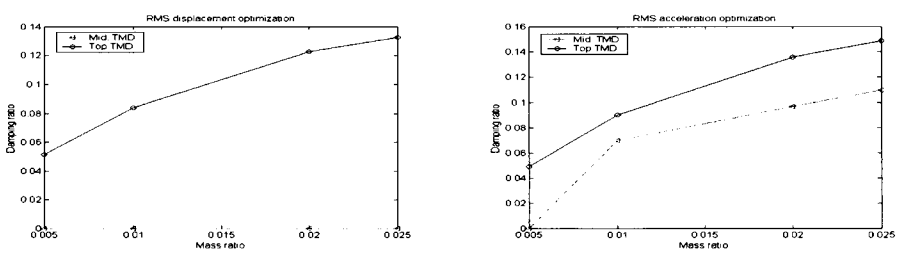
In actual application, the gross mass of multi-TMDs should be limited and is generally taken within five percent of the total mass of the building. In this present study, the upper limit of the ratio of the TMD's mass to the building mass is set as 0.005, 0.01, 0.02 and 0.025, respectively. For each case, the optimization to maximize reduction of RMS displacement and acceleration responses at the top floor is carried out. Fig. 2 shows the maximum reduction of RMS responses versus mass ratio. It is evident that the control effectiveness of multi-TMDs, i.e., the reduction in structural response, increases with the TMD masses for both displacement and acceleration responses.

Under various mass ratios, the optimal damping ratios and frequency ratios are obtained as shown in Figs. 3 and 4, respectively. It is observed that the value of reduction index for acceleration is always greater than that for displacement. This means that TMDs perform better for suppressing acceleration than displacement. It is seen from Fig. 3(a) that when displacement optimization is concerned, the



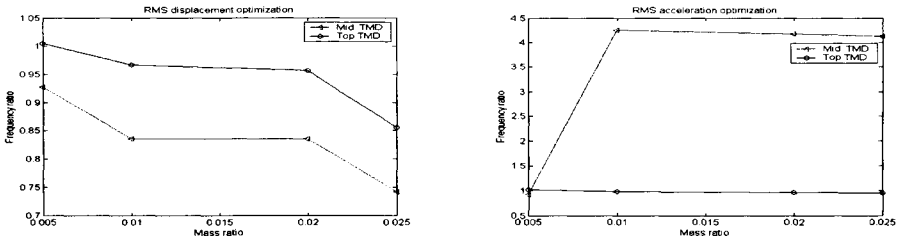
(a) Displacement optimization (b) Acceleration optimization

Figure 2: Reduction of RMS responses at the top floor



(a) Displacement optimization (b) Acceleration optimization

Figure 3: Optimal damping ratio versus mass ratio



(a) Displacement optimization (b) Acceleration optimization

Figure 4: Optimal frequency ratio versus mass ratio

TABLE 2
RESPONSE REDUCTION DUE TO SLIGHT CHANGE IN MASSES OF MULTI-TMDS

Case No.	$\frac{M'_{d1}}{M_{d1}}$	$\frac{M'_{d2}}{M_{d2}}$	Reduction in displacement				Reduction in acceleration			
Mass ratio			0.005	0.01	0.02	0.025	0.005	0.01	0.02	0.025
(1)	1.00	1.00	0.2016	0.2256	0.2610	0.2778	0.2601	0.2938	0.3748	0.4021
(2)	1.01	1.01	0.2019	0.2264	0.2612	0.2785	0.2607	0.2948	0.3760	0.4033
(3)	1.02	1.02	0.2022	0.2271	0.2614	0.2791	0.2614	0.2959	0.3772	0.4045
(4)	1.05	1.05	0.2029	0.2290	0.2618	0.2808	0.2633	0.2991	0.3807	0.4081
(5)	1.05	1.02	0.2018	0.2272	0.2609	0.2791	0.2609	0.2962	0.3776	0.4049
(6)	1.05	1.01	0.2014	0.2266	0.2606	0.2786	0.2601	0.2953	0.3765	0.4039

optimal damping ratio of the TMD at the top floor increases with the mass ratio. However, the optimal damping ratio of the TMD at the middle (25th) floor takes zero for all mass ratios. In the case of acceleration optimization, the optimal damping ratios of both TMDs increase with the mass ratio. The optimal damping ratio of the TMD at the top floor is always greater than that of the TMD at the middle (25th) floor. It is seen from Fig. 4(a) that when displacement optimization is concerned, the optimal frequencies of both TMDs decrease with the mass ratio and are around the first mode natural frequency of the building. However, in the case of acceleration optimization, except for mass ratio equal to 0.005, the optimal frequency of the TMD at the middle (25th) floor is around the second mode natural frequency of the building, indicating that higher modes play significant role in acceleration optimization. By comparing Figs. 3 and 4, it is observed that the optimal damping ratio is much more sensitive to the TMD mass than to the TMD frequency.

Table 2 shows the response reduction at the top floor due to a slight increase in the TMD masses while keeping the damping ratios and frequency ratios as their optimal values invariably. Here M'_{d1}/M_{d1} and M'_{d2}/M_{d2} are the masse increment ratios of the TMDs at the middle and top floors, respectively. It is seen that increasing the TMD masses in a same proportion will consistently improve the performance of the multi-TMDs. However, when the masses of the two TMDs are increased in different ratios, the performance of the multi-TMDs might be enhanced or degraded.

CONCLUSIONS

A general method for analyzing wind-induced random response of tall buildings installed with multi-TMDs is formulated in consideration of high order modes of the building and spatial correlation of wind force. The parameter optimization of multi-TMDs for wind-excited vibration control of tall buildings is conducted by means of the genetic algorithm (GA). The case study of a 50-storey building

in Hong Kong draws the following conclusions: (i) The maximum reduction ratio of RMS response increases with the increase of the TMD masses; (ii) The reduction ratio of acceleration is always larger than that of displacement; (iii) The optimal frequency ratio is not sensitive to the TMD masses; (iv) The displacement and acceleration optimizations provide different results in both reduction indices and optimal TMD parameters; and (v) The optimal frequencies of the multi-TMDs may be around the first mode natural frequency of the building or around the higher mode natural frequency.

ACKNOWLEDGEMENT

The work presented in this paper was supported by a grant from The Hong Kong Polytechnic University through the Area of Strategic Development Programme (Research Centre for Urban Hazard Mitigation). This support is gratefully acknowledged.

References

Abe M. and Fujino Y. (1994). Dynamic characterization of multiple tuned mass dampers and some design formulas. *Earthquake Engineering and Structural Dynamics* **23**, 813-835.

Code of Practice on Wind Effects (1983). Building Development Department, Hong Kong.

Breukelman B. and Haskett T. (2001). Good vibrations. *ASCE Civil Engineering* **71:12**, 55-59.

Davenport A.G. (1961). The spectrum of horizontal gustiness near the ground in high winds. *Journal of Royal Meteorological Society* **87**, 194-211.

Igusa T. and Xu K. (1994). Vibration control using multiple tuned mass dampers. *Journal of Sound and Vibration* **175**, 491-503.

Jangid R.S. and Datta T.K. (1997). Performance of multiple tuned mass dampers for torsionally coupled system. *Earthquake Engineering and Structural Dynamics* **26**, 307-317.

Kareem A. and Kline S. (1995). Performance of multiple mass dampers under random loading. *ASCE Journal of Structural Engineering* **121**, 348-361.

Kitagawa Y. and Midorikawa M. (1998). Seismic isolation and passive response-control buildings in Japan. *Smart Materials and Structures* **7**, 581-587.

Kwok K.C.S. (1984). Damping increase in building with tuned mass damper. *ASCE Journal of Engineering Mechanics* **110**, 1645-1649.

Kwok K.C.S. and Samali B. (1995). Performance of tuned mass dampers under wind loads. *Engineering Structures* **17**, 655-667.

McNamara, R.J. (1977). Tuned mass dampers for buildings. *ASCE Journal of the Structural Division* **103**, 1785-1798.

Rana R. and Soong T.T. (1998). Parametric study and simplified design of tuned mass dampers. *Engineering Structures* **20**, 193-204.

Ueda T., Nakagaki R. and Koshida K. (1992). Suppression of wind-induced vibration by dynamic dampers in tower-like structures. *Journal of Wind Engineering and Industrial Aerodynamics* **41-44**, 1907-1918.

Yamaguchi H. and Harnpornchai N. (1993). Fundamental characteristics of multiple tuned mass dampers for suppressing harmonically forced oscillations. *Earthquake Engineering and Structural Dynamics* **22**, 51-62.

CONSTRUCTION TECHNOLOGIES:

STRUCTURAL SYSTEMS AND DESIGN

This Page Intentionally Left Blank

Advances in Building Technology, Volume 2
M. Anson, J.M. Ko and E.S.S. Lam (Eds.)
© 2002 Elsevier Science Ltd. All rights reserved

Steel Joists for Cost Effective Flooring System

Aladesaye[1] M, Al-Jumaily[1] AM, and Coubray[2] B

[1] Diagnostics and Control Research Centre
Auckland University of Technology
Auckland, New Zealand

[2] Howick Engineering Ltd
Howick, Auckland,
New Zealand

ABSTRACT

Steel can be used as a substitute for timber and, in addition, can provide many significant advantages; however, the cost differential fluctuates. Steel has traditionally been slightly more expensive on a material basis, but savings offset this in greater structural efficiency, rapid assembly and reduction in rework costs experienced with poor quality timber. Increased global timber demand and diminishing resources are causing erratic timber price increases that are threatening the traditional raw material competitiveness. Steel has a fairly static international base cost. There is also a minimal waste of base material during manufacture, with steel having 1-2% wastage and Timber 5-11% wastage. In this research two steel joist systems are proposed, designed and engineered for flooring and based on manufacturing, design and serviceability criteria are assessed. Practical conclusions are made.

KEYWORDS

joist, flooring, top-hat, c-shape, design criteria

INTRODUCTION

In recent years a number of alternatives to wood as the primary framing material in residential construction have emerged. One of the most promising of these alternatives is the use of light gauge steel framing members as a replacement for dimensional lumber. Today, as the demand for wood products holds strong and the number of old-growth forest diminishes, it is paramount that we continue to search for alternative materials for wood and improve replacements that have been identified.

A wake up call for the residential construction industry came about in late 1992 as the composite price for framing lumber shot up almost 100% in a period of only five months. The composite fell back to earth by July of 1993 only to shoot back to record levels by the end of that year [4]. The warning signs were loud and clear. The rapid use of old-grown forests to produce long, large dimensioned lumber and plywood had reached the breaking point. All that was left, of a once endless supply of lumber, were a

few remaining old-grown forests located on government land and subject to federal logging restrictions [2].

The U.S. Department of Housing and Urban Development aided by the National Association of Home builders spearheaded an effort to identify emerging technologies that had the potential to replace wood. Housing and Urban Development identified a number of alternative materials including [1] foam core, panels, light-gauge steel framing, welded-wire sandwich panels, concrete forming systems and concrete block.

Steel's strength, weight, uniform manufacture, recyclability, termite resistance, and non-combustibility marked it as one of the most promising alternatives to wood in residential steel framing [3]. Now is the time to focus on improving alternatives to wood instead of waiting for the boom of skyrocketing prices to wake us up again. In order to improve the competitiveness of alternative materials we must look outside the box and explore new process and technology. The use of light gauge steel framing in residential construction present the opportunity to apply modern technological concepts and process improvement to the field of construction. Because of steel's high strength and design flexibility, innovative systems are possible which are not possible using other materials. It can span greater distances offering larger open spaces and increased design flexibility without requiring intermediate columns or load bearing walls. The structural integrity and overall quality of light gauge framing is well recognized amongst designers and builders in the residential construction industry as a superior building material. Light gauge is specified in an increasingly larger percentage of new housing starts especially where seismic and high wind loadings are a consideration. Because a steel framed home can be resistant to natural forces, some homeowners may save as much as 30% insurance premiums.

The higher quality and dimensional stability is responsible for eliminating virtually all nail pops and squeaky floors. The environmental benefits of light gauge steel framing are also significant. Among these are the fact that steel is inert and will not contribute to poor indoor air quality, it can be manufactured using 100% scrap steel, is 100% recyclable without material property degradation and does not contribute fuel to fire like wood [5]. The environmental arena is one of the fastest changing segments of society today. Experts in many fields are looking for new building strategies and technologies that will help sustain affordable growth into the next century. Steel is one for those building materials. By selecting recyclable materials for the structures built today, we can "precycle". Our descents will be able to re-use the steel we use today.

Based on engineering principles and certain manufacturing, design and serviceability criteria of two system steel joists, C -shape and Top-hat are proposed, designed and tested to determine their performance and liability for flooring industries. Special recommendations are given for best use.

MANUFACTURING CRITERIA

One of the most quantifiable and perhaps the most influential factors in the decision making process when choosing between two different steel materials is the initial cost of each one. The components of the total cost can be classified into four categories [6]: Material costs, fabrication cost, erection labour cost and other costs which include outside services other than erection, shop drawings and the additional costs associated with risk, the need for contingency, and the schedule requirements of the project.

It is seldom feasible to use more than one or two combinations of bolts diameters and grades on a project. The use of different diameters for different grades simplifies the quality assurance task of ensuring that each strength grade was used in the proper location [7, 9]. It allows more shop efficiency in the drilling or punching operations. Material that will involve many joints, bends, components, will

require more time to fix the numerous bolts during installation. Top hat purlins will take less time to install.

Stacking and handling are considered two crucial factors in any manufacturing process. Top hat is easy to stack on top of each other, which is also an advantage over other shapes.

DESIGN CRITERIA

Cold-formed steel (CFS) floor joists are normally treated as simply supported or continuous span bending members subjected to uniform and/or concentrated loads. Floor joists are also designed considering the compression flanges (top flanges) to be continually braced by the sub-flooring, thus providing lateral restraint. For the design of floor joists, any one of several criteria may control the design depending on the configuration of the section, thickness of material and member length. Six design checks are usually performed when designing CFS floor joists [8]. These are deflection, bending moment, shear, web, crippling, combined bending and web crippling and combined shear and bending.

Deflection limits imposed on the design of floor joist to minimize the impact on the finish material can significantly impact allowable joist spans. Deflection limits have to be carefully considered and justified. The amount of deflection that a joist member experiences under a certain uniform load is determined by the joist moment of inertia, Ix. The moment of inertia can be obtained from manufacture's catalogues or calculated in accordance with the American Iron and Steel Institute (AISI) Specification.

The grade of steel and the effective section modulus of the joist, Se, determine the allowable bending moment. The type of steel should be obtained from the manufacturer. The section modulus can be either calculated or obtained from the manufacturer. The calculation of the section modulus may be complex sometimes, as the effective widths for the compression components of the web, flanges, and lips have to be determined. Consequently, the effective section involves removal of portions of the compression flange, web and lip if each is sufficiently slender.

Web shear normally does not control the design of CFS floor joists for simple spans unless the members have a large web height to steel thickness ratio (h/t). However, the AISI specification requires web shear to be checked for all floor joists. The nominal shear strength, (Vn), of a web consisting of two or more sheets is calculated as the sum of the nominal shear strength of each sheet (web). Each sheet is considered as a separate element carrying its share of the shear force.

CFS joists have thin webs that are susceptible to localized web buckling at concentrated loads or bearing locations. AISI Specification section C3.4 provides design equations for single-web and I-sections with stiffened or partially stiffened flanges and un-stiffened flanges [8, 10]. These equations are limited to joists with web height to thickness (h/t) ratio of less than or equal to 200. Joists with (h/t) ratios greater than 200 shall be provided with adequate means of transmitting concentrated loads and/or reactions directly into web, the thickness of the steel, and the length of the bearing are the most critical components in the AISI web crippling equations. Other factors such as steel material, and bend radius play a lesser role.

The critical location for web crippling is at the member's ends for single joist spans and at the member's ends and intermediate supports for multiple spans. Most manufacturers tabulate the web crippling strength of simply supported joist spans in their technical catalogs. The design equations of the AISI Specification section C3.4 can be used if this information is not readily available [8,10].

AISI specification section C3.5 requires a combined bending and web crippling check for un-reinforced joist webs. Three equations are provided in AISI Specification Section C3.5: Single un-reinforced webs,

multiple unreinforced webs (such as I-beams), and Two nested Z-shapes (support point). Interaction equation for shapes having single unreinforced webs is normally used to design floor joist [8].

The combination of a bending stress and a shear in a web produces a further reduction in the capacity of the web. The degree of the reduction depends upon whether the web is stiffened or not. The presence of negative moment (reversed bending) at the interior supports of multiple span joists require certain measures to be taken to ensure the joists are not overstressed. AISI Specification section C3.3 requires combined shear and bending check for multiple span joists. The interaction equation for unstiffened webs is a circular formula based upon an approximation to theoretical interaction of local buckling resulting from shear and bending. The interaction equation for stiffened webs is linear and not as severe because of the greater post- buckling mode. The un-reinforced web equation is normally used when designing floor joists [8, 10].

The floor is designed to carry the specified loads within the acceptable deflection and vibration. The floor is designed for the combinations of live and dead loads. The floor may not be designed for wind and snow loads. The acting load must not be more than the strength of the materials and must not deflect joist more than required nor cause unnecessary vibration. Loads are primary considerations in any building design because they define the nature and magnitude of hazards or external forces that a building must resist to provide reasonable performance (i.e. safety and serviceability) throughout the structures useful life. The anticipated loads are influenced by a building's intended use (occupancy and function), configuration (size and shape), and location (climate and site conditions). Ultimately, the type and magnitude of design loads affect critical decisions such as material selection, construction details, and architectural configuration. Thus, to optimize the value (i.e. performance versus economy) of the finished product, it is essential to apply design loads realistically. High strength materials will be able to carry loads effectively.

SERVICEABILITY

Careful considerations must be addressed to serviceability issues, which arise with any floor system, of any type. The design of any floor is governed by serviceability limit states, which include deformation or deflections affecting the appearance or effective use of the floor and vibrations causing discomfort to people or damage to finishes or fixtures.

The dynamic (bounce) of flooring systems is a limiting state in design. The response can result in shaking or rattling.

ASSESSMENT

Two systems of joists, figure 1, are designed in this research, top-hat purlins and C-shaped member. Their specifications are summarized in Table 1.

The method used to calculate the strength of the joust is based on the uniform distributed load equivalent W, using the standard equation that governs floor design [11].

$$W = 1.2G + 1.6Q \tag{1}$$

Then the maximum bending moment M^* is determined by using the following formula for simply supported boundary conditions.

$$M^* = \frac{wl^2}{8} \tag{2}$$

The dead and live loads applicability limits for first floor are 0.48KN/m^2 and 1.92KN/m^2 respectively [12].

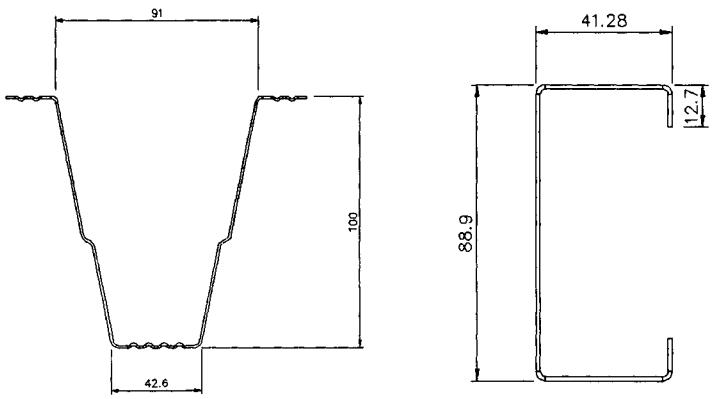


Figure 1: Joist Geometric Shapes: (a) – Tophat (b) – C-shaped

TABLE 1
JOIST SPECIFICATIONS

Specifications	Top-hat purlin	C-shape
Thickness (mm)	0.95	0.95
Web (mm)	100	88.9
Yield strength (Mpa)	345	228
Finish	Galvanized	Galvanized
Designation/Grade	HST250	ASTM A525
E (GN/m^2)	200	200
Spacing (mm)	1700	1200
Span (m)	2	2
Y_{max} (m)	56.6	44.45
I_x (mm^4)	386861.2	294347.9
Flange (mm)	42.6	41.28
Lip/Toe (mm	35	12.7

The limiting moment is determined using the formula

$$\phi_b M_n = \phi_b S_e f_y \tag{3}$$

with

$$S_e = \frac{I_x}{y_{max}} \tag{4}$$

The serviceability, however, is determined by calculating the maximum dead load deflection δ_G,

$$\delta_G = \frac{5w_G L^4}{384EI} \tag{5}$$

and the live load deflection as

$$\delta_Q = \frac{5w_Q L^4}{384EI} \tag{6}$$

Then calculating Δ_T

$$\Delta_T = \delta_G + 0.7\delta_Q \tag{7}$$

The vibration is checked by determining the deflection Δ using the formula for simply supported beam with a concentrated load as follows:

$$\Delta = \frac{wL^3}{48EI} \tag{8}$$

The results are summarised in Table 2 for the two joists.

TABLE 2
DESIGN PARAMETERS

	Design Parameter	Top-hat	C-shaped
Strength	$\phi_b M_n$ (kNm)	2.12	1.36
Deflection	Dead Load Deflection (mm)	8.41×10^{-5}	1.11×10^{-4}
	Live Load Deflection (mm)	3.23×10^{-4}	4.25×10^{-4}
	Δ_T (mm)	8.33×10^{-3}	8.33×10^{-3}
Vibration	Δ (mm)	0.0148	0.018
	Δ_{limit} (mm)	1	1

DISCUSSION AND CONCLUSION

Comparing the calculated variables with the design variables indicates that the strength, serviceability and vibration for the two joists are within the limits; however, some remarks are due as summarised in Table 3.

TABLE 3
COMPARISON BETWEEN TOP-HAT PURLINS AND C-SHAPED

FACTORS	Hat Purlins	C-shaped
Cost	Cheaper	
Time	Quicker to Install	Installation will take longer
Stacking/Handling	Better	Intricate
Appearance	Better	Good
Strength	56% Better	
Deflection	24% Better	
Vibration	18% Better	

The data presented and the conclusion drawn in this paper, represent only the beginning of a long-term industrial research for obtaining an efficient and economical steel joist. A larger database of tested different shapes of steel joist materials for flooring is needed to improve the accuracy of the proposed design criteria. It will be reasonable to investigate more shapes of joist manufactured by other companies.

REFERENCES

1. Alternative Framing Materials in Residential Construction: Three Case Studies, U.S. Department of Housing and Urban Development, Washington D.C., July 1994.

2. Alternatives to Lumber and Plywood in Home Construction: U.S. Department of Housing and Urban Development, Washington D.C., April 1993.

3. Chini, S. Abdol and Gupta, Kavita. (1995). A Cost Comparison Study Between Steel and Wood Residential Framing Systems. Shimberg Center for Affordable Housing, University of Florida, Gainesville, Florida.

4. Random L. (1998). Random Lengths Framing Lumber Composite Price, poster. Random Lengths Publications.

5. Barbour E. (1994). Thermal Performance of Steel-Framed Walls. NaHb Research Center nc.

6. Lorenzo R.F. (1983). Some Economic Considerations for Composite Floor Beams, Engineering Journal, 2nd Quarter, AISC, Chicago, IL, USA.

7. Murray, T.M. (1991). Use of Snug-Tightened Bolts in End-Plate Connections Proceedings of the second International Workshop on Connections in Steel Structures, Pittsburgh, PA, April 10-12.

8. Reyman, W.P , LRFD Cold formed steel design manual, American Iron and Steel Institute, 1991

9. HST Purlins and Girts, Steel and tube technical design guide for purlins and girts. Pg.1.

10. Technical note on cold-formed steel construction. Tech. Note (552). Light gauge steel engineers Association. Nashille, TN.

11. New Zealand Standard NZS4203 : 1992. Page 19.

12. Prescriptive method for residential cold-formed steel framing, second edition: NAHB research center Upper Marlboro, MD: 1997.

APPENDIX -Symbols and Definitions

Symbols	Definitions
Se	Elastic section modulus of effective section
E	Young's Modulus of elasticity
I_x	Moment of inertial
F_y	Yield stress
W_G	Dead load
W_Q	Live load
M*	Maximum Bending moment
W	Load
L	Span
M_n	Nominal flexural strength
ϕ_b	Resistance factor for buckling strength
δ_G	Dead load deflection
δ_Q	Live load deflection
Δ	Deflection
Δ_T	Total deflection

Advances in Building Technology, Volume 2
M. Anson, J.M. Ko and E.S.S. Lam (Eds.)
© 2002 Elsevier Science Ltd. All rights reserved

ANALYSIS PLANE STEEL FRAME WITH SEMI-RIGID CONNECTIONS AND RIGID-ZONES WITH CONSIDERATION OF THE SECOND ORDER EFFECT

Vu Quoc Anh

Faculty of Civil Engineering – Hanoi Architectural University
Km 10 Nguyen Trai, Thanh Xuan, Hanoi, Viet Nam

ABSTRACT

The most recent European and American Codes allow the actual response of joints to be incorporated in frame design [3]. AISC -LRFD specification (1994) designed two types of construction according to the level of connection rigidity. There are Type FR (Fully Restrained) and Type PR (Partially Restrained) constructions. Type FR frames can be designed based on the specification in which the second order effects are considered to estimate column end moments and frame drift. However, even though semi-rigid frames (Type PR) must be designed considering flexible connections as well as second order effects, the specification has not described the design procedure for this type of structure in detail. The main objective of this technical note is to present a practical and accurate method for analysis of plane steel frames with semi-rigid connections and considering the second order effects.

KEYWORDS

Semi-rigid connections, Second order effect, Rigid zones (Rigid offsets), Stiffness matrix, Geometric stiffness matrix, Geometric nonlinearity

1. INTRODUCTION

For most building structures, especially tall steel buildings, the P-Delta effect most concern occurs in the columns due to gravity load, including dead load and live load. The column axial forces are compressive, making the structure more flexible against lateral loads. The P-Delta analysis accounts for the effect of a large axial load upon the transverse bending behavior of frame elements. Axial compressions reduce the flexural stiffness of frame elements, and axial tension stiffens them.

Comparing with reinforced concrete structure, member rigidity of steel structure is less, and displacement of steel structure is larger than that of reinforced structure, so the secondary moment due to axial force has to be considered, i.e., the problem of second order effects. In steel framed structures the lateral deflections along each element span (i.e., P-δ effects), the relative drift between the element

ends (i.e., P-Δ effects), and the effects of flexural moments on the axial stiffness cause nonlinear behavior with additional moments and displacements. There nonlinear geometrical effects alter not only the stiffness matrix of each element and that of structure as the whole, but the stability of each element and that of entire structure. For instance, the P-δ effects may lead to individual member buckling or local collapse, while P-Δ effects may lead to overall structural instability or story buckling.

One aspect that we have so far neglected is extremely important for practical applications. In most frames, the joints are not perfectly rigid but flexible, that is, the ends of the beam column can rotate with regard to the joint. This means that one must introduce an effective rotational spring at each end of the beam-column to take the deformability of the connection into account [5]. One must then distinguish between the rotations of the ends of the beam-column and of the joint, and add to the system of equations of the springs deformation relations involving these rotations.

2. TO ESTABLISH THE GEOMETRIC STIFFNESS MATRIX $[k_\sigma^*]$ AND STIFFNESS MATRIX $[k^*]$ FOR BEAM ELEMENT WITH SEMI-RIGID CONNECTIONS AND RIGID ZONES

To incorporate the connection rigidity into the member stiffness, it is a common practice to model the semi-rigid connection as massless and zero length rotational spring. Although semi-rigid connections exhibit nonlinear response characteristics throughout their whole loading history, it is generally accepted that under service loading conditions the semi-rigid connections can be assumed to behave linearly [4].

Structural model of beam with semi-rigid connections, Fig. 1, beam with semi-rigid connections and rigid-zones, Fig. 2. Where:$\{X\}$ vector of nodal point displacements of beam with semi-rigid connections;$\{F\}$vector of nodal point forces of beam with semi-rigid connections; e_1, e_2 length of rigid-zones (rigid offset) of connections; $\{X^*\}$ vector of nodal point displacements of beam with semi-rigid connections and rigid-zones ;$\{F^*\}$ vector of nodal point forces of beam with semi-rigid connections and rigid-zones ; k_1; k_2 rotation spring stiffness of connections;

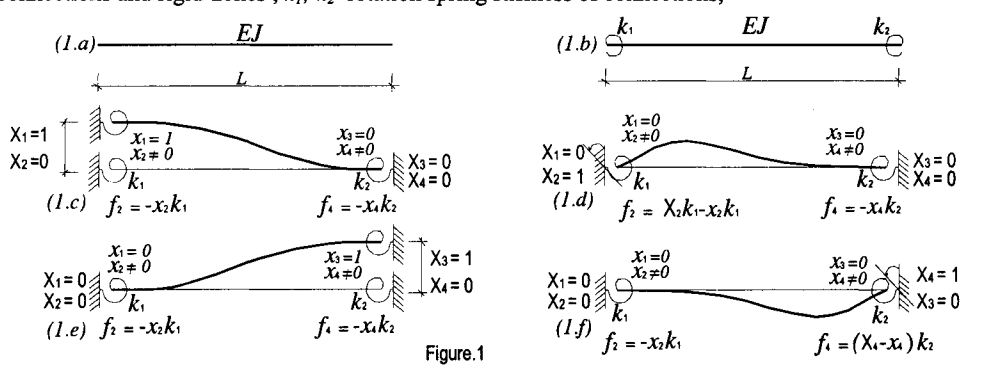


Figure.1

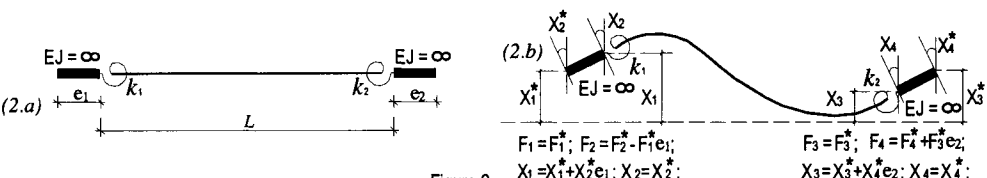


Figure.2

For a single element with semi-rigid connections and rigid-zones, the work balance with consideration of P-delta effect becomes

$$\int_{e}\{\delta\varepsilon\}^{T}[E]\{\varepsilon\}dV+\{\delta u_{k}\}^{T}[k_{k}]\{u_{k}\}+\int_{e}\{\delta u^{\cdot}\}^{T}[S]\{u^{\cdot}\}dV=\int_{e}\{\delta u\}^{T}\{q\}dV \tag{3.1}$$

Where $\{\delta u\}$ and $\{\delta\varepsilon\}$ are respectively small arbitrary displacements and their corresponding strains, [E] is the material property matrix, $[k_k]$ is the stiffness matrix of the springs, $\{\delta u_k\}^T$ are the small displacement of the springs, $\{q\}$ are body forces, and volume integration is carried out over the element volume V_e.

Using usual notation, we have for displacement field $\{u\}$ (which is a function of both space and time)

$$\{u\}=[N]\{x\};\qquad \{x\}=[T]\{X\};\qquad \{X\}=[e]\{X^{*}\};$$

$$\{u\}=[N][T][e]\{X^{*}\};\quad \{u^{\cdot}\}=[G]\{x\}=[G][T][e]\{X^{*}\};\quad \{u_{k}\}=\begin{bmatrix}x_{1}^{k} & x_{2}^{k} & x_{3}^{k} & x_{4}^{k}\end{bmatrix}^{T}; \tag{3.2}$$

$$\{\varepsilon\}=[B]\{x\}$$

$$\{\delta u_{k}\}^{T}[k_{k}]\{u_{k}\}=\delta x_{2}^{k}.k_{1}.x_{2}^{k}+\delta x_{4}^{k}.k_{2}.x_{4}^{k}=\begin{bmatrix}\delta x_{1}^{k} & \delta x_{2}^{k} & \delta x_{3}^{k} & \delta x_{4}^{k}\end{bmatrix}\cdot\begin{bmatrix}0 & 0 & 0 & 0\\ 0 & k_{1} & 0 & 0\\ 0 & 0 & 0 & 0\\ 0 & 0 & 0 & k_{2}\end{bmatrix}\begin{bmatrix}x_{1}^{k}\\ x_{2}^{k}\\ x_{3}^{k}\\ x_{4}^{k}\end{bmatrix}$$

$$\{u_{k}\}=\{X\}-\{x\}=\{X\}-[T]\{X\}=([I]-[T])\{X\}=([I]-[T])[e]\{X^{*}\} \tag{3.3}$$

$$\begin{aligned}&[k]\cdot\{x\}_{1}=[k_{k}]\cdot[\{X\}_{1}-\{x\}_{1}];\quad [k]\cdot\{x\}_{2}=[k_{k}]\cdot[\{X\}_{2}-\{x\}_{2}]\\ &[k]\cdot\{x\}_{3}=[k_{k}]\cdot[\{X\}_{3}-\{x\}_{3}];\quad [k]\cdot\{x\}_{4}=[k_{k}]\cdot[\{X\}_{4}-\{x\}_{4}]\end{aligned} \tag{3.4}$$

In general we have :

$$[k]\cdot\sum_{i=1}^{4}\{x\}_{i}=[k_{k}]\cdot\sum_{i=1}^{4}[\{X\}_{i}-\{x\}_{i}] \tag{3.5}$$

Where:

$$\{x\}_{i}=[T]\cdot\{X\}_{i}\Rightarrow\sum_{i=1}^{4}\{x\}_{i}=[T]\cdot\sum_{i=1}^{4}\{X\}_{i}=[T]\cdot[1\quad 1\quad 1\quad 1]^{T} \tag{3.6}$$

$$[k]\cdot[T]\cdot[1\quad 1\quad 1\quad 1]^{T}=[k_{k}]\cdot[1\quad 1\quad 1\quad 1]^{T}-[k_{k}]\cdot[T]\cdot[1\quad 1\quad 1\quad 1]^{T} \tag{3.7}$$

$$[k]\cdot[T]=[k_{k}]\cdot([I]-[T])\Rightarrow[k_{k}]=[k]\cdot[T]\cdot([I]-[T])^{-1} \tag{3.8}$$

In Eqs. (3.2), shape functions [N] are functions of space [2], [T] and [e] are transformation matrices (see [1]). Thus Eqs. (3.2) represent a local separation of variables. Combination of Eqs. (3.1) and (3.2) yields

$$\begin{aligned}&\{\delta X^{*}\}^{T}[\int_{e}[e]^{T}[T]^{T}[B]^{T}[E][B][T][e]\{X^{*}\}dV+[e]^{T}([I]-[T])^{T}[k_{k}]([I]-[T])[e]\{X^{*}\}+\\ &\int_{Ve}[e]^{T}[T]^{T}[G]^{T}[S][G][T][e]\{X^{*}\}dV]=\{\delta X^{*}\}^{T}[\int_{e}[e]^{T}[T]^{T}[N]^{T}\{q\}dV]\end{aligned} \tag{3.9}$$

Since $\{\delta X^*\}$ is arbitrary, Eq (3.3) can be written as:

$$[k^*]\{X^*\}+[k_\sigma^*]\{X^*\}=([k^*]+[k_\sigma^*])\{X^*\}=\{F^*\} \tag{3.10}$$

Where $[k^*],[k_\sigma^*]$ are the stiffness matrix, geometric stiffness matrix of the element with semi-rigid connections and rigid-zones; $\{F^*\}$ are external load vectors; $\{X^*\}$ is the displacement vector of the element with semi-rigid connections and rigid-zones;

The stiffness matrix, geometric stiffness matrix and external load vectors of the beam element with semi-rigid connections and rigid-zones are defined as:

$$\begin{aligned}
[k^*] &= \int_{Ve}[e]^T[T]^T[B]^T[E][B][T][e]dV+[e]^T([I]-[T])^T[k_k]([I]-[T])[e] \\
&=[e]^T[T]^T[\int_{Ve}[B]^T[E][B]dV][T][e]+[e]^T([I]-[T])^T[k_k]([I]-[T])[e]= \\
&[e]^T([T]^T[k][T]+([I]-[T])^T[k_k]([I]-[T]))[e]= \\
&=[e]^T([T]^T[k][T]+([I]-[T])^T[k][T][I]-[T])^{-1}([I]-[T]))[e]=[e]^T[k][T][e]
\end{aligned} \tag{3.11}$$

$$\begin{aligned}
[k_\sigma^*] &= \int_{Ve}[e]^T[T]^T[G]^T[S][G][T][e]dV=[e]^T[T]^T[\int_{Ve}[G]^T[S][G]dV][T][e] \\
&=[e]^T[T]^T[k_\sigma][T][e]
\end{aligned} \tag{3.12}$$

$$\{F^*\}=[e]^T[T]^T\{f\};\ \text{Where [2]}\ \{f\}=\int_{Ve}[N]^T\{q\}dV \tag{3.13}$$

3. COMPUTATIONAL ALGORITHM FOR A PROBLEM HAVING GEOMETRIC NONLINEARITY

The structure is divided into finite elements in the usual way. We can begin with zero initial displacements, $\{X^*\}_0=\{0\}$, or with a better estimate for $\{X^*\}_0$ if one is available. The load $\{F^*\}$ is applied and the corresponding $\{X^*\}$ is sought by iteration as follows. Computational details are explained subsequently [2].

1. Form the tangent-stiffness matrix $[K^*_t]$ of the structure in the current configuration $\{X^*\}_t$ (which is $\{X^*\}_0$ initially, $\{X^*\}_1$ after the first computational cycle, etc.).
2. Use displacements $\{X^*\}_t$ to form resisting loads $\{F^*_R\}_t$, which are loads applied to structure nodes by the deformed elements. (In the first computational cycle, these loads are zero if $\{X^*\}_0=\{0\}$.)
3. Solve for displacement increments $\{\Delta X^*\}_{t+1}$ and update the configuration to $\{X^*\}_{t+1}$

$$\{X^*\}_{t+1}=\{X^*\}_{t+1}+\{\Delta X^*\}_{t+1}\ \text{ where }\ \{\Delta X\}_{t+1}=[K^*_t]^{-1}(\{F^*\}+\{F^*_R\}_t)$$

Net loads $\{F^*\}+\{F^*_R\}_t$ are an imbalance between externally applied and internally generated nodal loads. The load imbalance drives the structure toward a configuration that reduces the imbalance. In an equilibrium configuration, the imbalance is zero.

4. Check for convergence; for example, see if $\|\Delta X^*_{i+1}\|<e\|X^*_{i+1}\|$, where e is a small number chosen by the analyst. If not converged, return to step 1.

5. NUMERICAL EXAMPLE TO VERIFY

A two-story, three bay frame is analyzed with rigid and semi-rigid connections, and with and without geometric nonlinearity. Fig 3 shows the frames configuration (I_{beam} = 8356 cm^4, I_{column} = 5696cm^4, E = 210+E6), dimensions, loading and numbering of members and joints. And instead of the spring stiffness the joint stiffness ration α= k/i_x is used; k spring stiffness (kNm/rad).The results of the analysis are presented in table 1 and 2. This example is taken in order to demonstrate the validity of the program written by Pascal language following the $[k_\sigma^*]$ and $[k^*]$ created in part 2. It also shows the effects of connection flexibility and geometric nonlinearity on displacements and moments.

Connection flexibility effects both force distribution and deformation in beams and columns of the frame, and must be accounted for in a structural analysis. This can be done by conducting a second-order analysis of the frame, one that addresses both geometric nonlinearity and connection flexibility. The softening of the connections results in the large increase in the building drift.

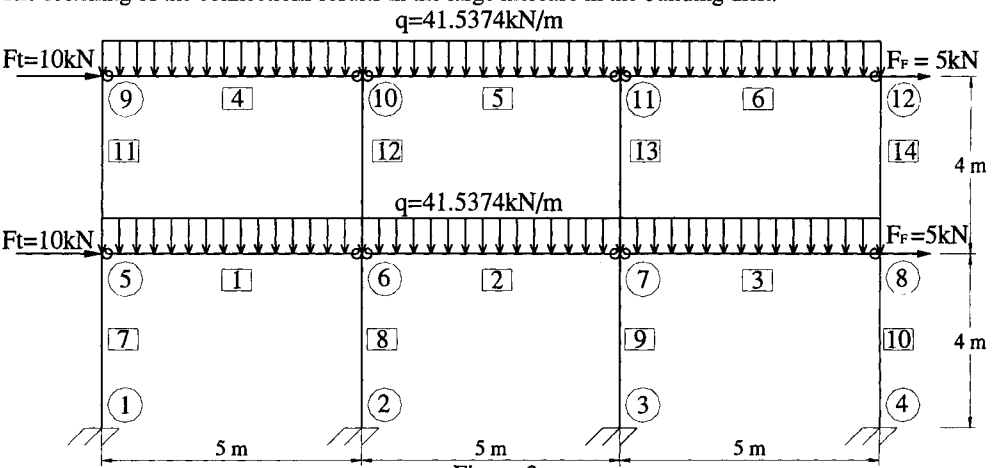


Figure 3

TABLE 1 (kN/m)
MOMENT OF SEMI RIGID STEEL FRAME WITH CONSIDERATION OF P-DELTA EFFECT

Element	Moment Sign	Section	Pin connectio	Steel Frame with Semi-rigid Connection & P-Delta effect							Fixed connetion
			Sap 2000 & P-Delta	α = k/i_x							Sap 2000 & P-Delta
				0.001	0.5	1	2	4	10	1000	
1	2	3	5	6	7	8	9	10	11	12	13
1	+	1	0	0.04	8.96	17.32	27.21	35.83	42.59	46.65	46.64
	-	2	129.8	129.91	112.93	102.1	88.90	76.15	63.75	51.75	51.66
	+	3	0	0.01	24.79	38.11	54.51	71.38	89.44	109.4	109.62
2	+	1	0	0.001	9.83	19.81	33.05	46.86	61.30	76.46	76.66
	-	2	129.8	129.81	112.46	100.9	86.44	71.91	57.15	42.08	41.90
	+	3	0	0.08	24.78	37.88	53.54	68.82	83.95	98.96	99.15
3	+	1	0	0.02	9.81	19.87	33.49	48.19	64.31	82.27	82.49
	-	2	129.8	129.73	112.58	101.5	87.76	74.54	61.70	49.37	49.29
	+	3	0	0.11	24.47	36.76	50.39	62.15	71.74	78.49	78.51

4	+	1	0	0.02	8.49	16.78	25.88	33.14	38.31	41.05	41.01
	-	2	129.8	129.88	113.79	103.6	91.46	79.70	68.25	57.08	56.92
	+	3	0	0.03	24.00	36.04	51.30	67.50	85.17	104.7	104.9
5	+	1	0	0.01	10.70	22.20	37.19	52.66	68.76	85.58	85.80
	-	2	129.8	129.82	112.64	101.1	86.39	71.33	55.66	39.32	39.08
	+	3	0	0.09	23.92	35.61	49.95	64.53	79.66	95.42	95.62
6	+	1	0	0.03	10.69	22.38	38.03	54.76	72.91	92.77	92.99
	-	2	129.8	129.76	113.06	102.7	90.31	78.50	67.06	55.96	55.81
	+	3	0	0.12	22.95	32.13	41.22	48.10	52.80	55.11	55.08
7	Column Elements	1	70.01	69.80	27.72	20.69	15.10	11.04	7.95	5.72	5.74
		2	-27.7	-27.51	-2.81	-2.52	-4.27	-6.60	-8.77	-10.3	-10.3
8		1	68.51	68.30	30.99	26.20	23.13	21.36	20.33	19.90	19.90
		2	-27.1	-26.92	4.70	9.08	12.08	14.11	15.93	17.94	17.96
9		1	68.50	68.31	31.02	26.23	23.07	21.00	19.31	17.59	17.60
		2	-27.1	-26.89	4.74	9.12	11.94	13.40	13.91	13.46	13.45
10		1	70.00	69.80	32.83	29.26	27.86	27.67	27.88	28.04	28.02
		2	-27.7	-27.48	7.30	14.38	20.87	26.15	30.49	33.75	33.80
11		1	27.65	27.47	-6.15	-14.8	-22.9	-29.2	-33.8	-36.4	-36.36
		2	0	-0.02	-8.49	-16.8	-25.9	-33.1	-38.3	-41.0	-41.01
12		1	27.06	26.91	10.26	9.22	9.39	10.40	12.22	14.99	15.00
		2	0	0.04	13.29	13.84	14.11	14.84	16.41	19.09	19.10
13		1	27.06	26.99	10.23	8.89	8.11	7.23	5.73	3.22	3.21
		2	0	0.12	13.23	13.22	11.92	9.77	6.74	2.65	2.63
14		1	27.66	27.59	17.17	22.38	29.52	36.00	41.25	44.74	44.71
		2	0	0.12	22.95	32.13	41.22	48.10	52.80	55.11	55.08

TABLE.2
LATERAL DISPLACEMENT (cm)

Joints	Pin connection	Steel Frame with Semi-rigid Connection & P-Delta effect							Fixed connection
	Sap 2000 & P-Delta	$\alpha = k/i_x$							Sap 2000 & P-Delta
		0.001	0.5	1	2	4	10	1000	
1	4	5	6	7	8	9	10	11	12
5	3.820	3.8048	1.3236	0.9972	0.7834	0.6528	0.5619	0.4942	0.496
9	11.753	11.704	3.3283	2.2993	1.6618	1.2944	1.0506	0.8762	0.878
6	3.820	3.8042	1.3236	0.9974	0.7837	0.6533	0.5625	0.4949	0.497
10	11.752	11.704	3.3272	2.2979	1.6602	1.2924	1.0485	0.8740	0.876
7	3.819	3.8041	1.3237	0.9977	0.7843	0.6540	0.5632	0.4955	0.497
11	11.752	11.704	3.3265	2.2970	1.6589	1.2909	1.0469	0.8724	0.875
8	3.820	3.8042	1.3241	0.9983	0.7851	0.6549	0.5643	0.4966	0.498
12	11.752	11.704	3.3262	2.2963	1.6579	1.2897	1.0455	0.8709	0.873

6. SUMMARY AND CONCLUSIONS

The linear elastic analysis assumes that the deformations are relatively small, and the equilibrium equations can be formulated with respect to initial geometry. When increasing applied loads cause

significant changes in the structure's geometry, the equilibrium and compatibility equations are nonlinear and the resulting stiffness matrix contains terms that are functions of axial forces and deformations. The stiffness matrix to represent this behavior must include the effect of geometric nonlinearity. In addition, for members with flexible connections at the ends, the stiffness matrix must be modified to account for the effect of connection flexibility.

The first-and second-order stiffness matrices of beam column of double symmetrical cross section with semi-rigid connections and rigid zones are derived in classical manner. The derived matrices can be used in the stability, first- and second-order elastic analysis of steel frames with semi-rigid connections and rigid zones.

Connection flexibility and geometric nonlinearity influence the distribution of forces in the structure. Both effects contribute to a significant increase in the drift of the frame. The semi-rigid connections cause a shift in moments from the beam ends to the span; and as a result, the overall maximum moments decrease in beams. The connections may be used to balance positive and negative moments in beams to effect economic designs.

REFERENCES

[1]. Anh Vu Quoc. (2001). Stability Analysis of Steel Frames with Semi-rigid Connections and Semi-rigid Connections with Rigid-Zones. *Viet Nam Journal of Mechanics* **23:3**, 134 – 148.

[2]. Cook, R. D., Malkus, D. S., and Plesha, M. E., (1989). *Concepts and Applications of Finite Element Analysis*, Third Edition, John Wiley and Sons, Inc, ISBN 0-471-84788-7, USA.

[3]. Chen. W.F., Yoshiaki Goto and J.Y. Richard Liew. (1996). *Stability design of Semi-Rigid Frames,* A Wiley-Interscience Publication, John Wiley & Sons, INC, USA.

[4]. Mak Wai-hing, Simon. (1996). Natural Frequencies of Steel Structures with Semirigid Connections. *Advances in Steel Structures (Procceding of International Conference on Advances in Steel Structures).* Vol II, 1101-1106, ISBN 0-08-042830-4, Hong Kong.

[5]. Zdenek P. Bazant and Luigi Cedolin. (1991). *Stability of Structures (Elastic, Inelastic, Fracture, and Damage Theories)*, Oxford University Press, UK.

This Page Intentionally Left Blank

Advances in Building Technology, Volume 2
M. Anson, J.M. Ko and E.S.S. Lam (Eds.)
© 2002 Elsevier Science Ltd. All rights reserved

POST-TENSIONED CONCRETE FLOOR SYSTEMS IN AUSTRALIA

A. Charalambous[1], P Ashford [2] and R.B. Sandie [3]

[1] Director, The O'Neill Group Pty Ltd, Consulting Engineers,
Melbourne, Victoria 3000, Australia
[2] Faculty of Architecture, Building and Planning, University of Melbourne,
Parkville, Victoria 3052, Australia
[3] Formerly Head of Civil Engineering and Building, Swinburne University of Technology,
Hawthorn, Victoria 3122, Australia

ABSTRACT

In Australia, post-tensioned concrete floor systems are now the preferred type of construction for many large buildings, for reasons of economy and superior performance. The authors review relevant current Australian code requirements, design methods and construction practices and illustrate some typical design details for post-tensioned floors. After considering anticipated building trends in Australia, the authors conclude that the use of post-tensioned concrete floor systems will continue to increase.

KEYWORDS

Post-tensioned concrete, Performance based design, Partially prestressed, Load balancing, Bonded tendons, Internal stressing pockets.

INTRODUCTION

In Australia, since the mid nineteen eighties, post-tensioned concrete floor systems have become the preferred type of construction for many large buildings, including high-rise residential and office buildings, hotels, car parks, shopping centres and warehouses. This increase in popularity of post-tensioned floors has come about because, compared with more traditional reinforced concrete and structural steel floor systems, they offer advantages of:

Economy: The higher initial costs of the post-tensioning steel are more than off-set by cost savings arising from reduced floor thicknesses (which save materials and space and reduce column and footing loads), faster construction cycles, and lower on-going maintenance costs.

Performance: Post-tensioned floors are reliable and safe and provide excellent control of concrete cracks and deflections. They also have superior performance under heavy wheel and racking loads, such as occur in warehouses. At the time of transfer of full prestress loads to a floor, it is subjected to the highest loads it is likely to encounter and has virtually been 'proof loaded".

Design Flexibility: Post-tensioned floors permit buildings to be designed with large column free and wall free open spaces. Building services are not restricted in location by large beams intruding into ceiling spaces. There is considerable design flexibility in positioning openings and ducts.

Ease of Analysis: Another important factor which has increased the popularity of post-tensioned concrete is the ready availability of commercial software design computer programs (e.g RAPT: Reinforced and Post-Tensioned Concrete Design, introduced in Australia in 1987). Before such programs came onto the market, design methods were tedious, and largely the province of specialist prestressing firms.

AUSTRALIAN CODES FOR POST-TENSIONED CONCRETE

In Australia, all concrete structures, whether unreinforced, reinforced or prestressed, are covered by a single standard, AS 3600: Concrete Structures (2001), which contains design and detailing rules and performance criteria. The current third edition of AS3600 was issued in May 2001, to incorporate some amendments and rule changes, pending a major review of the code, now underway.

The code is supplemented by a commentary, AS3600.1 (1994), which explains the intent of the major elements of the code. AS 3600 also references about thirty other related Australian codes covering areas such as requirements for materials, material testing, admixtures, formwork, and loads on structures.

AS 3600 replaced earlier separate codes for prestressed and reinforced concrete and moved substantially from "prescriptive" to "performance" based design, in which designers have increased freedom to select design parameters. Whilst experienced designers can use this freedom to produce more efficient and economical design solutions, there is some potential for designers without experience in prestressed concrete to make serious mistakes, particularly if they do not understand some of the limitations of the computer design packages now widely available.

Australian code requirements for post-tensioned concrete floors are discussed where relevant in following sections of the paper.

AUSTRALIAN DESIGN METHODS FOR POST-TENSIONED FLOORS

Post-tensioned floors are invariably designed with bonded (grouted) tendons, since AS 3600 prohibits the use of unbonded tendons except for slab-on-ground construction.

AS 3600 permits a range of structural analysis methods for slabs. These include the use of moment coefficients, design strips, idealised frames, linear elastic analysis, and plastic analysis using lower bound and yield line methods. For post-tensioned concrete slabs, designers normally use computer programs, with increasing use of finite element analysis in place of methods based on design strips and idealised frames.

Partially prestressed design of slabs (in which some concrete tension is permitted) is normal, using load balancing techniques to control deflections and the levels of prestress for economical design solutions. Post-tensioned tendons are used to provide for overall load capacity. Reinforcing is added in combination with tendons to provide ultimate strength capacity and crack control. This approach

is found to provide more economical floors than fully prestressed designs, (where concrete tension under working loads is eliminated).

Shear stresses in post-tensioned slabs are analysed by using truss analogy models, as in many other countries. AS 3600 has more liberal shear reinforcing requirements that some overseas codes. Shear reinforcing is rarely needed for band-beam structures, except to resist shear due to specific severe loads. In practice, some shear reinforcing is normally placed adjacent to columns, whether needed or not.

Slab movements under prestressing forces are accommodated by careful detailing around stiff elements, such as lift and stair cores, to prevent cracking. Movement joints are usually provided at 30 to 35 metre centres.

DEFLECTION CRITERIA

Deflections usually govern the design of post-tensioned concrete floor slabs. Deflection criteria need to be chosen carefully and with due regard to the use of the structure, since they have considerable effect on the economy of the design.

Load balancing techniques are used for design, to keep deflections within specified limits under dead loads and some part of the live load. The portion of full live load depends on the type of structure and its occupancy.

AS 3600 limits calculated long-term and incremental deflections for beams and slabs under the design loads for serviceability to span/250 generally, and to span/500 for members supporting masonry partitions, where provision is made to minimise the effects of movement, or to span/1000 otherwise. There is a trend to adopt these stricter limits for other situations, particularly residential apartments, where occupants of expensive apartments expect very high performance standards and are alarmed by noticeable deflections in tiled floors, by vibrations and by any cracking of brittle wall and ceiling materials.

AS 3600 requires the effects of vibrations on concrete structures and elements to be considered. Except where there are known sources of vibrations, control is normally achieved by limiting ratios of span/overall depth for post-tensioned slabs to less than 40, and for beams to less than 30. Specific vibration problems may require dynamic analysis of the structure, normally accomplished by using proprietary computer programs.

AUSTRALIAN CONSTRUCTION PRACTICES FOR POST-TENSIONED CONCRETE FLOORS

In Australia, many high rise buildings are erected without external scaffolding. In these situations, Occupational Health and Safety Regulations require post-tensioning to be carried out from inside the buildings. To accommodate this, slabs and beams are designed to incorporate internal prestressing pockets, as shown in Figures 1 and 2.

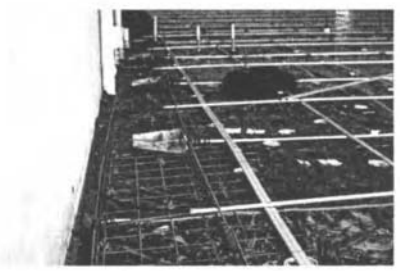


Figure 1: Prestressing Pockets in place

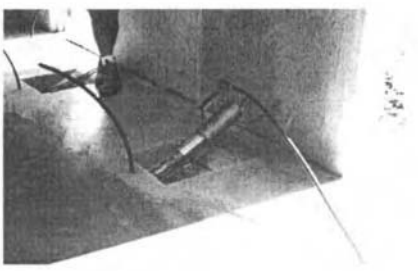


Figure 2: Internal Stressing Pocket

Typical construction cycles for high rise post-tensioned floors, from pouring to stripping of formwork, are five to six days. Typically, floor designs are based on 32 MPa compressive strength concrete. Twenty four hours after a post-tensioned floor is cast, it is usual to apply 25% of the prestressing forces to mitigate against shrinkage cracking. The remaining prestress is applied when the concrete achieves a compressive strength of 22.5 MPa, generally four to five days after pouring. Full prestress can be applied in as little as two to three days with special mix designs and the use of additives. For tall multi-storey buildings, this can reduce construction times by several months, with substantial costs savings when compared with reinforced concrete systems.

Formwork can be stripped immediately after full prestress is applied. Back propping may be required to support the weight of wet concrete from the next floor to be poured. Installation of services can commence as soon as formwork is removed.

For slabs "onion" type anchorages are preferred to swaged end anchors and end plates, for reasons of cost and ease of placement. However, onion anchorages have more potential to fail by pulling through the concrete, so need to be properly detailed and installed to separate individual strands and to ensure concrete can be easily placed and properly vibrated in the region of the anchors. Anti-burst reinforcement is provided at the live and dead end anchorages by helical ligatures around the anchors or by other reinforcing systems. Swaged end plates are preferred for beams, because of the concentration of strands in a small area. Typical end anchorage details are shown in Figures 3, 4 and 5.

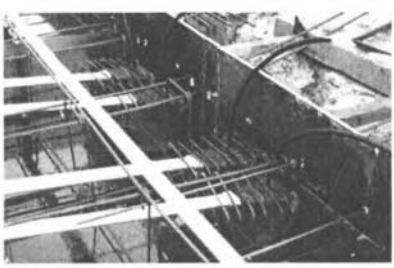


Figure 3: End Anchors with helical anti-burst reinforcement

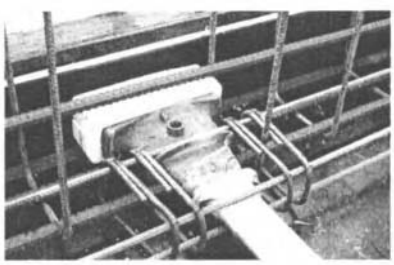


Figure 4: End anchor with anti-burst reinforcing

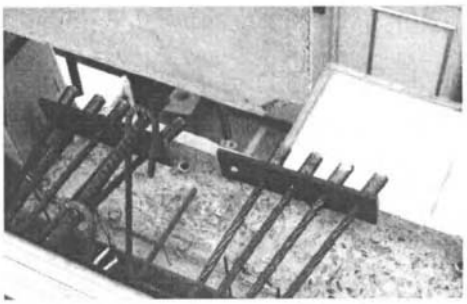


Figure 5: Swaged end anchors with end plates

Some typical details of suspended slabs follow. For a 200 mm thick slab, the main prestressing tendons are spaced at 1500 mm centres. Low levels of transverse prestress, from 0.7 MPa to 2.5 MPa, are applied by transverse cables spaced at 2.5 to 3 metres, to control concrete cracking. Prestressing tendons consist of stress-relieved bundled wire strands, with typical overall diameters of 12.7 mm and 15.2 mm, and ultimate tensile strengths (UTS) of 1840 MPa and 1750 MPa respectively. The tendons are stressed up to a maximum of 85% of their UTS. Tendons are stressed using hand-held hydraulic jacks and each strand is stressed individually.

Mutli-strand ducts are typically 19mm deep by 200 mm wide for four strand applications and 250 mm wide for five strands. Prefabricated cast-steel live anchors are available in sizes to match the ducts. Multi-strand circular ducts are not commonly used in Australia, except where very high prestressing forces are required in large transfer beams support podiums etc.

LONG SPAN POST-TENSIONED FLOORS

Post-tensioned concrete floor systems become increasingly more economical than other floor systems for spans from 8 metres to 12 metres, although they can be used for spans down to about 5 metres for small areas which do not justify any change in the reinforcement systems. For spans of 8 metres and above, the savings in floor thickness can be used to reduce building heights or provide extra space, even extra floors, within the building envelope. For typical post-tensioned suspended floors of spans from 8 to 12 metres, slab thicknesses for residential buildings range from 180 mm to 250 mm.

ONE AND TWO-WAY BANDED FLOOR SYSTEMS

One-way banded floor systems are widely used in Australia for commercial and retail buildings and offices. The building layout may dictate the choice of one or two-way action, but two-way post tensioned floor systems are much less common because of construction difficulties arising from clashes between crossing tendons running in different directions. Post-tensioning permits good control of deflections for band beams (strong bands of tendons), which are typically 2.4 metres wide to suit the available lengths of plywood sheets used for formwork.

Reinforced concrete slabs are used between post-tensioned band beams, for infill spans up to about 6 metres, because required reinforcement levels are low and the high costs of prestressing cannot be justified for such short spans. "Bondek" steel formwork, which remains in place and forms part of the slab reinforcement, can also be used when formwork costs are prohibitive.

In Melbourne, particularly for residential apartments, it is usual to construct single thickness floors, with the "strong bands" of tendons accommodated within the overall slab depth. Formwork is simple and service pipes, ducts, etc, can be installed without being restricted by the structure.

Designers usually avoid steps to balconies, because of difficulties in profiling and placement of tendons. An upstand concrete hob at the junction of the main slab and the balcony is provided for ease of weather proofing

POST-TENSIONED CAR PARK STRUCTURES

Nearly all recent Melbourne multi-storey car parks have used post-tensioned concrete floors for reasons of economy, since they permit large column-free spans which suit typical car parking layouts. There is a move from enclosed to open deck car parks because the fire restrictions are less onerous for the latter.

Typically, car bays are 2.4 to 2.6 metres wide. Band beams are at 8.5 metre centres and span 10 metres or more, with cantilever overhangs of up to 2.5 metres. Slab thicknesses are 160 to 180 mm and beams are 250 to 400 mm (10m span). Design live loads are 3 kPa.

SLAB-ON-GROUND CONSTRUCTION

Post-tensioned slabs-on-ground have proven to be very effective for heavily loaded industrial floors of large dimensions and with large pour areas. Cracks can be controlled and construction joints can be eliminated or reduced, avoiding the effects of impact wheel loads at joints and reducing long-term maintenance. Reinforced slabs typically have joints at 5 to 6 metre spacings in both directions, whereas post-tensioned slabs are poured in bays of 35 metres square, or even larger, without joints.

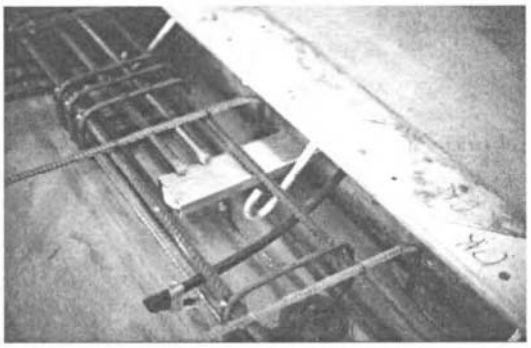
Tendons are not required to be bonded. Large slabs are usually analysed using commercial computer programs as plates on elastic foundations (eg. on a semi-infinite elastic half space). Since it is notoriously difficult to quantify the elastic properties of subgrades, sensitivity analysis is carried out by increasing and reducing soil parameters by a factor of 10.

Slab-on-ground thicknesses are typically 125 mm up to 250 mm. A recent Melbourne example is a wharf container terminal, with wheel loads from a 35 tonne forklift carrying a 20 tonne container and with containers stacked four high over large areas.

For large areas which require multiple pours, both movement and construction joints must be carefully detailed. Slabs rest on double membranes or single membranes on sand, to reduce subgrade drag and to permit shortening under prestressing with minimum prestressing losses. A typical movement joint is shown in Figure 6.

Most floors are poured inside already erected precast wall panels and, for aesthetic reasons, it is usual to have a 1.2 metre wide pour-strip at each end of the slab to accommodate stressing anchors,

rather than using stressing pockets and to avoid having to cut off exposed grout tubes. The pour-strips are eventually filled with reinforced concrete.



CONCLUSION

In Australia's largest cities there is ongoing movement of residents back to the city centres. Housing needs are being satisfied by construction of high quality and expensive residential buildings on prime sites. Occupants want large column-free and wall-free spaces, and expect their apartments to be crack free. Commercial properties and warehouses are becoming larger and owners are looking for economic solutions and low ongoing maintenance costs.

Post-tensioned concrete floor systems are safe, reliable and provide economic and performance advantages for many of these buildings. Consequently it is anticipated that the use of such floors will continue to increase in Australia in response to market forces.

REFERENCES

Australian Standard AS 3600-2001. (2001). *Concrete Structures,* Standards Australia, Sydney, Australia.

Australian Standard AS 3600.1. (1994). *Concrete Structures Supplement 1 – Commentary,* Standards Australia, Sydney, Australia.

This Page Intentionally Left Blank

Advances in Building Technology, Volume 2
M. Anson, J.M. Ko and E.S.S. Lam (Eds.)
© 2002 Published by Elsevier Science Ltd.

HIGH-TECH OR MOCK-TECH : STRUCTURAL RATIONALITY OF THE HIGH-TECH MOVEMENT IN BUILDING

James G A Croll

Chadwick Professor of Civil Engineering,
University College London, London WC1E 6BT

ABSTRACT

With their abundance of glass, exposed, celebrated, and often muscular structural steelwork and building services, many of the motifs of, so-called, high-tech buildings are being adopted by an increasing circle of architects and engineers. The new aesthetic that is being created is often characterised as providing rational structural solutions. This paper examines the validity of this claimed rationality. It develops a simple approach to the assessment of structural performance by considering comparative estimates of primary structural material volumes of alternative structural solutions. Not only does this methodology allow assessment of the rationality of high-tech building, but it also provides a general approach of immense potential benefit in the conceptual design of structures. Its reliance upon straightforward, physically based structural models, and the consideration that it is amenable to simple hand calculation, make this approach a powerful supplement to the increasing dependence upon computer analysis to inform even conceptual design.

KEYWORDS

Architecture, buidings, engineering, function, form, high tech, rationality, structures.

BACKGROUND

Traditional building construction evolved through a process of trial and error to produce building structures that often present a natural harmony of material, structural form, function and aesthetics. The accumulated craft skills that became amortised in, say, the traditional timber-framed temple of China or the masonry Gothic Cathedrals of Europe, provide convincing support to this argument. In their struggle to come to terms with the disharmony resulting from the development and use of the new strong materials at the beginning of the 19th century, both Pugin[1] and Viollet le Duc[2] in their different ways attempted to evolve an aesthetic appropriate to these new materials. Both were witnessing a disjuncture

not only between structure and form but also in the organisation and institutionalisation of the professions that evolved from the previously united craft traditions.

Increasingly, what one was to actually see in a building was not that required to allow it to stand up. Over a period of time structure was to become more and more implicit, often hidden behind façades that expressed the building's aesthetic qualities. Structure became the preserve of a group who formed themselves into the engineering professions, while form and the aesthetic qualities became the domain of the architectural profession. So it has remained for the past 200 years. Indeed, by the late 20th century the increasing use of glass façades meant that even the cladding of many buildings became implicit, with the ultimate absurdity that both structure and form became invisible. In a lecture which alluded to this aesthetic absurdity, Roger Scruton discussed a new glass building development (over what had been the fine Georgian Tolmer Square) just north of Euston Road. In some revealing images he opined that the only redeeming aesthetic qualities of this building were the somewhat distorted reflections from it of the remnants of a Georgian terrace on the south side of Euston Road.

Seen against this background, the high-tech movement can be viewed as an attempt to 'put Humpty Dumpty back together again'. Within the architecture of Rogers, Foster, Hopkins, Grimshaw, and many others, structure was again to become explicit. No longer hidden from view but celebrated in sometimes muscular forms, structure could once again be read as part of the aesthetic of the building. Making use of steel tubes for compression, rods and cables for tension, cable nets, pylons, cable-stays, metallic castings, counterbalanced spans, ... buildings started to look more like the products of bridge engineering. At one level this is surely a healthy return to the traditional harmonies. Structure and form can be interpreted as being once again reunited, helping to create a new aesthetic of buildings. However, if this harmony is to be complete, in the sense laid down by Ruskin[3] or Viollet le Duc[2], the structural systems being adopted would need to represent a rational and "best use" of the materials being adopted.

Amongst the claims made for high-tech buildings (see for example Davies[4]) is the assertion that their structures are rationally based. With the design often involving collaborations between some of the most respected architects and engineers of our age, it might be anticipated that these claims are firmly based. But are they? This paper examines a limited selection of archetypical high-tech buildings from the perspective of whether they do represent a logical and materially efficient integration of structure and form. It extends a methodology used recently by Croll[5] to examine the relative efficiencies of cable-stayed and catenary-type suspension bridges. This methodology will show that serious questions need to be addressed as to whether the high-tech movement really does represent a rational re-harmonisation of material, structure and form within a new aesthetic of building.

METHODOLOGY

To allow assessment of the structural effectiveness, an extension of the method recently used to compare the relative merits of cable-stayed and catenary-type suspension bridges[5] will be adopted. In this earlier study, the primary load paths all involved pure membrane action, either in the form of compression forces, $C_j(x)$, or tension forces, $T_j(x)$, where x is the axial position along member j. Based upon characteristic material strengths, σ_C and σ_T, for respectively compression and tension, the volume of the primary membrane structural elements may be represented as

$$V_C = \sum_j \left[\int \frac{C_j(x)}{\sigma_C} dx \right]$$

$$V_T = \sum_j \left[\int \frac{T_j(x)}{\sigma_T} dx \right] \tag{1}$$

Both (C_j, T_j) are taken to be positive. For the case of the suspension bridge, the primary structural behaviour could be represented by integrations of the type indicated by eqn (1), since bending behaviour is generally of local, secondary importance. However, in most structures a combination of bending and membrane behaviour must be considered.

Where bending is present, it will be assumed that the structural elements take the form of components in which the dominant bending resistance is in flanges. This would be the case where, say, universal beam or column sections, or hollow rectangular sections, are used in steel construction. In these cases, the volume of steel required to resist the bending moments $M(x)$ would be given by

$$V_B = 2 \int \frac{|M(x)|}{\sigma_B d} dx \tag{2}$$

where σ_B is a characteristic bending stress, and d, the effective depth between the flanges. To this must be added the material volume of the web required to resist the shear force, $Q(x)$.

$$V_Q = \int \frac{|Q(x)|}{\tau_Q} dx \tag{3}$$

where τ_Q is the characteristic shear strength of the web. Very similar relationships would apply for the quantities of steel reinforcement in a reinforced concrete beams. The main differences for concrete beams are that the bending steel volume would be half that given in eqn (2), and d would represent the effective depth between the centroids of the tension reinforcement and the concrete compression block. In the following, just buildings constructed from steel structural components will be considered.

To keep the analyses to simple and explicit forms, use will be made of statically admissible distributions of force. From the static theorem of plasticity, this will result in safe estimates of ultimate state behaviour, with the consequence that material volumes will be slight overestimates of those that would be predicted from more precise analyses which also take into account the requirements of strain compatibility. By careful choice of statically admissible force flows through the systems being analysed, primary material volumes should be reliably predicted and certainly should provide a basis for comparing alternative structural systems.

Before looking at the following examples, it is worth noting the close relationship between the assessment of membrane material volumes of eqn (1), and the concepts of 'pertinacity' introduced by Maxwell.[6] In a remarkable contribution, Maxwell showed that the sum of the algebraic pertinacities of the tension and compression members of a membrane frame is dependent only upon the nature of the position and magnitude of the loading that is applied to the frame. Two pertinacities can be defined:

$$\begin{aligned} \text{PER}_C &= -\sum_j \int C_j \, dx = -\sum_j C_j \cdot l_j \\ \text{PER}_T &= +\sum_j \int T_j \, dx = +\sum_j T_j \cdot l_j \end{aligned} \tag{4}$$

where the second equality applies when (C_j, T_j) are constant over the length l_j of the member j. For any two frames, A and B, having load position and magnitude fixed, the algebraic sum of the pertinacities

$$\text{PER} = \text{PER}_T + \text{PER}_C \tag{5}$$

will be found to be the same. This remarkable lemma was used by French[7] to show an error in my contribution in reference (5). For the situation where the characteristic strengths in tension and compression can be taken as equal, the material volumes for the membrane action, as given by eqn (1), can be seen to be proportional to the sum of the absolute values of the pertinacities, so that

$$V = V_T + V_C \propto |PER_T| + |PER_C| \tag{6}$$

I am grateful to Profession French for drawing my attention to this lemma and for the other insights it opens up in the field of optimisation. Its results and implications deserve to be rather better known.

CASE STUDIES OF CABLE-STAYED BUILDINGS

Single Asymmetric Stays

As an example of an archetypical high-tech building, consider a cable-stayed industrial building of the form shown in Figure 1. This structural solution has, for example, been used in the Grimshaw, 1987, Brentford superstore. It embodies many of the motifs of high-tech architecture: pylons supporting cable-stays to the roof that are in turn counterbalanced by tension back-stays. The echoes of bridge engineering are self-evident.

For the statically admissible distribution of local bending in the roof, it is assumed that the moments at quarter-span are equal to the continuity moment at mid-span; this has the effect of keeping bending steel volumes to a minimum by virtue of ensuring a relatively uniform level of $|M|$, as shown in Figure 1(b). A minimum volume of bending steel will result when $\int |M| dx$ is a minimum. This will be closely approximated when the positive and negative levels of moment are roughly equal.

Associated with the above distribution of bending in the roof girder, the membrane force flow is shown in Figure 1(b). For illustration purposes, angles $(\vartheta_1, \vartheta_2)$ and roof height-to-span h_r/l, and girder depth-to-span ratio, d/l, will be used to characterise the cable-stayed roof geometry. Based upon equations (1) – (3), the total primary steel volumes will, where l_j represents the length of member j, be given as

$$V_T = \sum_{j=1}^{3} \frac{T_j l_j}{\sigma_T} = \frac{ql^2}{\sigma_T}\left[\frac{7}{12}\left(\frac{1}{\sin 2\vartheta_1} + \frac{1}{\sin 2\vartheta_2} + \frac{\tan\vartheta_2}{\tan\vartheta_1}\cdot\frac{h_r}{l}\right)\right]$$

$$V_C = \sum_{j=4}^{7} \frac{C_j l_j}{\sigma_C} = \frac{ql^2}{\sigma_C}\left[\frac{7}{12}\left(\frac{1}{\sin 2\theta_1} + \frac{1}{\sin 2\theta_2} + \frac{\tan\theta_2}{\tan\theta_1}\cdot\frac{h_r}{l}\right) + \frac{h_r}{l}\right]$$

$$V_B = \int \frac{|M|}{\sigma_b d} dx = \frac{23}{18\times 48}\cdot\frac{ql^3}{\sigma_b d}$$

$$V_Q = \int \frac{|Q|}{\tau_Q} dx \approx \frac{ql^2}{8\tau_q} \tag{7}$$

which for the case of w/l = 0.125, $h_r / l = 0.2$, $\sigma_T/\sigma_B = 1.1$, $\sigma_T/\sigma_C = 1.2$, $\sigma_T/\sigma_Q = 1.6$ and $\vartheta_1 = 25^o$ (that corresponds with the minimum total primary steel), the steel volume is given by

$$V_{\text{single stay}} = \alpha[4.640 + 0.0293\, l/d] \tag{8}$$

This may be contrasted with the primary steel required for a more conventional portal frame, shown in Figure 2. To eliminate any uncertainty in total cost that would arise from the provision of foundations having horizontal shear capacity, it has been assumed that a steel tension tie proves the horizontal thrust at the base of the columns. For the purposes of producing a reasonably optimised bending moment distribution in the portal frame, the statically admissible moment distribution has again been taken to

have equal positive and negative moments; the moment and shear force take the form shown in Figure 2(b). For this frame, the various components of primary steel volume are

$$V_T = \frac{T_j l_j}{\sigma_T} = \alpha \left[\frac{1}{16} \cdot \frac{l}{h_r} \right]$$

$$V_C = \sum_{j=2}^{3} \frac{C_j l_j}{\sigma_C} = \alpha \left[\frac{1}{16} \cdot \frac{l}{h_r} + \frac{h_r}{l} \right] \left(\frac{\sigma_T}{\sigma_C} \right)$$

$$V_M = \int \frac{|M|}{\sigma_b d} dx = \alpha \left[0.0771 \frac{l}{d} + 0.125 \frac{l}{d} \cdot \frac{h_r}{l} \right] \left(\frac{\sigma_T}{\sigma_b} \right)$$

$$V_Q = \int \frac{|Q|}{\tau_Q} dx = \alpha \left[0.375 \right] \left(\frac{\sigma_T}{\tau_Q} \right) \tag{9}$$

which, for the same geometric and material properties as were used for the example of Figure 1, gives a total primary steel volume of

$$V_{\text{portal}} = \alpha \left[1.528 + 0.1123 \frac{l}{d} \right] \tag{10}$$

As a function of the span-to-depth ratio, Figure 3 shows that over almost the entire range of practical *l/d* ratios the standard portal frame requires considerably less total primary structural steel than does the cable-stay roof system. At *l/d* = 20, the cable-stayed roof system can be seen to involve 25% more primary steel for the super-structure than the equivalent portal frame. When the foundations are taken into account, the situation becomes considerably worse for the cable-stayed roof.

Whereas the portal frame requires foundations capable of generating just *ql* of vertical compression, the cable-stayed solution requires a compression foundation totalling *3.334ql*; that is, the compression foundation needs to be 233% larger than that for the conventional portal frame. If this foundation disadvantage of the cable-stayed roof system were not enough, it is important to remember that it is also required to develop a tension foundation having capacity of *2.334ql*, some 133% more than the compression capacity required of the foundations for the equivalent portal frame. Allowing for the increased cost of providing tension as compared with compression foundations, it is clear that the foundation costs of the cable-stayed solution will be considerably greater than that for the more conventional portal frame. If for example it is assumed that tension foundation is, force for force, say three times the cost of compression foundation, then the total foundation cost for the cable-stayed frame of Figure 1(a) would be around ten times higher than the equivalent portal frame.

Double Symmetric Stays

An even more common solution for the cable-stayed building is shown in Figure 4. Such a topology has been used by, among others, Rogers, 1979, in a laboratory building in Cambridge and Grimshaw, 1984, in the Oxford ice rink (both cited in Reference (4)). In this case the primary steel volumes are given by

$$V_T = \sum_{j=1}^{3} \frac{T_j l_j}{\sigma_T} = \frac{ql^2}{\sigma_T} \left[0.467 \left(\frac{1}{\sin 2\vartheta_1} + \frac{1}{\sin \vartheta_2} + 1.577 \frac{\tan \vartheta_2}{\tan \vartheta_1} \cdot \frac{h_r}{l} \right) \right]$$

$$V_C = \sum_{i=4}^{7} \frac{C_i l_i}{\sigma_C} = \frac{ql^2}{\sigma_C} \left[0.467 \left(\frac{1}{\sin 2\theta_1} + \frac{1}{\sin 2\theta_2} + 1.577 \frac{\tan \theta_2}{\tan \theta_1} \cdot \frac{h_r}{l} \right) + \frac{h_r}{l} \right]$$

$$V_B = \int \frac{|M|}{\sigma_b d} dx = 0.01032 \cdot \frac{ql^3}{\sigma_b d}$$

$$V_Q = \int \frac{|Q|}{\tau_Q} dx \approx 0.196 . \frac{ql^2}{\tau_q} \tag{11}$$

Support cables have been positioned to provide the optimum distribution of bending moment in the roof girder. This is shown in Figure 4(b) to involve a statically admissible moment distribution having equality of sagging and hogging moments. In this case the total primary steel for the same geometric and material properties as the above examples, with the exception that $\theta_l = 30^o$ is chosen to produce the least steel volume, will be

$$V_{double\ stay} = \alpha \left(3.663 + 0.0114 \frac{l}{d} \right) \tag{12}$$

Although providing a somewhat better super-structural material volume than the single asymmetric cable-stay of eqn (8), it is clear from Figure 3 that this solution is also considerably less efficient than the conventional portal frame, for the same overall scantlings, over a wide range of girder depth to span ratios, *d/l*. With the foundations being required to carry *3.972ql* of compression and *2.972ql* of tension the disadvantages from the additional costs for foundations are however, even more extreme than those for the single asymmetric cable-stay.

To overcome this excessive additional foundation disadvantage in the use of cable-stayed roof systems, a solution along the lines of Figure 5 has sometimes been adopted. This form has been used in for example Ahrends' 1984 supermarket in Canterbury (cited in Davies[4]) and Croydon railway station. However, this solution to the foundation problems can only be adopted for the case of the double symmetric cable-stays. Avoiding the need for tension piling by connecting the lower back-stay to the foot of the pylon has the effect of increasing forces T_3, C_5, and increasing the lengths over which they act. It also requires the development of horizontal foundation forces at the bottoms of the pylons, which, to keep comparisons on the same basis, are assumed to be developed with a self-equilibrating tie connecting the pylons at foundation level. For interest, a symmetric cable-stayed system as shown in Figure 5 would, for the same material and geometric parameters as above, and again with $\theta_l = 30^o$, require a total primary super-structural material volume given by

$$V_{double\ stay} = \alpha \left(5.229 + 0.0114 \frac{l}{d} \right) \tag{13}$$

This can be seen in Figure 3 to compare even less favourably with the equivalent portal frame. However, this solution does have the distinct advantage over the single asymmetric cable-stay of Figure 1 or the double symmetric cable-stay of Figure 4, of requiring a foundation delivering just *ql* of compression, identical with that of the portal frame. A symmetrically placed pair of cable-stays, as shown in Figure5, also has the advantage of offering bracing resistance to horizontal load, whereas those of Figure 1 and 4 would require additional bracing.

Single Symmetric Stays

Another class of cable-stayed sheds is worthy of consideration. When in the form shown in Figure 6, the double-span cable-stay system will require a primary material volume

$$V_{\text{cable-stay}} = \alpha \left(3.340 + 0.0487 \frac{l}{d} \right) \tag{14}$$

while in this case an equivalent double-span portal frame of Figure 7 requires

$$V_{\text{portal}} = \alpha\left(2.855 + 0.1971\frac{l}{d}\right) \tag{15}$$

Given that both of these cases will require foundations having $2ql$ worth of compression capacity and recalling that neither requires either tension or horizontal shear capacity in the foundations, it is clear from the comparison shown in Figure 8 that at practical levels of l/d, the balanced cable-stay has considerable material advantage over the equivalently dimensioned portal frame. It most certainly has considerable structural rationale as compared with the situations where the back stays are not themselves being used to support primary structure, such as the examples of Figures 1, 4 and 5 discussed above. This might be anticipated, given that situations like that shown in Figure 6 are close to the structures often used for major bridge crossings. In contrast with many later adaptations, some of the first high-tech uses of cable-stayed buildings (see for example Rogers 1982 factory in Newport, Wales, or his 1984 laboratory in Princeton, USA, both cited in Reference (4)) were of this single symmetric form. In a slightly modified form involving two cable-stays per span, Grimshaw, 1988, also adopted this form for the leisure centre at Stockbridge.

CABLE-STAYED BRIDGES

These latter single symmetric cable-stayed buildings are very similar to the geometries adopted for cable-stayed bridges. In an earlier article, together with its subsequent discussion, the the cable stayed bridge of form similar to that shown in Figure 9 has over wide parametric ranges been shown (see Reference (5)) to have considerable material advantage as compared with the usual parabolic cable suspension bridge. However, in both the parabolic and cable-stay suspension bridges treated in Reference (5), it was necessary to provide end anchorages that were capable of developing horizontal thrusts of $ql^2/2h_t$. This allowed valid comparisons in situations where the parabolic cable suspension bridge is necessarily required to develop such an end anchorage force. However, if all of the horizontal thrust from the inclined cables of the cable-stayed system, shown in Figure 9, is carried by self-equilibrating compression forces in the deck, then the primary steel volumes (where material below roof level is neglected, since this is common for all systems of this class) can be shown to be

$$V_{\text{stay}} = \frac{2\alpha}{\sin 2\theta}(1+\beta) \tag{16}$$

where $\beta = \sigma_T / \sigma_C$. Equation (16) displays a minimum when $\vartheta = 45°$. It is interesting to compare this with the Michell minimum weight structure, shown in Figure 10. Strictly, this Michell structure would apply only when $\beta = 1$, but with a little licence it can be shown that the optimum Michell truss has a material volume

$$V_{\text{Michell}} = \frac{\pi\alpha}{2}(1+\beta) \tag{17}$$

Compared with the optimum structure, the least weight cable-stay system of Figure 9 can be seen to have 27.3% more material. Allowing for the $2ql$ compression load to be taken over the roof height $0.2l$, assumed for the examples of Figures 1 – 7, and using $\beta = 1.2$, the volumes of materials required for the various two-span systems are

$$V_{\text{stay (minimum)}} = 4.88\alpha$$
$$V_{\text{Michell}} = 3.94\alpha \tag{18}$$

Including these in Figure 8, it can be seen that both the above pure membrane optima can, over certain (admittedly impractical geometries) ranges of l/d, involve greater primary material volumes than the more conventional portal frame and the single cable-stay solution. An explanation for this is that even

for relatively inefficient bending action, if the load path is short it may be more economic to resist the load through bending than to provide a greatly extended membrane load path.

DISCUSSION AND CONCLUSIONS

The question of what constitutes an optimum structural solution, when both bending and membrane primary load resistance are present, is clearly not straightforward. Even for the simple classes of single-span and double-span cable-stayed roofs, the results can be surprising. What is not surprising is the extreme inefficiency of using pylons that do not derive their stability from a functional and symmetrically supported roof. This was the case for the examples treated in Figures 1 and 4. For these cases it is not just the considerable additional super-structural primary structural material that is needed, but crucially, the considerably increased costs of foundations.

There are many structures that adopt similar principles to those considered in Figure 1 and 4. The Hong Kong and Shanghai Bank in Hong Kong, the Centre Pompidou building in Paris, and, closer to my own home, the Camden Town Sainsbury's building in London, all involve very similar structural actions. Space does not permit a full analysis of the structural rationale of these systems. Nevertheless, it is clear, even from the above, that many systems being adopted within the high-tech building movement use structural forms that involve very inefficient use of primary structural material. At the very least this raises interesting questions as to whether the claims often made for the structural solutions for high-tech buildings are entirely rational or whether in many cases they are solutions that merely mock those adopted for rational reasons in other engineering applications.

REFERENCES

1 Pugin, A W N. The True Principles of Pointed or Christian Architecture, London (1841). See also, Davey, P. Pugin Pointed the Way, *Architectural Review*, May (1984), 20-23.

2 Viollet-le-Duc, E. Entretiens sur l'architecture, Paris (1858-1872); English translation, Discourses on Architecture, London (1875).

3 Ruskin, J. The Seven Lamps of Architecture, London (1849)

4 Davies, C. High Tech Architecture, *Thames and Hudson*, London (1988).

5 Croll, J G A. Thoughts on the structural efficiency of cable-stayed and catenary suspension bridges, *The Structural Engineer*, 75(10), (1997), 173–175. See also discussion by French, M J and Dalton, H C. *The Structural Engineer*, 75(19),(1997), 345-347 .

6 Maxwell, J C. Scientific Papers II, 175, Cambridge, *Cambridge University Press*, (1840).

7 French, M J. Engineering Design: the Conceptual Stage, London, *Heinemann*, (1971).

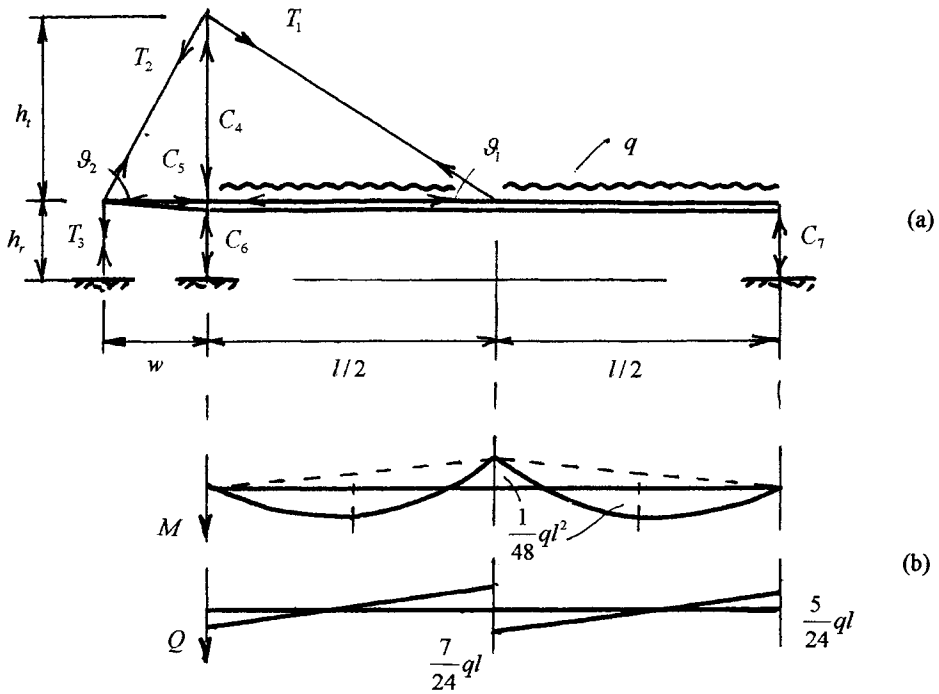


Figure 1 : Single asymmetric, single span, cable-stayed building, showing : (a) primary membrane force flow, and (b) distribution of bending moment and shear force over roof beam.

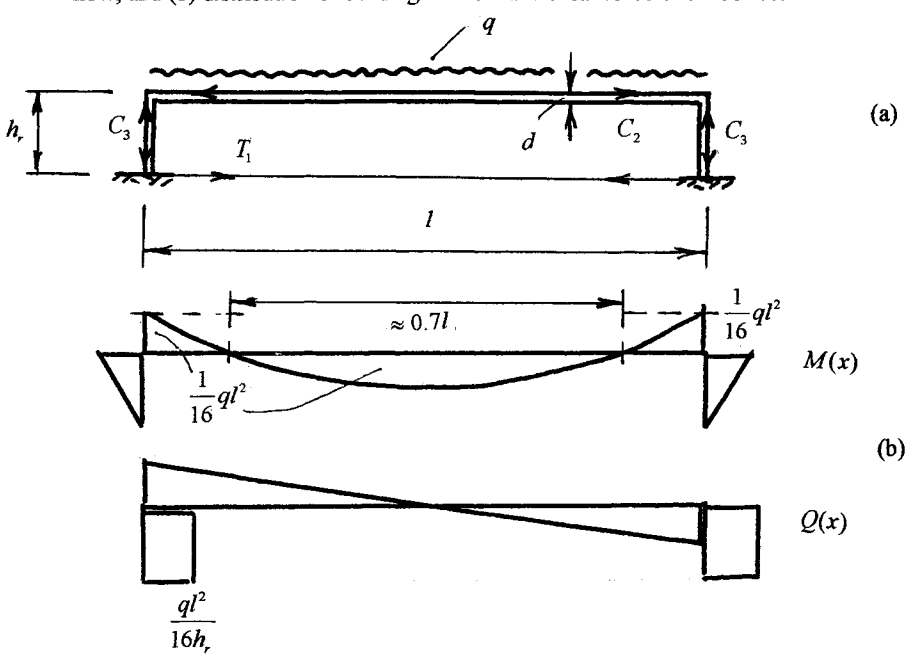


Figure 2 : Single span portal frame showing : (a) primary membrane force flow, and (b) distribution of bending moment and shear force over frame.

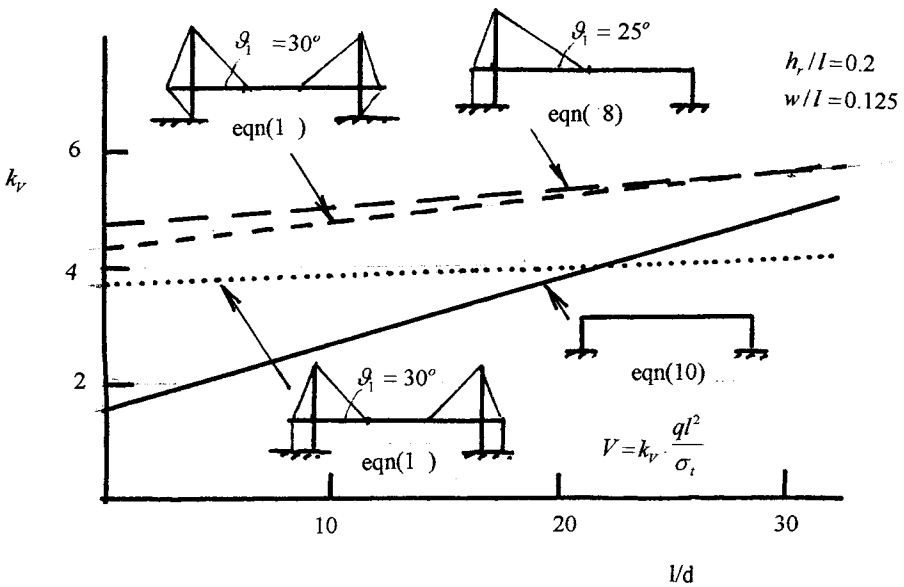


Figure 3 : Comparisons of primary material volumes required for various cable-stayed and conventional single span portal frame roof systems

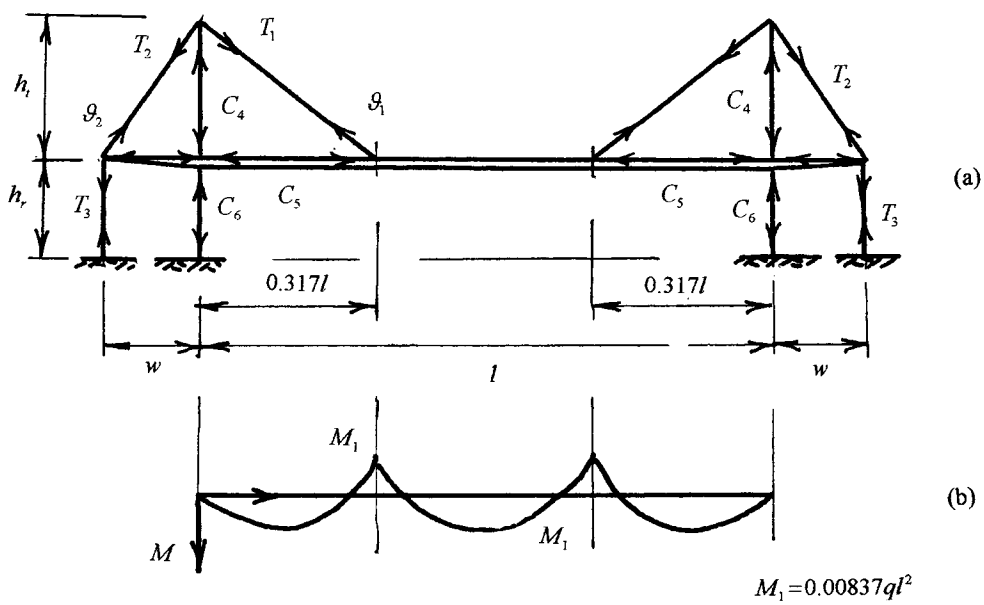
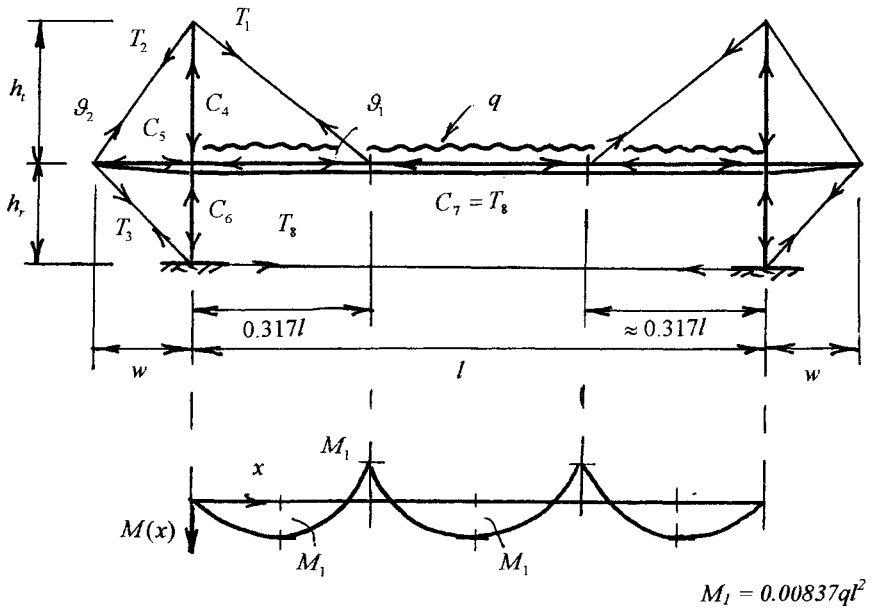


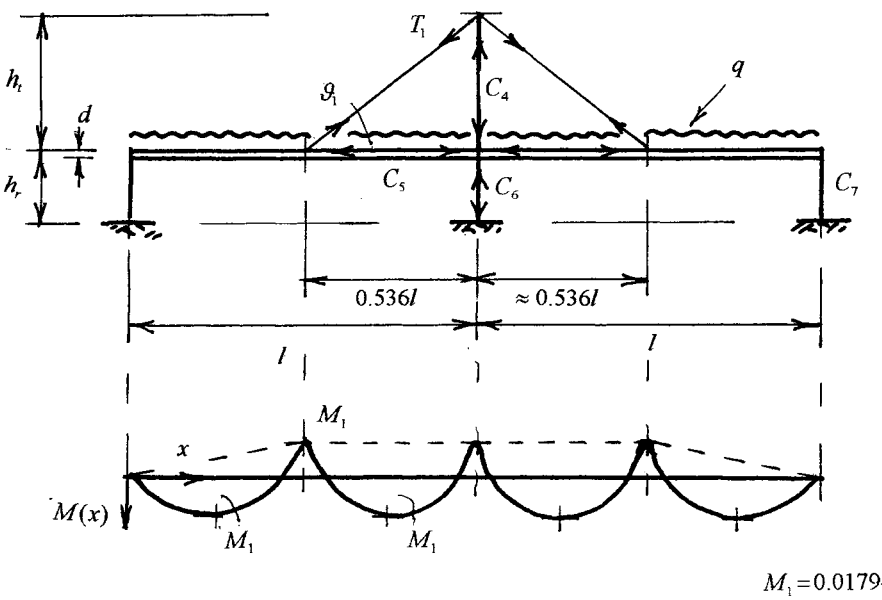
Figure 4 : Double symmetric, single span, cable-stayed building with vertical counter ties, showing : (a) primary membrane force flow, and (b) distribution of bending moment over roof beam.



(a)

(b)

Figure 5 : Double symmetric, single span, cable-stayed building with inclined counter ties, showing : (a) primary membrane force flow, and (b) distribution of bending moment over roof beam.



(a)

(b)

Figure 6 : Single symmetric, double span, cable stayed roof, showing : (a) primary membrane force flow, and (b) distribution of bending moment over roof beam.

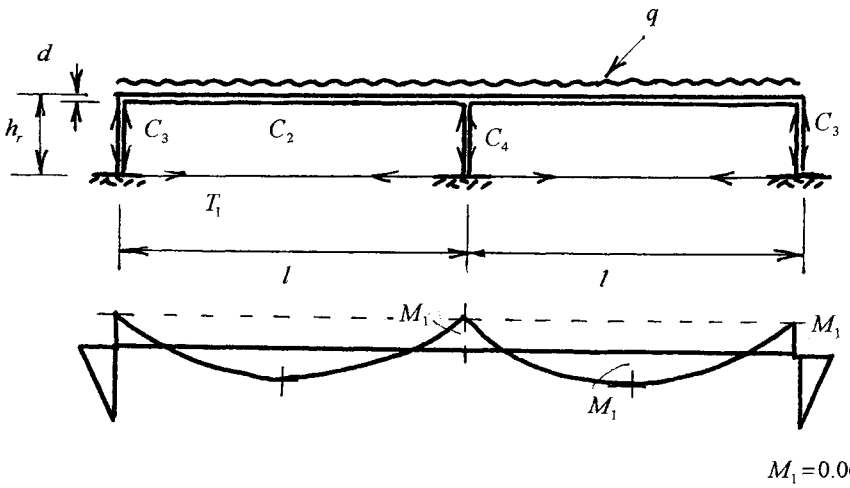


Figure 7 : Double span portaal frame, showing : (a) primary membrane force flow, and (b) distribution of bending moment and shear force over frame.

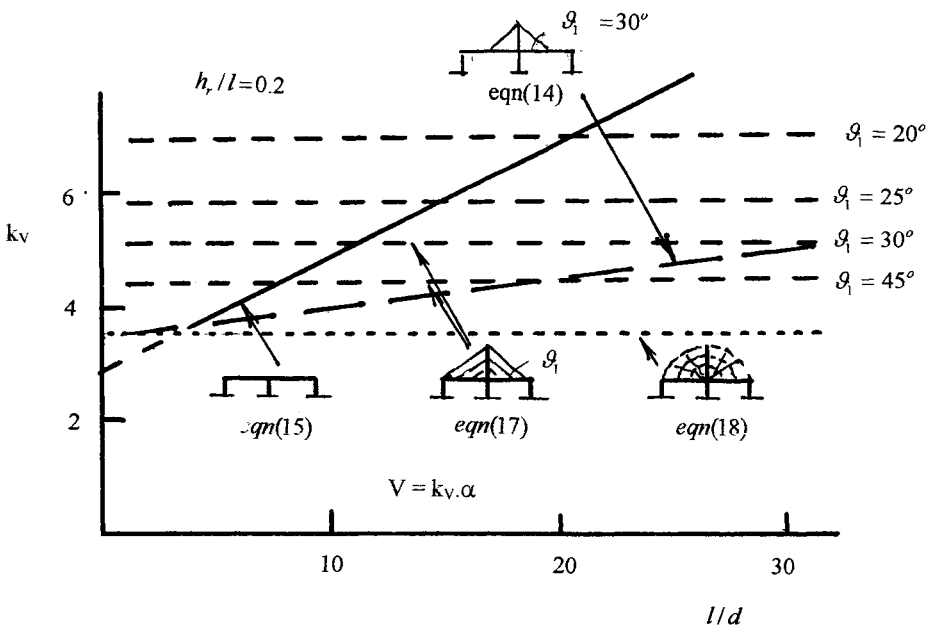


Figure 8 : Comparisons of primary material volumes required for various cable-stayed and conventional double span portal frame roof systems.

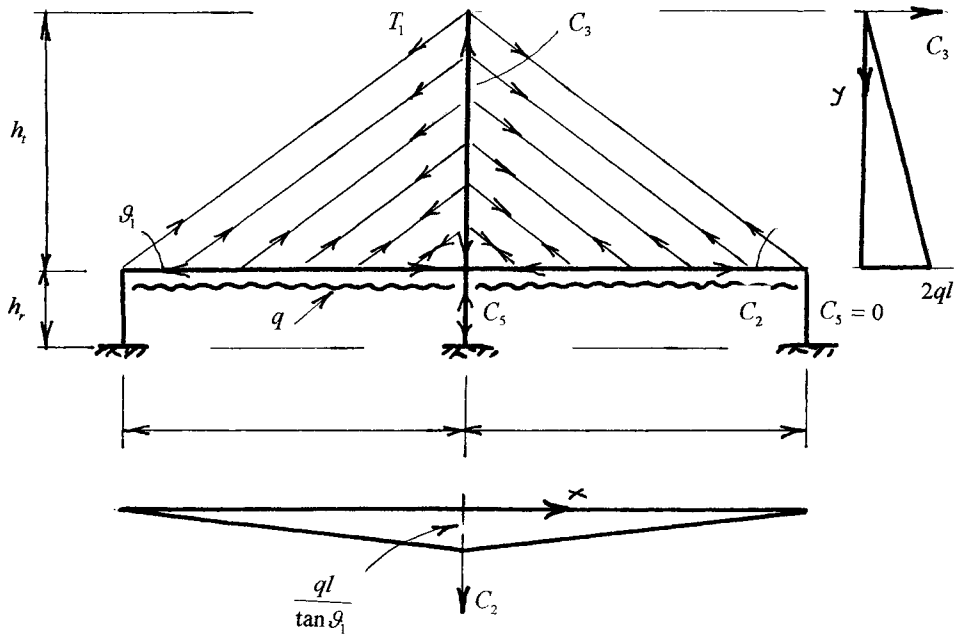


Figure 9 : Balanced cable stay bridge showing primary membrane force flow.

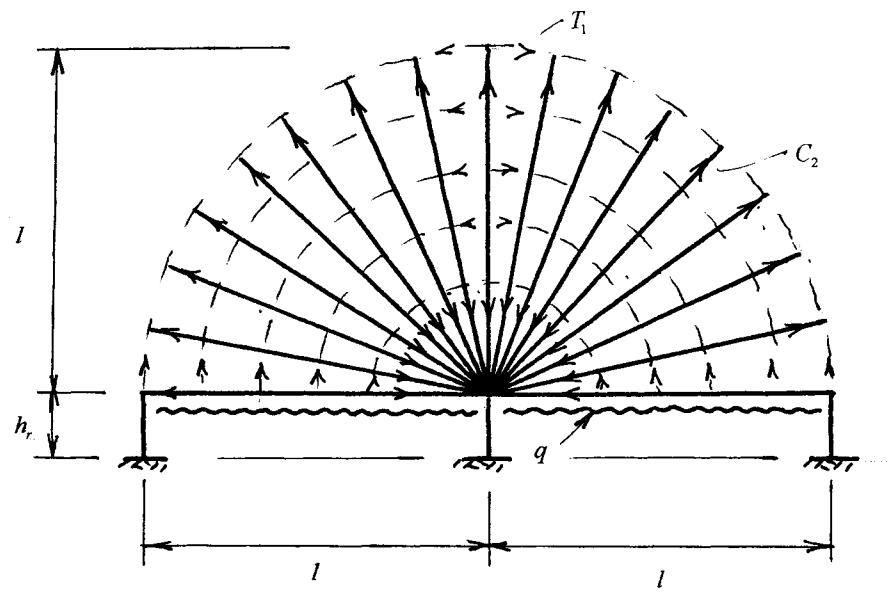


Figure 10 : Balanced Michell-type optimum truss system.

This Page Intentionally Left Blank

Advances in Building Technology, Volume 2
M. Anson, J.M. Ko and E.S.S. Lam (Eds.)
© 2002 Elsevier Science Ltd. All rights reserved

THE GAMMON SKANSKA CONSTRUCTION SYSTEM

Ted Lawton, Peter Moore, Ken Cox and John Clark

Gammon Skanska Construction Ltd.
Devon House, Quarry Bay, Hong Kong

ABSTRACT

This paper presents the revolutionary and unique "Gammon Skanska Construction System", which is the product of an in house research and development programme into modular construction extending for more than three years. The vision of the programme is to take the construction industry forward to levels of efficiency found in the oil, ship and automobile industries. Heavy investment has been made into the Research and Development programme for the System, including the full scale building of a modular three-storey mock up in Dongguan (see Appendix 1), two modular show flats for the Integer Exhibition at the Tamar site in Hong Kong and the preparation of a promotional video. After two years of patent searching, it would appear that this is the first time that a precast modular design may be readily and economically used for high-rise construction, without compromising structural integrity or weatherproofing.

KEYWORDS

Tang Committee Report, Gammon Skanska Construction System, Precast, Modular, High-rise, Economy, Sustainability, Maintainability, Environmental & Safety.

INTRODUCTION

The Construction Industry Review Committee report on the Hong Kong construction industry, released in January 2001, supports the need for change. The Committee called on the industry to improve its performance, finding that it produced a finished product that was seldom defect-free and in a manner that was labour-intensive, at times dangerous and polluting.

The reality for contractors is that they must now produce high quality products at ever-lower prices, whilst minimising the community impact. Using substantially its own in-house design, engineering and production resources to develop the Gammon Skanska Construction System, Gammon Skanska has learnt, that one way to improve productivity levels and quality is by moving the construction process away from site and into factory controlled conditions.

The system is based on building high quality modular units that are fully fitted out in the factory and then transported to the site for erection. This approach reduces on site work and allows buildings to be delivered more quickly, safely, with much less waste and thus a reduced impact on the local environs where construction work is being undertaken.

The concept behind the Gammon Skanska Construction System is summarised on the general layout of a typical cruciform block, contained within Appendice 2.

CONSTRUCTION METHOD

Container sized, precast concrete modules are firstly manufactured and then fully fitted out in factory-controlled conditions, including M & E, joinery, tiling, bathrooms, kitchens, decoration, fixtures and fittings, before being delivered to site. Modules are then erected and concrete is poured between them, to create vertical in-situ walls, which lock the modules together and also to become the main load bearing structure of the building. The entire core area, including stair wells, lift shafts and lobby areas can be modularized to match the wings, to enable a uniform construction method across each floor.

Unprecedented rates of site construction can thus be achieved, such as a two to three day floor cycle, instead of a six-day floor cycle, which is primarily due to the fact that no floor slab construction and very little wall formwork are required. Additional time is subsequently saved due to the 70% reduction in building finishing works at site. A comparison programme between a traditionally constructed and a modular system construction project are shown in the Appendix 3.

DESIGN PHILOSOPHY

Modular Construction has generally met with limited success and construction has generally been limited to less than twenty storeys, because of the problems associated with jointing, structural integrity and the cumulative weight of stacked modules. Existing solutions to these problems appear to render systems not workable or commercially viable. This system is based on existing, routine Hong Kong construction methods, using only conventional reinforced concrete to form the modules and structure of the building, to produce a homogeneous building, without the use of specialist grouting techniques, welded or bolted

connections. This approach is intended to simplify development and approvals from the relevant Authorities, and to ensure that there will be no future unproven, long-term inspection and maintenance liabilities.

Using professional experience from a wide range of disciplines, a variety of concepts and methods have been used, to integrate and develop the system into a seamless method of Modular Construction. These include: -

Architecture	-	Complimentary floor plans, features and finishes.
Building	-	Precast facade production, enabling the provision of factory produced features and finishes.
Civil Engineering	-	Match-casting of segmental bridge decks, enabling the quick, precision handling and jointing of sets of adjoining modules.
Steelwork Fabrication	-	Accurate dimensional control of casting beds, enabling the casting of sets of modules with repeating precision, for subsequent ready assembly on site.
Structural	-	Innovative integration of specialist designs for high-rise buildings, segmental bridges and precast concrete systems.
Building Services	-	Complimentary cable routing, risers and specially designed connections.

DESIGN DETAILS

Detailed commercial designs have been completed, including tower blocks of over 40 storeys, under the guidance of an RSE, according to all relevant design standards and BD requirements for Hong Kong.

Building Structure

Module walls combine with the in-situ wall pours to generate significant composite structural strength and stiffness, which enhances structural integrity. With the aid of reinforcing bar starters from the module floor slabs, these pours further lock the ends of these slabs together and generate monolithic sections of floor slab. Shear keys on the sides of the slab sections, enhance the generation of global structural floor plate shear action, in a similar, but in much less onerous manner to that of precast segmental bridge construction. Similarly they are suitably preloaded in compression, to ensure load distribution across slab joints without differential movement or cracking of finishes. A building of similar nature and strength to that of a conventional high-rise building is thereby created, consisting of floor plates, shear walls and core where required.

Modules

Each module is designed to span between and individually shed vertical load into the in-situ concrete walls, so that modules do not support their cumulative weight from above. This enables efficient high-rise construction and also ensures that the possibility of resistance to progressive collapse is at least as good, if not higher, than that of conventionally constructed building.

Jointing Method

A precision interlocking jointing system has been developed to readily join sets of modules together, to generate totally open plan rooms of the required size with minimal in-situ work. It is this in-situ work which has historically rendered other modular systems impractical, with regard to maintaining structural integrity, alignment and waterproofing.

ECONOMY AND SUSTAINABILITY

Modular Construction as a direct comparison with traditional construction, is often more expensive, mainly due to the capital costs of the factory and high transportation costs. However, an overall cost study in the SAR/PRC areas, indicates that the shorter construction period of a typical 40 storey residential tower of between 4 and 6 months, can result in savings amounting to millions of dollars (HK) due to the interest saved on capital investment.

Due to the higher level of factory installed products and more focused quality control methods at the factory floor, it is considered that the assembly of the precision engineered units by a skilled workforce will greatly enhance the overall sustainability of tomorrows housing stock providing a much higher durable product.

The modular units have clear uninterrupted space as all beams, wall thickenings and columns are externally designed, providing sustainable accommodation whereby rooms may be partitioned in ways and with products that can be undertaken at any time, to suit Client/End Users requirements. The resulting ability to change from say 2 to 3 bedroom layouts, without moving home or re-building, is a current goal of Hong Kong environmentalists.

MAINTAINABILITY

Potential cracking between modular joints is eliminated by a suitable amount of preload, shear keys, and epoxy glue, as with segmental bridges and also by the in-situ concrete pours. Between modules there is a double floor slab, providing a vented, drained void, which provides a barrier to any water leaks from the flat above to the flat below. Horizontal and vertical joints of the modules are designed for minimum maintenance and traditional sealants, requiring no more maintenance than facade systems.

ENVIRONMENTAL FRIENDLINESS

Modular construction vastly improves the environmental friendliness of construction in Hong Kong. The system enables faster site construction, thereby reducing the impact on neighbouring areas, during the construction process. This is achieved by a number of factors, including a reduced workforce and limited site activities, such as 70% less site placed concrete, whilst the revolutionary slab construction (in that, no supporting falsework and formwork is required), eliminates the consumption of materials, such as timber, steel and aluminum on site, and since the modules are fully fitted out off-site at the factory, there are consequently significantly less waste materials to dispose of. In addition vehicles entering and leaving site are reduced by at least 40% with consequently less noise and reduced impact to the surrounding roads.

For future owners of the completed units, the air void between double floor slab, reduces vertical noise transmission between flats by half, and contributes towards savings in thermal transmission losses, providing benefits in reduced energy requirements.

The environmental benefits of the system are of sufficient merit to warrant being featured in the international Integer Exhibition at the Tamar site in Hong Kong. This includes two modular show flats with alternative internal layouts, a conference room and a rest room facility. Two primary features are clearly demonstrated, the provision of sustainable accommodation, whereby a set of modules may be readily used or repartitioned at any time to provide alternative functions and the units are demountable for use elsewhere, eliminating the demolition process.

SAFETY

The modular solution is a safer method of construction. Due to the dead weight of the modules they are inherently more stable during erection, relatively simple to assemble and the modules act as a working deck for the connection process of the units, with a perimeter access scaffold being provided around the perimeter of the building. Workers follow up with minor riser pipe work and finishing works on the levels immediately below, working safely within the confines of the modular tower. These processes are repetitive and therefore with a trained workforce, the number of operatives working on site is significantly reduced compared to traditional construction works.

APPLICABILITY AND RELEVANCE TO HONG KONG

The Tang Committee Report has called for the Hong Kong Construction Industry to take a leap forward and improve its practices. The Gammon Skanska Construction System does indeed take this substantial step from the current practice of prefabricated facades, floor panels, stairs and prefabricated bathroom pods, to a total modular system and currently the Government led trend, towards providing incentives for developers by the introduction of floor area concessions for precast innovation, mean that the time is right to develop the initial pilot project in Hong Kong and move the next generation of housing design forward.

WHO WINS AND WHAT ARE THE BENEFITS

To summarise, there are many benefits associated with the modular construction and a few of the winners are: -

Developers

- Quicker completion means earlier occupancy ... which means earlier sales and rentals and lower financing costs resulting in tens of millions of dollars in savings for a typical residential development.
- High quality finish – at no more cost than traditional construction – that commands a premium price and reduces maintenance costs.

Residents

- High quality factory produced finishes.
- Air-void between flats reduces sound transmission by half.
- All internal walls are non-structural so they can be moved at anytime.

Workers

- Construction process is inherently safer because it comprises far fewer, more repetitive site-based actions.
- Working environment is generally more pleasant and conducive to safe, productive activity, less noise, dust, pollution and waste.

The Environment

- 75 per cent less construction noise.
- 40 per cent less vehicle movements on-site.
- 60 per cent less dust and noise pollution.

CONCLUSION

The Hong Kong Construction Industry is currently reviewing its practices, in order to adopt the changes affecting our industry. It is believed that the Gammon Skanska Construction System addresses many of the change issues, by taking the production process away from site into a factory controlled climate whereby, quality can be achieved by using a skilled trained workforce and improvements in the time to procure a new project can be achieved by implementing system construction.

With continued ongoing development, the second generation Gammon Skanska Construction System design is currently examining reduced maintenance on future towers with such item as:

- Self finish external wall treatments with materials such as monolithic wall tiles, or self-cleaning coloured concrete.
- Maintaining risers, plumbing and drainage within the building envelope.
- Reduced thermal transmission through facades.
- The use of lightweight, self-compacting high strength concrete, utilising recycled aggregates.

These enhancements will be incorporated into designs on current potential pilot projects.

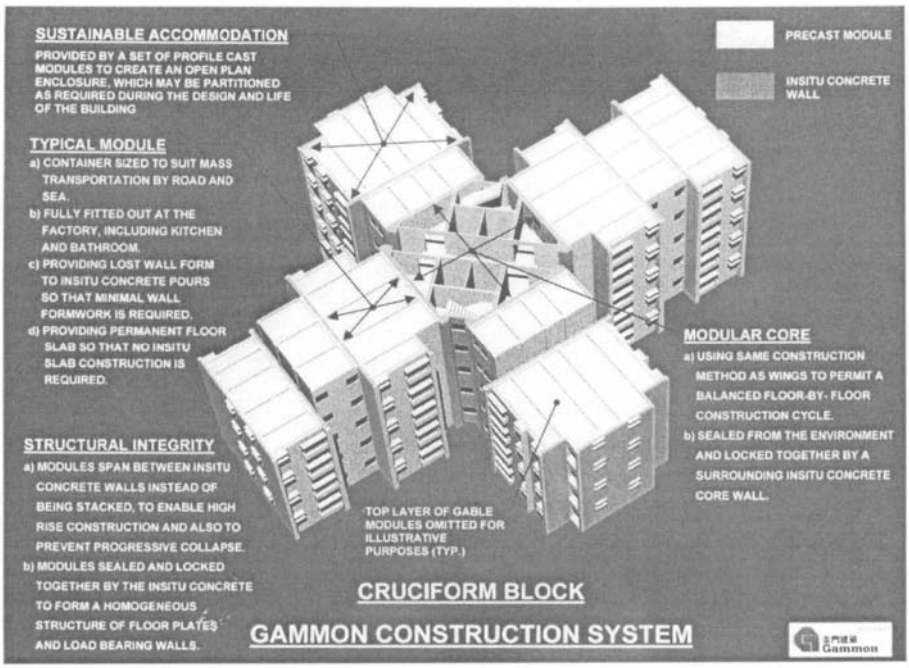
The Gammon Skanska system is equally appropriate for other types of buildings including, hotels, educational facilities, prisons, or, linear type developments and can be designed for demountable and re-usable functions.

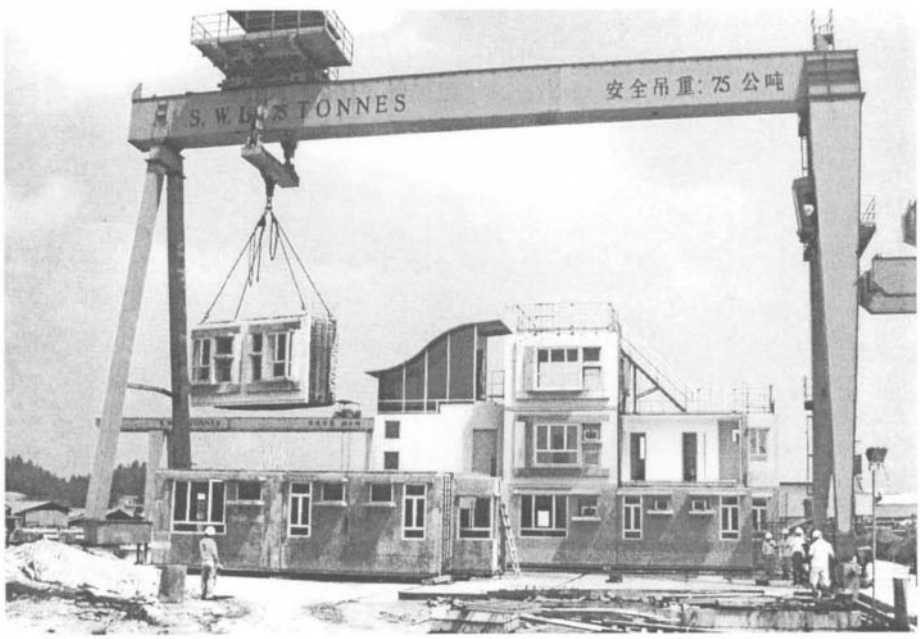
The system is available for licence both here in South East Asia and elsewhere in the world.

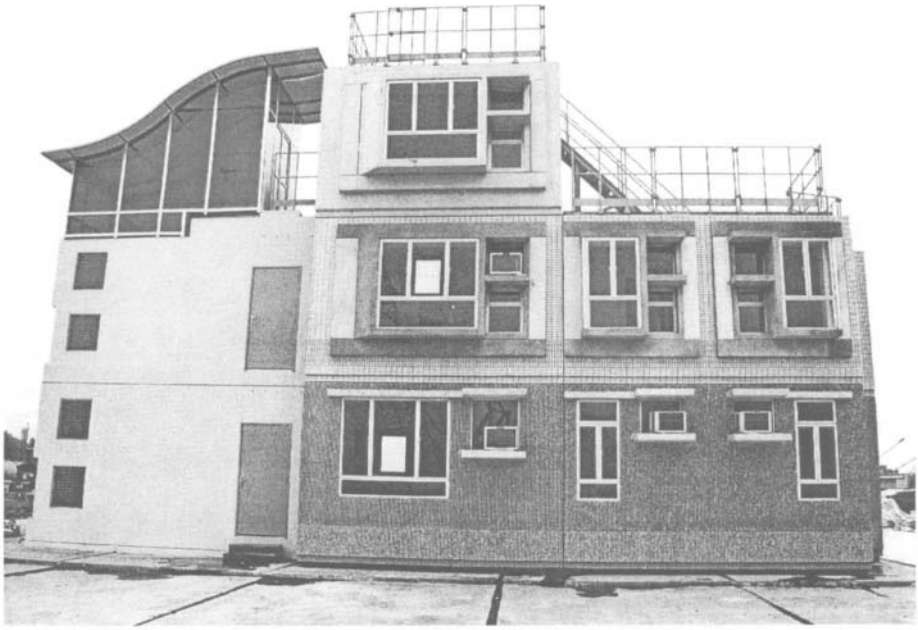
APPENDICES

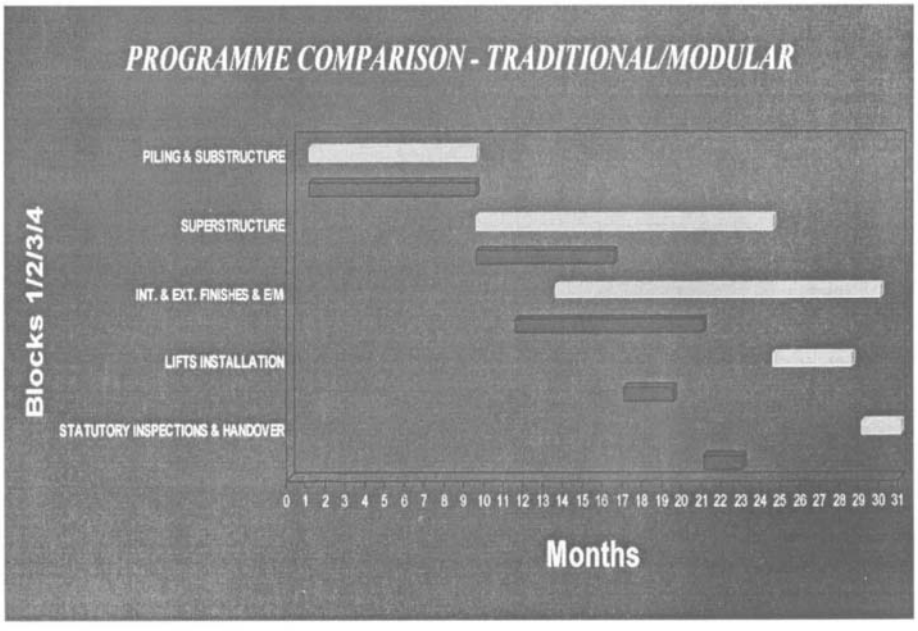
Attached for references are the following documents: -

- Photograph of the Gammon Skanska Construction System Prototype – Appendix 1.
- The Gammon Skanska Construction System – Cruciform block layout features – Appendix 2.
- Comparison programme – conventional construction to a modular system – Appendix 3.


SUSTAINABLE ACCOMMODATION
PROVIDED BY A SET OF PROFILE CAST MODULES TO CREATE AN OPEN PLAN ENCLOSURE, WHICH MAY BE PARTITIONED AS REQUIRED DURING THE DESIGN AND LIFE OF THE BUILDING
TYPICAL MODULE
a) CONTAINER SIZED TO SUIT MASS TRANSPORTATION BY ROAD AND SEA.
b) FULLY FITTED OUT AT THE FACTORY, INCLUDING KITCHEN AND BATHROOM.
c) PROVIDING LOST WALL FORM TO INSITU CONCRETE POURS SO THAT MINIMAL WALL FORMWORK IS REQUIRED.
d) PROVIDING PERMANENT FLOOR SLAB SO THAT NO INSITU SLAB CONSTRUCTION IS REQUIRED.
STRUCTURAL INTEGRITY
a) MODULES SPAN BETWEEN INSITU CONCRETE WALLS INSTEAD OF BEING STACKED, TO ENABLE HIGH RISE CONSTRUCTION AND ALSO TO PREVENT PROGRESSIVE COLLAPSE.
b) MODULES SEALED AND LOCKED TOGETHER BY THE INSITU CONCRETE TO FORM A HOMOGENEOUS STRUCTURE OF FLOOR PLATES AND LOAD BEARING WALLS.
PRECAST MODULE
INSITU CONCRETE WALL
TOP LAYER OF GABLE MODULES OMITTED FOR ILLUSTRATIVE PURPOSES (TYP.)
MODULAR CORE
a) USING SAME CONSTRUCTION METHOD AS WINGS TO PERMIT A BALANCED FLOOR-BY- FLOOR CONSTRUCTION CYCLE.
b) SEALED FROM THE ENVIRONMENT AND LOCKED TOGETHER BY A SURROUNDING INSITU CONCRETE CORE WALL.
CRUCIFORM BLOCK
GAMMON CONSTRUCTION SYSTEM
Gammon


S.W.L. 75 TONNES
安全吊重: 75 公吨




PROGRAMME COMPARISON - TRADITIONAL/MODULAR
Blocks 1/2/3/4
PILING & SUBSTRUCTURE
SUPERSTRUCTURE
INT. & EXT. FINISHES & E/M
LIFTS INSTALLATION
STATUTORY INSPECTIONS & HANDOVER
0 1 2 3 4 5 6 7 8 9 10 11 12 13 14 15 16 17 18 19 20 21 22 23 24 25 26 27 28 29 30 31
Months

Advances in Building Technology, Volume 2
M. Anson, J.M. Ko and E.S.S. Lam (Eds.)
© 2002 Elsevier Science Ltd. All rights reserved

THE DEVELOPMENT OF FACTORY PRODUCED HOUSING

Miles, J.[1], Badger, D.[2], Rose, J.[3] , Geeson, P[4], and Donelan. P[5]

[1]Arup Group Ltd, London, UK
[2]Arup Group Ltd, Midlands Campus, UK
[3]Arup Associates, London, UK
[4]Arup Group Ltd, Warsaw, Poland
[5]Arup Japan Ltd, Tokyo

ABSTRACT

This paper addresses the need to build high quality, sustainable housing in a rapidly expanding urban environment like Hong Kong. In order to build faster, yet maintain quality and reduce costs, it is suggested that a step-change in construction technology will be required. The potential for Off-Site Fabrication, in the form of a factory-produced concrete modular system, is described and examples are cited of demonstration buildings in the U.K which suggest that such a system is viable.

KEY WORDS

Community, Construction Technology, Energy, Environmentally responsible, Factory, Housing, Innovation, Manufacturing, Modular Construction, Multidisciplinary, Prefabrication, Sustainability, Value.

1. SETTING THE SCENE

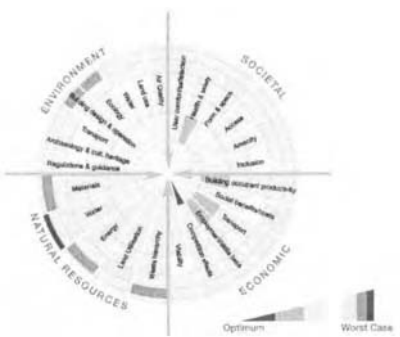
1.1 Background

Hong Kong is a vibrant, expanding city. With 3.3 million people living inside 125 sq.kms, the area around Hong Kong Island and Kowloon is one of the most densely populated urban centres in the world. The continued economic development of Mainland China, and particularly the Special Economic Zone around Shenzen, means that the regional population is likely to increase significantly over the next 20 years as trade and commercial development gathers pace. All the signs, despite the recent economic slowdown, are that the medium-term trend is growth-oriented and the authorities in the region must plan for an increasing population. The need for high quality, cost-effective, environmentally responsible, residential construction has never been greater. How can this need best be fulfilled?

Within the above context, conventional methods of design and construction have limited attraction. From a quality point-of-view, the need to build more quickly and within tighter budgets pressures contractors to reduce construction quality. From an environmental point-of-view, traditional design approaches have shortcomings and are and in need of improvement. The Hong Kong authorities have clear ambitions in both of these directions and are actively encouraging the development of new ideas and innovative techniques in planning, design and construction. The challenge is to develop communities living in high quality, environmentally friendly, buildings which are swift to construct at economical prices. In every sense of the word, this elusive combination may be described as '**Sustainable Housing**' and this paper puts forward some thoughts on the road to realisation of this ideal.

1.2 The Methodology

The delivery of sustainable housing requires a multidisciplinary and balanced approach to the development of new designs. There are many variables which must be considered simultaneously under the four primary headings of Social, Environmental, Natural Resources, and Economic. Good design requires the harmonisation of all of these. Some form of systematic and disciplined appraisal is therefore necessary if the appropriate balance is to be achieved. Several tools have been developed over recent years for this purpose and, within Arup, the SPeAR system has found widespread favour. Use of a tool such as this can be invaluable if adopted at the outset of a project and used regularly to assess the developing characteristics of a scheme as it goes through the various stages of project development. Fig 1 illustrates this essentially graphic approach, which has been endorsed in the UK recently as an independent tool for assessing residential development schemes (Ref 1).



SPeAR is a sustainability assessment tool which allows the multiple variables being assessed to be presented in a simple visual form. Colour coding utilises green (near the centre of the circle) and red (near the circumference) to represent good and poor performance respectively. A progressive change of colour at intermediate radii deals with cases between the extremes. The circle is divided into four headline zones (Environment; Societal; Natural Resources; Economic). Within each zone, a range of relevant issues are represented as segments and coloured according to assessed performance.

Fig 1: The SPeAR Sustainability Assessment Tool

1.3 Construction Technology

There have been impressive advances in construction technology in Hong Kong over recent years. The construction cycle-time for high-rise dwellings has been systematically reduced to 6 days per storey (and, even to 4 days) by increasingly sophisticated organisation and management on site, plus the widespread adoption of Off-Site Fabrication (OSF) techniques. Principal amongst these is the use of pre-cast concrete for facades. However, there are limits to what can be achieved and there is a danger that the single-minded pursuit of speed can lead to compromises in finished quality and site-safety. In any case, the cycle-times referred to above relate only to the single storey completion time for *structure;* the figures make no allowances for services, finishings and fittings – all of which take a

great deal longer to complete than structural work. And not only do these tasks take longer. It is here that the majority of 'value' is brought to the building. Clearly, if a step-change is to be brought to the *overall* construction/completion cycle, something more all-embracing than pre-cast concrete structure alone must be considered. It is this thinking that leads to the conclusion that factory-built modular housing might be attractive.

Off-site fabrication of volumetric, interior- finished, dwelling units has the following potential advantages

- It allows maximum value to be installed in the factory, thereby allowing capital costs and transport costs to be amortised more easily over any given number of dwellings.
- It allows factory standards of manufacture, finish and reliability to be achieved.
- It removes the maximum possible fraction of labour from site, thereby reducing the likelihood of poor workmanship, accidents, and errors.
- It significantly speeds up the construction/completion cycle, thereby increasing the return on capital employed for developers and reducing the duration and intensity of annoyance to site neighbours.
- It provides secure, safe, factory-based, jobs for the workforce in preference to the relatively dangerous, insecure, site-based jobs, normally associated with the construction industry.

For all of the above reasons, OSF and, particularly, volumetric modular construction, has received a great deal of attention in recent years. In the U.K., the trend began with clients from the hotel and fast-food industries wanting buildings of higher quality and reliability, delivered and commissioned within shorter timescales. Clients in these sectors recorded impressive gains for their businesses (some fast-food retailers claiming a factor of 10 improvement in the installation and commissioning timescale for a typical roadside restaurant). The obvious success of these initiatives prompted interest amongst a wider circle of clients, and residential buildings are a large segment of the construction industry with a potential for big gains.

The next two sections of this paper examine the recent development of a particular sustainable modular housing system in the UK and its potential extension for application to high rise system for Hong Kong and East Asia.

2. MODULAR CONSTRUCTION – CASE STUDIES FROM THE UK

This section outlines two prototype residential buildings which utilise factory-built concrete modular products developed by Meteor Systems (a consortium of Arup, Peabody Enterprises and Taylor-Woodrow). The concept is founded on the following basic precepts:

- The product must be the right price (i.e. it must meet or beat conventional build costs).
- The product must satisfy customer needs
- The product must satisfy the demands of the regulatory and financial bodies (i.e it must satisfy regulated performance criteria and it must be mortgageable/insurable).
- The product must be sustainable when measured against the headline parameters identified in Section 1.2.

To deliver a product which meets all of these needs simultaneously requires a 'first-principles' approach to design and production. The materials used, and the production processes, must be developed as an integral part of the product design exercise. Working through this cycle, the defining characteristics of the production facility are found to be:

(i) A flexible manufacturing regime (must produce a wide variety of different products, sometimes in quite small batches and in random sequences).

(ii) Elasticity of output (must be able to cope with peaks and troughs in demand without undue fluctuations in selling price).

(iii) Low capital investment (volumes of production are not sufficient to accommodate mass consumer product levels of capital intensity).

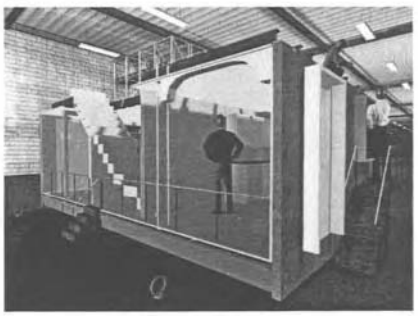
This trio of requirements is unlike the pattern found in 'standard' solutions from other industries. It is not possible, therefore, to transplant an accepted process from elsewhere. The factory design and process layout has been a particular challenge, and the key elements of the system which has been devised are summarised in Fig 2:



(a)



(b)



(c)

*Initially, flat-panels are produced on high quality (but very simple) shuttering **(a)**. Panels can be of arbitrary length and breadth. The panels are then assembled into boxes (modules) using purpose... designed equipment **(b)**. The boxes then pass down a moving fit-out line where internal equipment is installed and finishings applied.*

Fig 2 : Key Elements of Meteor Systems Production Concept

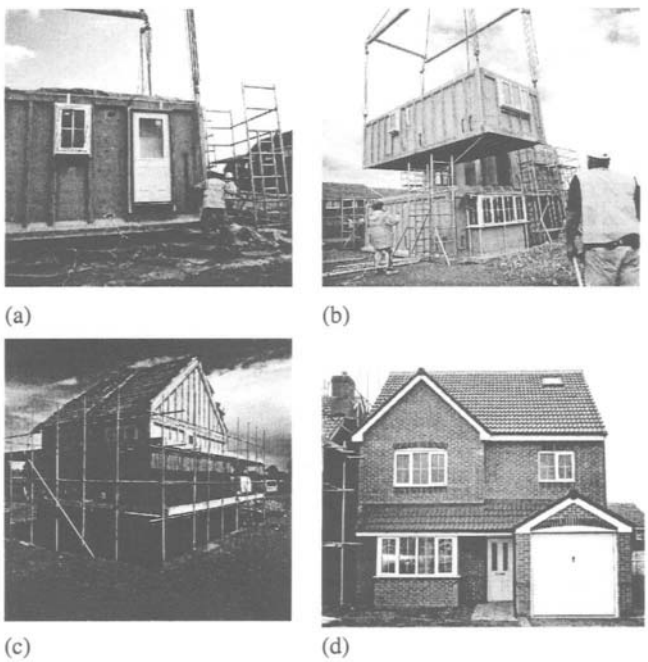
Based on the principles outlined above, a prototype production facility has been set up and the production of two buildings has been embarked upon. These buildings deliberately represent two extremes of the UK housing market in order to demonstrate the flexibility and design potential of the Meteor System. The first (built in Northampton for one of the UK's leading private housebuilders and completed in the Summer of 2001) is based on an entirely conventional design, un-modified in its layout and appearance from a conventionally-built counterpart. The second is an unconventional, architect-designed terrace of apartments and townhouses, in which an environmentally responsible approach to design has been emphasised. This building has recently won an RIBA design award and

is about to move into construction on site. It will be built at Acton in North London for Peabody Trust. Both Projects are associated with low-rise developments.

2.1 Detached House – Northampton (for Bellway Homes)

This project utilised Meteor Systems' concrete modules to provide a volumetric solution to a traditional requirement. The concrete modules provide a robust, high-quality infrastructure which is overclad with traditional bricks and roof-tiles. The modular solution is flexible enough to accommodate all the 'idiosyncrasies' of a typical design (i.e. the builder's standard layouts were not modified to accommodate factory-imposed inflexibilities). However, the truss-free roof allowed significant improvements to the available space over the basic layout, turning a standard three-bedroom, two-story house into a four-bedroom, three-storey house with additional en-suite facilities.

The concrete solution provides high thermal mass and good sound insulation. This house has excellent energy-in-use characteristics with a SAP rating in excess of 106. SAP (Standard Assessment Procedure) is part of the UK building regulations for checking energy usage by checking efficiency of the heating system, the insulation and the building leakage. A SAP rating of 106 is very good. It also has measured sound attenuation characteristics which are well in excess of those measured in traditionally built versions of the same design nearby on the same site.



*The modules for this house were installed within 10 working hours, providing a fully finished, weather tight interior ready for completion of interior joints and overcladding **(a)**; **(b)**. The exterior cladding (bricks and roof tiles) were then applied in a conventional fashion **(c)**. It is estimated that this approach, once established, could reduce typical build times from around 16 weeks to three weeks **(d)**.*

Fig 3 : Construction Sequence for Conventional Detached House

2.2 Terrace of Apartments/Town Houses (for Peabody Trust)

This small development builds on the technical achievements of the Northampton project and seeks to demonstrate the potential of the Meteor System to accommodate a variety of design demands (e.g. unconventional facades; double-height interior spaces; low energy in use; irregular layouts; etc). Comprising some 30 modules, it is intended to be delivered and completed on site within 6 working

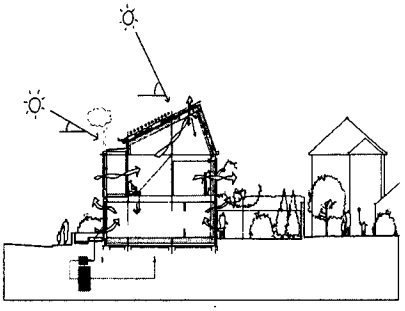
weeks – a very substantial reduction from the 40 week programme estimated for the conventional construction of the same building.



(a)



(b)



(c)

This RIBA award-winning design for a small terrace of town-houses and apartments ***(a)*** *will have unconventional facades and dramatic forms of interior layout* ***(b)****. There will also be a heavy emphasis on low energy-in-use and other environmentally responsible design issues* ***(c)****. The application of the Meteor System to this project demonstrates the flexibility of the concept.*

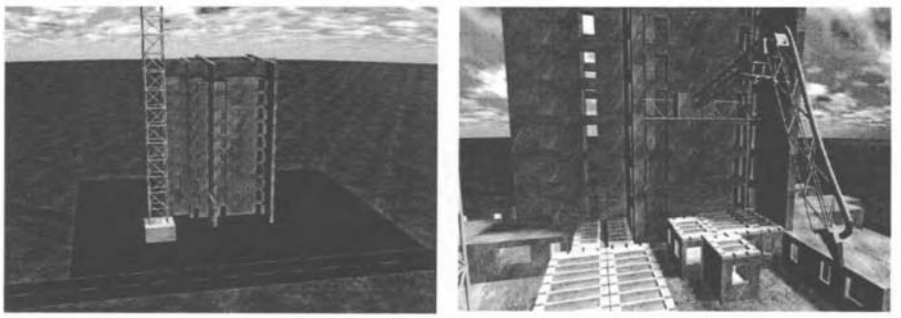
Fig 4 : Environmentally Responsible Design – Town Houses/Apartments to be built in Acton, North London

3. EXTENTION TO HIGH RISE APPLICATIONS FOR EAST ASIA

The basic system for producing high quality, low-cost modular products has already been developed in the U.K. A factory for producing fully-finished modules has been designed, and funding for a pilot factory is being raised.

With some modifications to the engineering design of the modules themselves, the system could be adapted and extended to cope with high-rise situations. Feasibility studies have been conducted which have examined structures up to 40 storeys, and concept designs have been produced. It should be possible to produce a great majority of the design-types most widely seen in Hong Kong (both public and private types) at prices which would compete with conventional delivery. It has been calculated that the completion time of the superstructure of a 35 storey block could be reduced to the order of 12-15 weeks, with on-site labour running at around 25% of conventional levels. The benefits in terms of reduced potential for accidents, errors and poor workmanship are obvious, as is the improvement in return on capital employed for the developer/contractor.

Fig 5 illustrates the concept. The system employs a hybrid approach to construction, using in-situ techniques for the core (slip-forming) and factory-built products for the residential elements. There is also a degree of site automation (for example, the grouting robot used to provide a 'bed' for incoming modules – illustration 5(b)).



(a) (b)

Hybrid construction techniques are proposed for high-rise variants of the concrete modular concept. The core of the building will be slipformed ***(a)*** *with modules shipped to site and placed around the core using heavy lift cranes. The 'grouting arm'* ***(b)*** *is illustrative of the type of site automation which is envisaged.*

Fig 5 : High Rise Solution Concept for Hong Kong

Further extensions of the concept have been developed for deployment in other climates (e.g. Singapore). Sustainable neighbourhoods were a key theme in the scheme illustrated in Fig 6. Layouts incorporating sky-gardens; passive cooling; renewable energy sources; and neighbourhood 'clusters'; were developed for high-rise communities. Again, this concept could be built to higher standards, and very much faster, than the conventional counterpart.

4. CONCLUSIONS

Off-Site Fabrication (OSF) has an important contribution to make in the continued development of the construction industry. There is a great interest, worldwide, in the pursuit of factory-built quality and environmentally responsible design. The realisation of these goals simultaneous with the achievement of an economic price and social benefit, represents the holistic ideal of sustainable housing design.

Substantial development work in the UK suggests that these ideals can be delivered in a low/medium rise context. Extension to the high-rise context has also been shown to be feasible, and concept designs have been developed and costed. An important barrier, however, to the further progress of these ideas is the capital investment required to complete the detailed designs and set-up a pilot production facility. This demand for investment is faced daily by the major manufacturers of consumer products (cars; white goods; electronic components; etc), but it is an alien concept to the construction industry. In relative terms, the capital at risk is small (a pilot factory, capable of producing some 10,000 modules per year, might cost 120M HK$. A car production facility might cost 50-100 times this amount!). Nevertheless, the risk is real and, without a step of faith, the first move will not be made.

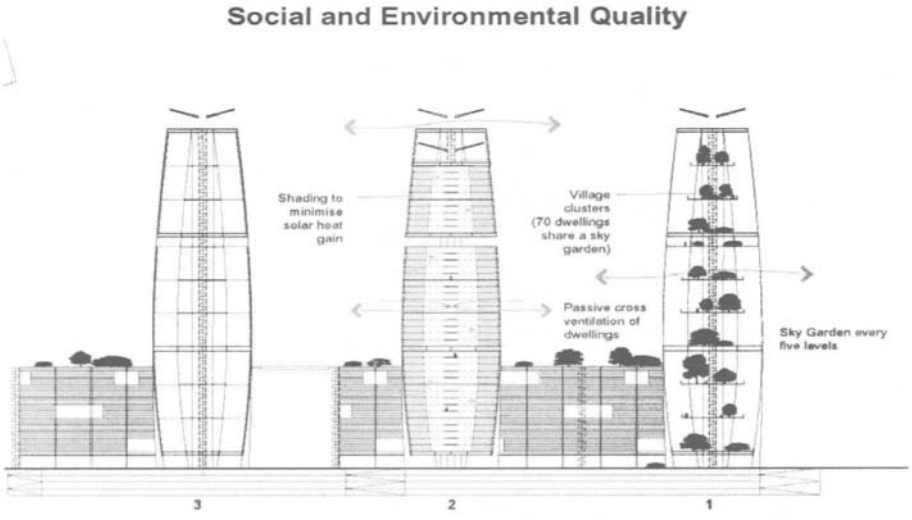
The benefits, if successful, are clear. What is less clear is whether the appetite of the industry is sufficient to make it take the risk and start the ball rolling.



(a)



(b)



(c)

The development of Sustainable Communities is addressed by this high-rise concept for Singapore ***(a)***, ***(b)***. *Dwellings are arranged in Village Clusters around Sky Gardens. Passive cross-ventilation, solar shading and roof-mounted P.V. arrays and water collectors all feature as part of the design concept* ***(c)***.

Fig 6 : Sustainable Housing for High Rise Communities

5. ACKNOWLEDGEMENTS

The authors gratefully acknowledge the visionary and definitive contributions of Paul Harbard and Dicken Robinson at Peabody Trust; and Roger Blundell and Roger McAnoy at Taylor Woodrow; in the development and realisation of the Meteor System prototypes and the detailed design of the factory.

6. REFERENCES

"The e-factor: Six Guiding Principles to Improving Sustainability in Housebuilding". The Housing Forum; 108-110 Judd St., London, WC1H 9NT. May 2000.

"Homing in on Excellence". The Housing Forum, 108-110 Judd Str., London, WC1H 9NT. March 2002.

This Page Intentionally Left Blank

Advances in Building Technology, Volume 2
M. Anson, J.M. Ko and E.S.S. Lam (Eds.)
© 2002 Elsevier Science Ltd. All rights reserved

RECENT RESEARCH ON STEEL-CONCRETE COMPOSITE SHELL ROOFS

J.G. Teng[1], H.T. Wong[1], Z.C. Wang[2], S.L. Dong[3]

[1]Department of Civil and Structural Engineering
The Hong Kong Polytechnic University, Hong Kong, China
[2] Research Centre of Spatial Structures, Shanghai Jiaotong University, Shanghai, China
[3] Department of Civil Engineering, Zhejiang University, Hangzhou, China

ABSTRACT

Steel-concrete composite shell roofs (Comshell roofs) are formed by pouring concrete on a thin stiffened steel base shell which serves as both the permanent formwork and the tensile steel reinforcement. The thin steel base shell, constructed by bolting together open-topped modular units consisting of a base plate with surrounding edge plates, is a steel shell with thin stiffeners in both directions. The new system retains all the benefits of thin concrete shells, but eliminates the need for temporary formwork and minimises the required falsework. Intensive research is currently being conducted by the authors on the behaviour and design of these composite shell roofs. This paper provides a description of this new structural system and a summary of current research on the various possible failure modes of this system.

KEYWORDS

Shells, Roofs, Concrete Shells, Bolted Steel Shells, Composite Construction, Modular Construction, Wet Concrete Loading, Buckling, Design

INTRODUCTION

Many thin concrete shells have been built around the world as large span roofs, but their use has gradually declined over the past few decades. This decline has been due mainly to the high cost of construction and removal of temporary formwork and associated falsework for concrete casting in the construction of a thin concrete shell. This labour intensive and costly process of construction, coupled with the increasing ease in analysing complex skeletal spatial structures offered by advances in computer technology, has made concrete shells much less competitive than they were a few decades ago.

Over the years, there have been several attempts aimed at eliminating the need for temporary formwork in constructing thin concrete shell roofs, but these have met with only limited success. An excellent review of these attempts and other developments of thin concrete shell roofs has been given by Medwadowski (1999) who concluded that forming "remains the great, unsolved problem of construction of concrete thin shell roofs. Any and all ideas should be explored, without prejudice." The latest development in the forming of thin concrete shell roofs is the Conshell roof system proposed by Teng (2001) which is believed to be a very promising solution to this difficult problem. In this paper, this new structural system

is first briefly introduced, followed by a summary of the intensive current research being conducted at The Hong Kong Polytechnic University in collaboration with Shanghai Jiaotong University and Zhejiang University.

THE COMSHELL SYSTEM

The Comshell roof is a steel-concrete composite shell roof formed by pouring concrete on a thin stiffened steel base shell which serves as both the permanent formwork and the tensile steel reinforcement. A brief description of the system is given here, but further details are available elsewhere (Teng, 2001).

The steel base shell is constructed by bolting together modular steel units in the form of an open-topped box consisting of a flat or slightly curved base plate surrounded by edge plates (Figure 1). By adopting different shapes for the base, different shell forms can be achieved but this paper is limited to cylindrical shell roofs only (Figure 2) as they are the easiest to construct by this modular approach.

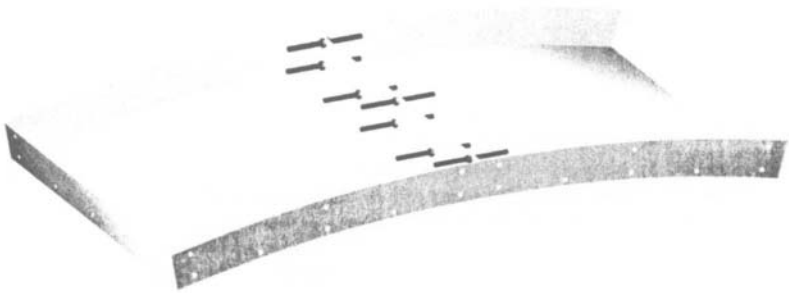


Figure 1: Modular units and bolted connection

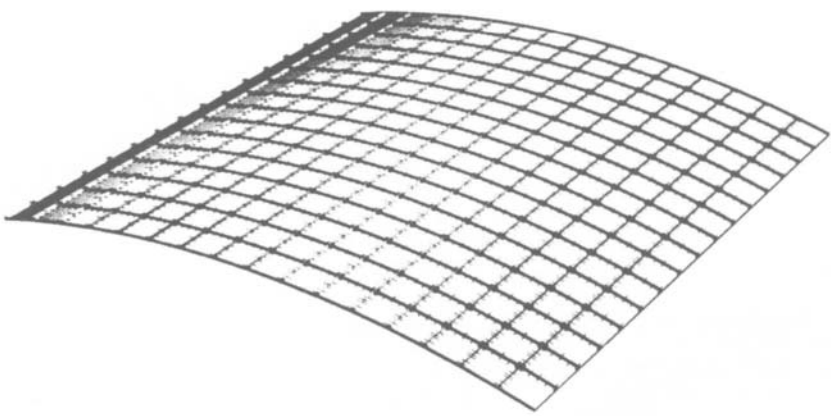


Figure 2: Steel base shell formed from modular units

The modular units for cylindrical shell roofs are made with two of the edge plates slightly inclined, so that when they are assembled using bolts, a curved profile of desired curvature results (Figures 1 and 2). Holes are drilled on the edge plates for bolt connections to adjacent units, and the bolted-together edge plates form stiffeners in both directions (Figure 2). The circular profile of the shell can be either approximated by flat bases, or exactly followed by slightly curved bases with all edge plates being perpendicular to the base. In fact, the base may be convex or concave, and slightly corrugated if required, for enhanced resistance to local buckling.

ADVANTAGES OF THE COMSHELL SYSTEM

The Comshell system has many advantages over existing roof systems, which has been fully discussed by Teng (2001) and is thus not repeated here. This modular approach of construction also has many advantages over a more conventional approach of composite construction in which the roof is constructed using large cold-formed thin curved sheets with corrugations running in one direction and with shear studs welded on before concrete casting. These include: (a) mass factory production of the units of a few standard sizes and curvatures is possible, and shells of desired spans and curvatures can be built easily; (b) transportation to and handling on site is easy, and units can be bolted together to form big panels (e.g. half-span arch panels) for lifting; (c) the steel shell so built has many thin stiffeners formed from edge plates, as a result its buckling resistance is greatly enhanced so shoring during construction will be substantially reduced; (d) the stiffeners can prevent wet concrete from flowing down the shell surface; (e) the stiffeners together with bolts act as shear connectors between the steel shell and the concrete, so additional welded shear connectors are unlikely to be required; and (f) the stiffeners can be used as spacers to ensure accurate positioning of reinforcing bars to resistant hogging moments.

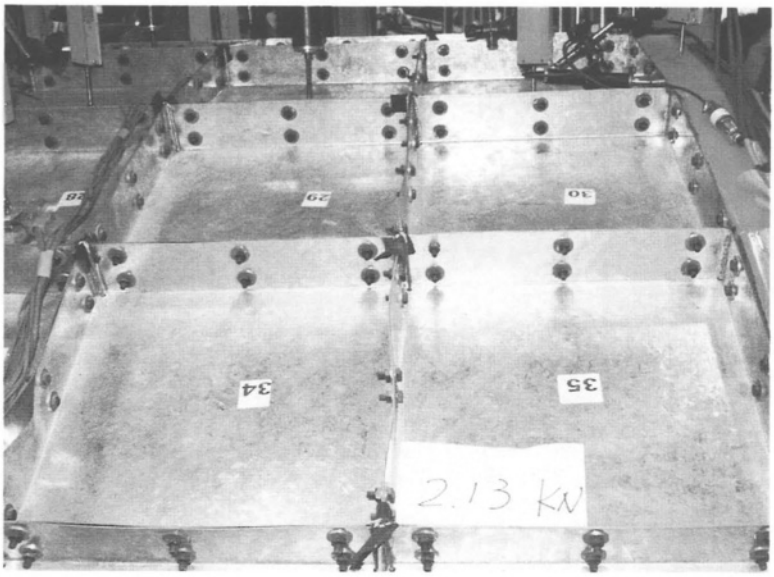
With the appropriate use of small corrugations when necessary, steel sheets of 1-2 mm in thickness are expected to be sufficient for the base plate of the modular unit to carry wet concrete loading without excessive deformations, stresses or local buckling. Due to this small thickness, the units can be press formed easily with precise geometric control. The units can be assembled into arch panels on ground before lifting, ensuring a tight control of the geometric shape of the assembled shell and limiting shoring requirement.

FAILURE MODES AND CURRENT RESEARCH

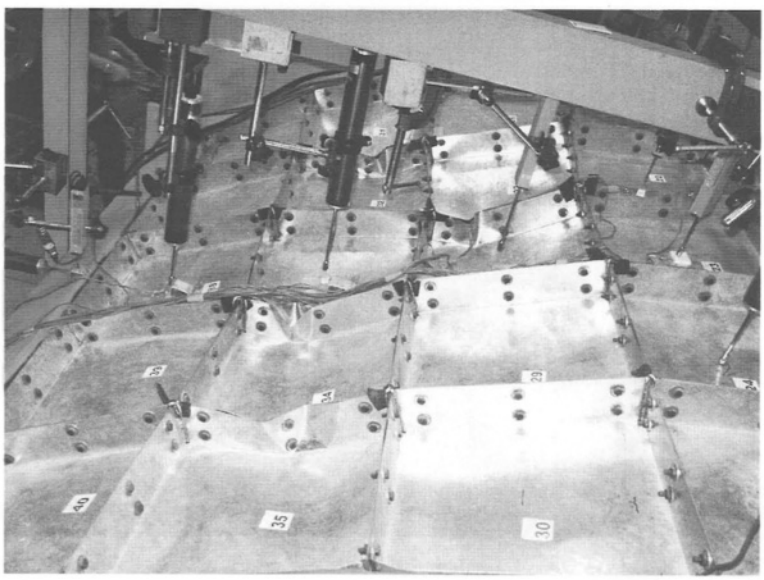
For the Comshell system to be widely used in practice, many issues have to be studied to establish a sound understanding of the behaviour and strength of these shells, and to develop suitable design methods. At the present, a number of failure modes have been identified, and each needs a great amount of research. These failure modes are associated with either the construction stage or the service stage and are currently being investigated at The Hong Kong Polytechnic University in collaboration with Shanghai Jiaotong University and Zhejiang University. These failure modes and associated current research are outlined below.

Construction Stage

During the construction stage, the wet concrete acts as loading on the bolted steel base shell which can fail by either local buckling or overall buckling. Local buckling is in one of two modes: buckling of the bolted stiffeners formed from edge plates and bucking of the base of the modular unit. Figure 3a shows the local buckling mode of stiffeners in a model steel base shell during laboratory experiment (plan size: 2 m x 2m). The particular geometry of this model shell dictated that local buckling occurred before overall buckling, nevertheless the model shell finally collapsed in an overall buckling mode after large post-local buckling deformations of the stiffeners (Figure 3b).



(a) Local buckling



(b) Overall buckling

Figure 3: Buckling modes of a steel base shell

The local buckling mode has a stable postbuckling path, so it does not signify the exhaustion of the load carrying capacity of the shell. Nevertheless, it can lead to excessive deformation which can impair the visual quality, serviceability and strength of the shell. The overall buckling mode leads to the collapse of the shell and is thus a more dangerous mode. Interaction between the two modes is likely to be significant, as local buckling can reduce the resistance of the shell to overall buckling. The sheeting thickness of the steel base shell and hence the economy of the entire system is controlled by these buckling modes. A number of possibilities exist to enhance these buckling loads without increasing the sheeting thickness, including the use of small corrugations for the base plates, the provision of stiffeners to the edge plates, and the casting of concrete in two stages (Teng 2001, 2002).

A program of tests on model steel base shells is currently underway where both the overall buckling mode and the local buckling mode are considered. A scaling problem exists in conducting buckling tests on small-scale models (e.g. using models of 2 m x 2m in base size to simulate real shells with a base size of 20 m x 20 m). Given that the main uncertainty in the behaviour of these bolted steel shells lies in the behaviour of the bolted joints, the purpose of these tests, which are both costly and time-consuming, is mainly to provide test data for the verification of a finite element model which can capture the behaviour of these joints. Once a reliable finite element model is established and verified, numerical analyses can be conducted for a wide range of shell geometries far beyond the confines of small-scale laboratory tests.

Service Stage

Once the shell has been constructed, the main loading on the structure is its self weight, snow loading, wind loading, and seismic loading if the shell is located in a seismically active area. The wind loading is uplifting, provided the shell is not a deep one, so in general, it is beneficial. Self weight, together with snow loading if the structure is located in a cold region, is probably the most important loading condition for a large span Comshell roof. Seismic loading is another important consideration.

The base plate is subject to complex distributions of membrane and bending stresses at the end of concrete casting. After the curing of concrete, the base plate is subject to additional stresses as a result of any additional loading such as snow loading and the removal of any shoring and the long term creep deformations of concrete. The base plate is biaxially stressed and is subject to one of the various combinations of compressive and tensile membrane stresses in addition to bending stresses. It should be noted that if the final stress state of the base plate is compressive in at least one direction, then unilateral buckling of the base plate is a likely failure model. Creep deformations of the concrete under self weight loading will not have the devastating consequence of changing the overall shape of the shell, as the steel base shell controls its overall shape, however they are still important as they will lead to redistribution of stresses between the steel shell and the concrete shell above it. A study of the unilateral buckling of the base plate will be carried out in the near future.

Overall buckling of Comshell roofs under gravity loading is probably the most important controlling failure mode for large spans. The strength in this failure mode is likely to be controlled by the bolted joints which are the weak links in bending resistance in the composite shell. Given the complexity of the buckling problem, the first step must be the development of a nonlinear finite element model and the experimental verification of such a model. The key to the success of such a finite element model lies in its ability to model the behaviour of the joints under combined axial force and bending. To this end, a series of tests have been carried out on slabs and arches with a bolted steel base featuring various types of connections. Figure 4 shows a steel base arch with long connection bolts. Figure 5 shows load defection curves of two composite arches, one (Arch A) constructed using the bolted steel base arch shown in Figure 4 and another constructed with a base arch in which very short connection bolts were employed. Although there is a small difference in the concrete properties of the two arches, the main difference between them lies in the connection bolts: one featured connections with long bolts which were anchored in the cast in-situ concrete and one with short bolts which thus did not have anchorage in the concrete. The strengths and load-deflection curves of the two arches are very different although the failure mode is similar (Figure 6). These tests illustrate the importance of connection details in determining the overall response of such composite arches.

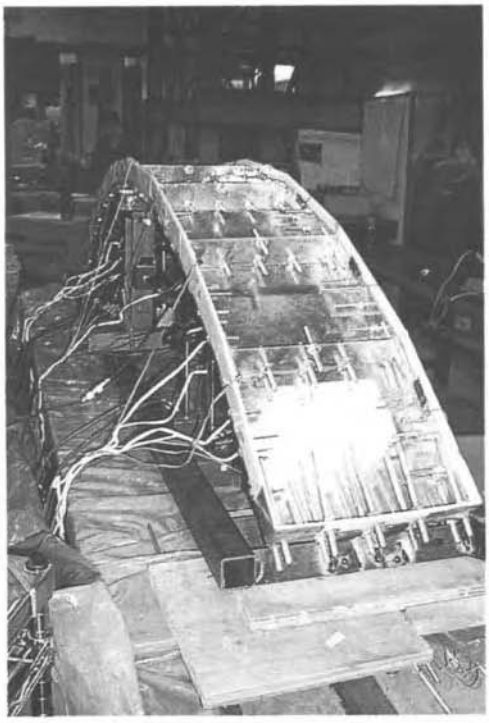


Figure 4: Steel base arch with long connection bolts

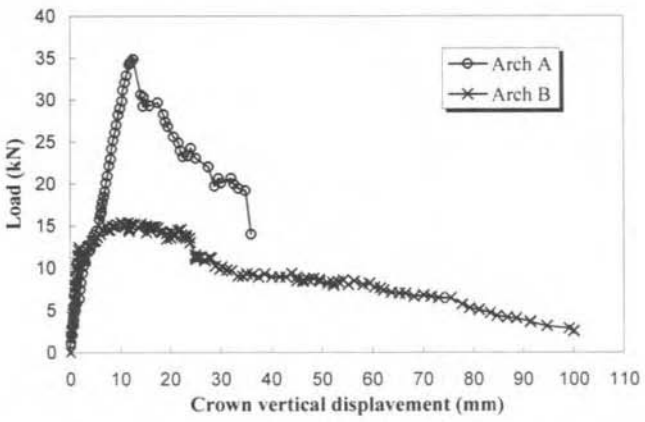


Figure 5: Load-deflection curves of two composite arches

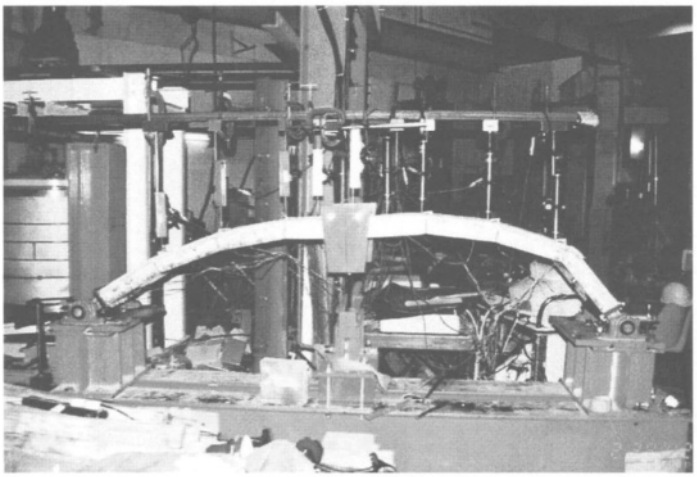


Figure 6: Failure mode of a composite arch

In addition to these arch tests, a series of tests on bolted composite joints has also been completed to study the behaviour and strength of these joints subject to eccentric loading. A method for the modelling of these joints is being developed, which will be compared with the test results. This method, after verification using the joint test data, will be applied to the prediction of the behaviour of the test arches. In the near future, a large-scale model Comshell roof will be built and tested at the Research Centre of Spatial Structures of Shanghai Jiaotong University, which will provide not only insight into the behaviour of the Comshell system, but also test data for the verification of a finite element model incorporating the simple joint modelling method currently under development. Once the finite element model is shown to predict the arch and model shell test results satisfactorily, it will be used to study the buckling behaviour of Comshells with full-scale dimensions.

CONCLUSIONS

This paper has presented an innovative structural system, namely steel-concrete composite shell roofs (Comshell roofs), for enclosing large spaces. These composite shells are formed by pouring concrete on a thin stiffened steel base shell which serves as both the permanent formwork and the tensile steel reinforcement. The thin steel shell, constructed by bolting together modular units consisting of a base plate with surrounding edge plates, is a steel shell with thin stiffeners in both directions. The structural design of this new system is controlled by a number of failure modes that may arise during either the construction or the service stage. These failure modes have been discussed in this paper. A summary of intensive current research has also been given. It is expected that by the end of this research program, the basic behavioural characteristics of the system will have been defined, and suitable numerical methods for analysing these shells established. Sufficient knowledge will also have been developed by then to enable the system to be applied in practice, although a great deal of further research will be required to establish a clear understanding of all major behavioural aspects, refine the construction process, and formulate simple design methods.

ACKNOWLEDGEMENTS

This work has been supported by the Research Grants Council of the Hong Kong Special Administrative Region, China (Project No: PolyU 5059/99E) with additional support provided through a research studentship for Mr. H.T. Wong. The authors are grateful for this support.

REFERENCES

Medwadowski, S.J. (1998). Concrete Thin Shell Roofs at the Turn of the Millennium. *Current and Emerging Technologies of Shell and Spatial Structures, Proceedings of an IASS Symposium*, April, pp. 9-22.

Teng J.G. (2001). Steel-Concrete Composite Shells for Enclosing Large Spaces. *Proceedings, International Conference on Steel and Composite Structures*, Pusan, Korea, 14-16 June, pp. 403-409.

Teng J.G. (2002). Steel-Concrete Composite Shells: a New Structural System for Enclosing Large Spaces. To be published.

Advances in Building Technology, Volume 2
M. Anson, J.M. Ko and E.S.S. Lam (Eds.)
© 2002 Elsevier Science Ltd. All rights reserved

EFFECT OF THE SHEAR WALL CUTOFF ON STOREY DRIFTS OF FRAME-SHEAR WALL STRUCTURES

Quanfeng Wang
Department of Civil Engineering, Huaqiao University, 362011 Quanzhou, Fujian, China.

ABSTRACT

In references (Wang et al 1999) and (Wang et al 2001), the seismic responses of frame-shear wall structures with shear wall cutoff have been studied and it is concluded that not all frame-shear wall structures need to extend their shear walls to the height of the entire structure. Continuing from references (Wang et al 1999) and (Wang et al 2001), in this paper the structures are to be analyzed using a member system-storey model under simulated earthquake excitations. The magnitude of interstorey drift is a key index to the amount of structural and nonstructural damage expected in a given storey. Therefore, the study is aimed at determining numerically the effect of shear wall cutoff on storey drifts in frame-shear wall. Contrasting the results to the result from the shaking table, it has an agreement with each other. Finally, a conclusion is given that terminating the wall at the midheight does not affect earthquake response detrimentally, if the shear wall is taller, the effect on the storey drifts is not significant.

KEYWORDS

Frame-shear wall structures, shear wall cutoff, member system-storey model, storey drift, simulated earthquake excitations.

INTRODUCTION

Reinforced concrete structural walls are frequently used to provide lateral stiffness for frame-shear wall buildings. Often the walls are interrupted to accommodate a large space for building function. Structural engineers have developed confidence in the design of buildings in which the distributions of weight and stiffness in the vertical direction are more or less uniform. The confidence is reasonably well founded, having been derived from numerous structures and research observations. To the best of our knowledge, there is no work described in the literature aimed at developing a simple method for the earthquake response of a frame-shear wall structure in which the shear wall does not continue up to the roof. Consequently, traditional analytical methods for frame-shear wall system need to be modified or new approaches need to be developed for the accurate assessment of the response of these structures subjected to static and dynamic loadings. In references [1] and [2], the seismic

responses of frame-shear wall structures with shear wall cutoff have been studied and it is concluded that not all frame-shear wall structures need to extend their shear walls to the height of entire structure. Continuing from references [1] and [2], this paper describes the structures analyzed using a member system-storey model under simulated earthquake excitations. Both structural and nonstructural damage sustained during earthquake ground motion are produced primarily by lateral displacement. Thus, adequate damage control can be achieved if lateral deformations are controlled by providing enough lateral stiffness. Drift resistance is a major factor in assessing whether a proposed structure is suitable for a tall building. The taller the building, the greater the need to mobilize all the structural interaction that can contribute to drift resistance. The magnitude of interstorey drift is a key index to the amount of structural and nonstructural damage expected in a given storey. Therefore, the study is aimed at determining numerically the effect of shear wall cutoff on storey drifts in frame-shear walls. The numerical analyses of the structures use the finite element technique with a base motion having peak base accelerations of 0.41g. Contrasting the results to these from a shaking table, these are in agreement with each other. The conclusion given is that terminating the wall at midheight does not affect the earthquake response detrimentally, and if the shear wall is taller than that, the effect on the storey drifts is not significant.

ANALYTICAL METHOD

Motion Equation

Consider a multi-degree-of freedom system excited by a generalized force, $Q^*(t)$, if the viscous damping theory and the Lagrange equation are used, the differential equation of motion is given by

$$[M]\{Y''\}+[C]\{Y'\}+[K]\{Y\}=[M]\{a_g(t)\} \tag{1}$$

in which *[M], [C]* and *[K]* is the mass; damping and stiffness matrices of the system, respectively; *{Y}, {Y'} and {Y''}* is the lateral displacement, velocity and acceleration vectors of the mass, respectively, and $\{a_g(t)\}$ is the ground acceleration vector.

The equation of motion of the (j)th mode in normal coordinates, η, may be written as (Argyris 1991)

$$\eta_j''+2\,\nu_j\omega_j\,\eta_j'+\omega_j^2\,\eta_j=Q_j^*(t) \tag{2}$$

in which ν_j, ω_j are the modal damping ratio and angular frequency of (j)th mode respectively, and

$$Q_j^*(t)=\int_0^H q(t,x)Y_j(x)\,dx \,/\, M_j^* \;;$$

$$M_j^*=\int_0^H m(x)Y_j^2(x)\,dx \;;$$

$q(t, x)$ is the random loading; $Yj\ (x)$ is the function of mode at the (j) th mode; $m(x)$ is the distributed density of the structural mass.

Solution of the Motion Equation

Numerical implementation would be necessary for complicated earthquake-like excitations. In modeling buildings for earthquake response analysis, the "shear beam model" has been used extensively. This simple method, however, is not always practical or accurate since it neglects important effects such as: (1) The flexure of structural system; (2) the interaction between adjacent stories, and various failure modes are not exhibited by the model. Alternatively, member-by-member analysis of frames is frequently used to model structures that exhibit elasto-plastic state of each member at any time due to earthquake excitations. However, there is an excessive number of degrees of freedom in the model. This paper uses an alternative procedure: member system-storey model (Clough 1972 and Muto 1979) that combines the advantages from "shear beam model" and member-by-member analysis of frames to estimate the earthquake responses of frame-shear wall structures with shear wall cutoff. The complete structure stiffness matrix is obtained from the individual frame and frame-shear wall stiffness matrices. The results to be presented later were obtained by numerically integrating Eq.2 using the Wilson - θ method. The time step was chosen to be 0.02 sec. and small enough to provide accurate results.

SEISMIC RESPONSES OF FRAME-SHEAR WALL STRUCTURES WITH SHEAR WALL CUTOFF

Here, the example is assumed to be similar to the test specimens in Moehle (1984), and makes it possible to compare, at least qualitatively, the finding from this study with the observations made in the experimental research. Four small-scale reinforced concrete test structures were constructed. These are identified by the designations FW9, FW4, FW1, and FW0. Each structure is assumed to consist of two identical parallel nine-storey, three-span frames and a central shear wall built parallel to the frames (Moehle 1984). Wall height varies for different structures as explained later on. The material properties are assumed to be the same as the measured values for the test specimen with the nine-storey structure. The concrete has a modulus of elasticity of 19,000 MPa. It is assumed the mass lumped at each level is 470 kg. Structure FW0 comprises the frame only. The structure FW9 includes two nine-storey, three-bay frames and a nine-storey prismatic wall. The other structures FW1 and FW4 are nominally identical to structure FW9 except that the wall extends only to the first and fourth floor levels respectively. Because of the continuity provided by the full height wall, structure FW9 can be considered to represent a building having a reasonably uniform distribution of stiffness over the entire height. In contrast, structures FW1 and FW4 have the wall cutoff at the first and fourth floor levels, respectively.

The Maximum Displacements

The structures are subjected to the first 10 seconds of the NS single horizontal component of the EI Centro recorded during the 1940 Imperial Valley Earthquake. The amount of viscous damping is fixed at 2% of critical value, which is thought to be representative of a concrete structure. The numerical analyses of the structures follow the finite element technique with a base motion having peak base accelerations of 0.39g, 0.34g, 0.41g and 0.32 g for FW0, FW1, FW4 and FW9, respectively. Computed displacement curves of the four structures are plotted

in Fig. 1. Structure FW0 behaves obviously with a typical shear deformation character. In contrast, structures FW1, FW4 and FW9 behave obviously with a typical shear-flexure deformation character corresponding to theoretical prediction. The maximum top-level displacements obtained by the experiments (Moehle1984) and by the analysis method proposed in this paper are summarized in Table 1. With respect to the maximum top-level displacements, the analytical results are in good agreement with the experimental results except for structure FW9, but are considered as an acceptable estimate. The correlation between the two methods suggests that the numerical method proposed in this paper is adequate for representing the dynamic response of the structures with shear wall cutoff.

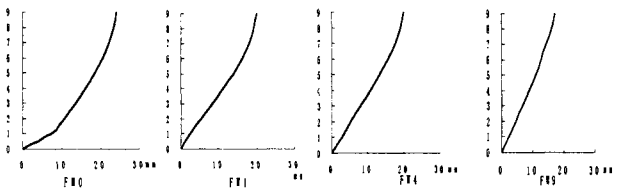


Figure 1: Computed displacements of the four structures

TABLE 1

THE MAXIMUM TOP-LEVEL DISPLACEMENTS (mm)

Structures	Measured d_m	Calculated d_c	d_c/d_m
FW0	26.3	24.2	0.92
FW1	22.4	20.2	0.90
FW4	23.2	20.1	0.87
FW9	26.1	17.1	0.66

The numerical analyses for the structures FW1, FW4 and FW9 use the same base motion having peak base accelerations of 0.41g, the resulting computed top-level displacements are as shown in Table 2. Comparison of the maximum top-displacement responses with simulated earthquake excitations (Table 2) does not show any significant variation between FW4 and FW9 under the strong earthquake but significant variation does exist between FW1 and FW9. What is clear, however, is that the shear wall should not be interrupted at the bottom of the structure. The values in parentheses in the table are ratios of quantities between the part height and the full height shear walls.

TABLE 2

EFFECT OF SHEAR WALL HEIGHT ON TOP-LEVEL DISPLACEMENTS (mm)

Structures	FW1	FW4	FW9
d_c	24.2 (1.18)	20.1 (0.98)	20.5

Storey Drifts

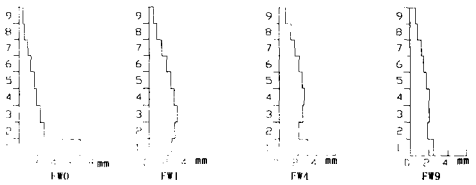


Figure 2: Computed storey drifts of the four structures

Distributions of computed storey drifts are plotted in Fig.2. For structure FW0, the discontinuity in the frame system in the first storey results in concentrations of interstorey drift and possible damage in that storey, interstorey drift in the first storey is many times that of the top-level drift. For structure FW9, the same irregularity as the frame FW0 is smoothed out by the shear wall that is continuous over the height of the structure. As a result, interstorey drifts for FW9 are nearly uniform over the full height. Structures FW1 and FW4 include shear walls to cover the first and fourth stories respectively, but a possible discontinuity is introduced at the locations of the wall cutoffs. Observed responses indicate that the larger drift is preset in the third storey for FW1. For the same shear wall cutoff in a different storey as in FW4, there is no apparent distress. Apparently, the location of the wall cutoffs affects the value of storey drift. It can be seen from Fig.2 that the drift shape of FW4 is almost the same as the drift shape of FW9 and the distributions of interstorey drifts for FW4 are more uniform over the entire height than for FW1. From Fig.2, it can also be seen that structures having the same stiffness cutoff, but occurring in different stories, do not perform equally. Using maximum drift as a criterion for comparison, terminating the wall at the midheight (as in FW4) does not affect response detrimentally. In contrast, terminating the same wall at a lower level of the structure FW1 results in behavior that is not significantly better than observed for the structure with no wall. It is means that a higher location of the wall cutoffs is better than a lower location for earthquake response. Drift distributions in FW4 do not reflect the apparent discontinuity in the lateral load resisting system. However, it should be noted that the drift at top level for FW4 is smaller than the drift for FW9 as shown in Fig.2. This means structure FW9 with the full height shear walls is subjected to more earthquake excitations than structure FW4. As mentioned above, the larger the stiffness of a structure, the more earthquake excitation (Wang 1991).

CONCLUSIONS

Four small-scale reinforced concrete frame-shear wall structures with and without shear wall cutoff, subjected to simulated earthquake excitations, have been studied and the analytical responses compared with experimentally measured responses. The study is aimed at determining analytically the effect of shear wall cutoff on storey drifts in the frame-shear wall structures with shear wall cutoff. Results from the shaking table are in agreement with the analytical results. Finally, it can be concluded that terminating a wall at midheight does not affect earthquake response detrimentally. If the shear wall is taller than that, the effect of the cutoff on the storey drifts is not significant. It is noted that these conclusions are based solely on the study reported in this paper, and further study of this topic is recommended.

References

Argyris, J.H. (1991). Dynamics of Structures, Elservier Science Publication Co., New York.

Beckett, R. and Hurt, J. (1967). Numerical Calculations and Algorithms, McGraw-Hill Book Co., New York.

Clough, R.W., & Bathe, K.J. (1972). Advances in Computational Methods in Structural Mechanics and Design: Finite Element Analysis of Dynamic Response, The University of Alabamain Huntsville.

Moehle, J.P. (1984). Seismic analysis of R/C frame-wall structures. Journal of Structural Engineering, ASCE, 1984, **110:11**, 2619- 2635.

Muto, K. (1979). Comments on Dynamic Design Procedure of Muto Institute and Newly Proposed Seismic Codes of Japan and U.S.A., Muto Inst. Structural Mechanics, Tokyo.

Wang, Quanfeng, Wang, Lingyun, and Liu, Qiansheng (1999). Seismic response of stepped frame-shear wall structures by using numerical method. Int. J., Computer Methods in Applied Mechanics & Engineering, **173:1-2**, 31-39.

Wang, Quanfeng, Wang, Lingyun, and Liu, Qiansheng (2001). Effect of shear wall height on earthquake response. Int. J., Engineering Structures, **23:4**, 376-384.

Wang, Quanfeng (1991). CAD for the member of shear wall in frame-shear wall tall building, Proceedings of Int. conference on Computational Engineering - Science, 1167-1169, ICES Publications, Melbourne, Australia.

CONSTRUCTION TECHNOLOGIES:

WIND ENGINEERING

This Page Intentionally Left Blank

Advances in Building Technology, Volume 2
M. Anson, J.M. Ko and E.S.S. Lam (Eds.)
© 2002 Elsevier Science Ltd. All rights reserved

HILBERT-HUANG TRANSFORM FOR DAMPING RATIO IDENTIFICATION OF STRUCTURES WITH CLOSELY SPACED MODES OF VIBRATION

J. Chen and Y. L. Xu
Department of Civil and Structural Engineering, The Hong Kong Polytechnic University
Hung Hom, Kowloon, HongKong

ABSTRACT:

This paper investigates the possibility of using the Hilbert-Huang transform method for modal damping ratios identification of the structure with closely spaced modal frequencies. A 2-story shear building under an impact excitation is studied for a wide range of dynamic properties from well-separated modal frequencies to very closely spaced modal frequencies. The damping ratio identification error by the HHT method as well as FFT method are compared with the theoretical value and then expressed as the function of normalized frequency space. The results show that the HHT method is superior to the FFT method in the identification of damping ratio of the structures with closely spaced modes of vibration. The HHT method seems to be a promising tool for parameter identification of linear structures.

KEYWORDS

System identification, closely spaced modal frequencies, modal damping ratio, the HHT method, the FFT method, random decrement technology

INTRODUCTION

The identification of damping ratios of a civil engineering structure is an important task toward the accurate dynamic response prediction and the reliable dynamic design of the structures. For a linear lightly-damped structure with well-separated modal frequencies, the Fast Fourier transform (FFT) method in conjunction with the bandwidth method are the most popular approach for identifying the modal damping ratios of the structure from the measured structural response time histories (Bendat and Piersol, 1993). This approach, however, may encounter difficulties when applied to structures with closely spaced modes of vibration.

Recently, a new data processing method named as Hilbert-Huang transform (HHT) has been proposed by Huang and his co-workers (1998), which consists mainly of empirical mode decomposition (EMD) and Hilbert transform (HT). Yang and Lei (1999, 2000) then successfully applied the HHT method to identify the modal parameters of linear structures based on the measured response data. They concluded that the HHT method offers a simple, effective and accurate tool for parametric

identification of linear structures. However, the example structures considered in their work are generally those with well-separated modal frequencies. The applicability of the HHT method to identify the structures with closely spaced modes of vibration has not been investigated yet.

Thus, the focus of this paper is to explore the possibility of using the HHT method to identify modal damping ratios of structure with closely spaced modes of vibration. The procedure suggested by Yang and Lei (1999) for modal damping ratio identification is adopted with some degrees of modification in respect of intermittency check. It is then applied to a 2-story building under impact load for a wide range of dynamic properties from well-separated modes of vibration to very closely spaced modes of vibration. The computed time-history of dynamic response of the system is first decomposed using the EMD with intermittency check to obtain the two modal free response time-histories of the system. The HT is then applied to each modal free response time history to estimate the natural frequency and modal damping ratio. The two modal damping ratios identified by the HHT method are finally expressed as the function of the function of the normalized frequency space and compared with those from the dynamic theory and those identified using the FFT method with the bandwidth method. These comparison show that the HHT method seems to be a promising tool for parameter identification of linear structures.

HHT FOR DAMPING RATIO IDENTIFICATION

Principle of HT for Parameters Identification of SDOF Structure

Application of Hilbert transform (HT) for modal parameters identification has been conducted for either linear or non-linear dynamic system (Feldman 1985, 1994; Hammond 1987). Considering a linear SDOF structure under the impulsive loading, for example, the impulse displacement response function of the structure is

$$v(t) = \begin{cases} 0, & t < 0 \\ A_0 e^{-\xi\omega_0 t} \sin \omega_d t, & t \geq 0 \end{cases} \tag{1}$$

where ω_0, ω_d =natural and damped circular frequency of the structure; ξ is the damping ratio; A_0 is a constant decided by the intensity of impulsive loading and the mass and frequency of the structure. To meet the requirement of applying the Hilbert transform, the impulse response function can be extended to the negative domain by considering its mirror image.

$$v(t) = A_0 e^{-\xi\omega_0|t|} \sin \omega_d t, \quad -\infty < t < \infty \tag{2}$$

The Hilbert transform of a real-valued function $y(t)$ in the range $-\infty < t < \infty$ is a real-valued function $\tilde{y}(t)$ defined by (Bendat and Piersol, 1986) as

$$\tilde{y}(t) = H[y(t)] = \frac{1}{\pi} P \int_{-\infty}^{\infty} \frac{y(s)}{(t-s)} ds \tag{3}$$

where H denotes the Hilbert transform operator, P indicates Cauchy principal value. An analytic signal $Y(t)$ associated with $y(t)$ can then be defined as follows. An analytic signal means a signal having no negative frequency components with Fourier transform.

$$Y(t) = y(t) + i\tilde{y}(t) = A(t)e^{i\theta(t)} \tag{4}$$

$$A(t) = [y^2(t) + \tilde{y}^2(t)]^{1/2} \qquad \theta(t) = \tan^{-1}\left[\frac{\tilde{y}(t)}{y(t)}\right] \tag{5}$$

where $A(t)$ and $\theta(t)$ are defined as the amplitude and instantaneous phase angle of $y(t)$, respectively; and i is the imaginary unit. The instantaneous frequency $\omega(t)$ is then given by

$$\omega(t) = d\theta(t)/dt \tag{6}$$

Similarly, the corresponding analytic signal $z(t)$ for $v(t)$ of Eq. (2) can be obtained using Eq. (4) as

$$z(t) = v(t) + i\tilde{v}(t) = A(t)e^{-i\theta(t)} \tag{7}$$

For special case that ξ is small and ω_0 is fairly large, the amplitude $A(t)$ and the phase angle $\theta(t)$ for the SDOF system can be obtained as follows (Yang and Lei, 1999).

$$A(t) = A_0 e^{-\xi\omega_0 t} \tag{8}$$

$$\theta(t) = \omega_d t - \pi/2 \tag{9}$$

By introducing the logarithmic and differential operators to Eqs. (8) and (9) respectively, one obtains

$$\ln A(t) = -\xi\omega_0 t + \ln A_0 \tag{10}$$

$$\omega(t) = \frac{d\theta(t)}{dt} = \omega_d \tag{11}$$

Clearly, the damped natural circular frequency ω_d can be identified from the slope of instantaneous phase function $\theta(t)$. With the identified ω_d and the slope $-\xi\omega_0$ of the straight line of the decaying amplitude $A(t)$ in a semi-logarithmic scale, the damping ratio ξ can be identified from the function $\omega_d = \omega_0\sqrt{1-\xi^2}$. Considering that the instantaneous frequency may fluctuate around its mean value due to the amplitude variation of the signal (Huang, 1998) and that the requirement of small damping ratio may limit the application of the HT method, Yang and Lei (1999) suggested to determine the slope ω_d of the phase function $\theta(t)$ and the slope $-\xi\omega_0$ by applying the linear least-square fit technique to the linear function represented by Eq. (9) and Eq. (10).

Damping Ratio Identification Using HHT for MDOF Structure

For a linear MDOF system, its dynamic displacement response $v(t)$ caused by the external excitation $\boldsymbol{P}(t)$ can be expressed as the superposition of modal displacement responses.

$$v(t) = \sum_{j=1}^{N} v_j(t) = \sum_{j=1}^{N} \boldsymbol{\Phi}_j Y_j(t) \tag{12}$$

where N is the number of modes of vibration involved; $v_j(t)$ is the jth modal displacement response vector; $\boldsymbol{\Phi}_j$ is the jth mode shape; and $Y_j(t)$ is the jth modal response which can be computed from the following uncoupled modal equation.

$$\ddot{Y}_j(t) + 2\xi_j\omega_j\dot{Y}_j(t) + \omega_j^2 Y_j(t) = P_j(t)/M_j, \quad j = 1,2,...N \tag{13}$$

where ξ_j and ω_j are the jth modal damping ratio and natural circular frequency, respectively; and $P_j(t)$ and M_j are the jth modal force and modal mass, respectively.

It is seen from Eq. 12 that measured dynamic response time history of a MDOF consists of contributions from different vibration modes. Thus, directly application of the above mentioned identification procedure to MDOF structure can cause ambiguous meaning of instantaneous frequency as defined in Eq. (11). In general, band-pass filtering technology is necessary for the measured response in order to obtain a monocomponent signal that suitable for HT identification. Unfortunately, this filtering procedure may fail especially for structures with closely spaced modes of vibration (Staszewski, 1998). The EMD method is thus introduced to deal with this problem.

The empirical mode decomposition (EMD) is the key part of HHT method, which can decompose a complex signal into a series of intrinsic mode functions (IMF). This decomposition is based on the direct extraction of the energy associated with various intrinsic time scales of the time history itself (see detail in Huang et al, 1998). After EMD decomposition, the analyzed signal, e.g. $x(t)$ is finally expressed as the sum of the IMFs plus a final residue.

$$x(t) = \sum_{j=1}^{N} c_j(t) + r(t)_N \tag{14}$$

where N is the number of IMF components; and r_N is the final residue. An intrinsic mode function satisfies the following two conditions: (1) within the data range, the number of extrema and the number of zero-crossings are equal or differ by one only; and (2) the envelop defined by the local maxima and the envelop defined by the local minima are symmetric with respect to the mean.

Typically, different IMF has different time scale and the first IMF has the finest scale. However, when the analyzed data contain intermittency, directly application of EMD decomposition may cause mode mixing, which means that different time scales are contained in one IMF. Huang et al. (1999) then suggested a criterion called intermittency check to avoid mode mixing. The criterion works by specifying a cutting frequency ω_c for each IMF during EMD decomposition. Data having frequencies lower than ω_c will be removed from the resulting IMF.

It is pointed out by Huang et al. (1998) that the definition of instantaneous frequency for a signal has physical significance if it is an IMF. Thus we can use the EMD method to decompose the measured response of a MDOF structure into sum of IMF that admits well-behaved Hilbert transform. Therefore, the HHT method can be applied to identify ξ_j and ω_j ($j = 1, \cdots, N$) of a MDOF structure from the measured response time histories of the system under impulsive loading. The measured response time history is first decomposed into the IMFs using EMD method with intermittency check to obtain modal response time histories. The cutting frequencies used in EMD decomposition are determined from the power spectrum of the measured response time history. Then, for each of identified modal response time histories, the HT identification procedure for a SDOF system can be applied to identify the modal parameters ξ_j and ω_j.

NUMERICAL RESULTS

To explore the possibility of applying the aforementioned HHT method to identify the modal damping ratios of a structure with closely spaced modal frequencies, a 2-story shear building under an impulsive loading is studied for a wide range of dynamic properties from well-separated modal frequencies to very closely spaced modal frequencies. The equation of motion of the building can be expressed as follows:

$$\begin{bmatrix} m_1 & 0 \\ 0 & m_2 \end{bmatrix} \begin{Bmatrix} \ddot{x}_1 \\ \ddot{x}_2 \end{Bmatrix} + (a \begin{bmatrix} m_1 & 0 \\ 0 & m_2 \end{bmatrix} + b \begin{bmatrix} k_1 + k_2 & -k_2 \\ -k_2 & k_2 \end{bmatrix}) \begin{Bmatrix} \dot{x}_1 \\ \dot{x}_2 \end{Bmatrix} + \begin{bmatrix} k_1 + k_2 & -k_2 \\ -k_2 & k_2 \end{bmatrix} \begin{Bmatrix} x_1 \\ x_2 \end{Bmatrix} = \begin{Bmatrix} 0 \\ \delta(t) \end{Bmatrix} \tag{15}$$

where m_1 and m_2 are the two masses; k_1 and k_2 are the two stiffness coefficients; $\delta(t)$ is the impulsive load; it is equal to 1 when t=0 and equal to zero when $t \neq 0$; and the damping factors a and b are so decided that the two modal damping ratios are the same, which is

$$a = \frac{2 f_1 f_2}{f_1 + f_2} \xi \qquad b = \frac{2}{f_1 + f_2} \xi \tag{16}$$

Three typical levels of modal damping ratio of ξ=1%, 3% and 5% are considered in this investigation to see the effects of modal damping ratio on the applicability of the HHT method.

By changing the structural parameters m_1, k_1, m_2 and k_2 of the system, the difference (space) between the two natural frequencies are altered. To present a measure of the space (difference) between the two undamped natural frequencies f_1 and f_2, a space index (MSC NASTRAN, 1983) is adopted here.

$$\gamma = (f_2 - f_1)/(f_2 + f_1) \tag{17}$$

The index γ varies in a [0,1] range; a large value corresponds to well-separated modes of vibration while a small value denotes closely spaced modes of vibration. The maximum index considered in this application is 0.75 with f_1=1.10Hz and f_2=7.71, and the minimum index is 0.046 with f_1=3.39Hz and f_2=3.72Hz. The space index less than 0.046 is hardly achieved for the 2DOF structure investigated.

Fig.1 and Fig2 show the acceleration response time history of mass1 and its power spectrum for the case of structure with well-separated modal frequencies. In this case, the structural parameters are m_1=1 kg, m_2=2 kg, k_1=2256 N/m, and k_2=250 N/m. The two undamped natural frequencies are f_1=1.68Hz and f_2=7.99Hz with a corresponding space index of 0.66. The first two modal damping ratios are set as 5% using Eq. (16). From the power spectrum, the two natural frequencies and modal damping ratios can be easily identified using the FFT method in conjunction with the bandwidth method. The results are listed in Table 1. To identify the modal damping ratios of the system using the HHT method, the EMD method with the intermittency check is applied to the acceleration response time history of mass 1 with the cutting frequency of 4.39 Hz, which is the trough between two peaks of the spectrum. Since it is a 2DOF system, only one cutting frequency for the first IMF component is designed in the implementation of intermittency check during the EMD. A total of 5 IMF components are obtained by EMD. The first and second IMF components are plotted in Fig.3 and 4, respectively, together with the theoretical second and first modal responses of mass 1 of the system correspondingly.

It can be seen from Fig. 3 and Fig. 4 that the first IMF and second IMF component are nearly the same as the second and first modal response of mass 1 of the structure. Then, by applying the Hilbert transform to the first two IMF components, the instantaneous phase angle and amplitude of each IMF component can be obtained as the function of time. Shown in Fig. 5 and 6 are the instantaneous phase angle and amplitude of the first IMF component together with the fit lines using the linear least-square fit technique. The modal damping ratio and natural frequencies can then be identified from the slopes of the two fit lines, and the results are listed in Table 1. It is seen from Table 1 that the modal damping ratios identified by the FFT method are slightly smaller than the theoretical values, but the modal damping ratios identified by the HHT method are very close to the theoretical values.

TABLE 1 2-STORY STRUCTURE WITH WELL-SEPARATED MODAL FREQUENCIES

	Damped Frequency (Hz)			Damping ratio		
	Theoretical Value	FFT	HHT	Theoretical Value	Bandwidth Method	HHT
First Mode	1.68	1.71	1.68	5%	4.62%	5.02%
Second Mode	7.98	7.99	7.99	5%	4.81%	5.01%

For the case of structures with very closely spaced modes of vibration, acceleration response time history of mass 2 of the structure and its power spectrum are shown in Fig. 7 and Fig.8. Here, the structural parameters are selected as m_1=11.6 kg, m_2=0.1kg, k_1=3256 N/m, and k_2=30N/m. The two modal damping ratios are set as 5%. The two undamped natural frequencies are computed as f_1=2.58Hz and f_2=2.85Hz giving a space index of 0.050. It is seen from Fig. 8 that there are two peaks corresponding to the two damped natural frequencies. However, these two peaks are too close to each other to identify the two modal damping ratios using the bandwidth method. Thus, the HHT method is applied to the acceleration response time history of mass 2 to identify the modal damping ratios. The used cutting frequency in the EMD is 2.68 Hz. A total of 6 IMF components are obtained, the first and second IMF components are plotted in Figs. 9 and 10, respectively, together with the second and first modal responses of mass 2. It is seen that due to the closely spaced modes of vibration, the first two IMF components deviate from the theoretical modal responses to some extents. The instantaneous phase angles and amplitudes obtained by the HHT method and their linear least-square fits are shown in Figs 11 and 12 for the first IMF component. The identified natural frequencies and

modal damping ratios by the HHT method are listed in Table 2 together with the theoretical values. It is seen that the natural frequencies identified by the HHT method and the FFT method are quite close to the theoretical values. The two modal damping ratios identified by the HHT method are larger than the theoretical values but less than 10%. The FFT method together with the bandwidth method, however, fails to identify the modal damping ratios.

TABLE 2 2DOF SYSTEM WITH VERY CLOSELY SPACED MODAL FREQUENCIES

	Damped Frequency (Hz)			Damping ratio		
	Theoretical Value	FFT	HHT	Theoretical Value	Bandwidth method	HHT
First Mode	2.58	2.56	2.54	5%	-----	5.48%
Second Mode	2.85	2.87	2.83	5%	-----	5.36%

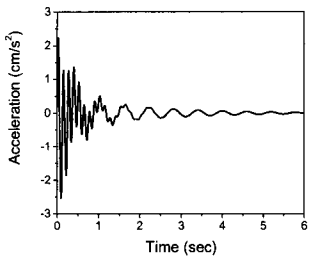


Fig. 1 Acceleration time history for well-separated modes of vibration

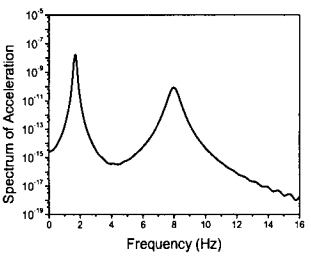


Fig. 2 Power spectrum for the time history shown in Fig.1

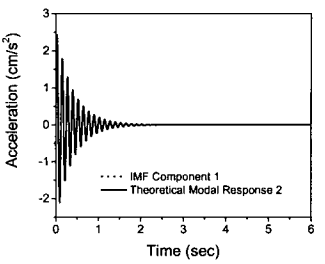


Fig. 3 The First IMF component and the second modal response (well-separated mode)

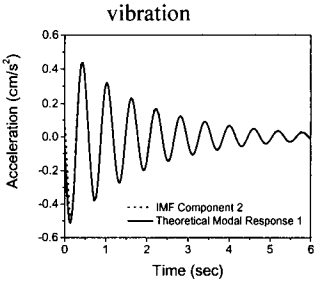


Fig.4 The second IMF component and the first modal response (close spaced mode)

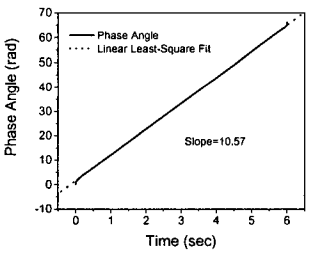


Fig.5 Phase angle and linear least-square fit (well-separated mode)

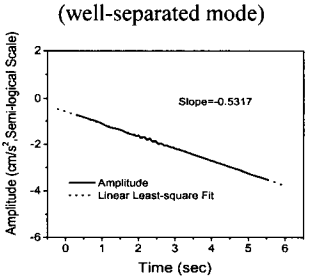


Fig. 6 Amplitude and linear least-square fit (well-separated mode)

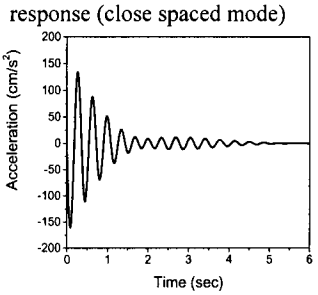


Fig. 7 Acceleration time history for close-spaced modes of vibration

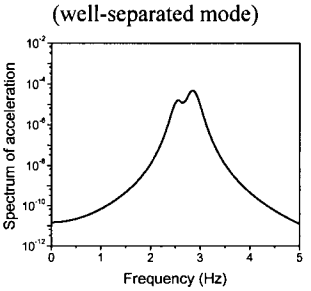


Fig. 8 Power spectrum for the time history shown in Fig.7

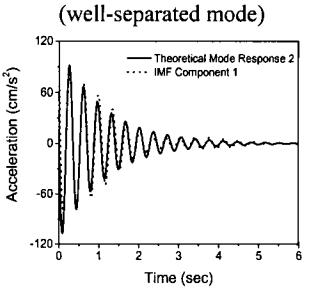


Fig. 9 The First IMF component and the second modal response (well-separated mode)

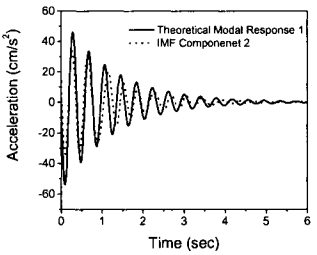


Fig.10 The second IMF component and the first modal response (close spaced mode)

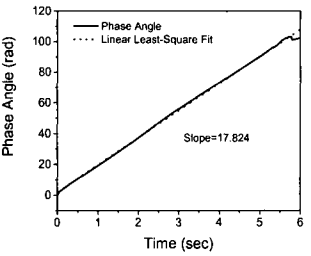


Fig.11 Phase angle and linear least-square fit (close spaced mode)

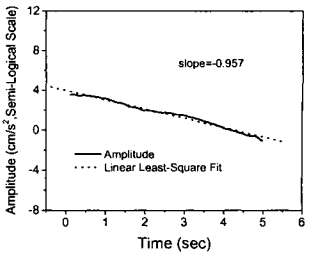
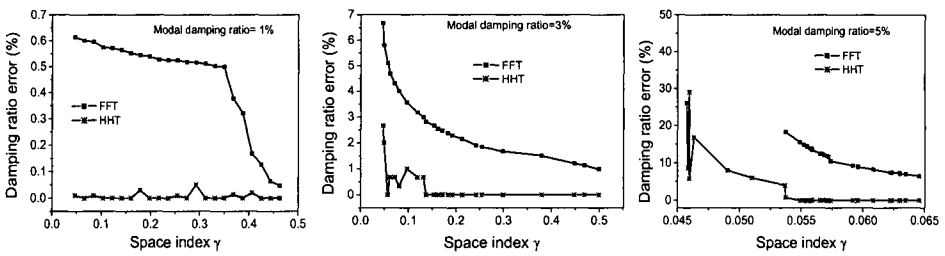


Fig. 12 Amplitude and linear least-square fit (close spaced mode)

To examine further the applicability of the HHT method for the identification of modal damping ratios, the identified results of the first modal damping ratio using both HHT method and FFT method are shown, in terms of the relative damping ratio error against the space index, in Figs.13a, 13b, and 13c for the cases of the theoretical modal damping ratio of 1%, 3% and 5%, respectively. The relative damping ratio error is defined as the ratio of the absolute value of the difference between the identified damping ratio and the theoretical value to the theoretical value.

It is seen that for the case of 1% modal damping ratio, the modal damping ratio identified by the HHT method is almost the same as the theoretical value and independent of the space index. The relative damping ratio error caused by the FFT method, however, increases with the decrease of space index but the relative error is smaller than 0.7%. For the case of 3% modal damping ratio, the modal damping ratio identified by the HHT method is almost the same as the theoretical value if the space index is less than 0.13. Then, with the decrease of space index, the relative error increases but it is less than 3% within the concerned range. The deviation of the modal damping ratio identified by the FFT method increases with the decrease of space index but the maximum error in the concerned space index range is less than 7%. For the case of 5% modal damping ratio, the FFT method with the bandwidth method fails to identify the modal damping ratio when the space index γ becomes less than 0.053 but the HHT method is still workable. Though the relative damping ratio error becomes large for the case of 5% modal damping ratio, it is less than 10% when γ is larger than 0.05 when using the HHT method. The HHT method seems more robust than the FFT method for different levels of structural damping. The results clearly demonstrate that the HHT method is superior to the FFT method in the identification of modal damping ratios of the structure with closely spaced modes of vibration.



(a) $\xi = 1\%$ (b) $\xi = 3\%$ (c) $\xi = 5\%$

Fig. 13 Variation of damping ratio error with space index

CONCLUDING REMARKS

This paper investigates the identification of modal damping ratio using Hilbert-Huang transform with emphasis on the structures with closely spaced modes of vibration. Application of the HHT method for damping ratio identification of a 2-DOF structure under impact load has been conducted for a wide range of dynamic properties from well-separated modal frequencies to very closely spaced modal frequencies. The identified results are compared with that obtained by FFT method, showing clearly that the HHT method is superior to the FFT method in the identification of damping ratio of the structures with closely spaced modes of vibration. The HHT method performing in the frequency-time domain seems to be a promising tool for system identification of linear structures. Further works are needed to investigate its practical application for noise-included measurements.

ACKNOWLEDGMENTS

The writers are grateful for the financial support from the Hong Kong Polytechnic University through its Area of Strategic Development Programme in Structural Health Monitoring and Damage Detection to the second writer. The authors would like to thank Dr. Ray R. Zhang of Colorado School of Mines for his valuable discussion and suggestions.

REFERENCES

Bendat J.S. and Piersol, A.G. (1986), "Random Data: Analysis and Measurement Procedures", 2nd Edition, John Wiley & Sons, NY.

Bendat J.S. and Piersol, A.G. (1993), "Engineering Applications and Correlation and Spectral Analysis""2n^{d} Edition, John Wiley & Sons, NY.

Cohen, L., (1995), Time-frequency analysis, Engelwood Cliffs., NJ: Prentice-Hall.

Feldman M. (1985), "Investigation of the natural vibrations of machine elements using the Hilbert transform", Soviet Machine Science, 2, 44-47.

Feldman M.(1994), "Non-linear system vibration analysis using the Hilbert transform—I. Free vibration analysis method 'FREEVIB'", Mech. Syst. Signal Process. 8, 309-18.

Hammond J. K. and Davis P. (1987), "The use of envelope and instantaneous phase methods for the response of oscillatory non-linear systems to transients". Proc. of the 5th IMAC, London, 1460-1466.

Huang, N.E., Shen Z., Long S. R., Wu M. J. C., Shih H. H., Zheng Q. No., Yen N. C., Tung C. C., and Liu H. H. (1998), "The Empirical mode decomposition and the Hilbert spectrum for nonlinear and non-stationary time series analysis", Proc. R. Soc. Lond. A, Vol. 454, pp. 903-995.

Huang, N. E., Shen, Z. and Long, S.R. (1999), "A new view of nonlinear water waves: the Hilbert spectrum", Annu. Rev. Fluid Mech., 31:417-457.

MSC/NASTRAN (1983), "User's Manual", Macnal-Schwendler Corp.

Staszewski, W. J., (1998), Identification of non-linear systems using multi-scale ridges and skeletons of the wavelet transform, J. of Sound and Vibration, 214(4), 639-658

Yang J. N. and Lei Y. (1999), "Identification of natural frequencies and damping ratios of linear structures via Hilbert transform and empirical mode decomposition", Proc. of Int. Conf. on Intelligent Systems and Control, IASTED/Acta Press, Anaheim, CA, 310-315.

Yang J. N. and Lei Y. (2000), "System identification of linear structures using Hilbert transform and empirical mode decomposition", Proc. of 18th Int. Modal Analy. Conf.: A Conference on Structural Dynamics, San Antonio, TX, Society for Experimental Mechanics, Inc., Bethel, CT, Vol.1, 213-219.

Advances in Building Technology, Volume 2
M. Anson, J.M. Ko and E.S.S. Lam (Eds.)
© 2002 Elsevier Science Ltd. All rights reserved

APPLICATION OF HHT METHOD TO SYSTEM IDENTIFICATION OF DI WANG BUILDING DURING TYPHOON YORK

S.W. Chen[1,2], Y.L. Xu[1], R.C. Zhang[3] and G.Q. Li[2]

[1]Department of Civil and Structural Engineering, The Hong Kong Polytechnic University, Hung Hom, Kowloon, Hong Kong
[2]Department of Building and Structural Engineering, Tongji University, Shanghai, China
[3]Division of Engineering, Colorado School of Mines, Golden, Colorado, USA

ABSTRACT

The wind and structural monitoring system installed in the Di Wang Building timely recorded wind and structural response data during Typhoon York in September 1999. The newly emerged Hilbert-Huang transform (HHT) method together with the random decrement technique (RDT) is applied in this paper to the measured data to identify dynamic characteristics of the building. A series of natural frequencies and modal damping ratios of the building under different wind speeds in different directions are identified and compared with those from the fast Fourier transform (FFT)-based method. The results show that the natural frequencies identified by the HHT method and the FFT method are almost the same, but the modal damping ratios identified by the two methods are different to some extent. The results also show that the total modal damping ratios increase with increasing wind speed and vibration amplitude but the situation is reversed for the natural frequency.

KEYWORDS: Di Wang Building, system identification, HHT, RDT, FFT method, comparison

INTRODUCTION

For tall buildings, the most popular approach for identifying natural frequency and modal damping ratio is to carry out ambient vibration measurement and then apply the fast Fourier transform (FFT)-based method to the measured building response time histories. However, this method often overestimates modal damping ratios due to bias errors involved in the spectral analysis (Litter and Ellis, 1995) though it can identify natural frequencies quite accurately. This approach will become more questionable to identify the modal damping ratios when the building response is non-stationary. The random decrement technique (RDT) may be an alternative to identify building modal damping ratios (Tamura 1996) but the same constraints on the data source (stationary, well separated modes of vibration) make it difficult to use effectively (Jeary, 1986).

Recently, Huang and his co-workers (1998) proposed the Hilbert-Huang transform (HHT) method, which consist of mainly the empirical mode decomposition (EMD) and the Hilbert transform (HT). The most powerful feature of the HHT method is capable of analyzing nonlinear and non-stationary time histories in the frequency-time domain. Yang and Lei (1999, 2000) successfully applied the HHT method together with the random decrement technique (RDT) to identify the modal parameters of linear

structures. They concluded that the HHT method offers a simple, effective and accurate tool for parametric identification of linear structures. However, this approach has not been examined yet using the field measurement data of real tall buildings under strong winds.

This paper thus applies the HHT method to the field measurement data of the Di Wang Building during Typhoon York to identify the dynamic characteristics of the building. The natural frequencies and modal damping ratios identified by the HHT method are then compared with those obtained by the FFT-based method to evaluate the applicability and superiority of the HHT method. The changes of natural frequencies and damping ratios with wind speed and building vibration amplitude are also investigated.

WIND AND STRUCTURAL RESPONSE DATA

The Di Wang Building, located in the downtown Shenzhen City of China, is one of the tallest composite buildings in the world. The height of the main structure is 310m and the width and depth of the building are 70 m and 37m respectively. On 16 September 1999, Typhoon York, which is the strongest typhoon since 1983 and the typhoon of longest duration on record, attacked Hong Kong and Shenzhen. The wind and structural monitoring system installed in Di Wang Building timely recorded both wind and structural response data. The detailed information on the Di Wang Building, Typhoon York and the monitoring system can be found in Xu and Zhan (2001).

The recorded time histories of 38 hours duration starting from 17:20 HKT, 15 September 1999 to 8:20HKT, 17 September 1999 are used for analysis in this paper. From the recorded wind speed and direction data at a height of 348m, it is found that the wind direction changes from the north-east to the south-west in clockwise and then remains almost constant. The high mean wind speeds occur during the transition period of wind direction, 4:00 to 19:00 on September 16. The maximum hourly mean wind speed is 33.80 m/s, which occurs between 6:00 to 7:00 HKT on September 16.

By averaging the signals from the north and south lateral displacement transducers, one may have the averaged lateral dynamic displacement response of the building with respect to its shear center, for these two transducers are symmetrically installed to the lateral axis on the 69th floor. The torsional dynamic displacement response can be obtained as the difference of the two lateral displacement responses divided by the distance between the two transducers. The longitudinal displacement response is taken directly from the channel installed on the longitudinal axis. The lateral, longitudinal, and torsional acceleration responses can be obtained n a similar way. Figs. 1 shows the lateral acceleration response time history of one hour duration from 16:00 to 17:00 HKT on 16 September 1999.

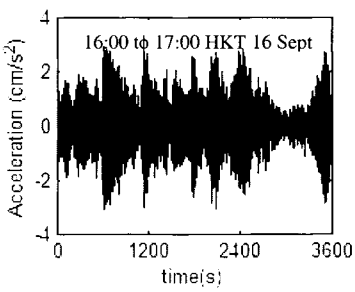


Fig. 1 Lateral Acceleration Response Time History

THE HHT METHOD FOR MODAL IDENTIFICATION

The Hilbert-Huang transform (HHT) method was proposed by Huang et.al. (1998). The basic procedure of using the HHT method to identify the natural frequencies and modal damping ratios from the measured response time histories can be followed in three steps. The measured structural response time history is first decomposed into the intrinsic mode functions (IMFs) using the empirical mode decomposition (EMD) method with the intermittency check to obtain modal response. The random decrement technique (RDT) is then applied to each of the modal response to extract the free modal response. Finally, the Hilbert transform (HT) is applied to each of the free modal response time histories to obtain the corresponding natural frequency and modal damping ratio.

Empirical Mode Decomposition (EMD)

By applying the EMD method, a complicated time history can be decomposed into a series of IMFs, $c_j(t)$, that admit well-behaved Hilbert transforms. The original time history $x(t)$ can be then expressed as the sum of the IMFs plus the final residue,

$$x(t) = \sum_{j=1}^{N} c_j(t) + r(t)_N \tag{1}$$

where N is the number of IMFs; and r_N is the final residue.

To avoid the mode mixing during the sifting process, a criterion was suggested by Huang et al. (1999) to separate the waves of different periods into different modes based on the modal frequencies. This criterion is named as the intermittency check, decided by the lower limit of the frequency ω_c that will be included in any given IMF component. The intermittency check, however, should be applied with care, for any additional criterion introduced in the sifting process implies an intervention with a subjective condition.

Random Decrement Technique(RDT)

When applying the random decrement technique (RDT) to each of the modal response time histories (Ibrahim, 1977), a threshold level should be selected to obtain N segments. The j^{th} free modal response $\ddot{x}_j^f(t)$ can be then obtained from the ensemble average of all segments as

$$\ddot{x}_j^f(i\Delta t) = \frac{1}{N}\sum_{k=1}^{N} \ddot{x}_j^t(t_k + i\Delta t); \quad i = 1,2,...,m \tag{2}$$

where $\ddot{x}_j^t(t)$ is the j^{th} modal response; t_k is the starting time for each segment; and $m\Delta t = t$ with t being the duration of each segment.

Hilbert Transform

The Hilbert transform (HT) has long been used to study linear and nonlinear dynamic systems and to identify their modal parameters in the frequency-time domain (Feldman 1985, 1994; Hammond 1987). The Hilbert transform of a real-valued function $v(t)$ in the range $-\infty < t < \infty$ is a real-valued function $\tilde{v}(t)$. By applying the HT method, the analytical signal $z(t)$ for $v(t)$ can thus be obtained as

$$z(t) = v(t) + i\tilde{v}(t) = A(t)e^{-i\theta(t)} \tag{3}$$

where $A(t)$ is the amplitude and $\theta(t)$ is the phase angle. The frequency-time distribution of the amplitude is designated as the Hilbert amplitude spectrum. Yang and Lei (1999) suggested the following procedures for the system identification of SDOF systems based on the HT method: (1) determine the damped frequency ω_d from the slope of the phase function $\theta(t)$ by the linear least-square fit technique; and (2) determine $\xi\omega$ by applying the linear least-square fit technique to the decaying amplitude $A(t)$ in a semi-logarithmic scale. After ω_d and $\xi\omega$ have been got, the natural frequency ω and damping ratio ξ can be obtained consequently.

COMPARISON OF MODAL FREQUENCIES AND DAMPING RATIOS

Data base

The time histories of acceleration response of one-hour duration are used to identify the first two natural frequencies and modal damping ratios. It is found that the structural response may vary considerably

within one-hour duration, which may affect the true change of natural frequency and modal damping ratio with hourly mean wind speed and hourly response standard deviation. To solve this problem, ten-minute standard deviations of structural displacement response in one-hour time history and the maximum difference between these six standard deviations are computed. If the maximum difference exceeds a specified value, the corresponding histories will not be included in the modal identification. As a result, a total of 14 one-hour time histories in different directions are selected for the subsequent modal identification. The time histories in lateral direction are listed in Tables 1. In the tables, "sep15" means "September 15" and "t19" denotes time "19:00 to 20:00 HKT" for instance.

Data analysis

The HHT method is applied to each selected acceleration response to obtain the Hilbert spectrum in the frequency-time domain. A typical Hilbert spectrum for the acceleration time history shown in Fig.1 is presented in Fig.2. From this Hilbert spectrum, the first two instantaneous frequencies can be easily found around 0.2 Hz and 0.7 Hz, respectively. The cutting frequencies required by the imtermittency check for the first two modal responses are then determined as 0.125 Hz, 0.25 Hz, and 0.9375 Hz. The first three-minute duration of the resulting first two modal response time histories are plotted in Fig.3 for the acceleration time history shown in Fig. 1. It is seen that each modal response is dominated by only one frequency and almost symmetric with respect to the horizontal line at zero level.

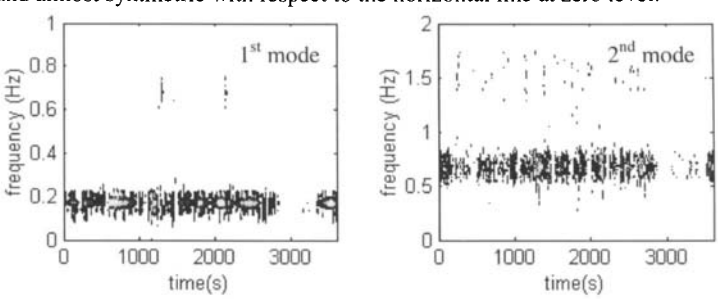


Fig. 2 Hilbert Spectra of Lateral Acceleration Response

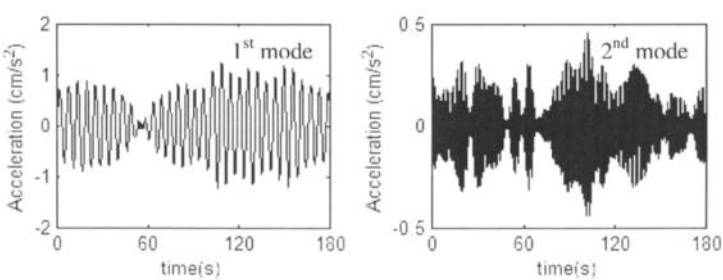


Fig. 3 First Two Total Modal Acceleration Response

Then random decrement technique (RDT) is the applied to the total modal responses to extract the free modal responses. The optimal threshold level used in the RDT would be in the range from 1.0σ to 1.5σ, where σ is the standard deviation of the time history. In this study, the threshold level is chosen as $1.5\ \sigma$. The duration of segment can be determined in such a way that the RDT function is fully decayed. The durations used in this study are 90 seconds and 25 seconds for the 1st and 2nd lateral modes of vibration, 100 seconds and 25 seconds for the 1st and 2nd longitudinal modes of vibration, and 60 seconds and 20 seconds for the 1st and 2nd torsional modes of vibration. The number of segments used in the RDT for each total modal response time history must be large enough. The number of segment used in this study is more than 270, 354, and 420 for the 1st lateral, longitudinal, and torsional mode of vibration. The number of segment for the 2nd lateral, longitudinal, and torsional mode of

vibration is more than 1103, 1127, and 1571, respectively. Fig. 4 depicts the 1st and 2nd free modal response time histories resulting from the 1st and 2nd total modal response time histories shown in Fig. 3 by the RDT.

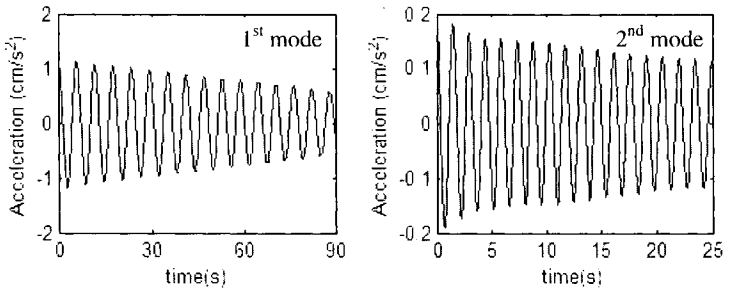


Fig. 4 First Free Total Modal Acceleration Response

The last step is to apply the HT method to each of the free modal response time histories to yield the instantaneous phase angle and amplitude functions and then the modal frequencies and modal damping ratios. Table 1 lists the first two natural frequencies and modal damping ratios of the Di Wang Building identified by the HHT method for different time periods in lateral direction. The results in longitudinal and torsional directions are omitted due to the space limitation.

To assess the applicability and superiority of the HHT method, the FFT method is also used to obtain the dynamic characteristics. The data number of each FFT is taken as 8192. The half-power bandwidth method is then applied to find the modal frequencies and modal damping ratios. The results identified by the FFT-based method for different time periods in lateral direction are shown in Table 1.

Table 1 Identified natural frequencies and modal damping ratios in lateral direction

Time	Frequency(Hz)						Modal damping ratio(%)					
	1st			2nd			1st			2nd		
	FFT	HHT	FFT/HHT	FFT	HHT	FFT/HHT	FFT	HHT	FFT/HHT	FFT	HHT	FFT/HHT
sep15.t19	0.1734	0.1739	0.9971	0.6880	0.6885	0.9993	0.84	0.74	1.14	0.57	0.70	0.81
sep15.t20	0.1731	0.1744	0.9925	0.6878	0.6872	1.0009	0.99	0.72	1.38	0.60	0.43	1.40
sep16.t03	0.1725	0.1723	1.0012	0.6861	0.6855	1.0009	1.74	1.08	1.61	0.49	0.58	0.84
sep16.t05	0.1705	0.1701	1.0024	0.6802	0.6803	0.9999	1.06	1.04	1.02	0.40	0.49	0.82
sep16.t06	0.1707	0.1705	1.0012	0.6826	0.6816	1.0015	1.25	1.02	1.23	0.75	0.59	1.27
sep16.t12	0.1696	0.1689	1.0041	0.6774	0.6783	0.9987	2.06	0.98	2.10	0.70	0.65	1.08
sep16.t13	0.1693	0.1701	0.9953	0.6790	0.6779	1.0016	1.27	0.91	1.40	0.73	0.56	1.30
sep16.t14	0.1695	0.1697	0.9988	0.6805	0.6795	1.0015	1.13	0.50	2.26	0.69	0.62	1.11
sep16.t15	0.1700	0.1702	0.9988	0.6807	0.6793	1.0021	1.90	0.78	2.44	1.28	0.55	2.33
sep16.t16	0.1702	0.1702	1.0000	0.6819	0.6819	1.0000	1.07	0.66	1.62	0.64	0.38	1.68
sep16.t17	0.1710	0.1713	0.9982	0.6834	0.6822	1.0018	1.03	0.51	2.02	0.35	0.38	0.92
sep16.t19	0.1713	0.1716	0.9983	0.6837	0.6837	1.0000	1.75	1.00	1.75	0.53	0.51	1.04
sep17.t01	0.1720	0.1725	0.9971	0.6851	0.6845	1.0009	1.77	0.60	2.95	0.69	0.67	1.03
sep17.t07	0.1722	0.1715	1.0041	0.6863	0.6859	1.0006	1.34	0.84	1.60	0.37	0.43	0.86
Mean value	0.1711	0.1712	0.9992	0.6831	0.6826	1.0007	1.37	0.81	1.75	0.63	0.54	1.18

Comparison

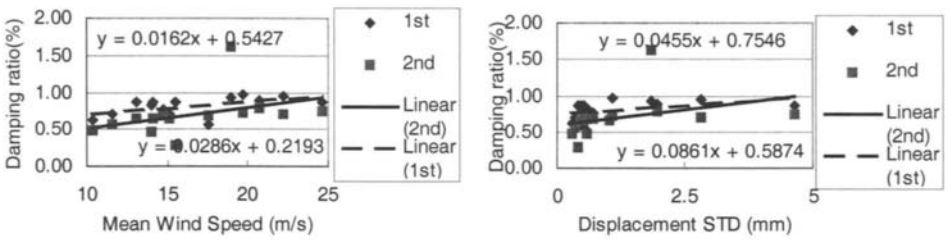
It is seen from the table that the modal frequencies identified by the HHT method are almost the same as those identified by the FFT method. In the lateral direction, the ratio of the 1st modal frequency identified by the FFT method to that identified by the HHT method ranges from 0.9925 to 1.0041, having a mean value of 0.9992. The ratio of the 2nd modal frequency ranges from 0.9987 to 1.0021, having a mean value of 1.0007. Similar frequency ratios are obtained in the longitudinal and torsional directions. However, the modal damping ratios by these two methods are different. The ratios of the modal damping ratio identified by the FFT method to that identified by the HHT method range from 1.02 to 2.95 for 1st mode and from 0.81 to 2.33 for the 2nd mode in the lateral direction. The corresponding mean values are 1.75 and 1.18 respectively. The FFT method seems to overestimate the modal damping ratio. Similar results have been obtained in the other two directions.

In consideration of the inherent drawback in the FFT-based half-power bandwidth method performed in the frequency domain and the adaptive nature of the HHT method performed in the frequency-time domain for modal damping ratio identification, the modal damping ratios identified by the HHT method may be more reliable than those by the FFT method. Thus, the investigation of the variations of modal frequency and damping ratio with vibration amplitude and wind speed are based on the results obtained from the HHT method.

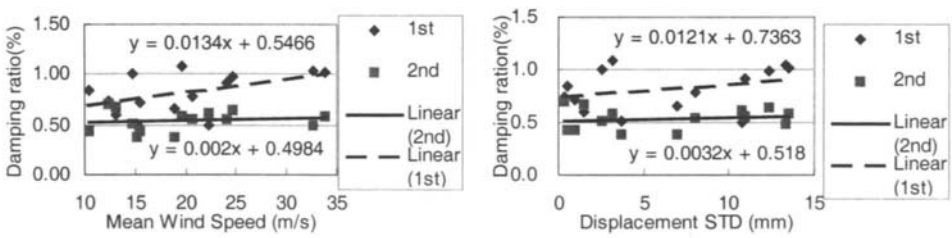
VARIATIONS OF MODAL PROPERTIES WITH WIND SPEED AND RESPONSE AMPLITUDE

Variations of total modal damping ratio with wind speed and response amplitude

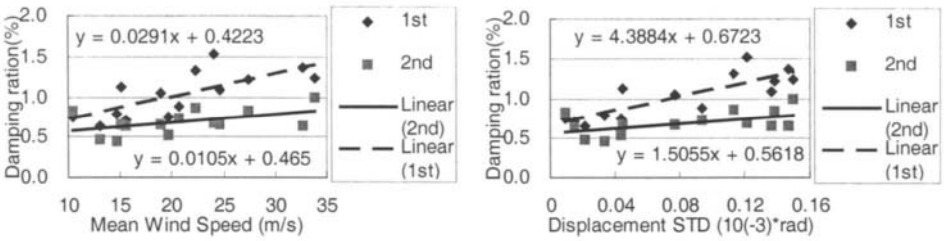
The variations of the first two total modal damping ratios with hourly mean wind speed and hourly standard deviation of displacement response in different directions are plotted in Fig 5. The linear least-square fits to these data are also plotted in the figure. It is seen that the total modal damping ratios increase with the increase of hourly mean wind speed and displacement standard deviation.



(a) Longitudinal



(b) Lateral

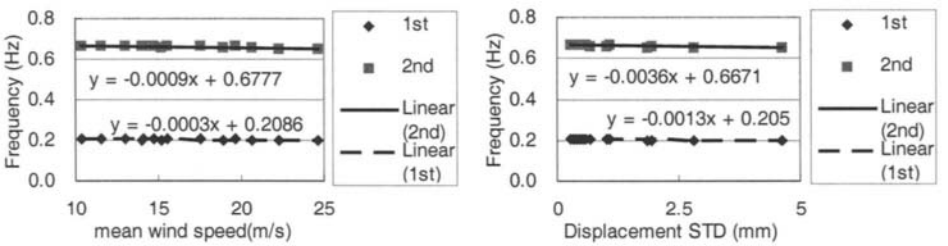


(c) Torsional

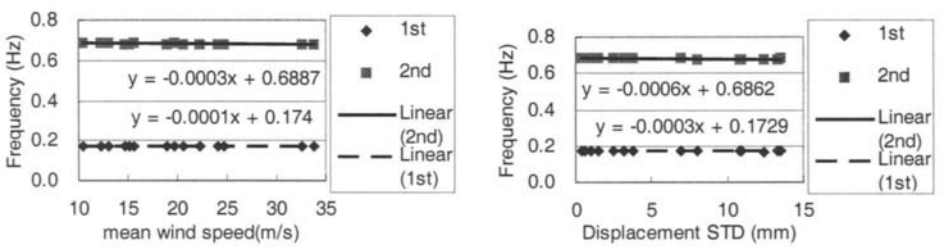
Fig. 5 First Two Total Modal Damping Ratios vs. Mean Wind Speed and Vibration Amplitude

Variations of natural frequencies with wind speed and response amplitude

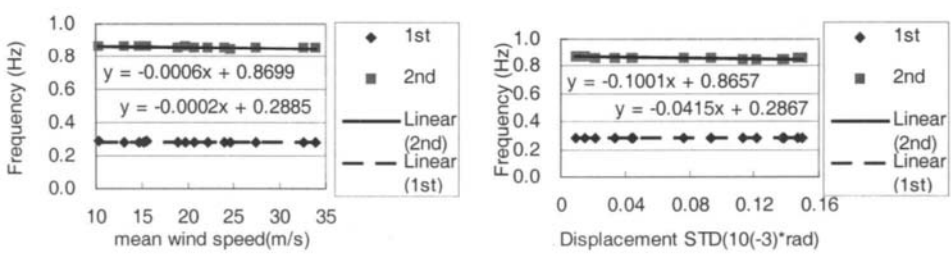
The changes of the first two natural frequencies with the hourly mean wind speed and the hourly standard deviation of displacement response, plus with their linear least-square fits are shown in Figs.6. It is seen that all the modal frequencies decrease very slightly with increasing hourly mean wind speed and the displacement standard deviation.



(a) Longitudinal



(b) Lateral



(c) Torsional

Fig. 6 First Two Modal Frequencies vs. Mean Wind Speed and Vibration Amplitude

CONCLUSIONS

The Hilbert-Huang transform (HHT) method has been applied to the measured wind and structural response data of the Di Wang Building to identify its dynamic characteristics. A series of natural frequencies and modal damping ratios of the building under different wind speeds in different directions have been identified and compared with those by the FFT-based method. The results show that the natural frequencies identified by the HHT and FFT method are almost the same. The modal damping ratios identified by the HHT method indicate that the FFT-based bandwidth method may significantly overestimate the modal damping ratios. The total structural modal damping ratio increases slightly with increasing wind speed and vibration amplitude but the situation is reversed for the natural frequency.

ACKNOWLEDGMENTS

The writers are grateful for the financial support from The Hong Kong Polytechnic University through its Area of Strategic Development Programme in Structural Health Monitoring and Damage Detection to the second writer.

REFERENCES

Feldman M., 'Investigation of the natural vibrations of machine elements using the Hilbert transform', *Soviet Machine Science*, 2, 44-47 (1985).

Feldman M., 'Non-linear system vibration analysis using the Hilbert transform—I. Free vibration analysis method 'FREEVIB'', *Mech. Syst. Signal Process.* 8, 309-18 (1994).

Hammond J. K. and Davis P., 'The use of envelope and instantaneous phase methods for the response of oscillatory non-linear systems to transients', *Proc. of the 5th IMAC*, London, 1460-1466 (1987).

Huang, N.E., Shen Z., Long S. R., Wu M. J. C., Shih H. H., Zheng Q. No., Yen N. C., Tung C. C., and Liu H. H., 'The Empirical mode decomposition and the Hilbert spectrum for nonlinear and non-stationary time series analysis', *Proc. R. Soc. Lond. A,* Vol. 454, pp. 903-995 (1998).

Huang, N. E., Shen, Z. and Long, S.R., 'A new view of nonlinear water waves: the Hilbert spectrum', *Annu. Rev. Fluid Mech.*, 31:417-457 (1999).

Ibrahim, S.R., 'Random Decrement Technique for Modal identification of Structures', *J. Spacecraft*, 14(11), 696-700 (1977).

Jeary, A.P. , 'Damping in tall buildings-a mechanism and predictor,' *Earthquake Engineering and Structural Dynamics,* Vol. 14, 733-759 (1986).

Littler, J.R. and Ellis, B.R., 'Measuring the dynamic characteristics of prototype structures,' A State of the Art in Wind Engineering, Krishna, P. Edited, 133-154 (1995).

Tamura, Y. and Suganuma, S.Y., 'Evaluation of amplitude-dependent damping and natural frequency of buildings during strong winds,' *J.Wind. Eng.Ind. Aerodyn.* Vol.59, 115-130 (1996).

Xu Y.L. and Zhan S., ' Field measurements of Di Wang Tower during Typhoon York', *Journal of Wind Engineering and Industrial Aerodynamics,* Vol. 89, No.1, 73-93 (2001).

Yang J. N. and Lei Y., 'Identification of natural frequencies and damping ratios of linear structures via Hilbert transform and empirical mode decomposition', *Proc. of Int. Conf. on Intelligent Systems and Control*, IASTED/Acta Press, Anaheim, CA, 310-315 (1999).

Yang J. N. and Lei Y., 'System identification of linear structures using Hilbert transform and empirical mode decomposition', *Proc. of 18th Int. Modal Analy. Conf.: A Conference on Structural Dynamics*, San Antonio, TX, Society for Experimental Mechanics, Inc., Bethel, CT, Vol.1, 213-219 (2000).

Advances in Building Technology, Volume 2
M. Anson, J.M. Ko and E.S.S. Lam (Eds.)
© 2002 Elsevier Science Ltd. All rights reserved

DISCUSSION ON DYNAMIC COEFFICIENTS FOR WIND-RESISTANT DESIGN IN SINGLE-LAYER RETICULATED SHELLS

Y. Q. Li

Department of Structural Engineering, Tongji University,
Shanghai 200092, People's Republic of China

ABSTRACT

Wind load is an important load in structural design of large-span single-layer reticulated shells. In order to consider the effects of fluctuating component of wind in a quasi-static wind-resistant design method, dynamic coefficients are usually used. In this paper, a method using artificial simulated wind load to estimate the coefficients has been presented. Based on wind load code of China, a Kiewitt type single-layer reticulated spherical shell was used as an example to investigate the dynamic coefficients, which is named wind-excited vibration coefficients in this code. Through a comparison between dynamic time-history analysis results and quasi-static analysis results, it is proved that the wind-excited vibration coefficients should be paid much attention to for wind-resistant design in large-span single-layer reticulated shells.

KEYWORDS

large-span single-layer reticulated shells, wind-excited vibration coefficient, artificial simulated wind load, *p*-order auto-regressive simulation technique

INTRODUCTION

The single-layer reticulated shell is an excellent large-span spatial structural system, which has been widely used. However, this system is very sensitive to the distribution of external load, and stability problem is dominant for structural safety. Considering the fluctuating and random characteristics of wind load, wind action becomes a very important load for the structural design of large-span single-layer reticulated shells, which should be paid more attention to than earthquake action in most cases. Therefore, it is necessary to estimate wind load more reasonable for this structure. In order to consider the effects of fluctuating components of wind in quasi-static wind-resistant design methods, dynamic coefficients are usually used. At present, a quasi-static method is used in GBJ 99-87 (1989), as the same as in wind-resistant design of other structures, such as tall buildings. Thus, the quasi-static wind load is estimated by following equation:

$$w_k = w_0 \mu_z \beta_z \mu_s \tag{1}$$

Where w_0 is the basic wind pressure in site, μ_z is the height coefficient, β_z the wind-excited vibration coefficient, and μ_s is the shape coefficient.

In Eq.(1), the result of ($\mu_z \mu_s w_0$) can be taken as the mean wind pressure for a corresponding point, where μ_z is a modifying coefficient for the height of the point and μ_s is another modifying coefficient for the place of the point on the surface of shell. Therefore, the wind-excited vibration coefficient β_z is a dynamic coefficient using to reflect the effect of fluctuating components of wind.

Up to now, widely accepted rules for estimating the values of wind-excited vibration coefficient in wind-resistant design of large-span single-layer reticulated shells do not exist in wind load code of China. Generally, empirical values for the coefficients were used for all the nodes of the structure. In fact, the coefficients will be different according to many parameters of single-layer reticulated shells, including the geometrical shape and flexibility of shell, the rise to span ratio, and even the spatial effects of wind load with the increase of span. Therefore, it is necessary to do further research on how to determine the suitable wind-excited vibration coefficients for such structural system. In this paper, considering the time and spatial correlation of natural wind, the artificial wind speed processes were simulated by an *p*-order autoregressive-type simulation method, and the super-relaxation iteration method was chosen to solve the large-scale matrix of regressive coefficients during the simulation. Through a comparison analysis on the characteristics of simulated wind, it was proved reasonable. Using the artificial simulated wind load, the wind-excited vibration responses of an single-layer reticulated spherical shell were investigated as an example with dynamic time-history analysis. Then, a statistic method was used to deal with the response variables including wind loads, displacements of nodes and internal forces of elements. At the same time, the quasi-static method suggested by wind load code was also used to analyze the same shell. Based on a comparison of the results from two methods, the suitable values of wind-excited dynamic coefficients were discussed.

SIMULATION OF WIND LOAD

Estimation of wind load is the first step for wind-resistant analysis. In this paper, time series of wind forces at each node of single-layer reticulated shells will be generated from artificial simulated wind. Many works have been done on how to simulate the spatial distribution of windspeed (Kareem, A. (1999)). Provided the windspeed processes abide by Gaussian distribution, mainly there are two kinds of simulation method, one is the spectral technique including CAWS (the Constant Amplitude Wave Superposition) and WAWA (Waves with Weighted Amplitude), the other is the time series methods including the autoregressive (AR) scheme, moving average (MA) scheme and their combination method ARMA. Anyways, for a practical project of large-span single-layer reticulated shells with so many degrees of freedom (DOFs), it's always a painstaking thing to simulate the windspeed at each joint. In this paper, the *p*-order auto-regressive filter technique is used to simulate the time series of windspeed, which was proved efficient for large DOFs problems (Li Y.Q. (2000)).

Brief introduction of the simulating process

In the *p*-order AR method, M multi-correlated random processes as $[u(t)] = [u^1(t) \quad \cdots \quad u^M(t)]^T$ can be generated by following equations (Iannuzzi, A.and Spinelli, P. (1987)):

$$[u(t)] = \sum_{k=1}^{p} [\Psi_k][u(t - k\Delta t)] + [N(t)] \tag{2}$$

Where, $[u(t-k\Delta t)]=[u^1(t-k\Delta t) \cdots u^M(t-k\Delta t)]^T$; $N(t)=[N^1(t) \cdots N^M(t)]^T$, $N^i(t)$ is a Gaussian white noise random process, $i=1,\cdots,M$; $[\Psi_k]$ is a $M\times M$ matrix of autoregressive coefficients, $k=1,\cdots,p$.

From Eq.(2), we can obtain the relationship between the covariance matrix $R_u(j\Delta t)$ and regressive coefficient matrix Ψ_k as follow:

$$[R]=[\overline{R}][\Psi] \tag{3}$$

Where,

$$[R]_{pM\times M}=\left[R_u{}^T(\Delta t),\cdots,R_u{}^T(p\Delta t)\right]^T \tag{4}$$

$$[\Psi]_{pM\times M}=\left[\Psi_1^T,\cdots,\Psi_p^T\right]^T \tag{5}$$

$$[\overline{R}]_{pM\times pM}=\begin{bmatrix} R_u(0) & R_u(\Delta t) & \cdots & R_u[(p-2)\Delta t] & R_u[(p-1)\Delta t] \\ R_u(\Delta t) & R_u(0) & \cdots & R_u[(p-3)\Delta t] & R_u[(p-2)\Delta t] \\ \vdots & \vdots & \ddots & \vdots & \vdots \\ R_u[(p-2)\Delta t] & R_u[(p-3)\Delta t] & \cdots & R_u(0) & R_u(\Delta t) \\ R_u[(p-1)\Delta t] & R_u[(p-2)\Delta t] & \cdots & R_u(\Delta t) & R_u(0) \end{bmatrix} \tag{6}$$

$$[R_u(j\Delta t)]_{M\times M}=\begin{bmatrix} R_u^{11}(j\Delta t) & \cdots & R_u^{1M}(j\Delta t) \\ \vdots & \ddots & \vdots \\ R_u^{M1}(j\Delta t) & \cdots & R_u^{MM}(j\Delta t) \end{bmatrix}, j=1,\cdots,p \tag{7}$$

$$[\Psi_j]_{M\times M}=\begin{bmatrix} \Psi_j^{11} & \cdots & \Psi_j^{1M} \\ \vdots & \ddots & \vdots \\ \Psi_j^{M1} & \cdots & \Psi_j^{MM} \end{bmatrix}, j=1,\cdots,p \tag{8}$$

Based on Wiener- Khintchine Equation, the relationship between the covariance and power spectrum density can be obtained as

$$R_u^{ik}(j\Delta t)=\int_0^\infty S_u^{ik}(n)\cos(2\pi nj\Delta t)dn\ ,\quad i,k=1,\cdots,M \tag{9}$$

In order to resolve Eq. (3), A super-relaxation iteration method was chosen in the paper to solve the large-scale matrix equation group of regressive coefficients.

$$x_{ij}^{k+1}=\omega[(-\sum_{l=1}^{i-1}r_{il}x_{lj}^{k+1}-\sum_{l=i+1}^{N}r_{il}x_{lj}^{k}-y_{ij})/r_{ii}]+(1-\omega)x_{ij}^{k},\quad \begin{matrix} i=1,\cdots,N \\ j=1,\cdots,M \end{matrix} \tag{10}$$

Where ω is a relaxation factor. It has been proved that the calculation will be steadily convergent if $0<\omega<2$. Specially, if $\omega=1$, it become to the Gauss-seidel iteration method. For the super-relaxation iteration method, $1<\omega<2$.

Provided ε is the convergent limit, a convergent rule can be used as follow:

$$\left|\sum_{l=1}^{N}x_{lj}^{k+1}x_{lj}^{k+1}-\sum_{l=1}^{N}x_{lj}^{k}x_{lj}^{k}\right|\le\varepsilon\ ,\quad j=1,\cdots,M \tag{11}$$

As for $[N(t)]$, it can be calculated from a Cholesky's factorization, $[R_N]=[L][L]^T$, as follows:

$$[R_N] = [R_u(0)] - \sum_{k=1}^{p} [R_u(k\Delta t)] \tag{12}$$

$$[N(t)] = [L][n(t)] \tag{13}$$

Thus, we can obtain M spatially correlative discrete random processes with interval Δt and mean value of zero. Usually, windspeed at one point can be divided into two parts, the mean wind speed $\overline{V}$ and the fluctuating component $v(t)$. Here, the simulated random processes $u(t)$ can be taken as the fluctuating component $v(t)$ as follows

$$V(t) = \overline{V} + v(t) = \overline{V} + u(t) \tag{14}$$

Based on wind load code, we can obtain the basic wind pressure w_0. According to the relationship between wind speed and wind pressure, the basic mean windspeed can be calculated by

$$\overline{V} = \sqrt{2w_0 / \rho} \tag{15}$$

Where ρ is the density of air.

Examples of windspeed simulation

An example was used to check the reasonability of simulated results, as shown in Fig.1. Here, the mean windspeed $\overline{v}_{10}$=25m/s, the roughness length z_0=0.2m, the time interval Δt=0.1s, and the order p=4. Simulated time series of windspeed at Point A and B are given in Fig.2. Fig.3 gives a comparison of power spectrum density (PSD) of simulated results with target PSD, the well-established Von Karman spectrum formula (Von Karman, T.(1948)). It can be seen that the PSD of simulated processes are well consistent with the target PSD.

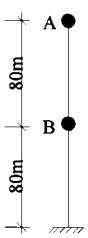


Figure1: A example with two pints

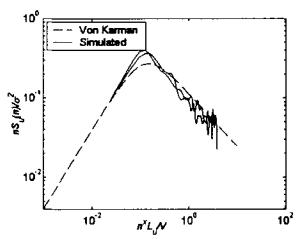
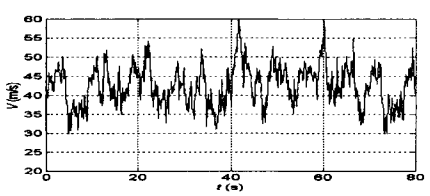
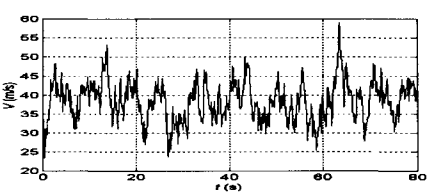


Figure3: Comparison of PSD



(a) Point A



(b) Point B

Figure 2: Simulated time-series of windspeed

DYNAMIC ANALYSIS OF A SINGLE-LAYER RETICULATED SPHERICAL SHELL

As an example, a Kiewitt type (K6-12) single-layer reticulated spherical shell was used to investigate the wind-excited vibration coefficients, as shown in Fig.4. The span L is 100m and the rise f is 40m. The height of bottom is 40m. All the elements are 180mm diameter tubes with 5mm thickness. $\bar{v}_{10}$=25m/s, z_0=0.4m. Fig.5, 6, 7 and 8 gave a part results about the simulated time series of windspeed and wind force, the responses of node displacement and element internal force, respectively.

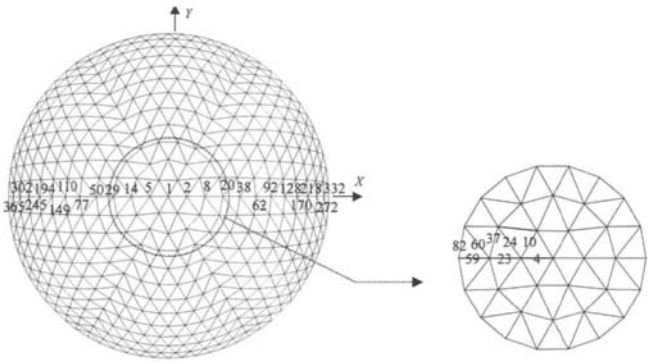
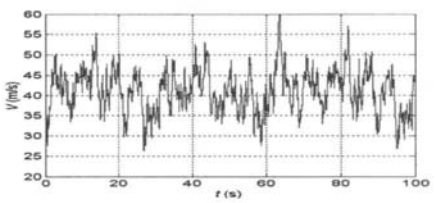
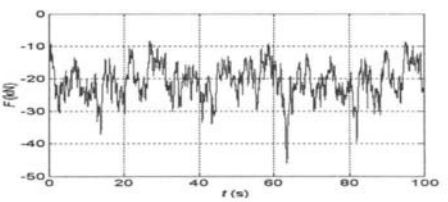


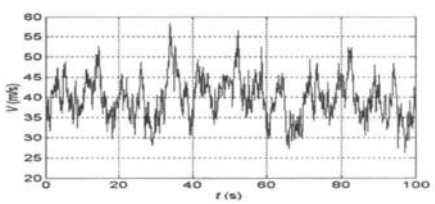
Figure 4: A Kiewitt type shell and number of some joints and members in central area



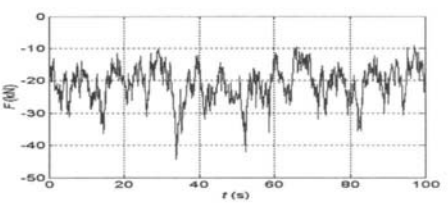
(a) Node No. 1



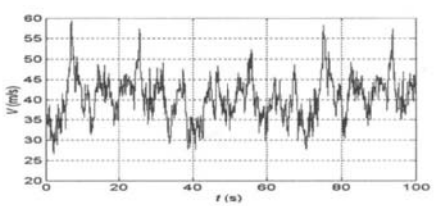
(a) Node No.1



(b) Node No. 92

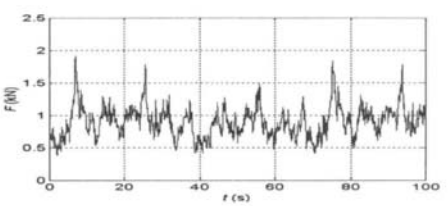


(b) Node No.92



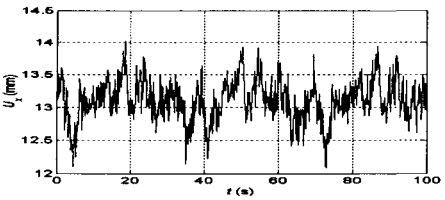
(c) Node No. 110

Figure 5: Time series of windspeed

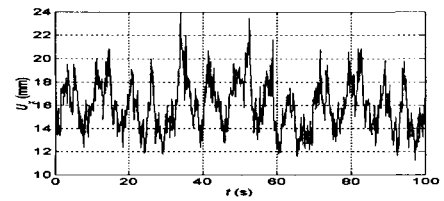


(c) Node No.110

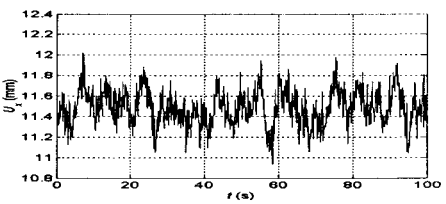
Figure 6: Time series of wind force



(a) Node No. 1

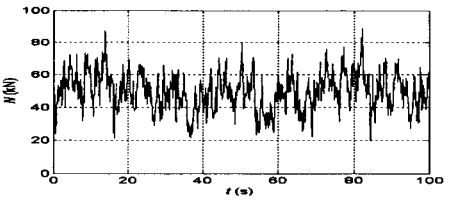


(b) Node No. 92

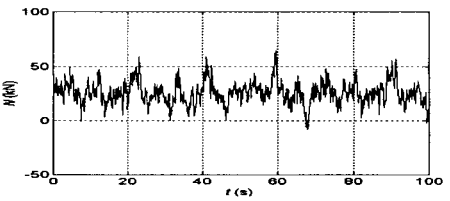


(c) Node No. 110

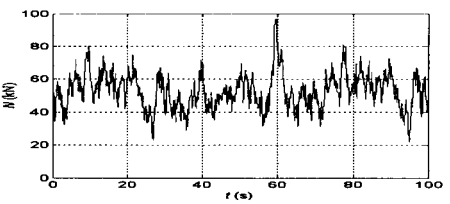
Figure 7: Time series of displacement



(a) Element No.4



(b) Element No.10



(c) Element No.23

Figure 8: Time-series of axial force

COMPARISON WITH QUASI-STATIC ANALYSIS RESULTS

Based on wind load code, a quasi-static method was used to analyze the same shell. According to Eq.(15), the basic wind pressure is 0.391 kN/m^2 at $\overline{V}$ =25 m/s. The wind-excited vibration coefficient β_z was equal to 2.0 temporarily. On the other hand, we can calculate the coefficients from dynamic results. To a variable u with a confidence interval [$\bar{u}$ - d, $\bar{u}$ + d] corresponding to a certain confidence level (1-α), a dynamic coefficient can be obtained as follows:

$$\beta = ((\bar{u})_d \pm d)/(\bar{u})_s \tag{16}$$

Where $(\bar{u})_d$ is the mean value of u from dynamic analysis, $(\bar{u})_s$ is the corresponding result from quasi-static analysis. α is the probability that the value of u is out of the confident interval [$\bar{u}$ - d, $\bar{u}$ + d], this is, $\alpha = P\{u < \bar{u} - d \quad or \quad u > \bar{u} + d\}$. If u is a response variable, β is called as the dynamic to static ratio of u, which is often used in structural analysis. While if u is the wind force, β will have the same function with the gust factor (Solari G. (1990)), although the calculation methods are different. Anyways, the value of β can be taken as an estimation of the wind-excited vibration coefficient.

According to Eq.(15), the values of β according to wind forces, displacement of node and axial force of element with a confidence level of 95% are given in Table 1, 2 and 3, respectively. It should be pointed out that in quasi-static analysis we had used a temporal dynamic coefficients of 2.0.

TABLE 1: Dynamic coefficients of part nodes according to wind force

Node No.	Dynamic analysis results (kN)		β	Quasi-static analysis results (kN)
	Mean wind force	σ of wind force		
1	-20.77	5.38	1.70	-24.83
2	-27.25	7.198	1.70	-32.54
5	-14.03	3.70	1.76	-16.24
8	-26.39	6.82	1.69	-31.80
14	-12.059	3.05	1.70	-14.40
20	-26.539	6.92	1.76	-30.61
29	-9.699	2.49	1.71	-11.51
38	-24.179	6.23	1.69	-29.05
50	-6.729	1.76	1.76	-7.77
62	-22.619	5.83	1.69	-27.22
77	-2.89	0.75	1.69	-3.47
92	-20.989	5.46	1.69	-25.23
110	0.909	0.24	1.75	1.05
128	-19.39	5.16	1.70	-23.18
149	4.63	1.26	1.73	5.44
170	-18.32	5.05	1.76	-21.19
194	7.91	2.16	1.72	9.38
218	-16.30	4.42	1.71	-19.36
245	10.82	3.04	1.75	12.55
272	-14.75	4.07	1.69	-17.77
302	12.23	3.41	1.69	14.71
332	-13.66	3.89	1.69	-16.46
365	13.42	3.94	1.74	15.70

TABLE 2: Dynamic coefficients of part nodes according to displacement in X and Z directions

Node No.		Dynamic analysis results (m)		β	Quasi-static analysis results (m)
		Mean displacement	σ of displacement		
1	X	0.01310	0.00031	1.70	0.01548
	Z	0.00673	0.00256	1.75	0.00788
2	X	0.01381	0.00048	1.69	0.01633
	Z	0.01058	0.00343	1.72	0.01256
5	X	0.01277	0.00037	1.70	0.01509
	Z	0.00353	0.00182	1.67	0.00436
20	X	0.01525	0.00127	1.71	0.01788
	Z	0.01010	0.00329	1.78	0.01157
29	X	0.01162	0.00054	1.69	0.01377
	Z	0.00384	0.00132	1.72	0.00456
62	X	0.01582	0.00194	1.68	0.01895
	Z	0.00805	0.00278	1.64	0.01001
77	X	0.01116	0.00029	1.70	0.01319
	Z	0.00292	0.00042	1.68	0.00350
128	X	0.01580	0.00222	1.73	0.01847
	Z	0.00614	0.00210	1.76	0.00714
149	X	0.01226	0.00064	1.69	0.01452
	Z	0.00057	0.00062	1.81	0.00067

TABLE 3: Dynamic coefficients of part elements according to axial force

Element No.	Dynamic analysis results (kN)		β	Quasi-static analysis results (kN)
	Mean axial force	σ of axial force		
4	49.73	11.40	1.76	57.47
10	25.61	10.68	1.65	31.86
23	52.74	10.75	1.58	67.72
24	18.37	12.34	1.71	22.41
37	19.05	9.70	1.68	23.41
59	48.72	9.37	1.70	58.06
60	10.24	6.14	1.69	12.57
82	12.66	7.41	1.80	14.57

From Table 1, we can find that with the confident level of 95%, the wind-excited vibration coefficients are about 1.7 according to wind force. If according to node displacement with the same confident level, the wind-excited vibration coefficients become a little larger, as shown in Table 2. While if based on the axial force of elements with the same confident level, the wind-excited vibration coefficients are varying between 1.58 and 1.80.

CONCLUSIONS

Wind-excited vibration coefficients are important in generating wind force of each node in wind-resistant design of large-span single layer reticulated shells. This paper just presents a simple ideal about how to obtain the coefficients. However, other factors, such as the effects of geometrical nonlinear characteristics, the interaction between wind and shells, are also necessary to be considered, especially with the increase of span or flexibility. Furthermore, wind tunnel model tests should be carried out to measure the simultaneous pressure distribution on the surface of shell with different rise to span ratios. On the other hand, such tests can be used to check the reasonability of simulated wind pressure distribution of shell surface, especially the spatial correlation. From the analysis results in this paper, the values of wind-excited vibration coefficients according to wind forces and wind-induced vibration responses are different. To the example shell used in this paper with a rise to span ratio of 0.4, the wind-excited vibration coefficients from wind force is about 1.7, while based on the response variables, it will become a little larger. From the point of view of a structural designer, it is better to consider the values of wind-excited vibration coefficients based on the responses of shells.

REFERENCES

GBJ 99-87. (1989). *China Loading Code for Buildings*. China Plan Press. (in Chinese)

Iannuzzi, A., Spinelli, P. (1987). Artificial Wind Generation and Structural Response. *Journal of Structural Engineering, ASCE*, 113:12.

Kareem, A. (1999). Analysis and Modeling of Wind Effects: Numerical Techniques. *Wind Engineering into the 21st Century*, Larsen, Larose & Livesey, Eds., Balkema, Rotterdam, 43-54.

Li Y.Q. (2000). *Wind-Resistant Theoretical Research of Large-Span Reticulated Shell Structures and Discussion on Several Practical Problems*. Postdoctoral Research Report of Zhejiang University. (in Chinese)

Solari G. (1990). A Generalized Definition of gust Factor. *Journal of Wind Engineering and Industrial Aerodynamics* 36, 539-548.

Von Karman, T.(1948). Progress in the Statistical Theory of Turbulence. *In Proceedings of National Academy of Science*, Washington DC, 530-539.

Advances in Building Technology, Volume 2
M. Anson, J.M. Ko and E.S.S. Lam (Eds.)
© 2002 Elsevier Science Ltd. All rights reserved

WIND MODELING IN *BLWT* AND DISCUSSION ON SEVERAL PROBLEMS

Y. Q. Li, Y. Tamura, A. Yoshida and A. Katsumura

Dept. of Architectural Engineering, Tokyo Institute of Polytechnics,
Atsugi, Kanagawa 243-0297, Japan

ABSTRACT

In this paper, wind modeling in the new boundary layer wind tunnel of Tokyo Institute of Polytechnics (TIP) was introduced briefly. Based on the test results, windspeed profiles and turbulence intensity profiles corresponding to different terrains defined by the loading code of Japan were simulated successfully. With comparative analysis of the measured data, the effects of blocks and spires on the profiles in this BLWT were presented. Several problems, including the optimal shape of spires, the consistency of power spectral density and the calculation methods for length scales were discussed. Finally, some advices about modeling wind in BLWT and processing the measured data were given for future reference.

KEYWORDS

boundary layer wind tunnel (BLWT), wind modeling, approach flow, windspeed profile, turbulence intensity profile, power spectral density, length scale

INTRODUCTION

At present, wind tunnel tests are widely used in many aspects, including obtaining overall or local wind load distribution of buildings, observing the wind-induced vibration responses of structures, evaluating pedestrian level winds, simulating the dispersion of pollutants, studying the characteristics of wind flow above special site, etc.. To structural engineering, it is a great help for wind-resistant design of some special structures vulnerable to wind load. In order to obtain the wind-effect data representative of full-scale conditions from a model test, the quality of the simulated approach flow in Boundary Layer Wind Tunnel (BLWT) is prerequisite. The simulated wind field should be approximate enough in basic characteristics to natural wind in the practical site, such as windspeed profiles, turbulence intensity profiles and power spectra density of windspeed with a certain length scale. In this paper, wind modeling of approach flow in the new boundary layer wind tunnel of Tokyo Institute of Polytechnics (TIP) was introduced briefly. Windspeed profiles and turbulence intensity profiles corresponding to four types of terrains defined by Architectural Institute of Japan (AIJ, 1996) were simulated successfully. With comparative analysis of the measured data, the effects of block size

and density, spire number and shape on windspeed profiles, turbulence intensity profiles, PSD and length scales in the BLWT were investigated. Several problems were discussed, including the optimal shape of spires, the consistency of power spectral density with existing spectrum models and the calculation methods for length scales. Finally, several advices about modeling wind in BLWT and processing the measured data were given for future reference.

WIND MODELING

Brief introduction of the BLWT in TIP

The new wind tunnel of Tokyo Institute of Polytechnics is a closed low-speed boundary layer wind tunnel. The test section of the wind tunnel is 1.8m high and 2.2m wide, with a length of about 19m. The available windspeed is from 0.5m/s to 15.0m/s, the uniformity of windspeed distribution is more than 99% and the center turbulence intensities are less than 1%. The fluctuating pressure measuring system can be used to measure multi-point pressures simultaneously with a maximum of 128 channels. High frequency force balance techniques can be used in the BLWT.

Wind modeling for four types of terrains

The widely used spire-roughness technique is implemented to simulate the required four types of wind profiles. Four kinds of triangular spires are used: Type 1: 1.0 m high and 0.15m wide in base, Type 2: 1.0 m high and 0.25 m wide in base, Type 3: 1.5 m high and 0.20 m wide in base, and Type 4: 1.5 m high and 0.30 m wide in base. The roughness of floor was adjusted by cube blocks with different sizes and densities. The sizes of three kinds of cube blocks are 30×30×30 mm, 60×60×60 mm and 90×90×90 mm, respectively. As for the density of blocks, three kinds were used with intervals of 600×400 mm (sparsely), 400×400 mm (commonly) and 400×200 mm (densely), respectively.

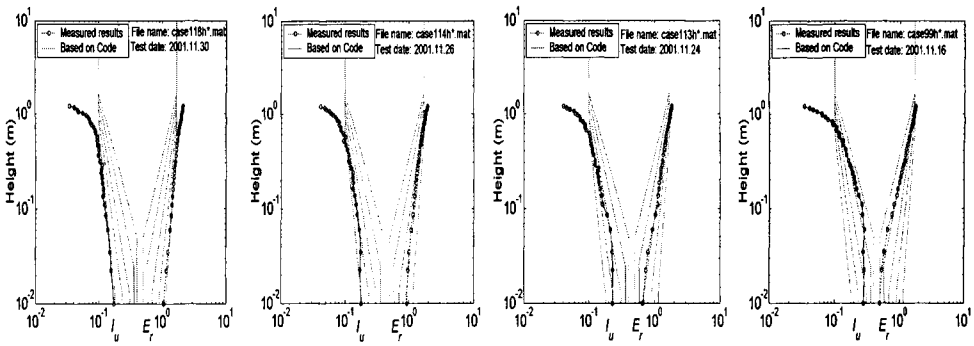
Many cases were tested with different combinations between spires and blocks. Finally, four types of terrains defined by AIJ (1996) were simulated successfully by trial and error. The windspeed profiles and turbulence intensity profiles for these terrain types are given in Fig.1. In the figure, the continuous lines without marks are based on AIJ (1996), as described in Table 1. $E_r = U(z)/U_{10}^{\mathrm{II}}$, is the vertical distribution coefficient of windspeed in the flat uniformly rough (FUR) terrain, U_{10}^{II} is the windspeed at 10m high above Terrain type II. E_r, the turbulence intensity I_u, the length scale ${}^{x}L_u$, the corresponding roughness length Z_b, the gradient height Z_G and the exponent α for four types of terrains given by AIJ (1996) are also shown in Table 1. For the measured data in a case that does not belong to type II, there is no a corresponding value of U_{10}^{II} directly. Therefore, it is necessary to change U_{10}^{II} to U_{10}^{I}, U_{10}^{III} and U_{10}^{IV} respectively based on "the power law". Provided the actual scale is 1:L, the values of E_r can be calculated as

$$E_r(z) = \frac{U(z)}{U(10/L)} * \lambda \qquad (1)$$

Where λ is a coefficient between U_{10} on measured terrain type with U_{10}^{II}, which is equal to 1.232, 1.000, 0.794 and 0.576 corresponding to terrain type I, II, III and IV, respectively.

TABLE 1
Descriptions for different terrains by AIJ

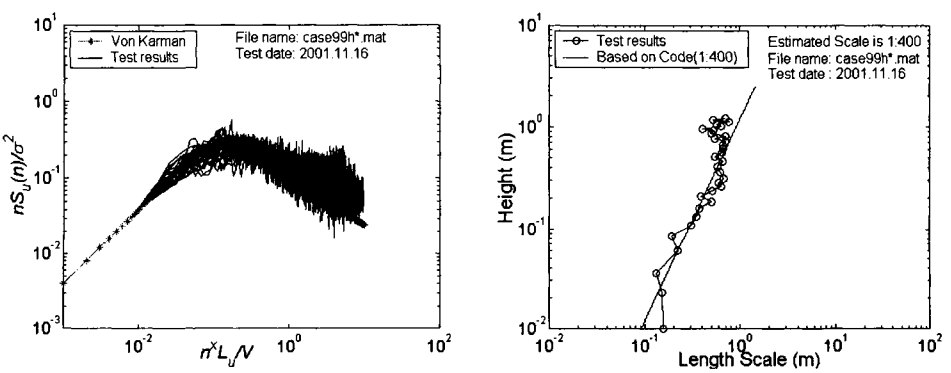
Terrain types		I	II	III	IV
E_r	$Z \le Z_b$	1.15	0.90	0.69	0.58
	$Z_b < Z \le Z_G$	$1.7(Z/Z_G)^{\alpha} = U_z/U_{10}^{\mathrm{II}}$			
I_u	$Z \le Z_b$	0.18	0.23	0.31	0.36
	$Z_b < Z \le Z_G$	$0.1(Z/Z_G)^{-\alpha-0.05}$			
${}^{x}L_u$		$100(Z/30)^{0.5}$			
Z_b		5	5	5	10
Z_G		250	350	450	550
α		0.10	0.15	0.20	0.27



(a) α =0.10 (b) α =0.15 (c) α =0.20 (d) α =0.27

Figure 1: Windspeed and turbulence intensity profiles for four simulated terrain types

Fig.2 gives an example of the distribution of power spectral density (PSD) and length scale along height in a case that belongs to terrain type Ⅳ. The distributions of PSD in all the cases are well consistent with Von Karman spectrum model (Von Karman, 1948), which is widely used. The distribution of length scale along height in this case is well consistent with the formula recommended by AIJ (1996), as given in Table 1. It should be noted that not all the test cases have such well consistent results for length scale. All the results show that, as the exponent α decreases, the slope of distribution of length scale along height will increase gradually as well as the values of length scales near to the wind tunnel floor, as shown in Fig.3a and 3b.



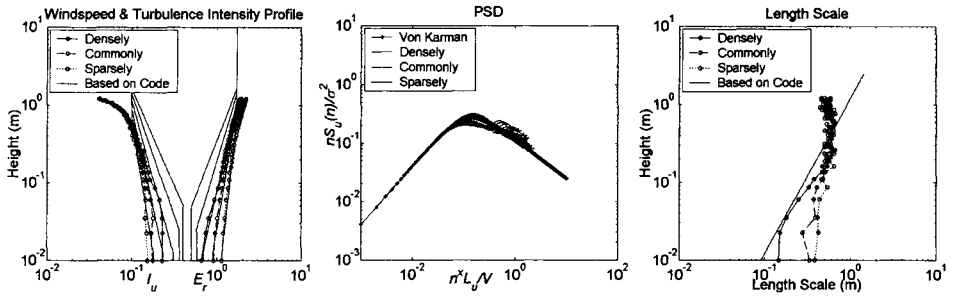
(a) PSD $S_u(z,n)$ (b) Length scale ${}^xL_u$

Figure 2: PSD and length scale in a case (Terrain type Ⅳ)

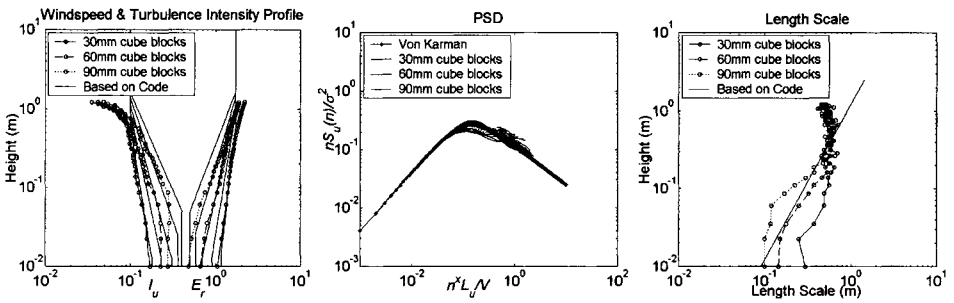
DISCUSSION ON SEVERAL PROBLEMS

Effects of Blocks and Spires

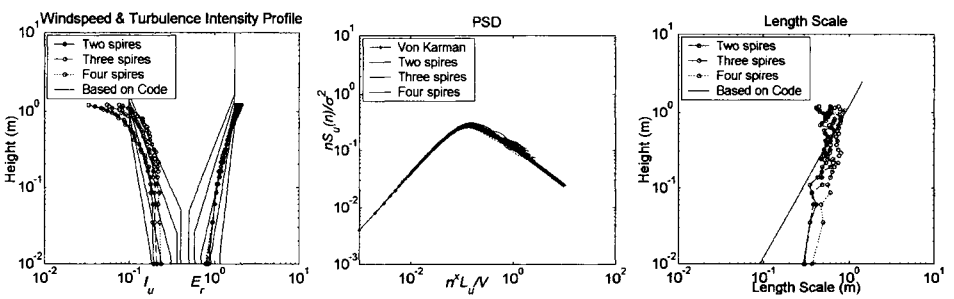
Many comparisons had been carried out to investigate the effects of blocks and spires in the wind tunnel, including the effects of block size and density, the effect of spire number and shape, etc.. A part of results is given in Fig.3. It should be pointed out that herein we used an autoregressive (AR) method to smooth the curves of PSD directly resulted from the multidimensional discrete fast Fourier translation (FFT) method shown in Fig.2a. The consequent difference in the results of length scales is shown in Fig.6 later on.



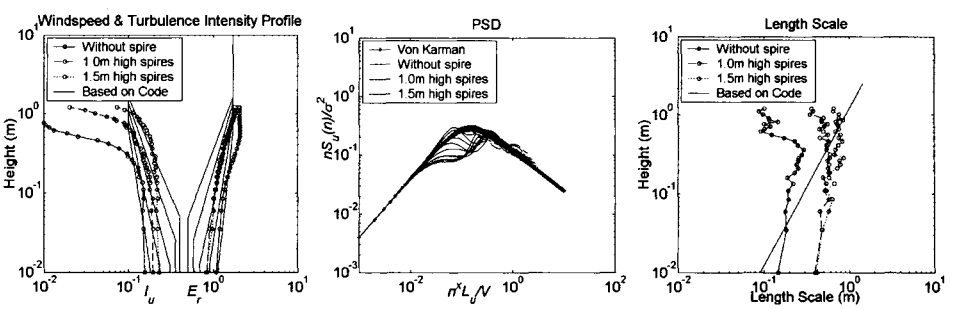
(a) Density effects of 60×60×60 mm blocks with four 1.5m high spires (Type 3)



(b) Size effects of Blocks placed densely with four 1.5m high spires (Type 3)



(c) 90×90×90 mm blocks placed commonly with two, three and four 1.5m spires (Type 4)



(d) Four spires (Type 4) with 60×60×60 mm blocks placed densely

Figure 3: Effects of blocks and spires

Based on the comparison, following results can be found: (1) With the same block size, the increase of block density gives obvious effects on windspeed profiles, turbulence intensity profiles and length scale near to the wind tunnel floor, but little on PSD. If the block size increases, the effects of block density will increase correspondingly. The same regularity can be seen for the effects of block density. (2) The difference between two and three spires is very small in the BLWT, but compared with four spires, there are obvious difference in the results of turbulence intensity profiles and length scale, and little to windspeed profiles and PSD. (3) The effects of spire height on the results of windspeed, turbulence intensity and length scale profiles are obvious. As the height of the spire increases, the gradient height of simulated wind field, or the thickness of boundary layer will increase, too.

Determination of the spire shape

The spire shape has a great effect on the measured results, which can be proved in Fig.3(c) and 3(d). Therefore, how to determine the shape of spires initially for a new BLWT is really a problem. One method for designing spires was presented by Irwin (1981). An empirical relation among the height of spires h, the thickness of boundary layer δ and the power-law exponent α was used as follow:

$$h = 1.39\frac{\delta}{1+\alpha/2} \tag{2}$$

Then, based on a momentum balance analysis, the base width to height ratio b/h of triangular spires can be estimated by the following equation:

$$\frac{b}{h} = 0.5[\frac{\psi(H/\delta)}{1+\psi}](1+\frac{\alpha}{2}) \tag{3}$$

Where, H is the height of test section. The coefficient ψ can be calculated by following equations:

$$\beta = (\frac{\delta}{H})(\frac{\alpha}{1+\alpha}) \tag{4}$$

$$\psi = \beta\frac{\frac{2}{1+2\alpha}+\beta-\frac{1.13\alpha}{(1+\alpha)(1+\alpha/2)}}{(1-\beta)^2} \tag{5}$$

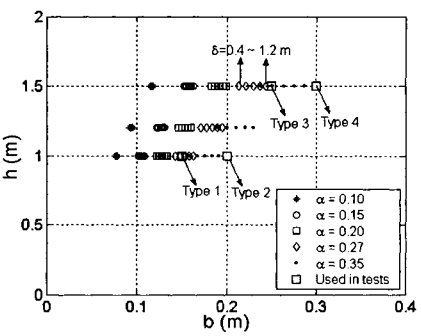


Figure 4: Optimal shape analysis of spires

According to above method, optimal base width of spire, b, corresponding to three kinds of spire height, 1.0m, 1.2m and 1.5m, for the BLWT are given in Fig.4, considering five different exponent α, 0.1, 0.15, 0.2, 0.2 and 0.35, respectively. To each kind of exponent, five kinds of thickness of boundary layer, δ, are analyzed, including 0.4 m, 0.6 m, 0.8 m, 1.0 m and 1.2 m. At the same time, four types of spires used in the tests are shown in the figure. From Fig.4, it can be found that the spires Type 2 and Type 4 are not suitable to our tests theoretically. That was proved by the test results, too.

Comparison on PSD

There are many different spectrum models used to describe the distribution of PSD. Based on the theory of isotropic turbulence, Von Karman (1948), presented a spectrum formula as follow:

$$\frac{nS_u(z,n)}{\sigma_u^2} = \frac{4n^x L_u/V}{[1+70.8(n^x L_u/V)^2]^{5/6}} \tag{6}$$

Where n is the frequency in Hertz, ${}^xL_u$ is the length scale of longitudinal turbulence in X direction, V is the mean windspeed of longitudinal component u and σ_u is the root mean square (RMS) value of V.

Another spectrum model proposed by Kaimal et al. (1972) with the reduced frequency $f = nz/V(z)$, as

$$\frac{nS_u(z,n)}{\sigma_u^2} = \frac{32.0f}{(1+50f)^{5/3}} \tag{7}$$

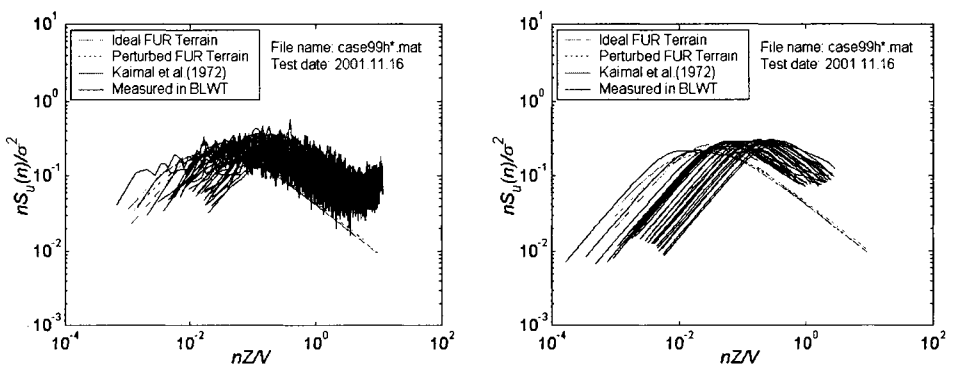
Tieleman (1992) developed spectral equations for the longitudinal component u as follows:
For the ideal flat uniformly rough (FUR) terrain:

$$\frac{nS_u(z,n)}{\sigma_u^2} = \frac{20.53f}{1+475.1f^{5/3}} \tag{8}$$

For the Perturbed FUR terrain:

$$\frac{nS_u(z,n)}{\sigma_u^2} = \frac{40.42f}{(1+60.62f)^{5/3}} \tag{9}$$

As an example, a comparison between above spectrum expressions and PSD distributions resulted from measured data in one case is shown in Fig.5. In Fig.5(a), the PSD is calculated directly with the FFT method, while the curves of PSD in Fig.5(b) are smoothed with the AR method. From Fig.2 and Fig.3, it can be found that the PSDs from measured data are well consistent with the distribution described by Von Karman expression. However, there are increasing errors with other expressions as the height increases, as shown in Fig.5. This reason is that the reduced frequency $f_m = nz/V(z)$ corresponding to the maximum of PSD increases along the height, which can be proved in Fig.5(b). In Eq.(6), such regularity has been considered, but neglected in Eq.(7) to Eq.(9).



(a) Without smoothed (b) Smoothed with the AR method

Figure 5: Comparison of PSD distributions with existing spectrum formulas

Estimation of Length Scale

The length scale ${}^xL_u$ is a measure of the most energetic gust size used widely in wind engineering practice. It is also a necessary value for designing the test model. The values of length scale will be different at different height or above different terrains. There are several methods can be used to calculate the values of length scale from measured data. Harris (1986) gave extensive discussions about the equations for calculating length scale deduced from existing spectrum formulas. However, these formulas have several parameters, which are not easy to be used for processing the measured data in wind tunnel tests. In this paper, three kinds of methods are chosen to estimate the values of length scale from the measured data.

The physical definition of length scale at a measured point is given as follow:

$$^{x}L_u(z) = \overline{V}\,^{x}T_u = \overline{V}\int_0^{\infty} R(\tau)d(\tau) \tag{10}$$

Where, $^{x}T_u = \int_0^{\infty} R(\tau)d(\tau)$, is the time scale of longitudinal turbulence in x direction, $\overline{V}$ is the mean windspeed, and $R(\tau)$ is the cross-correlation function of measured time history data.

Except for the definition, Length scale can be estimated based on the existing spectrum expressions. For example, An equation for estimating length scale can be obtained from the well-established Von Karman spectrum formula (Eq.(5)) at the frequency $n = 0$ as follow:

$$^{x}L_u(z) = \frac{V(z)S_u(z,0)}{\sigma_u^2(z)} \tag{11}$$

Where $S_u(z,0)$ is the value of power spectral density function at frequency $n = 0$ at height z. During the data processing, the first part of PSD was used as the representative value of $S_u(z,0)$.

In addition, simple empirical formulas also can be used to estimate of the values of $^{x}L_u$. An empirical is recommended to estimated the length scales in the Atmospheric Surface Layer (ASL) by American Society of Civil Engineers (ASCE, 1999) as follow:

$$^{x}L_u(z) = \frac{z}{2\pi f_m} \tag{12a}$$

Where $f_m = nz/V(z)$ is the reduced frequency for which $nS_u(z)$ is a maximum.

Architectural Institute of Japan (AIJ, 1996) also gives an almost the same simple equation as follow:

$$^{x}L_u(z) = \frac{1}{6.87}(V/n)_{peak} \tag{12b}$$

Where $(V/n)_{peak}$ means the values of $V(z)/n$ for which $nS_u(z)$ is a maximum.

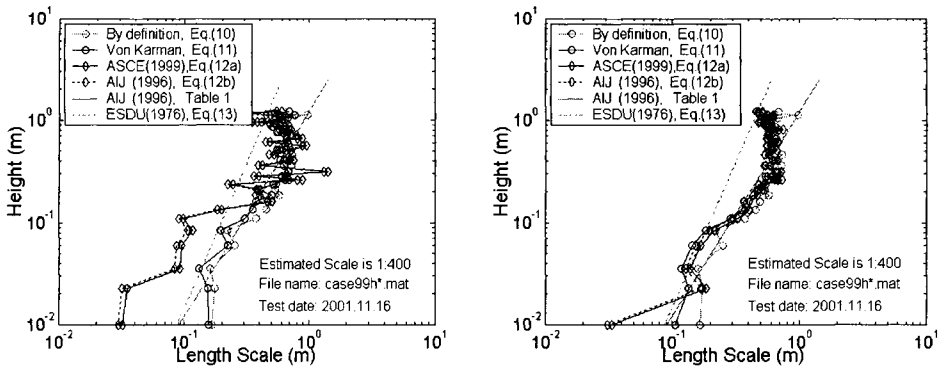
The difference between Eq.(12a) and Eq.(12b) is just a constant, the former is 2π and the latter is 6.87.

A comparison of the results of length scale calculated from above mentioned equations is given in Fig.6. In Fig.6(a), the values of length scale are based on the PSDs resulted directly from the FFT method, while in Fig.6(a), the values of PSD used are smoothed with the AR method. In Fig.6, the continuous lines without marks are based on AIJ (1996), as shown in Table 1; the dashed lines without marks are from E.S.D.U. (1976), as given by following equation:

$$^{x}L_u(z) = 25(z^{0.35}/Z_b{}^{0.063}) \tag{13}$$

From Fig.6, it can be found that the calculated results of length scale from Eq.(10) and Eq.(12) are very near to each other, and the difference becomes smaller and smaller as the height increases. Anyway, all of the results from above mentioned methods are approximate and acceptable.

Regarding to the lines recommended by codes, it should be noted that the formula proposed by AIJ (1996) does not consider the effect of terrain types on length scale. In fact, the slope of length scale data along height is different according to the roughness length, which can be observed from the measured results in the wind modeling tests.



(a) Using PSDs without smoothed (b) Using smoothed PSDs with the AR method

Figure 6: Estimation of length scales

CONCLUSIONS

Based on the test and discussion, several conclusions can be drawn as follows:
(1) The spire-roughness technique is efficient way for wind modeling in wind tunnel. However, it seems not easy to control the results with theoretical analysis. Trial and error is necessary for the test.
(2) The effect of spires to the characteristics of simulated wind is dominant, while the size and density of blocks have obvious effects on the wind flow near to the floor of wind tunnel. The method proposed by Irwin (1981) can be used as a reference to determine the shapes of spires initially.
(3) The peak of PSD to the reduced frequency moves with the increase of height obviously, so Van Karman spectrum model is better to describe the characteristics of simulated wind in the wind tunnels.
(4) Regarding the calculation of length scale, Both Eq.(10) Eq.(11) and Eq.(12) are simple and suitable with approximate results, especially based on the smoothed PSDs with the AR method.

REFERENCES

American Society of Civil Engineers (ASCE). (1999). *Wind Tunnel Studies of Buildings and Structures, ASCE Manuals and Reports on Engineering Practice No. 67*, Task Committee on Wind Tunnel testing of Buildings and Structures. Aerodynamic Committee Aerospace Division. Published by ASCE, American Society of Civil Engineers.
Architectural Institute of Japan (AIJ). (1996). *Recommendations for Loads on Buildings*, Published by AIJ, Architectural Institute of Japan. (In Japanese)
ESDU. (1976). *Characteristics of Atmospheric Turbulence near the Ground, Part III: Variations in Space and Time for Strong Winds (neutral atmosphere), Item75001*, ESDU International Ltd., London.
Harris R.I. (1986). Longer Turbulence Length Scales. *Journal of Wind Engineering and Industrial Aerodynamics* 24, 61-68.
Irwin H.P.A.(1981). The Design of Spires for Wind Simulation. *Journal of Wind Engineering and Industrial Aerodynamics* 7:3, 361-366.
Kaimal, J.C., Wyngaard, J.C., Izumi, Y. and Cote, O.R. (1972). Spectral Characteristics of Surface-layer Turbulence. *Q. J. Royal Meteorol. Soc.* 98, 563-589.
Tieleman H.W.(1992). Wind Characteristics in the Surface Layer over Heterogeneous Terrain. *Journal of Wind Engineering and Industrial Aerodynamics* 41-44, 329-340.
Von Karman, T.(1948). Progress in the Statistical Theory of Turbulence. *In Proceedings of National Academy of Science*. Washington DC, 530-539.

Advances in Building Technology, Volume 2
M. Anson, J.M. Ko and E.S.S. Lam (Eds.)
© 2002 Elsevier Science Ltd. All rights reserved

WIND-INDUCED DYNAMIC RESPONSE AND WIND LOAD FACTOR FOR FLEXIBLE ROOF STRUCTURES WITH MEDIUM DEFORMATION

W. J. Lou[1], F. Lu[2] and B. N. Sun[1]

[1]Department of Civil Engineering, Zhejiang University, Hangzhou 310027, P. R. China
[2]The Second Institute of Project Planning & Research, Ministry of Machinery Industry, Hangzhou 310006, P. R. China

ABSTRACT

This paper carries out comparative study of wind tunnel test and theoretical analysis on wind-induced responses and wind load factors for flexible roof structures with medium deformation. Flexible roof structures with medium deformation refer to a kind of roofs that the wind-structure-coupling effects can be neglected. Fluctuating wind pressure records from rigid model wind tunnel tests are taken as wind loads acting on roof structure, then wind-induced responses and wind load factors are analyzed in the time domain. For comparison, the spectral analysis based on quasi-steady theory is also used to predict wind responses of the same roof structure. It is found that the results predicted by the time domain method well agree with those obtained by the perfect aeroelastic model wind tunnel tests. On the other hand, the results predicted by spectral analysis based on quasi-steady theory are the same with test results only in tendency, but far more than test results in value. Hence, a modified coefficient is introduced when the spectral analysis method based on quasi-steady theory is used to estimate the wind effects on flexible roof structures with medium deformation.

KEYWORDS

Long-span roof structure, wind-induced response, wind load factor, wind effect factor, time domain method, quasi-steady theory; spectral analysis.

INTRODUCTION

The wind load has recently become a major concern in wind-resistant design of long-span roof

structures due to their characteristics: light, flexible, lightly damped, low natural frequency and so on. Furthermore, these kinds of structures are relatively low, located in the high turbulence intensity region of the atmospheric boundary layer where wind velocity varies widely with elevation. The roof shapes are generally so irregular that the airflow and aerodynamic effects are complicated. Consequently, the structures become quite sensitive to wind load, particularly to its dynamic effect.

The roof structures, in terms of their stiffness, can be divided into three categories: rigid roof structures, flexible roof structures with medium deformation and flexible roof structures with large deformation. For rigid roof structures, wind-induced dynamic response can be neglected. For flexible roof structures with large deformation (i.e. membrane structures), the coupling action between structure movement and approach flow should be considered. For flexible roof structures with medium deformation, on one hand, since the amplitude of vibration is on the small side, the coupling action between the structure and approach flow can be neglected; on the other hand, vibration-induced inertia force should be taken into account. As flexible roof structures with medium deformation are widely used in Civil Engineering, it is of particular importance to investigate wind effects on these structures.

Most of the previous investigations were made for the characteristics of the mean and fluctuating wind pressures acting on roofs with various shapes, such as hip roofs (Xu and Reardon,1998), gable roofs (Case and Isyumov,1998), flat roofs with parapets (Kareem and Lu, 1992) and stadium annular covering (Marighetti *et al.*, 2000). In their works, the roofs were reasonably regarded as rigid covers since the roof span is relatively small. However, as the roof span increases, the flexibility of roof and its dynamic effects have to be considered. Heretofore, several researches on wind response of flexible roof structures with medium deformation have been carried out by means of wind tunnel test combined with computer numerical analysis. For example, Yasui (1999), based on the data obtained from a stiff model wind tunnel test conducted for a long-span structure, simulated a multi-point fluctuating wind pressure time series by the Monte Carlo method. Then a time series response analysis was carried out using the wind pressure time series. Uematsu (1997) measured the modal force of the first vibration mode (i.e. the modal force is regard as a sum of the point pressures multiplied by weighting factors) through a rigid model wind tunnel test, and then, the gust loading factor or so-called wind effect factor, defined as the ratio of maximum peak displacement response to the mean displacement response in a time duration, was computed. Although this method enjoys a distinct advantage of simple and immediate computation, in this study, only the first modal force is considered for estimating the gust-loading factor; neither effects of high order mode of vibration nor the non-linear properties of structure are considered. The researches of China mainly adopt spectral analysis based on quasi-steady theory to analyze wind responses of long-span roof structures (Lou et al., 2000). But, since the wind pressure applied on the roof are chiefly generated by pneumatic separation and reattachment, whether the quasi-steady theory is still suitable should be further discussed and the expression of wind-induced force on the roof is also a problem. In the present study, wind-induced dynamic responses and wind load factors of roof structures are analyzed in the time domain based on wind pressure records from rigid model wind tunnel tests. For comparison, the spectral analysis based on quasi-steady theory is also used to predict wind responses of the same roof structure. It indicates that time domain method has high accuracy, but quasi-steady theory is not well suitable to predict wind-induced responses of roof structures.

SPECTRAL ANALYSIS BASED ON QUASI-STEADY THEORY

Based on quasi-steady theory, fluctuating component of the wind force acting on roof structure is expressed as (Simiu and Scanlan, 1986):

$$F_i(t) = \frac{1}{2}\rho V^2 A_i \left[C_{Li} \frac{2v(t)}{V} + \left(\frac{\mathrm{d}C_{Li}}{\mathrm{d}\alpha} + C_{Di} \right) \frac{w(t)}{V} \right] \tag{1}$$

where V and $v(t)$ are the horizontal mean wind speed and horizontal fluctuating wind speed at roof level respectively; $w(t)$ is the vertical fluctuating wind speed at roof level. In order to compare with the wind tunnel test results, in this study the vertical fluctuating wind speed $w(t)$ is neglected. The Eqn.1 then is simplified as

$$F_i(t) = \rho C_{Li} A_i V v(t) \tag{2}$$

in which ρ is air density; C_{Li} is the mean lift force coefficient of pressure pat i obtained from wind tunnel test; A_i is the roof surface area corresponding to node i.

A long-span flat roof subjected wind excitation vibrates like as elastic thin plate, and so can be divided into orthogonal elements. Using thin plate bending element stiffness and mass matrices, the finite element vibration equations of a long span roof structure under wind excitation are assembled as

$$[M]\{\ddot{X}\} + [C]\{\dot{X}\} + [K]\{X\} = \{F(t)\} \tag{3}$$

In similar as the spectral analysis of wind responses for high-rise building, the RMS displacement response of node q on roof is given by (Lou et al., 2000)

$$\sigma_{x_q}^2 = \sum_{j=1}^{n} \varphi_{qj}^2 \frac{\sum_{r=1}^{n}\sum_{k=1}^{n} \varphi_{rj}\varphi_{kj}\rho^2 V_r V_k C_r C_k A_r A_k}{M_j^2} \times \int_0^\infty \frac{\sqrt{S_v^r(\omega) S_v^k(\omega)} \cdot \mathrm{coh}(r,k,\omega)}{(\omega_j^2 - \omega^2)^2 + (2\beta_j \omega_j \omega)^2} \mathrm{d}\omega \tag{4}$$

and then the RMS acceleration is

$$\sigma_a = \sqrt{\sum_{j=1}^{n} \omega_j^4 \sigma_{xj}^2} \tag{5}$$

where, $S_v(\omega)$ and $\mathrm{coh}(r, k, \omega)$ are spectral density and coherence function of the horizontal fluctuating wind velocity respectively. Spectral density and coherence function reported by Davenport are adopted in this investigation.

TIME DOMAIN METHOD

Commonly, the analysis of wind response in the time domain is conducted in the following three steps. First, fluctuating wind speed time history is simulated from fluctuating wind speed spectrum by means of harmonic synthesis and linear filter; Next, the time history of fluctuating wind load acting on the structure is determined through transforming the time history of wind speed into that of wind load based on quasi-steady hypothesis. Third, the response is calculated by the time domain six-order Runge-Kutta method. However, the airflow sweeping past the roof structure will create complicated pneumatic separation and reattachment, and so it will bring about errors that the quasi-steady theory is adopted to describe the wind load acting on the long-span roof structure. Accordingly, in the present

study, dynamic wind pressure records obtained by stiff model wind tunnel tests through simultaneous technique are taken as wind loads applied on roof structure. And then, wind responses and wind load factors are analyzed by the time domain six-order Runge-Kutta method. The fluctuating wind load $F_i(t)$ acting on node i of roof structure can be ascertained by pressure tap i as follows:

$$F_i(t) = \frac{1}{2} C_{pi}(t) \rho V^2 A_i \tag{6}$$

where $C_{pi}(t)$ is the lift force coefficient time history of node i; A_i is the roof surface area corresponding to node i.

Combined Eqn.3 with Eqn.6, the wind-induced response time history of roof structures can be calculated by direct integral approach such as six order Runge-Kutte method. Then, the statistical information (maximum value, mean value and RMS) of responses and the wind load factor are easily obtained.

WIND-INDUCED DYNAMIC RESPONSE AND WIND LOAD FACTOR

In order to verify the accuracy of the above time domain method, a square flat roof, simply supported on a closed building, with ratio of height to span L/H = 3.0 and with 30m span, is selected as an example for numerical analysis, rigid model and perfect aeroelastic model wind tunnel tests. The computed first six natural frequencies of this prototype are 2.03Hz, 5.07Hz, 5.07Hz, 8.13Hz, 10.15Hz, and 10.15Hz. The rigid model was made with the geometry scale of 1/50. The perfect aeroelastic model was designed with the same geometry scale of 1/50. In order to satisfy Froude number similarity, Cauchy number similarity and mass distribution similarity requirements, the model is finally made of aluminum plate with 1.5mm thickness. In wind tunnel tests, the mean wind velocity reference height for the tests was set 20cm above the floor of the wind tunnel, just the height of roof surface. The reference wind velocity is 12m/s for fluctuating pressure measurement tests and varies from 8m/s to 12 m/s with 1m/s interval for acceleration measurement tests. Due to satisfaction of Froude number similarity, the accelerations of the aeroelastic model were just equal to those of the prototype roof.

RMS Acceleration Response

The roof RMS acceleration responses are obtained by three approaches: spectral analysis based on quasi-steady theory, time domain method and aeroelastic model wind tunnel tests respectively. In calculation, the damping ratio of the first mode is set to be 1.0% that is near to the aeroelastic model damping ratio. The wind pressure coefficients are obtained from the stiff model wind tunnel tests. The first six modes are taken into account in order to consider the effects of high order modes on acceleration responses of the roof when spectral analysis based on quasi-steady theory is used.

Fig. 1 and 2 show the RMS acceleration responses at quarter-span pints under different wind speeds and wind directions. The curves as shown in Fig. 1 and 2 are obtained by the above three approaches respectively. It is clear from the figures that the results predicted by the time domain method well agree with those obtained by the perfect aeroelastic model wind tunnel tests. It also found that the results predicted by spectral analysis based on quasi-steady theory are the same with test results only in tendency, but far more than test results in value. Consequently, spectral analysis based on quasi-steady theory is not well suitable to the analysis of the wind-induced responses of roof structures.

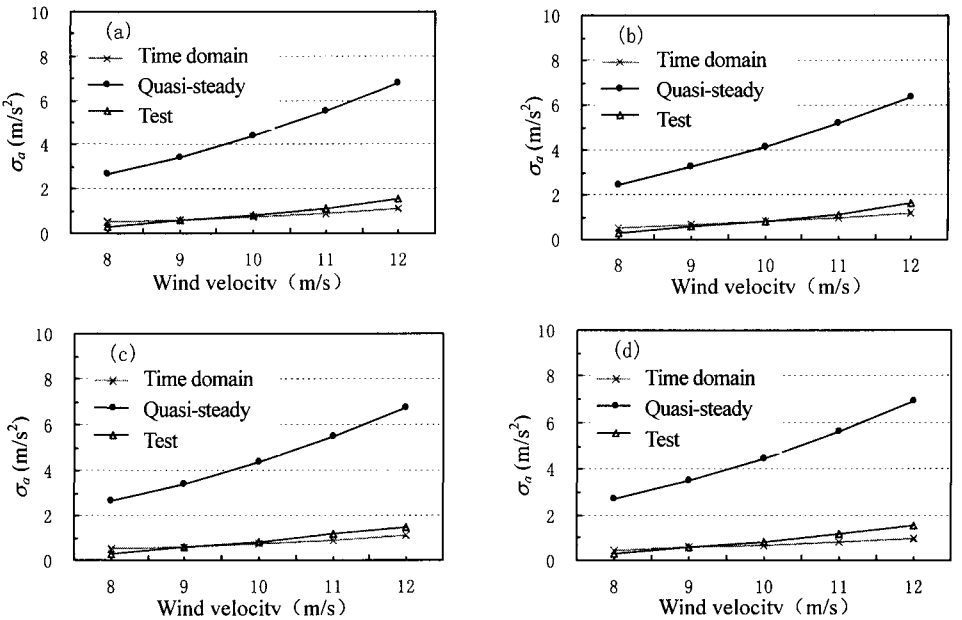


Figure1. RMS acceleration response of roof at left quarter span under different wind velocities:
(a) 0° wind direction ; (b) 15° wind direction ; (c) 30° wind direction; (d) 45° Wind direction

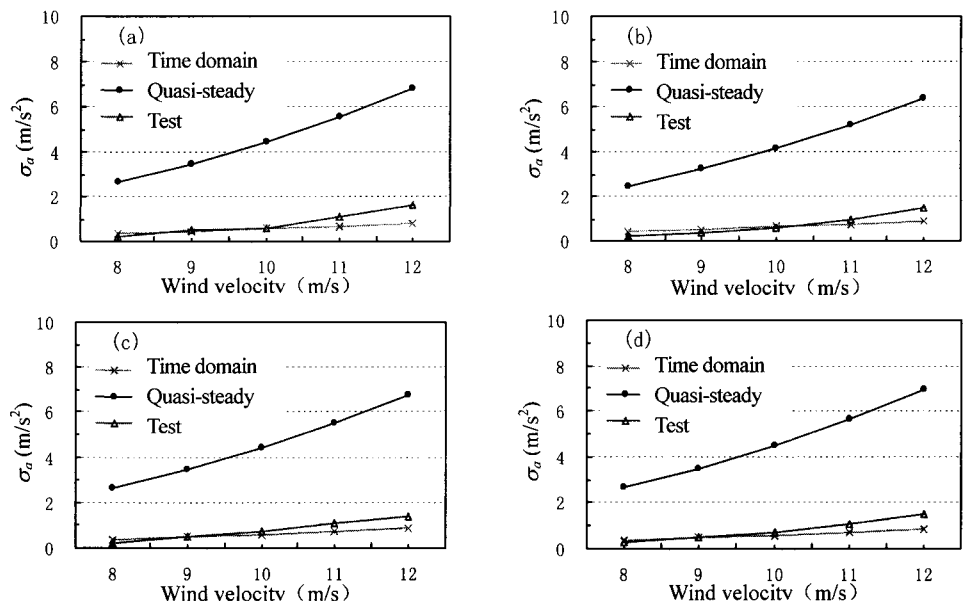


Figure2. RMS acceleration response of roof at right quarter span under different wind velocities:
(a) 0° wind direction ; (b) 15° wind direction ; (c) 30° wind direction; (d) 45° Wind direction

Wind Load Factor

It is common practice to evaluate wind effects on structures using an equivalent static wind load. The equivalent static wind load for a flexible roof may be expressed as the product of the mean wind pressure and a wind load factor. In China Building Load Code (GBJ9-87), wind load factor is specified as the ratio of maximum wind-induced force to static component of wind force acting on the roof. In the previous paper of authors (Lou et al., 2000), it has been pointed out that wind load factor significantly varies with positions on a roof. It indicated that the distribution of wind load factor on the whole roof is a curve surface similar to the first mode shape. Therefore, the wind load factor is not convenient to be used. In fact, if defining a coefficient as the ratio of maximum wind-induced effect (including static and dynamic effect) to wind-induced static effect, such as the ratio of maximum peak displacement response to the mean displacement response in a time duration, this coefficient is denoted as wind effect factor expressed as follows

$$\beta_D = 1 + \frac{U_D}{U_s} = 1 + \frac{\mu\sigma_x}{U_s} \tag{7}$$

where β_D is the wind effect factor of the roof; U_D and U_s are displacement response induced by dynamic component and static component of wind load respectively; σ_x is RMS displacement response of the roof; μ is the peak coefficient of response, inhere, μ is approximately set to be 3.0.

The computed results demonstrate that wind effect factor is almost uniform on the whole roof, and so wind effect factor is prior to wind load factor in estimating wind-induced response. Table 1 shows the wind effect factors of the example prototype roof at the wind velocity of 70.7m/s and under the different wind directions. In this table, the results predicted by time domain method and by spectral analysis based on quasi-steady theory respectively are listed. The following features can be seen: (1) The wind effect factors predicted by spectral analysis based on quasi-steady theory are far more than those predicted by time domain method, (2) The variation of wind effect factor with the wind direction is not significant.

TABLE 1

COMPARISON OF WIND EFFECT FACTORS

Wind direction		0°	15°	30°	45°
Wind load factor	Time domain method	1.30	1.32	1.31	1.30
	Spectral analysis	2.46	2.63	2.49	2.36

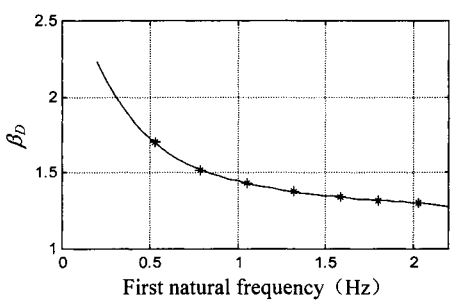


Figure 3: Wind effect factors at different first natural frequency

Further investigation suggests that the wind effect factor depend primarily on stiffness (or frequency) of roof structures. The variation of wind load factor of the example flat square roof with its first natural frequency is shown in Figure 3.

Modification of the Spectral Analysis Based on Quasi-Steady Theory

The spectral method based on quasi-steady theory is used to estimate wind-induced responses of tall buildings due to its simplicity. Can this method still estimate wind-induced responses of roof structures by introducing a modified coefficient to the result obtained by this method? Carefully comparing the curves shown in Fig.1 and Fig.2, it is seen that if the ratio of the result predicted by time domain method to that predicted by this method is near to a constant value, this constant value can be taken as the modified coefficient. For the convenience of practical application, the ratios of the wind effect factors by two methods under different wind velocities and roof stiffness are investigated. As shown in Table 2 and Table 3, the ratios in all cases are near to 0.6, and so the modified coefficient of wind effect factor can be approximately set to be 0.6 when the spectral analysis method based on quasi-steady theory is used to estimate the wind effects on flat roofs with medium deformation.

TABLE 2

MODIFIED COEFFICIENTS OF WIND EFFECT FACTOR UNDER DIFFERENT WIND SPEEDS IN THE CASE OF 2.03Hz ROOF FIRST FREQUENCY

Wind velocity (m/s)	56.6	63.6	70.7	77.8	84.9
Modified coefficient	0.57	0.55	0.53	0.52	0.50

TABLE 3

MODIFIED COEFFICIENTS OF WIND EFFECT FACTOR UNDER DIFFERENT ROOF FREQUENCYS IN THE CASE OF 30m/s WIND SPEED

First frequency (Hz)	0.53	0.79	1.05	1.58	2.03
Modified coefficient	0.593	0.615	0.628	0.634	0.635

CONCLUSIONS

The following conclusions are drawn from comparisons of analytical and test results: (1) The RMS accelerations of the roof under various wind speeds and directions predicted by time domain method well agree with those of the perfect aeroelastic model wind tunnel tests. On the other hand, the results predicted by spectral analysis based on quasi-steady theory are the same with test results only in tendency, but far more than test results in value; (2) A modified coefficient must be introduced for the purpose of that the spectral analysis method based on quasi-steady theory is suitable to estimating wind effects on roofs; (3) The modified coefficient of wind effect factor is approximately set to be 0.6 when the spectral analysis method based on quasi-steady theory is used to predict the wind effects on flat roofs with medium deformation.

ACKNOWLEDGEMENT

The financial support of the National Science Foundation of China through Grant 59978044 for this work is gratefully acknowledged.

References

Case P. C. and Isyumov N. (1998). Wind loads on low buildings with 4:12 gable roofs in open country and suburban exposures. *Journal of Wind Engineering and Industrial Aerodynamics* **77-78**, 107-118.

Kareem A. and Lu P.C. (1992). Pressure Fluctuations on Flat Roofs with Parapets. *Journal of Wind Engineering and Industrial Aerodynamics* **41-44**, 1775-1786.

Lou, W. J. Lu F. and Sun B. N(2000). Study on buffeting response for flexible roof structures. *Advances in Structural Dynamics,* J. M. Ko and Y. L. Xu (eds.), Elsevier Science Lid. Oxford. UK, **2**, 1519-1526.

Marighetti J., Wittwer A., Bortoli M.D., Natalini B., Paluch M. and Natalini M. (2000). Fluctuating and Mean Pressure Measurements on a Stadium Covering in Wind Tunnel. *Journal of Wind Engineering and Industrial Aerodynamics* **84**, 321-328.

Simiu E. and Scanlan R. H. (1986), *Wind Effects on Structures*. 2th ed., John Wiley & Sons. Inc, USA.

Uematsu Y., Yamada M. and Karasu A (1997). Design Wind Loads for Structural Frames of Flat Long-span Roofs: Gust Loading factor for a Structurally Integrated Type. *Journal of Wind Engineering and Industrial Aerodynamics* **66,** 155-168.

Xu Y. L.and Reardon G. F. (1998). Variations of Wind Pressure on Hip Roofs with Roof Pitch. *Journal of Wind Engineering and Industrial Aerodynamics* **73**, 267-284.

Yasui H., Marukawa H., Katagiri J., Katsumura A., Tamura Y. and Watanabe K. (1999). Study of wind-induced response of long-span structure. *Journal of Wind Engineering and Industrial Aerodynamics* **83**, 277-288.

Advances in Building Technology, Volume 2
M. Anson, J.M. Ko and E.S.S. Lam (Eds.)
© 2002 Elsevier Science Ltd. All rights reserved

THE EFFECTS OF WIND-INDUCED DYNAMIC RESPONSE BY ADDED AIR MASS FOR MEMBRANE STRUCTURES

B. N. Sun[1], J. M. Wang[2] and W. J. Lou [1]

[1]Dept. of Civil Engineering, Zhejiang Univ., Hangzhou 310027, China
[2]Dept. of Civil Engineering, Zhejiang Univ. of Science and Technology, Hangzhou, China

ABSTRACT

Based on the characteristics of the wind load and response of membrane structures, the thin airfoil aerodynamic theory is applied to calculate air inertia load of the membrane structures for unsteady flows in the paper. Vortex method is used to derive the formula of added air mass of membrane and the theoretical results are gained at the first time. Some useful results are obtained through analyzing the effects of inertial load caused by the added air mass for dynamic response properties of membrane structures.

KEYWORDS

Membrane structures; Vortex method; Added air mass; Vortex-induced vibration

INTRODUCTION

Among the analyses of wind-induced dynamic responses of long-span roof structures, small deformation is often assumed and the added air mass induced by structural vibration in the unsteady flows is generally neglected. Because membrane structures belong to the light-flexible and small damping structures, large deformation will be produced under the action of wind load. Great turbulence in the boundary layer of atmosphere can cause the vortices to break off and the flows to convert in the process of viscosity diffusion and wake, and the turbulence-induced vibration in this process can't be neglected. Therefore, the added air mass on the membrane structures must be considered by the knowledge of unsteady flows, which is difficult to analyze and not settled well heretofore. In past decade, a few papers analyzed nonlinear wind-induced dynamic responses for membrane structures. But the added air mass is usually not considered in the their theoretical

calculation. Some studies(Harrod 1981, Zhang1990) suggested to use indiscriminately Morison Equation obtained from ocean building dynamics to solve the wind-induced dynamic responses of membrane structures.

In order to study this problem deeply, the thin airfoil aerodynamic theory(Arnold 1976) is applied to calculate added air mass of membrane structures. The vortex sheet of thin airfoil theory fitted to membrane structures in unsteady flows is established. The vortex filaments are used to calculate added mass action on membrane structures. These theoretical results are obtained by some techniques, such as coordinate mapping and Mathematical denotation integral, and the formulae of added air mass for the membrane structures are convenient to study the flexible roofs including long-span structures. Finally, the inertia loads induced by the added air mass are used to analyze the dynamic response of the membrane structures in time domain, and some important results of wind-induced vibration of the membrane structures are obtained.

VORTEX SHEET OF AIRFOIL AERODYNAMICS

The vortex sheet, shown schematically in Fig.1, may be thought of as an infinite number of vortex filaments, each has infinitesimal strength and extends to infinity or to boundary of the flow. The strength of the vortex sheet, γ_m, termed the circulation density, is defined as a limiting form of Stokes's theorem:

$$\gamma_m = \lim_{\Delta s \to 0} (\frac{1}{\Delta s} \int \vec{\mathbf{V}} d\vec{\mathbf{S}}) \tag{1}$$

Where Δs is the width of the sheet enclosed by the contour. If the circulation is clockwise, γ_m is a positive value.

No discontinuities occur anywhere in the velocity field except at the sheet itself. It could be proved (Arnold 1976) that the velocity component parallel to the vortex surface jumps by an amount equal to the strength of the sheet at the point where the contour crosses the sheet surface, i.e.:

$$\gamma_m(x,t) = u_2 - u_1 \tag{2}$$

Suppose a plane membrane is horizontally supported in a static state, the distance between the supports of the membrane is l, the mass per unit area is m. Membrane is assumed to be undergoing a natural vibration continuously in two-dimensional space. The maximum vibration amplitude is H, as shown in Fig.1, and the expression of the dynamic displacement $h(x,t)$ at any point x and time t is:

$$h(x,t) = 4H \frac{x(l-x)}{l^2} \cos \omega t \qquad (0<x<l) \tag{3}$$

The complex velocity potential Φ_z induced by a vortex filament at any position $z = x + iy$ $(i = \sqrt{-1})$ can be expressed as:

$$\Phi_z = i \frac{\gamma_m(\xi,t) d\xi}{2\pi} \ln(z - \xi) \tag{4}$$

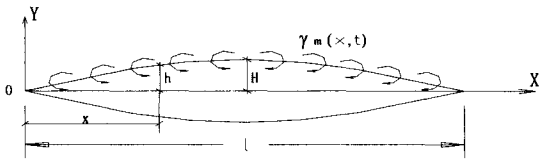


Fig.1 Deformation of membrane and model of vortex sheet schematically

The components of velocity in the x- and y-directions induced by the circulation density $\gamma_m(\xi,t)$ at any point on the membrane can be obtained from equation (4) as $\mathrm{Re}[\partial\Phi_z/\partial z]_{z=x}$ and $\mathrm{Im}[-\partial\Phi_z/\partial z]_{z=x}$, respectively. The total velocity components distributed along the whole membrane are given as follows:

$$\begin{cases} \dfrac{1}{2}(u_1+u_2)=[u]_{y=0}=0 \\ \dfrac{1}{2}(v_1+v_2)=[v]_{y=0}=\dfrac{1}{2\pi}\displaystyle\int_0^l \frac{\gamma_m(\xi,t)}{\xi-x}d\xi \end{cases} \quad (0<x<l) \tag{5}$$

Where u_1, u_2 are the vibration velocity components of the membrane in the x-direction and v_1, v_2 are vibration velocity components in the y-direction respectively, shown in Fig.2. Therefore, v_1, v_2 can be expressed as:

$$\begin{cases} v_1=\dfrac{\partial h}{\partial t}+u_1\dfrac{\partial h}{\partial x} \\ v_2=\dfrac{\partial h}{\partial t}+u_2\dfrac{\partial h}{\partial x} \end{cases} \tag{6}$$

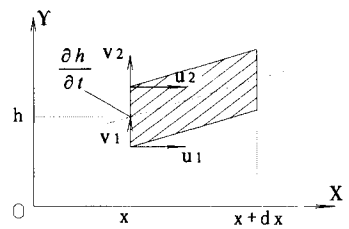


Fig.2 Speed amount of membrane

Applying equations (5) and (6), an integral equation can be obtained as follows:

$$\frac{\partial h}{\partial t}=\frac{1}{2\pi}\int_0^l \frac{\gamma_m(\xi,t)}{\xi-x}d\xi \qquad (0<x<l) \tag{7}$$

Now substituting equation (3) into the equation (7) and integrating, the solution $\gamma_m(x,t)$ will be:

$$\gamma_m(x,t)=-\frac{2H\omega}{\pi}\sin(\omega t)\left[\sqrt{\frac{l-x}{x}}\int_0^l\sqrt{\frac{\xi}{l-\xi}}\frac{4x(l-x)}{l^2}\frac{}{x-\xi}d\xi+\frac{Cl}{\sqrt{x(l-x)}}\right] \tag{8}$$

Where C is an integral constant. Introducing the coordinate transformation:

$$\begin{cases} x=\dfrac{l}{2}(1-\cos\theta_x) \\ \xi=\dfrac{l}{2}(1-\cos\theta_\xi) \end{cases} \tag{9}$$

and substituting equation (9) into equation (8), the solution γ_m becomes as:

$$\gamma_m = -\frac{2H\omega}{\pi}\sin\omega t\left[-\pi\sin\theta_x(1+\cos\theta_x)+\frac{2C}{\sin\theta_x}\right] \tag{10}$$

Because the flow pattern is symmetric with respect to $x = l/2$, the solution γ_m should satisfy a boundary condition:

$$\gamma_m(\frac{l}{2},t) = 0 \qquad or \qquad \gamma_m(\frac{\pi}{2},t) = 0 \tag{11}$$

The integral constant C, determined by above boundary condition, is $\pi/2$. Finally, we get the solution:

$$\gamma_m = 2H\cdot\omega\cdot\sin\omega t\cdot ctg\theta_x\cdot(\sin^2\theta_x - \cos\theta_x) \tag{12}$$

ADDED AIR MASS ON MEMBRANE

According to the definition of velocity potential Φ and generalized Bernoulli's equation, we have:

$$\left[\frac{\partial\Phi}{\partial t}\right]_1 + \frac{1}{2}(u_1^2+v_1^2) + \frac{p_1}{\rho} = \left[\frac{\partial\Phi}{\partial t}\right]_2 + \frac{1}{2}(u_2^2+v_2^2) + \frac{p_2}{\rho} \tag{13}$$

Then, the pressure difference Δp is as follows:

$$\Delta p = p_1 - p_2 = \rho\frac{\partial h}{\partial t}\frac{\partial h}{\partial x}\gamma_m(x,t) + \rho\frac{\partial}{\partial t}\int_0^x \gamma_m(\xi,t)d\xi \tag{14}$$

Where ρ is mass density of the airflow. Also, substituting equations (3) and (12) into the equation (14) and applying coordinate transformation equation (9), the pressure difference Δp can be expressed as:

$$\begin{aligned}\Delta p &= \rho\left(-H\omega\sin^2\theta\sin(\omega t)\right)\left(4H\frac{\cos\theta}{l}\cos(\omega t)\right)\left(2H\omega\sin(\omega t)ctg\theta(\sin^2\theta-\cos\theta)\right)\\ &\quad + 2\rho H\omega^2\cos(\omega t)\int_0^{\theta} ctg\theta_\xi\left(\sin^2\theta_\xi - \cos\theta_\xi\right)\left(\frac{l}{2}\sin\theta_\xi\right)d\theta_\xi\\ &= \frac{8\rho H^3\omega^2}{l}\sin^2(\omega t)\cos(\omega t)(\sin\theta\cos^3\theta - \sin^3\theta\cos^2\theta)\\ &\quad + \rho Hl\omega^2\cos(\omega t)(\frac{1}{3}\sin^3\theta - \frac{1}{2}\theta - \frac{1}{4}\sin 2\theta)\end{aligned} \tag{15}$$

Based on the energy conservation, the kinetic energy increment dT_f of the air should be equal to the work done on the whole membrane by the force corresponding to Δp during time period dt. This relation could be expressed as:

$$\begin{aligned}dT_f &= \int_0^l \Delta p ds\,\frac{\partial h}{\partial t}dt = \int_0^l \Delta p\sqrt{1+\left(\frac{\partial h}{\partial x}\right)^2}dx\,\frac{\partial h}{\partial t}dt \approx \int_0^l \Delta p\left[1+\frac{1}{2}\left(\frac{\partial h}{\partial x}\right)^2\right]dx\,\frac{\partial h}{\partial t}dt\\ &= \rho H^2 l^2\omega^3\sin(\omega t)\cos(\omega t)dt\left\{\frac{11\pi}{96}+0.674132\left(\frac{H}{l}\right)^2\cos^2(\omega t)+\frac{\pi}{64}\left(10+24\left(\frac{H}{l}\right)^2\cos^2(\omega t)\right)\left(\frac{H}{l}\right)^2\sin^2(\omega t)\right\}\end{aligned} \tag{16}$$

Denoting the added air mass per unit area of the membrane as m_a, the kinetic energy increment dT_f of the vibration membrane can be expressed as:

$$\begin{aligned} dT_f &= \frac{\partial}{\partial t}\left[\frac{1}{2}m_a\int_0^l\left(\frac{\partial h}{\partial t}\right)^2 dx\right]dt = m_a\int_0^l\frac{\partial h}{\partial t}\frac{\partial^2 h}{\partial t^2}dxdt \\ &= \frac{8}{15}H^2 l\omega^3\sin(\omega t)\cos(\omega t)dt\cdot m_a \end{aligned} \tag{17}$$

From the equation (16) and equation (17), we can obtain the added air mass per unit area m_a:

$$m_a = \rho l\left(\frac{55\pi}{256}+1.0922\left(\frac{H}{l}\right)^2+0.1718\left(\frac{H}{l}\right)^2\cos(2\omega t)+0.5522\left(\frac{H}{l}\right)^4\sin^2(\omega t)\right) \tag{18}$$

It is a theoretical formula of the added air mass for the membrane structures, which shows that the added air mass m_a depends on air density ρ, distance l between the supports, maximum vibration amplitude H, circular frequency ω and time t. Since H/l is less than 0.1 in most cases, the forth term of the equation (18) is the quartic small quantity and could be neglected. Also the third term is far less than the sum of the first and second terms in equation (18). So it is adequacy to hold the first two terms. Then equation (18) could be approximately expressed as:

$$m_a = \rho l\left(\frac{55\pi}{256}+1.0922\left(\frac{H}{l}\right)^2\right) \tag{19}$$

Thus, the added air mass m_a can be considered as independent on circular frequency ω and time t. The non-dimensional form of the equation (19) will be:

$$\overline{m}_a = \frac{55\pi}{256}+1.0922\overline{H}^2 \tag{20}$$

Where $\overline{m}_a$ and $\overline{H}$ are non-dimensional parameters and they are equal to $m_a/\rho l$ and H/l respectively.

From equation (20), it is shown that $\overline{m}_a$ is quadric function of $\overline{H}$. When $\overline{H}$=0, $\overline{m}_a$=0.6750, and $\overline{H}$=0.1, $\overline{m}_a$=0.6859, the $\overline{m}_a$ only increases a small value (1.6%). By the numerical integral calculation for some H、ω and t, Minami(1998) indicated that $\overline{m}_a$ does not depend on H、ω and t and suggested that $\overline{m}_a$ equal 0.68. But from the theoretical equations (18) and (20) obtained from present study, the non-dimensional added air mass $\overline{m}_a$ increases with the $\overline{H}$ as power function. Only when high-order small terms are neglected, m_a becomes independent on ω and t. When $\overline{m}_a$=0.68, $\overline{H}$ is equal to 0.068, which means that the amplitude of structure vibration reaches as high as 6.8% of the distance between the supports. Since varying range of $\overline{m}_a$ is small in general cases, the value of $\overline{m}_a$ could be taken as a constant, which corresponds to the numerical results by Minami(1998). In this case, the added air mass on membrane is directly proportional to the product of air density ρ and span l. The larger span between the supports of the membrane structures is, the greater added air mass and the air inertia loads on the structures, and more sensitive to fluctuation wind loads on the membrane structures.

So how to reduce the distances between the local supports should be taken into account in resisting-wind design of membrane structures.

WIND LOADS OF THE MEMBRANE STRUCTURES

The wind loads of the membrane structures are composed of fluctuated wind loads and inertia loads induced by the added air mass. The general formula on a point i of the membrane structures is given by:

$$P_i(t) = \frac{1}{2}\mu_{si}\rho A_i V_i^2(t) - m_a A_i \frac{\partial^2 h}{\partial t^2}$$
$$= \frac{1}{2}\mu_{si}\rho A_i V_i^2(t) + \left(\frac{55\pi}{64} + 4.3688\left(\frac{H}{l}\right)^2\right)\rho A_i \frac{H}{l}\omega^2 x_i(l - x_i)\cos(\omega t) \tag{21}$$

Where the first term of right side of expression (21) is resistance force, i.e. the so-called general wind load, in which μ_{si} is the wind body-shape coefficient, ρ is the air density, A_i is the correlative area, $V_i(t)$ is the fluctuated wind speed and could be artificially generated by linearly filter method of self-regression model through application of Kaimal spectral density. In this paper, we selected the Kaimal constant is 0.4, the roughness length is 0.2m, the time step length is Δt=0.1061s, the time step numbers is N=1024 and self-regression step is p=4. The second term of equation (21) is the inertia loads of the added air mass on the membrane structures in unsteady vortices.

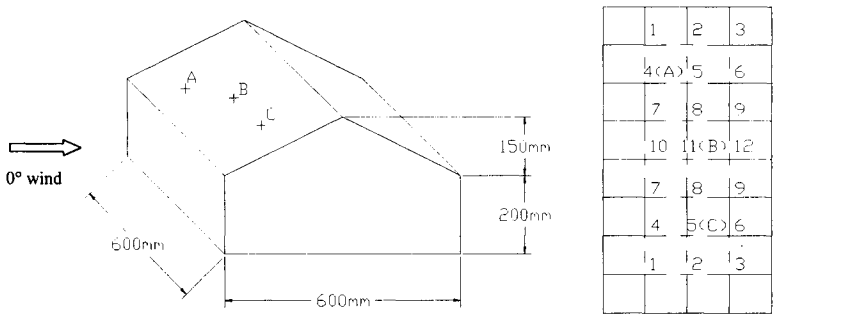
The equation (21) is the wind load equation for membrane structures in which the vortex-induced air inertia load is calculated when membrane structures vibrate in unsteady flows. From the equation we can see that the loads are related to air density ρ, span l, vibration amplitude H, the position x_i and circular frequency ω. But the air inertia loads acting on the cylinder in unsteady flows or from the Morison Equation are a constant in any position of the structures, that means independent of structural vibration. Generally, since the direction of inertia loads is not consistent with that of flows, the inertia loads of cylinder structures and from Morison equation can't be indiscriminately applied to the membrane structures. Here equation (21) indicates that the inertia loads vary with the point position of the structures, which truly reflects the basic characteristics of air inertia loads acting on the membrane structures.

ANALYSIS OF VORTEX-INDUCED VIBRATION IN THE TIME DOMAIN

The movement equation of the membrane structures is

$$\boldsymbol{M}\ddot{\boldsymbol{u}}(t) + \boldsymbol{C}\dot{\boldsymbol{u}}(t) + \boldsymbol{K}\boldsymbol{u}(t) = \boldsymbol{P}(t) \tag{22}$$

Where $\boldsymbol{M}$ and $\boldsymbol{K}$ is the mass and stiffness matrix respectively. Assuming damping matrix $\boldsymbol{C}$ is Rayleigh damping and the damping ratio is 0.055. $\boldsymbol{P(t)}$ is the wind loads acting on membrane structures and the equation (21) is taken as its expression.



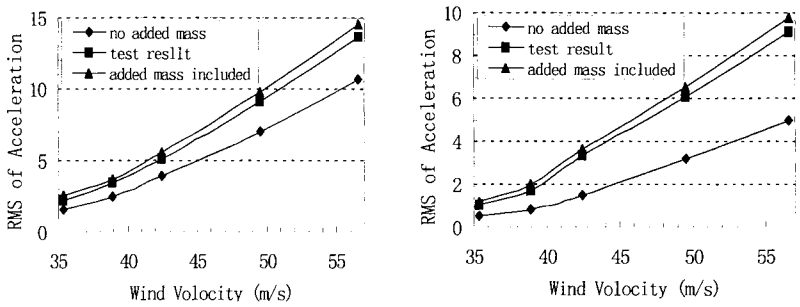
(a) Calculation modal (b) Position number

Fig.3 Computation modal of membrane structures

Taking a double-slope roof membrane structures as an example, as shown in figure 3, the time domain analysis is applied to calculate dynamic responses of windward roof of membrane structures when the around walls of the structure are closed and wind angle is equal to 0°.

Figure 4(a) and 4(b) represent acceleration RMS at point A and B for different wind velocities and the analytical results are compared with that obtained from aeroelastic modal test(Wang 2001) when added air inertia is applied or not respectively. When the first term of equation (21) is only used to calculate structural response, i.e. does not include added air mass, acceleration RMS in time domain is evidently less than that obtained from wind tunnel test. Its calculated error is quite large, especially in lower positions of the structures, for example at point A. The reason is that Bernoulli Equation is based on hypothesis of quasi-steady flows, in which wind pressure fluctuation entirely is attributed to wind turbulence. From the knowledge of gradient wind, the wind velocity at point A is relatively small and its fluctuation is small too. Therefore, the corresponding wind pressure and its wind-induced vibration are small. When the added air mass is taken into account, the calculating acceleration RMS increases evidently and its value is close to or somewhat greater than result obtained from wind tunnel test.

When wind velocity is equal to 42.43m/s, wind angle is 0° and around walls of double-slop roof structure are closed, as shown in fig. 3, the added air mass is included to calculate displacement and acceleration RMS of windward roof for the structure. The results show that the influence of added air mass for displacement average of the structures is very small. But the influence of displacement RMS and acceleration RMS are evidently great. Taking the center point of the structure as an example, when added air mass is taken into account, the displacement RMS increases from 5.14cm to 8.32cm by 1.619 times. For the other positions, the displacement RMS also increase by 1.567~2.766 times. Also, the acceleration RMS of the structures evidently increases by 1.360~2.830. It is shown that the vortex-induced dynamic response is a main influence factor of membrane structural vibration and cannot be neglected in wind-resisting design.



(a) Measure point A (b) Measure point B

Fig.4 Acceleration RMS on point A and B at different wind velocity

CONCLUSIONS

In the present study, the theoretical formulae of the added air mass for the membrane structures are derived and are applied to analyze the wind-induced dynamic response of large-span flexible roof. The FEM and time domain analysis is also applied to study vortex-induced vibration of the membrane structures. Some main conclusions are obtained as follow:

1. The added air mass is approximately independent on natural frequency of the membrane structures and time, but varies directly with the ratio of product $\rho \cdot l$.

2. The inertia loads caused by added air mass is related not only with air density ρ and span l, but also with the position x_i, vibration amplitude H and frequency ω.

3. The added air mass has little influence on displacement average, but has greatly influence on displacement RMS and acceleration RMS. It means that the added air mass is a main factor for increasing the response of membrane structures and can't be neglected in resisting-wind design.

ACKNOWLEDGEMENT

The financial support of the National Science Foundation of China through Grant 59978044 for this work is gratefully acknowledged.

References

Arnold M. Kuethe and Chuen-Yen Chow(1976). *Foundations of Aerodynamics: Bases of Aerodynamic Design.*

Harrod M. G. et al(1981), Translated by Hou Guoben et al. Ocean building dynamics. Ocean Publishing Company.

Minami H.(1998), Added Mass of a Membrane Vibration at Finite Amplitude. *Journal of Fluids and Structures* **12**, 919-932.

Wang Jimin, Sun Bingnan, Lou Wenjuan(2001), The Characteristics of Wind Load and Wind-Induced Vibration of Membrane Roof by Wind Tunnel Experiments. *Chinese Journal of Space Structures* **7:3**, 18-25.

Zhang Xiangting(1990). *Wind Load Theory of Engineering Structures and Wind-resisting Handbook* Tongji University Publishing Company, CHINA.

ENVIRONMENTAL TECHNOLOGIES:

ADVANCED PERFORMANCE MODELLING

This Page Intentionally Left Blank

Advances in Building Technology, Volume 2
M. Anson, J.M. Ko and E.S.S. Lam (Eds.)
© 2002 Elsevier Science Ltd. All rights reserved

PARAMETERIZATION STUDY ON THE OPERATING EFFICIENCY OF AIR-COOLED CHILLERS

K.T. Chan and F.W. Yu

Department of Building Services Engineering
The Hong Kong Polytechnic University, Hong Kong, China

ABSTRACT

The chiller plants for providing cooling in buildings in a dense urban environment, as is Hong Kong, often require heat rejection by air-cooled condensers. Improved efficiency of air-cooled reciprocating chillers requires knowledge of the behaviours of the operating parameters. A parameterization study aiming at exploring such behaviours was carried out with the hybrid use of the operating data from an installed chiller in an existing building and the predicted data by a validated chiller model. The chiller efficiency generally increases with the chiller part load ratio. A close relationship between the evaporator performance and the chiller part load ratio was observed, but varying the chilled water flowrate and the evaporating temperature shows a diverse effect on the evaporator performance. Multiple steps of capacity control would result in fluctuating compressor power input. Evaluation of the condenser performance indicates that the performance cannot be simply represented by any one of the control parameters: part load ratio, refrigerant mass flow, heat rejection airflow and condensing temperature. The opportunity of reducing the condensing temperature at below-design outdoor conditions for better efficiency and energy saving was exploited through the evaluation of the boundary and the means to achieve the lowest possible working condensing temperature.

KEYWORDS

Air-cooled chiller, reciprocating compressor, operating efficiency, condensing temperature

INTRODUCTION

The chiller plants for providing cooling in buildings in a dense urban environment, as is Hong Kong, often require heat rejection by air-cooled condensers. Energy consumption using different heat rejection methods has been reported, e.g. Yik, et al. (2001). The electricity consumption by chiller plants is large, and imposes a direct impact on the peak demand load on the power station. Improving the operating efficiency of the chillers would lead to less electricity consumption and hence less emission of global warming gases from power stations, which contributes to the overall scheme for building energy effectiveness.

The operating efficiency of a chiller can be expressed in kW/ton, which is the chiller consumption per ton of refrigeration output. Chan and Yu (2002) reported that the cooling effectiveness is penalized by the high electricity consumption by the chillers running at low efficiency as they work at a high condensing temperature of about 50°C based on the design outdoor condition of 33°C. Similar finding was stated by Smith and King (1998). Poor chiller efficiency also results from the oversized chillers running at part loads most of the time, and the inappropriate matching of operating chillers to the building cooling load based on the experience of the plant operators. Improving the chiller efficiency requires knowledge of the behavior of each operating parameter on the chiller consumption and the cooling output. Nevertheless, there is a lack of culture in keeping in-situ chiller operating parameters, which poses the difficulties in verifying the chiller performance over the manufacturer specification and developing optimum control strategies for improved chiller efficiency.

This parametric study explores the behaviors of the operating parameters of direct air-cooled chillers with reciprocating compressors from a local chiller plant. Study is made on the key operating parameters: evaporating and condensing pressures, chilled water flow rate, supply and return chilled water temperatures and entering and leaving condenser air temperatures, as well as the chiller power together with other predicted parameters from a chiller system model. It is intended to exploit further how the chiller efficiency can be improved by reducing the condensing temperatures under the local mild weather. Results of the parametric analysis will be useful in three ways. Firstly, the relative significance of each parameter on the chiller efficiency can be identified, which will provide a gateway for the chiller system simulation study and to verify the confidence levels on the prediction of the chiller component performances by simulation. Secondly, the understanding of the characteristic relations within the performance and operating parameters can help to trace out a set of chiller efficiency curves under different weather-load conditions for the optimal combinations of chillers and the evaluation of the year round consumption. Thirdly, the results support the need of developing control of lowering the condensing temperature by making full use of the below-design outdoor temperature conditions for maximizing the chiller efficiency, taking into account the likely effects and boundaries of other operating parameters.

THE STUDIED CHILLER PLANT AND THE CHILLER MODEL

The Studied Chiller Plant

The studied chiller plant consists of seven identical sets of air-cooled reciprocating chillers using refrigerant R-22 with rated capacity of 120 tons of refrigeration (420 kW). The loading and unloading of chillers are manually controlled with reference to the return chilled water temperature, chiller running ampere and outdoor air temperature. At a particular cooling demand, the chilled water flow rate through each chiller may be equal to or greater than the design flow rate by operating more pumps than necessary.

Each single chiller typically composes of three semi-hermetic reciprocating compressors with cylinder unloaders for capacity control, a thermostatic expansion valve for regulating the refrigerant feed to the evaporator, a shell-and-tube evaporator and an air-cooled condenser of finned coils with multiple condenser fans. There are six steps of capacity control with a minimum of 33% rated capacity by staging the three compressors with cylinder unloaders. Each operating compressor is interlocked with 3 constant-speed condenser fans. The required heat rejection when adopting head pressure control can be obtained by cycling the condenser fans.

Hourly operating parameters of the individual chillers were obtained from the manually recorded readings from the built-in instruments. The operating parameters include: evaporating and condensing pressures, P_{ev} and P_{cd} (kPa), chilled water flow rate m_w (kg/s), supply and return chilled water

temperatures, T_{chws} and T_{chwr} (°C), entering and leaving condenser air temperatures, T_{cdae} and T_{cdal} (°C) and chiller running ampere, I_{ch}. Field measurements using portable instruments for the running ampere, power factor and chilled water flow rate were also carried out to substantiate the accuracy and reliability of the recorded data.

The Chiller System Model and Parameter Evaluation

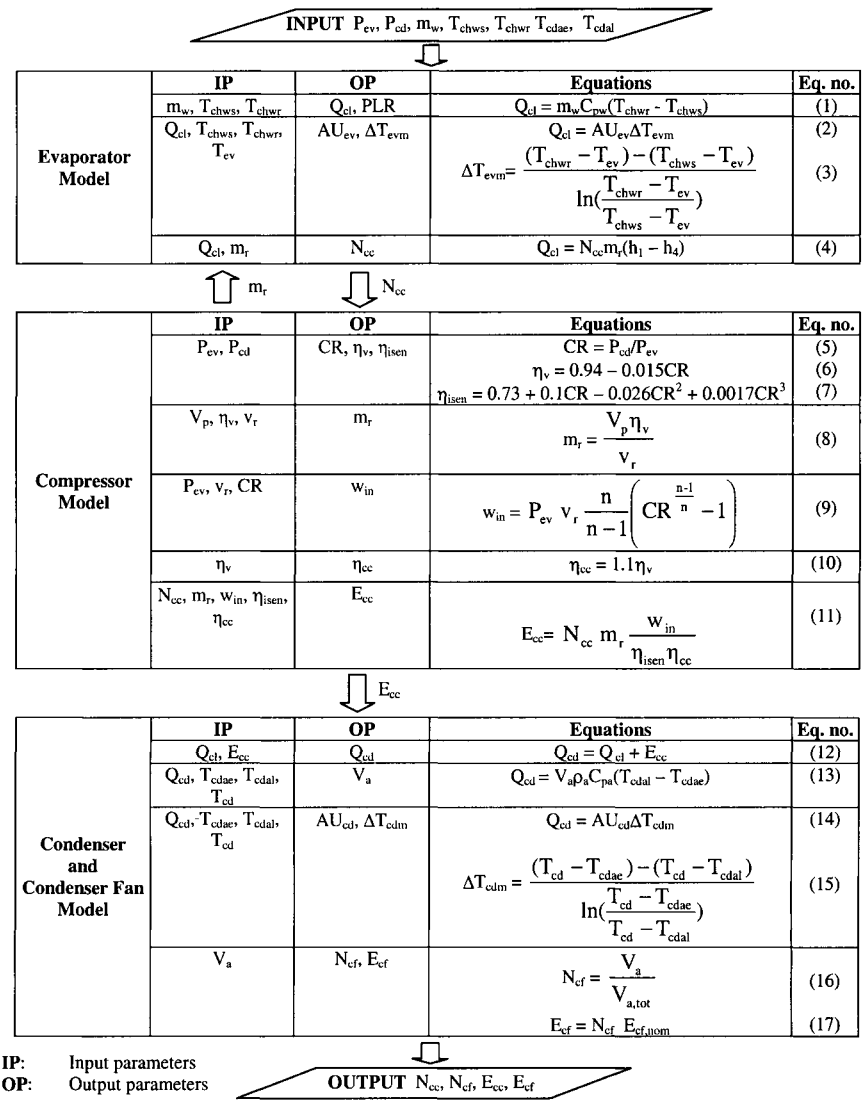


Figure 1: The chiller system model.

In the vapor compression cycle of chiller operation, the thermodynamic states of the refrigerant can be determined from the state equations of the refrigerant. Figure 1 shows the system model containing

different sets of empirical, mass and energy equations (1) to (17) within the chiller components. The hourly operating data (i.e. P_{ev}, P_{cd}, m_w, T_{chws}, T_{chwr} T_{cdae}, and T_{cdal}) constitute the independent input parameters to evaluate the predicted parameters that cannot be directly monitored but influencing the chiller consumption. It is expected that the predicted parameters would satisfy with real operating conditions as the range of the input parameters complies with the actual operating conditions. The chiller part load ratio, PLR was used to indicate the cooling load. The procedures and assumptions for the evaluation of the predicted parameters are described as below.

For the compressor model, the piston displacement of a compressor, V_p (m^3/s) in Eqn. (8) relating to the cylinder diameter, stoke of the piston, cylinder number per compressor and the revolution per second is regarded as a constant and can be evaluated by using the manufacturer data at the rated condition. For a typical reciprocating compressor, the volumetric efficiency, η_v is related to the compression ratio, CR by the empirical Eqn. (6) (Wang 2001). The refrigerant mass flow rate per capacity control step, m_r can be determined from the known parameters of η_v and the specific volume of refrigerant at the compressor suction state, v_r. The predicted m_r is then used to evaluate the required number of capacity control steps, N_{cc} for a certain cooling load using Eqn. (4) in the evaporator model.

The isentropic compression efficiency, η_{isen} is empirically governed by the compression ratio, CR in Eqn. (7) (Tassou, et al. 1998). Since there is no mathematical relation governing the compressor efficiency, η_{cc}, it is firstly approximated to be the volumetric efficiency with additional 10% to offset the power loss due to the mechanical friction in the compressor as given by Eqn. (9). Subsequent calibration to the η_{cc} can be carried out by comparing the results of the predicted output parameters with the operating data to give a derating factor as a function of the part load ratio.

For a specific cooling load the required heat rejection, Q_{cd} (kW) is readily calculated using Eqn. (12) upon the cooling load, Q_{cl} (kW) and the compressor power input, E_{cc} (kW) are evaluated from the evaporator and compressor models. The calculated Q_{cd} can then be used to find out the required condenser airflow, V_a (m^3/s) and the number of operating condenser fans and hence the fan power, E_{cf} (kW) based on the modeling equations in the condenser model.

The predicted power consumption of an operating chiller, E_{ch} by the system model is given by Eqn. (18), whereas the actual chiller power consumptions were obtained from the hourly recorded data.

$$E_{ch} = E_{cc} + E_{cf} \tag{18}$$

RESULTS AND DISCUSSION

Model Validation

Model validation can be accomplished by comparing the predicted data with the operating data and calibrating the empirical model equations so that the discrepancy falls within ±10% of the operating data. The chiller efficiency curve defined as a plot of the kW/ton against the chiller part load ratio was used here for the validation process. Figure 2 shows the existing data, the predicted data by the model after calibrating the compressor efficiency, the regression line of the existing data of chiller efficiency together with the ±10% boundary lines.

Nearly all the predicted values lie within the ±10% boundary lines. Parametric analysis can then be carried out based on the operating parameters and the predicted parameters from the validated model.

In the existing chiller plant studied the efficiency exceeded 1.3 kW/ton most of the time, indicating that the chiller operation cannot meet the minimum COP of 2.7 (i.e. 1.3 kW/ton) required for air-

cooled reciprocating chillers under the code of practice for energy efficiency of air-conditioning installations implemented by the government (EMSD, 1998). This low part-load efficiency of the air-cooled chiller deserves the exploration of optimum control strategies to minimize the compressor power at the below-design conditions.

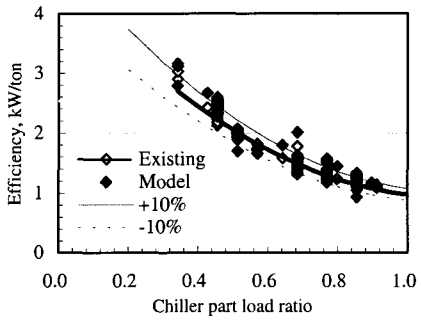


Figure 2: Chiller efficiency curve obtained from existing data (with modeled data for comparison)

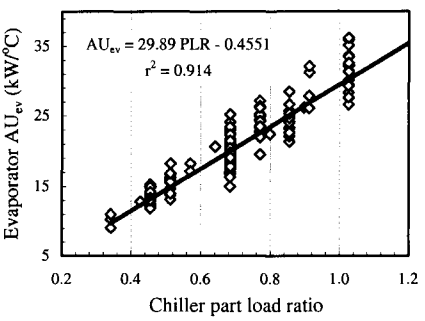


Figure 3: Correlation of the evaporator performance with the chiller part load ratio

Parametric Analysis

Having identified that the chiller efficiency is dependent on the part load ratio, it is necessary to exploit the change of the performance parameters of the chiller components in response to the part load ratio and the relative significance of the control parameters on the performance.

As can be seen in Figure 3, the evaporator performance parameter expressed by the heat transfer coefficient, AU_{ev} closely relates to the chiller part load ratio, with a coefficient of determination of 0.91. For a certain cooling capacity, the AU_{ev} can be explicitly predicted by the regression equation. Such explicit equation is preferable in developing the chiller system model for steady-state simulation when the ease of computation prioritizes over the accuracy. Precise prediction on the evaporator performance should resort to the mechanistic relations on the shell-and-tube heat exchanger involving the shell side and tube side heat transfer coefficients together with the specific parameters on the evaporator geometric and fluid properties. The coefficients associated with the chilled water mass flow, m_w and the cooling capacity, Q_{cl} would introduce implicit equations, under which all the parameters have to be solved by the iterative approach.

It is expected that the AU_{ev} of the evaporator and cooling capacity are enhanced with larger chilled water flowrate. The trade-off between the enhanced cooling capacity and the increased pump power incurred by larger water flow should be investigated, especially at the low part load condition when the pump power may outweigh the compressor power. Another operating strategy is to raise the evaporating temperature by setting the supply chilled water temperature at a higher value under the part load condition. Nevertheless, from the parametric analysis, appreciable improvement in the evaporator performance cannot be obtained by increasing the evaporating temperature during the part load operation. There exists a wide range of the AU_{ev} at a particular evaporating temperature and a clear trend between the two cannot be observed.

The results of the parametric analysis on the evaporator side indicates that varying the control parameters of chilled water flow and the evaporating temperature shows a diverse effect on the chiller operating efficiency, as they do not bear a close relationship with the evaporator heat transfer coefficient. It suggests that the mechanistic relation of chilled water flow rate on the AU_{ev} will be dominant at the tube side heat transfer coefficient, whereas it produces fluctuating effect on the shell

side heat transfer coefficient. The direct relation between the chiller efficiency and the part load ratio becomes justified if the operating chiller is maintained at constant chilled water flow.

Figure 4 depicts the capacity control steps by staging compressors and unloading cylinders in response to different part load ratios. Referring to Figure 5, at a constant part load ratio, the compressor power and work of compression exhibits a linear relationship. However, the compressor power values shift up and down with changes of part load ratio. This explains for the need of applying a derating factor as a function of part load ratio to the compressor efficiency in the prediction of actual compressor power. This modeling approach is common to mechanistic models in which the mechanistic relations employ empirical functions to predict performance of the modeled components and to simplify the required geometric parameters.

It is noted that fluctuating compressor power occurs at part load ratio of around 0.8 at which the 4th and 5th capacity control steps coexist, and higher compressor power occurs at lower part load ratios handled by half-load operating compressors. This situation can be improved by using variable compressor speed to modulate the refrigerant flow on continuous basis, but is not feasible for the reciprocating chillers where the refrigerant flow is intermittently controlled by unloading cylinders and staging of compressors.

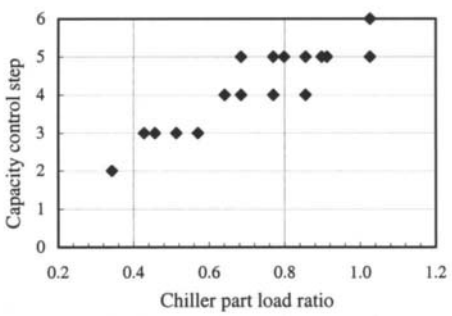


Figure 4: Required capacity control step for various chiller part load ratio

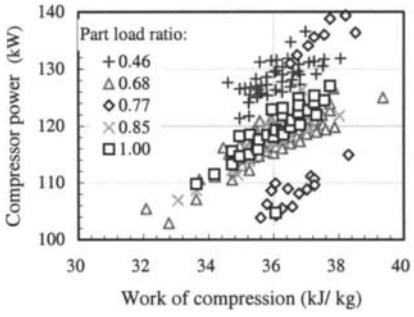


Figure 5: Compressor power vs. work of compression at various part load ratio

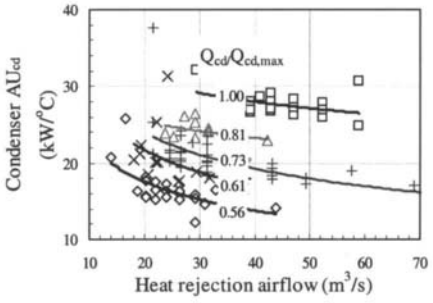


Figure 6: Effect of heat rejection airflow on the condenser performance

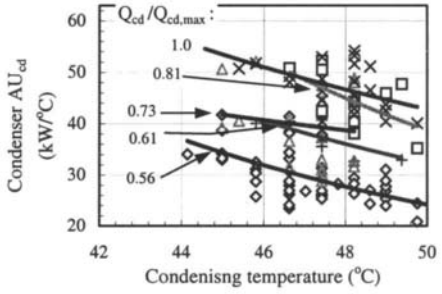


Figure 7: Effect of condensing temperature on the condenser performance

Similar to the behavior of the evaporator performance, the condenser performance in terms of the condenser heat transfer coefficient, AU_{cd} increases with the chiller part load ratio, but the correlation is much weaker than in the evaporator. Further parametric analysis illustrates that the condenser performance cannot be simply represented by any one of the control parameters: total refrigerant mass

flow, m_r, heat rejection airflow, V_a and condensing temperature, T_{cd}. As shown in Figure 6, the condenser performance increases with the normalized heat rejection ratio (i.e. $Q_{cd}/Q_{cd,max}$), but unexpectedly, the increase in condenser airflow would depress the condenser performance at any particular heat rejection ratios.

Since the refrigerant mass flow and the heat rejection airflow are constrained by the operating balances of the cooling load and the required heat rejection, they are not controllable for energy efficiency under varying weather-load conditions. As seen in Figures 7 and 8, the condenser performance and the chiller efficiency are improved with downward shift of condensing temperature at below-design outdoor temperature even though the operation is under head pressure control.

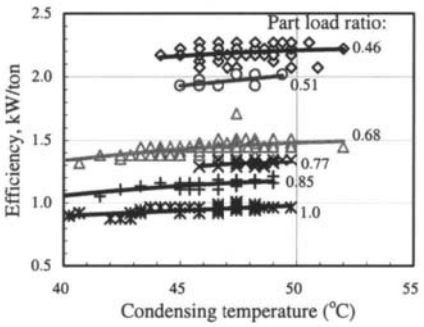


Figure 8: Relationship between the chiller efficiency and the condensing temperature

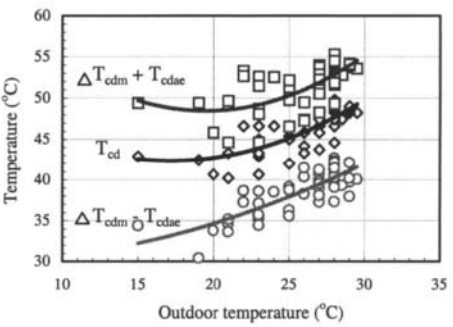


Figure 9: Boundaries for the condensing temperature at various outdoor temperatures

Opportunity of Reducing the Condensing Temperature

For a certain heat rejection, the condensing temperature can be reduced by cycling on more condenser fans to increase the heat rejection airflow. To exploit the likely boundary conditions experienced by the condensing temperature, two specific parameters: $\Delta T_{cdm} + T_{cdae}$ and $\Delta T_{cdm} + T_{cdal}$ are plotted together with the condensing temperature, T_{cd} against the outdoor temperature, T_{cdae} as shown in Figure 9. The condensing temperature data lie within the $\Delta T_{cdm} + T_{cdal}$ and the $\Delta T_{cdm} + T_{cdae}$ at any outdoor temperature. The two parameters form the upper and lower boundaries, and that the condensing temperature follows the inequality below:

$$\Delta T_{cdm} + T_{cdae} < T_{cd} < \Delta T_{cdm} + T_{cdal} \tag{19}$$

It is desirable to control the condensing temperature close to the lower boundary by making full use of the lower outdoor temperatures during the mild season. The condensing temperature tends to drop slightly with decreasing outdoor temperature under the head pressure control by cycling on more condenser fans to induce larger heat rejection airflow. But this drop of condensing temperature, as seen in Figure 9, is small. The potential of reducing the condensing temperature can be greater if the head pressure control method is discarded.

The constraint of lowering the condensing temperature lies on whether ΔT_{cdm} can be reduced, which can be achieved through the enhancement of the condenser heat transfer coefficient, AU_{cd}.The existing control makes the condenser operate at the ceiling of ΔT_{cdm} (i.e. 20°C) with the condensing temperature of above 50°C most of the time, which is undesirable for energy efficiency.

The maximized chiller efficiency occurs at the lowest possible condensing temperature governed by

the outdoor temperature and the condenser performance. However, the lower boundary for the condensing temperature is constrained by the requirement for lubrication oil return and for the thermostatic expansion valve to work properly. Further experimental and simulation studies are required to develop the control algorithm to achieve the lowest possible condensing temperature making use of the low outdoor temperatures available during the mild weather, and taking into account the operational constraints. Quantification of the improved chiller efficiency and the year round energy saving can then be made from a set of chiller efficiency curves generated by a chiller system simulation together with the anticipated weather-load conditions.

CONCLUSIONS

A parameterization study aiming at exploring the behaviors of the operating parameters of the air-cooled reciprocating chillers by the hybrid use of the operating data of an existing chiller and predicted data by a chiller system model has been carried out. A chiller system model taking into account the thermodynamic properties of the vapor compression cycle and the operating balances with the chiller components was developed and validated to predict other parameters influencing the chiller efficiency.

Increasing the chilled water flow and the evaporating temperature to enhance the evaporator performance is likely to be offset by the additional pump power and a trade off study between the two should be carried out. The constraints of the chilled water temperature reset control for improved efficiency lie on the limited enhancement on the evaporator performance and the additional pump power from the increased chilled water flow. The realistic compressor power performance can be predicted using an empirical expression of compressor efficiency relating to the part load ratio. Fluctuating compressor power and chiller efficiency by the multiple number of capacity control steps was identified.

Evaluation of the condenser performance indicates that the chiller efficiency as well as the condenser performance can be improved by reducing the condensing temperature. The analysis on two specific parameters: $\Delta T_{cdm} + T_{cdae}$ and $\Delta T_{cdm} + T_{cdal}$ from the operating data confirms that the condensing temperature is lower bounded by $\Delta T_{cdm} + T_{cdae}$ and upper bounded by $\Delta T_{cdm} + T_{cdal}$. The condensing temperature can be brought down by lowering the upper boundary through introducing additional heat rejection airflow by driving more numbers of condenser fans. It can also be reduced by lowering the ΔT_{cdm} through the enhancement of the heat transfer coefficient, AU_{cd}.

ACKNOWLEDGEMENTS

This study is supported by the HKSAR Research Grant Council, grant no. PolyU5018/00E.

REFERENCES

Chan K.T. and Yu F.W. (2002). Part load efficiency of air-cooled multiple-chiller plant. *Building Serv Eng Res & Tech* **2:3**, 31-41.

EMSD, The Government of the HKSAR. (1998). *Code of practice for energy efficiency of air conditioning installations*. Printing Department, HKSAR.

Smith M. and King G. (1998). Energy saving controls for air-cooled water chillers. *Building Services Journal,* April, 47-48

Tassou S.A., Ge Y.T., Datta D. and Chan K.Y. (1998). Modeling and control of multi-compressor food retail refrigeration systems. *IMechE Seminar Publication* **15**, 53-66.

Wang S.K. (2001). *Handbook of air conditioning and refrigeration*. New York: McGraw-Hill.

Yik F.W.H., Burnett J. and Prescott I. (2001). Predicting air-conditioning energy consumption of a group of buildings using different heat rejection method. *Energy and Buildings* **33**, 151-166.

Advances in Building Technology, Volume 2
M. Anson, J.M. Ko and E.S.S. Lam (Eds.)
© 2002 Elsevier Science Ltd. All rights reserved

THE DESIGN OF HIGHLY GLAZED FACADES AND THEIR ENVIRONMENTAL IMPACT

Phil Jones

Welsh School of Architecture
Cardiff University, Cardiff CF10 3NB

ABSTRACT

Thermal comfort and energy use in modern office type spaces is closely related to the thermal performance of the glazed façade. The ability to provide shading and thermal insulation can influence the type of environmental system for cooling and ventilation. This paper will describe the use of computer modelling to predict glazing performance in relation to modern office environments. A combination of dynamic thermal modelling and spatial airflow modelling has been used in the design of a range of glazed facades. The paper will draw on experience of real façade design projects based on new and existing offices in Europe, involving different combinations of glazing treatments and internal environmental systems. The appropriateness for such systems in Hong Kong is discussed.

KEYWORDS

Facades, energy efficient design, thermal modelling, airflow modelling, chilled surface cooling.

INTRODUCTION

In recent years there have been interesting developments in façade design in Europe. This has largely been in response to the design of 'climate selecting' or 'passive' buildings that can provide comfort conditions with the efficient use of energy. Many such buildings have highly glazed facades to provide daylit spaces, visual contact between inside and outside, and to provide aesthetically pleasing elevations. However, thermal conditions and energy use in modern office type spaces is closely related to the performance of the glazed façade. Its ability to provide shading and thermal insulation can influence the type of environmental system for cooling and ventilation. The façade is increasingly becoming a major component of environmental design and its performance needs to be carefully assessed during design in relation to the heating and cooling loads on the space and the associated systems.

A well designed façade can significantly reduce the cooling load of a building. In Switzerland, for example, there is a tight control over the use of air-conditioning, and in most cases it is restricted to mechanical ventilation with some comfort cooling. Air conditioning is only allowed if the design can

demonstrate that the solar gains are minimised through the facade. Sometimes additional cooling may be provided through active cooled surfaces, such as chilled beams and ceilings. These new innovative combinations of façade design, low level ventilation and surface cooling, provide energy efficient thermally comfortable solutions for modern office environments. The question is, to what extent are these solutions appropriate to the Hong Kong environment, typified by, high levels of internal heat gains from people and processes, and high external temperatures, solar radiation and relative humidity.

THERMAL DESIGN OF FACADES

The aim of the thermal design of facades is to control heat gain and heat loss. The solar heat gain can be from direct and diffuse solar radiation. In hot weather, there will also be some transmission heat gains from high external temperatures. Controlling solar gains is more difficult for west and east facades where the sun angle is lower.

The problem of controlling solar gains can be addressed through innovative shading, often of a dynamic nature, moving into position only when the sun is incident on the façade. A typical European requirement could be that the internal air temperature does not exceed 26°C in summer and the internal glass surface temperature should be within 5°C of the space air temperature. Glazing g-values (that is, a coefficient that describes the total solar transmission through a facade) should be less than 0.15 and there must be an internal mass greater than 350kgm^{-2} of floor area. The facade has to be carefully designed to minimise solar heat gains, not only to the space but also to the glazing system and avoiding high glass temperatures. Even for facades with low g-values, there have been problems associated with excessive heat gains and high internal glass surface temperatures (greater than 40°C), making the internal glazing effectively a 'low temperature' radiator.

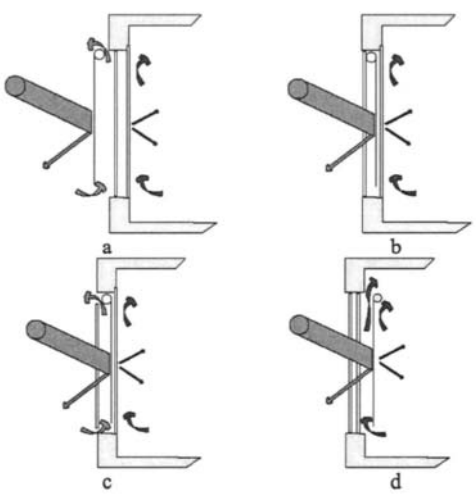


Figure 1: Illustration of different glazing shading strategies indicating convective and radiant heat exchange for, a) external shading, b) middle sealed shading, c) middle ventilated shading, and d) internal shading.

So, if large areas of glazing are to be used, some form of shading is required. This can be located (see figure 1):

- On the external façade: sometimes moving into position only when the sun is on the façade. This is usually considered the best approach, as the solar heat gains are kept external to the space and glazing system.
- In the middle: within the glazing system. If the system is sealed then the solar heat gains can be trapped within the glazing system and can result in high internal glass temperatures. If the glazing system is ventilated then the heat gains can be exhausted to outside, but still the glazing system is subject to some gains which can give high temperatures, especially if the ventilated glazing extends for a number of floors.
- On the inside: This is the worst case to control as the heat gains are allowed to enter the space. Although some are reflected back and absorbed by the shading system most of the heat will be contained in the space either as convective gains or long wave radiant gains.

COOLED SURFACES AND MECHANICAL VENTILATION

The façade design should be integrated as part of the overall environmental design. This will often include the ventilation and thermal capacity aspects of thermal design. The façade design should control solar gains and minimise external heat gains. This should be accompanied by measures to reduce internally generated heat gains from lights and small power. Ventilation can often be reduced to the minimum for occupation and where necessary, other means of cooling applied. A strategy is outlined in figure 2.

1. Reduce internal gains
   - Internal gains 25-35 W/m^2
2. Provide solar control façade
   - g-value less than 0.15
3. Reduce ventilation to minimum for occupancy. Expose thermal mass to stabilise heat gains (usually with night cooling).
   - Exposed mass cooling 5-10W/m^2
   - Ventilation rate 2-3ac/h at 18°C
4. If heat gains are higher, provide mass cooling with a water or air chilled slab
   - Chilled mass cooling 30-35W/m^2
5. If heat gains are higher provide cooling with chilled beams
   - Chilled beam cooling < 80W/m^2

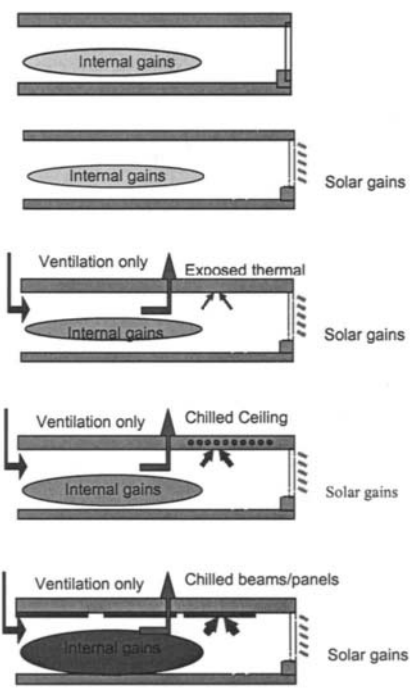


Figure 2: Chilled surface and mechanical ventilation options

Mechanical ventilation systems should have low pressure drop distribution to minimise fan power. In the UK, building regulations specify a specific fan power of 2W/l/s for new buildings [Part L2, UK Building Regulations 2002]. Ventilation systems are often of the displacement type, using floor delivery systems with extract at high level.

PREDICTIVE TOOLS

The accurate prediction of the performance of integrated environmental systems is needed for design. The glazing system performance must be integrated with other environmental aspects, such as passive or active cooled surfaces and displacement ventilation. There is therefore a need to be able to predict the time varying performance of facades under varying external conditions of temperature and solar radiation. This can be achieved using a dynamic energy model. The model HTB2 used in the work described here was developed at the Welsh School of Architecture (Alexander 1997) and is in use in a number of academic and industrial organisations. It can be used to predict internal space and glass surface temperatures (Lang et al 2000). It models the system as a set of nodes, each node associated with a space temperature or a surface (or 'finite difference' temperature within a construction). The only assumed information is the ventilation rate of the space and this has to be input to the model. Figure 3 presents the nodal description of a simple space with a blind on the inside.

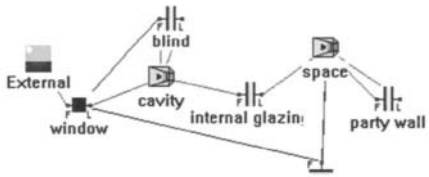


Figure 3: A nodal representation of an office space with an internal blind. The gap between the blind and the glazing is modelled as a separate space.

The ventilation rates associated with individual spaces and the spatial variation of temperatures and air movement can be predicted using an airflow model. The most widely used airflow models are now generally computational fluid dynamics (CFD) models. They can predict the spatial variation of temperatures and air movement. Airflow models are generally used to predict conditions at a point in time, often using surface temperature boundary conditions generated by dynamic models, which can account for thermal mass effects (Jones and Kippenburg 2000). Figure 4 presents an example of an airflow model predicting the airflow and internal temperatures for an internal blind system.

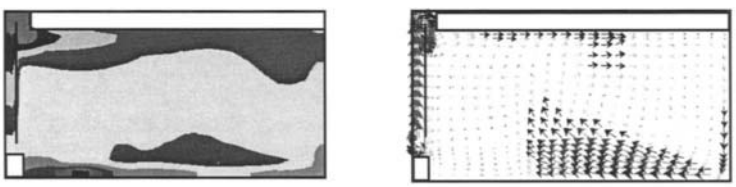


Figure 4: A vertical section through a space with an internal blind and displacement ventilation, showing the temperature contours and air velocity vectors.

APPLICATION TO SHADED GLAZED FACADES

The above tools have been used to predict the performance of the glazing systems shown in figure 1. In each case the system was approximated to a system of nodes, with the inside shading option indicated in figure 3. The ventilation rates associated with the three ventilated shading systems (cases 1a, 1c, and 1d in figure 1) were estimated from airflow prediction (similar to figure 4). The results are presented in figure 5 (a to d).

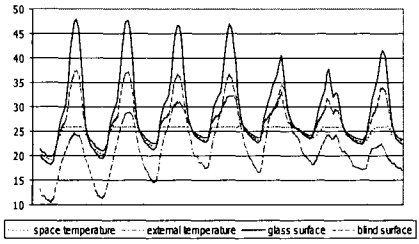


Figure 5a: Internal blind.

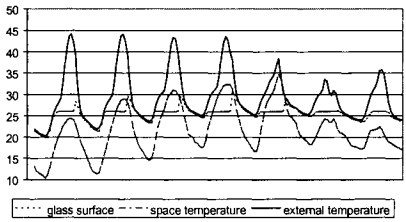


Figure 5b: Middle blind in sealed glazing system.

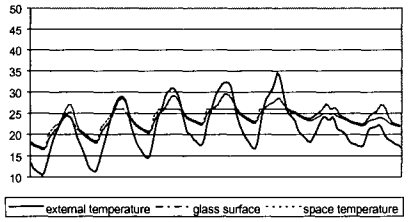


Figure 5c: Middle blind in ventilated glazing system

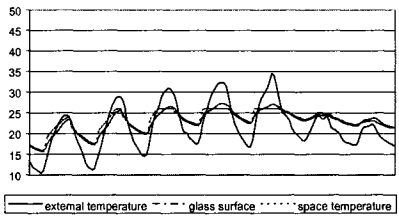


Figure 5d: External blind.

The results of the simulated blind performance indicate the internal glass (or blind in figure 5a) temperature for the different systems. For example, with the internal blind and middle sealed blind the internal glass surface temperature is relatively high, peaking at 36.5°C and 43.5°C respectively, which is well above the desired 5°C limit above the internal space temperature.

When considering these results it should be noted that they relate to specific window systems, with particular blind and glazing properties. They are therefore only indicative of the performance of these types of systems and should considered in this context.

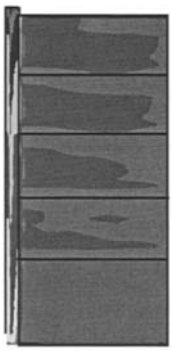


Figure 6: Double skin façade on five floors.

In some cases the blind system will extend over the whole façade and it will be necessary to predict the façade performance at this scale. In such cases the airflow model can be applied to predict peak or typical conditions. Figure 6 shows an example of a simulation of a double skin façade indicating the rise in air temperature with height, imposing an increasing cooling load and internal glass surface temperature on floors at higher level.

APPLICATION TO OTHER CLIMATES

The above discussion has related mainly to building designs in northern Europe. The application to other climates such as Hong Kong is considered below in relation to the main differences in climate.

- Higher external air temperatures: If the façade is well insulated and well sealed, in relation to air leakage, the increase in transmission heat gain should not give rise to a significant increase in the heat load on the space. The coolin load relating to the ventilation air supply will be higher but the supply air temperature and flow rates to the internal spaces need not change as they then only relate to the occupancy levels, internal heat gains and solar gains.
- Increased solar radiation: If a low g-value façade is used then the solar heat gain should be well controlled. For example a double skin ventilated façade with shading should provide sufficient solar control.
- Higher external humidity: The supply air must have humidity control, and the building should be well sealed to minimise air leakage and consequential effects on internal relative humidity levels. The internal sources of moisture in Hong Kong, that is, people, should be no different from other parts of the world.

So, the indication is that the integrated façade and environmental systems described in this paper can be used in Hong Kong without much alteration. The main differences for the Hong Kong situation will be in relation to increased cooling and dehumidifying of the external ventilation air supply.

CONCLUSION

The modelling of facades is important in relation to controlling solar gains. There is potentially a wide range in performance for different glazing shading systems. The main aspect of successful design is to exhaust the solar heat gains trapped by the glazing system. This is a problem for internal and sealed glazing blind systems.

The design of the integrated environmental system will depend on the level of internal heat gains. The system should aim to minimise ventilation cooling and provide chilled surface cooling as appropriate to the internal heat gains.

Such systems will work in Hong Kong provided the building is well sealed and the ventilation supply air has humidity control.

A combination of dynamic thermal modelling and CFD airflow modelling provides a means of predicting system performance and integrating the glazing system with other environmental systems, for example, thermal mass and ventilation.

References

Approved Document L2, Conservation of fuel and power, UK Building Regulations, April 2002.
Alexander, D K (1996; revised 1997) 'A Model for the Thermal Environment of Buildings in Operation, release 2.0c', Welsh School of Architecture, Cardiff University.
Lang, W, Herzog, T, Hausladen, G, Kippenberg, K, and Jones, P, (2000) 'Adjustable Solar Shading and Heat Conservation Louvres For Transparent, Multi-Layered Glass Facades'. Proceedings of the Eurosun 2000 Conference, Kopenhagen, Denmark.
Jones, P J and Kippenberg, K (2000) 'Effect of Thermal Mass on the Airflow and Ventilation in Passive Building Design', Roomvent 2000, 273-279.

This Page Intentionally Left Blank

Advances in Building Technology, Volume 2
M. Anson, J.M. Ko and E.S.S. Lam (Eds.)
© 2002 Elsevier Science Ltd. All rights reserved

LOCAL STUDY OF THE INFLUENCE OF A NUMERICAL THERMAL MANIKIN ON THE AIR FLOW PATTERN AND TEMPERATURE FIELD OF A SPACE

Kaja Kippenberg-Kretzer and Phil Jones
Welsh School of Architecture, Cardiff University, Wales, UK

ABSTRACT

This paper presents the first results of a numerical thermal manikin implemented into a Computational Fluid Dynamics (CFD) code whose position in the simulated space can be easily changed in successive steady-state calculations. The mobility allows for local studies of the influence of human heat release and body shape on the air flow pattern and temperature field of a space.

The body of the manikin consists of 14 segments, with a simple body shape. For the study presented here constant skin temperatures were assumed. A more refined thermo-physiological model is currently developed. The manikin is a simulation tool that can be run on a standard desk top computer or notebook with reasonable computation time.

Three different positions of the manikin were simulated: One with the manikin standing near the internal wall, one with the manikin in the centre of the space and one with the manikin standing near the window. For all three positions simulations for summer and winter conditions were performed, respectively. Thus, all in all 6 cases are presented. The simulations clearly show the influence of the position of the manikin on the air flow pattern and temperature field of the space, using a relatively course grid manikin.

KEYWORDS

CFD, thermal manikin, mobile manikin, thermal comfort, local prediction, air flow

INTRODUCTION

Heat release and shape of the human body influence the air flow pattern and the temperature field of a space. Depending on the purpose of a space occupants might move around or be more static. The less active people are, the more sensitive they usually are towards the thermal environment, (ASHRAE (1993)). Thus, the importance of the influence of their heat release on the thermal environment increases with decreasing activity levels, e.g. for sedentary activities in a typical office space.

Indoor thermal environments often are non-uniform throughout a space. Recent research of thermal comfort has investigated the ability of the human body to adapt to a wide range of thermal conditions as well as behavioral adaptation of occupants to their thermal environment (Brown & Jones (1993)), (Humphreys & Nicol (1988)). Recent studies showed that people might even prefer a thermal environment that varies in time and space (Xia, Zhao & Wu (2000)), (Conceicao (2000)), (Nakamura, Mizuno & Ida (2000)) to a static and uniform one.

When innovative low energy heating and cooling systems or passive building design, for which often no previous experiences of performance exist, are to be developed, the examination of the achieved thermal environment and adjustment of design during the design process is important. With advancing computer technology, numerical manikins are increasingly employed for the investigation of thermal comfort and indoor thermal environments. Several manikins with complex thermo-physiological models exist (Murakami, Kato & Zeng (2000)), (Huizenga, Hui & Arens (2001)), (Miyanage, Urabe & Nakano (2001)), and one of them is integrated into a CFD code (Murakami, Kato & Zeng (2000)). However, numerical manikins have been very detailed requiring large CFD grids and simulation times.

The manikin employed in this study is implemented within a CFD code (Jones & Waters (1993)) using a relatively course grid structure. Its position in the simulated space can be chosen at the start of each run of a steady-state simulation, whereby the geometry and layout of the simulated space are conserved. The mobility of the numerical manikin is of great advantage for the examination of non-uniform indoor thermal environments. The layout of the manikin and the simulated space is explained in detail below.

The aim of the work is the development of a numerical manikin simulation tool that can be used on a standard desktop computer or notebook with reasonable computation time. It should be possible to perform a study with different positions of the manikin quickly. Thus, the grid is rather coarse and the shape of the manikin very simple.

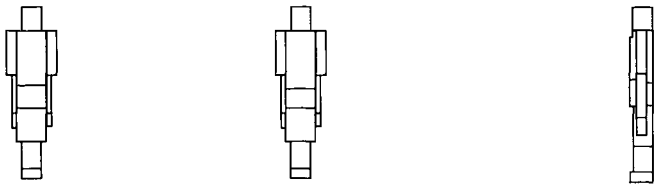
In this paper six case studies of a space similar to an office space are presented: The first one with the manikin standing near an internal wall, the second one with the manikin standing in the centre of the space and the third one with the manikin standing near the window. For all three positions simulations for summer and winter conditions were performed, respectively. The aim was to investigate the influence that the position of the manikin has on the air flow pattern and temperature field under varying thermal conditions.

THE MODEL

For the study presented here a standard CFD code was used (Jones & Waters (1993)) which has been adapted to incorporate a numerical manikin. The code employs finite volume method with hybrid differencing scheme. Turbulence is modelled with a constant eddy viscosity of 200 x laminar. Currently the model only deals with convective heat exchange but in the future a radiant component will be added.

The body of the manikin is displayed in Figure 1. The heat exchange with the environment is modelled by defining constant skin temperatures. Values were taken from an experimental physical manikin (Myers, Hosni & Jones (1998)) consisting of 16 body parts. For simplicity at this stage this study uses only 14 body parts; feet, calves and thighs are defined as blocks. For left and right body parts mean values of the

skin temperature values in (Myers, Hosni & Jones (1998)) were used. The constant skin temperatures are displayed in Table 1.



a) b) c)

Figure 1: Schematics of the manikin body segments: a) front, b) back, c) side

TABLE 1
SKIN TEMPERATURE OF THE DIFFERENT BODY SEGMENTS OF THE MANIKIN

Body Part	Skin Temperature [°C]
Feet	29.6
Calves	31.6
Thighs	31.5
Lap	32.9
Buttocks	32.3
Chest	30.6
Back	32.4
Head	28.3
Upper Arms	30.5
Lower Arms	30.8
Hands	29.5

Currently the shape of the manikin is very simple, with the arms attached to the torso and the legs being one rectangular block. The influence of this simplification on the air flow pattern will be investigated later, and necessary changes will then be made.

The whole simulated space including the body of the manikin is built of a rectangular grid with varying cell sizes. Around the manikin the grid is finer than in areas further away from the manikin that are of lesser interest. The grid lines extend through the whole space causing refinement of the grid not only at the position of the manikin but also in the extrapolation of the manikin body along the respective directions. The side lengths of cells around the manikin are 0.05m to 0.10m, those of cells further away are up to 0.20m. This grid is rather coarse and was chosen so to keep computation time low. The dimensions of the simulated space are 3m x 6m x 2.7m. The space has only one wall to external, the whole area of which is treated as a window. Mechanical ventilation was employed, with supply and

extract opening sizes of 0.2x0.2 m^2. The inlet opening is located in the upper centre of the 3m internal wall, opposing the window. The outlet is located in the ceiling, centred around the long axis with a distance of 2 m to the window. The u-value of the window was chosen to be 3W/m^2. All enclosures have differing surface temperatures as displayed in Table 2. Those temperatures were calculated by thermal dynamic simulation, employing HBT2, a thermal dynamic simulation computer program developed at the Welsh School of Architecture, (Alexander (1996)).

TABLE 2
SPACE SETUP

	Summer	Winter
Date	18/7; 16am	9/12; 8am
External Air Temperature [°C]	28.7	-1.6
Ventilation Rate [m^3/s; ac/hr]	0.0405; 3	0.027; 2
Supply Air Temperature [°C]	18.0	30.0
Floor/ Ceiling Surface Temperature [°C]	25.1	20.7
Wall Surface Temperature [°C]	25.6	20.5
Window Surface Temperature [°C]	28.4	13.0
Av. Space Air Temperature [°C]	24.9	20.8

At the start of a simulation the user first has to enter the location and size of the ventilation openings in multiples of the largest cell side length for each direction. If the geometry of the space does not allow a chosen opening the computer displays an error message and advice on choices of smallest possible modifications of either decreasing the size of the respective opening or changing its location. After the openings are accepted by the program the user is asked to enter the position of the manikin as distance to the origin, as well in multiples of the largest cell side length for each direction. The program then adjusts the grid accordingly. If the position of the manikin which constitutes the layout of the grid does not comply with the chosen geometry of the space (e.g. space dimensions or size and location of openings) the user will be advised on the nearest possible position of the manikin. With the current grid the correction of the manikin position is usually not larger than about 0.2m. To allow a large number of positions of the manikin variation of cell sizes is constrained to each cell size being an integer multiple of the next smaller one.

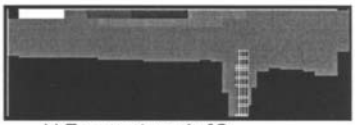
CASE STUDIES

The air flow patterns and temperature distributions of the case studies are displayed in figures 2.1 to 2.3. for the winter cases and figures 2.4 to 2.6 for the summer cases. The results show that the location of the manikin significantly affects both the distribution of air velocities and (in the case of the summer time) the air temperatures.

Winter



a) Velocities in m/s

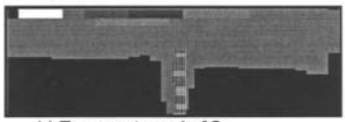


b) Temperatures in °C

Figure 2.1: Manikin near window, winter case

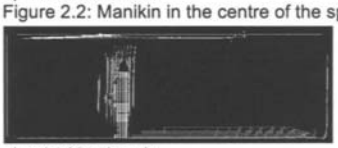


a) Velocities in m/s

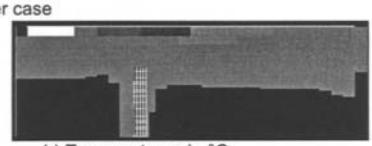


b) Temperatures in °C

Figure 2.2: Manikin in the centre of the space, winter case



a) velocities in m/s



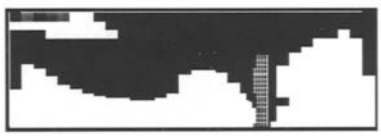
b) Temperatures in °C

Figure 2.3: Manikin near internal wall, winter case

Summer

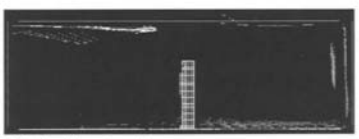


a) Velocities in m/s

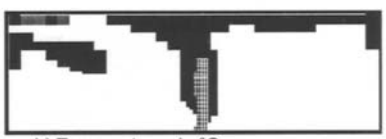


b) Temperatures in °C

Figure 2.4: Manikin near window, summer case



a) Velocities in m/s

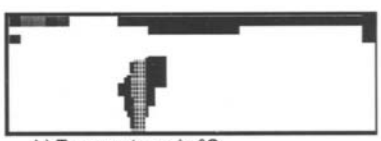


b) Temperatures in °C

Figure 2.5: Manikin in the centre of the space, summer case



a) Velocities in m/s



b) Temperatures in °C

Figure 2.6: Manikin near internal wall, summer case

CONCLUSIONS

- The influence of the position of the manikin on the air flow pattern and temperature field of the simulated space can clearly be seen. The study shows the advantage of a mobile manikin over a static one in the examination of non-uniform thermal environments.
- It would be useful to construct a seated manikin and allow for the user to choose the posture of the manikin at the start of a simulation run since the heat release pattern and body shape of a seated manikin will be different from that of a standing one.
- A more refined thermo-physiological model of the manikin is currently developed and will be validated with experimentally measured data from a physical THERMAL MANIKIN used by a research group at Hong Kong Polytechnic University. The CFD code will be coupled with a radiation model, enabling a more accurate prediction of convective and radiant heat exchange. With the refined thermo-physiological model local predictions of thermal comfort that include several comfort parameters shall be performed for non-uniform thermal environments.
- The manikin shall be simple enough to allow the program to be run on a standard computer with reasonable calculation time so that local studies may be performed for everyday design processes. A systematic study needs to be performed to find out how much precision in each part of the model (e.g. grid, heat release) is needed in order for the results to be useful for the design process.
- The refined manikin model will allow the investigation of further questions of interest, among them the distinction of air-conditioned and passive design buildings from simulations point of view.

References

Alexander, D.K. (1996, rev. Nov. 1997). *A Model for the Thermal Environment of Buildings in Operation, release 2.0c*, Welsh School of Architecture R&D, Cardiff, UK.

ASHRAE. (1993), Chapter 8, *1993 ASHRAE handbook – Fundamentals*, American Society of Heating, Refridgerating and Air-Conditioning Engineers, Inc., Atlanta, USA.

Brown, J.C. and Jones, P.J. (1993), Thermal Comfort in Modern Industrial Buildings. *CLIMA 2000.*

Conceicao, E.Z.E.(2000). Evaluation of Thermal Comfort and local Discomfort Conditions by numerical Modelling of Human and Clothing Thermal Systems. *Air Distribution in Rooms, Ventilation for Health and Sustainable Environment, ROOMVENT 2000.* Awbi, H.B., Ed., Elsevier, Oxford, UK, Vol.1, 131-136.

Huizenga, C., Hui, Z. and Arens, E. (2001). A model of human physiology and comfort for assessing complex thermal environments. *Building and Environment* **Vol.36:6**, 691-699.

Humphreys, M.A. and Nicol, J.F. (1988), Understanding the Adaptive Approach to Thermal Comfort. *pre-publication draft for ASHRAE Transactions.*

Jones, P. and Waters, R. (1993). The Practical Application of Indoor Airflow Modeling. *Modeling of Indoor Air Quality and Exposure, ASTM STP 1205*, Niren L. Nagda, Ed., American Society for Testing and Materials, Philadelphia, USA, 173-181.

Miyanage, T., Urabe, W. and Nakano, Y. (2001). Simplified human body model for evaluating thermal radiant environment in a radiant cooled space. *Building and Environment* **Vol.36:7**, 801-808.

Murakami, S., Kato, S. and Zeng, J. (2000). Combined simulation of airflow, radiation and moisture transport for heat release from a human body. *Building and Environment* **Vol.35:6**, 489-500.

Myers, J.B., Hosni, M.H. and Jones, B.W. (1998), Interaction of Air Motion with the Human Body. *ASHRAE Transactions* **Vol.104: Part 1B**, 863-882.
Nakamura, Y., Mizuno, M. and Ida, D. (2000), Study on Prediction of Thermal Comfort in unsteady and Inhomogeneous Thermal Environment. *Air Distribution in Rooms, Ventilation for Health and Sustainable Environment, ROOMVENT 2000*, Awbi, H.B., Ed., Elsevier, Oxford, UK, Vol.1, 47-52.
Xia, Y., Zhao, R. and Wu, W. (2000), Human Thermal Sensation to Air Movement Frequency. *Air Distribution in Rooms, Ventilation for Health and Sustainable Environment, ROOMVENT 2000.* Awbi, H.B., Ed., Elsevier, Oxford, UK, Vol.1, 41-46.

This Page Intentionally Left Blank

Advances in Building Technology, Volume 2
M. Anson, J.M. Ko and E.S.S. Lam (Eds.)
© 2002 Elsevier Science Ltd. All rights reserved

VALIDATION OF THE SIMULATION MODELS OF THE DOUBLE SKIN FACADE

W.J. Stec & A.H.C. van Paassen

Indoor Climate Technology, Sub Faculty of Mechanical Engineering, TU Delft,
Mekelweg 2, 2628 CD, Delft, The Netherlands. Email: w.j.stec@wbmt.tudelft.nl.

ABSTRACT

A mathematical model of the double skin façade (DSF) is validated with two test facilities.
A simplified version of the double skin façade was constructed in the laboratory. It is focused on defining its heat performance including convection (free or mixed), conduction, radiation and transportation heat transfer. Measurements and simulations were made at steady state conditions thus no real weather conditions were taken into account. The flow through the model is driven by the buoyancy effect and/or by fan.
Results from the laboratory test facility are used in modeling a test cell with a double façade situated outside the laboratory. This model is validated by experiments on this test cell under real weather conditions.
Validated model of the building with the double skin façade can be used to analyze the performance of different configurations of the double skin façade and related control.

KEYWORDS

Validation of thermal and airflow model of the double skin facade. Simulations.

INTRODUCTION

In the recent past several studies of the double skin façade (DSF) were done. Some of them were based purely on the simulations (Todorowic & Cvjetkovic 2001, Stec & Van Paassen 2001, Di Maio 2000, Mastrullo & Mazed & Vigo 1983, Moots & Benzin 1996). Some of the studies were also based on the experimental approach (Ziller 2000, Chic & Shako 2001, Spinnler 2002, Jones & Message & Li 2000, Sealens & Hens 2001). All those works introduce the heat and flow performance inside of the double skin facade (DSF) under steady state or unsteady conditions. None of these studies gives a validated thermal and air flow model of the double skin façade together with detailed analysis of its performance. In this work current result of the validation the simulation models of the double skin facade together with the building behind are presented.

Validation work is divided into two parts:

- Validation of the simulation model of the DSF with the laboratory test facility.
- Validation of the simulation model of the DSF together with the building done with the use of the test cell outside the laboratory

With a laboratory test facility thermal and airflow performance is tested under steady state conditions. That means that no changing outside weather conditions are taken into considerations. With this facility the buoyancy effect and free convection heat transfer are studied.
The results from the laboratory facility are used in simulation of the behavior of a full-scale test cell with DSF placed outside the laboratory. The performance of this test cell is monitored and compared with double skin facade and building is tested under real weather conditions.

SIMULATIONS OF THE LABORATORY TEST FACILITY

Measurements

The test facility is constructed out of the wood with steel frame and one glass wall (figure 1.). All walls apart from the glazed one are insulated with the 50 mm tick polystyrene. The back wall substitutes the basic wall of the building and the front glass plate simulate outside glass skin of the building. Back wall and glass skin create the air cavity in which a heating mat is situated. Heating mat gives up to 500 W/m^2 constant heat flux.
T-type thermocouples (36) were installed to examine temperature distribution. The temperatures of each surface and cavity on three heights are measured.

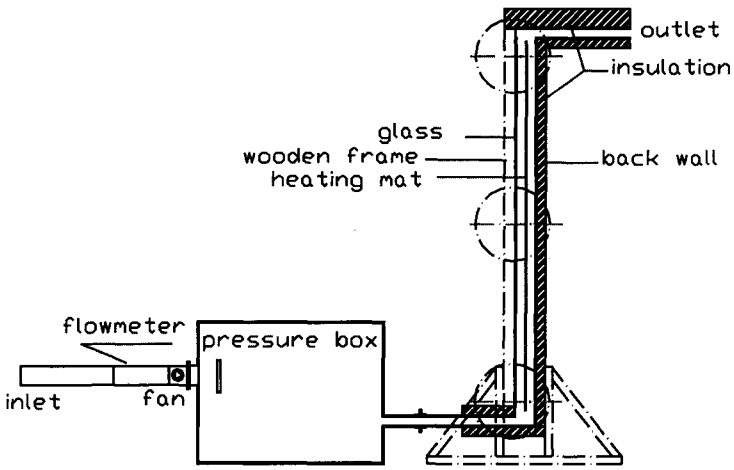


Figure 1. Test facility of the DSF at TU Delft

The flow measurement is realized with the use of the pressure box and flow meter connected to the inlet of the model. The pressure box supplies air to the cavity, which should be equal to that, induced by buoyancy effect. The flow meter installed on the inlet to the pressure box measure the total airflow through the system. Its accuracy is approximately 5%.
The fan connected with the pressure box compensates the resistance of the pressure box and flow meter (see figure 1). It can also be used for experiments with forced airflow through the cavity.

Simulations

The mathematical model consists of two parts: the airflow model and the thermal model.
These two models are simultaneously interacting one with each other.
The model was realized with the use of the MATLAB™. The model is static what in this case does not decrease its quality with comparison to the dynamic one (Di Maio 2001).
During the measurements the test facility was protected from any disturbances, so movements of the surrounding air are neglected and variations of temperature are very slow.
The airflow is driven by the buoyancy effect and is calculated according to Van Paassen &Voorden 2000. The average difference between calculated and measured flow shows to be 4.17% what is inside of the accuracy of the flow measurement.
The thermal model was built based on the network of heat exchange between each skin of the model (Stec 2002). The conduction, convection, radiation and transportation heat transfer was considered (see fig. 2). The problem that was to be solved was to select the solutions for the convection and transportation heat transfer.

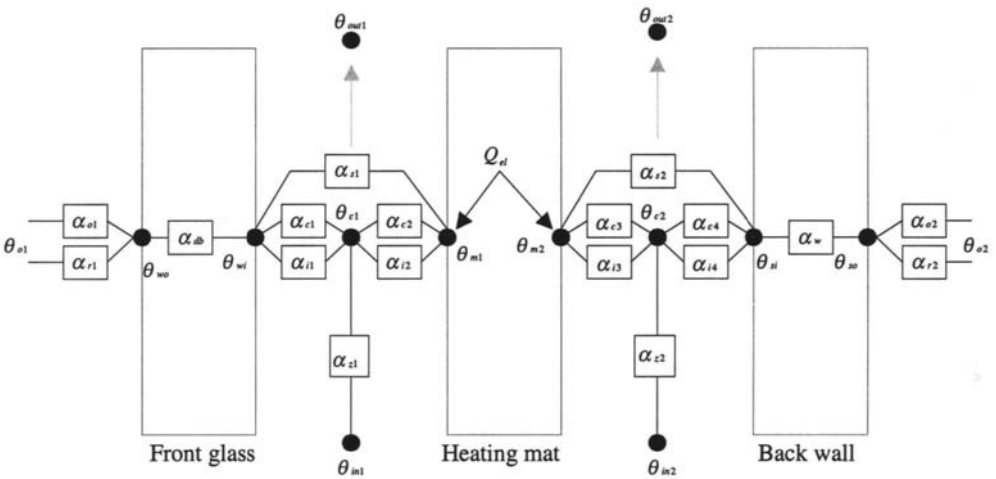


Figure 2. Network of heat exchange in the model of DSF.

Where,

$\alpha_{o(1,2)}$ -	Convection heat transfer coefficients between external surfaces of the model and outside air
$\alpha_{c(1,2,3,4)}$ -	Convection heat transfer coefficients between each skin and air inside of the model
$\alpha_{z(1,2)}$ -	Transportation heat transfer coefficients that represent the heat flow in the cavity from a lower to a higher node in the network.
$\alpha_{i(1,2,3,4),adb,w}$ -	Conduction heat transfer coefficients
$\alpha_{s(1,2),r(1,2)}$ -	Radiation heat transfer coefficients

By regression values of the transfer coefficients are defined giving the best fit with the measurements (table 1). Also ranges of values for each coefficient are given using the heat transfer relations found in literature.

Table 1. Values of specified heat transfer coefficients found by regression and with the formulas.

heat transfer coefficient	Values defined by regression	Final values defined with formulas
α_{o1}	8.80	8.20 – 8.50
α_{o2}	6.30 – 6.50	6.40 – 6.60
α_{c1}	5.00 – 5.80	4.90 – 5.90
α_{c2}	10.60 – 10.80	10.40 – 10.43
α_{c3}	6.70 – 6.80	6.50 – 6.60
α_{c4}	5.60 – 5.70	5.60 – 5.66
α_{z1}	10.90 – 11.25	11.20 – 11.40
α_{z2}	12.60 – 13.40	12.90 – 13.44

The formula of Knudsen & Katz for free convection along the vertical plate was selected as the one that gives the best fit of the calculations with measurements.

$$Nu = 0.52(Gr \cdot \Pr)^{0.25} \qquad [1]$$

The transportation heat transfer coefficient was defined analytically and is given by equation [2]

$$\alpha_z = \frac{\dot{m} \cdot c_p \cdot (\theta_{out} - \theta_{in})}{A_m \cdot (\theta_c - \theta_{in})}, \qquad [2]$$

where;

$A_m[m^2]$– Area of the heating mat,

$\dot{m}[kg/s]$– Mass flow through the cavity,

$\theta_{out}[C]$– Temperature of the air leaving the cavity

$\theta_{in}[C]$– Temperature of the air entering the cavity

$\theta_c[C]$– Temperature in the cavity (in the middle of the height),

$c_p\left[\frac{J}{kg \cdot K}\right]$- Specific heat of the air,

Results

With the simulation model the total performance of the double skin façade was simulated. The calculations and measurements were made for the following data:

H = 2 m. – Height of the DSF

B = 1 m. – Width of the DSF,

D = 0.1 m. – Distance between the back wall and front glass

Q_{el} = 500 W/m^2. – Power of the heating mat. It is placed in the middle between the back wall and front glass.

With these inputs the average difference on temperature between the air in the cavity and outside air is 14.78 °C.

Standard deviations between the temperatures (measured and calculated) are in range between 0.3879 and 0.1824.
Correlation coefficients are in range of 0.9184-0.9822. Comparison of the cavity temperature for the period of 6 days is shown in figure 3.

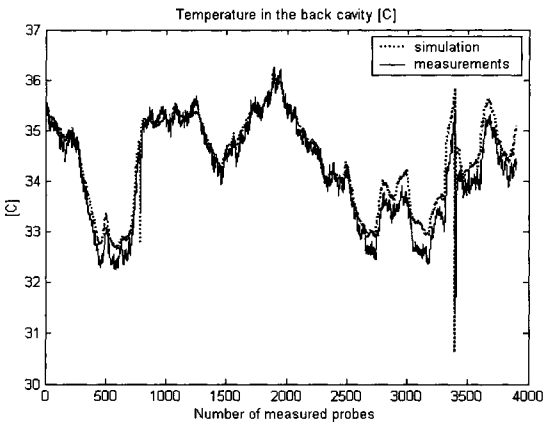


Figure 3. Comparison of the temperature (measured and simulated) in the back cavity

SIMULATIONS OF THE DOUBLE SKIN FAÇADE WITH THE BUILDING BEHIND UNDER THE REAL WEATHER CONDITIONS

Measurements

The measurements were done with the test cell at TU Delft (see figure 4). Test cell is equipped with following elements:



Figure 4. Test cell at TU Delft

- The double skin façade constructed from:
  - Basic wall with motorized windows
  - Additional glass skin on the outside of the wall

    - Venetian motorized blinds situated in the cavity between the wall and glass façade
    - Valves on the bottom of the façade
- Air handling split level unit
- Mechanical ventilation system with two modes of control: supply air or extract air from the cavity by making an over- or under pressure in the cell.
- Weather station and monitoring system with the measurements of:
    - Solar radiation (On the horizontal surface, the vertical inclined wall and inside of the test room)
    - Temperature. In total 48 thermocouples were placed outside and inside of the cell and in every layer and on different heights of the double skin façade.
    - Wind velocity and direction

With these measurements simulations of buildings with double skin facades can be tested.

Simulations

Simulation was made with Simulink^{tm} and it is divided into
- Simulations of the double skin façade
- Simulations of the building.

To build the model of the double skin façade results from the laboratory test facility are used. Additional components taken here into consideration are:
- Wind effect
- Airflow distribution in function of the position of the blinds, windows and valves controlling the airflow in the cavity
- Distribution of the solar radiation heat gains in the structure of the façade. This include also different properties of the blinds in function of the angle of the blades

The wind effect is considered based on the solutions proposed by Van Paassen & Voorden (2000) and Di Maio (2001). It is closely related with the airflow through the model. The airflow is calculated based on the network of flow exchange (Di Maio 2001). The influence of the construction of the façade and its components needs to be improved to reflect precisely the real behaviour of the façade. Calculations of the solar radiation and its distribution in the structure of the façade are carried out with the following steps:
- Calculating of the solar radiation falling on the vertical plate from the solar radiation falling on the horizontal plate
- Creating the network of the distribution of the solar radiation in the structure of the façade
- Defining the properties of each skin (absorption, reflection and transmission coefficient)
- Calculating ratios of the solar radiation absorbed on by each skin and transmitted to the inside of the building

Calculations of the vertical solar radiation from the horizontal solar radiation were made according to the Orgill 1977 and Brink 1987. The calculation results were compared with the relevant measurements. Calculations agree fairly well except the diffuse radiation at cloudy days.
The network of distribution of the solar radiation in the facade was build with double reflection of the rays inside of the façade. Properties of materials were defined based on tables found in literature and with the program WIS (Bakker 1996).
With such a constructed model of solar radiation final solar radiation transmitted through the façade to inside was calculated (Stec 2002). To improve the results more studies of the properties of materials

are necessary. Especially it is important with defining the properties of blinds as a function of the blades' angle.
The simulation model of the building behaviour was based on the models of Di Maio (2001) and Groninger (2000). All enclosing walls, one point air model, HVAC and internal heat gains are taken into account.

Results

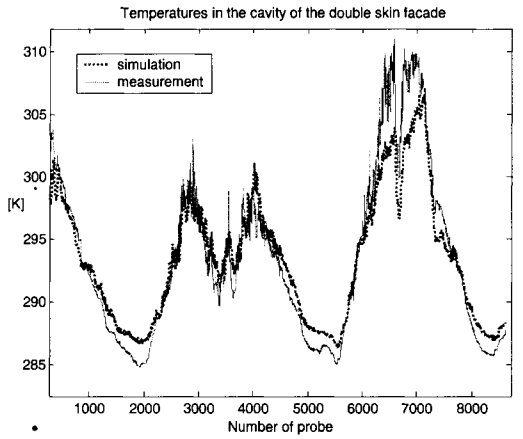


Figure 5. Comparison of the temperature (measured and simulated) in the cavity of the double skin façade

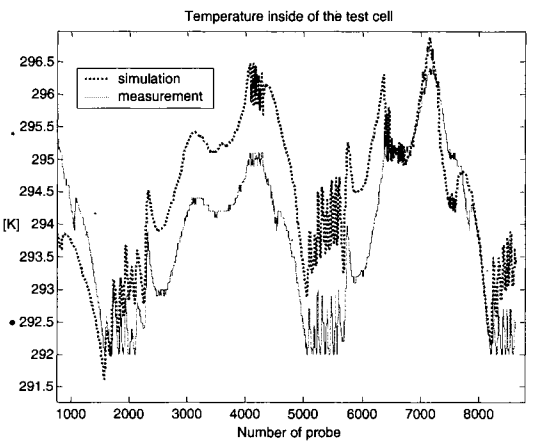


Figure 6. Comparison of the room air temperature (measured and simulated)

Calculations of the temperature in the cavity and inside the test cell are compared with the measurements (see figure 5 & 6). Both subsystems (DSF and room) have better correlations with measurements when the outside conditions are stabilized.
In general simulation model of the double skin façade shows a good fit. Nevertheless model needs some adjustments to be more flexible for different weather conditions and settings of the blinds and valves.
Thermal behaviour of the room shows to be correct. Still some adjustments are needed to simulate the influence of the window openings and HVAC system.

CONCLUSIONS

- Models of double skin façade (DSF) are validated using measurements of the laboratory test facility and the test cell under real weather conditions
- In general models of DSF agree quite well with the experiments
- After necessary improvements simulation model of the building with the double skin façade will be used to examine the thermal and airflow performance for different configurations of the building and DSF.

ACKNOWLEDGEMENT

Autors would like to thank to the several companies involved in the project: Novem (financial support), Unica (HVAC installation co.), Rollecate (facades design & construction), Klima Delft (consulting).

REFERENCES

1. Bakker L., Plokker W., van Dijk D.(1996). WIS User's guide, incl. Tutorial. *TNO Building and Construction Research*
2. Brink van den G.J. (1987). Validation of solar radiation models and recommendations of the model for Dutch climatological circumstances. *TPD TNO – TH, Report No. 314.266 – 3 and 514.015,* Delft, The Netherlands.
3. Chiu Y. and Shao L. (2001). A parametric study of solar double skin façade on energy saving effect. *Clima 2000 – Napoli 2001*, Italy
4. Di Maio F. (2001). Integration of double facades and ventilation systems in buildings. PhD Thesis. TU Palermo.
5. Groninger B. (2000). Cooling with natural ventilation in office buildings. *Internal Report KK –* 1145. TU Delft
6. Jones J. and Messadi T. and Li S. (2000). Experimental Study of the cooling season performance of ventilated double-glass envelope cavities. *International building physics conference*. TU Eindhoven, The Netherlands p357-365.
7. Mastrullo R., Mazzei P. and Vigo P. (1983). The performance of a natural – circulation solar air heater. *ASHRAE Transactions*. 89, No. 1A, pp. 288-298.
8. Mootz F. and Bezian J. (1996). Numerical study of a ventilated façade panel. *Solar energy*, Vol. 57, No. 1, pp. 29 – 36.
9. Orgill J. F., Hollands H.G.T.(1977). Correlation equation for hourly diffuse radiation on a horizontal surface, *Solar Energy, Vol. 19, pp 357 – 359.*
10. Sealens D. and Hens H. (2001).Experimental evaluation of the airflow in naturally ventilated active envelopes. *Journal of Thermal Env. & Bldg. Sci.,* Vol 25-October 2001
11. Spinnler M., Blumenberg J., Heuss S., Zollner A. (2002). Decentral energy supply for buildings with double skin facade. *Sustainable development of energy, water and environment systems.* June 2-7,2002, Dubrovnik, Croatia.
12. Stec W. (2002). Draft of the final report from the project "Performance of the double skin façade". TU Delft.
13. Todorovic B. and Cvjetkovic T. (2001). Glass envelope above the basic one, influence on energy demand. *Clima 2000 - Napoli 2001*, Italy,
14. Van Paassen A.H.C. and Stec W. (2001). Controlled double facades and HVAC. *Clima 2000 - Napoli 2001*, Italy,
15. Van Paassen A.H.C., and Van der Voorden M.(2000). Development of simplified tools for evaluation energy performance of double facades. *International building physics conference*. TU Eindhoven, The Netherlands p347-355.
16. Ziller C. and Sedlacek G. (2000). Natural ventilation of rooms with twin – façade systems. *International building physics conference*. TU Eindhoven, The Netherlands p367-374.

Advances in Building Technology, Volume 2
M. Anson, J.M. Ko and E.S.S. Lam (Eds.)
© 2002 Elsevier Science Ltd. All rights reserved

MODELLING OF A CLOSE-COUPLED PHOTOVOLTAIC HEAT PUMP

C. P. Underwood and A. D. Jones

School of the Built Environment & Sustainable Cities Research Institute,
Northumbria University, Newcastle upon Tyne NE1 8ST, UK

ABSTRACT

The close coupling of a conventional compression heat pump evaporator with photovoltaic modules is proposed, thus ensuring a higher power generating efficiency from the PV modules than would be the case in conventional installations. The power generated is used to power the heat pump compressor for the generation of domestic hot water in cool northern latitude climates. A mathematical model of the plant is described and the model is applied to a system scaled at 6kW – capable of generating all hot water needs of a large family home with a surplus available for space heating when needed. Results show that the plant is capable of generating all such energy needs in summer, with a significant power surplus, and about 40% of these needs on sunny winter days.

KEYWORDS

Thermal modelling; heat pump; photovoltaics; system simulation; domestic hot water; module temperature

LIST OF SYMBOLS

H	Enthalpy ($kJkg^{-1}$)
T, T'	Temperature (K, °C)
Q	Heat transfer rate (kW)
W	Work transfer rate (kW)
P	Pressure (bar(a))
V	Volume (m^3)

ρ	Density (kgm^{-3})
C	Thermal capacity (kJK^{-1})
m	Mass flow rate (kgs^{-1})
A	Area (m^2)
U	Thermal transmittance coefficient ($kWm^{-2}K^{-1}$)
x	Vapour quality (fraction)
I	Total solar radiation (kWm^{-2})
C_{FF}	Fill factor constant (Km^2)
σ	Stefan-Boltzman constant ($5.67\times10^{-11}kWm^{-2}K^{-4}$)
α	Solar absorptivity (fraction)
ε	Surface emissivity for long-wave radiation (fraction)
n	Index of compression (taken as 1.3 for R134a)
R	Characteristic gas constant ($0.08149kJkg^{-1}K^{-1}$ for R134a)
η	Efficiency (fraction)
P_{HP}	Heat pump coefficient of performance (dimensionless)
c	Specific heat capacity ($kJkg^{-1}K^{-1}$)

SUBSCRIPTS

e,c,a,p	Refer to evaporator, condenser, accumulator and compressor respectively
mod	Module
r,w	Refer to refrigerant and water respectively
s	Surface (solar when used with "mod")
i,o	Refers to inlet, outlet respectively
crit	Critical refrigerant state
f,fg,g	Refer to liquid, saturated vapour and gaseous phases respectively

INTRODUCTION

Several sources have identified substantial potential for power from photovoltaics (PV) within buildings (for a summary, see for example Gregory & McNelis (1994)). The performance of PV-cladding might be optimised through load targeting to particular loads within a building (Bailey et. al. (1993)). One area of particular promise lies in the integration of PV with heat pumps for space heating, principles of which have been identified by Underwood (1995).

The electrical conversion efficiency of a PV module is currently around 15%, most of the excess energy is converted to waste heat. The utilisation of this waste heat as heat pump source energy gives the additional benefit of lowering PV module temperature, leading to increased PV power conversion efficiency, which varies inversely with the temperature of the PV material by approximately $0.35\%K^{-1}$. Thus a reduction in PV material temperature of 30°C would improve power generation by 10%. In typical UK summer conditions, PV modules operate at around 30-40°C. Maintaining the module temperature at a reasonable frost margin (e.g. 5°C) ensures that this 10% improvement in power generation is a practical and feasible target.

In this work, a close-coupled PV compression heat pump is described as a basis for the sustainable generation of domestic hot water in cool northern latitude climates such as the UK. A dynamic thermal model for the system is developed and the model is applied to samples of UK weather data. Conclusions are drawn about the performance of the system in relation to the conventional heating of domestic hot water.

CLOSE-COUPLED PV HEAT PUMP

Figure 1 is a system diagram of the proposed close-coupled PV heat pump for domestic heating. The PV modules are mounted on the roof of a typical house. In normal daytime operation a combination of energy in surrounding ambient air plus solar radiation to the PV surface provides the necessary source energy to sustain the heat pump. The evaporated refrigerant is piped to the compressor from which superheated refrigerant enters the condenser where heat is given up to the hot water store. The fluid leaving the condenser then expands through a throttle before returning to the PV modules. Coincidentally, a low body temperature for the PV substrate will be maintained due to heat exchange with the evaporator (maintained at 5°C to give a frost margin) ensuring high power conversion efficiency.

The key target load for the system will be domestic hot water – increasingly becoming the dominant thermal energy load in modern airtight and well-insulated houses. However, by inter-connecting the house space heating through an annular heat exchanger and a two-position three way valve, the heat pump condenser can provide heat input to the space heating during those times in which the hot water thermal store is satisfied.

In the model described below, the hydrofluorocarbon working fluid R134a is adopted.

SYSTEM MODELLING

PV-Evaporator

The module energy balance was adapted from a model proposed by Jones (1999). Consequently, energy balances about the PV-evaporator give:

$$\frac{\mathrm{d}T_{\mathrm{mod}}}{\mathrm{d}t} = \left[Q_{\mathrm{mods}} - (Q_{\mathrm{modr}} + Q_{\mathrm{modc}} + Q_{\mathrm{er}} + W_{\mathrm{mod}})\right] / C_{\mathrm{mod}} \tag{1}$$

$$\frac{\mathrm{d}H_{\mathrm{ero}}}{\mathrm{d}t} = \left[m_{\mathrm{er}}(H_{\mathrm{eri}} - H_{\mathrm{ero}}) + Q_{\mathrm{er}}\right] / (V_{\mathrm{er}}\rho_{\mathrm{er}}) \tag{2}$$

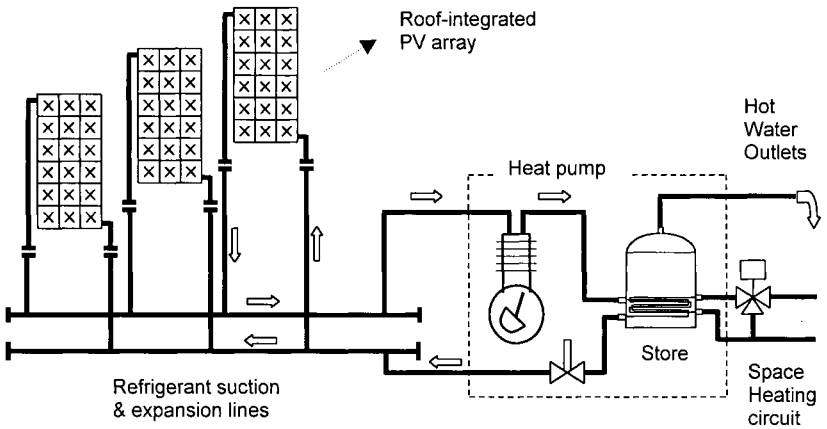


Figure 1: Conceptual system schematic

The various energy rates are:

$$Q_{\text{mods}} = A_{\text{mod}}\alpha_{\text{mod}}I_{\text{s}} \tag{3}$$

$$Q_{\text{modr}} = A_{\text{mod}}\sigma(\varepsilon_{\text{mod}}T_{\text{mod}}^4 - \varepsilon_{\text{sky}}(T_{\text{o}} - 20)^4) \tag{4}$$

$$Q_{\text{modc}} = A_{\text{mod}}h_{\text{c}}(T_{\text{mod}} - T_{\text{o}}) \tag{5}$$

$$Q_{\text{er}} = A_{\text{modi}}U_{\text{er}}(T_{\text{mod}} - T_{\text{er}}) \tag{6}$$

$$W_{\text{mod}} = C_{\text{FF}}I_{\text{s}}\ln(kI_{\text{s}})/T_{\text{mod}} \tag{7}$$

The refrigerant quality leaving the PV-evaporator will be:

$$x_{\text{ero}} = (H_{\text{ero}} - H_{\text{erf}})/H_{\text{erfg}} \tag{8}$$

$$\text{And when } x_{\text{ero}} > 1 \text{ then } T_{\text{ero}} = T_{\text{er}} + (H_{\text{ero}} - (H_{\text{erf}} + H_{\text{erfg}}))/c_{\text{erg}} \tag{9}$$

$$(\text{Otherwise } T_{\text{ero}} = T_{\text{er}})$$

Refrigerant properties were obtained from ICI (1996). In general:

$$H_{\text{erf}}, H_{\text{erfg}}, c_{\text{erg}} = \text{f}(T_{\text{er}}, T_{\text{crit}}) \tag{10}$$

It was assume that the evaporator, controlled to a constant pressure condition, would experience at all times:

$$P_{er}, T_{er}, \rho_{er} = \text{constant} \tag{11}$$

An algorithm was developed to calculate the boiling heat transfer coefficient within the PV-evaporator tubes based upon a method proposed by Collier & Thome (1999). However this proved computationally demanding and it was noted that the dominant independent variables were refrigerant mass flow rate and heat exchange surface temperature for the constant pressure (and temperature) conditions anticipated. A curve fit was therefore obtained based on results from the algorithm, giving a more convenient result with little loss of accuracy:

$$\begin{aligned} U_{er} &= 3.5237 + m_{er}(3.57892 - 0.34108T'_{mod} + 0.00756T'^2_{mod}) + \ldots \\ m^2_{er}&(-3.59294 + 0.36268T'_{mod} - 0.00833T'^2_{mod}) - 1.03174T'_{mod} + 0.08085T'^2_{mod} \end{aligned} \tag{12}$$

Compressor

The displacement, work transfer and leaving enthalpy can be expressed as follows based on the standard equations for a single stage reciprocating compressor (see for example McQuiston et. al. (2000)):

$$m_{pr} = V_{ps}\rho_{er}(1 - V_{pd}/V_{ps}) \times \left[(P_{cr}/P_{er})^{1/n} - 1 \right] \tag{13}$$

$$W_{pr} = m_{pr} R T_{ero} \left[n/(n-1) \right] \times \left[(P_{cr}/P_{er})^{(n-1)/n} - 1 \right] \tag{14}$$

$$W_p = W_{pr}/\eta_p \tag{15}$$

$$H_{pro} = H_{ero} + W_{pr}/m_{pr} \tag{16}$$

The dynamics of the refrigerant flow rate in the evaporator and compressor were neglected. Hence:

$$m_{er} = m_{pr} \tag{17}$$

Condenser and Accumulator

Energy and continuity balances about the condenser give:

$$\frac{dT_{cwo}}{dt} = \left[m_{cw} c_w (T_{cwi} - T_{cwo}) + Q_c \right] / C_c \tag{18}$$

$$\frac{d\rho_{cr}}{dt} = (m_{pr} - m_{cr})/V_{cr} \tag{19}$$

The refrigerant state leaving the condenser was assumed to be a saturated liquid at all times and the condensing rate dynamics were neglected. Hence by a steady-state energy balance on the refrigerant side:

$$m_{cr} = (Q_c + m_{pr} H_{pro}) / H_{cro} \tag{20}$$

Energy and continuity balances about the accumulator give:

$$\frac{dH_{aro}}{dt} = \left[m_{cr} H_{cro} - m_{pr} H_{aro} \right] / (V_{ar} \rho_{cr}) \tag{21}$$

$$\frac{dV_{ar}}{dt} = (m_{cr} - m_{er}) / \rho_{cr} \tag{22}$$

The condenser heat transfer rate was obtained from:

$$Q_c = A_c \left[1/U_{cr} + 1/U_{cw} \right]^{-1} \times (T_{cwo} - T_{cr}) \tag{23}$$

The condensing heat transfer coefficient was based on a correlation obtained from Collier and Thome (1999) for condensation outside tubes. Once again, in the interest of computational efficiency, a curve fit was obtained based on this method related to the two dominant independent variables involved; T_{cr} and m_{cr}:

$$\begin{aligned} U_{cr} &= 0.37081 - 0.0017 T_{cr} + m_{cr}(2.858878 - 0.01306 T_{cr}) + \ldots \\ & m_{cr}^2 (0.01093 T_{cr} - 2.39208) \end{aligned} \tag{24}$$

To close the equation set, an algorithm was written to calculate the refrigerant properties based on the extended Antoine equation (ICI (1996)), from which:

$$T_{cr} = f(\rho_{cr}) \tag{25}$$

$$P_{cr} = f(T_{cr}) \tag{26}$$

Finally, the heat pump coefficient of performance:

$$P_{HP} = m_{cw} c_w (T_{cwo} - T_{cwi}) / W_p \tag{27}$$

MODEL APPLICATION AND RESULTS

The model equations were assembled into blocks using Simulink in the Matlab environment. Four Matlab functions were written. Two of these were used to pre-process boiling and condensing heat transfer data (subsequently reduced into the simple correlations of equations (12) and (24)). The third Matlab function was used to calculate condensing refrigerant properties (equations (25) and (26)) and the fourth function was used to pre-process solar data. The latter was read from a file of global horizontal solar radiation measurements at 10-minute intervals. The global values were first split into direct and diffuse components, then corrected to equivalent surface-normal total solar radiation using a procedure described by Jones (1999). The measurements (including 10-minute external air temperatures) were taken in Newcastle upon Tyne during 1995-1997.

Model differential equations were solved using a 4th-order Runge-Kutta method and the model was applied to the input data set summarised in Table 1 which is based on a plant scaled to 6kW of condenser output at design. The plant would be capable of generating all hot water needs for a large family home with a surplus for space heating use at certain times. To service this load, 52 modules each of 0.63m^2 would be needed – sufficient to cover the south-facing pitch of the typical house referred to, thus forming part of the roof covering. The model was run during two daytime periods – a clear August day and a clear January day, for the daytime period 07:00-17:00hrs in order to demonstrate the potential of the plant during the main daytime hours of sunshine. Results are summarised in Figures 2 and 3.

DISCUSSION AND CONCLUSIONS

Figures 2 (c) & (d) show the simulated module power generation and corresponding compressor power use. In clear summer conditions, the module-generated power satisfies the compressor for most of the operating day with a significant excess available for other uses. In winter, the module-generated power satisfies about 40% of the compressor power requirement necessitating top-up power at other times of the day. The corresponding heat pump coefficient-of-performance profiles are shown in Figures 2 (a) & (b). Figures 3 (a) & (b) show that the module temperature remains fairly close to the constant evaporating conditions (5°C), ensuring high module power generating efficiencies at all times. With heat pump operation, the mean module temperature on a clear winter day is 5.06°C and the solar conversion power efficiency is 12.79%. This contrasts with 18.21°C and 12.21% without heat pump operation. However in summer, the corresponding module data are 7.16°C and 13.74% with heat pump operation and 46.67°C and 11.95% without. Clearly a significant module performance improvement can be expected with close-coupling especially in warmer weather conditions.

Figures 3 (c) & (d) indicate the temperature available for hot water heating. For all occasions in which the module power matches or exceeds the compressor power demand, heat is being generated "free" and in a sustainable manner. With the addition of a thermal store, it will be possible to achieve this sustainable heating of hot water throughout most of the operating year, except winter, though in winter a significant contribution can be expected. Further work needs to be done on the design of a thermal store and associated plant controls.

It is concluded that the close-coupling of PV modules with a conventional compression heat pump evaporator offers considerable potential for sustainable domestic hot water heating in the cooler northern latitude climates.

REFERENCES

Bailey B, Doty J R, Perez R, Stewart R, Donegan J (1993) Evaluation of a demand side management photovoltaic system *IEEE Transactions on Energy Conversion* **8:4** 621-627

Collier J G, Thome J R (1999) *Convective Boiling and Condensation* Oxford Science Publishers, Oxford

Gregory J A and McNelis B (1994) Photovoltaics in the UK *Proc. Northsun '94: Solar Energy at High Latitudes* James & James, London

ICI (1996) *Klea 134a Physical Property Data Sheet* ICI Klea, Runcorn

Jones A D (1999) Computer Modelling of the Power Supply and Demand of a Photovoltaic Building (PhD Thesis: University of Northumbria at Newcastle)

McQuiston F C, Parker J D, Spitler J D (2000) *Heating, Ventilating and Air Conditioning* John Wiley & Sons, New York

Underwood C P (1995) Scenarios for the Utilisation of Power by HVAC Plant from Photovoltaic Cladding on Buildings *Proc. CIBSE National Conference, Eastbourne, Vol. I* 118-126

ACKOWLEDGEMENTS

Thanks are due to the Newcastle Photovoltaics Application Centre at the School of Engineering, Northumbria University, for the supply of solar and external temperature data.

TABLE 1
MODEL INPUT DATA

Data Type: Symbol	Value	Data Type: Symbol	Value
Parameter: V_{er}	$0.1m^3$	Parameter: c_w	$4.2kJkg^{-1}K^{-1}$
Parameter: A_{mod}	$32.76m^2$	Parameter: A_c	$6.0m^2$
Parameter: A_{modi}	$9.8m^2$	Parameter: V_{cr}	$0.003m^2$
Parameter: ε_{sky}	0.95	Input constant: P_{er}	3.5355bar(a)
Parameter: ε_{mod}	0.9	Input constant: T_{er}	5^oC
Parameter: h_c	$0.002kWm^{-2}K^{-1}$	Input constant: ρ_{er}	$17.325kgm^{-3}$
Parameter: C_{FF}	$63.44Km^{-2}$	Time series: $I_s(t)$	From input file
Parameter: K	$109m^2kW^{-1}$	Time series: $T_o(t)$	From input file
Parameter: α_{mod}	0.7	Input constant: m_{cw}	$0.412kgs^{-1}$
Parameter: C_{mod}	$187.5kJK^{-1}$	Input constant: T_{cwi}	45^oC
Parameter: V_{ps}	$2.7962\times10^{-3}m^3s^{-1}$	Initial cond: $H_{ero}(0)$	Sat. gas at P_{er}
Parameter: V_{pd}	$1.3658\times10^{-4}m^3s^{-1}$	Initial cond: $T_{mod}(0)$	7^oC
Parameter: N	1.3	Initial cond: $T_{cwo}(0)$	55^oC
Parameter: η_p	0.68	Initial cond: $\rho_{cr}(0)$	Sat. liquid at P_{cr}
Parameter: R	$0.08149kJkg^{-1}K^{-1}$	Initial cond: $V_{ar}(0)$	$0.001m^3$
Parameter: U_{cw}	$0.404kWm^{-2}K^{-1}$	Initial cond: $H_{aro}(0)$	H_{cro}
Parameter: C_c	$15kJK^{-1}$		

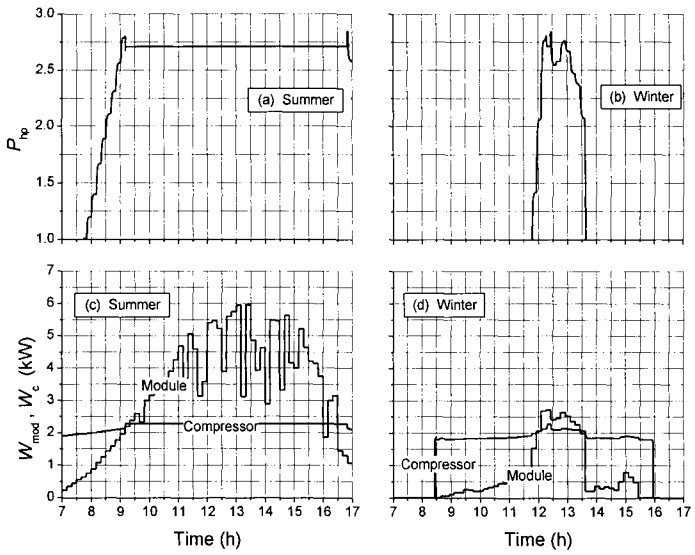


Figure 2: Simulated performance and power utilisation

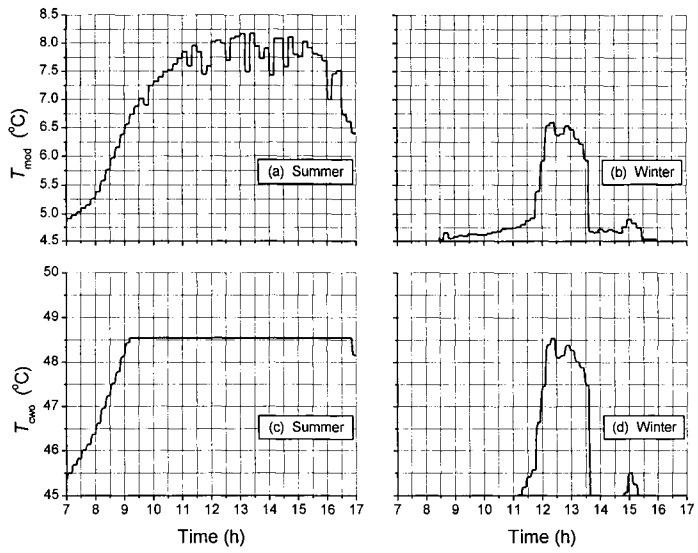


Figure 3: Simulated module and condenser water temperature

This Page Intentionally Left Blank

Advances in Building Technology, Volume 2
M. Anson, J.M. Ko and E.S.S. Lam (Eds.)
© 2002 Elsevier Science Ltd. All rights reserved

ANALYSIS OF NATURAL VENTILATION EFFECT FOR AN OFFICE BUILDING CONSIDERING MOISTURE ABSORPTION BY MATERIALS

Yoshida Harunori[1] and Kono Tetsuya[1]
[1]Department of Global Environment Engineering, Kyoto University,
Yoshida Honmachi, Sakyo-ku, Kyoto 606-8501, Japan.

ABSTRACT

Natural ventilation of buildings is becoming one of the major design approaches for sustainable buildings all over the world; however, the control strategies of vents or windows have not been well established especially when applied to hot and humid climate such as the Asian summer. In humid weather natural ventilation accelerates the absorption of water vapor by books, papers, materials used for furniture and furnishing, etc. This effect may increase the air-conditioning load when ventilation is performed intermittently in an air-conditioned building. Therefore it is important to determine ventilation control strategies on how and when vents or windows should be open and closed. For this analysis the authors developed a simulation code that can calculate air-conditioning load and room conditions by taking both natural ventilation and moisture flow analysis into account. In the present paper how much the vent schedules and quantities of moisture absorbing materials affects air-conditioning loads and room thermal conditions is evaluated and investigated. The results show that the natural ventilation controlled by temperature plus humidity ratio during nighttime is the best scenario among the considered scenarios, but enthalpy based control is not adequate contrary to expectation. Air-conditioning load is reduced by 37% in comparison to that for the no ventilation scenario.

KEY WORDS

Natural ventilation, Simulation, Moisture absorption, Air-conditioning load, Energy conservation, Asian climate

INTRODUCTION

Natural ventilation has come to international attention as a means to harmonize buildings with the natural environment and achieve energy conservation. Traditionally residential buildings relied deeply on natural ventilation for environmental control but other types of buildings depend mostly on HVAC systems. Recently however a number of naturally ventilated nonresidential buildings with a new concept can be found especially in European countries and the number of this type of project is increasing in Japan (Enomoto, Yoshida and Morita (1988) and Sako et. al. (1999)) and other countries as well. Most of the time in those buildings natural ventilation is achieved with the provision of specific features like vent shafts and automatically controlled vents instead of providing only manual opening/closing of windows.

Utilizing natural ventilation for controlling building environment and achieving energy conservation is a conventional technology but at the design stage comparing several design ideas and determining optimal control strategies for vents to maximize natural ventilation advantage is not an easy task. For the best design sophisticated computer simulation should be used to predict airflow rates and wind speed distributions in compartments. However the

research work related to determining an optimal control strategy is insufficient and the implications for different control strategies are not clarified. In addition, especially in a humid climate such as in Asia, natural ventilation may increase the absorption of water vapor by the books, papers, materials used for furniture and furnishing, etc. (Takahashi and Yoshida (2000)), and consequently air-conditioning load may increase when air-conditioning and ventilation take place alternately.

Since most available simulation codes are limited in performance, the authors developed a simulation tool that can calculate air-conditioning load and room conditions by incorporating the simultaneous analysis of natural ventilation and moisture absorption/desorption by materials. In this paper firstly the configuration of the tool is described. Then it is evaluated how moisture absorption/desorption and different control strategies affect air-conditioning loads and room thermal conditions using the tool, and a pseudo-optimal ventilation strategy is proposed.

SIMULATION CODE

The simulation code was developed by modifying the HASP/ACLD, Japanese heating/cooling load calculation program where the algorithm is based on the internationally used response factor method, by adding two major parts; 1) calculation of natural ventilation rates for a building with multiple compartments, and 2) calculation of heating and cooling loads considering simultaneous heat and moisture flow in building and existing materials in compartments.

Calculation of Airflow Rates

In most of the available codes to calculate natural ventilation for a multi compartment building, airflow through an opening between two compartments is calculated assuming the opening as a point orifice without size. This simplification implies that air flows always only one-way even though two-way airflow may occur along a vertical opening like a window and a door due to buoyancy effect. The governing equations used for evaluating the airflow through a vent opening are as follows by assuming a steady state (See Figure 1).

$$G_U = sign(\rho_b - \rho_a) \cdot \frac{2}{3} \cdot pq \cdot \sqrt{2g\rho_a |\rho_b - \rho_a|} \cdot \{h_2 - h_n\}^{3/2} \quad (1)$$

$$G_L = sign(\rho_b - \rho_a) \cdot \frac{2}{3} \cdot pq \cdot \sqrt{2g\rho_a |\rho_b - \rho_a|} \cdot \{h_n - h_1\}^{3/2} \quad (2)$$

$$G = G_U + G_L \quad (3)$$

$$h_n = (-P_a' + P_b')/\{(\rho_b - \rho_a)g\} \quad (4)$$

Where, G_U and G_L are the airflow rate of upper and lower part of the opening and G is the net airflow. ρ_a and ρ_b are the air density of the space A and B. h_1, h_2 and h_n are the height of the upper and lower ends of the opening, and the neutral pressure level from the reference floor height. g is the acceleration due to gravity. p, q are the height and width of the opening. *sign* is the sign of the term inside the parentheses. In Figure 1 P_a' and P_b' are the space pressures at the reference height.

Net airflow rate for a compartment or space must be zero because of the conservation of mass. i.e. $\sum G = 0$. When N compartments exist in a building N-th order nonlinear simultaneous equations are obtained (Eq. 5). In our study the equations are solved by applying a nonlinear programming approach known as the Gauss-Newton method with line-search , that is, by minimizing the objective function Eq. 6 regarding pressures P_1 through P_N.

$$\mathbf{G}(P_1, P_2 \cdots, P_N) = \mathbf{0} \quad (5)$$

$$\min_{\mathbf{P}} G_T = G_1^2 + G_2^2 + G_3^2 + \cdots + G_N^2 \quad (6)$$

Calculation of Air-conditioning Loads Considering Moisture Absorption and Desorption

Although simultaneous heat and moisture transport in building materials is not taken into account in most air-conditioning load calculation codes, it might have a large effect on the loads when natural ventilation is used

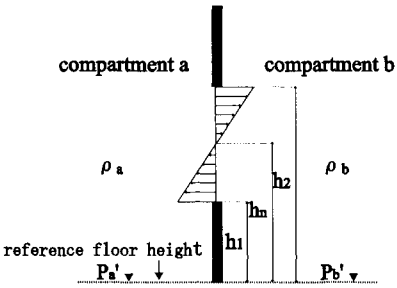


Figure 1: Model of airflow through an opening

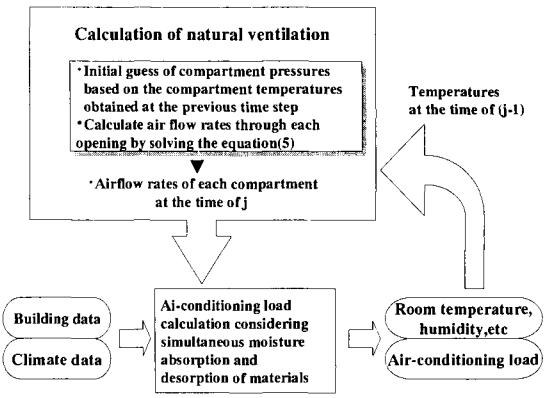


Figure 2: Configuration of the whole simulation

extensively and intermittently. One of the authors had developed a method for calculating transient responses considering the phenomenon of multi-layered construction based on discrete Fourier transform, Yoshida (1991) and Yoshida et al. (1994). For the present study a new simulation code incorporating this feature was developed. The method is briefly summarized as follows. The overall response of a multilayer construction is expressed by the equation (7), where $\mathbf{P} = (X\ \Theta)^T$, $\mathbf{F} = (W\ Q)^T$, and $X\ x\theta wq$, Θ, W and Q are the s-domain variables of humidity x, temperature θ, moisture flow w and heat flow q. $\mathbf{K}$ is called a 2 by 2 admittance matrix with the elements
of s-domain function $K(s)$. Inverse discrete Fourier transform is applied to obtain the time domain response $k(t)$ for a triangular input. Eight kinds of response $k(t)$ are defined as shown in Table.1. Using the $k(t)$ the equations governing heat and moisture balance of a room are formulated as equation (8) and they can be solved by differentiating them with respect to time.

$$\begin{Bmatrix} \mathbf{F}_1 \\ \mathbf{F}_2 \end{Bmatrix} = \begin{bmatrix} \mathbf{K}_{11} & \mathbf{K}_{12} \\ \mathbf{K}_{21} & \mathbf{K}_{22} \end{bmatrix} \cdot \begin{Bmatrix} \mathbf{P}_1 \\ \mathbf{P}_2 \end{Bmatrix} \tag{7}$$

$$m_r \frac{dx_r}{dt} = M_g + M_{ac} + m_v(x_o - x_r) + \sum_{L=1}^{L} A_L \sum_{j=0}^{\infty} k_{22,12}(j\Delta)\theta_o(t - j\Delta) - \sum_{I=1}^{I} A_I \sum_{j=0}^{\infty} \left\{ k_{22,11}(j\Delta)x_r(t - j\Delta) + k_{22,12}(j\Delta)\theta_r(t - j\Delta) \right\}$$

$$m_r c_p \frac{d\theta_r}{dt} = H_g + H_{ac} + m_v c_p(\theta_o - \theta_r) + \sum_{L=1}^{L} A_L \sum_{j=0}^{\infty} k_{21,22}(j\Delta)\theta_o(t - j\Delta) - \sum_{I=1}^{I} A_I \sum_{j=0}^{\infty} \left\{ k_{22,21}(j\Delta)x_r(t - j\Delta) + k_{22,22}(j\Delta)\theta_r(t - j\Delta) \right\} \tag{8}$$

TABLE 1 Transfer function coefficients of simultaneous heat and moisture transport

			Heat/mass flow response	
	Input	Output	Penetrating	Absorbing
Direct response	temperature θ	heat flow q	$k_{21,22}$	$k_{22,22}$
	humidity x	moisture flow w	$k_{21,11}$	$k_{22,11}$
Cross response	temperature θ	moisture flow w	$k_{21,12}$	$k_{22,12}$
	humidity x	heat flow q	$k_{21,21}$	$k_{22,21}$

Configuration of Whole Simulation

The whole simulation is comprised of the above two methods. In the course of simulation temperatures of

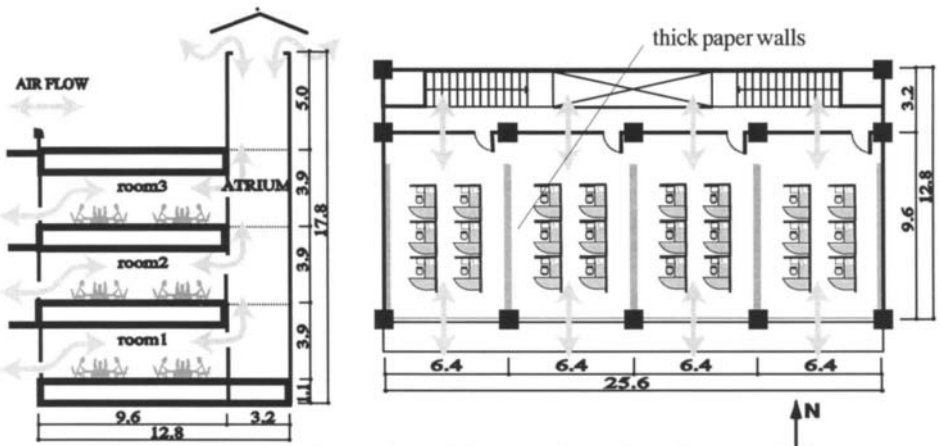


Figure 3: Building model used for simulation [m]

TABLE 2 Conditions of model building

NAME	MATERIALS FROM INSIDE TO OUTSIDE (mm)				
exterior wall	gypsum board (12)	fiberglass (50)	concrete (120)	cement (25)	ceramic tile (8)
glazing	heat absorbing glazing (8)				
beam facing exterior	concrete (300)	cement (25)	caramic tile (8)		
paper wall	paper (150)	plywood (6)	air (70)	plywood (6)	paper (150)
inner wall	plywood (6)	air (70)	plywood (6)		
floor (ceiling)	carpet (6)	cement (20)	concrete (130)	air (930)	rock wool board (15)

NAME	AREA(m²)	NAME	AREA(m²)
exterior wall(south)	27.4	exterior beam(west,east)	10.6
glazing	31.2	paper wall	322.6 (2.8H×7.2W×8)
vebt opening	13.1 (0.8H×4.1W×4)	inner wall	58.6
exterior wall(west,east)	26.9	floor (ceiling)	245.8
exterior beam(south)	28.2		

air conditioning hour	8:00 -- 18:00				
artificial lighting load (20W/m²)	9:00 -- 17:00 (90%)	18:00 (70%)	19:00 -- 21:00 (30%)		
people load (0.18 /m²)	9:00 -- 11:00 (80%)	12:00 (40%)	13:00 -- 17:00 (80%)	18:00 (35%)	19:00 -- 21:00 (10%)
equipment load (4.65 kW)	9:00 -- 19:00 (35%)				

compartments are fixed as those of the previous time when calculating airflow rates, then by using the airflow rates the air-conditioning loads and compartment temperatures at current time are calculated. For the exact calculation these two steps must be performed alternately until the airflow rates, the loads and the temperatures converge at the current time. However, to reduce of computation time this process is not performed. The effect of this simplification is not significant because compartment temperatures do not change drastically with time. The outline of the whole simulation process is schematically shown in Figure 2.

BUILDING MODEL FOR SIMULATION

For the present study a small office building shown in Figure 3 is used for simulation. Openings located below the windows and an atrium or a vent shaft with a top opening are provided enhancing natural ventilation. This feature is one of the typical ways for designing a naturally ventilated building. The wind pressure coefficients of each opening are determined according to the position of the opening and current outside wind direction. Attaining optimum utilization of natural ventilation all the openings are assumed to be controlled by Building Energy Management System (BEMS) based on a given scenario. Commonly used interior finishing such as gypsum and rock wool boards, carpets, etc. is put on ceilings, walls and floors and these materials are good moisture absorbing materials. Besides theses, hypothetical thick paper walls are located inside the room representing documents or books on bookshelves. The maximum size of the hypothetical wall is 7.2 by 2.8 m for each span and 8 rows are specified altogether. Other conditions of the building are summarized in Table 2. The weather data used are those

of the Reference Year of Osaka, Japan where the climate is hot and humid in summer.

Natural ventilation scenarios are abbreviated by combinations of letters. The first letter represents ventilation strategy: R means non-natural ventilation with daytime air-conditioning, D is for daytime ventilation only, N for nighttime only and air-conditioned during daytime, B for both night and daytime. The second letter represents the control strategy of opening/closing of the vents: N means no control, T for opening/closing vents control based on temperature, E for based on air enthalpy and H for based on air temperature in daytime and both temperature and humidity ratio in nighttime. The third letter is optional. If letter n is added no moisture absorption is taken into account in simulation, and if number 2 is used the paper wall area is 2/3 of the maximal area and number 1 is for the area of 1/3.

The strategy of vent control is as follows;

T is for controlling based on temperature. Daytime: open when $22 \le T_i \le 28°C$, $18 \le T_o \le 26°C$ and $T_o \le T_i$ are all satisfied. Nighttime: open when $20°C \le T_i$, $10 \le T_o \le 28°C$ and $T_o \le T_i$ are all satisfied. Where T_i is room temperature and T_o is outside air temperature.

E is for controlling based on enthalpy. Daytime open when $12.6 \le E_i \le 33.6\,J/g$, $8.2 \le E_i \le 29.4\,J/g$ and $E_o \le E_i$ are all satisfied. Nighttime: open when $16.8\,J/g \le E_i$ and $E_o \le E_i$ are satisfied. Where E_i is room air enthalpy and E_o is outside air enthalpy.

The above strategy is made by averaging the strategies applied for several real projects. At present there is no standardized and well established way of securing an optimal control strategy, therefore a real project is designed by rule of thumb and tuned at the operation stage. Rationally finding an optimal control strategy is an important future issue.

RESULTS AND DISCUSSIONS

The simulation results for each scenario are compared and analyzed below mainly by showing the total air-conditioning loads of three rooms. The duration of the simulation is the six months from June to October.

Effect on Air-conditioning Loads by Moisture Absorption

As previously stated simultaneous heat and moisture transfer is not taken into account in commonly used air-conditioning load calculation codes, and the effectiveness generated by natural ventilation enhancement is usually analyzed by similar codes. Therefore evaluating the difference caused by whether the effect into account is taken into account or not is necessary and gives valuable information. As seen in the Table 3 giving results for the scenario of RNn (non-simultaneous transfer) and RN, RN2 and RN1 (with simultaneous transfer), the total loads increase about 15% by taking the effect into account; more precisely 16%, 14% and 12 % for RN, RN2 and

TABLE 3 Seasonal Total Load for Scenario R (effect of simultaneous transfer)

Scenario	Cooling Load(GJ)	Ratio to RNn
RNn	62.8	1.00
RN	73.2	1.16
RN2	72.0	1.15
RN1	70.6	1.12

TABLE 4 Seasonal Total Load for Scenario T (controlled based on temperature)

Scenario	Cooling Load(GJ)	Ratio to RN
RN	73.2	1.00
DT	50.1	0.69
NT	53.6	0.73
BT	47.6	0.65

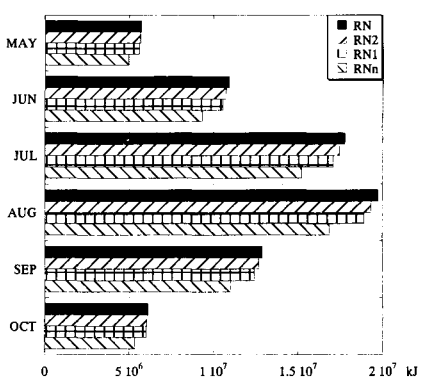


Figure 4: Monthly loads for scenario R

RN1 respectively. The differences caused by quantities of moisture absorbing materials are smaller than those caused by the consideration of the absorption effect. The reason for the increase is mainly due to the large latent load during the start-up period when the effect is considered. This is created by the stored moisture in materials due to moist air leakage in the nighttime. To investigate it more precisely the loads for each month are shown in Figure 4. However the increases are almost the same, roughly 17%, for all months. Buildings intended to enhance natural ventilation usually have many openable vents which tend to create large leakage area and to create much air leakage. Therefore, careful consideration must be taken to minimize the leakage area and a load calculation code that can handle the simultaneous transfer must be used.

Thermal Load Reduction by Temperature Based Natural Ventilation Control

The thermal load reduction by the temperature based natural ventilation control, which is abbreviated as T and defined previously, is evaluated. The results are shown in Table 4 by comparing to the reference operation RN, that is the non-natural ventilation scenario. The reduction of all the scenarios, DT, NT and BT, is approximately

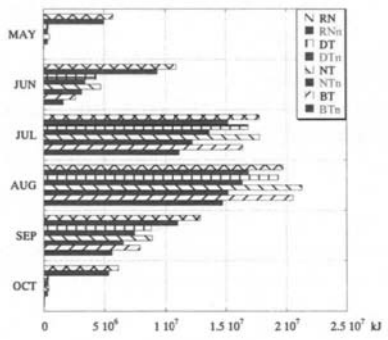


Figure 5: Monthly loads for scenario T

TABLE 5 Load comparison for scenario T and E

Scenario	Cooling Load(GJ)	Ratio to BT
BT	47.6	1.00
BE	51.0	1.07
Scenario	Cooling Load(GJ)	Ratio to DT
DT	50.1	1.00
DE	55.3	1.10

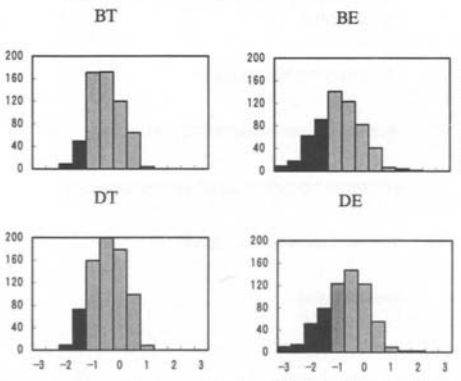


Figure 7: Distribution of PMV for scenario T and E (B: whole day ventilation, D: day time ventilation)

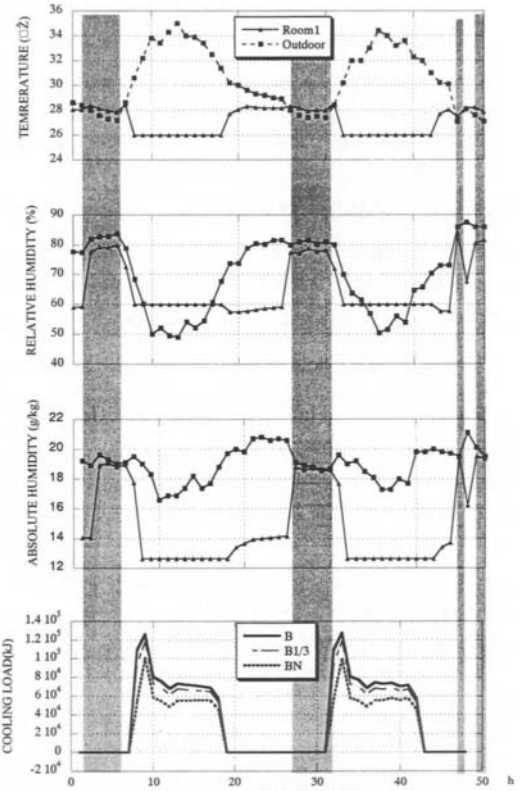


Figure 6: Example of adverse effect by nighttimeventilation

TABLE 5 Load comparison for scenario T and H

Scenario	Cooling Load(GJ)	Ratio to RN
RN	73.2	1.00
BT	47.6	0.65
BE	51.0	0.70
BH	45.9	0.63

30%. The best strategy in terms of load reduction is BT (35%), namely ventilation both for daytime and nighttime, followed by DT (31%); daytime ventilation only, and then NT (27%); nighttime only. It can be seen that the effectiveness of nighttime ventilation is not so significant. To investigate the reason, the monthly base loads are shown in Figure 5, and all the loads of scenario DT; daytime only, are smaller than those of RN; however the load in August of scenario NT; nighttime only, is only 8% larger. This adverse effect is generated because there is a higher possibility that outside temperature is lower than the room temperature, but outside humidity is quite high during the night, and this causes load increase. The specific and extreme example is shown in Figure 6: The halftone parts indicate naturally ventilated periods and during the times when the room air humidity becomes very high but the room is not well cooled.

Thermal Load Reduction by Enthalpy Base Natural Ventilation Control

As the air-conditioning load for processing air is directly related to enthalpy rather than dry bulb temperature, enthalpy based natural ventilation is more appropriate so that thermal load reduction should be improved. However determination of the thresholds is not straightforward because people cannot directly sense enthalpy. In the present study, therefore, the thresholds were determined by trial and error so as to make the opening time of vents as close as possible to that, about 30% opening duration per season, of the temperature based control scenario. The thresholds found are those explained previously. Simulation results for the whole day ventilation scenario, however, did not show improvement contrary to our expectation. Rather the load increased by 7% as shown in Table 5. This can still be due to moisture absorption. In addition, as the distribution PMV shows in the upper part of Figure 7, even the thermal condition of the rooms is worse than that for scenario BT. To avoid the problem a day time only scenario DE was investigate, but improvement was not achieved.

Additional Improvement on Temperature Base Control

To improve scenario T, additional control is added. That is, ventilation is activated only when the humidity ratio of the outside air is lower than that of room air to suppress moisture absorption. This scenario is named BH. By this modification additional a 2% load reduction can be attained. The improving effect is very small but large difference was found in total ventilation time, of about 60 % of the scenario BT. The comparisons of scenario RN, BT, BE and BH are shown in Table 6.

CONCLUSION

Many successful buildings with enhanced natural ventilation can be found especially in Europe and they represent one of the types known as green buildings. It is getting popular in Asian countries as well, but in a humid climate it may not always be adequate because moisture absorption by building materials when vented causes substantial additional thermal load when air-conditioning is in operation again after ventilation.

To investigate this issue the authors developed a computer program which combines the calculation of airflow rates by natural ventilation for a multiple compartment building and the calculation of intermittent air-conditioning loads and room temperatures considering simultaneous heat and moisture transfer. Applying this code to a naturally vented small office building several control strategies for ventilation ware investigated. Although the results are not necessarily universal to any building many general and important findings are obtained as follows.

1) By incorporating calculation of simultaneous moisture absorption and desorption into the simulation algorithm, it was found that air-conditioning load increases by about 15%. Although in common load calculation codes this effect is not considered.

2) As the basic and commonly applied ventilation strategy, a temperature based control strategy was investigated. Comparing three natural ventilation scenarios, namely daytime only,

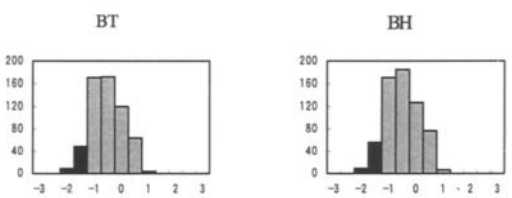


Figure 8: Distribution of PMV for scenario T and H (B: whole day ventilation, D: day time ventilation)

nighttime only and whole day, it was found that nighttime ventilation is not as effective as expected. This is because humid air is brought in by ventilation during the night and moisture accumulation takes place. In general it appears that the effectiveness of the whole day ventilation is not significant.

3) In order to improve ventilation effectiveness by avoiding moisture absorption issue, enthalpy based control was investigated. However, a load reduction was not attained. On the contrary the load increased and room environment evaluated by PMV became even worse. The result indicates that determination of the appropriate thresholds is difficult, even though this control strategy is used on some real projects of a naturally ventilated building.

4) Furthermore to improve the temperature based control strategy, humidity ratio based control, added during nighttime only, can decrease load by 5% over the purely temperature based control strategy.

ACKNOWLEDGMENT

The present study was supported by a grant-in-aid from the Ministry of Education and Science Japan. The authors are deeply grateful for this aid.

References

Enomoto G., Yoshida H. and Morita Y. (1998). Study on natural ventilation by window operation in a high-rise office building. *Summaries of Technical Papers of Annual Meeting,* Architectural Institute of Japan, **D:1**, 1017-1018.

Sako H. et al. (1999). Field measurement of a thermal environment and an energy conservation in the office building utilizing night purge system and natural ventilation. *Annual Report of The Society of Heating Air-Conditioning and Sanitary Engineers of Japan*, 1577-1580.

Takahashi T. and Yoshida H. (2000). Verification and Selection of Moisture Absorbing Materials Considering Simultaneous Heat and Moisture Transfer Effect. *Summaries of Technical Papers of Annual Meeting.* Architectural Institute of Japan, **D:2**, 311-312.

Yoshida H. (1991). Calculation Method of the Triangle Response of a Multi-layer Wall with Simultaneous Heat and Moisture Transfer by Discrete Fourier Transform. *Transactions of The Society of Heating Air-Conditioning and Sanitary Engineers of Japan,* **No.46**, 21-29.

Yoshida H., Terai T. and Sueyoshi H. (1994). Transient Analysis of Air-Conditioning Load and Room Conditions Considering Simultaneous Heat and Moisture Transport of Multi-Layered Constructions. *Building and Environment,* **Special Issue:29.3**, 337-343.

Yoshida H. and KonoT. et al. (2001). Room Temperature Mitigation and Cooling Load Reduction by the Aid of Natural Ventilation. *Summaries of Technical Papers of Annual Meeting.* Architectural Institute of Japan, **D:2**, 491-494.

Crawley D. B. (2001). EnergyPlus New Capabilities in a Whole-building Energy Simulation Program. **BS2001.** *IBPSA*, 51-58.

Yoshida H. and Kono T. (1991). Simulation of Temperature and Humidity Fluctuation of a Room with Moisture Absorption and Desorption, *21th Symposium on Thermal and Environmental Issues —Analysis and Design related to Building and Moisture Issues*, Architectural Institute of Japan, 65-74

ENVIRONMENTAL TECHNOLOGIES:

ENERGY/WATER CONSERVATION IN BUILDINGS

This Page Intentionally Left Blank

Advances in Building Technology, Volume 2
M. Anson, J.M. Ko and E.S.S. Lam (Eds.)
© 2002 Elsevier Science Ltd. All rights reserved

FRIENDLY INTERFACE AND DATA TRANSFER FOR ENGINEERING ASSESSMENT OF BUILDING DESIGN OPTIONS AT SKETCH DESIGN STAGE *"ENERGYSAVE"*

A.Bennadji[1], N.M.Bouchlaghem[1], D. Loveday[1], M.Holmes[2],
J. Shaffery[2] and R.van Zyl[3], A.Hallam[4]

A.Bennadji@lboro.ac.uk, N.M.Bouchlaghem@lboro.ac.uk, D.L.Loveday@lboro.ac.uk,
michael.holmes@arup.com, Joseph.Shaffery@arup.com, robert.vanzyl@amec.com,
adrian.hallam@member.riba.org

[1]Department of Civil and Building Engineering
Loughborough University, Loughborough, Leicestershire LE11 3TU, UK
[2]Arup Research & Development, 13 Fitzroy Street, London W1T 4BQ, UK
[3]Amec Capital Projects, Warwickshire, CV37 9NJ, UK
[4]RIBA, Ark DM Ltd, 15 Napier Street, Sheffield, S11 8HA, UK

ABSTRACT:

At present, during the early design stage of a building, different options are assessed using simple tools (tables, graphs and software) that contain a large number of assumptions the very nature of which can bias choice or possibly lead to an inappropriate solution. It can be argued that the only way to provide a rational assessment of options is to use calculation methods that represent in detail the physical processes involved; this usually involves the use of dynamic thermal models. Furthermore if this tool is also used during detailed design it would introduce a consistency that is normally absent from the analytical design process. Many designers are of the opinion that, because not all details are known, then such tools are not suitable for application at early stages in the design. This view can be challenged because, even at the concept stage, a great deal is known about a building.

This project aims to show that a general description of the building can be used to generate sufficient data to drive a valid analysis using a detailed thermal model at the early sketch stage of the design process. The paper describes the philosophy, methodology and the interface developed to achieve this aim. The interface guides the user through the input process using a series of screens giving options for keywords used to describe the building; comprehensive default data built into the software are then attached to these keywords. The resulting data file is a building description that is the best possible interpretation of the design intent. This can then be used to assess options and guide towards a final design.

Whilst naturally ventilated buildings are currently considered to be the ideal solution to low energy design in the UK, there remain a large proportion of buildings for which air conditioning offers the

only practical solution. This project is intended to provide a means to assess design options for such buildings at a very early stage in the design and in particular address the selection of the most appropriate system. The form of the interface is still developing and while it has been demonstrated to designers no third party tests have yet been carried out.

KEYWORDS

Architecture, Engineering, Energy, Assessment, Sketch stage, Design process, Data transfer and XML.

1. INTRODUCTION

There have been a number of projects that aim to provide simple interfaces to assist the designer, for example:

- The 'NATVENT' project (Natural ventilation for Offices. BRECSU March 1999);
- The 'Office Design Tools' (Building Services Journal, December 1999);
- The 'Building Design Advisor (BDA)' (Papamichael, K. et al. Decision making through use of interoperable simulation software, Building Simulation '97. Fifth International IBIPSA Conference, Prague 1997).

The complex nature of ventilation, and the very uncertain nature of the boundary conditions (wind environment, pressure coefficients, for example) justify the simple nature of the analytical models used in the first two examples. The third is a way of using a detailed thermal model to analyse design options. The main difference between this proposal and the BDA lies in the interface. The BDA uses a graphical tool that requires each space to be specified in some detail. It is therefore close to a conventional analysis tool and as such is not suitable for studies at the sketch stage of the design. The method by which results are presented is however one example that will be examined during the project. Members of the *EnergySave* team have visited the Laurence Berkley Laboratory in California and are therefore fully aware of the strengths and weaknesses of the BDA.

The intention of the *EnergySave* project is to make use of available software and skills. In particular, whilst a detailed thermal model is necessary for the implementation of the method there is no intention to develop that model. It is however important that the source code of that model is available to the team. The model selected is ENERGY2. This program has been developed in Arup Research and Development and has been exposed to the International Simulation Community by means of the IEA Annex 21 (a task shared project related to quality assurance and validation of thermal models).

In order to facilitate energy calculations it was necessary to develop generic system models. These are based upon those described in the CIBSE Energy Code 2, 'Energy demands for air conditioned buildings'. Arup Research and Development were involved in the drafting of this code and made significant inputs into the building description application of climatic data and testing of early versions. Although these models are very simple they capture the essential features of the systems. This means that the major inefficiencies are accounted for.
At present, during the early design stage of a building, different options are assessed using simple tools (tables, graphs and software) that contain a large number of assumptions the very nature of which can bias choice or possibly lead to an inappropriate solution. It can be argued that the only way to provide a rational assessment of options is to use calculation methods that represent in detail the physical processes involved; this usually involves the use of dynamic thermal models. Many designers are of the opinion that, because not all details are known, then such tools are not suitable for application at early stages in the design. This view can be challenged because, even at the concept stage a great deal is known about the building, for example:

- Size;
- Number of floors;
- Occupancy;
- Preferred glazed areas;
- Insulation standards;
- Thermal mass;
- Required internal environmental conditions.

Not withstanding this there is still resistance to the application of simulation, typical reasons given are:

- Too time consuming to input the necessary data;
- The program is not user friendly;
- Manual methods are quite adequate;
- Programs cannot be trusted;
- Do not understand how the program works.

Arups had already recognized the need to address these issues and encourage the use of simulation throughout the life cycle of the building and so, at their own expense, joined the International Energy Agency (IEA), Building and Community Systems, Annex 30 (Bringing Simulation to Application). Arup Research and Development was the official UK Participant.

The IEA project demonstrated the value of simulation throughout the design process, the value of good quality default data and the need for software validation. However despite identifying user friendliness as an important issue in increasing the uptake of simulation throughout the construction industry, it did not make a serious attempt to address that issue. One objective of *EnergySave* is to redress this.

2. ENERGYSAVE CONCEPT

The second objective for the *EnergySave* interface is to capture the essential elements of a design in an unambiguous way to enable a valid energy analysis at the concept stage of a design. The use of a detailed thermal model[1] at both this stage and later stages in the design process would bring a consistency to the analysis through out design. A third and equally important objective is to provide a mechanism to bring simulation to those who believe it to be too complex for their needs and far to difficult to use. This is done in several ways:

- The use of extensive, intelligent defaults to minimise the amount of data that are required;
- The use of a pictorial based input system to identify the main input parameters;
- The use of minimum data to describe building;
- A critical assessment of the most significant features that can affect the energy consumption of the building.

An example of the later is the way solar shading is described. In the case of passive buildings it is particularly important to ensure that the effect of any purpose built shade is accurately represented. In the case of air-conditioned buildings this is less necessary because energy consumption is far more

[1] A detailed thermal model is usually a simulation program capable of calculating the performance of both building and HVAC systems at hourly intervals for the period of a year. In the UK context design programs based upon the CIBSE Admittance method are not considered to be detailed thermal models.

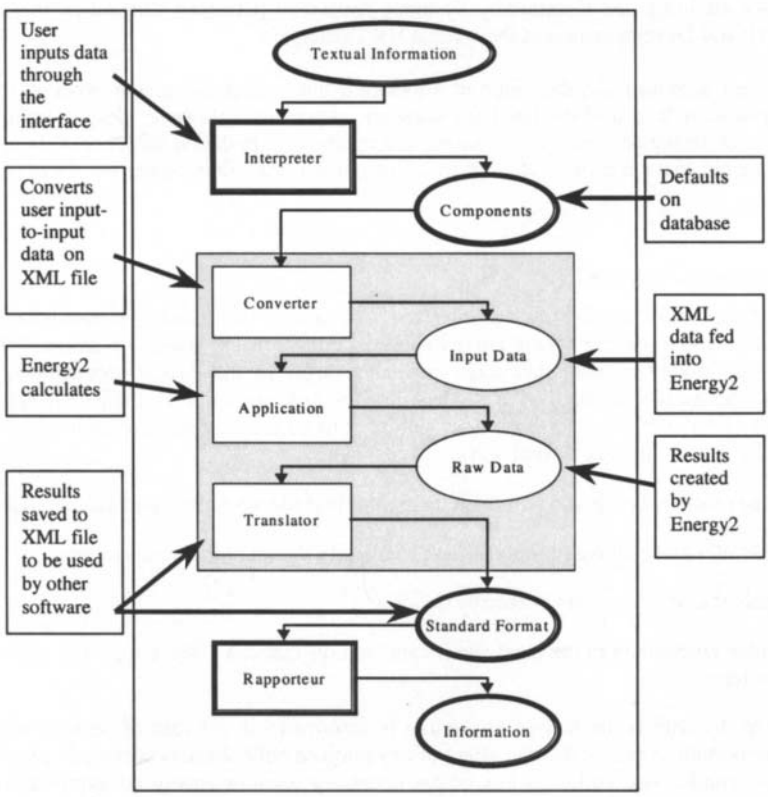
closely related to systems and controls. *EnergySave* does not ignore external shade but on the other hand does not encourage users to be obsessed with complex representations. The form of the building is simplified, at present to a rectangle. While this is recognised to be a limitation it is also felt that the majority of buildings can be adequately represented. *EnergySave* is intended to apply to the norm. Section 4 (Overview of the interface) demonstrates the principles described above.

A fundamental to the system is to use what is already available, thus the main database used is a commercial product chosen because the majority of PC users will have access to it. Intermediate data transfer uses an XML Schema taken from the public domain (Green Building Schema).

It is important to realise the *EnergySave* **does not** contain a calculation engine. It is intended that the XML file be described in sufficient detail to allow the use of third part 'engines'. This is in direct contrast to the development of public domain engines in the USA.

3. STRUCTURE

The following flow diagram shows the form of the system.



The interface between *EnergySave* and the application is the XML file. This Section briefly describes the system.

3.1 The Interpreter

The written descriptions are converted into components using rules developed from discussions with designers from the industrial partners, Amec, Ove Arup and RIBA, who have also provided default data based upon previous projects. These are combined with user specific data into building and system components and written to a standardised data file. The data structure produced by this process is to be specified in sufficient detail to allow any developer to use their model in conjunction with this system. One function of the interpreter is convert simple descriptions into physical layers that are suitable for use in a detailed thermal model. Examples are:

- Opaque walls. Input U value and response time – output layers in the construction and the physical properties of those layers.
- Glazing. Input shading coefficient – output layers and basic properties such as transmission and absorption at normal incidence for each.

The 'Interpreter' combines the default data taken from the database and combines that with the user input to write the XML file. It is important that a single XML file contains ALL options investigated. This can be done by specifying each as a new building on the same site (campus in the Green Building Schema).

3.2 The Converter

This is specific to the simulation model used and it would be written by the application vendor to convert the data on the XML file to that required by the program.

3.3 The Application

In this case the Arup ENERGY2 program will be used. It could however be any appropriate model.

3.4 The Translator

This is specific to the program used in the analysis and is used to convert the predictions (raw data) into a standard format. This format is specified in detail to allow the system to be used by other software developers. The output from the 'translator ' is to the XML file.

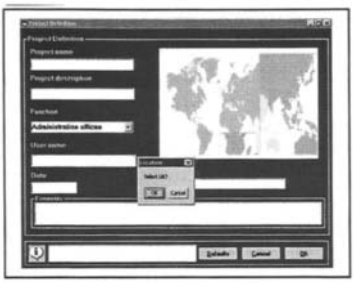
3.5 The Rapporteur

The nature of the output from an energy simulation requires specialist knowledge for a valid interpretation, in particular where comparisons are to be made. The rapporteur provides a facility to compare and interpret design options. It is hieratical in nature so the user is first offered overall energy (and CO_2 figures). It is then possible to delve deeper to looking order to develop an understanding of the performance indicated. Automatic comparison of options will be available. The 'Rapporteur' is currently under development.

4. THE INTERFACE

This Section shows some of the essential elements of the interface and where appropriate how they can be used to set defaults. It is intentional that the screens – or forms –presented to the user do not have the appearance of a conventional Windows interface. It is inappropriate to display the complete

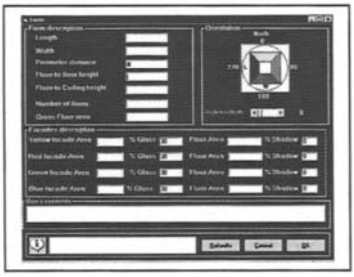
interface, the sample 'forms' presented here are intended to highlight the main principles behind *EnergySave*.



Project Definition
In addition to capturing the standard inputs such as project description and user, the location and function of the building are defined. Location sets insulation standards via local building regulations and occupancy patterns and internal gains are set by the function. A default building is generated.

Location
The country map is displayed. Each region contains a link to a climatic data file. Software vendors can enter their particular file names on the database. Exposure is also identified. Because this can be done in several ways, an advanced option allows an alternative definition, terrain type. This is intended to provide data for software that requires some means to describe wind shading for infiltration and ventilation calculations.

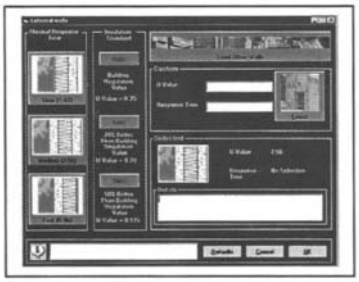




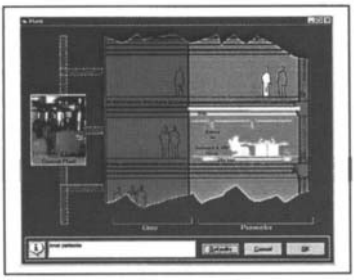
Building's form
A simple model of a building is created, using zones based on the façades. The user inputs the length, width, floor-to-floor height, and the number of floors. Simple solar shading is also set here, another input (not illustrated here) allows for individual window shade to be entered.



Internal Gains
Internal loads are defined by 'level', very high to very low. The defaults corresponding to these levels are displayed and it is possible for the user to make changes.



External Walls
Materials used in external walls can be selected. The variations are labelled by their U-Value and thermal response time (Admittance). The user can select the closest type of wall or alternatively create a custom wall using the advanced option. Similarly other input screens allow input of parameters for windows, partitions etc.



HVAC Systems

A side view cut out section of the building is split into the core, inner perimeter and outer perimeter. Each section can be "filled" with heating and cooling systems. This is shown in the green section with the under-floor VAV system. As the user enters data, options are limited for other sections so that inappropriate combinations cannot be selected.

5. CONCLUSION

The *EnergySave* project is intended to bring simulation to a wide range of building design professionals. To do this it has been necessary to make many simplifications to the description of a building and the associated HEVAC systems. These are based upon the relative importance of each element upon energy consumption. It is believed that the weightings used will result in meaningful predictions. *EnergySave* differs from other approaches to simplified energy analysis in that simplifications are made in the way data are described to the analytical engine and not in the engine.

6. ACKNOWLEDGEMENT

EnergySave is part funded by the United Kingdom Department of Trade and Industry.

BIBLIOGRAPHY

AIA, (1999), Understanding the Design Process, AIA.

Baker, N.V. (1994), The LT Method 2.0 –An energy design tool for non-domestic building, K.Steemers, Editor. Royal Institute of British Architects: Cambridge Architecture Research Limited.

Baker,N.V., Fanchiotti,A and Steemers,K. "Daylighting in Architecture: A European conference Book". CEC, JamesX James Ltd., London.

Baker, N.V. (1994), Energy and environment in non-domestic buildings, Royal Institute of British Architects, London.

Broadbent,G.H. (1966), The design process, Portsmouth college of Technology –School of Architecture.

Brown.J, Palmer.J. (1991), Occupancy profiles and incidental gains in thermal simulation programmes Databuilt, report to BRE, September.

CIBSE guide. (1986), The Chartered Institution of Building Services Engineers, London.

Hyde, R.A. and A. Pedrini (1999), The (LTV) Architecture Design Tool: Critique of Planning Strategies for Energy Efficiency. In ANZAScA, Sydney.

Szokolay.S.R. (1980), Environmental science handbook for architects and builders, the construction press.

This Page Intentionally Left Blank

Advances in Building Technology, Volume 2
M. Anson, J.M. Ko and E.S.S. Lam (Eds.)
© 2002 Elsevier Science Ltd. All rights reserved

THE DEVELOPMENT OF A PROTO-TYPE PV DECK-SHADING SYSTEM AS THERMAL BUFFER AND ELECTRICITY GENERATOR

J.Close[1], KH Lam[1] and YH Wong[1]

[1]Department of Architecture, University of Hong Kong, Pokfulam Rd, HK SAR China

ABSTRACT

A Copper Indium Diselenide (CIS) technology photovoltaic deck-shading system has been designed for the sub-tropical climate to generate electricity, act as a thermal buffer and provide naturally lit shaded recreation or teaching-space at deck level. The system has been designed for pre-wiring and pre-fabrication techniques to allow the increased quality control of factory production plus reduced site installation costs. The system has a wider range of applications but is customized to the 7.5m x 9.6m planning grid of Hong Kong (HK) Schools. The system is suited to 330x 1300mm dimensioned modules, and particularly the ST40 CIS module manufactured by Siemens Solar. The robust, lightweight and low-maintenance system is particularly designed for latitude 22° where high altitude sun permits close-spacing of the modules that can, with 33% increased module area, maximise summer electricity yield. Performance under high wind-load has been a critical factor in the design necessitating wind tunnel measurements and module wind-loading tests. The module supporting system consists of factory pre-fabricated stainless steel trusses supporting paired strings of modules. Each truss interlocks to the preceding truss through the hub containing the customized electrics junction box. The system and its electrical components are intended as starters to the development of a local PV components industry. Simulation studies for the new 36 class Ma Wa School, to be completed in 2003, indicate that a 6-bay system provides a modest 2.8% saving on the annual cooling load and the electricity yield contributes 9.79% to the estimated annual classroom electricity demand. Tendered costs indicate the total system construction at approximately US$681/m^2 with module costs representing about 61% of the system costs.

KEYWORDS

Copper Indium Diselenide (CIS) Photovoltaic (PV) deck-shading system, thermal buffer, electricity generator, pre-fabrication, low- maintenance

INTRODUCTION

Hong Kong (HK) is a vertical city but its schools are a building sector with a more pronounced horizontal than vertical character thus offering scope for optimizing PV applications with a generous area for PV arrays. New HK schools conform to a 7.5m x 9.6m planning grid providing the opportunity for product standardization and also PV commercialization due to the size of the Schools Construction Programme administered by the HK Government. A PV roof deck shading system has been designed for HK schools and six bays are to be included in the Ma Wan Primary School, a government/utility funded PV demonstration project currently under construction, Close (2001). The deck shading proto-type design is a self-supporting system that acts as a thermal buffer to the building envelope as well as generating electricity. It offers, at roof-deck level, additional sheltered space for equipment, recreation or teaching while its open north-light design ventilates the space and the PV modules.



Fig. 1 : Model of Ma Wan Primary School, Hong Kong Construction from January 2002-mid 2003

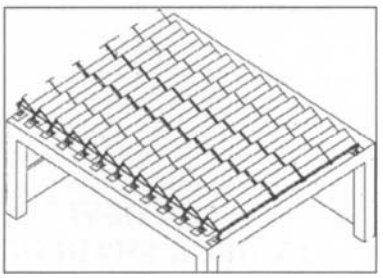


Fig. 2 : 7.5m x 9.6m bay of roof deck shading system with double module of Siemens Solar ST40 CIS technology

APPROACH

The design of the deck-shading system included these factors:

- Selection of PV technology (performance in sub-tropical climate), manufacturer & module
- Truss spacing + dimensional relationship to the 7.5m x 9.6m planning grid
- Wind-load capacity of selected module
- Detailed structural design for pre-fabrication, low-maintenance + long life
- Integration of the electrical sub-system.

1. PV TECHNOLOGY & MODULE SELECTION

Cost and relative efficiency are still the major factors in PV module selection. Performance monitoring in real outdoor conditions indicates the related effects of high ambient air temperature and high cell temperature on lowering PV module efficiency of mono & polycrystalline modules in the sub-tropical climate of Hong Kong. Their high cost also inhibits large area application for Building Integrated Photovoltaic (BIPV) applications. Amorphous Silicon (a-Si) technology is considerably lower cost but its long-term stability is still under review and improved efficiency above maximum 8% peak rate is not yet achieved. Copper Indium Diselenide (CIS) is a relatively new thin-film technology now coming into commercial production that has similar lower material/production costs as a-Si but a higher efficiency, Siemens Solar has produced the first production line CIS modules, independently tested and rated at 10.2% efficiency and warranted for 10years by the manufacturer. Siemens Solar advises the end-2002 price for ST40 (40watts peak) is US$120 per module which is comparable to US Utility electricity charge of US$3 per watt - the prevailing benchmark.

CIS PV technology appears to offer the potential of improved performance over amorphous silicon, yet without the efficiency losses in high temperature conditions of mono or poly-crystalline technologies or their higher cost. A recent paper by Durisch, Lam & Close, (2) records the performance in real outdoor conditions of an early production module of Siemens ST40 in temperate climate from which a general model for performance in all climate conditions was developed. Table1 adjacent, indicates the relatively small efficiency drop (2%) over cell temperature range of 35-85° C. This is particularly important in HK's high summer temperatures. At these cell temperatures, mono or polycrystalline cell efficiency can drop substantially, to 5% below rated efficiency for some products. Also, the relatively high efficiency is maintained for irradiance levels varying between 200-1000 W/m^2 at only 2% variation.

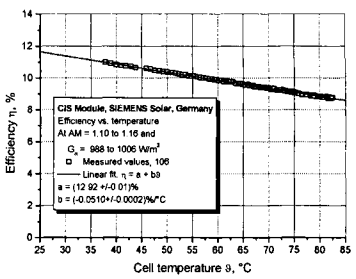


Table 1 : Siemens ST40 performance under high cell temperatures -HK conditions

2. SYSTEMS DESIGN : TRUSS SPACING + MODULE AREA

An open deck-shading system promotes ventilation, and, in the northern hemisphere, if correctly north/south orientated, provides indirect (cool) daylight. It also provides maximum solar access for south-facing modules. The opaque Siemens Solar module dimensions 329 x 1293mm, permitting 5 modules per 7.5m bay width. The design pairs them to form two adjacent strings. The 25 degrees truss design angle is best for all-year performance at HK's latitude. For the 9.6m bay length the closer spacing between truss centres of 800mm, compared with the initial 1066mm, permits 12 trusses per bay compared with 9, give an increased module area of 33%. During winter months, with sun angle below 40°, there will be mutual shading of the lower part of the truss but by-pass diodes limit the shading impact on the total electricity generated. Simulation with various programmes has estimated the annual yield, though only PVSYST allows for mutual shading losses. (The differences in the PVSYST annual yields results from the weather database range.) Yield and contribution to a school's annual electricity consumption as reported by Close, Wong, Chan & Kwok (3) is based on 6 bays of the deck-shading system and the 36 classroom, Ma Wan School design that also incorporates other PV installations and energy-saving School Building Energy Management System (BEMS).

Design: Open ventilated truss + maximum module area	Modules Per 6- bay	Module Area M^2	Total at peak rate kW	Estimated Annual Yield kWhrs
25 degree tilt at **1,066mm** ccs **double** module	540	231.6	21,600 kW	24,370kWhrs
25 degree tilt at **800mm** ccs **double** module + **by-pass diode**	720	308.8	28,800 kW	32,432 kWhrs

Fig 3 : Comparison of truss spacing, module area and estimated annual yield

Tech + Ref	PVCad 2.1d	PVSyst 3.0 preliminary + Met 2 '81/90 (Synth)	PVSyst 3.0 project + Met 2 '81/90 (Synth)	PVSyst 3.0 project + Met 4 HKO '81/90 + 61/90	HKU Logged Data + '84/94 HKO Met
CIS ST40	**31** MWh	**21.1** MWh	**34** MWh	**27.9** MWh	**32.4** MWh

Figure 4 : Comparison of simulated yield from different programmes and weatherbases

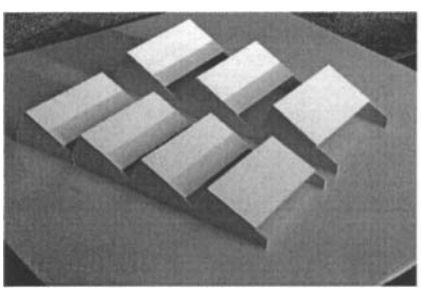


Fig 5: Comparison of truss spacing : 800mm + 1066mm spacing

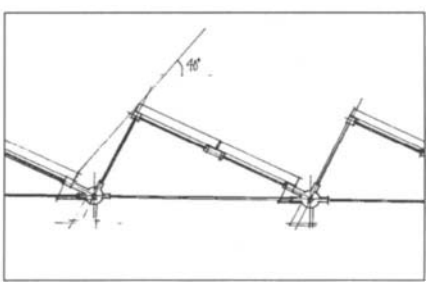


Fig 6: 800mm truss centres with mutual shading below 40°

3. WIND-LOAD

Hong Kong is a city subject to summer typhoons with high wind speeds. The HK Building Department imposes a wind-load code on all installations related to their exposure and building height. Additionally the context of low-rise Ma Wan School with high-rise surrounding buildings is known to produce turbulent and unexpected conditions. The extent of these conditions and likely loading on the PV deck system was

simulated in wind tunnel tests carried out at The Wind Tunnel Facility of the HK University of Science & Technology (HKUST) in December 2001. The wind pressure conditions were determined by carrying out both a wind tunnel topographical study of the Ma Wan island location and also the cladding pressure tests on a 1:100 scale model of the Ma Wan School (See Figure 7 below).

The Wind Tunnel tests simulated the loading under the extreme conditions of mean hourly gradient wind velocity of 64m/second as stipulated by the HK Practice Note (PNAP150). The wind pressure measurements on the 1:100 scale model were taken at pressure taps located through the six bays of deck-shading system and at 10 degree intervals of incident wind direction over the full 360 degrees. The suction, or negative pressure, measured greater than the positive pressure and the leading edge of the array received the brunt of the pressure. See diagram in Figure 8 below. The largest positive differential pressure measured 2.33kPa and the largest negative differential pressure measured -7.28kPa.

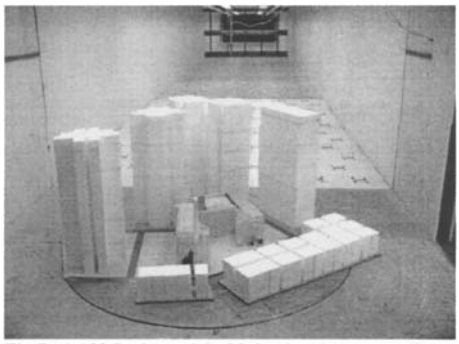


Fig 7 : 1:100 Scale model of School with surrounding high buildings in HKUST Wind Tunnel

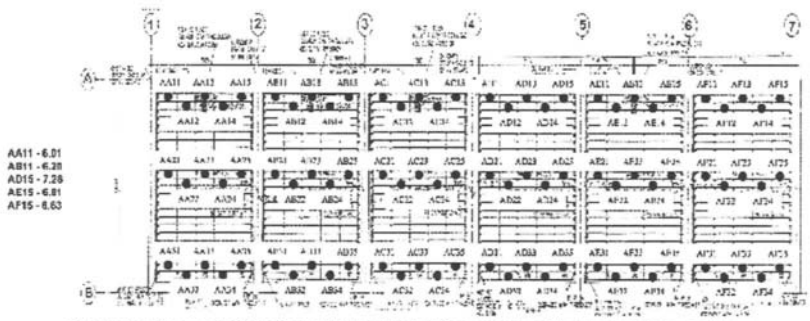
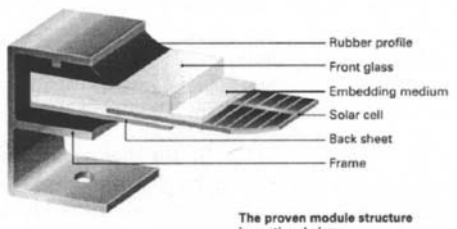


Figure 8 : Diagram of the 6-bay PV deck-shading system with pressure tap positions. Maximum negative pressure positions identified

4. MODULE STRENGTH

The selected module, the Siemens Solar ST40, is a standard module in the PowerMax range. The product literature gives insufficient construction detail for structural calculations , see brochure detail below, and the meaning of the various certificates, IEC 61215, UL 1703, TUV safety class II, etc, is not identified.



Reference to the manufacturer established the construction as

Cover glass – Tempered Solite glass 3.05-3.40mm thick
3 Sheets EVA encapsulate
Raw CIS module – Untempered glass 1.8-2.1mm thick
1 Sheet EVA encapsulate
1 Sheet TPAT (Tedlar Polyester Aluminium Tedlar)
34mm deep aluminium frame on all four sides

Figure 9 : Siemens Solar brochure image of the ST40 module construction with manufacturer's description adjacent

In view of the large negative pressures possible on the module in extreme conditions it was decided to test the module's wind-loading capacity at a Test Facility certified by the HK Government. A standard production module, ST40 was tested for a cyclic pressure test in accordance with HK Practice Note PNAP 106 incorporating a 1.25 safety factor at the Research Engineering Development Façade Consultants Ltd, Yuen Long, HK. The ST40 module maintained its structural integrity at +1.50kPa Positive Pressure and at -3.3kPa Negative Pressure. In view of the far higher pressures measured in the wind tunnel test, the module was next tested with a continuous negative loading in 0.50kPa increments from 1-8.0kPa, held for 10 seconds, and subsequently in 1kPa increments, held for 10 seconds. The module maintained its structural integrity up to -17kPa Negative Pressure, more than double the maximum wind pressure measured in the wind tunnel test, and no further tests were done. Subsequently, the same structurally tested module was electrically tested and found to be in working order and not electrically affected by the deflections of the pressure test.

5. STRUCTURAL SYSTEM DESIGN

Since the standard Siemens Solar ST40 module meets the wind-loading demands, the supporting system was then refined. The system is required to be robust yet also lightweight, low maintenance and with visual appeal. Further the system should be designed for wiring integration, factory pre-fabrication, easy transportation, resulting in a sensibly-priced final product with a long-life.

HK's extremely corrosive marine climate influenced the selection of stainless steel over galvanized steel, paint-protected steel or structural aluminium. The projected 50+ year life of school premises and low maintenance needs were major factors. The shading system consists of a standard truss design linking cast stainless steel circular sections and high tensile stainless steel rods. The trusses interlock at the hub with a specially designed gusset plate. The hub is bolted to the upstanding support suited to the Ma Wan school application but capable of modification for other conditions.

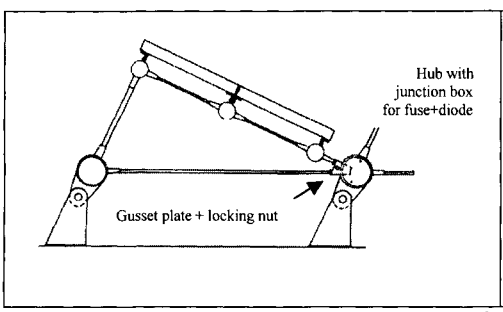


Figure 10 : Truss design with inter-locking gusset plate and hub

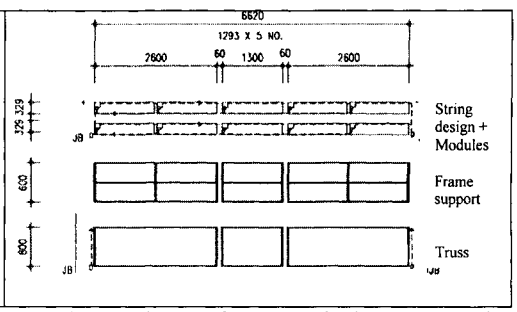


Fig 11 : Diagram of the prefabrication & wiring string

6 ELECTRICAL DESIGN

A further design aim was the integration of the electrical system wiring to minimize site labour and this resulted in the design of a customized junction-box. Upper and lower lines of modules each form a string. As shown in Figure 11. The modules being connected with pre-wired push-fit connectors. The hub that interlocks the trusses also houses the customised junction box. This incorporates two sets of connector, fuse and bypass diode, one set for each string of modules per truss as shown in Figure 12 below. For Ma Wan School the junction boxes will be linked via customised branch cables to the inverter sited on the wall below. The Centre for Advanced Product Development Technologies (CAPDT) at HKU assisted in the 3d solid modeling of the interlocking hub that links the trusses together and locks with the upstand support. The rapid tooling technique is the means of generating the proto-types of complex parts directly from 3D Computer Aided Design (CAD). Approaches are presently being made to electrical contractors in HK to collaborate on the detailed design and small-scale manufacture of the customized junction boxes

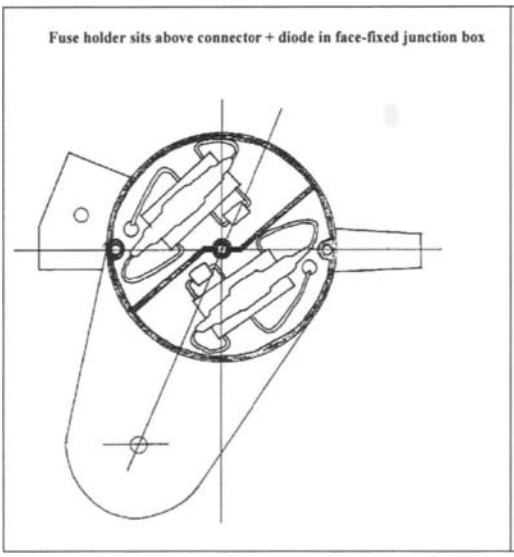


Fig 12 : Plan of the customised junction box with fuse & diode sets

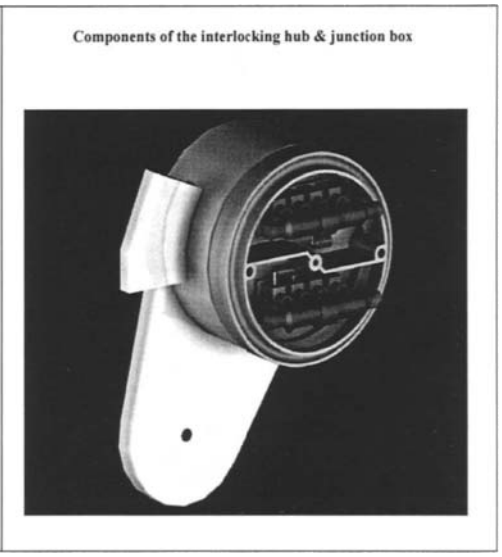


Fig.13 : Solid 3D modeling of the hub for rapid proto-typing

7 COSTS

The PV deck-shading system is one of four PV installations included in the new school at Ma Wan. Prices submitted in the tender procedures indicate the following costs:

Construction (no overheads)	%	Total %
General Contractor (GC)		
Modules	61	
Truss system	5.6	
GC's Building Services Interface	4.5	
Protection	2.5	
Wind-load test	3.3	
Struct/Elect. Design checks	2.6	
Extras	2.5	
Total GC		**82**
Electrical Contractor		
Inverter	11	
Junction boxes, isolators and cables etc	7	
Total Electric Contractor		**18**
Total		**100**

Fig 14 : Indicative percentage costs of the PV Deck-shading system

The truss support system is a relatively small proportion of the total cost despite the choice of stainless steel material. 7% total allowance for General Contractors' interface with the building services and extras indicates the lack of experience of contractors in this construction as does the additional 6% for wind-load tests and more particularly the structural design and electrical design checks. As is frequent in construction today, the contractor carries the 'Design and Build' responsibility. The electrical costs exclude monitoring system costs. The approximate total cost of both general contractor and electrical contractor's work is about HK$5316/m^2 (US$681.5/m^2).

8 SCIENTFIC INNOVATION & RELEVANCE

The outdoor testing in sub-tropical conditions (Hong Kong) indicates the suitability of CIS technology for our high ambient temperatures in summer and also the consistent conversion performance in lower solar radiation conditions. The Siemens Solar module's lightweight yet robust construction also suits the high

wind-load demands of typhoon regions. The lightness allows the supporting structure of the deck-shading system to be correspondingly lightweight. The stainless steel construction is low-maintenance and its construction easily pre-fabricated and pre-wired. The specially designed and integrated junction box includes by-bass diodes and fuses. No such junction box is presently commercially available to the knowledge of these authors. Local electrical industries are being encouraged to manufacture small quantity PV components for the PV industry. Although the system has been designed for schools it has wider applications as a shading structure for markets, car-parking, petrol stations, bus terminals etc. As a system, it can be easily reduced or extended. As a system design it has the potential, through greater familiarity and experience of PV integration, to lower initial manufacture and installation costs.

RESULTS & CONCLUSION

Priced at US$3 per watt and with performance in real conditions expected to be close to the rated STC efficiency, the Siemens Solar ST40 module offers good value. The module presently has a 10year limited manufacturer's warranty. At the time of writing, Siemens Solar has advised of their intention to modify the construction of the module from that tested by reducing the EVA sheet encapsulation of the raw module and also the backing sheet. Structural calculations based on the new construction details indicate the revised module would meet the wind-loading requirement. A proto-type truss, the width of a bay (7.5m) will be manufactured in preparation for the full test of the module plus supporting system required by the local building authority. A study of the production, construction and life-cycle analysis costs is underway. A local electrical components manufacturer has expressed interest in the junction box production. 6 bays of the system will be installed in the Ma Wan Primary School in the Spring of 2003 with 12 months monitoring to follow. The tendered construction costs include approximately 14% extra covering unknown work. This highlights the higher costs of work outside a contractor's normal building experience and the unknown shared scope of work with the electrical contractor identifying the need for construction professionals to be educated and trained in PV building integration.

Acknowledgements:

The Ma Wan Primary School BIPV demonstration project is carried out with funding from the Hong Kong Government's Innovation and Technology Commission and the CLP Research Institute.
The following advice and contributions are gratefully acknowledged:

Building energy simulation by PC Chan & WS Kwok of Dept of Architecture, Chinese University, HK
Structural engineering advice provided by Ove Arup & Partners (HK) Limited
Technical module construction details from Siemens Solar
Wind Tunnel Tests carried out by the CLP Wind/Wave Tunnel Facility, HKUST
Module Wind-loading tests carried out by Research Engineering Development Façade Consultants Ltd
3D solid modeling and rapid tooling processes by Tony Yeung at the Dept of Architecture, University of Hong Kong,

References:

1. Close, J., (2001) *The HK Schools Solar Education Programme,* proceedings of PVSEC-12, Cheju, Korea.
2. Durisch. W., Lam, K.H. & Close, J., (2002) *Behaviour of a Copper Indium Diselenide module under Real Operating Conditions*, presented at WREN VII, Cologne, July 2002.
3. Close, J., Wong, Y.H., Chan. P.C. & Kwok, W.S., (2001) *Hong Kong Energy Re-regulation and the role of the HK Schools Solar Education Programme*, 17th European PV Conference & Exhibition, Munich.

This Page Intentionally Left Blank

Advances in Building Technology, Volume 2
M. Anson, J.M. Ko and E.S.S. Lam (Eds.)
© 2002 Elsevier Science Ltd. All rights reserved

INTEGRATION OF DOUBLE FACADES AND VENTILATION SYSTEMS IN BUILDINGS

F. Di Maio and A.H.C. van Paassen

Laboratory for Refrigeration Engineering and Indoor Climate Technology,
Delft University of Technology, Delft, The Netherlands.

ABSTRACT

Nowadays the awareness concerning the environmental pollution and the demand of transparent facades in architecture, lead research in finding new solutions to increase the energy performances of the building and the installations as well. Among those, different kind of Double Skin Facades have been studied and several laboratories are still working on them to find a suitable way to apply this technology in new buildings and in the restructuring of old ones. To find out how the constructive parameters affect the performances of the Second Skin Façade and for the purpose of energy saving in building this paper studies the modelling of systems made up by Double Façade coupled with a building. These interactions between the building, the Double Facade and the external environment have been simulated using the simulation code Simulink.
The model has been set up to answer questions about: (a) the gradient of pressure along the facades; (b) flow and temperature along the façade; (c) find out the necessity for control; (d) how to split up the Double Facades in compartments in order to have benefits without serious overheating problems. The effect of the depths of the cavity has been shown to influence the Double Façade's performances.
It has found that due to the pressure gradient, different airflow at different temperature enter the room facing the Double Skin Façade. A control system is then necessary to synchronize all the components involved.

KEYWORDS

Second Skin Façade, simulation, Simulink, pressure gradient, airflow, thermal balance, stack effect, wind pressure, overheating.

INTRODUCTION

The demand of transparent facades in architecture, has given new impulse in finding new way to improve the energy performance of the buildings. Among those, different kind of Double Skin Facades have been studied and several laboratories are still working on them to find a suitable way to apply this technology in new buildings and in the restructuring of old ones.

In traditional buildings the outdoor climate is considered as an enemy, whose influence must be controlled by the Heating, Ventilation and Air-Conditioning system. The technology of the Double Skin Façade coupled with an HVAC system is an attempt to achieve the opposite, namely to use the solar radiation and the wind, in an advantageous way to reduce the energy consumption and to improve the comfort at the same time. Actually the Double Skin Facades can reduce the solar gain in summer and provide thermal insulation in winter. Moreover, it can be used as a solar collector to preheat the ventilation air. The intelligent controlled façade tries to use outdoor climate as much as possible for all indoor climatic aspects. These aspects include cooling and heating to maintain a required indoor temperature, the supply of fresh air and the guarantee of a certain lighting level. The solar radiation is used in addition to heating and lighting and the natural ventilation can be used for fresh air supply and for cooling. Although this seems an attractive building philosophy, there are problems because the advantage of the outdoor climate is often not available at the right time or in the required amount. Consequently, the Double Skin Facades of the building should be equipped with components that can be controlled such that the best use is made of the outdoor climate. This requires intelligent controlled façades (Paassen, 1999).

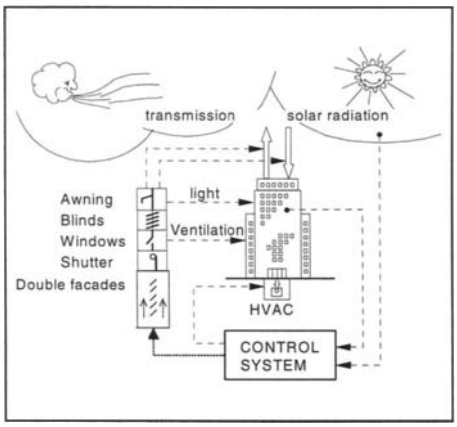


Figure 1 - Building with an intelligent façade.

Figure 1 shows in a schematic way the relation between the Double Facades, the building, the HVAC system and the weather conditions. In order to get a good integration the controlled facades should be equipped with the following components:

1) Shading devices. For the applications in the Double Skin Façade the more effective shading devices are the venetian blinds placed between the external glass element and the glass element facing the room. They act as solar collectors supplying the stack effect that is one of the main driving forces moving air inside the cavities. Exterior shading device (as awnings, rolling shutters and shades but no second skin) could show equivalent performance in summer and could therefore be used to prevent high cooling load. They have some disadvantages due to the risk they can be blown away by the wind especially in the high buildings.

2) Louvers with adjustable slats can also control sunlight entering the rooms. Consequently they can be used as well for shading as controlling daylight.

3) Adjustable vent windows for ventilation and cooling with outdoor air. Cool outside air, especially during the night, could be forced by wind and "chimney" effect would push warm air out so that built-up heat would be removed. All these components have the capability to influence the contribution of

the outdoor climate to the indoor climate aspects such as indoor air temperature, fresh air supply and lighting.
In case the indoor climate conditions cannot be maintained with the use of the passive components and the outdoor climate, the following active components should be available:
4) Auxiliary heater and/or cooler.
6) Artificial lighting.
The HVAC system should be equipped with heat recovery units connected with the double facades' cavities as well. The Double Skin Facades can be used as heat recovery for the HVAC system (Stec & van Paassen 2001).

MODELLING

The model used in these simulations is make up by many subsystems but as shown in figure 2 the main framework can be regarded as an interaction between the Second Skin Façade subsystem and the Thermal Model subsystem. As schematically shown in figure 2 the output variables of the Double Façade model are used as input of the Thermal Model of the Building.
The heat transfer coefficients related to external surfaces of the façade walls and the one related to the external surfaces of the double glasses are considered to be the same. They are implemented in the Alpha Generator subsystem inside the Double Façade model (Di Maio & van Paassen 2001).
The Thermal Model of the building uses these variables as inputs together with the weather data and the ventilation heat flows computed in the Ventilation Generator subsystem (see figure 2) to perform the calculations needed to calculate the air temperatures and the walls temperatures of the rooms. Iteratively the Double Façade model uses results of these calculations as inputs together with the weather data.
As an output of the coupled model, the air temperatures inside the rooms are stored in the Matlab workspace and can be plotted as shown later on.
The way the Second Skin Façade subsystem works can be found in literature Di Maio & van Paassen (2001).

The Thermal Model

The purpose of the model

The thermal model calculates the indoor temperatures and the wall's temperatures in all rooms of the building. The inputs necessary to perform these calculations are the weather data, the ventilation heat flows from the Ventilation Generator, the internal glass' temperatures and the average air temperatures in the cavity from the Double Facade subsystem. The Thermal Model of the rooms receive the airflows rate and their temperatures flowing in the cavities from the Double Façade model subsystem together with the temperatures of the glass panes facing the rooms. Convective heat exchanges take place between the glass' surfaces and the air in the rooms. Radiative heat exchanges take place between the glass' surfaces and the rooms' surfaces.
The Double Façade model receives the air and surfaces temperatures of the rooms from the Thermal Model of the rooms. The subsystems showed in figure receive the weather data from the Matlab workspace.

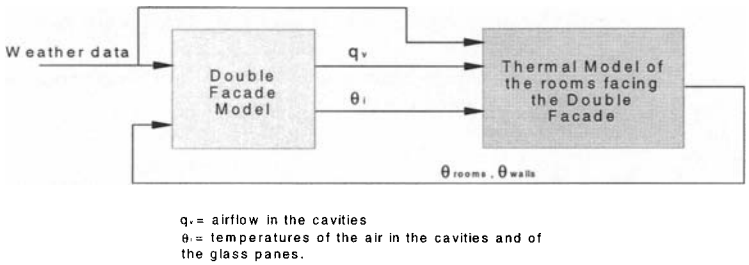


Figure 2 - Model of the rooms modelling the building's room and the Double Façade.

Model hypotheses

A network as shown in figure 3 can illustrate the heat transfer process occurring in a room. It represents the heat transfer in a room which is surrounded on both sides and above and below by identical rooms. This standard room has three interior walls in addition to the roof and the floor. The exterior wall is facing the double façade which is provided with a venetian blind as solar shading device.
Due to the complexity of the thermal network simplifications are necessary to build the model. It is assumed a good mixture of the air inside the rooms, so that only one temperature ("homogeneous temperature distribution" model usually called "One-point model") depicts the thermal response of the room to the heating and cooling loads caused by the internal sources and by the flows calculated in the Ventilation Model subsystem. Each interior surface of the room is depicted by one node. The latter assumption has been verified by Mitalas (1965). About the first one especially in unconditioned rooms, temperature gradients have been observed. These gradients depend strongly on the air circulation inside the room (Chen, 1988). Nevertheless this assumption has been accepted for the purpose of this thesis. A resistance network connecting the nodes represents the heat exchange by radiation between the various surfaces and the heat exchange between these surfaces and the room air. For each node a heat balance can be set up. These heat balances result in a set of differential equations that are solved simultaneously together with the others contained in the subsystem named Double Façade model (see fig. 3).
Three types of heat transfer are taken into consideration in the modelling process. There is convective heat transfer from the window's glass, the walls, the floor and the ceiling to the room air. There is a radiative heat transfer from the window's glass to each wall's surface, to the floor and the ceiling. There is conduction heat transfer inside the walls, floors and the ceilings of the building. The heat balances of all the surfaces in the room do not take into account the radiative heat transfer between the surfaces themselves but a virtual surface having the mean temperature of the surfaces inside the room and a view factor equal to $(1-F_{s,g})$ (where $F_{s,g}$ represents the view factor between the surface and the glass), exchanges radiative energy with the walls' surface. A ventilation heat flow from the Double Façade subsystem or from the air-handling unit is present in order to maintain the comfort condition inside the rooms. Moreover during the working time there is an internal load inside the rooms due to the people, the lightning and the equipments. Solar radiation falls on the Double Façade. Part of it enters the room through the glasses and the sunshine device and it is assumed to be evenly divided on the entire area of the room and it will be indicated by q_{si}. It was supposed that the entire surface facing the cavity is made by glass. Actually part of that surface ($1.1 \cdot 3.6$ m^2) is made by brick. Due to the shading device it does not receive a lot of solar radiation $(A3+A4) \cdot q_s$. Further investigations should be done in order to estimate the real approximation and its thermal influence on the system.
Each wall in the model is simulated according to the scheme shown in figure 4.

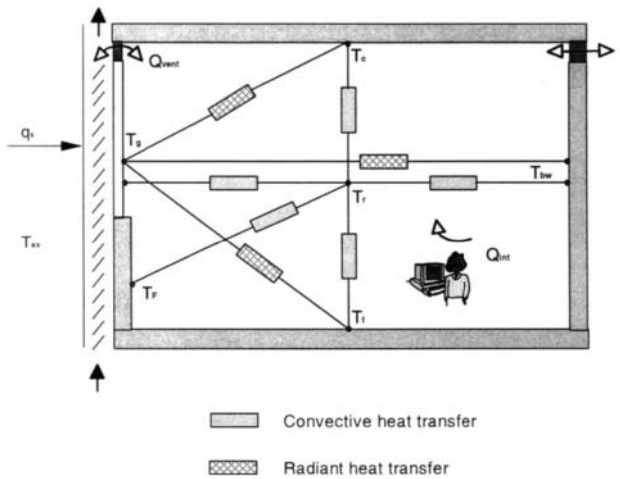


Figure 3 – Physical model of the thermal behaviour of the room

Lumped parameter assumption is adopted. This is realized by splitting the wall into some layers. In each layer, the parameters, like temperature, specific heat and conductivity, are the same. Since the parameters are actually different, the more layers the wall is split, and the closer the model is to the reality. However, too many layers make the models more complicated and lower simulation speed.
On both side of a wall there is a convection heat transfer to the air temperature (T_r), a radiant heat transfer to the surrounding surfaces and a solar load (q_{si}) depending on the surface that is taken into account. Conductive heat transfer is present inside the walls. Each wall itself is divided into three layers having its own conductivity *k*, density ρ, specific heat *c* and thickness Δx. It was assumed a good connection between the different surfaces of the wall so that no additional resistances the thermal energy has to meet through the wall. Running the simulation it is possible to know the temperatures in the four points in the wall.

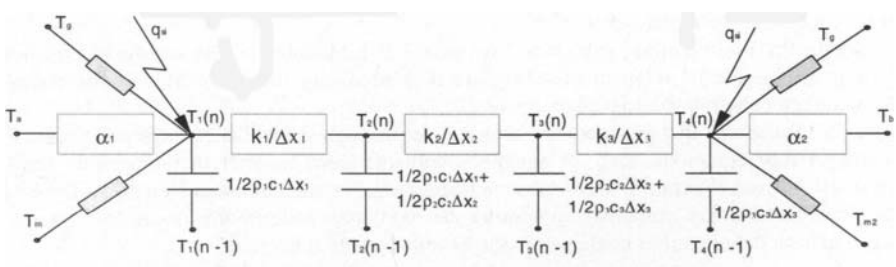


Figure 4 –Electrical R-C representation of the wall.

Where:

α_i = convective heat transfer; i = 1, 2	[W/m^2 K]
k_i = conductivity of the ith layer; i = 1, 2, 3	[W/m K]
ρ_i = density of the ith layer; i = 1, 2, 3	[kg/m^3]
c_i = specific heat of the ith layer; i = 1, 2, 3	[J/kg K]
Δx_i = thickness of the ith layer; i = 1, 2, 3	[m]

T_a = air temperature in the room and/or in the cavities [K]
T_b = air temperature in the room [K]
T_i = temperature inside the walls; i = 1, 2, 3 [K]
T_g = temperature of the glass [K]
T_m = mean temperature of the walls [K]

Decomposition into subsystems

The system is composed of a segment for each storey. Each of them has basically the following subsystem:

- The Wall, Floor, Ceiling subsystems
- The Alpha Generator subsystem
- The average Wall Temperature subsystem
- The Ventilation Generator subsystem
- The One Point Air Model subsystem

Because the subsystems are almost the same for each floor, only those ones concerning the second storey will be discussed in detail. Figure 6 shows the second storey subsystem.

The wall, floor, ceiling subsystems

There are 21 of these subsystems in the model. Each of them has to compute the temperature on both side of the layer (wall, floor or ceiling). The temperatures between the layers in which the wall, floor or ceiling are divided are monitored as well.
There are five *Floor-Ceiling subsystems* in the model. As far as the second storey subsystem is concerned, the subsystem designed to compute the temperature of the ceiling is the same as the one computing the temperature of the third storey's floor. The inputs are the weather data, the glass' temperatures of the windows on the third storey and on the second storey from the Double Façade subsystem, and the third and second room's air temperature from the One Point Air model subsystem. The small differences concerning the fourth storey ceiling and the first storey floor will be discussed later on.
The equations implemented in the Floor-Ceiling subsystem are derived from heat balances made on the system schematically shown in figure 4.
When data for the Floor-Ceiling subsystem (contained in a Matlab file) are substituted in these four equations it is possible to solve them. Therefore it is necessary to load a Matlab file contains the physical parameters before to run the simulation.
There are 21 subsystems that calculate the heat transfer through the walls, ceilings and floors. Each of them contains four equations, then 84 equations with the same number of temperature have to be simultaneously solved in order to know those temperatures. For each iteration step this is done together with the four heat balance equations computing the room's air temperature in the four rooms of the building, and with the equations contained in the Double Façade subsystem.

The One Point Air model

From a heat balance for the system showed in figure 3 it is possible to derive the differential equation 1 which calculates the air temperature in the room.

$$\rho_a c_a V_{r2} \frac{dT_{r2}}{dt} = Q_{int} A_{fl} + Q_{vent} + \alpha_{r2}(T_{g2} - T_{r2}) A_g + \alpha_{r2}(T_F - T_{r2}) A_F +$$
$$+\alpha_{r2}(T_{sw1} - T_{r2}) A_{sw1} + \alpha_{r2}(T_{sw2} - T_{r2}) A_{sw2} + \alpha_{r2}(T_{bw} - T_{r2}) A_{bw} + \alpha_{fl}(T_{fl} - T_{r2}) A_{fl} + \quad (1)$$
$$+\alpha_c (T_c - T_{r2}) A_c$$

Where:

A_g =	total glass area	[m^2]
A_F =	internal façade wall area	[m^2]
A_{sw1} =	internal side wall 1 area	[m^2]
A_{sw2} =	internal side wall 2 area	[m^2]
A_{sw2} =	internal back wall area	[m^2]
A_F =	floor area	[m^2]
A_c =	ceiling area	[m^2]
ρ_a =	air density in the room	[Kg/m^3]
c_a =	specific heat of air in the room	[J/Kg·K]
V_a =	volume of the room	[m^3]
Q_{vent} =	ventilation heat flow	[W]
Q_{int} =	internal heat load	[W/m^2]

Solving this equation the results are the air temperature in the rooms.

RESULTS

Several simulations have been carried out on the coupled model in order to investigate the usage of night cooling by opening the vents windows facing the Double Façade. The simulations have been carried out for a four-storey, west oriented building:

-Height 13.2 m;
-Width 3.6 m;
- Depth of the cavity 0.4 m;
- Ventilation opening area 3.2×0.155 m^2;
- Opening angle of vent windows 45°, 25°, 15°, 0°.
- Internal load 500W in each room;
- Pressure in the room –2 Pa;

Figure 5 shows the room temperatures at each floor together with the external temperature and the airflows through the ventilation openings (45 degree). After a four-day period with bright and warm weather eventually the temperature on the fourth floor reaches about 40 °C. With opening angles of vent windows 45° the temperature on the same floor could be reduced to about 30 °C.

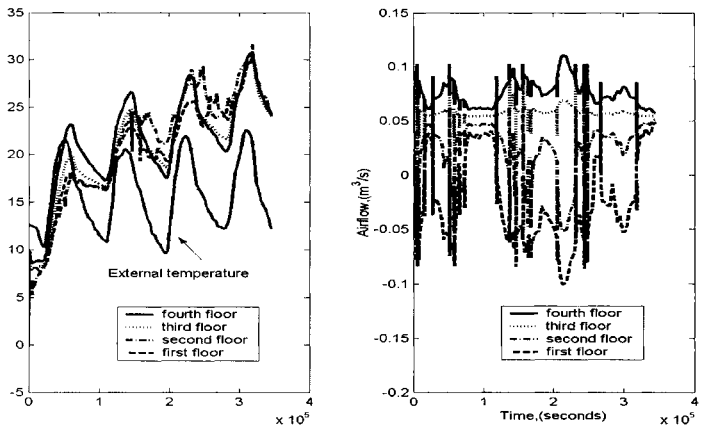


Figure 5 – Indoor and outdoor temperature. Opening angle 45°. Airflows through ventilation openings. Due to the pressure gradient along the façade, air is extracted from the rooms in the first and second storey and supplied into the above rooms.

The neutral zone of the façade is placed somewhere between the second and the third storey. Due to the pressure gradient along the cavity, air is extracted from the rooms in the first and in the second storey and supplied into the above rooms. The result is that the average indoor temperature are higher at the highest floor due to supply of warm air from the cavity, while in the first and second floor cooler air is supplied from the corridor and exhausted through the cavity.

CONCLUSIONS

The temperatures inside the rooms at different floors have been shown to be different. Highest floors have higher temperatures. Moreover, the pressure gradient and its effect on the ventilation rate through vent openings suggests a proper control of the ventilation openings and partitioning of the Double Façade to avoid overheating problems. The simulations shown that the Double Skin Facades can have a flexible use as (a) supply fan or exhaust fan; (b) preheating device for ventilation systems with natural supply through openings in the inner façade; (c) supplier of preheated fresh air for a central air handling unit.

REFERENCES

Chapman A.J., (1984), *"Heat transfer"* Macmillan, New York.

Stec, W., Paassen, van A.H.C. (2001).

Chen, Q., (1988),*"Indoor airflow, air quality and energy consumption of buildings"*, Thesis, Delft University of Technology", Delft, The Netherlands.

Di Maio F. and Paassen van A.H.C., (2001). *"Simulation of Air Conditioning Systems assisted by Double Facades"*, Proceedings of the 7th Clima 2000 World Congress, Napoli, Italy.

Mitalas, G. P., (1965), *"An assessment of common assumptions in estimating cooling loads and space temperatures"*. ASHRAE Transactions, 71 part II.

Paassen, van A.H.C. (1999). *"Integration of intelligent facades and HVAC in low energy buildings"*, Proceedings of the 3th International Symposium on HVAC, pp.1-11, Shenzhen, China.

Stec, W., and Paassen van A.H.C., (2001). *"Controlled Double Facades and HVAC"*, Proceedings of the 7th Clima 2000 World Congress, Napoli, Italy.

Advances in Building Technology, Volume 2
M. Anson, J.M. Ko and E.S.S. Lam (Eds.)
© 2002 Elsevier Science Ltd. All rights reserved

MECHANICALLY VENTILATED DOUBLE SKIN FAÇADES

M. Kragh, PhD

Permasteelisa, Via Friuli 10, 31020 San Vendemiano (TV), Italy

ABSTRACT

With the growing interest in environmentally friendly architecture and transparency, the development has lead to still more advanced building envelope concepts. Double skin façades pose an interesting alternative as they allow large transparent areas without compromising occupant comfort and energy consumption. The paper introduces different mechanically ventilated double skin configurations in terms of engineering and performance characterisation. The two main concepts discussed are the Active Wall, a double skin façade mechanically ventilated with the return air from the indoor environment, and the Interactive Wall, which is ventilated with outdoor air by means of small fans incorporated in the façade. System performance characterisation becomes increasingly complex as the function of the building skin adapts to the environmental requirements. The paper discusses ways of characterising the façade in order to provide adequate input for HVAC system sizing, a field currently lacking guidelines and standardisation coverage. The way these advanced façade systems act as filters between indoor and outdoor environments allows for not only transparency and daylighting, but also implementation of soft cooling technology. Successful implementation, however, depends closely on an integrated design approach from the early, schematic phases of design, where the Architect should collaborate with both façade engineers and M&E engineers in order to create a truly synergetic overall building design scheme.

KEYWORDS

Multiple skin façades, double skin facades, transparent architecture, integrated building design, comfort, energy consumption, performance characterisation, financial implications.

BACKGROUND

The present paper deals with advanced façades for commercial buildings, but many of the considerations will apply to other applications as well. Growing awareness of environmental issues is currently leading to more sustainable architecture on a global level with local differences depending on climate, market trends and legislation. After having relied on HVAC to handle the indoor climate and to a much lesser extent designing *with* the climate, architects and engineers are now explicitly re-discovering fundamental principles and facing the challenge of realising sustainable architectural designs and indoor spaces with high levels of occupant comfort without inferring excessive energy consumption.

A current architectural trend – the pursuit of fully transparent buildings – are pushing the boundaries of design, in turn leading to innovative concepts and generally more adaptive and responsive façade configurations. Multiple skin façades can be conceived as a response to the demand for transparency and occupant comfort in a sustainable context. Whereas the present paper deals specifically with the façade configurations, it is noted that true design optimisation is only possible when local climatic conditions, building orientation and thermal mass are duly taken into account during schematic design.

All too often, the façade design is developed when fundamental decisions, for instance pertaining to HVAC system scheme, have already been taken. At this point, it can be too late to fully benefit from an advanced façade solution. If façade and environmental system are engineered as two parts of the same solution, not only will the performance most likely be superior – both initial and running costs may moreover be reduced significantly. Successful application of these systems depends closely on the adoption of an integrated design approach from the early, schematic phases of a given project. Moreover there is a pronounced need for a common language in order to characterise and communicate the performance of innovative systems such as the mechanically ventilated façades. Quantities such as U-value and solar heat gain coefficient are not readily applicable when the façade interacts with the ventilation system, and traditional ways of designing HVAC systems may not be adequate when assessing possible application of innovative solutions such as soft-cooling.

ADVANCED FAÇADE CONCEPTS

Façade Types

In order to introduce the adopted terminology, four fundamentally different façade categories are described briefly in the following.

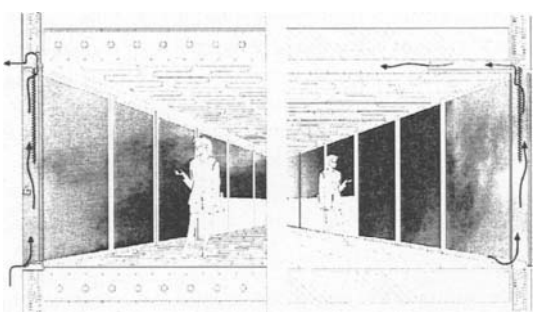


Figure 1: Schematic – Interactive Wall (left) and Active Wall (right)

Conventional, fully glazed, façade

In this context, the conventional façade is the base case, typically incorporating insulating glazing units and either external or internal shading devices. Coated glass is used to modify thermal and solar glazing performance.

Naturally ventilated façade (a.k.a. double skin façade or flue wall)

The glazing configuration is composed of an external single layer of glass and an internal insulating glazing unit. The cavity between the two skins is naturally ventilated with outdoor air through openings in the external skin. The cavity can be continuous over one or more floors.

Active Wall (a.k.a. airflow window or climate wall)

The glazing system is composed of an external insulating glazing unit and an internal single layer of glass. The cavity between the two skins is ventilated with return room air, which is extracted from the room at the base of the glazing and returned to the air-handling unit at the top. (Refer to the schematic in Figure 1). Figure 2 shows the Headquarters of ABN AMRO, a large-scale application of the Active Wall concept.

Interactive Wall

In this case the glazing configuration is composed of an external single layer of glass and an internal insulating glazing unit. The cavity between the two skins is ventilated with outdoor air, which is introduced at the base of the glazing and returned to the outside at the top by means of temperature-regulated micro-fans located in the façade itself (Refer to the schematic in Figure 1). The Interactive Wall is currently being adopted at the new headquarters of ST Microelectronics in Geneva (Figure 2).

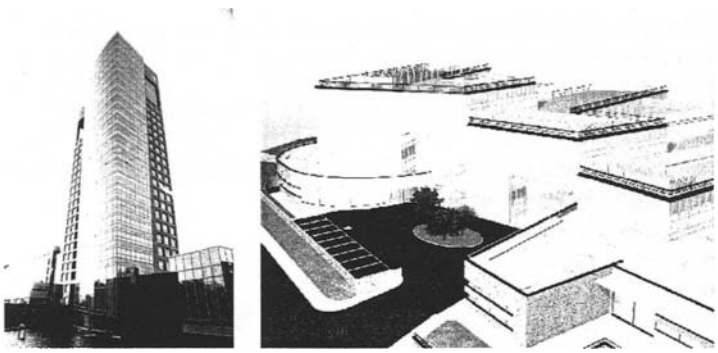


Figure 2: Left / ABN AMRO Headquarters, Amsterdam, Active Wall,
Right / ST Microelectronics, Geneva, Interactive Wall (in progress)

Smart façades

As the building envelope is increasingly acting as an adaptive filter it is also increasingly integrated with the environmental system of the building. The various components of the building envelope are connected to the building management system (BMS) for example as parts of the overall ventilation or daylighting strategies. Whereas smart systems as such are beyond the scope of the present paper it is noted that, whereas the term *Smart* denotes that the façade responds with a certain logic, the term *Intelligent* somehow implies a system with a learning capacity. Such systems are actually being developed, for instance control of shading devices can be engineered to adopt a certain occupant behavioural pattern, but there is a general tendency to ascribe more intelligence to products than what is actually justified given this terminology.

Comparison

Energy loads and occupant comfort are two determining factors in terms of both environmental quality and economy (directly in terms of reduced cooling/heating loads and indirectly in terms of increased occupant comfort and productivity). Comparing the performance of the different systems is complex, but can be summarised as follows:

The *Active* façade is preferred in climates where occupant comfort close to the façade during cold periods is a concern. Since the façade is integrated with the building ventilation system and ventilated with indoor air,

the indoor surface temperature is close to room air temperature, reducing downdraught and the sensation of 'cold radiation'. Moreover, the system allows for heat-recovery on sunny days in heating mode. The transmission heat loss is low due to the three layers of glass.

The *Interactive* façade, on the other hand, is preferred when cooling loads are the major concern. Its low solar heat gain coefficient is comparable to that obtained by means of external shading, yet without the potential drawbacks associated with these (aesthetics, cost, wind resistance, maintenance). The solar heat gain coefficient is a central parameter when dealing with large transparent areas in office buildings with high internal gains. The solar heat gain coefficient of the Interactive Façade is roughly half that of the Active Façade, which has a considerable impact on the solar gains. In cold periods with heating loads, the micro-fans in the façade are switched off and the façade has a low transmission heat loss. Another potential benefit is that the façade system is 'stand-alone', as there is no physical integration between façade and building ventilation system.

Due to the extra layer of glass, the acoustic insulation of the double skin façades is improved compared with conventional façades. However, special glazing configurations are usually employed in cases with strict requirement in terms of acoustic insulation.

The three main building physics parameters characterising a façade are the following:

g	the solar heat gain coefficient (SHGC) – the fraction of irradiant solar energy transmitted to the indoor environment	[-]
U	the thermal transmittance	[W/m²K]
τ_{vis}	the light transmittance	[-]

Besides the glazing configuration itself (Active/Interactive), the system performance depends closely on glass types, blinds setting and reflectance, airflow rates, panel dimensions and design details in general. Whereas g and τ_{vis} are usually specified for the glazing, U can be specified for the glazing and/or the whole system, including framing members and spandrel zones. Moreover, the *internal glazing surface temperature* is an important comfort parameter, which is frequently considered part of the system performance. In order to allow a rough comparison, a set of indicative performance parameters is given in the following table.

TABLE 1
INDICATIVE PERFORMANCE PARAMETERS (WHOLE FAÇADE)

Façade Type	Light Transmittance τ_{vis}	Solar Heat Gain coeff. g	Thermal Transmittance U	Acoustic Insulation R_w
Conventional fully glazed	0.50 – 0.60	0.30 – 0.40	2.0W/m²K	32 – 34dB(A)
Active Wall	0.60 – 0.70	0.15 – 0.25	1.4W/m²K	36 – 40dB(A)
Interactive Wall	0.60 – 0.70	0.10 – 0.20	1.2W/m²K	36 – 40dB(A)

Energy and comfort

It is important to note that any measure of energy performance should always be assessed in conjunction with a measure of the corresponding comfort performance. In other words: for a given set of project conditions, a given level of occupant comfort results in a certain energy consumption, depending on façade and HVAC system design.

ENGINEERING AND PERFORMANCE ASSESSMENT

Engineering of Advanced Façades

As façade designs become increasingly complex and façades tend to interact with environmental systems of buildings, a timely, well defined and adequate façade performance characterisation is still more instrumental to successful overall building design. Moreover, the façade characterisation should be communicated in time for M&E contractors to account for the façade performance in a sufficiently detailed way to consider alternative and potentially innovative schemes.

In the following it is assumed that structural integrity of the façade systems is secured. This is not to say that structural aspects are less important in any way, but the paper is deliberately focusing on concepts and building physics related aspects pertaining to energy and comfort.

Advanced façades act as filters between the outdoor environment and the controlled environment indoor, responding to combinations of occupant requirements and climatic situations, modifying their configuration and characteristics. Hence the static values applicable to conventional, passive building components are rendered obsolete if the true potential of advanced façades is to be taken into account. In less abstract terms this means that the performance of a ventilated façade incorporating solar shading depends on both *airflow rates* and the *setting of the shading device*, parameters which may change according to the requirements.

In the following, the approach currently adopted by Permasteelisa Research & Engineering is introduced in order to illustrate the need for thorough analysis and characterisation of double skin façades. The method is based on commercially available software and simplifications are introduced in recognition of the intrinsic complexity – the problems are essentially 3-dimensional and include airflow – which cannot be dealt with in an operational way as part of normal project engineering. However, the methods presented in the following are found to yield acceptable accuracy.

Framing and spandrel are modelled by means of 2-dimensional finite element methods. Permasteelisa is currently utilising the THERM software (THERM, 2000), but various similar tools are commercially available. A steady state analysis is carried out according to standards and/or project specifications. Heat fluxes and temperature distributions are determined on the basis of a relatively detailed model of a given section. Since the objective is always to assess system performance, the frames are modelled including the edge of the glazing taking 2-dimensional edge effects into account

Conventional glazing system characteristics are usually provided and certified by the glazing supplier. As mentioned, insulating glazing units – or single layers of glass – can be modelled by means of the Window software (Window, 1994). For more *complex glazing systems*, such as ventilated double skin façades incorporating solar shading, Permasteelisa is currently using the WIS software (WIS, 1996). Apart from the fundamental principles of the model, the main limitation of the tool is the availability of product data. Permasteelisa is currently part of the *WinDat* Thematic Network, funded in part by the European Commission, aiming at improving WIS product libraries and making the software available through the Internet (visit www.WinDat.org for information).

Theoretical Assessment Procedure: Thermal and Solar Performance

In the following, the estimation procedure is briefly introduced using an Active Wall as an example. The method can be divided into five steps as follows

I. Window modelling of glazing units

Glazing systems are combined of different layers stored in the Window glass library. Subsequently these

glazing systems can be imported into a given THERM model.

II. THERM modelling of frames/spandrel

A finite element model is created and thermal properties are assigned to the various elements (materials) of the section. The program calculates the U-values of different parts of the model and the temperature distribution depending on environmental conditions.

III. WIS modelling of the glazing centre

By means of the WIS software, the glazing system can be modelled including both solar shading and ventilated cavities. In order to adequately characterise the glazing performance, the systems are usually modelled, *varying both blind setting and airflow rates*. Moreover, *different environmental conditions* are modelled in order to determine U-value and solar heat gain coefficient as well as glazing surface temperatures for different design conditions. The nature of the airflow is not simulated as in computational fluid dynamics (CFD). Application of CFD is beyond the scope of normal performance assessment and poses a series of problems in terms of boundary conditions. Research is in progress and it is possible that future models will be based on CFD methods, but currently the WIS tool is found to yield acceptable approximations whilst being user- friendly and operational.

IV. Estimation of overall system performance

The *system overall U-value* (frame, spandrel, glazing centre) is estimated by area-weighting the component U-values. A series of U-values are computed for different airflow rates to enable M&E engineers to analyse different scenarios. For the glazing system, the performance is estimated for different façade cavity airflow rates, blind settings and environmental conditions. The U-value will usually be specified for night-time conditions without ventilation as well as daytime conditions with ventilation. The solar heat gain coefficient is specified for different airflow rates and blind settings as input for optimisation.

V. Condensation risk assessment

The *condensation risk* is assessed determining the minimum internal surface temperature under design conditions. If the indoor ambient temperature and the minimum internal surface temperature are known, the critical indoor relative humidity can be specified. In order to operate with a façade characterisation, which is independent of environmental conditions, the *Temperature Factor* is defined as follows (EN ISO 13788, 2001):

$$f_{Rsi} = \frac{\theta_{si} - \theta_e}{\theta_i - \theta_e}$$

Where

f_{Rsi}	is the temperature factor	[-]
θ_{si}	is the internal surface temperature	[°C]
θ_i	is the indoor temperature	[°C]
θ_e	is the outdoor temperature	[°C]

Façade / HVAC

When dealing with the Active Wall configuration (indoor/indoor ventilation), the integration with the building ventilation system is a central issue. Usually, the ventilation of the façade is based on the required air-change of the indoor environment, which under normal conditions corresponds roughly to the optimum façade airflow rate. In situations with cooling loads, which is the normal situation in commercial buildings with large transparent areas and low U-values, the air is expelled when extracted from the indoor

environment. In periods with heating loads, two situations are considered. When solar irradiation is heating up the air in the façade, the heat can be recovered by means of heat exchangers, whereas the air will be cooled in absence of solar irradiation. Thus, the overall energy performance depends on the overall building HVAC/façade scheme. Along with the U-value, the temperature of the air leaving the façade cavity is usually specified, enabling M&E engineers to account for enthalpy changes. The term *equivalent U-value (or apparent U-value)* is adopted to indicate that it applies to the façade when ventilated

Project-Specific Testing

Verification of project-specific design details is an essential part of the engineering process. Full-scale mock-up testing is used to secure correct airflow distribution - air velocities are measured and smoke is used to visualise the nature of the flow. The condensation risk may, moreover, be assessed in a climatic chamber as part of subsequent general performance testing.

Full-Scale Test Rooms

At Permasteelisa's Headquarters in Italy, a series of advanced façade solutions have been realised in conjunction with innovative HVAC systems. Currently, a total of 12 full-scale test rooms are operative and another 2 rooms are in progress. The measurements yield direct comparisons between different solutions exposed to identical climatic conditions and provide a basis for validation of both simplified and detailed engineering tools. The building envelope configurations comprise double skin façades (naturally ventilated, mechanically ventilated indoor-indoor and outdoor-outdoor). The environmental systems comprise variations of radiant systems as well as displacement ventilation. For comparison, the innovative systems are installed side-by-side with conventional systems adopting high performance glazing and fancoil cooling/heating. The rooms are continuously monitored in terms of energy consumption, ambient temperatures and humidity as well as surface temperatures across the façade and solar radiation transmitted through the façade. Moreovcr, daylight measurements can be carried out in one room at a time. A meteorological station records the climatic conditions from the roof of the building. A more detailed description of the test rooms can be found in (Kragh, 2001).

FINANCIAL IMPLICATIONS

First Costs and Running Costs (Energy and Maintenance)

Also in terms of *first costs*, the building should be analysed as a whole. When contemplating application of high-performance, advanced façade designs, decision makers should carefully analyse implications in terms of potentially reduced HVAC requirements. Downsizing ducting and air-handling units results in direct savings in terms of components and installation, and indirect savings in terms of an increasing net-lettable area. HVAC system downsizing and utilisation of radiant systems reduce the required equipment maintenance. Case studies such as the UCB Center in Brussels have demonstrated that innovative solutions can be realised at the same overall building cost as conventional solutions and result in increased comfort, reduced maintenance and 30% energy savings (Kragh, 2000 and 2001).

Productivity

Energy-efficient building and office design offers the possibility of significantly increased worker productivity. By improving lighting, heating, and cooling, workers can be made more comfortable and productive. The Rocky Mountain Institute has carried out a series of case studies of new buildings and retrofits, all demonstrating the correlation (Romm and Browning, 1998).

Tax Incentives and Building Codes

In the UK, Government initiatives to secure best value have lead to changes from normal development, making 'cost in use' a key factor in the design. The Authorities need to take into account whole life costing of the service or element. Both central and local government is thus undergoing significant change. Similar strategic changes are also taking place in the private sector. The purchase decision is moving away from the lowest tendered costs with the focus being more on the cost in use benefits whoever the tenant is going to be. This issue is particularly relevant in the selection of an appropriate façade design. The tax laws in the United Kingdom are uniquely favourable to technical development in environmental engineering generally and active façades in particular. UK tax relief is given by way of capital allowance on plant and machinery that writes off the capital value effectively within 8-9 years (Glanville, 2000).

Added Value

Summarising, it could be concluded that the integrated design of high performance building envelopes in conjunction with innovative HVAC systems can result in significant *added value at contained costs*. At present, energy savings may not be economically significant on all markets, but legislation and incentives will gradually lead to more sustainable designs from a political hold. However, the added value in terms of increased occupant comfort and productivity, downsizing of mechanical plant, increased net-lettable area, lower running costs and last, but not least, improved (corporate) image may well turn out to be far more powerful drivers in the future.

REFERENCES

EN ISO 13788 (2001). *Hygrothermal performance of building components – Internal surface temperature to avoid critical surface humidity and interstitial condensation – Calculation method*

Glanville, G. (2000). Financial Implications of Modern Architectural Envelopes in Office Buildings. *Modern Façades for Office Buildings* (in Dutch: Moderne Gevelarchitectuur voor Kantorbouw), October 26, 2000, ed. Renckens, J., Delft Technical University, The Netherlands

Kragh, M. (2000). Building Envelopes and Environmental Systems. *Modern Façades for Office Buildings* (in Dutch: Moderne Gevelarchitectuur voor Kantorbouw), October 26, 2000, ed. Renckens, J., Delft Technical University, The Netherlands

Kragh, M. (2001). Monitoring of advanced Façades, Proceedings of *The Whole-life performance of façades*, University of Bath, CWCT, 18-19 April 2001, Bath, UK

Romm, J.J. and Browning, W.D. (1998). *Greening the Building and the Bottom Line – Increasing Productivity Through Energy-Efficient Design*, Rocky Mountain Institute, Colorado, USA

THERM (2000). *THERM 2.1 NFRC Simulation Manual.* Windows and Daylighting Group. Lawrence Berkeley National Laboratory, USA

Window (1994). *Window 4.1 Program description* and Optical Data Library. Windows and Daylighting Group. Lawrence Berkeley National Laboratory, USA

WIS (1996). Advanced Windows Information System. *WIS 1.0 Reference Manual & User's Guide.* TNO Building and Construction Research. The Netherlands. Funded in part by the European Commission, Joule II programme, EU

Advances in Building Technology, Volume 2
M. Anson, J.M. Ko and E.S.S. Lam (Eds.)
© 2002 Elsevier Science Ltd. All rights reserved

CASE STUDIES OF THE APPLICATION OF INNOVATIVE ENERGY-EFFICIENT EQUIPMENT IN BUILDINGS

C.K. Lee, K.K. Lam and Martin K.T. Wu

Energy Efficiency Office
Electrical & Mechanical Services Department
Government of the Hong Kong Special Administration Region

ABSTRACT

The Energy Efficiency Office (EEO) of Electrical and Mechanical Services Department is actively exploring means to reduce energy consumption in buildings and a series of initiatives are being implemented to achieve the goal. One of the initiatives is to investigate advanced and innovative energy saving equipment and technologies via series of pilot projects in government buildings with a view to promote the wider use of these technologies in public and private sectors of the construction industry. The investigation covers innovative equipment for lighting, air conditioning, lifts and escalators, etc. The paper will present details of two case studies of the pilot projects, one for lighting and one for air-conditioning, carried out by EEO in government buildings. The pilot lighting project involved the application of high output T5 lamps and luminaires in an indoor games hall. Aspects on both energy and visual performance will be presented for the new lighting system and comparison will also be made with the existing high bay lighting system using High Intensity Discharge (HID) lamps. For the case study in air-conditioning, focus will be on the application of indirect evaporating pre-cooling system for fresh air intake to building. The otherwise waste exhaust air and waste condensate water form the building air-conditioning system were used for heat reclaim through an integrated heat exchanging and evaporating unit in this pilot project. Significant energy saving have been recorded in both cases.

KEYWORDS

Energy Efficiency, High Output T5 Lamps, Games Hall Lighting, Indirect Evaporating Cooling.

PILOT T5 LIGHTING PROJECT AT EAST KAI TAK INDOOR GAMES HALL

As part of the Pilot Energy Management Opportunity (EMO) Implementation Programme using innovative energy efficient equipment, Energy Efficiency Office (EEO) of Electrical and Mechanical Services Department (EMSD) has completed a pilot lighting project at East Kai Tak (EKT) Indoor Games Hall. The new lighting system made use of the latest T5 lighting technology for illuminating the high ceiling games hall. As compared with the existing high-bay lighting using High Intensity Discharge (HID) lamps, the new high output T5 lighting system was found to be more energy

efficient and offered many other benefits which provide users of the games hall a more comfortable visual environment for their sporting activities. There were totally 48 high-bay HID luminaries existing in the game hall. Half of the lamps were 400W metal halide and the rests were 250W high pressure sodium (SON) lamps. The new T5 lighting system included 56 special impact resistant luminaries accommodating 3x49W high output T5 lamps and electronic ballasts (168 T5 lamps in total). Power consumption was 17.2kW for the existing lighting system. Measurement on site for the new T5 lighting system was 8.7kW, which represents a power reduction of almost 50% in lighting. The average illuminance measured at floor level was found to be 760 lux and 480 lux for the new T5 lighting system and the existing high-bay lighting system respectively. Other than the 58% increase in illumination level, improvement in the lighting quality in terms of glare, colour appearance and colour rendition were also recorded. Surveys were also carried out to collect users' opinion on the new lighting system. Majority of the users' feedback was in favour of the new T5 lighting system. General comments included brighter than before, more comfortable, less glare, softer visual environment and better colour appearance.

Existing Lighting System in EKT Indoor Games Hall

The existing lighting installation in EKT Indoor Games Hall consists of 24 numbers 400W metal halide lamps and 24 numbers 250W high pressure sodium (SON) lamps mounted inside the industrial type high-bay luminaries with parabolic reflectors. Fig. 1 shows the existing lighting layout plan and Fig. 2 shows a photograph of the existing lighting environment with HID lamps. The metal halide and SON luminaries were designed to mount in pair (Fig. 3) adjacent to each other for colour blending. All existing HID lamps were switched on for the whole opening hours of the game hall because these HID lamps need at least 5 minutes warming up period to start up and instant re-strike after switching off or a power interruption is also not possible. The colour appearance of metal halide lamp is typical cool white in colour (6000°K) and that for SON is yellow (2000°K). Neither metal halide lamps (too cool) nor SON lamps (too warm) are suitable to be used alone for indoor games halls lighting and they are therefore employed in pair for colour mixing and to create an appropriate visual environment for sporting purposes. Metal halide lamps are also characterised by their good colour rendering property (essential for live TV broadcasting) but less efficacy (76 lm/W). SON lamps have relatively poorer colour rendition (rich in yellow/orange spectrum) and possible shift of colour appearance in operation but much higher efficacy (100 lm/W).

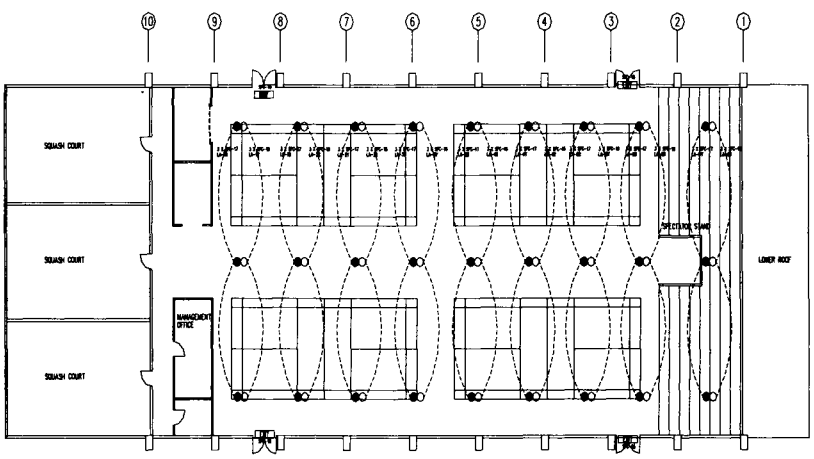


Fig. 1: Existing HID lighting layout at EKT Indoor Games Hall



Fig. 2: Existing lighting environment with HID lamps at EKT Indoor Games Hall

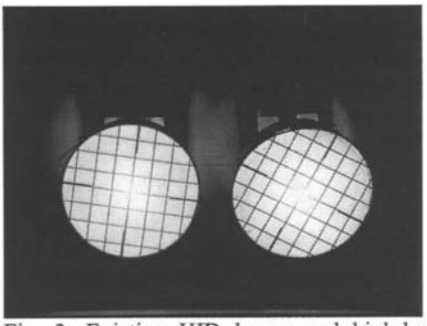


Fig. 3: Existing HID lamps and high-bay luminaries at EKT Indoor Games Hall

New High Output T5 Lighting System

The new pilot T5 fluorescent lighting system we used in EKT Indoor Games Hall consisted of 4 rows of 14 specially designed impact resistance luminaries complete with 3x49W high output T5 lamps and electronic ballasts (Fig. 4 and Fig. 5). The design illuminance was 500 lux at floor level as recommended by CIBSE Lighting Class II for indoor sports and mid-level competition such as regional or local club competition, which generally involved medium size spectators capacity with medium viewing distances. High-level training can also be included in this class.

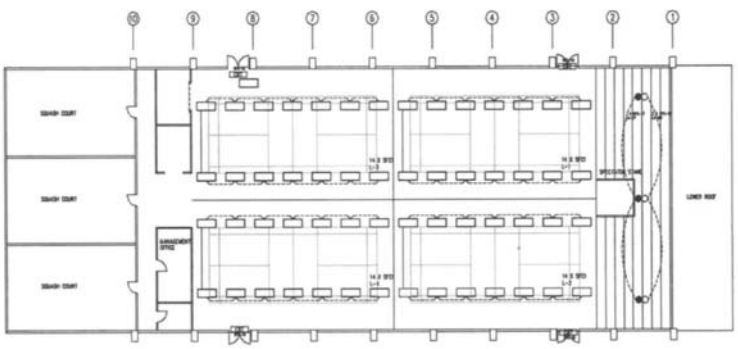


Fig. 4: Lighting layout of the new high output T5 lighting at EKT Indoor Games Hall

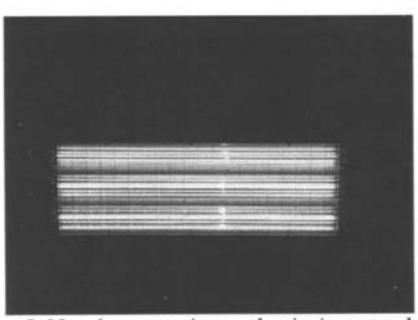


Fig. 5: New impact resistance luminaires complete with 3x49W T5 lamps and electronic ballasts at EKT Indoor Games Hall



Fig. 6: Visual environment of the new T5 lighting at EKT Indoor Games Hall

Unlike HID lamps, T5 fluorescent lamps could be switched on and off instantly without a long warming up period. Operation of the new T5 lighting system could then be arranged to suit the schedule of game hall booking and the switching circuits have also been arranged in 4 separate zones to tie in with the layout of the 4 badminton courts.

Energy Performance

Energy performance of the two lighting systems was measured on site on 23 July 2001. The measured results were summarised in Table 1. It was found that the total power reduction for the new T5 lighting system was 8.5kW (49%) and improvement in current THD was also very apparent (reduced from 23.6% to 4.7%). As the games hall is fully air conditioning, reduction in heat gain from lighting would also decrease cooling load of the AC plant. The estimate reduction in cooling load would be about 30% of the reduced lighting load (i.e. 2.5kW).

TABLE 1
ENERGY PERFORMANCE OF THE EXISTING HID AND NEW T5 LIGHTING SYSTEMS

	Existing HID Lighting System	New T5 Lighting System	% Difference
Active Power (kW)	17.2 kW	8.7 kW	- 49%
Power Factor.	0.97	0.99	+ 2%
Current THD	23.6%	4.7%	- 80%
Lighting Power Density	26.3 W/m^2	13.3 W/m^2	- 49%

Visual Performance

Illuminance in lux (i.e. lumen/m^2) of a point at a horizontal plane illuminated by a lighting system is one of the most important parameter defining the quantity of light received at the point. The horizontal illuminance at floor level was measured on 22 May 2001 with both HID and T5 lighting systems. Results of the measurements indicated that the average illuminance measured for the existing lighting system was 479 lux with a maximum of 642 lux occurred at the centre of the games hall. For the new T5 lighting system, the average measured illuminance was 760 lux and the maximum illuminance occurred at centre of the hall was 998 lux. There was an average increase of 58% in illumination when the games hall was lit by the new T5 lighting system. The uniformity found for both old and new lighting systems were 0.48 and 0.51 respectively. The minor improvement was due to the closer spacing of T5 luminaires at ceiling level.

Glare is a major concern in an indoor games hall for both players and spectators alike. The concentrated point source of HID lighting can cause problematic glare. The condition occurs whenever someone looks directly or very close to an HID lamp in the line of sight. When the eye "sees" the extremely bright light source, the pupil becomes very small. Then, when the eye looks elsewhere, it cannot focus properly for a few seconds. The situation is similar to your eye responses when a camera flash blinds your subjects during a photo shoot. The linear and diffused light source of T5 lamp does not create the same problem. Although they are quite bright, T5 lamps are not "blinding" like the HID lamps.

Glare caused by a light source is directly proportional to its brightness. Luminance in candela per square meter (cd/m^2) is a physical measure of a surface brightness caused by light emission or reflection. Luminance for both HID and T5 luminaries had been measured at various observation angles. Because of the parabolic effect, maximum luminance (1.160 x 10^5 cd/m^2) occurred at about 60° for 250W SON luminaries, which is almost 11 times brighter than the new T5 luminaire at the same

observation angle. As far as disability glare is concerned for players viewing upward in the game hall, HID luminaries would create more serious problem than T5 luminaires.

Other then the measurable parameters above for assessing the quality of the visual environments of the two lighting schemes, colour temperature and colour rendition properties could also play their parts in the appraisal. The light colour of a lamp is expressed as colour temperature in Kelvin (K). The T5 lamps used have a colour temperature of 4000°K (i.e. cool white) and could maintain the colour appearance throughout their lives. Metal halide and SON lamps have an initial colour temperature of 6000°K (daylight) and 2000°K (yellow) respectively and their colour appearance could deviate during their operation lives resulting in a non-consistent colour appearance among lamps.

Measured to a scale of 0 to 100, the colour rendering index (CRI) describes the capability of a light source to accurately render a sample of eight standard colours relative to a standard source. Light sources that exhibit higher CRIs render colour better than sources with low CRIs. The T5 fluorescent lamp used in this project has CRI above 80 and those for metal halide and SON lamps are 65 and 27 respectively. A CRI of at least 60 is recommended by CIBSE Lighting Guide 4 for multi-purpose sport halls to reveal the correct colour pitch markings.

The average rated life for HID lamp is about 20,000 hours and for T5 lamps is 16,000 hours. They lose some of their light output as they age. Expressed quantitatively, it is common for the output of HID sources to degrade by nearly 40 percent over their lifetime, whereas T5 lamps exhibit lumen depreciation as low as 5 percent. The T5 lighting scheme would therefore maintain a much more consistent lighting level throughout their lifetime than their HID counterparts. If the economic lamp life (i.e. 30% depreciation) were taken into account for bulk lamp replacement schedule, the advantage of longer lamp life for HID lamps would then be diminished.

INDIRECT EVAPORATING PRE-COOLING SYSTEM AT KOWLOON PARK

As one of the pilot projects using innovative energy efficient equipment, we have completed in September 2001, the installation of an indirect evaporative cooling (IEC) system at Kowloon Park Swimming Pool Complex. The IEC module is basically an indirect evaporating pre-cooling unit for fresh air intake to building. The otherwise waste exhaust air and waste condensate water form the building air-conditioning system are used for heat reclaim through this module.

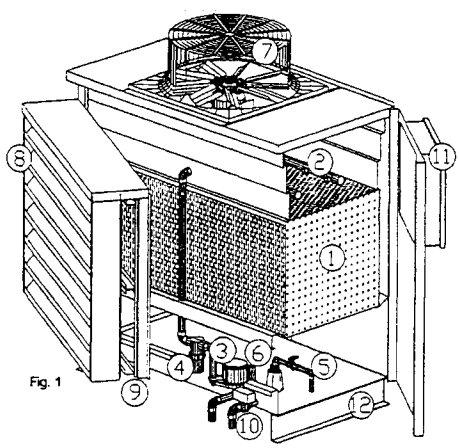


Fig. 7: Construction of the Indirect Evaporating Cooling Module

As shown in Fig. 7, the module consists of an extended surface cross-flow wet plate heat exchanger, nozzle sprays, an indirect pump, strainers, a vaporiser air fan, solenoid valves and control panel. The heat exchanger is constructed of non-corrosive polymeric materials. Exchanger plate spacing controlled by air turbulence spines is designed to enhance heat transfer, water distribution and efficiency. Primary and secondary airflows are separated by polymeric adhesive and rubber seals. Primary airflow is horizontal and vaporiser airflow is vertical in a cross-flow pattern.

System Description

The IEC module is originally designed for outdoor application using direct outdoor air and water mains as energy sources for pre-cooling fresh air. In our pilot project, the module was installed inside the Air Handling Unit (AHU) plant room in Kowloon Park Swimming Pool Complex. The existing exhaust and fresh air duct inside the plant room were modified and connected into the module for heat reclaim before leaving the building. The cool condensate water condensed from the AHUs are collected in a small tank and pumped into the IEC module via a small submersible pump for evaporating cooling. The ductwork and pipe work arrangement at the vicinity of the IEC module are shown in Fig. 8 with various temperature, humidity and flow sensors installed and connected to the computer for data logging.

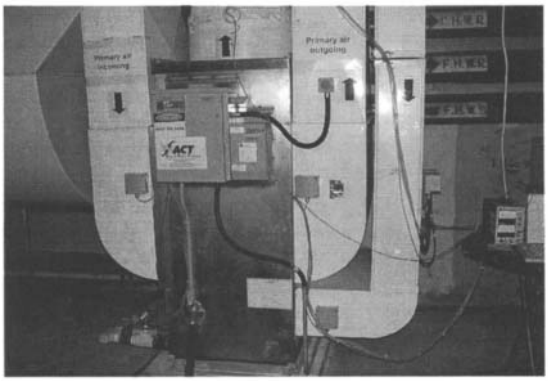


Fig. 8: Ductwork Connection to the Indirect Evaporating Cooling Module

Strategy for Testing

In order to accurately assess the energy performance of the IEC module installed in Kowloon Park Swimming Pool Complex for different climatic and weather conditions throughout the year, the following measurement instrument and testing equipment have been installed for collecting data and logged into a computer. The Department of Building Services Engineering of PolyU was appointed as consultant for the whole testing process including the installation of monitoring equipment.

1. Temperature and humidity sensors and transducers at inlet and outlet positions of the exhaust and primary/fresh air ducts.
2. Air flow sensors and transducers at intake air ducts of exhaust air and primary air.
3. Temperature sensors and transducers at inlet and outlet of the condensate water pipes.
4. Water flow sensors at flow of condensate water pipe.
5. A package of data logging system for collecting data every 10 minutes for 1 whole year starting from October 2001

The schematic line diagram of the complete testing system is shown in Fig. 9. The location of some

sensors and transducers could also be identified in Fig. 8. All instrument installed were calibrated in the laboratories of PolyU before installing on site.

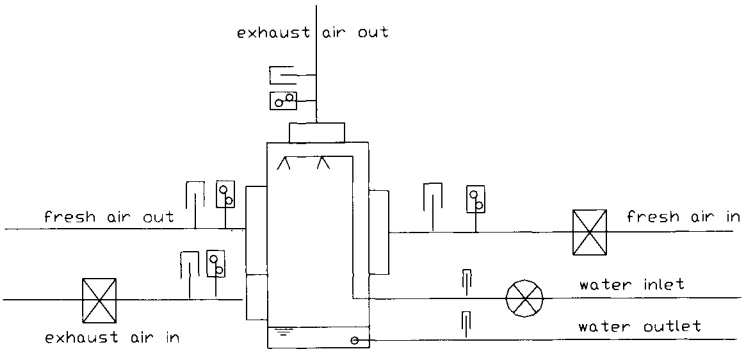


Fig. 9: Schematic Diagram of the Testing System

Preliminary Test Results

The basic mathematical model for the energy performance analysis of this IEC system is:

$$Q_p = Q_e + Q_c$$

Where Q_p, Q_e, and Q_c are the absolute values (sensible and latent heat) of the energy change for primary air, exhaust air and evaporation of the condensate water. These quantities could be calculated from the measured dry bulb temperature, relative humidity or wet bulb temperature and volume flow rate of the primary air and exhaust air before and after the heat exchanger together with evaporation of the condensate water. Test data have been collecting on site since October 2001. Data collected in November and December 2001 and January 2002 were not good enough due to very low primary air temperature. We are expecting good results in summer with a wider temperature differential of the primary and exhaust air.

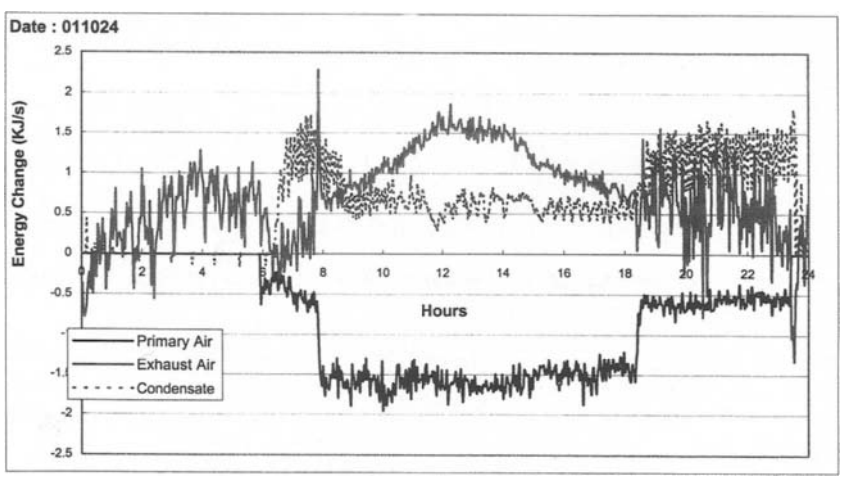


Fig. 10: Absolute Energy Changes measured on 24/10/2001

In order to demonstrate the effectiveness of the system, data collected on 24/10/2001 were used for analysis of energy transferred amount primary air, exhaust air and evaporating water. The absolute value of energy of the three items were plotted against time as shown in Fig. 10. From these data plot, the energy gain for the primary air is more or less equal to the total energy change for both exhaust air and condensate water. The measured values at 2:00 p.m. on 24/10/2001 were extracted from the data logger and highlighted in Table 2 below.

TABLE 2
EXTRACT OF DATA LOGGED AT 2:00 P.M. ON 24/10/2001

	Temp. IN	Temp. OUT	RH IN	RH OUT	Flow Rate
Primary Air	29°C	27°C	59.5%	65.5%	608 l/s
Exhaust Air	26.5°C	25°C	57.5%	71.5%	332 l/s
Condensate Water	17.5°C	20°C	--	--	4 l/min

The site measurements are still ongoing on site until end of summer in 2002. It is too early to draw any conclusion yet. The overall energy performance of the system will then be analysed for different weather conditions. Nevertheless, the use of exhaust air and condensate water, which are generally available free of charge in all air conditioned spaces, to pre-cool the outside primary air load is extremely beneficial for air conditioning systems in both existing or new buildings.

ACKNOWLEDGEMENT

The authors would like to thank Dr. T.M. Chung and Dr. H.X Yang of Department of Building Services Engineering, the Hong Kong Polytechnic University and their research students, in particular Mr. Kenneth Lo and Mr. An, for carrying out the measurements on sites.

Advances in Building Technology, Volume 2
M. Anson, J.M. Ko and E.S.S. Lam (Eds.)
© 2002 Elsevier Science Ltd. All rights reserved

A DYNAMIC MODEL OF COMMERCIAL GAS AND OIL BURNED BOILERS

Z. Liao and F. Parand
Building Research Establishment (BRE), Bucknalls Lane, Watford, WD25 9XX, UK

ABSTRACT

A dynamic model of commercial hot water boilers has been developed and integrated with other heating system component models to create a simulator of central heating systems. Detailed experimental data were obtained to validate the boiler model. The validation results indicate that the model can accurately simulate both transient and steady state performance of such boilers as installed in central heating systems. The model development was carried out under a European Commission project with the aim to improve the overall efficiency of water heating systems. The simulator was subsequently used to develop an innovative boiler controller that has been tested in simulation, emulation, a test building and field trials in real buildings with successful results. This paper presents the mathematical boiler model and its implementation in Simulink™. The validation of the model is also discussed.

KEYWORDS

Energy efficiency, boiler, control, model, simulation, validation, central heating systems.

INTRODUCTION

In common with many other types of building services plants, boilers in heat systems are often considerably oversized in order to provide a substantial margin of capacity [Gardner, 1984]. Therefore it is essential to operate such boilers under part load with high efficiency. Most boilers deliver hot water satisfactorily but in most cases do so under undetected inefficiency when managed by the presently installed control devices and systems [Liao and Parand, 2001]. This is because boilers in heating systems are normally controlled such that a certain temperature setpoint of the hot water supply, which may be fixed or compensated with the external temperature [Levermore, 1992], is maintained. The variation of heating load at the terminal is not considered comprehensively in most existing boiler control schemes. As a result, the overall energy performance is normally far below the level that would otherwise be obtained if the control of boilers could be optimised [Liao and Parand, 2001].

An European Union project, funded under the CRAFT programme, in which BRE and other research partners worked as the Research and Development arm of a number of industrial companies, investigated this problem and developed an innovative control technology for the optimal control of boilers in heating systems. The boilers investigated in this project are commercial gas or oil burned boilers with a normal heating capacity ranging from 20 kW to 300 kW, which are widely used in heating systems in Europe. The investigation was carried out in both simulation and field trials. A simulation platform of

central heating systems has been developed for this purpose, in which a dynamic model of gas or oil burned boilers found an important role to play. Over last 40 years a number of boiler models have been developed [Lu, 1993; Lang, 1992]. Some of these models have been integrated with some thermal simulation software packages well established. However, no model is suitable for the purpose of this project because:

- These models do not cover the type of boilers investigated.
- Rigorous validation is not exhibited therefore misleading may occur if these models or methods were directly employed in this project.

Therefore of fundamental importance to the reliability of the simulation platform is to develop a dynamic model of the targeted boilers and cross-validate the model using experimental data obtained from different sources.

METHODOLOGY

The methodology adapted for developing and validating the boiler model is briefly summarised as below:

- Survey study of gas or oil burned boilers used in heating systems in Europe. This study was carried out in three European countries, including UK, Germany and Italy. The objective is to collect technical information of the targeted boilers and to understand how they are installed and operated in the current practice. Through this study a number of typical boiler structures have been identified.
- Develop the mathematical model. The typical boilers were analysed to identify essential heat transfer processes. A simplified boiler model was developed.
- Implement the model in Simulink™ for validation and utilisation.
- Validate the model. The validation was carried out using experimental data obtained from different sources. These data sources include the operation data of real systems obtained through the survey study mentioned above, experiments carried out respectively in a test rig specially built in BRE, UK for this project and a testing facility in ICITE, Italy.

MATHEMATICAL MODEL

Figure 1 presents a simplified structure of targeted boilers.

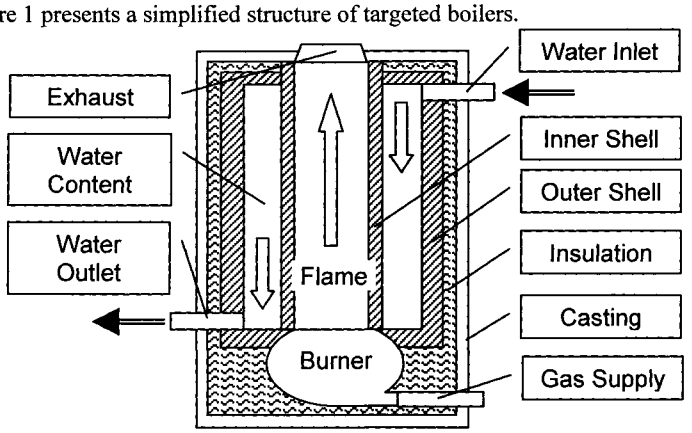


Figure 1 A simplified structure of gas or oil burned boilers

As shown in Figure 1, a gas or oil burned boiler consists of the following major components:

- A burner where fuel (gas or oil) is combusted to release heat.
- A flame tunnel along which flame loses heat energy and cools down to as low as 150°C at the exhaust.
- An inner shell that separates the flame and the water content.
- A water tunnel where water is heated.
- An outer shell.
- An insulation fabric.
- Casting shell.

The heat transfer within the boiler includes:

- Fuel is combusted in the burner to release heat that is transferred to the inner shell through both radiation and convection.
- Heat conducts through the inner shell and transfer to the water content through convection.
- Water enters the boiler at a lower temperature at the inlet and is heated while it flows through the water tunnel. Water discharges from the outlet at a higher temperature.
- Water loses heat to the outer shell that in turn transfer heat to the insulation layer. The heat lost from the insulation layer is then conducted through the casting shell and transferred into the ambient.

This can be translated to an electrical circuit as presented in Figure 2.

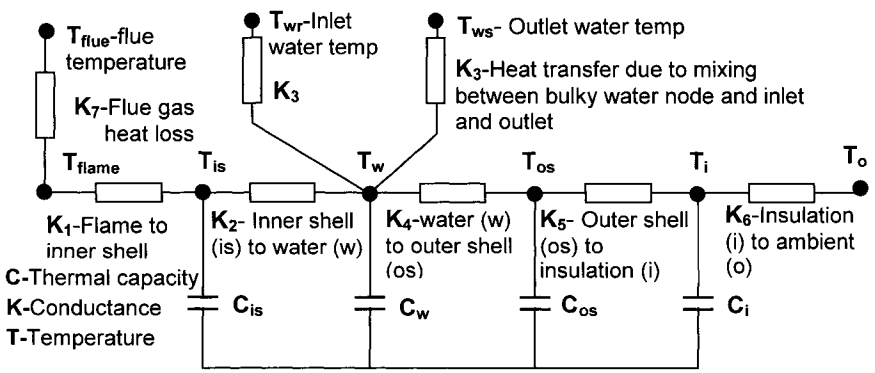


Figure 2 Electrical circuit model of a gas or oil burned boiler

The dynamics of the inner shell (T_{is}) is governed by:

$$C_{is} \cdot \frac{dT_{is}}{dt} = Q_{burner} - K_2 \cdot (T_{is} - T_w) \tag{1}$$

where:

Q_{burner} is the heat transfer from the flame to the inner shell.

Heat transfer between the flame and the inner shell is through both convection and radiation, therefore Q_{burner} can be calculated by:

$$Q_{burner} = E_c \cdot (T_{flame} - T_{is}) + E_r \cdot (T_{flame}^4 - T_{is}^4) \tag{2}$$

Alternatively, Q_{burner} can be treated as a constant determined by the normal heating capacity and efficiency of the boiler. In this paper, Q_{burner} is treated as a constant but of different values for different boiler operations. In general the cycle of boiler operation can be distinguished into three steps, as below:

- Idle: the burner is not firing and the ventilation fan is not running. During this period, the inner shell may lose heat to the air naturally ventilated through the combustion chamber and flame tunnel.
- Purge: the burner is not firing yet but the ventilation fan is running. During this period, the inner shell may lose heat to the air forcedly ventilated through the combustion channel and flame tunnel.
- Firing: the burner is firing and the ventilation fan is running. During this period, heat is transferred to the inner shell from the flame.

Therefore, Q_{burner} is given as:

$$Q_{burner} = \begin{cases} Q_{idle} & Idle \\ Q_{purge} & Purge \\ Q_{fire} & Firing \end{cases} \tag{3}$$

The dynamics of the water node (T_w) is governed by:

$$C_w \cdot \frac{dT_w}{dt} = K_2 \cdot (T_{is} - T_w) - K_4 \cdot (T_w - T_{os}) - \dot{m} \cdot (c\rho)_w \cdot (T_{ws} - T_{wr}) \tag{4}$$

The lumped water temperature (T_w) is related to the water temperature at the inlet (T_{wr}) and outlet (T_{ws}) of the boiler through the following equation [Niu, 1994]:

$$T_w = \alpha \cdot T_{wr} + (1-\alpha) \cdot T_{ws} \tag{5}$$

where α is a constant ranging from 0 to 1.0.

The dynamics of the outer shell (T_{os}) is governed by the following equation:

$$C_{os} \cdot \frac{dT_{os}}{dt} = K_4 \cdot (T_w - T_{os}) - K_5 \cdot (T_{os} - T_i) \tag{6}$$

Finally the dynamics of the insulation layer and the casting shell (T_i) is governed by:

$$C_i \cdot \frac{dT_i}{dt} = K_5 \cdot (T_{os} - T_i) - K_6 \cdot (T_i - T_o) \tag{7}$$

IMPLEMENTATION IN Simulink™

Two versions of the boiler models have been implemented in Simulink™ for investigation. In the first version, all components presented in Figure 1 and 2 are presented by a number of single lumped variables. For example, the water content is presented by a lumped water temperature (T_w) and a total thermal capacity of water content (C_w). In the second version, the boiler is equally divided into five sections and each section is treated in the same manner as how a whole boiler is treated in the first version. Therefore in this version, each component property is represented by five lumped variables. For example, the water temperature is represented by five sectional water temperature ($T_{w1}, T_{w2}, T_{w3}, T_{w4}, T_{w5}$). This is illustrated in Figure 3.

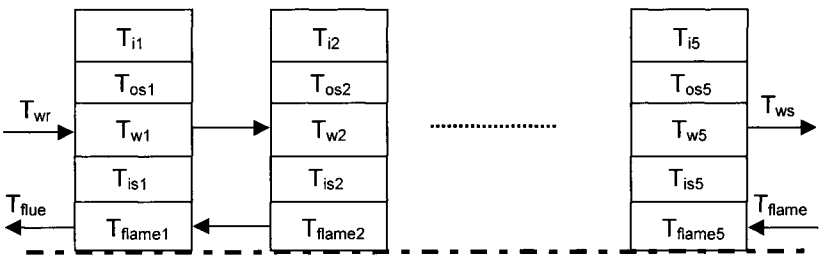


Figure 3 Sectional boiler model (5 sections)

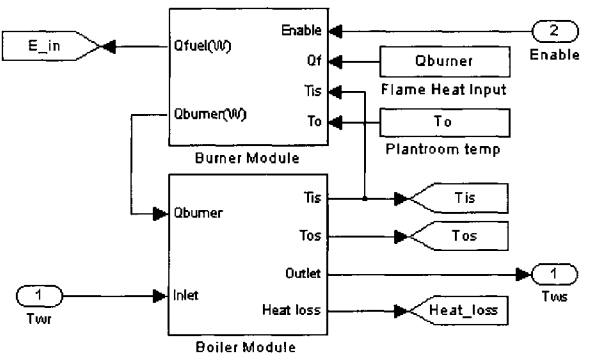


Figure 4 Simulink implementation of the boiler model

Figure 4 presents an overview of the Simulink implementation of the boiler mode. It shows that there are two essential modules, including a Burner Module and a Boiler Module. The Burner Module deals with the control of burner and calculates the heat energy transferred from the flame to the inner shell (Equation 3). The Boiler Modules accommodates the dynamic equations of the inner shell (Equation 1), water content (Equation 4), outer shell (Equation 6) and insulation layer (Equation 7). The constants presented in the model are calculated on the basis of the technical data of boilers. For each given boiler, a set of these constants are described in a data file. Different boilers can be simulated in this implementation by associating relevant boiler data file with it.

VALIDATION

The boiler model has been rigorously validated using experimental data obtained from different sources. These sources include:

- Survey study. During the survey study that was aimed to identify typical boilers used in heating systems in Europe, a number of site measurements have been made to produce the data related to the performance of selected boilers in real operation.
- Experiments carried out in a boiler test-rig in BRE, UK. This rig consists of three major parts, including two boilers with a total heating capacity of 100 kW, a hydraulic system simulating the heating load and a software simulated building.
- Long-term testing in ICITE (Italy). A commercial boiler with 40 kW of heating capacity was installed in a fully instrumented testing facility in ICITE to test the long-term performance of the boiler.

Figure 5 presents how the experimental data is used to validate the boiler model. It shows that the recorded data of the water parameters at the inlet of boiler (flow rate and temperature) and the boiler control signal are fed into the boiler model that in turn simulates the water parameters at the boiler outlet (Outlet_sim). The simulated outlet parameters are compared with the experimental data of the outlet water (Outlet_test). The comparison shows how accurate the model can simulate the dynamic performance of the boiler.

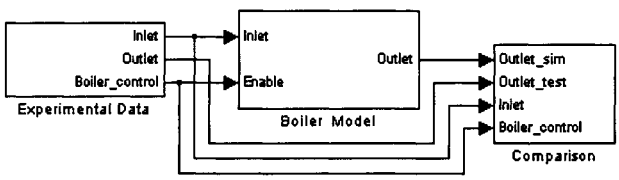


Figure 5 Validating the boiler model using experimental data

Figure 6 presents an example of validating the model using the experimental data monitored in a real installation (Building B14 in BRE) through the survey study. A good agreement can be observed between simulated and tested outlet water temperature.

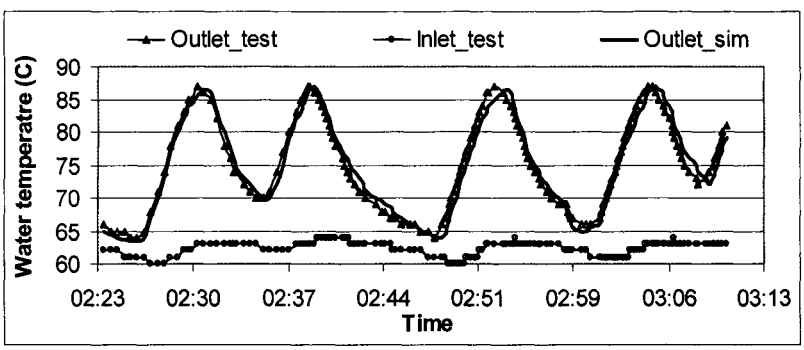


Figure 6 Validating the boiler model using experimental data monitored in a real installation

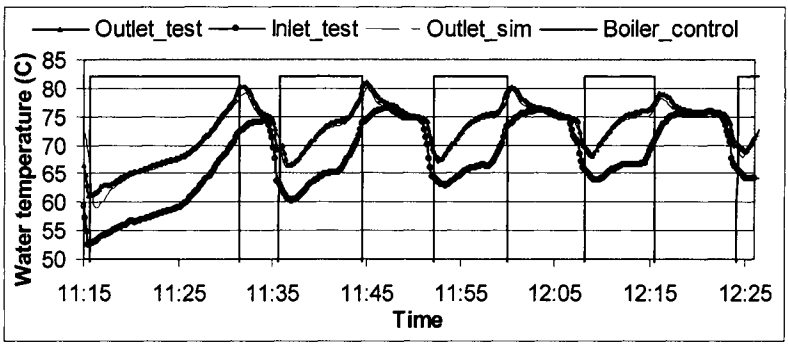


Figure 7 Validation by test-rig data (floating Inlet temperature)

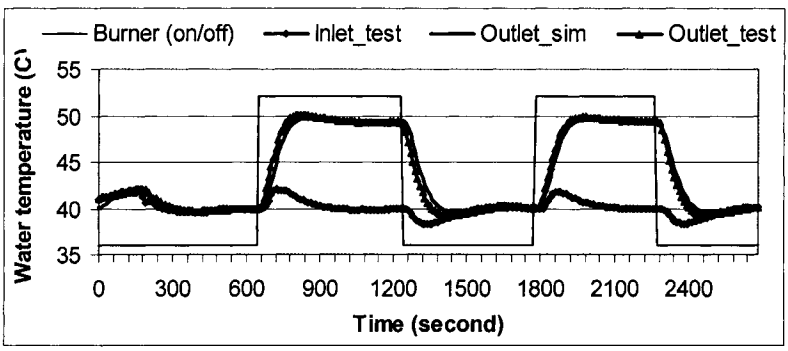


Figure 8 Validation by test-rig data (constant Inlet temperature)

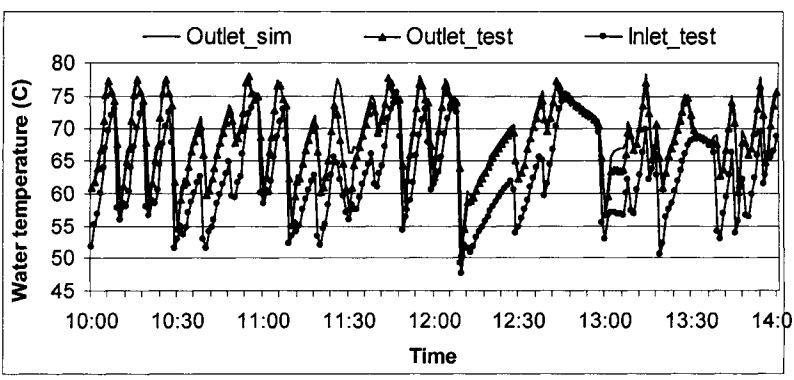


Figure 9 Validation by ICITE data (an example)

Figure 7 and 8 present the validation results using the data recorded in the test-rig experiments. Two scenarios were considered, including:

- The test rig is driven by the building simulator to mimic a real operation. In this case the Inlet water temperature varies as linked in the distribution loop (Figure 7).

- The Inlet water temperature is controlled at a constant value and the boiler is turned on and off to test the transient performance of the boilers (Figure 8).

Figure 7 and 8 indicates that the boiler model can accurately simulate the performance of the boilers installed in the test rig.

The test in ICITE lasted for two heating seasons and all recorded data was used to validate the boiler model as well as for other purposes. Figure 9 only presents a snapshot of this validation. A good agreement between the simulated and recorded outlet water temperature can be observed, consistently over the entire testing period.

CONCLUSION

A simplified model has been developed to simulate the dynamic performance of commercial gas or oil burned boilers that are commonly used in heating systems in Europe. Two versions of the model have been implemented in Simulink™. The model has been rigorously validated using experimental data obtained from different sources. The validation results show that the model can simulate the dynamic performance of the targeted boilers with high accuracy. This model had been integrated with a simulation package of central heating systems, which was used for the development of a novel boiler controller [Liao and Parand, 2001].

ACKNOWLEDGEMENTS

The work presented in this paper was financially supported by EU through Craft programme (contract number: JOE3-CT98-7010) and the participating industrial partners, including Brittech Controls (UK), ISC (Germany) and Digital Controls (Italy). The authors would like to thank Dr. John Crabb from University of Exeter, UK for his fundamental analysis of heat transfer processes in the targeted boilers, which makes the development of the model presented in this paper possible. Special thanks also go to ICITE (Italy) for carrying out the long-term testing that have provided the experimental data used to validate the model.

REFERENCES

P. Gardner. (1984). Energy Management Systems in Buildings. Energy Publications, ISBN 0-905332-34-2.

P. Lang. (1992). Models for Use in Power Plant Operation. J. Elect. Power and Energy Systems, 14(5), pp321-335.

G. J. Levermore. (1992). Building Energy Management Systems – An Application to Heating and Control. E & FN Spon, ISBN 0-419-15290-3.

Z. Liao, F. Parand. (2001). Final Report of EU Craft Project: JOE3-CT98-7010: Controller Efficiency Improvements for Commercial and Industrial gas or oil burned boilers.

S. Lu. (1999). Dynamic Modelling and Simulation of Power Plant Systems. Proc Instn Mech Engrs, Vol 213 Part A.

S. Lu, B. W. Hogg and N. Li. (1993). An integration Average Model for Boiler Evaporation System Simulation. SCS Simulation Ser., powered by gas or oil burned boilers, 25(4), pp169-174.

J. L. Niu. (1994). Modelling of Cooled-Ceiling Air-Conditioning Systems. Ph.D thesis, The Delft University of Technology, Netherlands.

Advances in Building Technology, Volume 2
M. Anson, J.M. Ko and E.S.S. Lam (Eds.)
© 2002 Elsevier Science Ltd. All rights reserved

LOW ENERGY BUILDING MATERIALS: AN OVERVIEW

A. M. Omer

The School of Built Environment
University of Nottingham, University Park
Nottingham NG7 2RD, United Kingdom

ABSTRACT

Sustainability has acquired great importance due to the negative impact of various developments on the environment. The rapid growth during the last decade has been accompanied by active construction, which in some instances neglected the impact on the environment and human activities. The impact of developments on the traditional heritage has not been taken into consideration although the latter represents a rich resource for sustainable building practices.

KEYWORDS

Building materials, energy efficiency, sustainable development, environment impacts

INTRODUCTION

Within the last decade sustainable development and building practices have acquired great importance due to the negative impact of various development projects on the environment. In line with a sustainable development approach, it is critical for practitioners to create a healthy, sustainable built environment [1,2]. In Europe, 50% of material resources taken from nature are building-related, over 50% of national waste production comes from the building sector, and also 40% of energy consumption is building-related [3,4]. More attention should be directed towards establishing sustainable guidelines for practitioners. Furthermore, the rapid growth in population has active construction that, in some instances, neglected the impact on the environment and human activities. At the same time, the impact on the traditional heritage, an often-neglected issue of sustainability, has not been taken into consideration, despite representing a rich resource for sustainable building practices.

Sustainability has been defined as the extent to which progress and development should meet the need of the present without compromising the ability of the future generations to meet their own needs [5]. This encompasses a variety of levels and scales ranging from economic development, and agriculture, to the management of human settlements and building practices. This general definition was further development to include sustainable

building practices and management of human settlements. During the Rio Earth Summit in 1992 [6], the following issues were addressed:

- The use of local materials and indigenous building sources.
- Incentive to promote the continuation of traditional techniques, with regional resources and self-help strategies.
- Regulation of energy-efficient design principles.
- International information exchange on all aspects of construction related to the environment, among architects and contractors, particularly non-conventional resources.
- Exploration of methods to encourage and facilitate the recycling and reuse of building materials, especially those requiring intensive energy use during manufacturing, and the use of clean technologies.

This study investigates sustainable building practices. The objectives of the study aims to:

1. Develop a comprehensive definition of sustainability that includes socio-cultural, bio-climate, and technological aspects.
2. Establish guidelines for future sustainable architecture.
3. Predict the CO2 emissions in buildings.
4. The proper architectural measure for sustainability is efficient, energy use, waste control, population growth, carrying capacity, and resource efficiency.
5. Establish methods of design that conserve energy and natural resources.

A building inevitably consumes materials and energy resources, the technology is available to use methods and materials that reduce a building's environmental impacts, increase operating efficiency, and increase durability. Literature on green buildings reveals a number of principles that can be synthesised in the creation of the built environment that is sustainable. According to one source, these are: land development, building design and construction, occupant considerations, life cycle assessment, volunteer incentives and marketing programmes, facilitate reuse and remodelling, and final disposition of the structure [7]. These parameters and many more are essential for analysis, making them an important part of the design decision-making process. Today architects should prepare for this, but they have to deal with existing buildings with many unfavourable urban environmental factors: many spaces have no choice of orientation, and are often set in noisy streets, with their windows opening into dusty and polluted air and surrounding buildings overshadowing them.

BUILDING AND CO_2 EMISSION

To achieve urban dioxide (CO_2), emission targets more fundamental changes have been suggested [8]. The actual performance of buildings must also be improved to meet the emission targets, To that end, it has been suggested that the performance assessment should be introduced o ensure that the quality of construction, installation and commissioning achieve the design intent. Two key parameters, air-tightness and the commissioning of plant and controls, are the main elements of assessing CO_2 emission. Air-tightness is important as uncontrolled air leakage wastes energy. Uncertainties over infiltration rates are often the reason for excessive design margins that result in oversized and inefficient plants.

Commissioning to accepted procedures would significantly improve energy efficiency. The slow turnover in the building stock means that improved performance of new

buildings will only cut CO_2 emissions significantly in the long term. Consequently, the performance of existing buildings must be improved. For example, improving 3% of existing buildings would be more effective in cutting emissions than, say, improving the fabric standards for new non-domestic buildings and improving the efficiency of new air conditioning and ventilation systems.

BUILDINGS AND ENERGY USE

Buildings consume energy mainly for cooling, heating and lighting as shown in Table 1. The energy consumption must be based on the assumption that the building operates within ASHRAE-thermal comfort zone, during the cooling and heating periods [9]. Most of the buildings incorporate energy efficient passive cooling, solar control, photovoltaics, lighting and day lighting, and integrated energy systems. It is well known that thermal mass with night ventilation can reduce the maximum indoor temperature in buildings in summer [10]. Hence, comfort temperatures may be achieved by proper application of passive cooling systems. In addition, energy can be saved if an air conditioning unit is used [11]. The reason for this is that in summer, heavy external walls delay the heat transfer from the outside into the inside spaces. Moreover, if the building has a lot of internal mass the increase in the air temperature is slow. This is because the penetrating heat raises the air temperature as well as the temperature of the heavy thermal mass. The consequence is a slow heating of the building in summer and the maximal inside temperature is reached only during the late hours when the outside air temperature is already low. The heat flows from the heavy walls inside can be removed with good ventilation in the evening and night. The capacity to store energy also helps in winter, since energy can be stored in walls from one sunny winter day to the next cloudy one. Here defined four levels of thermal mass as follows:

1. Light building: no thermal mass, like a mobile home.
2. Medium-light building: light walls, but heavy floor, like cement tiles on concrete floor, and concrete ceiling.
3. Semi-heavy building: heavy floor, ceiling and external walls (20 cm concrete blocks) but light internal partitions (Gibsum boards).
4. Heavy building: heavy floor, ceiling, external and internal walls (10 cm concrete blocks, with plaster on the both sides).

The exact reduction in the maximum indoor temperature depends on the amount of thermal mass, the rate of night ventilation, and the temperature swing the site between day and night.

SUSTAINABLE PRACTICES

With increasing urbanisation in the world, cities are growing in number, population and complexity. At present 2% of the world's land surface is covered by cities and yet the people living in them 75% of the resources consumed by mankind. Economic and social imperatives often dictate that cities must become more concentrated, making it necessary to increase the density to accommodate the people, to reduce the cost of public services, and to achieve required social cohesiveness. Tabe 2 shows the effect of urban density on city's energy demand.

TABLE 1
ENERGY-SAVING IN BUILDINGS

Passive Comfort Measures	Active Comfort Measures	Climatic zones			
		Mediterranean	Subtropical	Tropical	Desert
Natural ventilation		6	7	7	7
	Mechanical ventilation	4	5	6	6
Night ventilation		6	7	7	7
	Artificial cooling	3	5	5	6
Evaporative cooling		3	2	2	7
	Free cooling	5	6	6	7
Heavy-weight construction		6	2	2	6
Light-weight construction		3	5	5	4
	Artificial heating	4	0	0	1
Solar heating		6	0	0	0
	Free heating	5	0	0	0
Incidental heat		4	0	0	0
Insulation/permeability		5	0	0	4
Solar control/shading		6	6	6	7
	Daytime artificial lighting	3	3	3	2
Daylighting features		6	5	5	4

* 0 = not important, 4 = important, and 7 = very important (importance is rated from 0 to 7).

TABLE 2
EFFECTS OF URBAN DENSITY ON CITY'S ENERGY DEMAND

Positive effects	Negative effects
Transport: • Promote public transport and reduce the need for, and length of, trips by private cars. Infrastructure: • Reduce street length needed to accommodate a given number of inhabitants. • Shorten the length of infrastructure facilities such as water supply and sewage lines, reducing the energy needed for pumping. Thermal performance: • Multi-storey, multiunit buildings could reduce the overall area of the building's envelope and heat loss from the buildings. • Shading among buildings could reduce solar exposure of buildings during the summer period. Natural lighting: Energy systems: District cooling and heating system, which is usually more energy efficiency, is more feasible as density is higher. Ventilation: • A desirable in flow pattern around buildings may be obtained by proper arrangement of high rise building blocks.	Transport: • Congestion in urban areas reduces fuel efficiency of vehicles. Vertical transportation: • High-rise buildings involve lifts, thus increasing the need for electricity for the vertical transportation. Ventilation: • A concentration of high-rise and large buildings may impede the urban ventilation conditions. Urban heat island: • Heat released and trapped in the urban areas may increase the need for air conditioning. • The potential for natural lighting is generally reduced in high-density areas, increasing the need for electric lighting and the load on air conditioning to remove the heat resulting from the electric lighting. Use of solar energy: • Roof and exposed areas for collection of solar energy are limited.

Buildings are significant users of energy and materials in a society and energy conservation in buildings plays an important role in urban environmental sustainability. A challenging task of architects and other building professionals today is to design and

promote low energy buildings in a cost effective and environmentally responsive way. Passive and low energy architecture has been proposed and investigated in different locations of the world [12,13]; design guides and handbooks were produced for promoting energy efficient buildings [14-17]. However, at present, little information is available for studying low energy building design in density populated areas. Designing low energy buildings in high-density areas requires special cure to the planning of urban structure, co-ordination of energy systems, integration of architectural elements, and utilisation of space. At the same time, the study of low energy buildings will lead to a better understanding of the environmental conditions and improved design practices. This may help people study and improve the quantity of built environment and living conditions.

MAJOR CONSIDERATIONS FOR LOW ENERGY BUILDINGS

1. Efficiency Use of Energy

- Climate responsiveness of buildings.
- Good urban planning and architectural design.
- Good house keeping and design practices.
- Passive design and natural ventilation.
- Use landscape as a means of thermal control.
- Energy efficiency lighting.
- Energy efficiency air conditioning.
- Energy efficiency household and office appliances.
- Heat pumps and energy recovery equipment.
- Combined cooling systems.
- Fuel cells development.

2. Utilise Renewable Energy

- Photovoltaics.
- Wind energy.
- Small hydros.
- Waste-to-energy.
- Landfill gas.
- Biomass energy.
- Biofuels.

3. Reduce Transport Energy

- Reduce the need to travel.
- Reduce the level of car reliance.
- Promote walking and cycling.
- Use efficient public mass transit.
- Alternative sources of energy and fuels.

4. Increase Awareness

- Promote awareness and education.
- Encourage good practices and environmentally sound technologies.
- Overcome institutional and economic barriers.

- Stimulate energy efficiency and renewable energy markets.

CONCLUSION

Many towns around the world are facing the problem of increasing urban density and energy demand. As towns represent a significant source of growth in global energy demand, their energy use, associated environmental impacts, and demand for transport services create great pressure to our planet. Low energy design of urban environment and buildings in densely populated areas requires consideration of a wide range of factors, including urban setting, transport planning, energy system design, and architectural and engineering details. It is found that densification of towns could have both positive and negative effects on the total energy demand. With suitable urban and building design details, population should and could be accommodated with minimum worsening of the environmental quality.

REFERENCES

[1] Celik Z. (1994). Urban preservation as theme park: the case of Sogukcesme Street. In: Celik Z., Favro Z., and Ingersoll R., editors. Streets: critical perspectives on the public space. Berkeley (CA): University of California Press, p. 83-94.
[2] Naga A.M., and Amin M. (1996). Towards a healthy urban environment in hot-humid zones-information systems as an effective evaluation tool for urban conservation techniques. In: Proceedings of XXIV IAHS World Congress; Ankara, Turkey.
[3] Anink D., Boostra C. and Mark J. (1996). Handbook of sustainable buildings: an environmental performance method for selection of materials for use in construction and refurbishment. UK: James and James.
[4] Naga A.M., Alsallal K., and Eloliasty R. (1997). The impact of city urban patterns on building energy consumption in hot climates: Alain city as a case study. In: Proceedings of ISES Solar World Congress; Taejon, South Korea, p. 170-81.
[5] Steele J. (1997). Sustainable architecture: principles, paradigms, and case studies. New York: McGraw-Hill Inc.
[6] Sitarz D. editor. (1992). Agenda 21: The Earth Summit Strategy to save our planet. Boulder (CO): Earth Press.
[7] Lobo C. (1998). Defining a sustainable building. In: Proceedings of 23rd National Passive Conference, ASES'98. Albuquerqul (USA): American Solar Energy Society.
[8] EIBI (Energy in Building and Industry). (1999). Constructive thoughts on efficiency, building regulations, inside committee limited, InsidEnergy: magazine for energy professional. UK: KOPASS, p.13-14.
[9] ASHRAE. (1993). Energy efficient design of new building except new low-rise residential buildings. BSRIASHRAE proposed standards 90-2P-1993, alternative GA. American Society of Heating, Refrigerating, and Air Conditioning Engineers Inc., USA.
[10] Kammerud R., Ceballos E., Curtis B., Place W., and Anderson B. (1984). Ventilation cooling of residential buildings, ASHRAE Trans: 90 Part 1B.
[11] Shaviv E. (1989). The influence of the thermal mass on the thermal performance of buildings in summer and winter. In Steemers TC, Palz W., editor. Science and Technology at the service of architecture. Kluwer Academic Publishers, p. 470-2.
[12] Yuichiro K., Cook J., and Simos Y. editors. (1991). Passive and low energy architecture. In: Special Issue of Process Architecture, Tokyo (Japan).
[13] Givrni B. (1994). Passive and low energy cooling of buildings. New York: Van Nostrand Reinhold.

[14] CIBSE. (1998). Energy efficiency in buildings: CIBSE guide. London: Chattered Institution of Building Services Engineers.
[15] FSEC. (1984). Principles of low energy building design in warm, humid climates. Cape Canaveral (FL): Florida Solar Energy Centre (FSEC).
[16] State Projects. (1993). Building Energy Manual. Australia: NSW Public Works.
[17] Watson D. editor. (1993). The energy design handbook. Washington (DC): American Institute of Architects Press.

This Page Intentionally Left Blank

Advances in Building Technology, Volume 2
M. Anson, J.M. Ko and E.S.S. Lam (Eds.)
© 2002 Elsevier Science Ltd. All rights reserved

BUILDING HVAC SYSTEMS ECONOMIC PERFORMANCE EVALUATION USING NEURAL NETWORK METHOD AT BEGINNING OF DESIGN

Fulin Wang[1], Yi Jiang[2] and Harunori Yoshida[1]

[1]Department of Global Environment Engineering, Kyoto University,
Yoshida Honmachi, Sakyo-ku, Kyoto 606-8501, Japan
[2]Department of Building Science & Technology, Tsinghua University,
Beijing 100084, P. R. China

ABSTRACT

Two aspects need to be done to assess the performance of building Heating Ventilation and Air Conditioning (HVAC) systems. One is to evaluate the extent to which an HVAC scheme satisfies the air conditioning requirement. The other is to evaluate the economic characteristics of several HVAC schemes, all of which can satisfy the air conditioning demand. It is difficult to evaluate the economic performance of HVAC systems because economic evaluation involves some factors that frequently change and often unknown such as equipment price, especially at the beginning of the design stage. Furthermore, there is a conflict between the situation of knowing few information of HVAC system and the demand of detailed information to evaluate economic characteristics at design beginning stage. Neural network method can solve these problems for its self-adaptive ability and convenient multi-variable input-output function. ADLINE neural network model is analyzed and used to evaluate the economic characteristics of HVAC systems. The compare between the value predicted by ADLINE and the value calculated in detail shows that the relative error is less than 6% and the economic performance evaluation using ADLINE neural network model can satisfy the demand of actual HVAC project design.

KEYWORDS

Building HVAC Systems, Economic Performance, Evaluation, Prediction, Neural Network Method, ADLINE

INTRODUCTION

In order to assess the performance of building Heating Ventilation and Air Conditioning (HVAC) systems, actually two aspects need to be done, one of which is to evaluate the extent to which an HVAC scheme satisfies the air conditioning requirement and the other of which is to evaluate the economic characteristics of several HVAC schemes that can satisfy the air conditioning demand.

Many scholars have studied much about the assessment of the extent to which an HVAC scheme satisfies the air conditioning requirement. But there are few researches about evaluating the economic characteristics of the HVAC systems, especially combining the economic evaluation into design stages. It is difficult to evaluate the economic performance of HVAC systems because economic evaluation involves some factors that frequently change and often unknown such as equipment price, especially in the design beginning stage. However, at design beginning stage it is important to know the economic performance of several feasible schemes. Because some big decision, such as scheme of heating and cooling source, need to be decided before design. Only after determining the design content could the design be in progress. Reasonable economic evaluation can help the managers of a building and designers make good decision and prevent to repeat and waste work.

Design beginning stage is the beginning of the HVAC systems design. At this stage, the known information is about the building, such as building area, building use, building envelope parameter and so on. Besides these parameters, the HVAC scheme and refrigeration scheme can also influence the economic characteristic. But to calculate the economic parameters in detail, such as initial investment and operation cost, the information above is far from adequacy. In order to calculate the economic parameters in detail, at least the size and amount of the HVAC equipments and materials need to be known. However at the the beginning of the design stage this information is impossible to be obtained. So there is a conflict between the situation of knowing few information of HVAC system and the demand of detailed information to evaluate economic characteristics at the beginning of the design stage.

For the purpose of solving this conflict, some economic prediction method is needed other than detailed calculation. The prediction method should be able to process multi-variable problem because at the beginning of the design stage there are many variables that might influence the economic characteristic, such as building area, building use, building envelope parameters, the HVAC scheme and refrigeration scheme. Neural network method can solve this kind of problems for its self-adaptive ability and convenient multi-variable input-output function.

Neural network is 'a network of interacting simple units together with a rule to adjust the strength of the connections between these units in response to externally supplied data', Lisboa (1992). There are two phases to use a neural network:

(a) Training phase, which is to determine the weight of the connection between two neurons by inputting the parameters of training samples and comparing the output given by the neural network and the samples' output and adjusting the weight according to a certain study algorithm.
(b) Recall phase, which is to use the trained neural network to predict the value of an unknown object corresponding to its input parameters.

This paper will discuss how to apply neural network method to predict the economic parameters of a

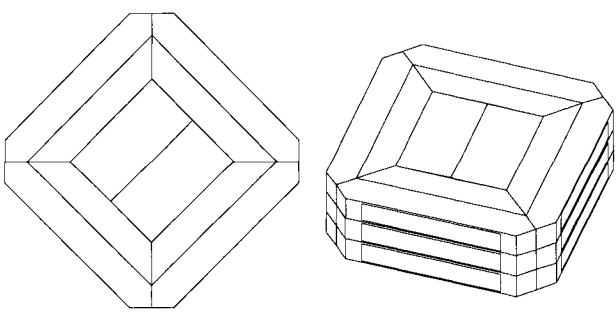
building's HVAC systems at the beginning of the design stage.

NEURAL NETWORK TRAINING

The first step of using a neural network is to train it. For the sake of training a neural network, training samples need to be determined. The training samples are a series of data vectors, every of which is consisted of input vector and output vector. For the aspect of economic characteristics of a building 's HVAC systems, the input vector contains the parameters that can influence the economic characteristics, such as building area, building use, building envelope parameter, and the output vector is the economic parameters, i.e. initial investment and operation cost of the HVAC systems. Because there are too many variables that might influence the economic characteristics, sensitivity analysis needs to be implemented to determine the important variables and eliminate the variables that influence the economic characteristics very slightly.

Sensitivity Analysis

This article analyzed a building as shown in Figure 1 and studied the economic sensitivity to the change of building area, building use, building envelopment, rate of window to wall, shape factor (rate of length to width), opening hours, outside air supply scheme, cooling and heating source scheme, HVAC scheme. The initial investment and operation cost of the sample building at 25 kinds of different situation w ere calculated by changing the parameters mentioned above.



Plan Perspective

Figure 1: Sample building for sensitivity analysis

Building use is divided into three types according to the indoor heat generation: 1) hotel (including residential buildings), 2) office building (including library and hospital buildings), 3) shopping center (including restaurant, dancing hall, exhibition hall and gymnasium). Two kinds of window are analyzed, 1) single layer aluminum alloy window, 2) double layer aluminum alloy window. Two kinds of outside air supply scheme are analyzed, 1) constant outside air rate which is 0.1, 2) variable outside air rate which is from 0.1 to 1. Three kinds of regular HVAC scheme were analyzed: 1) FCU, 2) CAV, 3) VAV. Five kinds of regular cooling and heating source scheme were analyzed: 1) Compression refrigerator driven by electric power and water boiler burning gas, 2) Compression refrigerator driven by electric power and water boiler using electric power, 3) LiBr absorber driven by vapor and boiler burning gas, 4)

LiBr absorber burning gas, 5) Air source heating pump.

Sensitivity analysis of initial investment

The sensitivity analysis showed that building area has prevailing influence to HVAC initial investment. Rate of window to wall and length to width cause the same scale of influence to HVAC investment. The change of building use can change HVAC initial investment 40%. Different window type can make HVAC initial investment change 8% and the influence of window type can be ignored. HVAC scheme can change the initial investment 50%. Cooling and heating source can change the initial investment 30%.

Figure 2 shows the change of the HVAC initial investment caused by the changing of the factors mentioned above except building area which is prevailing, compared with the building in standard condition. The standard condition is a office building, whose rate of window to wall is 0.7, rate of length to width is 1, single layer aluminum alloy windows are used, HVAC sch eme is FCU, cooling and heating source is scheme (1).

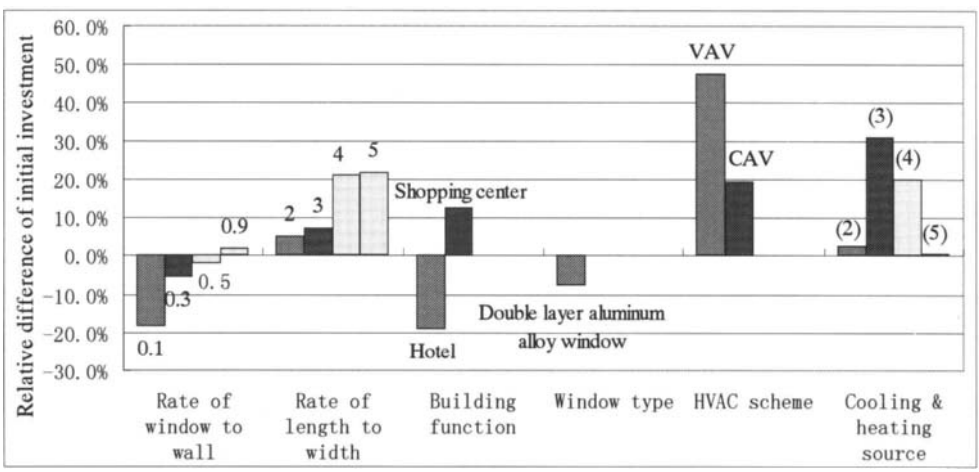


Figure 2: Change of initial investment caused by different factors

From the analysis above we can determine that the sensitive factors of initial investment are building area, building use, rate of window to wall, rate of length to width, HVAC scheme, cooling and heating source scheme. The change of window type cause little influences to the initial investment and can be ignored.

Sensitivity analysis of operation cost

Sensitivity analysis shows that the change of building area and opening hours overwhelmingly influence the operation cost of HVAC systems. The rate of window to wall and length to width can change the operation cost about 20%. Building use can change the operation cost 2~3 times. Window type can change the operation cost 6%. The operation cost of constant outside air rate system is 30% higher than that of variable outside air rate. HVAC scheme can change the operation cost change 50%~100%.

Cooling and heating source scheme can change the operation cost 20%.

Figure 3 shows the HVAC systems operation cost change caused by changing the factors mentioned above except building area and opening hours which are prevailing, compared with the building in standard condition.

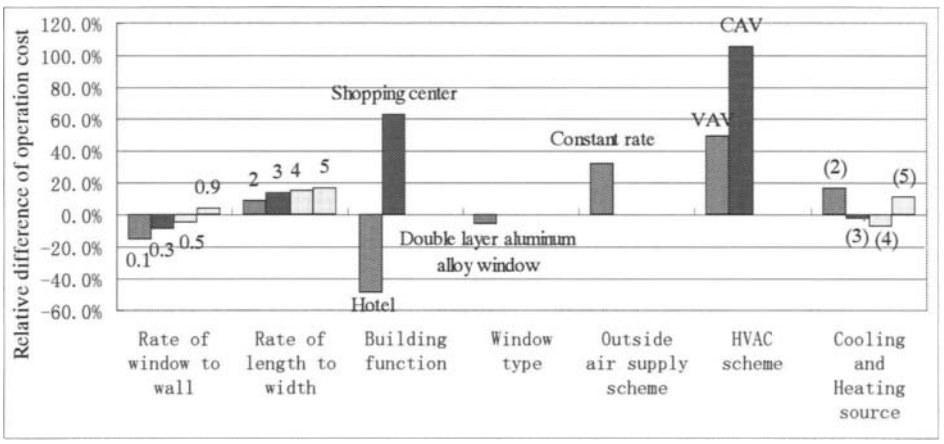


Figure 3: Change of operation cost caused by different factors

According the analysis above we can determine the sensitive factors of HVAC systems operation cost are building area, opening hours, building use, rate of window to wall, rate of length to width, HVAC scheme, cooling and heating source scheme. The change of window type has little influence to the operation cost and can be ignored.

Selection of Neural Network Model

There are near 60 different types of neural network depending on the structure and the algorithm u sed to define them, (Cai, 1998). Among these neural network models, Adaptive Linear Element (ADLINE) is proper to predict economic characteristics. One reason is that E. Shoneburg had successfully used ADLINE to predict the changing of several stocks (Hu, 1993). Another reason is that the initial investment and operation cost of HVAC systems have obviously linear relationship with the building area, which has the overwhelm influence to the economic characteristics according to the sensitivity analysis. The difference between ADLINE and linear regression method is that ADLINE uses iterative method to calculate the weight of every variable, which is convenient for calculating using computer. Furthermore, it is convenient to adjust weights when new samples are added to the sample set.

Figure 4 shows the structure of the ADLINE model. $(x_0, x_{1k}, x_{2k}, \cdots, x_{nk})^T$ is input vector. $(w_0, w_1, w_2, \cdots, w_n)^T$ is weight vector. The continuous output is

$$Y_k = X_k^T W = W^T X_k \tag{1}$$

During training phase, the Least Mean Square (LMS) algorithm is used to adjust the weight to adapt the

neural network to the characteristics of training samples. The error between neural network predicted value and expected value at time t is

$$E_k(t) = \frac{1}{2}[d_k - y_k(t)]^2 = \frac{1}{2}\varepsilon_k(t)^2 \tag{2}$$

The weight vector at time t+1 is

$$W(t+1) = W(t) - \eta \frac{\partial E_k(t)}{\partial W(t)} \tag{3}$$

Let $\eta = \dfrac{\alpha}{\|X_k\|_2^2}$, then

$$W(t+1) = W(t) + \frac{\alpha}{\|X_k\|_2^2}\varepsilon_k(t)X_k = W(t) + \frac{\alpha}{\sum_{i=0}^{n}|x_{ik}|^2}\varepsilon_k(t)X_k \tag{4}$$

Where,

W (t+1) — Weight vector at time t+1,

W (t) — Weight vector at time t,

α — Learning speed, when 0< α <2, the iterative computation is convergent, (Cai, 1998).

X_k — Input vector,

ε_k — Error between neural network predicted value and expected value, $\varepsilon_k = d_k - y_k = d_k - X_k^T W_k$

When the total error of all training samples is less than the preset least error, the training processing is finished.

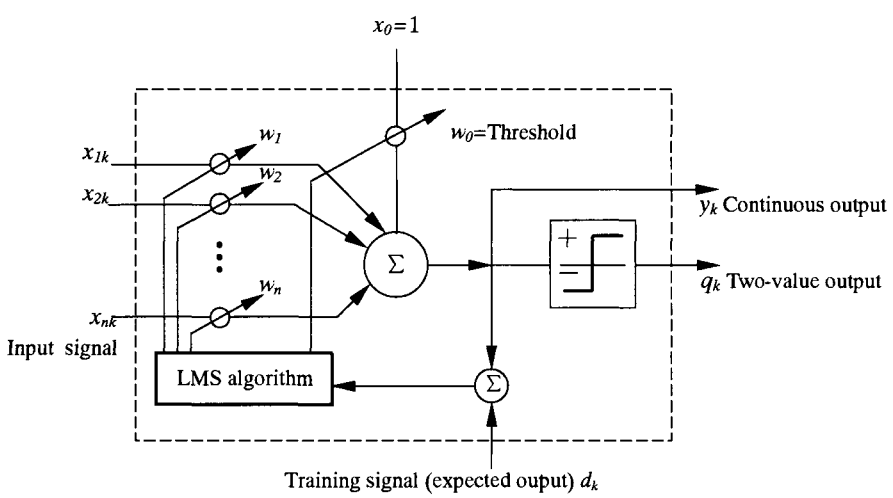


Figure 4: Structure of ADLINE

Because ADALINE is a linear model, the influence of inconsecutive variables, such as building use, HVAC scheme, cooling and heating source scheme, can only be reflected through using amending coefficient which is determined according to the sensitivity analysis. The consecutive variables are the input parameters of the neural network. Because the operation cost is in direct ratio to the opening hours, operation cost can be calculated through multiplying the predicted operation cost per hour and opening hours.

The training samples are 21 selected buildings. Firstly the initial investment and operation cost of these samples are calculated in detail. DeST (Chen, 1999), a simulation software developed by Tsinghua University is used to simulate the whole year performance of a HVAC design. Through simulation we can obtain the size and quantity of HVAC equipment and materials and the hourly operation parameters. So the initial investment and operation cost can be calculated according to the simulation results. Then economic parameters of these samples are used to train a neural network. Figure 5 shows the changing of relative error accompanying the iterative times.

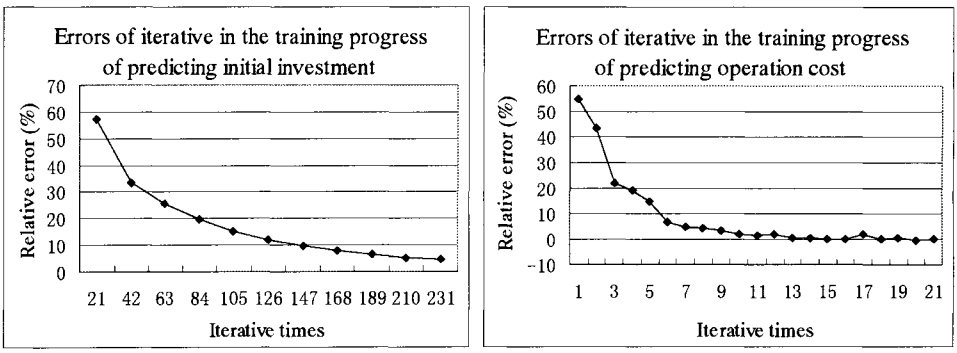


Figure 5: Relative error change along with iterative

NEURAL NETWORK PREDICTION

After the neural network training is finished, the characteristics of the samples are stored in the neural network. When we input the parameters of the building to be predicted, the neural network will output the HVAC systems' initial investment and operation cost as the prediction result according to the characteristics stored in it. Figure 6 shows the difference between the detailed calculation value and neural network prediction value of initial investment and operation cost of 5 real buildings, which are not the training sample buildings.

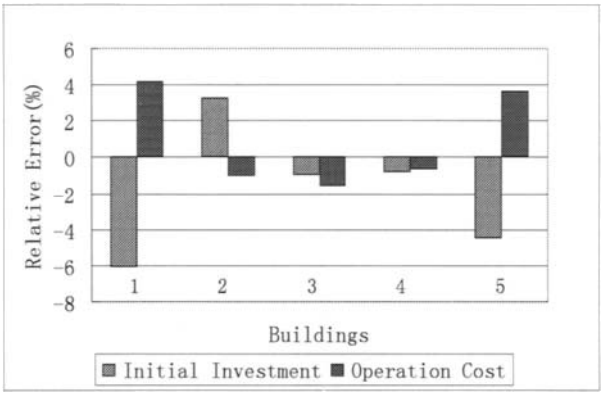


Figure 6: The difference between neural network prediction and detailed calculation value

DISCUSSION

The biggest predominance of prediction using neural network is the self-adaptive function, which make it can adapt to the change of some factor such as price.

Because the training of neural network is to adjust the weight between the nodes according to the input samples, the trained neural network reflects the mean character of the samples. If the deference among the samples is too big, the training process cannot converge to relatively high accuracy. Then more detailed input variables are needed to obtain high accuracy of training.

CONCLUSION

For the purpose of make good decision of HVAC scheme, it is important to evaluate the economic performance of several feasible HVAC schemes at the beginning of the design of a building's HVAC systems. Neural network method is suitable to predict the economic parameters at the beginning of the design stage for the lack of detailed information of HVAC equipments and materials. The analysis of this paper shows that the ADLINE neural network method can successfully predict the economic characteristics of HVAC systems at the the beginning of the design stage.

REFERENCES

Chen F., Deng Y., Xue Z., and Wu R. (1999). DeST - Toolkit of Buil ding Artificial Environment Simulation. *HV & AC,* 1996:5, 32-35.

Cai K. (1998). *Realization Technology of Neural Networks,* Press of Guofang University, Changshai, China.

Hu S. (1993). *Application Technology of Neural Networks,* Press of Guofang University, Changshai, China.

Lisoa P. G. J. (1992). *Neural Networks - Current Applications,* Chapman & Hall, London, UK.

Advances in Building Technology, Volume 2
M. Anson, J.M. Ko and E.S.S. Lam (Eds.)
© 2002 Elsevier Science Ltd. All rights reserved

A REVIEW OF RESEARCH CONCERNING THE USE OF PCMS IN AIR CONDITIONING AND REFRIGERATION ENGINEERING

Fuqiao Wang[1], Graeme Maidment[1], John Missenden[1], Robert Tozer[2]

[1] *South Bank University, School of Engineering, 103 Borough Road, SE1 0AA, London, U K.*
[2] *Waterman Gore-Mechanical and Electrical Consulting Engineers, Versaillers Court, 3 Paris Garden, SE1 8ND, London, U K*

ABSTRACT

Phase Change Materials (PCMs) found considerable application in the 1980s and early 1990s in large air conditioning schemes. PCMs were primarily used to introduce capacitance within the system to enable it to take account of fluctuations in the daily cooling load. The main benefits of this are lower capital expenditure through smaller chiller size and lower revenue costs through greater use of off peak electricity. This paper reviews recent research into phase change materials applied to refrigeration and air conditioning (RAC). The specific research areas it addresses are methods for improving heat transfer within the PCM, optimum control techniques and novel methods of integration.

KEY WORDS: PCM, Cooling storage, Heat Transfer, Refrigeration, Air Conditioning, TES

INTRODUCTION

Thermal energy storage (TES) systems have played an important role in energy management, and have been used extensively in RAC systems. Water was commonly employed as a sensible energy storage material. In the early 1970s, they were used to produce capacitance within the cooling systems by minimizing the fluctuations in daily cooling load. TES systems are now developed as a demand side management (DSM) tool for electric load management and for supply side management (SSM) allowing efficient and economical power production. In buildings, DSM utilises smaller capacity cooling equipment resulting in smaller capital costs of plant and lower running costs through the greater use of off peak electricity. SSM allowed the existing national grid to be more efficient and effective, reducing the requirement for new capital intensive power stations. More efficient use of power stations also resulted in environmental benefits through reduced greenhouse gas emissions.

In the UK, buildings consume approximately 40% of the total energy used (Beggs, 1997), and a significant reduction of emissions from the building sector is a key Government priority in the fight against global warming (Kulkarni 1994). The incorporation of TES in building systems has been reported to directly result in 10-20% reductions of carbon dioxide emissions (Beggs, 1995, 1997). TES has also been integrated into renewable energy schemes allowing better use of intermittent natural energy sources and reducing the requirement for fossil fuel generated electricity and heat.

Phase Change Materials PCMs, which are an alternative to sensible storage, subsequently found considerable application in the last two decades in large air conditioning schemes. The main advantage of latent storage over sensible storage mechanisms is their ability to store large quantities of energy in

small volumes and to produce a constant source temperature. However, the literature suggests that PCMs, like sensible storage systems are not problem free. Common drawbacks of these storage designs are the low heat transfer rate within the phase change material partly due to the effect of super cooling. Despite these limitations, phase change materials have found application in a number of new building services technologies. This paper reviews the state of the art of PCM systems including difficulties in applying PCM in refrigeration and air conditioning, and the novel methods of application.

THE MAIN PROBLEMS AND RESEARCH FOR BETTER PCM APPLICATION

The main difficulties associated with the application of PCMs in RAC system reported in the literature are low heat transfer rate, the effect of super cooling and poor system design/ control. These difficulties and research to overcome them is discussed in the paper.

Other problems that have been cited are less generic and are not reported here in detail. These include the effect of incongruence on one type of PCM, salt hydrates, which result in a short life for the PCM (see EPSLtd design guide). Also problems of corrosion of heat exchanger surfaces with some PCM types is not reviewed but discussed elsewhere (ASHRAE 1997).

Low Heat Transfer Rate and Improvements

The low heat transfer rate within PCMs occurs for a number of reasons. Firstly as the solid/liquid boundary moves away from the heat transfer surface, the thermal resistance increases. Secondly, in the solid region, this is further increased by heat transfer being solely by conduction and this is low due to the low thermal conductivity of PCMs. Heat transfer enhancement techniques, include the following:

Larger heat exchanger surface

As a PCM heat exchanger, the main heat transfer resistance is on PCM side, the use of extended surfaces on this side can effectively reduce the thermal resistance. For the shell-and-tube type, a number of researchers reported their results. Lacroix (1993) implemented the investigation of the PCM around a finned tube in both radial and axial directions by numerical and experimental methods, the results showed that annular fins are most effective for moderate mass flow rate and small inlet temperatures of the heat transfer fluid. Choi et al. (1996) found that the enhancement of heat transfer by thin finned-tube over the unfinned-tube is negligible, the heat transfer coefficient in the thick finned-tube system is approximately two times higher than that in the unfinned-tube system. Sadasuke (1991) investigated the performance of a finned flat wall in contact with Paraffin wax under solidification, a mathematical model showed good agreement with the test results. The numerically study on fins can also be found in Velraj (1997) and Costa et al. (1998) work.

Thermal conductivity enhancement

A) *By using metal matrix* Hoogendoorn and Bart (1992) have reported that the low value of the thermal conductivity of the PCMs could be greatly improved by embedding a metal matrix structure in them. Tong et al (1996) numerically investigated increasing the heat transfer rate during ice melting and freezing by inserting a metal matrix into water. They concluded that inserting an aluminium matrix into a low thermal conductivity PCMs could achieve an exponential increase in the inner wall heat flux and similar decrease in the total melting and freezing time. The parameter dominating heat transfer enhancement is the metal matrix volume fraction, while geometric sizes play minor roles.

B) *By using heat pipes* The heat pipe is a passive heat transfer device with a thermal conductivity equivalent to approximately 500 times that of copper (Reay 1995). Heat pipes can help the PCM charging and discharging with in short time, and make the storage system controllable, which helps to

improve the system efficiency. In 1987 a new air-conditioning system using a heat pipe ice storage system was installed in Yokohama in Japan, the new system achieved a COP equivalent to a water chiller system (CADDET). In 1994, a heat-pipe ice thermal storage system for air conditioning was installed by another Japanese company, which showed a coefficient of performance for cooling of 2.79 for ice storage and 3.08 for space cooling. These COPs are equivalent to water storage systems (Kawamaki, 1996). A mathematical model based on a heat pipe latent heat storage system was developed by Horbaniue et al.(1996,1999).

C) *By using high conductivity materials combined with PCMs* Seigel (1977) studied the improvement in solidification rate in molten salt dispersed with high conductivity particles. For a reasonable fraction (20% by volume) of these particles in PCM, moderate improvement (17%) in heat transfer rate is achieved. Chow and Zhong (1996) proposed two thermal-conductivity enhancement techniques, the first technique focused on placing encapsulated PCMs of various shapes in a liquid metal medium. The second technique involves a metal/phase-change material composite. Specifically, 5%Ni was added uniformly to the PCM (LiH), the later method gave a better enhancement in thermal conductivity. Compared to the pure PCM, the melting time was halved. Velray et al. (1999) reported three methods of improving the thermal conductivity in PCM, of which both the numerical solution and test results showed that using lessing rings can enhance the thermal conductivity by several times but it also reduces the PCMs storage capacity.

Using PCMs with different melting temperature- Big temperature difference

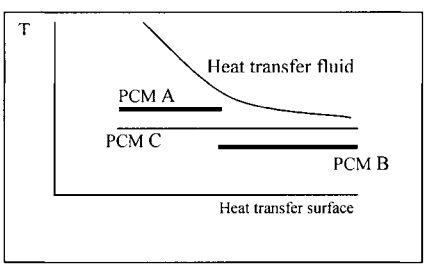


Figure 1 The temperature distribution along heat transfer surface with different PCM

The mechanism to enhance heat transfer rate by using different melting PCM can be explained by figure 1. Using PCMs A and B instead of PCM C, there is a great improvement in temperature difference along the whole heat transfer surface, and then a better heat transfer rate achieved. Farid was the first to use this method of enhancing heat transfer in thermal storage capsules containing paraffin waxes (Farid et al 1990)

Farid (1994) tested his theory on a system employing direct contact latent heat storage method, and chose $Na_2S_2O_3 \bullet 5H_2O$ and $Na_2CO_3 \bullet 10H_2O$ as PCMs, which have different phase change temperatures. Heat transfer fluid flowed from the first $Na_2S_2O_3 \bullet 5H_2O$ solution to the second $Na_2CO_3 \bullet 10H_2O$ during heat charging process. The use of two columns connected in series for heat storage gave higher rates of heat transfer during heat charge and discharge, when compared to a single column. Gong et al. (1996, 1997) through numerical investigation, found that the heat transfer rate could be increased by 30%-35% using five PCMs than using a single PCM. Domanski and Fellah (1996) found that by using two PCMs in the same storage tank could improve the second-law efficiency of the system significantly (31.4% for two PCMs system compared to 22.4% for a single PCM system). Wang et al (1999) also found that the phase change time of composite PCMs with the optimum linear phase change temperature distributions used in thermal storage systems can be decreased by as much as 25-40% by selecting the segmented numbers of composite PCMs as compared with that of single PCMs.

Direct contact

Etherington was thought (Farid et al 1994) the first to introduce the idea of using direct contact heat transfer between an immiscible heat transfer fluid and solution of hydrated salt. Light mineral oil as a heat transfer fluid was bubbled through a solution of sodium phosphate dodecahydrate. Heat was exchanged between the bubbles and the solution efficiently without the requirement of expensive

metallic heat transfer surface. Subbaiyer et al. (1990) showed a simulated result of a refrigeration unit with a direct contact evaporator. The unit consumed only 50-60% of electrical energy compared with a cooling coil ice generator. Kiatsiriroat et al.(1998) developed a direct contact evaporator system, which uses an injection of R12 refrigerant into the water tank to exchange heat with water directly, cooled the water to freezing point and ice was formed, the ice was used for producing chilled water for air conditioning, the coefficient of performance was about 3.4-3.6 which is higher than that of conventional system. Kiatsiriroat et al (2000) also investigated a sodium thiosulphate pentahydrate storage exchanging heat directly with heat transfer oil during discharging process; high heat transfer was obtained with direct contact heat exchange method.

Royon et al. (1997) first presented a new material, formed from two solutions, the first was a solution of acrylamid and bisacrylamid and the other was a starting-solution (potassium persulphate), the mixture is maintained at 313K, and the polymerization is complete after about 12 hours. The material has two contradictory constraints: maximum water for high thermal capacity and maximum polymer for better rigidity, which can contact directly with heat transfer materials, and does not need any envelope. It also can include other PCMs in a tridimensional network of polymer by using the polymerising process. They found that the new material appears to be very promising for practical applications involving the recovery of low level thermal energy.

Electrohydrodynamics (EHD)

Crystallization which occurs during phase change processes, consists of two separate processes, namely, nucleation and crystal growth. Based on diffusion-reaction theories, the rate of crystallization from a liquid depends on the rate of heat transfer from the crystal surface to the bulk of the liquid, and the growth rate of crystallization then depends on the rate of mass transfer. When an electric field is present in a dielectric crystal-melt system, the bulk liquid is be polarised. The force acting on the dipole by electric field will have a strong effect on the stagnant or effective film in the bulk melt. This will result in instability in the film and reduce the thickness so that the film coefficient is increased; as a result, the rate of crystallisation from the liquid is significantly increased. Yan et al (1997) found that the time for appearance of crystals reduced by 50% at 15KV than that at zero fields, and more stable crystals appear earlier under the action of an electric field. It means that heat and mass transferred from the crystal surface to the bulk mixture is enhanced than without an electric field

Super Cooling and Improvements

A further factor that results in lower system efficiency is the phenomenon of super cooling. This is the presence of liquid below freezing point. System efficiency is reduced with super cooling since it causes the effective temperature difference between the phase change material and the heat transfer temperature to be reduced, and prolongs the charging and discharging time.

The addition of nucleating agents to the PCM (for example ice), iron ore, iron chips and silver iodide can effectively improve the probability of nucleation (Chen et al 1998). Different materials have different nucleating agents. Saito et al. (1990) thought Vonnegutwas was the first to report the use of AgI and PbI_2 as the nucleating agents for super cooled water droplets in the atmosphere, and found that these agents greatly improved the super cooling phenomenon of small water droplets. They later found that in ice storage systems, the surface roughness affected the degree of super cooling (for ice formation). The super cooling state can be minimised by applying a certain roughness on the surface such as the electrolytically polished surface or the porous surface.

Super cooling does not occur with organic compounds, such as paraffin wax which presents no super cooling. However, they have a disadvantage of low thermal conductivity.

System Design and Control

Due to the complexity of the phase change process, few software are available which can precisely predict the behavior of PCM systems. Hence, contemporary designers faced great difficulty in the design and control of systems. This led to oversized or undersized PCM storage systems of which the former were uneconomical and inefficient due to long charging and discharging times, hence were hard to control. This also reflected on the smaller sized PCM storage systems, which did not offset the output load.

Knebel (1995) believes that with total shifting type PCM schemes storing the optimum quantity of energy at night to satisfy the following days demand is very important in terms of operating efficiency. As the building load varies depending on the time of year occupancy pattern etc, however, accurate predication of demand is complex. Keeney (1994) used an intelligent control system based upon weather forecast and utility tariffs to optimise operational performance of a PCM cooling scheme. Rupanagunta et al. (1995) developed a 24-hour load-forecast model to achieve dynamic system response to the variations in the ambient weather conditions. They designed an optimal controller for the storage system's operating cycle to minimise the running costs of the storage facility. The saving of the control storage system under optimal control was 4.3% over an alternative ice-priority control strategy when perfect foresight is assumed.

NOVEL APPLICATION OF PCM IN AIR CONDITIONING AND REFRIGERATION

The review of the literature has made it apparent that the problems with PCM applications, in particular the low effectiveness needs to be resolved. To improve the energy saving potential of PCMs, recent research has reported novel methods of applying phase change materials in cooling systems. These techniques consist of evaporative cooling, night radiation cooling and direct integration of PCM heat exchanger, which are discussed below.

Evaporative Combined PCM in HRAC System

Asrael et al (2000) reported a scheme where thermal storage was incorporated into the cooling tower circuit as shown in figure 2, this enabled the system to charge the thermal store at night when there are lower wet bulb temperatures. The stored cold energy is released into the heat rejection circuit during the day, which produces lower condensing temperatures and higher efficiency. According to Asrael this method can reduce both peak energy and power use by as much as 35%.

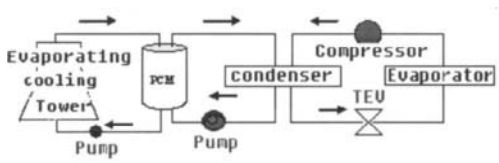


Figure 2: Night evaporative cool with PCM system

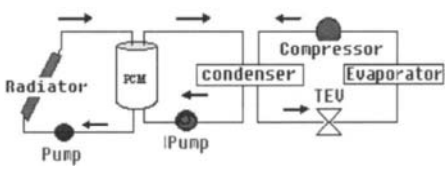
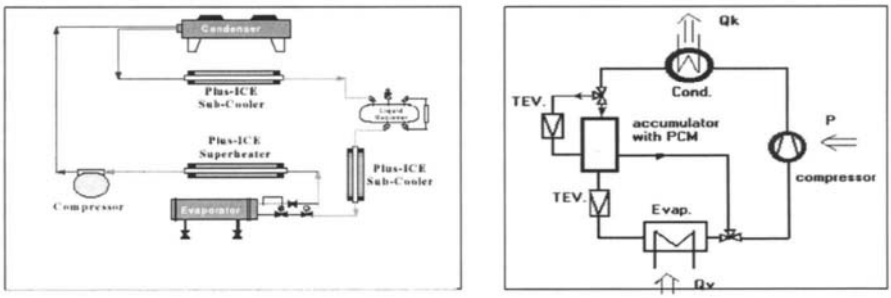


Figure 3: Night sky radiation cool with PCM system

Night-sky Radiant Cooling Combined PCM in HRAC System

A number of papers reported schemes which use night sky radiant cooling within the heat rejection water circuit as shown in Fig 3. The lower effective temperature of the night sky is used as a heat sink with long wave radiation taking place between the condenser water and the night sky. With the use of thermal storage cold energy can be released during daytime hours to improve energy efficiency. CADDET reported a case in USA on night sky radiant cooling system combined the PCM storage

system, the net annual cooling energy savings are over 50%.



(a) (b)

Figure 4 PCM integrated directly into refrigeration system

PCM Integrated Directly in Refrigeration System

Ure (1997) reported (Fig4 (a)) refrigeration system incorporating phase change material heat exchangers in contact with the suction and liquid lines. The purpose of the liquid line PCM exchanger is to enable the refrigeration system to benefit from lower night-time ambient conditions. At night lower temperatures generate lower condenser pressures as well as increased liquid sub-cooling. The use of a PCM in the liquid line provides an artificial load on the condenser, which often avoids the necessity for inefficient condenser control, as well as allowing the night-time cold energy to be stored for release during daytime operation. Ure does not qualify the benefit of this technology when applied to a real system, but states that a 15K increase in sub-cooling levels leads to a 10% improvement in peak plant efficiency. The purpose of the suction line PCM exchanger is to limit the superheat in the suction line by providing thermal capacitance. Again Ure gives a peak efficiency improvement of 15% for a 5K reduction in superheat, but this is not quantified under applied condition.

HAVELSKÝ (2001) (fig.4 b) numerically investigated another system shown in Fig.4(b), which uses a PCM integrated directly in a heat pump cycle. By controlling the three way valves, the accumulator with PCM stored energy from refrigerant coming through the condenser will act as an evaporator when the outside temperature is less than the balance point temperature. With this system, the numerical results showed that the average energy saving was nearly 20%.

PCM Integrated into Thermoelectric Cooling (TEC) System

Omer et al (2001) studied the application of PCM integrated with a TEC system. They found that heat sink with large heat storage is crucial to the performance of TEC system. They employed an encapsulated PCM as a cold sink in thermoelectric system, and integrated the PCM with heat pipes, which prevented the heat flow back to the cold space during off power periods as shown in Fig 5. It was found that the COP of the new system with PCM increased by a factor of two than without PCM.

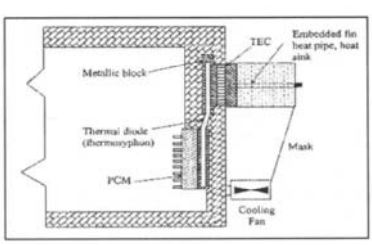


Figure5 PCM integrated into thermoelectric refrigeration system

CONCLUSIONS

A comprehensive literature has been reviewed in this paper. New PCM materials, heat transfer enhancement technology, nucleating and super cooling preventing techniques, combined new technology and system optimal control technology have been developed progressively.

Low heat transfer rate, as a main drawback of PCMs, has been recognized. Many heat transfer enhancement methods are investigated extensively and summarized in this paper. These methods provide effective ways of overcoming heat transfer problems in practice. Meanwhile system design requires sophisticated software to help designers with efficiency system in design stage. It is necessary to build a mathematical model to predicate and optimise the behavior of the systems. In order to increase the energy saving potential of PCMs in system, the novel use PCMs in RAC systems is also discussed in this paper.

Acknowledgements-The authors gratefully acknowledge the Engineering and Physical Science Research Council in the UK for supporting this research.

REFERENCES

Abraham, M. M. (1997). Optimization of the storage process for a cool thermal storage system, *Journal of Energy Resources Technology, Transactions of the ASME* **119: 4**, 236-241.

Akiya, T, (1991). Novel cool storage system using HCFC-141b gas clathrate. *Proc. of the IECEC* **6**,115-119

Asreal J., Phelan, P.E., Wood, B.D. (2000). Feasibility of lowering the condenser's inlet water temperature of a chiller using thermal water storage. *Applied Energy* **66**, 339-356

ASHRAE, 1997, *Fundamentals.* American Society of Heating, Refrigerating and Air-conditioning Engineers, 1791 Tullie Circle, N.E., Atlanta, GA 30329.

Banaszek, J., Domanski, R., Rebow, M. and El-Sagier, F. (1999). Experimental study of solid-liquid phase change in a spiral thermal energy storage unit. *Applied Thermal Engineering* **19: 12**, 1253-1277.

Banaszek, J., Domanski, R., Rebow, M. and El-Sagier, F. (2000). Numerical analysis of the paraffin wax-air spiral thermal energy storage unit. *Applied Thermal Engineering* **20: 4**, 323-355

Beggs C. B., (1997). ICE thermal storage: Impact on United Kingdom Carbon dioxide emissions. *Building Serv.Eng.Res.Technol* **15:1**, 11-17

Beggs, C. B, (1997). Ice thermal storage: Theoretical study of environmental benefits, *Building Serv.Eng.Res.Technol* **18: 3**, 157-160.

Beggs, C. B. (1995). Ice thermal storage: application to demand-side management in the United Kingdom, *Building Serv.Eng.Res.Technol* **16: 1**, 25-31.

Choi, J.C., Kim,S.D. and Han,G.Y. (1996). Heat transfer characteristics in low-temperature latent heat storage system using salt-hydrates at heat recovery stage. *Solar Energy Materials and Solar Cells* **40: 1**, 71-87.

Chen S.L., Wang P.P., Lee T. S. (1998). An experimental investigation of nucleation Probability of supercooled water inside Cylindrical capsules. *Experimental Thermal and Fluid Science***18:4**, 299-306

Chow L.C. and J.K. Zhong (1996). Thermal conductivity enhancement for Phase Change Storage Media. *Int. Comm. Heat Mass Transfer* **23:1,** 91-100

Das, S. and Dutta, T. K. (Nov 1993). Mathematical modeling and experimental studies on solar energy storage in a phase change material. *Solar Energy* **51: 5**, 305-312.

Dini S. and Saniei, N. (1992). Refrigerant hydrate as a cool storage medium. *ASME, HTD* **215**, 63-72.

Domanski, R. and Fellah, G. (1996). Exergy analysis for the evaluation of a thermal storage system employing PCMS with different melting temperatures. *Applied Thermal Engineering* **16:11**, 907-919.

EPSLtd design guide, EPSLtd website **http://www.EPSLtd.co.uk**

Farid, M. M. (Feb 1994). Performance of direct contact latent heat storage units with two hydrated

salts. *Solar Energy* **52: 2**, 179-189
Farid, M. M., Hamad, F.A. and Abu-arabi, M. (1998). Phase change cool storage using dimethyl-sulfoxide. *Energy Conversion and Management* **39: 8**, 819-826.
Farid, M. M., Kim, Y., Kansawa, A. (1990). Thermal performance of a heat storage model using PCMs with differnt melting temperature: experimental. *ASME J.Energy Res. Technol* **111**, 125-131
Gong, Z. X., and Mujumdar, A. S. (1996). Cyclic heat transfer in a novel storage unit of multiple phase-change materials, *Applied Thermal Engineering* **16:10**, 807-815
Gong, Z-X and Mujumdar, A. S. (Mar 1996). Enhancement of energy charge-discharge rates in composite slabs of different phase change materials, *Int. J. of Heat and Mass Transfer* **39: 4**, 725-733.
HAVELSKÝ, V. (2001). Possibilities of Primary Energy Savings in Heat with Thermal Storage. *Clima 2000/Napoli 2001 World Congress_Napoli (I)* **15-18** September
Henze, G. P. (1998). Simulation environment for the analysis of ice storage controls, *ASHRAE Trans.* **104**, 41-47
Horbaniuc, B., Popescu, A. and Dumitrascu, G. (1996). Correlation between the number of fins and the discharge time for a finned heat pipe latent heat storage system. *Renewable Energy* **9:1-4**, 604-608
Ito, H. and Miura, N. (1991). Heat transfer enhancement by fins in latent heat thermal energy storage devices. *ASME-JSES-JSME Int. Solar Energy Conference* **1991,** 223-228
Keeney,Kevin and Braun,James (1996). Simplified method for determining optimal cool control strategies for thermal storage in building mass. *HVAC&R Research* **2:1**, 59-78
Kiatsiriroat, T., Siriplubpla, P. and Nuntaphan, A. (1998). Performance analysis of a refrigeration cycle using a direct contact evaporator. *Int. J. of Energy Research* **22:13**, 1179-1190.
Kiatsiriroat,T., Tiansuwan, J., Suparos, T., and Thalang, K N. (2000). Performance analysis of a direct-contact thermal energy storage-solidification. *Renewable Energy* **20:2**, 195-206.
Kulkarni, P. P. (1994). Soalr absorption cooling for demand-side management. *Energy Eng.* **91:5**, 29
Lacroix M.. Study of heat transfer behavior of a latent heat thermal energy unit with a finned tube. *Int.J. HMT* **36**, 2083-2092.
Najafi, M., Schaetzle W.J., and Huang J.T. (1991). Latent heat storage applications in heat pump, *Proceedings of the IECEC* **4**, 122-127.
Omer, S.A., Riffat S.B., X. Ma, (2001). Experimental investigation of a thermoelectric refrigeration system employing a phase change material integrated with thermal diode (thermosyphons), *Applied Thermal Engineering* **21**, 1265-1271
Royon L.,Guiffant. G., and Flaud, P. (1997). Investgation of heat transfer in a polymeric phase change mateial for low level heat storage. *Energy Conversion Management* **38:6,** 517-524
Rupanagunta, P., Baughman, M.L., Jones, J.W. (1995) Scheduling of cool storage using non-linear programming techniques. *IEEE Transactions on Power Systems* **10: 3**, 1278-1285
Saito, A., Utaka, Y., Okawa, S. (1990). Investigation of an effect of characteristics of surface and cooling rate on a freezing temperature of super-cooled water. *Int. J. of HMT* **33:8**, 1697-1709.
Sari A. and Kaygusuz K. (2001). Thermal performance of myristic acid as a phase material for energy storage application, *Renewable Energy* **24**, 303-317
Subbaiyer, S. (1990). Computer simulation of a vapor-compression ice generator with a direct-contacted evaporator. *ASHRAE Trans.***96:1**,118-126.
Tong, X. L, Khan, J. A., and Amin, M. R. (1996). Enhancement of heat transfer by inserting a metal matrix into a phase change material, *Numerical Heat Transfer; Part A: Applications* **30:2,** 125-141
Velraj, R.. (1999).Heat transfer enhancement in a latent heat storage system, *Solar Energy* **65:3**, 171
Wang, J., Chen, G., and Zheng, F. (1999). Study on phase change temperature distributions of composite PCMs in thermal energy storage systems, *Int. J. of Energy Research* **23:4**, 277-285.
Yan, Y.Y. (1997). The effect of an electric field on heat and mass transfer for dielectric crystallization. *Trans IChemE* **75:A**, 668-671

Advances in Building Technology, Volume 2
M. Anson, J.M. Ko and E.S.S. Lam (Eds.)
© 2002 Elsevier Science Ltd. All rights reserved

Water and Energy Conservation of Rainwater Collection Systems on Building Roofs

H. X. Yang, W.H. Chow and J. Burnett

Department of Building Services Engineering,
The Hong Kong Polytechnic University, Hong Kong

ABSTRACT

In this study, an investigation on the rainwater catchment systems for domestic supply and commercial supply were conducted for Hong Kong Conditions. The focus of this study is the water and energy conservation of rainwater collection on building roofs in Hong Kong. The amount of rainwater supply mainly depends on the amount of rainfall, the collection area (i.e. normally roof area), runoff coefficient and the size of collection tank. The main parameters and their relationships have been established to estimate the amount of rainwater collected in different roof areas and different sizes of tanks based on the amount of rainfall recorded by the Hong Kong Observatory. The investigations of the supply and utilization of rainwater for different types of buildings such as residential, commercial and other developments were made. The results of the investigations such as supply, the demand of flushing, feasibility, reliability and energy saving of using rainwater supply are summarised in this paper.

KEYWORDS

Water, Energy, Conservation, Rainwater, Collection, Building, Roofs, Hong Kong

1. INTRODUCTION

Water conservation is regarded as more important than energy conservation on earth nowadays. Water

shortage occurs in a lot of areas in the world. Significant amount of fresh water in Hong Kong is supplied from Shenzhen as well. The necessity for water conservation is obvious. One of the methods which can save water as well as energy is the rainwater collection technique on building roofs. The collected rainwater can be used for different purposes, such as drinking, cooking, cleansing, irrigation, toilet flushing and heat rejection of refrigeration systems in buildings.

In Hong Kong, the Government makes use of reservoirs for collection and storage of rainwater. After sterilization and purification process, the water collected by reservoirs can be provided as fresh water to people. Nowadays, water supply from solely the collection of rainwater is insufficient compared to the increasing demand. Therefore, another water source is the water pipe transportation supply from Guangdong, which accounts for a capacity of 1,100 million cubic metres per year [1]. Beside fresh water supply, the Water Supply Department (WSD) also provides seawater for flushing toilets for about 70% of the total area in Hong Kong [2]. It means that fresh water is also used for flushing toilets in some rural areas. In this paper, a case study of rainwater collection is investigated for different types of building to find the feasibility and reliability of using rainwater for flushing toilet and other possible areas.

Energy could be saved if rainwater is used in a building as the energy use for water transportation could be reduced and energy saving for water-cooling refrigeration systems can also be achieved. Thus, the energy saving due to rainwater application is also studied in this paper.

2. THE RAINWATER COLLECTION SYSTEM IN KFBG

The new reception building of the Kadoorie Farm and Botanic Garden (KFBG) in the New Territory has been built. A number of environmental-friendly and energy saving techniques are applied in the design, such as solar energy application, rainwater collection and grass roof. Rainwater is collected on the roof of the building and is used for flushing toilet. There is no city water supply in the farm as the farm locates in the rural area of Hong Kong. Spring water is used for all the activities so that water saving is very important. The schematic diagram of the rainwater collection and flushing water supply system in KFBG is shown in Figure 1. A rainwater tank of $1m^3$ on the roof is provided to collect rainwater by the roof catchment as shown in Figure 2. A break tank is used for toilet flushing, which consists of two numbers of ball float valves, one for rainwater and another for fresh water. The ball float valve level setting for rainwater supply is higher than the ball float valve for fresh water. If the rainwater supply

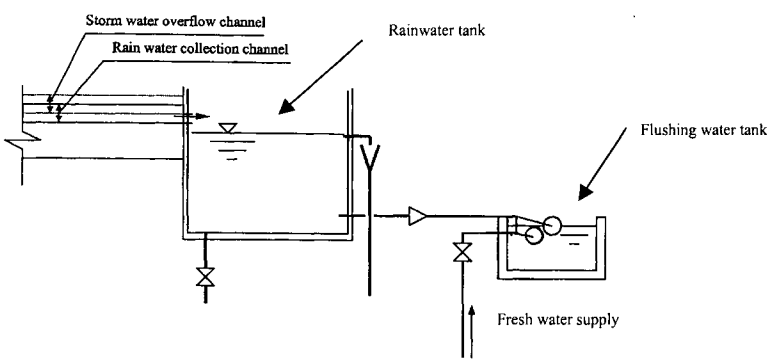


Fig.1 Schematic diagram of the rainwater collection system at KFBG

is not sufficient or the rainwater tank is empty, fresh water supply will fill up the tank for toilet flushing. If the supply of rainwater is greater than the demand of flushing, the rainwater collection tank will become full and then overflow. The excess rainwater will be drained to the traditional rainwater drainage system.



Fig.2 The rainwater collection tank on the building roof in KFBG

3. RAINWATER COLLECTION IN HONG KONG

Hong Kong is characterized as a sub-tropical weather. The mean annual rainfall is around 2215mm, which is based on the recorded data from the Hong Kong Observatory from 1961 to 1990. The wettest month is August and the driest month is January. In August, rain occurs about four days in seven days and the average monthly rainfall is 391.4mm. In January, the average monthly rainfall is only 23.4mm and rain occurs only for about six days in a month [2]. Figure 3 shows the five-day normal mean rainfall (1961 to 1990) in a year. These data can be used for calculating the potential amount of rainwater collected on building roofs.

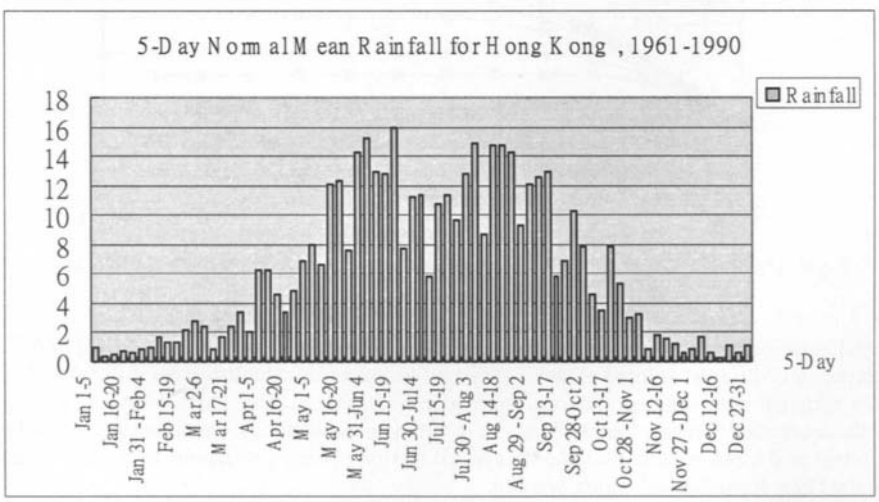


Fig.3 Five day normal mean rainfall in Hong Kong (1961-1990)

The amount of rainwater supply depends on the amount of rainfall, the collection area and the run off coefficient. Equation 1 gives the potential supply of rainwater. The runoff coefficient (Cr) is the ratio of the volume of water runs off a surface to the volume of rainfall that falls on the surface as shown in Equation 2. Due to the losses from leakage, evaporation and overflow, Cr is normally taken as 0.8 for a well-constructed roof harvesting system [4].

$$S = R \times A \times Cr \tag{1}$$

$$\text{Run off coefficient (Cr)} = \frac{\textit{Volume of runoff}}{\textit{Volume of rainwater}} \tag{2}$$

where S = Mean rainwater supply, i.e. the amount of rainwater collected, m^3;
R = Mean rainfall, (mm);
A = Collection area, m^2;
Cr = Run off coefficient.

Since the rainfall in Hong Kong varies and is not evenly distributed throughout a year, the rainwater collection tank is required to store the rainwater for daily use. If a small tank is chosen, the tank is easily fully charged and then overflows quickly during heavy rainfall. This leads to a result of water loss and decrease of catching efficiency. If the tank size is large, of course, rainwater can be collected close to or even the same as the potential rainwater supply amount. However, it will occupy a large space and also high construction cost will be involved. As a result, choosing suitable size of rainwater storage tank is very important. The amount of rainwater collected against different collection areas based on runoff coefficient 0.8 is calculated and presented in Figure 4. It shows that the maximum amount of rainwater collected is directly proportional to the collection area.

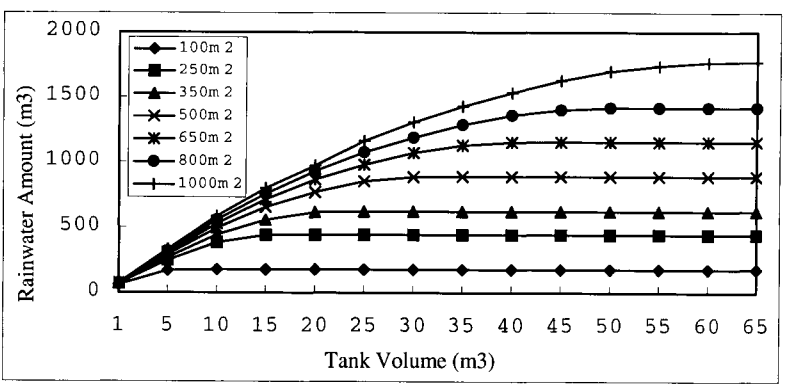


Fig.4 The amount of rainwater collected for different size of tanks and roof areas

The general equations have been established to estimate the amount of rainwater collected in different collection area and different volume of tanks. Different formulas are established for different collection areas with different conditions, which are summarized in Table 1. Those equations can be used to estimate the amount of rainwater quickly and easily with two assumptions. One is assumed that the run off coefficient is 0.8 and another one is only applied to Hong Kong's situations because the data are based on the Hong Kong historic rainfall record.

Table 1 Summary of equations to estimate the amount of rainwater

Collection Area (m^2)	General Equation	Condition
100	$Y = -51.98X^2 + 267.14X - 156.44$	$1 \leqq V \leqq 10$ and $0 \leqq Y \leqq 177.16$
250	$Y = -30.86X^2 + 279.48X - 182.34$	$1 \leqq V \leqq 20$ and $0 \leqq Y \leqq 442.90$
350	$Y = -25.47X^2 + 298.56X - 198.32$	$1 \leqq V \leqq 25$ and $0 \leqq Y \leqq 620.06$
500	$Y = -19.33X^2 + 291.10X - 204.95$	$1 \leqq V \leqq 35$ and $0 \leqq Y \leqq 885.80$
650	$Y = -15.52X^2 + 209.59X - 205.26$	$1 \leqq V \leqq 45$ and $0 \leqq Y \leqq$ 1151.54
800	$Y = -12.93X^2 + 289.71X - 202.41$	$1 \leqq V \leqq 55$ and $0 \leqq Y \leqq$ 1417.28
1000	$Y = -10.56X^2 + 288.40X - 198.30$	$1 \leqq V \leqq 65$ and $0 \leqq Y \leqq$ 1771.60

where : Y = Amount of rainwater (m^3), V = Volume of collection tank (m^3)

($V = 5(X-1)$ for X=2, V = 1 when X=1 and V=5 for X=2)

4. RAINWATER CONSUMPTION

The supply of the rainwater collected on different roof areas with different sizes of tanks for several locations were investigated for three major categories: residential high-rise buildings, commercial buildings, industrial buildings and small houses. According to the Plumbing Engineering Services Design Guide[7, the demands of flushing for different buildings were investigated and summarized in Table 2. It is found that the supply of rainwater is insufficient for toilet flushing demand especially for residential high rise buildings. Most of them have only less than 10% of demand. The insufficient rainwater supply is due to the limited roof area. It is also not practicable to use large collection tank such as $65m^3$ tank to collect more water due to the space consumption, increase of structure loading and cost. Therefore, suitable and reasonable sizes of collection tank should be selected.

The reliability for commercial and small houses is much better than that of residential high-rise buildings. The rainwater supply and consumption is illustrated in Figure 5 for commercial buildings. The reliability of supply for commercial, small house and other places are listed in Table 3.

5. COST ANALYSIS

According to the information from WSD, the cost for supplying fresh water is around HK\$8/m^3 including the purchasing cost from Guangdong, operation, maintenance (O&M) and administration costs. The cost for supplying seawater is around HK\$1.68/m^3. The annual saving for using rainwater supply is shown in Table 3. The figures in brackets in table 3 show the costs or savings when the fresh water charge is \$4.58/ m^3. The government subsides users for fresh water and seawater supply (the sea water supply for toilet flushing is free of charge). Therefore, the end users pay less than the real cost.

The payback is also estimated s shown in the table. Due to the amount of saving was not significant, longer payback period was found. The construction cost is much greater than the cost of water saved due to the limited roof area.

Table 2 Summary of investigations

A) High-rise residential buildings

Estate	Tse Man Est. Phase 2	Un Chau Estate Phase 3	New Kwai Fong Gardens	Kwai Chung Plaza
Roof area (m^2)	674	1019	410	506
No. of flat / floor	10	20	8	8
No. of storey	40	40	31	27
Collection tank volume (m^3)	45	65	25	30
Rainwater supply annually (m^3)	1194	1805	725	893
Flushing demand annually (m^3)	17885	36792	9505	8278
% of demand	6.7	4.9	7.6	10.8
Cost of fresh water (HK$)	9,552 / (5,469)	14,440 / (8,267)	5,800 / (3,321)	7,144 / (4,090)
Cost of sea water (HK$)	2,006	3,232	1,218	1,500
Energy saving for transportation of fresh water (kWh)	478	722	290	357
Energy saving for transportation of sea water (kWh)	506	794	319	393
Construction Cost (HK$)	110,000	155,000	62,700	72,600
Pay back period (Years)	12 / (20)	11 / (19)	11 / (19)	10 / (18)

B) Commercial and industrial buildings

Location	Redevelopment of Park Theatre	Office Tower I, Metropolis	Comweb Plaza	Lee Hang Industrial Bldg.
Roof area (m^2)	417	1587	480	1152
No. of storey	20	15	25	11
No. of flushing point	107	165	122	154
Collection tank volume (m^3)	25	65	25	65
Rainwater supply annually (m^3)	736	2464	826	2016
Flushing demand annually (m^3)	2643	6160	3204	7726
% of demand	27.9	40	25.8	26
Cost of fresh water (HK$)	5,888 / (3,371)	19,712 / (11,285)	6,608 / (3,783)	16,128 / (9,233)
Cost of sea water (HK$)	1,236	4,140	1,388	3,387
Energy saving for transportation of fresh water (kWh)	294	986	330	806
Energy saving for transportation of sea water (kWh)	324	1084	363	887
Construction Cost (HK$)	52,800	155,000	62,700	155,000
Pay back period (Years)	9 / (16)	8 / (14)	10 / (17)	10 / (17)

C) Small houses, apartments & others

Location	Small House at rural area	House at Mount David's Road	Custom Examination Facilities Bldg.	New reception building of Kardoorie Farm
Roof area (m^2)	70	177	1424	192
No. of storey	3	3	2	1
Collection tank volume (m^3)	2	10	65	1
Rainwater supply annually (m^3)	87	310	2332	66
Flushing demand annually (m^3)	102	128	2664	35
% of demand	85	85	87.5	95.9
Cost of fresh water (HK$)	696 / (398)	2,480 / (1,420)	18,656 / (10,681)	528 / (302)
Cost of sea water (HK$)	146	521	3917	NIL
Energy saving for transportation of fresh water (kWh)	35	124	933	26
Energy saving for transportation of sea water (kWh)	38	136	1026	NIL
Construction Cost (HK$)	7,500	30,000	155,000	4800
Pay back period (Years)	11 / (19)	12 / (21)	9 / (15)	9 / (16)

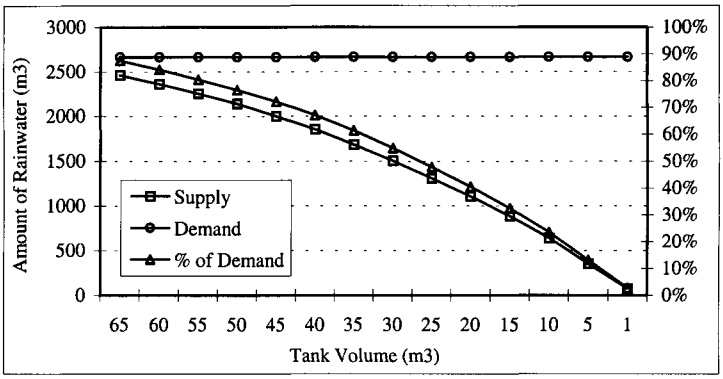


Fig.5 Rainwater supply and demand for a commercial building

Table 3 Reliability of rainwater supply for different sizes of collection tanks

Tank Volume (m^3)	Un Chau Estate Phase 2		Office Tower I, Metropolis		Custom Examination Facilities Building, Tsing Yi	
	Rainwater Supply (m^3)	% of Flushing Demand	Rainwater Supply (m^3)	% of Flushing Demand	Rainwater Supply (m^3)	% of Flushing Demand
65	1805	4.9	2464	40.0	2332	87.5
60	1797	4.9	2363	38.4	2243	84.2
55	1766	4.8	2253	36.6	2144	80.5
50	1720	4.7	2137	34.7	2036	76.4
45	1644	4.5	2000	32.5	1921	72.1
40	1548	4.2	1851	30.0	1784	67.0
35	1440	3.9	1682	27.3	1632	61.3
30	1315	3.6	1503	24.4	1460	54.8
25	1166	3.2	1310	21.3	1275	47.9
20	992	2.7	1108	18.0	1080	40.5
15	800	2.2	886	14.4	865	32.5
10	586	1.6	640	10.4	628	23.6
5	333	0.9	352	5.7	348	13.1
1	73	0.2	73	1.2	73	2.7

6. ENERGY CONSERVATION

Energy can also be saved from rain water collection as shown in Table 3. If rainwater is used for irrigation or cleansing, the same amount of fresh water must be saved. According to the information given by the Water Services Department of the HKSAR, the energy consumption for treatment and transportation of fresh water is 0.4 kWh/m^3. On the other hand, if the collected rainwater is used for flushing purpose and the energy consumption for treatment and pumping sea water for flushing is 0.44 kWh/m^3, the annual energy saved for treatment and transportation of water for different purposes were presented in Table 3. The energy saving was only for treatment and transportation of the water from source to users.

7. CONCLUSIONS

The supply and demand of using collected rainwater for toilet flushing were investigated for different

type of buildings in Hong Kong. It was found that the collected rainwater is insufficient for the demand of toilet flushing for the high rise buildings. The supply might only cover 10% of the demand because the rainwater catching area (i.e. roof area) is limited for high-rise residential buildings. For commercial buildings of fifteen to twenty-five storeys, the reliability of supply was found better than the high rise domestic buildings. It is because the supply increases and the demand decreases compared with high rise domestic buildings. However, the reliability of rainwater supply for small houses or buildings with large floor areas is very good.

Although using larger rainwater collection tank can collect much water, it would not be practicable as it will occupy more space and increase structure loading and construction cost. The flushing or irrigation system in a building cannot just rely on rainwater, but also on fresh water supply as well.

REFERENCES

[1] Water supply data of Hong Kong, Water Supplies Department, The Hong Kong SAR Government.

[2] Data of Meteorological Observations in Hong Kong, Hong Kong Observatory, The Hong Kong SAR Government.

[3] Gould John, Rainwater catchment systems for domestic supply, Design, construction and implementation, pp3-32,45-60

[4] Texas water development board in cooperation with the center for maximum potential building systems - Texas guide to rainwater harvesting

[5] Lanka rainwater harvesting forum - Household water security in Sri Lanka Using Domestic roof water harvesting

[6] Lanka rainwater harvesting forum - Current rural water security practices with domestic roof water harvesting

[7] FAKT :1999 - Domestic rainwater harvesting: Perception of water professionals, The Institute of Plumbing – Plumbing Engineering Sevices Design Guide

[8] HKBEAM 3/99, An Environmental Assessment Method for New Residential Buildings. CET 1999

Advances in Building Technology, Volume 2
M. Anson, J.M. Ko and E.S.S. Lam (Eds.)
© 2002 Elsevier Science Ltd. All rights reserved

THE INFLUENCE OF ENVELOPE CHARACTERISTICS TO THE ENERGY BEHAVIOUR OF HIGH-RISE RESIDENTIAL BUILDINGS

Yik, F., Bojic, M., Wan, K.

Research Centre for Building Environmental Performance, Department of Building Services Engineering, The Hong Kong Polytechnic University, Hung Hom, Kowloon, Hong Kong SAR, China

ABSTRACT

This paper presents the results of several studies on the influence of different envelope characteristics to the energy behaviour of flats in high-rise residential buildings in Hong Kong. These studies investigated into the effects of various conventional façade treatments, including variations in the wall thickness, the window-to-wall area ratio and the shading coefficient of window glass, and the provision of shading devices, such as overhang and side-fins. In addition, the effects of applying thermal insulation at different positions within walls, partitions and doors, and of insulated walls and doors in different parts of the building fabric were investigated. The impacts of these factors on the yearly cooling load were evaluated using the software HTB2, which is a detailed building heat transfer model. These studies showed that the use of glazing of better performance would be the most effective in reducing the yearly cooling load in a residential building, by up to 13%, and applying thermal insulation could lead to a reduction in this load by up to 10%. Key considerations to be given in determining where to put insulation are described and areas for further investigations are outlined.

KEYWORDS: High-rise residential, Envelope design, Thermal insulation, Annual cooling load, Simulations

INTRODUCTION

The residential sector is responsible for about a quarter of the annual electricity use in Hong Kong, which is equivalent to about one-sixth of the total primary energy requirement of the city. To cope with the projected housing demand, tens of thousands of new public and private residential units are produced each year (HKHA, 1995). This will further increase the electricity use of the residential sector, and the associated green house gas emissions, in the coming years. It is therefore important to also target for a higher level of building energy performance while attempting to realise the quantity target.

Energy use in high-rise commercial buildings in Hong Kong has been actively researched into (Chau et al, 2000), but much less so for residential buildings. In the past, the majority of residential flats were not equipped with air-conditioners but the situation is now reversed – air-conditioning has become the

dominant energy end-use in residential buildings and the major cause for the rapid rise in electricity consumption of the residential sector in the past decade. Therefore, more active research studies into means for enhancing the energy performance of residential building design is needed. Simulation predictions showed that the annual cooling requirement in residential buildings, which is proportional to the electricity consumption, is dominated by the heat gains through the building envelope (Yik et al, 2000). Careful consideration should, therefore, be given to the energy performance of the building envelope in designing energy efficient residential buildings.

This paper presents the results of several simulation studies on high-rise residential buildings in Hong Kong that were undertaken at the Hong Kong Polytechnic University. These studies investigated into the influence to the space cooling load when the building envelope was incorporated with different characteristics. The studied characteristics include a range of conventional façade treatments and the less conventional method of applying thermal insulation to walls and doors in buildings in subtropical climate.

THE SIMULATION SOFTWARE HTB2

The simulation tool used in the study was HTB2, which is a dynamic building energy model that can predict the heating and cooling loads and the environmental conditions in a building. In HTB2, the dynamic heat conduction through the building envelope is modelled using an explicit finite difference numerical scheme (Lomas et al, 1997; Jones & Alexander 1999). HTB2 can model dynamic heat transfer through multi-layered walls, roofs and partitions and through glazing taking into account variations in the solar transmittance and absorptance with different solar incident angles. The model can predict the thermal performance of a building when it is subject to the influence of outdoor temperature, solar gain, shading, and ventilation and infiltration. It also allows the user to define complex cooling and heating schedules, occupancy, lighting and internal load intensity patterns, and to vary control settings during run-time, to mimic realistic occupation conditions.

THE MODEL BUILDING

Figure 1 shows the layout of an intermediate floor in a typical high-rise residential building in Hong Kong, which comprises eight apartments per storey. Unlike commercial buildings, few residential buildings are equipped with central air-conditioning systems. In residential buildings, window-type and split-type air-conditioners are widely used. Within a residential apartment, air-conditioners would be provided for some rooms, such as living rooms and bedrooms, but some other rooms, such as bathrooms and kitchens, would not be equipped with air-conditioners. The common lobby on each floor is also not air-conditioned. Survey studies showed that the operation pattern of air-conditioners in residential buildings would basically follow the occupation pattern of the rooms (Lam, 1993; Leung, 2002). Air-conditioners serving living and dining rooms would be turned on most often in the evenings, sometimes during daytime as well, but would be switched off at night. Those serving bedrooms, however, would be run starting from late evening till early in the morning in the next day.

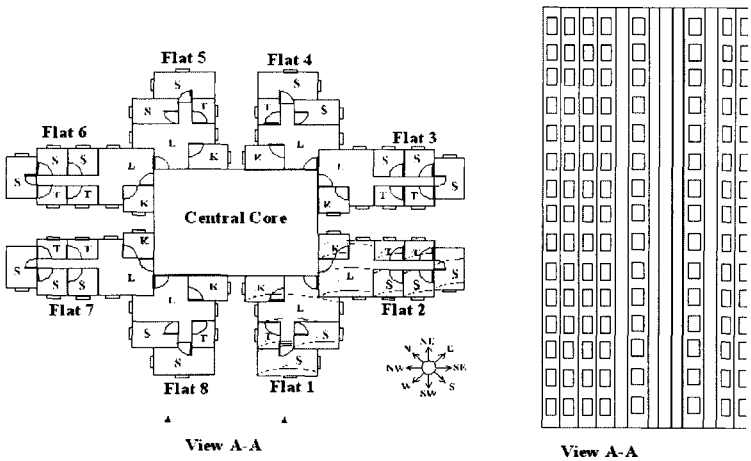


Figure 1: Floor plan and elevation of the model residential building

CONVENTIONAL FAÇADE TREATMENTS

Some of the results obtained from studies on the effects of varying individual features of the building envelope design are summarised below. In these studies, the model building was assumed to comprise 40 storeys of residential flats with a floor layout as shown in Figure 1.

Table 1 summarises the values of the parameters assigned to the envelope design of the model building that were chosen as the reference case (Case 0), and the value of the parameter varied in each of the additional cases studied (Cases 1 to 6). The parameters varied include the wall thickness (Case 1); the window-to-wall area ratio (Case 2); the shading coefficient of window glass (Case 3); inclusion of an overhang at each window (Case 4); and inclusion of a side-fin at the left-hand side (Case 5) and the right-hand side (Case 6) of each window. The side-fin dimensions were denoted by the parameter called external shading multiplier, which was calculated according to the standard method defined in the Handbook for overall thermal transfer value (OTTV) calculations (Building Authority, 1995).

TABLE 1
BUILDING FAÇADE FEATURES VARIED IN THE PARAMETRIC STUDY (IN BOLD FACE)

Case	0	1	2	3	4	5	6
Wall thickness (mm)	100	**300**	100	100	100	100	100
Window to wall area ratio	0.65	0.65	**0.25**	0.65	0.65	0.65	0.65
Shading coefficient of window glass	0.95	0.95	0.95	**0.25**	0.95	0.95	0.95
Shading (external shading multiplier)	0	0	0	0	**OH 0.5**	**LF 0.5**	**RF 0.5**

Notes: OH 0.5 denotes overhang with an external shading multiplier of 0.5; LF 0.5 denotes side-fin at the left-hand side with an external shading multiplier of 0.5; and RF 0.5 denotes side-fin at the right-hand side with an external shading multiplier of 0.5.

Figure 2 shows a comparison of the annual cooling loads of the building pertaining to the cases studied. As can be seem from this figure, replacing clear glass with a shading coefficient of 0.95 by reflective glass with a shading coefficient of 0.25 (Case 3) would result in a rather significant

reduction in the annual cooling load of the residential building, by 13%. Each of the other features studied would contribute to a reduction in the annual cooling load by several percent.

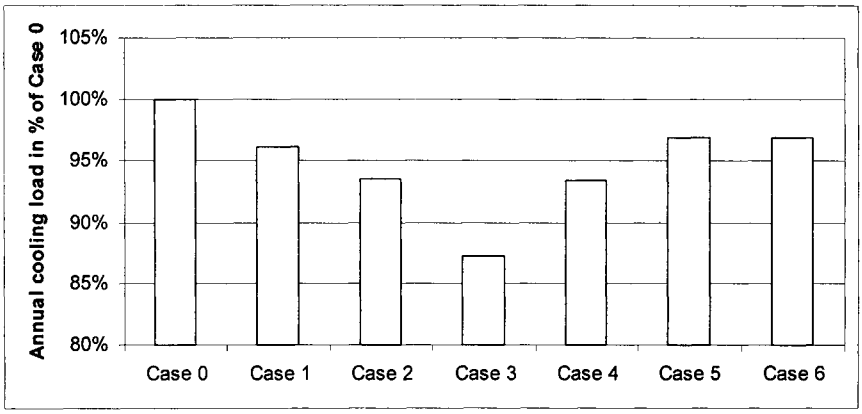


Figure 2: Comparison of the effect on the annual cooling load of the residential block due to different façade treatments (refer to Table 1 for details of the Cases shown)

THERMAL INSULATION

At present walls and doors in residential buildings in Hong Kong are not thermally insulated at all. Studies have been performed to investigate if providing thermal insulation to the building fabric would be effective in improving the energy performance of residential building designs. In these studies, the flats, as shown in Figure 1, with their original construction design were taken as the base-case model. Modifications to the base-case model were then made on the walls and doors, which included inserting a layer of thermal insulation into different locations within the walls, and applying these modified walls to different parts of the fabric.

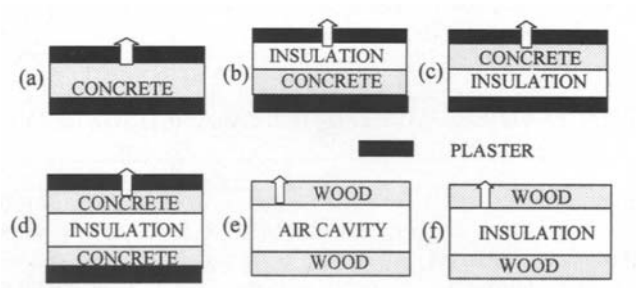


Figure 3: Thermal insulation position in a wall and a door: (a) wall without thermal insulation; (b) wall with thermal insulation at the outer side; (c) wall with thermal insulation at the inner side; (d) wall with thermal insulation in the middle; (e) door without thermal insulation; and (f) door with thermal insulation. The arrows designate the outside face of slabs

Since the layout of each pair of apartments is simply a mirror image of the other pairs of apartments on the same floor (Figure 1), the simulation study was based on the layout of Flats 1 and 2 only. The

thermal insulation material for the walls was assumed to be polystyrene (thermal conductivity, k, = 0.034W/Km) and the study investigated into having this insulation layer inserted into three different locations in a wall slab, as shown in Figure 3. The thermal insulation material for the doors was assumed to be mineral wool (k = 0.053W/Km), which would form the middle layer in a door (Figure 3).

The effects of applying thermal insulation to different combinations of the walls and doors enclosing the two flats were also studied. Figure 4 shows four cases of walls and doors arrangements: F, W, L, and B. In the F arrangement, the thermal insulation layer was inserted at the outer side of the walls, and all the external walls as well as the walls and the main entrance doors that separate the flats from the common lobby were insulated. In the W arrangement, all walls between air-conditioned rooms and non-air-conditions rooms were insulated. In the L arrangement, the walls circumscribing the living room and the connected corridors were insulated. In the B arrangement, only walls enclosing the bedrooms were applied with thermal insulation.

Details about the study on the influence of the arrangement of the thermally insulated walls and doors on the space cooling load in the two modelled residential units have been reported in Bojic et al (2002c). In that study, the walls were applied with a 50mm thick thermal insulation, at the outer side of the concrete layer, and a range of thickness of the concrete layer in the walls, up to 400mm, was covered. The thickness of the thermal insulation layer applied to the modified doors was 38mm. The yearly cooling load (Q) of the two flats, when incorporated with the base-case design and when having the building fabric design modified according to each of the four wall and door arrangements F, W, L & B (Figure 4), and with different combinations of the thickness of the concrete layer in the walls, were predicted using HTB2.

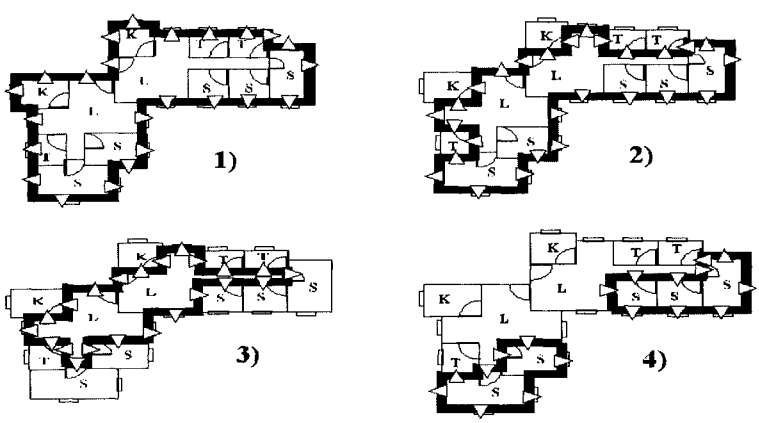


Figure 4: Walls and doors arrangements: 1) F, 2) W, 3) L, and 4) B. Here, S denotes a bedroom, L a living and dining room, K a kitchen, and T a toilet. The tip of each arrow indicates the side of concrete where the insulation layer was placed.

Figure 5 shows one set of the results, including the difference between the yearly cooling loads of the modified cases from that for the base-base. The simulation predictions indicated that the optimal insulation arrangement would be to apply insulation only to those walls circumscribing the living room and the connected corridors (arrangement L). A reduction in the yearly cooling load of the two flats by up to 8% could be achieved for this arrangement.

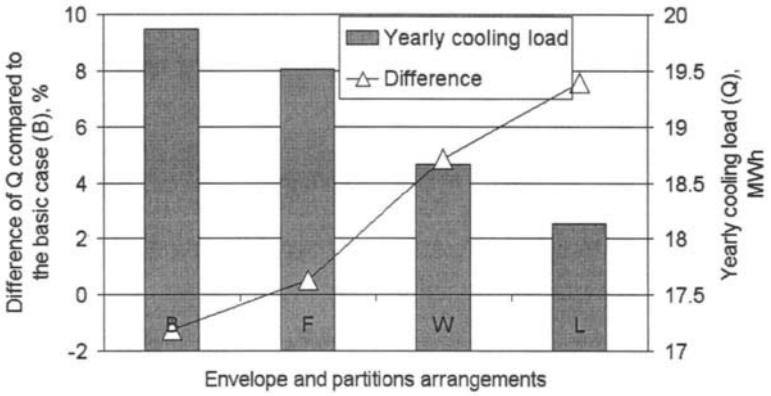


Figure 5: Yearly cooling load and cooling load difference as functions of the arrangement of thermally insulated walls and doors. Difference of cooling load is compared to that of the basic case. Here, modified walls have 50mm of thermal insulation, and 400mm of concrete.

The effect of varying the location of the insulation layer within the wall has been studied based on arrangement F (Bojic et al, 2001; 2002a). In that study, the thermal insulation layer, up to 150mm thick, was placed either at the inner side, or at the outer side, or at the middle of the walls (Figure 3). The thickness of the concrete layer covered in the study was up to 400mm. Some of the simulation results are shown in Figure 6, which shows the variation in the yearly cooling load (Q) with the thickness and position of the thermal insulation layer for Flat 1, when its windows were facing southeast. It can be seen that inserting the thermal insulation layer at the outer side and in the middle could lead to an increase in the cooling load; the location of the insulation layer in the walls of this flat should, therefore, be at the inner side of the concrete layer in order that a reduction in the cooling load could be achieved. Other results obtained in the study showed that placing the insulation layer at the outer and middle positions could still lead to a reduction in the cooling load if the windows were oriented toward a different direction, but still less significant than placing the insulation at the inner surface. Moreover, further increasing the insulation layer thickness beyond 50mm would lead to virtually intangible incremental effects, which was a general observation among the cases studied. A reduction in the yearly cooling load by up to 7% could be achieved when the 50mm thick thermal insulation layer was inserted at the inner side of the concrete layer.

Other observations made from the simulation study results include:

- For a residential building in hot climate regions, which is air-conditioned primarily in the evening and in the night-time, adding thermal insulation and thermal mass to external walls could lead to counteracting effects. Adding thermal mass would increase the heat storage in the fabric leading to an increased cooling load in the evening. The cooling load could be reduced by also increasing the thermal insulation to reduce the heat transfers into the walls through the outdoor surface, which would be effective when the thickness of the wall is around 250mm. However, increasing the thermal insulation of a thin wall would reduce the rate that the stored heat could be dissipated back to the outdoor, leading to an increase in the cooling load.
- The best strategy of providing thermal insulation in the building fabric of residential buildings would be to insulate the partitions so as to minimise heat transfer from non-air-conditioned spaces into the living room, which would be cooled in the evening, as for arrangement L

(Figure 4). However, for bedrooms, which would be cooled in the late evening and overnight, adding insulation, as for arrangement B (Figure 4) would lead to the opposite effect.

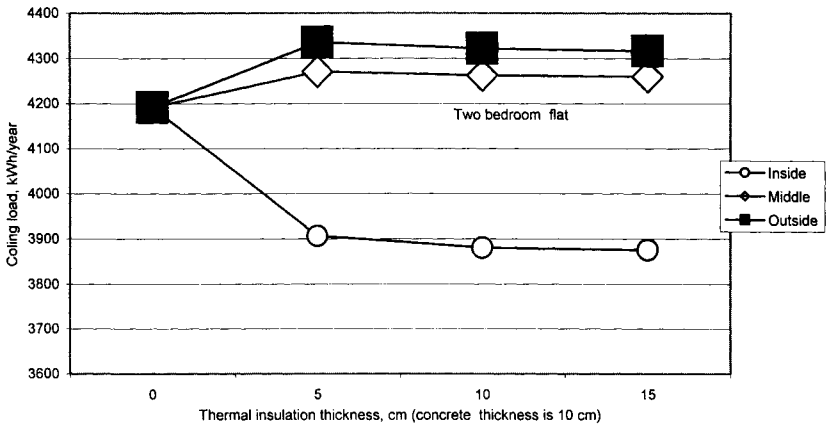


Figure 6: Cooling Load as a function of the thermal insulation thickness and the position of thermal insulation inside the F-walls (thickness of concrete is 100mm).

CONCLUSION

In this paper, a summary is given of the findings of several investigations performed on the thermal performance of the envelope design of high-rise residential buildings in Hong Kong when the building envelope was incorporated with different characteristics. These investigations were based on the yearly cooling load predicted using the detailed building heat transfer simulation program HTB2.

The results presented include the effects of several conventional treatments at the façade for improving the energy performance of the envelope of a residential building, including increasing the wall thickness, reducing the window-to-wall area ratio, reducing the shading coefficient of the window glass and inclusion of overhangs and side-fins at windows. Simulation predictions showed that the use of a glazing type of better thermal performance would be effective in reducing the yearly cooling load in the air-conditioned spaces. Other treatments at the façade could each yield a reduction in the yearly cooling load by several percent.

The simulation studies on the effects of applying thermal insulation to the building fabric elements showed that the insulation layer to be applied would lead to a significant effect up to thickness of 50mm, but further increasing its thickness would lead to intangible incremental benefit. Among the results for the investigated scenarios of applying thermal insulation to different elements of the building fabric, the maximum reduction in the yearly cooling load was found to be about 8%. The best strategy of applying thermal insulation would be to insulate those partitions between spaces that would be air-conditioned in different periods and between air-conditioned and non-air-conditioned spaces. Inserting the insulation layer at the inner surface of the concrete layer would, in general, lead to beneficial results. Inserting the layer at other positions, e.g. the inner side or at the middle of the wall could lead to the opposite effect depending on the exposure direction of windows and external walls in the flat.

As the yearly cooling load of a flat would be proportional to the annual electricity use for air-conditioning the flat, a reduction in the yearly cooling load means a reduction in the electricity consumption of a similar order, which will be accompanied also by a reduction in the primary energy consumption and in environmental impact.

Further studies should be made into how the building envelope design could be optimised, taking into account of the trade offs among cooling energy use, lighting energy use, availability of daylight and natural ventilation, and economic viability of the improvement measures.

ACKNOWLEDGEMENTS

The work was undertaken within the Research Centre for Building Environmental Performance, Department of Building Services Engineering. The authors wish to acknowledge the financial support provided by The Hong Kong Polytechnic University under the Area of Strategic Development in the Faculty of Construction and Land Use.

REFERENCES

Bojic, M., Yik, F., Sat, P. (2001). Influence of Thermal Insulation Position in Building Envelope on the Space Cooling of High-Rise Residential Buildings in Hong Kong. *Energy and Buildings* **33:6,** 569-581.

Bojic, M., Yik, F., Leung, W. (2002a). Thermal Insulation of Cooled Space in High-Rise Residential Buildings in Hong Kong. *Energy Conversion and Management* **43:2** 165-183.

Bojic, M., Yik, F., Sat, P. (2002b). Energy Performance of Windows in High-Rise Residential Buildings in Hong Kong. *Energy and Buildings* **34:1,** 71-82.

Bojic, M., Yik, F., Wan, K., Burnett, J. (2002c). Influence of Envelope and Partition Characteristics on the Space Cooling of High-Rise Residential Buildings in Hong Kong. *Building and Environment* **37:4,** 347-355.

Building Authority (1995). *Code of practice for overall thermal transfer value in buildings*, Building Authority, Hong Kong.

Chau, C.K., Burnet, J., Lee, W.L. (2000). Assessing the Cost Effectiveness of an Environmental Assessment Scheme. *Building and Environment* **35,** 307-320.

HKHA (1995). *Housing Millions*, Community Relations Section, Hong Kong Housing authority, Hong Kong.

Jones, P. J., Alexander, D. (1999). Modelling building performance, Proceedings of The 3rd International Symposium on Heating, Ventilation and Air Conditioning, Shenzhen, China, 237-244.

Lam, J.C. (1993). A survey of electricity consumption and user behaviour in some government staff quarters. *Building Research and Information,* Vol. 21, No. 2, pp.109–116.

Leung, W.W.H. (2002). *Trade-off between temperature and air-movement for reducing air-conditioning energy use in residential buildings in Hong Kong*, MPhil Thesis, Department of Building Services Engineering, The Hong Kong Polytechnic University (Submitted for examination).

Lomas, K.J., Eppel, H., Martin, C.J., Bloomfield, D.P., (1997). Empirical validation of building energy simulation programs, Energy and Building, 26, 253-273.

Yik, F.W.H., Wan, K.S.Y., Burnett, J. (2000). Assessment of envelop energy performance in HK-BEAM for residential buildings, *Transactions*, Vol.7 No.2, p.49-55, The Hong Kong Institution of Engineers.

Advances in Building Technology, Volume 2
M. Anson, J.M. Ko and E.S.S. Lam (Eds.)
© 2002 Elsevier Science Ltd. All rights reserved

TOTAL OPTIMAL OPERATION FOR HVAC SYSTEM WITH HEAT SOURCE AND DISTRIBUTION SYSTEM

Yoshida Harunori[1], Iguchi Yuuya[2], Matsuoka Ippei[1] and Wang Fulin[1]

[1]Department of Global Environment Engineering, Kyoto University,
Yoshida Honmachi, Sakyo-ku, Kyoto 606-8501, Japan.
[2]Nikken Sekkei, Inc, 2-1-3 Koraku, Bunkyo-ku, Tokyo 112-8565, Japan.

ABSTRACT

Operation of building systems after occupancy is getting to be recognized as a key issue for substantial reduction of energy use and CO_2 emission. Especially optimal operation of HVAC systems is very important because of their large energy consumption. Many methodologies for the purpose have been proposed, however most of the reported results are based on the simulation with the assumption that the performance of each component and subsystem is known or prescribed. In this paper an optimal operation scheme of HVAC systems for existing buildings is proposed and the test results of applying the scheme in a real office building are shown and investigated. The scheme is divided into two steps: the first is to identify the parameters of the mathematical model of each component such as a fan, a pump and a heat pump, and the second is to optimize total energy consumption of HVAC system operation. Mathematically the second step is a non-linear optimization process which is to be embedded into a BEM system.

KEYWORD

Optimization, Identification, Simulation, HVAC, BEM system, Energy saving, Methodology test.

MODEL IDENTIFICATION

Operation of building systems is increasingly to be recognized as a key issue for substantial reduction of energy

use and CO_2 emission, especially the operation of HVAC systems because of their large energy consumption. So it is important to determine proper HVAC systems' models to optimize the operation. We would suggest the way to get good models using real operation data of system components, which we give the name of 'model identification'. Figure 1 shows a HVAC system. This system has energy storage, one heat pump unit, one secondary pump, and four air handling units which have two fans (but energy storage and four constant speed fans in air handling unit are not considered in optimization). The following parts of this paper will discuss how to identify the models of these equipments.

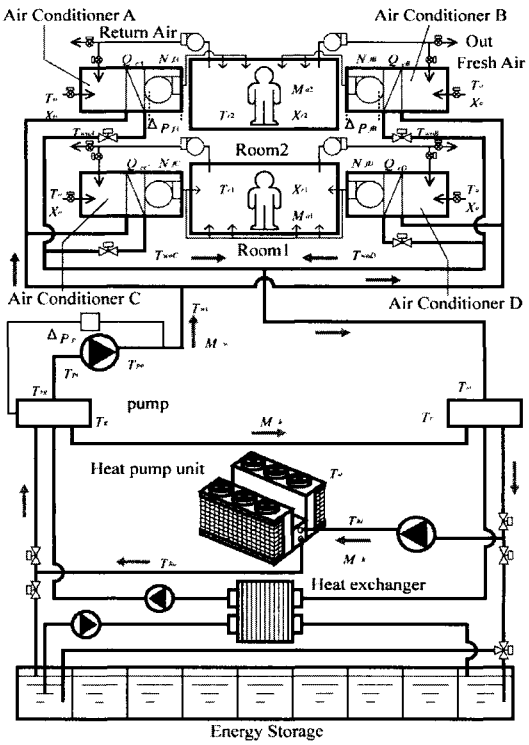


Figure 1 : HVAC system assumed in the research

Secondary Pump and Fan in AHU

Pump and fan model is composed of following equations.

$$C_f = \frac{M}{\rho N D^3} \tag{1}$$

$$C_h = \frac{1000 \times \Delta P}{\rho N^2 D^2} \tag{2}$$

$$C_h = a_0 + a_1 C_f + a_2 C_f^{\,2} + a_3 C_f^{\,3} + a_4 C_f^{\,4} \tag{3}$$

$$\eta = b_0 + b_1 C_f + b_2 C_f^{\,2} + b_3 C_f^{\,3} + b_4 C_f^{\,4} \tag{4}$$

$$E = \frac{M \Delta P}{\eta \rho} \tag{5}$$

C_f :dimensionless coefficient of water or air flow rate, C_h :dimensionless coefficient of pressure difference, D :equivalent diameter, M :water or air flow rate, ρ :water or air density, N :revolution speed, ΔP :pressure difference, E :electric energy consumption, η :efficiency of a pump or fan. Model identification of pump and fan are to decide the values of parameters a_i and b_i in equation (3) and (4) using Least Square Approximation method. First, these parameters were decided according to specification data supplied by the manufacture. Second, water or air flow rate , pressure difference ΔP , revolution speed , and electric energy consumption were to be measured, then parameters were corrected to minimize the difference between measured data and simulation data. Electric energy consumption of pump and fan of measured data and simulation data are shown in TABLE 1 and 2. The ratios of error of mean square to designed energy consumption are shown, too.

TABLE 1
ELECTRIC ENERGY CONSUMPTION OF SECONDARY SUPPLY PUMP

	mean of electric energy consumption[kW]	error of mean square of electric energy consumption[kW^2]
measured data	0.90	-
simulation data before corrected	1.15	0.484 (22.0%)
simulation data after corrected	0.96	0.264 (12.0%)

TABLE 2
ELECTRIC ENERGY CONSUMPTION OF SUPPLY AND RETURN FAN

	mean of electric energy consumption [kW]	error of mean square of electric energy consumption [kW^2]		mean of electric energy consumption [kW]	error of mean square of electric energy consumption [kW^2]
measured data of supply / return fan A	0.96 / 0.55	-	measured data of supply / return fan B	1.34 / 0.67	-
simulation data of supply / return fan A before corrected	0.53 / 0.19	0.488(22.2%) / 0.393(26.2%)	simulation data of supply / return fan B before corrected	0.85 / 0.30	0.521(23.7%) / 0.377(25.2%)
simulation data of supply / return fan A after corrected	0.96 / 0.55	0.148(6.74%) / 0.066(4.38%)	simulation data of supply / return fan B after corrected	1.34 / 0.67	0.087(3.95%) / 0.035(2.34%)

Heat Pump

Heat pump model is composed of the following equations.

$$\frac{Q_h'}{Q_{hd}} = \left(e_0 + e_1 T_{hi} + e_2 T_{hi}^2\right)\left(e_3 + e_4 T_o + e_5 T_o^2\right) + e_6 \tag{6}$$

$$\frac{E_h'}{E_{hd}} = \left(g_0 + g_1 T_{hi} + g_2 T_{hi}^2\right)\left(g_3 + g_4 T_o + g_5 T_o^2\right) + g_6 \tag{7}$$

$$r_q = \frac{Q_h}{Q_h'} \tag{8}$$

$$E_h = r_e \cdot E_h' \tag{9}$$

$$T_{ho} = T_{hi} - \frac{Q_h}{M_h c_w} \tag{10}$$

M_h :water flow rate in heat pump cycle, Q_h :cooling load, Q_{hd} :rated value of cooling capacity, T_{hi} :inlet water temperature, T_{ho} :outlet water temperature, T_o :outdoor air temperature, E_{hd} :rated value of electric energy consumption, and c_w :water specific heat capacity, Q_h' :the maximum cooling capacity, E_h' :the maximum energy consumption, r_q :a rate of partial load, r_e :a rate of real electric energy consumption, and r_q :supposed to be equal to r_e .

Heat pump model identification is to decide parameters e_i , g_i in equation (6) and (7). Basically, the method of identification is same as pump and fan. Errors between before and after models corrected are shown in TABLE 3. Rated value of cooling capacity Q_{hd} and rated value of electric energy consumption E_{hd} are constant. Where outdoor temperature T_o and cooling load Q_h are measured by the BEM system and known.

TABLE 3
ELCTRIC ENERGY CONSUMPTION OF HEAT PUMP

	mean of electric energy consumption[kW]	error of mean square of electric energy consumption[kW^2]
measured data	20.8	-
simulation data before corrected	22.0	1.64(5.7%)
simulation data after corrected	20.8	1.08(3.8%)

Cooling Coil

Cooling coil model is composed of the following equations.

$$Q_c = Q_d + Q_w \tag{11}$$

$$Q_d = U_d A_d T_{md} \tag{12}$$

$$Q_w = U_w A_w h_{mw} \tag{13}$$

$$\frac{1}{U_d A_d} = K_{od} + K_{td} + K_{id} + \frac{F}{A_{id}} \tag{14}$$

$$\frac{1}{U_w A_w} = K_{ow} + K_{tw} + K_{iw} + \frac{F}{A_{iw}} \tag{15}$$

$$T_{wo} = f_{two}(X_{ai}, M_w, T_{wi}, T_{ai}, M_a) \tag{16}$$

Equation (16) is refered to coil model in the paper, reference 3).

Q_i :cooling load, U_i :total heat transfer rate, A_i :surface area of coil, K_{od}, K_{ow}, K_{td}, K_{tw}, K_{id}, K_{iw} :terms related to heat transfer, X_{ai} :inlet air humidity ratio, M_a :outlet air flow rate, M_w :water flow rate through coil,

T_{ai} :inlet air dry bulb temperature, T_{wi} :inlet water temperature.

Coil model identification is to decide a coefficient F which is dirty ratio of coil in equation (14) and (15). The method of identification of coil is same as other equipments. Then a numerical subscript d means dry part, w means wet part. Errors between before and after cooling coil models corrected are shown in TABLE 4.

TABLE 4

LOAD OF COOLING COIL

	cooling load[kW]		cooling load[kW]
AHU A before corrected	1.72(5.47%)	AHU C before corrected	4.07(12.1%)
AHU A after corrected	1.48(4.72%)	AHU C after corrected	1.13(3.34%)
AHU B before corrected	1.84(5.87%)	AHU D before corrected	4.15(12.3%)
AHU B after corrected	1.18(3.75%)	AHU D after corrected	1.59(4.73%)

TOTAL OPTIMAL OPERATION

In Total Optimal Operation, optimal set points, which are water flow rate of secondary pump, air flow rate of supply fan in AHU, and outlet water temperature from heat pump are determined by solving an optimal problem of which the objective function is energy consumption of whole HVAC system shown as follows.

$$E = E_f + E_p + E_h \tag{17}$$

E:total energy consumption, E_f:consumption of fan, E_p:consumption of pump, E_h:consumption of heat pump unit. E_f:the function of supply air flow rate M_a, E_p is of M_w, and E_h is of M_a, M_w, and T_{sg}. T_{sg} is secondary supply water temprature, and is assumed to be equal to T_{ho}. Therefore E is the function of M_a, M_w, and T_{sg}. There are following four conditions and constraints in the optimization.

1) To satisfy cooling demand.
2) HVAC system operation is proper.
3) HVAC system operation and loads are at a steady state.
4) There is no heat loss from pipes and ducts.

Applying Total Optimal Operation to the real system is tested. The outdoor temperature, outdoor humidity, and cooling load of the test day are shown in Figure 2 and 3, in which case N1 and N2 is normal operation, case O1 and O2 is Total Optimal Operation. In the test, real time cooling load, outdoor temperature, outdoor humidity, and room temperature, room humidity are substituted into the equations of HVAC model. Then the equations are solved to find the each setpoint. The system is controlled based on the setpoints. The results are shown in TABLE 5. From TABLE 5, the comparing of case O1 and case N2, both of which have the same cooling load, shows that Total Optimal Operation can reduce 30.3% of the energy

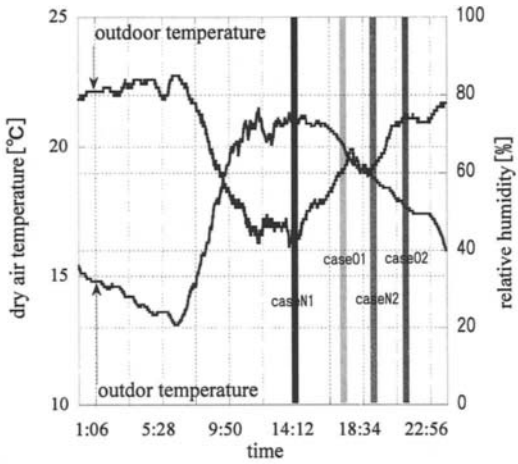


Figure 2 : outdoor temperature and humidity in the test day

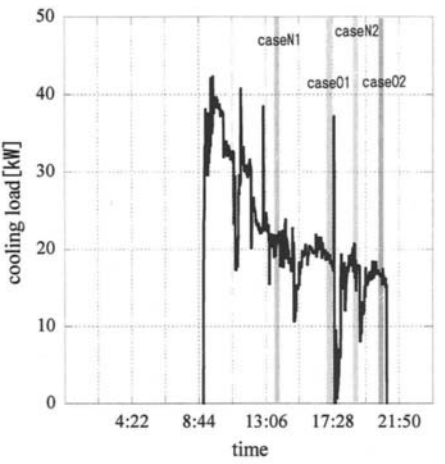


Figure 3 : cooling load in the test day

TABLE 5
RESULTS OF TOTAL OPTIMAL OPERATION

	caseN1	caseO1	caseN2	caseO2
cooling load [kW]	20.7	18.7	18.7	16.3
supply water temperature [°C]	7.7	12.5	7.7	13.4
water flow rate [l/min]	24.6	41.6	21.7	43.6
air flow rate in AHU A [m3/h]	2078	1440	2635	1440
air flow rate in AHU B [m3/h]	2703	2410	3657	2410

	electric energy consumption[kW]			
	caseN1	caseO1	caseN2	caseO2
heat pump	6.86	5.77	5.87	4.64
secondary supply pump	0.83	0.21	0.83	0.20
AHU A	0.63	0.33	0.99	0.32
AHU B	1.76	1.50	3.53	1.59
total	10.1	7.81	11.2	6.75

	heat pump	secondary supply pump	AHU A	AHU B	total
CASE N2	5.87	0.83	0.99	3.53	11.2
CASE O1	5.77	0.21	0.33	1.5	7.81
reduced electric energy consumption[kW]	0.10(1.70%)	0.62(74.7%)	0.66(66.7%)	2.03(57.5%)	3.39(30.3%)
ratio of each reduced electric energy consumption to total reduced one[%]	2.9	18.3	19.5	59.3	-

consumption of case N2.

RESULTS AND DISCUSSION

Total Optimal Operation was tested in 27/10/2001, when cooling load was small. The percentage of reducing energy consumption can be expected to be lower when it is in a peak load season. Because the optimal operation cuts down the excessive energy consumed by normal operation. When it is in peak load season, the excessive energy is not as much as in low load season. So the expected energy saving effect of optimal operation is not as much as that in low load season. To investigate this point, optimal operation in a high load season is compared with normal operation in the season by using simulation models.

Comparison in a High Load Season

A high cooling load given by simulation, outdoor temperature and humidity on 23rd Aug in 2001 are shown in Figure 4 and 5. The results of simulation are in TABLE 6. From TABLE 6, it is found that the rate of reducing energy consumption by Total Optimal Operation on the high load day is 7.4%, much smaller and about one fourth of 30.3%, which is that of the test day. However, the amount of reducing energy consumption by Total Optimal Operation on the high load day is 1.51kW, about one half of 3.39kW, which is that of 27/10/2001. The result is that even on the high load day, the reduction of energy consumption is about one half of that on a low load day. Considering an operation on high load days, middle and low load days suitable to optimal operation, considerable energy consumption is to be reduced by Total Optimal Operation. The result of simulation, on the assumption that the number of days of high, middle, and low load is same, shows that 8.76% of energy consumption can be reduced through July, Augusy, and Septem-

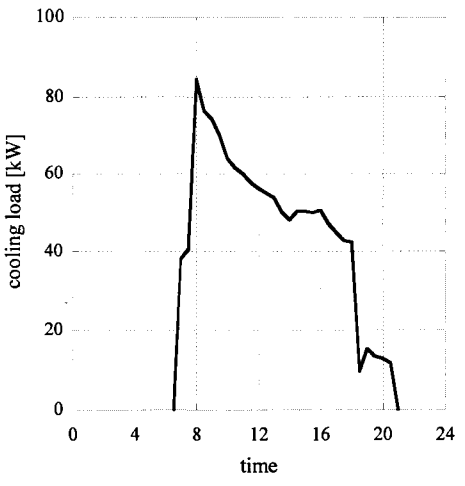


Figure 4 : cooling load in the hottest day

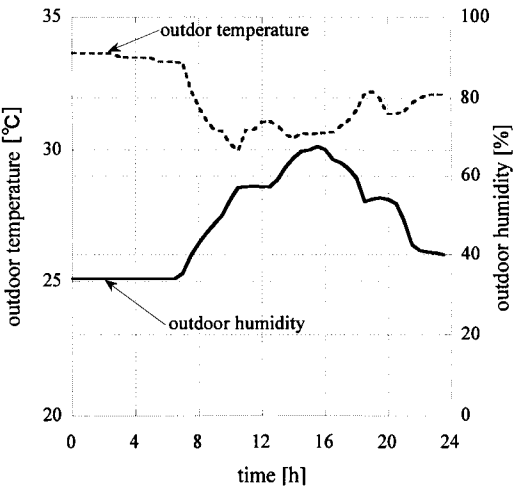


Figure 5 : outdoor temperature and humidity in the hottest day

TABLE 6
RESULTS OF SIMULATION IN A HIGH COOLING LOAD DAY

	heat pump [kW]	secondary supply pump [kW]	supply / return fan in AHU A [kW]	supply / return fan in AHU B [kW]	total [kW]
normal operation	18.9	0.75	0.49 / 0.28	0.88 / 0.44	21.8
Total Optimal Operation	18.4	0.12	0.45 / 0.26	0.64 / 0.31	20.2
energy consumption reduced [kW]	0.55	0.63	0.04 / 0.02	0.24 / 0.13	1.61
rate of energy consumption reduced [%]	0.29	84.5	7.7 / 7.1	27.0 / 29.8	7.4
ratio of each reduced electric energy consumption to total reduced one[%]	34.2	39.1	2.48 / 1.24	14.9 / 8.08	-

ber.

CONCLUSION

The feasibility of the proposed method was tested in a real HVAC system of an office building and the following results were obtained: 1) Parameter identification can be performed successfully by using mathematical models used in common simulation software such as TRNSYS, HVACSIM+ and HASP/ACLD. 2) No small errors in the model performance were found at some operating points. however, about 13.3% energy conservation was able to be attained by the optimal operation method as a whole.

REFERENCES

1)Yoshida H., Koga S., and Terai T. (1990). Optimal Design of Heat Source using a Statistical Method of Calculating *Heat Load. AIJ Kinki Chapter Architectural Research Meeting* **30,** 113-116.

2)Mark A. Cascia.(2000). Implementation of a Near-Optimal Global Set Point Control Method in a DDC Controller. *ASHRAE Transaction* **106:1,** 249-263.

3)A.H.Elmahdy et al(1997). A Simple Model for Cooling and Dehumidifying Coils for Use in Calculating Energy Requirements for Buildings. *ASHRAE Transaction* **83:2.**

Advances in Building Technology, Volume 2
M. Anson, J.M. Ko and E.S.S. Lam (Eds.)
© 2002 Elsevier Science Ltd. All rights reserved

MODEL-BASED FAULT DETECTION AND DIAGNOSIS ON AN OFFICE ROOM

B. Yu[1], A. H. C. van Paassen[1] and S. Riary[2]

[1]Lab of Refrigeration Engineering & Indoor Climate Control, Department ME&MT, Delft University of Technology, 2628 CD Delft, the Netherlands
[2]Techniplan, the Netherlands

ABSTRACT

Energy comsumption in Building Heating, Ventilation and Air-Conditioning (HVAC) systems is growing quickly. Fault detection and diagnosis (FDD) is necessary for the modern office building since it can be used to trace the cause of the decrease of energy efficiency in an HVAC system or the decrease of the thermal comfort level in the rooms. This paper studies a model-based FDD on an office room. By analyzing the physical relations between all the parts of an office room, the models for the room are built with Simulink®. Two types of fault are studied in this paper: an opening window and a jammed radiator valve. By introducing a characteristic parameter, these two faults are able to be detected and diagnosed.

KEYWORDS Model-based; Fault detection and diagnosis; Simulink; HVAC system; office building

INTRODUCTION

As a result of economic, business and population growth, energy use in buildings has grown quickly in the recent decades. More and more residential and commercial buildings have been built and have contributed increasing service demands, e.g. more air-conditioning, more computers, larger rooms.

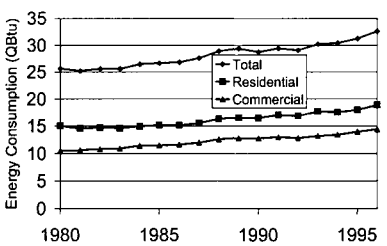


Figure 1: Building Energy Use, 1980-96, U.S.

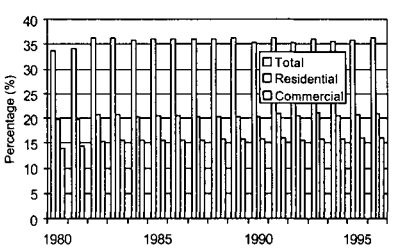


Figure 2: Percentage of Buildings Energy Consumption to the Total Energy Consumption, 1980-96, U.S.

Some useful information can be acquired from statistics for the United States. As shown in Figure 1, according to the review of U.S. Department of Energy (1999) from 1980 to 1996, the energy use of buildings increased about 27%. Therein, the increased amount for residential building is about 25% and for commercial building is about 36%. It is shown in Figure 2 that building energy use in the U.S. accounts for over one-third of U.S. total energy consumption. Therein, residential building accounts for one-fifth and commercial building accounts for one-sixth of U.S. total energy consumption. For the energy use in EU, similar conclusion also can be drawn (Vreuls, 1998). As an energy crisis approaches rapidly, research into energy saving for buildings is quite significant and is being developed from different point of view.

In order to achieve a comfortable working environment, thanks to the rapid development of computers and information & communication technology, modern office buildings increasingly supply integrated, complicated and intelligent services. People want better indoor climate quality and network facilities. Therefore, Heating Ventilation and Air-Conditioning (HVAC) system, automatic control systems and Building Energy Management Systems (BEMS) have been gradually installed in buildings. Since the building control system and HVAC system could not run under optimal condition and sometimes faults or disturbances appear in the different stage of design, commissioning and operation, this increases the complaints level from tenants and the energy consumption level. Hence fault detection and diagnosis (FDD) is necessary.

Model-based FDD has been studied for the past twenty years. It shows good results in some applications. Usoro et al. (1985) presented a nonlinear mathematical model of HVAC system plus an extended Kalman filter to detect faults. A computer program that implements this method was successfully used to detect various simulated faults in the HVAC system. Vaezi-Nejad et al. (1992) used ARX models to diagnosis energy abnormal consumption as a window left opened in a building. Because the opening of a window in a room results in a quick transient variation of the internal temperature, the paper used a model following the behaviour of the inner temperature. Dexter et al. (1996) described two model-based schemes for detecting and diagnosing faults in HVAC system. The first scheme uses a "first principles" model and a rule-based classifier to identify the faults. The second scheme uses a set of fuzzy models and a classifier based on fuzzy matching for fault diagnosis. Peitsman et al. (1994, 1996) presented a black-box model to build an FDD system for a reciprocating chiller. Wang and Wang (1999) presented a law-based sensor fault diagnosis and validation on a central chiiling system. They use a validated dynamic simulation package to evaluate their FDD method. Peitsman (1997) discusses black-box-model-based diagnosis for real-time systems. The diagnosis tool can perform a fast evaluation of a given situation, provided that conflict detection and diagnosis are both performed on the same level of detail. However, the diagnosis tool lacks some robustness. This is caused by the uncertainty in some of the ARX models. Benouarets et al. (1994), Dexter et al. (1997), Ngo and Dexter (1998) introduce fuzzy reference model-based FDD. It is a semi-qualitative method. The feasibility of FDD based on semi qualitative generic reference models has been demonstrated. No training on the actual plant is needed and the faults in a simulated AHU can be successfully identified. Diagnosis based on generic fuzzy models will be slightly less sensitive than diagnosis based on fuzzy models of an individual design.

Model-based FDD is applied on an office room. The simulation model is first built and validated. (Yu and van Paassen, 2001). The physical model calculates the reference value for the room temperature.

The procedure for model-based FDD system is simply shown as figure 3. The system uses residuals to realize the FDD process. Residuals come from the difference between real system output and model output.

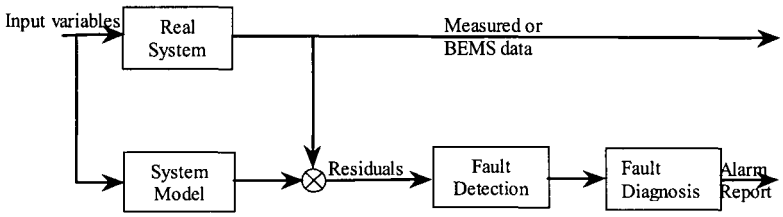


Figure 3: Procedure for model-based FDD system

Two faults are studied on this model-based FDD system. They are: 1) an open window; and 2) a jammed radiator valve. In order to simulate and test the FDD system and physical model, a room is chosen in the office building of the Kropman company in Rijswijk (Netherlands).

SYSTEM ANALYSIS

Modeling Structure

The structure of the model-based FDD for the office room is shown as Figure 4.

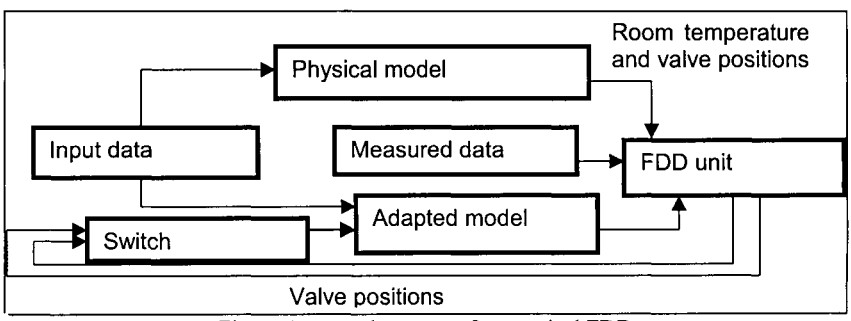


Figure 4: general structure for practical FDD

The components in the stucture are

1. Physical model; predicts the correct room temperature as a result of the dynamic simulation of the thermodynamic behavior of the air in the room.
2. Real state; gives the measured air temperature in the room
3. Adapted model; gives a prediction of the air temperature when the radiator valve jams.
4. Input data; consists of the weather data and technical data from the air-conditioning unit, such as the temperatures of warm and cold water supply.
5. Switch; it has the task, when necessary, to switch over from the theoretical valve position (calculated by physical model), to an estimated valve opening. This happens when FDD suspects the presence of a fault. Doing this, we can simulate a faulty situation

Fault type

With regard to faults in the air temperature, we classify into two types.

1. Fault type I causes an increase in the room temperature.
2. Fault type II causes a drop in the room temperature.

The first step in the FDD process is identifying these two types of faults. The difference has to do with the weather condition, e.g. during a hot summer day an open window results in a fault type I whereas in the wintertime it results in a fault of type II.

In this paper the winter situation with the following two faulty conditions are considered:
1. an open window
2. a jammed radiator valve

Effects of the fault on air temperature

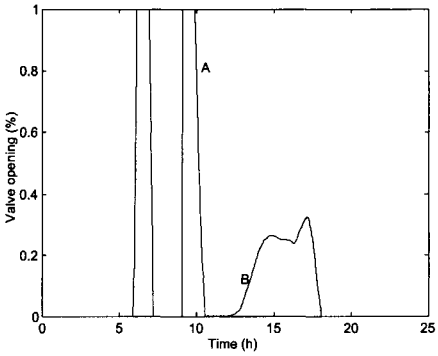


Figure 5: variation of valve opening for one day

For the raditors valve case, the effects are mostly dependent on the direction of the valve movement (closing/ opening). The variation of the valve opening in a workday in November is shown in figure 5.

Points A and B are two points with different characteristics. On point A the valve is closing and on point B the valve is opening. Jamming the valve on point A results in a fault type I and jamming on B results in a fault type II.

With the assumption that during the winter the outside temperature is most of the time below the indoor comfort temperature, it is concluded that an open window will results in a fault type II. The designed FDD component takes account of the type of the fault and activates different criteria.

For the sake of fault detection, information acquired from the measurement plays an important role. In an office building, usually the room temperature is the only measurement, which is directly available for fault detection. Another valuable variable is the output of the controller present in the room. In a faultless situation, it is assumed that the radiator valve position (X) is equal to the normalized value of the output signal (x) from the controller (thermostat), for example, $x = 50\% \Rightarrow X = 0.5$.

X is not a measured value, but a system parameter. Th physical model calculates both room temperature and the output of the controller. The phsysical model creates the diagram in Figure 5. Because of the inaccuracy of the model, some differences arise between calculated room temperature results, $T_{air,model}$ (Tm) and valve position X_{model} (Xm) and their real values of them, $T_{air,real}$ (Tr) and X_{real} (Xr).

$$r\ (\text{residuals}) = (Tr) - (Tm) \tag{1}$$

$$\Delta X = (Xr) - (Xm) \tag{2}$$

Variations of these two variables are shown in figures 6 and 7 for a test period of 11 days on November. Figure 8 shows the variation of Xr for the same day as in figure 5.

Figures 6 and 7 show how the calculated results of Tm and Xm deviate from their real values. Fault detection algorithm should consider these deviations in such a way that fewer false alarms happen. From the result in Figure 4, it can be concluded that the physical model gives a reasonable approximation of the real room temperature. The differences between real and calculated values for

room temperature are mostly limited between ±1 degree Kelvin. In this case, a threshold of 1 degree can be taken to be one indication of a faulty condition.

$$\left.\begin{array}{l} r > 1 \\ r < -1 \end{array}\right\} \quad \text{faulty condition} \tag{4}$$

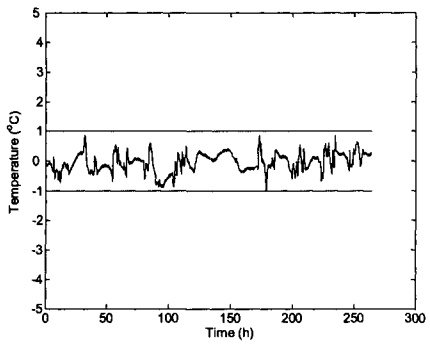


Figure 6: variation of residue during 11 days

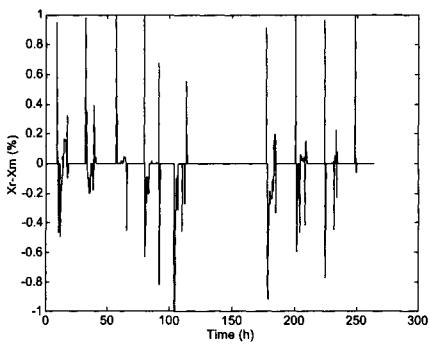


Figure 7: variation of ΔX during 11 days

However, it seems this variable is not a complete detection parameter from the simulation results for the following reasons:

1. Temperature drop caused by an open window could be compensated by an increase in the radiator valve opening.
2. In practice, the threshold to trigger the alarm has to be at least equal to 1.5 degrees. Smaller values of threshold increases the possibility of false alarm due to the natural fluctuation in the room. It is remarkable that the order of magnitude of faults is the same as that due to disturbances.
3. Heat capacity of the walls strongly delays the effect of a fault type II on room temperature.

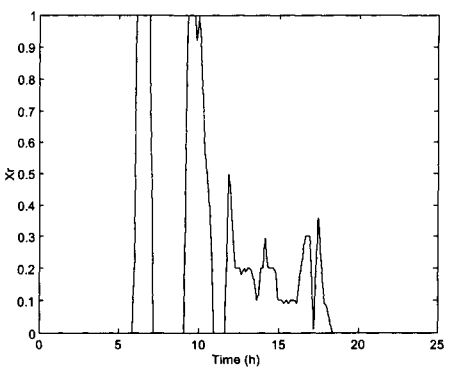


Figure 8: variation of controller output for one day

The simulation results show that only using condition (4) for fault detection will lead to big delays between the occurence of a fault and its detection. This can affect the online character of the FDD system in a bad way. To make the detection happen earlier, another characteristic parameter is needed. This parameter not only uses the r variable as a detection criterion, but also make use of the differences between valve positions calculated by physical model (Xm) and output of the controller in the real condition (Xr). This parameter should be insensitive to the within tolerance deviations between the valve positions. The tolerable deviations are those fluctuations as a result of uncertainties and inaccuracies in the physical model (Figure 5).

FAULT DETECTION ANALYSIS

Type 1:

When a fault occurs which results in a temperature drop in the room (fault type II), the difference

between Xr and Xm or ΔX, will grow quickly. After occurrence of a fault type II the controller tries to compensate for the temperature drop by an increase in the output signal to the radiator. In the mean time the valve position calculated by the model follows a direction leading to the faultless situation. Integration of ΔX over time is considered as one the characteristic parameter. Another variable, which also reflect the effect of fault type II, is the fraction Toutside/Tinside. A temperature drop caused by a fault type II makes the value of the fraction increase. A characteristic parameter which is a combination of above two effect is introduced as:

$$P = \left|\frac{T_{outside}}{T_{inside}}\right| \int |X_r - X_m| \, dt \tag{5}$$

if $|T_{outside}| < 1$, then $\left|\frac{T_{outside}}{T_{inside}}\right| = \left|\frac{1}{T_{inside}}\right|$

The parameter P for a faultless situation is shown in Figure 9. P is made by an integrator, which undergoes a reset every morning at 4 o'clock. Doing this the value of P is set to zero at 4 o'clock every morning. When a fault type II happens, P begins to grow quickly. Passing a limit ε, which P does not exceed in a healthy (faultless) situation, indicates a fault. Figure 10 shows the P values when a window is open with 100m^3/h airflow after 13.5hour.

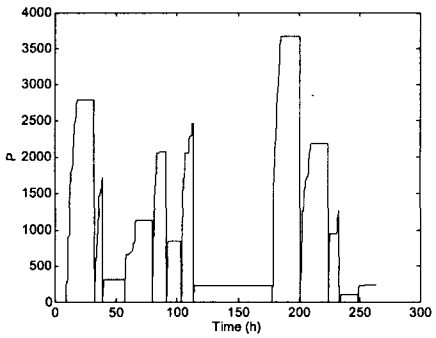


Figure 9: variation of variable P during a test period of 11 days

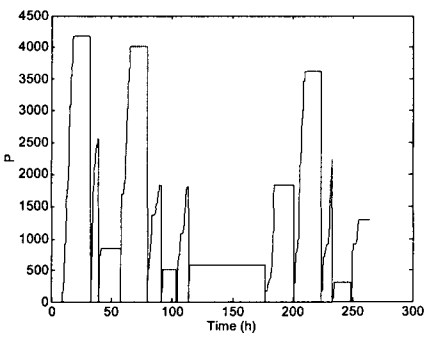


Figure 10: Variation of parameter P when a window open 100m^3/h after 13.5hour

From Figure 9, the cautious threshold is 3500 but this could introduce a longer delay in detection. Choosing a smaller threshold will improve the speed of detection but a lower value enlarges the chance of false alarms. An optimum value for ε is chosen as 3000. Although by this choice the chance of false alarm still exists, we will try to reduce this possibility by using redundant conditions during detection and diagnosis. One of these conditions is the residual of room temperature. When a fault type II arise, the residued (Tr-Tm) is smaller than –0.5 and in the case of a fault type I, it is greater than 0.7 degree. This condition prevents a false alarm on the 8th day of the test period where P>3000.

Type 2:

When the result of a fault is a temperature increase in the room (fault type I), our conclusion can be a jammed radiator valve during getting closing. Detection of a fault type I occurs by establishing a remarkable increase in the residual. Considering the available heat power of the radiators, a (during closing period) jammed radiator valve results almost immediately (1-2 hours) in a increase of more than 1.5 degree in residual. This is the case when the valve position has been bigger than 50%.

When residue reaches a value bigger than 1.5 degree, an alarm report shall occur. It is obvious that in this case, detection and diagnosis happen at the same time.

Type 3:

There is another type II fault which can be detected quickly by the criterion 'residual has crossed the limit of −1.5 degree'.
This is the case when in the early morning the valve refuses to open. Because of the compensation heat from the radiators, this limit can hardly be crossed by another faulty condition, open window.

DIAGNOSIS

A fault type II can be a result of 1) a radiator valve that is jammed during opening; or 2) an open window.

When a fault type II occurs, the characteristic parameter P increases and the detection threshold (ε=3000) will be crossed. The next step is to diagnose of the fault source. Here an open window and a jammed valve are considered as condidates. An adapted model is used to for the diagnosis (Figure 4). This model calculates a fictitious room temperature (Ta), as soon as the variable P crosses the limit of ε = 3000.

When P > 3000, a sample and hold action is started by which the theoretical position of the radiator valve (Xm) gets sampled and held. This value is considered as the manipulated valve position (Xa), which will be sent to the adapted model via the switch. Switch changes from Xm over to Xa when P > ε. The room temperature calculated by adapted model is an indicative temperature for the real case wherein the radiator valve is jammed on (Xr). Because of the delay between the fault arising and crossing the limit of e > 3000, it is not possible to calculate the exact position of the jammed valve by sample and hold. Actually the average of the valve position is used. The average period is 30 min and the estimated Xa is

$$X_a = X_{n+1} = \frac{X_n + X_r}{2} \tag{6}$$

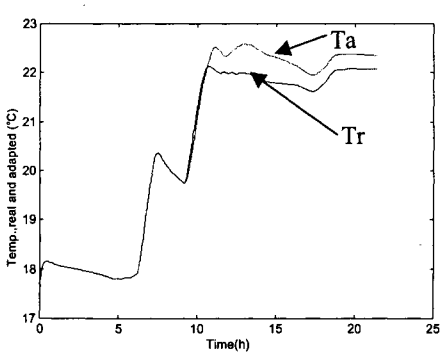


Figure 11: Curve of Treal & Tadapted when a jammed valve fault

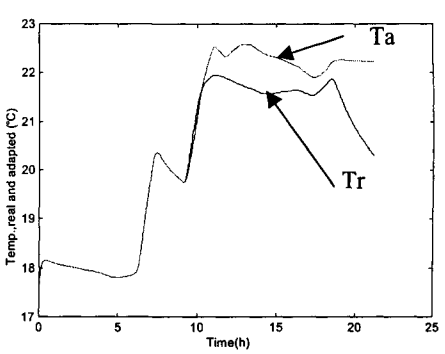


Figure 12: Curve of Treal & Tadapted when a open window fault

By means of the adapted model the faulty behavior of the room temperature as a result of a jammed radiator valve is simulated. Fiugre 11 and Figure 12 are two different results when the P overshot the threshold to indicate a fault.

- When a jammed valve causes a temperature drop in the room, Tr and Ta will develop in a parallel way. This is shown in Figure 11. The shift is due to the difference between Xavr. and Xr. The difference remains smaller than 1 degree.
- When the temperature drop comes from an open window, the difference between Tr and Ta will keep growing as shown in Figure 12. It will continue to grow until it become bigger than 1.5 degree, which results in an alarm.

CONCLUSION

Energy comsumption in office building is growing quickly in recent decades. Faults which appear in a building HVAC system lead to more energy comsumption and worse thermal comfort. Model-based fault detection and diagnosis has been studied for an airconditioned room in one office building. The effects of two types of fault, an open window and a jammed radiator valve, have been explored. A characteristic parameter P which allows for the compensation effect of the radiator and the influence of outside temperature has been presented. When the above two types of fault appear, P can be used as the fault detection criterion and the adapted model is used for the fault diagnosis. The results achieved are good.

REFERENCE

[1] Benouarets, M. and Dexter, A.L. (1994). Model-based approaches to fault detection and diagnosis in air- conditioning system, *Proceedings 4th Int. Conf. System simulation in Buildings*, Liege: Univ. of Liege

[2] Dexter, A.L. and Benouarets, M. (1996). A generic approach to identifying faults in HVAC plants, *ASHRAE Trans.*, **102:1**, pp. 550-556

[3] Dexter, A.L. and Ngo, D. (1997). Fault diagnosis in large-scale air-conditioning systems, *IFAC Fault Detection*, Supervision and Safety for Technical Processes, pp. 727-732

[4] Ngo, D. and Dexter, A.L. (1998). Fault diagnosis in air-conditioning systems using generic models of HVAC plant, *Proc. The 5th Int. Conf. System simulation in Building '98*, Liege, Belgium, pp. 446-457

[5] Peitsman, H.C., et al. (1994). Application of ARMA-models and neural networks to a reciprocating chiller for fault detection, *Proceedings 4th int. conf. System simulation in buildings*, Liege: Univ. of Liege

[6] Peitsman, H.C., et al. (1996). Application of black-box models to HVAC systems for fault detection, *ASHRAE Trans.*, **102:1**, pp. 628-640

[7] Peitsman, H.C., et al. (1997). ARX models and real-time model-based diagnosis, *ASHRAE Winter Meeting*, Philadephia, Jan. 25-29

[8] U.S. Department of Energy. (1999). Energy Information Administration. Monthly Energy Review. DOE/EIA-0035(99/05), Washington DC

[9] Usoro, P.B., et al. (1985). An innovation-based methodology for HVAC system fault detection, *Trans. of ASME, J. of dynamic systems, measurement and control*, **107**, pp. 284-289

[10] Vaezi-Nejad, H., et al. (1992). Detection of an open window in building, IEA Annex 25, Centre scientifique et technique du B atiment, Marne-la-Vallee, pp. 1-12

[11] Vreuls, H.H.J. (1998). Novem Energiegids, Novem. - 2e ed.

[12] Wang, S. and Wang, J.B. (1999). Law-based sensor fault diagnosis and validation for building air-conditioning systems, *Int. J. HAVC&R*, **5:4**, pp. 353-380

[13] Yu, B. and Paassen, A.H.C. van (2001). Modeling with simulink and bond graph method for fault detection in an air-conditioned room, *Proc. 4th Int. Conf. Indoor Air Quality, Ventilation & Energy Conservation in Building*, Changsha, Hunan, China, pp. 1163-1170

Advances in Building Technology, Volume 2
M. Anson, J.M. Ko and E.S.S. Lam (Eds.)
© 2002 Published by Elsevier Science Ltd.

The Applications of Solar Heat Transfer & Solar Electricity Transfer in Building

Zhang Wei[1]and Yuan Huizhou[1]

[1] Department of Building Engineering, Shenzhen Polytechnic,
Shahe Road West, Shenzhen, 518055,China

ABSTRACT:

The fossil energy (e.g. fossil oil, natural gas, coal) in the world is limited. It would be unavailable if fossil energy is consumed in the same increasing rate as that of today. In our country, the possession of fossil energy per person is only one-third of its world average, and 95% of energy is imported to the Taiwan area. One of the major environmental problems, at present, is green-house effect in the whole globe, which results from a large amount of carbon dioxide. The more fossil energy is used, the more carbon dioxide is given off. In many cities in North China, the concentration of aerosol is 9.6 times as much as the Acceptable Concentration Level set by the World Health Organization(WHO), and acid rain has been found in many areas. Solar energy is a new power source with a long history, which is characterized by large quantity, easy to obtain, safety, cleanness. Therefore, it has little effect in destroying the ecology balance. Thus world exploitation and utilization of solar energy is an urgent solution to the green-house problem. Solar energy can be used in many fields, including such as in electric power generation, but still today there is relatively mature commercial technology usage except in solar heat transfer. Consequently, this paper inquires into not only solar heat transfer but solar electricity transfer.

KEYWORDS:
solar energy, solar PV, building integrating PV, solar heat transfer, solar electricity transfer, solar building

ONE: CONTEMPORARY APPLICATION IN SOLAR HEAT TRANSFER

As solar energy research & utilization is taken seriously by international society , in the National

Development Planning Program of 1995-2010 for new energy and heat reuse applications , China raised a government policy of " enterprise should be up to a larger scale; technology should be up to higher level; quality should be up to higher grade and market should be up to better standards." Since 1987, when Professor Yin Zhiqiang, of Tsinghua University, obtained the vacuum heat-transfer tube patent, the quality and technology level of our solar products have reached international advanced level. The solar heater industry has become a new business with good prospects.

In the mainland, the number of solar heaters is about ten million, family utilization ratio is 4%, among which Yunnan has more than 20%. Our solar heater products are of the full-automatic type, hold-pressure type, balcony-hanging style and slope-roof style since 1992. They are also exported to Japan, Korea, Singapore, Malaysia and other places. During the six years from 1985 to 1992, the method of reward was carried out in order to popularize solar heating systems. During these years, the area of solar heat collector in use was increased with 80,000 m^2 in 1992 compared with 40,000 m^2 to 50,000 m^2 for earlier years, furthermore, the figure was over 90,000 m^2 in 1995. During these more than ten years, the total output value for solar heaters was up to nearly $10,000,000,000, the total area of heat collector was as much as 870,000 m^2 and the utilization ratio was about 3.1%. Hence thousands of employment opportunities were created in the solar industry.

As indicated in table 1-1, the total area of heat collector in the mainland and Taiwan still has large latent capacity compared with that of relative advanced nations and states. In Taiwan, the area of installed heat collector system (both family heater and industry heater) is up to 18,000,000 m^2. It is estimated that 116,300 equivalent litres of fossil energy has been saved every year and 4204,000 tons less of carbon dioxide has been output.

TABLE 1-1

THE SOLAR USUAGE DATA OF STATES AND AREAS IN THE WORLD

States and areas	Famiy utilization ratio(%)	Total solar collector area(m^2)
America	60	
Japan	15	
Israel	80	
Taiwan(China)	3.1	87
Mainland(China)	4	1000
Kunming(China)	20	6 5

TWO:PRINCIPLES AND INTEGRATED SYSTEM OF SOLAR-HEAT TRANSFER & SOLAR ELECTRICITY TRANSFER

Put simply, the principle of solar-heat transfer is to collect heat through a heat collector and conducting that heat to water. The system is mainly made up of a heat collector, a hot-water box, a auto-controlled auxiliary calorifier and a temperature-control pump.(See Fig 2-1)

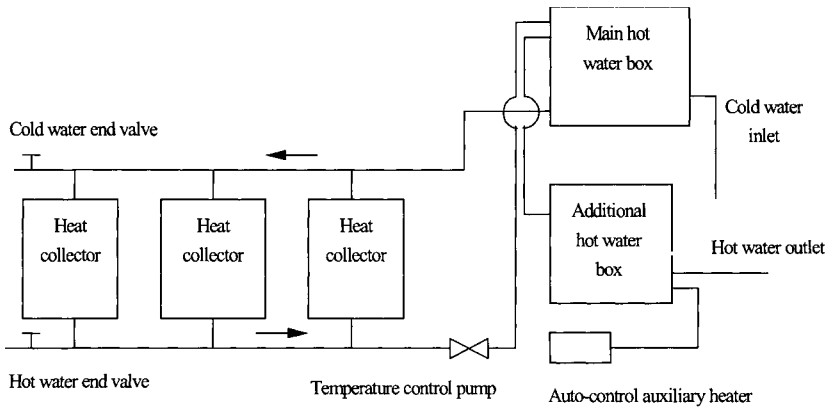


Figure 2-1 The principle of solar heat transfer

The heat collector is in the core position and the key technology of solar-heat transfer. It can be divided into the flat style and the vacuum tube style according to the difference of structure.(See Fig 2-2 and Fig 2-3). The flat style is composed of many copper-aluminum cores, characterized by simple manufacture and with low cost of construction. However, with low outside temperature, when the heat collected by the copper plate is conducted to water, part of the heat is lost to air. Therefore, the heat efficiency drops in the cold season. The outside tube is high of boron-silica glass which can resist heat and can resist hail stones. The inside tube is glass or metal. The exterior of the inside tube is made by a magnetron spatter vacuum plating process, the plating having a higher absorption rate and lower radiation rate. The reflection plate is able to gather solar energy between the tubes. Thus the solar utilization ratio is improved. The temperature of the tubes can be raised to over 200°C when they are exposed to the sun without water. The temperature of water in box can go up to 70°C-90°C, the average thermal efficiency is over 40% and the heat dissipation value is below 3 $W/m^2 \cdot °C$.

There is a temperature controller in the auto-controlled auxiliary heater. When the temperature of hot water is below the demand on a cloudy day or rainy day, the auto-controlled auxiliary heater will heat water in the box, in the usual way with electricity, liquefied gas or diesel oil. Which way is used depends on the customer's circumstances.

The temperature-control pump will open automatically when the temperature of water on one side of the heat-collector is higher than that of the hot water box, the water is pumped into the water box from the heat-collector, and so the water's temperature in the box is rising. This cycling will not be stopped until the temperatures of the two sides are equal.

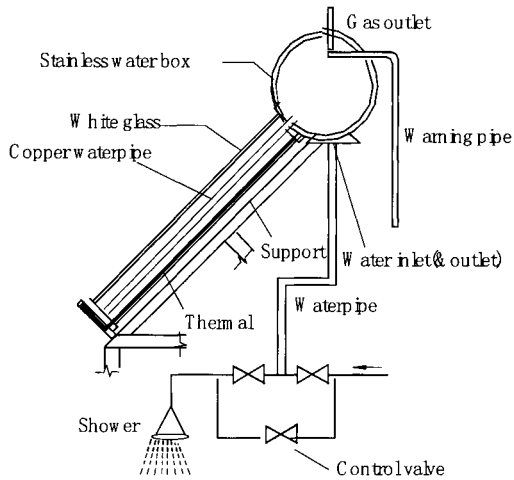


Figure 2-2 Flat style solar collector

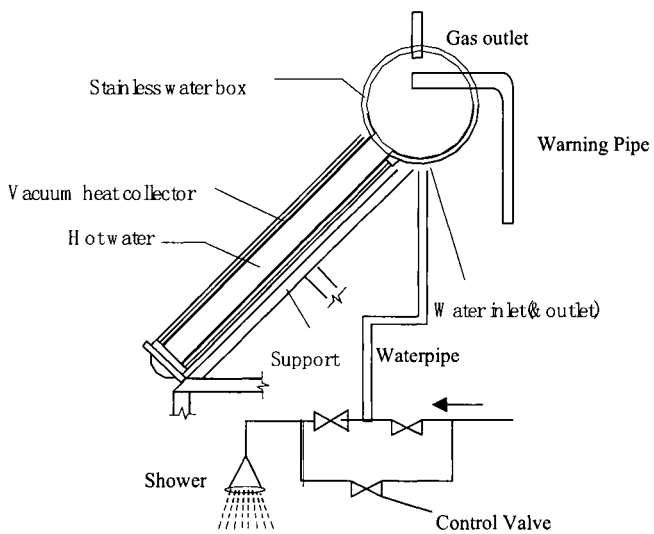


Figure 2-3 Vacuum tube style solar collector

The solar battery was invented in 1954 by an American scientist, Pearson et al.. At first America used it to power an artificial satellite, Vanguard. At that time, because it was very expensive, it was limited to sea-islands or remote places where laying a cable was really difficult. Then, along with the invention of non-crystal solar battery, it became possible for solar energy to generate electricity in building.

The solar battery uses the principle of photoelectricity. An electron is created when the surface of a

semiconductor is subjected to solar radiation. Described in more detail, the solar batter contains overlay P-model semiconductors and N-model semiconductors. This combination will create negative electrons and positive electrons when radiated. The negative electron is absorbed by its N-model semiconductor and the positive by its P-model and a voltage comes into being between the two surfaces of those two kinds of semiconductor. The current emerges when they are wire connected.

Several kinds of semiconductors are used in producing solar batteries, the most common is silicon, the rest are cadmium sulphide, gallium arsenide, etc. If a silicon semiconductor is employed, it can be made into a monocrystal, polycrystal and non-crystal by different manufacture methods.

Solar electricity is coming in at a high level and a large scale, among which PV technology applications are the main popular aera at present. From the report of the international energy institution, solar building will become the most important new industry. As to integrating buildings and PV, the Building Integrating PV(BIPV) can be divided into two kinds: one is a PV system integrating building, the other is a PV device integrating building. These two kinds have their own characteristics respectively.

THREE:EXAMPLES IN ENGINEERING

One college in Shenzhen has ten student-dormitories(500 students in each). These buildings adopted solar-heat systems of the copper-aluminia flat style. The design hot water consumption is 50 kiloliters per student every day. According to the meteorological data of Shenzhen in the last ten years, the sunny days are 210 a year, while the cloudy days and rainy days are only 155 per year. On a sunny day, one square meter of heat-collector can heat at least 100 kiloliters water from 20°C to 50°C. If it was done by liquefied gas, it would consume 0.3 kilograms and give off 0.9 kilograms carbon dioxide. The cost of construction and the discharged volume of carbon dioxide by solar and liquefied gas each dormitory are reported in table 3-1.

TABLE 3-1
THE COMPARISON OF THE COST OF CONSTRUCTION

	Solar collector area(Water heater)	Unit price (YuanRMB)	Cost of equipement($\times 10^4$Yuan RMB)	Operation cost per year ($\times 10^4$Yuan RMB)	Amount of carbon dioxide discharge(Tons)	Total cost(equipemeng and operation 15years) ($\times 10^4$ Yuan RMB)
Solar	250 (m^2)	1000	25	1	0	40
Liquefied gas	100	2000	20	3	47.25	65

As table 3-1 indicates, the primary cost of a solar system(about 250,000 Yuan RMB) is a little higher than that of a liquefied gas system(about 200,000 Yuan RMB), but if calculated over 15 years, the former's total cost for ten dormitories will be 2,500,000 Yuan RMB less than the latter's, and what is more, the solar system will not discharge 472.5 tons carbon dioxide a year, favourable to reducing the green-house effect.

FOUR: PROBLEMS TO SOLVE

Even though solar-heat transfer has been applied widely, there are still some problems to be solved urgently:

1.There are many enterprises in this industry, but there are less than 10 enterprises with a large scale production and over 50,000,000 Yuan RMB output value a year. However, there are over 500 enterprises whose output is less than 1,000,000 Yuan RMB. Accordingly, there are too many products varieties and this is not good for establishing a good service system.

2.The government must build up products test centers and in addition work out product quality levels and engineering acceptance quality regulations, which will enhance enterprise healthy development.

3.During the design of most buildings, the solar-heat systems are not considered as an integral part of the buildings, but are only treated as equipments for later installation. Thus the installation of solar-heat systems will damage the construction of the building outside to some extent. If installed on a roof, it may cause the roof to leak. Therefore, it is important that architects understand the nature of solar-heat systems, which will lead them to consider their standard water proofing integration during the design.(for example, for protection of a balcony, the heat conservation of a roof, etc) This also will lead to installing the solar systems more extensively in a building.

4.Need legislation. It is necessary that solar systems should be designed and installed compulsorily as part of residential architecture for the purpose of reducing carbon dioxide discharge.

CONCLUSION

Along with the appearance of higher efficiency vacuum heat tubes and the usage of auto-controlled auxiliary calorifiers, solar-heat transfer systems can be used in practice on a large scale. This is not only technologically feasibile, but brings better economic benefits than conventional fossil energy systems. The most important additional function is reduction CO_2 discharge. Energy is in short supply in the mainland, especially electricity. At present, over 20 countries still have no electricity supply, where many people live. Taiwan is so short of energy that over 95% is imported, which not only consumes a large amount of foreign exchange but also affects the economy stability. We have abundant solar resources for two-third of the area with sunshine for over 2000 hours a year and the amount of radiation is also over 5,020,000 KJ/m^2 a year. The development and utilization of solar energy not only reduces the green-house effect but also reduces the energy gap between supply and demand. It is beneficial to both the economy and the environment protection if the cleanness of solar energy is widely used, the legislation is strengthened by government, and the quality of solar products and their installation quality are supervised.

References

Nu Ximing etc.(2000).The Development and Potential Application of Recycle Energy in Taiwan. *Engineering Magazine* 26:2,22-31.

Qu Jingsong etc.(1989). The Policy of New Energy and Recycle Energy in UK. *Quarterly Magazine of Energy* 22:1,17-22.

ENVIRONMENTAL TECHNOLOGIES:

FIRE SAFETY ENGINEERING

This Page Intentionally Left Blank

Advances in Building Technology, Volume 2
M. Anson, J.M. Ko and E.S.S. Lam (Eds.)
© 2002 Elsevier Science Ltd. All rights reserved

INTUMESCENT FIRE PROTECTION COATING THICKNESS FOR SHALLOW FLOOR BEAMS

W. Sha and T. M. Chan

Metals Research Group, School of Civil Engineering, The Queen's University of Belfast, Belfast BT7 1NN, UK

ABSTRACT

To design for fire protection required for universal beams and columns the British Standard provides a formula relating the protection thickness to section factors, thermal conductivity, fire resistance and limiting temperature. However, this formula does not apply to the shallow floor beams, which are almost totally contained within the concrete slab. This paper is to derive an alternative relationship for determining the thickness of intumescent fire protection coating required for shallow floor beams, using existing fire test data. The results clearly show that the required thickness of fire protection to the shallow floor beams is thinner than to the regular steel beams. The formula derived can be used for quick, simple design calculation for the required thickness of fire protection. For safety reason in design there should be a safety factor used in conjunction with the formula. The analysis based on fire test data is supplemented with calculations based on beam temperature obtained from heat transfer models.

KEYWORDS

Intumescent coating, fire protection, shallow floor, fire engineering, fire test, asymmetric beam, thermoconductivity, steel structure, section factor.

INTRODUCTION

Providing adequate fire protection to steel structure (columns and beams) is the traditional way to prevent failure and to ensure that the structural steel member can meet the required fire resistance standard. The most common types of fire protection in building structures are board protection, concrete encasement and intumescent coating. However, these protections can increase the cost of construction by about 50% of the structural section member and the depth of the section by up to some 6-cm [Todd (1996)]. Sometimes different types of fire protection can be used together to achieve a better fire resistance.

The development of shallow floor construction is an excellent example of the use together of different concepts of fire protection to give a better performance of fire resistance. In this type of construction,

a beam is contained almost totally within the depth of a concrete floor. Only the bottom flange or a plate welded to the bottom flange is exposed outside of the concrete floor. Therefore, intumescent coating can be applied on the exposure area at the bottom flange.

In the recent years, Corus (formerly British Steel) with the collaboration of the Steel Construction Institute (SCI) in England has developed two types of new shallow floor beams, the fabricated SLIMFLOR beam and the ASYMMETRIC SLIMFLOR beam. In addition, TOPHAT beam was developed in Scandinavia [Sha (1997a,b), (1998), (2001), Sha & Lau (2001), Ngu (1999)].

Shallow floor construction provides a solid, flat-slab appearance similar to reinforced concrete construction. The fabricated SLIMFLOR beam is based on a Universal Column section, with a single horizontal plate welded to its bottom flange, shown in Figure 1. The ASYMMETRIC SLIMFLOR beam (ASB) does not require welding of an additional plate and achieves optimum properties for design. The TOPHAT beam is formed by four plates welded together to make a shape like a hat. The floor can be constructed of pre-cast concrete units or long span composite slabs with deep profiled steel decks.

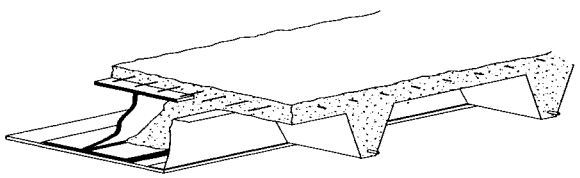


Figure 1: Fabricated Slimflor beam

Because the beams are almost totally contained within the floor slab, they have inherently good performance in fire and in most cases can achieve 60 minutes fire resistance without applied protection. However, if the fire resistance requirement is more than 60 minutes then protection must be applied to the bottom plate. Thin film intumescent coatings are ideal in this respect because they add a negligible amount to the depth of the section. Typically, thickness of about 1 mm is used for protecting conventional steelwork. For shallow floor beams, the required thickness is expected to be lower due to the intrinsically good fire resistance of the construction.

In the British Standard, a formula is given to calculate the required thickness of fire protection to regular steel section depending on the fire resistance rating and on the limiting temperature of the member. However, this formula does not apply to the three new shallow floor beams. The aim of this work is to derive a new formula to calculate the required thickness of fire protection for the new shallow floor beams from fire test data.

Intumescent coatings are paint-like materials which are inert at normal temperature but, when subjected to heat, swell to form an insulating char, stable over a limited period of time in fire conditions. Their thermoconductivity value varies with temperature, and is estimated at around 0.5 W/m°C. These materials provide thermal protection to the underlying surface through the absorption of heat by endothermic chemical reactions and through the insulating properties of the final char [Butler (1997)]. The two commonly used intumescent coatings manufactured by Nullifire Ltd., England are S605 and S607. S605 has been marketed by Nullifire for a number of years and is a hydrocarbon solvent-based system. It contains 10–25% xylene, 2.5–10% C9 alkylbenzenes and 50–75% proprietary resins, pigments and fillers. It has been fully assessed for conventional beams and columns using the procedures of the Association of Specialist Fire Protection (ASFP) [Fire (1992)]. Specifically, it has been fire tested utilising structural sections after extensive accelerated and natural ageing. The assessment of S605 for shallow floor systems can therefore gain confidence from the

earlier assessment. S607 is a newer water based product developed from S605. Is contains proprietary resins, water and fillers. It does not have the same level of test evidence on conventional steelwork to support the assessment but it has been tested in Norway on a shallow floor system and performed in a very similar manner.

PROCEDURE

The three types of shallow floor beams used in previous fire tests are the Slimflor beam, Asymmetric Slimflor beam and Top-Hat beam. By using the previous fire tests result data [Sha (1997a,b), Sha & Lau (2001), Ngu (1999)] a formula can be derived to calculate the required thickness of fire protection for these beams. The previous fire tests data include the sizes of the shallow floor beams tested, the coating thickness, the testing time and the temperatures measured at the bottom flange or at the plate welded to the bottom flange. The important data from the fire tests are shown in Table 1. This contains all the fire test data.

TABLE 1
FIRE TEST DATA FOR THE FIVE TESTS AT NULLIFIRE, THREE TESTS AT SINTEF AND THE WARRINGTON TEST

Beam	H_p (m)	A (m^2)	Coating	Thickness (mm)	Temperature (°C)		
					60 min	90 min	120 min
Slimflor	0.436	0.01372	S607	0.166	687	802	903
	0.436	0.01372	S605	0.343	559	714	818
	0.436	0.01372	S605	0.651	483	605	718
	0.436	0.01372	S605	0.993	388	498	609
ASB	0.316	0.01267	S605	0.285	469	630	717
	0.316	0.01267	S605	0.774	-	462	587
Top-Hat	0.470	0.01104	S607	0.179	721	823	915
	0.470	0.01104	S607	0.179	718	811	868
	0.470	0.01104	S607	0.537	532	673	747
	0.420	0.00893	S607	0.418	-	-	800

Nullifire Ltd. carried out fire tests on four unloaded Slimflor beams and a Top-Hat beam protected using S605 and S607 intumescent coatings manufactured by the same company. The test furnace was approximately 1-m cube. Protection was only applied on the plate welded to the bottom flange (Slimflor) or the bottom flange (Top-Hat). This was directly exposed to fire and the rest of the section was buried in sand, Figure 2 [Sha (1997a), Sha & Lau (2001)]. Temperatures were measured along the beams at two sections, each approximately one third of the exposed beam length (approximately 1 metre) from the end of the beams. "K" type thermocouples were used, with a diameter of 1.5 mm, in a sheath. The variation in the coating thickness was within about 7.5 μm.

In Table 1 the last three Top-Hat beams were tested at Norwegian Fire Research Laboratory (SINTEF) [Task (1993)]. All tested Top-Hat beams have a lower-flange thickness of 10 mm. The bottom face of the beams was protected using the S607 intumescent coating. The furnace temperature was measured with thermocouples of shielded type as described in Figure 4 of International Maritime Organization

(IMO) Resolution A.754 (18) Section 7.2.1 [FTP (1998)]. The diameter of the thermocouples was 6 mm.

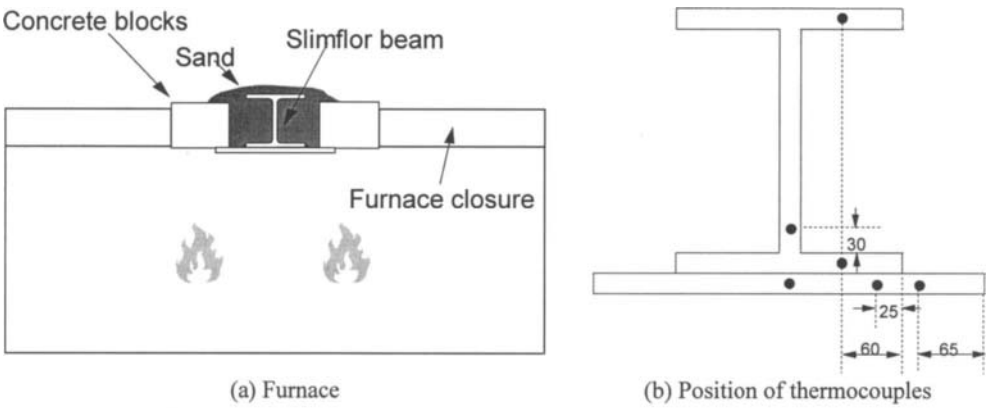
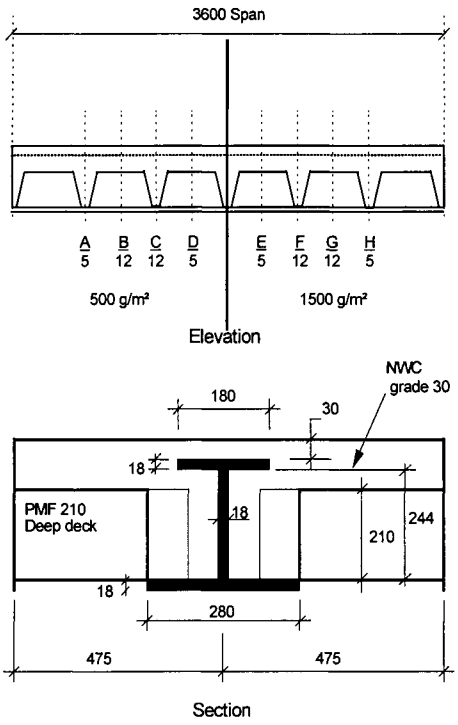


Figure 2: Test at Nullifire Ltd.

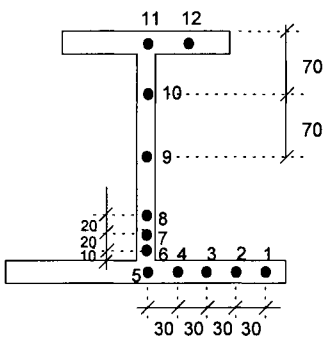
An unloaded asymmetric Slimflor beams was tested at Warrington Fire Research Centre, England. The bottom face of the beams was protected using the S605 intumescent coating. In the test, only the bottom flange was directly exposed to fire, and the rest of the section was surrounded by concrete. Half of the beam on the left-hand side was coated with a relatively thin layer of S605 coating, at a density of 500 g/m^2 (thickness = 0.285 mm). The coating for the right-hand side was relatively thick, 1500 g/m^2 (thickness = 0.774 mm). The furnace at Warrington Fire Research Centre was much larger than the one used in Nullifire Ltd. The furnace was 3.6 m long and 0.95 m wide. Figure 3 shows the elevation and section views of the test assembly [Sha (1997b)]. 3 mm diameter mineral insulated "K" type thermocouples, Ni-Cr/Ni-Al, with insulated hot junctions and Inconel sheaths were used. The Warrington data were also used in the paper (Table 1), undistinguished from the Nullifire data. It is difficult to directly compare the results with the tests at Nullifire in a smaller furnace as the beams were different, but earlier work has demonstrated that tests at the two laboratories give comparable outcome [Sha (2001a)].

As mentioned above, these beams are almost contained within the floor slab. They have very good performance in fire and in most cases can achieve 60 minutes fire resistance without applied protection. For more than 60 minutes fire resistance, protection must be applied to the bottom flange or the plate welded to the bottom flange. Therefore the fire test data at 60 minutes are not used for this paper.

The required thickness of fire protection to the steel section depends on the rate of heating of the section and on the limiting temperature of the member. For enclosed members with box or profile protection the heat flow depends on the section factor (H_p/A) of the member and on the properties of the fire protection material. The introduction of the section factor concept enables a broader use of fire test data to be made, leading to economy while maintaining the required performance standard. A steel section with a large perimeter (H_p) will receive more heat than one with a smaller perimeter. In addition, the greater the cross-sectional area (A) of the section, the greater is the heat sink. It follows therefore that the increase in temperature for a small thick section will be slower than for a large thin one. Section factor is thus a measure of the rate at which a section will heat up in a fire. The higher its value the greater will be the protection thickness required.



(a) Elevation and section views



(b) Position of thermocouples

Figure 3: The ASB test beam

According to BS 5950: Part 8, the thickness of fire protection for the regular beams, d_i, is determined from the formula [Newman & Lawson (1991)]:

$$d_i = (H_p/A)\,\lambda_i\,[t_e/(40(\theta_s - 140))]^{1.3}\,F_w \qquad (1)$$

where λ_i = thermal conductivity of the fire protection material; t_e = fire resistance (min); θ_s = limiting temperature of the section; F_w = modification factor (<1) due to the density of the protection material; H_p = perimeter of section exposed to fire (m); and A = cross sectional area of the steel member (m^2).

Because the shallow floor beams have a different cross sectional shape compared to the regular steel section the thickness of fire protection required might be different from what is obtained using the above formula. To derive the formula for shallow floor beams the first task is to calculate the section factors of the shallow floor beams used in the previous fire tests. Now rearranging the formula like the following:

$$d_i/(H_p/A) = \lambda_i [t_e/(40(\theta_s - 140))]^{1.3} F_w \quad (2)$$

As the d_i, H_p, A, θ_s and t_e are known the plot of $d_i/(H_p/A)$ against $[t_e/(\theta_s - 140)]^{1.3}$ should yield a linear relationship. θ_s is the section temperature measured at time t_e in the fire test, t_e being 90 and 120 minutes. The values of these and the other parameters are listed in Table 1. From this the combined coefficients of λ_i, F_w and $40^{-1.3}$ can be found.

RESULTS AND DISCUSSION

Table 1 includes the values of d_i, H_p and A calculated with the beam condition used in the fire tests. Figure 4 shows the graph of $d_i/(H_p/A)$ against $[t_e/(\theta_s - 140)]^{1.3}$. The 19 data points in the figure are from the 19 temperature values in the last two columns of Table 1. It may be noted that in the last row of Table 1, there is no datum collected in the fire test corresponding to 90 minutes, resulting in the odd number of the total data points. Both coatings, from the three test facilities, are shown in the figure, as little difference was found in their performance. The figure also displays a best-fit line, which has a coefficient of determination (R^2) of 0.89. As mentioned before, these shallow floor beams are almost contained within the floor slab. They have very good performance in fire and in most cases can achieve 60 minutes fire resistance without applied protection. The graph in Figure 4 only includes the values of $d_i/(H_p/A)$ plotted against the values of $[t_e/(\theta_s - 140)]^{1.3}$ at 90 and 120 minutes fire resistance. The equation for the best-fit line represents the required thickness of fire protection to the shallow floor beams:

$$d_i/(H_p/A) = 0.263 [t_e/(\theta_s - 140)]^{1.3} - 0.016 \quad (3)$$

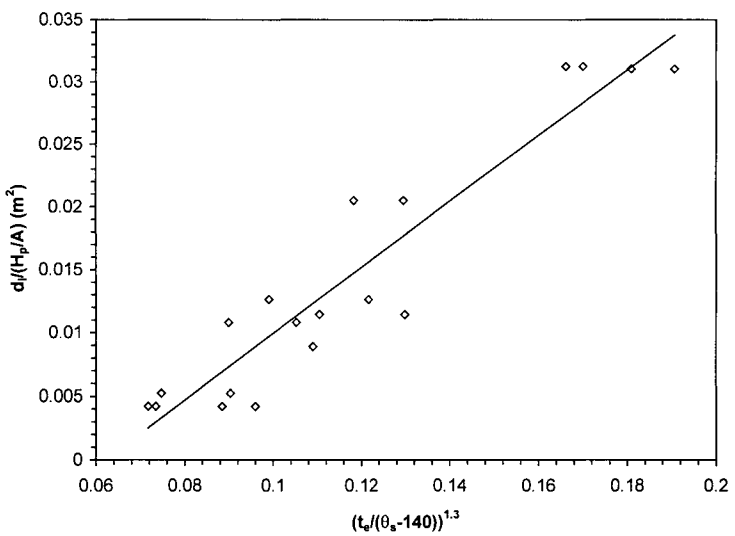


Figure 4: $d_i/(H_p/A)$ against $[t_e/(\theta_s - 140)]^{1.3}$ from fire test data

Obviously the combined coefficients of λ_i, F_w and $40^{-1.3}$ are represented in 0.263. The significant difference between this formula and the original formula for the regular section (Eqns. 1 and 2) is that this formula has a negative constant (–0.016) added into it. This indicates that the required thickness of fire protection for the shallow floor beams is thinner than for the regular steel beams. This formula is useful for the engineers for quick determination of the required thickness of fire protection.

The steel temperatures at various parts of a shallow floor beam can also be calculated from heat transfer models [Sha (2001b)]. This was carried out with a Slimflor beam of the same dimension as used in the fire tests [Sha & Lau (2001)]. Figure 5 shows the calculation results, in the form of the plot of $d_i/(H_p/A)$ versus $[t_e/(\theta_s - 140)]^{1.3}$. The thermoconductivity of the intumescent coating used in the calculations was 420 W/m°C. The typical variance in the thermal conductivity (λ) of steel is included in the program, in the form of $\lambda = 54 - 0.033\ (T - 20)$ where T is the steel temperature in Celsius. When T is greater than 829°C, λ remains at 27.3 W/m°C. The relationship between $d_i/(H_p/A)$ and $[t_e/(\theta_s - 140)]^{1.3}$ for plate is:

$$d_i/(H_p/A) = 0.186\ [t_e/(\theta_s - 140)]^{1.3} - 0.021 \tag{4}$$

and for flange:

$$d_i/(H_p/A) = 0.345\ [t_e/(\theta_s - 140)]^{1.3} - 0.031 \tag{5}$$

The coefficients of determination (R^2) are 0.9997 and 0.995 for plate and flange, respectively. The value 140, embedded in Eqns. 4 and 5, is an assumption.

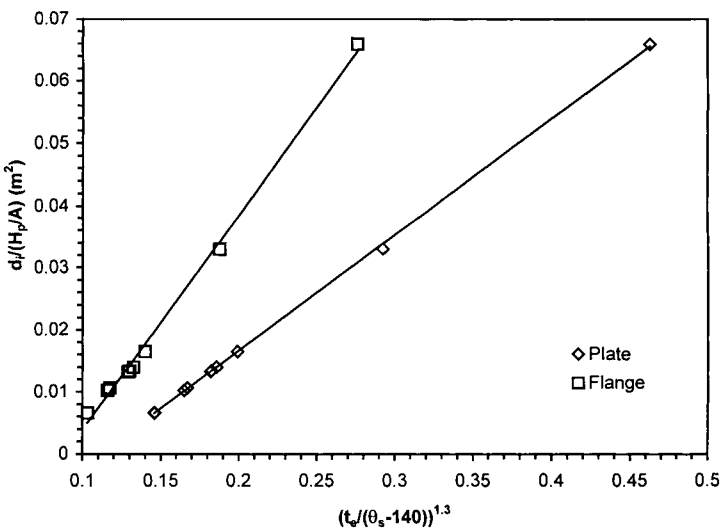


Figure 5: $d_i/(H_p/A)$ against $[t_e/(\theta_s - 140)]^{1.3}$ from heat transfer model calculation

SUMMARY

From fire test data the required thickness of intumescent coating for fire protection of shallow floor beams is derived. The thickness is thinner than for regular steel beams because of a negative constant. The formula can be used for quick, simple design calculation for the required thickness of fire protection. For design purposes there should be a safety factor used in conjunction with the formula.

REFERENCES

Butler K.M. (1997). Physical Modelling of Intumescent Fire Retardant Polymers. *ACS Symposium Series*, vol. 669, ch. 15, Science and Technology, ed: K.C. Khemani, American Chemical Society, Washington, pp. 214–230.

Fire Protection for Structural Steels in Buildings (1992). 2nd edn., Association of Specialist Fire Protection Contractors and Manufacturers (ASFPCM), Aldershot, UK.

FTP Code: International Code for Application of Fire Test Procedures (Resolution MSC.61(67)) Including Fire Test Procedures Referred to in and Relevant to the FTP Code (1998). International Maritime Organization, London, UK.

Newman G.M. and Lawson R.M. (1991). *Fire Resistance of Composite Beams*, Steel Construction Institute, Ascot, UK, p. 37.

Ngu T. L. (1999). *Modelling of Fire Resistance of Steel Floor Structures*, Appendix D, Project for BEng in Civil Engineering, The Queen's University of Belfast, Belfast, UK.

Sha W. (1997a). *The Fire Resistance of Slimflor Beams Protected Using Intumescent Coatings S605 and S607*, Report to Nullifire Ltd., Document RT629, Steel Construction Institute, Ascot, UK.

Sha W. (1997b). *The Fire Resistance of Asymmetric Slimflor Beams Protected Using Intumescent Coatings S605 and S607*, Report to Nullifire Ltd., Document RT655, Steel Construction Institute, Ascot, UK.

Sha W. (1998). Fire Resistance of Floors Constructed with Fire-resistant Steels. *Journal of Structural Engineering* **124:6**, 664–670.

Sha W. (2001a). Fire resistance of slim floors protected using intumescent coatings. *Proceedings of The Eighth International Conference on Civil and Structural Engineering Computing*, ed: B.H.V. Topping, Civil-Comp Press, Stirling, UK, Paper 65.

Sha W. (2001b). Heat transfer in fire across a wall in shallow floor structure. *Journal of Structural Engineering* **127:1**, 89–91.

Sha W. and Lau N. C. (2001). Temperature development during fire in slim floor beams protected with intumescent coating. *Structural Engineering, Mechanics and Computation*, vol. 2, ed: A. Zingoni, Elsevier Science, Oxford, UK, pp. 1103–1110.

Task Report (1993). Task No. 250000.10/93.015, SINTEF NBL Norwegian Fire Research Laboratory.

Todd A. (1996). *Steel or concrete, the economics of commercial buildings*, British Steel Sections Plates & Commercial Steels, Cleveland, UK.

ENVIRONMENTAL TECHNOLOGIES:

INDOOR ENVIRONMENTAL CONTROL

This Page Intentionally Left Blank

Advances in Building Technology, Volume 2
M. Anson, J.M. Ko and E.S.S. Lam (Eds.)
© 2002 Elsevier Science Ltd. All rights reserved

THE AIRFLOW AROUND AND INSIDE HIGH-RISE RESIDENTIAL BUILDINGS IN HONG KONG

Bojic, M., Yik, F., Burnett, J.,

Research Centre for Building Environmental Performance, Department of Building Services Engineering, The Hong Kong Polytechnic University, Hung Hom, Kowloon, Hong Kong SAR, China

ABSTRACT

The airflow around and inside high-rise residential buildings in Hong Kong has been studied, with focus put on four major aspects: pedestrian wind environment, air-conditioner heat rejection, natural ventilation, and indoor air movement. The pedestrian wind studies showed that CFD simulation is an appropriate and effective method essential to designs of estate layouts to avoid excessive wind amplification and stagnant regions. The heat rejection studies showed that the dimension of recessed spaces should be checked taking account of the positions of window-type air conditioners and the amount of the rejected heat to avoid energy wastage and cooling capacity loss. Methods have been proposed to mitigate the problem. The natural ventilation studies assessed availability of natural ventilation in a typical building design. The indoor air movement studies looked into the impacts of the installed location of a window-type air conditioner on the indoor air movement pattern and thermal comfort of occupants.

KEYWORDS

CFD, pedestrian wind, recessed spaces, air-conditioner performance, natural ventilation, indoor air movement

INTRODUCTION

Good environmental performance of high-rise residential buildings is of vital importance to Hong Kong because an enormous number of residential units already exist and tens of thousands of new units are developed each year. To enhance their performance, we should evaluate and improve new designs of rooms, flats, entire buildings, and entire estates. The Hong Kong Building Environmental Assessment Method (HK-BEAM), which is a voluntary assessment scheme available in Hong Kong, provides good practice guides, including a list of issues of importance and benchmarks of building environmental performance (BEC, 1999). Research studies are ongoing in support of further development and enhancement of these guidelines, and to provide advice on improved new designs to ensure good thermal comfort and air quality inside and outside the residences, and to minimise adverse impacts on the environment in the global, local and indoor scales.

One of the major areas being pursued has been on the airflow around and inside high-rise residential buildings. The study on indoor and outdoor airflows were performed primarily using computational fluid dynamics (CFD) simulation, with the use of software packages such as FLUENT 5.0, FLOVENT, and a multi-zone airflow model COMIS. The research studies on airflow around buildings concerned with wind flow within an entire estate and the buoyant flow inside recessed spaces immediately outside high-rise buildings due to heat rejection by air conditioners. The aims of the studies include to ensure comfort of pedestrians and users of amenities; and to minimise impact of the confined recessed space on the electricity consumption of air conditioners. Research has also been done on airflow inside buildings, looking into utilisation of natural ventilation in residences for enhancing indoor air quality and minimising energy use for comfort control, and into airflow inside rooms for enhancing thermal comfort. This paper reviews these studies, summarizing their results, drawing some conclusions, and giving recommendations for their use in practice. For details of these studies and applied techniques, the reader is directed to recent papers dealing with specific topics.

FLOW AROUD A BUILDING

Airflow on Pedestrian Level (Lee, 2001)

Wind induced airflow within an estate on the pedestrian level should provide pedestrians and users of amenities with both thermal comfort and quality air. When channelled to flow around a group of buildings, the wind will accelerate or decelerate to an extent that depends on the layout of building blocks in the estate and the shape of the buildings. High wind speeds cause thermal discomfort to pedestrians and in the extreme cases could be dangerous to them whereas stagnant air causes pollution problem and deposition of debris in amenities areas.

The results of the CFD study on an existing high-rise estate in Tseung Kwan O of Hong Kong are presented here (Lee, 2001). The estate is shown in Fig. 1. In the CFD study, the flow was computed by using roughly 500,000 cells in the 3D meshes (shown in Fig.2). Then, the software FLUENT 5.0 was used in conjunction with the standard k-ε model. The velocity vectors and wind amplification factor distributions for the case with Northeasterly wind on the horizontal plane 2m above ground, as obtained from the CFD simulation, are shown in Fig.3 and Fig. 4. With these results, areas exposed to high and low-speed wind can be clearly seen. These CFD predictions agreed well with the results from an erosion test in a wind tunnel (CU, 2000). They also agreed in an order of magnitude with measurements at the actual site. Note, that the boundary conditions set at CFD simulations were the same as that set in the wind tunnel.

Air-Conditioner Heat Rejection in Recessed Spaces (Bojic et al, 2001a&b, 2002 a-f)

The heat discharged by condenser units of window-type air conditioners into a recessed space may lead to excessive use of electricity by air conditioners at higher levels, which should be avoided. Some typical locations of these air conditioners inside the recessed spaces are shown schematically in Fig.5. A photo of one recessed space containing four window-type air-conditioners per storey is shown in Fig.6. The CFD code FLUENT 5.0 and the k-ε model were used to predict the temperature and flow fields inside different recessed spaces. The results show that there would be powerful rising hot air streams inside these spaces. A velocity field on a horizontal plane inside the recessed space is shown in Fig.7. This figure has been selected as the cover page figure for the journal *Energy and Buildings*. The velocity and temperature field on a vertical plane is shown in Fig.8.

The effects of varying the height (Bojic et al, 2001a), depth (Bojic et al, 2002a), locations of air conditioners (Bojic et al, 2001a), and the amount of rejected heat (Bojic et al, 2002a,b) in a recessed

space were studied. The results show that condenser units of air-conditioners at the top levels would draw less air at an elevated temperature, and, therefore, would consume much more electricity than



Figure 1: Tseung Kwan O Site

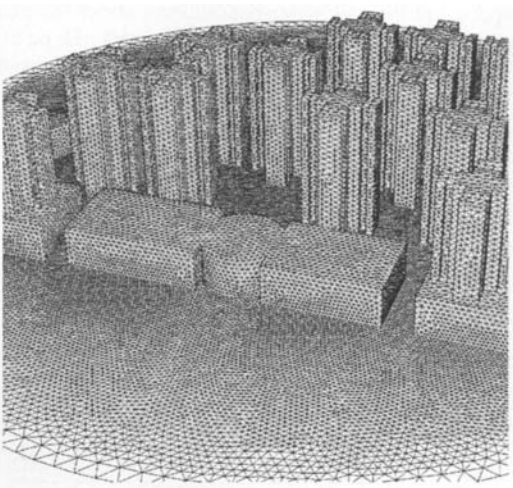


Figure 2: The unstructured grid of the Tseung Kwan O site

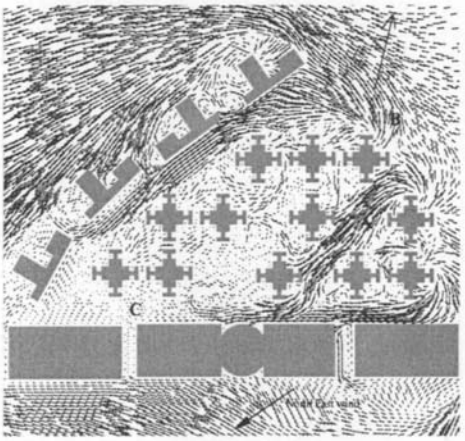


Figure 3: The velocity vector plot based on the CFD results of a 3D simulation.

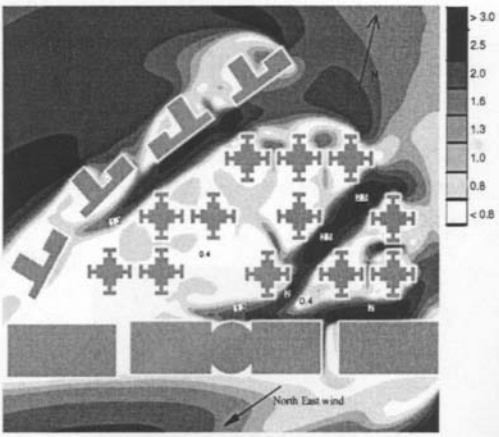


Figure 4: The contour of the wind amplification factor predicted by a 3D simulation.

they should, and would at the same time suffer from reduced output capacity. The energy consumption of the topmost units could be reduced by around 10% with a reduction in the height of the recessed space by five stories, or a reduction in the rejected heat by 5%, or an increase in the air conditioner distance from the corner wall by 1.1m. However, the energy consumption would not change with a variation in the depth of the recessed space.

Furthermore, the provision of horizontal plates inside the recessed space has been proposed as a mitigation measure, which would divert the hot air plume from below to flow outside the recessed space and thus allow air-conditioners above the plate to draw in cool outdoor air for condenser heat removal. The effects of installing one plate (Bojic et al, 2002c) and several plates (Bojic et al, 20002d) have been studied. Provision of one plate inside the recessed space would on average lower the electricity consumption of the topmost air conditioners by 15%, and provision of two plates by 48%. These results would inform design for the avoidance of excessive use of electricity by air conditioners in recessed spaces.

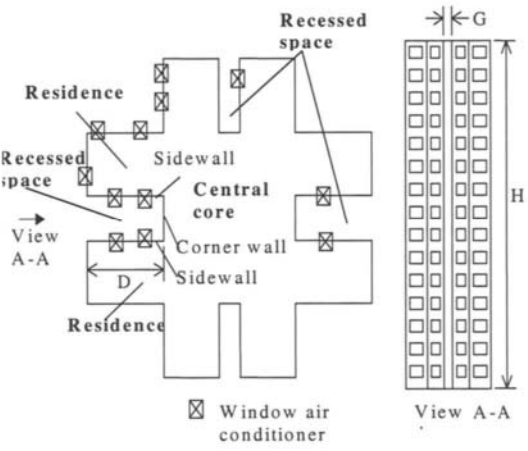


Figure 5: Layout of a Recessed Space of a High-rise Residential Building

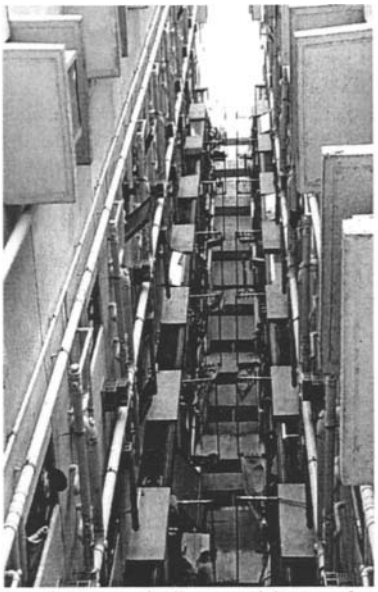


Figure 6: Photo of a Recessed Space of a High-rise Residential Building

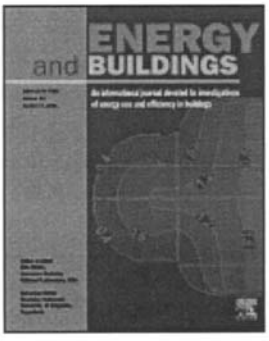


Figure 7: Cover Page of Energy and Buildings journal - Velocities contours at a horizontal plane

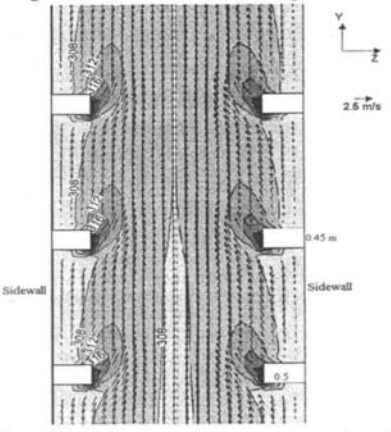


Figure 8: Velocity and temperature at vertical symmetry plane

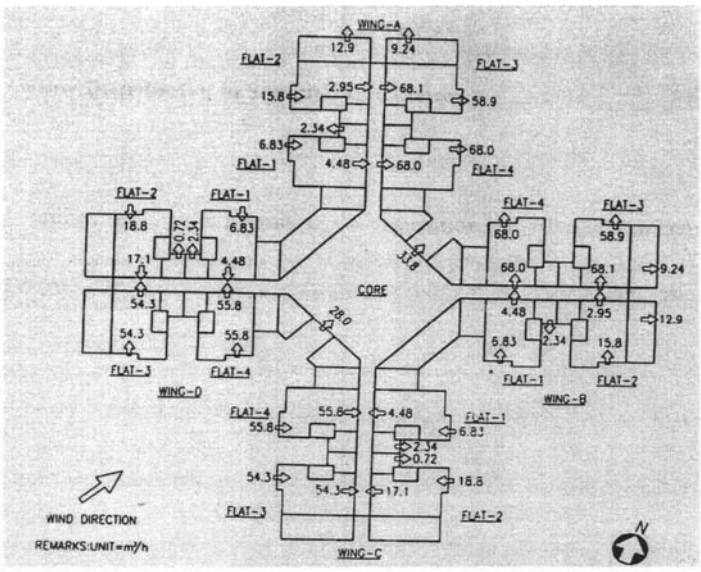


Figure 9: Flow distribution for 10th floor at the wind speed of 4m/s with inside/outside temperature difference of 12^0C

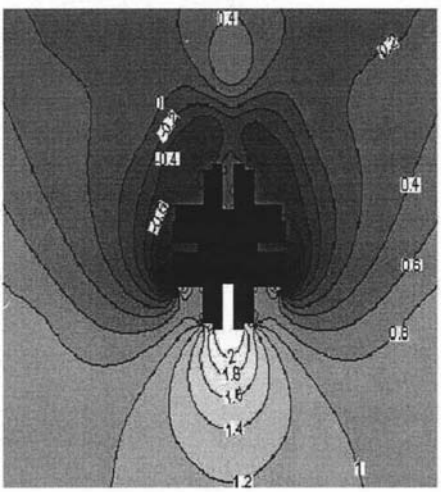


Figure 10: Result of FLUENT on wind pressure coefficient.

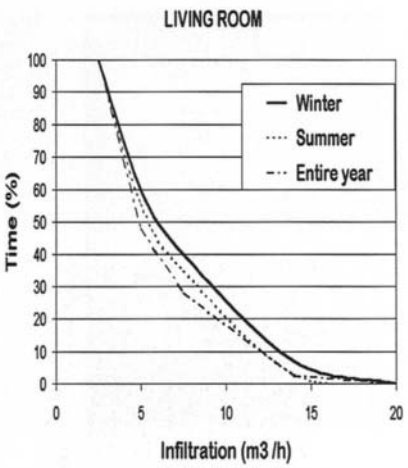


Figure 11: Cumulative time of occurrence of various infiltration rates inside a living room

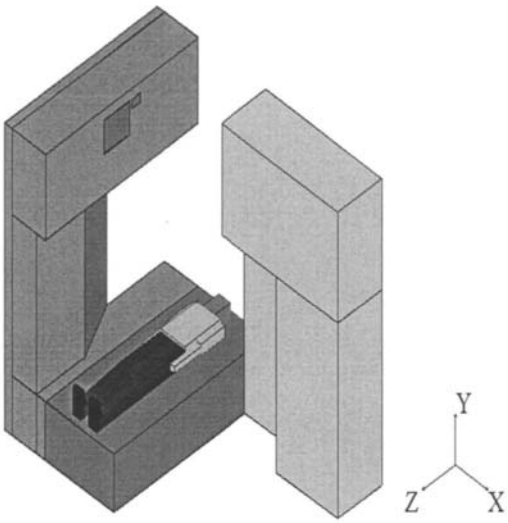


Figure 12: Three dimensional scheme of the investigated room

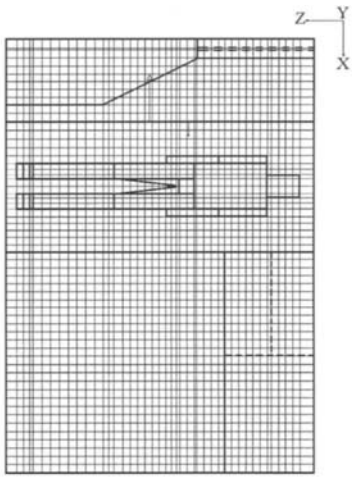


Figure 13: Plan view of grid applied in the investigated room

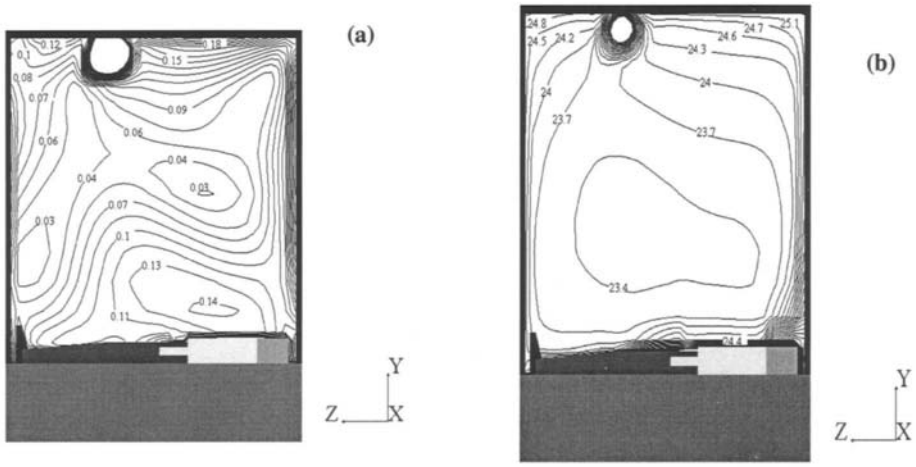


Figure 14: Contours of (a) velocity and (b) temperature on the symmetry plane of the sleeping man.

FLOW INSIDE A BUILDING

Natural Ventilation (Chan, 2001)

Ventilation provision in residential units is essential, for dilution of indoor air pollutants, such as radon, odours, and moisture, so as to ensure acceptable indoor air quality. For minimising the

associated energy use, sufficient ventilation should, as far as possible, be achieved by natural ventilation, although mechanical ventilation or air-conditioning would still be required for quick purging of pollutants at high concentration levels or for thermal comfort control in hot summer days.

As an example, the result of applying the multi-cell airflow simulation program COMIS to modelling the airflows in the flats on one floor of a typical residential building is presented here. This study was performed for summer and winter and for several wind speeds that may be expected at the building site. The floor plan of the studied building is shown in Fig. 9. Wind pressure coefficients were first determined from a CFD simulation of the outdoor airflow using FLUENT, as shown in Fig. 10. The air movements between indoors and outdoors and from room to room inside the flats on the 10^{th} floor of the building, as predicted by COMIS, are shown in Fig. 9. The result shown was pertaining to a wind speed of 4m/s and an indoor/outdoor temperature difference of 12°C. The result shows that in the four building wings, Flats 3 and 4 would enjoy good natural ventilation, while Flats 1 and 2 would be poorly ventilated. However, Flats 3 and 4 of wings A and B would have ventilation air ingression from the lobby, which would not be fresh outdoor air but could have already been partially polluted as the air passed through other flats.

The COMIS simulation results also allowed the cumulative time of occurrence of various rates of infiltration in a room to be determined. Fig. 11 shows the result for one of the living rooms in the studied building. As the ventilation requirement for this room was $5m^3/h$, it can be seen that this requirement would be satisfied only for 50% of time in the year, meaning that infiltration alone would not provide adequate ventilation for that room throughout the year. This suggests that changes to the floor layout design, or the use of devices for enhancing natural ventilation (e.g. trickle vents) or mechanical ventilation, would be required.

Room Cooling (Bojic et al, 2001b, 2002f)

For rooms equipped with air-conditioners, the location for installation of the air conditioners should be carefully chosen in relation to the room and furniture layout and the position of the occupants to avoid poor air circulation and draft, which affect thermal comfort of the residents. This would be critical to relatively small rooms.
This issue has been investigated into by the application of the CFD software FLOVENT and the k-ε turbulence model to model the airflow and temperature fields in a bedroom for three positions of an air-conditioner. The room layout studied was as shown in Fig. 12. A plan view of the 80,000 cells used for the simulation domain is shown in Fig. 13. Fig.14 shows the air velocity and temperature distributions on a vertical plane inside the room obtained in the simulation study. Such results would inform building designer of the optimal location for installing the air-conditioner for providing the maximum degree of thermal comfort for the occupant.

CONCLUSION

This paper presented the results of several studies done at the Hong Kong Polytechnic University on the airflows around and inside high-rise residential buildings in Hong Kong. These studies were on airflow by using CFD; first on pedestrian level due to wind; second, inside recessed spaces due to air conditioner heat rejection; third, inside high-rise buildings due to natural ventilation; and finally inside a room due to operation of the air-conditioner. As CFD approach is restricted due to limited computer memory and speed, problems of scaling, and that of turbulence modelling, CFD and multi zone analysis used at design stage would give order of magnitude values that are consequences of such a design.

For a new estate design, a CFD analysis of the layout of building blocks would help to avoid exceedingly high wind amplifications or stagnant zones. The results of such a study will provide a

visualisation of the wind environment, allowing the master layout design of a new estate to be fine-tuned.

For a new building design, a CFD analysis of the recessed space would help to avoid excessive use of electricity and decrease in cooling capacity when the residential flats are cooled. Next, for a new building design, a COMIS and CFD analyses on assisting of natural ventilation in dwellings would help to enhance indoor air quality and minimize energy use for comfort control. Finally, for a new building design, a CFD analysis on adequate provisions for installation of air-conditioners taking into account possible locations of furniture in a room would help to enhance thermal comfort control.

Generally, the results from such studies would inform design of estate, building, residences, and interior of rooms leading to better indoor and outdoor environmental conditions and more environmentally sustainable housing development.

Acknowledgements

The work is being undertaken within the Centre for Building Environmental Performance, Department of Building Services Engineering. The authors wish to acknowledge the financial support provided by The Hong Kong Polytechnic University under the Area of Strategic Development in the Faculty of Construction and Land Use.

References

BEC (1999). *HK-BEAM An Environmental Assessment for New Residential Buildings*, Business Environment Council (formerly Centre of Environmental Technology Limited).

Bojic, M., Lee, M., Yik, F. (2001a). Flow and Temperatures outside a High-Rise Residential Building due to Heat Rejection by Its Air- Conditioners. *Energy and Buildings*, **33:7,** 737-751.

Bojic, M. Yik, F. Lo, T.Y. Lee, M. (2001b) Locating Air-Conditioners and Furniture inside Residential Flats, In: Indoor Environment Technology Towards A Global Approach, 7th Rehva World Congress: Clima 2000, Napoli 2001, Naples, Italy, September 15 to 18, HVAC Systems and Equipment, C06, 72-81.

Bojic, M., Lee, M., Yik, F., (2002a). Influence of a Depth of a Recessed Space to Flow Due to Air-Conditioner Heat Rejection. *Energy and Buildings*, **34:1** 33-43.

Bojic, M., Yik, F., Lee, M., (2002b). Influence of Heat Rejected by Air Conditioners to Flow Inside a Recessed Space. *Building research and information*, Article in press.

Bojic, M., Yik, F., Lee, M., (2002c). Influence of Heat Rejected by Air Conditioners to Flow Inside a Recessed Space with One Plate. *Transactions of ASHRAE*, Article in press.

Bojic, M., Yik, F., Lee, M. (2002d). Influence of Plates on Flow inside a Recessed Space Generated by Rejected Heat. *Building and Environment*, Submitted article.

Bojic, M., Yik, F., Lo T.Y. (2002e). Locating Air-conditioners and Furniture inside Residential Flats to Obtain Good Thermal Comfort. *Energy and Buildings*, 34/7 (2002) 745-751.

Chan, K.M., (2001). *Application of COMIS to Investigate the Ventilation of Residential Units in High-Rise Residential Units in High-Rise Residential Building in Hong Kong*. Meng. Dissertation, The Hong Kong Polytechnic University.

CU (2000). Environmental Studies of High Rise Residential Buildings in Hong Kong, Tseung Kwan O area 59, Cardiff University, The Hong Kong Polytechnic University.

Lee, M.M. (2001). Application of CFD to Improve the Design of High-Rise Estates. *HKIE transactions*, **8:1,** 13-22.

Advances in Building Technology, Volume 2
M. Anson, J.M. Ko and E.S.S. Lam (Eds.)
© 2002 Elsevier Science Ltd. All rights reserved

BUILDING VENTILATION 'HEALTH' CHECKS

Phil Jones
Welsh School of Architecture,
Cardiff University

ABSTRACT

This paper describes the production of a Ventilation Check Technical Memorandum produced by the Chartered Institute of Building Services Engineers (CIBSE) through a UK government funded Partners in Innovation (PII) project. The procedure comprises a checklist and standard method that outlines the tasks and procedures necessary to maintain a ventilation system in good working order. It is designed to highlight areas of inefficient performance of a system to enable remedial action to be taken. The tool provides a standardised approach to ventilation system maintenance that is applicable to the non-domestic building stock, and supports the adoption of good practice across the building services profession.

KEYWORDS

Ventilation, check-list, non-domestic buildings, performance testing.

INTRODUCTION

This paper describes a new CIBSE Technical Memorandum (TM) for carrying out regular checks on ventilation systems in non-domestic buildings. Most buildings require ventilation, whether by natural means through purpose made openings, or with mechanical assistance. Regular inspection and maintenance of a ventilation system is essential to ensure that it is operating effectively and efficiently. It should provide good air quality for the health, comfort and productivity of the occupants, or appropriate to any process, whilst optimising energy efficiency.

The concept of ventilation checks is not new. Compulsory ventilation performance checks have been undertaken in Sweden since 1991 and are based mainly on two Swedish law acts; the Swedish Planning and Building Act (PBA 1987:10) and the Swedish Work Environment Act (1977:1160). Both apply to a good indoor climate and the owner of the building is responsible for ensuring this

The TM provides guidance for building owners or operators and facilities managers to carry out a regular performance check of a building ventilation system with reference to health and safety, and energy use. It is designed as a guide to check that the ventilation system installed in the building is

clean and delivers the correct volume and reasonable quality of air into the spaces where it is required..

The TM outlines a range of measures for inspecting a building and its ventilation system. These are selected to highlight areas where systems may be performing poorly and require remedial action. These measures are set out in checklists that are applicable to any non-domestic building. The anticipated benefits through using the TM include:

- Identification of poorly performing systems
- Validation of properly performing systems
- Enhanced occupant satisfaction.
- Improved productivity due to effective operation of ventilation systems
- Reduced energy costs

BACKGROUND

The technical knowledge and professional experience needed to maintain ventilation systems are widely available. However, owners and operators of buildings do not always appreciate the need for regular maintenance and the negative impact that poorly maintained systems has on energy efficiency and the indoor environment.

Poor indoor air quality may adversely affect productivity (CIBSE TM24, 2001) and inefficient operation will waste energy. Even well designed buildings may be compromised throughout their working life by poor and inefficient operation. Problems may also arise if the function of the ventilation system is not properly considered when buildings undergo a change of use or layout. Also, it is generally recognised that air-conditioned buildings require high levels of maintenance to maintain efficient operation and, for example, reduce the risk of sick building syndrome (Ventilation and health in non-industrial Environments, 2001).

The use of the TM relates directly to satisfying the requirements of UK Health and safety at work legislation, which requires the provision of effective and suitable ventilation, and that systems should be regularly and properly cleaned, tested and maintained (Workplace health, safety and welfare, 1992). They should deliver minimum recommended ventilation rates (CIBSE Guide B2 2001) should not cause uncomfortable draughts for occupants and within reason remove odours.

In addition the TM responds to new requirements from Part L (Building Regulations Approved Document Part L2, 2002) of the UK Building Regulations, and proposed European legislation on energy performance in buildings. Approved Document L2 of the Building Regulations introduces a requirement that 'the owner/occupier of a building should be provided with details of the installed building services plant and controls, their method of operation and maintenance, and other details that collectively enable energy consumption to be controlled.' These details include the basic information about the building that is required to undertake this ventilation system check. Approved Document L2 also allows for air leakage tests be carried out on certain building types, and sets new requirements for specific fan power in new and refurbished buildings.

The proposed Directive of the European Parliament and of the Council on the energy performance of buildings (Directive of the European Parliament and of the Council on the energy performance of buildings, 2001) will cover *'specific inspection and assessment of boilers and heating/cooling installations'*. It includes installed equipment for air-conditioning and ventilation and regular maintenance of air conditioning systems

THE VENTILATION CHECK

The procedure contains two levels of survey (Figure 1). Before these are carried out it is advised that base data on the building, its installations and usage in the form of a building log book is compiled.

Building Description

The new Part L2 introduces a requirement that 'the owner/occupier of a building should be provided with details of the installed building services plant and controls, their method of operation and maintenance, and other details that collectively enable energy consumption to be controlled.' These details will almost always include the basic information about the building that is required to undertake a ventilation system check. The log book is only required for new buildings granted planning consent after 1st April 2002. It is also likely to be provided for some refurbishment works approved after that date. In all other cases the basic information for the ventilation checklist will have to be assembled. Ideally this will be made available by the client prior to any visit to the site. Details of the building for inclusion in the building log book should be collected under the following headings:

- The building
- Ventilation system
- Occupancy and building use

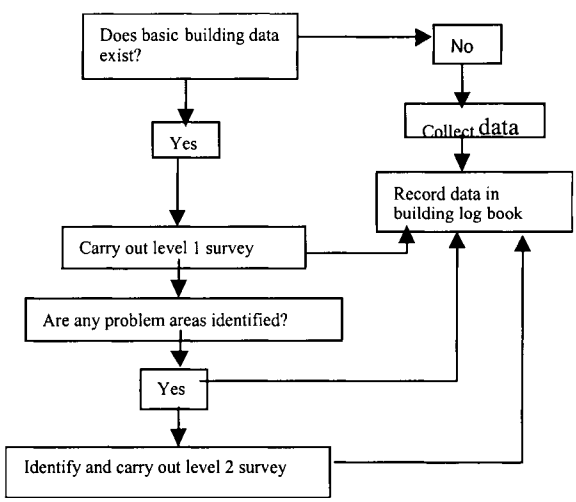


Figure 1: Diagram of survey procedure

Level 1 survey

This survey provides a basic assessment of performance. It is of the form of an annual 'walk-through' survey using observation and instantaneous measurements. On most buildings it should be possible to carry out a Level 1 survey within one working day, providing the building log book information is available and good access is provided. This survey provides a basic assessment of performance.

The use of a camera to record any relevant issues is advisable. Simple spot check measurements may be used to validate performance where appropriate, for example, to check temperatures, RH, CO_2 levels, air velocities, static pressure etc.

The survey will provide the following information:

- Indoor Air Quality
    - *Occupancy Satisfaction:*
    - *Fresh air supply:*
    - *Pollutant audit:*
- Comfort
- Air Leakage
- Room Air Delivery
- Cooling and Heating
- Energy Efficiency
- Equipment
- Cleanliness

The building should be ranked as follows:

1) needs major remedial action immediately
2) certain areas need attention without delay
3) system satisfactory

Factors that need to be addressed at a level 2 survey should be identified.

- An update information in the building log book,
- A report on the effectiveness building ventilation system,
- Any recommendations for remedial or repair work,
- The need for more detailed surveys where appropriate.

Level 2 surveys

These involve more detailed surveys that may be undertaken as a matter of routine or may be identified as required under the Level 1 survey to address specific problem areas or dealing with complex ventilation systems. Level 2 surveys include a more detailed survey of the performance of the ventilation system, which might include monitoring conditions over a period of time and undertaking occupancy surveys. Actions that might be carried out under a Level 2 survey might include:

- Comfort and air quality measurements:
    - *Occupant surveys*
    - *Carbon Dioxide Monitoring*
    - *Gaseous sampling –*
    - *TVOC's*
    - *Formaldehyde*
    - *Microbial sampling*
    - *Particulate measurement -*
    - *Cleaning*
- Energy measurement:
    - *Specific fan power*
    - *Energy audit*

- Check on Control Equipment

BENCHMARK INFORMATION

The ventilation system can be checked against:
- current good practice
- current best practice

For older buildings that may not be designed to current good practice, the survey will identify what action is needed to bring them to current good practice standards. This may be targeted to take place during a programme of refurbishment.

The benchmark data relating to current good and best practice is listed below in Table 1 for the test criteria.

TABLE 1
BENCHMARK DATA

Criteria	**Benchmark**	**Good practice**	**Best practice**
Indoor Air Quality	Carbon Dioxide (CO_2) (ppm)	1000	< 600
	Occupant Dissatisfaction	10-20%	5-10%
	Fresh Air Supply (l/s)	8 l/s	12 l/s
Criteria	**Benchmark**	**Good practice**	**Best practice**
Comfort	Air Velocity (m/s)	<0.15 (80%)	0.15 m/s (100%)
Air Leakage	Refer to CIBSE TM 23	/	/
Room Air Delivery	Ventilation Effectiveness		
	Mixing system	>80%	>90%
	Displacement system	>100%	>110%
Energy Efficiency	Specific Fan Power $kW/(m^3/s)$	<3	<2
Cleanliness	Cleanliness of system	no visible dust	regular cleaning & filter changes

References

CIBSE TM24, (2001)
Ventilation and health in non-industrial Environments. Report from a European Multi-disciplinary Scientific Consensus Meeting Clima 2001 September 2001.
Workplace health, safety and welfare, Workplace regulations 1992
CIBSE Guide B2 (2001)
Building Regulations Approved Document Part L2 (2002)
Directive of the European Parliament and of the Council on the energy performance of buildings 2001 COM (2001)266 (Draft)

This Page Intentionally Left Blank

Advances in Building Technology, Volume 2
M. Anson, J.M. Ko and E.S.S. Lam (Eds.)
© 2002 Elsevier Science Ltd. All rights reserved

Application of Titanium Dioxide in Refuse Collection Point

K.F. LAU, Andy M.T. SUEN, Arthur C.C. TANG

Building Services Branch, Architectural Services Department,
Government of the Hong Kong Special Administrative Region

ABSTRACT

Photo-catalysis is an advanced oxidation process for decomposing organic pollutants in water and air. Titanium Dioxide (TiO_2) is a semiconductor and it has been proved to be the best among the other semiconductor materials tested for photo-catalysis due to its strong oxidizing power under UV illumination and also its chemical stability. Extensive scientific studies on photo-catalytic chemistry of Titanium Dioxide have been carried out over the past 25 years. The studies done so far have proved that Titanium Dioxide is very effective in the removal of organic and inorganic compounds from contaminated water and air. Recently, the Architectural Services Department of the HKSAR Government has carried out a pilot project on the application of Titanium Dioxide where the internal wall surfaces of a newly completed Refuse Collection Point (RCP) were coated with this material. The indoor air quality (IAQ) of this RCP was then measured and the results were compared to the indoor air quality of another RCP of similar construction and locality but without Titanium Dioxide wall coating. This paper presented the measured IAQ data of the two RCPs and the data are also compared and discussed. The paper also looked at the way forward for the application of Titanium Dioxide in the construction industry.

KEYWORDS

Photo-catalysis, Semiconductor, Titanium Dioxide (TiO_2), Air Pollutants, IAQ.

INTRODUCTION

Global environmental pollution has long been an undeniable social problem that needs to be addressed imminently. According to researchers, Titanium Dioxide (TiO_2) has the ability to combat pollution due to its photo-catalytic property and this technology is becoming more and more appealing to the industry today.

When TiO_2 is applied to a surface, the surface will have the effects of self-sterilizing, anti-bacteria, anti-virus, anti-fungi, self-cleaning, anti-fogging, stain-proof and easy cleaning. Experiments also showed that when TiO_2 is used, the low-intensity UV radiation from various types of indoor lighting fixtures such as fluorescent lamps is already sufficient to photo-catalytically decompose nearly all

pollutants in indoor environments. If the pollutants are carbon compounds like aldehydes, they will be completely decomposed to carbon dioxide and leaving nothing behind. If the pollutants are those containing nitrogen and sulphur, their products such as nitric acid and sulphuric acid would stay on the TiO_2 surface [1].

Titanium Dioxide

Titanium Dioxide is a solid semiconductor. It is a colourless material and begins to melt at over 1800 ^0C [2]. It is one of the most basic materials in our daily life. Due to its high refractive index, durability, strength, non-toxicity, dispersion, tinting, and chemically inert nature, it has been widely used for coatings, enamels, paints, lacquers, inks, leather finishes and ceramics. Normally, it has to be developed to a particle size of about 0.3 microns so that one may realize its special properties. It has also been proved to be the best among the other semiconductor materials tested for photo-catalysis due to its strong oxidizing power under UV illumination and also its chemical stability.

Photo-catalytic Action

Photo-catalysis is an advanced oxidation process for decomposing organic pollutants in water and air. Extensive scientific studies on photo-catalytic chemistry of TiO_2 have been carried out over the past 25 years. The studies done so far have proved that TiO_2 is a very effective photo-catalyst in the removal of organic and inorganic compounds from contaminated water and air.

There are three prerequisite conditions for the photo-catalytic action to function satisfactorily. Firstly, the decomposition reaction only occurs when light energy (ultra-violet portion) is utilized by the catalytic action of TiO_2. Secondly, the photo-catalytic reaction will not take place unless a substance of interest is brought into contact with the surface of TiO_2. Thirdly, which is also most important, the reactions only take place when UV light reaches the TiO_2 surface. When all these three conditions are satisfied, the photo-catalytic activity of TiO_2 plays a positive role which decomposes organic materials such as dirt, grime, malodorous chemicals, irritants, toxic chemicals, smoke residues, bacteria, etc. that come into contact with it. This effect gives rise to the well-known phenomenon of paint chalking, where the organic components of paint break down as a result of photo-catalytic action [3].

Due to the complexity of the chemical reaction involved in the photo-catalytic mechanisms, the details of the chemical reactions will not be covered in this report. In essence, a photo-catalyst is a substance that would be activated by a photon. Activation of the chemical reaction of a semiconductor photo-catalyst is achieved through the absorption of a photon of ultra-band energy, which results in the promotion of electrons from the filled level to the vacant level, generating an electron-hole pair. This electron-hole pair is the primary photoproduct formed upon the excitation of a semiconductor and has a finite lifetime to allow a separate site for the oxidative and reductive half-reactions to occur [4].

PILOT TiO_2 PROJECT

The Architectural Services Department is responsible for the design and construction supervision of Refuse Collection Points (RCPs) for the Food and Environmental Hygiene Department. As there are staff/workers who would stay inside the RCPs for a long period of time everyday, the indoor air quality (IAQ) inside RCPs has always been one of our main concerns. As such, sufficient mechanical ventilation as well as various types of air purification equipment such as water scrubbers, electrostatic filters, UV sterilizers and bio-oxygen generators, etc. are provided at these RCPs to improve the indoor air quality.

To further enhance the IAQ of RCPs, we have carried out a pilot project recently on the application of TiO_2 where the internal wall surfaces of a newly completed RCP were coated with this material. The air pollutants concentration in this RCP was then measured and the results were compared to the air pollutants concentration of another RCP of similar construction and locality but without TiO_2 wall coating.

The Refuse Collection Points

A Refuse Collection Point (RCP-1) located at Kowloon Tong is a newly completed two-storeyed building and consists of a refuse collection chamber on ground floor and offices and plantrooms on the upper floor. The refuse collection chamber has a floor area of $160m^2$ approximately. Ducted mechanical ventilation system is provided inside the refuse collection chamber which is connected to a water scrubber system. The water scrubber system is provided to ensure that smelly exhaust air from the RCP will not cause nuisance to the residents nearby. As the indoor air quality inside the refuse collection chamber is one of our main concerns, electrostatic air filter, UV sterilizer and bio-oxygen generator are installed inside the refuse collection chamber. In addition, all the internal wall surfaces of the refuse collection chamber were applied with TiO_2 coating.

In order for the photo-catalytic action to take place, presence of UV light is vital. High intensity discharge (HID) lamps are installed at ceiling level of the refuse collection chamber and the UV contents from these discharge lamps would provide the necessary light energy for the photo-catalytic action of TiO_2.

A second Refuse Collection Point (RCP-2) that was used for comparison is located at Tai Kok Tsui and its construction and M&E provisions are similar to the previous RCP-1 except that there is no TiO_2 coating on the wall surfaces of the refuse collection chamber.

Application of TiO_2 Coatings

The use of correct method and procedures for applying TiO_2 coating is very important as it will directly affect the durability of the coating as well as its effectiveness of air pollutants removal. In this pilot project, TiO_2 solution was used and the solution was prepared in the factory and then delivered to site by the supplier. First of all, the wall tiles where TiO_2 coating would be applied were washed and cleaned with fresh water to remove all grease and dust particles. The walls were then let to dry thoroughly before the TiO_2 coating was applied. A pressurized airbrush using compressed air was used to spray the TiO_2 solution onto the surface of the wall tiles. When the first layer of TiO_2 solution was dried a second layer was then applied and all together three layers of TiO_2 solution were applied. The solution was then left to dry for 24 hours so as to achieve a rigid attachment of the TiO_2 coating on the wall surfaces.

Measurement Instrumentations

Carbon Monoxide Measurement - An Air Quality Monitor for continuous and simultaneous monitoring of 5 primary IAQ parameters including CO was used. The instrument has an electro-chemical sensor for the measurement of CO. This sensor, coupled with microprocessor and proprietary software, provide reliable, reproducible and accurate data for evaluation, assessment and control of air quality parameters.

TVOC Measurement - A ppbRAE monitor is used for the measurement and monitoring of TVOC. This equipment is installed with a microprocessor control and uses photo-ionization detector to detect a

wide range of organic vapors. Organic vapours passing through a UV lamp are photo-ionized and the ejected electrons are detected as current. The default calibration gas is Isobutylene.

On-Site Measurements

The on-site measurements at the two RCPs include two main parts, i.e. visual inspection and pollutants measurements. Before conducting on-site measurements at the RCPs, the indoor environments of the RCPs were visually inspected with great care to search for stains and blots on wall tiles. A walk through of RCP-1 and RCP-2 were carried out and locations where dirt accumulated were noted. In particular, the locations inspected included wall surfaces above drainage channels, wall surfaces close to exhaust duct air inlets and areas where garbage containers were located. The staff/workers inside the RCPs were also interviewed and their views recorded.

On-site measurement of pollutants concentration was then conducted. Due to resources constraints, the measured parameters included only carbon monoxide (CO) and Total Volatile Organic Compound (TVOC) and using culture-based sampling method. It was realized that samplings by culture-based method have their limitations it does not provide a continuous profile of monitoring [5]. However, due to time and resources constraints, culture-based methods were considered to be the most practical approach for this exercise. A measuring period of 10 minutes for each location and a logging interval of 1 minute were used.

RESULTS

Visual Inspection

For the two premises investigated, tiles on walls of RCP-1 were white in colour and were maintained in a rather clean condition even after being put into operation for almost a year. The wall surfaces appeared to have no mould growth or stain. From the interview with the staff/workers of RCP-1, it was also noted that the wall tiles required little cleaning.

On the contrary, the overall impression of RCP-2 was less favourable. Walls of this RCP were not as clean as RCP-1 and stains and blots could be seen in many wall surfaces inside the RCP even though the RCP had just been cleaned before our site measurement.

Pollutants Measurements

Several on-site measurements for CO and TVOC concentrations including indoor and outdoor locations at RCP-1 and RCP-2 were taken and recorded. The concentration profiles of CO at four measurement points of RCP-1 and RCP-2 and the concentration profiles of TVOC at three measurement points of RCP-1 and RCP-2 are taken and recorded. A comparison between the averaged air pollutants concentration data for RCP-1 and RCP-2 is summarized in table 1 below:

TABLE 1
COMPARISON OF INDOOR AND OUTDOOR AIR POLLUTANTS CONCENTRATION FOR RCP-1 AND RCP-2

	Types of Indoor Air Pollutants	Average Indoor Concentration (A)	Average Outdoor Concentration (B)	Percentage Increase at Indoor (C)
RCP-1	Carbon Monoxide	0.98ppm / (1136.5ug/m^3)	0.92ppm / (1066.9ug/m^3)	6.5%
RCP-2	Carbon Monoxide	1.24ppm / (1438.0ug/m^3)	1.07ppm / (1240.9ug/m^3)	15.9%
RCP-1	TVOC	177ppb / (409.1ug/m^3)	150ppb / (346.7ug/m^3)	18%
RCP-2	TVOC	320ppb / (739.7ug/m^3)	262ppb / (605.6ug/m^3)	22%

FINDINGS AND DISCUSSIONS

Less Stains and Easy Cleaning

As both RCPs had been put into operation for a certain period of time, it was reasonable to find dirt or stain on wall surfaces inside such an operational environment. However, from the visual inspections, wall tiles of RCP-1 where TiO_2 was applied were found to be in a better condition than those in RCP-2. Therefore, 2-fold effects could have been resulted from the TiO_2 coating. Firstly, dirt or other matters that reached the surface of the coating oxidized to become gaseous compounds and left nothing behind on the wall surfaces. Secondly, substances left behind on the coating surface had been cleaned and washed away easily.

Removal of Air Pollutants

From the data as summarized in Table 1 above, the increases in average indoor CO concentration for RCP-1 and RCP-2 are 6.5% and 15.9% respectively and the differences between the two are quite substantial. The smaller increase in average indoor CO concentration level in RCP-1 could have been resulted from the application of TiO_2 coating on the wall surfaces which removed some of the air pollutants.

As for TVOC, the increases in average indoor TVOC concentration for RCP-1 and RCP-2 are 18% and 22% respectively. Although only a small difference was observed between the two RCPs, TiO_2 could have induced some effects on the reduction of TVOC content of RCP-1.

Shortfall of this Investigation

As the two measured RCPs are not exactly identical in terms of locations as well as operational conditions, it is in fact not appropriate to have direct comparison on the measured data for RCP-1 and RCP-2. It would be more meaningful if the investigation could have been carried out at one single RCP where the site measurements could be taken at the RCP before and after the application of TiO_2 wall coating. However, due to technical and operational constraints, this was not possible at the time of this pilot project. As such, in this investigation, we can only discuss the effect of TiO_2 on the removal of indoor air pollutants with respect to the concurrent outdoor conditions for the RCPs.

THE WAY FORWARD

As a matter of fact, the effectiveness of TiO_2 in the removal of air and water pollutants has been proved and verified in many scientific researches and laboratory tests. Apparently, the pilot project carried out by the Architectural Services Department as mentioned above has also indicated that TiO_2 could have some effects in the removal of indoor air pollutants. However, it would be useful if more extensive and in-depth investigations could be carried out in future to verify the effectiveness of TiO_2 in practical applications. Incidentally, other possible applications of TiO_2 in the Building Services Industry could also be explored. The following are some of the suggested areas where such applications can be further investigated:

Ductwork and PipeWork

TiO_2 coating can be applied on the internal surfaces of air ducts or water pipes provided that the ducting or piping system has equipped with appropriate UV light source to enable the photo-catalytic reaction to take place. With TiO_2 coating, the formation of dirt or scale on the internal surfaces of the ductwork or pipework would be reduced and the frequency of ductwork or pipe work cleaning required would thus be reduced. As for water pipework system, reduced scaling on internal pipe surfaces would also reduce the necessary pump power required which means savings in electricity operating cost.

Lighting Fittings

In lighting design and installation, the maintenance factor is one of the main factors that would affect the number of light fittings to be provided and thus the electricity operating cost. When TiO_2 is applied to the internal surfaces of a luminaire and/or the external surface of a light bulb, the amount of dirt/dust that would attached to the surfaces of these lighting equipment would be greatly reduced. The maintenance factor of the luminaire would thus be improved and subsequently the number of light fittings required to achieve the same illumination level would then be reduced. This would result in savings in not only initial equipment cost but also in electricity operating cost. One obvious example would be the application in vehicle tunnels. If TiO_2 were applied to the lighting fittings (or even to all internal surfaces) of a tunnel, it would not only increase the maintenance factor of the luminaries but also help removing some of the air pollutants and thus improving the indoor air quality inside the tunnel.

REFERENCES

[1] A. Fujishima, K. Hashimoto, T. Watanabe (1997). Ti02 Photocatalysis – Fundamental and Applications, BKC, Japan

[2] http://pearl1.lan1.gov/periodic/elements/22.html

[3] S.P Pappas, R.M. Fischer, J. Paint Technol. 46 (1974) 65.

[4] N. Serpone, P. Ezio (1989). Photocatalysis: fundamentals and applications, Wiley, New York

[5] Stern MA, Allit U, Corden J, Millington W. The investigation of fungal spores in intrameural air using a Burkard continuous recoding air sampler. Indoor & Built Environment 1999;8:40-8

Advances in Building Technology, Volume 2
M. Anson, J.M. Ko and E.S.S. Lam (Eds.)
© 2002 Elsevier Science Ltd. All rights reserved

THE MEASUREMENT OF SURFACE MASS TRANSFER COEFFICIENTS IN A STANDARD FLEC

J. L. Niu, L. Z. Zhang, T. K. Wan

Department of building services engineering, the Hong Kong Polytechnic University, Hunghom, Kowloon, Hong Kong, China

ABSTRACT

FLEC (field and laboratory emission chamber) is becoming a standard method to characterize pollutant emissions from building materials. Up until now, only the emission rate profiles are obtained, which are useful for the comparison and ranking of emission strength from different materials. However, to use the chamber emission test data to model pollutant concentrations in real buildings, and also to evaluate the effects of various control strategies, mass transfer model is required. As the first step, surface convective mass transfer coefficients are essential. In this study, a first series of direct measurements of surface mass transfer coefficients using distilled water at 5 air flow conditions ranging from 186ml/min to 509ml/min in a standard Flec is conducted. Mass transfer data inside the Flec is correlated by a dimensionless equation.

KEYWORDS

Flec, Mass transfer, Emission, Model, Experiment, Water

INTRODUCTION

There is an increasing awareness regarding the potential impact of indoor air pollution on health and comfort, in particular, the emission of volatile organic compounds (VOCs) from building materials and products. This has resulted in various technical guides for emission testing. The current state-of-the-art involves two types of devices: emission test chamber and emission cell. The emission test chamber is defined as an enclosure with operational parameters for the determination of VOCs emitted from building products. Typical chamber volumes cover a range from 20 L to 1m^3 (Spiker, Hosker, and Corner et al., 1992). In case of the emission cell, the surface of the test specimen itself becomes the integral part of the cell and it has a high sensitivity due to large loading ratio (surface area/volume). To-day, the best described and most frequently used tool is the so-called Field and Laboratory Emission Cell-FLEC (Wolkoff, 1996). The emission cell is portable and user-friendly, therefore, FLEC has become a standard for emission testing in Europe (CEC, 1998; Uhde, Borgschulte and Salthammer, 1998).

There have been many tests with FLEC involving various building materials. ClenΦ and co-workers (Clenϕ, Clausen, and Weschler et al., 2001) measured the ozone removal rates by selected building products. Wolkoff and Nielsen (Wolkoff and Nielsen, 1996) obtained the diffusion profiles of trans-2-nonenal with Flec data from carpet and hexane from sealing material, to name but a few. In these researches, emission rate profiles are obtained for a given air volumetric flow rate. These results are test-specific. However, to use these emission test data to model pollutant concentrations in real buildings, and also to evaluate the effects of various control strategies, more detailed mass transfer model is needed. A complete emission model should include three mechanisms: convective mass transfer on surfaces, diffusion in solids, and sorption-desorption with building materials. As the first step, in this study, the surface convective mass transfer coefficients in a standard FLEC are obtained experimentally. Such work has not been found in the open literature. Correlations are summarized to estimate the mean and local Sherwood numbers using dimensionless parameters governing the transfer and flow properties.

EXPERIMENTAL PROCEDURE

The Flec cell is circular and made of stainless steel with a diameter of 150mm and a maximum height of 18mm. The flow geometry is shown in Fig.1. The cell in our experiment is composed of two parts: cap and lower cavity. The deepness of the lower cavity is 10mm. When testing, the material is placed on the bottom surface of the lower cavity and becomes an integral part of the emission cell. The air is supplied through the cap. It is introduced through two diametrically positioned inlets (symmetrically placed) into a circular-shaped channel at the perimeter from where the air is distributed over the test surface through the circular air slit. The flow geometry of the cell is shown in Fig.1 and the pictures of the Flec in Fig.2. The cell is supplied with clean and humidified air from air supply unit. After mass transfer, the air leaves the cell at the top of its center. A more detailed description of the structure and parameters of the cell can be found in (CEC, 1998). The complete test rig is shown in Fig.3.

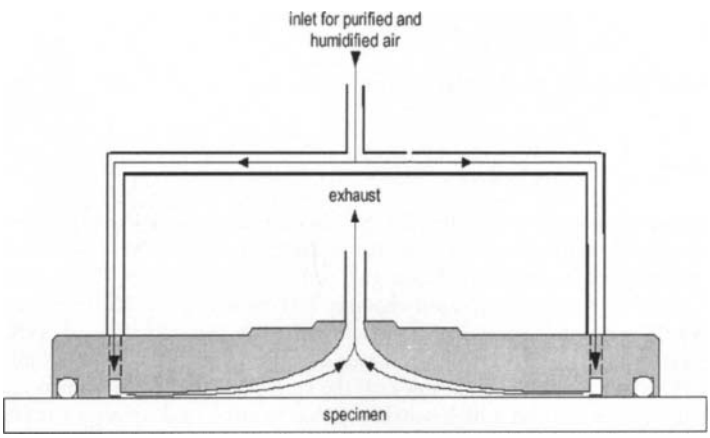


Figure 1: A schematic showing the flow geometry of the Flec

The supply air flows from a compressed air bottle and is divided into two streams. One of them is humidified through a bubbler immersed in a bottle of water and subsequently it is mixed with the other dry air stream. The humidity of the mixed air stream is controlled to the set points by adjusting the proportions of air mixing. The air-flow rates are controlled by two air pumps/controllers at the inlet and outlet of the Flec. To prevent outside air from infiltrating into the Flec, a manometer is installed to monitor the pressure inside the Flec and ensure the inside pressure positive. The humidities and temperatures in and out the Flec are measured by the built-in RH and temperature sensors in the pumps/controllers. The measuring accuracies are respectively 2% for relative humidity and 0.2°C for temperature and 2.5% for air flow rate.

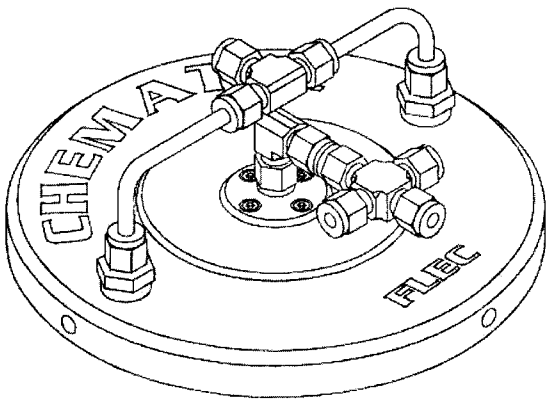


Figure 2: Pictures of the Flec, showing the cap

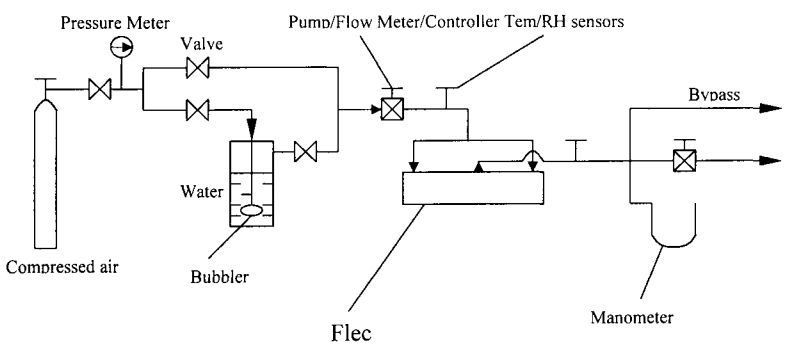


Figure 3: The set-up of the test apparatus

In this experiment, distilled water is used as the loading material. Rather than directly measuring emission rate profiles of VOCs from building materials, convective surface mass transfer coefficients are calculated by measuring the humidity differences between the inlet and outlet of an air stream, which flows through the Flec and exchanges moisture with water on the lower surface. To investigate the mean and local mass transfer coefficients at different Flec radius, five glass discs with thickness of 10mm and diameters ranging from 130 to 148mm are prepared. In each test, a disc is placed onto the bottom surface and distilled water is filled in the space between the cell wall and the disc. Special care is given to ensure the water has the same height with the disc and doesn't wet the disc's upper surface. When the air is pumped, it exchanges moisture with the water and is humidified. Since the RH of water on water surface is 100%, by calculating the humidity differences, the mean convective mass transfer coefficients across the water surface can be calculated. Different discs provide the mean mass transfer coefficients at various Flec radius. To investigate the influences of different gases, both air and N_2 are used in the experiment.

Once the humidity differences are measured, the mean mass transfer coefficient is calculated by

$$Sh_m = \frac{2k_m\delta}{D_v} = \frac{V\Delta\omega}{A_t(\omega_s - \bar{\omega})} \tag{1}$$

where V is the volumetric air flow rate to the Flec (m^3/s), $\Delta\omega$ is the humidity ratio differences between air inlet and outlet (kg/kg), A_t is the transfer area between air and water surface (m^2), ω_s is humidity ratio on the water surface (kg/kg), and $\bar{\omega}$ is the mean humidity ratio of air in Flec (kg/kg), D_v is vapor diffusivity in air mixture (m^2/s), Sh is Sherwood number and k_m is the mean mass transfer coefficient (m/s). The Reynolds number used to characterize the airflow rate is based on the height of the air inlet slit, δ, and given by

$$\mathrm{Re} = \frac{2u_m\delta}{\nu} \tag{2}$$

where ν is the kinematic viscosity (m^2/s) and u_m is the mean air velocity at the slit, and it is calculated by

$$u_m = \frac{V}{2\pi r_0\delta} \tag{3}$$

where r_0 is the maximum radius of the emission surface (m).

RESULTS AND DISCUSSION

Table 1 lists the experimentally obtained mean Sherwood numbers with different radius glass discs. Two types of gases, air and nitrogen, are available. Seven diameter discs are used. A correlation has been summarized to calculate the mean Sherwood numbers from the experimental data with regression techniques as following:

$$Sh_m = 0.8171\mathrm{Re}^{0.8578}Sc^{0.6790}\left(\frac{r_0 - r}{2\delta}\right)^{-0.6761} \tag{4}$$

where Sc is the Schmidt number.

TABLE 1
EXPERIMENTALLY OBTAINED SHERWOOD NUMBERS

Air					
r_0 (mm)	V (ml/min)				
	186	245	316	420	509
74	0.81391	1.03057	1.19082	1.37914	1.46617
72	0.43780	0.56455	0.64878	0.83161	0.90868
70	0.28898	0.37821	0.47548	0.61128	0.68202
67.5	0.19596	0.26686	0.32558	0.44335	0.52334
65	0.15243	0.20342	0.27078	0.35473	0.44313
60	0.10811	0.14691	0.17809	0.24095	0.29400
55	0.08623	0.11304	0.14412	0.19490	0.23350
N_2					
r_0 (mm)	V (ml/min)				
	186	245	316	420	509
74	0.91957	1.03340	1.17637	1.32567	1.55477
72	0.47904	0.57112	0.68604	0.85910	0.98332
70	0.31088	0.40202	0.49329	0.59180	0.66532
67.5	0.22056	0.27714	0.34385	0.45679	0.55953
65	0.17872	0.23797	0.30671	0.41255	0.48580
60	0.13079	0.17036	0.21523	0.28729	0.34831
55	0.10244	0.13481	0.17059	0.22644	0.27193

The comparisons between the experimentally obtained and the calculated Sh numbers are plotted in Flg.4. It is seen that the correlation fits the experimental data well. The largest deviation happens when the Sh is very large, namely, in the position near air slit. This phenomenon may result from the influences of inlet flow conditions. Generally speaking, the correlation can be used to represent the

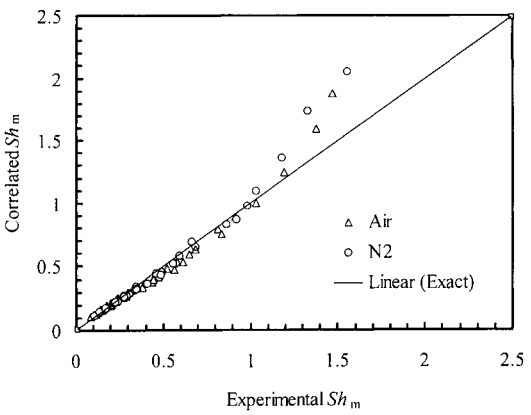


Figure 4: Comparisons of Sh numbers correlated and experimentally obtained

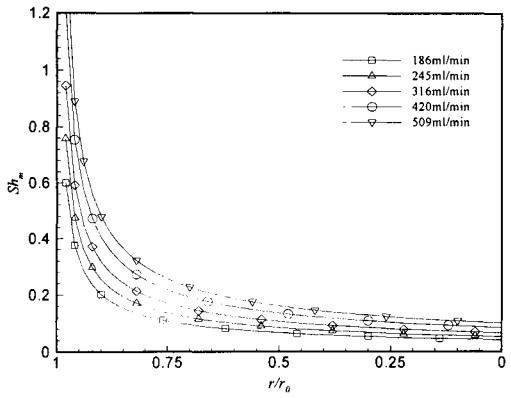


Figure 5: Mean Sherwood numbers in relation to Flec radius

mean Sherwood numbers. The calculated mean Sh numbers from the above equation in relation to Flec radius are shown in Fig.5 for air. It is disclosed that the Sherwood numbers decrease with the flow progressing. The higher the air flow rates, the larger the Sh numbers. For air flow rate ranging from 186 to 509ml/min, the mean Sherwood numbers on the whole Flec emission surface change from 0.05 to 0.2.

CONCLUSIONS

In this experiment, the mean mass transfer coefficients in a standard Flec cell are measured. A correlation is summarized to calculate the Sherwood numbers along the chamber radius. The results indicate that the mean Sherwood numbers on the whole emission surface change from 0.05 to 0.2, depending on the air volumetric flow rates. Locally, the mean Sh numbers decrease with radius decreasing.

ACKNOWLEDGEMENTS

The authors acknowledge the funding from the Research Grant Council of the Hong Kong SAR government.

REFERENCES

CEC-Commission of the European Communities. (1998). prENV 13419-2, Building products-determination of the emission of volatile organic compounds- Part2: Emission test cell method, Brussels: European Committee for Standardization.

Clenϕ J.G., Clausen P.A., Weschler C.J., and Wolkoff P. (2001). Determination of ozone removal rates by selected building products using the Flec emission cell. *Environmental Science Technology* **35**, 2548-2553.

Spiker E.C., Hosker R.P., Corner V.J., White J.R., Were R.W., Harmon F.L., Gandy G.D., and Sherwood S.I. (1992). Environmental chamber for study of the deposition flux of gaseous pollutants to material surfaces. *Atmospheric Environment* **26A,** 2885-2892.

Uhde E., Borgschulte A. and Salthammer T. (1998). Characterization of the filed and laboratory emission cell- FLEC: flow field and air ve ocities. *Atmospheric Environment* **32:4,** 773-781.

Wolkoff P. and Nielsen P.A. (1996). A new approach for indoor climate labeling of building materials-emission testing, modeling, and comfort evaluation, *Atmospheric Environment* **30,** 2679-2689.

Wolkoff P. (1996). An emission cell for measurement of volatile organic compounds emitted from building materials for indoor use- the filed and laboratory emission cell FLEC. *Gefahrstoffe-Reinhaltung der Luf* **56,** 151-157.

This Page Intentionally Left Blank

Advances in Building Technology, Volume 2
M. Anson, J.M. Ko and E.S.S. Lam (Eds.)
© 2002 Elsevier Science Ltd. All rights reserved

COMPARISON OF SUMMER AND WINTER THERMAL ENVIRONMENT IN TRADITIONAL VERNACULAR HOUSES IN SEVERAL AREAS OF NEPAL

H. B. Rijal[1] and H. Yoshida[1]

[1]Department of Global Environment Engineering, Kyoto University,
Yoshida Honmachi, Sakyo-ku, Kyoto 606-8501, Japan

ABSTRACT

To evaluate and improve the thermal environment in traditional vernacular houses of the Banke, Bhaktapur, Dhading, Kaski and Solukhumbu districts of Nepal, an indoor thermal investigation and a questionnaire survey were conducted in the summer and winter. They were analyzed in terms of 1) the mitigation of thermal environment by residents, 2) the relation between living-space temperature and climate, 3) the temperature control effects by building materials, 4) the relation between indoor and outdoor temperature difference and altitude, and 5) a comparison of indoor and outdoor temperature difference in existing studies.

The findings on the thermal environment of investigated houses are as follows. 1) Residents mitigate the thermal environment by moving between indoor, semi-open and front yard spaces. 2) Living-space temperature was found to be very high in the sub-tropical climate in the summer (32.0 °C) and very low in cool climate in winter (6.5 °C). It is different according to climatic zones and seasons, which suggests that people have adapted to live with their natural environment. 3) The room temperature was 3.2K lower than the outdoor temperature during summer daytime, and 3.8-5.5K higher during winter nighttime. This is due to the effect of cool radiation in summer and heat storage in winter by the earth floor, stone walls and brick walls of the houses. 4) The indoor and outdoor temperature difference (T_{in}-T_{out}) was small in the low altitude location and large in the high altitude location. This is due to presence of open-type houses in low altitude locations and closed-type houses in high altitude locations. 5) Compared to Japanese houses, Nepalese houses are similar in T_{in}-T_{out}. This could be due to limitations of local building materials and the construction methods of traditional houses. The T_{in}-T_{out} of Nepalese and Japanese houses was 1.2K in summer which is 1K smaller than in winter. The reason for this could be that residents open the openings in summer and shut them in the winter.

KEYWORDS

Nepal, Altitude, Sub-tropical climate, Temperate climate, Cool climate, Traditional vernacular houses, Indoor and outdoor temperature difference, Regional difference

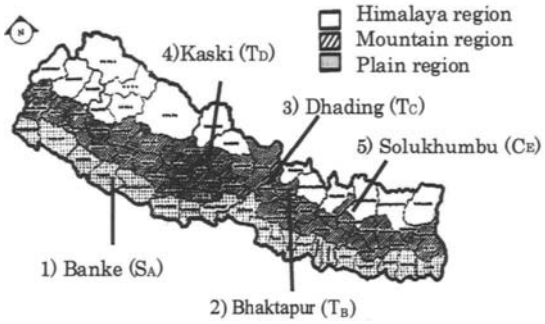


Figure 1: Locations of survey areas

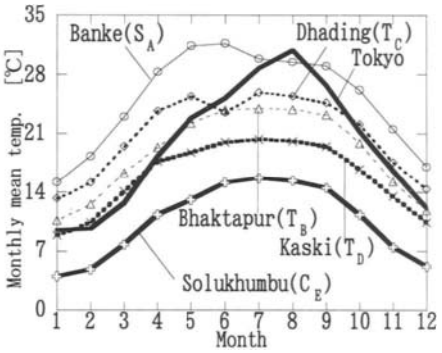


Figure 2: Monthly average outdoor air temp.

TABLE 1
OUTLINE OF INVESTIGATED DISTRICTS

District	Address	Altitude [m]	Climate	May*	January*
1)Banke (S_A)	Mahadevpuri VDC-1 Mahadev Goun	≒150	sub-tropical (S)	31. 4	15. 2
2)Bhaktapur (T_B)	Bhaktapur Municipal-1 Tachapal Tole	≒1350	temperate (T)	22. 2	10. 6
3)Dhading (T_C)	Jyamrung VDC-1 Salle Goun	≒1500	temperate (T)	25. 4	13. 3
4)Kaski (T_D)	Dhampus VDC-5 Sude Goun	≒1700	temperate (T)	18. 8	8. 9
5)Solukhumbu (C_E)	Salleri VDC-1 Chiwang Khop Goun	≒2600	cool (C)	13. 1	4. 0

*: H.M.V. of Nepal (1995, 1997, 1999), monthly mean outdoor air temp. [°C] (mean of 1987-1996), meteorological station: S_A; Nepaljung (reg.off.), T_B; Kathmandu airport, T_C; Dhunibesi, T_D; Lumle, C_E; Chialsa

INTRODUCTION

Nepal is a small country with a 147,181km^2 land area, but the climate varies from sub-tropical to frigid due to the wide altitude difference of 60m to 8848m. Therefore, different types of traditional houses, which have a variety of ideas to mitigate inside thermal conditions can be found. The examples are, 1) eaves or roofs cutting down sunshine, 2) effective ventilation, 3) semi-open spaces, and 4) thermal mass by using materials such as stone and soil. However, problems can also be found. For example, neither the windows nor doors have glass and, as a result, excessive openness effects the winter room conditions. In addition, a gradual increase of modern building materials are being used, such as corrugated iron, which make the indoor environment worse.

A qualitative understanding can easily be made from the information above, however, a quantitative analysis is necessary to improve the indoor thermal conditions by using modification or renovation methods. But, no such study can be found, therefore this study focuses on the thermal environment in traditional houses in Nepal. Summer and winter measurements were analyzed and summarized based on indoor and outdoor thermal environments and the regional differences. The objectives of this study are as follows. 1) To clarify the mitigation of the thermal environment of residences, such as use of space and duration of time spent in them. 2) To quantify the relation between living-space temperature and climate. 3) To find out the temperature control effect of houses, such as indoor and outdoor temperature difference. 4) To identify the house types according to altitude in terms of indoor and outdoor temperature difference. 5) To evaluate the thermal characteristics of traditional houses by comparing with them existing research.

THE STUDY AREA

The study areas are located in the Banke (A), Bhaktapur (B), Dhading (C), Kaski (D) and the Solukhumbu (E) districts of Nepal (Figure 1, Pandy, 1995). The climatic zone of A is sub-tropical (S). B, C and D are temperate (T), and E is cool (C). These are abbreviated as S_A, T_B, T_C, T_D and C_E. Study areas are chosen according to the altitude, climate, topography, ethnicity, energy, and housing conditions in Nepal (Table 1).

In Nepal, summer is in May and winter is in January (Figure 2). Because of the landlocked nature of the country, the climate is dry and hot in summer. Nepal lies in low latitudes (26°-30° north), therefore the solar radiation is high in winter. Bhaktapur is an urban area and the other districts are rural areas. In rural areas, agriculture is the main occupation and firewood is used for cooking and heating. Table 2 shows the outline of investigated houses. The types of houses are: one-story mud houses in S_A, 4-5 story brick houses in T_B, 2-3 story stone houses in T_C, T_D and C_E. The thickness of mud, brick and stone walls are approximately 10cm, 50cm and 50cm respectively. The typical house spaces are as follows. 1) S_A has kitchen, bed room, prayer room and veranda (semi-open) in 1F. 2) T_B has shop, water space and toilet in 1F, bed and store room in 2F, bed and living in 3F, kitchen in 4F, and store and terrace in 5F. 3) T_C has veranda, kitchen and bed in 1F, storage, bed room and balcony in 2F, and store in 3F. 4) T_D has veranda, kitchen and bed in 1F, and storage in 2F. 5) C_E has cattle shed in 1F, kitchen, bed room and prayer room in 2F, and store and bed room in 3F. The house is constructed by natural material which is available in the village. But, recently, because of modernization, the thatched roof is being changed to a corrugated iron roof. In the temperate climate (T_C, T_D), the kitchen room is used not only for cooking but also for living, dining, sleeping, etc. But, in other climates the kitchen is not used for sleeping. In the cool climate (C_E), because of low temperatures, people spend most of their time in the kitchen burning firewood.

INVESTIGATIONS

Investigations were conducted in summer (April to May 2000) and in winter (December 2000 to January 2001). Air temperature, relative humidity, globe temperature, surface temperature, solar radiation, wind velocity and direction were measured. The main outdoor and indoor measurement points were 1.5m above the ground level (in T_B 1.5m above the roof level) and 0.6m above the floor level respectively. Air temperature was also measured at 0.1m above the floor level and 0.1m below the ceiling level. Surface temperature was measured in the middle of the floor, wall, ceiling and roof. All data were measured in 5 minutes intervals and recorded by a data logger. Measured data were calibrated. Questionnaire survey related to thermal mitigation was conducted with 10(S_A), 12(T_B), 17(T_C), 19(T_D) and 9(C_E) subjects.

RESULTS AND DISCUSSION

Mitigation of Thermal Environment by Residents

Figure 3 shows the percentage of space used and duration of time spend in indoor, semi-open, front yard and outdoor spaces in a day. It can be divided into a) S_A, b) T_B, C_E and c) T_C, T_D. In summer, people spend most of their time in the semi-open spaces and front yard to feel cool atmosphere in S_A, T_C and T_D. Conversely, T_B and C_E have no semi-open spaces and people spend time mostly indoors. The T_B is a city area and people do more activity indoors. The C_E is a cool climate, and people have a habit of living indoors even in the summer. Because of low temperatures in winter, people spend more time indoors than they do in the summer (Table 2). Duration of time spent indoors in summer and winter is similar in the T_B and C_E areas, while a difference of 3.2-9.2h in other districts. During winter nights, residents of T_C sleep in the semi-open spaces, where very little indoor and outdoor temperature difference exists.

TABLE 2
OUTLINE OF INVESTIGATED HOUSES AND DURATION OF TIME SPEND IN EACH SPACE

District	No. of story	Wall types	Roof types	Roof material	Duration of time spend (summer/winter) [h/day]				
					n	indoor	semi-open	front yard	outdoor
a)Banke (S_A)	1	mud	gable	thatch, mud tile	10	5.7/14.9	5.2/1.8	7.2/1.7	5.9/5.6
b)Bhaktapur (T_B)	4-6	brick	gable	mud tile, CI	12	15.3/15.9	-	1.5/1.9	7.2/6.2
c)Dhading (T_C)	2-3	stone	gambre	thatch, slate, CI	17	7.4/12.5	7.1/3.1	2.4/2.6	7.1/5.9
d)Kaski (T_D)	2	stone	gambre	thatch, slate, CI	19	10.7/13.9	4.1/2.7	2.1/1.8	7.2/5.6
e)Solukhumbu (C_E)	1-3	stone	gambre	wooden board, CI	9	15.1/16.2	-	2.1/2.0	6.8/5.8

CI: corrugated iron, n: number of subject, indoor: inside the house, semi-open: veranda, balcony, front yard: front garden, roof terrace, cattle shed, outdoor: farm, jungle

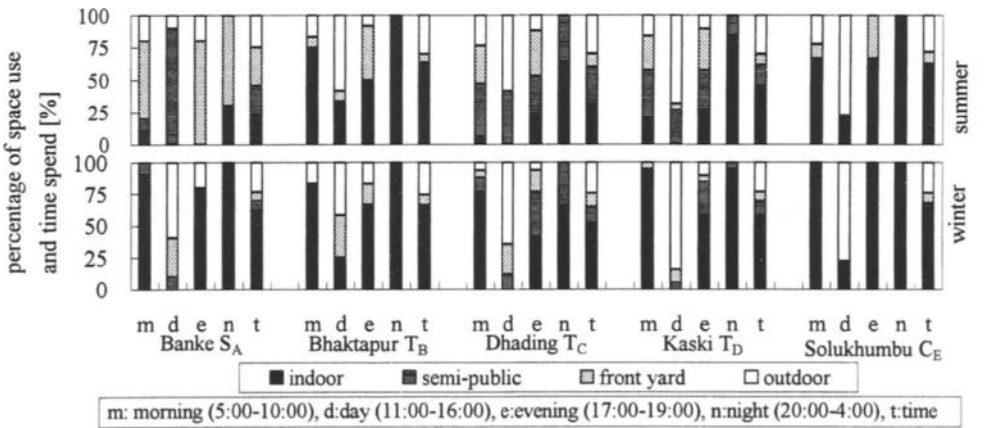


Figure 3: Percentage of space use and duration of time spend in each space in a day

Because of their habit to live in nature, their thermal sensation is different from thermal comfort standard. This hypothesis can be described by summer lifestyle, where residents of S_A sleep in the front yard to feel the cool atmosphere at night. It can be said that people mitigate the summer and winter thermal environment by moving in indoor, semi-open and front yard areas, and by considering the period of time spent in each space.

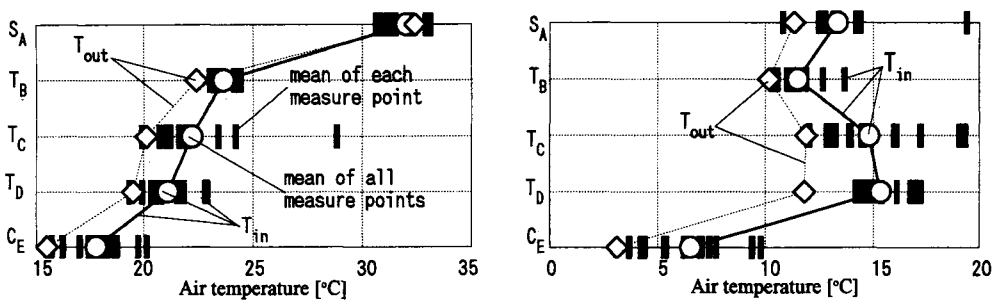
Living Space Temperature and Climate

Table 3 shows the mean thermal environment of investigated houses. Figure 4 shows the daily mean outdoor (T_{out}) and indoor (T_{in}) air temperature in summer and winter. The indoor air temperature i.e. living-space temperature was found to be very high in the sub-tropical climate in the summer (32.0 °C), medium in the temperate climate (11.5-23.6 °C) and very low in the cool climate areas in the winter (6.5 °C). It is an uncomfortable thermal environment from the thermal comfort point of view, but people have accustomed themselves to these environments. The summer and winter living-space temperature difference was 5.8°C (T_D) to 18.7°C (S_A), which showed a big seasonal difference. T_C and T_D have less seasonal difference in living-space temperature, because people burn firewood year around for cooking and heating on the ground floor and heat rise to all upper floor of the house. It can be concluded that living-space temperature is found to be different according to climatic zones and seasons, which suggests that people have adapted to live with their natural environments.

TABLE 3
MEAN THERMAL ENVIRONMENT OF INVESTIGATED HOUSES

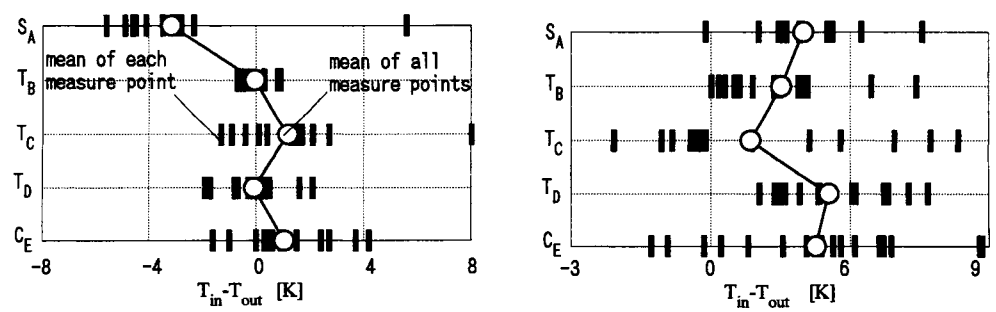
Study	No. of house	n	T_{out} [°C]		T_{in} [°C]		T_{in}-T_{out} [K]				r ± SD	
			s	w	s	w	s*	s**	w*	w**	s	w
a)Banke (S_A)	10	13	32.4	11.3	32.0	13.3	-3.2	2.0	-1.0	5.0	0.6±0.1	0.7±0.3
b)Bhaktapur (T_B)	5	14	22.4	10.1	23.6	11.5	-0.1	2.4	-1.9	4.5	0.3±0.1	0.3±0.1
c)Dhading (T_C)	8	15	20.1	11.9	22.2	14.8	1.2	2.8	2.0	3.8	0.8±0.4	0.8±0.4
d)Kaski (T_D)	7	15	19.5	11.8	21.1	15.3	-0.1	3.4	1.6	5.5	0.6±0.1	0.6±0.1
e)Solukhumbu (C_E)	6	16	15.5	3.1	17.8	6.5	1.0	3.5	1.5	5.2	0.6±0.3	0.7±0.3

n: number of indoor measurement points, T_{out} & T_{in}: daily mean outdoor & indoor air temp., s: summer, w: winter, *: day mean (6:00-18:00), **: night mean (0:00-6:00& 18:00-24:00), SD: standard deviation
r: T_{in}(max.-min.)/T_{out}(max.-min.)



(a) Summer (daily mean) (b) Winter (daily mean)

Figure 4: Indoor and outdoor air temperature



(a) Summer (day mean) (b) Winter (night mean)

Figure 5: Indoor and outdoor air temperature difference

Temperature Control Effect by Building Materials

Figure 5 shows the indoor and outdoor temperature difference (T_{in}-T_{out}) in summer daytime and winter nighttime. The indoor air temperature was 3.2K (S_A) lower than outdoors in the summer daytime and 3.8K (T_C) to 5.5 K (T_D) higher than outdoors in the winter nighttime (Table 3). The ratio of daily range of indoor and outdoor air temperature (r) was small (0.3-0.7) in summer and winter. Compared to indoor air temperature, the daily mean floor and wall temperature was 3.6K (T_C) and 2.8K (T_C) lower in summer and 3.4K (C_E) and 7.4K (C_E) higher in winter respectively. The results showed that earth and wooden floors, mud, brick and stone walls are effective in keeping houses cool in summer and warm in winter.

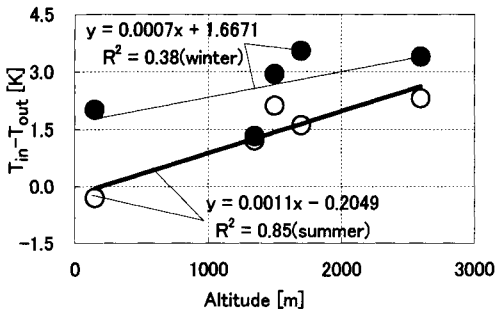


Figure 6: Relation between indoor and outdoor temp. difference and altitude

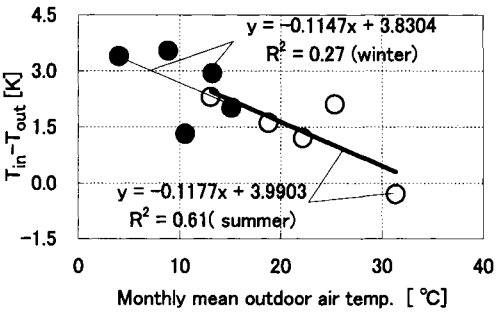


Figure 7: Relation between indoor and outdoor temp. difference and monthly mean outdoor air temp.

Relation between Indoor and Outdoor Temperature Difference and Altitude

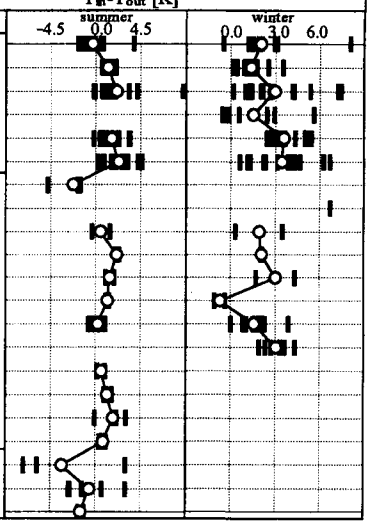
Figure 6 shows the relation between daily mean indoor and outdoor temperature difference (T_{in}-T_{out}) and altitude. Figure 7 shows the relation between T_{in}-T_{out} and the monthly mean outdoor air temperature. In summer, T_{in}-T_{out} was small (-0.3K) in the low altitude area (S_A, 150m) and large (2.3K) in the high altitude area (C_E, 2600m) (Table 4). T_{in}-T_{out} were highly correlated with the altitude and monthly mean outdoor air temperature. In winter, T_{in}-T_{out} was higher than in summer. However, a summer and winter both recorded similar trends in regards to altitude and monthly mean outdoor air temperature (see figure 6 and 7). Because of different methods of firewood usage for heating, the correlation coefficient is weaker in winter than summer. In the T_B (1350m), people do not burn the firewood for heating, therefore it has a smaller T_{in}-T_{out} than in the low altitude areas (S_A). The results showed that T_{in}-T_{out} is different according to altitude. The reasons could be that in the low altitude areas (sub-tropical climate), the open-type houses are suitable for high summer temperatures. In contrast, in the high altitude areas (cool climate), the closed-type houses are more suitable for low winter temperatures. In the medium altitude areas (temperate climate), the semi-open (veranda) and semi-closed (a window without a door) type houses are suitable in summer and winter.

Comparison of Indoor and Outdoor Temperature Difference

Table 4 shows the comparison of indoor and outdoor temperature difference (T_{in}-T_{out}) in Nepal, Japan and China. Nepalese houses are compared with Japanese houses because the latitudinal climatic variations of Japan is similar to the altitudinal climatic variations of Nepal. For reference, Chinese underground houses are also included. Traditional houses share a common point in their use of local materials and construction methods, therefore they can be compared in different areas. In Nepal, T_{in}-T_{out} was -0.3 to 2.3K in summer and 1.3 to 3.5K in winter. Compared to an existing study, T_{in}-T_{out} was lower in study areas 1, 13, 14, 15 (summer) and 6 (winter) than in this study (Table 4). If these values are excluded, the indoor and outdoor temperature difference of Japanese houses are in the range of Nepalese houses. It shows that the thermal characteristic of Nepalese and Japanese traditional houses are similar. This could be due to limitations in local building materials and construction methods of traditional houses. However, it should be noted that as we explained above, traditional houses have a high temperature control effect in summer daytime and winter nighttime. Focusing in microclimate, T_{in}-T_{out} is also different according to altitudes.

TABLE 4
COMPARISON OF INDOOR AND OUTDOOR TEMPERATURE DIFFERENCE

Country	Study area	No. of house	Measure points	T_{out} [°C] s	w	T_{in}-T_{out} [K] s+	w+
Nepal	a)Banke(S_A)	10	13	32.4	11.3	-0.3	2.0
	b)Bhaktapur(T_B)	5	14	22.4	10.1	1.2	1.3
	c)Dhading(T_C)	8	15	20.1	11.9	2.1	2.9
	cc)Dhading(T_C)	3	7	-	14.0	-	1.5
	d)Kaski(T_D)	7	15	19.5	11.8	1.6	3.5
	e)Solukhumbu(C_E)	6	16	15.5	3.1	2.3	3.4
Japan	1)Yamagata	1	5	24.1	-	-2.3	-
	2)Hokaido	1	1	-	-2.8	-	6.7△
	3)Yamanashi	1	2	26.0	6.4	0.5	1.9
	4)Yamanashi	1	2	23.9	5.0	2.1	2.1
	5)Yamanashi	1	2	21.3	3.5	1.4	3.0
	6)Yamanashi	1	2	20.6	3.6	1.2	-0.8
	7)Gifu	1	11	27.1	6.4	0.2	1.5
	8)Shimane	1	6	-	3.7▲	-	3.0
	9)Okayama	1	2	24.7	-	0.6	-
	10)Kochi	1	3	29.8	-	1.2	-
	11)Kagoshima	2	5	27.6*	-	1.8	-
	12)Kagoshima	2	4	27.3	-	0.8	-
China	13)Luoyang	2	3	29.3	-	-3.4	-
	14)Sanmenxia	3	5	26.7	-	-0.6	-
	15)Lanzhou	2	3	22.1	-	-1.5	-



T_{out} & T_{in}: outdoor & indoor air temp., s: summer, w: winter, *: mean of two days, Matsue meteorological station, △: 1 measure point, 1: mean of each measure point, +, ○: mean of all measure points, a)-e): This study, cc): Rijal et al.(2001), 1): Ichikawa et al.(1970), 2): Kubota et al.(1989), 3)-6): Miyano et al.(1990), 7): Yanase et al.(1969), 8): Igarashi et al.(1971), 9): name in Japanese(1969), 10): Akamatsu et al.(1972), 11): Oshiyama et al.(1972), 12): Morita et al.(1972), 13)-15): name in Japanese (1987).

To find the summer and winter difference of Nepalese and Japanese houses, the average of T_{in}-T_{out} is taken in summer and winter. The results were 1.2K in summer and 2.2K in winter, which is 1K greater in winter. The reason could be that residents adjust the opening, for example doors and windows are opened in summer and shut in winter.

CONCLUSION

In this study an indoor thermal investigation and a questionnaire survey were conducted in summer and winter for the traditional houses in the Banke, Bhaktapur, Dhading, Kaski and Solukhumbu districts of Nepal. The results are as follows.

1) Residents mitigate the thermal environment by moving between indoor, semi-open and front yard spaces.
2) Living temperature is found to be different according to climatic zones and seasons.
3) The room temperature was 3.2K lower than the outdoor temperature in summer daytime, and 3.8-5.5K higher in winter nighttime. The results showed that earth and wooden floors, mud, brick and stone walls are effective in keeping houses cool in summer and warm in winter.
4) The indoor and outdoor temperature difference was small in the low altitude location and large in the high altitude location.
5) Compared with Japanese houses in existing studies, Nepalese houses had similar indoor and outdoor temperature differences. The indoor and outdoor temperature difference of Nepalese and Japanese houses was 1.2K in summer which is 1K smaller than in winter.

ACKNOWLEDGEMENTS

We would like to thank The Kurata Memorial Hitachi Science and Technology Foundation for its financial support, the investigated households for their cooperation and our families and friends for their encouragement.

References

Akamatsu T, Nashiro M, Kondo Y, Yanase T, and Hanaoka T (1972). Studies on Microclimate of Folk Houses in Japan Part 11 An Observation on House Climate in Summer of Ferro-concrete, Concrete-block and Wooden Houses in Warm-wet District of Japan (Southern Sea-side of Shikoku). *Research Journal of Living Science* **19:2,** 129-138.

H.M.G. of Nepal (1995, 1997, 1999). *Climatological Records of Nepal, 1987-1990, 1991-1994, 1995-1996.* Ministry of Science and Technology Department of Hydrology and Meteorology Kathmandu, Nepal.

Ichikawa K, Kaneko K, Yanase T, and Hanaoka T (1970). Studies on Microclimate of Folk House in Japan Part 5 On the Thermal Conditions in Folk House of Doza Style in Yamagata. *Research Journal of Living Science* **17:1,** 91-96.

Igarashi Y, Yanase T, and Hanaoka T (1971). Studies on Microclimate of Folk House in Japan Part 7 On the Effects of the Shelter-belt for a Site upon the Indoor Climate. *Research Journal of Living Science* **18:2,** 127-133.

Name in Japanese (1969). Title in Japanese. *Hausklima* **1,** 32-33.

Name in Japanese (1987). Title in Japanese. *AIJ Tokai Chapter Architectural Research Meeting* **25,** 245-248.

Kubota H, Kayano S, Kishishita K, and Ogasawara Y (1989). Heating Environment of Ainu People' s Traditional House "Chisett". *Transactions of the Society of Heating, Air-conditioning and Sanitary Engineers of Japan* **41,** 1-10.

Miyano N, Asami M, and Miyano A (1990). Studies on the Living Environment from the Viewpoint of variations between Temperature and Humidity in Bedrooms and Toilet Rooms A Case Study of Traditional Wooden Private Houses in Yamanashi Prefecture. *Jpn. J. Biometeor* **27:2,** 57-70.

Morita S, Ichikawa K, Yanase T, and Hanaoka T (1972). Studies on Microclimate of Folk Houses in Japan Part 9 On the Indoor-climate of Native House of Ranging Huts System in Amami Island, Kagoshima Prefecture and the Comparison between the House-climates of it and of Concrete House. *Research Journal of Living Science* **19:1,** 36-45.

Oshiyama M, Furuyama K, Ichikawa K, Yanase T, and Hanaoka T (1973). An Observation on House Climate in Summer of Two-ranging Huts System House in Osumi. *Research Journal of Living Science* **20:2,** 161-171.

Pandy R K (1995). *Development Disorders in the Himalayan Heights Challenges and Strategies for Environment and Development Altitude Geography.* 53, 290, Ratna Pustak Bhandar, Baghbazar, Kathmandu Nepal.

Rijal H B, Yoshida H, and Umemiya N (2001). Investigation of Winter Thermal Environment in Traditional Vernacular Houses in a Mountain Area of Nepal. *J. Archit. Plann. Environ. Eng. AIJ* **546,** 37-44.

Yanase T, Imamura F, Ichikawa K, and Hanaoka T (1969). Studies on Microclimate of Folk House in Japan Part 4 On the Thermal Conditions in Folk House of Steep Gable (Gassyo) Style in Shirakawa. *Research Journal of Living Science* **16:1.2,** 64-73.

Advances in Building Technology, Volume 2
M. Anson, J.M. Ko and E.S.S. Lam (Eds.)
© 2002 Elsevier Science Ltd. All rights reserved

MAXIMIZING THE VENTILATION RATE FOR COOLING ENERGY REDUCTION

M. Udagawa[1] and H. Roh[2]

[1] Department of Architecture, Kogakuin University
Nishi-Shinjuku, Shnjuku-ku,
Tokyo 163-8677, Japan
[2] Systech Environmental Research Laboratory
Koenji-Minami, Suginami-ku,
Tokyo 166-0003, Japan

ABSTRACT

It is widely recognized that to minimize the ventilation rate will reduce the energy consumption of air conditioning systems in both heating and cooling seasons. However, the temperature difference between indoor and outdoor air temperatures in the cooling season is not so large in comparison with that in the heating season. In addition, there are many hours when the outdoor air temperature in the cooling season is lower than the design space air temperature.

Therefore, to minimize the ventilation rate may not be important for energy reduction in cooling with air conditioning systems. Better indoor air quality may be provided without increasing the energy requirements by increasing the ventilation rate during the cooling operation. Energy reduction in air conditioning system operation can be also expected depending on the temperature and humidity conditions required in the cooling season.

Appropriate ventilation rates and a basic control strategy are discussed using simulation results of a typical office building with the climatic conditions of Japan where the space cooling consumes larger amount of energy than the space heating in most major cities. The simulation results of the model office building in Tokyo show that the energy requirements for the cooling are almost the same wheather the ventilation rate is set to a minimum outdoor air requirement or to a maximum ventilation rate for all outdoor air without mixing with the return air from conditioned space. This simulation results show the potential of the outdoor air as a cooling source in the cooling season. Control strategies of the ventilation rate in practical design and operation of the air conditioning systems are discussed using the energy requirements obtained by the system simulation.

KEYWORDS

Cooling, office building, simulation, ventilation, energy conservation, air conditioning, heat load

INTRODUCTION

Ventilation rate and heat loads in cooling system is discussed from the view point of possibility of maximizing the ventilation rate including an all fresh air system without return air. It is widely recognized to minimize ventilation rate for reducing the energy consumption of air conditioning systems in both heating and cooling season. However, the difference between indoor and outdoor air temperatures in the cooling season is not so large in comparison with that in the heating season. In addition, there are many hours when the outdoor air temperature in the cooling season is lower than the design space air temperature required.

Therefore, to minimize the ventilation rate may not be important for energy reduction in the cooling operation of air conditioning systems. Better indoor air quality may be provided without increasing the energy requirements by increasing the ventilation rate in cooling operation.

Using the system simulation tool, this study examined the possibility of a cooling system to use outdoor air for cooling source as well as for better indoor air quality.

COOLING SYSTEM WITH MAXIMUM VENTILATION RATE

For example, in Tokyo the average outdoor air temperature of six months, from May to October when mechanical cooling is necessary, is 22.2 °C which is lower than the room set air temperature of 26.0 °C. Due to room heat load of office buildings in Tokyo, space cooling is required throughout the year caused by internal heat generation from lighting, office equipment and occupants in the space. Except for midsummer, the outdoor air temperature is lower than the room set point temperature. In such conditions, an all fresh air

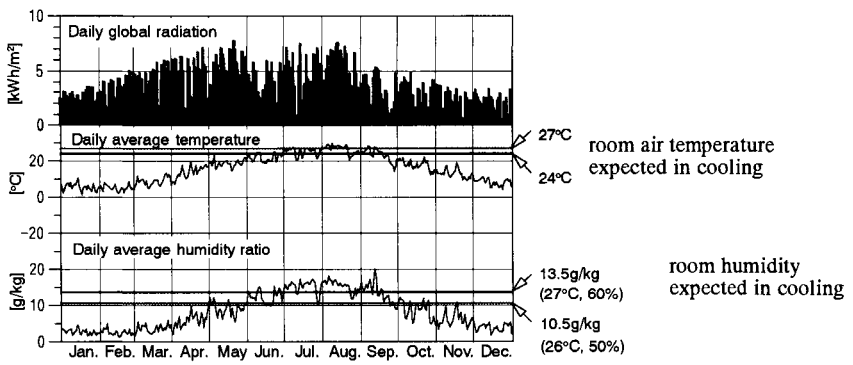


Figure 1: Annual variation of weather data and room thermal environment expected in cooling

system, in which 100% of cooling air supply from outdoors may be more advantageous than the cooling operation with minimum ventilation rate.

Figure 1 shows the year round variation of the weather data in Tokyo. The temperature difference between the expected conditioned room air temperature range in summer is small in comparison with the temperature difference in winter. This means that the sensible heat load of the cooling coil caused by ventilation air is not expected to be large, while the latent heat should be carefully considered as shown in Figure 1 in which the difference of the humidity ratios between outside air and the room conditions is rather large.

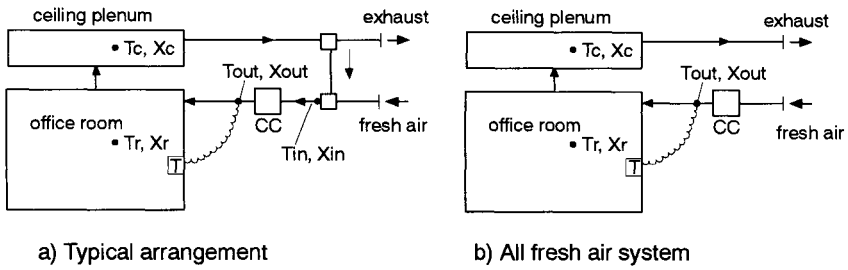


Figure 2: Office room cooling system schematic diagram

Figure 2a shows an example of a usual system with the return path making use of recirculation of the excess room air after exhausting the ventilated air. In this case, the ventilation rate is considered to be minimum or an appropriate value and the mixture of the ventilation outdoor air and the return air is introduced to the cooling coil. To examine the cooling coil load of the air conditioner including the ventilation cooling load at the extreme conditioned, the cooling system with all fresh air system shown in Figure 2b is assumed. The system is very simple, since there is no return path from the conditioned room to the air conditioner.

SIMULATION PROCESS

The system simulation of the cooling coil load of the air conditioner for three Cases was carried out for the model building shown in Figure 3. The simulated building had been designed as a typical office building for the simulation studies related to the room heat load and energy consumption by the air conditioning systems proposed by Takizawa(1985). For the typical floor, two office spaces are separated each other with the core space in the center. The floor area of each office space is 303m ^{2} and the volume is 787 m ^{3} with 2.6 m ceiling height.

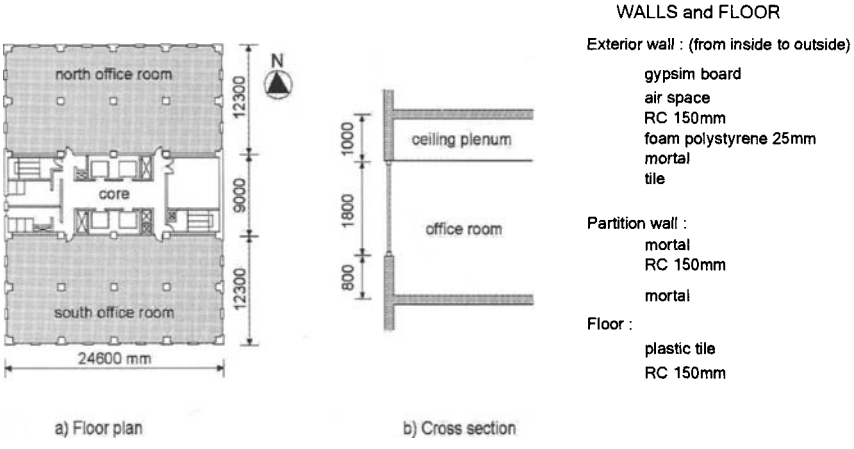


Figure 3: Model office building

TABLE 1
DESCRIPTION OF SIMULATION CASES

Case		Ventilation air ratio	Ventilation rate [m^3/h]	Cooling air supply[m^3/h]
Case 1	Base case(Fig. 2a)	25%	1200	4800
Case 2	Increased case(Fig. 2a)	50%	2400	
Case 3	All fresh air (Fig. 2b)	100%	4800	

The south room was used to discuss the simulated results, while the whole typical floor had been used as the simulation model. Since the tendency of the simulation results of the south room and the north room showed very similar.

The air conditioning systems of Figure 2 are assumed with the ventilation rate of the three cases. TABLE 1 shows the combination of ventilation rates. The supply air flow rate from the air conditioner, 1.6 kg/s (4800 m^3/h) was determined using the room sensible cooling load at the peak condition. Case 1 in Table 1 is the minimum outdoor air case. The ventilation rate of the minimum out door air case is 0.4 kg/s (1200 m^3/h) calculated from the recommended minimum ventilation rate for the office building in Japan based on 4 m^2/h per floor area which implies 20 m^3/h per person. In this case 25% of the supply air rate is the ventilation rate. Case 3 shows the all fresh air case in which 100% of supply air is outdoor air. In Case 2, 50% of supply air is outdoor air.

The building envelopes are considered as typical designs used in the Tokyo area. Light colored internal blinds are supposed to be used for shading direct solar radiation to the office space. The room internal heat generation from lights and appliances are 20 W/m^2 and 10 W/m^2, respectively and 0.2 person/m^2 of space are assumed. The internal heat generation as well as cooling operation from 8:00 to 18:00 is assumed. The room temperature set point is 26 °C throughout the cooling season. The room air humidity is free floating, as the constant outlet humidity model is used in the simulation model of cooling coils in the simulation tool EESLISM. The typical year weather data of Tokyo edited from AMeDas weather data set were used. Whereas the cooling period can be considered as lasting a whole year for the office building in Tokyo, it is assumed in this study that a cooling period of six months from May to October ia a sufficient period for mechanical cooling and summer weather conditions.

The simulation was carried out using a generalized simulation tool EESLISM developed by Udagawa(1990 and 1999). EESLISM can be used to simulate the whole building thermal system consisting of building thermal models and mechanical heating and cooling systems. The authors have used EESLISM for the simulation study of office buildings as well as residential houses(2001). The rooms to be simulated and the heating and cooling systems are defined as system components and the air flow path is used to connect the related system components. Using the information of each system component and their relationship, a set of simultaneous equations for the temperature and humidity ratios describing heat and mass balance of whole system components is set up and solved at each time step of the simulation process.

COOLING COIL LOAD AND ROOM THERMAL ENVIRONMENT

The results of the simulation are shown in Figures 4 through 7. Because of the internal heat generation and solar radiation through the envelopes, the room heat load shows the requirement for cooling as shown in Figure 4. As the room cooling loads are the same for the three Cases, Figure 4 can be used to examine the tendency of the room cooling loads commonly for all simulation cases. The daily coil cooling loads for the three Cases can be compared using Figure 5. The coil load is normalized for the room floor area. While Case 1, the minimum ventilation rate case shows the smallest daily loads among the three Cases in midsummer from early July to middle of September, Case 3, all fresh air case shows the smallest in June and late

September. It is very obvious that the latent cooling load for Case 3 in midsummer is very large in comparison with the base case, Case 1, whereas the sensible cooling coil loads of the three Cases show only small differences. Except for midsummer both sensible and latent cooling loads show smaller differences in spite of the large difference in the ventilation rate.

Figures 6 and 7 show the hourly simulation results for a week in midsummer, from end of July to beginning of August. The room thermal environment are also shown in Figure 6. The air temperature and humidity variations of the room air and the coil inlet air are similar for all cases, since the room air temperature is kept to the set point and the coil outlet air temperature is controlled to keep the room set point temperature. As the constant outlet relative humidity model is used in the simulation, the room humidity can not be kept to a constant value even in the air conditioned hours. The relative humidity of the cooling coil of the outlet air was assumed to be 90%. Under the controlled outlet air temperature with CAV control scheme,

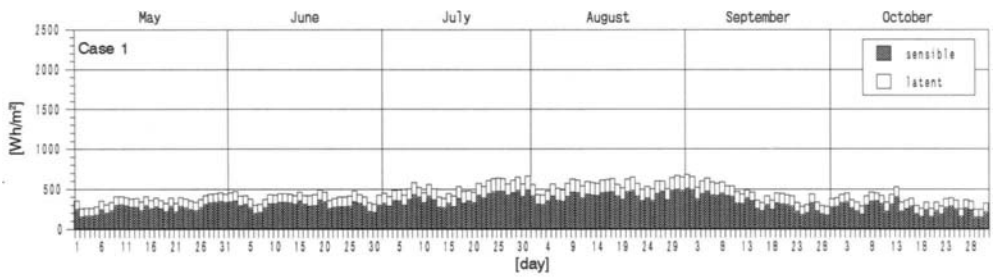


Figure 4: Variation of daily room cooling load of Case 1

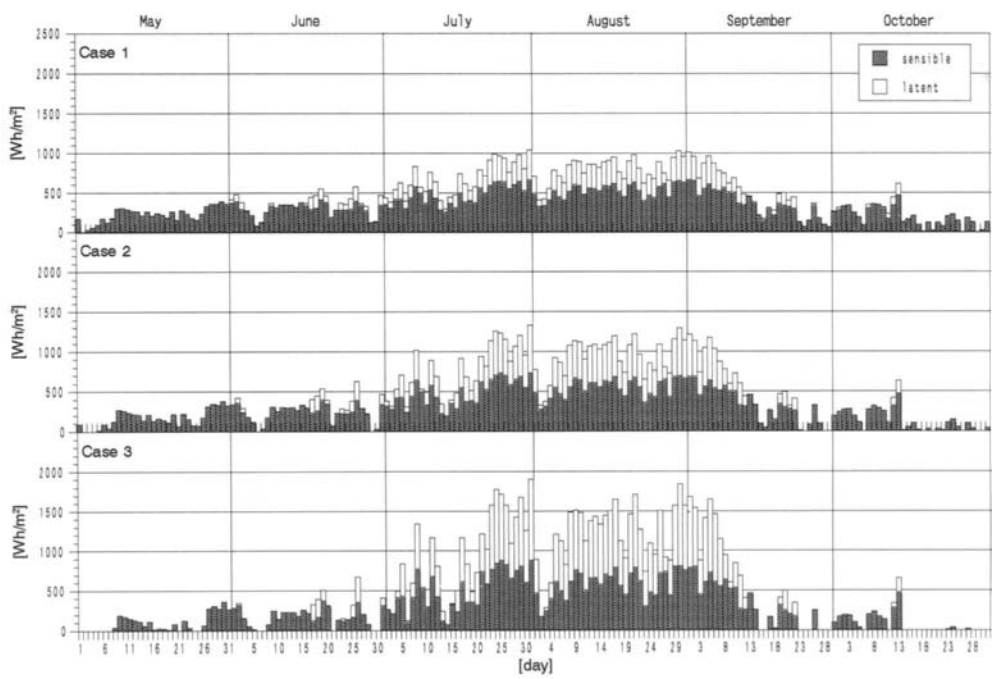
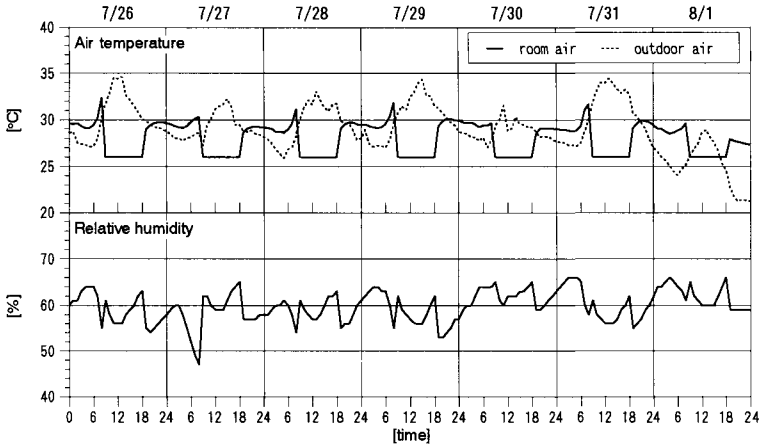


Figure 5: Comparison of dairy cooling coil loads



Figiure 6: Hourly variation of room air temperature and humidity
(Case 1, from July 26 to August 1)

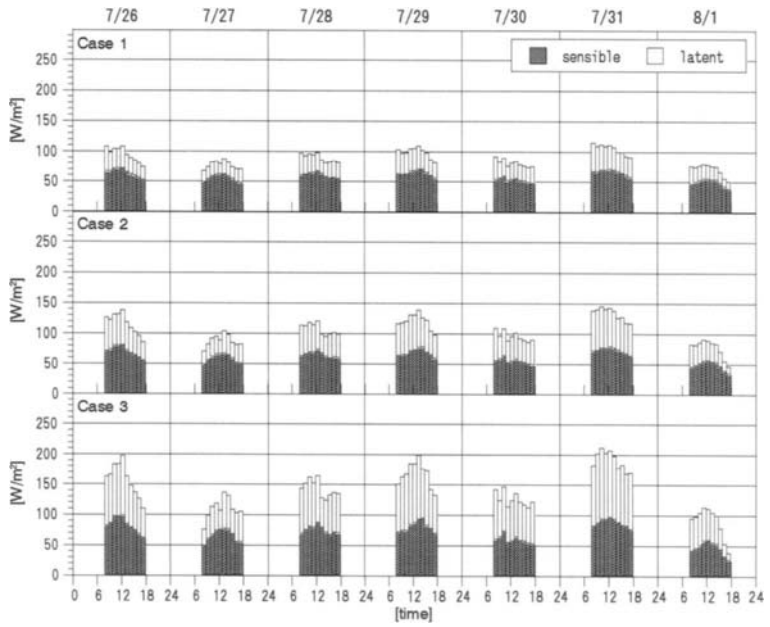


Figure 7: Comparison of hourly cooling coil loads in midsummer
(from July 26 to August 1)

the room air humidity is around 60% in the air conditioning hours for all Cases.

The peak coil load is observed on July 31 with the maximum outdoor air temperature of 34.4 °C. The hourly coil loads are shown in Figures 7 for the comparison of Cases 1 to 3. Figure 7 shows almost twice

TABLE 2
COMPARISON OF MONTHLY AVERAGE COOLING COIL LOADS (kWh/㎡month)

	Cooling season May - October			Midsummer July and August		
	sensible	latent	total	sensible	latent	total
Case 1	10.1	3.3	13.4	15.0	7.3	22.3
Case 2	9.3	4.3	13.6	15.6	10.0	25.6
Case 3	8.5	6.6	15.1	16.6	15.6	32.2

the latent cooling coil load when comparing Cases 1 and 3. When comparing Cases 1 and 2 the latent load of Case 2 is larger than that of Case 1 by 20%. For the sensible coil loads, only small differences are shown, while Case 3 shows the largest load.

DISCUSSION ON VENTILATION RATE IN COOLING

Comparison of coil cooling loads for the entire cooling season is shown in TABLE 2. The total seasonal cooling loads consisting of sensible and latent loads express small differences considering the large difference in ventilation rate. The seasonal total cooling load is almost the same comparing Case 1 with Case 2, while a 13% increase exists comparing Case 1 with Case 3. However, increase of the latent heat load is remarkably close to increase of the ventilation rate especially in midsummer, July and August. The difference of the latent load between Case 1 and Case 2 is 37% of Case 1 in the midsummer. As shown in Figure 5, even in June and September, monthly heat loads of the three Cases do not show significant differences. Even in winter, cooling is often required for room heat load base in many office buildings in Tokyo. The difference in the total annual cooling coil load due to the increased ventilation rate is considered to be very small.

When increasing the ventilation rate during the cooling operation, the increase of the latent coil load to remove moisture from outdoor air is an important problem in midsummer. In considering the hourly cooling load, this tendency is emphasized as shown in Figure 7. For the cooling system, the ventilation rate is not necessary to be set at a minimum value for energy conservation even in midsummer, if the latent heat is removed effectively. The effect of the ventilation rate strongly depends on the difference in indoor and outdoor air humidity ratios. As shown in the results for June and September, the applications to the office building might be expected during a climate of low humidity in midsummer or when the buildings require cooling at night.

The all fresh air system using a heat recovery component using total heat exchanger with high effective latent heat exchange may be considered as a possible technology to reduce the latent heat load in midsummer. A latent heat exchanger with an efficiency of 75% can reduce the latent load of Case 3 to that of Case 1.

It is a well known practical way to use a minimum ventilation rate in the peak hours in midsummer and a maximized appropriate ventilation rate for the free cooling or the economizer cycle. Nevertheless, an all fresh air system has the possibility for the design of a simple duct system since the return duct system can be neglected. An all fresh air system may also be extended to examine the possibility of hybrid ventilation system combine with natural ventilation and a mechanical cooling system.

CONCLUSION

The effect of ventilation rate on the cooling coil load was examined for an office building assumed to be built in Tokyo to study the possibility for using outdoor air as a cooling source as well as for the preservation of better indoor air quality.

The simulation results for three Cases using three different levels of ventilation rate from the minimum to an all fresh air input showed that the total seasonal cooling coil loads are almost same. From the view point of energy consumption in cooling, the all fresh air system has a possibility to be used as a simple system and would provide better indoor air quality compared with the minimum ventilation case.

The latent coil load significantly increases corresponding to the ventilation rate in midsummer, July and August, while there is no significant difference for the sensible cooling coil loads. Therefore, dehumidification is very important when examining the relationship between cooling energy and ventilation rate during the hot and humid summer period.

Advantageous applications should be examined considering the factors influencing the cooling coil load. Latent heat recovery systems, climatic conditions, types of building and required room environment in cooling operation are the key variables to be balanced in designing effective applications.

REFERENCES

Roh H. and Udagawa M.(2001), Simulation study on the performance of a fabric heat storage system, Journal of Architecture, planning and environmental engineering, AIJ, No. 544 31-38

Takizawa H.(1985), Proposal of a typical office building for heat load simulation, Proc. of the 15th Symposium on Heat, AIJ(Architectural Institute of Japan) 35-42

Udagawa M. (1990), Simulation of room thermal environment and energy use of residential buildings, Proc of Inernatinal CIB W67 Symposium, 1990

Udagawa M. and Satoh M.(1999), Energy simulation of residential houses using EESLISM, Proc. of Building Simulation '99(Sixth International IBPSA Conference, 1999, Kyoto) 91-98

Advances in Building Technology, Volume 2
M. Anson, J.M. Ko and E.S.S. Lam (Eds.)
© 2002 Published by Elsevier Science Ltd.

THERMAL INDOOR CLIMATE AS A BUILDING PERFORMANCE

Proposal for new criteria, design aids and assessment methods in The Netherlands

A.C. van der Linden[1], A.C. Boerstra[2] and S.R. Kurvers[3]

[1] Delft University of Technology, Faculty of Civil Engineering and Geo Sciences, Department of Building Engineering, P.O. Box 5048, 2600 GA Delft, The Netherlands, e-mail: a.c.vanderlinden@citg.tudelft.nl ; web site: http://www.BnB.citg.tudelft.nl
[2] BBA Indoor Environmental Consultants, Rotterdam, The Netherlands
[3] High Performance Buildings, Gouda, The Netherlands

ABSTRACT

In the assessment of thermal indoor climate in the Netherlands, the directives commonly used, are the ones given in 1979 and 1991 by the Government Buildings Agency (GBA). The criteria formulated in 1991, expressed in 'weighted excess hours' were a subject for debate. This paper treats these directives and their backgrounds, but above all, a proposal for new guidelines is presented. It incorporates the new notions about desired comfort temperature as described by "adaptive models" as given by De Dear and Brager.

KEYWORDS

Indoor climate, thermal comfort, thermal comfort performance criteria, building thermal performance, performance assessment, adaptive models.

INTRODUCTION AND BACKGROUND

One of the main characteristic performances of a building is its thermal indoor climate. The indoor climate should optimally support the activities of the people within the building. In The Netherlands more than 20 years of experience exist with performance specifications on Thermal Indoor Climate, formulated by the Dutch Government Buildings Agency (GBA), Van der Linden et al. (2002). Using Fanger's Predicted Mean Vote (PMV), these specifications are based on the central starting point that a in a "good" building the thermal climate exceeds at most 10% of the working time the limits of $-0,5 < PMV < 0,5$, Rijksgebouwendienst (1979). In computer simulations on a yearly bases, the hours that the indoor climate exceeds these limits are counted and the hours are weighted in relation to the extend the climate exceeds the limits. The design value is 150 weighted hours. For an average office building i.e. this means that the indoor operative temperature exceeds a limit of 25°C for at most 100 hours a year (about 10% of the working time in the summer period of about six months).
Weighing the hours the climate exceeds the desired limits was considered necessary regarding the difference in thermal capacity of different buildings. This can be plainly noticed: in the case of a small thermal capacity, the mean temperature of a room during the *excess hours* will be definitely higher

than in that of a heavy building. It can also be assumed without further argumentation, that in such situations the thermal load experienced by people will also be higher. Fanger's Predicted Percentage of Dissatisfied (PPD) was applied as a criterion to calculate the extent of excess temperatures. During the period in which it exceeds a PMV = +0.5 (PPD = 10%), a weighting directly proportional to the PPD is applied. In other words, 1 hour with 20% 'dissatisfied' counts twice as heavily as 1 hour with 10% 'dissatisfied'.
The weighting hours method also provides the possibility to consider the way in which people adjust to higher indoor temperatures, whether by modifying their clothing or increasing the air circulation (opening windows). These changes and the influence of different building types and building services, are automatically included in the input data for the execution of computer simulation calculations.
However consultants and designers widely apply the GBA-method in practice, in combination with other criteria. The debate that is taking place about the method shows the difficulty of optimally communicating its content with occupants and owners of the building.
Furthermore the method works very well in assessing buildings in the design stage by using temperature simulation programs. Assessing buildings in use is much more complicated because it is hardly possible to have temperatures measured during the complete six months summer period. So measurements of two days or two weeks periods have to be used.
Members of the Dutch construction industry and the research world came together to discuss some of these items during a workshop in Delft. The workshop report, De Wit et al. (1999), which includes a bibliography and interviews, constitutes the basis for a new project. The Technical University of Delft in collaboration with BBA/HPB (see authors) and ISSO (Dutch Institution for Study and Research in the field of Building services) is carrying out this project with the support of NOVEM (Dutch Organisation on Energy and Environment) and the Government Buildings Agency. This project will re-examine the current criteria, taking into account the recent research results on adaptive models and will develop new design and assessment instruments for practical use, Van der Linden (2000).

INTERNATIONAL DEVELOPMENTS; ADAPTIVE MODELS

The indoor climate criteria discussed up to now are based on steady state comfort models based on work with large groups of individuals in a laboratory situation.
In the Netherlands, people's adaptive behaviour in practice - changing clothing or physical conditions i.e. increase the air velocity by opening windows - has been taken into account for over 10 years now, Brouwers (1989). In indoor climate computer simulations at higher indoor temperatures (Ti > 25 °C) the summer value of $I_{clo} = 0.7$ is reduced by 0.2 points to $I_{clo} = 0.5$ and v_{air} is set to 0.25 m/s. As a matter of comparison, these actions cause the limit temperature to shift from 25.5°C to above 27°C.
The chosen values are plausible, but have not been validated by serious research.

Besides the effects of adjusting the physical conditions, new findings based on field studies gathered by Brager and De Dear (1998) show another additional effect which indicates a psychological adaptation to a higher indoor temperature in relation to the one outdoors in a preceding period and to people's expectations. This effect counts especially for naturally ventilated buildings, situations in which people have a stronger relation to the outdoor climate and, to certain extent, are able to influence their own thermal indoor climate.
These findings provide well-founded information on the magnitude of the combined effects. They form the basis for an adaptive model in which de indoor comfort temperature is given in relation to the mean outdoor effective temperature in the preceding (one month) period.
Figures 1 shows the results that are already familiar to people working in this field.
In buildings with natural ventilation and options for individual control of the indoor climate, the comfort temperature in relation to the outdoor temperature varies to a larger extent than the PMV-model can explain. The adaptation of the clo-value and the increase in air circulation during periods with higher temperatures, represent only half of the observed difference.

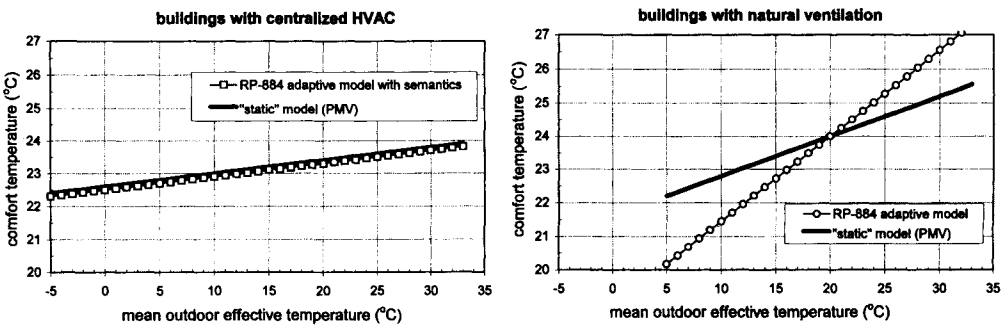


Figure 1: Comfort temperature in relation to the mean outdoor temperature in buildings without operable windows and with centralised temperature control and buildings with natural ventilation and with individual possibilities to influence the indoor climate, De Dear (1998).

In their article De Dear and Brager suggest that the other half of the difference is related to people's psychological adaptation to an indoor climate that follows the outdoor climate to a much higher degree than in an air-conditioned building. This leads to the conclusion that people's recent thermal experiences, together with their expectations concerning the premises concerned, play an important part in their assessment.

Recent analysis, Kurvers et al. (2001), of data found in 61 buildings in the Netherlands some 10 years ago, Preller et al. (1990), shows that a higher percentage of satisfied people is found in buildings with operable windows and natural or mechanical ventilation but without mechanical cooling, than in HVAC buildings, figure 2.

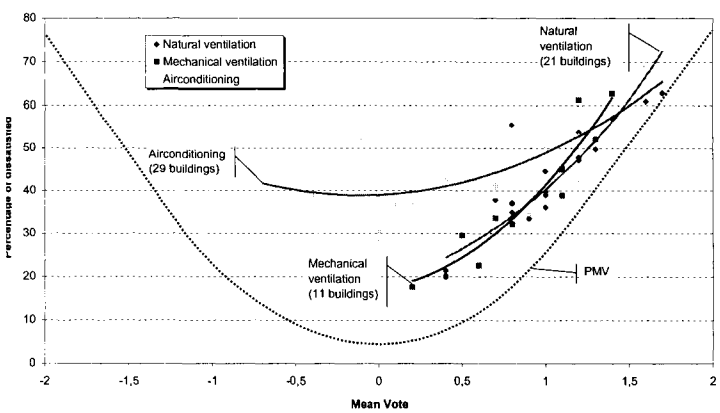


Figure 2: Relation between MV and PD in summer, Kurvers et al. (2001)

Figure 3 (next page) shows that the satisfaction in non air conditioned buildings, expressed in the percentage of satisfied people, is greater - although these people experience the climate as hotter (MV = +0.97 and +0.91) - than of people in air conditioned buildings (MV = +0.51).
This means that the statistical distribution of the votes is quite different in the two situations.
It is important to know that the percentage of dissatisfied people is fixed by counting the people that vote +2 and +3. Furthermore, the votes were not asked for instantaneously. The questions about summertime experiences were put in the context of a broader Sick Building Survey, carried out in

January and February. So the respondends' reactions were based on long-term experience and expectations. The results are consistent with Brager and De Dear's findings and illustrate the necessity for an adjustment of the current Dutch guidelines.

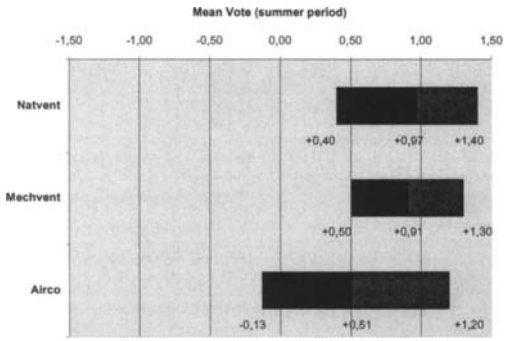


Figure 3: Mean Vote in summer as found in three building categories, Kurvers et al. (2001-1)
The values given represents P10, average and P90; number of buildings see figure 2.

PROPOSAL FOR A NEW DUTCH GUIDELINE ON THERMAL INDOOR CLIMATE

Based on a extensive literature review, Kurvers et al. (2001-2) a proposal for a new thermal comfort guideline is made. Note that this is just a proposal under discussion in the Dutch research group working on the subject. The thermal comfort model used, is the adaptive model developed by Aucliciems et al (Oseland & Humpfreys, 1994).
Basis for the assessment of the quality of the indoor thermal climate in practice are the lines given in figure 4. The quantitative data that these comfort limits are based upon are derived from De Dear et al (1997). These lines represent the upper limit of the 90% satisfaction area. Exceeding these lines means PPD > 10%. Following the work of De Dear et al. the comfort temperature varies with the outdoor temperature. This outdoor temperature is described by RMOT*, see intermezzo.

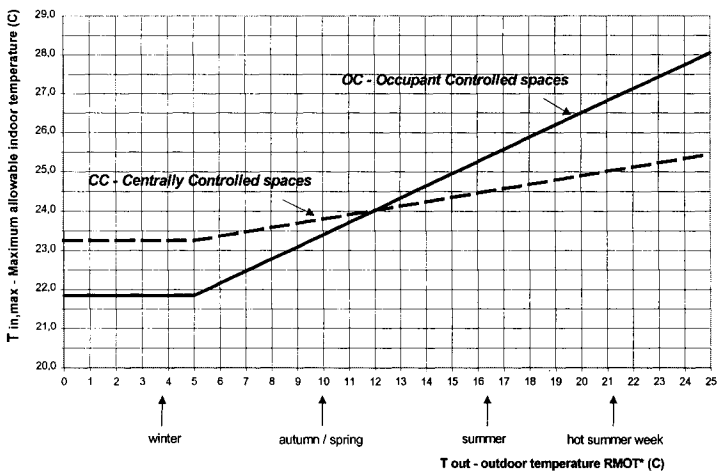


Figure 4: Upper comfort limits for the effective indoor temperature (based on the PPD=10% lines of De Dear et al, 1997) for occupant controlled and centrally controlled spaces in relation to outdoor temperature (see also Intermezzo RMOT*).

The comfort criterion for occupant controlled building spaces is less severe than the criterion for centrally controlled indoor climate and also less severe than the existing criteria as given by the Dutch GBA for both occupant controlled and centrally controlled buildings. This means less need for mechanical cooling (less complicated building services) and less energy use. But there is a strong need to give a very clear definition on "when a building space can be considered as occupant controlled".

Building performance with respect to thermal indoor climate

To assess the performance of a building with respect to the thermal indoor climate the response of the building (a room in the building) to the outdoor climate of a whole year is considered. In designing new buildings this is common practice; the use of thermal simulation computer models is wide spread. It is important to use the same basis. In The Netherlands the outdoor Climate of the year 1964/65 is used as a reference. To assess buildings in use is quite another topic. This is treated shortly further on in this paper

In a computer simulation, the hours (during working time) that the comfort limit of figure 4 is exceeded are counted. This is more or less the same as was done in the GBA-method, described before. The great difference is the basis of the criterion for the momentary comfort in which people adaptive behaviour is now taken into account.

To take into account the difference in thermal behaviour of buildings with different thermal mass and different types of building services, resulting in a stable or a more fluctuating indoor climate, also the extend to which the limit is exceeded is counted and the average is calculated. In this way a classification of building performance with respect to indoor thermal climate as given in table 1 can be made.

TABLE 1
PERFORMANCE CLASSIFICATION PROPOSAL

classification	% of time limit is exceeded	exceeded with (avg.)
excellent	0%	-
good	0-10%	<1 °C
moderate	0-10%	>1 °C
poor	>10%	-

Optimising communication

Nowadays it is quite normal for a consultant to translate the employer/client's functional requirements, often formulated in abstract terms, into quantitative ones; subsequently, the consultant will suggest one or more solutions that comply with the quantitative requirements. The client may then make a decision based on other preconditions and performances.

Even if the account is rendered to the client in quantitative terms, the actual communication takes place in the domain of (non-quantified) functional requirements. The client has to rely completely on the consultant for a translation into technical solutions.

To achieve proper communication regarding the thermal indoor climate, a qualification as given in table 1, will be of great help. Because these qualifications are still formulated in a rather abstract way, it probably will be necessary to translate them into figures that can be more intuitively comprehended.

Assessing buildings in use

Work is to be done on an instrument that can directly assess buildings, based on measurements of indoor and outside temperatures during a limited period of time (one or two days and up to a week).

Once the indoor climate quality during a shorter period will be related to the indoor climate for the whole year for different building prototypes and for a number of outdoor climate prototypes during one or two weeks, this should be possible. This relation may be found by means of large number of computer simulation calculations.

Intermezzo: RMOT*

Analysis of field studies (e.g. De Dear, 2001; Oseland & Humpfreys, 1994) showed that the amount of clothing people wear inside correlates strongly with the Running Mean Outside Temperature (RMOT), which is an 'artificial' outdoor temperature that can be described as an integrated temperature over the day of exposure and a couple of days before. It was assumed that in general the time-dimension of thermal adaptability is of the same order as the time-dimension of clothing adaptation. For practical reasons a numerical simplification of the RMOT is introduced, called RMOT*. In formula:

$$RMOT^* = \frac{1 \times T_{out,\ today} + 0.80 \times T_{out,\ yesterday} + 0.4 \times T_{out,\ day\ before\ yesterday} + 0.2 \times T_{out,\ 2\ days\ before\ yest}}{1 + 0.8 + 0.4 + 0.2}$$

With the remark that as 'outdoor temperature' on a certain day (today, yesterday etc.) once should calculate the average from the maximum and minimum outdoor temperature that can be collected from weather stations.

OCCUPANT CONTROLLED BUILDING SPACES

Because of the great difference between the two comfort limits it is very important to develop a clear definition to judge whether a building space can be considered occupant controlled.
Windows that can be opened (natural ventilation) are very important, but are of no use when the building occupants can not use them the way they want to. About the same can be said of individual control of building services. One of the parameters that limit the extend to what individual control can be practiced is the number of people in a room. A field study in 13 Dutch office buildings (about 12000 occupants in total) shows a big difference in the number of complaints in relation to the number of people in a room (figure 5), Kurvers et al. (2001-1).

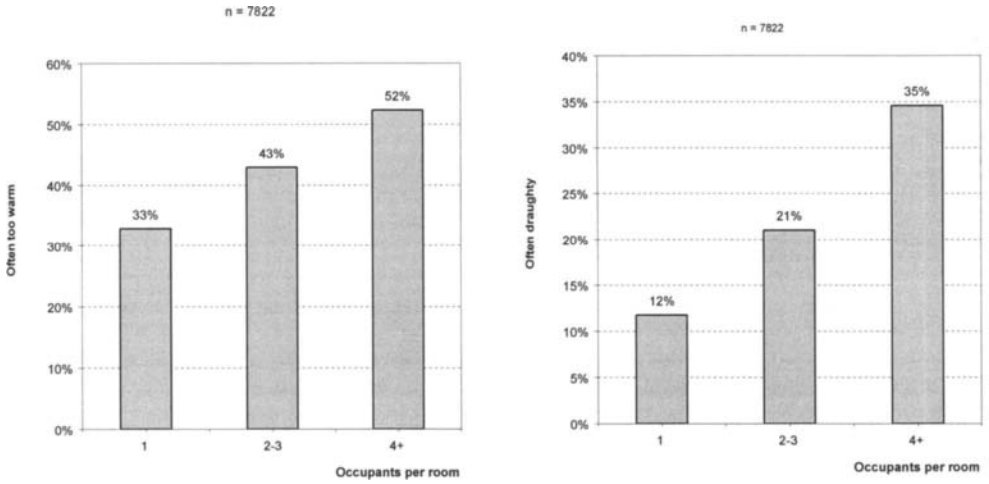


Figure 5: Relation between number of occupants per room and the percentage of occupants perceiving their workplace as "often too warm" (left) or "often draughty" (right) in 13 Dutch office buildings.

Perception of health, air quality, acoustical and visual comfort shows the same effect. Office rooms for 4 occupants or more lead to 1.5 – 3 times more complaints compared with the situation that rooms are occupied by just one person.

A part of the population was also asked about their perception of the possibilities of individual temperature control and the possibility of opening windows. Figure 6 shows 3.5 times more occupants in larger office rooms don't have the opportunity to open a window compared to single person rooms. About 4 times more occupants judge the possibility of individual temperature control insufficient.

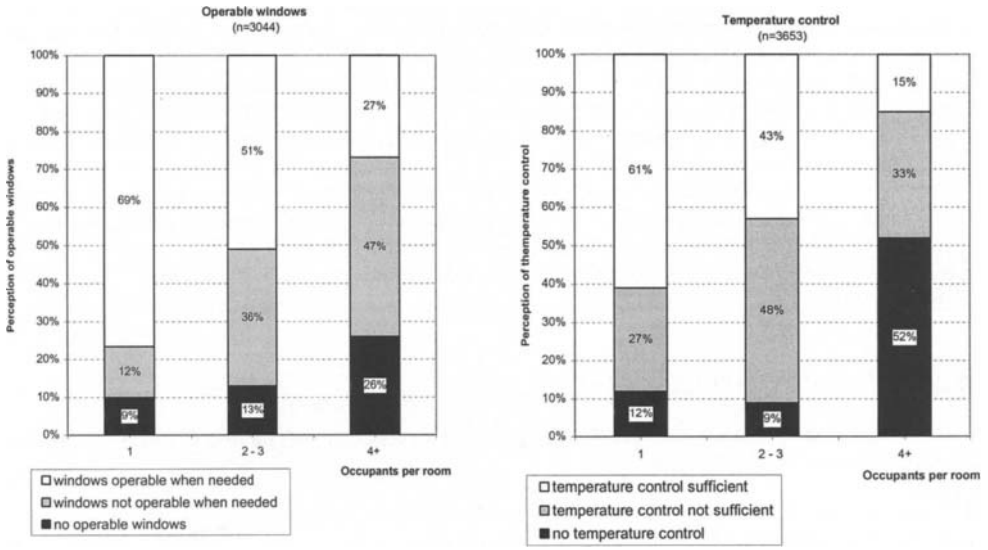


Figure 6: Number of occupants per room and the perception of the effect of operable windows (left) and the perception of the effect of temperature control (right) in 8 Dutch office buildings.

DISCUSSION

Based on a thorough review of the literature, Kurvers et al. (2001) and workshops with Dutch IEQ experts, a proposal for a new Dutch guideline for thermal comfort performance of indoor spaces is presented. Some aspects of the proposal are still 'under discussion', e.g. the RMOT* concept. Another question is: what requirements to use when outside air temperatures are below 5 °C, and what to do with the 5-12 °C range where requirements for occupant controlled spaces are now more stringent than those for centrally controlled and often artificially cooled spaces?

Furthermore lot of work has to be done on developing a good definition of "occupied controlled building space".

The final version of the guideline will be established the second half of the year 2002. This final version will present guidance on *how* to use the new requirements, not just in a design context (computer simulations), but also for evaluation purposes (measurement analysis).

In addition to the new guideline a format for field studies will be presented to evaluate the new guideline during the coming years.

ACKNOWLEDGEMENTS

This paper is based on the outcomes of a study carried out by Delft University of Technology and ISSO, the Dutch institution for the Study and Research in the field of Building Services in co-operation with BBA Environmental Consultants and High Performance Buildings.

The project is funded by NOVEM, the Dutch organisation on Energy and Environment and the Rijksgebouwendienst, the Government Buildings Agency of the Netherlands.

CONCLUSION AND IMPLICATIONS

A draft guideline for thermal comfort performance evaluation is presented. It's properties:

- The new guideline distinguishes between requirements for centrally controlled and for occupant controlled indoor environments, following De Dear's meta-analysis results.
- The new guideline will define 'suitable occupant control': e.g. requirements for effective operable windows, clothing policies, group size per room, etc.
- The upper temperature limits are set in terms of maximum allowable operative indoor temperatures. These increase with increasing outside temperature (RMOT*). Thus anticipating on adaptive effects (both behavioural and psychological) in relation to season and weather conditions. See figure 4 and Intermezzo RMOT*.
- The building's performance is characterized by the 'percentage of occupancy time that the allowable maximum indoor temperature is exceeded' and the 'average amount of degrees that the upper-limit is exceeded during these hours of excess'.
- It defines different levels of thermal performance quality in 4 categories. See table 1.
- Once established, the new guideline will be evaluated on the basis of well defined field research

LITERATURE AND REFERENCES

Brouwers, G.F.M. and A.C. van der Linden (1989), Assessment of Indoor Climate (in Dutch), *Klimaatbeheersing* **18:7**, 257-264.

De Dear R.J., G.S. Brager and D. Cooper (1997), Developing an Adaptive Model of Thermal Comfort and Preference, final report ASHRAE RP-884, Atlanta, USA.

De Dear, R.J. and G.S. Brager (1998), Developing an adaptive model of thermal comfort and preference, *ASHRAE Transactions*, Technical paper for the Winter Meeting.

De Dear, R.J. (2001), Clothing in relation to weather patterns, *personal memo*, unpublished.

De Wit, M.S., A.C. van der Linden and A.K. Raue (1999), Evaluation of performance indicators for thermal comfort in buildings (in Dutch), report PG-110, ISSO, Rotterdam, The Netherlands.

Kurvers, S.R., A.C. van der Linden, A.C. Boerstra (2001-1), Individual control, less energy use, healthier, more comfortable and productive indoor environment (in Dutch), *Facility Management Magazine*, **14:96**, 57-65.

Kurvers, S.R., A.C. van der Linden, A.C. Boerstra (2001-2), Thermal Indoor Climate as a Building Performance; literature review (in Dutch), Delft University of Techn. CiTG/GBT, The Netherlands

Oseland, N.A. and M.A. Humphreys (ed) (1994), Thermal comfort: past, present and future; Proceedings of a conference at the Building Research Establishment, Garston, BRE, UK.

Preller, L., T. Zweers, J.S.M. Boleij, B. Brunekreef (1990), Complaints on health and indoor climate in office buildings (in Dutch), report S83, Dir. Generaal van de Arbeid, The Hague, The Netherlands.

Rijksgebouwendienst (1979), Indoor Climate in Office Rooms of new Buildings, Hoofdafd. Bouw, afd. Warmte- en Luchttechniek, Dutch Government Buildings Agency, The Hague, The Netherlands.

Van der Linden, A.C., A.K. Raue and A.C. Boerstra (2000), Thermal Comfort and Building Performance, International Building Physics Conference, Eindhoven, The Netherlands.

Van der Linden, A.C., A.C. Boerstra and S.R. Kurvers (2002), Thermal Indoor Climate; building performance characterised by human comfort response, *Energy and Buildings*, spring 2002.

Advances in Building Technology, Volume 2
M. Anson, J.M. Ko and E.S.S. Lam (Eds.)
© 2002 Elsevier Science Ltd. All rights reserved

IMPROVEMENTS OF INDOOR HUMIDITY PERFORMANCE BY A NOVEL AIR-CONDITIONING SCHEME: CHILLED-CEILING COMBINED WITH DESICCANT COOLING

L. Z. Zhang, J. L. Niu

Department of Building Services Engineering,
The Hong Kong Polytechnic University, Kowloon, Hong Kong, China

ABSTRACT

A novel HVAC system, chilled-ceiling combined with desiccant cooling is proposed for an office room in hot and humid climates in Hong Kong. Studies found that improved indoor humidity performance can be obtained in comparison with a traditional all-air conditioning system. Actually, for conventional constant volume all air system, the minimum RH is in July and the RHs are well controlled to around 50% in summer season. In winter and transient seasons, the RHs rise up. RHs bigger than 70% occasionally occur in these seasons. In contrast, the chilled ceiling combined with desiccant cooling system controls indoor temperature and humidity independently. The variations of monthly averaged RH are relatively small and they are in phase with outside humidity fluctuations: maximum in August and minimum in February.

KEYWORDS

Radiant cooling, Humidity, Desiccant cooling, all-air system.

INTRODUCTION

There have been increased interests of radiant cooling in North America and Asian countries due to its inherent advantages of increased thermal comfort with reduced energy use (Feustel and Stetiu, 1995; Stetiu 1992; Niu, Kooi Ree 1995). However, up until now, most of the works concerning radiant cooling are focused on its thermal analysis, while indoor humidity, which is equally important as thermal performance, is neglected. The scarcity of knowledge in this area has limited the applications of chilled-ceiling systems to hot and humid regions, where the risk of condensation on the chilled ceiling surfaces represents a significant problem. This is understandable considering Hong Kong has a hot and humid summer with an average dew point exceeding 22°C. Consequently, indoor moisture levels need to be carefully controlled in this climate, not only for thermal comfort purposes, but also for condensation reasons. It is inevitable that air dehumidification and ventilation must be well combined with chilled ceiling panels and the resulting indoor humidity performance should be evaluated, in addition to building thermal performance analysis.

In this paper, the indoor humidity behaviors associated with a system combining chilled-ceiling and desiccant cooling (CC+DC) are investigated and compared with a traditional constant volume all-air system (CAV). Some operational measures to prevent water condensations on ceiling panels are recommended.

SYSTEM DESCRIPTIONS

Traditional air-conditioning system is constant volume all-air system. In such a system, both the sensible and latent load is treated by coiling coils in an AHU (Air Handling Units). To use the concept of radiant cooling, a new system, namely, a system combi ıing chilled-ceiling with desiccant cooling, is proposed, as shown in Fig.1 for schematics and Fig.2 for psychrometrics, respectively. With this system, the latent load is treated by the desiccant cooling system and most of the sensible load is treated by ceiling panels. The water flow rate to ceiling panels is kept fixed, while the inlet water temperature is controlled instead to maintain a pre-fixed indoor environment.

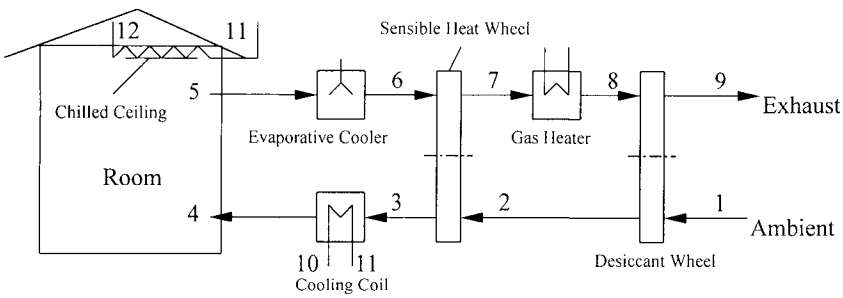


Figure 1: Schematics of the system combining chilled-ceiling with desiccant cooling.

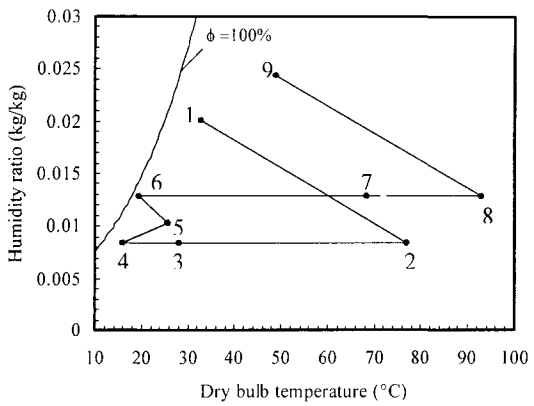


Figure 2: Psychrometrics of air handling in desiccant cooling.

The main purpose of desiccant cooling is for fresh air ventilation and dehumidification. Ambient outdoor air at state 1 enters the supply air duct. This air passes through a desiccant wheel and hot, dry air exits at state 2. This increase in temperature is due to the heat of sorption and some sensible heat transfer. The hot, dry supply air transfers much of this heat to the return air stream in process 2 to 3 involving a sensible heat wheel. Unlike a commonly used desiccant cooling, where air at state 3 is evaporatively cooled to state 4, in this system, the warm, dry air at state 3 is cooled by a cooling coil to around 18°C, to keep the dryness of supply air at state 4. The cool, dry air at state 4 is then distributed to the room. After accepting the building latent load and a small amount of sensible load, the air then returns to the desiccant system through return air ducting. This is the state of the air which corresponds to state 5. This somewhat cool, fairly dry air is evaporatively cooled to as low a temperature as possible at state 6. This cold, damp air is then preheated by the rotary sensible wheel to state 7 while cooling the supply air stream. State 7 is the state of the moist air as it enters the heating coil. Hot, humid air exits at state 8 and regenerates the desiccant wheel. Warm, very humid air at state 9 is then exhausted to the surroundings. In this combined system, εn evaporating temperature as high as 15°C is needed for the water-chiller, which means a much raised *COP*.

METHODS

Thermal performance is evaluated by a special cooling load program for cooled ceiling systems ACCURACY (Niu and Kooi 1994) which is developed and validated previously at Delft University of Technology in Netherlands. The program calculates not only the cooling load, but also the required supply water or air temperatures for different panel installation areas. The program also works out the respective convective and radiant heat extractions by cooling panels, and the radiant and convective heat from all the window and wall surfaces. Adopting such building dynamics simulation techniques, year round simulation of rooms with or without chilled-ceilings provides hour-by-hour data of cooling/heating loads, and temperatures of room air and other components.

Moisture balance in the room is calculated by,

$$\frac{V_r \rho_r dw_r}{d\tau} = -\dot{v}_s \rho_s (w_r - w_s) + ACH \cdot V_r \rho_o (w_o - w_r) + \dot{m}_s - \dot{m}_{ad/de} \quad (1)$$

where V_r is the room volume (m^3), ρ is air density (kg/m^3), w is humidity ratio (kg/kg), τ is time (hr), $\dot{v}_s$ is supply air volumetric flow rate (m^3/h), ACH is air infiltration rate (h^{-1}), $\dot{m}_s$ is indoor moisture generation rate (kg/h), subscripts "r", "o", "s" refer to "room", "outside", and "supply" respectively. The last term $\dot{m}_{ad/dc}$ is moisture adsorption and absorption by room surfaces and furniture (kg/h). In general, the moisture adsorption/absorption properties of building materials are less understood, therefore, overall, precision of moisture prediction lags behind that for thermal prediction. In this study, the indoor surface and furniture adsorption and desorption effects are not included. In reality, such effects may help smooth the RH fluctuations, but will not significantly affect the hourly averages (Niu and Burnett 1998). In simulations, thermal analysis is coupled with moisture analysis to take into account the interactions between thermal and moisture performance. The performance of the desiccant cooling system is predicted with a model proposed by (Jurinak, Mitchell, and Beckman 1983)

A typical office room in a south-facing high-rise building in Hong Kong (22°N, 114°E) is simulated in this study. The office is 5.1m long, 3.6m wide, and 2.6m high. The thickness of the envelope is 260mm and the resulting heat transmission coefficient U for the opaque part of the facade is $2.91 W/m^2K$. The glazing area is $2.88m^2$ with double-pane windows of which center-of-glass U value is 1.31 W/m^2K. Louver curtain is installed behind windows. It is determined that about 70% of the

ceiling is covered by radiant ceiling panels when the radiant ceiling panel system is applied. An occupancy pattern of 2 persons with a schedule from 9 to 18h is simulated in the office. When present, each person generates 75W sensible heat and 57.6g/h moisture. Of the sensible heat generated, 50W is radiative and 25W is convective. Besides, constant loads of 459W of equipment and lighting with a schedule from 9 to 18h are modeled in the room. Half of these loads are considered as radiative and half convective. The operating hours of the ceiling panels and ventilation systems are also from 9 to 18h. However, as will be discussed later, dehumidification/ventilation prior to the operation of chilled-ceilings would be required in summer to prevent condensation on panel surfaces. Air infiltration rates ranging from 0.05 to 0.4 ACH are modeled during the time when the ventilation system was switched off and the building is not pressurized.

The supplied chilled water flow rate to the ceiling panels is 0.5t/h, resulting a temperature rise of about 1.6°C through the panels. The ventilation fresh air is supplied at a rate of $67m^3/h$, which complies with ASHRAE standard 62 (ASHRAE 1999). For all-air systems, the ratio of return/fresh air is 3.4, resulting a supply air flow rate of $300m^3/h$. The operative temperature is set to 25°C in summer and 23°C in winter.

RESULTS AND DISCUSSION

The distribution of indoor relative humidity during working hours are shown in Fig.3 for CAV and CC+DC. The optimum zone is from 40% to 60%RH and 50% RH is ideal for building occupants to avoid the hazards of fungi, bacteria, viruses, and respiratory difficulties. The figure shows that the all-air system has the least annual hours in the comfort region, and has the most hours in either the dry (<40%) or the humid (>60%) regions. The chilled-ceiling combined with desiccant cooling controls the indoor humidity best: 90% of annual operating hours is in the optimum region.

The monthly averaged relative humidity is illustrated in Fig.4 for CAV and CC+Dc. For conventional constant volume all air system, the minimum RH is in July and the RHs are well controlled to around 50% in summer season. In winter and transient seasons, the RHs rise up. RHs higher than 70% occasionally occur in these seasons. This phenomenon is due to the fact that in a conventional all air system, temperature is intentionally controlled, while the humidity is passively controlled, because the supply air state is determined by the sensible load. In winter and transient seasons, sensible load becomes smaller and air is not sufficiently dehumidified. The result of this approach is a loss of humidity control while the temperature is maintained at set point. In contrast, in a CC+DC system, both the temperature and the indoor humidity are well controlled around set points, since they are decoupled and intentionally controlled independently. The variations of monthly averaged RH are relatively small and they are in phase with outside humidity fluctuations: maximum in August and minimum in February. It can be concluded that chilled-ceiling systems have better indoor humidity controls with reduced energy use than their all-air counterparts.

Even though chilled-ceiling systems realize independent humidity control with reduced energy use, when used in hot and humid regions, condensation on ceiling panels remains a troublesome issue. To prevent condensation, room air needs to be dehumidified prior to the operation of ceiling panels. A one-hour in advance dehumidification/ventilation strategy is simulated in which ceiling panels are operated from 9:00-18:00 and the AHU is operated from 8:00-18:00. The room moisture levels are substantially pulled down during the first dehumidification hour, and when the ceiling panels begin to operate, the maximum RHs are below 90%. Therefore, water condensation is prevented. The larger the air infiltration rates at night, the earlier it requires for air dehumidification, to prevent condensation. Generally speaking, a one hour in advance dehumidification could prevent condensation for most buildings except those that have very high air infiltration rates. On the other hand, if a building is well enclosed and the air infiltration rate is less than 0.05 at night, no condensation occurs

even for simultaneous dehumidification and ceiling cooling. The condensations with desiccant cooling are similar to those with AHU.

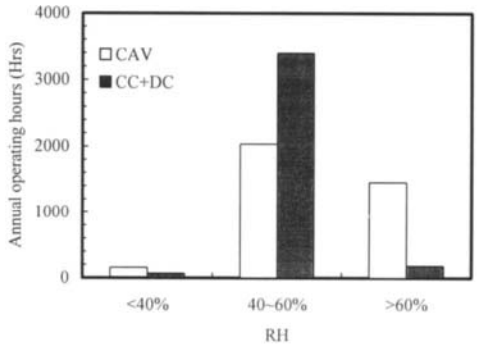


Figure 3: Indoor humidity distributions of two systems: CAV and CC+DC.

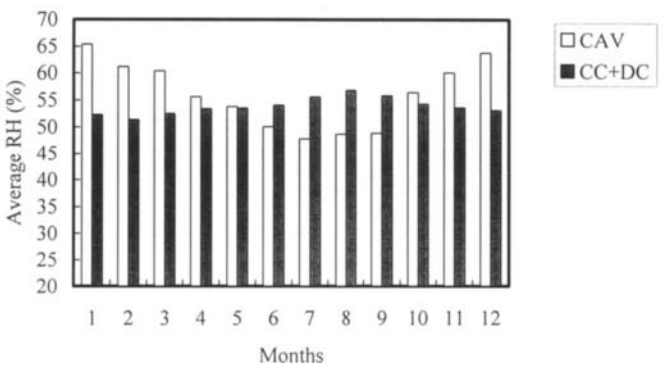


Figure 4: Monthly averaged relative humidity: CAV and CC +DC

CONCLUSIONS

The conventional constant volume all air system passively controls the indoor humidity. The result of this approach is a loss of humidity control while the temperature is maintained at set point in transient seasons. In contrast, in a system combining chilled-ceiling with air dehumidification, the temperature and the indoor humidity are decoupled and intentionally controlled independently. As a result, more annual hours are in the comfort region.

Air dehumidification and ventilation system should be operated at least one hour earlier than the operation of ceiling panels. Otherwise, condensation may occur. However, if a building is well sealed and the air infiltration rate is less than 0.05 at night, no condensation occurs even without in advance dehumidification.

ACKNOWLEDGEMENTS

This research is funded by the Research Grant Council of the Hong Kong SAR government, project No. B-Q222, and the Postdoctoral Fellowship of the Hong Kong Polytechnic Unicversity, G-YC34.

REFERENCES

ASHRAE. (1999). *ANSI/ASHRAE Standard 62-1999, Ventilation for acceptable indoor air quality.* Atlanta: American Society of Heating, Refrigerating and Air-Conditioning Engineers, Inc.

Feustel H.E., Stetiu C. (1995). Hydronic radiant cooling-preliminary assessment. *Energy and Building* **22:3**, 193-205.

Jurinak J.J., Mitchell J.W., Beckman J.W. (1983). Open cycle desiccant air conditioning as an alternative to vapor compression cooling in residential applications, *Proceedings of the ASME Solar Energy Division 5th Annual Conference*, 374-381. Orlando, FL, USA.

Niu J.L. and Burnett J. (1998). Integrating radiant/operative temperature controls into building energy simulation programs. *ASHRAE Transactions* **104:2,** 210-217.

Niu J.L. and Kooi J.v.d. (1994). Indoor climate in rooms with cool ceiling systems. *Building and Environment* **29:5,** 283-290.

Niu J.L., Kooi J.v.d. and Ree H.v.d. (1995). Energy saving possibilities with cooled-ceiling systems. *Energy and Buildings* **23:2,** 147-158.

Stetiu C. (1992). Energy and peak power savings potential of radiant cooling systems in US commercial buildings. *Energy and Buildings* **30:2,** 127-138.

ENVIRONMENTAL TECHNOLOGIES:

RECYCLING TECHNOLOGIES

This Page Intentionally Left Blank

Advances in Building Technology, Volume 2
M. Anson, J.M. Ko and E.S.S. Lam (Eds.)
© 2002 Elsevier Science Ltd. All rights reserved

THE ECO-COSTS/VALUE-RATIO

Ch.F. Hendriks, Mrs. ir. Gabriëlla M.T. Janssen and J. Vogtländer

Faculty of Civil Engineering and Geosciences, Delft University of Technology,
PO Box 5048 2600 GA Delft, The Netherlands

ABSTRACT

The basic idea of the EVR (Eco-costs/Value Ratio) model is to link the 'value chain' (Porter, 1985) to the ecological 'product chain'. In the value chain, the added value (in terms of money) and the added costs are determined for each step of the product 'from cradle to grave'. Similarly, the ecological impact of each step in the product chain is expressed in terms of money, the so-called eco-costs.
The eco-costs are 'virtual' costs: these costs are related to measures which have to be taken to make (and recycle) a product *'in line with earth's estimated carrying capacity'*. These costs have been estimated on the basis of technical measures to prevent pollution and resource depletion to a level which is sufficient to make our society sustainable. The ratio of eco-cost and value, the so-called Eco-costs/Value Ratio, EVR, is defined in each step in the chain as:

$$EVR = \frac{eco\text{-}costs}{value} \tag{1}$$

The five components of the eco-costs have been defined as 3 'direct' components plus 2 'indirect' components:

- virtual pollution prevention costs, being the costs required to reduce the emissions of the production processes to a sustainable level (Vogtländer et al., 2000);
- eco-costs of *energy*, being the price for renewable energy sources;
- *materials* depletion costs, being (costs of raw materials) * (1-α), where α is the recycled fraction;
- eco-costs of *depreciation*, being the eco-costs related to the use of equipment, buildings, etc.;
- eco-costs of *labour*, being the eco-costs related to labour, such as commuting and the use of the office (building, heating, lighting, electricity for computers, paper, office products, etc.).

Based on a detailed cost-structure of the product, the eco-costs can be calculated by multiplying each cost element with its specific Eco-costs/Value Ratio, the EVR. These specific EVRs have been calculated on the bases of LCAs.

KEYWORDS

eco-costs, value, recycling, prevention, land use, materials, pollution

1 INTRODUCTION

In the Preface of 'Our common future' of the World Commission on Environment and Development, G.H. Brundtland wrote in 1987:
'The downward spiral of poverty and environmental degradation is waste of opportunities and of resources. In particular it is a waste of human resources. These links between poverty, inequality, and environmental degradation formed a major theme in our analysis and recommendations. What is needed now is a new era of economic growth – growth that is forceful and at the same time socially and environmentally sustainable.'(Brundtland, 1987).

But what do these rather philosophical definitions of our future aim mean to governmental authorities business managers, designers and engineers in terms of the practical decisions they take?
There is a need to resolve simple questions like: What is the best architectural design in terms of ecological impact? What is the best concept of buildings in a city in terms of sustainability? What is the best spatial planning?

For that reason, the Delft University of Technology developed the eco-costs/value model as a practical tool for decision-making, based on the LCA methodology, and comprising the following features:

- one single indicator for the 3 major groups of environmental impacts (materials depletion, fossil energy consumption, toxic emissions) and land-use;
- a relatively simple and well defined allocation model to cope with the typical LCA difficulties in the building industry (in the building industry LCAs are characterized by many 'indirect' environmental impacts, like the environmental impact of the manufacturing of building equipment which are shared by many other external systems);
- an indicator which shows the degree of delinking of economy and ecology (eco-costs) of a product, which can be applied when a designer is asked to design a product (a house, a road, a city) within a given budget; the issue is then to create maximum value for the end-user at a minimum of environmental burden (eco-costs).

The basic idea of the model is to link the 'value chain' (Porter, 1985) to the ecological 'product chain'. In the value chain, the added market value (in terms of money) and the added costs are determined for each step of the product 'from cradle to grave'. Similarly, the ecological impacts of each step in the product chain are expressed in terms of money as well: the so called eco-costs. See Figure 1.

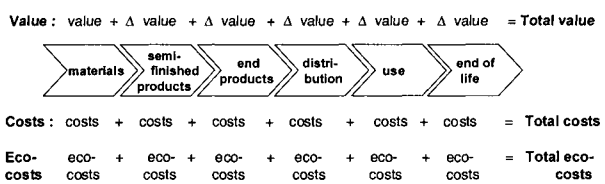


Figure 1: The basic idea of combining the economic and ecological chain: 'the EVR chain'.

The eco-costs are 'virtual' costs: these costs are related to measures which have to be taken to make (and recycle) a product *'in line with the earth's estimated carrying capacity'*. These eco-costs are the sum of the 'marginal prevention costs' of each 'class' (type) of pollution, see chapter 3.1, and the costs of measures for prevention of material and energy depletion, see chapter 3.2 and 3.3.
Since our society is yet far from sustainable, the eco-costs are 'virtual': they have been estimated on a 'what if' basis. The costs of the required prevention measures are not yet fully integrated in the current costs of the product chain (the current Life Cycle Costs). It is expected that, *in future,* the eco-costs

will become part of the product costs (by means of 'eco-tax', 'tradable emission rights', or other governmental measures), since our society will not continue to accept consequences unsustainable situations in the long term.

2 THE VALUE, COSTS AND ECO-COSTS OF A PRODUCT

Now we look into one step of the production chain.
The value ('fair price') of a product is determined by:

- product quality;
- service quality;
- image.

These 3 components of value are described in more detail by the 'eight dimensions' of Garvin (Garvin, 1988).

The cost-structure of a product comprises:

- the purchased materials (or components);
- the required energy;
- depreciation (of equipment, buildings, etc.);
- labour.

For each company in the production chain, the tax + profit equals the value minus the costs.

The direct eco-costs have been defined as sum of the following elements:

- virtual pollution prevention costs, being the costs required to reduce the emissions in the product chain (from cradle to grave) to a sustainable level;
- eco-costs of energy, being the price for sustainable energy sources;
- eco-costs of materials depletion, being (costs of raw materials)x(1-α), where α is the recycled fraction of materials to *make* a product (for details on the 'end of life' and recycling phase, see Section 4).

The indirect eco-costs are:

- eco-costs of depreciation, being the eco-costs related to the use of equipment, buildings, etc.;
- eco-costs of labour, being the eco-costs related to commuting and the use of the office (building, heating, lighting, electricity for computers, paper, office products, etc.).

This is depicted in Figure 2.

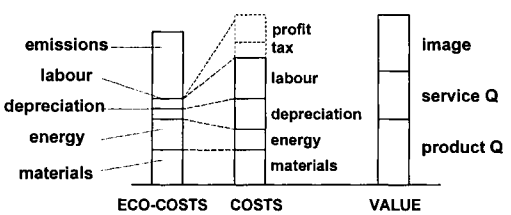


Figure 2: The decomposition of 'virtual eco-costs', costs and value of a product

Along the production chain the value, the costs and the eco-costs can be added up, as depicted in Figure 3.

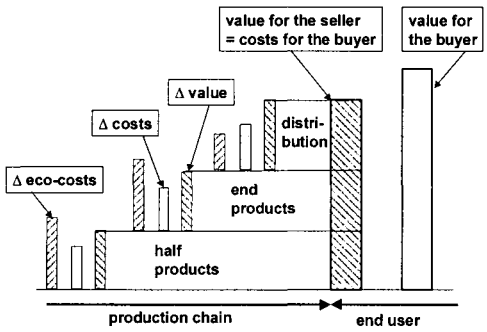


Figure 3: The decomposition of the value in the chain

Characteristic for each process, product or service is the ratio of the value and the eco-costs.
We can define this Eco-costs/Value Ratio, EVR, at every aggregation level of the production chain:
EVR = eco-costs/value.

A low EVR indicates that the product is fit for use in a future sustainable society. A high EVR indicates that the value/costs ratio of a product might become 'less than one' in future (since 'external' costs will become part of the 'internal' cost-structure), so there is no market for such a product in future.
Later in this article we will show how we might apply the EVR model for economic allocation in the LCA of a complex product-service system, but first we will define and describe the eco-costs.

3 THE COMPONENTS OF THE ECO-COSTS

As mentioned in Chapter 2, we define the eco-costs as the sum of 3 direct (toxic emissions, energy and materials depletion) and 2 indirect elements (depreciation and labour).
All these elements are calculated according to the LCA method, as defined in ISO 14041, as described hereafter.

3.1 The virtual pollution prevention costs

For toxic emissions, the marginal prevention costs are assessed for seven emission effect classes on the basis of prevention measures which are based on readily available technologies. The costs of the required marginal prevention measures are based on current West European price levels:
6.40 Euro/kg SO_x equivalent for acidification;
3.05 Euro/kg PO_4 equivalent for eutrophication;
50.0 Euro/kg VOC equivalent for summer smog;
12.3 Euro/kg fine dust for winter smog;
680 Euro/kg Zn equivalent for heavy metals;
12.3 Euro/kg PAH equivalent for carcinogenics;
114 Euro/1000 kg CO_2 equivalent for global warming.

3.2 The eco-costs of energy

The calculation method to determine the eco-costs of energy is based on the assumption that fossil fuels have to be replaced by sustainable energy sources. For details see (Vogtländer, 2001). The 'eco-costs of energy' is equal to the costs of the renewable energy system which has to replace the current system.

3.3 The eco-costs of materials depletion

With regard to the depletion of materials, the main approach in the model is:
- the eco-costs of materials depletion are set equal to the market value of the raw materials when the materials are not recycled;
- when a fraction α of the sourced material is recycled, a factor $(1-\alpha)$ is applied to the market value of the raw material for the new product to calculate the eco-costs of materials (for the general concept and its details see Section 4),

therefore

$$\textit{eco-costs of materials depletion} = \textit{'market value of the raw material'} \times (1-\alpha) \qquad (2)$$

The underlying assumption is that the (average) market value of the virgin material for *metals* reflects the fact whether the material is scarce or hard to find and/or mine (e.g. platinum, gold, silver), or whether that will happen in the foreseeable future.

For *plastics* however, the situation is different, since the source of it is crude oil.
It is more in line with the general philosophy of this model to avoid the use of fossil fuels and use biomass instead as source material for plastics. Therefore, in the EVR model the price of feedstock for plastics based on biomass has been chosen for the eco-costs of materials depletion. This price is estimated at 0.6 Euro/kg.
The fraction α has to be applied to the materials used for the new product (and *not* as a fraction of materials from the old product at the End of Life), *after* the upgrading process (if applicable).

3.4 Indirect eco-cost: the eco-costs of labour

The eco-costs of labour are indirect eco-costs, since labour as such is hardly causing any environmental burden. However, there is some environmental burden related to labour, such as the environmental impacts of heating, lighting, computers, commuting, etc.
The calculations of these eco-costs are specific for the type of labour.
A good guess for in offices is that the eco-costs for labour are approx. 10% of the costs. Calculations on labour outside offices (shop floor personnel in factories, sales people, truck drivers, etc. show that the eco-costs will vary in a range of 5% - 15% of the costs, where the eco-costs of commuting and use of electricity play a rather dominant role. Therefore it is recommended to make an LCA assessment in each typical case.

3.5 Indirect eco-costs: the eco-costs of depreciation of production facilities

The eco-costs related to the fact that fixed assets are used to make a product, are indirect eco-costs.
The calculations on the eco-costs of the use of fixed assets have the same characteristics as cost estimates for investments: for each individual situation, calculations have to be made on the applied materials and the required manpower.

The basic idea behind the 'eco-costs of depreciation' is that the eco-costs of the production equipment (or production facilities) have to be allocated to the products which are made by means of this equipment or in these facilities. The standard procedure is:

1. Calculate the eco-costs of the equipment or facility.
2. Divide the eco-costs of step 1 by the lifetime T (in years) of equipment or facility. In the EVR model the 'economic lifetime' has to be applied instead of the 'technical lifetime', which is 'safe side' since the economic lifetime is usually shorter than the technical lifetime.
3. Divide the outcome of step 2 by the quantity of products N which are produced per year.

In formula:

$$\textit{eco-costs of depreciation} = (\textit{eco-costs of the production facility})/T/N \tag{3}$$

It is obvious how to apply equation [3] to a production facility for prefab floor slabs, doors, prefab walls and other components for buildings.
But this equation is also applied to determine in more complex situations. As an example, this allocation procedure is applied to the use of an office building per m^2 per annum. Note that different facilities or different subsystems of facilities might have a different lifetime, T.
The same methodology can be used to analyse whether it is better to renovate specific old office buildings, rather than demolish these buildings and build new ones.
Since the EVR model applies the economic lifetime of the facility, equation [3] has a high similarity with the normal, linear equation for production costs related to depreciation:

$$\textit{costs of depreciation} = (\textit{value of the production facility})/T/N \tag{4}$$

Combining equation [3] and [3]:

$$\textit{eco-costs of depreciation} = (\textit{costs of depreciation}) \times (\textit{eco-costs/value})_{\textit{production value}} \tag{5}$$

The meaning for equation [5] is that the eco-costs of depreciation can be derived from the normal costs of depreciation by multiplying it with the EVR of the production facility. In situations where more than one type of product is produced in a complex production system, and where a 'cost break down structure' of the product is available, equation [5] can provide an easy way out of a rather complex allocation problem.
Calculations show the following characteristics for the eco-cost/value ratio:

- complex machines 0.3
- luxurious buildings (offices) 0.3
- low cost offices 0.4
- processes in stainless steel 0.4
- refineries 0.5
- steel structures 0.6
- warehouses 0.6

In general:

- the use of steel (and other metals) is related to a high EVR (because of high pollution prevention costs);
- complex systems have a low EVR (because of a high labour content).

4. THE ISSUE OF LAND-USE

The increasing use of land (urban areas, industrial areas, road infrastructure, etc.) is a major cause of degradation of our environment. In the last decades there is a growing concern about this negative aspect of a growing population and a growing economic wealth. So, most of the designers feel the need for incorporating the negative aspects of 'land-use' in spatial planning. But how?

The so called 'eco-costs of land conversion' is proposed as a single indicator, being the marginal costs of prevention (or compensation) of the negative environmental effects of change of land-use. These 'eco-costs of land conversion' are based on four sustainability characteristics of land (before and after the conversion):

1. the botanical aspects (the species richness and the rarity of ecosystems and vascular plants);
2. the aspect of 'scenic beauty';
3. the aspect of production of food and biomass;
4. the aspect of the H_2O cycle.

For the situation of The Netherlands (and the Western part of Europe), the eco-costs of the aspects 1 and 2 appear to be dominating.

4.1 The botanical aspects

'Habitat for plants, animals and other species' is one of the two major aspects with regard to conversion of land. The issue here is that 'biodiversity' is degraded by the expansion of urban areas. Although both flora and fauna are effected, flora has been widely accepted to classify the subject of land-use (Lindeijer, 2000), since it is easier to characterize than fauna (indicators for fauna are still under development), and since it is argued that there is a link between both types of biodiversity.

Species richness is characterized by the number of species of vascular plants at a certain area, S. It is one of the most applied measures of characterizing the botanical aspects of land in LCAs (Lindeijer, 2000).
For many Western European countries, data on S are available. For The Netherlands field data are available on a grid of 1 km^2.

In the EVR model, land-use is expressed in terms of 'actual m^2 'x' quality factor' of land before and after the change. The quality factor is defined as the counted total number of vascular plant species, S, divided by the quality norm for it, $S_{ref.}$, where $S_{ref.}$ is the number of species for 1 km^2 of nature.
The category indicator for species richness of land, *SRI* ('Species richness Indicator') is introduced, which is expressed in terms of the area, A (m^2), multiplied by the quality factor for it, $S/S_{ref.}$.

$$SRI = A \times S/S_{ref.} \tag{6}$$

So *SRI* is expressed in terms of 'equivalent m^2 of nature'.
The environmental effect of the change of land-use is described now as

$$\Delta SRI \times A \times AS/S_{ref.} \tag{7}$$

where Δ denotes the difference of S and *SRI* before and after the change.

For the quality norm of S in The Netherlands, $S_{ref.}$, a value of 250 vascular plants species for 1 km^2 is proposed. S is more than 250 for 9% of the total area of The Netherlands. (Areas above 300 are very scarce: 3.5% , areas above 200 are quite common: 21%).

For Germany, England and the northern part of France, the same quality norm of 250 species for 1 km^2 is proposed, since the species richness in these countries is in the same order of magnitude as in The Netherlands (Barthlott et al.,1998). For species richness of other countries, see (Vogtländer, 2001).

The total costs of compensation, the eco-costs of species richness, are:

$$eco\text{-}costs\ of\ species\ richness = \Delta SRI \times 4 \quad (Euro) \tag{8}$$

Where Δ *SRI* is the difference between *SRI* before and after the conversion.
A much more subtle methodology of botanical characterization on the basis of counting of species (vascular plants), is a methodology developed by Witte (Witte, 1998). This methodology takes the rarity of plants and ecosystems into account.
Although species richness is an indicator for botanical value ('when there are many species, there are normally valuable species as well'), it is a logical step forward to distinguish between species which are important and species which are less important. In this system, 'rarity of eco-systems' is the main measure of importance.
Since this method has been operationalised for The Netherlands only, the method is not described in this article. For a description of the methodology, see (Vogtländer et al., 2001) and (Vogtländer, 2001).

References

[1] Barthlott, W., Winiger M. (1998). *Biodiversity, a challenge for development research and policy,* Springer-Verlag, Berlin
[2] Brundtland, G.H., Khalid, M. (1987). World Commission on Environment and Development, *Our Common Future*, Oxford University Press, Oxford – New York
[3] Garvin, D.A. (1988). *Managing Quality,* Free Press, New York
[4] Henley, N., Shogren, J.F. White, B.(1997). *Environmental Economics, in theory and in practice,* Basingstoke, MacMillan
[5] Lindeijer, E. (2000). *Review of land-use impact methodologies,* Journal of Cleaner Production, **8**, 273-281
[6] Pearce, D.W., Turner, R.K. (1990). *Economics of natural resources and the environment,* Harvester Wheatsheaf, New York, 1990
[7] Porter, M.E. (1985). *Competitive advantage,* Free Press, New York
[8] Vogtländer, J.G. (2001). *The model of the Eco-costs/Value Ratio,* a new LCA based decision support tool, Thesis, Delft University of Technology, DfS, Delft
[9] Vogtländer, J.G. Lindeijer, Witte, J.P.M,. Hendriks, Ch.F. (2001) *Characterizing the change of land-use on the basis of species richness and rarity of vascular plants and ecosystems,* Journal of Cleaner Production (accepted)
[10] Witte, J.P.M. (1998), *Natural Water Management and the Value of Nature,* PhD thesis, University of Wageningen

Advances in Building Technology, Volume 2
M. Anson, J.M. Ko and E.S.S. Lam (Eds.)
© 2002 Elsevier Science Ltd. All rights reserved

SUSTAINABLE USE OF RECYCLED MATERIALS IN BUILDING CONSTRUCTION

Mrs. ir. Gabriëlla M.T. Janssen and Ch.F. Hendriks

Faculty of Civil Engineering and Geosciences, Delft University of Technology,
PO Box 5048 2600 GA Delft, The Netherlands

ABSTRACT

This contribution focuses on the importance of sustainability in the building sector. The underlying idea being that sustainability and durability must be considered jointly. Different models are presented to determine the degree of sustainability, focussing on: the degradation factor, life cycle assessment, the Delft ladder of priorities, high-grade applications, design for recycling, design for disassembly, and the ecocost-value ratio. Examples are given of case studies in which these models have been applied successfully.

KEYWORDS

materials, recycling, life cycle assessment, high grade application, degradation, ecocosts

INTRODUCTION

The term 'sustainability' was introduced in the UN report *Our Common Future* (Brundlandt). The NEPP describes sustainable development as that which meets the needs of the current generation, without endangering the opportunities for future generations to meet their particular needs. The concept encompasses not only the environment, but also social and economic interests such as health and wellbeing, safety, care for living space, prosperity, sufficient employment and a fair distribution of resources. To ensure real sustainable development, these interests must be combined at all levels. Sustainable construction could therefore be described as a way of designing and constructing buildings that support human health (physical, psychological, and social) and which is in harmony with nature, both animate and inanimate.
For the importance of sustainability the model of factor 20 is proposed.
The so-called 'Factor 20' is a metaphor, a guideline for sustainable development and to make specific steps forwards. The metaphor can also be used for sustainable construction. Factor 20 refers to the aim to have the environmental impact per unit of prosperity reduced by a factor of 20, thus meeting social needs 20 times as environmentally efficiently – in this case building housing and other property. There are also a number of variants to this factor, e.g. using the less stringent factors 4 and 10. Assuming

that both the population and worldwide economic developments will continue increasing, it is quite some challenge to reduce the environmental pressure. To answer the question 'how great is the environmental load that mankind is asserting on the environmental capacity?', the American biologist and environmental expert Barry Commoner (1972) described the environmental load using the following formula:

$$EL = P \times PP \times E \quad (1)$$

where:

EL	=	environmental load
P	=	population size
PP	=	average prosperity per person
E	=	environmental load per unit of prosperity

Let us assume the (not unreal) scenario that in 50 years time the world's population will have doubled, the average prosperity per person will be fivefold (the poor countries have a lot of catching up to do), and we want to halve the total environmental pressure. This means that the environmental impact per unit of prosperity must be reduced by a factor of 20. To implement changes of this size, a number of trends will have to be reversed. However, such reductions cannot easily be achieved by (improving) existing systems and technologies. In addition to technological innovations, people's behaviour and perceptions will also have to change. Technological solutions can only succeed if they fit in with social and cultural developments.

What is sustainable and what is sustainable construction?

There are many descriptions of the term 'sustainable', but there is no single definitive meaning. Most descriptions also provide a very limited view of the subject. We should not think that 'sustainable' merely focuses only on the environment. The processing industry understood this far earlier: environmental aspects should not be placed alongside or opposite other aspects or interests, but should be 'part of the concept as a whole', or as part of an integral approach. Here we should note that, in relation to the word 'construction', the term 'sustainable' has two meanings, i.e. both durable and sustainable.
Durable refers to the property of a material, building section or construction that can resist any unacceptable deterioration of relevant functional characteristics through specific chemical, physical and mechanical loads, over a certain period of time.
Sustainable refers to the general property of a material, building section or construction that indicates whether or not specific demands are met for affecting the air, water and soil qualities, for influencing the health and wellbeing of living organisms, for use of raw materials and energy, and even for scenic and spatial aspects, as well as for creating waste and nuisance.

Errors often occur when only one of these meanings is taken into consideration for sustainable construction or, worse still, if one meaning has priority over the other. Such errors can and must be prevented by integrating both aspects into the development and knowledge transfer with regard to sustainability.

Starting points

Decisions concerning integral sustainability, which include both meanings of the term, should be based on the following three starting points.
- An integral approach to (raw) material use in the construction industry should be based durability as well as sustainability.

- The application should be optimised based on the entire life cycle, including several life cycles for reused material.
- The application should be such that recycled material is used for the next best purpose possible within the building chain. This means that these materials must be used in such a way that they can be easily recognised and separated.

Degree of sustainability

Various instruments have been developed to measure or calculate the sustainability of materials.

Degradation factor (DF)
Using the design specifications as starting point and taking into account (variants for) material use and the required lifespan, including repair and maintenance scenarios, an image can be formed of the expected degradation, as a function of time and conditions of application. This is also important in the decision-making process when considering possible variants for reuse and recycling once the end of the lifespan has been reached.

Life-cycle thinking (LCA method)
Life cycle thinking is based on the fact that decisions taken in one phase (design, implementation, management, maintenance, demolition and reuse) should always be set against the background of the consequences for the following phases. The intention is to minimise the environmental interventions over the entire life cycle. The most suitable method for this is the life-cycle analysis (LCA), which has now received both national and international (ISO: International Organisation for Standardisation) recognition.

TABLE 1
OVERVIEW OF ENVIRONMENTAL PROBLEMS IN THE LCA METHOD

Depletion	Pollution	Deterioration
Depletion of raw materials	Greenhouse effect	Deterioration of landscape
Abiotic and biotic depletion	Deterioration of ozone layer	Deterioration of ecosystems
	Human toxicity	Deterioration of habitats
	Ecotoxicity	Victims
	Smog	Dehydration
	Acidification	Fragmentation
	Eutrophication	
	Radiation	
	Rejected heat	
	Odour	
	Noise	
	Working conditions	

Waste management
Until recently, the Dutch approach was based on the so-called 'Lansink's ladder', i.e. prevention – reuse of building elements – reuse of materials, incineration with energy recovery – incineration – disposal.

Lansink's ladder dates back to the end of the 1970s, when the legislation concerning waste products was first being written. However, looking back with hindsight, we notice several things. Firstly, the number of opportunities has increased, i.e. the scale of these opportunities (construction, building elements and materials) and there are new insights regarding immobilisation (using chemical or physical methods to prevent the spread of contaminants). Secondly, Lansink's ladder includes a clear order of preference. Methods are now available concerning life-cycle analysis (LCA), eco-costs (costs of ensuring a system or process meets sustainability criteria, including the so-called hidden costs) and value assessment. In particular, the results of the LCA methods and the EVR (eco-costs/value ratio) are applicable for making the best choice as to which rung on the ladder should be used in a specific situation. The result is thus an 'eco-ladder' or 'sustainability ladder' for the building sector, in which the order up the steps is 'tailor made'. This new dynamic ladder is depicted below, under the name 'Delft's ladder'.

TABLE 2
THE 'DELFT'S LADDER'

The 10 steps	Consequences
Prevention	'Design for recycling' (DFR), recovery, based on remaining lifespan (technical and economic)
Reuse of constructions	DFR, oversizing, selective dismantling, remaining lifespan
Reuse of building elements	DFR, selective dismantling, reprocessing, return system
Reuse of materials	DFR, selective dismantling, reprocessing, return system, leaching and content of contaminants
Useful application as residue	Quality equal to reference (with regard to leaching)
Immobilisation with useful application	Leaching and content of contaminants
Immobilisation without useful application	Dumping conditions
Incineration with energy generation	Emission limitation
Incineration	Emission limitation
Dumping	Dumping conditions

The return system refers to building elements or building materials that are returned to the original supplier and are processed (cleaned, repaired etc.), thus allowing them to be reused for the same purpose.

The Dutch Building Materials Decree specifies acceptable compositions and leaching, while the Dumping Decree defines the regime with which dumping sites must comply. Immobilisation means that the dosage rate for leaching (leaching rate) must be drastically reduced once the material has been treated (thermally, chemically or by adding a binder).

High-grade

The term 'high-grade reuse' is becoming clearer. It is often said that, although a lot of construction and demolition waste is reused, this is mostly low-grade waste that is only suitable for building roads. High-grade therefore means reuse in concrete or other building products, as the economic return is much higher for roads than for concrete buildings.

Based on the Delft's ladder, and with the exception of the most desired option, how can the high-grade level be defined? The key can be found by answering the following 10 questions as accurately as possible. By performing this exercise for all recycling options, the results can be easily compared. However, just as when using the life-cycle analysis to select a material, we see that none of the options receives a perfect score, but weighing the criteria further usually leads to the desired choice.

TABLE 3
HIGH-GRADE LEVELS FOR REUSE

High-grade applications: definition of the functional unit as per the LCA	Choices or actions
Applications meet all existing requirements, according to both private and public law	Yes or no
Technical lifespan is greater than economic lifespan	Yes or no
Applications require little maintenance	Express in mass quantities of maintenance materials per functional unit
Maximum potential for future reuse	State the various opportunities for reuse
Minimum degradation during the usage phase	No longer usable due to degradation
Applications are material-extensive	Materials required per functional unit
Applications are energy efficient	Energy required per functional unit
Applications have minimum harmful emissions	Emissions per functional unit
Applications have minimum non-reusable residual waste	Amount of unusable waste in kg per functional unit
Applications conform to market standards	Yes or no

Design for recycling (DFR)

Most primary raw materials are natural substances and are homogeneous, e.g. sand, gravel, clay, oil (including the production of plastics), wool, cotton and wood (for various applications in the building sector, but also for paper), and ores (for metal production). This homogeneity often makes it possible, with relatively simple preparation, to use these raw materials in the production process.

However, this is not true for secondary raw materials, i.e. mainly discarded products, mostly material conglomerates the composition of which is often so complex that reuse is only possible after extensive processing.
Recycling secondary raw materials generally requires a series of processes, of which recognition, sorting, size reduction, and separating are the most important.
Housing or construction demolition rubble must first have the iron, wood, mastic, bitumen, cardboard, chipboard, plastics, aluminium, zinc, copper etc. removed before the aggregate from the rubble crusher is suitable for use as secondary material. Asphalt and concrete from broken-up road pavings is also contaminated with road dirt, salt and oil residues etc. that must be removed before the recycling process can begin.
During the past decades, mechanical 'reprocessing' systems have largely replaced manual processes, primarily in the metal sector but also for construction and demolition waste (CDW), so that CDW can now be used on a large scale in the construction sector.
Not only the recycling sector, but also the government, came under increasing pressure to implement 'design for recycling' (DFR), i.e. designing items in such a way that they can be recycled. DFR means:
- using fewer materials;
- using parts that can be easily dismantled;
- marking all the plastic parts used so that they can be readily identified during dismantling and can be easily separated for further processing.

Governments, both in the Netherlands and elsewhere, are promoting DFR through certification, subsidies, 'return to supplier' obligations and levies on non-recyclable materials or scarce primary raw materials.

For a definite DFR design the following categories of materials must be capable of being recycled and separated.

Concrete
- according to VBT concrete specifications (meets national standards)
- non-standard compositions (for use in concrete)

Masonry
- bricks, sand-lime brick and concrete brick with mortar (for use in roads or concrete)
- aerated concrete
- crushed brick used as such or in brick (without mortar)
- crushed sand-lime brick for use in sand-lime brick
- crushed concrete brick for use in concrete brick

Bituminous materials
- asphalt without modified binders
- asphalt with modified binders
- roofing materials

Wood
- hardwood
- unpreserved wood
- preserved wood

Plastics
- thermosetting and thermoplastic agents should be used separately

Design for disassembly (DFD)
When using constructions and materials the criterion applies that, regardless of whether or not materials can be disassembled in an economic fashion, they can be separated for later reuse, if necessary. The following provides a basis for this strategy.
- Inspection and sampling.
- Specifications.
- Maintenance inventory.
- Conditions of use.

Some elements and materials should have been previously removed: flue pipes, gypsum blocks, gypsum walls, aerated concrete, bituminous roofing containing tar, asbestos and materials mixed with dangerous waste.
Mixing with (contaminated) soil should be avoided where possible.
With regard to the various categories of materials that should be recycled and separated, the comments in the section 'Design for recycling (DFR)' concerning concrete, masonry, metals and wood, also apply here.
Glass should be separated independently or in combination with concrete or masonry.
Plastics should be split into thermosetting and thermoplastic agents.

When demolishing roads and hydraulic engineering constructions the DFD method is fairly simple as the various materials are usually applied in layers.

Eco-costs/Value Ratio (the EVR model)
This model describes 'sustainability' (in the ecological sense) from a management systems approach, in which sustainability means the strive for eco-efficiency, as defined by the World Council for Sustainable Development: 'the delivery of competitively priced goods and services that satisfy human needs and bring quality of life while progressively reducing ecological impacts and resource intensity through the life cycle, to a level at least in line with earth's estimated carrying capacity' (WTCSD, 1993).

This business-oriented definition connects the thinking of the modern manager ('the delivery of competitively priced goods and services ... ... quality of life') to the need for a sustainable society ('while progressively reducing ... ... to ... ... earth's carrying capacity'). But what does this definition mean in practice for managers and designers, with regard to the many decisions taken daily? This is why a numeric model has been designed that is based on this definition, whereby well-founded choices can be made during the design phase with respect to the sustainability of the design, which is then used as a basis for setting out an entrepreneurial strategy.

The first section of the definition describes the 'value' of a product, the second section describes the impact on the environment, or 'eco-costs'. The basic idea behind the model is to couple the 'value chain' (Porter, 1985) to the 'product chain' as defined in the life cycle assessment. The added value and the costs are defined in the value chain for every step (from raw material to client, the usage phase and the 'end-of-life' phase). The environmental impact is also defined in monetary terms for each step in the chain, i.e. the eco-costs. If the usage phase and 'end-of-life' phase are also added to the chain, this gives the 'Total Costs of Ownership' (this approach is common in the car industry and for structural and civil-engineering and civil projects). The 'Total Eco-costs of Ownership' are therefore defined in a similar way in the model.

The eco-costs are 'virtual' costs, i.e. the hidden costs required to manufacture and use a product in a sustainable manner, or 'in line with earth's carrying capacity'. These costs are estimated based on the costs of technical measures to prevent undesired emissions and based on depletion of fossil energy and raw materials. As our society is nowhere near sustainable, the eco-costs are 'virtual', or not yet integrated into existing costs of the product chain (the existing life cycle costs). The eco-costs therefore consist of costs that have yet to be made to reduce the environmental impact (emissions and depletion) to a sustainable level. The eco-costs/value ratio (EVR) is defined as: EVR=eco-costs/value. The composition of eco-costs, costs and value is shown in Figure 1.

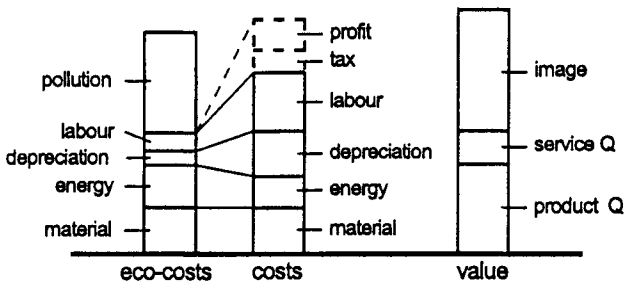


Figure 1: The value, costs and eco-costs of a product

A low EVR means that a product is suitable for a future sustainable society. A high EVR means that the economic value/cost ratio will worsen along the road to a sustainable society (and may even drop below 1.0) due to the required prevention measures, so that there will be no market for these goods in a future sustainable society.

Advances in Building Technology, Volume 2
M. Anson, J.M. Ko and E.S.S. Lam (Eds.)
© 2002 Elsevier Science Ltd. All rights reserved

STRENGTH OF CONCRETES PREPARED WITH NATURAL AND RECYCLED AGGREGATES AT DIFFERENT MOISTURE CONDITIONS

C.S. Poon, Z. H. Shui and L. Lam

Department of Civil and Structural Engineering,
The Hong Kong Polytechnic University, Kowloon, Hong Kong, China

ABSTRACT

The influence of moisture conditions of natural and recycled aggregates on the properties of the strength of the hardened concretes was highlighted in this study. Natural and recycled aggregates were incorporated into concrete in different combinations. The aggregates were controlled at air-dried, oven-dried and saturated-surface dried (SSD) states respectively prior to use. The results show that replacements of up to 50% of natural aggregates by recycled aggregates do not have significant detrimental events on the strength of the concrete produced. The effect of the moisture states of the aggregates on the strength of the concretes prepared with oven-dried and SSD-state aggregates at early age (i.e. 3 and 7 days) was noticeable. The concrete prepared with the air-dried aggregates achieved the highest average strength values at various ages. For the concrete prepared with recycled aggregates at the SSD condition, the increase in proportion of recycled aggregates significantly reduced the splitting tensile strength. The results suggested that an air-dried aggregate that contains not more than 50% recycled aggregate is optimum for producing normal strength recycled aggregate concrete.

KEYWORDS

Concrete, recycled aggregates, moisture state, strength development

1. Introduction

In Hong Kong, the construction industry produces about 37,000 tonnes of construction and demolition (C&D) waste everyday, which is roughly four times higher than that of municipal solid waste. But the shortage of land for new landfills and the end of major land reclamation projects in the near future have setup alarm in Hong Kong to find alternative uses of the C&D waste [1]. The government has adopted a policy to support innovative programmes that will promote the reuse of recycled aggregates. Recently, a few open storage-sites have been set up for temporary storing C&D waste and producing recycled aggregates, such as in Tseung Kwan O and at the old Kai Tak airport site. A development is being made to produce bricks and blocks with recycled C&D wastes [2]. To further develop the use of recycled aggregates in concrete production in Hong Kong, a systematic research programme is being carrying out at The Hong Kong Polytechnic University.

A number of past research has studied the properties of concrete made with recycled aggregates [3-5]. Hendriks and Pietersen [6] and Hendriks and Nijkerk [7] outlined the application issues of recycled aggregates in Europe, and described the main processes and equipment. Travakoli and Soroushian [8] highlighted the key factors that influence the strength characteristics of recycled aggregate concrete, such as the strength, size distribution and water absorption of the original concrete. Larbi et al [9] tried a thermal treatment method to improve the quality of recycled aggregate, and they found that after thermal treatment at 800°C, the recycled aggregate was reasonably comparable to conventionally used river-dredged aggregates.

Due to the high water absorption capacity of recycled concrete aggregates, the influence of the moisture states of the recycled aggregates on the properties of the fresh and hardened concrete prepared with recycled aggregates has received some research interest. Pre-wetted and saturated recycled aggregates were used in several studies [3, 10] in order to prevent a rapid decrease in concrete workability. These studies concluded that there was no obvious impact of the pre-wetted recycled aggregates on the mechanical properties of concrete. And this pre-wetting method has been recommended by several researchers [3]. However, Fleisher and Ruby [11] indicated that wet processing (i.e. pre-spraying) is not necessary for technological reasons, as long as the natural moisture of the aggregates is taken into account during the mix design. Also, it is suggested that it is hardly possible to pre-spray the recycled aggregate uniformly at a level of work that can still be justified. Oliveira and Vazquz [12] found that the compressive strength of the concrete made from dry and saturated recycled aggregates was slightly lower than the reference concrete. The decrease was especially noticeable in flexural strength of the concrete prepared with the saturated aggregates. And the concrete prepared with saturated and dry recycled aggregates exhibited poorer freeze thaw resistance whereas better results were obtained from the concrete made with the semi-saturated aggregates.

This study aims to increase the insight of the effects of the moisture states of the recycled aggregates on compressive and splitting tensile strength of the hardened concrete so as to promote the practical application of recycled aggregates in concrete production.

2. Experiments

2.1 Materials

Cement and fine aggregate

The cement used in this study was a locally produced Ordinary Portland cement equivalent to ASTM Type I Portland cement. The density of the cement was 3.16 g/cm^3 and the specific surface was 3,519 cm^2/g. The chemical composition of the cement is shown in Table 1. No chemical and mineral admixture was used in this study. The fine aggregate used was a natural river-sand with a fineness modulus of 2.11.

Coarse aggregates

Both natural and recycled aggregates were used in this study. The natural aggregate was a crushed granite with nominal sizes of 10 mm and 20 mm. The recycled aggregate was a crushed and graded unwashed recycled concrete aggregate obtained from a single source at the old Kai Tak airport in Hong Kong. The recycled aggregate was generated by the demolition activity of a number of reinforced concrete buildings and the concrete runway. The recycled aggregate was divided into two types in terms of their maximum nominal sizes,

i.e. 10 mm and 20 mm. The physical and mechanical properties of the recycled aggregate are shown in Table 2, where the porosity of the aggregates was determined using mercury intrusion porosimetry (MIP). In the concrete mixtures, the 10 mm and 20 mm coarse aggregates were used in a proportion of 1: 2.

2.2 Preparation of concrete mixtures

The concrete mixes were prepared with the use of natural and recycled coarse aggregates in four combinations; i.e., 100% natural, 80% natural + 20% recycled, 50% natural + 50% recycled and 100% recycled. These proportions of the concrete mixes were designed using the absolute volume method by assuming the aggregates were at a saturated surface-dried (SSD) condition. Adjustments were sequentially made according to the moisture contents and water absorption capacity of the respective aggregates. All the mixes had a free water content of 205 kg/m^3, a free water-to-cement ratio (w/c) of 0.57, and a fine aggregate to total aggregate ratio of 0.375. As the densities of the natural and recycled coarse aggregates were different, the actual amounts of fine and coarse aggregates in the mixes were slightly different.

In the study, the moisture states of the natural or recycled coarse aggregates were controlled at three states, i.e., air-dried (AD), oven-dried (OD), and SSD, while the fine aggregate was used at the as- received moisture state. Thus, in total, twelve concrete mixes were prepared with different combinations of natural and recycled aggregates in different moisture states. The oven-dried aggregates were prepared by drying them in an 105°C oven for 24 hrs, and they were cooled down to room temperature prior to mixing in the mixer. SSD aggregates were prepared by removing the surface moisture from the aggregates with a moistened cloth after immersing the aggregates in water for 24 hrs. The detached cement mortar during the soaking process was carefully collected and returned into the mixture.

To maintain the designed mix proportioning unchanged, the amounts of water and aggregates used in mixing were adjusted according to the actual moisture contents of the aggregates. When the air-dried and the oven-dried aggregates were used, an additional amount of water was needed to saturate the aggregates. Also, as the recycled aggregate had a higher water absorption capacity, the amount of water added to the mix increased as the percentage of recycled aggregate increased when they were used in the AD and OD states. The actual amounts of water and materials used in these twelve mixes are given in Table 3, and the moisture contents of the aggregates used in these mixes are given in Table 4. All the concrete mixtures were mixed for about 5 minutes in a Croker concrete mixer before casting into moulds and compaction on a vibrating table.

2.3 **Tests**

The compressive strength of the hardened concrete was determined at the ages of 3, 7, 28 and 90 days on 100mm cubes. The splitting tensile strength of these concretes were determined at the same ages on ϕ100×200mm cylindrical specimens. These specimens were removed from the moulds after 1 day and were cured in water at 27°C before testing.

3. Results and discussions

The compressive strengths of the concrete mixes are shown in Figure 1. It can be observed that all the concrete mixes achieved the target compressive strength of 35 MPa at the age of 28 days. However, the effects of the moisture states of the coarse aggregates on the compressive strength of the concrete were quite different for different combinations of coarse

aggregates. When only crushed granite was used as the coarse aggregate, the mixes prepared with the coarse aggregate in the AD and SSD states had similar compressive strength values at all tested ages, while the strength of the mix prepared with the coarse aggregate in the OD state was much lower. The use of recycled aggregate as a replacement of the crushed granite seemed to have a positive effect on the mixes prepared with the coarse aggregates in the OD state but a negative effect on those prepared with the coarse aggregates in the SSD state. Fig. 1 shows that while the strength of the AD mixes almost maintained unchanged as the percentage of recycled aggregate increased, the strength of the OD mixes increased, but the strength of the SSD mixes decreased. As a result, the OD mix showed a higher compressive strength than the SSD mix at all tested ages when all the crushed granite was replaced by the recycled aggregate. It can be seen that the 90-days compressive strength of concrete prepared with 50% and 100% SSD-recycled aggregate was lower than that of the others. It is interesting that the 28 days strength of AD-aggregate concrete at various recycled aggregate contents were higher than the strengths of the OD-aggregate concrete at the age of 90 days. And the 90 days strength of 50% recycled aggregate concrete prepared at the SSD state was lower than that of 28 days strength of 50% AD-recycled aggregate concrete. For the concretes prepared with 100% recycled aggregate, the 90 days strength of SSD aggregate concrete was lower than that of 28 days strength of AD- and OD-aggregate concretes.

The splitting tensile strength data are shown in Fig.2. The development of splitting tensile strength of concretes with various aggregate combinations up to 28 days was similar to that of the compressive strength. However, at the age of 90 days, the difference between the SSD series of concretes and the other two series of concretes become more significant. The splitting strength of the AD and OD series concretes was more or less similar to each other whereas the splitting strength of the SSD series concretes was obviously lower. The value further decreased with increasing percentages of recycled aggregate replacement. This result is consistent with the study described in Ref. [12].

It is well known that the strength of concrete depends on the strength of the cement matrix, the aggregates, and the interfacial bond between the cement matrix and the aggregates. For concrete prepared with crushed granite, the difference in strength development between the OD mix and the SSD mix might be related to the development of the interfacial bond strength. Wong et al [13] found that saturated-surface dried granite had a better bond with cement than the dried one in the initial period of curing. This may account for the lower strength of the concrete prepared with the OD granite than that with the SSD granite, although the high initial w/c ratio in the OD mix may also reduce the strength of the cement matrix.

The situation in the concrete prepared with recycled aggregates is different. The results of the present study reveals that compared with the crushed granite, the moisture states of the recycled aggregate had an opposite effect on the strength development of the concrete, and the use of the recycled aggregate in the SSD state is not preferred. The low compressive strength of the concrete prepared with the SSD recycled aggregate may be attributed to the bleeding of concrete, which was observed during compaction of the concrete cubes on the vibrating table. During vibration, the water inside the recycled aggregate particles may tend to move toward the cement matrix, creating a relatively high local W/C in the vicinity of the particles. This process can weaken the bond between the recycled aggregate and the cement matrix. On the contrary, when the recycled aggregate is used in the OD state, water and may tend to move from the bulk cement matrix toward the recycled aggregate particles, and cement particles may accumulate around the recycled aggregate particles. As a result, a

stronger bond may be formed between the cement matrix and the aggregate particles particularly at the early age.

Conclusion

1. For the concrete mixtures prepared with the incorporation of recycled aggregates, the air-dried aggregate concretes exhibited the highest compressive strength. The SSD recycled aggregates seemed to impose the largest negative effect on the concrete strength, which might be attributed to "bleeding" of excess water in the pre-wetted aggregates in the fresh concrete.
2. The long-term splitting tensile strength of concrete with 50% or more SSD-recycled aggregate was considerably lower than that of the other concretes.
3. Based on the results of this study, aggregates in the air-dried (as-received) state and contain not more than 50% recycled aggregate should be optimum for normal strength recycled aggregate concrete production.

Acknowledgement

The authors wish to acknowledge the financial support of The Hong Kong Polytechnic University, through the funding of IGARD and ASD-Advanced Building Technology. The Civil Engineering Department of the Hong Kong SAR Government is thanked for providing the recycled aggregate samples.

References

[1] C.S. Poon and S. Azhar, An investigation on the scope and applications of recycled aggregates in the Hong Kong construction industry, Proceedings, One Day Annual Seminar on Environmentally Friendly Structure, The Hong Kong Institution of Engineers Structural Division, Hong Kong, 2000.

[2] C. S. Poon, S. C. Kou and L. Lam, Use of Recycled Aggregates in Moulded Concrete Bricks and Blocks, accepted by Construction and Building Materials for publication.

[3] T.C. Hansen, RILEM Report 6—Recycling of Demolished Concrete and Masonry, Published by E & FN Spon, Bodmin, UK, 1992.

[4] C.S. Poon, Z.H. Shui, L. Lam and S.C. Kou, Microstructure and Compressive Strength of Concrete Prepared with Recycled Aggregates, submitted to Construction and Building Materials for possible publication.

[5] I.B. Topcu, Physical and mechanical properties of concretes produced with waste concrete, Cem. Concr. Res. 27(12) (1997), 1817-1823.

[6] Ch.F. Hendriks, H.S. Pietersen, RILEM Report 22—Sustainable Raw Materials—Construction and demolition waste, Edited by The Publishing Company of RILEM, 2000.

[7] Ch.H. Hendriks, A.A. Nijkerk, The Building Cycle, Aneas technical publishers, The Netherlands, 2000.

[8] M. Tavakoli and P. Soroushian, Strength of recycled aggregate concrete made with using field-demolished concrete as aggregate, ACI materials Journal, 93(2) (1996), 182-190.

[9] J.A. Larbi, W.M.M.Heijnen, J.P. Brouwer and E. Mulder, Preliminary laboratory investigation of thermal treated recycled concrete aggregate for general use in concrete, Waste Materials in Construction-WASCON 2000, Edited by G.R. Wooley, etc., England, May and June (2000), 129-139.

[10] K.K. Sagoe-Crentsil, T. Brown and A.H. Taylor, Performance of concrete made with commercially produced coarse recycled concrete aggregate, Cem. Concr. Res. 31(2001) 707-712.

[11] W. Fleischer and M. Ruby, Recycled aggregates from old concrete highway pavements, Exploiting wastes in concrete-Proceedings of Int. Seminar, Edited by R.K. Dhir and T.G. Jappy, Dundee, Scotland (1999), 151-161.

[12] M.B. de Oliveira and E. Vazquez, The influence of retained moisture in aggregate from recycling on the properties of new hardened concrete, Waste Management, 16 (1996) 113-117.

[13] Y.L. Wong, L. Lam, C.S. Poon and F.P. Zhou, Properties of fly ash-modified cement mortar-aggregate interface, Cem. Concr. Res. 29 (1999), 1905-1913.

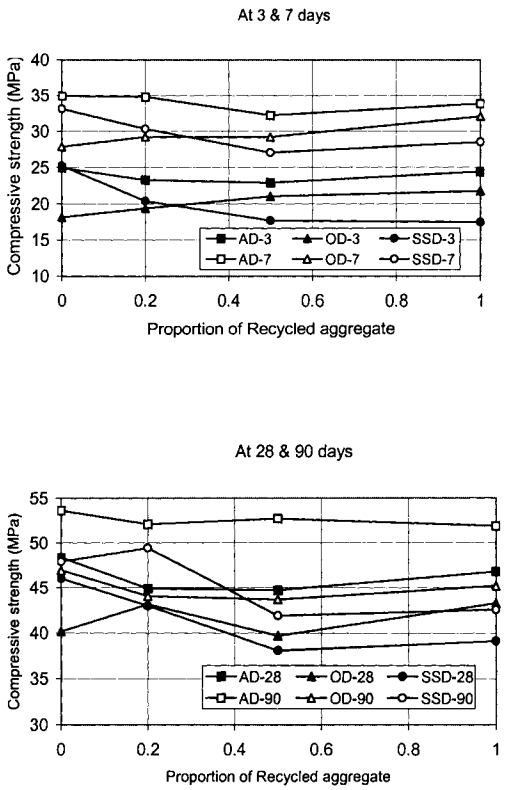


Fig. 1 Effect of recycled aggregate content on compressive strength of concrete mixes

Table 1 Chemical composition of cement (%)

CaO	SiO_2	Al_2O_3	Fe_2O_3	MgO	SO_3	L.O.I.
63.15	19.61	7.32	3.32	2.54	2.13	2.97

Table 2 Properties of natural and recycled coarse aggregates

Type	Nominal size	Density (kg/m^3)	Water absorption (%)	Strength (10% fines) KN	Porosity (%)
Crushed granite	10mm	2620	1.25	159	1.60
	20mm	2620	1.24		
Recycled aggregate	10mm	2330	7.56	117	10.45
	20mm	2370	6.28		

Table 3 Actual mass of water and materials used in different mixes

Mix	Combination of coarse aggregate	Moisture state of coarse aggregate	Proportions (kg/m^3)						
			Water	Cement	Sand	Crushed granite		Recycled aggregate	
						10 mm	20 mm	10 mm	20 mm
AD1	100% crushed granite	AD	214	353	667	362	724		
OD1		OD	221	353	667	360	720		
SSD1		SSD	209	353	666	364	729		
AD2	80% crushed granite + 20% recycled concrete	AD	217	353	660	287	574	70	139
OD2		OD	230	353	661	284	569	67	135
SSD2		SSD	206	353	661	288	576	72	144
AD3	50% crushed granite + 50% recycled concrete	AD	229	353	647	176	351	170	343
OD3		OD	247	353	647	175	349	164	332
SSD3		SSD	207	353	649	177	354	177	354
AD4	100% recycled concrete	AD	241	353	625			330	663
OD4		OD	271	353	625			317	642
SSD4		SSD	209	353	625			342	684

Table 4 Moisture contents of aggregates for mix preparation (%)

Mix	Moisture content (%)				
	Sand	Crushed granite		Recycled aggregate	
		10 mm	20 mm	10 mm	20 mm
AD1	0.61	0.70	0.66	3.70	2.90
OD1	0.61	0.00	0.00	0.00	0.00
SSD1	0.40	1.25	1.24	7.16	6.14
AD2	0.76	0.78	0.85	3.84	3.22
OD2	0.82	0.00	0.00	0.00	0.00
SSD2	0.82	1.25	1.24	7.16	6.14
AD3	0.45	0.72	0.42	3.28	3.15
OD3	0.45	0.00	0.00	0.00	0.00
SSD3	0.76	1.25	1.24	7.16	6.14
AD4	0.40	0.65	0.48	3.65	3.02
OD4	0.42	0.00	0.00	0.00	0.00
SSD4	0.42	1.25	1.24	7.16	6.14

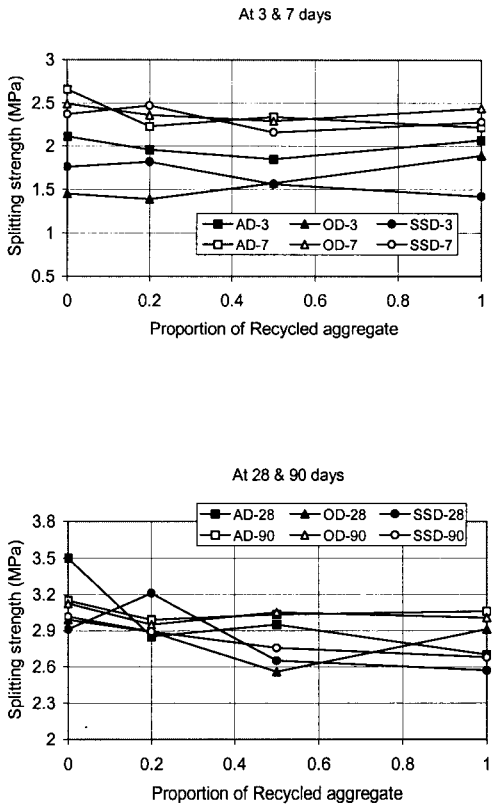


Fig. 2 Effect of recycled aggregate content on splitting strength of concrete mixes

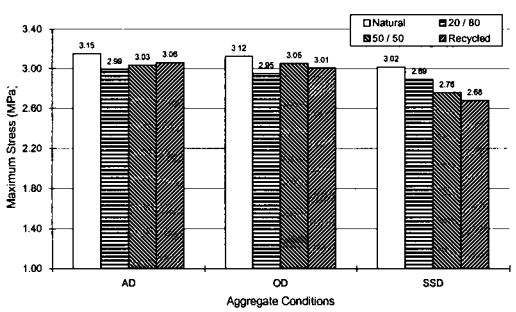


Fig. 3 Splitting tensile strength of concrete at 90 days

Advances in Building Technology, Volume 2
M. Anson, J.M. Ko and E.S.S. Lam (Eds.)
© 2002 Elsevier Science Ltd. All rights reserved

CLAY-BRICK RECOVERY FROM MASONRY DEBRIS BY MEANS OF A THERMAL PROCESS

K. van Dijk[1], A. Fraaij[1], Ch.F. Hendriks[1], E. Mulder[2]
[1] Delft University of Technology, faculty of Civil Engineering, department material science, the Netherlands
[2] TNO Environment, Energy and Process Innovation, department of Chemical Engineering, the Netherlands

ABSTRACT
In the Netherlands more than 95 percent of all stony fraction of building demolition debris is being reused as a road building material. Twelve million tons on yearly base and each year the amount is growing. To avoid problems in future, alternatives should be created for future recycling of building materials. For masonry debris, clay-bricks should be recovered and reused for future brick laying. A thermal process might be a possibility of recovering clay-bricks from masonry. In this research first a model is made, which can calculate the forces in masonry and the shear stress on the clay-brick mortar interface. Then laboratory experiments are performed in which pieces of masonry are thermally treated in order to determine the required temperature. In the next laboratory research the strength of the clay-brick mortar interface is being measured. The research project is being evaluated by doing a full scale test in the clay-brick factory. The research shows that clay-brick recovery can be very successful, but it strongly depends on the way of dismantling the masonry from the building.

KEYWORDS
Masonry, building demolition debris, recycling, clay-bricks, recovery, thermal process, the Netherlands

INTRODUCTION

Clay-bricks from masonry constructions are reused on a very small scale in the Netherlands. The mortar is chipped from the bricks, which is a very labor intensive job. To make clay-brick recovery on larger scale possible a new technology should be introduced.

A thermal process might be a suitable technology to recycle clay-bricks. Clay-brick mortar separation can be achieved by heating to a temperature of 850 °C. At this temperature cement mortar decomposes. Lime decomposes at a temperature of 400 °C. In this laboratory research the quality of clay-brick that are

recovered from masonry debris by giving it a thermal treatment is determined. The effect of a temperature treatment on the properties of the clay-brick will also be determined.

The recovered clay-brick must be checked on internal cracking. Internal cracking will influence the mechanical properties of the clay-brick, which can be checked by measuring the tensile and compressive strength.

The difference in linear expansion coefficient between mortar and clay-brick causes shear stresses on the clay-brick mortar interface. The mortar is compressed and in the clay-brick there are tensile stresses, if there is still a bond between the two components. The mortar clay-brick interface is the weakest part of masonry and therefore might break by shear stresses. The temperature for collapsing of the interface depends on the properties of the clay-brick related tot the properties of the mortar and the resistance of the interface for shear stresses.

When the temperature in the oven is increasing, water in the open pores starts to evaporate. It is possible that cracking occurs by thermal strains in the clay-brick. This will decrease the mechanical quality of the clay-brick. It is also possible that the cracking already occurred during technical life span of the masonry. The strains in the product can reach a maximum caused by frost/thaw loads or mechanical loads during the technical life span. This can cause damage to the clay-brick and make it unsuitable for reuse.

THEORETIC MODEL

The situation of strains caused by thermal loads is modeled as a composite material, consisting of a layer of mortar and a layer of clay-brick. The difference in expansion coefficient between clay-brick and mortar introduces tensile and compressive stresses when thermally loaded. At the clay-brick mortar interface a shear stress is introduced (figure 1).

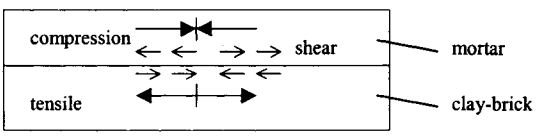


figure 1: Schematic view of strains in the clay-brick mortar interface caused by a temperature load

Now the boundary conditions for this loading situation can be made up. The total expansion (formula 1) of a material is the sum of thermal expansion and expansion caused by strains. The tensile or compressive load can be written as a function of expansion. The strain (formula 2) the thirst derivative of the change in length in a certain direction.

$$\varepsilon = \alpha T + \frac{N}{EA} \qquad (1)$$

$$\varepsilon = \frac{\partial u}{\partial x} \qquad (2)$$

This results in an equilibrium with a main force, which is a function of the expansion coefficient (ε) and the thermal expansion coefficient (α). The shear stress (q) is the thirst derivative of the main force in the x direction.

$$q = -\frac{\partial N}{\partial x} \qquad (3)$$



Figure 2: Material model of the clay-brick and mortar interface

In figure 2 the material model of clay-brick - mortar interfacial zone is shown. Both layers have a Youngs modulus, surface area and thermal expansion coefficient. The effective thickness of the mortar layer is 8 millimeters and for the clay-brick it is 50 millimeters.
Until the clay-brick mortar interface is broken, there is an internal equilibrium. The compression force in the mortar layer is equal to the tensile force in the clay-brick. The expansion for both materials is equal. For this loading situation a parallel system is valid, which means that the stiffness of both materials must be summed. Using formula 1 together with the second boundary condition results in formula 4.

Boundary conditions:

$$N_I + N_{II} = 0$$
$$\varepsilon_1 = \varepsilon_2 = \varepsilon \qquad \frac{N_1}{EA_1} + \alpha_1 T = \frac{N_2}{EA_2} + \alpha_2 T \qquad (4)$$
$$EA = EA_1 + EA_2$$

The solution is found by using boundary condition 1 and 3 with formula 4.

$$N_1 = -N_2 = \frac{EA_1 \cdot EA_2}{EA}(\alpha_2 - \alpha_1) \cdot T \qquad \text{and} \qquad \varepsilon = \frac{EA_1\alpha_1 + EA_2\alpha_2}{EA} \cdot T$$

Resulting in a total thermal expansion coefficient: $\alpha = \frac{EA_1\alpha_1 + EA_2\alpha_2}{EA}$

The shear stress (q) is the thirst derivative of the main force in the x direction. Because the main force N is undependable of x, the shear stress on the clay-brick mortar interface must be constant. From literature values can be found for the thermal expansion coefficient and Youngs modulus both for clay-bricks and mortar.

Clay-brick: $\alpha_1 = 3 - 9 \cdot 10^{-6} K^{-1}$ and $E_1 = 10 - 20 \cdot 10^9 Pa$

Mortar: $\alpha_2 = 10 - 12 \cdot 10^{-6} K^{-1}$ and $E_2 = 20 - 40 \cdot 10^9 Pa$

The huge variation in values for different clay-bricks and mortars results in a big range in shearing stress at certain temperatures. For example, when the temperature is 540°C than the shearing stress ranges between 0,35 and 5,60 N/mm^2 for the extreme values of the thermal expansion coefficient and the Youngs modulus.

LABORATORY EXPERIMENTS

Description samples

The masonry pieces came from a recycling plant. The demolition companies deliver their building demolition debris to the plant and the stony fraction is being crushed in order to produce granulate for building road foundations. Different types of masonry pieces are being collected, which came from different buildings, that were being demolished by different demolition companies. The masonry pieces, consisting 3 or 4 whole clay-bricks are being transported to the laboratory. In the laboratory both a gas heated chamber kiln and a electric heated kiln are being used for clay-brick recovery tests.

Temperature treatment

For the first experiment an electric heated kiln is been used. With the electric heated kiln it is impossible to use a forced cooling. The real temperature development during cooling is not measured. The gas heated kiln is suddenly heated when the burning gas is flowing in. The difference in temperature in the beginning of the temperature treatment is about 70°C.

TABLE 1: Experiments on clay-brick recovery

Experiment	Heating time	Max temperature/time	Cooling time	Sample	Results:
1	0:30	600 / 2:00	Non forced	softmud clay-brick red + Portland cement mortar	clay-bricks are cracked in two pieces, with a size of half a clay-brick
				hand molded clay-brick + lime mortar	lots of cracks in the clay-bricks
				plastered masonry	clay-bricks are broken in two pieces, the cracks on the mortar clay-brick interface can be seen clearly
2	0:30	400 / 1:00	Non forced	softmud clay-bricks red + Portland cement mortar	no visible cracks, clay-brick recovery is not successful even with mechanical force
				hand molded clay-brick + lime mortar	cracks are visible on clay-brick mortar interface, the clay-bricks can be recovered after a soft hit with a hammer
				plastered masonry	cracks on clay-brick mortar interface
3	2:00	600 / 1:00	Non forced	softmud clay-bricks red + Portland cement mortar	masonry part falls apart, the clay-bricks are totally cracked
				hand molded clay-brick + lime mortar	idem
				plastered masonry	idem
4	2:00	500 / 2:00	Non forced	softmud clay-bricks red + Portland cement mortar	the clay-brick can not be recovered
				hand molded clay-brick + lime mortar	the clay-brick mortar interface is cracked, the clay-bricks are recovered
				plastered masonry	the clay-brick mortar interface is cracked, the clay-bricks are recovered
Gas heated kiln					
5	2:00	540 / 1:00	Non forced	softmud clay-bricks red + Portland cement mortar	the clay-brick mortar interface is cracked, some clay-bricks are broken in two, some pieces of mortar are still stuck to the clay-brick
				hand molded clay-brick + Portland cement mortar	same result, some clay-bricks are recovered
6	2:00	540 / 1:00	Non forced	softmud clay-bricks red + Portland cement mortar	Cracks on clay-brick mortar interface, recovered
				hand molded clay-bricks red + Portland cement mortar	Cracks on clay-brick mortar interface, recovered
Electric kiln					
7	2:00	540 / 1:00	Non forced	softmud clay-bricks red + Portland cement mortar	The clay-bricks are totally cracked

Table 1 shows the results of the experiments that are done. In the first experiment the electric heated kiln is used to heat the clay-bricks to 600°C in half an hour. Then the temperature is stabilized during two hours. The cooling time depends on the heat capacity of the kiln, but is not measured. When the clay-brick mortar interface is cracked, the clay-bricks can be recovered easily, without damage. Both hand molded clay-bricks, which have a rough surface and softmud clay-bricks, which have a smooth surface are easily recovered.

Conclusions

The most effective clay-brick recovery can be realized at a temperature of 540°C. A higher temperature than 570°C results in damage to the clay-bricks. The clay-bricks are cracked, because of the sudden expansion during the quartz phase transformation.
The firing time is one hour at 540°C, the total firing time including heating and cooling down takes 5 hours. The firing time might be decreased, especially during cooling. The heating phase is more critical, because of the tensile forces in the clay-brick.
It can be concluded that the recovery of clay-bricks from masonry with Portland cement is more effective than with lime mortar. Less mortar is stuck to the surface of the clay-bricks. The Youngs modulus and thermal expansion coefficient are higher and therefore the shear stress in the clay-brick mortar interface will also be higher.

The results of the gas heated kiln, were better than for the electric heated kiln. This might be a result of the heating process. In an electric kiln the masonry is heated by radiation. In the gas heated kiln, the masonry is heated in the flames. Electric heating might result in a higher temperature coefficient in the masonry, as a result of which the clay-bricks crack.

Measuring the strength of the mortar clay-brick interface

Description of the research

Different mortars are made consisting of Portland cement CEM I 32,5. The mortars are being prepared with the same consistence by using the vibration table (according to the standard NEN 3534). The composition of the mortars is shown in TABLE 2.

TABLE 2: composition off the mortars

	p.c. A.	sand	lime	water	other substitutes
1	1	4	0.6	1.2	none
2	1	4	0	1.15	0.6 fly ash (EFA)
3	1	4	0	1	a.e. water reducing agent (30 cc/50kg cement)
4	1	4	0	0.9	a.e. water reducing agent (90 cc/50kg cement)
5	1	4	0	0.75	a.e. water reducing agent (300 cc/50kg cement)

For every type of mortar samples are being made in order to measure the strength of the mortar. The samples have a standard size of 40.40.160 mm^3. The samples are being stored for 28 days and then the three point bending test and compression test is being performed.

For two clay-brick types ('klinker' and 'hardgrauw') three 'shear stress' samples are being made for all the mortar types. The clay-bricks have a sanded site that was in the mold and an unsanded site. This layer of sand will have influence on water suction of the clay-brick and therefore differences are made in sample preparations.

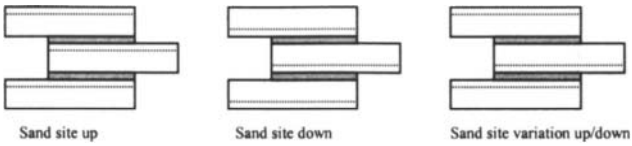


Figure 3: samples for shear stress measurements

After 28 days of hardening the samples are being tested. The mortar clay-brick interface will be loaded on shear stress. The load is increased slowly, until one of the interfaces brakes. Then the load is increased until the other interface also collapses.

The shear stress in the clay-brick mortar interface is: $\tau = \frac{P}{2 \cdot b \cdot l}[N/mm^2]$

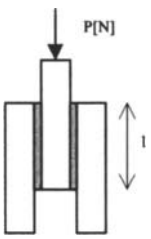


Figure 4: loading situation of the samples

TABLE 3: Strength of the mortars and of the clay-brick mortar interface

			clinker	hardgrauw	Air [%]
mortar	Compressive strength	3 p.b. strength	shear stress	shear stress	
1	12.5	3.4	0.9	1.2	7.8
	0.6	0.4	0.2	0.3	
2	14.6	4.3	1.4	1.4	3.0
	1.9	0.3	0.5	0.2	
3	4.8	2	0.7	0.8	17.5
	0.5	0.2	0.3	0.4	
4	5.3	2	0.4	0.3	24.5
	1.2	0.1	0.2	0.1	
5	4.3	1.9	0.5	0.2	20.3
	0.7	0.2	0.1	0.1	

The density of the mortars is calculated by measuring the volume and the weight of the mortar bars. With the mixture composition the 'real' volume of cement, water and sand can be calculated. Also the percentage of water can be calculated.

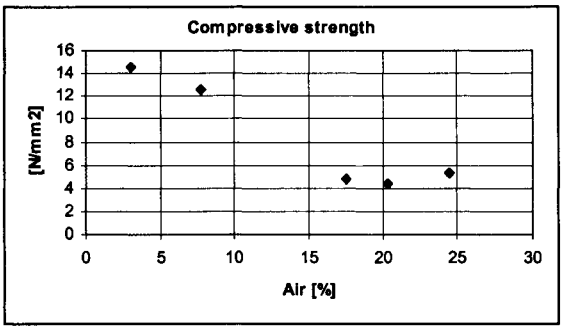


Figure 5: Compressive strength of the mortar samples

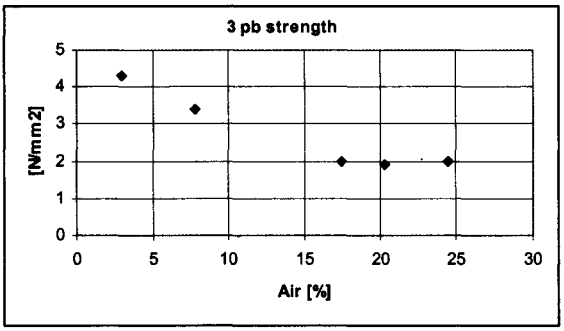


Figure 6: 3 pb strength of the mortar samples

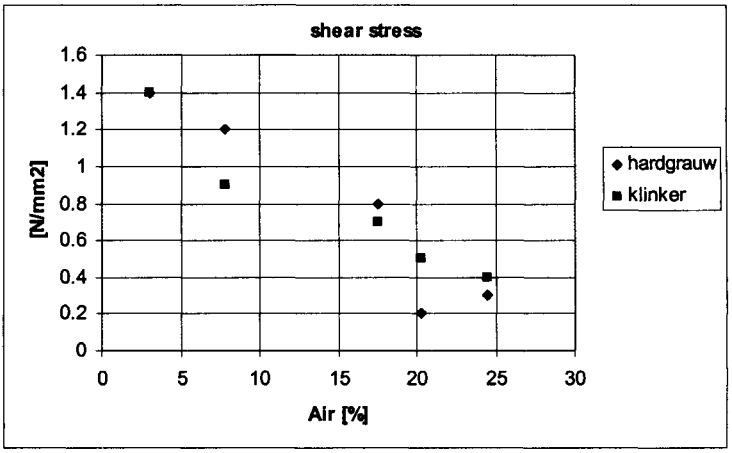


Figure 7: Shear stress of the masonry samples

From the theoretic model (figure 1) was concluded that the compression force in the mortar is equal to the tensile force in the clay-brick. The shear stress is the first derivative in x direction. It can be concluded that the clay-brick mortar interface is the weakest part, no values were found higher than 1,4 N/mm^2. The shear stress can vary between 0,35 and 5,60 N/mm^2, according to the model.

Conclusions

Mortars with fly ash require less water. The density is higher and the compressive strength, 3pb strength and strength of the clay-brick mortar interface are higher. A higher air content results in a lower density and a lower strength. The strongest type of mortars have a shear strength of 1.4 N/mm^2. The hardness of the clay-brick does not influence the strength of the clay-brick mortar interface. Some values for the shear strength were higher for the harder type of clay-brick and some values for the softer clay-brick. The lowest value (0.2 N/mm^2) was found for mortar type 5, with the harder type of clay-brick.
To evaluate the results from the laboratory research, a test has been performed in a clay-brick factory. The masonry has been selectively deconstructed from a building in Rotterdam.



Photo 1: Demolition of the railway building 'de Boezembocht' in Rotterdam

The interior and exterior walls are connected by anchors, therefore it is hardly impossible recover big parts of masonry from the walls. The pieces of masonry break before being recovered from the demolition object. In total 2,500 kg of masonry is collected and being transported to the factory. In the factory the masonry is put on wagons and transported to the chamber kiln. In the chamber kiln the masonry is thermally treated, in 10 hours to 540°C than 20 hours constant and then 10 hours cooling. The result is:

- 900 kg clay-bricks are recovered
- 900 kg clay-bricks are damaged
- 220 kg clay-bricks are broken
- 505 kg of mortar

The recovery rate is about 45 percent of the input, but this result strongly depends on the way of dismantling the masonry.

References

Bouma A.L. (1989). Mechanica van constructies: elastostatica van slanke structuren, VSSD, Delft University Press, The Netherlands

Advances in Building Technology, Volume 2
M. Anson, J.M. Ko and E.S.S. Lam (Eds.)
© 2002 Elsevier Science Ltd. All rights reserved

EFFECTIVE WASTEWATER TREATMENT / RECYCLING TECHNOLOGIES FOR CONSTRUCTION INDUSTRY – A LOCAL EXPERIENCE

Kenny S. W. Wong

Environmental Management Division, Hong Kong Productivity Council,
EMD, HKPC Building, 78 Tat Chee Avenue, Kowloon Tong, Hong Kong

ABSTRACT

During the construction / demolition period of a site, various types of wastewater will be generated and discharged. These various types of wastewater are, but not limited to, water from bore piling operation, rain water and ground water collected, spray water for dust removal, truck cleaning water, sewage and kitchen wastewater, etc. In most of the construction sites, government foul sewers will not be connected to the site premises during the construction period, hence the wastewater will have to be discharged to storm water drain, inland and coastal waters, etc. In this regard, the quality of discharged effluent will be controlled to very stringent limits, such as suspended solids (SS) to 30mg/L, oil and grease (O&G) to 20mg/L, biochemical oxygen demands (BOD_5) to 20mg/L, chemical oxygen demands (COD) to 80mg/L, etc. Without proper treatment, the discharged wastewater will exceed the discharge limits, resulting from not only polluting the environment, but also leading to heavy penalty to the construction companies.

This paper will focus on presenting appropriate technologies to tackle different types of wastewater from construction sites. They are:

1. Effective chemical coagulation and sedimentation system for treating high solids content construction runoff / wastewater from construction activities;
2. Biological wastewater treatment system in continuous operation for treating organic waste bearing wastewater from site office toilets, etc;
3. Biological wastewater treatment system in batch operation for treating highly polluted organic waste bearing wastewater from kitchens and canteens;
4. Automatic wheels washing machine for cost effective management of truck wheels cleaning process.

KEYWORDS

Construction wastewater, recycling, coagulation, sedimentation, biological treatment, anaerobic and aerobic treatment, sequencing batch reactor, automatic wheel washing machine

INTRODUCTION

Construction Industry is one of the largest industries in Hong Kong. The trade has been contributing to Hong Kong's success into one of the World's most famous cities by building effective transportation & communication networks, constructing landmark buildings and forming large infrastructures, such as the Chep Lap Kok International Airport, Disneyland, CyperPort, Science Parks, etc. However, during the construction period of a site, various types of construction operations will discharge potential environmental pollutants creating air, noise, waste, wastewater pollution, etc. Without proper handling and treatment methodologies, the discharged pollutants will exceed HKSAR Government's discharge standards, thus resulting from not only polluting the environment, but also leading to heavy penalty to the construction companies and interruption of construction activities. This paper will concentrate on the presentation of appropriate technologies which are utilized locally in dealing with the discharged wastewater from various types of construction operations.

Local Legislation - Water Pollution Control Ordinance (WPCO)

The Water Pollution Control Ordinance (Chapter 358) was enacted in 1980 and amended in 1990 and 1993. It provides the main statutory framework for the declaration of water control zones to cover the whole Hong Kong Territories. The whole Hong Kong territories are divided into 10 water control zones and the last control zone was declared on 1995. Within each control zone, all discharges or deposits are controlled by a licensing system. The Environmental Protection Department (EPD) of the HKSAR Government is responsible for the issuance of licence as well as enforcement of the licensing conditions. Depending on the water receiving bodies of the discharged premises, EPD will set discharge limits to the potential pollutants of the effluent that make acceptable to foul sewer, storm

drain, inland and coastal waters, etc. Upon issuance of the discharge licence, the licence holder is responsible to meet the effluent discharge standards, which are set out according to the Technical Memorandum (TM) issued under the WPCO. The TM is a guide issued by EPD in determining standards for effluents. It sets standards that differ in different areas and between surface waters and sewers. The standards also vary with the rate of effluent flow and the standard in the higher flow ranges are normally more stringent than those in the lower flow ranges.

Over the entire period of a typical construction site, especially in those new development areas, foul sewers are not normally connected until the very late stage of the project. The effluent will be discharged to storm drain, inland and coastal waters, etc. without subsequent treatment by the authority. Hence the quality of the discharged effluent from a construction site is controlled to very stringent limits, in most of the areas, suspended solids to 30mg/L, oil and grease to 20mg/L, biochemical oxygen demands to 20mg/L, chemical oxygen demands to 80mg/L, etc.

All effluent discharged from a construction site is subject to control, and the maximum penalties are:

(a) For illegal discharges : 6 months imprisonment, and
   - for a first offence, a fine of HK$200,000;
   - for a second of subsequent offence, a fine of HK$400,000;

   in addition, if the offence is continuing offence, a fine of HK$10,000 is applicable for each day.

(b) For discharges of poisonous or noxious matter :
   - for a first offence, a fine of $400,000 and imprisonment for 1 year;
   - for a second or subsequent offence, a fine of HK$1,000,000 and imprisonment of 2 years;

   in addition, if the offence is a continuing offence, a fine of HK$40,000 is applicable for each day.

(c) For contravention of the conditions of a licence :
   - a fine of HK$200,000 and imprisonment for 6 months

Construction runoff / wastewater discharged from construction activities

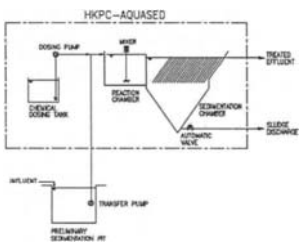
The largest amount of wastewater discharged from a typical construction site is highly turbid muddy wastewater. The wastewater sources are generally classified as construction runoff, rainwater or ground water collected within the site, spray water for dust suppression, equipment or vehicle cleaning water, and wastewater generated from construction activities, such as air lifting process of bore piling. The discharged quantity can be ranged from only $10m^3$/day (superstructure) up to over $100m^3$/hr (foundation – bore piling process). The concentration of suspended solids in the wastewater can be ranged from 100mg/L (normal runoff) to over 30,000mg/L (bore piling wastewater). In the past, the construction companies used plain sedimentation tanks to treat the muddy wastewater. Some of the sites even add gravity sand filters for improving the solids removal efficiency. However the performance of those sedimentation tanks and filters were far from satisfactory because of poor design and low hydraulic retention time (HRT) which was insufficient to allow sedimentation of suspended particles. From the past experience, a HRT of more than 10 hours is required to settle the majority of

solid particles from the wastewater. Moreover, it is quite normal that the wastewater discharged from a typical construction site is slit-clay laden and therefore it cannot be separated effectively even for long HRT. It is because most of the fine suspended particles carry the same polarity of charge making them very difficult to combine into larger particles of settleable sizes. In order to overcome the problem, chemical agent which carries an opposite charge should be applied to agglomerate with the suspended particles for enhancing the effectiveness of sedimentation and a carefully designed tilted plate / tube settler should be put in place to separate the flocculated particles from the cleared wastewater. As many construction sites in Hong Kong are very congested and there is lack of space for the installation of huge sedimentation tanks for long HRT, it is necessary to design a fully automatic and self-contained system comprising the above features to treat the discharged wastewater in compliance with the government's discharge standards.



AquaSed

A self-contained wastewater treatment system for the construction site (herein after named as AquaSed) was developed by the Hong Kong Productivity Council and its flow schematic diagram is presented on the right. Untreated wastewater is pumped into the preliminary sedimentation pit from some low points within the construction site premises. In addition to acting as the centralized wastewater collection tank within the site, the main purpose of the preliminary sedimentation pit is to allow the settlement of relatively large and heavy particles (e.g. sand, grit, etc.) from the wastewater inside the pit, thus reducing the loading as well as the chemical consumption of AquaSed. The transfer pump is mounted at the middle level of the pit so that the settled solids will not be pumped up. When the wastewater is pumped into AquaSed, the system is turned on automatically. The mechanical mixer in the reaction chamber turns at an optimum speed to facilitate effective coagulation of the chemical with the suspended particles to form larger size flocs. Then all the wastewater is transferred into the sedimentation chamber, where the large flocs are settled at the bottom of the chamber and the cleared water is discharged through the V-notch weir at the top of the sedimentation chamber. A carefully designed tube settler is placed in the sedimentation chamber to enhance sedimentation of relatively smaller flocs. The design of the V-notch weir is to facilitate even distribution of wastewater rising up to the entire surface of the sedimentation chamber. Through measuring the height of water above the bottom of the V-notch weir, the flow rate of the wastewater pumped into AquaSed is easily monitored. After treatment, the concentration of suspended particles in the discharged effluent would be reduced to below 30mg/L.



Apart from suspended solids, the pH value is also an important parameter that is easy to exceed the discharge limit, especially when concreting process is being executed within the site. Because of the properties of the concreting agents, the pH value of the wastewater is usually very high, and sometimes up to 13. A specially designed Neutralization Unit can be adopted to adjust the pH value of the wastewater discharged from the AquaSed into acceptable range. Through proportional dosage

controlling mechanism, when the pH value of the wastewater is far beyond the set point, alkali or acid will be dosed at full speed to bring up or down the pH value respectively. When the pH value approaches the set point, the dosing rate will be reduced automatically so as to reduce the consumption of acid or alkali and to prevent overshooting of the effluent pH value. After treatment, the pH value of the effluent will be within the range of 6-9.

By the combination of AquaSed and Neutralization Unit, the suspended solids concentration and the pH value of the effluent can be treated to below 30mg/L and within the range of 6-9 respectively, which complies to the very stringent government discharge standards. In fact the system can be readily accommodated in construction sites of various sizes. The compact design of the AquaSed and Neutralization Unit enhance mobility of the system and it can be transported easily to different locations by standard trailer. However, the compact design does not affect the treatment capacity, standard models of AquaSed can handle continuous wastewater inflow rate from $10m^3$/hr to $120m^3$/hr.

With the superb quality of treated effluent, many construction sites are recycling the effluent for various types of construction activities, such as air lifting process for bore piling, equipment & truck wheels cleaning, dust suppression etc. The recycling of treated effluent will help the construction companies to achieve huge saving of water charge. Our experience revealed that some of the construction sites can recycle about 50% of the wastewater, and the monetary saving can be as high as HK$5,000 a day (i.e. monthly saving of HK$130,000, assuming 26 working days a month). Hence the payback period on the capital cost of AquaSed can be less than 3 months.

The incredible design of the system has been widely accepted by the construction industry. In addition it has gained important professional recognition. The AquaSed has won the CMA Certificate of Merit Award in the 2000 Hong Kong Awards for Industry and its has got one Hong Kong Short Term Patent approved and two other international patents pending approval.

Wastewater discharged from site toilets

The wastewater discharged from site toilets generally is part of normal sewage from household activities. Unlike sewage from household activities that can discharge directly to government foul sewer without treatment, the quality of toilet wastewater from construction sites will have to meet the stringent government discharge standards on storm drain, inland and coastal waters if they are discharged. It is because foul sewer is normally not connected until the end of the construction project. The wastewater has high concentration of pollutants, normally BOD_5 at 150-250mg/L, SS at 200-400mg/L, COD at 200-400mg/L and E-coli at over 100,000count/100ml respectively.

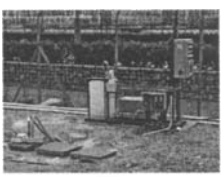
Traditionally the wastewater discharged from the site toilets was handled by two different ways:

- Build a septic tank to collect and treat the toilet wastewater and then discharge through a soak away pit. However, the septic tank is not effective enough to treat the wastewater to acceptable

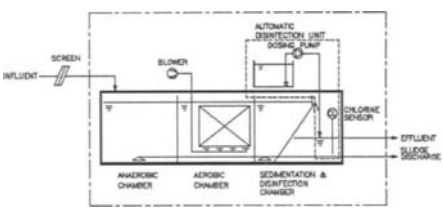
level for discharge. Due to the fluctuation of soil properties from one site to another, in many occasions the discharged wastewater from the septic tank cannot be penetrated away through the soak away pit. Overflow of septic tank is more likely to occur during rainy reason.

- Collect all the toilet wastewater into collection tanks and arrange tanker to pump the waste away from site periodically. Although no on-site treatment is required, the pump-away cost is very high and the construction company has to ensure that the collection tank does not overflow before calling upon the tanker.

To provide a more cost effective choice against the above methods, a self-contained package sewage treatment system (herein after named as STS) was developed for handling wastewater generated from construction site toilets. STS consists of an anaerobic chamber, an aerobic chamber and a sedimentation & disinfection chamber. Through different stages of continuous biological treatment, the BOD_5, SS, COD and E-coli can be reduced significantly to a level that complies to the discharged limits. A copy of the flow schematic diagram of STS is shown on the right. The wastewater from the toilets is firstly discharged into the anaerobic chamber for digestion and decomposition. After that, wastewater will be overflowed into the aerobic chamber for the aerobic treatment process. In the aerobic chamber, soluble and suspended organic matters in the wastewater are absorbed and assimilated by the microorganisms growing on the surface of fill media. After aerobic treatment, the wastewater enters into the sedimentation and disinfection chamber in which sedimentation will take place and then disinfecting agent will be dosed automatically to the treated effluent before discharge. The discharged effluent will be able to achieve acceptable concentrations of 20mg/L, 30mg/L, 80mg/L and 1,000count/100ml on BOD_5, SS, COD and E-coli respectively. Apart from the excellent treatment performance, STS generates very little sludge. Normal desludging frequency will be about 1-2 times a year. This will assist the construction companies to save a lot of money from an average of weekly tanker away of untreated sewage from the site.



STS



To enhance operation efficiency and effectiveness, STS can be floor mounted, buried wholly or half-submerged. The reactor is made of Fibre Reinforced Plastic (FRP) and it is light weight, high strength, anti-corrosion and highly durable, such that it can withstand very harsh environment on a construction site.

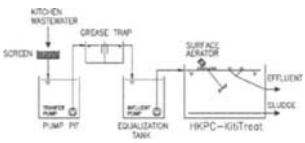
Wastewater discharged from site kitchens and canteens

Wastewater discharged from the site kitchens and canteens contains high oil and grease content and high concentration of other organic pollutants, normally O&G at over 300mg/L, BOD_5 at

150-500mg/L, SS at 80-150mg/L and COD at 500-1300mg/L respectively. Similar to the management of wastewater from other construction activities and site toilet wastewater, the quality of the kitchen and canteen wastewater from construction sites will have to meet the stringent government discharge standards on storm drain, inland and coastal waters. Normally the site kitchens and canteens will install in-situ grease trap to remove O&G and other insoluble pollutants. However, it is ineffective because of low hydraulic retention time and the standard design of the grease trap is unable to meet the discharge standards of storm drain, inland and coastal waters.



KitiTreat



Since the organic content of the kitchen and canteen wastewater is much higher than those of toilet wastewater, a batchwise biological treatment system (herein after named as KitiTreat) was developed for handling wastewater generated from construction site kitchens and canteens. KitiTreat employs the latest Sequencing Batch Reactor (SBR) technology in which the wastewater will be fed batchwise into the system at where the biological removal of pollutants will be taken place under optimum operating conditions and in fully automatic fashion. By batchwise operation, KitiTreat operates one or two cycles a day for removing O&G, BOD_5, SS and COD to a level that complies to the discharged limits. A copy of the flow schematic diagram of KitiTreat is shown on the right. After passing through the standard designed grease trap, the wastewater is stored in the equalization tank. The operating cycle of KitiTreat begins with automatic control of fill action. Through the control of programmable logic controller (PLC), the wastewater is fed into KitiTreat reactor and aeration will be carried out simultaneously. The organic matters in the wastewater are absorbed and assimilated by the microorganisms inside the reactor. After the aeration process, aeration stops and allows the activated sludge to settle. Then the clean supernatant will be discharged from the floating discharge weir. The discharged effluent will be able to achieve acceptable concentrations of 20mg/L, 20mg/L, 30mg/L, 80mg/L on O&G, BOD_5, SS and COD respectively. The KitiTreat is operated in fully automatic fashion and no chemical is required for normal operation. In addition it can be easily transported from one site to another by standard trailer.

Truck cleaning wastewater

Traditionally manual cleaning of truck wheels by using water hose was performed at the exit of a construction site. By doing so, extensive labour force and huge amount of fresh water were consumed. In many occasions, the mud and grit adhered to the base chassis and the inner wheels of the trucks could not be removed effectively. By manual cleaning, the cleaning time for the wheels of a dirty truck would take approximately 8-10 minutes. For some very heavy traffic site, the truck cleaning process will become the bottleneck of the construction operations, which sometimes resulted in a truck queue waiting for cleaning before exiting the site.



EnviroWash





In order to provide a cost effective way to manage the truck wheel cleaning operation on construction sites, a specially designed truck wheel washing machine (herein after named as EnviroWash) was developed. By using EnviroWash, the wheels cleaning operation for a vehicle on exiting the construction site can be performed automatically and the vehicles can be cleaned thoroughly from outside, inside and below the wheels. As the cleaning operation is very efficient, the typical cleaning time for a standard truck is only 1-2 minutes. Hence the cleaning time is greatly reduced and at the same time the cleaning performance is much better when comparing to manual cleaning. After cleaning, the water can be collected, treated and recycled thus reducing the water consumption and eliminating the effluent disposal problem. Because of the fully automatic operation of EnviroWash, the labour force for manual cleaning can also be eliminated. By eliminating the labour force and achieving significant saving in water charge on using EnviroWash, a typical construction site can easily save for HK$14,000 per month. Hence the payback period on the capital cost of EnviroWash is only about 8 months. Apart from noticeable financial savings, the special features of EnviroWash indeed assisted the construction industry to better manage their truck wheels cleaning process. Examples of the special features are, but not limited to, its high performance water jets offers superb cleansing effect; it has equipped with smart inducation lamps to provide user friendly instruction of operation; its specially designed weight activated mechanical sensor safeguards transiting personnel from high pressure jet; its highly effective coagulation unit to remove the solid particles from the recycling water.

Similar to the AquaSed wastewater treatment system, the genius design of the EnviroWash has also gained important professional recognition. The EnviroWash has won the CMA Certificate of Merit Award in the 2001 Hong Kong Awards for Industry and its has got one Hong Kong Short Term Patent approved and another China patent pending approval.

CONCLUSION

With the above 4 systems in place, the construction companies will not only be able to compile with the most stringent environmental requirements, but also can achieve huge monetary savings and improvement of company's corporate image by devoting more efforts on environmental protection.

References

Environmental Protection Department (1991), *Technical Memorandum – Standards for Effluents Discharged into Drainage and Sewerage Systems, Inland and Coastal Waters.*

Environmental Protection Department (1995), *Water Pollution Control Ordinance – Victoria Harbour (Phase Two) Water Control Zone Information Booklet.*

Advances in Building Technology, Volume 2
M. Anson, J.M. Ko and E.S.S. Lam (Eds.)
© 2002 Elsevier Science Ltd. All rights reserved

BALANCE THEORY FOR RECYCLING OF CONSTRUCTION AND DEMOLITION WASTES

E.O.W. Wong and R.C.P. Yip

School of Professional and Continuing Education, The University of Hong Kong, Pokfulam Road, Hong Kong

ABSTRACT

The key to reduce construction and demolition wastes (C&D wastes) lies in finding a way to make them valuable. Recycling of C&D wastes into profitable commodities is one of the effective means.

Balance of the supply of C&D wastes and the demand of recycled C&D waste products (Balance Theory) is recommended in new developments. The maturity of Balance Theory requires gradual establishment of recycling facilities. These facilities are capable to accept and handle not only inert materials but also other C&D wastes like wood and wood products, cardboard, metal, plastics etc. The Balance Theory rouses construction workers to adopt the idea of reduction of wastes. They are educated to clean their working places constantly and collect all construction wastes they generated into separate collection spots within the construction site. The site management personnel is required to establish site facilities and set up conditions in employment contracts and subcontracts for workers and subcontractors to follow. The culture of separating wastes at sources must be established and widely adopted so that Balance Theory could be realised.

All in all, Balance Theory advocates the amount of wastes generated from a construction project and sent for recycling process must be equivalent (or proportional) to the amount of the recycled C&D products imported and used as construction materials for that project. Evaluation of the Balance Theory can be extended to a group of developments within a district or even augmented to a city as a whole. Zero C&D wastes sent to landfill may be too idealistic, however, minimisation of C&D wastes could be realised if Balance Theory is enforced.

Appropriate actions taken by the Government may be needed to encourage the execution of the Balance Theory when recycling facilities and the green working culture of construction participants are well developed. Balance Theory can be first carried out in government projects as pilot scheme. The proportion of imported and exported amount of C&D wastes be reviewed and adjusted to suit the adoption and development of the Balance Theory.

KEYWORDS

Recycling, Sustainable Development, Construction & Demolition Waste, Balance Theory, Waste Management, Material Management.

BACKGROUND

Since 1987, the notion of "Sustainable development" was introduced in the Brundtland Report. Sustainable development or sustainability is generally defined as a constraint on present consumption to ensure that future generations will inherit a resource base no less than the previous generation inherited. In meeting this intergenerational goal, sustainability is concerned with two types of limits the environment imposes on growth or development – source limits and sink limits. Source limits refer to the environment's finite capacity to provide resources – both renewable and nonrenewable, and both mere production inputs and essential, non-substitutable "natural" services. The sink limit refers to the environment's capacity to assimilate the wastes that economic growth and development cause.

Environmental Protection Department of the Hong Kong Special Administrative Region (EPD 1998) defined construction and demolition (C&D) materials as a mixture of surplus materials arising from any excavation, civil/building construction, site clearance, demolition activities, road works and building renovation. Statistical information from the EPD 2000 showed that the average daily C&D materials produced was 4 times as much as that of municipal solid waste. This reflected that the construction industry generated a substantial high proportion of solid waste in Hong Kong.

The aim of this article is to arouse the significance of sustainable development in the culture of the construction industry. On national level, sustainability is a resource management and pollution control problem. On the global level, sustainability is concerned with intragenerational equity, cross-boundary pollution, the loss of biodiversity, and the aesthetic value of nature. Although definitions of sustainability vary, there are some important common themes: a concern for the environment, an appreciation of the crucial difference between development and growth, and most importantly, a concern for both inter- and intra-generational equity. In order to achieve the global aim, there are several ways that have to be achieved in the construction industry:

- to minimise the amount of construction & demolition wastes through better planning and design;
- to recover those unavoidable C&D wastes into secondary material;
- to employ the secondary materials in construction projects.

ESTABLISHMENT OF BALANCE THEORY

The composition of C&D waste materials disposed at landfill sites in Hong Kong in 1995 is shown in Table 1 (Source: EPD 1995). It is noted that the asterisked inert materials can be easily recyclable into secondary materials if they are properly sorted and re-employed in construction site as temporary works and permanent works. The other C&D waste, except the ferrous metals, being sent to landfills can also be re-used if they are properly handled through recycling processes. Recent research indicated that the recycled inert materials of the C&D wastes were largely re-used for reclamation, road sub-base, bituminous macadam, and concrete of lower structural grade. Demolished ferrous metal can be sent to steel mill for processing as recycled steel. The scrap metal market in Hong Kong has successfully collected and recovered over 90% of ferrous metal wastes

from construction site. This scrap metal was largely shipped aboard for reproduction as other metal products and partially recycled locally as reinforcement bar, and in turn being used in local construction projects. Wood wastes in construction site include wood products, bamboo, trees and vegetation (mainly obtain from over-site activities in civil engineering works). If wood wastes are properly handled, the recycled products are basically cellulose products in chip and powder form. These recycled products can be used as raw material for chipboard, paper pulp, daily cover in landfill and mulch for moisture retention in landscaping works. Hence, though the construction industry produces quite significant amount of C&D wastes, we could recover them and re-use them into construction projects and benefit the community as a whole.

TABLE 1

COMPOSITION OF CONSTRUCTION & DEMOLITION WASTE DISPOSED OF AT LANDFILLS IN 1995 (SOURCE: EPD 1995)

Component	Composition of each category of construction & demolition waste received at landfill sites (% by weight)				
	Road work material	Excavated soil	Demolition waste	Site Clearance	Renovation Waste
Soil/Sand*	23.0	73.8	21.5	33.0	19.4
Concrete/Mortar*	16.9	1.2	10.8	4.6	7.4
Rock/Rubble*	14.4	12.5	27.7	15.0	38.8
Reinforced concrete*	14.2	0.4	5.8	0.9	7.0
Brick/Tiles*	0.8	0.4	12.1	1.4	9.6
Sub-total	**69.3**	**88.3**	**77.9**	**54.9**	**82.2**
Slurry & mud	1.8	9.7	1.5	1.0	3.1
Asphalt	24.7	0.0	0.0	0.2	0.0
Cement contaminated	1.7	0.4	3.2	15.6	3.3
Wood	0.6	0.9	10.5	13.3	7.1
Ferrous metals	0.5	0.0	0.6	1.0	1.3
Non-ferrous metals	0.0	0.0	0.7	0.2	0.1
Others (include bamboo, trees, glass, plastics, bulky wastes /fixtures, organics & garbage	1.4	0.7	5.6	13.8	2.9
Total	**100.0**	**100.0**	**100.0**	**100.0**	**100.0**
Percentage of total quantity of C&D waste landfilled	5.2	59.4	8.5	14.6	12.3

Note: * Inert materials which are considered suitable for public filling areas
The above figures are estimated by visual inspection of 3060 trucks loads delivering construction & demolition waste in 1995. They should be regarded as indicative only rather than actual composition of construction & demolition waste during the year.

The basic principle of Balance Theory is to acquire the equilibrium between the supply of the C&D wastes and the demand of the recycled C&D secondary materials. The Theory requires gradual achievement in Balance Ratio as defined:

$$\text{Balance Ratio (BR)} = \frac{\text{C\&D Secondary Materials Employed (by weight)}}{\text{C\&D Wastes Produced (by weight)}}$$

If a construction project acquires a high Balance Ratio (BR), that means it does not produce too much C&D wastes. Even if it produces much wastes, it is able to absorb quite a high proportion of the secondary materials.

From Table 1, it reflects that quite a high amount of C&D materials can be re-used or recycled into construction secondary materials even in different natures of projects. Hence, if a project can achieve 70% BR, it arrives a satisfactory level. If a project can achieve 80% or higher, it acquires at commentary level.

PLANNING & DESIGN

Balance Theory advocates that the amount of C&D wastes generated from a construction project is equivalent (or proportional) to the use of recycled C&D products. In order to obtain a commentary level, reduction of wastage is a fundamental step to achieve this purpose.

Waste minimisation can be greatly achieved at design stage. A good design saves considerable amount of wastages. Considerations of the dimension in design approach in one way complies with the functional requirements and on the other way focuses on minimising the cutting wastage of materials. Minimisation of discrepancies in construction information by careful coordination of all design components enables reduction of unnecessary abortive and redundant works. Standardisation of building elements allows repeated use of standard components such as system formwork, pre-fabricated units and precast units. Selection of environmental friendly materials and environmental friendly construction methods will be determinants of sustainability.

Largely adoption of recycled materials in temporary works and permanent works is another essential step to increase the balance ratio. EPD 2000 revealed that 80% of C&D inert materials were sent to public filling area as reclamation material. However, if better sorting process is undertaken, some of these materials could be retrieved to re-use or recycle as usable materials for construction aspects. It is, for instance, concrete fragments of smaller size in C&D wastes are treated by crushing and sieving processes. They can be used as aggregate in road formation, bituminous macadam, concrete blocks or lower structural grade concrete (RILEM recommendation 1992). The other 20% of C&D wastes which were sent to landfill can also be retrieved to a large extent by better sorting process for re-use through recycling. Wood waste can be re-used in producing wood chip products and paper pulp products. Gypsum board wastes can be reproduced as gypsum board or other gypsum products. Plastic wastes can be turned out as plastic raw materials. Consideration should be given to the cost, energy consumption and waste generation during the process of sorting, retrieval and recycling of these wastes. Cost-benefit analysis approach to evaluate the actual financial and environmental benefits must be taken into account. Selection of recycled materials in the design of temporary and permanent works enhances the achievement of a higher Balance Ratio. Preference should be given to recycled materials in design stage to ensure a certain amount of recycled materials is used in the proposed project. When new materials must be used, consideration should be given to the selection of material that is recyclable and re-usable after demolition.

WASTE MANAGEMENT AT WORK

Recent study of construction wastes (Poon et al 2001) revealed that public housing projects generated less construction wastes when compared to private residential projects. Table 2 shows the significance of wastes by trade in these two categories of projects.

From the figures, it reflected that standardised public housing project, due to its repetitive nature, provides better condition for site management which enhances reduction of construction wastes. It is evident that the design and conscious waste reduction implementation affects greatly the outcome of waste management. Other than the nature of project, adoption of a stringent waste management plan on site will greatly reduce the level of wastage and in turn reduces the resources require to handle the wasted materials.

TABLE 2
WASTE PERCENTAGE IN DIFFERENT TRADES FOR PUBLIC HOUSING PROJECT VS. PRIVATE RESIDENTIAL PROJECT

		Public Housing Project	Private Residential Project
Trade	**Material**	**Percentage Wastage**	**Percentage Wastage**
Concrete	Concrete	3-5%	4-5%
Formwork	Timber board	5%	15%
Reinforcement	Steel bars	3-5%	1-8%
Masonry	Brick & Block	6%	4-8%
Dry wall	Fine aggregates	5%	6-10%
Wall screeding	Ready mixed concrete	7%	4-20%
Floor screeding	Ready mixed concrete	1%	4-20%
Wall plastering	Plaster	2%	4-20%
Ceiling plastering	Plaster	2%	4-20%
Floor tiling	Tiles	6%	4-10%
Wall tiling	Tiles	8%	4-10%
Installation of bathroom fittings	Sanitary fittings	2%	1-5%
Installation of kitchen fittings	Kitchen fittings	1%	1-5%

Waste Management Plan can be categorised into three assertions:

a) Waste Preventive and Reduction Action at Design Stage

   i) Coordinate with designer to ensure dimension of material is well considered to avoid cutting wastage;
   ii) Adoption of pre-fabricated precast building components;
   iii) Design to suit system formwork or large panel formwork to reduce the use of timber formwork;
   iv) Designer and specification writer to willfully adopt recycled secondary materials in new development.

b) Waste Preventive and Reduction Action during Site Operations

This plays an important role to minimise unnecessary waste and fulfill recycling. It requires full devotion of site management and supervisory staff to propel all kind of waste preventive and reduction plans to push workers and subcontractors to implement. These plans are not limited to:

i) carefully plan ahead of all works to avoid mistakes, abortive works and double handling;
ii) establish site facilities for collection and sorting of C&D wastes;
iii) centralise material cutting and storage areas so that reusable pieces can be easily located;
iv) educate workers to be "green" construction consciousness by reducing unnecessary cutting of materials, cleaning working spots constantly, collect and sort all their construction wastes into the designated collection spots;

c) Material Management to Avoid Unnecessary Wastage

Material management to avoid unnecessary wastage should be the joint effort of site management and head office policy.

i) Adopt just-in-time material ordering and consumption system to manage material to avoid unnecessary wastage due to stockpile and transportation damage within site areas;
ii) Consider environmental friendly alternatives like cut-to-size, and/or pre-mixed materials to avoid in-situ cutting and mixing;
iii) Adopt to use as much recycled materials when condition permits;
iv) Establish corporate policy to enforce waste management plan and enforce its implementation by means of incentive or penalty system.

CULTURE AND EDUCATION

The strategy in setting up a successful waste management plan to achieve high Balance Ratio, relies much on the partnership between government, industry and consumers and on shared responsibilities among the main actors. Economic constraints, lacking technical specifications for the recycled materials as well as unclear legislation with respect to secondary materials constitute obvious barriers in the development of the use of recycled materials. Hence, specific actions have to be undertaken in order to give the evident opportunities a chance:

Information and sensibilisation of all the parties involved is a necessary. Responsibilities have to be refined. On site, the site manager is "a king" who also decides whether the waste is separated or not. Up to now, even the economical benefits have not made them start separation and few even consider starting it for environmental reasons. To start source separation on a large scale seems to require an order from waste officials.

Economic bottle necks have to be relaxed. Indeed, how strong the social concern about the environment may ever be, the final motivation for using recycled materials will always stay an economic one. As long as there is no real economic interest in using recycled materials instead of virgin raw materials the use of the former will last marginal.

The sustainability paradigm presents challenges as well as opportunities for the construction industry. It will mean higher costs for polluting materials, disposal methods, and processes. It will put a

premium on recycling. Sustainability also opens up new markets for those firms willing to take the initiative and gain the expertise. As business becomes aware that reducing waste and pollution means more profits, new markets are created for the industry. These opportunities include: installing more efficient, less polluting energy systems in power plants; providing environmental upgrades for existing factories; incorporating new more efficient, less polluting technologies into new facilities; and making buildings more energy efficient. Firms with this expertise, particularly those emphasising at the source reduction, will be in demand.

Specifications which relied thus far for a great extent on past experience with virgin materials of well known geological origin have to be reviewed and adapted. Moreover, the standard forms of building contracts are recommended to be revised to address environmental issues and that building professionals need to become aware of the importance of sustainable construction and tailor their professional services accordingly.

GOVERNMENT ENACTMENT AND ENCOURAGEMENT

Support and encouragement from the Government is essential to stimulate a new industry – sustainability development. There are mainly twofold of functions that the Government should play for the initiation and the subsequent growing industry. First and most essential encouragement the Government could give is to provide project funding in developing recycling facilities and the employment of the recycled secondary materials. Bonus can be awarded to those projects achieving commentary or even satisfactory level of the Balance Ratio. It could support private enterprises to enter into the recycling businesses like sorting, classification of wastes, processing and transportation.

On the other fold, the Government can legitimate more stringent rules to enforce the use of recycled materials as well as set up codes of practice for construction participants to carry out the Environmental Management Systems (EMS). In Ontario, the new waste management regulation enforces source separation to be part of the demolition projects over 2000 square metres. The EMS aims to provide a comprehensive framework for achieving sustainability during the construction stage of projects. Similar codes are published by the South African Bureau of Standards (SABS 1993). In the preface to this Code of Practice, the SABS acknowledges the valuable assistance derived from "Specification for Environmental Management Systems", published by the British Standard Institution (BSI 1992). In South Africa, most formal EMS have been implemented by large industrial and business organisations. It provides a comprehensive checklist which should improve the practice of environmental management of construction.

CONCLUSION

Construction industry must inevitably change its historic methods of operating with little regard for environmental impacts to a new mode that makes environmental concerns a centerpiece of its efforts. A proactive, involved industry that addresses environmental effects squarely will have a far better chance of addressing issues and finding solutions prior to government involvement on a scale that has negative consequences for the industry. The Balance Theory as well as the proposed Balance Ratio can be used as a means for establishing the goals of sustainable or green construction. The era of sustainability, perhaps more than anything else, is establishing that we need to synthesize and integrate information to provide future generations with their own sustainable environment.

REFERENCES

Alexander, J. (1993). Making Job-Site Recycling Work, *Journal of Light Construction*, **12:2**, 28-29.

Crushed Concrete Rubble and Masonry Rubble as Aggregate for Concrete - Betonpuingranulaat en metselwerkpuingranulaat als toeslagmateriaal voor beton (1986). The Netherlands: Dutch Centre for Civil Research and Codes (CUR), Gouda.

Fuggle, R.F. & Rabie, M.A. (1992). *Environmental Management in South Africa.* South Africa: Cape Town.

Gardener, J.E. (1989). Decision Making for Sustainable Development: Selected Approaches to Environmental Assessment and Management, *Environment Impact Assessment Review*, **9:4**, 337-366.

Global Environment Facility: Work Program Fiscal Year 1993 – Fourth Tranche. (1992). Washington: UNDP/World Bank/UNEP.

Hong Kong Environmental Protection Department. (1995). *Monitoring of Solid Waste in Hong Kong 1995.* Hong Kong: Environmental Protection Department.

Hong Kong Environmental Protection Department. (1998). *Monitoring of Solid Waste in Hong Kong 1998.* Hong Kong: Environmental Protection Department.

Hong Kong Environmental Protection Department. (2000). *Monitoring of Solid Waste in Hong Kong 2000.* Hong Kong: Environmental Protection Department.

Hong Kong Environmental Protection Department. (2000). Publication in World Wide Web, http://www.info.gov.hk/epd/pub/solidwaste/fig0.5.htm, 2000.

Hong Kong Environmental Protection Department. (2000). Publication in World Wide Web, http://www.info.gov.hk/epd/pub/solidwaste/fig0.6.htm, 2000.

Poon, C.S., Yu, T.W. & Ng, L.H. (2001). *A Guide for Managing and Minimizing Building and Demolition Waste.* Hong Kong: The Hong Kong Polytechnic University.

Robinson, N.A. (1989). A Legal Perspective of Sustainable Development. *The Legal Challenge of Sustainable Development.* Ottawa: Carswells.

Steele, M.W. & Kazushi Wakita. (1994). *Energy-Related Technologies: Five Technologies for Lower Energy Demand and Decreased Air Emissions.* Cambridge: The Consortium of Global Environment and Construction Industry.

Van den Honert, E.L. (1993). Environmental Management Plans and Environmental Monitoring: Input During Detailed Design and Construction, *Proceedings of the Annual Transportation Convention*, Vol. 1A, paper 2, Pretoria.

Advances in Building Technology, Volume 2
M. Anson, J.M. Ko and E.S.S. Lam (Eds.)
© 2002 Elsevier Science Ltd. All rights reserved

IMPROVE THE QUALITY OF CONSTRUCTION AND DEMOLITION WASTE BY SEPARATION TECHNIQUES

W. Xing, H. Pietersen, Ch. Hendriks, and P. Rem

Faculty of Civil Engineering & Geo-sciences, Delft University of Technology,
P. O. Box 5048 2600 GA Delft, The Netherlands

ABSTRACT

In the Netherlands, each year about 16 million tons of construction and demolition waste (CDW) is produced, which locally is the largest solid waste stream. Nowadays, about 90% (by weight) of construction and demolition waste is being reused. However, most of it is reused in road foundations, embankments, and so on. Therefore, construction and demolition waste is still recycled in relatively low technical applications. In order to recycle CDW at a high technical level, the two main materials from CDW—concrete rubble and brick (masonry) rubble—should be recycled/reused in the concrete industry and in the brick industry respectively, and proper quality control is an important step to ensure qualified products without environmental risks. This study focuses on effective separation techniques to improve the quality of CDW, based on differences in physical properties and chemical compositions between concrete/mortar and brick. In the laboratory study, both dry and wet separation techniques were used to obtain concentrates of concrete/mortar rubble and brick rubble. The results show that magnetic separation, jigging, spiral separation, and color separation can be successfully applied for treating construction and demolition waste, and clean products can be obtained of satisfactory.

KEY WORDS

Construction and demolition waste, quality improvement, separation techniques, recycling, concrete rubble, brick rubble, physical behavior, chemical composition

INTRODUCTION

In the Netherlands, each year around 16 million tons of construction and demolition waste (CDW) is produced. It is one of the solid wastes with large quantities in the Netherlands. Because of the limited natural raw materials resources and high population density, the reuse and recycling of secondary materials is strongly encouraged by Dutch authorities and industry. In 1994, Dutch government published the "Environmental Management Act" and stipulated an order of preference for waste treatment that was referred to as "Lansink's ladder". After several years, the "Delft ladder" was put forward by Delft University of Technology. The Delft ladder covers all options of waste treatment.

Current practice of most CDW processing plants in the Netherlands is to reuse CDW in useful applications. Since it has been forbidden to dump recyclable CDW by the Dutch Construction and Demolition Waste Dumping Ban in 1997, more and more CDW is reused. Nowadays, about 90% (by weight) of CDW is being reused. Dutch government aims to further increase the percentage of CDW recycling in the next few years.

In order to reuse or recycle waste materials without environmental risks, the Dutch Building Materials Decree (BMD) gives the maximum acceptable risk for soil and ground water contamination in terms of the leaching values of building materials for inorganic compounds, and chemical composition for organic compounds. When CDW is reused as a building material, its environmental quality should meet the requirements of the Building Materials Decree. In addition, for the sake of the labor health, dangerous substances in CDW, like asbestos, polycyclic aromatic hydrocarbons (PAH), are governed by specific regulations. For example, according to the "asbestos safety module", asbestos must be removed selectively by certified companies in the building before it is demolished. All regulations ensure a minimum of environment and health risks with the recycling of CDW in construction.

The construction and demolition waste can be reused/recycled in three ways, recycling, up cycling, and down cycling. When a material from one chain is reused in the same chain, it is called recycling. When a material is reused in another chain, if it is for a lower-grade application, it is called down cycling; if it is for a higher-grade application than its original one, it is called up cycling. At present, the construction and demolition waste is mostly reused as road foundation and embankment materials. This means that the recycling of CDW is still in a relatively lower technical level. In order to reuse CDW as building materials and avoid down cycling, the quality of the materials must be improved to meet the requirements of quality standards. For this purpose, the separation techniques that have being applied in the mining industry can be used to treat CDW.

The largest fraction of CDW consists of hard stony material such as concrete and masonry/ clay brick; a minor part consists of wood, metals, paper, plastics, and so on. In order to reuse the two main materials from CDW, concrete rubble and brick rubble, respectively, suitable techniques were chosen according to the differences between the two materials. After separation, concrete rubble and brick rubble concentrates were obtained with high purity.

CONSTRUCTION AND DEMOLITION WASTE

Construction and demolition waste can be considered as two parts, reusable materials and waste material. The reusable materials can be divided into two different groups, i.e., stony materials and non-stony materials. Stony materials, like concrete and masonry/clay brick, constitute the majority of CDW (see Table 1). Non-stony materials include wood, plastics, paper, metals and so on. The waste includes harmful materials for the environment or people's health like asbestos, tar, organics, chlorides, and the materials containing these contaminants. The stony materials are usually reused as secondary aggregates in construction.

TABLE 1
COMPOSITION OF CDW (WEIGHT PERCENTAGE)

Composition	Concrete	Brickwork	Asphalt	Wood	Gravel	Metal	Packaging	Other
Percentage (%)	41	29	20	2	2	1	1	4

In the Netherlands, there are three main types of recycled aggregates: concrete aggregates, masonry aggregates, and mixed aggregates. Only a very small amount of the recycled aggregates is used in its own chain cycle again. From the point of view of "life cycle management", treated products from

CDW should be reused/recycled for their original application, this means that concrete rubble should be reused in concrete, and masonry/brick rubble should be reused in brick. In other words, CDW is desired to be recycled at a high technical level. The aim of this study is to improve the quality of the stony materials in order to reuse them in their original applications as qualified products.

In this study, two types of materials were used. One was actual construction and demolition waste taken from a Dutch CDW processing plant of "Theo Pouw" (Utrecht, the Netherlands); another was a mixture of brick and Portland cement mortar/lime mortar that was prepared in the laboratory.

Actual Construction and Demolition Waste

The construction and demolition waste was crushed in the processing plant, and the fraction with particle size smaller than 4mm was removed. After treating in the plant, the material contains concrete, clay brick, and a very small amount of pollutants like lime, asphalt, and wood.

By sieving analysis according to Dutch standard NEN2560, it is found that about 50 percent of the material is bigger than 8mm and about 10 percent is smaller than 4mm. The material was wet sieved into five fractions: 2 to 5mm, 5 to 10mm, 10 to 19mm and larger than 19mm. Samples were taken from each fraction and sorted by hand sorting into two fractions, namely the brick fraction and concrete fraction. The results are shown in Figure 1.

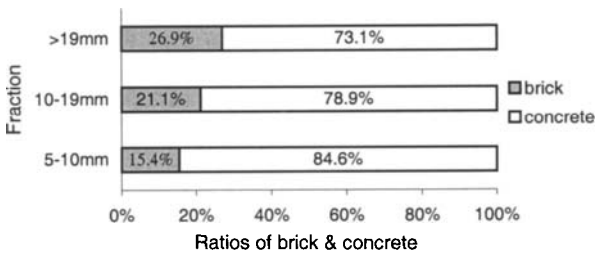


Figure 1: Proportions of brick and concrete with different particle sizes

From the above analysis, it is known that the amount of concrete in this material is about 80%, and the amount of masonry around 20%.

Mixtures of Brick and Mortar

Samples were made by mixing Portland cement mortar that had been hardened for 28 days with clay bricks in different ratios. In order to know the influence of the type of material, lime mortar was also used to make the mixture. In addition, three kinds of bricks were used, normal brick with a red color, brick with a yellow color, and hard fired brick with a dark red color. Mortar and brick were crushed and sieved respectively, then they were mixed in the different weight ratios of 50% to 50%, 30% to 70%, and 70% to 30% with the particle size between 0.15 to 2.36mm.

Properties of Concrete/mortar and Brick

The concrete rubble and brick rubble are the two main components in CDW. In order to recycle them respectively, the mixed granulate that was obtained from the plant must be further treated, and the two materials must be separated from each other to ensure qualified products. How to choose a suitable

separation technique? The differences of physical or chemical properties between the two materials are the basis. These differences are described in Table 2.

TABLE 2
DIFFERENCES BETWEEN CONCRETE AND BRICK & SUITABLE TECHNIQUES

Property	Brick	Concrete /Mortar	Techniques
Magnetic behavior	3 to 4% of Fe_2O_3	0 to 1% of Fe_2O_3	Magnetic separation
Density	1.6 to 1.8 g/cm^3	2.3 to 2.5 g/cm^3	Jigging, fluidized bed method, spiral separation
Color	Red or yellow	Grey	Color separation

A separation technique that works based on material density difference, or magnetic behavior, or color difference can be applied to separate concrete/mortar and brick from each other. The possible techniques are also shown in Table 2.

QUALITY UPGRADING AND DISCUSSION

The samples from actual CDW were separated by jigging, Humphrey spiral separation, and color separation techniques. The laboratory prepared samples were tested by a magnetic separator.

For bricks that are bound by mortar, a thermal process can be used to break mortar off brick. Applying a temperature of about 400°C for five minutes, mortar was removed from brick completely.

Separation of Actual CDW

Jigging

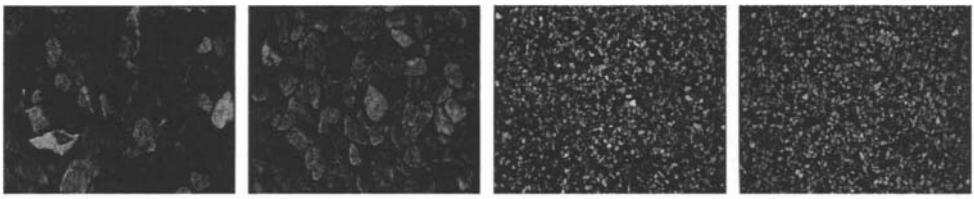
The ratio of the apparent densities in water for concrete and clay brick is bigger than that in air. Therefore, gravity separation will be more effective in water. Jigging is such a method. In a jig, the separation of materials with different densities is accomplished in a bed which is rendered fluid by a pulsating current of water. When water is put under pressure by a plunger, the particles fall with different speeds to the bottom, depending on their densities. The heavy fraction will sink first and be discharged from the bottom of the apparatus.

Four fractions, with particle sizes of 2 to 5mm, 5 to 10mm, 10 to 19mm, and >19mm, were separated by a jig. For each fraction, two concentrates were obtained, i.e., one on the top of the container and another on the bottom of the bed. The upper concentrate is the brick fraction and the lower is the concrete fraction. A good separation is easily obtained with larger particle size. For the fraction with particle size larger than 19mm, both brick fraction purity and concrete fraction purity are high (with similar color). This can be seen in Figure 2. For the fraction with the smallest particle size (2 to 5mm), a good separation is obtained by an asymmetric stole at lower frequency. The results show that jigging is an effective wet method to separate light and heavy stony fractions from CDW, especially for coarse particles. After jigging, the concrete fraction can be cleaned enough and recycled as concrete aggregates directly, but the brick fraction should be dried before recycling.

Humphy spiral separation

The fraction with a particle size smaller than 2.5mm was tested using the Humphrey spiral. The principle of the spiral technique is based on the gradient that exists when particles with different densities are transported by a water stream. The separation result depends on the difference in density,

particle size, particle shape and porosity. From this test, it is known that concrete fraction can be separated from soil and fine sand fraction successfully. Figure 3 shows the separation result.



Brick fraction | Concrete fraction | Brick fraction | Concrete fraction

Figure 2-a: Particle size > 19mm

Figure 2-b: 2mm < particle size <5mm

Figure 2: Separation by jigging



Figure 3: Separation by Humphrey spiral

Color separation

There is a clear difference between the colors of concrete and brick. Figure 4 shows the result of color analyzing by a computer. This is an effective method. However, it is expensive, and it is only effective when the material is cleaned, all particles are in their original colors.

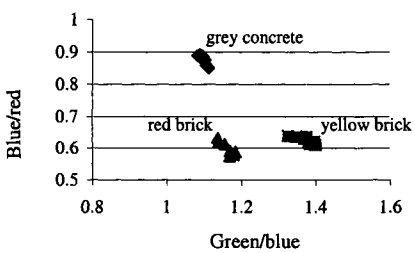


Figure 4: Color separation

Separation of Mortar and Brick by Magnetic Separation

The content of Fe_2O_3 in brick is higher than that in concrete/mortar as shown in Table 2. In the case that brick is considered as a magnetic material, concrete/mortar can be considered as a non- or weakly magnetic material. Ideally, the particles of brick should end up in the magnetic fraction and the particles of mortar end up in the non-magnetic fraction. Table 3 shows the separation results. The

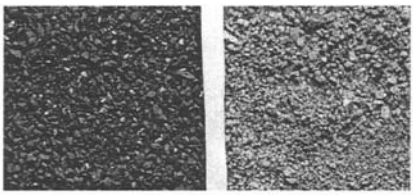
results show that when the ratio of brick to mortar is 1:1 at the machine angles of 15° and 17° with 1.2A current, good separations can be obtained. For the mixture of brick and mortar with ratio of 3:7, a good separation can be obtained at 17°, while for the mixture of brick and mortar with ratio of 7:3, a good separation can be obtained at 15°.

TABLE 3
MAGNETIC SEPARATION WITH THE MIXTURES OF BRICK AND MORTAR

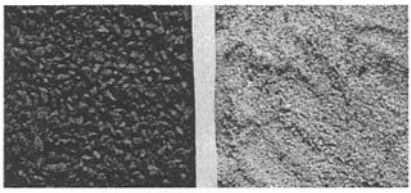
Sample	Current I (A)	Machine angle α	Percentage of brick (%)	Purity of brick	Purity of Mortar
hard red brick : mortar = 50% : 50%	1.5	15	63.51	Pure	Purest
	1.5	17	55.67	Pure	Purest
	1.2	12	67.68	Non-pure	Pure
	1.2	15	54.91	Pure	Purest
	1.2	17	53.62	Pure	Purest
	1.0	9	73.18	None	Non-pure
hard red brick : mortar = 30% : 70%	1.5	15	41.45	None	Purest
	1.5	17	37.55	Non-pure	Pure
	1.2	15	35.40	Non-pure	Purest
	1.2	17	33.37	Pure	Pure
hard red brick : mortar = 70% : 30%	1.5	15	72.46	Non-pure	Pure
	1.5	17	70.28	Pure	Pure
	1.2	15	70.65	Purest	Purest
	1.2	17	67.34	Pure	Non-pure
red brick : mortar = 50% : 50%	1.2	17	56.62	Purest	Purest
	1.2	15	55.62	Pure	Purest
red brick : mortar = 30% : 70%	1.2	17	36.22	Pure	Purest
	1.2	15	36.30	Pure	Purest
red brick : mortar = 70% : 30%	1.2	15	70.6	Purest	Purest
yellow brick : mortar = 50% : 50%	1.2	15	56.22	Pure	Purest
yellow brick : mortar = 30% : 70%	1.2	15	40.50	Pure	Purest
yellow brick : mortar = 70% : 30%	1.2	15	72.83	Purest	Purest
red brick : lime mortar = 50% : 50%	1.2	15	48.94	Purest	Purest
red brick : lime mortar = 30% : 70%	1.2	15	29.71	Purest	Purest
red brick :lime mortar = 70% : 30%	1.2	15	66.17	Purest	Purest

The purity of produced product was checked by visual examination of color. There are four cases: "purest" means that all particles are in their own colors; "pure" means that the color is mixed with a few pieces of other color particles; "non-pure" means that the color is mixed with some pieces of other color particles; and "none" means the color is mixed with other particles.

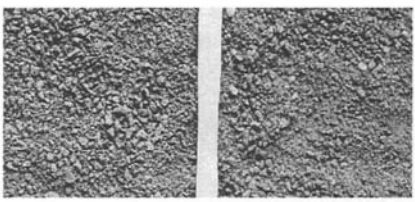
In order to know how pure the separated brick or mortar/lime mortar fraction is, the separated brick fraction and mortar fraction were compared with the mixtures that were prepared in the laboratory according to their colors. In Figures 6-b and 7-b, the separated brick fraction and mortar fraction are the same as those in Figure 5-a. The color of prepared mixture (Figure 6-a) is similar to that of the separated brick (Figure 6-b). Hence, the purity of the separated brick is around 93%. Similarly, the purity of the separated mortar is around 87% (Figure 7). From this experiment, it is clear that magnetic separation is an effective method to separate brick and mortar from each other.



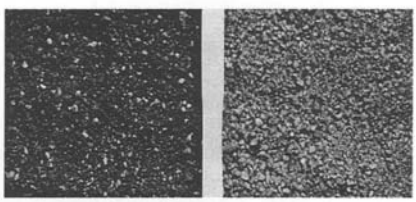
5-a: Red brick & Mortar



5-b: Red brick & Lime mortar

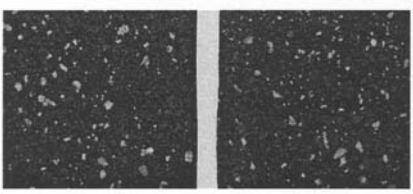


5-c: Yellow brick & Mortar



5-d: Hard red brick & Mortar

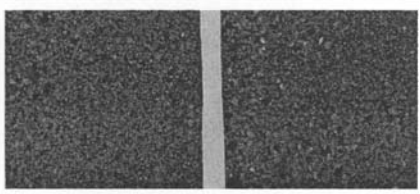
Figure 5: Magnetic separation with different mixtures



6-a 6-b

6-a: Prepared brick with purity of 93.2%
6-b: Separated brick fraction

Figure 6: Purity of brick fraction



7-a 7-b

7-a: Prepared mortar with purity of 87.2%
7-b: Separated mortar fraction

Figure 7: Purity of mortar fraction

CONCLUSIONS

The only way to recycle CDW to a higher technical level is to improve the quality, especially to improve the quality of stony materials from CDW. From the laboratory study, it is known that magnetic separation, jigging, Humphrey spiral and color separation are suitable to treat construction and demolition waste. For the coarse fraction, a good separation of concrete and brick from each other can be obtained by jigging. For the fraction with particle size smaller than 3mm, a good separation can be obtained by either using Humphrey spiral or using magnetic separator. For color separation, a good separation can be obtained only with clean materials. The costs of color separation are higher than for the other three methods. Both jigging and Humphrey spiral are wet separation methods. The advantage of a wet method is that concrete rubble is washed at the same time so that it can be reused directly. However, it costs money to dispose of the slurry.

REFERENCES

1. Eikelboom, R. T., Ruwiel E. and Goumans J. J. J. M. (2001). The Building Materials Decree: an example of a Dutch regulation based on the potential impact of materials on the environment. *Waste Management* **21:3**, 295-302.
2. Hendriks, Ch. F. and Pietersen, H. S. (2000). Sustainable raw materials—construction and demolition waste. *State-of-the-Art Report of RILEM Technical Committee* **165-SRM**, 10-11 and 122-137.
3. Hendriks, Ch. F. and Raad, J. S. (1997). Report: Principles and background of the Building Materials Decree in the Netherlands. *Materials and Structures* **30:Jan.-Feb.**, 3-10.
4. Lauritzen, E. K. (1993). Demolition and reuse of concrete and masonry. *Proceedings of the Third International RILEM Symposium on Demolition and Reuse of Concrete and Masonry*, Denmark. 5-8 and 455-463.
5. Nijkerk A. A. and Wijnand L. D. (2001). Handbook of recycling techniques. 166-168.
6. O'Mahony, M. M. and Milligan, G. W. E. (1991). Recycling of construction waste, *Waste materials in construction*. 225-231.
7. Robert B. L. (1995). Separation processes in waste minimization. 91-101.
8. Xing, W. (2001). Upgrading the quality of construction and demolition waste—the key to recycle CDW at a high technical level. *Proceeding of International Conference on Environmental Concerns and Emerging Abatement Technologies*, China. Oral-33, 1-4.

ENVIRONMENTAL TECHNOLOGIES:

SUSTAINABLE BUILDING

This Page Intentionally Left Blank

Advances in Building Technology, Volume 2
M. Anson, J.M. Ko and E.S.S. Lam (Eds.)
© 2002 Elsevier Science Ltd. All rights reserved

SUSTAINABLE BEARING STRUCTURES

M.J.P. Arets & A.A.J.F. van den Dobbelsteen

Delft University of Technology, Faculty of Civil Engineering and Geosciences,
Department of Building Engineering, P.O. Box 5048, 2600 GA Delft, The Netherlands.
M.J.P.Arets@citg.tudelft.nl

ABSTRACT

Aiming at a factor 20 reduction of the environmental load of buildings in 2040, it is necessary and logical to start by reducing the environmental load of the most important aspects of a building. The bearing structure is responsible for the second largest part of the environmental load of the building; the energy consumption is responsible for the greater part, assuming the life span of a building is 75 years (van den Dobbelsteen & van der Linden, 2000). The bearing structure consists of the foundation, columns, beams, floor and roof structure, and sometimes walls and facades. The horizontal elements of the bearing structure, consisting of the floor and roof structure and beams, are causing about 80% of the environmental load of the total bearing structure. Especially the floor and roof structure play a very important role (Arets, 2000). Therefore, optimisation of the floor structure will lead to an important environmental improvement of the whole office building. The question which structural material is ecologically or economically best, depends on the span the building design needs. For each floor type, for structural spans between 4.8 and 16.8 m, the environmental load and cost have been determined, resulting in a clear overview of best solutions for different spans.
Besides using the best floor types from an environmental point of view, given a certain building span, there are three other possibilities of diminishing the environmental load of the bearing structure:

- using the right material for the right function
- use of new materials for bearing structures
- innovative solutions for bearing structures

This paper describes how to determine the most sustainable floor types and how these other three possibilities contribute to diminishment of the environmental load of the bearing structure.

KEYWORDS

Sustainability, factor 20, environmental assessment, environmental impact, environmental load, environmental cost, innovation, sustainable building, bearing structure, floors, building materials.

1. INTRODUCTION

1.1 Factor 20 improvement

In 1987 the 'Brundtland Commission' released the report 'Our Common Future' in which the definition of sustainable development was an important topic. This definition made a connection between environmental and social goals in the world. In the year 1990 Ehrlich & Ehrlich and Speth re-introduced a formula, which makes it possible to quantify this connection between both goals:

$$\mathbf{EP = P \times W \times E}$$

In this formula EP stands for environmental pressure, which was said to be too high and had to be halved in 50 years from 1990. P stands for the world population, which is predicted to double within 50 years. W stands for the average welfare rate of a world citizen, which is predicted to improve with factor 5 in 50 years. Therefore E, the environmental impact by welfare per citizen, equals:

$$\mathbf{½ = 2 \times 5 \times \underline{1/20}}$$

The calculation shows that by the year 2040 the environmental load has to decrease by 95%, a factor 20. This factor 20 can be used as a goal and guiding line for the environmental performance of for instance buildings.

1.2 The environmental importance of the bearing structure

When analysing the environmental load of (office) buildings it turns out that the greater part of the environmental load is caused by energy consumption during the lifespan of the building (assuming the lifespan of a building is 75 years). The bearing structure is responsible for the second largest part of the environmental load of the building (van den Dobbelsteen & van der Linden, 2000).
Buildings often don't achieve a lifespan of 75 years; offices are functionally obsolete after 25-35 years. The shorter the lifespan the bigger the share of the bearing structure in the environmental load of buildings.
If we want to achieve a factor 20 improvement in 2040, a focus on the parts that contribute the most to the environmental load is necessary. Therefore, sustainability in building technology should be concentrated on improving the bearing structure and energy consumption. In this paper environmental improvement of the bearing structure is elaborated.

1.3 Four steps to improve the bearing structure

There are four ways to improve the environmental load of the bearing structure, in order of impact:

1. Finding the best materials given a certain bearing structure span
2. Making optimal combinations of bearing materials
3. Finding new materials for bearing structures
4. Developing innovative solutions for bearing structures

In the next four chapters these four principles are elaborated.

2. THE BEST MATERIALS GIVEN A CERTAIN BEARING STRUCTURE SPAN

2.1 The functional unity

In order to find the best material or structure variant a functional unity has to be defined. This functional unity forms the basis for comparison of different materials, without it a proper comparison isn't possible.
The functional unity consists of structural, safety and comfort requirements;

- load
- deformation
- dimensions
- fire safety (of the construction)
- thermal isolation
- sound isolation

Before comparing the alternatives, the requirements have to be quantified and the alternatives have to be designed in a way they meet all the requirements.

2.2 Horizontal elements of the bearing structure

When improving the bearing structure, consisting of the foundation, columns, beams, floor and roof structure and sometimes walls and facades, the first question is which part of the bearing structure is determining the greater share of the environmental load of the bearing structure. It turns out that the horizontal elements of the bearing structure (beams, floor and roof structure) determine about 80% of the environmental load caused by the bearing structure. Especially the floors (including roof, ground-floor and storey floors) are an important part of the environmental load (Arets, 2001).

2.3 Different floor types and their environmental load

Floors play an important role in the environmental load of the bearing structure. Therefore the environmental load of different floor types at different spans has been determined. These floors are:

- hollow core slab
- composite floor-plate (reinforced)
- composite floor-plate (pre-stressed)
- TT-slab
- steelplate-concrete floor
- bubbledeck floor
- wooden floor

In order to compare these floors, the functional unity is defined:

- load: 2,5 kN/m^2 (excl. construction weight)
- deformation: in conformance with the Dutch standards
- fire safety: 120 minutes
- sound isolation: in conformance with the Dutch standards for dwellings
- span: 4,8 to 16,8 m (with steps of 0,6 m), without intermediate beams

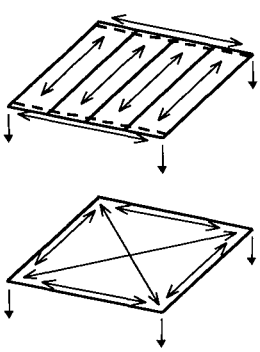


Figure 1: Load bearing capacity of floors in one and two directions

An important difference between the bubbledeck floor and the other floors is that the bubbledeck floor has a load bearing capacity in two directions. The other floors have a bearing capacity in one direction and beams are necessary to lead the load to the columns, this is shown in figure 1. These beams are not taken into account while determining the environmental load and cost.

For different spans the dimensions of the floors have been calculated meeting the requirements as defined in the functional unity. The wooden floor is equipped with plaster slabs to improve its fire safety up to 120 minutes. All floors have finishing.
Knowing the dimensions of the floors, the environmental load of the different floor types at different spans have been calculated. Therefore the database of GreenCalc (a Dutch computer program which calculates the environmental load of buildings; GreenCalc is LCA-based) is used. GreenCalc expresses the environmental load as environmental cost, making it possible to compare the economic and the ecological cost. The environmental cost are the cost necessary to prevent environmental effects and to restore the damage caused by the environmental effects.
The results are shown in figure 2. This graphic shows that the wooden floor and the hollow core slab have the lowest environmental cost for short spans and for lager spans the concrete TT-slab has the lowest environmental cost. This indicates that, based on the mentioned requirements, from an environmental point of view these floor types are the best for these spans.

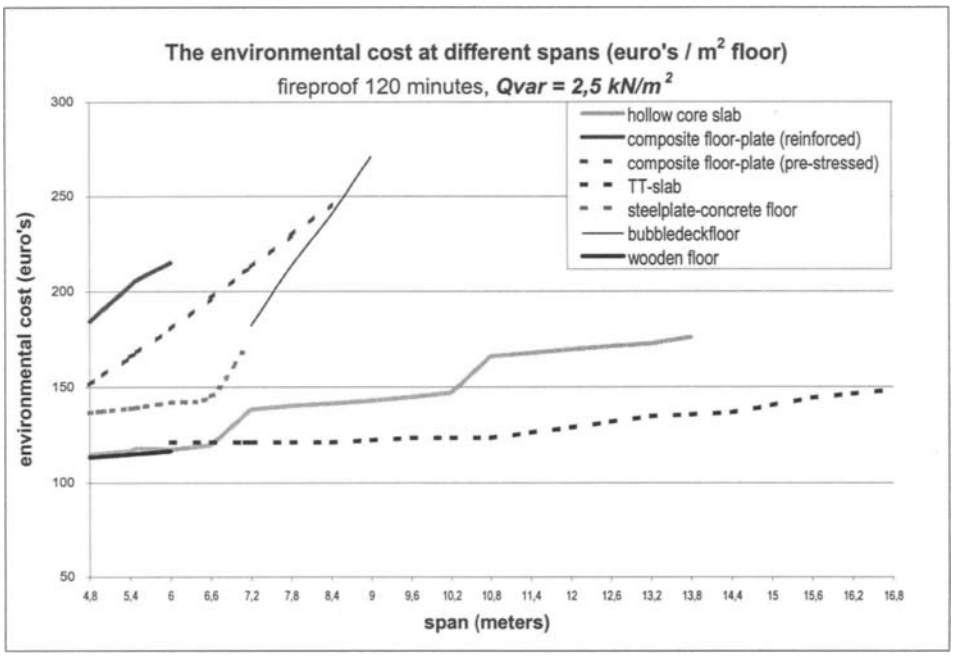


Figure 2: The environmental cost of different floor types

But not only the environmental cost is interesting, the economic cost of the different floor types play an important role in the decision making. Therefore the economic cost of these floors at the different spans has been calculated and added to the environmental cost, leading to the integral cost. The integral cost of the different floors is shown in figure 3. When looking at this graphic it's obvious that from environmental and economic point of view for short spans the hollow core slab is the most profitable and for larger spans the TT-slab is the most profitable (Arets, 2001).
There are a few things to keep in mind:

- these conclusions are only valid for the functional unity as mentioned earlier
- the economic and environmental cost are calculated for the Netherlands
- the cost (environmental and economic) is influenced by made assumptions; therefore it's more important too look at the difference in cost between the floor types than too look at the value of the cost.

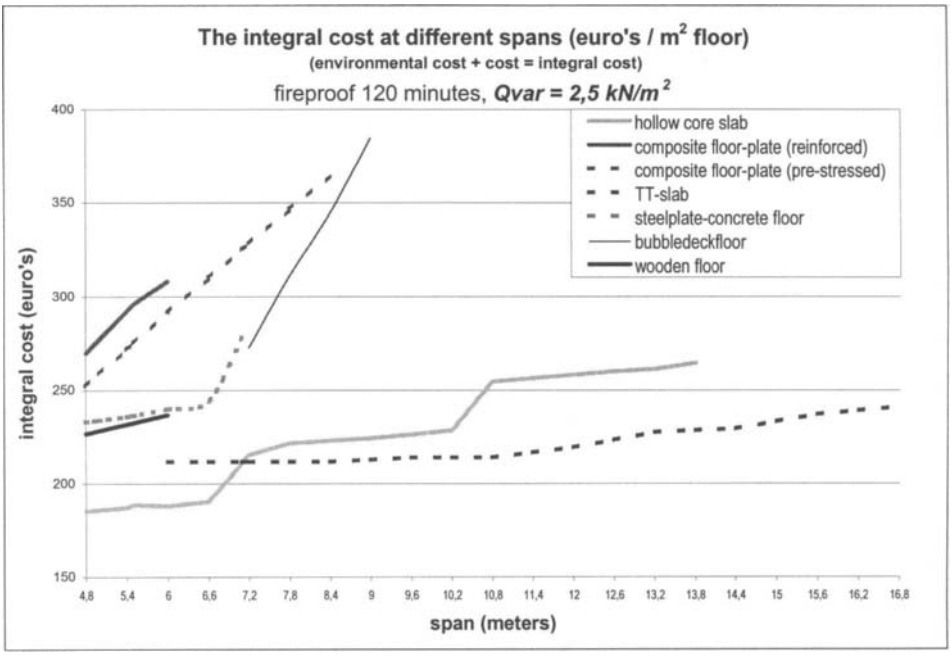


Figure 3: The integral cost of different floor types

3. THE RIGHT MATERIAL FOR THE RIGHT FUNCTION

Concrete, steel and timber are mostly used for the bearing structure. These materials have different qualities with respect to tensile-strength, compression-strength, bending-strength, shear-strength and so on. In order to use as less material as possible it's logical to use a material of which the qualities fit the appearing strain. But to diminish the environmental load there is more then just minimizing the use of materials. It's also important that one uses materials with a low environmental impact. The combination of using less material and materials with low environmental impact should lead to the use of the right material for the right function. In order to find out which material should be used from an ecological point of view the environmental cost of concrete, steel and timber have been calculated for a different manner of loading. The premises are:

Concrete: -B35 (tensile-strength: 1,4 N/mm^2; compression-strength: 21 N/mm^2; modulus of elasticity: 31000 N/mm^2)
-B65, precast (tensile-strength: 2,15 N/mm^2; compression-strength: 39 N/mm^2; modulus of elasticity: 38500 N/mm^2)

Steel: -Fe E 235 (tensile-strength: 235 N/mm^2; compression-strength: 235 N/mm^2; modulus of elasticity: 210000 N/mm^2)

Timber: -K24 (tensile-strength: 8,17 N/mm^2; compression-strength: 12,25 N/mm^2; modulus of elasticity: 7400 N/mm^2)
-K24, glulam (tensile-strength: 10,2 N/mm^2; compression-strength: 15,3 N/mm^2; modulus of elasticity: 9250 N/mm^2)

The environmental cost for the mentioned materials is calculated en indexed. The material with the lowest environmental cost get index 100. In table 1 the results are shown. Looking at the table it's clear that steel has high environmental cost. Although, for example the compression-strength of steel is much better than the compression-strength of concrete and timber, the environmental cost are so big that the index is 5 times higher than the environmental cost of the 'best choice'.

TABLE 1
ENVIRONMENTAL COST (INDEXED) - FOR DIFFERENT MANNERS OF LOADING

		weight	volume	compression-strength	tensile-strength	deformation by compression	deformation by tension
Concrete	B35	100	200	186	--	124	--
	B65	100	200	100	--	100	--
Steel	Fe E 235	964	620	515	217	571	327
Timber	K24	261	100	160	101	261	101
	K24, glulam	324	124	158	100	259	100

Concrete without any reinforcement metal is almost never put into practise. With reinforcing metal the compression-strength and the tensile-strength of concrete get better, but due to the high environmental cost of steel the environmental cost of reinforced concrete rise. If the concrete is pre-stressed, the material qualities will improve more than if it's reinforced, meaning that the environmental cost of pre-stressed concrete is lower then of reinforced concrete (Arets, 2001).

When applying the materials as construction, the shape of construction elements is also important. To get an impression of the environmental cost and the integral cost of beams, made of different materials and applying the most common shape for that material, the dimensions of the beams are calculated (Hogeslag, 1995). The span is 8 meter with one intermediate point of support; the load (without construction weight) is 15 kN/m. Knowing the dimensions, it's possible to calculate the environmental cost and the integral cost (in euro's). The results are shown in table 2.

TABLE 2
ENVIRONMENTAL COST FOR DIFFERENT BEAMS

Material	Dimensions	Environmal cost / meter	Index
reinforced concrete	250 mm x 490 mm	88	251
prestressed concrete	200 mm x 450 mm	65	186
steel	HE 260 A	190	543
timber (glulam)	100 mm x 800 mm	35	100
aluminium	HE 240 A + 4 studs (15x30)	193	553
Material	**Dimensions**	**Integral cost / meter**	**Index**
reinforced concrete	250 mm x 490 mm	114	114
prestressed concrete	200 mm x 450 mm	106	105
steel	HE 260 A	231	229
timber (glulam)	100 mm x 800 mm	101	100
aluminium	HE 240 A + 4 studs (15x30)	284	282

The results in table 2 show that from economical and environmental point of view timber (glulam) is the best solution and pre-stressed concrete is just a little bit worse.

Analysis of the relation between material qualities and their environmental cost leads to these conclusions:

- ⇨ High strength concrete (like B65) has the lowest environmental cost with regard to compression-strength.
- ⇨ Timber (especially glulam) has the lowest environmental cost with regard to tensile-strength.
- ⇨ For short spans timber (glulam) has the lowest environmental and integral cost; pre-stressed concrete is just a little bit worse.

Important for the environmental load of elements of the bearing structure is the shape of the element. As is well know an I-profile is much more effective (for bending, buckling, etc.) then a massive cross-section with the same amount of material.

4. NEW MATERIALS FOR BEARING STRUCTURES

4.1 Diminishing the environmental load of materials

In order to achieve the factor 20, the environmental load of the bearing structure has to decrease. Two ways have been mentioned, but there are more possibilities:

- ⇨ decrease material use with 95%
- ⇨ use material with 95% less environmental load
- ⇨ prolonging the lifespan by factor 20

An example of decreasing the amount of material are the concrete floor slabs. Using hollow core slabs or bubbledeck floors instead of massive floors, the amount of concrete is decreased from about 20% up to 45%. Decrease of material use can also be achieved by using the right material for the right function. Note that one has to be careful; although some materials are more suited for a function then others, the environmental load can be much higher.
Recycled materials and 'natural' materials have less environmental load than 'standard' materials. Note that when using these recycled or 'natural' materials, they have to meet the same requirements as 'standard' materials.
Prolonging the lifespan is possible on different levels. First of all the lifespan of the whole bearing structure (whole building) can be prolonged. Second the lifespan of elements of the bearing structure can be prolonged. This requires elements that are demountable and not polluted and that they are re-used in a sustainable way. Third the lifespan of the materials can be prolonged.
The greatest step towards the factor 20 is combining the three mentioned principles. Use less material and make sure that the used materials have a low environmental load and that they have a long lifespan (Arets, 2001).

4.2 'New' materials

As said before, in the western world concrete, steel and timber are commonly used materials for bearing structures. There are also other materials with specific qualities like glass, synthetic materials, bamboo and all kinds of other natural materials, for instance round timber from young trees.
It will take time to find out what the exact qualities of these materials are and how to use them in a way their qualities are utilised.
The search for 'new' materials which meet the same requirements and have a less environmental impact goes on.

5. EXAMPLES OF INNOVATIVE SOLUTIONS FOR BEARING STRUCTURES

Prefab demountable concrete constructions could be a solution for the shortening lifespan of buildings. The bearing structure consists of prefab pre-stressed concrete elements, put together at the construction site. The connections are mostly bolted and therefore demountable. Examples of these constructions are: the SMT system, the CD-20 system and the Bestcon system (Straatman, 2000).
A similar kind of construction is developed by Prof. van Herwijnen. It consists of specially developed TT-slabs, steel-concrete beams and concrete columns. All the elements are prefab and all connections are bolted and demountable (van Herwijnen, 2000).
One of the problems with this kind of construction is the question who is willing to take the used elements back, approve of them and use them in another building.

An example of an innovative solutions for floors is the IXO-floor. This floor consists of a three dimensional steel frame, with plates on both sides as ceiling and floor. The service-pipes can run through the frame. The floor construction can be demounted as far as cubic elements from about 600 mm and these elements can be demounted further (IXO Sustainable Technology, 2001).

The last example comes from 'historical' constructions, it's an 'under-stressed construction'. In these constructions the occurring tension and compression while bending is disengaged, and a large lever arm is created. Through this large lever arm the construction is very resistant for bending. And because of the disengaging different materials can be used; where there is tension, for instance timber, where there is compression, for instance concrete. Applying this principle in new constructions, floors could be under-stressed as well.

Just like the innovation in materials, the innovation in bearing structure needs to continue. More research of the whole bearing structure is needed. Also research on other building elements, on prolonging the lifespan and more efficient use of the building is necessary.

REFERENCES

Arets, M.J.P. (2001), *Milieuvergelijkingen van draagconstructies ('Environmental comparison of bearing structures')*, Master thesis, Delft University of Technology, Faculty of Civil Engineering and Geosciences, Department of Building Engineering, The Netherlands.

van der Dobbelsteen, A.A.J.F. & van der Linden, A.C. (2000). Finding the most effective sustainable measures, *Proceedings Sustainable Building 2000 Maastricht, The Netherlands,* 667-669.

Ehrlich, P. & Ehrlich A. (1990), *The Population Explosion*, Hutchinson: London, UK.

van Herwijnen, F. (2000), Development of a new adaptable and demountable structural system for utility buildings, *Proceedings Sustainable Building 2000 Maastricht, The Netherlands,* 378-380.

Hogeslag, A.J. (1995), *Algemene constructieleer - deel III: Hout*, Delft University of Technology, Faculty of Civil Engineering and Geosciences, The Netherlands.

IXO-Sustainable Technology (2001), *brochure IXO-floor*, Amersfoort, The Netherlands.

Speth, J.G.(1990), Can the world be saved? *Ecological economics*, **vol. 1**, 289-302.

Straatman, R. (2000), *Environmental related issues in precast demountable construction*, Master thesis, Delft University of Technology, Faculty of Civil Engineering and Geosciences, Department of Building Engineering, The Netherlands.

World Commission on Environment and Development (1987), *Our common future*, Oxford University Press, Oxford/New York.

Advances in Building Technology, Volume 2
M. Anson, J.M. Ko and E.S.S. Lam (Eds.)
© 2002 Elsevier Science Ltd. All rights reserved

DELIVERING SUSTAINABILITY THROUGHOUT THE BUILDING PROCESS: A STUDY OF THE UK CEMENT AND CONCRETE SECTOR

J. Glass [1] and D.N. Pocklington [2]

[1] Oxford Centre for Sustainable Development, Oxford Brookes University, Gipsy Lane, Oxford, OX3 0BP, UK
[2] British Cement Association, Century House, Telford Avenue, Crowthorne, Berkshire, RG45 6YS, UK.

ABSTRACT

Sustainability is becoming an increasing influence on the way buildings and infrastructure are designed, constructed and occupied. With its emphasis on the 'triple bottom line' issues of environmental protection, economic growth and social progress, the principle of sustainability forms the basis of an increasing number of mandatory and voluntary initiatives within the EC and its Member States. Within the UK, sustainable development, (and its implications for energy use, materials, resources and social equity), is encouraged by government through the use of sectoral strategies and its incorporation in government policy relating to construction.

Within this policy context, this paper will consider the UK cement and concrete sector on a number of levels from compliance with European and national legislation to voluntary improvements to manufacturing performance. For example, the industry has been proactive in its early uptake of environmental management systems such as EMAS and ISO 14000 and its development of life cycle assessment of products. More recently, these have been extended to the inclusion of sustainability, and the development of company and sectoral sustainability strategies. However, with the construction industry producing almost 20% of the UK's waste and the occupation of buildings accounting for about 50% of UK CO_2, this paper will also focus on efforts to reduce the burden on UK plc via good practice using cement and concrete in construction. There will be a discussion of the use of fabric energy storage capacity of concrete to reduce or remove the need for air conditioning in buildings, recycled or waste materials within concrete and various methods to reduce waste.

KEYWORDS

Buildings, Cement, Concrete, Construction, Design, Environmental Management Systems, Sustainability.

INTRODUCTION

Sustainability is becoming an increasing influence on the way buildings and infrastructure are designed, constructed and occupied. With its emphasis on the 'triple bottom line' issues of environmental protection, economic growth and social progress, the principle of sustainability forms the basis of an increasing number of mandatory and voluntary initiatives within the European Community and its Member States. This development of EU legislation has reflected the growing environmental awareness within the Community, and the early reliance on 'command and control' has now been supplemented with 'producer responsibility' legislation, economic instruments and voluntary agreements (Pocklington, 1995; 2000). Within the UK, sustainable development, (and its implications for energy use, materials, resources and social equity), is encouraged by government through sectoral strategies and its incorporation in government policy relating to construction (DETR 1999a; 1999b; 2000a). Many of the European and UK directives in this area are related to the global issue of climate change and the targets determined within the Kyoto Protocol, which has resulted in more stringent controls, measures and taxation on 'energy intensive' industries. The UK cement and concrete industry is considered to be energy intensive (it produces approximately 2% of UK CO_2) and as such is subject to environmental legislation. It is also part of the £58bn construction industry in the UK, which is said to account for almost 20% of all waste. At first glance, these statistics indicate why this sector has been a key target for improvement, if the UK is to meet its commitments to the Kyoto Protocol. However with the construction and occupation of buildings accounting for about 50% of UK CO_2, it is clear that there are perhaps more significant results to be gained elsewhere. Perhaps by combining legislation invoking producer/manufacturer responsibility with a much more concerted effort to reduce the burden on UK plc by good practice in design and construction, this imbalance can be redressed.

This paper outlines the policy context associated with the manufacture of cement and the production of concrete. It will show that, in addition to compliance with European and national legislation in this area, the UK cement and concrete industry has been proactive in the improvement of its own performance and diligent in investing in energy efficiency improvements. Adoption of environmental management systems (i.e. EMAS, ISO 14000) has been accompanied by the development of life-cycle product assessment and the development of company and sectoral initiatives. However, there are also significant benefits to be gained in sustainability terms by better employing cementitious materials within the built environment to reduce the operational energy burdens associated with buildings. This issue will be examined in relation to property development, procurement and design, construction and building use. In particular, there will be a discussion of the use of fabric energy storage capacity of concrete to reduce or remove the need for air conditioning in buildings, recycled or waste materials within concrete and various methods to reduce waste (in terms of materials, time and energy).

RESPONSES TO GLOBAL ENVIRONMENTAL ISSUES – POLICY AND PRACTICE

As a consequence of the 5th EU Environmental Action Programme, sustainability is now one of the objectives of the Community, being incorporated formally into its legislative regime in the early 1990s. Further features of the Programme were the concept of shared responsibility between all stakeholders and the switch in emphasis from environmental protection by control of the environmental media (air, water, and land) to a consideration of the effects of all the environmental implications on various sectors of the economy. These provided the stimulus for broadening the scope from purely legislative controls to 'horizontal measures' (i.e. market-based instruments, horizontal, supporting instruments, and financial support measures). These measures have been imposed (in addition to statutory legislation) and the UK cement industry has been obliged to invest significant sums (c. £500M) to ensure its compliance, notably in relation to Integrated Pollution Prevention and Control (IPPC). In addition, there are a number of major instruments and measures that are currently affecting the UK cement and concrete industry related directly to environmental sustainability. These tend to be climate

change/CO_2-focused measures, as the UK strives towards honouring its commitments under the Kyoto Protocol. Global warming is the most significant environmental issue to be addressed, and the control of greenhouse gas emissions is an area that has been subject to the development of 'horizontal measures'. The UK has provided leadership in this area with the development of its Climate Change Programme, including the innovative combination of fiscal measures and negotiated agreements within the Climate Change Levy (CCL) and the market mechanism of the Emissions Trading Scheme (ETS) (Pocklington, 2001a).

Cement production is regarded as an energy intensive process, being associated with the generation of large quantities of carbon dioxide through the burning of fossil fuels within the kiln, and from the decomposition of limestone. Globally, these sources account for 5% of man-made CO_2 emissions, although in Europe the figure is closer to 2%. Under the UK CCL scheme, a levy is imposed on the industrial use of energy (although there are a number of excluded energy uses, exempted fuels, and activities subject to half-rate levy). An 80% reduction in CCL payments is available to companies whose sectors make commitments to energy efficiency improvements or reductions in CO_2 emissions. This discount is limited to 'energy intensive industries' falling within the IPPC regime and is conditional on the establishment of negotiated agreements with government. The UK cement industry is committed to improve energy efficiency by 25.6% from 1990 to 2010. This exceeds the government's aspirational target of 20%, its legally binding Kyoto commitment of 12.5%, and is substantially higher than a number of comparable sectors. Whilst the CCL scheme may be regarded as a technical success (set to achieve 2.56 MtC of carbon savings, DETR, 2000b). However, when viewed in terms of its equitability to business, a different conclusion is reached: the scheme is complex and there are significant discrepancies between the contributions of different sectors (Pocklington, 2001a; 2001b).

Details of the UK Emissions Trading Scheme were announced shortly after the CCL became effective, and it started in Spring 2002. In addition to CO_2, the ETS includes five more greenhouse gases (methane, CH_4; nitrous oxide, N_2O; hydrofluorocarbons, HFCs; perfluorocarbons, PFCs; sulphur hexafluoride, SF_6) providing that suitable protocols for measuring and verifying emissions can be developed. The ETS is expected to yield a minimum of 2.0MtC, i.e. of a similar order to the CCL, however, it is a simpler, more flexible system, in which there are no limits on who may trade and so commentators are more optimistic about its success. The Scheme is open to those already in the CCL regime and voluntary 'Direct Entrants', which must bid for part of an annual incentive of £30M, available over five years and are given 'allowances' permitting the holder to emit given quantity of greenhouse gases. Participants will trade these allowances ('cap and trade'), on 31st December 2002, compliance with targets will be assessed, and incentive payments made in April 2003. The process will be repeated annually.

Another recent economic instrument is the UK's Aggregates Tax, the objectives of which are to address the environmental impact associated with quarrying operations, to reduce the demand for virgin aggregate, and encourage the use of recycled materials. From April 2002, a tax of £1.60/tonne was imposed on sand, gravel and crushed rock subjected to commercial exploitation in the UK. The formal basis of the taxation includes a comprehensive range of exemptions (for other quarried or mined products such as coal, metal ores, industrial minerals etc. and for limestone used in the production of lime and cement). Despite this, the tax is expected to generate approx. £385m revenue in its first year, all of which will be returned to business through a cut in employer National Insurance Contributions and a new Sustainability Fund to deliver environmental benefits, similar to that within the Landfill Tax (Pocklington, 1998). The Aggregates Tax has attracted significant criticism from certain sections of the industry regarding its introduction, applicability and likely effectiveness at delivering the stated objectives. It is not yet clear to what extent it will result in genuine environmental improvements or to what degree it will effectively promote imports to the UK of materials not subject to the tax.

Indeed, there are two aspects to consider when assessing the effects of such environmental taxation. First, its efficiency in generating an environmental benefit and secondly, its overall environmental effectiveness (in terms of the alternatives available (e.g. Emissions Trading *vs.* CCL), the scope of the measure (e.g. addressing CO_2 emissions during manufacture when majority are associated with use); and other 'knock-on' effects of the measure (Oxford Economic Reporting, 2001; Centre for Economics and Business Research, 2001). This is well demonstrated by the CCL; although it is expected to result in a significant reduction in CO_2, the scheme is inefficient in its bureaucratic, restricted nature and pundits suggest that a similar result could have been produced through the ETS alone. In sum, cement and related concrete materials are subject to both the CCL and the Aggregates Tax. In addition to the likely impact on jobs and materials prices, it is anticipated that there will be an adverse effect on the UK infrastructure, where products are sold into areas with fixed budget allocations (e.g. local authorities). The impact will be significantly greater in areas such as Northern Ireland and the South East, where the locations favour imports from counties/countries not subject to the additional taxation.

Although the UK cement and concrete industry has been subject to an increasing number of fiscal and legislative environmental controls, it has nevertheless been proactive in the improvement of its environmental performance through voluntary initiatives. Initially introduced on the basis of ensuring environmental compliance, environmental management systems (EMSs) are now viewed in terms to their potential benefits to the company in areas such as stakeholder involvement, ethical investments, insurance, and purchasers of their goods or services. There is a strong business case for good environmental performance, and all cement plants within the UK have ISO 14000, and over 65% additionally have EMAS, with its commitment to public reporting. Concomitant with the uptake of EMSs has been company involvement in areas beyond their direct control, both upstream and downstream from their operations. In addition to controlling their interfaces with third parties, as required for most EMSs, organisations have developed expertise in supply chain management and life cycle assessment. The latter is of particular relevance, for it provides the basis for linking the costs and impacts of the production of cement to the use of concrete products. Recent work in this area has demonstrated that the 'use' phase of buildings and structures has a much greater environmental impact than that of the preceding processes associated with their provision. This confirms that greater benefits can be achieved via improvements in planning and design of buildings.

The cement and concrete sector has also been approached by government, with a view to develop and publish a 'sector sustainability strategy'. Since the sustainability of cement is strongly linked to its use in concrete products, buildings and structures, it was decided that a strategy for concrete in construction would be more appropriate than one for the cement industry in isolation. An inaugural meeting of the sector group was held in July 2001, following which representatives of interested parties met to draw up a programme of work. The British Cement Association are providing project management, and are sponsoring a supporting R&D programme at the University of Surrey. Additional inputs will include life cycle data on a range of concrete products, from a programme undertaken by Cembureau, and information from the ambitious two-year programme, 'Toward A Sustainable Cement Industry', undertaken by the World Business Council on Sustainable Development.

Having examined the cement and concrete sector, as an example of an 'energy intensive' industry that forms a major part of the UK construction industry, the next section of this paper considers the realms of the various actors and organisations involved in the realisation of the built environment. This will show that the onus to implement change (e.g. responding to climate change) has been, to date, placed squarely with the production side of the construction industry and how the procurement and design side is yet to be as significantly affected. However, it will also demonstrate that change is afoot, particularly within the UK context.

TOWARDS SUSTAINABLE DEVELOPMENT – THE ROLE OF DECISION MAKERS

The issue of how to use land sustainably is becoming more important in European and UK policy and is a matter of concern for planners and property investors (Williams et al, 2000). At the level of planning policy, sustainability is being woven carefully into the content of key documents, but for the layperson this may be a difficult trend to distinguish because it affects and interlinks so many diverse aspects of policy. One response to these issues has been the development of 'sustainable site selection' methods, which are being used by local authorities and private companies. As sustainability is addressed more comprehensively by policy, it will become clear that sustainability-linked EIA methodologies and in-use assessment methods will need to be developed and adopted as standard. This may require a significant effort to integrate social aspects of sustainability sufficiently. For sustainable property development, 'behind the scenes' characters are at least as important as the government and its regulatory building and planning framework in producing more sustainable buildings. Individuals and institutions that invest in property on a regular basis (i.e. not owner-occupiers) effectively control the location, nature and (sustainability) value of development. Institutional investors, such as pension funds, dominate property investment and long term financial performance is the single most important criteria against which they judge success.

Research within the London property investment industry suggests that 'environmental' factors will be a greater matter for concern for tomorrow's investors, but never for today's[1]. In the meantime such investors' decisions will continue to be based almost solely on the basis of long-term rental returns. This is unproductive as regards sustainability and singularly unhelpful in terms of operational efficiency to reduce CO_2 emissions, for example the highest rental returns in commercial office properties are associated with buildings featuring air conditioning as standard. This unwillingness to take a lead, forcibly or voluntarily, on sustainable property development is unlikely to change unless the government proffers a fiscal 'carrot' and a tax 'stick' to alter the situation in the same way as it has implemented appropriate measures affecting the production of building materials. With about 50% of the UK's CO_2 emissions arising mainly from the occupancy of buildings, designers, clients, building users, materials suppliers and contractors have major parts to play in the responsible design, construction and use of the built environment. Therefore, it has been suggested that development decisions for buildings should actually be based on the following 'rules' (Institution of Structural Engineers, 1999):

- Refurbish, adapt and re-use existing buildings (in preference to greenfield development). If not, design and construct new buildings that are adaptable to different users and functions and therefore offer longer life.
- Use recycled components and materials or those from sustainable sources.
- Minimise energy needed to operate buildings by essentially passive design.
- Use or recycle waste produced during construction, operation and deconstruction.

This list supports the notion that a discussion of the need to build should always be preceded by a discussion of the re-use/refurbishment options. Rehabilitation of existing buildings and structures is a very worthwhile option as is examining design life expectancy and maintenance/ replacement cycles in more detail. Within the sustainability debate there is also much discussion about the relative merits of re-use versus new build. There is no clear answer – as for most issues in the sustainability remit, it is a matter of balance. That said, research on the re-use and rehabilitation of older concrete frame buildings has revealed the inherent benefits of a structural frame with longevity, enabling creative refurbishment to buildings in high value, prestigious city centre locations (Gold & Martin, 1999).

---

[1] Keeping, M.: Oxford Centre for Real Estate Management, Oxford Brookes University, including Parnell, P. & Sayce, S. (1999) Attitudes towards financial incentives for green buildings, Drivers Jonas, London, UK.

Despite calls for change, sustainable methods of property valuation have yet to emerge within the mainstay of the traditional real estate sector. Until such conventions are overturned, then the sector's environmental credentials are unlikely to improve.

EVALUATING THE ALTERNATIVES – THE NEED FOR ECO-ACCOUNTING

The use of partnering and non-competitive forms of procurement is becoming more popular in building construction. There is an increasing incidence of 'blue chip' companies and regular construction clients choosing to establish long term contractual arrangements (and relationships) to create a more stable, trusting and ultimately productive working environment. There are several major benefits to this type of approach that impact positively in sustainability terms, not least the eradication of lengthy and intensive tendering routines. In addition, the establishment of long term working relationships facilitates better compilation and analysis of project data on the 'triple bottom line' factors. For example, the project partners can engage in 'continuous improvement' more easily where they have a series of ongoing projects and can work together to improve performance (e.g. by reducing construction waste or improving site standards), linking sustainability with good business practice.

There is a powerful tendency for the UK construction industry at large to rely on a 'first-cost culture'. This stems from a traditional approach to building procurement whereby one-off clients sought the lowest price for their one-off building and valued this criterion above most others. There is now growing concern that the short-term attitude to costing is undermining long-term sustainability for both the procurers and the occupiers of buildings. A more equitable and integrated approach is required, which does not simply presume at the outset that "green buildings cost 10-20% more to build, so we won't build green". However, there has not yet been significant growth in the use of whole-life costing (i.e. life-cycle costing, LCC). Life-cycle costing is a step forward in better eco-accounting, but it is still not sufficient on its own. At a slightly different level, eco-accounting in the form of life-cycle assessment (LCA) of a building and its component parts is becoming an increasingly appropriate means to measure and compare the environmental impacts caused by all aspects of production, design, construction, use, recycling and demolition. By the same token, the methods for appraising the practical aspects of construction are also under development.

The UK government has launched a strategy for sustainable construction, which was intended to give appropriate guidance to the various actors within the sector. The strategy aimed 'to provide a catalyst for change' by promoting awareness and stimulating action, in particular to reduce waste (the construction industry produces almost 20% of all UK waste). One example from the concrete sector was the Princess Margaret Hospital in Swindon, a major new building built on (cement) remediated land, designed to use 30% less energy during occupation than a conventional hospital, which generated 50% less waste during construction than typical sites (Glass, 2001). The in-situ concrete frame structure and precast concrete cladding were designed and built within a tight project framework (devised by a specialist sustainability consultant) to prove beyond doubt that all the triple bottom line issues could be addressed on a major public sector project. Indeed, the ability to measure and compare performance via appropriate indicators is an increasingly popular means of expressing tangible progress. A number of indicators have been taken forward under the Movement for Innovation (M4i) initiative in the form of environmental performance indicators (EPIs) for sustainable construction (Movement for Innovation, 2001):

- Operational carbon dioxide emission (kg CO_2/m^2/year)
- Embodied carbon dioxide (kg CO_2/m^2)
- Water (m^3/person (equivalent)/year)
- Waste in the construction process (measured in $m^3/100m^2$ floor area)
- Biodiversity (TBC; possibly area of habitat preserved or change in species index)
- Transport (TBC; possibly transport km or number of movements)

Having agreed on the most appropriate indicators, the effective comparison of live project data to industry benchmarks will now be possible – given that project managers are able to facilitate the collection and manipulation of such data.

DELIVERING RESULTS – FABRIC ENERGY STORAGE WITH CONCRETE

Indicators are a measurement tool, that is agreed, but it is the relative weighting or ranking associated with those indicators that will determine how success is to be judged on a project-by-project basis. To demonstrate this and relate it to global warming, take CO_2 amongst a basket of other key environmental indicators associated with climate change – doing so, a clear hierarchy emerges (in order of increasing magnitude):

- Initial construction impacts
- Refurbishment impacts
- In-use impacts: energy use and maintenance
- Urban development and infrastructure
- Society: people and their activities (including car travel)

The impacts from buildings are mainly from their use and the CO_2 associated with the generation of energy for heating, lighting and cooling. Only about 10% of operational (in-use) impacts are from the energy notionally embodied within building materials. The dominance of operational impacts means that designers, planners and constructors must keep in perspective the fact that sustainability is a matter of balance, and as such their efforts should be squarely on the long-term aspects of building performance. For instance, recent changes to UK Building Regulations are in direct response to global targets in terms of reductions in CO_2 and other greenhouse gas emissions. Operational energy efficiency in buildings is of the highest concern to UK government, and this is why such aspects of building construction are held up as the industry's most significant problem in terms of sustainability. One of the greatest concerns is the increasing use of air conditioning, which is very energy intensive and requires regular maintenance and short-term replacement cycles. This is in direct contrast to natural ventilation (passive) design strategies that are designed for long-life and minimal expenditure in terms of upkeep.

This is one area where concrete construction can make a very significant contribution (Glass et al, 1999). The use of concrete's thermal mass (called fabric energy storage) can result in 50% lower operational energy consumption and 20% lower capital construction costs, compared to 'comfort cooling'. Examples of major buildings throughout the UK demonstrate that building owners and occupiers can reap long term savings by exposing the undersides of the concrete floor slab (and other elements) to reduce and delay the onset of peak internal air temperatures. The building construction cost can be reduced by 5% simply on the basis of removing suspended ceiling systems. Exposed concrete offers a stunning example of the architectural opportunities for the building client. To give an indication of the scale of cost savings involved, a 32,000m^2 public sector building in Scotland was designed to achieve a £185,000 energy saving per annum by using concrete's fabric energy storage properties. As a dense material for floor and wall surfaces, concrete also offers a major benefit in terms of building health. The inert nature of concrete provides a better level of indoor air quality (IAQ). In combination with good natural ventilation and natural daylight, productivity improvements of at least 10-15% have been documented, and with the UK's current figure of £600m worth of days lost due to the symptoms of sick building syndrome, there is a clear business case. A simple ratio (1:5-10:200)[2] can be used to describe the orders of magnitude involved, for example in commercial office developments, where 1 = the cost of construction; 5-10 = the operational cost to run the building, and 200 = the salaries of people within it.

[2] After Peter Rogers (Stanhope) and Robin Nicholson (Construction Industry Council).

CONCLUSIONS

Despite the environmental importance of energy consumption and CO_2 emissions, the legislative and fiscal measures introduced to date have been restricted in their efficiency and effectiveness, and have tended to focus on production-related issues – a relatively small contribution in relation to emissions during use. The cement and concrete sector is making major inroads towards the practical and measurable delivery of sustainability throughout the building process, but it is no longer only within the realm of the 'energy intensive' industries to provide tangible results. Having complied with new economic instruments and voluntarily adopted environmental management systems, the sector is quickly reaching the limits of a 'reasonable response'. Rather, the time has come for sweeping changes to practice; to overhaul what in sustainability terms is an antiquated way of producing the built environment, but the onus must now be placed downstream of manufacturing activities.

An holistic approach involving whole-life assessments must be central to any future measure, and the construction industry has a vital role to play in providing such an analysis. Such an approach will be one outcome of the sectoral sustainability initiative on concrete in construction, which will build upon existing industry expertise in life-cycle analysis and supply chain management, and other sustainability initiatives. However, these must be complemented by a re-assessment of other drivers including the whole issue of material standards, Building Regulations, and initiatives relating to the operational energy associated with building use. Improvement to the long-term energy performance of buildings is a key part of sustainability and there is a clear business case for specifying concrete. However, the UK construction industry currently lacks tools with sufficient breadth of functionality and data to best evaluate and appraise the economic, social and environmental aspects of sustainable construction. It is unreasonable to expect the design team for a building project to be able to weigh up (unaided) the myriad pieces of evidence relating to sustainability indicators. An integrated eco-accounting methodology that is able to balance the 'triple bottom line' business case and compare it with 'business as usual' in an equitable fashion is vital to move the industry forward. These tools are being developed by some major construction firms, to provide the best response to the government's sustainable development and sustainable construction strategies. However, they will not be sufficient in their own right to deliver the changes deemed necessary – these will be effected only by major fiscal 'carrots' and tax 'sticks' to drive change forward. Indeed, it has been suggested that the magnitude of incentive necessary may be of an unprecedented order, for example with energy costs needing to be set at 40 times their current levels to fundamentally affect decision making processes.

REFERENCES

Centre for Economics and Business Research (2001) *A tax policy without concrete foundations?,* (a report for the British Cement Association, the Quarry Products Association, the Construction Products Association and the British Precast Concrete Federation).

Department of the Environment Transport & the Regions, DETR (now DTLR):
DETR (1999a). *A better quality of life, a strategy for sustainable development*, HMSO, London, UK.

DETR (1999b). *Quality of life counts: Indicators for a strategy for sustainable development for the United Kingdom - a baseline assessment*, Government Statistical Service, London.

DETR (2000a). *Building a better quality of life, a strategy for more sustainable construction*, HMSO, London, UK.

DETR (2000b). *Climate change – the UK programme*, HMSO, London, UK.

Glass, J., Kendrick, C. & Baiche, B. (1999). Maximising opportunities for fabric energy storage, (in Dhir, R.K. & Paine, K.A., *Radical design and concrete practices*, Thomas Telford, London, UK), Creating with Concrete Congress Proceedings, University of Dundee, Scotland.

Glass, J. (2001). *EcoConcrete: the contribution of cement and concrete to more sustainable development*, British Cement Association, Crowthorne, UK.

Gold, C.A. and Martin, A.J. (1999). *Refurbishment of concrete buildings*, BSRIA Guidance Note GN9/99, BSRIA, Bracknell, UK.

Institution of Structural Engineers (1999). *Building for a sustainable future: construction without depletion,* ISE/SETO, London, UK.

Movement for Innovation, M4i (2001). *Environmental performance indicators for sustainable construction,* (Sustainability Working Group Report), M4i, Watford, UK.

Oxford Economic Reporting (2001). *The Climate Change Levy - its impact and proposals for change*, September, (a report for the Engineering Employers Federation, EEF).

Pocklington, D.N. (1995). The role of environmental action programmes in the development of EU Environmental Legislation. *Environmental Law and Management* **7:6,** p.221.

Pocklington, D.N. and Pocklington R.E. (1998). The EU Landfill Tax – externalities and external influences, *Journal of Planning and Environmental Law* **June**, p.529.

Pocklington, D.N. (2000). Progress towards Kyoto targets through an EU Environmental Agreement on CO_2 Emissions from Passenger Cars. *Environmental Law and Management* **12:2,** p.60.

Pocklington, D.N. (2001a). The UK Climate Change Levy – innovative but flawed, *EELR*, **10:7,** p.220.

Pocklington, D.N. (2001b). Industry soundings, *Environmental Law and Management*, **13:2,** p.81.

Williams, K., Burton, E. & Jenks, M. (2000). *Achieving sustainable urban form*, E & FN Spon, London, UK.

This Page Intentionally Left Blank

Advances in Building Technology, Volume 2
M. Anson, J.M. Ko and E.S.S. Lam (Eds.)
© 2002 Elsevier Science Ltd. All rights reserved

SERVICE LIFE PLANNING: DEFINITION OF CLIENT REQUIREMENTS

Rebecca Hooper[1], Kathryn Bourke[1], Josephine Prior[1] and David Richardson[1]

Building Research Establishment Ltd., Watford, WD25 9XX, UK

ABSTRACT

The paper aims to provide architects, designers, engineers, specifiers and contractors with an understanding of the information they need from clients in order to deliver functional, durable buildings and infrastructure that provide value for money. Service life planning is the mechanism by which the design and construction process sets out to achieve a required service life. Achieving a pre-defined service life is one indicator of the value provided by the facility and service life planning offers a mechanism to achieve the goals of value from construction procurement.

The recent UK Government reviews of the construction industry have highlighted the need for improvements in the construction process to ensure efficient delivery of effective facilities. By understanding and defining service life and performance requirements clients can greatly increase the likelihood of achieving the value that they need from the final facility. Considering the service life of a facility at an early stage of the construction procurement process can lead to:

- improved understanding and definition of expectations of the facility in use;
- increased likelihood of continuity of function over time;
- reduced risk of failure and consequent loss of business value;
- optimal capital and operational expenditure.

Factors that are important to the achievement of required service life and need to be considered by the client are:

- the purpose of the facility;
- demands placed upon the design (*must-haves*) such as corporate policies, aesthetic considerations, sustainability credentials and so on;
- the need for flexibility;
- the required service life and the effects of service life failure;
- the levels of repair and maintenance;
- project expenditure and whole life costing.

KEYWORDS

Service life; client; whole life cost; value, briefing.

INTRODUCTION

This paper introduces the principles behind the *Service Life Checklist for Clients* (BRE 2002). The *Checklist* has been developed as the first stage in the service life design process, under the project *Service life design to minimise whole life costs and promote sustainable construction*, funded by the Construction Industry Directorate of the UK Department of Trade and Industry. This paper aims to provide architects, designers, engineers, specifiers and contractors with an understanding of the information they need from clients in order to deliver functional, durable buildings and infrastructure (referred to as facilities in this paper) that provide value for money.

What is Service Life and Why is it Important?

BS ISO 15868-Part 1 (BSI 2000) defines service life as "*the period of time after installation during which a building or its parts meets or exceeds the performance requirements*". Achieving a pre-defined service life is, therefore, one indicator of the value provided by the building. Service life planning is the mechanism by which the design and construction process sets out to achieve the required service life. The planning process begins with the definition, by the client, users or other stakeholders, of the service life required for the final facility and any performance requirements that it is expected to meet or exceed. Yet, the client does not always provide the information required by the design/construction team to match their expectations. A recent consultation exercise demonstrated that where service life information is included in the client brief, designers check their designs against this information (Hooper and Rizzi 2001). Clearly, where this information is missing, these checks cannot be made.

The Changing Attitude of Construction Clients

The sole purpose of construction project is to fulfil a business or aspirational need. The success of a facility depends on how well it meets a client's needs and interests. Construction should not only be an answer to basic client requirements, but it should also enhance and facilitate the activities that it accommodates (Prior and Rizzi 2002).

Recent changes in client attitudes to construction are reflected in an increasing interest in through-life costs, that is, not only the capital costs but also the operational costs associated with delivery of functional performance for a defined life span (Kernohan et al 1996, RAE 1998). The client has a significant opportunity to improve the delivery of their facilities, though the definition of required service life and performance at the start of the construction procurement process. Clear vision and direction are important elements for success. By understanding and defining service life and performance requirements clients can greatly increase the likelihood of achieving the value that they need from the final facility.

UK construction initiatives, such as Rethinking Construction (Egan 1998), Constructing the Team (Latham 1994) and The Building Down Barriers Programme (Cain 2000) demonstrate that repeat construction clients have paid "*unnecessarily high costs for an inefficient process which all too often delivered functionally inefficient buildings and facilities*" (Cain 2000). The UK Government Construction Clients' Panel has committed to *Achieving Excellence* through (GCCP 1999):

- Procurement decisions based on value for money,
- Using risk and value management,
- Performance specifications,
- Whole life costing,
- Use of information technology and standardised document handling,
- Use of innovative procurement strategies based on integration of the supply chain.

Inefficiencies in procurement and management of construction projects can cost up to £600 million per year for the UK Government (NAO 2001) leading to innovative procurement mechanisms finding favour. These mechanisms include (NAO 2001):

- *Private Public Partnerships* (HM Treasury 1999), particularly *Private Finance Initiative* projects (HM Treasury 2000). The supplier is contracted to construct and then deliver the services that the facility is intended to provide.
- *Design and Build* (HM Treasury 1999). A single supplier is responsible for both the design and construction of the facility.
- *Prime Contracting* (Holti et al 1999). A form of design and build where the prime contractor is expected to have an established supply chain to encourage the provision of value for money and quality.

These changes in UK Government attitude, and the focus upon achieving value from construction over a defined lifetime, are reflected internationally. For example, The Construction 21 Report of the Singapore Government encourages increased construction procurement through Design and Build (Ministry of Manpower 1999). In the USA, it is Federal policy to use performance-based acquisition wherever practicable and the *Seven steps to performance-based services acquisition*, provides a web-guide to assist procurement stakeholders apply this policy (DOC 2002). All of these Government policies support the idea that efficiency and value gains can be made through improved procurement, particularly construction procurement. And yet there is very little direct consideration of service life in these performance related procurement routes.

CURRENT PRACTICES IN CLIENT BRIEFING

The Royal Institute of British Architects (RIBA 2000) defines *Appraisal* as the first stage in construction procurement. *Appraisal* is conducted by (or on behalf of) the client and includes *"Identification of client's requirements and of possible constraints on development."* It is at this stage of the procurement process that the service life of the building needs to be considered and information relating to service life identified so that it is available to form boundaries to the design and construction process as procurement progresses. Factors that might be considered during *Appraisal* include (RIBA 2000):

- *"Functional performance*
- *Programme for operational use*
- *Value for money"*
- *Quality, architectural profile, corporate image*
- *Available finance*

Of these factors, functional performance, architectural profile, corporate image, programme for operational use and available finance, all have service life implications. However, to use this information effectively, fundamental questions should be considered, such as, *how long will the facility be expected to last, how will it be looked after, how will it accommodate change?* The need for this critical information was highlighted in BS 7543:1992 (BSI 1992), *"The building owner should specify the required service life of the building in the initial brief"*. However, recent industry consultation demonstrates this is often not the case (Hooper 2001). The *Service Life Checklist for Clients* aims to facilitate the inclusion of service life information in the briefing process. Factors, important to service life, that need to be considered by the client are:

- the purpose of the facility;
- demands placed upon the design (*must-haves*) such as corporate policies, aesthetic considerations, sustainability credentials and so on;
- the need for flexibility;
- the required service life and the effects of service life failure;
- the levels of repair and maintenance;
- project expenditure and whole life costing.

THE PURPOSE OF THE FACILITY

Defining the purpose of the facility assists the design/construction team to focus their efforts on making sure the facility achieves its objectives over its required lifetime. Clients need to consider why the facility is important to them, what it needs to achieve and if it needs to do (or avoid doing) anything particularly special.

Example

- The client wants a new corporate headquarters (HQ) to house 500 office staff who use the latest IT equipment that is regularly upgraded. The building should reflect their high-tech corporate image. This could lead the design/construction team towards a design that not only allows for easy upgrading of IT equipment but also of interior finishes to maintain a modern look. The team may consider specifying finishes that are inexpensive, easy to replace and that are only intended to last a short life span.

MUST-HAVES

The client may have specific desires or be subject to particular obligations. This information is essential to the design/construction team, as it will constrain the design and construction process. These *must-haves* can include an already purchased site, a particular feature and business policies that have design implications. Only by clearly identifying these limits can the design/construction team work within them.

For example, sustainability is becoming an increasingly important facet of construction. From the client's perspective there may be corporate policy obligations to maximise the sustainability of the facility. Such obligations can include energy efficiency, the use of the materials generated from the site clearance in the construction, or a predominance of recycled materials in the facility. It is important that the client considers these aspects and makes any relevant sections of policy documents available to the design/construction team.

Example

- The client of the corporate HQ is a banking / investment house and therefore requires fail safe power supplies and back-up to computer systems, together with expensive security measures and archiving facilities.
- The client has already purchased a site in a major town. This location will influence the design as, in this case, materials and a suitably trained workforce will be readily available for construction and inspection, maintenance, repair and replacement activities.
- As the client is a major consumer of electricity there is a corporate policy to maximise energy efficiency of buildings to minimise the electricity costs. This relevant corporate policy needs to be made available to the design/construction team.

FLEXIBILITY

The risks of obsolescence within the required service life are difficult to foresee, but it is possible for the design to include flexibility. The client is better placed than the design/construction team to foresee future changes. The client needs to consider if there are likely to be any changes in the purpose of the facility over its lifetime or if there are likely to be major changes to the facility contents. Describing the potential changes assists the design/construction team to address the level

of flexibility of the facility, which helps to maximise the likelihood of continued function over the service life.

Example

- As the corporate HQ is for a growing company, allowances should be made for increasing staff numbers during the service life. This could be as simple as orientating the building to allow for further construction on the site. Additionally, consideration is given to the potential need for increased car parking to accommodate additional staff, again through careful consideration of the building orientation on the site.
- Equally, there are likely to be significant changes in the computing servers during the lifetime of the building. Hence, these pieces of equipment should be accessible for replacement without significant disruption to the business value of the building, probably on the ground floor close to a parking area.

THE REQUIRED SERVICE LIFE

In addition to assessing how long the facility needs to last to serve their own purpose, the client needs to consider if they will want to sell the facility on and if they intend to offer a warranty or achieve a premium price for it. All of these factors will affect the service life they require from the facility. Knowing the required service life will help the design/construction team to design, specify and build the parts of the facility that need to last its life-time. It is important for clients to remember that the required service life is related to the overall facility not to individual components and that some maintenance, repair or replacement should be expected.

Example

- The building of the HQ is a substantial investment expected to provide business value to the company for a period of 50 years. In this case, the structural elements and underground structures such as sewerage pipes would be expected to last the required service life. However, the client has determined that the interior of the HQ needs to echo a high-tech corporate image. A suggested mechanism is a design allowing for the regular replacement of internal finishes. Hence the required service life of the building typically exceeds the lifetime of the internal finishes.

THE EFFECTS OF SERVICE LIFE FAILURE

The client needs to consider how the facility might stop being of value. Highlighting factors that would lead to service life failure, and would have significant implications for the client, allows the design/construction team to minimise the risk of these happening during the required service life. Service life failure and the end of service life are often related to uneconomic function of the building (Hooper 2001), when the building is not cost-effective to run, or is too costly, to maintain, repair and operate. This indicates that maintaining function within commercial limits is important to meeting or exceeding the performance required over the service life.

Example

- The failure of internal finishes in the corporate HQ will not affect the business value of the building since routine replacement is anticipated and can be budgeted for. However, failure of the power supply to a central computer server would mean money lost in staff time or customer losses as well as the repair costs. Understanding the critical importance to the

business of maintaining the power supply should lead the design team to make all the necessary arrangements to ensure of the continuity and quality of the electricity supply.

INSPECTION, MAINTENANCE, REPAIR AND REPLACEMENT

Only with very temporary facilities is it likely that no inspection, maintenance, repair or replacement of components will be necessary. The strategies to conduct these operations will depend on many factors such as facility purpose, location and the intended facility management arrangements. Firstly, clients need to make a choice between a proactive or reactive approach. Essentially, do they want to keep the facility running smoothly (proactive) or fix it if it breaks (reactive)? Also, there may be specific requirements concerning the scheduling of repair and replacements. Knowing the approach to be adopted, and details of required scheduling, allows the design/construction team to create a facility that fits the client's needs.

Example

- Since the client intends to maintain a modern interior to the HQ building, the design accommodates this by regular replacement of internal finishes. However, the client also requires that any internal routine maintenance and replacement activities take place during the night or at weekends so that the business is not disrupted. Thus, the interior finishes need to be easy to replace in very short time scales. This leads designers away from specifying painted finishes which take time to apply, dry and cause a lingering odour. Instead the design team suggests covering the walls with a readily demountable patent partitioning system or dry board finish fixed with cups and screws. In this way, the internal wall finishes can be replaced in a phased sequence throughout the offices without disruption, odour or wet paint.

PROJECT EXPENDITURE

An initial budget may have been allocated for the construction in advance of the developed construction brief, but this will often be on a capital cost basis using typical historic square metre costs. Equally, unless specifically requested in the briefing document the design team will not necessarily conduct whole life cost analysis. Whole life costing (WLC) has been identified as a mechanism to deliver improved value for money and predictability of expenditure (CCC 1999).

Clients need to identify if the available budget is for capital costs only and if consideration of operating costs is required. The design/construction team can assess if the client requirements can be met within the initial budget. If WLC analysis is requested they can use the service life information to develop and select the most whole life cost-effective option by balancing the capital and operating costs within the boundaries placed upon the design.

Example

The corporate HQ is to have a prestigious entrance hall. Two options are under consideration are:

a) A stone floor that is hard wearing and would last the life of the building but has an increased risk of accidental damage which is expensive to repair and the potential for increased slip hazards in wet weather. Additionally, the floor is likely to allow dirt to be carried through the entrance hall to the interior offices.
b) A high quality carpet that would be less expensive initially but would require daily cleaning and regular replacement throughout the lifetime of the building, and thus would be associated with higher operational costs.

One optimised solution might be to provide replaceable entrance matting which would minimise the slip hazard on the stone floor but avoid dirt being tracked into the building and thus reduce cleaning costs in other areas beyond the entrance hall. This solution would partially offset the increased capital costs of the stone flooring by reducing operational costs elsewhere in the building.

SUMMARY

Considering the service life of a facility at an early stage of the construction procurement process can lead to:

- improved understanding and definition of expectations of the facility in use;
- increased likelihood of continuity of function over time;
- reduced risk of failure and consequent loss of business value;
- optimal capital and operational expenditure.

The key areas for consideration by the client are:

- The purpose of the facility:
  - Why are you considering a construction project?
  - What do you want the facility to achieve?
  - Why is the facility important to you or your business?
  - Do you want anything special?
- The *must-haves*:
  - Has a site been selected/purchased?
  - Do you want a particular feature?
  - Do you have any business policies that might affect the design or construction?
- The need for flexibility:
  - Can you foresee any changes in the purpose of the facility over its lifetime?
  - Will you want to make major changes to the facility contents during its lifetime?
- The required service life:
  - How long do you want the facility to last?
  - Will you want to sell it on?
  - Will you be offering a warranty?
- The effects of service life failure:
  - How might the facility stop being of value to you or your business?
  - Are you responsible for the facility throughout its service life?
- The levels of repair and maintenance:
  - Do you want to keep the facility running smoothly or fix it if it breaks?
  - Do you have specific requirements of the inspection, maintenance, repair or replacement?
- Project expenditure and whole life costing:
  - Is the budget just for capital costs?
  - Are you considering the whole life cost?

Acknowledgements

The Building Research Establishment is grateful to the UK Government Department of Trade and Industry for their support. Additionally, BRE would like to thank all the members of the project Consultative Group:

- B Bell (Rail Track)
- R Cather (Arup R&D)
- H Davies (Hywel Davies Consultancy)
- T Harrison (Quarry Products Association)
- B Law (Association of Planning Supervisors)
- G Somerville (UK Cares)
- G Bowskill (UK Highways Agency)
- L Clark (University of Birmingham)
- D Doran (David K Doran Consulting)
- E Kay (Halcrow Group Ltd,)
- J Maw (J Maw Consulting)
- R Wolstenholme (W S Atkins)

REFERENCES

British Standards Institution - BSI (1992). BS 7543:1992, *Durability of buildings and building elements, products and components*, BSI, London, UK.

British Standards Institution - BSI (2000). BS ISO 15686-1:2000, *Service life planning - Part 1: General Principles*, BSI, London, UK.

Building Research Establishment – BRE (due for publication 2002). *Service Life Checklist for Clients*, CRC Ltd., London, UK.

Cain, C. (2000). *The building down barriers programme explained - The building down barriers programme*, www.defence-estates.mod.uk/prime_contracting/building_down_barriers.htm, London, UK.

Construction Clients' Forum - CCC (1999). *Whole life costing, a clients guide*, Construction Clients' Forum, London, UK.

Department of Commerce - DOC (2002). *Seven steps to performance-based services acquisition,* http://oamweb.osec.doc.gov/pbsc/home.html, Washington, USA.

Egan, Sir J. (1998). *Rethinking Construction, report of the construction industry taskforce*, Department of the Environment, Transport and the Regions, London, UK.

Government Construction Clients Panel - GCCP (1999). *Constructing the best government client, Achieving excellence,* HM Treasury, www.ogc.gov.uk/embedded_object.asp?docid=240, London, UK.

HM Treasury (1999). *Procurement Strategies, Procurement Guidance, No.* 5, HM Treasury, porch.ccta.gov.uk/treasury/reports.nsf, London, UK.

HM Treasury (2000). *Treasury Taskforce Guidance: 1997-2000*, HM Treasury, www.ogc.gov.uk/pfi/, London, UK.

Holti, I., Nicolini, D., Smalley, M. (1999). *Prime contractor handbook of supply chain management, sections I & II,* Ministry of Defence, www.defence-estates.mod.uk/prime_contracting/bdbmay99.doc, London, UK.

Hooper, R., Rizzi, F. (2001). BR 428, *Durability assessment of building and structures: consultation exercise results*, CRC Ltd., London, UK.

Kernohan, D., Gray, J., Daish, J. (1996). *User participation in building design and management,* 2nd Edition, Butterworth Architecture, London, UK.

Latham, Sir M. (1994). *Constructing the team: final report of the government/industry review of procurement and contractual arrangements in the UK construction industry*, Her Majesty's Stationary Office, London, UK.

Ministry of Manpower (1999). *Construction 21 report*, MOM, www.gov.sg/mom/construction21/, Singapore.

National Audit Office - NAO (2001). *Modernising construction, Report by the comptroller and auditor general*, The Stationary Office, http://www.nao.gov.uk/publications/nao_reports/00-01/000187es.pdf, London, UK.

Prior, J. J., Rizzi, F. (Due for publication Summer 2002). *Getting it right: a Clients' guide to achieving functionality in construction*, Building Research Establishment, work in progress funded by UK Department of Trade and Industry, Watford, UK.

Royal Institute of British Architects - RIBA (2000). *The architects plan of work*, RIBA Publications, London, 2000.

The Royal Academy of Engineering – RAE (1998). *The long term costs of owning and using buildings*, RAE, London, U.K.

Advances in Building Technology, Volume 2
M. Anson, J.M. Ko and E.S.S. Lam (Eds.)
© 2002 Elsevier Science Ltd. All rights reserved

INNOVATIONS IN THE DESIGN OF HOUSING DEVELOPMENTS IN HONG KONG

Horsfield J.N.[1], Gibbons C.[1], Yau R.M.H.[1], Ip T.F.C.[2]

[1]Ove Arup and Partners (HK) Ltd, Hong Kong

[2]Tom Ip and Partners, Hong Kong

ABSTRACT

This paper presents recent developments in the design of high rise residential accommodation in Hong Kong. The role of government, and the business community is reviewed to explore how innovative design is being encouraged within the sector. There then follows a case study of the design of a Home Ownership Scheme public housing development, which incorporates innovative features aimed at addressing many of the problems associated with high density living in an urban environment. The case study demonstrates the strong emphasis that has been placed by Hong Kong people on providing affordable, environmentally responsible, and socially sustainable housing and how this can be realised through an innovative and integrated approach to architectural and engineering planning and design.

KEY WORDS

Community, Efficiency, Energy, Environmentally responsible, Innovation, Life-cycle cost, Multidisciplinary, Optimisation, Natural ventilation, Prefabrication, Stakeholder participation, Value

INTRODUCTION

Buildings are among the largest consumers of natural resources, generators of waste and consumers of energy. In 2000 Hong Kong's construction industry consumed more than HK$50 billion worth of materials, energy and water and was responsible for approximately 40% of all municipal waste flows (EPD, 2002). Completed buildings place an even greater demand on the environment. Lighting, ventilating and cooling Hong Kong's residential and commercial buildings consumes around 50% of all electricity produced for the territory (EMSD, 2001). Economic efficiency and environmental protection, if not yet synonymous, are certainly being seen as strongly linked as the quest for sustainable development gathers momentum. The building industry has a significant contribution to make as it begins to reflect on its current practices and seeks to implement processes of change that lead to more sustainable patterns of production and consumption. The term ecological modernisation has been used to describe the process by which markets re-orientate to capitalise on trends in more environmentally responsible behaviour (Mol, 1997). An essential feature of this trend is for governments to provide impetus through appropriate market intervention. It is then the purview of industry to seek out innovative ways of creating and capturing market share in the ensuing

environmentally responsible approaches to economic growth. Environmental and economic interests are therefore not necessarily mutually exclusive and benefits are best achieved through a multi-disciplinary approach to the development process. A strong emphasis must be placed on stakeholder participation throughout the process of design, construction and operation of buildings.

The Hong Kong construction industry is beginning to recognise these opportunities and a number of initiatives have been instigated by the government to promote more environmentally responsible behaviour. These initiatives are being supported by the local business community and are establishing a niche, which has the potential to change the way construction professionals approach their work.

THE ROLE OF GOVERNMENT, BUSINESS AND THE COMMUNITY

In his policy address of 1999 the Chief Executive of Hong Kong made a commitment to improve working practices in the construction industry and established the construction industry review committee. In March 2001 the committee issued its report Construct for Excellence which identifies key areas in the construction industry which need to be addressed by industry professionals and government in order to improve quality, safety, foster innovation and reduce environmental degradation.

In March 2001 and March 2002 the government, through the Planning Department, Buildings Department and the Land's Department, issued Joint Practice Notes No.1 and No.2 respectively. The practice notes aim to encourage construction professionals to adopt principles of design that lead to more liveable space in residential developments. Balconies for apartments, larger lifts and lift lobby areas, the introduction of sky gardens, natural ventilation of apartments and the use of prefabricated construction elements are all featured in the practice notes. The practice notes offer various incentives in the form of gross floor area (GFA) concessions to encourage developers to incorporate the features.

Non-government organisations (NGOs) also have a role to play. Traditionally, NGOs have taken a critical stance from outside of industry. More recently, however, NGOs are becoming involved with industry. In Hong Kong the non-profit making NGO BEC (Business Environment Council) administers the HK-BEAM (Hong Kong Building Environmental Assessment Method) scheme. This voluntary scheme rewards environmentally responsible design, construction and operation of buildings. Covering global, local and indoor issues the scheme awards credits based on exceeding legislative requirements for buildings. Depending on the number of credits achieved a building can gain a rating of fair, good, very good or excellent. While the scheme is currently voluntary, it is gathering momentum and many developers now require their buildings to be assessed. This clearly demonstrates that the construction industry is beginning to place value on environmentally responsible behaviour.

CASE STUDY - PUBLIC HOUSING DEVELOPMENT, HONG KONG

Introduction

This section presents a case study of a residential development in Hong Kong, which is planned to incorporate many of the initiatives discussed. The innovative use of architecture in the context of Hong Kong housing has led to a hierarchy of space aimed at creating a more liveable environment for the residents of the development. This has been further enhanced through the incorporation of the government GFA incentives. Innovative engineering has been incorporated into the design process in order to improve resource use efficiency, reduce waste generation and improve energy use efficiency. The entire design process has been conducted in an open manner, drawing on the expertise of the many different stakeholders and professional disciplines required to bring a project of this nature to fruition.

In Autumn 2000 the Hong Kong Housing Authority invited entries for a two stage architectural competition. The aim of the competition was to promote an environmentally responsible approach to the production of subsidised housing in Hong Kong. The Shui Chuen O Home Ownership Scheme development was chosen for the competition. Hong Kong based architect Tom Ip and Partners won the competition and design commenced in March 2001. The Shui Chuen O development will provide 2500 units in 7 domestic tower blocks with associated car parking, landscaping and non-domestic facilities. In keeping with the environmentally responsible theme of the competition the winning scheme incorporates many innovative architectural and engineering features, which continue the drive toward sustainable development.

Architecture

The architecture of the Shui Chuen O residential project develops a hierarchy of space, which seeks to create a living environment where residents can feel a sense of community. The layout of the spaces focuses around three main plazas that are ecologically themed with a high degree of variety in the landscaping and provides barrier free community space for all residents to enjoy. The main public entrance plaza (Sun Plaza) leads to the two semi-public plazas (Forest and Water) and onto covered bridges linking to the domestic entrance lobbies of each individual tower block. The edges of the plazas clearly define the pedestrian system and covered walkways running around the perimeter and interconnect to the semi-private spaces that offer a diversity of outdoor amenities while encouraging communication and leisure activities.



Figure 1 Proposed Home Ownership Scheme public housing development at Shui Chuen 0, Shatin.

The scheme incorporates sky gardens, balconies, urban-windows and integrates innovative architecture and engineering in an holistic manner which epitomises many of the principles of sustainable development.

The seven domestic blocks are arranged in an intelligent tri-modular form, which maximizes the view potential of the development and follows the natural topography of the site. A "Green Core" is positioned at the centre of each block, while the centre of each of the three wings contains a "Social Hub" linking the four apartments in each wing. Accessed directly from the lift lobby through a straight but short corridor, the hub spaces provide a departure from the conventional corridor approach to unit entrances with direct visual contact with the lift lobby. The green core contains the lifts and main service arteries for each block and is arranged such that every third level is a full floor with two levels of mezzanine above before another full floor is reached. These lofty, environmentally conscious and naturalistic spaces are enhanced by natural ventilation, day light and greenery and create a sense of neighbourhood within the blocks, which would otherwise become simply an access to a dwelling.

The development takes full advantage of the plot ratio and GFA incentives recently promoted by the Hong Kong Government. Additional social space, aimed at enhancing the neighbourhood concept, is provided in the form of the "Urban Window", the "Green Sky Walk" and "Sky Garden". The sky walks and gardens are located at the 18th Floor and on the roof of each block and are accessible to all residents of the tower blocks. The urban windows add interest to the architectural elevation and break up the visual impact of the development, providing visual cues to the mountain landscape beyond. Every apartment has a private balcony leading from the main living area. The balconies not only provide a high quality indoor environment but they also play a crucial role in improving the acoustic properties of the development, in particular attenuation of traffic noise from adjacent roads.

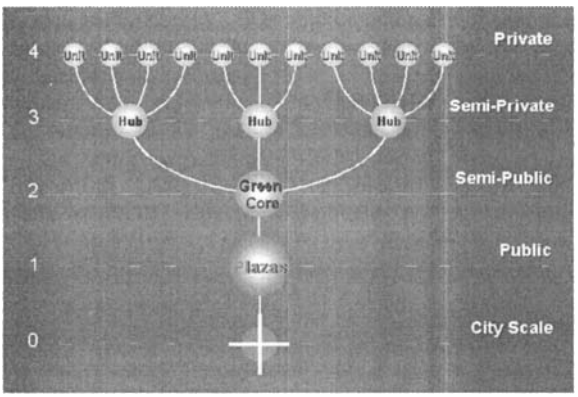


Figure 2 Spatial planning of the Shui Chuen O. Public Housing Project.

The diagram illustrates how the spatial planning hierarchy is conceptualised. Residents travel from the City Scale, urban space though the Public spaces and ultimately into the Private spaces.

Engineering

The engineering design for the Shui Chuen O development has proceeded in parallel with the architectural design. This approach has, as far as possible, allowed the engineering to "inform" the architecture, a process that has proceeded on two fronts. First a series of site specific engineering studies have been undertaken which have influenced the architectural planning. These studies have assisted in realising a design that has the potential to work in harmony with, rather than create a barrier against, the environment. Included are: natural ventilation and natural lighting studies which focus on reducing energy consumption; a traffic and acoustic study aimed at assisting with the architectural planning and arrangement of the domestic blocks; and an environmental wind study to assist in the development of a landscaping scheme that optimises human comfort in the common external areas. Second, engineering systems have been developed, which have the potential to increase efficiencies in resource use, energy use and waste handling. These include: an efficient structural system developed using innovative wind engineering and advanced structural optimisation techniques; the use of architectural precast concrete to capitalise on the dual function of material as structure and architectural finish; a photovoltaic system for the on-site generation of electrical power; a grey water recycling system for cleansing and irrigating common areas; and an automated refuse system to facilitate more efficient and hygienic refuse collection.

Engineering Studies

Natural Ventilation Study

In order to reduce the energy consumption of the development's mechanical ventilation systems, extensive use of natural ventilation has been promoted for the apartment units. Computational fluid dynamic analysis techniques were used to evaluate the innovative architectural design and recommendations made for areas where adjustments could be made to improve the natural ventilation characteristics of the development. Architectural features incorporated to improve the natural

ventilation of the common areas include the ventilated hubs, sky-walks and urban windows. The inclusion of wind wing walls and strategic positioning of operable windows will encourage natural ventilation within apartment units.

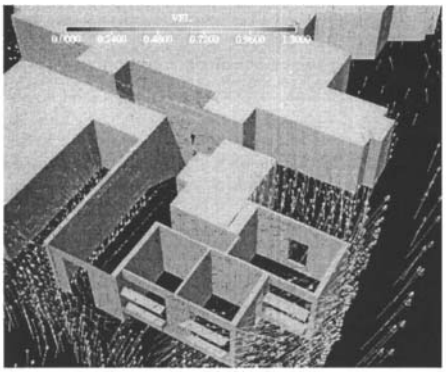


Figure 3. Natural Ventilation CFD Analysis

Natural ventilation is one of the most effective methods for reducing building energy consumption and the build up of indoor air pollutants. Computational Fluid Dynamics modelling has been used to analyse the effectiveness of natural ventilation within the development. By evaluating the specific architectural design and the meteorological condition, environmental benefits of the naturally ventilated indoor environment can be realised.

Natural Light Study

A computer modelling technique was employed to simulate the natural light penetration/reflection into each apartment unit. This process was able to inform the architecture in terms of window location and development of the detail of the facade to achieve optimum natural light performance in the context of other architectural constraints. Through these studies, it was possible to demonstrate compliance with the highest requirements of the sustainability tool HK Beam.

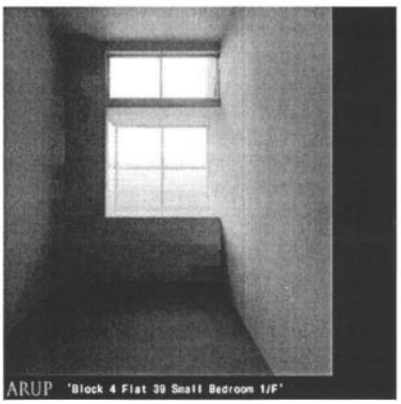


Figure 4. Radiance daylight simulation

Daylight is an energy efficient means of enabling appropriate room function. The requirements of HK-BEAM are set as the target for performance and by undertaking a daylight simulation daylight penetration within the rooms has been assessed. The daylight simulation is also used to access visual comfort and lumen distribution assisting in window and artificial lighting design.

Traffic Noise Study

The need for noise barriers around the development has been eliminated. This has been made possible through the close coordination of the environmental engineering, traffic engineering and architectural disciplines. By studying traffic flow data within the vicinity of the development it has been possible to determine those noise sensitive receivers that would be adversely affected by traffic noise. The arrangement of the affected apartments has been reviewed and adjustments made to the planning to reduce noise impact. Through the incorporation of balconies and bay windows into the noise impact assessment analysis it has been demonstrated that no apartment will experience noise levels in excess of 70dB(A).

Environmental Wind Comfort Study

The success of the outdoor areas of any residential development is in part dependent on the level of comfort associated with the wind environment. An environmental wind climate investigation demonstrated that pedestrian safety is maintained throughout the development. In addition to the safety criteria it has been possible to demonstrate that wind comfort levels appropriate to the activities to which the various areas are intended can be met. In those areas where wind comfort levels are not satisfactory, the environmental wind tunnel testing has furnished data allowing the location, form and function of the architecture and landscaping to be adjusted such that appropriate comfort levels can be achieved.

Engineering Systems

Structural Optimisation

Structural optimisation is an essential process in the design of building structures. The concept is not new, as structural engineers have traditionally sought to make the most efficient use of structural materials. The Shui Chuen O project has made use of advances in engineering technology to realise significant benefits in the efficiency of resource use. The use of computer aided structural optimisation and advanced wind engineering techniques have been instrumental in the realisation of these benefits.

The effects of local wind climate were established by testing a small-scale model of the surrounding topography in a wind tunnel. The data from this topographical test were then matched with a larger scale model of the buildings which was subsequently tested using an innovative multiple force balance technique to determine the wind loads to be used in the structural design. The wind loads predicted from the wind engineering study were found to be less than those predicted from a prescriptive code approach.

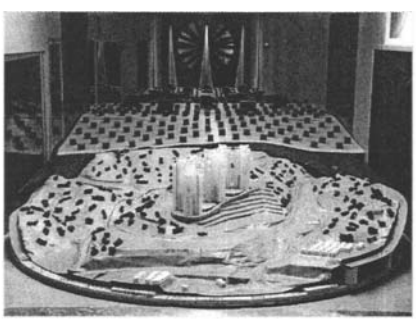


Figure 5. 1:400 scale model in wind tunnel.

The most common method of predicting structural wind loads is the high frequency force balance technique (HFFB). The testing of the Shui Chuen O model involved the simultaneous use of multiple HFFBs to measure loads and load distributions on the linked towers.

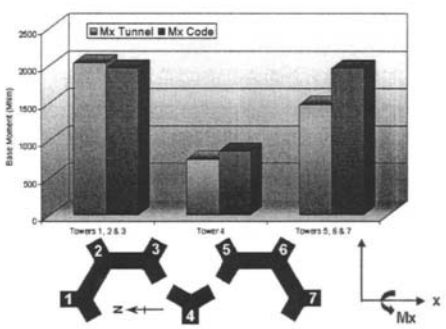


Figure 6. Comparison of wind tunnel test and code results.

The towers of the Shui Chuen O development are architecturally similar. However, due to topography and shielding they each experience different wind loads. Although there were some local increases in wind load compared with the code significant overall savings were achieved.

The loading derived from the wind tunnel testing was used to develop the structural design. Using computer aided structural optimisation technology the contribution of each element of the building to the overall stiffness of the structure is identified. Advanced algorithms determine the amount of structural material that can be redistributed such that the more efficient elements are increased in size while the less efficient elements are reduced. This optimisation process is controlled by a set of input parameters, which in the case of the Shui Chuen O project was based on structural material cost and value of useable floor space.

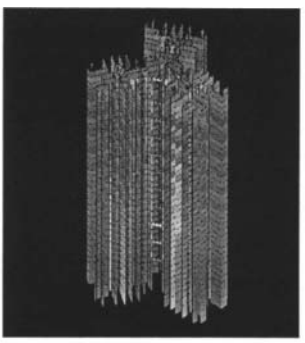


Figure 7. Identification of efficient elements

The relative cost efficiency of one of the towers of the Shui Chuen O development is illustrated graphically with the "hotter", lighter colours representing elements of higher efficiency and the "cooler", darker colours representing the less efficient elements.

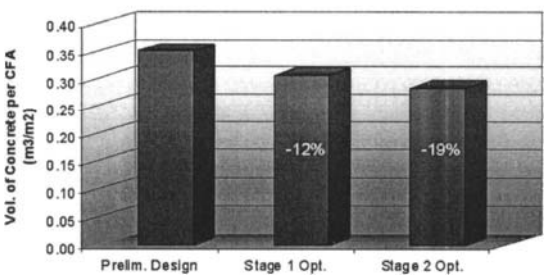


Figure 8. Savings in concrete volume through the optimisation process.

The process involves an initial preliminary optimisation based on code determined wind loads followed by a second optimisation using the wind loads generated by the wind tunnel testing. Significant savings in concrete volume have been realised.

The structural optimisation process has improved the cost efficiency of the structure while maintaining the overall structural performance (Horsfield etal, 2002). The potential value and environmental significance of these design processes is well illustrated through examination of the Hong Kong residential sector. In 1999 some 86,500 residential units were completed in Hong Kong (Hong Kong Housing Authority, 2001), with the primary construction material being reinforced concrete. If a 10% reduction in the use of these materials could be achieved, this would equate to the structural component of 25 no. 35 storey towers. The total volume of structural material in these towers would be approximately 700,000 tonnes. If one considers that construction today is a waste disposal problem of the future then initiatives that reduce construction material stored in current building stock should be encouraged.

Precast Facades

The Shui Chuen O project will adopt architectural precast facades. These façade units are prefabricated under factory conditions and delivered to site ready for immediate installation into the permanent works. The façade finish is achieved through the use of pigmented concrete and the application of specific surface treatments, which include acid etching a colourless surface sealant. This solution is particularly efficient in terms of material use as the structural substrate of the façade

performs the dual functions of structure and aesthetics. More significantly the need for finishing tiles is eliminated.

The elimination of traditional tiled finishes offers significant benefits in terms of future maintenance. A typical future maintenance regime for a building utilising tiled facades would include the need for local replacement of tiles that become de-bonded. There are also issues of safety as de-bonded tiles fall from building facades. Therefore, in addition to material use efficiency, and the potential to reduce capital costs, a life cycle cost approach yields additional benefits through the potential for reduced maintenance costs during operation.

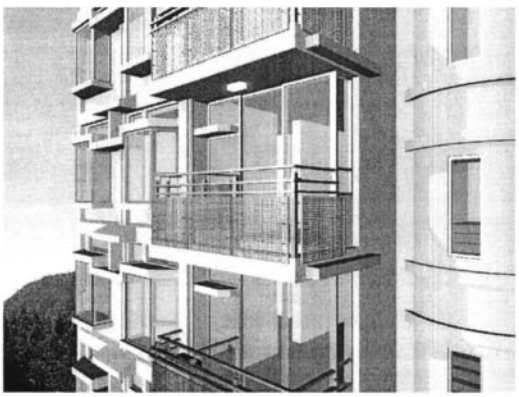


Figure 9. Precast façade.

Economic and environmental benefits derived through the efficient use of construction material

The structural concrete performs a dual role in providing strength and stiffness of the panel and the architectural finish.

A life cycle cost approach yields added benefits in terms of future maintenance effort.

Photovoltaic System

The most abundant form of energy on Earth is Solar energy from the Sun. While this source of energy is freely available it has also been traditionally difficult to collect in sufficient quantity to be of any commercial use. However, improvements in solar collector technology are beginning to have an impact on the power generation sector and commercially viable formats are now available. The Shui Chuen O development will to incorporate a system of photovoltaic (PV) cells to generate a portion of the electricity required for communal lighting within the green core areas. The PV cells are made almost entirely of silicon, which is one of the most abundant elements on Earth. The PV cells convert short-wave radiation from the sun into electricity in a thin layer of semiconductor material. By linking many PV cells together sufficient energy can be "harvested" to generate useful power.

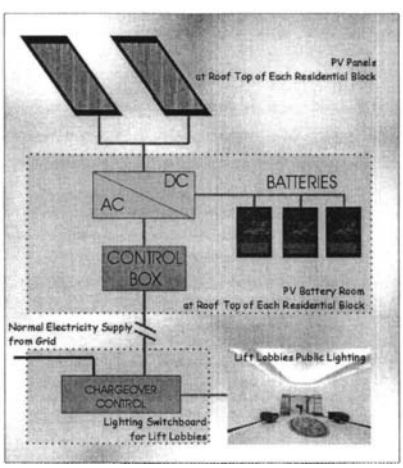


Figure 10. Schematic of the proposed photovoltaic system

Photovoltaic (PV) panels mounted at the roof level allowing greatest exposure to sunlight. Energy generated during the day is used to charge storage batteries for night-time discharge to power feature lighting within the Green Core.

The Shui Chuen O project will accommodate arrays of PV cells on the roof of each domestic block. The power generated from these arrays will run the communal, feature lighting within the green core of the lower 8 stories of each block.

The environmental benefits associated with implementation of the PV system are primarily associated with reduced emissions of so-called "green house" gases associated with more traditional methods of power generation. Such gases may contribute to global warming and climate change. Added benefits arise from the promotion of renewable energy systems, which foster further advancement of the associated technology and improvements in the economic viability of such systems.

Grey Water Recycling System

Estimates of the amount of fresh water available on Earth for human consumption range from 3 to 10 times current consumption levels (Tietenberg, 2002). These estimates combined with a world with expanding population and an uneven distribution of available water highlights the need to treat freshwater as a scarce resource and conserve its use where possible.

In order to reduce fresh water consumption the Shui Chuen O development will utilise a grey water recycling system. This system will collect and recycle grey water from baths, showers and wash basins from domestic bathrooms and utilise it for cleansing and irrigation purposes. It has been calculated that the grey water collected from all of the bathrooms of one block of the development will provide sufficient water to meet the entire development irrigation requirements for podium landscaping and all of the cleansing demand for the non-domestic areas at and below podium.

Water quality is a principle concern in the development of a water recycling facility. In Hong Kong there are currently no Government standards or codes of practice regulating the recycling of waste water from buildings. Water recycling regulations have, however, been developed in China and in some states in the USA. Regulations are based on the expected degree of human contact with and the intended use of the recycled water. The water quality levels adopted for the Shui Chuen O development exceed those recommended in the Chinese Standard GJ 25.1-89 (National Standard of the People's Republic of China, 1989).

Automated Refuse Collection System

The hygienic disposal of municipal waste is a common problem in modern living. This problem is magnified in the case of a high density, city development such as Shui Chuen O. To minimise the problem of odour and to create a controlled, low maintenance environment for the disposal of municipal waste an Automated Refuse Collection System will be implemented in the development. The system comprises a single refuse chute in each block with inlet doors on each floor. An underground network of pipes connects each building to a central collection station where refuse is compacted and stored in sealed containers. Residents dispose of refuse at a chute at each level of the residential block from where it is transferred to the central processing station via the underground pipe network controlled by a vacuum system. Therefore, once placed in the chute refuse is contained in a sealed environment for removal from site.

CONCLUSIONS

This paper has set out to illustrate some of the innovations that are being implemented in Public Housing developments in Hong Kong. Emphasis is also placed on the importance of adopting a multidisciplinary approach toward this kind of development. This is by no means a new idea, indeed project collaboration has been around for as long as projects. However, this paper has examined the role that government can play in encouraging and empowering the private sector to make more

environmentally responsible decisions in the development process. The paper has also examined how non-government organisations can exert pressure on industry to effect changes that contribute to this process. Finally this paper has presented a case study which illustrates the response of the construction industry to these pressures. The result is clearly a move in the direction of a more innovative and ultimately more sustainable construction industry.

ACKNOWLEDGEMENTS

The authors wish to give special thanks to Hong Kong Housing Authority and Tom Ip and Partners Architects for supporting the use of the innovative engineering technologies on the Shui Chuen O project. Also thanks to Man-Wah Chui of Ove Arup and Partners Hong Kong Ltd knowledge centre for assisting with data research and thanks to CM Chan of Hong Kong University of Science and Technology and Roy Denoon of Ove Arup and Partners Hong Ltd for their technical contribution.

References

Carley, M and Christie I (2000), *Managing Sustainable Development,* London, Earthscan.

EMSD (2001), *Hong Kong Energy End – use Data*, EMSD.

EPD (2002), Waste Reduction Guidelines. Retrieved 20th March 2002, from http://www.info.gov.hk/epd /waste/cdm/en_problem1.html

Hong Kong Government (2002), *Statistical table on Gross Domestic Product by economic activity.* Retrieved 20th March 2002, from http://www.info.gov.hk/censtatd/eng/hkstat/fas/nat_account/gdp

Hong Kong Housing Authority (2001). Stock of Permanent Residential Flats. Retrieved 19 December, 2001, from http://www/info.gov.hk/hd/eng/hd/stat_00/stock_f.htm

Horsfield, JN, Denoon, RO, Chan, CM, Gibbons, C (2002), Innovative Engineering, and its Contribution to Sustainable Development, *Proc. Innovative Building Symposium,* 37-48.

Mol, A P J (1997), Ecological Modernisation: industrial transformations and environmental reform, *The International Handbook of Environmental Sociology*, Cheltenham, Edward Elgar, 138-149.

National Standard of the People's Republic of China. GJ25.1-89: 生活雑用水水質標準 (Specification for Grey Water). National Standard of the People's Republic of China, 1989.

Tietenberg, TH (2000), *Environment and Natural Resource Economics*, New York, Addison Wesley.

Advances in Building Technology, Volume 2
M. Anson, J.M. Ko and E.S.S. Lam (Eds.)
© 2002 Elsevier Science Ltd. All rights reserved

Life-Cycle Analysis and Environmental Impact Assessment of Heating and Air-Conditioning Systems

M. Prek

University of Ljubljana, Faculty of Mechanical Engineering,
Askerceva 6, SI-1000 Ljubljana, Slovenia

ABSTRACT

During the design process of heating and air conditioning systems, the designer must analyse various factors in order to determine the best design options. Therefore, the environmental aspects of a product should be included in the analysis and selection of design options if an environmentally - aware design is to be produced. If one wishes to assess a product's environmental impact, its whole life cycle must be studied. The Life Cycle Assessment (or LCA) methodology is an example of one kind of environmental analysis which included the entire life-cycle of a product. However, this method has some limitations. It is unable to tackle the total environmental impact on a number of different levels (e.g. materials, energy, waste) at the same time. To overcome some problems in the LCA method, an alternative method, the so-called Eco-Indicator method has been proposed. Since it is based on a weighting method, only a single score for the total environmental impact is calculated. The application of this method for the optimisation of heating and air-conditioning systems is presented in this paper.

KEYWORDS

Environmental management, Environmental impact, Weighting method, Heating, Heating system, Air-conditioning, LCA method

INTRODUCTION

Life Cycle Assessment (LCA) is defined by ISO 14 series standards, e.g. ISO 14040 (1997), ISO 14041 (1998). They do not, however, give all the necessary information required for carrying out an LCA. The main phases of LCA are goal and scope definition, inventory, impact assessment and interpretation. The various applications of LCA are not regulated by the standard. The implementation of environmental assessment tools is complicated at all levels. It must, nevertheless, be an essential part of all the process, since every product impacts on the environment to some extent. Raw materials have to be extracted, the product has to be manufactured, distributed and packaged and ultimately it

must be disposed of. If we wish to assess a product's environmental impact, all its life cycle phases must therefore be studied; a life cycle assessment can be used in two ways:

1. To determine the total environmental impact of products or design alternatives with the aim of comparing them. For a designer an LCA can provide a solution if he has to choose between design alternatives or between different components or materials
2. To determine the most important causes of one product's environmental impact and a designer can then concentrate on these to achieve improvements here first.

A designer using a LCA in the design process has been faced by two major problems. The result of LCA is difficult to interpret. Within a life cycle assessment it is possible to determine the contribution of a product life cycle to the greenhouse effect, acidification and other environmental problems, while the total environmental impact remains unknown. The reason is the lack of mutual weighting of the environmental effects. In general, the careful collection of all the environmental data in a product's life cycle is complex and time-consuming. As a result extensive LCA usually cannot be carried out during a design process. Life Cycle Cost (LCC) calculations are an application of investment calculations which have been used in planning and design of products. These calculations are used as a routine for equipment comparison. It enables the purchase price and an estimate of the present value of the life cycle operating costs. In LCA calculations the present value of total costs (investment and operation) is calculated. In this case, the equation is as follows from ISO/DIS 14042 (1998):

$$\text{LCC(total)} = \text{Investment} + \text{Energy cost} + \text{Maintenance cost} + \text{Disposal cost} \tag{1}$$

LCC calculations are based on an equation of present values. Depending on the case, the calculations can be sensitive to the interest rate and the time of the calculation period (utilisation time or the life cycle of the device). In order to be able to optimise environmental performance, we need to weight different impacts to a common number. In LCA terminology, this is called weighting. In order to make weighting possible, we need to express environmental impacts via indicators that can be compared to some reference or valued. These indicators are called impact category indicators and may be chosen early or late in a cause-effect chain, but existing weighting methods today either use emissions or transformed emissions and compare with emission goals or use monetary valuation of damages. The Eco-indicator method, introduced by Goedekoop (1993) has resolved these problems as follows. The LCA method has been expanded to include a weighting method. This has enabled one single score to be calculated for the total environmental impact based on the calculated effects, as is shown by Goedekoop et al. (1993). During the development of the weighting method for the Eco-indicator much attention was given to defining the environmental impact. Into the account are taken the following environmental effects, as shown in Figure 1. The problem lies in determining the weighting factors. In this method, the so-called Distance-to-Target principle was chosen. This principle has been in use for some years in the Swiss Ecopoints weighting system Kortman et al. (1994). The procedure for determining the indicator value I can be expressed by the following equation:

$$I = \sum_i W_i \cdot \frac{E_i}{T_i} \tag{2}$$

where is W_i subjective weighting factor which expresses the seriousness of effect i, E_i is the contribution of the product life cycle to an effect i_i and T_i target value for effect i. In more general terms, the effect of a number of impacts can be written as:

$$I = D_k \cdot \sum_i \frac{E_i}{T_i} \tag{3}$$

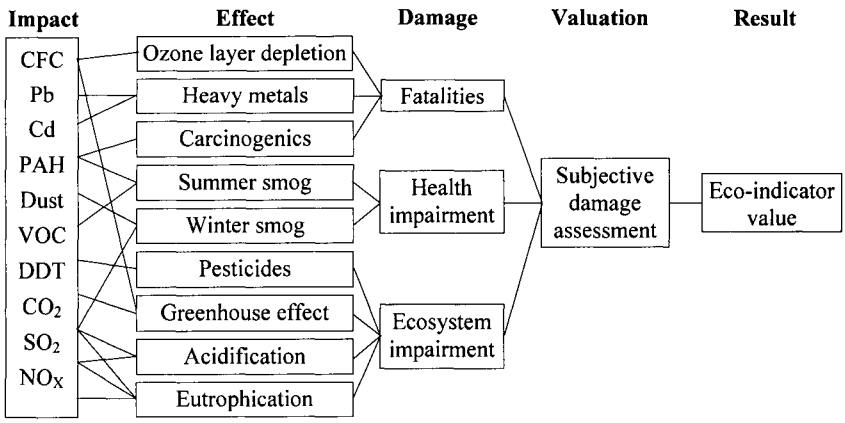


Figure 1: Eco-indicator weighting principle

In order to assess the overall impacts of trade-offs, the relative importance of various environmental problems must be determined. Following are criteria recommended to develop a weighted set of environmental problems, given in Table 1.

TABLE 1
WEIGHTING FACTORS FOR ENVIRONMENTAL EFFECTS

Environmental effect	Weighting factor	Criteria
Greenhouse effect	2,5	0,1 °C rise every 10 years, 5% ecosystem degradation
Ozone layer depletion	100	Probability of 1 fatality per year per million inhabitants
Acidification	10	5% ecosystem degradation
Eutrophication	5	Rivers and lakes, degradation of an unknown number of aquatic ecosystems (5% degradation)
Summer smog	2,5	Occurrence of smog periods, health complaints, particularly among asthma patients and the elderly, prevention of agricultural damage
Winter smog	5	Occurrence of smog periods, health complaints, particularly among asthma patients and elderly
Pesticides	25	5% ecosystem degradation
Airborne heavy metals	5	Lead content in children's blood, reduced life expectancy and learning performance in an unknown number of people
Waterborne heavy metals	5	Cadmium content in rivers, ultimately also impacts on people
Carcinogenic substances	10	Probability of 1 fatality per year per million people

The target level still embodies a major problem - what is a good target level and how can such a level be defined? To ensure that the target level is equivalent for different effects, a correlation must be established with the damage caused by the effect. The premise is that the target level for each effect yields uniformly serious damage. The following damage levels are assumed to be equivalent as defined by Goedekoop et al. (1993):

- the number of fatalities as a consequence of environmental effects (as acceptable, the chosen level is 1 fatality per million inhabitants per year)
- the number of people who become ill as a consequence of environmental effects. This refers in particular in winter and summer smog. (the acceptable level is that smog periods should hardly ever occur again).
- ecosystem degradation (a target level has been chosen at which only 5% ecosystem degradation will still occur over several decades).

To establish a correlation between damage levels and the effects, a detailed study was carried out of the actual state of the environmental in Europe. These data, given by Kortman et al. (1994) were used to determine the current level of an environmental problem and by what factor the problem must be reduced to reach an acceptable level. Table 1 lists the weighting factors and criteria applied. This table reveals that high priority must be given to limiting substances causing ozone layer damage and the use of pesticides. Furthermore, a great deal of consideration must be given to the diffusion of acidifying and carcinogenic substances.

There can be little doubt that buildings are important contributors to environmental deterioration. Buildings contribute 15% to 45% of the total environmental burden for each of the eight major LCA inventory categories. In any design, trade-offs must be made among solutions aimed to optimise building performance for various objectives. Environmental objectives are diverse, complex, interconnected, and frequently conflicted. Decision-making tools such as multiple attribute decision analysis can assist designers and their clients resolve conflicting project goals that normally are part of any project. Systematic analysis based on empirical data has provided the tools necessary for designers and other decision-makers to evaluate the trade-offs they must make between environmentally-friendly building features.

CASE STUDY

The purpose of the calculation is to establish priorities, or in other words - where can the designer best to achieve the greatest possible environmental profit? In the first instance it is possible to make fairly rough calculations and simplifications are permissible. In a life cycle perspective there is an optimum, where the incremental increase of impact from environmental performance and from equipment construction demands equals the incremental decrease of impacts from increasing efficiency – see Figure 2.

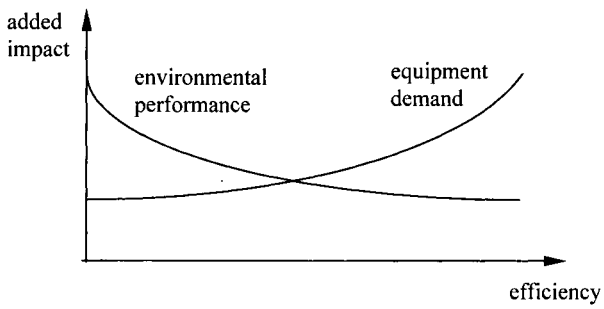


Figure 2: Optimisation of environmental performance of heating and air conditioning systems

Figure 3 shows ground plan of one building floor for heating or air conditioning system. In continuation of article it is shown the comparison between three different heating systems. For all these three different heating systems we took the same building floor for case study. Hence this the required heating/cooling power (11,8 kW) is the same for all heating systems.

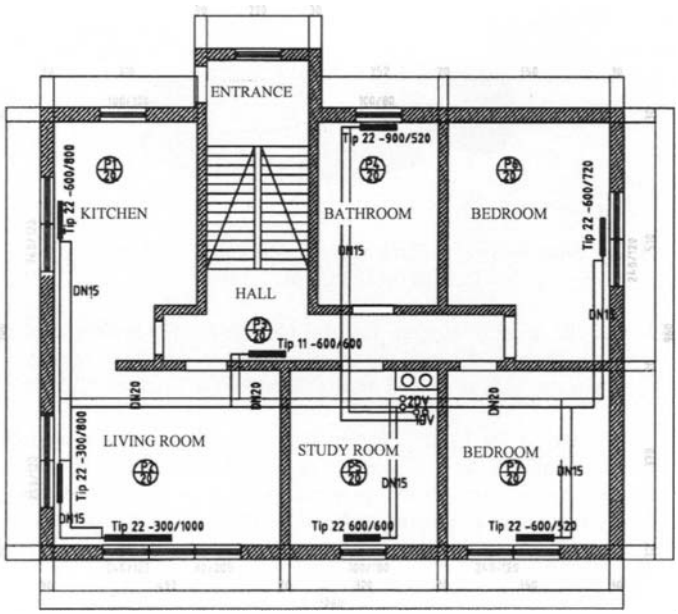


Figure 3: Simplified ground plan of one building floor for heating or air conditioning system

A simplified life cycle of heating or/and air-conditioning systems is given in Figure 4. Such a process tree provides a useful insight in further analysis.

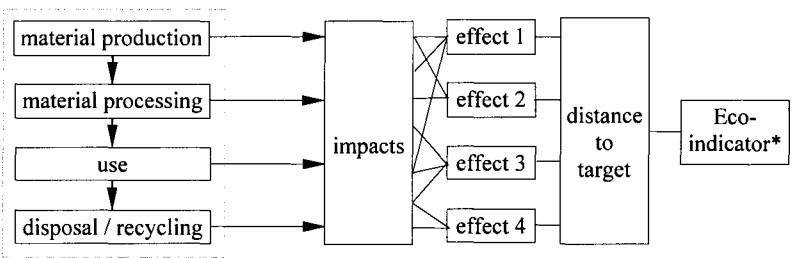


Figure 4: Example of simplified life cycle for heating and air conditioning system. The use phase determines the overall functional unit of a product. *The result is given in milli Eco-indicator point (mPt)

Radiator heating

In the case of radiator heating system, two different systems are analysed. The main difference was the chosen material for piping system (steel/copper) and for radiators – heating panels (steel/aluminium).

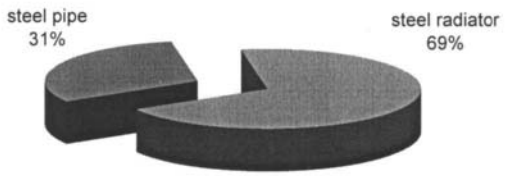


Figure 5: Eco-indicator value for steel radiator heating; pipe length 78,4 m, material for radiator 0,927 Pt, pipe 0,412 Pt, total 1,339 Pt

In Figure 5 is presented the result of analysis for steel radiator heating system with steel pipes, made by Eco-indicator method. The results reveal the great importance of radiator (greater mass of radiator than pipes) which presents the 70 % of overall impact. Total Eco-indicator is 1,339 Pt.

The results of similar analysis for heating system with aluminium radiators and copper pipes (as alternative) are shown in Figure 6. As it is seen in Figure 6, the copper pipes for aluminium radiator heating are dominant among the materials for environmental impact. Copper pipes represents 56 % of overall impact for the given example, despite smaller dimensions. Total Eco-indicator is 4,0 Pt, and is much more as for the steel system.

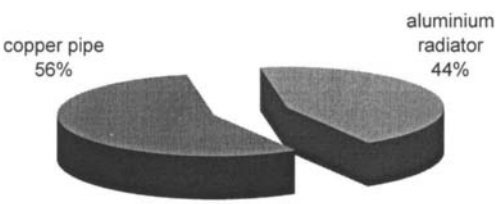


Figure 6: Eco-indicator value for aluminium radiator heating; pipe length 78,4 m, material for radiator 1,774 Pt, pipe 2,234 Pt, total 4,0 Pt

Floor heating

Eco-indicator value for polyethylene pipes, dimension 14×2, is 0,089 Pt and for polybutene pipes, dimension 16×2,2, is 0,111 Pt. Pipe length was 291 m and was the same for both systems. Difference was only in pipe material, while all other parameter were the same. While the heating demand is the same regardless the heating system, analysis results are comparable to other systems, since they are expressed in the form of Eco-indicator points. Smaller (better) eco-value for floor heating system is also the consequence of the fact that the extra building construction was not considered.

Fan coil convector

For the analysis, the exposed floor fan coil convector unit was chosen with average parts (valves, fittings etc). The base unit is made of 1,0 mm thick galvanized steel plate. Cold panels are insulated. The fan section is composed of a cross-flow tangential fan and special air discharge sections that ensures a uniform distribution of the airflow. The three-speed motor is mounted on flexible supports. Cabinet is made in five separate pieces, a front panel in 1 mm thick galvanized steel and painted with a durable baked polyester powder coating. Pipe coil is a copper tube and lanced aluminium fin construction. The convectors were chosen in accordance with heating power. The convectors are substitute for radiators, as is shown in Figure 3. For piping system, one could assume the same conditions as for the radiator heating system. Since the fan coil unit consists from various parts, we could determine the Eco-value for different part. In Figure 7 is shown the Eco-indicator value for different materials and in Figure 8 for different parts. From these figures the influence of different materials in different parts of unit is obvious.

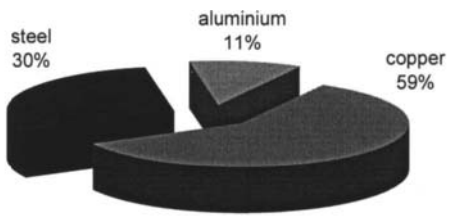


Figure 7: Eco-indicator value for fan coils (convector heating / cooling), by materials, total 3,126 Pt

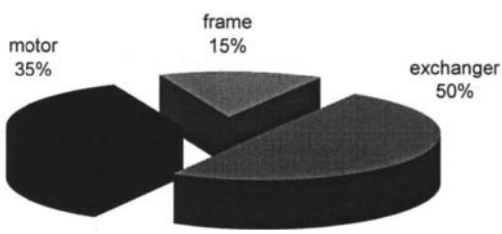


Figure 8: Eco-indicator value for fan coils (convector heating / cooling), by elements

In Figure 8 is presented the result of analysis for fan coil units. Heat exchanger is made of aluminium plates and copper pipes, which contributes the greater Eco-indicator (50 % of the whole unit). Total Eco-indicator is 3,126 Pt.

CONCLUSIONS

The Eco-indicator method has been used for the analysis and optimisation of heating and air conditioning systems. This method enables environmentally-aware design and is open working method with a platform on which both industry and science can integrate the environmental aspects into the design process. These design alternatives can be calculated in the same way with this method. The result permits the user or the designer to see how much environmental impact of these design alternatives will have. The designer can analyse the consequences of an idea quickly and effectively and establish clear selection criteria for an idea.

Prerequisites for a fair comparison of environmental characteristics of different heating and air conditioning systems are that the systems compared are equal and fulfil the functional requirements, the limits of the systems are drawn up by the same principles, technical characteristics and material data of the systems and equipment are reliable, environmental profiles of energies and materials used in the comparison are comparable. The weighting factors, used by the analysis, expresses the relation between an impact and the amount of damage either to human health or ecosystem quality. In used methodology they based on a combination of distance to target and damage function approach. Environmental impacts from production processes of products and materials are taken into account.

This research showed that three different concepts of heating systems with different construction materials varies the Eco-indicator value. We can see that for radiator heating system the Eco-indicator value is far superlative than for floor or fan coil convector heating system. Copper pipes and other copper parts contributes to the greatest environmental impact. Radiator heating Eco-indicator (1,339 Pt – steel pipes and 4,0 Pt – copper pipes) showed three times higher value for copper pipes than for the steel pipes despite smaller dimensions. The lowest values are obtained for floor heating systems, but no extra building construction was considered. Reasonable values are obtained for fan coil units (convector heating/cooling) with Eco-indicator value 3,126 Pt. Analysis show up, that heat exchanger (copper pipes) contributes the main part of the value. Nevertheless, the environmental aspect is only one of the evaluation criteria in addition to cost, aspects of use and standards.

REFERENCES

ISO (1997). Environmental Management - Life Cycle Assessment - Principles and Framework. ISO 14040:1997

ISO (1998). Environmental Management - Life Cycle Assessment - Goal and Scope Definitions and Inventory Analysis. ISO 14041:1998

ISO (1998). Environmental Management - Life Cycle Assessment - Life Cycle Impact Assessment. ISO/DIS 14042:1998

Goedekoop M.J. (1993). *The Eco-indicator 95, Final Report, NOH Report 9523*, Pré Consultants, Amersfoort, Nederland

Goedekoop M.J., Duif G.A.P. and Keijser I.V. (1993). *Eco-indicator, Development decision support tool for product development, NOH Report 9407*, Pré Consultants, Amersfoort, Nederland

Kortman J.G.M., Lindeijer E.W., Sas H. and Sprengers M. (1994). *Towards a single indicator for emissions, an exercise in aggregating environmental effects, Report No. 1994/2*, Ministry of Housing, Spatial Planning and the Environment (VROM), Nederland

Frischknecht R., Hofstetter P. and Knoepfel I. (1994). *Environmental inventories for energy systems*, ETH Zürich

Advances in Building Technology, Volume 2
M. Anson, J.M. Ko and E.S.S. Lam (Eds.)
© 2002 Elsevier Science Ltd. All rights reserved

QUANTITATIVE EVALUATION OF THE EFFECTS OF BUILT-UP GEOMETRY AND TREES ON DIURNAL AIR TEMPERATURE IN CANYON-TYPE COURTYARDS

LIMOR SHASHUA – BAR [1] and MILO E. HOFFMAN [1 2]

[1] Faculty of Architecture and Town Planning
[2] National Building Research Institute
Technion–Israel Institute of Technology, Haifa 32000 , Israel
mhoffman @ techunix.technion.ac.il

ABSTRACT

This paper attempts to place proper emphasis on the role of urban courtyards in passive cooling. The article is a part of a larger study in preparation on the sustainability design of urban streets and courtyards on passive cooling in the urban canopy layer (UCL). The passive design control elements studied are the courtyard's geometry and the density of shade trees. The study presents the case of attached canyon-type courtyards in residential buildings, using summer data in the Tel-Aviv metropolitan area near the Mediterranean sea coast, characterized by hot and humid climate during the summer season. Measurements of air temperature were taken hourly at 9:00, 15:00,and 18:00 h in two courtyards, situated in the same locality in Tel-Aviv. Both courtyards consist of a 20 – 25 meter open space enclosed between two stretches of buildings of about 12 m high. Simulations were conducted for each courtyard, with and without trees, using an analytical model, the "Green CTTC model", developed recently by the authors. The simulations provide quantitative evaluation of a courtyard's diurnal air temperature pattern over the course of 24 hours. The effects of changes in the courtyard's geometry and the density of shade trees were studied by simulations. The simulated values were compared with measurements in situ. The combined cooling effect of the two studied courtyards due to trees and deepening is found to reach 4.5 K at noon out of 9 K rise of air temperature from sunrise to noon in August. The illustrations of the simulations carried out on the two studied courtyards further the importance of sustainability consideration in courtyard designs, and thus show the potentially in AC energy saving. The Green CTTC model applied to urban courtyards provides a practical tool for this purpose.

KEYWORDS

Urban climate , Trees, Vegetation climatic effects, Green CTTC model, Urban courtyard design

1. INTRODUCTION

Open spaces usually cover more than two thirds of the urban area in modern architecture, hence their microclimate dominantely affects the urban canopy layer (UCL) climate. The case study presented here is a part of a study in preparation on the sustainability of different urban typologies on passive cooling. The typology presented in this paper is attached canyon-type courtyards in residential buildings. The control elements in passive design evaluated quantitatively in this study are the thermal effects of the courtyard's geometry and the density of shade trees. The latter is becoming an important issue as private courtyards are in the course of being converted for parking purposes due to urbanization and population growth [Rosenfeld et al. (1995), Wilmers (1988)].

Field observations were conducted in two canyon-type courtyards in Tel-Aviv city near the Mediterranean sea coast. The two courtyards are similar in geometry but slightly differ in tree density. The canyon-type courtyard is an urban open space enclosed between two stretches of buildings. It can be viewed as a connected unit of several typical single outdoor courtyards attached to apartment house buildings. The microclimate in such single courtyards is strongly influenced by background conditions, especially by the conditions prevailing in neighbouring courtyards such as vegetation, built-up geometry and albedo. The canyon-type is chosen here for analytical analysis in order to estimate the impact of design parameters on the microclimate of outdoor open courtyards.

The courtyard's diurnal air temperature pattern is evaluated quantitatively using an analytical model, the "Green CTTC model", developed recently by the authors [Shashua-Bar & Hoffman (2002)]. The model is based on the same principles as the Cluster Thermal Time Constant (CTTC) model, developed formerly by M. E. Hoffman and colleagues [Sharlin & Hoffman (1984), Swaid & Hoffman (1990/1)] and on the CC model - a modified CTTC model for enclosed courtyards [Mosseri (1990), Hoffman & Mosseri et al. (1994)], with additional effects of adjoining walls and shade trees. Simulations were conducted for each courtyard, with and without trees. The simulations provide prediction of air temperature pattern over the course of 24 hours including the diurnal thermal effect of the trees. The simulated cooling effects are compared with actual measurements in situ at 9:00, 15:00 and 18:00 h. In addition, simulations were conducted to assess the thermal effect of deepening the courtyards by raising the building height.

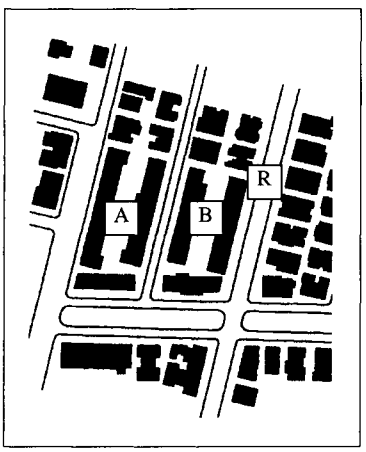
2. SITES AND EXPERIMENTAL DATA ANALYSIS

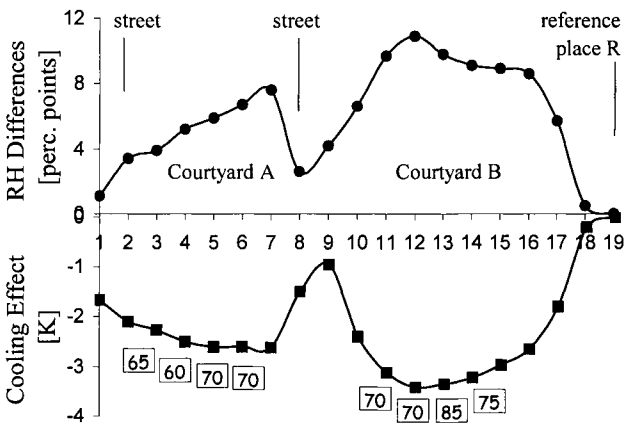
Data used in this paper are taken from a field study [Shashua-Bar & Hoffman (2000)] carried out by the authors on calm days in summer (July-August , 1996) on eleven green sites located in the Tel-Aviv metropolitan area. Two of the studied sites are canyon-type courtyards with trees. The Tel-Aviv metropolitan area is characterized by a hot and humid climate during the summer season with an average air temperature at noon about 29.7 °C and a relative humidity of 65.8%, as recorded in August 1996 at Sde-Dov , a near-by Meteorological station.

Nineteen observation places spaced at about 10 m were chosen along the two sites. Dry and wet bulb temperatures were measured at 9:00, 15:00, and 18:00 h, approximately at the height of 1.80 m. Besides the climatic variables, the partial shaded area (PSA) around each observation place in the site was also determined at 15:00 h (14:10 solar time), the time at which air temperature reaches its maximum in summer in the studied region.

The two courtyards are situated in Tel-Aviv in the same neighbourhood. Both sites consist of a 20-25 meter open space enclosed between two stretches of a 4-floor buildings of about 12 m high. Courtyards A and B are planted with a variety of shade trees of Olives, Poinciana and well-developed Ficus predominating. The PSA in courtyard A is about 66% and in B about 75%. The axis of both sites

are oriented close to North-South. The sites' map is given in Fig. 1, together with the patterns of the maximum cooling and humidity effects at noon.
The cooling effect of trees at each observation place, as determined by measurements in situ, was defined as the difference between the measured air temperature at the site and that at a nearby reference place, outside the site. The reference place was chosen to represent the sites' background microclimate, close to the site (50 to 100 m from it) with no trees. The humidity effect of the trees is evaluated in the same way, as the difference between the humidity (absolute or relative) of the site and that of its reference (op. cit. [Shashua-Bar & Hoffman (2000)]).





A = Courtyard A
B = Courtyard B
R = Reference place
[•] = PSA in %

Location of Observation Points
along Courtyards A and B . 15:00 h

Observation points : courtyard A = 4 , courtyard B = 4
Width of the sites : courtyard A = 20 m , courtyard B = 25 m
Length of the sites : courtyard A = 75 m , courtyard B = 67 m

Figure 1: Site maps, obs. plans and patterns of the maximum cooling effects [K] and humidity differences RH [percentage points] . Data : August 11-13 , 1996 . Time : 15:00 h (14:30-15:30)

In Fig. 1, the patterns of the cooling and relative humidity (RH) effects at 15:00 h indicate significant variations among the observation values. Statistical analysis indicates:

1st)An inverse relationship exists between the cooling and relative humidity effects. The relationship is strong (correlation r = -0.884). For every 1 K cooling, a rise of 3.1 percentage points in the relative humidity is expected at noon (the regression slope b = -3.1) .

2nd) The variation in the cooling effects along the site is explained mainly by the trees shade coverage. The relationship is highly significant (r = 0.830 , b = -3.37).

Daily average cooling and relative humidity effects in the two courtyards during the period of measurements (11-13, August 1996) are summarized in Tables 1 and 2. The air temperature and relative humidity at the reference place represent the daily background values.

At sunrise (6:00 h) and at midnight (24:00 h), no noticeable effects in air temperature and relative humidity were found in eleven green sites in the authors field study (op. cit. [Shashua-Bar & Hoffman (2000)]). The average temperature at sunrise (06:00 h), was 24.7 °C and the relative humidity 84%.

TABLE 1
DAILY AVERAGE COOLING EFFECTS ; [K]
(AVERAGES FOR THE DAYS OF MEASUREMENTS INSIDE THE SITES)

Site	09:00 h	15:00 h	18:00 h
Courtyard A	-1.31	-2.47	-2.29
Courtyard B	-1.78	-3.26	-2.50
Av. Reference Air Temp.[°C]	29.50	33.70	31.70

TABLE 2
DAILY AVERAGE HUMIDITY EFFECTS ; [PERC. POINTS]
(AVERAGES FOR THE DAYS OF MEASUREMENTS INSIDE THE SITES)

Site	09:00 h	15:00 h	18:00 h
Courtyard A	6.1	5.2	10.8
Courtyard B	8.6	10.9	12.7
Av. Reference RH [%]	71.4	69.1	70.3

3. ANALYTICAL ANALYSIS

3.1. *Outline of the Green CTTC model*

The quantitative evaluation of the courtyard's diurnal air temperature is obtained by simulations using the analytical Green CTTC model (op. cit. [Shashua-Bar & Hoffman (2002)]). It is based on the same principles as the Cluster Thermal Time Constant (CTTC) model, developed earlier by M. E. Hoffman and colleagues (op. cit. [Sharlin & Hoffman (1984), Swaid & Hoffman (1990/1), Mosseri (1990)]), with the additional effects of adjoining walls and shade trees.

The CTTC model incorporates design parameters related directly to the physical structure and properties of built-up forms (building density, shade areas, the cluster's open space geometry, etc.). It was validated against observed data gathered in the Mediterranean coastal region of Tel-Aviv [Sharlin & Hoffman (1984), Aizenberg & Hoffman (1992)] and of Jerusalem and Essen in Germany [Swaid & Hoffman (1990/1)].

In the CTTC model, the predicted air temperature of a cluster is calculated through the contribution of the heat received from external sources, mainly net solar radiation and anthropogenic heat-release. The Green CTTC model includes the additional effect of vegetation. Conceptually, the predicting equation of the cluster's air temperature at time t is :

$$T(t) = T_0 + \Delta T_{SOLAR}(t) - \Delta T_{NLWR}(t) - \Delta T_{GREEN}(t) + \Delta T_{AHR}(t) \quad (1)$$

where:

T_0 is the regional base (or background) temperature, which was found to be equal to the mean daily air temperature measured at a representative rural Meteorological station (op. cit. [Swaid & Hoffman (1990/1)]).

$\Delta T_{SOLAR}(t)$ is the contribution of solar radiation (direct and diffused) to air temperature variations.

$\Delta T_{NLWR}(t)$ is the contribution of net outgoing long-wave radiation flux to air cooling.

$\Delta T_{GREEN}(t)$ is the cooling contribution to air temperature by vegetation in the cluster.

$\Delta T_{AHR}(t)$ is the anthropogenic contribution to air temperature including effects of man-made nature such as heat release owing to transportation, fuel consumption for domestic use and so forth.

The thermal effect of shade trees, in $\Delta T_{GREEN}(t)$, is estimated considering the effect of solar radiation penetration and the intensity of evapotranspiration. For well developed Ficus trees, the reduction of insolation by the presence of shade trees was estimated in this study for the summer period to be about 40% of the global solar radiation intensity incident on the tree canopy (op. cit.[Shashua-Bar & Hoffman (2002)]). In other words, complete shade coverage by trees (PSA = 1), would still allow the cluster to receive 60% of the global solar radiation.

3.2. *Estimating the cooling effect of trees*

The Green CTTC model is applied to simulate the diurnal air temperature of the two courtyards, with and without trees, using the cluster's parameter values as follows:
The solar radiation absorptivity, *m*, was 0.7 for ground and 0.5 for walls in both sites.
The overall heat transfer coefficient of surface *h*, which is related to wind velocity, was on the average 12 [W / m^2 K] in both sites.
The Brunt number (effective atmosphere emissivity), Br which is related to vapour pressure and cloudiness of the climatic region was on the average 0.74 for both sites.
The ground surface thermal emissivity , e , was 0.92 for both sites.
Cluster Thermal Time Constant , CTTC [hours], was 8 for ground and 6 for walls, in both sites.
The tree shade coverage represented by the partial shaded area, PSA Tr, was 0.66 for courtyard A and 0.75 for courtyard B.

The simulated diurnal patterns of air temperature for the two studied courtyards, using the Green CTTC model, are shown in Figure 2. In each courtyard, the higher curve indicates the diurnal estimates of air temperature in the absence of trees, and the lower one the values in the presence of trees. The difference of air temperature between the levels of the two curves in each courtyard gives the estimated cooling effect of the trees. The measured air temperature values in situ at 9:00, 15:00 and 18:00 h, are indicated for comparison.

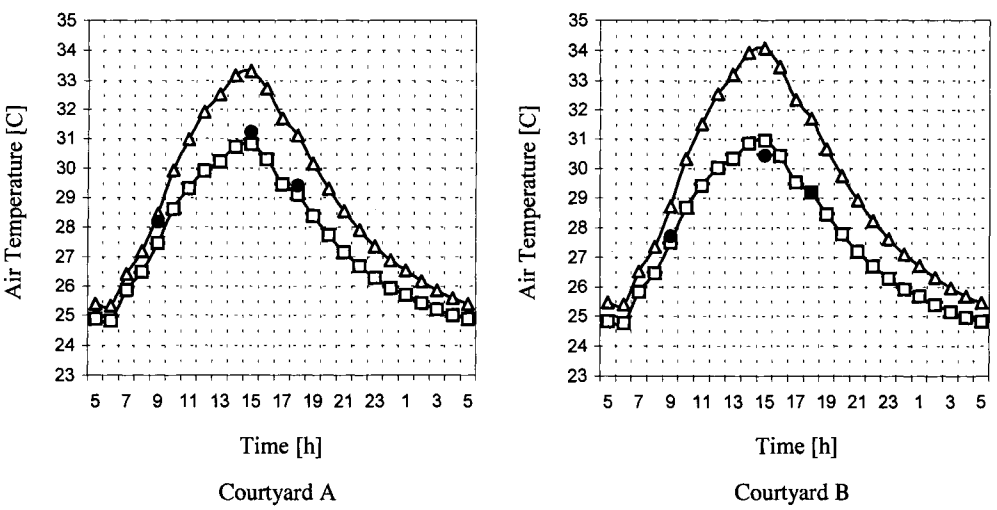


Figure 2 : Simulated patterns and measured in situ values of diurnal air temperature in courtyards A (H / W = 0.60) and B (H / W = 0.48) . Data : 11-13 August 1996
Δ Cluster without trees ◘ Cluster with trees ● Measured values in each courtyard

Table 3 shows the comparison between the measured values of cooling effects by trees and the simulated ones. A close fit was found between the measured and the simulated values. The bias at 15:00 and 18:00 h is less than 0.25 K, and at 9:00 h less than 0.5 K.

TABLE 3
COMPARISON BETWEEN MEASURED AND SIMULATED ESTIMATES OF COOLING EFFECTS ; [K]

Site	09:00 h	15:00 h	18:00 h
Courtyard A			
Measured	-1.31	-2.47	-2.29
Simulated	-0.97	-2.50	-2.00
Courtyard B			
Measured	-1.78	-3.26	-2.50
Simulated	-1.22	-3.12	-2.51

3.3. *Estimating the effect of courtyard deepening*

Vernacular architecture made much use of deep courtyards (high H / W ratio) and narrow open urban spaces to enhance cooling in hot and dry regions. Modern technology and traffic circulation led to reverse this trend. Lately, however, the need for residential housings is leading to high buildings on existing open spaces, thus to deepening but not necessarily on narrow spaces. Municipality ordinance are allowing increase in buildings' height from 3-4 floors to 6-8 floors in several streets in Tel-Aviv. The effect of this deepening process can be evaluated by simulations, using the Green CTTC model.
Figure 3 shows the simulated diurnal air temperature values for the two deepened canyon-type courtyards, by increasing their buildings' height to 20 m, from a 4 floor building to a 6 floor building, leaving the courtyard width unchanged (20-25 m).

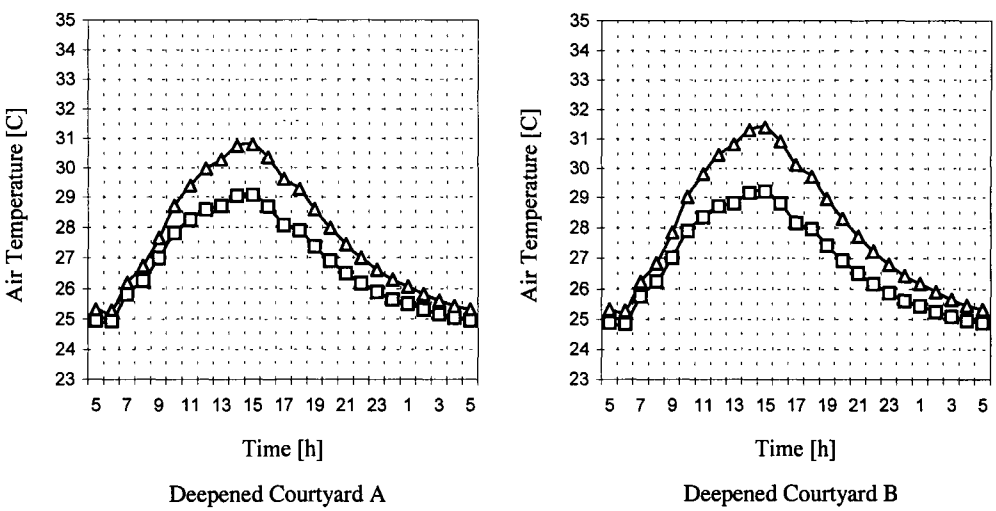


Figure 3 : Simulated patterns of diurnal air temperature in the two deepened courtyards A (H / W = 1.0) and B (H / W = 0.8)
Δ Deepened courtyard without trees ◘ Deepened courtyard with trees

The curves of the deepened two courtyards in Figure 3 show lower temperatures than the corresponding ones in Figure 2. The difference between the levels of the respective curves (actual 12 m height vs 20 m height) gives the cooling effect of deepening the courtyard. Table 5 summarizes these effects at 15:00 h.

The simulated effects in table 4 show that the air temperature lowering due to deepening is stronger in canyon-type courtyards without trees (about 2.6 K) than with trees (about 1.7 K). The effect of trees is also reduced by deepening. The reason is that the cooling effect of vegetation is used to cool a larger volume of air in the deep courtyard than in a shallow one.

TABLE 4

DEEPENING EFFECT [K] IN THE STUDIED COURTYARDS WITH AND WITHOUT TREES . 15:00 h

Site	Courtyard A	Courtyard B
Simulated cooling effect of Deepening		
In courtyard without trees (from H = 12 m to H = 20 m)	-2.51	-2.69
In courtyard with trees (from H = 12 m to H = 20 m)	-1.73	-1.74
Simulated Cooling effect of trees		
In courtyard with actual height (H = 12 m)	-2.50	-3.12
In deepened courtyard with raised height (H = 20 m)	-1.72	-2.18
Total Cooling effect of trees and deepening	-4.23	-4.87

The maximum combined cooling effect at 15:00 h due to trees and deepening in the two types of courtyard is estimated to be about 4.5 K (4.23 K and 4.87 K in courtyards A and B). This level of cooling is impressive considering the fact that the average rise in air temperature, from sunrise to noon, is about 9 K in August, in the hot-humid region of Tel-Aviv. The effect on indoor Air Conditioning (AC) energy saving following 4.5 K lowering of the surrounding air temperature is expected to be significant. Simulations run by Rosenfeld et. al (op. cit. [Rosenfeld et al. (1995)]) on sustainability design of building geometry, widespread use of cool surfaces and vegetation in cities indicate saving of up to 20% of cooling energy.

4. SUMMARY AND CONCLUSIONS

The Green CTTC analytical model, developed recently by the authors is applied to simulate diurnal air temperature patterns in canyon-type courtyards. The design control elements studied are the cooling effect of planted trees and thermal effects of deepening the cluster.
The main findings are:

1. The Green CTTC model is found to be suitable for predicting the air temperature inside an open outdoor canyon-type courtyard. Comparison with daily measurements in situ shows deviations less than 0.5 K.
2. The cooling effect of shade trees in such a courtyard in Tel-Aviv was found to be 3 K at noon, with shade tree coverage (PSA) of 75%. This level of cooling is significant considering the fact that the average rise in air temperature is about 9 K in August in the studied region.
3. Deepening the courtyard by raising the cluster's height lowers its air temperature as expected. The simulated effect of changing the height from 12 m (4 floors) to 20 m (6 floors) produces a cooling effect of about 2.5 K in a courtyard of 20-25 m wide. This effect is significant and even exceeds the cooling effect of trees.

4. The cooling effect of trees depends on the shade coverage (PSA level) as well as on the cluster's geometry. This effect is reduced by deepening the cluster, as the tree cooling energy serves a larger volume of air in a deep cluster than in a shallow one with an equal floor area.
5. The combined cooling effect in canyon-type courtyards due to trees and deepening is found to reach 4.5 K at noon in August. The implication on indoor AC energy savings from a 4.5 K cooling in the surrounding air temperature illustrates the benefits inherent in sustainability design.
6. The Green CTTC model applied to courtyards provide a practical tool for sustainability design in passive cooling through assessing the thermal impacts of various control elements defining the cluster's physical structure, properties of built-up forms and presence of shade trees. In this study, the model was applied, mainly, to assess the thermal impact of trees and of the cluster's deepening.

REFERENCES

1. Aizenberg A. (1992). *Development of climatic urban design guidelines based on the analytical CTTC model for prediction of air temperature variations* . M.Sc. Thesis (in Hebrew, English summary) , Technion , Haifa , Israel .
2. Hoffman M.E. and Mosseri A. and De-Urrutia O. and Wertheim I. (1994). The courtyard as a climatic design element -a quantitative approach. *Proceedings of PLEA Conference* , 2-8.
3. Holden T.S. (1961). Calculation of incident low terms radiation . *ASHRAE J.* , 51-54.
4. Mosseri A. (1990). *The inner courtyard as a climatic component in a residential area* . M.Sc. Thesis (in Hebrew, English summary) , Technion , Haifa , Israel .
5. Rosenfeld A.H. and Akbari H. and Bretz S. and Fishman B.L. and Kurn D.M. and Sailor D. and Taha H. (1995). Mitigation of urban heat islands : materials, utility programs, updates. *Journal of Energy and Buildings* **22** , 255-265 .
6. Sharlin N. and Hoffman M.E. (1984). The urban complex as a factor in the air temperature pattern in a Mediterranean costal region . *Journal of Energy and Buildings* **7** , 149-158 .
7. Shashua-Bar L. and Hoffman M.E. (2000). Vegetation as a climatic component in the design of an urban street . *Journal of Energy and Buildings* **31** , 221-235 .
8. Shashua-Bar L. and Hoffman M.E. (2002). The Green CTTC model for predicting the air temperature in small urban wooded sites . *Journal of Building and Environment* **BAE 638** in press.
9. Swaid H. and Hoffman M.E. (1990/91). Climatic impacts of urban design features for high and mid–latitude cities . *Journal of Energy and Buildings* **14** , 325-336 .
10. Swaid H. (1993). Urban climate effects of artificial heat sources and ground shadowing by buildings . *International Journal of Climatology* **13** ,797-812 .
11. Wilmers F. (1988). Effects of vegetation on urban climate and buildings . *Journal of Energy and Buildings* **15–16** , 507-514 .

Advances in Building Technology, Volume 2
M. Anson, J.M. Ko and E.S.S. Lam (Eds.)
© 2002 Elsevier Science Ltd. All rights reserved

SUSTAINABILITY NEEDS MORE THAN JUST SMART TECHNOLOGY

A.A.J.F. van den Dobbelsteen[1], A.C. van der Linden[1] & D. Klaase[2]

[1] Delft University of Technology, Faculty of Civil Engineering and Geosciences,
P.O. Box 5048, 2600 GA Delft, Netherlands
[2] MAB Project Developers, P.O. Box 19412, 2500 CK The Hague, Netherlands

ABSTRACT

The performance of the built environment is behind schedule on the way to factor 20 environmental improvement by 2040. A case study with government office buildings, discussed in this paper, stresses the importance of improving more than just building materials and services. Substantial improvement can be achieved by focussing on all three dimensions of sustainability: technological efficiency, efficient use of space and a long functional life span.
Space efficiency can be improved by intensive use of space, like innovative work concepts, and multiple use of space, like stacking and combining functions. These avoid claims on rural areas and diminish the amount of building materials and energy needed.
The life span of buildings can be prolonged by a sustainable building structure that has possibilities of adaptability to unforeseen future functional changes of the building. Short term contracting in the real estate market requires functional adaptability of office buildings. This functional adaptability is enabled by technical flexibility.

KEYWORDS

Sustainability, sustainable building, environmental assessment, environmental performance, environmental impact, environmental index, factor 20, intensive use of space, multiple use of space, adaptability, flexibility, real estate market.

INTRODUCTION

In the year 2040 factor 20 environmental improvement is necessary if we allow the whole world population high welfare standards [Ehrlich & Ehrlich, 1990; Speth, 1990]. In order to see whether sustainable building policy is effective or needs to be changed the environmental performance of buildings can be determined and related to this factor 20 target. If the performance were to develop linearly (an assumption open to discussion) factor 4.8 improvement would have been necessary in the year 2000. The relation of a building to a 1990 reference building, the environmental index, can also measure the performance. Hence, this index should have been 480 in the year 2000.

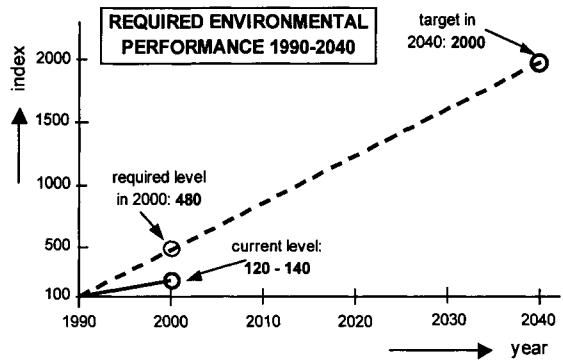


Figure 1: The factor 20 target line and recent performance of buildings.

Recent environmental assessments of sustainably built Dutch buildings show that, since the year 1990, the environmental quality of buildings has averagely improved factor 1.4 to 2.5 [Croes et al., 2001]. More specific conclusions can be drawn from an environmental assessment of 'normal' government office buildings [van den Dobbelsteen et al., 2002-2], in co-operation with the Dutch Government Buildings Agency (DGBA). The offices were compared to a well-defined 1990 reference office, based on the number of users (fte) of the studied office, the gross floor surface (gfs) or the office design itself. For more details about these references: see [van den Dobbelsteen et al., 2002-3].

Technical causes of the arrears

There are various causes for the environmental arrears of individual buildings. Sustainable building as a policy is focussed on small adaptations of traditional solutions. Technically, an environmental index of 800 is already possible, but the combination of measures necessary is expensive and complex.
Another reason for not meeting requirements, even in well-intented projects, might be caused by the approach on the building scale and by disregarding urban solutions. With a wider urban approach of sustainable building greater environmental profits can be achieved than just of an individual building.

Three dimensions of sustainability

The mentioned possible causes of insufficient environmental improvement are of a technological kind. Solutions tend to be automatically sought in that direction. The limited progress of environmental performance, however, shows that a focus solely on technological efficiency is not enough. Sustainability has more than one dimension. The factors space and time, largely independent from technology but important for the eventual environmental load, are often forgotten.
Improvement of the use of building space and prolonging the life span of buildings can be additional factors to technological efficiency, which together might enable factor 20 improvement of the built environment (the whole volume in Figure 3).

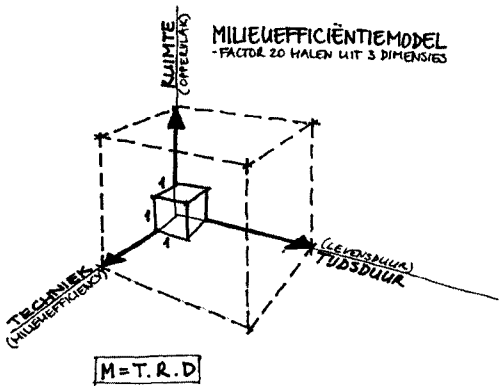


Figure 2 (in Dutch): Achieving factor 20 improvement by three dimensions of sustainability: technology (efficiency), space (surface) and time (life span).

In this paper solutions in all three dimensions will be elaborated. The case study of government office buildings will be used as illustration project for the different solution directions for sustainability: technology, space use and life span.

TECHNOLOGICAL EFFICIENCY

Results of the assessment of government office buildings [van den Dobbelsteen et al., 2002-2], all of them designed without special attention for sustainability, can be found in Table 1.

TABLE 1:
GOVERNMENT OFFICES ASSESSMENT RESULTS [AFTER: VAN DEN DOBBELSTEEN ET AL., 2002-2].

PROJECT					ENVIRONMENTAL COST			INDEX
name	built	renov	fte	total gfs	total	/fte	/m2 gfs	des ind
Food Inspection Department, Zutphen	2000	-	80	1.312 m2	€ 3.082.795	€38.535	€2.350	110
Mixed Office Pels Rijckenstraat, Arnhem	1965	1996	225	6.897 m2	€ 13.044.824	€57.977	€1.891	109
Tax Office, Gorinchem	1976	1995	270	6.342 m2	€ 12.642.825	€46.825	€1.994	110
New Geometry Department, Delft	2001	-	429	13.590 m2	€ 34.430.946	€80.259	€2.534	108
Ministry of Social Affairs and Employment, The Hague	1990	-	1800	57.812 m2	€ 100.877.247	€56.043	€1.745	116
Ministry of Housing, Spatial Planning and Environment, The Hague	1992	-	3260	92.097 m2	€ 184.114.991	€56.477	€1.999	91
Public Works Office (Johan de Witt monument house), The Hague	1655	1966	35	1.671 m2	€ 3.477.861	€99.367	€2.081	102
Traffic and Public Works Office ('The Artillery'), The Hague	1998	-	420	14.275 m2	€ 21.649.257	€51.546	€1.517	119
TOTAL AVERAGE	1947	1986	815	24.250 m2	€ 18.666.037	€60.879	€2.014	108

Beside general information about the buildings in Table 1 the environmental cost, an indicator for the environmental impact (calculated with the computer model GreenCalc) and an environmental index can be found. The environmental index results from comparison with the environmental cost of a

fictitious reference building, with the same design, same shape, but with different building materials and services. Hence, it assesses the applied building technology, given a certain building design. It is visible that the average improvement of the office buildings with respect to 1990 is 8%. The average construction or renovation year is 1992, but there is no particular tendency of improvement towards the year 2001: the index of older buildings is not particularly worse.

Energy consumption

Considering a reference life span of 75 years, about 60% of the environmental load is caused by energy consumption (see Figure 3). Since 1990 much effort is put into improving the energy efficiency of government buildings. Progress by energy conservation measures like thermal insulation and more efficient heating services has often been suppressed by a growth in computer use and cooling [Parap werkgroep, 2001].

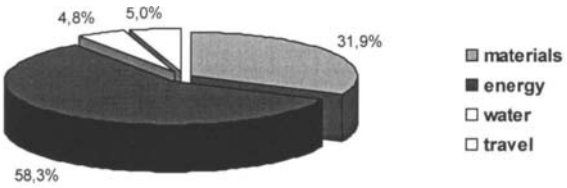


Figure 3: Environmental cost division of government offices [van den Dobbelsteen et al., 2002-2].

The environmental impact of energy consumption is dominated by energy for artificial lighting and heating, followed by apparatus like computers. Therefore, improvement should be focused on these aspects: more access of daylight, smart light switching and heat recovery systems. Further progress in the sustainability of technical services like energy, water and IT-supply can be made through collection of these functions, because of scale and efficiency advantages. One can think of cold and heat storage in the ground and a central heat pump, solar or power service.
Beside these short-term improvements a wide shift toward sustainable energy sources is necessary. Van der Linden & van den Dobbelsteen [2000] already highlighted this.

Building materials

Secondly important in the environmental load, growing of importance if the life span of the building is shortened and if the use of sustainable energy increases, is the use of building materials. The bearing structure is responsible for about 60% of the environmental load of building materials, dominated by the floor structure and beams.

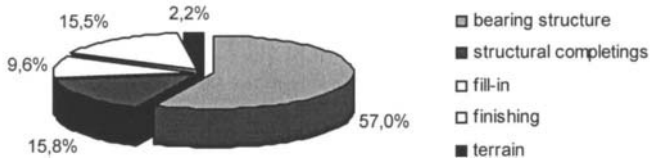


Figure 4: Environmental cost division of government offices [van den Dobbelsteen et al., 2002-2].

With this in mind, focussing on improvements in the building details is, however worthwhile, not effective. Putting effort in the improvement of the bearing structure will more effectively lead to better performance. For more information about the bearing structure: see [Arets et al., 2002].

IMPROVING THE USE OF SPACE

In Table 1 the design index only indicates the environmental impact of the applied materials and services. By using a different reference, 'constructing' a fictitious reference building based on the required gross floor surface (gfs index) or the number of users (fte index), the design efficiency and use of floor surface can be assessed (Table 2).

TABLE 2:
DIFFERENT ENVIRONMENTAL INDICES [AFTER: VAN DEN DOBBELSTEEN ET AL., 2002-2].

PROJECT name	INDEX des ind	gfs ind	fte ind
Food Inspection Department, Zutphen	110	121	181
Mixed Office Pels Rijckenstraat, Arnhem	109	118	109
Tax Office, Gorinchem	110	117	135
New Geometry Department, Delft	108	86	78
Ministry of Social Affairs and Employment, The Hague	116	119	105
Ministry of Housing, Spatial Planning and Environment, The Hague	91	102	102
Public Works Office (Johan de Witt monument house), The Hague	102	127	81
Traffic and Public Works Office ('The Artillery'), The Hague	119	139	120
TOTAL AVERAGE	108	109	103

Considering the design index as a measure for technical efficiency, the difference between the design index and gfs index tells something of the design efficiency (a space indicator). The difference between the fte index and gfs index gives an impression of the efficiency of floor surface use (a use indicator). If the fte index is less than the gfs index, too few people use the building. If it is greater, then there is efficient use of floor surface, compared to the 1990 reference. For instance, the building in the first row has an innovative office concept with shared and flexible desks. This turns out to be an important factor of improvement.

The FSI and surface indices

Another way of assessing space use is by indices for floor and ground surface use, again related to a reference building, or by the floor space index (FSI), the amount of floor area realised divided by the surface of the building area on which it is realised. In Table 3 these can be found for the assessed government buildings.
The index for floor use reflects the deviation from the 1990 average of 28 m^2 gfs per fte. The average shows the government uses more floor surface per employee, probably related to specific functions. Of the two positive exceptions the Food Inspection Department has an innovative office concept with shared and flexible workplaces.
In the indices for ground use there is a clear distinction between offices built in dense city areas and offices at the outskirts of town. Especially the ministries, located near nodes of public transport in the centre of The Hague, have a very efficient use of ground surface.

TABLE 3:

GOVERNMENT OFFICES SPACE USE RESULTS [AFTER: VAN DEN DOBBELSTEEN ET AL., 2002-2]. THE INDICES FOR FLOOR AND GROUND USE RESULT FROM COMPARISON WITH A REFERENCE BUILDING.

PROJECT	FLOOR USE			GROUND USE			FSI
name	total gfs	m2/fte	index	total	m2/fte	index	
Food Inspection Department, Zutphen	1.312 m2	16,4	173	1.546 m2	19,3	111	0,85
Mixed Office Pels Rijckenstraat, Arnhem	6.897 m2	30,7	92	3.871 m2	17,2	85	1,78
Tax Office, Gorinchem	6.342 m2	23,5	122	3.857 m2	14,3	99	1,64
New Geometry Department, Delft	13.590 m2	31,7	91	11.596 m2	27,0	60	1,17
Ministry of Social Affairs and Employment, The Hague	57.812 m2	32,1	88	11.088 m2	6,2	206	5,21
Ministry of Housing, Spatial Planning and Environment, The Hague	92.097 m2	28,3	99	13.519 m2	4,1	375	6,81
Public Works Office (Johan de Witt monument house), The Hague	1.671 m2	47,7	60	1.392 m2	39,8	72	1,20
Traffic and Public Works Office ('The Artillery'), The Hague	14.275 m2	34,0	84	2.855 m2	6,8	194	5,00
TOTAL AVERAGE	24.250 m2	30,5	92	6.216 m2	16,8	159	3,90

This example shows intensive use of space by efficient floor concepts (especially in offices), multi-functional use of buildings and multiple use of space in the third dimension reduce the urban space needed, and thus consumption of materials and energy. Furthermore, deterioration of nature through building extension outside the urban environment is prevented.

De Wilde [2002] introduced the following distinction between intensive and multiple use of space. Intensive use of space means intensifying use of surface for a certain function. Multiple use of space appears in three different forms with combinations being possible (see: figure 5). The first form is multiple use of space in the second dimension, the plain surface. Different functions are put next to each other, which is defined as *mixed use of space*. The second form is a differentiated form of mixed use of space, in which the different functions are put on top of each other: *multiple use of land*. The third form is *multiple use in time*, in which a set amount of floor area is used for different functions, one after the other.

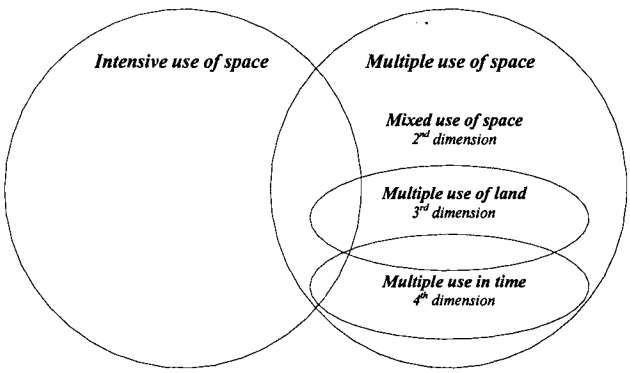


Figure 5: Different types of intensive space use [de Wilde, 2002]

PROLONGING THE LIFE SPAN

In the shown case study results life span consequences have not been taken into account; old buildings were considered as new buildings. With a limited look at sustainability a 'tight' building is the best solution for good environmental performance (a high environmental index): a smaller building envelope means less energy consumption and less building materials mean less environmental impact. However, with this approach future changes (new spatial requirements, different work forms etc.) are ignored, possibly shortening the eventual life span of the building.

Importance of the life span for sustainability

A part of the environmental load develops during the life span of a building (e.g. by energy and water consumption or travel); another part is mainly initial, imposed at the beginning of the life span of the building or urban area (e.g. use of building materials) or at the end of it (e.g. demolition waste). Because of the initial environmental load, in case of a short life span the environmental load per unit of time is bigger than with a long life span, taking a long lifetime as a reference.
Therefore, prolonging the life span of buildings and urban areas as a whole is an important means to diminish the environmental load. When buildings lose their function demolition is often the most feasible solution. Adaptability is a primal necessity, because functional changes can hardly be predicted.

Flexibility for adaptability

Sustainable buildings offer enough possibilities to undergo changes through times. In the real estate market adaptability starts with financial unboundness. The success and size of young companies is so fluctuating that they do not dare tie themselves to long-term contracts [van Eldonk et al., 2001]. This is also a tendency among bigger companies. For accommodation this means that the conditions might change completely within a few years. In that perspective it is dangerous to bet on a function that is boosting at the moment of decision. It is wiser to strive after multi-functionality, or functional flexibility. Technical flexibility forms the basis for functional flexibility. An overview of urban flexibility forms, the drive behind them and possible solutions can be seen in the table underneath.

TABLE 4
TYPES OF URBAN FLEXIBILITY [VAN DEN DOBBELSTEEN & KLAASE, 2002-1].

FLEXIBILITY TYPE and BACKGROUND	POSSIBLE SOLUTION
Financial flexibility	
Financial unboundness organisations are not tied to long financial obligations	• functional flexibility (see below) • short-term (hiring)contracts • buildings not tuned to current trends → sustainable quality
Functional flexibility	
Multi-functionality a building is adaptable to changing circumstances; it can accommodate different functions	• technical flexibility (see below) • reckon with growth • elaboration to the highest quality
Technical flexibility	
Oversizing/ overdimensioning the building structure has sufficient measurement for a dynamic and growing organisation	• high ceilings and large door openings • spacious floor plan, in which additions are possible • over-dimensioned floor structures for different functions
Extendibility parts can be added or removed on, under or next to the building	• reservation of space for later additions or adaptations • over-dimensioned bearing structure for additions • removable, dismantleable constructions
Re-arrangeability the building structure offers opportunities to vary the fill-in	• open bearing structure without obstacles • removable inner walls • comparting of technical functions and infrastructure • separability: additional entrances, stairs and elevator shafts

CONCLUSION AND DISCUSSION

Sustainable building should be focussed more on the intensification of space use and a longer useful life span of built areas, rather than solely improving technological efficiency. This paper gives an overview of conceptual solutions with which all factors can effectively add to a better environmental performance.

An important stimulance for solutions for efficient use of space and a long life span would be the assessibility of the environmental impact of these. At the moment only the use of building materials, energy and water, the technological efficiency, can be translated into environmental indicators. Space use can only be put into indices that visualise the difference with a reference, but comparison with the environmental impact of e.g. building materials is not possible yet. To estimate the eventual life span of a building, and thus the environmental impact of measures in that direction, is even more difficult. Therefore, development of assessment models for space use and life span are a necessity to make these factors of sustainability as important as the technological efficiency.

A final remark can be made about the relative importance of buildings within urban areas. Good buildings have no future in bad areas; a good urban plan however tolerates bad buildings. Therefore, it is important to have a good urban fabric as the foundation of sustainable building.

LITERATURE

- Arets M.J.P. & van den Dobbelsteen A.A.J.F. (2002). Sustainable bearing structures. *In these proceedings.*
- Croes H., Dewever M. & Haas M. (2001). *One number says it all* (poster), Dutch Government Buildings Agency: The Hague, Netherlands.
- van den Dobbelsteen A. & Klaase D. (2002-1). De broodnodige focus op een lange gebruiksduur van kantoren - The paradigm shift (2). *Real Estate Magazine* **20**.
- van den Dobbelsteen A.A.J.F., Arets M.J.P. & van der Linden A.C. (2002-2). *Milieubelasting van rijkskantoorgebouwen - Hoofdrapport*, Delft University of Technology: Delft, Netherlands.
- van den Dobbelsteen A.A.J.F., van der Linden A.C. & Ravesloot C.M. (2002-3). Defining the reference for environmental performance. *In these proceedings.*
- Ehrlich P. & Ehrlich A. (1990). *The Population Explosion*, Hutchinson: London, UK.
- van Eldonk A., Venema P. & de Vos tot Nederveen Cappel C. (2001). *Het Nationale Kantoren-marktonderzoek 2001*, Twynstra Gudde: Amersfoort, Netherlands.
- van der Linden A.C. & van den Dobbelsteen A.A.J.F. (2000). Building 2040, factor 20 less environmental load? *Proceedings Sustainable Building 2000, 22-25 October 2000, Maastricht, the Netherlands*, 598-600.
- Parap werkgroep. (2001). *Kantelpuntonderzoek*, Dutch Government Buildings Agency: The Hague, Netherlands.
- Speth J.G. (1990). Can the world be saved? *Ecological economics* **1**, 289-302.
- de Wilde Th.S. (2002). Meervoudig ruimtegebruik en binnenstedelijke verdichting rond treinstations. *Cement* **2**, 33-36.

Advances in Building Technology, Volume 2
M. Anson, J.M. Ko and E.S.S. Lam (Eds.)
© 2002 Elsevier Science Ltd. All rights reserved

DEFINING THE REFERENCE FOR ENVIRONMENTAL PERFORMANCE

A.A.J.F. van den Dobbelsteen[1], A.C. van der Linden[1] & C.M. Ravesloot[2]

Delft University of Technology,
[1] Faculty of Civil Engineering and Geosciences, P.O. Box 5048, 2600 GA Delft, Netherlands
[2] Faculty of Architecture, P.O. Box 5043, 2600 GA Delft, Netherlands

ABSTRACT

In the year 2040 factor 20 improvement of environmental impact is necessary. Measuring the environmental impact of building provides insight into the progress or decrease with respect to the factor 20. One environmental assessment type is determining the environmental index, by relating the environmental load of the studied building to that of a certain reference. There are three ways of defining a reference:

1. basing it on the design of the studied building, but changing the building materials and services
2. basing it on the gross floor surface and 'constructing' a fictitious reference building around it
3. basing it on the number of people for whom the building is designed and relating that to a reference floor surface, followed by the 'construction' of a fictitious reference building.

A case study with 12 government office buildings shows that the definition of the reference is stipulating for the resulting index. This paper describes the different reference types and presents results and conclusions of the government office buildings assessment.

KEYWORDS

Sustainability, sustainable building, environmental assessment, environmental performance, environmental impact, environmental cost, environmental index, factor 20, reference, reference building.

INTRODUCTION

Sustainability has become an important new performance factor in the over-all quality of building design. Many models have been developed in order to assess the environmental impact of building designs. For a broad perspective the calculated impact has to be related to a target for the future. The World Commission on Environment and Development (1987) stressed that sustainable development has to be achieved in synchronic attention for welfare and environment. Ehrlich & Ehrlich (1990) and Speth (1990) made this quantifyable by relating the pressure on the environment (EP) to the world population (P), their welfare rate (W) and the environmental impact of goods, also called metabolism (E).

$$EP = P*W*E \tag{1a}$$

$$1/2 = 2*5*1/20 \quad (1b)$$

With the objective to weaken the pressure on the environment and a growing population, while giving the poorer part of the world a comparable welfare rate as the western population, requiring factor 5 improvement, 50 years later, by the year 2040, the environmental impact has to be reduced by 95%.

In order to estimate the progress in sustainability the environmental performance of buildings can be related to that of a 1990 reference. Thus an environmental index can be deducted, showing the achieved factor improvement. The difficulty is to define this reference in a specific design, exact measures, building materials and services.

CALCULATION TYPES

Buildings can be compared through the absolute environmental load or through relative scores or environmental indices. Environmental indices offer extra opportunities:

- simple scores, in contrast with different effect scores in many digits
- comparability of aspects of sustainability, of which scores are put in different units
- insight into progress or arrears of the environmental performance, with respect to a reference year
- environmental improvement of buildings, with respect to a reference building or the factor 20
- insight into environmental differences between functionally unequal buildings
- categorisation of buildings according to the environmental index (see Table 1)
- diminishment of absolute errors in environmental assessments.

If the calculated absolute values (basis for the index) stay reasonably valid, the comparison can also give information about differences and causes of the environmental load of buildings.

TABLE 1:
THE ENVIRONMENTAL INDEX OF DIFFERENT BUILDINGS [AFTER: CROES, DEWEVER & HAAS, 2001].

building	city	year	index
Reference Building	-	1990	**100**
Tax Office	Roermond	1992	**109**
Police Headquarters	Leusden	1996	**113**
Public Works	IJmuiden	1998	**141**
Information centre De Hoep	Castricum	1998	**143**
WWF Dwelling	Apeldoorn	1999	**146**
Employment Bureau	Amsterdam	1996	**156**
Tax Office	Enschede	1996	**166**
Municipal Health Service	Tiel	1998	**168**
Project XX	Delft	1998	**168**
IBN-DLO Research Centre	Wageningen	1998	**173**
Dept Collection Agency	Leeuwarden	2001	**176**
BEAR Architects Office	Gouda	2000	**203**
Public Works	Terneuzen	1999	**219**
Court of Justice	Tiel	1998	**222**
Katreine Office Tower	Utrecht	1998	**224**
Dynamic Office	Haarlem	1997	**225**
Oxfam Building	Gent (B)	1998	**252**
DWA Consultants Office	Bodegraven	2000	**254**

An environmental index can be obtained by relating the environmental load of a building to the environmental load of a reference (see Figure 1).

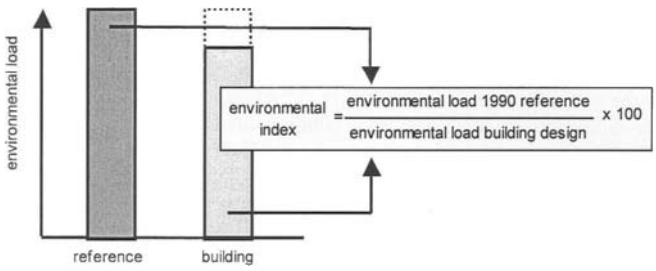


Figure 1: determination of the environmental index

In order to assess buildings in a correct way, comparisons based on the environmental index have to meet the following conditions.

1. Buildings should meet a *functional unity*, a collection of demands ensuring all assessed buildings have a comparable function and meet the same technical requirements.
2. An *input protocol* is necessary: the contemplated building elements or environmental aspects as well as the measure of input details should be equal for all studied buildings.
3. Different types of buildings can be compared. However, each building type demands its own reference and functional unity. A *functional conversion protocol* is necessary for slightly different buildings in a collection of buildings with one reference.

The most important part of a building comparison based on environmental indices is the definition of the reference, of which there are three different types.

REFERENCE TYPES

The design reference

In the design reference the design of the reference (shape, floor surface, façade fill-in, amount of building materials) is the same as the studied building. The design reference is based on a list of reference solutions for building materials, energy and water services. These reference data are pasted into the dimensions of the studied building design in the assessment model. The results of Table 1 were drawn in accordance with this approach. This reference type is appropriate for one specific building; every new building requires a new reference definition.

An index based on the design reference ('design index') only assesses the ecological quality of the applied building materials and services. The approach is quick and easy but in fact means working with a shifting reference, because the design, size, form, fill-in and building use change with each studied building. Hence, solely by the design index one building is not completely comparable with another.

The gfs reference

The floor surface reference is based on the *gross floor surface* (gfs) of the studied building or on spatial requirements in the original brief. The building geometry, façade and fill-in, however, are 'constructed' in accordance with a reference building design. The gfs reference is especially useful in case of design competitions, if different designs are made for the same building.

An index based on a gfs reference ('gfs index') assesses the environmental performance of the building design and the applied building materials and services. To get a picture of the building design alone, given certain material and service choices, the environmental index should be compared to an index based on the design reference.

The fte reference

In a fte reference the number of people (or *full time employment*, fte), for whom the building has been designed, forms the basis for comparison. With a fte reference the reference building is built from scrap, needing a definition of functions in a building, their reference floor surface and specific facilities, a standard fill-in, a standard bearing structure, façade design etc.

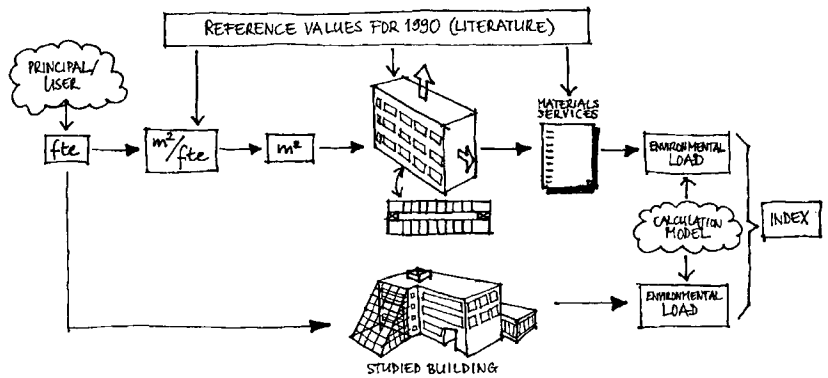


Figure 2: The determination of the fte reference, its environmental load and the environmental index.

With a fte reference more aspects of a building can be assessed than with a gfs reference, but the determination of it is more complex. The number of people using the studied building is not always known and can change during the lifetime of the building. Hence, the environmental performance will vary with different personnel data.
An index based on a fte reference ('fte index') assesses the complete environmental load of building use, building design and applied materials and services with respect to a fictitious building. To get an impression of the building use alone, given certain building design and materials and service, the fte index should be related to a floor surface index.

DEFINING DESIGN REFERENCES FOR OFFICES

Starting with the number of personnel using the studied building a next step is to determine the 1990 reference floor surface per fte, from which point the whole reference building can be defined.

Floor surface

There is no estimation of the floor surface use per employee explicitly for the year 1990. In the Netherlands in the year 1996 the average surface use was 27.9 m^2/employee, a value that dropped to 25.5 in 1999 and 23.8 in 2001 [van Eldonk et al., 2001]. If this trend already took place before 1996, in the year 1990 the average floor use must have been bigger than 27.9 m^2. However, in the Netherlands only around the year 1996 the first space-saving office innovation projects started [Rijksgebouwendienst, 1996]. Therefore, in 1990 the average gfs per employee can be assumed around 28 m^2.

Office concept

The fill-in of the required floor surface depends on the chosen office concept, which is a combination of organisational use and an architectural fill-in concept. In 1998 only 9% of the Dutch offices had an innovative concept [van Antwerpen & Hermans, 1998]; most had territorial workplaces. The largest

part of offices had a cell structured fill-in, of which 40% with 1 or 2 person rooms, 23% with 3 or 8 person rooms ('group offices') and 21% a combination of both. Therefore, it is reasonable to pick a territorial cell office as a reference for 1990.

Building depth and length

As many researchers found out, Dutch cell offices are mainly based on a floor module of 1.80 m x 5.40 m and a single middle corridor of 1.80 m. This means a common building depth for the 1990 reference building is 12.60 m.
Based on Dutch legislation rules for security exits a reference length of around 60 m can be chosen, or - with 32 bays of 1.80 m - rounded off to 57.60 m. Hence, the reference gfs per layer is 12.60 x 57.60 = 725.8 m^2. The exact building length can be tuned to an integer number of building layers. Reference offices with a gross floor surface of 725.8 m^2 and less have one building layer, the building length depending on the needed floor surface, rounded off upwards in order to fit the bay measure of 1.80 m.

Building height

In case of big floor surfaces a limited reference building length would lead to an unrealistic height, necessitating additional structural measures. Therefore, a maximum reference height has to be defined, based on a conventional concrete structure with a stiff core around the elevators. An assumed maximum height with this technique is 24 layers. A free floor height of 2.40 m is common [Boer et al., 1996], so with a construction and service height of 1.20 m the total reference floor height is 3.60 m. This means a maximum reference building height of 86.40 m. In case of a large reference office (20.000 m^2 and bigger, like a ministry) this maximum height is quickly attained, after which expansion of the reference floor surface can be found in an extension of the building length.

Calculation of the measurements for the reference building geometry

Following the definition of different reference measures the shape of the fictitious reference building for a studied office building can be determined from formulas (see Table 2).

TABLE 2:
REFERENCE LIST FOR ENVIRONMENTAL COMPARISONS [AFTER: VAN DEN DOBBELSTEEN ET AL., 2002].

number of fte (p)	p		
needed surface (A)	A=28*p		
total facade length (L_{tot})	L_{tot}=28*p/12,60=2,222*p		
	A<=725,8 →	A >725,8 →	
layers (y)		y=L_{tot}/57,60=0,0386*p	
		y<=24 →	y>24 →
number of layers (Y_{ref})	Y_{ref} = 1	Y_{ref}=A/57,60 round off upwards to integer	Y_{ref}=24
building height (H_{ref})	H_{ref}=3,60*Y_{ref}=3,60	H_{ref}=3,60*Y_{ref}	H_{ref}=3,60*Y_{ref}=86,40
needed surface per layer (a)		a=A/Y_{ref}	a=A/Y_{ref}
number of bays (t)	t=L/1,80 round off upwards to an integer	t=a/12,60/1,80=a/22,7 round off upwards to an integer	t=a/12,60/1,80=a/22,7 round off upwards to an integer
building length (L_{ref})	L_{ref}=1,80*t	L_{ref} = 1,80*t	L_{ref}=1,80*t
gross floor surface (A_{ref})	A_{ref}=12,60*L_{ref}	A_{ref}=12,60*Y_{ref}*L_{ref}	A_{ref}=12,60*Y_{ref}*L_{ref} =302,4*L_{ref}

This definition of reference design geometries looks complex but can be easily put in a spreadsheet model, as was done for the later presented case study of government offices.

Additional design references

For complete data input in an environmental assessment model the next additional features of the reference building were chosen, only presented briefly here.

- Having no statistical preference for the *orientation* of office buildings, the arbitrary choice the long elevations of the office were oriented on the west and east. The entry is at the eastern elevation.
- The east and west elevation are given a usual external *glass percentage* of 30%, the window-frame included. The short elevations on North and South are blind.
- A *cellar* is included, but it is not taken into account as functional space.
- The reference office has a flat roof without special facilities.
- The cell structured office floor has a modular fill-in based on a module of 1.80 m by 5.40 m. Based on databases of the Dutch Government Buildings Agency (DGBA) an average *internal wall surface* of 90% of the gross floor surface is chosen, of which 10 percent points internal doors.
- The *bearing structure* is a column structure with a stiff core of 3.60 m by 3.60 m.

References for building materials and services

Having the measures determined reference materials and building services can be defined (Table 3).

TABLE 3:
REFERENCE LIST FOR ENVIRONMENTAL COMPARISONS [AFTER: VAN DEN DOBBELSTEEN ET AL., 2002].

Building materials	
Bearing structure	foundation, columns, beams, floor structure, roof structure and bearing walls of concrete, cast on site, 40 mm EPS insulation of ground floor and roof
Facades	brick masonry - 50 mm rockwool - lime stone blocks, tropical timber windows with double panes, entrance of glass in tropical timber frames, security door of tropical plywood
Fill-in	25% massive lime sand block walls, 75% metalstud walls with 50 mm rockwool, honeycomb doors in tropical timber frames, concrete stairs
Finishing	cement decks, bituminous roofing with gravel ballast, gypsum ceiling panels, 90% lino and 10% ceramic tile floor covering, 10% ceramic tile wall covering and 90% lime plaster-work with acrylic paint
Terrain	50 mm asphalt pavement
Energy consumption	
Building use	opening times 8.00-20.00 h, 38 hours working week, 85% presence, 1 computer per person, no auto power-down,
Climatising	light walls, heavy facades and closed ceilings, conventional boiler, mechanic exhaust, 2.0 m^3/hm^3, no heat recovery, no ventilator control, no cooling
Warm tap water	conventional boiler with central heating, distribution by circulation
Lighting	conventional TL ceiling fittings, room switches, 40% of functional surface has daylight possibilities
Water consumption	
Facilities	restaurant, showers and greenery watering present, no air moistening
Sanitation	toilets with 9 liter reservoirs, standard taps and showers
Substitution	no substitution of tap water by rain water
Travel	
Site	town borders, 400-600 people/km^2, internal work (85% presence)
Public transport	railway station at 4 km, frequency 4 times per hour, bus abri at 500 m, frequency 4 times per hour
Private transport	motorway at 1 km, through traffic on service road, parking lots at 100 m, 0.6 lots per employee, pedestrian and bike paths separated from road by greenery

What does the fictitious reference building look like?

The reference office can be seen as a typical Dutch 'motorway office', located at the border of a town near a service road, with a rather large parking area and distant from public transport. The office design is rather traditional, with a concrete bearing structure and traditional brick masonry. It has a

cell-structured fill-in (every employee has his own desk). The building services and heat insulation are in accordance with 1990 legislation requirements.

THE CASE STUDY 'ENVIRONMENTAL LOAD OF GOVERNMENT OFFICES'

As part of the PhD research 'Effective sustainable accommodation of office work' government offices were assessed following the described methodology. With the computer model GreenCalc the environmental cost of the offices were determined and compared to those of a 1990 reference office. All three described reference types were applied so three different indices could be compared (Table 4).

TABLE 4:
ENVIRONMENTAL COST ASSESSMENT OF OFFICES [AFTER: VAN DEN DOBBELSTEEN ET AL., 2002].

PROJECT			ENVIRONMENTAL COST				INDICES		
name	fte	total gfs	fte ref	gfs ref	design ref	building	fte ind	gfs ind	des ind
Food Inspection Department, Zutphen	80	1.312 m2	€ 5.570.813	€ 3.741.298	€ 3.399.331	€ 3.082.795	181	121	110
Mixed Office Pels Rijckenstraat, Arnhem	225	6.897 m2	€ 14.207.590	€ 15.358.491	€ 14.183.908	€ 13.044.824	109	118	109
Tax Office, Gorinchem	270	6.342 m2	€ 17.028.197	€ 14.825.328	€ 13.847.414	€ 12.642.825	135	117	110
New Geometry Department, Delft	429	13.590 m2	€ 26.881.966	€ 29.642.722	€ 37.105.729	€ 34.430.946	78	86	108
Ministry of Social Affairs and Employment, The Hague	1800	57.812 m2	€ 106.381.111	€ 119.768.645	€ 117.243.867	€ 100.877.247	105	119	116
Ministry of Housing, Spatial Planning and Environment, The Hague	3260	92.097 m2	€ 186.903.684	€ 187.858.968	€ 167.259.442	€ 184.114.991	102	102	91
Public Works Office (Johan de Witt monument house), The Hague	35	1.671 m2	€ 2.809.185	€ 4.418.202	€ 3.560.588	€ 3.477.861	81	127	102
Traffic and Public Works Office ('The Artillery'), The Hague	420	14.275 m2	€ 25.983.913	€ 30.113.393	€ 25.754.837	€ 21.649.257	120	139	119
TOTAL AVERAGE	815	24.250 m2	€ 19.288.323	€ 20.286.352	€ 19.117.756	€ 18.666.037	103	109	108

The results show that environmental indices sometimes have a wide spread. Taking the first row of the Food Inspection Department in Zutphen as an example, interesting conclusions can be drawn.

- The design index mainly gives an impression of the environmental performance of the chosen building materials and services for energy and water. The design index shows 10% improvement with respect to the 1990 reference building. For a building realised 8 years after 1990 that's not a bad nor a good score. With the factor 20 target in mind it should have been better. Probably the zinc façade cladding is a cause of the limited improvement.
- The gfs index is better, meaning the building design efficiency improves the environmental performance by materials and services. To see the design efficiency alone, the gfs index has to be divided by the design index. Hence, a design efficiency improvement of 10% can be deducted, which can be explained by a relative compact geometry and sober fill-in.
- The fte index shows a large improvement with respect to the 1990 reference building. Related to the gfs index an extra improvement by factor 181/121=1.5 is achieved. This can be explained by the innovative office concept with shared and flexible working places; more people make use of the building than in the fictitious reference building. In case of a floor surface reference or - even worse - design reference, this measure would not have been taken into account.

Some of the office buildings show improvement in the gfs index, but worsening in the fte index. This means the building design is effective but, with respect to the standards in 1990, not enough people use it. In general, perhaps because of their specific function, in government offices more space is commonly used per employee than in commercial offices [van Eldonk et al., 2001].

CONCLUSIONS

The assessment of government offices also shows the environmental performance of common offices are far behind the target to achieve factor 20 environmental improvement in 2040.The case study also shows that the choice of a reference is stipulating for the results and their interpretation. Nevertheless, all index types retrieved from application of the different references are useful in environmental assessments of buildings, for every index unveals different aspects.
As a follow-up of the government office buildings assessment the average environmental load per m^2 or per fte can be deducted and applied as a reference performance demand in the nearby future. This performance per employee enables an easy fixation of the reference environmental load of a whole office organisation, apart from the chosen office concept, building design and applied technology. The principal and architect can use it improving the environmental quality of their project; society can deduct the achieved factor of improvement towards sustainability.

A consideration should be made about the factor time. Defining a reference building geometry and fill-in, a 'tight' building is the best solution for good performance (a high environmental index): a smaller building envelope means less energy consumption and less building materials mean less environmental impact. However, with this approach future changes (new spatial requirements, different work forms etc.) are ignored, possibly shortening the eventual functional life span of the building. In environmental assessment models the life span is usually fixed. Therefore, an extra factor should be taken into account, in which aspects like adaptability play a role. This factor could reflect the expectance of the functional life span of a building, with respect to reference life span. In the period of the case study such a time factor could not yet be enhanced.

LITERATURE

- van Antwerpen J. & Hermans W. (1998). *Huisvestingsvoorkeuren van kantoren*, INBO: Wageningen, Netherlands
- Boer J.R., Diehl P.J. & Koenders H. (1996). *Arbo-normenboek*, Samsom Bedrijfsinformatie: Alphen a/d Rijn, Netherlands
- Croes H., Dewever M. & Haas M. (2001). *One number says it all* (poster), Dutch Government Buildings Agency: The Hague, Netherlands
- van den Dobbelsteen A.A.J.F., Arets M.J.P. & van der Linden A.C. (2002). *Milieubelasting van rijkskantoorgebouwen - Hoofdrapport*, Delft University of Technology: Delft, Netherlands
- Ehrlich P. & Ehrlich A. (1990). *The Population Explosion*, Hutchinson: London, UK
- van Eldonk A., Venema P. & de Vos tot Nederveen Cappel C. (2001). *Het Nationale Kantorenmarktonderzoek 2001*, Twynstra Gudde: Amersfoort, Netherlands
- Rijksgebouwendienst. (1996). *Kantoorinnovatie*, Rijksgebouwendienst, The Hague, Netherlands
- Speth J.G. (1990). Can the world be saved? *Ecological economics* **1**, 289-302
- World Commission on Environment and Development. (1987). *Our common future*, Oxford University Press, Oxford, UK/New York, USA

INFORMATION TECHNOLOGIES:

BUILDING PROCESS INTEGRATION/COORDINATION

This Page Intentionally Left Blank

Advances in Building Technology, Volume 2
M. Anson, J.M. Ko and E.S.S. Lam (Eds.)
© 2002 Published by Elsevier Science Ltd.

CONSTRUCTING THE FUTURE

T. W. Broyd

Research & Innovation Director, WS Atkins plc, Epsom, KT18 5BU, England
Visiting Professor in Construction Management, University of Reading, RG6 2BU, England

ABSTRACT

Construction helps to shape the built environment and provides the infrastructure for society, yet despite the fact that it is an important industry in any country it is not good at planning for the future. In the UK the Government's Foresight programme has brought together business, government and science to identify the challenges and opportunities that face construction in the next twenty years. The Foresight report 'Constructing the Future' (2001) supports and extends other recent initiatives that are designed help improve and benefit the UK construction industry both now and in the future.

The Foresight study involved setting up a number of groups to examine the issues of housing; repair, refurbishment and re-use of facilities; sustainable materials; information and communication technology; business, globalisation and commerce; and safe construction. The final report was produced following extensive consultation and feedback. It indicated that the construction industry needs to embrace a wide range of new materials, technologies and innovative approaches in the future. These include: advances in components and materials (in particular nanotechnology), information and communications technology, and technologies that help to deal with the issues of sustainability. To ensure we fully benefit from these advances requires a shift in industry practices, attitudes and quality. The advantages include better housing and living conditions, environmental sustainability and lower construction costs. Action is needed urgently at every level of the sector because to meet the challenges most changes have to be substantially in place within 10 years .

The report made nine recommendations. To: promote 'smart' buildings and infrastructure; improve health and safety; enable supply chain integration; invest in people; improve existing built facilities; exploit global competitiveness; embrace sustainability; increase investment returns; and plan ahead.

Since publication, the UK's forward-thinking has continued, with a 'Blue skies', future scenario workshop and publication of a major review on Government construction R&D policies and practices.

KEY WORDS

Construction, research, foresight, future

INTRODUCTION

Construction is one of the most important industries in any developed country, not only in economic terms but also in the way it helps shape the built environment and provides the physical infrastructure for civilized society. Despite its sometimes tarnished image, the industry has always excelled at managing complex programmes, often involving groups of people necessarily brought together for one-off projects and working in hazardous or inhospitable places. As a result, the industry has developed both flexibility and good skills in problem solving. What it is not so good at, however, is planning for the future.

Until recently, this lack of forward thinking has been practically a virtue. With uncertain cycles of demand, the ability to respond quickly to changing economic drivers has perhaps rightly been seen as more important than scanning ahead. The signs are that that is now changing. With construction clients increasingly seeking 'lifetime' solutions provided by stable supply chains, and the growing importance of both sustainability and globalisation, there is now both the opportunity and the need for the industry to think ahead.

Within the United Kingdom, we are learning to use structured approaches within a national initiative known as 'Foresight'. It involves thinking intelligently about the issues that will affect the future - up to 20 years hence; not to predict what will happen, but rather to prepare for it and influence it as much as we can. In the past few years people from a broad spectrum of construction industry backgrounds have come together to develop sets of issues that will need to be addressed if the industry is to answer the needs of its customers, its users and its workers. The results are summarised in this paper

THE FORESIGHT PROGRAMME

Foresight (www.foresight.gov.uk) is not fanciful academic dreaming, but hard-nosed business reality. A Government programme, it brings together business, government, the science base and others to help identify the challenges and opportunities of the next twenty years. It includes a number of panels ranging from crime prevention and manufacturing, to financial services and healthcare. The Foresight study on construction, chaired by the author, also doubles as the futures theme group of CRISP, the UK Government supported Construction Research & Innovation Strategy Panel, through which it is linked to the entire construction industry. It is part of a number of initiatives – in particular, Latham (1994) and Egan (1998) - that have taken place in recent years to help assess and bring about substantial improvements to benefit the UK construction industry both now and in the future.

To determine the Foresight programme recommendations for the future of construction a number of issues groups were initially established to examine:

- Housing
- Repair, refurbishment and re-use of facilities
- Sustainable materials
- Information and communication technology
- Business, globalisation and commerce
- Safe construction

Working through a steering group, the feedback from these issues groups enabled the production of a consultation document which was made available to interested parties both from within and outside the construction sector. Their responses were taken into account in preparing the final report and recommendations published last year, Constructing the Future (2001).

CONSTRUCTION SCENARIO

As a sector of economic importance the UK construction sector business is worth £65 billion a year and employs over 1.4 million people. It comprises 186,000 SMEs and includes 165,000 private contracting firms. In the next ten to twenty years they will be faced with immense challenges as a result of new technologies and materials, different operational processes and intensifying cross border competition. The industry will also need to respond to a changing world, with climate change, traffic impact and a revolution in computers and information technologies, amongst other impacts, creating new and different demands, influencing demographic changes and altering life styles. The pace of change will be fast and all-embracing. It will create more business opportunities than ever before. It will also be highly dependent on information sharing, customer-centric thinking, electronic commerce and co-operation at every level throughout an integrated supply chain. It will embrace a changed cultural thinking that impacts on and benefits many aspects of the user environment.

Pointers to the future

There are numerous pointers to indicate that the construction sector is going to have to embrace a wide range of new materials, technologies and innovative approaches in the future. These include:

Advances in components and materials.

Amongst the many probable advances are: new composite materials such as fibre cement and light alloys; nanotechnology to impregnate building components with 'smart' solutions for identity, data collection and management; surface coatings that electronically change colour and warn of stress points; super-strong paint for crumbling concrete that cuts repair and maintenance costs; pre-wired looms which enable house wiring completion in one day.

Information and communications technology

Future construction teams will be process, not project-based, with integrated computer-aided design and data-sharing approaches linked by web-technology. Multi-dimensional modelling (x,y,z, time and cost) and visualisation will incorporate both design and client needs, whilst the Internet will enable fast 'intelligent' planning submission and approval. Remote data collection on the maintenance and operation of facilities will be the norm. The creation of supply-chain research partnerships between designers, constructors and component manufacturers are also very likely.

Methods and people

Amongst the changes that will impact on people within the industry will be the creation of innovation teams and technology clusters and extensive use of collaborative technology. Virtual reality and simulation will be used for safety purposes, whilst computers will provide on-site training and fitting guidance. Robots will increasingly become available, especially for hazardous or monotonous work. To protect workers intelligent clothing will help to communicate and react to changing conditions.

Sustainability

Advances will be made in many areas of sustainability. For example, a reduction in construction waste can be expected, with manufacturers required to collect and re-cycle materials. Efficient, low-cost micro power generators and fuel cells will provide local power networks. Embedded nanotechnology chips will monitor building conditions and contact repair and maintenance teams before breakdown, whilst 'smart' concrete will sense real-time vibration of structures and highlight early repair needs.

Gaining the advantages

To ensure we fully benefit from these advances requires a continuing shift in practices and attitudes within the construction sector and in the quality that the industry delivers. It also needs to overcome many existing problems with customer dissatisfaction and to improve the way its capability is perceived and understood by both public and private sectors.

The advantages of positive action are immense, delivering - amongst other things - better housing, improved living and working conditions, effective environmental sustainability, lower construction costs and a construction industry that is globally competitive and profitably sound. Yet, if the construction industry is to master this future, action needs to be taken now, for in construction planning terms twenty years is almost upon us. Consequently, if we are to see an improvement in the industry's value-added impact on the built environment in that time, then most of the influential changes required have to be in place within 10 years or less.

Furthermore, because the primary key to the future lies in achieving an integrated approach throughout the entire construction process, the changes that are needed cannot simply be each viewed in isolation. They require unified and collective responses, not piecemeal reaction, because the future of construction implies significant change at every level of the sector and not merely for the larger companies and the enlightened thinkers. This means that Government, professional and trade bodies, academia and financial institutions have to work closely with the industry to help deliver the changes that all of society can benefit from in the future.

RECOMMENDATIONS FOR ACTION

The Foresight report that resulted from our deliberations and the consultation exercise recommended nine areas where appropriate action was required. In priority order these are as follows:

Promote 'smart' buildings and infrastructure

Technology will enable almost anything, so deciding how best to apply it is the critical skill. Significant long-term advantages that benefit sustainability and improve design by feeding back information will be achieved by using intelligent, data gathering materials and components. Costs will be saved through use of standard components and factory-automated pre-assembled units. Innovation is the key to the future success of construction, using technology as the enabler. The industry therefore needs to embrace a complete technology and innovation culture change so that research and development is seen as the core value for the future and essential to business success.

Recommendation

Accelerate the introduction of new technologies, 'intelligent' products, standardised, pre-assembled components and advanced materials at all levels of the built environment. This will provide business opportunities, improve living/working environments and feedback to improve construction quality.

Improve health and safety

There are some 80 fatalities, 4,000 major injuries and 10,000 3-day injuries on UK construction sites every year, as well as an appreciable under-reporting of injuries and incidents of ill health.

Within 20 years it would be desirable to achieve zero deaths in construction and to reduce the number of serious injuries on site by at least 80%. For this to be feasible we need to undertake more research into the long-term health impacts of construction site working. Automation in the shape of pre-fabricated component manufacturing and on-site robotic assembly, together with site modelling and simulation, have a major role to play in improving construction safety. Nurturing the workforce and improving safety will enable better recruitment and retention of people. It is well known that a healthy workforce is a happy one. We also need to introduce a 'no blame / no fault' compensation system to encourage near-miss reporting and feedback on site-related health issues.

Recommendation

Improve the health and safety of people working on site. Enhance safety awareness and thinking throughout the construction process - design, manufacturing, build, operations and maintenance. Ensure better safety training, health monitoring and near-miss reporting, and introduce safety-driven construction automation. This will save lives, minimise health problems and improve productivity.

Enable supply chain integration

The integration of design into production and operation will join up areas such as quality of design, sustainability, standardisation, automated production and pre-assembly off-site, and lead to better supply chain management. Much of the industry currently deals with the construction project process as a series of sequential and largely separate operations undertaken by individual designers, constructors and suppliers who have no stake in the long-term success of the product and no commitment to its operating and maintenance costs. Supply chain improvements, enabled with new skills and talent will make a significant difference.

Individual supply chains within the construction industry need to seriously assess and understand their roles and responsibilities in being part of an integrated process. For example, information on all construction products and materials should be available over the Internet in the form of standard coded data (typically IFCs - Industry Foundation Classes) describing specifications, stock availability, prices etc. The skill in integration lies in how businesses manage and transform information, so that freedom of access and seamless interchange of shared information is an important issue. Standards for data exchange are crucial, in particular to enable communications between different IT platforms.

Recommendation

Advance technology-driven thinking and practice across design, production, build, operations and maintenance. Joining up web-enabled supply chain processes and communication standards will cut construction costs and promote seamless customer solutions throughout the construction lifecycle.

Invest in people

Construction firms need to become learning organisations, absorbing and using knowledge and providing for lifelong learning. Investing in human capital and knowledge awareness - a company's most important asset - will help to bridge the skills gap. Research and development will maintain competitiveness. The industry also needs to be responsible for assuring the health of its people, so that health monitoring / screening and better health and safety training are required.

In ten to twenty years the construction industry will require a complete range of different skills. To meet these needs a re-think is required in the way that construction education is organised. Computer integration of construction processes implies a need for cross-disciplinary education.

Recommendation

Re-think construction education. Define future people skills and integrate education, knowledge and learning across the entire construction process. Lifelong learning and knowledge management, will enhance industry standards, improve profitability and attract better people into the industry.

Improve existing built facilities

Half the UK's construction output consists of repairs and maintenance to existing facilities. New ways are needed to exploit alternative uses and innovative technology. The refurbishment 'process' needs clearer understanding and more efficient practices. Components need to be improved, with an emphasis on standardised, modular products. Much of the built environment was not designed for inclusivity, so there are few facilities easily accessible to the elderly and disabled. Obsolescence in existing facilities could be overcome by technical fixes or re-use. Data on operation and maintenance costs, and better asset management, will help to ensure the sustainability of existing facilities.

Recommendation

Improve renovation and repair methods and practices. Ensure research and development embraces technologies and components for repair and refurbishment. Better refurbishment 'processes' and standards for their supply will enhance living conditions and add value to existing built facilities.

Exploit global competitiveness

Global change needs to be faced and new strategies and alliances found to manage it. Opportunities exist for large and small firms to exploit global competitiveness through co-operation and information-sharing. UK component and construction suppliers don't understand their international competitiveness, and mid-size companies should dismantle their rigid structures and practices in favour of co-operative networks for greater flexibility. Today's technology can help achieve this.

Recommendation

Recognise the impact of globalisation and exploit flexible, collaborative, business frameworks and information sharing. Helping all construction businesses, from research and design to manufacturing and supply, to cope with globalisation and harness the technology required to manage it will improve business co-operation and create competitive advantage.

Embrace sustainability

Sustainability embraces long-term environmental viability as well as economic and social issues. Built environment design, construction and operation should be sustainable in use, re-use and recycling of materials and energy. Whole life thinking needs to prevail from design and manufacture, to build, operation, maintenance and disposal. Sustainability will increasingly be 'market-driven' and a concerted effort is required to change the embedded culture of construction industry thinking to embrace sustainability at every level. Sustainability needs to be clearly 'valued' and supported by the financial community, clients and public alike.

Recommendation

Sustainable construction and whole-life principles need to be client-driven. By shifting industry culture to embrace sustainable thinking at every level we can save energy, reduce waste and pollution and cut the lifetime costs of property ownership.

Increase investment returns

The perception of construction among financial institutions and the public needs to be changed to that of a high-tech industry delivering value through new methods of funding. To compete for funding the industry needs to be more innovative and show better assessment and understanding of risk. Increased risk sharing and greater profitability would make a notable difference to funders' attitudes. Investors need greater confidence in the ability of the construction sector to deliver results that reflect a sensible level of risk linked to reasonable returns. The existing image of construction as seen by institutional investors and the public is not good and there is a notable image problem.

Construction needs to change from being seen as a high-risk low-return sector to a low-risk high-profit industry. This will only come about through greater investment in innovation and in skilled people, higher standards, better quality and increased profitability. The move from public to private investment in infrastructure will continue but new ideas are needed to support and encourage this.

Recommendation

Seek innovative methods of demonstrating the value of built assets and lessening project risk. By better understanding 'risk and reward' principles the industry will increase profitability, improve the way it is perceived and valued and encourage new types of funding and investment.

Plan ahead

The industry needs to anticipate and plan for the future through long-term strategic thinking, better forecasting and investment, and new customer framework agreements. This requires the sector to change the business structure to reflect a longer term perspective. The industry needs to think about how buildings and facilities will be in twenty years, to consider future technology trends and impacts, and determine the future competition. These actions are needed so that construction companies can recognise and create new opportunities. The changing business structure should reflect local and global issues. It also needs to recognise the inherent lack of business skills within many smaller construction firms. Planning and preparing for the future will ensure it is always in the best possible position to manage economic downturns and remain globally competitive.

Recommendation

Anticipate and plan for change. Greater awareness of the cyclical nature of construction economics, long-term strategic thinking, future forecasting and co-ordinated planning will help the sector to better meet future customer needs, remain competitive and improve its contribution to the UK economy.

MAKING PROGRESS

Since publication of the Foresight report in Autumn 2001 we have continued to look ahead.

Future scenario

Earlier this year a joint workshop organised by Foresight, CRISP and the Foundation for the Built Environment, brought together 45 industry delegates representing a wide range of industry views, to consider how changes in a world in twenty years time might impact on the construction sector and what should be done to embrace the challenges and opportunities presented.

Participants first gave their views on possible and likely future trends in areas, such as lifestyles and attitudes, environmental issues, political and social issues, and scientific and technical developments. They were then asked to identify the top five aspects that they thought the construction industry should focus on. Their collective responses indicated that top priorities should be placed on:

- New technologies – especially nanotechnology, robotics and artificial intelligence
- Engagement and understanding with users and a better value proposition for society
- Addressing and mitigating environmental impact
- Building on the basis of whole-life performance
- Addressing human resource limitations, training and cross-profession fulfilment

Finally the participants were asked to determine the implications and indicate what needed to be done now to prepare for the future. Amongst the key suggested actions to emerge were the need for:

- A strategic forum to engage the financial institutions and government in developing an alternative value measurement system for construction
- A future 'blueprint' for construction, with consistent principles
- Political champions
- Best practice examples from other countries
- A single institution for construction
- A strategic forum to develop a future vision for the industry

Construction research

In support of the requirement to advance construction innovation and research and thereby improve the overall construction process, the UK Government earlier this year published a review of relevant Government R&D policies and practices, Fairclough (2002). This took into account many of the recommendations of the Foresight report and supported the views that both the Government and industry needed greater and more collaborative investment in construction research.

It proposed a new forum to play a pivotal role in strategic research thinking and called for a strategic vision for construction that acknowledged the construction sector's contribution to the 'quality of life' agenda. It also called for recognised centres of construction research excellence, longer-term and multi-disciplined university-industry research programmes for the built environment and greater support designed to encourage innovation throughout the industry.

IN CONCLUSION

Examining the future and determining what needs to be done now in order to prepare for it, is proving to be a catalyst for action. It remains for the construction sector in the UK to continue to adopt a proactive, rather than reactive approach to the constantly changing world that surrounds it and for which it has the responsibility for ensuring a sound and sustainable built environment for the future.

REFERENCES

DTI, Foresight (2001). *Constructing the Future*. HMSO, London.
Egan, J. (1998). *Re-thinking Construction*. DETR, HMSO, London
Fairclough, J. (2002). *Rethinking Construction Innovation and Research*. HMSO, London.
Latham, M (1994). *Constructing the Team*. HMSO, London.

Advances in Building Technology, Volume 2
M. Anson, J.M. Ko and E.S.S. Lam (Eds.)
© 2002 Elsevier Science Ltd. All rights reserved

ENGINEERING PERFORMANCE IMPROVEMENT USING A HYBRID ARTIFICIAL INTELLIGENCE SYSTEM

Luh-Maan Chang and Lei Zhang

School of Civil Engineering, Purdue University,
West Lafayette, IN 47906, USA

ABSTRACT

Industrial construction projects have been experiencing serious problems such as cost overrun and schedule delay. While seeking for the causes of the problems, people have come to realize the impacts of engineering activities on a successful project implementation. Improving engineering performance can lead to better project outcomes. Former studies on engineering performance improvement have either focused on the promotion of certain techniques or products, or looked at specific engineering processes or areas. There is a lack of a systematic and analytical approach that improves engineering performance based on the understanding of the relationships between engineering inputs and project outcomes. The paper proposes a generic model, which integrates genetic algorithms with artificial neural networks, for modeling engineering performance measurement and improvement on industrial construction projects. Due to its robust and efficient search ability in complex situations, genetic algorithms are employed to search for solutions to improving engineering performance with the searching criteria, fitness function, being the neural networks that have been trained to predict performance for given engineering inputs. To make suggestions for possible engineering performance improvement, the research introduces the idea of self-comparison evaluation, which compares a project's actual engineering performance to its possible better performance searched by genetic algorithms.

KEYWORDS

Engineering Performance, Engineering Performance Improvement, Artificial Neural Networks, Genetic Algorithms

BACKGROUND

For a long time, industrial construction projects have been experiencing unsuccessful implementation of projects. An industry survey (Post 1998) reported that one-third of the projects surveyed was over budget and nearly half was delivered late.

The development of an industrial facility spans over five stages: pre-project planning, detailed design, procurement, construction, and start-up and commissioning (CII 1997). Early researches addressed the impact of engineering performance on the overall outputs of a project. For example, design errors, changes and omissions could constitute approximately 10% of the total installed costs of a project while construction mistakes account for only about 2% (Davis *et al* 1989). 25% of the

facility owners surveyed by Post (1998) ranked detailed design as the weak link in the process of facility development.

The Research Team 156 (RT-156) of Construction Industry Institute (CII) conducted a research project to measure engineering productivity and establish the cause-effect relationship between engineering inputs and project outputs. The team studied the industrial project data collected by CII Benchmarking and Metrics (BM&M) Committee. The study reported that the detailed design phase was a prime source of project schedule delays and that about half of the project scope and development changes were initiated during the detailed design phase. The report also pointed out that design errors were the utmost source of field rework and that design-related field rework surpassed that initiated by both owner and constructor (Georgy *et al* 2000).

PROBLEM STATEMENT AND RESEARCH OBJECTIVES

Since industrial projects involve huge amount of investment, even a small percentage of cost overrun or schedule delay will result in serious economic loss. Therefore, there is an urgent need to improve project outputs through improving engineering performance. This research aims at searching for approaches to improve engineering performance on industrial construction projects through integrating genetic algorithms with artificial neural networks. Engineering refers to the detailed design phase of an industrial project. The following objectives are to be achieved:

- To explore the power of genetic algorithms and artificial neural networks in improving engineering performance.
- To construct a plausible approach to evaluating engineering performance

PREVIOUS STUDIES ON ENGINEERING PERFORMANCE

Engineering Performance Measurement

Engineering is a systematic process with inputs and outputs. Engineering performance measurement deals with the output side. The ability to successfully perform the engineering and design activities on an industrial construction project depends on various project input variables (i.e., project attributes and conditions), which are essential in driving its engineering performance. There was a lack of analytical scheme that can approximate the cause-effect relationship between engineering inputs and outputs until the research work of CII RT-156.

CII RT-156 identified a total of 25 engineering input variables and ten engineering performance measures, as shown in Table 1 and Table 2 respectively. Figure 1 illustrates RT-156's framework. The first part is a framework for establishing the relationships between engineering inputs and engineering performance measures through neuro-fuzzy networks. The second part evaluates engineering performance via a composite index, which is the value of a multi-attribute utility function with the engineering performance measures being the variables (Chang *et al* 2001).

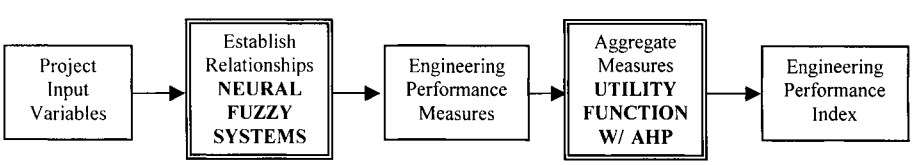


Figure 1: CII RT-156's Framework

TABLE 1
ENGINEERING INPUT VARIABLES

Category	Variables
General project attributes	Project size (total installation cost)
	Contract type
	Relative size of project compared to projects of the same industry type
	Relative level of complexity
	Site conditions
	Legal and environmental conditions
General owner attributes	Owner profile and participation
	Newness of process technology to owner
	Owner previous experience with designer
General designer attributes	Split engineering practices
	Designer qualifications and capacity
	Newness of process technology to designer
Project schedule	Design schedule
	Design-construction overlap
Project information inputs	Completeness of scope definition
	Completeness of objectives and priorities
	Completeness of basic design data
	Quality of constructor input and constructability
	Quality of vendor data
Level of automation	Use of 3D CAD modeling
	Use of Integrated Databases (IDB)
	Use of Electronic Data Interchange (EDI)
Project changes	Percent TIC scope changes
	Change management procedure
	Change communication system

TABLE 2
ENGINEERING OUTPUT VARIABLES (ENGINEERING MEASURES)

Category	Variables
Detailed design value	% design rework
	Design document release commitment
	% detailed design schedule delay
	% detailed design cost overrun
Fabrication and construction value	% fabrication and construction schedule delay due to design deficiencies
	% fabrication and construction cost overrun due to design deficiencies
	% construction hours for design problem solving and field design
	% estimated dollar savings due to constructability
Start-up and commissioning value	% start-up schedule delay due to design deficiencies
	% start-up cost overrun due to design deficiencies

Engineering Performance Improvement

Researchers in the past tried various approaches to improve engineering performance, but most of their approaches are qualitative in nature and have certain limitations. The limitations come from the fact that some approaches promote the use of a specific technique or product and some look at specific areas of engineering and design activities (Armentrout 1986, Atkin and Gill 1986, Breen and Kontny 1987, Choi and Ibbs 1990, Ginn and Barlog 1993, Teicholz 1996). There is a lack of a systematic and analytical approach that looks at improving engineering performance based on the understanding of the relationship between engineering performance and its driving factors (Tables 1 and 2).

THEORETICAL FOUNDATION

Artificial Neural Networks (ANNs)

ANNs emulate the behavior of human neurons as well as their learning ability. Their basic element is also called neuron (or node). All neurons are organized in layered structure and connected with weighted links. There is always an input layer where the initial stimulus happens, and an output layer where the final reaction of the system is shot out. There could be more than one hidden layer. ANNs' two major functions are learning and recall. Learning is the process of adapting the connection weights in an ANN to produce the desired outputs in response to inputs. Recall is the process of producing outputs in accordance to specific inputs using the knowledge obtained through learning (Tsoukalas and Uhrig, 1997).

Genetic Algorithms (GAs)

GAs are robust general-purpose search program based on the mechanism of natural selection and natural genetics (Holland 1972). Genes and chromosomes are the fundamental elements in GAs. A chromosome is a string of genes. In a real problem, genes are the variables that are considered influential in controlling the process being optimized, and a chromosome is a solution to the problem. GAs search for the optimal solution from populations of chromosomes. In this research, the genes will be the 25 input variables in Table 1. A chromosome is a set of the 25 input variables. There is an objective function (preferably called fitness function) in GAs. The search process seeks the maximum or minimum value of the fitness function. Crossover and mutation are two basic operations in GAs. Crossover is a process of producing new individuals by recombining the information contained in two parents. Mutation alters individuals randomly by changing the value of some of the variables.

MODELS

The fundamental approach of the research is to employ GAs to search for the engineering performance inputs that lead to optimal engineering performance. The neural network system shown in Figure 1 serves as a complicated fitness function. Three models were built.

- Engineering Performance Index Model (EPI Model).
- GA-ANN-Integrated Search Model (GA-ANN Model).
- Engineering Performance Evaluation Model (EPE Model).

EPI Model

EPI model is in essence the framework of CII RT-156. As illustrated in Figures 2a and 2b, EPI model is comprised of two parts. The first part is 10 neural networks that establish the relationships between the 25 engineering inputs and the 10 engineering performance measures respectively. The

second part is a multiple attribute utility function that takes the outputs from the 10 neural networks in the first part as its inputs and translates them into a composite utility score, called engineering performance index.

The 10 neural networks, after being trained, can predict performance measures for given engineering inputs. The 10 engineering performance measures depict, from different perspectives, the quality of outputs of engineering activities. However, if it is required to evaluate a project or to compare it with another one, it will be hard to make the judgment when 10 varying measures are presented. Therefore, there comes the need for a single composite measure that indicates the overall level of engineering performance and contains the information embedded in the 10 measures. Through multiple attribute utility function, an engineering performance index is defined on the scale of [0, 1] with 0 depicting the poorest engineering performance and 1 the best performance.

Thus, through the trained neural networks in EPI model, if given engineering inputs, EPI model can make prediction on engineering performance through both a group of 10 different measures and an overall engineering performance index. The set of 10 measures gives a comprehensive view of engineering performance. The engineering performance index will be used as fitness function value in the following GA-ANN model and EPE model.

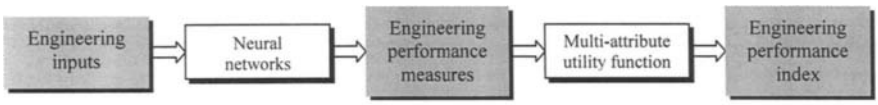


Figure 2a EPI Model -- General Idea

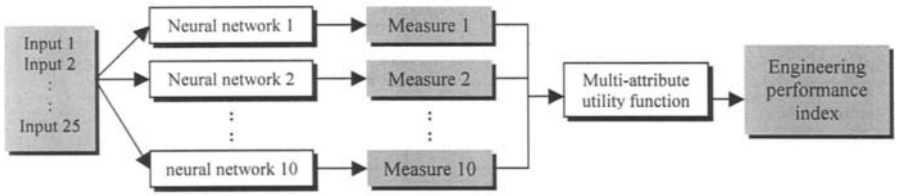


Figure 2b EPI Model -- Breakdown

GA-ANN Model

GA-ANN model, as shown in Figure 3 on the next page, depicts a typical genetic search process. The most distinguished feature of GA-ANN model is its fitness function, EPI model. This is where the GA-ANN integration happens.

The genetic search starts with an initial population. The initial population is comprised of a number of individuals. Each individual is a chromosome consisting of 25 genes, each of which corresponds to an engineering input. Then, all the individuals in the initial generation are evaluated through the fitness function, EPI model. Each individual, a set of 25 engineering inputs, is presented to the trained neural networks. The fitness function value will be the predicted engineering performance index. Then the initial generation goes through the genetic operations: selection, crossover and mutation, during which individuals with higher fitness values get selected, reproduced, crossed over and mutated. Thus, the second generation is formed, and the fitness values are assessed for its individuals, ... This process keeps going on until a certain termination criterion is met. Usually the termination criterion can be a desired fitness value, the maximum number of generations or

computation time. By the time the process stops, one or more sets of engineering inputs will be identified as the ones that can lead to an engineering performance levels close or equal to the desired one.

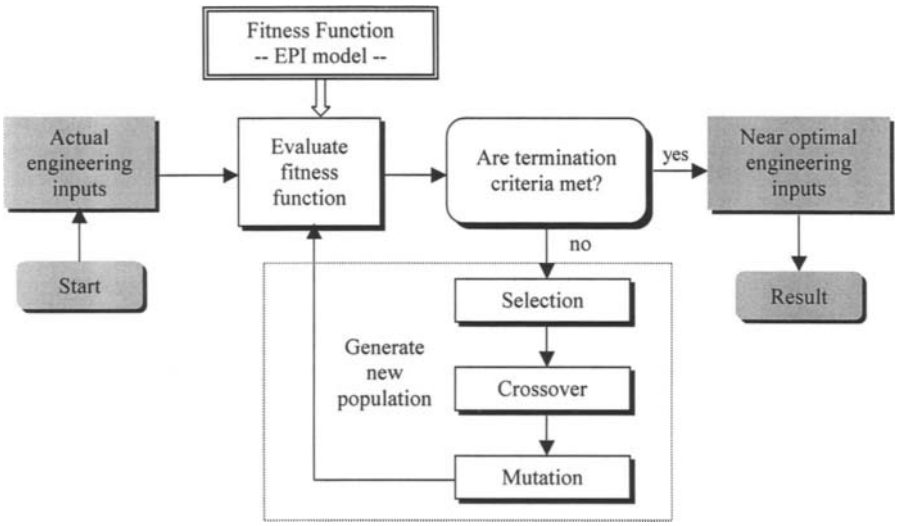


Figure 3 GA-ANN Model

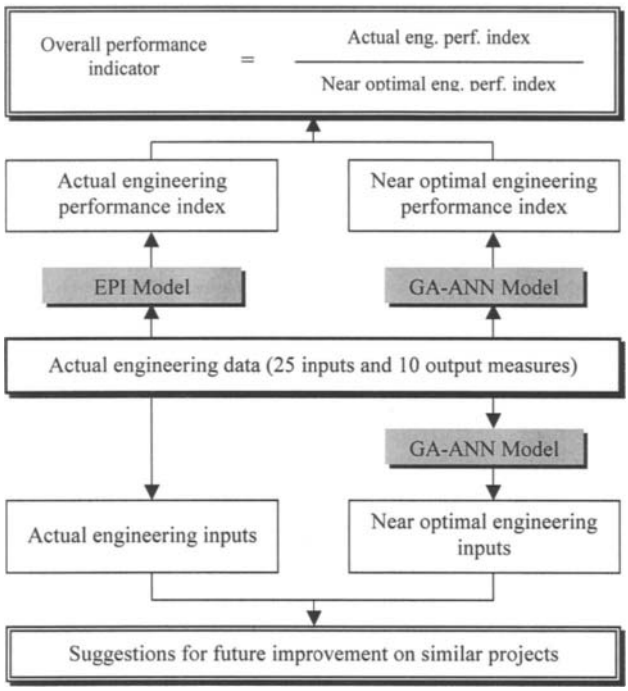
EPE Model

EPE model is the implementation of both EPI model and GA-ANN model, as shown in Figure 4. The fundamental idea of EPE model is a self-comparison concept. The following explains the idea.

As shown by the up-arrows in Figure 4, through EPI model, a project can get an engineering performance index that to some extent indicates its actual level of performance. The same project can also obtain a near optimal engineering performance index through GA-ANN model. The self-comparison compares the actual index with the near optimal one and uses the ratio as an overall performance indicator to indicate how much of the engineering performance potentiality has been realized on this project.

Thus, the evaluation is made by comparing what has been done to what could have been done on the project rather than by comparing the project to a common standard. Previous studies tried to find or create a common standard and made evaluations by comparing actual projects to the standard. However, industrial construction projects differ significantly from project to project, and clients and contractors keep a stable and long-term partnership that makes their projects highly customized. Therefore it is not appropriate to find a common standard for all projects even in the same category of heavy processing facility construction. This justifies the self-comparison idea.

EPE model does another self-comparison shown by the down-arrows in Figure 4. For a project, GA-ANN model can search for the near optimal engineering inputs. Comparing the actual engineering inputs and the near optimal ones may point out where improvements should be made on similar projects in future.



How the Models Work Together

EPI model, GA-ANN model and EPE model work together in a relationship shown in Figure 5. EPI model is the foundation that provides fitness function for GA-ANN model and serves as prediction model for both GA-ANN model and EPE model. GA-ANN model does near optimal search for EPE model. EPE model is the implementation of EPI model and GA-ANN model based on the self-comparison concept.

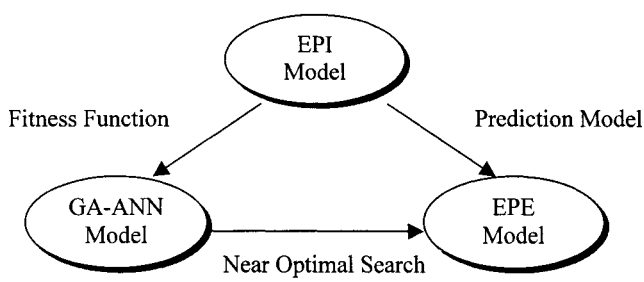


Figure 5 Relationships between Models

ANTICIPATED APPLICATIONS OF THE MODELS

For past projects, GA-ANN model and EPI model together search the near optimal engineering performance and the corresponding engineering inputs, and EPE model makes the overall engineering performance evaluation and points out what could have been done to achieve better engineering performance.

For future projects, GA-ANN model looks for the possible near optimal engineering inputs and outputs for the project. These anticipated project inputs and outputs might act as the guideline and goal at the actual implementation stage.

DATA ANALYSIS

The project data for validating the proposed models are being collected by the authors.

SUMMARY

This paper proposed a systematic approach to improving the practice of engineering performance. The fundamental idea is to find the possible best practice of engineering activities for a given project. To pursue this, artificial intelligence techniques are employed to build the models. Artificial neural networks provide the ability to establish the relationships between engineering activity inputs and engineering performance outputs, and genetic algorithms serve as a search engine to find the possible best engineering practice based on the relationships between engineering inputs and outputs identified through artificial neural networks.

REFERENCES

Armentrout D. R. (1986). Engineering Productivity Management and Performance Measurement. *Journal of Management in Engineering* **2:3**, 141-147

Atkin B. L. and Gill E. M. (1986). CAD and Management of Construction Projects. *Journal of Construction Engineering* **112:4**, 557-565

Breen W. C. and Kontny V. L. (1987). Automation's Impact on Engineering Design Progress. *Journal of Management in Engineering* **3:4**, 275-287

Chang L. M.,, Georgy M. E. and Zhang L. (2001). *Engineering Productivity Measurement.* Research Report, RR156-11, Construction Research Institute, Austin, TX

Choi K. C. and Ibbs C. W. (1990). Costs and Benefits of Computerization in Design and Construction. *Journal of Computing in Civil Engineering ASCE* **4:1**, 91-106

CII (1997). Determining the Impact of Process Change on the EPC pprocess: A Model to Quantify Time Cost Improvements. *Report, IR125-2*, Construction Industry Institute, Austin, TX

Davis K., Ledbetter W. B. and Burati J. L. (1989). Measuring Design and Construction Quality Costs. *Journal of Construction Engineering and Management ASCE* **115:3**, 385-400

Georgy M., Chang L. M. and Walsh K. (2000). Engineering Performance in Industrial Construction. *Proceedings for Construction Congress VI*, ASCE, Orlando, FL

Ginn D. and Barlog R. (1993). Reducing Complexity and Working with Bottlenecks Improves an Oil Refinery's Engineering Performance. *National Productivity Review*, Winter 1993/1994, 63-77

Holland J. (1975). *Adaptation in Natural and Artificial Systems,* The University of Michigan Press

Post N.M. (1998). Building Teams Get High Marks. *Engineering News Record* **240:19**, 32-39

Tsoukalas L. H. and Uhrig R. E. (1997). *Fuzzy and Neural Approaches in Engineering,* John Wiley & Sons, Inc.

Advances in Building Technology, Volume 2
M. Anson, J.M. Ko and E.S.S. Lam (Eds.)
© 2002 Elsevier Science Ltd. All rights reserved

LIFE-CYCLE INTEGRATED MANAGEMENT INFORMATION SYSTEM (LMIS) OF CONSTRUCTION PROJECT

HE QING-HUA

Research Institute of Project Administration and Management, Tongji University
Shanghai, 200092, P. R. China

ABSTRACT

Information systems, which are almost separately developed for Development Management in the decision phase, Project Management in the implementation phase and Facility Management in the operation phase, just serve their own separate management purposes and are established in different project languages and work platforms. Flexible, effective and efficient information communication is difficult to realize and this causes many potential disadvantages. The paper puts forward the concept of the Life-cycle Integrated Management Information System (LMIS); and focuses on the framework of the information model, and the level and method of system integration.

KEYWORDS

Life-cycle, Integrated management, LMIS, Information model, System integration

The Life-cycle period of a Construction Project is composed of a decisions phase, an implementation phase and an operations phase. Each phase has a corresponding management method, Development Management (DM), Project Management on behalf of the owner (OPM) and Fkacility Management (FM). The Development Management Information System (DMIS) used in the decision phase, the Project Management Information System (PMIS) used in the implementation phase and the Facility Management Information System (FMIS) used in the operation phase are almost independent and isolated, only serving their self-management and not able to share and integrate information and data. The main ineffectiveness are presented bellows:

(1) Because the owner's management in the decision phase, the implementation phase and the operation phase are almost separated, the information that should be inter-related is created by individual information system. The data just serves special phase and could not be applied in other phases directly.

(2) Information systems for the different phases have different data structures and platforms. The data created in different phases cannot be shared, which causes the same data to be input several times. Resource waste and a lot of unnecessary mistakes are caused.

(3) During the information communication in different phases, much valuable information is easily omitted. Because of the separation of the DMIS, PMIS and FMIS, many communication obstacles occur and effective information is attenuated. Information cannot meet the needs of the information receptors.

(4) Information communication in different phases easily distorts the information also. When information is transferred between different users, such as a development manager, the project manager and the facility manager, the original meaning will be altered in many cases.

(5) Information transferred through different phases is delayed or interrupted [2].

(6) The cost of information processing is increased.

(7) Information transparency is reduced [13].

(8) The Information system cannot assist in the realization of the planning and life-cycle control aims.

(9) It leads to information content overload in communication in the different phases, and also makes it difficult for management the documentation in different version [3,4].

1 DEVELOPMENT TREND OF MIS APPLIED IN CONSTRUCTION PROJECT

With the rapid development of communication technology and information technology, more and more attention is paid to the applications of Management Information Systems in the construction industry. In general, five key points are as follows:

(1) Among the different Management Information Systems (such as PMIS and FMIS), and the Management Information System subsystems (such as the finance management subsystem, cost control subsystem, contract management subsystem), research into systems integration has been paid more and more attention. Information sharing and data efficiency could be reached through using a uniform data structure and a more effective Documentation Management System [5,15].

(2) The integration of Management Information Systems applied in the construction industry and other computer-aided systems are being improved. Examples include the integration between FMIS and CAD system, and between cost control systems and CAD systems [6].

(3) With the adoption of a unified and open standard technology, such as TCP/IP protocol and java language platform, an openness is greatly improved. The reliability of the Management Information System on special software and hardware platforms will be reduced, its transplantable ability and inter-operation will continuously improve, making extension and application easier.

(4) A Management Information System attaches more emphasis to the integration of a computer network platform, so that different location projects can be managed conveniently, such as linear infrastructure projects [1,12,14].

(5) Management Information Systems are adopting more advanced systemic methods (such as the technology of Object-Oriented system analysis and design) and emphasizing users' participation which improve efficiency and agility in developing the systems [5.15].

2 THE CONCEPT OF LMIS

Based on the analysis of trends in development and the weakness in traditional Management Information Systems applied in the construction industry, the paper puts forward the concept of Life-cycle Integrated Management Information System (LMIS) for construction project. LMIS may be defined as an integrated human-computer interoperability system serving the investor, developer, operators, development managers, project managers, facility managers; it uses software, hardware, network communication equipment and other office equipment, and its aim is to realize the objective of the life-cycle management target (including cost objectives, schedule objectives, quality objectives, etc.) . It enables all the different participants to acquire and process life-cycle information accurately, on time, efficiently and effectively in supporting them to plan and control the project.

LMIS should possess the following characteristics.

(1) Integration
Interior and exterior integration are the two main aspects of the LMIS integration. Combined with Text data and Graphic data in the system, LMIS maintains the integration of the data by cooperative working with different function models in different phases of the life-cycle period. To reach this goal, the best method is to put all the data for the different phases of the life-cycle period into the same central database. LMIS should have an openness of input and output which can link to exterior systems so as to achieve integration with outside data.

(2) Openness
LMIS should have good compatibility with other systems and could examine the reliability of outside data to ensure safety. The GRANID system developed by GIB engineering consulting company in Germany has many merits to be referenced. The system is able to process data with different formats, such as inputting graphic data with DXF and DWG, inputting text data with PCX and ASC II , using SQL to exchange data with RDBMS, and receiving PDS, DXF, DWG, HPGL, HTML, ASC II .

(3) Better communication
In the decision making for, implementation and operation of modern construction projects, different involved participants provide service in different locations. To realize the life-cycle objective, LMIS should possess strong communication capability. Distributed database's Client-Server systems could be applied to organize information created in different phases during the life-cycle period. Users in different locations use the same central database independently and harmoniously as in a virtual LIMS' office. Consistency, continuity, integration, safety, reliability of data in a central database could be ensured through the definition of centralized and distributive working processes. By using data safety and security technology, data safety on a network platform could be achieved.

3 INFORMATION MODEL OF LMIS

A unique information model is necessary for information communication and processing among different phases and involved participants. But, LMIS should receive information such as CAD files, and other information and data from designers, contractors and suppliers. This could be realized through interface processing programs.

Using the unified information model to integrate information in different phases and between different participants has been paid more and more attention in recent years. The paper analyzes and compares the following information models focusing on the establishment of a unified information model: Building Construction Core Model (BCCM), Information Reference Model for AEC (IPMA), Building Project Model (BPM), information models in Information/Integration for Construction (ICON),

Unified Approach Model (UAM), General Construction Object Model (GenCOM), ATLAS LSE Project type Model (PtM), Generic Reference Model for life-cycle facility management 【2,3,9,10,11,16,17,18】.

The BCCM is suited for ISO STEP and has more advantages compared to other models. Figure 1 is the framework of BCCM information model 【9】.

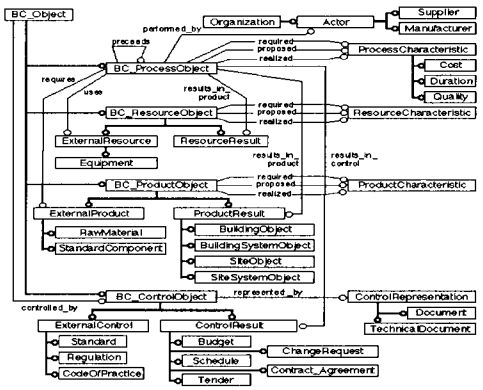


Figure 1: Framework of BCCM information Model

The BCCM information model reflects the relationships among the parts of a project. It could be used as a carrier for all the information in life-cycle management. Thus the central database can be defined and this database is surely well integrated. Meanwhile, the BCCM information model has good adaptability. It is suited for all different kinds of construction projects. It could be used as the basis of the LMIS information system design. To satisfy the character and requirement of LMIS, the BCCM information model should be adjusted in the following ways.

(1) The Product object is the description and definition of the construction project physically including the space usage. It will be adjusted until it is identical to the project, and used as the core of the LMIS information model. The Product object may be defined using a project breakdown structure and code system.

(2) Information objects for life-cycle integrated management is made from procedure objects, control objects and resources objects. Every information object is defined through several attributions.

(3) Building the relationship between project breakdown structure and all the information objects. Any node of the project breakdown structure may become a carrier of a certain information object and its attribution. So all the management functions can be linked through a project breakdown structure, and the data used for the same management function is integrated and the data from different management function is integrated too if necessary.

(4) The project breakdown structure based on product objects and information objects is a two dimensional information model of LMIS. Thus all the information in a construction project's life-cycle phase is integrated with the help of a project breakdown structure, and could be integrated in different ways for certain information objects such as contract, time, cost. etc..

According to the principles and methods just discussed, the system structure of an LMIS information model should be established as in Figure 2.

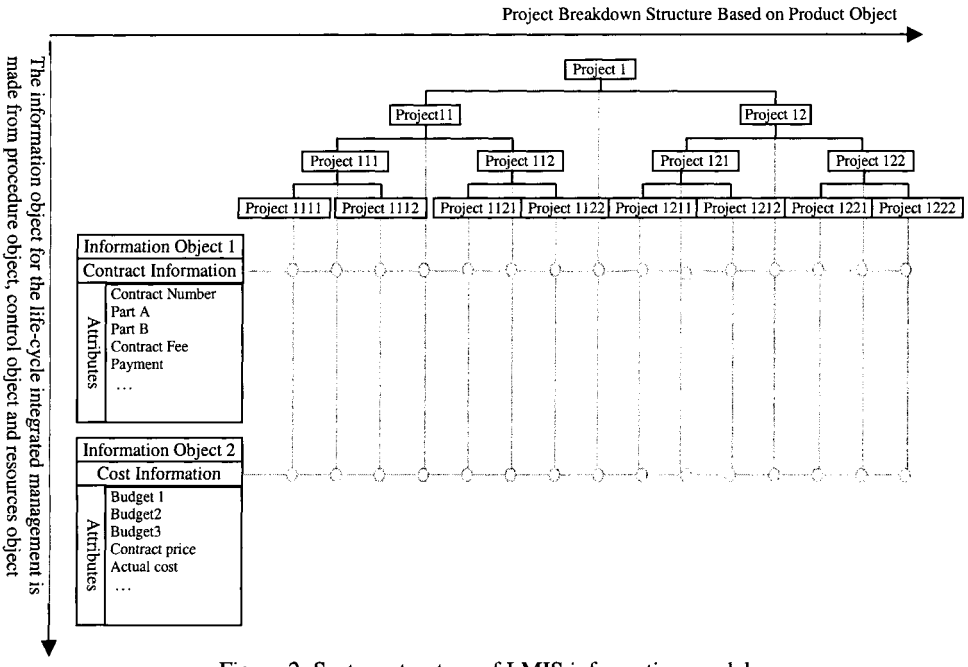


Figure 2: System structure of LMIS information model

4 INTEGRATION LEVEL AND METHODS OF LMIS DEVELOPMENT

Generally, the development of an LMIS follow two basic methods: integration based on a single project database and the integration based on an interfacing approach [15]. The integration level of the former is higher and the system has uniform information models and databases, and the integration level of the latter is lower. The latter comprises only communication between systems, and there is no uniform information model connecting different programs, databases, interfaces and project views. Normally the programs exchange data by links or an integrating environment [19]. After a comparison and analyses of many similar systems, the OPIS (Object-model based Project Information System) and GRANID system have significant advantages for studying the approaches and levels of LMIS.

Thomas Frose, who pursued his Ph.D. degree in Standford University, first declared the OPIS system in 1992. The main aim of OPIS is to realize computer-aided management integration through shared Object Oriented Models. Figure 3 shows the Integration levels and structure of the OPIS system [18].

OPIS system has four integration levels.

(1) System-level object. It includes system-level control and shared objects and allows users to switch between different applied models through an interface.

(2) Shared central database. It is shared by all applied models and is the core of the system. The system uses the database to store all information related to different applied models. The database has applied Objective-C for the writing of Shared Object Libraries for managing the system.

(3) Modules application. This has the ability to input and analyze the input data. The applied models defined in the OPIS system include libraries browsers, planning based on expert systems, cost-control, schedule-control and CAD links.

(4) Stand-alone Applications. This level introduces Stand-alone Applications, such as CAD to the OPIS system by the created linking models.

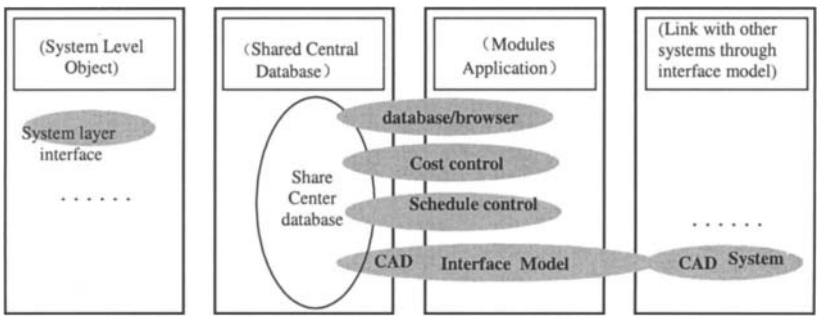


Figure 3: Integration levels and structure of the OPIS system

The GRANID system is developed by the GIB Engineering Consulting Company in Germany. It is integrated software approximately achieving the philosophy of a life-cycle integrated management information system. The application modules of the system include: strategic planning of project decision-making, project management and control, and facility management. [9]. Integration Levels and Methods of the GRANID system are shown in figure 4 [9].



Figure 4: Integration levels and method of GRANID system

The core functions of the GRANID system, such as cost-control, schedule control and strategic control, CAD management and housing handbooks, are based on a central database and ensure the consistency of the data for the Life-cycle period. The core functions include:

(1) Linking. In order to achieve flexible integration and process data with other applied systems.

(2) Reliability verification. In order to verify the data read by other applied systems and ensure the data input meet the applied requirement of the GRANID system.

(3) Report system. To provide different detailed-level reports to different users.

(4) Search system. To provide on-line search facilities and allow users to search by different combinations of methods.

(5) Management Information System. This is a user interface to the Report System and Search System, to provide a series of visualization express tools for such as figures, traffic lights [7].

The integration levels and method of LMIS are as follows based on the analysis of the OPIS system, GRANID system and other similar system.

(1) The life-cycle integrated management information system of a construction project should be based on a central database. Through the building of the central database, is achieved a management function including Development Management in the decision phase, Project Management in the implementation phase and Facility Management in the operation phase, which leads to efficient integration of data for different function models and ensures the consistency of data in different stages of the Life-cycle. The definition of the central database must use uniform information models.

(2) The data exchange between LMIS and other mature applied business software applied for designers, contractors and suppliers can be achieved by input-linked programs.

(3) LMIS will provide decision support information through data collection, transfer, processing, storage, updating and maintenance. According to the needs, a report system could output in terms of mature office software formats such as Microsoft Office format. The data exchange between mature office software and LMIS could be realized by an output-linked program.

Integration diagram of the LMIS system is shown in figure 5.

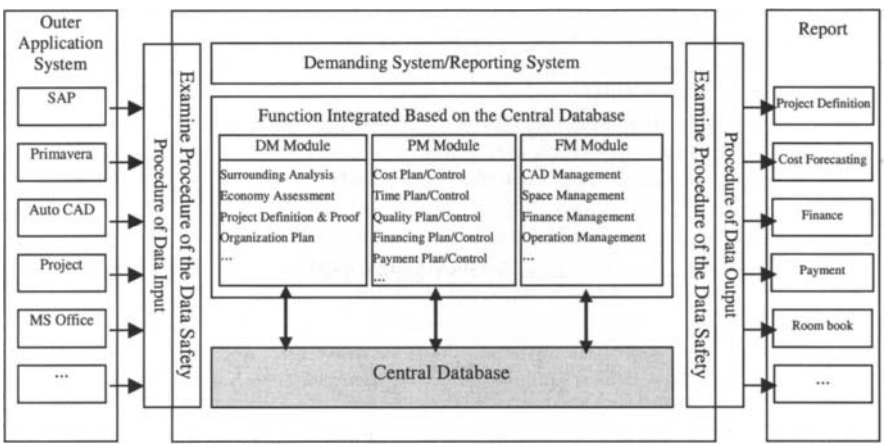


Figure 5: Integration chart of the LMIS system

5 SUMMARY

Recently, with the rapid development of management theories, information technology and communication technology, many researchers have tried to reform the traditional information management methods using different integration means, including product data integration, process integration, multi-disciplinary and supply-chain integration, tools integration and intra-business integration and so on. Compared with other industry, such as the mechanical manufacturing industry and motor industry, the application level of information technology in the construction industry is

much lower. The concept of LMIS uses a systematic view to integrate information in different stages. The aim is to overcome the weaknesses of the current isolated management information systems. The paper studies the key problem of LMIS system development, including the design of an information model, the integration levels and structure of LMIS.

REFERENCES

【1】 Alan Hecht.A (1998). Web-based project management framework. PM Network[R].

【2】 Aouad G. et.. (1994). Integration of construction information, Final report, University of Salford[R], UK

【3】 August-Wilhelm Scheer (1994). Wirtschaftsinformatik-Informationssusteme im Industriebetrieb[R], Shanghai Scientific Publishing Company

【4】 Bjork B. C. (1992). A unified approach for modeling construction information[R], Building and Environment, Vol.27, No. 2.

【5】 Chimay J. Anumba (2001). Integrated system for construction: challenges for the millennium[R]. International conference on construction information technology. Hong Kong.

【6】 Conrad Wong (2000). Computer-aided quantity survey software Vhstation[R], International conference on construction information technology 2000. Hong Kong. 2000.1.17-18.

【7】 Dr. -Ing Greiner Ingenieurberatung mbH (1999). Graphisches und alphanumeriche informations- und dokumentationssystem brochure[R].

【8】 Dr.-Ing Greiner Ingenieurberatung mbH Homepage (2001)[EB/OL]. http://www.gib-muc.com.

【9】 ISO. Building Construction Core Model (2002)[EB/OL].http://www.bre.co.uk.

【10】 Luiten G., Froese T., Bjoerk B. C., Cooper G., Junge R., Karstila K. & Oxman R. (1993). An information reference model for architecture, engineering and construction[R]. The first international conference on the management of information technology for construction. Singapore.

【11】 Luiten G. (1994). Computer aided design for construction in the building industry[R], Ph.D. thesis. Delft University of Technology. Netherlands.

【12】 Mesa systems guide Inc. Homepage (2002)[EB/OL]. http://www.mesasys.com.

【13】 Miler C. & Bock T.(1995). DISYNC-Distributed intelligent information system is construction[R]. 6th international conference on computing in civil and building engineering. Berlin.

【14】 Miroslaw Skibiewski (2001). Web-based project management for construction: search for utility assessment tools[R]. International conference on construction information technology. Hong Kong.

【15】 Mustafa Alshawi (2000). Integrated construction environments: technology & implementation[R]. International conference on construction information technology. Hong Kong.

【16】 Reschke R. & Teijgler H. (1994). Generic reference model for life cycle facility management[R]. ISO TC184/SC4/WG3 document N351.

【17】 Tolman F., Bakkeren W. & Boehms M.. Atlas LSE project type model (1994)[R], ESPRIT Project 7280-ATLAS/WP1/Task 1500 document D106-Ic.

【18】 Thomas Froese (1992). Integrated computer-aided project management through standard object-oriented models[R], Ph.D.thesis. Stanford University.

【19】 Thomas Froese(2002). Challenges and a vision for computer-integrated management systems for medium-sized contractors [EB/OL]. http://www.civil.ubc.ca/tfroese

Advances in Building Technology, Volume 2
M. Anson, J.M. Ko and E.S.S. Lam (Eds.)
© 2002 Elsevier Science Ltd. All rights reserved

INFORMATION REUSE MECHANISM FOR A MANAGEMENT INFORMATION SYSTEM: EPIMS

Ma Zhiliang[1], Yang Jun[1] and Yoshito Itoh[2]

[1] Department of Civil Engineering, Tsinghua University,
Beijing 100084, P.R. China
[2] Center for Integrated Research in Science and Engineering,
Nagoya University, Japan

ABSTRACT

The mass information generated in the construction phase includes documents such as a bill of quantities and drawings, records of construction and so on. Since this set of information covers the whole construction process of the project and all parties related to the project, it is expected to be useful after the project is finished. A management information system named EPIMS has been developed to support the collaborative work and the sharing of project information through Internet among the multi-party in constructive phase. This paper focuses on the reuse of the project information from EPIMS. The information reuse mechanism is established, and then a system approach to the information reuse is proposed. Finally, a prototype system called EXPLYZER is analyzed and the relative important issues are clarified.

KEYWORDS

Construction Projects, Information Reuse, XML

INTRODUCTION

Computer systems are becoming indispensable tools in Architecture/Engineering/Construction (AEC) industry nowadays. Even in such a narrow field as construction projects, many kinds of software system have been developed and applied. For example, various software systems have been used for cost estimating, scheduling, construction planning, information management etc.

There are two aspects concerning the application of computer systems in construction projects according to the scope of users. One aspect is the application in each party, such as within a constructor company or within an engineer company, and the other aspect is the application among the concerned parties of the project. Although the former is advocated for many years, no single system covers the whole construction process up to now. As a result, the format of information set obtained in the construction process differs from project to project depending on what separate software systems

the party uses in the project, and few standards or regulations have been put forward for managing the format of the information set. On the other hand, as far as the latter is concerned, the use of Internet has made it possible for the multi-party in a construction project to share a software system as a platform of project management.

Two authors of the paper et al. have succeeded in developing such a system called EPIMS (Electronic Project Information Management System 2002). By using the system, the participants of a construction project from different party may submit and reply information through Internet and the information are stored in the database server. Thus the participants can collaborate and share the information according to his role in the whole construction process. As a result of using EPIMS for project management, a uniform set of information is expected to accumulate in the database server in the end of the project. Since this set of information covers the whole construction process of the project and all parties related to the project, it is expected to be useful after the project is finished.

Zantout & Marir (1999) analyzed electrical document management systems (EDMS) used in industry. Dany & Simaan (2000) conducted a study on integrating document management with project and company data based on EDMS. These studies dabbled into but did not solve this problem completely. Yunsik, Mark & Robert (2002) for the first time used the word "Building Documents" to regard the information that can be reused and clarified some basic issues.

This paper focuses on the reuse of the project information that is accumulated during the project by using EPIMS. EPIMS is reviewed with the emphasis on the structure of database. Then the mechanism of information reuse is analyzed. Finally, the system model is established for a prototype system called EXPLYZER and the prototype system is currently under development. Although the discussion in the paper is around EPIMS, the methodology is applicable for similar systems.

REVIEW OF EPIMS

Traditionally, some party needs to submit paper documents in the critical steps in the construction process according some regulations or in response to some request for some other parties to check. For example, when the contractor are prepared on the construction, he needs to submit a report using a specified form possibly with some appendix documents to the engineer in order to start the construction. As a reply, the engineer fills some comments in the report, and then returns it to the contractor.

EPIMS is devoted for the collaboration of multi-party in the management of construction projects through Internet. It provides the mechanism of workflow so that by using EPIMS in the management of construction, the above-mentioned information is submitted and processed through Internet in an efficient way. That is, if the information needs to go through several participants before the process is finished, then it is automated according to the system settings that reflect the regulations. It also provides the functions of browsing the information from several different views, such as by information type, submission date etc. so that the participants can easily look up the information according to his role. In addition, it contains functions of arbitrary querying and graphic representation of query results. If it is used with a spreadsheet software such as Microsoft Excel, the statistics of the query results can be obtained.

In EPIMS, three types of information are dealt with, i.e. report form, reference to report form and appendix documents. Among them, the report form corresponds to the traditional ones, while the reference to report form and appendix documents correspond to the traditional appendix documents, because a copy of the report form has to be appended when it is used as an appendix.

A hybrid scheme of database structure is used to store the three types of information in the system. Namely, XML files and relational database are used to store the first two types of information and normal files such as Microsoft Word files are used to store the last type of information, because the first two types of information are structured and the last one is not. The reason why XML is adopted in the storage of information is that it can better accommodate complex structured information and facilitate the change of report forms without changing the programming code of the system. The reason why relational database is used along with XML files is to raise the efficiency of the system, because XML is less efficient when dealing with simple structured information.

REUSE MECHANISM OF INFORMATION FROM EPIMS

The information accumulated in the construction phase normally includes documents summarized in Table 1. When a project is completed, participants need to extract relative information from the database that contains these documents and conserve it as construction archives for information reuse. This demand is driven mainly by two aspects. One is that companies want to preserve the relative documents for future reference, and the other is that the government forces the owner to submit construction comprehensive information in order to preserve construction evidence and use it in the urban management.

TABLE 1
INFORMATION IN ARCHIVES

Classification	Description	Examples
Project Information	Fundamental description of a construction project	Bidding Documents Drawings Contracts
Construction Information	Information to record various segments of construction activity	Construction Records Quality Control Records Test Records Job Cost Records
Management Information	Information of strategy, activity in management	Conference Records Supervisal Monthly Statements
Other Information	Other aid information	Specifications Licenses

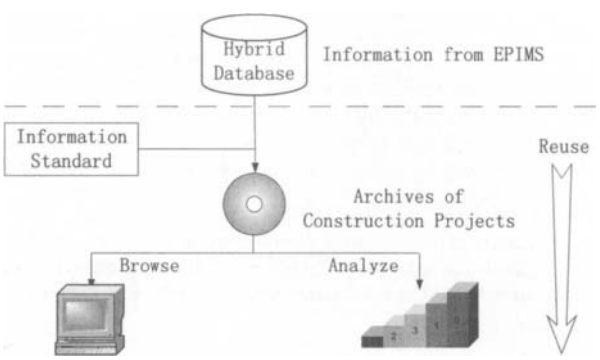


Figure 1: Information Reuse Mechanism in Construction Projects

Figure 1 illustrates the information reuse mechanism in construction projects, where the archives stand for the information in the construction phase that can be reused. To cope with different complete environments of participants, the archives should abide by information standard. Participants in construction projects obtain their archives from EPIMS based on their rights. Participants may reuse the information in their archives for different purposes. The comparison of information reuse among different participants is shown in Table 2.

TABLE 2
INFORMATION REUSE AMONG PARTICIPANTS

	Participant	Purpose	Reuse Method
Common	All	Archives to reconstruct various segments of a project's activity long after it has been completed	Browse Query
Special	Owner	Reference for operating the facility	Analyze
	Engineer Contractor	Consultant when similar jobs with similar problems are encountered in other projects	
	Government	Administration in construction industry	

The minimum objective of information reuse should be to ensure that archives are human-readable so that participants can reuse the information just as the archives in paper form. By using information technology, more efficient method for information reuse method is made possible. Two aspects can be expected. First of all, the function of query can be provided to help users find the desired information quickly. Secondly, the function of analysis can be provided to process the accumulated information to obtain information in the form of statistics, summary etc. to use them in decision-making. As a special case of analysis, artificial intelligence technology can be used to learn from the archives so that a system that can replace expert or at least can assist expert can be developed to cope with the requirements for experience from complex construction projects.

SYSTEM APPROCH ON REUSE OF INFORMATION FROM EPIMS

Conceptual Model of EXPLYZER

Based on the information reuse mechanism, we established the model of EXPLYZER, a prototype system that is named after Explorer and Analyzer, the two main components of the system. The conceptual model is illustrated in Figure 2. A component called Extractor will be developed and embedded in EPIMS to extract relative data from the system database according to the right of the participant. Explorer is the browser for the archives, by using which users can view or query information conveniently, and it can meet the common purpose of information reuse. On the other hand, Analyzer is the component by using which the information is analyzed to provide the users with information for the special purpose.

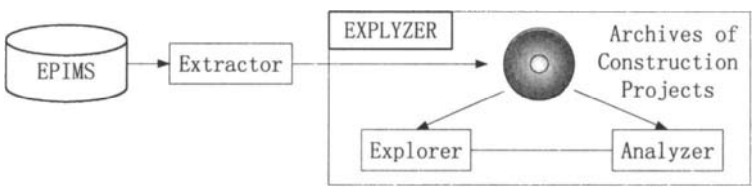


Figure 2: Conceptual Model of EXPLYZER

Structure of Archives

Archives should be a set of stored information. In order to make them be consistent with EPIMS and independent exclusively from a particular database management system, XML is adopted as the standard language in the archives. Namely, while EPIMS uses hybrid database to store the information in construction projects, the derived archives thus consists of mainly XML files without any relational database files.

The archives are formed in a hierarchical structure with 3-tire architecture shown as Figure 3. The core layer is the template layer that contains a set of schemata with corresponding XSL. Each schema can be viewed as the definition of a data container for a type of information, and the XSL file is the corresponding style format (Harold 2000). In this sense, the schema file and the style file together can be regarded as the template of information in construction projects. These templates can be derived based on that in EPIMS. The index tree of archives is described in the upper layer and data instances that conform to the schemata in the bottom layer. In addition, the normal files are connected with the data records through hyperlinks. In this way, any information entry can be retrieved from top to bottom.

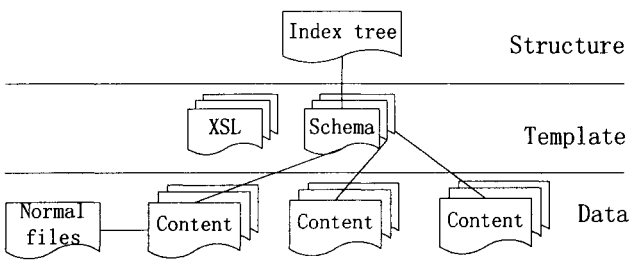


Figure 3: Hierarchical Structure of Archives

In order to efficiently and automatically retrieve the set of documents related to a given project, indexing data is included in the XML files. As shown in Figure 4, the indexing data in documents is directly derived from the reference to report form in relational database in EPIMS and contains references to project, participant, activity and other relative documents.

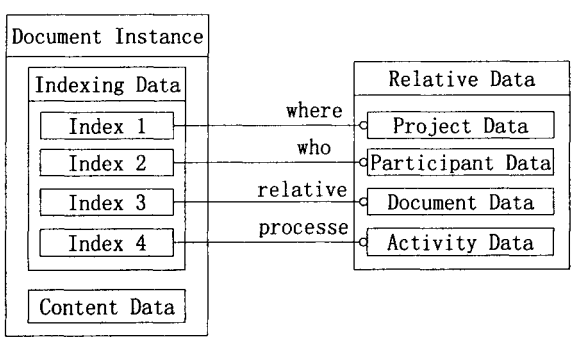


Figure 4: Document Indexing Structure

For example, an inspection record for a concrete beam takes the following form. In the part of indexing data, the information about this record such as the location, the constructor and supervisor of

the beam is described. The relationship between this document and others is represented by hyperlinks, which indicates the complementary information about the beam.

```
<? xml version="1.0">
……
<IndexingData>
    <ProjectData>
        <Location>
            <Division>division 2</ Division>
            <Floor>3</Floor>
        </Location>
        ……
    </ProjectData>
    <ParticipantData>
        <Contractor>ZhongGuanCun Construction Company</Contractor>
        <Supervisor>FangYuan Inc.</Supervisor>
    </ParticipantData>
    <DocumentData>                                          <!-- hyperlink -->
        <! ATTLIST RelativeDocument1 xlink:href="/test/ConcreteTestReportNo 24.xml" >
        <! ATTLIST RelativeDocument2 xlink:href="/test/SteelTestReportNo 24.xml" >
        <! ATTLIST RelativeDocument3 xlink:href="/photo/BeamPhoto.jpg" >
    </DocumentData>
    <ActivityData>
        <Submitter>Tom</Submitter>
        <SubmitDate>2001-9-6</SubmitDate>
        ……
    </ActivityData >
</IndexingData>
<ContentData>
    <ConstructDate>2001-8-17</ConstructDate >
    <InspectDate>2001-9-7</InspectDate>
    ……
    <InspectResult>qualified</InspectResult>
</ContentData>
……
```

Information Query in Explorer

In EXPLYZER, three methods for information querying are available. They use hierarchical structure; document indexing data and document contents respectively to query. The corresponding algorithms are summarized in Figure 5.

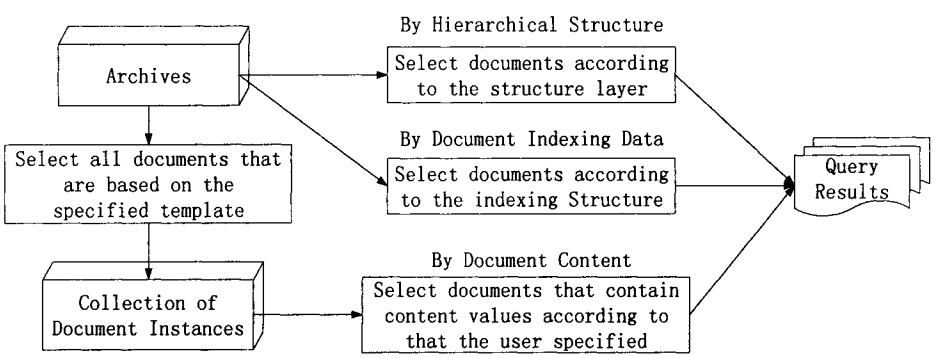


Figure 5: Query Algorithms for Three Supported Methods

The three methods of querying offer increasing detail of information query but with decreasing efficiency. Proper combination of these methods will achieve the balance between function and efficiency. For example, when structural cracks occur in several beams during the operation of the facility, the owner may need to inspect all beams constructed by the same contractor in the same period. He can do this in the following way. Firstly, he finds out the collection of document instances of inspection records in the project with the first method. Then he refines the collection according the contractor with the second method. Finally the required documents are selected by parsing the information item "ConstructDate" with the third method.

Case-Based Reasoning Model in Analyzer

In the experience-oriented construction industry, knowledge and judgments of past experience are critical to solving problems that may reoccur. Traditional mediums for transferring experience such as paper-based documents, photographs, and oral discussions have been found to be inadequate for transferring experience (Manavazhi, 1995). The shortcoming may be overcome by applying new technologies in the Artificial Intelligence domain, such as Case-Based Reasoning (CBR) and Data Mining (DM). Yang & You (1996) discussed the ability of CBR for providing suggestions for the current problem by remembering and learning from results of the past cases. DM is used in knowledge discovery to reveal new pieces of knowledge from large databases (Krzysztof 1998). Based on the CBR process, we establish the conceptual model of the Analyzer component shown as Figure 6.

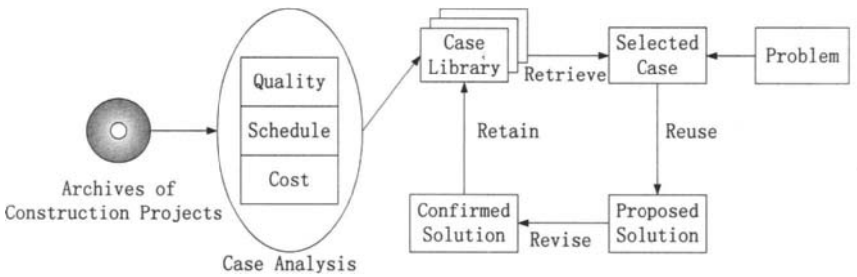


Figure 6: Conceptual Model of CBR in Analyzer

A case library is derived from the archives through case analysis at first. In this step, DM is used to mine the required information hiding in the mass data. Then a suitable case is retrieved from the case library by matching indexes established for the new case (or problem case). The information and knowledge in the selected case is then reused to provide an initial solution to the problem. When it does not fully satisfy the problem specification the proposed case is revised (or adapted) using domain rules and/or human intervention. The revised case is then evaluated and criticized to assess the suitability through the solution and is retained if suitable.

Quality assurance, schedule control and cost management are the major aspects of construction project management and the relative documents constitute the major body of facility archives of the project. So the function of Analyzer will to provide assistant information in these aspects of construction project management.

Now EXPLYZER is under development. The further work will be reported in future papers.

CONCLUSION

This paper focuses on the reuse of the information that is accumulated in construction projects by using EPIMS. The information reuse mechanism is established and then a system approach is proposed. In the approach, a prototype system named EXPLYZER is analyzed and the important reuse are clarified. EXPLYZER provides functions such as browse, query and analysis, which make it possible to reuse the information stored in the archives efficiently.

REFERENCES

Dany Hajjar & Simaan M. AbouRizk 2000, Integrating Document Management with Project and Company Data, Journal of Computing in Civil Engineering, Vol. 14, No. 1, ASCE, pp.70-77.

Harold, E.R. 2000, XML bible, IDG Books Worldwide.

Krzysztof Cios, Witold Pedrycz & Roman Swiniarsk 1998, Data Mining Methods for Knowledge Discovery, Kluwer Academic Publishers.

Ma Zhiliang, Yang Jun and Wu Jianfeng, 2002, A Web-Based Management Information Systemfor Multi-Party in Construction Projects, 9th International Conference on Durability of Building Materials and Components.

Manavazhi Mohan 1995, Capture and utilization of project experience through case-based reasoning and hypermedia technologies, Computing in Civil Engineering (New York) 2 Jun 5-8 1995, ASCE pp. 1294-1301

Srinath Pereraa & Ian Watsonb 1998, Collaborative case-based estimating and design, Advances in Engineering Software Vol. 29, No. 10, pp. 801–808.

Yang, Jyh-Bin & You, Nie-jia 1996, Applications of case-based reasoning in construction engineering and management, Computing in Civil Engineering (New York), pp. 663-669.

Yunsik Song, Mark J. Clayton & Robert E. Johnson 2002, Anticipating reuse: documenting buildings for operations using web technology, Automation in Construction, vol. 11, pp. 185–197.

Zantout, Hind & Marir, Farhi 1999, Document management systems from current capabilities towards intelligent information retrieval: an overview, International Journal of Information Management, Vol. 19, Issue: 6, pp. 471-484.

Advances in Building Technology, Volume 2
M. Anson, J.M. Ko and E.S.S. Lam (Eds.)
© 2002 Elsevier Science Ltd. All rights reserved

MOBILE COMMUNICATIONS – THE NEXT GREAT MODIFIER OF OUR HOMES, WORKPLACES AND CITIES

Bill Southwood

Arup Communications, Ove Arup & Partners Hong Kong Limited

ABSTRACT

There have been many technological advances that have modified our cities – the passenger lift, air conditioning and the motor car for example. The revolution in communications between people and machines on the move promises (or threatens) to be the next.

The time taken to travel between, for example, one's home and workplace depends on both distance and mode of travel used. Communications changes the access model radically by allowing work to be conducted at either place or in "third places" such as transport facilities and coffee shops.

Whilst it is too early to gauge fully the effect on the city and its buildings, there are some early conclusions to be drawn. There is the direct impact – antennas on roofs, space for IT equipment, demands for highly serviced work spaces. Secondly there is the effect on peoples' movement – mobile telephones have had a profound effect on peripatetic workers. Finally IT is making an impact on the design of the airports, railway stations, community areas in housing estates and shopping malls. The most advanced are now incorporating cabled and wire-less information access to allow visitors to be continually connected.

KEYWORDS

Information technology, mobile communications, intelligent building.

THE CITY – A COMMUNICATIONS PERSPECTIVE

The city has always been a powerful vehicle for communication. Lyon, at the confluence of the Rhone and Saone rivers, also became a hub for a network of Roman roads linking together parts of the greatest empire the world had known. The natural geography of Hong Kong's harbour, sheltered from typhoons and with entries to the east and west, made it an attractive place for the British Empire to trade in East Asia. Singapore, a trading city-state of great distinction, now seeks to replace trade in goods with trade in information – it sees many similarities.

Up to the end of the 18th century the dominant forms of communication involved sending a letter or emissary (or both) on horseback, coach or sailing ship. The 19th century brought steam to power rail and sea transport. These demanded faster communication, and the electric telegraph was developed. Suddenly it was possible to communicate to the other ends of the country and the planet instantaneously.

The 20th century added the automobile and aeroplane. These were mirrored by the rise of the telephone, firstly in the local environment but rapidly complemented at metropolitan, national and global levels. Telegraph evolved into the telex service which oiled business until the last decade of the century. The telephone dominated both as a means of voice communication and later as a bearer for data. The century also saw wireless communication thrive as a means of point to point communication, broadcast radio and television, and, most significantly in mobile communications.

Communications networks, by their very nature, are more valuable as more entities are connected to them. Your connection to the Internet increases the value of mine without costing me a cent, a true economic externality. Telecommunications networks therefore tend naturally to grow from the center and, as a result, have the potential to change the city's access model dramatically.

As well as allowing access the city also functions as a hub for social intercourse. Edward Lloyds 18th century coffee house allowed men of affairs to meet and found the insurance industry. The 20th century equivalent is the dealing room where men and women of affairs conduct business with their counterparts around the world. Another candidate for the title of heir to the coffee shop might be the internet café.

INFORMATION AND COMMUNICATIONS TECHNOLOGIES

The digital global economy was heralded by IBM's launch of the personal computer in 1980. But this is not necessarily the most important development. The 1970s had been long distance direct dialling become efficient and increasingly economical. People became accustomed to communicating casually over long distances. A relatively primitive and unsatisfactory technology, facsimile was the third major influence, with a boom in almost instantaneous written message transmission.

By the early 1990s fax had created a demand that brought email to the fore. With the growth of worldwide web the PC, previously a device for writing or calculating with, became a communications tool as important as the telephone. The final pieces of jigsaw came in the mid 1980s with the first generation of mobile phones. Although the early examples were heavy and coverage was patchy the industry responded to a demand for mobility in ways which could not have been anticipated.

The synthesis of these technologies is imminent and is about to make the greatest change to the way we live, work and play since the automobile. Third generation (3G) wireless communication promises to deliver all of our information, email, entertainment, multi-media to us "on the move". It will have three levels of mobile cells, the smallest being the pico cell which may cover an area as small as an office floor or a portion of a shopping mall. 3G users will thus be located to within a few meters. Apart from the concerns over civil liberties, the opportunities for providing useful location based information are tantalising. You need never again be lost in a city; you will always know where to obtain a decaffeinated latte; as you walk into the airport terminal your Personal Digital Assistant (PDA) which contains full details of your flight booking will tell the airline you are there, check you in and direct you to the appropriate lounge where your favourite drink will be waiting.

Two fundamental problems arise in the scenario: the first is the sheer volume of information with which people may be confronted. The second problem is security- are you happy to have the information on your Digital Assistant being constantly accessed by others?

The growth in power and speed

In the late 1960s Intel's chief scientist, Charles Moore, predicted that the growth in the power of a computer processor would double every 18 months[1]. This has proven remarkably robust and shows no sign of being invalidated in the next. This implies a 60% compound annual growth. Less well known is a "Law" published in 1998 by Jacob Nielsen[2] which states that bandwidth available for connection to the internet grows at 50% per annum. Thus computer power will continue to outstrip connection speeds. One can extrapolate both of these laws back by 150 years and see that bandwidth has been growing exponentially since the earliest days of the telegraph in the mid 19th century[3]. Figure 1 shows ICT analysed by its bandwidth and the distance over which it can operate. Distance can conveniently be divided into four zones:

- The personal area of a few metres supported by the personal area network (PAN)
- Local area covering an office or building (LAN), in a university or school this may be considered a teaching area network (TAN)
- Metropolitan area (MAN) and its variant for a campus (CAN)
- Wide area network connecting cities and countries (WAN)

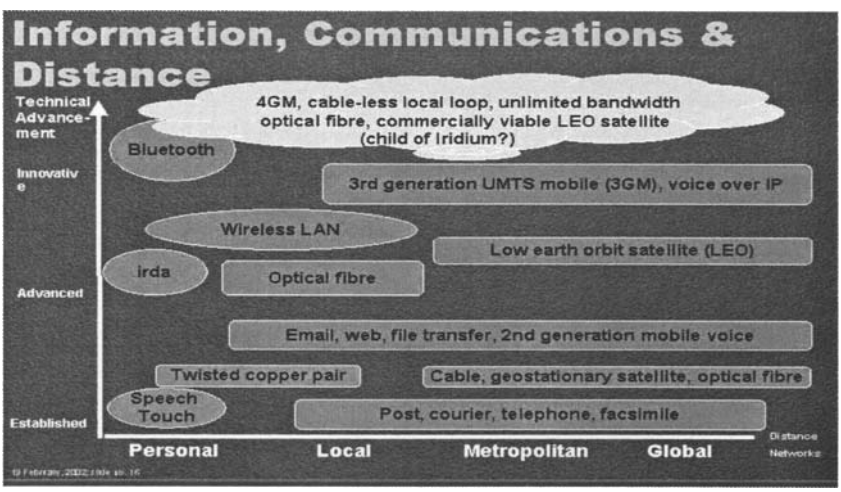


Figure 1: Bandwidth and distance for a range of technologies[4]

Copper cable

Copper has been written off as a transmission medium twice in the last forty years. The first time was in the 60s when the geo-stationary satellite first provided high quality affordable international communications. Submarine cable companies all but closed down in the face of this competition until demand for bandwidth brought cable back into the equation.

Copper survived a second attack from optical fibre a decade later and, once again, survived. For the final connection to the home or workplace, copper is affordable and, able to provide for all but the most bandwidth hungry applications.

Optical fibre cable

Optical fibre is a technologist's dream, having effectively unlimited bandwidth and very low loss making it ideal for long-haul routes between cities or for submarine cables. It is also almost impossible to tap into undetected, made from cheap materials, very strong if correctly installed and terminated and free from corrosion. Termination is complex and more expensive than copper, making it less suitable in the local area where copper is likely to continue to prevail in the foreseeable future.

Wireless communication

Line of sight microwave is a quick and convenient way of connecting over the wide area. It is a convenient way of covering the "last mile", and a number of companies are using it to deliver broadband connections to homes and businesses. For the reasons stated earlier, it is likely to be replaced by cable as the market matures and bandwidth demand increases. Radio and television broadcasting is a major user of the radio frequency spectrum. Not needing any physical connection to the receiver makes it an economical method of dissemination. However demands from competing businesses such as mobile communications operators means that more and more broadcast services are going to be provided over cable to free up spectrum. This reverses the pattern of the last sixty years where your phone was wired and your TV set had an antenna.

The ICT revolution is most evident in the growth in wireless mobile. Nonexistent as a commercial product twenty years ago the mobile handphone has surpassed and in many countries, the wired telephone as the preferred means of voice communication. The implications on our cities are many and various, and include:

- Sites for base stations, masts and antennas are increasingly in demand.
- The user becomes increasingly dependent on the service.
- Mobile communications has liberated people as diverse as plumbers, doctors and travelling sales executives from the tyranny of the fixed office phone.
- The technology is starting to encourage true m-businesses (e-business for mobiles), initially in low speed data applications such as share price information or sporting results.

The Internet and email

The explosive growth of the Internet in the last decade is well documented[5], the Internet and World Wide Web having become the information source of choice for increasing numbers of people. Email has similarly replaced paper and facsimile as the dominant medium of communication.

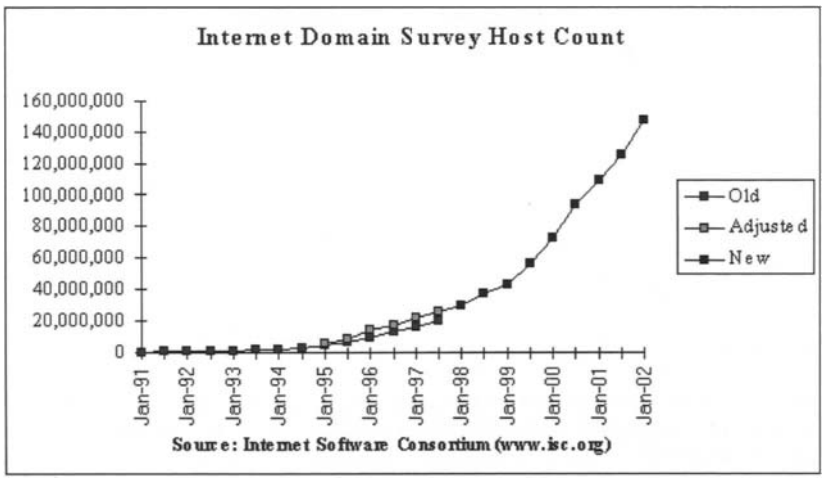


Figure 2: Internet growth

IT, THE URBAN LIFESTYLE AND CITY PLANNING

Good architecture can be said to display three fundamental characteristics: its function or commodity which makes a building or a city work; its firmness which makes it stand up; and delight, an almost impossible parameter to measure but one easily recognized, particularly when absent. In his two seminal books[6] on information and architecture, MIT's Bill Mitchell maps these onto the new age:

- Function is replaced by information, the *raison d'être* of more and more industry;
- Firmness is represented by the network that (more or less) reliably connects organizations in cyberspace (cyborgs) to one another;
- Delight Mitchell sees all around in the endless ways in which the cyborg can work or play in his or her garden.

This trend has both a baleful influence on the city and the potential to re-vitalise it. Technology alienates and fragments - it replaces banks with cash tills, post offices with email, shopping with web browsing, transport with video conferencing, the school with e-learning, the soccer pitch with electronic games and the theatre with a web-delivered video. But using the same technology we are free to re-define our boundaries and interact with a whole new community of people (and other entities). The unexpected success of the short message service over mobile phones is evidence of people subverting the technology in unexpected ways.

Faced with the need to be seen as thoroughly modern, city planners and commercial developers alike have sought to enter partnerships with ICT companies to give their patch a real (or at least perceived) competitive advantage. However even in the late 1990s, well before that decade's whirlwind romance with all things internet went sour, cautionary notes were being sounded. A paper in the British Town Planning Review [7] argued against seeing a technological "quick fix" to issues such as road pricing, access control and advanced commercial development. However others have continued to seize onto the opportunity. London's Chiswick Park has a web site which sums up a cyber-enabled philosophy - www.enjoy-work.com/chiswick-park/index.html.

The intelligently designed building and city

The term "Intelligent Building" tended to be technology focussed. But the building must meet the needs of its owners and occupants. Intelligent does not mean necessarily overwhelmed by technology. Competition for talented staff will be intense; digitally enhanced productivity will be the key to financial success; rapid and radical change organisations will require buildings to adapt and the ownership/rental models change.

The European Commission has funded a multi-disciplinary project SANE – Sustainable Accommodation for the New Economy[8] – to look into these issues and construction. SANE, with representation from organisations in Germany, Norway, Spain and the United Kingdom, will design and develop a work place model within which the different needs of business can be met. This will include the need for both "real" space but will also include "virtual" spaces – the work place I create when I spend time in an airport lounge communicating with my project team 10,000 kilometres away. The synthesis of these two ideas will bring together the thinking which Arup has been developing, often in conjunction with project leader DEGW, in projects such as The Intelligent Building in South East Asia (1995 to 1998)[9]

The Office

Today's office is broadband enabled. From any fixed point a worker can connect over copper or optical fibre cable with high speed data to allow access to multi-media information. The office will be able to change at will to re-locate people into project teams, work groups or individual study locations. The office will be linked to global broadband networks by a combination of optical fibre, line of sight microwave, infra red and satellite – the user will not know (and will not even care) which technology, telephone company or quantity of bandwidth is being used to connect to remote information bases.

Wireless local area networks will complement (but not replace) cabled solutions, providing similar communications to people working in offices, on conference tables or waiting in the lobby. Concern will be expressed over the increased radiation levels at the work place brought about by the systems. This will be particularly important in hospitals where sensitive and life critical processes are underway. The issue of security, both to protect personal information from intruders and to protect systems from damage by viruses, will become increasingly important.

Project teams will need to ensure that the right decisions are taking at the right time so that the building can adapt to this technology. The designs therefore must allow for cable, antennas and equipment – above all producing buildings which can adapt.

Transport nodes

The railway station and the airport terminal present two interesting communications challenges. Both have mission critical systems to enable them to carry out their primary function – to transfer people, goods and information between land and vehicle. In addition however they are places where people spend time and money and also where people will expect increasingly to be connected. The Cathay Pacific lounge at Chek Lap Kok in Hong Kong includes consoles where travellers may swipe their boarding pass through an elegant computer terminal, gain access to flight details, destination city, email or the web.

The back of house systems to support airport and rail terminals are both safety critical and vital to the terminal business. The opportunity to use mobile communications to speed the process of checking in a passenger whilst increasing the level of security can be achieved today – third generation mobile and other technologies will locate the passenger within a few metres.

Once on the aircraft or train the traveller is going to expect to work or play, constantly connected to the information used back at wherever "base" is today. They will also expect to have access to any other media – internet access in the aircraft seat or the rail carriage will become the norm.

Health Care institutions

Like the airport the hospital contains life critical systems which must be resilient, reliable and robust. At the same time they are places where people can spend considerable amount of time. The Hospital Authority of Hong Kong commissioned a study into all aspects of communications within and between their forty-three hospitals. They asked that maximum integration be achieved between, for example the nurse call buttons at the beds, the nurse stations the wards, the physician on the move between hospitals, the pathologist analysing data in a laboratory and the admissions staff. Wireless local area networks combined with the fixed links will allow a radical change to the way patient records are displayed to clinical staff in the laboratory or at the bed side.

Educational institutions

Universities around the world are delivering courses outside their own geographical patch. Almost every major institution in Europe, the United States, Asia and Australasia is linked in some way to provide technical and management courses. The Higher Education Funding Council of England is now implementing a e-University.

The Imperial College School of Medicine in London has used broadband communications, multi-media and audio-visual techniques to resolve the problem of how to teach trainee surgeons and have them available for work in hospital wards at the same time. Video cameras in operating theatres linked to video displays in lecture theatres link the lecturer, surgeon and students, giving unparalleled opportunity for many to participate in operations. There is nothing to prevent this information being transmitted to students anywhere in the world.

The shopping mall

The pico cell knows that you are within two minutes of a range of shops, food outlets and entertainment venues. Your PDA knows that you require a pair of shoes, a bowl of noodles and two tickets to a musical. It shows you which escalators to use to reach them, the options you have and the prices you will be charged. This is possible because the shopping mall has been "wired" with an internal radio network (IRN) which enables it to deliver all of the wireless information services to both the business and the customers within the shopping mall. The search engine will direct you to the commodities – the business will have better and quicker access to its customers.

The home

Research in Japan shows that people open their refrigerator door twenty-seven times more than their front door. The Japanese response has been to experiment with internet enabled refrigerators which tell you the content and age of the food, suggest recipes for your next meal and place orders with your local supermarket for delivery of your next order of vegetables.

People will expect the same high quality broadband connection to their homes as they enjoy in all other places where they live, work or are entertained. The home will be linked by broadband fibre, copper or microwave to a range of global networks. Landlords and local communities are providing portal services to give residents information about transport, security, forthcoming events and local news.

The design of the home, like the office before it, will need to accommodate these technologies efficiently and unobtrusively. The use of wireless will allow devices to communicate without cables, a huge advantage in the domestic environment. Public housing projects such as Shui Chuen O in Hong Kong are looking to adopt sensible levels of communication in both the developments' public spans and individual dwelling units.

The city

The city itself becomes part of this virtual living environment. Different users spend time in different parts of the city – the worker has communication needs while travelling between home and wherever the work place may be today. The home worker will venture out into the city with a different set of needs. Those caring for children, the elderly or the disabled will be more empowered by availability of information about services which are relevant to them. Those being cared for will be less discriminated against. The best modern cities are already universally wired and covered with wireless networks. The latter can cause aggravation as inconsiderate mobile phone users disrupt the tranquility of a park, restaurant or even a concert performance. Technological solutions to these fundamentally human and societal problems, such as jamming, are doomed to fail. Society will adopt a new set of norms, a new definition of "good manners" to define what behaviour is acceptable and what is not. In the meantime the city must ready to embrace the information which is travelling on optical fibres beneath its streets, within the pools of infra red and wireless connection within coffee shops and railway station waiting rooms.

CONCLUSION

Interaction between people, the built environment and the technologies is complex. The key is sustainability, the concept of using less of the earth's resources than we give back. Information technology, mobility and globalisation all have a part to play –a video conference can replace five long distance air journeys; a virtual team can work between a design office in London, a coffee shop in Manhattan and apartment in Hong Kong. Technology in the hands of imaginative people will allow us to work together developing our environment at internet speed without destroying the planet. This view of the future is not just promising, it is essential to the survival of our societies, businesses and life styles.

---

[1] See history on http://www.intel.com/research/silicon/mooreslaw.htm
[2] See details on http://www.useit.com/alertbox/980405.html
[3] Arup on Engineering, David Dunster (Ed), Ernst & Sohn circa 1996, Bill Southwood "The world wired up" p141
[4] Source Arup Communications 2001
[5] Data available on http://www.isc.org/ds/hosts.html and further links on the Library of Congress site at http://lcweb.loc.gov/global/internet/inet-stats.html - collections
[6] Mitchell, William J. (1995) City of bits: space, place and the infobahn. - Cambridge, Mass., London. MIT Press. 0262133091 (see also http://mitpress2.mit.edu/e-books/City_of_Bits); and Mitchell, William J. (1999) E-topia: urban life, Jim -but not as we know it. - Cambridge, Mass.; London : MIT
0262133555
[7] Dr Steven Graham and Dr Simon Marvin, "Planning cyber-cities? Integrating Telecommunications into urban planning", Town Planning Review 1999
[8] Information available on www.saneproject.com
[9] Intelligent Buildings in South East Asia, Andrew Harrison, Jim Read and Eric Loe, E & FN Spon 1998

Advances in Building Technology, Volume 2
M. Anson, J.M. Ko and E.S.S. Lam (Eds.)
© 2002 Elsevier Science Ltd. All rights reserved

ONLINE REMOTE CONSTRUCTION MANAGEMENT (ORCM)

A. Weippert
Queensland University of Technology, Brisbane, Australia.

S.L. Kajewski
Queensland University of Technology, Brisbane, Australia.

P.A. Tilley
CSIRO Building, Construction and Engineering, Brisbane, Australia.

ABSTRACT

Unlike many other industries, construction is highly fragmented with numerous design firms, consultants, contractors, subcontractors and suppliers involved in almost any project. Due to the construction industry not having a coherent and integrated computer system that encompasses the whole of the construction process from design through construction to final account and facilities management, even though the today's technology can make this possible, data exchange between project participants is still largely undertaken on paper. In an attempt to bring the unique talents of various construction industry project participants together in a more productive and integrated manner, the Online Remote Construction Management (ORCM) project commenced in July 1999 proposing to test, field trial and/or evaluate online information and communication systems on up to 5 case study projects over a 2-year period. The ORCM research project aims to demonstrate leadership in facilitating the use of online technologies for the design, management and construction of building and civil construction projects, by identifying and implementing appropriate communication and information technology solutions that will ultimately improve resource management, support and integrate total project life cycle considerations, increase efficiencies on projects, reduce overall cost and improve project outcomes. This paper provides final results, findings and recommendations obtained through the implementation of two ORCM Surveys on one of five ORCM case study projects investigated.

KEY WORDS

Construction industry; information technology (IT); internet; communication systems; remote.

INTRODUCTION

The nature of building and civil construction projects requires team members to attend the construction site to resolve issues that arise during the design, documentation, and construction stages of a project. Australia, in particular, is a large country with dispersed projects and team members usually headquartered in the major cities and regional centres. Extensive travel is therefore necessary, with inefficiencies in time and delays in decision-making. Arguably one of the most significant problems presently facing the construction industry is communication. The industry is characterised by inaccurate and untimely communications that often results in costly delays to the progress of a construction project. If the current level of international research activities are any guide, Internet-based communication and information technology (IT) tools, systems and techniques is seen by many as a potential solution to the communication problems – i.e.: allowing seamless collaboration between project consortiums, promoting rapid resolution of ongoing project issues, and thereby reducing the need for unnecessary travel time and cost overruns. Yet, despite advances in computing and IT, the construction industry is making insufficient use of transferring project data and information electronically. McCaffer et al (1991) argue that data exchange between project participants is largely undertaken on paper. This 'traditional' paper-based form of project communication is still common today.

RESEARCH AIM AND OBJECTIVE

The Online Remote Construction Management (ORCM) project - a collaborative research project funded and supported by a number of Australian (Queensland) industry, government and university based project partners - commenced in July 1999 aiming, in general, to develop, trial and/or evaluate communications systems on up to five case study projects over a two-year period (1999 - 2001), allowing collaborative design and construction to be undertaken between members of a geographically dispersed construction project consortium. Thereby fostering the expansion of communication and information technologies in the building and civil construction sectors, and stimulating the use of such technologies in building and infrastructure projects, resulting in an increase in IT knowledge, awareness and skills of companies in both the public and private sector. Additionally, the project aimed to demonstrate leadership in facilitating the use of online technologies for the design, management and construction of building and civil construction projects, by identifying and implementing appropriate communication and information technology solutions that will ultimately: improve resource management, support and integrate total project life cycle considerations; increase efficiencies on projects; and reduce overall cost and improve project outcomes.

PROJECT SIGNIFICANCE

New South Wales Government (Australia) comments that a $10 million project with monthly cash-flows of $500,000 might have as many as 50 contracts, 5 different consultants, 200 tenders, 600 final drawings, 3,000 amended drawings, 150 contract variations, 600 site instructions, and 6 meetings per week. The use of appropriate IT would be invaluable in improving the efficiency and productivity of such projects. Further, the New South Wales Government indicates that even a 1% improvement in productivity on their annual expenditure of approximately $6 billion could fund the equivalent of 1 major hospital or 20 primary schools per annum. Nationally, the construction industry is valued at approximately $30 billion per annum and with preliminary studies indicating

that with appropriate utilisation of IT a 1% improvement in productivity may be conservative, the potential benefit for the construction industry is considerable (Fujitsu Centre, 1998).

CHALLENGES FACING THE CONSTRUCTION INDUSTRY

Love et al, (1996) comments that construction organizations are faced with many new challenges, including the need to: change current work practices; become more client orientated; more competitive as well as productive. These challenges are attributable to the many factors that effect the working environment, such as: globalisation of the economy; greater performance expectations from the clients; increased competition between local contractors; continued restructuring of work practices, and industrial relations. Better information sharing between disciplines and the automation tools used can ensure large improvements in the efficiency, productivity and quality of the building industry (Howell, 1996). It is proposed that more innovative IT (Internet-based) communication tools/systems could be used to help improve the flow of project communications to ensure that communications occur in a controlled, timely and less costly manner than would traditionally be the case, ensure that information leakage is kept to an absolute minimum, and thus ensuring that all members of the project consortia are in possession of the most up-to-date and accurate project information (Figure 1).

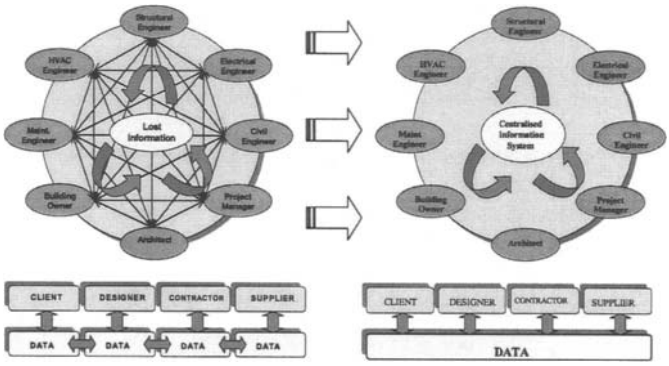


Figure 1: Traditional v Central Project Communication

ORCM CASE STUDY PROJECT (CSP1)

Queensland Department of Main Roads (QDMR) identified and provided access to a truly 'remote' ORCM case study project (referred to as CSP1). The project was completed with the full support of the client and contractor for the project's use as an ORCM case study project. A general description of CSP1 statistics is provided in TABLE 1:

TABLE 1

CSP1 PROJECT STATISTICS

Statistics	CSP1
Client	: QMDR
Project description	: Widening & overlay of Highway
Value at completion	: $ 4.1 million
Contract delivery system	: Traditional
Contract time	: 220 calendar days
Completion date	: March 2001
Primary Contractor	: PNC
Information Technology	: projectCentre

COMMUNICATION TOOL/SYSTEM USED AND INVESTIGATED

The implementation and use of projectCentre (http://www.projectcentre.net/) was examined as the Internet-based IT/communication medium for project communications and document control throughout the various phases of the CSP1 project. projectCentre is a "project web portal" or web-based project management system for construction industry projects. A web browser was all that was required by the project team to gain secure access with the use of a username and password, and/or transmit project documents from any location where Internet services are provided. Project team members sent, received and managed correspondence, requests for information, instructions, variations, drawings and many other documents involved in the construction process.

INFORMATION TECHNOLOGY (IT) ANALYSIS SURVEY

As a part of the ORCM project, research was required into the benefits of IT and (Internet-based) communication tool/system implementation into the construction industry. To ensure an 'Information Technology Analysis Survey' could be administered on the five ORCM case study projects without delay - i.e.: for the evaluation of IT implementation, as well as the benefits, advantages and barriers to that implementation - it was proposed that that the original 'Information Technology Analysis Framework' (Tucker et al, 2000) developed and implemented on the Acton Peninsular Project' be utilised (with publication authors' permission).

ORCM case study project participants, who made use of the various Internet-based IT tools and/or communication systems (including projectCentre), and who completed both sections of the 'ORCM IT Analysis Survey', included: Architects; Consultants; Contract Administrators; Contractors; Engineers; IT Implementation Managers; Managers/Directors; Project Managers; IT tool/system Representatives; Site Foremen; Superintendents; and Superintendent Representatives: In Section 1 ORCM researchers asked project participants, to provide a general background to their role in the project as well as provide a record of past and/or existing levels of IT 'exposure' and/or experience on projects. To determine project and organisational levels of IT implementation and application, as well as identify potential benefits, advantages and/or barriers experienced by that implementation, Section 2 of the ORCM IT Analysis Survey specifically examined IT implementation from 7 different but inter-connected perspectives (TABLE 2).

TABLE 2

SEVEN PERSPECTIVES DESCRIBED

#	Perspective	Description
1	Information Technology	*: Focusing on IT tools used and their technical aspects.*
2	User Utility	*: User satisfaction and perceived value of IT use - based on the extent to which it helps the user do the job more efficiently and effectively.*
3	Project Organisation	*: Role IT plays in facilitating integration of project participants.*
4	Project Management Functions	*: Impact of IT on project management functional goals - information needs, quality and timeliness, and construction.*
5	Benefits	*: Link between IT implementation and any project-related short-term benefits - both tangible and intangible benefits.*
6	Value-adding	*: Relationship between IT implementation and overall project delivery process - perceived value-added aspect of process in terms of generating business value to the client and project stakeholders.*
7	Strategic Positioning	*: Impact on the organisation at the strategic level. It is concerned with how lessons learned in this project are disseminated and hence contributed to the strategic positioning of the organisation.*

IT ANALYSIS SURVEY – RESULTS

In the first section of the ORCM IT Analysis Survey, ORCM researchers asked case study project participants and/or users of the various IT tools and/or Internet-based communication systems implemented on the five ORCM case study projects, to provide a general background to their individual roles/responsibilities in the project, as well as a record of past and/or present levels of IT 'exposure' and/or experience on projects. Results obtained from CSP1 project participants and/or users of the projectCentre system are summarised in Figure 2:

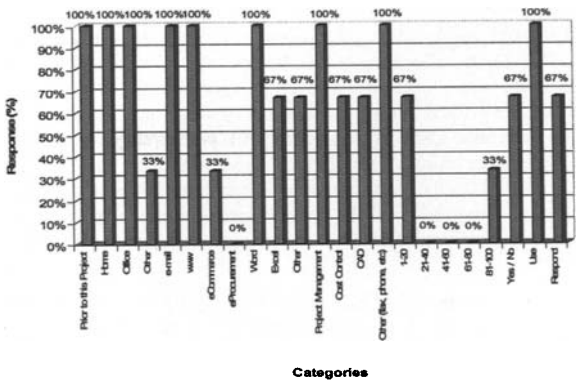


Figure 2: CSP1 Results - General Information

Similarly (for comparison purposes), Figure 3 summarises the combined/average result (%) calculated from responses provided by project participants and/or users of the same or similar IT tools and/or Internet-based communication systems implemented on the remaining four ORCM case study projects for the same 'General Information' criteria.

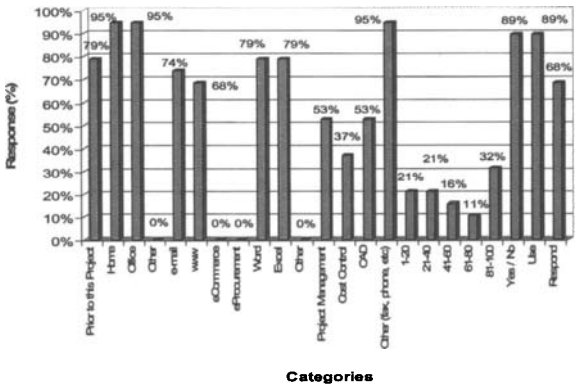


Figure 3: Combined Results of Remaining Four ORCM Case Study Projects - General Information

CSP1 results verify majority of percentages calculated for each criterion (Figure 2), exceed the combined/average percentage scores calculated from the remaining four ORCM case study project participant responses (Figure 3). This comparison provides a reasonable indication as to how CSP1 participants compared against the participants of the remaining four ORCM case study projects, i.e.: in relation to their individual IT strengths, weaknesses, levels of computer and software 'exposure', experience and/or usage, etc.

CSP1 project participants and/or users of projectCentre were also asked to score each of the 7 perspectives (TABLE 2), by allocating a number between 1 (lowest) and 5 (highest) to each (weighted) criteria listed within each of the seven perspectives. ORCM researchers then combined and 'manipulated' the individual scores to obtain an overall percentage (%) or rating for each perspective - i.e.: to determine CSP1 project participants perceived (overall) level of satisfaction for each perspective. Percentage ratings for each perspective were then 'ranked' to help illustrate CSP1 project participants' overall level of satisfaction and perceived influence the implementation and use of projectCentre had on the project (TABLE 3). Project participant responses, ratings, comments and/or suggestions were analysed and assessed in accordance with the framework proposed in Kajewski, et al (1999).

TABLE 3

CSP1 –RANKING OF SEVEN PERSPECTIVES

Rank	Perspective	Rate	User Satisfaction and Influence On Project
1st	Information Technology	68%	Highest

2nd	Project Management	62%	Above average
3rd	User Utility	58%	Average
4th	Strategic Positioning	56%	Low to average
5th	Value Adding	55%	Low
6th	Project Organisation	53%	Low
7th	Benefits	52%	Lowest

ORCM 2ND QUESTIONNAIRE

Additionally, research and analysis was required of a more 'qualitative' or 'descriptive' nature - i.e.: to help determine levels of personal 'impact' and/or influence each project participants perceived the implementation of an IT tool and/or Internet-based communication system (ICS) had on each of the five ORCM case study projects. This was achieved by implementing the 'ORCM 2nd Questionnaire', made up of fifteen questions, summarised in TABLE 4.

TABLE 4

ORCM 2ND QUESTIONNAIRE

#	Question
1	What has gone well with the use of [*ICS*] in this project?
2	What has not gone so well?
3	What problems have you had with implementing and using [*ICS*]?
4	How have the above problems been addressed?
5	Has the use of [*ICS*] improved communications in the contract?
6	How have you and/or your organisation overcome administrative and legal issues associated with using electronic as opposed to traditional methods of communication?
7	What types of communication are most suited to a [*ICS*] process?
8	What types of communication would you recommend that one should not use a [*ICS*] process for?
9	Has [*ICS*] improved efficiency on the project?
10	Has [*ICS*] assisted relationships on the project?
11	Would you recommend the use of [*ICS*] on future construction projects?
12	Would [*ICS*] be useful for pre-construction or maintenance activities?
13	If so, how?
14	What should one do to more effectively use [*ICS*]?
15	Kindly include any additional comments, recommendations, etc. that you may have regarding the implementation of [*ICS*].

CRITICAL SUCCESS FACTORS

In summary, based on the assessment by the researchers involved with the CSP1 project, combined with the comments provided during interviews and responses from project participants to the two ORCM questionnaires ('ORCM Information Technology (IT) Analysis Survey'; and the 'ORCM 2nd Questionnaire'), a list as a of critical success factors were made to help ensure successful implementation of IT tools and/or Internet-based communication systems (including projectCentre)

and/or processes for similar geographically dispersed (remote) civil and building projects, including:

- Main stakeholders need to strategically plan the implementation - creating a feeling of trust (reliability, relevance etc) to the potential user.
- Ease of use / compatibility- both client and contractor wants to learn only one system for ease of use - commonality of access, features and data entry is most important.
- Quality and accuracy of any project related communication or information (electronic or paper based) is still directly dependant on the user of the IT tool and creator of that piece of information or correspondence.
- Training and system support are a must, including on-demand onsite, or on-line demonstrations of the proposed IT tool or communication system.
- Trailing an incomplete system or one that has not had much exposure to users should be treated as a 'special case' and not left to the users to solve the problems. Best practice would be to adopt a 'proven' simple to use systems, or systems compatible with most other IT products and/or systems used in the industry which will not be unfamiliar to "new" users - potentially saving overall project time, cost, labour, errors, etc.
- Any implementation of a new system should be fully resourced to ensure that all aspects are covered during the early stages of development - reassuring users there is a corporate commitment (including hardware / communications provisions, and IT 'Help Desk' support).
- Reliability and adequacy (including sufficient speed) of the communications is essential to gain commitment from potential users. If it works well, new technology will be taken up so cutting costs on critical parts of a new system should not be considered.
- User is a key factor in gaining advantage from an IT system - taking only the type or potential advantages of a newly developed IT tool or communication system into consideration, is not enough during implementation on any remote project site; users needs must be a prime focus.
- Legal issues such as electronic signatures and requirements for hard copies need to be clarified.
- All project participants and stakeholders need to be fully committed to using the new IT tool or communication system, with "buy in" at the highest level within the participating companies. The project Superintendent (or equivalent) should be the driver of IT uptake for a project.

CONCLUSION

The Online Remote Construction Management (ORCM) findings help reinforce the need for further research and monitoring of IT tools and Internet-based communication systems development and level of adoption within the construction industry. Ensuring over time, all building and civil construction sectors project stakeholders realise the benefits of IT adoption thus overcoming barriers to changing existing organisational behaviours; people (culture); communication processes; structures and tasks. *"Without doubt the ability to bring people and technologies together in two-way communication will have major social impact and integrate the world in a way that we have never experienced before"* (Brandon, 2000).

ACKNOWLEDGEMENTS

The ORCM project was a major research project undertaken by the Queensland University of Technology (QUT) Commonwealth Scientific Industrial Research Organisation (CSIRO) Construction Research Alliance, based at the Queensland University of Technology, Brisbane, Queensland, Australia - jointly funded (July 1999 to December 2001) by the Queensland

Government Information Industries Bureau (IIB) Department of Communication and Information, Local Government, Planning and Sport; the Queensland Department of Main Roads (QDMR); the Queensland Department of Public Works (DPW); and the Queensland University of Technology.

REFERENCES

Brandon, P. 2000: Construction IT: Forward To What? INCITE 2000 Conference, Implementing IT To Obtain a Competitive Advantage in the 21st Century, The Hong Kong Polytechnic University, January.

Fujitsu Centre 1998: Information Technology in the Building and Construction Industry: Current Status and Future Directions, A Report for the National Building and Construction Committee Department of Industry, Science and Resources, Australian Graduate School of Management and Building Research Centre, Faculty of the Built Environment, University of New South Wales, August.

Howell, I. 1996: The Need For Interoperability In The Construction Industry. In Proceedings of the InCIT 96 International Construction Information Technology Conference, Sydney, Australia, April.

Kajewski, S., Weippert, A. and Tilley, P. 1999: Online Remote Construction Management (ORCM) Data Collection Methodology Report, , Queensland University of Technology, School of Construction Management and Property, Brisbane Australia, January.

Love, E.D. and Mac Sporran, C. 1996: The Use of Information Technology By Australian Construction Contractors. The Chartered Building Professional, June.

McCaffer, R., Baldwin, A., Carrillo, P. and Thorpe, A. 1991: The Future of IT In Construction - An Academic Viewpoint. Technical Information Service. The Chartered Institute of Building, TIS No. 132.

Paulson, B.C. 1995: Computer Applications In Construction, McGraw-Hill, Inc., Singapore.

ProjectCentre, 2001: Web Site -http://www.projectcentre.net/

Tilley, P.A. 2000: Communication and Information Flow in Construction: Methodology for the On-Line Remote Construction Management (ORCM), Project Steering Committee, CSIRO / QUT, Australia.

Tucker, S.N., Mohamed, S. and Ambrose, M.D. 2000: Information Technology Analysis Framework for Acton Peninsular Project, Report for Department of Industry, Science and Resources, CSIRO and QUT.

Weippert, A., Kajewski, S. and Tilley, P.A. 2000: Online Remote Construction Management (ORCM) IT in Construction: Benchmark Methodology Report, QUT Brisbane, Australia.

This Page Intentionally Left Blank

Advances in Building Technology, Volume 2
M. Anson, J.M. Ko and E.S.S. Lam (Eds.)
© 2002 Elsevier Science Ltd. All rights reserved

COMPUTER-AIDED-CONSTRUCTION-MANAGEMENT, A NEW PARADIGM

Conrad Tin-Cheung WONG[1], Hubert Mak[1] and Heng Li[2]
[1]VHSoft Technologies Co. Ltd. Fl 29-30, Chinachem Century Tower, 178 Gloucester Road, Wanchai, Hong Kong.

[2]Department of Building and Real Estate, The Hong Kong Polytechnic University, Hung Hom, Kowloon, Hong Kong

ABSTRACT
This paper presents our experience gained from developing an industry-university collaboration through conducting research projects based on the use of computer-aided construction technologies. A research project, which is to develop the VHBuild (a Web-based project management system, is analyzed as a case study from the viewpoint of collaborative efforts of university researchers and industrial practitioners. The case study reveals many issues and discussions related to the current growing interest in developing IT applications to the construction industry.

KEYWORDS
Industry-University collaboration, innovation and development, construction IT.

INTRODUCTION

Yau Lee Construction Ltd (Yau Lee) is a medium-size contractor in Hong Kong. Because of its size and previous successes in investing in advanced construction technologies, the company was convinced, in early 1997, of the necessity to have sufficient in-house Construction IT expertise to be able to gain a competitive advantage in the Hong Kong construction market. Since then, Yau Lee actively pursued the adoption and development of advanced construction technologies and IT technologies. An early example is the design and implementation of a 4-day construction cycle which incorporates the use of prefabricated window facades, semi-prefabricated floors, prefabricated partition walls and staircases. Later on, this 4-day cycle was further improved by the introduction of fully prefabricated bathrooms which is the result of a collaboration with Yau Lee and the Hong Kong Polytechnic University.

At the same time, Yau Lee started several initiatives on the use of IT systems in its construction projects. From the very beginning, the company understands the IT research and development can not be as productive as it would need to be in the construction production business. Akin to any high-tech endeavor, the risk of failure is high, but even if there are only 3-5% of the projects are successful, the benefits and profit-returns can cover the entire investments.

Realising there wasn't sufficient expertise and technical strengths in the Company, the management of Yau Lee contacted Professor Heng Li (the academic partner) in the Department of Building and Real Estate at the Hong Kong Polytechnic University. The first collaborative project was the development of a computer system to integrate the preparation and visualization of interior designs, estimation of costs of interior designs, and virtual walk-through of the designs so that project participants can get a realistic appreciation of the project before the commencement of the construction. During this collaboration, the company provided the necessary funding support, users requirements, testbeds and feedbacks on the various developmental stages of the system. The academic partner was responsible for the system design and implementation of the system. As the academic partner is abreast with the most recent information and developments in the topical area, he can ensure that the technologies embedded in the system are the most suitable and updated.

The initial collaborations between Yau Lee and the academic partner enabled them to build a strong sense of trust and better understanding of the collaborative roles. This has proven to be crucially important for the continuing success of upcoming collaborations. Among other projects, the major collaboration has been the development of the VHBuild system which is a Web-based construction project management system.

VHBUILD: AN EXAMPLE OF INDUSTRY-UNIVERSITY COLLABORATION

VHBUILD can serve as a repository for project-specific information that can be accessed by all project participants. It can also acquire knowledge from previous cases of critical issues and experiences using data mining techniques. In order to clearly describe this system, it is necessary to firstly describe the computational model of VHBUILD, which is followed by the introduction of the knowledge management module embedded in the system.

Information Flow Model

An information flow model is developed for VHBUILD in order to define system components and their interactions within the overall information flow and sharing process. The model is based on a repository of all project information at different stages. The repository, or database, resides on a main server to ensure the security and integrity of data. The model is composed of four main components. The daily site report (DSR) component collects and stores information regarding daily site activities and produces schedule data. The schedule control (SC) component enables updating schedule and produces schedule reports. The document management (DM) component provides a convenient tool for users to manage different project files generated during the projects. The critical issues (CI) model keeps a track record of all important issues occurred or might occur during the projects. The model components and their interactions are illustrated in Figure 1.

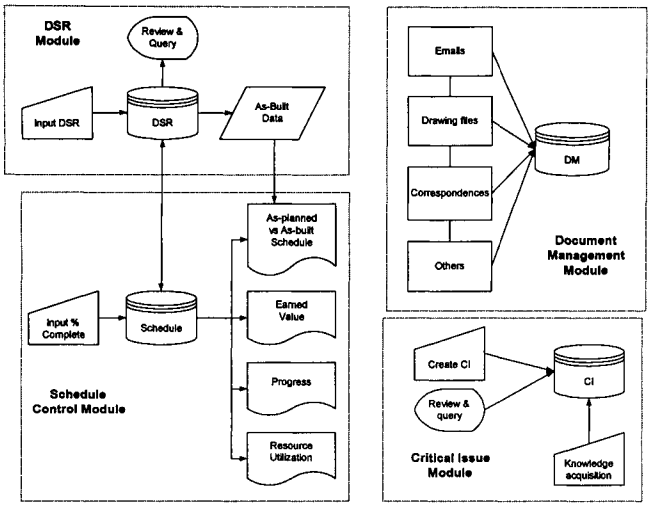


Figure 1: Components of VHBUILD (Modified after Abdelsayed and Navod 1999)

The four components are further described in the following sections.

Daily Site Report Module

Daily site report (DSR) provide project managers with a comprehensive record of site activities. The reports are prepared by creating and completing electronic forms. The format and content of the electronic forms are determined by users based on the level of details they required. The DSR allows users to register information regarding the types and descriptions of work done on a daily basis, and problems encountered. It can also keep track of periods of no work or inactivity. In addition, the DSR can keep records of types and quantities of resources allocated and used. Figure 2 shows an example of daily site report.

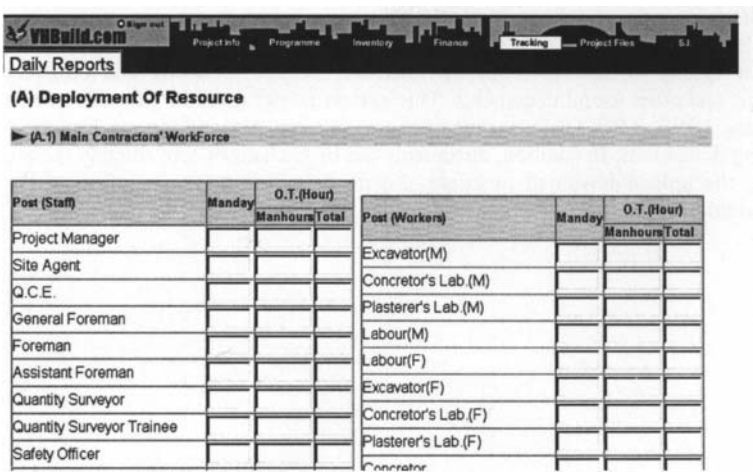


Figure 2: An example of DSR

Information collected from daily site reports can be used to generate as-built factual data. The availability of daily site reports allows project participants to review project information in real time, because these site reports are available at the end of a day rather then at the end of each month.

Schedule Control Module

The schedule control module provides access to "on-line" schedule information. Users have the option to select the level of details of the schedule to view. Typically, the schedule control module an present the percentage of an activity either in an-hours or dollars. The as-built schedule data, which is collected using daily site reports, an be summarized and incorporated into the schedule to form the realistic as-built representation of an activity's progress.

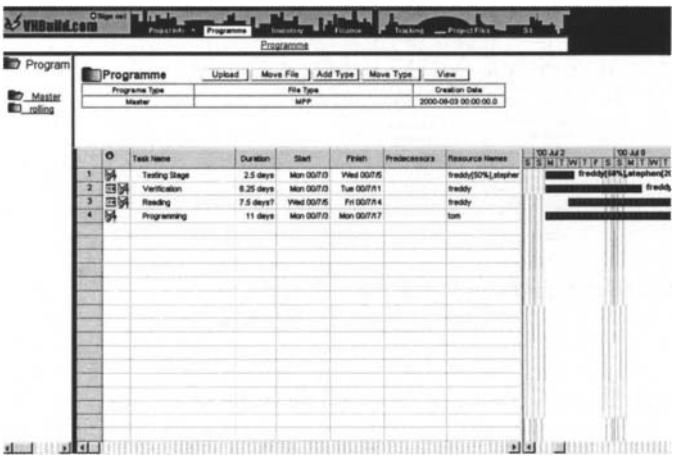


Figure 3: Schedule Control

Figure 3 is a screen dump of the schedule control module. From Figure 3, it can be seen that the comparison between the as-built and as-planned is presented graphically.

Document Management Module

A document management system is developed for the users to manage incoming and outgoing correspondences, drawings, and other useful documents. This system allows users to view documents in various formats including DWG, MSWORD, scanned images, and etc. A searching mechanism is also available for retrieving documents. In addition, documents can be exchanges conveniently among project participants using the upload/download functions. Figure 4 indicates the interface of the document management module.

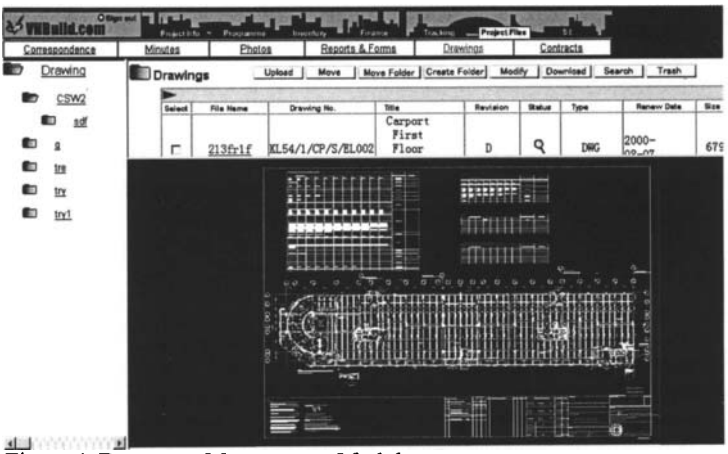


Figure 4: Document Management Module

The availability of the document management module maintains the integrity of project documents.

Critical Issue Module

The critical issue module enables project managers to record critical issues and/or events which have occurred or might occur during the project. By entering the nature of the critical issues which includes the consequences, reasons and related descriptions and files, the system can store the critical issues for further use. These critical issues can be important site instructions from architects, potential hazards and threats to the projects. The critical issue module has the following major functions:

- Store and retrieve critical issues
- Advise the project managers on how to handle the critical issues
- Automatically update its knowledge base on the arrival of new critical issues using data mining techniques.

When a new critical issue is prepared and entered into the system, it is stored as a case that can be retrieved and reasoned using case-based reasoning techniques (Li 1996).

Knowledge Management: Case-Based Reasoning Approach

Case-based reasoning (CBR) is a problem solving strategy which is based on re-use of past solutions to address a new problem. Instead of representing knowledge as rules in rule-based expert systems, a case-based reasoning system maintains a case base that stores cases previously solved. When a new problem is encountered, the system retrieves cases similar to the new problem from its case base, selects the most similar one, and then converts the old solution to a new one for the new problem (Kolodner 1988). This technique is appealing because humans often make decisions in similar ways, and many attempts have been made to address CBR as a scientific cognitive model (Kolodner 1988).

There are two important operators in a case-based reasoning system: select and adapt. Select is the means of retrieving the most similar case from the case base according to the features of the new problem. A weighted count of matching features provides one way to select the best case; however, this does not take into account the fact that the case itself may determine the importance of a feature. Some approaches to finding the best cases are: preference heuristics (Kolodner 1988), dimensional analysis (Rissland and Ashley 1988), and dynamically-changing weighted evaluation function

(Stanfill 1987). Once the best case has been selected, it is necessary to adapt the solution of the case to fit the new problem as closely as possible. In adaptation, decisions have to be made about what stays the same and what changes. The two alternatives for reusing a previous construction situation are to replay the operators that produced the solution and to reuse the construction situation itself. These are identified by Carbonell (1986) as derivational analogies and transformational analogies. The second transfer the solution of an old case directly to that it satisfies the criteria of a new problem; whereas a derivational analogy modifies the problem-solving processes or techniques of an old case to construct paths that result in solutions to the new problem.

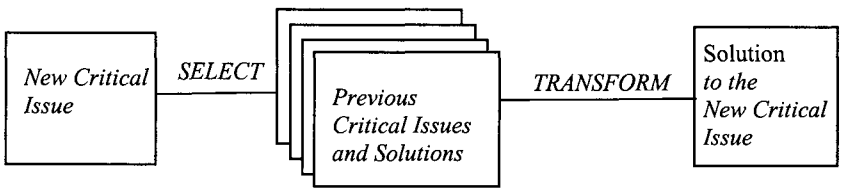


Figure 5: Case Based Reasoning Mechanism

A critical issue case is an abstract of information about a previous situation. The content of each case should include information that facilitates its reuse but not necessarily all the detail of the critical issue itself. Cases can be developed from a collection of previous critical issues. For our project, a critical issue case contained (1) case number and indexing keywords, (2) situational description addressing the background of the critical issue, (3) parties involved, (4) related documents, files and reasons for invoking the critical issue, (5) expected or actual results. A case has a root node indicating its indexing number and keywords representing important issues involved in the case. The retrieving process is based on searching for and matching keywords.

The retrieval and selection among cases entails the recognition of the relevance of each case to a new critical issue. The case base is indexed by the keywords of each case. When a new critical issue is defined as a set of issues and goals, the system traverses the cases according to the new definition of critical issue, and identifies the similarities between the cases and the new critical issue. The case with the highest similarity is then selected as a basis for generating a solution for the critical issue. To model this selection process, a weighted count of matching keywords can be applied. User interaction allows the set of matching keywords and their relative importance to be modified.

Case adaptation in VHBUILD forms the essence of solution generation. As a CBR model, the system assumes that case selection provides a specific case that is close to an acceptable solution and adapts those aspects of the case that are inconsistent. The selected case should contain most issues and goals that define the problem of a critical issue to be resolved. Knowledge used in case adaptation includes heuristics, common senses and issues, case base, and proportional relations. Modify reservation values, introduce new issues/goals, and select additional cases are three techniques of case adaptation.

Experience and lessons gained from the VHBILD collaboration

The VHBuild system has been in trial use for a number of housing projects commissioned by the Hong Kong Housing Authority. In the collaboration of VHBuild, the division of work between the academic partner and the industrial partner has been clear. The academic partner was responsible for the design of the information flow model and the module for knowledge management. Relying on his extensive contacts with international research communities and previous research experience, the academic partner has devised an information flow model which takes into considerations of the construction

practices in Hong Kong as well as the state-of-the-art research results. Because of this, the information flow model is perceived to be a useful one as it not only allows individual project participating companies to own and manage their information and data, but also maps out the flow of information in the same way as the conventional flow of information.

On the other hand, the industrial partner, Yau Lee Construction Ltd., has realized the full potential of Construction IT, and established a subsidiary company called VHSoft Technologies Ltd. (VHSoft). In order to ensure the strong support of the top management of its parent company, Yau Lee designated a senior manager to operate this new subsidiary. Since 1999, VHSoft has maintained an office of over 50 employees including programmers, sales consultants and administrative staff. In order to provide the first-hand experience and feedbacks on the use of Construction IT systems, the senior managers have led the trial use and implementations of the systems developed by the VHSoft. For example, the VHBuild was firstly used in one of the housing projects contracted to Yau Lee. The feedback information was crucial to the VHBuild development team in debugging, refining and gauging its usefulness.

Because both the academic partner and industrial partner understand clearly their relative strengths, the collaboration has been smooth and successful. In retrospect the following points emerge as being critical in maintaining an industry-university collaboration.

1. The academic partner should understand that not all of the collaborative projects are of high academic value. This also implies that not all of the collaborative projects can lead to high-level academic publications.
2. The management of intellectual property rights requires careful arrangement and consideration to avoid problems.
3. The industrial partner should understand that not all collaborative projects can have immediate and tangible benefits.
4. In order to achieve a successful collaboration, the industry and universities should better understand their relative strengths and work closely and productively together.

CONCLUDING REMARKS

Industry-university collaboration can allow both sides to share ideas, strengths and resources. Through the collaboration, the university researchers can find real-life research problems and additional resources to work with. The outcomes can not only bring about new discoveries and knowledge, but also enrich the contents of teaching materials. The industry, however, can obtain state-of-the-art technologies and solutions for their problems at hand, as well as trained personnel for future problem-solving. In the increasingly competitive operating environment in construction, the industry must try to obtain the best technologies, to educate and train the very best people, then make sure that they are employed effectively in the interests of the construction industry and of the society as a whole.

In order to sustain a longer term collaboration, the industry and universities should find answers to the problems emerging from the collaborative process, based on trusts and mutual benefits.

REFERENCES

Abdelsayed, M and Navon, R (1999) An Information Sharing, Internet-based, System for Project Control. *Civil Engineering and Environmental Analysis*, **16**, pp. 211-233.

Carbonell, J. G. (1986) Derivational Analogy: A Theory of Reconstructive Problem Solving and Expertise Acquisition. In Michalski, Carbonell and Mitchell (eds) *Machine Learning: An Artificial Intelligence Approach*. Morgan Kaufmann Publishers, Los Altos, CA, Vol 1, pp. 137-162.

Edwards, D J, Shaw, T and Holt, G D (1996) Electronic document management systems and management of UK construction projects. *Journal of Building Research and Information* **24**(5), pp. 87-292.

Goldberg, D E (1989) Genetic Algorithms in Search, Optimization and Machine Learning. Addison Wesley, Massachusetts.

Kolodner, J. L. (1988) Retrieving events from a case memory: a parallel implementation, *Proceedings of the DARPA Workshop on Case-Based Reasoning*, Morgan Kaufmann, Clearwater, Florida.

Li, H. (1996) Case Based Reasoning for Intelligent Support of Construction Negotiation. *Information and Management Journal*. **30**, pp. 231-238.

Rissland, E. L. and Ashley, K. D. (1988) Credit assignment and the problem of competing factors in case-based reasoning, *Proceedings of the DARPA Workshop on Case-Based Reasoning*, Morgan Kaufmann, Clearwater, Florida.

Rushdi, H and Retik, A (1997) The use of VR for design coordination in distributed environment. The *First International Conference on Concurrent Engineering in Construction*, London.

Stanfill, C. (1987) Memory-based reasoning applied to English pronunciation, *Proceedings of the Sixth National Conference on Artificial Intelligence*, Seattle, Washington.

Veshosky, D (1998) Managing innovation information in engineering and construction firms, *Journal of Management in Engineering*, ASCE, **14**(1), pp. 58-66.

Advances in Building Technology, Volume 2
M. Anson, J.M. Ko and E.S.S. Lam (Eds.)
© 2002 Elsevier Science Ltd. All rights reserved

RAISED FLOOR SYSTEM: A PARADIGM OF FUTURE OFFICE BUILDING FITOUT?

G. Zhang, J. Yang and A. C. Sidwell

School of Construction Management and Property, Queensland University of Technology, Brisbane, QLD 4001, Australia

ABSTRACT

The ever-changing nature of the business environment requires office buildings to respond to organizational, technological and environmental changes. In addition to the latest technologies such as IT and telecommunication, interior configuration and reconfiguration of new office buildings will become a crux of the issue (Barber, 2001). However, conventional approaches to office building fitout, cannot always meet these diverse requirements on a cost-effective basis. Raised floor systems (RFS), also known as access floor systems and adopted in many intelligent buildings (IB) applications (Harrison et al., 1998), can satisfy these requirements because of its high flexibility, speedy installation process and wide adaptability with other building components. RFS technology is also capable of largely reducing fitout time and operation costs in retrofit projects, while allowing more ergonomic considerations for the workplace. This paper introduces current research on the RFS and relevant comparative studies of the conventional approaches to office fitout. The research includes product specification, life cycle costing, construction processes, system integration, and facility management during reconfiguration using the RFS systems. Attempts are also being made to identify appropriate RFS design, installation, implementation, monitoring and maintenance procedures. The paper aims to provide evidence that RFS will replace conventional approaches for office building fitout for many applications in the near future.

KEYWORDS

Raised floor system, office building, intelligent building, fitout, retrofit, comparative study, flexibility.

INTRODUCTION

Traditional office buildings were generally designed to satisfy the essential work requirements, such as provisions of desks, chairs and telephones. Today, new office buildings not only need to facilitate the basic functions, more importantly they must be able to cope with changing requirements of their owners and occupants. This can be reflected in three aspects.

- New and emerging IT and telecommunication technologies have caused a fundamental shift in business activities away from simple clerical processes and towards more communication-

based, managerial and creative work. As a result, new requirements of office buildings are emerging continuously, such as office automation, modularity, integration and ergonomics, to make office work more efficient for the organization and comfortable for the individuals.

- Organisational flexibility, perceived to be an important feature by many corporate owners and tenants of office buildings, demands an ability in these buildings to reconfigure quickly and economically. This flexibility can be evaluated by churn rate, the percentage of the organization that moves work location during a year, which directly reflects the volatility of the organization (Harrison et al., 1998).
- The role of facilities management is also changing today. It now must include distributed information systems and information exchange between systems to reach more effective management decisions, thus resulting in more savings in the optimised operations of the building components and systems (Flax, 1991).

Many existing office buildings in Australia, with fitout facilities and systems commissioned more than a decade ago, cannot meet these changing requirements. Fixed structures, rigid mechanical and HAVC systems, and quickly obsolete data connectivity are common problems (SRIA 1994). Alternative fitout methods, such as ones using raised floor systems (RFS), appear to be able to respond to these potential challenges. However, RFS is still in its infancy of development. Its advantages are yet to be realised by the vast majority of office building occupants and owners. How they compare to traditional fitout methods and what advantages they can bring about is the topic of a research project being undertaken in the Queensland University of Technology (QUT), Australia. This paper discusses the problems of conventional approaches to office building fitout before presenting the benefits of intelligent building systems and RFS. Based on these findings, this paper introduces the QUT research project, covering the initiation of research, research plans and methodology, main focuses, as well as on-going development processes.

CONVENTIONAL APPROACHES TO OFFICE BUILDINGS FITOUT

Offices were once designed to keep people apart, and space planning was based on the ruthless divisions of hierarchy and status (Myerson and Ross, 1999). In the conventional approach to office fitout, the aim is to provide staff with a place to work. According to their seniority and responsibility, the floor space is divided by dry walls into single rooms for managers and open place for junior staffs. Interior fitout is so simple that it may only include space dividers, desks, chairs, bookshelfs and telephones. When information technology is gradually adopted in the workplace, the office environment needs to accommodate desktop computers and peripherals, scanners and plotters, facsimiles and more recently, Internet based facilities. However the cumbersome wires and cables of these technologies, often requires additional work to office fitout when first installed, and can subsequently make relocation and reconfiguration costly and time consuming. Air conditioning, an important aspect of HVAC, presents another example. Its cooling units and fans are usually installed at the end of corridors, and the air from the central plant and cooling tower is delivered to rooms through inlets in the corridor walls or perforated ceilings. Very often the whole level of office space gets cold or heated air regardless whether they are required only for individual rooms or areas. Air is diffused with the same temperature, velocity and direction, without users' own control. Therefore it cannot provide a comfortable workspace.

Changing business requirements originating from innovations and advancement of IT and telecommunication, also demand more flexibility in office relocation and asset renewal or upgrades, as well as in facilities management. As we know, primary mechanical systems have a typical life span of 20-25 years, electrical systems 10-15 years, interior partition 5-10 years, telecommunications and IT technology 3-5 years (Yang, 2001). When the occupants upgrade the

systems with short life spans, the rigid partition, cables and wiring built in conduits cannot support the upgrade due to their fixed structure, limited capacity and quality. Shifts towards corporate downsizing and frequent physical relocation of employees to meet organizational uncertainty are reinforcing the trend towards the integration of building systems. The abilities to save energy costs and to reconfigure workspace on a cost-time effective basis are believed to be among the most critical issues of contemporary building design and construction. Furthermore, HVAC, especially air conditioning, are neither ergonomic nor healthy under the conventional installation. In the open office space, pollutants may be circulated continuously through the system. Air temperature, speed and direction cannot be adjusted to suit individual comfort levels. Staff may develop fatigue in such unhealthy environment. Lack of shared tenant services (STS), a problem common in conventional office buildings, will inevitably bring about the redundancy in facility acquisition and disorder in facility management processes. Finley et al. (1991) pointed out that the *raison d'etre* of STS is the economics of scale allowing many tenants access to services that they would not be able to afford on their own. All these problems will directly depreciate the functionality of the office building thus its marketability.

In summary, it is evident that conventional approaches to office building fitout are increasingly incapable of meeting the changing requirements of the occupants and owners in the era of rapidly advancing technologies. Intelligent buildings (IB) and new fitout approaches are now predicted to better serve the purpose of improving office productivity, comfort levels, and organisational flexibility.

INTELLIGENT BUILDINGS AND RFS APPLICATIONS

Intelligent Buildings and Their Development

An intelligent building is one that creates an environment that maximizes the efficiency of the occupants of the building, while at the same time allowing effective management of resources with minimum life cycle costs (Cho and Fellows, 2000). Intelligent buildings, also known as smart buildings, were originated in the early 1980s in the USA. Initially denoting buildings which incorporated sophisticated IT and telecommunications facilities, IB development was once closely linked to the growth of IT. However, the conception of intelligent building is far beyond the convergence of high technologies. In fact, a high-tech "intelligent building" cannot be regarded as intelligent unless these high technologies are integrated to foster creativity, productivity, dynamic intellectual stimulation, and information exchange as well as environment to promote mental and physical health. Intelligent buildings must also be able to respond to new changes, and learn and adapt to new operating patterns through usage. Therefore, "the intelligent buildings must be understood as a concept, not as a product. Needs are constantly evolving; Intelligent buildings is a direction, not a destination" (Moult, 1998). Another important feature of intelligent building is its cost-effectiveness, i.e., its lower installation cost of building control systems, reduced churn operational cost, lower renovation cost as well as reduced energy consumption costs, and most importantly, lower 'whole of life' cost. These advantages will undoubtedly add values to these office buildings.

Components of Intelligent Buildings

Intelligent buildings often integrate a wide range of services and systems into a unified whole. Table 1 lists the common components of intelligent buildings in the three categories of systems, structures and services.

Intelligent buildings can integrate advanced components to make office work more efficient and ergonomic, the occupants more comfortable and productive, the owners more cost-effective and

flexible, and the environment safer and healthier. These advantages can be achieved on the premise that the intelligent building's structure, skin, connectivity, service system and interior system work in orchestrated harmony as well as provide optimal performance for their functionality. Nowadays, the structure and skin may provide spatial adaptability with individual access to the natural environment, optimize design to reduce material use, and facilitate better constructability and no-waste construction processes. The connectivity systems can highlight the importance of just-in-time connectivity vs. redundancy; user-based reconfigurability of outlets, dynamically located shared services, flexible density of data, power and voice, and compatibility. The service systems can strengthen the applications of shared tenant services. The interior systems may provide a spatially flexible, individually conditioned, connected and healthy environment, and at the same time, ensure low energy use and other resource consumption (Loftness, et al., 1997). Within the office building's context, one aspect remains critical to realize these advantages, i.e., an infrastructure that integrates these components for the maximum benefits. To this end, interior fitout using raised floors has become a recent highlight.

Table 1 Common Component of Intelligent Buildings

Services and systems in intelligent buildings		
Building systems	Building structures	Tenants services
1. Direct digital control system 2. Fire safety system 3. HVAC system 4. Lifts and escalators 5. Lighting system 6. LAN system 7. Power system 8. Security system 9. Telecommunication backbone system	1. Structure design with flexibility 2. External skin system 3. Intelligent flooring system 4. RFS	1. Communal antenna broadcast distribution system 2. Private automatic branch exchange 3. Public address system 4. Satellite services 5. Video conference 6. Office automation

Raised Floor Systems (RFS)

The origins of raised floor can be traced back to 1954, when Tom Tremer, an American inventor, designed a special floor to accommodate the weighty mainframe computers under development at IBM's test facility in Endicott, New York (Ellison and Ramsey, 1989). Tremer's floor offered a strong, level surface for the large computers and a way of storing the bulky cables. For this sole purpose however, the cost of raised floor was much higher than other methods. Therefore raised floors did not attract widespread attention until the last two decades when they were designed to integrate cable management, HVAC, plumbing and fire protection as a whole. This new approach not only reduced the initial cost largely compared to the other methods such as power pole (PP) or poke-through and cellular deck but also lowered the life cycle cost of office buildings. Figure 1 presents the life cycle cost (LCC) comparison for a building between the options of using RFS and PP systems with or without HVAC. This was a study done by Ellison and Ramsey (1989) on a 35,000 sq ft, open plan office building project based on the LCC of 65% computer usage and 20% relocation annually over 10 years life span. It indicates that RFS is has the cost advantage over PP without HVAC; however, it is much more much favourable than PP if the system included HVAC.

How RFS can respond to the emerging demands of office buildings can be illustrated through two examples:

- Flexibility: in most buildings the relocation of power and communication wiring is usually accomplished by cutting carpets, drilling holes on slabs, chasing walls and removing ceilings

panels. The ongoing maintenance and retrofit costs are high and can directly affect rental returns. RFS can simplify the relocation process and reduce expenses. The floor-mounted air diffusers and fan units require no ductwork and can be easily transferred to a new location. Conduit layouts and utilities can be accommodated within as little as 15cm of the underfloor plenum.

- Ergonomics: in the traditional HVAC system, the temperature in an open plan office environment remains constant to all occupants, who may have individual preference to air temperature, direction and strength of airflow. In the RFS environment, with task air from personal diffusers on the floor panel, each individual's preference can be met, thus maintaining a healthier work environment, reducing fatigue and uplifting productivity.

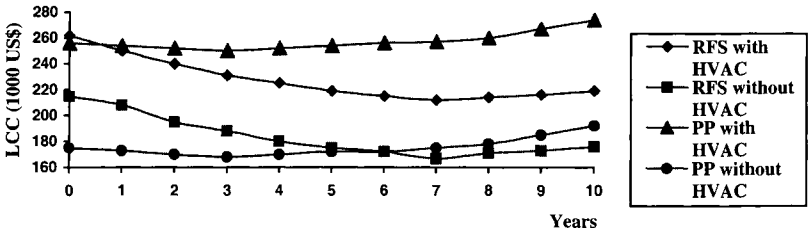


Figure 1. Life cycle cost comparison between RFS and PP
(based on data from Ellison and Ramsay research)

The effectiveness and economics of RFS are also due to its flexible design and construction process. Generally, RFS consists of structural components, panel support systems, finishes and accessories. Installations often include the following steps. First, the pedestals are laid on the floor surface, which can be either the rough slab of a new building or the original floor in a refurbishment project. The modular panels fixed by bolting, gravity, or corner lock and snap-on stingers, are then placed side by side on the top of pedestals forming a uniform smooth surface with the appearance of a solid floor. The stringers are optional in developing the panel strength while resisting horizontal loadings or seismic forces. Second, carpets, vinyl, cork and other surfacing materials are covered on the panels to protect their corrosion, avoid pedestrian slipping, reduce noise, as well as to meet aesthetic requirement. The resulting space between the RFS panels and the original surface can then be used to facilitate the layout of various cables, ducts, pipes and distribution box, with the added bonus of easy access for servicing and relocation. Finally, all other accessories including cable carriers, floor edging, ramps, diffusers, sockets, data and voice outlets, are installed to form the integrated RFS. Figure 2 illustrates the advantages of adopting RFS in office fitout and its association with other building components.

APPLICATION POTENTIAL OF RFS IN RETROFIT PROJECTS

RFS also has promising applications in retrofit projects in Australia. Many office buildings constructed during 1970s to 1980s in Australia adopted the conventional design for fitout and service utilities and had few considerations for office automation, connectivity and other induced innovations (SRIA 1994). These buildings will soon enter a stage of major upgrades of their service systems and subsystems and on a long-term basis, face substantial retrofit costs if using the conventional fitout method. RFS based applications, with reasons mentioned above, can play a major role in the upgrades of these office buildings if their advantages and benefits, and especially the LCC based cost savings, are commonly realised. Moreover, emerging new technologies,

changing requirements in the workplace and business routines and practice will lead to the retrofit of all office buildings on a more frequent basis. Trends in the US and Europe have already indicated resurgence of RFS applications. Given time and more exposure, RFS will prove to be a new and viable option for retrofitting Australian commercial buildings.

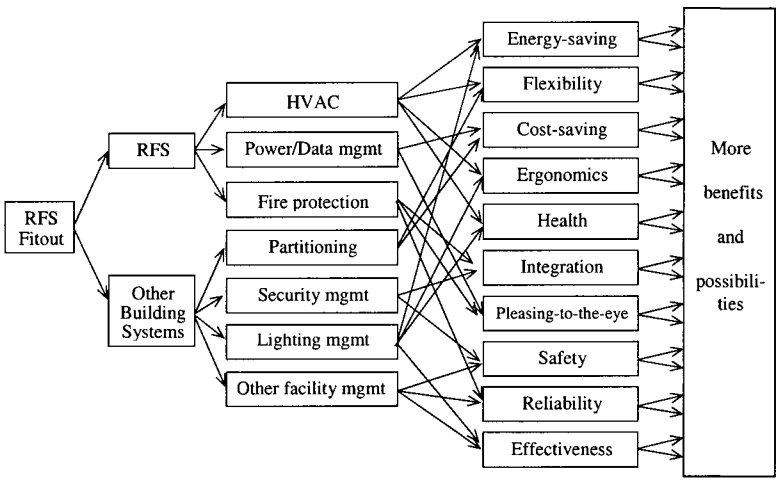


Figure 2. Advantages of RFS to office buildings fitout

A COMPARATIVE STUDY AT QUT

Research Initiation

The research originated from the authors field observation of the office fitout and retro-fit construction practice in Australia and was further inspired through their research work in the US and Europe between 1999 and 2001. A recent trend of practice of some of the largest corporate tenants of office buildings in the US and Europe is moving towards just-in-time office space provision, integrated services, organizational flexibility and maximized individual comfort levels (Barber, 2001). Pilot projects of new and retrofit office buildings in these regions have been equipped with IB technologies which incorporate RFS as a core component. While the initial response is encouraging, a question arises for many building professionals, especially owners and corporate tenants. That is, how does the RFS approach compare with the conventional suspended ceiling and floor furnishings, in terms of development and lifecycle costs, constructability, maintenance, and facility management? Given that Australia is often influenced by the economy and business trends in the US and Europe, it is vital to identify these issues before interests develop into urgent demands. The research project reported here aims to investigate and respond to these issues on a comparative study basis.

Research Focuses

Emphasis of this research is not on the actual development of RFS itself. Rather, it focuses on the integration of RFS with other building components to provide the RFS enabled environment to meet changing office building requirements. In particular, the research involves studies on RFS specification, constructability, system integration and procurement and other construction management issues associated with RFS implementation. Lifecycle costing analysis will be an

integral part of the study. A vital component of this research is a comparative study on some of the attributes mentioned above between RFS and the conventional fitout approaches. This will provide a much needed validation of the RFS potentials.

Research Plan and Methodology

The research will be carried out from both theoretical and practical respects. Literature reviews on previous RFS research, studies on RFS design and application specifications, and rationalization of RFS installation processes will form the basis of theoretical establishment in this research. The research will also be aided by a live experimental laboratory to provide first hand information on RFS installation and application issues. Field visits and observations will be conducted to verify and enrich findings. In the overall research process, comparative studies of RFS vs. conventional approach will be carried out in two stages: initial procedural study and comprehensive study on major cost and benefits issues. Figure 3 illustrates the overall research plan, which is scheduled for three years.

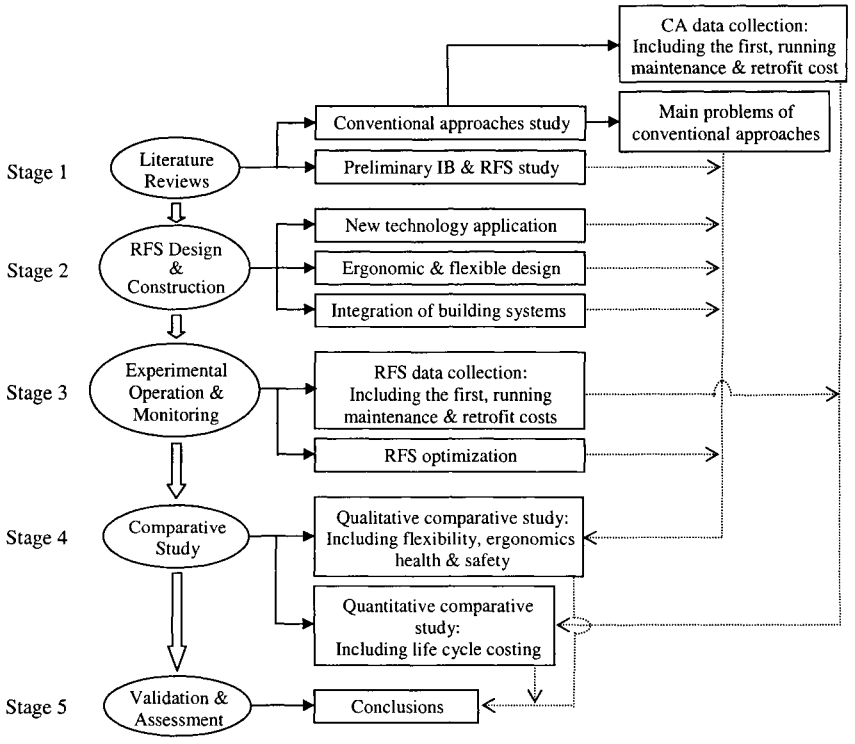


Figure 3. Research model of RFS study

Expected Outcome and Significance

The research will bridge a gap between emerging IB and RFS technologies and the relative lack of understanding thus implementation of these technologies and products. It will provide sufficient evidence and answers to lifecycle costing of RFS applications, their comparisons to conventional floor applications, and at the same time, identify a model of the optimal RFS practice for its

implementation and integration with other components. This will enable building professionals from clients to contractors to gain better understanding of the RFS application in order to identify the best options for commercial office fitout practice.

CONCLUSIONS

With the evolving requirements of the occupants and owners of office buildings, and with the emerging IT and telecommunication technologies, intelligent buildings will become increasingly popular for office buildings in the years to come. RFS, as a core component of intelligent building system and with its ability to integrate building control, wire and cable management, HVAC, power, connectivity, fire protection, security, asset management, etc. into a whole system, has the potential of meeting these evolving requirements. As RFS applications are becoming an integral module of intelligent building systems adopted in office buildings in the US and Europe, it is necessary to explore the potential and benefits of RFS under Australian conditions. A RFS research with Australian local characteristics is now being carried out at QUT, Brisbane, including product specification, whole of life cost-benefit analysis, constructability, utilities and system integration, and facility management during reconfiguration. Ongoing study may involve RFS installation, implementation, monitoring and maintenance procedures. It is expected that the outcomes of this research will justify the popularity of RFS applications and accelerate their implementation process in Australia.

REFERENCES

Barber, C. (2001) Brand New Workplace. *Facilities Design & Management,* 20(4), p28.

Ellison, J. and Ramsey, B. (1989) Access Flooring: Comfort and Convenience and Be Cost-justified. *Building Design and Construction for Tate Access floors Inc.(April),* USA

Flax, B. M. (1991). Intelligent Buildings. *IEEE Communications Magazine* Vol 4, 24-27.

Harrison, A., Loe, E. and Read, J. (1998) *Intelligent Buildings in South East Asia*, London: E & FN Spon, UK

Loftness, V., et al (1997) The Intelligent Workplace Retrofit: Investing in the Hidden Infrastructures for Workplace Flexibility and Performance. *IB/IC Conference* March, Israel

Finley, M. Jr., Karakure, A. and Nbogni, R. (1991). Survey of Intelligent Building Concepts. *IEEE Communications Magazine,* Vol 4, 18-23.

Cho, M. and Fellows, R. (2000) Intelligent Building Systems in Hong Kong Offices, *Facilities* 18(5/6), p225

Moult, R. (1998) Integrating Building Systems Implementing the Intelligent Building Concept. *Proceedings 2nd International Symposium on Intelligent Buildings (Oct)*, Beijing

Myerson, J. and Ross, P. (1999). *The Creative Office*, Gingko Press Inc., USA

SRIA (1994) Australia's 100 Tallest Buildings, Reinforced Concrete Digest, No. 16, Steel Reinforcement Institute of Austarlia (SRIA).

Yang, J. and Peng, H. (2001) A Decision Support System for the Application of Intelligent Building Technologies. *International Journal of Renewable Energy* Vol 22, 67-77.

INFORMATION TECHNOLOGIES:

GRAPHICS AND VIRTUAL REALITY APPLICATIONS

This Page Intentionally Left Blank

Advances in Building Technology, Volume 2
M. Anson, J.M. Ko and E.S.S. Lam (Eds.)
© 2002 Elsevier Science Ltd. All rights reserved

A NEW 3D RECONSTRUCTION TECHNIQUE AND ITS APPLICATION IN MEASURING BUILDING QUANTITIES

Cao Yang[1] and Li Heng[2]

[1,2] Department of Building and Real Estate, The Hong Kong Polytechnic University
Hong Kong

ABSTRACT

3D reconstruction technique deals with developing 3D models from three 2D orthographic views. This paper reviews existing algorithms in terms of their relative advantages and weaknesses. Then, a new method developed to reconstruct 3D models from 2D construction drawings is presented. The method is unique in the sense that it combines knowledge based system with drawing interpretation so that engineering components can be recognized and reconstructed from simplified descriptions presented in the engineering drawings. The method is evaluated through the application of automatic measurement of quantities from drawings.

KEYWORDS

Feature recognition, 3-view drawing, 3D reconstruction, stretch object.

1 INTRODUCTION

In the construction industry, 2D drawings are used to describe the 3D construction components. Although there are CAD packages which allow users to draw 3D components, construction professionals are so accustomed to 2D drawings that it is very difficult, if not impossible, to persuade them to change from 2D to 3D drawings. Usually, if a 3D component is easy to describe and understand, then it is represented by a single 2D drawing, otherwise partial section drawings are added to assist the user to comprehend the details of the component. The process of reading and comprehending a drawing involves mentally reconstructing the 3D component from different 2D orthographic views. For example, the practice of quantity surveying requires the surveyor to be able to mentally reconstruct the 3D model so that relevant quantities can be measured. The process of taking off quantities from 2D drawings is very tedious and prone to errors. In order to develop a computer system to automatically measure quantities from 2D drawings, it is essential and important to be able to automatically reconstruct the 3D model from 2D orthographic views.

The first research of 3D reconstruction probably dates back in 1972, and from then onwards many studies have been carried out on this theme (Nagendra and Gujar 1988). Most of the algorithms developed are able to generate three dimensional objects only containing planar faces, as objects with curved faces are much more difficult to generate from 2D views (Aldefeld 1983, Sakurai and Gossard 1983). Although the developed algorithms are different in various aspects, the following major steps are generally adopted in the task of generating 3D models from 2D orthographic views:

Step 1: Transformation of 2D points to 3D vertices;
Step 2: Generation of 3D edges from 3D vertices;
Step 3: Construction of faces from 3D edges; and
Step 4: Formation of a 3D polyhedron from faces.

However, Step 3 creates a surface model which may include non-existent (false) vertices, edges and faces, how to efficiently detect and remove such elements from the intermediate model against the exponential increase of the number of the combination of candidate faces is a challenging issue in the development of algorithms for 3D reconstruction.

On the other hand, the characteristics of construction drawings also present difficulties in developing 3D reconstruction algorithms. Construction drawings have many components, such as reinforcement steel bars, that are very difficult and troublesome to draw in their true dimensions. Because of this, designers often use simplified ways to represent these components. For example, the reinforcement bars are represented by one line with attached text to indicate the numbers and sizes of the bars. These simplifications make it more difficult to recognize and reconstruct a 3D model from 2D orthographic views.

To solve the difficulties mentioned above, we developed a feature-based recognition method to recognize and interpret the symbols and elements in construction drawings (CDs). Then, based on the recognition and interpretation result, a 3D reconstruction method is presented. At last, its application in QS is implemented based on the reconstruction results.

2 CHARACTERISTICS OF CONSTRUCTION DRAWINGS

Construction drawings possess many characteristics which make the task of 3D reconstruction challenging and complex. For example, the 3D information of one construction component is often indicated by several 2D orthographic views and these orthographic views are often separated in several drawings. Information can be either described as graphics or texts in the drawings. If some components share the same features, then the shared features will only be represented once at a certain location of the drawings in the form of annotation.

Moreover, in the construction drawings, structurally connected components often have overlapped region in the graphic descriptions. This brings difficulties to the 3D reconstruction. Additional work is needed to correct this overlapped region. Sometimes, well-known information about standard components are omitted from drawings. This requires domain knowledge from experienced engineers so that the entire component can be reconstructed.

Because of these characteristics of construction drawings, existing systems or algorithms for 3D automatic reconstruction need excessive manual data input before they can generate a useful 3D models

from 2D orthographic views, not mentioning that these systems perform poorly in handling imprecise or error representations which are not uncommon in construction drawings. The feature-based recognition method developed by us

3 AUTOMATIC RECOGNITION OF CONSTRUCTION DRAWINGS

Before a 3D model of a construction component can be built, it is important that the 2D orthographic views are automatically recognized. This section presents how to automatically recognize construction drawings. Main components of a building include columns, beams, walls, slabs, and staircases. A construction drawing is used to describe the structural information of these components by the boundary projections of the components in the three orthogonal 2D views including the components' top view F(t), front view F(f), and section view F(s). In each of the 2D views, in addition to the boundary projection, information such as special symbols, descriptive texts are also attached. Thus, the task of recognizing a construction drawing must include recognizing both graphical and textual descriptions which will be elaborated below.

Before construction drawings can be automatically recognized, it is necessary to define some terminologies to be used in describing drawings. Graphic primitives (GPs) are basic graphic elements such as lines, circles, etc. A graphics primitive composition (GPC) refers to the combination of a GP and its relationships with other GPs. A GPC contains specific and sufficient information about a GP, such as the boundary of the GP, related symbols, annotations and so on. Analyzing each GPC can obtain useful features which are used to distinguish one particular GP from others.

In a CD, a construction component is composed of many GPs. It is therefore important to correctly identify all the GPs in the component as the recognition process is based on the recognition of GPs and their relationships in the component (Dori 1990). Specifically, the recognition process starts with recognizing the projection boundaries of the component that can be obtained by removing the GPCs representing the steel bars, the symbols, and descriptive texts. In Fig 1, the projection boundaries of a beam from its top view, front view and section views are presented.

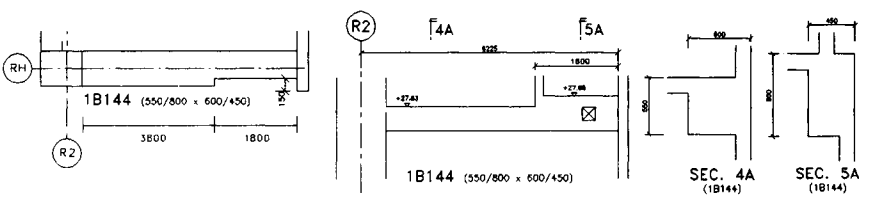


Figure 1: Projection boundaries of a beam from top, front and section views.

A single object's projection boundary in a 2D view is made of one or several closed polygons. Frequently, the projection of a component includes parts of other components' projections to show that it is connected with these parts. This results in unclosed polygons as redundant GPs are included. It is therefore necessary to remove the redundant GPs and enclose the polygons. For example, after removing the redundant GPs from the projection boundaries in Figure 1, the projection boundaries of the beam are as shown in Figure 2.

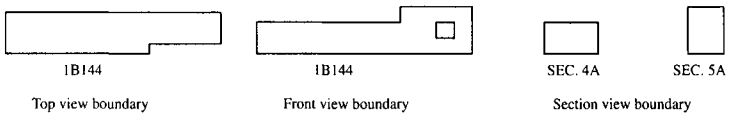


Figure 2: Projection boundaries after removing redundant CPs

A construction drawing contains many important symbols and texts. For example, the grid symbols are the reference for view matching; texts describing the sizes of components are indispensable. Thus, after the recognition of projection boundaries the associated information are extracted by analyzing the symbols, texts and boundaries of adjacent components.

The extracted data about the projection boundaries, as well as the associated information, are stored in a database structure indicated below.

The database structure of the projection boundaries:

```
{
    Component name;
    Size;
    Top view height (if it exists);
    Project view;
    Group of vertex G (v);
    Group of edge G (e);
    Group of Grid symbol G (g);
    Group of adjacent components G (E);
}
```

This database contains the essential information for drawing recognition. Once the projection boundaries of the 2D views are recognized, they form the basis of 3D reconstruction which is presented next.

4 3D RECONSTRUCTION OF OBJECTS

The availability of the recognized projection boundaries of the 2D orthographic views can be used to reconstruct a 3D object. Among all the reconstruction methods, the method for reconstructing stretch objects is the most commonly used one. A stretch object is defined as follows. Given the three orthographic views of an object, if there are at least two of the three views have rectangular projection boundaries, then the object is called a stretch object, or 2.5D object. The stretch object is regarded as an object that is created by stretching a plane along an appointed track. The plane to be stretched is called the stretch plane (Nezis and Vosniakos 1997).

In construction engineering, almost all the components/objects are designed as stretch objects or a composition of several stretch objects.

Because of this, the reconstruction method based on stretch of objects becomes very useful. This method requires to divide a composite object into a group of simple stretchable objects which can be reconstructed individually. The composition of the simple stretchable objects results in a complicated

object. The flow chart of the reconstruction method is shown in Figure 3.

In addition to the stretch objects, there are also other 3D objects that can be considered as special stretch objects. For example, prism and truncated cone are regarded as the special stretch objects, and can be reconstructed by the method. Although the sphere and objects with spherical surface cannot be reconstructed by the method, fortunately they appear only in the upholster, not in the structural components. Thus, the stretch method can cope with the reconstruction of most construction components and objects.

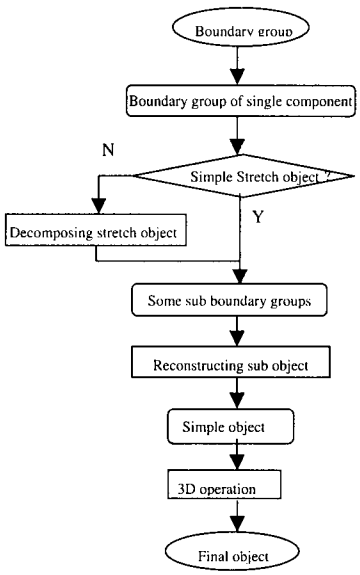


Figure 3 The 3D reconstruction method based on stretch of objects

4.1 Automatic regeneration of the absent projection

In construction drawings, some standard parts are often represented by their code names, with the graphical details omitted from the drawings. In order to obtain the complete 3D components, the absent parts have to be automatically regenerated after analyzing the existing projection boundaries and the code names (symbols and texts etc.). The regeneration process is controlled by the following two rules:

(1) If the missing part is a column or slab, and only the top projection exists, then draw the circumscribed rectangle R(out) of the top projection. The front projection is regenerated as a rectangle and the length of it is the length of the R(out), and the width of it is the height of the column (the data is obtained from the text information). The section projection is regenerated as another rectangle and the length of it is the width of the R(out), and the width is the height of the column.
(2) If the missing part is a beam or wall, and there exist two projections, then project the two projection boundaries to the third view, and the projections are two lines. The third projection is regenerated as a rectangle and the length of it is the length of one of the lines; the width is the length of the other line.

4.2 *Decomposition of complex projections*

If there are holes/voids in an object, the holes are shown as closed boundaries in the projections. The holes can be separated from the projections. For example, let us assume that there is a hole O(f) in object F(f), then the following procedure can separate the hole from the object.

(1) Project the O(f) into F(t), and the projection is a line L. From each end point draw a line that is orthogonal with F(f), then the two lines divide F(t) into three regions. The region that includes the line L is called the projection region (PR) of O(f) in F(t). The part of the boundary that in the PR is O(f)'s projection in F(t), called O(t).
(2) The O(f)'s projection in F(s) that called O(s) is obtained as in (1).
(3) {O(t), O(f), O(s)} is the projection group of the hole O. A hole flag is added to the projection group.
(4) Remove the O(f) from the F(t).

After identifying all holes' projection group from the main projection group, the projection group for the holes is removed from the object which can be reconstructed using the stretch method.

4.3 *Recomposition of simple stretch objects*

After the decomposition and reconstruction of individual stretchable objects, these objects have to be recomposed to form the actual construction component. This is achieved in a two-step process: aggregation of simple objects and removal of false objects.

For example, if a construction component is composed of three objects which include two true objects and one false object as shown in Figure 4.

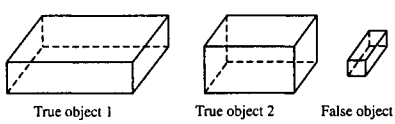


Figure 4: Decomposed and reconstructed 3D objects of a construction

Because all the objects are reconstructed by the stretch method in the same coordinate system, the objects are simply aggregated and 3D operations can be applied directly to obtain the actual construction component. Specifically, all the true objects are integrated by the 3D plus operation to obtain a temporary object. Then, using the 3D minus operation, the temporary object is reduced by the volumes of the false objects. The actual construction component is thus resulted as shown in Figure 5.

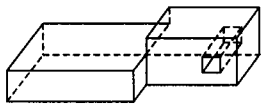


Figure 5: Actual construction component resulted from recomposition

5 REMOVAL OF EXCRESCENT PARTS

The reconstructed 3D objects of adjacent components based on the stretch method often have inter-penetrations at the joints. As a result, excrescent parts occur which should be removed.

A building is composed of many components that support each other. Different kinds of materials and joints are used according to the different mechanical relations. For the purpose of 3D reconstruction, the mechanical relations can be simplified into the following three cases.

- Non-mechanical connection (NMC) is that the two components are adjacent, but there is no mechanical relation between them.
- Horizontal traction connection (HTC) is that the two components are adjacent, and there is a horizontal pressure/tension through the surface.
- Vertical traction connection (VTC) is that the two components are adjacent, and there is a vertical pressure/tension through the surface.

The method to remove the excrescent parts is given as:

(1) If the mechanical relation of the components is NMC or HTC, then select a component arbitrarily, and remove the excrescent parts from it, keep the other component intact.

(2) If the mechanical relation of the components is VTC, then select the component which is relatively on the top or higher, and remove the intersectant parts from it, keep the lower one intact.

After this operation, the reconstruction of a construction component is completed and finalized.

6 CONCLUSIONS

This paper reviews existing algorithms in terms of their relative advantages and weaknesses. Then, a new method developed to reconstruct 3D models from 2D construction drawings is presented. The method is unique in the sense that it combines knowledge based system with drawing interpretation so that engineering components can be recognized and reconstructed from simplified descriptions presented in the engineering drawings.

The method is evaluated through the application of automatic measurement of quantities from drawings. As once the 3D models of construction components are resulted, measurement of quantities becomes a simple task, as the quantities are measured in volumes and/or surface areas of the components which are automatically obtained from any 3D software system.

References

Aldefeld, B (1983) On automatic recognition of 3D structures from 2D representations. *Computer Aided Design*, **15**(2), pp.56-64.

Dori D (1990) Preprocessing of Engineering Drawings for 3D Reconstruction, *Proc. IEEE First International Conference on Systems Integration (ICSI '90)*, pp. 284-292, Morristown, New Jersey.

Idesawa, M (1972) A system to generate a solid figure from three views. *Transaction of the Japan Society of Mechanical Engineers*, **38**(310), pp. 1267-1276.

Nezis K, and Vosniakos G (1997) Recognizing 21/2D shape features using a neural network and heuistics, *Computer-Aided Design*, **29**(7), pp. 523-539.

Nagendra, I V and Gujar U G (1988) 3D objects from 2D orthographic views, a survey. *Computer and Graphics*, **12**(1), pp. 111-114.

Sakurai, H and Gossard D C (1983) Solid model input through orthographic views. *ACM/SIGGRAPH*, **17**(3), pp. 243-252.

Advances in Building Technology, Volume 2
M. Anson, J.M. Ko and E.S.S. Lam (Eds.)
© 2002 Elsevier Science Ltd. All rights reserved

Virtual Planning Environment Based on Internet

Chen Nengcheng [1], Gong Jianya[1] and Li Deren [1]

[1] National Laboratory for Information Engineering in Surveying, Mapping and Remote Sensing, Wuhan University, 129 Luoyu Road, Wuhan, China, 430079

ABSTRACT

"Virtual Reality Model Language (VRML)" combined with Java3D and XML is one of the key technologies which enable the new generation of Three Dimensional World Wide Web (Web-3D) to come true. With the supplement of three dimensional virtual scenery, the VRML can visualizes information in 3D means and carries them in Internet. And also, the development of VRML technology will become the noticeable focus to which urban planners will pay much attention. It will enables urban planning work a new look by helping to introduce planning information and display planning work in INTERNET and attracting more and more people to care for and join in urban planning job.Virtual Planning Environment(VPE) based on Internet is an interactive ,distributed and 3D Virtual Geographical Environment(VGE) which is a N-tiers complicated system running with multiple interfaces .In server side, The GIS business logical process constructed by J2EE is presented to provide spatial data and geo-processing services .In client side ,there are many approaches such as VRML,Java3D, Chromeffects to implement the visualization of spatial data ,The VRML method combined with Java3D is described in detail in this paper. The prototype of VPE in the virtual city zone under P2P network environment is studied. Moreover, how to organize distributed spatial data and process instant geo-spatial information is explained. In the end, some conclusions are drawn and some suggestions are proposed for later construction of VPE.

KEYWORDS

GIS, Internet GIS, VRML, 3DGIS, Java3D, J2EE

INTRODUCTION

The impact of the Internet, specifically the World Wide Web, on our future becomes more profound each day. The number of users and the amount of information increase at a phenomenal rate. The Web can now be found in our homes, in our children's schools and even in our places of employment. Many businesses are beginning to adopt Internet principles and apply them to their corporate Intranet. Those people proficient with Internet tools will be more valuable to their current or future employers.

With the popularity of new technology in virtual planning environment, it is a convenient way to publish the information of urban on Internet and universal accepted by people. However, there is existing some limitation in user interface because of its static and raster expression, that is to say, the user interface based on html is some collection of text, image and multimedia. For urban planning, the much more information is based on 3D besides law, principle and urban schema, which can't be represented by 2D static image. Therefore, it is difficult to make common people know these information .It is urgent to adopt new technology to render and transmit 3D information on Internet by WWW.

With the development of 3D technology, it is possible to solve the above problems. VRML is the combination of WWW, 3D computer graphics interface " Open Inventor " and enabled scenery description language. Java3D is another effective way provided by Sun and was designed with several goals in mind. Chief among them is high performance. Several design decisions were made so that Java 3D implementations can deliver the highest level of performance to application users.

Until now, we assumed that the GIS database server and its clients are connected by a fast local network and use the same operating system. Irrespective of whether the database is stored using a file system or a real database system, the communication between client and server is transparent and the only difference between working on the client and working on the server is a somewhat reduced performance due to networking overhead.

In fact, network is neither transparent nor changeless. With rapid scientific development and further exploration towards the network, the human kind gets to know that network is trustless, latency unequal to zero, bandwidth is limited, network is not security, topology is volatile, system is no only an administrator and transmission need cost.

Java, being robust, security, easy to use, easy to understand, and automatically downloadable on a network, is an excellent language basis for distributed applications. The Java 2 Platform, Enterprise Edition (J2EE) is a robust suite of middleware services that make life very easy for server-side application developers. For VGE, what's need is to develop a distributed application system in accordance with J2EE standard.

This paper provides the concept and features of VPE. Moreover, it explains architecture construction for VPE, accessing, displaying and analyzing planning data on Internet. It includes three portions: Presentation, Application server and Data server. Presentation tier finishes rendering different data source (vector, image, attribute, video) on universal information device (PC, PDA). Application server tier executes kinds of business logic (data access, extract data from spatial database, encode image data, encrypt data). Data server manages and stores planning data in file or database styles. And then, A case study on how to manage and render a small planning area is presented. Lastly, it comes to some conclusion about VPE.

VIRTUAL PLANNING ENVIRONMENT

Distributed virtual environments are the integrations of virtual environments and network. Distributed virtual geo-environments are virtual environments for studying geo-phenomena and geo-process. Virtual Planning Environment (VPE) based on Internet is an interactive, distributed and 3D Virtual Geographical Environment (VGE) which is a N-tiers complicated system running with multiple interfaces. VPE has the following features:

Distributed information system. One advantage of Internet is permitted to access distributed database and perform distributed operations. VPE based on Internet succeed to benefit of Internet, it may be a distributed system. In this system, the planning data may locate at different data server and planning operations consist in different application server. Consequently, data and analysis tool must be single component or module, Once user need any of them, it can be discovered and loaded on any node of Internet.

Universal device support. Both wire Internet users and wireless Internet users can access this system. Thus, It is available not only in different operation system (Microsoft, Unix, Solaris, Linux, POS) but also in different device (PC, PDA, MOBILE).

Real time system. Real time means the corresponding time. The System must reduce the round-trip time so that the remote operation reaction is same as local operation. For instance, If end user add a mark point, application must insert this information into database quickly and correctly and inform everyone on-line.

Interactive. The System must provide well user interface, which permit user who don't know GIS can perform operations in conformity to tips.

Multiple render styles. The information of urban planning must express in different style, which includes text, graphics, video, movie and so on. Just as figure 1 shows, Graphics can be rendered into image, vector, three dimension and VRML.

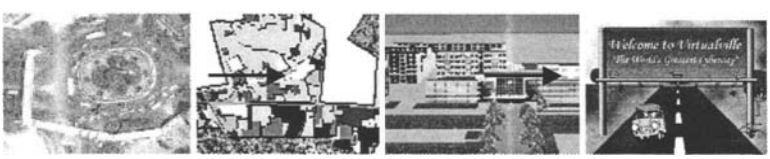


Figure 1:Four different rendering style of Graphics

ARCHITECTURE

In essential, VPE based on Internet is a web application service system, which includes URL, HTTP, HTML (XML), web server and web browser. In a sense, the internal meaning of web is a hypertext information system constructed on Internet and increasing extended information space is the external web resource mark mechanism, application protocol and data format.

The architecture of a web application service system is based on distributed N-tiers environment and includes client, web application server and data server. See figure 2, the architecture of VPE based on Internet includes client, web application server and data server. In this model, each application logic and business services are separated into different components, which communicates with each other by means of network. In general, it may be described as three-tiers computational model in logical.

Client tier: It is user interface that shows and operate planning data. It may run on PDA, information device based on J2ME, PC computer based on J2SE.It may be three kind of client just as table 1 shows. For thin client, in client side, Java Applet is loaded from Server, displays image, raster data and performs basic operation (zoom in, zoom out, pan and send request), Server side performs query

client side displays image, raster, vector and three dimension data and performs basic operations ir common or custom-built browser. For fat client, server side only execute spatial querying and send th prearranged spatial data selection to client, client receives the selection and analysis, renders and displays by means of Java Applet or Plug-ins in common or custom-built browser.

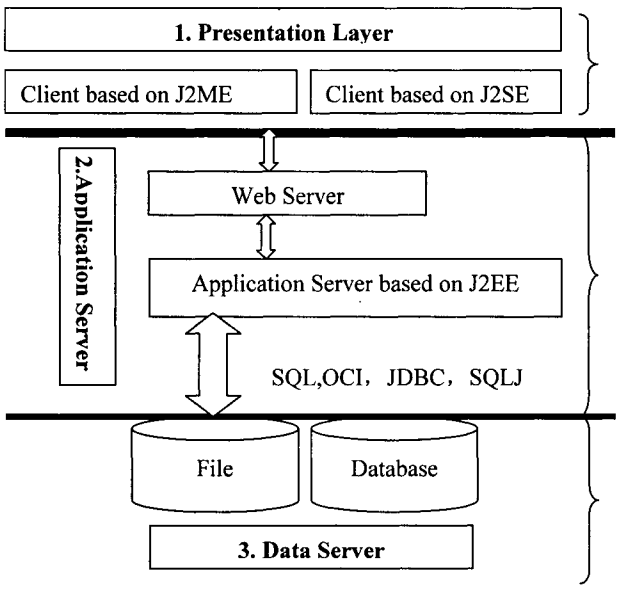


Figure 2: Architecture of VPE based on Internet

TABLE 1
COMPARISION AMONG THREE DIFFERENT CLIENTS

Client	Function	Protocol	Browser	Server	Running program
Thin	Display	HTTP	Common	Render, DEG, Filter	Applet, ASP+Applet, JSP+JavaBean
Medium	Display Render	HTTP RMI IIOP	Common custom-built	Render, DEG Filter	Applet,Application JavaBean
Fat	Display Render DEG	HTTP RMI IIOP	Common custom-built	Filter	Applet,Application JavaBean CORBA

Application server tier: Namely logical business tier, it executes critical business processing whic'. costs much more time. For example, coordinate transform service, geo-spatial encode, address matching and so on. As figure 3 shows, there is an instance of servlet engine which runs in web server, Meanwhile it is RMI client of application server. Applet in browser communicates with application server by means of servlet engine. The servlet engine accepts client's request and transmits it to application server, application server processes the request and return results to browser.

Data server tier: The planning data is stored in this tier, which includes file server ,database sever and existing information system. Application Server access data by means of JDBC, ODBC, SQLJ or SQL.

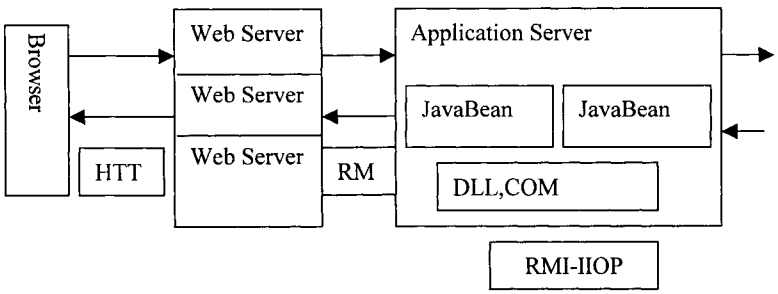


Figure 3: Application Server based on Servlet

CASE STUDY

In this section, a region is provided to explain how to create virtual planning environment based on Internet. It contains two phrases: design and implementation of entities, aviation implementation.

Design and implementation of entities: Abstraction of basic object is referenced to four domain guidelines of land use during the procedure of region design in the virtual planning scenery. As figure 4 shows, flat must be embodied into door, window, balcony and so on.

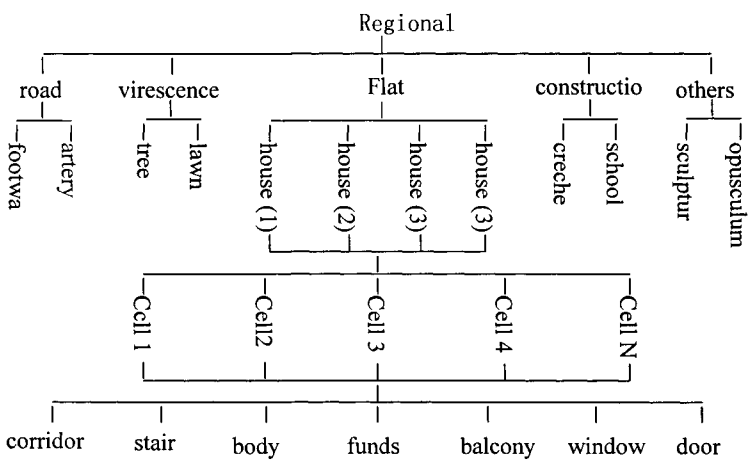


Figure 4: The Objects' Hierarchy Graphic In Regional Scenery

Aviation implementation: The navigation route was designed for purpose so that visitor can roam about in the virtual scenery. We think that footway and artery as the navigation route and viewpoint of visitor is consistent with that of "intelligent agent" (the representation of user in the scenery), visitor will feel scene changing by means of intelligent agent's moving on the route. The event during the procedure can be generalized into the following five phases: logical, engine, trigger, time and target phase. Trigger phase contains two portions: Global position variable is used to track and keep the current position (coordination, orientation) of viewpoint of intelligent agent in scenery. Road stop is used to store the beginning and end position information of road, answer the mouse event by means of touch sensor and realize intersection choose. Logical phase is composed of script nodes which can be used to accept data, send it to orientation interpolator and

position interpolator, startup time phase and bind viewpoint into scenery. In time phase, orientation and position interpolator in engine phase brings variety at specific time interval , sends and changes parameters of viewpoint in target phase, so that causes change of viewpoint of visitor. In target phase, parameters of current viewpoint is stored in global position variable pertain to trigger phase and used to the next interaction. Five phase revolves and aviation is in incessancy.

Example: Figure 5 expatiates the demonstration of scenery result.

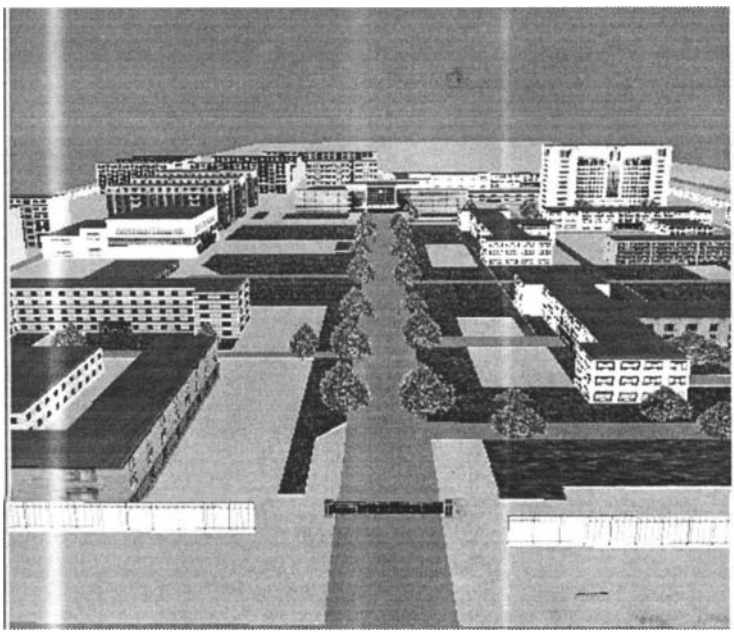


Figure 5 :the demonstration of scenery result

CONCLUSION

VPE is not only a distributed web application system but also virtual scenery based on three dimension technology. From the design and implementation of experimental regional scenery, it is proven that combination among J2EE, Java3D and VRML is an effective way to construct virtual planning environment.

ACKNOWLEDGMENTS

We are grateful to the support from CNSF for LIESMARS Grant No.49871066.

REFERENCES

GONG Jianya(2001).Design and Implementation of an Internet GIS.GEO-SPATIAL INFORMATION SCIENCE.04:2,1-7.
CHEN Nengcheng and GONG Jianya(2001).King George Island Spatial Data model. GEO-SPATIAL

Advances in Building Technology, Volume 2
M. Anson, J.M. Ko and E.S.S. Lam (Eds.)
© 2002 Elsevier Science Ltd. All rights reserved

MODELING OF COMPLICATED STRUCTURES IN A VIRTUAL REALITY ENVIRONMENT

Aizhu Ren[1], Yang Wen[2], Shougong Li[3], Yun Xu[4]

[1,2,4] Department of Civil Engineering, Tsinghua University, Beijing, 100084, China
[3] Department of CAD Engineering, China Academy of Building Research, Beijing, 100013, China

ABSTRACT

Two-dimensional modeling has been employed in most currently available pre-processor for the structural analysis. It is not suitable for those complicated structures that are irregular in their shape, and the conflict parts of structural components cannot be easily discovered by manual examinations before construction. In this paper, a new method for the three-dimensional modeling of complicated structures in a virtual reality environment is presented. By employment of this method, users can specify beams, columns and other components in a three-dimensional space as if they are being constructed in the real world. Joints of components will be visible to users, and the clashed parts of components can be located in the virtual world. The solutions on modeling of complicated structures in a virtual reality environment are illustrated. Principles of computer-aided intersection testing of structural components in a virtual reality environment are also presented.

KEYWORDS

Structure modeling, Virtual Reality, Intersection Testing, AutoCAD, WTK, 3D modeling, ObjectARX.

INTRODUCTION

Two-dimensional (2D) modeling has been employed in most currently available pre-processor for the structural analysis. When the users work with those systems, they must draw the structural plans in a predefined 2D planar space first, specify the locations, sizes, and other relevant data of the cross sections of structural components, and then attach altitude parameters of each component to the corresponding

cross section, and finally all these information should be combined together to make the model of the structure applicable for analysis.

Such a modeling method is originally developed for the modeling of regular structures. It is still reasonable to use it when a structure is simple and regular in its shape. But structures have become more and more complicated, since many advanced technologies have been used in building industry. The 2D modeling method is then no longer suitable. For instance, it would be impractical to create a whole structure model of the steel-framed greenhouse of Beijing Arboretum to employ 2D modeling method, since the greenhouse is irregular and hard to represent in a planar space when it is seen from the plan view or the elevation view.

To construct models of complicated structure efficiently, three-dimensional (3D) modeling should be employed to handle all sorts of structures, especially irregular ones. Unfortunately, creating 3D models with existing CAD technologies is still unsatisfactory. For example, 3D models created by traditional CAD system are often unable to be manipulated in real-time, and attempts to use such models to explore different stages of construction process is also unfeasible. In order to solve these problems, a new method of 3D modeling based on the virtual reality (VR) and traditional CAD modeling technologies is presented in this paper.

Virtual Reality is a technology that generates simulative environment of real world by computers. In this environment, through different kinds of sensors, users are involved in such an artificial virtual environment and can interact with it directly and naturally. Virtual reality systems can be classified as three categories, that is, involved systems, non-involved systems and mixed systems. The equipments used in an involved VR system, including head-mounted displays, data gloves, and data dresses, would be so costly that the expense of equipments would be unacceptable to most users. Therefore, non-involved VR systems are employed to be integrated into 3D modeling systems to enhance their performance at reasonable costs.

The solutions on modeling of complicated structures in a virtual reality environment and the implementation details are presented in the following sections.

SYSTEM DESIGN

The so-called "complicated structures" in this paper refer to those structures with knightheads, oblique beams or columns, walls with holes, or arc-shape components. The structural system and the components in it are hard to be represented clearly on 2D CAD drawings. Therefore, the modeling process is carried out in a 3D space.

The functions of our system is designed as follows:

— Provide a real 3D design space, in which the locations and sizes of structural components can be described in the desired precision. Users are able to position the structure system with the most convenient coordinate system, observe the structure system from arbitrary view.

— The input of geometry of a component can be accompanied with assigning of attributes, which are

indispensable for further computation and design. During the modeling process, all these attributes can be queried, displayed and modified.

— In order to improve the efficiency of modeling, "group" input mode is provided. Components that meet the requirement of some specific rules will be viewed as a "group", and thus can be created or modified simultaneously. In this way, repetitive work is avoided and the tedious human effort of creating models can be reduced considerably.

— Intelligent processors to exam intersections by the computer are developed for the designers to find conflict parts.

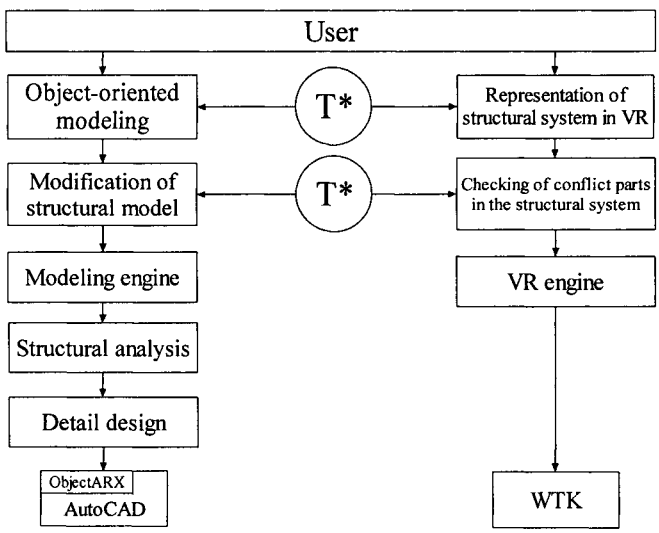


Figure1: System architecture
(*: T represents a "Transformer")

World Tool Kit (WTK) is selected as the platform for VR environment. WTK is an advanced cross-platform development environment for high-performance, real-time 3D graphics applications. With the high-level application programmer's interface (API), end-users of WTK can write codes to call the functions in WTK function library, and then create the virtual world. WTK also provides a 3D modeling tool, called World Up Modeler (WUM), which generates files known as NFF format. WUM is designed to create geometric models; consequently it is not inherently adapted to the modeling of structural components, because each of these components will contain not only geometric information, but also other attributes. All these attributes should be combined with the geometric model of the component, and be viewed as a single object. It is obvious that customized application should be developed to implement this idea. Unfortunately, WUM does not provide a powerful programming interface for developers to implement modeling with non-geometric attributes. Accordingly it is necessary for us to include another platform, AutoCAD, which can provide more convenient extension programming interface as well as stronger supports for 3D modeling. As one of the most popular CAD software, AutoCAD provides for its users the ObjectARX programming environment, an object-oriented C++ API, to use, customize, and extend AutoCAD. The ObjectARX libraries comprise a versatile set of

tools for application developers to take advantage of AutoCAD's open architecture. In an ObjectARX application, we can customize the graphics system, derive custom entities classes, and add extension data to the entities, and thus implement the modeling of building structures and the input of all other relevant data at the same time.

Employment of both AutoCAD and WTK may help us to build more powerful and efficient application of 3D modeling. Figure 1 shows the system architecture we discuss above.

To add and modify data of CAD models in a VR environment, a two-way data transformer between VR and CAD environment should be implemented. When the models are modified on AutoCAD, corresponding data in the VR environment should be automatically updated, and vice versa. Since the modeling functions of AutoCAD will be directly utilized, making changes to the structural models under AutoCAD will be convenient. Although data translation from CAD to VR will be done by WTK without much effort, the opposite directional data conversion, namely, modifying the structural models in VR environment and then updating the corresponding data in CAD, cannot be implemented simply by WTK. As a result, a VR engine should be developed.

IMPLEMENTATION OF OBJECT-ORIENTED MODELING IN AUTOCAD

Abstraction and Definition of Elementary-Component Classes

Object-oriented method has been employed when we try to define the types of elementary components. First of all, it can be easily noticed that different kinds of structural components usually share some attributes of the same types. Thus we may set up a base class to manage these attributes. In the class hierarchy of ObjectARX programming environment, AcDbEntity is the base class for all geometric entities, namely those database objects having a graphical representation. Accordingly, our base class for all structural components will also be derived from AcDbEntity. This class will be in charge of the material type of a component, the style, size and direction of its cross section, and other commonly shared properties.

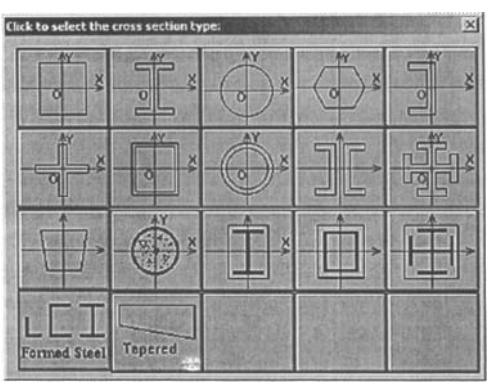


Figure2: Cross section types defined by the system

The system has predefined 9 sorts of material types, including brick, wood, concrete, and steel. And 17

cross section types, such as rectangular, circular, H-shaped, etc., are also predefined, as shown in Figure 2. In addition, user-defined section types are supported. Each type will have a corresponding code in the system, making the access to these types easier and faster.

The size and the normal vector of a cross section are also necessary for a complete description of the cross section. Hence they should be represented by member variables of the base class.

Any given kind of structural component can be defined as a component class, derived from the base class. Beams, columns and knightheads are examples of simple components that can be directly derived from the base class without making many changes. Given the axial line that passes through the central point of it cross section, any object of these three classes will be fully determined if the length or height is also specified. Walls, prefabricated slabs, stairs, and other structural components can be defined in a similar way except that their geometric parameters are more complicated.

The relationship of elementary-component classes is shown as Figure 3.

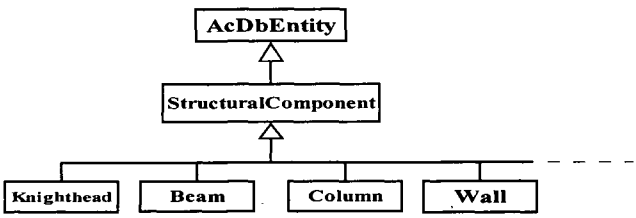


Figure 3: Relationship of elementary-component classes

Assembling of the Structural System from Elementary-Component Classes

Once the elementary-component classes have been implemented, the users can construct the 3D models according to their designs. The modeling process is similar to those commonly used 3D CAD systems. Generally what a user should do is just to draw each part of the whole structural system through keyboard and mouse, by adding, modifying or deleting objects of those elementary-component classes.



Figure 4: The dialogue box of selecting a method to lay a group of beams.
(Other parameters of the beams may be also specified in this dialogue box.)

For the convenience of users, the system provides a fast approach, depending on the use of axes, to create structural models of the same kind. Here is an example of laying several beams in the system. Suppose two orthogonal groups of parallel axes lines have been drawn in advance and formed 6 rectangular reference grids. The first step is to pick up the desired cross section type, and then specify the length of each side of the cross section. A dialogue box is then shown (as in Figure 4), and one of the four available methods to add the beams can be selected:

— Grid Mode: to add a beam along one specified side of a certain reference grid;
— Axis Mode: to add beams along each segment of a specified axis;
— Window Mode: to add beams along all the reference grids inside a user-specified window;
— Two-point Mode: to add a beam, the two end-points of which should be specified by the user.

Figure 5 illustrates the results of using the "window mode" to lay beams on each segment of the six reference grids. There are altogether 17 beams, and each beam is corresponding to a segment of axis line. The cross sections of these beams are the same. We may notice that these beams are 3D entities, thus it is possible to observe them from any desired view if we properly make use of the system.

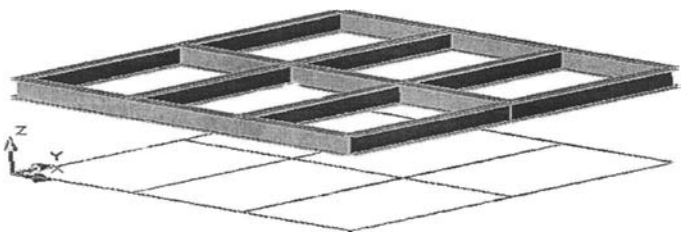
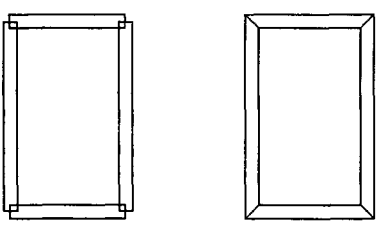


Figure 5: Results after "window mode" is used

The cross section of walls is simpler than those of beams and columns, but wherever a column or knighthead breaks the wall, special attention should be paid, since in a structure system a wall should be viewed as two independent parts once it is separated by another structural component. Consequently the system should recognize this situation and regenerate the wall. What's more, the connection point of several walls and the adjacent profiles should be recalculated to make display better, as shown in Figure 6.



(a) Before recalculation (b) After recalculation
Figure 6: recalculation of the profile of wall

DISPLAY OF THE MODEL IN A VIRTUAL REALITY ENVIRONMENT

In order to display the 3D models in a VR environment, data of models generated from AutoCAD must be translated into one of the formats that WTK can process. That is, after constructing the models under AutoCAD, users should save them in a DXF format file at first, and then use the WUM to open this DXF file, and make further conversion or map textures.

Since WUM does not support geometric entities other than polylines and 3D faces, we have to write extra codes to convert the original models to a set of polylines and 3D faces before they are exported as

a DXF file.

The geometric profile of a structural model is often complicated and sometimes even delicate, and the number of faces of a model is quite large. As a result, mapping texture will turn out to be rather time-consuming. Generally speaking, in most projects, engineers and their clients do not pay much attention to the texture of the surface of the structure. Then using proper colors to characterize the structural components, which can save a lot of time, will be a practical approach and be satisfactory enough.

When the NFF file is obtained, we may present the structural models in VR environment by applying WTK library.

Theoretically the detailed representation of sophisticated joints can be implemented in a similar way: The joint will be modeled under AutoCAD, and then converted to a NFF format file. After that, the detailed model will be viewed in WUM or our VR application. Because of the limitation of the length of this paper, further discussion will be carried on in another paper.

INTERSECTION TESTING IN A VIRTUAL REALITY ENVIRONMENT

Principle of Intersection Testing

Since the design for structure engineering projects is often accomplished by a number of engineers, design conflicts may be produced and would result in expensive construction mistakes if they were not discovered in advance. Traditionally, testing for design conflicts is done by experienced experts in every engineering profession who bring useful data together, check the plans and make oral discussions. Definitely much effort is required. In the modeling system discussed in this paper, users can not only examine the models intuitionally in the 3D VR environment, but leave this boring task to the system's automatic intersection testing utility as well.

The principle of computer-aided intersection testing is not too complex. Use computer programs to find out whether the structural components and pipes or other equipment in a structure have interfered with one another. If there is any undesired intersection, the model may have design errors and revision is needed.

Scheme for Implementation of Intersection Testing

The implementation of computer-aided intersection testing in our system includes the four steps: data digging, data analysis, data visualizations, errors feedback and modification.

Data digging means the collection of useful data related to the intersection testing. In the system discussed in this paper, data for intersection testing come from the models constructed under AutoCAD and their counterparts in VR environment. Structural components such as walls, beams and columns are geometrically made up of simple solids such as cubes, spheres, cylinders, etc. Since the CAD model of a structural component in our system contains all of its geometric data, we can calculate the size and position of each solid that constitutes the component.

In the data analysis step, the system will check the obtained simple solids for intersection in certain sequence. Mathematically speaking, to check whether two static solids intersect with each other or not is to find out whether the corresponding equations set has at least one reasonable solution. But solving these solutions is usually incredibly difficult. Fortunately we can take advantage of some powerful functions of intersection testing in the WTK library to simplify this problem.

The conflict parts of structure can be expressed in special color effects intuitionally in the VR environment. By real-time roaming, users will be able to discover these sites with ease.

By finding out the conflicts parts, designers may set out to make modifications. But the direct modifications of VR models are not currently practical because of two main reasons. On one hand, the technique of two-way data exchange between VR and CAD has yet to reach maturity and should make further optimization. On the other hand, nowadays most available personal computers still lack of the computation ability to achieve the data conversion from VR to CAD in an acceptable time limit. In this paper an indirect approach is contrived to replace the direct modification. Structural components that have conflict parts will be traced in the CAD platform and the original corresponding objects in the CAD models are obtained. Then the modifications will be applied to the CAD models, and finally new VR models will be regenerated using the revised data of CAD models. If the CAD and VR platforms had been integrated into one single software, and the computers were capable enough, then modifying VR models directly would become much easier.

CONCLUSION

Traditional 2D modeling method could hardly generate complicated 3D structural models immediately and check the consistency of input data intuitionally. By using ObjectARX to custom and extend AutoCAD, precise 3D models of various structures can be conveniently constructed. Making full use of WTK library allows us to view the 3D models in a VR environment and process the automatic intersection testing. Thus the complexity of modeling is largely reduced and the efficiency is greatly improved. Designers who take advantage of such a 3D modeling system will be able to fix their attention not on the modeling process itself but on their designs.

REFERENCES

1. Lewis R. and Séquin C. (1998). Generation of 3D building models from 2D architectural plans. *Computer-Aided Design* **30:10,** 765-779.
2. Shougong L., Dailin C., Kaili Z. and Aizhu. R. (2001). Research on a software for joint check up on building design. *China Civil Engineering Journal* **35:5,** 105-110.
3. Whyte J., Bouchlaghem N., Thorpe A. and McCaffer R. (2000). From CAD to virtual reality: modeling approaches, data exchange and interactive 3D building design tools. *Automation in Construction* **10:1,** 43-55.
4. Yang W. and Aizhu R. (2002). The 4D model of massive reinforced-concrete under construction. *Computer Engineering and Design* **23:1,** 29-33.
5. *AutoCAD2000 ObjectARX Developer's Guide,* Autodesk, Inc. USA
6. *World Tool Kit Reference Manual Release 7,* Sense 8, CA, USA

INFORMATION TECHNOLOGIES:

GIS/GPS APPLICATIONS

This Page Intentionally Left Blank

Advances in Building Technology, Volume 2
M. Anson, J.M. Ko and E.S.S. Lam (Eds.)
© 2002 Elsevier Science Ltd. All rights reserved

A NEW GENERATION OF MULTI-ANTENNA GPS SYSTEM FOR LANDSLIDE AND STRUCTURAL DEFORMATION MONITORING

X.L. Ding[1, 4], D.F. Huang[2, 4], J.H. Yin[2, 4], Y.Q. Chen[1, 4],
C.K. Lau[3, 4], Yuwen Yang[2, 4], Y.R. Sun[1], W. Chen[1]

[1]: Department of Land Surveying and Geo-Informatics
[2]: Department of Civil and Structural Engineering
Hong Kong Polytechnic University, Hong Kong, China
[3]: Fong On Construction & Engineering Co., Ltd.
[4]: Corporative Research Centre (CRC) for Ground Engineering and Technology

ABSTRACT

As an advanced navigation and measurement technology, GPS has been in the past two decades extensively applied to many fields and disciplines. One of the prominent applications of GPS is the precise monitoring of deformations of, e.g., engineering structures and the crust of the Earth. A limiting factor for large-scale use of GPS in such applications is however its high hardware cost. For continuous monitoring of deformations, each point to be monitored needs equipped with a set of geodetic quality GPS instruments. This makes many applications such as routine monitoring of landslides too expensive in most cases. A multi-antenna GPS system has been developed and tested by the research team aiming at significantly reducing the cost of GPS when used for monitoring deformations of objects such as slopes. The system uses special hardware and software components to allow one GPS receiver to be connected to a number of GPS antennas. One set of such equipment can therefore be used to monitor a number of points. The system reduces the cost of GPS hardware by many folds. This paper describes a new generation of the multi-antenna GPS system that has been developed by the research team. The system consists of integrated hardware and software components for data acquisition, transmission, processing, analysis and visualization. Integration of the GPS system with conventional slope monitoring systems will also be discussed in brief.

KEYWORDS

Slope deformation, GPS, multi-antenna GPS, landslides

INTRODUCTION

Many man-made and natural structures such as buildings and slopes undergo various forms of deformations. It is useful to study such deformations to understand the response of the structures to such factors as typhoons and groundwater level changes and to assess the safety and health conditions of the the structures.

As an example, Hong Kong has a large number of slopes. Some of the slopes may potentially fail and result in landslides. Since World War II, more than 470 people have lost their lives because of landslides. Monitoring of the progressive deformations of slopes and other parameters such as changes in groundwater levels, together with comprehensive analysis of the monitoring data, should help to prevent unexpected landslides.

GPS has been in the past two decades or so extensively applied to many fields and disciplines and proven to be a very useful tool for monitoring deformations of both man-made and natural structures. GPS offers many advantages over traditional surveying techniques that measure relatively geometric quantities (i.e., distance, angles and height differences) between selected points. In general, GPS is more accurate, efficient, highly automatic and low labor intensive. However, a limiting factor for large-scale use of GPS in such applications has been its high hardware cost. For continuous monitoring of deformations, each monitored point needs equipped with a set of geodetic quality GPS instruments. This makes many applications such as the routine monitoring of landslides too expensive in most cases.

In collaboration with researchers in Australia and China, we have developed in our past work a concept of using multiple GPS antennas with one GPS receiver to form the so-called multi-antenna GPS system, particularly for monitoring structural deformations (Tsakiri et al., 1998; Chen et al., 2000; Ding et al., 2000). The first system developed by the research team uses a standard commercial off-the-shelf GPS receiver together with a speically designed GPS multi-antenna switch (GMS) to enable multiple GPS antennas to be attached to the receiver so that all the points occupied by the antennas can be monitored with the system (Fig. 1). As a result of the devlopment, the cost of the GPS hardware per monitored point is grossly reduced, a multi-fold reduction in fact, making GPS a much more affordable technology for many applications.

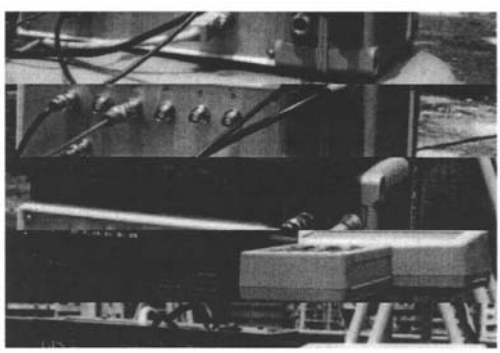


Figure 1: The first generation multi-antenna GPS system developed at the Hong Kong Polytechnic University

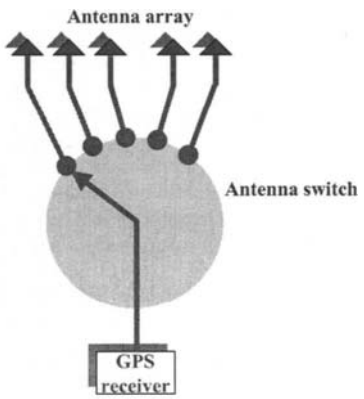


Figure 2: The design of the GPS multi-antenna switch (GSM)

To further reduce the cost of the system and to improve its performance, a second generation of the system has been developed. The new system includes tighter integration of the different hardware and softwre components and the employment of more advanced data processing and management algorithms. This paper first briefly reviews the design concept of the multi-antenna GPS system and then introduces the features of the hardware and software components of the new system.

THE CONCEPT OF MULTI-ANTENNA GPS SYSTEM

For standard GPS systems, one GPS receiver uses one antenna. Therefore, only one point as defined by the position of the antenna can be measured when using such a standard GPS system. Such GPS systems are widely used in navigation, surveying and many other applications. When using the standard GPS system to continuously monitor deformations, either the deformation of the Earth's crust or that of the various engineering structures such as slopes, each GPS system can only be used to monitor the movement of one point.

For the multi-antenna GPS system, on the other hand, a time-sharing concept is used to allow each of the antennas attached to the system to be connected to the receiver sequentially to collect GPS observations. The concept is realised by the use of a specially designed GPS multi-antenna switch (GMS) (Fig. 2). The data from each of the antennas can be used to compute the position, and therefore the movement of the corresponding antenna.

The configuration of a complete multi-antenna system when used in the differential mode is illustrated in Fig. 3 where a second receiver is used on a known station (reference station) to increase the positioning accuracy of the multi-antenna GPS system.

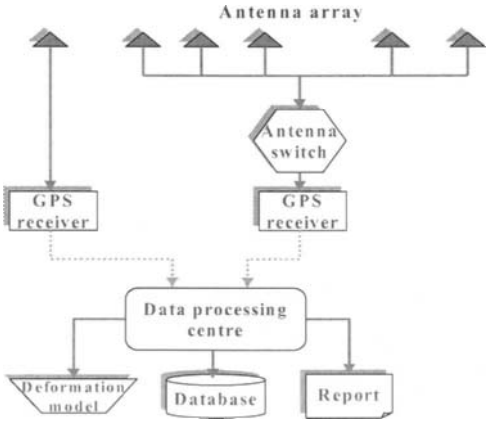


Figure 3: Configuration of a differential multi-antenna system

DESIGN OF THE NEW MULTI-ANTENNA GPS SYSTEM

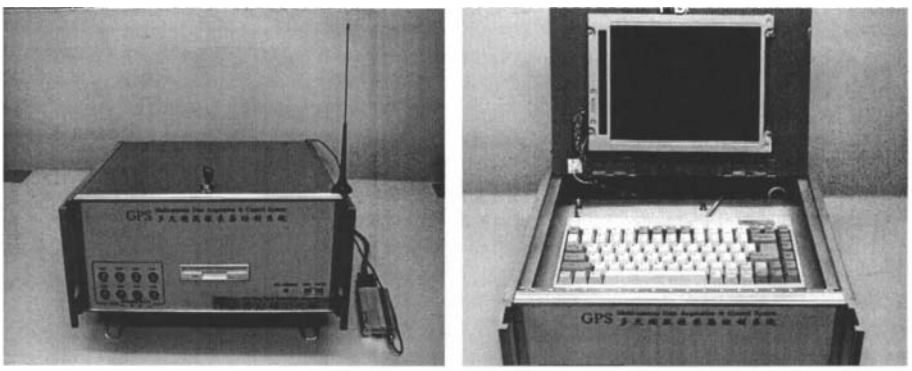
In order to make the multi-antenna GPS system more robust, compact and cost-effective and easier to install, maintain and operate, impovement to the hardware, software and data processing algorithms of the earlier system has been made.

Hardware Components

The new system more tightly integrates the GPS receiver, the GMS and the data communication system through the use of a field industrial PC (Fig. 4). Instead of a standard geodetic quality GPS receiver, a GPS OEM board is used to ease the integration with other components and to further reduce

the cost of the system. There is a wide choice of GPS OEM boards available on the market that can be used with such a system. The main considerations for choosing a GPS board are the data sampling rate of the board and whether it is of single or dual frequency.

Either a fixed telephone line, a dedicated data line, a wireless GSM data line or radio transmitters can be used as the communication link between the office and the site GPS systems. The radio transmitters usually require direct line of sight between the site and the office or intermediate transmitting stations have to be used (e.g., Ding et el., 1996). Fiber optic cables are the best data links although the setting up cost is relatively high.



(a) (b)

Figure 4: Integrated GPS receiver, GMS and data communication system. (a) shows the front side of the unit with eight-channel antenna connectors, a floppy disk driver and telephone line sockets. A GSM modem and antenna connected to the unit are also shown. (b) shows the screen and keyboard of the industrial PC.

Data Processing and Analysis Algorithms and Software

The software package developed for the new system is for remotely controlling the operation of the system, calculating the positions and movements of the GPS antennas attached to the multi-antenna GPS system and for assessing the risks of the monitored object. The main menu of the software is shown in Fig. 5.

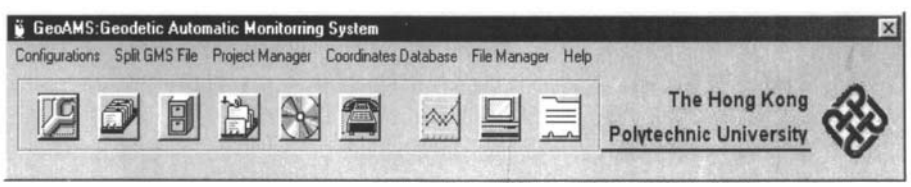


Fig.5: Main menu of the system software

The structure of the data processing and management software is shown in Fig. 6. Once the system is set up initially in the filed, its operation can be controlled remotely through the data communication system. The most important parameters that determine the operation of the system include the data

sampling rate of the system, the satellite cut-off angle, the time that the receiver connects to each of the antennas in each rotation loop, and how the data should be transmitted to the office, i.e., in real-time or at fixed time intervals.

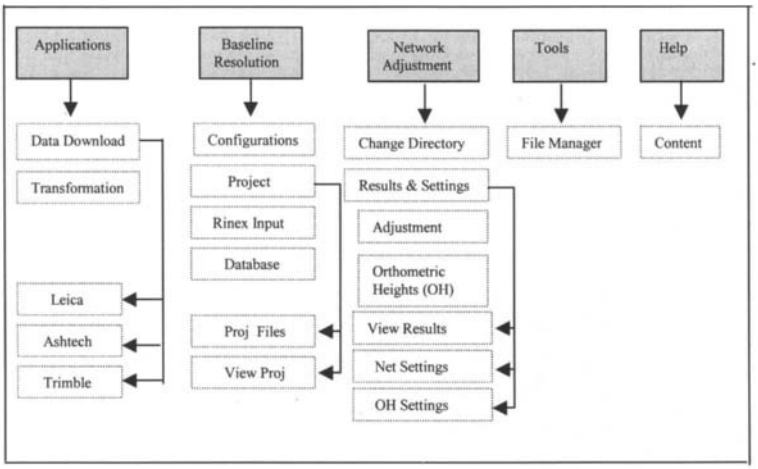


Figure 6: The structure of the data processing and management software

Fig. 7 shows the screen where the antenna channels to be used are selected, and the data sampling interval, satellite cut-off angle, time interval for each channel in a rotation loop and the form of data transmission are determined.

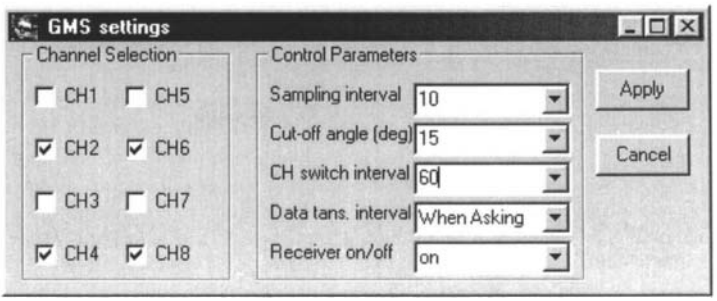


Figure 7: Setting up of some system parameters

Fig. 8 is a screen of the software that shows the system operation status, including the status of each channel, the number of the satellites that are currently being tracked, and the azimuth and elevation angle of the each of the satellites.

The software accepts the commonly used GPS data formats such as the RINEX, Leica, Ashtech and Trimble formats. The software can process GPS baselines, carry out GPS network adjustment and

transform ellipsoidal height into orthometric height. The system can work either in the static or the kinematic (RTK, real time kinematic) mode. The former offers milimeter positioning accuracy but requires a longer observation time period, from about 15 minutes to longer than half an hour depending on the site conditions and the length of the baseline, while the latter offers centimeter positioning accuracy and requires shorter observation time, i.e., near real-time to a few minutes.

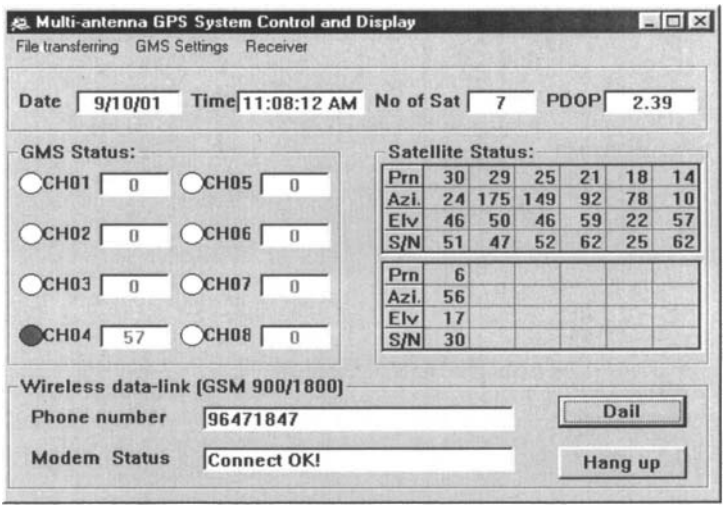


Figure 8: Screen showing system operation status

The well known LAMDA (Least squares Ambiguity Decorrelation Adjustment) method (Teunissen, 1995; Teunissen et al., 1997) method for the resolution of the carrier phase ambiguity is used in the software.

Fig. 9 shows a screen of the software that displays the movement of a monitored point in the forms of the 3D coordinate variations and of the plane view of the point positions.

INTEGRATION WITH TRADITIONAL MONITORING INSTRUMENTS

GPS has a number of advantages over traditional slope monitoring technologies. It provides accurate information on point positions and the changes in the point positions in a global reference frame that is not affected by local deformations. Besides, GPS works 24 hours and under any weather conditions. It is also highly automatic and cost-effective in the case of the multi-antenna system developed.

GPS however also has its shortcomings. The foremost is that it can only measure surface deformations. Besides, it is affected by the site conditions, e.g., the visibility to the sky.

GPS is therefore complementary in a number of aspects with the traditional landslide and structural monitoring techniques. It is advantageous to integrate GPS and other monitoring technologies in practical applications to utilise their respective advantages. Research is currently being carried out to optimally integrate the technologies (see Yin et al., 2002).

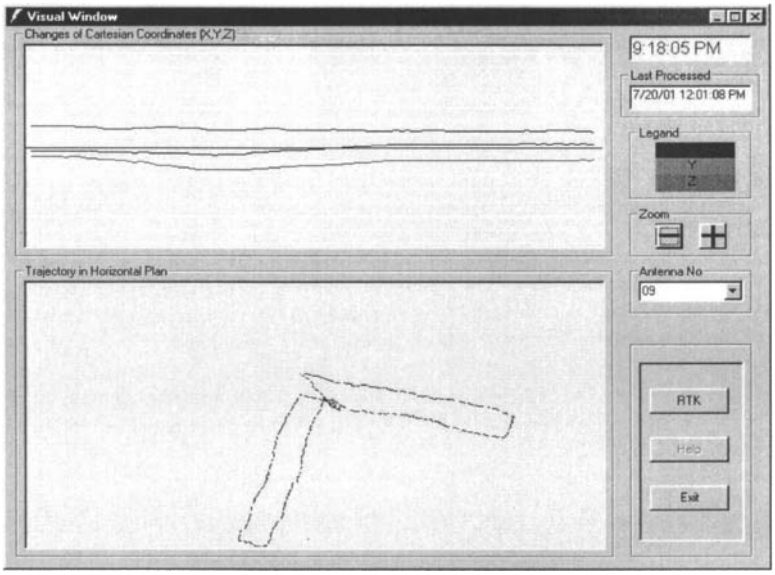


Figure 9: Visualisation of point movement

CONCLUSIONS

A multi-antenna GPS system developed for the monitoring of landslides and structural deformations has been introduced, including its conceptual design, and its hardware and software components. The multi-antenna design makes the cost of GPS hardware much lower than the standard GPS systems when used for monitoring landslides and structural deformations, and makes GPS a technology viable for many applications that have in the past been considered impossible. Besides the reduction in the cost of GPS equipment, the newly developed multi-antenna GPS system has also more tightly integrated the various components of the system and therefore much easier to install, operate and maintain.

ACKNOWLEGEMENTS

The research work presented was supported by grants (Project Nos.: PolyU5051/98E and CRC 4/99) from the Research Grants Council of the Hong Kong Special Administrative Region Government and The Hong Kong Polytechnic University.

Reference

Chen, Y.Q., Ding, X.L., Huang, D.F. and Zhu, J.J. (2000) A multi-antenna GPS system for local area deformation monitoring, *Earth, Planets and Space*. Vol. 52, No. 10, pp. 873-876.

Ding, X.L., Ren, D., Swindells, C., Montgomery, S.B., Jewell, R.J. (1996) An intelligent data acquisition system for pit slope deformation monitoring, Proc. 8th FIG International Symposium on Deformation Measurements, Hong Kong, 25-28 June, pp. 339-344.

Ding, X.L., Chen, Y.Q., Huang, D.F., Zhu, J.J., Tsakiri, M. and Stewart, M. (2000) Slope monitoring using GPS: a multi-antenna approach, *GPS World*, No. 3, Vol. 11, pp. 52-55.

Teunissen, P.J.G. (1995) The least-squares ambiguity decorrelation adjustment: a method for fast GPS integer ambiguity estimation. *Journal of Geodesy*, 70:65-82

Teunissen, P.J.G., P.J. de Jonge, C.C.J.M. Tiberius (1997) The least-squares ambiguity decorrelation adjustment: its performance on short GPS baselines and short observation spans, *Journal of Geodesy*, 71:589-602

Tsakiri, M., Stewart, M. and Ding, X.L. (1998) System design for GPS steep slope deformation monitoring, Western Pacific Geophysics Meeting, American Geophysical Union, Taipei, July 21-24. Abstract in Supplement to EOS Transactions, American Geophysical Union, Vol. 79, No. 24, P. W11.

Yin, J.H., Ding, X.L., Yuwen Yang, Lau, C.K., Huang, D.F., Chen, Y.Q. (2002) An integrated system for slope monitoring and warning in Hong Kong, Proc. Advances in Building Technology (ABT 2002), 4-6 December, Hong Kong.

Advances in Building Technology, Volume 2
M. Anson, J.M. Ko and E.S.S. Lam (Eds.)
© 2002 Elsevier Science Ltd. All rights reserved

ULTRA HIGH RESOLUTION REMOTE SENSING FOR URBAN INFORMATION SYSTEMS AND 3D CITY MODELING

Manfred Ehlers[1], Jochen Schiewe[1] and Matthias Möller[1]

[1] Research Center for Geoinformatics and Remote Sensing (FZG)
University of Vechta
P.O. Box 1553, D-49364 Vechta, Germany
[mehlers,jschiewe,mmoeller]@fzg.uni-vechta.de

ABSTRACT

This paper presents how ultra high resolution remote sensing data can be used within a GIS environment for the development of urban information systems and 3D city modeling. The paper concentrates on techniques to use digital surface models (DSM's) from remotely sensed data for the creation of highly accurate digital terrain models (DTM's). DSM's can be obtained from digital stereo scanner data or from laserscanning. It can be demonstrated that DSM'S from laserscanning are better suited for 3D city analysis. Using GIS techniques, however, also DSM's from stereo matching can be improved to produce highly accurate DTM's. Together with image and GIS (e.g. digital cadastral) data, these DTM's form a 3D urban information system which can be used for pollution modeling or telecommunication planning.

KEYWORDS

Ultra high resolution remote sensing, laserscanning, urban information systems, 3D city modeling, GIS, digital surface models, data fusion techniques

INTRODUCTION: GIS AND REMOTE SENSING FOR URBAN INFORMATION SYSTEMS

Geographic Information Systems (GIS) are more and more seen as an integral part of the modern information and communication society. Improved methods for data access and integration have accelerated this process. Consequently, GIS technology serves as the basis for the development of urban information systems (UIS). Remotely sensed image data can be used to generate the necessary current, accurate and synoptic information for the GIS databases. Due to the high spatial resolution requirements for UIS aerial photography has been used as standard imaging input. The advent of the new satellites with a resolution of better than 1m (e.g., IKONOS, Quickbird) and digital airborne scanner sensors with a high geometric fidelity and spatial resolutions (e.g., HRSC, ADS, DMC) in the cm range, however, challenges the analog airphoto techniques.

These airborne and spaceborne high resolution sensors offer an advanced potential for generating and updating GIS databases especially for urban areas. Moreover, digital airborne stereo sensors are capable of producing digital surface models (DSM) by automated techniques. Coupled with differential GPS and inertial navigation systems (INS), these sensors generate georeferenced ultra high resolution multispectral image data together with their accompanying DSM. Another way of creating this type of information is the use of laser scanning technology coupled with a multispectral imaging device. With these ultra high resolution sensors, however, the user community faces a new problem in the analysis of this type of image data. Standard techniques have to be augmented for an appropriate analysis because the necessary pixel homogeneity can no longer be achieved by the integration effect of large pixel sizes (e.g., 10 – 80 m). Due to their high spatial resolution the information content of the ultra high resolution data in such heterogeneous regions is very complex. Hence, the integration of the increasing amount of available GIS and/or elevation data (e.g., from stereo or laser scanners) as well as novel and efficient analysis techniques become a mandatory requirement for efficient processing and analysis.

We propose an integrated processing approach which fuses image analysis (e.g., segmentation or classification) and GIS (e.g., overlay or intersection) techniques. With that the heterogeneous properties of the objects of interest can actually be considered. The paper will present experimental results using high-resolution image and elevation data of two air-borne systems (HRSC-A, TopoSys II) which clearly demonstrate the benefits of introducing available GIS information for the classification and updating process for urban areas as well as the possibility of generating 3D city models for telecommunication industries or emission/immission modeling.

REMOTE SENSING PROGRAMS

There are many ways to distinguish between remote sensing systems. The most common one is probably the differentiation between space/satellite and airborne systems. Other possible taxonomies include spatial/spectral resolution, recording mode or spectral coverage (Table 1).

TABLE 1
TAXONOMY OF REMOTE SENSING SYSTEMS (FROM: EHLERS ET AL., 2002)

Taxonomy of Remote Sensing Systems						
Recording Platform	Satellite/Shuttle		Aircraft/Balloon		Stationary	
Recording Mode	Passive (Electrooptical, Thermal Infrared, Thermal Microwave)			Active (Laser, Radar)		
Recording Medium	Analog (Camera, Video)			Digital (Whiskbroom, Line Array, 2D CCD)		
Spectral Coverage	Visible/Ultraviolet	Reflected Infrared		Thermal Infrared	Microwave	
Spectral Resolution	Panchromatic 1 Band	Multispectral 2 – 20 Bands		Hyperspectral 20 – 250 Bands	Ultraspectral > 250 Bands	
Radiometr. Resolution	Very High (> 12 bit)	High (8-12 bit)		Medium (6 – 8 bit)	Low (< 6 bit)	
Spatial Ground Resolution	Ultra High < 1m	Very High 1 – 4 m	High 4 – 10 m	Medium 10 – 50 m	Low 50 – 250 m	Very Low > 250 m

Satellite Systems

Today, a wide variety of systems are used to detect energy patterns which provide information about the earth, its atmosphere, oceans, and land surfaces. The bulk of satellite remote sensing data is currently acquired by multispectral scanners such as Landsat TM and linear array devices such as SPOT HRV and IRS LISS sensors in the visible and near infrared positions of the electromagnetic spectrum.

With the advent of commercial high-resolution satellite programs from companies such as Space Imaging, Digital Globe or Orbview, new application fields have been opened for space based remote sensing. This includes – for the first time – operational applications for urban areas where the spatial resolution requirements are higher than for any other areas. Table 2 shows the characteristics of the two currently available commercial very high resolution sensors in space.

TABLE 2
SELECTED VERY HIGH RESOLUTION SATELLITE MISSIONS

Company	Digital Globe		Space Imaging	
System	QuickBird 2		Ikonos	
Mode	Pan 11 bit	Multispectral 4 bands 11 bit.	Pan 11 bit	Multispectral 4 bands 11 bit
Spatial Resolution	0.61 m	2.44 m	1 m	4 m
Spectr. Resolution (nm)	450-900	450 - 520 (b) 520 - 600 (g) 630 - 690 (r) 760 - 900 (nir)	450-900	450 - 520 (b) 520 - 600 (g) 630 - 690 (r) 760 - 900 (nir)
Suitable Scale for Applications	1:25,000 – 1:5,000			
Swath Width	16.5 km	16.5 km	11 km	11 km
Image Scene Size	16.5 x 16.5 km² Strip: 16.5 x 165 km²		11 x 11 km²	
Orbit Height	450 km		681 km	

Besides North America, Europe, India and Japan, other countries such as Israel, Brazil, China or Korea have been successful in launching their own national remote sensing satellites and challenge the established remote sensing nations.

Airborne Programs

Advanced technologies such as GPS coupled navigation systems and improved digital sensor technologies have the potential to overcome the strongest impediment of aircraft scanners: the lack of geometric stability. Public and private research concentrates on the development of digital line array or matrix scanners that will serve as successors to the 'classical' air cameras. Companies such as LH Systems or Zeiss Imaging are offering first commercial systems, research centers such as the German Space Establishment (DLR) fly their own prototypes. Such systems have to establish their market somewhere between the satellite image user seeking higher resolution and the airphoto user seeking digital input and GIS compatibility. Consequently, airborne scanner systems have to offer stereo capability and multispectral recording. The HRSC-A (High Resolution Stereo Camera - Airborne) is a narrow-angle digital multispectral stereo scanner for photogrammetric and remote sensing applications (Wewel and Scholten, 1999).

The camera was originally developed for the Russian Mars-96 space mission and later modified for airborne remote sensing applications. Especially the peripheral digital electronics were re-designed for use on aircraft. The system is mounted on a Zeiss T-AS stabilization platform. The HRSC uses the linear array imaging principle. Nine CCD line detectors are mounted in parallel at the focal plane behind one single optics and perpendicular to the flight direction. Nine images of the same strip are recorded almost simultaneously as a result of the forward motion of the aircraft. Five of the nine CCD lines of the HRSC-A are arranged at specific viewing angles (fore-aft-nadir) to provide stereo and photometric viewing capability; four of the nine CCD lines are covered with different filters for the acquisition of multispectral images (Tab. 3).

TABLE 3
SELECTED ULTRA HIGH RESOLUTION STEREO AIRCRAFT SCANNERS

	HSRC-A	HRSC-AX
Focal length	175 mm	151 mm
Total field of view	38° x 12°	41° x 29°
Number of CCD lines	9	9
Sensors per CCD line	5.272	12.172
Sensor size	7 µm x 7 µm	6.5 µm x 6.5 µm
Spatial resolution at 3000 m flying height	15 cm	20 cm
Radiometric resolution	8 bit	12 bit
Suitable application scale	1:500 (dep. on flying height)	1:500 (dep. on flying height)
Spectral resolution / band numbers	1 - Blue: 395- 485 nm 2 - Green: 485- 575 nm 3 - "Red": 730- 770 nm 4 - NIR: 920-1020 nm 5 - Nadir/stereo (Pan): 585- 765 nm	1 - Blue: 450 – 510 nm 2 - Green: 530 – 576 nm 3 - Red: 642 – 682 nm 4 - NIR: 770 – 814 nm 5 - Nadir/stereo (Pan): 520 – 760 nm
Read-out frequency	450 lines/sec	1640 lines/sec

A fully automatic photogrammetric and cartographic processing system was developed that allows that the system can work basically without ground control points (GCP's). This system makes use of DGPS and inertial navigation system technologies (Wewel and Scholten, 1999). For the generation of digital surface models (DSM's) a digital multiple correlation process is performed. The resulting identical image points are converted into object points by ray intersections. Finally, based on the DSM's digital orthoimages are generated and multispectral orthomosaics are produced. As a spin-off, an extended narrow-angle system (HRSC-AX) has been developed by the DLR providing higher radiometric resolution, larger swath width and re-designed multi-spectral bandwidths which are better suitable for terrestrial applications (see Tab. 3) (Neukum et al., 2001).

During the last couple of years, laserscanning systems have reached maturity due to the enhanced performance of GPS/IMU solutions for capturing orientation data of the associated moving platforms. Just recently the TopoSys company released their airborne TopoSys II system which simultaneously produces elevation data through laserscanning and multispectral imagery employing a line array scanner. The laser scanner operates with a glass fibre array producing a parallel acquisition pattern. First and last pulse elevation data with a height accuracy of about ± 0.2 m are delivered in a raster of 0.5 m x 0.5 m or 1 m^2, respectively. The imaging sensor produces four bands in the visible and near infrared spectrum with a ground pixel size of 0.5 m at a radiometric resolution of 8 bit (TopoSys, 2002).

SEGMENTATION APPROACH FOR THE ANALYSIS OF MULTI-SENSORAL DATA

As already pointed out, standard techniques have to be augmented for an appropriate analysis of the

available ultra-high resolution data for urban applications. In this context, we will firstly concentrate on the integration of the increasing amount of available multi-sensor data (multi-spectral imagery and elevation data, with the emphasis on the latter) as well as on the use of novel analysis approaches (in particular, segmentation methods). It should be noted that this rather data driven approach can be further extended to a hybrid procedure, i.e. it is able to integrate a priori knowledge from GIS databases and other sources.

Tasks

From an application point of view we will concentrate in the following on two key processing steps in the context of urban analyses which are the estimation of object and terrain surface heights and the separation of buildings from other objects. With respect to the first task, most elevation evaluation systems (like stereo matching or laserscanning) yield the respective largest values above a position, i.e. a *Digital Surface Model (DSM)*. However, for some applications (e.g., for hydrological modeling) those objects that stand clearly above the terrain surface (e.g., buildings, trees) are not of interest, i.e. the *Digital Terrain Model (DTM)* is required. Furthermore, for object extraction purposes and 3D city modeling the absolute height values of objects above the terrain surface (i.e., the difference between DSM and DTM) are required. Because in practice a DTM is not always available, not sufficiently accurate or reliable (or just too expensive) a substitute has to be estimated (*estimated DTM, eDTM*). The means, that a *normalization* has to take place. For this task, a couple of geometrically based algorithms have been developed (for an overview see Schiewe, 2001), but none of them have succeeded to an operational status so far. This is mainly due to the limited quality (especially for inclined terrain) and the missing grade of automatization (especially due to abstract thresholds). Thus, an application dependent combination of methods incorporating rather high interactive efforts for controlling and editing are presently applied in practice.

Also, the automated classification of topographical objects in urban scenes is still far from maturity. But for a couple of applications not a detailed but rather rough interpretation is sufficient. If, for example, the analysis of object heights has separated relatively high objects (i.e., building and trees) from lower ones, the recognition task might be reduced to the separation of the first mentioned classes.

Methodology overview

In the following we want to present a novel region-based, multi-scale approach for urban and landscape modeling purposes from multi-sensor data with the emphasis on elevation information. The procedure can be divided into two major parts: Firstly, the segmentation of multi-sensor data is performed which in analogy to a visual interpretation can be done at various scales. In order to attach semantical meanings to the obtained geometrical regions (e.g., terrain or non-terrain surfaces for the first task, or buildings or trees for the second), a classification using a fuzzy-logic approach takes place in a second next step.

Segmentation

Segmentation methods are well known from Computer Vision since the 1980's and have been applied in many disciplines. However, due to several reasons their use for the analysis of remotely sensed data has been rather limited (Schiewe et al., 2001). From the general strategies, we prefer a region-growing approach which from our experiences shows a good tolerance against noise and produces closed borders as well as sufficiently homogeneous segments with respect to relevant attributes. General goal of the segmentation step is an accurate delineation of the desired regions (terrain and non-terrain areas, buildings and trees, respectively). Obviously we also demand for the membership of one and only one class (which will be determined later on) to one segment. To achieve these goals, a proper choice of *homogeneity criteria* has to be applied. In the case of the DSM normalization we follow the hypothesis that regions which have to be reduced to the terrain surface are characterized by strong altitude gradients and curvatures (Schiewe, 2001). By extending the complexity presented so far by additionally introducing mul

tispectral or panchromatic image data, we have experienced worse segmentation results due to irregular and inaccurate border lines. This effect is mainly due to a strong affection of image data by noise and shadows. The region growing process is now controlled by a comparison of the obtained homogeneity measures of neighboring primitives with a user-defined threshold. Varying this threshold, one can influence the grade of generalization: The lower the value the less primitives are merged and the larger the total number of segments becomes.

Classification

For the interpretation of the obtained segments we apply a *fuzzy logic* classification approach. There are several reasons for introducing partial rather than crisp memberships in this context (see, for example, Cheng, 2002): On the one hand, the description of the real phenomenon is neither geometrically sharp nor certain. On the other hand, the limited spatial sampling rates and measurement errors (the latter being mostly unknown) also lead to indeterminate boundaries. As input for the classification we can use several application dependent features for every extracted segment. For each feature the membership function to a category is computed (fuzzification). Because a generic determination of these functions seems to be impossible we apply tolerance intervals from logical considerations and a linear function in order to describe the partial memberships. Finally, the assignment to one and only one class (de-fuzzification) is based on a comparison of the maximum of the obtained single membership values with a threshold. As *features* in the case of the normalization task the mean of altitude gradients (pointing to forest areas) and the 90% percentile of gradients (pointing to steep edges likes in buildings) can be taken into account. In order to handle the problem of flat roofs (i.e., segments with low gradients), we also consider the 90% percentile of gradients of all surrounding segments (referring to a building edge with high gradients). Finally, the mean difference between first and lust pulse laser scanning measurements, if available, can be considered for each segment (also pointing to wooded areas and building outlines). For the task of separating buildings from trees not only the object height but in particular the Normalized Difference Vegetation Index (NDVI) and the spectral texture (in panchromatic imagery) are meaningful features.

Examples

The multi-sensor data set which covers a settlement near the City of Ravensburg (Germany) consists of simultaneously acquired laserscanning and multispectral image data of the TopoSys II-sensor. Fig. 1 illustrates the processing results applying the described region based approach. As an example, the fuzzification result for the feature "mean gradient" demonstrates the desired high membership values of wooded areas to the class of non-terrain areas as well as the necessity of taking also the gradients of surrounding segments of roof regions into account. Comparing the achieved results for both tasks - normalization and separation of buildings and other objects - no omission errors were found. The number of commission errors is below 2% of the entire number of segments. Critical regions within the terrain surface estimation process are small clearings within wooded areas whose slope behavior in contrast to the surrounding trees could not be sufficiently separated. Applying the segmentation and the following classification not only at one, but at multiple scales, reduces the number of commission errors with decreasing generalization level. However, this scaling process must not be performed as far as possible because the number of omission errors would increase and in the extreme case one would end up with an undesired point-wise classification.

Significantly worse results have been obtained using elevation data derived from an automated matching using imagery of the HRSC-A sensor for the test site of the City of Osnabrück (Germany). Due to the stereo matching procedure that is used to create the elevation data, segments are produced that do not coincide well with actual borders. While the number of omission errors was quite low (about 2 %), the number of commission errors (ca. 40 %) was definitely too high. Also the integration of image data could not improve the resulting quality. It becomes obvious that without additional information (i.e., human or

GIS based knowledge) an *automated* procedure as presented here cannot compensate for the limited input data quality.

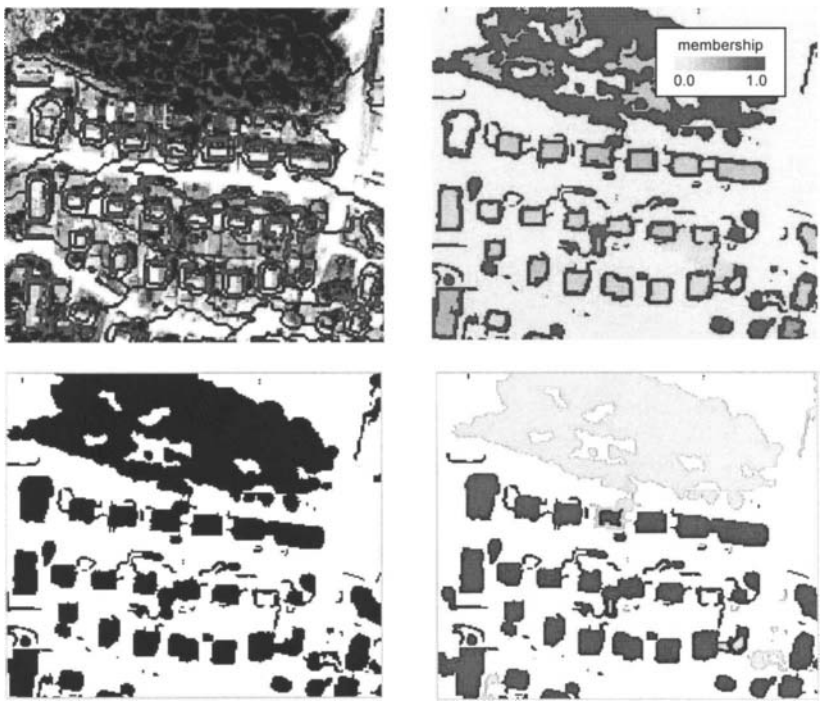


Figure 1: Results of multi-sensor data processing: segmentation (upper left), fuzzification based on feature "mean gradient" (upper right), classification of terrain surfaces (in gray; lower left), classification of buildings vs. wooded areas (in red and green, respectively, lower right)

URBAN ANALYSIS WITH DTM's FROM OPTICAL SCANNER DATA

DTM Generation

Despite the failure in the automated segmentation process, elevation data from stereo matching of digital image data can be improved by manual techniques if no laserscanning data are available. A number of automated (or semi-automated) methods have been developed for DTM extraction from laser DSM data. Unfortunately, they do not work well with HRSC-DSM-data (see above and also Baltsavias, 1999, von Hansen and Vögtle, 1999). This is caused by the representation of 3D objects in the HRSC DSMs. The edges of 3D objects do not appear as vertical lines but rather as slopes with a tent-like behavior (fig. 2). This effect is caused by the 18.9° fore and aft stereo bands and the employed stereo matching algorithm. In our test area, the city of Osnabrück (Germany), we obtained HRSC digital orthoimages with a ground resolution of 0.15 m data in addition to the DSM data. The imaging products had a geometric accuracy of $\pm$one pixel in x- and y-direction. They were directly integrated into a GIS environment. We used the orthophotos as GIS background information for on-screen digitizing of reference points (RP's). These RP's represented exact ground truth (e.g., streets, meadow, yards or parks). About 400 equally distributed

RP's per km² were found yielding a density of about one point per 2,500 m². This density is well suited for the representation of a terrain with a moderate morphology and without any steep slopes.

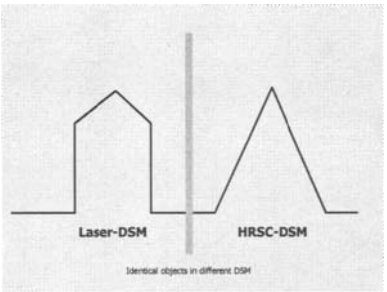


Figure 2: Object Representation in DSM's from laserscanning (left) and HRSC data (right)

In the next step, elevation values were assigned to the RP's from the underlying DSM using the GIS focal function operator. At last, the terrain surface can be interpolated from the RP elevation values using an inverse distance weighting (IDW) algorithm. For the calculation of each DTM point, the 12 next neighbor RP's were used. The accuracy of the interpolated DTM was checked from a total of 669 check points (CP's). These CP's were terrestrially measured with a very high accuracy. The average difference in height was about 1 m which represents an excellent accuracy. The maximum difference was 12.1 m which was caused by shadowed areas where no gray values can be used for the calculation of the HRSC DSM.

Assigning elevation to objects

Using the described techniques, it could be proved that both type of elevation measurements (i.e. DSM's by stereo matching and laserscanning) can be used as a basis for 3D urban information systems. Building heights are needed, for example, for the modeling of traffic noise and of the spreading of radio waves for mobile telecommunication purposes. For building height extraction, we combined a priori knowledge about house location and extension from the digital German cadastral database (ALK) with the HRSC DTM's in a GIS environment. The centroids of these building were extracted as GIS point layer and the DTM and DSM values were assigned to the points using the GIS overlay operator. The actual height of each building could then be calculated by subtracting the DSM value from the DTM value. The resulting elevation is the height at the centroid point of the building which can be linked directly to the respective building. The 3D data set can be exported from the GIS into a WWW compatible format using the VRML technology and can be visualized in every common internet browser.

This technique was used to demonstrate the effects of newly constructed buildings on the urban climate in Osnabrück. Fig. 3 shows that new large buildings (outlined in yellow) block the nightly cool air which comes from the outside of the city toward its center (indicated by blue arrows). This 3D view - if constructed in advance in an urban information system - allows planners and decision makers to visualize and simulate effects of city developments on its climate. With this, negative climatic and pollution effects in urban areas could be avoided or at least minimized.

CONCLUSIONS

Using advanced image processing, data fusion, and GIS techniques it could be demonstrated that ultra high

resolution image data from airborne scanners are an important information source for urban information systems. Accurate, current and high resolution DTM's can be generated from airborne scanners using direct laser techniques or indirect stereo matching algorithms of electro-optical image data. These DTM's can be used for 3D applications such as noise and pollution simulation or telecommunication planning.



Figure 3: 3D view of Osnabrück: Newly constructed buildings (yellow outline) block the flow of cold and fresh air toward the center of the city

References

Baltsavias, E. (1999): A comparison between photogrammetry and laser scanning. *ISPRS Journal of Photogrammetry and Remote Sensing*, Elsevier Science, **Vol. 54**, 83-94.

Cheng, T. (2002): Fuzzy objects: their changes and uncertainties. *Photogrammetric Engineering & Remote Sensing* **68(1)**, 41-49.

Ehlers, M., R. Janowsky and M. Gähler (2002): New Remote Sensing Concepts for Environmental Monitoring, in: Ehlers, M. (Ed.) *Remote Sensing for Environmental Monitoring, GIS Applications, and Geology*, Proceedings of SPIE **Vol. 4545**, Bellingham, WA, 1-12.

Neukum, G. and HRSC-Team (2001): The airborne HRSC-AX cameras: evaluation of the technical concept and presentation of application results after one year of operation, *Photogrammetric Week 2001*, Stuttgart, 117-130.

Schiewe, J. (2001): Ein regionen-basiertes Verfahren zur Extraktion der Geländeoberfläche aus Digitalen Oberflächen-Modellen. *Photogrammetrie - Fernerkundung - Geoinformation* **(2)**, 81-90.

Schiewe, J., Tufte, L., Ehlers, M. (2001): Potential and problems of multi-scale segmentation methods in remote sensing. *GIS - Geographische Informationssysteme* **14(6)**, 34-39.

TopoSys (2002): www.toposys.de, accessed February 20, 2002

von Hansen, W. and Vögtle, T. (1999): Extraktion der Geländeoberfläche aus flugzeuggetragenen Laserscanner-Aufnahmen. *Photogrammetrie - Fernerkundung - Geoinformation*, **(4)**, 229-236.

Wewel, F. and F. Scholten (1999): High Resolution Stereo Camera (HRSC): Multispectral Data Acquisition and Photogrammetric Data Processing, *Proc. 4th International Airborne Remote Sensing Conference and Exhibition*, Ottawa, **Vol. 1**, 263-271.

This Page Intentionally Left Blank

Advances in Building Technology, Volume 2
M. Anson, J.M. Ko and E.S.S. Lam (Eds.)
© 2002 Elsevier Science Ltd. All rights reserved

Data Model and 3D Visualization of Underground Pipeline

Qingquan Li, Yong Yan, Bisheng Yang, Xianghong Hua
Wuhan University, Wuhan, Hubei
P.R.China, 430079

ABSTRACT

Pipelines are part of the infrastructure of any city and research about the 3D representation of pipelines is very important for integrating into 3D building models, road models and terrain models. These models are all indispensable components in a digital city. In this paper, the reality of managing pipelines is introduced first. Second, a Layer Model and data structure of a 3D pipeline object is proposed, which can meet the requirements of 3D spatial representation and interactive operation. Third, the paper illustrates how to build the 3D underground pipeline model and introduces the method of subsection calculation. Finally, an experimental system prototype is developed based on C++ and OpenGL, and several experimental results are illustrated.

KEYWORDS

3D pipeline model, visualization, interactive operation, layer model

1 INTRODUCTION

For a long time, the management and maintenance of pipelines has been performed manually and with low efficiency. Therefore much research about managing pipeline with computer assistance has been done. Now most systems of managing pipelines exploit programming language integrated with GIS software such as MAPINFO and ARC/INFO. Researchers and users trust them for they have strong basic function of GIS and have experienced the baptism of the market. Several systems of managing pipelines are based on GIS platforms developed independently such as GeoStar and MAPGIS. These systems include the professional function of managing a pipeline besides basal functions, but most of them are based on 2D or 2.5D and they cannot represent the spatial relation of complicated pipelines. Even some pipes vertical to the surface of the earth are difficult to handle. As a result, many approaches and systems for 3D pipeline models have been developed. Some famous GIS software such as MAPINFO and ARC/INFO can represent a simple 3D object, but they cannot depict and analyze 3D relations of the complex objects in detail. Furthermore, they cannot implement modeling of a 3D pipeline. In China, several corporations have been researching the 3D representation of pipelines such as ZONDY and LinTu. They have made achievements in virtual 3D image browsing and

roaming, and this is inadequate for managing a 3D pipeline. Based on close-range photogrammetry and CSG model, 3D pipeline model can be constructed(Bürger,2000, ERMES,2000). This method is useful for the representation of complicated objects aboveground, but cannot adapt to underground pipelines.

The increasing quantity of pipelines requires data management and storage to be powerful and efficient. At present, data models used in commercial GIS are mainly Topology-Relationship Model and Space-Entity Models. Topology-Relationship Models mostly adopt the POLYVRT structure, which can save memory because data does not overlap. But the structure is so complicated that data is difficult to edit and maintain. Though Space-Entity Models make data stored repeatedly, it enhances the maintenance of data. According to the types of pipeline data, the author combines the virtues of the two models and put forward a data structure named Layer Model, which not only saves memory but also is easy to edit and maintain the pipeline data.

The following sections are arranged as follows. First, the reality of pipeline management is introduced. Second, the Layer Model and data structure of the 3D pipeline object is proposed, which can meet the requirements of 3D spatial representation and interactive operation. Third, the paper illustrates how to build the 3D underground pipeline model and introduces the method of subsection calculation. Finally, an experimental system prototype is developed based on C++ and OpenGL, and several experimental results are illustrated.

2 ORGANIZATION OF PIPELINE DATA

Underground city pipelines can be sorted into seven classes such as pipelines for feed water and for drainage. Every class can be subdivided. For instance, pipelines of feed water include pipelines for industry, for homes and for fire protection.

2.1 Layer Model

The complexity and large amount of pipeline data requires an efficient management mechanism for spatial data. Therefore, a Layer Model of pipeline data is developed that can not only meet the requirements of 3D spatial representation, but can also meets the requirements of interactive operation with 3D objects. Figure 1 illustrates the Layer Model.

According to the different classes of pipeline, all data is organized and managed by different layers, which include layer of feed water, drainage, burning gas pipeline, and so on. The shapes of most pipelines are branching, orbital and radial, so a pipeline can be decomposed to several pipeline sections according to junctions or points of changing radius. At a joint, pipelines attachments such as T-junction and intersection junction are used to connect the pipeline sections. So we can consider that every pipeline is composed of pipeline sections and attachments, as figure 1 illustrates. And the most basic data about pipelines are points that marked the attachments and used to construct continuous pipeline sections. These basic data can be called "points on pipelines".

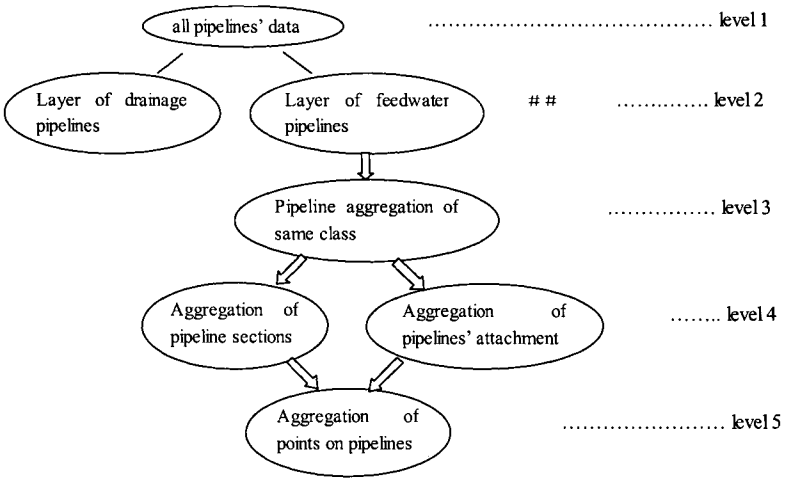


Figure 1: Layer Model of pipeline data

2.2 Data Structure

Based on the Layer Model, the structure of storing data is reticular that is close to a tree structure. The data type of every class has a little discrimination, but their structures are the same basically. Taking the data of feed water pipelines as an example, from figure 1, we can see these data comprise a reticular structure too. All nodes in the network denote the aggregation of some data, which is stored in the tables or files. The data in the same node is stored separately as spatial data and attributive data. Attributive data includes the material of the pipeline, time of burying, and so on. It is stored in the relative database and used to afford detailed information when inquiring or indexing. Coordinates, color and radius are spatial data, which are used for modeling and 3D visualization. It is stored in files with special format. Spatial data connects with Attributive data by the same identity.

This mode of storing data has several advantages:

- It can reduce overlapping data and save memory.
- It can be easy to edit and maintain.
- It makes quick data indexing, so the system can run fluently.

For the purpose of query and analysis, a pipeline index must be provided to speed up data retrieval. The R^+-tree index (Storcebraker, 1986) proves to be a useful index. When querying and analyzing, the identities of pipeline sections chosen are decided by the R^+-tree index first. Then the files of spatial data are indexed. It's a multilevel index, so depending on the identities of pipeline sections, we can decide which pipelines are chosen through indexing the files of pipelines, and which layers of pipelines can be decided subsequently.

3 3D PIPELINE MODELING

OpenGL is an excellent program interface for creating 3D Real-time graphics. With it, complicated objects are constituted by drawing basic figures such as dots, lines and polygons. The author uses numerous quadrangles to simulate the surface of pipeline object. Before modeling, enough data for calculation needs must be obtained. Through dealing with all the files of points on pipelines, we can obtain the 3D coordinates of all the nodes on the Centre Line Of Pipelines. Centre Line Of Pipeline means the conduit axes. These 3D coordinates, together with radius and color of pipeline, are initial

data ready for the 3D modeling and representation.

3.1 Surface Differential (Liu, 1999)

A pipeline is usually represented with a line on the plan. In 3D rendering, a pipe is represented with a column. The axis of column is the Centre Line Of Pipeline, and the radius of the column is the pipe's radius. The surface of column is divided into several quadrangles just as figure 2b illustrates. Some experiments indicate that the more quadrangles the more realistic is simulated pipe. At the same time, the speed of system running becomes slower. With a simulated pipe divided into coarser, the speed of system running is faster. When the surface of column is eight quadrangles, the speed of system running and the quality of display are in balance.

Figure 2a: 2D representation of pipe

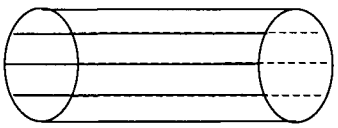


Figure 2b: 3D representation of pipe

3.2 Simulation of Pipeline Section

In plan, a pipeline section will be represented with a polyline which has no height (Fig.3a). In 3D rendering, we divide a pipeline section into several columns (figure 2b) and are simulated though connecting these columns. There are several problems to be noticed. If every column is composed by eight quadrangles and if columns are not connected well then gaps between columns will appear easily. The correctness of those quadrangles' coordinates is important too. The wrong coordinates may lead the vertexes of the quadrangles to be not coplanar and the simulated pipeline will look twisty. So the author has advanced an arithmetic named Subsection Calculation to solve the above problems. The arithmetic is first to calculate the coordinates of vertexes on the brim of node (node 1 or 15 in Fig 4), then to calculate the coordinates of vertexes on the brim of other node (node 2 to 14 in Fig 4) in turn. This is illustrated in detail below.

- Arcing the corner of Center Line Of Pipeline (Fig. 3b)

Centre Line Of Pipeline is a polyline that has height. It is ready to simulate the pipeline and it does not be shown eventually. At a corner, the value of radian changes with the angle. The radius of the circle including the radian equals to the radius of pipeline section.

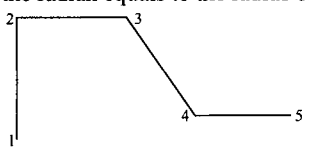


Figure 3a: polyline in the plan

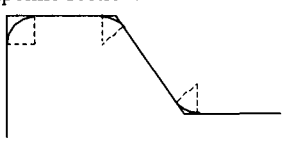


Figure 3b: Arcing Centre Line Of Pipeline

- Dividing the Center Line Of Pipeline into subsections (Fig. 4)

According to the value of radian, the number of subsections in the corner is decided. In figure 4, the node 1 to 15 serial numbers denotes the spots where the Center Line Of Pipeline is divided. The 3D coordinates of these spots will be calculated from the initial data.

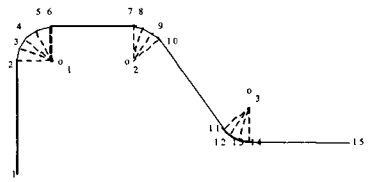


Figure 4 : dividing the Center Line Of Pipe

- Calculating the coordinates of vertexes on the brim of pipe (node 1 or 15) (Fig 5)

In figure 5, O-XYZ is a 3D Cartesian System. The reference frame (o-xyz) is defined below. Its origin superposes the first node (node 1) of the Center Line Of Pipeline. Its z-axis is parallel to the first line (node 1 to 2) of the Center Line Of Pipeline. Its x-axis is perpendicular to the Z-axes of Cartesian System.

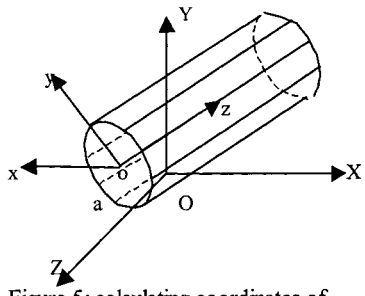


Figure 5: calculating coordinates of vertexes on the brim of port

Through rotation and translation, the reference frame can be change into the 3D Cartesian System. Known from the spatial analytic geometry, the arbitrary vertex "a" (Fig 5) at the brim of pipe has the relation in the reference frame and Cartesian System given formula (1). Its matrix form is given formula (2).

$$\begin{cases} X = a_1x + a_2y + a_3z + x_0 \\ Y = b_1x + b_2y + b_3z + y_0 \\ Z = c_1x + c_2y + c_3z + z_0 \end{cases} \quad \ldots(1) \qquad \begin{pmatrix} X \\ Y \\ Z \end{pmatrix} = \begin{pmatrix} a_1 & a_2 & a_3 \\ b_1 & b_2 & b_3 \\ c_1 & c_2 & c_3 \end{pmatrix} \begin{pmatrix} x \\ y \\ z \end{pmatrix} + \begin{pmatrix} x_0 \\ y_0 \\ z_0 \end{pmatrix} \quad \ldots(2)$$

In the two coordinate transforms, (x_0, y_0, z_0) is the coordinate of the origin of the reference frame located in the Cartesian System. Nine coefficients are the orientation cosines of two axes, i.e.

$$\begin{pmatrix} a_1 & a_2 & a_3 \\ b_1 & b_2 & b_3 \\ c_1 & c_2 & c_3 \end{pmatrix} = \begin{pmatrix} \cos Xx & \cos Xy & \cos Xz \\ \cos Yx & \cos Yy & coxYz \\ \cos Zx & \cos Zy & \cos Zz \end{pmatrix} \quad \ldots(3)$$

The coordinates of the vertexes on the brim of pipe are easy to calculate in the reference frame. It, together with the nine coefficients and (x_0, y_0, z_0), are added to formula (2). Then the coordinates of vertexes on the brim of pipe in the Cartesian System, i.e. true 3D coordinates, are calculated.

- Calculating the coordinates of vertexes on the brim of other nodes

When calculating in turn, there are two possible circumstances met. One is "beeline" such as node 1-2 (Fig 6a). The other is "siphon" such as node 2-3, node 3-4 (Fig 6b).

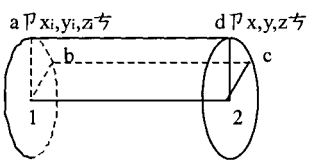


Figure 6a: calculation on the beeline

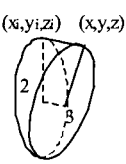


Figure 6b: calculation on the siphon

For the beeline (Fig 6a), the coordinates (x_i, y_i, z_i) of vertexes on the brim of port (node 1) have been obtained in the last step. The coordinates of node 1 to 15 also have been calculated in the before-mentioned step. So the coordinates (x,y,z) of vertexes on the brim of next node (node 2) can be

calculated as a rectangle. For the siphon (Fig 6b), the coordinates (x_i,y_i,z_i) of vertexes on the brim of node 2 have just been gained. The coordinates (x,y,z) of vertexes on the brim of next node (node 3) can be calculated as an isosceles trapezoid. By analogy in turn, the coordinates of all the vertexes on the brim can be obtained. Connecting them as rectangles 'abcd' in figure 6a, a pipeline section will be formed (Fig 7).

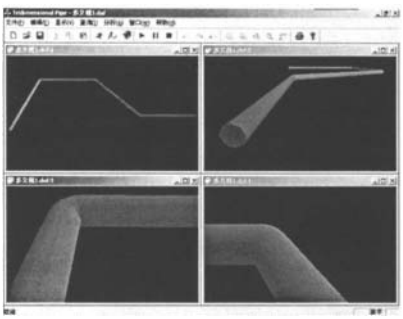


Figure 7: simulation of pipeline section

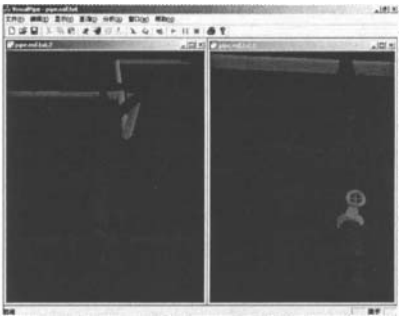


Figure 8: connection of pipeline sections

3.3 Connection of Pipeline Sections

In fact, there are attachments such as T-junctions, valves to connect pipeline sections. Therefore, the author abstracts them as 3D symbols and combines these simulated attachments with pipeline sections (Fig 8). Because there are so many attachments and varieties attachments, it's difficult to build all of them. If each attachment has only one uniform 3D symbol, it will affect the reality of pipeline. For improving the speed and quality of 3D visualization, what instrument of modeling for these attachments should be used? These problems await more research.

4 EXPERIMENT

Combined Layer Model of data and the method of modeling, a system has been developed using Visual C++ and OpenGL. The 3D system represents the underground pipeline mainly. The primary buildings are created with simple model and 3D character to mark it. The translucent allow the visibility of the underground pipeline. A existing pipeline model or a plan about burying pipeline, creating new pipeline model, analysis and query the attribute data of pipelines, walk through or fly through along a defined route or navigate by mouse and keyboard can all be visualized. Some experimental results are shown below in Fig 9.

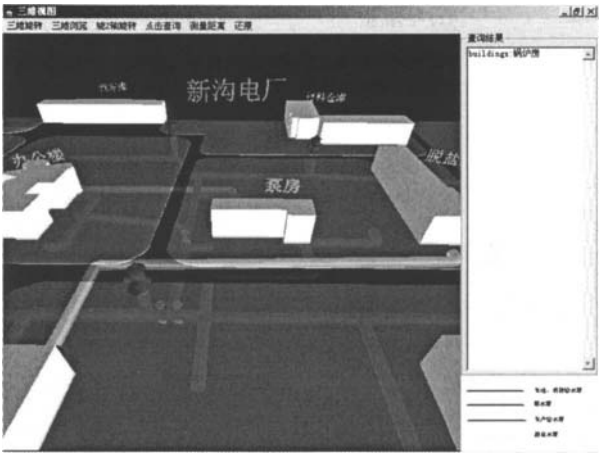


Figure 9: 3D pipeline model

5 CONCLUSION

Research on the 3D representation of pipelines is very important, for integrating into 3D building models, road models and terrain models. These models are all indispensable components in a digital city. The 3D pipeline model is very useful in many fields (management of plant, urban planning etc). This paper has introduced some researches about creating and storing 3D pipeline models. Many experiments are finished and several conclusions are drawn as follows:

- The Layer Model for pipeline data can not only decreases the volume of data storage but is also easy to edit and maintain the pipeline data.
- Subsection Calculation, not depending on the program language, makes the simulated pipeline fully connected with no gaps and with a realistic representation.
- Because a pipeline is modeled as several pipeline sections, spatial analysis can be used to define the topologic relation between pipeline sections.
- The method of data organization and pipeline modeling can be used for pipelines above the ground. But it isn't efficient enough to model most intricate pipelines in workshops.
- The problem of how to represent attachments more realistically needs more research.

REFERENCES:

Bürger Thomas, Busch Wolfgang,2000. Using knowledge about shape and position of plant elements in Photogrammetric As-Built-Documentation. International Archives of Photogrammetry and Remote Sensing. Vol. XIXIII, partB5. Amsterdam 2000.
Cui Binguang, Sun Hu, Zhu Zhaoguang, 1991. Photogrammetry. Mapping Publishing Company.

ERMES Pierre,2000. Constrains in cad models for reverse engineering using Photogrammetry. International Archives of Photogrammetry and Remote Sensing. Vol. XIXIII, partB5. Amsterdam 2000.

Frank A.VAN DEN HEUVEL,2000. Trends in CAD-Based Photogrammetric measurment. International Archives of Photogrammetry and Remote Sensing. Vol. XIXIII, partB5. Amsterdam 2000.

Liu Zongwei,1999. Research of construction and application of large scale DEM in urban site planning. Wuhan Technical University of Surveying and Mapping thesis of master's degree.

Li Xiang, Li Manchun, Yu Yousheng, Yi Hong, 1999. A useful GIS data structure of urban underground pipeline. Remote Sensing Information. No.3, 1999.

Tang Wei, Weng Jingnong , Zhang Shubing, 2001. GIS-based Hydraulic Calculations of Water-supplying Pipe Network. China International Conference on Digital City Construction Technology & Forum on Digital City in 21st Century.

Tian Yinzhong, Zhang Zhenglu, Yang Xu,1997. Detection and information management of underground pipeline net. Mapping publishing company.

Yu Hailong, Wang Nong, Xie Gangsheng, 2001. Research on constructing the topology structure of the urban underground pipeline based on MapInfo. Mine Measure No.1, 2001.

The brief introduction and resolution to application of VRMap2.0. www.lingtu.com

Advances in Building Technology, Volume 2
M. Anson, J.M. Ko and E.S.S. Lam (Eds.)
© 2002 Elsevier Science Ltd. All rights reserved

A FAST GPS-BASED SYSTEM FOR SURVEY CHECK OF ROAD ALIGNMENTS

Esmond Mok

Department of Land Surveying and Geo-Informatics,
The Hong Kong Polytechnic University, Hunghom, Kowloon,
HONG KONG, SAR CHINA

ABSTRACT

Survey check of road alignments is an important quality assurance procedure in road construction. Before the kerb lines are actually laid, engineering surveyors have to set out road alignment reference marks and indicators. The positions of these indicators would be checked independently by consultant surveyors to ensure that they are set out according to design parameters. Many surveying methods can be adopted to set out and carry out survey check of road alignments. The most commonly used approach is by radiation with a total station [see e.g. Uren J. and Price W.F., (1978), Schofield W. (1993)]. This conventional surveying method has the disadvantage of requiring a sufficient number of intervisible control points near the survey area. To fulfill this requirement, sufficient control points have to be maintained inside the project area throughout the project period, which is a difficult task for surveyors in complicated construction site environments.

When consultant surveyors carry out the survey check of road alignments with the conventional method, they always encounter the same difficulty that request for survey check of setting out work is in a rather short notice, the results of which have to be reported as quickly as possible in order not to delay the progress, however, time is required to re-establish control points and to carry out data processing of survey check results. In order to alleviate this pressure imposed on consultant surveyors, a fast GPS-based system for survey check of road alignments is proposed. This system combines the GPS positioning techniques with an automatic database search and computational algorithm. With the high precision GPS Real-Time Kinematic (RTK) [see e.g. Hofmann W. (1992), Leick, A. (1995) and Misra P. et al. (2001)] positioning results fit into the processing engine, survey check results can be reported on-site.

KEYWORDS

GPS, Survey Check, Road Alignment.

INTRODUCTION

Setting out of design features and survey check of setting out work are essential roles of an engineering surveyor. As a quality assurance procedure, it is a common practice in Hong Kong that alignments set out by contracting companies are checked by a consulting company employed by the client. Therefore, in road construction projects, the contractor would, according to the design geometry, set out kerb line positions at regular chainage such as 100, 105, 110; and these positions will be checked by consulting company. To ensure independence, the consultant would survey positions as if the chainage information is not known. Although such information is normally shown, it is recorded for reference only. The actual chainage of the positions surveyed and their deviations from the design geometry are then determined. If any points are outside the acceptable tolerance, the contractor has to carry out necessary remedial work.

Many surveying methods can be adopted to set out and conduct survey check of road alignments. The most commonly used approach is by radiation with a total station [see e.g. Uren J. and Price W.F., (1978), Schofield W. (1993)]. This conventional approach has the disadvantage that control points are needed near the project area. Therefore, very often, additional field procedures have to be carried out to connect the distant controls to the project site. Consultant surveyors adopting this conventional surveying method would require additional efforts to re-establish the control points if they are destroyed or disturbed, or their visibility is obstructed. The situation may become worse if the request for survey check is in short notice and the survey check results have to be reported as quickly as possible in order not to delay the progress. In order to alleviate this pressure imposed on consultant surveyors, a fast GPS-based system for survey check of road alignments is proposed. This system combines the GPS positioning techniques with an automatic database search and computational algorithm. It is well-known that GPS positioning has the following advantages over classical surveying techniques:

1. Intervisibility between ground stations is not required. For GPS positioning, it is only necessary for the receivers to be able to track satellite signals in a fairly open area, which is normally the case in road construction sites.
2. GPS positioning can be carried out under all weather conditions.
3. Separation between stations within 10 km is considered as "short baseline" in GPS positioning. Therefore, establishment of one GPS reference station would well serve different survey activities inside the10km radius.

With the high precision GPS Real-Time Kinematic (RTK) [see e.g. Hofmann W. (1992), Leick, A. (1995) and Misra P. et al. (2001)] positioning results fit into the processing engine, survey check results can be reported immediately on-site. This paper discusses the configuration of the proposed system and the computational methods adopted for automatic processing of survey check results.

SYSTEM CONFIGURATION

Figure 1 below shows the configuration of the GPS-based road alignment survey check system. A GPS receiver with RTK capability is connected to a data storage and processing unit. This unit can either be a notebook or PDA type computer. RTK positioning results may either be referenced to the WGS84 coordinate system, or have been transformed to the grid coordinate system adopted for carrying out the project, depending on the settings of the GPS device and availability of transformation parameters. If the device output is in WGS84 coordinate system, they will be transformed to the relevant grid coordinate system before performing alignment check computation.

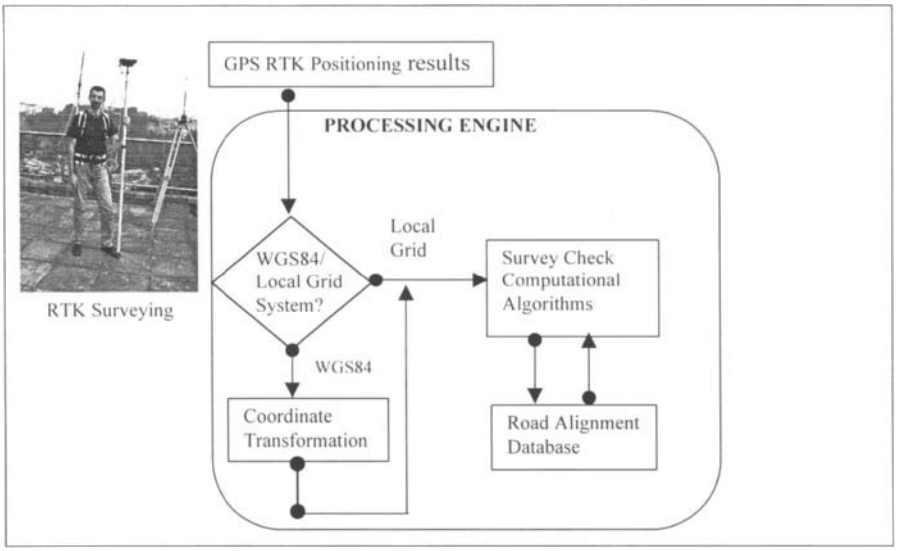


Figure 1: Configuration of the GPS-based Survey Check System

The database component of the processing engine contains information about type of alignment (straight, circular or transition), their start and end chainages, and geometrical parameters. With the GPS positioning result, an automatic search for the correct road section is performed and relevant road alignment parameters are extracted for alignment check computation. Details of the computational method is described below.

ALIGNMENT CHECK COMPUTATION

Straight Alignment

Computational check for straight and circular curve alignments are quite straight forward. For the case of straight alignment shown in Figure 2, P is the point requiring survey check. The bearing of the straight alignment; α_T, chainage at the tangent point T; CH(T), and the coordinates of T ; (N_T, E_T) are known design parameters extracted from the database.

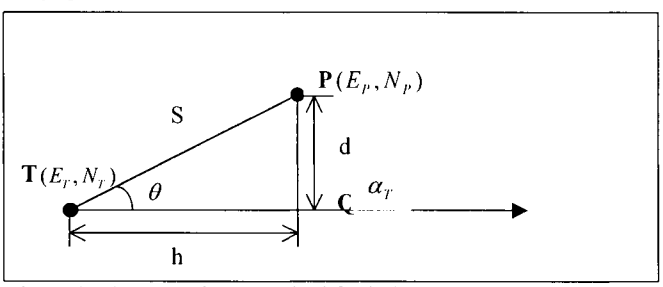


Figure 2: Computational method for independent check of straight alignments.

With the angle θ and distance S derived from coordinates of T and P, the chainage of point P and its perpendicular offset from the design alignment, denoted by CH(P) and OS(P) can be expressed as,

$$\begin{aligned} CH(P) &= CH(T) + h = CH(T) + S \cdot \cos\theta \\ OS(P) &= d = S \cdot \sin\theta \end{aligned} \qquad (1)$$

Circular Curve Alignment

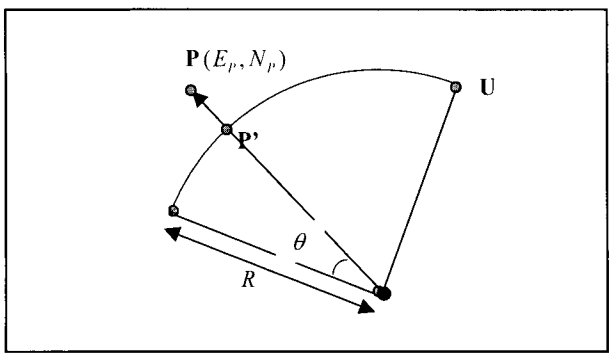


Figure 3: Computational method for independent check of Circular curve alignment.

Figure 3 shows a section of circular alignment TU. To determine the chainage of P' which is the projection of P on arc TU, the following simple mathematics are applied.

$$\begin{aligned} CH(P') &= CH(T) + arc\ TP' = CH(T) + R \cdot \theta \\ OS(P) &= CP - CP' = CP - R \end{aligned} \qquad (2)$$

where θ is obtained by subtracting bearings CP and CT, and the distance CP is determined from the known coordinates of C and P.

Transition Spiral

Survey check of transition spiral is not as straight forward as the above two cases. The computational approach suggested below requires iteration. Another approach based on the Method of Lagrange Multipliers was suggested in Mok, E. (1997).

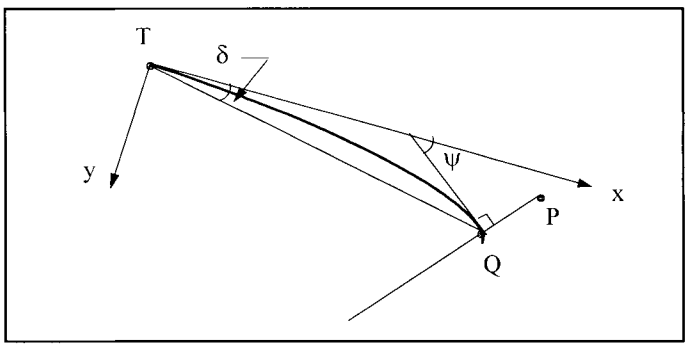


Figure 4 : Diagram showing a section of transition spiral. The chainage and offset of point P referring to the proposed alignment is to be determined.

A typical transition curve geometry is shown in Figure 4. Point P is the point surveyed whose chainage and offset with respect to the design alignment is to be determined. The tangent bearing; α_T, grid coordinates of T; (N_T, E_T), chainage of T; CH(T) and the transition spiral's RL value (R is the minimum radius of curvature and L is the total spiral length) are the four basic elements to define the geometry and orientation of a transition spiral. With this information, coordinates of P at any chainage can be deduced from the following well-known transition curve formulae.

$$\psi = \frac{s^2}{2RL} \qquad \text{(a)}$$

$$x = s - \frac{s^5}{40(RL)^2} + \frac{s^9}{3456(RL)^4} - \frac{s^{11}}{224640(RL)^6} + \cdots \qquad \text{(b)}$$

$$y = \frac{s^3}{6RL} - \frac{s^7}{336R(RL)^3} + \frac{s^{11}}{42240(RL)^5} - \cdots \qquad \text{(c)}$$

$$\tan\delta = \frac{y}{x} \qquad \text{(d)}$$

$$c = \sqrt{x^2 + y^2} \qquad \text{(d)} \qquad (3)$$

s is the spiral length from the tangent point T to the point of interest;
c is the chord length from T to the point of interest;
x, y are the x and y-coordinate of the point of interest referred to the spiral's coordinate system with the origin at T.

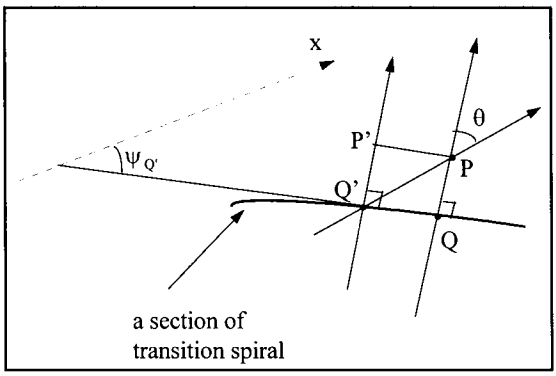


Figure 5 : Amplification of a section of transition spiral

As shown in Figure 5, the offset of P from Q and the chainage of Q are to be determined, with the spiral length of Q considered not exactly known initially. Therefore an estimation is needed to determine the initial position of Q and its normal bearing, denoted by Q' and bearing Q'P'. The estimated chainage of Q' can be readily obtained from the chainage information recorded on site, or by using the distance computed from the coordinates of T and P. Therefore

$$\alpha_{Q'P'} = \alpha_T + \psi_{Q'} - 90^\circ \tag{4}$$

$$\begin{aligned} N_{Q'} &= N_T + c_{TQ'} \cdot \sin(\alpha_T + \delta_{TQ'}) \\ E_{Q'} &= E_T + c_{TQ'} \cdot \cos(\alpha_T + \delta_{TQ'}) \end{aligned} \tag{5}$$

If the spiral length is correct, Q' would coincide with the correct position Q, then θ and distance PP' will be equal to zero. Based on this condition both θ and the distance PP' can be used as indicators to check if the iteration process has converged to the correct position Q. At the beginning of the iteration process, position of Q', the corresponding θ and distance PP' are computed. If PP' is outside the specified tolerance, say 1mm, the spiral length will be updated by adding or subtracting one-half of the distance PP', i.e.

$$s_{Q'}(i+1) = s_{Q'}(i) \pm \frac{1}{2} \cdot PP'(i) \tag{6}$$

and the new position of Q' is computed. This process continues until either PP' or angle θ is within the acceptable tolerance. It should be noted that the addition or subtraction of PP' to the spiral length depends on the position of Q' relative to Q as well as the increasing chainage direction. Suppose Q' is on the left of Q as shown in Figure 5, and the direction of increasing chainage is also from left to right, then the updated spiral length will be the previous length plus one-half of the length PP'. However if Q' is on the right of the Q with the same increasing chainage direction, one-half of PP' will be subtracted from the previous spiral length.

CONCLUDING REMARKS

Road alignment setting out provides important reference marks and indicators for workers to lay kerbs in accordance to design alignments, and any mistakes would significantly affect the road construction project. A GPS-based system suitable for survey check of road alignment in complex and rapidly changing construction sites has been proposed. The system helps consultant surveyors to obtain road alignment survey check results quickly on site. If there are any suspicions on the setting out work, a resurvey can be carried out for verification without delay.

The key factors that would affect the effectiveness of RTK positioning are the radio communication system used and its transmission power. The line of sight requirement for UHF and VHF radio links and the restricted use of high transmission power in some cities have limited the effective range of RTK positioning. As wireless communication through mobile phone's data link service has become increasingly popular, some GPS manufacturers have started integrating mobile communication with RTK to maximize the performance of RTK. Without doubt, such integration would enhance the effectiveness of the survey check system.

Finally, although the system proposed is for alignment check. With a little modification of the database design and processing software, the system can further be developed to become a system for checking structural and civil engineering works such as check for slope and pipe alignment, and pile location.

REFERENCES

Hofmann-Wellenhof, B. Lichtenegger,H., and Collins, J. (1992). *GPS Theory amd Practice*, Springer, New York.

Lam, K. and Mok, E. (1996). Real-Time Processing System for Road Alignment Setting Out. *Proceedings of Geoinformatics "96 Wuhan" - International Symposium on the Occasion of the 40th Anniversary of Wuhan Technical University of Surveying and Mapping (WTUSM)*, pp585 - 592.

Leick, A. (1995), *GPS Satellite Surveying*, 2nd Edition, John Wiley & Sons, New York..

Misra P. and Enge P. (2001), *Global Positioning System, Signals, Measurements, and Performance*, Ganga-Jamuna Press, Missachusetts.

Mok, E. (1997). A Survey Check of Transition Curve Alignments. *Journal of the Civil Engineering Surveyors*, 1997 Year Book, 49 - 57.

Oliver J.G. and Clendinning, J.(1978), *Principle of Surveying, Vol. 1, Plane Surveying*, Van Nostrand Reinhold, Berkshire, U.K.

Schofield W. (1993). *Engineering Surveying*, Butterworth-Heinemann, Oxford, U.K.

Uren J. and Price W.F., (1978), *Surveying for Engineers*, Macmillan Press, Hampshire, U.K.

This Page Intentionally Left Blank

Advances in Building Technology, Volume 2
M. Anson, J.M. Ko and E.S.S. Lam (Eds.)
© 2002 Elsevier Science Ltd. All rights reserved

GPS NAVIGATION AND GUIDANCE SYSTEMS FOR CONSTRUCTION INDUSTRY

Günther Retscher [1] and Esmond Mok [2]

[1] Department of Applied and Engineering Geodesy, Vienna University of Technology, Gusshausstrasse 27-29, A – 1040 Wien, Austria,
Tel.: +43/1/58801 12847, Fax: +43/1/58801 12894, E-mail: gretsch@pop.tuwien.ac.at

[2] Department of Land Surveying and Geo-Informatics, The Hong Kong Polytechnic University, Hung Hom, Kowloon, Hong Kong SAR, China,
Tel.: +852/2766 5953, Fax: +852/2330 2994, E-mail: lsemok@polyu.edu.hk

ABSTRACT

New applications for the use of GPS have emerged especially in construction industry in recent years. The applications are ranging from navigation of trucks in fleet management, the guidance of construction machines to precise surveying, setting out and monitoring of engineering structures. Thereby GPS can be employed in many different modes where the suitable method is selected depending on the accuracy requirements for position determination. Most of these applications require also the possibility for continuous position determination in real-time. If this is the case, nowadays modern real-time kinematic GPS (RTK-GPS) can be employed. The use of these modern surveying and positioning techniques facilitates also the development of new machinery and system processes in construction industry. Especially for the guidance of construction machines, systems have been developed to increase the productivity of construction works. Commercial systems are available nowadays from several companies, e.g. for the guidance of graders, dozers and caterpillars. In general, the systems use 3-D surveying systems for position determination mostly in combination with other sensors.

Following a brief description of satellite positioning modes, their major applications in construction industry will be highlighted and common features of modern 3-D machine guidance systems based on RTK-GPS will be outlined in this paper. Finally the 3-D machine guidance systems are compared with common conventional systems and their advantages summarized.

KEYWORDS

GPS, Satellite Positioning, Navigation, Fleet Management, Machine Guidance, Construction Machines, 3-D Machine Guidance Systems

1 INTRODUCTION

Whether the given application is in general construction, earthmoving or civil engineering, nowadays advanced surveying techniques using lasers, total stations and GPS positioning solutions and software are available that can provide more control over the job task and site. For site preparation, powerful software for design and estimating takeoff as well as a complete line of machine control systems for the smallest skid steer to the largest bulldozer can be employed. Thereby modern machine control systems use a variety of technologies, either in combination or alone, including laser, GPS systems, total station, sonic or laser tracers and software. Using advanced machine control systems operators have the information they need in the cab, allowing them to significantly increase productivity, reduce material overages and work with greater precision. Starting from a short description of the principle of operation of modern satellite positioning and navigation methods, the use of GPS in construction industry and machine guidance will be described more in detail in this paper.

2 GPS POSITIONING AND NAVIGATION

Satellite positioning systems have been developed to provide the possibility for continuous position determination worldwide. New systems are currently under development or at the stage of launching their satellites into orbit. All of them have in common, that they were developed following the concept of the successful U.S. NAVSTAR-GPS (**Na**vigation **S**ystem with **T**ime **a**nd **R**anging – **G**lobal **P**ositioning **S**ystem). The development of this system started already in the 1970's by the Department of Defence (DoD) of the U.S.A. Therefore the system was primarily installed for military navigation. Besides the U.S.A., also the former Soviet Union States developed a similar system, the so-called GLONASS (Russian's Global Navigation Satellite System). In the 90's, the integration of GPS and GLONASS was one step towards a future Global Navigation Satellite Systems (GNSS). Strategic goals of the GNSS were to create a system that is independent from any military or national control, to guarantee the continuity of service over a certain time period, and to offer an improved service compared to GPS which is affordable. Mainly because of military reasons and the disagreement of the U.S. government to allow international control for GPS, the European community also started to develop an own global satellite navigation system at the end of last century. This system is called GALILEO and should be fully operable at the end of 2008.

2.1 Basic Concept of Satellite Positioning

As the concept of satellite positioning systems is very similar it will be easy to understand the concept of others with the knowledge of the concept of one system. The design concept of a satellite positioning system has to fulfil the following requirements:

> The system must guarantee 3-D positioning determination anywhere in the world, at any time and during any weather condition with the specified positioning accuracy. In addition to position determination, for many applications also the determination of the velocity and acceleration of the moving receiver must be possible.

In general, the satellite positioning systems consists of three segments, i.e., the space segment (satellites in orbit), the ground control segment (monitoring stations and master control station) and the user segment (receiver and antenna). For identification and distance measurements, the satellites broadcast code sequences which are modulated on carrier phase signals. In the case of GPS, two

sinusoidal carrier phase signals, L1 and L2[1], and two PRN (pseudo-random noise) codes, the precise P-code and the C/A-code[2], are broadcasted. For the future generation of GPS satellites, it is planned to add a third civilian and another military frequency. The satellite orbits are determined by a network of monitor stations around the world. These so-called broadcast ephemeris are then transferred to the user from the satellites in the navigation message to obtain real-time position determination. The user segment can be broadly classified into users for military and civilian applications. There are various types of GPS receivers available on the market to suit different applications such as surveying and mapping, vehicle navigation and recreation. Further information about their principle can be found in books about satellite positioning, e.g. (Hofmann-Wellenhof et. al., 1992; Leick, 1995; Wells, 1986; Seeber, 1993; Mok & Retscher, 2000).

2.2 Observation Types and Positioning Modes

Position determination is done by distance or range measurements. Depending on the type of observation used, pseudorange measurements with the code phases (P-code or C/A-code) or carrier phase measurements (signal L1 or/and L2) can be carried out. Thereby positioning accuracies in the range of 0.3 to 40 m can be obtained using code observations. Higher accuracy position determination up to the centimetre level, however, can only be achieved using carrier phase measurements. The accuracy spectrum of different methods is compared graphically in Fig. 1. As can be seen, different satellite positioning techniques offer a wide range of positioning accuracies. After distinguishing between code and phase observations, the methods can be categorised into absolute and relative positioning techniques. The term absolute or single-point positioning is used to describe positioning techniques using only one receiver in stand-alone mode. This technique is usually applied for navigation. For relative positioning, however, at least two receivers are required. Due to the use of differencing techniques, the positioning accuracy can be increased for simultaneous observations of two receivers to at least four satellites. These techniques are usually applied in surveying, for mapping applications and also for precise navigation.

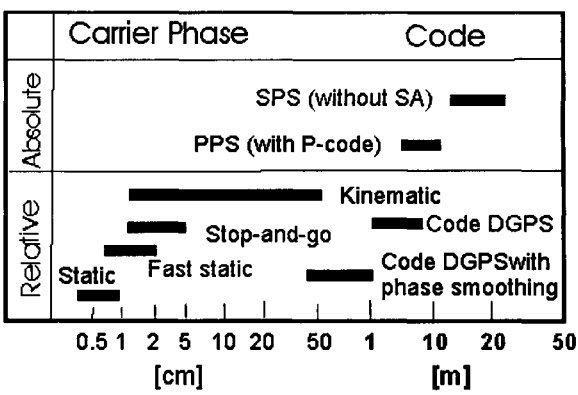


Figure 1: Accuracy spectrum and different modes of satellite positioning [3]

[1] The signals L1 and L2 are electromagnetic waves in the L-band with frequencies of 1575.42 MHz and 1227.60 MHz.

[2] P-code stands for Precise code and C/A-code for Coarse/Acquisition code. The PRN code is a random signal of '+1' and '-1' code sequences.

[3] SPS stands for Standard Positioning Service using the C/A Code and PPS for Precise Positioning Service with the P-code.

2.3 GPS Positioning Modes for Surveying

Positioning methods used in surveying are usually relative positioning techniques with carrier phase observations to achieve a high level of precision. In general, it can be distinguished between static positioning, rapid (or fast) static positioning, stop-and-go, reoccupation and kinematic positioning. The modes differ mainly in their observation time and whether the receivers are static or moving throughout the entire observation period. The highest positioning accuracy can be obtained using the static positioning technique. In this case, both receivers are stationary on their points over a certain period of time. The length of the observation period depends on the number of satellites, the precision requirements, the length of the line, the type of receiver (single L1 or dual frequency receiver L1 and L2), and the atmospheric conditions. Static observations are taken over a time span of 30 minutes up to several hours and rapid static observations within a few minutes up to 20 minutes. If more than two receivers are used, the static method can be employed for many survey applications, especially for the establishment of control networks very economically. Satellite positioning techniques have therefore nearly replaced conventional surveying techniques for this type of application. The survey work is very easy and the processing of the results is usually done in post mission. These technique is employed e.g. for the establishment of control points for engineering projects (construction of a tunnel or bridge). For the rapid static or stop-and-go observations, the limited factor is the short observation time of a few minutes or only seconds. Due to recent developments in satellite receiver technology, however, these methods can be replaced by modern real-time kinematic (RTK) positioning techniques. The above methods require that two receivers are stationary for a short time period. In the kinematic mode, the second or so-called rover receiver is moving and collects data continuously. Then position determination has to be done separately for each measurement epoch. Depending on the speed of the moving receiver, positioning accuracies on the few centimetre up to decimetre level can be achieved (see Fig. 1).

3 USE OF GPS IN CONSTRUCTION INDUSTRY

Satellite positioning and navigation can be employed in the construction industry for many different tasks. Especially in the navigation mode, nowadays GPS has become a standard tool to manage a large truck fleet or to perform vehicle navigation and guidance (see Fig. 2). These system have been developed due to the integration of GPS in common systems based on other sensors more than one decade ago and their application has become quite popular with professional and private users (see e.g. Krakiwsky, 1991). The combination with other sensors such as dead reckoning (DR) and map matching, however, is required as GPS for position determination in stand alone mode only works well for open areas. In the case of obstruction of the satellite-receiver visibility, either the position accuracy is bad or no position determination is possible. Especially in cities with high-rise buildings, the satellite visibility is a very critical issue for vehicle navigation systems (see Retscher and Mok, 2001).

Using precise methods with carrier phase measurements (see section 2.2) very high accuracies for continuous position determination can be achieved. Recent system developments include so-called attitude determination systems where also the orientation (or heading) and the current position of a truck or vehicle can be determined using one GPS system. In this case a L1/L2 RTK GPS receiver with dual-antenna is employed that provides precise position, heading and speed of a dynamic platform. The receiver achieves horizontal positioning accuracies of 20 mm and vertical accuracies of 30 mm up to 20 times per second as well as heading accuracies of 0.03° RMS (root mean square

error) at 10 times per second (Trimble 2002). Typical application areas are in the fields of construction, dredging, marine survey, commercial marine, and general machine guidance.

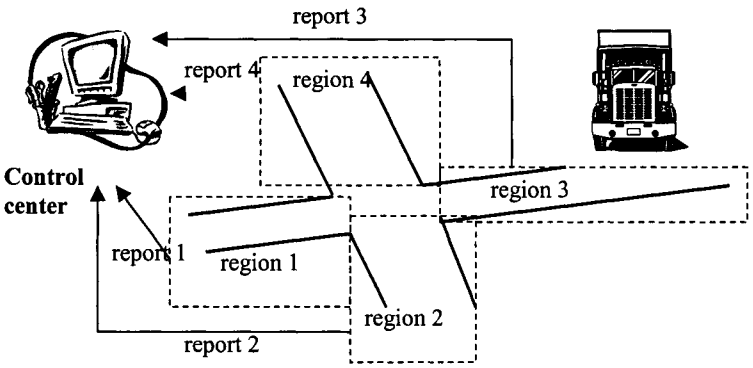


Figure 2: Operation principle of a fleet management service

4 MACHINE GUIDANCE AND CONTROL

Different types of construction machines are available that can be employed for different tasks. Dozers are usually employed for bulk earthworks and earthmoving, the construction of abutments and ramps, embankments, etc. For fine grading, course grading of materials, sub base formation or sideslope work usually motor graders are employed. The asphalt or concrete surface of a road can be built using paving equipment. The methods developed for the guidance of these machines can be distinguished depending on the level of automation they achieve. The highest level of automation is achieved with modern 3-D guidance systems and automatic blade control. In this case, the navigation parameters and deviations of the machine blades from the designed surface are obtained from a comparison with the given alignment of the road. The given alignment is usually based on a digital terrain model. If a correction is required, the parameters are automatically sent to the machine hydraulics to maintain the design elevation and cross slope. Visual control is provided for the machine operator using a navigational display. Some machinery employ also manual blade control where the guidance of the blades is controlled by the operator.

4.1 Components of Machine Guidance Systems

The main component of 3-D guidance system is a positioning unit which is able to track the machine movements continuously. Due to the availability of modern RTK GPS systems and total stations with automatic targeting and tracking such systems could be developed. They are able to determine the 3-D position of the machine continuously with a high frequency of up to 10 Hz, i.e., 10 times per second. The kinematic sequence of machine positions represents the trajectory of the machine. Fig. 3 shows the main components of a 3-D machine guidance system. Apart from the positioning unit, usually additional sensors are included into the system design, e.g. electronic inclinometer or tiltmeter to measure the pitch and roll of the machine or the blade. Inclinometers or tiltmeters are employed to measure the longitudinal and transversal tilt (i.e., pitch and roll) of the machine and/or its blade. The longitudinal sensor (so-called long slope sensor) measures the vehicle pitches in the direction of travel and hub for all system sensors. The transversal sensor is a highly

dynamic measuring unit that determines current lateral blade inclination for exact control of lateral inclination. In addition, a precise determination of blade rotation using a so-called rotation compensator provides for optimum lateral inclination compensation (see e.g. Moba, 2002). This sensor is in principle an electronic gyro compass or heading sensor. All the sensors are integrated with the positioning unit in the sense of a multi-sensor system (Retscher, 2002).

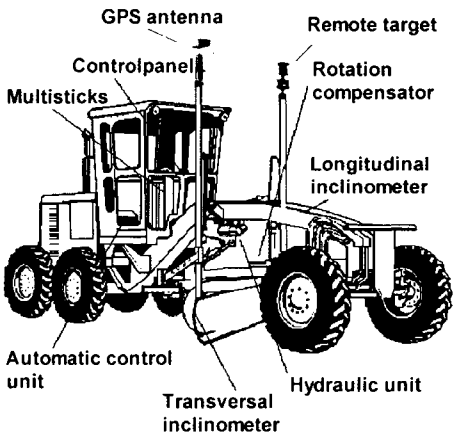


Figure 3: Main Components of 3-D Machine Guidance Systems

4.2 Comparison of 3-D Guidance with Conventional Systems

Table 1 compares the 3-D guidance systems using total stations and RTK GPS with traditional methods based on string lines and stakes or the use of rotating lasers. The conventional systems require surveyors to provide the interface between the engineering design and the machine operator on site. This can be achieved by using grade stakes that are placed at strategic locations around the site and indicate the level of cut and fill required at that point. Machine operators then have to use their experience to interpolate the grade between the stake locations. Grade stakes can be replaced by string lines (see Fig. 4) where the machine is guided along the line using detectors such as ultrasonic or laser tracers. Their main disadvantages, however, are that grade stakes or string lines are often knocked out by the machines during the course of the daily work and that they are very labour intensive in setting out and maintenance. On-site surveyors are required to stake and re-stake, to check the resulting surface, to calculate the volumes of earth moved and deviations from the desired design surface (see e.g. Carlson et al., 1999; Anderson 1999). The use of rotating laser systems shown in Fig. 5 has led to an increase in productivity and cost-savings. With the rotating laser beam a horizontal plane is defined and the deviations from the plane can be observed. The laser detectors are usually mounted on the blade of the machine. Using laser systems, height control can be performed with high precision. Their application, however, is limited for areas with small changes in gradient. Otherwise new setups of the laser instrument are required very frequently. Rotating laser systems are mainly employed for precise height control of graders.

The major applications for 3-D machine guidance systems can be found in construction industry and mining for the guidance of dozers, graders, excavators, scrapers as well as in agricultural applications for the guidance of tractors and harvesters (see Table 1). Depending on the accuracy

TABLE 1
COMPARISON OF MACHINE GUIDANCE SYSTEMS

	String lines or Stakes	Rotating Laser Systems	Robotic Total Station	GPS
Dimensions	3-D	1-D (height only)	3-D	3-D
Reference stations required per site	Many tachymeter stations required for setting out	One or more; site dependent	One per machine	One
Setups per construction site	Not applicable	Multiple times per site	Multiple times per site	One
No. of machines supported by reference station	Not applicable	Unlimited in one plane	One per total station	Unlimited
Maximum range	Sensors work in close-range	up to 300 m depending on line of site	up to 700 m depending on line of site	Several kilometres
Usability under bad visibility conditions	Not affected	Reduced	Reduced	Not affected
Accuracy	mm - level	mm - level	mm - level to cm - level	cm - level
Major applications	Guidance of road and slipform paving machines	Precise height control for graders; Guidance of road and slipform paving machines	Guidance of graders, excavators, scrapers or dozers	Guidance of dozers and scrapers, Precise Farming



Figure 4: Guidance of paving machines using string lines (after Anderson, 1999)

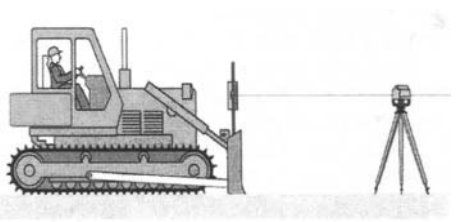


Figure 5: Operation principle of rotating laser systems

requirements, RTK GPS systems or robotic total stations are employed. Systems are available on the market from several companies (e.g. Leica, 2002; Gomaco, 2002; Trimble, 2002). The high precision requirements for the guidance of road and slipform paving machines, however, are still very challenging for 3-D guidance systems. In recent case studies 3-D systems using two robotic total stations (see Gomaco, 2002) or dual antenna GPS systems (see Trimble 2002) have been tested. The systems still need further improvements that conventional and labour intensive methods can be replaced totally. For the determination of the movements of the construction machine a new algorithm has been developed. For further information the reader is referred to (Retscher, 2001 and 2002).

5 CONCLUSIONS AND OUTLOOK

Due to the use of modern surveying techniques in combination with advanced software new application areas in construction industry have emerged. Nowadays construction machines can mainly be controlled and guided automatically. 3-D guidance systems will significantly reduce times for surveying and therefore achieve cost savings while increasing productivity of construction works. Thereby satellite positioning methods play an important role. To achieve very high precision requirements especially in the vertical in the course of fine grading and paving, however, a combination with other sensors and methods is still required. On the other hand, where precision requirements are low GPS systems are most commonly used in stand alone mode for navigation of machinery and truck fleets.

References

Carlson B., H. Baertlein, R. Eckels, S. Lyle (1999): Dozer 2000 – A Revolution in Machine Guidance. in: Leica Dozer 2000 Presentation CD-Rom, Leica Geosystems, Heerbrugg, Switzerland.

Gomaco (2002): Stringless Guidance System. Technical Notes, Gomaco Corporation, Ida Grove, Iowa, USA. http://www.gomaco.com/Resources/leica.html (Last visited: January 2002)

Hoffmann-Wellenhof B., B. Lichtenegger, J. Collins (1992): GPS, Theory and Practice. Springer Verlag, Wien.

Krakiwsky E. J., 1991. GPS and Vehicle Location and Navigation. GPS World, May 1991, pp. 50-53.

Leica (2002): Machine Guidance and Control, Technical Notes, Leica Geosystems, Heerbrugg, Switzerland. http://www.leica-geosystems.com/machine/index.htm (Last visited: January 2002)

Leick A. (1995): GPS Satellite Surveying. 2nd Edition, John Wiley & Sons, New York, 560 pgs.

Moba (2002): Machinery Control. Technical Notes, MOBA Mobile Automation GmbH, Elz, Germany. http://www.moba.de/e/bau/index.htm (Last visited: January 2002)

Mok E., G. Retscher (2000): Satellite-based Positioning. Chapter 7 in: Chen Y.-Q., Y. C. Lee (Eds.): Geographic Data Acquisition. Springer Verlag, Wien, New York, pp. 99-119.

Retscher G., E. Mok (2001): Integration of Mobile Phone Location Services into Intelligent GPS Vehicle Navigation Systems. in: Papers presented at the 3rd Workshop on Mobile Mapping Technology, January 3-5, 2001, Cairo, Egypt.

Retscher G. (2001): Trajectory Determination for Machine Guidance Systems. in: Papers presented at the KIS2001 Symposium, June 5-9, 2001, Banff, Canada. http://info.tuwien.ac.at/ingeo/pub/papers/kis.pdf (Last visited: January 2002)

Retscher G. (2002): Multi-Sensor Systems for Machine Guidance and Control. in: Papers presented at the FIG 2002 conference in Washington DC, USA, April 19-26, 2002.

Seeber G. (1993): Satellite Geodesy. Walter de Gruyter, Berlin, New York, 531 pgs.

Trimble (2002): Rugged Dual-Antenna GPS Receiver for Precise Heading and Position. Product Information. http://www.trimble.com/ms860.html (Last visited: Feb. 2002)

Timble (2002 a): Machine Control: Earthmoving and Highway Construction. Technical Notes, Trimble Navigation Ltd., Dayton, Ohio, USA. http://www.trimble.com/civilengineering.html (Last visited: January 2002)

Trimble (2002 b): Site Vision GPS: 3D GPS Grade Control System. Technical Notes, Trimble Navigation Ltd., Dayton, Ohio, USA. http://www.trimble.com/sitevision.html (Last visited: January 2002)

Advances in Building Technology, Volume 2
M. Anson, J.M. Ko and E.S.S. Lam (Eds.)
© 2002 Elsevier Science Ltd. All rights reserved

THE USE AND FUTURE POTENTIAL OF GIS BASED APPROACHES TO BUILDING DESIGN AND BUILDING MANAGEMENT

M.I. Wallace, V. Lau, C. Gibbons

Ove Arup and Partners Hong Kong Ltd.,
5th Floor, 80 Tat Chee Avenue, Kowloon Tong,
Hong Kong

ABSTRACT
This paper introduces the concept of Geographical Information Systems (GIS) to the application of building design and management. In particular, it addresses the benefit of visualisation techniques to the better management of buildings in Hong Kong through a visual and animated building database of building components.

Keywords: Geographical Information Systems, GIS, Building Design, Building Management, Visualisation, Database.

INTRODUCTION

The use of GIS based tools to provide design and total database management for buildings is becoming more feasible. Simple information systems for buildings based upon GIS software are already being used in many areas including space management, human resource management and facility management. The concept of 3D GIS for buildings is in its infancy and as buildings become more complex the amount of data generated, analysed and stored will increase. Significantly GIS is able to aid visualisation of the data. It can be customised to meet specific building management and user requirements and can link with various databases of stored data.

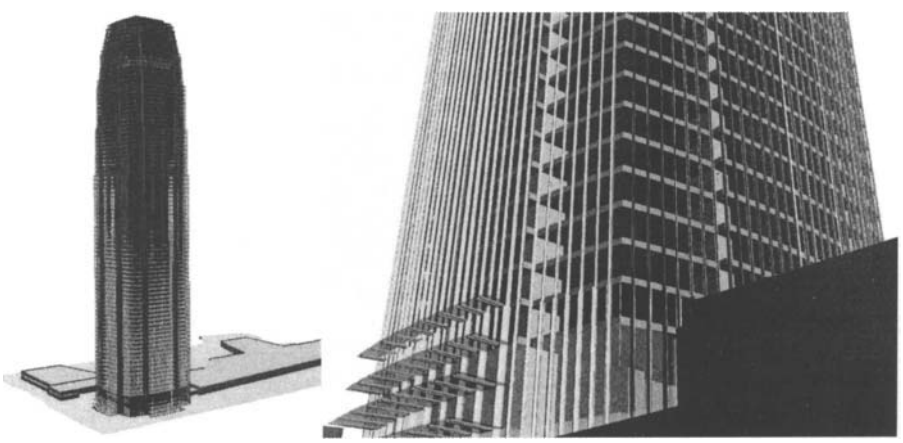


Figure 1: Tall Building 3D GIS Model

A conceptual 3D building GIS has been developed for a typical tall building, see Figure 1. This structure comprises over 100 storeys and will contain a large amount of systems and data. A 3D GIS could be developed for tall buildings or complex buildings such as combined office and retail and residential properties to store, monitor and provide a management system for the facility or a series of facilities. GIS technology provides a platform to manage spatial data and when linked to standard co-ordinate systems allows external data to be analysed and assessed within the same reference frame. GIS can be applied to various databases and information already gathered for various buildings and building design alternatively through the visualisation element of GIS it can be applied to simple display of spatial data to the complex analysis of relationships and responses to change within the system.

The future of GIS for buildings can be seen by looking at the images in Figures 1 and 2. Think of them as databases of building elements. Information can be embedded into each surface, cube, polygon, line etc and each can respond by varying its colour, transparency or texture to display current information about its condition. Obviously this requires feedback from data gathering within the building which could be carried out manually or from sensor arrays or monitoring equipment. This information could be selective depending on the tasks and analysis required or automated depending on the nature of the building.

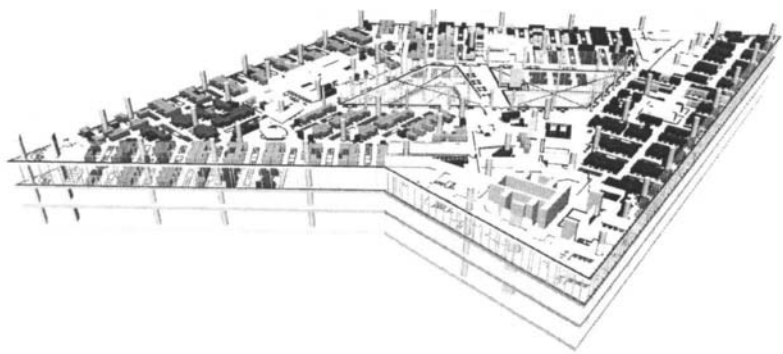


Figure 2: 3D Workstation Space Management System

The visualisation element of the technology allow data to be tagged to visible features within the virtual building. In Figure 3 the 3D building model shows how information has been extracted from selecting the desk to display the information stored on that individual workstation.

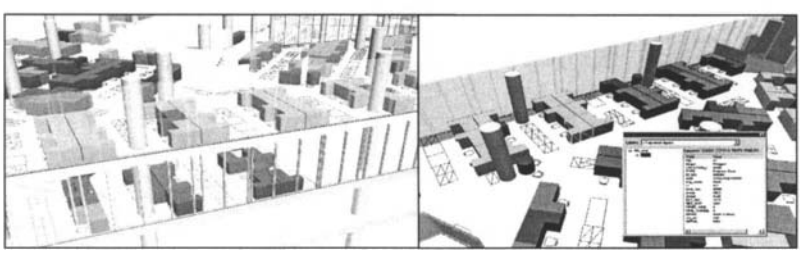


Figure 3: Data embedded within the 3D workstation

The 3D database system shown on Figures 2 & 3 can present various elements within a database to display information such as workstation user, their group affiliation and simple telephone directory information about that workstation. It can also display the current group layout of staff within the office by colour and identify any un-allocated desks to target efficient use of space within the office.

WHY GIS ?

The use of GIS within the building management field should increase due to the higher degree of flexibility of the software. The added value benefits of analysing and assessing various building performance attributes from database information is becoming more feasible. The spatial relationship of the building, its components and the interaction of the building with its surroundings can be modelled from the initial design process through to the entry of tenants and the human behaviour and activity within the building. It is most useful in the areas of building and facility management where managers have a large stock of property which require monitoring and control.

At present most large high rise buildings and other complex properties that combine office, retail and occasionally residential elements within the development have tailored building management systems (BMS). These BMS are usually built around the core building processes of electrical, environmental and mechanical systems such as heating, cooling, security, lighting, lift and escalator controls etc. Information from various sources are currently fed back into the system to provide information to make basic decisions, which are usually undertaken automatically such as for ventilation and air-conditioning when pre-set limits are exceeded. BMS are generally passive and are criteria driven in their logic.

GIS systems can be more easily developed to identify the cause and effect of changes within a building such as "increased air conditioning output" may be a result of open doors or windows. They can also determine more easily trends and change within a building and highlight this to the management. With an efficient inventory and reporting system, defects and poor quality systems or equipment within the building can be identified and quantified. This may be clear from increasing maintenance requirements or other cause and effect elements such as increased power consumption for example. If the data has been collected in a systematic and logical manner then the various forms of analysis can be undertaken to aid the decision process. GIS models can target the various office elements to visualise the layout and distribution of office information such as desk allocation and use of space as shown in Figure 2. They can also store as archival information all the associated building plans, reports, digital photographs and other details for easy retrieval through pop up displays and selective interrogation of the 3D virtual building.

As Information Technology advances, the use of local wireless network systems and controls will become cheaper, more accessible and more readily available. IT systems are already an essential element as well as an integral part of our buildings. The further development of local wireless networks and accurate positioning systems within buildings will allow information to be gathered more easily and efficiently from anywhere within a building. Security and reliability of these systems will be the key to integrating them into a GIS based building management system.

CAD systems are already available that incorporate 3D design elements within their systems to allow better visualisation of design as well as identification of conflicts between drawings

and designs within their 3D models. This is the future of better building design where computer simulation and drawing generation based upon these models can be issued directly to the contractor. Finishes as well as structural elements and interfaces for the various E&M and internal fixings can be seen within the model and rectified at an early stage of the design process. These systems are likely to realise substantial savings in time and cost on procurement of building projects. They can also be directly fed into a GIS system.

Where a building management system has been developed to gather and store data in connection with the building the real benefit of GIS is in the early development of the database structure and the linking of this with final required use and logic of the GIS. Development of the data structure and final output should be designed to allow sufficient query and interrogation of the GIS to aid the decision process.

Where several buildings contain the same database attribute information they can be compared to identify differences that may in part lead to cost savings due to early identification of efficiencies or deficiencies in each building. Procurement and maintenance costs could be reduced by combining resource for efficient ordering of supplies where building databases are linked together.

External influences on the building can also be more easily modelled such as sunlight and viewable area from office floors. This sort of information assists in the decision making on the suitability of the floor or aspect of the windows.

Other external influences can also be considered such as pedestrian and local traffic flow models in assessing various demands on the building for access and exits. A GIS based approach gives greater flexibility and ease of reference for the data stored for a building.

The GIS interface can be customised to present typical report generation and can be accessed through WEB servers or intranets to allow multi user query on the system. The benefits for this depend on how the data within the building needs to be displayed and presented and the user levels and requirements. Essentially this can be varied to suit particular objectives of the system.

TALL BUILDING 3D GIS MODEL

To test the potential for such a system a 3D GIS has been developed to model the building structure and the various elements and data layers likely to be required for a working and compatible system. The conceptual physical model for the structure was based upon the building plans and the architectural layout plans. Further detail was added for a few floors to determine the complexity and explore any limitations to the exercise.

Development Platform

The model was developed using ESRI ArcGIS 8.1 package with its extension 3D Analyst providing three-dimensional analysis and visualisation. The whole development process from data preparation, conversion and 3D model construction were carried out within this platform. Other GIS software are just as likely to be used to develop such a system. The hardware used to process and develop the system comprised a Pentium P4 1.5GHz PC with 512MB RAM incorporating an NVDIA Quadro 2 Pro 64MB display card.

Data Conversion and Preparation

Data preparation is always the most critical part of the model development. Usually the preparation of accurate and consistent data for a GIS model takes the majority of the development time. Appropriate data must be collected while irrelevant data must be excluded from the model. System structure is dependent on the overall objective of the system and the data to be embedded within it. The data conversion process and analysis is presented in Figure 4.

Data was collected from digital architectural and structural drawings in AutoCAD file format. The table below highlights the data development flow and details. This process was carried out for each of the individual layers within the model. The exterior and interior structural and

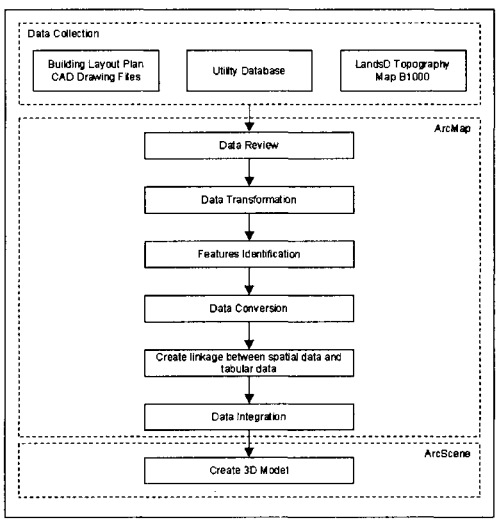


Figure 4: Data Model Development Flow

architectural layout as well as utilities plans, services function etc was assessed for each individual floor and podium. These were then converted into various GIS layers. Each layer contains a single element of the building data such as core wall, conduit, sprinkler layout etc and any surface, line, wall or element can have data embedded into the model. Figure 5 displays how the various complex floor layouts were developed for the building.

Complications with the model were mostly encountered with the merging of reference co-ordinate systems to local Hong Kong Grid as well as ensuring that the data was clean with connecting lines and points. The Hong Kong grid was used in preference to a local building grid to allow the data and model to be linked to external data if necessary.

The choice of data was also focussed at presenting visually acceptable and meaningful data for future development of the model. Identical floor layouts were linked together to minimise the size of the model. For visualisation duplicate floors shared the same data set and layout referencing to the database was linked to floor number to allow quicker interrogation of the various floor attributes. The lifts serving various floors and levels within the structure were also identified and the location and referencing system for these lifts were embedded into the

model so that lifts could be identified for each floor as through lifts or as lifts servicing that particular floor.

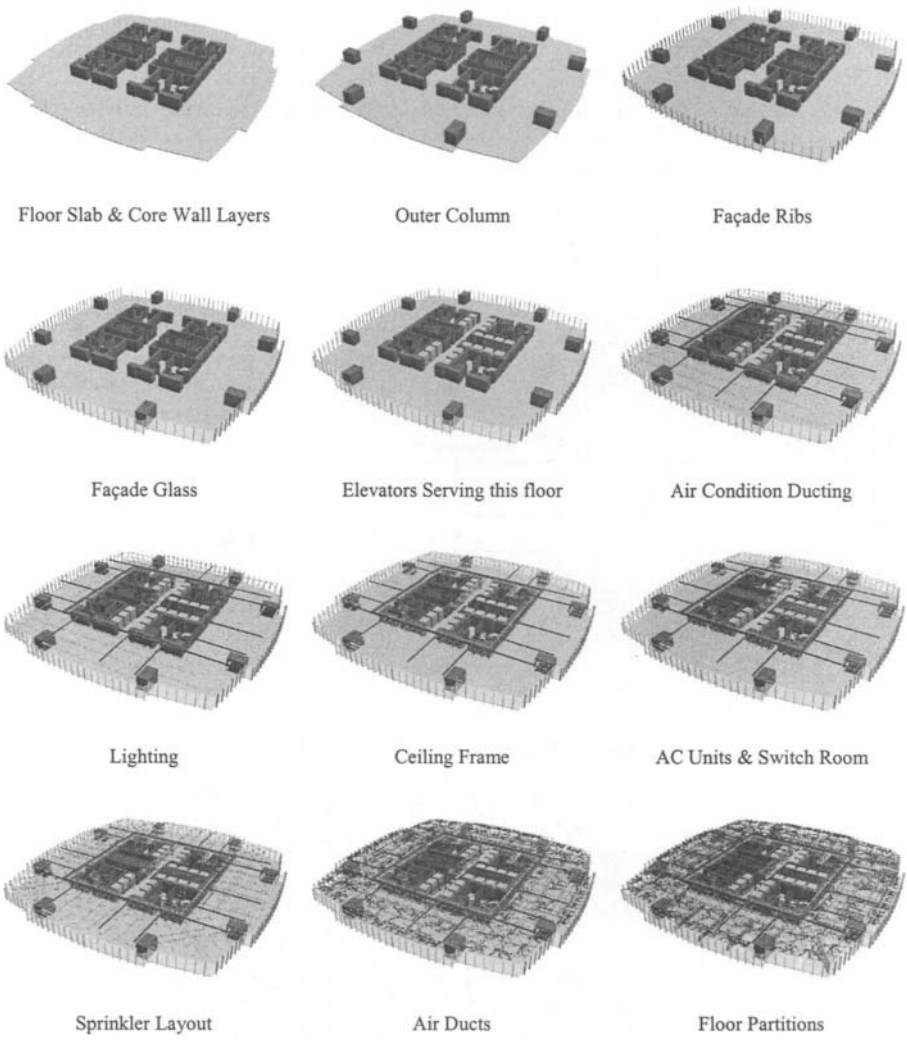


Figure 5: Complex Floor Data Layers

Features that had different functions and behaviour were separated into different layers for facility management and visualisation purpose. Individual structural features of the building were converted into the GIS as separate layers to allow each building element or layer to be switched off to display only that individual item requiring interrogation to be displayed for easier and quicker viewing of the information.

Additional data was added to the 3D model to simulate a working floor model to determine the benefit and capability of the GIS in displaying the floor plan layout. A seating plan comprising desk workstation polygons, partition walls and filing cabinets were included. Information can be tagged to any element within the 3D scenes by applying reference locations to the 3D model surfaces, polygons, lines and layout.

To link the building to its surroundings a digital terrain model (DTM) of the surrounding area was generated from local digital map data. This was incorporated to identify the surrounding aspect and position of the building to provide a reference to adjacent features. The model could be further expanded with the incorporation of external data such as surrounding infrastructure and associated facilities such as utility connections at pavement and road level.

3D Model Development

Layers are then added into the 3D GIS environment to build the 3D building model. The base height or floor number for each feature was assigned during data preparation. These layers were then offset or extruded vertically at their particular floor level. Appropriate colour and levels of transparency were set for each feature layer to present the best visual effect.

The speed of image rendering and display of information at the buildings simplest level comprising the structural frame and general layout of the building was smooth and acceptable. Zooming and display functions worked well. As further layers and seating plans were added to the model there was a marked decrease in speed of the system. This occurred when we developed a single complex floor plan.

Where only one or two elements of the system were needed to be displayed in the 3D environment the model appeared to perform well and as such further development could be targeted at processing and displaying only the data layers of interest.

As computer speed increases the capability of whole display of the building will improve and with better software development and storage of 3D data and rendering the future of this technology should be assured.

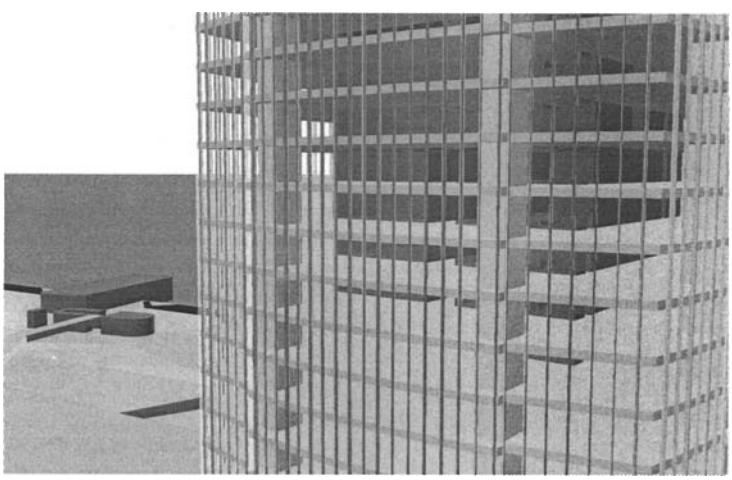


Figure 6: Close up of core wall, column and glass frame

One of the floors of the building was selected to display all the layers described in Figure 5. A full set of utility layers were added plus the building exterior and interior structure including core wall, void, glass frame, life shaft, life, washing closet, AC room as well as the seating plan for the floor. Various internal and external views of this floor level are shown on Figures 6 and 7.

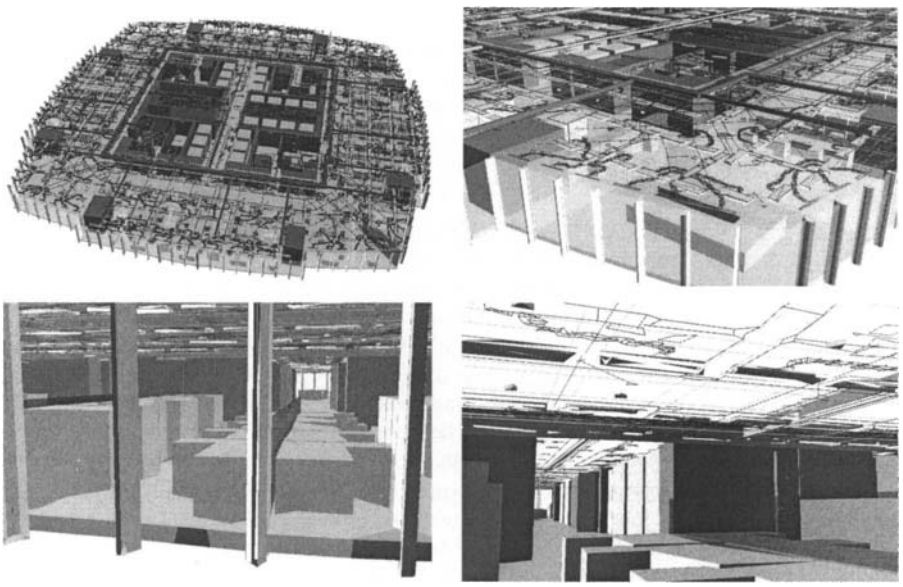


Figure 7: Images of Complex Floor

CONCLUSIONS

It has been demonstrated from the model that the use of 3D GIS for buildings is feasible and becoming more practicable. Improved speed and performance of the software and hardware will enhance the development of this tool in the future. The need to store ever increasing amounts of data and the trend to develop intelligence and data integration within buildings provides a sound basis for visual database as well as human interaction analysis within GIS.

The need for building GIS systems will be driven by developers and property management operators. The combined use of large building stock and facility management are inherent in the technology and with increased and cheaper sensor technology linked to wireless intranets, the feedback time and analysis of the system can be improved. Whether the system is used simply as a visual database or as a complex analysis tool depends on the user requirements. If data is generated, stored and presented with a view to presenting and easier understanding of the data then the potential uses and benefits of the system may be explored in ways not already realised.

ACKNOWLEDGEMENTS

The concepts and ideas included in this paper are based on a series of projects carried out by Ove Arup and Partners over recent years. The insight, contribution and constructive suggestions of all the team members involved have been greatly appreciated by the authors.

Advances in Building Technology, Volume 2
M. Anson, J.M. Ko and E.S.S. Lam (Eds.)
© 2002 Elsevier Science Ltd. All rights reserved

AN INTEGRATED SYSTEM FOR SLOPE MONITORING AND WARNING IN HONG KONG

J.H. Yin[1,4], X.L. Ding[2,4], Yuwen Yang[1,4], C.K. Lau[3,4], D.F. Huang[1,4], and Y.Q. Chen[2,4]

[1]: Department of Civil and Structural Engineering
[2]: Department of Land Surveying and Geo-Informatics
The Hong Kong Polytechnic University, Hong Kong, China
[3]: Fong On Construction & Engineering Co., Limited, Hong Kong
[4]: Centre for Ground Engineering and Technology

ABSTRACT

This paper presents an integrated system for monitoring and warning of landslides. The system consists of an automatic conventional slope monitoring package and a multi-antenna Global Positioning System (GPS) package. The automated slope monitoring package has (a) different types of sensors and (b) a remote data acquisition/control system connecting an office computer to datalogger for data communication and control with visual software. Sensors include (in-place inclinometers, (b) piezometers, (c) a rain gauge and (d) a Time Domain Reflectometer (TDR). The multi-antenna GPS is a special technology newly developed for monitoring surface movements of a slope. The two packages or sub-systems can work independently or jointly to monitor a slope. When working together, the two sub-systems can be set up at the same slope site. The conventional sub-system mainly measures the sub-surface ground movements and pore water pressures and the GPS sub-system mainly measures the surface ground movements. The data from the two sub-systems can be transferred to the same office computer, processed and analyzed together. The integrated data can be automatically retrieved, temporarily stored and transmitted from the two sub-systems. Software can perform data download, storage, analysis and real-time display. All data from in-place inclinometers, piezometers, a rain gauge, a TDR and the GPS are integrated in the process. A database has also been developed. Some preliminary monitoring data are also presented in the paper.

KEYWORDS

Slope, landslide, monitoring, warning, movement, pore water pressure, global positioning system, inclinometer, piezometer, rainfall gauge ,time domain reflectometer

INTRODUCTION

Hong Kong is a hilly region with normally heavy rainfalls in the summer. Heavy rainfalls can easily induce slope failures or landslides. Other factors such as human activities, rock weathering and ground water rising may also contribute to the landslides. Landsides still impose a great

danger to human life and property, despite much efforts made, like the carrying out of slope maintenance and stabilization measures. In Hong Kong, many buildings, plants and important facilities are either very close to or even on the hillside. In a landslide, life and property may be at risk. Therefore, any pre-warning of slope failure will allow time for people to evacuate and take other preventive measures.

According to Malone (1998), many landslides in Hong Kong have a deep seated slip and noticeable displacement may occur prior to failure. Sometimes, the landslide is progressive in nature. It is possible to forewarn a landslide by monitoring any pre-failure displacement.

Therefore real-time slope monitoring may potentially play an important role in landslide warning and prevention. Parameters, such as slope displacement, pore water pressure and rainfall intensity that may be directly related to a landslide are particularly relevant. The data of these parameters once obtained needed to be interpreted and analysed in order to establish any trend that may be used as an indication of any potential slope failure. Before a slope failure takes place, people likely to be affected may be notified in advance and evacuated accordingly. Engineering stabilization measures may also be implemented in order to prevent or slow down the impending slope failure. In this paper, an integrated slope monitoring system is introduced. The system consists of an automatic conventional slope monitoring sub-system and a multi-antenna GPS sub-system. The method integrating the two sub-systems will be explained in the paper.

AUTOMATIC CONVENTIONAL SLOPE MONITORING PACKAGE

In Hong Kong, rainfalls induce most man-made or natural slope failures. The surface rainfall runoffs will cause the surface soil wash out and erosion. The rainfall infiltration will cause the reduction of suction (a stabilising stress) in the soil mass, ground water table rising, reduction of effectives stresses, all of which may cause a reduction in soil strength and slope movements. When the movements reach a certain limit, slope failure or collapse will occur. When a slope fails, very often a clearly defined slip surface in the soil mass is developed. To obtain data on the slope movements, it is necessary to monitor (a) rainfalls, (b) pore water pressures, (c) soil mass movements, especially down hill lateral movements, and (c) the location of the slip surface. Yin and Ding (1999) have proposed an integrated automatic system for monitoring all the four factors that may cause a slope to fail.

The automatic conventional slope monitoring system adopted in the project has the following features:

(a) Automatic data acquisition/control: remote data acquisition, storage data retrieval from a monitoring site to an office computer;
(b) Monitoring of slope movements, pore water pressure and rainfall intensity;
(c) Locating the slip surface in the slope mass by measuring relative displacements in the slipping zone;
(d) Detecting both small (a few mm) and large displacement (from 100 mm to more than one metre);
(e) High resolution or accuracy; and
(f) Reliable even under high temperature and high humidity weather conditions.

The conventional sub-system consists of (a) in-place inclinometers, (b) piezometers, (c) a rain gauge and (d) a Time Domain Reflectometer (TDR). The sub-system has a datalogger, a M20T modem, a power supply and software. Details of the instruments are presented in the following sections.

In-place Inclinometer



Figure 1. An in-place inclinometer

In-place inclinometers (model 906 'little dipper', biaxial and high-gain version) are adopted in this project (see Figure 1). Their specifications are: angular range ±12.5 degrees, response time of 0.15 second and operating temperature ranges from 10°C to 50C. The 'little dipper' inclinometer can also measure temperature with scale factor of 0.1°C/mV and an accuracy of ±0.75°C (User's Manual[1]).

In-place inclinometers are installed in boreholes, generally at depths less than 45m for purposes of monitoring ground movement. The inclinometers can be installed in a standard inclinometer access tube with an internal diameter of 2.75 inches. They can detect the rotation angles at different depths, which are used to obtain slope lateral movements and direction. After the inclinometers have been installed at a slope site, readings can be taken automatically by a data acquisition/ control system.

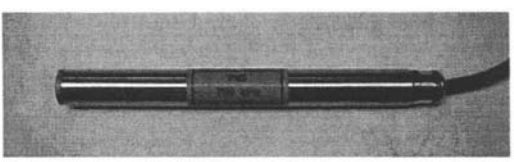


Figure 2. A piezometer

Piezometer

Vibrating wire (VW) piezometers made in Canada are selected in the project (see Figure 2). A VW piezometer can allow remote measurements of piezometric level and pore pressure over a long period of time. It also measures the temperature of the gauge and its surrounding soil. These piezometers have a measurement range of 750 kPa of pore water pressure at the maximum water depth of 76.53m. .

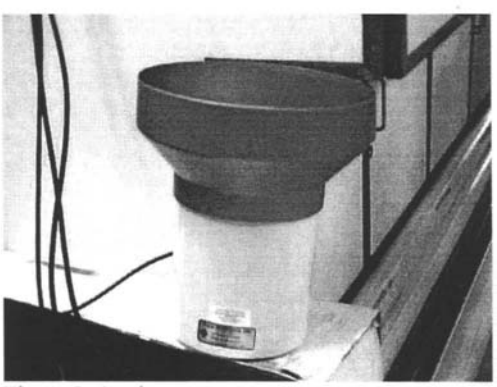


Figure 3. A rain gauge

Rainfall gauge

A rain gauge of type TE525 MM is selected to monitor rainfall intensity at a slope site (see Figure 3). It is a standard weather bureau tipping bucket rain gauge. Main specifications are: accuracy of ±1% (rainfall rate up to 1 inch/hour); infinite in increments of tip of rainfall; environmental limits from 0° to +50°C; humidity range from 0 to 100% (User's Manual[2]).

TDR 100 set

A Time Domain Reflectometer (TDR) is a new technology, which is very effective and accurate in locating a slip surface in the slope mass. Model TDR 100 is selected as a part of the automated integrated slope monitoring sub-system. The TDR consists of TDR 100 tester (see Figure 4), SDMX 50 multiplexer and one TDR cable. TDR 100 contains the pulse generator for the signal applied to TDR cable. The performance specifications of TDR 100 are: pulse generator output, 250 mV into 50 ohms; waveform sampling, 20 to 2048 waveform values over a chosen length;

range of up to 2100 metres, 0 to 7 microseconds; resolution of 1.8 millimetre and 6.1 picoseconds; operation temperature ranges from -20°C to 50°C. The SDMX 50 is a 50 ohms, eight-to-one, coaxial multiplexer to minimize signal attenuation. All channels have equal transmission line lengths (User's manual[3]).

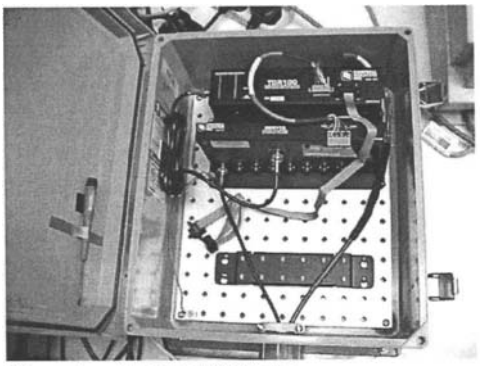


Figure 4. A TDR 100 Tester

The basic principle of TDR is similar to that of radar. TDR's original usage is to monitor breakage in communication or power lines. This technique has now been applied successfully in many applications in geotechnical engineering. One of the applications is to monitor the depth of a slipping surface.

The relative magnitude and location of the localised shear zone (or slip surface) can be detected immediately from the waveform when a TDR tester is connected to the TDR cable (see Figure 4). The size of the spike increase correlates roughly with the magnitude of movement in the slip surface.

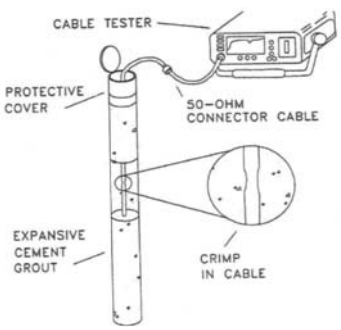


Figure 5. Coaxial cable installation and a TDR cable tester

Slope Sentry

A Model 798-B-TDR Slope Sentry (User's manual[4]) is a stand-alone datalogger for monitoring up to 10 inclinometers, up to 16 vibrating wire piezometers, a tipping bucket rain gage and up to 8 TDR cables (see Figure 6). Its main hardware consists of a CR10X datalogger, an M20 terminal modem, an AVW4 vibrating wire interface and a PS12 power supply. The Slope Sentry provides electric power to all instruments, manages measurement schedule, records the output readings from all instruments and transfers data from the monitoring site to a computer in the office.

Two external 12 volts batteries can be used to supply electric power to the Slope Sentry. In addition, two solar panels can be connected to perform automatic daily charging of both the external batteries and an internal battery in PS12, which is for emergency use only. An AVW4 interface is enclosed for signal transfer between a piezometer and a datalogger. A CR10 X datalogger performs data recording, sensing of alarm limits and control of an alarm system.

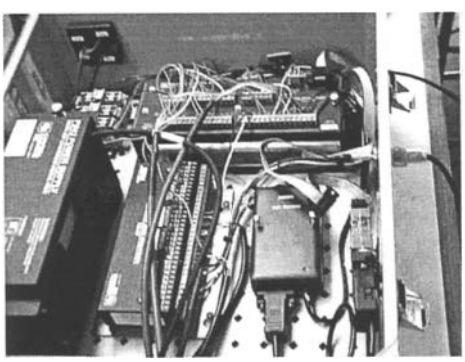


Figure 6. Slope Sentry

An M20 terminal modem is used to transmit data remotely. This modem allows transfer of data across a GSM900 digital cellular phone

network. The M20T is a GSM digital transceiver, which is considered to be a GSM mobile telephone without a handset. The M20T has an extra interface to allow a data device to be connected and can be used to collect data from a datalogger at a speed of a land-based 9600 baud modem, which closely emulates a standard "Hayes style" telephone modem. Through the M20T modem and the GSM communication technology, temporarily-stored data in the datalogger can be transferred to a computer in the office. Main specifications of the M20 Terminal modem are: standard RS 232 serial port; operating temperature ranges from -29°C to +55°C (User's manual [5]).

MULTI-ANTENNA GPS AND INTEGRATION WITH THE CONVENTIONAL SLOPE MONITORING PACAKGE

Among GPS instruments, the GPS receiver is the most expensive component. At present, one GPS receiver is used to monitor the movement of one point only. If there are ten points to monitor, ten GPS receivers are needed. This makes GPS monitoring more expensive than conventional geotechnical instruments. The one-receiver-to-one-point approach adopted in the standard GPS is the main reason of the high cost using GPS for monitoring.

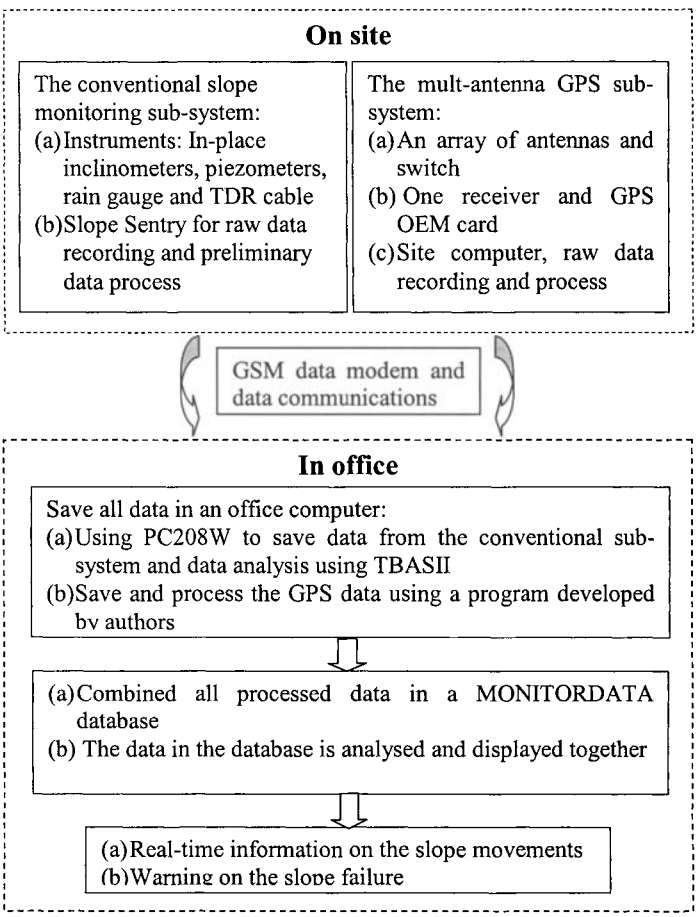


Figure 7. Illustration of the integration of the two sub-systems

In our newly developed GPS technology (Ding et al. 2002), a multi-antenna-switch is added to one GPS receiver to build up a multi-antenna GPS array, in which there are eight input ports (antenna) and one output port. After the receiver has got signal from one port, the receiver automatically switches to the next port until data from all ports are received. The one receiver in the multi-antenna GPS works in the same way as that of a standard GPS. Since only one receiver is used instead of 10 receivers, the multi-antenna GPS is much cheaper that the standard GPS with a resulting cost saving of about 80 %.

The authors have integrated the multi-antenna GPS with the conventional slope monitoring package as presented in the proceeding sections. The conventional package monitors mainly the sub-surface soil movements and pore water pressures while the multi-antenna GPS mainly

monitors the surface movements of a slope at an array of points. The integrated Slope Monitoring and Warning System (SMWS) combines and enhances the advantages of the conventional sub-system and the multi-antenna GPS. Data of the subsurface movements, pore water pressures and the slip location from the conventional sub-system plus rainfall measurements are combined with the data of the three-dimensional (3-D) movements of a large number of points on the slope surface to give a complete set of data, a whole picture, and better understanding of the slope movement. The integrated system can give a more comprehensive understanding of a slope and may give a more reliable warning before the slope starts to fail.

The method of integrating the multi-antenna GPS with the conventional sub-system is described here. In our design each sub-system can work separately and independently. The two sub-systems can also be integrated together and work jointly. When integrated, the two sub-systems are installed at the same slope site:

(a) The conventional sub-system is installed at a number of selected locations mainly sub-surface. The number of locations depends on the slope size and importance. The in-place inclinometers are placed in a vertical (or inclined) borehole with an access tube (a PVC pipe) at one-metre intervals, down through the potential slip surface. The TDR cable sensor is also installed through a vertical (or inclined) borehole through the potential slip surface at a location near to or away from the inclinometer borehole. A number of piezometers are installed at selected points in the soil mass. The rain gauge is normally placed on the ground surface at or near the slope site.

(b) An array of antennas are placed on poles (or small concrete blocks) on the slope surface. Special cables connect the antennas to one GPS receiver.

An illustration of the integration of the two sub- systems is shown in Figure 7.

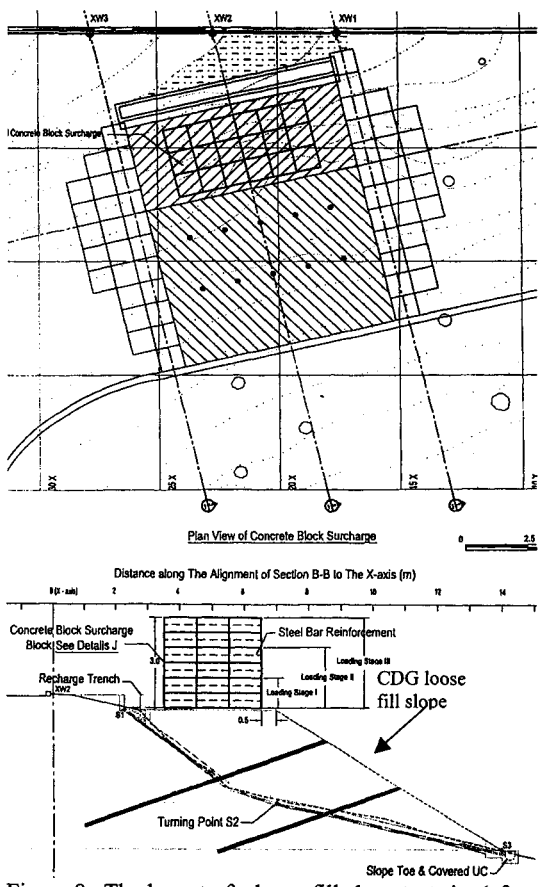


Figure 8. The layout of a loose fill slope test site (after Department of Civil Engineering of the University of Hong Kong (2002))

SITE TRIAL

The above integrated Slope Monitoring and Warning System (SMWS) has been installed at a loose fill slope test site in Hong Kong. The loose fill slope site is located in Kadoorie Agriculture Research Centre in Yuen Long of Hong Kong and constructed by the Department of Civil Engineering of the University of Hong Kong (2002) (see Figure 8). Completely Decomposed Granite (CDG) has been loosely placed to form the test slope. The natural ground below the test slope has a slope angle of 15°. The CDG loose fill slope has a slope angle of 33°. In plan view, the

slope area is 9.0m (width)×11.7m (length) with a maximum height of 4.5m. Two rows of soil nails are installed. There is a platform of 3m ×6.0m (see Figure 8) at the crest platform. Precast concrete blocks are to be used as surcharge acting on the crest platform. The concrete blocks will be placed gradually. Ground water table will also be raised. The idea is to cause the fill slope to fail under a control condition.

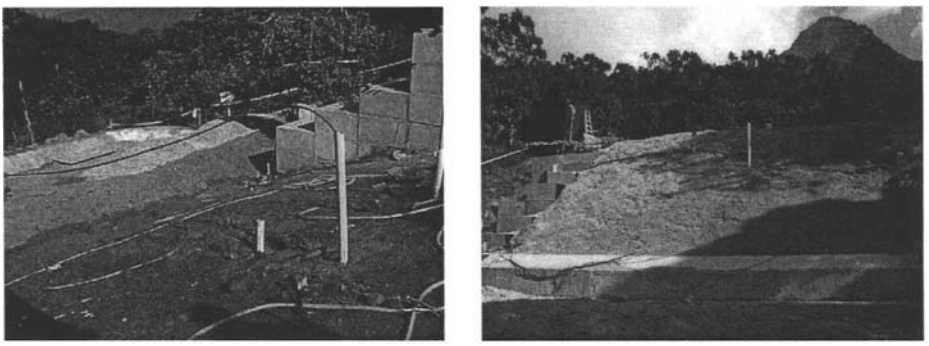


Figure 9. Installation of in-place inclinometers and TDR cable in two vertical boreholes – a down slope view (left) (partially built) and an upper slope view (right) (the final shape)

At the slope site, five in-place inclinometers have been installed in one vertical borehole of 6.3m in depth into the natural ground beneath the test slope (see Figure 9). One TDR cable is embedded in another near-by vertical borehople of 6.5m depths (see Figure 9). One piezometer is directly buried at the interface between the CDG fill and the natural ground next to the TDR and inclinometer boreholes. An array of five steel poles are installed on the sloping surface. The top of each pole supports one GPS antenna. Two further foundations on the stable ground support a portable station and a base reference station. The Slope Sentry, TDR tester, GPS receiver, switch box and other instruments are placed in a small shed close to the monitoring site. DC power battery supplies electric power to all instruments.

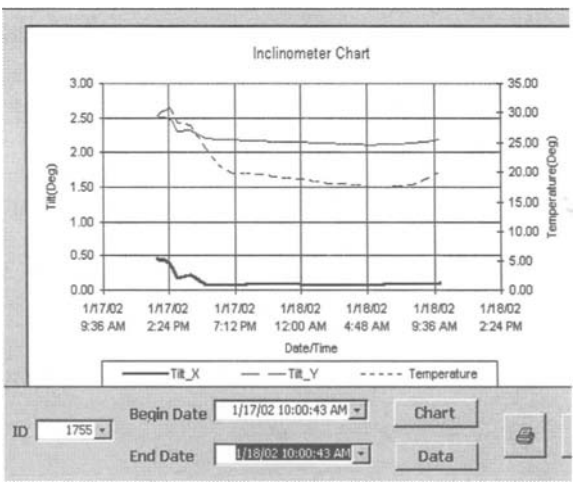


Figure 10. Graphical display of monitoring data in a database

A MONITORDATA database has been established for this particular site. Figure 10 shows the graphical display of data from Inclinometer No 1755 - relation of tilting angle and temperature with time on January 17, 2002 in the MONITORDATA database.

SUMMARY AND REMARKS

An integrated Slope Monitoring and Warning System (SMWS) is introduced in this paper. The method for integration of a conventional slope monitoring sub-system and a multi-antenna GPS

sub-system is described. The SMWS has been installed at a CDG loose fill slope test site in Hong Kong. Based on the work to date, the following main points can be summarised:

(a) The integrated SMWS can give a complete set of data on the slope under monitoring – subsurface and surface movements, pore water pressure, location of the slip surface and rainfall intensity. All these will provide more comprehensive information on the slope conditions and thus give a more reliable warning before the slope fails.
(b) The integrated system combines and enhances the advantages of the conventional sub-system and the GPS sub-system. Furthermore, the integrated system is more cost-effective for slope monitoring.
(c) The integration method is flexible. The two sub-systems can also work separately and independently if so required.

The functions, reliability, and accuracy of the integrated system need field verification. The field trial verification is currently still in progress and the findings will be reported in the near future.

ACKNOWLEDGEMENT

The research work in this paper is supported by grants (Project No. - CRC 4/99, A/C:3-ZB39 and Project No. - PolyU5090/98E) from the Research Grants Council of the Hong Kong SAR Government and The Hong Kong Polytechnic University. The project team is grateful to the Department of Civil Engineering of the University of Hong Kong for allowing us to use their loose fill test slope site for the field trial. Mr. Jeff N. Schuyler has provided valuable advice to us on the project. All the supports and advice given are gratefully acknowledged.

Reference

Department of Civil Engineering of the University of Hong Kong (2002). Drawings of the "Full-scale Field Tests of Loose Fill Slope Stabilised with Soil Nails at Kadoorie Argicultural Research Centre, Lam Kam Road, Shek Kong, Yuen Long".

Ding, X.L., J.H. Yin, Y.Q. Chen, C.K. Lau, Z.L.Li, D.F. Huang, Y. R., Sun, and Y.W. Yang. A new generation of multi-antenna GPS system for landslide and structural deformation monitoring. In proceedings of Advances in Building Technology (ABT 2002), 4-6 December 2002 in Hong Kong.

Malone A. (1998). Slope movement and failure: evidence from field observation of landslides associated with hillsides cuttings in saprolite. in Hong Kong. Proceedings 13th Southeast Asia Geotechnical Conferences, Taipei.

User's manual[1]: Model 906 Little Dipper, Applied Geomechanics, 2001

User's manual[2]: TE525 Tipping bucket rain gage, Campbell Scientific, 2001

User's manual[3]: TDR100 Instruction manual, Campbell Scientific, 2001

User's manual[4]: Slope –Sentry, Applied Geomechanics, 2001

User's manual[5]: Siemens M20T GSM digital transceiver - instructions for use, Campbell Scientific, 2001

Yin, J-H. and Ding, X.L. (1999). Research Proposal - Integrated Intelligent Slope Monitoring and Warning System, CRC-Centre for Ground Engineering and Technology(C-GET), the Faculty of Construction and Land Use, The Hong Kong Polytechnic University.

INFORMATION TECHNOLOGIES:

PROJECT MANAGEMENT SUPPORT SYSTEMS

This Page Intentionally Left Blank

Advances in Building Technology, Volume 2
M. Anson, J.M. Ko and E.S.S. Lam (Eds.)
© 2002 Elsevier Science Ltd. All rights reserved

DECISION MODEL FOR THE SELECTION OF DEMOLITION TECHNIQUES

A. Abdullah and C. J. Anumba

Department of Civil and Building Engineering, Loughborough University, Loughborough, LE11 3TU, UK

ABSTRACT

The demolition of structures is governed by a number of criteria. The changing natures of demolition criterion from one demolition project to another makes the selection of demolition techniques very risky and time-consuming for the contractor. This paper describes the development of a multiple-criteria decision support system using Analytic Hierarchy Process (AHP) for the selection of the most appropriate demolition technique. The AHP comprises three parts: hierarchic structure, prioritization procedure, and calculation of results. A postal questionnaire and interview survey was conducted with demolition contractors in the United Kingdom to identify the criteria and the alternatives for the development of the hierarchic structure. There are six major influential criteria identified: Structure characteristics; Site conditions; Cost; Past experience; Reuse & recycling and Time. These criteria used to select three main alternatives: progressive demolition; deliberate collapses mechanism and deconstruction. An example is presented to illustrate the potential application of the proposed model using computerized decision support software, namely Expert Choice 2000.

KEYWORDS

Analytic hierarchy process (AHP), demolition technique selection model, multiple criteria, intelligent system and decision-making process.

INTRODUCTION

Selecting a demolition technique is one of the most important tasks faced by a demolition contractor at the tender stage. The changing nature of parameters from one structure to another makes the selection of demolition techniques difficult for the contractor. Before selecting any type of demolition technique, the demolition contractor needs to consider a set of criteria and assess their relevance to the demolition work to be undertaken in order to arrive at the most appropriate demolition technique. There are no sets of criteria, which uniquely and completely determine the appropriate demolition technique for a particular project (Fesseha, 1999). Furthermore, demolition techniques are continually evolving, becoming faster, safer and more cost effective (Atkinson &

Faulkner, 2000). The number of different demolition techniques in the demolition industry has increased over the last decade. In the past, the basic tools of demolition were wrecking ball, crane and front-end loader. Today, standard equipment used includes the hydraulic excavator with many attachments such as, hammers, shears, grapples, pulverisers and multi-purpose attachments. Implosion or using an explosive to demolish a structure is also an option. This has resulted in an increasing demand for systematic methods of selecting the most appropriate technique for a specific demolition project.

The nature of the problem involves a multicriteria decision-making ability. It requires an effective decision making technique to systematically evaluate demolition techniques against a number of criteria, which will help the individual or project team to select the most appropriate demolition technique from the alternatives available. The decision is based on experience, skill and knowledge and its varies from one to another decision-maker. Even with an experienced and knowledgeable decision-maker, their procedures are kept confidentially. From the literature search, there is still no systematic procedure by experts that can help in evaluating the selection of demolition technique.

With regards to the problem mentioned, the Analytical Hierarchy Process (AHP) was chosen for this study to gives the decision maker the framework needed to model a complex decision scenario, therefore allowing for a better understanding of the problem, its criteria and possible choice. Muralidhar, Santhnam, and Wilson (1990) support the belief that the AHP caters specifically for decision making with multicriteria attributes. This paper therefore presents the development of a theoretical framework using AHP for the selection of the most appropriate demolition technique.

RESEARCH METHODOLOGY

In this study, both questionnaires and interviews were used to elicit essential information from demolition contractors. The aim of the survey is to identify the criteria and alternatives used to select the demolition techniques.

Postal Questionnaires

The population for this research is the demolition contractors in United Kingdom (UK). National Federation of Demolition Contractors (NFDC) UK provides the sampling frame of this research. There were 157 demolition contractors as a corporate member registered with NFDC (Atkinson & Faulkner, 2000). All the contractors from the sampling frame were contacted by telephone to make sure the willingness and confirmation of address before the questionnaire were send by post. Finally, about 100 out of 157 demolition contractors were interested to be included in this research as a sample. The response rate for the survey was 37 per cent, out of 100 questionnaires delivered, of which 94.6 per cent of the represented usable replies and 5.4 per cent unusable replies. The experience and position of the respondents in the company stimulated confidence in the result of the survey. About 86 percent of the respondents has more than 10 years of experience and represents top-level management in the respondent's company.

The experts assessed each criterion in the questionnaire by ranking their relative importance to each other. Statistical analysis was carried out to refine these criteria with the purpose of identifying the relative degree of importance of each criterion. Table 1 shows the selection criteria for demolition techniques identified by the respondents.

TABLE 1
SELECTION CRITERIA FOR DEMOLITION TECHNIQUES (RANKING FOR RELATIVE IMPORTANCE)

Criteria	Ranking
Health and safety	1
Stability of the structure	2
Location and accessibility	3
Presence of hazardous material	4
Environmental consideration	5
Shape and size of the structure	6
Client specification	7
Structural engineer approval	8
Time constraint	9
Extent of demolition	10
Financial Constraint	11
Recycling consideration	12
Transportation consideration	13
Availability of plant or equipment	14

Structured Interview

Structured interviews (6 interviews) with key experts were conducted after the entire postal questionnaire returned. The refined criteria that resulted from the postal questionnaire were given to the key experts for reassessment and to ensure the relevance of the identified criteria. Statistical analysis was carried out to refine the criteria, which were used directly in the AHP method, to develop a proposed hierarchic structure.

THE DEMOLITION TECHNIQUES

The actual demolition starts when the structural elements demolished. There are three main types of demolition techniques, which are progressive demolition; deliberate collapse mechanisms and deconstruction. These are the alternative technique that can be selected by the contractor in the selection process conducted in the tendering stage.

Progressive demolition

The progressive demolition is the controlled removal of sections of the structure, at the same time retaining the stability of the remainder and avoiding collapse of the whole or part of the structure to be demolished. Progressive demolition is particularly practical in confined and restricted areas and may be considered for the majority of sites. The progressive demolition includes progressive demolition by machine i.e. Excavator attached with boom and hydraulic attachments such as pulverisers, crushers and shears; and Progressive demolition by balling which involves the progressive demolition of a structure by the use of a iron ball that is suspended from a lifting appliance and then released to impact the structure, repeatedly, in the same or different locations.

Deliberate collapse mechanisms

Demolition by deliberate collapse is the removal of key structural members to cause complete collapse of the whole or part of the building or structure. This method usually employed on detached, isolated, fairly level sites where the whole structure is to be demolished. A sufficient space must be allocated to enable removal of equipment and personnel to a safe distance. The demolition by deliberate collapse includes deliberate collapse by explosive and deliberate collapse by wire rope pulling.

Deconstruction

Deconstruction process reverses the sequence of construction, dismantling a structure that proceeds from roof to ground in a general trend. The structures are carefully dismantled in order to maximize the recovery of valuable building resources for reuse and recycling. This technique can be used, for example as part of renovation or modification work and prepare the way for deliberate collapse. The elements to be removed should be identified and the effects of removal on the remaining structure fully understood and included in the method statement, with the elements to be removed marked on site. If instability of any of the remainder might result in a possible risk to personnel on the site and to other people nearby, sections of the structure should not be removed. The deconstruction can be done by hand or machines.

MODEL DEVELOPMENT

Several methods are available to evaluate the multiple criteria decision-making problem i.e. ranking, weighting, rating, and paired comparison. Since the contractor bases judgement on experience and knowledge, the AHP method agree with the behavior of the decision process. The computerized decision support software (Expert Choice 2000) was used to structure the demolition technique selection model and will be discussed in the following section. One actual demolition project was used to illustrate the model development process (Table 2).

TABLE 2
THE PROJECT CHARACTERISTICS

Project Characteristics	Explanations
Type of structure	3-storey car park constructed from concrete beam, which are laid onto concrete supporting columns. The structure demolished because of the redevelopment project involved in the area.
Location	The car park located in the town centre where health and safety of the public is the main concern. The site can be easily access by road. The nearest adjacent structure is about 20 meter. There is a main road beside the car park, which have a high traffic volume during the peak hour.
Contractor background	Many years' experience demolished a concrete structure whether in urban or rural areas generally by using progressive and deliberate removal of element demolition techniques. Have several experiences demolish a structure by using explosive.
Reuse & Recycling	The only materials that can be recycled are rebar as a scrap iron and concrete debris as a fill material.
Time	Proposed project completion date is three months.

Analytic Hierarchy Process (AHP)

AHP has been applied to many types of decision problem, since its introduction by Thomas L. Saaty in the mid-1970s. Partovi (1994) described AHP as 'a decision-aiding tool for dealing with complex, unstructured and multi-attribute decision'. Fundamentally, the AHP works by developing priorities for alternatives and the criteria used to judge the alternatives (Saaty, 1994). Analytic hierarchy process takes into account judgements based on people's feeling and emotions as well as their thoughts (Saaty, 1994). Golden (1989) described AHP as *analytical* by using numbers, *hierarchical* by structuring the decision problem into levels, and *process*-oriented because its step-by step approach. Application can be found in such diverse fields as portfolio selection, transportation planning, manufacturing system design, and artificial intelligence (Saaty, 1994).

The number and diversity of AHP applications has grown rapidly with the introduction of its PC implementation, Expert Choice (Person, 2001). Expert Choice is intuitive, graphically based and

structured in a user-friendly way so as to be helpful for conceptual and analytical thinkers, novices and category experts. Because the criteria are presented in a hierarchical structure, decision-makers are able to practice their level of expertise, and apply judgments to the criteria consider important to their personal or organizational objectives. At the end of the process, decision-makers are fully aware of how and why the decision was made, with results that are meaningful and practical. Thousands of businesses and government agencies use Expert Choice to structure, justify and optimize critical group decisions (Person, 2001). The majority of these applications have introduced analytical solutions for the problems that involved both quantitative and qualitative criteria (Skibniewski & Chao, 1992), which is related to the selection process that is the objective of this study. There are three basic steps in using AHP: hierarchic structure, prioritization procedure, and calculation of results (Fong & Choi, 2000).

Hierarchic structure

A complex decision problem is expressed as a hierarchy structure (Saaty, 1994). Structure the hierarchy from the top (the overall objective or goal from a decision-maker's viewpoint), through the intermediate levels (the criteria or objectives affecting the decisions), to the lowest level (sub-criteria and decision alternatives are on each descending level of the hierarchy).

The selection of the most appropriate demolition techniques was the goal of the decision-makers and is located at level 0 of the model to serve as the goal node. The criteria which affecting the demolition technique selection was the result taken from the questionnaires survey and interview. These criteria had been classified into 6 categories, and inserted in level 1 of the model to serve as main criteria. The criteria for each category were inserted in level 2 of the model to serve as sub-criteria nodes. Statistically, level one; and two of the hierarchy consists of a total of 6, and 16 nodes respectively. Finally, the alternative solutions occupied the lowest levels to serve as the choice available for the decision-makers in the last screening stage. The hierarchy structure for the proposed model shows in Figure 1.

Prioritization procedure

The second step is to weight or to judge (define) the priority of each criterion. At each level pairwise comparisons are conducted for each category with the one in the adjacent upper level, and the weight are entered into a comparison matrix. The elements on the second level (Structure characteristics, site conditions, cost, past experience, reuse and recycling, and time) are arrange into matrix, and the decision makers make judgements about the relative importance of the elements with respect to the overall goal of selecting the most appropriate demolition technique. The judgements are entered using the fundamental scale for pairwise comparisons (see Table 3).

TABLE 3
SCALE OF RELATIVE IMPORTANCE USED BY (SAATY, 1994)

Intensity of Importance	Definition	Explanation
1	Equal importance	Two activities contribute equally to the objective
3	Weak importance of one over another	Experience and judgement slightly favor one activity over another
5	Essential or strong importance	Experience and judgement strongly favor one activity over another
7	Demonstrated importance	An activity is strongly favored and its dominance demonstrate in practice
9	Absolute importance	The evidence favoring one activity over another is of the highest possible order of affirmation
2,4,6,8	Intermediate values between the two adjacent judgements	When compromise is needed
Reciprocals of above nonzero	If activity i has one of the above nonzero numbers assign to it when compared with activity j, then activity j has the reciprocal value when compared with i.	

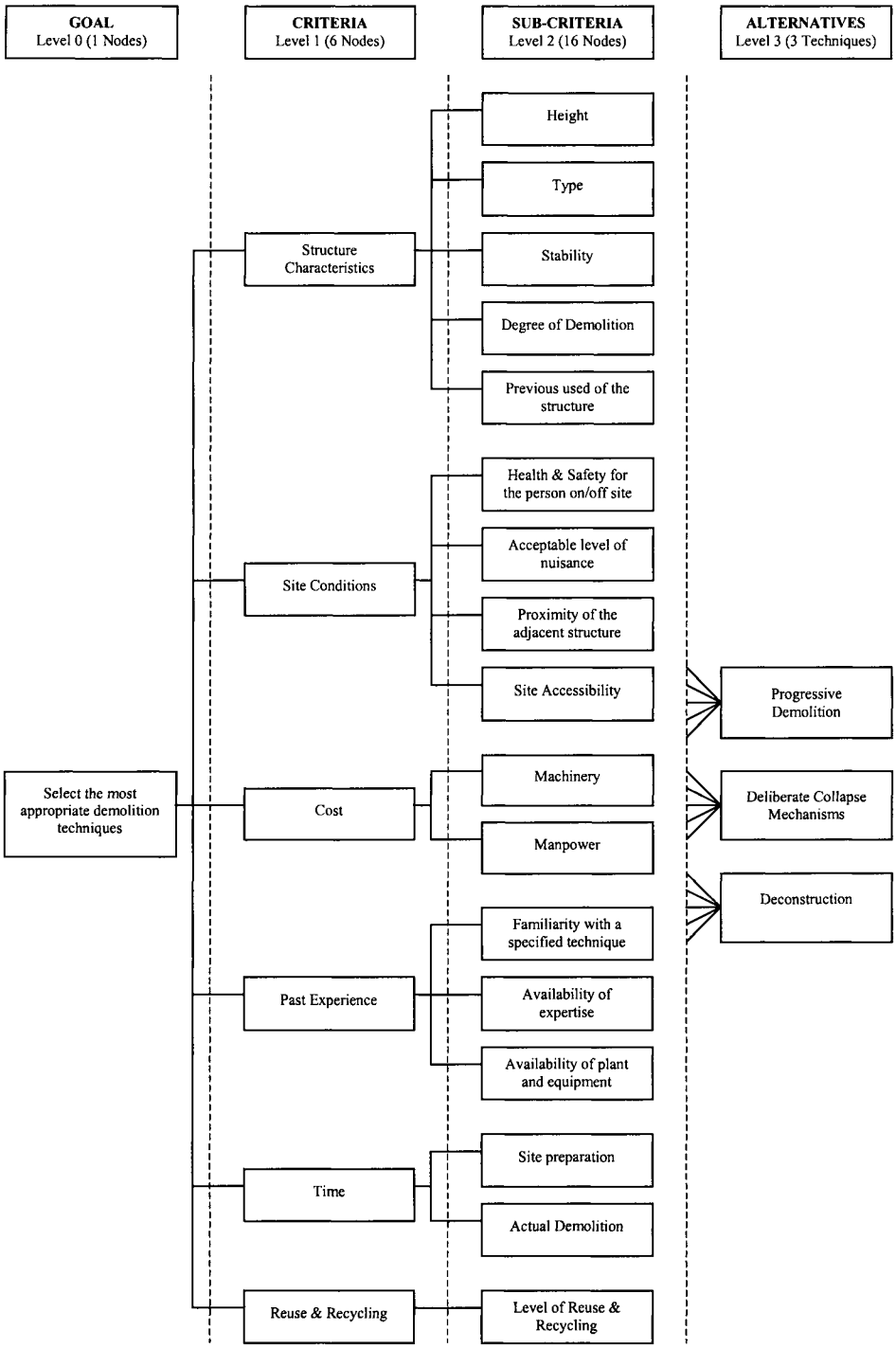


FIGURE 1: HIERARCHY STRUCTURE FOR THE SELECTION OF DEMOLITION TECHNIQUE

Saaty (1994) describes pairwise comparison as 'the element that appears in the left-hand column is always compared with the element appearing in the top row, and the value is given to the element in the column as it is compared with the element in the row. If it is regarded less favorably, the judgment is a fraction. The reciprocal value is entered in the position where the second element, when it appears in the column, is compared with the first element when it appears in the row'. For example, when judging the relative preference of factors located in level 1 with respect to the goal (level 0), a rating of 5 is assigned in the comparison with structure characteristics and site conditions. This indicates essential or strong importance or experience and judgment strongly favor structure characteristics over site conditions. In comparing cost with past experience with respect to the goal, the rating of 3 assigned. This means cost is weak importance of one over past experience. The same procedure repeated when the rating of 7 assigned in comparing site conditions with time with respect to goal. Intensity of importance (7) assigned for this matrix can be explains, as a site condition is strongly favored if compared with time. All the remaining pairwise comparison matrices among the nodes in the hierarchy can be established by following the same procedure. Table 4 presents the start of pairwise comparison of level 0 with level 1. Similar pairwise comparison tables exist for level 1 with level 2 and level 2 with level 3.

TABLE 4
START OF PAIRWISE COMPARISON OF LEVEL 0 WITH LEVEL 1

Demolition technique selection criteria (1)	Structure characteristics (2)	Site conditions (3)	Cost (4)	Past experience (5)	Reuse & recycling (6)	Time (7)
Structure characteristics	1	5	5	5	7	8
Site conditions	1/5	1	5	5	5	7
Cost	1/5	1/5	1	3	3	5
Past experience	1/5	1/5	1/3	1	1	3
Reuse & recycling	1/7	1/5	1/3	1	1	3
Time	1/8	1/7	1/5	1/3	1/3	1

Calculation of results

The next step is to perform synthesis process from the model global goal. This process converts all the local priorities into the global weights of alternatives. Saaty (1996) remarks that 'if there are more than two levels, the various priority vectors can be combined into priority matrices, which yield one final priority vector for the bottom level'. Local priority is the priority relative to its parent or upper level, while global priority, also called final priority, is the priority with respect to the goal. Table 5 shows the local and global priority of each criterion in the final selection of demolition technique. The table format was adapted from (Fong & Choi, 2000). As a result from the pairwise comparison matrices, the overall priorities of model's main criteria were determined (see Table 6). AHP provides a measure to test out the degree of inconsistency by the decision-makers called Consistency Index (CI). In general, a consistency index < 0.10 is acceptable. The CI can be calculated for each matrix as follows (Saaty, 1994):

The Consistency Index $CI = (\lambda\text{-}n) / (n\text{-}1)$; n = Matrix size, and λ = Eigenvalue

The contractors can select three alternatives for the demolition techniques (Progressive demolition, deliberate collapse mechanisms and deconstruction). These three techniques must be compared pairwise for each criterion. This process is similar to the procedures that used to develop the normalized eigenvector of criteria. Finally the synthesis with respect to goal, which is to select the most appropriate demolition technique, is presented in Table 7. The order of prioritization is progressive demolition, deliberate collapse mechanisms, and deconstruction (from the most to the least appropriate demolition techniques to be used in the project example).

TABLE 5
THE PRIORITY OF EACH CRITERION IN THE SELECTION OF DEMOLITION TECHNIQUE

Criterion	Local priority [a]	Global priority [b]	Subcriterion	Local priority [a]	Global priority [b]
Structure characteristic	0.491	0.491	Height	0.107	0.052[c]
			Type	0.054	0.027
			Stability	0.525	0.258
			Degree of demolition	0.281	0.138
			Use of structure	0.034	0.017
Site conditions	0.255	0.255	Health and safety for the person on and off site	0.057	0.148
			Acceptable level of nuisance	0.110	0.028
			Proximity of the adjacent structure	0.241	0.061
			Site accessibility	0.071	0.018
Cost	0.113	0.113	Machinery	0.750	0.085
			Manpower	0.250	0.028
Past experience	0.058	0.058	Familiarity with a specified techniques	0.268	0.016
			Availability of plant and equipment	0.117	0.007
			Availability of expertise	0.614	0.036
Time	0.028	0.028	Site Preparation	0.167	0.005
			Actual demolition	0.833	0.024
Reuse & recycling	0.054	0.054	Level of reuse and recycling	1.000	0.054

[a] Local priority is derived from judgement with respect to a single criterion
[b] Global priority is derived from multiplication by the priority of the criterion
[c] The result is obtained as follows: 0.491 X 0.107 = 0.052

TABLE 6
RELATIVE PRIORITY OF CRITERIA

Criterion	Relative priority
Structure characteristic	0.491
Site conditions	0.255
Cost	0.113
Past experience	0.058
Reuse & recycling	0.054
Time	0.028

Consistency index = 0.09

TABLE 7
OVERALL PRIORIZITATION OF THE THREE ALTERNATIVES

Criterion	Relative priority
Progressive demolition	0.534
Deconstruction	0.262
Deliberate collapse mechanisms	0.204

Consistency index = 0.07

CONCLUSION

The demolition contractor faces a problem in selecting the most appropriate demolition technique for a specified project because it involves a multicriteria decision-making ability. The characteristics of the problem require an effective decision making method to systematically evaluate the demolition techniques available against a number of influential criteria. With regard to this problem, computerised decision support software called Expert Choice 2000, which implements the AHP methodology was used to structure the demolition technique selection model.

A questionnaire survey and expert interview survey involving contractors and demolition experts in the UK were used to establish the influential criteria in selecting demolition techniques. The criteria

finally grouped into six main categories. The result shows that the structural characteristics followed closely by the site conditions are the main influential criteria to select a demolition technique. The most appropriate technique selected for the demolition project based on the weighting inserted during the pairwise comparison, is progressive demolition. The same technique also selected in the actual demolition project. Therefore the proposed model can be very helpful to assist the demolition contractor in selecting the most appropriate demolition technique in any given situation.

REFERENCES

Atkinson, J., and Faulkner, G. (2000). NFDC Yearbook 2000, *The latest in plant and specialist demolition equipment up for grabs*. Surrey: Contract Journal.

British Standards Institution. (2000). *Code of Practice for Demolition*. British Standard BS 6187:2000. London: BSI Standards.

Fesseha, T. (1999). *Criteria for Selection of Demolition Techniques*. M.Sc. Dissertation. , Loughborough: Loughborough University.

Fong, P. S. W., and Choi, S. K. Y. (2000). Final contractor selection using the analytical hierarchy process. *Construction Management and Economics*, **18(5)**, 547-557.

Golden, B. *et al.* (1989). *The Analytic Hierarchy Process: Application and Studies*. London: Springer-Verlag.

Muralidhar, K., Santhnam, R., and Wilson, R. L. (1990). Using the analytic hierarchy process for information system project selection. *Information and Management,* **(Feb)**, 87-95.

Partovi, F. Y. (1994). Determining what to benchmark: An Analytic Hierarchy Process Approach. *International Journal of Operations and Production Management,* **14(6)**, 25-39.

Person, A. H. (2001). *Expert System*, [Internet]. Available: http://www.expertchoice.com/productbrief [1 September 2001].

Saaty, T. L. (1994). *Fundamentals of decision making and probity theory with the analytic hierarchy process* (First ed. Vol. VI). Pittsburgh, USA: RWS Publications.

Saaty, T. L. (1996). *Multicriteria Decision-Making*. Pittsburgh: RWA Publications.

Skibniewski, M., and Chao, L. (1992). Evaluation of advanced construction technology with AHP method. *Journal of Construction Engineering and Management, ASCE,* **118**, 255-261.

This Page Intentionally Left Blank

Advances in Building Technology, Volume 2
M. Anson, J.M. Ko and E.S.S. Lam (Eds.)
© 2002 Elsevier Science Ltd. All rights reserved

DEVELOPING AN EXPERT SYSTEM FOR PROJECT PROCUREMENT

Albert P.C. Chan[1]

Department of Building and Real Estate, Hong Kong Polytechnic University,
Hung Hom, Hong Kong, HKSAR, PRC

ABSTRACT

It is claimed that the correct choice of a building delivery method will lead to the success of a building project. Hence selecting an appropriate procurement system is an essential step in any construction project process. If a client makes a wrong choice, the penalty may be time and cost overrun and a general dissatisfaction. Despite considerable research into the choice of appropriate procurement systems for construction projects, no generally applicable solutions have been found. This paper reports a research study carried out in Hong Kong on procurement selection. The study aims to develop an expert system to aid the selection of the most appropriate procurement system. A procurement categorization is developed to reflect the current procurement practice in Hong Kong. The model is based on a set of criteria and utility factors derived from ten local experts through 4 rounds of Delphi survey. A statistically significant consensus on the weighting of the utility factors for each procurement system was obtained. The results vividly reveal that Delphi method is a powerful and appropriate technique in deriving objective opinions in a rather subjective area such as the multi-attribute model for the selection of procurement system.

KEYWORDS

Expert system, procurement selection, multi-attribute model.

INTRODUCTION

The construction industry in Hong Kong is rather conservative and not innovative. In contexts where there are no specific incentives or benefits for being innovative, most construction clients rely on traditional systems of design-bid-build to deliver their projects. This has been the case in Hong Kong for the last two to three decades, particularly for clients with mass building programs such as the Hong Kong Housing Authority (HKIA, 1998).

Many clients, however, are becoming increasingly dissatisfied with the traditional form's operational characteristics and seek other methods of procurement, organisation and management to meet their

more exacting needs (Griffith, 1989). Integrated procurement system and management-oriented system are approaches that can be used to help dealing with the problems associated with the traditional system (Masterman, 1992).

It is known that procurement methods play a major role in defining and shaping contractual and work relationships between parties involved in the construction process. It is also claimed that the correct choice of a building procurement method will lead to the success of a building project (Bennett & Grice, 1990). A project may be regarded as successful if the building is delivered at the right time, at the appropriate price and quality standards, and provides the client with a high level of satisfaction (Barclay, 1994). If the client makes an inappropriate choice, the penalty may be time and cost overrun and a general dissatisfaction.

Previous research (Chan & Fung, 1996) found that clients and their advisers often refer to past experience and personal preference in selecting procurement systems for their projects. Research regarding systematic procurement selection techniques and their application to the industry in Hong Kong is rather limited. Research by Skitmore & Marsden (1988), Bennett & Grice (1990), and Chan (1995) have developed similar procurement selection model. However, Tsoi (1997) has found that none of this model is applicable to the unique Hong Kong construction industry. Thus, in order to enhance the applicability of these models, future research should be directed to develop a Hong Kong based model by taking the local construction industry into account.

This paper, based on the earlier work by Chan et al (2001), reports the development of an expert system to guide the client in selecting an appropriate procurement method for a building project in Hong Kong. A multi-attribute model will be used to obtain the most appropriate choice of procurement system for a building project in Hong Kong. The model is based on a set of utility factors derived from a panel of local experts through the application of the Delphi methods.

DEFINING BUILDING PROCUREMENT

Franks (1998) described a "building procurement system" as "the amalgam of activities undertaken by a client to obtain a building". Masterman (1992) defined a "building procurement system" as "the organisational structure adopted by the client for the management of the design and construction of a building project."

Previous studies (Chan, 1994, 1995, 1996; Chan & Tam, 1994; Chan & Lam, 1995) suggest that alternative procurement systems can be used successfully on building projects and provide time and cost benefits to both clients and contractors. However, no one single system will suit every conceivable type of project (Chan & Tam, 1994). The selection of a system appropriate to the unique facets of a particular project is a critical determinant of the ultimate success of the project (Chan, 1996). Chan et al (2001) identify that the most popular procurement systems adopted in Hong Kong include sequential traditional, accelerated traditional, competitive design and build, enhanced design and build, novation, and management contracting.

Nahapiet (1985) found out that there is no one best contractual arrangement for building projects. The most appropriate choice of procurement system depends on the individuality of the particular project and its client. The key to successful procurement system is the identification of the clients' objectives and project characteristics and matching of these to the most appropriate procurement system.

One of the fundamental needs to ensure the successful delivery of a building project is the correct choice of method for managing the relationships between the different organisations and specialists that will form the project team (Masterman, 1994).

DEVELOPING A PROCUREMENT SELECTION MODEL BASED ON THE DELPHI TECHNIQUE

Delphi technique is being increasingly used in many complex areas in which a consensus is to be reached. Some of these areas included the development of residential areas (Anatharajan and Anataraman, 1982), theory and design application (Corotis and Harris, 1982), and bridge condition rating and effects of improvements (Saito and Sinha, 1991). Moreover, the Delphi method is a highly formalized method of communication that is designed to extract the maximum amount of unbiased information from a panel of experts. Therefore, it would be appropriate to adopt the Delphi technique for obtaining a set of universal utility factors for the selection model of procurement system.

Delphi Background

The Delphi concept was developed from the American defense industry. Project Delphi was the name of a study done by the Rand Corporation for the U.S. Air Force in the early 1950's concerning the use of expert opinion (Robinson, 1991). The objective of the study was to "obtain the most reliable consensus of opinion of a group of experts by a series of intensive questionnaires interspersed with controlled opinion feedback" (Linstone and Turoff, 1975). It was originally developed for market research and sales forecasting purposes (Goldfisher, 1992).

The Delphi method can be characterised as a method for structuring a group communication process so that the process is effective in allowing a group of individuals as a whole to deal with complex problems. Delphi is primarily a communication device, which is applied when the consensus of experts on an uncertain issue, often intangible is desired (Linstone and Turoff, 1975). It is conducted by rounds interspersed with group opinion and information feed back in the form of relevant statistical data. Delphi is an iterative forecasting procedure characterized by three features (Dickey and Watts 1978): 1) anonymity, 2) iteration with controlled feedback, and 3) statistical response.

Panel members remain unknown to one another and respond to a series of questionnaires. The iterative nature of the procedure generates new information for panelists in each round enabling them to modify their assessments and project them beyond their own subjective opinions. It can represent the best forecast available from a consensus of experts (Corotis, Fox, and Harris, 1981).

The Delphi approach offers an additional advantage in situations where it is important to define areas of uncertainty or disagreement among experts. In these instances, Delphi can highlight topics of concern and evaluate uncertainty in a quantitative manner. Group evaluation of belief statements made by panel members is an explicit part of Delphi (Robinson, 1991). Goldstein (1975) correctly points out that, while the group view has a higher probability of being correct than an individual, its success depends principally on the careful selection of the panel and formulation of questions. The major difficulties of Delphi, however, lie in maintaining the high level of response and in reaching and implementing a consensus (Robinson, 1991).

Format of Delphi Rounds

Ten experts were selected to provide opinions on the suitability of a certain procurement path for a given criterion. The ten members of the panel represent a wide distribution of professional, with four from the public client organisations; three from the private consultant groups and three are academics in the Universities in Hong Kong. The composition of this group of experts provides a balanced view for the Delphi survey. The Delphi method adopted in this research consisted of four rounds. In the first and second round of Delphi questionnaire, it was intended to gather a set of exclusive selection

criteria for the procurement system in the Hong Kong construction industry. The respondents were asked to provide a minimum of five criteria for the selection of the most appropriate procurement system in the first round Delphi. The second round of the questionnaire dealt with all the criteria provided in the first round and experts were asked to state the importance for each of the criterion. In the third round of questionnaire, a list of criteria with corresponding questions were presented and the respondents were requested to assess the suitability of each procurement system against each selection criterion.

While analysing the data, the focus should be on the opinion of the group rather than that of individuals. Therefore a Concordance analysis, which measures the consistency of the experts' responses over successive rounds of the Delphi, is adopted. In the fourth round of Delphi, respondents were provided with results in round three. They were asked to re-consider the scores of the utility factors and see whether they would adjust them. The consistency of the results improved significantly over the last two rounds. Full details of the Delphi survey are recorded in Chan et al's paper (2001).

THE MULTI-ATTRIBUTE MODEL

By the application of the Delphi method, a set of sufficiently consistent utility factors was obtained after the final round of Delphi questionnaire. The set of selection criteria and the corresponding utility factors are used to develop a procurement selection model. The multi-attribute model consists of the following set of client's criteria, which are re-phrased as priority questions.

1. *Price competition*: How important is it to choose your project team by price competition, so increasing the likelihood of a low price?
2. *Time available*: How important is early completion to the success of your project?
3. *Time predictability*: To what extent do you require a specific completion date at the start of the project?
4. *Availability of competent contractors*: How important is it to have a plentiful supply of competent contractors to work for the procurement system?
5. *Clear end user's requirements*: How capable is the client able to state his or her requirements clearly and precisely at the tender stage?
6. *Complexity*: Is the project highly specialized, technologically advanced or highly serviced?
7. *Certainty of cost without fluctuation*: How important is a firm price at the beginning of construction needed?
8. *Flexibility for changes*: To what extent do you expect the project to have frequent changes in the design and construction once the work has begun on site?
9. *Risk management*: To what extent do you need risk avoidance in the event of time, cost, design liability and quality slippage?
10. *Responsibility*: To what extent do you wish to have a single point of responsibility for the completion of the design and construction of the project?
11. *Familiarity*: How important is it for the client to choose a familiar system to deliver the project?

The priority questions will allow the users to prioritize the criteria according to a specific project and the user's specific requirements (Skitmore and Marsden, 1988; Bennett and Grice, 1990; Chan, 1995; Love et al., 1998). Figure 1 shows the multi-attribute model with the mean values of the utility factors for the each procurement system against each selection criterion.

The Use Of The Selection Model

The selection model can be applied by following the procedures laid down below (Chan and Yung, 2000; Skitmore and Marsden, 1988):

1) The user reads all the priority questions and enters the relative importance of each criterion in the table on a scale of 1 to 5, 1 being the least important, and 5 being the most important. The prioritisation exercise enables the users to specify their requirements according to the project needs and circumstantial factors.
2) Each priority rating is taken in turn and multiplied by each of the utility factors, the results being entered into the appropriate columns. This is compared for all the criteria.

The totals of each of the result columns, under each procurement path, are calculated, and ranked in descending order. The most appropriate procedure should have the highest total result.

Selection Criteria	Utility Factors													
	Traditional system					Integrated system						Management		
	Client's Priority Rating	Sequential		Accelerated		Competitive design & build		Enhanced design & build		Novation		Management contracting		
W significant at 0.05 level		U.F.	Score	U.F.	Score	U.F.	Score	U.F.	Score	U.F.	Score	U.F.	Score	
1. **Price Competition** • How important is it to choose your project team by price competition, so increasing the likelihood of a low price?		85.6		68.1		91.9		88.1		76.3		55		
2. **Time Available** • How important is early completion to the success of your project?		51.9		76.3		84.4		75.6		76.3		86.3		
3. **Time Predictability** • To what extent do you require a specified completion date at the start of the project?		77.5		70.6		93.8		86.9		87.5		71.3		
4. **Availability of Competent Contractors** • How important is it to have a plentiful of supply of competent contractors to work for the procurement system?		92.5		83.8		66.9		68.1		65.6		51.3		
5. **Ability to State Clear End user's requirements** • How capable is the client able to state the employer's requirements precisely at the tender stage?		93.8		75		87.5		95		95		56.3		
6. **Complexity** • Is the project highly specialized, technologically advanced or highly serviced?		70		55		73.1		85.6		85.6		83.1		
7. **Certainty of Cost without Fluctuation** • How important is a firm price at the beginning of construction is needed?		73.8		46.9		93.8		88.1		87.5		41.3		
8. **Flexibility for Changes** • To what extent do you expect frequent changes in design and construction once the work has begun on site?		66.3		65.6		50.6		55.6		55.6		88.1		
9. **Risk Management** • To what extent do you need risk avoidance in the event of time, cost, design liability, and quality slippage?		75.6		59.4		90		82.5		82.5		58.1		
10. **Responsibility** • To what extent do you wish a single point of responsibility for the completion of the programme, design and construction of the project?		66.9		57.5		100		93.8		89.4		58.1		
11. **Familiarity** • How important is it for the client to choose a familiar system to deliver a building project?		96.3		60.6		80.6		75.6		46.9		51.3		
Total														
Order of preference														

Figure 1: Multi-attribute Procurement Selection Model (Chan et al, 2001).

CONCLUSION

Building projects in Hong Kong have been managed mainly in the traditional way. In the last two decades, alternative procurement systems have been mainly used in the public sector in Hong Kong, such as the Architectural Service Department (ASD) and the Hospital Authority. After a close investigation of the prevailing procurement system in Hong Kong, it was found that there is not a systematic and disciplined way to aid the client in selecting the most appropriate system. Clients in the public sector mainly based their choice on previous experience; the traditional system, being the most familiar, was usually chosen. These findings vividly support the aim of this research in which the development of a systematic procurement selection model for Hong Kong is essential in order to reduce the possibility of selecting the incorrect procurement system.

The application of the Delphi method in deriving a procurement selection model was shown to be an appropriate technique. It enables a sufficient consistency to be reached in a rather subjective area. With the aid of this model, construction clients can adopt a more reliable and objective approach to select an appropriate procurement system for a construction project.

ACKNOWLEDGEMENT

The author gratefully acknowledges the Hong Kong Polytechnic University for providing funding to support this research effort.

REFERENCES

Anatharajan, T. and Anataraman, V. (1982). Development of residential areas – Delphi Technique for decision making. *International Journal for Housing Science and Its Applications*, **v.6 no.4**, 1982, 329-341.

Bennett, J and Grice, A (1990). Procurement systems for buildings. In Brandon, PS (Ed.), *Quantity Surveying Techniques: New Directions*, BSP Professional Books, Oxford.

Chan, A.P.C. & Fung, C.Y. (1996). Procurement systems in Australia, *1996 CIB Beijing International Conference*, October 21-24, 1996 Beijing, China.

Chan, A.P.C. & Lam, P. (1995). Novation contract - an innovative variation to design build, *International Congress on Construction*, Singapore, 5-6 October 1995, 197-203.

Chan, A.P.C. & Tam, C.M. (1994). Design and build through novation, *CIB W92, Procurement Systems - Symposium 1994*, Hong Kong, 4-7 December 1994, 27-36.

Chan, A.P.C. (1994). Evaluation of novation contract, *National construction and Management Conference*, Sydney, Australia, 17-18 February, 1994, 129-142.

Chan, A.P.C. (1995). Towards an expert systems on project procurement. *Journal of construction procurement*, **Volume 1, no.2**, November 1995, 124-149.

Chan, A.P.C. (1996). *Determinants of project success in the construction industry of Hong Kong*, Unpublished PhD Thesis, University of South Australia.

Chan, APC and Yung, EHK (2000). *Procurement selection model for Hong Kong*. Research Monograph. The Hong Kong Polytechnic University. ISBN 962-367-285-3. 143 pages.

Chan, APC, Yung, EHK, Lam, PTI, Tam, CM, and Cheung, SO (2001). Application of Delphi method in selection of procurement systems for construction projects, *Construction Management and Economics*, **Vol.19, No.7**, 699-718.

Chan, APC, Yung, EHK, Ma, TYF, and Lam, PTI (2001). An overview of procurement systems in Hong Kong, *Creative Systems in Structural and Construction Engineering*, Edited by Singh, A, AA Balkema, 2001, 221-225.

Corotis, R. Fox, R. and Harris, J. (1981). Delphi methods. Theory and design load application. *Journal of the Structural Division*, **v.107, no.6**. 1095-1105,1981.

Dickey, J. and Watts, T (1978). *Analytic techniques in urban and regional planning*. McGraw-Hill Book Company, New York, N.Y.

Franks, J. (1998). *Building Procurement systems, A client's guide*, 3rd edition Addison Wesley Longman Limited and the charted Institute of Building, 1998.

Goldfisher, F. (1992). Modified Delphi: a concept for new product forecasting. *Journal of Business Forecasting* (JBT), **11(4),** 10-11.

Goldstein, N. (1975). A Delphi on the Future of the Steel and Ferroalloy Industries. *The Delphi Techniques and Applications*, Addison Wesley, Reading, Mass, 1975, 210-226.

Griffith, A. (1989). *Design-build procurement and buildability*, CIOB TIS No. 112.

Linstone, H. & Turoff, M. (1975). *The Delphi method: Techniques and Applications*, Addison-Wesley, Reading, Mass., 3-12.

Love, PED, Skitmore, M. & Earl, G. (1998). Selecting a suitable procurement method for a building project. *Construction Management and Economics* **Volume 19**, 221- 233.

Masterman, J.W.E (1992). *An Introduction To Building Procurement Systems*, E& FN Spon, London. 1992.

Masterman, J.W.E. (1994). Client characteristics and needs in relation to their selection of building procurement systems, *CIB W92 East Meets West, Procurement Systems Symposium, 1994*. Hong Kong. 79-87.

Nahapiet, J.(1985). *The management of construction projects, Case studies form the USA and UK*, CIOB, 1985.

Robinson J. B.L. (1991). Delphi Technology for Economic Impact Assessment. *Journal of Transportation Engineering*, **Vol.117, No.3** May/June, 1991.

Saito, M. and Sinha, K. (1991). Delphi study on bridge condition rating and effects of improvements. *Journal of Transportation Engineering*, **v.117, no.3**, 320-334, 1991.

Skitmore, M and Marsden, DE (1988). Which procurement system? Towards a universal procurement selection technique. *Construction Management and Economics*, **6**, 71-89.

Tsoi, P.K. (1997). *Applicability of the procurement selection technique in Hong Kong -Multi-attribute approach*, Unpublished BSc Thesis, The Hong Kong Polytechnic University.

Advances in Building Technology, Volume 2
M. Anson, J.M. Ko and E.S.S. Lam (Eds.)
© 2002 Elsevier Science Ltd. All rights reserved

SUPPORT SYSTEM FOR PROJECT MANAGEMENT AND PRODUCTION OF CONCRETE PRECAST ELEMENTS

E.Dassori[1] and M.Frasani[2]

[1]Department of structural and geotechnical engineering, University of Genoa
16145 Genoa, Italy
[2] CSG Information Technology
29017 Fiorenzuola d'Arda (PC), I

ABSTRACT

The paper presents the most important information system now used by Italian producers for project management and production of concrete precast elements. It is an information system developed for the automation and integration of activities affecting the duration of the order, for the co-ordination of the commercial office, technical office, production, transport and assembly, in order to optimise the use of resources and to increase the quality both of the services and the elements manufactured. The control of the order keeps all these phases under observation verifying the efficiency of the various areas and thereby reducing the time taken for the order.

KEYWORDS

Project management, production, concrete, precast, elements.

Introduction

The Italian market of precast elements in reinforced concrete (normal and pre-compressed) is characterised by strong demand and by the high quality of the components being produced, which are: plinths, mono and multi-level pillars, beams (9-40 m), floors (different typologies for lights between 3 and 10 m), joists (floors and coverings for lights from 10 to 25 m), non-load bearing wall elements (solid, lightened and sandwich).
Regarding demand, in Italy precast elements in concrete (non-load bearing external walls and structures) cover between 70% and 95% of the production of buildings for offices, commerce and industry. For housing there is a modest use only of linear structural elements (pillars and beams) in that, for this typology, on site solutions in concrete and load bearing walls in brick blocks are preferred.
The companies producing these components operate in a technically complex and highly competitive scenario and for this reason more and more they feel the need to use advanced management instruments that allow them to increase productivity and the quality level of their performance.
With this in mind the information system that we are dealing with here was designed and, at this moment in time, is the most widely used in Italy; it has also been chosen by firms operating in other countries of the European Community. The present version of the program offers an enormous range of performances that go from support to project management and control of production and that are the fruit of more than 20 years of research and applications.

Data flow

Figure 1 describes the flow of data within the information system, which as can be seen, covers all the areas concerned in the order: the commercial office, technical office, production structures, transport and assembly.

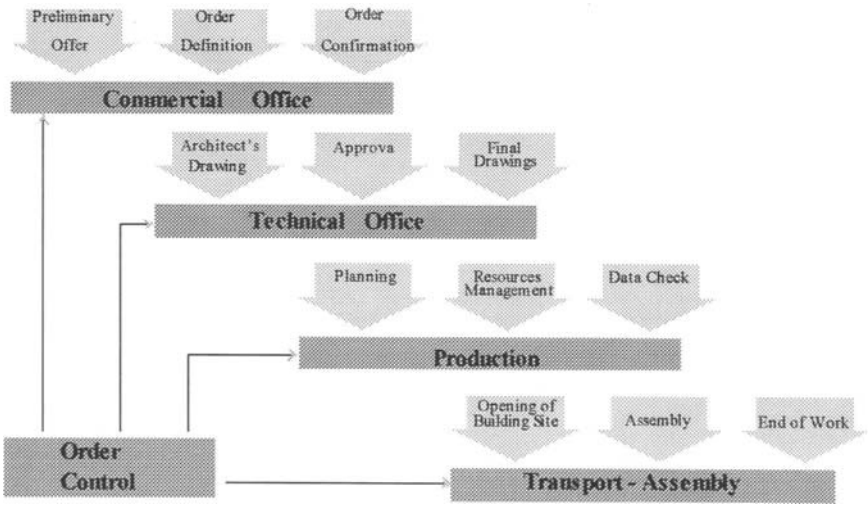


Figure 1:The flow of data in the information system

One of the most important characteristics of the system of management budgeting and control is that it does not use a price list but employs *"rules of cost"* that permit a better assessment of direct and indirect costs throughout the process. These also consider the quantity parameter, which, as a function of the repetitiveness of the same or similar items, allows optimisation of the administration of resources.
The information system sees departments as single entities structured like "small companies" that work together to reach the general objectives of the whole company. For each process planning (budget of costs and times) is therefore defined in such a way as to rapidly and globally check the expenses and the programmed/perceived deadlines.

The structure of the program

The system is based on two integrated software modules called LEGO-CAD and P2000, the first being destined to the technical functions and the second to management ones. Figure 2 shows the active functions in detail in the two programs and the way they interface.
Instead, the integrated flow of the system is shown in Figure 3, where the functions carried out by the modules are those listed in the following.

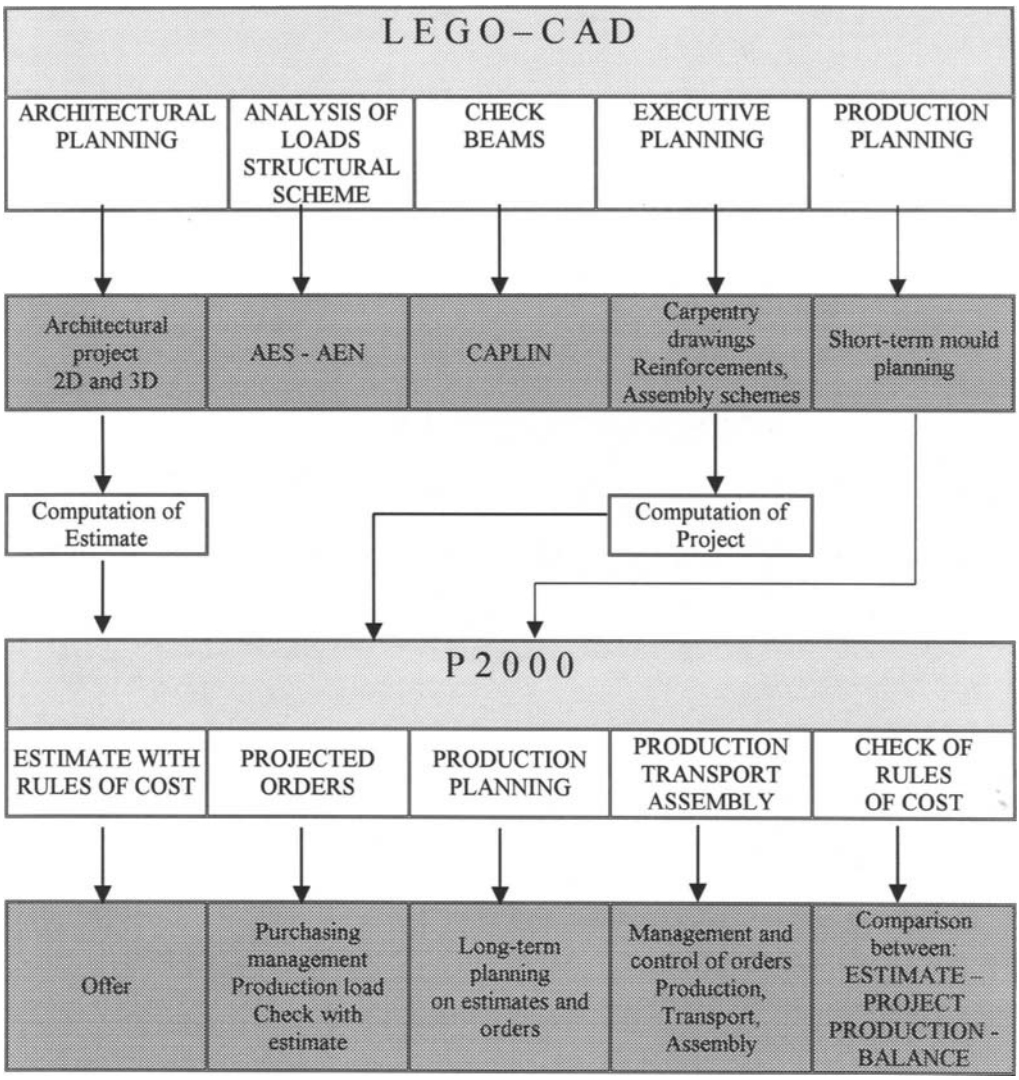


Figure 2: Integration and functions of the LEGO-CAD and P2000 modules

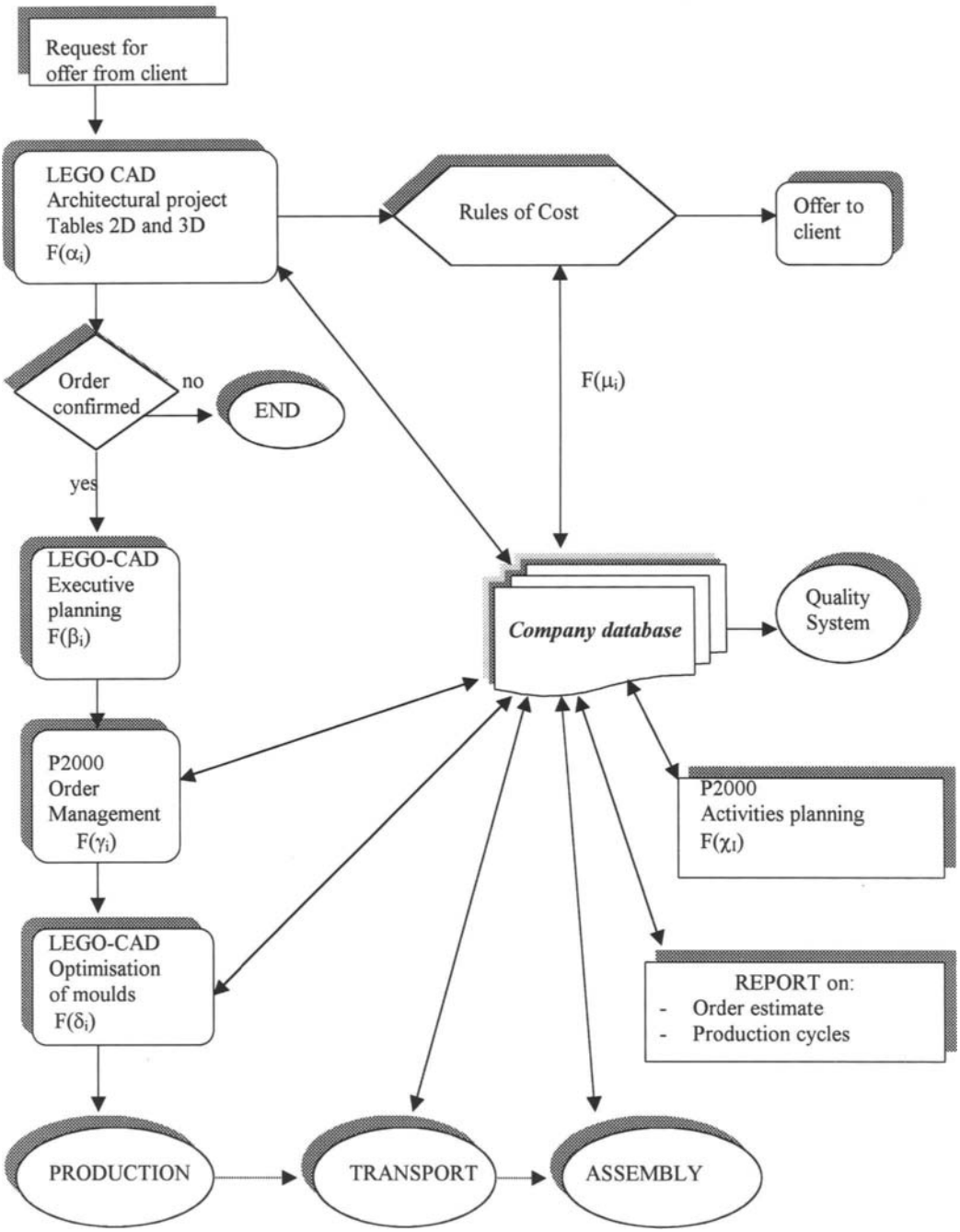


Figure 3: Integrated flow of the system

$F(\alpha_i)$ Architectural project for budget whose output is:

- Plant drawings, sections and complete prospects of automatic dimensioning
- Three-dimensional model of the structure
- Computation of the elements
- Cost analysis for each type of component
- Analysis of transport, assembly and complementary services
- Analysis of loads and static schematisation as output for generic structural solution finders (SAP,...)
- Printout of the offer

$F(\beta_i)$ Executive project whose output is:

- Definition of connections with metal inserts
- Production of the drawings for building of the moulds
- Production of the drawings for metal reinforcements
- Assembly schemes
- Summary of materials
- Computation of the designed products
- Data transfer to order management module
- Analysis of order costs and comparison with the approved estimate

$F(\gamma_i)$ Medium and long-term programming whose output is:

- General planning of production expressed in the form of a Gantt diagram.

The order is inserted in the general programming of medium and long-term production. This planning temporarily concerns the confirmed orders already designed, already confirmed orders but not yet designed and estimates in the acquisition phase.

To operate this programming and obtain the diagram, the necessary resources are defined and the order delivery priorities and those of the selected estimates are assigned.

$F(\delta_i)$ Short-term programming (10-15 working days) whose output is:

- Printout of the production plan with allocation of resources
- Visualisation of state through Gantt diagrams for every mould and for the group of orders. Graphically each order is identified with a colour, the alternation of colours shows the rhythm of work for each individual mould
- Order requests for the raw materials necessary for the production plan
- Printout of the cards for the automation of the production, transport and assembly phases
- Information for medium and long-term management control

The function aims at optimisation of the use of moulds. This phase is managed directly by the head of production. He operates virtually in a graphic environment using the executive project and the planimetrical scheme of the factory with the layout of the moulds. Simply by using the mouse, the person in charge takes the components from the executive drawings and drags them to the moulds. The program arranges to suggest the best position on the basis of the data concerning production in progress, the resources available and the general production deadlines.

$F(\chi_i)$ Activity programming whose output is:

- General programming of the activities shown by means of a Gantt diagram
- Programming and management of transport and assembly
- Information elements for the company database

The function is integrated with the optimisation module of the moulds and elaborates the data relative to daily production.

$F(\mu_i)$ Feedback

Through the structure of the company database a feedback function relative to validation of the rules of cost is active. The procedure detects real times and costs and compares them with the corresponding elements on which the rules of cost were set. Their congruence is thereby controlled in real time and

not at the end of the financial years. The comparison takes place on accurate values and not averages distributed over all the typologies in production that, in cases like these, would not be very significant. The company database supplies all the elements necessary for process controls that are guided by the company Quality System implemented according to ISO 9001/2000.
Figure 4 describes the structure of the only production, programming module:

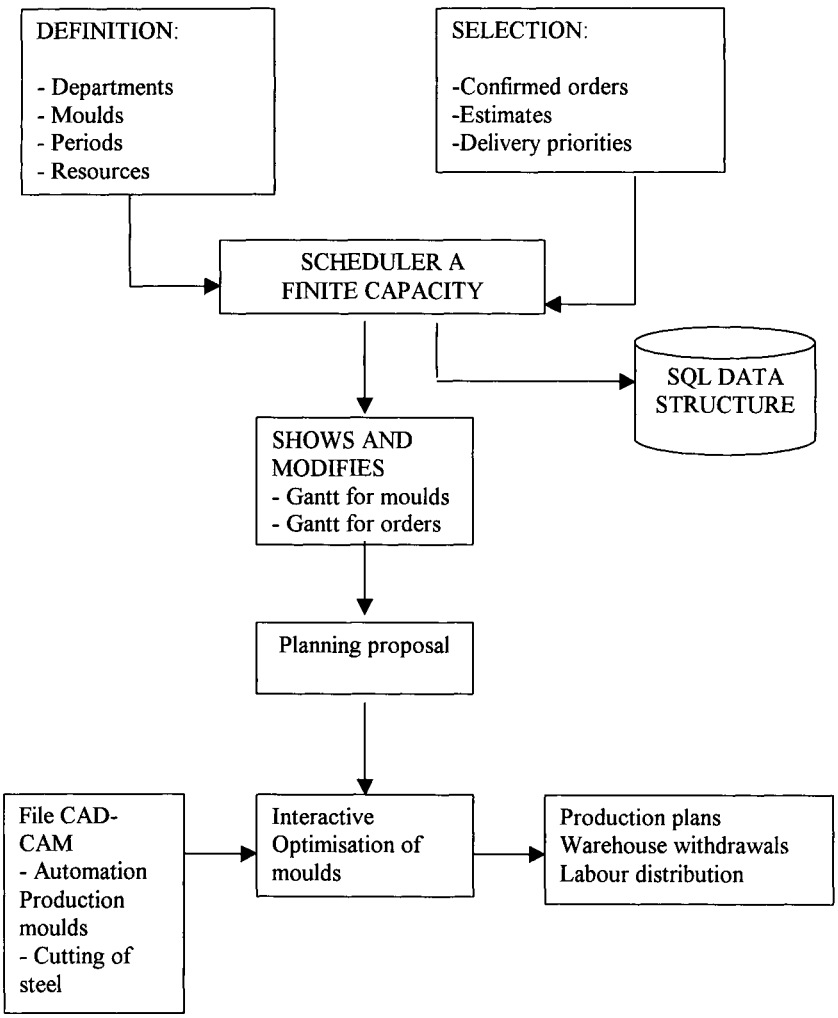


Figure 4: Structure of the production, programming module

The output of this phase is: printout of the general layout of production by date of pouring, printout of the executive forms of the products made in the same order as their positioning on the belt, printout of the summaries of concrete, inserts, polystyrene, lifting devices, printout of the reinforcement by profile and by diameter of each product in the mould, file CAD-CAM in UNITEC format to govern the robot

for the design of products and the positioning of the separators and sides, file CAD-CAM to cut the metal reinforcement bars, printout of the labels with barcode. The label with the barcode that is printed in the same order as the products are positioned on the belt. The label is in double format so that one part stays in the company while the other is automatically attached to the piece and goes with it the whole of its future life becoming the fundamental element for the traceability of the product (ISO 9001/2000).
Figures 6 and 7 show the Gantt diagram for the mould and the order Gantt.

The structure of the software

The analysis of the software starts from the complete knowledge of the problems of the sector. In practice the structure of the software envisages a database in which the different program modules are inserted. In this way the structure of the software offers total integration between the existing parts while maintaining a very high degree of elasticity compared to the needs of the users and the possibility of further developments.
Figure 4 shows the blocks that make up the structure of the software and that have the functions described in the following:

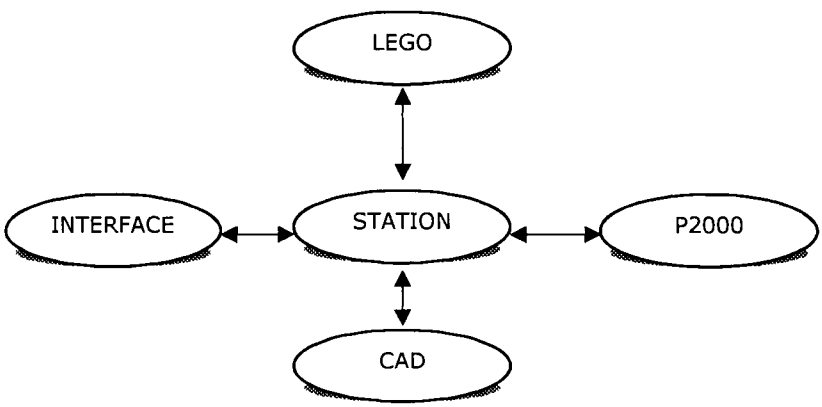


Figure 5: Structure of the software

STATION	Server of messages that makes the programs communicate with each other
LEGO	Design interface made up of different modules for architectural planning, executive planning and optimisation of moulds
INTERFACE	Manages the interface toward the user
CAD	Graphic motor
P2000	Management program

Development of these programs started with the Fortran language and HP computers. The modularity of the programs has allowed evolution over time of the different operating systems (RTE-A, DOS, UNIX, Windows from release 3.11 to present versions). The structure of the data is based on ASCII files for the graphic environment and on SQL relational database for management. These data structures envisage the archiving of any type of document produced even from other programs (Word, Excel,...).

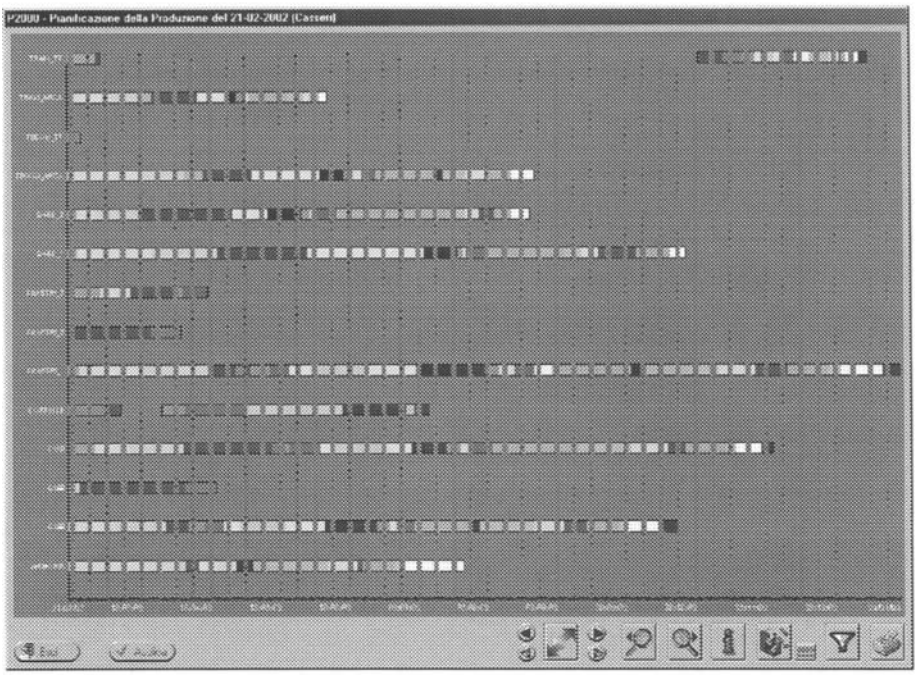
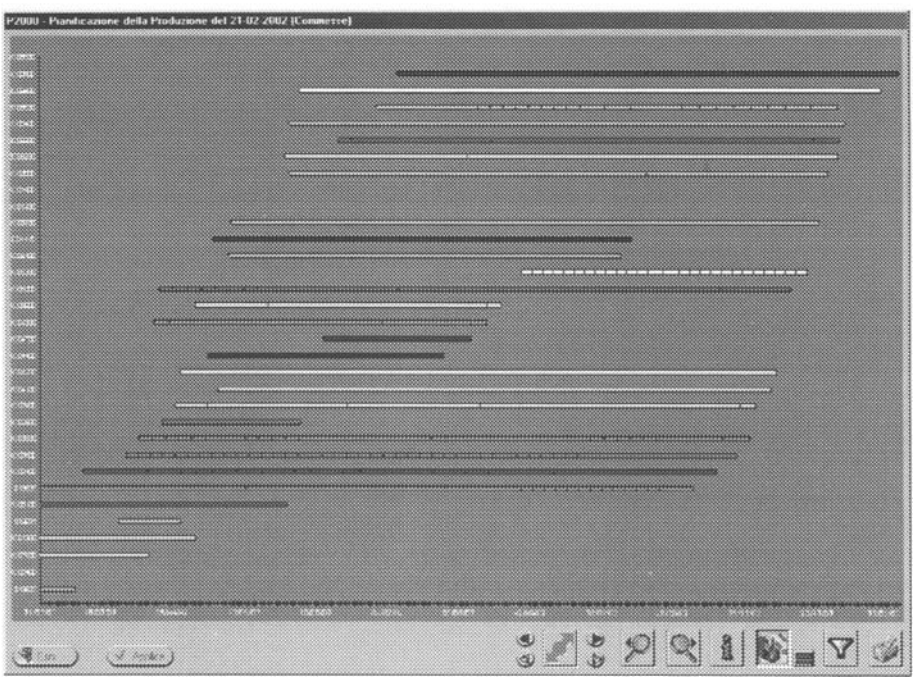


Figure 6 (above): Gantt diagram of the mould. Figure 7 (below): Order Gantt



Advances in Building Technology, Volume 2
M. Anson, J.M. Ko and E.S.S. Lam (Eds.)
© 2002 Elsevier Science Ltd. All rights reserved

A SURVEY MANAGEMENT SYSTEM FOR ADVANCED BUILDING CONSTRUCTION

Steve Y. W. Lam and Conrad H. W. Tang

Department of Land Surveying and Geo-Informatics,
The Hong Kong Polytechnic University,
Kowloon, Hong Kong SAR, China

ABSTRACT

This paper provides engineering surveyors with a practical and concise explanation of the concepts and techniques needed for managing the scope, project organization, quality, costs, time and risks in advanced building construction in Hong Kong and other parts of the world. It reviews briefly some of the key management concepts governing the survey operations, and describes how to apply the theory into practice in accordance with the ISO 9001:2000 standard.

KEYWORDS

Advanced building construction, engineering surveys, project-based survey management system, total quality management system, ISO 9001:2000.

INTRODUCTION

In the past decade, the authors observed four revolutionary changes in advanced building construction. Firstly, construction organizations manage construction teams on project basis as the more efficient way to accomplish their goals and strategies. Secondly, the adoption of total quality management (TQM) system under ISO 9001:2000 to deal with organizational and technical problems has been proved successful in managerial processes. Thirdly, the demand for high accuracy standards in engineering surveying is highlighted by the increasing adoption of precast and prefabricated components for modern building structures, and the setting-out of computerized construction machines being used in building projects. Fourthly, the integration of application software, 3D modeling and simulation, multimedia systems and robotics technologies are becoming technically and economically feasible in engineering survey operations and building construction.

Engineering survey operations required of building construction projects are given in Figure 1. In the projects, engineering surveyors are responsible for geodetic control surveys, detail mapping for alignment design and geometric modeling of building design, setting-out of the new structures, and deformation monitoring of buildings and ground displacements. They are the front line workers particularly in setting-out the precise geometric models of structures during construction. In fact, survey operations are required from start to finish in building projects.

To cope with rapid advancement of construction technology and managerial processes associated with the survey operations in advanced building construction, six functions of a project-based survey management system are briefly described in this paper. These management functions are managing the scope, project organization, quality, costs, time and risks (Turner 1999).

Early in Year 2001, ISO 9001:2000 officially replaced ISO 9001:1994, ISO 9002:1994 and ISO 9003:1994, and asserted the role of the well-known standard as a quality management model, in stead of, as a quality assurance model of the previous version. ISO 9001:2000 adopts the principles of TQM, and requires a construction organization to demonstrate ability in fulfilling four main aspects and eight principles of the quality management.

The four aspects of the TQM emphasized by ISO 9001:2000 are:
1. management commitment,
2. process-based approach,
3. customer service, and
4. continuous improvement.

The eight principles specified by ISO 9000:2000 are:
1. customer focus,
2. leadership,
3. involvement of people,
4. process approach,
5. system approach to management,
6. continual improvement,
7. factual approach to decision making, and
8. mutually beneficial supplier relationship.

Quality control elements of the TQM system under ISO 9001:2000 are given in Table 1. Details of implementing some of the quality control elements for managing engineering surveys in building construction are discussed in the following sections.

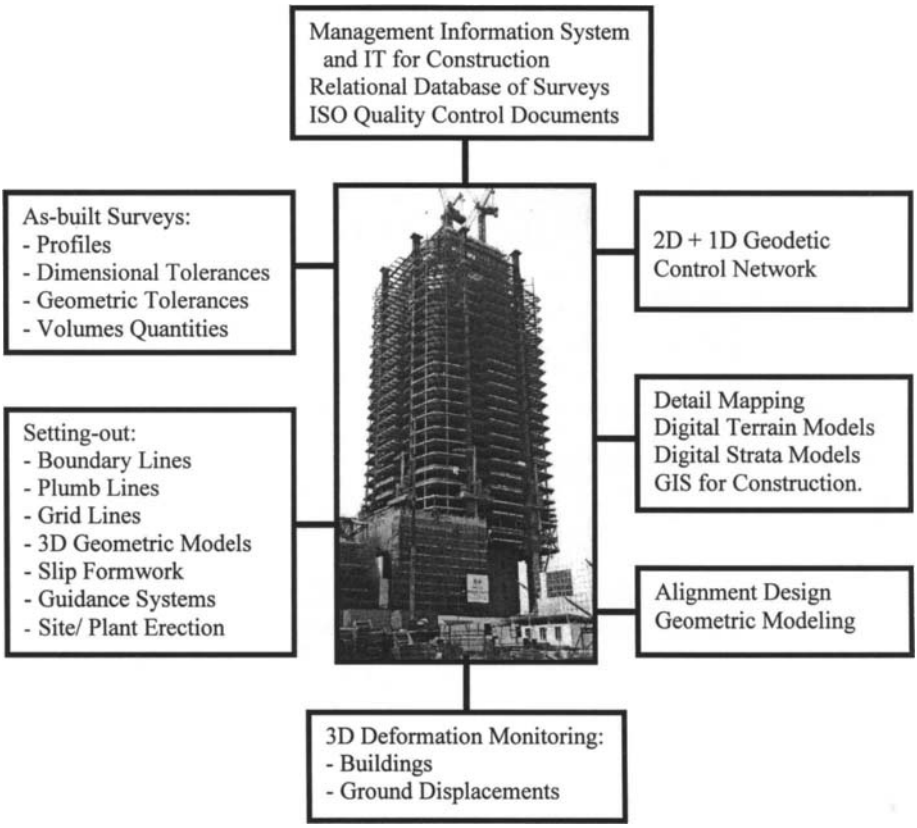


Figure 1: Engineering Survey Operations in Building Construction Projects

TABLE 1
QUALITY CONTROL ELEMENTS OF ISO 9001:2000 (ISO 9001:2000, Table B.2)

Item	Quality Control Elements
1	Scope 1.1 General 1.2 Application
2	Normative reference
3	Terms and definitions
4	Quality management system 4.1 General requirements 4.2 Documentation requirements
5	Management responsibility 5.1 Management commitment 5.2 Customer focus 5.3 Quality policy 5.4 Planning 5.5 Responsibility, authority and communication 5.6 Management review
6	Resource management 6.1 Provision of resources 6.2 Human resources 6.3 Infrastructure 6.4 Work environment
7	Product Realization 7.1 Planning of product realization 7.2 Customer-related processes 7.3 Design and development 7.4 Purchasing 7.5 Production and service provision 7.6 Control of monitoring and measuring devices
8	Measurement, analysis and improvement 8.1 General 8.2 Monitoring and measurement 8.3 Control of non-conforming product 8.4 Analysis of data 8.5 Improvement

MANAGING THE SCOPE AND PROJECT ORGANIZATION

Scope management is defined as the function of ensuring that enough, but only enough, work is undertaken to deliver the project's purpose successfully (Turner 1999). In the process of scope management, project requirements and organizational objectives are converted into statements of work to produce the expected benefits (ISO 9001:2000, Item 7.1). These scope statements must be published in the quality control documents of the organization (ISO 9001:2000, Item 4.2). The quality control documents include quality manuals, quality procedure manuals, department/section manuals, operation/work instruction manuals and quality control records (Lam and Tang 2000).

As different projects may have different contract requirements and customer expectation, project quality plans (PQP) and survey quality plans (SQP) are published to supplement the scope documents. In practice, a project engineering surveyor is responsible to design and establish SQP, and to integrate them into the overall milestone plan of the project. In building construction, a milestone is an event that marks the completion of a group of related tasks or the completion of a phase of the project. Three columns are usually found on a milestone plan form (MPF) having the planned dates on the first column, the milestone schedule and networks (e.g. flowcharts, bar charts, CPM charts and PERT charts) on the second column and the detailed description of the milestone on the third column. It is easy to create MPFs and modify a set of milestones for the survey tasks on personal computer systems by using Primavera Project Planner®, Microsoft Project® or other construction management software adopted by the project organization.

In managing a project survey team, an engineering surveyor has to control human, material and financial resources provided by the human resources department of the organization. Under ISO 9001:2000, it is the responsibility of an engineering surveyor to establish responsibility charts for each project to define:

1. the organizational structure of the survey team;
2. all necessary human resources policies and procedures to enable the survey organization to achieve its objectives; and
3. the job description and responsibilities of named survey workers and subcontractors to achieve a particular milestone.

Survey responsibility charts are then integrated into an overall responsibility chart of the project organization to expedite human resources management and achieve business objectives.

MANAGING THE QUALITY

To achieve high quality and profit on the survey operations, survey services must be completed on time, within budget, and meet the customer's requirements with satisfaction (ISO 9001:2000, Items 5, 7.1 and 7.2). All the positional, dimensional and geometric tolerances of survey measurements must be acceptable with respect to accuracy standards which are specified in the contract documents of the project. In building construction, contract

documents include government building standards and regulations, construction drawings and suppliers' specifications.

It is required that field notes and survey data of quality practices must be kept in traceable records. It is the responsibility of an engineering surveyor to ensure that all survey documents are properly labeled and addressed in files or computer systems so that the records are retrievable easily to meet particular demand or purpose, and that wrong use and loss of important data can be avoided. Use of relational database software, management information system for construction (MISC), E-commerce networks and computer systems are recommended for the document control process.

During the project period, survey staffs are responsible for ensuring that inspection work is carried out according to management procedures, approved method statements, inspection and testing plans, work instructions and other procedure manuals. All measuring and test equipment must be controlled, calibrated and well maintained (ISO 9001:2000, Item 7.6). This is to ensure that all survey measurements are consistent with the accuracy standards. It should be noted that test certificates and calibration of all survey instruments must be traceable to national or international standards, and in accordance with documented procedures.

In order to assure quality of survey services in the long run and to keep pace with rapid advancement of surveying technology we are experiencing in building construction, continuous improvement and life-long learning attitude of survey employees are needed. Therefore, training should be provided to ensure workers to capably accomplish the tasks correctly and productively. The survey of Dulaimi and Beckingsale (2001) on construction workers indicates that, under the Investors in People (IiP) Standard of the United Kingdom, employees are motivated by keeping their quality and skill level in line with the business objectives through long-term staff development. Under (ISO 9001:2000, Item 6.2), it is not enough for the company to provide training to its survey employees; the company has to evaluate whether the training produces competent people for the job.

A quality system for managing the survey operations should be reviewed at regular intervals by internal auditors of the project (ISO 9001:2000, Item 8). Any deficiency or non-conformance found in the audit should be recorded and brought to the person who is responsible for the problem to carry out corrective action with preventive measures for future operations (ISO 9001:2000, Item 8.3). Guidelines for performance improvements and establishing effective rewarding system are given in ISO 9004:2000.

MANAGING THE COSTS, TIME AND RISKS

During the life cycle of a building construction project, an engineering surveyor is often involved in cost planning and cost control processes. Cost planning is implemented during the feasibility study and design stage of a project, and it involves a breakdown of proposed total expenditure into allowances to be made for various cost targets of the project. Cost control is one of the most vital management functions that takes place throughout complete duration of a project. It is a systematic recording of costs incurred in the construction and their critical comparison among the planned cost of the scheduled work, the planned cost of the completed

work and the actual cost of the completed work by plotting them against duration on S-curves. A comparison of the planned cost of the completed work with the original estimates helps to control elapsed time (Turner 1999).

In a modern integrated cost-engineering system (e.g. Primavera Expedition®), standard cost codes and project cost codes are used to referencing and documenting items such as labor, materials, pants and equipment, subcontracts, procurement items, accounting items and human resources items to facilitate cost estimation, tendering and construction of the project. The database of the system enables surveyors and other members of the construction team to monitor project costs at any stage and time schedule of the project.

Turner (1999) lists the five steps of risk management as to:
1. identify the sources of risk;
2. determine impact of individual risks including its potential consequence or damage;
3. assess overall impact of risks;
4. determine how the risk can be reduced by avoidance, deflection and contingency plans; and
5. control the identified risk items by monitoring their potential consequence and risk resolution progress.

By experience, contingency approach to survey management is always emphasized in building projects because most of the projects have to be completed within tight budgets and short periods of time. Three types of contingency encountered are money (allowance in budget), time (allowance in schedule) and performance/ quality (allowable tolerances). Surveyors should develop a set of backup plans (contingency plans) which will be used when the original plan can not be implemented or when a crisis happens. Further management applications on identifying project risks, risk analysis techniques and overcome factors of risks in building construction are found in, for instances, (Salzmann and Mohamed 1999) and (Toakley 1995).

CONCLUSION

This paper describes briefly the methods and applications for managing the scope, project organization, quality, costs, time and risks associated with engineering survey operations under ISO 9000:2000 in building construction projects. Undoubtedly, the adoption of ISO 9000:2000 and the TQM system in surveying, construction and other industrial sectors will continue to grow. Whoever is able to supply better quality products at lower cost will capture more local and global market share. And TQM is a very necessary tool in pursuit such excellence and profitability in both the surveying and construction industry.

REFERENCES

Dulaimi M. and Beckingsale T. (2001). Adopting Investors in People (IiP) Standard and its Potential Impact on Motivation. *Asia Pacific Building and Construction Management Journal.* **6**, 37-43.

ISO 9000: 2000 Quality Management Systems – Fundamentals and vocabulary. International Organization for Standardization.

ISO 9001: 2000 Quality Management Systems – Requirements. International Organization for Standardization.

ISO 9004: 2000 Quality Management Systems – Guidelines for performance improvements. International Organization for Standardization.

Lam S. and Tang C. (2000). Responsibilities of Engineering Surveyors under ISO 9000 Certification in Hong Kong Construction Industry. *Journal of Geospatial Engineering.* **2:1**, 67-78.

Salzmann A. and Mohamed S. (1999). Risk Identification and Interaction in International BOOT Projects. *The Australian Institute of Building Paper.* **9,** 101-114.

Toakley A. (1995). Risk Analysis Techniques. *The Australian Institute of Building Paper.* **6,** 69-75.

Toakley A. (1995). Risk Management Applications – A Review. *The Australian Institute of Building Paper.* **6,** 77-87.

Turner R. (1999). *The Handbook of Project-based Management.* McGraw-Hill, London.

Advances in Building Technology, Volume 2
M. Anson, J.M. Ko and E.S.S. Lam (Eds.)
© 2002 Elsevier Science Ltd. All rights reserved

CHARACTERIZE CONCRETE DEMAND IN BORED-PILE CONSTRUCTION THROUGH SIMULATION

Ming Lu[1] and K.C. Ying[2]

[1]Asst. Prof., Dept. of Civ. & Struct. Engrg, Hong Kong Polytechnic University, Hong Hom, Hong Kong
[2]Res. Asst., Dept. of Civ. & Struct. Engrg, Hong Kong Polytechnic University, Hong Hom, Hong Kong

ABSTRACT

The in-situ concreting process involves both the site contractor and the readymixed concrete supplier. In practice, an inevitably imperfect concrete supply, causing interrupted site operations, often lowers the site productivity. Meanwhile, an oversupply of truckmixers by the concrete supplier to guarantee continuous site operations is not a solution since excessive queuing of concrete truckmixers on site not only results in underutilized resources but also increases the chances of concrete being unfresh. As found out from previous studies, the complexities and uncertainties involved in the concreting operations on site make it difficult for the site to accurately convey the temporal demand of concrete to the concrete supplier in advance, which, in turn, contributes to lack of coordination between the plant and the site.

The objective of this research is to characterize the concrete demand on a bored-pile construction site by simulating the entire concreting operations on an ongoing railway station project in Hong Kong. The well-known CYCLONE technology is used to illustrate the processes and the interaction of resources that define the method of concreting a bored pile. Further, the same bored-piling operations are modeled using a newly developed Simplified Discrete-Event Simulation Approach (SDESA) in order to precisely characterize the concrete demand. A comparison of the CYCLONE model and the SDESA model demonstrates the simplicity and effectiveness of SDESA in modeling complex construction systems. A comparison of the actual supply pattern, which is obtained from site QA records, against the SDESA-characterized demand pattern, has justified the frequent queuing of truckmixers as observed on the site. The outcome of the research will be of immediate help for local concrete plants to match the supply to bored-pile concreting sites and for local contractors to plan bored-pile construction activities.

KEYWORDS

Operations simulation, readymixed concrete, bored pile construction, CYCLONE, SDESA

INTRODUCTION

The heavy demand for ready mix concrete (RMC) in Hong Kong is among the most intensive in the world with an output of the order of 1.5 m3 per capita per annum for the existing population of 7 million when construction activity is at high levels. Thus, enhancing the operational efficiency, resource utilization and delivery service of Hong Kong's concreting industry is important to the improvement of productivity and competitiveness of the entire construction industry. Meanwhile, the in-situ concreting process involves both the site contractor and the readymixed concrete supplier. In practice, an inevitably imperfect concrete supply, causing interrupted site operations, often lowers the site productivity. On the other hand, an oversupply of truckmixers by the concrete supplier to guarantee continuous site operations is not a solution since excessive queuing of concrete truckmixers on site not only results in underutilized resources but also increases the chances of concrete being unfresh.

To provide local concrete producers with a simulation-based decision-support tool for the resource provision planning and the production planning of a RMC plant, so as to meet given demands at a number of sites for concrete over a working day, a computer platform for simulation modeling and analysis of Hong Kong's one-plant-multi-site RMC production system, called HKCONSIM, has been developed in-house based on the latest construction simulation research outcome, and validated by real-life operations data in Hong Kong (Lu et al, 2002). Demand at each site is expressed by quantity and timing. The emphasis of the simulation modeling is on the interactions of multiple sites with the plant, and the objective is to improve the supply service levels and the utilization of truckmixer resources. One significant improvement achieved via the research is that to simulate the RMC production operations with HKCONSIM does not require familiarity by the user with any software-specific terminology and modeling schematics, in contrast with existing commercial simulation packages. The process of constructing a simulation model is reduced to specifying the details for each pour and each site and allocating the plant and truckmixer resources available on self-explanatory on-screen forms. HKCONSIM produces quantitative performance measures of system operational efficiency and delivery service level as outputs for evaluating the simulated scenarios, and thereby, helping to optimize the simulated system in terms of pouring schedules on each site and resource provisions. Therefore, by experimenting on a HKCONSIM produced model the user, being a practitioner in the concreting industry, can readily study complicated relationships between the pattern of demand for concrete, the plant and truckmixer resources available to the system, and both the service levels achieved on sites and the utilization levels achieved for the resources involved.

By using HKCONSIM on an experimental, but realistic basis a local concrete producer helped validate the potential benefits that HKCONSIM can bring about to readymixed concrete producers in terms of enhancing efficiency, resource utilization, and the delivery service level. Nevertheless, one major barrier, which has been encountered in both the real system and the simulated one, has prevented the further optimization of the system performance: in general, the site could not clearly specify to the concrete supplier the temporal demand of concrete in terms of truckmixer arrival times due to the complexities and uncertainties involved in the concreting operations on site. For example, as normally practiced, on the day prior to the pour the site would only inform the plant on the first truckmixer arrival time (i.e. when the pour commences) and the average inter-arrival time of succeeding truckmixers (i.e. an approximate straight-line relationship between the time and the truckmixer arrivals). The temporal demand of concrete for keeping continuous site operations is actually highly non-linear depending on a number of uncertain or dynamic factors related to the concrete placing methods and site specific conditions, thus rendering it difficult to be predicted in

an accurate and quantitative way. Even the approximation of the linear relationship has so far relied on the knowledge, judgment, and intuition of experienced site personnel.

The objective of this research is to characterize the temporal demand of concrete on a bored-pile construction site by simulating the entire concreting operations on an ongoing railway station extension project in Hong Kong. The well-known CYCLONE technology is used to illustrate the construction processes and the interaction of various resources in concreting a bored pile. Further, a newly developed Simplified Discrete-Event Simulation Approach (SDESA) has been implemented to model the bored-pile processes aimed at predicting the arrival times of truckmixers to ensure continuous concrete supply and undisturbed site operations. The remaining sections first brief on the simulation methodology, followed by an elaboration on the variables of the simulation models including some physical properties of the pile and the technical specifications on the construction method. A comparison of the CYCLONE model and the SDESA model is made to demonstrate the simplicity and effectiveness of SDESA in modeling complex construction systems. A comparison of the actual supply pattern, which is obtained from site QA records, against the SDESA-characterized demand pattern, is also made to justify the frequent queuing of truckmixers as observed on the site. Finally, a conclusion is given for the research.

CONSTRUCTION OPERATIONS SIMULATION

Construction planning is the most crucial, knowledge-intensive, ill-structured, and challenging phase in the project development cycle due to the complicated, interactive, and dynamic nature of construction processes. The methodology of discrete-event simulation, which concerns "the modeling of a system as it evolves over time by a representation in which the state variables change only at a countable number of points in time" (Law and Kelton, 1982), provides a promising alternative solution to construction planning by predicting the future state of a real construction system following creation of a computer model of the real system based on real life statistics and operations. Ever since the inception of CYCLONE technology (Halpin, 1977), simulation models for typical construction systems have been delivered as electronic realistic prototypes for engineers to experiment on, eventually leading to productive, efficient and economical field operations. Nonetheless, operations simulation has lagged spreadsheets, databases, scheduling packages, and other types of software in acceptance and implementation in the construction industry because of the complexities and time requirements involved in constructing a model (Paulson, 1995).

The latest research endeavor on construction simulation has been driven to make simulation methods easier to users. Shi (1999) adapted the activity-based simulation approach to a construction simulation model with one single "activity" element. Hajjar and AbouRizk (2000) developed application frameworks that encapsulate reusable codes as well as common design patterns for a specific class of applications in order to expedite and simplify the development of special-purpose construction simulation tools. As a new attempt Lu (2001) proposed a simplified discrete-event simulation approach (SDESA). Compared with the existing event-based and activity-based approaches, SDESA has significantly streamlined the queuing structures and resources management in simulation by (1) reducing the queuing structures at individual activities into one single dynamic queue of flow entities for the whole simulation model; and (2) distinguishing disposable resource entities from reusable ones and managing all types of resources utilized in the simulation model with a dynamic queue of resource entities (Lu, 2001). A prototype of SDESA has been coded into a computer system using Microsoft Access, which is a relational database system with supporting VB macro programs. SDESA has been applied to model the one-plant-multi-site readymixed concrete supply system in Hong Kong (Lu et al, 2001), a granular base-course construction system featuring both cyclic and linear processes and an asphalt paving construction system with complicated technological/logical constraints (Lu, 2002). This paper reports a new case of applying SDESA to a

bore piling construction project in Hong Kong. In addition, the SDESA-based model is compared with the CYCLONE-based model for demonstrating the simplicity and usefulness of SDESA in complex construction planning.

BORED-PILE CONCRETING METHOD

Bored-pile construction using readymixed concrete supplied by a remote plant is the common piling construction practice in Hong Kong. The entire bored-pile construction method consists of (1) site formation (pre-drilling), (2) excavation (grabbing & chiseling), (3) Concreting, (4) testing and (5) finishing. The main contractor generally sublets the work packages to different specialty sub-contractors without overlapping them; hence, each may be treated as an independent process. The simulation of the complete bored-pile concreting process is based on the ongoing Sha Tin railway station extension project, as part of the Hong Kong's Kowloon-Cantoon Railway Corporation (KCRC) East Rail Extension Project, with over 200 piles to be constructed. Data for simulation modeling were collected through site investigation from September to November in 2001. Experienced site engineers were interviewed to elicit useful information on the construction method for building simulation models. The major variables for the bored-pile concreting simulation model are the length of the pile, which ranges from 30 to 60 meters dependent on the underground soil conditions and the diameter of the pile, which ranges from 1m to 3m depending on the loading capacity of the pile. In this paper, the simulation models are set up for concreting a pile of 50 meters long and 2 meters in diameter, which can be readily adapted to piles of any length and diameter in a more general sense. 7 m^3 truckmixers are used to carry concrete from the plant to the site, with each truckmixer delivery to raise the bottom level of the pile by about 2 m (i.e. $h = \frac{7}{\pi(1)^2}$) where 10% concrete loss is acceptable by the specification. Theoretically, the bottom level of the pile rises by 10 meters with the completion of placing five truckloads of concrete, at which time the temporary steel casing is lifted and truncated.

Each pile should be concreted as soon as practicable after obtaining the permission of the A/E engineer. By technical specifications, the entire process of concreting a pile should be conducted within a day and without interruptions. Resources utilized in concreting a bored pile include (1) truckmixers delivering concrete from the concrete plant to the site; (2) temporary steel casing bolted up with uniform sections, each being 2m in diameter and 6m in length; (3) one mobile crane controlled by one operative; (3) one hopper (7 m^3); (4) one oscillator to raise temporary casing; (5) termie pipe for directing concrete to the bottom of pile; (6) one Q/A inspector; (7) concreting crew of four to five workers; and (8) a general worker to help concreting.

The process starts once the first truckmixer arrives on the site. Following the concrete quality checking by the Q/A inspector, the truckmixer moves into the unloading position. When the hopper, the crane and a general worker are ready, the truckmixer unloads concrete into the hopper; the volume capacity of the truckmixer and the hopper is usually 7 m^3. After unloading concrete and washing out, the truckmixer leaves the site for the concrete plant. On the other hand, the crane lifts up the hopper and moves to the bored pile position for the working crew to pour concrete into the pile through the tremie pipe, which prevents the segregation of concrete due to the free fall effect. Next, the crane moves the empty hopper back to the truckmixer unloading position, and the above hopper-concreting cycle is repeated. In addition, one temporary casing section would be lifted up and truncated after five hopper-concreting cycles for constructing a 2m-diameter pile. When cutting the temporary steel casing, the crane is preempted from hooking up the hopper so as to hold straight the casing section being severed. The crew, usually made up of five skilled workers, unscrews the casing joints once the tremie pipe is temporarily removed and the casing has been withdrawn by the

oscillator. After releasing the casing section in a storage area, the crane hooks up the hopper again for a new hopper-concreting cycle. In constructing a 50m long bored pile, 5 cut-casing cycles and 25 hopper-concreting cycles are to be repeated.

CYCLONE MODEL VS SDESA MODEL

The CYCLONE model for the bored-pile concreting process as described is shown in Fig. 1. Note that the distributions of activities' duration as simulation input models are fitted using site-recorded data.

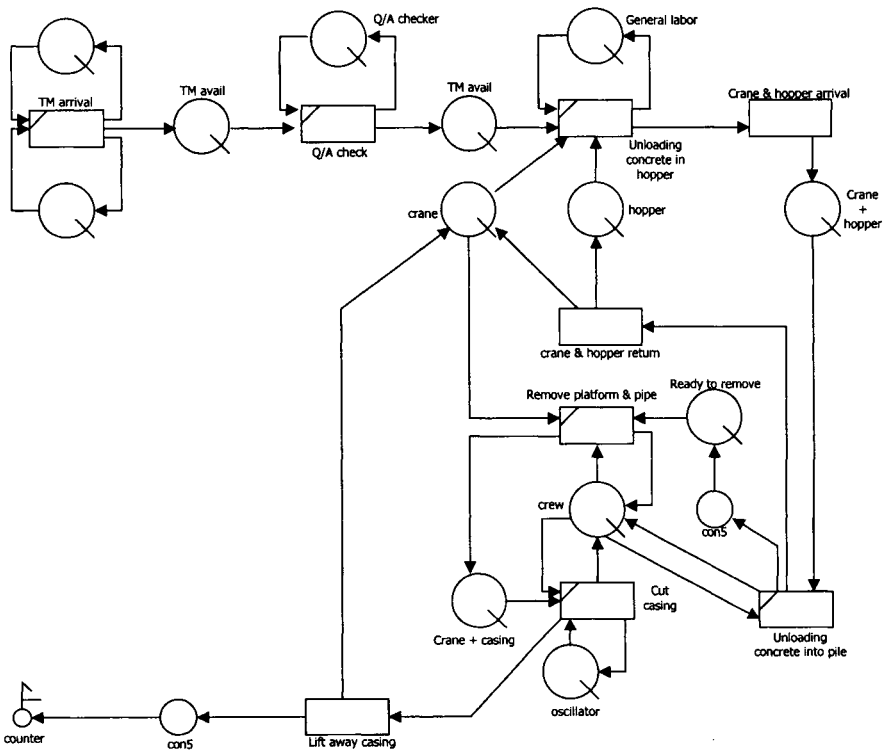


Figure 1. CYCLONE model for bored-pile concreting operations

In Figure 1, truckmixers are inserted into the system at the head of the model according to the supply pattern that is actually observed on site. The concrete supply was observed to be more than adequate in keeping continuous concreting operations on site, with truckmixers waiting to be unloaded most of the time. The mobile crane is used on three COMBI activities, i.e. "Remove platform & pipe" for cutting the steel casing, "Unloading concrete into hopper", and "Unloading concrete into pile". The crew resource (i.e. the "Crew" QUEUE) is shared by three COMBI activities, i.e. "Remove platform & pipe", "Unloading concrete into pile", and "Cut casing". One function node (CON5 after COMBI "Unloading concrete into pile") is used to control the initiation of withdrawing and cutting the casing, and another one (CON5 after NORMAL "Lift away casing") to control the completion of the bored-pile concreting.

For comparison, the counterpart SDESA model has also been constructed as illustrated in Fig. 2, which contains three production lines, the top line corresponding to the hopper-concreting cycle, the middle line for the cut-casing cycle, and the bottom line simply for controlling the completing of the whole process. In Fig. 2, the flow entities to be processed by each production line are marked with dashed diamonds, the resource entities requested by one activity are marked down at the left top corner of each activity block, with the resource entities released by one activity at the right top corner, and the disposable resource entities generated by one activity at the right bottom corner highlighted with quotation marks and dashed rectangles. Note that various production lines or cycles are logically connected with the disposable resources entities representing intermediate products or command units that are produced at the end of certain activities and can be used for once only.

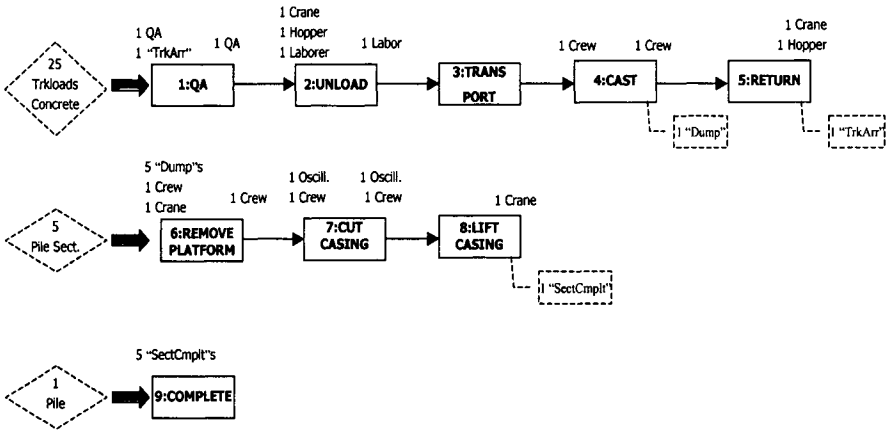


Figure 2. SDESA model for bored-pile concreting operations

The SDESA model is preferred over the CYCLONE model for two reasons: (1) simulating with SDESA does not require familiarity by the user with any software-specific terminology and modeling schematics as with CYCLONE; the process of building a SDESA model for complex construction operations is as simple as the CPM planning, thus allowing fast development of complicated models by common practitioners, which is in particular of significance to construction planning. (2) User outputs can be easily customized by running Access queries on simulation data, as the prototype of SDESA has been coded into a computer system using Microsoft Access, which is a relational database system with supporting VB macro programs. The finish times of the resources for concreting a 50-meter long bored pile are around 570 minutes after running the SDESA model on a PIII 850 PC, which takes only 15 seconds computer time. This fits closely with the 9-10 working hours for actual site operations. Next, the SDESA-characterized temporal demand of concrete are presented and discussed in detail.

SIMULATED DEMAND PATTERN VS ACTUAL SUPPLY PATTERN

Table 1 shows the temporal demand of concrete that has been characterized by running the SDESA model for three independent times. The start times of unloading concrete into the hopper for the 25 truckmixers are given under the "StartUnload" columns, i.e. minutes after the start of site operations. The interval of truckmixer arrivals based on the "StartUnload" times is calculated under the "InterArr" columns. The slight variability of outputs from run to run is caused by the

indeterministic activity duration. The cross-column average can be used for the plant to dispatch truckmixers to site to ensure uninterrupted site operations.

TABLE 1.
TEMPORAL DEMAND OF CONCRETE CHARACTERIZED THROUGH SDESA SIMULATION

Trkmixer	Run 1		Run 2		Run 3		Avg.	
ID	StartUnload	InterArr	StartUnload	InterArr	StartUnload	InterArr	StartUnload	InterArr
1	5.3		3.8		4.0		4.4	
2	20.2	14.9	19.7	15.8	18.7	14.8	19.5	15.2
3	33.6	13.4	32.7	13.0	36.0	17.3	34.1	14.6
4	46.7	13.1	47.5	14.9	51.2	15.2	48.5	14.4
5	63.7	17.0	63.4	15.9	66.8	15.6	64.7	16.2
6	118.5	54.8	117.5	54.1	116.7	49.8	117.6	52.9
7	136.7	18.2	133.3	15.7	132.3	15.7	134.1	16.6
8	148.7	12.0	148.3	15.0	149.6	17.2	148.9	14.8
9	163.2	14.5	163.6	15.3	166.3	16.7	164.4	15.5
10	178.5	15.3	178.0	14.4	181.3	15.0	179.3	14.9
11	226.6	48.1	228.4	50.3	231.9	50.6	229.0	49.7
12	243.1	16.5	243.1	14.8	248.2	16.3	244.8	15.8
13	258.1	15.1	259.7	16.6	264.7	16.5	260.8	16.0
14	275.2	17.0	275.6	15.9	278.6	13.9	276.5	15.6
15	290.0	14.9	289.6	14.0	296.1	17.5	291.9	15.5
16	340.8	50.7	341.8	52.3	344.6	48.6	342.4	50.5
17	355.9	15.1	356.8	15.0	359.4	14.8	357.4	15.0
18	371.7	15.8	370.8	13.9	374.2	14.7	372.2	14.8
19	388.0	16.3	386.4	15.6	389.8	15.6	388.0	15.8
20	406.4	18.4	400.5	14.1	404.8	15.0	403.9	15.8
21	458.4	52.0	448.9	48.4	459.0	54.2	455.4	51.5
22	472.3	13.8	462.7	13.8	475.1	16.1	470.0	14.6
23	486.1	13.8	476.8	14.2	488.7	13.6	483.9	13.9
24	499.7	13.6	492.1	15.2	505.9	17.2	499.2	15.3
25	514.7	15.0	505.2	13.1	520.8	14.9	513.5	14.3

It is noted that the inter-arrival time is about 50 minutes every five-truckmixer deliveries, because the hopper-concreting cycle is halted due to the crane being occupied in cutting the casing. Hence, SDESA simulation model is capable of handling the subtle and dynamic resource interactions in piling operations and accounting for such effects in the concrete demand characterized.

Fig. 3 shows the histogram of the actual truckmixer inter-arrival times, which are calculated from the arrival times on site for 125 truckmixer deliveries logged in the site Q/A records. The inter-arrival time ranges from 3 to 10 minutes with the mode around 7 minutes. Obviously, the concrete plant has treated the piling site being studied as a highly important customer by committing significant truckmixer resources to ensure undisturbed site operations. However, the plant must pay a high price to deliver such outstanding service in that truckmixers often queue up on site before unloading, which is deemed as waste of plant resources. In a one-plant-multi-site setting, the level of service to other site clients may be compromised because of truckmixers being held up on this site. In addition, excessive queuing may also end up with unfresh concrete that is not suitable for use. Therefore, the demand of readymixed concrete in concreting a bored pile characterized through simulation experiments will be immediately of help to local concrete plants for matching the supply to site requirements and optimizing resource utilization.

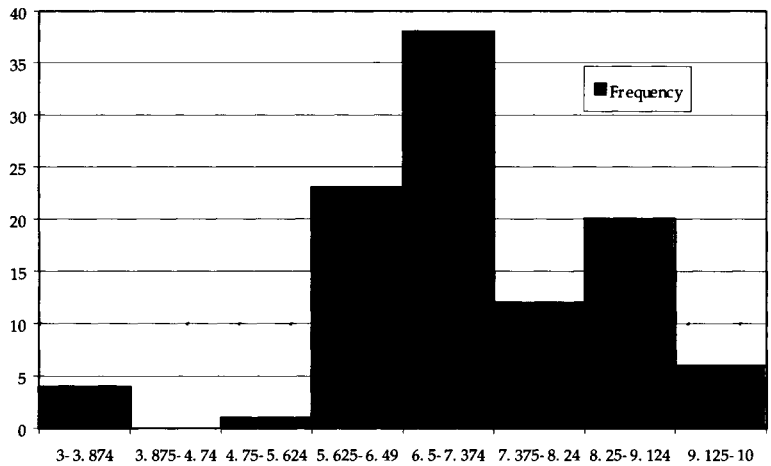


Figure 3: Histogram for actual supply pattern of concrete (inter-arrival times of truckmixers)

CONCLUSION

The concrete demand on a bored-pile construction site is characterized by simulating the entire concreting operations on an ongoing railway station project in Hong Kong with SDESA. A comparison of the CYCLONE model and the SDESA model demonstrates the simplicity and effectiveness of SDESA in modeling complex construction systems. A comparison of the actual supply pattern, which is obtained from site QA records, against the SDESA-characterized demand pattern, has justified the frequent queuing of truckmixers as observed on the site. The outcome of the research will be of immediate help for local concrete plants to match the supply to bored-pile concreting sites and for local contractors to plan bored-pile construction activities.

REFERENCE

Hajjar, D., and AbouRizk, S. (2000), "Application Framework for Development of Simulation Tools", *Journal of Computing in Civil Engineering*, ASCE, 14(3), 160-167.

Halpin, D.W. (1977). "CYCLONE-A method for modeling job site processes." *J. Constr. Div.*, ASCE, 103(3), 489-499.

Law A. and Kelton D. (1982). *Simulation Modeling and Analysis*, McGraw Hill, New York.

Paulson, B.C. (1995). *Computer Applications in Construction*, Wiley, New York.

Lu, M. (2001), "Simplified discrete-event simulation approach for construction simulation", *J. Constr. Engrg. And Mngmt.*, ASCE, accepted

Lu, M., Anson, M., Tang, S.L., and Ying, K.C. (2002), "Simulation-based e-learning and virtual training for complex construction planning", Proceedings of World Project Management Week 2002, Hong Kong.

Lu, M. (2002), "Simulate Road Construction Operations Using Simplified Discrete-Event Simulation Approach (SDESA)", Proceedings of First International Conference on Construction in the 21st Century (CITC2002), Miami, Florida, USA

Shi, J. (1999) "Activity-Based Construction (ABC) Modeling and Simulation Method", *J. Constr. Engrg. And Mngmt.*, ASCE, 125 (5), 354-360.

Advances in Building Technology, Volume 2
M. Anson, J.M. Ko and E.S.S. Lam (Eds.)
© 2002 Elsevier Science Ltd. All rights reserved

AGENT-BASED SPECIFICATION AND PROCUREMENT OF CONSTRUCTION PRODUCTS

E. A. Obonyo, C. J. Anumba and A. Thorpe
CICE, Department of Civil & Building Engineering Loughborough University,
Loughborough, Leicester, LE11 3TU, UK.

ABSTRACT

The specification and procurement of construction products is a key part of any construction project. Within an e-procurement environment, it is important that this function be automated to an appropriate degree. This paper is based on APRON, a project at Loughborough University focusing on agent-based specification and procurement of construction products. The paper starts with a brief introduction to specification and procurement of construction products, highlighting the main problems in these activities. It also introduces some key concepts in agent technology including a definition. The paper then gives an overview of other related projects. The main part of the paper uses six main themes to illustrate the need for agents in activities related to the specification and procurement of construction products. Each theme is discussed in terms of rationale and cues that may show that an application domain may benefit from an agent-based approach and these two concepts are extended into a case for agent-based specification and procurement of construction products. The paper ends with a brief discussion and concludes that the specification and procurement of construction products is an ideal application domain for the deployment of an agent-based solution.

KEYWORDS

Agent-based, specification, procurement, construction products.

INTRODUCTION

Specification of construction products involves defining constraints that have to be satisfied in a particular artefact. Procurement encompasses all activities involved in obtaining materials and services and managing their inflow into an organization towards the end user (Gebauer et al, 1998). When defined this way, there is a very thin line between specification and procurement. Obonyo et al (2001) point out that both activities rely heavily on retrieving information from sources have an open architecture with structures exhibiting dynamism.

Such problems can now be adequately addressed given that the latest developments in information technology model problems quite similar to fragmentation in the construction industry (Obonyo et al, 2001). Some emerging solutions are based on AI paradigms taking the form software agents.

DEFINING AGENTS

It is not easy to define the term 'agents.' Nwana et al (1996) advance a number of explanations for this difficulty: it is a common term in every day conversion; it encompasses a broad area: it is a meta-term and researchers in this area have come up with such synonyms as 'bots', 'spiders' and 'crawlers.' Various researchers have defined the term 'agent' in various ways (Brustolini, 1991, Jennings et al, 1998, Maes, 1994, Lieberman, 1997, Franklin and Graesser, 1996 & Ferber, 1999), but there is a general consensus that software agents exist in an environment and they have a perception of this environment. They can sense the conditions in the environment and such senses may affect how they act in future. Software agents are also perceived to be adaptive and capable of learning. They are also autonomous and proactive, exhibiting goal-directed behaviour. It, therefore, suffices to say that agents are systems capable of autonomous, purposeful action in the real world (Brustolini, 1991).

REVIEW OF RELATED WORK

Interest in Artificial Intelligence among people in the Construction Industry is nearly four decades old. As a matter of fact, the phrase 'Automated Design' preceded CAD (Howard, 1998). As early as the 1960s, various researchers in this industry had envisaged the use of Artificial Intelligence paradigms. Examples include such articles as 'On Evolution of Artificial Intelligence' presented at the 1964 IEEE Symposium on Human Factors and Benard Rudolfsky's 'Architecture without Architect' article published in the 1960s. Perhaps one of the greatest visionaries was Nicholas Negroponte of MIT who published an 'Architecture Machine' magazine in the 1970s documenting predictions on use of AI in construction. There are a number of recent related projects. ADLIB is a project at Loughborough University aimed at developing a multi-agent system framework for the representation of activities and processes involved in the collaborative design of light industrial buildings (Ugwu et al, 2000). A sister project at the same university focuses on the construction claims negotiation domain.

A CASE FOR AGENT-BASED SPECIFICATION AND PROCUREMENT OF CONSTRUCTION PRODUCTS

Various researchers have defined different matrices for determining when to use an agent-oriented software engineering paradigm (EURESCOM, 2000; O'Malley and DeLoach, 2001; Ferber, 1999; Wooldridge and Jennings, 1998; Paranuk, 1998; Heilmann, 1996 & Paranuk, 1996). The case presented in this paper is based on a review of such decision criteria.

Handling complex or diverse communication.

Rationale: Agent-based communication results in simpler interfaces, code reuse and analysis/ design reuse. This is beneficial in situations where complex or diverse type of communication is required.

Cues: The core activities in an ideal domain for an agent-based solution should be based on human-oriented communication. The problem should also require a solution that is more cognitive than computational by nature. Communication may be complicated by a need to integrate several heterogeneous, stand-alone applications and legacy systems. If the information required in the domain is only available as several, different limited portions, then there may be value in investing in agents.

Evaluating specification and procurement of construction products: Communication forms a vital part of this activity since it occurs in a naturally distributed and decentralised context. The problem is cognitive and involves a significant amount of intuition. Activities in this domain require tools that can

reason with uncertain or incomplete information because some information is only available during advanced stages of the project. Bielawski and Lewand (1991) point out that agents should solve problems that cannot be adequately solved by common sense reasoning. Many decisions made in the specification and procurement of construction products are based on the recommendation of an expert.

The disciplines involved in the specification of construction products use different programming languages, represent data with different representation languages and models, and operate on different computing platforms. In CICA's (Construction Industry Computing Association) 1996 Annual Report, there were 85 solutions specific to or customised for the construction industry listed under Software Directories. The use of heterogeneous tools makes communication a very complicated process.

The use of computing applications is further complicated by the fact that software development is very dynamic. Users need to make the existing applications future-proof, implying that when better tools become available, existing knowledge sources do not have to be redesigned. The legacy systems in the specification of construction products can benefit from being incorporated into a wider co-operating community using agent technology, allowing interoperability of all systems.

In addition, a construction product specifier needs to integrate information from various people. The tasks involved can thus be easily broken down into standalone processes and delegated to agents. It is evident from the above that the specification and procurement of construction products requires complex and diverse communication and will therefore benefit from the use of software agents.

A narrow, specific and restricted domain

Rationale: As explained in the previous sub-section, agents simplify communication. For this to be of any benefit to an organisation, this process of simplifying communication should be manageable. It should be possible to restrict the scope to agent tasks, which would not take an individual human being more than a few hours to solve otherwise writing rules for automation becomes a tedious and complicated task.

Cues: Greatest value from using software agents can be realised only when it is possible to precisely articulate the problem. The problem domain should be narrow and specific.

Evaluating specification and procurement of construction products: The best way to illustrate that the specification and procurement of construction products satisfies this requirement is to actually model an agent in this domain. A door specification agent is described below:

TABLE 1:
A Pseudocode for Door Specification

Scenario outline: Agent-based Door Specification
An APRON door specification agent is required to match Designer's requirements and the manufacturer's brochure. The building codes and the client's brief govern the choice, expense and type of product the Designer is allowed to use. Here we consider an agent, within a Designer's office, which the Designer can give product requirements to. The agent then explores the various product possibilities, within the scope of the Client's brief and the building codes. The agent asks the Designer to decide which options to pick generating a detailed specification for the product.

Door Specification Agent
Identity:
The agent is identified by the task of identifying door attributes and associating them with a Designer's requirement.

Roles:
Door requirements extraction and detailed door specification generation.

Interactions with environment:
Sensory input:
The Designer initiates the process by selecting a desired category of attributes, for example, fire rating, door style, surface performance and mode of operation. He then proceeds to specify a value for the selected attributes, for example 20 minutes fire rating.

Acquaintances:
In this scenario it has been assumed that the agent interacts with only one other agent, the Door Catalogue agent.

Resource ownership and access:
The Designer has read-only access to Manufacturer's Door brochures to enable the electronic viewing of product attributes.

Actions:
(Communicate) Get Door Attribute Category from the Designer (style, material, fire rating, mechanical strength, mode of operation etc).
(External) Gather information on options from Manufacturers' brochures.
(Internal) Evaluate the options and decide on the best selection based on the specified constraints.
(Communicate) Suggest options to the Designer.
(Communicate) Get choice from Designer.
(Communicate) Get a desired attribute value for the selected door attribute value (for example door fire rating could vary from 20 minutes to 30 minutes, 40 minutes, 60 minutes, 90 minutes etc).
(External) Gather information on various options from Manufacturer's brochures.
(Internal) Evaluate the options and decide on the best selection based on the specified constraints.
(Communicate) Suggest options to the Designer.
(Communicate) Get choice from Designer.
(Internal) Construct detailed specification for the product.

Mental state and behaviour:
Purpose:
The agent's goal is to extract door performance requirements from a Designer and to turn this into detailed product specification by suggesting alternatives to the user based on constraints imposed by the Designer and product availability as documented in the Manufacturers' door brochure. Once the Designer makes the choice, the agent generates a detailed product specification that can be used for bidding.

Behaviour:
The agent is not able to generate detailed door specifications without the Designer first confirming a choice.

Knowledge and beliefs:
How to generate specifications based on a Designer's requirements;
How to access and use information from a Manufacturer's product brochure.

From this example, it is evident that the specification and procurement of construction products as an application domain is narrow, specific and restricted enough to allow easy deployment of agents.

Worthiness of the Project

Rationale: The use of agents as opposed to other solutions should result in some identifiable value.

Cues: This criterion is very subjective because value means several things to different individuals and organisations. An organisation may invest in agent-based solution because it will result in a new and innovative way of handling problems and make a difference to the way the organisation operates. Agent-based solutions could also automate some functions thus freeing employees of performing routine tasks. This increases productivity and profits. Agents can also make the process of handling knowledge more efficient. They can be used to propagate and proliferate knowledge. When knowledge from previous projects is wrapped using an agent, it becomes easy to reuse them. Agents can therefore add value in a domain where it is necessary to preserve knowledge. Finally, domains that have multi-player or multi-criteria decision-making can ensure consistency through the use of software agents.

Evaluating specification and procurement of construction products: Construction project teams comprise a variety of disciplines with poorly integrated silos of knowledge. The 'dot-com' solutions solutions rapidly deliver more information through a bigger 'pipe' but there is a need to improve the quality of the information going through the pipe. Agent-based systems offer a means of using distributed artificial intelligence to model the distributed silos of knowledge and could improve the quality of information available for specification and procurement of construction products.

As pointed out earlier, the main problems in the specification of construction products emanate from the fragmentation in the industry. There is distribution of information across the disciplines; separation of the construction phases and spatial distribution on electronic networks as shown in Figure 1.

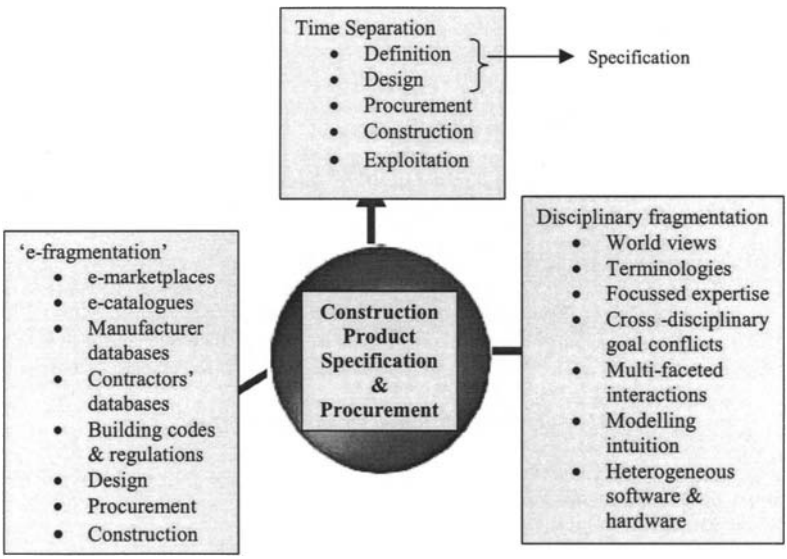


Figure 1: Dimensions of Fragmentation

Agents are capable of several things including making informed decisions; learning and adapting over time; communicating with other agents (including human agents) and integration with legacy systems. Agent services such as brokering, translation and coordination can be used to save time spent in gathering information. They can also handle the various dimensions of fragmentation and increase the knowledgebase. These can add value to the operations in the specification and procurement of construction products.

Impracticality or impossibility to specify system behaviour on a case-by-case basis.

Rationale: Agents have a goal-oriented behaviour and can therefore be used to develop a flexible system capable of adapting their behaviour patterns in a dynamic environment. Agent-based systems are highly modular. The agents can be 'easily' added or replaced and can therefore handle situations requiring systems that are likely to be expanded or modified or ones whose purpose may change.

Cues: An ideal domain for an agent-based solution should ideally require a system that will exist in an unknown environment in which it is impossible to foresee all future situations. Agent-based solutions also adequately model systems whose performances gracefully degrade as uncertainty increases.

Another identifying mark for an ideal application domain for agents is the existence of numerous ideal solutions to satisfy a goal depending on the prevailing circumstances. There should also be a need for systems that require dynamism.

Evaluating specification and procurement of construction products: The systems supporting the specification of construction products are ill-structured. There has been a significant shift to executing construction-related tasks on the Internet. The Internet is an open system whose structure dynamically changes. Therefore there is a need for open, distributed, heterogeneous and flexible architectures. Agents shift focus from systems with a particular configuration to the use of flexible agents 'that can be swapped in and out as the entities they represent are shuffled around' (Paranuk, 1996) enabling systems to adapt to changes in the context of operations and changes in needs. As the agent architecture permits re-use of existing code and self-configuration of the system, the cost and time for setting up a new unit in the electronic marketplace is reduced substantially.

In a construction project it is not possible to have a perfect view of what lies ahead. Agents address the problem of unavailability of all the necessary information at the initial design stage. The level of detail in a contract document depends on the amount of information available during design. The performance of the whole process therefore 'gracefully degrades with increase in uncertainty' and variations in product specifications are inevitable.

Every designer is faced with numerous options and each of them may be appropriate depending on the usage scenario. The use of agents can present designers with an intelligent way to query manufacturer databases on the properties of their products. Agent-based solutions can therefore enable systems in the specification and procurement of construction products to adapt their behaviour depending on the prevailing circumstances.

Handling negotiation, co-operation and competition among different entities.

Rationale: Agents in a multi-agent community communicate and collaborate. Their activities can be modelled into a grid of interdependencies.

Cues: Problems that require solutions that can handle concurrent execution of multiple tasks with conflicting goals are ideal for agent-based systems. Other qualifying features include the existence of multiple stakeholders with different interests and the existence of problems that are both too complex for a monolithic solution and too difficult to decompose into independent sub-problems.

Evaluating specification and procurement of construction products: Specification of construction products is executed as a multi-disciplinary operation meaning that in any project, there are different points of view. The various disciplines involved have compartmentalised themselves over time. Each of them has evolved a unique view of the world and developed special terminologies. Each discipline pursues built-in goals, which may conflict with the global goals of the design. Due to focussed expertise, certain solutions are only true *ceteris paribus* (all things held constant).

There are a number of stakeholders, the client wants a habitable space, the regulatory bodies demand compliance with stipulated codes and by-laws and the contracted companies seek to maximise their profits. In extreme situations parties quite remote to the contract may feature; For example, environmentalists and people concerned with maintaining a certain look and feel for heritage or cultural reasons.

Disciplinary design is presented in big chunks hiding details that may be necessary for integration (Shakeri, 1998). Further complexities arise from multifaceted interactions: multiple disciplines may focus on one parameter simultaneously. Also the designers have counter-intuitive behaviour. But modelling intuition is ineffective or adverse when constraints become active. Through modularity and abstraction, agents offer a means of dealing with such complexities.

Need for autonomous execution

Rationale: A core characteristic for agent-based systems is goal-directed, autonomous behaviour and negotiation. An ideal application domain must demonstrate a need for this advanced level of autonomy.

Cues: The deployment of agents in a given domain makes sense only when there is a need for a system that is capable of acting on behalf of a user.

Evaluating specification and procurement of construction products: The publicly indexable Web contained an estimated 800 million pages as of February 1999, encompassing about 15 terabytes of information or about 6 terabytes of text after removing HTML tags, comments, and extra whitespace (Lawrence and Giles, 1999). Specification of construction products requires searching, querying and filtering out 'noise' from this magnanimous library. Even within construction industry-specific Web sites there are numerous portals. By early 1999 there were 150 to 200 such companies (Valued Gateway Customer, 1999). (This number has subsequently shrunk). However, overwhelmed by 'information overload' (Maes, 1994), specifiers require agents to automate search processes.

DISCUSSION AND CONCLUSION

This paper has made a case for agent-based specification and procurement of construction products by pointing out the benefits that can be derived from the agents' ability to plan, set goals, reason about actions, and improve knowledge and performance through learning. The specification and procurement of construction products occurs in a collaborative environment and this fragments activities. The use of agents is justified by the existence of distributed teams. Information, which is very critical to the success of the project, is multi-dimensional by nature. The key questions in identifying the different dimensions of information are: who needs what information and in which format; who possess the information, where and in what format; when, where and how will the exchange occur? Existing technologies such as object-oriented techniques provide partial solutions that address distribution and dynamism. But as these solutions are becoming sufficiently developed, collaboration needs are advancing to a higher level and a potential 'killer-application' will have to model solutions that address all the possible dimensions of information. It has been demonstrated in this paper that the domain of construction product specification and procurement meets the six main criteria for potential agent-based applications.

REFERENCES

Bielawski, L and Lewand, R. (1991), *Intelligent Systems Design, Integrating Expert Systems, Hypermedia, and Database Technologies*, John Wiley & Sons, USA.

EURESCOM (2000), Model and Guidelines for assessing the suitability of agent technology adapted from Project P907-GI, MESSAGE, Deliverable 1.

Ferber, J. (1999), *Multi-Agent Systems, An introduction to Distributed Artificial Intelligence*, Addison-Wesley, An imprint of PEARSON EDUCATION, UK.

Franklin, S. and Graesser, A (1997), Is it an Agent, or just a Program? A Taxonomy for Autonomous Agent, *Intelligent Agents III*, ATAL 96, LNAI 1193, Springer-Verlag, Mller, J.P. and Wooldridge, M.J (eds.), 21-35.

Gebauer, J., Beam, C., Segev, A. (1998): *Impact of the Internet on Procurement*, in: Acquisition Review, Spring 1998, 167-181.

Howard, R.(1998), *Computing in Construction, Pioneers of the Future*, Butterworth Heinemann, UK.

Lawrence, S. and Giles, L. (1999), Accessibility and Distribution of Information on the Web, NEC Research Institute, *Excerpt from study presented in Journal Nature*: "Accessibility of information on the web", Nature, Vol. 400, 107-109.

Lieberman, L (1997), Autonomous Interface Agents, *In Proceedings of ACM Conference on Human Factors in Computing Systems (CHI)*, 67-74.

Maes, P. (1994), Agents that Reduce Work and Information Overload, *In Communications of the ACM*, Vol. 37 No. 7, 31-40.

Nwana, H. (1996), Software Agents: An Overview, *The Knowledge Engineering Review*, 11(3), 205-244.

Obonyo, E.A., Anumba, C.J., Thorpe, A. and Parkes, B. (2001), Specification and procurement of construction products: Potential role of intelligent agents, *In the Proceedings of* IAWTIC'2001, (ISBN 0858898489), Mohammadian, M. & Stonier, R.J. (Eds), Las Vegas, 268-279.

Obonyo, E.A., Anumba, C.J., Thorpe, A. and Parkes, B. (2001), Agent-based support for electronic procurement in construction, *Artificial Intelligence in Construction*, Anumba, C.J., Ugwu, O.O and Ren Z. (Eds), CICE, Loughborough University, UK, 99 – 113.

O'Malley S.A. and DeLoach S.A. (2001), Determining When to Use an Agent-Oriented Software Engineering Paradigm, *Proceedings of the Second International Workshop On Agent-Oriented Software Engineering (AOSE-2001)*, Montreal, Canada.

Paranuk, H. V. D. (1998), What Agents do in Industry, and Why? An overview of Industrial-Oriented R&D at CEC, Published in Klusch and Weiss, eds., *In Cooperative Information Agents II*, LNCS 1435, 1-18.

Paranuk, H. V. D. (1996), Applications of Distributed Artificial Intelligence in Industry, In O'Hare and Jennings, eds, *Foundations of Distributed Artificial Intelligence*, Wiley Inter-Science, 139-164.

Shakeri, C. (1998), Discovery of Design Methodologies for the Integration of Multi-disciplinary Design Problems, PhD Thesis, Mechanical Engineering Dept, Worcester Polytechnic Institute.

Wooldridge, M. and Jennings, N.R. (1998) Applications of Intelligent Agents, *In Agent Technology: Foundations, Applications, and Market,* Springer Verlag, Berlin: 3-28.

Ugwu, O. O., Anumba, C. J., Newnham, L. and Thorpe, A. (2000), The Application of DAI in the Construction Industry, CIB W78 - IABSE - EG SEA AI, *Construction Information Technology 2000 (CIT2000 Ed),* Reykjavik, Iceland.

Valued Gateway Customer (1999), Trends in the Building Industry: The Internet as your Platform, Presentation at CIFE, Stanford University, USA.

Advances in Building Technology, Volume 2
M. Anson, J.M. Ko and E.S.S. Lam (Eds.)
© 2002 Elsevier Science Ltd. All rights reserved

IVMS - AN INTERACTIVE SYSTEM FOR IMPROVING VALUE MANAGEMENT STUDIES IN CONSTRUCTION

Qiping Shen and Jacky K.H. Chung

Department of Building and Real Estate, The Hong Kong Polytechnic University
Hung Hom, Kowloon, Hong Kong Special Administrative Region, China

ABSTRACT

Value Management (VM) is an organised function-oriented systematic team approach directed at analysing the functions and costs of a system, supply, equipment, service or facility, for the purpose of enhancing its value, through achieving the required functions specified by the customers at the lowest possible overall cost, consistent with requirements for performance. Because of its strong potential in improving value for money for construction projects, client organisations in both the public and private sectors are using VM increasingly in their projects. However, a recent study has suggested that the special characteristics of using VM in Hong Kong, such as the large number of participants and short duration, have presented some unique difficulties in implementing VM studies. These difficulties also prohibit further applications of VM in the territory. One way to overcome these identified difficulties is to develop an interactive group decision support system that can facilitate the decision-making process in VM studies. This paper introduces such a system, entitled the Interactive Value Management System (IVMS), which is designed to improve the implementation of VM studies. It gives a detailed description of the structure and characteristics of the system and the support that it can provide, including information, communication and analysis. This is followed by the functionalities of the modules inside the system. Finally, the potential benefits and limitations of the system are discussed. It is concluded that IVMS is a very useful tool for improving VM studies in construction.

KEYWORDS:

Value Management, Group Decision Support Systems, Interactive Value Management Systems, Construction

INTRODUCTION

Value Management (VM) has been receiving increasing attention in Hong Kong, especially since the Asian financial crisis in 1997 (Shen and Kwok, 1999). There is a surge of interest in VM applications in the construction industry. Both the public and private sectors in Hong Kong have been using VM to ensure value for money for their projects during the preliminary project feasibility study stage. However, a recent survey suggested that VM users had encountered problems such as lack of active participation

and insufficient time/information in the decision analysis (Shen and Chung, 2000). There is a strong demand for improvements to the practice in order to maximise the benefits of using VM studies. One possible way to overcome the above difficulties is to apply information technology to facilitate VM studies. As a branch of information technology, GDSS has the potential to promote active participation, encourage interaction, and facilitate decision analysis in VM studies. To verify this hypothesis, a special GDSS prototype named the Interactive Value Management System (IVMS) is being developed at the Hong Kong Polytechnic University (Chung and Shen, 2001). This paper aims to introduce the conceptual framework of the IVMS and demonstrate how it can be applied to VM studies. It begins with an introduction of GDSS, including the definition, development and application, followed by a description of the system structure, its functionality, and the potential benefits of the IVMS.

GDSS, also known as Group Support Systems or Computer Support Cooperative Work Systems, is a computer technology which combines communication, computing, and decision support technologies to facilitate the formulation and solution of unstructured problems by a group of people (DeSanctis and Galluple, 1987). In short, GDSS is a computer-based system designed to support groups of people and to engage them in a common task through the interface of a shared environment (Aiken et al., 1995). It consists of hardware, software, people, and procedures. In the mid 1980s, GDSS research was mainly centralised in university research laboratories. The results, however, were inconsistent because of the different experimental settings and subjects adopted in studies. Nevertheless, the true effectiveness of GDSS in improving the group decision-making process has been assured by field studies. GDSS field studies have consistently shown positive results, and nearly all "real-world" users are extremely satisfied with the application of GDSS in meetings (Dennis et al., 1988). It is concluded that GDSS is highly useful in improving the group decision-making process (Dennis et al., 1988; Chun and Park, 1998). Today, the success of GDSS is gaining acceptance and it has been widely applied in many famous organisations, including the University of Arizona (GroupSystems), IBM (Team Focus), and Xerox (the Colab System).

THE INTERACTIVE VALUE MANAGEMENT SYSTEM

The IVMS is a specific GDSS system designed to enable team members to exchange information, make presentations, brainstorm and prioritise ideas in VM studies. It aims to:

- Improve collaboration between members
- Facilitate information management
- Promote exchange of ideas, opinions and preferences
- Improve the productivity and accuracy of data analysis

The IVMS is a web-based application in which software is essentially installed and operated on a server. It supports multi-platforms, including Windows 98, Windows 2000 and Mac OS, and allows users to access the system at any machine, anytime, and anywhere. The web interface is also user-friendly and assists users with varying levels of knowledge regarding computing and decision support.

In addition, the system is designed as a set of toolboxes, including a virtual team unit, an information unit, a communication unit, and an analysis unit, and a summary is given in Figure 3. This enables facilitators to decide what GDSS functions to use, and when and how to use them, so as to accommodate the various requirements in VM studies.

System Architecture

The design of the IVMS is based on the GDSS model proposed by DeSanctis and Galluple (1987). It is composed of users (members and facilitators), a user interface (web browser), software (IVMS toolbox), and hardware (input and output devices, databases, servers). A pictorial representation of the system architecture and a summary of the system components are given in Figure 1 and Table 1 respectively.

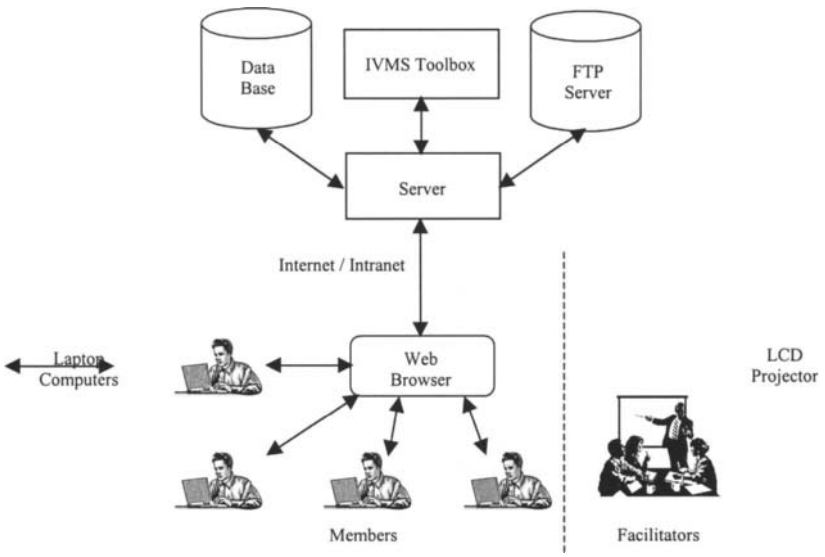


Figure 1: System Architecture of the IVMS

TABLE 1
COMPONENTS OF THE IVMS

Components	Description
Members and facilitators	Users
Laptop computer	An input and output device for users
Internet/Intranet	A connection link for laptop computers and the server
Web browser	An interface for users to operate the system
IVMS Toolbox	A set of GDSS tools
LCD projector	A public screen for information display
Server	A processor for data calculation and coordination
FTP server	A storage device for project information
Database	A storage device for data produced in meetings

The IVMS is designed to improve VM studies and its users include both members and facilitators of VM study teams. In a GDSS-supported VM study, the facilitator is responsible for the smooth operation of the IVMS and he/ she has to decide what GDSS functions to use, and when and how to use them in accordance with VM job plans. In order to share the additional workload, an assistant helps him/her to operate the system by starting and stopping the software, and provides technical support to members.

Figure 2 shows that members and facilitators are provided with laptop computers, which are used as input and output devices in workshops. The computers are connected to a server through the Internet or Intranet, and they allow members to operate the IVMS or carry out private work, such as text editing,

formatting, data file creation and modification. In addition, an LCD projector is provided so that facilitators and members can present the results of idea generation, voting, analysis, and private work on a public screen. A server, a database, and an FTP server are also included in the IVMS. The server is a computer processor which links up the workstations to the database and the FTP server. These storage devices are designed to manage all project information uploaded in the pre-study phase, and to record the generated ideas, collected comments, and voting results in meetings. For security reasons, the databases and servers can be placed in either the office of the client or that of the service provider, and maintained by assistants.



Figure 2: A Typical Setting of the IVMS in a Workshop Environment

The IVMS Toolbox

The IVMS is designed as a set of toolboxes comprised of four boxes, including a virtual team unit, an information unit, a communication unit, and an analysis unit. A detailed discussion of these toolboxes is given in Figure 3.

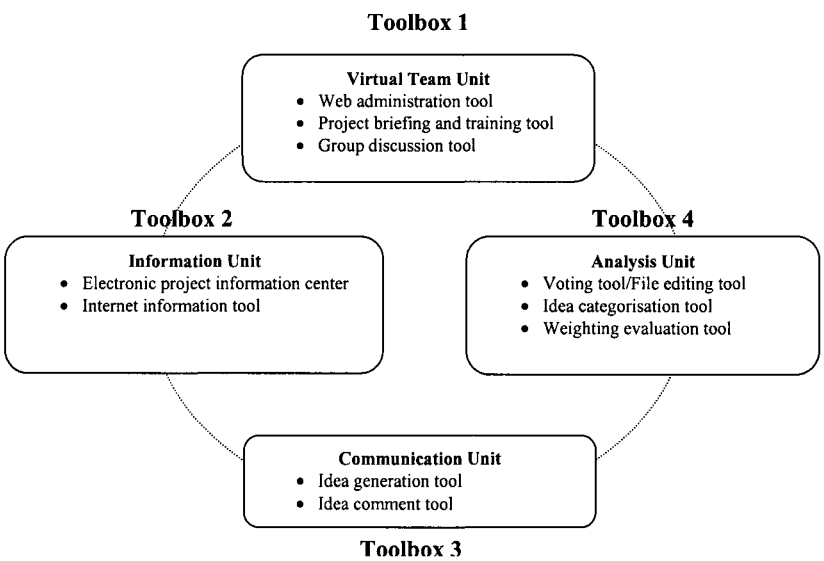


Figure 3: Toolbox of the IVMS

The toolboxes are designed to support a group of specific tasks: therefore, different toolboxes are applied to different phases of VM studies. As shown in Figure 4, Toolbox 1 (the virtual team) aims to improve the collaboration between team members, and mainly applies to the pre- and post-study phases. Toolbox 2 (information) aims to facilitate information management throughout the studies. Toolbox 3 (communication) aims to promote the exchange of ideas, opinions and preferences within groups and is mainly applied to the creativity and evaluation phases. Toolbox 4 (analysis) aims to improve the productivity and accuracy of data analysis and is mainly applied to the analysis, evaluation and development phases. These toolboxes are integrated into two modules, the Pre-meeting Module and the Meeting Room Module, in accordance with the SAVE 40-hour job plan. The following sections introduce these modules and illustrate how they can be applied to improve VM studies:

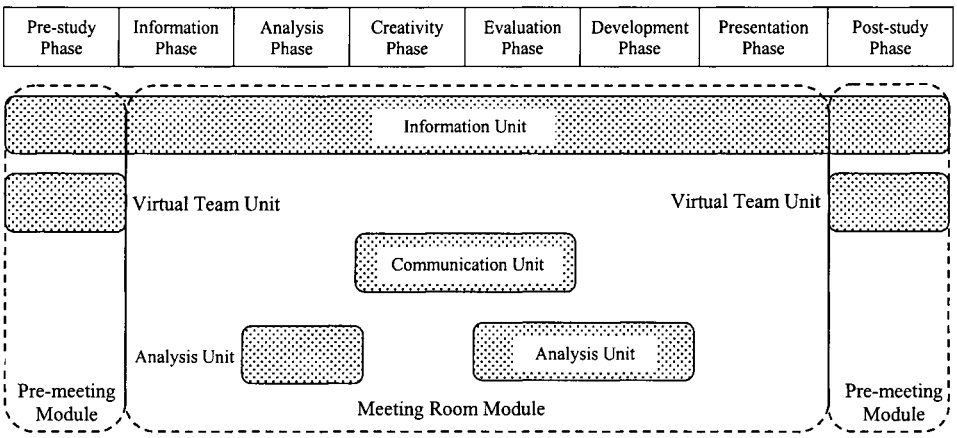


Figure 4: Toolboxes of the IVMS

Pre-Meeting Module

Virtual Team Unit

The virtual team unit aims to improve collaboration between team members in the pre- and post-study phases. It enables members to work together as a team at anytime and anyplace through the Internet, thus better coordination and preparation work can be achieved. It comprises three tools: a web administration tool, a group discussion tool, and a project briefing and training tool.

The group discussion tool is an electronic forum that allows members to enjoy group discussions before meetings. They can raise new topics or comment on other people's topics by posting messages on a newsgroup; the messages are then emailed to all the other members automatically. The project briefing and training tool assist clients or facilitators in conducting pre-meeting briefings. Besides the online PowerPoint presentation, the tool also provides a virtual site visit tour by the use of photos and online videos, in order to ensure that members have a better understanding before coming to meetings. Figure 5 illustrates this feature inside the virtual team unit of the IVMS.

Information Unit

The information unit aims to facilitate information management and improve the availability of information in VM studies. It includes an electronic project information centre and a set of Internet

information tools. Figure 6 illustrates the information tools that allow members to access to external information during the workshop. The electronic project information centre is a file exchange system which allows members to store and share project information on the Internet. Members are provided with web folders in an FTP server and they can simply use Internet browsers to upload or download the files, including correspondence, cost data and drawings, before meetings. If there is new information, a notice will be automatically sent to members so that they can download it through the system.

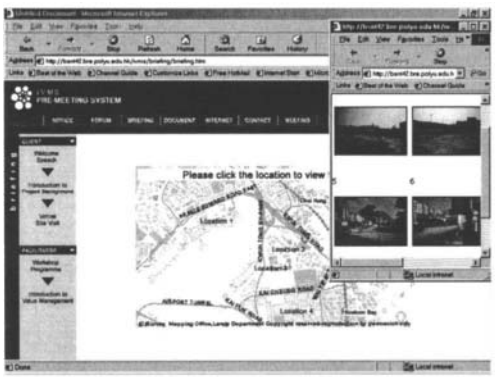


Figure 5: Virtual Site Visit Tour



Figure 6: A Set of Internet Information Tools

Meeting Room Module

Communication Unit

The communication unit aims to promote the exchange of ideas, opinions and preferences within groups. Research findings show that people feel freer to exchange ideas, comments and preferences in an anonymous environment. The communication unit makes use of this technique to promote participation and encourage interaction in VM studies; it is comprised of an idea generation tool and a comment tool.

Analysis Unit

The analysis unit is designed to improve the productivity and accuracy of data analysis in the analysis and evaluation phases. It is comprised of a set of analysis tools, including an electronic FAST diagram and voting tool, an idea categorisation tool, and an electronic weighting evaluation tool.

THE BENEFITS OF THE IVMS

(1) Facilitate Information Management in VM Studies

Previous survey findings suggest that lack of information is the most frequently encountered difficulty in VM studies (Shen and Chung, 2000). The project information centre can improve the quantity of information and make it available to other members through the Internet. It has simplified and centralised the information distribution process so that information can be easily shared among members to provide a common understanding of the project. The centre also facilitates the formation of a database of VM studies. As shown in Figure 7, the uploaded project information and meeting records can be combined to produce a completed record at the end of a VM study. The accumulated information becomes a good and reliable information source to support future studies.

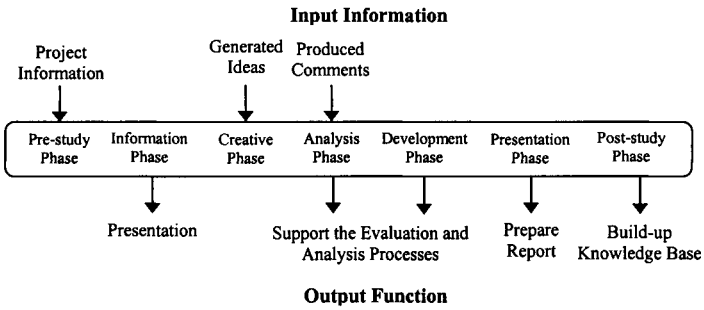


Figure 7: Input and Output of Electronic Information Centre

In order to further improve the availability of information, the centre provides an Internet connection during the workshops. Members can retrieve information such as government indexes and annual reports through the Internet, or directly connect to the desktop computers in their offices through the dial-up facilities, which overcome the constraints of the physical location.

(2) Improve the collaboration between team members

A VM team is normally comprised of people from different organisations. However, it is difficult to arrange an introductory meeting before the workshops because many clients are trying to shorten the duration of VM studies. The IVMS can improve collaboration among team members by enabling them to work together at anytime and anywhere through the Internet in the pre-meeting phase. In the virtual conference room, the Briefing Tools provide background information on the project. Members can gain a better understanding of the project objectives and limitations before attending the workshops. The Electronic Notice Board and Electronic Forum facilitate good communication between members and enable them to prepare better for VM workshops.

(3) Promote active participation and encourage interaction

Lack of participation and involvement of members is a typical problem in VM studies. Research findings show that people become free to exchange ideas, comments and preferences in an anonymous environment. The cyber forum creates such an environment to promote participation and encourage interaction in VM studies. It is especially useful in motivating those members who are afraid of speaking in public or worry about sounding stupid in front of a group of people. It is believed that members' active participation will lead to more ideas and comments in VM studies. The cyber forum reduces the conformance pressure on members (the fear of challenging a powerful player's bad idea), so that members can judge people's ideas solely based on their merits rather than other social factors.

The creative use of the cyber forum can assist facilitators to introduce new "group structuring techniques" into VM studies. For example, anonymous individual brainstorming can be integrated with face-to-face group brainstorming to form a new brainstorming technique. Ideas can be collected anonymously from individuals and then presented to the group to stimulate additional ideas. This approach can empower the process by utilising the strengths of both brainstorming methods. In short, the promoted active participation and enhanced interaction enable the group discussion to become more creative and vigorous, hence more good ideas and feasible solutions can emerge from the VM study.

(4) Assist the decision analysis in workshops

IVMS provides various computer tools to improve the productivity and accuracy of data analysis during workshops. The use of modelling tools can eliminate human errors and shorten the data processing time. The links to commonly used software packages enable members to use their familiarised tools to analyse different scenarios. These tools can assist members in responding to "what-if" questions quickly, by varying the data input and observing the impacts of different solutions.

CONCLUSION

This paper has demonstrated that the Interactive Value Management System can improve VM studies. A detailed description of the characteristics and structure of the system have been given, and the support that can be provided by the system has also been elaborated. The functionalities of the modules inside the system and the potential benefits of the system have been discussed. It is concluded that IVMS is a very useful tool for improving VM studies in construction.

ACKNOWLEDGEMENT

The authors wish to express their sincere gratitude to The Hong Kong Polytechnic University for financial support for the research project described in this paper.

REFERENCES

Aiken, M.; Vanjani, M.; and Krosp, J. (1995). Group decision support systems, Review of Business, Vol. 16, No. 3, pp. 38-42.

Chung, K.J. and Park, H.K. (1998). Examining the conflicting results of GDSS research, Information & Management, Vol. 33, pp. 313-325.

Dennis A.R.; George, J.F.; Jessup, L.M.; Nunamaker, J.F.; and Vogel, D.R. (1988). Information technology to support electronic meetings, MIS Quarterly, December, pp. 591-624.

DeSanctis, G. and Galluple, R. B. (1987). A foundation for the Study of group decision support systems, Management Science, Vol. 33, May, pp. 598-600.

Shen, Q.P. and Kwok, E. (1999). The Economic Downturn in Hong Kong: Crisis or Opportunity for Sustainable Value Management Applications? Proceedings of the 3rd International Value Management Conference, Hong Kong Institute of Value Management, Hong Kong Convention and Exhibition Centre, Hong Kong, 6-7 May, pp. 1-7.

Shen, Q.P. and Chung, K.H. (2000). Overcome difficulties in VM studies: The use of information technology. IN: Proceedings of the 4th HKIVM Int'l Value Management Conference, 22-23rd November, Hong Kong, pp. 28-36.

Shen, Q.P. and Chung, K.H. (2001). Using information technology to overcome difficulties in value management studies – Hong Kong's experience, Journal of Construction Research, Vol. 2, pp. 147-156.

Advances in Building Technology, Volume 2
M. Anson, J.M. Ko and E.S.S. Lam (Eds.)
© 2002 Elsevier Science Ltd. All rights reserved

PRODUCTIVITY EXCELLENCE THROUGH AN INTEGRATED CONSTRUCTION MANAGEMENT SYSTEM FOR THE BUILDING AND CONSTRUCTION INDUSTRIES

Peter Yan, Chief Executive Officer

Global e-Business Services Limited
30/F., MLC Millennia Plaza, 663 King's Road, North Point, HONG KONG

ABSTRACT

This paper describes the actual case of how an Integrated Construction Management application designed specifically for the construction industry can enhance productivity, efficiency and competitive advantage.

The application is an advanced web-based system covering construction tendering, procurement, workflow management, document management and project management functions. It is a full Internet based system with advanced PKI-based (public key infrastructure based) security features to ensure data confidentiality, data integrity and authenticity.

Among the users of various components and/or modules of the Integrated Construction Management system are the Hong Kong Government and various commercial enterprises.

In the paper, we will illustrate through describing one of our success cases, how various functions of the application have brought about the said improvements and elaborate on the quantitative achievement of such improvements. We will also illustrate the benefits of the application not only to the construction companies themselves but also how the implementation of such applications has improved the business partners of the construction companies, such as their subcontractors or suppliers.

In addition, we will also share with the audience the experiences we have in implementing such applications for various organisations. These include our assessment of the critical success factors, the challenges normally faced, the considerations of different stakeholders in the implementation process and the justifications for implementing such applications.

KEYWORDS

Integrated Construction Management System, Electronic Tendering, Bill of Quantity, Document Management, e-Procurement, Workflow, Project Management, Productivity

INTRODUCTION

In April 2000, the Chief Executive of the Hong Kong Special Administrative Region formed the Construction Industry Review Committee (CIRC) to review the current state of the industry and recommend improvement measures. The Committee has proposed items of improvement measures aiming for better performance of the industry. There were recommendations on certain areas which comprised of improvement on the existing tendering process and procurement logistics. This paper illustrates how information technology can be applied in real life situation through an Integrated Construction Management System (ICMS) to implement the recommendations of the CIRC review report and to improve companies in the construction industry in their productivity, efficiency and competitive advantage.

The paper starts by providing the background and characteristics of the construction industry, reinforcing the challenges faced by its practitioners and how ICMS applications could overcome such challenges. The paper concludes by illustrating a real case in Hong Kong – the Shui On Construction and Materials Limited, on how ICMS can achieve significant result in productivity and efficiency gain.

CHARACTERISTICS OF THE LOCAL CONSTRUCTION COMPANIES

The local construction industry is characterized by a high level of subcontracting. There are a small number of large local contractors while most local construction companies are usually small in size. More than 90% of the local construction companies had less than HK$10 million gross value of construction work performed in 1999. Many of them act as subcontractors to the large companies, that is, the main contractors. (Source: [July 2001] Profiles of Hong Kong Major Service Industries – Building and Construction, Hong Kong Trade Development Council). The industry is labour-intensive, traditional and old-fashioned. The result of such a manual characteristics is lengthy process and procedures in project administration, leading to loose control, increase cost and low productivity. Occurrence of several non-compliant construction incidents occurred in 2001 have increased much awareness and concern to improve existing practices in project management.

Since most of the companies are low in profitability, industry participants usually adopt a short-term vision. Many of them are resisting to invest in advanced construction technologies and more efficient work processes, it will ultimately decrease the industry's competitiveness in the long-term.

WHY IS A COMPREHENSIVE CONSTRUCTION MANAGEMENT SYSTEM REQUIRED FOR THE INDUSTRY?

According to the CIRC report, it is not uncommon that construction projects experience delays and exceed budget. In such cases, penalty would be incurred and results in financial loss and poor professional image. The reason behind as suggested by the report is due to a lack of accountability through the prevalence of many non-value adding multi-layered subcontractors with lax supervision (Source: [Jan 2001] Construct for Excellence, Report of the Construction Industry Review Committee).

When too many parties are involved in a construction project with the existence of a large amount of subcontractors in different stages, it is always be difficult to control the project progress since delivery of the construction products would be pieces by pieces. It is therefore recommended in the CIRC report that a structured site supervision system should be set up to safeguard the built quality. It allows the factors of consideration to be planned and designed at the very beginning

stage to facilitate downstream activities such that all processes and practices should be rationalized as far as possible to shorten the learning curve and to provide greater predictability over outcomes. To achieve this, IT solution will be required to improve the information flow among all project participants and to enhance project logistics management. For example, an on-line project management system would allow each construction sites situated in different locations to report project progress to head office. In this way, the most up-to-date project status can be readily compiled at the head office and travelling between the head office and the project sites will be greatly reduced.

Another highlight in the report is relating to the existing procurement and logistics practices. It points out that the method of procurement will directly affect the construction work quality and outcome. Focus has been imposed on two particular areas: pre-qualification of subcontractors and assessment of bids and contract award with a scoring system. However, the existing tendering system is much paper-based and traditional. There is low transparency and lack of openness to both tenderers (here refer to subcontractors) and the general public. The CIRC report suggested the use of prequalified tendering to identify the past performance and quality attributes of tenderers and use of a marking scheme to select the quality subcontractors.

To ensure that developers and contractors comply with the mechanism and to create an open and fair environment for industry players, the use of IT through a web-based electronic tendering solution is recommended. The CIRC report encourages the adoption of electronic tendering in the construction industry by endorsing the Works Bureau's initiatives in electronic tendering.

The CIRC report also advocates on the extensive use of information technology in other specific areas like document management system and workflow improvement processes. It concludes that an integrated system combining the above applications serving as a one-stop solution specifically designed for the industry is much desired in achieving significant productivity gain.

WHAT IS INTEGRATED CONSTRUCTION MANAGEMENT SYSTEM (ICMS)?

ICMS is a web-based application and is construction industry oriented. Users of the system require no proprietary software/hardware installation and the set up cost is minimal. It deploys strong encryption technology through PKI-based security framework to ensure extremely high level of data confidentiality, data integrity and authenticity.

The ICMS components include construction electronic tendering, procurement, workflow management, project management and document management functions. The characteristics of each component and their benefits to industry users are discussed below.

Electronic Tendering System



In the CIRC report, it stresses the importance of pre-qualification and bid assessment. To achieve this, an open and transparent tendering and procurement process is inevitable. The Electronic Tendering function, equipped with subcontractor pre-qualification exercise and on-line purchasing features, is able to improve industry users in daily tendering process. The suppliers and contractors registration management supports pre-qualification procedure by enabling the developers or main contractors to approve those qualified subcontractors with proven track records. Contracts could then be awarded to those industry participants with consistently good performance.

Features of Electronic Tendering System at a glance:

Suppliers and contractors Registration Management

- Online vetting for new and approved registration
- Pre-qualification of registered subcontractors
- Updates supplier's information for developer / main contractor's future assessments

Project based Tender Management

- Creation of project reference for new project
- Tender documents defined in individual project reference for easy identification

Refine project by Trade Management

- Categorizes project items in different trade, expandable sub-level and secondary sub-level
- Divides suppliers and contractors role according to their engaged business

Easy Site Purchase Management

- Direct site purchase requests from site office
- Simple and user-friendly instant online request for quotation

Other Features

- Supports open and registered tender posting
- Supports electronic security keys certified by Hong Kong Post
- Supports tender clarification, postponement, suspension and addendum posting
- Online Q&A enquiry box
- Real time service by synchronizing with the Hong Kong Observatory
- Consolidated tender submission by highly secured tender box program

Based on the experience in developing the ETS system (www.ets.com.hk) for the Government Supplies Department (GSD), the Electronic Tendering System offers the most secured platform to industry users in disseminating tender notice and documents arising from works projects. Contractors could, through a simple web-browser, instantly download and submit their tender offer to a highly secured tender box.

Bill of Quantity (BQ) System

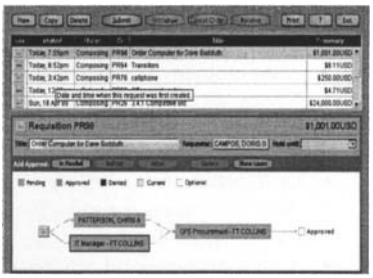


Integrated with the Construction Tendering System, the BQ (Bill of Quantity) Management System facilitates tender evaluation. The BQ summary report enables users to access all tender offers at a glance with automatic comparison process to facilitate bid evaluation.

Features of Tender BQ Management System

- Facilitates tender preparation and evaluation
- Displays in excel format
- Intelligent "waterloo" comparison of returned BQ Excel file to track unauthorized changes
- Discrepancy Report Generation to highlights only insertions / deletions / modifications
- Allows the import of returned BQ files from diskettes or CD-ROM with BQ summary report

Procurement and Workflow Management (e-Procurement)



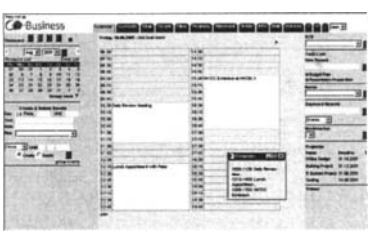
Traditional procurement involves manual paper-flow processes which are time consuming, difficult to control, non-productive and inefficient. e-Procurement can streamline those tedious processes, resulting in procurement cost reduction. It could significantly reduce purchasing cycle time and increase operation efficiency accordingly.

Workflow management also applies in various project stages, ranging from project initiating, suppliers record vetting, tender posting, document and suppliers' bid sharing. Information could be exchanged between headquarters and site offices without boundary. Site offices could perform approval requests directly and send them to Headquarters for approval.

Features of e-Procurement

- Electronic catalogues for product / site materials selection
- Pre-customized electronic forms for on-site procurement request
- Establishes dynamic sequence workflows for request, review and approval according to company structure
- Real-time status tracking and control of entire process
- Advanced reporting tools for data analysis and supplier evaluation in business negotiations and strategic planning

e-Project Management System (e-PMS)



e-PMS is a real-time management tool for multi-construction projects. It is proficient in categorizing projects with status highlighted as well as to allocate relevant parties and timeline. The features of e-PMS are described:

Group Calendar

- Organization of related activities and perform group schedules
- Update meeting status among group members
- Resources and time allocation for projects
- Alert box to remind upcoming event

Project Administration

- Role-based control for member's identity
- Allows administrator to manage resources, groups and users
- Assigns and shares events of current projects to group members

Group Communication

- Supports e-mail or fax sending with file attachments to select group members
- Contact Manager Tool to import directories from other formats
- Chat Forum for users to conduct on-line discussion
- Dialogues and data are displayed and stored as documentation for future retrieval

Request Tracker System

- Products and services support management
- Categorizes incoming request and automatically assign respective user
- Acknowledge request and online status checking for customers

- Views pending requests and assigns work time for billing calculation
- Forms a knowledge base for public searching or restricted for authorized access

Time Card System

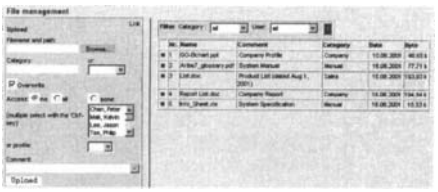
- Administrates working hours and assigns working days to several projects
- Actual measurement of working hour by out and back on duty
- Calculation of working hours for progress tracking and cost estimation

Other Benefits

- Multi-languages support – English, Chinese and up to 15 languages
- WAP and PDA access
- Online Help Support, FAQ and tips

e-Document Management System (e-DMS)

Traditional filing system results in numerous loose-leaf papers difficult for searching and sharing. The construction industry produces tones of documents, maps and diagrams everyday which makes filing more complex and time-consuming. DMS can improve the existing situation through the following features.



Features of DMS:

- Central repository for users to share files and documents
- Uploads files / intranet links and directories
- Assigns access right for relevant parties
- Adds remarks and comments on each document
- File sorting and searching by categories

The e-Project Management System (e-PMS) together with e-Document Management System (e-DMS) served as a real-time management tools for multi-location construction projects. This function facilitates the coordination of construction activities and enables the multi-location construction sites to report the project progress to its head office. All paper documents including sizable maps and diagrams can be uploaded from all locations to the system which serve as a central repository for authorized users to share. The e-PMS is also equipped with time card system for recording of "in" and "out" time for duty or work which assist in working hours calculation for progress tracking and cost estimation.

Through these features, industry users can be benefited by monitoring the cost and time spent by group members against budget and schedule in a real-time basis. Project manager can modify the project plan and reassign resources immediately with quick response to unexpected circumstances. It also facilitates the circulation and access of confidential documents and drawings.

ICMS provides audit trail for all actions taken and which parties have been involved. It increases control and accountability of personnel involved and reduces improper access and approval within the process. ICMS aims at reducing the project cycle time, increasing contractors relationship management, achieving operation efficiency and ultimately, increasing project compliance and control.

CASE STUDY: SHUI ON CONSTRUCTION AND MATERIALS LIMITED

Company Background



SOCAM.com Ltd. is a wholly owned subsidiary of the Hong Kong construction giant –Shui On Construction Materials Ltd. (HKSE: 983) of the Shui On Group. It is a leading Hong Kong company engaged in construction, construction materials and property development in Hong Kong and the mainland China.

Applied Applications:

SOCAM.com is developed by SOCAM.com Limited for providing total solutions in tendering and procurement logistics. Selected modules in the ICMS are applied. One of the key functions is the electronic tendering (e-Tendering) system, a web-based tool to conduct the entire tendering process based on a secured system. For those low value purchasing items where tender document is not necessary, ec-Purchasing function is available for instant quotation. The whole implementation and operation, including supplier enablement, training and hotline, of this platform is outsourced to an application service provider.

Useful Statistics:

The system has been in operation since September 2000. As of March 2001, the total number of registered suppliers in the system has already exceeded 500 which accounts for more than 60% of the active supplier base of Shui On Construction and Materials Limited. More than 18,000 visitors have been attracted to the site with more than 3,800 tender documents downloaded. It generated more than HK$380 million tender value through its electronic tendering and procurement portal. In November 2001, SOCAM.com has been enhanced to include the Shui On Plant and Equipment Services Ltd. (SOPESL) and the MIS department as system users.

Benefits to SOCAM:

- Achieved 1 per cent cost savings in production within 3 months after implementation
- Productivity gain with 10-30 per cent improvement
- Streamlining existing tendering process, increase communication between SOCAM and existing/potential partners e.g. clients, subcontractors and suppliers
- Prompt delivery: implementation timeframe within 3 months through a ready-to-market application
- Enabled internal staff from different sites and offices to access updated project information remotely which expedite for tracking and information/data retrieval
- Outsourcing non-core operations to outside party, such as application hosting; telemarketing; help desk; supplier vetting/recruitment and user/supplier training, allows the company to focus on its core business

Key Issues Encountered and How They Are Resolved:

Issue: The implementation of SOCAM.com requires re-engineering of existing procurement and tendering process.

Actions taken to resolve the issue:

- A dedicated business unit was set up to oversee the electronic tendering system and capitalize on the business opportunity of this system.
- Strong management support and commitment were demonstrated and communicated to the working level at various levels of management.
- The benefits of process re-engineering were communicated to all internally

- Mass internal training on IT usage to all employees were conducted prior to the rollout of the electronic tendering system
- Advises were solicited from the expert opinion of the application service provider that has numerous experiences in building electronic tendering systems.

Issue: SOCAM has faced resistance to change from its subcontractors and suppliers.
Actions taken to resolve the issue:

- Special offers were given to award first movers.
- The message that electronic tendering will replace traditional process in the long term was repeatedly communicated to the contractors and suppliers.
- A step-by-step implementation plan was devised, starting with the more ready and capable contractors/suppliers, then extending gradually to those less ready companies
- A comprehensive suite of supplier enablement services, including training and help desk, was solicited from the application service provider.
- A Pilot Run was conducted to ensure the full consideration of the supplier/subcontractors' requirements before implementation

Issue: Concerns from internal users and external suppliers regarding security.
Actions taken to resolve the issue:

- Strong encryption technology based on PKI-based security framework was deployed to ensure high level of data security, integrity and identity authentication.
- A reputable application service provider with track records of implementation experiences of similar platforms was selected for the development of the system.
- An independent third party (i.e. the Hong Kong Productivity Council) was employed to conduct comprehensive audit review on the provider's technical infrastructure.

CONCLUSION

Despite of the recent economic downturn in Hong Kong, there is still a lot of infrastructure and construction works ahead. The government has proposed to award construction and consultancy contracts worth about HK$280.8 billion by the end of 2002, subject to funding approval of the Legislative Council Finance Committee. Sizable projects are underway which include the redevelopment work for old Kai Tak Airport and adjacent areas, works arising from railway development, public and private sector housing construction, etc. As recommended in the CIRC report, the construction industry must improve its long-term competitiveness through the use of innovative technologies and more efficient work processes. The government has already taken the lead in encouraging the use of I.T. in various industries.

The China's accession to World Trade Organization (WTO) enabled local construction industry to capture the opportunities in the mainland real estate development and construction market. However, the local industry players must maintain its competitive edge against local and overseas competition. The ICMS provides a mean for local industry practitioners to achieve significant productivity gain through the application of information technology.

REFERENCES

Henry Tang and Construction Industry Review Committee (2001), Construct for Excellence – Report of the Construction Industry Review Committee

Profiles of Hong Kong Major Service Industries – Building and Construction, http://www.tdctrade.com/main/si/spcons.htm. Viewed on 1/10/2002.

SOCAM – Annual Report (2001)

Advances in Building Technology, Volume 2
M. Anson, J.M. Ko and E.S.S. Lam (Eds.)
© 2002 Elsevier Science Ltd. All rights reserved

4D-CSCW MODELING FOR CONSTRUCTION MANAGEMENT*

Zhang Jianping[1], Cao Ming[2] and Ren Aizhu[3]

[1]Associate Professor, Dept. of Civil Engineering, Tsinghua University, Beijing, China
[2] Ph.D. Student, Dept. of Civil Engineering, Tsinghua University, Beijing, China
[3] Professor, Dept. of Civil Engineering, Tsinghua University, Beijing, China

ABSTRACT

With the development of computer network technology, research in Computer Supported Cooperative Work (CSCW) systems is becoming popular. CSCW has the potential of providing the environment needed for groups of diverse users to cooperate in order to achieve their common goals. Our current research has mainly focused on those extensions to a 4DSMM (4D Site Management Model) concept necessary to provide a wider scope that also allows cooperative work and information sharing by Internet for different project teams, and the development of a new experimental system. This paper presents a new 4D-CSCW model for construction management through integrating CSCW technology with the existing 4DSMM, and discusses the features of this newly extended model based on studying the cooperative work and communication methods of construction management and the regulation of data flow in construction process. The techniques for applying the model in construction management practice are then described.

KEYWORDS

Construction management, 4D-CAD, CSCW, Cooperative Work

INTRODUCTION

Today, computer technology has achieved rapid development and is being widely used. However, most of the users work in an individual mode. Though these users can communicate

*This research is supported by Natural Science Foundation of China

with each other by local network or Internet and share some of the information, for data access, information processing and programming, all these works are separated and independent. In the modern information society, people's living style and working modes have the features of grouping, interaction, distribution and cooperation. There is an urgent need for a new computer system, which can support group activities and enable the group members to coordinate and cooperate with each other. This has lead to a new technical field: Computer Supported Cooperative Work (CSCW), which can be defined as group cooperative work to accomplish a common task in a computer-supported environment (CS).

The earliest CSCW research started in the 1960s, D.Eaglebart[1] first developed an experimental system called NLS/AUGEMENT, and implemented the concept of hypertext, which is an information network composed of information nodes and links between nodes. Since the 1980s, with the development of the related technologies such as computer networks, multimedia technology, data compression and storage, CSCW has become the focus of much work by many researchers. In 1984, Iren Grief of MIT and Paul Cashma[2] of Digital Equipment Corporation organized a workshop to explore technology's role in the work environment and coined the term "computer-supported cooperative work" to describe it. In the construction field, CIFE (Center for Integrated Facility Engineering) [3] of Stanford University has undertaken a series of research projects on Internet collaboration in construction management since 1999. But still, there is no practical CSCW system that can completely meet the requirements of project management, because of the wide dispersals of the many parties and the complexity of construction management.

As we all know, during the construction phases of a project, many different developer, designer, contractor project teams work together and various specialist sub-contractors. These teams usually work in different places and need to frequently exchange information. However, these are always obstructions in information exchange between working teams and personnel. As modern construction projects are getting larger in scale, and the regulations, limitations and complexity for construction organizing increase, these obstructions and the influence then exert have become serious. The requirement for more effective communication and real time sharing of information between distributed teams has become even greater. In project implementation, it is necessary to achieve united management, leading into CSCW and developing an effective computer information management system. The generation of a new cooperative management environment can reduce and even eliminate the communicate obstructions caused by space and time isolation, so as to fulfill the purpose of information sharing, improving the working environment, reducing working intensity, saving time and cost, and raising the efficiency and technical level of the construction engineering management.

During this research, a 4D site management model (4DSMM) has been generated, which links a 3D model of a construction project with a project activity schedule, each activity suitably annotated with its resource requirements including material, plant, cost and work space [4]. A computer system for the 4D Management of Construction Planning and Resource Utilization (4D-MCPRU) based on the 4DSMM has been also developed. This system achieves dynamic

construction planning and resource management including site space utilization at the project level and 4D visualization and decision-making support within the construction process, so that an environment for exchanging and sharing information can be provided among the various management departments of a construction contractor [5]. Our current research work has mainly focused on those extensions to the 4DSMM concept necessary to generate a new 4D-CSCW model for construction management through integrating the CSCW technology, which allows cooperative working and decision making, and communicating and sharing information by computer network for different project teams, and the development a new experimental system.

4D-CSCW MODEL

Concept of 4DSMM

4DSMM[4] consists of the 3D model of the project coupled with a construction schedule, and allows incorporation of the 4D model into the whole site management information system and for dynamic resource management at project level, through the provision of decision-making support. 4DSMM has construction progress information features added and performs a number of site management functions over space and time. 4DSMM provides an information platform that allows dynamic site planning through the 3D model and the schedule to implement construction planning, analysis of resource requirements for each construction activity, assignment of construction resources and displays of site utilization. Extra to the traditional 4D simulation, a most notable feature of 4DSMM is the mechanism of two-way data exchange between the 4D model and scheduling information, which enables dynamic resource management, including material, equipment and labor usage and cost control at project level. This means that project managers can adjust resources plans according to changes of schedule in a timely manner. Figure 1 describes the organization of the 4DSMM model.

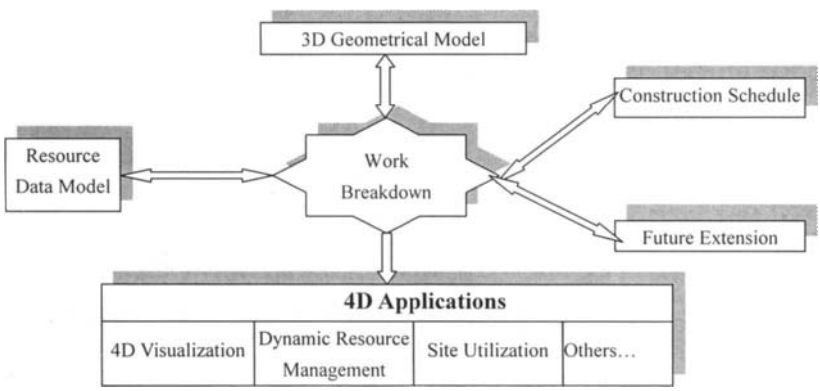


Figure 1: The 4DSMM Model

Architecture of 4D-CSCW

According to the architectures of popular CSCW systems, and considering the actual requirement and work flow in construction project management, the 4D-CSCW model adopts a centralized structure based on Client/Server mode. The 4D-CSCW involves a 4D application module, cooperation agent module, communication management module and a cooperative management module. The logical relationship between them is shown in figure 2.

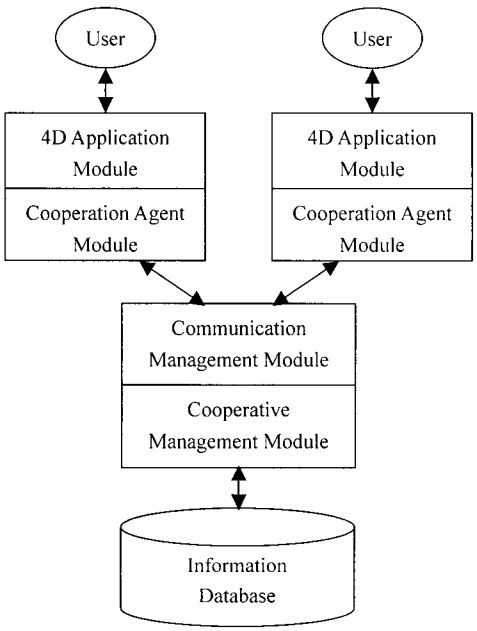


Figure 2: Architecture of 4D-CSCW

1. ***The 4D application module*** is user-oriented and concerned with how persons interact with the computer system in carrying out the overall function for inputting, modifying and browsing all project information including the generation of the 3D model of the project and the additional properties for any 3D object, manipulation of the Work Breakdown Structure (WBS) data, the access construction schedule information, the inquiry of various management data and so on. In this module, a 4D management engine is developed to link the 3D model with a project construction schedule automatically and describe the state of a site at any stage. It is pivotal for 4D simulation of the construction process, material quantities calculation, workspace analysis, and costs estimation. A graphical cooperation demonstration is also provided to complete real-time cooperative management based on sharing the application program and information.

2. ***Cooperation agent module*** is the core of the client in this system which can catch users'

operation commands with the event-driven program, transform them into a series of messages in a certain format and send them to the server of the system. The server can then transmit the messages to other cooperating parties. This module can also receive and process the operation messages from the server.

3. ***The communication management module*** is a message transmitter and manager on the server of the system. It mainly provided the functions for connecting and disconnecting users, responding to requests, and receiving, analyzing, processing and sending all messages.

4. ***The cooperative management module*** is the kernel of the whole cooperation system that resides on the server and completes the tasks of identifying the users, assigning responsibilities, controlling of user authorities and managing data.

Working Mode of 4D-CSCW

According to the spatiotemporal concept, group cooperation work can be classified into 4 work modes: (1) Synchronous mode cooperation work for common tasks at the same time and one place, such as mutual decision making, document compiling, computer aided design and indoor conferencing; (2) Distributed synchronous mode cooperation work for common tasks at the same time but different places, like co-design, co-editing, group decision making and video conferencing; (3) Asynchronous mode cooperation work for a common tasks at one place but not the same time, such as rotational working; (4) Distributed asynchronous mode cooperation work for the same task at different times and places, e.g. the development of a large-scale project.

Based on the characteristics of the construction industry with its usual requirements for project management and the need for maintenance of the system and reliability, 4D-CSCW uses two different working modes within a group and between various groups. The group members conduct real-time cooperative management with the synchronous mode within a group (i.e. design team, project management department), so as to exchange and share real-time information. Cooperative working between groups uses the distributed asynchronous mode, such as E-mail, WWW pages or Bulletin Board Systems for information release.

Database for Supporting Cooperative Work

Since the CSCW system possesses features for grouping, cooperation, distribution, and are dynamic, it is difficult to meet systems demands with a traditional relational database. A new database system that can support CSCW has been created to solve the problem on how to store, share and exchange data among systems for different purposes. The database contains a great deal of graphic data to represent the 3D geometrical model, non-graphic schedule data and all resource information, such as the WBS system, cost accounting, and material, equipment and labor management etc. Except for data storing and managing as above, this

database also has the following features for supporting CSCW:

1. **Man-man interaction** A predefined access interface is provided so that different modules will utilize the data for different purposes, and support the interaction between the group members. Each member can not only view, access and use the shared data, but also can be aware of any data operation by other members, and receive notification on data alterations.

2. **Management of nonstructural data** One significant enhancement of the database is the ability to organize, manage and access the nonstructural data by use of an index mechanism. This is to enable the effective storing and managing of complex information, such as multimedia data, special data, temporal data, complex objects, images, knowledge, ultra text.

3. **Synchronous and asynchronous working mode** The database can support the two working synchronous and asynchronous modes. A key objective is to provide real-time operation data for different purposes of the cooperative working.

4. **Cooperation work** Since the CSCW system involves the cooperation among several members, it is necessary to reserve past records for every member. The rollback ability of the cooperative working procedure is also needed in asynchronous mode.

Parametric 4D Construction Feature Model

In the 4DSMM model, the construction properties attached to the 3D solid model are used to provide the information about the structure components. They accurately and actually describe the shape and size of a structure component and finished state of the permanent work of a construction project. However this model, with its large amounts of stored information, is not suitable for network transmission. A new model description method is therefore needed to decrease the volume of data transmission.

A feature-based components model has been studied to establish a parametric construction features model. This model contains the geometry information for all structural components, CAD topology information, and components engineering information etc., and has the ability to greatly reduce the storage space needed by the model, and speed up network transmission. It can also be transformed into typical engineering drawings through a features database of the structure model, so as to achieve a graphical display of the features model.

In the features model, the following information must be included:

Global Information	—	Component Type
		WBS Code
		Component Shape and Size
		Component Position
Material Information	—	Material Type

		Material Specification
Construction Information	—	Working Flow Working Status Starting Time Finishing Time
Resource Requirement	—	Labor Material Equipment Site Space

Using a parametric features model also makes it possible to completely solve the problem of data exchange and sharing during construction progress including the construction schedule, quality control and resource management data, and to meet the requirements of 4D-CSCW for data sharing and transmission by computer network, so as to assure the consistency between geometric drawing and features data in the system. The object-oriented method also makes it possible to easily add new feature properties to the model, and is beneficial to the system extension.

KEY TECHNIQUES

System User's Role Control

Under the cooperative working environment, every one who enters the 4D-CSCW will act a certain role, and has different levels of authority to access different resources. How to control the user's authority limits is a very important problem. In the system, the controlling role-accessing right could solve this problem. First of all, the people who work for the same goal will be organized into a group, e.g. developer, contractor or specialized department, and sub-contractor, etc. In a working group, all the members are organized together with a certain type of relationship, e.g. equality relationship, master-slave relationship and client/server relationship. The different users act different roles with certain rights, which can be entrusted by data access authorities and cooperative operation authorities. There are several kinds of user role authority, such as accessing right, browsing right, modifying right, copying right or voting right, which determines whether the user can view the actual fact of the cooperation procedure, or whether the user can browse, modify related contents, can privately keep a copy of a common document, or whether the user has a voting right through cooperative discussion. With this role control measure, we can conveniently accept the dynamic change of a user's role and position, beneficial to both security and confidentiality in cooperation.

System Concurrent Control

In 4D-CSCW, one major feature is cooperative work among multi-users. Every user needs to

immediately perceive another user's operation for sharing data at the same time. To avoid the inconsistency of the sharing of objects, which occurs under multi-user concurrent operations, the system must provide concurrency control to solve conflicts caused by simultaneous operation.

The methods of achieving system concurrency control mainly are locking, centralized control, transaction mechanism, dependent test, reversible execution and operation conversion, etc. Two methods are designed and implemented in the 4D-CSCW for achieving system concurrent control. The locking and unlocking of the shared data is implemented and the concurrent operation of user by a locking mechanism control. However, this would affect rapid feedback to the user, but this locking control of shared data is effective and easy to operate and implement. The centralized control method is used to manage all the sharing objects operations to ensure consistency of the data, and to receive the users' data operation requests and broadcasts to all the users, so that orderly operations are enabled.

CONCLUSION

In view of the complexity of construction management with its many parties on different place and the requirement for more effective communication and real time sharing of information between distributed teams, a new 4D-CSCW model for construction management has been generated by integrating CSCW technology with the existing 4DSMM model developed by the authors. This model provides a cooperative working environment for cooperative working and decision-making, and for communicating and sharing information by computer network between different project teams and between managers. The application of the new model would reduce delays in the project schedule and losses caused by inefficient information transmission, and further improve information management in the construction domain.

REFERENCES

[1] Qing-hua ZHENG., Theory, Implementation & application of CSCW: Computer Science, 1996, 2 3(5): 18-22.

[2] Jonathan Grudin. Computer-supported cooperative work: History and focus. IEEE Computer, 1994, 21 (5): 19-26

[3] CIFE, Summaries of CIFE Research Projects for 1993 – 2002, Web page www.stanford.edu/group/CIFE/Publications/index.html

[4] Jian-Ping ZHANG, M. ANSON and Qian WANG, A New 4D Management Approach To Construction Planning and Site Space Utilization, Computing In Civil Engineering, 2000, pp15-22.

[5] J. P. Zhang, H. J. Wang, K.W. Chau and M. Anson, Towards 4D Management for Construction Planning and Resource Utilization, Computing in Civil Engineering, 2002, pp1281-1286.

Advances in Building Technology, Volume 2
M. Anson, J.M. Ko and E.S.S. Lam (Eds.)
© 2002 Elsevier Science Ltd. All rights reserved

THE IMPLEMENTATION OF KNOWLEDGE MANAGEMENT AND ORGANISATIONAL LEARNING IN CONSTRUCTION COMPANY

Dr Patrick X.W. Zou and Chie-Ann Lim

Faculty of the Built Environment, The University of New South Wales,
UNSW Sydney 2052, Australia; email: p.zou@unsw.edu.au

ABSTRACT

While organisational learning (OL) has been implemented in many companies, knowledge management (KM) has also become a new buzzword in the managerial world. Many commercial sectors have effectively adopted the concepts of KM and OL into their management system to improve their competency in the competitive business environment. However, construction company has not yet shown significant application of these concepts, despite it is also a competitive industry. This paper aims to encourage the implementation of KM and OL in construction company by providing an overview of the principles, along with a proposal of KM--OL model that is designed to best-fit the construction business environment.

KEYWORDS

Knowledge management, organisational learning, construction management, knowledge planning, knowledge organising, knowledge implementing, knowledge controlling, knowledge evaluating

INTRODUCTION

From the revolution of information technology, the technical capabilities that are available for storing, analysing, and transmitting information have been greatly increased. New information technology capabilities enable a company to improve its effectiveness in gaining, using or communicating knowledge from one person to another (Bernbom, 2001).

Knowledge is about understanding the meaning of information (Benson and Standing, 2002). As the 'knowledge era' grows and becomes more important, construction company needs to shift their focus from information management to KM. This paper focuses on the implementation of KM in construction company and discusses it in the context of encouraging OL culture. The paper also provides an overview of KM and OL principles, along with the proposal of a KM--OL model that fits construction business environment.

KNOWLEDGE MANAGEMENT

At present, there are no universally accepted definitions of KM. The intention of this section is to draw a definition for KM from a construction contractor's perspective. Numerous definitions of KM are collected from literature and these are summarised in Table 1.

TABLE 1 DEFINITIONS OF KNOWLEDGE MANAGEMENT

Authors	Definition
Spek and Spijkervet (1997)	'is the explicit control and management of knowledge within an organisation aimed at achieving the company's objectives.'
Webb (1998)	'the identification, optimisation and active management of intellectual assets to create value, increase productivity, and gain and sustain competitive advantage.'
Borghoff and Pareschi (1998)	'the management of the environment that makes knowledge flow through all different phase of organisational process life-cycle.'
Laudon and Laudon (1999)	'a process of systematically and actively managing the stores of knowledge in an organisation.'
Wiig (1999)	'the systematic and explicit management of knowledge-related activities, practices, programs, and policies within the enterprise.'
Beckman (1999)	'is the formalisation of and access to experience, knowledge, and expertise that create new capabilities, enable superior performance, encourage innovation, and enhance customer value.'
Rosenberg (2001)	'a system that supports the creation, archiving, and sharing of valued information, expertise, and insight within and across communities of people and organisations with similar interests and needs.'
Bernbom (2001)	'the fundamental about the discovery and capture of organisational knowledge, the filtering and arrangement of this knowledge throughout the organisation.'
Benson and Standing (2002)	'is concerned with automating and externalising explicit knowledge and devising support mechanisms to facilitate tacit knowledge transfer, including creation of knowledge.'

In fact, KM practices reach beyond the boundaries of computers and networks and it includes non-technical activities such as training and development, human resource management, intellectual property management (Bernbom, 2001), and organisational learning (Nonaka et al, 2001). In this paper, from the construction contractor's perspective, KM is described as:

'the management processes (including planning, organising, implementing, controlling and evaluating) of creating, capturing, transferring, sharing, retrieving, and storing of data, information, knowledge experiences, and skills by using appropriate information and network technology, with the endorsement of total involvement in organisational learning to enable knowledge acquisition throughout the processes.'

This concept addresses the viewpoint of 'it is the KM that facilitates and enables OL in a company', and this will be discussed in detail later.

ORGANISATIONAL LEARNING

There are articles suggest that not only KM itself is critical; OL is another issue that should also be addressed. Dixon (1999) states that 'knowledge is the result of learning and does ephemeral, constantly need to be revised and updated'. The author also claims that 'learning is the process that leads to knowledge'. In addition, Malhotra (2000) claims that '...information archived in a database doesn't ensure that people will necessarily see or use the information'. No matter how perfect a KM system being set up, it will just exist in name only if the organisation does not have a culture of 'willing to learn' and 'willing to share what's being learnt'. Thus, the concept of OL is recommended to balance any inadequate of KM implementation.

Organisation composes of intelligent adaptive agents and knowledge. Consequently, organisations themselves are synthetic agents in which knowledge and learning reside in the minds of the participant agents and in the connections among them (Carley and Hill, 2001). Nonaka et al. (2001) view an organisation as an entity that creates and utilises knowledge continuously and dynamically. They define OL as 'the interaction among individual learning which create knowledge in an organisation'. Further to this, Duncan and Weiss (1979) define OL as 'the process by which organisation members develop knowledge about action outcome relationships and the effect of the environment on these relationships, which leads to growth and change of organisational knowledge'. Other authors, such as Bennis and Nanus (1985) view OL as a set of processes used to obtain and apply new knowledge, behaviour, tools and values.

THE NEED OF KNOWLEDGE MANAGEMENT AND ORGANISATIONAL LEARNING IN CONSTRUCTION COMPANY

As the strategic management of intellectual assets (knowledge) is becoming major policy area for modern corporations (Neef, 1998), KM and OL are, therefore, not only key functions of the commercial world, they are also relevant and applicable to construction companies. In construction company, KM and OL are required to provide sustainable continuous improvement in its competitive and fragmented environment. If knowledge is the key of an organisation's long-term competitive advantage, it is incumbent upon organisations to help their employees to apply their knowledge and skills to the best.

Maxwell-Hart and Marsh (2001) have classified the modern construction management into 12 key roles. These include (1) corporate management, (2) business management, (3) financial and management system, (4) project management, (5) promotion and business development, (6) information and communication technology, (7) commercial and contractual practice, (8) communications and presentations, (9) health, safety and welfare, quality and environment, (10) respect for people, (11) client relationships, and (12) the construction profession in society. It is inevitable that every role requires the utilisation and application of skills, understanding, knowledge and experience in particular aspects. Maxwell-Hart and Marsh (2001) have then suggested four levels of competence for continuous improvement in management roles. These levels including:

- Appreciation – know what a term means and what its purpose and objective is.
- Knowledge – understand in detail the principles of the topic and how and where they applied to.
- Experience – have acquired working knowledge and skill.
- Ability – be able to fully apply skill with desired results.

It is clear that KM and OL has become an important issue in model construction management. KM and OL should be considered in each of these 12 key management roles, in order to achieve a higher level of competence and continuous improvement in a construction company.

A PROPOSED KM--OL MODEL FOR CONSTRUCTION COMPANY

In order to keep the business continuous growth, construction company is now required a specific tailored yet comprehensive KM and OL model. Thus, a KM--OL model is proposed to fit and fulfil these needs and this is shown in Figure 1 below:

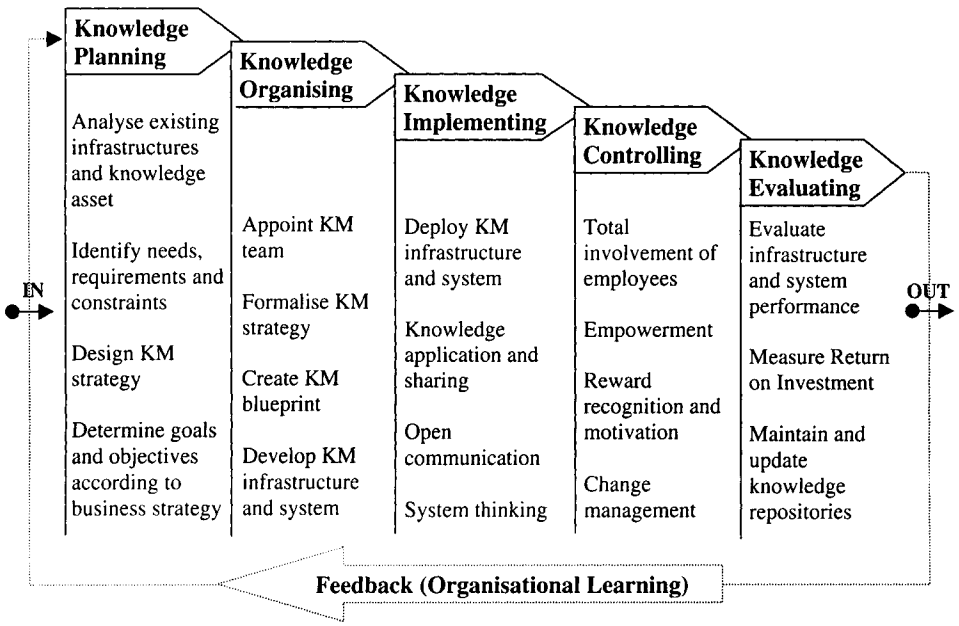


Figure 1: Proposed KM--OL Model for Construction Company

Knowledge Planning

The first stage for the application of KM and OL in construction company is the knowledge planning stage. How could knowledge be planned? This is just a concept. In the planning stage, the company management should analyse the existing infrastructures and knowledge assets they have, followed by identify the needs, requirements and constraints. Then, a primary KM strategy can be designed in accordance with the goals and objectives of business strategy determined. The knowledge infrastructures are the technologies used to facilitate KM in capturing, sharing, storing, retrieving and distributing knowledge throughout the company. They can be company existing intranet, data warehouse or project management tools. The analysis can be done by listing all existing infrastructures and systems in a checklist, including detail explanations of each infrastructure to be used in supporting KM. Besides, the existing knowledge asset, such as codified information, previous projects and historical records, should be identified in another checklist. This is to determine which type of knowledge is useful and can be reused in the company KM system. The understanding of these existing infrastructures and assets can assist in determine the needs of KM support as to identify the requirement for KM implementation. More crucially, it provides the ground for construction company to analyse its strength, weakness, opportunities and threats (SWOT) in application of KM and OL.

The design of KM strategy must be properly aligned with company business strategy so that both are able to drive each other toward the company goal and vision. Before that, a clear company vision is

essentially required. The company's vision can be effectively expressed to employees by using cryptic slogans. According to Nonaka (1998), cryptic slogans are highly effective tools for knowledge-creating companies in Japan. The key principle of this tool is the personal commitment which creates employees' sense of identity with the company and its mission. With the clear company vision, KM system can be designed in conjunction of both KM and business strategies. A well-designed KM system should include the following characteristics:

- Easy to use, easy to access at anytime and from anywhere,
- Flexible and scalable,
- Interoperatable,
- May be informal,
- Able to support collaborative works, and
- Support organisational learning.

Knowledge Organising

A cross-functional KM team, comprising senior management personnel and various representatives from company internal departments, should be established to analyse and integrate the knowledge asset within the company operations. The KM team has responsible to adapt the KM system in their departments so that knowledge can be fully utilised and best fit into the management systems. The development of KM infrastructure and system requires best practice knowledge repository which must include an appropriate knowledge resource navigator in the system to guide users in searching knowledge. Besides, the system must be able to support collaborative work by allowing e-conference and net meeting. The knowledge infrastructure can be organised by combination of different technologies. For instance, knowledge repositories, communication networks and collaborative platform (Tiwana, 2000) are suitable infrastructures to support KM. Knowledge repositories should contains both employees' knowledge and company's knowledge. Employees' knowledge, including their basic directories, skills, experiences, and expertises can be converted into company's knowledge, which comprise of company background information, operation experiences, and corporate visions. Thus, the knowledge that, perhaps, permanently stored in the repositories will become the company's valuable asset to enhance decision support system and case-based reasoning approach. The communication network should go beyond the company intranet system. The network system should be able to facilitate collaborative synergy, decision support, team learning and even informal conversation among users. In addition, knowledge servers should be used to provide the collaborative platform. This collaborative platform must include a comprehensive search engine that provides easy access to knowledge when acquired. Moreover, it should facilitate virtual meeting and conferencing on net so that tacit knowledge is able to communicate among users. In developing the KM infrastructures and systems, it is advisable to fully utilise the existing infrastructures and extend the facilities if necessary. Certainly, appropriate cost planning is required to keep the whole process in budget.

Knowledge Implementing

Once the KM infrastructures being set up, the capturing, transferring, sharing, storing and retrieving of knowledge can be deployed even if the systems have not yet been completed. Testing of the KM system can be carried out by studying on a pilot case or project to identify any pitfalls of the systems. From the testing process, KM system can be modified and upgraded to the preferences of the company. Knowledge application and sharing from the employees must be encouraged. Training is required for the employees to get familiar with the new systems. Employees should be familiar with the search engine and make use of it to search for knowledge they need while contributing their experiences and knowledge to the systems. Open communication must be encouraged in a successful KM system. Shared knowledge requires the creation of shared context (Tiwana, 2000). Every one in the company should be allowed to contribute and access to knowledge at anytime and from anywhere. Any new

knowledge updates should be immediately available to all users. However, confidential and private records must be protected. In addition, system thinking should be promoted among the employees for a complete implementation of KM system. System thinking is frequently used in problem solving, which emphasise on the aspects of the entire system surrounding a problem are taken into account and dealt with to satisfy all needs and constraints (Modarres and Bahrami, 1997). By applying system thinking, employees are able to consider and appreciate the full range of issues in establishing the KM system and generate innovative solutions to meet the new KM system.

Knowledge Controlling

Total involvement of all employees is essential to ensure the KM is deployed effectively. Ranging from office employees to construction site staffs, the understanding, participation and contribution to the vision of KM system should be thoroughly spread. If the member of company does not clearly understand the goals of the process, then commitment to a complete examination of the KM operations, processes, and future cannot be guaranteed (Chinowsky and Meredith, 2000). To a certain extent, employees should be empowered to participate in creating and modifying of company's decision support system through proposed KM system. The culture of knowledge sharing among employees should be encouraged. Thus, a strong reward recognition structure must be introduced in company to integrate the KM system into employees' learning culture. The employees who contribute to the KM system can be rewarded by financial incentive, evaluation, and promotion system. In addition to the reward recognition, appropriate motivation approaches should be used to enhance the employees' commitment to the new KM system. Organising knowledge campaigns, providing equal opportunities, allowing freedom of activity, upgrading working and learning environment, financial assistants, and medical allowances are some good approaches to motivate employees. After the KM system is built, the challenge is now shift to the management of cultural changes in the company's operations. Basically, managing change falls into three categories: structure, technology and people. This involves making an alteration in authority relations, coordination mechanisms, job redesign, changes in employee attitudes, skills, expectations, perceptions, and/or behaviour. To manage these changes, construction company should have change-development program interventions built on humanistic-democratic values that seek to improve the KM system's effectiveness and employee well-being. The program should include valuation of human and company growth, collaborative and participative processes, and a spirit of knowledge inquiry. Moreover, it should include sensitivity training, survey feedback, process consultation, team building, and intergroup development.

Knowledge Evaluating

The evaluation of KM performance can be conducted based on the measure of client's satisfaction levels, operational efficiency, staff motivation and competency, quality and improvement programs, employee turnover, and time taken in training (Edvinsson and Malone, 1997; Sveiby, 1997). The evaluation for Return on Investment (ROI) should be carried out in the way of expressing profit margin that comparing profits to value-added created, rather than to revenues. The measures should focus on resources such as the intellectual assets, which should consist of the following components (Sveiby, 1997):

- Growth/renewal – duration of experience, level of education, training costs, professional grading, and number of contracts secured from clients.
- Efficiency – ratio of professionals and value-added per professional.
- Stability – employee age, seniority ratio, and employee turnover rate.

A successful KM system must have the perspective on the past, present and future. Therefore, on-going management support and maintenance is needed for knowledge strategy and KM system in construction company.

Feedback (Organisational Learning)

The entire system learns as it interprets signals from the feedback of KM processes and enables planning for the future change. The feedback from KM system provides systematic and structured knowledge as the ground for OL. Therefore, construction company has the obligation to provide employees the opportunity to learn via shared knowledge, task assignments, and job rotation in the KM system. There is no generic solution in OL. However an approach can be modified from Kolb's Learning Cycle (cited by Bessant, 2000), as shown in Figure 2. This approach includes four phases – experiment, experience, reflection and conceptualisation.

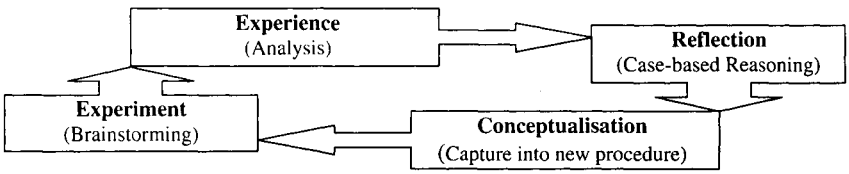


Figure 2: Modified Kolb's Learning Cycle

A good learning culture is vital for the establishment and development of a good KM system in construction company. The organisational cultural factors can eventually shape, underpin and support the overall effectiveness of the KM and OL model. The cultural factors to be taken into consideration include:

- Willing to share,
- High trust and mutual respect,
- Cooperation and collaboration, and
- Team learning – 'win-win' learning relationships.

KM--OL Model as Total Approach

As a whole, the KM--OL model described can be viewed as a total flexible approach that is suitable for construction company to implement KM in enhancing the ability to adequately respond to clients' requirements and its fragmented business environment. The model provides a mutually exclusive approach that is appropriate to use within the 12 roles of modern construction management described by Maxwell-Hart and Marsh (2001). This involves the creating, capturing, transferring, sharing, retrieving, and storing of knowledge, as well as learning, across different management roles in construction company and harnessing per capital knowledge from each construction project.

CONCLUSIONS

The paper has proposed a KM definition from construction contractor's perspective and a KM--OL model for construction company. The strategies and approaches that underpin the model have also been described. As the model indicates, OL can only be achieved when knowledge is captured and transferred. Therefore, it is the KM implementation that enables and improves the process of OL in construction company. The implementation of KM and OL should be focused mainly on the processes rather than solely on technology. Thus, the culture, behaviour and perspective towards the implementation of KM and OL should be placed at the first place. Although the KM--OL model is proposed, the viability is still inconclusive. Further research should focus on identifying and evaluating the real practical strategies of KM and OL application in construction company.

REFERENCES

Beckman, 1999, The Current State of Knowledge Management, in *Knowledge Management Handbook*, Liebowitz, CRC Press LLC.

Bennis W. and Nanus B., 1985, Organisational Learning: The Management of the Collective Self, *New Management*, 3 (1), 7-13.

Benson and Standing, 2002, *Information Systems: A Business Approach*, John Wiley & Sons Ltd.

Bernbom, 2001, *Information Alchemy – The Art and Science of Knowledge Management*, Jossey-Bass Inc., California, USA.

Bessant J., 2000, Learning and Continuous Improvement, *From Knowledge to Strategic Competence: Measuring Technological, Market and Organisational Innovation*, Joe Tidd, Imperial College Press.

Borghoff and Pareschi, 1998, *Information Technology for Knowledge Management*, Springer, Verlag Berlin Heidelberg, New York.

Carley and Hill, 2001, Structural Change and Learning within Organisations, in *Dynamics of Organisations: Computational Modelling and Organisation Theories*, AAAI Press/The MIT Press.

Chinowsky and Meredith, 2000, *Strategic Corporate Management for Engineering*, Oxford University Press, New York.

Dixon, 1999, *Common Knowledge – How Companies Thrive by Sharing What They Know*, Harvard Business School Press, USA.

Duncan R. and Weiss A., 1979, Organisational Learning: Implications for Organisational Design. *Research in Organisational Behaviour*, 1, 75-123.

Edvinsson L. and Malone M., 1997, *Intellectual Capital: Realising Your Company's True Value By Finding its Hidden Brainpower*, Harper Business Press.

Laudon and Laudon, 1999, *Essentials of Management Information Systems – Transforming Business and Management*, 3rd Edition, Prentice-Hall, Inc., New Jersey, USA.

Malhotra, 2000, *Knowledge Management for E-Business Performance: Advancing Information Strategy to Internet Time*, available at <http://km.brint.com>, [accessed March 2002]

Maxwell-Hart G. and Marsh G., 2001, *Management Development in the Construction Industry*, Institute of Civil Engineers, Thomas Telford Publishing, London.

Modarres M. and Bahrami A., 1997, Corporate Downsizing: Preserving the Core Knowledge Base by Utilising Expert Systems, Strategic Decision Support Systems, and Intelligent Agents, *Knowledge Management and Its Integrative Elements*, Liebowitz J. and Wilcox C., CRC Press.

Neef, 1998, *'The Knowledge Economy'*, Butterworth-Heinemann, USA.

Nonaka I., 1998, The Knowledge-Creating Company, in *Harvard Business Review on Knowledge Management*, Harvard Business School Press.

Nonaka I., Reinmoller and Toyama, 2001, Integrated Information Technology Systems for Knowledge Creation, *Handbook of Organizational Learning and Knowledge*, Oxford University Press.

Rosenberg, 2001, *E-Learning – Strategies for Delivering Knowledge in the Digital Age*, McGraw-Hill Companies, Inc., USA.

Spek and Spijkervet, 1997, Knowledge Management: Dealing Intelligently with Knowledge, in *Knowledge Management and Its Integrative Elements*, Liebowitz and Wilcox, CRC Press LLC.

Sveiby K., 1997, *The New Organisation Wealth: Managing and Measuring Knowledge-Based Assets*, Berrett-Koehler Publishers.

Tiwana, 2000, *The Knowledge Management Toolkit – Practical Techniques for Building a Knowledge Management System*, Prentice-Hall, Inc., New Jersey.

Webb, 1998, *Knowledge Management: Linchpin of Change – Some Practical Guidelines*, Aslib, The Association for Information Management, London.

Wiig, 1999, Introducing Knowledge Management into the Enterprise, in *Knowledge Management Handbook*, Liebowitz, CRC Press LLC.

This Page Intentionally Left Blank

Advances in Building Technology, Volume 2
M. Anson, J.M. Ko and E.S.S. Lam (Eds.)
© 2002 Elsevier Science Ltd. All rights reserved

A PROTOTYPE OF KNOWLEDGE-BASED DECISION SUPPORT SYSTEM FOR CONSTRUCTION COST MANAGEMENT

Patrick X.W. Zou [1] and Cynthia C.X. Wang [2]

[1] Faculty of the Built Environment, The University of New South Wales,
UNSW Sydney 2052, Australia; email: P.Zou@unsw.edu.au
[2] Faculty of Design, Architecture and Building, The University of Technology Sydney,
Broadway NSW 2007, Australia; email: cynthia.wang@uts.edu.au

ABSTRACT

With a broad literature review, this paper highlighted the need of high level decision support systems for the industry and the possibilities of developing such system that is provided by the current information technologies. It was revealed that a range of cost-control and cost estimating softwares are available in the market. However, these softwares are mainly low-level computer-based systems for data storage/retrieval and cost calculation, high-end softwares with ability of data analysis and managerial decision support are rare. The paper hypothesises that in the future software for cost management in construction should focus on the implementation of expert knowledge, *i.e.*, the ability and expertise to apply the cost rate and other data in cost control, along with construction experience and make correct decisions in the competitive market. The design of a prototype of such decision support system is presented in this paper. This system is web-based and is an integrated suite of tools employing four software sub-products, which link to a comprehensive knowledge database. This knowledge base is the backbone of the system, and is accessible from any level within the system to provide support for better decision-making in cost management.

KEYWORDS

Decision support system, construction cost management, knowledge base, statistical analysis, what-if analysis, system functions

INTRODUCTION

Construction managers make many of small or big decisions during the management of a construction project. Their decision making is based on information in a wide area, including legal requirements, building codes and standards, manufacturer's specifications, material costs, site-specific data, and experience gained from past projects, *etc.* As building construction is such an information intensive industry, it is necessary to develop computerised decision support tools/systems to improve their effectiveness in the planning stage of construction projects.

Due to the recent availability of highly sophisticated software development tools, more accurate process models and more effective decision support systems can now be developed much more quickly with reduced cost. The opportunity now exists to quickly identify the systems most needed and to develop the tools that will enable the participants in the construction industry to plan and function more effectively and efficiently.

In this paper, a broad literature review was conducted in the area of building construction for decision support systems and cost management systems. Based on the findings from the literature review, a design of the prototype of a knowledge-based decision support system for cost management is presented.

LITERATURE REVIEW

Decision Support System

The research on decision support system in construction industry only started recently. Applications on various areas in construction industry have been identified in the literature.

Couzen *et al.* (1993) presented an executive information system for construction contract bidding decisions. Brightman *et al.* (1999) have been working with managers from a number of construction firms in order to develop a decision support tool to inform and support strategic thinking. Their work led to the creation of a Construction Alternative Futures Explorer (CAFE) - a computer based package which provides a means of structuring and analysing soft data, about possible future business environments.

Leu *et al.* (2000) developed a prototype of a decision support system for construction resource levelling. Construction planners can interact with the system to carry out *ad hoc* analysis through "what-if" queries. Hegazy *et al.* (2000) developed a simulation model of the operations for an actual design firm, which enables the analysis of resource optimisation needs.

The Construction Primer is a computer-aided design decision support system which was used as a learning-aid for students of architecture and building in New Zealand and Australia. Burry *et al.* (2001) described it as a database-drivable interactive multimedia environment that provides readily updated access to many levels of information.

Rule-based expert systems and artificial neural networks are two major systems for developing intelligent decision support systems. Li and Love (1999) presented a computer based mark-up decision support system called InMES (integrated mark-up estimation system) that integrates both rule-based expert system and neural networks.

Rule-based systems can be applied to a number of problems. The primary strength of these systems lies in their capacity to provide explicit explanations to their output. The explanation capacity enables users to understand the logic reference of why and how the output is reached, and increased the user acceptance of the output. However, directly implanting knowledge into rule-based expert systems is a tedious and labour intensive task, recent studies have focused on the automatic acquisition of knowledge for developing knowledge bases (Quinlan, 1986 and Li, 1994).

In summary, there have been efforts in developing decision support systems in contract bidding, resource levelling, mark-up estimation, evaluating business environment and construction related teaching and learning, *etc.* The continual advances in computer technology have created a potential for further improvement of these systems and expand its usage to other areas in the construction industry. These areas include networking multidiscipline teams, planning construction activities, project cost management, project status-report, and assisting project transaction and communication processes, *etc.* The following sections will focus on construction project cost management systems.

Cost Related Computer Systems

An investigation of software usage in cost estimation and management has been conducted. The literature search reveals an enormous number of cost-related softwares available in the market (Web Ref. 1-18). Most of them are targeted for specific industries such as building construction (Web Ref. 2, 4, 7, 10,14, 15, 17), social service and telecommunications (Web Ref. 3), manufacturing (Web Ref. 6, 8, 13), airspace industry (Ref. 12), while some of them (Web Ref. 1, 5, 11, 18) are general-purpose software packages. Cost optimisation of construction projects reported in the literature is limited to critical path method (CPM) or CPM-like models of the project (Liu *et al.* 1995, and Feng *et al.* 1997).

The main functions included in these estimating packages can be summarised as follows:

1. Importing quantity data.
2. Assemblies.
3. Calculation sheets.
4. Subcontractor bid analysis.
5. Calculating costs.
6. Export to scheduling and cost management software.
7. Overheads and profits.
8. Presenting the data in various formats.

There are also some other softwares evolved from the traditional accounting and cost management software packages (*e.g.*, Web Ref. 7). They often have all the normal accounting facilities as well as the estimating functions mentioned above.

It is found that most of the cost-related softwares in construction industry are estimating softwares connected with a database (Web Ref. 2, 10, 13, 14, 15). They represent low-level software systems for data storage, data retrieval, and calculating processes. These softwares are very mature in terms of technologies and functionalities. However, in construction industry, it is not enough for project managers and cost engineers to merely have project data, the more important thing is to analyse the data and make use of it. In order to do this, knowledge on the data and its interpretation is essential. These findings indicate that the future software for cost management in building construction should focus on the implementation of expert knowledge, which is the ability and expertise to apply the cost rate and other data in cost control and make correct decision in the competitive market.

The scale and complexity of a decision support system is governed by the scale and complexity of the data and expert knowledge involved in the decision making. A common theme amongst designers and developers is that prototype models are essential to building a successful decision support system. Prototyping can help users who often find it hard to state their information needs. Analysts and software developers learn immense amounts from building prototypes and from the users' reaction to them. This paper aims at providing the design guidelines of a prototype of a knowledge-based decision support system for cost management in construction industry, which can be used for evaluation and refinement.

A PROTOTYPE OF KNOWLEDGE-BASED DECISION SUPPORT SYSTEM FOR CONSTRUCTION COST MANAGEMENT

Types of Knowledge and Knowledge-Based System

There are different classifications of knowledge proposed by different researchers (*e.g.*, Machlup, 1980 and Holsapple, 1995, *etc.*). In this paper, the knowledge types initially proposed by Holsapple (1995) is adopted. Six knowledge types are included in this classification and they are: descriptive, procedural, reasoning, linguistic, assimilative, and presentation knowledge.

Knowledge about the state of some world is called descriptive knowledge. It is more commonly referred to as data, or information. The historical bidding records, material price, labour costs, *etc.* are descriptive knowledge.

The procedural knowledge is concerned with a step-by-step procedure for accomplishing some tasks. The steps used to compute cost estimation, a procedure for calculating an expected demand for some product are examples of procedural knowledge.

A third major type of knowledge is reasoning knowledge. A piece of reasoning knowledge specifies the conclusion that can be drawn when a specified situation exists. A set of company regulations, rules that prescribe forecasting approaches are reasoning knowledge.

Linguistic knowledge is the basis for acquiring every other type of knowledge as well as for acquiring greater linguistic knowledge. It enables the decision maker to make sense out of what is observed. A vocabulary, grammar, knowledge of the meaning of special terminologies, and an understanding of graphing conventions are all examples of linguistic knowledge.

Assimilative knowledge is the basis for controlling the changes permitted to a knowledge storehouse. It is housekeeping knowledge governing the permissible contents, orderliness, and efficiency of a knowledge storehouse. Examples include knowledge about how long to retain the historical records or derived data, what to regard as irrelevant or not valid, and the impact of new additions on existing pieces of knowledge.

Presentation knowledge is the inverse of linguistic knowledge. It is the basis for packaging outgoing messages or reports. Customised and standard forms, templates, vocabularies, grammars, and knowledge about preparing graphs and reports are all presentation knowledge.

In the proposed knowledge-based decision support system, the relationships between different types of knowledge mentioned above are illustrated in Figure 1. The descriptive, procedural and reasoning knowledge form the core of the knowledge base. The other three types of knowledge form the interface between the system and the user.

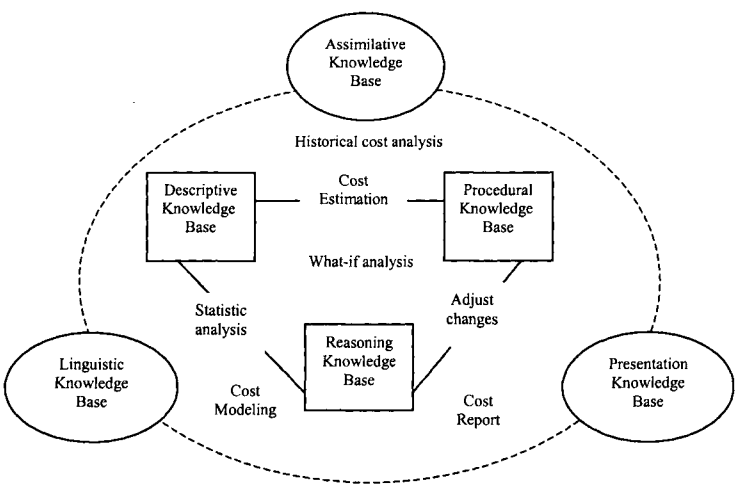


Figure 1 Structure of the knowledge base in decision support system

Functions of Proposed Knowledge-Based System

The proposed knowledge-base system is to support cost engineer and project managers in construction cost management. It is designed for two purposes: one is to offer estimating functionality and reliable cost

data while the other is to provide extensive knowledge base for cost control. The prototype of the system is expected to have basic estimating functions and advanced decision support functions, as discussed in the following sections.

For the basic functions, the system is supposed to assist the user to accurately calculate the cost of a construction project. It takes into account the bids and quotes from subcontractors, material suppliers, price mark-ups, taxation and cost analysis. These functions can be summarised as follows:

1. Estimation takeoff:
   (1) Lookup building items from the database, in categories;
   (2) Select items or add items if not available from database;
   (3) Assign quantities to items;
   (4) Assign notes to items;
   (5) Perform assembly (related items).
2. Estimation process:
   (1) Cost information displayed in categories;
   (2) Modify the material information;
   (3) Perform the estimate;
   (4) The above procedure can be repeated.
3. Report:
   (1) Dollar amount and percentage summary of the categories of work are given;
   (2) Apply percentage, lump sum and step mark-ups and other costs (tax, *etc.*);
   (3) Present the total net costs, mark-ups, and total costs for the job.

For the advanced decision-support functions, the proposed software system can access multiple knowledge rules base, prompting the user for necessary information, then optimising the cost modelling method based on the users' criteria. The optimising engine can generate the complete cost report.

The knowledge rules define the best possible, and other alternative ways, of making decision by asking a series of questions that an experienced cost engineer would normally consider. It also contains the engineer's expertise to convert the static data and the rates into useful information.

The advanced functions of the system include:

1.Present the database contents (can connected to multiple existing database);
2. Import/input quantity data from design drawing packages;
3. Use for variations and change control;
4. Use for interim payments to assess work in progress;
5. Analyse the priced tenders and use for future cost planning;
6. Obtain the material information from suppliers' web site;
7. Issue purchase orders and contracts (connect to the supplier through internet);
8. Monitoring cost and progress;
9. Provide appropriate levels of cost details for management reporting;
10. Support decision making (through knowledge rule-based system);
11. Compare predicted costs with real costs (graphs, curves);
12. Experiment with the workflow (in combination with a scheduling system);
13. Cost analysis (introducing statistic functions and cost modelling);
14. Automated cost estimating, cash flow model and documentation;
15. Automated cost and knowledge database development, search, and retrieval.

Structure and Implementation tool of the System

The structure of the system is designed based on the cost control cycle and can be clearly illustrated by Figure 2. The system is to be built as an integrated tool suite of some software sub-products which are specifically designed for the cost estimating, control and management in construction industry. The

software package is proposed to include four main sub-systems (details are given as follows), and each sub-system can be developed separately and linked to each other at the final stage.

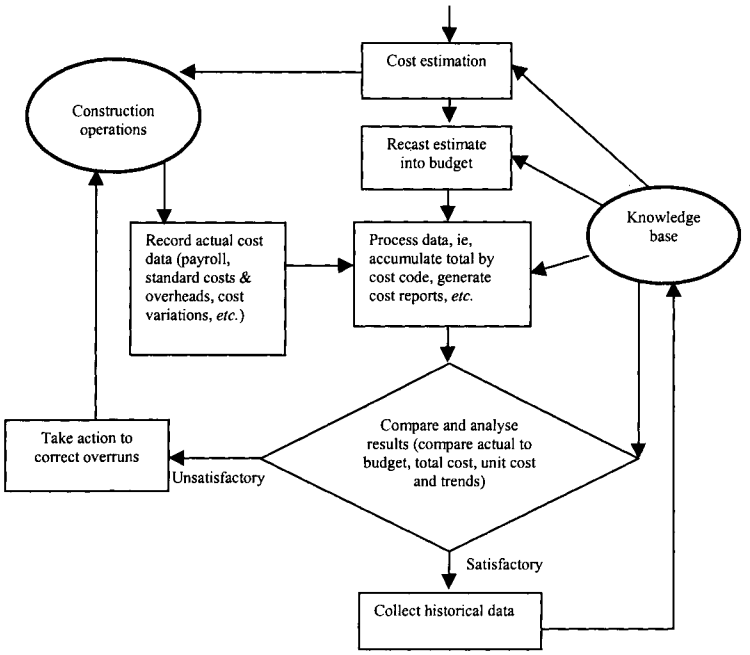


Figure 2 Structure of the proposed system

1. A sub-system for basic estimate functionalities, which integrates all the necessary cost estimating functions and allows the user to enter the process at any level. To save development time and costs, this sub-system can be introduced from existing estimating software packages.
2. Multiple databases to store the six types of knowledge as described earlier. This is the essential part of the system. The user can search the knowledge base for estimating methodologies. The knowledge base can also be built and/or customised by the user.
3. Statistical package to facilitate cost estimating relationship development and a uniquely designed spreadsheet that promotes structured, systematic model development. This system will be linked to the database to obtain maximum capabilities.

   The cost analysis statistical package will include most of the features contained in major statistics programs plus many tailored functions for the cost estimator. Within the system, the user can edit data obtained from other sources; review histograms and scatter plots; perform basic statistical analysis including linear, log-linear, and non-linear regression; fit beta curves; and fit learning curves both with and without rate effects.
4. A sub-system which has built-in inflation, time phasing, documentation, sensitivity/what-if, risk and other analysis capabilities. The results of the above analysis can be immediately integrated with the estimation and be automatically included in the estimate documentation. The results can also be used to populate custom knowledge database.

The prototype of the proposed decision support system are to be constructed with the latest computer technologies including Oracle database system, Enterprise JavaBean, JSP, XML, *etc.* Java is selected as the main programming language in building up the prototype, due to Java's full capability in working with the internet and Oracle database.

The software system is internet/web based. Internet technologies, including the web, web browsers, and search engines, have provided unprecedented opportunities for conducting business online. Together, these technologies enable the creation of web-based information systems. The web-based decision support system can overcome geographic and cost barriers to new markets, have access to worldwide communications and a global presence. It can also replicate and share scarce information by linking to data warehouses, and structure or restructure relationships both internally and externally.

A web-based system can provide latest information for material cost, labour cost, inflation data, foreign currency exchanging rates, *etc.* This is especially useful and efficient for large scale project. In another aspect, unlike many current software packages which must be used within the company's Intra-net, it is accessible from anywhere with Internet access.

CONCLUSIONS

This paper has focused on the use and development of decision support systems of cost management in construction industry. It is found that most of the cost-related softwares available in the market are estimating softwares, and usually they are connected with a database. They represented low-level computer-based systems for data storage and retrieval, with functions of calculating and estimation. High-level softwares with ability of data analysing and decision support are rare in building construction industry. It is predicted that next generation software for construction cost management will focus on the implementation of expert knowledge and supporting capabilities of managerial decision making.

The design of the prototype of knowledge-based decision support system for construction cost management is presented in the paper. The proposed knowledge-based decision support system is web-based, which provides global access and other service excellence. It is an integrated tool suite of several software sub-products, which is linked to the knowledge base which contains the six types of knowledge. The knowledge base is the backbone of the system. The structure of the knowledge base and the logistical design of the system are illustrated in the paper. The implemented system will help project managers to acquire timely and accurate information, carry out statistic analysis and what-if analysis, as well as access expert knowledge base, and this will lead to an improved decision making in construction cost management.

REFERENCES

Brightman, J. R., Eden, C., van der Heijden, K. and Langford, D. A., (1999), "The development of the construction alternative futures explorer", *Automation in Construction*, **8**, 613-623.

Burry, M., Coulson, J., Preston, J. and Rutherford, E. (2001), "Computer-aided design decision support: interfacing knowledge and information", *Automation in Construction*, **10**, 203-215.

Couzen, A., Thorpe, A., and Skitmore, M. (1993), "Executive information system for construction contract bidding decisions", in *Management of information technology for construction.* Edited by K.S. Mathur et al. World Scientific Publishing Co., Singapore, 149-165.

Feng, C.W., Liu, L., and Burns, S. A. (1997), "Genetic algorithms to solve construction time-cost trade-off problems", *J. Comp. in Civ. Engrg.*, ASCE, **11:3**, 184-189.

Hegazy, T., Grierson, D., Ayed, A., and Zaneldin, E. (2000), "Resource optimisation in a design office using simulation", *Project Management Journal*, **31:4**, 33-43.

Holsapple, C. W. (1995), Knowledge management in decision making and decision support. Knowledge and Policy: *The International Journal of Knowledge Transfer and Utilization*, **8:1**.

Leu, S. S., Yang, C. H., and Huang, J. C. (2000), "Resource levelling in construction by genetic algorithm-based optimisation and its decision support system application", *Automation in Construction*, **10**, 27-41.

Li, H. (1994), *Machine Learning of Design Concepts*, Computational Mechanics Press, UK.

Li, H. and Love, P.E.D., (1999), "Combining rule-based expert systems and artificial neural networks for mark-up estimation", *Construction Management and Economics*, **17**, 169-176.

Liu, L., Burns, S. A., and Feng, C. W. (1995), " Construction time-cost trade-off analysis using LP/IP hybrid method", *J. Constr. Engrg. and Mgmt., ASCE*, **121:4**, 446-454.

Machlup, F. (1980*), Knowledge: Its creation, distribution, and economic significance,* Vol. 1, Princeton, N. J.: Princeton University Press.

Quinlan, J. R. (1986), Induction of decision trees, *Machine Learning,* **1:1**, 81-106.

Tompkins, B. G. (1985), *Project Cost Control for Managers*, Gulf Publishing Co., Houston, Texas, pp.6.

WEB REFERENCES

1. Cost Analysis Strategy Assessment (CASA), (http://www.logsa.army.mil/alc/casa/).
2. Cost Estimating Guides (http://www.costbook.com).
3. Cost Xpert (http://www.costxpert.com/).
4. Cost Track (http://www.ontrackengineering.com/).
5. Crystal Ball (http://www.decisioneering.com/crystal_ball/index.html).
6. DeccaPro (http://www.deccansystems.com/DeccaPro.htm).
7. EMQUE's Perfect Project (http://www.emque.com).
8. Decision by Life Cycle Cost (D-LCC) (http://www.aac-usa.com/).
9. Success4 (http://www.uscost.com/success4.htm).
10. D4COST•2000 (http://www.d4cost.com/).
11. ForecastX (http://www.forecastx.com/).
12. JPL's Project Design Center Tools and Models (http://pdc.jpl.nasa.gov/newtools/public/newtools.html).
13. KAPES (Knowledge Aided Planning & Estimating System) (http://www.kapes.com/).
14. Means DemoSource (http://www.rsmeans.com/demo/demo.html).
15. Accu.Build - Construction Software (USA) (http://www.accu-build.com) .
16. Amlink Cost Estimating Lodex, Cost manage Lodex (http://www.amlink.com.au).
17. Buildsoft (http://www.buildsoft.com.au).
18. Cost Estimating Bid Team, Cost Manage Profit Maker (http://www.cdci.com).

INDEX OF CONTRIBUTORS

Volumes I and II

Abdullah, A. 1671
Agrawal, A.K. 489
Ahmad, I. 671
Aladesaye, M. 1035
Aleksyuk, S. 335
Alfano, J. 771
Al-Jumaily, A.M. 1035
Andre, P. 147
Anh, N.D. 937
Anh, V.Q. 1043
Anumba, C.J. 1671, 1713
Aouad, G. 55
Arets, M.J.P. 1449
Ashford, P. 679, 1051
Ashida, S. 339, 351
Azhar, S. 671

Badger, D. 1081
Balendran, R.V. 803
Beck, J.L. 457
Beckman, W.A. 165
Bennadji, A. 1209
Bergman, L.A. 513
Berry, P.A. 183, 199
Betts, M. 55
Bock, T. 339, 343, 351, 355
Boerstra, A.C. 1375
Bojic, M. 1289, 1331
Bonnaillie, L. 255
Bouchlaghem, N.M. 1209
Boulgakov, A. 355
Bourke, K. 1467
Boyd, A.J. 873
Bridge, R.Q. 191, 207
Broyd, T.W. 1519
Bulgakow, A. 335, 339
Burnett, J. 1281, 1331

Can, E. 255
Canino, I.R. 671
Cao, M. 1737
Cao, Y. 1587
Cao, Z. 595
Carlson, J.D. 545
Chai, J.C. 603
Chan, A.P.C. 687, 1681
Chan, D.W.M. 687
Chan, K.T. 1157
Chan, S.L. 621, 629
Chan, T.M. 1321
Chandler, A.M. 747
Chang, C.C. 529
Chang, L.M. 1527
Chapas, R. 255
Charalambous, A. 1051
Chau, K.T. 303, 319
Chen, A. 731
Chen, C.Q. 465
Chen, D.-Y. 913
Chen, G.D. 465
Chen, J. 1107
Chen, N.C. 1595
Chen, Q. 273
Chen, S.W. 1115
Chen, W. 1611
Chen, Y.Q. 1611, 1661
Chen, Y.Y. 555
Chen, Z.F. 797
Cheng, P.G. 1001
Chi, S.C. 771
Chin, C.S. 921
Chong, K.P. 3
Chow, W.H. 1281
Chu, A.Y.T. 621
Chung, J.K.H. 1721
Chung, K.F. 621, 629, 637, 661
Clark, J. 1073
Close, J. 1217
Cooper, R. 55
Coubray, B. 1035
Cox, K. 1073
Cox, S.S. 113
Cramer, S.M. 105
Croll, J.G.A. 1059
Cuevas, C. 147
Cui, H.Z. 859
Cyr, M.F. 17, 239

Dai, G.L. 695
Dai, J. 281
Dassori, E. 1689
Dexter, A.L. 157
Di Maio, F. 1225
Ding, X.L. 1611, 1661
Donelan, P. 1081
Dong, S.L. 1091
Drzal, L.T. 225
Du, X.L. 563, 571
Duan, Y.F. 1025
Ehlers, M. 1619
El-Ashkar, N.H. 233
Emerson, R.N. 97
Eminaga, A. 865

Fanger, P.O. 29
Fischer, G. 781
Fisher, J.W. 415
Flanagan, R. 39
Fraaij, A. 1415
Frasani, M. 1689
Friday, O.M. 105
Fu, Y.F. 845
Fujitani, H. 473
Fukuyama, H. 945

Garlock, M.M. 447
Geeson, P. 1081
Gero, J.S. 47
Gibbons, C. 703, 1475, 1653
Glass, J. 1457
Gong, J.Y. 1001, 1595
Gong, W.M. 695
Graybeal, B. 431
Guan, K. 375

Hagiwara, H. 481
Hallam, A. 1209
Hanser, A. 361
Hata, K. 473
He, Q.H. 1535
He, W.L. 489
Hendriks, Ch.F. 1391, 1399, 1415, 1439
Herrera, R. 439
Hiwatashi, T. 473
Hodgson, A.T. 113
Hoffman, M.E. 1493
Holmes, M. 1209
Hong, C. 255
Hong, H.P. 763
Hooper, R. 1467
Horsfield, J.N. 1475
Howes, R. 383
Hu, B. 255
Hu, Y.X. 303, 319
Hua, X.H. 1629
Huang, D.F. 1611, 1661
Huang, J.Z. 603

Huang, Y. 853
Huo, D. 611

Iguchi, Y. 1297
Ip, T.F.C. 1475
Ismail-Yahaya, A. 263

Janssen, G.M.T. 1391, 1399
Ji, L. 695
Jiang, J.B. 289
Jiang, Y. 1265
Jing, J. 739
Jones, A.D. 1189
Jones, P. 1165, 1173, 1339
Jung, H.J. 545

Kajewski, S.L. 1559
Katsumura, A. 1131
Kaufmann, E.J. 415
Kippenberg-Kretzer, K. 1173
Kitipornchai, S. 803
Klaase, D. 1501
Ko, J.M. 537, 953, 1001
Kono, T. 1199
Kowalsky, M.J. 247
Kragh, M. 1233
Krapivin, D. 335
Kreupl, K. 343
Kumar, D. 113
Kumar, V. 121
Kurata, N. 497
Kurtis, K.E. 233
Kurvers, S.R. 1375

Lacôte, P. 147
Lam, K.H. 1217
Lam, L. 789, 1407
Lam, L.C.H. 969
Lam, N.T.K. 747
Lam, S.S.E. 731, 755
Lam, S.Y.W. 1697
Lam. K.K. 1241
Lau, C.K. 1611, 1661
Lau, K.F. 1345
Lau, V. 1653
Lawton, T. 1073
Lebrun, J. 147
Lee, A. 55
Lee, A.C.C. 703
Lee, C.K. 1241
Lee, G.C. 405, 961
Lee, J.H.K. 969
Lee, J.N. 129, 137
Lee, P.K.K. 969
Lee, P.S. 157
Lee, S. 137
Lee, S.K.L. 797
Leung, A.Y.T. 803
Leung, C.K.Y. 797
Leung, H.Y. 803
Li, C.S. 731
Li, D.R. 1595
Li, G.Q. 1115
Li, H. 1025, 1569, 1587
Li, J. 289
Li, J.H. 747
Li, P.F. 579
Li, Q.Q. 1629
Li, S.G. 1601
Li, S.R. 375, 391
Li, V.C. 781
Li, W. 121
Li, X.L. 579, 587
Li, Y.Q. 1123, 1131
Li, Z.J. 811
Liang, Z. 961
Liao, Z. 1249
Lim, C-A. 1745
Lin, G. 771
Lin, S. 1017
Lin, Z.S. 853
Little, J.C. 113
Liu, F.T. 1009
Liu, H.J. 977
Liu, J.B. 297
Liu, X.H. 327
Liu, Z.Q. 755
Lo, T.Y. 859
Lou, W.J. 1139, 1147
Loveday, D. 1209
Lu, F. 1139
Lu, H.S. 303
Lu, L.W. 415
Lu, L.-W. 423
Lu, M. 637, 1705
Lu, X.L. 985
Luo, W.B. 311

Ma, Z.L. 1543
MacArthur, J.M. 703
Maidment, G. 1273
Mak, H. 1569
Mao, C. 415
Marshall-Ponting, A. 55
Matsui, M. 65
Matsuoka, I. 1297
McFarland, D.M. 513
Meden, H. 351
Mehta, G. 225
Memari, A.M. 865
Messac, A. 263
Miles, J. 1081
Mindess, S. 873
Misra, M. 225
Missenden, J. 1273
Mita, A. 481, 521
Mitchell, J.W. 165
Mohanty, A.K. 225
Mohr, B. 233
Mok, E. 1637, 1645
Möller, M. 1619
Moore, P. 1073
Mu, B. 239
Mudlock, M. 431
Muhummud, T. 439
Mulder, E. 1415

Nadella, K. 121
Nanko, H. 233
Ng, C.L. 993
Ni, Y.Q. 537, 953, 1025
Nimityongskul, P. 897
Niu, J.L. 1351, 1383

Obonyo, E.A. 1713
O'Donnell, A. 255
Oehlers, D.J. 819
Omer, A.M. 1257
Ouyang, Z.X. 905

Pan, S.W. 1017
Parand, F. 1249
Parshin, D. 355
Patrick, M. 183, 191, 199, 207
Perez, F.J. 423
Pessiki, S. 423, 431
Pietersen, H. 1439
Pircher, M. 215
Pocklington, D.N. 1457
Poon, C.S. 845, 1407
Prek, M. 1485
Prior, J. 1467
Pritchin, S. 335
Prochiner, F. 367

Qian J.R. 273, 289, 311, 739

Ravesloot, C.M. 1509
Reichler, M. 165
Rem, P. 1439
Ren, A.Z. 1601, 1737

Retscher, G. 1645
Riary, S. 1305
Richardson, D. 1467
Ricles, J.M. 415, 439, 447
Rijal, H.B. 1359
Roh, H. 1367
Rojas, P. 447
Rose, J. 1081
Rosenboom, O.A. 247

Sakino, K. 889
Sandie, R.B. 1051
Sause, R. 423, 439, 447
Schiewe, J. 1619
Seracino, R. 819
Sexton, M. 55
Sha, W. 881, 1321
Shaffery, J. 1209
Shah, S.P. 17, 239
Shashua-Bar, L. 1493
Shen, Q.P. 1721
Shen, W.G. 929
Shenton III, H.W. 255
Shi, W.Z. 1001
Shiozaki, Y. 473
Shui, Z.H. 1407
Sidwell, A.C. 1577
So, F. 645
Soda, S. 473
Sodeyama, H. 473
Southwood, B. 1551
Spencer, Jr. B.F. 537, 545
Stec, W.J. 1181
Su, R.K.L. 747, 969
Suen, A.M.T. 1345
Sun, B.N. 1139, 1147
Sun, Y. 889
Sun, Y.R. 1611
Sung, L. 3
Suwada, H. 945

Tahir, M.A. 827, 897
Takahira, S. 521
Tam, C.M. 399
Tamura, Y. 65, 1131
Tang, A.C.C. 1345
Tang, C.A. 845
Tang, C.H.W. 1697
Tang, J.M. 797
Tao, L.J. 579, 587
Teng, J.G. 789, 1091
Thorpe, A. 1713
Tilley, P.A. 1559
Tomura, T. 473
Tong, M. 405
Tong, Y.C. 661
Tozer, R. 1273
Tse, T. 529
Tu, J. 563, 571

Udagawa, M. 1367
Underwood, C.P. 1189
Uy, B. 835

Vakakis, A.F. 513
van den Dobbelsteen, A.A.J.F. 1449, 1501, 1509
van der Linden, A.C. 1375, 1501, 1509
Van Dessel, S. 263
van Dijk, K. 1415
van Paassen, A.H.C. 1181, 1225, 1305
van Zyl, R. 1209
VanLandingham, M.R 3
Vesey, D.G. 653
Viet, L.D. 937
Vogtländer, J. 1391

Wallace, M.I. 1653
Wan, C-W. 703
Wan, H.W. 853
Wan, K. 1289
Wan, T.K. 1351
Wang, C.C.X. 1755
Wang, F.L. 1265, 1297
Wang, F.Q. 1273
Wang, G.Y. 555
Wang, J.M. 1147
Wang, J.Y. 537
Wang, Q.F. 1099
Wang, S.S. 763
Wang, S.W. 173
Wang, X.S. 595
Wang, Y.M. 513
Wang, Z.C. 1091
Wang, Z.Y. 297
Wei, D.M. 1009
Weippert, A. 1559
Wen, Y. 1601
Wen, Z.P. 303, 319
Wheeler, A. 215
Wheeler, A.T. 199
Wong, C.T.C. 1569
Wong, E.O.W. 1431
Wong, H.T. 1091
Wong, K.S.W. 1423
Wong, K.W. 405
Wong, R.W.M. 713
Wong, Y.H. 1217
Wong, Y.L. 281, 731, 755, 845
Wool, R.P. 255
Wu, B. 755, 1009
Wu, M. 405
Wu, M.K.T. 1241
Wu, Q. 129, 137
Wu, S.P. 29, 905
Wu, W.J. 603
Wu, Y.H. 405

Xiao, J.-Z. 913
Xiao, R.Y. 921
Xiao, X.C. 771
Xie, L-L. 75
Xie, M. 723
Xie, Z.X. 723
Xing, W. 1439
Xu, Y. 1601
Xu, Y.L. 977, 985, 993, 1107, 1115
Xue, S.D. 595

Yan, P. 1729
Yan, Y. 1629
Yang, B.S. 1629
Yang, G. 545
Yang, H.X. 1281
Yang, J. 1543, 1577
Yang, J.N. 1017
Yang, J.R. 611
Yang, K.T. 83
Yang, R.L. 327
Yang, Y.W. 1611, 1661
Yang, Z. 985
Yang, Z.C. 977
Yau, R.M.H. 1475
Ye, L.P. 739
Yik, F. 1289, 1331
Yin, J.H. 1611, 1661
Ying, K.C. 1705
Yip, R.C.P. 1431
Yoshida, A. 1131
Yoshida, H. 1199, 1265, 1297, 1359
Yoshito, I. 1543
You, Q.Z. 695
Yu, B. 1305
Yu, F.W. 1157
Yu, W.K. 629, 637, 661
Yuan, H.Z. 1313
Yuen, K.-V. 457

Zeng, M. 905
Zhang, B.Y. 571
Zhang, D.S. 587
Zhang, G. 1577
Zhang, J.P. 1737
Zhang, L. 1527
Zhang, L.H. 579
Zhang, L.Z. 1351, 1383
Zhang, Q.X. 611
Zhang, R.C. 1115
Zhang, W. 1313
Zhang, Y.H. 571
Zhang, Z.J. 811
Zhang, Z.Y. 579
Zhao, Q. 853
Zhao, Q.L. 929
Zheng, G. 1025
Zhou, M.K. 905, 929
Zhou, X.T. 953
Zhou, X.Y. 327
Ziang, M.Z. 281
Zou, P.X.W. 1745, 1755

KEYWORD INDEX

Volumes I and II

Abrupt change, 297
ACBM, 239
Acceptable level for earthquake human mortality, 75
Active friction dampers, 465
Active variable stiffness system, 1009
Adaptability, 1501
Adaptive models, 1375
Added air mass, 1147
Adjacent buildings, 985
ADLINE, 1265
Advanced building construction, 1697
Advanced cementitious composites, 945
Agent-based, 1713
Air, 113
Air-conditioner performance, 1331
Air conditioning, 165, 1273, 1367, 1485
Air-conditioning load, 1199
Air-conditioning systems, 157
Air-cooled chiller, 1157
Airflow, 1173, 1225
Airflow modelling, 1165
Air pollutants, 1345
All-air system, 1383
Altitude, 1359
Anaerobic and aerobic treatment, 1423
Analytic hierarchy process (AHP), 405, 1671
Annual cooling load, 1289
Anti-earthquake optimum design, 555
Approach flow, 1131
Arch dam, 563, 571
Architecture, 1059, 1209
Artificial neural networks, 1527
Artificial simulated wind load, 1123
Asian climate, 1199
Assessment, 1209
ASTM E119, 105
Asymmetric, 281
Asymmetric beam, 1321
Atomic force microscope, 3
Augmented reality, 351
AutoCAD, 1601
Autoclaved aerated concrete, 865
Automated commissioning, 157
Automatic wheel washing machine, 1423
Axial compressive behavior, 289

Balance theory, 1431
Bamboo, 653
Bamboo columns, 661
Bamboo scaffolds, 629, 661
Barrier, 113
Based-isolated structure, 529
Base isolation, 473, 513
Base isolation principles, 961
Basement construction, 713
Basic mechanical properties, 637
Bay, 263
Bayesian inference, 457
Beams, 811, 819, 873
Bearing capacity, 603
Bearing structure, 1449
BEM system, 1297
Bending, 811
Bias errors, 157
Biaxial confinement, 873
Bill of quantity, 1729
Biocomposites, 225
Biological treatment, 1423
Biotechnology, 3
BNDWF, 771
Boiler, 1249
Bolted steel shells, 1091
Bond property, 811
Bond strength, 865
Bonded tendons, 1051
Borate, 129, 137
Bored pile construction, 1705
Boundary Layer Wind Tunnel (BLWT), 1131
Brick rubble, 1439
Bridge, 1001
Briefing, 1467
Buckling, 835, 1091
Buckling capacity, 215
Building demolition debris, 1415
Building design, 47, 1653
Building HVAC systems, 1265
Building integrating PV, 1313
Building management, 1653
Building management system, 173
Building materials, 121, 1257, 1449
Building processes, 343
Buildings, 113, 1059, 1281, 1457
Building systems, 343
Building thermal performance, 1375
Bump cutters, 679
Burnish finish, 679

CAD, 47
Calorimetry, 881

Case analysis, 611
Cement, 233, 1457
Cement Admixture, 853
Central heating systems, 1249
CFD, 1173, 1331
Check-list, 1339
Chemical composition, 897, 1439
Chilled surface cooling, 1165
Chilling system, 173
China, 375, 391
Chongqing, 391, 405
Circular concrete member, 889
Circular steel tube, 889
Civil infrastructure system, 555
Clay-bricks, 1415
Clay solution cementing, 723
Cleaning Robot, 339
Client, 1467
Closely spaced modal frequencies, 1107
Coagulation, 1423
Cold-formed steel frame, 375
Collection, 1281
Column buckling, 621
Column element, 273
Columns, 835
Comfort, 1233
Commissioning, 173
Common construction problems and solutions, 713
Communication systems, 1559
Community, 1081, 1475
Comparative study, 1577
Comparison, 993, 1115
Competitive advantage, 39
Complete quadratic combination rule, 763
Complete stress-strain curve equation, 289
Composite, 233, 781
Composite beam, 183, 207
Composite connection, 183, 199
Composite construction, 439, 703, 1091
Composite material, 255
Composite slab, 191
Composite structures, 835
Compressing consolidation, 723
Compression, 431
Compressive strength, 921
Computational agents, 47
Computer modeling, 637
Concrete, 233, 383, 423, 431, 789, 803, 1407, 1457, 1689
Concrete filled, 215
Concrete filled steel tubular column, 439
Concrete jacket, 827
Concrete mixing, 671
Concrete rubble, 1439
Concrete shells, 1091
Concrete structures, 297, 811, 835
Concrete uniformity, 671
Condensing temperature, 1157
Confined concrete, 889
Confined masonry, 247
Confinement, 431, 789
Confinement design, 889
Confinement effect, 889
Confocal microscopy, 3
Connection stiffness, 297
Connection system, 367
Connector, 367
Conservation, 1281
Construction, 367, 375, 1457, 1519, 1721
Construction and demolition waste, 1431, 1439
Construction cost management, 1755
Construction industry, 391, 1559
Construction IT, 55, 1569
Construction labour supply, 399
Construction-led design, 703
Construction machines, 1645
Construction management, 1737, 1745
Construction process improvement, 55
Construction process re-engineering, 687
Construction products, 1713
Construction projects, 1543
Construction sector, 39
Construction technologies, 687, 1081
Construction wastewater, 1423
Contaminant, 113
Continuity plates, 415
Continuous composite beam, 183
Contraction joint, 563
Control, 1249
Control algorithm, 993
Control strategy, 969
Conversion method, 695
Cool climate, 1359
Cooling, 1367
Cooling storage, 1273
Cooperative work, 1737
Copper gangue, 853
Copper Indium Diselenide (CIS), 1217
Cost, 361
Coulomb dampers, 465
Coupling beams, 755
Creep, 129
CSCW, 1737
c-shape, 1035
Cumulative damage, 913
Cyclic wall response, 247
CYCLONE, 1705
Cylinder splitting strength, 921

Damage assessment, 481
Damage detection, 1017
Damage free, 945
Damage index, 521
Damage reduction, 945
Damage tolerance, 781
Damper, 521
Damping device, 969
Data analysis techniques, 1017
Data fusion techniques, 1619
Data transfer and XML, 1209
Database, 1653
Decision-making method, 75
Decision support system, 1755
Deck-shading system, 1217
Deformability, 311
Deformation compatibility, 781
Degradation, 1399
Demolition technique selection model, 1671
Derivitized soybean oil, 225
Desiccant cooling, 1383
Design, 191, 263, 375, 431, 1091, 1457
Design agents, 47
Design criteria, 1035
Design development, 629, 637
Designer materials, 3
Design flexibility, 343
Design formulae, 921
Design innovations, 687
Design method, 611
Design of experiment, 121
Design process, 1209
Different elements, 361
Difficult construction environment, 713
Diffusion, 113
Digital map, 303
Digital surface models, 1619
Discontinuities, 579
Displacement, 747
Di Wang Building, 1115
Document management, 1729
Domestic hot water, 1189
Doppler sodar, 65
Double skin façades, 1233
Drift, 747
Drift-based design, 311
Drift decomposition, 311
Driving communications, 335
Dual structure system, 739
Ductility, 415, 755
Durability, 3, 233
Dynamic interaction, 563
Dynamic models, 355
Dynamic monitoring, 335
Dynamic properties, 297
Earthquake, 423, 439, 447, 571, 747
Earthquake economic loss estimation, 75
Earthquake response control, 473
Earthquake simulation test, 281
ECC, 781
Eccentrically loaded columns, 827
Eco-costs, 1391, 1399
Economic efficiency, 361
Economic performance, 1265
Economy, 1073
Effective damping, 505
Effective length coefficient, 621
Efficiency, 1475
Electricity generator, 1217
Electronic tendering, 1729
Elements, 1689
Embedded system, 351
Emission, 1351
End plate connection, 183
Energy, 1081, 1209, 1281, 1475
Energy concept, 739
Energy conservation, 1199, 1367
Energy consumption, 1233
Energy efficiency, 1241, 1249, 1257
Energy efficient design, 1165
Energy saving, 1297
Engineered structure, 653
Engineered wood construction, 97
Engineering, 1059, 1209
Engineering performance, 1527
Engineering performance improvement, 1527
Engineering surveys, 1697
Envelope design, 1289
Environment impacts, 1257
Environmental and safety, 1073
Environmental assessment, 1449, 1501, 1509
Environmental cost, 1449, 1509
Environmental impact, 1449, 1485, 1501, 1509
Environmental index, 1501, 1509
Environmental load, 1449
Environmentally responsible, 1081, 1475
Environmental management, 1485
Environmental management systems, 1457
Environmental performance, 1501, 1509
Epicentral distance, 319
e-procurement, 1729
Evaluation, 1265
Evolutionary power spectral density function, 763
Excavation, 611
Experiment, 731, 1351
Experimental study, 977
Experimental testing, 797
Expert system, 1681

External Reinforcement, 865
Extreme pressure distribution, 65
Extrusion, 17, 239

Façade cleaning, 339
Façades, 1165
Facility management, 351
Factor 20, 1449, 1501, 1509
Factory, 1081
Fail-safe, 497
Fatigue behavior, 913
Fatigue design, 913
Fatigue test, 913
Fault detection and diagnosis, 1305
Fault diagnosis, 157, 173
Feature recognition, 1587
FFT method, 1115
Fiber, 17, 233, 239, 255
Fiber-reinforced concrete, 239, 873
Fiber reinforced plastics, 797
Fiber reinforced polymer, 865
Financial implications, 1233
Fineness, 897
Finite element method, 603
Finite element model, 587
Fin plate, 199
Fire, 105
Fire engineering, 1321
Fire models, 83
Fire protection, 1321
Fire test, 1321
Fitout, 1577
Flatness and levellness, 679
FLEC, 1351
Fleet management, 1645
Flexibility, 361, 1501, 1577
Flexural loading, 215
Flexural strength, 803, 921
Flooring, 1035
Floors, 1449
Fluid damper, 985
Fluid viscous dampers, 327
Fly ash, 239, 881, 897, 929
Foresight, 1519
Form, 1059
Foundation, 563, 603, 723
Foundation rock, 571
Fracture, 415
Fragility curves, 319
Frame, 263, 383
Frame-shear wall structures, 1099
Frequency response function, 953
Frequency-time decomposition, 1017
Friction, 191
FRP, 789
FRP confined concrete column, 289
FRP plating, 819
FRP reinforcement, 781
FRP rod, 803
Full-scale measurement, 65
Full-scale models, 827
Full-scale tests, 661
Function, 1059
Future, 1519
Fuzzy sensors, 157

Games hall lighting, 1241
Gammon Skanska Construction System, 1073
Genetic algorithms, 1025, 1527
Geographical Information Systems (GIS), 1001, 1653
Geometric Nonlinearity, 1043
Geometric stiffness matrix, 1043
GFRP, 811
GIS, 303, 1595, 1619, 1653
Global positioning system, 1661
GPS, 1611, 1637, 1645
GPS Sonde, 65
Green construction, 629
Green CTTC model, 1493
Ground vibration, 587
Group decision support systems, 1721
Gypsum, 105

Health monitoring, 481, 497, 521
Heating, 1485
Heating system, 1485
Heat load, 1367
Heat pump, 1189
Heat transfer, 1273
Heterogeneity, 845
HHT, 1115
High grade application, 1399
High output T5 lamps, 1241
High performance concrete, 17, 913
High performance pavements, 679
High Performance Polymer (HPP), 921
High-rise, 1073
High-rise building, 731, 953
High-Rise residential, 1289
High slump concrete, 671
High-strength concrete, 889
High strength steel, 431, 439
High tech, 1059
High tech equipment, 977
Hilbert transform, 1017
Hong Kong, 303, 687, 1281
House, 367
Housing, 233, 391, 1081
Housing panels, 225

Humidity, 1383
HVAC, 1297
HVAC system, 1305
Hybrid base-isolated system, 327
Hybrid platform, 977
Hydration, 897
Hydration products, 881
Hysteresis model, 545

IAQ, 1345
Identification, 1297
Ill-conditioned equations, 273
Impact loading, 873
Inclinometer, 1661
Indirect evaporating cooling, 1241
Indoor, 113
Indoor air movement, 1331
Indoor air quality, 29
Indoor and outdoor temperature difference, 1359
Indoor climate, 1375
Industrial waste, 853
Industrialised housing, 375, 391, 405
Industrialized, 383
Industry-University collaboration, 1569
Inelastic, 281
Inelastic rotation, 415
Inelastic seismic response, 739
Information model, 1535
Information reuse, 1543
Information Technology (IT), 3, 1551, 1559
Innovation, 1081, 1449, 1475
Innovation and development, 1569
In-plane wall response, 247
In-situ test, 611
Integrated building design, 1233
Integrated construction management system, 1729
Integrated design method, 343
Integrated management, 1535
Intelligent bearings, 961
Intelligent building, 1551, 1577
Intelligent system and decision-making process, 1671
Intensive use of space, 1501
Interactive operation, 1629
Interactive value management systems, 1721
Inter-disciplinarity, 55
Interfacial bond, 781
Interior forces in nails, 611
Internal stressing pockets, 1051
Internet, 1559
Internet GIS, 1595
Intersection testing, 1601
Intumescent coating, 1321
Inverse dynamic model, 529
Irregular inclusion, 845
ISO 9001: 2000, 1697

J2EE, 1595
Java3D, 1595
Joining operations, 343
Joints, 653
Joist, 1035

Kinematics, 355
Knowledge base, 1755
Knowledge controlling, 1745
Knowledge evaluating, 1745
Knowledge implementing, 1745
Knowledge management, 1745
Knowledge organising, 1745
Knowledge planning, 1745

Labour market, 399
Landslides, 1611, 1661
Land use, 1391
Large-span single-layer reticulated shells, 1123
Laserscanning, 1619
Laser screeds, 679
Lateral load resistance, 97
Lateral seismic loading, 771
Lattice shell, 595
Layer, 113
Layer model, 1629
LCA method, 1485
LDV, 65
Leaching, 137
Length scale, 1131
Life-cycle, 1535
Life cycle assessment, 1399
Life-cycle cost, 555, 1475
Light-frame construction, 105
Lightweight aggregate, 859
Liquefying, 723
LMIS, 1535
Load balancing, 1051
Load proportion, 661
Local optimal feedback-feedforward control, 937
Local optimal location of counterforces, 937
Local prediction, 1173
Location, 355
Long period velocity pulses, 489
Longitudinal shear, 207
Long-span roof structure, 1139
Loss, 303
Low-cost housing, 375
Low-maintenance, 1217

Low-rise buildings, 747
LQR, 529
Lumps and balls, 671

Machine guidance, 1645
Machine learning, 481
Macro-model, 273
Magneto-Rheological (MR) fluid, 537
Magnetorheological fluid, 969
Maintainability, 1073
Manufacture, 391
Manufacturing, 1081
Masonry, 1415
Mass transfer, 1351
Material management, 1431
Material properties, 105
Materials, 113, 1391, 1399
Maximum paste thickness, 897
MCFT, 273
M-DOF systems, 961
Mechanical properties, 629
Mechanical resistance, 191
Mechano-sorptive, 129
Media- and electric wiring, 361
Member system-storey model, 1099
Membrane element, 273
Membrane structures, 1147
Metakaolin, 881
Metal plate connections, 97
Methodology test, 1297
Microcellular plastics, 121
Microelectronics, 3
Microelement, 853
Microstructure, 859
Mixture proportion, 905
Mobile communications, 1551
Mobile computers, 351
Mobile manikin, 1173
Modal damping ratio, 1107
Modal frequency, 481
Mode localization, 513
Mode Superposition, 1009
Model, 113, 1249, 1351
Model-based, 1305
Model test, 603
Model updating, 457
Modeling, 129, 165
Modular, 1073
Modular construction, 1081, 1091
Modular steel scaffolds, 621
Module temperature, 1189
Moisture absorption, 1199
Moisture state, 1407
Moment resisting connection, 447
Moment resisting frame, 447
Monitoring, 1661
Movement, 1661
MR dampers, 473, 529, 545
MR fluid, 473, 969
Multi-antenna GPS, 1611
Multi-attribute model, 1681
Multi-criteria decision making, 55
Multi-disciplinarity, 55
Multidisciplinary, 1081, 1475
Multiple criteria, 1671
Multiple seismic inputs, 595
Multiple skin façades, 1233
Multiple Tuned Mass Dampers (multi-TMDs), 1025
Multiple use of space, 1501
Multi-scale modeling, 3
Multi-story building, 993
Multi-support earthquake excitation, 595

Nacelle travelling, 339
Nanomechanics, 3
Nanotechnology, 3
Natural, 255
Natural ventilation, 1199, 1331, 1475
Navigation, 1645
nD modelling, 55
Near field and far field earthquakes, 319
Nearby traffic-induced ground motion, 977
Near-fault effect, 465
Near-fault ground motions, 489
Nepal, 1359
Neural network method, 1265
Neural networks, 637, 953
Nondestructive evaluation, 17
Non-domestic buildings, 1339
Non-ductile, 755
Nonlinear analysis, 439, 447
Nonlinear dynamic interaction, 571
Nonlinear dynamics, 513
Nonlinear normal mode, 513
Nonlinear seismic response, 563
Nonstationary, 595
Non-stationary excitation, 763
Non-supporting removable wall-unity, 361
Notch toughness, 415
Number of cycles, 913
Numerical modeling, 579
Numerical simulation, 845

ObjectARX, 1601
Office building, 1305, 1367, 1577
Operating efficiency, 1157
Operations simulation, 1705
Optimization, 263, 1297, 1475
Optimizing design, 905

Optimum seismic design load, 75
Organisational learning, 1745
OSB, 129
OTE algorithm, 327
Outriggers, 703
Overheating, 1225

Panel, 383
Panel zone, 415
Panfloats, 679
Paper, 233
Parameter estimation, 545
Parameter optimization, 1025
Parametric sensitivity, 771
Parametric study, 993
Partially prestressed, 1051
Passive friction dampers, 489
Passive viscous dampers, 489
Pavillion, 653
PCM, 1273
Peak response, 763
Peak sensor, 521
Pedestrian wind, 1331
Performance, 165
Performance assessment, 1375
Performance based design, 75, 1051
Performance-based engineering, 465
Performance characterisation, 1233
Performance evaluation, 465
Performance objective levels, 739
Performance testing, 1339
Personalized ventilation, 29
PGA input, 319
Phosphogypsum, 929
Photo-catalysis, 1345
Photovoltaic (PV), 1217
Photovoltaics, 1189
Physical behavior, 1439
Piezoelectric actuators, 465
Piezometer, 1661
Piled raft, 603
PIV, 65
Plastic foam, 121
Plates, 873
Plating, 819
POD, 65
Pollution, 1391
Polymer processing, 121
p-order auto-regressive simulation technique, 1123
Pore water pressure, 1661
Porosity, 859
Portland cement, 881
Post-tensioned concrete, 1051
Post-tensioned masonry, 247
Post-tensioning, 447
Poverty, 375
Power failure, 497
Power spectral density, 1131
Pozzolana, 897
Precast, 423, 1073, 1689
Prediction, 165, 1265
Prefabricated wall panels, 97
Prefabrication, 367, 399, 1081, 1217, 1475
Prefabrication systems, 343
Pressure gradient, 1225
Prestressed, 423
Prevention, 1391
Principal component analysis, 953
Probability, 763
Process, 367
Procurement, 1713
Procurement selection, 1681
Product hierarchy, 343
Production, 1689
Productivity, 29, 1729
Project management, 1689, 1729
Project-based survey management system, 1697
Pseudo-dynamic test method, 731
Pseudo excitation method, 595
Public housing, 687
Pulp, 233
Push-over analysis, 273
Put-and-slide-technology, 361

Quality improvement, 1439
Quasi-steady theory, 1139

Radiant cooling, 1383
Radiative transfer, 83
Rainfall gauge, 1661
Rainwater, 1281
Raised floor system, 1577
Random decrement technology, 1107
Random response analysis, 537
Random vibration, 595
Rationality, 1059
RC beam, 803
RC building structures, 945
RC frame, 311
RDT, 1115
Readymixed concrete, 1705
Real estate market, 1501
Recessed spaces, 1331
Reciprocating compressor, 1157
Recognizing, 351
Recovery, 1415
Recycled aggregates, 1407

Recycling, 1391, 1399, 1415, 1423, 1431, 1439
Reference, 1509
Reference building, 1509
Refrigeration, 1273
Regional difference, 1359
Rehabilitation, 819, 835
Reinforced concrete, 755, 797, 819
Reinforcement, 803
Reinforcing steel, 207
Reliability, 497, 555
Relocate systems, 361
Remote, 1559
Research, 1519
Resin, 255
Response reduction, 505
Restoring force characteristics, 945
Retrofit, 1577
Retrofitting, 819
RFID (Radio Frequency Identification), 351
Rheological technology, 545
Rheology, 239
Ride on helicopters, 679
Rigid rod, 985
Rigid zone (Rigid offsets), 1043
Risk, 303
Road alignment, 1637
Road base, 929
Robotic assembly systems, 343
Robot-oriented construction, 343
Robots, 355
Robust control, 457
Robust reliability, 457
Roofs, 255, 1091, 1281
Room fires, 83
RTK-GPS, 65

Sandwich structure, 255
Satellite positioning, 1645
Scattering metrology, 3
Scenario earthquake, 303
Scraping straight edges, 679
SDESA, 1705
Second order effect, 1043
Second skin façade, 1225
Section factor, 1321
Sedimentation, 1423
Seismic, 97, 255, 423, 731, 755
Seismic damage evaluation, 953
Seismic damage mitigation, 447
Seismic damages, 303
Seismic death control, 75
Seismic design, 247, 739, 1009
Seismic design criterion, 75
Seismic effectiveness, 465
Seismic excitations, 327
Seismic response, 281, 297, 595, 993
Seismic response control, 985
Seismic simulator, 985
Seismic vulnerability analysis, 75
Self-balanced test, 695
Self-compacting concrete, 17
Semi-active control, 473, 505, 529, 1009
Semi-active friction dampers, 465, 993
Semi-active hydraulic damper, 497
Semi-active/passive, 961
Semi-active structural control, 497
Semiactive variable dampers, 327
Semi-active vibration control, 969
Semiautomatic, 339
Semiconductor, 1345
Semi-continuous composite beam, 183
Semi-rigid connections, 1043
Sensor fault, 173
Separation techniques, 1439
Sequencing batch reactor, 1423
Service life, 1467
Shaking table test, 473
Shallow Floor, 1321
Shear, 191
Shear connector, 207
Shear strength, 921
Shear-torque relationship, 281
Shear wall, 273
Shear wall cutoff, 1099
Shells, 1091
Shrinkage, 17
Side resistance, 695
Simulated earthquake excitations, 1099
Simulations, 3, 47, 165, 1181, 1199, 1225, 1249, 1289, 1297, 1367
Simulink, 1225, 1305
Simultaneous multi-channel pressure measuring system, 65
Single-plate connection, 199
Site condition, 319
Sketch stage, 1209
Skyscraper, 339
Slabs, 819
Slip-form paving, 905
Slope, 1661
Slope deformation, 1611
Smart damping devices, 545
Smart structures, 457, 521
Soft clay, 603
Soil, 747
Soil-nailing, 611
Soil-pile dynamic interaction, 771
Solar building, 1313

Solar electricity transfer, 1313
Solar energy, 1313
Solar heat transfer, 1313
Solar PV, 1313
Solidified material, 929
Source, 113
Soy oil, 255
Spacing, 355
Spatial structure, 595
Specification, 1713
Spectral, 747
Spectral analysis, 1139
Spiral reinforcement, 431
Stability analysis, 579, 621
Stack effect, 1225
Stakeholder participation, 1475
Standards, 191
Static load test, 695
Statistical analysis, 1755
Steel, 383
Steel connection, 199
Steel decking, 191
Steel plating, 819
Steel rebar, 803
Steel reinforcement, 873
Steel structure, 1321
Stiffness, 137
Stiffness matrix, 1043
Storey drift, 1099
Strength, 137, 859, 897
Strength development, 1407
Strengthening, 827
Stress concentration, 297
Stress level, 129
Stress-strain model, 789
Stretch object, 1587
Structural bamboo, 629, 637, 661
Structural control, 327, 937
Structural health monitoring, 1017
Structural healthy monitoring system, 1001
Structural response control, 489
Structural responses, 505
Structural retrofitting, 797
Structural steel, 439, 447
Structure modeling, 1601
Structures, 1059
Substructure, 731
Sub-tropical climate, 1359
Superplasticizer, 921
Supplemental energy dissipation systems, 489
Support vector machine, 481
Surface conditions, 827
Surface tolerances, 679
Surrounding rockmass, 579
Survey check, 1637
Sustainability, 1073, 1081, 1449, 1457, 1501, 1509
Sustainable building, 1449, 1501, 1509
Sustainable development, 1257, 1431
Swelling, 137
System, 383
System functions, 1755
System identification, 457, 545, 1017, 1107, 1115
System integration, 1535
System simulation, 1189

Tall-buildings, 319, 537, 703, 1025
Tang Committee Report, 1073
Technology, 39
Temperate climate, 1359
Termites, 129, 137
TES, 1273
Test frame, 473
Testing, 255, 653
Tests, 191
The FFT method, 1107
The HHT method, 1107
The Netherlands, 1415
Thermal analysis, 881
Thermal balance, 1225
Thermal buffer, 1217
Thermal comfort, 29, 1173, 1375
Thermal comfort performance criteria, 1375
Thermal induced cracking, 845
Thermal insulation, 1289
Thermal manikin, 1173
Thermal modelling, 1165, 1189
Thermal process, 1415
Thermal radiation, 83
Thermal stress, 845
Thermoconductivity, 1321
Three-dimensional data model, 1001
Timber, 383
Time domain method, 1139
Time domain reflectometer, 1661
Time-history, 731
Tip resistance, 695
Titanium Dioxide (TiO_2), 1345
Top-hat, 1035
Torsional, 281
Total quality management system, 1697
Traditional, 383
Traditional material used in a modern way, 653
Traditional vernacular houses, 1359
Transfer, 747
Transfer plate, 731
Transparent architecture, 1233
Treated wood composites, 137

Trees, 1493
Truck-mixed concrete, 671
Trust, 55
Tubes, 215
Tuned Liquid Column Damper (TLCD), 537
Turbulence intensity profile, 1131

Ultimate condition, 789
Ultimate drift ratio, 755
Ultimate moment, 889
Ultimate strain, 789
Ultra high resolution remote sensing, 1619
Ultra-high-strength concrete, 17
Unbonded, 423
Underground channel, 335
Underground powerhouses, 579
Uniaxial confinement, 873
Unsaturated polyester resins, 225
Urban climate, 1493
Urban courtyard design, 1493
Urban information systems, 1619

Vacuum suction, 339
Validation of thermal and airflow model of the double skin façade, 1181
Validation, 1249
Value, 1391, 1467, 1475
Value management, 1721
Vegetation climatic effects, 1493
Ventilation, 29, 1339, 1367
Vibrating screeds, 679
Vibration control elements, 945
Vibration mitigation, 537
Vibration suppression, 1025
Virtual environments, 47
Virtual models, 47
Virtual reality, 1601
Viscosity, 239
Visualization, 1629, 1653
VOC, 113
Vortex-induced vibration, 1147
Vortex method, 1147
VRML, 1595
Vulnerability, 303

Walls, 263, 423
Warning, 1661
Waste management, 1431
Water, 1281, 1351
Water absorption, 859
Water flow consolidation, 723
Wave transmission, 587
Web-side-plate connection, 183, 199
Weighting method, 1485
Weld access hole, 415
Welded moment connection, 415
Wet concrete loading, 1091
What-if analysis, 1755
Whole life cost, 1467
Wind, 97, 255, 747
Wind effect factor, 1139
Wind excitation, 1025
Wind-excited vibration coefficient, 1123
Wind-induced excitation, 537
Wind-induced response, 1139
Wind load factor, 1139
Wind modeling, 1131
Wind pressure, 1225
Windspeed profile, 1131
Wireless, 521
Wood, 105, 263, 355
Wood composites, 129
Wood frame shear walls, 97
Workability, 905
Workflow, 1729
WTK, 1601

XML, 1543

3D city modeling, 1619
3DGIS, 1595
3-D machine guidance systems, 1645
3D modeling, 1601
3D pipeline model, 1629
3-D random analysis, 595
3D reconstruction, 1587
3-view drawing, 1587

4D-CAD, 1737